Špela Zajko

COMPREHENSIVE STUDY OF THE EFFECTS OF DIFFERENT STERILIZATION PROCEDURES ON THE OPTICAL SENSORS

DISSERTATION

Zur Erlangung des Akademischen Grades eines Doktors der Technischen Wissenschaften

Eingereicht an der Technischen Universität Graz



Betreut durch

Prof.Dr. Ingo Klimant

Institut für Analytische Chemie und Lebensmittelchemie

Technische Universität Graz

Graz, im Februar 2012

Deutsche Fassung:
Beschluss der Curricula-Kommission für Bachelor-, Master- und Diplomstudien vom 10.11.2008
Genehmigung des Senates am 1.12.2008

EIDESSTATTLICHE ERKLÄRUNG

Ich erkläre an Eides statt, dass ich die vorliegende Arbeit selbstständig verfasst, andere als die angegebenen Quellen/Hilfsmittel nicht benutzt, und die den benutzten Quellen wörtlich und inhaltlich entnommene Stellen als solche kenntlich gemacht habe.

Graz, am …… ……..
(Unterschrift)

Englische Fassung:

STATUTORY DECLARATION

I declare that I have authored this thesis independently, that I have not used other than the declared sources / resources, and that I have explicitly marked all material which has been quoted either literally or by content from the used sources.

…… ……..
date (signature)

COMPREHENSIVE STUDY OF THE EFFECTS OF DIFFERENT STERILIZATION PROCEDURES ON THE OPTICAL SENSORS

Abstract

Sterilization is a physical or chemical process that destroys or eliminates microbial life, including highly resistant bacterial spores. Critical objects like implantable medical devices require the highest sterility assurance level before application. However, all sterilization methods have their limitations and different compatibilities with materials. The sterilization process should be compatible with as many materials as possible. Consequently, there is no singular sterilization method that is capable with all healthcare and other products including drugs, polymers, devices and materials, because of the severity of a process to meet the sterilisation criteria and definition. For example, heat may distort and melt certain plastics, but may be compatible with many drugs; ethylene oxide can sterilise many plastics, but cannot typically sterilise liquids and leaves residues. Radiation may damage some electronics, some plastics and drugs, but is very penetrating and can sterilise very dense materials. It must be recognised that a variety of factors must be carefully considered for each sterilization method selected in order to achieve reproducible and repeatable processes without affecting product quality, material's chemistry and biocompatibility.

The sterility of sensors that are used in medical applications, for biochemical investigations, operation of biotechnological reactors, etc. is a necessary but difficult-to-achieve prerequisite for the use of sensors. The process of disinfection or sterilization can result in a damage of in the sensitive functional layers of sensors, which in turn may cause impairments of the sensor function. However, in the field of the sterilization effects on optical sensors there is a lack of reliable data. In this study the influences, effects and compatibility of diverse sterilization procedures, such as gamma and electron beam sterilization, steam sterilization, sterilization with ethylene oxide, sterilization with hydrogen peroxide gas and sterilization with low-temperature hydrogen peroxide plasma on optical sensors for oxygen, pH, ammonia and temperature were determined. Additionally, with the help of this study, the number of the materials for the development of the optical sensor, which should be sterilized before utilization, will be reduced at the very beginning of the sensor development.

All optical sensors were made of define indicator, immobilized in the polymer matrix, which is permeable for analyte of interest. The sensors and materials were exposed to diverse sterilization procedures, listed above. Afterwards, different analytical methods were utilized for characterization of the sensors and materials and also the response of the sensor was measured and compared before and after each sterilization method. All measurements with explained alterations in the form of graphs and tables are presented in the *database* of this study. The interesting changes and effects of define sterilization procedures on optical sensors are discussed and results are introduced. Likewise, an overview or summary of whether the impact of sterilant agents destroyed the optical sensor or the sensor should be re-calibrated before application or the sterilization method has no effect on sensor response is represented in this study.

Key words: sterilization, luminescence, polymers, indicators, optical sensors, oxygen sensor, pH sensor, ammonia sensor, temperature sensor.

STUDIE ÜBER DIE AUSWIRKUNG VERSCHIEDENER STERILISATIONSVERFAHREN AUF OPTICSCHE SENSOREN

Kurzfassung

Sterilisation ist ein physikalisches oder chemisches Verfahren zur Abtötung von Mikroorganismen sowie hoch resistenter bakterieller Sporen. Kritische Objekte, wie zum Beispiel implantierbare medizinische Produkte, sollten den höchsten Sterilitätssocjerjeotswert erreichen. Alle Sterilisationsmethoden haben Grenzen ihre Anwendbarkeit für verschiedene Materialien betreffend. Deshalb gibt es nicht die „eine" Sterilisationsmethode, die man bei allen medizintechnischen und anderen Produkten, wie Medikamenten, Polymeren, Geräten und Materialien, einsetzen kann, um alle Kriterien und Anforderungen an die Sterilisation zu erfüllen. Hitze, z. B. kann bestimmte Kunststoffe verformen und schmelzen, eignet sich aber eventuell gut für Medikamente; Mit Ethylenoxid wiederum können Kunststoffe gut sterilisiert werden, Flüssigkeiten jedoch nicht. Strahlung kann die Elektronik und das Material von Geräten und auch Medikamente schädigen, eignet sich wegen seiner Penetration jedoch gut für dichte Stoffe. Bei der Auswahl einer Sterilisationsmethode müssen eine Vielzahl von Faktoren berücksichtigt werden, damit man einen reproduzierbaren und wiederholbaren Prozess entwickeln kann, der die Produktqualität, die Chemie und die Biokompatibilität der Materialien nicht beeinträchtigt.

Die Sterilität von Sensoren, die in der Medizin eingesetzt werden, für biochemische Untersuchungen oder im Betrieb von biotechnologischen Reaktoren, usw., ist eine Notwendigkeit, die nicht einfach zu bewerkstelligen ist. Der Desinfektions- oder Sterilisationsprozess kann zu einer Schädigung einzelner Sensorschichten führen, die die Leistung des Sensors verringern. Trotzdem gibt es, was die Einflüsse der Sterilisation auf optische Sensoren betrifft, keine verlässliche Datengrundlage. Deshalb werden in dieser Arbeit die Einflüsse, Auswirkungen und Verträglichkeit verschiedener Sterilisationsmethoden, wie Gamma- und Elektrionenstrahlsterilisation, Dampfsterilisation, Sterilisation mit Ethylenoxid oder Wasserstoffperoxid und Sterilisation mit einem Niedrigtemperatur-Wasserstoffperoxidplasma, auf optische Sensoren für Sauerstoff, pH, Ammoniak und Temperatur untersucht. Zusätlich wird nach dieser Studie, die Auswahl von Materialien für die Entwicklung von optischen Sensoren, die sterilisiert werden sollten vor der Verwendung, bei Beginn der Entwicklung reduziert.

Alle optischen Sensoren, die in dieser Studie verwendet werden, bestehen aus einem bestimmten Indikator, immobilisiert in einer Polymermatrix, die für den Analyten durchlässig ist. Die Sensoren und deren Materialien wurden den oben genannten Sterilisationsverfahren ausgesetzt. Danach wurden die Sensoren und Materialien mit verschiedenen analytischen Methoden charakterisiert und das Ansprechverhalten des Sensors vor und nach der Sterilisation wurde verglichen. Alle Messungen, mit erklärten Abweichungen, werden in der Datensammlung der Studie in Form von Graphen und Tabellen angeführt. Interessante Veränderungen und Effekte bestimmter Sterilisationsverfahren an optischen Sensoren werden diskutiert. Zusätzlich gibt es eine Zusammenfassung, in der die Auswirkung der Sterilisation auf den Sensor beschrieben wird (ob der Sensor zerstört wurden, ob er nach der Sterilisation neu kalibriert werden muss, oder ob keine Einflüsse der Sterilisation befürchten sind).

Schlagwörter*:* Sterilisation, Lumineszenz, Polymere, Indikatoren, optische Sensoren, Sauerstoffsensoren, pH-Sensoren, Ammoniaksensoren, Temperatursensoren.

Acknowledgments

First of all, I would like to thank *Prof. Dr. Ingo Klimant*, who gave me the opportunity to complete my dissertation at the Graz University of Technology at the Institute for Analytical Chemistry and Food Chemistry and for supervising my thesis. His ideas, suggestions and helpful discussions made a major contribution to this work.

Without the help of *Gregor Trimmel* and the Institute for Chemistry and Technology of Materials I would not have been able to perform some investigations on the polymer materials. Therefore, I want to thank everyone who helped me at this institute. Likewise, I would like to thank *Dr. Gerhard Mohr* who took his time to read my work and evaluate it.

Special thanks go to my "roommate" in the office - *DI Babsi Nacht* for solving the problems related to my foreign languages, for discussion about private life and for creating a friendly and funny atmosphere.

I am equally thankful to my colleagues of the working groups *sensor materials* and *applied sensors* for help, support and for periodic "meetings" outside the work environment, which helped me to decrease my stress level – *Ph.D. Sergey Borisov, Dr. Torsten Mayr, Dr. Kerstin Waich, Farzaneh Moradi, DI Birgit Ungerböck, DI Barbara Enko, DI Elisabeth Scheucher, DI Klaus Koren, DI Tobias Abel, DI Daniel Aigner, DI Chrisoph Larndorfer, DI Philipp Lehner, Dr. Michela Quaranta, DI Jokic Tijana, DI Susanne Schutting, Wiener Erika, Fellner Günter, Eveline Maier, Christina Trenn and Yvonne Größinger* and the former colleagues *Dr. Gunter Zenkl, DI Wernfried Haas, Dr. Günther Mistlberger, Dr. Edit Marosits and DI Johanna Wiesbauer*.

Moreover, I want to thank all other *people working at the Institute of Analytical Chemistry and Food Chemistry* who made it easier and faster to accomplish some bureaucratic work, who offered me education on the new devices in the laboratories, when needed and for friendly smiles and greetings every morning.

I am also grateful to all *employees from BBraun in Graz*, where I could borrow devices to perform measurements for my study which greatly contributed to my work and be part of the development process of the optical glucose sensor.

Financial support of my work in the form of scholarship by the *Slovene Human Resources Development and Scholarship Fund Ad Futura* is gratefully acknowledged.

Finally, very special thanks go to my *family* and *friends*, which supported me in every step, for their trust as well as the possibility to pursue my own paths. Likewise, I am very grateful to *my mom* who drove me in the year 2007 to Graz, reduced the nervousness before first meeting with Prof. Dr. Ingo Klimant and convinced me that studying in Graz was the right decision. Thanks also to *my father,* who accompanied me on the first work day in Graz and always gave me additional encouragement and confidence to work in Austria. Unfortunately, *my grandfather* who was probably the reason, why is education in my family very important, did not live to see that his granddaughter become a doctor. However, I know that today he would be very proud.

TABLE OF CONTENTS

I INTRODUCTION **1**

1 STERILIZATION GENERAL **3**

1.1 RADIATION STERILIZATION 5
1.1.1 Sterilization Procedure with Gamma Rays 7
1.1.2 Sterilization Procedure with E-Beam Radiation 8
1.1.3 Comparison Between the Gamma and E-Beam Sterilization 9
1.1.4 Effects of Radiation Sterilization on Microorganisms 10
1.1.5 Effects of Radiation Sterilization on Materials 12
1.1.5.1 Formation of free radicals by radiation sterilization 12
1.1.5.2 Radiation Sterilization in Presence or Absence of Oxygen 13
1.1.5.3 Chemical Changes in Irradiated Polymers 14
Main-chain Scission and Crosslinking Formation 14
Formation of Volatile Products 16
Discolouration and Odour Appearance 16
Changes in Conductivity 16
1.1.5.4 General Consideration by Selection of Polymers for Radiation Sterilization 17
1.1.6 Validation of Radiation Sterilization 17
1.1.7 Application of Radiation Sterilization 18

1.2 STEAM STERILIZATION 18
1.2.1 Sterilization Procedure 19
1.2.2 Sterilization Cycles 20
1.2.3 Effects of Steam Sterilization on Microorganisms 21
1.2.4 Effects of Steam Sterilization on Materials 23
1.2.5 Validation of Steam Sterilization 23
1.2.6 Application of Steam Sterilization 23

1.3 GASEOUS STERILIZATION 25
1.3.1 Sterilization with Ethylene Oxide 26
1.3.1.1 Sterilization Procedure 27
1.3.1.2 Sterilization Cycle 29
1.3.1.3 Effects of Sterilization with Ethylene Oxide on Microorganisms 30
1.3.1.4 Effects of Sterilization with Ethylene Oxide on Materials 31
1.3.1.5 Validation of Sterilization with Ethylene Oxide 32

1.3.1.6 Applications of Sterilization with Ethylene Oxide 32
1.3.2 Sterilization with Hydrogen Peroxide Gas 32
1.3.2.1 Sterilization Procedure 33
1.3.2.2 Sterilization Cycle 34
1.3.2.3 Effects of Sterilization with Hydrogen Peroxide Gas on Microorganisms 35
1.3.2.4 Effects of Sterilization with Hydrogen Peroxide Gas on Materials 35
1.3.2.5 Validation of Sterilization with Hydrogen Peroxide Gas 35
1.3.2.6 Applications of Sterilization with Hydrogen Peroxide Gas 36
1.3.3 Low Temperature Hydrogen Peroxide Plasma Sterilization 36
1.3.3.1 Sterilization Procedure 36
1.3.3.2 Sterilization Cycle 37
1.3.3.3 Effects of Low Temperature Hydrogen Peroxide Plasma Sterilization on Microorganisms 38
1.3.3.4 Effects of Low Temperature Hydrogen Peroxide Plasma Sterilization on Materials 40
1.3.3.5 Validation of Low Temperature Hydrogen Peroxide Plasma Sterilization 40
1.3.3.6 Application of Low Temperature Hydrogen Peroxide Plasma Sterilization 40

2 OPTICAL SENSORS GENERAL 42

2.1 LUMINESCENCE-BASED OPTICAL SENSORS 43
2.1.1 Mechanisms of Sensing 45

2.2 OXYGEN OPTICAL SENSORS 46
2.2.1 Fluorescence Quenching 47
2.2.1.1 Molecular Oxygen as a Quencher 48
2.2.1.2 Derivation of the Stern-Volmer Equation 48

2.3 pH OPTICAL SENSORS 49
2.3.1 Colour change based sensing 51
2.3.2 Fluorescence based sensing 51
2.3.3 Photoinduced Electron Transfer 52

2.4 OPTICAL TEMPERATURE SENSORS 53

2.5 OPTICAL AMMONIA SENSORS 54

II EXPERIMENTAL SECTION **57**

3 MATERIALS **59**

3.1 POLYMERS 63
3.1.1 Polystyrene 63
3.1.2 Polystyrene-co-Acrylonitrile 64
3.1.3 Polystyrene-co-Maleic Anhydride 65
3.1.4 Polysulfone 65
3.1.5 Cellulose Acetate 66
3.1.6 Ethyl Cellulose 67
3.1.7 Polyurethane Hydrogel 68
3.1.7.1 Hydrogel HydroMedTM D4 and D7 70
3.1.7.2 HydroThane^{TM} with 5% and 25% water content 70
3.1.8 Poly(PhenylSilsesQuioxane) 71
3.1.9 PolyVinylidene Chloride-co-Acrylonitrile 72
3.1.10 PolyMethyl MethAcrylate 73
3.1.11 PolyMethAcryloNitrile 74
3.1.12 Poly(2-HydroxyEthyl MethAcrylate) 74
3.1.13 Poly(EthyleneTerepthalate) 75

3.2 INDICATORS 76
3.2.1 Coumarin Derivatives 76
3.2.1.1 pH Sensitive Coumarin 77
3.2.2 Lanthanides based Luminescent Probes 77
3.2.2.1 Eu(tta)$_3$DEADIT 78
3.2.3 Long-Lifetime Metal-Ligand Complexes 79
3.2.3.1 Iridium(III) Coumarin 80
3.2.3.2 Platinum(II) and Palladium(II) Porphyrin complexes 80
Platinum(II) meso-tetrakis-(pentafluorophenyl)porphyrin (=PtTFPP) 82
Platinum(II) OctaEthyl Porphyrin (=PtOEP) 82
Platinum(II) and Palladium(II) Benzoporphyrins 83
Platinum(II) meso-tetra(4-FluoroPhenyl) TetraBenzoPorphyrin (=PtTPTBPF) 84
Palladium(II)) meso-tetra(4-FluoroPhenyl) TetraBenzoPorphyrin (=PdTPTBPF) 84
3.2.3.3 Ruthenium Complexes 85
Ruthenium(II)-tris-4,7-diphenyl-1,10-phenanthroline dichloride (=Ru(dpp)$_3$Cl$_2$) 85
DiChloroTris(1,10-Phenanthroline) Ruthenium(II) Hydrate 86
3.2.4 Pyrene Derivative 86

3.2.4.1 1-HydroxyPyrene-3,6,8-tris-bis(2-Ethylhexyl)Sulfonamide (=HPTS(DHA)$_3$) 87
3.2.5 Perylene Derivatives 87
3.2.5.1 PET Perylene BisImide 88
3.2.6 Xanthen Derivatives 88
3.2.6.1 Eosin EthylEster 89
3.2.6.2 DiChloroFluorescein 89
3.2.6.3 2´,7´-DiHexyl-5(6)-*N*-Octadecyl-CarboxAmidoFluorescein (=DHFA) 90
3.2.6.4 2´,7´-DiHexylFluorescein OctadecylEster (=DHFE) 91
3.2.7 pH Sensitive Non-Luminescence Indicators 92
3.2.7.1 BromoPhenol Blue 92
3.2.7.2 Thymol Blue 93
3.2.7.3 BromoThymol Blue 94
3.2.7.4 Methyl Orange 94

4 METHODS 95

4.1 SENSOR PREPARATION 95

4.2 STERILIZATION PROCEDURES 95
4.2.1 Radiation Sterilization 95
4.2.2 Other Sterilization Procedures 96

4.3 CHARACTERIZATION OF MATERIALS 97
4.3.1 Characterization of Polymers 97
4.3.1.1 Solubility Test (Dissolution) 97
4.3.1.2 Ultraviolet-Visible Spectroscopy 98
4.3.1.3 Contact Angle Measurement 99
4.3.1.4 Fourier Transform Infrared Spectroscopy 100
4.3.1.5 Differential Scanning Calorimetry 100
4.3.2 Characterization of (Luminescence) Indicators and Optical Sensors 102
4.3.2.1 Measurements of Light Absorption and Luminescence 102
4.3.2.2 Measurement of Luminescence Lifetime based on Phase-Modulation Fluorometry 104

III RESULTS AND DISCUSSION 107

5 RADIATION STERILIZATION (GAMMA AND ELECTRON BEAM) 109

5.1 RADIATION STERILIZATION OF OPTICAL OXYGEN SENSORS 109

5.2 RADIATION STERILIZATION OF OPTICAL pH SENSORS 122

5.3 RADIATION STERILIZATION OF OPTICAL TEMPERATURE SENSORS 129

5.4 RADIATION STERILIZATION OF OPTICAL AMMONIA SENSORS 133

6 STEAM STERILIZATION 138

6.1 STEAM STERILIZATION OF OPTICAL OXYGEN SENSORS 138

6.2 STEAM STERILIZATION OF OPTICAL pH SENSORS 141

6.3 STEAM STERILIZATION OF OPTICAL TEMPERATURE SENSORS 143

6.4 STEAM STERILIZATION OF OPTICAL AMMONIA SENSORS 146

7 STERILIZATION WITH ETHYLENE OXIDE GAS 147

7.1 STERILIZATION OF OPTICAL OXYGEN SENSORS WITH EtO 147

7.2 STERILIZATION OF OPTICAL pH SENSORS WITH EtO 151

7.3 STERILIZATION OF OPTICAL TEMPERATURE SENSORS WITH EtO 154

7.4 STERILIZATION OF OPTICAL AMMONIA SENSORS WITH EtO 155

8 STERILIZATION WITH HYDROGEN PEROXIDE (GAS OR PLASMA) 157

8.1 STERILIZATION OF OPTICAL OXYGEN SENSORS WITH H_2O_2 157

8.2 STERILIZATION OF OPTICAL pH SENSORS WITH H_2O_2 163

8.3 STERILIZATION OF OPTICAL TEMPERATURE SENSORS WITH H_2O_2 166

8.4 STERILIZATION OF OPTICAL AMMONIA SENSORS WITH H_2O_2 168

9 SUMMARY **170**

9.1 OXYGEN OPTICAL SENSORS 170

9.2 pH OPTICAL SENSORS 174

9.3 TEMPERATURE OPTICAL SENSORS 178

9.4 AMMONIA OPTICAL SENSORS 179

IV CONCLUSION **179**

10 CONCLUSION **185**

11 REFERENCES **189**

DATABASE **197**

SECTION A: RADIATION STERILIZATION OF POLYMERS 199

SECTION B: RADIATION STERILIZATION OF (LUMINESCENCE) INDICATORS 247

SECTION C: RADIATION STERILIZATION OF OPTICAL SENSORS 315

SECTION D: STEAM STERILIZATION OF OPTICAL SENSORS 565

SECTION E: STERILIZATION OF OPTICAL SENSORS WITH ETHYLENE OXIDE 649

SECTION F: STERILIZATION OF OPTICAL SENSORS WITH HYDROGEN PEROXIDE (GAS AND PLASMA) 749

FIGURE LIST

Figure 1 – 1: Emitted types of radiation. 6
Figure 1 – 2: Cobalt-60 irradiator. 8
Figure 1 – 3: Typical material-handling system for electron beam sterilization. 9
Figure 1 – 4: Schematic diagram of a typical steam sterilizer (autoclave). 19
Figure 1 – 5: Typical steam sterilization cycle in autoclave. 21
Figure 1 – 6: Idealized heat-inactivation curves of bacterial spores. 22
Figure 1 – 7: Schematic diagram of typical ethylene oxide sterilizer. 28
Figure 1 – 8: A typical ethylene oxide sterilization cycle. 29
Figure 1 – 9: Representation of sterility isolator for sterilization with hydrogen peroxide gas. 34
Figure 1 – 10: The decontamination effect as a function of cycle phase at sterilization with hydrogen peroxide gas. 35
Figure 1 – 11: Sterrad® 50, Sterrad® 100 and 100S and Sterrad® 200. 37
Figure 1 – 12: Schematic diagram of the interior of the Sterrad® 100. 37
Figure 1 – 13: Sterrad® 100 typical sterilization cycle. 38
Figure 2 – 1: Composition of the optical chemical sensor. 42
Figure 2 – 2: The classification of luminescence molecular sensors. 44
Figure 2 – 3: Spectra observables for luminescence sensing. 45
Figure 2 – 4: Principle of pH sensing by fluorescent PET sensors. 52
Figure 3 – 1: Two mesomeric forms of coumarin. 76
Figure 4 – 1: Schematic view of the knife-coating device. 95
Figure 4 – 2: Block diagram of a UV/VIS spectrometer. 98
Figure 4 – 3: A cross-sectional view of the droplet, used by the contact angle measurements. 99
Figure 4 – 4: Schematic of the experimental set-up used to carry out DSC. 101
Figure 4 – 5: A typical DSC curve obtained for a polymer sample. 102
Figure 4 – 6: Schematic representation of spectrofluorometer. 103
Figure 4 – 7: Principles of phase-modulation fluorometry. 104
Figure 5 – 1: Yellowing of the polymer PSf after ionizing radiation and the corresponding absorption spectra. 110
Figure 5 – 2: Decrease of solubility of the polymer HydroThane with 5% water content after radiation sterilization. 111
Figure 5 – 3: Absorption spectra of the polymer PPSQ before and after radiation sterilization. 112
Figure 5 – 4: Absorption spectra of the indicator $Ir(C_s)_2(acac)$, gamma sterilized in solid state and in solution. 112
Figure 5 – 5: Absorption spectra of indicator PtTFPP sterilized in solution before and after gamma and electron beam sterilization. 113
Figure 5 – 6: Alterations induced by radiation sterilization of the indicator PtTFPP in solution with solvent toluene. 113
Figure 5 – 7: Comparison of Stern-Volmer plots of oxygen sensors made indicator Ir(Cs)2(acac) and immobilized in polymers CA and EC before and after gamma and electron beam sterilization. 114
Figure 5 – 8: Absorption and emission spectra of oxygen sensor made of indicator $Ir(C_s)_2(acac)$ and immobilized in polymer PS before and after gamma sterilization. 115

Figure 5 – 9: Calibration curves and Stern-Volmer plots of the oxygen sensor made of indicator $Ir(C_s)_2(acac)$ and immobilized in polymer PS before and after gamma sterilization. 115

Figure 5 – 10: Absorption and emission spectra of the oxygen sensor made of indicator $Ir(C_s)_2(acac)$ and immobilized in polymer PS-co-PAN before and after electron beam sterilization. 116

Figure 5 – 11: Alterations in the absorption spectra by oxygen sensors made of indicator PtTFPP and immobilized in diverse polymer matrices before and after electron beam sterilization. 117

Figure 5 – 12: Emission spectra of oxygen sensors made of indicator PtTFPP and immobilized in Hydrogel D4 before and after electron beam sterilization. 118

Figure 5 – 13: Comparison of the calibration curves of the oxygen sensors made of indicator PtTFPP and immobilized in polymers H5 and PS before and after electron beam sterilization. 118

Figure 5 – 14: Absorption spectra, calibration curves and Stern-Volmer Plots of oxygen sensors made of indicator PtOEP and mmobilized in polymer PS before and after electron beam sterilization. 119

Figure 5 – 15: Absorption spectra and calibration curves of oxygen sensors made of indicators PtTPTBPF and PdTPTBPF and immobilized in polymer PS before and after gamma sterilization, 120

Figure 5 – 16: The response of the oxygen sensor made of indicator $Ru(dpp)_3Cl_2$ and immobilized in polymer PS-co-PAN before and after electron beam sterilization. 120

Figure 5 – 17: Response of the oxygen sensors made of indicator $Ru(dpp)_3Cl_2$ and immobilized in polymers PSf and PPSQ before and after gamma sterilization,. 121

Figure 5 – 18: Absorption spectra of the oxygen sensors made of diverse indicators and immobilized in polymer PS before and after gamma sterilization. 122

Figure 5 – 19: Absortpion spectra of the indicators $HPTS(DHA)_3$, DHFE and DHFA before and after gamma sterilization in solid state. 123

Figure 5 – 20: Normalized absorption spectra of pH sensor made of indicator $HPTS(DHA)_3$ and immobilized in polymer hydrogel D4 before and after electron beam sterilization. 124

Figure 5 – 21: Calibration curves of the pH sensor made of indicator $HPTS(DHA)_3$ and immobilized in polymer Hydrogel D4 before and after gamma and electron beam sterilization in standard ambient conditions.. 125

Figure 5 – 22: Absorption spectra of the pH sensor made of indicator DHFA and immobilized in polymer hydrogel D4 before and after radiation sterilization in standard ambient conditions and in buffer solution. 125

Figure 5 – 23: Absorption spectra of the pH sensor made of indicator DHFE and immobilized in polymer pHEMA before and after electron beam sterilization. 126

Figure 5 – 24: Absorption and emission spectra of the pH sensor made of indicator pH sensitive coumarin and immobilized in polymer hydrogel D4 before and after electron beam sterilization in standard ambient conditions and buffer solution. 127

Figure 5 – 25: Calibration curves of the pH sensor made of indicator PET Perylene bisimide and immobilized in polymer hydrogel D4 before and after gamma sterilization in standard ambient conditions and in buffer solution. 128

Figure 5 – 26: Absorption spectra of the sulfonephthalein pH indicators immobilized in hydrogel D4 before and after gamma sterilization. 128

Figure 5 – 27: Absorption spectra of indicator methyl orange after gamma sterilization in solid state and when immobilized in polymer hydrogel D4. 129

Figure 5 – 28: Absorption spectra of the polymer PVC-co-PAN before and after gamma and electron beam sterilization. 130

Figure 5 – 29: Absorption spectra of the polymer PMAN before and after gamma and electron beam sterilization. 130
Figure 5 – 30: Absorption spectra of the indicator Eu(tta)$_3$DEADIT gamma sterilized in solid state and as solution. 131
Figure 5 – 31: Absorption spectra and calibration curves of temperature sensor made of indicator Eu(tta)$_3$DEADIT and immobilized in polymer PS-co-PAN before and after gamma and electron beam sterilization. 132
Figure 5 – 32: Absorption and emission spectra of indicator rutheinum(II) complex, electron beam sterilized in solid state and absorption spectra and calibration curves when immobilized in polymers PVC-co-PAN and PMAN. 133
Figure 5 – 33: Absorption and emission spectra of indicator eosin ethylester before and after gamma sterilization in the solid state. 134
Figure 5 – 34: Absorption and emission spectra of ammonia sensor made of indicator eosin ethylester and immobilized in polymer hydrogel D7 before and after gamma sterilization. 135
Figure 5 – 35: Absorption spectra of indicators dichlorofluorescein and bromophenol blue before and after electron beam sterilization in solid state and as solution. 136
Figure 5 – 36: Absorption and emission spectra of ammonia sensor made of indicator dichlorofluorescein and immobilized in polymer EC before and after gamma and electron beam sterilization. 137
Figure 6 – 1: Absorption spectra of oxygen sensors made of indicators Ir(C_s)$_2$(acac) and Ru(dpp)$_3$Cl$_2$ and immobilized in polymer CA before and after steam sterilization. 138
Figure 6 – 2: Calibration curves of oxygen sensors made of indicators Ir(C_s)$_2$(acac) and PtTFPP and immobilized in polymer EC before and after steam sterilization. 139
Figure 6 – 3: Absorption spectra and calibration curves of oxygen sensor made of indicator PtTFPP and immobilized in polymer PPSQ before and after steam sterilization. 139
Figure 6 – 4: Calibration curves and Stern-Volmer plots of oxygen sensor made of indicators Ru(dpp)$_3$Cl$_2$ and immobilized in polymer PS before and after steam sterilization. 140
Figure 6 – 5: Absorption spectra of oxygen sensors made of indicators Ru(dpp)$_3$Cl$_2$ and immobilized in polymers PS-co-PAN and PSMA before and after steam sterilization. 140
Figure 6 – 6: Absorption spectra of the pH sensors made of polymer hydrogel D4, which became turbid after steam sterilization. 141
Figure 6 – 7: Absorption spectra of pH sensor made of indicators HPTS(DHA)$_3$ and pH sensitive coumarin and immobilized in polymer hydrogel D4 before and after steam sterilization. 142
Figure 6 – 8: Emission spectra of pH sensor made of indicator PET Perylene bisimide and immobilized in polymer hydrogel D4 before and after steam sterilization. 142
Figure 6 – 9: Absorption spectra of pH sensor made of indicator thymol blue and immobilized in polymer hydrogel D4 before and after steam sterilization. 143
Figure 6 – 10: Absorption spectra of pH sensor made of indicator methyl orange and immobilized in polymer hydrogel D4 before and after steam sterilization. 143
Figure 6 – 11: Absorption spectra of temperature sensor made of indicator ruthenium(II) complex and immobilized in polymers PVC-co-PAN and PMAN before and after steam sterilization. 144
Figure 6 – 12: Emission spectra and calibration curves of temperature sensor made of indicator Eu(tta)3DEADIT and immobilized in polymers PS-co-PAN and PVC-co-PAN before and after steam sterilization. 145
Figure 6 – 13: Emission spectra and response of temperature sensor made of indicator ruthenium(II) complex and immobilized in polymers PS-co-PAN and PVC-co-PAN before and after steam sterilization. 145

Figure 6 – 14: Absorption and emission spectra of ammonia sensor made of indicator eosin ethylester and immobilized in polymer CA before and after steam sterilization. 146

Figure 7 – 1: Absorption spectra and sensor response of the oxygen sensors made of indicators $Ir(C_s)_2(acac)$ and $Ru(dpp)_3Cl_2$ and immobilized in polymer EC before and after sterilization with ethylene oxide. 148

Figure 7 – 2: Calibration curves of the oxygen sensors made of indicators $Ir(C_s)_2(acac)$ and PtTFPP and immobilized in polymer HydroThane™ before and after sterilization with ethylene oxide. 149

Figure 7 – 3: Calibration curves and Stern-Volmer plots of the oxygen sensors made of indicators Ir(Cs)2(acac) and Ru(dpp)3Cl2 and immobilized in polymer hydrogen D4 before and after sterilization with ethylene oxide. 150

Figure 7 – 4: Calibration curves and Stern-Volmer plots of the oxygen sensors made of indicator $Ir(C_s)_2(acac)$ and immobilized in polymer PPSQ before and after sterilization with ethylene oxide. 150

Figure 7 – 5: Stern-Volmer plots of the oxygen sensors made of indicators $Ir(C_s)_2(acac)$, PtTFPP and $Ru(dpp)_3Cl_2$ and immobilized in polymer PSMA before and after sterilization with ethylene oxide. 151

Figure 7 – 6: Absorption spectra of pH sensors made of indicators $HPTS(DHA)_3$, DHFA, DHFE and pH sensitive coumarin and immobilized in polymer hydrogel D4 before and after sterilization with ethylene oxide. 152

Figure 7 – 7: Absorption spectra and calibration curves of pH sensors made of indicators DHFA and DHFE and immobilized in polymer pHEMA before and after sterilization with ethylene oxide. 153

Figure 7 – 8: Emission spectra of pH sensors made of indicators PET Perylene bisimide and immobilized in polymer hydrogel D4 before and after sterilization with ethylene oxide. 153

Figure 7 – 9: Absorption spectra of pH sensors made of indicator Thymol blue and immobilized in polymer hydrogel D4 before and after sterilization with ethylene oxide. 154

Figure 7 – 10: Absorption spectra and calibration curves of temperature sensors made of indicators $Eu(tta)_3$DEADIT and ruthenium(II) complex and immobilized in polymers PS-co-PAN and PVC-co-PAN before and after sterilization with ethylene oxide. 155

Figure 7 – 11: Calibration curves of temperature sensors made of indicators $Eu(tta)_3$DEADIT and ruthenium(II) complex and immobilized in polymer PMAN before and after sterilization with ethylene oxide. 155

Figure 7 – 12: Emission spectra of ammonia sensor made of indicators eosinethyl ester and dichlorofluorescein and immobilized in polymer EC before and after sterilization with ethylene oxide. 156

Figure 8 – 1: Calibration curves and Stern-Volmer plots of oxygen sensor made of indicators $Ir(C_s)_2(acac)$ and $Ru(dpp)_3Cl_2$ and immobilized in polymer hydrogel D4 before and after sterilization with hydrogen peroxide gas. 158

Figure 8 – 2: Absorption spectra of oxygen sensor made of indicator PtTFPP and immobilized in polymer hydrogel D4 before and after sterilization with hydrogen peroxide gas and plasma. 158

Figure 8 – 3: Absorption spectra and calibration curves of oxygen sensor made of indicators $Ir(C_s)_2(acac)$ and $Ru(dpp)_3Cl_2$ and immobilized in polymer hydrogel D4 before and after sterilization with hydrogen peroxide plasma. 159

Figure 8 – 4: Absorption and emission spectra of oxygen sensor made of indicator $Ru(dpp)_3Cl_2$ and immobilized in polymer HydroThane 5 before and after sterilization with hydrogen peroxide gas. 160

Figure 8 – 5: Absorption and emission spectra of oxygen sensor made of indicator $Ru(dpp)_3Cl_2$ and immobilized in polymer PSf before and after sterilization with hydrogen peroxide gas and plasma. 161

Figure 8 – 6: Absorption, emission spectra and calibration curves of oxygen sensor made of indicator $Ru(dpp)_3Cl_2$ and immobilized in polymer PS before and after sterilization with hydrogen peroxide gas and plasma. 162

Figure 8 – 7: Absorption spectra of pH sensor made of indicator $HPTS(DHA)_3$ and immobilized in polymer hydrogel D4 before and after sterilization with hydrogen peroxide gas and plasma. 163

Figure 8 – 8: Absorption spectra of pH sensor made of indicator DHFE and immobilized in polymer pHEMA before and after sterilization with hydrogen peroxide gas and plasma. 164

Figure 8 – 9: Response curves of pH sensor made of indicator PET Perylene bisimide and immobilized in hydrogel D4 before and after sterilization with hydrogen peroxide gas and plasma. 165

Figure 8 – 10: Absorption spectra of pH sensor made of sulfonephthalein pH sensitive dye and immobilized in hydrogel D4 before and after sterilization with hydrogen peroxide plasma. 166

Figure 8 – 11: Absorption spectra and response curves of temperature sensor made of indicator ruthenium(II) complex and immobilized in polymer PMAN before and after sterilization with hydrogen peroxide gas. 166

Figure 8 – 12: Normalized absorption spectra of temperature sensor made of indicator $Eu(tta)_3$DEADIT and immobilized in polymers PS-co-PAN and PMAN before and after sterilization with hydrogen peroxide plasma. 167

Figure 8 – 13: Absorption spectra and response curves of temperature sensor made of indicators $Eu(tta)_3$DEADIT and ruthenium(II) complex and immobilized in polymer PVC-co-PAN before and after sterilization with hydrogen peroxide gas. 168

Figure 8 – 14: Absorption spectra and emission spectra of ammonia sensor made of indicators eosinethyl ester and dichlorofluorescein and immobilized in polymer hydrogel D7 before and after sterilization with hydrogen peroxide gas and plasma. 169

TABLE LIST

Table 1 – 1: Sterilization proceduress and their cycle specifications. 3

Table 1 – 2: Comparison between gamma and electron beam sterilization process. 9

Table 1 – 3: The radiation response and examples of microorganisms exposed to radiation sterilization 11

Tabel 1 – 4: The polymers which are susceptible to either crosslinking or scission. 16

Table 1 – 5: Representation of radiation suitable medial, pharmaceutical products, foodstuffs and animal feeds. 18

Table 1 – 6: The time-temperature relationships in thermal sterilization processes. 19

Table 1 – 7: Applications of steam sterilization processes. 24

Table 1 – 8: Physical properties of ethylene oxide gas. 26

Table 1 – 9: The optimal parameters for sterilization procedure with ethylene oxide. 28

Table 1 – 10: Physical properties of ethylene oxide gas. 33

Table 1 – 11: Spectrum of activity; vegetative bacterial, spores and fungi by low temperature hydrogen peroxide plasma sterilization. 39

Table 3 - 1: Applied materials.. 59

Table 3 - 2: Applied optical sensors.. 61

Table 4 – 1: Typical chromophores in UV-VIS spectroscopy commonly found for polymers. 98

Table 5 – 1: The glass transition temperature and corresponding specific heat capacity of polymer EC before and after gamma irradiation.....111

Table 9 – 1: Summary of stability, resistance and alterations of diverse oxygen optical sensors towards different sterilization methods.....170

Table 9 – 2: Summary of stability, resistance and alterations of diverse pH optical sensors towards different sterilization methods. 174

Table 9 – 3: Summary of stability, resistance and alterations of diverse tempearture optical sensors towards different sterilization methods.....178

Table 9 – 4: Summary of stability, resistance and alterations of diverse ammonia optical sensors towards different sterilization methods.....179

ABBREVIATIONS

BI	–	Biological indicators
SAL	–	Sterility assurance level
FDA	–	Food and Drug Administration
DNA	–	Deoxyribonucleic acid
RNA	–	Ribonucleic acid
DRT	–	Decimal reduction time
LED	–	Light-emitting diode
EtO	–	Ethylene Oxide
PS	–	Polystyrene
PS-co-PAN	–	Polystyrene-co-acrylonitrile
PSMA	–	Polystyrene-co-maleic anhydride
PSf	–	Polysulfone
CA	–	Cellulose Acetate
EC	–	Ethyl Cellulose
H5	–	Hydrothane with 5% water content
PPSQ	–	Polyphenylsilsesquioxane
PVC-co-PAN	–	Polyvinylidene chloride-co-acrylonitrile
PMAN	–	Polymethacrylonitrile
PMMA	–	Polymethyl methacrylate
pHEMA	–	Poly(Hydroxyethyl methacrylate)
$Eu(tta)_3$DEADIT	–	Europium(III) Complex with 4-(4,6-di(1H-indazol-1-yl)-1,3,5-triazin-2-yl)-N,N-DiEthyl Benzen Amine
$Ir(C_s)_2(acac)$	–	Iridium(III)((benzothiazol-2-ly)-7-(diethylamino)-coumarin))2(acetyl acetonat)
PtTFPP	–	Platinum(II)-5,10,15,20-tetrakis-(2,3,4,5,6-pentafluorphenyl)-porphyrin
PtOEP	–	Platinum(II)-2,3,7,8,12,13,17,18-OctaEthyl-21H, 23H-Porphyrin
PtTPTBPF	–	Platinum(II) meso-tetra(4-FluoroPhenyl) TetraBenzoPorphyrin
PdTPTBPF	–	Palladium(II) meso-tetra(4-FluoroPhenyl) TetraBenzoPorphyrin
$Ru(dpp)_3Cl_2$	–	Ruthenium(II)-tris-4,7-diphenyl-1,10-phenanthroline dichloride
$HPTS(DHA)_3$)	–	1-HydroxyPyrene-3,6,8-tris-bis (2-Ethylhexyl)Sulfonamide
DHFA	–	2´,7´-DiHexyl-5(6)-N-Octadecyl-CarboxAmidoFluorescein
DHFE	–	2´,7´-DiHexylFluorescein OCtadecyl Ester
PET	–	Photoinduce electron transfer

SIMBOLS

Bq	–	Becquerel
Gy	–	Gray
N_0	–	The initial bacterial/bioburden or spore population (prior sterilization)
N_t	–	The population surviving after exposure to the sterilising agent
$n(t)$	–	The number of excited molecules at time t following excitation
Φ	–	Phase shift
ω	–	Angular frequency
m	–	Modulation
D	–	Diffusion coefficient
k_q	–	Experimental quenching rate constant
$[M^*]$	–	Concentration of fluorophore in excited state
$[Q]$	–	Concentration of quencher
I_0	–	Fluorescence intensity in the absence of quencher
I	–	Fluorescence intensity in presence of quencher
τ_0	–	Fluorescence lifetime in the absence of quencher
τ	–	Fluorescence lifetime in presence of quencher
K_{SV}	–	Stern-Volmer quenching constant
a_{H^+}	–	Hydrogen ion activity
f_{H^+}	–	Activity coefficient
pH	–	Negative base 10 power of hydrogen ion activity
pK_a	–	Negative base 10 logarithmic acid dissociation constant
pK_b	–	Negative base 10 logarithmic base dissociation constant
pK_W	–	Negative base 10 logarithmic water dissociation constant
$Hind$	–	Acid form of the indicator
Ind^-	–	Conjugate base of the indicator
f	–	Modulation frequency
k_0	–	The temperature-independent decay rate
k_1	–	Pre-exponential factor
ΔE	–	Energy gap between emitting level and higher excited state level
R	–	Gas constant
$\varepsilon(\lambda)$	–	Molar absorption coefficient
c	–	Concentration of absorbing species
l	–	Absorption pathlength
$A(\lambda)$	–	Absorbance
$T(\lambda)$	–	Transmittance
θ	–	Contact angel
γ_S	–	Solid surface free energy
γ_L	–	Liquid surface free energy
γ_{SL}	–	Solid/liquid interfacial free energy
q	–	Heating rate
C_p	–	Heat capacity (at constant pressure)

I
Introduction

1 Sterilization General

Sterilization refers to any process that effectively kills or eliminates transmissible agents (such as fungi, bacteria, viruses, spore forms, etc) from a surface, equipment, article of food, medication, biological culture medium, etc [1].

Sterilization can be achieved through a number of agents capable of sterilizing the product or materials, such as:

- Radiation sterilization (gamma rays, electron beam, X-rays, ultraviolet etc.)
- Heat sterilization (dry, moist)
- Chemical sterilization (e.g. ethylene oxide, hydrogen peroxide, etc.)
- Sterile filtration

The most applied sterilization processes and their cycle specifications are presented in following table:

Table 1 – 1: Sterilization processes and their cycle specifications.

Sterilization Processes	Cycle specification
Gamma and E-Beam Radiation	2.5 Mrads (25 kGy)
Saturated Steam	15 min at 121℃
Dry Heat	2 min at 134℃ 30 min at 180℃ 1 h at 170℃ 2 h at 160℃
Sterile Filtration	Passage through a 0.22 µm membrane

All sterilising methods have one thing in common; they must remove or destroy microorganisms. If the chosen sterilization method was applied to a product, its sterility should be tested [2].

First, the sterility is defined as 100% freedom from all viable microorganisms under testing conditions. Therefore, when the tests for sterility are performed, there should be no evidence of microbial growth. In general, there are two basic ways to test the sterility:

(1) product sampling and product sterility testing
(2) the application and use of biological indicators (BI)

Product sampling and product sterility testing is performed by placing a sample of the sterilised product in a suitable bacteriological recovery media and monitoring the bacterial growth. Product sterility testing methods for drugs and medical devices are generally described in the United State Pharmacopoeia, ISO, AAMI standards, ISO-11737-2 and ISO 11137 [2].

Biological indicators are another form of sterility evaluation. BI generally consists of spores of highly resistant microbes which are placed on or in the product load prior to sterilization. These indicators generally have a high microbial population in excess of what is naturally occurring on the product. The combination of high microbial population and high resistance for a specific sterilisation method makes these indicators a reliable tool for determination of sterility [2]. The examples of BI used in different sterilization methods are following:

Radiation *Bacillus pumilus* E601 ATCC 27142

Saturation steam	*Geobacillus stearothermophilus* ATCC 7953 or ATCC 12980
	Clostridium sporogenes PA 3679 or ATCC 11437
	Bacillus coagulans FRR B666 or ATCC 51232
	Bacillus subtilis 5230 or ATCC 35021
Ethylene Oxide	*Bacillus atrophaeus (subtilis var niger)* ATCC 9372 or NCTC 10073

Regardless of which sterility test is used, it is always necessary to know and do:

- the number of contaminating microbes on a certain amount of material or number of bioburden,
- the kinetics of microbial inactivation so that adequate and reasonable statistics can be applied in the design,
- development and validation of the sterilisation process or product to eliminate the concern of erroneously passing a non-sterile lot.

As already mentioned, to evaluate a sterilizing agent, the knowledge of kinetics of microbial inactivation is required. Each type of microorganism responds differently to the various available sterilization processes. The death of a single microbial cell is a biochemical process and the dynamics of microbial inactivation reveals that microbes are destroyed in a logarithmic or first order rate. An explanation of this phenomenon is that the logarithmic order of death is due to an expression of a monomolecular reaction of protein penetration or damage (e.g. one DNA gene) essential to reproduction [3].

Statistics of sterilization are based on the assumption that all microorganisms die or are inactivated in a logarithmic first order reaction rate. In reality, most bioburdern consists of mixed cultures and microorganisms in these mixed cultures are in various stages of growth so a logarithmic order of death may not be demonstrated. However, the logarithmic death approach continues to be used and exploited to predict the probability of survivors. Therefore, the sterilization is consequentially expressed as the probability of a number of microorganisms capable of surviving [2].

The commonly used and recognised mathematical expression of microbial inactivation by all sterilization methods is the decimal reduction value, commonly referred to as the D-value. The D-value is the time or dose that is required for a sterilization process takes to inactivate a microbial population one logarithm or 90%, to a known sterilising condition, specified for each sterilisation method. A mathematical description of the D-value is:

$$D - \text{value} = \frac{\text{Exposure time of dose}}{\text{Log } N_0 - \text{Log } N_t} \tag{1.1}$$

where N_0 = the initial bacterial/bioburden or spore population prior to exposure to sterilising agent
N_t = the population surviving after exposure to the sterilising agent

The D-value provides a characterisation of the resistance of a particular microbial population to a sterilisation method [3].

Up to this point the definition of sterility has been the complete destruction of all microbes. However, in reality the term can never be absolute or 100% complete because a certain probability of survivors will always exist due to the logarithmic order of death that occurs with microbial inactivation. Therefore, to estimate or design a sterilisation process it is necessary to know what level of probability of survivor is required. The concept of sterility assurance level defines the certainty that an item is sterile. For example, an assurance of less than 1 change in 1000000 that viable microorganisms are present in a sterilized article or dosage form for invasive medical devices - sterility assurance level (SAL) 10^{-6}. A product containing a drug or food that can support microbial growth is typically a higher standard – SAL = 10^{-11} [4].

The concept of the SAL specifies a single target for all sterilization processes. It considers the different initial levels of contamination that may be encountered for different products manufactured in different places and under different circumstances. Compared to other standards for sterility, it places far greater demands on knowledge of the product's bioburden, its response to the sterilization treatment and the uniformity of the particular sterilization processes. Ultimately it relies on the confidence in the extrapolation required to demonstrate that the process is capable of achieving what it is supposed to achieve [2].

The most important step in achieving a reliable sterilization process with a desired sterility assurance level is the validation of the sterilization process. Process validation is a documented program that provides a high degree of assurance that a specific process will consistently produce a product meeting its predetermined specifications and quality attributes [3]. A validation program generally consists of four major steps:

(1) Installation or material/product qualification(s) – the control of sterilization begins with the design control of a product and the process. There must be a design quality assurance system in place to identify when design input occurs, to ensure that there are written specifications or procedures, personnel interfaces and that the design output and the design verification is documented.

(2) Sterilization cycle development – the sterilisation design is focused primarily on the product design, and the end use of the product. Here the D-values are considered and the process parameters are checked for their compatibility with the product to be sterilised.

(3) Sterilization performance qualification – during sterilisation, performance results of half cycle runs or sub process verification runs are performed that verify results of D-value calculations by showing complete or near complete inactivation typically out of 10-100 samples of microorganisms on product, to indicate that the desired probability of survivor is established. These runs eliminate the need for complete destruction of all products to prove sterility.

(4) Certification – it is purely documentation, formal review and approval. However, during the review of the validation it is acceptable to confirm and calculate the probability of survivors for the process. From this information, a sterilization process can be reliably shown to be sterile.

A variety of factors must be carefully considered for each sterilisation method selected in order to achieve reproducible and repeatable processes without affecting product quality, material's chemistry and biocompatibility [1]. In the following chapters, radiation, heat and gaseous sterilizations will be presented in details.

1.1 Radiation Sterilization

All matter is made up of atoms. In the centre of the atom the nucleus is circled by negatively charged orbiting electrons. The atomic nuclei is composed of positively charged protons and uncharged neutrons. All stable atoms are electrically neutral, which means that the number of protons is equal to the number of electrons. On the other hand, in radioactive materials the nucleus of the atoms is unstable, which are subject to spontaneous decay or disintegration by ejecting a particle in an endeavour to acquire a more stable configuration, thus forming ''daughter nuclei''. Radiation is emitted as particles are ejected [3].

Radioactive isotopes emit different types of radiation:

- Alpha particles: Alpha particles consist of two protons and two neutrons bound together into a particle identical to a helium nucleus, which is produced in the process of alpha decay. When alpha particles pass through materials, they knock off electrons

from nearby atoms, gradually slowing down and lose their energy. Alpha decay of an isotope may also lead to a release of gamma radiation

- Beta particles: A Beta particle is a high-velocity electron that loses its energy in the same way as an alpha particle. It arises from radioactive disintegrations, consists of electrons with a single negative charge and a low mass. The penetrating capability through materials is far further than for alpha particles. This type of radiation can be used for sterilization, and is produced usually from electron accelerators rather than from radioactive isotopes.
- Gamma rays: Gamma rays are photons of electromagnetic radiation with energies in the range of 1 keV to 10 MeV. They are very penetrative through matter. Gamma rays are able to pass through matter with the same energy as they had when they entered, just fewer of them emerge. This property of penetration is the first and most important property of gamma radiation since it provides a robust process for industrial sterilization.

Alpha, beta particles and gamma rays and their penetration capabilities are presented in figure 1 – 1:

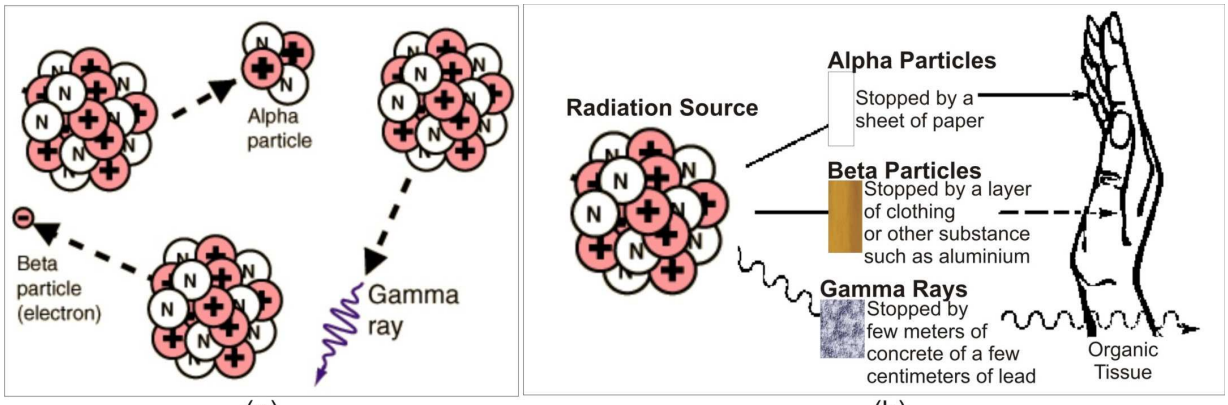

(a) (b)

Figure 1 – 1: Emitted types of radiation: alpha, beta particles and gamma rays and their penetration capabilities.

The industry-standard source of gamma radiation for industrial processing is cobalt-60. Consider the stable atom cobalt-59. It has 59 particles in its nucleus. When cobalt-59 is bombarded by neutrons, an extra neutron is added to the nucleus and the radioactive isotope cobalt-60 is formed. Radioactive decay of cobalt-60 is a single-stage process to stabilize to its daughter nucelei - nickel-60 [3]. Cobalt-60 first decays to excited nickel-60 by beta decay. Then the nickel-60 drops down to the ground state by emitting two gamma rays with energies of 1.33 and 1.17 MeV, respectively.

In practice, only gamma- and beta-rays have found usage as sterilization methods and a wide range of commercial medical products is now sterilized using either beta (electron beam) or gamma irradiation. Radiation sterilization is a highly reliable procedure, mostly due to its simplicity. In developed countries, radiation sterilization of disposable plastic medical items exceeds 50% of all such equipments. A major driver for conversion to radiation sterilization is the elimination of toxic chemical residue from the product, and also safety and environmental considerations in the sterilization process [5].

The lethality of radiation sterilization is dependent solely on one parameter – absorbed dose. In practice, absorbed dose is dependent upon the strength of the source, the apparent (bulk) density of the product packages being irradiated and the time of exposure. An empirical relationship must be determined for particular irradiators and products by means of measurement of dose (dosimetry). This is the key work that must be done in validating a particular irradiation sterilization process. The validation of the sterilization process is done to make certain that the products are rendered free of viable microorganisms and sterile. The

standards ensure certain predetermined criteria that validate sterilization procedure [4]. These criteria include:

- evaluation of materials to be used in the product and its packaging;
- determination of the products radiation stability;
- sterilization dose selection;
- product dose mapping;
- certification of the process;
- verification of the sterilization dose.

There are two types of units involved in quantitative measurement of nuclear radiation, those that measure physical nuclear radiation itself and those that measure the biological effect of nuclear radiation. Physical radiation units measure the activity of a source of radiation. The SI unit of physical nuclear radiation is the becquerel (Bq). Biological radiation units measure the effect of nuclear radiation on living tissue. The SI unit of biological radiation effect is the gray (Gy). One Gy corresponds to the transfer of 1 J of energy to 1 kg of living tissue [4].

The process of selecting a sterilization dose is intended to establish the minimum permissible dose necessary to provide the required or desired sterility assurance level (SAL), meaning the probability of a viable microorganism being present on a product unit after sterilization. The dose is dependent of the end use of the product and the microbial population existing on the product prior to sterilization. The Medical Devices Directorate has in 1993 determinate that the delivery of a radiation dose in excess of 25 kGy is accepted for radiation sterilization process for providing adequate assurance of sterility. According to the FDA (Food and Drug Administration), the medical device is labelled as sterile if the number of non-sterile devices is less than one in a million (SAL=10^{-6}). The dose of 25 kGy is based upon a consideration of the radiation resistance of microorganisms. It is also important to consider the number of bioburden before sterilization. The lower the bioburden, the more effective the process of sterilization will be. Therefore, the dose of 25 kGy would be sufficient provided that the bioburden does not exceed 100 microorganisms per item and that the organisms are not more resistant than *B.pumilus* [4].

1.1.1 Sterilization Procedure with Gamma Rays

Gamma irradiation as sterilization method for pharmaceutical products first appeared in the British Pharmacopoeia in 1963 and in the United States Pharmacopoeia in 1965. By the end of the 1970's, gamma sterilization had been adopted as regular sterilization method by large medical manufacturers, such as Baxter International, Becton Dickinson, Sherwood Medical, etc [3].

The properties required of a radioisotope as a source of gamma-rays suitable for sterilization are:

- availability of the isotope in large quantity
- provision of gamma-rays with sufficient energy to penetrate deeply into packages
- a half-life sufficiently long to maintain a reasonably steady processing. [6] The half-life is the time taken for the activity to fall to half of its original value. Cobalt-60 has a half-life of 5.3 years. Thus a radioactive isotope is decaying and losing activity at all times regardless of whether it is being used or not. This factor has economic implications for industrial-scale irradiation.

Gamma irradiation of a product is carried out in a batch operation or as a continuous process. The irradiation source is shielded with concrete to protect personnel and the environment. In a batch procedure, the product is placed close to the radiation source and its position changed at intervals. In the continuous process, items are loaded onto a mechanical conveyer which passes them through the irradiation chamber, shifting the position of the product relative to the radiation source to obtain even exposure. Each product box makes four complete transits through the irradiator starting on the lowest and finishing on the highest shelf. The intensity of the radiation decreases as it penetrates the product, 100 cm of

material with a density of 1 g/cm^3 reduces the intensity of radiation of cobalt-60 by 50%. The highest product temperature reached in industrial-scale gamma irradiators usually ranges from 30 to 40℃ depending on the source strength [4]. Cobalt-60 gamma irradiator is schematic depicted in figure 1 – 2.

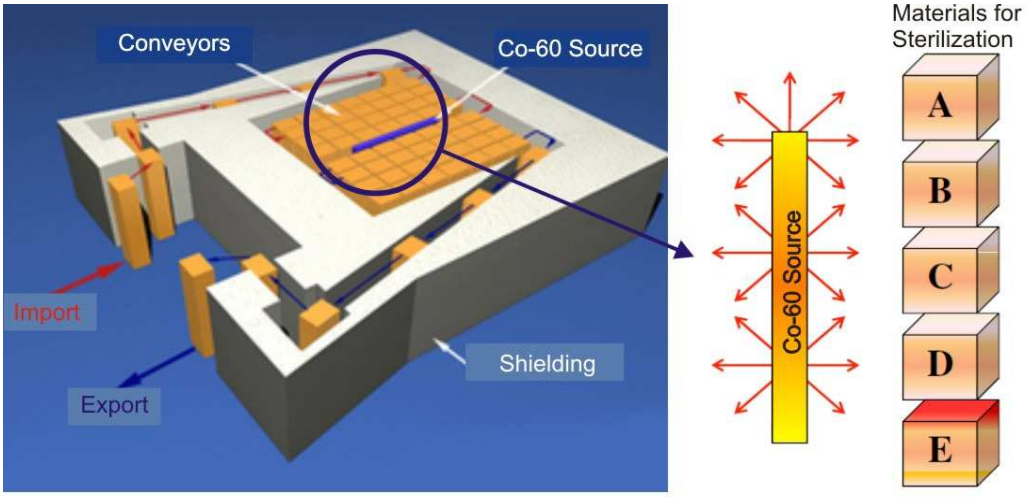

Figure 1 – 2: Cobalt-60 irradiator.

Gamma rays are pure energy with very short wavelengths and are highly effective in killing microorganisms. Likewise, they do not create residues nor have sufficient energy to effectively change the nuclei or to elicit neutrons of the atoms. The object never comes in contact with any radioactive material during the irradiation process. Consequently, most of the energy delivered during radiation sterilization simply passes through the object. The amount of energy that does not pass thought the object is negligible and is retained as heat. No radioactivity can be created or induced within the product, regardless of the absorbance dose [3].

Compared with all other methods of sterilization, gamma radiation has the overwhelming advantage of penetration through materials. The advantages of penetration extend through all aspects of medical products, from initial design to the final presentation of the products in their shipping packs. Another advantage of gamma radiation over other terminal sterilization processes is its reliability. The lethality of gamma radiation is dependent solely on dose. Therefore, controlling one parameter is simpler than to control more interaction or parameters and the processes that are easily controlled are more reliable than those that are not [2].

The greatest disadvantages of gamma irradiation are the deleterious effects of radiation on some polymers that might otherwise be preferred materials of manufacture, high initial capital cost, fear of radiation, extended length of time for qualifying irradiation materials and the disposal of radioactive waste [2].

1.1.2 Sterilization Procedure with E-Beam Radiation

The alternative to isotope sources of radiation is the production of accelerated electrons. Electron beam radiation was introduced in the 1970s and became an acceptable method of sterilization for healthcare products, such as syringes or cardiothoracic devices. The beam, a concentrated, highly charged steam of electrons, is generated by the acceleration and conversion of electricity. The electrons are generated by equipment referred to as accelerators which are capable of producing beams that are either pulsed or continuous - the greater the voltage, the faster the speed of the electrons; the faster the speed of the electrons, the greater their penetrative power through matter. Accelerators producing electron beams with energies of 5-10 MeV are suitable for radiation sterilization [3].

Accelerators have an economic advantage over isotopes that they can be turned off, when not required and electron beam is directional. Because they do not contain radioactive isotope, this provides the advantage from a public acceptance standpoint. Their disadvantage is in their poor penetrative properties in comparison to gamma rays [3].

When the electron beam is scanned through the product, the electrons interact with the device materials and create secondary energetic species such as electrons, ion pairs, and free radicals. These secondary energetic species are responsible for disrupting the DNA chains of microorganisms, inactivating them and rendering the product sterile [7]. When evaluating e-beam irradiation for the purpose of sterilization, product density, size, orientation, and packaging must be considered. In general, e-beam irradiation performs best when used on low-density, uniformly packaged products.

The modern material-handling system for e-beam sterilization is presented in figure 1 – 3:

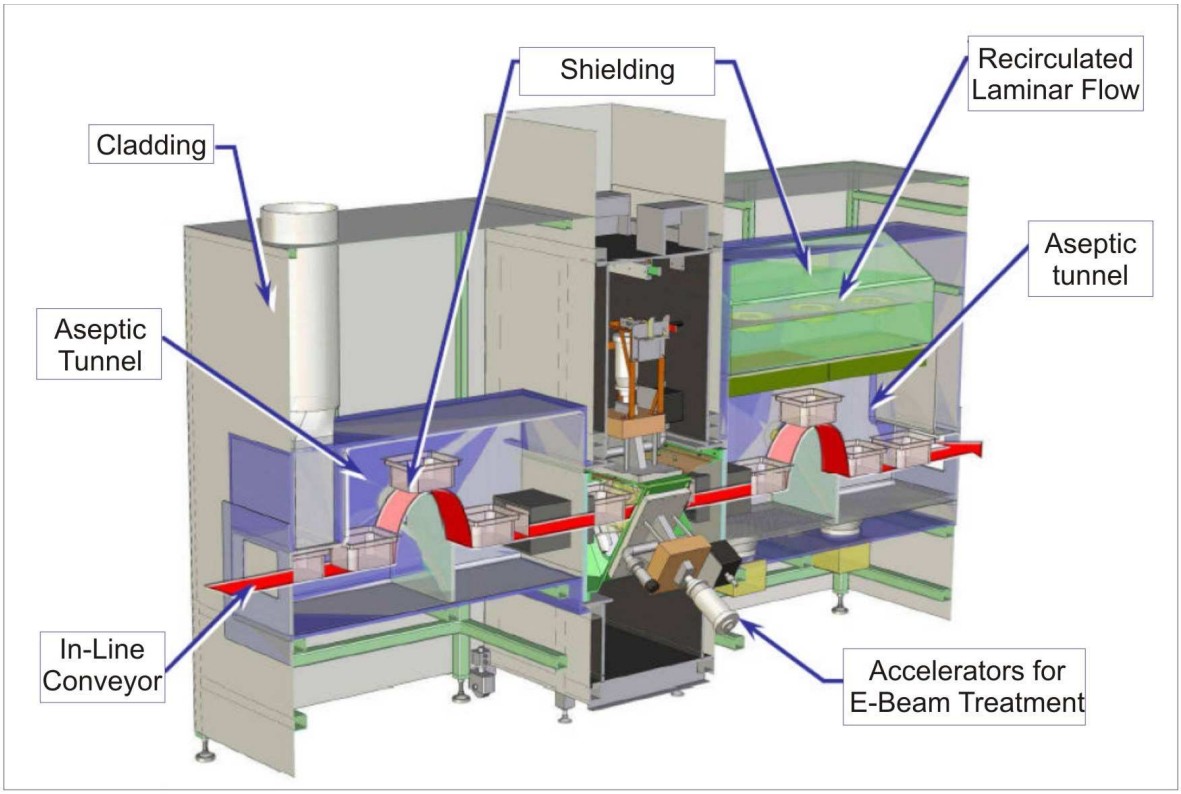

Figure 1 – 3: Typical material-handling system for electron beam sterilization.

Accelerators have an economic advantage over isotopes in that they can be turned off, when not required. The great advantage of e-beam sterilization is the shortest process cycle of any currently recognized sterilization method. In e-beam processing, overall process time, including time for transportation, averages from 5 to 7 minutes. With the use of established and recognized dosimetric release procedures, a product can be released from quarantine as sterile within 30 minutes [7].

1.1.3 Comparison between the Gamma and E-Beam Sterilization

In table 1 – 2, the comparison between gamma and e-beam sterilization is made:

Table 1 – 2: Comparison between gamma and electron beam sterilization process.

Consideration	Gamma Radiation	Electron Beam Radiation
Process type	Batch or continuous	Continuous

Sterilization Mechanism	Ionising radiation by gamma rays (deep penetration, low dose rates)	Ionising radiation by high energy electrons (low penetration, high dose rates)
Product Design	No restriction	Limitations with large components packages
Penetration	Complete penetration	Near-complete penetration
Product Packaging	The product density and package size are not concerned for most medical devices, because of the deep penetration capabilities of gamma radiation.	Penetration correlates directly to product density and carton size. Densely packaged materials and large cartons may more than one pass beneath the beam.
Controlled Parameters	Time	Beam current, width and energy; conveyor speed
Post-Sterilisation Testing	Not required Verification of sterility assurance level (SAL) is dosimetric	Not required Verification of sterility assurance level (SAL) is dosimetric
Post Sterilisation Quarantine Period	Not required	Not required
Residues	None	None

1.1.4 Effects of Radiation Sterilization on Microorganisms

Radiation damage to biological systems is caused by the energy absorbed from the radiation. The absorption of ionizing radiation in matter leads to numerous phenomena of high complexity [3]. In biological materials these can be categorized within four stages:

(a) A physical stage in which extremely unstable excited or ionized molecules (primary products) are produced from interaction of ionizing radiation with orbiting electrons.

(b) A physicochemical stage in which the primary products react spontaneously or in collision with each other, bonds are broken, and highly reactive ions, radicals and trapped charges are formed. It is the reaction of these reactive groups that produces observed changes.

(c) A chemical stage. This is the reaction and interaction of the reactive groups. It is a stage of achieving thermal equilibrium.

(d) The biological stage comprising a series of biochemical reactions at different levels of cellular organization, giving rise to observable biological effects. Loss of viability of the microbial cell is principally due to dimerization of DNA bases and scission and cross-linking of the sugar-phosphate backbone of DNA.

Microorganisms of a given type may respond differently to radiation according to different physical or chemical conditions existing within the cell or in its close environment. Microorganisms are more sensitive to radiation when oxygen is present during and after irradiation than in environments from which oxygen has been excluded. This is likely due to reaction of oxygen with free radicals formed by ionization of target molecules [3].

Water and organic molecules are altered upon being exposed to radiation energy [1]. Water is ionized and a hydrated electron (e_{aq}^-) is produced along or adjacent to the radiation track and depending on the reaction conditions, following speices could be also formed:

$$H_2O \rightarrow H_2O^+ + e_{aq}^-$$

$$H_2O \rightarrow H, e_{aq}^-, OH, H_3O^+, H_2O, H_2, H_2O_2, OH^-, HO_2, O_2, O_2^-, HO_2^-.$$

The free radicals produced in the more densely ionized portion of the track will recombine, whereas in the other portions of the track, where diffusion occurs, these radicals will react with solute [1].

In the presence of oxygen, significant quantities of the hydroperoxyl radical $\cdot HO_2$ are formed which produces H_2O_2:

$$2 \cdot HO_2 \rightarrow H_2O_2 + O_2$$

The longevity of the H_2O_2 molecule can be appreciable. Oxygen can be formed by other reactions involving the OH radical and H_2O_2. Hydrogen peroxide and the hydroperoxyl radical may act as oxidizing or reducing agents. In acid media, the OH_2 radical is undissociated and is a strong oxidant and a weak reducing agent, whereas the O_2 ion obtained from the dissociation of the OH_2 radical can act as a reducing agent. These species, i.e. $OH\cdot$, e_{aq}^-, and $H\cdot$, are capable of degrading and altering a variety of organic materials and biochemicals [1].

Inactivation of microorganisms occur either through direct ionization of a vital cellular molecule (DNA, key enzyme, etc.) or indirectly through the reaction of free radicals produced in the cellular fluid [8]. The main target sites of ionizing radiation in microorganisms are nucleic acids, principally DNA, but also RNA in RNA viruses. Additional damage may be caused to cell membranes and enzymes involved in nucleic acid repair [9]. As mentioned before, ionizing radiation produces highly reactive, short-lived hydroxyl radicals ($OH\cdot$) in water within microorganisms which, for example, cleave phosphodiester bonds in RNA, resulting in single-strand breaks or double-strand breaks. Damage to the sugars and bases may also occur. In complex aqueous media, such as biological products and finished pharmaceutical preparations, most changes originate from the recombination of radicals produced by the radiolysis of water. The final result depends on the microenvironment surrounding the irradiated object, such as the presence of water, oxygen, impurities, radicals absorbent, antioxidant, etc. The population of viable organisms decreases exponentially with increased dose. Hence, each species exhibits a specific sensitivity to irradiation [10].

In general, multicellular organisms are more sensitive to radiation than are unicellular organisms. Gram-negative bacteria are more sensitive than Gram-positive ones. The most radiation-resistant fungi are about as resistant as those bacterial spores having moderate radiation resistance, and viruses in general are more resistant than bacteria. The prions, which do not contain nucleic acid are extremely resistant and also the bacterial spores, with few exceptions, are resistant to radiation [1]. The table 1 – 3 represents the radiation response and the examples of microorganisms exposed to radiation sterilization.

Table 1 – 3: The radiation response and examples of microorganisms exposed to radiation sterilization

Radiation Response (D-value kGy)*	**Examples**
Sensitive (0.2 kGy)	Gram-negative bacteria
Moderately Resistant (0.5 - 0.6 kGy)	Moulds, yeasts and aerobic Gram-positive sporulating bacteria (e.g. *Bacillus Subtilis*)
Resistant (2.2 - 3.3 kGy)	Spores of anaerobic Gram-positive bacteria (e.g.*Clostridium botulinum, Clostridium tetani*) Enterococcus faecium (dried from serum broth) Deinobacter Radiodurans Most Viruses

Highly Resistant (4.5-50 kGy)	Foot- and mouth- disease virus Bacterial spores Prions (BSE)

* D-value denoted the radiation dose (kGy) necessary to reduce the viable cell number by 90%.

Microorganisms with a low resistance will not survive an exposure to a dose of radiation efficient enough to have a measurable influence on a very resistant microorganism, even when the number of sensitive cells is high. It must be noted that enzymes, pyrogens, toxins and antigens of microbial origin are in general very radiation resistant, compared with living cells. Therefore, the number of microorganisms present prior to radiation sterilization is of importance when dealing with medical products, regardless of the radiation resistance of the contaminating population [11]. The number of organisms present in the product being sterilized (the bioburden) determines the effective sterilizing does.

1.1.5 Effects of Radiation Sterilization on Materials

Ionizing radiation has been found to be widely applicable in modifying the structure and properties of polymers, and can be used to tailor the performance of either bulk materials or surfaces [12]. Therefore, some of the medical polymers undergo changes in structural and mechanical properties when subjected to radiation sterilization.

Certain classes of polymers are susceptible to chain scission mechanisms while others are altered through crosslinking processes. Likewise, the molecular weight of polymers and its distribution can be drastically altered by exposure to ionizing radiation. In general, the exposure of polymers to ionizing radiation will alter their basic molecular structure and associated macroscopic properties. Polymers are altered primarily through several basic schemes; electron absorption and subsequent cleavage that give rise to radical formation, radical combination resulting in the formation of crosslinks, or disproportionation to give scission and gas evolution [13].

Electron beam irradiation is typically gentler to polymers than gamma radiation, because the cycle for electron beams is so fast that oxidative effects are minimised. Gamma radiation is greater penetration and lower energy electrons (3 MeV) takes much longer cycle time (6-18 hours), giving time for more oxygen to permeate the polymers and produce oxidative degradation. [13]

1.1.5.1 Formation of free radicals by radiation sterilization

Trapped free radicals were discovered in irradiated polymers many years ago. Since the energies of ionizing radiation greatly exceed the ionization potential of atoms and molecules, ions and electrons are produced. Their lifetime at room temperature varies from fractions of a second to years. The radicals that are short-lived at room temperature can often be observed at liquid nitrogen temperature and their rate of disappearance measured on warming the sample [14].

The primary mechanism of modification of the polymer structure occurs via free radical formation. The damage is initiated with the ejection of a high-energy electron. The reactions are:

Generation of free electron: $R \Rightarrow R^+ + e^-$

Ionization: $e^- + R \rightarrow R^+ + 2e^-$

Highly excited electron states: $R^+ + e^- \rightarrow R^*$

The highly excited electron states may undergo radiationless or radioactive decay. They may also decay through a chemical pathway via heterolytic bond cleavage leading to the generation of ions or via homolytic bond cleavage resulting in the generation of free radicals:

Free radical formation: $RX^* \rightarrow R\cdot + X\cdot$

For polymers, it is the free radical generation that dominates. This leads to free radical reactions that depend on the chemistry of the polymer and may be coupled with the environment [13]. Such reactions can result in main chain scission, recombination, or disproportionation as exampled on polyethylene:

Main chain scission: $-(CH_2 - CH_2)- \rightarrow -(CH_2\cdot + \cdot CH_2)-$

Recombination: $-(CH_2\cdot + \cdot CH_2)- \rightarrow -(CH_2 - CH_2)-$

Disproportionation: $-(CH_2 - \cdot CH_2 + \cdot CH_2)- \rightarrow -(CH_2 = CH_2 + CH_3)-$

If the side group of the polymer is involved in scission, small radical fragments are generated, such as the hydrogen radical. The danger in this reaction is that this small radical is highly reactive and mobile, and it may be able to diffuse great distances triggering numerous reactions [13].

Energy-rich radiation created species can then undergo dissociation, abstraction and addition reactions in a sequence of reactions leading, ultimately to chemical stability. This stabilisation process, which occurs during, immediately after, or even days or weeks after irradiation, often results in physical and chemical changes in the polymers as a result of the stabilising recombination, crosslinking or chain scission that occurs. The resultant physical changes may include crosslinking, deterioration, discolouration, embitterment, formation of extractables, odour generation, stiffening, softening, chemical resistance, melt temperature, toxicological response and even destruction, e.g., Teflon polymer to powder [15].

The radiation effect on the properties and performance may also differ with location. As a polymer is irradiated, radicals are formed in the polymer proportional to the local dose. However, the associated stabilising chemical reactions that follow are proportional not only to the localised ionisation concentration but to the local concentration of reactants. Since the concentration of reactants differs by location (i.e. oxygen higher near exterior surfaces), the resultant radiochemical stabilising reactions are heterogeneous. In addition, orientation of molecular chains established during processing can have a profound effect on subsequent radiation damage. Molecular structures that fail during irradiation are always those molecules under the greatest combined stress from environment, load, solvent and residual moulding stress, i.e. normally at the surface [16].

Post-irradiation effects on polymers can be attributed to trapped free radicals, the presence of peroxides and possibly trapped gases. This has serious consequences for the industry that uses gamma radiation for sterilization and relies on stability of shelf storage prior application. First-, second- or third-order reactions based on the presence of several types of free radicals, i.e., antioxidant, polymer main chain scissoring, terminal end groups, side chains, pigments, processing aids, etc., may complicate determination of reaction rate equations [16].

1.1.5.2 Radiation Sterilization in Presence or Absence of Oxygen

The sterilization in presence and absence of oxygen has different effects on the polymer structure and degree of degradation. The difference depends on the chemical composition and morphology of the polymer. When ionizing radiation is performed in air there can be a severe propensity for structural degradation of the polymer. Most polymers, even those that crosslink in an inert environment, will have a tendency to undergo chain scission when oxygen is available during ionization. Also damage often occurs at much lower radiation doses, and degradation becomes a time dependent process [17].

Free radicals tend to oxidise easily, especially when oxygen is readily available such as at the surface of the polymer. In some cases inert gas, i.e., nitrogen, argon or a vacuum can be used to inhibit oxidation; antioxidants such as hindered amines are also useful in limiting oxidation. Fast dose rates from electron beam irradiation systems can minimise or limit

oxidative degradation of polymers by limiting the time of radical exposure to oxygen. Reducing oxidative degradation through one or more of the above mechanisms is important to keep in mind for oxidative sensitive materials containing thin profiles, such as films, coatings and fibres [17].

The time dependent mechanism of free radical reactions poses serious concern for radiation degradation of polymers. The free radical reactions in radiation-induced polymer oxidation as follows:

Initiation: $R - \gamma \rightarrow R\cdot$

Propagation: $R\cdot - O_2 \rightarrow RO_2\cdot$ $\quad RO_2\cdot - RH \rightarrow RO_2H + R\cdot$

Chain Branching: $RO_2H - RH \rightarrow RO\cdot + \cdot OH$ $\quad RO\cdot - RH \rightarrow ROH + R\cdot$

$\cdot OH - RH \rightarrow H_2O + R$

Scission and Crosslinking: $RO_2H, RO_2\cdot, R\cdot$

Termination: $2RO_2\cdot \rightarrow RO_2R + O_2$

The high diffusional mobility of oxygen provides a greater penetration into polymer and results in the generation of reactive free radicals that can be long-lived. Oxygen traps free radicals and drives reactions that are oxidative in nature. These chemical reactions result in the generation of oxidative products created within the polymer and include the formation of carboxylic acids, ketones, esters, alcohol derivatives, and peroxide based species. Free-radical reactions result in gaseous products, and in the presence of oxygen these can include carbon dioxide, carbon monoxide and water vapour. When peroxides degrade, chain branching is favoured and reactions result in further radical generation. This provides a pathway for the generation of numerous free radicals within the polymer. Additionally, the peroxide decomposition is temperature dependent. This results in a polymer that has both a time and temperature dependent degradation mechanism. Moreover, the depth of oxidation within the polymer depends on the oxygen-permeation rates and consumption rates per absorbed dose as well as the dose rate itself [13].

1.1.5.3 Chemical Changes in Irradiated Polymers

Density, molecular weight, chain length, entanglement, polydispersity, branching, pendant functionality and chain termination all contribute to the polymer's structure/property relationship, and each of these characteristics may be modified with radiation. Knowledge and understanding about the direction and magnitude of the changes brought about to each of these characteristics, as a function of the level of radiation exposure (dose), is crucial to prediction of performance and use of irradiation polymers [14].

The main chemical changes induced by ionizing radiation are:

(1) main-chain scission
(2) crosslinking formation
(3) volatile products formation
(4) discoloration and odour appearance
(5) changes in conductivity

The yields strongly depend on the chemical structure of the polymer.

Main-chain Scission and Crosslinking Formation

Understanding basic radiation chemistry may help to assess why a particular polymer is affected in a certain way. When a plastic is exposed to gamma radiation molecular bonds are broken. The polymer can either recombine into its original configuration or, if cross-scission occurs, the molecular weight of the molecules is reduced and the polymer is weakened. Conversely, where crosslinking occurs, a large three-dimensional matrix is formed and the polymer is strengthened. The effects of radiation on polymer are determined by the chemical

composition and formulation of the polymer, the morphology of the polymer (percentage of crystallinity, molecular weight and density), radiation dose and dose rate that is applied [18].

Polymers react to electron bombardment by crosslinking their molecular chains to become stronger and stiffer or by scissoring (breaking) the polymer chains which become weaker with reduced impact strength and lower elongation to break. Most materials do both (crosslink and scission) making prediction of physical performance more complex to forecast. Materials can be ranked by crosslink to scissoring ration [18].

Chain scission is the breaking of a polymer chain to create a polymer with two or more shorter chains. It is the most common structure change caused by chemical degradation. Because many physical and chemical properties are dependent on molecular weight, chain scission often results in a catastrophic loss in strength and toughness. The molecular weight of the polymeric component is very high and the breaking of just one out of every, e.g. 10000 bonds in a polymer backbone, will dramatically reduce its molecular weight and associated physical properties. Failure of the polymer will result if the degradation reaction continues unhindered [12].

Covalent chemical bonds that occur between macromolecules are known as crosslinks. The formation of crosslinks in a linear polymer causes two polymer chains to join, resulting in an increase in molecular weight. Linear polymers are most susceptible to crosslinking. Such degradation is detected as increased stiffness, brittleness and a decrease in solubility as the average molecular weight increases. The presence of crosslinks also influences the way in which these materials respond to heat. They cannot melt because of the constraints on molecular motion introduced by the crosslinks. Instead, at temperatures well above those at which thermoplastics typically melt, they begin to undergo irreversible degradation. Dissolution behaviour is also different by the crosslinked polymers because it will not dissolve. A high degree of crosslinking leads to the formation of an insoluble, infusible three-dimensional network [12].

Materials that crosslink more than they scissor generally do better in the radiation environment. Highly crystalline materials generally have higher resistance to molecular chain break-up by electron impact due to their strong, nested, compact, mutual reinforcement of polymer chains. Highly amorphous materials are generally resistant to radiation because the natural relaxed amorphous molecular configuration is capable of great ductility and elongation before break. Amorphous polymers can tolerate many scissions without breaking up [13].

The ratio of crosslinking and chain scission is critical and will vary from polymer to polymer and to some degree from part to part based on the chemical composition, e.g., aliphatic, aromatic, morphology of the polymer (% crystallinity, molecular weight, density), the design of the part (thick versus thin sections), the total radiation dose absorbed, the rate at which the dose was deposited, and to some degree the post-irradiation storage environment (temperature/oxygen). The ratio can also be significantly affected by residual stress processed into the part and the environment during irradiation (especially the presence or absence of oxygen) [13].

The nature of the polymer structure determines its response and physical change upon exposure to ionizing radiation. In general:

- Type A: $(CH_2 - CR´R´´)$ undergo a scission mechanism

- Type B: $(CH_2 - CHR)$ undergo a crosslinking

When the crosslinking and main-chain scission occurs simultaneously, one of the effects is predominant. An empirical rule has been proposed by Miller et al. to predict the behaviour of vinyl polymers during irradiation: when each carbon of the main chain carries at least one hydrogen atom, the net effect of irradiation is crosslinking, but if a tetra-substituted carbon atom is present, the polymer degrades. The presence of unsaturation in the polymer chain ads this effect and enhances the yield of crosslinking (for example natural rubber). Likewise,

the presence of aromatic groups lowers the yield of any reaction due to radiation. This rule is generally obeyed. The yield of main-chain scission and crosslinking depends on the temperature, the physical state and crystallinity of the polymer but not usually on dose rate [14].

If chain scission dominates, then very low molecular weight fragments, gas evaluation and unsaturated bonds may appear. Conversely, if crosslinking dominates, the result is an initial increase in tensile strength and toughness, will a resultant decrease in elongation with increased dose. Table 2 – 2 provides a summary of the general polymer schemes that are susceptible to either crosslinking or scission:

Tabel 1 – 4: The polymers which are susceptible to either crosslinking or scission.

Polymers prone to SCISSION	Polymers prone to CROSSLINKING
Poly(methyl methacrylate)	Polyethylene
Polyisobutylene	Polypropylene
Poly α-methylstyrene	Polystyrene
Poly(vinylidene chloride)	Polyacrylates
Poly(vinyl fluoride)	Polyamides
Polyacrylonitrile	Poly(vinyl chloride)
Polytetrafluoroethylene	Polyesters
Cellulose and derivatives	Unsaturated elastomers
DNA	Natural rubber

Formation of Volatile Products

Volatiles formed are mainly hydrogen and products arising from side-chain decomposition. Their yield also depends on the temperature and physical state of the polymer, and their formation often partly results in double bond formation. Vinyl and vinylidene double bonds, either initially present or formed during irradiation, often decay with a large yield owing to their high reactivity towards free radicals [14].

Discolouration and Odour Appearance

Undesirable effect in some polymers after irradiation is discoloration (usually yellowing) from the development of specific chromophores during the stabilising radiochemistry reactions or due to formation of conjugated double bonds, trapped ions and radicals. Colour development, which occurs at widely differing doses in various polymers, may diminish or increase with storage time after irradiation. Often discoloration appears prior to any measurable loss in physical properties. For example, radiation will induce yellowing conjugated double bonds in PVC at a dose much lower than is necessary to cause any reduction in its physical properties [15].

Therefore, irradiation often produces changes in the visible or UV absorption spectra of polymers. These changes also depend on the temperature of irradiation, post-irradiation treatment and the presence of additives. The discolouration of polymer samples has sometimes been used in dosimetry [14].

Another undesirable effect in some polymers is odour production as a result of specific radio-stabilising chemistries. The most common polymers with post-irradiation odour are polyethylene, PVC (rancid oil from oxidised soybean and linseed oils in the plasticiser) and PU [14].

Changes in Conductivity

Electrical conductivity strongly increases in many polymers during irradiation. This induced conductivity in polymeric insulating materials is often the cause of operational failure of electrical devices in intense radiation fields [14].

1.1.5.4 General Consideration by Selection of Polymers for Radiation Sterilization

Molecular chemical structure may contribute to radiation resistance: the benzene ring structure acts as ´electron bank´, rearranging itself to accept or lend an electron as needed without losing integrity – like a radiation shock absorber. Examples are styrenes, styrene alloys, polyester, polyurethane, polycarbonate and polysulfone [15].

Thick polymer sections are more resistant to oxidative radiation damage than thin films or fibres. Moisture content in the polymer can produce additional free oxygen and hydrogen by hydrolysis during irradiation. All polymers contain a finite amount of absorbed water. Moisture content is a variable that may need control [14].

The presence of additives can deeply affect the course of radiation-induced reactions. Some additives exhibit a protective effect while others sensitize the radiolysis or even completely modify the behaviour of the polymers during irradiation [14].

Many polymers show varying degrees of degradation and change with radiation that may create toxic by-products or leachables. Technological advances have done much to improve a material's resistance to radiation and radiation compatibility with the use of stabilisers, additives, antioxidants, etc.

All plastics are affected by radiation. Some effects are favourable or negligible, while others are not [15]. Some general considerations to be made in selecting polymeric plastics:

- Aromatic polymers, e.g., benzene rings, are more stable than aliphatic chains
- Polymers with low radical yields (G-values) after irradiation are more stable
- Phenolic antioxidants contained in most polymers are responsible for discoloration (the use of non-phenolic additives will usually eliminate the problem of discoloration)
- Most natural PP and PTFE are unstable upon irradiation
- PVC, polymethyl pentene (PMP) and PP should be specially stabilised to improve radiation compatibility
- High levels of antioxidants help radiation stability. In general, the antioxidant level may need to be increased if the product is to be radiation sterilised. Heat stabilisers tend to improve radiation resistance.
- Within a given polymer class, the lower the density the greater the radiation stability
- The elastic modulus is not greatly affected with one dose of sterilising radiation
- Fillers and reinforcing materials usually improve the radiation stability of adhesives, coatings and potting compounds
- Polymers used in adhesives, films, fibres, coatings and encapsulates react in much the same way to irradiation as the materials from which they are derived
- Addition of colour tints can minimise the discoloration effects of irradiation
- Modification of the polymer formula can reduce odours
- Extra care must be taken with nucleated polymers – nucleation increases embrittlement
- Most polymers are very tolerant of the mild dosages used to sterilise (200-400 Gy).

1.1.6 Validation of Radiation Sterilization

The radiation sterilization procedures were accepted by the U.S. Food and Drug Administration (FDA) due to the inherent reliability. The international standards for product, process and installation quantification for radiation sterilization are established in documents ISO 11137 Sterilization of Health Care Products – Requirements for Validation and Routine Control – Radiation Sterilization [19].

Biological indicators are not used for routine monitoring of ionizing radiation. The control of the irradiation plant must ensure that the recommended dose is delivered to all points within the product being sterilized. Radiation is accurately monitored by exposure of dosimeters within the load [4].

1.1.7 Application of Radiation Sterilization

The major uses of ionizing radiation are for the sterilization of thermolabile medical items, demonstrated in table 1 – 5.

Table 1 – 5: Representation of radiation suitable medial, pharmaceutical products, foodstuffs and animal feeds.

Type of Product	Ionizing radiation suitable for:
Medical and Pharmaceutical	Disposable syringes, labware, culture media Sutures Tissue grafts (cartilage, tendon, skin, heart valves, bone) Some types of powders Adhesive and other dressings Intravenous infusion sets
Foodstuffs and Animal Feeds	Ionizing radiation widely used in USA, but forbidden in EU except for dried herbs, spices and seasonings

Radiation sterilization has thus proved to be an invaluable industrial procedure. However, it must be pointed out that deleterious changes may occur in irradiated products, especially preparations in aqueous solutions. For this reason, radiation sterilization is usually reserved for articles in the dried state. The use of radiation for sterilization foodstuffs remains a contentious issue [4].

1.2 Steam Sterilization

The oldest and most recognized agent of destruction of microorganisms is heat. The first application of steam under pressure to microbial inactivation was used by Appert's food canning process. Moist and dry heats are sterilizing media. Moist heat includes either saturated steam or boiling water, where the latter is not a good sterilizing agent because of relatively low temperature. On the other hand, moist steam under pressure is inexpensive, sterilizes penetrable materials and exposed surfaces rapidly and leaves not residues. Steam sterilization works better than some other forms of sterilization because steam destroys most resistant bacterial spores in a brief exposure and heats rapidly because of mass heat transfer as it condenses. Therefore, when a requirement of sterility arises for a new type of medical device or pharmaceutical product, steam should always be given first consideration. Dry heat is better penetrative as steam, but is relatively slow, requires higher temperatures of application and is less efficient sterilizing media as moist heat. Dry heat as a means of sterilization is reserved for those products and materials that contain little or no water and cannot be sterilized with steam during the heating cycle [1].

The principle of steam sterilization is the displacement of air by steam within a pressure vessel, termed as autoclave, and has remained substantially the same for over 100 years. The classical autoclave is set to an internal pressure of approximately 1 atm above normal atmospheric pressure, affording a temperature of 121ºC. There is nothing particularly significant about the pressure or the temperature other than the availability of technology that can achieve these conditions and a conservative tendency to standardize thermal inactivation to conditions of known effectiveness. The sterilization by heat is most economical and the classical time proven method of inactivation of microorganisms. It is recognised for its simplicity, efficiency, effectiveness, low cost and speed of operation [2].

Typical steam process types are:

- Gravity (downward displacement)
- Pulsing (vacuum pulsing or pressure pulsing)
- High vacuum

- Superheat

Each type has its advantages and disadvantages. The selection of the particular process type is dependent upon a variety of factors such as the end use characteristic of the product.

1.2.1 Sterilization Procedure

The steam sterilization is carried out in the autoclave. Modern autoclaves may be specified and constructed to operate over a range of internal pressures, providing different temperatures determined by the temperature/pressure equilibrium for steam. For moist heat sterilization, the accepted range of sterilizing temperatures is 118-134℃. A number of time-temperature relationships were authorized by the British Pharmacopoeia, in year 1998 [1]. The table 1 – 6 shows the time-temperature relationships in thermal sterilization processes.

Table 1 – 6: The time-temperature relationships in thermal sterilization processes.

Process	Temperature [ºC]	Holding Period [min]
Moist heat (autoclaving)	121 126 134	15 10 3
Dry heat	160 170 180	120 60 30

The construction of a steam autoclave is shown in longitudinal cross section of figure 1 – 4.

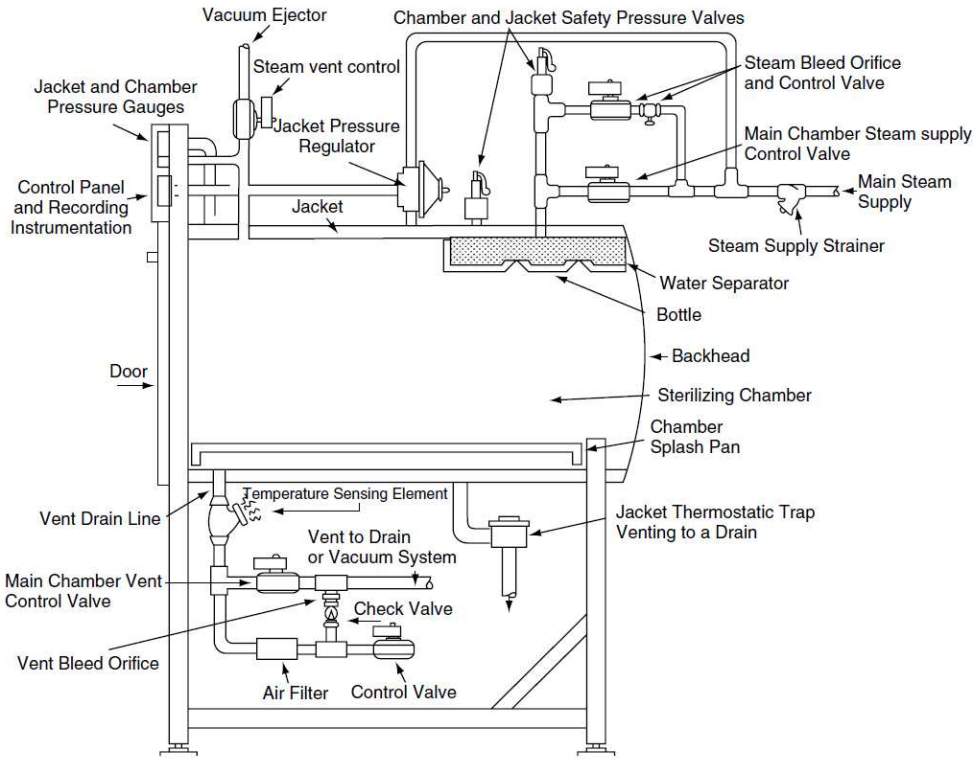

Figure 1 – 4: Schematic diagram of a typical steam sterilizer (autoclave).

The system consists of a steel shell equipped with a sealable door on one end and a permanent closure on the other end. A thermostatically trapped steam jacket surrounds the autoclave on all sides, except the backhead and the door. The main shell and the jacket are fed with steam through control valves, and both are equipped with pressure gauges and safety relief valves. A chamber temperature controller probe is generally located in the chamber drain vent line. Additional necessary design elements of the sterilizer are the baffle,

water separator and splash pan. Steam is supplied at high pressure from a steam generator to the jacket and directly to the rear of the chamber via a reducing valve. The incoming steam hits a baffle placed to prevent wetting of the load. Because it is hotter and lighter than air, the steam moves immediately upward and stratifies above the air in the chamber. With increasing pressure the steam forces the air out through the drain at the bottom of the chamber. A temperature sensor is strategically located at the coolest point in the drain line. The exposure period should be timed from when the equilibrium temperature that is correct for the pressure at which the autoclave has been set to operate is achieved in the drain line [3].

In the autoclave chamber, terminal sterilization is based on highly efficient heat transfer from the saturated steam to the autoclave load. Heat transfer occurs by the release of the latent heat from saturated steam under pressure as it condenses. Heat transfer has maximum efficiency at the phase boundary between steam and condensate at the same temperature. Steam at any point on the phase boundary has the same temperature as the boiling water from which it was produced and holds an extra load of latent heat, which is available for transfer when it condenses on to a cooler surface [3].

Heat penetration into items being sterilized by moist steam begins with the outside of each item having a layer of condensed steam adhering to it. Transfer of heat is by conduction from the steam to the condensate, to the walls of the container, and on into the fluid. Each stationary boundary layer presents its own resistance to heat penetration [4].

The major problems during the steam sterilisation are air removal, superheat, load wetness and material damage. Likewise, temperature, time and pressure are the critical parameters of the sterilization process and they depend on the specific loads or group of loads to be sterilized [19]. When air is present in a space with steam, the air will carry part of the load that the partial pressure of the steam reduced and the heating-up period will be prolonged. Therefore, the air removal is important in ensuring efficient autoclaving [20]. The entrapped air acts as a barrier to direct contact between steam and product. Sterilization by saturated steam is only effective for particular combinations of temperature and time in the absence of air.

Also, the steam quality affects the degree of sterilization and dryness of processed materials. When materials such as dressings, linens and outer wrappings are sterilized, the fabrics can become saturated with moisture. Excessive wetting of the materials hinders diffusion of air from the load. When the material is dry, air passes freely. When the material is wet, the diffusivity of air through the material decreases. Therefore, the quality of steam must be controlled during the sterilization cycle. Steam quality can be controlled in the autoclave chamber by using a steam separator and baffling. The quality of steam is the weight of dry steam present in a mixture of dry saturated steam and entrained water. Ideal steam for sterilization is 100% saturated steam. Factors such as boiler priming, poorly trapped steam supplies, and normal pipe wall condensation entrained by high-velocity steam flow all contribute to produce a steam quality that is less than 100% [1].

1.2.2 Sterilization Cycles

The choice of a cycle is ultimately dependent upon the heat-stability of the product, the type of primary container, the knowledge of heat penetration into the product, the autoclave technology available and the knowledge of the microbiological contamination prior to sterilization [3].

However, three approaches are used in designing sterilization cycles:

- Bioburden approach – based on determination of the number, type and resistance characteristics of the organisms contained in the bioburden. For heat-sensitive products, the heat exposure must be minimized in such a way to reach an optimum

balance between an acceptable degree of sterilization and an acceptable stability of the product after its sterilization.

- Overkill approach – is based on the concept that the sterilization process will inactivate a high microbiological challenge with an additional safety factor. Therefore, the biological indicator with a specific number of microorganisms (10^3-10^6) and a worst-case assumption is made that the heat resistance of the bioburden is equivalent to that of the biological indicator. Therefore, the cycle conditions established are more severe than those required to inactivate the real product bioburden.
- Combination of the two approaches – a combination of the two approaches is sometimes useful to reach a balance between the maximum acceptable SAL and the maximum allowable concomitant adverse effect upon the material to be sterilized, while the bioburden approach emphasizes the stability of the final product and the overkill approach places the emphasis on sterility.

Generally, a cycle comprises heating, sterilizing and cooling phases. Figure 1 – 5 illustrates the cycle typically used in the moist heat sterilization process.

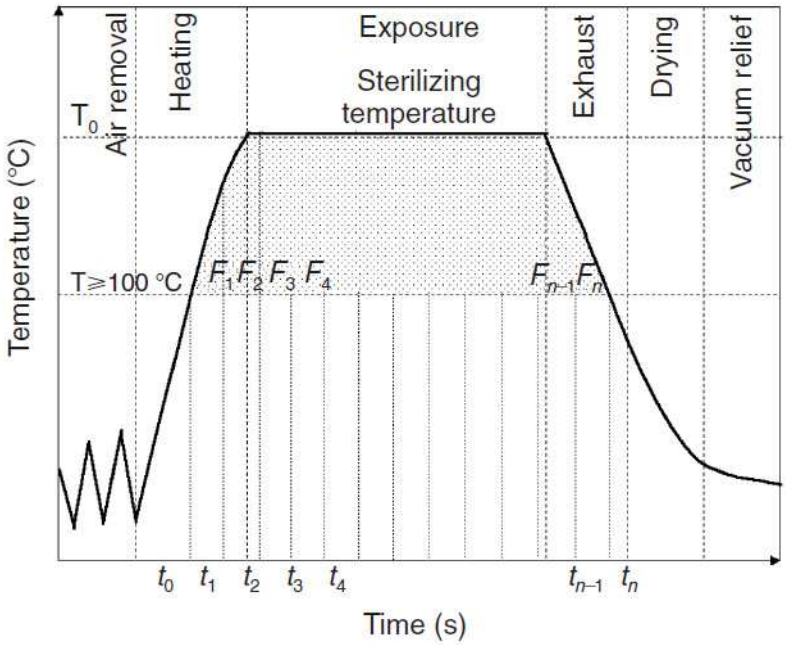

Figure 1 – 5: Typical steam sterilization cycle in autoclave.

The rate of heating and cooling a product in a container is a function of the container type and size, the viscosity of liquids, and the size and arrangement of the load. Therefore, to ensure sterilization efficiency, sterilization must begin after a certain equilibration time when the temperature of the material being sterilized has reached the set sterilizing temperature [3].

1.2.3 Effects of Steam Sterilization on Microorganisms

The goal of thermal processing for sterilization is to deliver sufficient heat to inactivate the organisms that might be present and to reduce the probability of survival of microorganisms to an acceptably low level. The destruction of the microorganisms begins to be significant at moist heat temperature above about 80°C and proceeds rapidly within the normal processing range of about 110°C to 140°C [4].

Thermal damage to biological systems is caused by absorption of heat energy. Well-controlled laboratory studies show that when pure cultures of microorganisms are held in

saturated steam at a constant sterilizing temperature there are linear relationships between the logarithm of the number of survivors and the time of exposure. The order of death is a first-order reaction mechanism that can be designated mathematically in several ways [4].

The three most important terms used to characterize thermal inactivation are the D-value, the z-value and the F-value:

1. The D-value – decimal reduction time (DRT) – is defined as the time in minutes at a particular constant temperature to reduce the viable population by 1log (i.e. to 10% of the initial value, or by 90%).
2. The z-value is defined as the temperature to bring about a 10-fold reduction in D-value; it is obtained from the slope of the curve in which the D-value on a logarithmic scale is plotted against temperature on an arithmetic scale.
3. The F-value expresses a heat treatment at any temperature as equivalent to that effect produced by a certain number of minutes at 121°C. F_0 is the F-value when z is 10°C.

In figure 1 – 6, the idealized heat-inactivation curves of bacterial spores are presented.

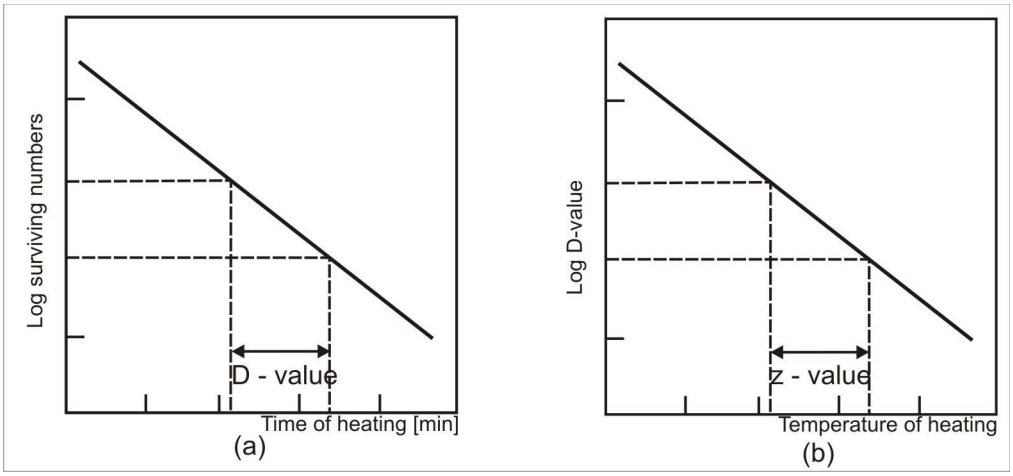

Figure 1 – 6: Idealized heat-inactivation curves of bacterial spores showing: (a) exponential decline in numbers of survivors during heating at constant temperature and the derivation of the D-value; (b) exponential decline in D-value with rise in temperature and the derivation of the z-value.

The thermal inactivation results from multiple events in microorganisms. There are several potential target sites in non-sporulating bacteria, ranging from the outer membrane of Gram-negative bacteria to the cytoplasmic membrane, ribonucleic acid (RNA) breakdown and protein coagulation. The principal mechanism for moist heat inactivation of spores is DNA denaturation. In bacterial spores, thermal injury has been attributed also to denaturation of vital spore enzymes, impairment of germination and outgrowth, membrane damage, increased sensitivity to inhibitory agents, structural damage and damage to the spore chromosome. Thus, the ability to repair DNA after heating must be an important aspect of heat tolerance [4].

Microorganisms show wide variation in their response to moist heat. Non-sporulating bacteria are usually destroyed at temperature of 50-60°C. The vegetative forms of yeasts and moulds show a similar response to most vegetative bacteria. Many viruses are sensitive to moist heat at 55-60°C, but for inactivation of viruses in association with blood and tissues, the recommended temperatures are higher. Spores of thermophilic bacteria are the most resistant. The resistance of spores to moist heat can be manipulated over several orders of magnitude by exposure to extreme pH values or cationic-exchange treatment. The content and location of water in the spore core play an important role but spore coats do not contribute to thermal resistance. The presence of organic matter can protect spores during heating. Peptone, albumin, nucleic acids, sugars and starch all provid protection at certain

concentrations. Also, spores occluded in crystal structures display a phenomenal resistance to destruction by heat. Prions are also highly resistant to steam [4, 21].

1.2.4 Effects of Steam Sterilization on Materials

Steam sterilization is predominantly used in hospitals and laboratories where reusable materials and products are frequently resterilised. The number of plastic materials and chemicals which can tolerate the high temperature and moisture of steam sterilization are limited. However, most metals, glass, ceramics and a large number of heat resistant polymers and plastic materials can be sterilized with steam. Some examples are; acetals, acrylonitrile-butadiene-styrene, aromatic polyurethanes, corrosion resistant metals, cotton, filters, glass, heat resistant liquids, solutions, drugs and parenterals, laboratory equipment (non-electrical lab equipment), muslin, nylon, polyallomer, polycarbonate, polypropylene, polysulfone, some polyvinyl chlorides, silicone, Teflon. Acrylics, styrene and many other heat sensitive polymers will melt and distort with steam and heat. Polyvinylchloride (PVC) may become cloudy, and typically softens significantly above 80°C. Many metals will eventually corrode due to moisture [2]. Paper, powders and oily materials that can get wet may not be completely compatible with moisture from steam.

1.2.5 Validation of Steam Sterilization

Steam sterilization can be validated either by indicators (chemical or biological) or physical measurements. When indicators are used for the validation, the humidity, temperature and time are important. For physical validation, only the measured temperature, pressure and time are available to validate the process [22]. Biological indicators are standardized preparations of specific microorganisms resistant to a sterilization process. The ineffectiveness/effectiveness of the sterilization process is provided with the biological indicators, on the bases of microorganism's survival. Frequently used biological indicators are: *Bacillus stearothermophilus* ATCC 7953, *Bacillus subtilis* 5230, *Clostridium sporogenes* PA 3679, *Bacillus coagulans* FRR B666; *Bacillus subtilis var. niger* ATCC 9372. Biological indicators must be reproducible and of a known resistance. They may be purchased as spore suspensions that can be inoculated onto test pieces or as ready-made test pieces on paper or aluminium strips. An incubation temperature of 55°C should be used to test for viability after exposure [3].

Many factors can impact the effectiveness of the process to destroy the microorganisms and must be considered in the validation program [23]. These factors include:

- qualification of the equipment
- resistance (D) value of the material to be sterilized
- thermal profiling of the chamber
- heat penetration of the load
- load sizes and configuration
- use and placement of biological indicators
- air removal

1.2.6 Application of Steam Sterilization

For an item to be suitable for steam sterilization it must be sufficiently heat-stable to withstand process temperature and it cannot be allowed to be susceptible to moisture damage, because sterilizing conditions will not be achieved in regions of the product that are not permeated by steam [2].

Products, which are sterilizable by saturated steam fall into three categories:

- Aqueous liquids – all of these types of product are filled into hermetically sealed nonporous containers. Those products that are terminally sterilized by saturated steam may be contained within glass ampoules, glass vials, glass syringes, glass bottles or flexible film infusion bags. There is no necessity for steam to penetrate into these containers or come into contact with the product. As long as the sterilizing temperature is obtained, the water content of the product itself will be sufficient to ensure that microbial inactivation is due to moist heat protein coagulation mechanisms.
- Nonporous solids – many medical devices are nonporous solids, for instance scalpel blades and rubber catheters, and may be sterilized by steam. In all cases of steam sterilization it is critical that the items are hermetically sealed into containers that are capable of serving two functions, to allow steam to penetrate and come into contact with all parts of the products, and to provide effective barriers to microbial ingress while still intact. Papers made to specifications appropriate for steam sterilization are available for wrapping items and as made-up bags.
- Porous solids – sterile dressings, filters and cellulosic materials are in general porous materials. It is generally problematic to ensure steam contact with all parts of porous materials because of entrapped air. Sterilizing temperatures will not be achieved in the presence of air. Avoidance of entrapped air is addressed through specific porous-load sterilization cycles rather than through any special packing or loading provision other than those constraining the sterilization of other solid products.

The table 1 – 7 shows the overview of application of moist heat as a sterilization process.

Table 1 – 7: Applications of steam sterilization processes.

Product or Equipment	Comment
Metal Instruments (including scalpels)	Dry heat preferred method; cutting edges should be protected from mechanical damage
Rubber Gloves	γ-radiation preferred method; if autoclave used, care with drying at end of process (little oxidation damage when high-vacuum autoclave used)
Respirator Parts	Steam sterilization recommended method; if disinfection required, low-temperature steam or hot water at 80℃ to be used
Surgical Dressings	Choice of sterilization method depends upon stability of dressings material to stress applied and nature of dressings components
Patenteral Products	Autoclaving is the approved method for sterilization of thermostable products
Non-patenteral sterile fluids	Sterile fluids suitable for clinical use; autoclaving process wherever possible
Ophthalmic solutions (eye-drops)	Autoclaving is the approved method for sterilization of thermostable products

1.3 Gaseous Sterilization

Medical practice in developed countries has been influenced by numerous modifications of medical devices, diagnostic and therapy methods in recent decades. Indeed, clinicians use increasing numbers of medical devices which are more complex and fragile, such as plastic devices and heat- and moisture sensitive microsurgery instruments. The approach to the patients has changed with the multiplication of minimally invasive procedures for diagnosis and therapy. Because of these changes, the need for new physical, physicochemical or chemical disinfection and sterilization procedures has increased. Therefore, the development of low temperature gaseous sterilization was the new alternative for sterilization of complex, heat- and moisture sensitive medical devices [4].

Among the gaseous sterilization technologies, ethylene oxide is one of the best alternatives possible. Ethylene oxide is the primary gas used in hospitals to sterilize items that cannot be sterilized by steam or that contain materials not compatible with radiation sterilization. The other gaseous agents such as propylene oxide, formaldehyde, methyl bromide, hydrogen peroxide and beta-propiolactone can be also used for the sterilization proposes of medical products, but these agents are more suitable for disinfection applications [1].

The properties that ideal gas for the sterilization proposes should have are:

- High efficacy: gas should be bactericidal, tuberculocidal, virucidal, fungicidal and sporicidal
- Rapid activity. Able to achieve sterilization quickly and below 65°C
- Organic material resistance: should withstand reasonable organic material challenge without loss of efficacy
- Strong penetrability: able to penetrate common medical device packaging materials and penetrate into the interior of device's lumens
- Material compatibility: should be compatible with a wide range of products and materials
- Non toxic: should present no health risk to the operators and patients, in particular leave no residues in sterilized products and no toxic by-products
- Environmental emission: should pose no hazard to the environment
- Monitoring capability: should be monitored easily and accurately with physical, chemical and biological process monitors
- Cost-effectiveness: should have reasonable cost for installation and for routine operation

There are two main categories of sterilizing agents by gaseous sterilization, which are distinguished by their antimicrobial actions:

- Alkylating agents – ethylene oxide, formaldehyde, methyl bromide, glutaraldehyde – alkylating agents are highly reactive and interact with many cell structures. There are many possible sites of alkylation such as the amino, sulphydryl and hydroxyl groups in proteins or the purine bases of nucleic acids. They have been referred to as radiomimetic poisons because their biological effects closely resemble that of ionizing radiations.
- Oxidizing agents - hydrogen peroxide, paracetic acid, ozone, chlorine dioxide, hydrogen peroxide gas-plasma – oxidation is characterised by the transfer of electrons from the target molecule to the oxidizing molecule, which plays the role of the electron acceptor.

In following chapters, the gaseous sterilization processes with ethylene oxide, hydrogen peroxide and hydrogen peroxide gas-plasma will be presented in details.

1.3.1 Sterilization with Ethylene Oxide

Ethylene oxide, also known as epoxyethane or dimethylene oxide, is a cyclic ether (C_2H_4O) with a boiling point of 10.7°C at atmospheric pressure. It is a colourless and virtually odourless gas. In its pure form ethylene oxide is highly flammable in air; in particular circumstances it may be explosive. In contact with water, it can transform into ethylene glycol and in the presence of chloride compounds into ethylene cyclohydrin. It reacts with many chemicals such as alcohols, amines, organic acids, and amides. The small size of the molecule as well as its very weak polarity gives it a high penetration power in narrow spaces. The ethylene oxide is not corrosive for metals. It can spontaneously decompose with the formation of methane, ethane and carbon dioxide. This decomposition is facilitated in special conditions such as the presence of air, temperature, pressure and some catalysts [24]. The following physical properties of ethylene oxide gas are presented in table 1 – 8.

Table 1 – 8: Physical properties of ethylene oxide gas.

ETHYLENE OXIDE	Properties
Molecular and Structure Formula	C_2H_4O 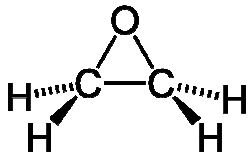
Molar Mass	44.05 g/mol
Appearance	Colourless gas
Density	0.882 g/mL
Melting Point **Boiling Point**	-111.3 °C 10.7 °C
Water Solubility	Complete
Main Hazards	Carcinogen

The advantages of ethylene oxide gas for hospital sterilization are that there is a wide range of materials that can withstand treatment without damage and it posseses high diffusivity and permeability. It is not used for pharmaceuticals. However, it is an extensively used alternative to irradiation as a method of cold sterilization for heat-labile medical devices and pharmaceutical packaging components. The significant disadvantages are its highly toxicity residuals if exposed patients and personnel (e.g. ethylene oxide, ethylene chlorohydrin and the less toxic ethylene glycol), flammability, explosively, carcinogenicity and high cost of handling and equipment. Ethylene oxide brings serious risks of chemical burns to body tissues if a device is not aerated after the sterilization cycle. The exposure to ethylene oxide vapours can generate small problems such as allergic reactions, headaches, dizziness, nausea and is linked to irritation of ocular and respiratory mucosa. In high concentration, risks include severe coughing and dyspnoea and neurological damage caused by a depressing effect on the central nervous system. In the liquid state, ethylene oxide can induce skin irritations and burns. The appearance of cataracts, polyneuropathies and memory impairment has been attributed to prolonged exposure to ethylene oxide. Ethylene oxide has been classified as a carcinogenic agent since 1994. Patient toxicity is related to the amount of residual gas present in the sterilized materials. Problems have been observed during the introduction of devices where the gas has not been evacuated, for example from outside body circuit. These problems are essentially blood abnormalities such as thrombopenia, fibrinolysis, allergic phenomenon, respiratory problems and cardio-vascular attacks [4]. Therefore, the use of ethylene oxide in hospitals is decreasing because of such

factors as risks to health, environmental concerns over waste sterilant disposal and longer turnaround time [1].

There are four ways in which ethylene oxide may be retained in products at the end of sterilization cycles. These are as gaseous ethylene oxide, as ethylene oxide dissolved in water, as ethylene oxide within but not attached to the product or packaging material and as molecularly adsorbed ethylene oxide. The total amount of residual ethylene oxide and the balance among the four forms of residue at the end of sterilization are functions of the sterilization process conditions, the composition of the product, the size of the product, the packaging materials and the packing density [25].

1.3.1.1 Sterilization Procedure

The three major elements in ethylene sterilization are:

(1) Preparation of the product
(2) Delivery of sterilization parameters
(3) The removal of the residual sterilizing agent

The product must be produced in such a manner as to control microbial contamination (bioburden). Other influencing factors to be considered are usually related to the complexity of the product in packaging and loading configuration. The product complexity is usually determined by the product engineers, who should be aware of requirement of the sterilization process. The objective in preparation of the product for sterilization is to provide uniform temperature and relative humidity [4].

The second major element is delivery of sterilization parameters to the product. The fact that a sterilization chamber operates at a specific temperature, pressure or gas concentration does not guarantee sterility. The factors important in delivery of sterilization parameters that influence sterility are number of bioburden, packaging, loading, mass, precycle conditioning, like heat and humidity, gassing time, gas concentration, exposure time, temperature and relative humidity, evacuation time and uniformity of conditions in the load [4].

The last major element in ethylene oxide sterilization is the removal of residual sterilizing agent. This is usually accomplished through sterilizer chamber evacuation with multiple air washes, with dedicated aeration chambers at elevated temperatures, or with both. A portion of the gas that is contained within the product at the conclusion of a sterilization cycle rapidly degasses from packaging components and thus is of concern to sterilizer worker safety, whereas it is the slower product desorption that poses concern to the patient. Factors that have an impact on the removal of residual agents are product, materials, configuration and packaging, loading, mass, exposure gas concentration, temperature, air washes, time and environment of aeration. Significant changes in any of these elements should be evaluated in terms of the influence on microbial lethality as well as influence on toxicity and safety to the worker and the user [1].

The basic scheme for an ethylene oxide gas sterilizer is represented in figure 1 – 7:

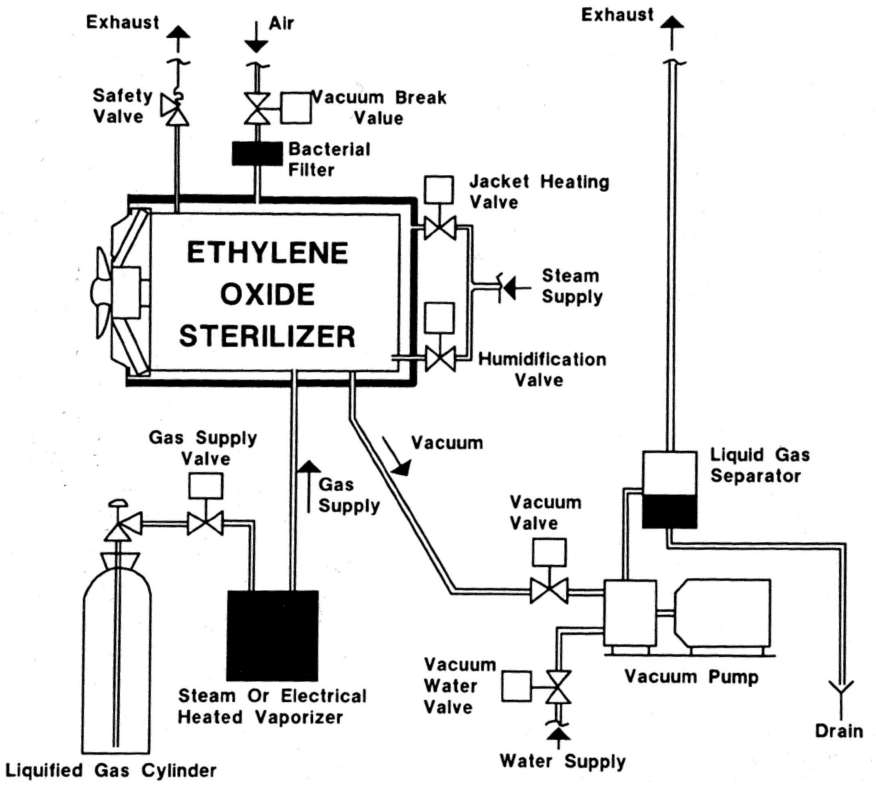

Figure 1 – 7: Schematic diagram of typical ethylene oxide sterilizer.

Sterilization is carried out in steel pressure vessels equipped with water or steam jackets to maintain the operating temperature. However, the vessels also contains a thermoregulation system (heated water, air or electrical), a vacuum system, a steam generator supplied with demineralised water and an antimicrobial filter in the air flow. The most economically way to sterilize with ethylene oxide use 100% ethylene oxide but it is also the most dangerous way because the gas is highly flammable and therefore extreme caution must be employed in process and control equipments. The ethylene oxide can be also mixed with an inert carrier gas, such as carbon dioxide. [1]

In sterilization processing there must be consistent assurance that multiple sterilization parameters – humidity, gas concentration, temperatures, and duration – are adequately controlled, monitored and documented. The optimal parameters for sterilization procedure with ethylene oxide are represented in table 1 – 9:

Table 1 – 9: The optimal parameters for sterilization procedure with ethylene oxide.

Parameter	Range of operation	Comments
Relative humidity	40 – 80% Optimal: 35%	The adsorption phenomenon could appear due to conditioning
Gas concentration	400-1000 mg/L	Higher concentrations create greater toxicity problems.
Temperature	40 – 50℃	The thermosensibility of medical devices must be considered
Duration	30 min – 10 h	The efficacy of the sterilization will depend on exposure duration, by constant parameters

Release of a load requires examination of the following parameters: graphic recording, process indicators and biological indicators. The graphic recording includes the pressure and

temperature as a function of time and must be similar to the nominal recording of the sterilizer. Process indicators use colour-changing ink and are directly printed on the packaging or on adhesive tapes. The indicators on sterilized and unsterilized devices have to be distinguished easily. Other indicators use the progressive modification of coloured ink through the presence of ethylene oxide, correct temperature and humidity rate. The biological indicators are usually paper strips or ready-to-use tubes containing a culture medium vial with colorimetric indicator. A biological indicator contains at least 10^6 *B.subtilis var. niger* spores. It must be placed in a critical part of the chamber and allows a true measure of the effect of the cycle on a known number of organisms introduced together with the load [2].

The International Standard ISO 10993-7 specifies the maximum threshold of ethylene oxide residues and their evaluation methods in medical devices. The acceptable thresholds take into account the patient/device contact time. In this way, the contact is classified as permanent when it exceeds 30 days; it is classified as long for a contact of between 1 and 30 days and limited when lower than 24 hours [26].

Preconditioning and post cycle aeration are used to aid the sterilisation process. Preconditioning facilitates the eventual humidity conditioning of significantly dry product loads and dehydrated bacterial spores, and post cycle aeration facilitates the removal of toxic residuals from materials treated with ethylene oxide [2].

1.3.1.2 Sterilization Cycle

A typical sterilization cycle begins with evacuation of the loaded sterilizer to a predetermined level. The sufficient vacuum must be achieved, not only because it may affect the settings for subsequent phases of the process but also because adequate air removal must be assured to avoid the formation of explosive mixtures with oxygen. A known amount of steam is then introduced and the sterilizer is left to soak for a short period. This is followed by injection of the sterilizing gas to its specified pressure. The sterilizer and its contents are then held under these conditions for the specified time of exposure. At the end of this period the gas is removed by evacuation and replaced by air that has passed through a bacterial-retentive filter [3]. A typical ethylene oxide sterilization cycle is depicted on figure 1 – 8:

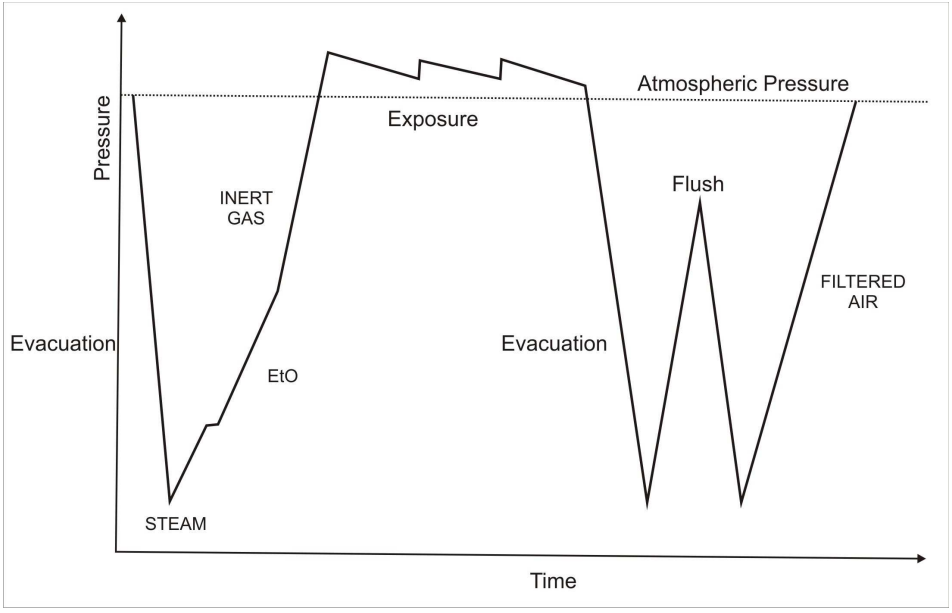

Figure 1 – 8: A typical ethylene oxide sterilization cycle.

The most important phase of the sterilization cycle is the introduction of steam under vacuum. Initial evacuation of the sterilizer is completely unavoidable. It is also potentially deleterious to microbial inactivation. During evacuation the load in the sterilizer loses heat, and more importantly it loses moisture. Steam injection restores the temperature and

moisture content of the load to its correct equilibrium [3]. This must be achieved before the sterilant gas is added due to the following two reasons:

(a) Ethylene oxide has a greater capacity to penetrate through materials than water has. If the two substances were to be injected into a sterilizer at the same time, the ethylene oxide molecules would permeate and diffuse through the load fastest, leaving the water molecules behind. Ethylene oxide is a comparatively poor sterilant in the absence of moisture.

(b) Water reacts with ethylene oxide. If the two substances were to be injected at the same time, the effective concentration of both systems would be reduced. This would have a deleterious effect on the rate of microbial inactivation.

There are different cycles for processes performed in a vacuum and those performed under pressure:

- Vacuum cycle: after an evacuation of the chamber, an essential phase is the ´pre-treatment´, which includes preheating and humidification of the load using short steam injections followed by evacuation. Ethylene oxide, pure or mixed with CO_2, is then injected. The contact between the load and the gas occurs at a pressure lower than atmospheric pressure. After an exposure time of over 1 h, the cycle is ended by repeated evacuations followed with filtered fresh air draining at constant sterilization temperature. High-efficiency particulate air filtered fresh air injection allows recovery of atmospheric pressure.
- Pressurized cycle: The exposure to the ethylene oxide lasts from 30 min to 2 hours. The pressure is always higher than atmospheric pressure.

The vacuum process has the advantage that ethylene oxide leaks are avoided. The advantages of the pressurized cycles are that they are shorter and inflammation risks are eliminated.

Repeated draining at the end of a cycle is not sufficient to achieve the correct desorption of ethylene oxide. For safe recovery, this desorption can be performed by simple storage in a ventilated room or by the use of special desorption enclosures where air ventilation is provided along with temperature regulation, temperature being the most important factor. The devices are loaded into baskets in order to ease ventilation of filtered warmed air, which is injected into the lower part of the enclosure and exhausted from the upper part [1].

1.3.1.3 Effects of Sterilization with Ethylene Oxide on Microorganisms

Inactivation and death of microorganisms results from alkylating effects on hydroxyl, sulfhydryl, carboxyl and amino groups within the cell. Ethylene oxide replaces labile hydrogen atoms in these groups and that causes the destruction of the normal cellular metabolism and ability to reproduce. Likewise, the reactions lead to denaturation of proteins, enzymes and nucleic acids. At the DNA and RNA, the alkylation of the guanosine triphosphate, guanine and adenine can appear. The degree of hydration of the microbes can play an important role in their destruction using ethylene oxide [1]. The main alkylation reactions are as follows:

$$R-OH + C_2H_4O \rightarrow R-O-CH_2-CH_2-OH$$

$$R-SH + C_2H_4O \rightarrow R-S-CH_2-CH_2-OH$$

$$R-COOH + C_2H_4O \rightarrow R-COO-CH_2-CH_2-OH$$

$$R-NH_2 + C_2H_4O \rightarrow R-NH-CH_2-CH_2-OH$$

Against prions, the ethylene oxide has no activity. The resistance of spores to ethylene oxide is less than ten times greater than the resistance of bacterial cells, yeasts and moulds. Bacterial spores can survive over a greater range of water activities and moisture contents than vegetative cells. They can withstand considerable degrees of desiccation. Spores with higher moisture contents and greater number of exposed active sites exhibit higher rates of

exchange of molecules with their immediate environment than do dry spores with low water activities. Ethylene oxide has also been shown to inactivate viruses [1].

The major factors that affect the efficiency of inactivation of microorganisms by ethylene oxide are:

- Gas concentration: Concentrations of less than 300 mg/L are insufficient to achieve sterility within practical process times. Very high gas concentrations imply very high pressures, which must correlate with increase in temperature within a sterilizer. For cold sterilization purposes, too high temperatures could be achieved. In practice, gas concentrations are usually with a range of 500 to 800 mg/L
- Temperature: Under constant conditions and within the range of limiting gas concentrations, ethylene oxide sterilization follows first-order chemical kinetics, i.e. the rate of inactivation is approximately doubled for every 10°C rise in temperature. The lowest temperature at which sterilization is theoretically possible is the temperature 10.7°C, because of the boiling point of ethylene oxide. The sterilization process normally operates with a cold sterilization range of 50–60°C.
- Humidity: Relative humidity has been recognized as critical factor in ethylene oxide sterilization. Ethylene oxide is quite ineffective against dehydrated microorganisms in a dry environment. Water acts as a carrier of ethylene oxide through permeable barriers of the cell. The water activity of the microbial cell and the relative humidity of the environment in which it finds itself are of critical importance to water movement and to the penetration of chemical sterilants to their target sites. The rate of microbial inactivation increases with increased relative humidity of the environment during exposure. By ethylene oxide sterilization, humidity levels are usually in the range of 50%–60% relative humidity.

Because gas concentration, temperature, humidity and the condition of the microorganisms can significantly affect a microorganism´s response to ethylene oxide, any microorganism used to evaluate the lethal effect of an ethylene oxide sterilization cycle should be standardized.

1.3.1.4 Effects of Sterilization with Ethylene Oxide on Materials

The ethylene oxide sterilization becomes the predominant sterilization method of sterilising heat sensitive polymer materials in healthcare products. The effects of ethylene oxide sterilization on materials:

- compatible with most polymeric materials
- some materials are sensitive to the humidity of the process (e.g. certain hydrophilic coatings)
- some materials can be more compatible with other methods under certain moulding, configuration and load conditions
- extremely temperature sensitive materials are not compatible at its higher temperatures

Ethylene oxide will sterilise most plastic materials including: acetals, elastomers, silicones, thermoplastic elastomers, natural rubber, urethane, nitrile butyl, styrene-butadiene, Teflons, polyamides, polyethylene, polyesters, polycarbonate, polysulfone, polyvinylchloride, polypropylene, polystyrene, thermosets, etc [2].

Polymeric materials are very permeable to ethylene oxide. Permeability is affected by the solubility of the gas in the polymer and the diffusivity of the polymer to ethylene oxide. Ethylene oxide is less soluble in polyethylene and polyesters than in celluloses or polyvinylchloride. Soft plastics and natural rubbers have higher diffusion coefficients for ethylene oxide than harder polymers such as acrylics and styrenes. Polymers with high diffusion coefficients will reach saturation solubility quicker than those with lower diffusion coefficients. A polymer that takes up residues slowly will release them slowly. Since devices may often be manufactured with several different types of polymeric material, it is difficult to

predict or quantify overall residue levels and practical rates of dissipation. A component such as the rubber plunger tip may as a result of its high diffusivity and thickness amount for most of the residues in a hypodermic syringe, although it is in itself only a minor component [27].

Due to its small size, ethylene oxide is able to be adsorbed by plastic materials. The factors affecting this adsorption are the type and size of polymeric material, the dimensions of the device and its packaging, as well as the sterilization parameters. For example, the thicker the surface is the greater the adsorption will be. Also, the adsorption is directly proportional to exposure time and concentration and reversibly proportional to the temperature.

In opposite to radiation and steam sterilisation, the ethylene oxide process can sterilise electronics or biomaterials without damage or destruction. Ethylene oxide can sterilise drug eluting stents that radiation and steam would damage.

1.3.1.5 Validation of Sterilization with Ethylene Oxide

Process validation is an essential part of ethylene oxide sterilization and it is described in detail in ISO 11135 and EN 550. Through the physical validation, the equipment and the proposed preconditioning and operating cycles must be carefully specified. Through biological validation, the gas concentration, humidity, temperature, time, sterilizer effects, load effects, etc. are determined. It must demonstrate that the SAL being obtained is no worse than 10^{-6}, it must demonstrate uniformity of treatment and it must provide the basis for routine monitoring. The microorganisms used for biological validation of ethylene oxide sterilization are the spores of *Bacillus subtilis* var *niger* [25]. A well-structured process design, its rigorous validation, and strict and efficient control of the sterilization cycle parameters are the key principles for the safe and efficacious release of the materials sterilized with ethylene oxide.

1.3.1.6 Applications of Sterilization with Ethylene Oxide

Ethylene oxide sterilization is suitable for small-scale and large-scale applications. It is primarily a method of cold sterilization and has so many associated complications that it is never used in preference to thermal sterilization for heat-stable materials. Sterilization by radiation is more reliable than ethylene oxide for cold sterilization, because it is simpler to control [4].

Ethylene oxide is penetrative. In order to inactivate microorganisms, ethylene oxide must come into contact with target sites in the microbial cell. Free movement of the gas to all parts and internal cavities is an essential prerequisite of the process. This imposes certain constraints on the design of product items, the design of packaging materials, the choice of packaging materials, and the manner in which products are packed in boxes, stacked, palletized and loaded into sterilizers. A basic prerequisite of product design is that sealed internal cavities should be avoided.

Some of the healthcare products that have been commonly sterilised with ethylene oxide are: bronchoscopes, catheters, dialysers, endoscopes, heart lung machines, laserscopes, rubber gloves, rubber tubing, scalpel blades, test tubes, stopcocks, syringes, vials, angioplasty devices, defibrillators, etc [2].

1.3.2 Sterilization with Hydrogen Peroxide Gas

Hydrogen peroxide is a powerful oxidizing agent with broad-spectrum activity and a good safety profile. Hydrogen peroxide is a colourless liquid with a nitrous smell. The chemical formula has the characteristic peroxide bridge –O-O-. The two O-H-bonds are not linear but in two orthogonal planes. Hydrogen peroxide was synthesized by the French chemist Thenard in 1818 and it became a very popular antiseptic for a time. Later, it was used as a disinfectant in the food industry, for the preservation of milk and water as well as fruit juice. Nevertheless, development of hydrogen peroxide vapour devices for sterilization proposes

did not occur until the 1990s [28]. Further physical properties of hydrogen peroxide are presented in the table 1 – 10:

Table 1 – 10: Physical properties of ethylene oxide gas.

HYDROGEN PEROXIDE	Properties
Molecular and Structure Formula	H_2O_2 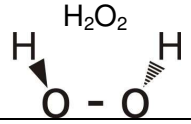
Molar Mass	34.0147 g/mol
Appearance	very light blue colour; colourless in solution
Density	1.114 g/mL (20℃; 30%) 1.450 g/mL (20℃; pure)
Melting Point **Boiling Point**	-0.43 ℃ 150.2 ℃
Water Solubility	Complete
EU Classification	Oxidant (O) Corrosive (C) Harmful (Xn)
Flash Point	Non-flammable

Hydrogen peroxide vapour is obtained through evaporation of a heated stock solution. This evaporation must take into account the fact that water in the solution is more volatile than the hydrogen peroxide itself. In order to obtain the required peroxide gas concentration, steam must be partially eliminated prior to the gas injection into the sterilization chamber. In order to obviate such a problem, a new method to generate hydrogen peroxide vapour from a non aqueous organic hydrogen peroxide complex instead of a stock solution has been proposed and a dual circuit generator designed which should also minimize this problem. Hydrogen peroxide gas is less stable and therefore less penetrating than ethylene oxide. [28]

Low concentrations, such as 3%, are widely available and legal to buy for medical use. Higher concentrations may be considered hazardous and is an aggressive oxidizes, which can corrode human skin. Direct contact toxicity is low, including the vapour phase which causes temporary irritation. Its effect is more acute on mucous membranes and the cornea while ingestion of a small quantity of a 35% solution can lead to lethal brain ischemia. Also, no carcinogenic activity has been established in humans [29].

1.3.2.1 Sterilization Procedure

The urgent need for low-temperature processes less harmful for operators and the environment than ethylene oxide has focussed the search by some investigators for a chemical whose benign byproducts are only oxygen and water alone. Vapour hydrogen peroxide technology has expanded, mostly in the food industry but also in biotechnology, pharmaceutical and scientific laboratory. In this technology a deep vacuum pulls hydrogen peroxide solution through a heated vaporizer and injects vapour into the sterilization chamber. An additional vacuum enhances gas penetration. The processing occurs at a temperature of 35-49℃ and the concentration of hydrogen peroxide is established around 10 mg/L. This concentration is obtained from a 35% solution [30].

The sterilization is accomplished in the sterility isolator. The schematic representation of sterility isolator is shown in figure 1 – 9.

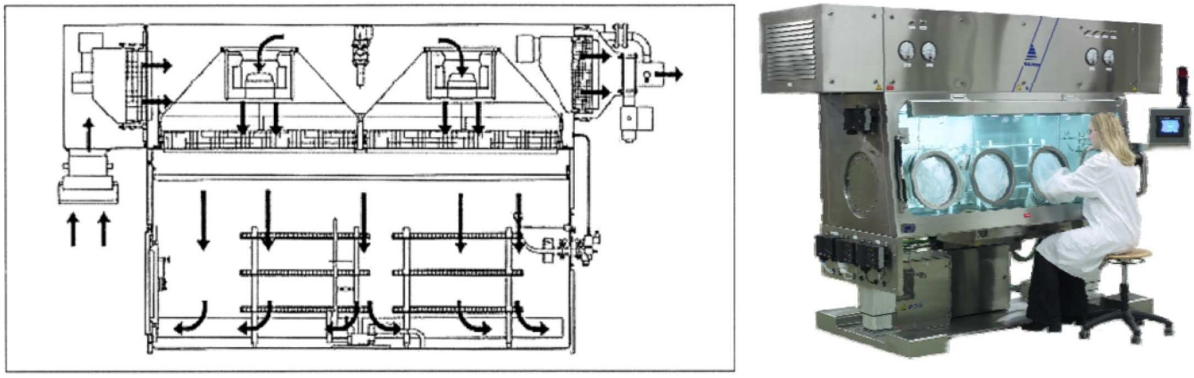

Figure 1 – 9: Representation of sterility isolator for sterilization with hydrogen peroxide gas.

1.3.2.2 Sterilization Cycle

The volume of the work chamber is about $1m^3$ and it is held under positive air pressure of about 60 Pa. Decontamination of the interior is performed with gaseous hydrogen peroxide. The isolator infrastructure holds a bottle with liquid 35% H_2O_2 on a balance. The gaseous H_2O_2 is entrained with the air steam of the recirculation fans and directed to the isolator work space through the terminal filters. During the conditioning phase of the isolator, prior to the proper decontamination phase, the relative air humidity is lowered to 20% to allow for an optimal take-up of the gaseous H_2O_2 in the decontamination phase. To initiate the decontamination process 70 g of 35% H_2O_2 are evaporated. Then, at intervals of 3 minutes each, additional 10 doses of 7 g H_2O_2 each are evaporated to maintain the decontamination effect and to obtain the required efficiency. After that process phase the isolator is purged with HEPA filtered air from the surrounding room in order to reach a final 1ppm H_2O_2 concentration within the work space of the isolator. This residual concentration allows the performance of sterility testing without any inhibiting effect. Total sterilization cycle time last approximately 2.5 hours [31].

The sterilization cycle is subdivided into four cycle phases, as follows:

(1) Preconditioning – the initial conditions required for decontamination are created in the chamber air. The parameters humidity and temperature of the chamber air must be monitored during this phase.

(2) Conditioning – is responsible for achieving a maximum bacterial reduction rate. The dose of gaseous H_2O_2 necessary to reach the desired decontamination effect is generated in the chamber. For this purpose, an initial quantity of H_2O_2 is vaporised from aqueous solution;

(3) Decontamination – the obtained effective dose is kept stable for the period of time that is necessary in order to achieve the desired decontamination result. In addition, the quantities of gaseous H_2O_2 that are no longer available in the chamber air due to adsorption and absorption on surfaces, used in bacterial reduction and decomposition are continuously made up;

(4) Purging – the required maximum residual concentration of H_2O_2 in the chamber is achieved through purging with fresh air.

Figure 1 – 10 illustrates the decontamination effect as a function of cycle phase.

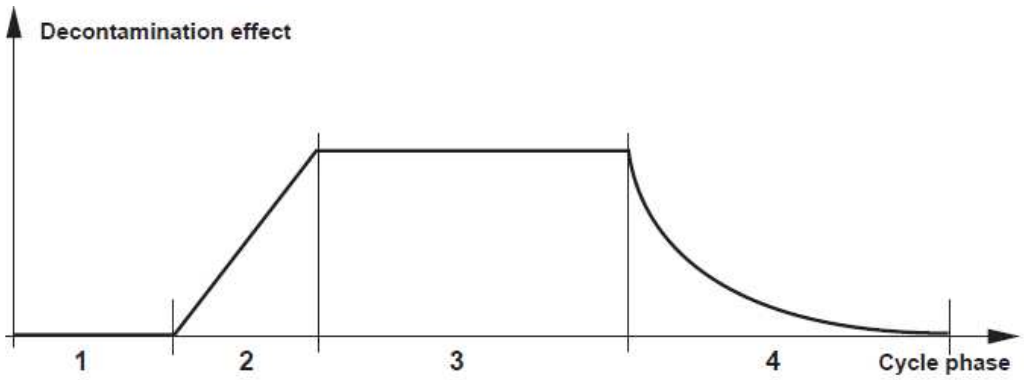

Figure 1 – 10: The decontamination effect as a function of cycle phase at sterilization with hydrogen peroxide gas.

1.3.2.3 Effects of Sterilization with Hydrogen Peroxide Gas on Microorganisms

Hydrogen peroxide is active against bacteria, fungi, yeast, spores and viruses. This activity is a function of concentration and contact time but seems to be rather independent of pH in the range from 2 to 10. Activity is greater against Gram-negative than against Gram-positive bacterial. Its sporicidal activity is greatly improved by increased temperature and concentration (between 25-60%) but does not seem to be affected by organic matter or salts [32].

In the vapour phase its activity seems to be greatly affected by water condensation on the target, which results in a lower local concentration. The maximum activity seems to occur at the start of the condensation process, i.e. at the dew point. Activity is also affected by decomposition due to catalytic action and adsorption of porous materials such as paper. [27]

The main mechanism of action seems to be the local formation of hydroxyl radicals, which are among the strongest oxidants known. These radicals could be produced under the action of superoxide ions by the reaction:

$$O_2^- + H_2O_2 \rightarrow OH\cdot + OH^- + O_2$$

Such highly active hydroxyl radicals are believed to react with membrane lipids, DNA, and double bonds of essential cell components.

1.3.2.4 Effects of Sterilization with Hydrogen Peroxide Gas on Materials

The ability to sterilize at low temperature is clearly a benefit in the reprocessing of temperature-sensitive devices and materials. On the other hand, certain materials absorb and break down peroxide, which can lead to inefficient sterilization process and longer aeration time. In general, peroxide is not suitable for the sterilization of large amounts of celluloses or other protein-based materials. Highly adsorbent or porous loads require special cycle development to ensure adequate sterilization, due to residuals. Peroxide gas also causes bleaching (or dulling) of coloured anodized aluminium [32].

1.3.2.5 Validation of Sterilization with Hydrogen Peroxide Gas

For the process validation, biological indicators with a specified resistance to H_2O_2 are applied. The testing of the H_2O_2 decontamination process use spores of *Bacillus stearothermophilus.* Likewise, during the routine, regular requalifications are required to guarantee proper operation. These include physical testing of all sensors (calibrations), inspection of the air handling system (qualification) and retraining the operators [31].

1.3.2.6 Applications of Sterilization with Hydrogen Peroxide Gas

Hydrogen peroxide gas based sterilization has been developed for various applications. A typical high-speed application can use 4.5 mg of hydrogen peroxide/liter at 40 to 45°C directly on a surface for less than 10 seconds exposure time and has the further advantage of producing minimal residues. In order to ensure the sterilization of packaged materials, like medical devices, porous materials or lumened and dead-ended instruments, it is necessary to remove air. In sterilization of healthcare products, the hydrogen peroxide gas is used to sterilise unwrapped metal instruments used for dental purposes. However, for applications where the SAL of 10^{-6} is required, the sterilization process only with hydrogen peroxide gas could not be applied [4].

1.3.3 Low Temperature Hydrogen Peroxide Plasma Sterilization

Plasma is defined as a fourth state of matter, after the solid, liquid or gaseous states. It can be produced by the action of either very high temperatures or electric and magnetic fields and it is composed of a cloud of ions, electrons and neutral species. Gases can be converted into plasma using a radiofrequency electromagnetic filed. For an ionized gas to be properly defined as plasma, the numbers of positively and negatively charged species present in the discharge need to be approximately equal [1].

Plasma can be divided into two categories. The first category is high-temperature plasmas, which includes plasmas that have temperatures about 5000°K. However, the plasmas used in sterilization processes belong to the second category, which are glow discharge or low temperature plasmas. They are created under reduced pressure conditions. The electrons or other species with sufficient energy disrupt the molecular bonds, while the temperatures of the atoms and molecules in the plasma are near ambient conditions. Because of these properties, the low-temperature plasma processes are well suited for the use in the sterilization of thermally sensitive materials [4].

The study of plasma to inactivate microorganisms began in the 1960s, but the commercialization of this technology did not occur until the early 1990s. At that time, many factors accelerated the development of sterilization processes employing plasma, such as need for a rapid, low-temperature, terminal sterilization process for growing number of heat- and moisture-sensitive devices [1]. Therefore, low-temperature hydrogen peroxide gas plasma sterilization has been applied in hospitals worldwide for almost a decade. Unlike ethylene oxide or formaldehyde steam sterilization, hydrogen peroxide is not toxic and does not leave residues on the sterilized instruments. Also, the instruments can be immediately used after sterilization [33].

1.3.3.1 Sterilization Procedure

The first commercial available apparatus for sterilization with low temperature hydrogen peroxide plasma was the Sterrad® 100 (Johnson&Johnson Medical Ltd), in year 1992. The commercial range has since diversified to include the Sterrad 100 S, Sterrad 50, Sterrad 200, Sterrad 100S/I GMP and Sterrad NX. Such a diversification was parallel to process improvements such as shorter cycles, adjustable volume of sterilizer chamber according to users' needs and dual doors. The Sterrad process is not strictly a cold plasma process as it is based on hydrogen peroxide, first in gas phase and then in plasma form [33].

The different Sterrad devices are represented in figure 1 – 11.



Figure 1 – 11: Sterrad® 50 (left), Sterrad® 100 and 100S (center) and Sterrad® 200 (right).

The sterilization procedure starts by placing the object to be sterilized in a vacuum chamber. The objects are wrapped in plastic sterilization pouches, to keep them sterile after processing. Articles have to be placed in packages which allow free penetration of hydrogen peroxide in order to ensure a contact with them while still providing an efficient sterile barrier. These materials can be made of polyethylene (Tyvek®), polypropylene or polycarbonate/polystyrene. As cellulose high absorbs hydrogen peroxide, all papers or derivatives must be avoided for packaging. In the chamber, the objects are placed on trays, which are entirely surrounded by a perforated, powered electrode [34]. Figure 1 – 12 shows the schematic diagram of the interior of Sterrad® 100 device.

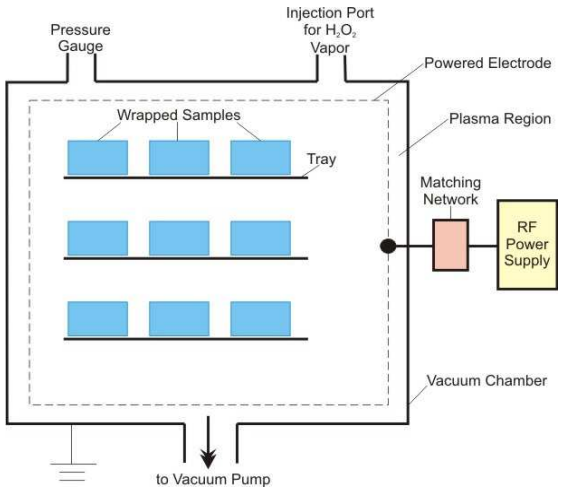

Figure 1 – 12: Schematic diagram of the interior of the Sterrad® 100.

1.3.3.2 Sterilization Cycle

The sterilization cycle lasts for at least 75 minutes with the chamber temperature maintained at 45°C. The cycle can be divided into five steps: an evacuation phase; an injection phase, a diffusion phase; a plasma phase and a final phase to re-establish atmospheric pressure.

The Sterrad 100 sterilization cycle is depicted in figure 1 – 13.

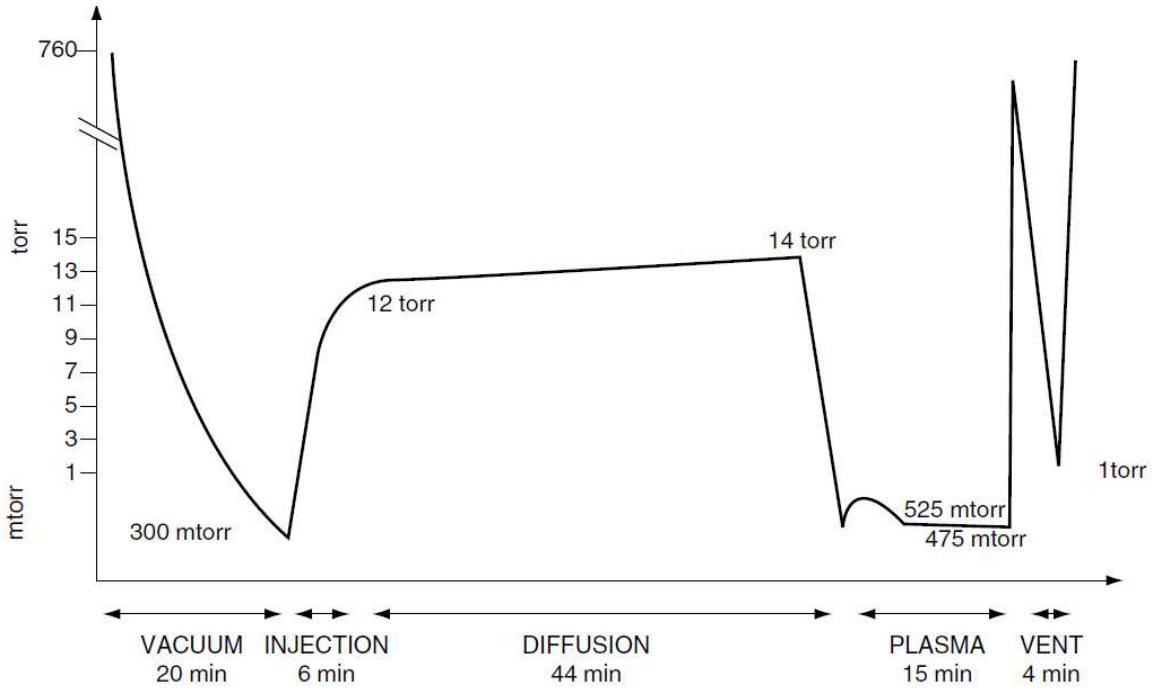

Figure 1 – 13: Sterrad® 100 typical sterilization cycle.

The sterilizing process is initiated by a vacuum of 300 mTorr to remove air and moisture. If any moisture is present on the objects to be sterilized the vacuum will not be reached and the cycle aborts. Then, hydrogen peroxide with a minimum concentration of 6 mg/L is injected and vaporized. It diffuses throughout the sterilizer load for 50 minutes [35]. An electrical filed created by a radio-frequency of 13.56 MHz generates a gas plasma from the hydrogen peroxide, which is broken down into free radicals:

$$\tfrac{1}{2}O_2 + H-O-H \xrightarrow{e^-} OH\cdot + OH\cdot$$

$$\tfrac{1}{2}O_2 + OH\cdot + H-O-H \xrightarrow{1\text{–}10eV} H_2O + O-O-H\cdot$$

$$H-O-O-H \xrightarrow{e^-} H-O-O-H'$$

$$H-O-O-H' \xrightarrow{e^-} H-O-O-H' + \text{radiation}$$

(visible or UV)

OH· = hydroxyl free radical
OOH· = hydroperoxyl free radical
H_2O_2' = excited hydrogen peroxide with high energy level electron

The radicals react with and kill the microorganisms. At the end of the plasma phase, the reactive species lose their high energy and recombine to form oxygen, water and other nontoxic byproducts. The sterilization chamber is returned to atmospheric pressure by introduction of high efficiency filtered air. The sterilized packs can then be handled safely, either for immediate use or storage without aeration [36,37].

1.3.3.3 Effects of Low Temperature Hydrogen Peroxide Plasma Sterilization on Microorganisms

By definition, a sterilization process must have the ability to inactivate a broad spectrum of microorganisms, including resistant bacterial spores. The Sterrad system contains a number of species (i.e. hydrogen peroxide, free radicals and ultraviolet radiation) that are known to be capable of reacting with molecules essential for the normal metabolism and reproduction

of microorganisms [38]. Three basic mechanisms are involved in the plasma inactivation of microbes:

- direct destruction of UV irradiation of the genetic material of microorganisms
- erosion of the microorganisms atom by atom, through intrinsic photodesorption by UV radiation to form volatile compounds combining atoms intrinsic to the microorganisms
- erosion of the microorganisms atom by atom, through etching, to form volatile compounds as a result of slow combustion using oxygen atoms or radicals emanating from the plasma. In some cases, etching is further activated by UV photons, increasing the elimination rate of microorganisms.

Microbicidal activity studies were conducted against vegetative bacterial (including mycobacteria), bacterial pores, yeasts, fungi and viruses. These organisms were chosen for their resistance to hydrogen peroxide, other chemical sterilants and disinfectants, or ionizing radiation. The microbicidal activity has been studied using shortened cycles with lowered hydrogen peroxide concentration and decreased diffusion times in the true vapour-phase or plasma periods. All of the organisms shown in table were found to be readily inactivated by an abbreviated Sterrad system cycle consisting of 20 minutes of diffusion with 2 mg/L of hydrogen peroxide and 5 minutes of plasma at a power of 300 W [38]. The test organisms, as well as the results of these tests are presented in table 1 – 11.

Table 1 – 11: Spectrum of activity; vegetative bacterial, spores and fungi by low temperature hydrogen peroxide plasma sterilization.

Microorganisms	**Type**	**Interest in testing**	**Results:** **No. positives /No. tested**
Bacillus Stearothermophilus	Bacterial spore	H_2O_2 resistant Steam indicator organism	0/9
Bacillus subtilis var. niger	Bacterial spore	H_2O_2 resistant EtO indicator organism	0/9
Bacillus Pumilus	Bacterial spore	Ionizing radiation resistant Radiation indicator organism	0/9
Staphylococcus aureus	Gram positive	H_2O_2 resistant Clinical significance	0/9
Deinococcus radiodurans	Gram positive	Ionization radiation resistant	0/9
Pseudomonas Aeruginosa	Gram negative	Clinical significance	0/9
Ercherichia Coli	Gram negative	Clinical significance	0/9
Serratia Marcescens	Gram negative	H_2O_2 resistant Clinical significance	0/9
Maroxella Osloensis	Gram negative	Ionizing radiation resistant	0/9
Mycobacterium Bovis	Acid fast	Chemical resistant Clinical significance	0/9
Candida Albicans	Yeast	H_2O_2 resistant	0/9
Candida Parapsilosis	Yeast	H_2O_2 resistant	0/9

		Clinical significance	
Trichophyton mentagrophytes	Filamentous mold	Clinical significance	0/9
Aspergillus Niger	Filamentous mold	H_2O_2 resistant Clinical significance	0/9

1.3.3.4 Effects of Low Temperature Hydrogen Peroxide Plasma Sterilization on Materials

According to the literature, hydrogen peroxide plasma is compatible with fewer materials than ethylene oxide gas [39]. Material decay can be caused by hydrogen peroxide, vacuum and the electrical energy of the plasma generator. The oxidizing action of hydrogen peroxide leads to modifications of polymers during sterilization and cause noticeable surface modifications. However, the Sterrad process has good material compatibility with a wide range of medical devices. It was reported that approximately 95% of over 600 resterizable devices tested were found to be compatible with the Sterrad process [40]. Most of the devices that appear incompatible exhibited a cosmetic change, such as fading of dyes, anodized aluminium compounds or a coloured plastic identification ring that did not affect the functionality of the devices. The Sterrad process has also been found not to have an adverse affect on the bulk properties of certain plastics materials that are degraded by exposure to radiation sterilization. The Sterrad process is also very compatible with metallic devices, containing the cutting edges.

Generally speaking, there is a good compatibility with metals such as aluminium, stainless steel and alloys or polymers such as polypropylene, polyethylene, polyvinyl chloride, silicone, polyurethane, vinyl acetate, polycarbonate and Teflon. Compatibility with glass is good, including optical fibres. Some other materials are not well suited to the Sterrad process, like cellulose, viscose, cotton, liquid, powders and foam devices. Hydrogen peroxide is absorbed by cellulose and that prevents that the normal cycle occur. In the same way, the presence of liquid interferes of proper vacuum formation [2].

1.3.3.5 Validation of Low Temperature Hydrogen Peroxide Plasma Sterilization

In order to verify that a load has been correctly sterilized, the parameters are controlled by using a series of indicators:

- Printing of the sterilization parameters (pressure, phase duration)
- recovery of coloured indicators (strips or adhesive tape)
- Verification of the analogy of the load with a validated analogous load
- Reading after 48 h of the biological indicators.

The most resistant organism in microbicidal studies was *B.Stearothermophilus* spores. In february of 1999, a self-contained biological using 10^6 of this spores have become available internationally for the routine monitoring of the Sterrad process. The required microbiological testing for sterilization with low temperature hydrogen peroxide plasma is described in details in ISO 14937. [33, 41]

1.3.3.6 Application of Low Temperature Hydrogen Peroxide Plasma Sterilization

The Sterrad 100 has been approved by The Food and Drugs Administration (FDA) for commercialization. It was established that the process allows a sterilization assurance level of 10^{-6} except for following material devices:

- polymer articles (1m ≤ length ≤ 2m and diameter ≥ 1mm)
- metal articles (length ≤ 40 cm and 1mm ≤ diameter ≤ 3mm)
- metal articles (40cm ≤ length ≤ 50 cm and 1mm ≤ diameter ≤ 3mm)

Sterilization of devices incorporating long and narrow lumens can be unreliable. To reduce these risks, an adapter booster is commercially available. This comprises a 59% hydrogen peroxide capsule to be fixed to one end of the device. However, one end-closed device cannot be processed [2].

Sterrad devices are recommended for the following situations:

- Sterilization of thermosensible medical devices in accordance with invalidated specifications and after results of biological indicator reading
- High level disinfection of thermosensible medical devices when steam cannot be used
- Medium-level disinfection or flexible endoscopes.

The features of the low-temperature hydrogen plasma sterilization procedure are:

- Appropriate sterilization procedure for heat- and moisture-sensitive devices
- Not toxic
- Does not leave residues on the material
- Instruments can be immediately used after sterilization

Numerous biocompatibility tests performed on raw materials as well as medical devices did not reveal any toxicity risks. The medical devices processed in the Sterrad sterilizer do not pose a risk to the health of patients or personnel handling the devices, because the hydrogen peroxide used in the process decomposes to form the nontoxic by-products, oxygen and water, during the course of the sterilization cycle [3].

The limitation is the weak penetrating power of plasma species. In the presence of organic residues, of packaging material, complex geometries, or of a large number of devices to be sterilized in a given chamber, the effectiveness of plasma is severely limited. Therefore, the researchers in the filed of plasma sterilization agree that plasma offers much promise a sterilizing technique, particularly toward prions and endotoxins, but its lack of penetrating power remains its greatest limiting factor [2].

2 Optical Sensors General

Chemical sensors are defined as follows: "*Chemical sensors are (small) devices capable of continuous recognizing concentration of chemical constituents in liquids or gases and converting this information in real-time to an electrical or optical signal.* [42]*"* A sensor works (in the ideal case) reversibly and continuously. Ideally, a sensor is placed in contact with the sample and the results are displayed over time.

Many types of sensors are known. They can be classified on the basis of the transducers as follows:

- Electrochemical and microelectronic sensors (potentiometric sensors, amperometric sensors, conductivity sensors);
- Optical sensors;
- Thermal sensors;
- Mass-sensitive sensors.

No universal basic principle exists for sensor´s development. Every practical task requires a specific adaptation of the measuring principle.

An optical chemical sensor consists of:

- A filter: improves selectivity and eliminates interferences;
- A receptor: the chemical sensitive layer - a recognition element – where a sensing element interacts with chemical components (analytes);
- A transducer: transforms the chemical information into an electrical or optical signal based on certain physical or physico-chemical principles and it also serves for amplification of the signal;
- An amplifier: data evaluation electronics.

The composition of optical chemical sensor is schematically presented in figure 2 – 1.

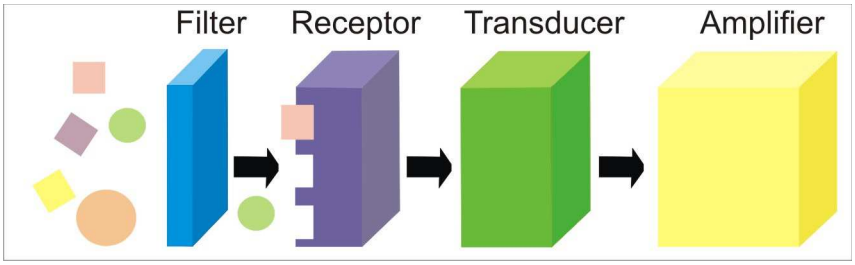

Figure 2 – 1: Composition of the optical chemical sensor.

Optical sensors are based on the measurement of changes in an optical quantity such as: refractive index, light scattering, reflectance, absorbance, fluorescence, chemiluminescene, etc. Therefore, the transducer in optical chemical sensors always has to be a configuration involving one or more photodetectors such as a photodiode or a CCD chip. Optical sensors have also been named optodes and optrodes; both terms are used to emphasize the fact that the information collected by such sensors involves optical measurements, in analogy with electrons as in case of electrodes [43].

The signal of optical sensors is generally derived from intrinsic or extrinsic optical signals. The spectral properties of the analyte are used for its determination. If the analyte does not display changes in optical properties, an indicator or label is used tocorrelate the analyte´s concentration with a useful optical signal.

The advantages of optical sensors over electrochemical sensors are:

- Ease of miniaturization;
- The materials and devices used, have become commercially available and cheaper;

- Not subjected to electrical interferences;
- An additional reference element is not required as in contrast to the electrodes;
- Remote measurements are possible, when using optical fibre sensors.

Optical sensors have also some drawbacks:

- Ambient light can interfere on optical properties;
- Narrow dynamic range compared to electrochemical sensors;
- Non-linear calibration;
- Limited long-term stability due to photobleaching or leaching of the immobilized indicator.

2.1 Luminescence-based Optical Sensors

A luminescence molecular sensor is a device, which measures the difference in the intensity of the signal of a fluorophore, when its fluorescence or phosphorescence characteristics change in presence of an analyte. The fluorophores acts as a signal transduced that, in the presence of the analyte, changes its photophysical characteristics which can be expressed as an optical signal and give information about the analyte. For measurements based on photoluminescence it is needed: a sensor, an optical measurement device – light source, an optical fibre (optional) and a detector connected with electronics which shows understandable results [44].

Numerous chemical and biochemical analytes can be detected by photoluminescence methods:

- Cations (H^+, Li^+, Na^+, K^+, Ca^{2+}, Mg^{2+}, Zn^{2+}, Pb^{2+}, Al^{3+}, Cd^{2+}, etc.);
- Anions (halide ions, citrates, carboxylates, phosphates, ATP, etc.);
- Neutral molecules (sugars, e.g. glucose, etc.);
- Gases (O_2, CO_2, NO, etc.).

Analytical techniques, based on fluorescence and phosphorescence detection are very popular because of their high selectivity and possibility of remote sensing with the use of optical fibres. When an analyte is fluorescent, direct fluorometric detection is possible at the appropriate excitation and observation wavelength [45]. However, most ions and molecules are not fluorescent therefore the following indirect methods need to be used:

- Derivatization that is a reaction of the analyte with a reagent leading to a fluorescent compound. It is often used in conjunction with a liquid chromatography with fluorescence detection;
- Formation of a fluorescent complex;
- Fluorescence quenching resulting from the collision of the analyte with fluorescent compound.

Very different techniques are used in the design of luminescence-based optical sensors. One can distinguish between passive and active modes of operation.

In the passive mode, the optical device measures the variation in luminescence characteristics (intensity, lifetime, polarization) of an intrinsically fluorescent analyte. In most cases the optical device involves an optical fiber – passive opt(r)ode.

In the active mode, the optical device uses for optical transduction the changes in the luminescence characteristics of a molecular sensor, which result from the interaction with an analyte [45]. The two main optical configurations are:

- In most cases, the photoluminescent molecular sensor is immobilized in a matrix that permits diffusion of the analyte. Any compound that interferes with the fluorophore has to be retained inside the sample and not leak into the matrix. The matrix does not only have to provide specificity but must also be stable and not dissolve into the sample. Specific fluorophores sensitive to the presence of many molecule

compounds like oxygen, hydrogen, or heavy metals exists and ensure a very robust sensing capability.

- The use of the continuous evanescent filed that exists at the surface of an optical fiber, where the cladding layer is replace by a layer containing the photoluminescent molecular sensor in a short portion of the optical fiber. At each reflection on the surface of the fiber core, the evanescent wave penetrates into the layer within a distance of the order of the wavelength of the propagating light. Fluorescence or phosphorescence emitted within this evanescent region can be reciprocally coupled back into the core and conveyed toward the detector.

The photoluminescence molecular sensors can be divided, on the basis of the type of fluorophore in three different classes [43]:

Class 1: Fluorophores that undergo quenching upon collision with an analyte (O_2, Cl^-, etc).

Class 2: Fluorophores that can reversibly bind an analyte. Fluorescence can be either quenched or enhanced upon binding.

Class 3: Fluorphores that are linked, with or without a spacer or not, to a receptor. The design of such sensors requires special care in order to fulfill the criteria of affinity and selectivity.

The above described sensors are shown on figure 2 – 2.

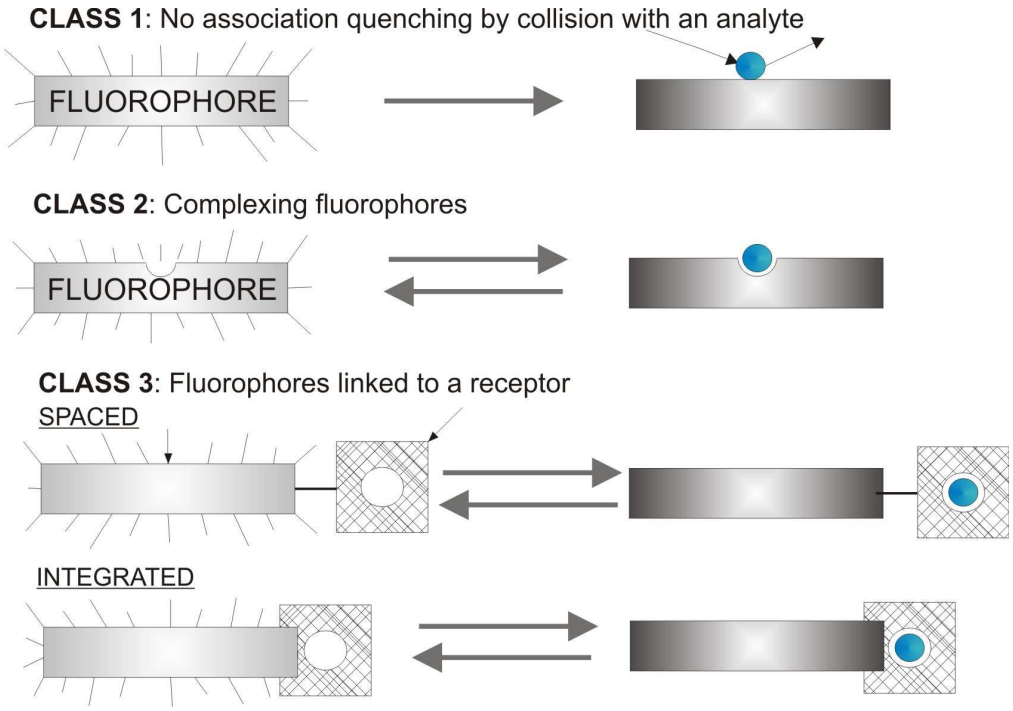

Figure 2 – 2: The classification of luminescence molecular sensors in three different classes, based on the fluorophore.

Measurements based on the photoluminescence are much more used than measurements based on absorbance. Light absorbance is measured as the difference between the light passing through the reference and the sample. In fluorescence the intensity is measured directly, without comparison with a reference beam. Fluorescence detection at 10^{-10}M is easily accomplished with most fluorometers, on the other hand in absorbance measurement, even with exceptional optics and electronics, such concentration would be very difficult to detect. The measurements, based on the fluorescence, are also widely used, because of their high selectivity and sensitivity, quick response time, local observation, remote sensing by using optical fibers, etc. Because the detected fluorescence signal is a direct response of the dye-analyte complex no reference measurement is required. All the described advantages of the fluorescence measurements have a great factor in their success [45].

However, in this study the sensors on which the effects of the diverse sterilization methods were determined are based on both methods; photoluminescence and absorbance.

2.1.1 Mechanisms of Sensing

Fluorescence intensity can be used to measure the concentration of the fluorescent species. However, the goal in the fluorescence sensing is not to measure the amount of florophore but the concentration a define analyte. Fluorescence sensing requires a change in the spectral properties of a fluorescent probe in response to the analyte. These changes can occur in the intensity, excitation spectrum, emission spectrum, anisotropy or lifetime of the sensing probe [43]. The spectral observables for fluorescence sensing are presented in figure 2 – 3.

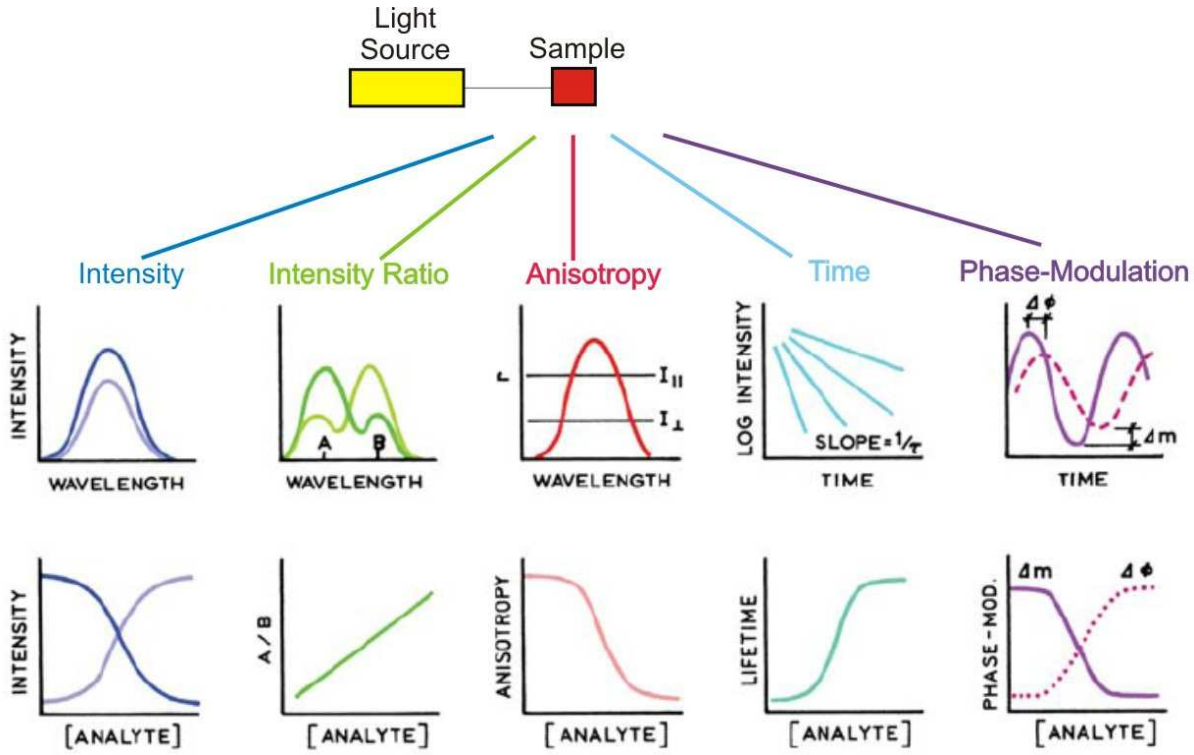

Figure 2 – 3: Spectra observables for luminescence sensing.

The most direct sensing method is the one which relies on the changes of the fluorescence intensity of the probe changes in response to the analyte. Such changes often occur for fluorophores that are subjected to collisional quenching by a relevant species such as oxygen. The quencher decreases the fluorescence intensity of the fluorophore. However, the quenching is only useful with a few clinically relevant analytes.

Fluorescence microscopy use wavelength-ratiometric probes because the ratios are independent of the probe concentration. The analyte concentration can then be determined from the ratio of fluorescence intensities measure at two excitation or emission wavelengths.

Another ratiometric method is fluorescence polarization or anisotropy. In this case the analyte causes a change in the anisotropy of the sample. Anisotropy measurements are frequently used in competitive immunoassays, in which the actual analyte displaces labeled analyte that is bound to the specific antibody. This results in a decrease in the anisotropy.

The most used method for photoluminescence sensing is the one based on changes in their lifetime of the fluorophore, which can be measured using either time-domain or frequency domain methods. A sample containing the fluorophore can be excited with an infinitely sharp pulse of light (δ-function). This results in an initial population (n_0) of the excited state of the fluorophore. The excited-state population decays with a rate k_r+k_{nr} according to:

$$\frac{dn(t)}{dt} = (k_r + k_{nr})n(t) \quad (2.1)$$

where n(t) = the number of excited molecules at time t following excitation
k_r = the radiation rate constant
k_{nr} = the non-radiation rate constant

Each excited fluorohpore has the same probability of emitting in a given period of time. This results in an exponential decay of the excited state population as follows:

$$n(t) = n_0 \exp(-t/\tau) \quad (2.2)$$

In a fluorescence experiment, the fluorescence intensity is rather observed as the number of excited molecules and the intensity and is proportional to the number of excited molecules. Therefore, for a single exponential decay, the equation can be rewritten:

$$I(t) = I_0 \exp(-t/\tau) \quad (2.3)$$

where I_0 = the intensity at time zero

The lifetime τ is the inverse function of the sum of the rates which depopulate the excited state:

$$\tau = (k_r + k_{nr})^{-1} \quad (2.4)$$

The fluorescence lifetime can be determined from the slope of a plot of log I(t) versus t or by fitting the data to assumed decay models.

The phase angle (Φ) and the modulation (m) can be also employed to calculate the lifetime using the following equations:

$$\tan\Phi = \omega\tau_\Phi \rightarrow \tau_\Phi = \omega^{-1}\tan\Phi \quad \text{by phase measurements} \quad (2.5)$$

$$m = \frac{1}{\sqrt{1+\omega^2\tau_m{}^2}} \rightarrow \tau_m = \frac{1}{\omega}\left[\frac{1}{m^2-1}\right]^{1/2} \quad \text{by modulation measurement} \quad (2.6)$$

where Φ = phase shift
ω = angular frequency
m = modulation

Intensity decays can be single-exponential, multi-exponential or non-exponential. For a single exponential decay in the time domain the actual lifetime is the time needed for the intensity to decay to 1/e of its initial value. For a multi-exponential decay, the 1/e time is typically not equal to any of the decay times [45].

2.2 Oxygen Optical Sensors

Oxygen determination is of utmost importance in many fields of science and technology, including biotechnology, medicine, food industry, etc. Various methods have emerged and been applied in manufacture, clinical monitoring, medical applications and biology. Among electrochemical oxygen sensors, the Clark oxygen electrode has been in the mainstream. However, a class of oxygen sensors based on fluorescence quenching has been extensively developed in last two decades. Optical oxygen sensors are expected to be inexpensive, easily miniaturized and simple to use, to have extraordinary sensitivity and reversibility and not to suffer from electrical interference or oxygen consumption. The use of optical oxygen sensors depends on three factors: optical sensing probes, supporting materials and determination methods [46].

Long lifetimes and excitation with red or near-infrared wavelengths are a property of organometallic complexes and such complexes have been frequently used in oxygen sensors. In organometalic complexes, the spin orbit coupling is enhanced because of the presence of the metal ion within the organic complex, which enables an efficient radiative decay from the lowest triplet state to the single ground state of the molecule - phosphorescence. Organometallic complexes present different phosphorescence lifetime which depend on the transient metal complex and the matrix material, typical values are in the range of microseconds, which is several orders of magnitude larger than the fluorescent excited state lifetime.

The diverse organometallic complexes are also useful for applications, such as oxygen sensing in blood or through skin because the autofluorescence from tissues or any biological sample is lower for longer excitation wavelengths. The use of longer wavelengths also avoids light absorption by hemoglobin and melanin. In the past there has been a limited number of fluorophores emitting at long wavelengths but the number of fluorophores that emit between 700 and 1000 nm has been growing and this region is sometimes called the therapeutic range [43].

An important feature for any sensor is selectivity. For oxygen, the selectivity is provided by a unique combination of the fluorophore and the supporting matrix. Desirable matrix properties also include high permeability for oxygen, adequate mechanical and chemical stability and high solubility for the indicator. Almost all fluorophores are collisionally quenched by oxygen, so that no fluorophore is completely specific for this analyte. The fluorescent probe should be sensitive to quenching by the oxygen. In order to obtain good sensitivity to low concentrations of oxygen, it is necessary to chose fluorophores characterilized by: long lifetime in the absence of oxygen, photostability, high luminescence quantum yields, efficient quenching, compatibility with solid-state light source and high molar absorbance.

2.2.1 Fluorescence Quenching

The intensity of fluorescence can be decreased by a wide variety of processes. Such decreases in intensity are called quenching. Quenching can occur by different mechanisms of which at least three mechanisms of quenching are known: and they are:

1. Intersystem crossing or the heavy atom effect
2. Electron exchange or Dexter interactions
3. Photoinduced electron transfer.

A collision between a fluorophore in its excited state and the quencher results a in radiationless deactivation and is called collisional or dynamic quenching. Collisional quenching occurs when the excited-state fluorphore is deactivated upon contact with some other molecule in solution, which is called the quencher. On the base of molecular interaction or contact between the quencher and the fluorophore, the latter returns to the ground state. In such process the molecules are not chemically altered. On the other hand, in the case of static quenching a complex is formed between the fluorphore and the quencher, and this ground state complex is nonfluorescent. Static quenching causes no change in the fluorescence decay time of the fluorophore, because the process takes place in the ground state [43].

However, the fluorescence characteristics (decay time and/or fluorescence quantum yield) of the excited fluorophore are affected by the presence of quencher as a result of the competition between its intrinsic de-excitation and these intermolecular processes:

- After excitation by a light pulse, the excited-state population of fluorophore and consequently the fluorescence intensity decreases more rapidly than in the absence of excited-state interaction with quencher;
- The fluorescence quantum yield is decrease in the presence of quencher.

The phenomenon of quenching provides a valuable context for understanding the role of the excited-state lifetime in allowing fluorescence measurements to detect various dynamic processes. The emission occurs over a longer period of time which provides an opportunity for interactions between the fluorophore and other molecules. Collisional quenching of fluorescence by, for example, molecular oxygen is an example of the expansion of time and distance provided by the fluorescence lifetime. Oxygen molecule diffuses in approximately 10^{-8}s or 10 ns. In 1 ns, the quencher can diffuse for about 15 Å. Einstein equation gives the diffuse distance of quencher during the lifetime of excited state:

$$\Delta x^2 = 2D\tau \tag{2.7}$$

where D – diffusion coefficient, cm^2/s.

2.2.1.1 Molecular Oxygen as a Quencher

A wide variety of substances act as quenchers of fluorescence. These are oxygen, halogens, amines, molecules with electron deficit, etc. One of the best-known collisional quenchers is molecular oxygen which quenches almost all known fluorophores. The most likely mechanism is that the paramagnetic oxygen causes the fluorophore to undergo intersystem crossing to the triplet state, which is promoted by spin-orbit coupling of the excited (singlet) fluorophore and the molecular oxygen [45].

The ground state of molecular oxygen is a triplet state (denoted $^3O_2$ or $^3\Sigma$) and it has two low-lying singlet states ($^1O_2$ or $^1\Delta$). Quenching of singlet or triplet states via energy transfer to produce $^1\Delta$ oxygen is thus possible:

$$^1A^* + {}^3O_2(^3\Sigma) \rightarrow {}^1A + {}^1O_2(^1\Delta) \text{ or } {}^3A^* + {}^3O_2(^3\Sigma) \rightarrow {}^3A + {}^1O_2(^1\Delta)$$

The contribution of oxygen quenching to the decay of an excited state can be expressed by a quenching term k_q [O_2], which is added to the rate constants of de-excitation. The longer the lifetime in the absence of O_2, the stronger the sensitivity to the presence of oxygen, and for some applications, solutions must be degassed by bubbling with nitrogen (or argon), or by the freeze-pump-thaw technique.

2.2.1.2 Derivation of the Stern-Volmer Equation

The fluorescence intensity observed for a fluorophore is proportional to its concentration in the excited state, M*. Under continuous illumination a constant population of excited fluorophores is established, and therefore dM*/dt = 0. The experimental quenching rate constant k_q is assumed to be time-independent. The time evolution of the concentration of M* is expressed by the following differential equation:

$$\frac{d[M^*]}{dt} = -\left(\frac{1}{\tau_0} + k_q[Q]\right)[M^*] \tag{2.8}$$

where k_q = experimental quenching rate constant,
τ_0 = lifetime of fluorophore in the absence of quencher,
[M*] = concentration of fluorophore in excited state,
[Q] = concentration of quencher.

Integration of differential equation (1.9) with the initial condition $[M^*] = [M^*]_0$ at t = 0 yields:

$$[M^*] = [M^*]_0 \exp\left\{-\left(\frac{1}{\tau_0} + k_q[Q]\right)t\right\} \tag{2.9}$$

The fluorescence intensity is proportional to the concentration of $[M^*]$ and is given by:

$$i(t) = k_r[M^*] = k_r[M^*]_0 \exp\left\{-\left(\frac{1}{\tau_0} + k_q[Q]\right)t\right\} = i(0)\exp\left\{-\left(\frac{1}{\tau_0} + k_q[Q]\right)t\right\} \quad (2.10)$$

where k_r = radiative rate constant of [M*].

The fluorescence decay is a single exponential whose time constant is:

$$\tau = \frac{1}{\frac{1}{\tau_0} + k_q[Q]} = \frac{\tau_0}{1 + k_q\tau_0[Q]} \quad (2.11)$$

Hence,

$$\frac{\tau_0}{\tau} = 1 + k_q\tau_0[Q] \quad (2.12)$$

This equation illustrates an important characteristic of collisional quenching, which is an equivalent decrease in fluorescence intensity and lifetime. For collisional quenching:

$$\frac{\tau_0}{\tau} = \frac{I_0}{I}, \quad (2.13)$$

where I_0 = fluorescence intensity in the absence of quencher,
I = fluorescence intensity in presence of quencher.

The form of Stern-Volmer equation is:

$$\frac{I_0}{I} = 1 + k_q\tau_0[Q] = 1 + K_{SV}[Q], \quad (2.14)$$

where K_{SV} – Stern-Volmer quenching constant.

Quenching data are usually presented as plots of I_0/I versus $[Q]$. It is expected, that the I_0/I is linear in dependence to the concentration of the quencher, with a slope is equal to K_{SV}. A linear Stern-Volmer plot is generally indicative of a single class of fluorophores, all equally accessible to the quencher.

2.3 pH Optical Sensors

pH is a convenient measure of the acidity/alkalinity of a system at a specified temperature. It is measured on a continuous scale from 0 to 14. Measurements of pH are carried out for a wide variety of purposes, for example on drinking water, to test a chemical against a specifications, as part of an analytical methods to monitor and control biochemical and physiological reactions, as process control in the chemical industry, for environmental monitoring of waste and effluents, etc [47].

The pH value of a given solution is a measure of the activity of the hydrogen ion, which is the effective concentration and is a measure of the ability of the hydrogen ion to move and combine with other ions [47]. The equations for calculating of hydrogen ion activity and pH are:

$$pH = -\log(a_{H^+}) \quad (2.15)$$

$$a_{H^+} = 10^{-pH} = f_{H^+}[H^+] \quad (2.16)$$

where a_H^+ = hydrogen ion activity
c_H^+ = hydrogen concentration

f_{H^+} = activity coefficient
pH = negative base 10 power of hydrogen ion activity

Water acts as both and acid and a base because upon dissociation it yields both a hydrogen ion and hydroxyl ion. Neutralization is the association of the hydrogen and hydroxyl ions to form water. A more general definition of an acid as a proton donor and a base as a proton acceptor is needed for non-aqueous solutions.

The titration curve is the essential tool for every aspect of pH system design and analysis. Therefore, to design of a pH system it is crucial to generate a titration curve at the process temperature with enough data points to cover the operational range and show the curvature within the control band – absolute magnitude of the difference between the maximum and minimum allowable pH.

Moreover, the dissociation constants are used to define the relationship between the activities of the components in equilibrium with each other. They also provide a measure of the strength of the acid or the base. In most applications, the stream concentration will be assumed to be dilute enough so that the charge balance equations that utilize these dissociation constants will be simplified by the omission of activity coefficients. The numerical value of the dissociation constant K typically falls in the same range as the hydrogen ion concentration, so that it is convenient to express it as a negative base ten logarithm as it is done for the pH. It is helpful to convert each pK_b to a pK_a via following equation:

$$pK_a = -\log K_a \tag{2.17}$$

$$pK_b = -\log K_b \tag{2.18}$$

$$pK_a = pK_w - pK_b \tag{2.19}$$

where pK_a = negative base 10 logarithmic acid dissociation constant
pK_b = negative base 10 logarithmic base dissociation constant
pK_W = negative base 10 logarithmic water dissociation constant

The acid or base strength increases as its pK_a or pK_b decreases. A pK_a or pK_b value less than zero means that the product of the ion activities is greater than the activity of the source molecule. Such acids and bases are called “strong” since they are essentially completely dissociated in the 0 to 14 pH range. Correspondingly, acids with a pK_a or pK_b greater than one are called “weak”. The relative weakness increases as the pK_a or pK_b increases. When the pH equals the pK_a, the negative acid ion activity is equal to the acid molecule activity. The dissociation is at the midpoint.

The conventional method used to measure pH is electrometric. It uses glass electrodes and is based on the measurement of the electromotive force of a cell which has a reversible electrode whose electrochemical potential depends on the activity of the hydrogen ions and hence on the pH. The use of such an electrode for pH measurement is limited. For example, it medicine where on-line monitoring of blood pH is desirable, the use of glass electrode was proved to be unpractical because of its large size, rigid design and possible electrical hazard. In addition, the presence of local electrical potentials in the body may affect the performance of the pH electrodes. Further, pH electrodes cannot be used for solutions through which an electrical current is flowing, for example in electrolysis cells and batteries. Other problems include susceptibility of wire leads and couplings to deterioration under corrosive conditions, or conditions of altering temperatures. Many of these problems can be overcome with the use of optical sensors along with spectroscopic techniques instead of glass electrodes [48].

Optical pH sensors are based on pH-induced reversible changes in optical or spectroscopic properties such as absorbance, reflectance, fluorescence, energy transfer, etc. The major component in an optical pH sensor is a pH sensitive layer/film that is prepared by immobilizing a pH sensitive dye into an appropriate polymer matrix, permeable for the protons or entrapped behind semi-permeable membranes. The pH probes are calibrated either either buffer solution of different pH or deionized water of different pH prepared by

using HCl and NaOH [48]. In pH optical sensors light is directed to the active end of the sensor, where it interacts with the pH sensitive indicator in the presence of fluid sample, which alters the intensity of the beam by absorption or fluorescence. The modified optical signal is then guided to the detector. [48]. The modes of pH sensing by optical sensors depends on the changes of the properties of pH sensitive indicators, which could be due to:

- colour change - measurements based on absorption;
- changes of the fluorescence properties of an indicator;
- quenching of the fluorescence intensity due to photoinduced electron transfer in the acidic environment.

2.3.1 Colour change based pH sensing

The most common optical measurements for pH value is based on the colour change of an indicator dye. There are a large number of pH sensitive indicator dyes, which have different pH ranges and colour changes. pH sensitive indicator dyes, based on colour changes are frequently weak acids or weak bases [49]. The general reaction scheme of a pH indicator can be formulated as follows:

$$HInd + H_2O \Leftrightarrow H_3O^+ + Ind^- \tag{2.20}$$

where Hind = acid form of the indicator
Ind^- = conjugate base of the indicator

The ratio of Hind and Ind^- determines the colour of the indicator and consequently the pH value. The Henderson-Hasselbalch equation for pH indicators can be written as:

$$pH = pK_a + \log\frac{[Ind^-]}{[HInd]} \tag{2.21}$$

Usually, the colour change is not instantaneous at the pK_a value, but there is a pH range where a mixture of colours is present. The pH range varies between indicators, but always falls between the pK_a value plus or minus one. This assumes that solutions retain their colour as long as at least 10% of the other species persists. For optimal accuracy, the colour difference between the two species should be as clear as possible and the narrower the pH range of the colour changes the better [50].

2.3.2 Fluorescence based pH sensing

Fluorescence based pH indicator offer much better sensitivity than the classical dyes based on colour change. Therefore, the pH value may be measured through the fluorescence emitted from pH sensitive fluorescent indicator. The simplest type of fluorescence pH sensor involves measuring the fluorescence intensity at a single wavelength [49].

Fluorophores can undergo chemical reactions when they are in their excited state. The most dominant type of an excited-state reaction is the loss or gain of photons. Such reactions occur because light absorption frequently changes the electron distribution within a fluorophore. Whether a fluorophore loses or gains a photon in the excited-state reaction is determined from the change in pK_a in the excited state. If the pK_a decreases ($pK_a^* < pK_a$) then the fluorophore will tend to lose a photon in the excited state. If the pK_a increases ($pK_A^* > pK_A$), then the fluorophore may pick up a photon in the excited state. Electron donors such as –OH, -SH, $-NH_2$ have a lone pair of electrons, and these electrons tend to become more conjugated to the aromatic ring system in the excited state, resulting in $pK_a^* < pK_a$. On the other hand electron acceptors such as $-CO_2^-$ and $-CO_2H$ have π orbitals in which electrons can be transferred in the excited state. This increased electron density results in weaker dissociation in the excited state: $pK_a^* > pK_a$ [45]. Water molecules acting as either a

proton acceptor or a proton donor are always in close contact with an acid or a base undergoing excited-state deprotonation or protonation, respectively [43].

Great care should be taken in the case of media containing high concentration of salts. Highly charged indicators are very sensitive to ionic strength. The pH error caused by ionic strength depends on the type of indicator used and on the concentrations of all ionic species in solution. The resulting errors are particularly significant when the composition of the sample solution differs significantly from that of the calibration solution or when it changes during measurements. Therefore, optical pH sensor cannot be applied to unknown sample solutions to give a reliable pH value. Further, the calibration curve of the pH sensor will also change if the temperature of the solution changes, resulting in giving wrong pH value [48].

For measurements of the pH value it is recommended to carry out ratiometric measurements, i.e. to determine the ratio of the fluorescence intensities measured at two wavelengths. These measurements are preferable because the ratio of the fluorescence intensities at two wavelengths is in fact independent of the total concentration of the indicator, photobleaching, fluctuations of the source intensity, sensitivity of the instruments, etc.

2.3.3 Photoinduced Electron Transfer

Another mechanism for sensing pH by optical means is based on photoinduced electron transfer (PET). This process involves a redox reaction between a fluorophore in the excited state and another functionality that can be found within the same molecule or units in close vicinity, but in most cases is not integrated into it. As PET is usually fast and fully reversible, it essentially constitutes a quenching process. In a typical PET sensor an aromatic fluorophore is covalently linked to an aliphatic amine, typically by a short methylene chain. The basic idea is that quenching by amines requires the lone pair of electrons localized on the nitrogen. When the fluorophore is in the excited state, these lone pair electrons are in a higher-energy orbital (HOMO), than the energy of the vacancy left by the excited electron. Hence, an electron from the nitrogen enters this lower energy orbital, effectively quenching the fluorescence. If the lone electron pair binds a photon the energy of this pair is lowered. Electron transfer is then inhibited and the fluorophore is not quenched [50]. Such probes are said to undergo photoinduced electron transfer (PET), which is the light-induced transfer of electron from the nitrogen into the aromatic ring. The amino group is capable of quenching only in the non-protonated state so that pH sensitivity is found if the pH is close to the pK_a of the amino group. At low pH the amino group is protonated and does not quenched the fluorophore. Spectral properties are determined by the fluorophore, whereas proton affinity (i.e. pK_a) is much more specific for the amino function [45]. The principle of pH sensing by fluorescent PET sensors is schematically presented in figure 2 – 4.

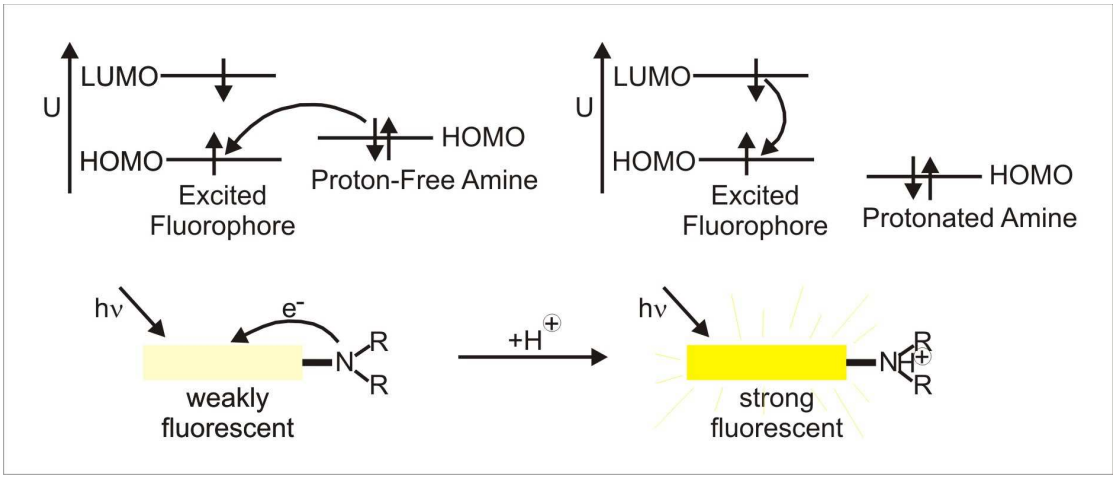

Figure 2 – 4: Principle of pH sensing by fluorescent PET sensors.

The excited fluorophore can be either the electron donor or acceptor. The direction of electron transfer in the excited state is determined by the oxidation and reduction potential of the ground and excited states. When discussing PET the term donor refers to the species that donates an electron to the acceptor. PET is predictable because the possibility of electron transfer can be assessed from the redox potentials of the fluorophore and quencher. The redox potentials can be determined by electrochemical measurements or by theoretical calculations using the energy levels of the LUMO (lowest unoccupied molecular orbital) and the HOMO [43].

2.4 Optical Temperature Sensors

Temperature is a key parameter in numerous fields of science and technology. While not a chemical parameter by itself, its knowledge is of higher significance since temperature affects the response of all chemical sensors. Sensing temperature by itself is also desirable in marine research, in underground geochemical studies, in diagnosis of diseases and in biotechnology. Luminescent temperature indicators have been employed lately as components for pressure sensitive paints in aircraft and car industry. Knowing temperature is particularly important in fluorescent sensing of oxygen since quenching by oxygen always is highly temperature dependent [51]. Optical temperature sensors are also used to provide an indication of the temperature where an optical output is required rather than an electrical output or where an electrical sensor will not withstand the environment being measured [52].

Lifetime-based luminescent temperature indicators have highly temperature-dependent luminescence and preferably they are immobilized in the gas-impermeable polymer matrices to avoid quenching by oxygen [53]. Excitation by visible light is strongly preferred in luminescent temperature sensing for the following reasons:

- LEDs which are available for the visible part of the spectrum are usually more efficient and less costly than non-LED based UV light sources;
- Visible excitation causes less back-ground fluorescence and thus less interferences;
- Visible light sources are well compatible with inexpensive plastic (PMMA) optical fibers, while UV excitation requires the use of much more expensive glass fibres.

Luminescent probes that display a strong temperature dependence of their luminescence lifetime include ruthenium complexes and complexes with lanthanide atoms, such as europium(III) complexes. The luminescent intensity of these indicators is highly temperature dependent and it significantly decreases at higher temperature are observed. Additionally, the long decay time of Europium complexes is another attractive feature [51]. Decay times could be determined with phase modulation technique using the following equation:

$$\tau = \tan\Phi / 2\pi f \qquad (2.22)$$

where f = modulation frequency

A principle of temperature sensing by luminescence is considered as follows. In general, emission intensity decreases as the temperature of the matter increases due to thermal activation: for example, a Eu^{3+} ion, the emission intensity decreases with increasing temperature due to thermal activation from the emissive Eu^{3+} $^5D_0$ level to a radiationless deactivated triplet level. Besides, energy transfer from ligand to Eu^{3+} would also be influenced by temperature. Europium emission is expected to change drastically with temperature [53]. Europium complexes are very promising for temperature sensing and imaging since, apart from their highly temperature-dependent luminescence and long luminescence decay times in order of several hundred microseconds which are only slightly affected by oxygen, they emit in the narrow optical window and posses [54].

The calibration plots for the temperature-sensitive materials are usually performed using Arrhenius-type equation (fitting with a correlation coefficient r^2>0.999):

$$\tau = (k_0 + k_1 \exp(-\frac{\Delta E}{RT})^{-1} \quad (2.23)$$

where k_0 = the temperature-independent decay rate for the excited state deactivation
k_1= pre-exponential factor
ΔE = the energy gap between emitting level and higher excited state level
R = gas constant

2.5 Optical Ammonia Sensors

Ammonia is ubiquitous in the atmosphere in low concentrations of low-ppb to sub ppb levels as a natural gas. Within earth's history it may have played an important role and has probably together with large amounts of liquid water and a chemically reducing atmosphere created the conditions which led to the origin of life on earth [55]. There are two natural pathways for atmospheric ammonia to enter the ecosystem. On the one hand nitrification is a direct deposition of ammonium and nitrate salts to the soil together with dust or rain water; on the other hand nitrogen is bound by specialised bacteria and released to the environment as ammonia. Nowadays large amounts of ammonium are added to the soils in form of fertilizer, which leads to acidification, eutrophication, change in vegetation and to an increase in atmospheric ammonia concentration.

Ammonification includes all metabolic activities that decompose organic nitrogen like excretion by plants and animals and decomposition of organisms and sewage by microorganisms. Through the fact that the number of domestic animals has risen steeply with industrialisation, released ammonia results mainly from agriculture and farming. Additionally chemical plants and motor vehicles have to be taken in account to summarize that most ammonia in our atmosphere is emitted directly or indirectly from anthropogenic sources [55].

High ammonia concentrations are a major concern in regions which are densely populated and with large number of farm animals. The sea and oceans act as a sink for ammonia. Acutely toxic concentrations cause a loss of equilibrium, hyperexcitability, increased breathing cardiac output and oxygen uptake and in severe cases convulsions, coma and death. An elevated ammonia concentration is one of the leading causes of fish-death. Ammonia oxidation in water can lower the dissolved oxygen concentrations, what impairs growth, leads to a delay of the development of fish and to increased larval fish mortality [56].

Unionized ammonia (NH_3) in water exists in equilibrium with the ammonium ion (NH_4^+) and the hydroxide ion (OH^-) as shown in the equation:

$$NH_{3,gas} + nH_2O_{liquid} \Leftrightarrow NH_{3,aqueous} \cdot nH_2O_{aqueous} \Leftrightarrow NH_4^+ + OH^- + (n-1)H_2O_{liquid}$$

Dissolved ammonia is $NH_{3,aqueous}$, the ionized form is the ammonium ion NH_4^+ and "total ammonia" refers to the sum of both. The equilibrium constant pK_a is around 9.5. The concentration of NH_3, increases with increasing pH and temperature.

In conventional analytical chemistry problems as to determine concentrations of ammonia below 100 µg/l are solved by the means of cost-intensive instruments in well-equipped laboratories with skilled persons. One of the drawbacks of these methods is that field measurements and continuous monitoring are not possible. At very beginning of ammonia sensor development, most of them work in gas phase because interferences such as pH, water itself and ionic strength would disturb their measurement principles. For measurements of dissolved ammonia the ammonia selective electrode is often used, as it offers the possibility for an online detection of ammonia at small concentrations. Usually, they are named as Severinghaus electrodes. The original design was developed specifically for

sensing of carbon dioxide but the principle on which these gas sensors operate is the same as for ammonia sensors. The key element is a small compartment into which the gas can penetrate through a semipermeable membrane. The gas undergoes a chemical transformation, for example, hydrolysis, in which some detectable ion or ions are produced. Thus, these sensors are based on measurement of localized changes in ion activity. Severinghaus electrodes have found wide application in clinical analysis. However, the electrochemical sensors suffer from major drawbacks, such as analyte depletion, biological material fouling and electrical interference susceptibility [57].

The sensing scheme for optical ammonia sensors is based on the deprotonation of the pH indicator by NH_3. The ratio between the protonated and the deprotonated form of the indicator is a function of ammonia concentration which can be deduced by measuring fluorescence at an appropriate wavelength. The presence of ammonia in the sensing layer leads to the deprotonation of the indicator resulting in a rise of the detected fluorescence intensity. The pH indicators are usually incorporated into polymer layers. The pK_a of the fluorescence indicator determines the dynamic range of the sensor. A low pK_a value results in a dynamic range for low ammonia concentrations [58]. The sensing scheme employed is based on the acid-base equilibrium between ammonia (pKa =9.24) and the dye is:

$$NH_{3,}(aq) + IndH \Leftrightarrow NH_4^+ + Ind^-$$

II
Experimental Section

3 Materials

The optical sensor materials chosen for the comprehensive study of the effects of diverse sterilization procedures could be divided into two large groups; indicators and polymers. Each indicator and each polymer were sterilized with gamma and electron beam sterilization methods and selected pairs were combined to obtain defined optical sensors. The optical sensors were additionally sterilized with steam, ethylene oxide, hydrogen peroxide gas and low-temperature hydrogen peroxide plasma. All materials used in this study are presented in table 3 – 1:

Table 3 - 1: Applied materials.

Materials	Availability	Remarks
Polymers		
Polystyrene (=PS, average Mw = 250 000)	SigmaAldrich <www.sigmaaldrich.com>	Polymer applied by optical oxygen sensors.
Polystyrene-co-Acrylonitrile (=PS-co-PAN; average Mw = 185 000, containing 30wt% polyacrylonitrile)	SigmaAldrich <www.sigmaaldrich.com>	Polymer applied by optical oxygen sensors.
Polystyrene-co-Maleic Anhydride (=PSMA93, average Mw = 224 000, containing 7wt% maleic anhydride)	SigmaAldrich <www.sigmaaldrich.com>	Polymer applied by optical oxygen sensors.
Polysulfone (=PSf, Mw = 26 000)	SigmaAldrich <www.sigmaaldrich.com>	Polymer applied by optical oxygen sensors.
Cellulose Acetate (=CA, Mw = 100 000)	Acros organics <www.acros>	Polymer applied by optical oxygen and ammonia sensors.
Ethyl Cellulose (=EC, ethoxy content 46%)	Fluka <www.sigmaaldrich.com>	Polymer applied by optical oxygen and ammonia sensors.
Polyurethane Hydrogel: Hydrogel Hydromed™ D4 Hydrogel Hydromed™ D7 HydroThane™ (5% H_2O cont.) HydroThane™ (25% H_2O cont.)	AdvanSource Biomaterials <www.advbiomaterials.com>	Polymers applied by optical oxygen, pH and ammonia sensors.
PolyPhenylSilsesQuioxane (=PPSQ, 100% phenyl, 4.5-6.5% OH)	ABCR <www.abcr.de>	Polymer applied by optical oxygen sensors.
PolyVinylidene Chloride-co-Acrylonitrile (=PVC-co-PAN, Mw = 150 000, containing 20wt% Acrylonitrile)	PolySciences <www.polysciences.com>	Polymer applied by optical temperature sensors.
PolyMethAcryloNitrile (=PMAN, Mw = 20 000)	Scientific Polymer Products <www.scientificpolymer.com>	Polymer applied by optical temperature sensors.
PolyMethyl MethAcrylate (=PMMA, Mw = 35 000)	Acros organics <www.acros>	Polymer applied by optical ammonia sensors.

Poly(2-HydroxyEthyl Methacrylate) (=pHEMA, Mv = 20 000)	SigmaAldrich <www.sigmaaldrich.com>	Polymer applied by optical pH sensors.
Poly(Ethylene Terephthalate) (Mylar®)	Goodfellow <www.goodfellow.com>	Support foil by sensors.
(Luminescence) Indicator		
Coumarin Derivatives:		
3-(2-benzothiazolyl)-7-hydroxycoumarin (=pH sensitive coumarin)	Prepared according to the literature procedure [59]	pH sensitive fluorescence indicator
Lanthanides based Luminescent Probes		
Europium(III) Complex with 4-(4,6-di(1H-indazol-1-yl)-1,3,5-triazin-2-yl)-N,N-DiEthyl Benzen Amine (=$Eu(tta)_3$DEADIT)	Prepared according to the literature procedure [54]	Temperature sensitive fluorescence indicator
Long-Lifetime Metal-Ligand Complexes		
Iridium (III)((benzothiazol-2-ly)-7-(diethylamino)-coumarin))2(acetylacetonat) (=$Ir(C_s)_2$(acac))	Prepared according to the literature procedure [60]	Oxygen sensitive phosphorescence indicator
Platinum(II)-5,10,15,20-tetrakis-(2,3,4,5,6-pentafluorphenyl)-porphyrin (=PtTFPP)	Frontier Scientific <www.frontiersci.com>	Oxygen sensitive phosphorescence indicator
Platinum(II)-2,3,7,8,12,13,17,18-OctaEthyl-21H, 23H-Porphyrin (=PtOEP)	Frontier Scientific <www.frontiersci.com>	Oxygen sensitive phosphorescence indicator
Platinum(II) meso-tetra(4-FluoroPhenyl) TetraBenzoPorphyrin (=PtTPTBPF)	Prepared according to the literature procedure [61]	Oxygen sensitive phosphorescence indicator
Palladium(II) meso-tetra(4-FluoroPhenyl) TetraBenzoPorphyrin (=PdTPTBPF)	Prepared according to the literature procedure [61]	Oxygen sensitive phosphorescence indicator
Ruthenium(II)-tris-4,7-diphenyl-1,10-phenanthroline dichloride ($Ru(dpp)_3Cl_2$)	Lancaster <www.lancastersynthesis.com>	Oxygen sensitive phosphorescence indicator
DiChloroTris(1,10-Phenanthroline) Ruthenium(II) Hydrate	SigmaAldrich <www.sigmaaldrich.com>	Temperature sensitive luminescence indicator.
Pyrene Derivatives		
1-HydroxyPyrene-3,6,8-tris-bis (2-Ethylhexyl)Sulfonamide (=$HPTS(DHA)_3$)	Prepared according to the literature procedure [62]	pH sensitive fluorescence indicator.
Perylene Derivatives		
PET Perylene BisImide	Prepared according to the literature procedure [50]	pH sensitive indicator based on Photoinduced Electron Transfer
Xanthen Derivatives		
2´,4´, 5´,7´-Tetrabromoeosin ethyl ester potassium salt	SigmaAldrich <www.sigmaaldrich.com>	pH sensitive fluorescence indicator.

(=Eosin EthylEster)		
2',7'-DiChloroFluorescein	SigmaAldrich <www.sigmaaldrich.com>	pH sensitive fluorescence indicator.
2´,7´-DiHexyl-5(6)-N-Octadecyl-CarboxAmidoFluorescein (=DHFA)	Prepared according to the literature procedure [63]	pH sensitive fluorescence indicator.
2´,7´-DiHexylFluorescein OCtadecyl Ester (=DHFE)	Prepared according to the literature procedure [63]	pH sensitive fluorescence indicator.
Sulphonephthalein Derivatives		
BromoPhenol Blue	Acros organics <www.acros>	pH sensitive indicator based on colour changes.
Thymol Blue	SigmaAldrich <www.sigmaaldrich.com>	pH sensitive indicator based on colour changes.
BromoThymol Blue	SigmaAldrich <www.sigmaaldrich.com>	pH sensitive indicator based on colour changes.
Azo Derivatives		
Methyl Orange	Fluka <www.sigmaaldrich.com>	pH sensitive indicator based on colour changes.

The optical sensors were prepared as combination of the selected indicator immobilized in the different polymeric matrices. The indicators were chosen on the basis of their sensitivity to defined analyte and the indicator class. On the other hand, polymer matrices were selected due to the permeability for defined analyte to the indicator and the frequency of the applications by development of optical sensor. In table 3 – 2 are reported all optical sensors which were sterilized with gamma, electron beam, steam, ethylene oxide, hydrogen peroxide gas and hydrogen peroxide plasma.

Table 3 - 2: Applied optical sensors.

Optical Sensors	
Oxygen Sensors	
Indicator	***Polymer***
Iridium (III)((benzothiazol-2-ly)-7-(diethylamino)-coumarin))2(acetylacetonat) (=Ir(C_s)$_2$(acac))(=Iridium(III)Coumarin)	Polystyrene Polystyrene-co-Acrylonitrile Polystyrene-co-Maleic Anhydride Polysulfone Cellulose Acetate Ethyl Cellulose Hydrogel Hydromed^{TM} D4 or D7 HydroThane^{TM} (5% H_2O content) PolyPhenylSilsesQuioxane
Platinum(II)-5,10,15,20-tetrakis-(2,3,4,5,6-pentafluorphenyl)-porphyrin (=PtTFPP)	Polystyrene Polystyrene-co-Acrylonitrile Polystyrene-co-Maleic Anhydride Polysulfone Cellulose Acetate Ethyl Cellulose Hydrogel Hydromed^{TM} D4 or D7 HydroThane^{TM} (5% H_2O content) PolyPhenylSilsesQuioxane
Platinum(II)-2,3,7,8,12,13,17,18-OctaEthyl-21H, 23H-Porphyrin (=PtOEP)	Polystyrene
Platinum(II) meso-tetra(4-FluoroPhenyl) TetraBenzoPorphyrin (=PtTPTBPF)	Polystyrene

Palladium(II) meso-tetra(4-FluoroPhenyl) TetraBenzoPorphyrin (=PdTPTBPF)	Polystyrene
Ruthenium(II)-tris-4,7-diphenyl-1,10-phenanthroline dichloride ($Ru(dpp)_3Cl_2$)	Polystyrene Polystyrene-co-Acrylonitrile Polystyrene-co-Maleic Anhydride Polysulfone Cellulose Acetate Ethyl Cellulose Hydrogel Hydromed™ D4 or D7 HydroThane™ (5% H_2O content) PolyPhenylSilsesQuioxane
pH Sensors	
Indicator	***Polymer***
1-HydroxyPyrene-3,6,8-tris-bis (2-Ethylhexyl)Sulfonamide (=$HPTS(DHA)_3$)	Hydrogel Hydromed™ D4
2´,7´-DiHexylFluorescein OCtadecyl Ester (=DHFE)	Hydrogel Hydromed™ D4 pHEMA
2´,7´-DiHexyl-5(6)-N-Octadecyl-CarboxAmidoFluorescein (=DHFA)	Hydrogel Hydromed™ D4 pHEMA
3-(2-benzothiazolyl)-7-hydroxycoumarin (=pH sensitive coumarin)	Hydrogel Hydromed™ D4 pHEMA
PET Perylene BisImide	Hydrogel Hydromed™ D4
BromoPhenol Blue	Hydrogel Hydromed™ D4
Thymol Blue	Hydrogel Hydromed™ D4
BromoThymol Blue	Hydrogel Hydromed™ D4
Methyl Orange	Hydrogel Hydromed™ D4
Temperature Sensors	
Indicator	***Polymer***
Europium(III) Complex with 4-(4,6-di(1H-indazol-1-yl)-1,3,5-triazin-2-yl)-N,N-DiEthyl Benzen Amine (=$Eu(tta)_3$DEADIT)	Polystyrene-co-Acrylonitrile Polyvinylidene Chloride-co-Acrylonitrile PolyMethAcryloNitrile
DiChloroTris(1,10-Phenanthroline) Ruthenium(II) Hydrate	Polyvinylidene Chloride-co-Acrylonitrile PolyMethAcryloNitrile
Ammonia Sensors	
Indicator	***Polymer***
2´,4´, 5´,7´-Tetrabromoeosin ethyl ester potassium salt (Eosin EthylEster)	Cellulose Acetate Ethyl Cellulose Hydrogel Hydromed™ D7 PolyMethyl MethAcrylate
2',7'-DiChloroFluorescein	Cellulose Acetate Ethyl Cellulose Hydrogel Hydromed™ D7
BromoPhenol Blue	Cellulose Acetate Ethyl Cellulose Hydrogel Hydromed™ D7 PolyMethyl MethAcrylate

3.1 Polymers

Each polymer applied for development of the defined optical sensor was gamma and electron beam sterilized and characterized. The different types of polymer applied in this study are listed in table 3 – 1. The properties and characteristic of each polymer are presented in the following sections.

3.1.1 Polystyrene

Polystyrene =(PS)	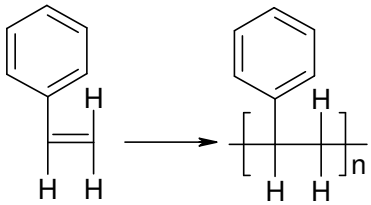 styrene polystyrene
Molecular Formula	$(C_8H_8)_n$
Molecular Weight	Typically n = 1000. A wide range of M_w is possible depending on the polymerisation conditions. General polystyrene has M_w = 100000-300000
Monomer	Styrene
Material Class	Thermoplastic
Glass-Transition Temperature, T_g	85-110°C

Polystyrene (Poly(1-phenylethane-1,2-diyl) (PS) is a relatively cheap thermoplastic resin with good processing properties. It therefore finds widespread use in the developed world. Among its features are: excellent colour range, transparency, rigidity and low water absorption. The mechanical properties depend on the molecular weight of the sample and the processing conditions [64].

The chemical makeup of polystyrene is a long chain of hydrocarbon in which every other carbon is connected to a phenyl group. Polystyrene is produced via anionic, cationic, Ziegler-Natta and free radical mechanisms using appropriate initiators. The free radical process is the most important commercially and it typically uses peroxide, persulfate or azo initiators. Free radical polystyrene can be produce by bulk, suspension or emulsion processes. Bulk polymerisation of styrene monomers may be accomplished by thermal initiation alone, without the addition of any initiator. Emulsion polymerisation is used on a semi-commercial scale for the production of polystyrene latex. Suspension polymerisation is used almost exclusively to produce expandable polystyrene. Bulk, suspension and emulsion polymerisation reactions can be performed in bathc while anionic polymerisation of styrene is limited for the production of narrow molecular weight distribution polystyrenes in laboratory quantities. Typical initiators are organolithium compounds. Cationic polymerization is used to produce low molecular weight resins and typically strong protonic acids such as Lewis acids are used as initiators. Polystyrene obtained with any heterogeneous Zigler-Natta catalyst is a mixture of products with different tacticities usually atactic and isotactic. Production methods include thermoforming and injection molding [64].

Polystyrene is generally flexible and can come in the form of mouldable solids or viscous liquids. PS is characterized by short range Van der Waals attractions between chains. Therefore, when the polymer is heated, the chains are allowed to take on a higher degree of conformation and slide past each other. The intermolecular weakness allows the polystyrene chains to slide along each other, rendering the bulk system flexible and stretchable. The ability of the system to be readily deformed above its glass transition temperature allows polystyrene to be easily softened and moulded with the addition of heat.

Solid polystyrene is used, for example, in disposable cutlery, plastic models, CD or DVD cases, smoke detector housings, toys, household goods, furniture etc. It is also used in a wide range of packaging applications. Heat resistant products are used for vending machine goods and for food and drink containers. Polystyrene Petri dishes and other laboratory containers such as test tubes and microplates play an important role in biomedical research and science. [65].

Oxygen plays a very important role in the degradation of polymeric polystyrene. Degradation mechanism involves depropagation. Thermal-oxidative products include benzaldehyde, benzoic acid, acetophenone, phenol, benzyl alcohol, styrene, styrene dimmer (diphenyl butane) and styrene trimer (triphenyl hexane). Antioxidants can be added to retard oxidative degradation by scavenging peroxy radicals as they are formed [66].

UV radiation at a wavelength of 254 nm is strongly absorbed and it can result in significant physical and chemical changes. Polystyryl radicals are formed from the scission of the tertiary CH bond. Cross-linkage between two polystyryl radicals results in rapid embrittlement of the polymer. Cross-linking is the dominant reaction occurring under short wavelength irradiation, in the absence of oxygen. In the presence of oxygen, short wavelength UV radiation causes yellowing of the polymer, which is primarily caused by the formation of conjugated polyene structures. Weathering may cause chain scission, yellowing and oxidation [66].

Polystyrene is highly resistance to gamma, electron beam and X-ray irradiation due to the protective action of the phenyl groups which dissipate the excitation energy without decomposing. In the absence of air flexural strength and tensile strength are not decreased by gamma irradiation with doses up to 5 MGy. Even in the presence of oxygen, changes in the properties and discoloration are negligible when applying the same dose range of gamma radiation used for sterilising medical supplies (20-30 kGy) [64].

3.1.2 Polystyrene-co-Acrylonitrile

Polystyrene-co-Acrylonitrile (=PS-co-PAN)	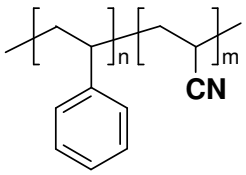
Molecular Formula	$(C_8H_8)_n(C_3H_3N)_m$
Monomer	Styrene, Acrylonitrile
Material Class	Thermoplastic, Copolymer
Glass-Transition Temperature T_g	105-125°C (T_g varies non-linearly with acrylonitrile content, with a maxima at 50%wt. acrylonitrile)

Polystyrene-co-acrylonitrile (PS-co-PAN) is a rigid, hard and transparent copolymer which is permeable for oxygen and water vapour. A typical composition is 76% of styrene and 24% of acrylonitrile. The mechanical properties are dependent on the acrylonitrile content. For example, acrylonitrile modified polystyrene possess a greater fatigue fracture resistance than unmodified polystyrene. Polystyrene-co-acrylonitrile is synthesized by emulsion, suspension or continuous bulk polymerization. The latter method is preferred for applications requiring high optical quality and gives better colour and haze. It may also be synthesized by free radical polymerization using a $ZnCl_2$ catalyst without initiator [64].

The applications of polystyrene-co-acrylonitrile are found in household appliances and goods – washing machine parts, refrigerator shelves, blenders, mixers, food trays, bottles and as bristle in brooms and brushes, in the automotive industry, such as batteries, lenses and interior trim [67].

Polystyrene-co-acrylonitrile is resistant to non-oxidising acids, aliphatic hydrocarbons, alkalis, (except KOH), vegetable oils, foodstuffs, detergents, gasoline, alcohol and some solvents. On the other hand, it is attacked by aromatic and chlorinated hydrocarbons, esters and ketones. The stability of the copolymer decreases with increasing acrylonitrile content. Maximal rate of decomposition occurs at 425°C with production of mainly NH_3 and HCN. Pyrolysis at 500°C under N_2 produces HCN, acetonitrile, acrylonitrile, styrene and toluene among other products. Outdoor exposure after 1 year reduces the impact strength of the copolymer by 75% and the bending strength by 50%. Gamma irradiation causes embrittlement and degradation of its physical properties [68].

3.1.3 Polystyrene-co-Maleic Anhydride

Polystyrene-co-Maleic Anhydride (=PSMA)	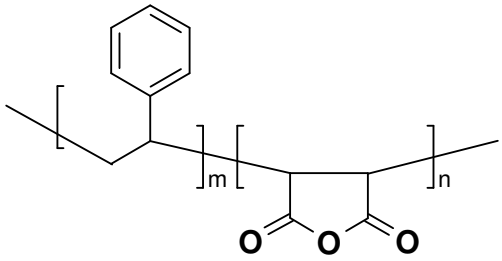
Molecular Formula	$(C_8H_8)_m(C_4H_2O_3)_m$
Monomer	Styrene, Maleic Anhydride
Material Class	Thermoplastic, Copolymer
Melting Temperature T_m	250-270°C
Glass-Transition Temperature T_g	135°C (depends on maleic anhydride content)

Polystyrene-co-maleic anhydride (PSMA) is a synthetic polymer, made of styrene and maleic anhydride monomers. The monomers alternate almost perfectly, making it an alternating copolymer. It is formed by a radical polymerization using organic peroxide as the initiator. It is available in a broad range of molecular weight and maleic anhydride contents [64].

PSMA are widely used in engineering plastic applications, normally in the impact modified and optional glass fibre filled variants. The specific reactivity of PSMA makes it a suitable agent for compatibility of normally incompatible polymers. PSMA copolymers also find good application niches in automotive interior, instrument panels, headliners, and in some appliance and business machine housing applications [67].

Polystyrene-co-maleic anhydride is characterized by transparent appearance, high heat resistance, high dimensional stability and the specific reactivity of the anhydride groups. The glass transition temperature is 20-60°C higher than the one of polystyrene; also the heat distortion temperatures are higher than the ones showed by polystyrene itself. The maleic anhydride co-monomer imparts rigidity to the styrenic backbone by raising the T_g by 2°C with each 1 wt% increase in the maleic anhydride content. In addition, the maleic anhydride co-monomer confers higher polarity to the styrenic backbone and hence, increases the modulus, strength, the solvent resistance and the adhesion to reinforce fillers and glass fibers [67].

3.1.4 Polysulfone

Polysulfone (=PSf)	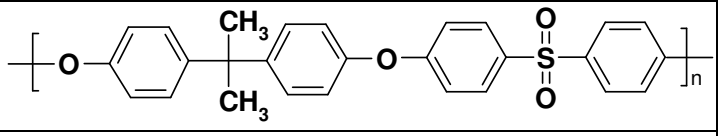
Molecular Formula	$(C_{27}H_{22}O_4S)_n$

Monomer	4,4´-Dichlorodiphenyl sulfone, Bisphenol A
Material Class	Thermoplastic
Polymer Synthesis	Polycondensation
Melting Temperature, T_m	310-390°C
Glass-Transition Temperature, T_g	185°C

Polysulfone (PSf) contains the subunit aryl-SO_2-aryl, the defining feature of which is the sulfone group. It is a high cost, rigid, amorphous material with low moisture absorption. In addition, polysulfones are characterized by high strength, very high surface-temperature limits, low creep, good electrical characteristics, transparency, self-extinguishing ability, and resistance to greases, to different solvents and to chemicals [69].

The primary uses of polysulfones include the manufacture of appliances and cookware. This polymer is also used in automotive and electronic industries. Filter cartridges made from polysulfone membranes offer resistance to extremely high flow rates at very low differential pressures when compared with Nylon or polypropylene media [24]. Polysulfone can be reinforced with glass fibers and can be used as a dielectric in capacitors. One unique application area for polysulfone is in membrane separation; in fact for example, asymmetric polysulfone membranes are used in ultrafiltration, reverse osmosis and ambulatory hemodialysis units. Polysulfone allows easy manufacturing of membranes, with reproducible properties and controllable size of pores down to 40 nanometers. Such membranes can be used for the following applications: hemodialysis, waste water recovery, food and beverage processing, gas separation and as filter media for filter sterilization [64].

Polysulfone is resistant to oxidizing agents therefore it can be washed with bleaches. Mechanically, polysulfone has high compaction resistance, which makes it suitable for uses under high pressures. It is also stable in aqueous acids and bases and many non-polar solvents [69]. Polysulfone has the highest service temperature of all melt-processable thermoplastics. Its resistance to high temperature and therefore can be used as a flame retardant. Its high hydrolysis stability allows its use in medical applications requiring autoclave and steam sterilization [64].

Polysulfone has poor resistance to UV light. Absorbance in the UV region occurs with attendant discoloration and losses in mechanical properties due to polymer degradation. For outdoor applications, the use of protective lacquers or grades of the material containing carbon black are recommended. According to the literature, polysulfone is resistant to most forms of radiation. Also, it has good resistance to bacterial and fungal attack and good dimensional stability [64].

3.1.5 Cellulose Acetate

Cellulose Acetate (=CA)	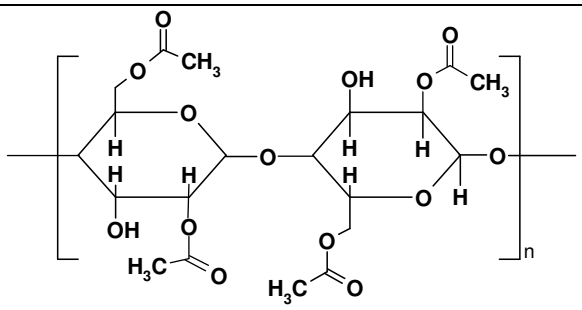
Molecular Formula	$(C_{11\text{-}12}H_{15\text{-}16}O_{7.5\text{-}8})_n$
Monomer	Base monomer unit glucose
Material Class	Polysaccharides
General Information	Thermoplastic polymer with excellent optical properties
Glass-Transition Temperature T_g	120°C

Melting Temperature T_m	230-250°C

Cellulose acetate (CA) is a modified natural polymer with a wide range of properties. It is the acetate ester of cellulose and is prepared by acetylation cellulose, according to following mechanism:

$$\text{Cellulose + Acetic Anhydride} \xrightarrow[-H_2O]{[H_2SO_4]/\Delta} \text{Cellulose Acetate}$$

Cellulose acetate has different applications: as a component in adhesives, as a film base in photography, for making a variety of consumer products including plastic films, cigarette filters and playing cards. It can be blended with different textiles, such as silk, cotton, wool, nylon, etc., to give to fabrics an excellent wrinkle recovery, handle, draping quality, quick drying, proper dimensional stability, cross-dye pattern potential, etc. [69].

Cellulose acetate has poor chemical resistance and it is attacked by acids and concentrated alkalis with subsequent production of corrosive acetic acid, which promotes autocatalysis. Hydrolytic breakdown is accelerated by metals, particularly copper. During degradation, cellulose acetate produces gaseous products which can initiate or accelerate the degradation of other organic materials [64]. A common chemical degradation mechanism of cellulose acetate is the primary reaction of hydrolysis, also known as deacetylation, during which hydroxyl groups replace acetate groups (CH_3COO) on the cellulose ring, with the concomitant formation of acetic acid (CH_3COOH). Simultaneously scission of the chains takes place, although the activation energy required to break bonds between cellulose rings is greater than the one required for deacetylation. Chain's scission results in a decrease in cellulose acetate's molecular weight and an increase in its solubility [64].

The photodegradation mechanism in the far UV-range comprises both a polymer chain scission of the glucosidic bond and a cleavage of side groups. In this case four different radicals were identified: the methyl radical, which results from the cleavage of the acetate side groups, and the three additional radicals types which are generated also from the irradiation of unsubstituted cellulose: the alkoxy radical at C_4 and the radical at C_1 which originates from the cleavage of the glucosidic bonds and the radicals from hydrogen abstraction from ring-carbons [14].

According to the literature, for carbon-based polymers, degradation predominates in those polymers whose main chain contains a quaternary carbon atom, that is, a $-CH_2CR_1R_2CH_2-$ unit, where R_1 and R_2 are groups other than H [14]. Such polymers have low heats of polymerization, are sterically stressed, and have somehow weaker C-C bonds at the quaternary carbon atom, which favors bond scission at this location. Therefore, the cellulose and its derivatives, tend to degrade upon irradiation with gamma and electron beam. Degradation results in a reduction in the average size (i.e. molecular mass) of the polymer [71]. The high-energy irradiation also caused the formation of carboxyl and carbonyl groups, which raised with increasing irradiation dosages. The DP of the samples decreased rapidly with increasing irradiation dosages. After the radiation, the gases can be formed, which are mainly H_2O with small amounts of CO_2 and CO [72].

3.1.6 Ethyl Cellulose

Ethyl Cellulose (=EC)	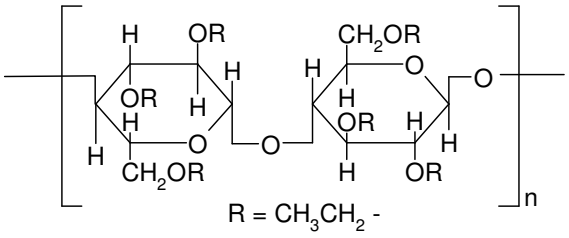
Monomer	Base monomer unit glucose

Material Class	Polysaccharides
General Information	Approximately 2.3 ethyl groups per monomer
Preparation	Cellulose + NaOH → Na-Cellulose (alkali cellulose) Na-Cellulose + C_2H_5Cl → Ethyl Cellulose + NaCl
Glass-Transition Temperature T_g	320°C
Melting Temperature T_m	135°C

Ethyl cellulose (EC) is a derivative of cellulose in which some of the hydroxyl groups on the repeating glucose units are converted into ethyl ether groups. The number of ethyl groups can vary depending on the manufacture. It is prepared from wood pulp or cotton by treatment with alkali and subsequent ethylation of the alkali cellulose with ethyl chloride. The content of ethoxy groups (-C_2H_5) are presented between 44% and 50% in the dried basis of polymer [64].

The polymer is applicable as adhesive, printing ink, lacquer, varnish, tablet coating and hot melt. Likewise, it is used in food, food packaging applications and as food additive. Ethyl cellulose is a water-insoluble polymer; it is used in controlled-release dosage forms. On the other hand it can take up water thanks to its hydrogen bonding capability which is due to the polarity difference between the oxygen atom and the ethyl group of the polymer [66].

Ethyl cellulose remains stable in water with neutral or slightly alkaline pH, as well as in a large number of organic liquids of different polarity, but is swollen in these media to a varying extent [72]. On the other hand, the polymer is susceptible to several routes of degradation. The degradation mechanisms are the following:

- Hydrolytic degradation in aqueous acid, as well as in non-aqueous, media by cleavage of the glucosidic bond;
- Hydrolytic cleavage of the glucosidic bond in water or in a moist environment catalyzed by cellulolytic enzymes of various fungi and bacteria; which is the basic process decomposition of cellulose;
- Oxidation processes proceeding via several pathways resulting in the introduction of carbonyl and carboxylic groups, and finally in chain cleavage to form various fragments; this process has to be avoided in cellulose bleaching with chlorine-containing bleach, as well as with chlorine-free oxidants;
- Thermal degradation at a temperature above 180-200°C along with various and rather complex reaction routes, leading to both gaseous products and char. This process that can be controlled and deliberately influenced by various flame retardant additives to cellulose fibres;
- Exposure to UV-VIS and high-energy radiation which induce degradation of the cellulose macromolecule.

The degradation of ethyl cellulose by gamma and electron beam radiation is characterized by a rapid decrease in DP. The primary process of bond cleavage, which is due to ionization, is followed by energy dissipation over rather long distances and secondary radical reactions, often proceeding as a radical chain reaction. The decisive radiochemicals processes are hydrogen abstraction leading to radical formation at the atoms C_1 and C_4, with subsequent cleavage of the glycosidic linkage and dehydration with elimination of H_2O, which frequently results in carbonyl group formation. Similar to all organic compounds, ethyl cellulose is known to yield low-molecular weight gaseous products, such as water vapour, carbon dioxide and carbon monoxide, upon irradiation [73].

3.1.7 Polyurethane Hydrogel

Hydrogels are made of three-dimensional network of a hydrophilic polymer and are capable of absorbing large amounts of water [76] Hydrogels are mainly produced by cross-linking of polymer chains – through physical, ionic or covalent interactions – by use of radiation processes, both UV and electron-beam [77]. In most cases, they are homogeneous materials

and their bulk properties are characterized and considered with regard to their applications [78]. Because of the presence of certain functional groups along the polymer chains, hydrogels are often sensitive to the conditions of the surrounding environment. For example, the swelling ration of these materials may be sensitive to the temperature, the pH or the ionic strength of the swelling agent, or even to the presence of a magnetic field or ultraviolet light [76]. The extent of the reversible swelling and deswelling properties of these materials is known to depend on the nature of both intermolecular and intramolecular cross-linking, as well as on the degree of hydrogen bonding in the polymer network.

Hydrogels formulated from polyurethanes are crosslinked with diisocyanate crosslinking agents or cured with radiation in the presence of a photoinitiator [79]. Crosslinked polyurethane hydrogels swell with water and organic solvents. The representation of a network arising from the reaction of poly(ethylene glycol with biscyclohexylmethane-4-4´-diisocyanate and 1,2,6-hexanetriol is illustrated in following reaction scheme:

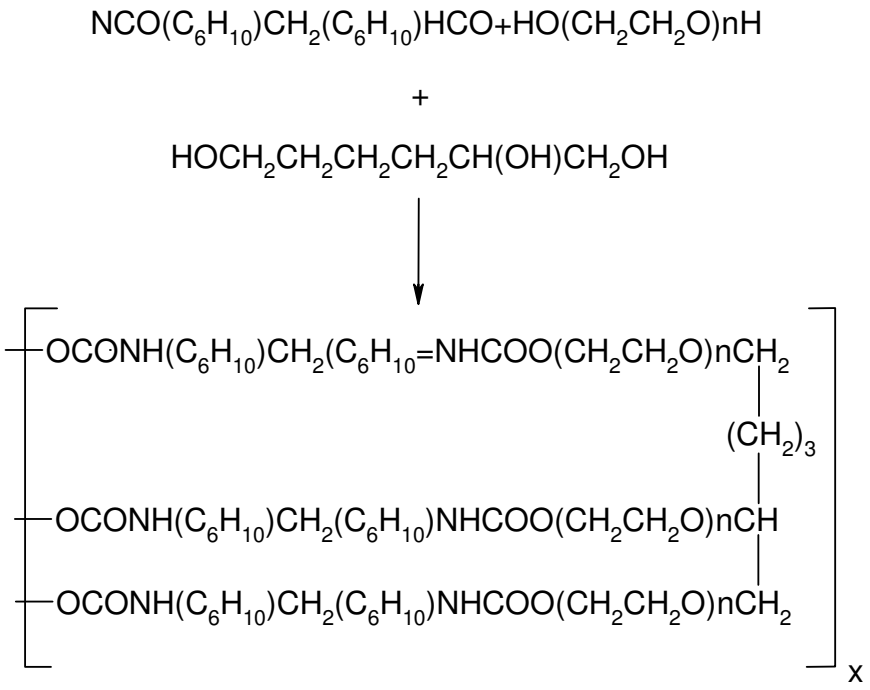

The combination of high water content and water insolubility makes these materials suitable for a number of biomedical applications [76], such as different devices, drug delivery and regenerative medicine. Hydrogels are already widely used as three-dimensional cell and tissue culture environments, as they are excellent mimics of the in vivo state. For these bio-related applications, the ability to control the synthesis of hydrogels to make structures with specific internal forms and shapes is an attractive prospect. For example, internal spaces created in hydrogels could be used to store cells or drugs and the three-dimensional structure of actual tissues and other in vivo components could be mirrored in the gel. Polyurethane hydrogels are biocompatible material. They can give appropriate response in defined applications, are not toxic and do not cause any damages on biological system [74].

Polyurethanes, especially those made using aromatic isocyanates, contain chromophores which interact with light. Increasing exposure time and/or light intensity during the storage under ambient laboratory conditions increased the amount of permanent set induced in some compression set tests – the samples did not fully return to their original size and/or shape. Higher-energy UV radiation promotes chemical reactions, some of which are detrimental to the foam structure [64].

The temperature at which thermal degradation starts can vary, as it is affected by the different heating processes and it depends on the types of polyurethanes used. When polyurethanes undergo thermal degradation some toxic chemicals may be produced. These

chemicals may include carbon dioxide, carbon monoxide, nitrogen oxides, hydrogen cyanide, isocyanates and amines [80].

Absorption of ionizing radiation causes free radical formation. The gamma sterilization procedure led to reduction in the swelling fraction of the hydrogel sheets. A decrease in the surface roughness was also observed in gamma sterilized samples [80].

3.1.7.1 Hydrogel HydroMedTM D4 and D7

HydroMed™ D4	
% Linear Expansion	50
% Water Content	50
Material Class	Hydrophilic Polyether Polyurethane
Melting Temperature T_m	104-126℃
HydroMed™ D7	
% Linear Expansion	10
% Water Content	30
Material Class	Polyether Polyurethane
Melting Temperature T_m	104-126℃

HydroMed D is a series of ether-based hydrophilic urethanes with excellent adhesive and cohesive properties. Water absorption level of each HydroMed in the series D depends upon end product target. These materials were designed to be used as coatings for a wide array of devices including catheters, guidewires, sutures, introducers, roads and valves. The HydroMed series can also be coated onto devices to reduce the absorption of white cells and proteins, thereby aiding in the analysis of blood and DNA. Processing of polymer is carried out by traditional solvent coating methods. The polymer granules can be dissolved in varying concentrations using most organic and inorganic solvent packages and the solutions can be dip coated or spray coated [81].

3.1.7.2 HydroThane™ with 5% and 25% water content

HydroThane™ with 5% and 25% water content (=H5; H25)	
Material Class	Hydrophilic Thermoplastic Polyurethane Elastomer
Melting Temperature T_m	200-220℃
Durometer Range Available	80 Shore A – 93 Shore A

HydroThane is a hydrophilic thermoplastic polyurethane elastomer, possessing water absorption rates ranging from 5% to 25%. This unique hydrophilic product line was designed to provide maximum physical properties for use in extruded or injection moulded components, while allowing for consistent single-step surface lubricity characteristics and a low friction coefficien. HydroThanes are available in aliphatic and aromatic versions and they have the ability to rapidly absorb water while maintaining high tensile strength and high elongation, resulting in a permanently lubricious polymer. Being hydrophilic, even when dehydrated, they should be sealed and stored in a cool, dry place. HydroThane can be processed using conventional extrusion or injection moulding equipment and are available in hardnesses of 80 Shore A and 93 Shore A [81].

3.1.8 Poly(PhenylSilsesQuioxane)

Poly(PhenylSilsesQuioxane) (=PPSQ)

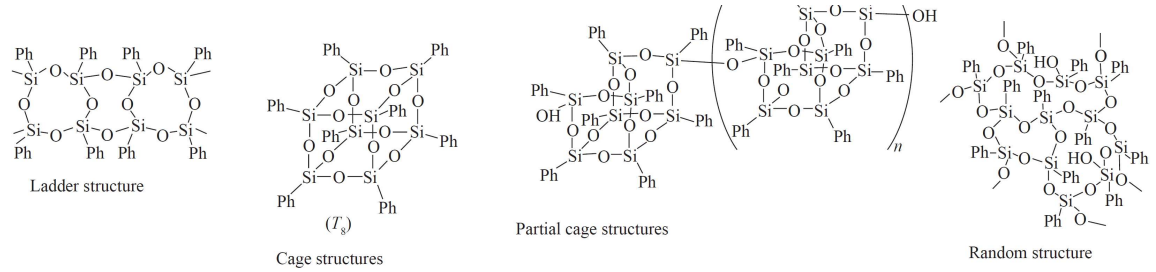

The structure of poly(phenylsilsesquioxane) depends upon the method of preparation. All structural types or combinations of the different types shown above may exist.

Molecular Formula	$(Ph\ Si\ O_{3/2})_n$
Polymer Type	Polysiloxanes/ Siloxane Ladder Polymers
Thermal Stability	>500°C

Poly(phenylsilsesquioxane) (PPSQ) is a brittle silicone resin and the most investigated polymer of the silsesquioxane class because of is solubility in common organic solvents and good thermal stability. The repeating unit consists of alternating silicon-oxygen atoms, in which two monovalent organic radicals (substituent) are attached to each of the silicone atom. Since the siloxane (Si-O) backbone is considered to be inorganic in nature, silicone polymers display both organic and inorganic character [82].

In general, silsesquioxanes have been obtained by the hydrolysis and polycondensation of trifunctional monomers, $RSiX_3$, where X can be a chloride, alkoxide or acetate group. The molecular weight and structure, as well as the thermal properties and solubility of these materials, are strongly influenced by different synthetic conditions such as the nature of the precursor, the polarity of the solvent, and the type of catalyst employed. The formation of PPSQ can be summarized by the following equation:

$$n\ PhSiX_3 + (3+x)\,n/2\ H_2O \rightarrow (PhSiO_{(3-x)/2}(OH)_x)_n + 3n\ HX \quad (X = -Cl, -OR, -OAc)$$

Ring-opening polymerization (ROP) of cyclic siloxanes is a process characterized by the transformation of a cyclosiloxane monomer into a linear siloxane polymer. Such process results from the cleavage of the SiOSi bond in the monomer ring and the subsequent reformation of this bond in the polymer chain. In contrast with the polycondensation, no low molecular weight side product is formed during the ROP process and the concentration of the reactive end groups remain at a low stationary level during the chain growth. A suitable monomer for the ROP of siloxanes may be any cyclic compound containing a reactive SiOSi group in its ring skeleton which is thermodynamically less stable when compared with its open chain structure [83].

Potential applications of this polymer include lithographic materials, gas-separation membranes, coatings for electric and optical devices, especially where high temperatures are required, thermostable glasslike photo-patternable films, insulating layers for semiconductors devices, second-harmonic generators, silicon oxycarbide precursors, binders for processing powders and as interlayer dielectric, high-temperature resins and organic antireflective coating [74].

PPSQ possess exceptional elasticity at unusually low temperatures. Since the glass transition is below -70°C, this makes these polymers extraordinarily good elastomers with a temperature range of potential applicability at least 200-250°C wider. Hence, polysiloxanes are the polymers of choice whenever applications either within an unusually broad range of temperatures, or at unusually high or unusually low temperature are required [84].

Pronounced stability of polysiloxanes at elevated temperatures is a direct consequence of a specific interplay of some of their fundamental properties including: inherent strength of the siloxane (Si-O) bond, pronounced flexibility of the -[Si-O]$_x$- chain segments and entropical higher stability of the low molecular weight cyclic siloxanes in respect to their high molecular weight open chain counterparts at degradation temperatures. Zhang et al. reported that PPSQ with a ladderlike structure is the most stable silsesquioxane polymer. They do not lose weight until 525℃ when heated in air. The decomposition reaction was mainly from loss of phenyl groups [83].

Silsesquioxanes contain β-electron withdrawing groups and they can be converted to silicon dioxide via elimination and hydrolysis at low temperatures or under UV exposure. The thermal reaction cascade for β-substituted silsesquioxanes leading to SiO_2-rich structures with a low level of carbon occurs at temperature above 180℃. UV exposure results in pure SiO_2 films and suggests that patterning β-substituted silsesquioxane films can lead to direct fabrication of dielectric architectures [84].

3.1.9 PolyVinylidene Chloride-co-Acrylonitrile

PolyVinylidene Chloride-co-Acrylonitrile (=PVC-co-PAN)	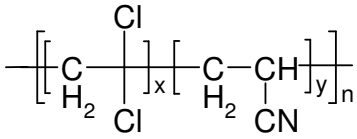
Molecular Formula	$(C_2H_2Cl_2)_x(C_3H_3N)_y$
Monomer	Vinly chloride/Acrylonitrile Copolymer
Material Class	Thermoplastic
Degradation Temperature	140℃

Polyvinylidene chloride copolymers possess the best combination of a high gas barrier and low moisture permeability. Copolymers of polyvinylidiene chloride are more easily processed than the homopolymer polyvinylidene. In polyvinylidene chloride-co-acrylonitrile (PVC-co-PAN), gas permeability increases with the acrylonitrile content, while the crystallinity decreases. The typical concentration of acrylonitrile in the polyvinylidene copolymer is between 5-15% [85].

Polyvinylidene chloride-co-acrylonitrile is prepared by radical polymerization, where the photochemical initiation is carried out with UV lamp [86]. It is frequently used as a thin layer between cellophane, paper and plastic packaging to improve barrier performance. Their ability to provide packaging with a barrier against gasses, odours, water, water vapours, oils and fats and their extraordinary ability to be easily heat-sealed has made them a widely used polymer in the food and medical packaging industries [74].

Copolymer polyvinylidene chloride-co-acrylonitrile is flame-proof, good resistant to sunlight, water acids and alkalis. It is not resistant to organic solvents, and it softens at lower temperature and it has a slightly lower strengths in respect to other materials that contain proportions of acrylonitrile. Polyvinylidene-co-acrylonitrile is unaffected by bacteria, fungi and insects [74].

During heating process, a two-step degradation of the polymer occurs. In the fist degradation region from 140-280℃, the weight loss occurrs due to the evolution of vinylidene chloride and due to the elimination of water, ethanol and the organic solvents. Also, the formation of conjugated unsaturated units gives yellow or brownish colouration. Upon further heating, the second stage of degradation takes place in the temperature range of 550-700℃, which results in the oxidative decomposition reactions of the organic copolymer, vinylidene chloride-acrylonitrile [85].

3.1.10 PolyMethyl MethAcrylate

PolyMethyl MethAcrylate (=PMMA)	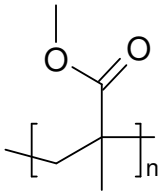
Molecular Formula	$(C_5H_8O_2)_n$
Monomer	Methyl Methacrylate
Material Class	Thermoplastic
Polymer Type	Acrylic
Glass-Transition Temperature T_g	85-115°C
Melting Temperature T_m	160°C

Poly(methyl methacrylate) (PMMA) is commercially the most important commercial member of the acrylate/methacrylate group of polymers. It was first introduced in 1936 and is available as cast and extruded sheet, tubes, rods, powders, pellets, solution, dispersion and emulsions. In addition to its use in sheet form, PMMA is also suitable for many extrusion and moulding applications, coating and surface treatments and has many industrial uses. It is non-toxic, odourless and tasteless and it is a clear, colourless, hard, brittle, fairly rigid material which can be drilled, carved or sawn and has exceptional optical clarity and resistance to degradation by UV light [87].

PMMA is manufactured by bulk, suspension, and solution or dispersion polymerisation. Above its glass-transition temperature PMMA is tough, pliable, extensible and easily bent or formed into complex shapes. At higher temperature, however, it is very susceptible to depolymerisation. Thermal degradation of an acrylic polymer, obtained by free-radical polymerization, proceeds in three steps of mass loss: the first and easiest is initiated by scissions of head-to-head linkages at about 160°C, representing one type of defect at the polymer backbone. The second by scissions at the chain-end initiation from vinylidene ends at around 270°C and the last by random scission within the polymer chain. Upon heating the PMMA above 300°C, an unzipping process occurs, which produces the monomer at >95% yield. The main products of combustion in a well-ventilated atmosphere are CO_2 and CO [14].

Degradation mechanism of PMMA as radical depolymerisation (unzipping) via chain scission is depicted on following reaction scheme:

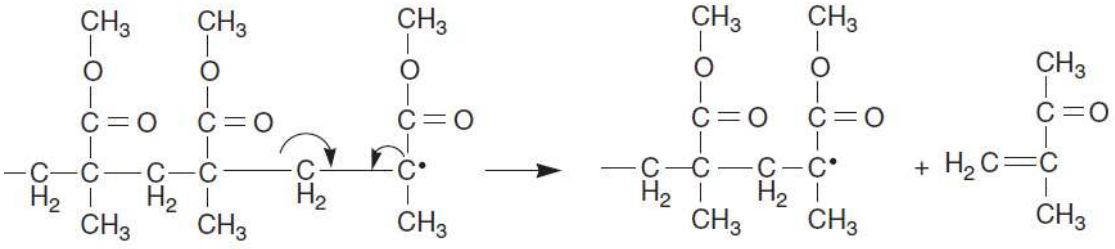

PMMA burns slowly with a blue, crackling flame and little smoke. It is resistant to environmental stress and oxidation at ambient temperature. PMMA may be crazed by solvents and organic compounds and ozonolysis causes degradation. UV radiation of thin films can cause a rapid decrease in Mw with the concomitant formation of small amounts of volatile products. The carbonyl group absorbs at 215 nm leading to chain scission and consequently degradation. Large doses of ionising radiation can cause brittleness, loss of strength, general reduction in physical properties and yellowing, but it does not influence its mechanical or electrical properties. Main chain fracture occurs during irradiation and gamma irradiation causes chain rupture leading to a decrease in T_g and intrinsic viscosity [88].

3.1.11 PolyMethAcryloNitrile

PolyMethAcryloNitrle (=PMAN)	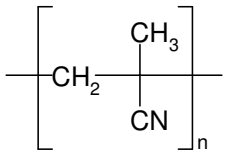
Molecular Formula	$(C_4H_5N)_n$
Monomer	Methacrylonitrile
Material Class	Thermoplastic
Polymer Type	Acrylic
Glass-Transition Temperature T_g	104-120°C
Melting Temperature T_m	>200°C

Polymethacrylonitrile (PMAN) is generally produced by free-radical polymerisation of methacrylonitrile [74]. The application of PMAN include electrode compositions, fuel cells, optical recording media, electrophotography, magnetorhelogical compositions, electromagnetic materials, sensors, oils, films, paint, adhesives, photoresists in x-ray lithography, thermal printing, moulding, biomedical applications. Thin films, produced by electrochemical polymerisation techniques, have potential applications in electronics, catalysis, corrosion inhibition, etc [64].

PMAN has a good mechanical strength and high resistance to solvents, acids and alkalis. This polymer at a lower temperature can either undergo a low-temperature colouration reaction or undergo depolymerisation to the monomer. The colouration reaction can be eliminated if the polymer is prepared using carefully purified monomer and AIBN initiator. Thermal degradation occurs by depolymerisation process to give the monomer in amounts greater than 90%. The presence of nitrile groups appears to prevent intramolecular H-transfer reactions. Degradation to monomer occurs above 200°C and is complete at 270°C [89]. Analytical studies of pure polymer show an almost quantitative degradation to monomer, with trace quantities of isobutene and HCN. Other studies show two initiation processes for polymer degradation in N_2, namely chain-end and random-scission initiation; internal cyclisation reaction leads to the formation of thermally stable residue having conjugated polyimide structure. Irradiation using high-energy radiation leads to main-chain scission without simultaneous cross-linking. Radicals produced by gamma irradiation are primarily the result of main-chain scission, hydrogen atom addition and abstraction [64].

3.1.12 Poly(2-HydroxyEthyl MethAcrylate)

Poly(2-HydroxyEthyl MethAcrylate) (=pHEMA)	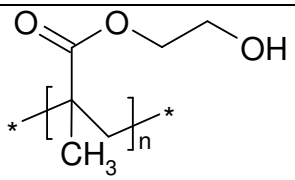
Molecular Formula	$(C_6H_{11}O_3)_n$
Monomer	Hydroxyethylene Methacrylate
Polymer Type	Vinylidene Polymers
Glass-Transition Temperature T_g	55-109°C

Poly(2-hydroxyethyl methacrylate) (pHEMA) functions as a hydrogel by rotating around its central carbon atom. In air, the non-polar methyl side turns outward, making the material brittle and easy to grind into the correct lens shape. In water, the polar hydroxyethyl side turns outward and the material become flexible. Other properties of the pHEMA are the

inertness, light specific weight, biocompatibility, permeability and case of preparation into various shapes, which contribute to its attractiveness for medical applications. Pure pHEMA yields lenses that are too thick for sufficient oxygen to diffuse through, therefore all contact lenses that are pHEMA based are manufactured with copolymers that make the gel thinner and increase its water of hydration. Other applications besides contact lenses are drug delivery systems, biomedical applications chromatographic columns, flocculating agents, etc. [90].

Under exposure to high temperatures, pHEMA degrades. It was reported that the first decomposition step of polymer was observed between ambient temperature and 340℃, while the second decomposition step from 340℃ to 400℃. At both decomposition steps the major product was this monomer which is formed because of depolymerisation reaction; while the side products, arising from ester decomposition were a six-membered glutaric anhydride type of ring, an oxolane, 2-isopropenyl ethyl methacrylate, methacrylic acid and carbon dioxide [91].

Under irradiation, the polymer of the type (CH_2-CR´R´´) such as pHEMA, will undergoes predominantly chain scission. The gamma irradiation promotes chain scission in pHEMA and strengthens the gamma relaxation, which suggests that the number of interchain hydrogen bonds decreases. [65]

3.1.13 Poly(EthyleneTerepthalate)

Poly(ethylene terephthalate) (Mylar®)	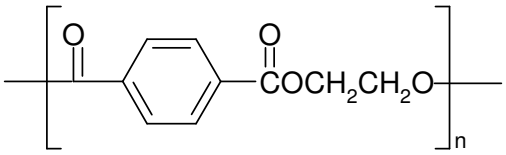
Molecular Formula	$(C_{10}H_8O_4)_n$
Monomer	DiMethyl Terephthalate, 1,2-Ethanediol
Material Class	Thermoplastic
Polymer Type	Polyester
Glass-Transition Temperature T_g	70-125℃
Melting Temperature T_m	245-280℃

Poly(ethylene terepthalate) (PET) is a thermoplastic polymer resin of the polyester family and it can exist as both as an amorphous and as a semi-crystalline polymer. The semicrystalline material might appear transparent or opaque and white depending on its crystal structure and particle size. It is semi-rigid to rigid, depending on its thickness, and it is very lightweight. PET is synthesized by two routes; reaction of dimethyl terephthalate with 1,4-ethanediol in the presence of a catalyst, usually acetate salts of zinc, calcium, manganese, magnesium and cobalt at 150-210℃. Higher M_w products can be obtained by solid-state post polymerisation process or by chain extension reactions [93].

Biaxially oriented PET film – known under trade name Mylar®, can be aluminized by evaporating a thin film of metal onto it to reduce its permeability and to make it reflective and opaque. These properties are useful in many applications, including flexible food packaging and thermal insulation. Because of its high mechanical strength, PET film is often used in tape applications, such as the carrier for magnetic tape or backing for pressure sensitive adhesive tapes [93].

A wide range of applications is possible because of the excellent balance of properties PET possesses and because the degree of crystallinity and the level of orientation in the finished part can be controlled. For packaging PET combines optimum processing, mechanical and barrier properties, which are adequate for the retention of carbon dioxide in packaging used for carbonated beverages. It also possesses good oxygen barrier properties which allow for

its use in many types of food containers. However, barrier properties are not sufficient for beer and foods that are highly sensitive to oxygen [64].

Mylar® foil is very resistant to oils and fats, organic alcohols, hydrocarbons, diluted acids and alkalis. It has poor resistance to phenols, ketones, ester, chlorinated organic solvents and concentrated bases. It can be recycled through depolymerisation. It is remarkably resistant to UV degradation [94]. The main types of degradation that can occur are hydrolytic, thermal and thermal oxidation. When PET degrades, several things happen: discoloration, chain scissions resulting in reduced molecular weight, formation of acetaldehyde and cross-linkage. Discoloration is due to the formation of various chromophoric systems following prolonged thermal treatment at elevated temperature. This becomes a problem when the optical requirements of the polymer are very high, such as in packaging applications. The thermal and thermooxidative degradation results in poor processiblity characteristics and performance of the material [94]. The ester group (-COO-) imparts susceptibility to chain scission after irradiation. Also the most abundant results from H atom abstraction from the chain end and the second is a substituted phenyl radical [14].

3.2 Indicators

All indicators which were sterilized and characterized before and after gamma and electron beam sterilization procedures and applied by construction of optical sensor are listed in table 3 - 3. The properties and characteristics of each indicator are presented in following chapters.

3.2.1 Coumarin Derivatives

Coumarins can essentially be described by two mesomeric forms, one nonpolar form with a low dipole moment and a more polar form with a higher dipole moment where a positive charge is located on the nitrogen atom and a negative charge is on the oxygen atom [44]. These two mesomeric forms of coumarin derivatives are presented on figure 3 – 1.

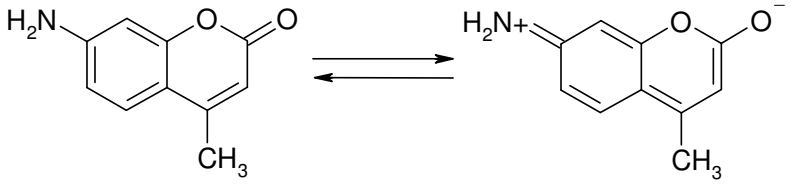

Figure 3 – 1: Two mesomeric forms of coumarin.

In the electronic ground state S_0 of coumarins, the nonpolar mesomeric structure is predominant and the polar form makes only a minor contribution to the actual π-electron distribution. The more polar mesomeric form is stabilized if the dye molecule is surrounded by polar solvent molecules. Therefore, the absorption maximum of coumarin dyes is generally shifted to longer wavelengths with increasing solvent polarity. In the electronic excited state S_1, the more polar mesomeric form is predominant. That is, the electronic dipole moment in coumarin dyes increases upon excitation. This induces the rearrangement of the surrounding solvent molecules and stabilizes the excited state, which lowers the energy of the excited state considerably. Therefore, coumarin derivatives exhibit a large Stokes shift as compared with, for example, rhodamine or oxazine dyes. Usually, coumarin derivatives are coupled covalently to biomolecules using activated carboxyl functions. As electron donating alkyl groups stabilize the positive charge on the nitrogen atom in the more polar mesomeric form, a shift in the absorption band occurs to longer wavelengths. Finally, it was found that the absorption and emission characteristics for coumarin derivatives can be further extended towards longer wavelengths if a heterocyclic substituent is introduced into the 3-position [44].

Derivatives of coumarin are also extensively used for intracellular pH measurement (4-methyl-7-hydroxycoumarin) because of its pK_a value of 7.8, the relatively large variation in its fluorescence intensity versus pH and its low toxicity [43].

3.2.1.1 pH Sensitive Coumarin

3-(2-benzothiazolyl)-7-hydroxycoumarin **(=pH sensitive Coumarin)**	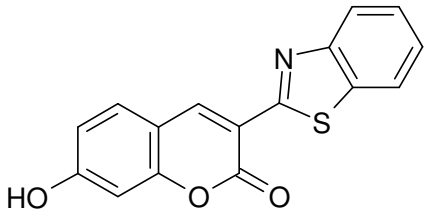
Net Formula	$C_{16}H_9NO_3S$
Molecular Weight	295.32
Chemical/Dye Class	Coumarin, pH sensitive fluorescence indicator
Appearance	Orange solid
Absorption Maximum	λ_{max}abs (acid) = 385 nm λ_{max}abs (base) = 485 nm λ_{max}em (acid) = 439 nm λ_{max}em (base) = 490 nm
pK_a	7.02

The absorption and fluorescence spectra of pH sensitive coumarin are highly pH-dependent in the near neutral pH range. While the fluorescence maxima do not change significantly with pH between 4 and 9, the relative intensities are around two times higher in alkaline solutions than in the acidic solution. The fluorescence of 7-hydroxycoumarin is almost invariably from the anion form in the pH 4-9 range, despite of photoexciting the undissociated species in acidic solutions. According to Förster, this can be interpreted in terms of photodissociation due to a decrease in pK_a in the first excited singlet state. Due to the pK_a value, the pH sensitive coumarin is useful longwave excitable and fluorescing indicator for measuring physiological pH values near-neutral pH´s (such as in blood) [59].

3.2.2 Lanthanides based Luminescent Probes

The lanthanides, such as europium (Eu^{3+}) and terbium (Tb^{3+}) are unique fluorescent probes, because they display line spectra from the individual atoms. The emission lifetimes are long, on the millisecond timescale, and arise from transitions between the f orbitals. These transitions are formally forbidden. The inner shell f orbital electrons are shielded from the environment, so that lanthanides do not display polarity-dependent spectral shifts and are not quenched by oxygen. The lanthanides can be sensitive to their environment, but in ways different from typical fluorophores. Their decay time depend on the number of coordinated water molecules [43].

The lanthanides posses low extinction coefficients, therefore they are not usually excited directly. The ions are at first bound to chelators that contain a fluorophore. The energy from the fluorophore can be efficiently transferred to the lanthanide. The chelators serve two other purposes; the chelator increases the quantum yield of the lanthanide by displacing the bound water molecules that act as quenchers and they also provide a means to bind the lanthanide to a biomolecule [45].

Lanthanides have found widespread use in high sensitivity detection. All biological samples display autofluorescence, which is usually the limiting factor in high sensitivity detection. The autofluorescence usually decays on the nanosecond timescale, as do most fluorophores. The lanthanides have long decay times and therefore continue to emit following disappearance of the autofluroescence [95].

For europium(III) complexes all emission emanates from the nondegenerate $^5D_0$ state. The strongest emissions are invariably observed in the $^5D_0 \rightarrow {}^7F_1$ and $^7F_2$ transitions regions, and

$^5D_0 \rightarrow {}^7F_4$ emission is frequently observed to have a moderate strong intensity. Emission intensities in the remaining $^5D_0 \rightarrow {}^7F_J$ transition regions are generally either very weak or unobservable. The excitation spectra involving direct radiative excitation of Eu^{3+} ions have the potential for providing very useful and sometimes unique structure information. In the near-ultraviolet and blue-visible regions, the excitation and absorption spectra may or may not mimic one another, depending upon the location and relaxation pathways of ligand-to-Eu^{3+} charge-transfer (CT) states [95].

When the chelator environment contains chromophores that are highly absorptive and luminescent in the near-ultraviolet or blue-visible regions of the spectrum, it is possible to sensitize Eu^{3+} luminescence via ligand-to Eu^{3+} nonradiative energy transfer processes. It involves a resonant coupling between the donor (ligand chromophore) and acceptor (Eu^{3+}) and two major criteria must be satisfied for this excitation:

- There must be some overlap between the luminescence spectrum of the donor and the absorption spectrum of the acceptor;
- The acceptor states of the Eu^{3+} ion must be identical with, or strongly coupled to the emitting states ($^5D_0$).

Most europium complexes comprised of chelators (ligands) of biological interest exhibit broad, relatively intense ligand-to-metal charge-transfer (CT) absorption bands in the ultraviolet region of the spectrum.

3.2.2.1 Europium(III) Complex with 4-(4,6-di(1H-indazol-1-yl)-1,3,5-triazin-2-yl)-N,N-DiEthyl Benzen Amine (=Eu(tta)$_3$DEADIT)

Europium(III) Complex with 4-(4,6-di(1H-indazol-1-yl)-1,3,5-triazin-2-yl)-N,N-DiEthyl Benzen Amine (=Eu(tta)$_3$DEADIT)	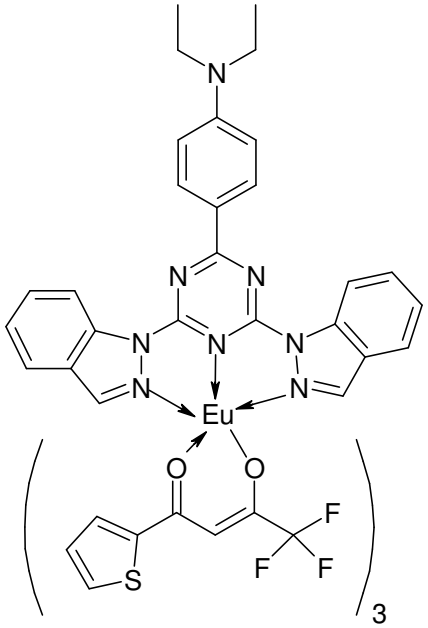
Net Formula	$C_{37}H_{28}O_2N_8SF_3Eu$
Molecular Weight	857.68
Chemical/Dye Class	Lanthanide based Temperature Sensitive Indicator
Appearance	Yellow Solid
Absorption Maximum	λ_{max}abs = 407 nm λ_{max}em = 620 nm
Quantum Yield	0.4
Brightness (ε·Φ)	>25,000

*[54]

Europium(III) chelators are applied for temperature sensing and imaging since they have high temperature-dependent luminescence. The features of lanthanide complexes are also

that they emit in a narrow optical window and possess long luminescence decay times in order of several hundred microseconds. The effect of the oxygen on the decay time of the Eu(III) complex is negligible. The temperature-dependent luminescence can be explained by deactivation of the $^5D_0$ state through a low-lying ligand to metal charge-transfer state. In case of Eu(tta)$_3$DEADIT the possible ways of deactivation are likely also to involve the antenna chromophore particularly by promoting the rotation of the diethylamino group. The luminescence intensity is much more temperature dependent than the decay time. Evidently, the decay time only reflects deactivation of the $^5D_0$ state, whilst higher temperature effect on the luminescence intensity represents the combination of two main processes including deactivation of the $^5D_0$ state of the europium ion, but also of the triplet excited state of the antenna chromophore [54].

The europium(III) chelate enables sensitization of the Eu^{3+} luminescence upon excitation with visible LEDs and can be successfully immobilized in polymer films. The Eu(tta)$_3$DEADIT possesses good photostability in the absence of oxygen. Although the photostabiltiy is substantially lower at air saturation it is still adequate for most applications if phase shift of luminescence is monitored. Therefore, Eu(tta)$_3$DEADIT is or could be applied by optical sensing of temperature and for compensating temperature effects of optical sensors [54].

3.2.3 Long-Lifetime Metal-Ligand Complexes

Long-lifetime metal-ligand complexes are of current interest for several reasons. They possess a relatively long-lived emission (microsecond to millisecond range), are highly stable, like covalent bonds, so there is no significant dissociation of the metal and ligands, are highly photostable and display large Stokes shifts. Because of these favourable properties, metal-ligand probes can have numerous applications in biophysical chemistry, clinical chemistry and DNA diagnostics [60].

The appropriate combination of metal and ligand results in a transition to a metal-to-ligand charge-transfer (MLCT) state. The transition is partially forbidden; therefore the decay times are long. Emission from these states is formally phosphorescence. However, these states are shorter lived than normal phosphorescent states, and thus can emit prior to quenching. The luminescence of metal-ligand charge complexes is thought to be short lived due to spin-orbit coupling with the heavy metal atom, which increases the allowedness of the normally forbidden transition to the ground state [43]. A Jablonski diagram for the metal-ligand complexes is shown in figure 3 – 2.

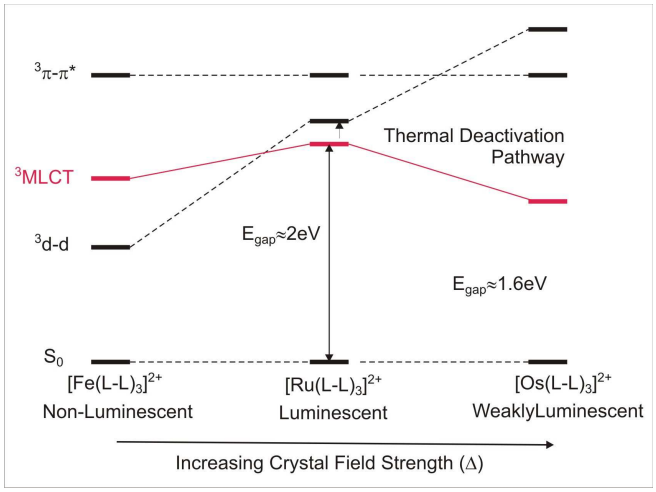

Figure 3 – 2: Lowest energy triplet states for metal-ligand complexes with increasing crystal field strength.

For a metal-ligand complex to be luminescent several criteria must be satisfied. The crystal field must be strong enough to raise the d-d state above the MLCT state. As the energy of the excited state decreases and is closer to the ground state, the rate of radiationless decay increases due to the energy gap law. The relative levels of MLCT and d-d state also determine the sensitivity of the metal-ligand complex decay times to temperature. If the d-d levels are close to the MLCT state, then the d-d states are thermally accessible. In these cases, increasing temperature results in decreased lifetimes due to rapid radiationless decay [43].

Viable oxygen indicators are almost exclusively represented by luminescent complexes of platinum(II) and palladium(II) with porphyrins or porphyrin derivatives such as e.g. porphyrin ketones or porphyrin lactones, by ruthenium(II) polypyridyl complexes and by iridium(III) coumarin complexes, which are presented in details in following chapters.

3.2.3.1 Iridium(III) Coumarin

Iridium (III)((benzothiazol-2-ly)-7-(diethylamino)-coumarin))2 (acetylacetonat) **(=Ir(C$_s$)$_2$(acac))**	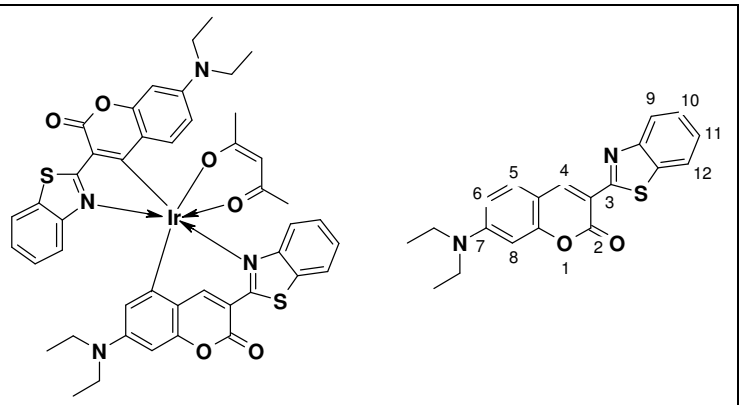
Chemical Formula	$C_{45}H_{41}IrN_4O_6S_2$
Molecular Weight	990.2 g/mol
Appearance	Yellow solid
Absorption Maximum Emission Maximum	λ_{max}abs = 450 nm λ_{max}em = 545 nm
Molar Absorbance	ε = 57100 $M^{-1}cm^{-1}$
Quantum Yield	0.53
Luminescence Lifetime (in the absence of the quencher)	τ_0 = 8.5 µs

The cyclometalated iridium(III) coumarin complex is often applied for optical oxygen sensing. It possesses efficient visible absorption and a high quantum yield, which results in high brightness. Likewise, it possesess low cross-sensitivity to temperature and suitability for both decay time-based and ratiometric measurements. Therefore, the complex is attractive for application in thin films for monitoring of fast processes and various types of nano- and microparticles, including magnetic beads with high signal-to-noise ratio. The disadvantage of the iridium(III) coumarin complex its low photostability, which restricts its application. If long-term measurements are not required, the probes can be successfully used for reliable monitoring of oxygen concentrations [60].

Spectral properties and oxygen sensitivity can be fine-tuned by varying the substitution of the coumarin ligand and using respective monomeric or dimeric complexes. Spectral properties depend on the nature of the substituent in the 3 position of the coumarin and are also determined by the nature of the donor group in the 7 position of the coumarin. The electron transitions in the complexes are the same nature as in the ligands, apart from the very high probability of intersystem crossing from the singlet excited state into the triplet state promoted by the presence of the “heavy atom” [60].

3.2.3.2 Platinum(II) and Palladium(II) Porphyrin complexes

Annulenes that contain four N-atoms within the ring perimeter are called porphyrins. Most natural porphyrins contain a skeleton of four pyrrole rings that are bridged in their α,α’-positions by four methane groups. Thereby, the macrocyclic inner ring contains only 16, and not 18 sp^2-hybridized atoms. Nevertheless, porphyrins are tetraaza[18]annulenes, because the β- and β’-C-atoms are conjugated methane groups that also contribute to the aromatic system. The NH groups also share their lone-pair p_y electrons with the aromatic system. The lone pairs of –N= groups reside in the plane of the ring system and do not overlap the

methane orbitals. Porphyrins bind metals to form complexes, which reside in the central N_4 cavity formed by the loss of two protons [96].

Porphyrins can coordinate metal atoms firmly to form metalloporphyrins. Porphyrins are very attractive for the design of sensors for molecule recognition. The flat and rigid structure of porphyrins offers the possibility for constructing various types of recognition sites. [97] They are used for the recognition of hydrophobic molecules, aminoacids, nucleobases, etc.

Pt- and Pd-porphyrins are used as highly efficient oxygen probes in optical oxygen sensors and enzyme biosensors. Excitation spectra of the porphyrins have an intense Soret band at about 400 nm and several bands in the region of 450-650 nm. Emission occurs in the region of 550-800 nm. Both spectra are very characteristic, but variable for different substituted porphines, metal derivatives, protometric and extra-ligand forms. The well-developed synthetic chemistry of porphyrin compound enables specific porphyrin probes to be designed and their spectral and physical properties (functional groups, solubility, hydrophobicity, etc.) adjusted for particular analytical applications [96].

In case of Pt- and Pd-porphyrins sufficient BSs are achieved only upon UV excitation into the Soret band, which is however highly undesirable for obvious reasons. Excitation in the Q-bands is significantly less efficient and overall intensities are approximately tenfold lower than for the iridium(III) complexes. Notably, the phosphorescence of Pd-porphyrins is quenched almost completely at air saturation so that very little emission is detected even under excitation into the Soret band [98].

Excited triplet states of metalloporphyrins are quenched effectively with dynamic quenchers, like molecular oxygen, nitrogen oxides, etc. Oxygen is the most valuable and dominating object for quenched-luminescence sensing of biologically active species. Platinum(II) porphyrin complexes have proved to be excellently suitable for oxygen sensing in the range from 0% to 100% air saturation. Luminescent oxygen-sensitive compositions are usually prepared in the form of thin (micrometer range) films which have uniform distribution of the probe throughout the film volume. True solid solutions of the dye molecule in an appropriate polymer are preferred. The material should be easily permeable for oxygen but not for any other species that could interfere with the probe luminescence and quenching with oxygen [99].

Following features of porphyrins can be summarized:

(1) Porphyrin oxygen probes have intense absorption bands in the visible spectral range of 480-580 nm. These bands essentially overlap with emission spectra of some light-emitting diodes, which are suitable for use as light sources. Therefore, porphyrins can be easily excited with a compact and low cost LED light source. The phosphorescence wavelengths of porphyrin are well separated from the excitation LED wavelength and thus the influence of excitation light source can easily eliminated.

(2) The intense red luminescence of metalloporphyrins having Stokes shifts of about 100 nm makes no special difficulties in filtering of the excitation and emission light.

(3) The chemical stability of Pt-porphyrins is very good

(4) The photostabiltiy is not as high as for polycyclic aromatics but quite satisfactory. In optical sensing applications with Pt-porphyrins, the photostability could be improved by:
    a. Decreasing the intensity of the excited light
    b. Providing conditions of total absorption of the excited light (i.e. when changes in dye concentration have no influence on the luminescent signal)
    c. Modifying the porphyrin macrocycle to produce photochemically more stable derivatives (e.g. polyfluorinated porphyrins)
    d. Oxygen sensing via lifetime measurements, which makes long-term signal drift quite insignificant.

Platinum(II) meso-tetrakis-(pentafluorophenyl)porphyrin (=PtTFPP)

Platinum(II)-5,10,15,20-tetrakis-(2,3,4,5,6-pentafluorphenyl)-porphyrin (=PtTFPP)	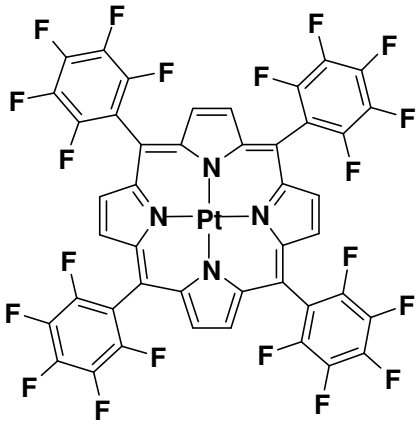
Chemical Formula	$C_{44}H_8N_4F_{20}Pt$
Molecular Weight	1168.62 g/mol
Appearance	Red solid
Absorption Maximum Emission Maximum	λ_{max}abs = 394, 509, 540 nm λ_{max}em = 649 nm
Molar Absorbance [$M^{-1}cm^{-1}$]*	394 nm: ε = 220000 509 nm: ε = 13400 540 nm: ε = 18100
Luminescence Lifetime (in the absence of the quencher)	τ_0 = 55 µs

*[61]

PtTFPP is very often an indicator of choice when designing optical oxygen sensors [100]. The Stokes shift between absorption and emission spectrum is relatively large (100-170nm). [101]. PtTFPP has also received much attention as photostable sensing materials. As the electron-withdrawing character of the perfluorophenyl substituents of PtTFPP strongly raises the redox potential and reduces the electron density of the porphyrin ring, PtTFPP is stable against photo-oxidation and photo-reduction [102].

Platinum(II) OctaEthyl Porphyrin (=PtOEP)

Platinum(II)-2,3,7,8,12,13,17,18-OctaEthyl-21H, 23H-Porphyrin (=PtOEP)	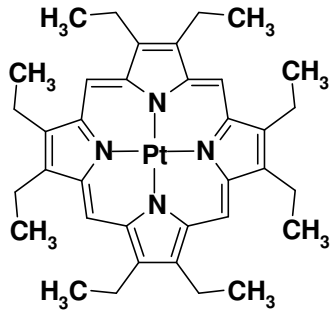
Chemical Formula	$C_{36}H_{44}N_4Pt$
Molecular Weight	727.84 g/mol
Appearance	Red solid
Absorption Maximum Emission Maximum	λ_{max}abs =382, 501, 536 nm λ_{max}em = 647 nm
Molar Absorbance [$M^{-1}cm^{-1}$]*	382 nm: ε = 286 000 501 nm: ε = 12 600 536 nm: ε = 62 400
Quantum Yield*	382 nm: Φ = 0.89 501 nm: Φ = 0.90 536 nm: Φ = 0.89

Luminescence Lifetime (in the absence of the quencher)**	τ_0 = 83 µs

*[61]

PtOEP was the first dye to be used in a polymer-based electrophosphorescent device. The emission is largely ligand based and possesses a relatively long lifetime. In general, excitation of the PtOEP dye will occur in parallel via energy- and charge-transfer processes [103]. The phosphorescence of PtOEP is effectively quenched by molecular oxygen; therefore immobilized in oxygen permeable polymers it is often applied for oxygen sensing. At high PtOEP concentration (>1.6 wt%) luminescence reduction was reported due to luminescence self-quenching. In neat films of PtOEP the phosphorescence spectrum was found to be strongly red-shifted. It is thought that aggregation occurs leading to triplet phosphorescent excimers, which cause the solid-state neat film behaviour [104].

Platinum(II) and Palladium(II) Benzoporphyrins

The complexes of platinum(II) and palladium(II) with meso-substituted benzoporphyrins can be excitable both in the blue and the red parts of the spectrum. Upon excitation in the blue region, the respective platinum complexes show even higher brightness than the iridium(III) coumarins. Considering excitation in the red region, the benzoporphyrin complexes absorb at longer wavelengths than the respective complexes of porphyrin ketones and porphyrin lactones. The indicators are nicely compatible with bright blue LEDs (425, 435 and also with a 450 nm LED in the case of PdTPTBPF) and a 625 nm red LED. This makes the indicators particularly promising for application in (fiber) optic sensors [105].

Pt(II) and Pd(II) benzophorphyrins can be excited at longer wavelengths than corresponding complexes of porphyrin-lactones and porphyrin-ketones. Generally, Pt(II) complexes are better suited for oxygen sensing due to their higher brightness and shorter phosphorescence decay time [61]. In fact, the general trend in photophysical properties of metalloporphyrins indicates that platinum(II) complexes possess 2-3 times higher emission quantum yields than the respective palladium(II) derivatives. They were found to benefit from intense absorption in the red region, very high luminescence brightness, but also high photostability. The photostabiltiy of the platinum(II) benzoporphyrins was found to be comparable to that of PtTFPP, which is known for its exceptional photostability [105].

However, the palladium(II) complexes show significantly higher sensitivity to oxygen than the respective platinum(II) dyes. Evidently, the palladium(II) complexes are more adequate for trace oxygen sensing, since their luminescence is quenched almost completely at air saturation. In the case of the palladium(II) complexes the temperature dependence of the triplet-state decay time (estimated in the absence of oxygen) is as high as 0.33-0.38%/K. On the other hand, the respective platinum(II) complexes show almost negligible thermal quenching (0.06-0.11%/K) [61].

The complexes of meso-substituted benzoporphyrins show very low tendency to aggregation in non-polar polymers such as polystyrene. Therefore, thin layers with a relative high concentration of indicator made and a layer of little thickness would respond virtually in real time to changes in oxygen concentration, but would still produce a very high signal because of the high emission quantum yields of the indicators. This property makes the benzoporphyrin complexes particularly suitable for ultrafast monitoring of oxygen tension [106]. Likewise, the NIR-emitting phosphorescent dyes were shown to be promising for applications in OLEDs and solar collectors. The platinum(II) and palladium(II) benzoporphyrins are therefore also suitable for measurements in blood and in subcutaneous tissue. Hence, the platinum(II) and palladium(II) benzoporphyrins are particularly promising for designing implantable oxygen and glucose sensors [61].

Platinum(II) meso-tetra(4-FluoroPhenyl) TetraBenzoPorphyrin (=PtTPTBPF)

Platinum(II) meso-tetra(4-FluoroPhenyl) TetraBenzoPorphyrin (=PtTPTBPF)	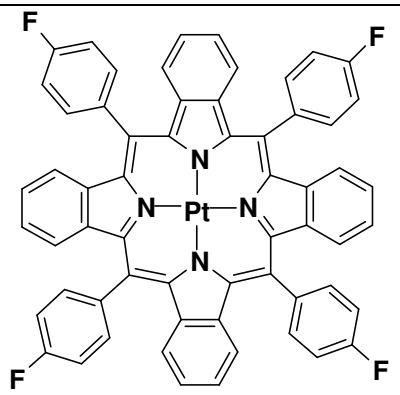
Net Formula	$C_{44}H_8N_4F_{20}Pd$
Molecular Weight	1078.95
Appearance	Green solid
Absorption Maximum Emission Maximum	λ_{max}abs = 430, 615 nm λ_{max}em = 773 nm
Molar Absorbance [$M^{-1}cm^{-1}$]*	430 nm: ε = 212000 615 nm: ε = 146000
Quantum Yield*	0.6
Luminescence Lifetime (in the absence of the quencher)	τ_0 = 1020 µs

*[61, 91]

Palladium(II)) meso-tetra(4-FluoroPhenyl) TetraBenzoPorphyrin (=PdTPTBPF)

Palladium(II) meso-tetra(4-FluoroPhenyl) TetraBenzoPorphyrin (=PdTPTBPF)	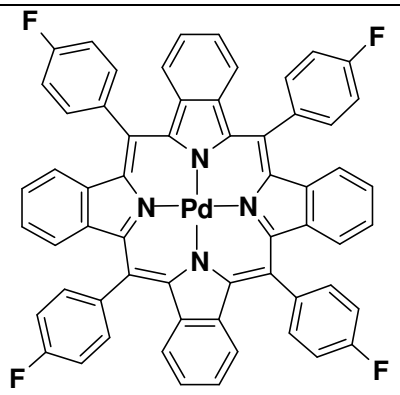
Net Formula	$C_{44}H_8N_4F_{20}Pd$
Molecular Weight	1078.95
Appearance	Green solid
Absorption Maximum Emission Maximum	λ_{max}abs = 443, 629 nm λ_{max}em = 800 nm
Molar Absorbance [$M^{-1}cm^{-1}$]*	443 nm: ε = 268000 629 nm: ε = 115000
Quantum Yield*	0.6
Luminescence Lifetime (in the absence of the quencher)	τ_0 = 350 µs

*[61]

3.2.3.3 Ruthenium Complexes

Ruthenium complexes have been the most popular oxygen probes. The fluorescence is strongly reduced by molecular oxygen due to dynamic quenching. Therefore, it is a viable oxygen probe based on either measurement of intensity or decay time [106]. Likewise, the ruthenium complexes are more photostable than porphyrins and when immobilized in polymer matrices, efficiently used as oxygen sensors, which can be excited by halogen lamps or blue LEDs only due to the favourable maxima absorption range [107]. The large Stokes' shift and the high fluorescence intensity allow for a cheap optical filter arrangement for suppression of stray light [108].

The ruthenium probes, however, exhibit only moderate brightnesses, which depend on the molar absorption coefficient and quantum yield. Although, the ruthenium complexes have been the most commonly used oxygen probe, they suffer from pronounced cross-sensitivity to temperature, since their triplet states are subject to severe thermal quenching. Because of great sensitivity to temperature, in this study, the dichlorotris(1,10-phenanthroline) ruthenium(II) hydrate was taken as the indicator for temperature sensor. Another inconvenience includes relatively short decay times of several microseconds, which results in low sensitivity unless highly oxygen permeable polymers are used.

Ruthenium(II)-tris-4,7-diphenyl-1,10-phenanthroline dichloride (=Ru(dpp)$_3$Cl$_2$)

Ruthenium(II)-tris-4,7-diphenyl-1,10-phenanthroline dichloride **(Ru(dpp)$_3$Cl$_2$)**	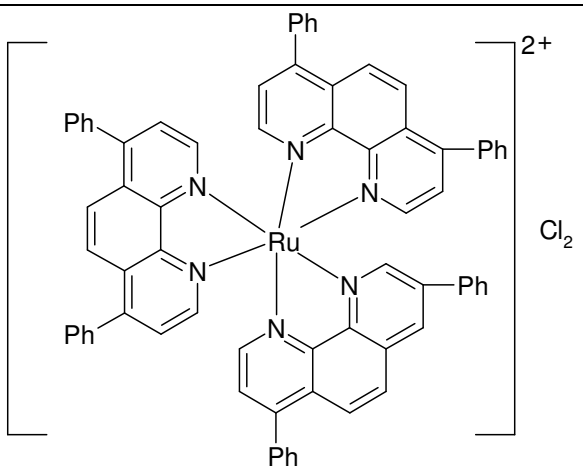
Net Formula	$C_{72}H_{48}Cl_2N_6Ru$
Molecular Weight	1169.17
Appearance	Orange solid
Absorption Maximum Emission Maximum	λ_{max}abs = 455 nm λ_{max}em = 613 nm
Luminescence Lifetime (in the absence of the quencher)	τ_0 = 5.1 µs

DiChloroTris(1,10-Phenanthroline) Ruthenium(II) Hydrate

DiChloroTris(1,10-Phenanthroline) Ruthenium(II) Hydrate	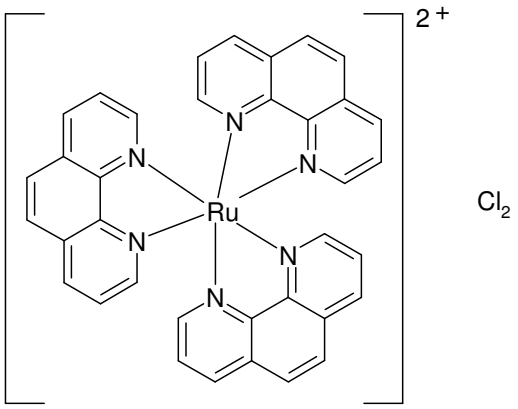
Net Formula	$C_{36}H_{24}Cl_2N_6Ru \cdot xH_2O$
Molecular Weight	712.59
Appearance	Orange solid
Absorption Maximum Emission Maximum	λ_{max}abs = 444 nm λ_{max}em = 590 nm

3.2.4 Pyrene Derivative

Pyrene derivative: 8-hydroxy-pyrene-1,3,6-trisulfonic acid trisodium salt (=HPTS) was first synthesized by Tietze and Baeyer at 1939 and is predominantly used as a fluorescent marker of neuronal growth and cell volume changes. The suitability of HPTS as a fluorescent indicator of pH was first proposed by Wolfbeis et al. in 1983. The study by Wolfbeis and colleagues showed that HPTS fluorescence was stable between pH 0 and pH 14, and was particularly useful for measuring pH in the physiological range [109].

The pH probe HPTS displays favorable properties as a wavelength-ratiometric probe. The sulfonate groups are for solubility in water and the hydroxyl group provides sensitivity to pH. A possible disadvantage of HPTS is that it undergoes ionization in the excited state-rather than at ground-state equilibrium. The fact that HPTS undergoes an excited-state reaction can be recognized by noting that the excitation spectra are comparable to the absorption spectra of both the phenol and phenolate forms, but that there is only a single long-wavelength emission spectrum. Another disadvantage of HPTS has been the relatively short excitation wavelength, particularly for the acid form [43].

Hulth et al. described a planar pH sensor incorporating the fluorescent indicator 8-hydroxypyrene-1,3,6-trisulfonic acid trisodium salt (HPTS) with cellulose acetate as matrix for 2-D pH mapping in early diagenetic studies of marine sediments. This system has two drawbacks. The given dynamic range does not match the average pH range in marine systems. Furthermore, this sensor based on HPTS is highly cross-sensitive towards IS changes. The lipophilic HPTS; 1-HydroxyPyrene-3,6,8-tris-bis(2-Ethylhexyl)Sulfonamide (=HPTS(DHA)3) show low cross-sensitivity to IS, which is not surprising since the charged sulfo-groups of the HPTS are here converted to the uncharged sulphonamide-groups [110]. Likewise, the brightness of the lipophilic HPTS is compared to that of the lipophilic fluorescein derivatives since the molar absorption coefficients of the fluoresceins are significantly higher and the HPTS derivatives in D4 are particularly promising for application in marine systems. Conveniently, the apparent pK_a of HPTS is 7.3, making it useful for clinical measurements [62].

3.2.4.1 1-HydroxyPyrene-3,6,8-tris-bis(2-Ethylhexyl)Sulfonamide (=HPTS(DHA)$_3$)

1-HydroxyPyrene-3,6,8-tris-bis(2-Ethylhexyl)Sulfonamide (=HPTS(DHA)$_3$)	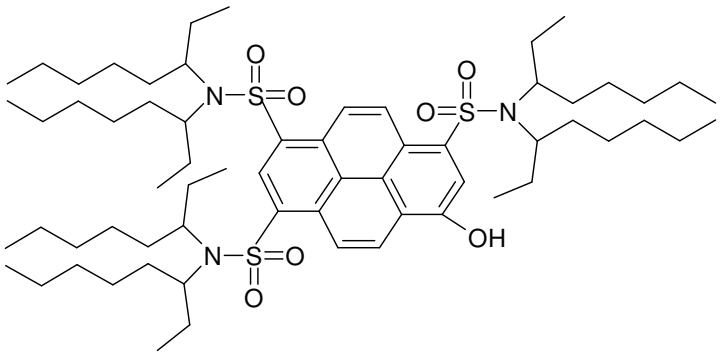
Net Formula	$C_{64}H_{109}O_6N_3S_3$
Molecular Weight	1139.73
Chemical/Dye Class	Pyrene based pH sensitive fluorescence indicator
Appearance	Yellow-Brownish Viscous Liquid
Absorption Maximum	λ_{max}abs (Acid) = 433 nm λ_{max}abs (Base) = 525 nm λ_{max}em (Acid) = 552nm λ_{max}em (Base) = 564 nm
pK_a	6.9

3.2.5 Perylene Derivatives

The perylene molecule consists of two naphthalene molecules connected by a carbon-carbon bond at the 1 and 8 positions on both molecules. In cell membrane cytochemistry, perylene is used as a fluorescent lipid probe. Perylene displays blue fluorescence [111]. Most perylenes are used primarily in high grade industrial paints, especially in original automotive finishes and in automotive refinishes. It is used as a blue-emitting dopand material in OLEDs, either pure or substituted. Perylene can be also used as an organic photoconductor [112].

Asymmetric perylene bisimide are suitable for the preparation of fluorescence chemosensors for pH. They carry one amino-functional substituent which introduces pH sensitivity via photoinduced electron transfer (PET) while the other one increases solubility. The excitation and emission spectra are diminished in intensity but not altered in shape as pH is increased. Perylene bisimides with selected PET functions can enlarge the dynamic range over 4 pH units. Tetra-tert-butyl-substituetd perylene bisimides yield more long-wave excitable sensors which feature excellent photostability. Cross-sensitivity to ionic strength is also negligible. Perylene bisimide dyes are known for their relatively high molar absorption coefficient 30000-90000 $M^{-1}cm^{-1}$, high quantum yield and excellent photostability [50].

3.2.5.1 PET Perylene BisImide

PET Perylene BisImide	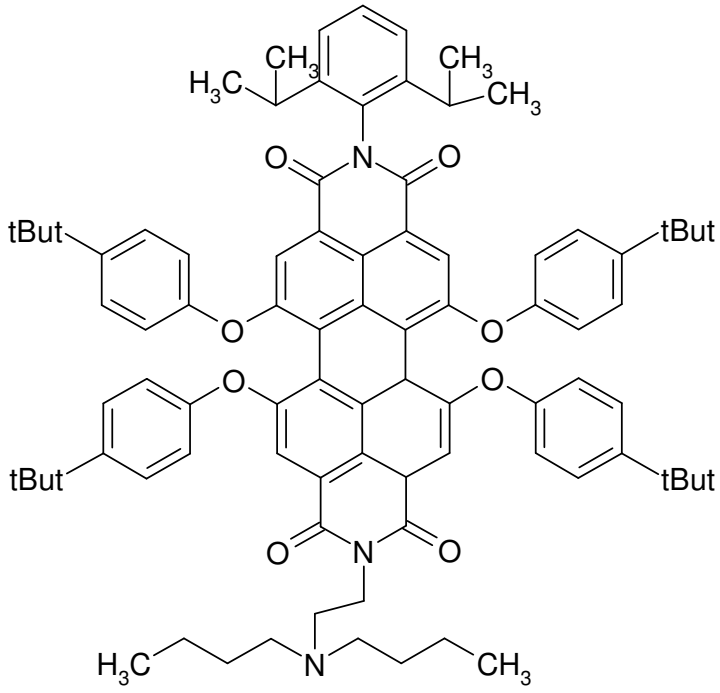
Net Formula	$C_{93}H_{95}N_3O_8$
Molecular Weight	1382.77 g/mol
Appearance	Red solid
Chemical/Dye Class	Perylene based fluorescent dye
Absorption Maximum Emission Maximum	λ_{max}abs = 452 nm; 542 nm and 582 nm λ_{max}em = 624 nm
pK_a	5.1
Quantum Yield	0.75 (protonated form); 0.11 (deprotonated form)

3.2.6 Xanthen Derivatives

Xanthene (9H-xanthene, 10H-9-ocaanthracene) is a yellow organic heterocyclic compound. Its chemical formula is $C_{13}H_{10}O$. Xanthene is used as a fungicide and it is also a useful intermediate in organic synthesis. Derivatives of xanthene include fluoresceins, eosins, rhodamines, pyronine, etc. Xanthene dyes tend to be fluorescent, yellow to pink to bluish red, brilliant dyes [113].

Xanthene dyes have been employed in various fieldsas following:

- Tracing agents in water pollution and aerial pesticide spraying studies;
- Colorant agents in drugs, cosmetics, textiles and inks;
- Laser dyes.

The spectral and thermodynamic properties of xanthene dyes are primarily governed by the substitution pattern of the xanthene structure, for instance, emission and absorption characteristics, the quantum yield and pK_a values. Generally, the substitution at the 2' and 7' position has little effect on the quantum efficiency, whereas substitutions at the 4' and 5' positions decrease the quantum yield. The emission characteristics of xanthenes also strongly depend on species formed by protonation or deprotonation [114].

3.2.6.1 Eosin EthylEster

2´,4´, 5´,7´-Tetrabromoeosin ethyl ester potassium salt (=Eosin EthylEster)	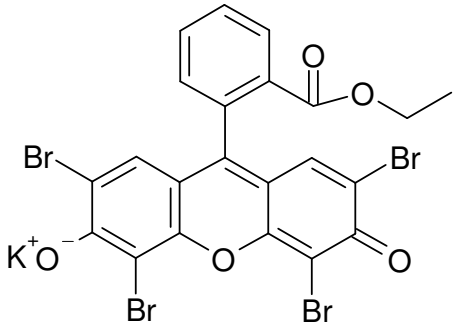
Net Formula	$C_{22}H_{11}Br_4KO_5$
Molecular Weight	714.03
Appearance	Red-brownish solid
Absorption Maximum Emission Maximum	λ_{max}abs (Acid) = 477 nm λ_{max}abs (Base) = 538 nm λ_{max}em (Acid) = 500 nm λ_{max}em (Base) = 560 nm
Chemical/Dye Class	Xanthene pH sensitive fluorescence indicator
pK_a	3.8
Quantum Yield	~0.5

Eosin is a red fluorescent dye in the form of triclinic crystals and it is a bromine derivative of fluorescein. The major applications of eosin are in dyeing textiles, ink manufacturing, in colouring cosmetics, in colouring gasoline and as a toner. Likewise, it is used in biology to stain cells due to strongly absorption by red blood cells, colouring them bright red. Recent studies have applied the eosin ethylester immobilized into the cellulose polymer as warning device for too high ammonia concentrations in lakes, fish farms, aquarium and the sea [115].

By ammonia sensors, a pH indicator is entrapped by gas-permeable membrane. The ammonia penetrating causes a change of pH that results in a colour or fluorescence change of the indicator dye [116]. Eosin has the lowest pK_a value of commercially available dyes and is therefore the most promising compound for trace measurements of ammonia [114].

3.2.6.2 DiChloroFluorescein

2',7'-DiChloroFluorescein	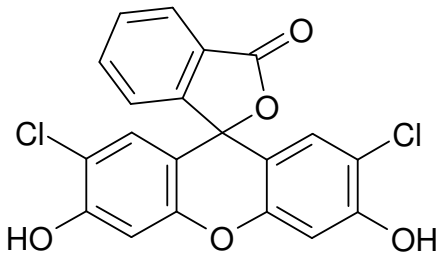
Net Formula	$C_{20}H_{10}Cl_2O_5$
Molecular Weight	401.20
Appearance	Light orange solid
Chemical/Dye Class	Xanthene pH sensitive fluorescence indicator
Absorption Maximum Emission Maximum	λ_{max}abs (Base) = 509 nm λ_{max}em (Base) = 520 nm
pH Range	4.0 – 6.0
Colour Change at pH	Weak green fluorescence (4.0) to intense green fluorescence (6.0)
pK_a	4.46
Quantum Yield	~0.9

Applications	Electroluminescent devices, sol-gel silica films, integrated circuits, photoresists, LED devices, solid-state dye laser, inks, fluorescent pH sensors, emissive probes, chemo- and photo-therapeutic treatment of disease,etc.

The dichlorofluroescein can be formed upon reaction of dichlorofluorescin with oxidizing species. Dichlorofluorescin is widely used to measure oxidative stress in cells. Upon appearance of fluorescent dichlorofluorescein, the fluorescence intensity can be easily measured and is the basis of the popular cellular assay for oxidative stress [117]. Likewise, dichlorofluorescein is often used in the Fajans method for the volumetric analysis of chloride.

The acidic forms of dichlorofluorescein are stronger acids than the corresponding forms of fluorescein. For the cationic and monoanionic acids, the difference in pK is 1.7; for the neutral acids, it is 0.9. The anionic acid of dichlorofluorescein is slightly weaker in their first excited singlet than in their ground states, the difference in pK being 0.2 [118].

3.2.6.3 2´, 7´-DiHexyl-5(6)-*N*-Octadecyl-CarboxAmidoFluorescein (=DHFA)

2´,7´-DiHexyl-5(6)-*N*-Octadecyl-CarboxAmidoFluorescein **(=DHFA)**	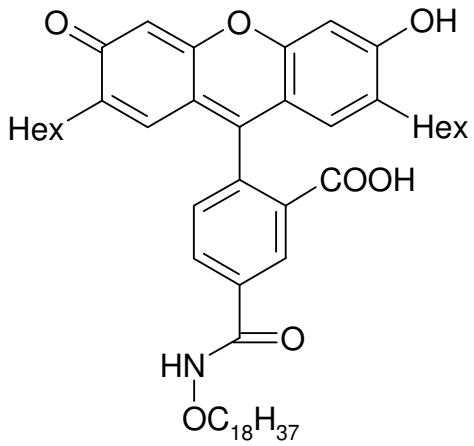
Net Formula	$C_{50}H_{73}O_7N$
Molecular Weight	800.13
Chemical/Dye Class	Xanthene pH sensitive fluorescence indicator
Appearance	Orange solid
Absorption Maximum	λ_{max}abs (Base) = 516 nm λ_{max}em (Base) = 545 nm
pK_a	7.3

Fluoresceins represent highly versatile indicators since: (a) their pK_a can be tuned in a wide range (which makes them suitable for a variety of applications), without significantly affecting the spectral properties and (b) they can be covalently attached to some polymers or made lipophilic to be entrapped in other matrixes. Lipophilization makes immobilization of an indicator virtually irreversible and prevents its leaching out of the sensor into the analyzed media [63].

The hexyl residues of lipophilic pH indicator DHFA fulfil two functions. Firstly, they have a positive inductive effect which diminishes the stability of the deprotonated form of the indicator, especially in nonpolar media and therefore shifts the apparent dissociation constant (pK_a´) to higher values. Secondly, they increase the lipophilicity of the dye. To obtain pH indicators which can be immobilisied in a lipophilic sensor matrix, the lipophilic character was further increased by amidation of the 5(6)-carboxyl group of DHCF with octadecylamine. Like most fluoresceins the protonated form of DHFA exists predominantly as lactone in a nonpolar surrounding [63].

DHFA exhibit slightly lower pK_a values than the respective non-substituted fluorescein derivatives. Such dependence can be explained by localization of the non-substituted indicators in regions of slightly lower polarity, which can presumably occur more easily due to sterics. Evidently, it is more difficult to penetrate these regions for the bulkier dihexylsubstituted derivatives. On the other side, in hydrogel D4 the situation is opposite and both dihexyl-derivatives possess the highest pK_a, approaching 8, indicating their localization in non-polar regions [119].

The cross-sensitivity of optical pH sensors towards IS originates in the fact that during pH measurements the proton activity of the solution is correlated to the concentration of the respective pH indicator species and not to their activities. The DHFA-containing sensors show a stronger IS effect due to the additional anionic charge of the dye and are therefore more useful for open sea measurements where the IS is high and nearly constant. The temperature cross-sensitivity was found to be small, especially for DHFA, it is almost negligible between pH 7.5 and 8.5 [119].

3.2.6.4 2´, 7´-DiHexylFluorescein OctadecylEster (=DHFE)

2´,7´-DiHexylFluorescein OctadecylEster (=DHFE)	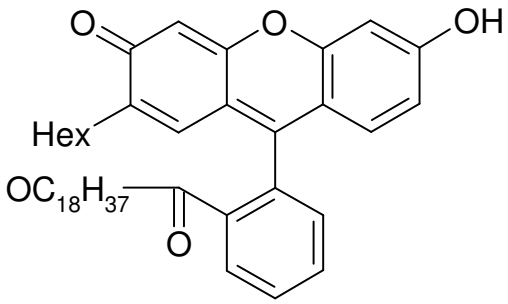
Net Formula	$C_{45}H_{60}O_5$
Molecular Weight	680.96
Chemical/Dye Class	Xanthene pH sensitive fluorescence indicator
Appearance	Yellow solid
Absorption Maximum	λ_{max}abs (Acid) = 498 nm λ_{max}abs (Base) = 524 nm λ_{max}em (Acid) = 523 nm λ_{max}em (Base) = 551 nm
pK_a	7.5

The indicator DHFE was made lipophilic by esterification of the carboxyl group with a C18 alkyl chain. By the lipophilic fluorescein derivatives and their esterification with long alkyl chains, there are three characteristic features: firstly, the number of charges is reduced to one negative charge because the carboxyl group became esterified; this results in a negligible cross-sensitivity towards ionic strength. Secondly, the modification of the carboxyl group prevents lactonization of the chromophore. Therefore, the indicators show different colours (wavelengths) for the basic and the acidic form, respectively. This is desirable with respect to internal referencing via ratiometric measurements. Thirdly, the lipophilic character of the dyes prevents their leaching from the polymer matrix. The indicators can be embedded in the hydrophobic blocks of a suitable polymer matrix. Thus, covalent coupling is not needed which facilitates sensor preparation [120].

DHFE was demonstrated to be nicely suitable for marine research because of the pK_a value of ≈8. Unfortunately, the photostabiltiy of DHFE is the poorest among all fluorescein derivatives, and this significantly limits its practical applicability [63].

3.2.7 pH Sensitive Non-Luminescence Indicators

A pH sensitive non-luminescencet indicator is a halochromic compound, with which the pH (acidity or basicity) can be determined visually. It is like a chemical detector for hydronium ions (H_3O^+) or hydrogen ions (H^+) in the Arrhenius model. As most naturally occurring organic compounds are weak protolytes, carboxylic acids and amines, pH indicators find many applications in biology and analytical chemistry. Moreover, pH indicators form one of the three main types of indicator compounds used in chemical analysis, along with complexometric indicators and redox indicators [121]. The colour change of an indicator occurs when the pH of the solution passes through its pK_a. The indicator is essentially measuring when the concentration of acid or base added is equal to the concentration of acid or base originally present in solution. Different pH indicators have different pK_a values and can therefore be used over various pH ranges in titration.

For colour change of pH sensitive non-luminescence indicators, a resonance of electron isomerism is responsible. Various indicators have different ionisation constants and therefore they show a change in colour at different pH intervals. Acid base indicators can be broadly classified into three groups:

1. The phthaleins and sulphophthaleins
2. Azo indicators
3. Triphenylmethane indicators.

The phthaleins are made by condensing phthalein anhydride with phenols. All of them suffer from irreversible breakdown in strong alkalis. The sulphophthaleins show sharpness of colour change. The examples are thymol blue, m-cresol purple, bromopheno blue, etc. The azo indicators are obtained by reacting aromatic amines with diazonium salt. They show colour change in strongly acid solution. The last group of indicators are triphenylmethane indicators, e.g. malachite green, crystal violet [122].

3.2.7.1 BromoPhenol Blue

BromoPhenol Blue	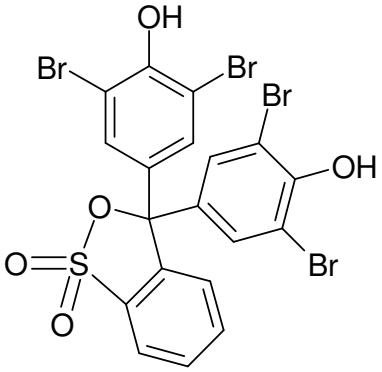
Net Formula	$C_{19}H_{10}Br_4O_5S$
Molecular Weight	669.96
Chemical/Dye Class	Sulfonephthalein pH sensitive dye
Appearance	Yellowish-brownish solid
Absorption Maximum	λ_{max}abs (Acid) = 426 nm λ_{max}abs (Base) = 603 nm
pH Range	3.0 – 4.6
Colour Change at pH	Yellow (3.0) to blue-purple (4.6)
pK_a	4.0, 3.85, 3.6

Bromophenol blue absorbs red light most strongly and transmits blue light. At low pH, the dye absorbs most strongly ultraviolet and blue light and appears yellow in solution. In solution at pH 3.6 obtained by dissolution in water without any pH adjustment, bromophenol

blue has a characteristic green red colour. This phenomenon is called dichromatic colour. Bromophenol blue is the substance with the highest known value of Kreft´s dichromaticity index. This means that it has the largest change in colour hue, when the thickness or concentration of observed sample increases or decreases [123].

Bromophenol blue is used as a colour marker to monitor the process of agarose gel electrophoresis and polyacrylamide gel electrophoreses. Since bromophenol blue carries a slight negative charge at moderate pH, it will migrate in the same direction as DNA or protein in a gel [123]. Other applications are in nanotechnology, semiconductors, sol-gel matrix, fuel cells, display device, paints, packaging system, diapers, contact lens, determining nucleic acids, water alkalinity, preserving genetic materials, detecting bacteria, etc. [124].

3.2.7.2 Thymol Blue

Thymol Blue	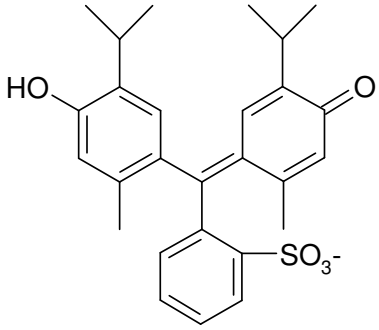
Net Formula	$C_{27}H_{30}O_5S$
Molecular Weight	466.59
Chemical/Dye Class	Sulfonephthalein pH sensitive dye
Appearance	Dark bluish-green to brownish solid
Absorption Maximum	λ_{max}abs (Acid) = 426 nm λ_{max}abs (Base) = 603 nm
pH Range	1.2 – 2.8; 8.0 – 9.6
Colour Change at pH	Red (1.2) to yellow (2.8); Yellow (8.0) to blue (9.6)
pK_a	1.65, 8.90

pH indicator thymol blue can be applied as convenient technique for flow visualization or the velocity measurement. Here a few drops of alkaline solution of the thymol blue are given to a region of interest in the flow and then the motion of the flow is observed. After the experiment, with addition of few drops of acid (HCl) the blue water becomes of light yellow colour and therefore it is possible to perform the next experiment without changing water in the tank [125]. Other applications are as display device, semiconductors, sensors, fuel cells, antimisting coating for glass, toys, corrosion inhibitor, correction fluid, textiles, packaging system, measurement of hydrogen ion concentration in swimming pool water, humidity-indicating agent, cosmetics, biostatic materials, determine bacteria growth, antidepressant drugs, dental impression material, etc. [77]

3.2.7.3 BromoThymol Blue

BromoThymol Blue	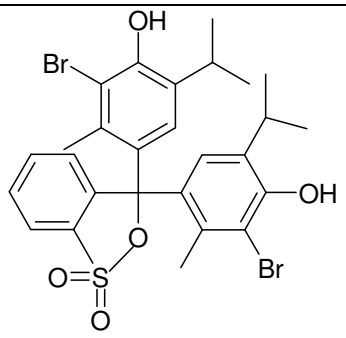
Net Formula	$C_{27}H_{28}Br_2O_5S$
Molecular Weight	624,38
Chemical/Dye Class	Sulfonephthalein pH sensitive dye
Appearance	Light pink or cream colored solid
Absorption Maximum	λ_{max}abs (Acid) = nm λ_{max}abs (Base) = nm
pH Range	6.0 – 7.6
Colour Change at pH	Yellow (6.0) to blue (7.6)
pK_a	7.0, 7.1

Bromothymol blue is mostly used in measuring substances that would have relatively low acidic or basic levels (near a neutral pH). It is often used in managing the pH of pools and fish tanks, for measuring the presence of carbonic acid in a liquid and also for observing photosynthetic activities or respiratory indicators. As carbon dioxide is absorbed from the breath into the solution, forming carbonic acid, the solution changes colour from green to yellow. Other applications are as sol-gel matrix, fuel cells, optical sensors, combustion gas detection system, paints, toys, cleaning products, detergents, textiles, food freshness sensor, detecting microorganisms, bacterial growth, dental materials, etc. [124].

3.2.7.4 Methyl Orange

Methyl Orange	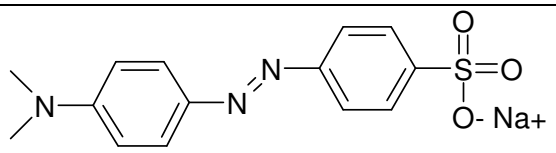
Net Formula	$C_{14}H_{14}N_3O_3SNa$
Molecular Weight	327.34
Chemical/Dye Class	Azo pH sensitive dye
Appearance	Orange solid
pH Range	3.0 – 4.4
Colour Change at pH	Red (3.0) to yellow (4.4)
pK_a	3.76, 3.40

Methyl orange is frequently used in titration because of its clear colour change. The dyes for titrimetric analyses are used to mark the end point of a titration, where exactly 1 equiv. of a titrant has been added to a given titrand. The colour change in an acidimetric titration usually takes place within an interval of ca. 1.2-2.2 pH units, the pH value of its middle-point corresponding to the pK_a value of the conjugate acid. Unlike a universal indicator, methyl orange does not have a full spectrum of colour change, but has a sharper end point [96]. Other applications are as liquid crystals, thin films, sensors, sol-gel matrix, waveguides, host-guest chemistry, display device, corrosion inhibitor, glass coatings, paints, pharmaceuticals, dental materials, measuring nucleic acid, etc. [124].

4 Methods

4.1 Sensor Preparation

The sensors were made onto support, poly(ethylene terephthalate) (Mylar®) foil. The ‘’cocktails’’ were prepared with respective indicator, polymer and solvent. The concentrations of the solutions were between 10 wt%-20 wt%, depending on the polymer used. The prepared solution was carried directly onto dust-free Mylar® foil. The layer was made by spreading the sensor solution onto a foil using a knife-coating device. It works under vacuum and enables the formation of homogeneous thick layers. The spacers are used for the appointment of the definite thickness of the sensor membrane layer. It must be considered, that the layer, which is made with the help of the knife-coating device, has the wet thickness and during drying, the solvent evaporates. Therefore, the effective thickness depends on the concentration of the polymer solutions and applied spacers. The knife-coating device is schematically shown in figure 4 – 1.

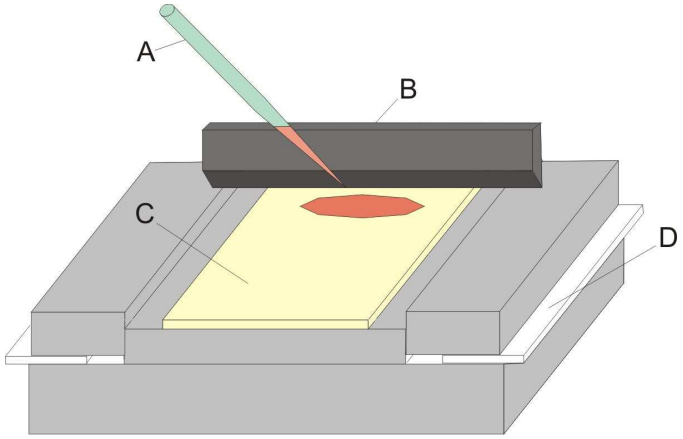

Figure 4 – 1: Schematic view of the knife-coating device: A = pipette containing define cocktail, B = coating device, C= polyester support (Mylar) and D= spacer.

4.2 Sterilization Procedures

4.2.1 Radiation Sterilization

The gamma and electron beam sterilization procedures were performed by the company MediScan GmbH& CoKG (www.mediscan.at). The polymers, indicators and sensors were exposed to the gamma rays and electron beam irradiation in normal ambient conditions, which are defines as at room temperature at 25℃, pressure at 1 bar and relative humidity between 40-60%. Gamma sterilization was performed with a Cobalt 60 source at doses 10, 25 and 50 kGy, respectively. The electron beam irradiation was carried out with a Rhodotron TT-100 10 MeV accelerator also at doses 10, 25 and 50 kGy. Irradiation doses were measured using Red Acrylic Perspex 4934 dosimeter.

Before sterilization, 1 g of each polymer in the solid form was weighed into a 4 ml Glass Clear Supelco Vial (www.sigmaaldrich.com). The vials were than packed into 7 cardboard

boxes. Three of them were exposed to gamma irradiation, three to electron beam irradiation and one to no irradiation, which served as the reference box before sterilization.

The indicators were also weighed into the 4 ml glass vials. However, the indicators have been radiation sterilized in solid state and in solution. Solid state means a form in which each indicator is purchased or synthesized. On the other hand, solution means that each indicator was weighed and dissolved with suitable solvent. The solvents were water, ethanol or toluene. When the indicator was completely dissolved in a solvent, 10^{-5} M solutions were prepared. In each of the seven cardboard boxes, the glass vial of certain indicator in solid state and in solution was placed. One box served as reference box before sterilization and the other six were gamma and electron beam sterilized with 10, 25 and 50 kGy, respectively. After the sterilization, the indicators in solid state were also dissolved and 10^{-5} M solutions were prepared so that absorption and emission measurements were possible and comparable before and after sterilization.

All optical sensors applied in this study were prepared according to chapter 4.1. Each type of sensor was equally made for seven times. One of them served as reference sensor before sterilization and the other six were packed into six different cardboard boxes and sterilized with gamma rays and electron beams with doses mentioned above. Additionally, the optical pH sensors were also gamma and electron beam sterilized in the buffer solution with pH 7.5. The sterilization in the buffer solution was chosen because the pH sensors are sometimes stored in humid surroundings before application. Therefore, the sterilization in the buffer solution will determine whether it is possible to radiation sterilize the sensors in the humid surroundings and whether the effects of gamma and electron beam sterilization on pH sensors are comparable to radiation sterilization in standard ambient conditions.

4.2.2 Other Sterilization Procedures

The optical sensors were also sterilized with other sterilization procedures; steam sterilization, sterilization with ethylene oxide, sterilization with hydrogen peroxide gas and sterilization with low-temperature hydrogen peroxide plasma. Likewise, for these sterilization procedures the optical sensors were prepared according to chapter 4.1. Five even sensors were prepared and each sensor was sterilized with each sterilization procedure mentioned above. One sensor served as reference before sterilization. The sensors were packed into five home-made plastic boxes, which could be opened during each sterilization procedure that the sterilization agent could come into contact with the sensors.

Steam sterilization was carried out in the autoclave at the institute of biotechnology and biochemical engineering, TU Graz (www.biote.tugraz.at). The sterilization procedure lasted for 15 minutes at temperature 121ºC. Afterwards, the sensors were dried in the oven (60ºC) for 24 hours.

The sensors were also sterilized with ethylene oxide gas. The procedure was performed by the company Wozabal GmbH&CoKG, Linz (www.wozabal.com). The mixture of ethylene oxide and carbon dioxide was used in the proportion 6% of EtO and 94% of CO_2. The average ambient temperature in the sterilizer with a volume of 500 litres was 45ºC and the pressure was 1,7 bar. The sterilization with ethylene oxide lasted 12 hours, of which 7 hours were spent for conditioning after the sterilization procedure.

The sterilization procedure with hydrogen peroxide gas was realized by the company Scan AG, Switzerland (www.scan.ch). The temperature in the isolator was 25ºC and the ambient humidity was 20% rF. The concentration of the hydrogen peroxide solution was 35.3% and the dosing capacity was 4.2 g/min. The decontamination phase lasted 12.2 minutes.

With Sterrad 100 NX the low-temperature hydrogen peroxide plasma sterilization was performed by the company Richard Wolf Endoscope GmbH, Germany (www.richard-wolf.com/) was performed. The sterilization cycle lasted 48 minutes and consisted of five phases. First, high vacuum was created in the chamber. A 59% hydrogen peroxide solution

was given into the evaporator. Hence, one portion of the water evaporates and 85-95% of the hydrogen peroxide solution was produced. Then the hydrogen peroxide solution was injected into the chamber, evaporates under high vacuum and diffuses in the chamber. By microwave frequency an electric field was established and hydrogen peroxide plasma was generated. The maximum chamber temperature was 55ºC. After that, the sterilization chamber was aerated with sterile filtered air.

4.3 Characterization of Materials

The effects of different sterilization procedures on optical sensor materials were defined with the application of diverse analytical procedures. Due to the great number of materials, the analytical methods, which are rapid and provided us with a lot of information, were chosen. All results measured with the analytical methods described in the following chapters were gathered and are presented in the *database* of this study. In the *database*, all the results of the measurements, the spectra, the alterations, etc. that appeared after sterilization methods are presented in the details.

4.3.1 Characterization of Polymers

A variety of techniques can be used to characterize the possible degradation mechanisms of polymers and the resulting products that are formed due to radiation sterilization. The following analytical methods are often employed for determining the effect of various mechanisms of degradation observed for polymers: solubility test (dissolution), infrared and Raman spectroscopy, electron spin resonance spectroscopy, ultraviolet-visible spectroscopy, thermal analysis, thermogravimetric analysis, such as differential scanning calorimetery, thermal mechanical analysis, etc. and pyrolysis gas chromatography.

The techniques that were used to understand and evaluate polymer degradation processes due to radiation sterilization were, in this study, solubility test (dissolution), contact angle measurements, for the determination of possible surface degradation processes, infrared spectroscopy, differential scanning calorimetry and ultraviolet-visible spectroscopy, which was also applied for the characterization of the (luminescence) indicators and optical sensors.

4.3.1.1 Solubility Test (Dissolution)

A control of polymer solubility provides a simple method of distinguishing polymers in the first instance. Dissolving a polymer in a solvent is a slow process which occurs in two stages: first, the solvent molecules slowly diffuse into the polymer to produce a swollen gel and then polymer-solvent interactions cause the gel to gradually disintegrate [18]. Solubility occurs when the free energy of mixing is negative, as follows:

$$\Delta G = \Delta H - T\Delta S < 0 \qquad (4.1)$$

A frequent effect of radiation sterilization on polymers is the cross-linking of the polymer chains. According to literature, the cross-linked polymers are not capable of dissolving [18]. They formed swollen gel. Therefore, the cross-linking of the polymer chains after radiation sterilization was proven with the solubility test. Solubility was determined by placing approximately 0.1 g of define polymer in a glass vial with 5 g of a particular solvent, which dissolved the polymer before radiation sterilization. The dissolution lasted 24 hours. If the polymer was not entirely dissolved after radiation sterilization, the cross-linking was evidenced.

4.3.1.2 Ultraviolet-Visible Spectroscopy

The absorption of ultraviolet or visible radiation by polymers leads to transitions among the energy levels and an electronic absorption spectrum results. Ultraviolet-visible spectroscopy can be used to identify chromophores such as benzene rings and carbonyl groups. It can also be used to determine the lengths of sequences of conjugated multiple bonds in certain polymers [18]. Chromophores are functional groups responsible for electronic absorption, with these groups undergoing $n \rightarrow \pi^*$ or $\pi \rightarrow \pi^*$ transitions. Table 4 – 1 lists some of the chromophores commonly found in polymers:

Table 4 – 1: Typical chromophores in UV-VIS spectroscopy commonly found for polymers.

Chromophore	Wavelength, λ_{max} [nm]	Molar Absorption Coefficient, ε_{max}
C = C	175 185	14000 8000
C ≡ C	175 195 223	10000 2000 150
C = O	160 185 280	18000 500 15
C = C – C = C Benzene Ring	217 184 200 255	20000 60000 4400 204

A UV-VIS spectrum is normally plotted as absorbance or transmittance versus wavelength. UV-VIS spectroscopy may be employed to identify the presence of any residual monomer remaining in a polymer sample or new formed chromophore or additional double bonds often formed in polymer after radiation sterilization.

For measurements of absorption spectrum the UV-VIS spectrometers are used. They consist of a light source. The most commonly used light sources are deuterium lamps in the region from 180 to 350 nm and tungsten filaments or halogen lamps in the region from 330 to 900 nm. A light source for the complete range is the xenon arc from 175 to 1000 nm. Usually are the monochromators by UV-VIS spectrometers is a prism or diffraction grating. A rotating sector mirror or rotating sector disc, referred as chopper, is used to generate a sample and a reference beam as well as to recombine them, which reached a sample and reference compartment. The standard detectors by spectrometers are photomultipliers and silicon diodes [13]. On figure 4 – 2, the block diagram of a UV/VIS spectrometer is presented.

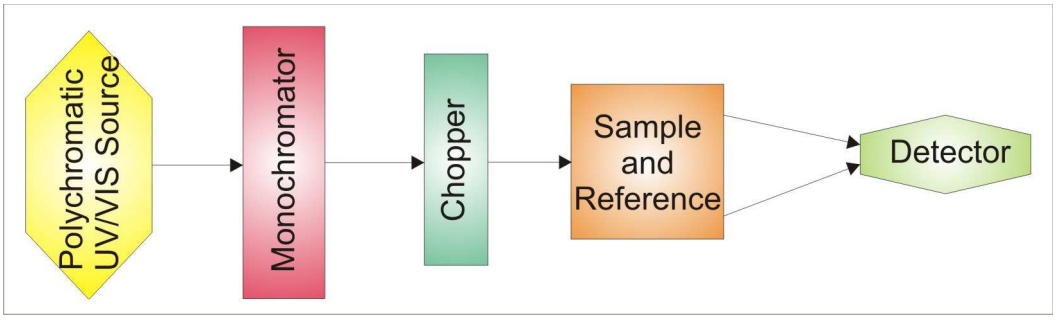

Figure 4 – 2: Block diagram of a UV/VIS spectrometer.

The efficiency of light absorption at a wavelength λ by absorbing medium is characterized by the absorbance or the transmittance [14]. In many cases, the absorbance of a sample follows the Beer-Lambert law, where the absorbance of a solution is directly proportional to the path length and the concentration of the absorbing molecule:

$$A(\lambda) = \log\frac{I_\lambda^0}{I_\lambda} = -\log T(\lambda) \quad \Rightarrow \quad T(\lambda) = \frac{I_\lambda}{I_\lambda^0} \qquad A(\lambda) = \log\frac{I_\lambda^0}{I_\lambda} = \varepsilon(\lambda)lc \qquad (4.2)$$

where $\varepsilon(\lambda)$ = the molar absorption coefficient
c = the concentration of absorbing species
l = the absorption pathlength

The radiation sterilized polymer was dissolved in the define solvent. The concentration of the polymer solution was 2 wt%. Absorption spectra were measured at a Cary 50 UV-vis spectrophotometer (www.lzs.concept.com) and the UV-VIS spectra were plotted as absorbance versus wavelength. The comparisons were made before and after each dose of radiation sterilization and the results are presented in *database section A.*

4.3.1.3 Contact Angle Measurement

The contact angle is the angle at which a liquid or vapour interface contact with a solid surface. A cross-sectional view of the droplet is represented on figure 4 – 3:

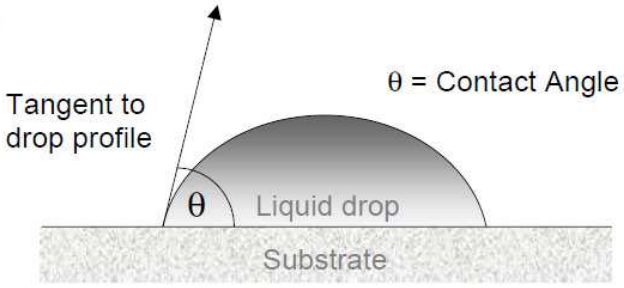

Figure 4 – 3: A cross-sectional view of the droplet, used by the contact angle measurements.

If the liquid is very strongly attracted to the solid surface the droplet will completely spread out on the solid surface and the contact angle will be close to 0°. That means that the solid surface is strongly hydrophilic. Less strongly hydrophilic solids will have a contact angle up to 90°. If the solid surface is hydrophobic, the contact angle will be larger than 90°. However, some materials with highly rough surfaces may have a water contact angle greater than 150° and are called superhydrophobic surfaces [126]

The theoretical description of contact arises from the consideration of a thermodynamic equilibrium between the three phases: the liquid phase of the droplet (L), the solid phase of the surface (S) and the gas/vapour phase of the ambient (G) [127]. The contact angle is a result of the interface/surface tensions (surface free energies) between liquid and solid surrounded by vapour and is measured according to the Young equation:

$$\gamma_S = \gamma_L \cdot \cos\theta + \gamma_{SL} \qquad (4.3)$$

where: θ = contact angel
γ_S = solid surface free energy
γ_L = liquid surface free energy
γ_{SL} = solid/liquid interfacial free energy

From the contact angle, physical properties of interaction between solid and liquid like wettability, affinity, adhesiveness and repellence can be studied.

For the measurements of the contact angle, the concentrated solutions of radiation sterilized polymers between 5 wt% to 20 wt% were prepared (depending on the polymer viscosity). The prepared polymer solution was spread onto standard glass microscope slide (76x26 mm, thickness 1 mm) (Carl Roth, www.carlroth.de) and the layer was made by a knife-coating device. The thickness of more than 20 µm was defined by the spacers. The contact angle of the certain polymer layer was measured with the Krüss Drope Shape Analyser 100

(www.kruss.de). The contact angles before and after define sterilization methods were compared and the graphs are presented in *database section A*.

4.3.1.4 Fourier Transform Infrared Spectroscopy

Infrared (IR) spectroscopy is a popular method for characterizing polymers. This technique is based on the vibrations of the atoms of a molecule. An infrared spectrum is obtained by passing infrared radiation through a sample and determining which fraction of the incident radiation is absorbed at a particular energy. The energy at which any peak in an absorption spectrum appears corresponds to the frequency of vibration of a part of the sample molecule [128].

Most infrared spectroscopy is carried out by using Fourier-transform infrared (FTIR) spectrometers. This method is based on the interference of radiation between two beams to yield an interferogram, i.e. a signal produced as a function of the change of pathlength between the two beams. The IR spectrum has inverse wavelength units (cm^{-1}) on the x-axis, which is wavenumber scale. The y-axis may be represented by % transmittance, with 100% at the top of the spectrum, which is traditionally used for spectral interpretation [129].

The infrared spectrum can be divided into three regions, namely the far infrared (<400 cm^{-1}), the mid-infrared (400-4000 cm^{-1}) and the near-infrared (4000-13000 cm^{-1}). In this study, the mid-infrared region was employed. Spectrum interpretation is simplified by the fact that the bands that appear can be assigned to particular parts of the molecule, thus producing what are known as group frequencies. The mid-infrared spectrum may be divided into the following four regions:

- X-H stretching region (4000-2500 cm^{-1}),
- Triple-bond region (2500-2000 cm^{-1}),
- Double-bond region (2000-1500 cm^{-1}),
- Fingerprint region (1500-600 cm^{-1})

The FTIR was used to investigate the changes and effects on polymers after radiation sterilization. The spectra were carried out with the Mattson 3000 FTIR Spectrometer (www.madisonir.com). The 2 wt% of the define polymer solution was made and 300 µl of that solution was spread on the Polyethylene InfraRed sample card (Aldrich, www.sigmaaldrich.com). Afterwards, the IR spectra before and after each sterilization procedure were compared and are presented in *database section A*.

4.3.1.5 Differential Scanning Calorimetry

Differential scanning calorimetry (DSC) involves examining the change in a property of a material on heating or cooling. DSC is used extensively to identify polymers and polymer blends and is a technique which records the energy necessary to establish a zero temperature difference between the sample and a reference material as a function of time or temperature. The two specimens are subjected to identical temperature conditions in an environment which is heated or cooled at a controlled rate. DSC curves are plotted as a function of time or temperature at a constant rate of heating. A shift in the baseline results from the change in heat capacity of the sample [18].

The basic equation used in DSC analysis is:

$$\Delta T = qC_p / K \qquad (4.4)$$

where ΔT = the difference in temperature between the reference material and the sample
q = the heating rate
C_p = the heat capacity (at constant pressure)
K = a calibration factor for the particular instrument being used

The schematic of the experimental set-up of differential scanning calorimeter is presented in figure 4 – 4.

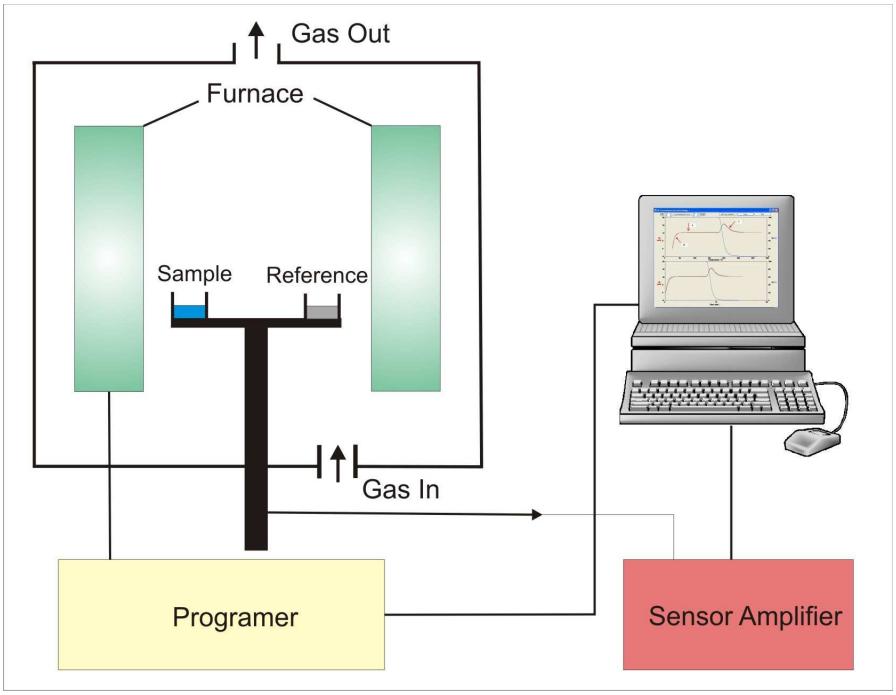

Figure 4 – 4: Schematic of the experimental set-up used to carry out differential scanning calorimetry.

The glass transition (T_g) and the melting temperature (T_m) of a polymer are detected with DSC measurements. The glass transition temperature is detected as an endothermic shift from the baseline is observed at the T_g in the traces of crystallisable polymers. Such a change results from an increase in heat capacity due to the increased molecular motions in the material. It should be noted that the T_g value will depend greatly on the heating and cooling rates used in a DSC run. At the melting point of a polymer, change from the solid to liquid state appears and this transition gives rise to an endothermic peak in the DSC curve. The width of the melting peak provides an indication of the range of crystal sizes and also their perfection [18].

Hence, DSC is used for measuring the enthalpy involved in polymer transitions. The peak area between the curve and the baseline is proportional to the enthalpy change (ΔH) in the sample. This enthalpy change can be determined from the area of the curve peak (A) by using the following relationship:

$$\Delta H \cdot m = K \cdot A \tag{4.5}$$

where m = mass of the polymer sample
K = a calibration factor for the particular instrument being used

The important transitions temperatures in the polymer that can be detected with DSC are presented in the figure 4 – 5.

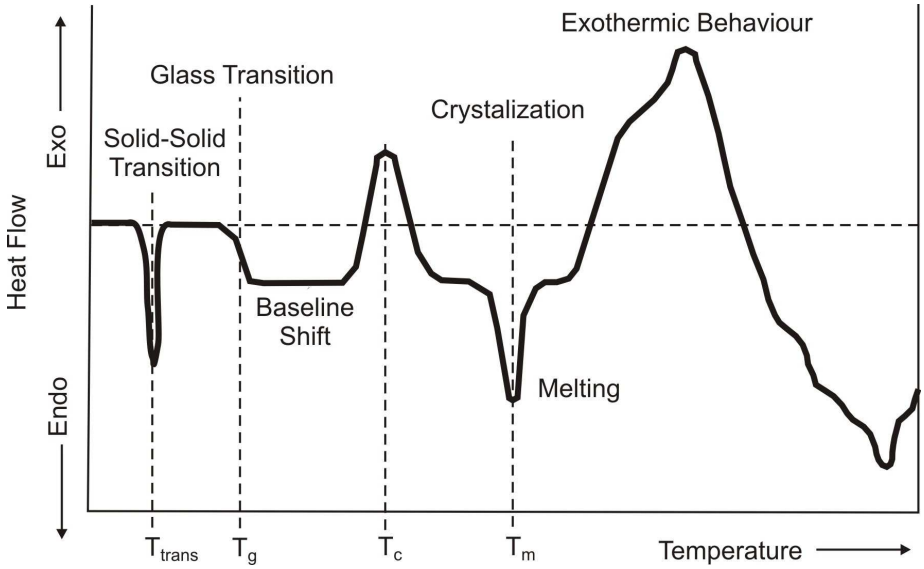

Figure 4 – 5: A typical DSC curve obtained for a polymer sample.

Proper sample preparation that maximizes the contact surface between the pan and the sample will reduce the resistance of the sample to heat flow though the DSC temperature sensors and will result in maximum peak sharpness and resolution. For this test, between 5-10 mg of define polymer sample was placed in an open aluminium sample pan and secured on the thermoelectric disk of the DSC cell. The heat required to increase the temperature was compared with the heat required to increase the temperature of an identical, empty pan. The different scanning calorimetry measurements were carried out on a Perkin-Elmer Pyris Diamond (www.perkinelmer.com) under a nitrogen flow of 20 ml/min. The heating rate was 10℃. Glass transition temperatures were read as the midpoint of change in heat capacity and the melting temperature as the peak area between the curve and the baseline as a function of enthalpy changes. The measured glass transition temperatures of polymer polystyrene, polystyrene-co-acrylonitrile, polystyrene-co-maleicanhydride, polysulfone, ethyl cellulose, polyvinylidene chloride-co-acrylonitrile, polymethyl methacrylate and melting temperature or support Mylar® foil before and after gamma sterilization are presented in *database section A*.

4.3.2 Characterization of (Luminescence) Indicators and Optical Sensors

4.3.2.1 Measurements of Light Absorption and Luminescence

The absorption spectra of indicator solutions and optical sensors were recorded as polymer solutions and the UV-VIS spectrometry is described in chapter 4.3.1.2. Emission and excitation spectra are measured using a spectrofluorometer. The optical module contains various parts, which are a light source, monochromator for selecting of the excitation wavelength and for analysis of fluorescence light, a sample holder, optical elements, like polarizers, a beam splitter, shutters, etc., photoelectrical detector and electronic and calculation technique for data acquisition and for saving them.

The excitation source is a lamp emitting a constant photon flow and is usually a deuterium or xenon lamp. The beam of light passes through a monochromator, which passes only a selected wavelength. The fluorescence is dispersed by another monochromator and detected by a photomultiplier tube. Scanning the excitation monochromator gives the excitation spectrum and scanning the fluorescence monochromator gives the fluorescence or

emission spectrum [16]. The schematic representation of spectrofluorometer is shown on figure 4 – 6:

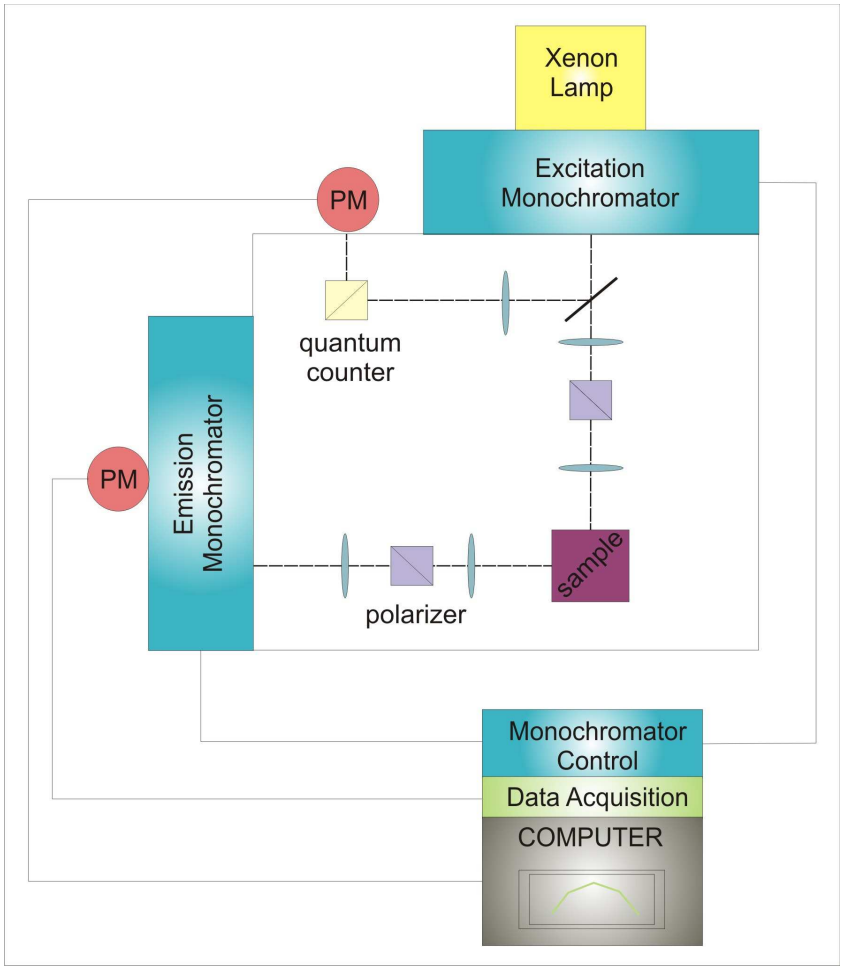

Figure 4 – 6: Schematic representation of spectrofluorometer.

Fluorometry is a very sensitive technique-up to 1000 times more sensitive than spectrophotometry. This is because the fluorescence intensity is measured above a low background level whereas in the measurement of low absorbances, two large signals that are slightly different are compared. Because of the outstanding progress in instrumentation, it is now possible in some cases to even detect a single fluorescent molecule [45].

Absorption spectra were measured at a Cary 50 UV-vis spectrophotometer (www.lzs.concept.com). Excitation and emission spectra were acquired on a Hitachi F-7000 fluorescence spectrometer (www.inula.at) equipped with a red-sensitive photomultiplier tube (PMT) R 928 from Hamamazu (www.hamamatsu.com). According to the spectral response characteristics of the PMT, its sensitivity at 650 nm is approximately 15% less than at 500 nm.

The indicators were radiation sterilized in solid state and as 10^{-5} M solution. The indicators sterilized in solid state were dissolved after sterilization and also the 10^{-5} M solutions were prepared. All indicator solutions were characterized with measurements of absorption and emission before and after certain radiation sterilization procedure. The spectra were evaluated, compared and are presented in *database section B*.

The optical sensors were also characterized with absorption and emission spectra before and after each sterilization procedure. Additionally, the spectra of diverse pH sensors were taken in three buffer solutions with different pH, where one pH was below, one around and one above the pK_a value of the indicator. Also, sigmoidal shape curves were obtained from emission intensity changes of the base peak intensity ratio versus pH. The absorption and emission spectra were measured by ammonia sensors in the acid and base environment.

The acid environment was performed with the acetic acid and the base environment with the ammonia solution. One drop of particular solution was putted into the polystyrene cuvette, with ammonia sensor and was sealed with parafilm. The solutions evaporated for 30 minutes and the acidic/basic environment in the cuvette was reached. Afterwards, the absorption and emission spectra were measured.

4.3.2.2 Measurement of Luminescence Lifetime based on Phase-Modulation Fluorometry

Phase-modulation fluorometry uses modulated light at variable frequency and gives the harmonic response of the sample, which is the Fourier transform of the δ-pulse response. The sample is excited with light that is intensity modulated at a high frequency comparable to the reciprocal of the lifetime. The emission is also intensity modulated at the same frequency. However, the emission does not precisely follow the excitation, but rather shows time delays and amplitude changes that are determined by the intensity decay law of the sample. The time delay is measured as a phase angle shift between the excitation and emission. The peak-to-peak height of the modulated emission is decreased relative to the modulated excitation, and provides another independent measure of the lifetime.

The phase shift and modulation of the emission depend on the relative values of the lifetime and the light modulation frequency. As the light modulation frequency increase, the phase shift of the emission increases and the modulation of the emission decreases. The dependence of the phase angle Φ and modulation m on the light modulation frequency is used to recover the intensity decay of the sample. The phase-modulation fluorometers operate over a wide range of light modulation frequencies and excitation wavelengths. The principles of phase-modulation fluorometry are presented in figure 4 – 7:

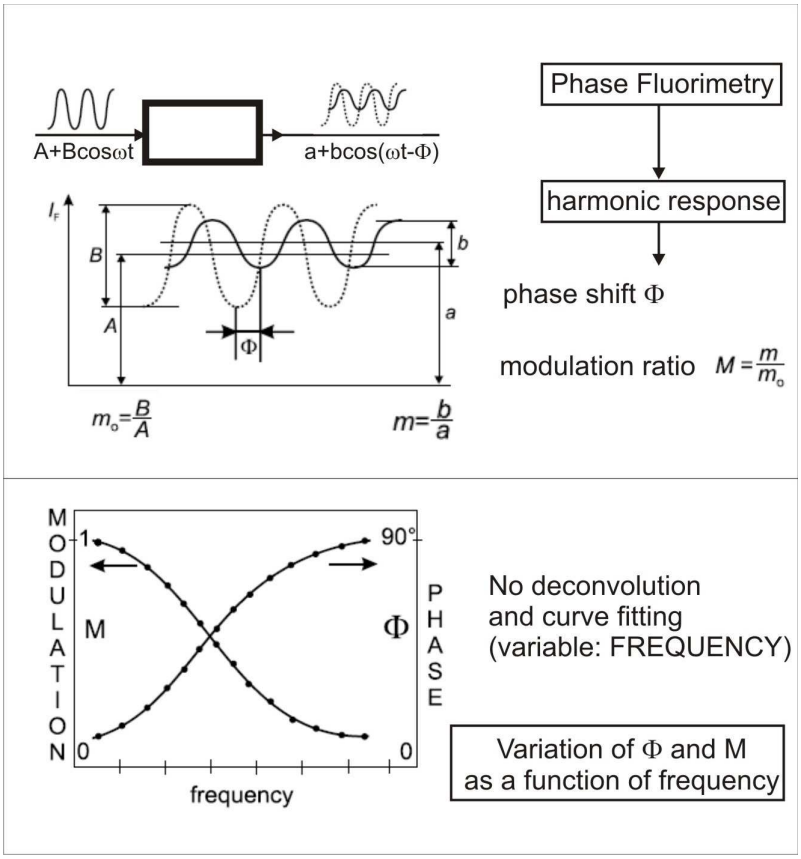

Figure 4 – 7: Principles of phase-modulation fluorometry.

Luminescence phase shifts were measured and consequently, the lifetime was calculated before and after sterilization of the optical oxygen and temperature sensors. They were measured with a two-phase lock-in amplifier (SR830, Stanford Research Inc.,

www.thinksrs.com). The sensor films containing the iridium(III) complex or ruthenium(II) complex ($Ru(dpp)_2Cl_2$ and dichlorotris(1,10-phenanthroline) ruthenium(II) hydrate) were excited with the light of a blue light-emitting diode (LED) (λ_{max} 470 nm, www.roithner-laser.com) which was sinusoidally modulated at a frequency of 20 kHz in the case of the iridium(III) complex, or at a frequency of 45 kHz in the case of the ruthenium(II) complex. The sensor films containing PtTFPP or PtOEP were excited with the light of 540 nm LED and a modulation frequency of 5 kHz was used. The same modulation frequency was used by the characterization of the oxygen sensors containing indicator PtTPTBPF. The Pt(II)- and Pd(II)-benzoporphyrins were excited with 630 nm LED and the modulation frequency by PdTPTBPF was 1 kHz. The temperature sensors with indicator $Eu(tta)_3$DEADIT were excited with the 425 nm LED, which was sinusoidally modulated at a frequency of 700 Hz.

A bifurcated fiber bundle was used to guide the excitation light to the sensor film and to guide back the luminescence after passing the define filter, which by majority of sensors was the OG 550 (Schott, www.schott.com). The filter before detector by the benzoporphirins was RG9 and by the europium(III) complex was OG 590. The luminescence was detected with a PMT (H5701-02, Hamamatsu, www.sales.hamamatsu.com).

Gas calibration mixtures were obtained using a gas mixing device (MKS, www.mksinst.com). The responses of the oxygen sensors before and after sterilization were measured at the 0, 50, 100, 150 and 212 hPa pO_2. Afterwards, the calibration curves and Stern-Volmer plots were calculated and compared. Temperature was controlled at 25ºC by a thermostat Thermo Haake DC50 cryostat (www.thermo.com). With the same thermostat, the temperature optical sensors were characterized at temperatures 15, 25 and 35ºC, respectively. Likewise, the calibration curves (luminescence lifetime) were calculated and compared.

The results, absorption/emission spectra and graphs of the sensor response before and after certain sterilization are presented in details in the *database sections C, D, E, F.* There, by each spectra or graph calculation were made for how much the absorption/emission intensity increases or decreases and which alterations are observed when caomparing the sensor response before and after certain sterilization method. Some interesting results and observations are presented and discussed in the following chapters.

III
Results and Discussion

5 Radiation Sterilization (Gamma and Electron Beam)

The effect of irradiation on different materials involves a very complicated set of processes which are:

- Multicompontent – several chemically active species are involved;
- Heterogeneous – the nature and intensity of processes differs;
- Involve species which diffuse and react in the material following generation of some active species in it.

The interaction of gamma and electron beam radiation with materials produces free electrons, positive ions and excited molecules. These primary products react to form a second generation of active intermediates containing excited molecules, positive and negative ions, free radicals and their combinations. During irradiation, most of the ejected electrons are captured again by the parent ions, leading finally to the formation of free radicals and irradiation that result mostly in various radicals with differing mobilities. It is generally believed that the alterations in the materials exposed to irradiation are mainly due to free radical reactions.

Prior to using gamma or electron beam radiation for the sterilization of diverse optical sensors, it is essential to determine the effects of radiation sterilization. Each material reacts differently to ionizing radiation, therefore it is important to define the compatibility of optical materials, the general effects on sensors, the influences on sensor response, the maximum doses which could be used for radiation sterilization of certain materials and optical sensors, etc.

In this study, the optical materials were gamma and electron beam sterilized with doses 10 kGy, 25 kGy and 50 kGy. The sterilized optical materials were polymers and indicators, which were sterilized in solid state and as solution. The polymers and indicators were used as basic component for optical oxygen, pH, ammonia and temperature sensors, which were also sterilized with gamma rays and electron beams. All results are gathered and presented in a *database:*

- Section A – Radiation sterilization of polymers

- Section B – Radiation sterilization of (luminescence) indicators

- Section C – Radiation sterilization of optical sensors

Important and interesting results are discussed and shown in the following chapters.

5.1 Radiation Sterilization of Optical Oxygen Sensors

The optical oxygen sensors were developed from diverse indicators and polymer matrices. The polymer matrices utilized in this study were cellulose materials; cellulose acetate (CA) and ethyl cellulose (EC), polystyrene (PS), polystyrene-co-acrylonitrile (PS-co-PAN), polystyrene-co-maleicanhydride (PSMA), polysulfone (PSf), polyurethane hydrogels; HydroMed^{TM} hydrogel D4/D7 and HydroThane with 5% water content (H5) and poly(phenyl silsesquioxane) (PPSQ). These polymers respond differently to ionizing radiation.

Ionizing radiation, especially gamma rays, has great penetration capability through material. Therefore, the polymers undergo alterations of either bulk or surfaces when subjected to

radiation sterilization. The nature of the polymer structure determines its response and physical change upon exposure to ionizing radiation. Polymers are altered through radical formation in the environment of radiation sterilization process or in the polymer structure. Since the concentration of reactants differs by location, the resultant radiochemical stabilising reactions are heterogeneous. However, some classes of polymer are susceptible to chain scission mechanisms while other are altered through cross-linking processesThey can also appear simultaneously, which makes the interpretation even harder. According to the rule, proposed by Miller et al; when each carbon of the main chain carries at least one hydrogen atom, the cross-linking predominates, but if a tetra-substituted carbon atom is present, the polymer degrades [14]. For example, polystyrene is susceptible more to cross-linking, while poly(methyl methacrylate), cellulose materials or polyacrylonitrile are prone to chain-scission. Other changes often observed on polymers after irradiation are deterioration, discolouration, embitterment, odour generation, stiffening, softening, chemical resistance, toxicological response and even destruction.

Likewise, the sterilization in the presence and absence of oxygen has different effects on the polymer structure and degree of degradation. However, in the presence of oxygen, electron beam radiation is typically gentler method to polymers than gamma because the sterilization cycle is fast and the oxidative effects are minimized. The gamma sterilization procedure gives more time for oxygen to permeate the polymers and produce oxidative degradation. Oxygen traps free radicals and chemical reactions of oxidative nature results in the generation of oxidative products created within the polymer and include the formation of carboxylic acids, ketones, esters, alcohol derivatives and peroxide based species. When peroxides degrade, chain branching is favoured and reactions result in further radicals generation of numerous free radicals within the polymer.

The polystyrenes; PS, PS-co-PAN and PMAN have the largest resistance to radiation sterilization compared to other polymers in this study. In general, polymers containing aromatic rings, systems of conjugated bonds and other structural elements ensure the dissipation of ionizing radiation exhibit high radiation stability. In these structures, internal radiation protection takes place due to benzene rings in the structure, which act as an “electron bank” and can rearrange itself in order to accept or lend an electron as needed without losing integrity – as a radiation shock absorber.

Likewise, polysulfone contains benzene rings and therefore is resistant to forms of radiation. However, ionizing radiation induces yellowing of PSf, which is shown in figure 5 – 1. Yellowing occurs when specific chromophores are formed. They usually appear prior to any measurable loss in physical properties. In polysulfone, the radiation absorbed by the sulfone groups initiates photo-oxidation processes involving free radical chain reactions, which are responsible for colouration of the polymer after radiation sterilization.

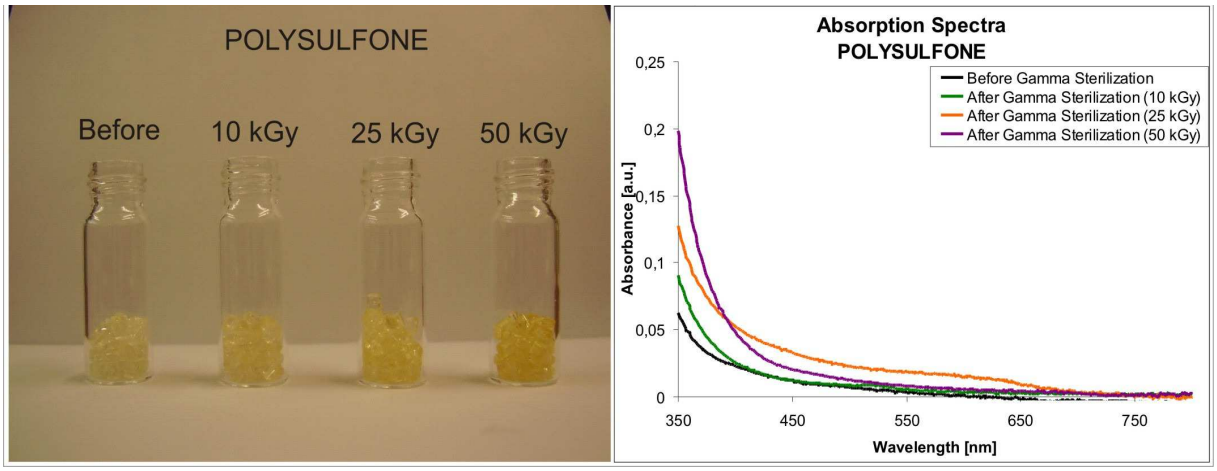

Figure 5 – 1: Yellowing of the polymer PSf after ionizing radiation (seen on the photo) and the corresponding absorption spectra.

The high-energy irradiation of cellulose materials caused the formation of carboxyl and carbonyl groups and the hydrogen abstraction led to radical formation of atoms C_1 and C_4 of cellulosic materials with subsequent cleavage of the glycosidic linkage. Similarly, after gamma and electron beam sterilization of cellulose materials, chain-scission of the main polymer chain occurs. The decrease of the glass transition temperature after gamma sterilization of the polymer ethyl cellulose with doses 25 and 50 kGy was evidence for chain-scission. The flexibility of the side chains was altered after radiation and the molecular weight was reduced. Therefore, the glass transition temperature became lower. The values of the glass transition temperature, measured with differential scanning calorimetry (DSC), before and after gamma sterilization of ethyl cellulose are presented in table 5 – 1.

Table 5 – 1: The glass transition temperature and corresponding specific heat capacity of polymer EC before and after gamma irradiation.

	T_g	Δc_p
BeforeS	140,21 °C	0,0879 J/g °C
10 kGy	140,53 °C	0,1370 J/g °C
25 kGy	136,91 °C	0,0894 J/g °C
50 kGy	136,17 °C	0,0831 J/g °C

The solubility test of the polyurethane hydrogels demonstrated that cross-linking takes place in the polymer HydroThane with 5 % water content after radiation sterilization with dose 25 kGy and in the polymers hydrogel D4/D7 with dose 50 kGy. These polymers were no longer soluble in the same solvent as before gamma and electron beam sterilization. According to the literature, the cross-linked polymers are not capable to dissolve [18]. The solvent molecules slowly diffused into the polymer and produced a swollen gel. However, the second stage of the dissolving process did not occur. Figure 5 – 2 shows the decrease of solubility by the polymer HydroThane with 5% water content with increasing irradiation doses.

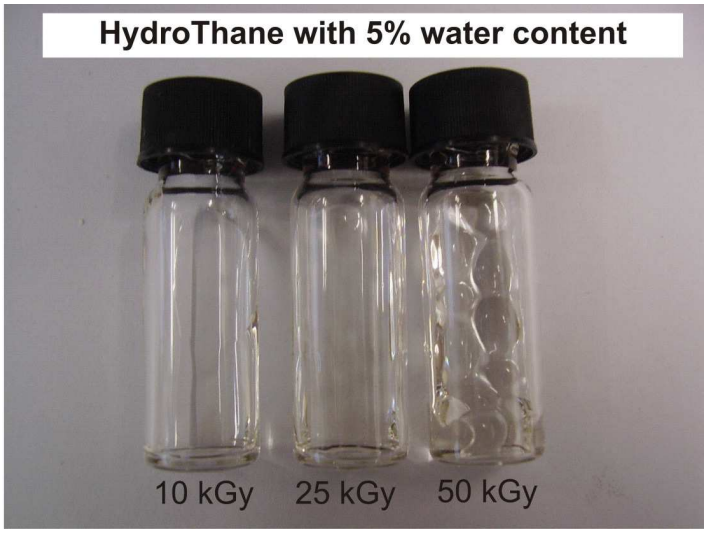

Figure 5 – 2: Decrease of solubility of the polymer HydroThane with 5% water content after radiation sterilization.

Silsesquioxanes contain beta-electron withdrawing groups and they can be converted to silicon dioxide via elimination after radiation sterilization. The alterations in the absorption spectra after radiation sterilization of the polymer PPSQ were also observed and are presented in figure 5 – 3.

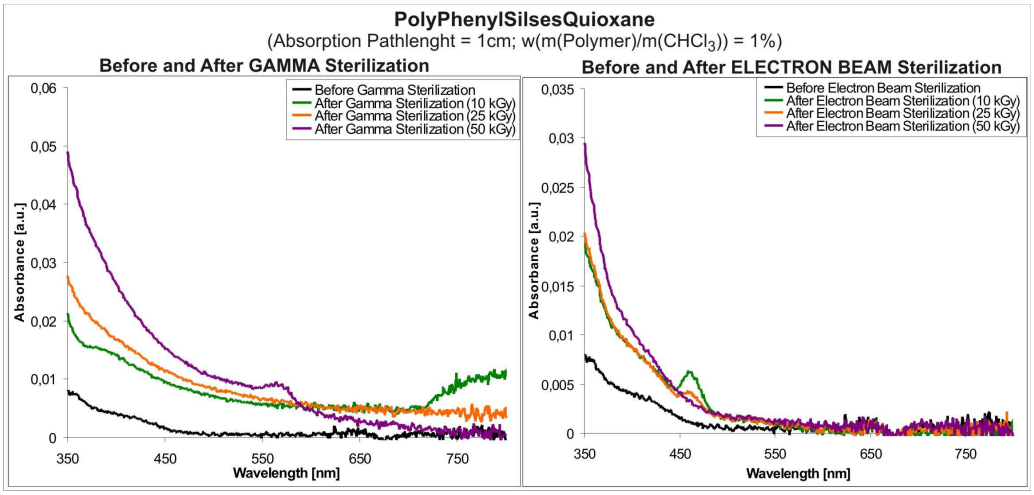

Figure 5 – 3: Absorption spectra of the polymer PPSQ before and after radiation sterilization.

All oxygen sensitive indicators; iridium(III) coumarin ($Ir(C_s)_2(acac)$), porphyrine complexes; PtTFPP, PtOEP, PtTPTBPF, PdTPTBPF and ruthenium(II) complex ($Ru(dpp)_3Cl_2$) applied in this study remain stable, when sterilized with gamma rays and electron beam in solid state. However, some alterations were observed, when the indicators were radiation sterilized as solution.

The iridium(III) coumarin was no longer capable of photo-emission after sterilization. The reactions that appeared were similar to the oxidation reactions of the indicator $Ir(C_s)_2(acac)$ induced by light. The common processes by oxidation reactions are the loss of one or more electrons from a chemical species as a result of photo-excitation of species or the reaction of a substance with oxygen under the influence of light. The mechanism of photobleaching is rather a transformation of the coumarin ligand in the complex in which a new phosphorescent product is produced. Probably, upon irradiation the radicals were formed in the solvent, which reacted and induced similar effects in the indicator structure as in the case of the mechanism of the photobleaching. The spectral properties were consequently changed after radiation. The comparison of the absorption spectra of the indicator $Ir(C_s)_2(acac)$ gamma sterilized in solid state and in solution are shown in figure 5 – 4.

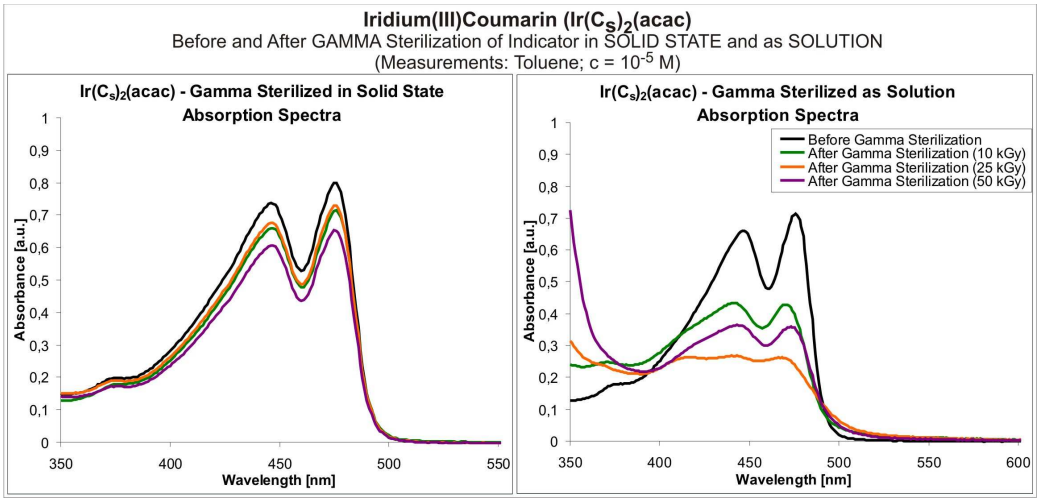

Figure 5 – 4: Absorption spectra of the indicator $Ir(C_s)_2(acac)$, gamma sterilized in solid state and in solution.

When the solution of indicator $Ru(dpp)_3Cl_2$ was irradiated the dissociation of the ligand appeared because a bathochromic shift of the absorption maximum was observed. Ionizing radiation of the porphyrin PtTFPP in toluene solvent also induced the alterations in the absorption spectra. New absorption peaks at longer wavelength were observed (see figure 5 – 5) after gamma and electron beam sterilization of the indicator PtTFPP.

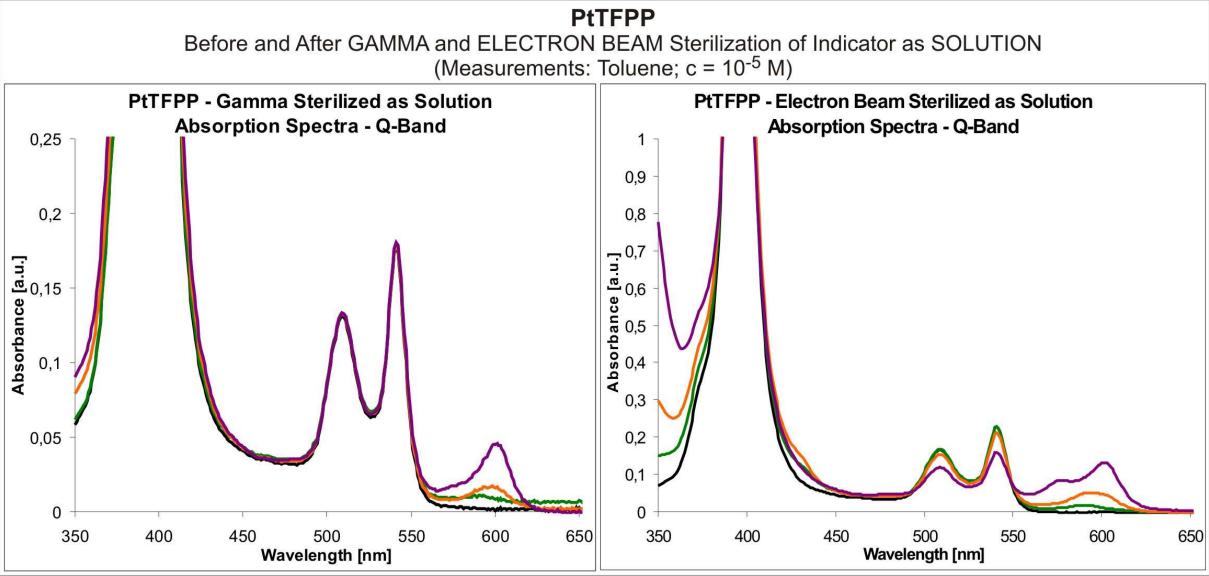

Figure 5 – 5: Absorption spectra of indicator PtTFPP sterilized in solution before and after gamma and electron beam sterilization.

The radiated solution of the indicator PtTFPP was additionally characterized with mass spectroscopy measurement. The results have shown that after electron beam radiation with 50 kGy of the indicator PtTFPP in solvent toluene, the reactions occurred between the radicals formed in the environment of the sterilization and the indicator structure (figure 5 – 6). The hydroxyl, hydrogen, oxygen radicals and toluene reacted with the porphyrine structure and the additional oxygen atoms on the structure induce the alterations in the spectra.

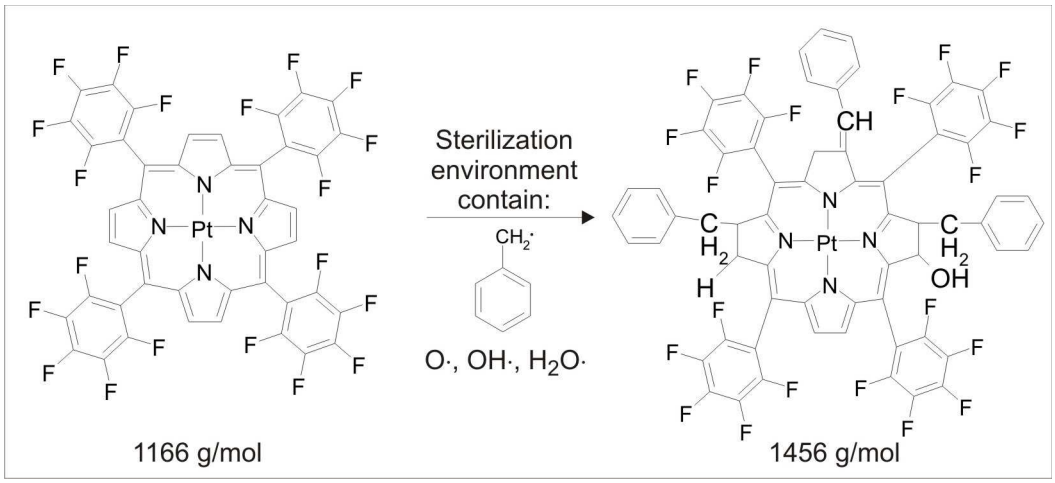

Figure 5 – 6: Alterations induced by radiation sterilization of the indicator PtTFPP in solution with solvent toluene.

After irradiation of other porphyrins as solution, alterations in the absorption spectra between 400-450 nm were observed. This absorption could be due to the reduction of the porphyrin structure. Generally, the electron beam sterilization induced greater changes than gamma rays in the porphyrin structure. Consequently, the porphyrin structure was reduced due to more reducing capability of the electron beam sterilization method comparable to gamma.

When these indicators were immobilized in polymer matrices, the impact on the sensor response was various. The gamma radiation of the oxygen sensors made of indicator $Ir(C_s)_2(acac)$ and immobilized in CA induced large changes after sterilization with dose 50 kGy. The polymer matrix was affected and alterations such as cleavage of the acetate groups which has influence on the sensor response. However, the electron beam sterilization method had lower impact on the sensor than gamma rays. Likewise, when EC was applied as the polymer matrix similar results were observed. The ether groups of the polymer EC dissociate which has influence on the quenching constant. The response of the oxygen sensors after radiation sterilization made of cellulose materials are presented in figure 5 – 7.

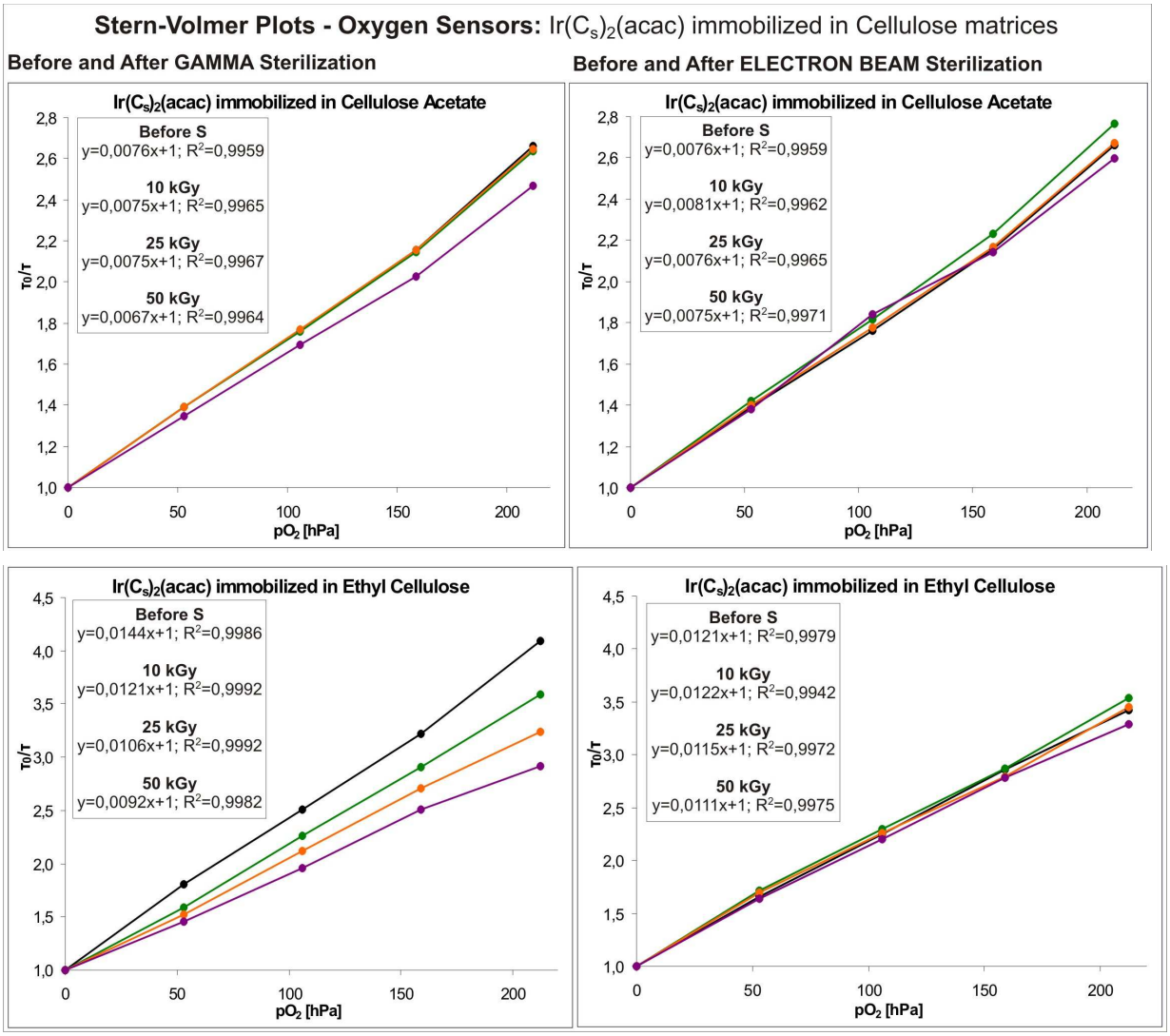

Figure 5 – 7: Comparison of Stern-Volmer plots of oxygen sensors made indicator Ir(Cs)2(acac) and immobilized in polymers CA and EC before and after gamma and electron beam sterilization.

Generally, after radiation sterilization of the indicator $Ir(C_s)_2(acac)$ immobilized in other polymer matrices, such as PS, PS-co-PAN, PSMA, PSf, PPSQ and polyurethane hydrogels, additional quenchers were formed, which was observed as uniform decrease of phosphorescence lifetime after sterilization. The quencher could be formed either in the polymer matrices or due to cleavage of the indicator structure. However, the absorption and emission capabilities of the sensor remained similar before and after sterilization. Figures 5 – 8 and 5 – 9 show an example of the oxygen sensor made of indicator $Ir(C_s)_2(acac)$ and immobilized in polystyrene, where the additional quenchers have influence on the sensor

response after radiation sterilization but the absorption and emission intensities and curve shapes remained similar.

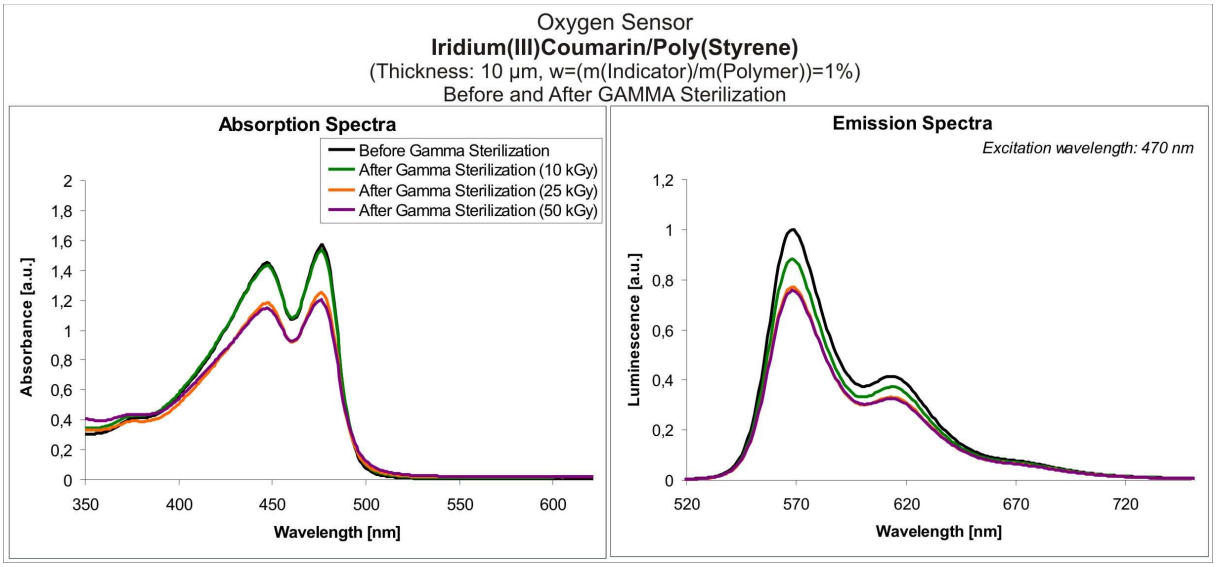

Figure 5 – 8: Absorption and emission spectra of oxygen sensor made of indicator $Ir(C_s)_2(acac)$ and immobilized in polymer PS before and after gamma sterilization.

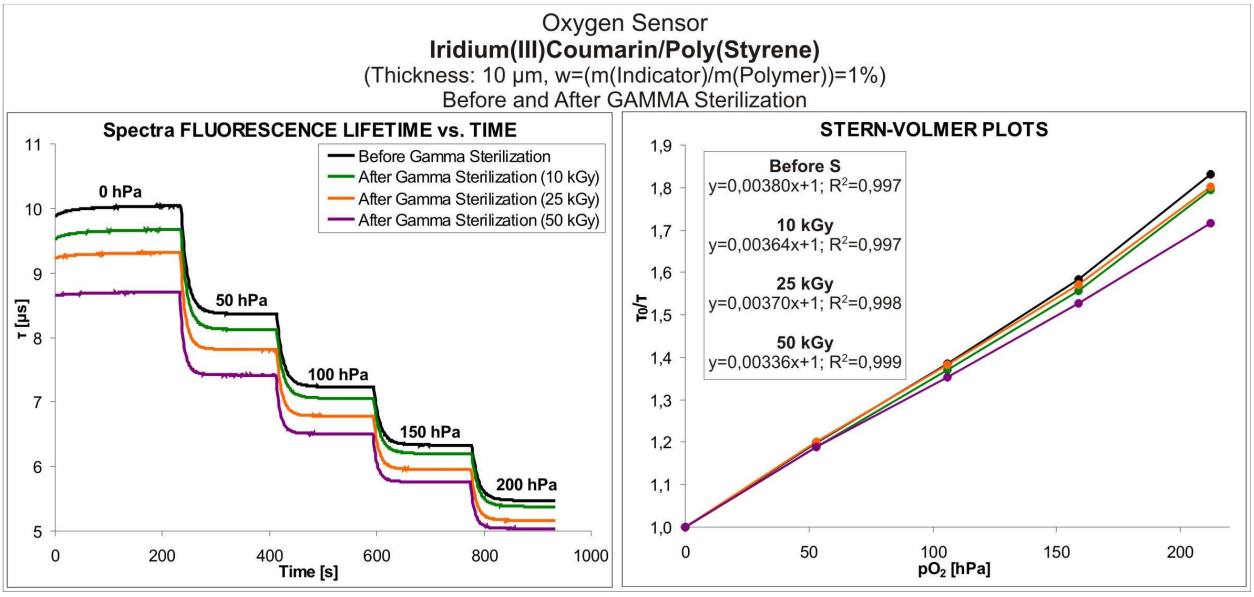

Figure 5 – 9: Calibration curves and Stern-Volmer plots of the oxygen sensor made of indicator $Ir(C_s)_2(acac)$ and immobilized in polymer PS before and after gamma sterilization.

When PSf was used as polymer matrix, a decrease of lifetime was also observed. The polymer became yellowish after radiation sterilization, which could induce greater background level in the phase-modulation measurements, which influences the lifetime. The radiation sterilization of the oxygen sensor made of polymer polystyrene-co-acrylonitrile led probably to dissociation of the cyano group in the polymer structure. The polarity of the matrix was changed as alterations in the absorption and emission curve were observed after sterilization with 25 kGy (presented in figure 5 – 10).

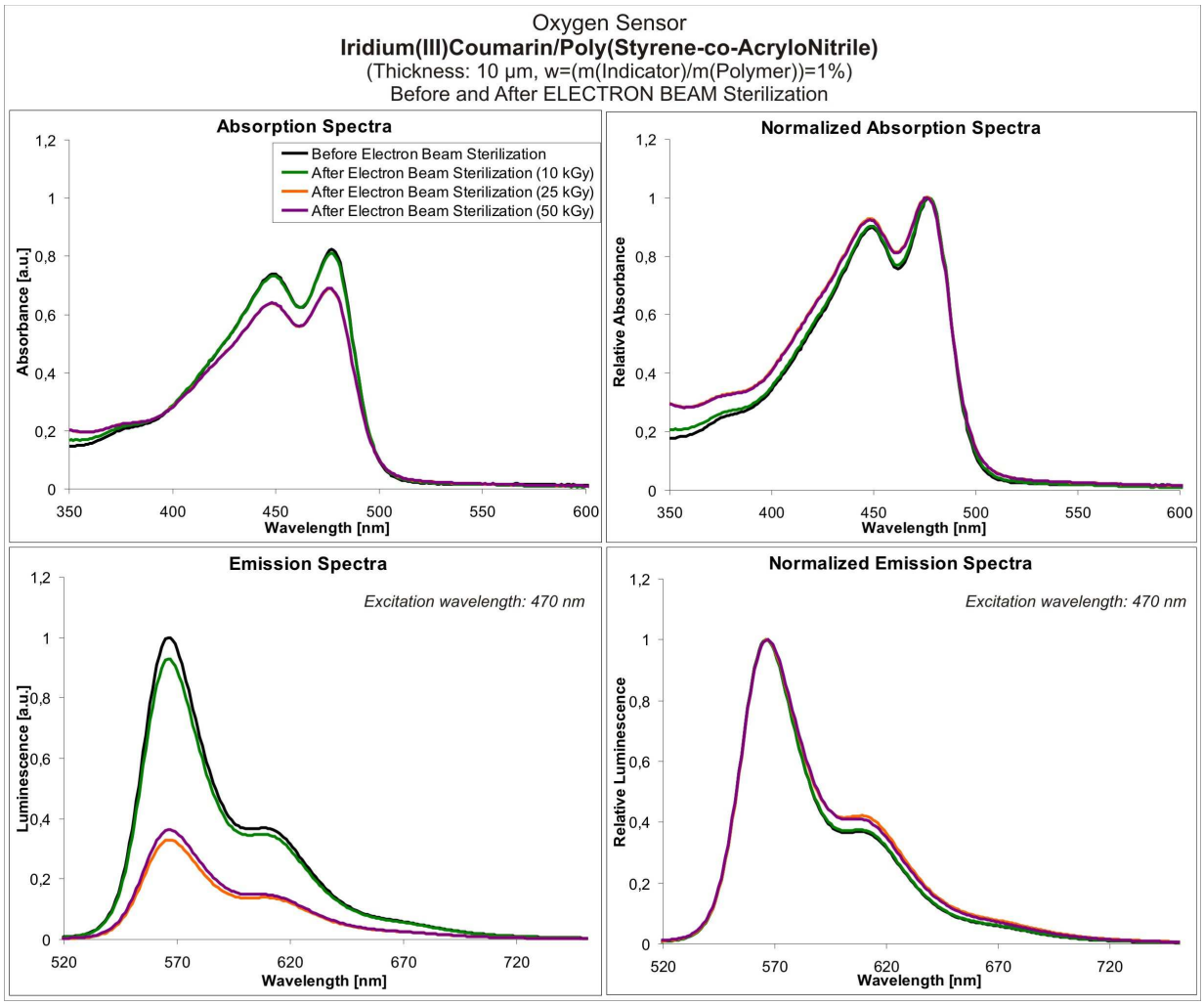

Figure 5 – 10: Absorption and emission spectra of the oxygen sensor made of indicator $Ir(C_s)_2(acac)$ and immobilized in polymer PS-co-PAN before and after electron beam sterilization.

The gamma and electron beam sterilizations have great affect of the oxygen sensor made of indicator PtTFPP. The observed alterations were similar to the ones after radiation sterilization of this indicator as solution. The additional peak(s) was/were observed in the absorption spectra in the majority of polymer matrices with exception of PS and PSf after gamma sterilization. Likewise, the electron beam induced greater alterations than gamma rays. The oxygen sensors were radiation sterilized in the environment with oxygen where the hydroxyl, hydrogen and oxygen radicals are frequently formed. In the polymer matrices, which are not resistant to irradiation the indicator PtTFPP was not shielded from these radicals and therefore the reactions between them and indicator structure appeared. That led to observed alterations in the absorption spectra. Figure 5 – 11 shows the alterations in the absorption spectra of oxygen sensors, where indicator PtTFPP was immobilized in diverse polymer matrices and sterilized with electron beams.

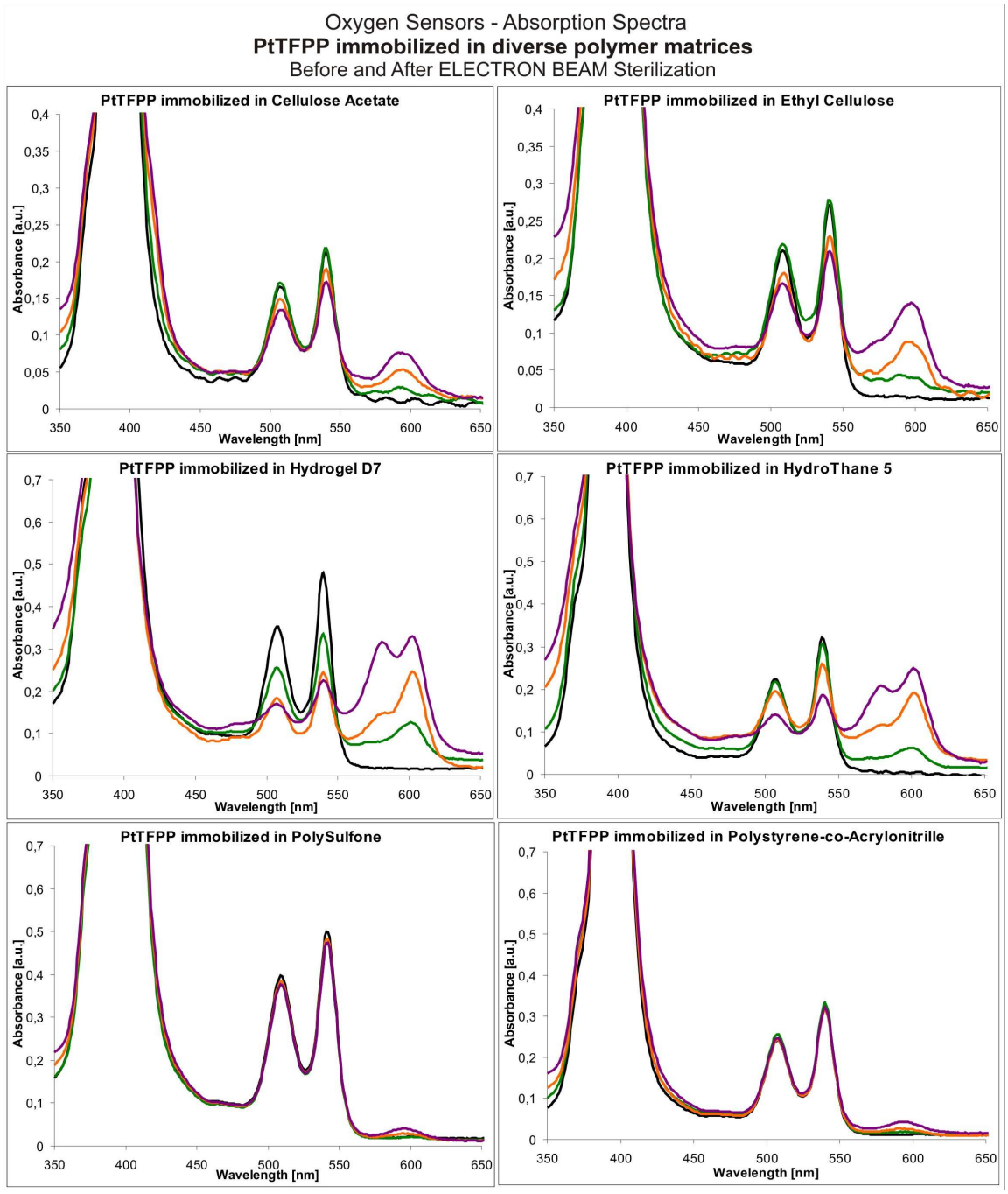

Figure 5 – 11: Alterations in the absorption spectra by oxygen sensors made of indicator PtTFPP and immobilized in diverse polymer matrices before and after electron beam sterilization.

The radiation sterilization induced similar alterations on indicator PtTFFP in some of the polymer matrices as when the indicator solution where the solvent was toluene was radiation sterilized (see figure 5 – 6). However, the emission capabilities of the oxygen sensors, which were altered after irradiation sterilization, were also changed. The emission spectra of oxygen sensors made of indicator PtTFPP immobilized in polymer matrix hydrogel D4 before and after electron beam sterilization with 50 kGy were measured with three different excitation wavelengths: 540 nm, 580 nm and 600 nm. They correspond to the absorption maximum of the Q-band of PtTFPP and absorption maxima of newly formed absorption peaks after electron beam sterilization. The absorption spectra of the sensors made of PtTFPP and hydrogel D7 were shown in figure 5 – 11. The corresponding emission spectra are presented in figure 5 – 12.

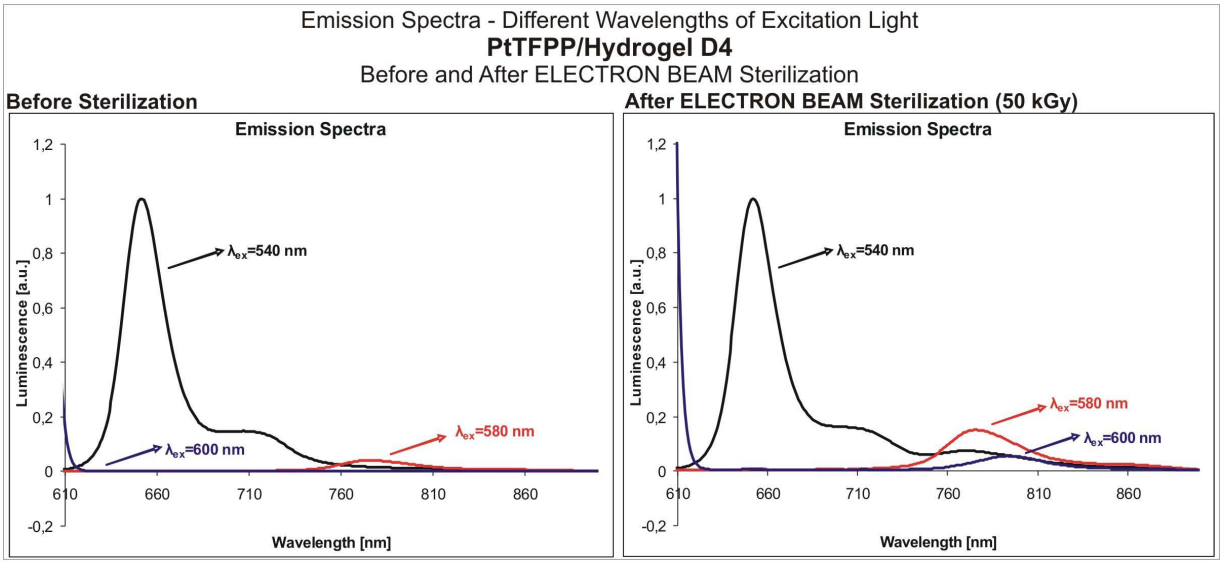

Figure 5 – 12: Emission spectra of oxygen sensors made of indicator PtTFPP and immobilized in Hydrogel D4 before and after electron beam sterilization.

The alterations of indicator structure of PtTFPP in certain polymer matrix also caused a decrease of the phosphorescence lifetime, which was only observed by sensors where an additional absorption peak was observed. Figure 5 – 13 shows the comparison between polymer matrix HydroThane with 5% water content, where alterations in the absorption spectra were observed, and polymer matrix polystyrene, where the electron beam sterilization had no impact on the PtTFPP structure.

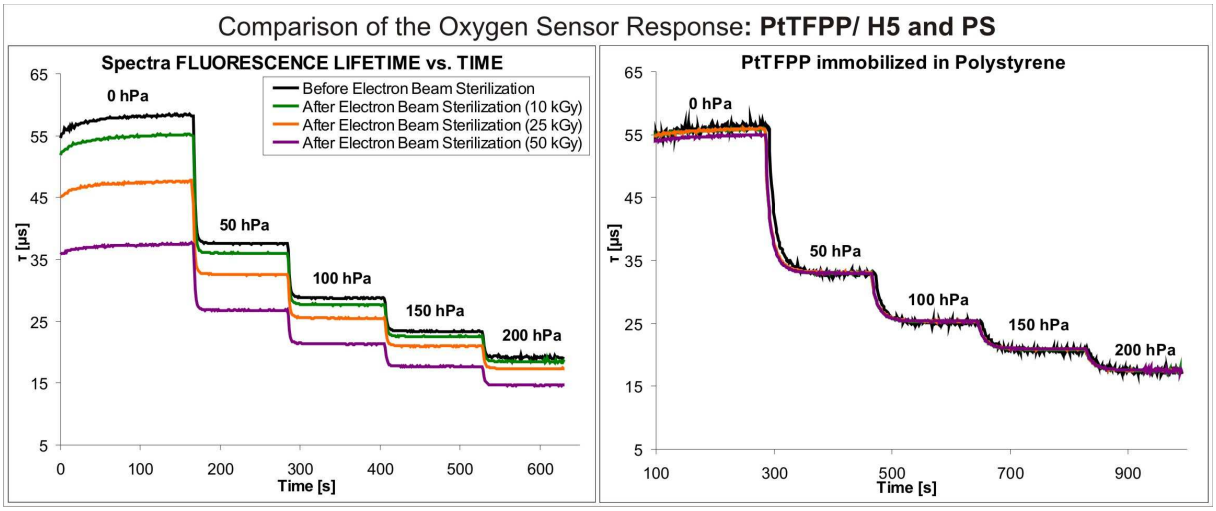

Figure 5 – 13: Comparison of the calibration curves of the oxygen sensors made of indicator PtTFPP and immobilized in polymers H5 and PS before and after electron beam sterilization.

The indicators PtOEP, PtTPTBPF and PdTPTBPF were only immobilized in the polymer matrix polystyrene. Radiation sterilization of the indicator PtOEP in polystyrene with oxygen in the environment is not recommended due to oxidation of the indicator structure, which was observed in the absorption spectra. Additionally, the phosphorescence lifetime of the sensor made of indicator PtOEP also decreased after radiation sterilization with a 25 kGy dose, which was due to formation of additional quenchers in the polymer structure. The absorption spectra, calibration curves and Stern-Volmer plots of oxygen sensor made of indicator PtOEP and immobilized in PS are presented in figure 5 – 14.

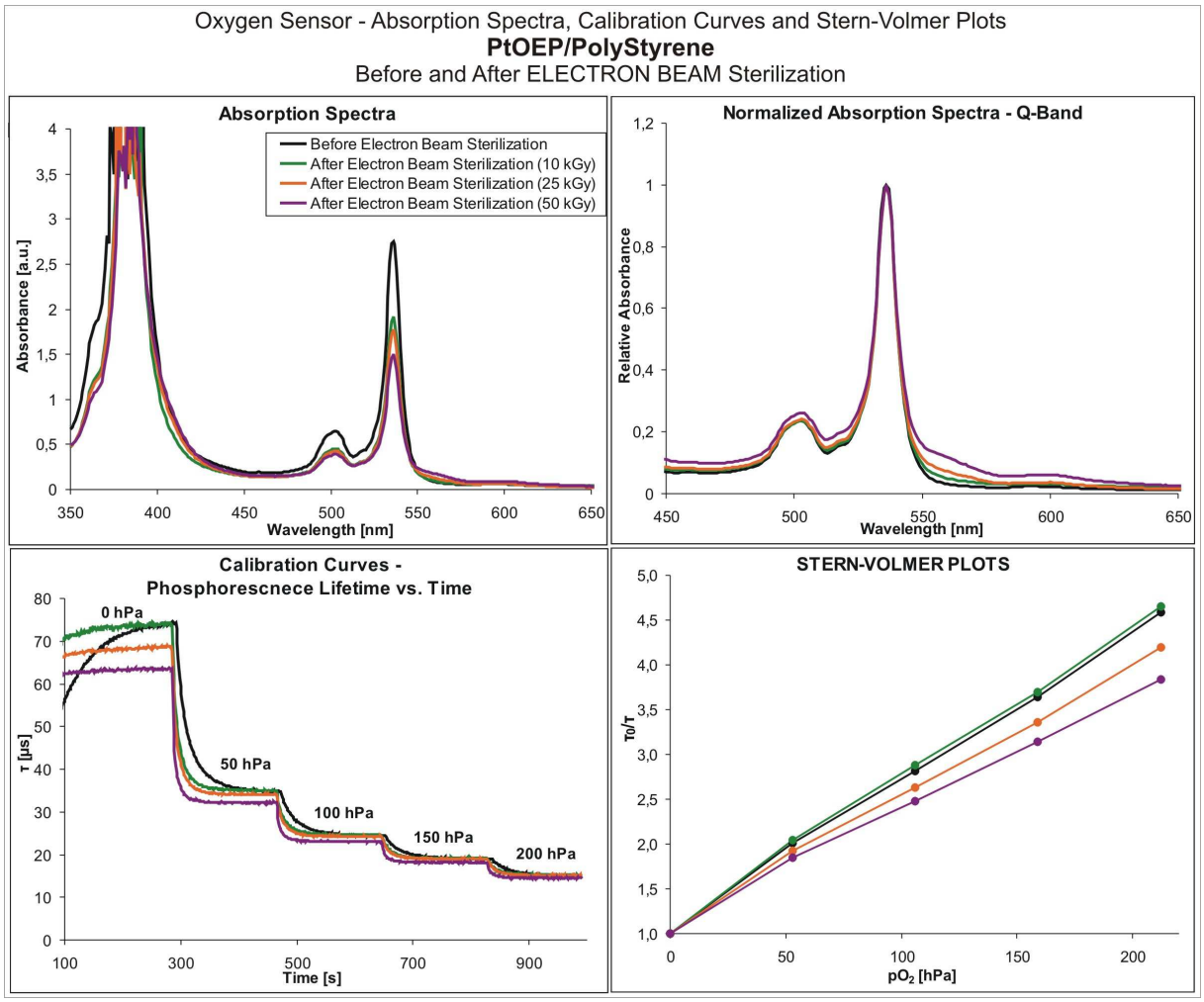

Figure 5 – 14: Absorption spectra, calibration curves and Stern-Volmer Plots of oxygen sensors made of indicator PtOEP and mmobilized in polymer PS before and after electron beam sterilization.

The Pt- and Pd- benzoporphyrin indicators remained stable when immobilized in PS after radiation sterilization. However, alterations in the response of the sensor were observed. A decrease of phosphorescence lifetime occured due to the formation of additional quenchers in the polystyrene matrix. Figure 5 – 15 shows the absorption spectra and calibration curves of PtTPTBPF and PdTPTBPF immobilized in polymer PS.

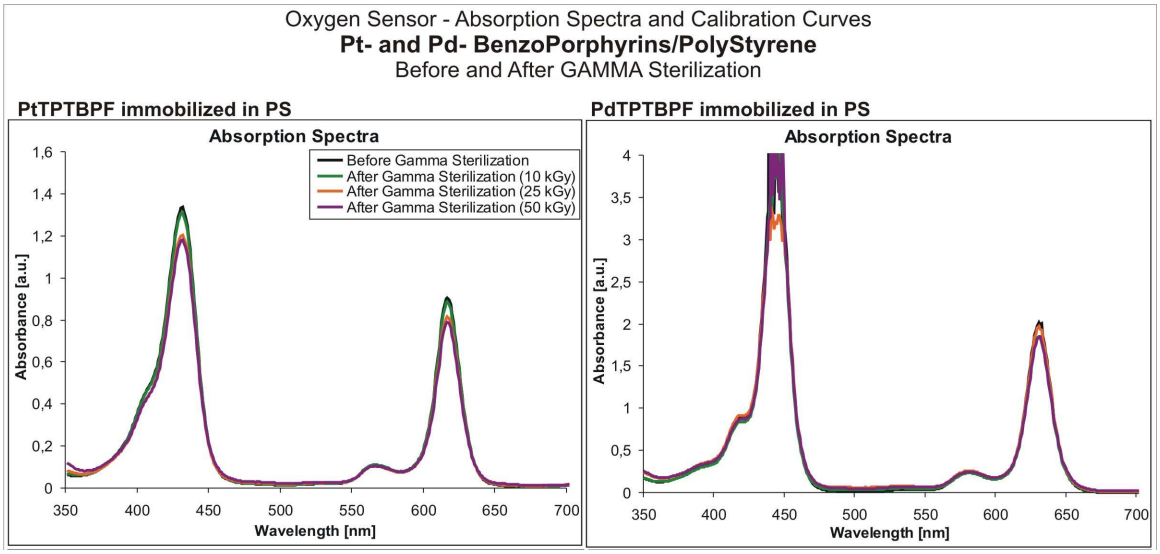

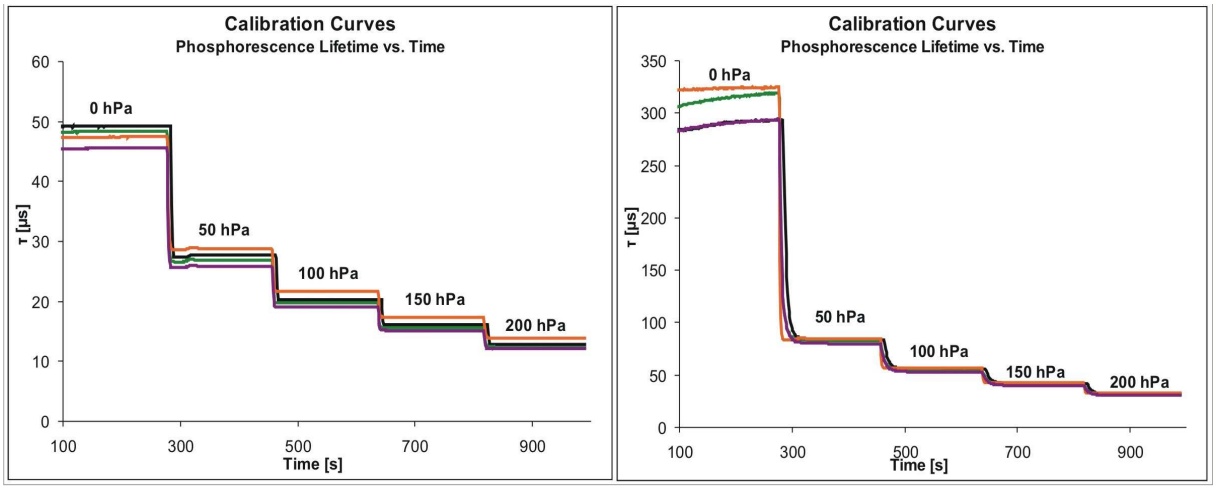

Figure 5 – 15: Absorption spectra and calibration curves of oxygen sensors made of indicators PtTPTBPF and PdTPTBPF and immobilized in polymer PS before and after gamma sterilization,

When the indicator $Ru(dpp)_3Cl_2$ was immobilized in diverse polymer matrices dissociation of the indicator's ligands appeared after radiation sterilization which was observed as a bathochromic shift of the absorption/emission maxima. By cellulosic materials, additional cleavage of acetate (by cellulose acetate) and ether (by ethyl cellulose) after radiation sterilization had influence on the response of the oxygen sensor. Likewise, in polyurethane hydrogels, hydrogel D7 and HydroThane™, additionally quenchers were formed, which lowered the phosphorescence lifetime.

Radiation sterilization of oxygen sensors made of polystyrenes (PS, PS-co-PAN, PSMA) also induced the formation of additional quencher of the ruthenium complex at higher doses seen as the decrease of the phosphorescence lifetime. The greatest decrease (for about 5%) among polystyrenes was observed when the indicator was immobilized in polystyrene-co-acrylonitrile due to dissociation of cyano groups, which additionally may act as quencher of the $Ru(dpp)_3Cl_2$ (Figure 5 – 16).

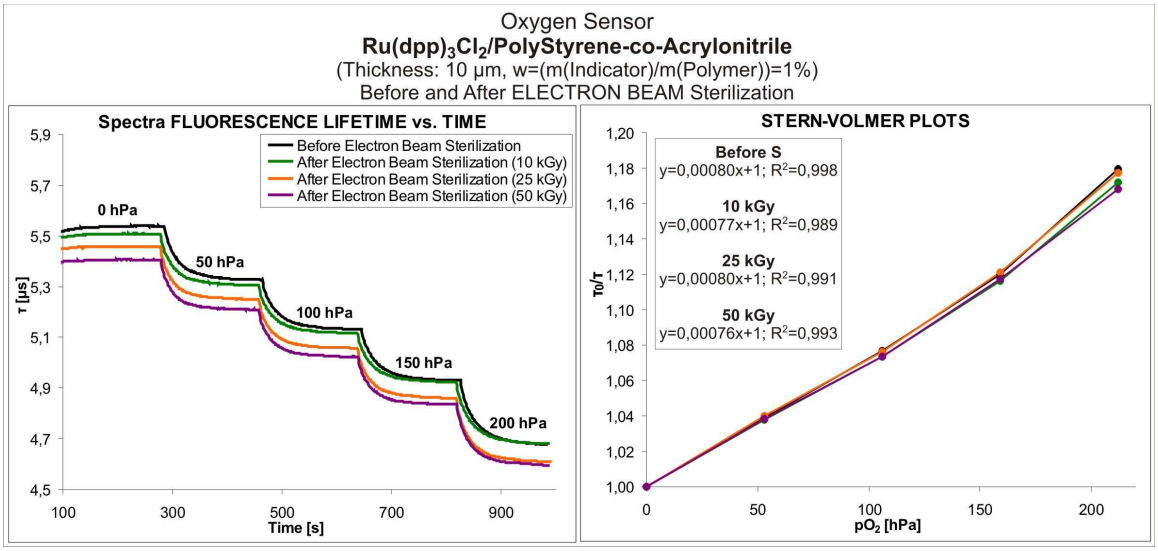

Figure 5 – 16: The response of the oxygen sensor made of indicator $Ru(dpp)_3Cl_2$ and immobilized in polymer PS-co-PAN before and after electron beam sterilization.

Radiation sterilization of the indicator $Ru(dpp)_3Cl_2$ and immobilized in matrices such as polysulfone and poly(phenylsilsesquioxane) had almost no impact on the sensor response and absorption/emission capabilities. Therefore, these two matrices are the most appropriate

for immobilizaation of indicator $Ru(dpp)_3Cl_2$, when the oxygen sensor with this indicator should be radiation sterilized. The responses of the sensors are presented in figure 5 – 17.

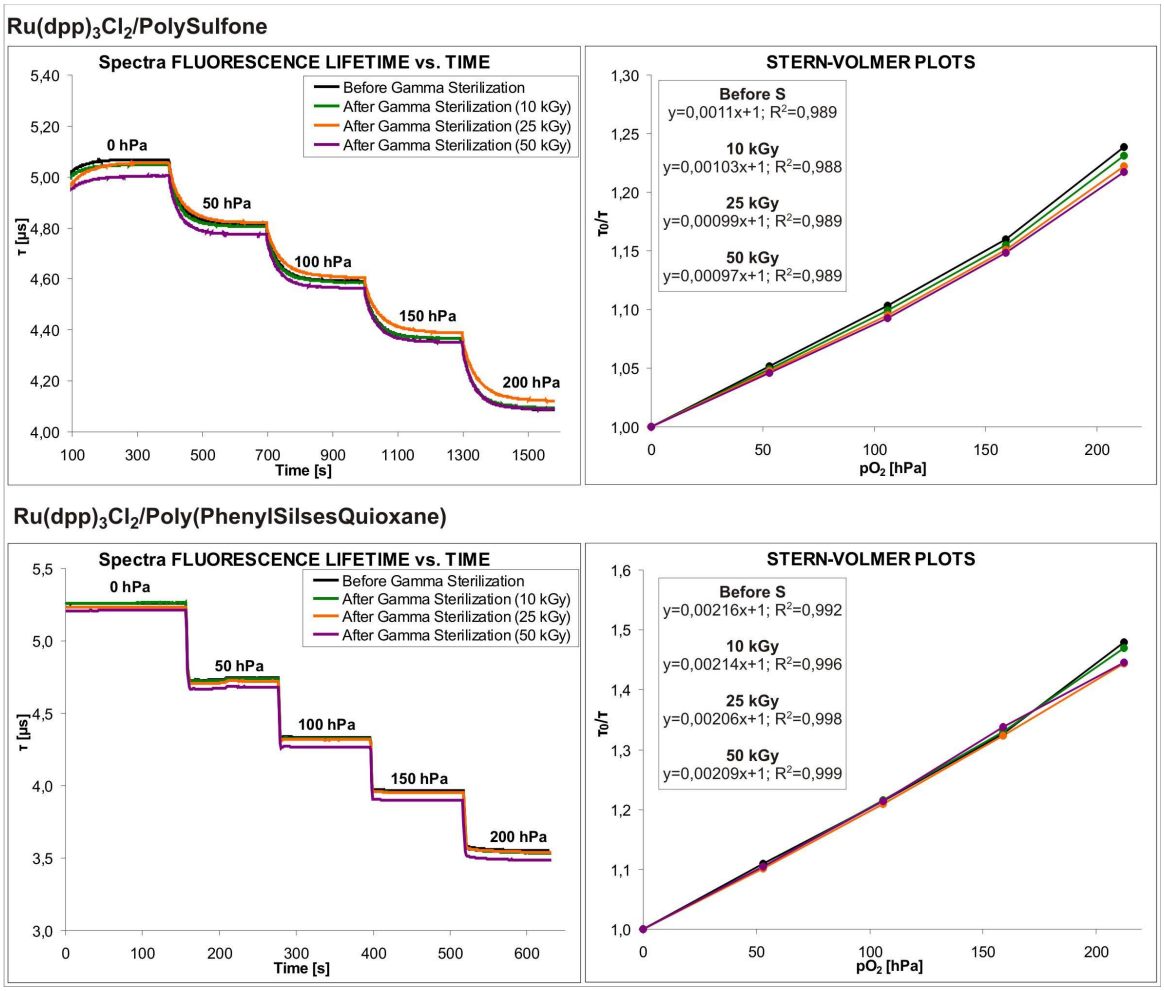

Figure 5 – 17: Response of the oxygen sensors made of indicator $Ru(dpp)_3Cl_2$ and immobilized in polymers PSf and PPSQ before and after gamma sterilization,.

To summarize, oxygen sensors have responded differently to radiation sterilization. Generally, the polymer matrix plays a major role in the stability of the sensor. If the polymer is resistant against gamma rays and electron beams, also the indicator is shielded from alterations. If the radiation sterilization has an impact on the polymer matrix, the changes can also affect the indicator structure and consequently the sensor response. Likewise, quenchers formed in the oxygen sensor structure after radiation sterilization were responsible for decreas of the phosphorescence lifetime by many oxygen sensors. Therefore, the majority of the sensors should be re-calibrated after the application of electron beam and gamma sterilization procedures. Figure 5 – 18 shows the comparison of the absorption spectra of oxygen sensors applied in this study. As already mentioned, the polymer PS is very resistant to radiation sterilization and therefore the indicators were protected from alterations. The exception was indicator PtOEP, where the radiation sterilization in the environment with oxygen and the formed radicals induced the oxidation of the indicator structure.

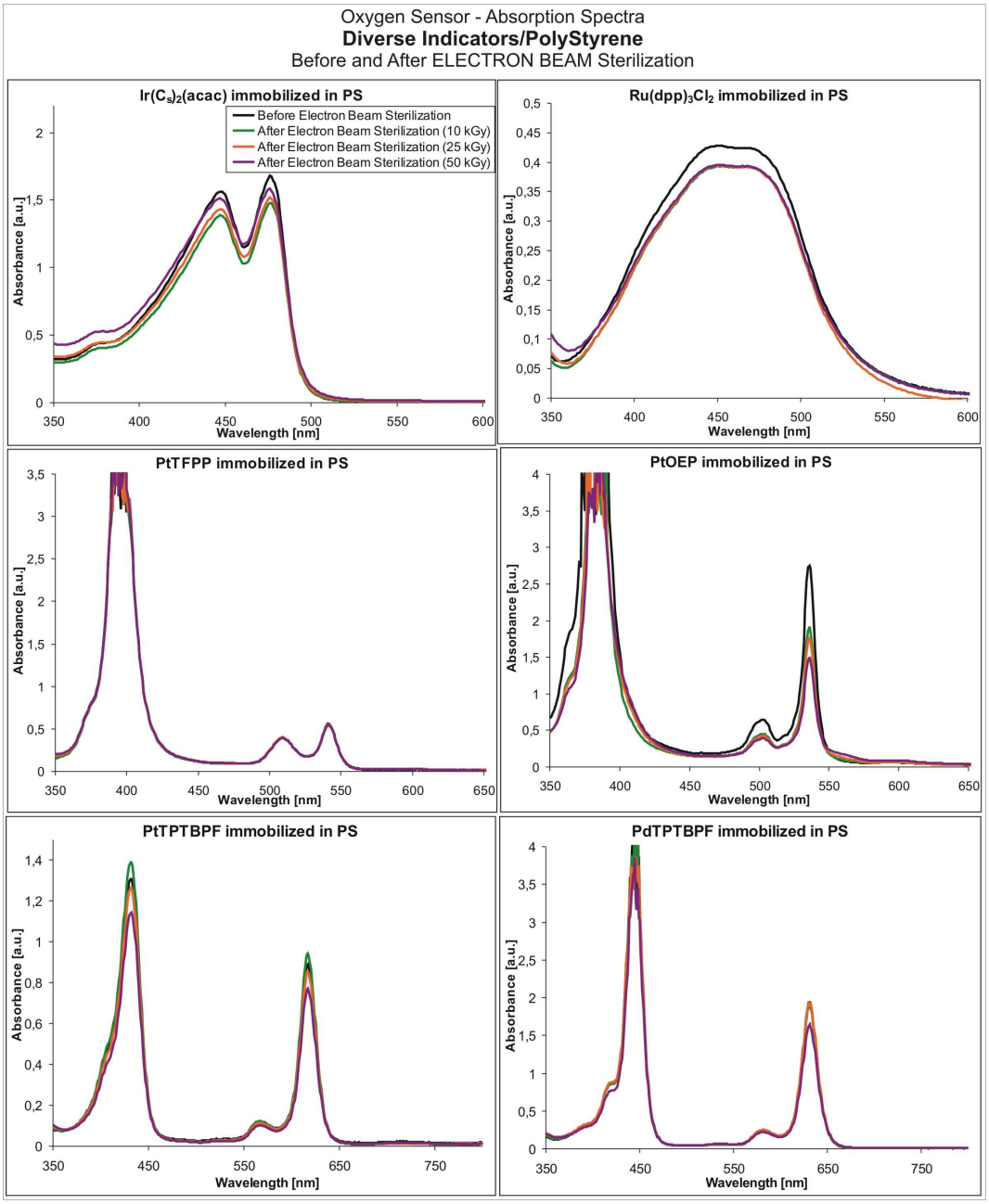

Figure 5 – 18: Absorption spectra of the oxygen sensors made of diverse indicators and immobilized in polymer PS before and after gamma sterilization.

5.2 Radiation Sterilization of Optical pH Sensors

Many optical fluorescence pH sensor, found in the literature, based on indicators 8-hydroxypyrene-1,3,6-trisulfonate (HPTS) and its derivatives, fluorescein or coumarin derivatives. These indicators possess considerably different spectral properties in the protonated and deprotonated state. However, pH sensitivity can also be introduced over photoinduced electron transfer and also the pH indicators based on colour changes are often applied. Therefore, in this study, two lipophilic fluorescein derivatives 2´,7´-DiHexylFluorescein OctadecylEster (=DHFE) and 2´,7´-DiHexyl-5(6)-*N*-Octadecyl-CarboxAmidoFluorescein (=DHFA), lipophilic HPTS 1-HydroxyPyrene-3,6,8-tris-bis(2-Ethylhexyl)Sulfonamide (=HPTS(DHA)$_3$) and coumarin derivative 3-(2-benzothiazolyl)-7-

hydroxycoumarin (=pH Sensitive Coumarin) were chosen as pH indicators, which have different spectra properties in the protonated and deprotonated state. The PET Perylene bisimide was selected as example of the pH indicator based on photoinduced electron transfer. The representatives for pH indicators based on colour changes were bromophenol blue, thymol blue, bromothymol blue and methyl orange.

By the development of the optical pH sensors, often appears that the sensors should be stored in the humid surrounding until application because the responses of the pH sensors remain identical by this mode of storage. Therefore, the pH optical sensors, based on fluorescence, were additional radiation sterilized in the buffer solution with pH 7.5 to determine whether or not is possible to radiation sterilized the pH optical sensor directly in humid surrounding.

All pH sensitive indicators were immobilized in the polymer matrix made of HydroMed^{TM} Hydrogel D4. Additionally, the lipophilic fluoresceins and pH sensitive coumarins were also immobilized in polymer matrix Poly(2-hydroxyethyl methacrylate) (pHEMA). The other fluorescence indicators, listed above, are too lipophilic for this type of polymer matrix.

The radiation sterilization induced alterations in the structure of indicators HPTS(DHA)$_3$, DHFE and DHFA, when sterilized in the solid state. The chromophores of indicators were more and more affected with increasing radiation doses. The radicals that were formed in the sterilization environment reacted with indicator structures and change the part of the molecule in which the electronic transition is responsible for a typical spectral band in the spectrum. Therefore, gradually decrease of the absorption and emission intensity was observed but the typical curve shapes remained the same. The absorption spectra before and after gamma sterilization of indicators HPTS(DHA)$_3$, DHFE and DHFA are presented in figure 5 – 19.

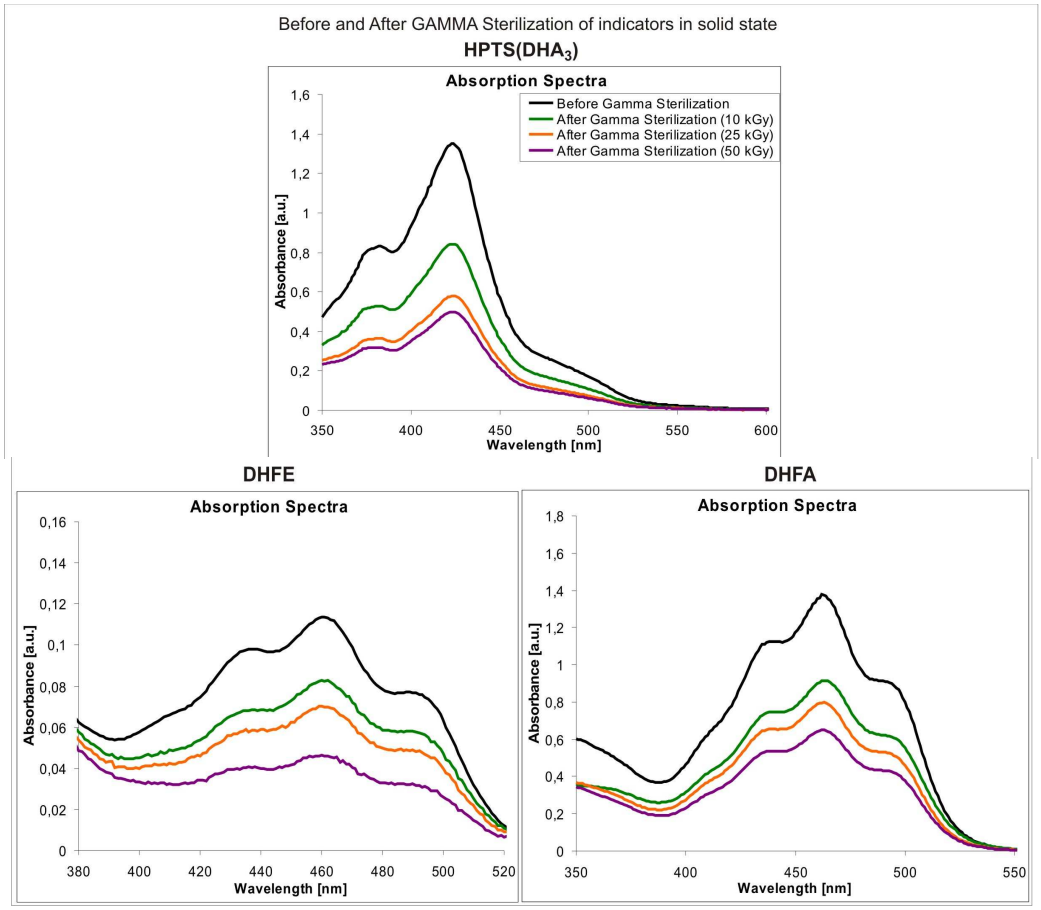

Figure 5 – 19: Absortpion spectra of the indicators HPTS(DHA)$_3$, DHFE and DHFA before and after gamma sterilization in solid state.

When the same indicators were immobilized in polymer matrices, the effects were not the same. The indicator HPTS(DHA)$_3$ was more stable and resistant when radiation sterilized in polymer matrix hydrogel D4 as without it. However, the capability of the deprotonation of the indicator was affected, which was observed as alterations in the protonation/deprotonation peaks ratio. The protonation peak was still observed in the absorption spectrum at pH 9.5, when sterilized with higher doses than 25 kGy. However, at pH 12 the protonation peak disappeared, which indicated that the hydroxyl group of the indicator was not altered after sterilization. Hence, the rate for the indicator to undergo the ionization was altered and the attainability of the indicator for the proton was more hindered after radiation sterilization due to alterations in the polymer structure. The permeability of the polymer D4 for the proton was changed after radiation sterilization and therefore the protonation peak was still observed in the absorption spectrum at pH 9.5. The effects of radiation sterilization on protonation/deprotonation capability of the indicator is shown in figure 5 – 20.

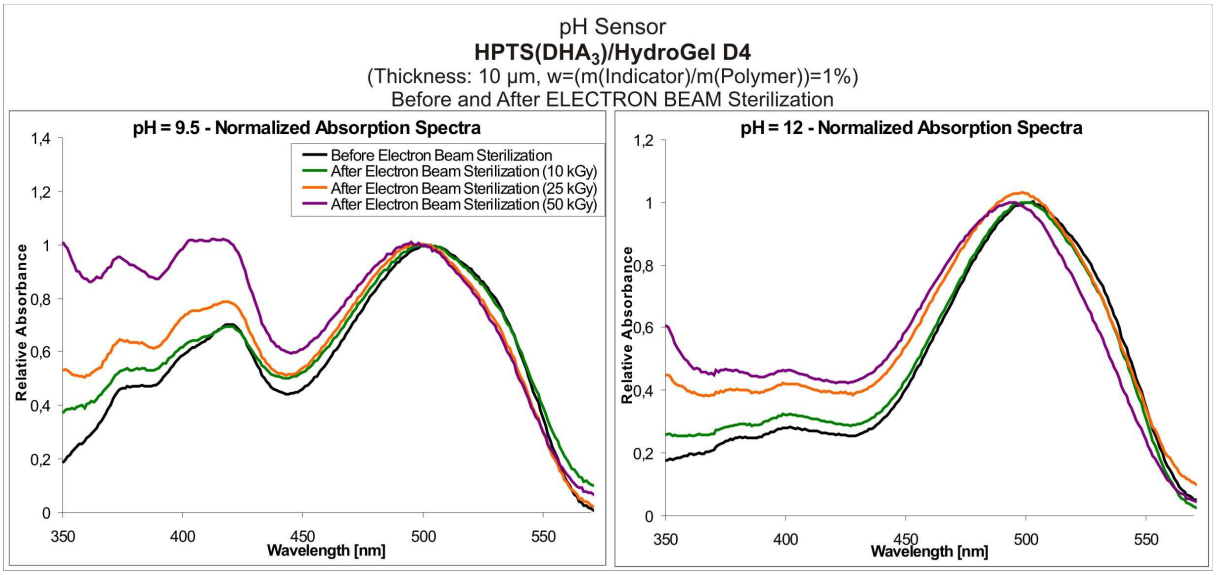

Figure 5 – 20: Normalized absorption spectra of pH sensor made of indicator HPTS(DHA)$_3$ and immobilized in polymer hydrogel D4 before and after electron beam sterilization.

Another effect, after sterilization with electron beam in standard ambient conditions and in buffer solution and gamma sterilization in buffer solution, was detected. The hypsochromic shift of the absorption maximum after sterilization with 25 and 50 kGy was observed. This effect is also presented on figure 5 – 20 and could appear due to radiation affect on pendant groups of lipophilic HPTS or due to migration of the indicator in more hydrophilic parts on the polymer hydrogel D4. The radiation sterilization of pH sensor made of indicator HPTS(DHA)$_3$ in the buffer solution induced the hydrolysis, which could be also responsible for the shift of the absorption maximum.

Hence, after radiation sterilization of the pH sensor made of indicator HPTS(DHA)$_3$ and immobilized in polymer Hydrogel D4 the sensor was still capable to absorb and emit the photons and the response was still pH dependent. However, the pK_a values were changed after sterilization, which could be due to migration of the indicator more hydrophobic (by increase of the pK_a) or more hydrophilic (by decrease of the pK_a) in the polymer matrix hydrogel D4. Therefore, after radiation sterilization the sensor should be re-calibrated before application. The calibration curves after gamma and electron beam sterilization in standard ambient conditions are presented in figure 5 – 21.

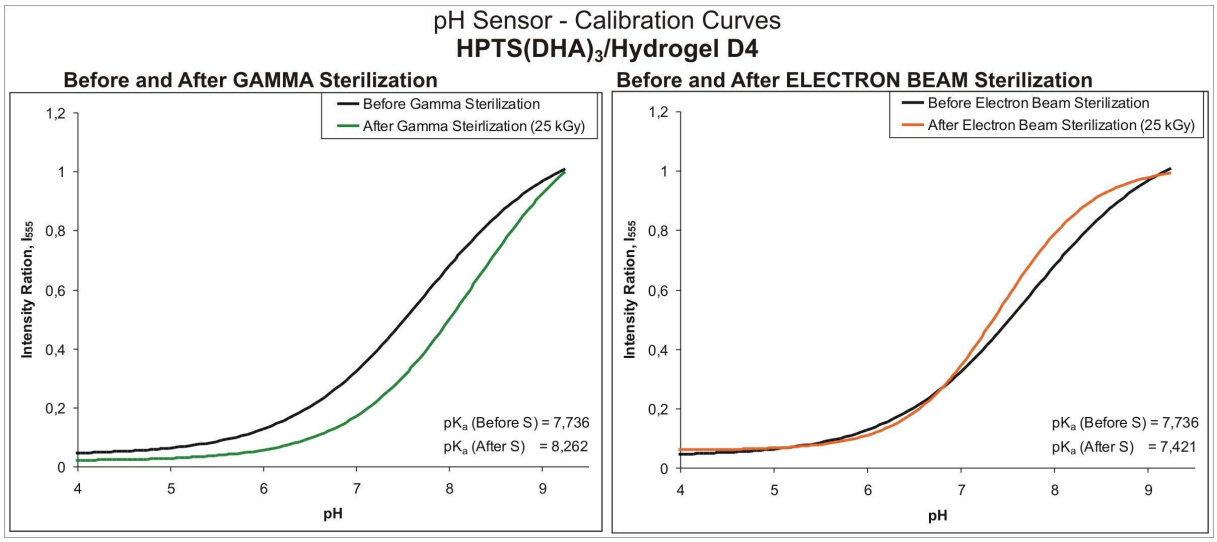

Figure 5 – 21: Calibration curves of the pH sensor made of indicator HPTS(DHA)$_3$ and immobilized in polymer Hydrogel D4 before and after gamma and electron beam sterilization in standard ambient conditions..

The lipophilic fluoresceins were immobilized in the polymer matrices made of polymers hydrogel D4 and pHEMA. When the indicators DHFA and DHFE were immobilized in hydrogel D4, the radiation sterilization with dose 50 kGy are too large because the typical absorption and emission curve forms in the spectra disappeared. After the sterilization with lower doses, the pH sensor should be re-calibrated. Additionally, the responses of the sensors sterilized in standard ambient conditions and in buffer solution were similar by indicator DHFE. However, the sterilization of the pH sensor in the buffer solution made of indicator DHFA and immobilized in hydrogel D4 should be avoided due to great decrease - for more than 60% after sterilization with 10 kGy and more than 90% after sterilization with 25 kGy - of the absorption and emission intensity. Figure 5 – 22 shows the comparison of absorption spectra between the pH sensor radiation sterilized in the standard ambient conditions and buffer solution.

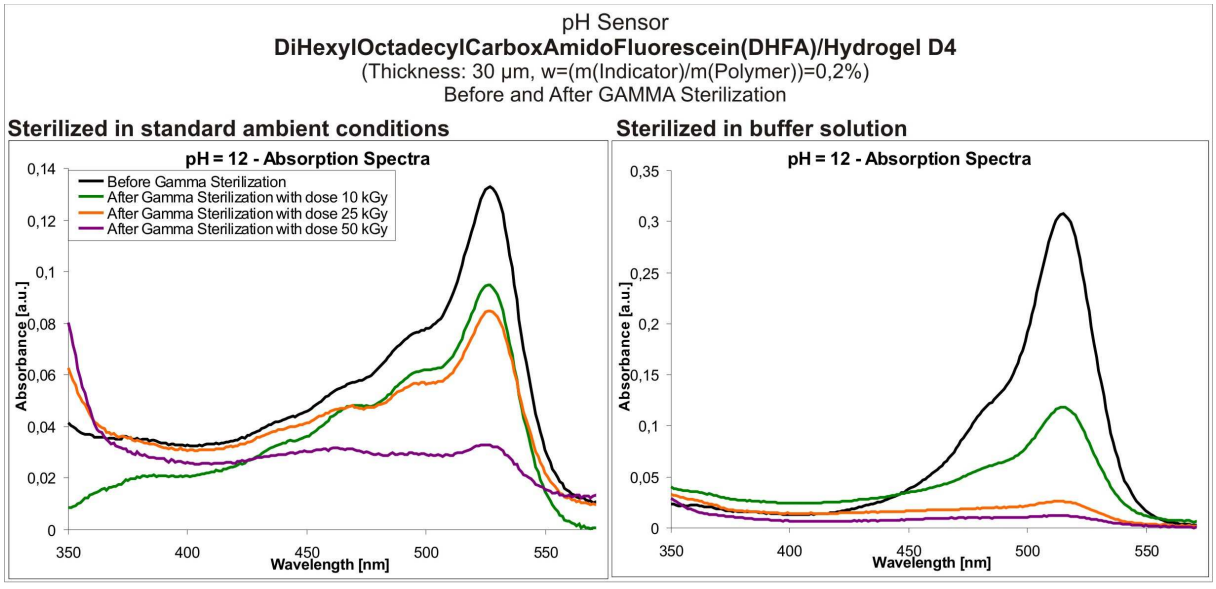

Figure 5 – 22: Absorption spectra of the pH sensor made of indicator DHFA and immobilized in polymer hydrogel D4 before and after radiation sterilization in standard ambient conditions and in buffer solution.

When the indicator DHFA and DHFE were immobilized in polymer pHEMA effect on polymer matrice was observed. When the sensor was sterilized in standard ambient conditions, the

sensor became turbid after characterization in the buffer solution, which was observed in the increase of the absorption and that is presented in figure 5 – 23.

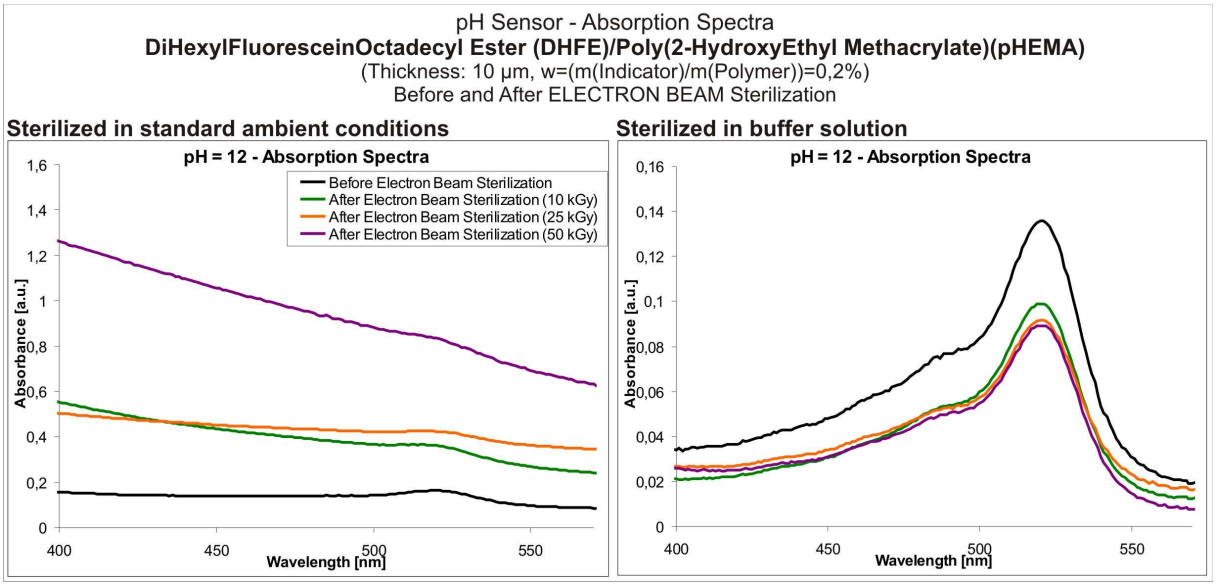

Figure 5 – 23: Absorption spectra of the pH sensor made of indicator DHFE and immobilized in polymer pHEMA before and after electron beam sterilization.

Consequently, the concentration of water uptake was altered and greater by polymer pHEMA after radiation sterilization. In general, the increase in equilibrium water content of the polymer after sterilization is a sign of chain-scission or re-conformation of polymer chains. According to the literature, under irradiation, the polymer of the type (CH_2-CR´R´´) such as pHEMA, undergo predominantly chain scission [92]. The irradiation promotes chain scission in pHEMA homopolymer and strengthens the relaxation, what suggest that the number of interchain hydrogen bonds decreases.

However, when the same sensor was sterilized in the buffer solution these effects on polymer pHEMA were not observed and the sensor did not become turbid after characterization. Accordingly, the chain-scission may be suppresses due to different environment during radiation sterilization and conformation of different radicals in the surrounding of sensor.

The indicators HPTS$(DHA)_3$ and lipophilic fluoresceins were not very resistant to radiation sterilization, when sterilized in solid state. However, the immobilization in the polymer matrix makes these indicators more stable and resistant to gamma rays and electron beam. On the contrary, the indicator pH sensitive coumarin was more stable after gamma and electron beam sterilization in the solid state because the absorption and emission intensity remained the same before and after sterilization. When the pH sensitive coumarin was immobilized in the polymer matrix hydrogel D4 or pHEMA, the indicator structure was very affected. The absorption and emission exceedingly decreased after sterilization and after dose 50 kGy the characteristic absorption and emission curve shapes were no longer observable. When the sensor was sterilized in water even greater alterations appeared. Due to the fact that the pH sensitive coumarin was stable when solely sterilized with gamma and electron beam in the solid state, the polymers hydrogel D4 and pHEMA were responsible for introducing the alterations in the indicator structure. After radiation sterilization, the radicals were formed in the polymers that reacted with the indicator and caused the gradually destruction of the cromophore structure. Hence, the exactly structure of the hydrogel D4 is not known but the structure of pHEMA is. Consequently, the radicals like hydroxyl or methyl could be formed in the polymer matrix and have impact on the chromophore of the indicator pH sensitive coumarin. Additionally, the methyl radical could be also responsible for the alterations when the indicator was radiation sterilized as the solution where the solvent was toluene. The

absorption spectra of the pH sensor made of pH sensitive coumarin and immobilized in hydrogel D4 and radiation sterilized in standard ambient conditions and buffer solution are shown in figure 5 – 24.

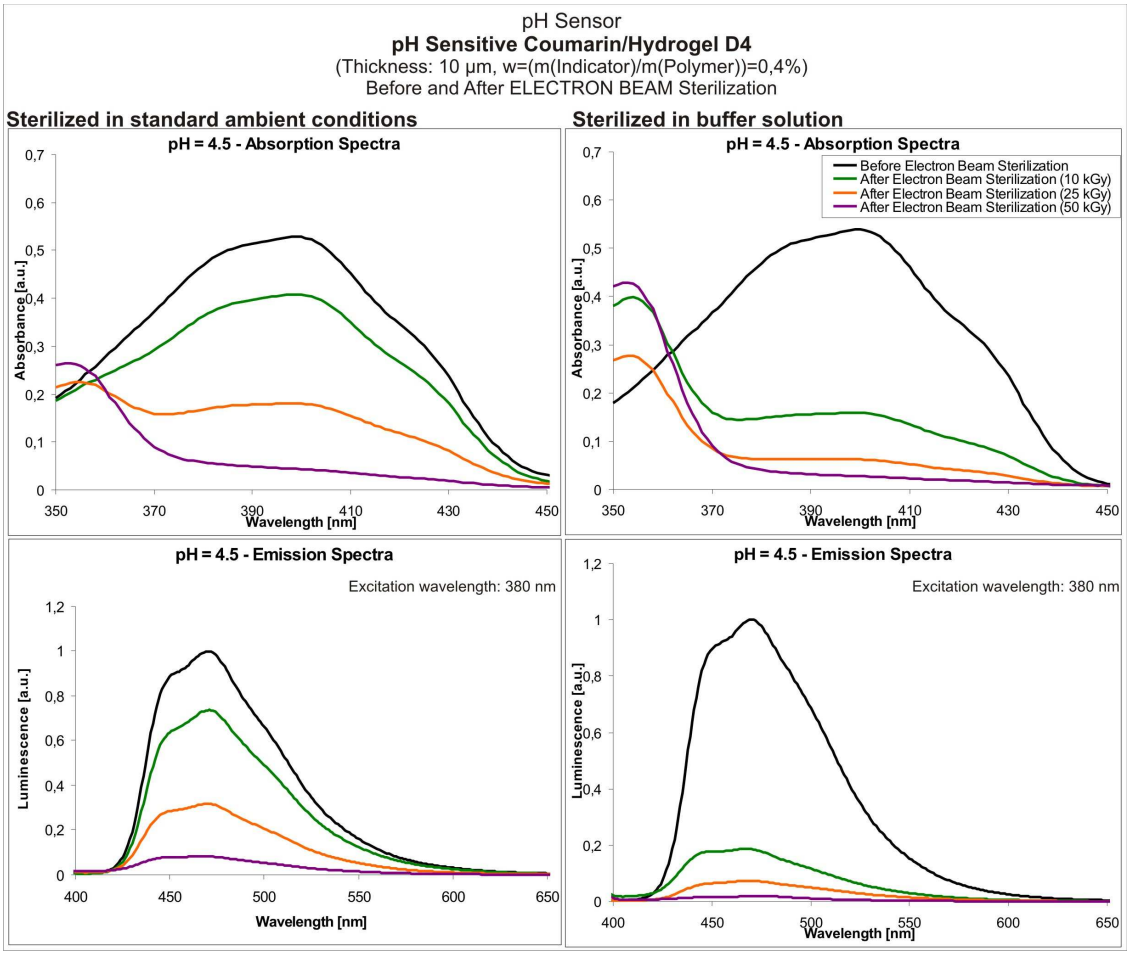

Figure 5 – 24: Absorption and emission spectra of the pH sensor made of indicator pH sensitive coumarin and immobilized in polymer hydrogel D4 before and after electron beam sterilization in standard ambient conditions and buffer solution.

After radiation sterilization in normal environment of pH indicator PET Perylene bisimide immobilized in hydrogel D4, where the pH sensitivity is introduced over photoinduced electron transfer (PET), the pH sensitivity was no longer observable. Therefore, the amino moiety, which is capable of quenching the indicator in the non-protonated state, was affected and the luminescence intensities were randomly distributed. On the other hand, when the same sensor was gamma sterilized in buffer solution at pH 7.5, pH sensitivity via PET was still observed and the PET efficiency was not affected. Therefore, the sterilization in the buffer solution protects the amino moiety from the alterations or the radicals formed in the buffer solution did not reacted with the indicator structure. However, after electron beam sterilization the pH sensitivity was observed when the sensor was sterilized in the standard ambient conditions and in buffer solution. Consequently, the electron beam sterilization procedure is more appropriate sterilization method for sterilization of this type of pH sensor as sterilization method with gamma rays. The response of the sensor made of indicator PET Perylene bisimide and immobilized in hydrogel D4 after gamma sterilization in the standard ambient conditions and in buffer solution is presented in figure 5 – 25.

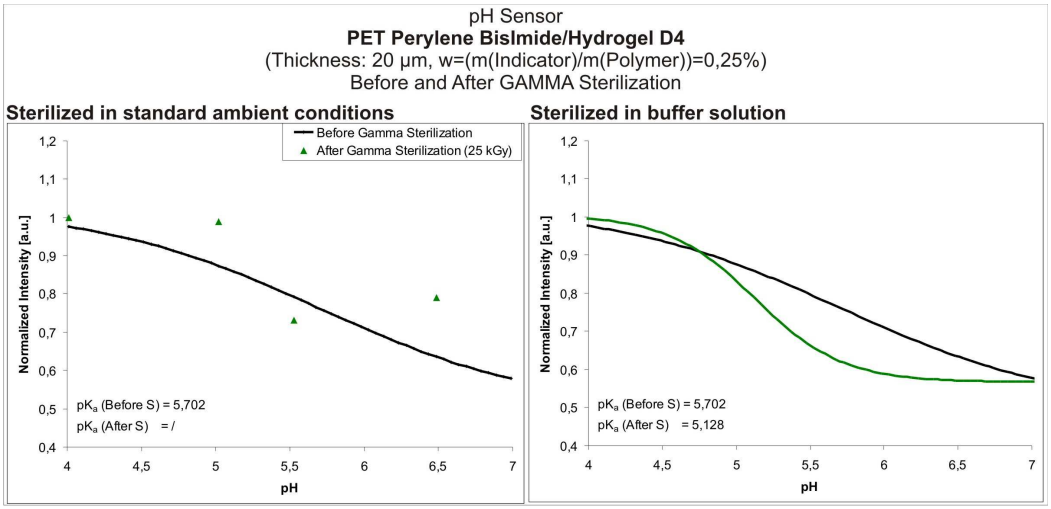

Figure 5 – 25: Calibration curves of the pH sensor made of indicator PET Perylene bisimide and immobilized in polymer hydrogel D4 before and after gamma sterilization in standard ambient conditions and in buffer solution.

The sulfonephthalein pH indicators, such as bromophenol blue, bromothymol blue and thymol blue, based on colour changes are irradiation resistant pH indicators, when sterilized in solid state and when immobilized in matrix hydrogel D4. The resistance of sulfonephthalein pH indicators to gamma and electron beam increase with increasing electron density of the indicators – the tymol blue is at least and bromophenol blue the most resistant. The absorption spectra of indicators immobilized in hydrogel D4 are presented in figure 5 – 26.

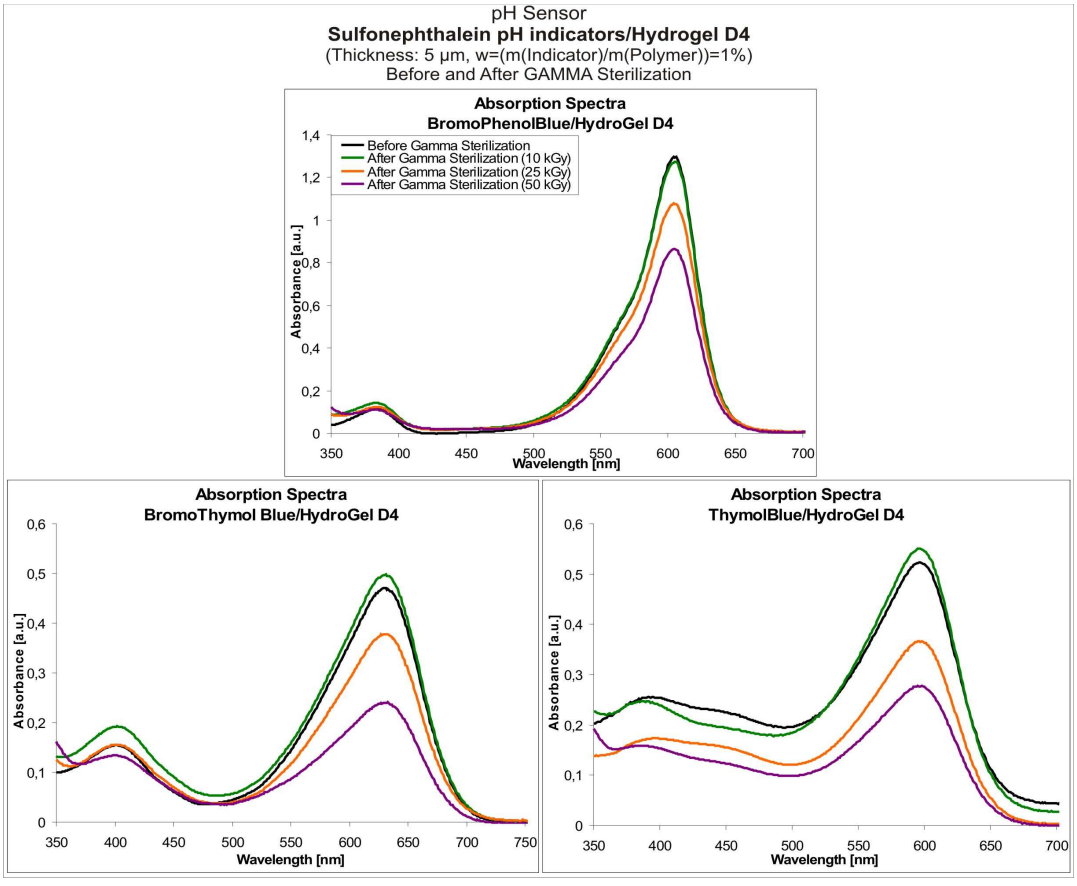

Figure 5 – 26: Absorption spectra of the sulfonephthalein pH indicators immobilized in hydrogel D4 before and after gamma sterilization.

The azo pH sensitive dye methyl orange is resistant to gamma rays and electron beam up to dose 50 kGy when sterilized in solid state. On the other hand, the sterilization of indicator in polymer matrix hydrogel D4 introduced great alterations due to decrease of the absorption (for about 40% of initial intensity) and changes in the curve shapes. Probably, the radiation sterilization induced the formation of the radicals in the polymer structure that reacted with the indicator structure, which have influence on the absorption ability of the indicator. The absorption spectrum of indicator methyl orange sterilized in solid state and when immobilized in hydrogel D4 is shown on figure 5 – 27.

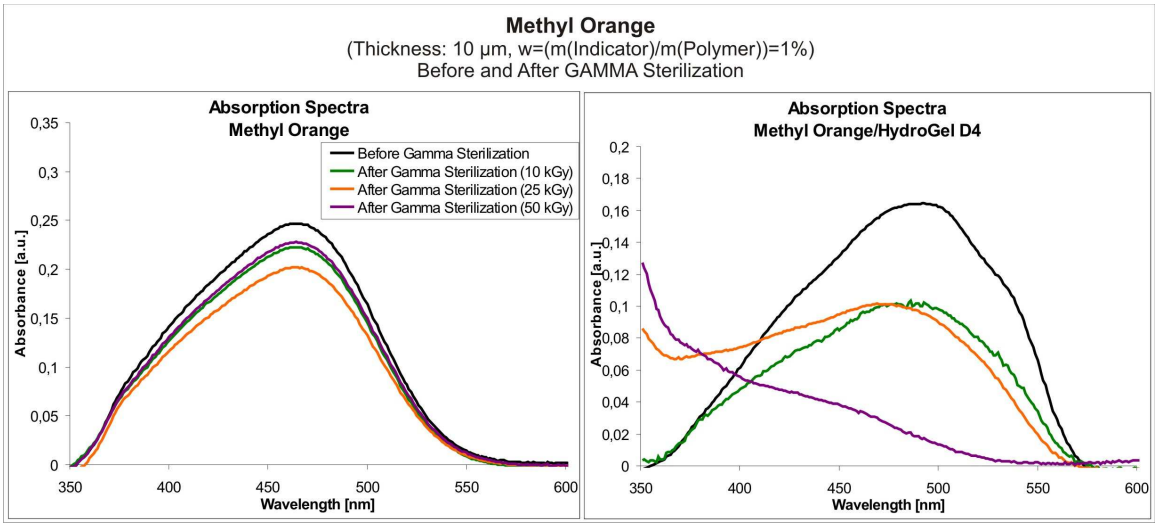

Figure 5 – 27: Absorption spectra of indicator methyl orange after gamma sterilization in solid state and when immobilized in polymer hydrogel D4.

5.3 Radiation Sterilization of Optical Temperature Sensors

Temperature is a key parameter in numerous fields of science and technology. While not a chemical parameter by itself, its knowledge is of higher significance since temperature affects the response of all chemical sensors. Luminescence probes that display a strong temperature dependence of their luminescence lifetime include ruthenium(II) complexes and europium(III) complexes. Therefore, the optical temperature sensors utilized in this study were made of indicators Europium(III) complex with 4-(4,6-di(1H-indazol-1-yl)-1,3,5-triazin-2-yl)-N,N-diethyl benzen amine (=Eu(tta)$_3$DEADIT) and dichlorotris(1,10-phenanthroline) ruthenium(II) hydrate.

The most sensor materials consist of an indicator contained in a polymeric matrix that serves as a solid support and as a selectively permeable membrane. The polymers that were employed as a polymer matrices were polyvinylidene chloride-co-acrylonitrile (PVC-co-PAN), polymethacrylonitrile (PMAN) for both indicators mentioned above and polystyrene-co-acrylonitrile (PS-co-PAN) for Eu(tta)$_3$DEADIT, since the ruthenium complex was not soluble in it.

The irradiation of polymers with gamma rays and electron beam has affect on the polymers. The PS-co-PAN is the most resistant to ionizing radiation among polymers used for optical temperature sensors. After irradiation of polymer PVC-co-PAN, the additional chromophore was formed which absorb light between 350-500 nm. The formation of conjugated unsaturated units, which gives the yellow to brownish colouration to the polymer matrix was observed in the absorption spectrum of the polymer PVC-co-PAN and is presented in figure 5 – 28.

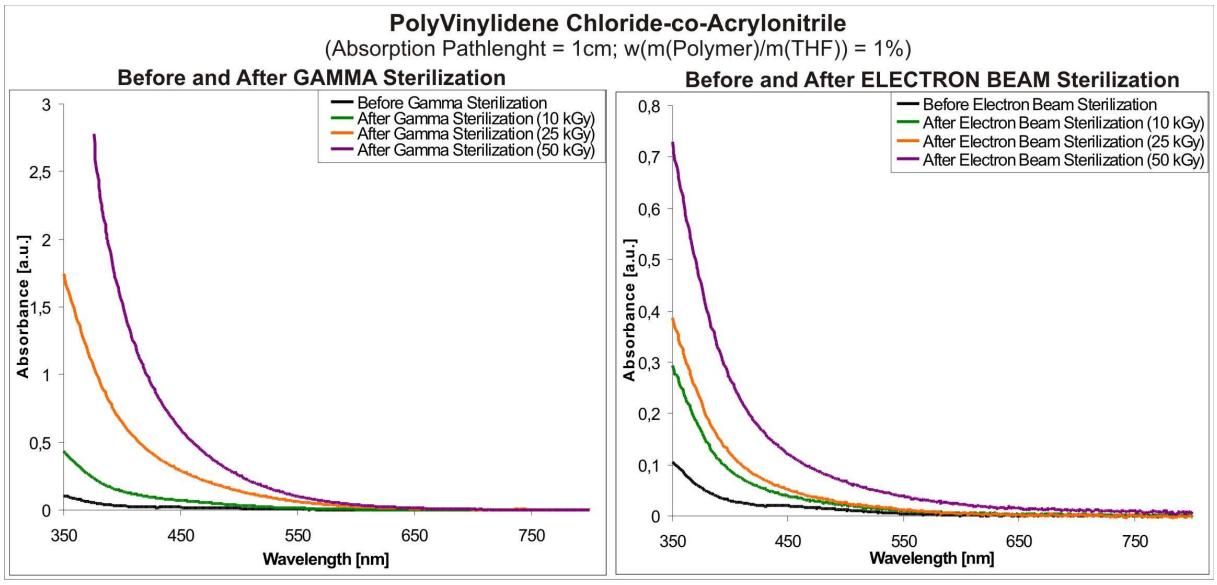

Figure 5 – 28: Absorption spectra of the polymer PVC-co-PAN before and after gamma and electron beam sterilization.

According to the literature, the irradiation of polymer polymethacrylonitrile (PMAN) leads to main-chain scission without simultaneous cross-linking [71]. Radicals are produced which are primarily the result of main-chain scission, hydrogen atom addition and abstraction. Hence, the chain-scission of the polymer induced the changes in the absorption capacity of the polymer PMAN after gamma and electron beam sterilization and the alteration was measured as the increase of the absorption (figure 5 – 29).

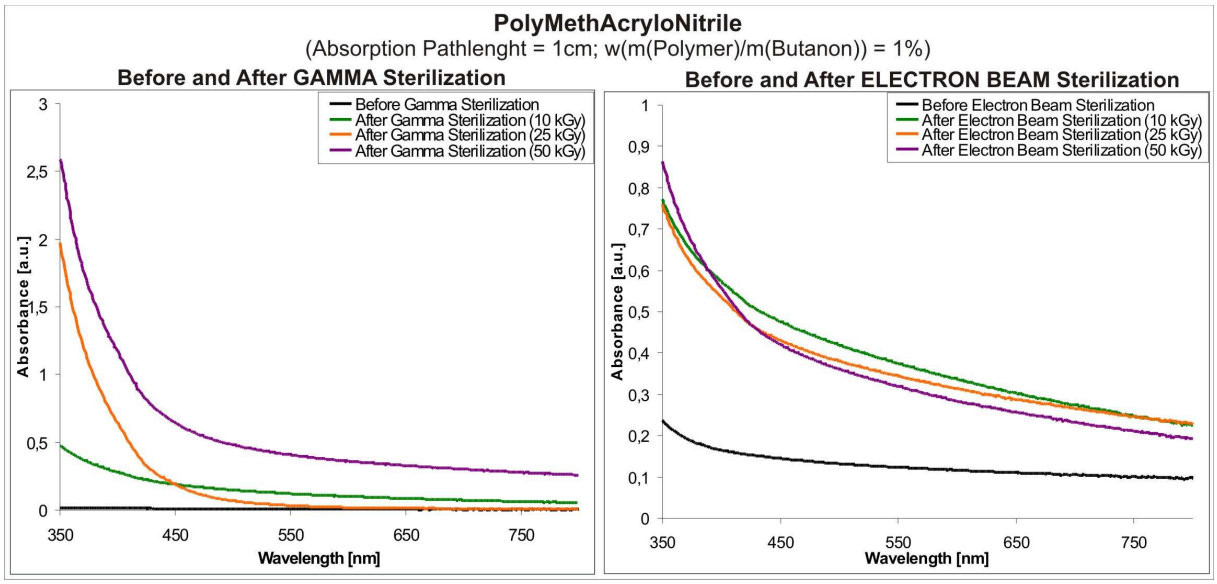

Figure 5 – 29: Absorption spectra of the polymer PMAN before and after gamma and electron beam sterilization.

However, all polymers PS-co-PAN, PVC-co-PAN and PMAN possess the cyano group in the structure. During irradiation this group could dissociate from the polymer main-chain and form a radical, which could additionally reacted and altered the characteristics of it. Additionally, the PVC-co-PAN contains chlorine and the radiation sterilization could also induce the cleavage of the chlorine atom, which also represent the danger for alterations of indicator structure.

The gamma and electron beam irradiation of the indicator Eu(III) complex in the solid state and in solution caused the alterations. The sterilization of Eu(III) complex with gamma and

electron beam led to reduction of the Eu(III) to Eu(II). However, the complex between the europium atom and ligand did not dissociate. On the other hand, when the same indicator was sterilized in the solution, where the solvent was toluene, more alterations appeared. The Eu(III) complex was also reduced and simultaneously the dissociation between $Eu(tta)_3$ complex and ligand DEADIT appeared. Figure 5 – 30 shows the alterations in the absorption and emission spectra of the indicator $Eu(tta)_3$DEADIT gamma sterilized in solid state and as solution.

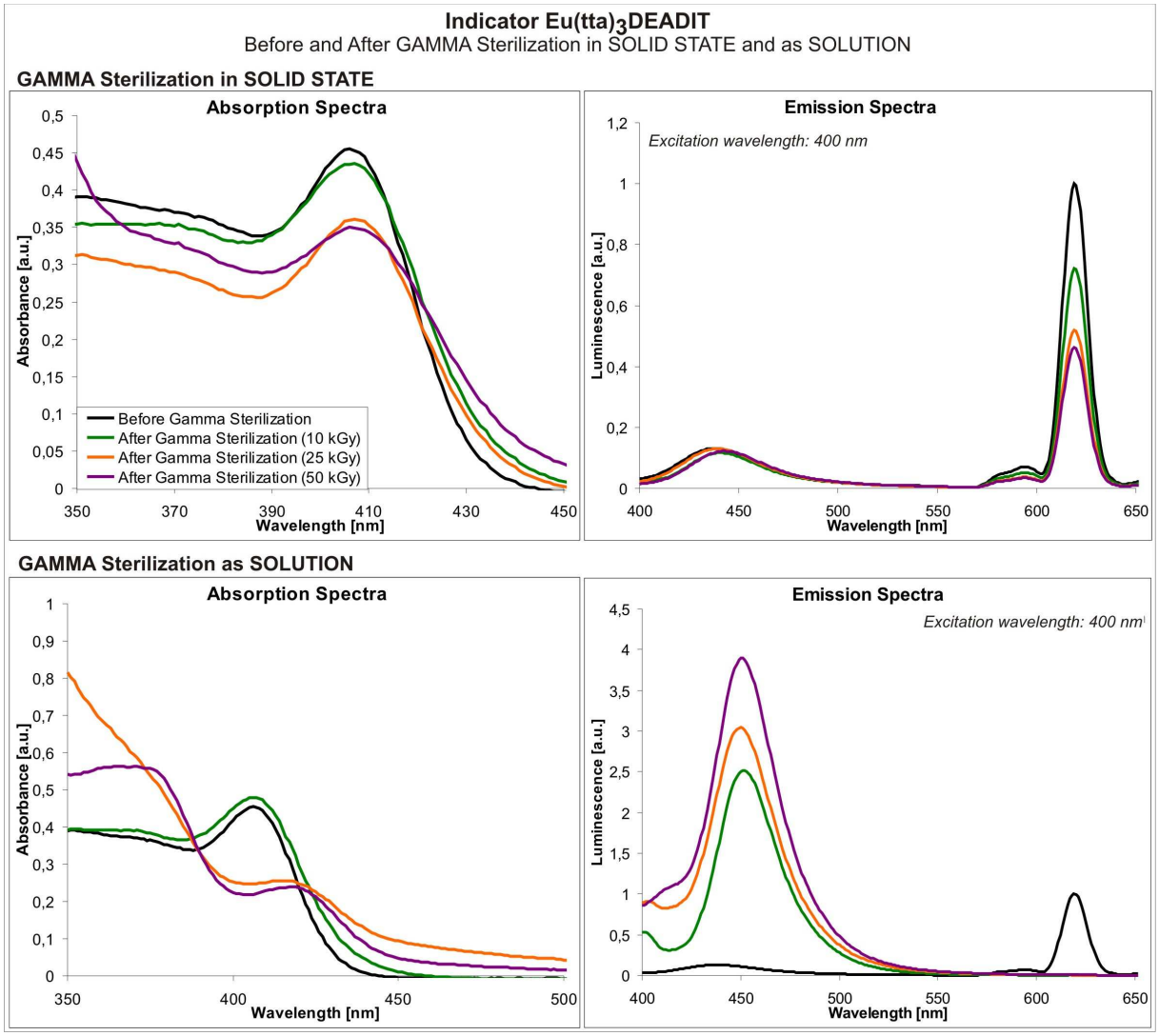

Figure 5 – 30: Absorption spectra of the indicator $Eu(tta)_3$DEADIT gamma sterilized in solid state and as solution.

When the same indicator $Eu(tta)_3$DEADIT was immobilized in the polymer matrix made of PS-co-PAN, the indicator was similar affected as when radiation sterilized in solid state. In the absorption spectra was observed that the Eu(III) complex was reduced to Eu(II). However, the electron beam has lower affect on the indicator as gamma rays and the sensitivity of the sensor toward temperature remained the same. The absorption spectra and calibration curved of temperature sensor made of PS-co-PAN and $Eu(tta)_3$DEADIT are presented in figure 5 – 31.

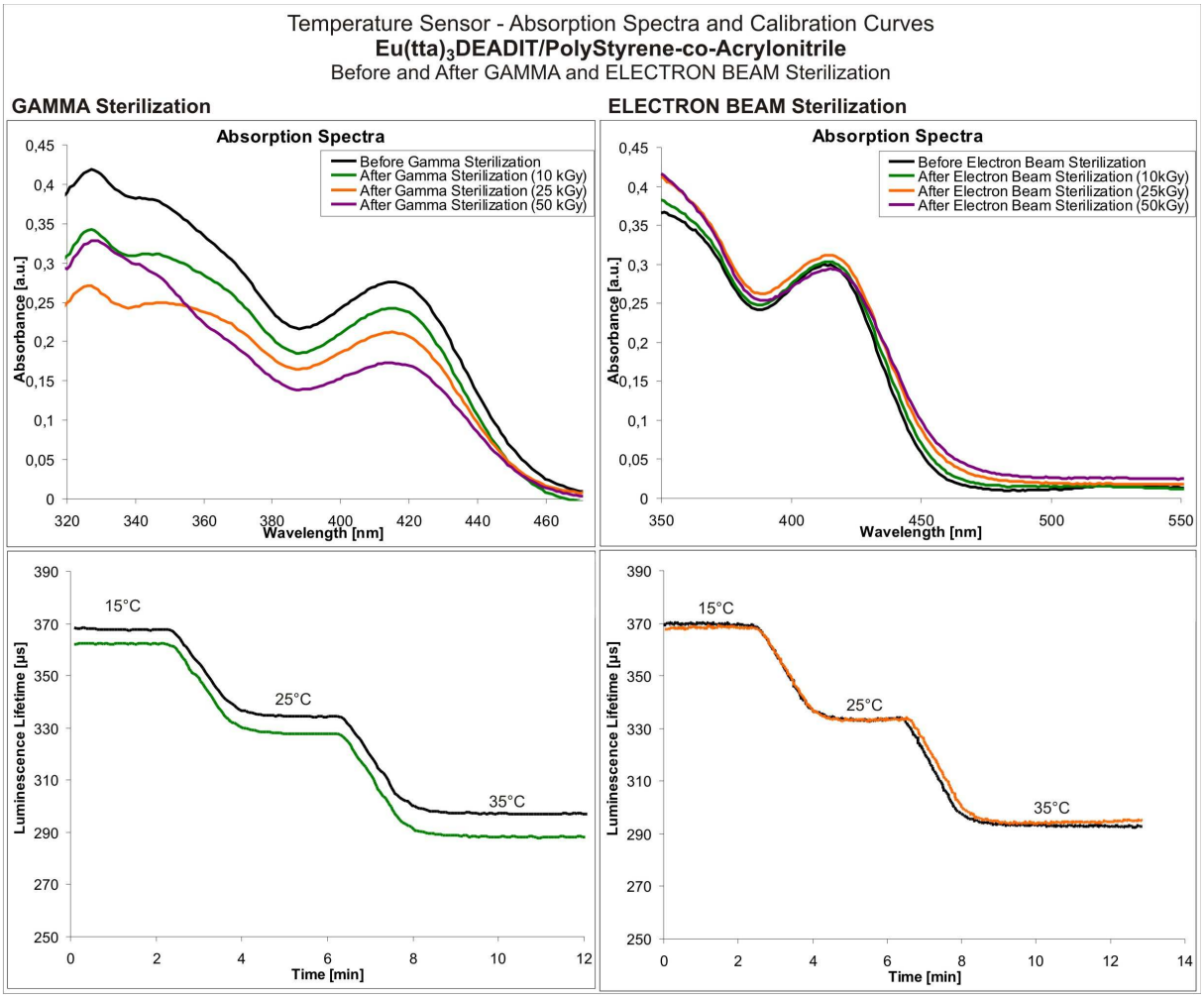

Figure 5 – 31: Absorption spectra and calibration curves of temperature sensor made of indicator Eu(tta)$_3$DEADIT and immobilized in polymer PS-co-PAN before and after gamma and electron beam sterilization.

The radiation sterilization of temperature sensors made of Eu(III) complex and polymer PVC-co-PAN and PMAN induce greater alterations in the absorption, emission spectra and sensor response. The gamma rays and electron beam reduce the Eu(III) complex, the cleavage of the chlorine atom in polymer matrix made on PVC-co-PAN and the dissociation between Eu(tta)$_3$ complex and ligand DEADIT appeared. Therefore, the polymer matrices PVC-co-PAN and PMAN are not appropriate for the temperature sensors with indicator Eu(tta)$_3$DEADIT when they should be radiation sterilizied.

The temperature sensitive indicator dichlorotris(1,10-phenanthroline)ruthenium(II) hydrate remained stable after sterilization with the gamma rays when sterilized in solid state. On the other hand, the electron beam sterilization with doses higher than 25 kGy caused the ligand dissociation due to the appearance of new absorption peak in the absorption and emission spectra. However, when the ruthenium(II) complex was immobilized in polymer PVC-co-PAN, the temperature sensors was resistant to gamma and electron beam sterilization. Hence, the sterilization of temperature sensors made of the same indicator and immobilized in PMAN also induce the dissociation of the ligand by the indicator because the changes were observed in absorption, emission and calibration curve after gamma and electron beam sterilization. Figure 5 – 32 shows the absorption and emission spectra of indicator rutheinum(II) complex, electron beam sterilized in solid state and when immobilized in polymers PVC-co-PAN and PMAN.

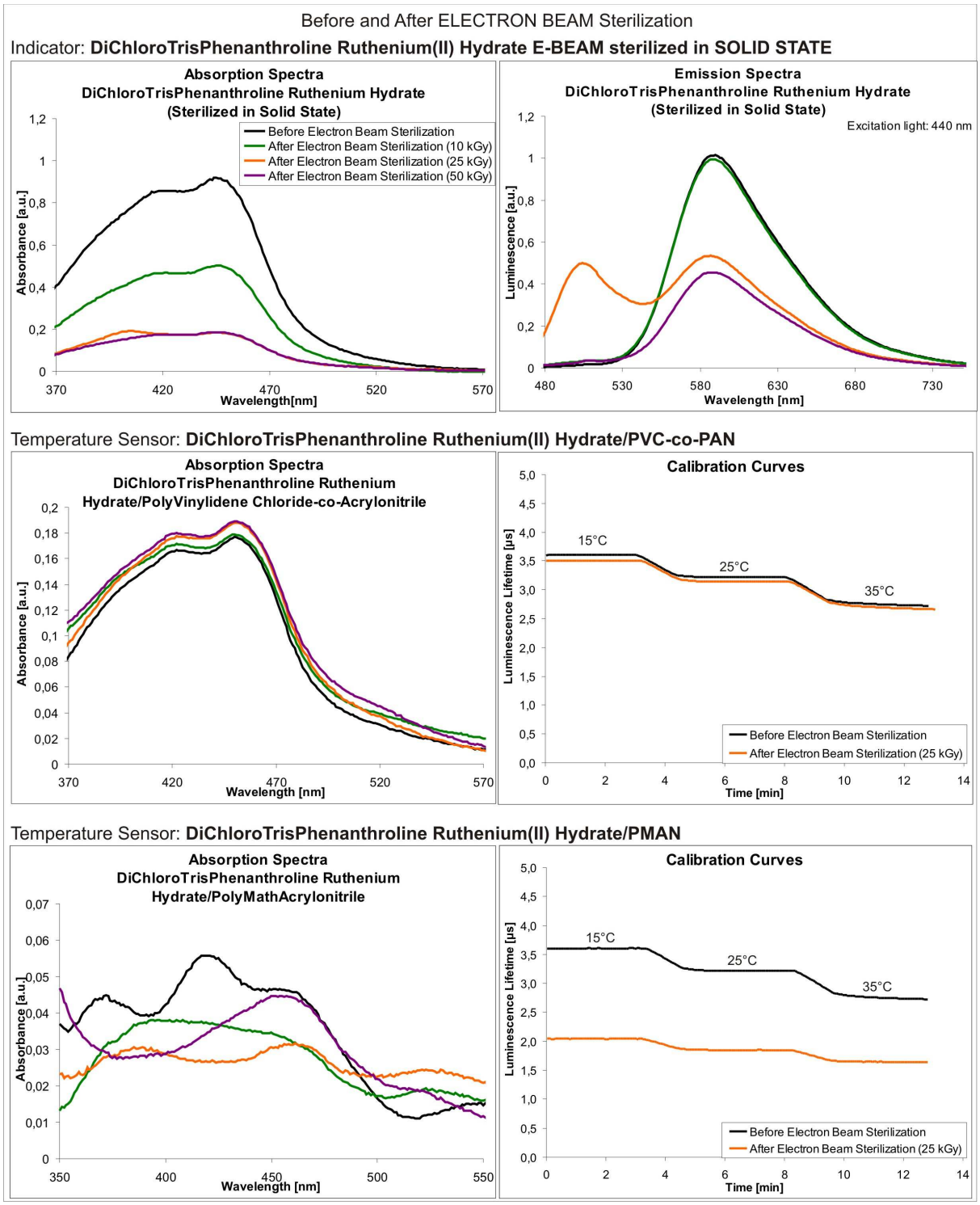

Figure 5 – 32: Absorption and emission spectra of indicator rutheinum(II) complex, electron beam sterilized in solid state and absorption spectra and calibration curves when immobilized in polymers PVC-co-PAN and PMAN.

5.4 Radiation Sterilization of Optical Ammonia Sensors

The optical ammonia sensors based on the principle of pH measurement. A pH indicator is entrapped by a gas-permeable membrane. The ammonia penetrating causes a change of pH

that results in a colour or fluorescence change of the indicator dye. Hence, fluorescent pH indicator eosin ethylester with of pK_a value of 3.8 and dichlorofluorescein having a higher pK_a value of 4.5 and bromophenol blue are often used and they were also applied and sterilized in this study. The ratio of the protonated to deprotonated form of the indicator is a function of ammonia concentration which can be deduced by measuring absorption or fluorescence at an appropriate wavelength.

The polymer matrix used for developments of optical ammonia sensors were cellulose materials; cellulose acetate (CA) and ethyl cellulose (EC), polymethyl methacrylate (PMMA) and HydroMed^{TM} hydrogel D7. The exposure of cellulose materials to ionizing radiation induced some degradation. The frequently chemical degradation mechanism of cellulose materials is reaction of deacetylation, during which hydroxyl groups replace acetate groups on the cellulose ring with the evaluation of the acetic acid. Simultaneously to the deacetylation, the chain-scission takes place. The chain-scission was determined with the differential scanning calorimetry (DSC) measurements of glass transition temperature of the polymer ethyl cellulose. The chain-scission involves the separation of the intermolecular connections. This increase the chain mobility and consequently, the T_g of polymer decrease. The results of the DSC measurements before and after gamma sterilization of polymer EC were already shown in table 5 – 1. The alterations after gamma and electron beam radiation of the sensors made of cellulose materials have different impact on the absorption/emission capabilities and sensor respond.

The irradiation of polymer PMMA also led to chain-scission. However, the decrease of the T_g was not observed by DSC measurements. Therefore, irradiation with lower doses than 50 kGy did not have influence on this type of polymer. Contrary, after gamma and electron beam sterilization with dose 50 kGy of polymer HydroMed^{TM} hydrogel D7, cross-linking appeared. This was determined due to the decreased solubility and appearance of the swollen gel after solubility test.

The indicators by optical ammonia sensors respond different to ionizing radiation. The eosin ethylester was resistant to electron beam sterilization in the solid state. On the other hand, the gamma rays have greater impact on indicator structure. The decrease of the emission intensity for approximately 80% was observed already after gamma sterilization with dose 10 kGy. Probably, during gamma irradiation, the indicator residues act as the quenchers, which decreased the emission intensity. However, the absorption was comparable before and after sterilization. The absorption and emission spectra of the indicator eosin ethylester after gamma sterilization in the solid state are presented in figure 5 – 33.

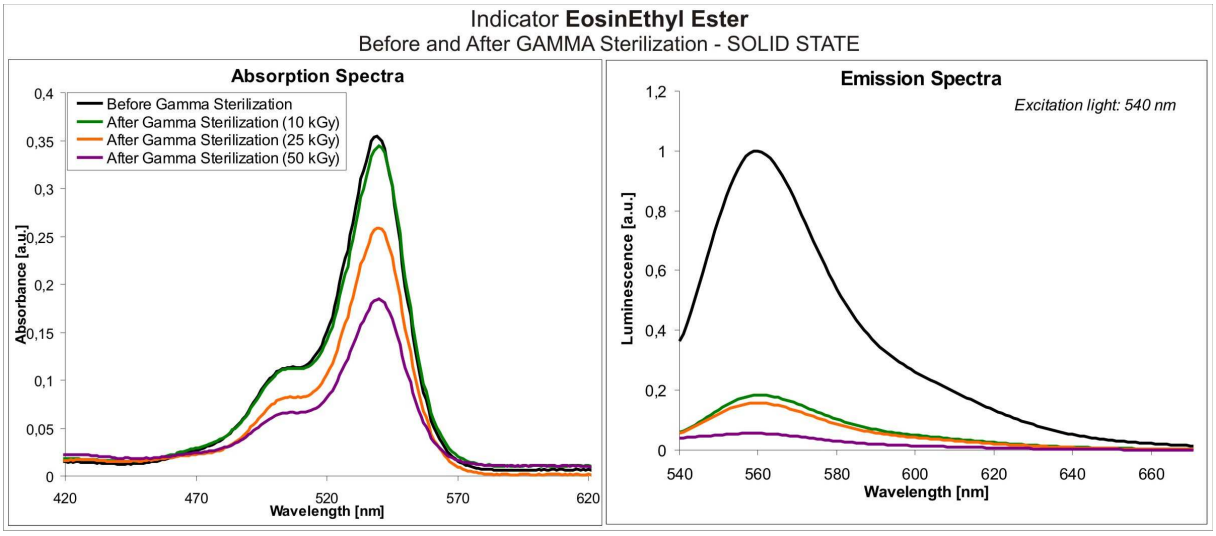

Figure 5 – 33: Absorption and emission spectra of indicator eosin ethylester before and after gamma sterilization in the solid state.

Similar impact as the radiation sterilization of indicator eosin ethylester in solid state have gamma rays and electron beam on sensors made of this indicator and immobilized in diverse polymer matrices. The absorption was not affected, but decrease for more than 50% of the emission intensity was observed by all polymer matrices with exception of PMMA. Therefore, the quenchers of indicator eosin ethylester were formed after radiation sterilization and the de-excitation of excited state occur without emission of the photons. The absorption and emission spectra of the ammonia sensor made of eosinethyl ester and immobilized in polymer hydrogel D7 are presented in figure 5 – 34.

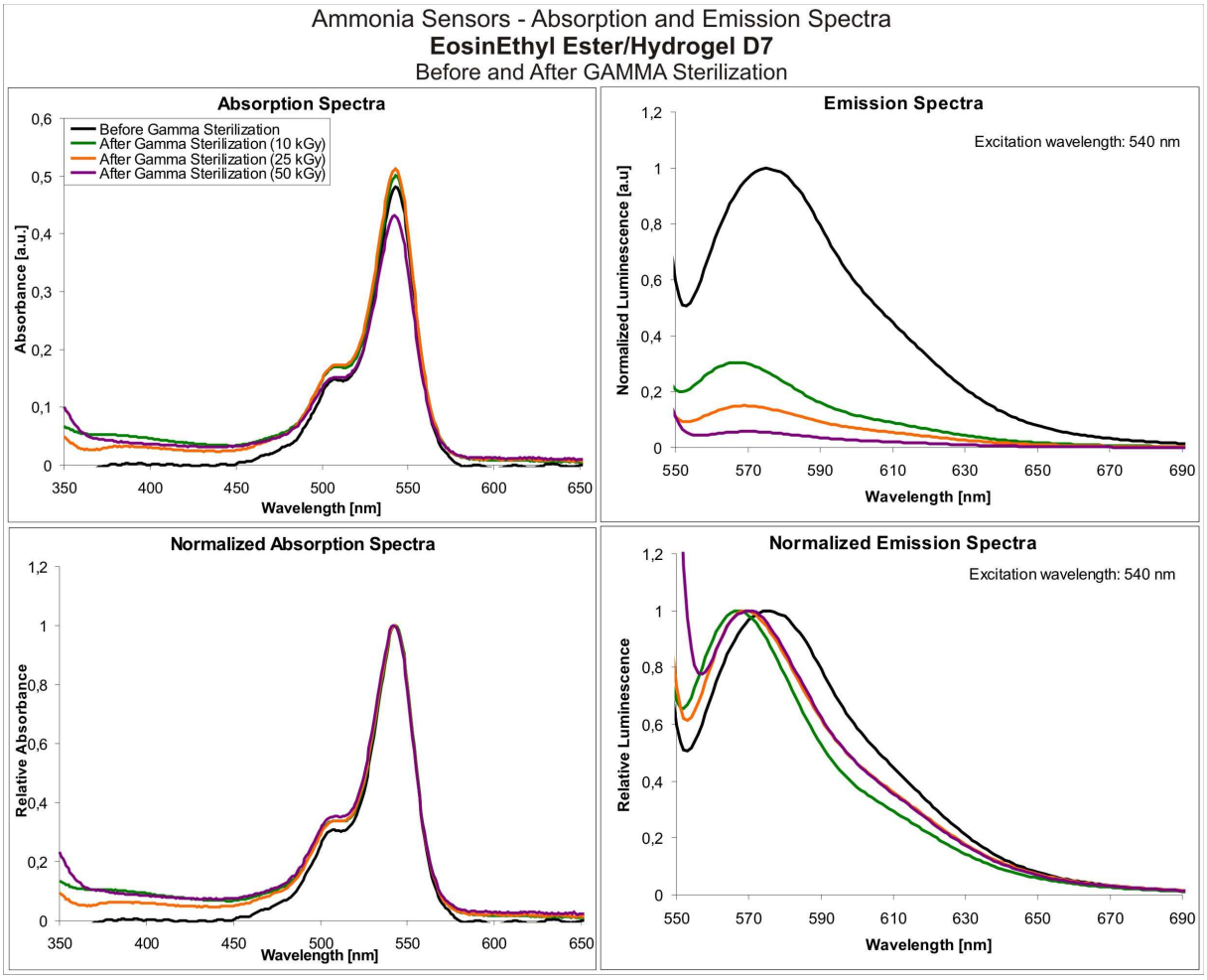

Figure 5 – 34: Absorption and emission spectra of ammonia sensor made of indicator eosin ethylester and immobilized in polymer hydrogel D7 before and after gamma sterilization.

Additionally, the hypsochromic shift of the emission maximum was observed after sterilization of the sensor with indicator eosinethyl ester and hydrogel D7, which is also shown in figure 5 – 34. Consequently, the polarity of the polymer matrix was altered after radiation sterilization or because the hydrogel D7 contains both hydrophilic and hydrophobic parts, the irradiation induced the changes in the position of the indicator in the polymer matrix. This effect was observed as solvatochromic shift in the emission maximum. The solvatochromic shift of the emission maximum was also detected after sterilization of the ammonia sensor made of cellulose acetate, where the polarity of this polymer matrix was slightly changed after radiation sterilization.

The other two indicators utilized for development of ammonia sensors, dichlorofluorescein and bromophenol blue, were unaffected when gamma and electron beam sterilized in the solid state. Contrary, all indicators were destroyed after radiation sterilization of indicator solutions, where the solvent was ethanol or water. Figure 5 – 35 shows the absorption

spectra of dichlorofluorescein and bromophenol blue after electron beam sterilization in solid state and solution.

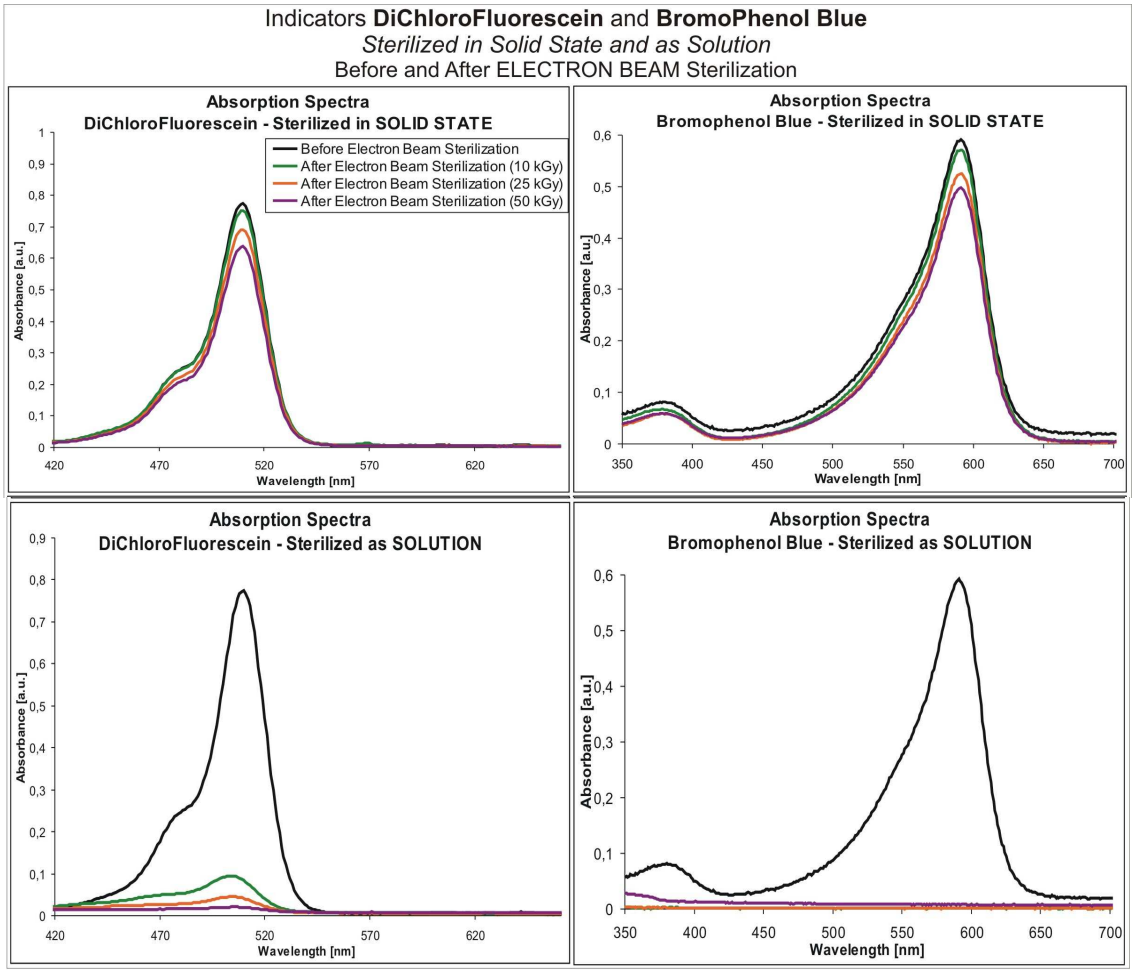

Figure 5 – 35: Absorption spectra of indicators dichlorofluorescein and bromophenol blue before and after electron beam sterilization in solid state and as solution.

The absorption capabilities of ammonia sensors made of indicator dichlorofluorescein and immobilized in diverse polymer matrices were similar before and after radiation sterilization. However, the emission intensity decreased also by this type of indicator. Probably, indicator dichlorofluorescein was reduced after irradiation due to reduction capabilities of electron beam and gamma rays and that could have influence on emission intensity. Consequently, the electron beam has more reduction capabilities as gamma rays. Therefore, greater decrease (for about 50%) and more alterations were observed after electron beam than gamma sterilization procedure. The example, shown in figure 5 – 36, is ammonia sensor made of indicator dichlorofluorescein and immobilized in polymer ethyl cellulose.

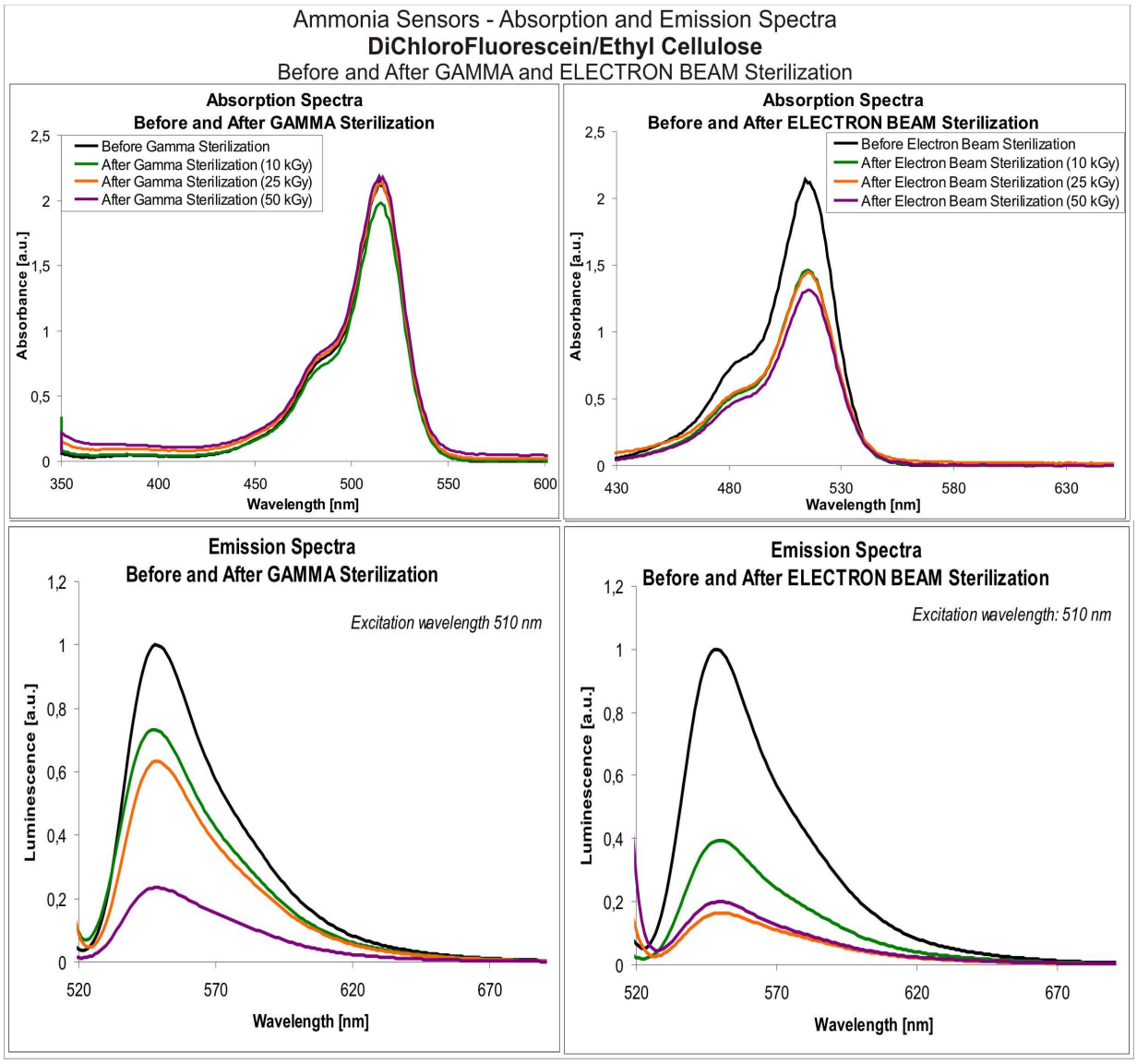

Figure 5 – 36: Absorption and emission spectra of ammonia sensor made of indicator dichlorofluorescein and immobilized in polymer EC before and after gamma and electron beam sterilization.

The indicator bromophenol blue immobilized in all polymer matrices applied in the study for ammonia sensors, was very resistant to radiation sterilization. The absorption curve forms remained the same and consequently, no reactions appeared that would have influence on the sensor response.

6 Steam Sterilization

Sterilization with saturated steam is the method that provides the best combination of flexibility in operation, safe results and low plant and running costs. In the science of sterilization, one of the considerations is the rate of material degradation relative to the rate of biological inactivation. Hence, steam sterilization demonstrates broad-spectrum antimicrobial activity and has a significant safety factor built into them to ensure lethality. However, steam sterilization is not suitable for temperature- or pressure- sensitive materials. In some cases, despite their resistance to heat, some materials may demonstrate stress cracking, turbidity, interferences or other effects after single or repeated steam sterilization and drying cycles.

In this study, the materials utilized by development of optical sensors were steam sterilized in autoclave and characterized afterwards. All results are gathered and presented in a database:

- *Section D – Steam sterilization of optical sensors*

Important and interesting results are discussed and shown in following chapters.

6.1 Steam Sterilization of Optical Oxygen Sensors

The number of polymers which can tolerate the high temperature and moisture of steam sterilization are limited. Therefore, the alterations were observed on the polymers applied in this study for the optical oxygen sensors. Among them were cellulose materials and Hydrothane™, which became turbid after sterilization method at 121ºC. To define, turbidity is the optical property that causes light to be scattered and absorbed rather than transmitted in straight lines through the sample [128]. Therefore, the turbidity of polymer was observed as the increase of the absorbance and that is presented in figure 6 – 1.

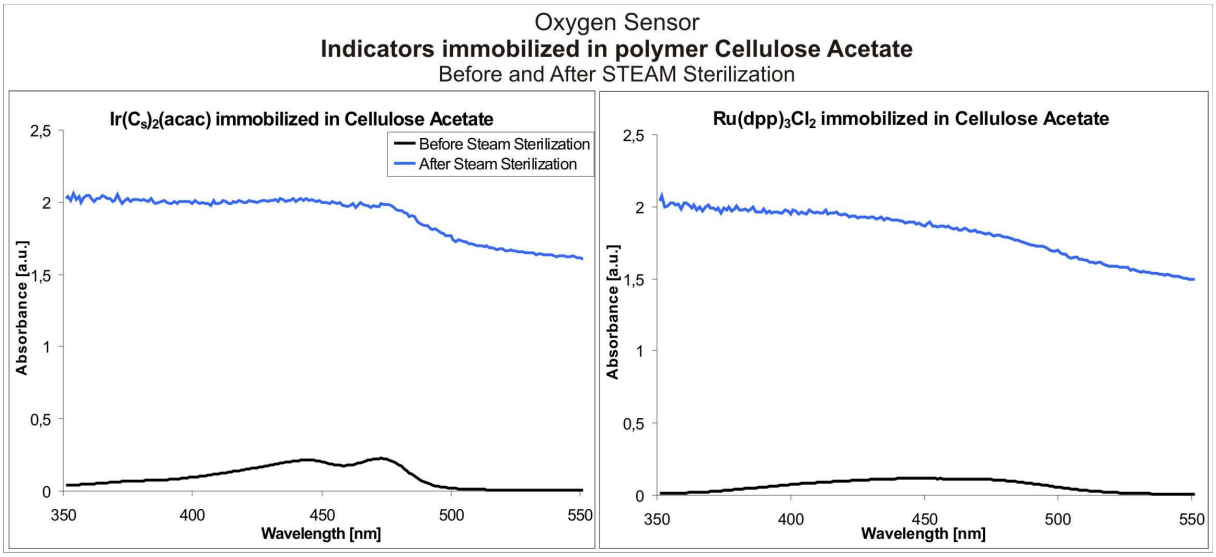

Figure 6 – 1: Absorption spectra of oxygen sensors made of indicators $Ir(C_s)_2(acac)$ and $Ru(dpp)_3Cl_2$ and immobilized in polymer CA before and after steam sterilization.

The response and luminescence lifetime of the oxygen sensors that became turbid were lower or changed after steam sterilization, but the response to the different concentrations of oxygen was still observed. However, before application, the sensors should be re-calibrated after steam sterilization. Figure 6 – 2 shows the calibration curves of the oxygen sensors which became turbid after steam sterilization.

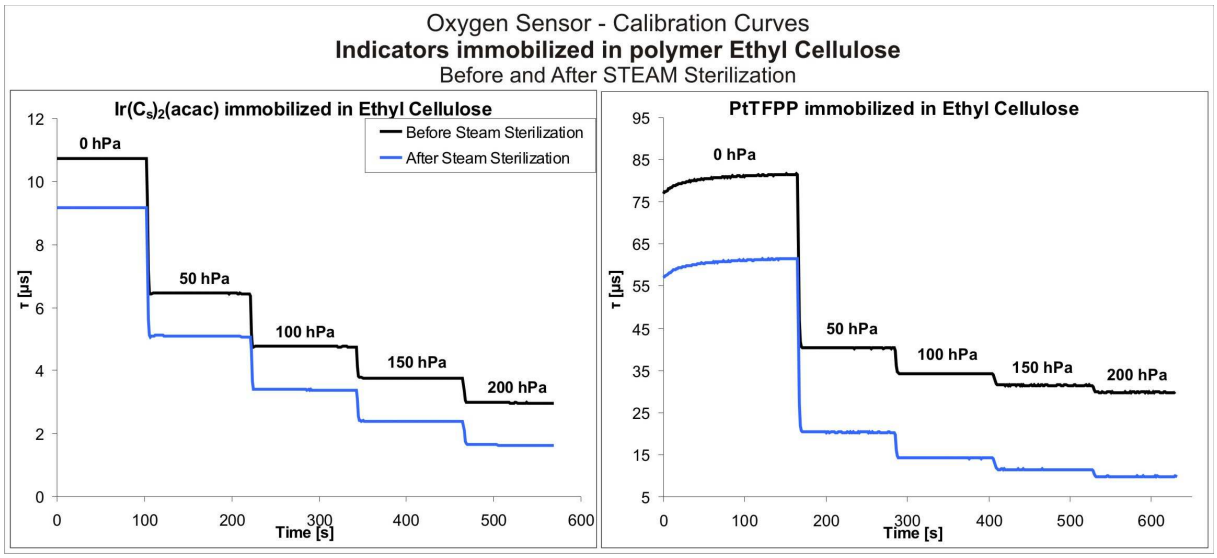

Figure 6 – 2: Calibration curves of oxygen sensors made of indicators $Ir(C_s)_2(acac)$ and PtTFPP and immobilized in polymer EC before and after steam sterilization.

The most affected by steam were oxygen sensors made of polymer PPSQ. The absorption spectra were altered and the response of the sensor, where the indicator was PtTFPP was no longer observed. By other indicators, the sensor response was changed after steam sterilization. According to the literature, the PPSQ polymer is very resistant to high temperatures. However, the moist could have affect on the polymer structure and the hydrolysis of Si-O-Si bond could appear [82]. The absorption spectra and calibration curves of the oxygen sensor made of polymer PPSQ and indicator PtTFPP is presented in figure 6 – 3.

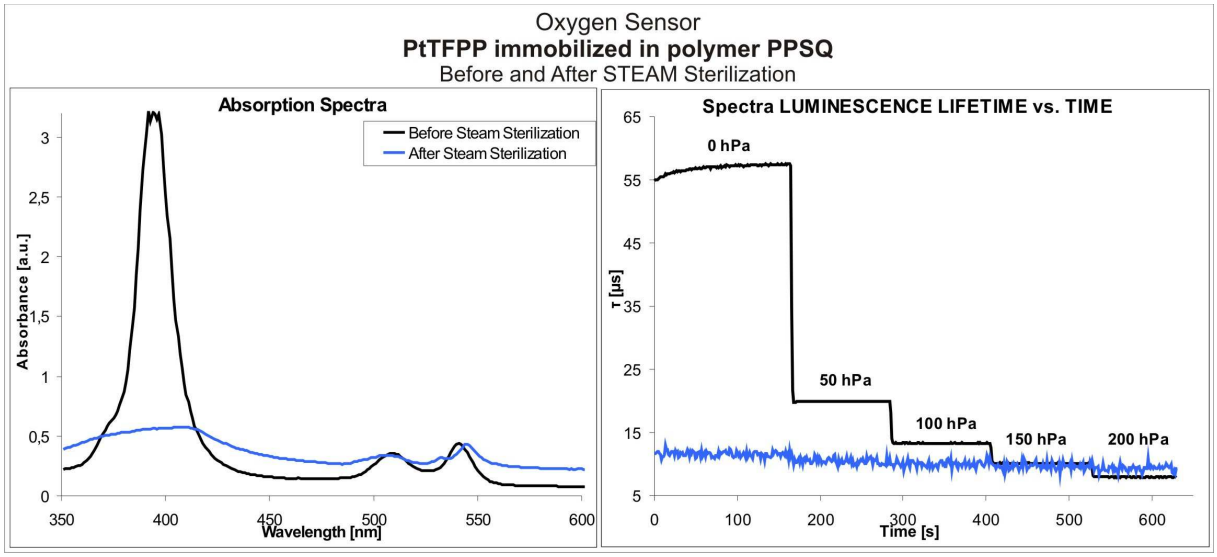

Figure 6 – 3: Absorption spectra and calibration curves of oxygen sensor made of indicator PtTFPP and immobilized in polymer PPSQ before and after steam sterilization.

The oxygen sensors made of indicators $Ir(C_s)_2(acac)$ and PtTFPP and polymers polystyrenes, polysulfone and hydrogel D4 were quite stable and resistant to steam

sterilization. However, small alterations were observed in the spectra and calibration curves. Therefore, before utilization the sensors should be re-calibrated. By the oxygen sensors made of the indicator $Ru(dpp)_3Cl_2$, more alterations were induced when this indicator was immobilized in polystyrene matrices. After steam sterilization of indicator $Ru(dpp)_3Cl_2$ immobilized in PS, the bathochromic shift of the emission spectra was observed and the response of the sensor was altered. When the same indicator was immobilized in PS-co-PAN and PSMA, the increase in the absorption was measured and typical curve form was no longer observed. Therefore, when the sensors are made of ruthenium(III) complex and immobilized in polystyrene matrices, they should not be sterilized with steam. The calibration curves of the oxygen sensor made of indicator $Ru(dpp)_3Cl_2$ and immobilized in PS and the absorption spectra, when immobilized in PS-co-PAN and PSMA are presented in figures 6 – 4 and 6 – 5.

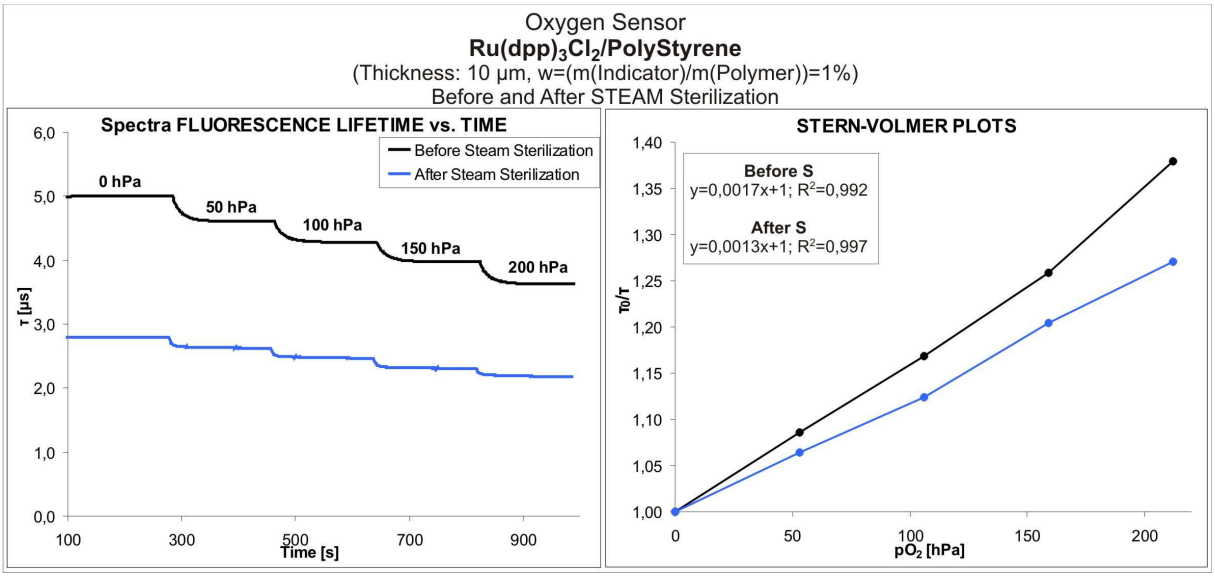

Figure 6 – 4: Calibration curves and Stern-Volmer plots of oxygen sensor made of indicators $Ru(dpp)_3Cl_2$ and immobilized in polymer PS before and after steam sterilization.

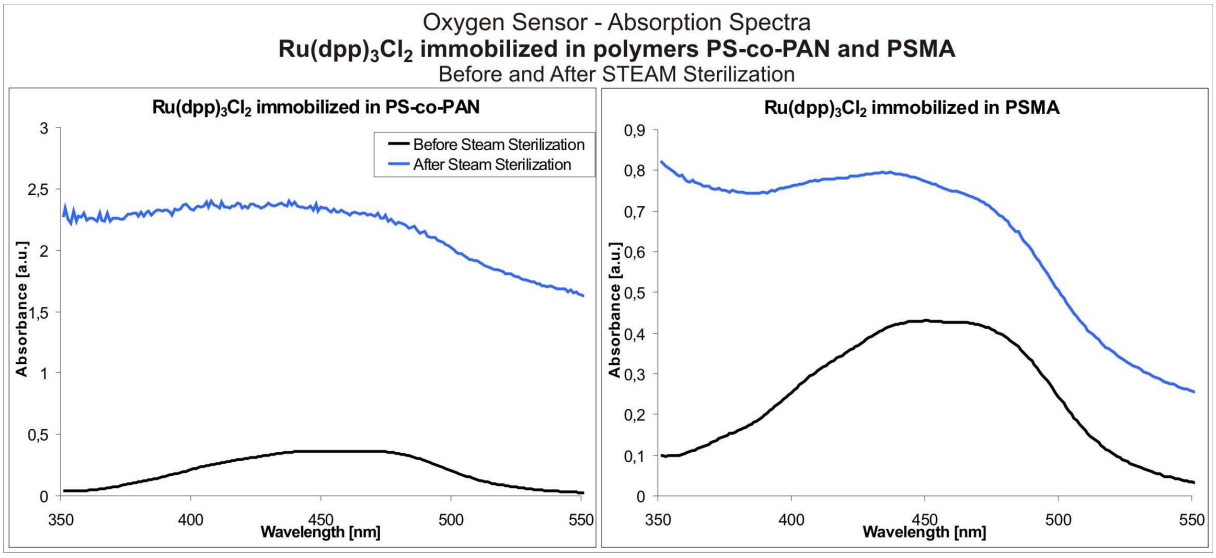

Figure 6 – 5: Absorption spectra of oxygen sensors made of indicators $Ru(dpp)_3Cl_2$ and immobilized in polymers PS-co-PAN and PSMA before and after steam sterilization.

6.2 Steam Sterilization of Optical pH Sensors

By steam sterilization the materials are exposed to harsh conditions such as heat, pressure and humidity. Hence, this sterilization procedure has a great impact on the polymer materials. The polymer matrices used by optical pH sensors were HydroMed^{TM} hydrogel D4 and Poly(2-Hydroxyethyl methacrylate)(pHEMA). The hydrogel D4 matrix became slightly turbid after steam sterilization, which was observed in the absorption spectra (figure 6 – 6).

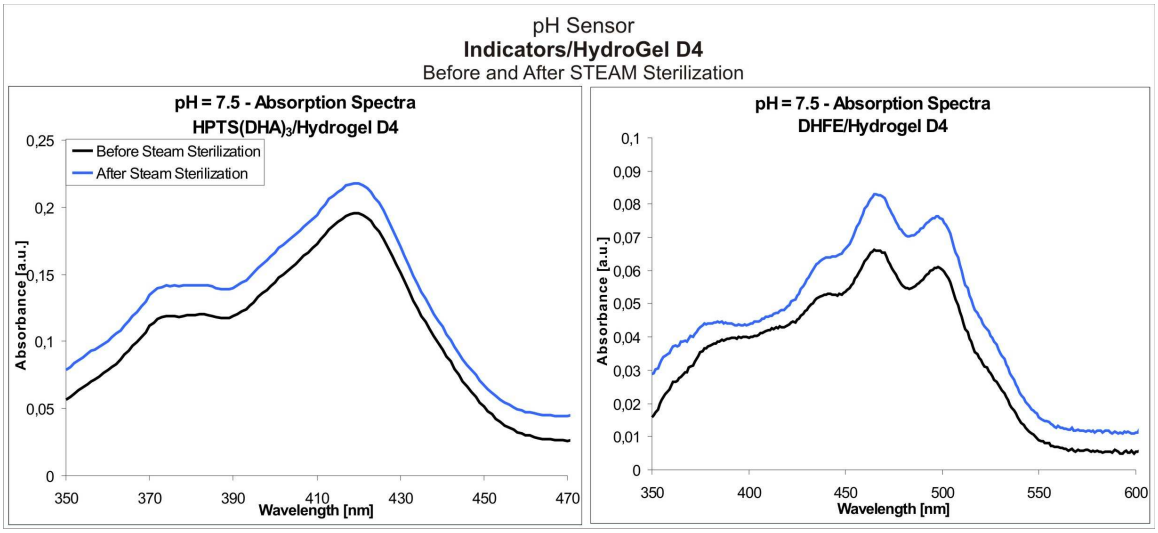

Figure 6 – 6: Absorption spectra of the pH sensors made of polymer hydrogel D4, which became turbid after steam sterilization.

The hydrogel D4 is a block copolymer containing both hydrophilic and hydrophobic domains. Steam sterilization had an influence on the orientation of these domains and the refractive index could be altered. Likewise, a slight melting of polymer was detected and therefore the inhomogeneities in the sensor layer could appear after the application of steam. On the other hand, pHEMA completely melts after applications of temperatures of 121ºC and steam. Consequently, steam sterilization is not an appropriate method for sensors, where the polymer matrix is made of the polymer pHEMA.

Although the polymer hydrogel D4 became turbid after sterilization, the shapes of the absorption and emission curves were comparable before and after sterilization. However, some alterations in the ratio between protonation and deprotonation absorption and emission peaks were observed. Therefore, steam has also an influence on the polymer permeability for the proton to the hydroxyl group of the indicator and the velocity of the protonation and deprotonation of the indicator was altered after steam sterilization. The alterations in the protonation/deprotonation ratio were observed by pH sensors made of the indicators HPTS(DHA)$_3$ and pH sensitive coumarin and are shown in figure 6 – 7.

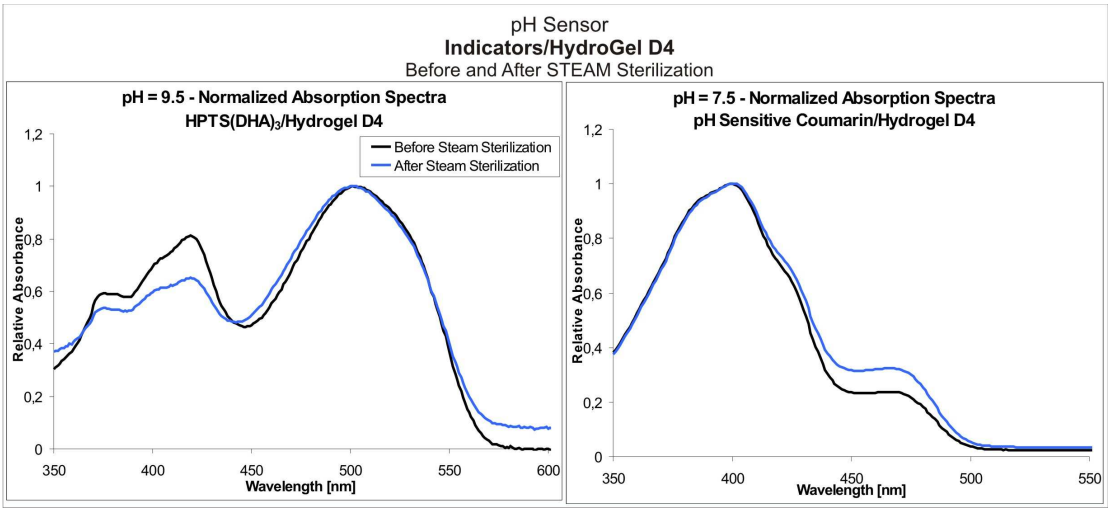

Figure 6 – 7: Absorption spectra of pH sensor made of indicators HPTS(DHA)$_3$ and pH sensitive coumarin and immobilized in polymer hydrogel D4 before and after steam sterilization.

When the PET Perylene bisimide was immobilized in hydrogel D4 and sterilized with steam, the indicator has migrated into the Mylar® support foil. The indicator PET Perylene bisimide is highly lipophilic and therefore the indicator has the tendency to migrate to more lipophilic polymer. At high temperatures the Mylar® became softer which accelerated this migration. Consequently, the pH sensitivity of PET Perylene bisimide was no longer observable and the fluorescence intensity increased after steam sterilization. The effects of the steam sterilization method on the indicator PET Perylene bisimide immobilized in the polymer matrix hydrogel D4 are presented in figure 6 – 8.

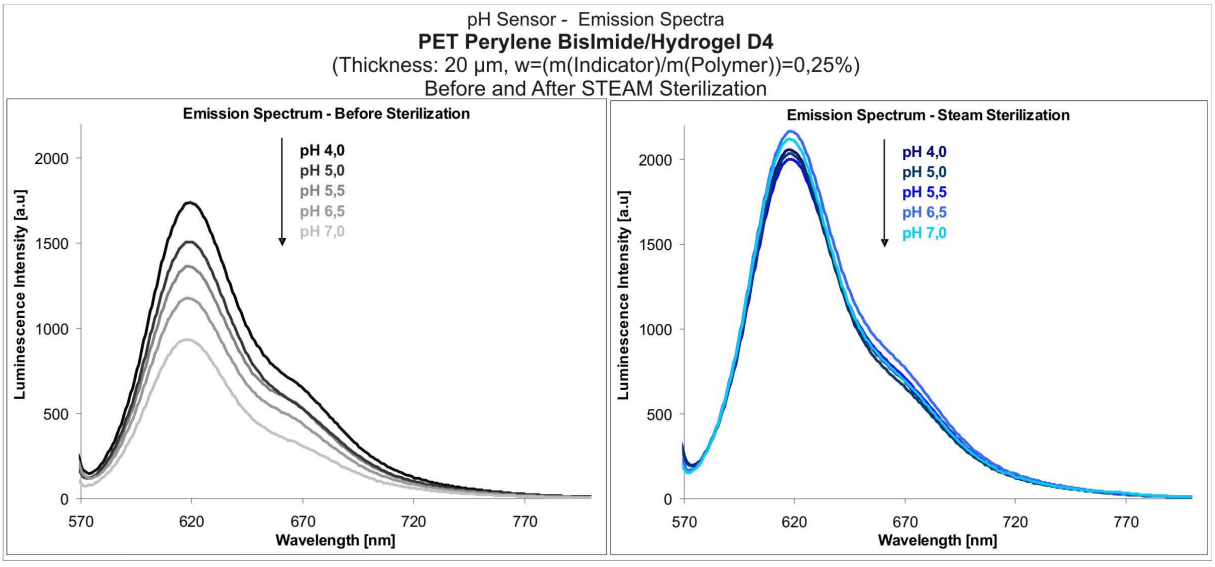

Figure 6 – 8: Emission spectra of pH sensor made of indicator PET Perylene bisimide and immobilized in polymer hydrogel D4 before and after steam sterilization.

The sulfonephthalein pH sensitive indicators immobilized in hydrogel D4 are less resistant to steam sterilization than to radiation sterilization methods. The decrease of the absorption was observed by all types of sensors. However, these decreases were not uniform when characterized in acid and base environment. Possibly, the slight melting of the polymer hydrogel D4 after the application of steam at 121ºC induced inhomogeneous parts in the sensor layer. Therefore, the sensor's parts for characterization could differ in acid and base environment and also before and after steam sterilization. Consequently, the dissimilar decreases of the absorption were observed. Figure 6 – 9 shows the inhomogeneous

decreases in absorption by the sulfonephthalein pH sensitive indicator thymol blue immobilized in the polymer hydrogel D4 after steam sterilization.

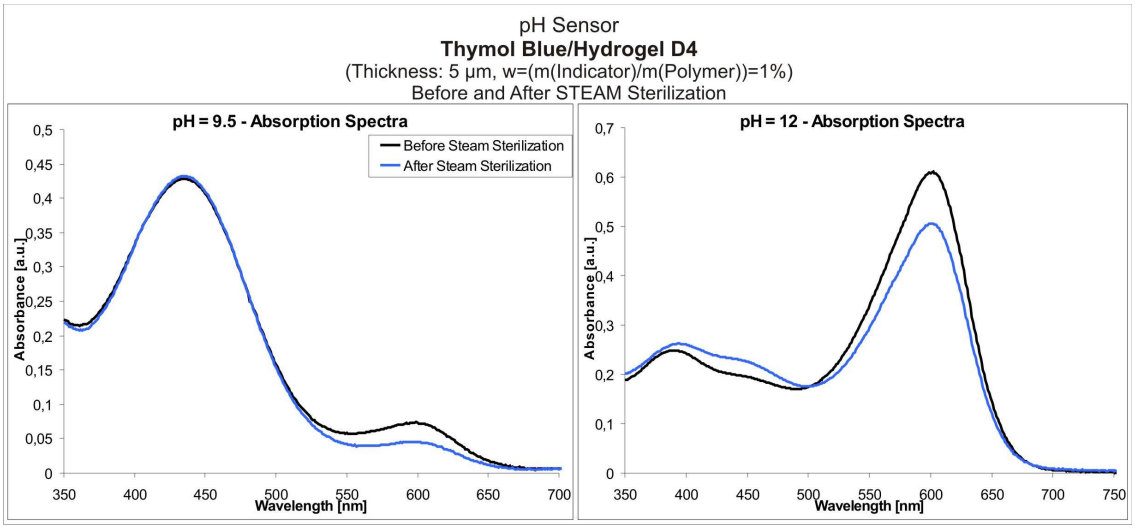

Figure 6 – 9: Absorption spectra of pH sensor made of indicator thymol blue and immobilized in polymer hydrogel D4 before and after steam sterilization.

Steam sterilization is also an inappropriate sterilization method for the azo pH sensitive dye methyl orange because the characteristic curve form was no longer observed after steam sterilization. The absorption spectra of methyl orange before and after steam sterilization are presented in figure 6 – 10.

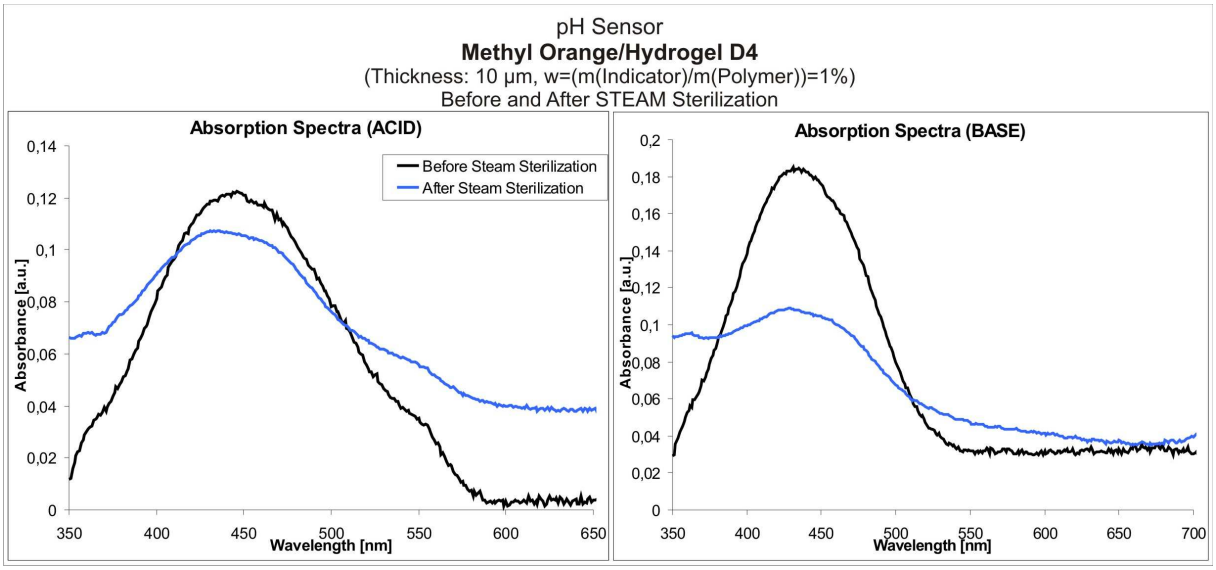

Figure 6 – 10: Absorption spectra of pH sensor made of indicator methyl orange and immobilized in polymer hydrogel D4 before and after steam sterilization.

6.3 Steam Sterilization of Optical Temperature Sensors

All polymers applied for the development of optical temperature sensors, in this study, became turbid after steam sterilization at 121ºC for 15 min. Figure 6 – 11 presents the increase of absorption, what is evidence for turbidity of the polymer matrix, by all temperature sensors made with the indicator dichlorotrisphenanthroline ruthenium(II) hydrate.

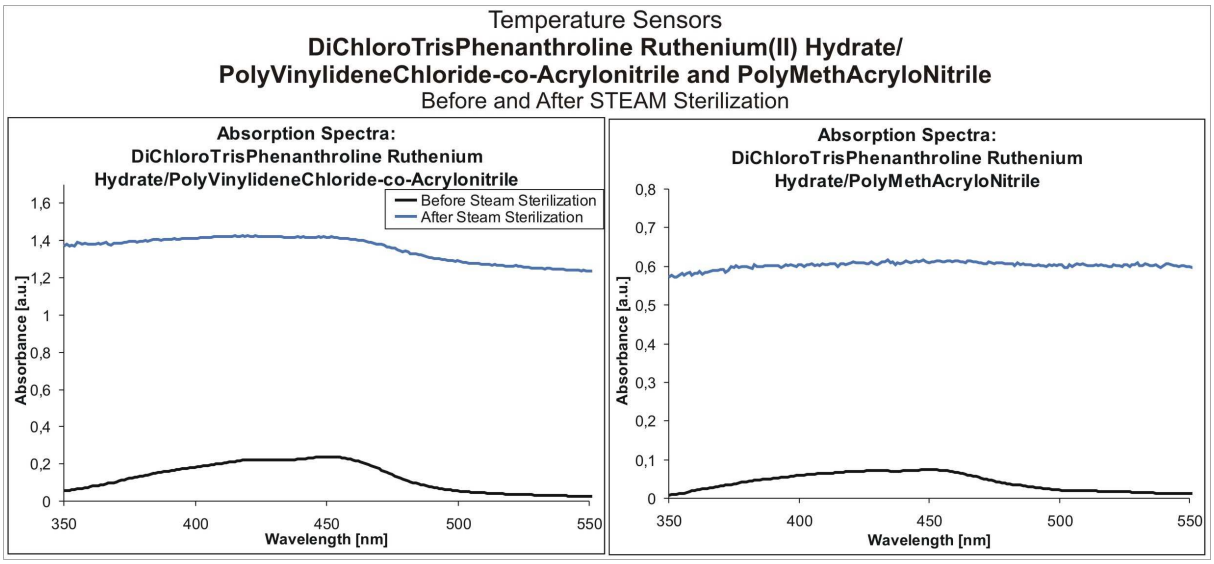

Figure 6 – 11: Absorption spectra of temperature sensor made of indicator ruthenium(II) complex and immobilized in polymers PVC-co-PAN and PMAN before and after steam sterilization.

However, the sensor emission intensity and response were not greatly altered with the exception of temperature sensors made of the Eu(III) complex and the polymer PVC-co-PAN, where the emission and the response of the sensor were no longer observed after steam sterilization. When the temperature sensors were made of the polymer PMAN, the luminescence lifetime decreased after steam sterilization due to induced hydrolysis. On the other hand, the response and emission remained similar by other temperature sensors and although the polymers became turbid after steam sterilization, the sensors with re-calibration of its respond could still be utilized. The calibration curves and emission spectra of the temperature sensors after steam sterilization are presented in figures 6 – 12 and 6 – 13.

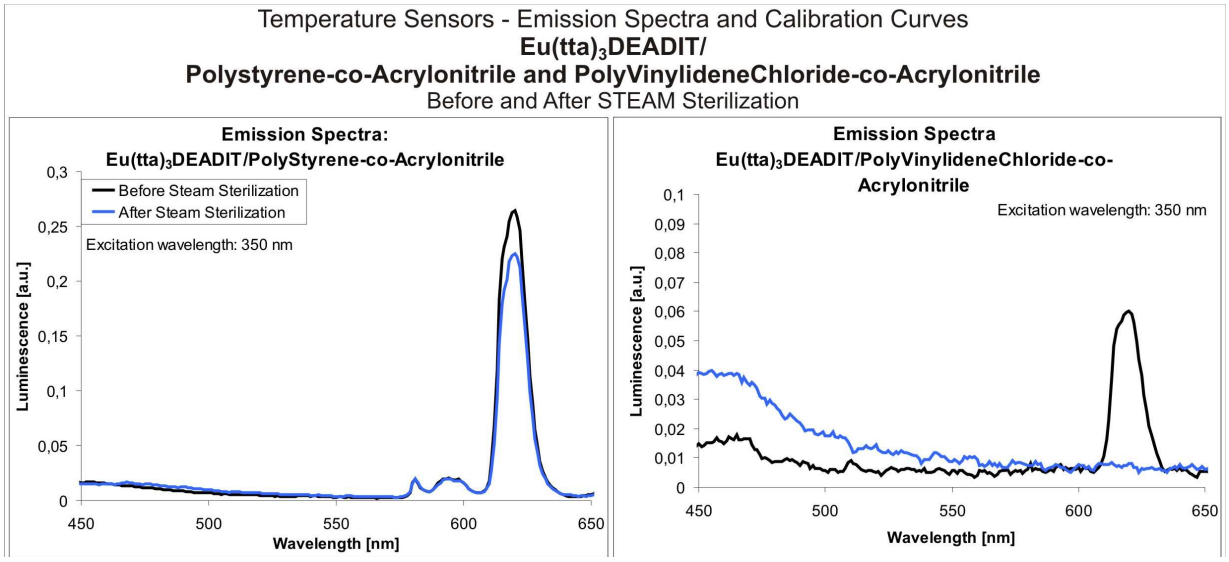

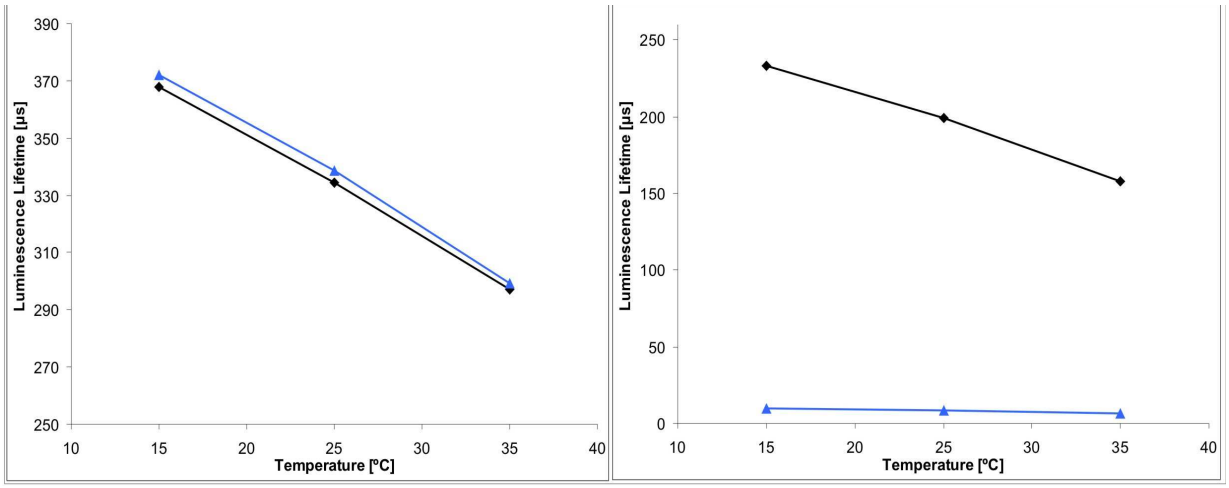

Figure 6 – 12: Emission spectra and calibration curves of temperature sensor made of indicator Eu(tta)3DEADIT and immobilized in polymers PS-co-PAN and PVC-co-PAN before and after steam sterilization.

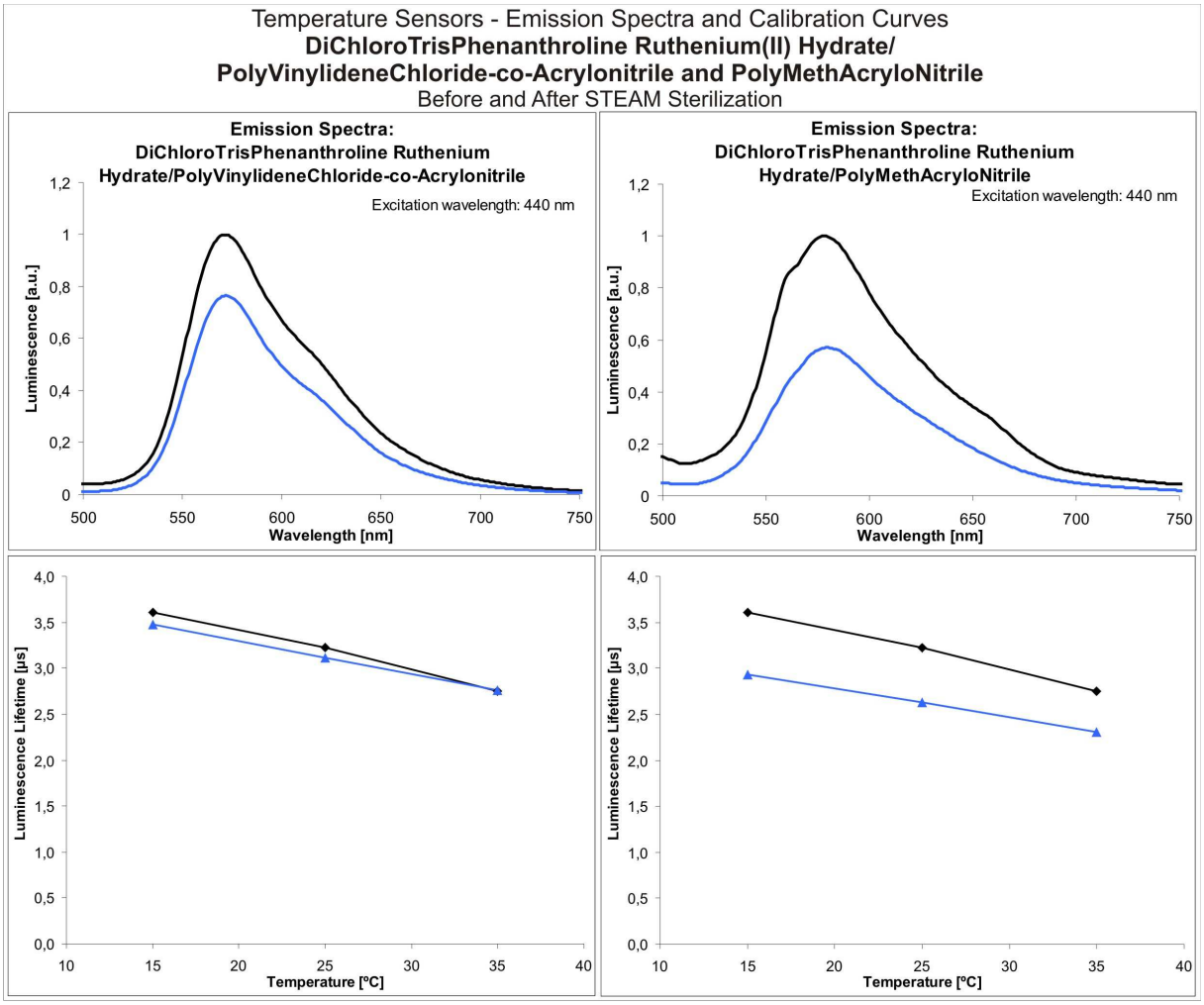

Figure 6 – 13: Emission spectra and response of temperature sensor made of indicator ruthenium(II) complex and immobilized in polymers PS-co-PAN and PVC-co-PAN before and after steam sterilization.

6.4 Steam Sterilization of Optical Ammonia Sensors

The optical ammonia sensors were made of the polymers CA, EC, PMMA and hydrogel D7. Cellulosic materials such as cellulose acetate and ethyl cellulose are not appropriate polymer matrices for sensors that should be sterilized with steam because they became turbid after sterilization. Likewise, the solvatochromic shifts of the emission spectra were observed, therefore the cellulose materials could undergo a hydrolysis reaction during sterilization in autoclave and that had an influence on the changes in the polarity of the polymer. Figure 6 – 14 shows the example of the absorption and emission spectra after steam sterilization of the ammonia sensors made of cellulose materials.

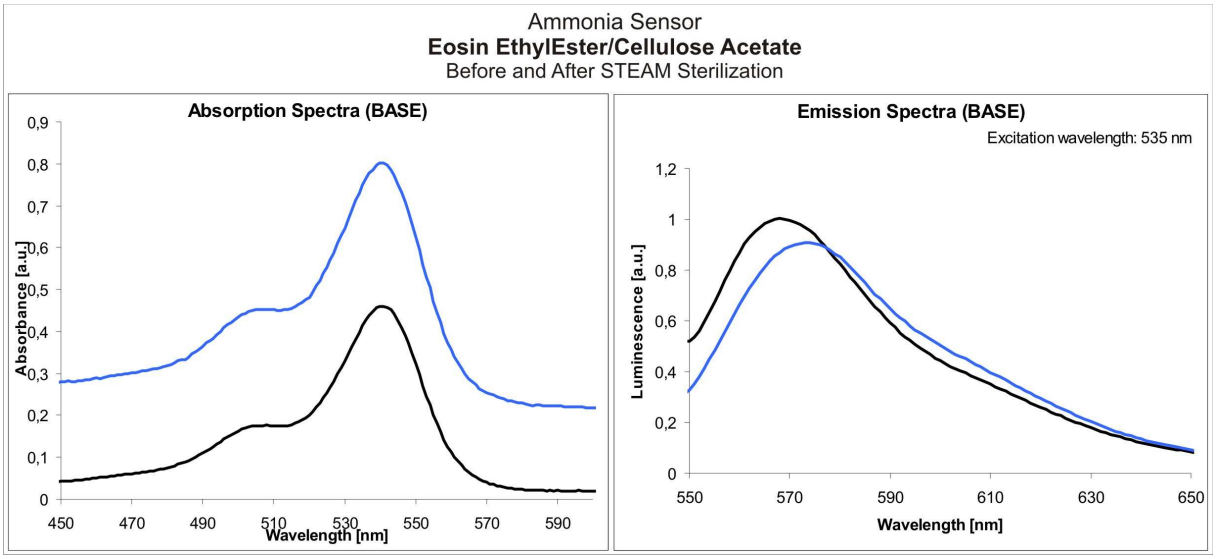

Figure 6 – 14: Absorption and emission spectra of ammonia sensor made of indicator eosin ethylester and immobilized in polymer CA before and after steam sterilization.

On the other hand, the ammonia sensors made of polymer hydrogel D7 remained stable after steam sterilization. However, some solvatochromic shifts of the emission maximum were also observed. Probably, after application of heat the position of the indicator in the polymer matrix changed due to hydrophobic and hydrophilic polymer composition and therefore, the sensor should be re-calibrated after application of the steam sterilization method. When the indicators were immobilized in PMMA the alterations and decrease of the absorption were observed. Therefore, steam sterilization is not an appropriate method when diverse indicators are immobilized in polymer PMMA.

7 Sterilization with Ethylene Oxide Gas

The efficiency of sterilization with ethylene oxide depends upon stringent control of process conditions, including humidity, duration and temperature. When properly performed, ethylene oxide has shown to effectively sterilize the materials and also to be capable for surface sterilization applications, including lumened devices and applications where the devices are constructed of permeable polymers. Likewise, complex medical devices evolved that are temperature and humidity sensitive, could be sterilized with ethylene oxide.

Many materials are compatible with the sterilization method that applies ethylene oxide gas. Therefore, by the sterilization of the heat sensitive polymer materials it is predominant. Most polymeric materials are very permeable to ethylene oxide and due to its small size it is able to be adsorbed by polymers. The factors affecting this penetration and adsorption are the type and size of polymeric material, the dimensions of the device and its packaging, as well as the sterilization parameters. For example, the thicker the surface is the greater the adsorption will be.

In this study, the optical sensors were sterilized with ethylene oxide. All results are gathered and presented in the database:

- *Section E – Sterilization of optical sensors with ethylene oxide*

The important and interesting results are discussed and shown in the following chapters.

7.1 Sterilization of Optical Oxygen Sensors with EtO

The ethylene oxide sterilization method induced some alterations in the oxygen sensor response. The oxygen sensors made of the indicators Iridium(III) coumarin, PtTFPP and ruthenium(III) complex and immobilized in cellulose materials such as cellulose acetate and ethyl cellulose were not resistant to ethylene oxide. Ethylene oxide probably reacted with hydroxyl groups of the polymer matrix which had an influence on the sensor response. Additionally, the alterations of the sensor made of polymer ethyl cellulose were greater than in the case of cellulose acetate, which could be due to etherification reactions induced by ethylene oxide gas. However, the response to the different concentrations of oxygen by described oxygen sensors was altered but the absorption and emission intensities were not. The absorption spectra and sensor response of the oxygen sensors made of the iridium(III) coumarin and ruthenium(III) complex and immobilized in ethyl cellulose are presented in figure 7 – 1.

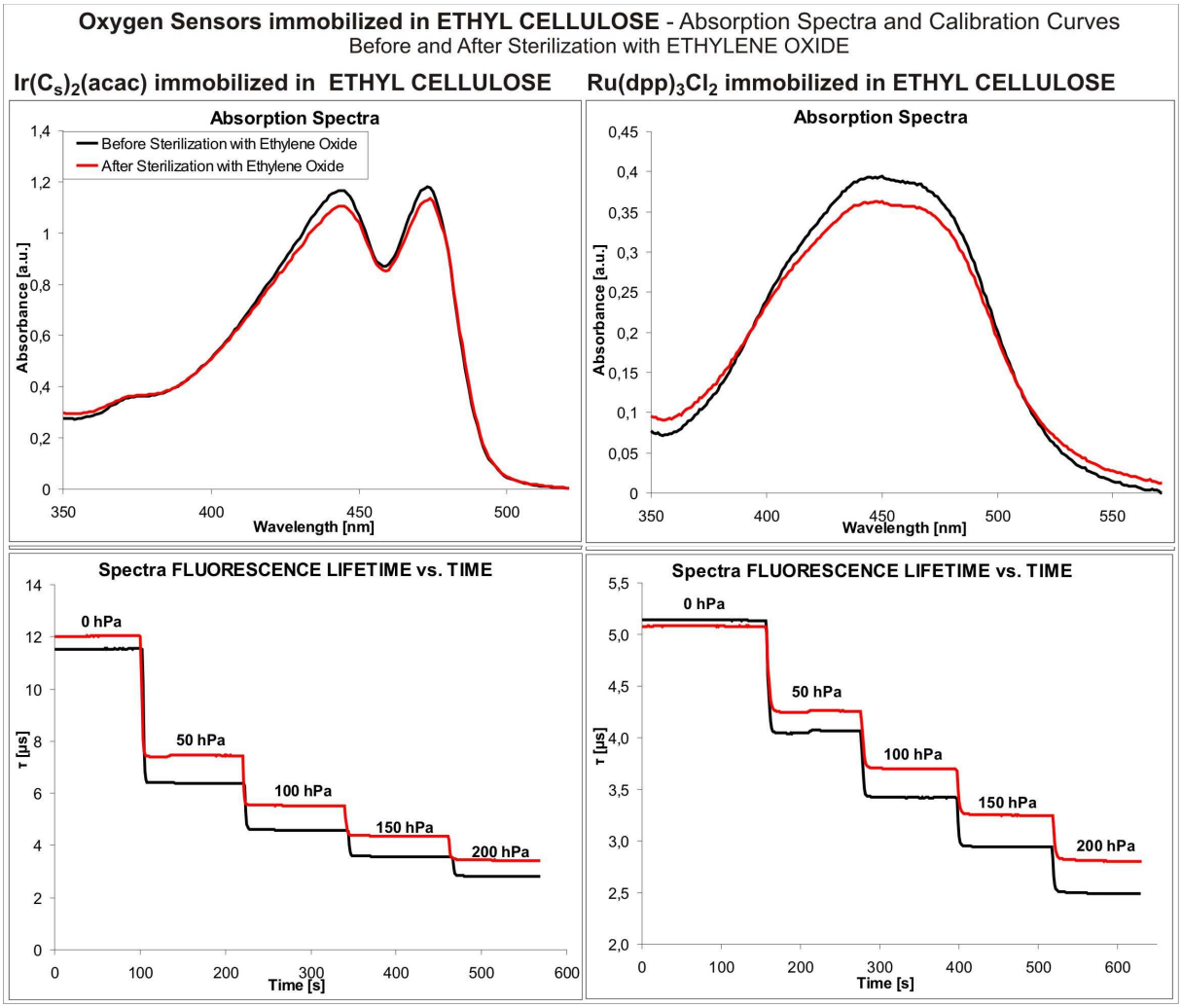

Figure 7 – 1: Absorption spectra and sensor response of the oxygen sensors made of indicators $Ir(C_s)_2(acac)$ and $Ru(dpp)_3Cl_2$ and immobilized in polymer EC before and after sterilization with ethylene oxide.

Similar alterations as those of oxygen sensors made of cellulose materials were observed when the polymer matrix was made of HydroThane with 5% water and indicator iridium(III) coumarin and ruthenium(III) complex. However, when the indicator PtTFPP was immobilized in the HydroThane with 5% water content, the response of the sensor remained the same before and after sterilization. That could be because additional alterations appeared or the indicator structure hindered the reactions between polymer and ethylene oxide because. Figure 7 – 2 shows the comparison of the sensor response made of the polymer HydroThane^{TM} and the indicators Iridium(III) coumarin and PtTFPP.

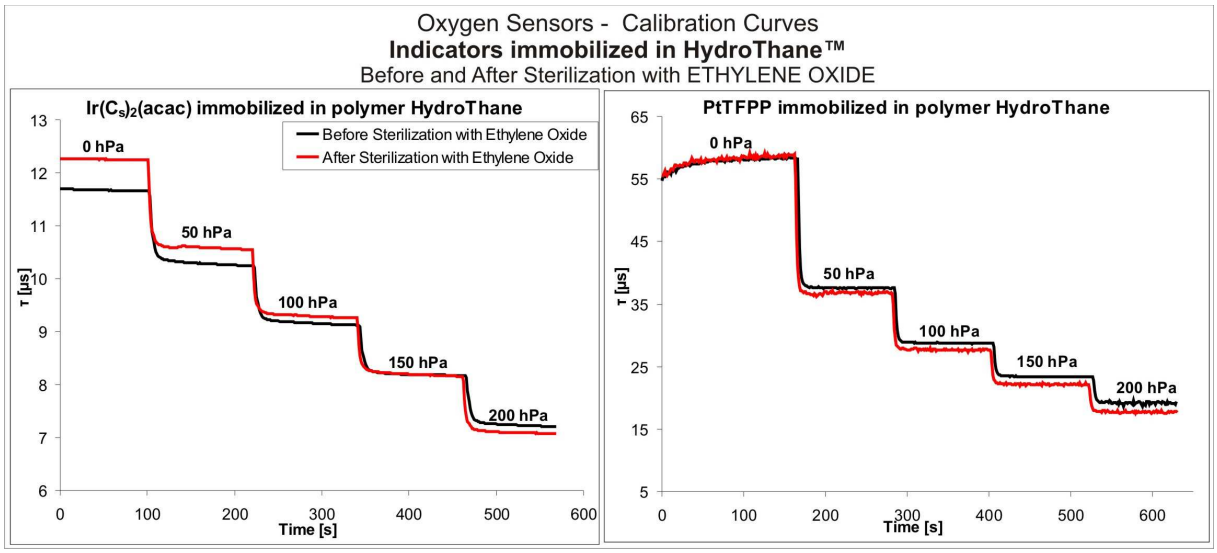

Figure 7 – 2: Calibration curves of the oxygen sensors made of indicators $Ir(C_s)_2(acac)$ and PtTFPP and immobilized in polymer HydroThane™ before and after sterilization with ethylene oxide.

On the other hand, among oxygen sensors made of the polymer Hydrogel D7 additional quencher were formed after sterilization with ethylene oxide due to an observed uniform decrease of thephosphorescence lifetime, which is presented in figure 7 – 3.

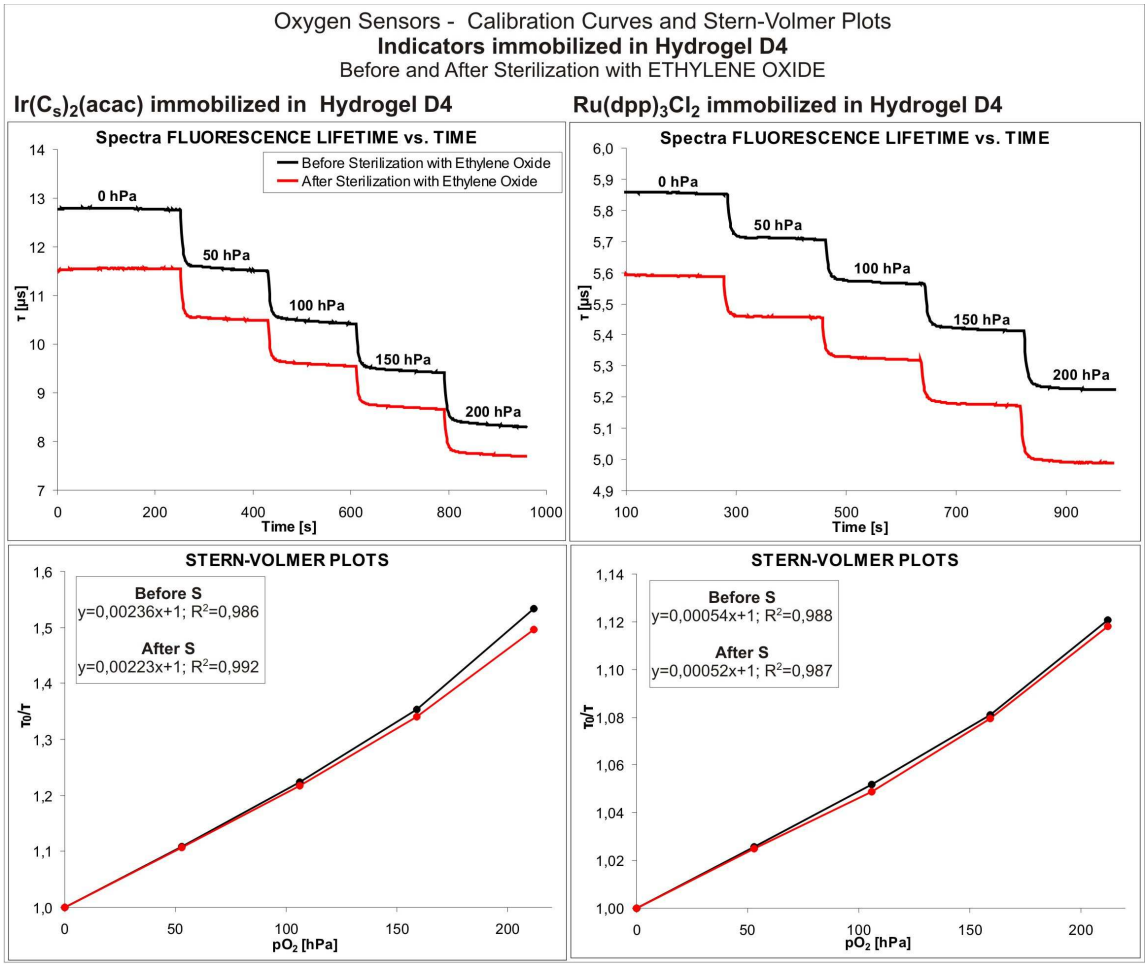

Figure 7 – 3: Calibration curves and Stern-Volmer plots of the oxygen sensors made of indicators Ir(Cs)2(acac) and Ru(dpp)3Cl2 and immobilized in polymer hydrogen D4 before and after sterilization with ethylene oxide.

However, the ethylene oxide also reacted with the polymer PPSQ, which possesses hydroxyl groups in the structure, and has altered the permeability capabilities of the indicator. Here, the luminescence lifetime remained the same in the absence of the oxygen, but was longer in the presence of the oxygen after sterilization. Therefore, the polymer matrix became less permeable for the quenchers. The response of oxygen sensors made of PPSQ after sterilization with ethylene oxide is presented in figure 7 – 4.

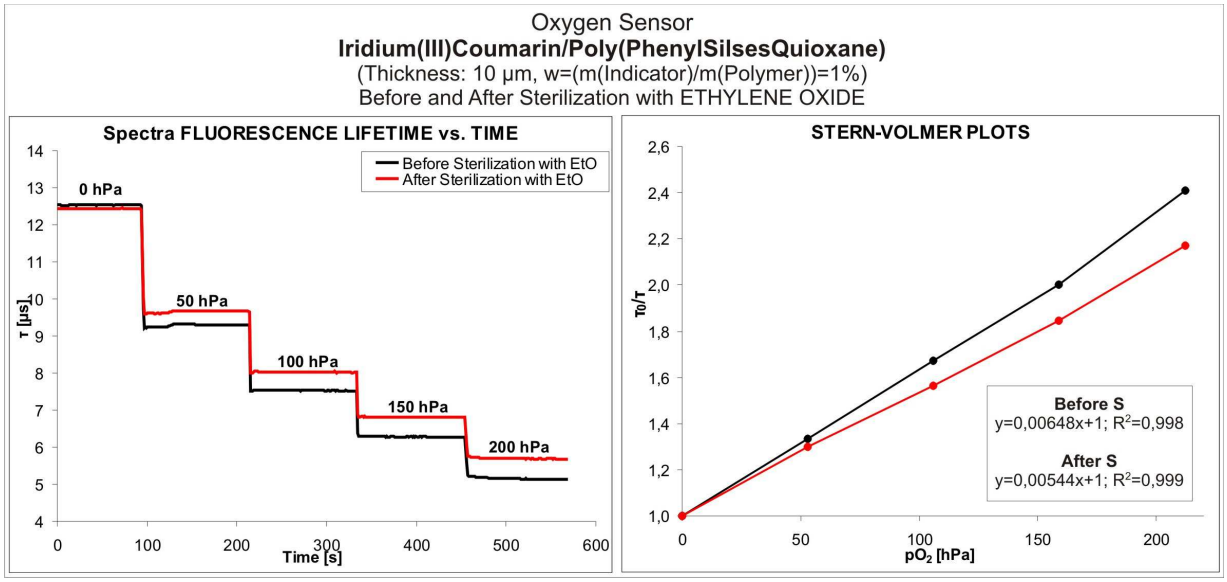

Figure 7 – 4: Calibration curves and Stern-Volmer plots of the oxygen sensors made of indicator $Ir(C_s)_2(acac)$ and immobilized in polymer PPSQ before and after sterilization with ethylene oxide.

The most resistant oxygen sensors to ethylene oxide are the polymers PSf, PS, PS-co-PAN and PSMA. The alterations of these sensors were negligible. The absorption, emission intensities and sensor response remained the same after sterilization with ethylene oxide. Figure 7 – 5 shows the example of the oxygen sensor response before and after sterilization with ethylene oxide made of the polymer PSMA and diverse oxygen sensitive indicators.

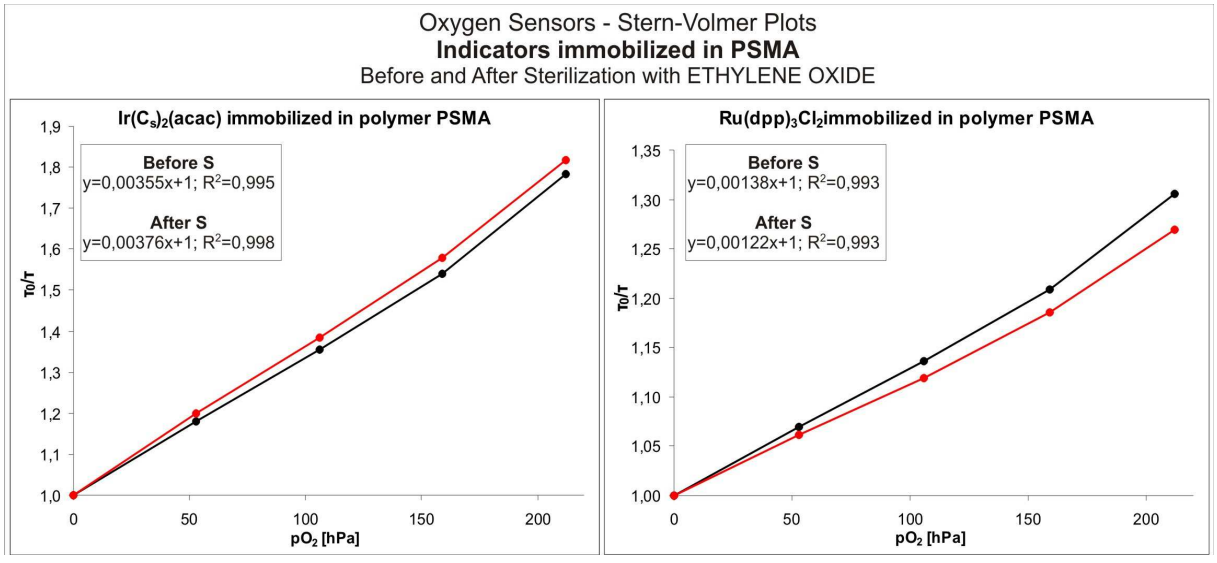

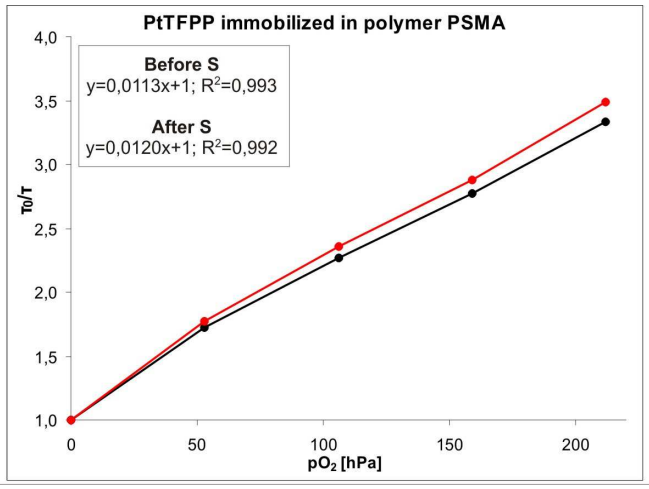

Figure 7 – 5: Stern-Volmer plots of the oxygen sensors made of indicators $Ir(C_s)_2(acac)$, PtTFPP and $Ru(dpp)_3Cl_2$ and immobilized in polymer PSMA before and after sterilization with ethylene oxide.

7.2 Sterilization of Optical pH Sensors with EtO

The sterilization method with ethylene oxide gas is an effective, low temperature chemical sterilization method. Additionally, from all sterilization methods it has the least effect on the polymers. That was also confirmed after ethylene oxide sterilization of optical pH sensors, based on fluorescence, because this sterilization procedure caused the least amount of alterations on the polymers from all procedures applied in this study.

After the sterilization with ethylene oxide of the pH sensors made of indicator lipophilic HPTS, lipophilc fluoresceins and pH sensitive coumarin immobilized in hydrogel D4, the decreases in the absorption were negligible. Hence, the chemical reactions between ethylene oxide and the hydroxyl group of the indicators did not appear. Therefore, the protonation/deprotonation capabilities were not altered. The absorption spectra before and after sterilization with ethylene oxide are shown in figure 7 – 6.

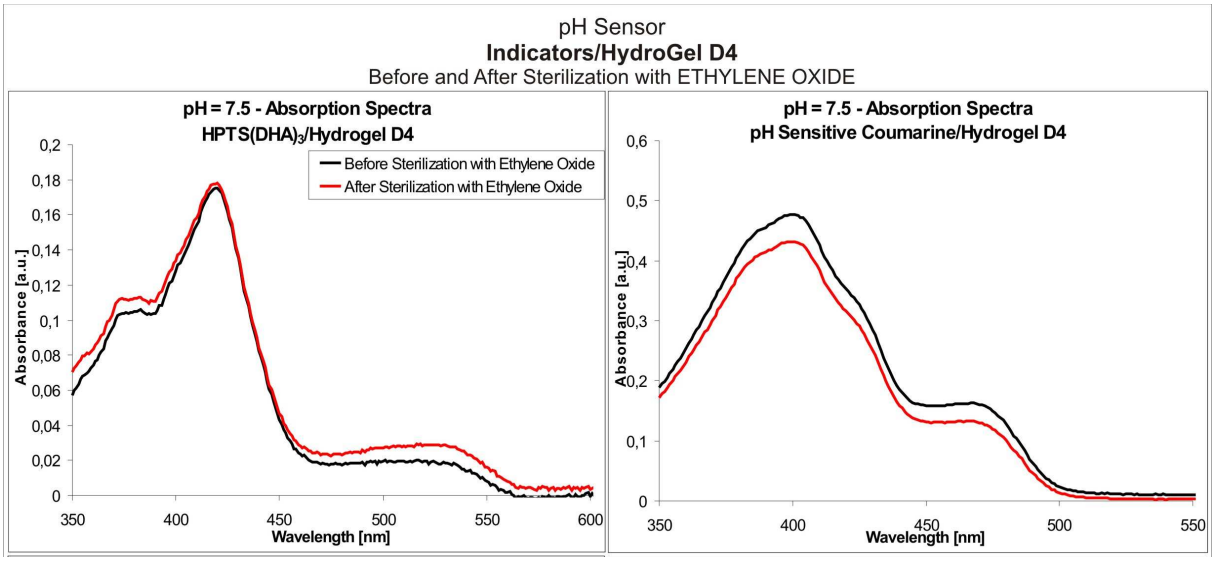

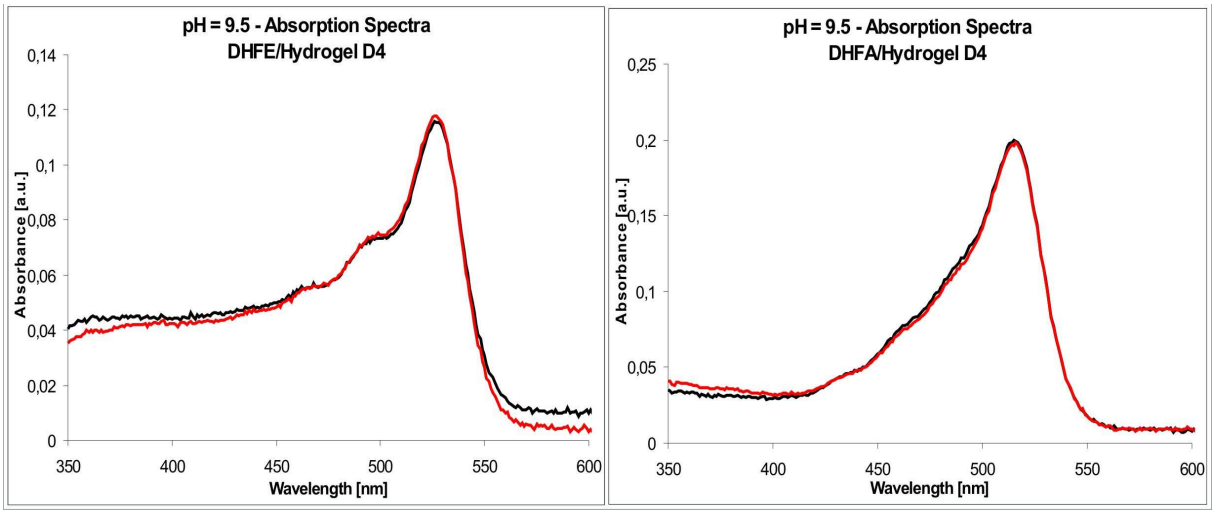

Figure 7 – 6: Absorption spectra of pH sensors made of indicators HPTS(DHA)$_3$, DHFA, DHFE and pH sensitive coumarin and immobilized in polymer hydrogel D4 before and after sterilization with ethylene oxide.

When the lipophilic fluoresceins were immobilized in the polymer pHEMA, the alterations in the absorption spectra were observed. Accordingly, some reactions between ethylene oxide and polymer matrix pHEMA occurred, since the absorption spectra were altered outside the absorption maximum region. The ethylene oxide probably reacted with pHEMA according to the following reaction scheme:

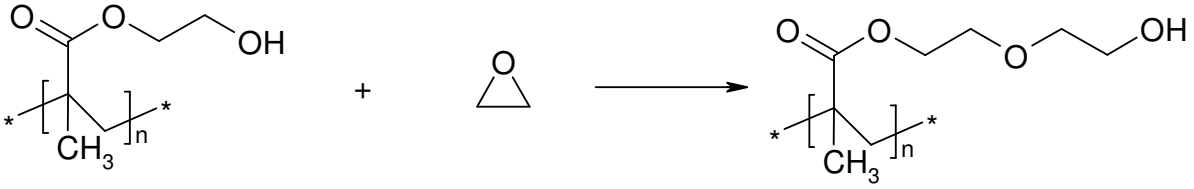

The reactions have the influence on the alterations that were observed in the absorption spectra and calibration curves of the pH sensors made of lipophilic fluoresceins and polymer pHEMA and are presented in figure 7 – 7.

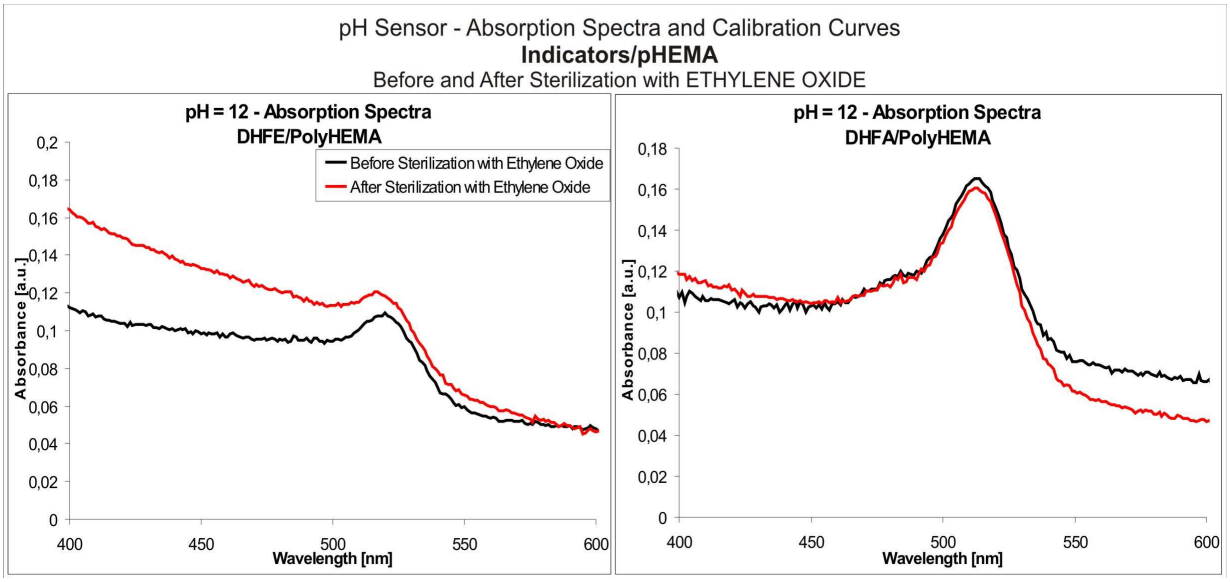

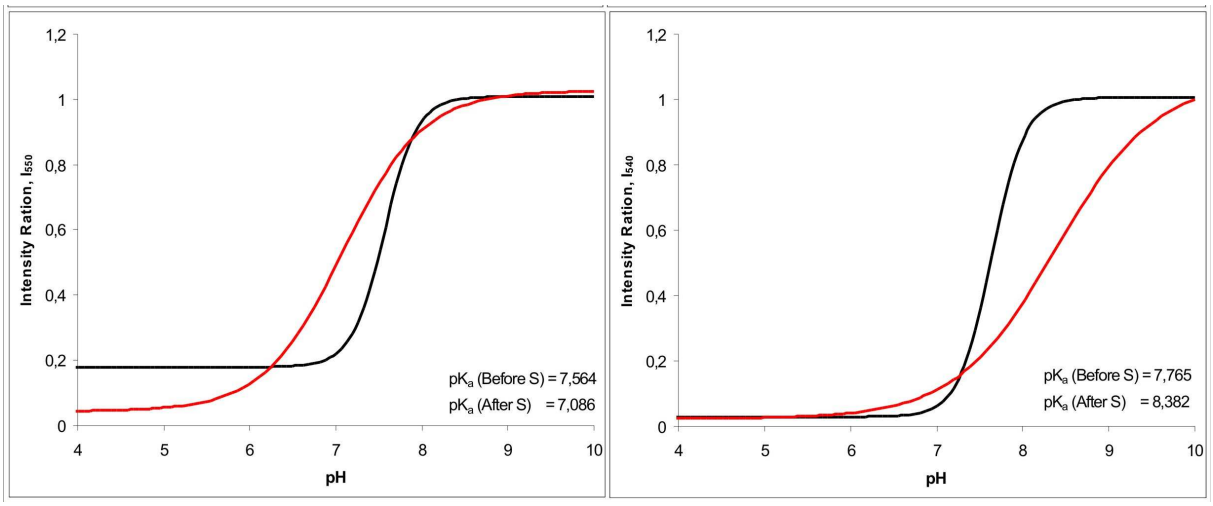

Figure 7 – 7: Absorption spectra and calibration curves of pH sensors made of indicators DHFA and DHFE and immobilized in polymer pHEMA before and after sterilization with ethylene oxide.

However, the ethylene oxide also has an influence on the indicator PET Perylene Bisimide, because the decrease of the luminescence intensity was observed and no pH dependence of the indicator. The ethylene oxide could react with the amino moiety responsible for the photoinduced electron transfer (PET) process. This hindered the PET process and consequently the pH dependent luminescence intensity was no longer observed. Figure 7 – 8 presents the decrease of the luminescence intensity and the non-existing pH dependence of the indicator PET Perylene bisimide immobilized in polymer hydrogel D4 after sterilization with ethylene oxide.

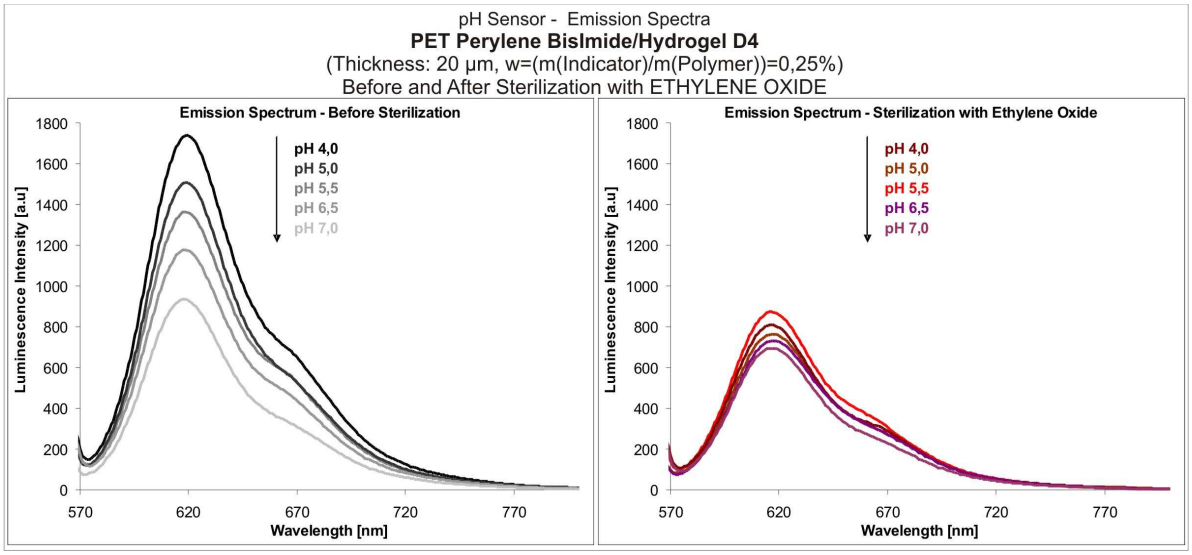

Figure 7 – 8: Emission spectra of pH sensors made of indicators PET Perylene bisimide and immobilized in polymer hydrogel D4 before and after sterilization with ethylene oxide.

Ethylene oxide gas has some influence on the sulfonephthalein pH sensitive dyes due to the decrease in the absorption. Likewise, the protonation and deprotonation capabilities were altered. That could be explained on the basis that the indicators were shifted to more hydrophobic parts of the polymer matrix hydrogel D4 after sterilization with ethylene oxide or some reactions between polymer and ethylene oxide appeared and that could alter the permeability capabilities for the proton to the indicator. The absorption spectra of the indicator thymol blue immobilized in hydrogel D4 before and after sterilization with ethylene oxide are shown in figure 7 – 9.

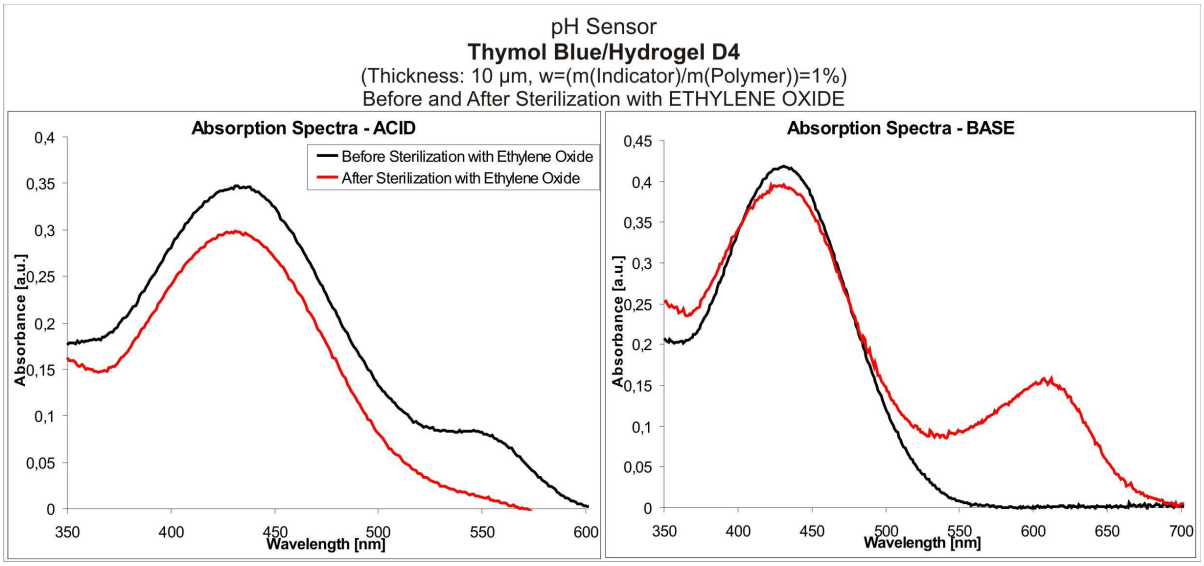

Figure 7 – 9: Absorption spectra of pH sensors made of indicator Thymol blue and immobilized in polymer hydrogel D4 before and after sterilization with ethylene oxide.

The sterilization with ethylene oxide of the indicator methyl orange immobilized in hydrogel D4 has the smallest effect on the sensor among all sterilization procedures applied in this study. Therefore, the sterilization with the ethylene oxide is the most appropriate method for the sterilization of pH sensors made of methyl orange and polymer hydrogel D4.

7.3 Sterilization of Optical Temperature Sensors with EtO

The sterilization method with ethylene oxide is recommended for the temperature sensors made of the indicator Eu(tta)$_3$DEADIT and immobilized in the polymer PS-co-PAN and sensors made of the indicator ruthenium(II) complex and immobilized in the polymer PVC-co-PAN because the absorption, emission and response of the sensors were not altered. The absorption spectra and calibration curves of these temperature sensors are presented in figure 7 – 10.

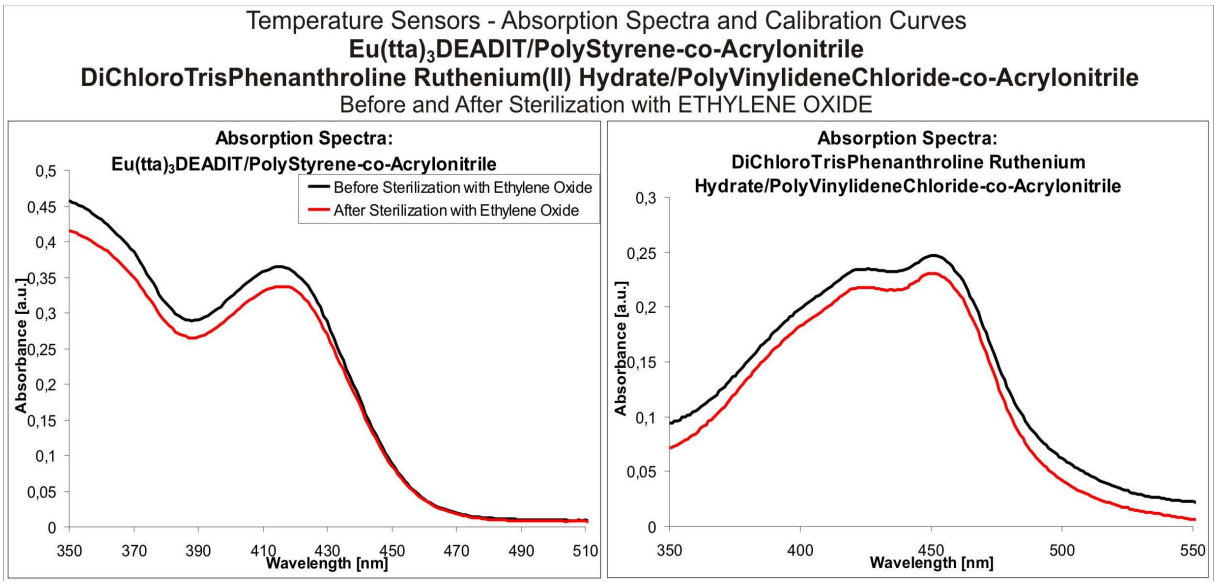

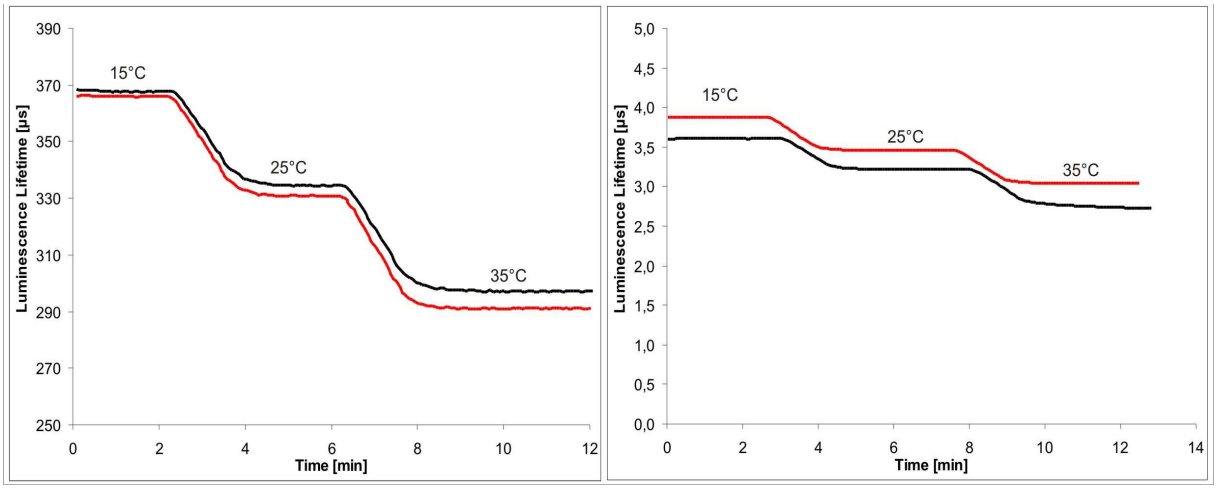

Figure 7 – 10: Absorption spectra and calibration curves of temperature sensors made of indicators Eu(tta)$_3$DEADIT and ruthenium(II) complex and immobilized in polymers PS-co-PAN and PVC-co-PAN before and after sterilization with ethylene oxide.

On the other hand, the luminescence lifetime of temperature sensors immobilized in PMAN decreased after the sterilization with ethylene oxide. However, the sensitivity of the sensor to the temperature was still observed. Hence, these temperature sensors should be re-calibrated after sterilization with ethylene oxide. Figure 7 – 11 shows the response of the temperature sensors before and after sterilization.

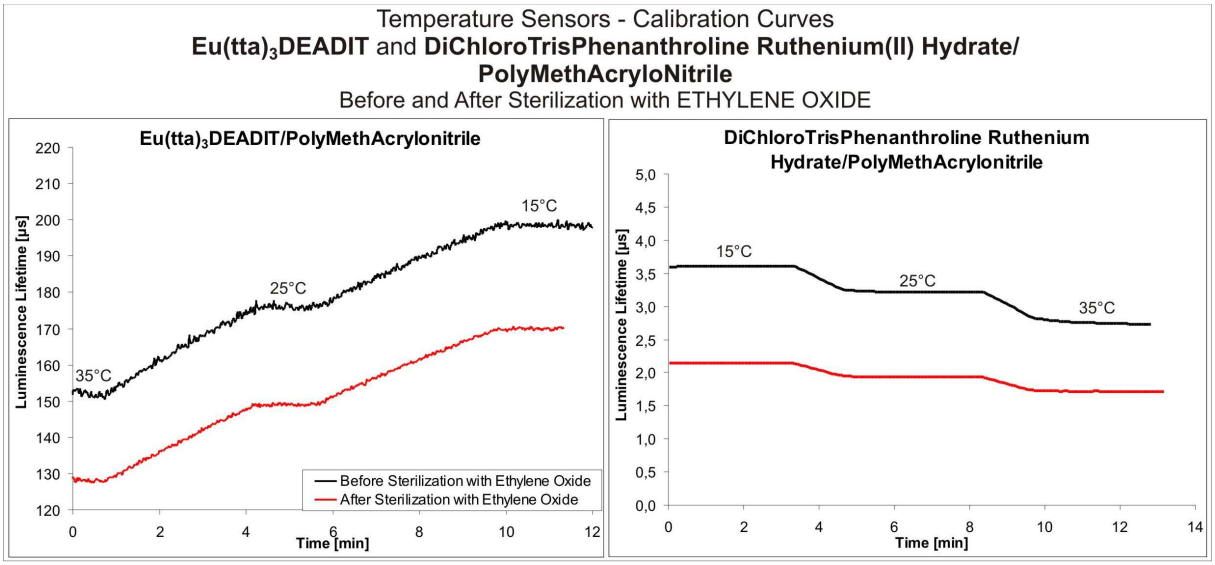

Figure 7 – 11: Calibration curves of temperature sensors made of indicators Eu(tta)$_3$DEADIT and ruthenium(II) complex and immobilized in polymer PMAN before and after sterilization with ethylene oxide.

7.4 Sterilization of Optical Ammonia Sensors with EtO

The sterilization with ethylene oxide is the most appropriate sterilization procedure in the case of ammonia sensors, because the least modifications were observed. However, some alterations were detected such as a solvatochromic shift of the emission maximum after sterilization of sensor made of polymer EC. Therefore, the ethylene oxide probably reacted with the polymer matrix and changed its polarity. The bathochromic shifts of the absorption and emission maximum are presented in figure 7 – 12.

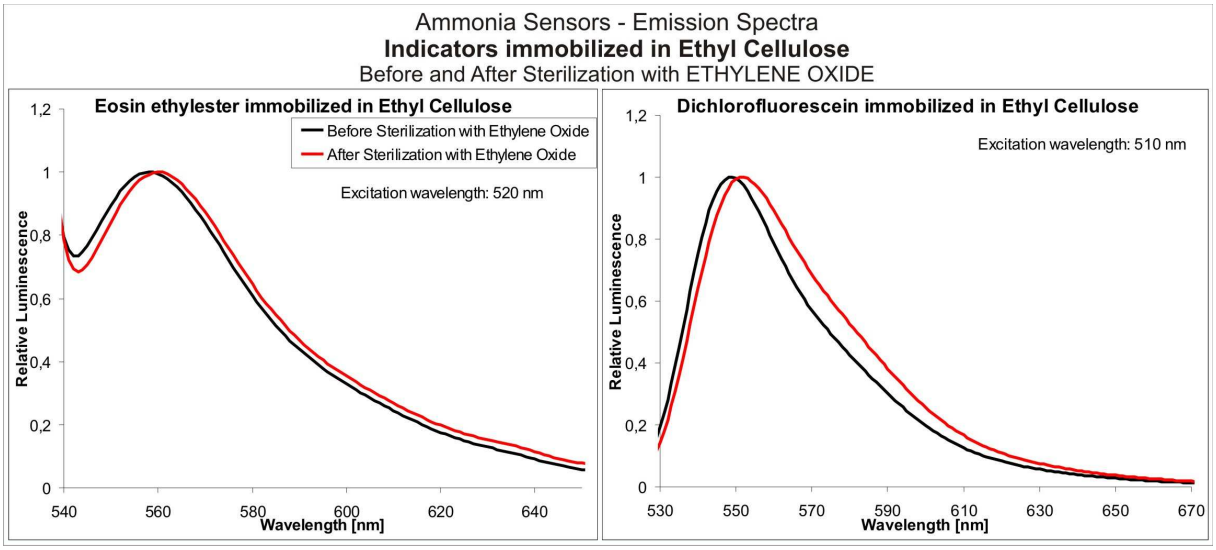

Figure 7 – 12: Emission spectra of ammonia sensor made of indicators eosinethyl ester and dichlorofluorescein and immobilized in polymer EC before and after sterilization with ethylene oxide.

The other ammonia sensors had a comparable response before and after sterilization and could therefore be sterilized with ethylene oxide.

8 Sterilization with Hydrogen Peroxide (Gas or Plasma)

Hydrogen peroxide is compatible with fewer materials than ethylene oxide gas. The oxidizing action of hydrogen peroxide leads to modifications of materials during sterilization and cause noticeable surface modifications on polymer matrices. Likewise, certain materials absorb and break down peroxide, which can lead to inefficient sterilization process and longer aeration time. Additionally, by plasma sterilization, material decay can be caused by UV radiation, vacuum and the electrical energy of the plasma generator. The sterilization procedure with low-temperature hydrogen peroxide plasma has also been found not to have an adverse affect on the bulk properties of ceratin polymeric materials that are degraded by exposure to radiation sterilization.

The sterilization procedure with hydrogen peroxide gas is a more gentler method than sterilization procedure with low-temperature hydrogen peroxide plasma and is more defined as the disinfection procedures because the sterility assurance level (SAL) of 10^{-6} could not be reached solely with the application of hydrogen peroxide gas. With the addition of hydrogen peroxide plasma, the SAL for medicine or pharmaceutical products is achieved. The procedure with hydrogen peroxide gas has shown the effects of hydrogen peroxide gas on optical sensor materials. The hydrogen peroxide plasma has additionally shown the effects of UV irradiation and free radicals that are formed due to the utilization of plasma.

All results and comparisons before and after the sterilization with hydrogen peroxide gas and plasma are gathered and presented in the database:

- *Section F – Sterilization of optical sensors with hydrogen peroxide (gas or plasma)*

Important and interesting results are discussed and shown in the following chapters.

8.1 Sterilization of Optical Oxygen Sensors with H_2O_2 (Gas or Plasma)

Hydrogen peroxide is absorbed by certain materials. Cellulosic materials such as cellulose acetate and ethyl cellulose, applied in this study, highly absorb hydrogen peroxide, thereby preventing the normal pressure changes during a sterilization cycle and causing it to abort. Therefore, optical sensors whose polymer matrix was made of cellulose materials were not sterilized with hydrogen peroxide (gas and plasma) sterilization methods.

Oxygen sensors made of the polymer Hydrogel D4 and the indicators iridium(III) coumarin, PtTFPP and the ruthenium(III) complex were affected by hydrogen peroxide gas and plasma. After sterilization with hydrogen peroxide, additional quenchers appeared that lower the luminescence lifetime and response of the sensors which is shown in figure 8 – 1.

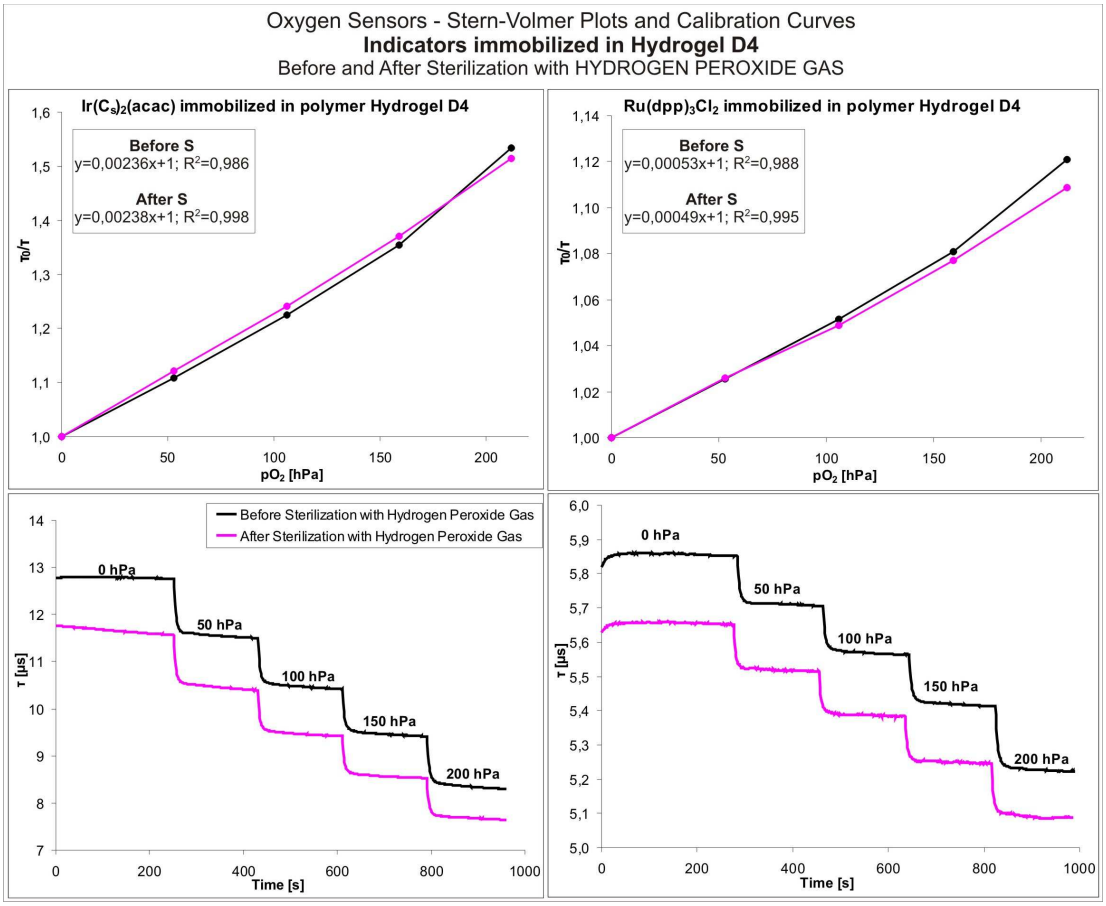

Figure 8 – 1: Calibration curves and Stern-Volmer plots of oxygen sensor made of indicators $Ir(C_s)_2(acac)$ and $Ru(dpp)_3Cl_2$ and immobilized in polymer hydrogel D4 before and after sterilization with hydrogen peroxide gas.

Since the hydrogen peroxide is one of the most powerful oxidizers known, it induces oxidation reactions in the indicator structure. The iridium(III) coumarin indicator sustains the oxidizing action of the hydrogen peroxide. On the other hand, the PtTFPP and the ruthenium(III) complex were more susceptible in some polymer matrices. The ruthenium(III) complex was oxidised to the ruthenium(II) complex and the oxygen radicals also reacted with porphyrine structure PtTFPP during sterilization procedure. The alterations due to oxidation were observed in the absorption and emission spectra and are presented in figure 8 – 2.

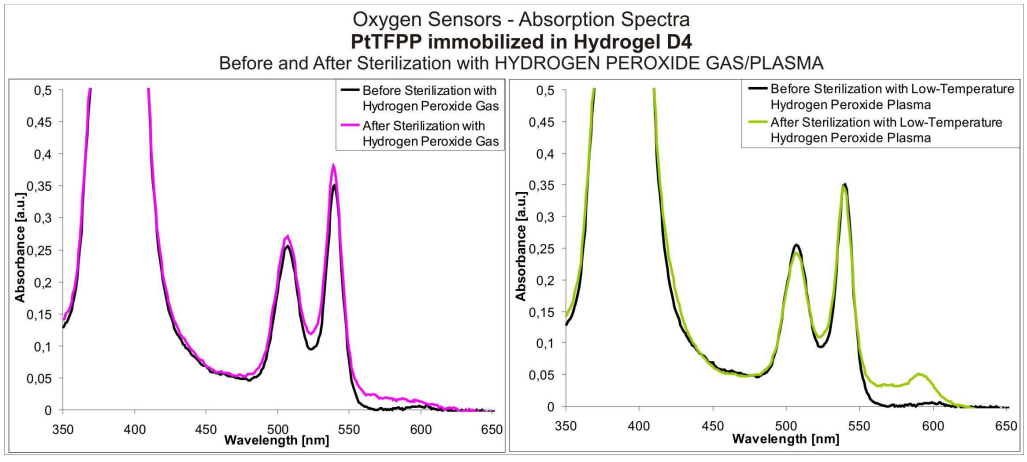

Figure 8 – 2: Absorption spectra of oxygen sensor made of indicator PtTFPP and immobilized in polymer hydrogel D4 before and after sterilization with hydrogen peroxide gas and plasma.

As already mentioned, the low-temperature hydrogen peroxide plasma induces the microorganism destruction and consecutive material decay with additional UV radiation with a wavelength of λ = 254 nm. The indicators iridium(III) coumarin and ruthenium(III) complex were very affected during UV radiation. Consequently, radiation during the sterilization cycle had an influence on the absorption, emission capabilities and response of the sensors. Figure 8 – 3 shows the alterations of the absorption spectra of the indicators iridium(III) coumarin and ruthenium(III) complex immobilized in hydrogel D4 after sterilization with hydrogen peroxide plasma.

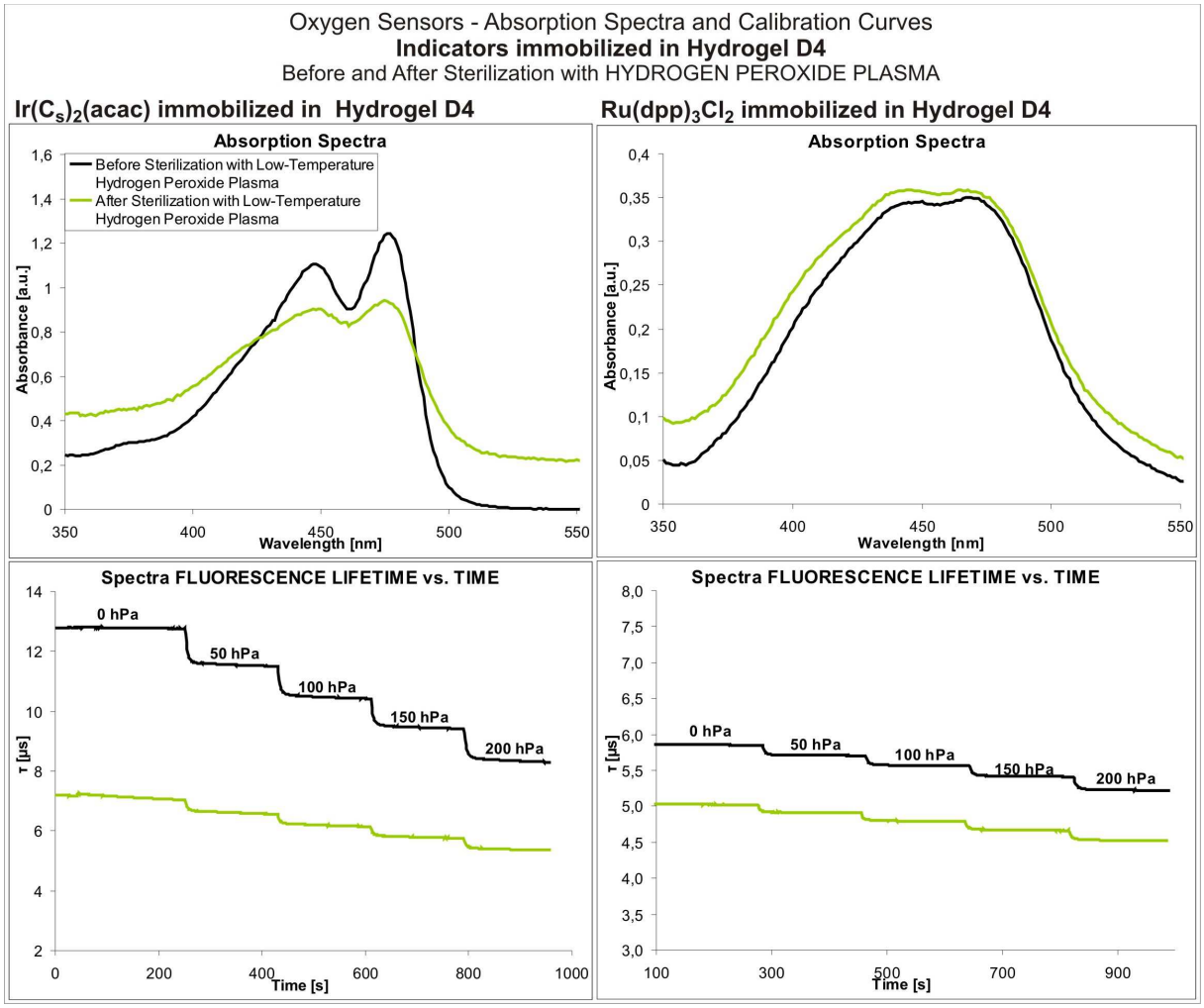

Figure 8 – 3: Absorption spectra and calibration curves of oxygen sensor made of indicators $Ir(C_s)_2(acac)$ and $Ru(dpp)_3Cl_2$ and immobilized in polymer hydrogel D4 before and after sterilization with hydrogen peroxide plasma.

When the oxygen sensors were made of Hydrothane with 5% water content, the indicator PtTFPP was protected from the oxidizing action of the hydrogen peroxide because the alterations in the absorption spectra were not observed. On the other hand, the polymer matrix PPSQ did not shield the indicator PtTFPP from oxidation. However, the indicator ruthenium(III) complex was oxidized in both matrices to the ruthenium(II) complex due to alterations in the absorption and emission spectra, which are presented in figure 8 – 4.

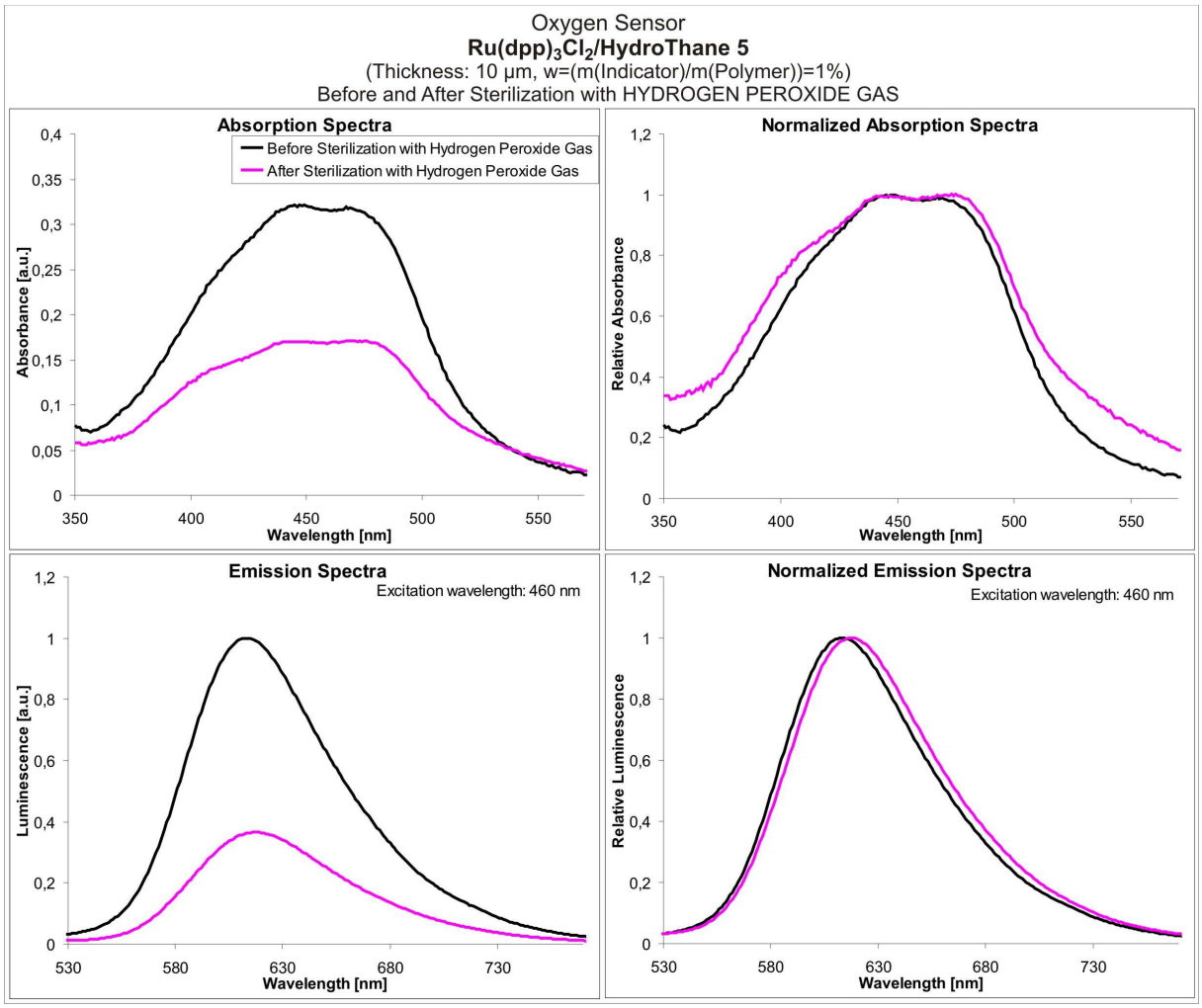

Figure 8 – 4: Absorption and emission spectra of oxygen sensor made of indicator $Ru(dpp)_3Cl_2$ and immobilized in polymer HydroThane 5 before and after sterilization with hydrogen peroxide gas.

However, the polymer PSf contains function groups in the structure that absorb UV radiation. Therefore, the iridium(III) coumarin and the ruthenium(III) complex were less affected by UV radiation than in other polymer matrixes after sterilization with hydrogen peroxide plasma. However, the ruthenium complex was although oxidized by hydrogen peroxide gas in the polysulfone matrix. The absorption spectra of the sensor made of the ruthenium(III)complex and polysulfone after sterilization with hydrogen peroxide gas and plasma are shown in figure 8 – 5.

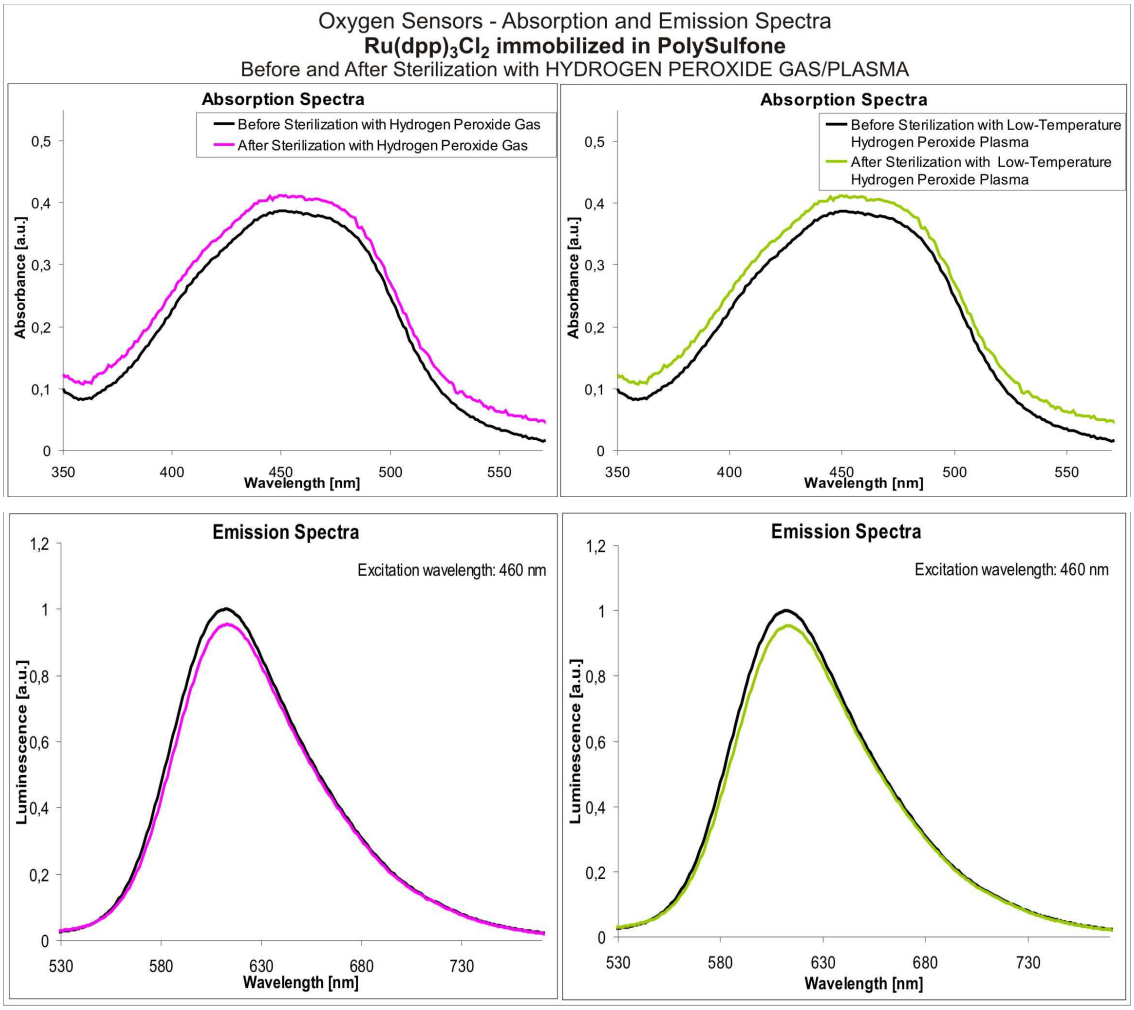

Figure 8 – 5: Absorption and emission spectra of oxygen sensor made of indicator $Ru(dpp)_3Cl_2$ and immobilized in polymer PSf before and after sterilization with hydrogen peroxide gas and plasma.

The ruthenium(III) complex was UV and oxidation resistant when immobilized in the polymers PS and PS-co-PAN. However, in these polymer matrices the additional quenchers appeared due to the uniform decrease of the luminescence lifetime after sterilization. The absorption, emission and response curves of the ruthenium(III) complex immobilized in PS are presented in figure 8 – 6.

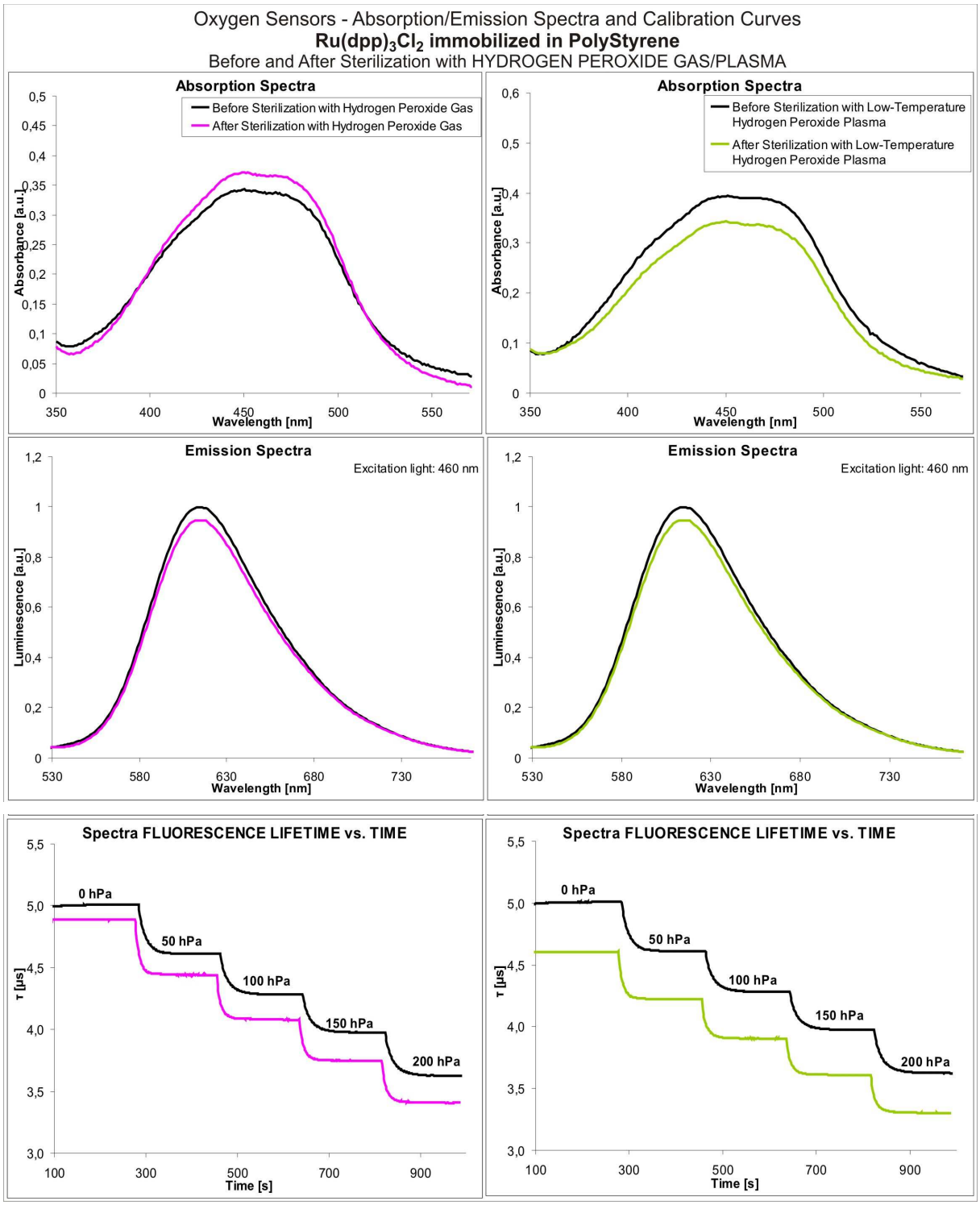

Figure 8 – 6: Absorption, emission spectra and calibration curves of oxygen sensor made of indicator $Ru(dpp)_3Cl_2$ and immobilized in polymer PS before and after sterilization with hydrogen peroxide gas and plasma.

When the indicators were immobilized in PSMA, the alterations, such as an oxidation of the indicators PtTFPP and ruthenium(III) complex and alterations due to UV irradiation were also determined after sterilization with hydrogen peroxide gas and plasma.

8.2 Sterilization of Optical pH Sensors with H_2O_2 (Gas or Plasma)

The alterations and reactions with the hydrogen peroxide gas were observed by the pH sensors made of the indicator HPTS(DHA)$_3$ and immobilized in hydrogel D4. The absorption decreased after sterilization and solvatochromic shifts of the absorption and emission maximum were observed. Consequently, the polarity of the hydrogel matrix could be altered due to oxidation modifications of polymer during sterilization or the hydrogen peroxide reacted with a pendant sulphonamide group, which could also be responsible for the solvatochromic shifts of the absorption and emission maxima. The alterations in the absorption spectra of pH sensors made of HPTS(DHA)$_3$ and hydrogel D4 are presented in figure 8 – 7.

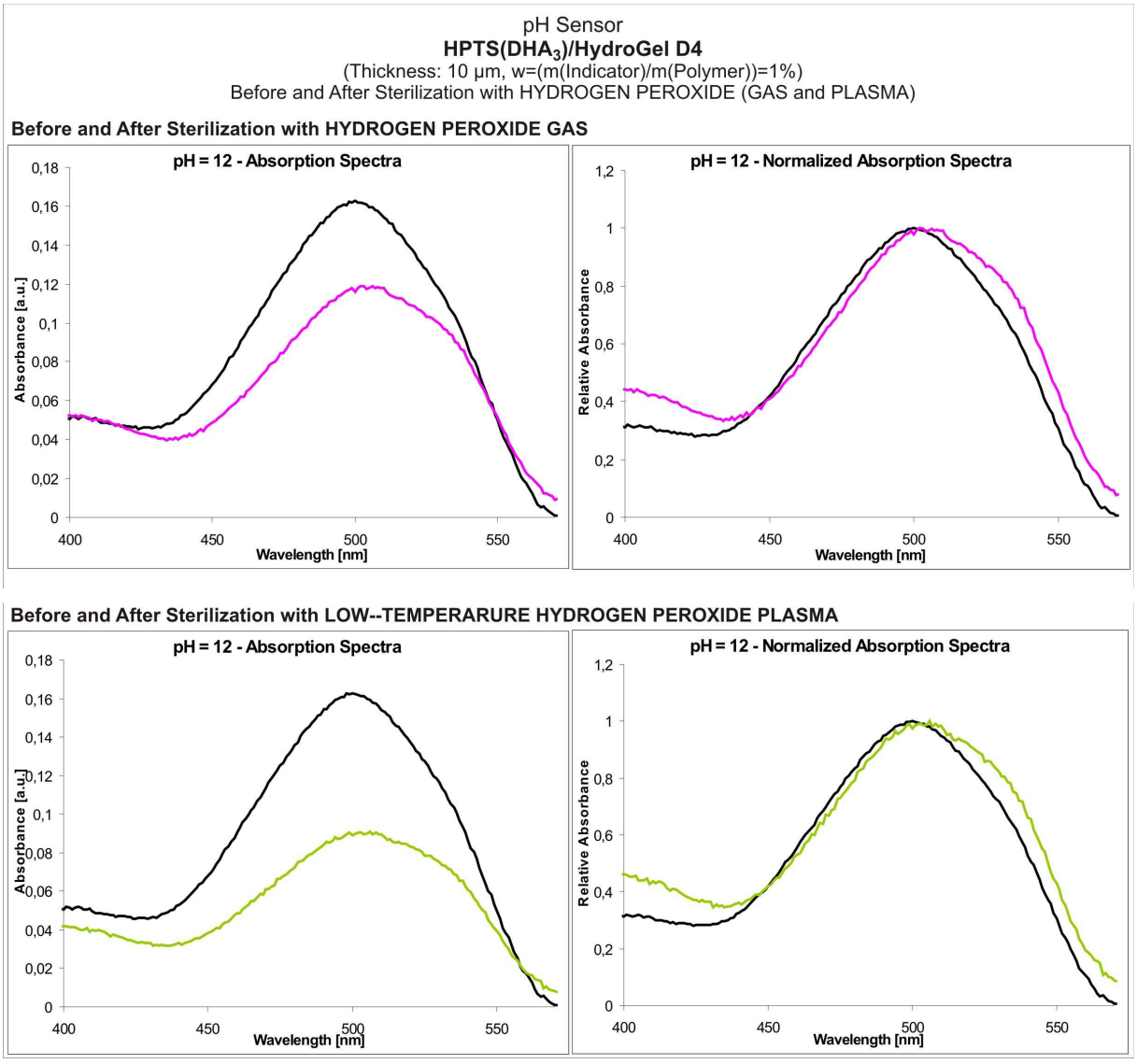

Figure 8 – 7: Absorption spectra of pH sensor made of indicator HPTS(DHA)$_3$ and immobilized in polymer hydrogel D4 before and after sterilization with hydrogen peroxide gas and plasma.

The lipophilic fluoresceins were very resistant towards sterilization with hydrogen peroxide gas and plasma when immobilized in hydrogel D4. On the other hand, regarding the sterilization of the DHFE, when immobilized in pHEMA, the quencher of the luminescence intensity appeared. The emission was no longer observed after sterilization with hydrogen

peroxide gas and plasma but the absorption was still detected. Figure 8 – 8 shows the decrease of the emission after sterilization of the indicators DHFE and pHEMA.

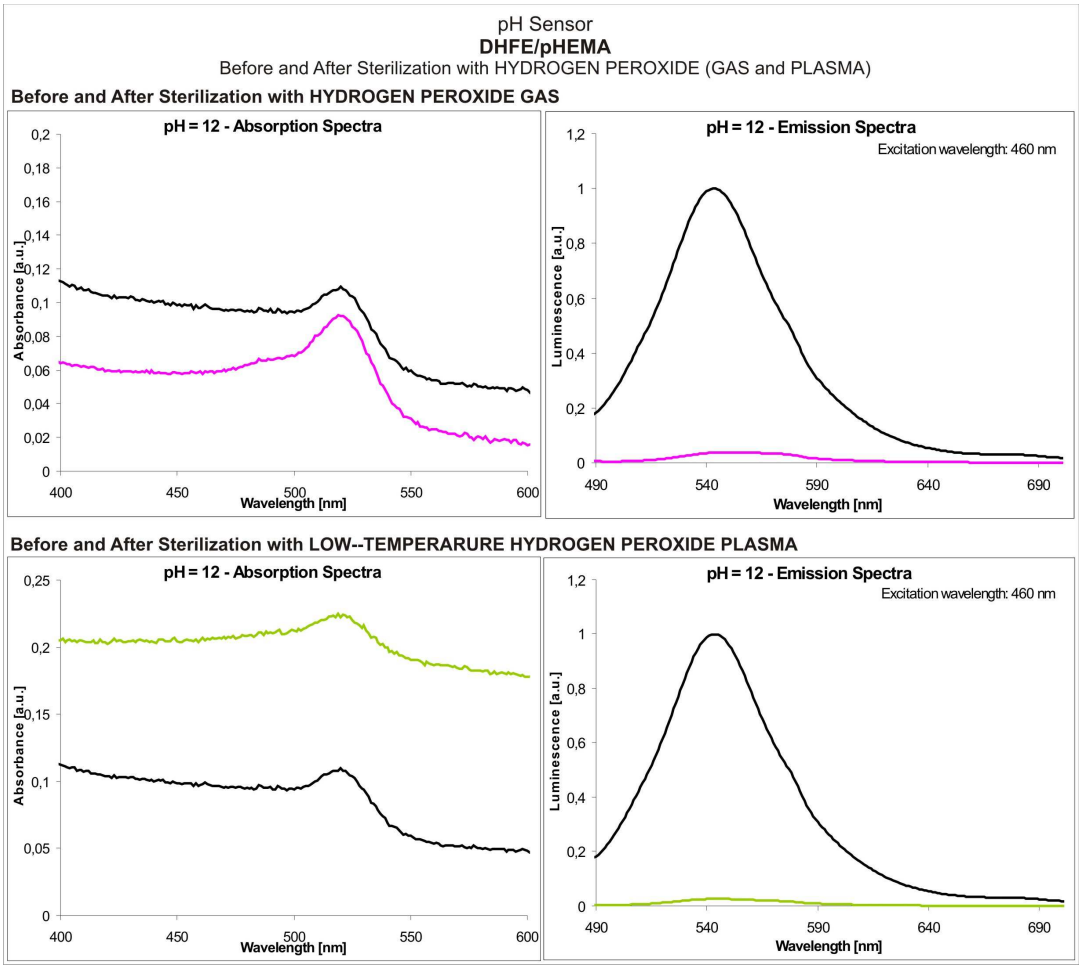

Figure 8 – 8: Absorption spectra of pH sensor made of indicator DHFE and immobilized in polymer pHEMA before and after sterilization with hydrogen peroxide gas and plasma.

Hence, the quencher did not appear after the sterilization of lipophilic fluorescein DHFA immobilized in pHEMA and the emission was still observed.

The pH sensitive coumarin immobilized in hydrogel D4 and pHEMA could be sterilized with hydrogen peroxide gas and plasma because the smallest alterations in the absorption and emission spectra among all sterilization methods applied in this study were observed. On the other hand, the sterilization with hydrogen peroxide gas and plasma of the PET Perylene bisimide in the hydrogel D4 has similar effects on the sensor response as sterilization with ethylene oxide. The pH sensitivity was no longer observed. Therefore, the hydrogen peroxide also oxidized the amino group, which is capable of quenching the indicator in the non-protonated state. The calibration curves before sterilization and the response of the sensor after sterilization with hydrogen peroxide gas and plasma are presented in figure 8 – 9.

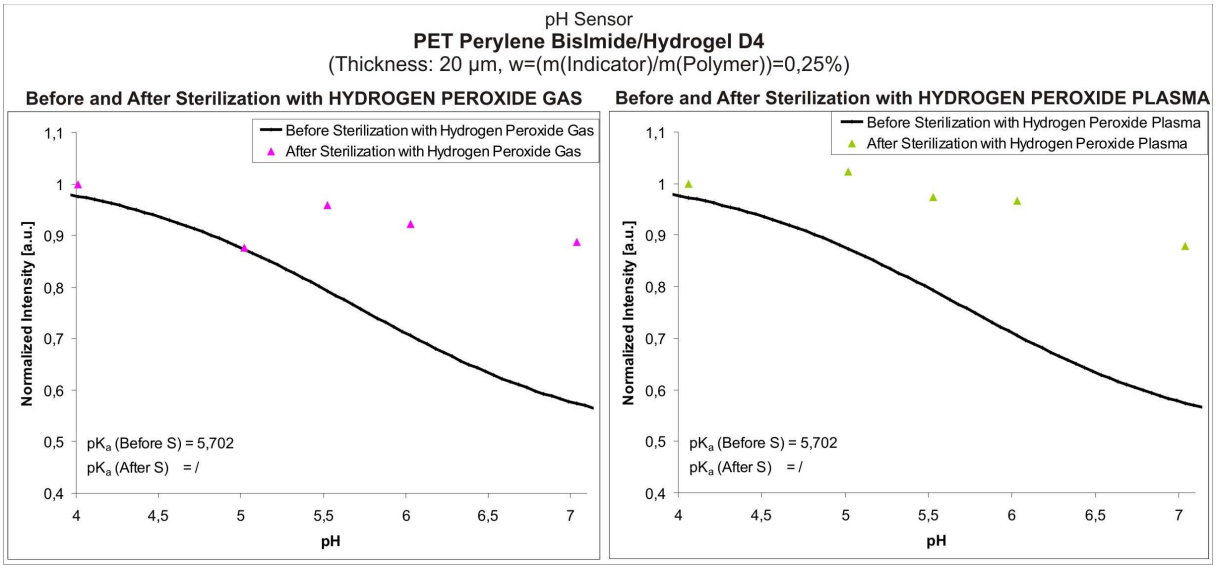

Figure 8 – 9: Response curves of pH sensor made of indicator PET Perylene bisimide and immobilized in hydrogel D4 before and after sterilization with hydrogen peroxide gas and plasma.

The pH sensors made of sulfonephthalein pH sensitive dye were resistant to sterilization with hydrogen peroxide gas. However, the indicator thymol blue immobilized in hydrogel D4 was destroyed after sterilization with hydrogen peroxide plasma. Consequently, of all sulfonephthalein pH indicators applied in this study, thymol blue is the most subjected to the oxidation and is therefore not resistant to photo-oxidation induced by UV radiation during sterilization with hydrogen peroxide plasma. The absorption spectra after sterilization with hydrogen peroxide plasma are shown in figure 8 – 10.

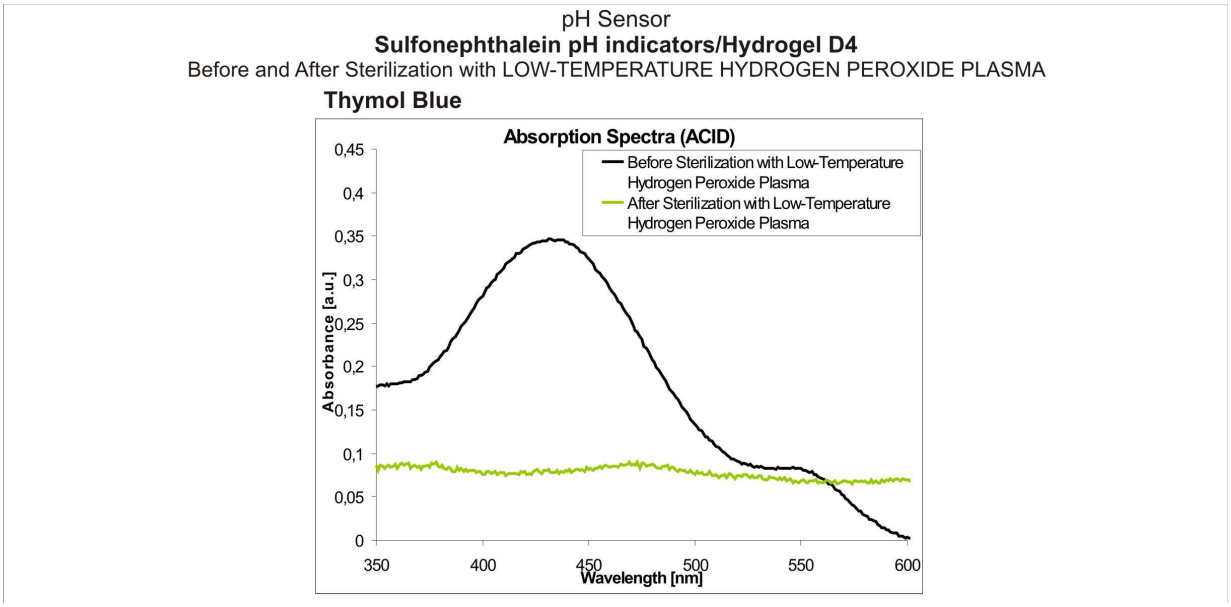

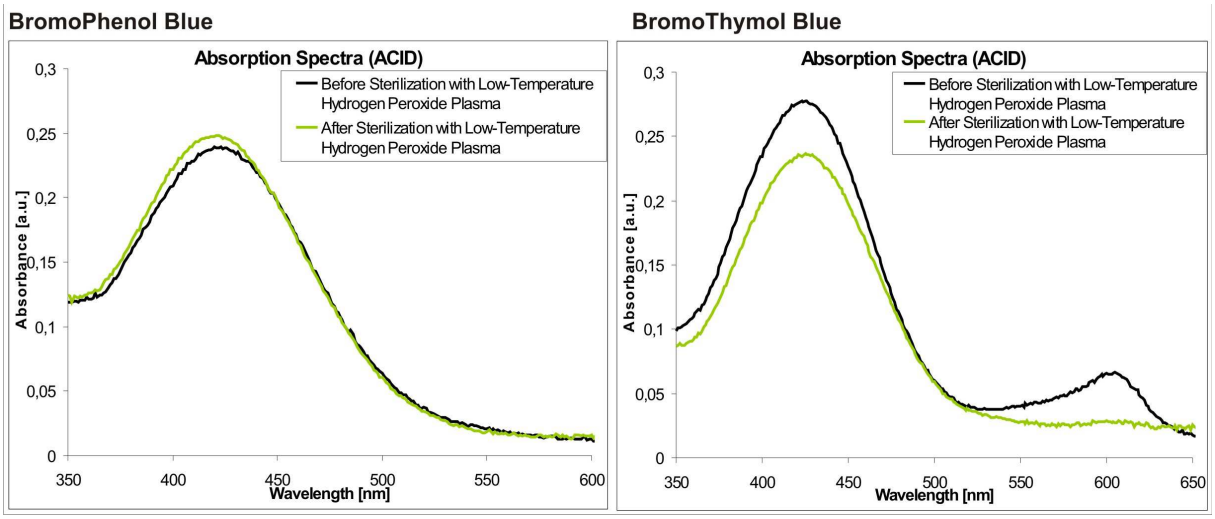

Figure 8 – 10: Absorption spectra of pH sensor made of sulfonephthalein pH sensitive dye and immobilized in hydrogel D4 before and after sterilization with hydrogen peroxide plasma.

8.3 Sterilization of Optical Temperature Sensors with H_2O_2 (Gas and Plasma)

The sterilization with hydrogen peroxide gas has no effects on the optical temperature sensors with the exception of the ruthenium(II) complex that was being immobilized in the PMAN. Here, the reactions between sensor and hydrogen peroxide appeared which have changed the absorption, emission and respond of the sensor after sterilization with hydrogen peroxide gas and also plasma. The absorption spectra and response curves are presented in figure 8 – 11.

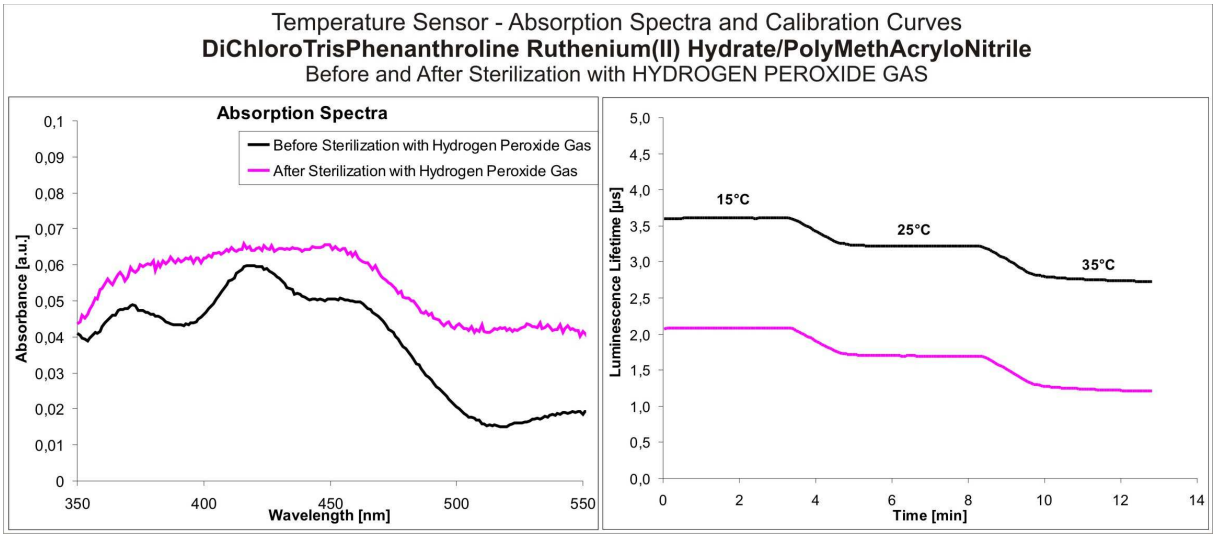

Figure 8 – 11: Absorption spectra and response curves of temperature sensor made of indicator ruthenium(II) complex and immobilized in polymer PMAN before and after sterilization with hydrogen peroxide gas.

When the temperature sensors were made of the indicator Eu(III) complex and sterilized with low-temperature hydrogen peroxide plasma, the complex $Eu(tta)_3$ was altered and affected. That could appear due to application of UV radiation because changes in the absorption

curve forms between 350-390 nm were observed. Figure 8 – 12 shows these alterations in the absorption spectra.

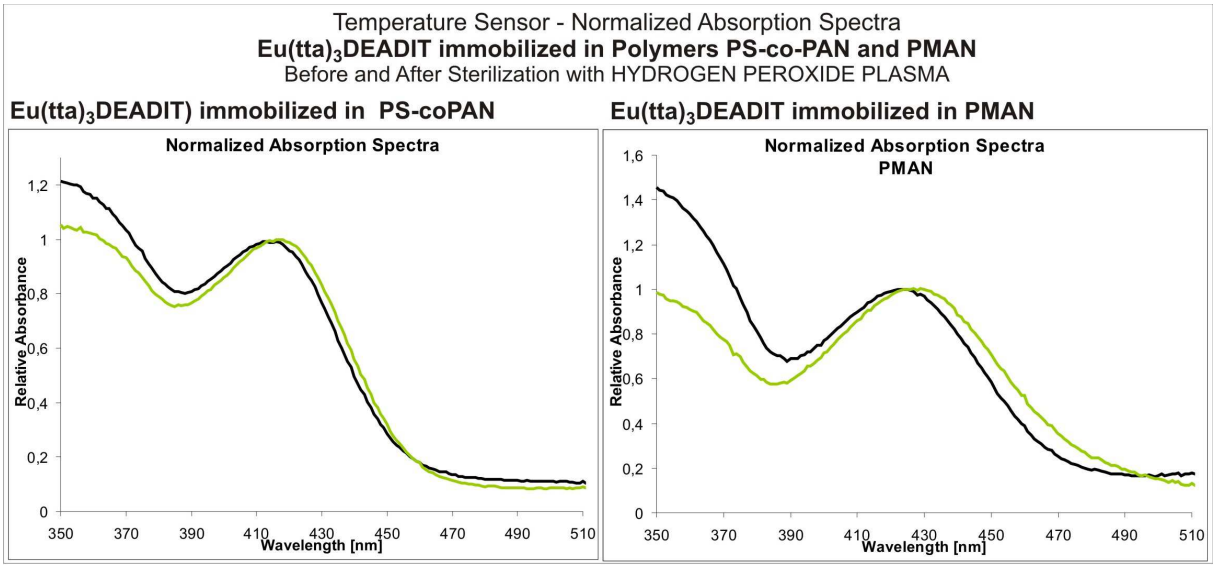

Figure 8 – 12: Normalized absorption spectra of temperature sensor made of indicator $Eu(tta)_3$DEADIT and immobilized in polymers PS-co-PAN and PMAN before and after sterilization with hydrogen peroxide plasma.

However, the sterilization with hydrogen peroxide gas caused no changes by temperature sensors made of the indicator Eu(III) complex immobilized in all polymer matrices and of the indicator ruthenium(II) complex immobilized in the polymer PVC-co-PAN. On the other hand, the sterilization method with low-temperature hydrogen peroxide plasma induced more alterations. Therefore, the sensors made of the Eu(III) complex should be re-calibrated after this sterilization method. The only sensor that remained stable after sterilization with hydrogen peroxide plasma was made of the ruthenium(II) complex immobilized in the polymer PVC-co-PAN. The absorption spectra and response curves of optical temperature sensors made with polymer PVC-co-PAN after sterilization with hydrogen peroxide gas and plasma are presented in figure 8 – 13.

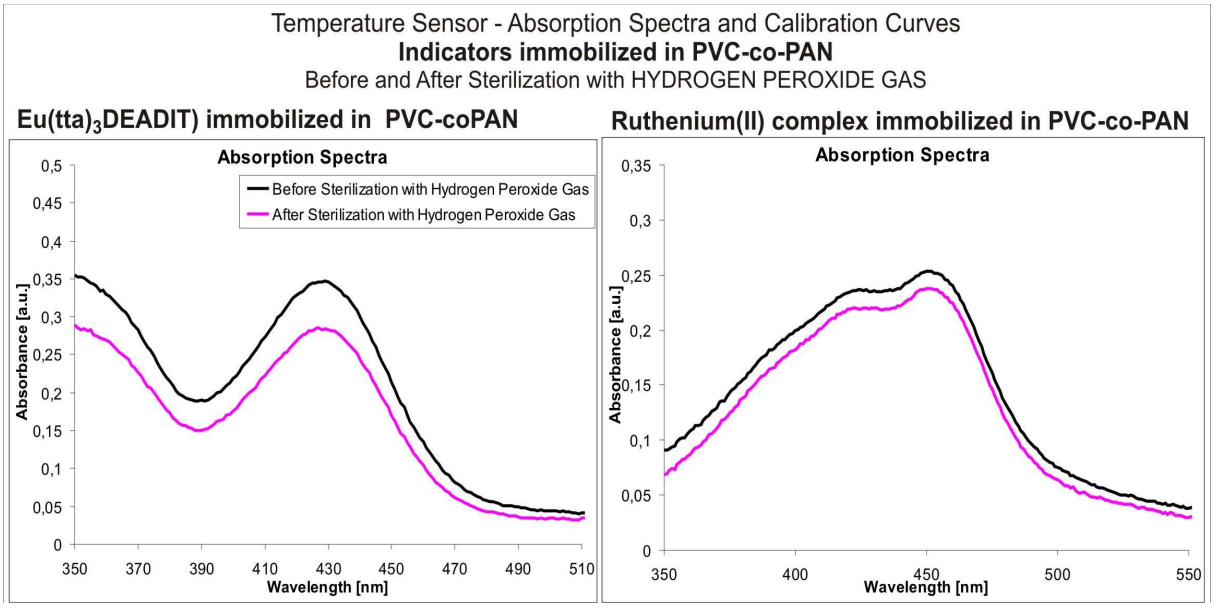

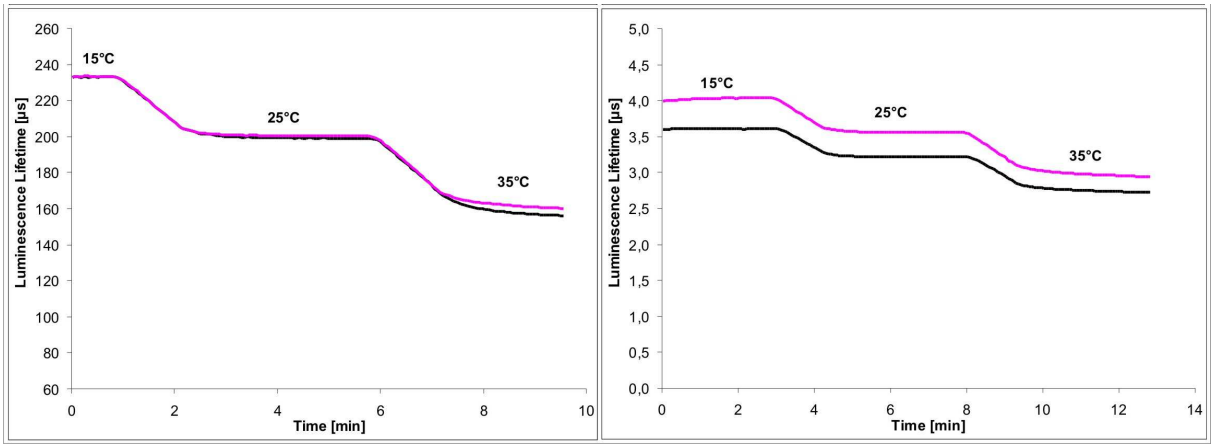

Figure 8 – 13: Absorption spectra and response curves of temperature sensor made of indicators Eu(tta)$_3$DEADIT and ruthenium(II) complex and immobilized in polymer PVC-co-PAN before and after sterilization with hydrogen peroxide gas.

8.4 Sterilization of Optical Ammonia Sensors with H_2O_2 (Gas and Plasma)

Hydrogen peroxide is absorbed by cellulose materials thereby preventing normal pressure changes during a sterilization cycle and causing it to abort. Consequently, ammonia sensors made of CA and EC polymer matrices could not be sterilized with any sterilization methods that contain hydrogen peroxide.

The absorption spectra of ammonia sensors made of polymer hydrogel D7 were not altered after sterilization. However, the hypsochromic shift of the maximum was observed by emission spectra. Therefore, the hydrogen peroxide reacted with polymer matrix and changed its polarity. The absorption and emission spectra of ammonia sensor made of polymer hydrogel D7 are presented in figure 8 – 14.

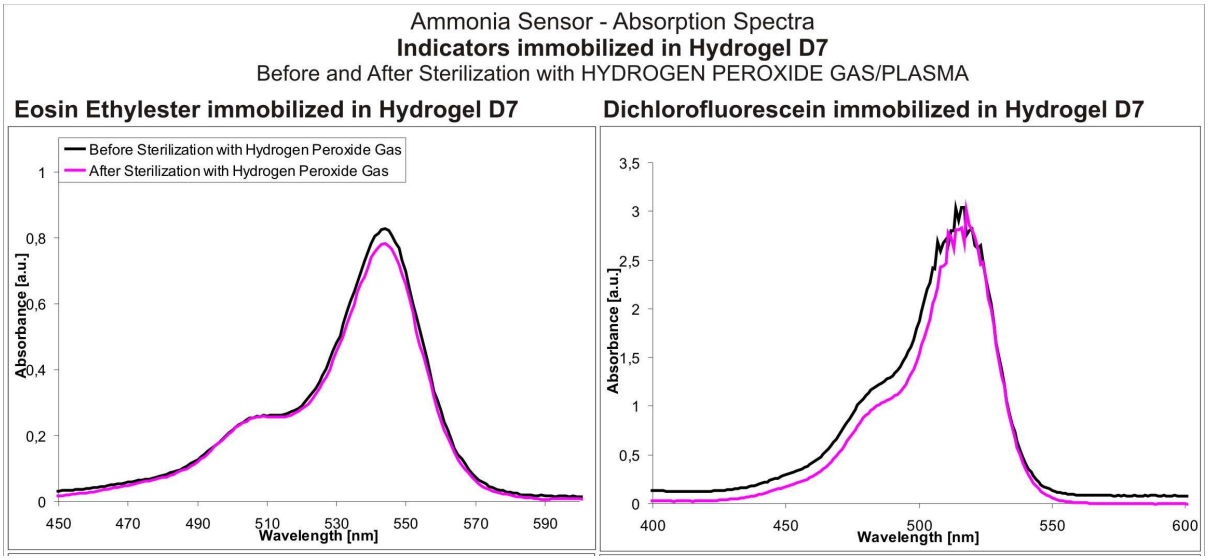

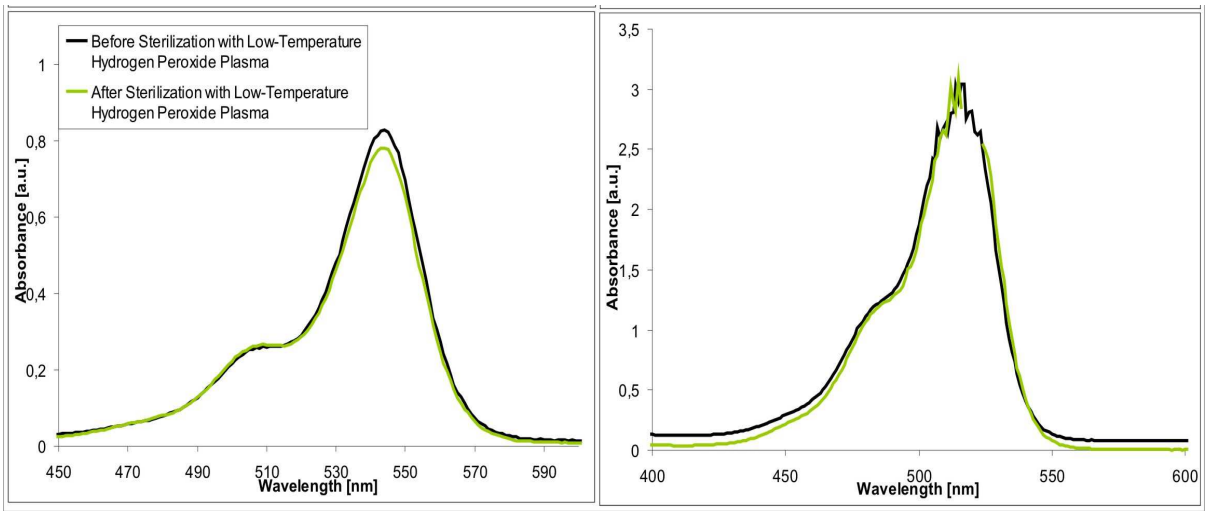

Figure 8 – 14: Absorption spectra and emission spectra of ammonia sensor made of indicators eosinethyl ester and dichlorofluorescein and immobilized in polymer hydrogel D7 before and after sterilization with hydrogen peroxide gas and plasma.

Hydrogen peroxide gas and plasma have also an impact on polymer PMMA because the polymer matrix became turbid after sterilization. That was observed in the absorption spectra of the ammonia sensor made of PMMA. However, the emission curve form and intensity remained similar after sterilization with hydrogen peroxide gas and plasma.

9 Summary

The following tables summarize the stability, resistance and alterations of oxygen, pH, temperature and ammonia optical sensors, respectively, towards different sterilization methods. A division was made as recommendation of certain sterilization methods, on the basis of how they affect the sensor response, absorption and emission. The colours in the tables represent the following:

Recommended sterilization method for optical sensor

Recommended sterilization method, but re-calibration of optical sensor should be made after sterilization method

Recommended sterilization method, but alterations in the absorption and emission spectra of optical sensor should be considered

Not recommended sterilization method for optical sensor

9.1 Oxygen Optical Sensors

Table 9 – 1: Summary of stability, resistance and alterations of diverse oxygen optical sensors towards different sterilization methods.

Sterilant	GAMMA			E-BEAM			Steam	Ethylene Oxide	H_2O_2 Gas	H_2O_2 Plasma
OXYGEN SENSOR	10	25	50	10	25	50				
$Ir(C_s)_2(acac)$ CA									/	/
$Ir(C_s)_2(acac)$ EC									/	/
$Ir(C_s)_2(acac)$ D4/D7										
$Ir(C_s)_2(acac)$ H5										
$Ir(C_s)_2(acac)$ PSf										
$Ir(C_s)_2(acac)$ PPSQ										
$Ir(C_s)_2(acac)$ PS										
$Ir(C_s)_2(acac)$ PS-co-PAN										
$Ir(C_s)_2(acac)$ PSMA93										
PtTFPP CA									/	/

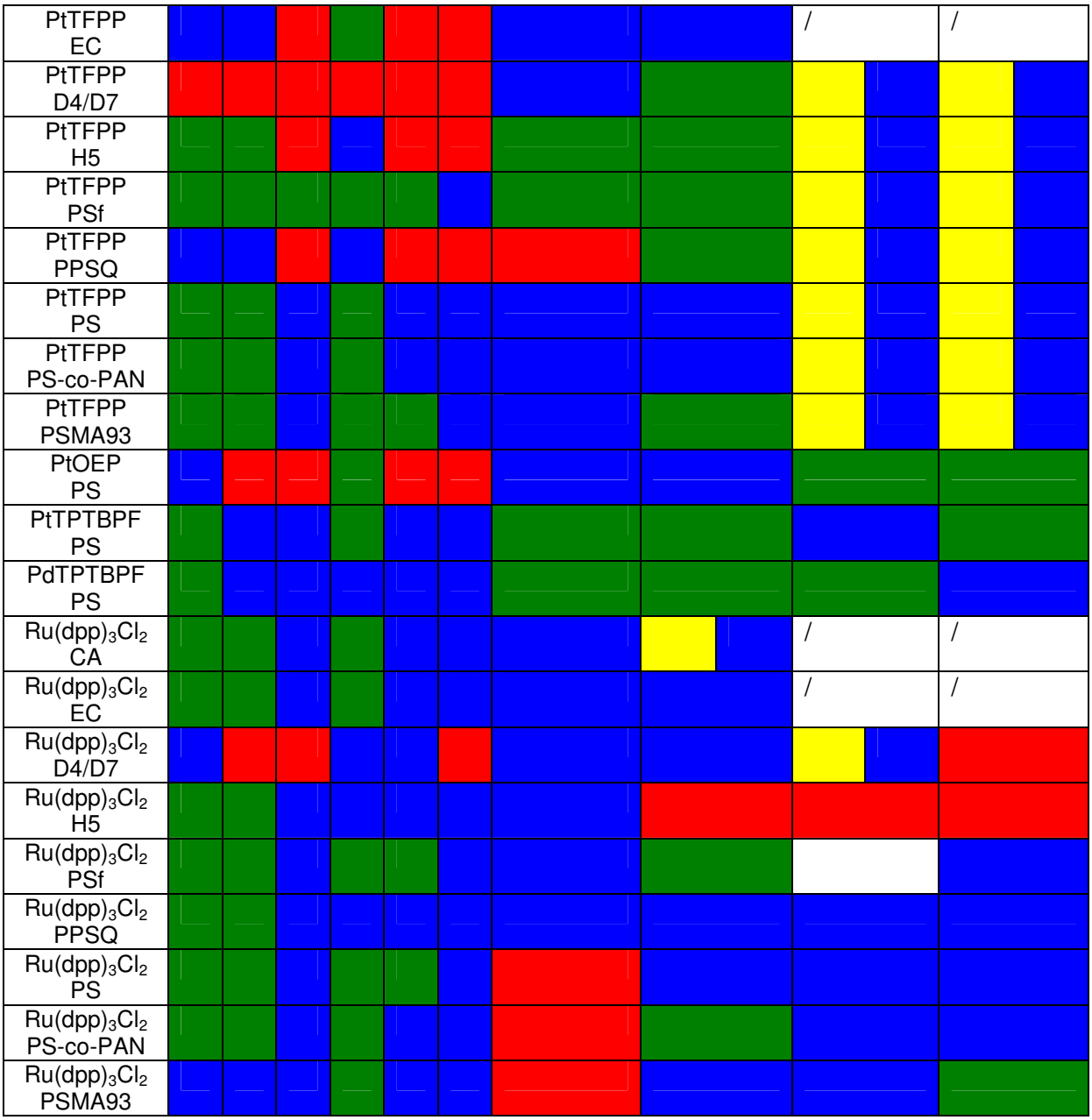

The majority of the oxygen sensors are radiation sterilizable with doses up to 25 kGy. However, the radiation sterilization induced some alterations and some of them should be re-calibrated after application of the radiation sterilization procedure. When the oxygen sensors were made of the polymers PS, PS-co-PAN, PSMA, PSf, PPSQ, the quenchers of the excited state were observed. Additionally, by cellulosic materials the acetate groups of the CA and ether group of the EC dissociate which has an additional influence on the quenching constant. Likewise, the radiation sterilization of the oxygen sensor made of PS-co-PAN led to cleavage of the cyano group in the polymer structure and that further lowers the phosphorescence lifetime.

Oxygen sensors made of the indicator PtTFPP were greatly affected by the gamma and electron beam sterilization. Additionally, the electron beams induced greater alterations than the gamma rays due to the more reducing capability of the sterilization procedure. Therefore, the sensor response made of porphyrins and sterilized with electron beams should be already re-calibrated at lower radiation doses in comparison to gamma sterilization. Higher doses are not recommended, especially for oxygen sensors made of the indicator PtTFPP and immobilized in hydrogel D7.

The least stable indicator towards the radiation sterilization and immobilized in PS was PtOEP. Radiation sterilization of this type of oxygen sensor with doses greater than 10 kGy should be avoided. The Pt- and Pd- benzoporphyrin indicators remained stable when immobilized in PS and radiation sterilized. However the alterations in the response of the sensors were also observed. The decrease of the phosphorescence lifetime was due to the formation of an additional quencher in the polystyrene matrix and the sensors should be re-calibrated after radiation sterilization with doses greater than 10 kGy.

Oxygen sensors made of the indicator $Ru(dpp)_3Cl_2$ were the most resistant of all indicators to gamma sterilization. Therefore, all oxygen sensors, with the exception of $Ru(dpp)_3Cl_2$ being immobilized in hydrogel D4 and PSMA, could be radiation sterilized up to 25 kGy without a re-calibration of the sensor response afterwards.

Steam sterilization has great effects on the polymers. The polymers CA, EC and Hydrothane™ became turbid after steam sterilization. However, the sensors still respond to a different concentration of oxygen. Therefore, oxygen sensors could be applied, but the re-calibration should be considered.

Oxygen sensors made of the polymer PPSQ were the most affected by steam. The absorption spectra were altered and the response of oxygen sensor with the indicator PtTFPP was no longer observed. Therefore, steam sterilization of the sensors made of PPSQ should be avoided. On the other hand, oxygen sensors made of the indicators $Ir(C_s)_2(acac)$ and PtTFPP and the polymers polystyrenes, polysulfone and hydrogel D4 were stable and resistant to steam sterilization. However, by some of these sensors small alterations were observed and these sensors should be re-calibrated before application.

When indicators were immobilized in polystyrene matrices, the least resistant indicator towards the steam sterilization was the indicator $Ru(dpp)_3Cl_2$. A bathochromic shift of the emission spectra was observed and the response of the sensor was altered. When it was immobilized in PS-co-PAN and PSMA, an increase in the absorption was measured and the typical curve shape could no longer be observed. Therefore, when the oxygen sensors are made of the ruthenium(III) complex and immobilized in polystyrene matrices, the steam sterilization is not recommended as sterilization procedure for these types of sensors.

After the sterilization method with ethylene oxide gas, the response and the duration of the phosphorescence lifetime of some of the oxygen sensors were changed afterwards. The cellulosic materials reacted with the ethylene oxide which had an influence on the sensor response. Therefore, the sensors with cellulosic matrices should be re-calibrated before application. Similar alterations as by oxygen sensors made of cellulose materials were observed when the sensors were made of the polymer matrix HydroThane™ and the indicators $Ir(C_s)_2(acac)$ and $Ru(dpp)_3Cl_2$. Consequently, re-calibration of the sensor response should be considered. However, when the indicator PtTFPP was immobilized in HydroThane™, the response of the sensor remained the same before and after sterilization. Therefore, additional calibration is not necessary.

On the other hand, by oxygen sensors made of the polymer Hydrogel D7 an additional quenchers were formed due to a uniform decrease of the phosphorescence lifetime after sterilization with ethylene oxide. Ethylene oxide also reacted with the polymer PPSQ, because the polymer matrix became less permeable for the oxygen. Likewise, these types of oxygen sensors should be re-calibrated. However, the polymers PSf, PS, PS-co-PAN and PSMA and consequently the sensors made of them were resistant to ethylene oxide gas. The alterations by these sensors were negligible and the sterilization method with ethylene oxide is recommended for these types of sensors.

The sterilization procedures with hydrogen peroxide gas or plasma induced more alterations on the sensor materials than ethylene oxide gas. Oxygen sensors made of the polymer Hydrogel D4 should be re-calibrated after sterilization with hydrogen peroxide gas because additional quenchers appeared which lower the phosphorescence lifetime. On the other

hand, hydrogen peroxide plasma induced additional alterations by the indicator iridium(III) coumarin and the ruthenium(III) complex due to UV irradiation. However, when these indicators were immobilized in polymer matrices that additionally absorb UV rays, such as PSf, the indicator structure of the indicators iridium(III) coumarin and the ruthenium(III) complex were less affected.

Hydrogen peroxide gas is an efficient oxidizing agent and therefore induced oxidation reactions in the indicator PtTFPP and the ruthenium(III) complex when immobilized in define polymer matrices. When the oxygen sensors were made of Hydrothane™, the indicator PtTFPP was protected from the oxidizing action of the hydrogen peroxide. On the other hand, the polymer matrix PPSQ did not shield the indicator PtTFPP from oxidation. However, the indicator ruthenium(III) complex was oxidized in both matrices to the ruthenium(II) complex. However, a response to the different oxygen concentrations could still be observed by these oxygen sensors. Therefore, with re-calibration after radiation sterilization the sensors could be applied. Additionally, the ruthenium(III) complex was UV and oxidation resistant when immobilized in the polymers PS and PS-co-PAN. However, in these polymer matrices the additional quenchers were formed and therefore these sensors should also be re-calibrated after sterilization with hydrogen peroxide gas and plasma.

The most appropriate sterilization method(s) for define optical oxygen sensor is(are):

$Ir(C_s)_2(acac)$_CA:	Gamma radiation up to dose 25 kGy, electron beam;
$Ir(C_s)_2(acac)$_EC:	Gamma radiation and electron beam up to dose 25 kGy;
$Ir(C_s)_2(acac)$_D4/D7:	Electron beam up to dose 10 kGy;
$Ir(C_s)_2(acac)$_H5:	Gamma radiation up to dose 25 kGy and electron beam up to dose 10 kGy;
$Ir(C_s)_2(acac)$_PSf:	Sterilization with ethylene oxide;
$Ir(C_s)_2(acac)$_PPSQ:	With re-calibration: Gamma and electron beam radiation up to dose 25 kGy, sterilization with ethylene oxide and hydrogen peroxide gas and plasma.
$Ir(C_s)_2(acac)$_PS:	Gamma radiation and electron beam up to dose 10 kGy, sterilization with ethylene oxide and hydrogen peroxide gas;
$Ir(C_s)_2(acac)$_PS-co-PAN:	Sterilization with ethylene oxide;
$Ir(C_s)_2(acac)$_PS:	Electron beam radiation up to dose 10 kGy, steam sterilization, sterilization with ethylene oxide, hydrogen peroxide gas and plasma;
PtTFPP_CA:	With re-calibration: Gamma radiation up to dose 25 kGy, electron beam radiation up to dose 10 kGy, steam sterilization, sterilization with ethylene oxide.
PtTFPP_EC:	Electron beam radiation up to dose 10 kGy;
PtTFPP_D4/D7:	Sterilization with ethylene oxide;
PtTFPP_H5:	Gamma radiation up to dose 25 kGy, steam sterilization, sterilization with ethylene oxide;
PtTFPP_PSf:	Gamma radiation up to dose 50 kGy, electron beam radiation up to dose 25 kGy, steam sterilization, sterilization with ethylene oxide;
PtTFPP _PPSQ:	Sterilization with ethylene oxide;
PtTFPP _PS:	Gamma radiation up to dose 10 kGy, electron beam radiation up to dose 10 kGy;

PtTFPP_PS-co-PAN: Gamma radiation up to dose 10 kGy, electron beam radiation up to dose 10 kGy;

PtTFPP_PSMA: Gamma radiation and electron beam radiation up to dose 25 kGy, serilization with ethylene oxide;

PtOEP _PS: Sterilization with hydrogen peroxide gas and plasma;

PtTPTBPF _PS: Gamma and electron beam radiation up to dose 10 kGy, steam sterilization, sterilization with ethylene oxide and hydrogen peroxide plasma;

PdTPTBPF _PS: Gamma radiation up to dose 10 kGy, steam sterilization, sterilization with ethylene oxide and hydrogen peroxide gas;

$Ru(dpp)_3Cl_2$_CA: Gamma radiation up to dose 25 kGy, electron beam radiation up to dose 10 kGy.

$Ru(dpp)_3Cl_2$_EC: Gamma radiation up to dose 25 kGy, electron beam radiation up to dose 10 kGy.

$Ru(dpp)_3Cl_2$_D4/D7: With re-calibration: Gamma radiation up to dose 10 kGy, electron beam radiation up to dose 25 kGy, steam sterilization, sterilization with ethylene oxide.

$Ru(dpp)_3Cl_2$_H5: Gamma radiation up to dose 25 kGy;

$Ru(dpp)_3Cl_2$_PSf: Gamma and electron beam radiation up to dose 25 kGy, sterilization with ethylene oxide;

$Ru(dpp)_3Cl_2$ _PPSQ: Gamma radiation up to dose 25 kGy;

$Ru(dpp)_3Cl_2$ _PS: Gamma and electron beam radiation up to dose 25 kGy;

$Ru(dpp)_3Cl_2$_PS-co-PAN: Gamma radiation up to dose 25 kGy, electron beam radiation up to dose 10 kGy; sterilization with ethylene oxide;

$Ru(dpp)_3Cl_2$_PSMA: Electron beam radiation up to dose 10 kGy, serilization with hydrogen peroxide plasma.

9.2 pH Optical Sensors

Table 9 – 2: Summary of stability, resistance and alterations of diverse pH optical sensors towards different sterilization methods.

Sterilant	GAMMA			E-BEAM			Steam	Ethylene Oxide	H_2O_2 Gas	H_2O_2 Plasma	
pH SENSOR	10	25	50	10	25	50					
$HPTS(DHA)_3$ D4											
$HPTS(DHA)_3$ D4 (Buffer S)											
DHFE D4											

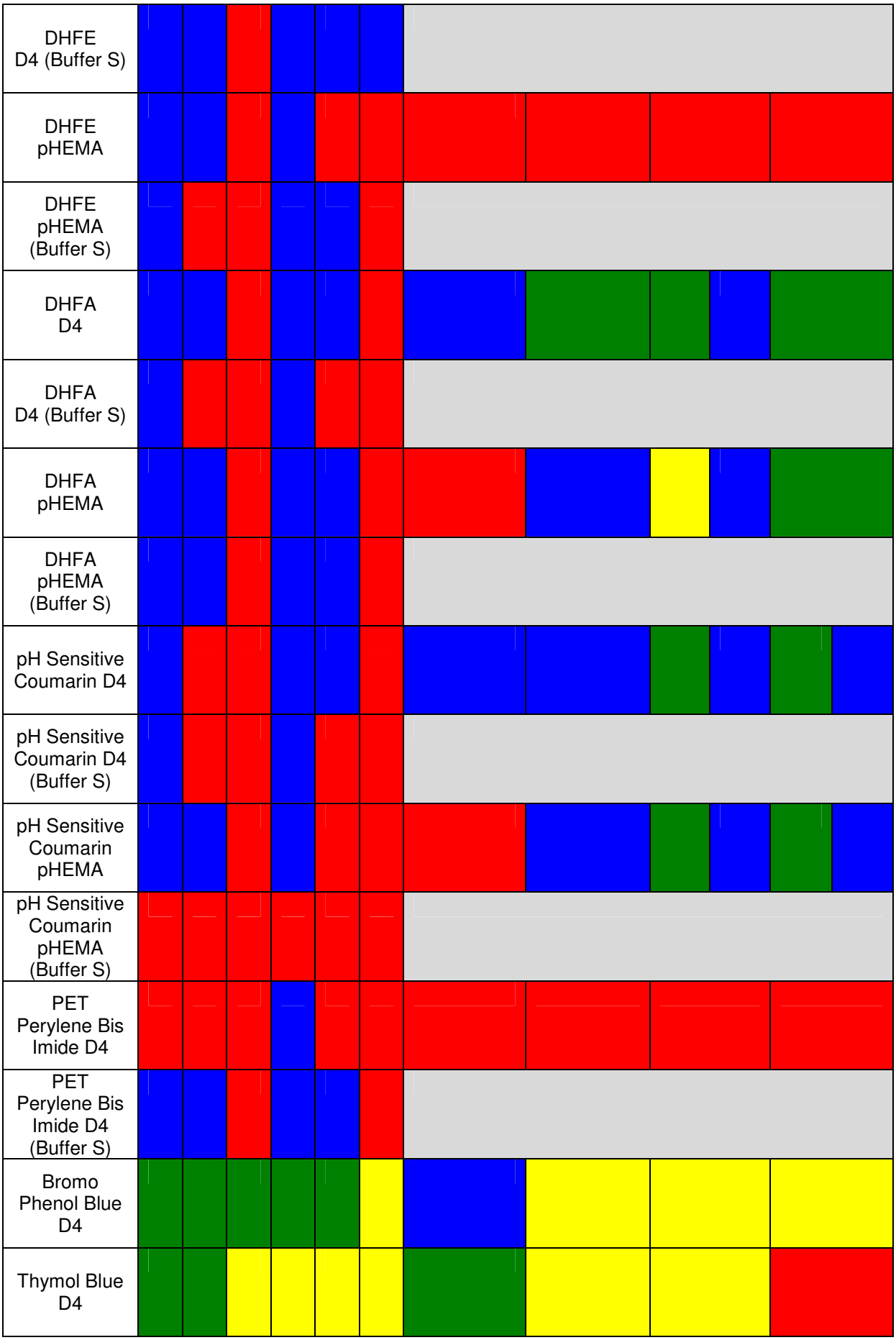
DHFE D4 (Buffer S)
DHFE pHEMA
DHFE pHEMA (Buffer S)
DHFA D4
DHFA D4 (Buffer S)
DHFA pHEMA
DHFA pHEMA (Buffer S)
pH Sensitive Coumarin D4
pH Sensitive Coumarin D4 (Buffer S)
pH Sensitive Coumarin pHEMA
pH Sensitive Coumarin pHEMA (Buffer S)
PET Perylene Bis Imide D4
PET Perylene Bis Imide D4 (Buffer S)
Bromo Phenol Blue D4
Thymol Blue D4

Bromo Thymol Blue D4	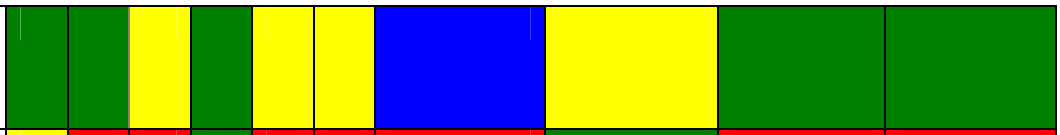
Methyl Orange D4	

The majority of pH sensors should be re-calibrated after the application of gamma and electron beam sterilization. Radiation sterilization has a great impact on optical pH sensors based on fluorescence. When the fluorescence pH sensitive indicators were immobilized in the polymer hydrogel D4, radiation sterilization had an impact on the protonation/deprotonation capability. Additionally, the migration of the indicator to more hydrophobic/hydrophilic parts of the polymer hydrogel D4 appeared which reduced or increased the pK_a value after sterilization. However, the sensors were still capable to absorb and emit the photons and the response was still pH dependent. Therefore, the pH sensors immobilized in hydrogel D4 should be re-calibrated after radiation sterilization.

Gamma and electron beam sterilization has affected the sensors made of the polymer matrix pHEMA. The concentration of the water uptake by the polymer pHEMA was greater after radiation sterilization, which is an indication of chain-scission or re-conformation of polymer chains. When the sensors made of pHEMA were sterilized in standard ambient conditions, the sensors became turbid after characterization in the buffer solution. However, when the same sensors were sterilized in the buffer solution, these effects on the polymer pHEMA were no longer observable and the sensors did not become turbid after characterization.

After gamma sterilization of the pH indicator PET Perylene bisimide immobilized in the hydrogel D4 in normal environment, the PET process was depressed and therefore the pH sensitivity was no longer observable. On the other hand, when the same sensor was gamma sterilized in a buffer solution, pH sensitivity via PET was still observed up to sterilization with dose 25 kGy. However, the sensor should be re-calibrated after sterilization because the PET efficiency was changed. Electron beam sterilization is a slightly more appropriate sterilization method for this type of pH sensor. Nevertheless, the sensor should also be re-calibrated and the doses should not exceed 10 kGy in standard ambient conditions and 25 kGy when sterilized in a buffer solution.

The most stable pH sensors against radiation sterilization were made of sulfonephthalein pH indicators based on colour change, such as bromophenol blue, bromothymol blue and thymol blue. However, the resistance of sulfonephthalein pH indicators to gamma and electron beam increases with an increasing electron density of the indicators – the tymol blue is the at least and bromophenol blue the most resistant. On the other hand, the azo pH sensitive indicator based on colour change – methyl orange – was not irradiation resistant to doses higher than 10 kGy.

By steam sterilization, both polymer matrices hydrogel D4 and pHEMA were affected by harsh conditions such as heat, pressure and humidity. The hydrogel D4 matrix became slightly turbid and parts of it melted after steam sterilization. Therefore, the inhomogeneities of the sensor layer appeared. Additionally, when the indicators based on fluorescence were immobilized in hydrogel D4 the changes in protonation/deprotonation absorption and emission peaks were observed. Therefore, all pH sensors made of hydrogel D4 should be re-calibrated after the application of steam. On the other hand, the polymer pHEMA melted after the utilization of temperature 121°C and is therefore not an appropriate polymer matrix for steam sterilization.

pH sensors made of PET Perylene bisimide and immobilized in hydrogel D4 should not be sterilized with steam due to a migration of the indicator to the more lipophilic support foil - Mylar®. Likewise, the steam sterilization is not an appropriate sterilization method for the azo

pH sensitive dye methyl orange because the characteristic curve shape could no longer be observed after steam sterilization.

Sterilization with ethylene oxide gas caused the least alterations on the absorption and emission capabilities by the pH optical sensors based on fluorescence and immobilized in hydrogel D4. However, the response curves were not exactly the same before and after sterilization with ethylene oxide gas with the exception of the pH sensor made of the indicator DHFA and immobilized in the polymer hydrogel D4. Therefore, re-calibration before the applications should be considered.

When the indicators were immobilized in the polymer pHEMA, greater alterations in the absorption spectra and response curves could be observed. Therefore, the sensors should also be re-calibrated after sterilization with the exception of pH sensors with the indicator DHFE where this mode of sterilization is not recommended. When the indicator PET Perylene bisimide was immobilized in hydrogel D4, the ethylene oxide probably reacted with the amino moiety of the indicator, which is responsible for PET process. Therefore the sensor was no longer pH dependent and the sterilization procedure with ethylene oxide is not appropriate.

Ethylene oxide gas has an impact on the absorption capabilities of the sulfonephthalein pH sensitive dyes. Additionally, the protonation and deprotonation peak ratios were altered. However, these sensors could still be utilized with re-calibration of the sensor response after the sterilization procedure. For sensor made of azo pH sensitive indicator methyl orange and immobilized in hydrogel D4, the sterilization method with ethylene oxide is the most appropriate sterilization procedure in comparison to all other applied in this study.

Hydrogen peroxide gas has an impact on pH sensors made of the indicator HPTS$(DHA)_3$ and immobilized in hydrogel D4. Alterations were observed in the absorption spectra and also in the response of the sensor. Therefore, after the application of the hydrogen peroxide gas and plasma as sterilization method, these sensors should be re-calibrated. The absorption and emission capabilities of lipophilic fluoresceins were similar before and after sterilization with hydrogen peroxide gas and plasma when immobilized in hydrogel D4. On the other hand, at the sterilization of the DHFE, when immobilized in pHEMA, the quenchers of the luminescence intensity appeared and the emission was no longer observed. Therefore, sterilization with hydrogen peroxide gas and plasma is not recommended for this type of sensor. On the other hand, the pH sensor made of lipophilic fluorescein DHFA and immobilized in pHEMA remained stable after the application of hydrogen peroxide and the quenchers were not observed.

The pH sensitive coumarin immobilized in hydrogel D4 and pHEMA could be sterilized with hydrogen peroxide gas and plasma, but re-calibration should be considered afterwards. On the other hand, sterilization with hydrogen peroxide gas and plasma of sensors made of PET Perylene bisimide and hydrogel D4 is not recommended due to an oxidation of the amino moiety and consequently the disappearance of pH sensitivity of the indicator.

The sulfonephthalein pH sensitive dyes are resistant to sterilization with hydrogen peroxide gas when immobilized in hydrogel D4. On the other hand, the indicator thymol blue immobilized in hydrogel D4 was destroyed after sterilization with hydrogen peroxide plasma due to UV radiation. The others were more resistant but also slightly affected. Therefore, re-calibration of these pH sensors should be considered after the application of hydrogen peroxide plasma.

The most appropriate sterilization method(s) for define optical pH sensor is(are):

HPTS$(DHA)_3$_D4:	With re-calibration: All sterilization methods;
DHFE_D4:	Sterilization with hydrogen peroxide gas and plasma;
DHFE_pHEMA:	With re-calibration: Gamma and electron beam radiation up to dose 10 kGy.

DHFA_D4: Sterilization with ethylene oxide and hydrogen peroxide gas and plasma;

DHFA_pHEMA: Sterilization with hydrogen peroxide plasma;

pH Sensitive Coumarin_D4: Sterilization with hydrogen peroxide gas and plasma;

pH Sensitive Coumarin_pH: Sterilization with hydrogen peroxide gas and plasma;

PET Perylene bisImide_D4: Electron beam radiation up to dose 10 kGy;

Bromophenol blue_D4: Gamma radiation up to dose 50 kGy, electron beam radiation up to dose 25 kGy.

Thymol blue_D4: Gamma radiation up to dose 25 kGy, steam sterilization;

Bromothymol blue_D4: Gamma radiation up to dose 25 kGy, electron beam sterilization up to dose 10 kGy, sterilization with hydronge peroxide gas and plasma;

Methyl Orange_D4: Electron beam radiation up to dose 25 kGy, sterilization with ethylene oxide.

9.3 Temperature Optical Sensors

Table 9 – 3: Summary of stability, resistance and alterations of diverse tempearture optical sensors towards different sterilization methods.

Sterilant	GAMMA			E-BEAM			Steam		Ethylene Oxide	H_2O_2 Gas	H_2O_2 Plasma
Temperat. SENSOR	10	25	50	10	25	50					
$Eu(tta)_3$ DEADIT PS-co-PAN											
$Eu(tta)_3$ DEADIT PVC-co-PAN											
$Eu(tta)_3$ DEADIT PMAN											
Ru(II) complex PVC-co-PAN											
Ru(II) complex PMAN											

The indicator $Eu(tta)_3$DEADIT was resistant to gamma and electron beam sterilization when immobilized in the polymer PS-co-PAN. However, greater alterations in the absorption, emission and sensor response were observed when the indicator $Eu(tta)_3$DEADIT was immobilized in the polymers PVC-co-PAN and PMAN. Therefore, the sensors should be re-calibrated after radiation sterilization up to dose 25 kGy. Higher doses are not appropriate for these types of temperature sensors. On the other hand, the indicator dichlorotris(1,10-phenanthroline) ruthenium(II) hydrate could be radiation sterilized when immobilized in PVC-co-PAN. However, the polymer matrix PMAN is not an appropriate matrix for both temperature sensitive indicators, when the sensors should be radiation sterilized with doses higher than 10 kGy.

After steam sterilization, all polymers applied in this study for the development of optical temperature sensors became turbid. However, the sensor emission intensity and response were still observed by the majority of the sensors with the exception of temperature sensors made of $Eu(tta)_3$DEADIT and the polymer PVC-co-PAN, where the emission and the response of the sensor could no longer be observed after steam sterilization. The other temperature sensors could still be utilized after steam sterilization, but the sensor response should be re-calibrated.

The sterilization method with ethylene oxide is recommended for temperature sensors made of the indicator $Eu(tta)_3$DEADIT and immobilized in the polymer PS-co-PAN and sensors made of the indicator ruthenium(II) complex and immobilized in the polymer PVC-co-PAN. On the other hand, the response of the temperature sensors immobilized in PMAN was altered after sterilization with ethylene oxide. Therefore, re-calibration should be made before applying these types of sensors.

All temperature sensors, with the exception of the sensor made of the indicator ruthenium(II) complex and the polymer matrix PMAN were sterilizable with hydrogen peroxide gas. On the other hand, the sterilization method with low-temperature hydrogen peroxide plasma induced more alterations. The only sensor that remained stable after sterilization with hydrogen peroxide plasma was made of the ruthenium(II) complex immobilized in the polymer PVC-co-PAN. However, the sensor response of the sensors made of $Eu(tta)_3$DEADIT and the polymers PS-co-PAN and PVC-co-PAN should be re-calibrated after sterilization and the sensors could still be utilized afterwards.

The most appropriate sterilization method(s) for define optical temperature sensor is(are):

$Eu(tta)_3$DEADIT_PS-co-PAN:	Gamma radiation up to 25 kGy, electron beam radiation up to 50 kGy, steam sterilization, sterilization with ethylene oxide and hydrogen peroxide gas;
$Eu(tta)_3$DEADIT_PVC-co-PAN:	Sterilization with hydrogen peroxide gas;
$Eu(tta)_3$DEADIT_PMAN:	Sterilization with hydrogen peroxide gas;
Ru(II) complex_PVC-co-PAN:	Gamma radiation up to 25 kGy, electron beam radiation up to 50 kGy, steam sterilization, sterilization with ethylene oxide and hydrogen peroxide gas and plasma;
Ru(II) complex_PMAN:	With calibration: Gamma radiation up to 10 kGy, electron beam radiation up to 25 kGy, sterilization with ethylene oxide.

9.4 Ammonia Optical Sensors

Table 9 – 4: Summary of stability, resistance and alterations of diverse ammonia optical sensors towards different sterilization methods.

Sterilant	GAMMA			E-BEAM			Steam	Ethylene Oxide	H_2O_2 Gas	H_2O_2 Plasma
AMMONIA SENSOR	10	25	50	10	25	50				
Eosin Ethyl Ester CA									/	/
Eosin Ethyl Ester EC									/	/

Eosin Ethyl Ester D7										
Eosin Ethyl Ester PMMA										
DiChloro Fluorescein CA									/	/
DiChloro Fluorescein EC									/	/
DiChloro Fluorescein D7										
Bromo Phenol Blue CA									/	/
Bromo Phenol Blue EC									/	/
Bromo Phenol Blue D7										
Bromo Phenol Blue PMMA										

Gamma and electron beam sterilization has a small effect on the absorption capabilities of ammonia sensors. However, the emission intensity decreased for more than 80% after irradiation by sensors made of the indicators eosin ethylester and dichlorofluorescein, which appeared due to the formation of the quencher for eosin ethylester and due to a reduction of the indicator dichlorofluorescein. Therefore, alterations in the emission intensity of ammonia sensors made of these two indicators should be considered. On the other hand, ammonia sensors made of the indicator bromophenol blue were very resistant to gamma and electron beam sterilization. Therefore, radiation sterilization is recommended for these types of sensors.

Ammonia sensors made of cellulosic materials, such as cellulose acetate and ethyl cellulose are not the most appropriate polymer matrices for steam sterilization because they become turbid afterwards. Additionally, the polarity of these polymer matrices was changed, which was observed as solvatochromic shifts of the absorption and emission maxima. However, the ammonia sensors made of the polymer hydrogel D7 remained stable after steam sterilization with the exception when the indicator eosin ethylester was immobilized in it. When the indicators were immobilized in PMMA, the alterations and a decrease of the absorption were observed. Therefore, steam sterilization is not an appropriate method when indicators are immobilized in the polymer PMMA.

The sterilization with ethylene oxide induced the least alterations on the ammonia sensors among all sterilization procedures applied in this study,. Some small alterations were detected when the polymer EC was used as polymer matrix. Here, the solvatochromic shift in the emission spectra was observed, which could be due to alterations in the polymer polarity. By other ammonia sensors, the changes in the absorption and emission spectra were negligible and therefore the sterilization method with ethylene oxide gas is recommended for these types of optical ammonia sensors.

Sterilization methods with hydrogen peroxide could only be applied to ammonia sensors made of the polymer matrices hydrogel D7 and PMMA. The absorption spectra of ammonia sensors made of the polymer hydrogel D7 were not altered after sterilization with hydrogen

peroxide gas and plasma. However, the emission spectra were. Therefore, re-calibration of these types of ammonia sensors should be considered. On the other hand, ammonia sensors made of the polymer matrix PMMA became turbid after sterilization with hydrogen peroxide gas and plasma. Similarly, hydrogen peroxide plasma has an effect on the emission capabilities of the sensor. Therefore, ammonia sensors made of the polymer PMMA should not be sterilized with hydrogen peroxide plasma.

The most appropriate sterilization method(s) for define optical ammonia sensor is(are):

Eosin ethyester_CA:	Gamma radiation up to 10 kGy, electron beam radiation up to 25 kGy, sterilization with ethylene oxide;
Eosin ethyester_EC:	Gamma radiation up to 10 kGy, electron beam radiation up to 25 kGy;
Eosin ethyester_D7:	Sterilization with ethylene oxide;
Eosin ethyester_PMMA:	Gamma radiation up to 25 kGy, electron beam radiation up to 10 kGy; sterilization with ethylene oxide;
Dichlorofluorescein_CA:	Gamma radiation up to 10 kGy, electron beam radiation up to 50 kGy, sterilization with ethylene oxide;
Dichlorofluorescein _EC:	Gamma radiation up to 25 kGy, electron beam radiation up to 10 kGy;
Dichlorofluorescein _D7:	Gamma radiation up to 10 kGy, electron beam radiation up to 50 kGy, steam sterilization, sterilization with ethylene oxide and hydrogen peroxide gas and plasma;
Bromophenol blue_CA:	Gamma radiation up to 25 kGy, electron beam radiation up to 50 kGy, sterilization with ethylene oxide;
Bromophenol blue _EC:	Gamma and electron beam radiation up to 50 kGy;
Bromophenol blue _D7:	Gamma and electron beam radiation up to 50 kGy; steam sterilization, sterilization with ethylene oxide;
Bromophenol blue _PMMA:	Gamma and electron beam radiation up to 50 kGy, sterilization with ethylene oxide.

IV
Conclusion

10 Conclusion

The effects of different commercial sterilization methods on the measuring function of the optical sensor were investigated. The sterilization procedures used have diverse effects on the sensor response.

Generally, the gamma and the electron beam sterilization method have a similar impact on the materials. However, the systems that are subject to the reduction are more affected through electron beam sterilization due to a greater capability for reduction than gamma rays. Even though, the doses around 50 kGy by both methods have a great impact on the sensor structure and response; therefore, lower doses are preferable. The polymer matrix plays a major role in the stability of the sensor towards radiation sterilization. Therefore, the polymers resistant to gamma rays and electron beams also protect the indicator structure from alterations. On the other hand, radiation sterilization has an impact on the polymer matrix changes were also observed in the indicator structure or in the sensor response.

After radiation sterilization of oxygen optical sensors in some polymer matrices, an additional quencher was formed, which decreased the luminescence lifetime. However, the oxygen sensors were responsive and could be utilized with re-calibration of the sensor respond after radiation sterilization. Likewise, the indicator PtTFPP was greatly affected by gamma and electron beam sterilization. The reactions that occurred during the irradiation between PtTFPP and its environment led to a new form of porphyrine which absorbed and emitted photons at longer wavelengths than before sterilization. Other oxygen sensitive indicators were in a different way resistant to gamma and electron beam sterilization. The indicator PtOEP was the least stable indicator towards radiation sterilization when immobilized in the polymer PS. On the other hand, the most stable indicator was $Ru(dpp)_3Cl_2$ when immobilized in diverse polymer matrices and radiation sterilized.

By radiation sterilization of optical pH sensors based on fluorescence, the protonation/ deprotonation rates were altered and by application of the polymer matrix hydrogel D4, the indicator migrated into more hydrophobic or hydrophilic parts of the matrix, which had an influence on the pK_a value of the sensor. Therefore, the majority of pH sensors made of fluorescence based pH sensitive indicators immobilized in hydrogen D4 should be re-calibrated after radiation sterilization.

The polymer pHEMA, which was the second polymer matrix applied for pH optical sensors, was affected through gamma rays and electron beams, when sterilized in standard ambient temperature, pressure and humidity. As far as the polymer pHEMA is concerned, the concentration of water uptake increased after radiation sterilization, which is a consequence of chain-scission or re-conformation of polymer chains. Therefore, after characterilization in buffer solution, turbidity of the sensor was observed. On the other hand, when the same sensor was radiation sterilized in buffer solution, these processes and effects on the polymer pHEMA were suppressed. Of all pH sensitive indicators, the indicator pH sensitive coumarin was the least stable against radiation sterilization. Contrary, the sulfonephtalein pH indicators based on colour change were the most stable one.

Temperature sensors made of the indicator $Eu(tta)_3$DEADIT immobilized in PS-co-PAN and the indicator dichlorotris(1,10-phenanthroline) ruthenium(II) hydrate immobilized in PVC-co-PAN were resistant to gamma and electron beam sterilization. On the other hand, the polymer matrix PMAN was the least appropriate when these temperature sensors should be radiation sterilized.

Gamma and electron beam sterilization have a small effect on the absorption capabilities of the ammonia sensor but a great effect on the emission. Quenchers were formed by sensors

made of the indicator eosin ethylester, which reduced the emission intensity. On the other hand, a reduction of the fluorescein structure appeared by sensors made of the indicator dichlorofluorescein, which has also an influence on the emission intensity. However, ammonia sensors made of the indicator bromophenol blue were very resistant to gamma and electron beam sterilization.

Steam sterilization procedure has an influence on some polymer materials which melted or became turbid during the sterilization process. Despite alterations in the polymer matrices, the response to the define analyte was still observed by some sensors. Therefore, by re-calibration of the sensors after the application of steam, the sensors could be utilized. However, the polymer matrix made of PPSQ was too affected and is therefore not recommended for this type of sterilization. On the other hand, the polymer matrices PS and PSf are resistant to high temperature, humidity and pressure and for these polymers the steam sterilization method could be applied. Moreover, if the indicator $Ru(dpp)_3Cl_2$ was the most stable indicator towards radiation sterilization, it was the least stable among oxygen sensitive indicator to steam sterilization. The sterilization of this indicator in polystyrene matrix is not recommended.

After steam sterilization of the pH sensors, the polymer matrix hydrogel D4 matrix became slightly turbid and parts of it melted, which induced inhomogeneities in the sensor layer. Therefore, all pH sensors made of hydrogel D4 should be re-calibrated after the application of steam. The polymer matrix pHEMA completely melted and is therefore not an appropriate polymer matrix for steam sterilization. Likewise, the pH sensor made of PET Perylene bisimide should not be sterilized with steam because a migration to the Mylar® support foil appeared and the PET process was no longer observable.

All polymers - PS-co-PAN, PVC-co-PAN and PMAN - used by optical temperature sensors became turbid after steam sterilization. This has an effect on the absorbance of the sensors. On the other hand, the emission and sensor response were still observed. Therefore, by re-calibration the sensors could be used despite of the turbidity. The exception was a sensor made of $Eu(tta)_3$DEADIT and immobilized in PVC-co-PAN, where the sensor was destroyed after the application of this type of sterilization. The steam also has an affect on the polarity of the polymer matrices applied for ammonia sensors. Therefore, the solvatochromic shifts in the absorption and emission spectra were observed. However, the best polymer matrix for ammonia sensors that can be sterilized with steam is hydrogel D7.

Sterilization with ethylene oxide gas had the least influence on the sensor materials and response. Overall, ethylene oxide gas has reacted with those polymer matrices that possess hydroxyl groups in their structure which changed the response of the sensor. Amongst oxygen sensors the response and the duration of the phosphorescence lifetime of the oxygen sensors were changed at cellulose acetate, ethyl cellulose, hydrothane with 5% water content and PPSQ. Therefore, the re-calibration after sterilization with ethylene oxide is necessary for these types of oxygen sensors. Likewise, sensors made of hydrogel D7 should be re-calibrated because the additional quenchers were formed. Amongst the polymers PSf, PS, PS-co-PAN and PSMA, no reactions with ethylene oxide were observed. Therefore, sterilization of the sensors made of these polymers with ethylene oxide is appropriate.

The majority of the pH sensors should be re-calibrated after sterilization with ethylene oxide gas because of the effects on the response curves which appeared due to reactions between ethylene oxide and polymer matrices. However, the indicator PET Peryelen bisimide should not be sterilized with ethylene oxide due to reactions that appeared between the sterilizing agent and the amino moiety of the indicator that suppressed the PET process. The pH sensor made of methyl orange remained the most stable when sterilized with ethylene oxide in comparison to all other sterilization procedures applied in this study.

Temperature sensors, with the exception of those made of the polymer matrix PMAN, were not affected by ethylene oxide gas. Similarly, ammonia sensors were affected the least by

this mode of sterilization. Alterations were observed when the sensors were made of ethyl cellulose. Amongst other ammonia sensors, the alterations were negligible.

The sensors were also compatible with hydrogen peroxide gas sterilization procedure. Generally, alterations were observed due to the oxidation action of hydrogen peroxide. However, sterilization solely with hydrogen peroxide gas does not provide a sterility assurance level (SAL) of 10^{-6}. Therefore, this mode of sterilization can only be applied when greater SAL numbers are required. SAL of 10^{-6} could be achieved with an additional utilization of hydrogen peroxide plasma. Hence, sterilization procedure with low-temperature hydrogen peroxide plasma induced more alterations than with hydrogen peroxide gas. Indicators sensitive to UV irradiation were affected and the absorbing and emitting capabilities of these indicators were changed after sterilization with hydrogen peroxide plasma. The oxygen sensitive indicators, ruthenium(III) complex and iridium(III) coumarin were affected in some polymer matrices due to UV irradiation. These indicators were the most stable when immobilize in the polymer PSf because the polymer contains the functional group that additionally absorbs UV light, which shielded the indicator against alterations.

As already mentioned, hydrogen peroxide gas is an oxidizer and the indicators PtTFPP and the ruthenium(III) complex were oxidized in some polymer matrices. However, a response to the different concentrations of the oxygen was still observed and with re-calibration of these sensors, utilization is still possible.

However, sterilization methods with hydrogen peroxide are not appropriate for cellulosic materials. Therefore, sensors where the indicators were immobilized in CA or EC were not sterilized with hydrogen peroxide gas and plasma.

Optical pH sensors were also affected by hydrogen peroxide gas and plasma sterilization method and the majority of the pH sensor response should be re-calibrated. For pH sensors, sterilization procedure with hydrogen peroxide is not appropriate. Likewise, for sensors made of the indicator PET Perylene bisimide the hydrogen peroxide sterilization methods are not appropriate due to an oxidation of the amino moiety, and consequently the pH sensitivity of the indicator could no longer be observed. The resistance of the sulfonephtalein pH indicators towards sterilization methods with hydrogen peroxide plasma was dependent on the electron density of the indicator. Therefore, the indicator thymol blue was subjected the most to oxidation of all sulfonephthalein pH indicators applied in this study and is therefore not resistant to UV radiation during sterilization with hydrogen peroxide plasma.

All temperature sensors, with the exception of the sensor made of the indicator ruthenium(II) complex and the polymer matrix PMAN, are sterilizable with hydrogen peroxide gas. Hydrogen peroxide plasma has more effects on these temperature sensors. More precisely, the only temperature sensor stable against hydrogen peroxide plasma was made of the ruthenium(II) complex and immobilized in polymer PVC-co-PAN. However, the response of the other sensors should be re-calibrated after sterilization with hydrogen peroxide plasma.

With hydrogen peroxide gas and plasma, only the ammonia sensors made of the polymer matrices hydrogel D7 and PMMA could be sterilized. However, amongst ammonia sensors made of hydrogel D7 the absorption capabilities were not altered, but the emission intensities were. On the other hand, sensors made of PMMA became turbid after the application of hydrogen peroxide and due to great alterations in the emission spectra, the sensors made of PMMA should not be sterilized with hydrogen peroxide gas and plasma.

To conclude, this study provides a general overview of the effects of the different sterilization methods on the optical sensors and materials. The sterilization methods described have different impacts as well as compatibilities with materials. Radiation sterilization can induce the formation of additional quenchers, altered the permeability of the polymer matrix for the analyte of interest or oxidized/reduced the indicator structure. The appearance of polymers is greatly affected by the application of steam. However, a response of some sensors was still observed and with re-calibration the sensors could still be utilized. The sterilization procedures with ethylene oxide induced the least changes on the sensors. Hence, amongst

polymers with hydroxyl groups the reactions could be observed and some of the sensors should also be re-calibrated. Hydrogen peroxide gas is an oxidizer and in some materials oxidation was observed. Additionally, after hydrogen peroxide plasma the indicators were destroyed due to UV radiation.

There is no sterilization procedure that would be appropriate for all materials and optical sensors. However, if re-calibration of the optical sensors after sterilization procedure is possible, the spectrum of recommended sterilization methods is quite extensive. Due to the great number of materials, additional studies on certain materials and interpretations of the effects are desirable. Therefore, this study only serves as the framework. Additional content of interest should be investigated in the future.

11 References

[1] Seymour, S.B. *Disinfection, Sterilization and Preservation*. 5th edition. Philadelphia, USA: Lippincott Williams&Wilkins, 2001.

[2] Wayne, R. *Sterilisation of Polymer Healthcare Products.* Shrewsbury, UK: Rapra Technology Limited, 2005.

[3] Nigel, A.H. *Achiving Sterility in Medical and Pharmaceutical Products.* New York: Marcel Dekker Inc., 1994

[4] Fraise, A.P., Lambert, P.A. and Maillard, J.Y. *Russell, Hugo & Ayliffe´s Principles and Practice of Disinfection Preservation and Sterilization*. 4th edition. United Kingdom: Blackwell Publishing, 2004.

[5] Clough, R.L. *High-energy Radiation and Polymers: A Review of Commercial Processes and Emerging Applications.* Nuclear Instruments and Methods in Physics Research. 2001; **185**, 8-33.

[6] Herring, C.M. and Saylor, M.C. *Chapter 8: Sterilization with Radioisotopes, Sterilization Technology: A Practical Guide for Manufacturers and Users of Health Care Products*. Morrissey, R.F and Phillips, G.B. (ed.). New York: Van Nostrand Reinhold, 1993.

[7] Calhoun, L.R., Allen, J.T., Shaffer, H.L, Sullivan, G.M. and Williams C.B. *Electron-Beam Systems for Medical Device Sterilization.* Medical Plastics and Biomaterials Magazine. 1997.

[8] Bridges, B.A. *Survival of Bacteria following exposure to ultraviolet and ionizing radiations.* 26th Symposium of Society for General Microbiology. Cambridge: Cambridge University Press, 1976.

[9] Moseley, B.E.B. *Ionizing Radiation: Action and Repair, Mechanisms of Action of Food Preservation Procedures.* Gould, G.W. (ed.). London: Elsevier Applied Science, 1989.

[10] World Health Organization. *Good Manufacturing Practices for Pharmaceutical Products.* PHARM/99.412. TRS 823, Annex 1. Geneva, 1999.

[11] Christensen, E.A. *The role of microbiology in commissioning a new facility and in routine control, in Sterilization by Ionizing Radiation.* Gaughran, E.R.L. and Goudie, A.J. (ed.), Vol. II, Montreak, Quebec, Canada: Multiscience Publishers, 1977.

[12] Ebewele, R.O. *Polymer Science and Technology.* Boca Raton, Florida: CRC Press LLC, 2000.

[13] Pruitt, L.A. *The Effects of Radiation on the Structural and Mechanical Properties of Medical Polymers, in Radiation Effects on Polymers for Biological use.* Kausch. H (ed.). Germany: Springer – Verlag Berlin Heidelberg, 2003.

[14] Bamford, C.H. and Tipper, C.F.H *Coprehensive Chemical Kinteics. Volume 14: Degradation of Polymers.* Oxford, UK: Elsevier Ltd., 1975.

[15] Wayne, R. *Sterilisation of Polymer Healthcare Products.* Shrewsbury, UK: Rapra Technology Limited, 2005.

[16] IAEA-TECDOC-1420. *Advances in Radiation Chemistry of Polymers.* Austria: International Atomic Energy Agency, 2004.

[17] Wookds, R.J. and Pikaev, A.K. *Applied Radiation Chemistry: Radiation Processing.* New York: John Wiley & Sons, Inc., 1994.

[18] Shashoua, Y. *Conservation of Plastics. Materials Science, Degradation and Preservation.* Oxford, UK: Elsevier Ltd., 2008.

[19] Matthew, F.B. *Clinical Environment, in Clinical Engineering Handbook.* Dyro, J.F. (ed.). Burlington, USA: Elsevier Academic Press, 2004.

[20] Scruton, M.W. *The Effect of Air with Steam on the Temperature of Autoclave Contents.* Journal of Hospital Infection. 1989; **14**, 249-262.

[21] Sykes, G. *The Basis for Sufficient of a Suitable Bacteriostat in Injections.* Journal of Pharmacy and Pharmacology. 1958; **10**, 40-45.

[22] Boca, B.M., Pretorius, E., et.al. *An Overview of the Validation Approach for Moist Heat Sterilization.* Pharmaceutical Technology, 2002. <www.pharmtech.com>

[23] Wayne, C., Conway S. G., et.al. *Reducing the Risk of Contamination of Sterile Parenteral Products via Ready-to-Use Closure Components.* AAPS PharmSciTech. 2010; **11**, 1572-1579.

[24] McKetta, J.J. and Cunningham, W.A. *Encyclopedia of Chemical Processing and Design.* Volume 20. New York: M. Dekker, 1984.

[25] Mendes, G.C.C., Brandao, T.R.S., et.al. *Ethylene Oxide Sterilization of Medical Devices: A review.* Am. J. Infect Control. 2007; **35**, 574-581.

[26] ISO 10993-1, *Biological Evaluation of Medical Devices – Part 1: Evaluation and Testing*, 2003.

[27] Manning, C.R. *Controling Ethylene Oxide Residues from the Manufacture of Medical Products.* Medical device and diagnostic industry Magazine. 2007; **11**, 136-144.

[28] Patnaik, P. *Handbook of Inorganic Chemicals*. New York: The McGraw-Hill Company, Inc., 2003.

[29] Jones, C.W. *Applications of Hydrogen Peroxide and Derivatives*. Cambridge, UK: Royal Society of Chemistry., 1999.

[30] Sigwarth, V. and Moirandat, C. *Development and Quantification of H_2O_2 Decontamination Cycles.* PDA Journal of Pharmaceutical Science&Technology. 2000; **54**, 286-304.

[31] Stärk, A. *Minimizing the Risk of Secondary Contaminations Through the Use of Isolators for Sterility Testing.* Pharm. Ind. 2009; **8**, 1429-1436.

[32] Sigwarth, V. and Stärk, A. *Effect of Carrier Materials on the Resistance of Spores of Bacillus stearothermophilus to Gaseous Hydrogen Peroxide.* PDA Journal of Pharmaceutical Science&Technology. 2003; **57**, 3-11.

[33] Okpara-Hofmann, J., Knoll, M. et.al. *Comparison of Low-Temperature Hydrogen Peroxide gas Plasma Sterilization for Endoscopes using Various Sterrad™ models.* Journal of Hospital Infection. 2005; **59**, 280-285.

[34] Lerouge, S., Wertheimer, M.R. et.al. *Plasma Sterilization: A Review of Parameters, Mechanisms and Limitations.* Plasmas and Polymers. 2001; **6**, 175-188.

[35] Spry, C. *Low-Temperature Hydrogen Peroxide Gas Plasma – Atomic Age Sterilization Technology.* Todays Surgical Nurce. 1998; **20**, 25-28.

[36] Murali, N.B., Mickelsen, S. et.al. *Safety and Efficacy of Hydrogen Peroxide Plasma Sterilization for Repeated Use of Electrophysiology Catheters.* JACC. 1998; **32**, 1384-1388.

[37] Kyi, M.S., Holton, J. and Ridgway, G.L. *Assessment of the Efficacy of a Low Temperature Hydrogen Peroxide Gas Plasma Sterilization System.* Journal of Hospital Infection. 1995; **31**, 275-284.

[38] Moisan, M., Barbeau, J. et.al. *Low-Temperature Sterilization Using Gas Plasmas: a Review of the Experiments and an Analyse of the Inactivation Mechanisms.* International Journal of Pharmaceutics. 2001; **226**, 1-21.

[39] Anon. *Choosing a Low-Temperature Sterilization Technology.* Health Devices. 1999; **28**, 430-455.

[40] Feldman, L.S. and Hui, H.K. *Compatibility of Medical Devices and Materials with Low-Temperature Hydrogen Gas Plasma.* Medical Device and Diagnostic Industry. 1997; **19**, 57-62.

[41] William, A.R., Gergen, M.F. and Weber, D.J. *Comparative Evaluation of the Sporicidal Activity of New Low-Temperature Sterilization Technologies: Ethylene oxide, 2 Plasma Sterilization Systems, and Liquid Peracetic Acid.* AJIC. 1998; **26**, 393-398.

[42] Kellner, R., Otto, M., Widmer, H.M. and Mermeet, J.H. *Analytical Chemistry.* Weinheim: Wiley-VCH, 1998.

[43] Lakowicz, J.R. *Principles of Fluorescence Spectroscopy.* 3rd ed., New York: Springer, 2006.

[44] Sauer, M., Hofkens, J. and Enderlein, J. *Handbook of Fluorescence Spectroscopy and Imaging*. Weinheim: Wiley/VCH Verlag, 2011.

[45] Valeur, B. *Molecular Fluorescence: Principles and Applications.* Weinheim: Wiley/VCH Verlag Gmbh, 2001.

[46] Wang, B. and Anyslyn, E.V. *Chemosensors. Principles, Strategies and Applications.* New Jersey: John Wiley&Sons, Inc., 2011.

[47] McMillan, G.K. and Cameron, R.A. *Advanced pH Measurement and Control.* ISA: Research Triangle Park, 2005.

[48] Gupta, B.D. *Fiber Optic Sensors: Principles and Applications.* New Delhi: New Indica Publishing Agency, 2006.

[49] Grattan, L.S. and Meggitt, B.T. *Optical Fiber Sensor Technology Applications and Systems.* Berlin: Springer Verlag, 1999.

[50] Aigner, D., Borisov, S.M. and Klimant, I. *New Fluorescent Perylene, Bisimide Indicators – A platform for Broadband pH optodes.* Anal. Bioanal. Chem. 2011; **400**/**8**, 2475-2485.

[51] Borisov, S.M. and Wolfbeis, O.S. *Temperature-sensitive Europium(II) probes and their use for simultaneous luminescent sensing of temperature and oxygen.* Anal.Chem. 2006; **78**, 5094-5101.

[52] John, L.N. and Corner, N.A. *Optical Temperature Sensors*. Patent Number: 5,180,227. 1991.

[53] Borisov, S.M., Vasylevska, A.S., Krause, Ch. and Wolfbeis, O.S. *Composite luminescent material for dual sensing of oxygen and temperature.* Adv.Funct.Mater. 2006; **16**, 1536-1542.

[54] Borisov, S.M. and Klimant, I. *Blue LED Excitable Temperature Sensors Based on a New Europium(III) Chelate.* J. Fluoresc. 2008; **18**, 581-589.

[55] Timer, B., Olthuis, W. and Van der Berg, A. *Ammonia sensors and their applications – a review*. Sens.Actuators B, 2005; **107**, 666-667.

[56] United States Environmental Protection Agency. *Water quality standards for the 21st century.* Washington: Office of water, 1991.

[57] Geschke, O., Klank, H. and Telleman, P. *Microsystem engineerign of Lab-on-a-chip devices.* Weinheim: Wiley-VHC Verlag GmbH, 2004.

[58] Waich, K., Mayr, T. and Klimant, I. *Fluroescence sensors for trace monitoring of dissolved ammonia.* Talanta. 2008, **77**, 66-72.

[59] Wolfbeis, O.S., Koller, E. and Hochmuth, P. *The unusually strong effect of a 4-cyano group upon electronic spectra and dissociation constants of 3-substituted 7-hydroxycoumarins.* Bull. Chem.Soc. J. 1985, **58**, 731-734.

[60] Borisov, S.M. and Klimant, I. *Ultrabright Oxygen Optodes Based on Cyclometalated Iridium(III) Coumarin Complexes.* Anal. Chem. 2007; **79**, 7501-7509.

[61] Borisov, S.M., Nuss, G. and Klimant, I. *Red Light-Excitable Oxygen Sensing Materials Based on Platinum(II) and Palladium(II) Benzoporphyrins.* Anal. Chem. 2008; **80**, 9435-9442.

[62] Mohr, G.J, Werner, T. and Wolfbeis, O.S. *Application of a novel lipophilized fluorescent dye in an optical nitrate sensor.* J. Fluoresc. 1995; **5**, 135-138.

[63] Borisov, S.M, Herrod, D.L and Klimant, I. *Fluorescent poly(styrene-block-vinylpyrrolidone) nanobeads for optical sensing of pH.* Sensors and Actuators B: Chemical. 2009; **139**, 52-58.

[64] Ellis, B. and Smith, R. *Polymers. A property database*. 2nd Ed. New York: CRC Press Taylor&Francis Group, 2009.

[65] Natta, F., Corradini, I.W. and Bassi, I.W. *Crystal structure of isotactic polystyrene.* Nuovo Cimento, 1960; **15**, 68-82.

[66] Bandyopadhyay, A. and Basak, A.C. *Studies on photocatalytic degradation of polystyrene.* Materials Science and Technology, 2007; **23**, 307-317.

[67] Brandrup, J., Immergut, E.H. and Grulke, E.A. *Polymer Handbook*. 4th Ed. New York: John Wiley & Sons, Inc., 2003.

[68] Utracki, L.A. *Polymer Blends Handbook.* Dordrecht, Netherland: Kluwer Academic Publisher, 2002.

[69] Ullman, F. and Gerhartz, W. *Ullmann's Encyclopedia of Industrial Chemistry.* Weinheim: Wiley-VHC, 2002.

[70] *Polysulfone.* Polymer Plastics Company, LC. 2011 <http://www.polymerplastics.com/performance_polysul.shtml>

[71] Scott, G. *Degradable polymers: principles and applications.* 2nd Ed. Dordrecht, Netherland: Kluwer Academic Publisher, 2002.

[72] Brown, R.M. and Saxena, I.M. *Cellulose: Molecular and structural biology. Selected Articles on the Synthesis, Structure, and Applications of Cellulose.* Dordrecht, Netherland: Springer, 2007.

[73] Gopal, N.G.S. *Radiation Sterilization of Pharmaceuticals and Polymers.* Radiat. Phys. Chem., 1978; **12**, 35-50.

[74] James, E.M. *Polymer Data Handbook*. UK: Oxford University Press, 1999.

[75] Han, J. H., Taylor, J. D., Kim, D. S., Kim, Y. S., Kim, Y. T., Cha, G. S. and Nam, H. *Glucose biosensors with hydrophilic polyurethane (HPU) blended with polyvinyl alcohol/vinyl butyral copolymer (PVAB) outer membrane.* Sensors and Actuators. 2007; **123**, 384-390.

[76] Gümüsderelioglu, M. and Topal, I.U. *Vinyl ether/acrylic acid terpolymer hydrogels synthesized by gamma-radiation: characterization, thermosensitivity and pH-sensitivity.* Radiat. Phys. Chem., 2005; **73**, 272-279.

[77] Drobny, J.G. *Radiation Technology for Polymers.* Dordrecht, Netherland: Springer, 2007.

[78] Elisseeff, J. *Structure starts to gel.* Nature Materials. 2008; **7**, 271-273.

[79] Domb, A.J. and Kumar, N. *Biodegradable Polymers in Clinical Use and Clinical Development.* New York: John Wiley & Sons, Inc., 2011.

[80] Kanjickal, D., Lopina, S., Evancho-Chapman, M.M. and Donovan, D. *Effects of Sterilization on Poly(ethylene Glycol) Hydrogels.* Journal of Biomedical Materials Research Part A. 2008; **7**, 608-617.

[81] *HydroMed™, HydroThane™.* AdvanSource Biomaterials Corp. 2010 <http://www.advbiomaterials.com/>

[82] Prado, L., Radovanovic, Patore, H.O. et al. *Poly(phenylsilsesquixoane)s: Structureal and Morphological Characterization.* Journal of Polymer Science. 2000; **38**, 1580-1589.

[83] Jones, R.G., Wataru, A. and Chojnowski, J. *Silicon-Containing Polymers: The Science and Technology of Their Synthesis and Applications.* Dordrecht, Netherland: Kluwer Academic Publisher, 2000.

[84] Smaihi, M. and Jermoumi, T. *Structural Study of Poly(phenylsilsesquixoane) Sol-Gel Materials.* Chem. Mater. 1995; **7**, 2293-2299.

[85] Hwang, T., Pu, L., Kim, S.W. et al. *Synthesis and barrier properties of poly(vinylidene chloride-co-acrylonitrile)/SiO_2 hybrid composites by sol-gel process. Journal of Membrane Science*. 2009; **345**, 90-96.

[86] Beswick, R.H and Dunn, D.J. *Plastics in Packaging – Western Europe and North America.* Shrewsbury, UK: Rapra Technology Limited, 2002.

[87] Myer, K. *Handbook of Materials Selection.* New York: John Wiley & Sons, Inc., 2002.

[88] Chalmers, J.M. and Meier, R.J. *Molecular Characterization and Analysis of Polymers.* Amsterdam, Netherlands: Elsevier, 2008.

[89] Graddie, N. and McNeill, C. *Thermal Degradation of Polymethacrylonitrile. Part II. The coloration reaction.* Journal of Polymer Science. 1958; **27**, 207-218.

[90] Rather, B.D. *Biomaterials science: an introduction to materials in medicine.* London: Elsevier Inc. 2004.

[91] Pielichowski, K. and Njuguna, J. *Thermal degradation of polymeric materials.* Shawbury, UK: Rapra Technology Limited. 2005.

[92] Diego, R.B., Sanchez, M.S., Ribelles, J.L.G. and Pradas, M.M. *Effect of gamma-irradiation on the structure of poly(ethyl acrylate-co-hydroxyethyl methacrylate) copolymer networks for biomedical applications.* J. Mater. Sci.. 2007; **18**, 693-698.

[93] Speight, J.G. and Large, N.A. *Large's Handbook of Chemistry.* 16th Ed. New York: McGraw-Hill, 2005

[94] Harper, C.A. *Handbook of plastics technologies: the complete guide to properties and Performance.* New York: The McGraw-Hill Companies, Inc., 2006.

[95] Richardson, F.S. *Terbium(III) and Europium(III) Ions as Luminescent Probes and Stains for Biomolecular Systems.* Chem. Rev. 1982; **82**, 541-552.

[96] Zollinger, H. *Color Chemistry. Syntheses, Properties, and Applications of Organic Dyes and Pigments.* 3rd ed. Zürich: Verlag Helvetica Chimica Acta, Weinheim: Wiley/VCH, 2003.

[97] Adler, A.D., Longo, L.R., et al. *A simplified synthesis for meso-tetraphenylporphine.* J. Org. Chem. 1967; **32**/**2**, 476.

[98] Borisov, S.M. and Klimant, I. *Luminescent nanobeads for Optica Sensing and Imaging of Dissolved Oxygen.* Microchim Acta. 2009; **164**, 7-15.

[99] Papkovsky, D.B. *Luminescent Porphyrins as Probes for Optical (bio)sensors.* Sensors and Actuators B. 1993; **11**, 293-300.

[100] Borisov, S.M., Lehner, P. and Klimant, I. *Novel optical trace oxygen sensors based on platinum(II) and palladium(II) complexes with 5,10,15,20-meso-tetrakis-(2,3,4,5,6-pentafluorphenyl)-porphyrin covalently immobilized on silica-gel particles.* Anal. Chimica Acta. 2011; **690**, 108-115.

[101] *Database of Fluorescence Dyes Properties and Applications.* Graz: University of Technology, 2011. <fluorophores.mgfb.at>.

[102] Orellana, G. and Moreno-Bondi, M.C. *Frontiers in Chemical Sensors. Novel Principles and Techniques.* Berlin Heidelberg: Springer-Verlag, 2005.

[103] Hartmut, Y. *Highly Efficient OLEDs with Phosphorescent Materials.* Weinheim: Wiley/VCH Verlag, 2008.

[104] Bansal, A.K., Holzer, W. et al. *Absorption and emission spectroscopic characterization of Platinum-octaethyl-porphyrin (PtOEP).* Chemical Physics. 2006; **330**, 118-129.

[105] Borisov, S.M., Papkovsky, D.B. et al. *Photophysical Properties of the new Phosphorescent platinum(II) and palladium(II) complexes of benzoporphyrins and chlorines.* Journal of Photochemistry and Photobiology A: Chemistry. 2009; **206**, 87-92.

[106] Klimant, I. and Wolfbeis, O.S. *Oxygen-Sensitive Luminescent Materials Based on Silicone-Soluble Ruthenium Diimine Complexes.* Anal. Chem. 1995; **67**, 3160-3166.

[107] Klimant, I., Belser, P. and Wolfbeis, O.S. *Novel Metal-Organic Ruthenium(II) Diimin Complexes for use as Longwave Excitable Luminescent Oxygen Probes.* Talanta. 1994; **41**/**6**, 985-991.

[108] Trettnak, W., Gruber, W., Reininger, F. and Klimant, I. *Recent progress in optical Oxygen Sensor Instrumentation.* Sensors and Actuators B. 1995; **29**, 219-225.

[109] Spry, D.B., Goun, A. and Fayer, M.D. *Deprotonation Dynamics and Stokes Shift of Pyranine (HPTS).* J. Phys. Chem. A. 2007; **111**, 230-237.

[110] Borisov, S.M, Herrod, D.L and Klimant, I. *Fluorescent poly(styrene-block-vinylpyrrolidone) nanobeads for optical sensing of pH.* Sensors and Actuators B: Chemical. 2009; **139**, 52-58.

[111] Donaldson, D.M., Robertson, J.M. and White, J.G. *The crystal and molecular structure of perylene.* Proc. R. Soc. Lond. A Math. Phys.Sci. 1953; **220**, 311-321.

[112] Faulkner, E.B. and Schwartz, R.J. *High Performance Pigments.* Weinheim: Wiley/VCH Verlag, 2009.

[113] *European chemical substances information system..* EU: European Commission Joint Research Centre. Institute for Health and Consumer Protection, 2011. <esis.jrc.ec.europa.eu>.

[114] Waich, K., Mayr, T. and Klimant, I. *Fluorescence Sensors for Trace Monitoring of Dissolved Ammonia.* Talanta. 2008; **77**, 66-72.

[115] Jocelyn, H. and Bruce-Gregorios, M.D. *Histopathologic Techniques.* Quezon City, Philippines: JMC Press Inc., 1974.

[116] Waich, K., Borisov, S., Mayr, T. and Klimant, I. *Dual Lifetime Referenced Trace Ammonia Sensors.* Sensors and Actuators B: Chemical. 2009; **139**, 132-138.

[117] Rota, C., Chignell, C.F. and Mason, R.P. *Evidence for Free Radical Formation during the oxidation of 2´,7´-dichlorofluorescin to the fluorescent dye 2´-7´-dichlorofluroescein by horseradish peroxidise: possible implications for oxidative stress measurements.* Free Radical Biology&Medicine. 1999; **27**, 873-881.

[118] Leonhardt, H., Grodon, L. and Livingston, R. *Acid-Base Equilibria of Fluorescein and 2´,7´-Dichlorofluorescein in their ground and fluorescent states.* The Journal of Physical Chemistry. 1971; **75**/**2**, 245-249.

[119] Schröder, C.R., Weidgans, B.M and Klimant, I. *pH fluorosensors for use in marine systems.* Analyst. 2005; **130**, 907-916.

[120] Weidgans, B.M, Krause, C., Klimant, I. and Wolfbeis, O.S. *Fluorescent pH sensors with negligible sensitivity to ionic strength.* The Royal Society of Chemistry. 2004; **129**, 645-650.

[121] *pH-measurements-indicators*. pH-meter.info. 2005. <www.ph-meter.info>.

[122] Khopkar, S.M. *Basic Concepts of Analytical Chemistry.* 2nd ed. New Delhi: New Age Internationl, 2004.

[123] Kreft, S. and Kreft, M. *Quantification of dicromatism: a characteristic of colour in transparent materials.* Journal of the Optical Society of America A. 2009; **26**, 1576-1581.

[124] Sabnis, R.W. *Handbook of acid-base indicators.* Boca Raton, FL: CRC Press, 2007.

[125] Patnaik, P. *Dean´s Analytical Chemistry Handbook.* Columbus,OH: The McGraw-Hill Companies, Inc., 2004.

[126] Förch, R. Schönherr, H. and Jenkins, A.T.A. *Surface Design: Applications in Bioscience and Nanotechnology.* West Sussex, UK: John Wiley & Sons Ltd., 2009.

[127] De Gennes, P.G. *Wetting: Statics and Dynamics.* Reviews of Modern Physics, 1985; **57**, 827-863.

[128] Nicholson, J.W. *The Chemistry of Polymers. 3rd edition.* Cambridge, UK: RSC Publishing, 2006.

[129] Clayden, J., Greeves, N., Warren, S. and Worthers, P. *Organic Chemistry.* New York: Oxford University Press Inc., 2008.

D A T A B A S E

A
Radiation Sterilization of Polymers

TABLE OF CONTENT

A RADIATION STERILIZATION OF POLYMERS **199**

A.1 Polystyrene **201**
A.1.1 Absorption Spectra 201
A.1.2 Contact Angle Measurement 201
A.1.3 Infrared Spectra 202
A.1.4 Differential Scanning Calorimetry 203

A.2 Polystyrene-co-Acrylonitrile **205**
A.2.1 Absorption Spectra 205
A.2.2 Contact Angle Measurement 205
A.2.3 Infrared Spectra 206
A.2.4 Differential Scanning Calorimetry 207

A.3 Polystyrene-co-Maleic Anhydride **209**
A.3.1 Absorption Spectra 209
A.3.2 Contact Angle Measurement 209
A.3.3 Infrared Spectra 210
A.3.4 Differential Scanning Calorimetry 211

A.4 Polysulfone **213**
A.4.1 Absorption Spectra 213
A.4.2 Contact Angle Measurement 213
A.4.3 Infrared Spectra 214
A.4.4 Differential Scanning Calorimetry 215

A.5 Cellulose Acetate **217**
A.5.1 Absorption Spectra 217
A.5.2 Contact Angle Measurement 217
A.5.3 Infrared Spectra 218

A.6 Ethyl Cellulose **219**
A.6.1 Absorption Spectra 219
A.6.2 Contact Angle Measurement 219
A.6.3 Infrared Spectra 220
A.6.4 Differential Scanning Calorimetry 221

A.7 Hydrogel HydroMed™ D4 and D7 **223**
A.7.1 Absorption Spectra 223
A.7.2 Contact Angle Measurement 224
A.7.3 Infrared Spectra 225

A.8 HydroThane™ with 5% and 25% water absorption **227**
A.8.1 Absorption Spectra 227
A.8.2 Contact Angle Measurement 228
A.8.3 Infrared Spectra 229

A.9 PolyPhenylSilsesQuioxane **231**
A.9.1 Absorption Spectra 231
A.9.2 Contact Angle Measurement 231
A.9.3 Infrared Spectra 232

A.10 PolyVinylidene Chloride-co-Acrylonitrile **233**
A.10.1 Absorption Spectra 233

A.10.2 Contact Angle Measurement 233
A.10.3 Infrared Spectra 234
A.10.4 Differential Scanning Calorimetry 235

A.11 PolyMethyl MethAcrylate 237
A.11.1 Absorption Spectra 237
A.11.2 Contact Angle Measurement 237
A.11.3 Infrared Spectra 238
A.11.4 Differential Scanning Calorimetry 239

A.12 PolyMethAcryloNitrile 241
A.12.1 Absorption Spectra 241
A.12.2 Contact Angle Measurement 241
A.12.3 Infrared Spectra 242

A.13 Poly(2-HydroxyEthyl MethAcrylate) 243
A.13.1 Absorption Spectra 243
A.13.2 Contact Angle Measurement 243
A.13.3 Infrared Spectra 244

A.14 Poly(Ethylene Terepthalate) (Mylar®) 245
A.14.1 Differential Scanning Calorimetry 245

A.1 Polystyrene

A.1.1 Absorption Spectra

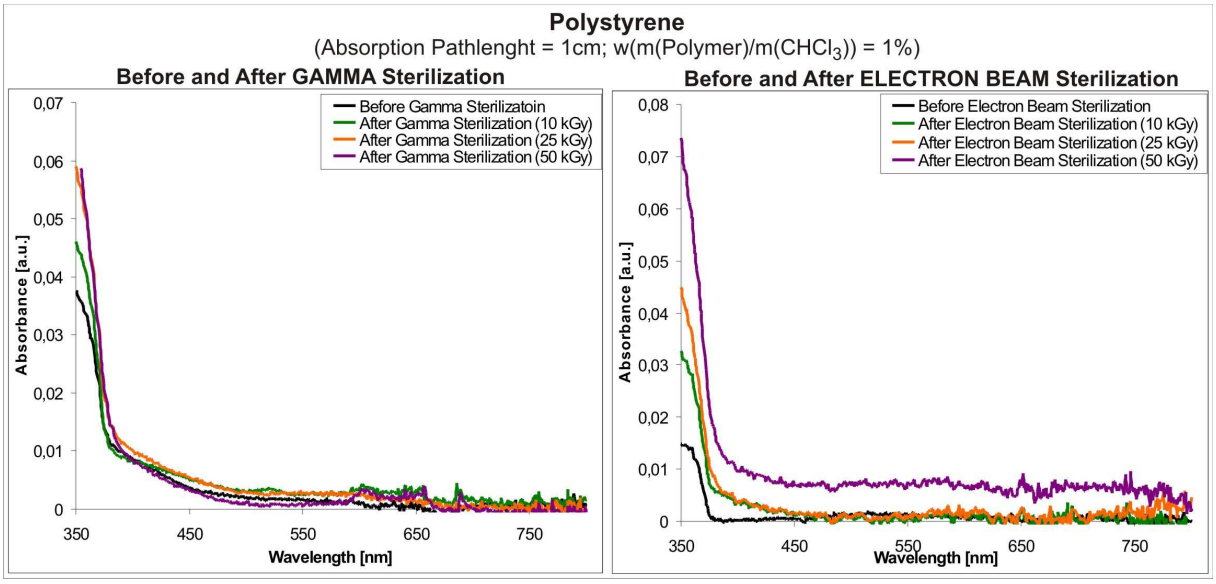

A.1.2 Contact Angle Measurement

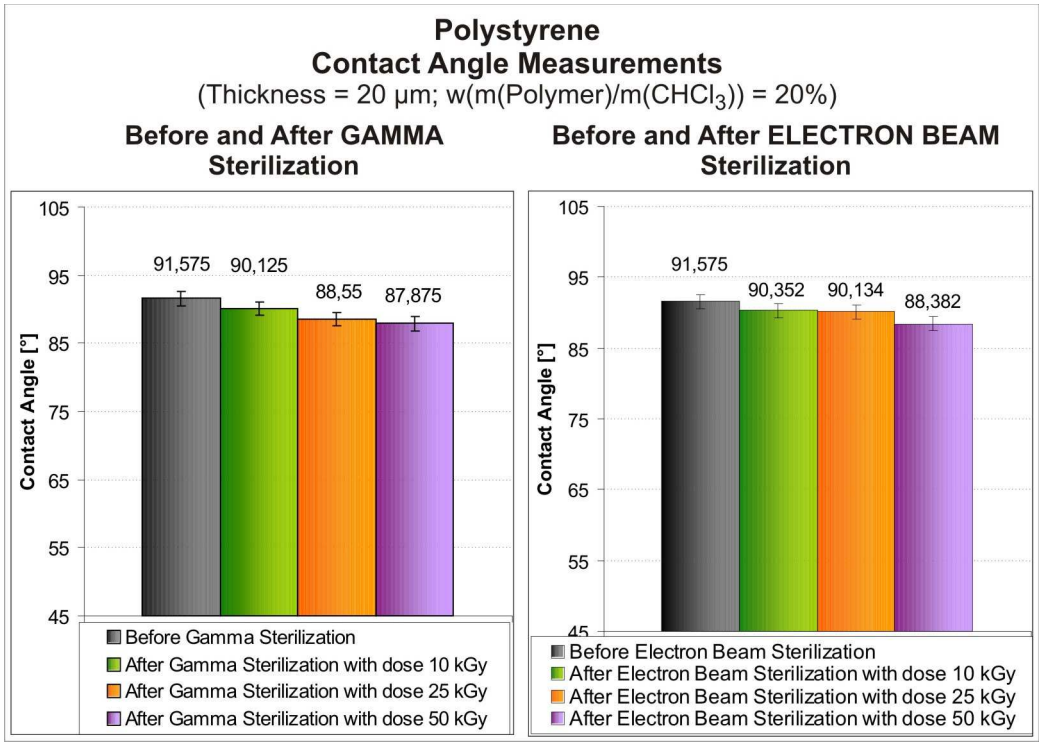

A.1.3 Infrared Spectra

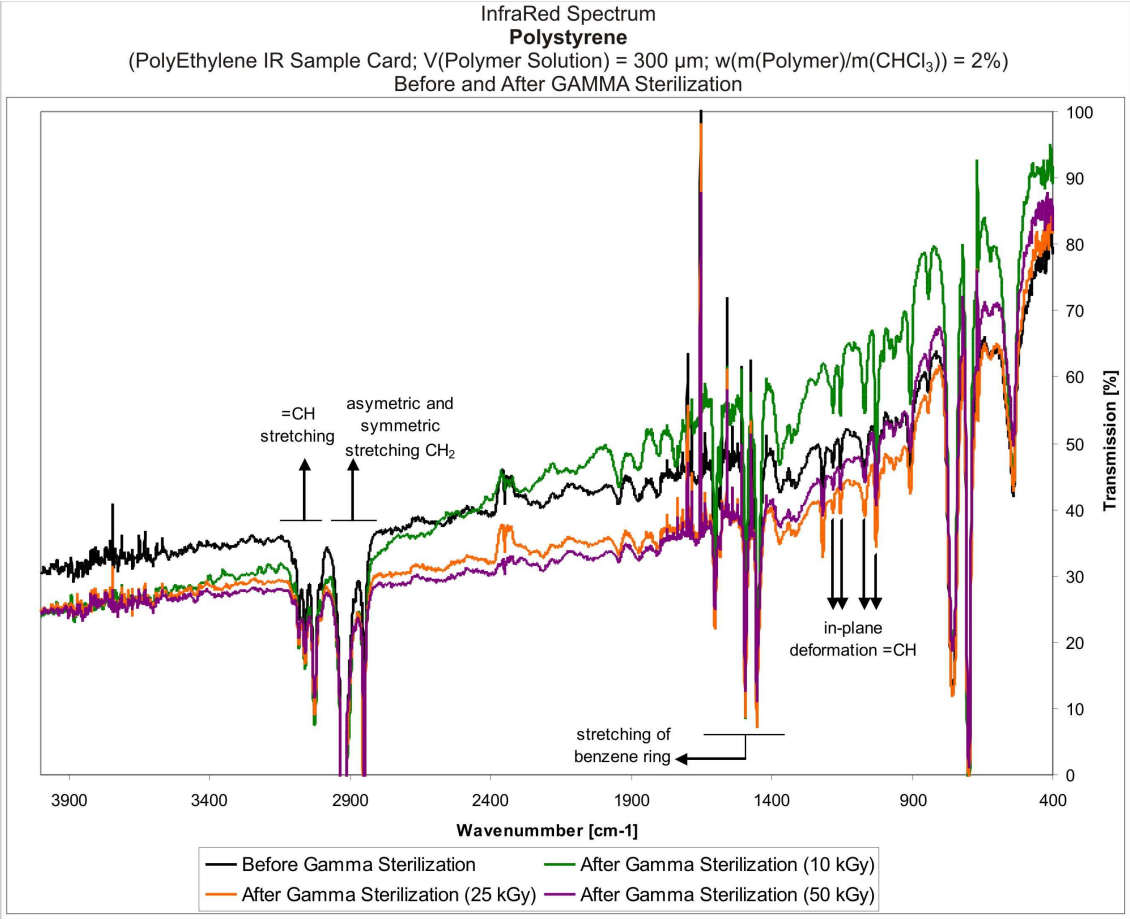

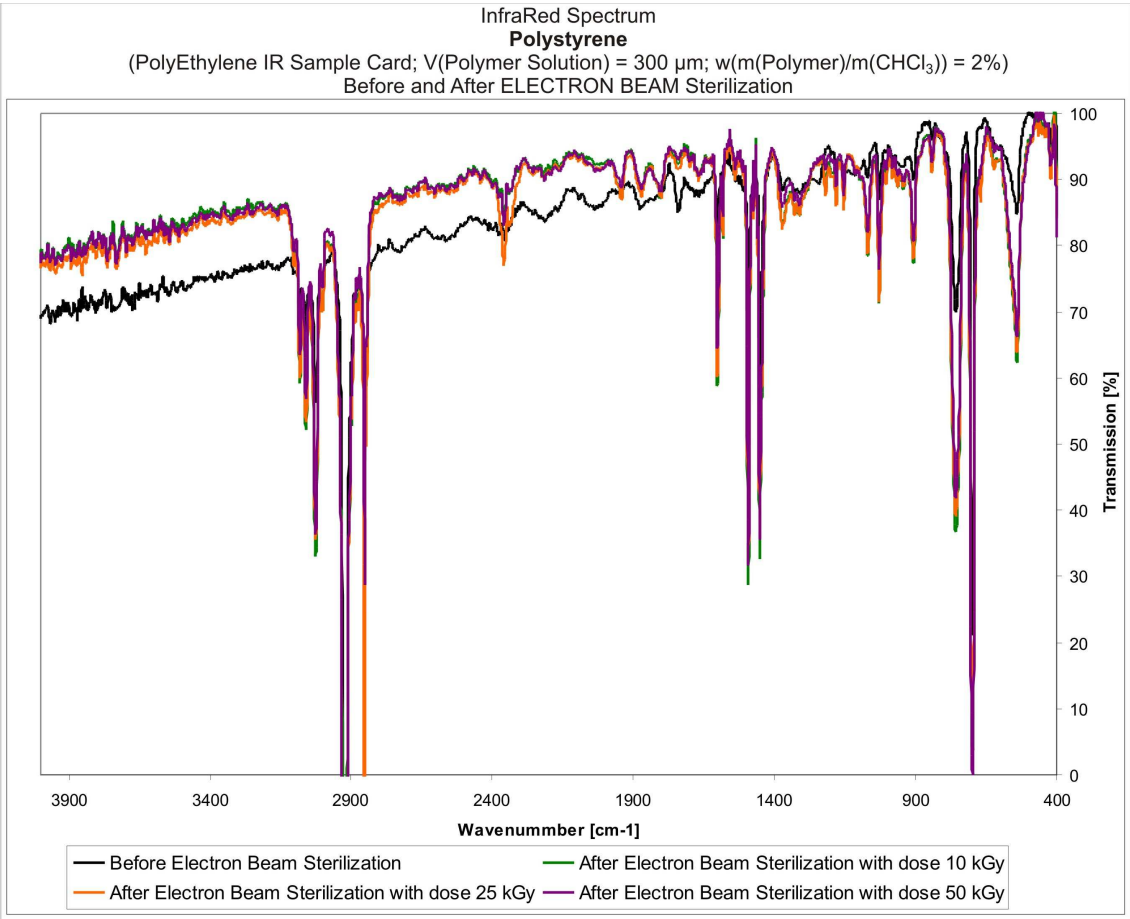

A.1.4 Differential Scanning Calorimetry

DSC Program:

30 °C – 150 °C 20 °C/min
150 °C – 30 °C 10 °C/min
30 °C – 150 °C 20 °C/min

	T_g	Δc_p
BeforeS	107,56 °C	0,253 J/g °C
10 kGy	107,60 °C	0,290 J/g °C
25 kGy	106,71 °C	0,249 J/g °C
50 kGy	105,64 °C	0,252 J/g °C

Before sterilization

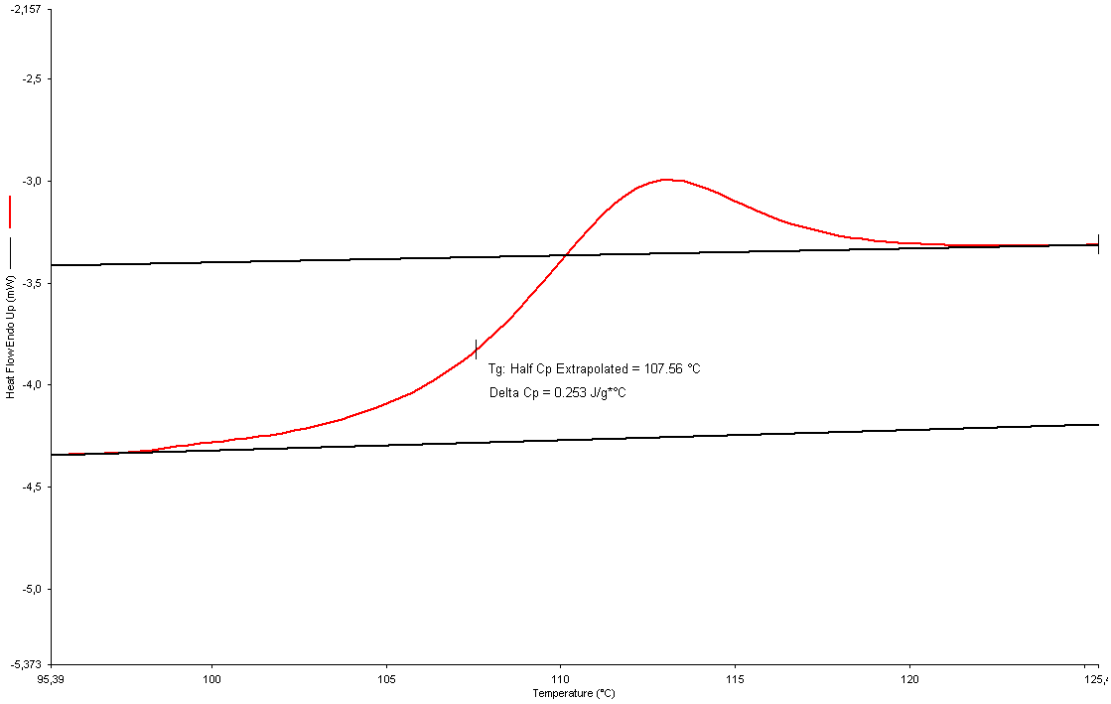

After GAMMA sterilization with 10 kGy

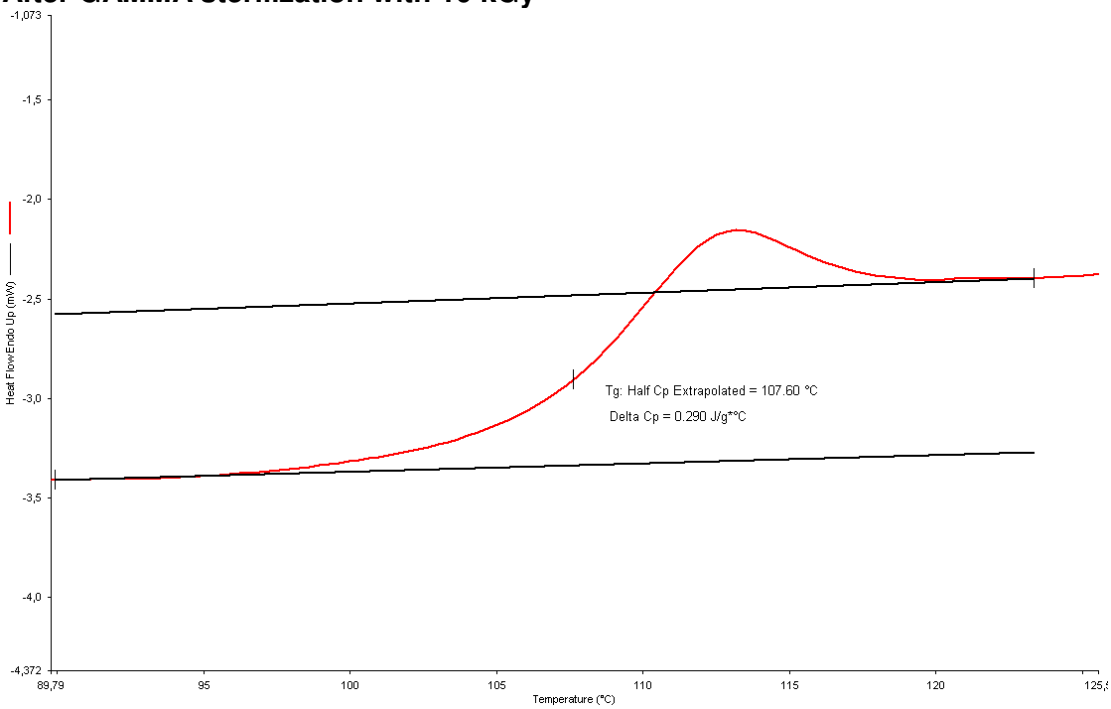

After GAMMA sterilization with 25 kGy

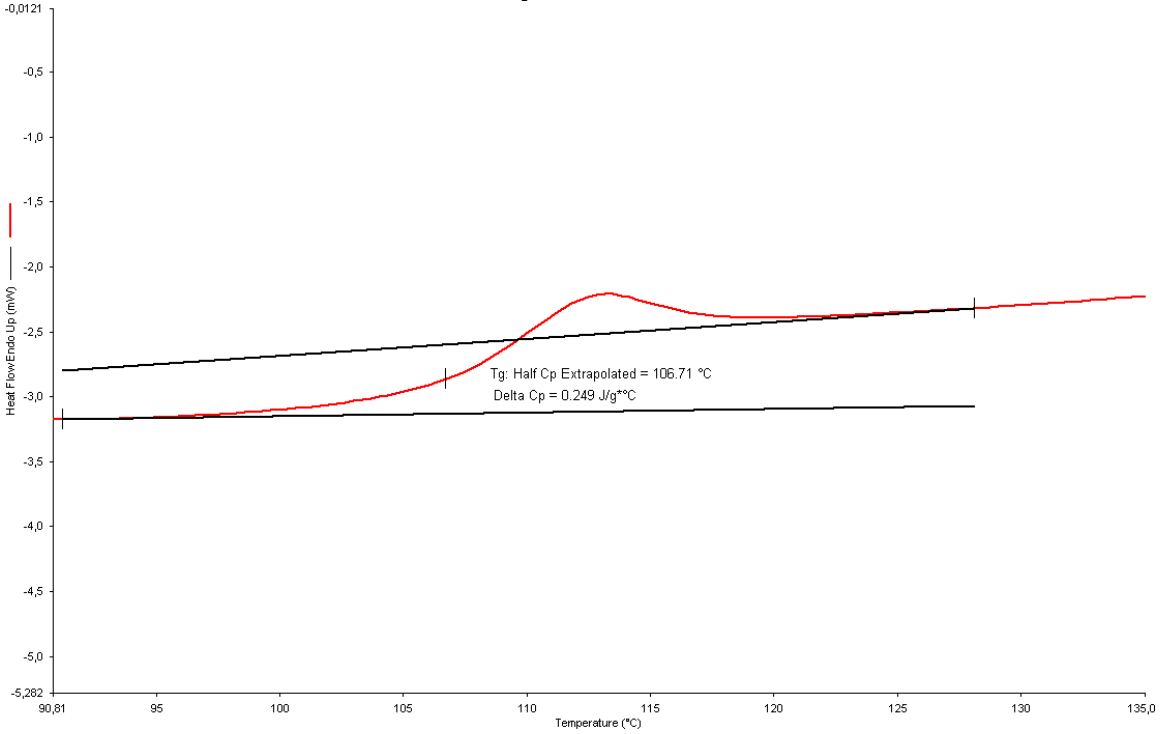

After GAMMA sterilization with 50 kGy

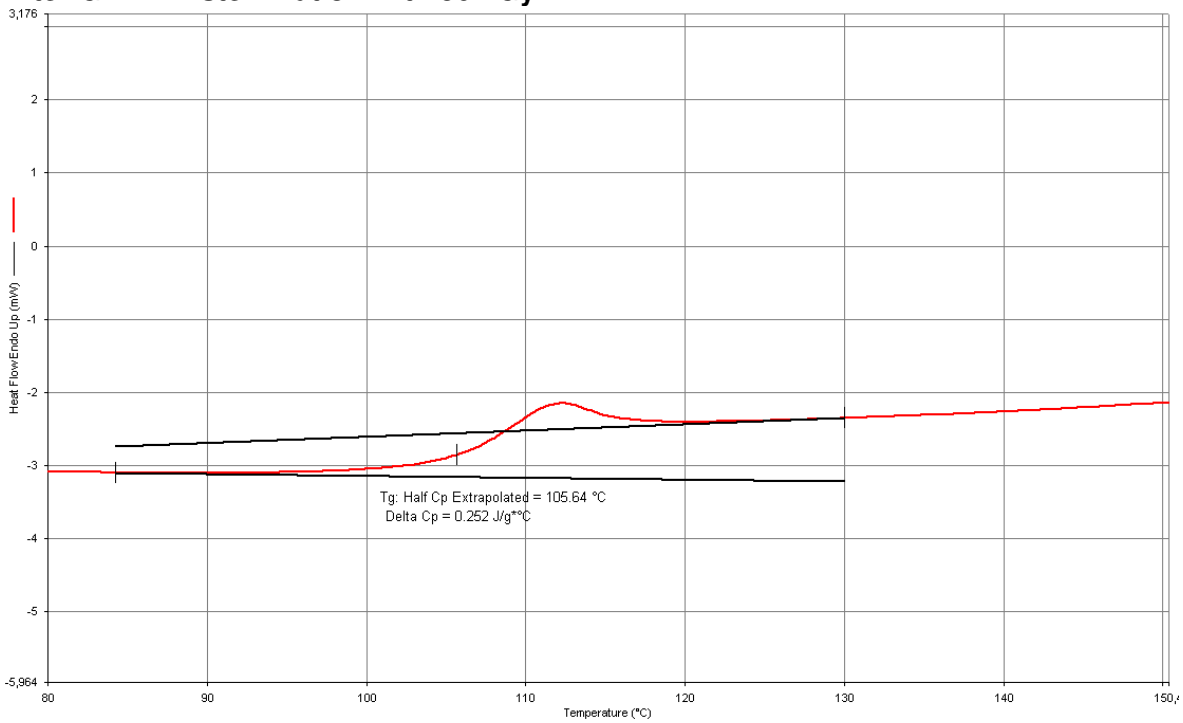

A.2 Polystyrene-co-Acrylonitrile

A.2.1 Absorption Spectra

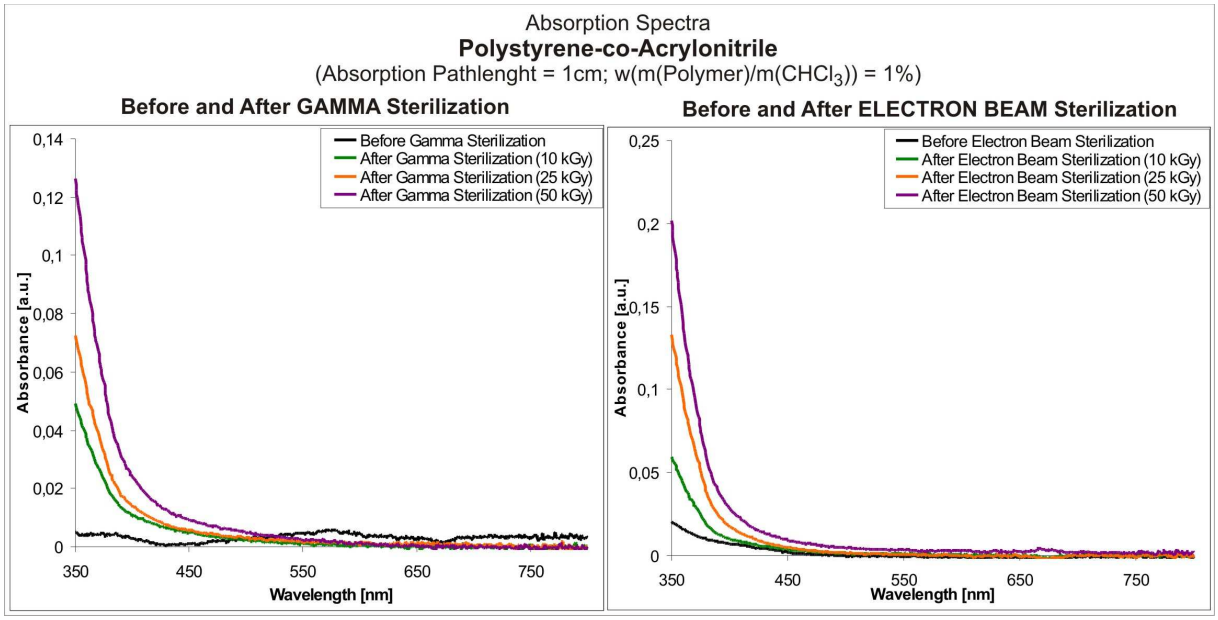

A.2.2 Contact Angle Measurement

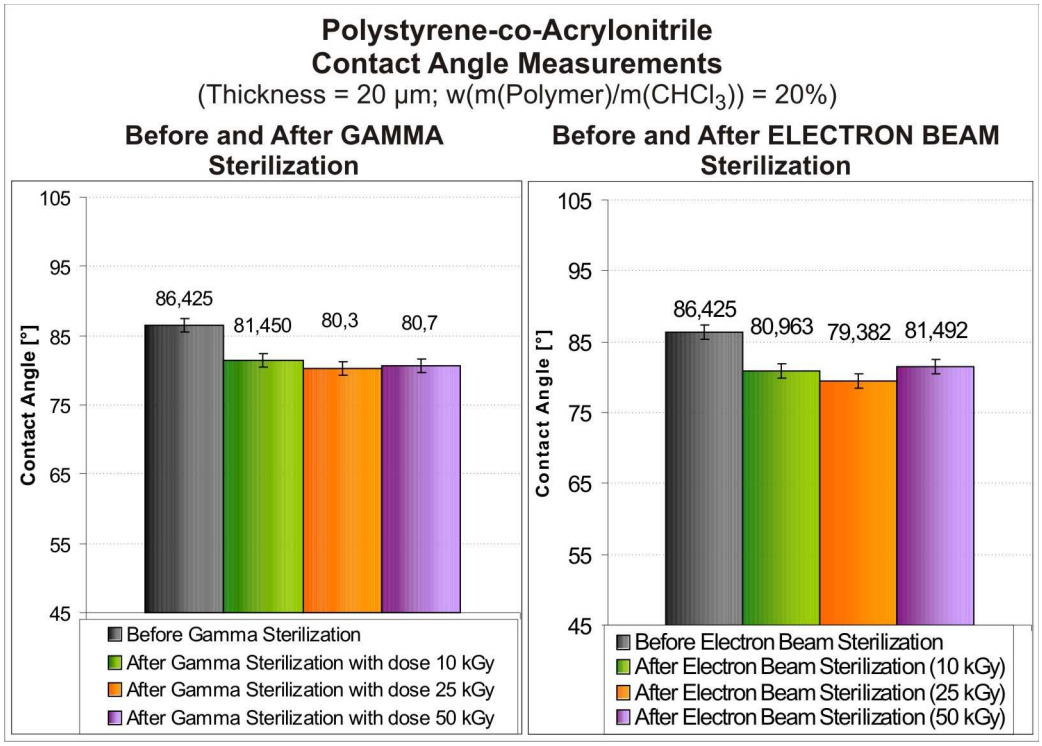

A.2.3 Infrared Spectra

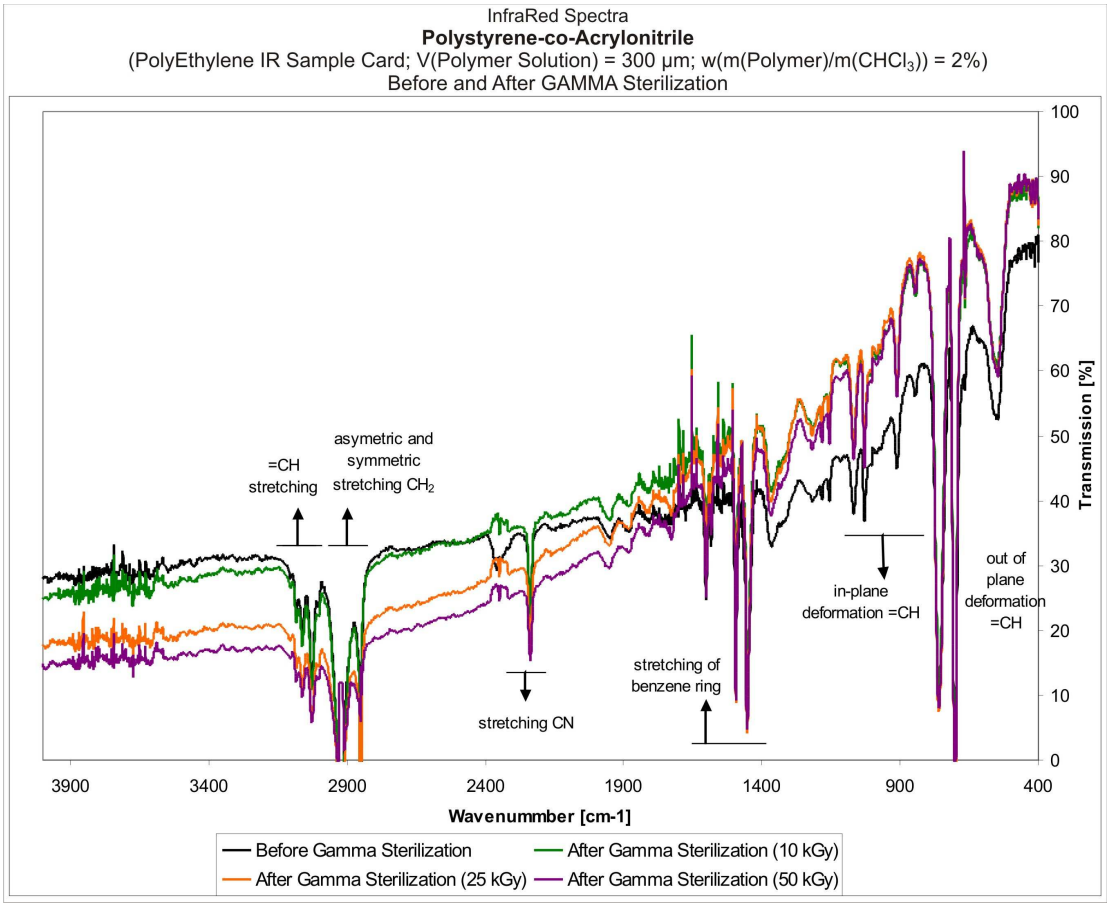

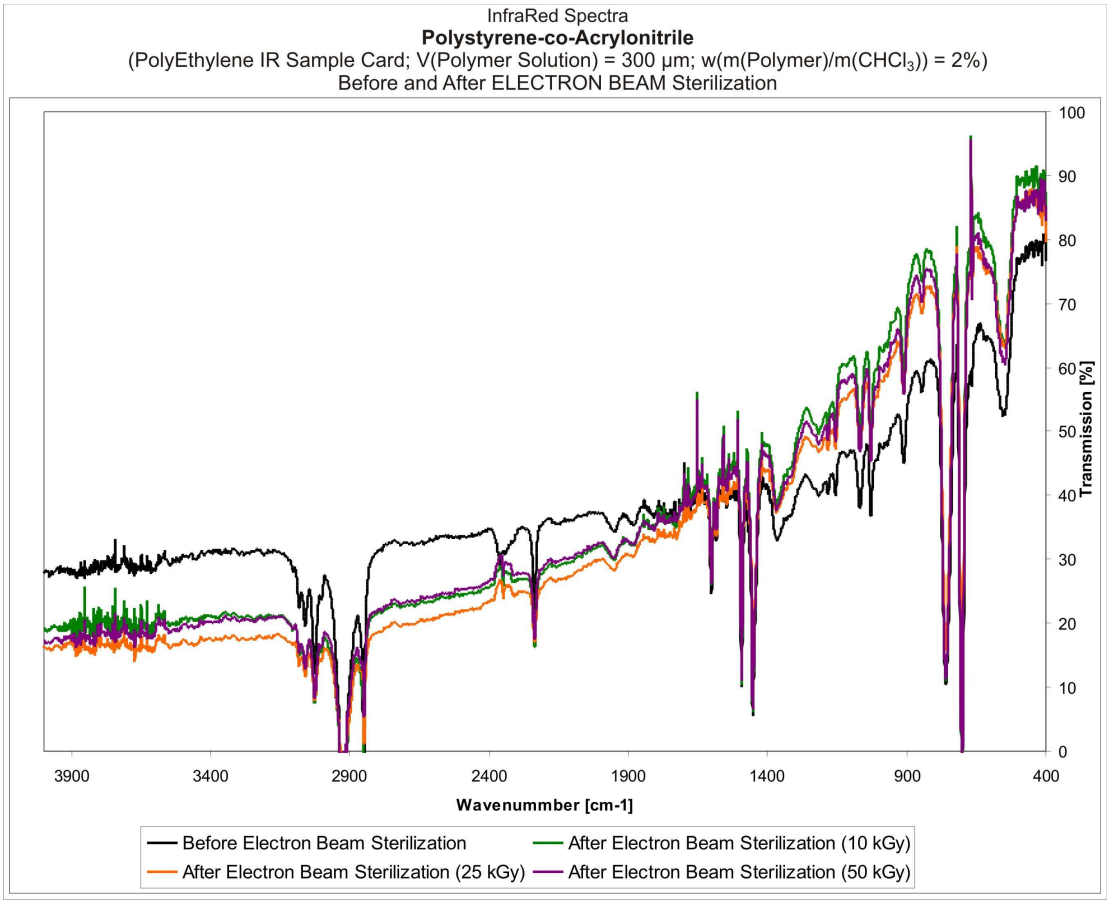

A.2.4 Differential Scanning Calorimetry

DSC Program:

30℃ – 150℃ 20℃/min
150℃ – 30℃ 10℃/min
30℃ – 150℃ 10℃/min

	T_g	Δc_p
BeforeS	111,19℃	0,292 J/g℃
10 kGy	107,58℃	0,306 J/g℃
25 kGy	106,54℃	0,364 J/g℃
50 kGy	108,02℃	0,252 J/g℃

Before sterilization

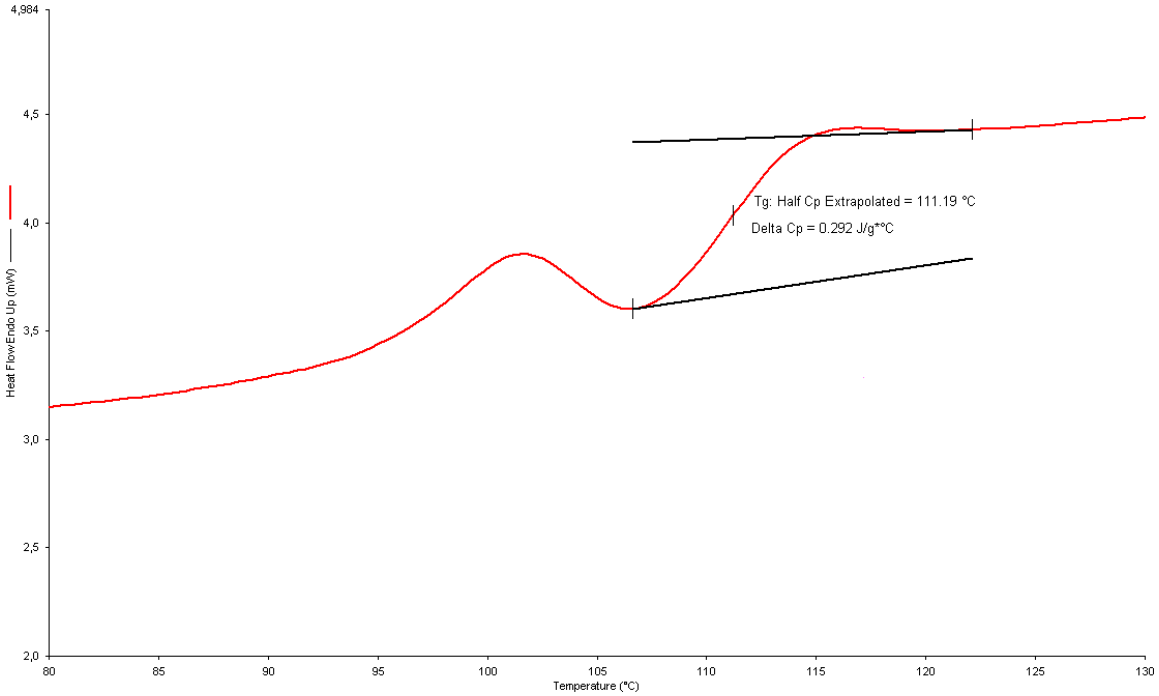

After GAMMA sterilization with 10 kGy

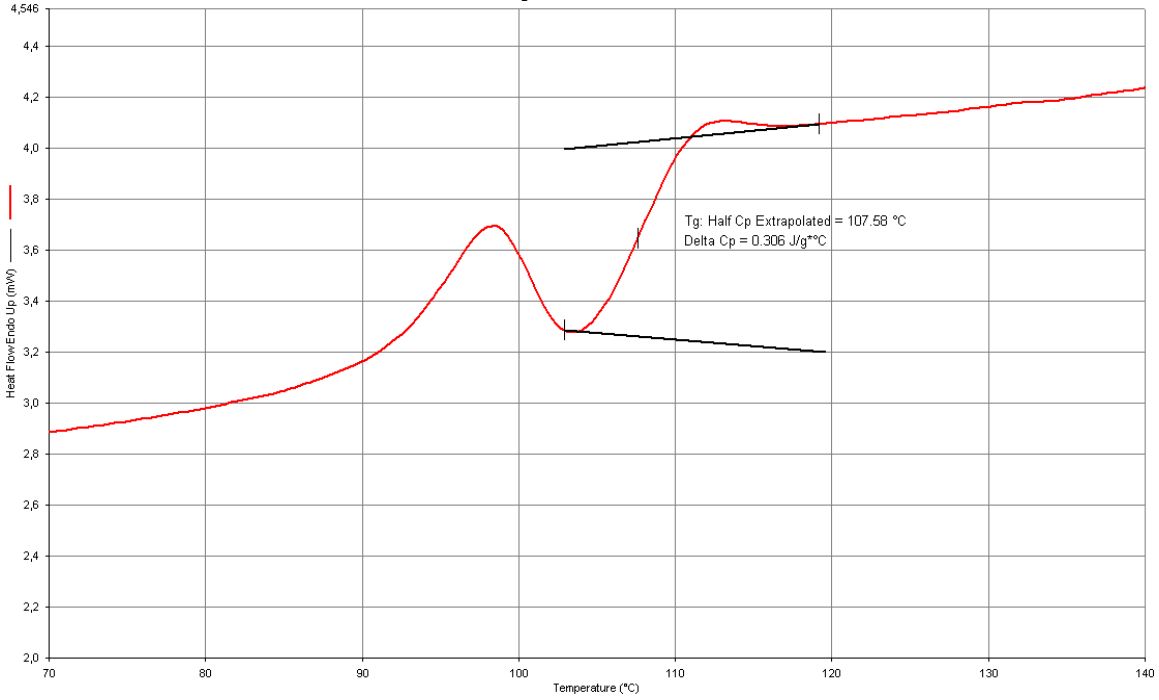

After GAMMA sterilization with 25 kGy

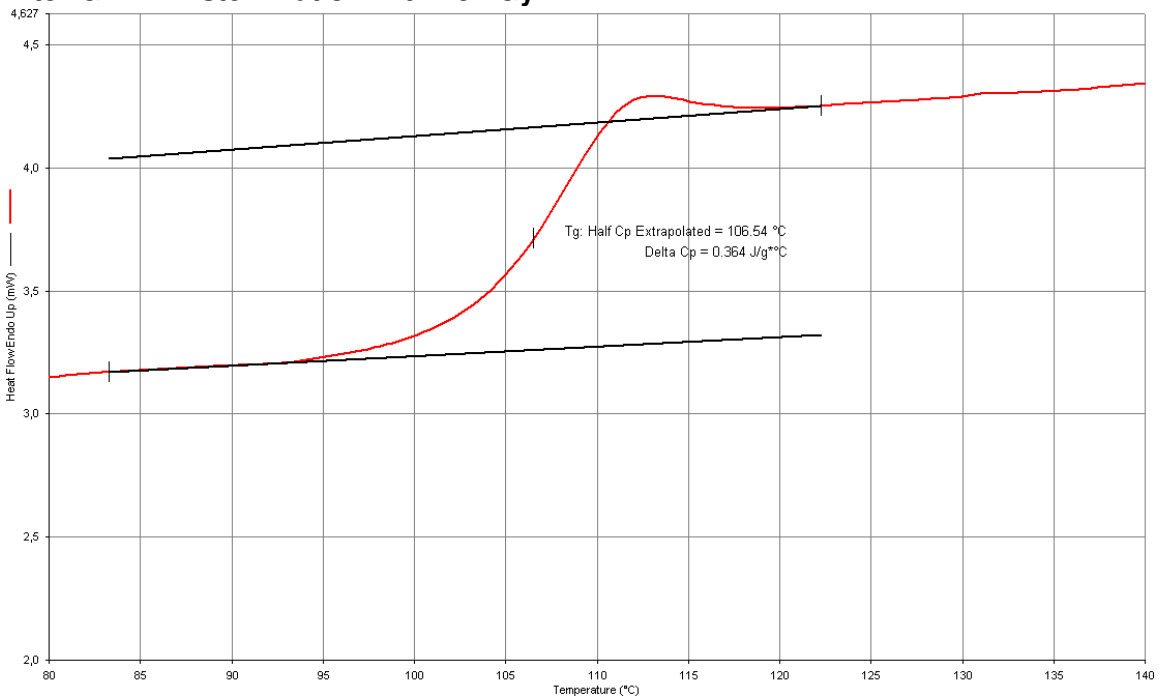

After GAMMA sterilization with 50 kGy

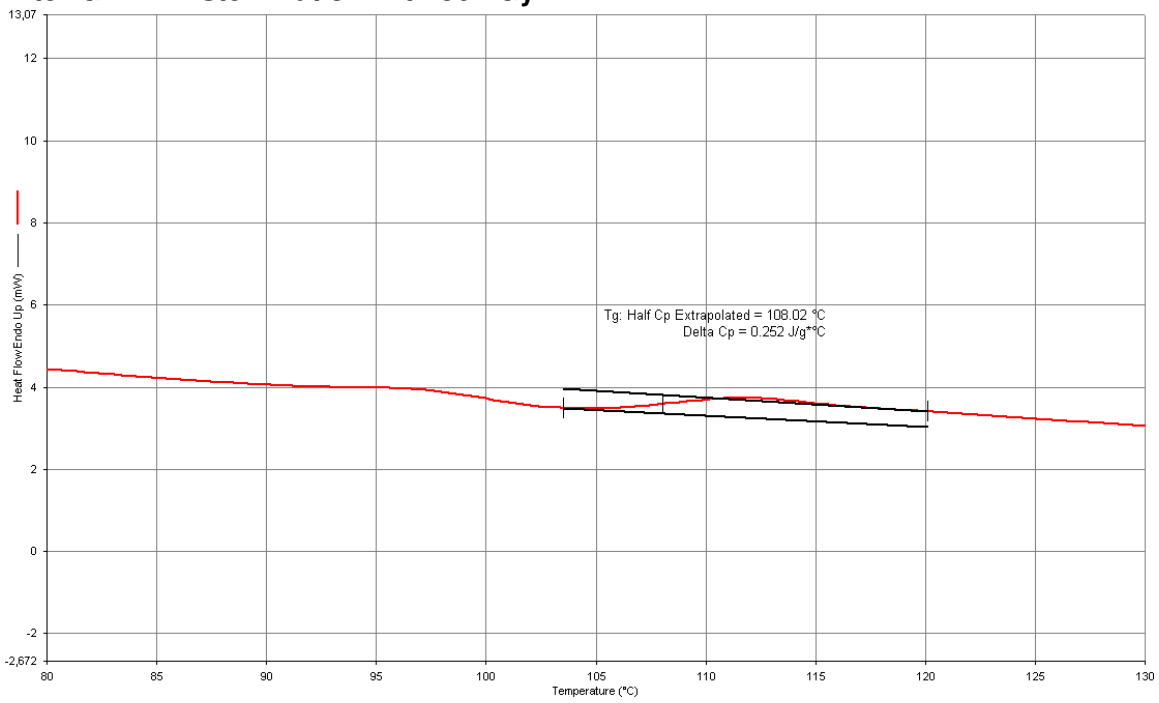

A.3 Polystyrene-co-Maleic Anhydride

A.3.1 Absorption Spectra

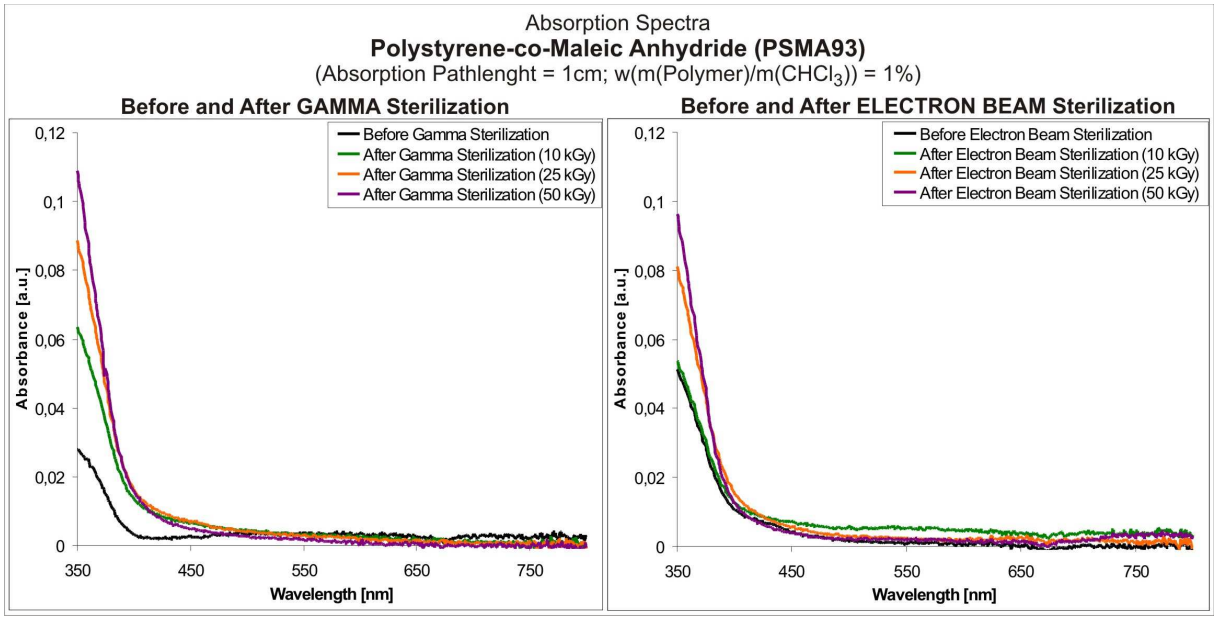

A.3.2 Contact Angle Measurement

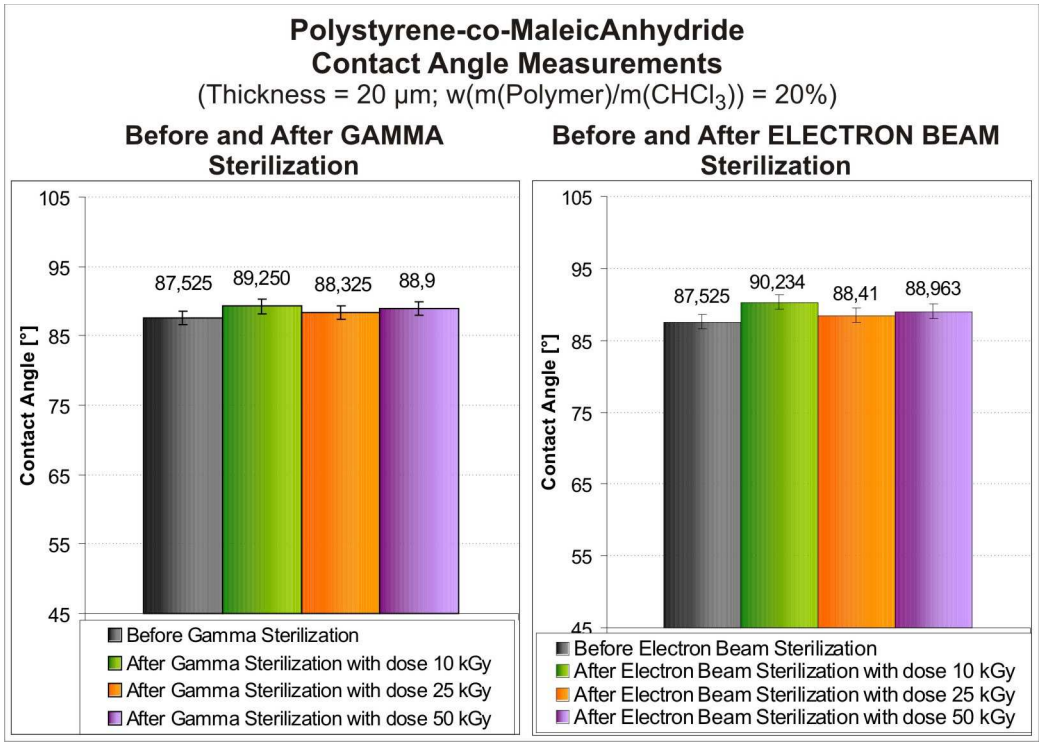

A.3.3 Infrared Spectra

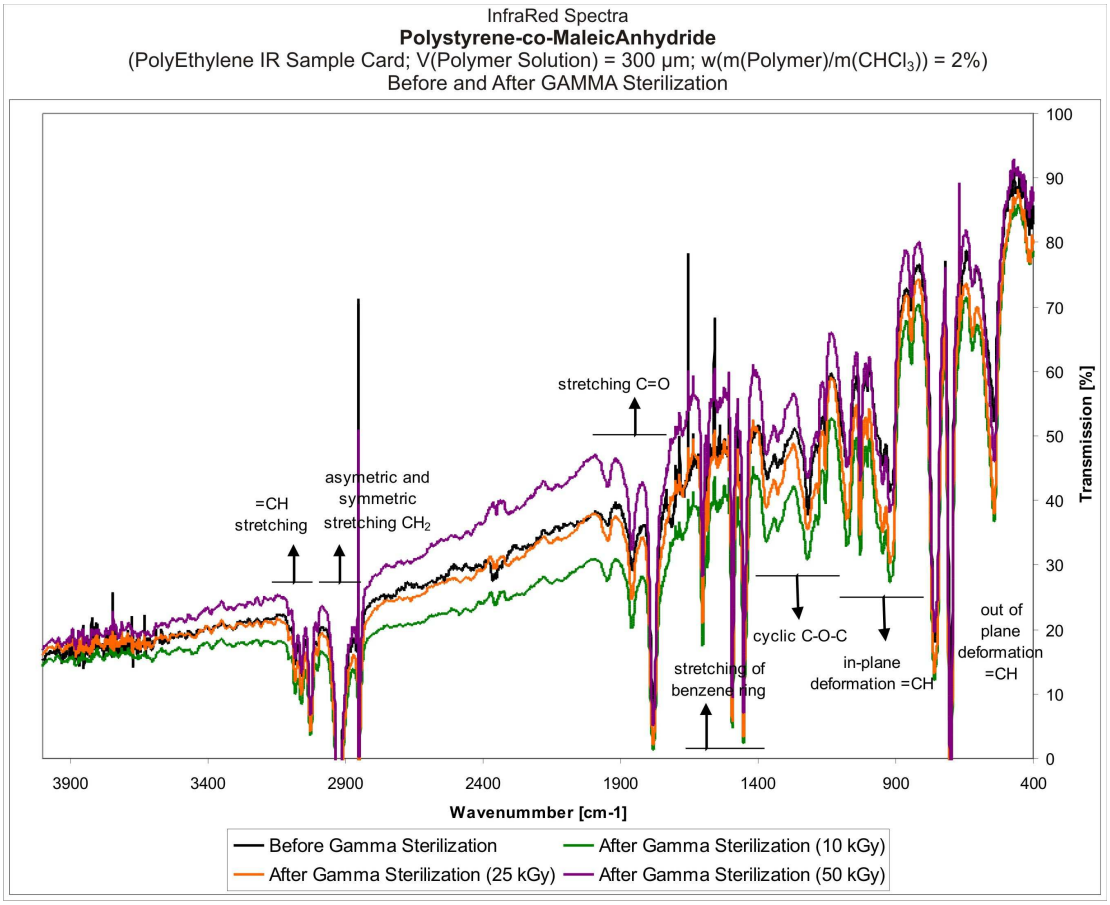

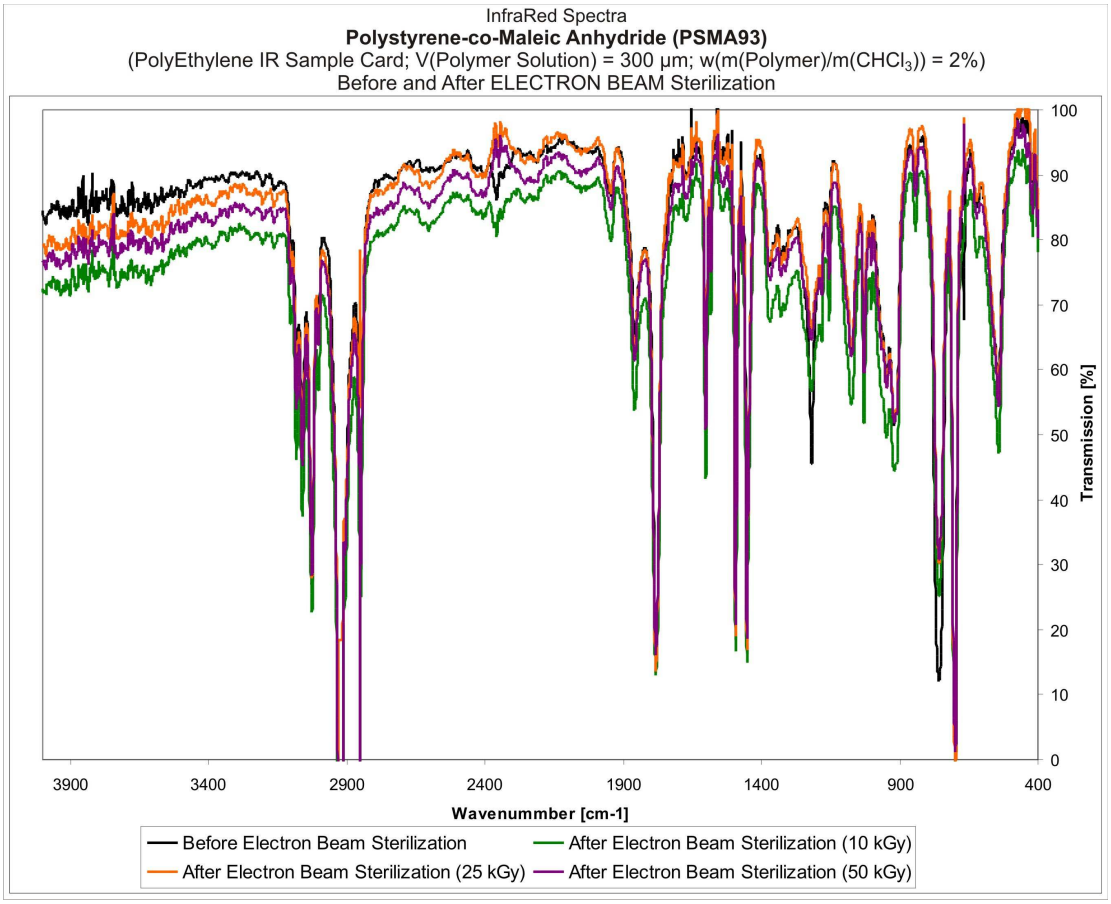

A.3.4 Differential Scanning Calorimetry

DSC Program:

30 °C – 180 °C 20 °C/min
180 °C – 30 °C 10 °C/min
30 °C – 180 °C 10 °C/min

	T_g	Δc_p
BeforeS	120,70 °C	0,320 J/g °C
10 kGy	121,90 °C	0,252 J/g °C
25 kGy	121,74 °C	0,232 J/g °C
50 kGy	120,47 °C	0,369 J/g °C

Before sterilization

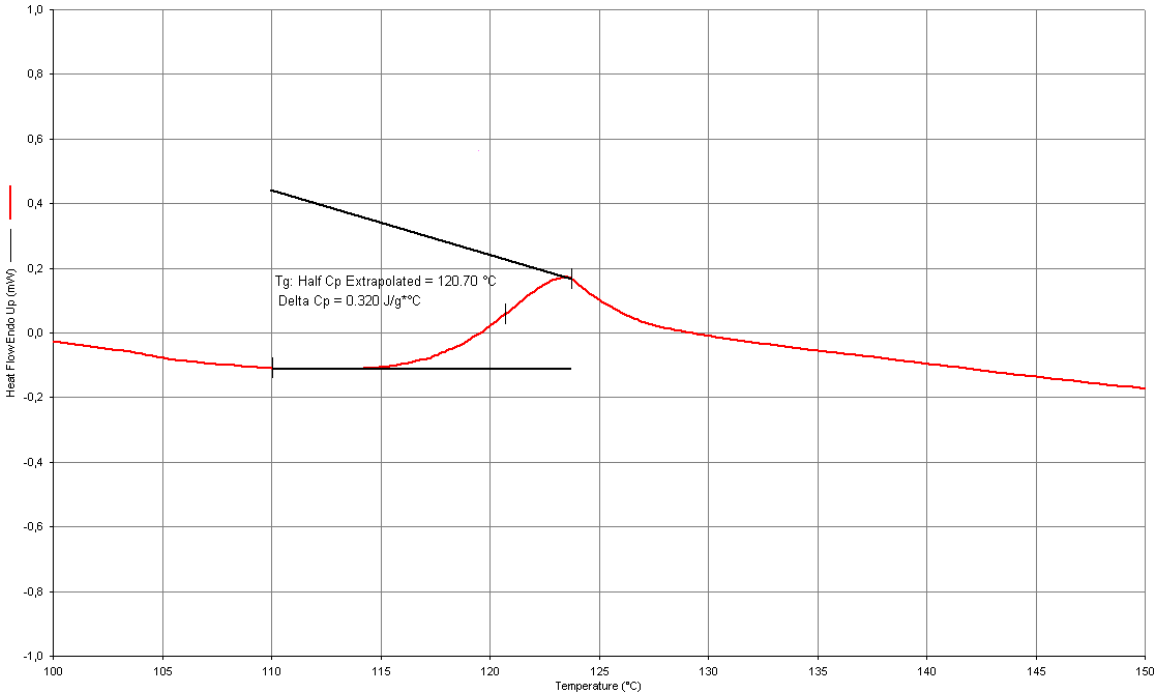

After GAMMA sterilization with 10 kGy

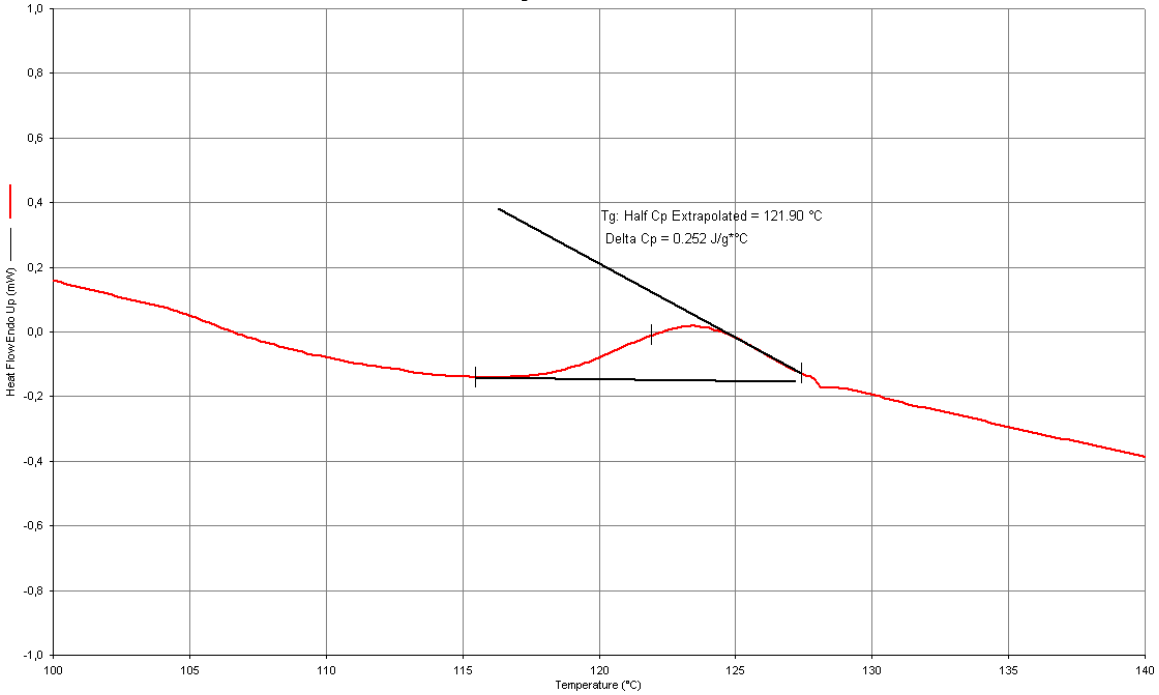

After GAMMA sterilization with 25 kGy

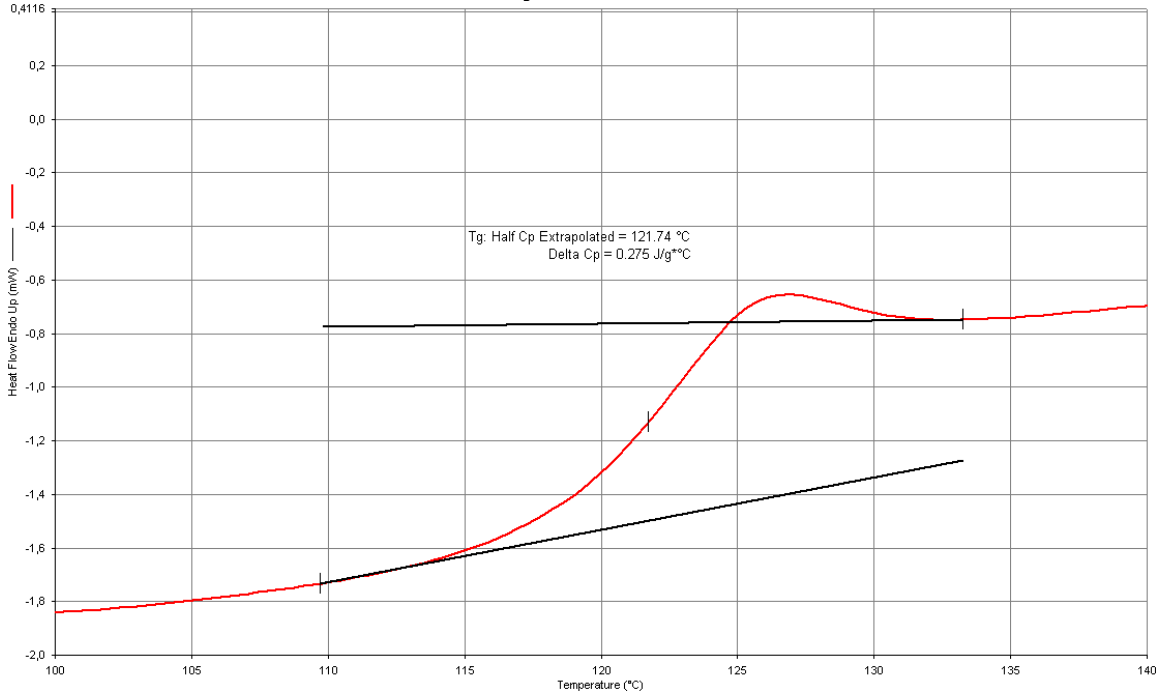

After GAMMA sterilization with 50 kGy

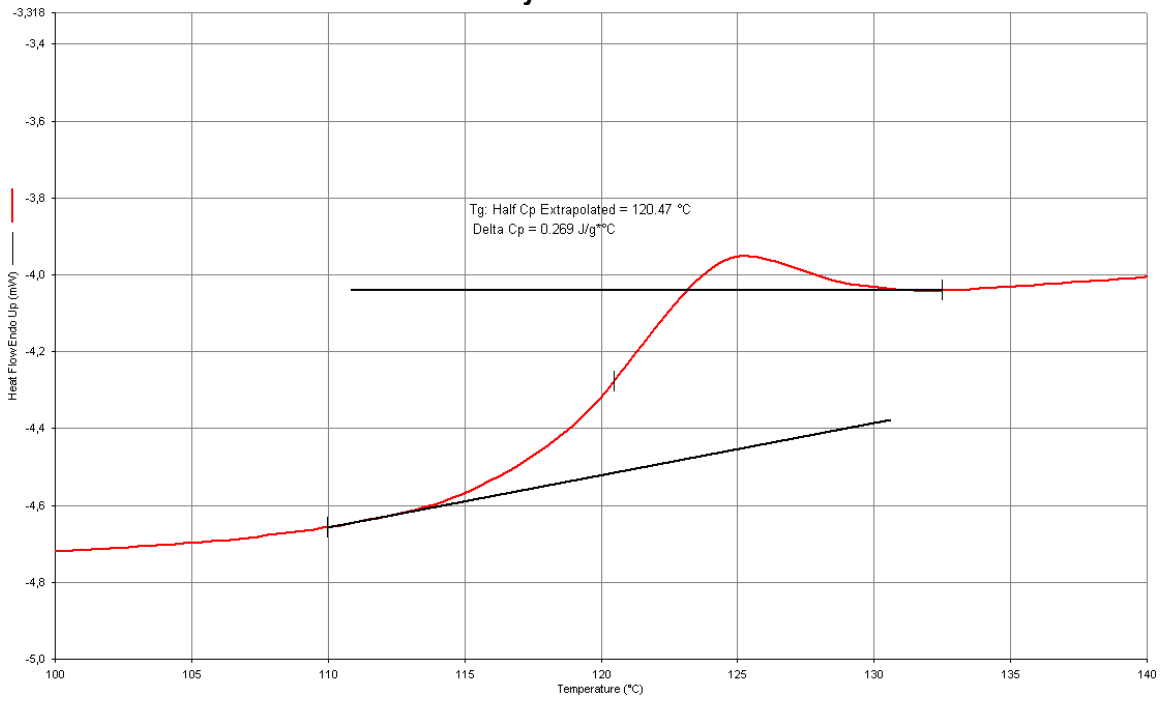

A.4 Polysulfone

A.4.1 Absorption Spectra

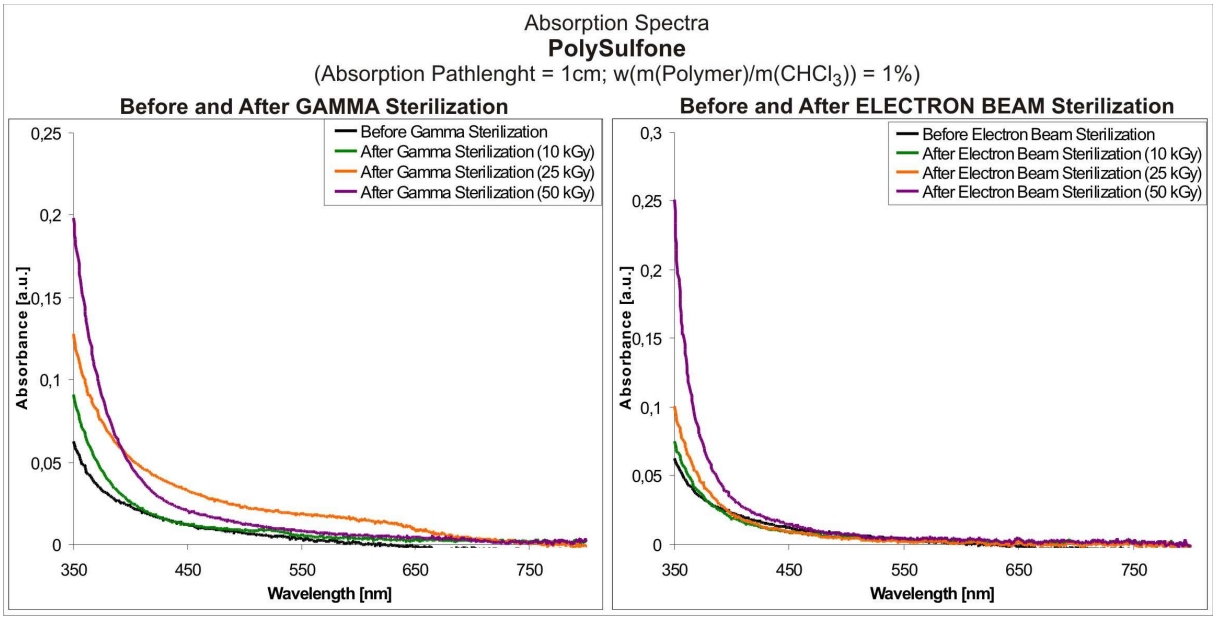

A.4.2 Contact Angle Measurement

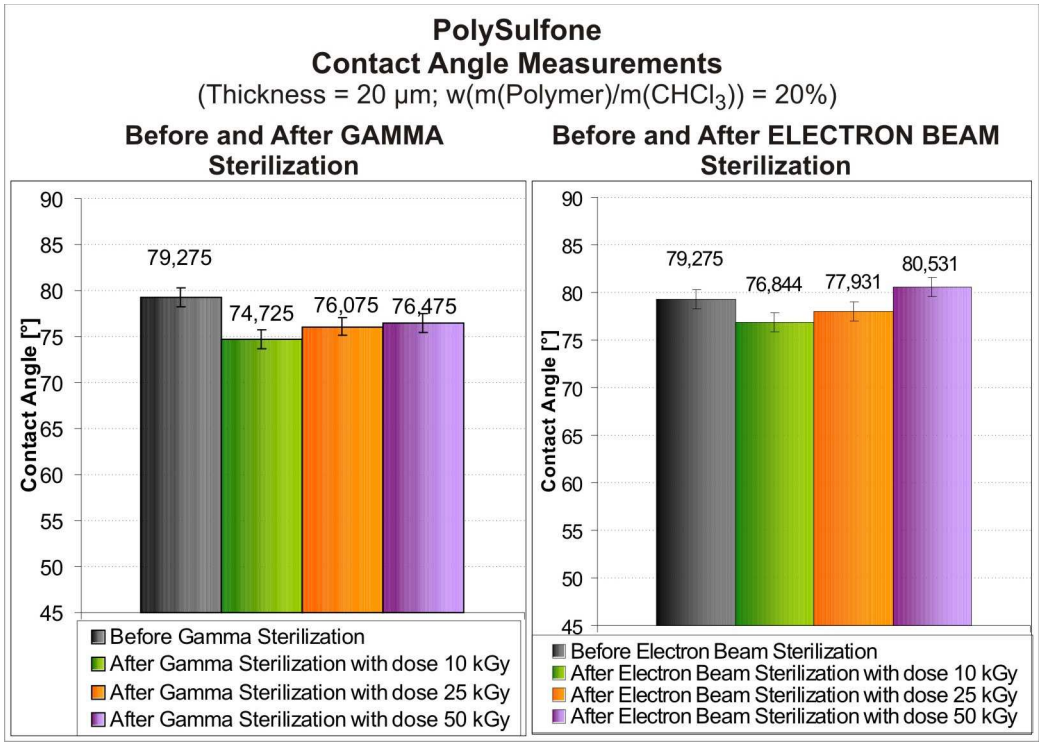

A.4.3 Infrared Spectra

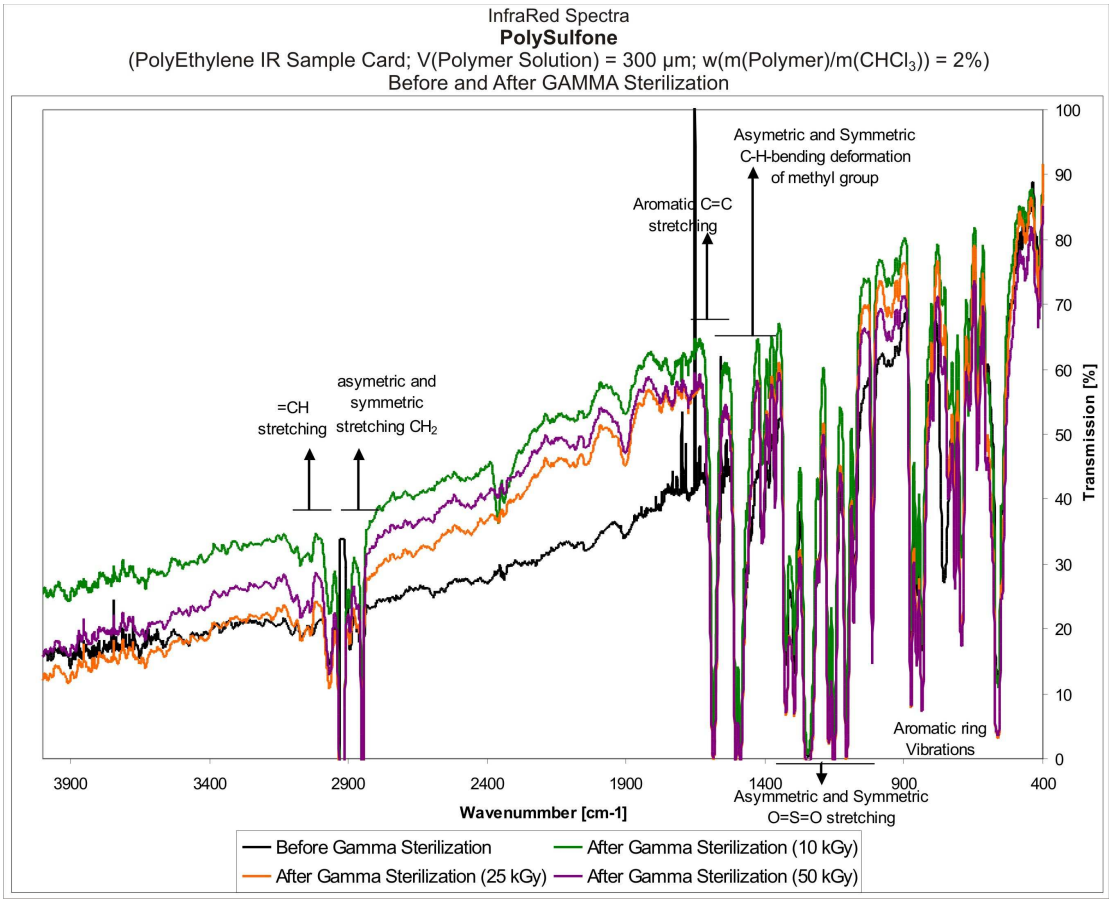

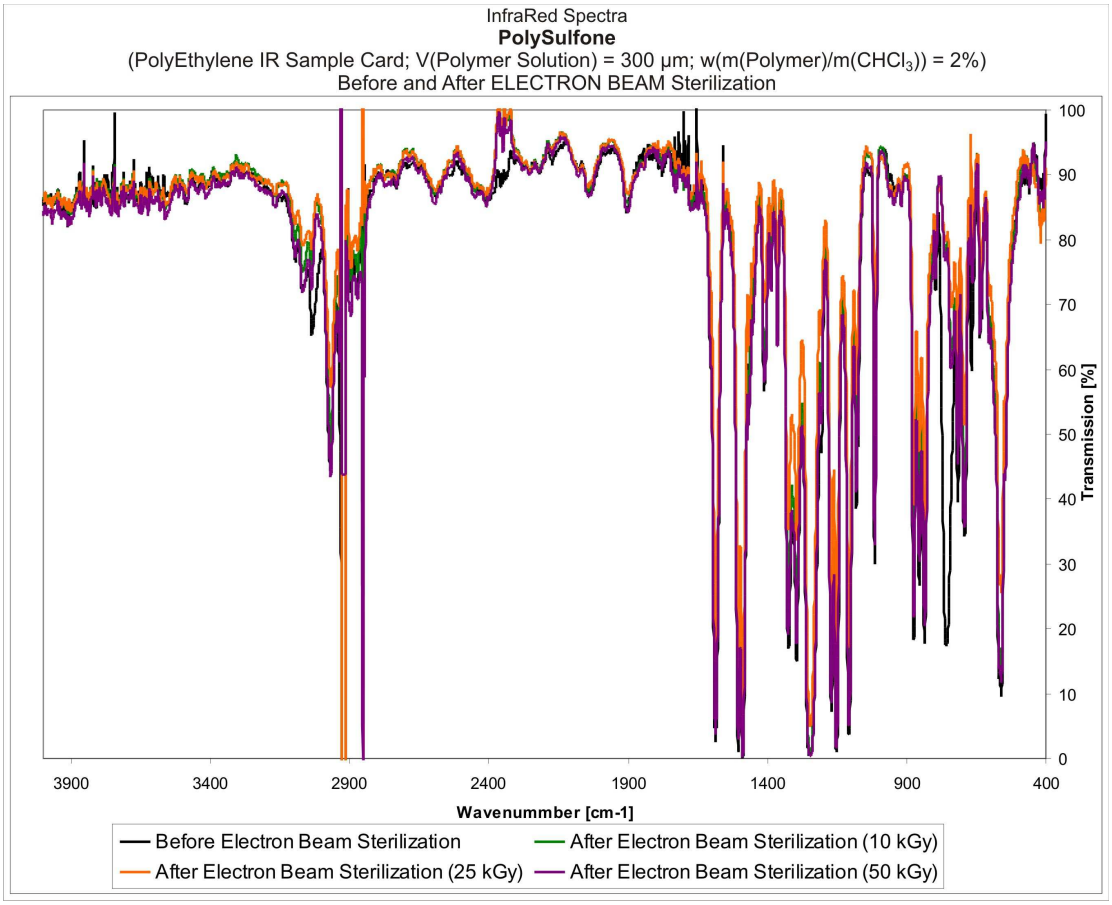

A.4.4 Differential Scanning Calorimetry

DSC Program:

30 °C – 220 °C 20 °C/min
220 °C – 30 °C 10 °C/min
30 °C – 220 °C 10 °C/min

	T_g	Δc_p
BeforeS	195,19 °C	0,173 J/g °C
10 kGy	190,17 °C	0,127 J/g °C
25 kGy	189,39 °C	0,230 J/g °C
50 kGy	187,24 °C	0,187 J/g °C

Before sterilization

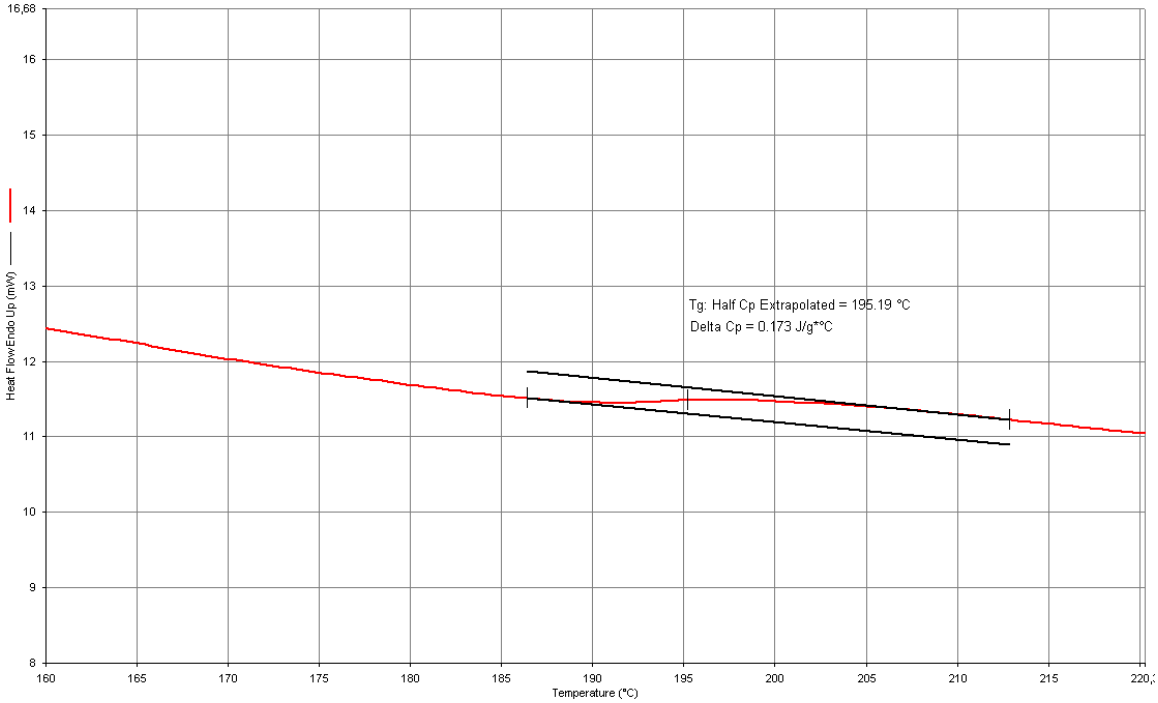

After GAMMA sterilization with 10 kGy

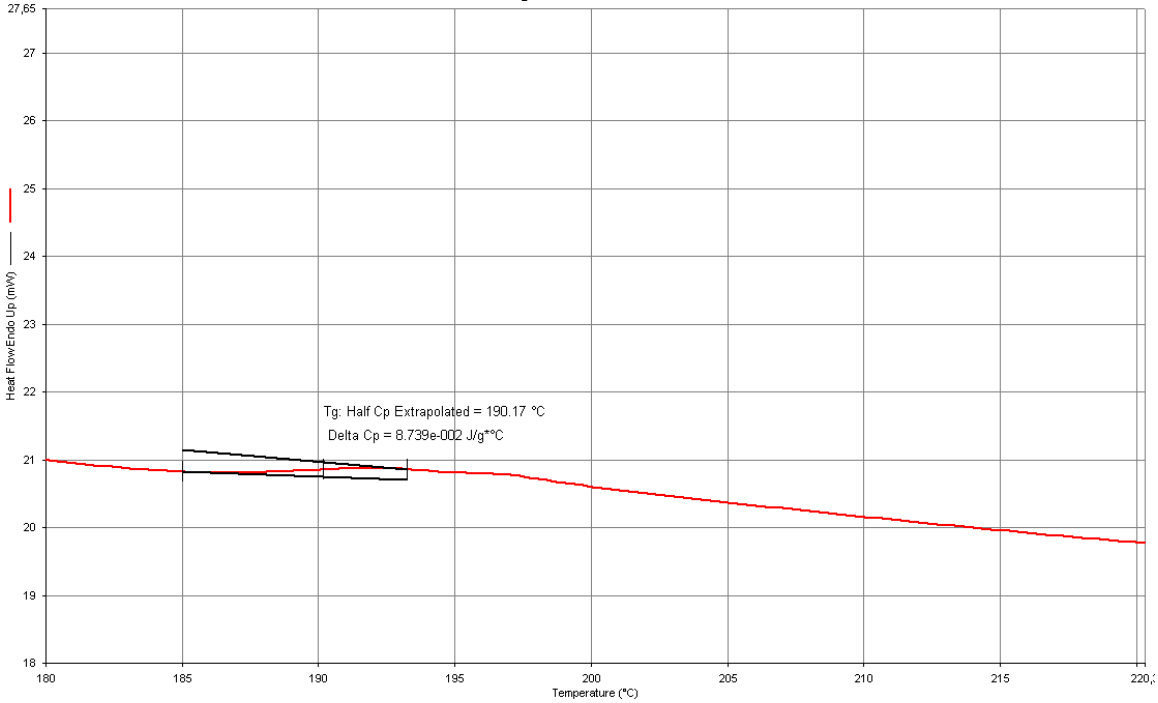

After GAMMA sterilization with 25 kGy

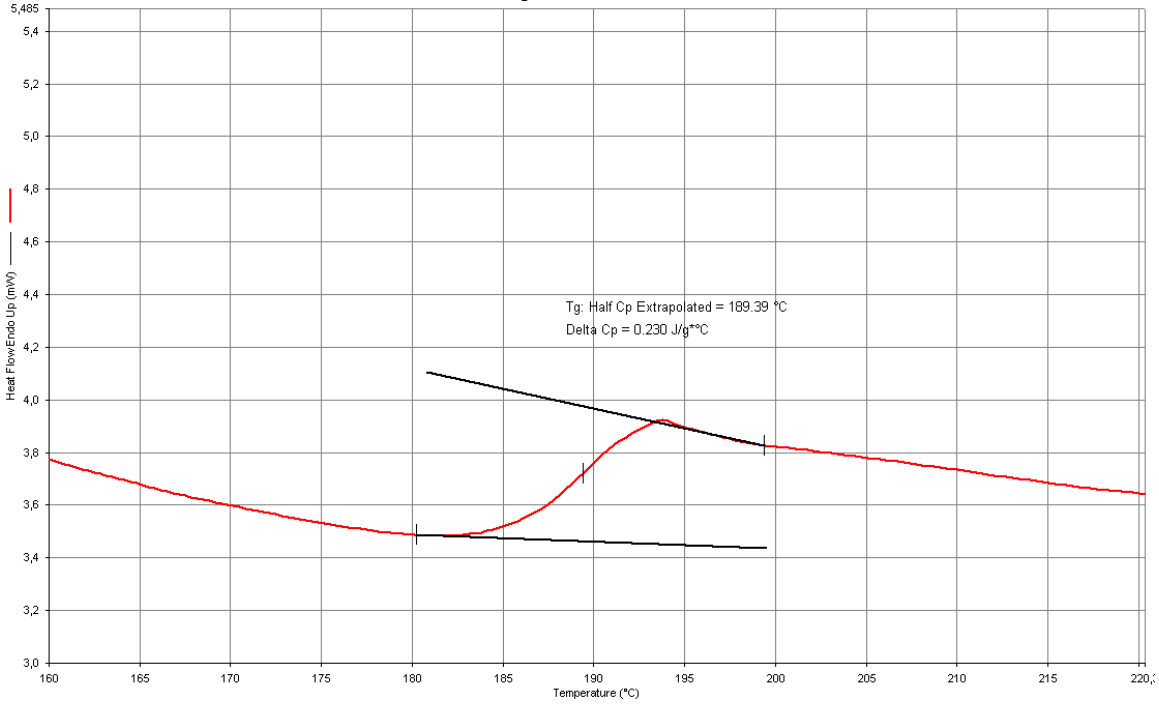

After GAMMA sterilization with 50 kGy

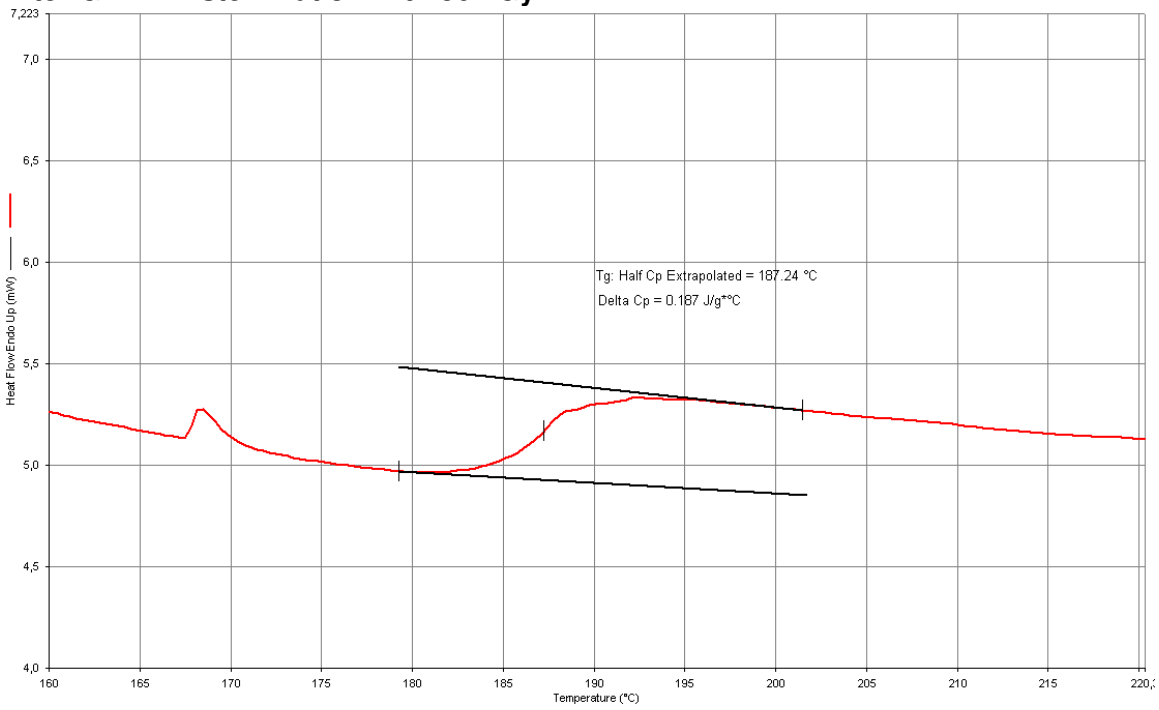

A.5 Cellulose Acetate

A.5.1 Absorption Spectra

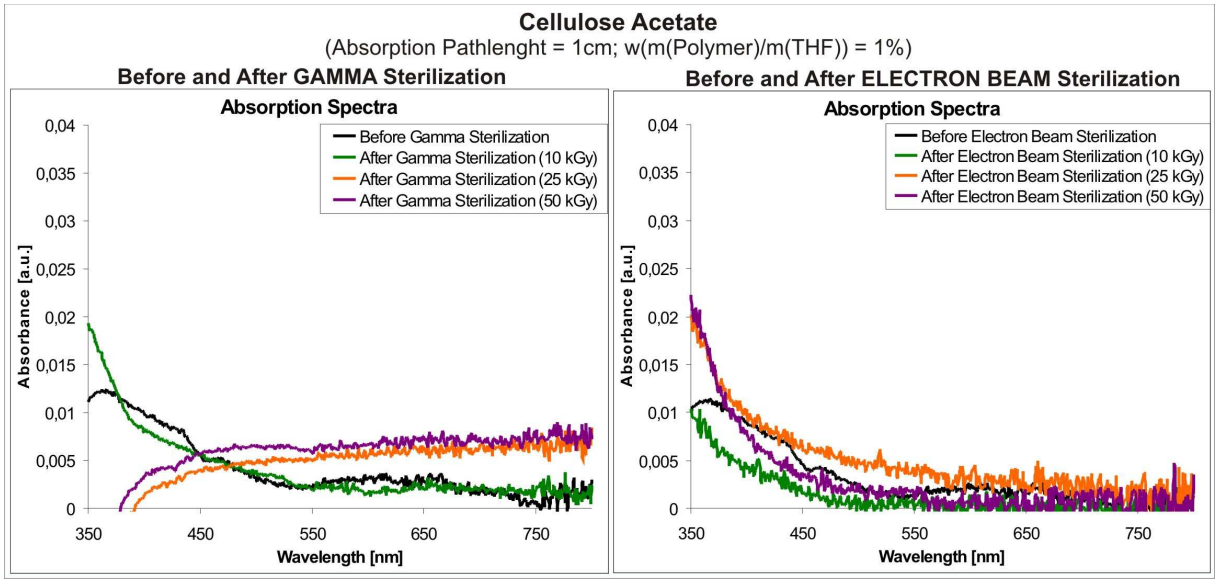

A.5.2 Contact Angle Measurement

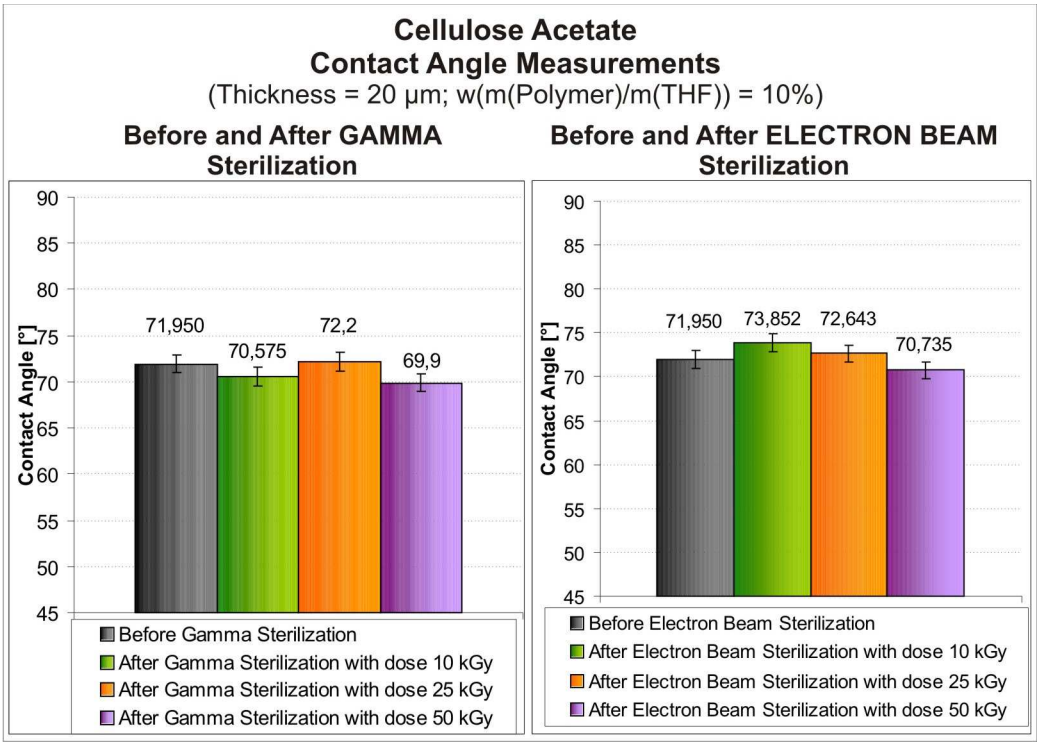

A.5.3 Infrared Spectra

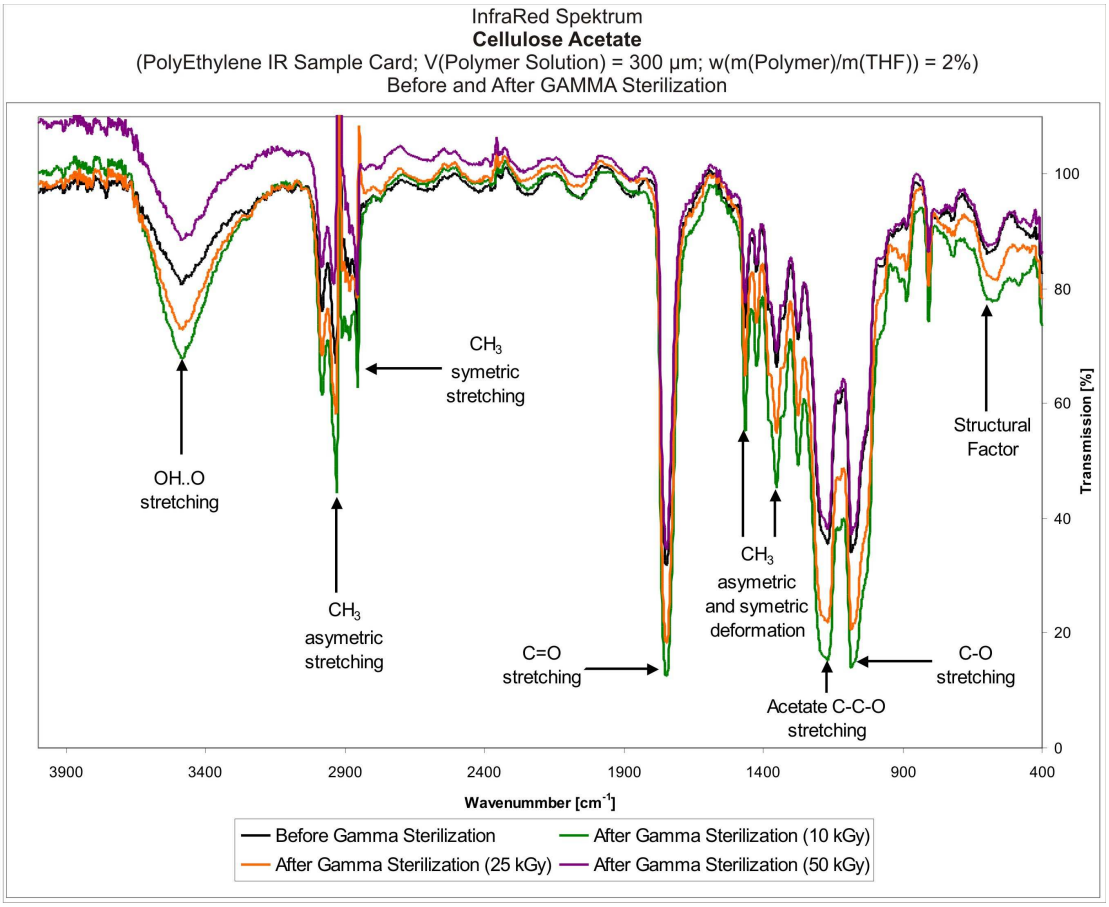

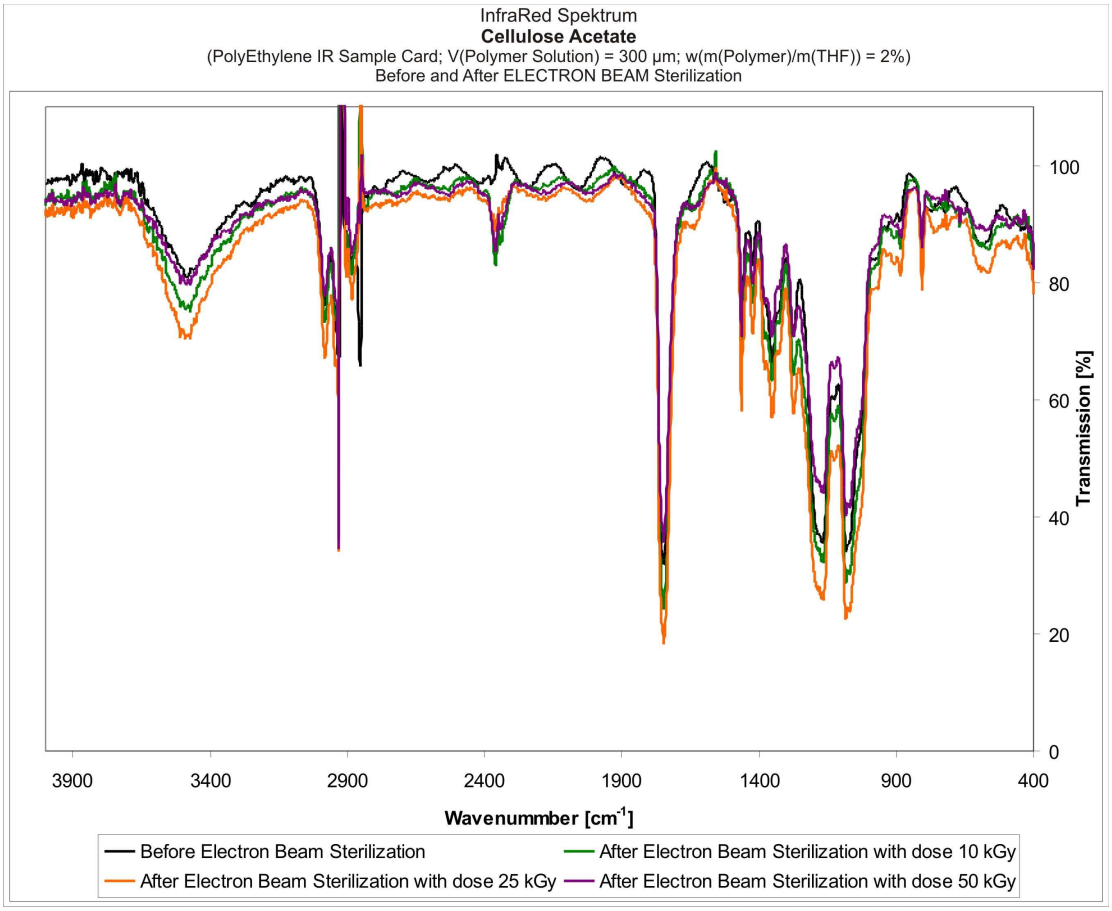

A.6 Ethyl Cellulose

A.6.1 Absorption Spectra

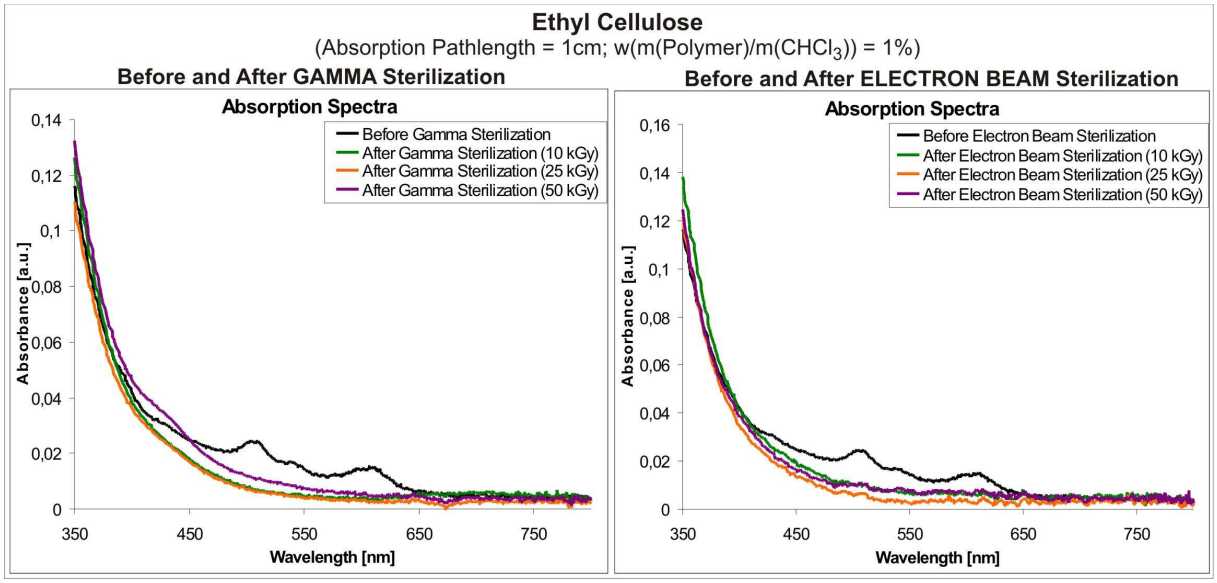

A.6.2 Contact Angle Measurement

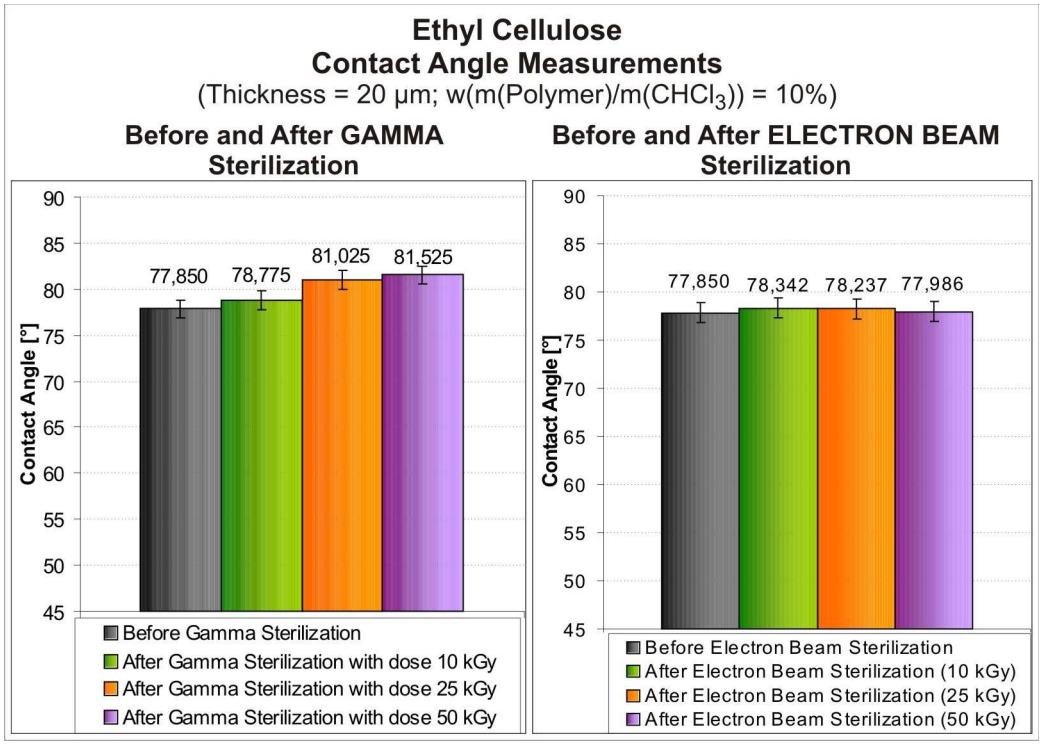

A.6.3 Infrared Spectra

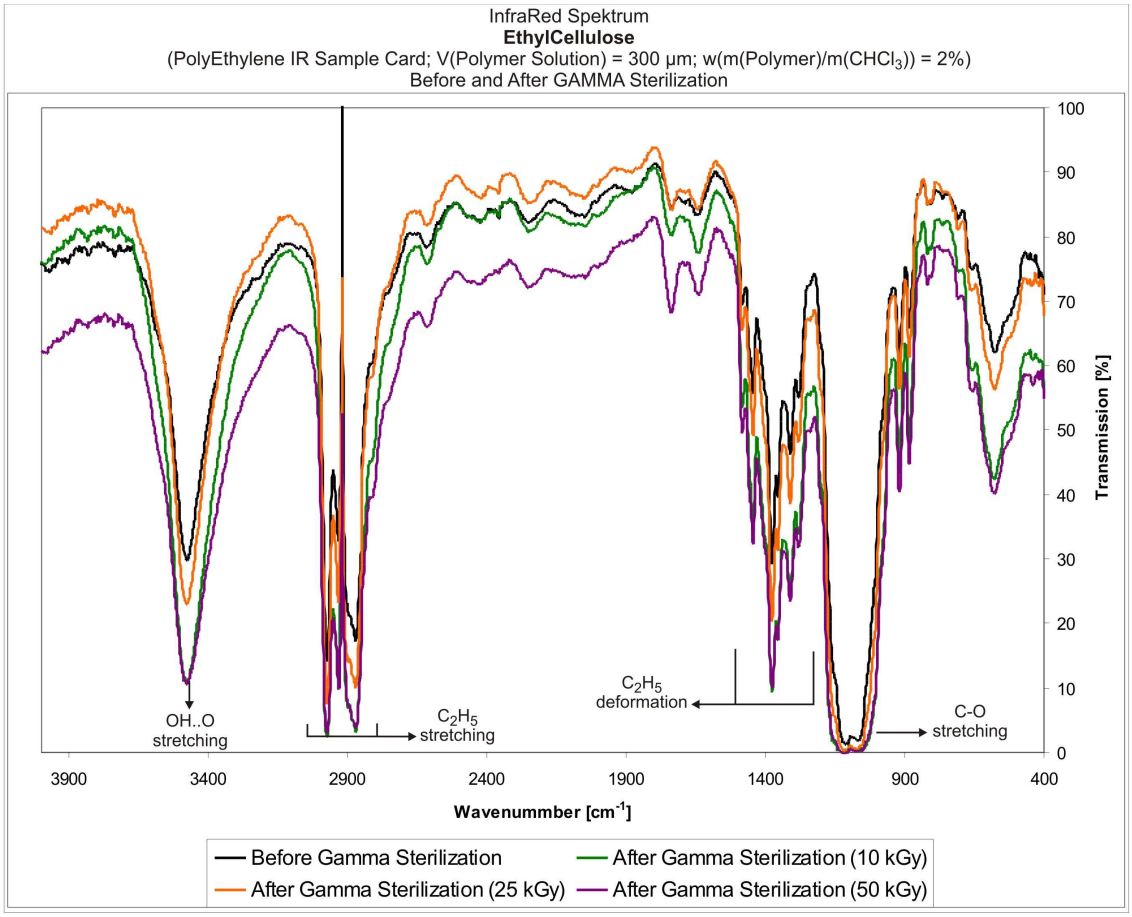

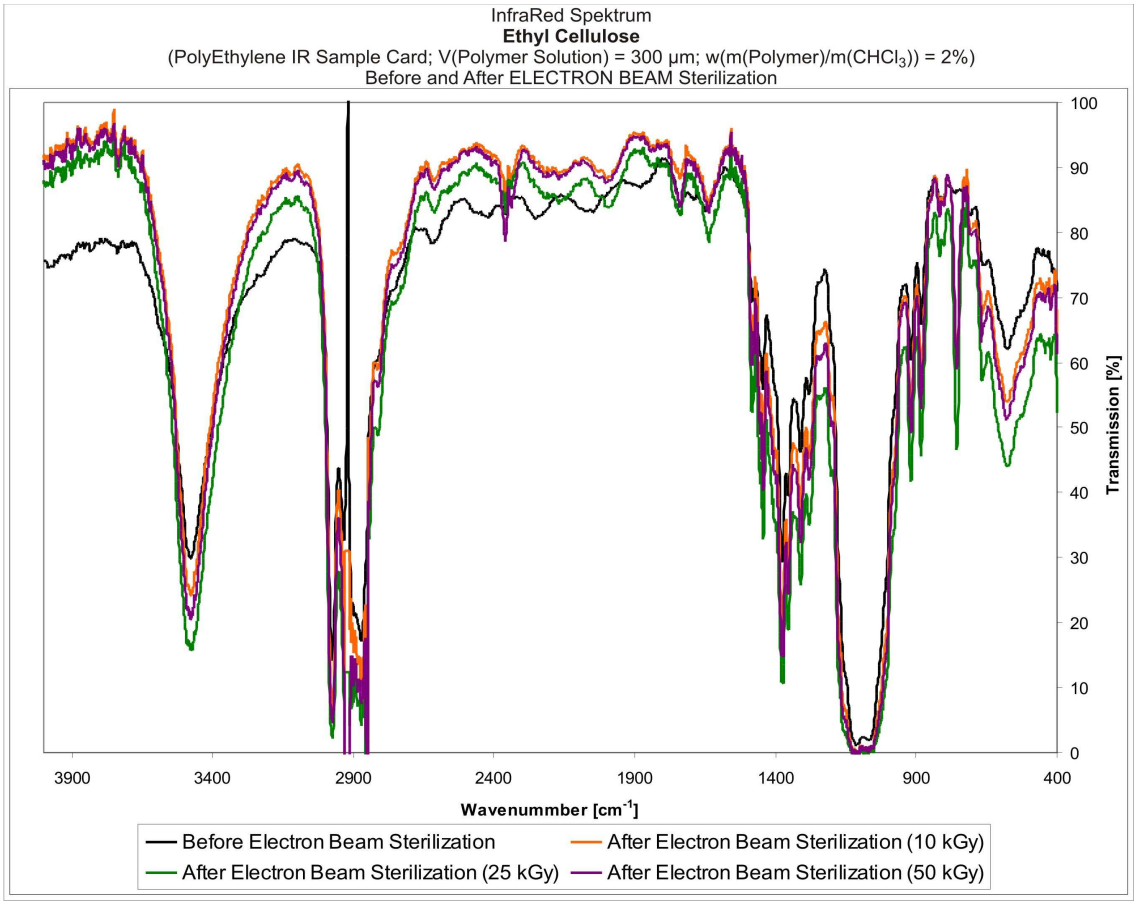

A.6.4 Differential Scanning Calorimetry

DSC Program:

30 °C – 250 °C 20 °C/min
250 °C – 30 °C 10 °C/min
30 °C – 250 °C 10 °C/min

	T_g	Δc_p
BeforeS	140,21 °C	0,0879 J/g °C
10 kGy	140,53 °C	0,1370 J/g °C
25 kGy	136,91 °C	0,0894 J/g °C
50 kGy	136,17 °C	0,0831 J/g °C

Before sterilization

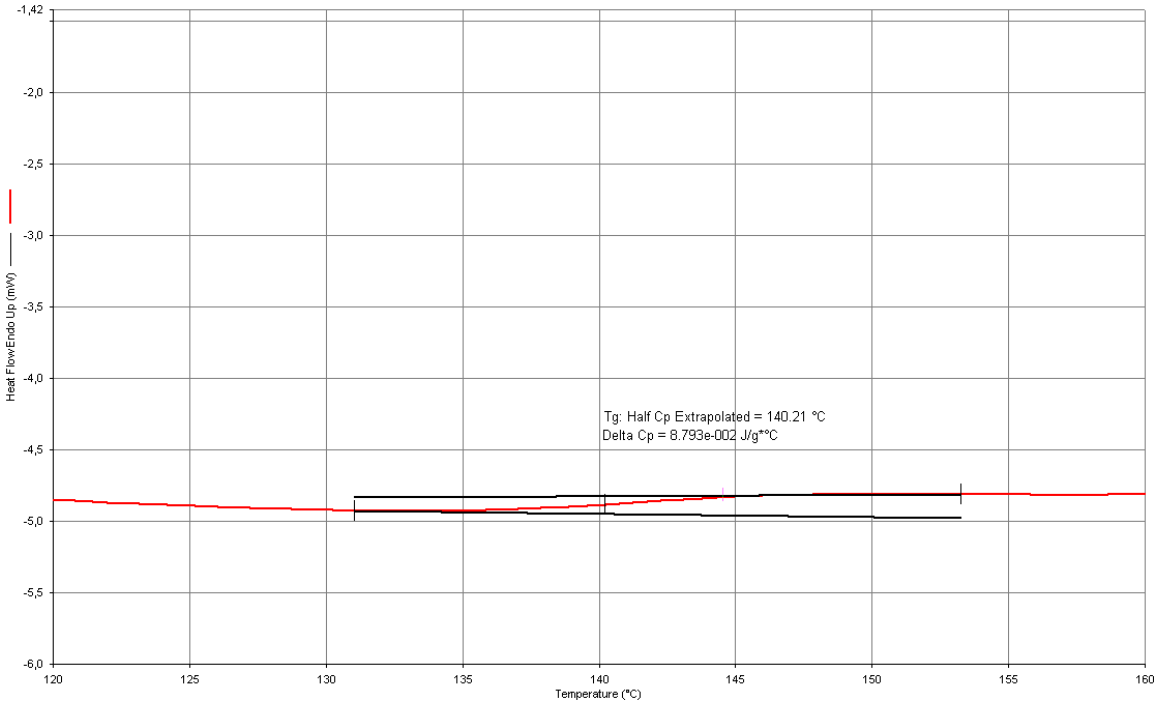

After GAMMA sterilization with 10 kGy

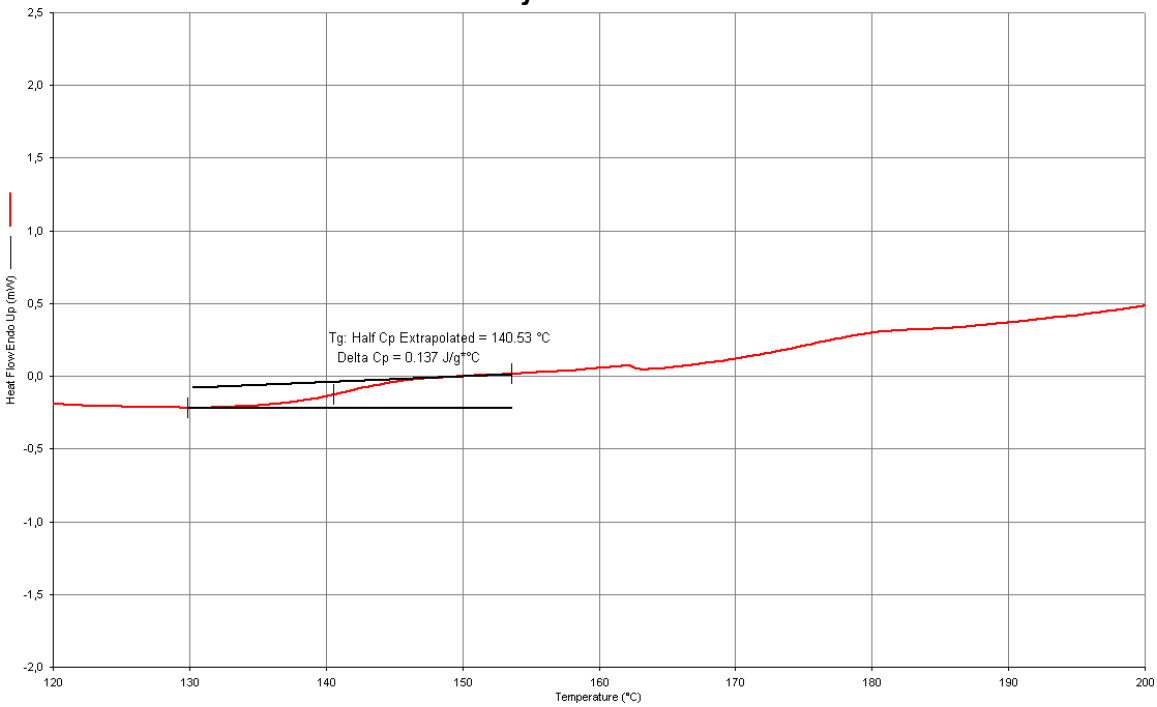

After GAMMA sterilization with 25 kGy

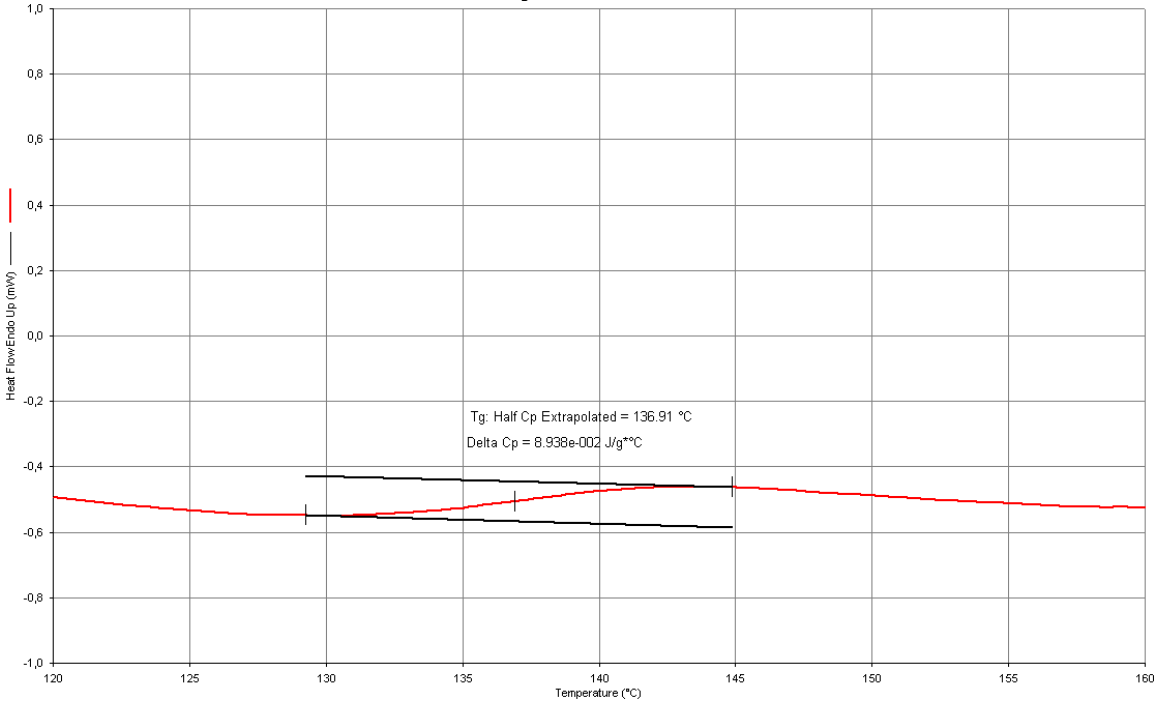

After GAMMA sterilization with 50 kGy

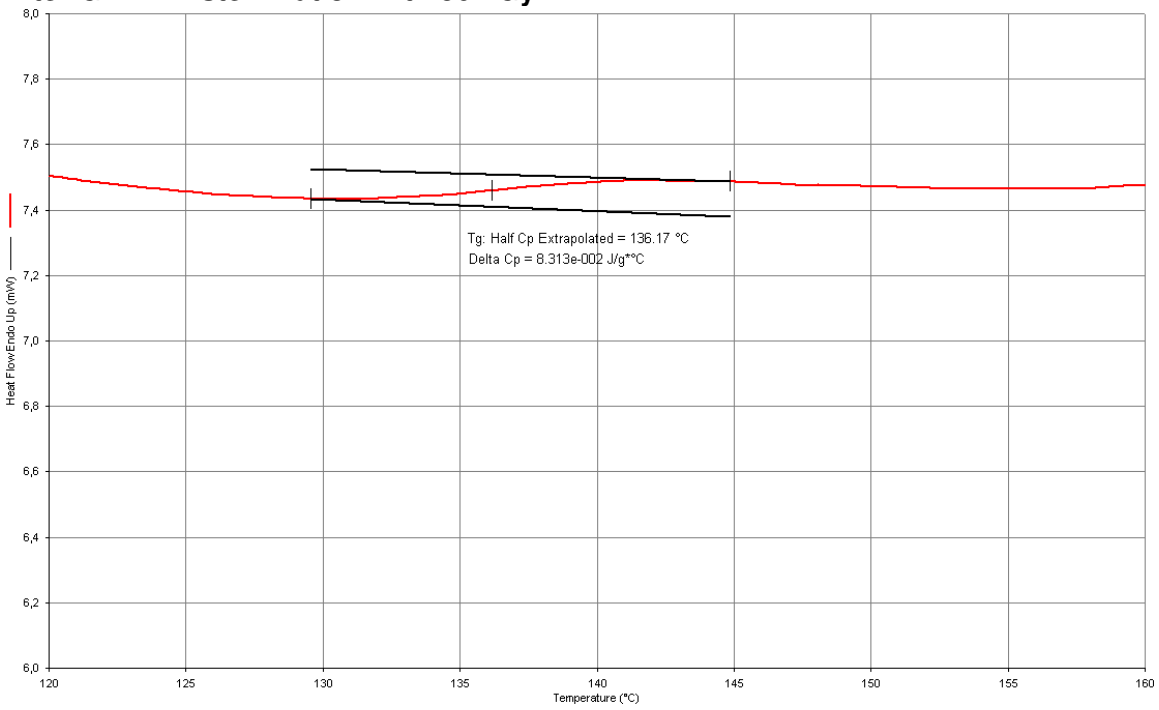

A.7 Hydrogel HydroMed™ D4 and D7

A.7.1 Absorption Spectra

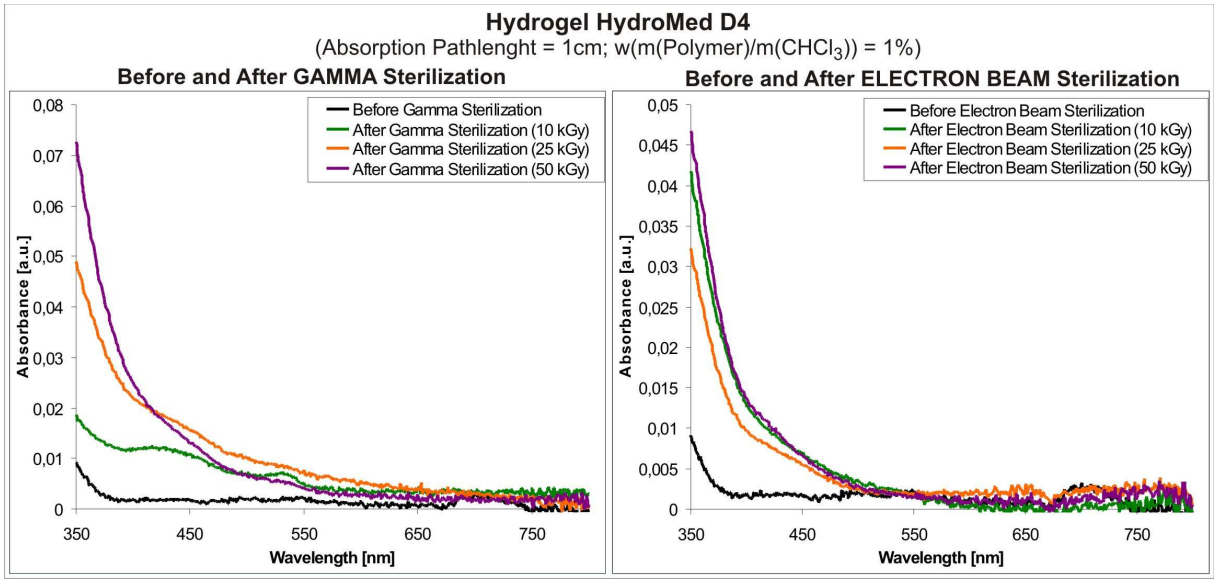

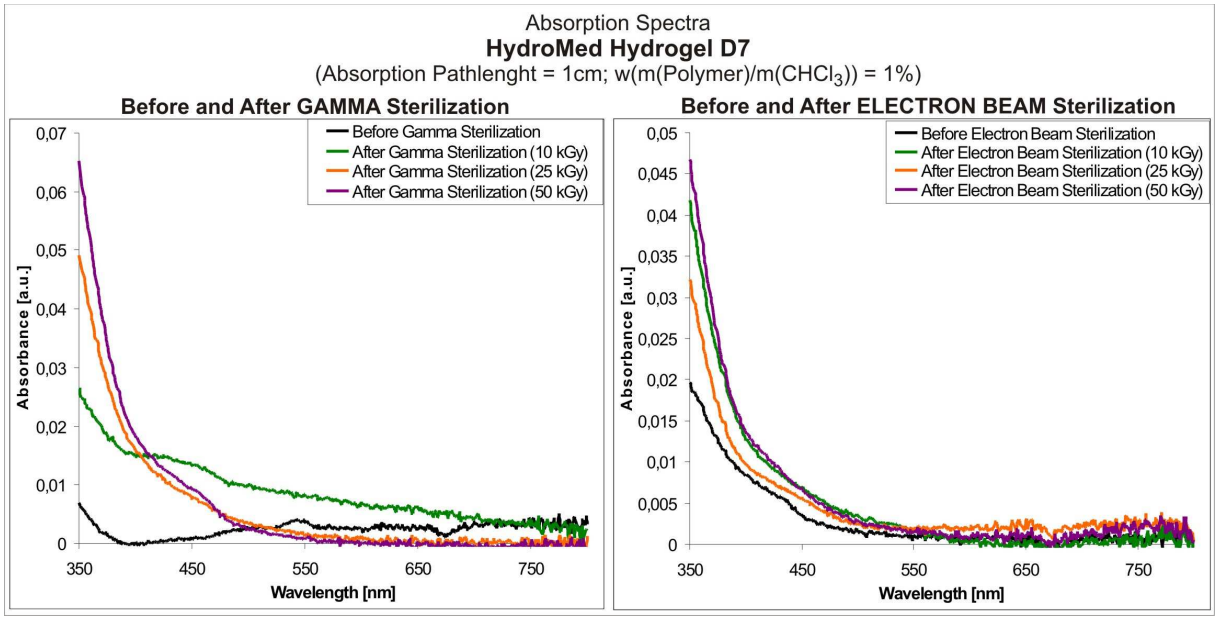

A.7.2 Contact Angle Measurement

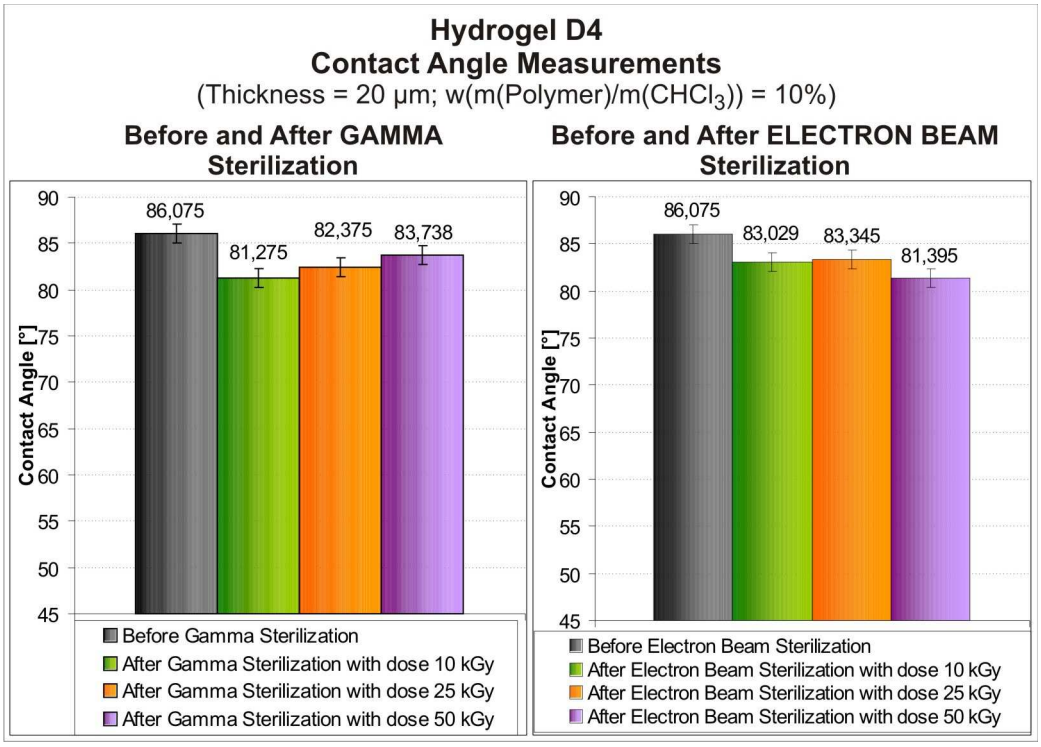

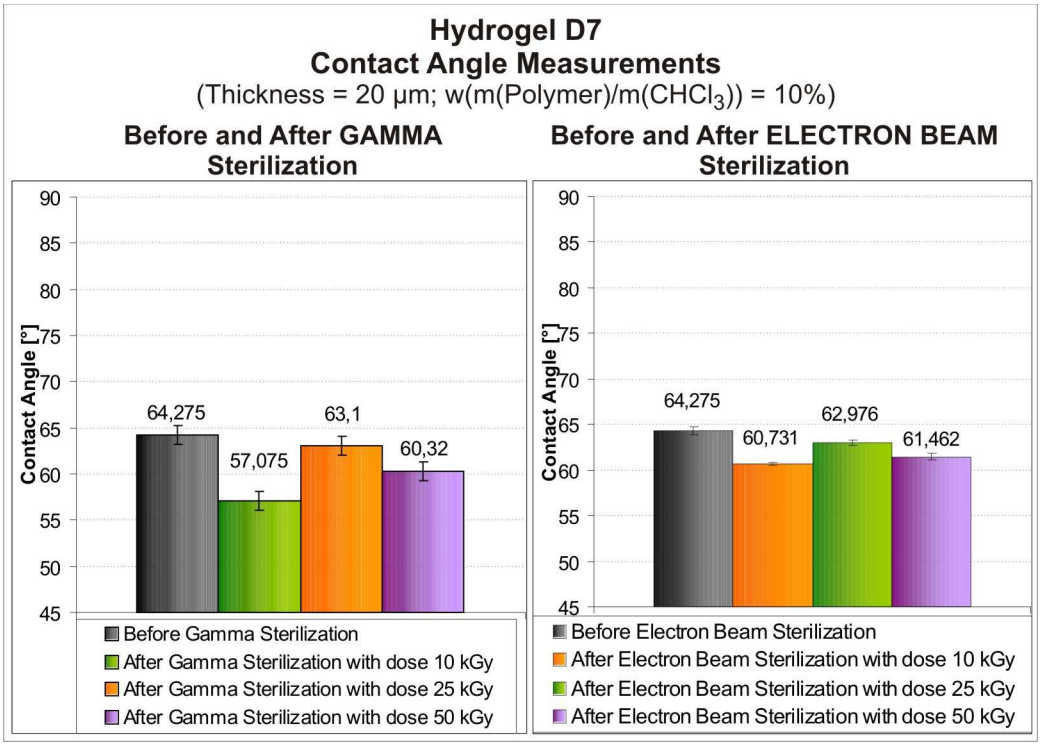

A.7.3 Infrared Spectra

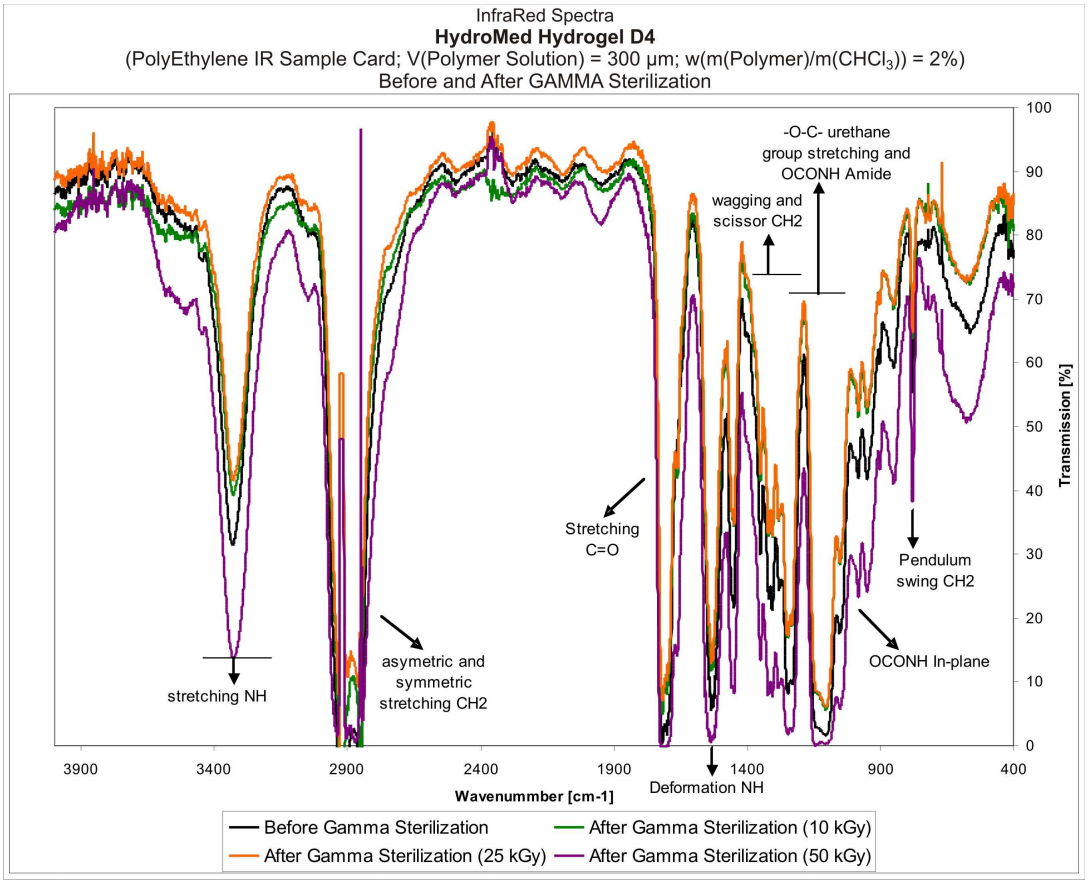

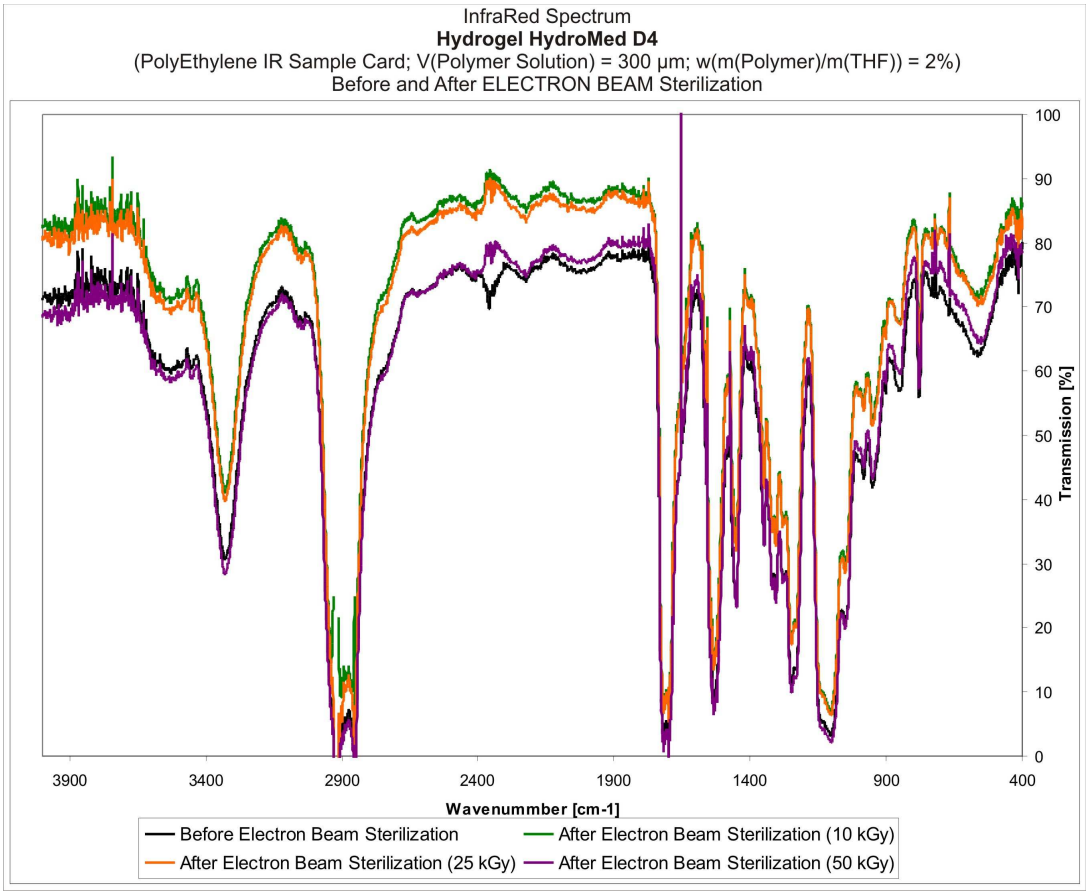

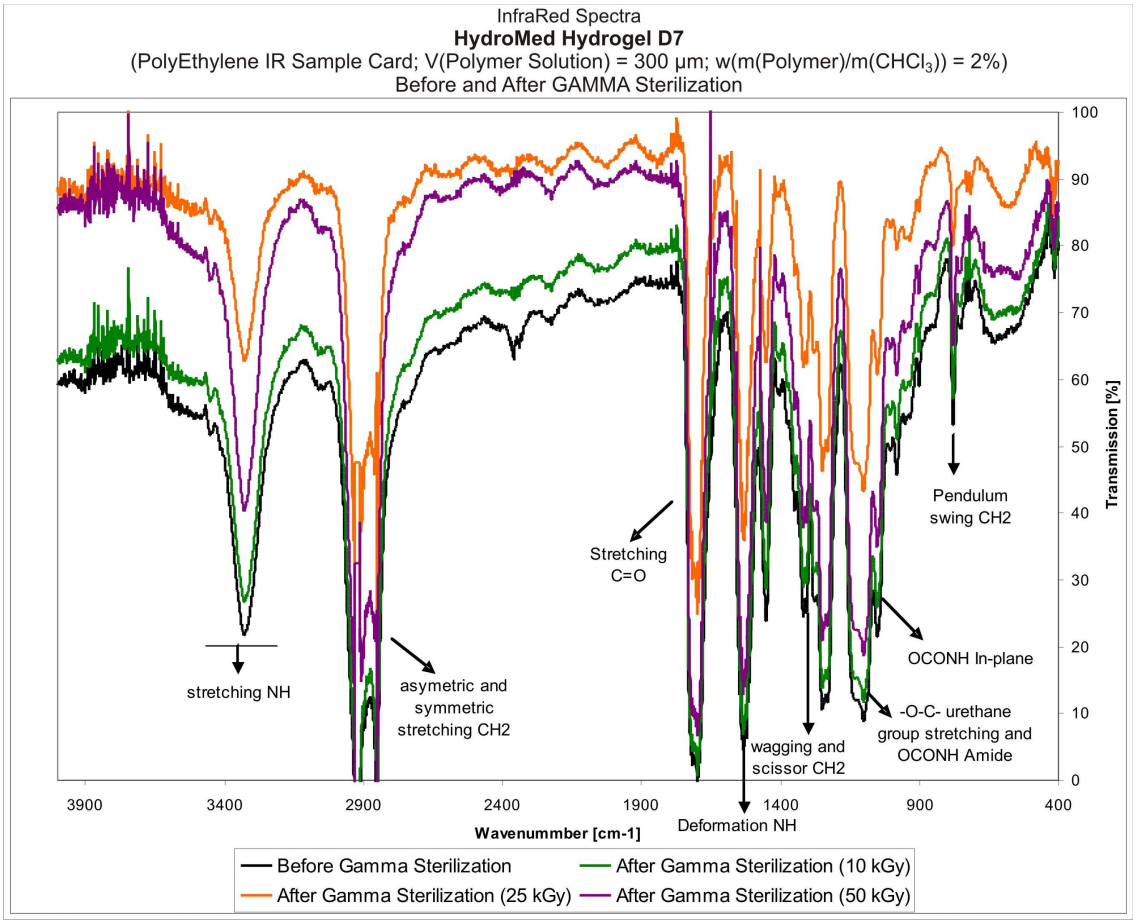
InfraRed Spectra
HydroMed Hydrogel D7
(PolyEthylene IR Sample Card; V(Polymer Solution) = 300 µm; w(m(Polymer)/m(CHCl3)) = 2%)
Before and After GAMMA Sterilization
stretching NH
asymetric and symmetric stretching CH2
Stretching C=O
wagging and scissor CH2
Deformation NH
Pendulum swing CH2
OCONH In-plane
-O-C- urethane group stretching and OCONH Amide
Wavenummber [cm-1]
Transmission [%]
Before Gamma Sterilization
After Gamma Sterilization (10 kGy)
After Gamma Sterilization (25 kGy)
After Gamma Sterilization (50 kGy)

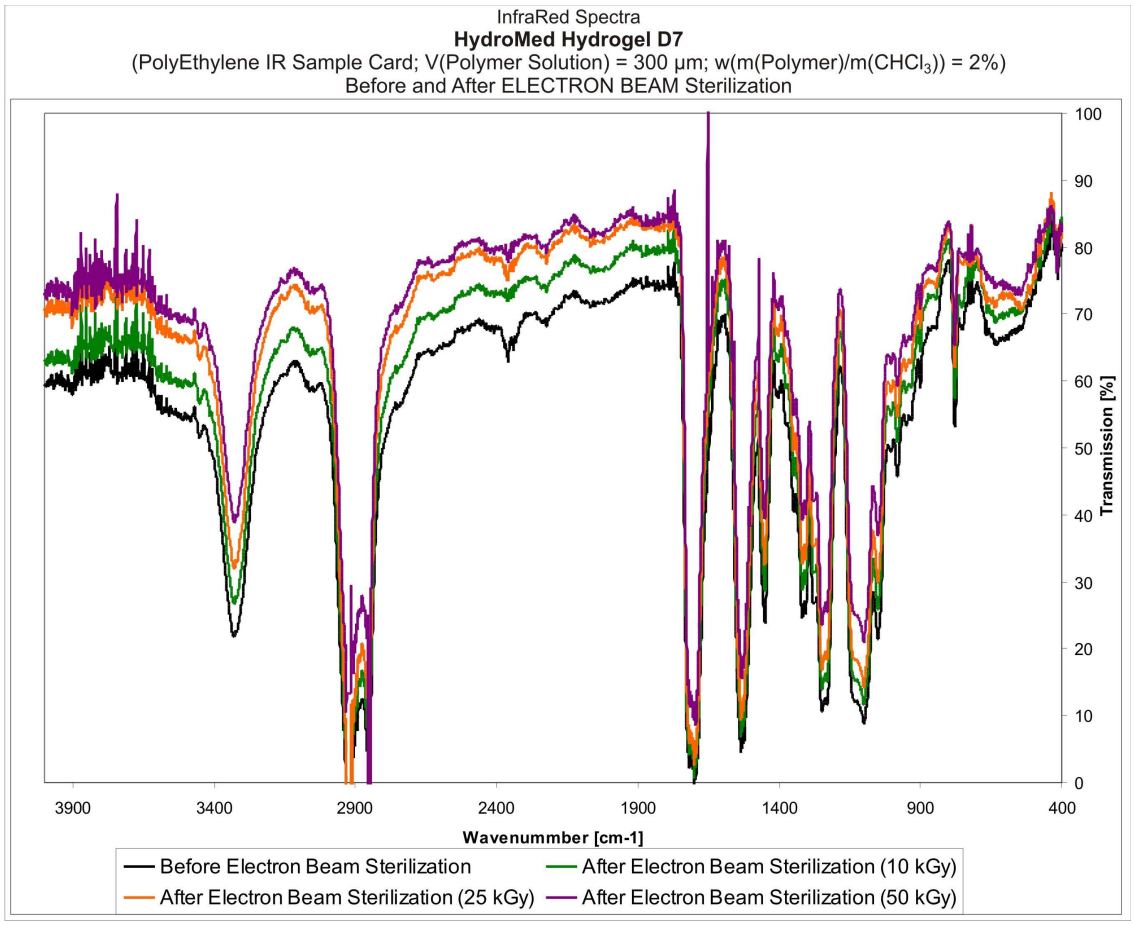
InfraRed Spectra
HydroMed Hydrogel D7
(PolyEthylene IR Sample Card; V(Polymer Solution) = 300 µm; w(m(Polymer)/m(CHCl3)) = 2%)
Before and After ELECTRON BEAM Sterilization
Wavenummber [cm-1]
Transmission [%]
Before Electron Beam Sterilization
After Electron Beam Sterilization (10 kGy)
After Electron Beam Sterilization (25 kGy)
After Electron Beam Sterilization (50 kGy)

A.8 HydroThane™ with 5% and 25% water absorption

A.8.1 Absorption Spectra

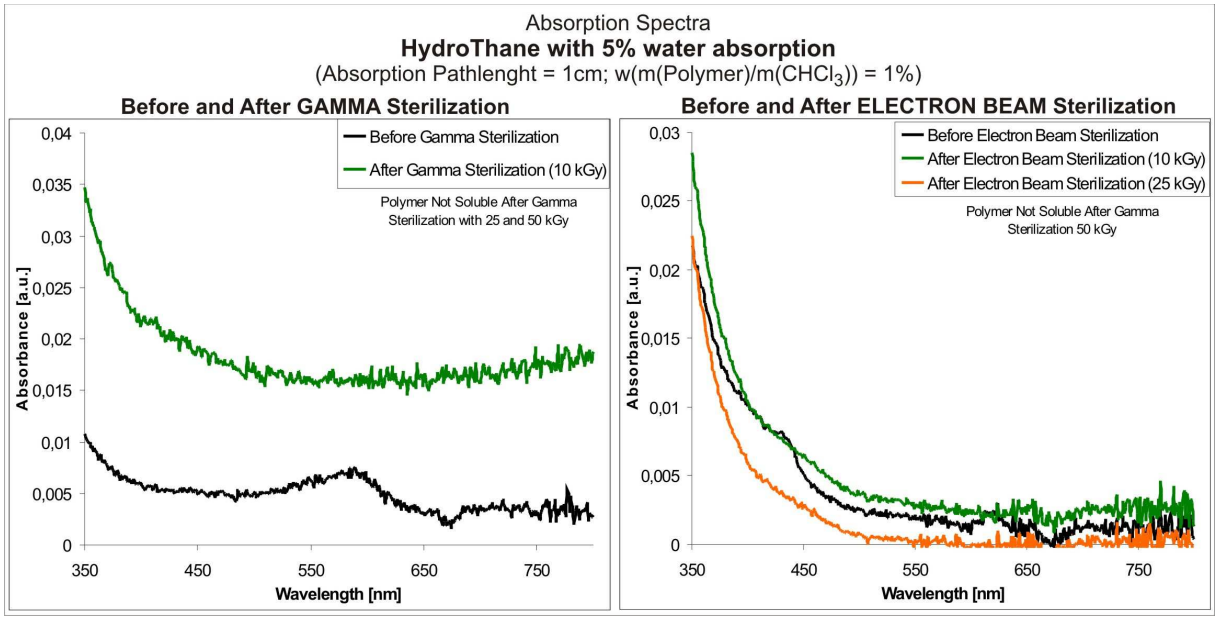

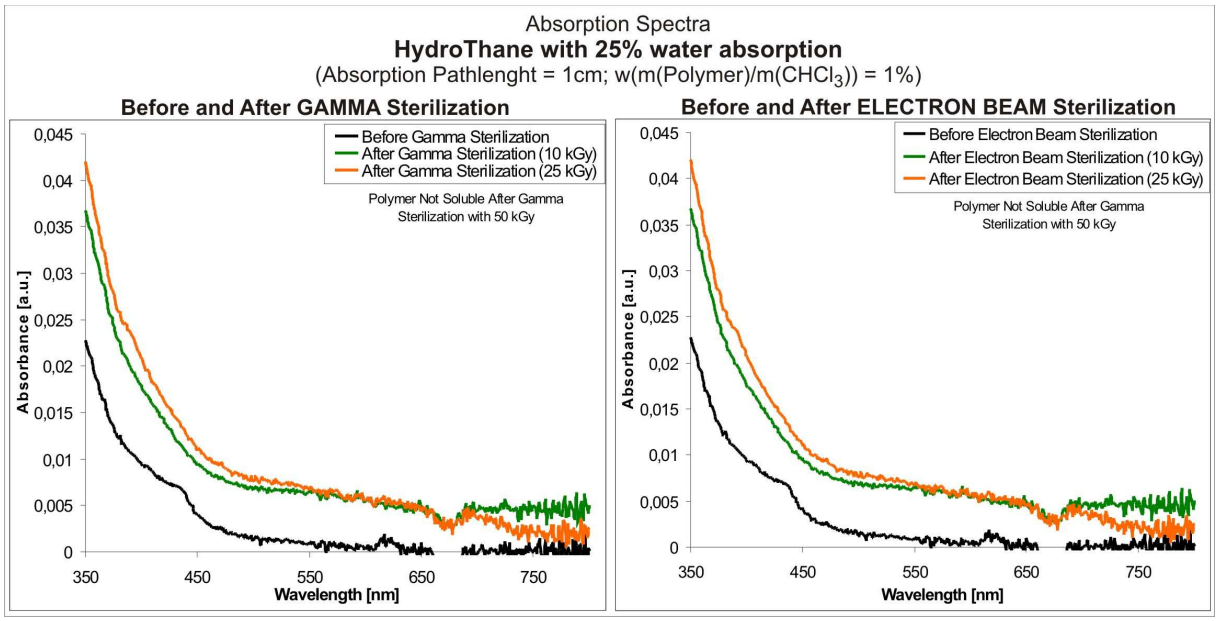

A.8.2 Contact Angle Measurement

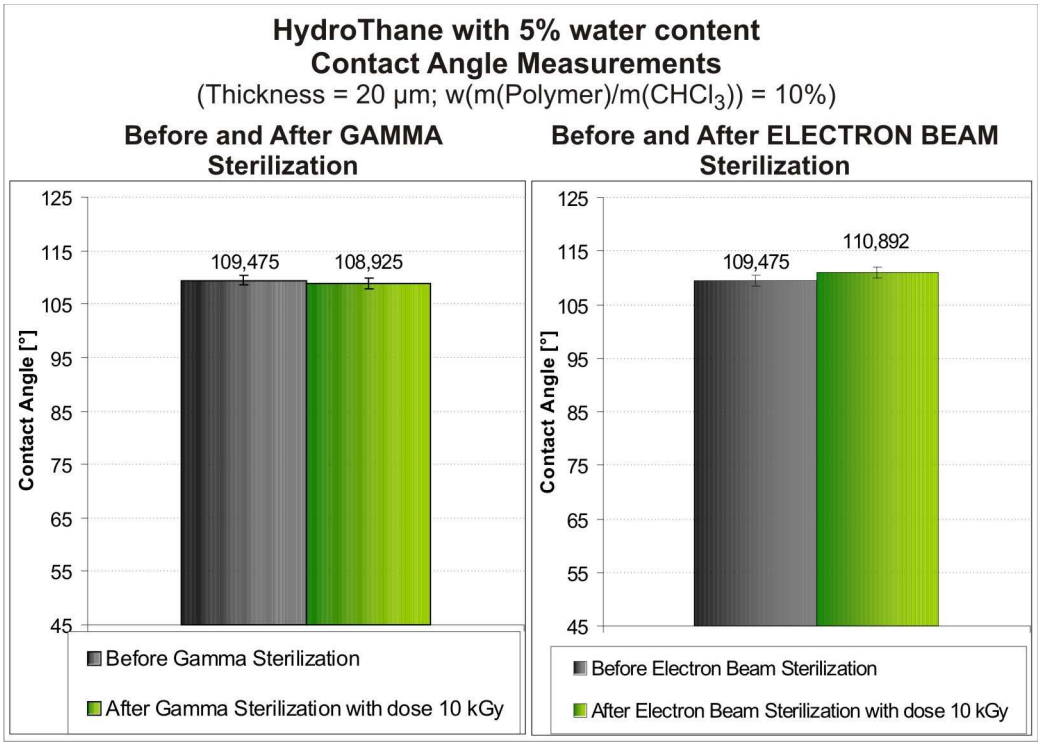

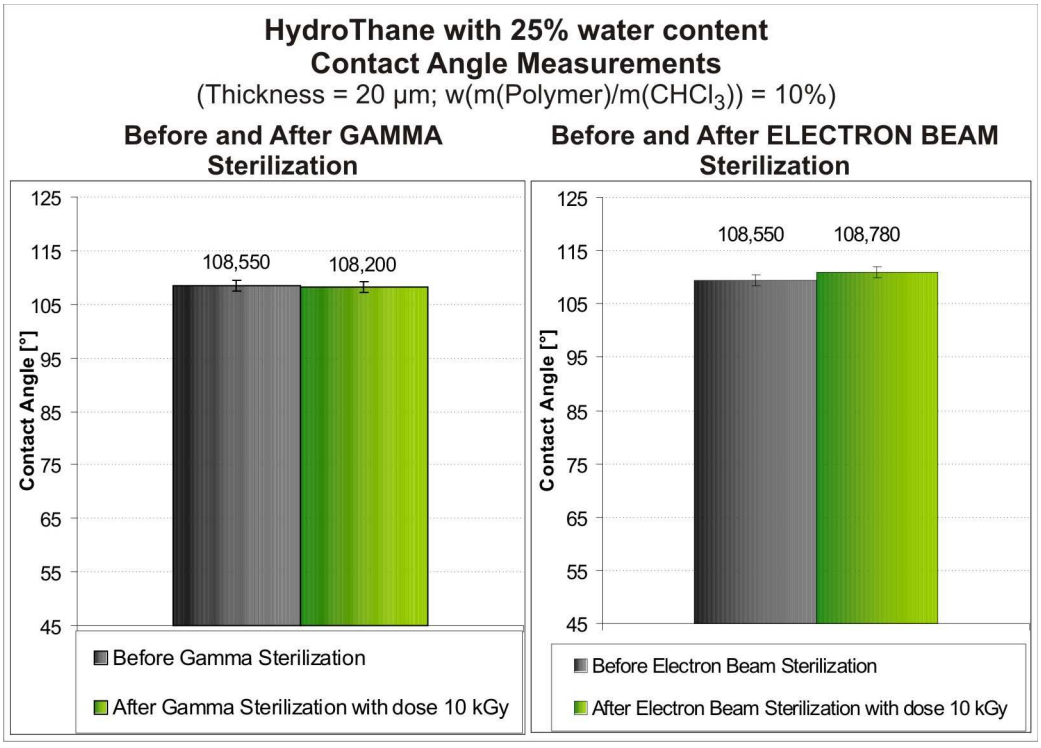

A.8.3 Infrared Spectra

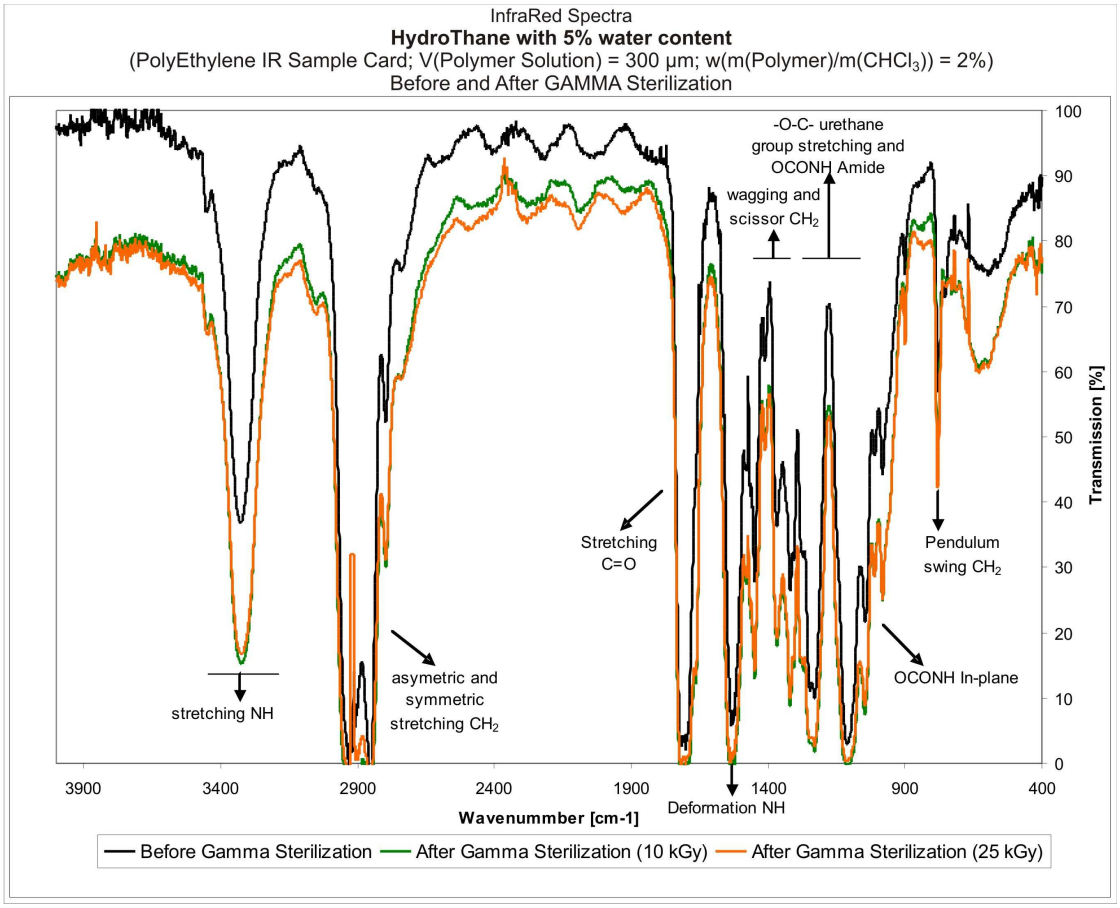

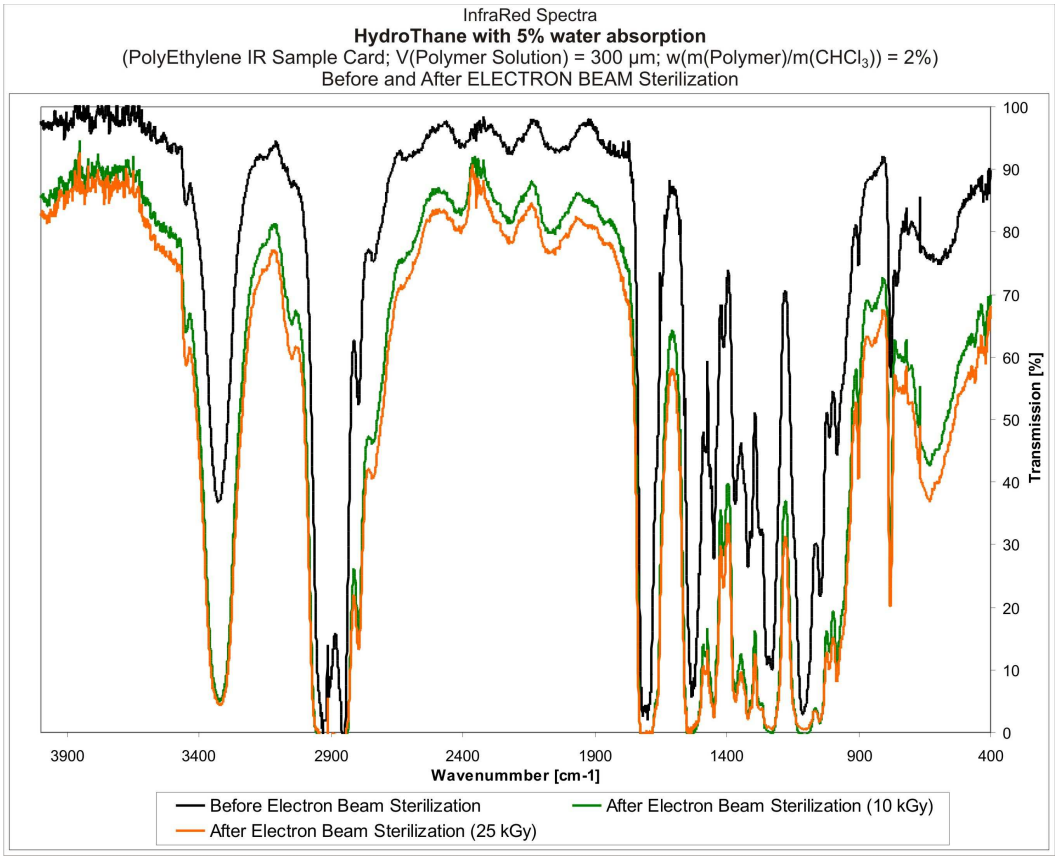

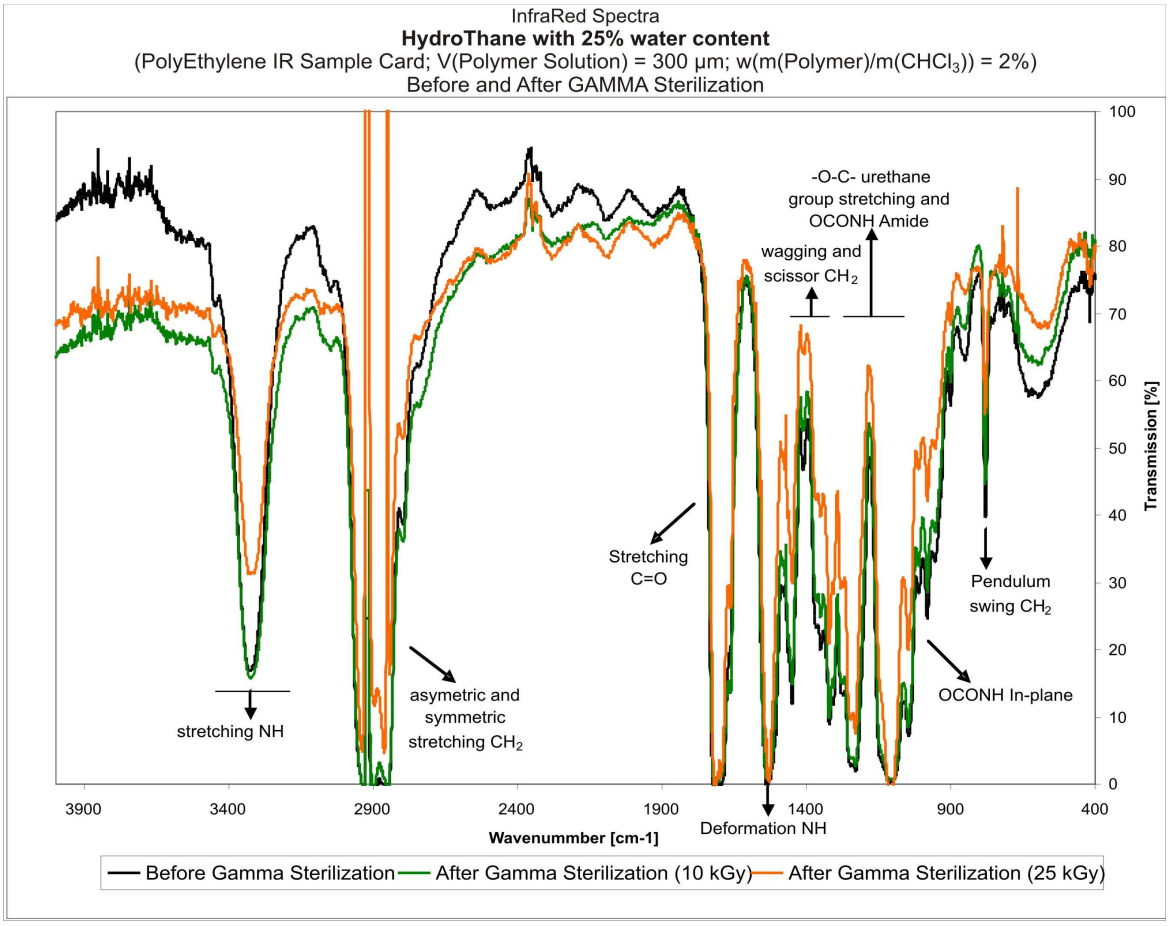
InfraRed Spectra
HydroThane with 25% water content
(PolyEthylene IR Sample Card; V(Polymer Solution) = 300 µm; w(m(Polymer)/m(CHCl3)) = 2%)
Before and After GAMMA Sterilization
-O-C- urethane group stretching and OCONH Amide
wagging and scissor CH2
Stretching C=O
Pendulum swing CH2
OCONH In-plane
asymetric and symmetric stretching CH2
stretching NH
Deformation NH
Transmission [%]
Wavenummber [cm-1]
Before Gamma Sterilization
After Gamma Sterilization (10 kGy)
After Gamma Sterilization (25 kGy)

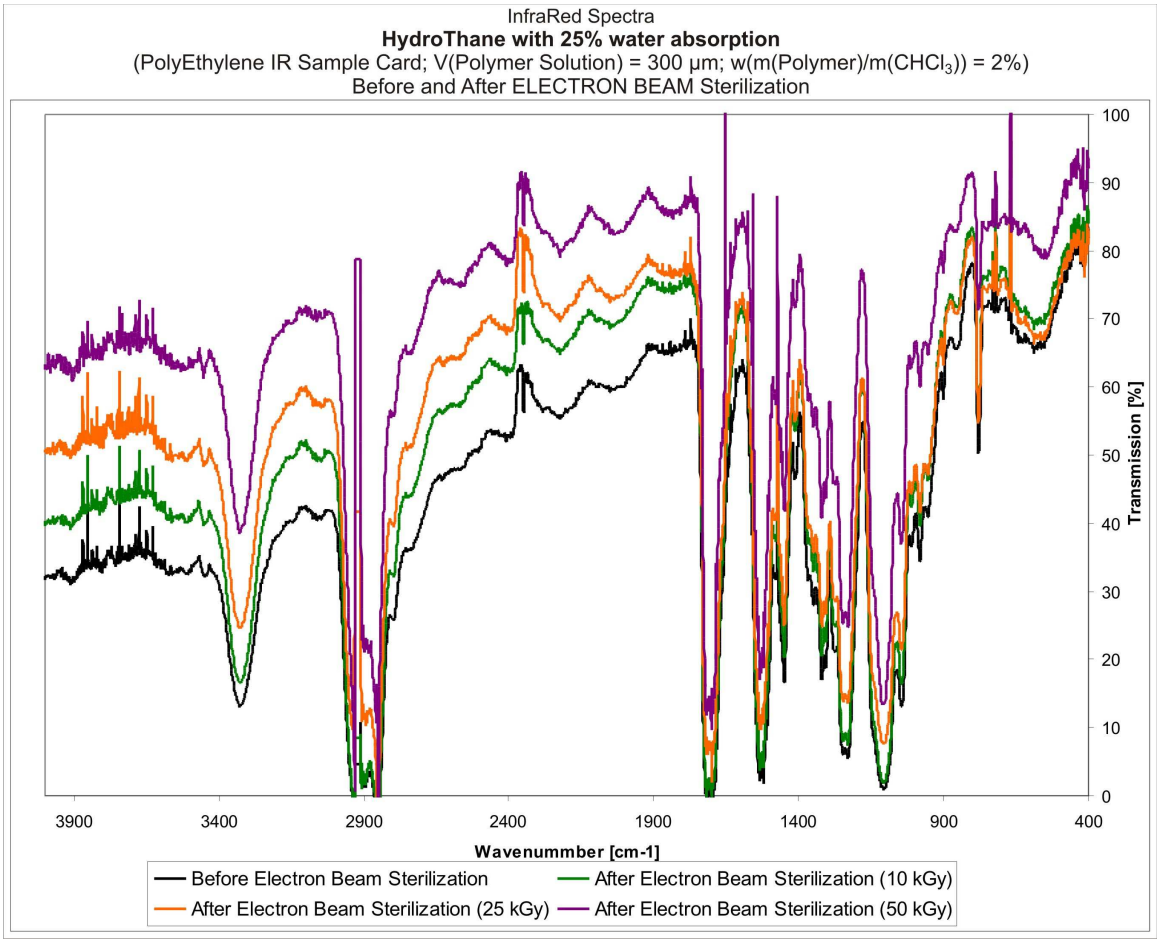
InfraRed Spectra
HydroThane with 25% water absorption
(PolyEthylene IR Sample Card; V(Polymer Solution) = 300 µm; w(m(Polymer)/m(CHCl3)) = 2%)
Before and After ELECTRON BEAM Sterilization
Transmission [%]
Wavenummber [cm-1]
Before Electron Beam Sterilization
After Electron Beam Sterilization (10 kGy)
After Electron Beam Sterilization (25 kGy)
After Electron Beam Sterilization (50 kGy)

A.9 PolyPhenylSilsesQuioxane

A.9.1 Absorption Spectra

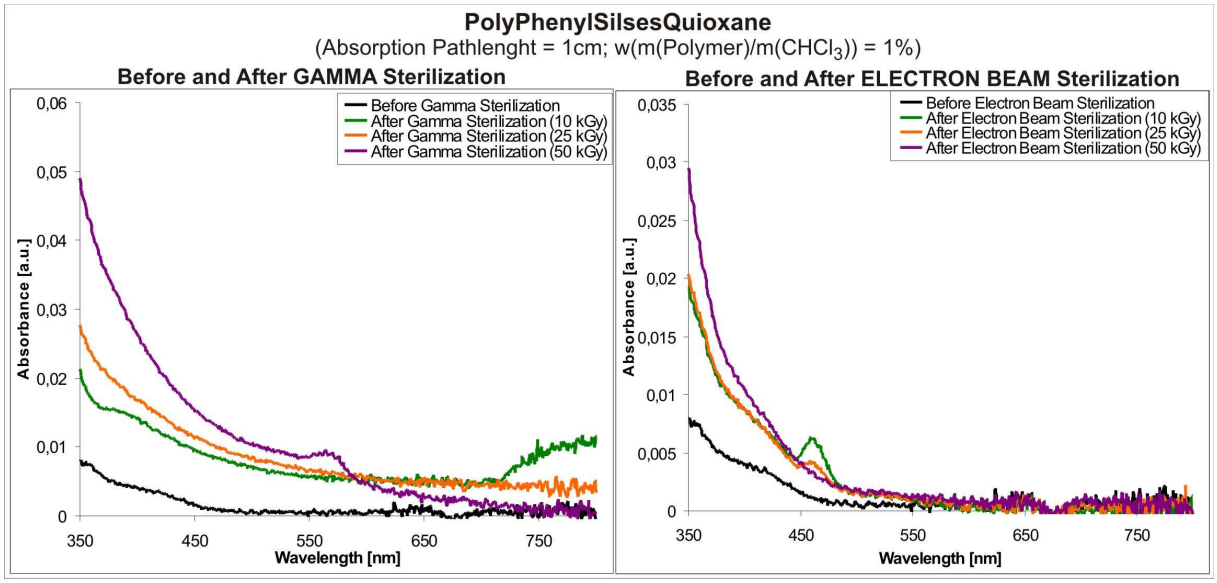

A.9.2 Contact Angle Measurement

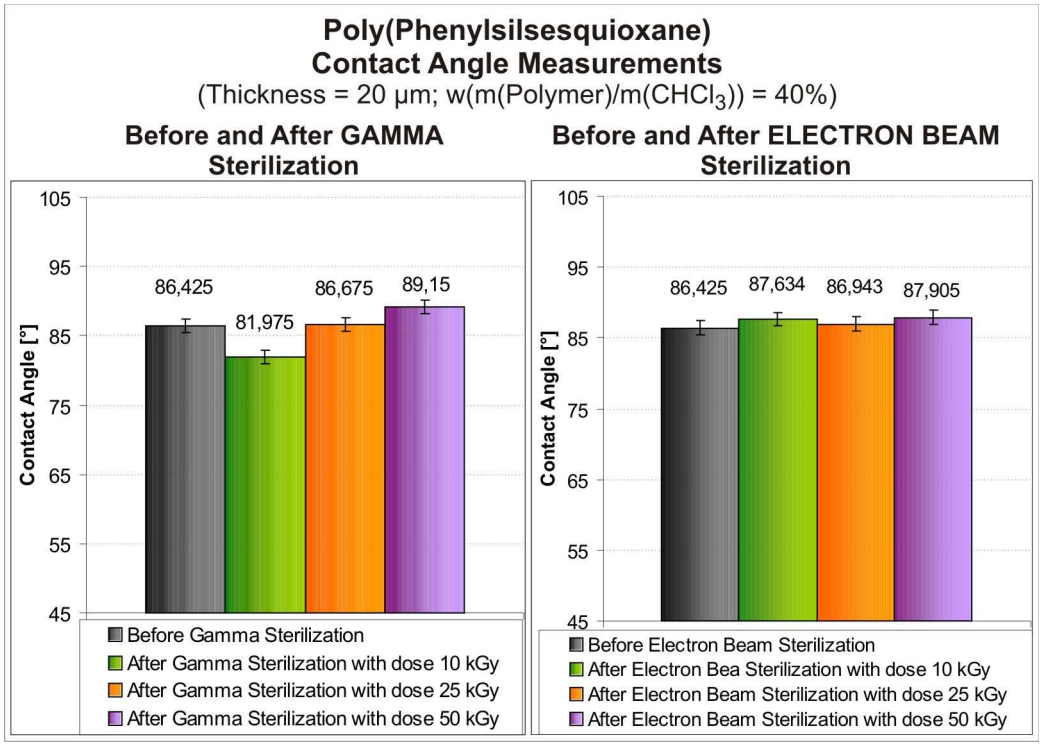

A.9.3 Infrared Spectra

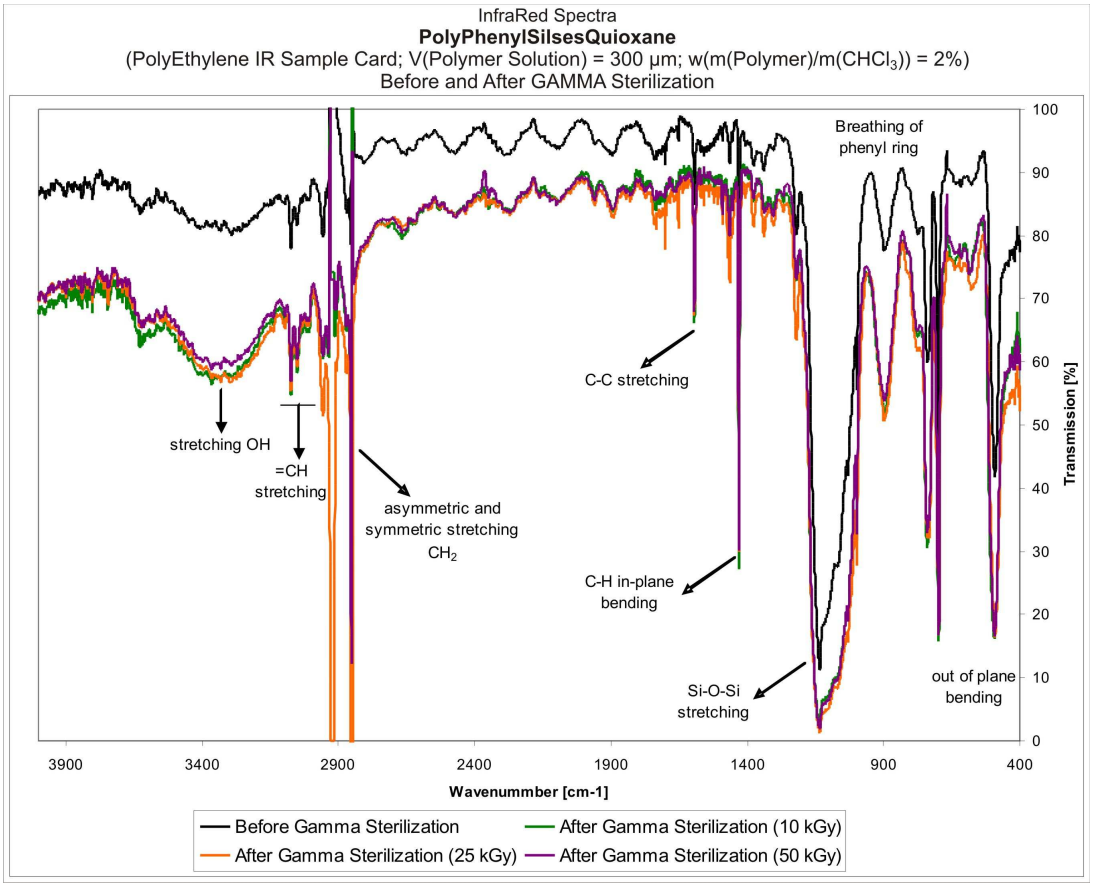

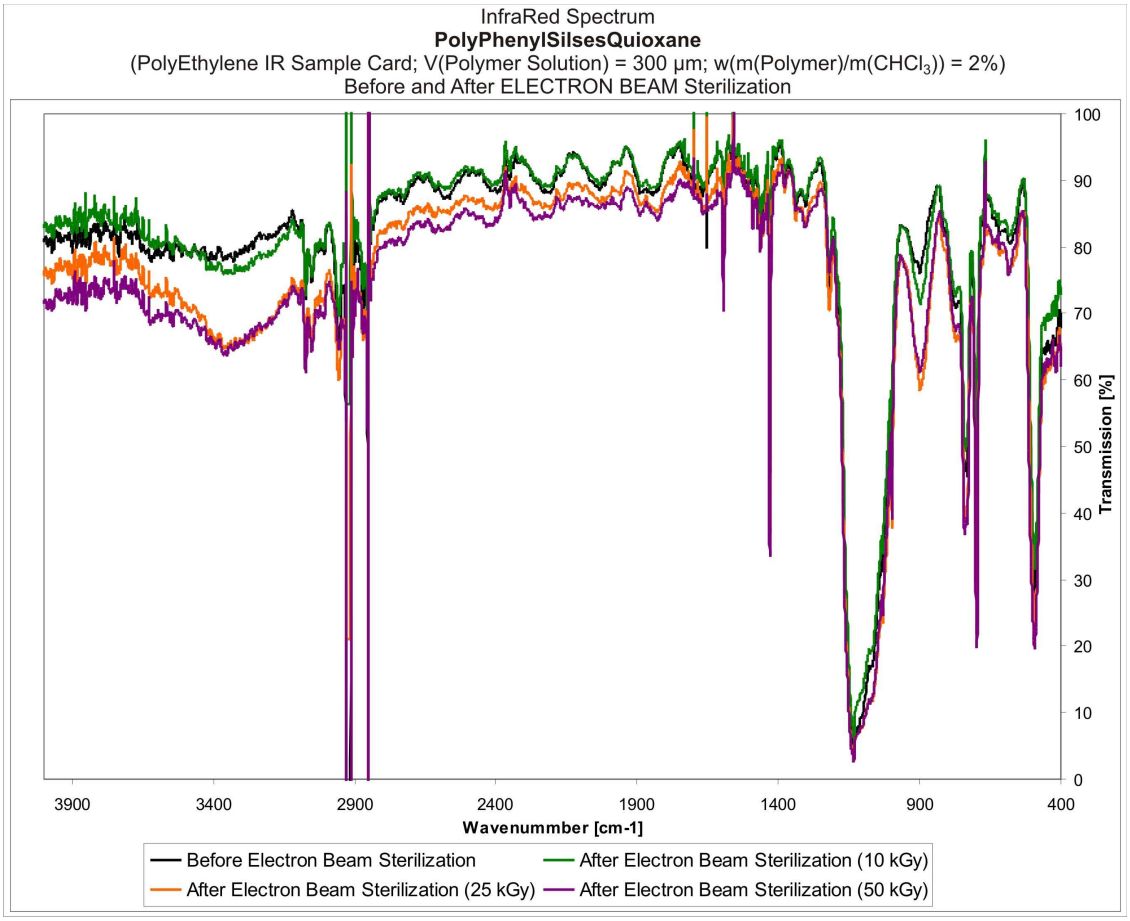

A.10 PolyVinylidene Chloride-co-Acrylonitrile

A.10.1 Absorption Spectra

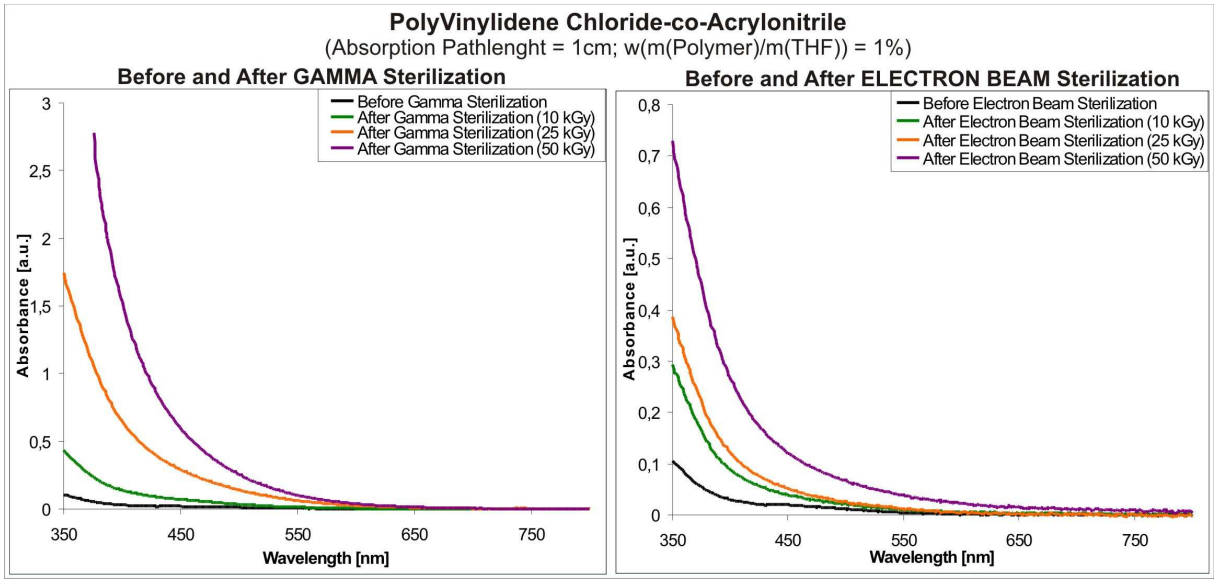

A.10.2 Contact Angle Measurement

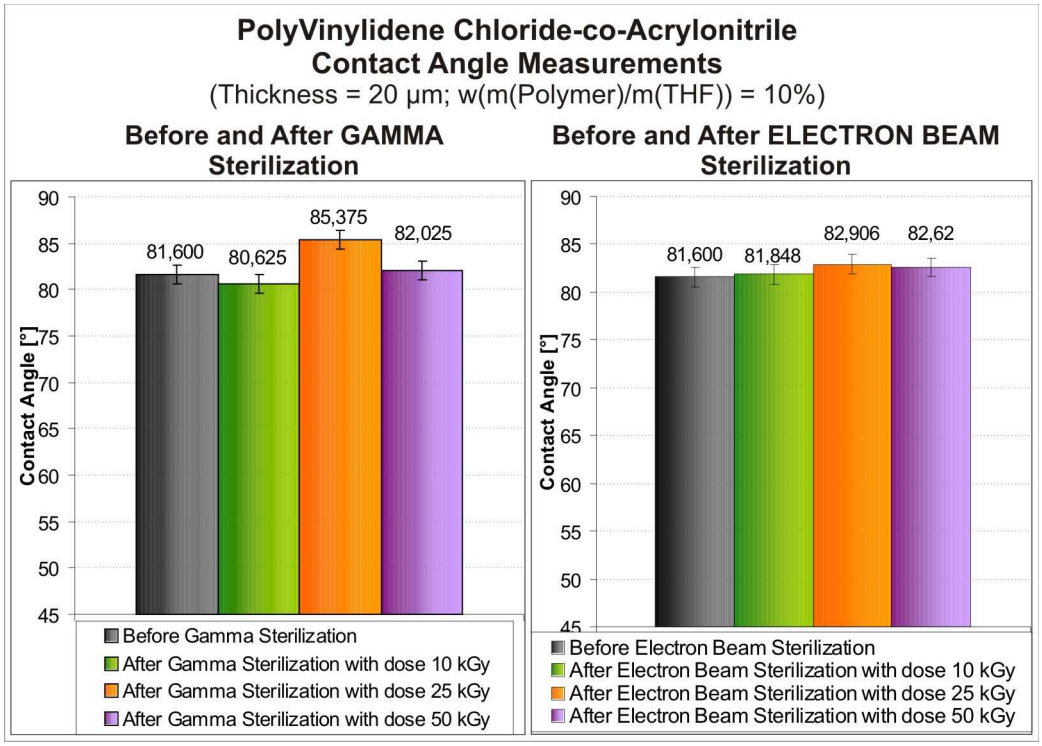

A.10.3 Infrared Spectra

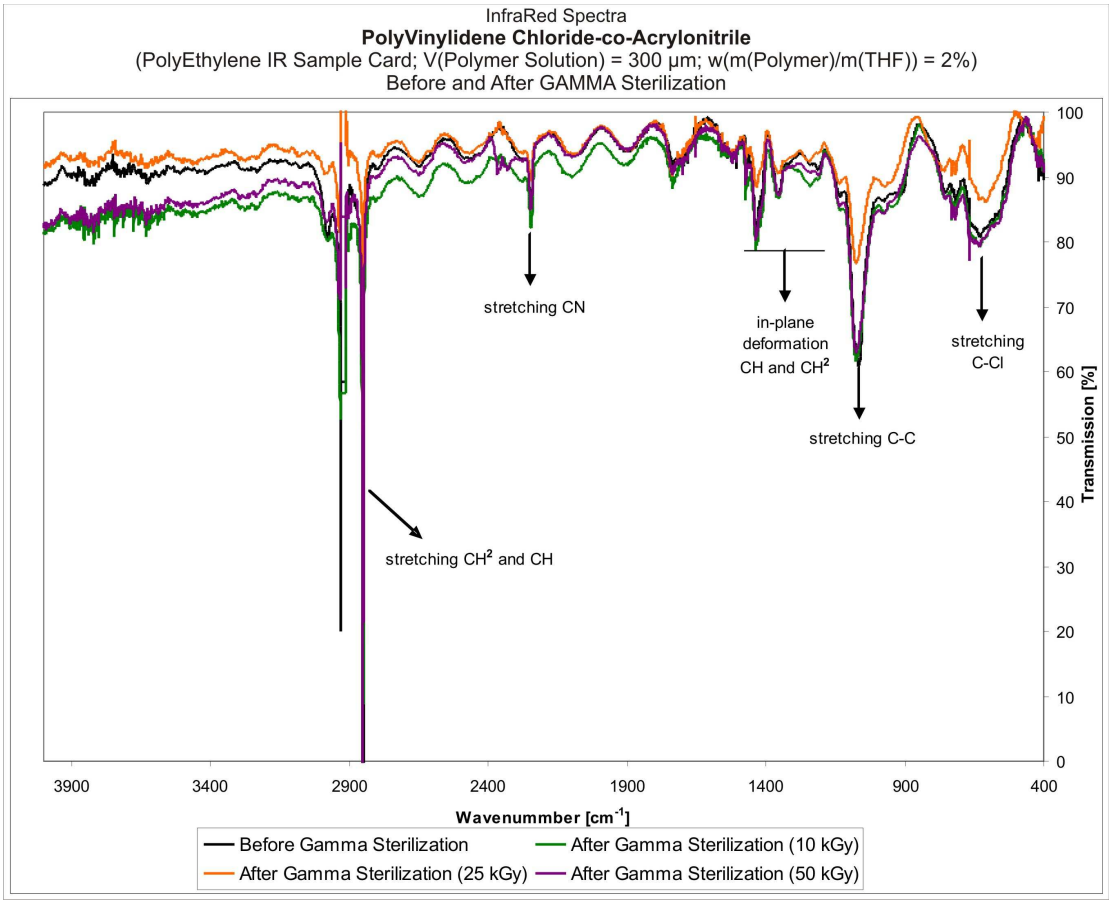

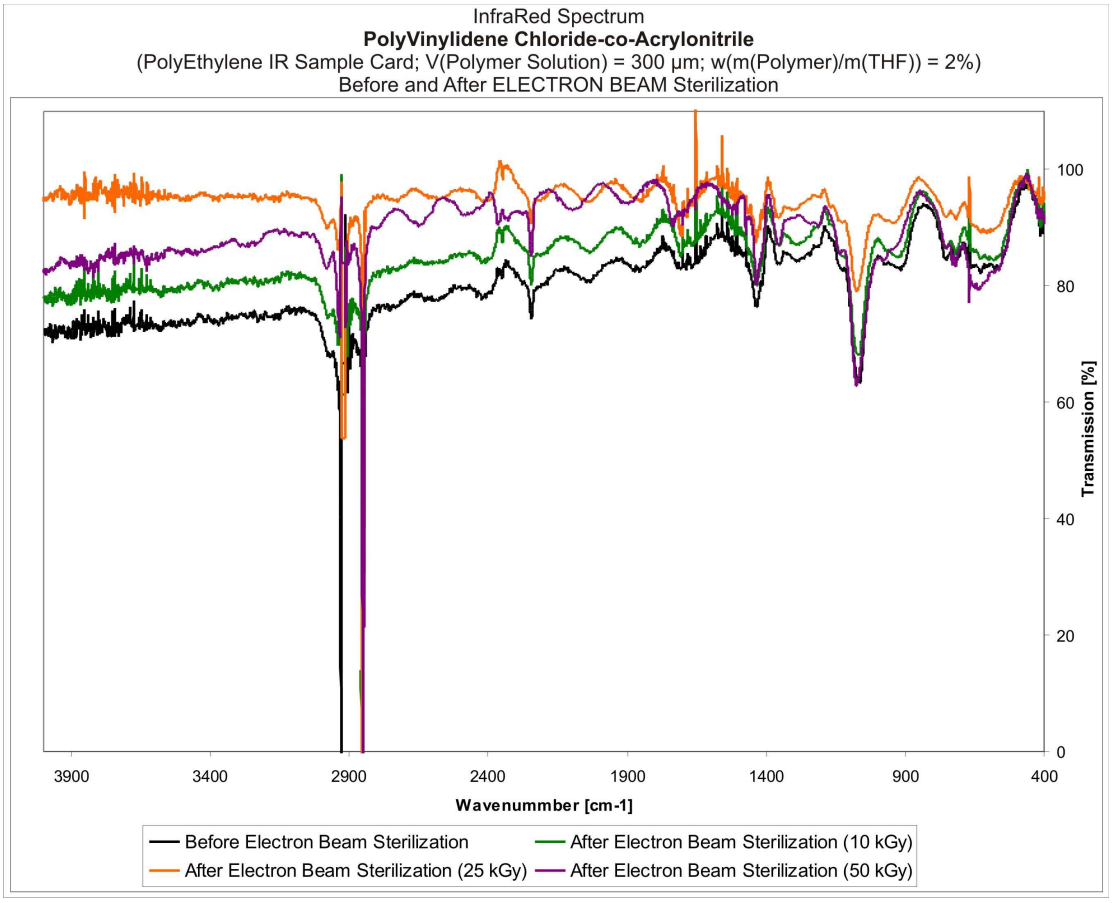

A.10.4 Differential Scanning Calorimetry

DSC Program:

0 °C – 120 °C 20 °C/min
120 °C – 10 °C 10 °C/min
0 °C – 120 °C 10 °C/min

	T_g	Δc_p
BeforeS	55,17 °C	0,234 J/g °C
10 kGy	55,20 °C	0,222 J/g °C
25 kGy	55,88 °C	0,209 J/g °C
50 kGy	56,04 °C	0,190 J/g °C

Before sterilization

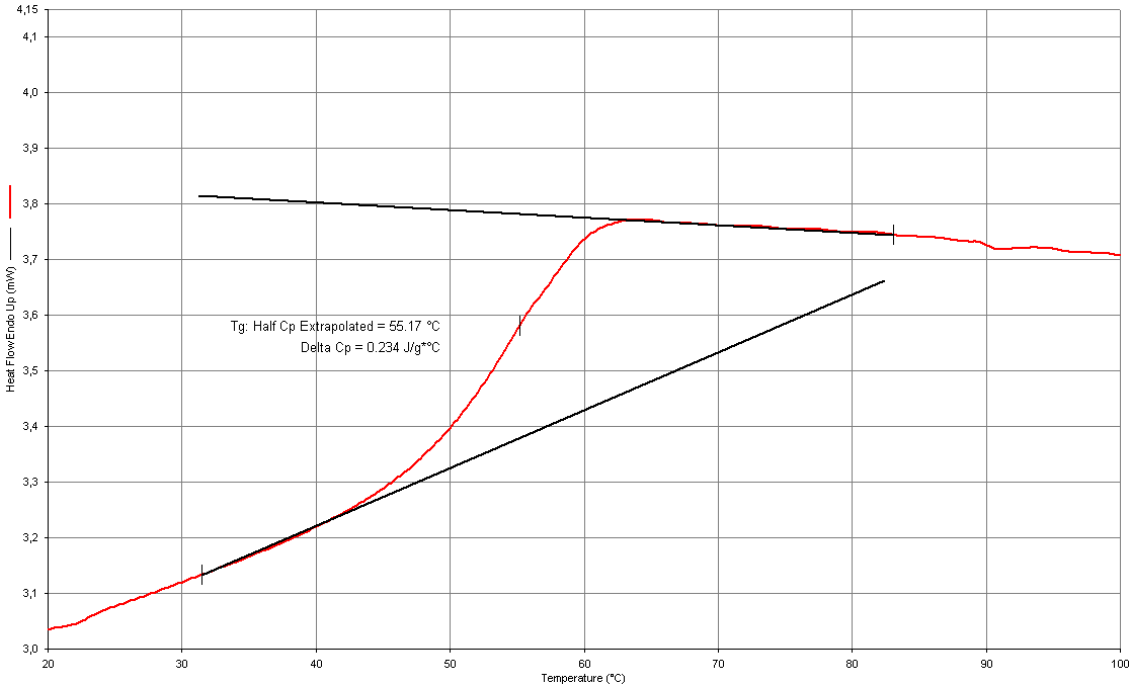

After GAMMA sterilization with 10 kGy

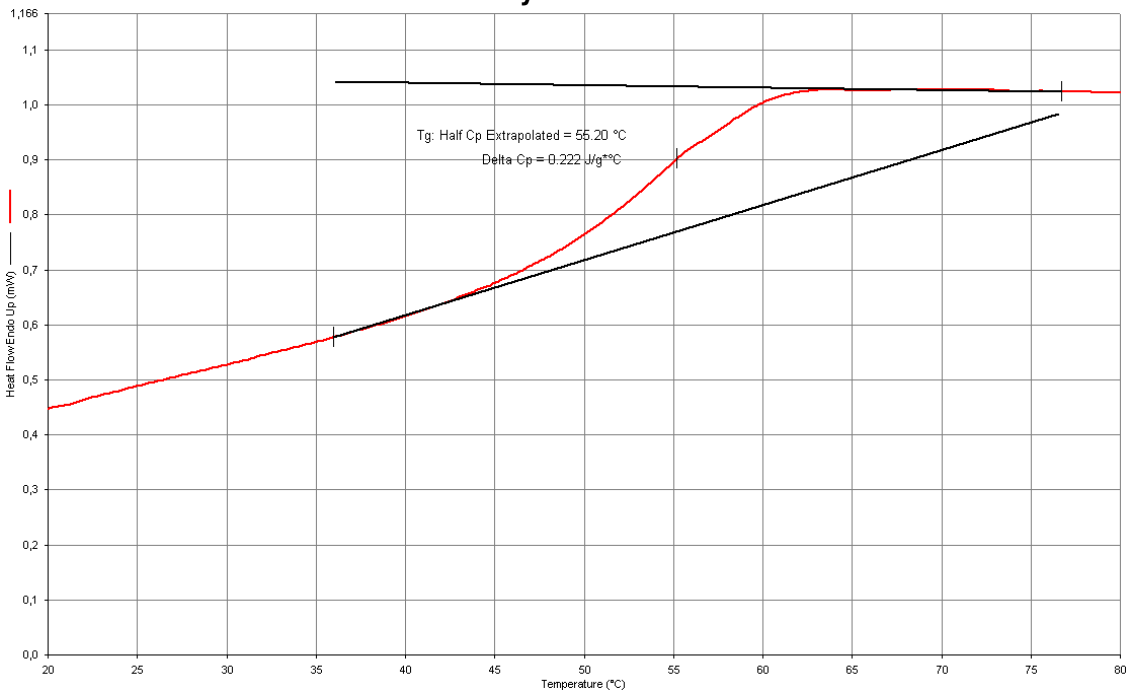

After GAMMA sterilization with 25 kGy

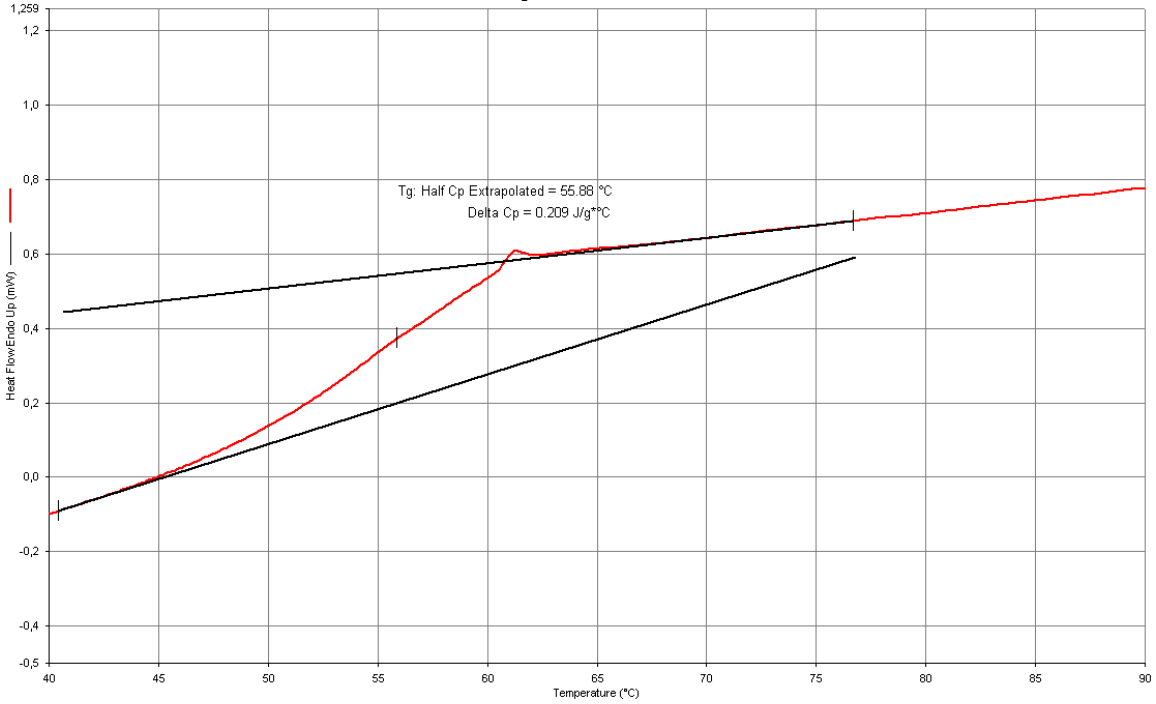

After GAMMA sterilization with 50 kGy

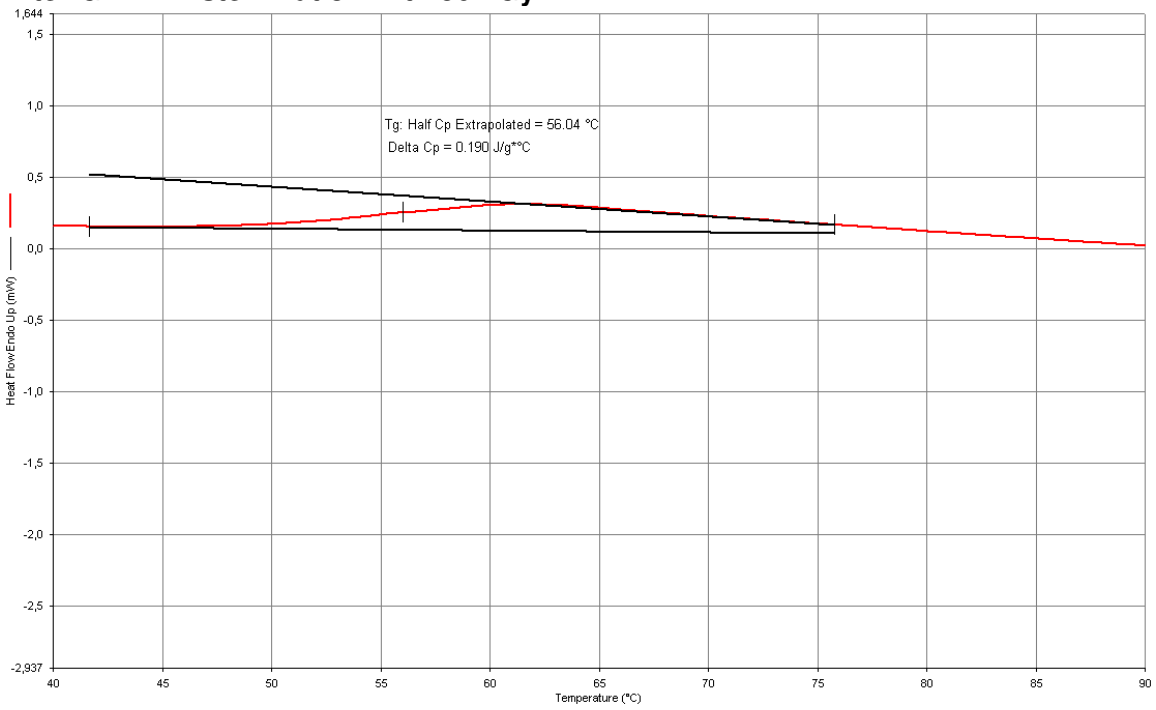

A.11 PolyMethyl MethAcrylate

A.11.1 Absorption Spectra

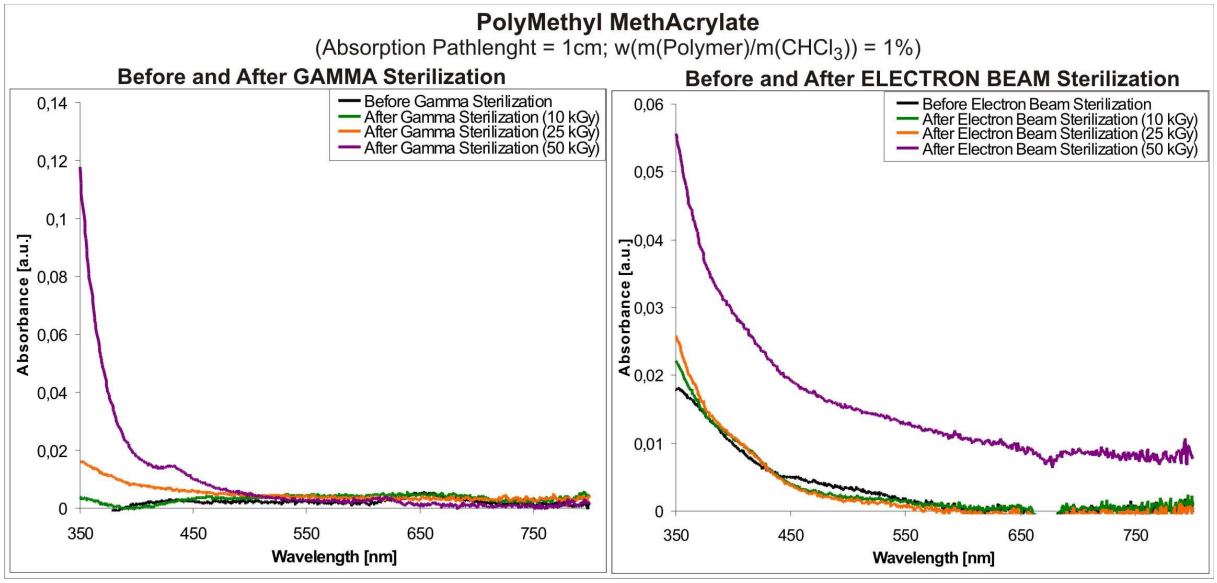

A.11.2 Contact Angle Measurement

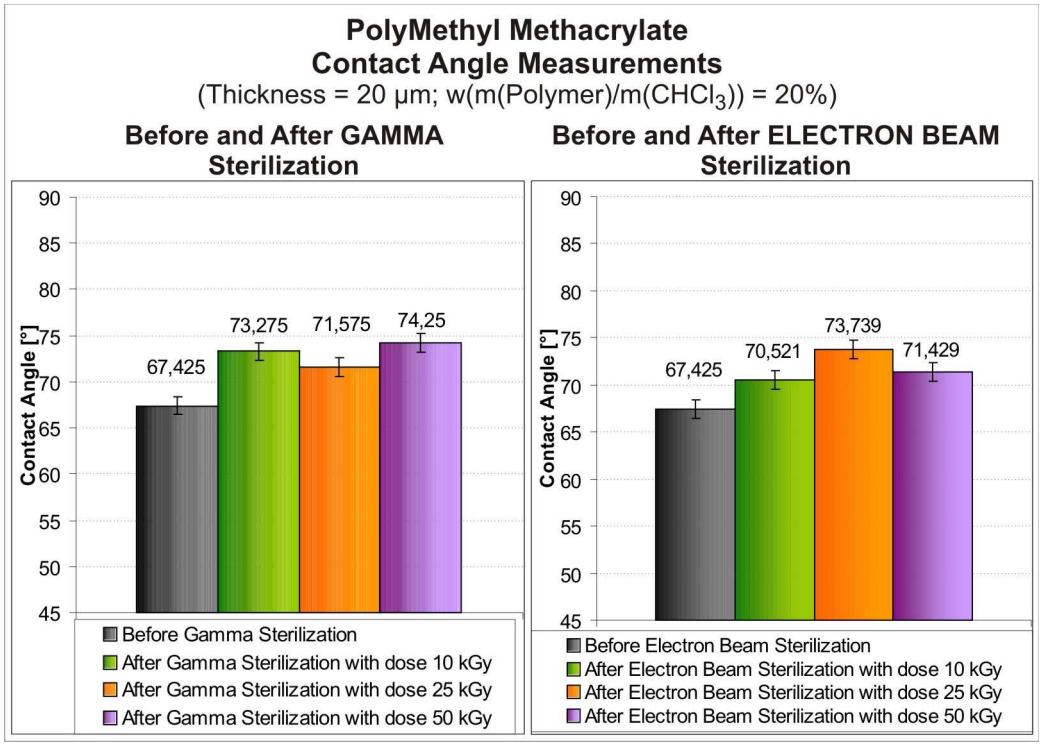

A.11.3 Infrared Spectra

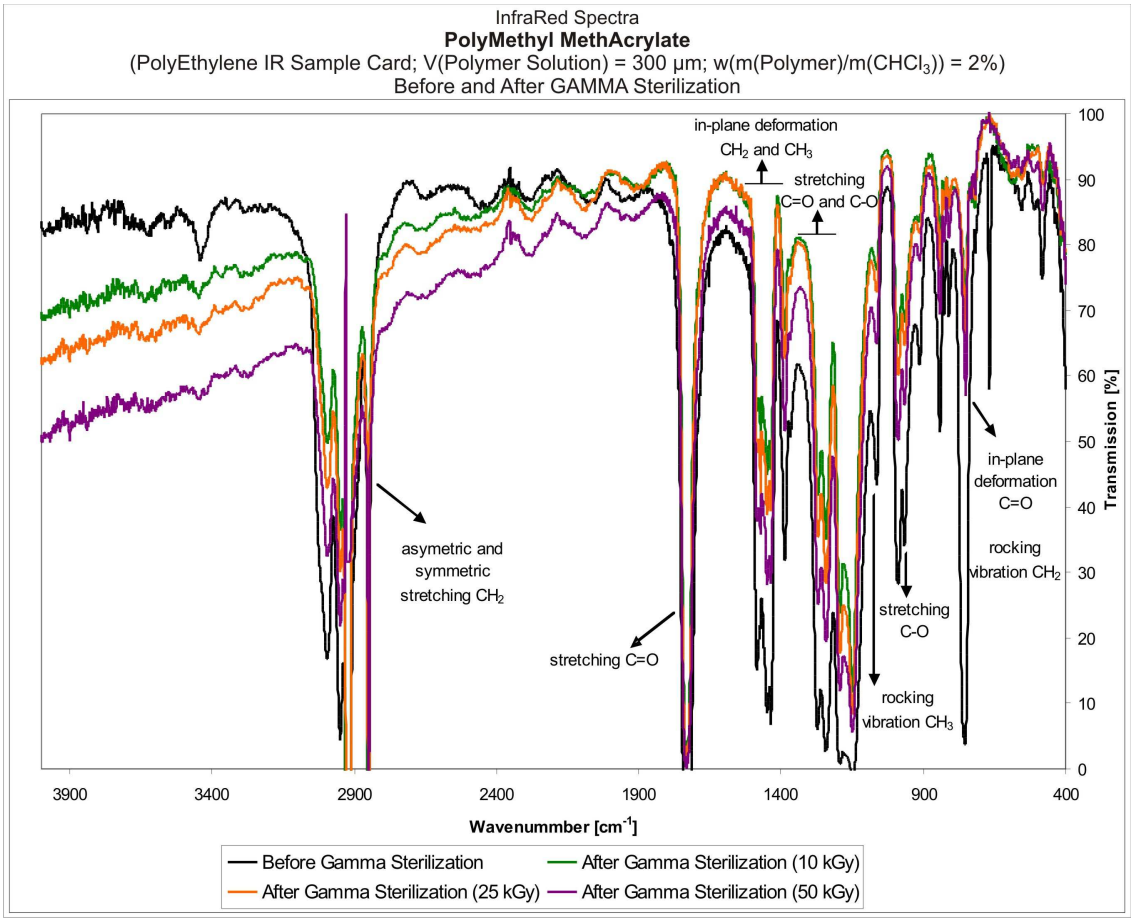

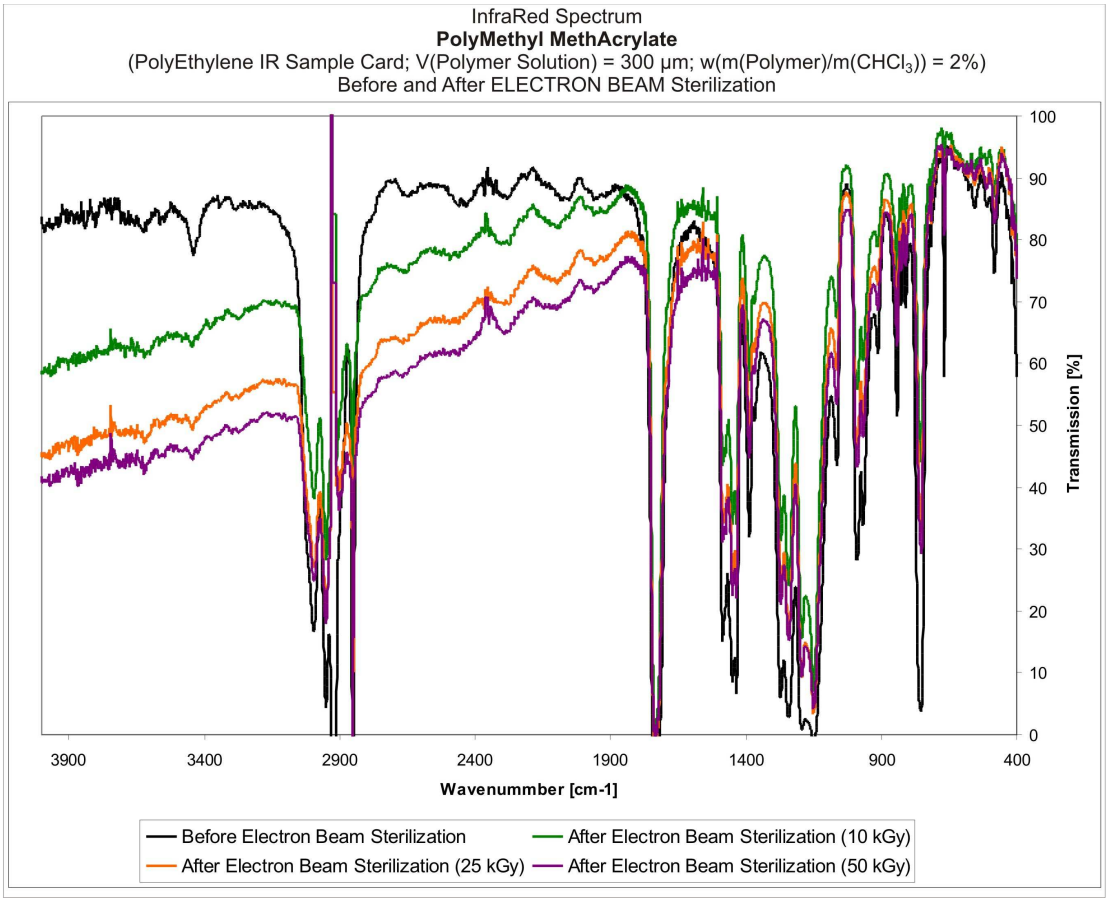

A.11.4 Differential Scanning Calorimetry

DSC Program:

30 °C – 160 °C 20 °C/min
160 °C – 30 °C 10 °C/min
30 °C – 160 °C 10 °C/min

	T_g	Δc_p
BeforeS	114,09 °C	0,212 J/g °C
10 kGy	115,76 °C	0,150 J/g °C
25 kGy	115,08 °C	0,201 J/g °C
50 kGy	114,64 °C	0,255 J/g °C

Before sterilization

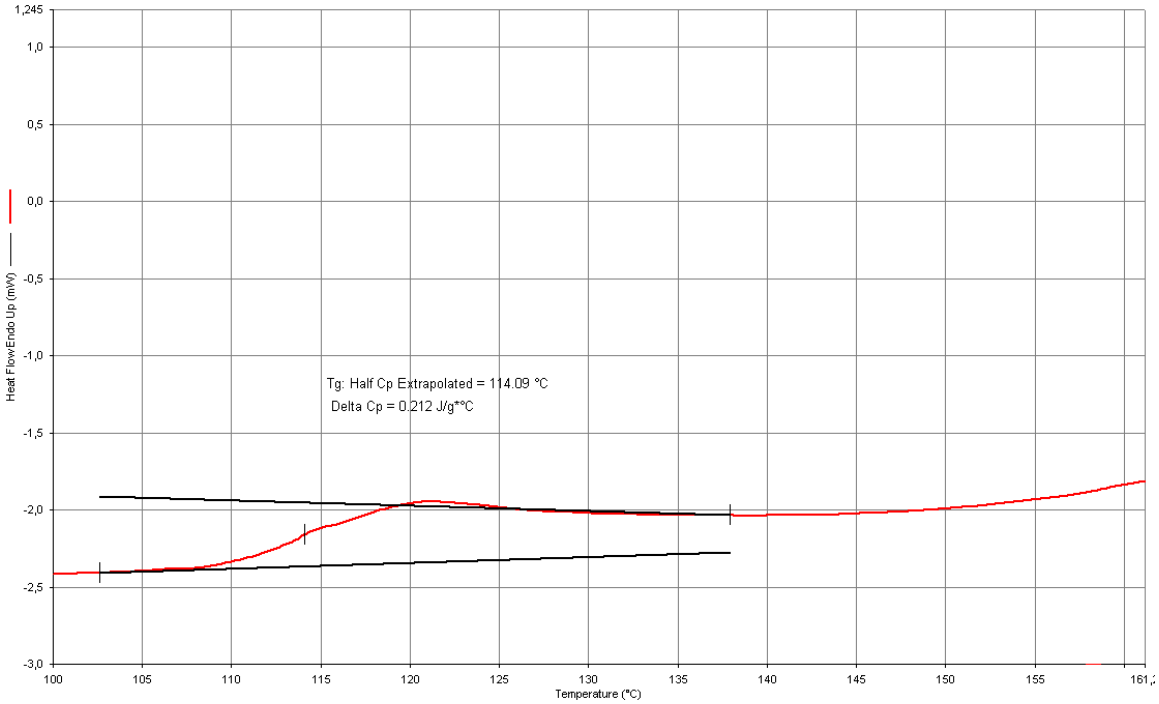

After GAMMA sterilization with 10 kGy

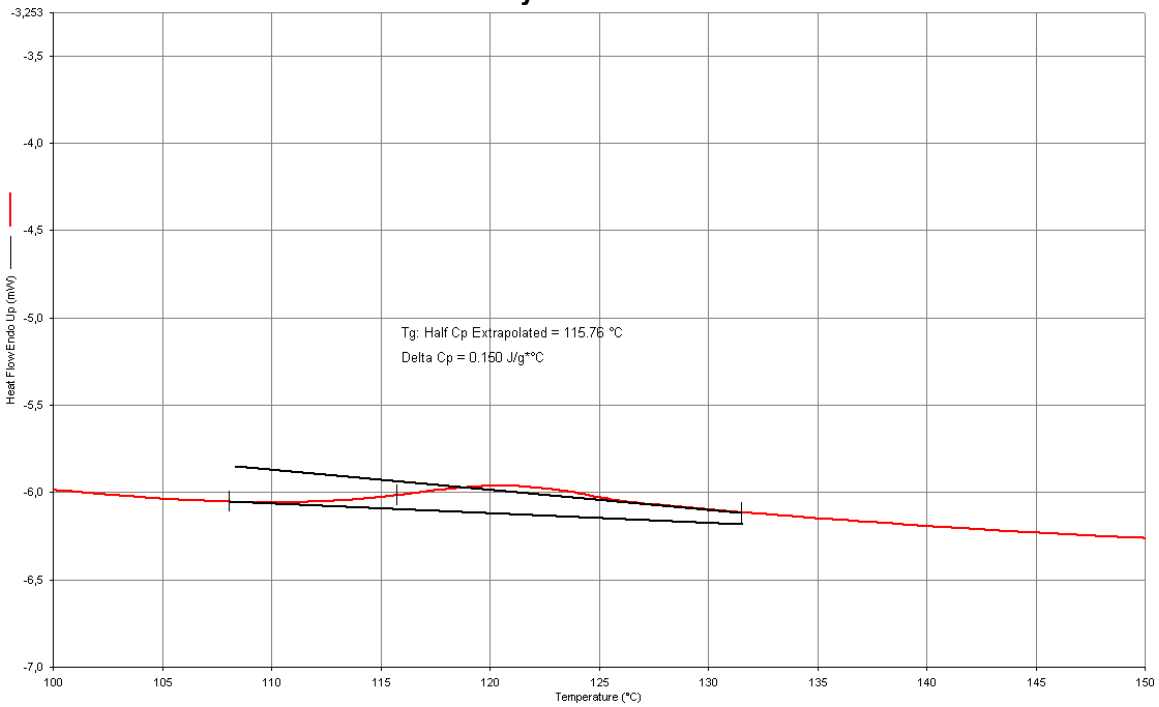

After GAMMA sterilization with 25 kGy

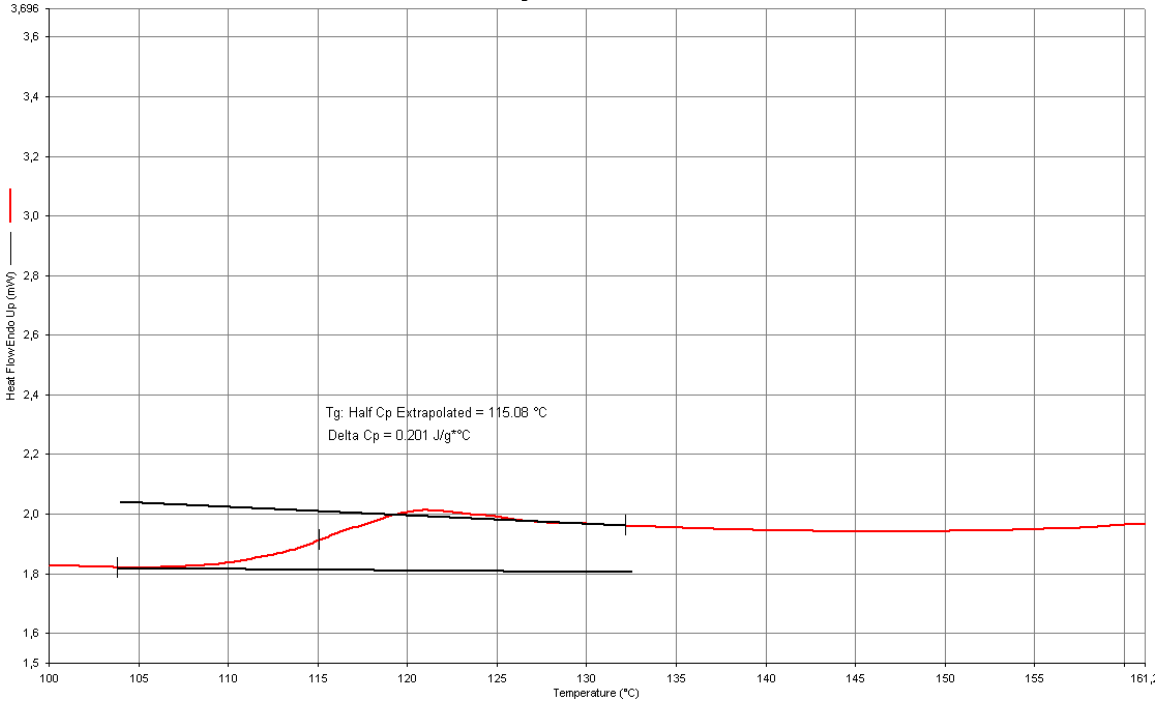

After GAMMA sterilization with 50 kGy

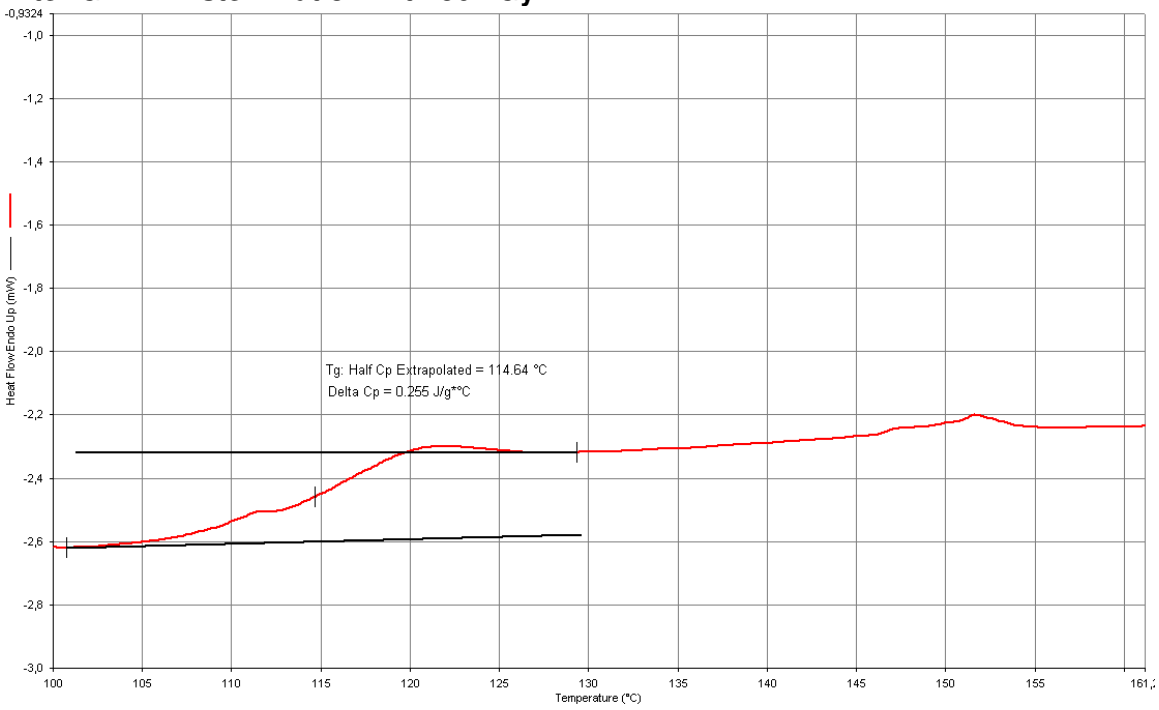

A.12 PolyMethAcryloNitrile

A.12.1 Absorption Spectra

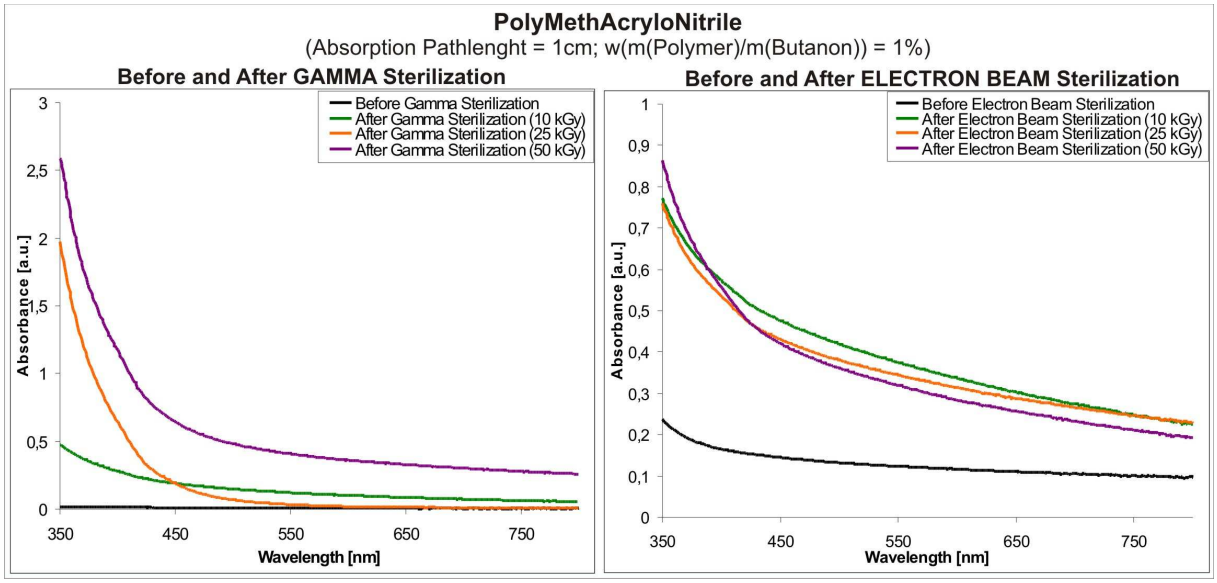

A.12.2 Contact Angle Measurement

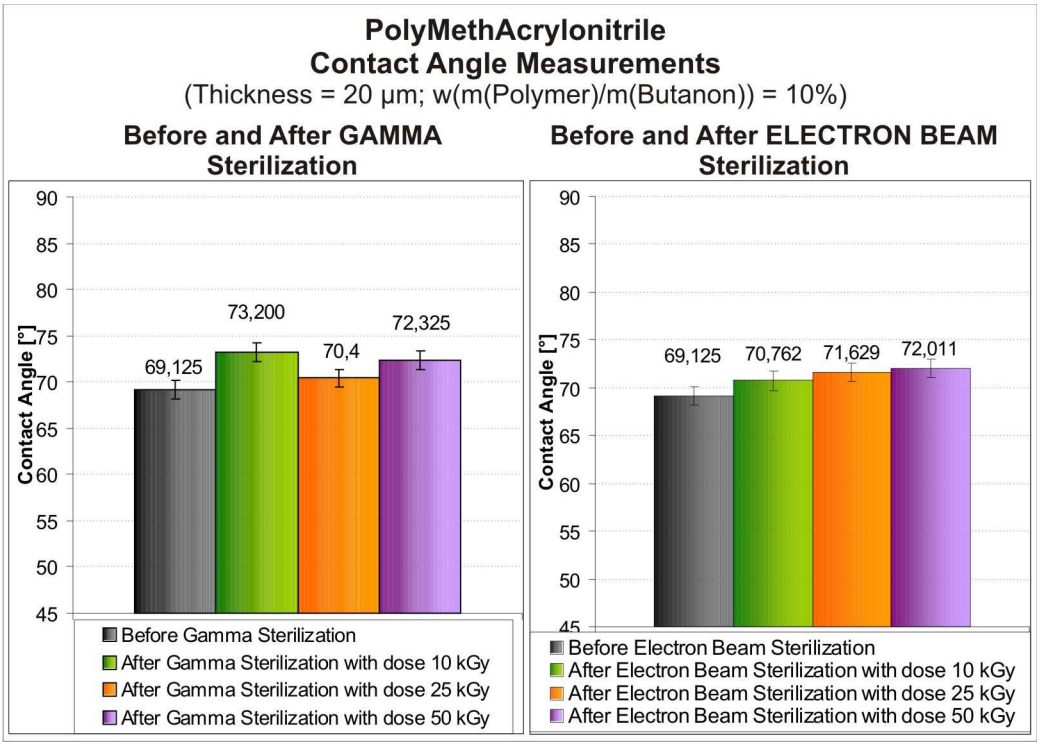

A.12.3 Infrared Spectra

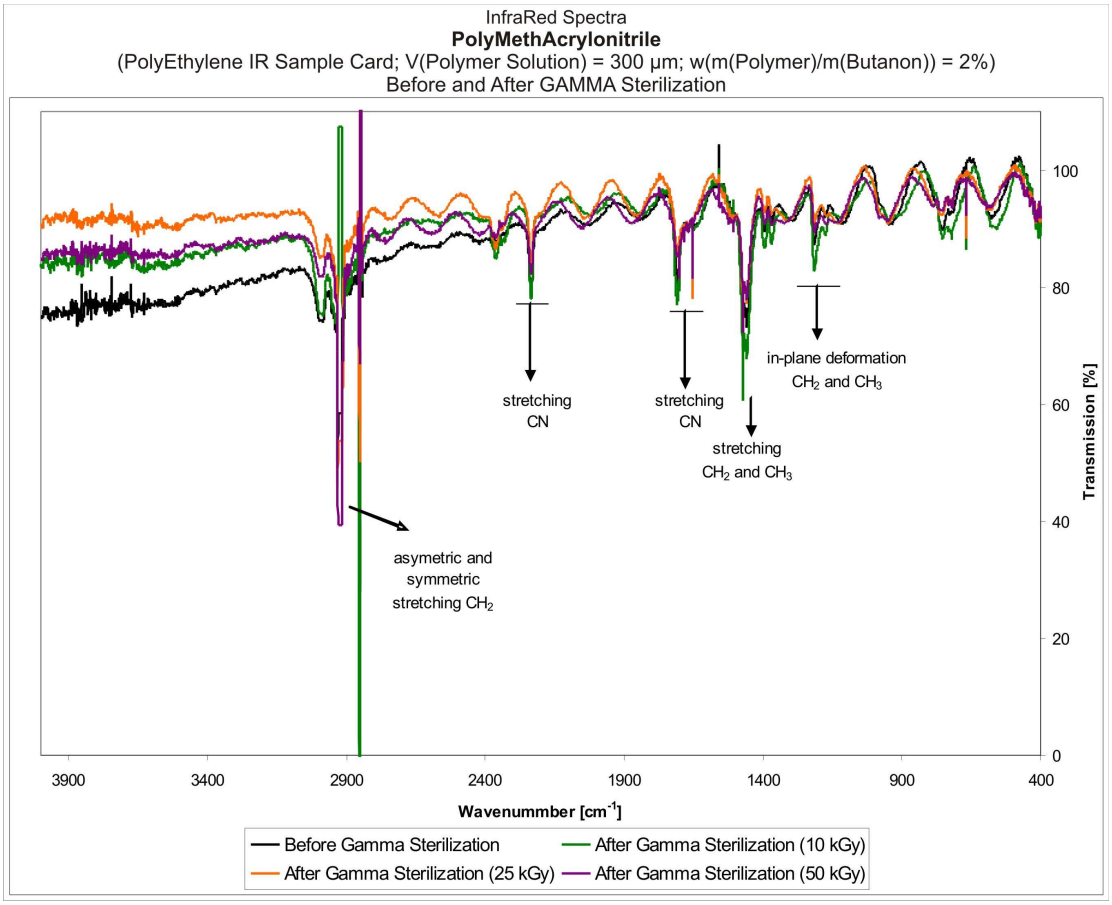

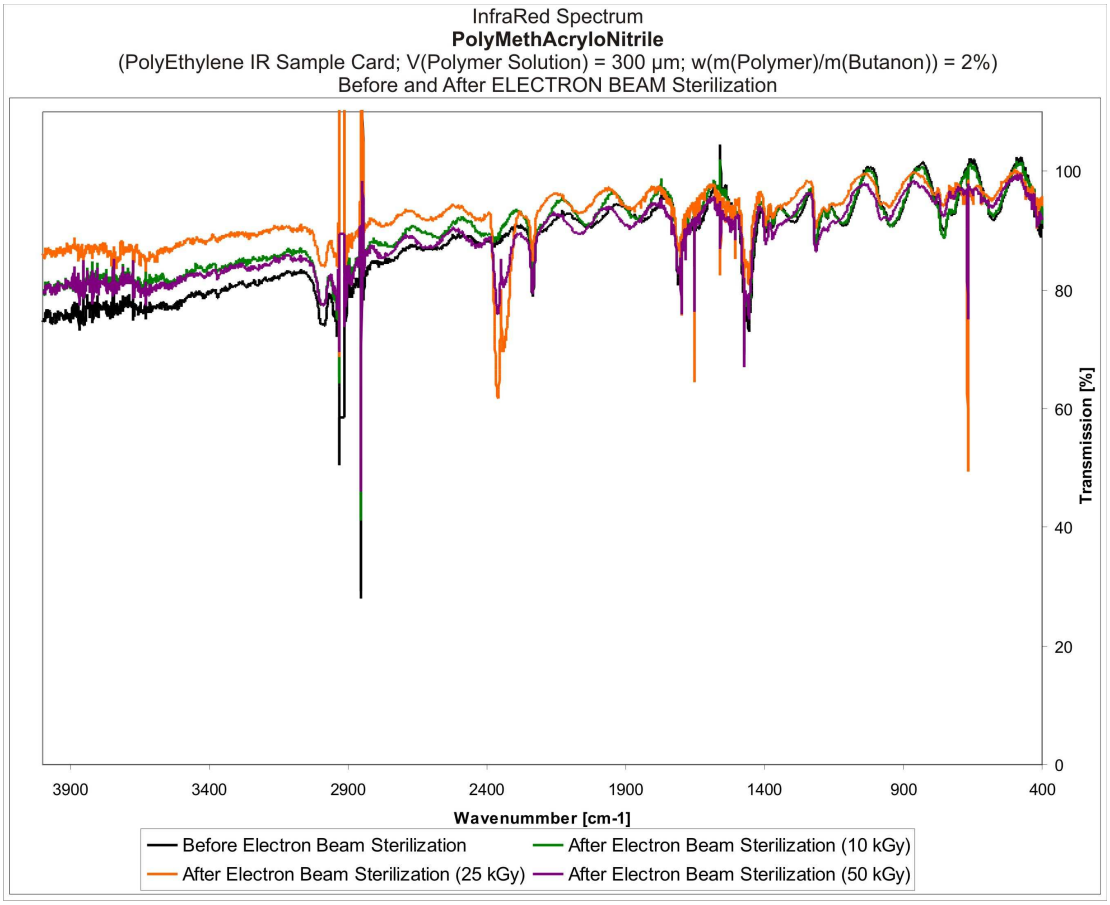

A.13 Poly(2-HydroxyEthyl MethAcrylate)

A.13.1 Absorption Spectra

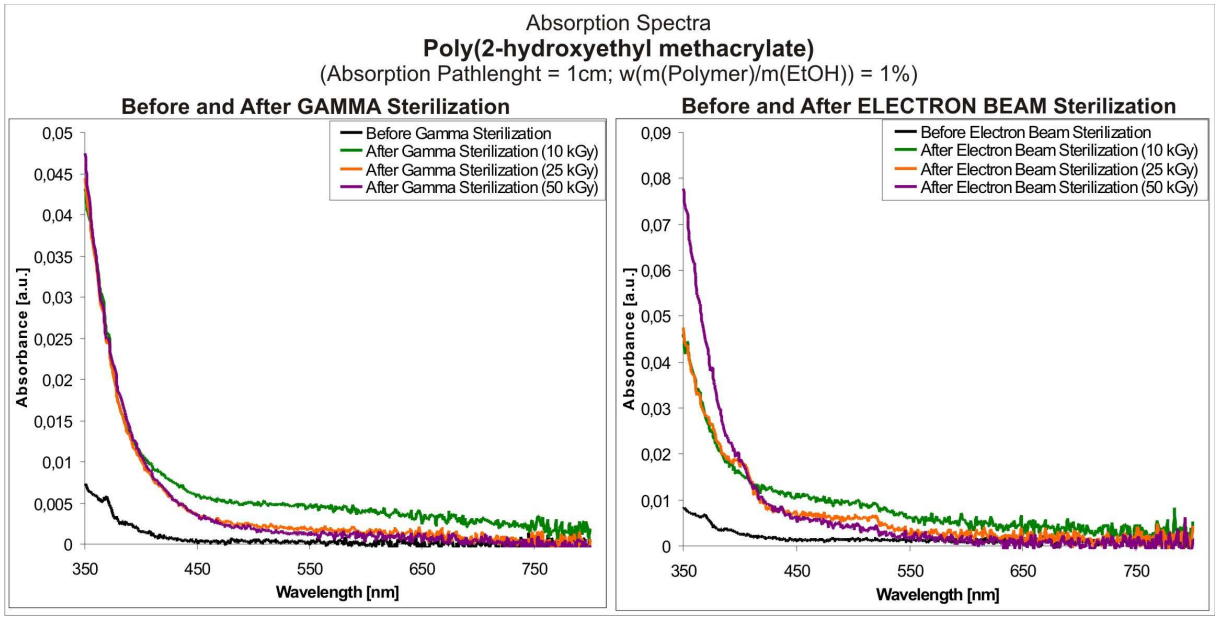

A.13.2 Contact Angle Measurement

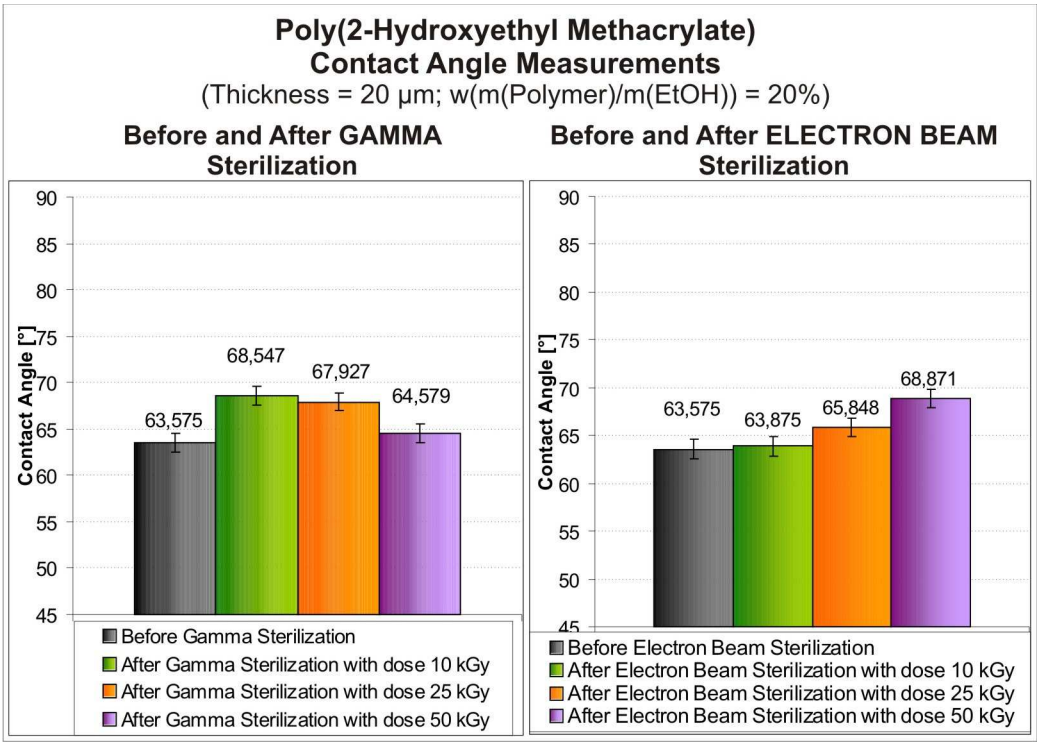

A.13.3 Infrared Spectra

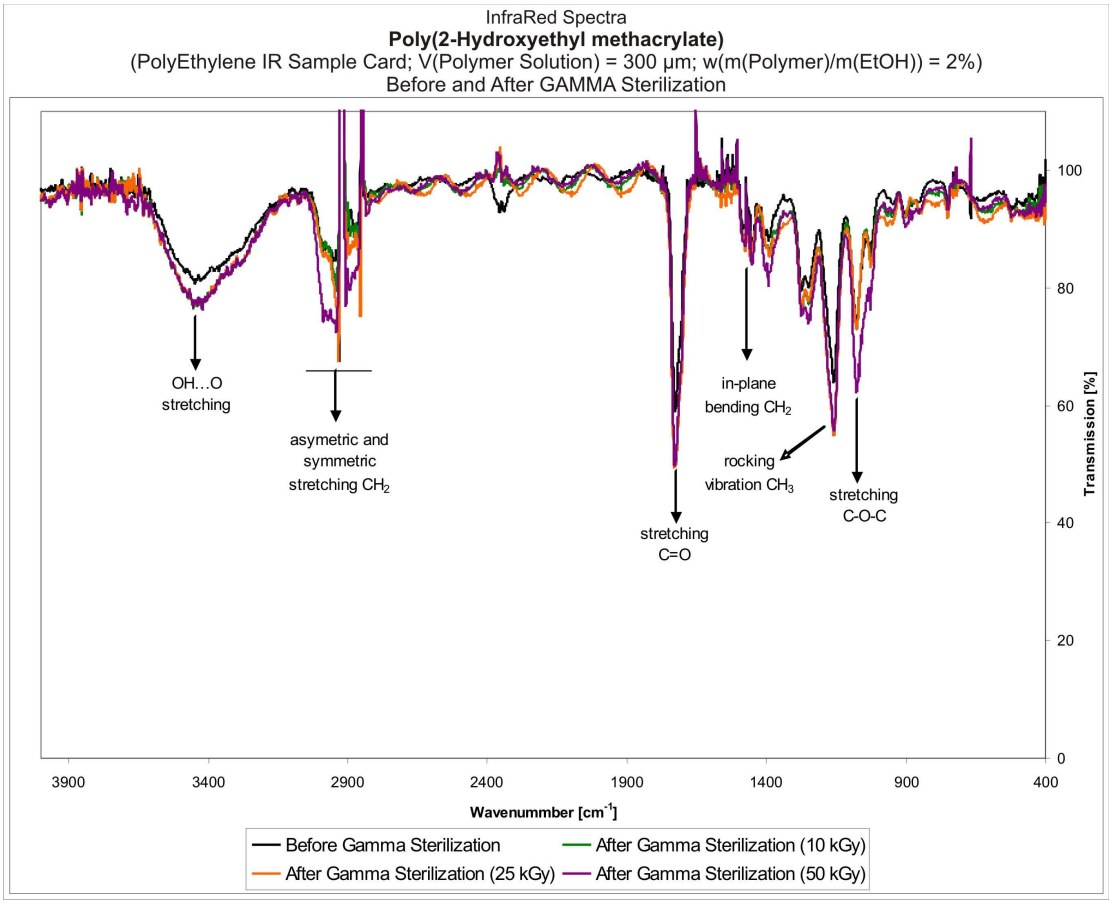

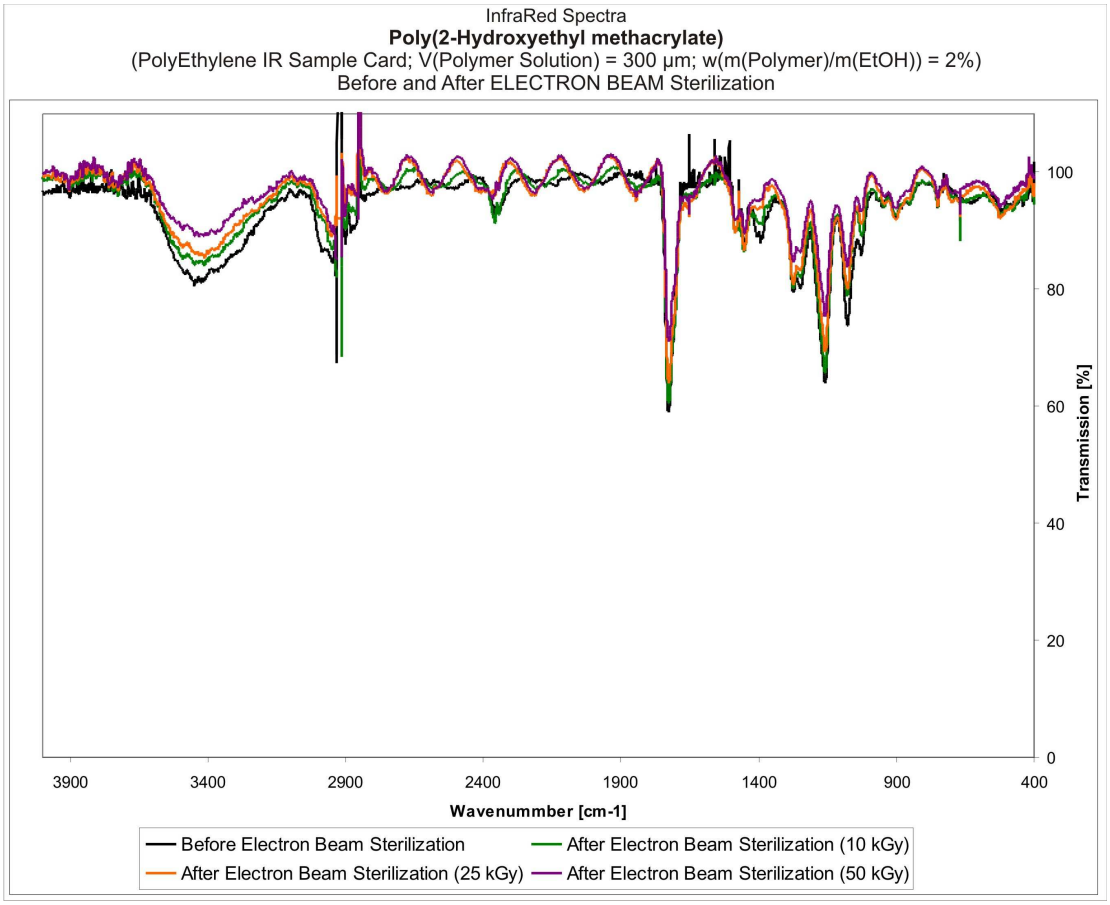

A.14 Poly(Ethylene Terepthalate) (Mylar®)

A.14.1 Differential Scanning Calorimetry

DSC Program:

30 °C – 290 °C 20 °C/min
290 °C – 30 °C 10 °C/min
30 °C – 290 °C 20 °C/min

	T_m	ΔH
BeforeS	201,59 °C	-48,194 J/g
10 kGy	200,26 °C	-52,171 J/g
25 kGy	200,31 °C	-44,144 J/g
50 kGy	200,18 °C	-57,358 J/g

Before sterilization

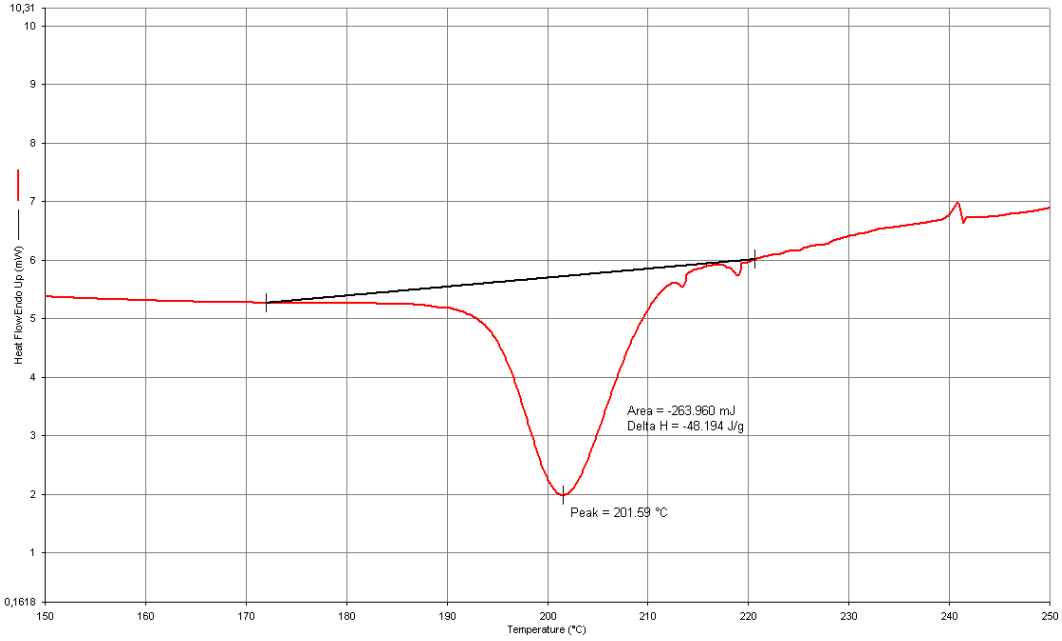

After GAMMA sterilization with 10 kGy

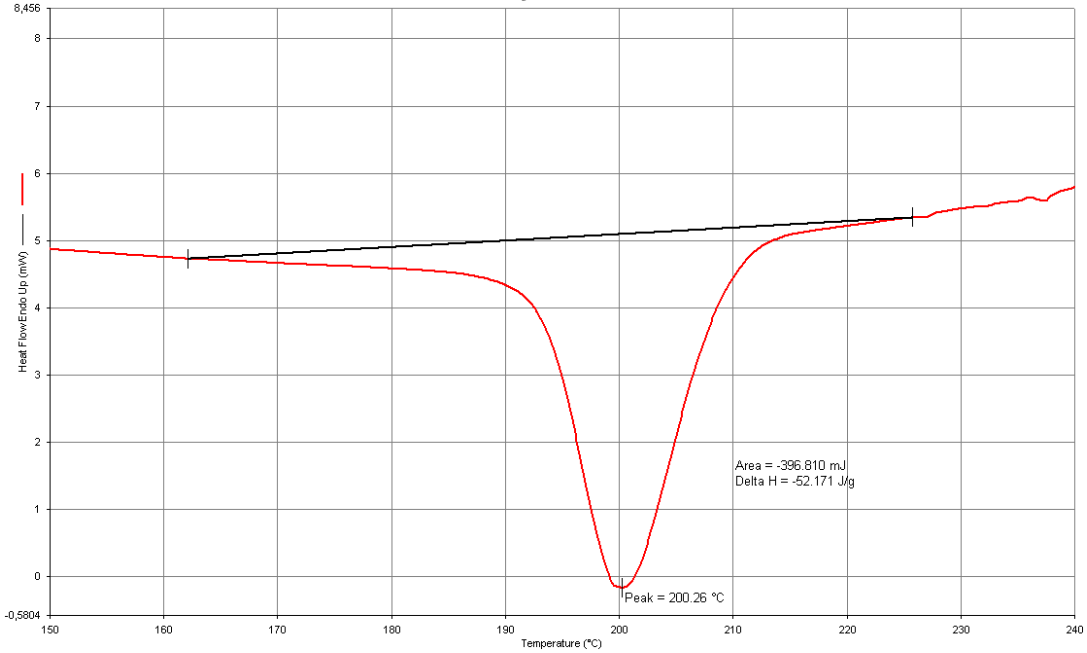

After GAMMA sterilization with 25 kGy

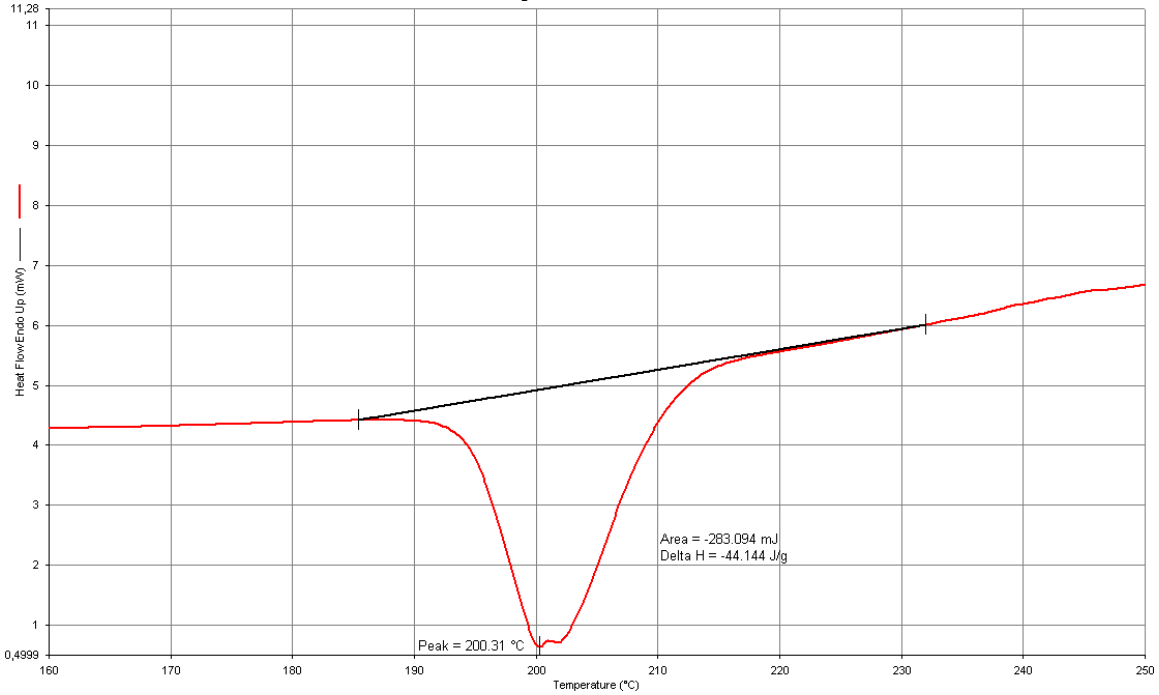

After GAMMA sterilization with 50 kGy

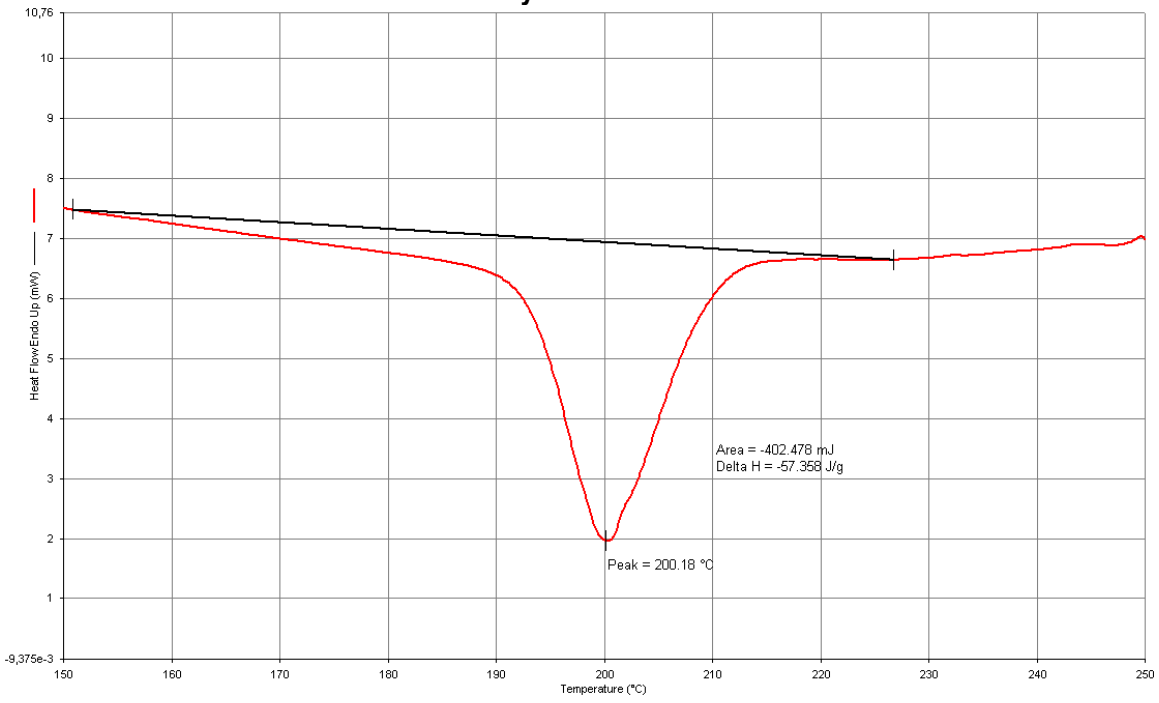

B
Radiation Sterilization of (Luminescent) Indicators

TABLE OF CONTENT

B RADIATION STERILIZATION OF (LUMINESCENT) INDICATORS 247

B.1 3-(2-benzothiazolyl)-7-hydroxycoumarin (=pH Sensitive Coumarin) 251
B.1.1 Gamma Sterilization 251
B.1.2 Electron Beam Sterilization 253

B.2 Eu(tta)$_3$DEADIT) 255
B.2.1 Gamma Sterilization 255
B.2.2 Electron Beam Sterilization 257

B.3 Iridium(III) Coumarin 259
B.3.1 Gamma Sterilization 259
B.3.2 Electron Beam Sterilization 261

B.4 Platinum(II) meso-tetrakis-(pentafluorophenyl)porphyrin (=PtTFPP) 263
B.4.1 Gamma Sterilization 263
B.4.2 Electron Beam Sterilization 265

B.5 Platinum(II) OctaEthyl Porphyrin (=PtOEP) 267
B.5.1 Gamma Sterilization 267
B.5.2 Electron Beam Sterilization 269

B.6 Platinum(II) meso-tetra(4-FluoroPhenyl) TetraBenzoPorphyrin (=PtTPTBPF) 271
B.6.1 Gamma Sterilization 271
B.6.2 Electron Beam Sterilization 273

B.7 Palladium(II) meso-tetra(4-FluoroPhenyl) TetraBenzoPorphyrin (=PdTPTBPF) 275
B.7.1 Gamma Sterilization 275
B.7.2 Electron Beam Sterilization 277

B.8 Ruthenium(II)-tris-4,7-diphenyl-1,10-phenanthroline dichloride (=Ru(dpp)$_3$Cl$_2$) 279
B.8.1 Gamma Sterilization 279
B.8.2 Electron Beam Sterilization 281

B.9 DiChloroTris(1,10-Phenanthroline) Ruthenium(II) Hydrate 283
B.9.1 Gamma Sterilization 283
B.9.2 Electron Beam Sterilization 285

B.10 1-HydroxyPyrene-3,6,8-tris-bis(2-Ethylhexyl)Sulfonamide (=HPTS(DHA)$_3$) 287
B.10.1 Gamma Sterilization 287
B.10.2 Electron Beam Sterilization 289

B.11 PET Perylene BisImide 291
B.11.1 Gamma Sterilization 291
B.11.2 Electron Beam Sterilization 292

B.12 Eosin EthylEster 293
B.12.1 Gamma Sterilization 293
B.12.2 Electron Beam Sterilization 295

B.13 2´,7´-DiChloroFluorescein 296
B.13.1 Gamma Sterilization 296
B.13.2 Electron Beam Sterilization 297

B.14 2′,7′-DiHexyl-5(6)-*N*-Octadecyl-CarboxAmidoFluorescein (=DHFA) **299**
B.14.1 Gamma Sterilization 299
B.14.2 Electron Beam Sterilization 301

B.15 2′,7′-DiHexylFluorescein OctadecylEster (=DHFE) **303**
B.15.1 Gamma Sterilization 303
B.15.2 Electron Beam Sterilization 305

B.16 BromoPhenol Blue **307**
B.16.1 Gamma Sterilization 307
B.16.2 Electron Beam Sterilization 308

B.17 Thymol Blue **309**
B.17.1 Gamma Sterilization 309
B.17.2 Electron Beam Sterilization 310

B.18 BromoThymol Blue **311**
B.18.1 Gamma Sterilization 311
B.18.2 Electron Beam Sterilization 312

B.19 Methyl Orange **313**
B.19.1 Gamma Sterilization 313
B.19.2 Electron Beam Sterilization 314

B.1 3-(2-benzothiazolyl)-7-hydroxycoumarin (=pH Sensitive Coumarin)

B.1.1 Gamma Sterilization

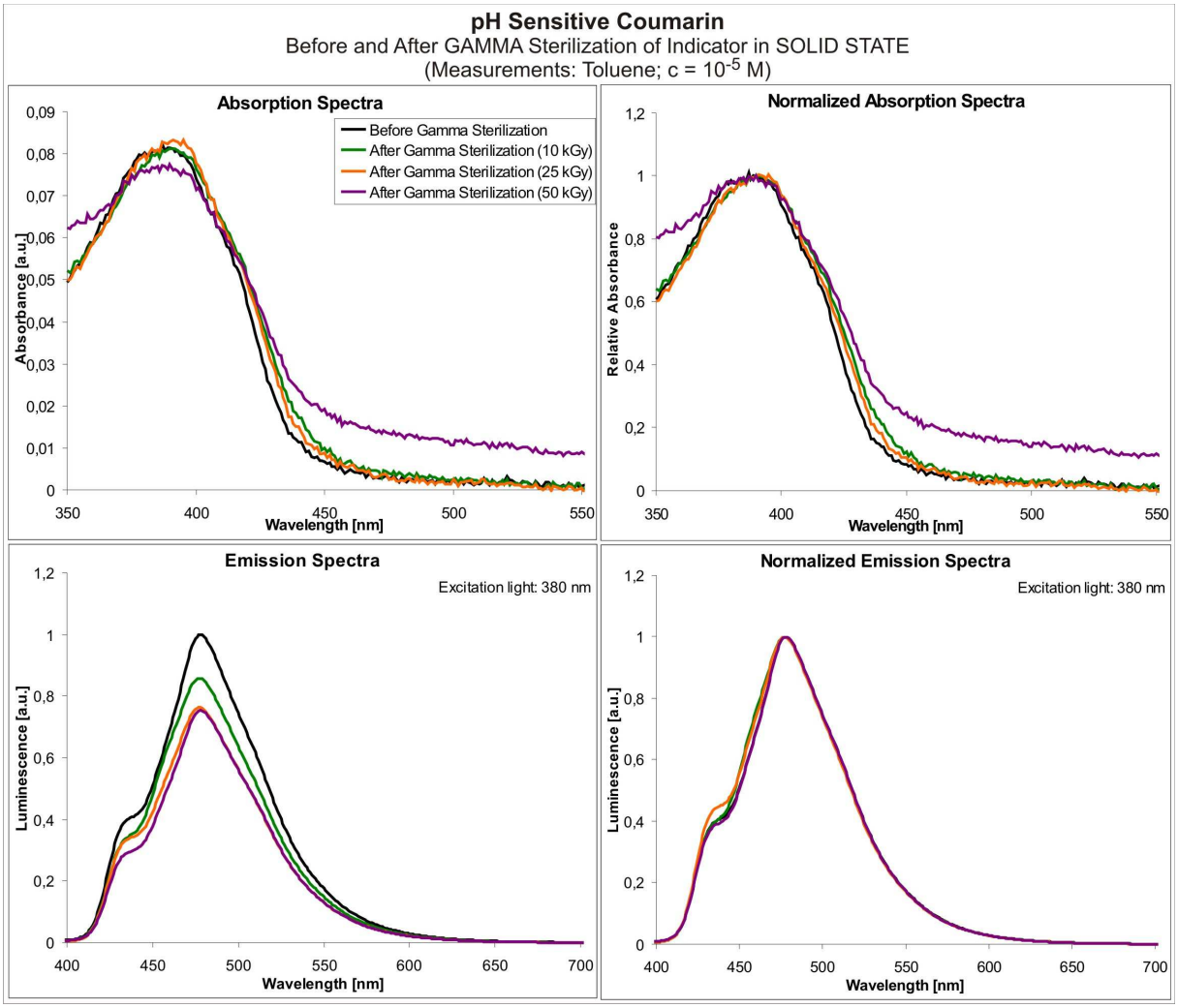

GAMMA/SOLID STATE	Absorption Spectra		Emission Spectra	
Alterations in Absorption/Emission Intensity	10kGy	0,37% decrease	10kGy	14,21% decrease
	25 kGy	1,60% increase	25 kGy	23,64% decrease
	50 kGy	5,08% decrease	50 kGy	24,67% decrease
Alterations in Absorption/Emission Curve Form	10kGy	Unaltered	10kGy	Unaltered
	25 kGy	Unaltered	25 kGy	Altered emission between 428-444 nm
	50 kGy	Increased absorption between 430 and 800 nm	50 kGy	Unaltered

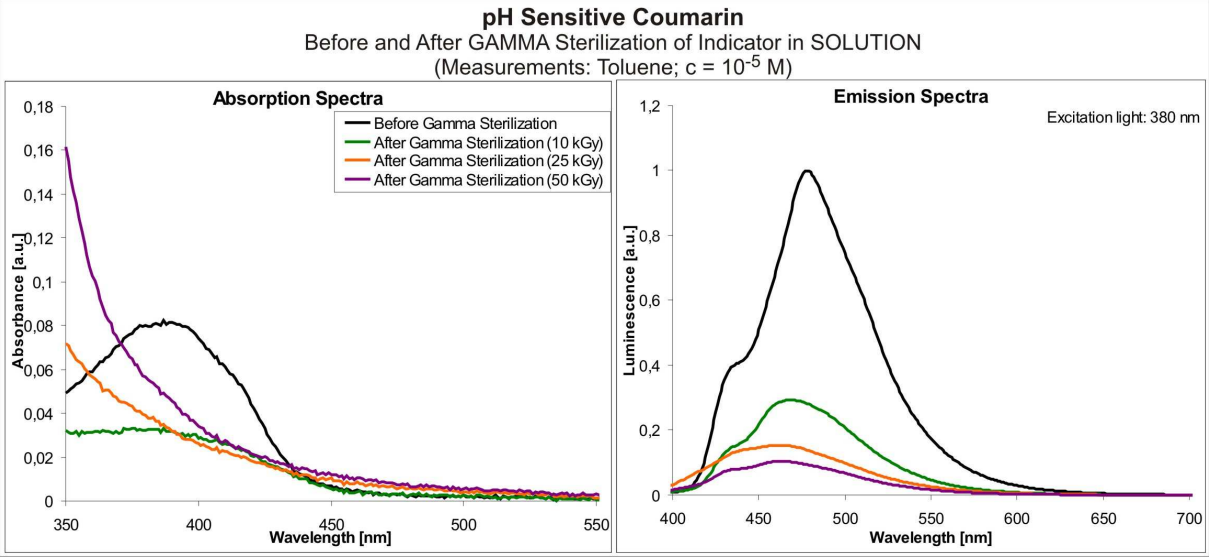

GAMMA/SOLUTION	Absorption Spectra		Emission Spectra	
Alterations in Absorption/Emission Intensity	10kGy	61,20% decrease	10kGy	71,57% decrease
	25 kGy		25 kGy	Decrease
	50 kGy		50 kGy	Decrease
Alterations in Absorption/Emission Curve Form	10kGy	Disappearance of characteristic curve form of pH Sensitive Coumarin	10kGy	Disappearance of characteristic curve form of pH Sensitive Coumarin
	25 kGy	Disappearance of characteristic curve form of pH Sensitive Coumarin	25 kGy	Disappearance of characteristic curve form of pH Sensitive Coumarin
	50 kGy	Disappearance of characteristic curve form of pH Sensitive Coumarin	50 kGy	Disappearance of characteristic curve form of pH Sensitive Coumarin

B.1.2 Electron Beam Sterilization

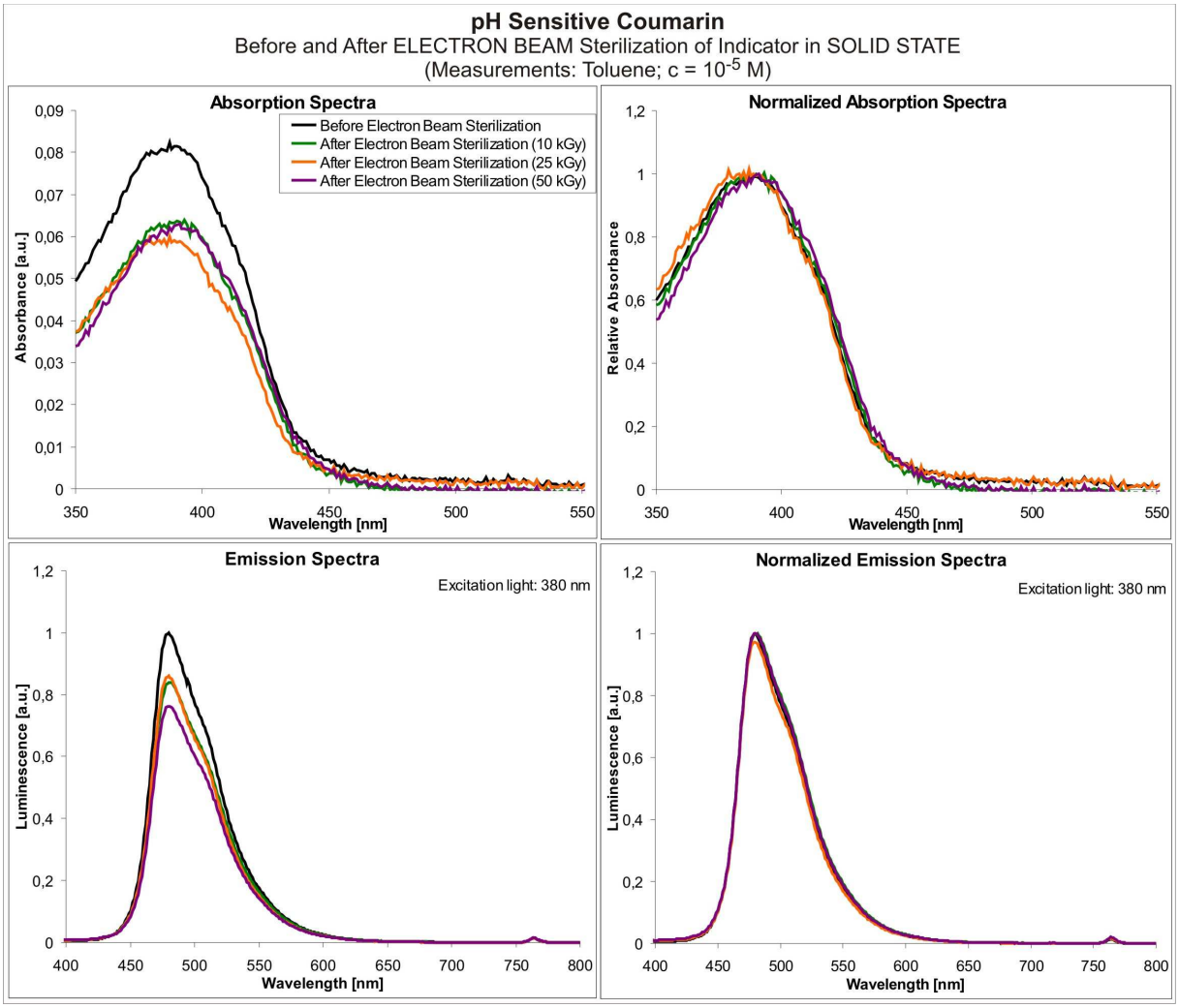

E-BEAM/SOLID STATE	Absorption Spectra		Emission Spectra	
Alterations in Absorption/Emission Intensity	10kGy	22,76% decrease	10kGy	15,99% decrease
	25 kGy	28,26% increase	25 kGy	11,70% decrease
	50 kGy	23,42% decrease	50 kGy	23,70% decrease
Alterations in Absorption/Emission Curve Form	10kGy	Unaltered	10kGy	Unaltered
	25 kGy	Unaltered	25 kGy	Unaltered
	50 kGy	Unaltered	50 kGy	Unaltered

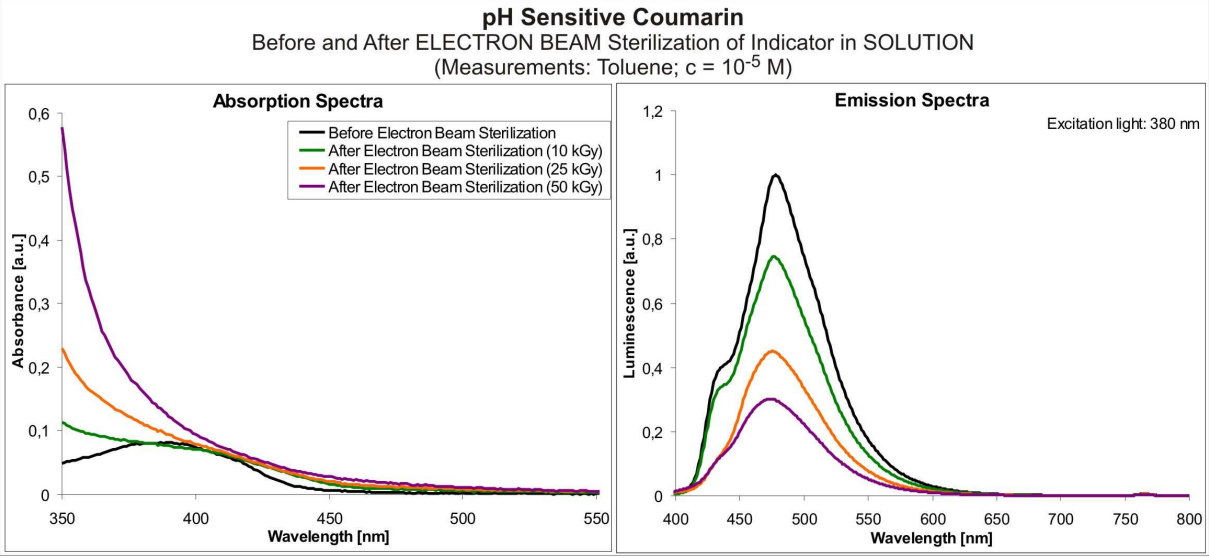

E-BEAM/SOLUTION	Absorption Spectra		Emission Spectra	
Alterations in Absorption/Emission Intensity	10kGy		10kGy	25,46% decrease
	25 kGy		25 kGy	54,97% decrease
	50 kGy		50 kGy	69,78% decrease
Alterations in Absorption/Emission Curve Form	10kGy	Disappearance of characteristic curve form of pH Sensitive Coumarin		
	25 kGy	Disappearance of characteristic curve form of pH Sensitive Coumarin		
	50 kGy	Disappearance of characteristic curve form of pH Sensitive Coumarin		

B.2 Europium(III) Complex with 4-(4,6-di(1H-indazol-1-yl)-1,3,5-triazin-2-yl)-N,N-DiEthyl Benzen Amine (=Eu(tta)$_3$DEADIT)

B.2.1 Gamma Sterilization

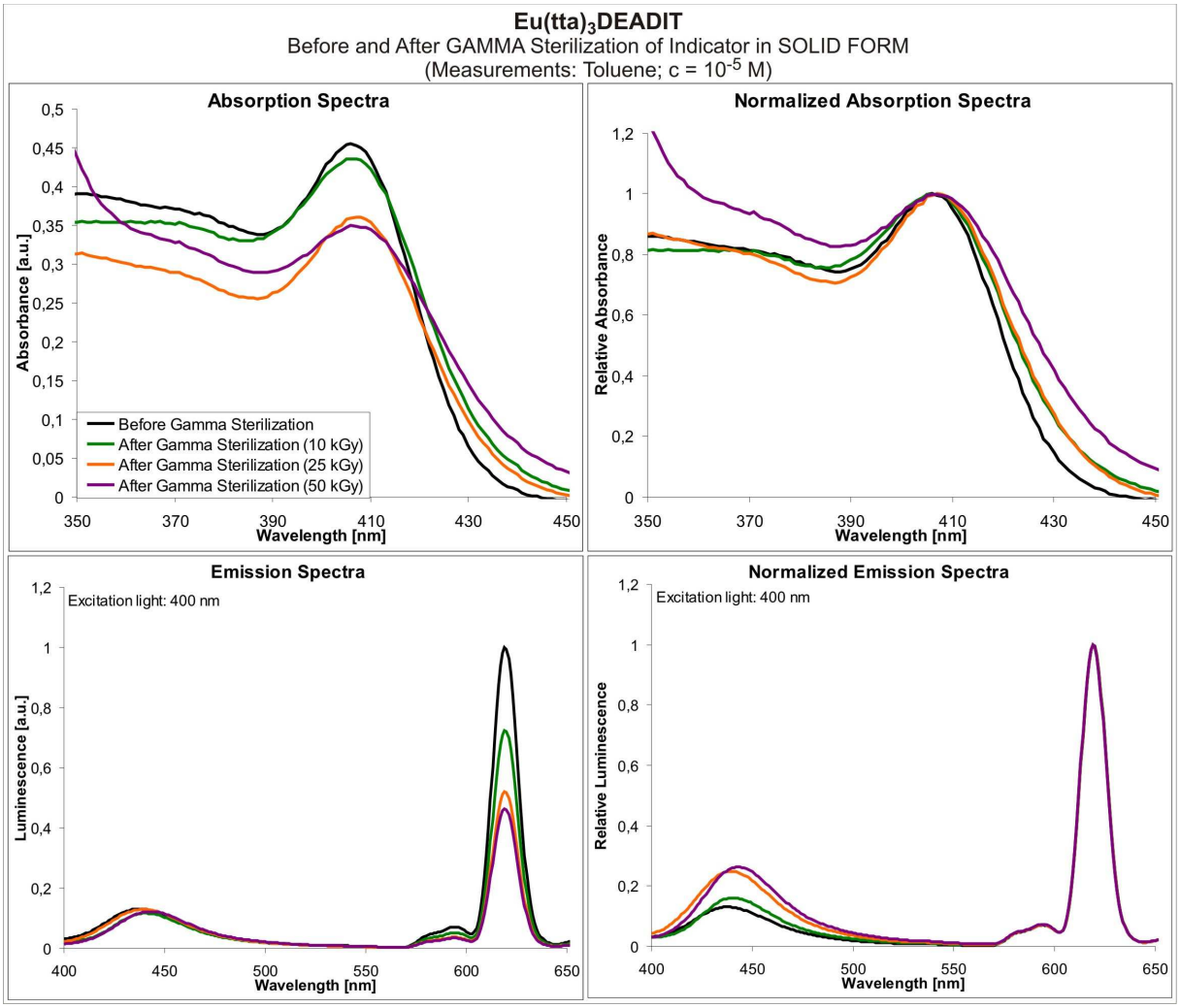

GAMMA/SOLID STATE	Absorption Spectra		Emission Spectra	
Alterations in Absorption/Emission Intensity	10kGy	4,30% increase	10kGy	27,75% decrease
	25 kGy	20,60% decrease	25 kGy	47,94% decrease
	50 kGy	23,09 decrease	50 kGy	53,65% decrease
Alterations in Absorption/Emission Curve Form	10kGy	Altered absorption between 350-370 nm; 385-400 nm and 415-450 nm.	10kGy	Increased emission of chelator´s peak for 18,3% Bathochromic shift of chelator´s peak for 3 nm
	25 kGy	Altered absorption between 370-400 nm and 415-450 nm.	25 kGy	Increased emission of chelator´s peak for 49,2%
	50 kGy	Altered absorption between 350-400 nm and 415-450 nm.	50 kGy	Increased emission of chelator´s peak for 50,1% Bathochromic shift of chelator´s peak for 6 nm

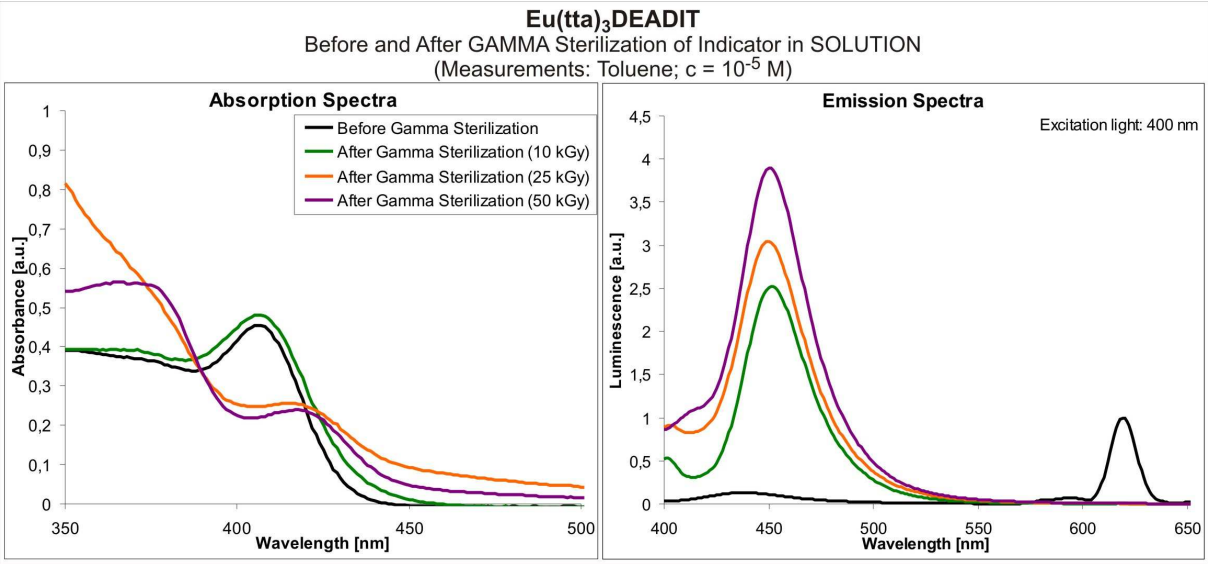

GAMMA/SOLUTION	Absorption Spectra		Emission Spectra	
Alterations in Absorption/Emission Intensity	10kGy	5,28% increase		
Alterations in Absorption/Emission Curve Form	10kGy	Altered - increased absorption.	10kGy	Increased emission of chelator´s peak with λ_{max} = 452 nm. Disappearance of characteristic peak of $Eu(tta)_3$DEADIT at 620 nm.
	25 kGy	Disappearance of characteristic curve form of $Eu(tta)_3$DEADIT. New peaks with λ_{max} = 417 nm.	25 kGy	Increased emission of chelator´s peak with λ_{max} = 452 nm. Disappearance of characteristic peak of $Eu(tta)_3$DEADIT at 620 nm
	50 kGy	Disappearance of characteristic curve form of $Eu(tta)_3$DEADIT. Two new peaks with λ_{max} = 367 nm and λ_{max} = 419 nm.	50 kGy	Increased emission of chelator´s peak with λ_{max} = 452 nm. Disappearance of characteristic peak of $Eu(tta)_3$DEADIT at 620 nm

B.2.2 Electron Beam Sterilization

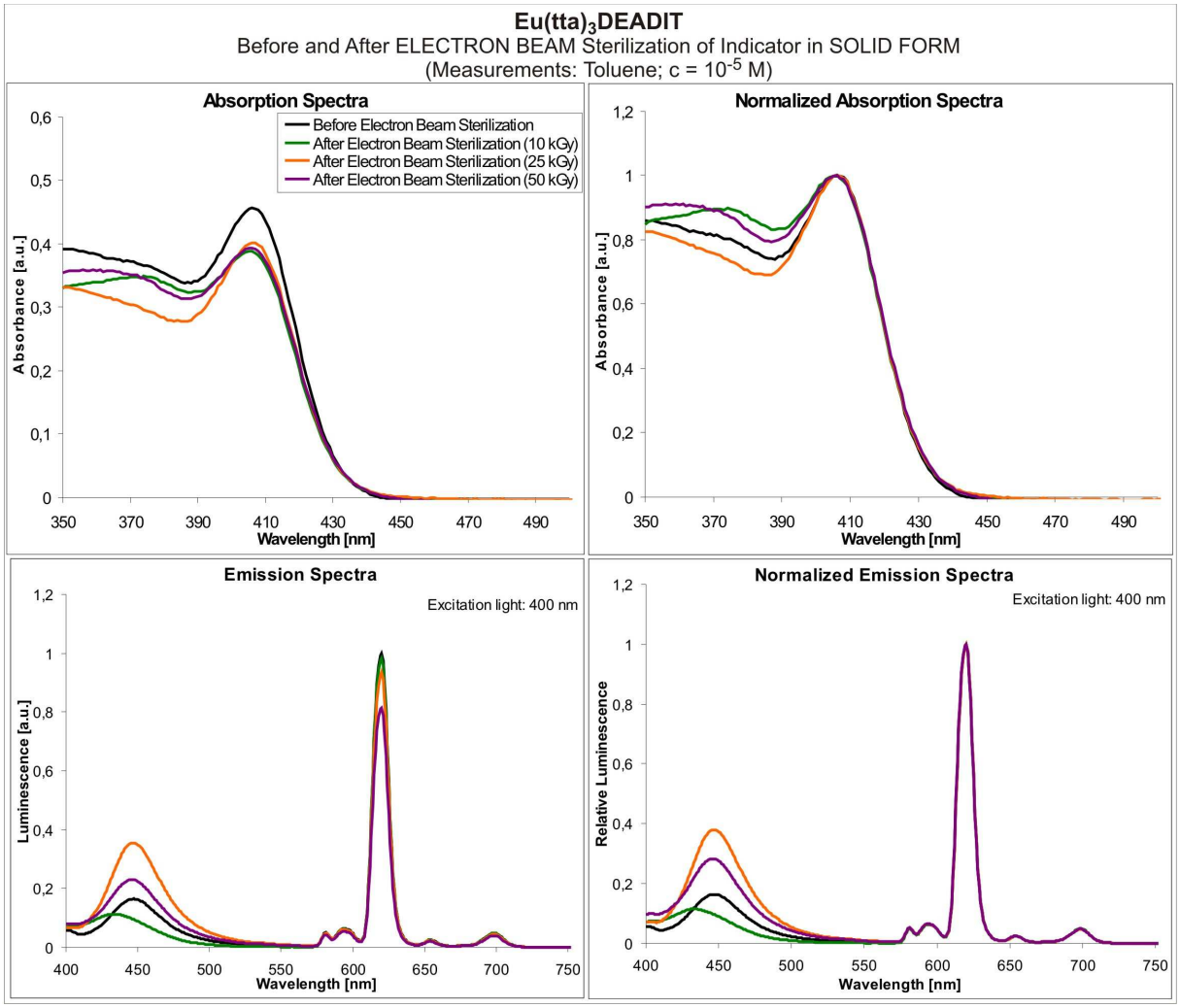

E-BEAM/SOLID STATE	Absorption Spectra		Emission Spectra	
Alterations in Absorption/Emission Intensity	10kGy	14,89% decrease	10kGy	0,39% decrease
	25 kGy	11,97% decrease	25 kGy	6,64% decrease
	50 kGy	13,69% decrease	50 kGy	18,69% decrease
Alterations in Absorption/Emission Curve Form	10kGy	Altered absorption between 350-400 nm.	10kGy	Hyprochromic shift of chelator´s peak for 14 nm. Decreased emission of chelator´s peak for 12%
	25 kGy	Altered absorption between 350-400 nm.	25 kGy	Increased emission of chelator´s peak for 53,6%
	50 kGy	Altered absorption between 350-400 nm.	50 kGy	Increased emission of chelator´s peak for 27,8%

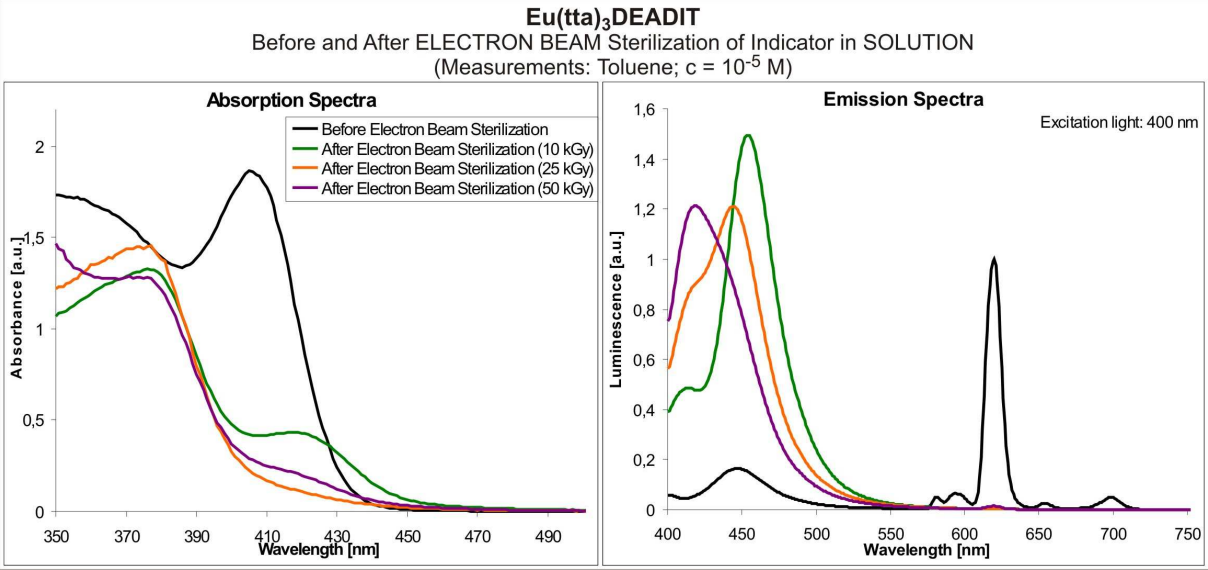

E-BEAM/SOLUTION	Absorption Spectra		Emission Spectra	
Alterations in Absorption/Emission Curve Form	10kGy	Disappearance of characteristic curve form of $Eu(tta)_3$DEADIT. Two new peaks with λ_{max} = 375 nm and λ_{max} = 420 nm.	10kGy	Increased emission of chelator´s peak with λ_{max} = 456 nm. Disappearance of characteristic peak of $Eu(tta)_3$DEADIT at 620 nm.
	25 kGy	Disappearance of characteristic curve form of $Eu(tta)_3$DEADIT. New peaks with λ_{max} = 375 nm.	25 kGy	Increased emission of chelator´s peak with λ_{max} = 445 nm. Disappearance of characteristic peak of $Eu(tta)_3$DEADIT at 620 nm
	50 kGy	Disappearance of characteristic curve form of $Eu(tta)_3$DEADIT. New peaks with λ_{max} = 375 nm..	50 kGy	Increased emission of chelator´s peak with λ_{max} = 420 nm. Disappearance of characteristic peak of $Eu(tta)_3$DEADIT at 620 nm

B.3 Iridium(III) Coumarin (=Ir(C_s)$_2$(acac))

B.3.1 Gamma Sterilization

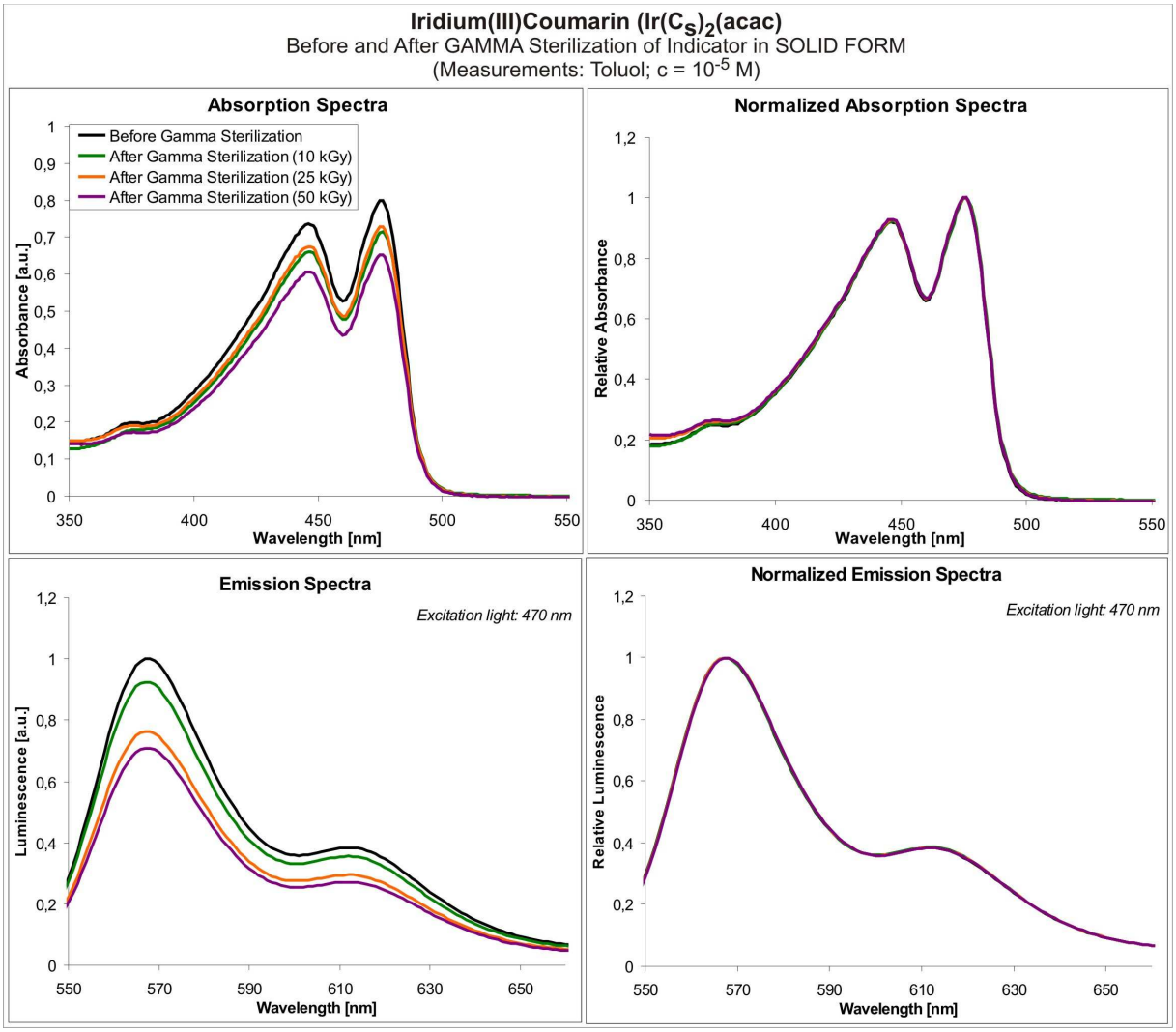

GAMMA/SOLID STATE	Absorption Spectra		Emission Spectra	
Alterations in Absorption/Emission Intensity	10kGy	10,60% decrease	10kGy	7,55% decrease
	25 kGy	8,83% decrease	25 kGy	23,69% decrease
	50 kGy	14,64% decrease	50 kGy	29,20% decrease
Alterations in Absorption/Emission Curve Form	10kGy	Unaltered	10kGy	Unaltered
	25 kGy	Unaltered	25 kGy	Unaltered
	50 kGy	Unaltered	50 kGy	Unaltered

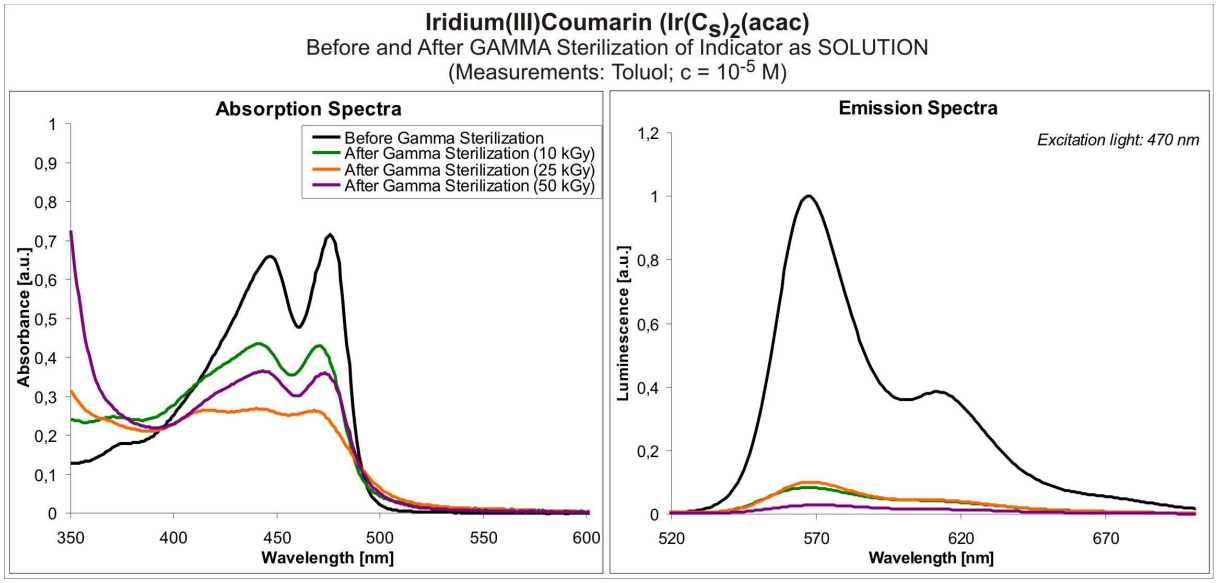

GAMMA/SOLUTION	Absorption Spectra		Emission Spectra	
Alterations in Absorption/Emission Intensity	10kGy	34,21% decrease	10kGy	91,67% decrease
	25 kGy	59,29% decrease	25 kGy	89,93% decrease
	50 kGy	44,81% decrease	50 kGy	97,12% decrease
Alterations in Absorption/Emission Curve Form	10kGy	Altered – increased absorption between 350-390 nm and 490-530 nm; Hypsochromic shift of λ_{max} for 7 nm.		
	25 kGy	Altered - increased absorption between 350-390 nm and 490-540 nm; Disappearance of two characteristic maximum peaks for Ir(Cs) 2(acac);		
	50 kGy	Altered - - increased absorption between 350-390 nm and 490-540 nm; Hypsochromic shift of λ_{max} for 5 nm.		

B.3.2 Electron Beam Sterilization

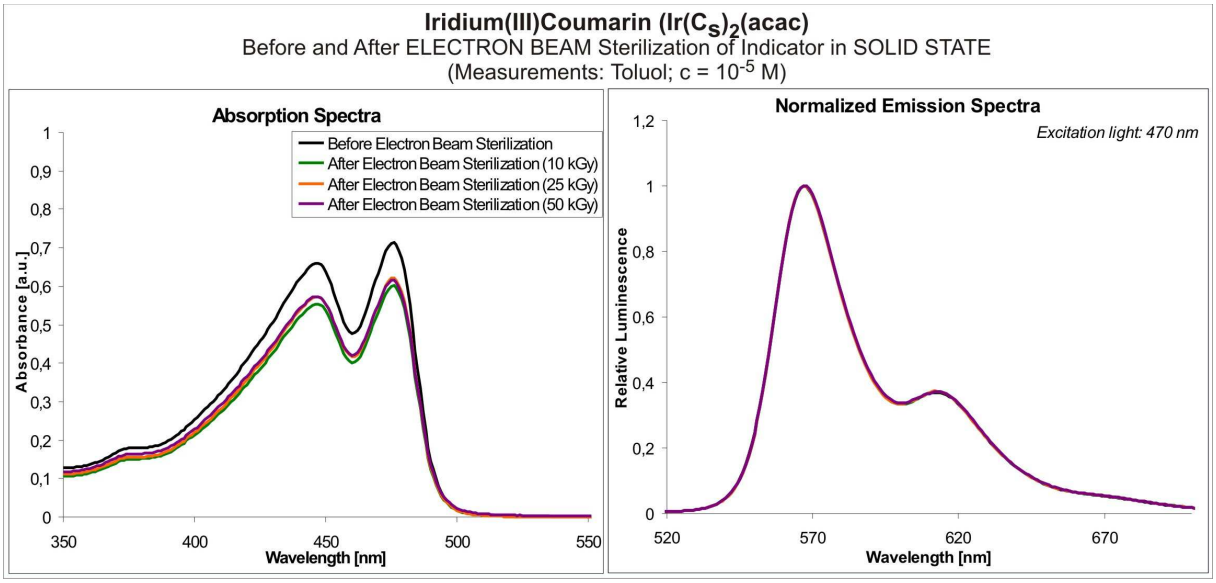

E-BEAM/SOLID STATE	Absorption Spectra		Emission Spectra	
Alterations in Absorption/Emission Intensity	10kGy	15,88% decrease		
	25 kGy	12,94% decrease		
	50 kGy	13,85% decrease		
Alterations in Absorption/Emission Curve Form	10kGy	Unaltered	10kGy	Unaltered
	25 kGy	Unaltered	25 kGy	Unaltered
	50 kGy	Unaltered	50 kGy	Unaltered

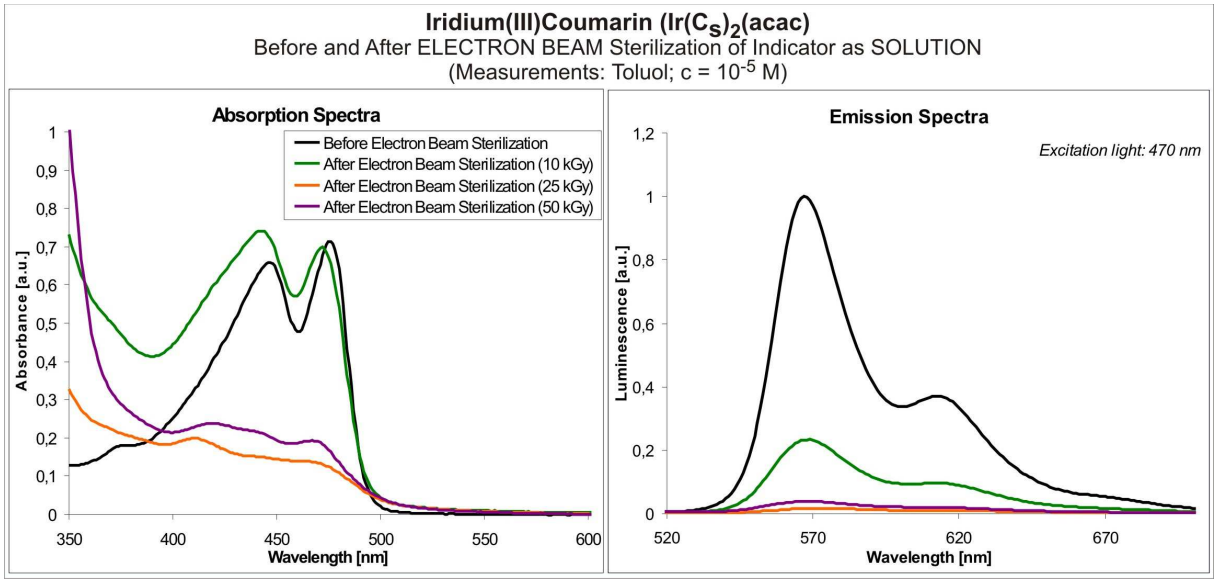

E-BEAM/SOLUTION	Absorption Spectra		Emission Spectra	
Alterations in Absorption/Emission Intensity			10kGy	76,66% decrease
			25 kGy	98,25% decrease
			50 kGy	96,15% decrease
Alterations in Absorption/Emission Curve Form	10kGy	Altered – first characteristic peaks for Ir(Cs) 2(acac) become absorption maximum; increased absorption between 350-470 nm and 495-530 nm; Hypsochromic shift of λ_{max} for 4 nm.		
	25 kGy	Altered - increased absorption between 350-390 nm and 490-530 nm; Disappearance of two characteristic maximum peaks for Ir(Cs) 2(acac);		
	50 kGy	Altered - - increased absorption between 350-390 nm and 490-540 nm; Disappearance of two characteristic maximum peaks for Ir(Cs) 2(acac);		

B.4 Platinum(II) meso-tetrakis-(pentafluorophenyl)porphyrin (=PtTFPP)

B.4.1 Gamma Sterilization

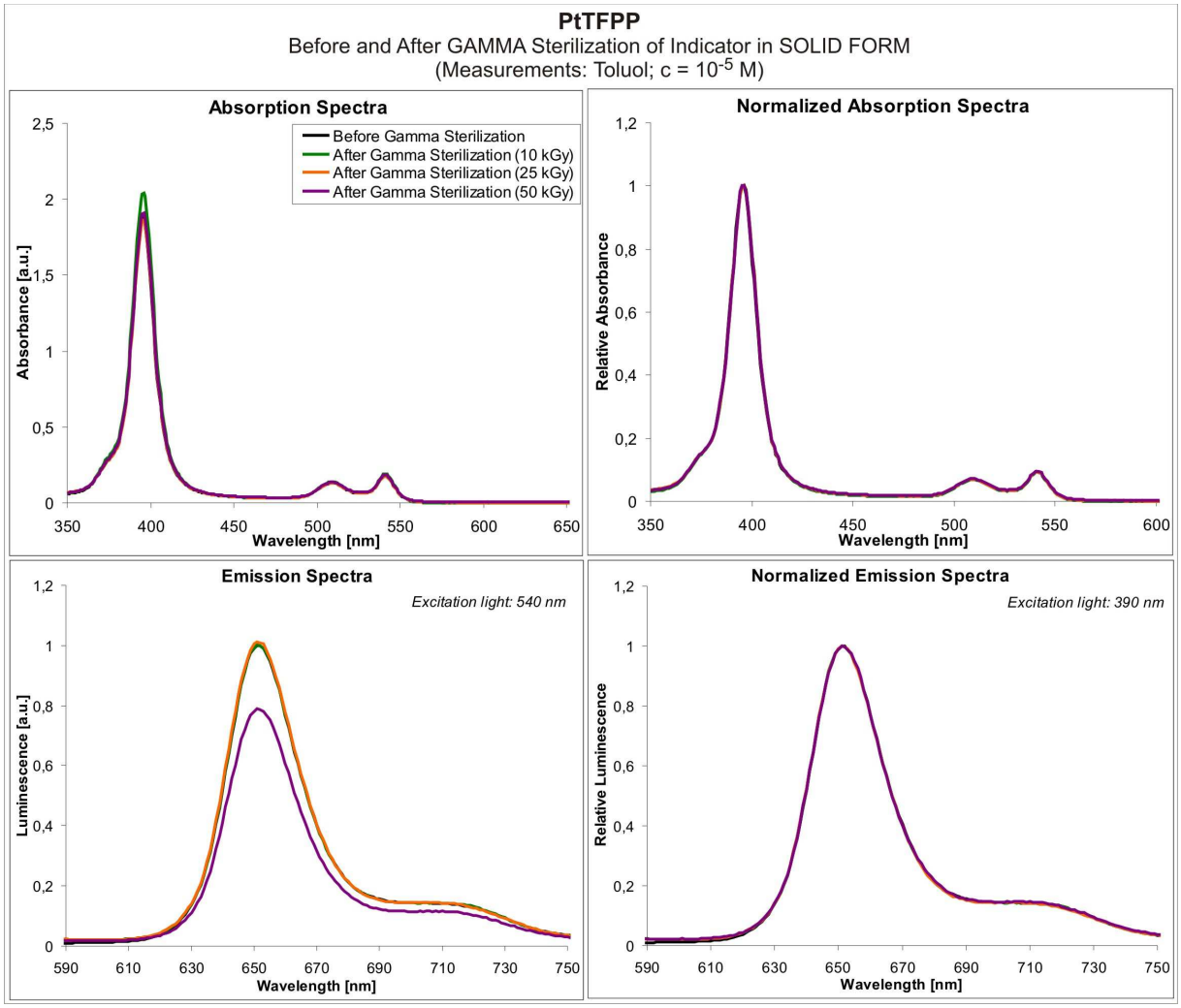

GAMMA/SOLID STATE	Absorption Spectra		Emission Spectra	
Alterations in Absorption/Emission Intensity	10kGy	7,95% increase	10kGy	0,23% increase
	25 kGy	0,83% decrease	25 kGy	1,31% increase
	50 kGy	1,36% increase	50 kGy	21,03% decrease
Alterations in Absorption/Emission Curve Form	10kGy	Unaltered	10kGy	Unaltered
	25 kGy	Unaltered	25 kGy	Unaltered
	50 kGy	Unaltered	50 kGy	Unaltered

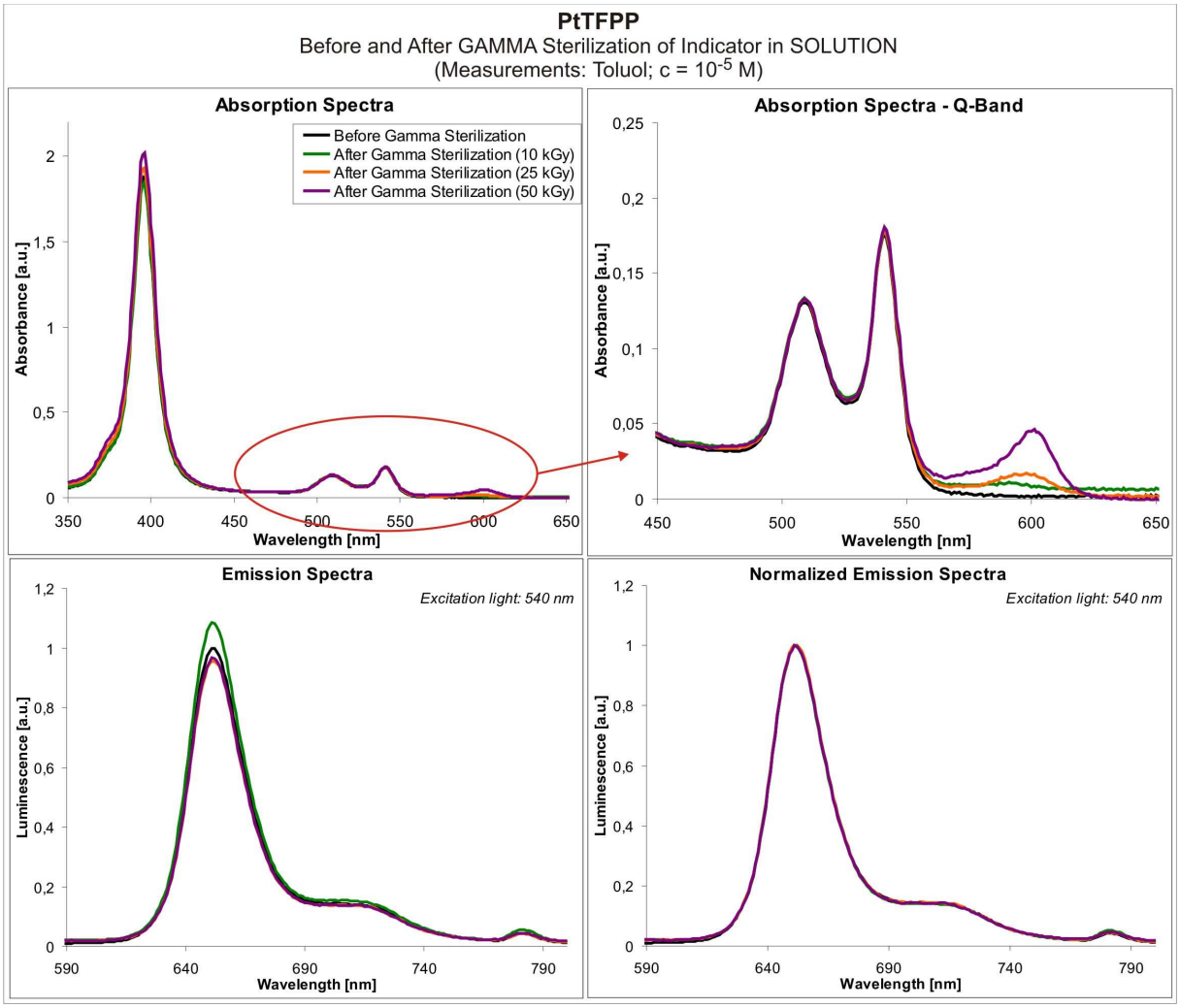

GAMMA/SOLUTION	Absorption Spectra		Emission Spectra	
Alterations in Absorption/Emission Intensity	10kGy	1,71% decrease	10kGy	0,23% increase
	25 kGy	2,57% increase	25 kGy	1,31% increase
	50 kGy	6,84% increase	50 kGy	21,03% decrease
Alterations in Absorption/Emission Curve Form	10kGy	Unaltered	10kGy	Altered – new peak with λ_{max} = 782 nm
	25 kGy	Altered – new peak with λ_{max} = 597 nm; Increased absorption between 350-365 nm.	25 kGy	Altered – new peak with λ_{max} = 782 nm
	50 kGy	Altered – new peak with λ_{max} = 599 nm; Increased absorption between 350-365 nm.	50 kGy	Altered – new peak with λ_{max} = 782 nm

B.4.2 Electron Beam Sterilization

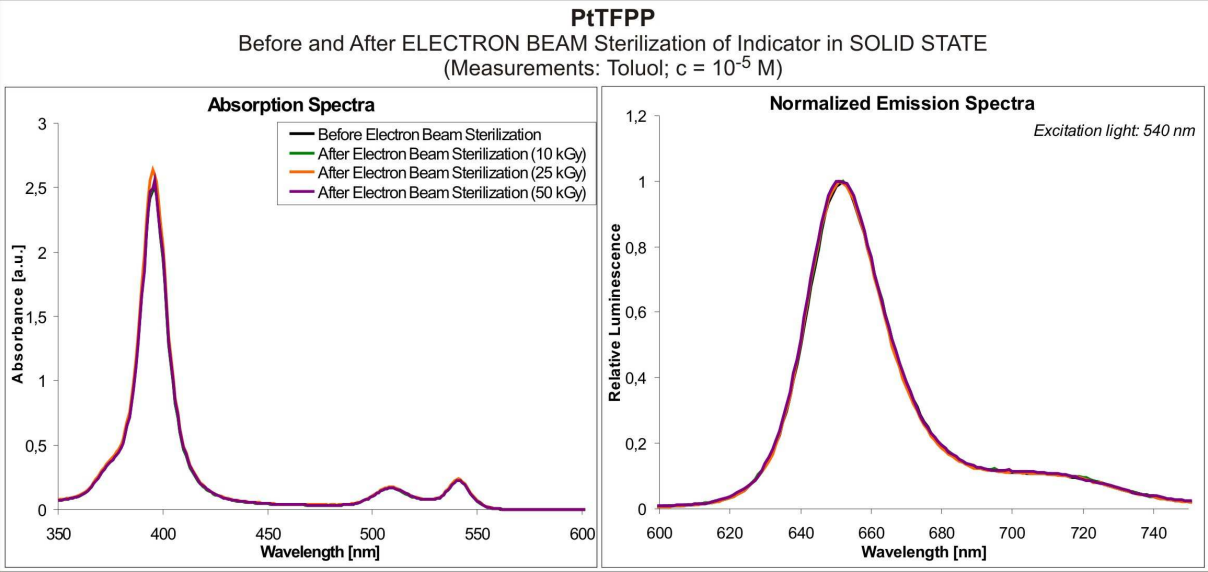

E-BEAM/SOLID STATE	Absorption Spectra		Emission Spectra	
Alterations in Absorption/Emission Intensity	10kGy	0,45% increase		
	25 kGy	5,14% increase		
	50 kGy	2,33% increase		
Alterations in Absorption/Emission Curve Form	10kGy	Unaltered	10kGy	Unaltered
	25 kGy	Unaltered	25 kGy	Unaltered
	50 kGy	Unaltered	50 kGy	Unaltered

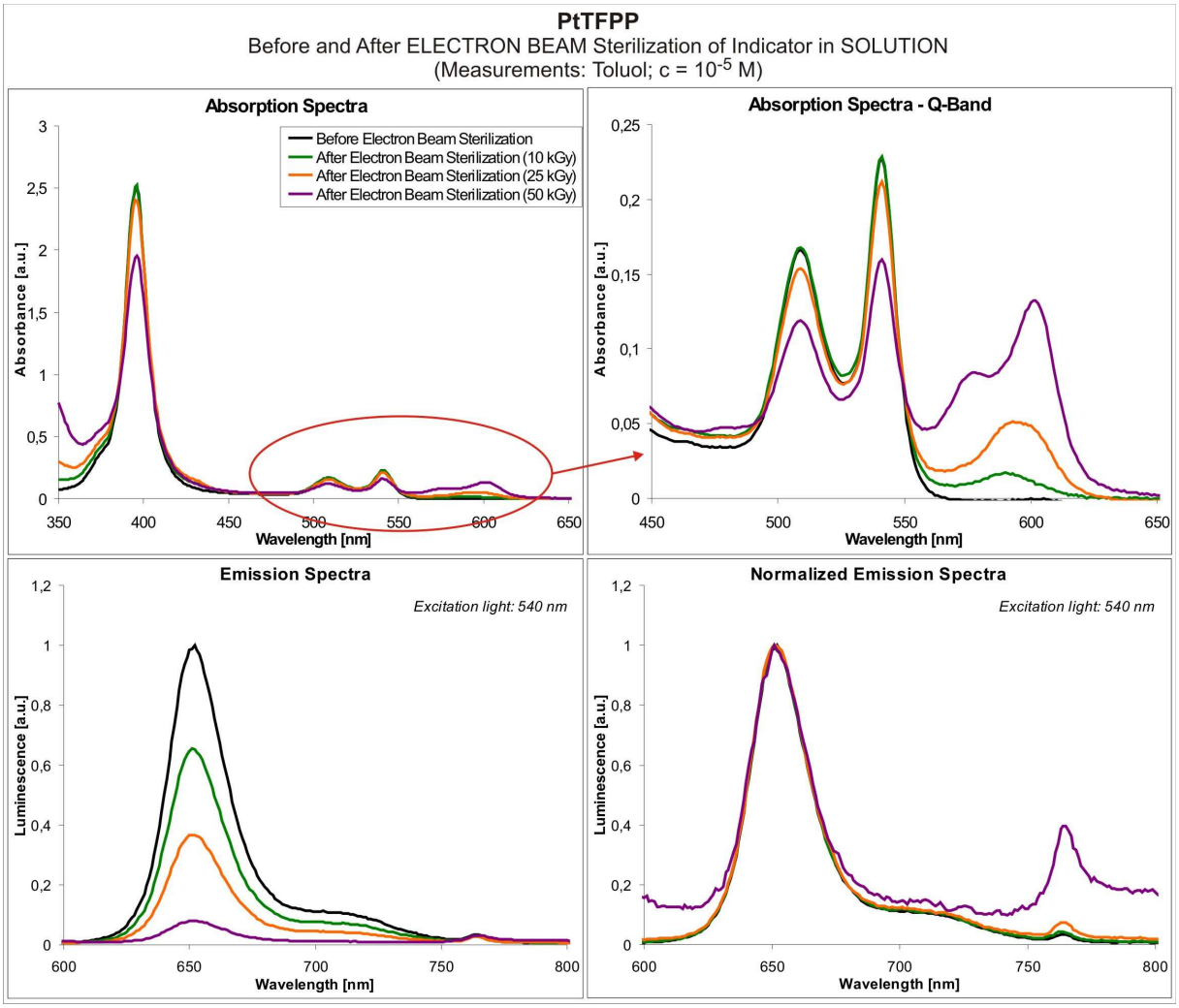

E-BEAM/SOLUTION	Absorption Spectra		Emission Spectra	
Alterations in Absorption/Emission Intensity	10kGy	0,87% increase	10kGy	34,41% decrease
	25 kGy	3,92% decrease	25 kGy	63,28% decrease
	50 kGy	21,85% decrease	50 kGy	91,86% decrease
Alterations in Absorption/Emission Curve Form	10kGy	Altered – new peak with λ_{max} = 589 nm; Increased absorption between 350-380 nm and 420-455 nm.	10kGy	Altered – new peak with λ_{max} = 765 nm
	25 kGy	Altered – new peak with λ_{max} = 593 nm; Increased absorption between 350-380 nm and 415-455 nm.	25 kGy	Altered – new peak with λ_{max} = 765 nm
	50 kGy	Altered – 2 new peak s with $\lambda_{max(1)}$=574nm, $\lambda_{max(2)}$=600nm; Increased absorption between 350-380 nm and 415-480 nm.	50 kGy	Altered – new peak with λ_{max} = 765 nm The form of the curve is altered between 600-640 nm and 676-800 nm

B.5 Platinum(II) OctaEthyl Porphyrin (=PtOEP)

B.5.1 Gamma Sterilization

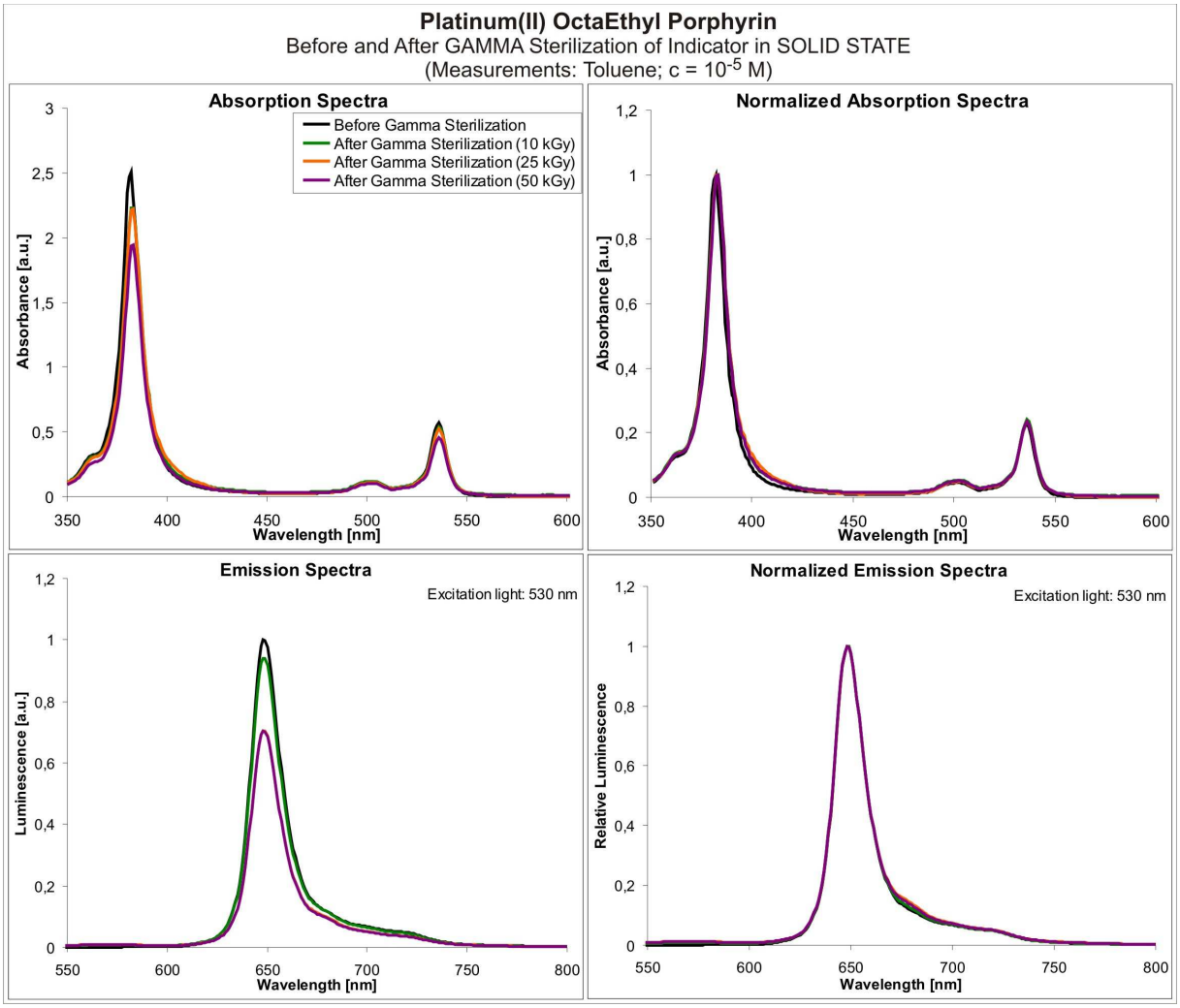

GAMMA/SOLID STATE	Absorption Spectra		Emission Spectra	
Alterations in Absorption/Emission Intensity	10kGy	10,94% decrease	10kGy	5,89% decrease
	25 kGy	11,32% decrease	25 kGy	29,50% decrease
	50 kGy	22,37% decrease	50 kGy	29,66% decrease
Alterations in Absorption/Emission Curve Form	10kGy	Increased absorption between 360-365 nm; 395-435 nm and 545-560 nm.	10kGy	Increased emission between 670-705 nm.
	25 kGy	Increased absorption between 360-365 nm; 395-435 nm and 545-560 nm	25 kGy	Increased emission between 670-705 nm.
	50 kGy	Increased absorption between 360-365 nm; 395-435 nm and 545-560 nm	50 kGy	Increased emission between 670-705 nm.

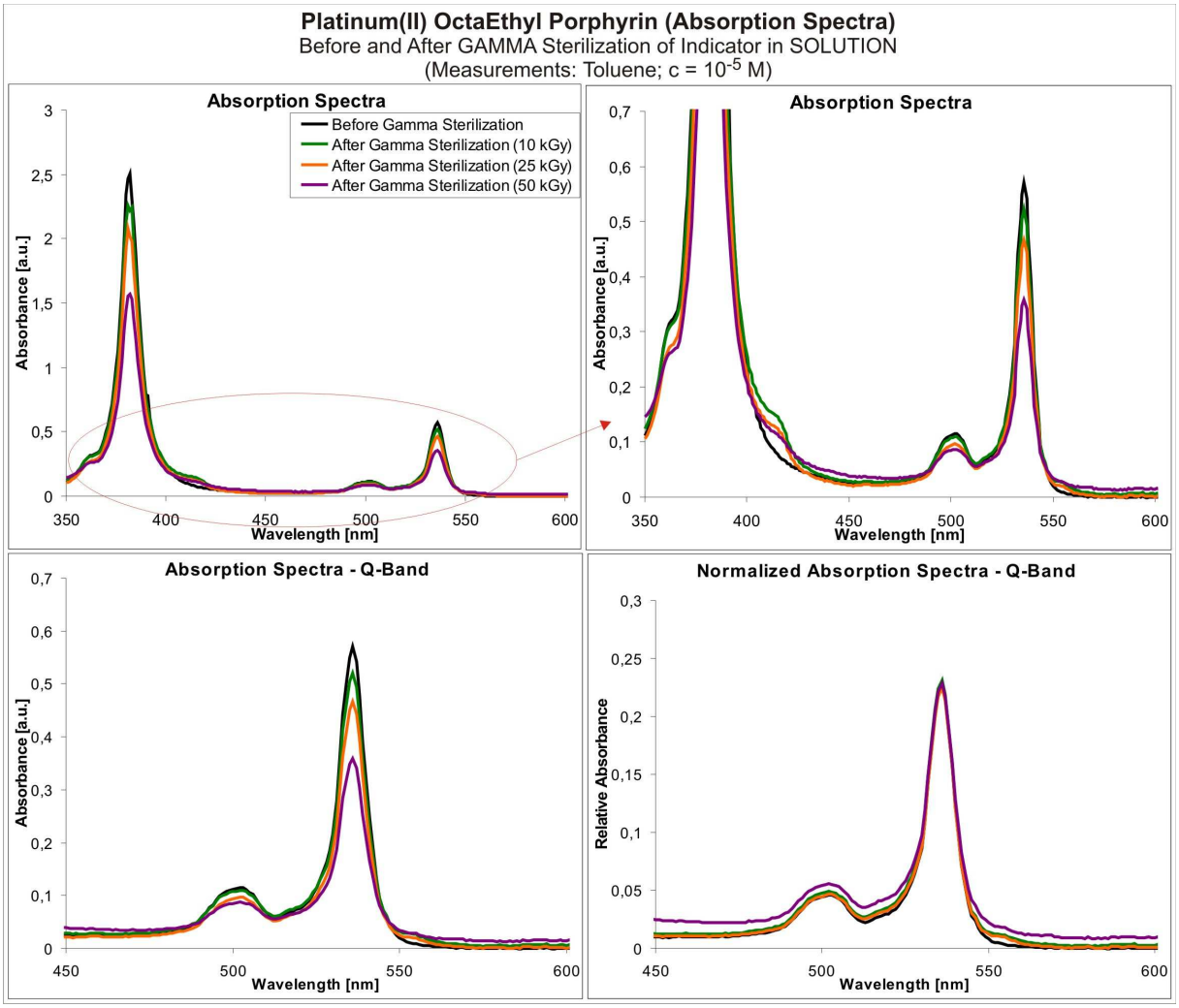

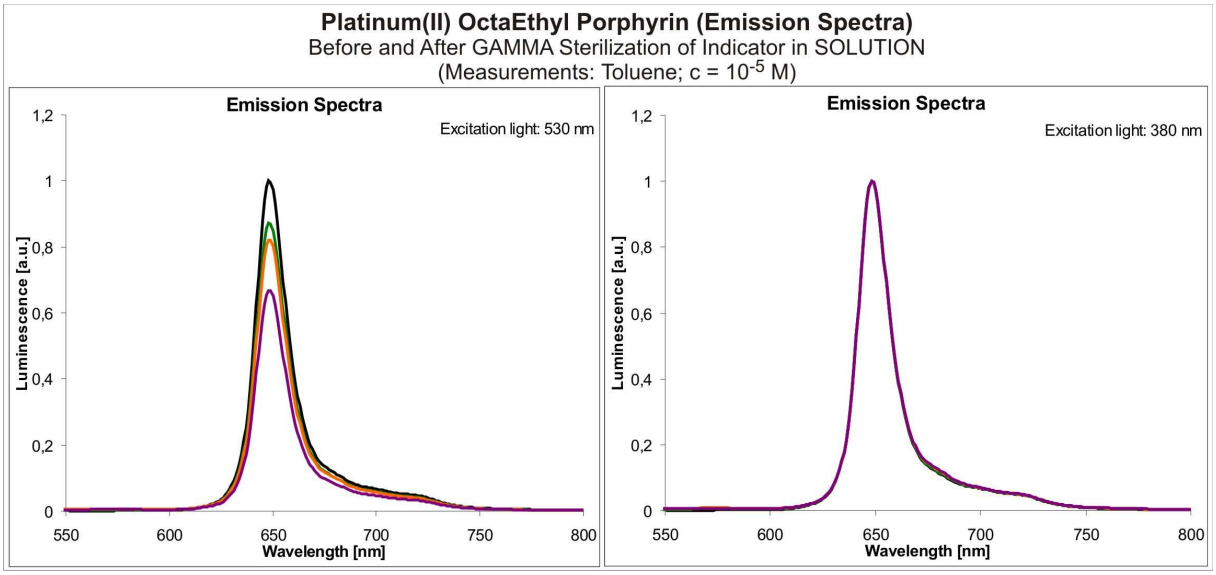

GAMMA/SOLUTION	Absorption Spectra		Emission Spectra	
Alterations in Absorption/Emission Intensity	10kGy	9,97% decrease	10kGy	12,75% decrease
	25 kGy	17,03% decrease	25 kGy	17,86% decrease
	50 kGy	37,29% decrease	50 kGy	33,14% decrease

Alterations in Absorption/Emission Curve Form	10kGy	Decreased absorption between 360-370 nm Increased absorption between 400-430 nm and 550-560 nm.	10kGy	Unaltered
	25 kGy	Decreased absorption between 360-370 nm Increased absorption between 400-430 nm and 550-560 nm.	25 kGy	Unaltered
	50 kGy	Decreased absorption between 360-370 nm Increased absorption between 400-480 nm and 550-600 nm.	50 kGy	Unaltered

B.5.2 Electron Beam Sterilization

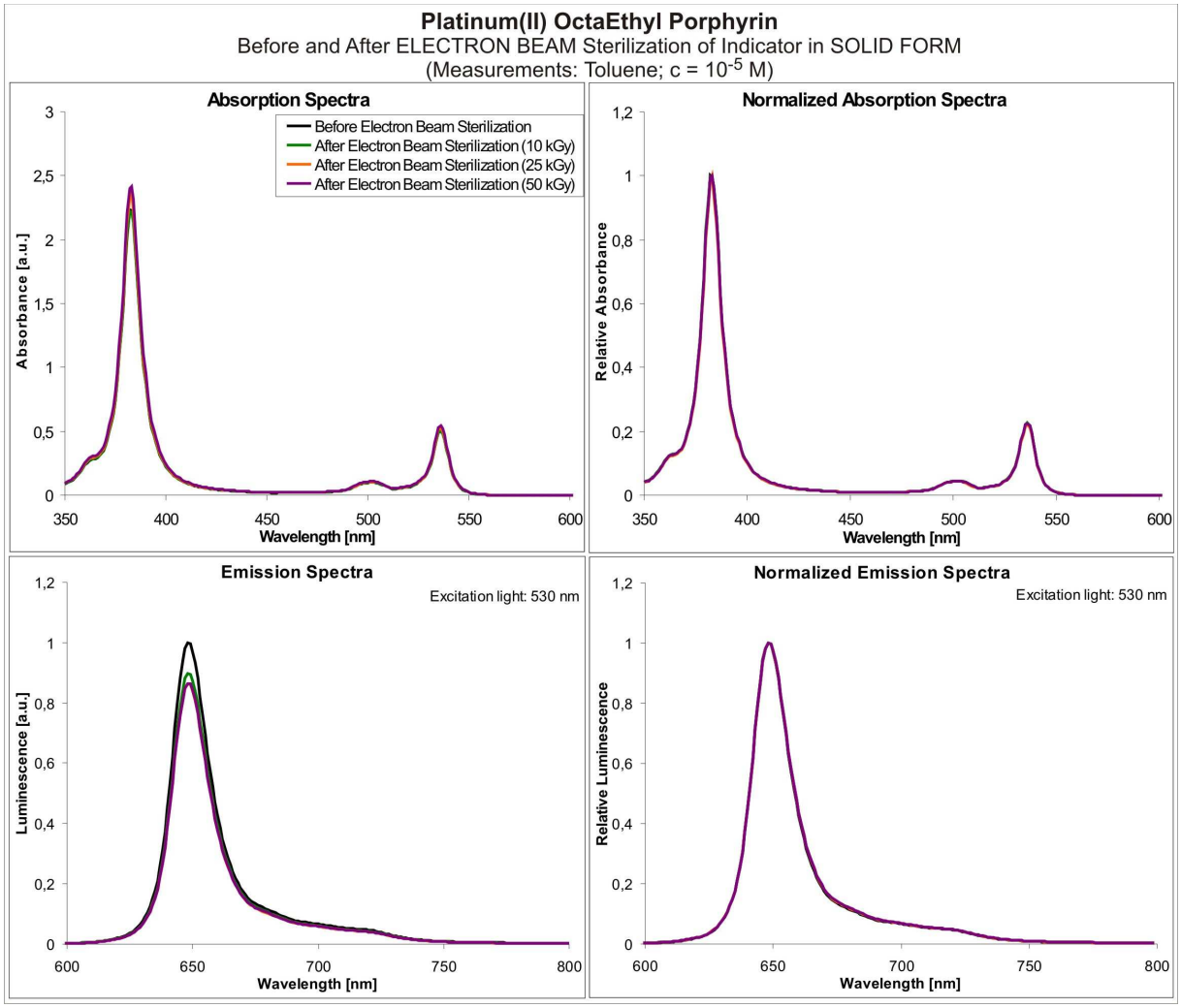

E-BEAM/SOLID STATE	Absorption Spectra		Emission Spectra	
Alterations in Absorption/Emission Intensity	10kGy	0,70% decrease	10kGy	10,13% decrease
	25 kGy	5,81% increase	25 kGy	13,55% decrease
	50 kGy	7,47% increase	50 kGy	13,55% decrease
Alterations in Absorption/Emission Curve Form	10kGy	Unaltered	10kGy	Unaltered
	25 kGy	Unaltered	25 kGy	Unaltered
	50 kGy	Unaltered	50 kGy	Unaltered

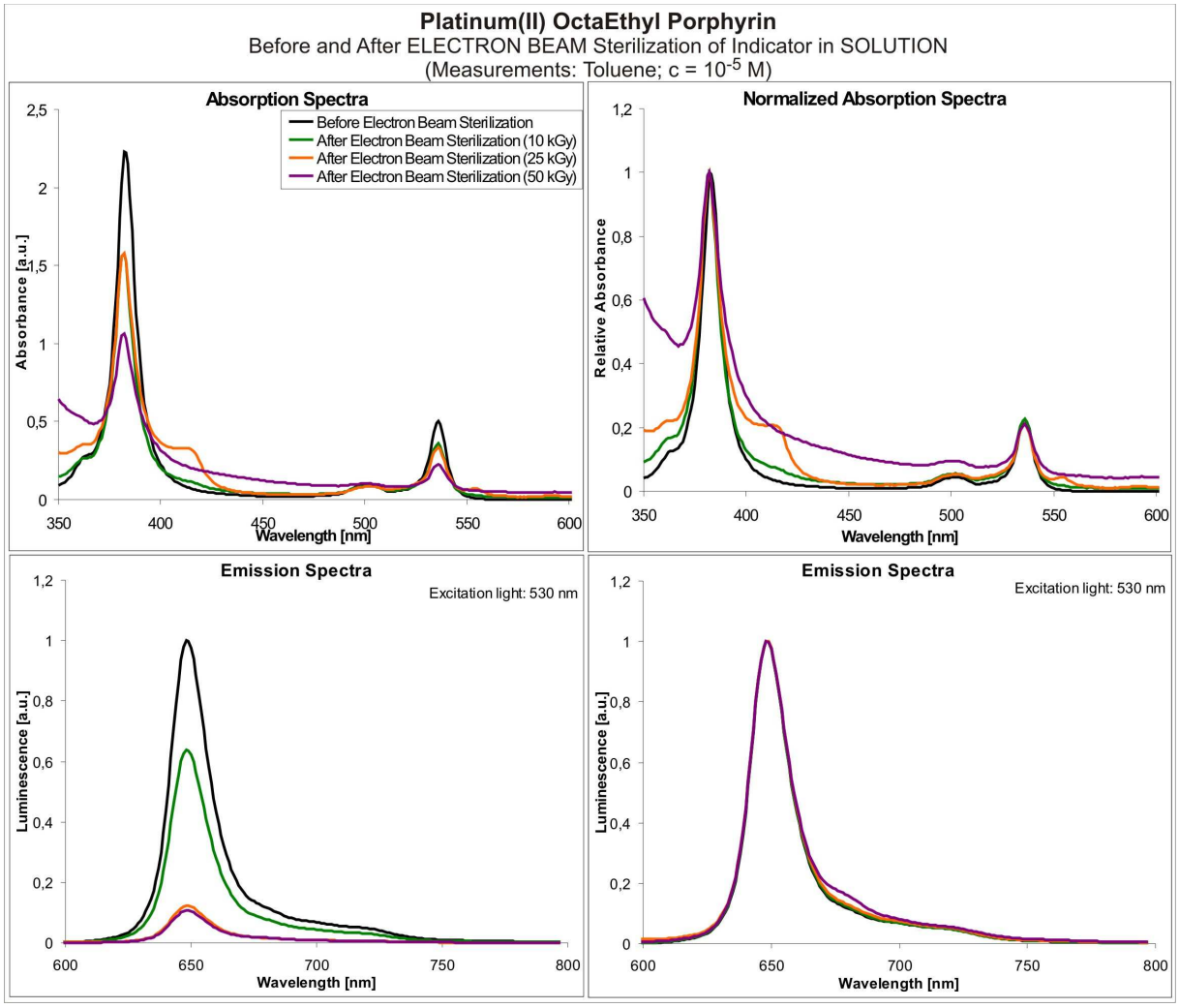

E-BEAM/SOLUTION	Absorption Spectra		Emission Spectra	
Alterations in Absorption/Emission Intensity	10kGy	9,97% decrease	10kGy	36,09% decrease
	25 kGy	17,03% decrease	25 kGy	87,75% decrease
	50 kGy	37,29% decrease	50 kGy	89,32% decrease
Alterations in Absorption/Emission Curve Form	10kGy	Increased absorption between 350-370 nm; 400-440 nm and 545-570 nm.	10kGy	Unaltered
	25 kGy	Increased absorption between 350-370 nm. Altered – 2 new peak s with $\lambda_{max(1)}$=414nm, $\lambda_{max(2)}$=553nm;	25 kGy	Unaltered
	50 kGy	Increased absorption between 350-380 nm; 390-520 nm and 540-800 nm.	50 kGy	Increased emission between 670-700 nm.

B.6 Platinum(II) meso-tetra(4-FluoroPhenyl) TetraBenzoPorphyrin (=PtTPTBPF)

B.6.1 Gamma Sterilization

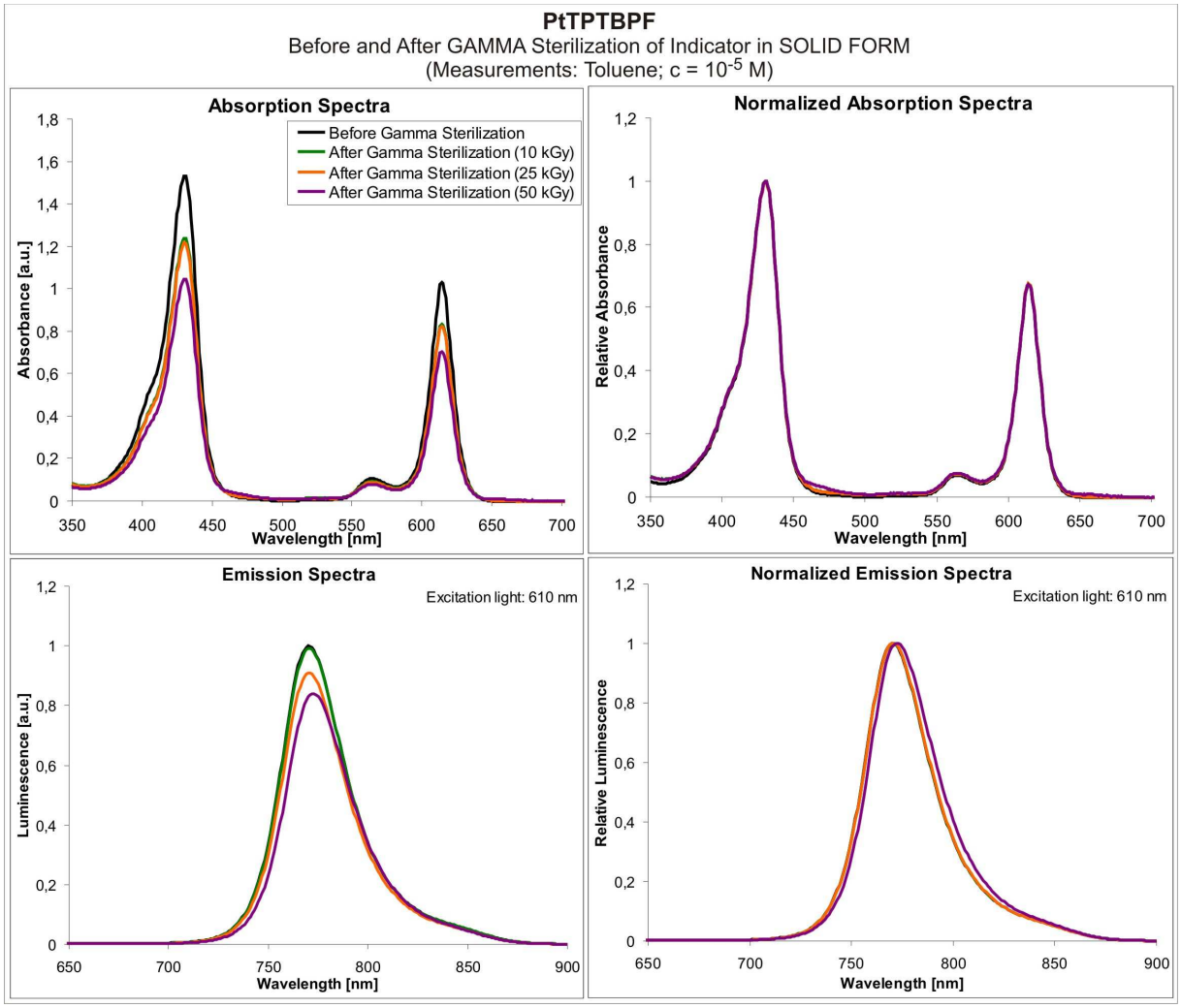

GAMMA/SOLID STATE	Absorption Spectra		Emission Spectra	
Alterations in Absorption/Emission Intensity	10kGy	19,03% decrease	10kGy	0,78% decrease
	25 kGy	20,36% decrease	25 kGy	9,20% decrease
	50 kGy	31,56% decrease	50 kGy	16,07% decrease
Alterations in Absorption/Emission Curve Form	10kGy	Unaltered	10kGy	Unaltered
	25 kGy	Unaltered	25 kGy	Unaltered
	50 kGy	Increased absorption between 455-480 nm.	50 kGy	Bathochromic shift of λ_{max} for 2 nm.

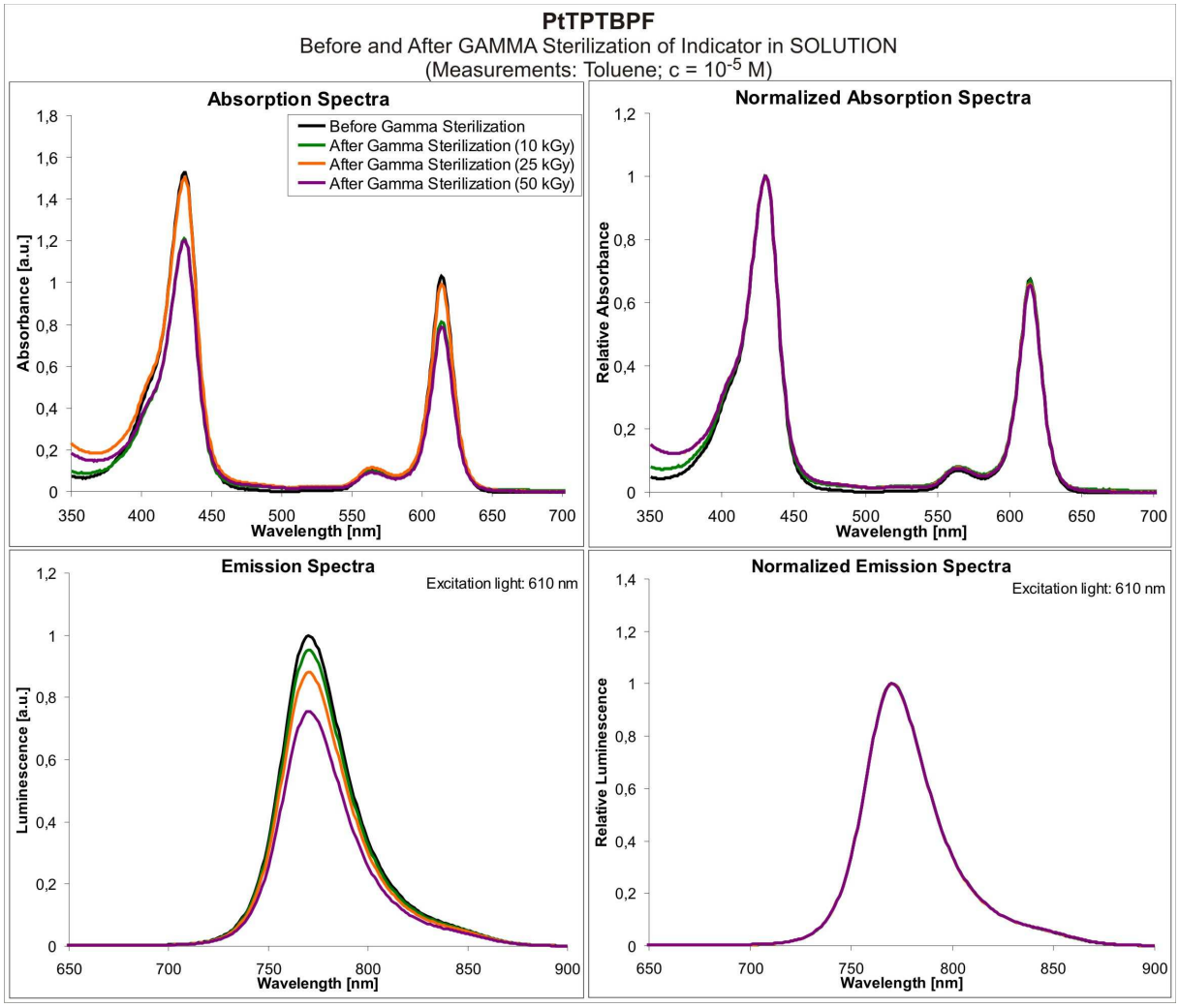

GAMMA/SOLUTION	Absorption Spectra		Emission Spectra	
Alterations in Absorption/Emission Intensity	10kGy	20,89% decrease	10kGy	4,75% decrease
	25 kGy	1,66% decrease	25 kGy	11,79% decrease
	50 kGy	21,31% decrease	50 kGy	24,43% decrease
Alterations in Absorption/Emission Curve Form	10kGy	Increased absorption between 350-390 nm and 455-500 nm.	10kGy	Unaltered
	25 kGy	Increased absorption between 350-390 nm and 455-500 nm.	25 kGy	Unaltered
	50 kGy	Increased absorption between 350-390 nm and 455-500 nm.	50 kGy	Unaltered

B.6.2 Electron Beam Sterilization

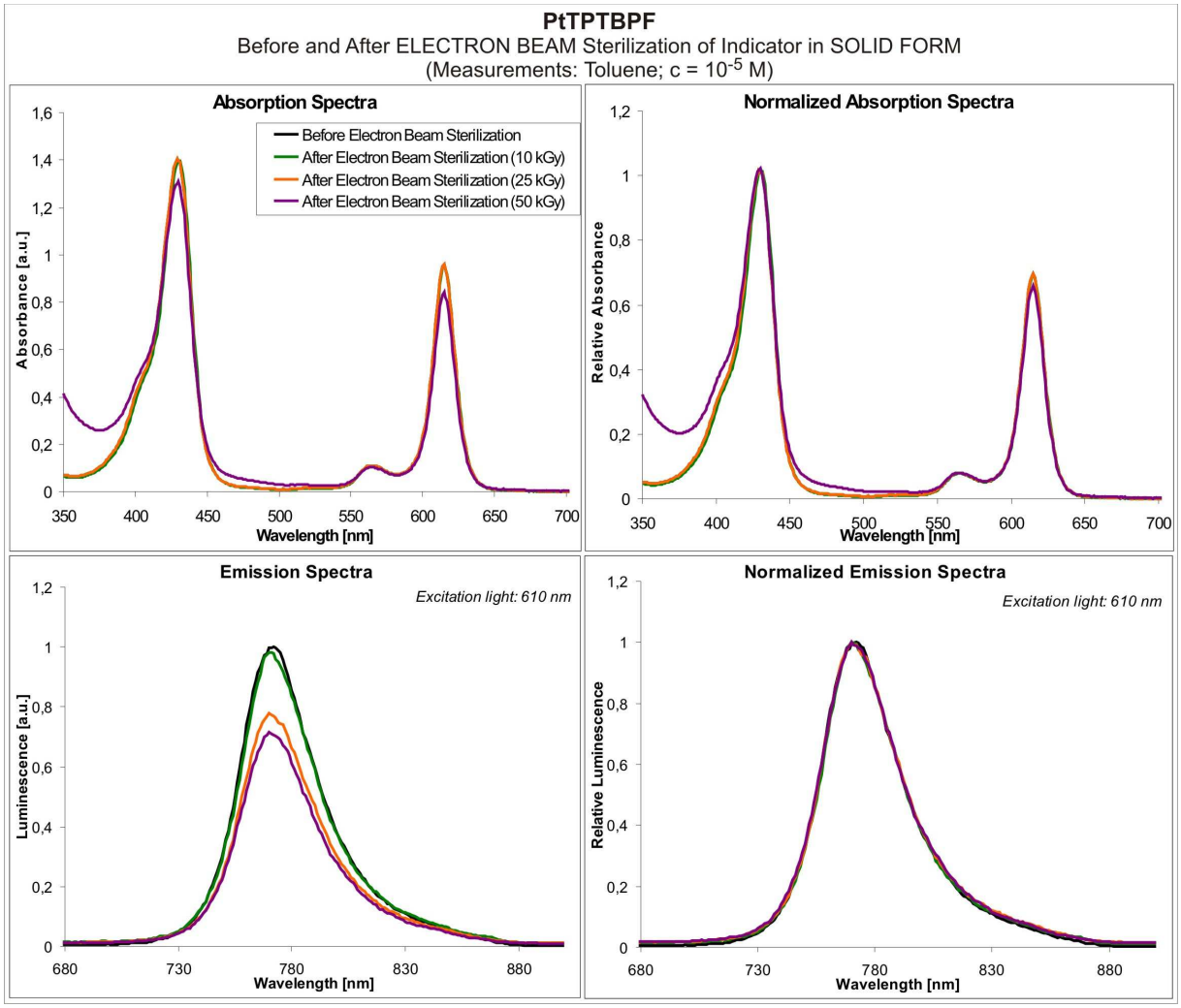

E-BEAM/SOLID STATE	Absorption Spectra		Emission Spectra	
Alterations in Absorption/Emission Intensity	10kGy	0,41% decrease	10kGy	1,71% decrease
	25 kGy	0,22% decrease	25 kGy	22,24% decrease
	50 kGy	6,68% decrease	50 kGy	28,48% decrease
Alterations in Absorption/Emission Curve Form	10kGy	Unaltered	10kGy	Unaltered
	25 kGy	Unaltered	25 kGy	Unaltered
	50 kGy	Increased absorption between 350-410 nm and 450-515 nm.	50 kGy	Unaltered

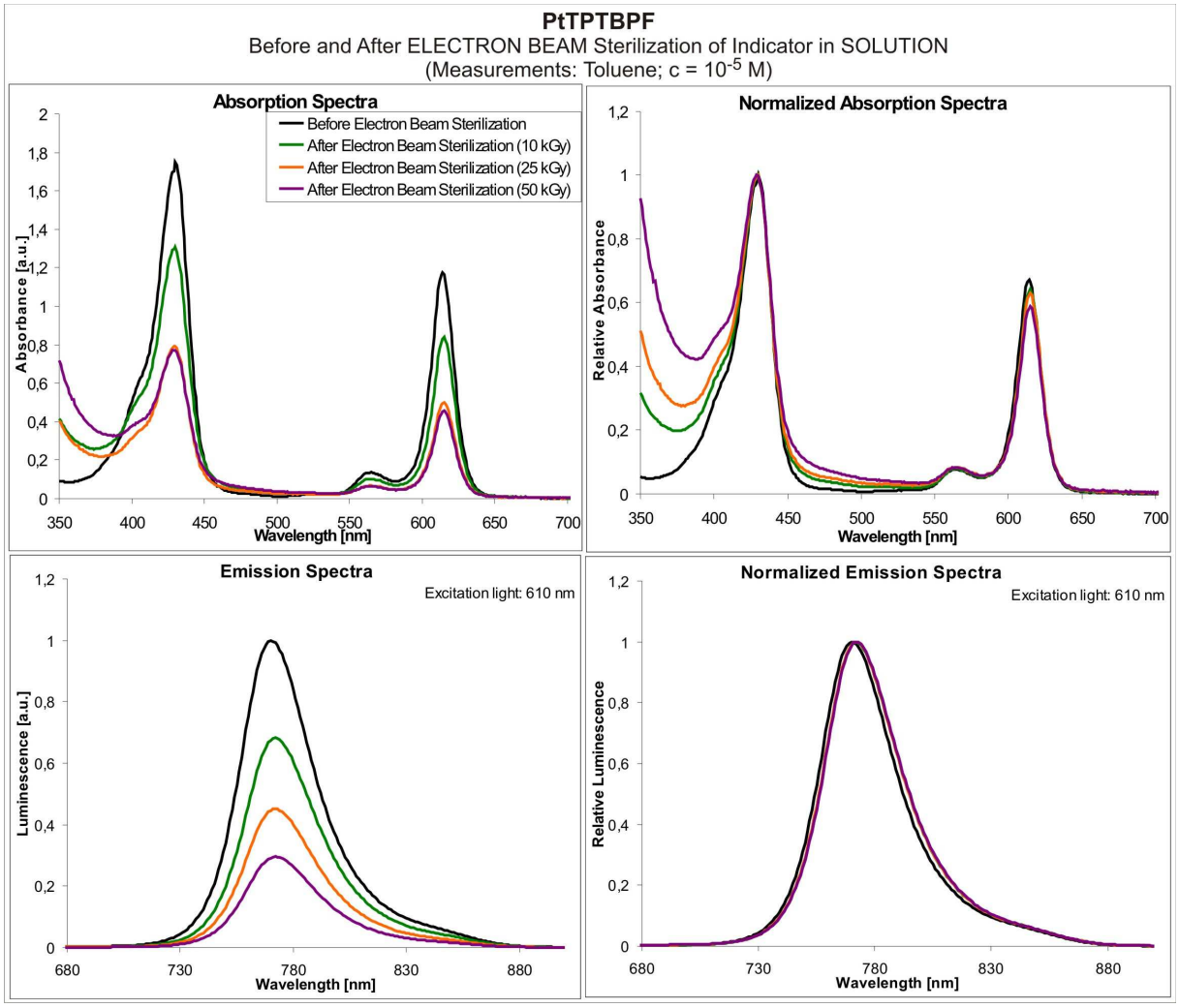

E-BEAM/SOLUTION	Absorption Spectra		Emission Spectra	
Alterations in Absorption/Emission Intensity	10kGy	25,10% decrease	10kGy	31,71% decrease
	25 kGy	54,62% decrease	25 kGy	54,92% decrease
	50 kGy	55,77% decrease	50 kGy	70,46% decrease
Alterations in Absorption/Emission Curve Form	10kGy	Increased absorption between 350-415 nm and 450-550 nm.	10kGy	Bathochromic shift of λ_{max} for 2 nm.
	25 kGy	Increased absorption between 350-415 nm and 450-550 nm.	25 kGy	Bathochromic shift of λ_{max} for 2 nm.
	50 kGy	Increased absorption between 350-415 nm and 450-550 nm.	50 kGy	Bathochromic shift of λ_{max} for 2 nm.

B.7 Palladium(II) meso-tetra(4-FluoroPhenyl) TetraBenzoPorphyrin (=PdTPTBPF)

B.7.1 Gamma Sterilization

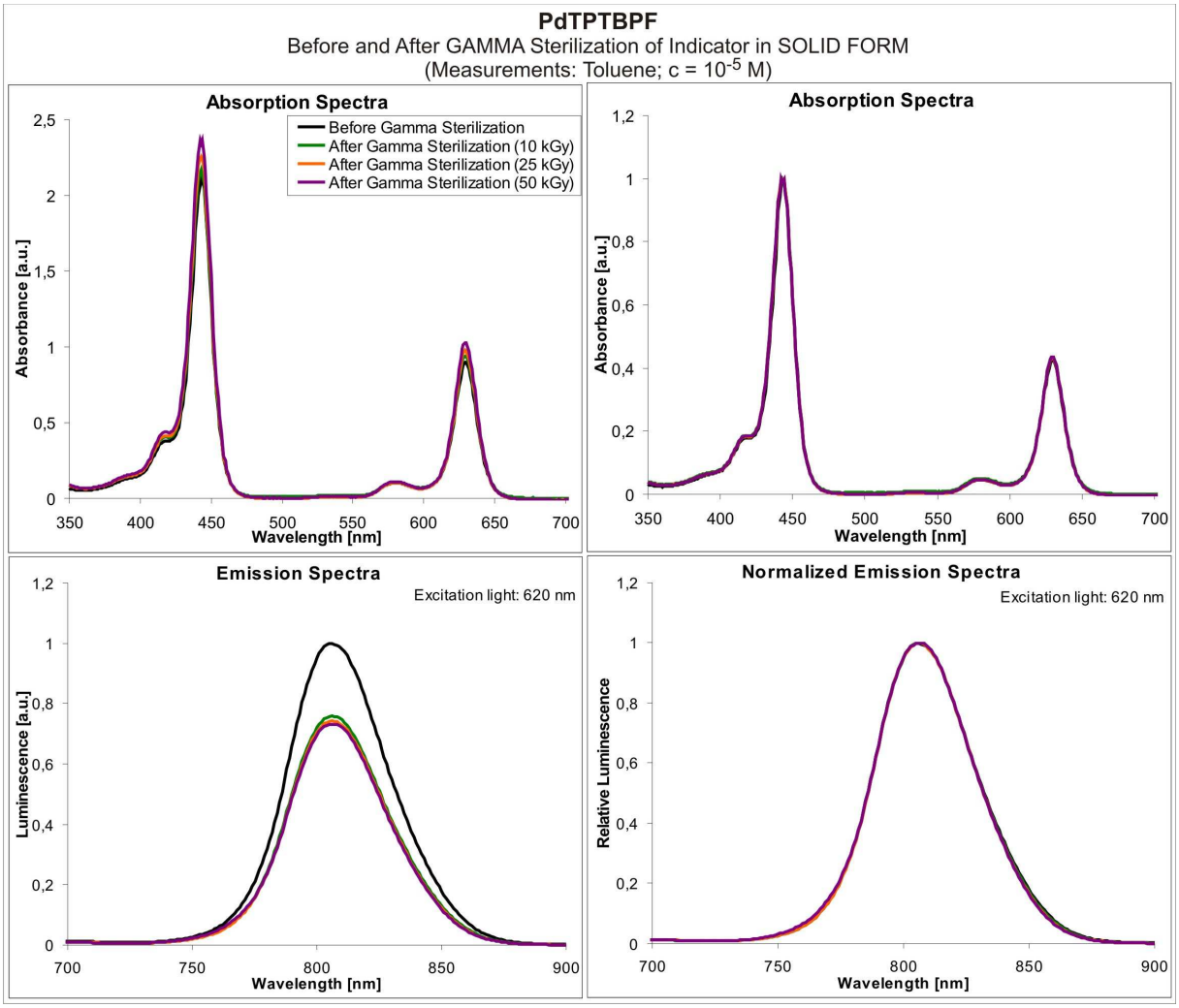

GAMMA/SOLID STATE	Absorption Spectra		Emission Spectra	
Alterations in Absorption/Emission Intensity	10kGy	2,19% increase	10kGy	24,19% decrease
	25 kGy	6,11% increase	25 kGy	25,67% decrease
	50 kGy	10,39% increase	50 kGy	26,77% decrease
Alterations in Absorption/Emission Curve Form	10kGy	Unaltered	10kGy	Unaltered
	25 kGy	Unaltered.	25 kGy	Unaltered
	50 kGy	Unaltered	50 kGy	Unaltered

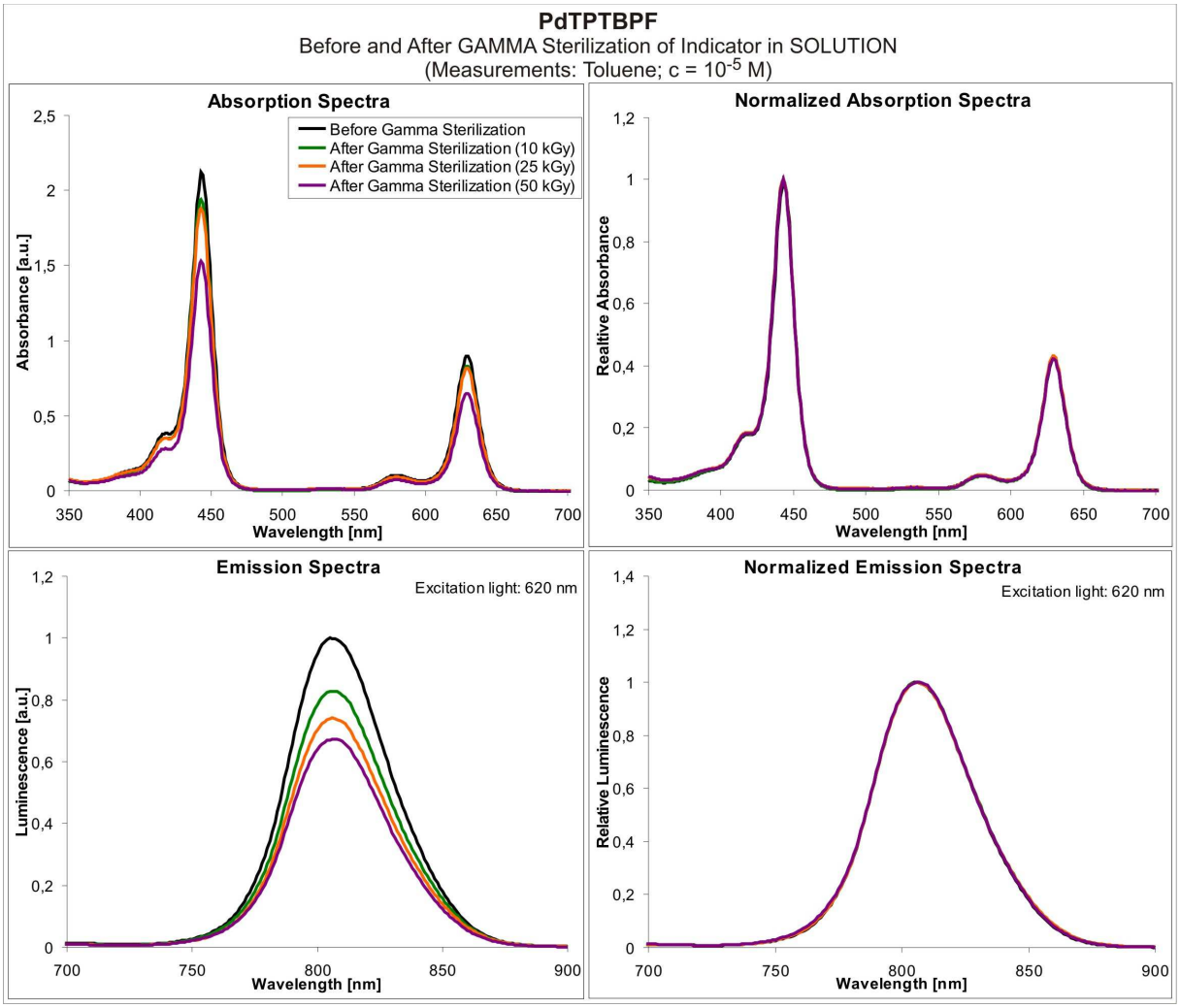

GAMMA/SOLUTION	Absorption Spectra		Emission Spectra	
Alterations in Absorption/Emission Intensity	10kGy	8,57% decrease	10kGy	17,22% decrease
	25 kGy	11,42% decrease	25 kGy	25,89% decrease
	50 kGy	27,81% decrease	50 kGy	32,69% decrease
Alterations in Absorption/Emission Curve Form	10kGy	Unaltered	10kGy	Unaltered
	25 kGy	Unaltered.	25 kGy	Unaltered
	50 kGy	Unaltered	50 kGy	Unaltered

B.7.2 Electron Beam Sterilization

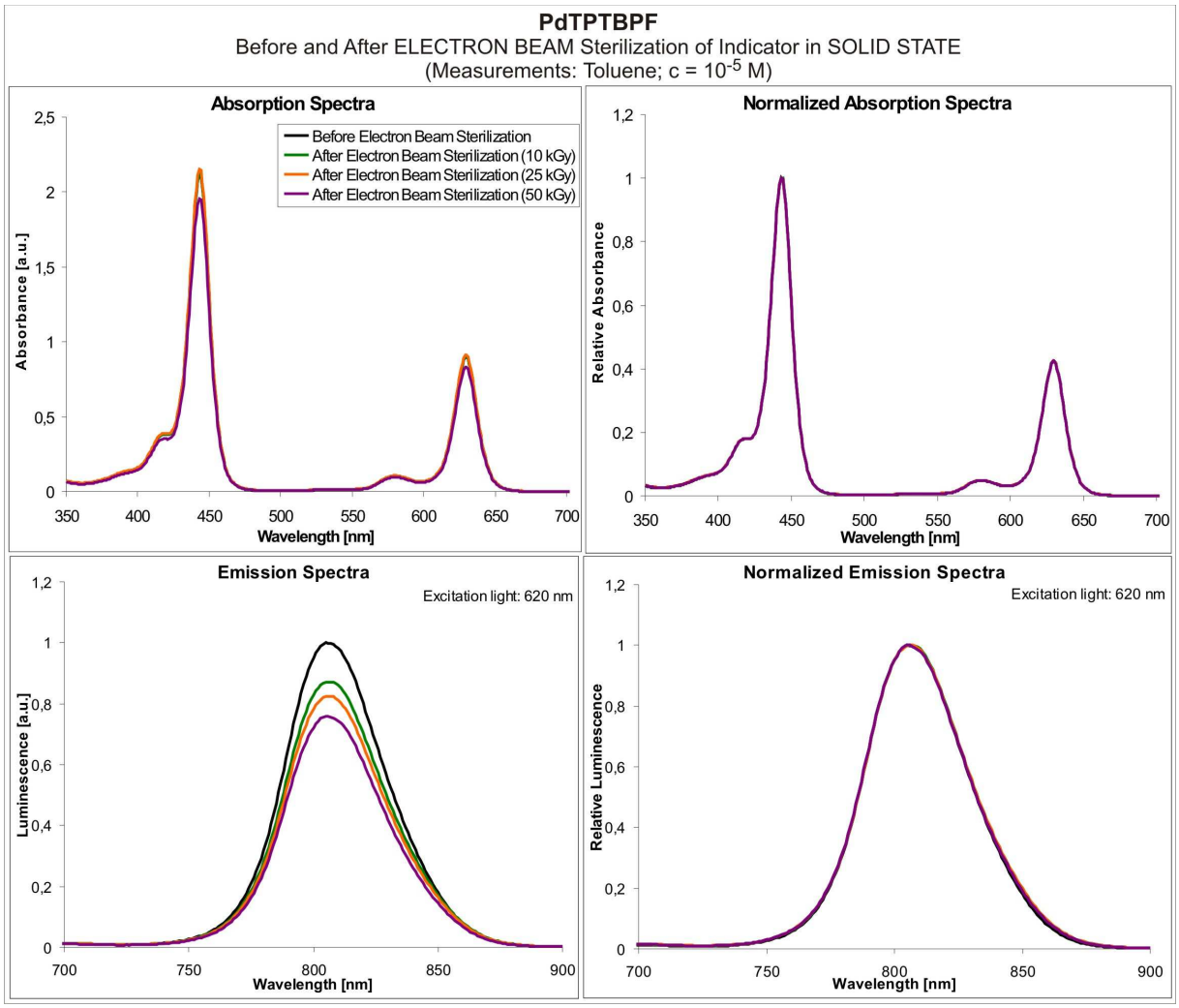

E-BEAM/SOLID STATE	Absorption Spectra		Emission Spectra	
Alterations in Absorption/Emission Intensity	10kGy	0,11% increase	10kGy	12,89% decrease
	25 kGy	1,45% increase	25 kGy	17,61% decrease
	50 kGy	7,81% decrease	50 kGy	24,08% decrease
Alterations in Absorption/Emission Curve Form	10kGy	Unaltered	10kGy	Unaltered
	25 kGy	Unaltered.	25 kGy	Unaltered
	50 kGy	Unaltered	50 kGy	Unaltered

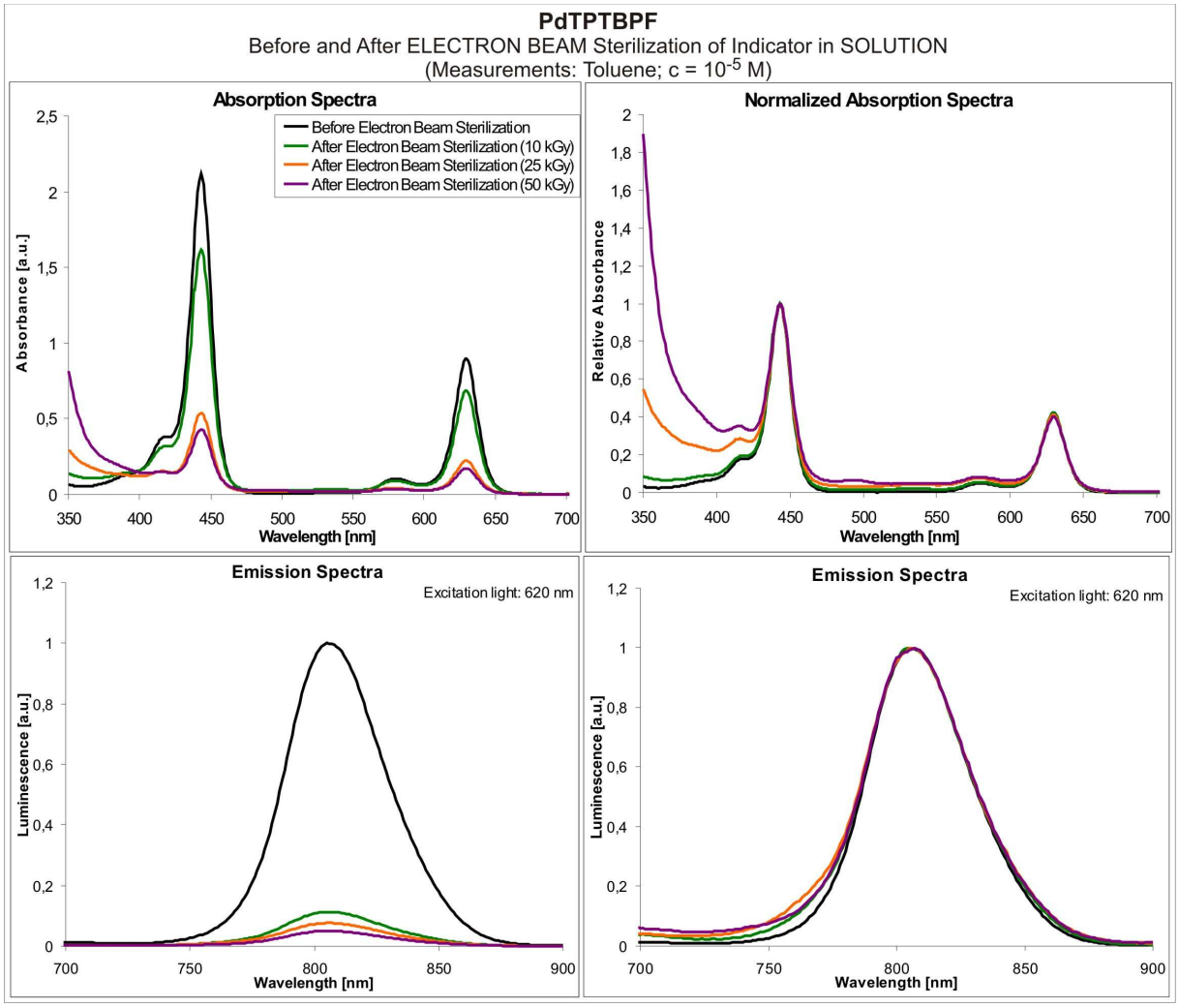

E-BEAM/SOLUTION	Absorption Spectra		Emission Spectra	
Alterations in Absorption/Emission Intensity	10kGy	23,65% decrease	10kGy	88,73% decrease
	25 kGy	74,55% decrease	25 kGy	92,37% decrease
	50 kGy	79,77% decrease	50 kGy	94,98% decrease
Alterations in Absorption/Emission Curve Form	10kGy	Increased absorption between 350-390 nm	10kGy	Changed curve form between 700-780 nm
	25 kGy	Increased absorption between 350-390 nm	25 kGy	Changed curve form between 700-780 nm
	50 kGy	Increased absorption between 350-390 nm	50 kGy	Changed curve form between 700-780 nm

B.8 Ruthenium(II)-tris-4,7-diphenyl-1,10-phenanthroline dichloride (=$Ru(dpp)_3Cl_2$)

B.8.1 Gamma Sterilization

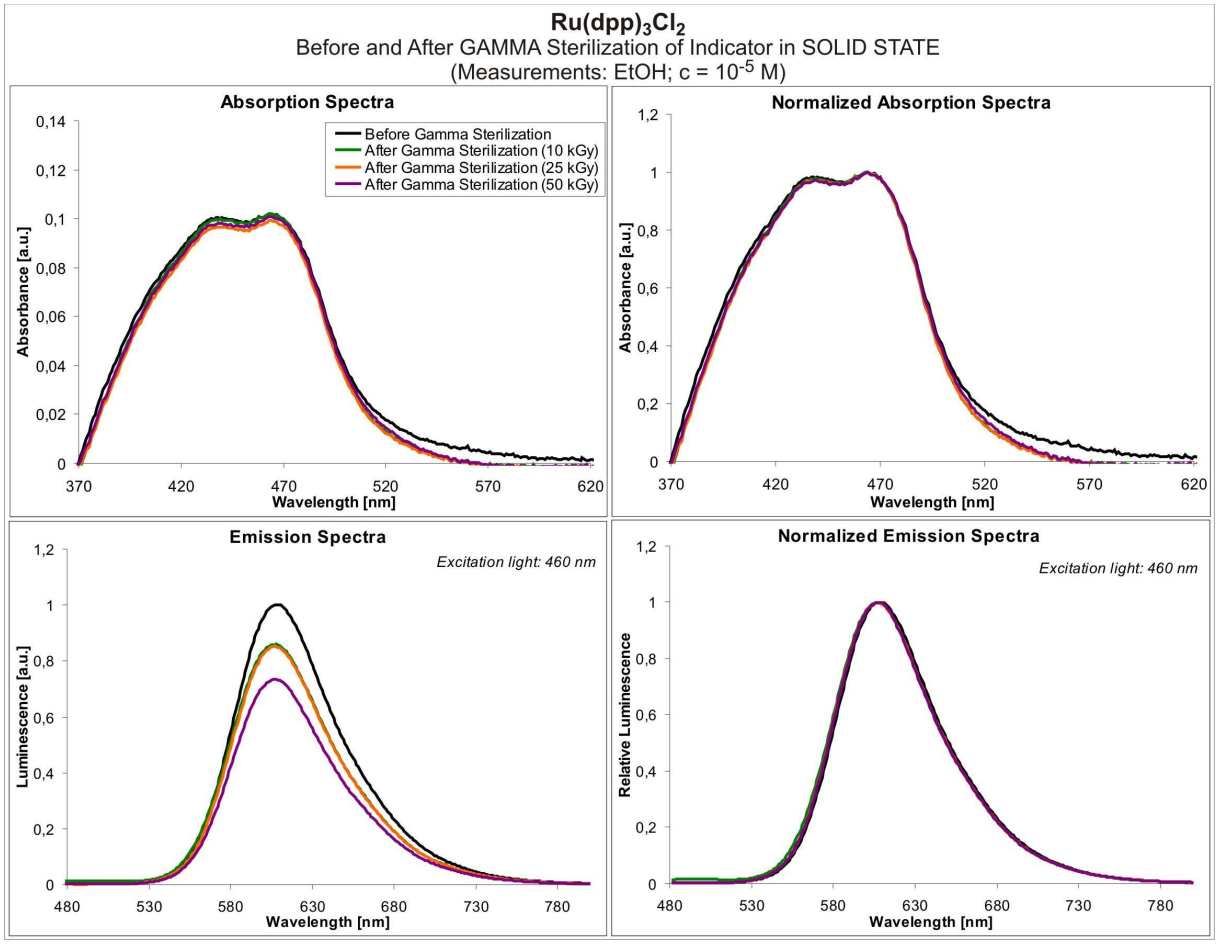

GAMMA/SOLID STATE	Absorption Spectra		Emission Spectra	
Alterations in Absorption/Emission Intensity	10kGy	0,49% decrease	10kGy	14,00% decrease
	25 kGy	2,60% decrease	25 kGy	14,73% decrease
	50 kGy	1,05% decrease	50 kGy	26,53% decrease
Alterations in Absorption/Emission Curve Form	10kGy	Decreased absorption between 520-620 nm	10kGy	Unaltered
	25 kGy	Decreased absorption between 520-620 nm	25 kGy	Unaltered
	50 kGy	Decreased absorption between 520-620 nm	50 kGy	Unaltered

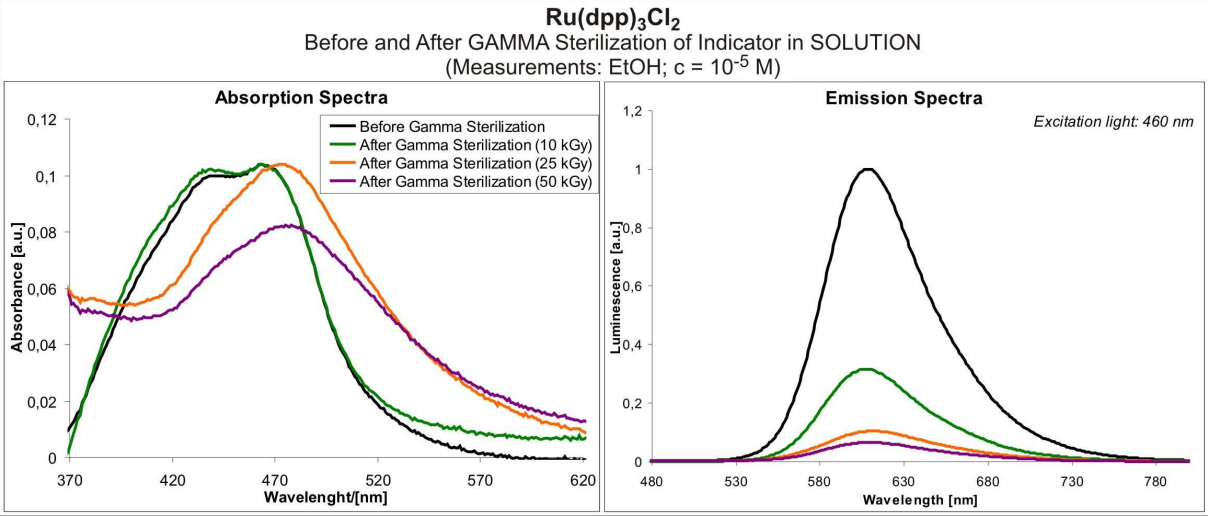

GAMMA/SOLUTION	Absorption Spectra		Emission Spectra	
Alterations in Absorption/Emission Intensity	10kGy	0,12% increase	10kGy	31,55% decrease
	25 kGy	/	25 kGy	89,52% decrease
	50 kGy	/	50 kGy	93,32% decrease
Alterations in Absorption/Emission Curve Form	10kGy	Increased absorption between 370-420 nm and 520-800 nm.		
	25 kGy	Disappearance of characteristic curve form of $Ru(dpp)_3Cl_2$ Altered – new peaks with λ_{max} = 472 nm – bathochromic shift of the absorption maximum for 13 nm.		
	50 kGy	Disappearance of characteristic curve form of $Ru(dpp)_3Cl_2$ Altered – new peaks with λ_{max} = 475 nm – bathochromic shift of the absorption maximum for 16 nm.		

B.8.2 Electron Beam Sterilization

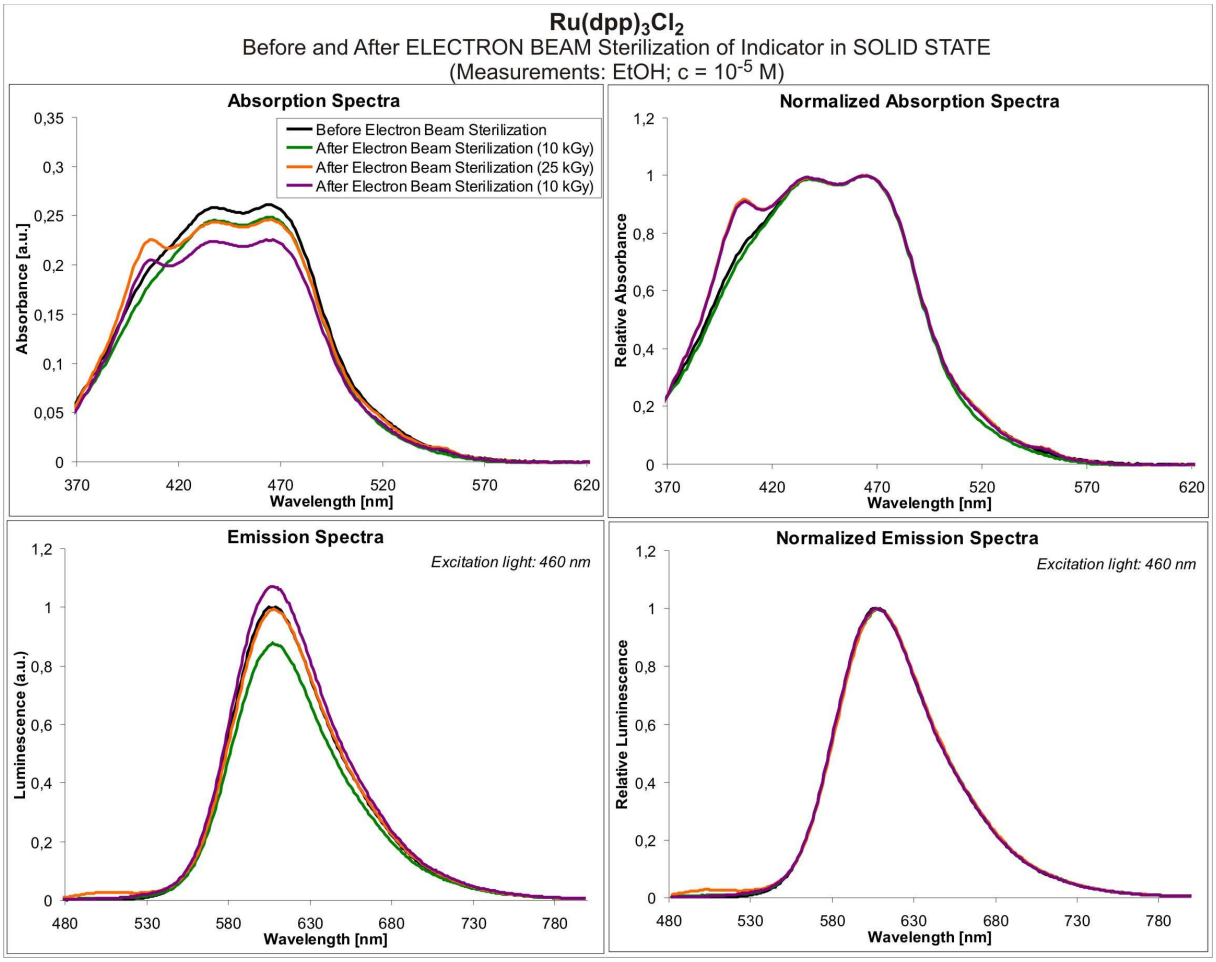

GAMMA/SOLID STATE	Absorption Spectra		Emission Spectra	
Alterations in Absorption/Emission Intensity	10kGy	4,82% decrease	10kGy	12,22% decrease
	25 kGy	5,84% decrease	25 kGy	0,69% decrease
	50 kGy	13,66% decrease	50 kGy	6,74% increase
Alterations in Absorption/Emission Curve Form	10kGy	Unaltered	10kGy	Unaltered
	25 kGy	Altered – new peak with λ_{max} = 405 nm	25 kGy	Unaltered
	50 kGy	Altered – new peak with λ_{max} = 405 nm	50 kGy	Unaltered

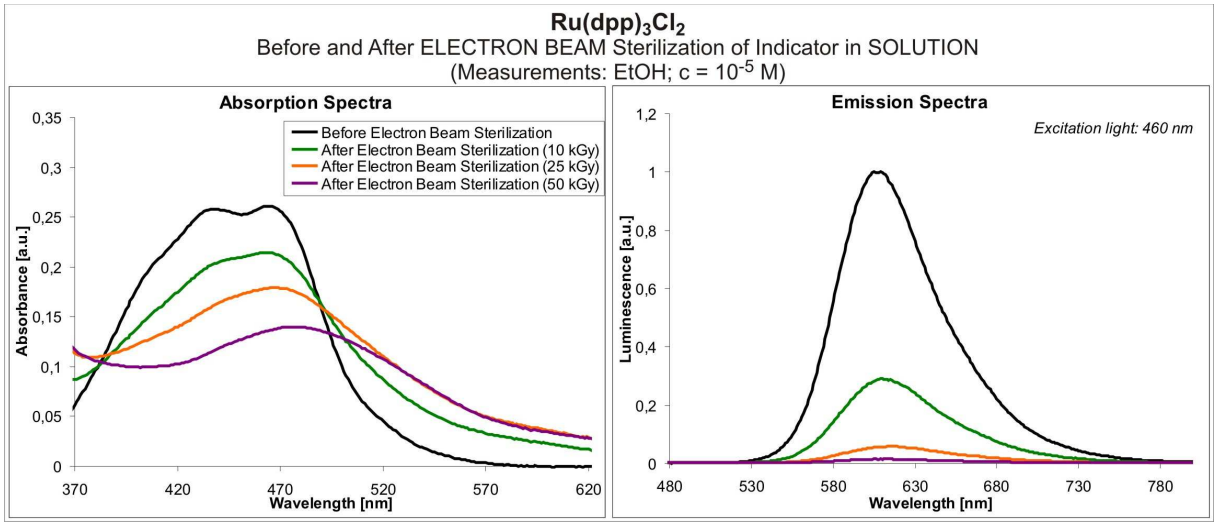

E-BEAM/SOLUTION	Absorption Spectra		Emission Spectra	
Alterations in Absorption/Emission Intensity	10kGy	Decrease	10kGy	70,91% decrease
	25 kGy	Decrease	25 kGy	94,20% decrease
	50 kGy	Decrease	50 kGy	98,47% decrease
Alterations in Absorption/Emission Curve Form	10kGy	Disappearance of characteristic curve form of $Ru(dpp)_3Cl_2$ Increased absorption between 490-800 nm		
	25 kGy	Disappearance of characteristic curve form of $Ru(dpp)_3Cl_2$ Altered –bathochromic shift of the absorption maximum for 4 nm.		
	50 kGy	Disappearance of characteristic curve form of $Ru(dpp)_3Cl_2$ Altered – new peaks with λ_{max} = 475 nm – bathochromic shift of the absorption maximum for 16 nm.		

B.9 DiChloroTris(1,10-Phenanthroline) Ruthenium(II) Hydrate

B.9.1 Gamma Sterilization

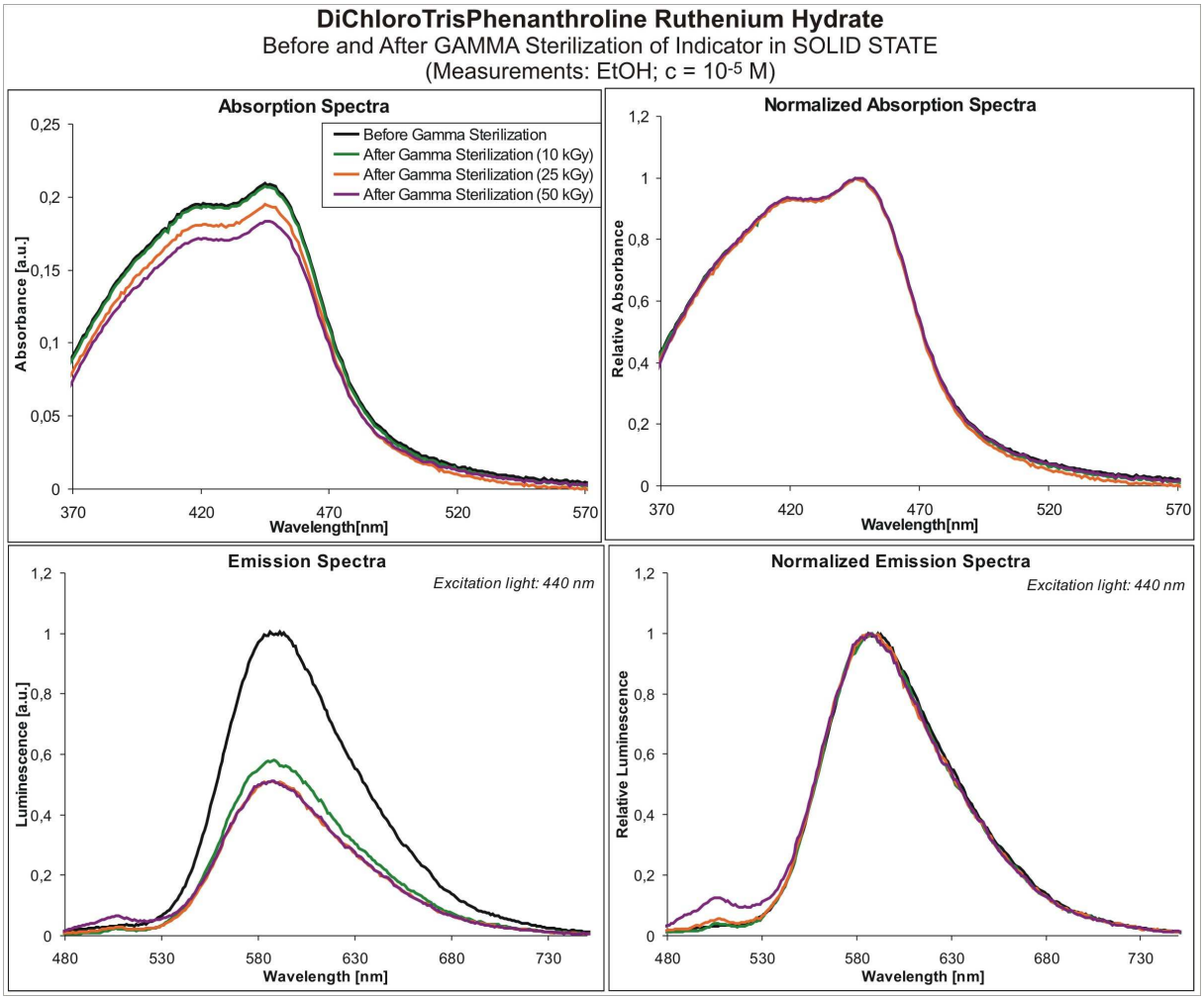

GAMMA/SOLID STATE	Absorption Spectra		Emission Spectra	
Alterations in Absorption/Emission Intensity	10kGy	0,95% decrease	10kGy	42,29% decrease
	25 kGy	6,98% decrease	25 kGy	49,20% decrease
	50 kGy	12,54% decrease	50 kGy	49,08% decrease
Alterations in Absorption/Emission Curve Form	10kGy	Unaltered	10kGy	Unaltered
	25 kGy	Unaltered	25 kGy	Altered – new peaks with λ_{max} = 509 nm
	50 kGy	Unaltered	50 kGy	Altered – new peaks with λ_{max} = 509 nm

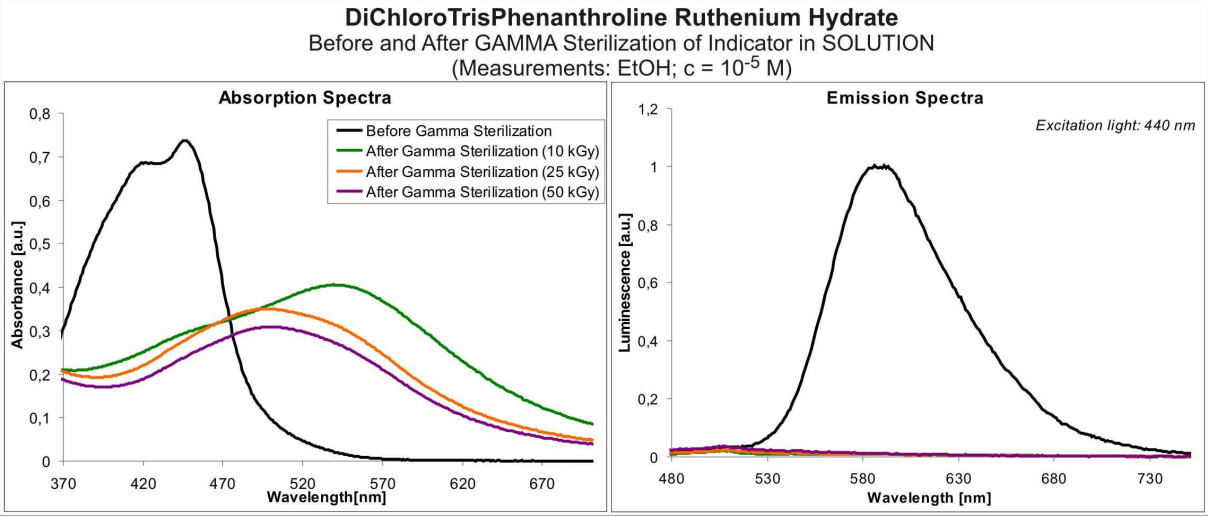

GAMMA/SOLUTION	Absorption Spectra		Emission Spectra	
Alterations in Absorption/Emission Intensity	10kGy	Decrease	10kGy	70,91% decrease
	25 kGy	Decrease	25 kGy	94,20% decrease
	50 kGy	Decrease	50 kGy	98,47% decrease
Alterations in Absorption/Emission Curve Form	10kGy	Disappearance of characteristic curve form of $Ru(dpp)_3Cl_2$ Altered – new peaks with λ_{max} = 540 nm – bathochromic shift of the absorption maximum for 96 nm The new colour of solution is deep purple		
	25 kGy	Disappearance of characteristic curve form of $Ru(dpp)_3Cl_2$ Altered – new peaks with λ_{max} = 493 nm – bathochromic shift of the absorption maximum for 49 nm. The new colour of solution is deep purple		
	50 kGy	Disappearance of characteristic curve form of $Ru(dpp)_3Cl_2$ Altered – new peaks with λ_{max} = 496 nm – bathochromic shift of the absorption maximum for 52 nm. The new colour of solution is deep purple		

B.9.2 Electron Beam Sterilization

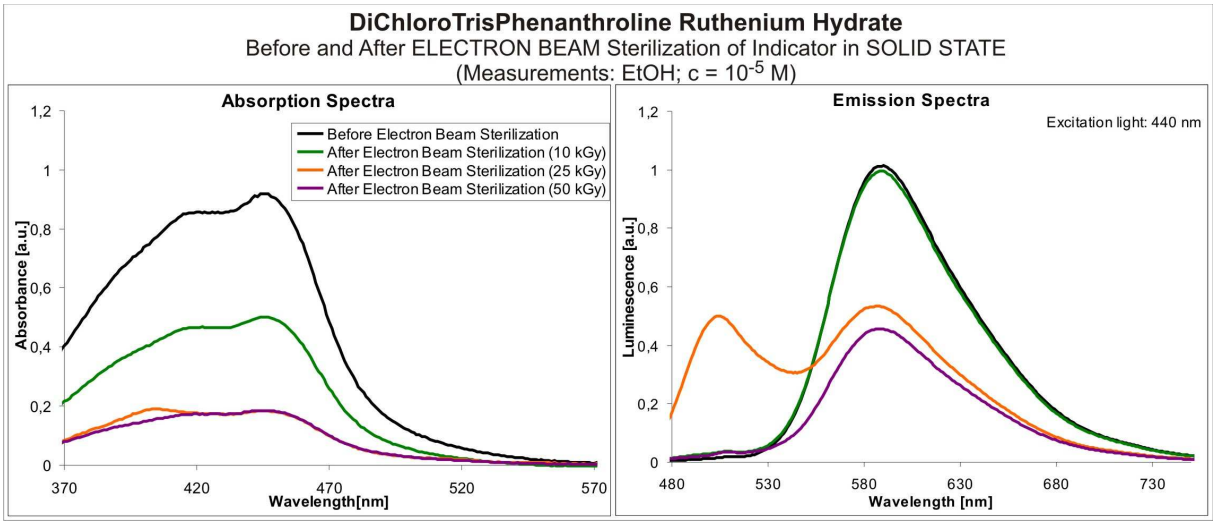

E-BEAM/SOLID STATE	Absorption Spectra		Emission Spectra	
Alterations in Absorption/Emission Intensity	10kGy	45,35% decrease	10kGy	1,83% decrease
	25 kGy	79,81% decrease	25 kGy	47,24% decrease
	50 kGy	79,82% decrease	50 kGy	55,16% decrease
Alterations in Absorption/Emission Curve Form	10kGy		10kGy	Unaltered
	25 kGy	Altered – new peaks with λ_{max} = 509 nm	25 kGy	Altered – new peaks with λ_{max} = 504 nm
	50 kGy		50 kGy	

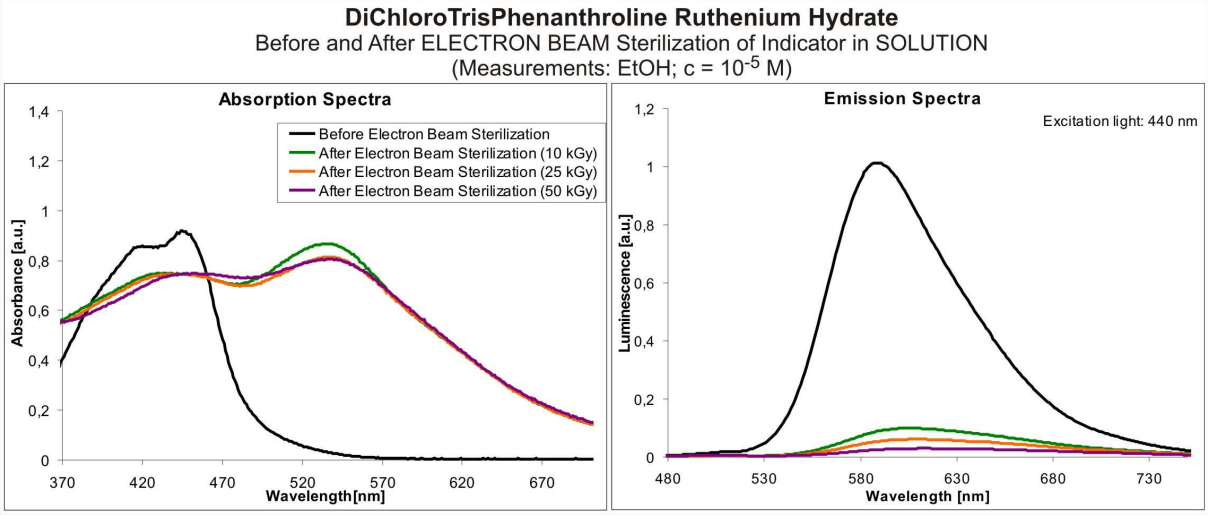

E-BEAM/SOLUTION	Absorption Spectra		Emission Spectra	
Alterations in Absorption/Emission Intensity			10kGy	90,16% decrease
			25 kGy	93,91% decrease
			50 kGy	97,03% decrease
Alterations in Absorption/Emission Curve Form	10kGy	Disappearance of characteristic curve form of $Ru(dpp)_3Cl_2$ Altered – new peaks with λ_{max} = 534 nm – bathochromic shift of the absorption maximum for 90 nm. The new colour of solution is deep purple		
	25 kGy	Disappearance of characteristic curve form of $Ru(dpp)_3Cl_2$ Altered – new peaks with λ_{max} = 534 nm – bathochromic shift of the absorption maximum for 90 nm. The new colour of solution is deep purple		
	50 kGy	Disappearance of characteristic curve form of $Ru(dpp)_3Cl_2$ Altered – new peaks with λ_{max} = 534 nm – bathochromic shift of the absorption maximum for 90 nm. The new colour of solution is deep purple		

B.10 1-HydroxyPyrene-3,6,8-tris-bis(2-Ethylhexyl)Sulfonamide (=HPTS(DHA)$_3$)

B.10.1 Gamma Sterilization

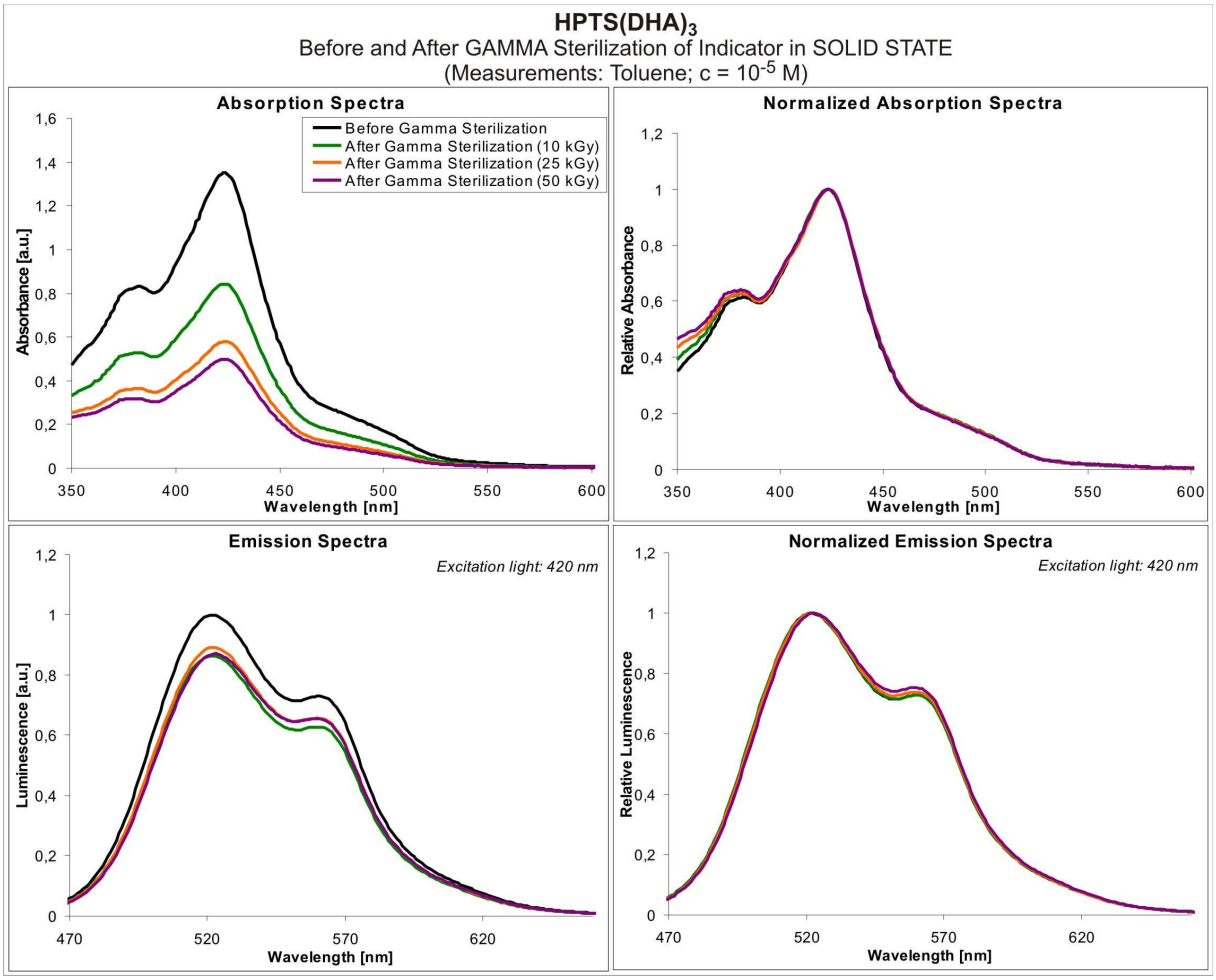

GAMMA/SOLID STATE	Absorption Spectra		Emission Spectra	
Alterations in Absorption/Emission Intensity	10kGy	37,67% decrease	10kGy	13,65% decrease
	25 kGy	57,08% decrease	25 kGy	10,92% decrease
	50 kGy	63,11% decrease	50 kGy	12,90% decrease
Alterations in Absorption/Emission Curve Form	10kGy	Altered between 350-380 nm	10kGy	Unaltered
	25 kGy	Altered between 350-380 nm	25 kGy	Altered between 550-565 nm
	50 kGy	Altered between 350-380 nm	50 kGy	Altered between 545-565 nm

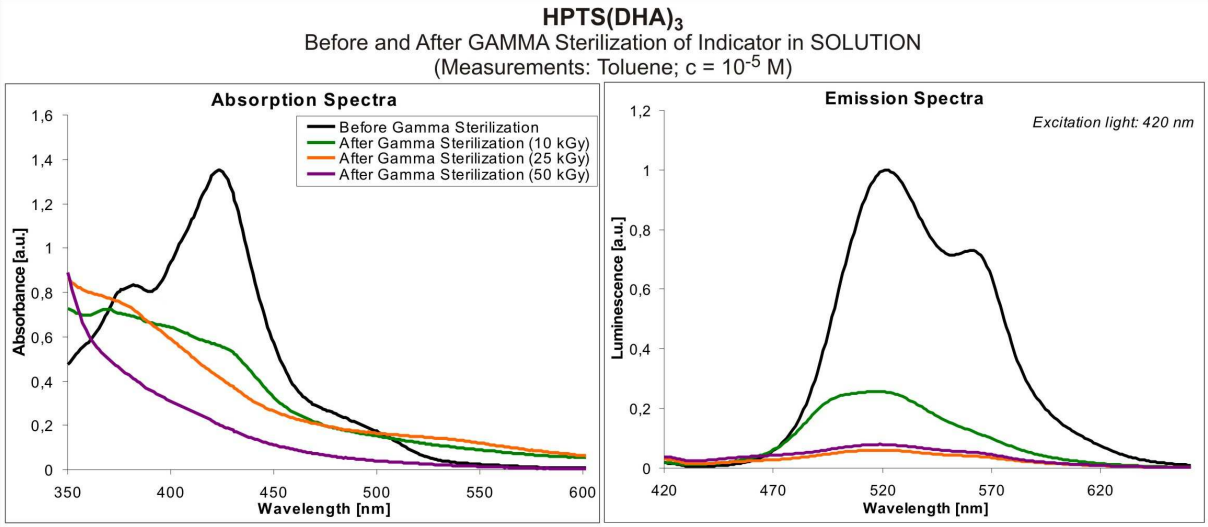

GAMMA/SOLUTION	Absorption Spectra		Emission Spectra	
Alterations in Absorption/Emission Intensity	10kGy	58,68% decrease	10kGy	74,39% decrease
	25 kGy	Decrease	25 kGy	Decrease
	50 kGy	Decrease	50 kGy	Decrease
Alterations in Absorption/Emission Curve Form	10kGy	Disappearance of characteristic curve form of $HPTS(DHA)_3$	10kGy	Disappearance of characteristic curve form of $HPTS(DHA)_3$
	25 kGy	Disappearance of characteristic curve form of $HPTS(DHA)_3$	25 kGy	Disappearance of characteristic curve form of $HPTS(DHA)_3$
	50 kGy	Disappearance of characteristic curve form of $HPTS(DHA)_3$	50 kGy	Disappearance of characteristic curve form of $HPTS(DHA)_3$

B.10.2 Electron Beam Sterilization

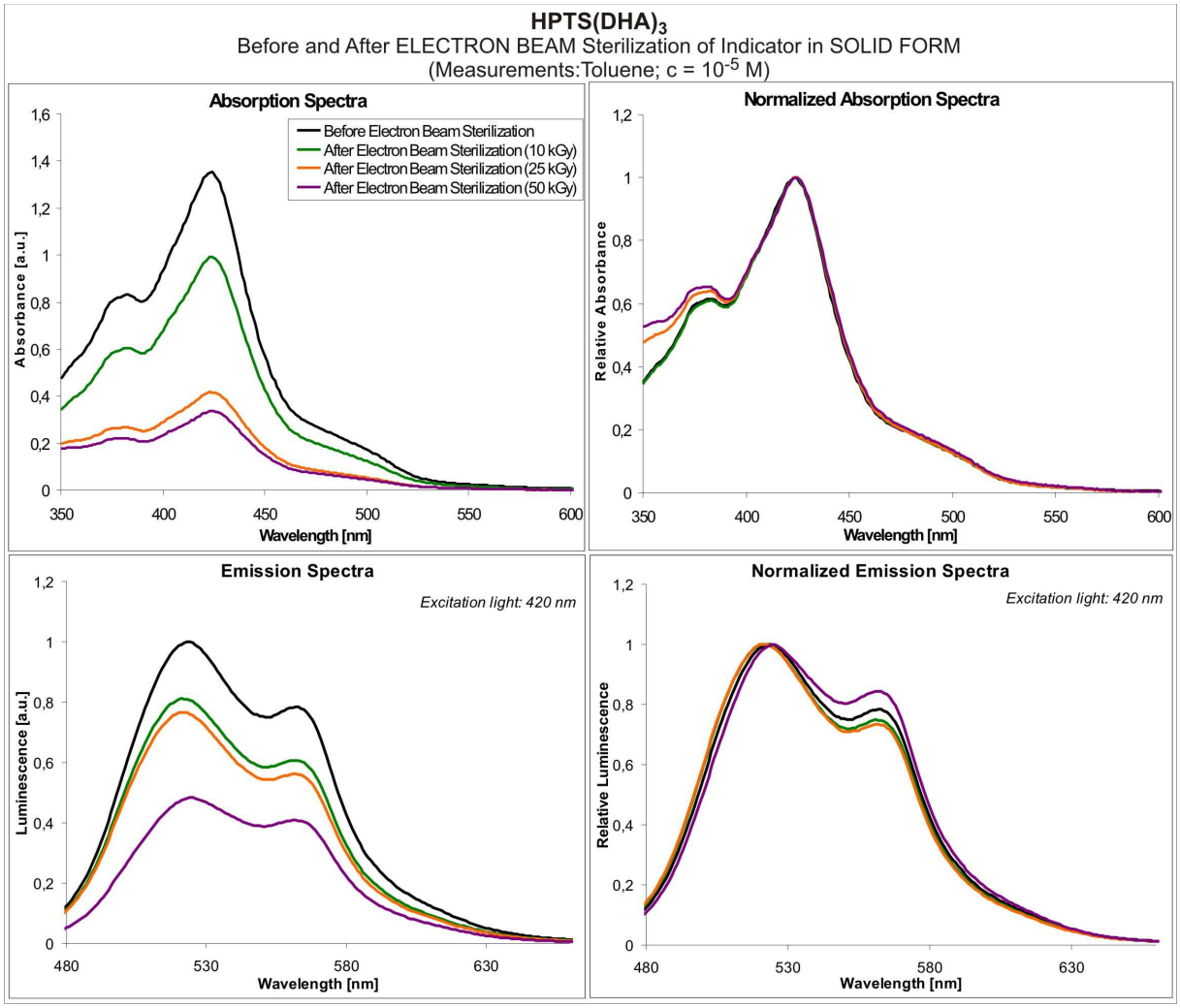

E-BEAM/SOLID STATE	Absorption Spectra		Emission Spectra	
Alterations in Absorption/Emission Intensity	10kGy	26,70% decrease	10kGy	18,84% decrease
	25 kGy	69,21% decrease	25 kGy	23,44% decrease
	50 kGy	75,12% decrease	50 kGy	51,61% decrease
Alterations in Absorption/Emission Curve Form	10kGy	Unaltered	10kGy	Altered between 540-570 nm
	25 kGy	Altered between 350-390 nm	25 kGy	Altered between 540-570 nm
	50 kGy	Altered between 350-390 nm	50 kGy	Altered between 530-575 nm

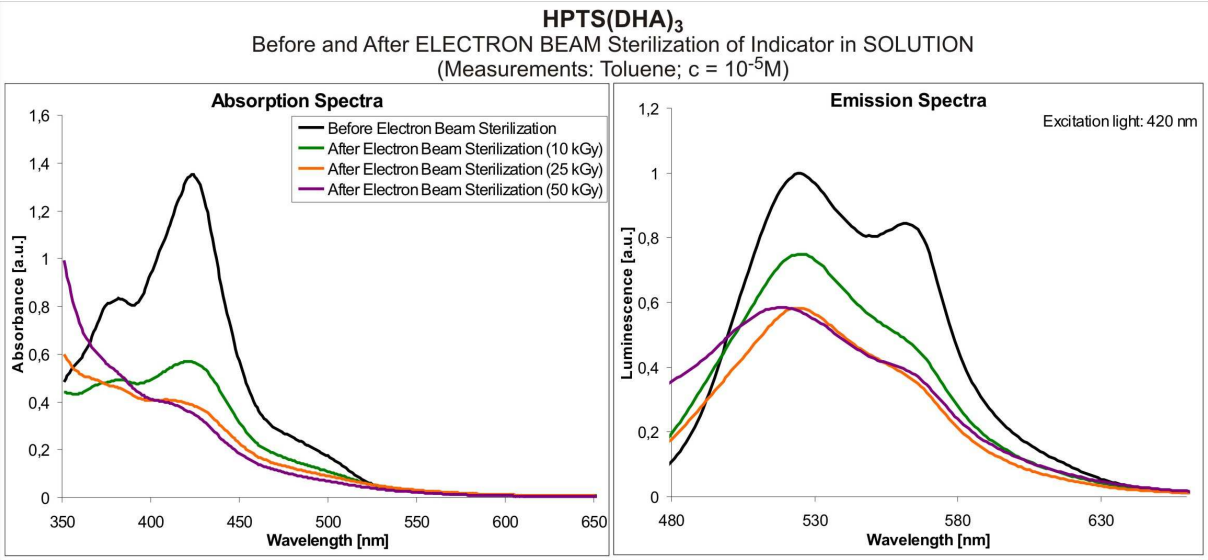

E-BEAMSOLUTION	Absorption Spectra		Emission Spectra	
Alterations in Absorption/Emission Intensity	10kGy	57,79% decrease	10kGy	35,61% decrease
	25 kGy	Decrease	25 kGy	39,54% decrease
	50 kGy	Decrease	50 kGy	38,97% decrease
Alterations in Absorption/Emission Curve Form	10kGy	Disappearance of characteristic curve form of $HPTS(DHA)_3$	10kGy	Disappearance of characteristic curve form of $HPTS(DHA)_3$
	25 kGy	Disappearance of characteristic curve form of $HPTS(DHA)_3$	25 kGy	Disappearance of characteristic curve form of $HPTS(DHA)_3$
	50 kGy	Disappearance of characteristic curve form of $HPTS(DHA)_3$	50 kGy	Disappearance of characteristic curve form of $HPTS(DHA)_3$

B.11 PET Perylene BisImide

B.11.1 Gamma Sterilization

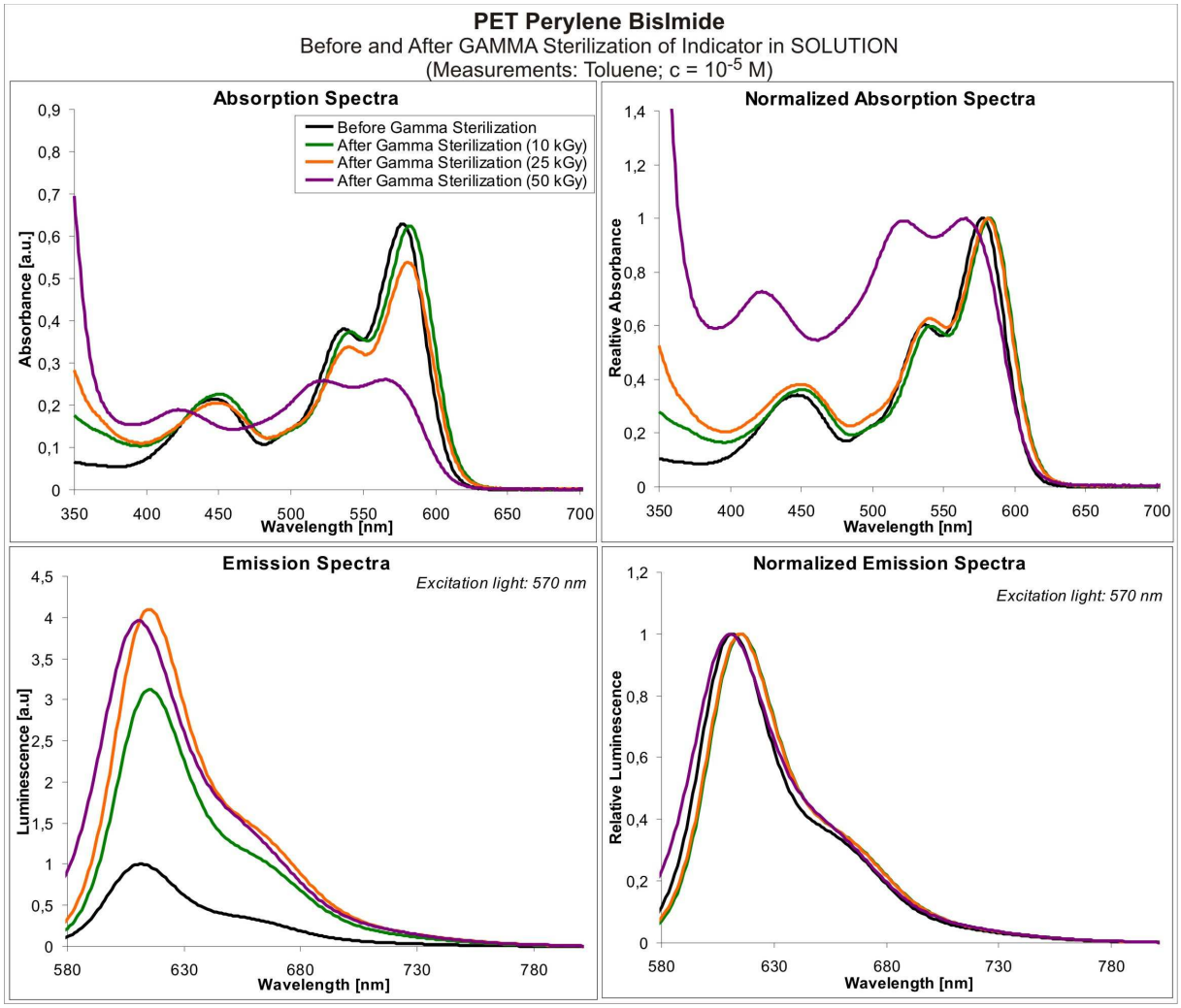

GAMMA/SOLUTION	Absorption Spectra		Emission Spectra	
Alterations in Absorption/Emission Intensity	10kGy	0,90% decrease	10kGy	312% increase
	25 kGy	14,41% decrease	25 kGy	410% increase
	50 kGy	58,56% decrease	50 kGy	396% increase
Alterations in Absorption/Emission Curve Form	10kGy	Increased absorption between 350-420 nm Bathochromic shift of the absorption maximum for 4 nm	10kGy	Bathochromic shift of the emission maximum for 3 nm.
	25 kGy	Increased absorption between 350-420 nm Bathochromic shift of the absorption maximum for 4 nm	25 kGy	Bathochromic shift of the emission maximum for 3 nm.
	50 kGy	Disappearance of characteristic curve form of PET Perylene BisImide Altered – new peaks with λ_{max} = 421 nm, λ_{max} = 517 nm and λ_{max} = 564 nm.	50 kGy	Hypsocromic shift of the emission maximum for 1 nm.

B.11.2 Electron Beam Sterilization

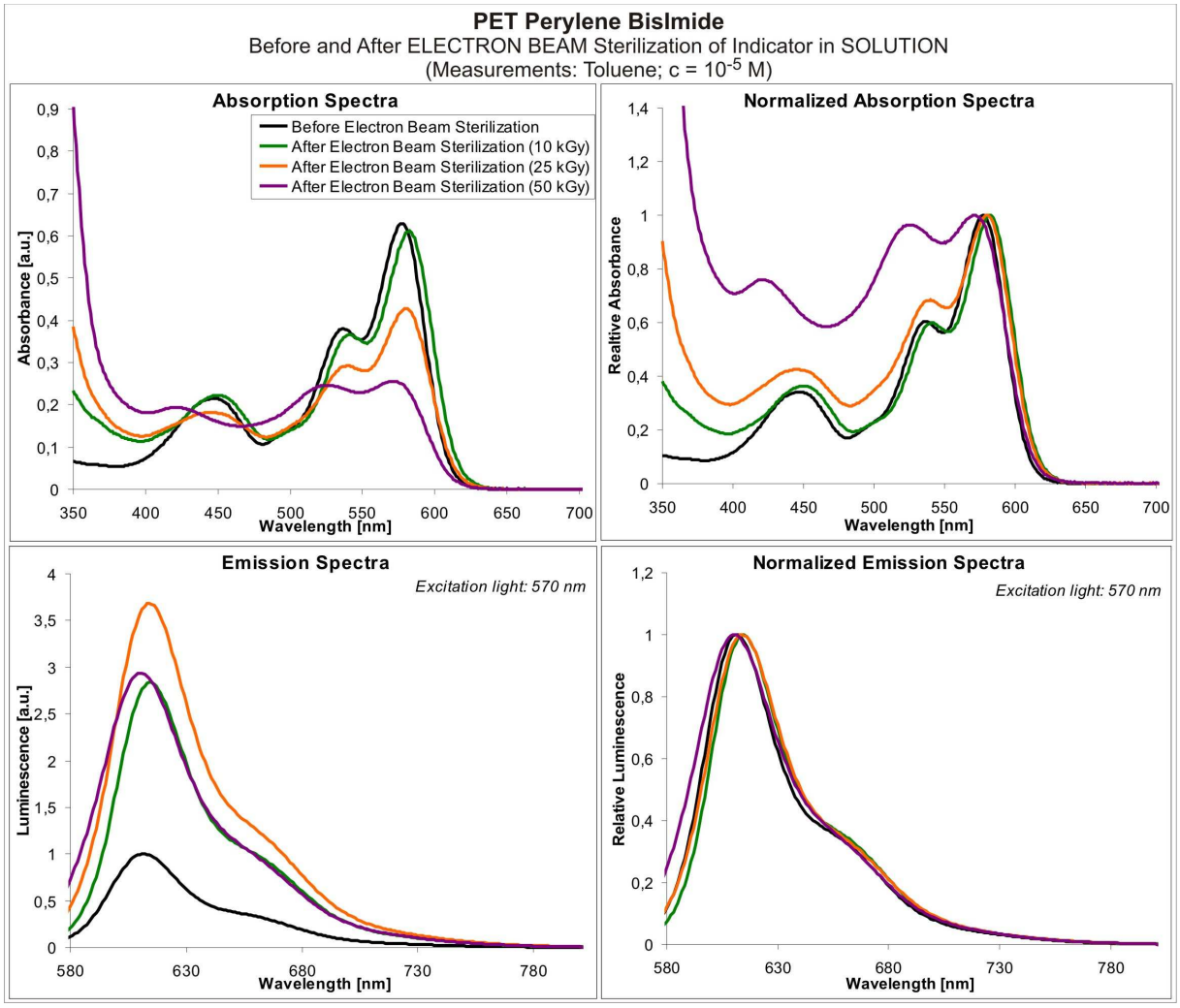

E-BEAM/SOLUTION	Absorption Spectra		Emission Spectra	
Alterations in Absorption/Emission Intensity	10kGy	2,97% decrease	10kGy	284% increase
	25 kGy	32,07% decrease	25 kGy	368% increase
	50 kGy	59,36% decrease	50 kGy	294% increase
Alterations in Absorption/Emission Curve Form	10kGy	Increased absorption between 350-420 nm Bathochromic shift of the absorption maximum for 6 nm	10kGy	Bathochromic shift of the emission maximum for 2 nm.
	25 kGy	Increased absorption between 350-550 nm Bathochromic shift of the absorption maximum for 2 nm	25 kGy	Bathochromic shift of the emission maximum for 2 nm.
	50 kGy	Disappearance of characteristic curve form of PET Perylene BisImide Altered – new peaks with λ_{max} = 419 nm, λ_{max} = 522 nm and λ_{max} = 570 nm.	50 kGy	Hypsocromic shift of the emission maximum for 2 nm.

B.12 Eosin EthylEster

B.12.1 Gamma Sterilization

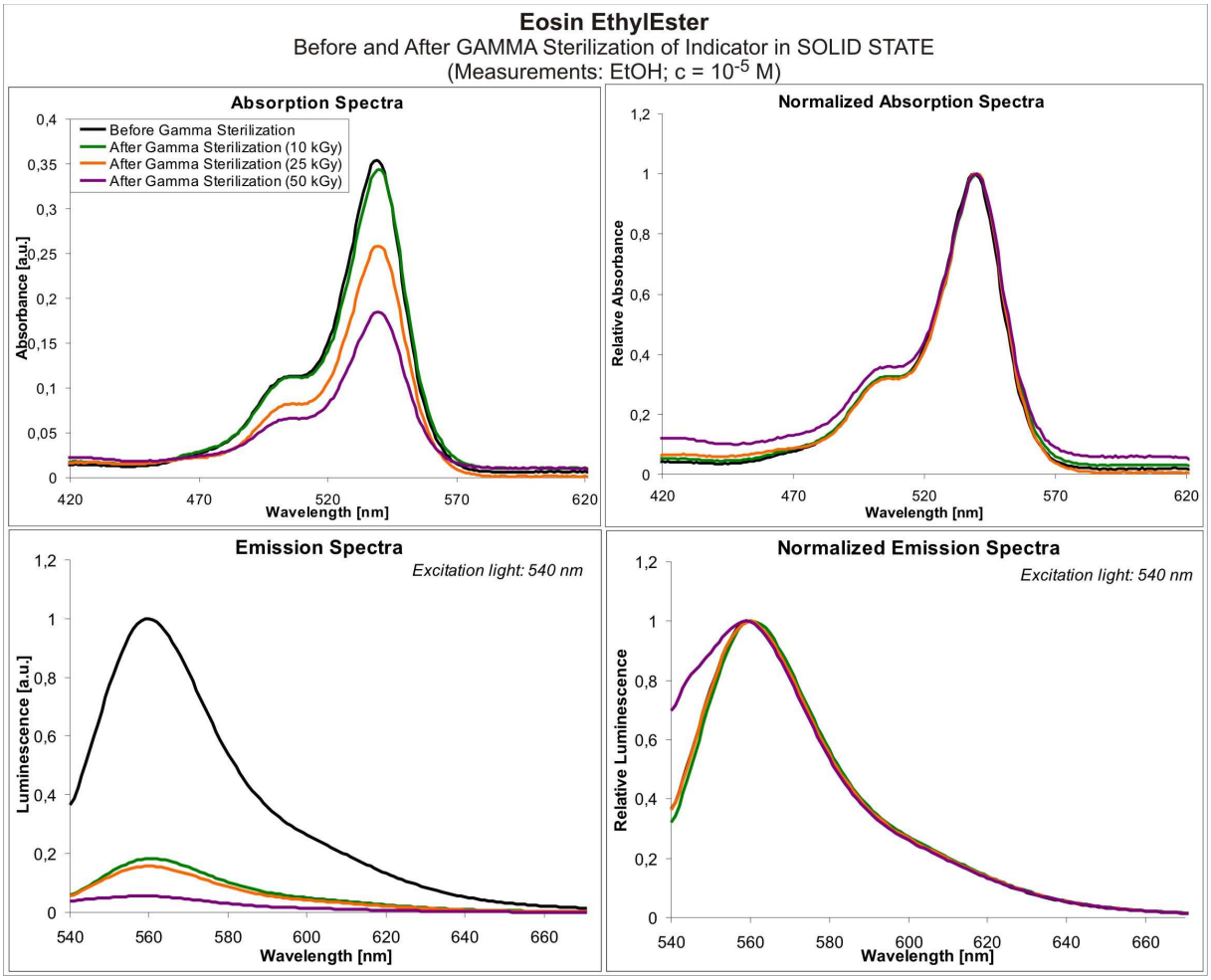

GAMMA/SOLID STATE	Absorption Spectra		Emission Spectra	
Alterations in Absorption/Emission Intensity	10kGy	2,92% decrease	10kGy	81,68% decrease
	25 kGy	27,05% decrease	25 kGy	84,20% decrease
	50 kGy	47,90% decrease	50 kGy	94,59% decrease
Alterations in Absorption/Emission Curve Form	10kGy	Bathochromic shift of the absorption maximum for 1 nm.	10kGy	Unaltered
	25 kGy	Bathochromic shift of the absorption maximum for 1 nm.	25 kGy	Unaltered
	50 kGy	Altered between 350-520 nm and 570-800 nm Bathochromic shift of the absorption maximum for 1 nm.	50 kGy	Altered between 540-560 nm

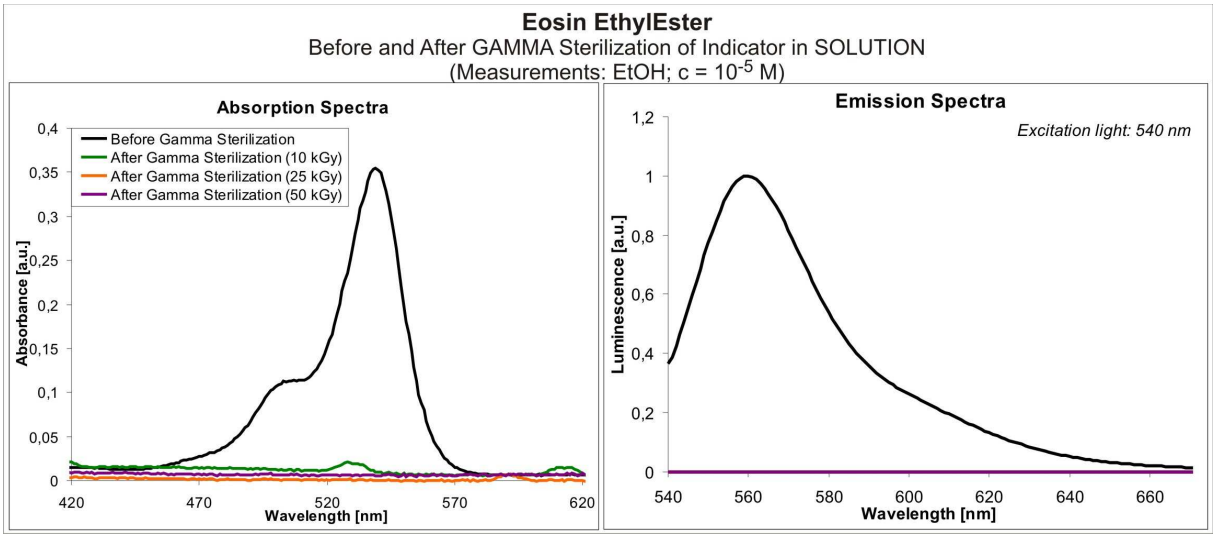

GAMMA/SOLUTION	Absorption Spectra		Emission Spectra	
Alterations in Absorption/Emission Intensity	10kGy	97,19% decrease	10kGy	99,98% decrease
	25 kGy	99,96% decrease	25 kGy	99,99% decrease
	50 kGy	98,46% decrease	50 kGy	99,99% decrease

B.12.2 Electron Beam Sterilization

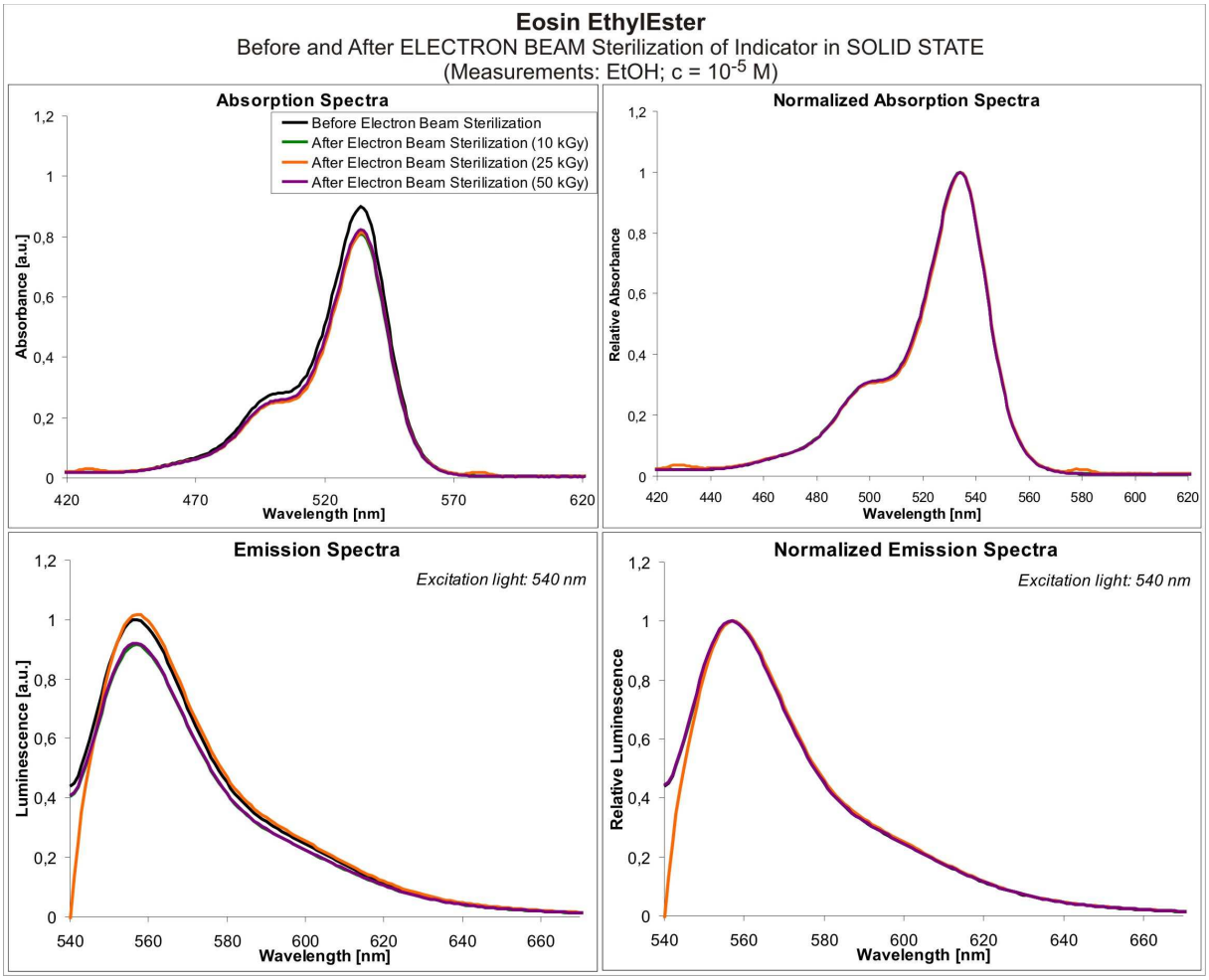

E-BEAM/SOLID STATE	Absorption Spectra		Emission Spectra	
Alterations in Absorption/Emission Intensity	10kGy	10,06% decrease	10kGy	8,50% decrease
	25 kGy	9,47% decrease	25 kGy	1,81% increase
	50 kGy	8,89% decrease	50 kGy	7,92% decrease
Alterations in Absorption/Emission Curve Form	10kGy	Unaltered	10kGy	Unaltered
	25 kGy	New peaks with λ_{max} = 427 nm and λ_{max} = 579 nm	25 kGy	Unaltered
	50 kGy	Unaltered	50 kGy	Unaltered

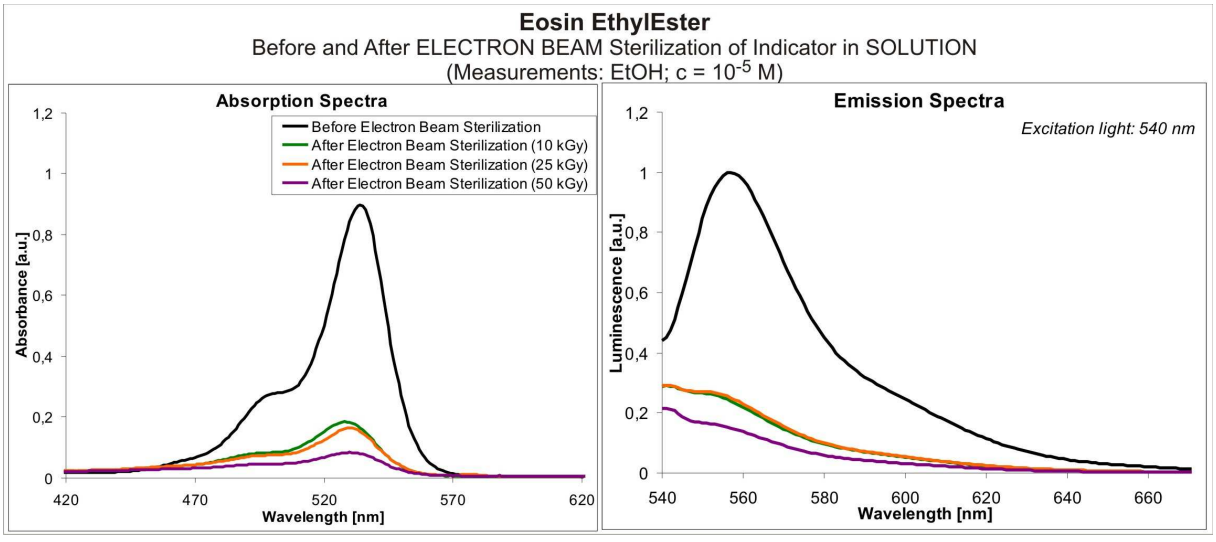

E-BEAM/SOLID STATE	Absorption Spectra		Emission Spectra	
Alterations in Absorption/Emission Intensity	10kGy	81,74% decrease	10kGy	Decrease
	25 kGy	82,96% decrease	25 kGy	Decrease
	50 kGy	91,07% decrease	50 kGy	Decrease
Alterations in Absorption/Emission Curve Form			10kGy	Disappearance of characteristic curve form of Eosin EthylEster
			25 kGy	Disappearance of characteristic curve form of Eosin EthylEster
			50 kGy	Disappearance of characteristic curve form of Eosin EthylEster

B.13 2´,7´-DiChloroFluorescein

B.13.1 Gamma Sterilization

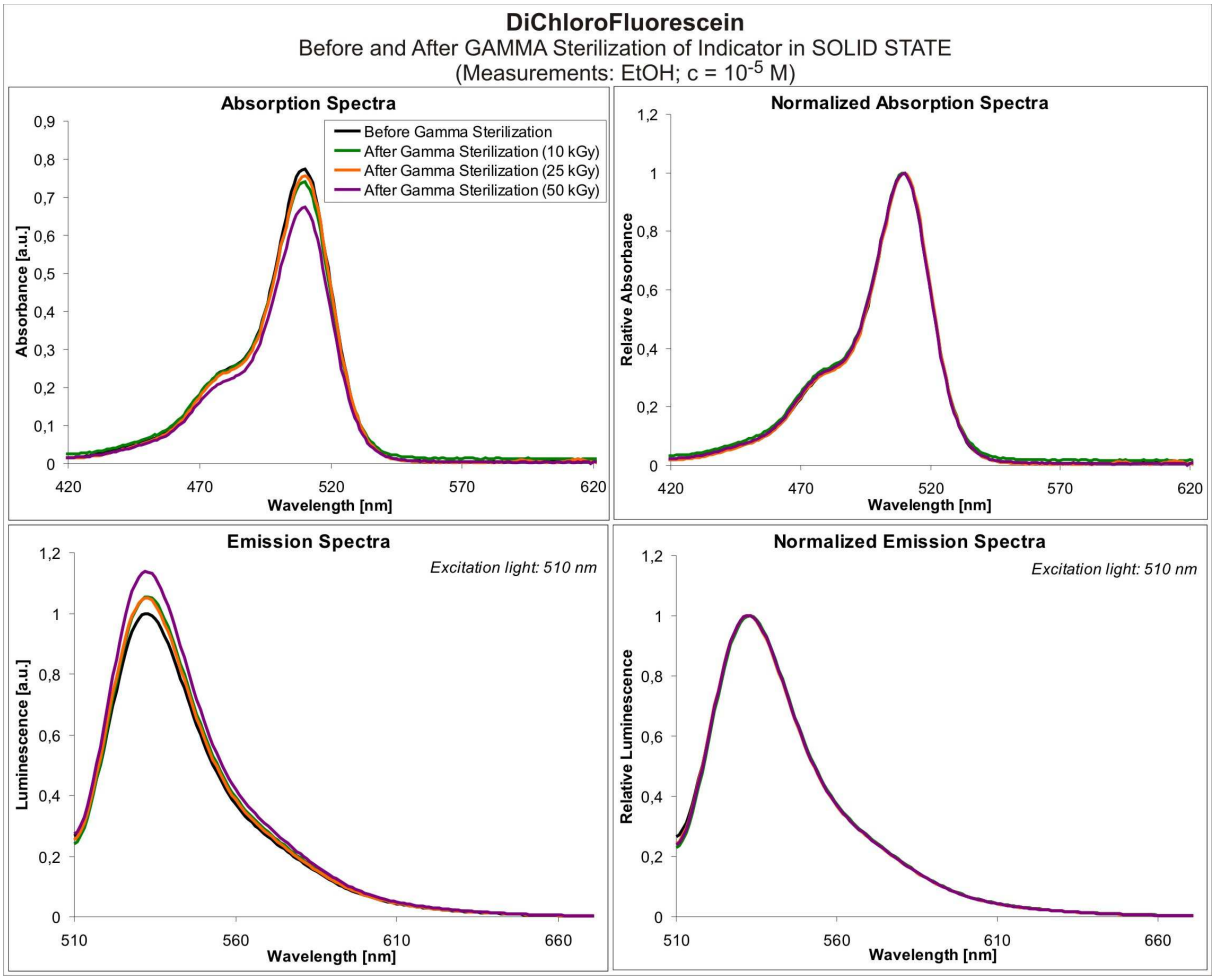

GAMMA/SOLID STATE	Absorption Spectra		Emission Spectra	
Alterations in Absorption/Emission Intensity	10kGy	4,50% decrease	10kGy	5,15% increase
	25 kGy	2,32% decrease	25 kGy	4,70% increase
	50 kGy	13,02% decrease	50 kGy	12,06% increase
Alterations in Absorption/Emission Curve Form	10kGy	Unaltered	10kGy	Unaltered
	25 kGy	Unaltered	25 kGy	Unaltered
	50 kGy	Unaltered	50 kGy	Unaltered

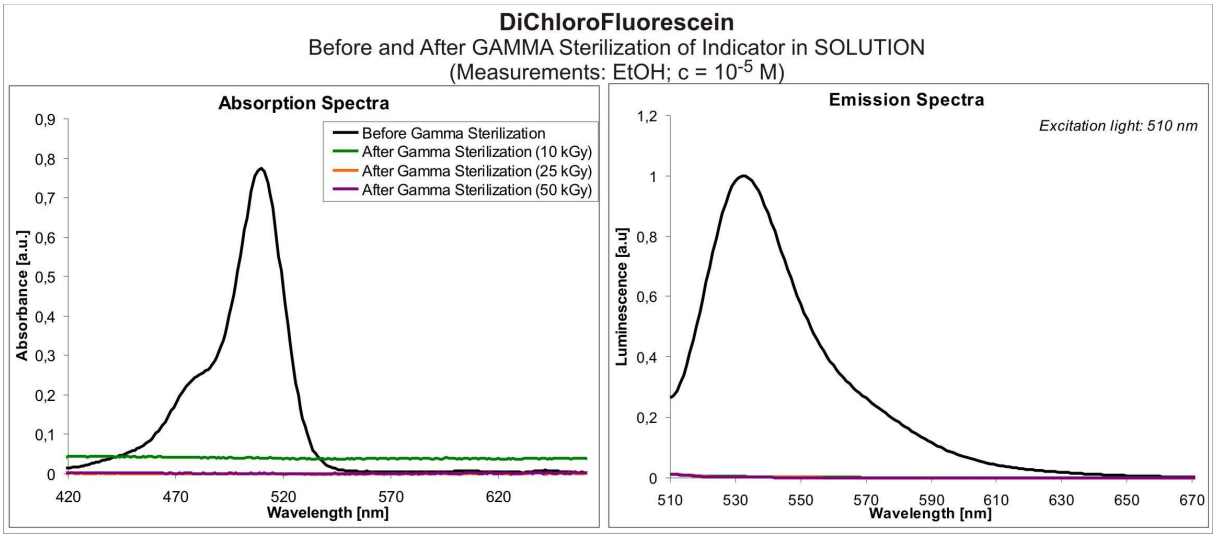

GAMMA/SOLUTION	Absorption Spectra		Emission Spectra	
Alterations in Absorption/Emission Intensity	10kGy	Decrease – no Absorption	10kGy	Decrease – no Emission
	25 kGy	Decrease – no Absorption	25 kGy	Decrease – no Emission
	50 kGy	Decrease – no Absorption	50 kGy	Decrease – no Emission

B.13.2 Electron Beam Sterilization

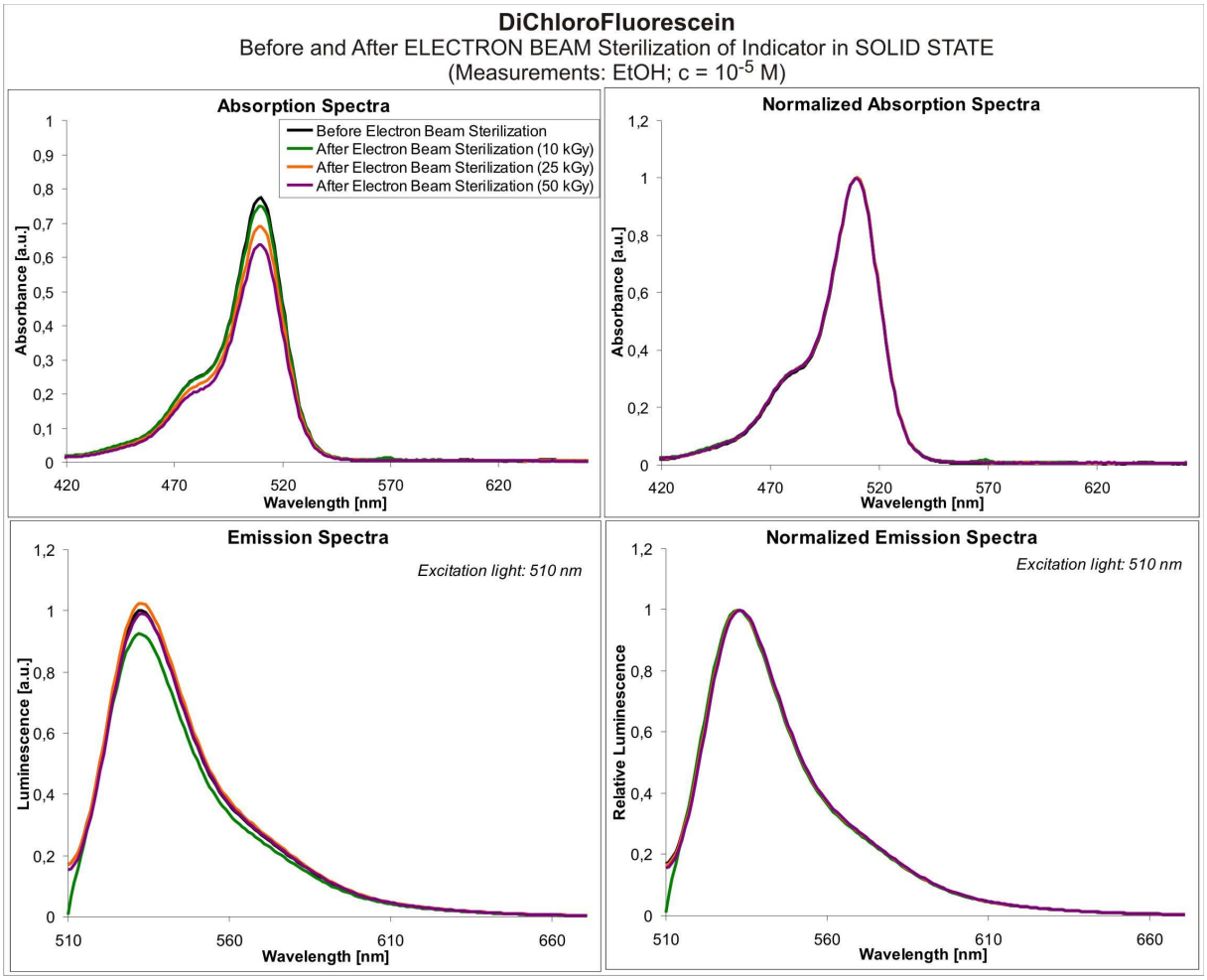

E-BEAM/SOLID STATE	Absorption Spectra		Emission Spectra	
Alterations in Absorption/Emission Intensity	10kGy	3,21% decrease	10kGy	7,50% decrease
	25 kGy	11,02% decrease	25 kGy	2,49% increase
	50 kGy	17,76% decrease	50 kGy	0,91% decrease

Alterations in Absorption/Emission Curve Form	10kGy	Unaltered	10kGy	Unaltered
	25 kGy	Unaltered	25 kGy	Unaltered
	50 kGy	Unaltered	50 kGy	Unaltered

DiChloroFluorescein

Before and After ELECTRON BEAM Sterilization of Indicator in SOLUTION

(Measurements: EtOH; c = 10^{-5} M)

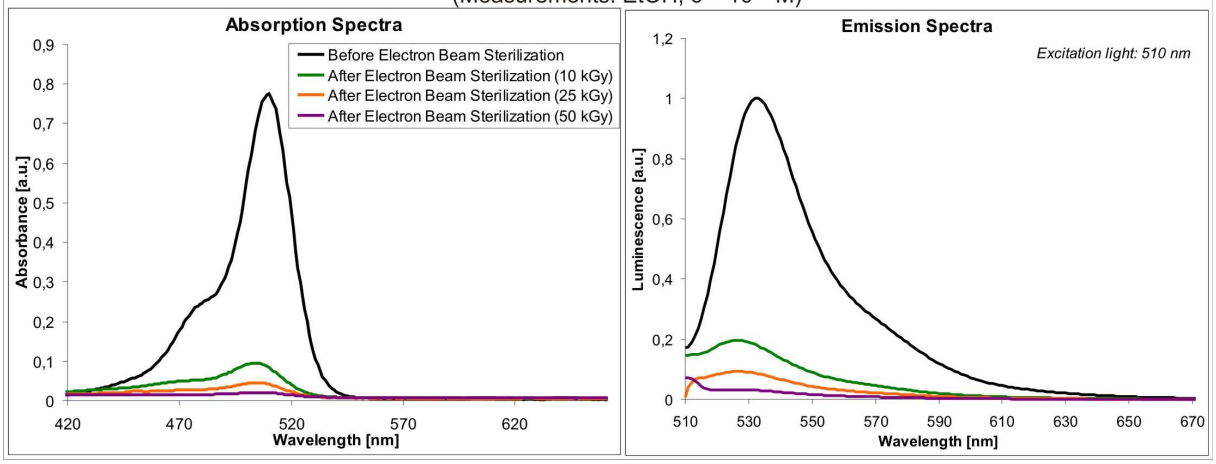

E-BEAM/SOLUTION	Absorption Spectra		Emission Spectra	
Alterations in Absorption/Emission Intensity	10kGy	87,83% decrease	10kGy	80,57% decrease
	25 kGy	Decrease	25 kGy	Decrease
	50 kGy	Decrease	50 kGy	Decrease
Alterations in Absorption/Emission Curve Form	10kGy	Disappearance of characteristic curve form of DiChloroFluorescein	10kGy	Disappearance of characteristic curve form of DiChloroFluorescein
	25 kGy	Disappearance of characteristic curve form of DiChloroFluorescein	25 kGy	Disappearance of characteristic curve form of DiChloroFluorescein
	50 kGy	Disappearance of characteristic curve form of DiChloroFluorescein	50 kGy	Disappearance of characteristic curve form of DiChloroFluorescein

B.14 2´,7´-DiHexyl-5(6)-*N*-Octadecyl-CarboxAmidoFluorescein (=DHFA)

B.14.1 Gamma Sterilization

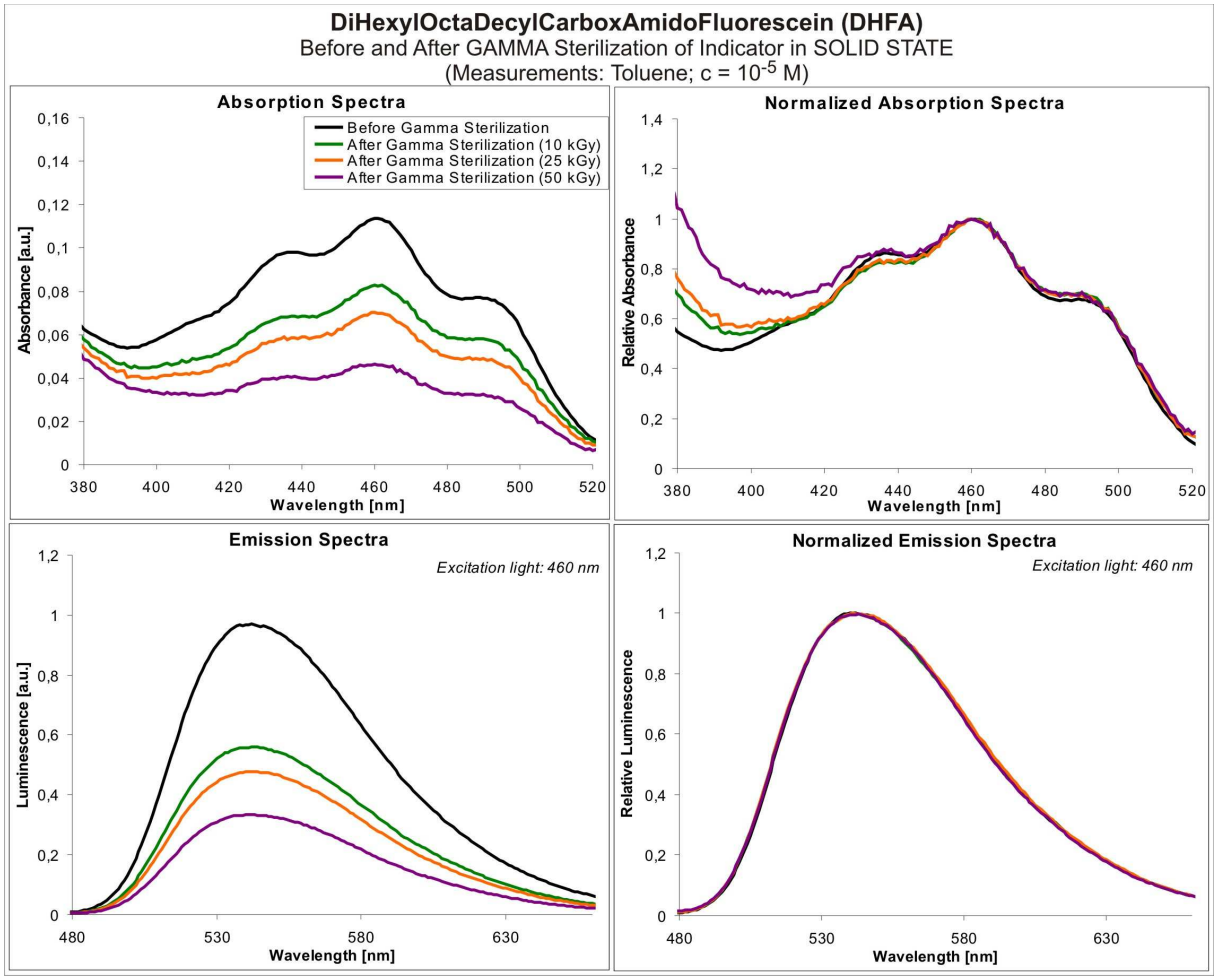

GAMMA/SOLID STATE	Absorption Spectra		Emission Spectra	
Alterations in Absorption/Emission Intensity	10kGy	27,22% decrease	10kGy	43,81% decrease
	25 kGy	38,17% decrease	25 kGy	52,21% decrease
	50 kGy	59,25% decrease	50 kGy	66,51% decrease
Alterations in Absorption/Emission Curve Form	10kGy	Altered between 350-410 nm	10kGy	Unaltered
	25 kGy	Altered between 350-410 nm	25 kGy	Unaltered
	50 kGy	Altered between 350-430 nm	50 kGy	Unaltered

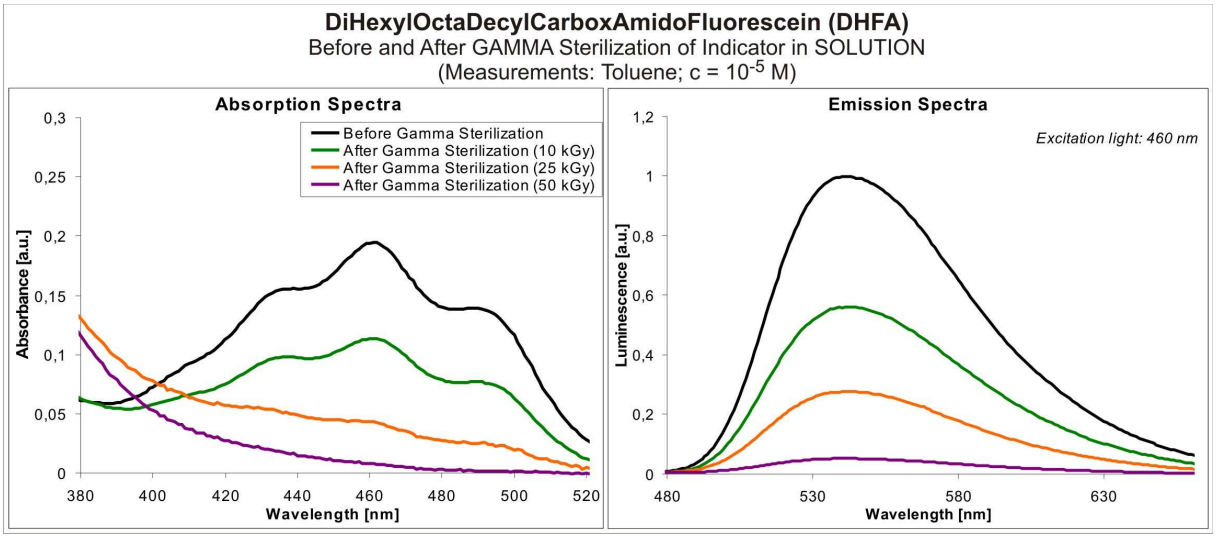

GAMMA/SOLUTION	Absorption Spectra		Emission Spectra	
Alterations in Absorption/Emission Intensity	10kGy	42,86% decrease	10kGy	43,90% decrease
	25 kGy	76,20% decrease	25 kGy	72,29% decrease
	50 kGy	92,56% decrease	50 kGy	94,65% decrease
Alterations in Absorption/Emission Curve Form	10kGy	Altered between 350-420 nm.		
	25 kGy	Disappearance of characteristic curve form of DHFA.		
	50 kGy	Disappearance of characteristic curve form of DHFA.		

B.14.2 Electron Beam Sterilization

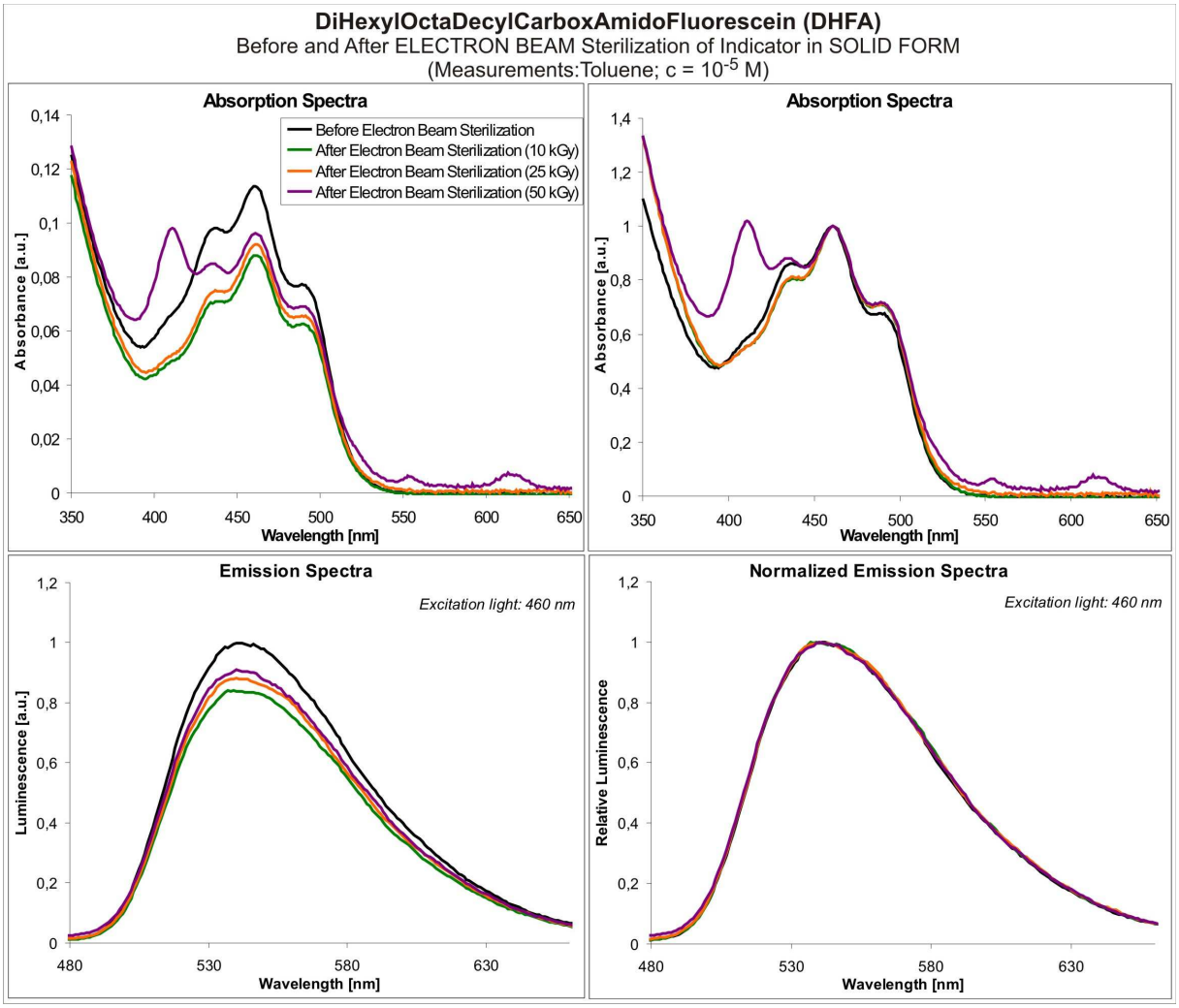

E-BEAM/SOLID STATE	Absorption Spectra		Emission Spectra	
Alterations in Absorption/Emission Intensity	10kGy	22,57% decrease	10kGy	15,76% decrease
	25 kGy	18,92% decrease	25 kGy	11,79% decrease
	50 kGy	15,31% decrease	50 kGy	9,10% decrease
Alterations in Absorption/Emission Curve Form	10kGy	Altered between 350-450 nm	10kGy	Unaltered
	25 kGy	Altered between 350-450 nm	25 kGy	Unaltered
	50 kGy	Altered between 350-450 nm and 510-650 nm Altered – new peaks with λ_{max} = 409 nm, λ_{max} = 552 nm and λ_{max} = 613 nm.	50 kGy	Unaltered

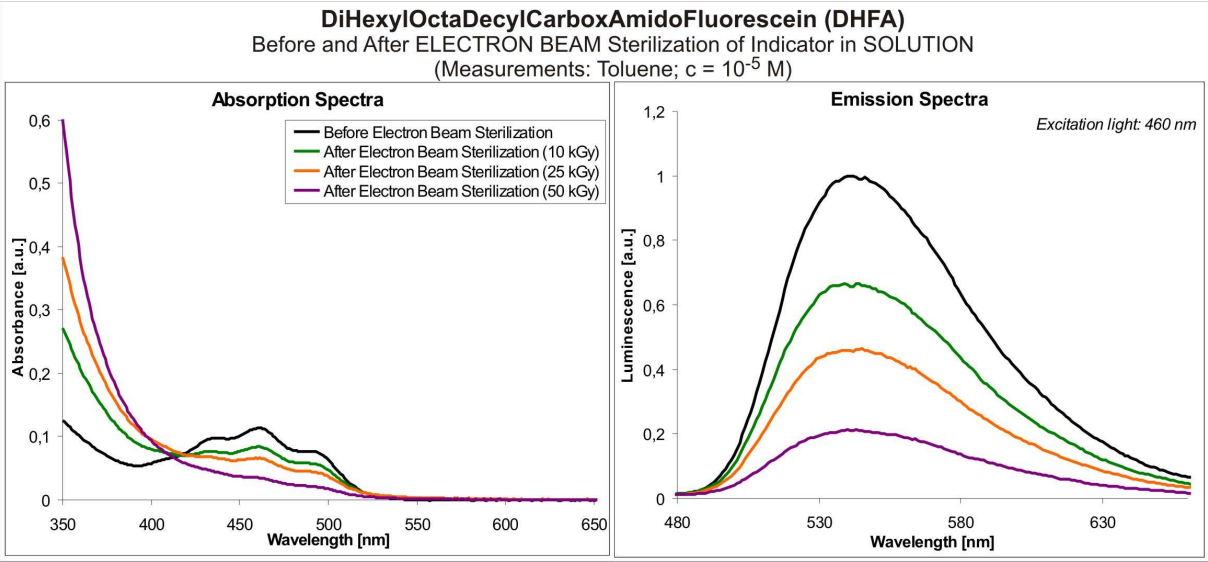

E-BEAM/SOLUTION	Absorption Spectra		Emission Spectra	
Alterations in Absorption/Emission Intensity	10kGy	26,52% decrease	10kGy	33,38% decrease
	25 kGy	42,15% decrease	25 kGy	53,98% decrease
	50 kGy	69,20% decrease	50 kGy	78,76% decrease
Alterations in Absorption/Emission Curve Form	10kGy	Altered between 350-415 nm		
	25 kGy	Altered between 350-415 nm		
	50 kGy	Disappearance of characteristic curve form of DHFA.		

B.15 2´,7´-DiHexylFluorescein OctadecylEster (=DHFE)

B.15.1 Gamma Sterilization

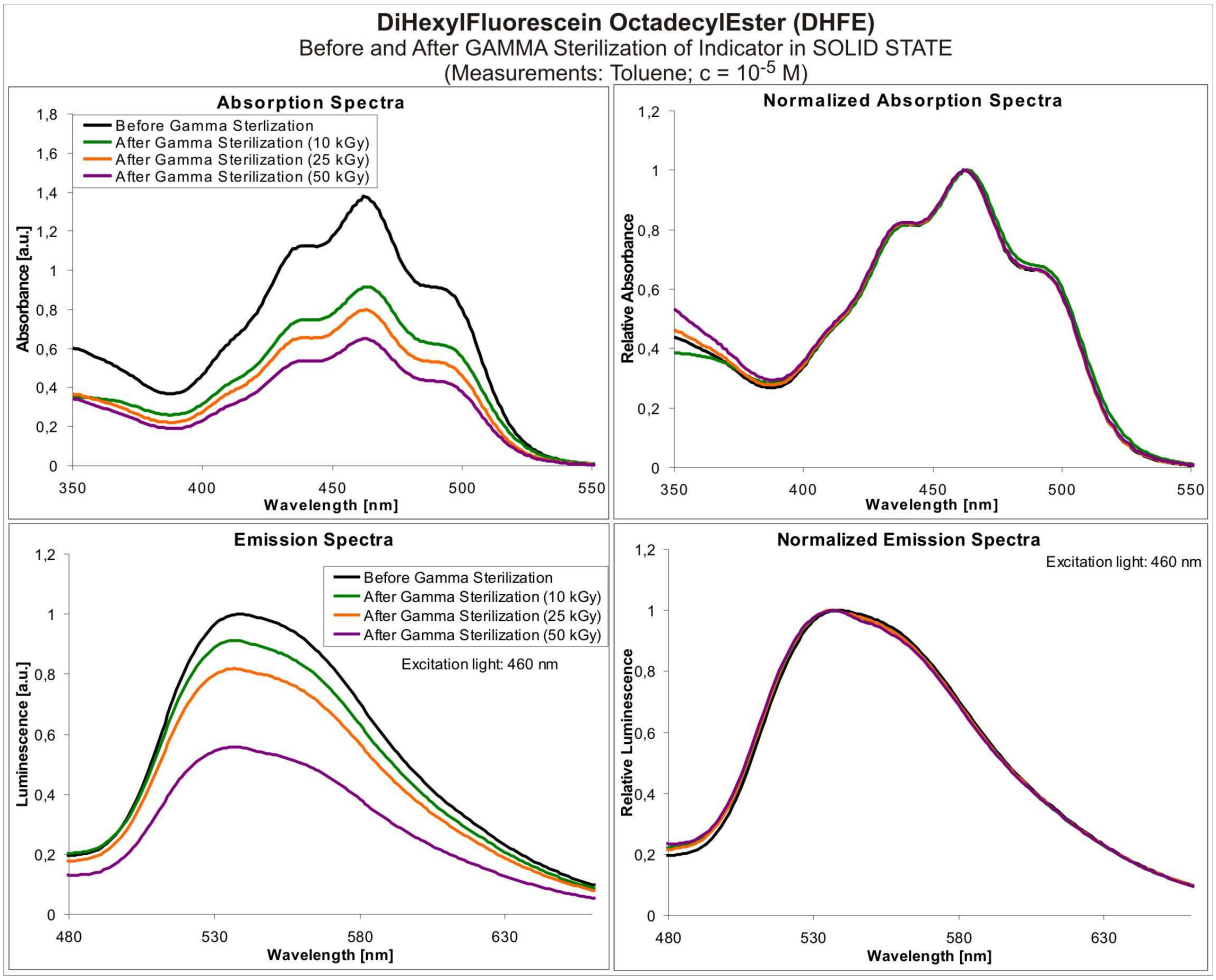

GAMMA/SOLID STATE	Absorption Spectra		Emission Spectra	
Alterations in Absorption/Emission Intensity	10kGy	33,44% decrease	10kGy	8,67% decrease
	25 kGy	42,06% decrease	25 kGy	18,13% decrease
	50 kGy	52,77% decrease	50 kGy	44,18% decrease
Alterations in Absorption/Emission Curve Form	10kGy	Altered between 350-370 nm	10kGy	Unaltered
	25 kGy	Unaltered	25 kGy	Altered between 540-570 nm
	50 kGy	Altered between 350-380 nm	50 kGy	Altered between 540-570 nm

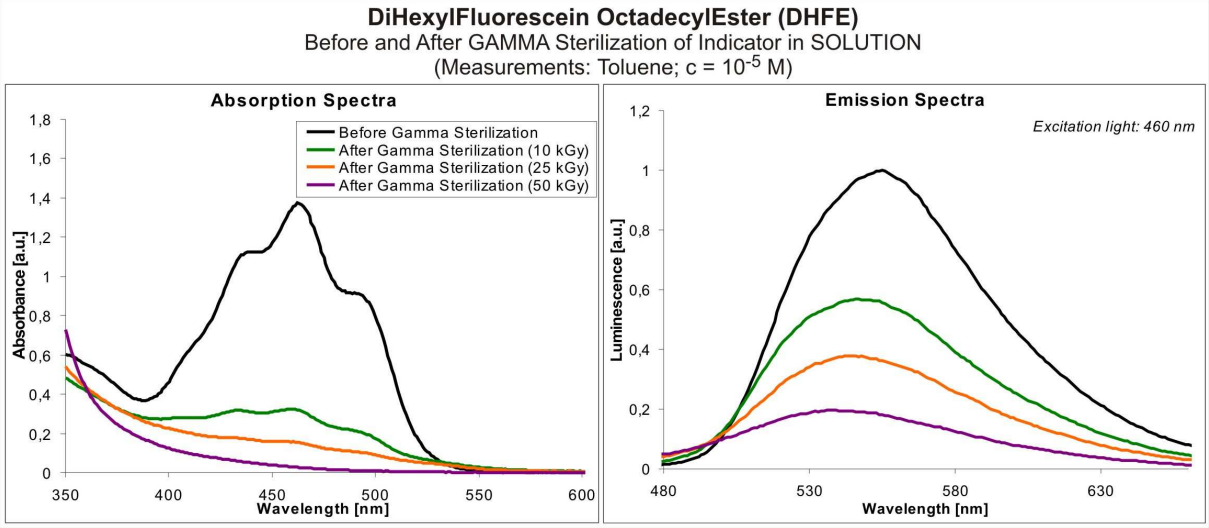

GAMMA/SOLUTION	Absorption Spectra		Emission Spectra	
Alterations in Absorption/Emission Intensity	10kGy	76,76% decrease	10kGy	44,39% decrease
	25 kGy	Decrease	25 kGy	63,80% decrease
	50 kGy	Decrease	50 kGy	81,86% decrease
Alterations in Absorption/Emission Curve Form	10kGy	/		
	25 kGy	Disappearance of characteristic curve form of DHFE		
	50 kGy	Disappearance of characteristic curve form of DHFE		

B.15.2 Electron Beam Sterilization

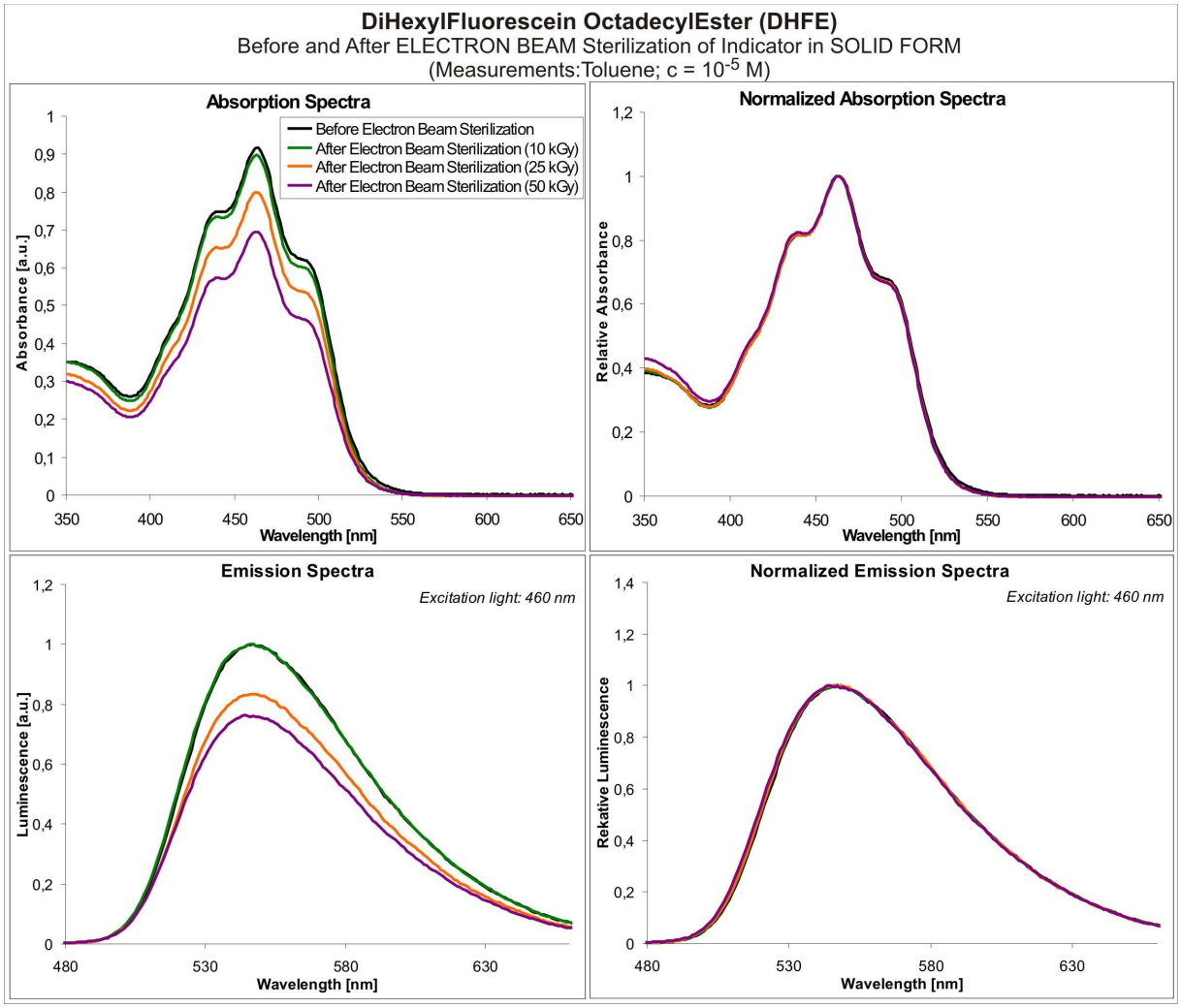

E-BEAM/SOLID STATE	Absorption Spectra		Emission Spectra	
Alterations in Absorption/Emission Intensity	10kGy	2,03% decrease	10kGy	0,22% increase
	25 kGy	12,74% decrease	25 kGy	16,68% decrease
	50 kGy	24,07% decrease	50 kGy	23,71% decrease
Alterations in Absorption/Emission Curve Form	10kGy	Unaltered	10kGy	Unaltered
	25 kGy	Unaltered	25 kGy	Unaltered
	50 kGy	Altered between 350-380 nm	50 kGy	Unaltered

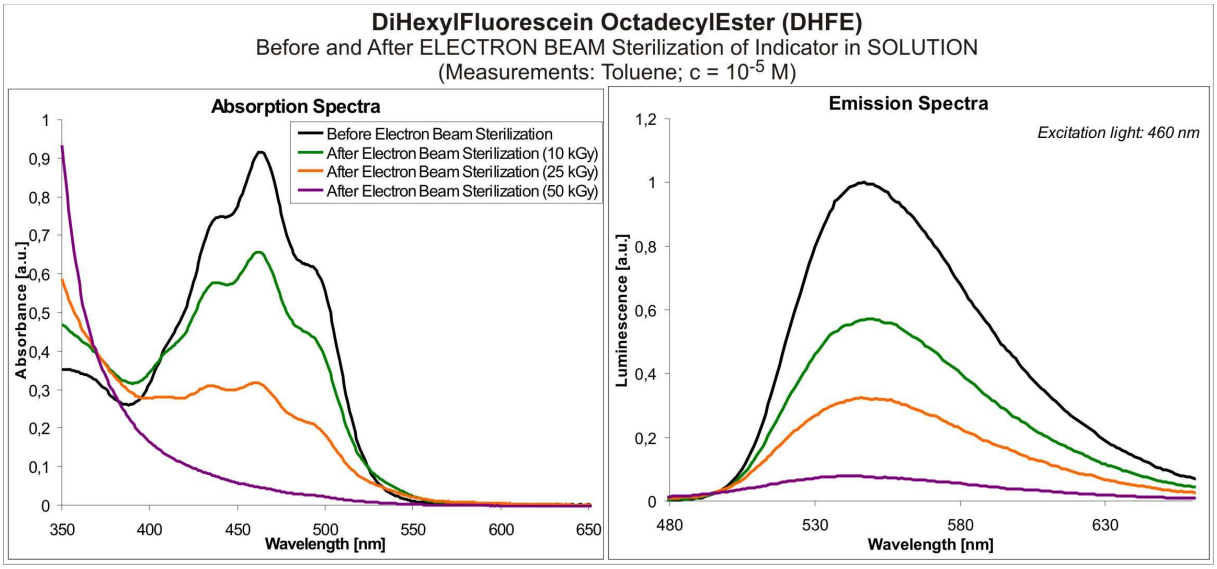

E-BEAM/SOLUTION	Absorption Spectra		Emission Spectra	
Alterations in Absorption/Emission Intensity	10kGy	28,63% decrease	10kGy	43,13% decrease
	25 kGy	65,85% decrease	25 kGy	67,87% decrease
	50 kGy	Decrease	50 kGy	92,25% decrease
Alterations in Absorption/Emission Curve Form	10kGy	/		
	25 kGy	/		
	50 kGy	Disappearance of characteristic curve form of DHFE		

B.16 BromoPhenol Blue

B.16.1 Gamma Sterilization

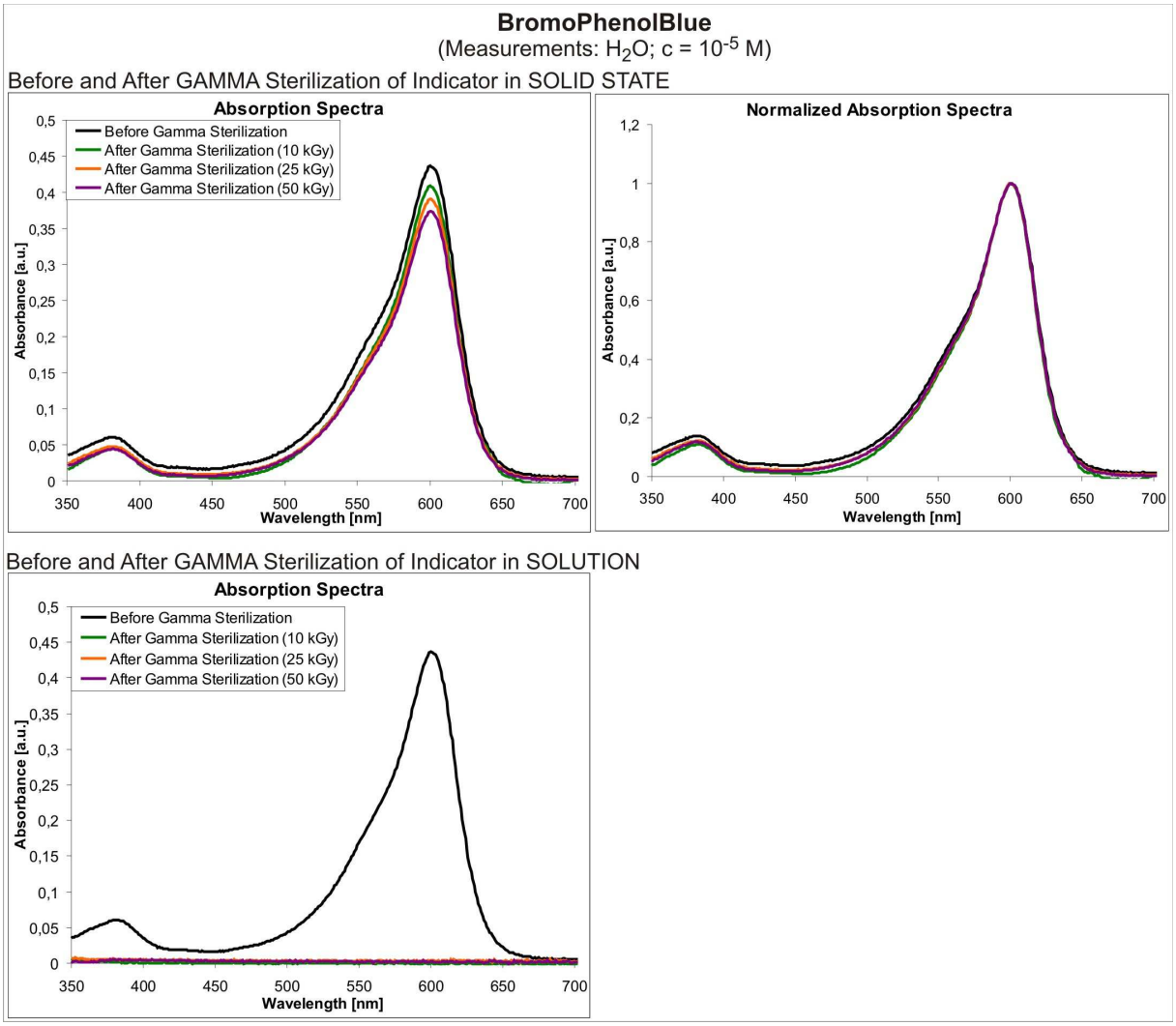

Solid State

GAMMA S.	Absorption Spectra			Alterations	
Alterations in Absorption /Emission Intensity	10 kGy	6,45% decrease	Alterations in Absorption /Emission Curve Form	10 kGy	Unaltered.
	25 kGy	10,69% decrease		25 kGy	Unaltered.
	50 kGy	14,52% decrease		50 kGy	Unaltered.

Solution

GAMMA S.	Absorption Spectra			Alterations	
Alterations in Absorption /Emission Intensity	10 kGy	99,54% decrease	Alterations in Absorption /Emission Curve Form	10 kGy	Disappearance of the characteristic absorption curve form.
	25 kGy	Decrease		25 kGy	Disappearance of the characteristic absorption curve form.
	50 kGy	Decrease		50 kGy	Disappearance of the characteristic absorption curve form.

B.16.2 Electron Beam Sterilization

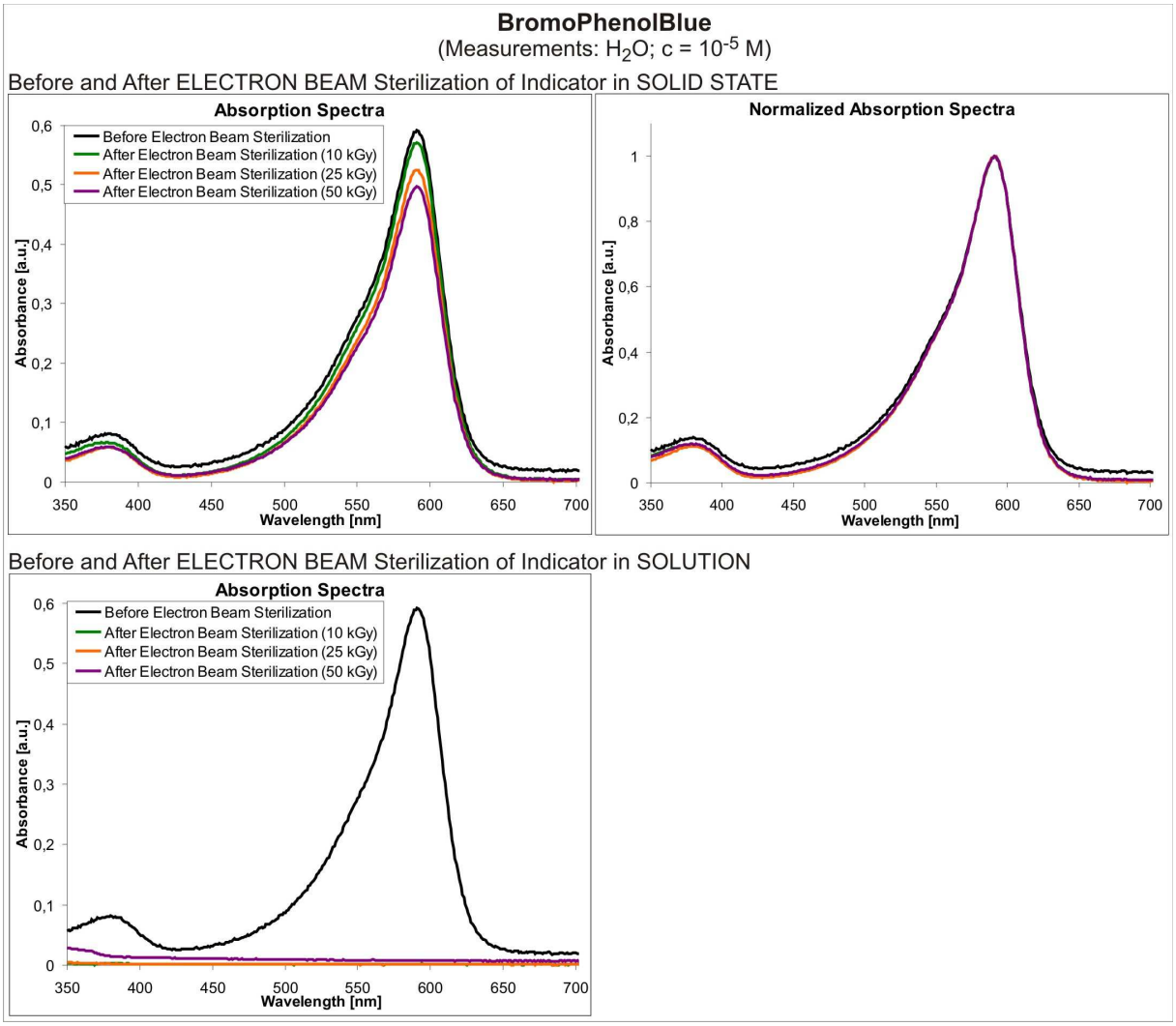

Solid State

E-BEAM S.	Absorption Spectra			Alterations	
Alterations in Absorption /Emission Intensity	10 kGy	3,45% decrease	Alterations in Absorption /Emission Curve Form	10 kGy	Unaltered.
	25 kGy	11,34% decrease		25 kGy	Unaltered.
	50 kGy	16,02% decrease		50 kGy	Unaltered.

Solution

E-BEAM S.	Absorption Spectra			Alterations	
Alterations in Absorption /Emission Intensity	10 kGy	98,75% decrease	Alterations in Absorption /Emission Curve Form	10 kGy	Disappearance of the characteristic absorption curve form.
	25 kGy	Decrease		25 kGy	Disappearance of the characteristic absorption curve form.
	50 kGy	Decrease		50 kGy	Disappearance of the characteristic absorption curve form.

B.17 Thymol Blue

B.17.1 Gamma Sterilization

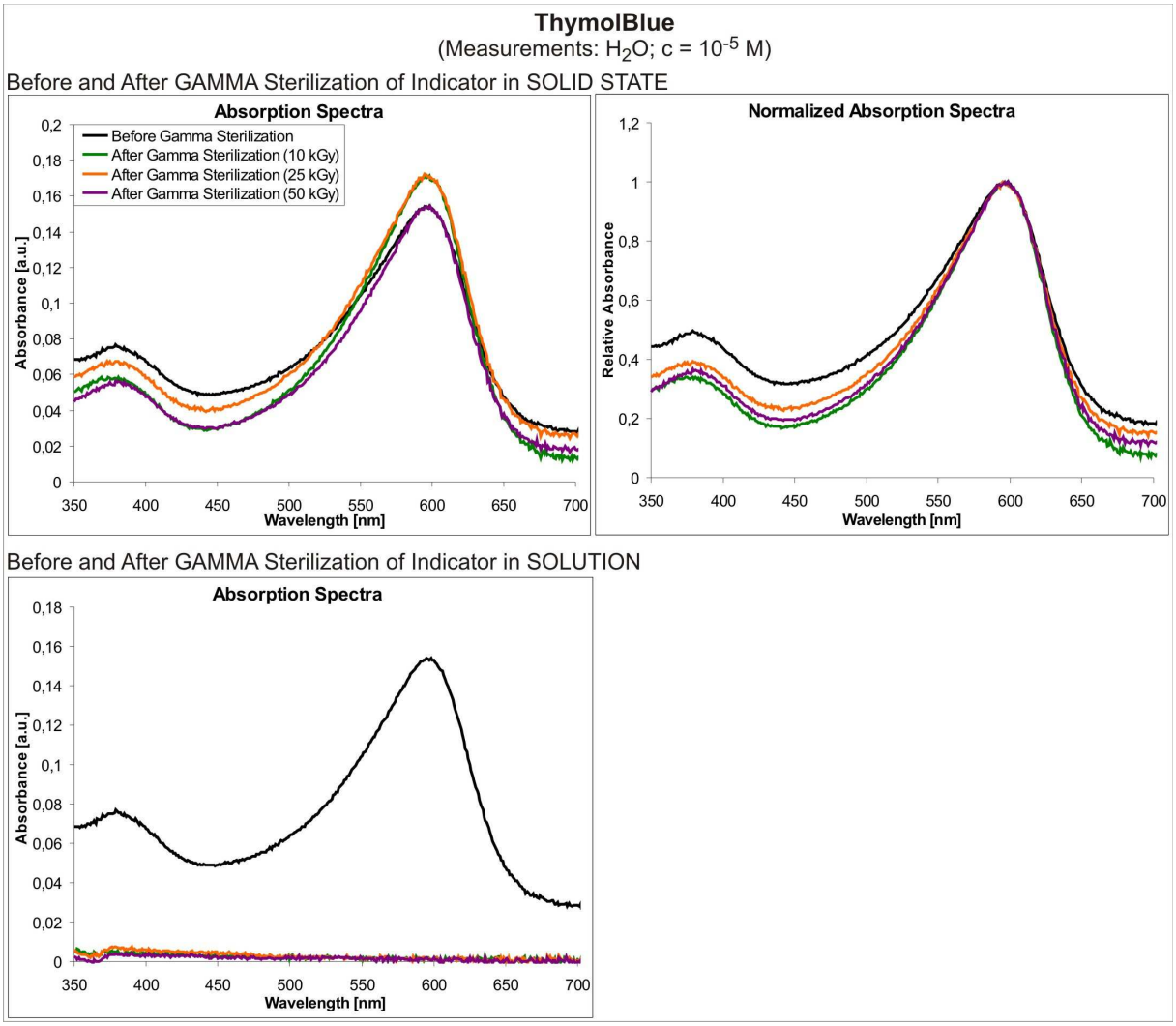

Solid State

GAMMA S.	Absorption Spectra			Alterations	
Alterations in Absorption /Emission Intensity	10 kGy	10,16% increase	Alterations in Absorption /Emission Curve Form	10 kGy	Lower absorption between 350-560 nm and 650-800 nm.
	25 kGy	10,62% increase		25 kGy	Lower absorption between 350-560 nm and 650-800 nm.
	50 kGy	0,11% increase		50 kGy	Lower absorption between 350-560 nm and 650-800 nm.

Solution

GAMMA S.	Absorption Spectra			Alterations	
Alterations in Absorption /Emission Intensity	10 kGy	99,60% decrease	Alterations in Absorption /Emission Curve Form	10 kGy	Disappearance of the characteristic absorption curve form.
	25 kGy	Decrease		25 kGy	Disappearance of the characteristic absorption curve form.
	50 kGy	Decrease		50 kGy	Disappearance of the characteristic absorption curve form.

B.17.2 Electron Beam Sterilization

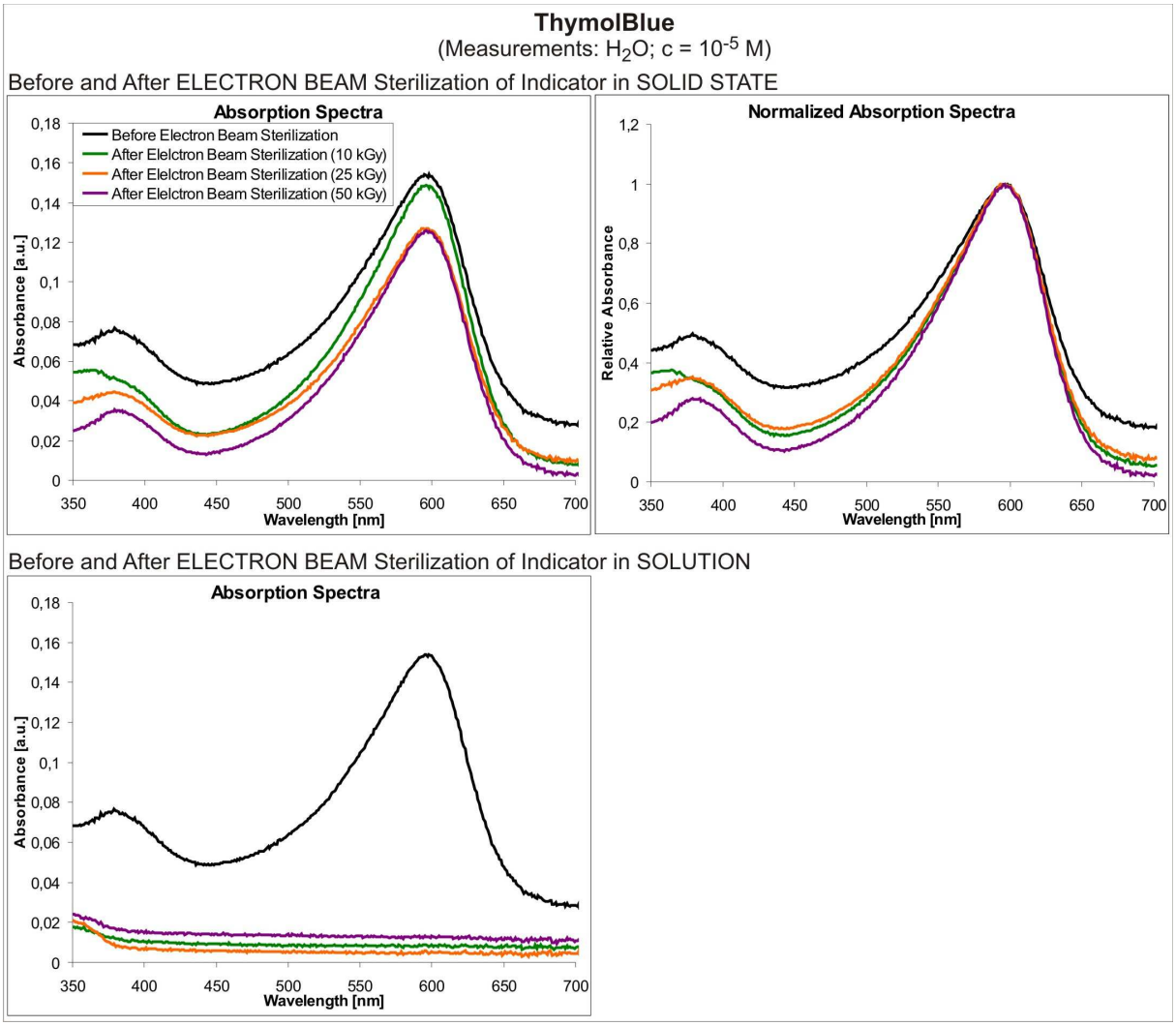

Solid State

E-BEAM S.	Absorption Spectra			Alterations	
Alterations in Absorption /Emission Intensity	10 kGy	3,47% decrease	Alterations in Absorption /Emission Curve Form	10 kGy	Altered absorption between 350-580 nm and 630-800 nm.
	25 kGy	17,52% decrease		25 kGy	Altered absorption between 350-580 nm and 630-800 nm.
	50 kGy	18,12% decrease		50 kGy	Altered absorption between 350-580 nm and 630-800 nm.

Solution

E-BEAM S.	Absorption Spectra			Alterations	
Alterations in Absorption /Emission Intensity	10 kGy	94,92% decrease	Alterations in Absorption /Emission Curve Form	10 kGy	Disappearance of the characteristic absorption curve form.
	25 kGy	Decrease		25 kGy	Disappearance of the characteristic absorption curve form.
	50 kGy	Decrease		50 kGy	Disappearance of the characteristic absorption curve form.

B.18 BromoThymol Blue

B.18.1 Gamma Sterilization

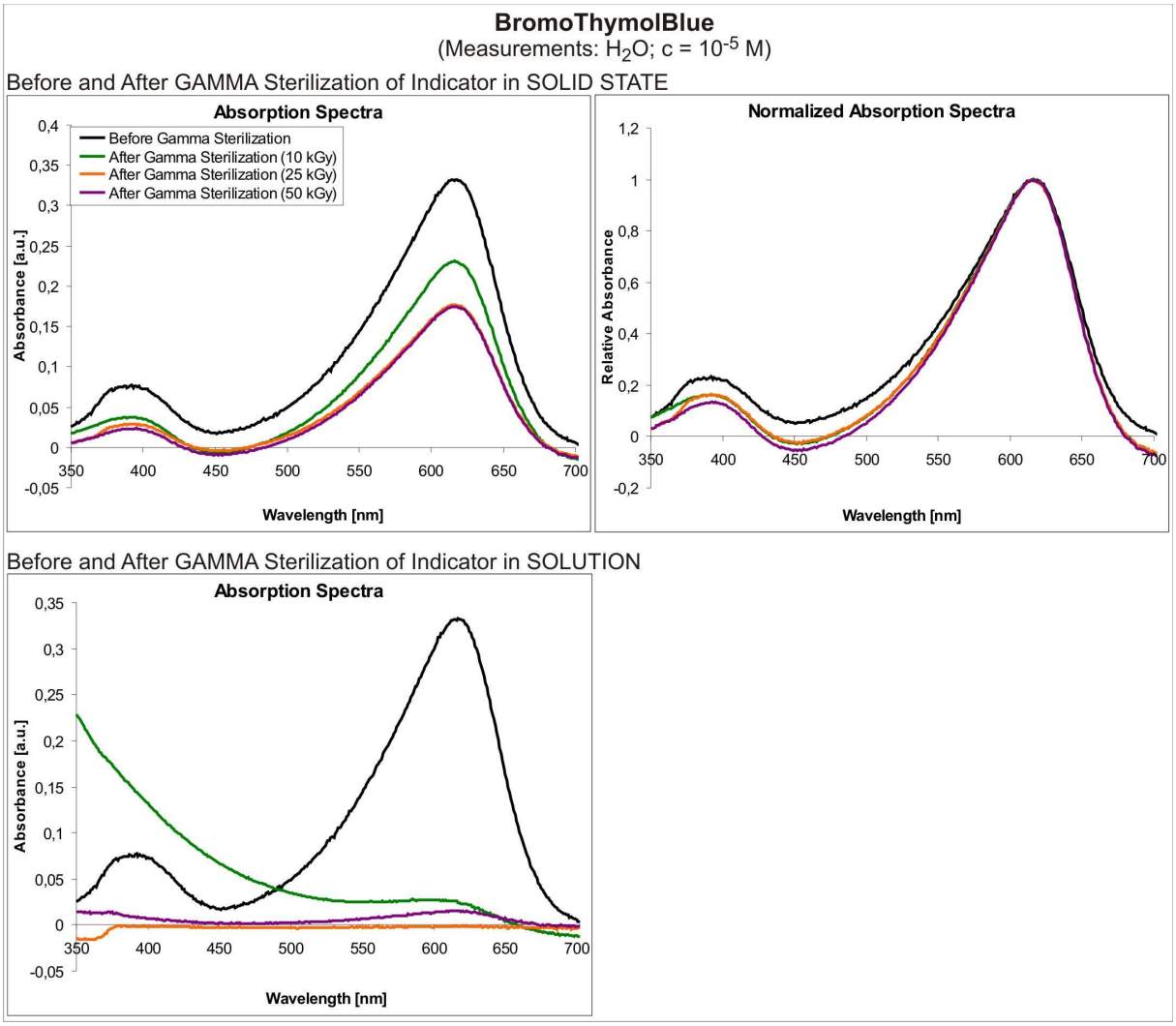

Solid State

GAMMA S.	Absorption Spectra			Alterations	
Alterations in Absorption /Emission Intensity	10 kGy	30,62% decrease	Alterations in Absorption /Emission Curve Form	10 kGy	Lower absorption between 350-550 nm and 650-800 nm.
	25 kGy	46,65% decrease		25 kGy	Lower absorption between 350-550 nm and 650-800 nm.
	50 kGy	47,38% decrease		50 kGy	Lower absorption between 350-550 nm and 650-800 nm.

Solution

GAMMA S.	Absorption Spectra			Alterations	
Alterations in Absorption /Emission Intensity	10 kGy	91,92% decrease	Alterations in Absorption /Emission Curve Form	10 kGy	Disappearance of the characteristic absorption curve form.
	25 kGy	Decrease		25 kGy	Disappearance of the characteristic absorption curve form.
	50 kGy	Decrease		50 kGy	Disappearance of the characteristic absorption curve form.

B.18.2 Electron Beam Sterilization

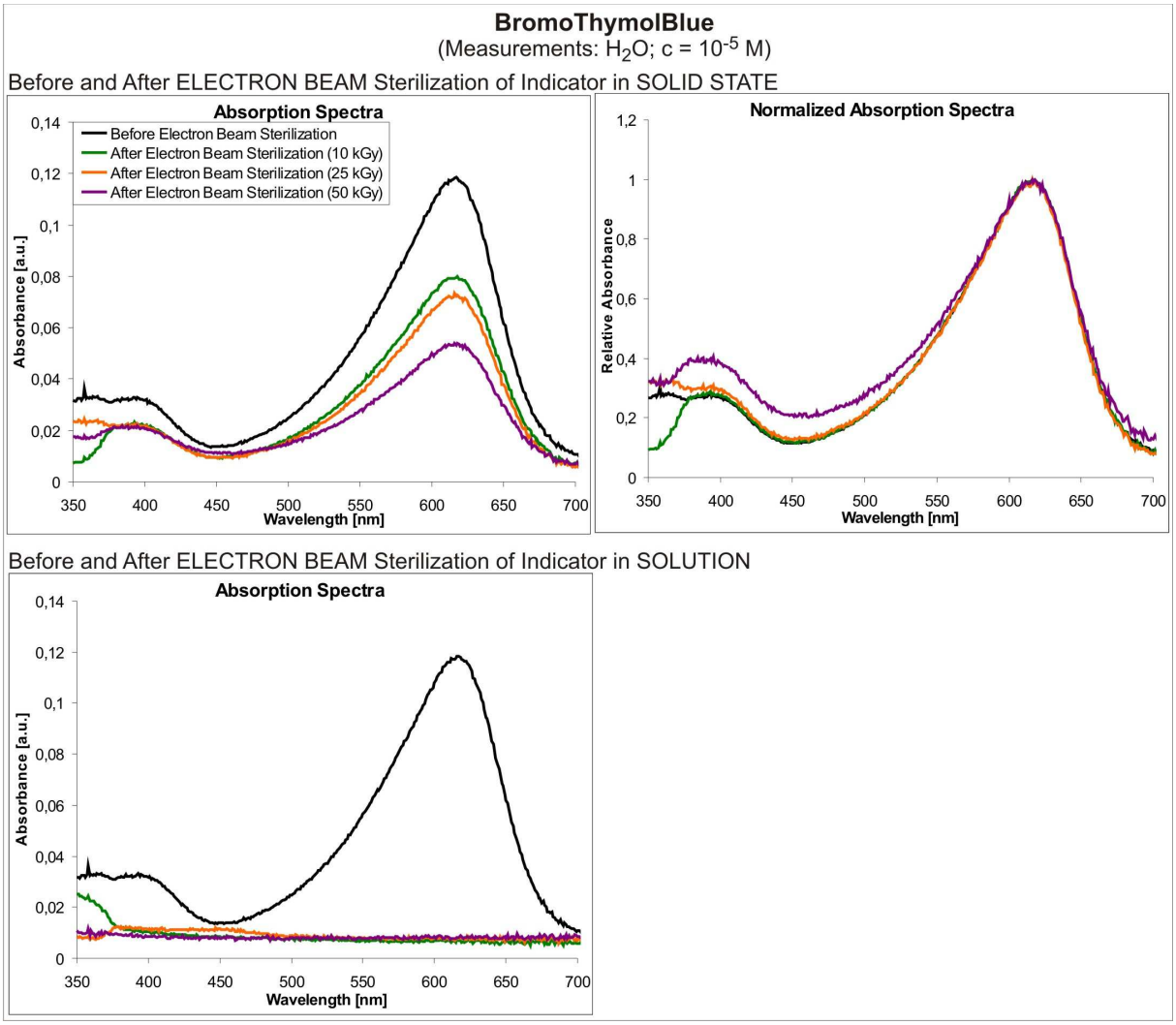

Solid State

E-BEAM S.	Absorption Spectra			Alterations	
Alterations in Absorption /Emission Intensity	10 kGy	32,56% decrease	Alterations in Absorption /Emission Curve Form	10 kGy	Unaltered.
	25 kGy	38,02% decrease		25 kGy	Unaltered.
	50 kGy	54,46% decrease		50 kGy	Altered absorption between 350-570 nm.

Solution

E-BEAM S.	Absorption Spectra			Alterations	
Alterations in Absorption /Emission Intensity	10 kGy	93,37% decrease	Alterations in Absorption /Emission Curve Form	10 kGy	Disappearance of the characteristic absorption curve form.
	25 kGy	Decrease		25 kGy	Disappearance of the characteristic absorption curve form.
	50 kGy	Decrease		50 kGy	Disappearance of the characteristic absorption curve form.

B.19 Methyl Orange

B.19.1 Gamma Sterilization

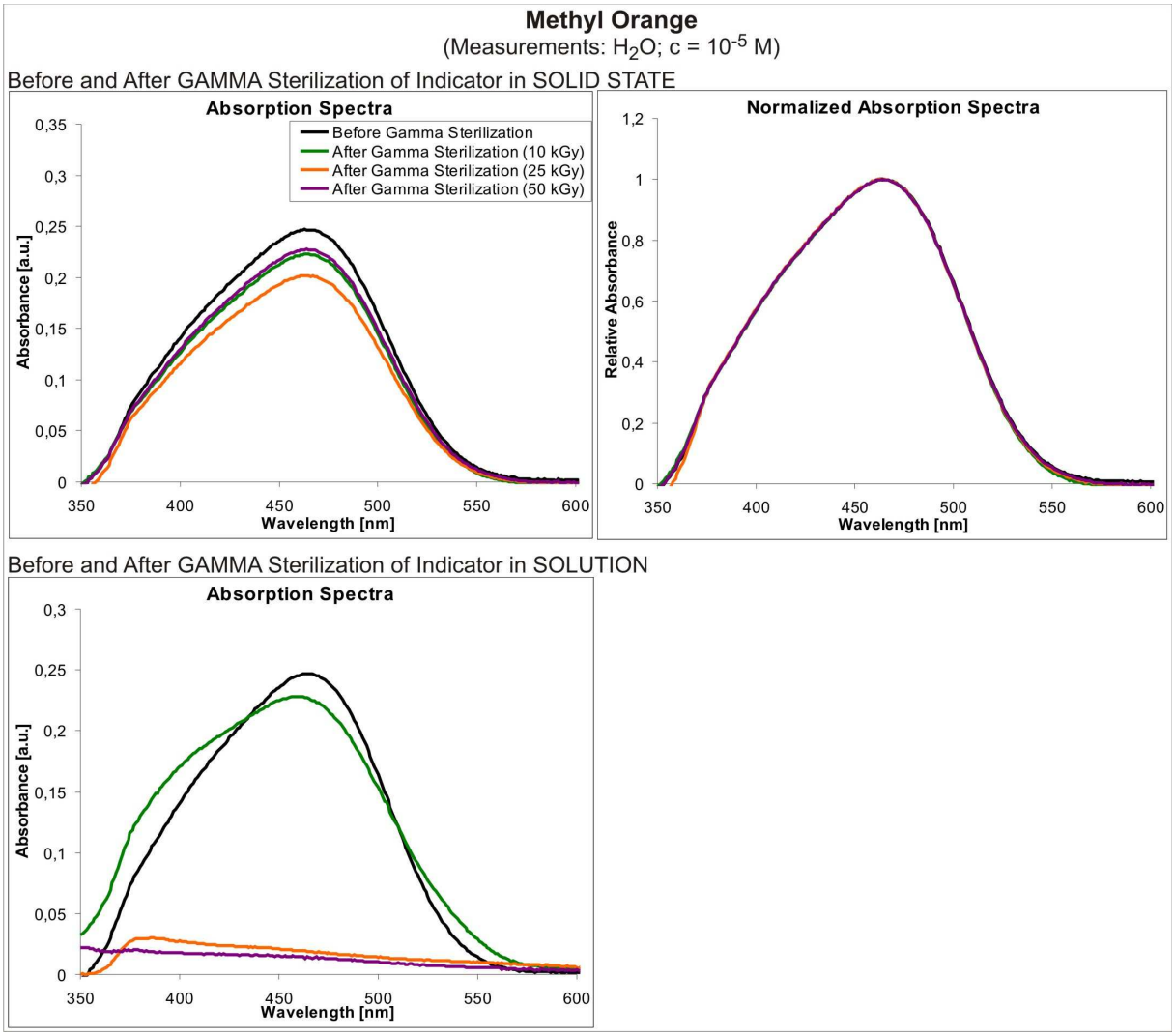

Solid State

GAMMA S.	Absorption Spectra			Alterations	
Alterations in Absorption /Emission Intensity	10 kGy	9,83% decrease	Alterations in Absorption /Emission Curve Form	10 kGy	Unaltered.
	25 kGy	18,29% decrease		25 kGy	Unaltered.
	50 kGy	7,81% decrease		50 kGy	Unaltered.

Solution

GAMMA S.	Absorption Spectra			Alterations	
Alterations in Absorption /Emission Intensity	10 kGy	7,69% decrease	Alterations in Absorption /Emission Curve Form	10 kGy	Altered absorption curve form between 350-450 nm and 520-800 nm. Hypsochromic shift of the absorption maximum.
	25 kGy	91,19% decrease		25 kGy	Disappearance of the characteristic absorption curve form.

	50 kGy	Decrease		50 kGy	Disappearance of the characteristic absorption curve form.

B.19.2 Electron Beam Sterilization

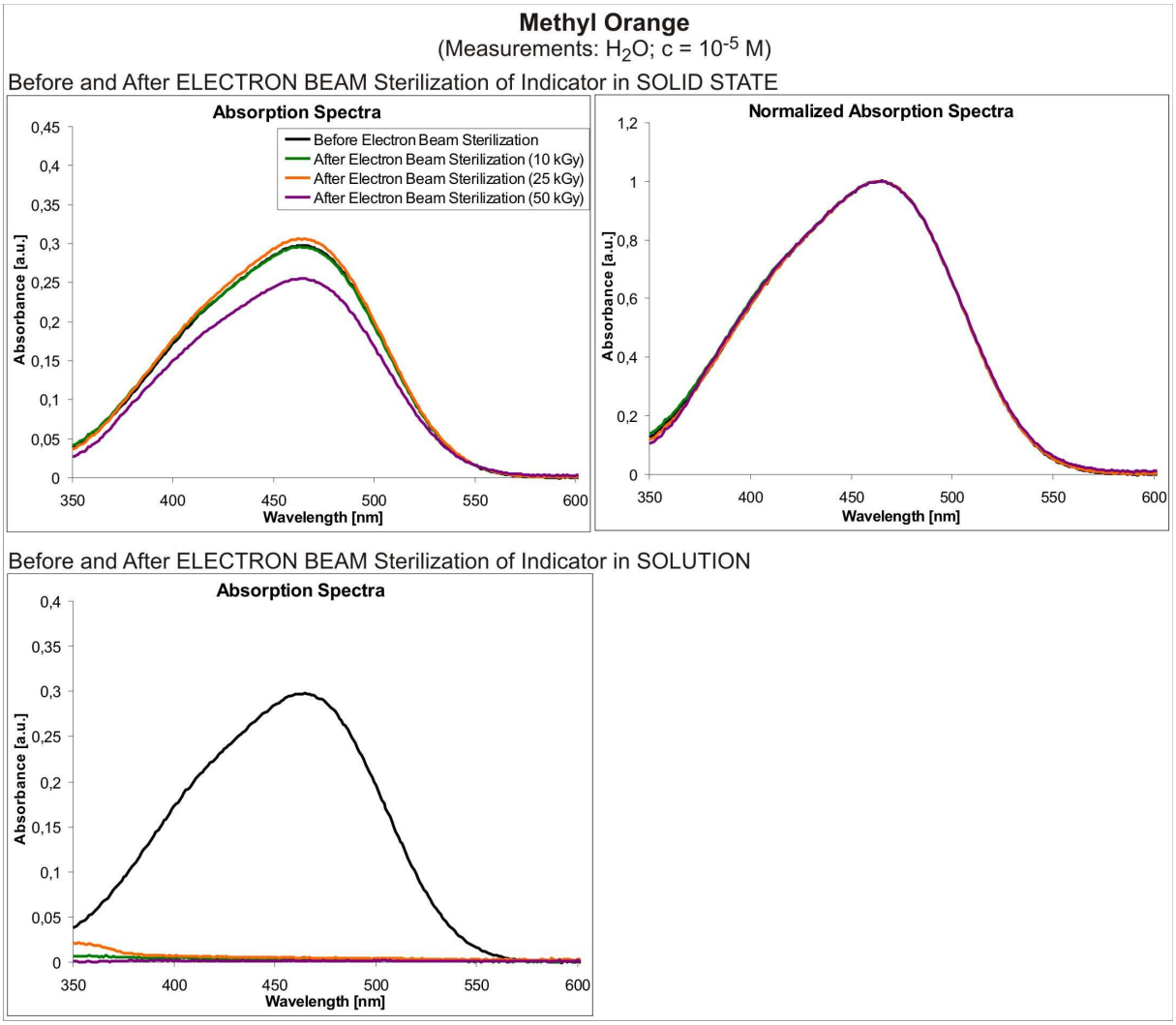

Solid State

E-BEAM S.	Absorption Spectra			Alterations	
Alterations in Absorption /Emission Intensity	10 kGy	0,57% decrease	Alterations in Absorption /Emission Curve Form	10 kGy	Unaltered.
	25 kGy	2,76% decrease		25 kGy	Unaltered.
	50 kGy	14,28% decrease		50 kGy	Unaltered.

Solution

E-BEAM S.	Absorption Spectra			Alterations	
Alterations in Absorption /Emission Intensity	10 kGy	99,45% decrease	Alterations in Absorption /Emission Curve Form	10 kGy	Disappearance of the characteristic absorption curve form.
	25 kGy	Decrease		25 kGy	Disappearance of the characteristic absorption curve form.
	50 kGy	Decrease		50 kGy	Disappearance of the characteristic absorption curve form.

C
Radiation Sterilization of Optical Sensors

TABLE OF CONTENTS

C RADIATION STERILIZATION OF OPTICAL SENSORS **315**

Optical OXYGEN SENSORS **323**

C.1 Iridium(III) Coumarin Complex immobilized in Cellulose Acetate **323**
C.1.1 Gamma Sterilization 323
C.1.2 Electron Beam Sterilization 325

C.2 Iridium(III) Coumarin Complex immobilized in Ethyl Cellulose **327**
C.2.1 Gamma Sterilization 327
C.2.2 Electron Beam Sterilization 329

C.3 Iridium(III) Coumarin Complex immobilized in HydroGel HydroMed D4/D7 **331**
C.3.1 Gamma Sterilization 331
C.3.2 Electron Beam Sterilization 333

C.4 Iridium(III) Coumarin Complex immobilized in HydroThane with 5% water content **335**
C.4.1 Gamma Sterilization 335
C.4.2 Electron Beam Sterilization 337

C.5 Iridium(III) Coumarin Complex immobilized in Poly(Sulfone) **339**
C.5.1 Gamma Sterilization 339
C.5.2 Electron Beam Sterilization 341

C.6 Iridium(III) Coumarin Complex immobilized in Poly(PhenylSilsesQuioxane) **343**
C.6.1 Gamma Sterilization 343
C.6.2 Electron Beam Sterilization 345

C.7 Iridium(III) Coumarin Complex immobilized in Poly(Styrene) **347**
C.7.1 Gamma Sterilization 347
C.7.2 Electron Beam Sterilization 349

C.8 Iridium(III) Coumarin Complex immobilized in Poly(Styrene-co-AcryloNitrile) **351**
C.8.1 Gamma Sterilization 351
C.8.2 Electron Beam Sterilization 353

C.9 Iridium(III) Coumarin Complex immobilized in Poly(Styrene-co-MaleicAnhydride) **355**
C.9.1 Gamma Sterilization 355
C.9.2 Electron Beam Sterilization 357

C.10 Platinum(II)Tetrakis(PentaFluorPhenyl)Porphyrin (PtTFPP) immobilized in Cellulose Acetate **359**
C.10.1 Gamma Sterilization 359
C.10.2 Electron Beam Sterilization 361

C.11 Platinum(II)Tetrakis(PentaFluorPhenyl)Porphyrin (PtTFPP) immobilized in Ethyl Cellulose **363**
C.11.1 Gamma Sterilization 363
C.11.2 Electron Beam Sterilization 365

C.12 Platinum(II)Tetrakis(PentaFluorPhenyl)Porphyrin (PtTFPP) immobilized in HydroGel D4/D7 **367**

C.12.1 Gamma Sterilization 367
C.12.2 Electron Beam Sterilization 369

C.13 Platinum(II)Tetrakis(PentaFluorPhenyl)Porphyrin (PtTFPP) immobilized in HydroThane 5 371
C.13.1 Gamma Sterilization 371
C.13.2 Electron Beam Sterilization 373

C.14 Platinum(II)Tetrakis(PentaFluorPhenyl)Porphyrin (PtTFPP) immobilized in PolySulfone 375
C.14.1 Gamma Sterilization 375
C.14.2 Electron Beam Sterilization 377

C.15 Platinum(II)Tetrakis(PentaFluorPhenyl)Porphyrin (PtTFPP) immobilized in PolyPhenylSilses Quioxane 379
C.15.1 Gamma Sterilization 379
C.15.2 Electron Beam Sterilization 381

C.16 Platinum(II)Tetrakis(PentaFluorPhenyl)Porphyrin (PtTFPP) immobilized in PolyStyrene 383
C.16.1 Gamma Sterilization 383
C.16.2 Electron Beam Sterilization 385

C.17 Platinum(II)Tetrakis(PentaFluorPhenyl)Porphyrin (PtTFPP) immobilized in PolyStyrene-co- Acrylonitrile 387
C.17.1 Gamma Sterilization 387
C.17.2 Electron Beam Sterilization 389

C.18 Platinum(II)Tetrakis(PentaFluorPhenyl)Porphyrin (PtTFPP) immobilized in PolyStyrene-co-MaleicAnhydride (PSMA93) 391
C.18.1 Gamma Sterilization 391
C.18.2 Electron Beam Sterilization 393

C.19 Platinum(II) OctaEthyl Porphyrin (=PtOEP) immobilized in PolyStyrene 395
C.19.1 Gamma Sterilization 395
C.19.2 Electron Beam Sterilization 397

C.20 Platinum(II) meso-tetra(4-FluoroPhenyl) TetraBenzoPorphyrin (=PtTPTBPF) immobilized in PolyStyrene 399
C.20.1 Gamma Sterilization 399
C.20.2 Electron Beam Sterilization 401

C.21 Palladium(II)meso-tetra(4-FluoroPhenyl) TetraBenzoPorphyrin (=PdTPTBPF) immobilized in PolyStyrene 403
C.21.1 Gamma Sterilization 403
C.21.2 Electron Beam Sterilization 405

C.22 Ruthenium(II) DiPhenylPhenanthroline DiChloride ($Ru(dpp)_3Cl_2$) immobilized in Cellulose Acetate 407
C.22.1 Gamma Sterilization 407
C.22.2 Electron Beam Sterilization 409

C.23 Ruthenium(II) DiPhenylPhenanthroline DiChloride ($Ru(dpp)_3Cl_2$) immobilized in Ethyl Cellulose 411
C.23.1 Gamma Sterilization 411
C.23.2 Electron Beam Sterilization 413

C.24 Ruthenium(II) DiPhenylPhenanthroline DiChloride ($Ru(dpp)_3Cl_2$) immobilized in HydroGel D4/D7 **415**
C.24.1 Gamma Sterilization 415
C.24.2 Electron Beam Sterilization 417

C.25 Ruthenium(II) DiPhenylPhenanthroline DiChloride ($Ru(dpp)_3Cl_2$) immobilized in HydroThane5 **419**
C.25.1 Gamma Sterilization 419
C.25.2 Electron Beam Sterilization 421

C.26 Ruthenium(II) DiPhenylPhenanthroline DiChloride ($Ru(dpp)_3Cl_2$) immobilized in PolySulfone **423**
C.26.1 Gamma Sterilization 423
C.26.2 Electron Beam Sterilization 425

C.27 Ruthenium(II) DiPhenylPhenanthroline DiChloride ($Ru(dpp)_3Cl_2$) immobilized in PolyPhenyl SilsesQuioxane **427**
C.27.1 Gamma Sterilization 427
C.27.2 Electron Beam Sterilization 429

C.28 Ruthenium(II) DiPhenylPhenanthroline DiChloride ($Ru(dpp)_3Cl_2$) immobilized in PolyStyrene **431**
C.28.1 Gamma Sterilization 431
C.28.2 Electron Beam Sterilization 433

C.29 Ruthenium(II) DiPhenylPhenanthroline DiChloride ($Ru(dpp)_3Cl_2$) immobilized in PolyStyrene-co-Acrylonitrile **435**
C.29.1 Gamma Sterilization 435
C.29.2 Electron Beam Sterilization 437

C.30 Ruthenium(II) DiPhenylPhenanthroline DiChloride ($Ru(dpp)_3Cl_2$) immobilized in PolyStyrene-co-MaleicAnhydride (PSMA93) **439**
C.30.1 Gamma Sterilization 439
C.30.2 Electron Beam Sterilization 441

Optical pH SENSORS **443**

C.31 HPTS(DHA_3) immobilized in HydroGel D4 **443**
C.31.1 Gamma Sterilization 443
C.31.1.1 Sterilization in Buffer Solution 446
C.31.2 Electron Beam Sterilization 449
C.31.2.1 Sterilization in Water 452

C.32 2´,7´-DiHexylFluorescein OctadecylEster immobilized in HydroMed Hydrogel D4 **455**
C.32.1 Gamma Sterilization 455
C.32.1.1 Sterilization in Water 457
C.32.2 Electron Beam Sterilization 459
C.32.2.1 Sterilization in Water 461

C.33 2´,7´-DiHexylFluorescein OctadecylEster immobilized in Poly(2-HydroxyEthyl MethAcrylate) (=pHEMA) **463**
C.33.1 Gamma Sterilization 463
C.33.1.1 Sterilization in Water 466
C.33.2 Electron Beam Sterilization 468
C.33.2.1 Sterilization in Water 470

C.34 2´,7´-DiHexyl-N-Octadecyl-CarboxAmidoFluorescein (=DHFA) immobilized in HydroMed Hydrogel D4 **472**
C.34.1 Gamma Sterilization 472
C.34.1.1 Sterilization in Water 474
C.34.2 Electron Beam Sterilization 476
C.34.2.1 Sterilization in Water 478

C.35 2´,7´-DiHexyl-N-Octadecyl-CarboxAmidoFluorescein (=DHFA) immobilized in Poly(2-HydroxyEthyl Methacrylate) (=pHEMA) **480**
C.35.1 Gamma Sterilization 480
C.35.1.1 Sterilized in Water 483
C.35.2 Electron Beam Sterilization 485
C.35.2.1 Sterilization in Water 487

C.36 pH Sensitive Coumarin immobilized in HydroMed Hydrogel D4 **489**
C.36.1 Gamma Sterilization 489
C.36.1.1 Sterilized in Water 492
C.36.2 Electron Beam Sterilization 494
C.36.2.1 Sterilization in Water 496

C.37 pH Sensitive Coumarin immobilized in Poly(2-HydroxyEthyl Methacrylate) (=pHEMA) **498**
C.37.1 Gamma Sterilization 498
C.37.1.1 Sterilization in Water 501
C.37.2 Electron Beam Sterilization 503
C.37.2.1 Sterilization in Water 505

C.38 PET Perylene BisImide immobilized in HydroMed Hydrogel D4 **506**
C.38.1 Gamma Sterilization 506
C.38.1.1 Sterilization in Water 509
C.38.2 Electron Beam Sterilization 512
C.38.2.1 Sterilization in Water 515

C.39 BromoPhenol Blue immobilized in HydroMed Hydrogel D4 **518**
C.39.1 Gamma Sterilization 518
C.39.2 Electron Beam Sterilization 519

C.40 Thymol Blue immobilized in HydroMed Hydrogel D4 **520**
C.40.1 Gamma Sterilization 520
C.40.2 Electron Beam Sterilization 522

C.41 BromoThymol Blue immobilized in HydroMed Hydrogel D4 **523**
C.41.1 Gamma Sterilization 523
C.41.2 Electron Beam Sterilization 525

C.42 Methyl Orange immobilized in HydroMed Hydrogel D4 **526**
C.42.1 Gamma Sterilization 526
C.42.2 Electron Beam Sterilization 527

Optical TEMPERATURE SENSORS **528**

C.43 Europium(III) Complex with 4-(4,6-di(1H-indazol-1-yl)-1,3,5-triazin-2-yl)-N,N-DiEthyl Benzen Amine (=Eu(tta)$_3$DEADIT) immobilized in PolyStyrene-co-Acrylonitrile **528**
C.43.1 Gamma Sterilization 528
C.43.2 Electron Beam Sterilization 529

C.44 Europium(III) Complex with 4-(4,6-di(1H-indazol-1-yl)-1,3,5-triazin-2-yl)-N,N-DiEthyl Benzen Amine (=Eu(tta)$_3$DEADIT) immobilized in PolyVinylideneChloride-co-Acrylonitrile **531**
C.44.1 Gamma Sterilization 531
C.44.2 Electron Beam Sterilization 532

C.45 Europium(III) Complex with 4-(4,6-di(1H-indazol-1-yl)-1,3,5-triazin-2-yl)-N,N-DiEthyl Benzen Amine (=Eu(tta)$_3$DEADIT) immobilized in PolyMethAcryloNitrile **534**
C.45.1 Gamma Sterilization 534
C.45.2 Electron Beam Sterilization 535

C.46 DiChloroTrisPhenanthroline Ruthenium(II)Hydrate immobilized in PolyVinylideneChloride-co-Acrylonitrile **537**
C.46.1 Gamma Sterilization 537
C.46.2 Electron Beam Sterilization 538

C.47 DiChloroTrisPhenanthroline Ruthenium(II)Hydrate immobilized in PolyMethAcryloNitrile **540**
C.47.1 Gamma Sterilization 540
C.47.2 Electron Beam Sterilization 541

Optical AMMONIA SENSORS **542**

C.48 Eosin EthylEster immobilized in Cellulose Acetate **542**
C.48.1 Gamma Sterilization 542
C.48.2 Electron Beam Sterilization 543

C.49 Eosin EthylEster immobilized in Hydrogel D7 **544**
C.49.1 Gamma Sterilization 544
C.49.2 Electron Beam Sterilization 545

C.50 Eosin EthylEster immobilized in Ethyl Cellulose **546**
C.50.1 Gamma Sterilization 546
C.50.2 Electron Beam Sterilization 547

C.51 Eosin EthylEster immobilized in PolyMethylMethAcrylate (=PMMA) **548**
C.51.1 Gamma Sterilization 548
C.51.2 Electron Beam Sterilization 549

C.52 DiChloroFluorescein immobilized in Cellulose Acetate **550**
C.52.1 Gamma Sterilization 550
C.52.2 Electron Beam Sterilization 551

C.53 DiChloroFluorescein immobilized in Hydrogel D7 **552**
C.53.1 Gamma Sterilization 552
C.53.2 Electron Beam Sterilization 553

C.54 DiChloroFluorescein immobilized in Ethyl Cellulose **554**
C.54.1 Gamma Sterilization 554
C.54.2 Electron Beam Sterilization 555

C.55 BromoPhenolBlue immobilized in Cellulose Acetate **556**
C.55.1 Gamma Sterilization 556
C.55.2 Electron Beam Sterilization 557

C.56 BromoPhenolBlue immobilized in Hydrogel D7 **558**
C.56.1 Gamma Sterilization 558

C.56.2 Electron Beam Sterilization 559

C.57.BromoPhenolBlue immobilized in Ethyl Cellulose 560
C.57.1 Gamma Sterilization 560
C.57.2 Electron Beam Sterilization 561

C.58 BromoPhenol Blue immobilized in PolyMethylMethAcrylate (=PMMA) 562
C.58.1 Gamma Sterilization 562
C.58.2 Electron Beam Sterilization 563

Optical OXYGEN SENSORS

C.1 Iridium(III) Coumarin Complex immobilized in Cellulose Acetate

C.1.1 Gamma Sterilization

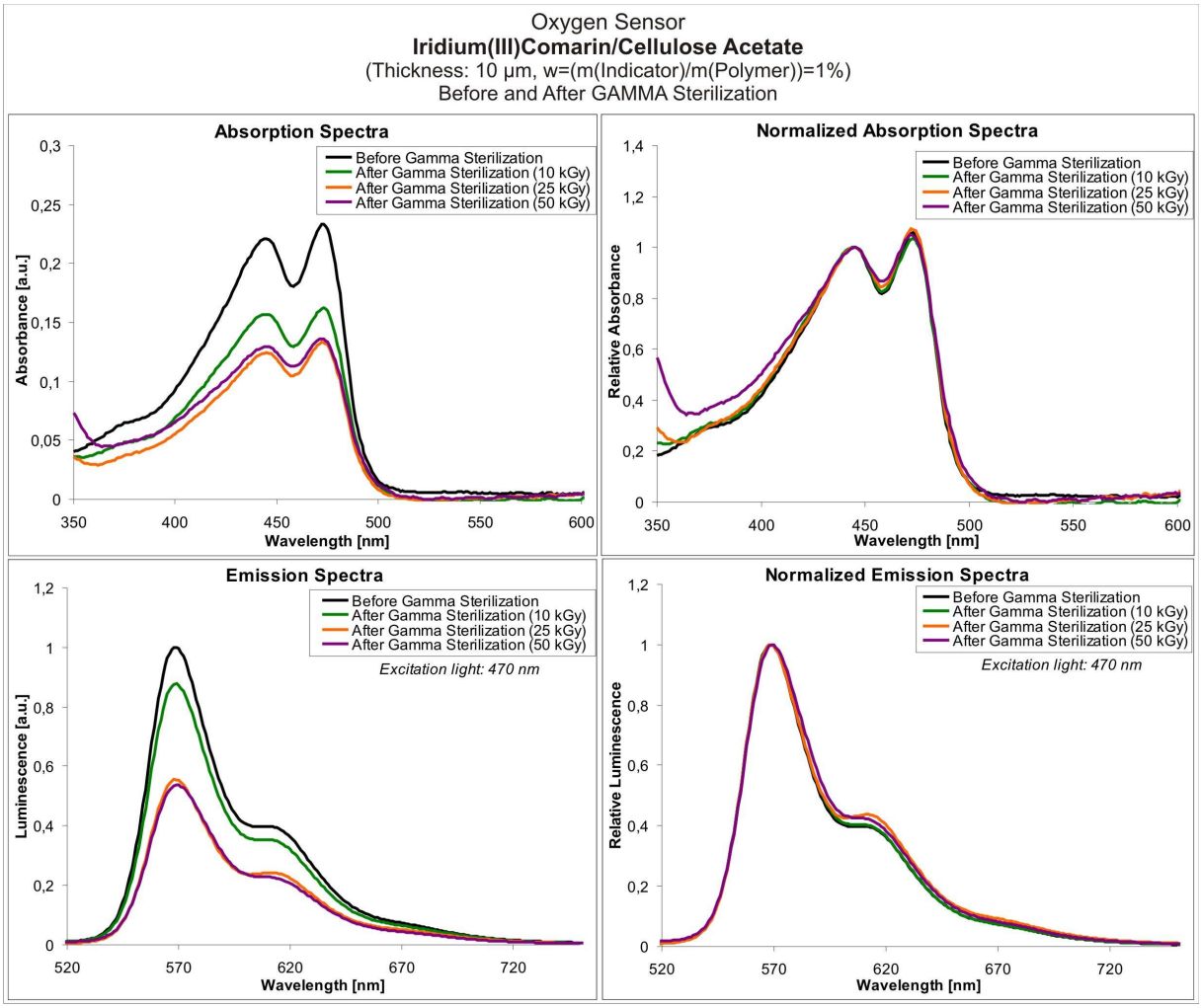

GAMMA Sterilization	Absorption Spectra		Emission Spectra	
Alterations in Absorption/Emission Intensity	10kGy	28,93% decrease	10kGy	12,30% decrease
	25 kGy	43,75% decrease	25 kGy	44,44% decrease
	50 kGy	41,18% decrease	50 kGy	46,25% decrease
Alterations in Absorption/Emission Curve Form	10kGy	Unaltered	10kGy	Unaltered
	25 kGy	Unaltered	25 kGy	Altered emission between 600-630 nm
	50 kGy	Altered absorption between 350-420 nm.	50 kGy	Altered emission between 600-630 nm

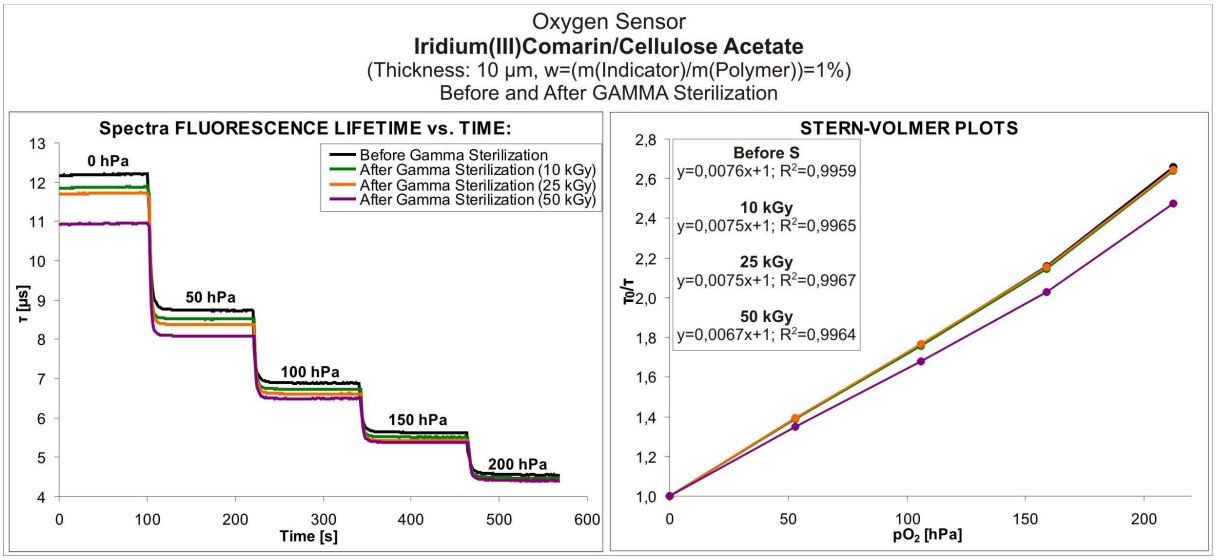

GAMMA Sterilization	Luminescence Lifetime		Stern-Volmer Plot	
Alterations in Luminescence Lifetime and Slope	10kGy	2,46% decrease of τ_0	10kGy	1,31% decrease of slope
		2,41% decrease of τ at 50 hPa		
		2,32% decrease of τ at 100 hPa		
		2,13% decrease of τ at 150 hPa		
		1,97% decrease of τ at 200 hPa		
	25 kGy	4,98% decrease of τ_0	25 kGy	1,31% decrease of slope
		4,12% decrease of τ at 50 hPa		
		4,06% decrease of τ at 100 hPa		
		3,37% decrease of τ at 150 hPa		
		3,51% decrease of τ at 200 hPa		
	50 kGy	9,84% decrease of τ_0	50 kGy	11,84% decrease of slope
		7,33% decrease of τ at 50 hPa		
		5,80% decrease of τ at 100 hPa		
		4,44% decrease of τ at 150 hPa		
		3,51% decrease of τ at 200 hPa		

C.1.2 Electron Beam Sterilization

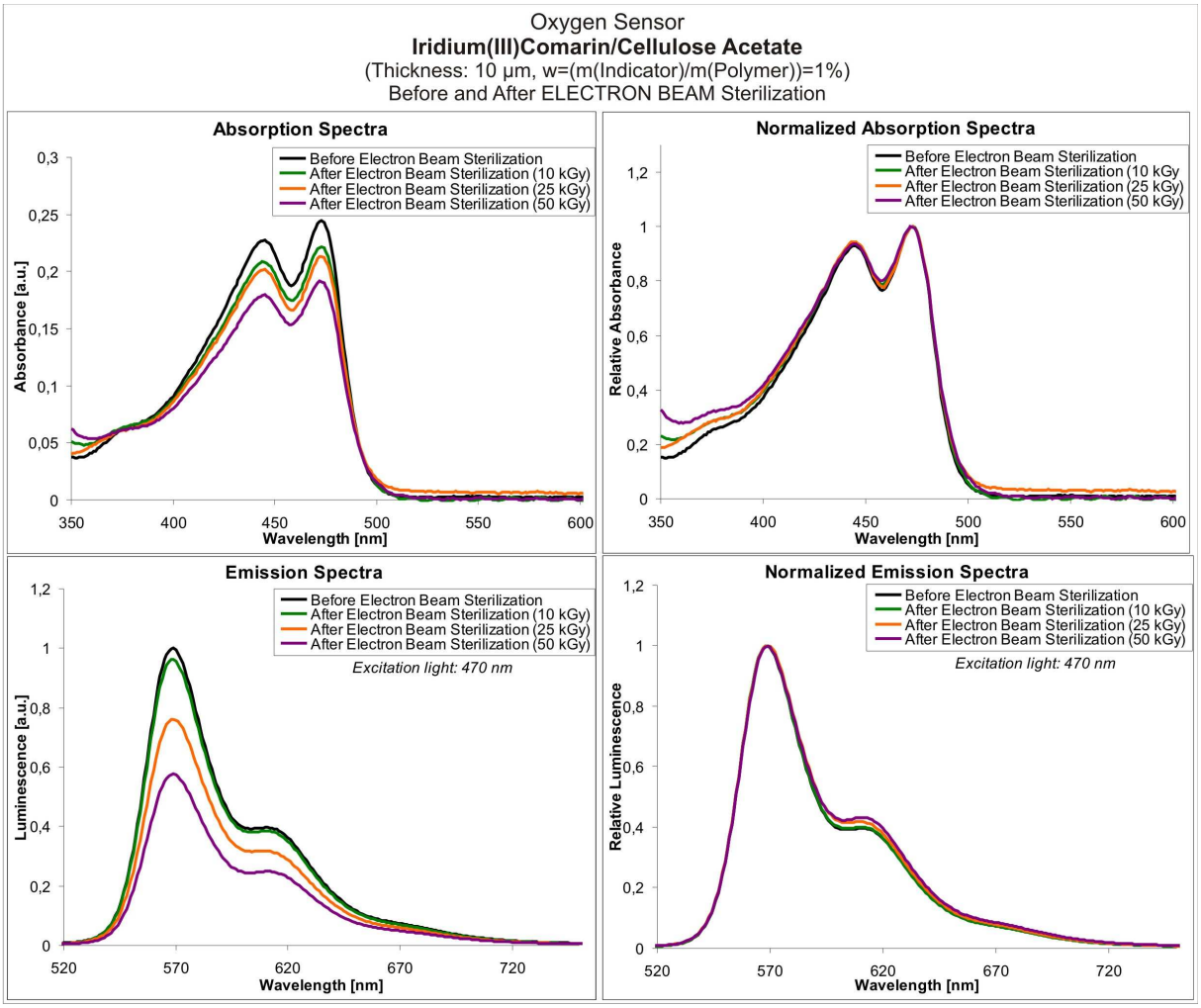

E-BEAM Sterilization	Absorption Spectra		Emission Spectra	
Alterations in Absorption/Emission Intensity	10kGy	9,46% decrease	10kGy	3,81% decrease
	25 kGy	12,70% decrease	25 kGy	23,96% decrease
	50 kGy	21,69% decrease	50 kGy	42,34% decrease
Alterations in Absorption/Emission Curve Form	10kGy	Altered absorption between 350-400 nm.	10kGy	Unaltered
	25 kGy	Altered absorption between 350-400 nm.	25 kGy	Altered emission between 600-630 nm
	50 kGy	Altered absorption between 350-400 nm.	50 kGy	Altered emission between 600-630 nm

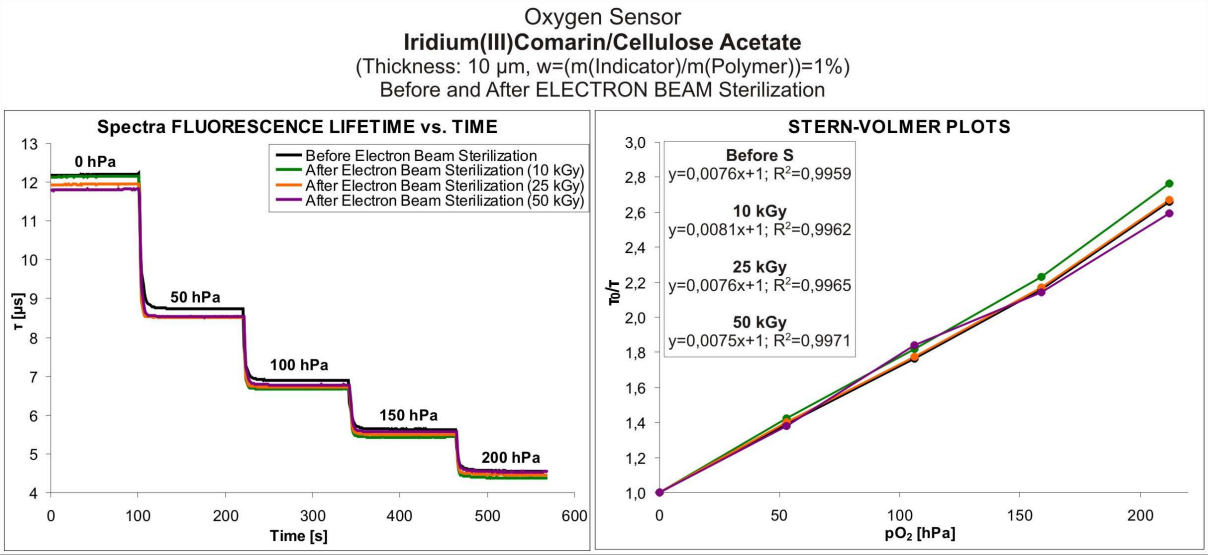

E-BEAM Sterilization	Luminescence Lifetime		Stern-Volmer Plot	
Alterations in Luminescence Lifetime and Slope	10kGy	0,82% decrease of τ_0	10kGy	6,17% increase of slope
		2,40% decrease of τ at 50 hPa		
		3,19% decrease of τ at 100 hPa		
		3,55% decrease of τ at 150 hPa		
		4,15% decrease of τ at 200 hPa		
	25 kGy	2,46% decrease of τ_0	25 kGy	Unaltered
		2,41% decrease of τ at 50 hPa		
		2,47% decrease of τ at 100 hPa		
		2,31% decrease of τ at 150 hPa		
		2,40% decrease of τ at 200 hPa		
	50 kGy	3,28% decrease of τ_0	50 kGy	1,31% decrease of slope
		2,30% decrease of τ at 50 hPa		
		1,60% decrease of τ at 100 hPa		
		1,24% decrease of τ at 150 hPa		
		0,87% decrease of τ at 200 hPa		

C.2 Iridium(III) Coumarin Complex immobilized in Ethyl Cellulose

C.2.1 Gamma Sterilization

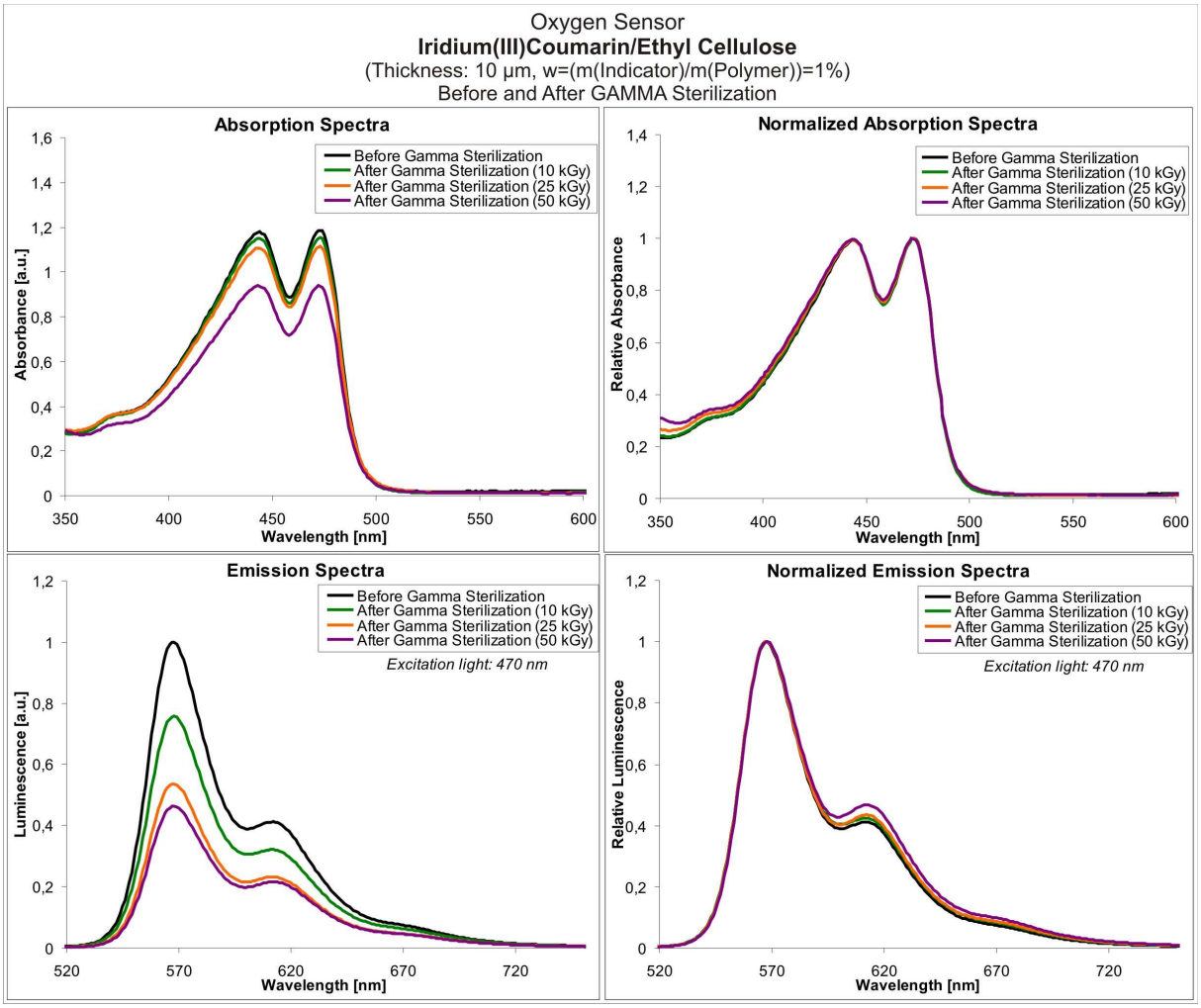

GAMMA Sterilization	Absorption Spectra		Emission Spectra	
Alterations in Absorption/Emission Intensity	10kGy	2,78% decrease	10kGy	24,24% decrease
	25 kGy	6,18% decrease	25 kGy	46,38% decrease
	50 kGy	20,83% decrease	50 kGy	53,64% decrease
Alterations in Absorption/Emission Curve Form	10kGy	Unaltered	10kGy	Unaltered
	25 kGy	Unaltered	25 kGy	Unaltered
	50 kGy	Unaltered	50 kGy	Altered emission between 595-680 nm

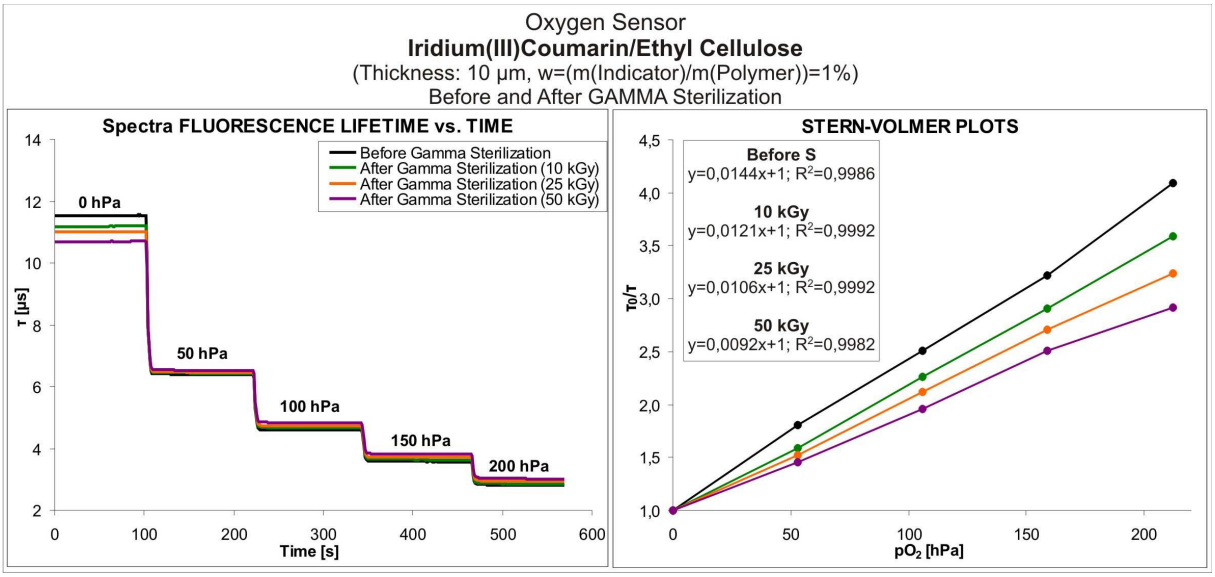

GAMMA Sterilization	Luminescence Lifetime		Stern-Volmer Plot	
Alterations in Luminescence Lifetime and Slope	10kGy	2,61% decrease of τ_0	10kGy	15,97% decrease of slope
		0,77% increase of τ at 50 hPa		
		3,19% increase of τ at 100 hPa		
		3,55% increase of τ at 150 hPa		
		4,15% increase of τ at 200 hPa		
	25 kGy	4,35% decrease of τ_0	25 kGy	26,39% decrease of slope
		1,24% increase of τ at 50 hPa		
		2,75% increase of τ at 100 hPa		
		3,50% increase of τ at 150 hPa		
		4,27% increase of τ at 200 hPa		
	50 kGy	6,96% decrease of τ_0	50 kGy	36,11% decrease of slope
		2,15% increase of τ at 50 hPa		
		4,76% increase of τ at 100 hPa		
		6,28% increase of τ at 150 hPa		
		6,95% increase of τ at 200 hPa		

C.2.2 Electron Beam Sterilization

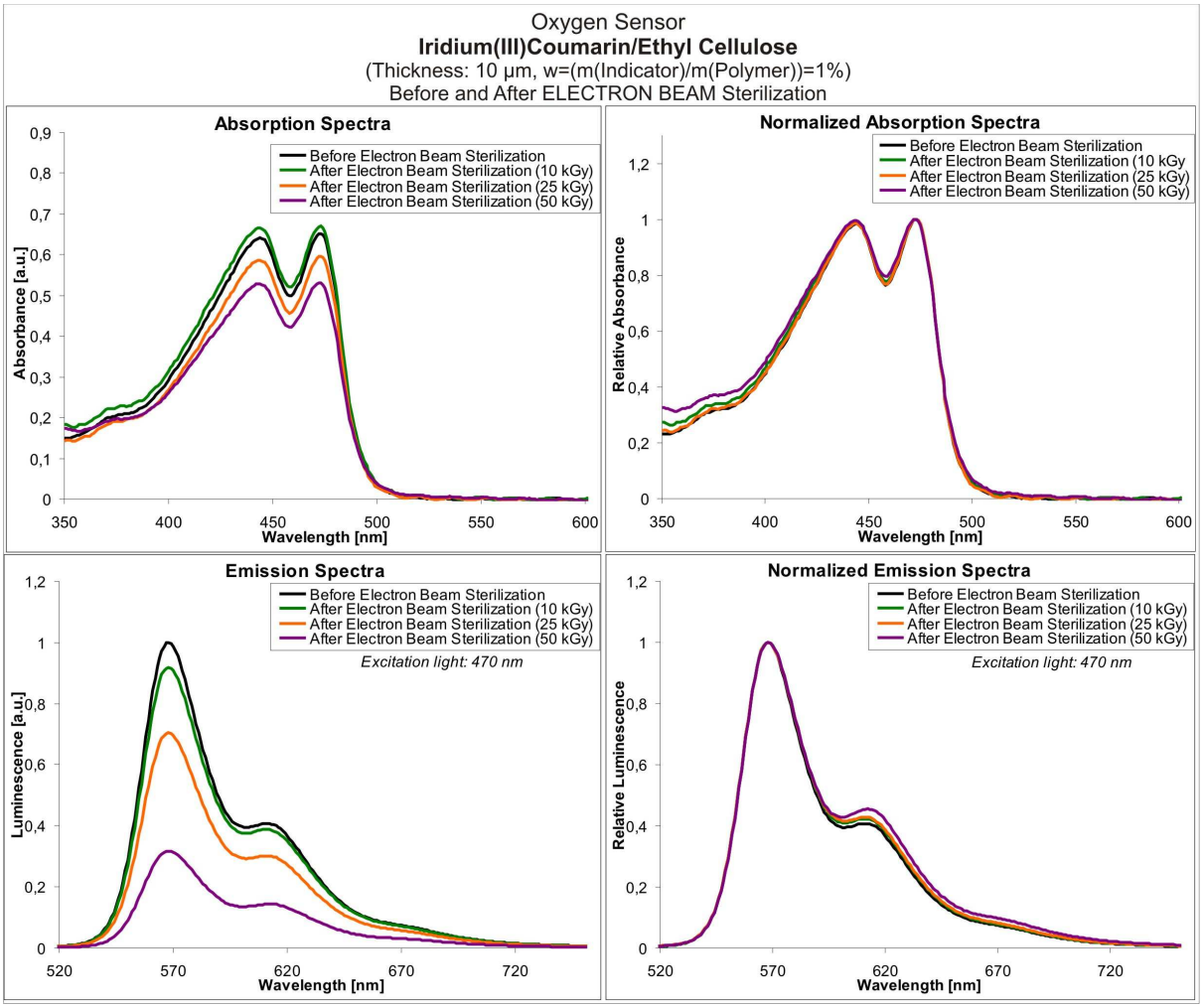

ELECTRON BEAM Sterilization	Absorption Spectra		Emission Spectra	
Alterations in Absorption/Emission Intensity	10kGy	2,68% increase	10kGy	8,23% decrease
	25 kGy	8,60% decrease	25 kGy	29,53% decrease
	50 kGy	18,55% decrease	50 kGy	68,31% decrease
Alterations in Absorption/Emission Curve Form	10kGy	Unaltered	10kGy	Unaltered
	25 kGy	Unaltered	25 kGy	Unaltered
	50 kGy	Altered absorption between 350-400 nm.	50 kGy	Altered emission between 590-720 nm

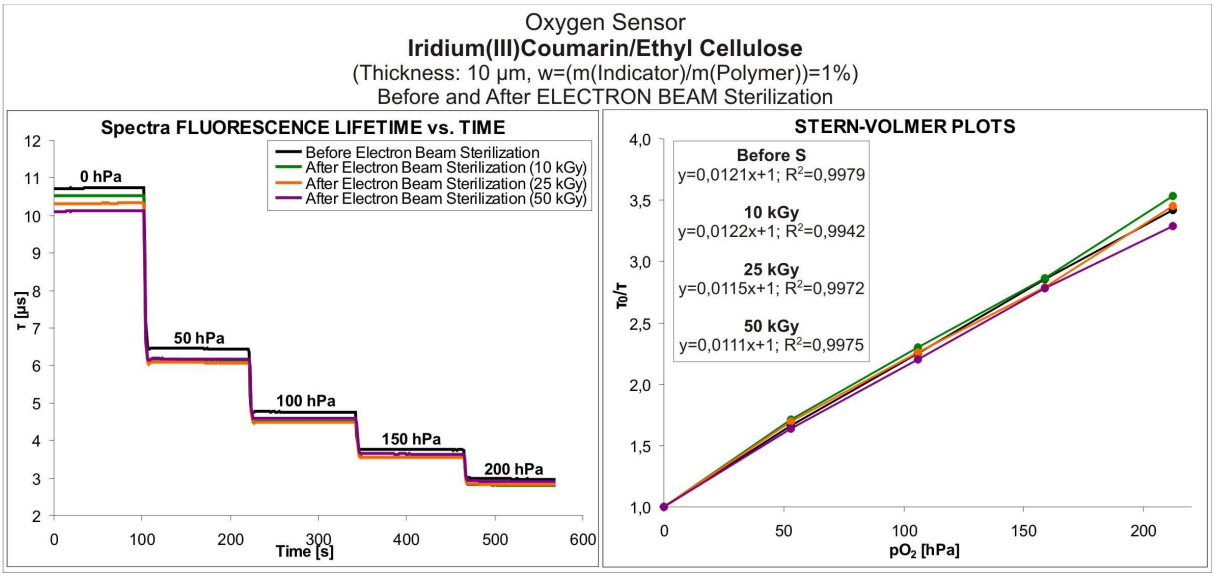

GAMMA Sterilization	Luminescence Lifetime		Stern-Volmer Plot	
Alterations in Luminescence Lifetime and Slope	10kGy	1,87% decrease of τ_0	10kGy	0,83% increase of slope
		4,64% decrease of τ at 50 hPa		
		5,24% decrease of τ at 100 hPa		
		5,59% decrease of τ at 150 hPa		
		5,39% decrease of τ at 200 hPa		
	25 kGy	3,74% decrease of τ_0	25 kGy	4,96% decrease of slope
		5,73% decrease of τ at 50 hPa		
		6,08% decrease of τ at 100 hPa		
		5,85% decrease of τ at 150 hPa		
		4,71% decrease of τ at 200 hPa		
	50 kGy	5,61% decrease of τ_0	50 kGy	8,26% decrease of slope
		4,33% decrease of τ at 50 hPa		
		3,77% decrease of τ at 100 hPa		
		2,92% decrease of τ at 150 hPa		
		2,36% decrease of τ at 200 hPa		

C.3 Iridium(III) Coumarin Complex immobilized in HydroGel HydroMed D4/D7

C.3.1 Gamma Sterilization

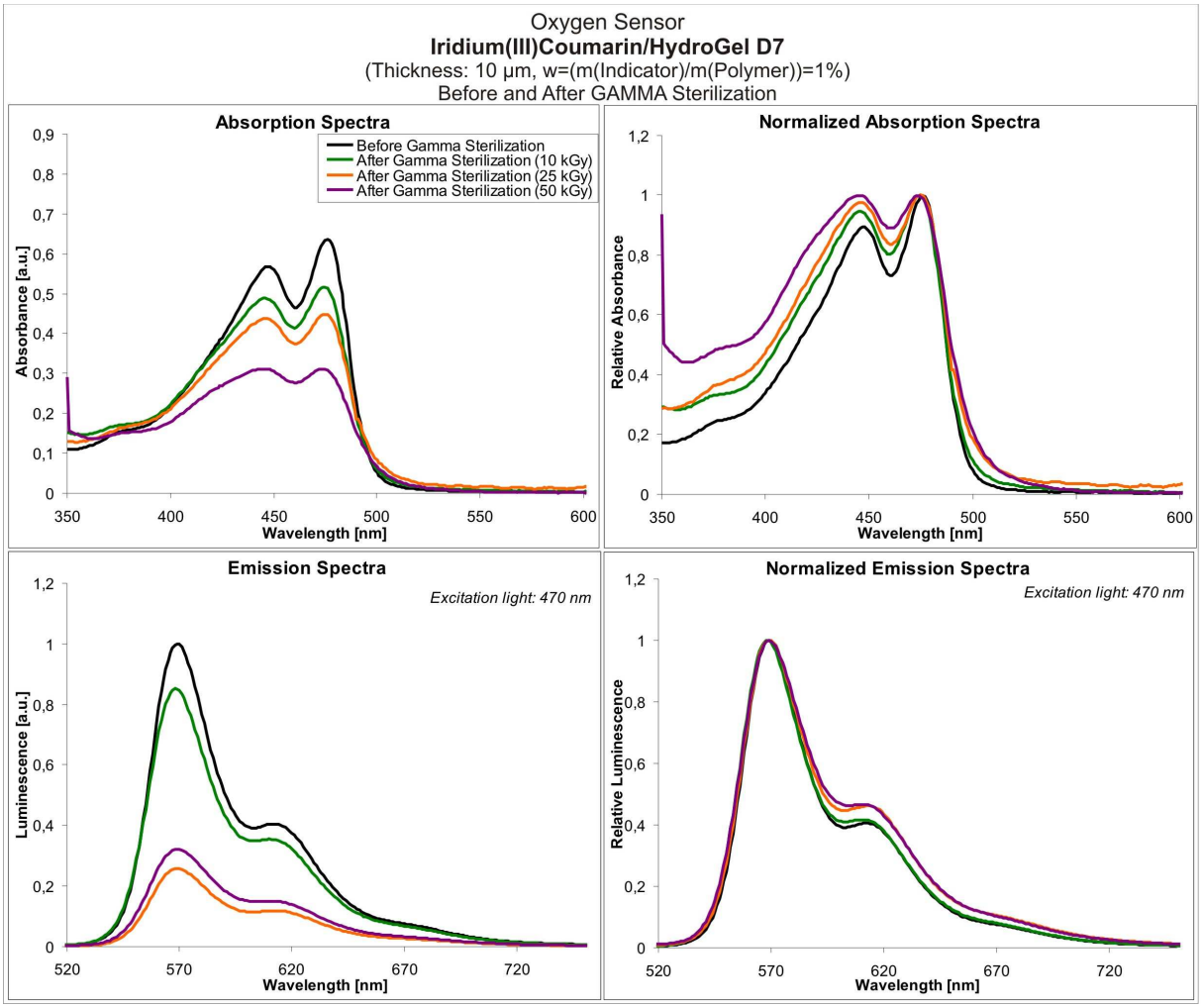

GAMMA Sterilization	Absorption Spectra		Emission Spectra	
Alterations in Absorption/Emission Intensity	10kGy	18,88% decrease	10kGy	14,85% decrease
	25 kGy	29,62% decrease	25 kGy	74,30% decrease
	50 kGy	51,00% decrease	50 kGy	67,74% decrease
Alterations in Absorption/Emission Curve Form	10kGy	Altered absorption between 350-470 nm and 500-535 nm. Hypsochromic shift of absorption maximum for 2 nm	10kGy	Altered emission between 597-612 nm
	25 kGy	Altered absorption between 350-470 nm and 490-600 nm. Hypsochromic shift of absorption maximum for 2 nm	25 kGy	Altered emission between 585-715 nm
	50 kGy	Altered absorption between 350-470 nm and 490-550 nm. Hypsochromic shift of absorption maximum for 2 nm	50 kGy	Altered emission between 585-715 nm

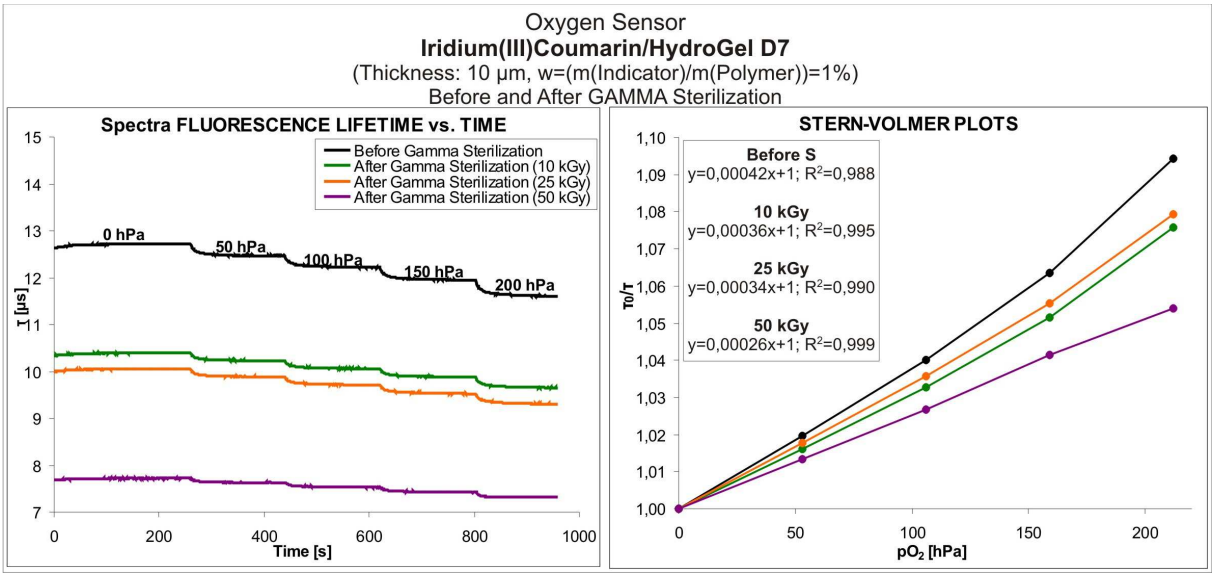

GAMMA Sterilization	Luminescence Lifetime		Stern-Volmer Plot	
Alterations in Luminescence Lifetime and Slope	10kGy	18,11% decrease of τ_0	10kGy	14,29% decrease of slope
		18,40% increase of τ at 50 hPa		
		17,21% increase of τ at 100 hPa		
		17,58% increase of τ at 150 hPa		
		16,64% increase of τ at 200 hPa		
	25 kGy	20,47% decrease of τ_0	25 kGy	19,33% decrease of slope
		20,88% increase of τ at 50 hPa		
		20,33% increase of τ at 100 hPa		
		20,50% increase of τ at 150 hPa		
		19,66% increase of τ at 200 hPa		
	50 kGy	39,21% decrease of τ_0	50 kGy	43,11% decrease of slope
		38,96% increase of τ at 50 hPa		
		38,20% increase of τ at 100 hPa		
		38,08% increase of τ at 150 hPa		
		36,89% increase of τ at 200 hPa		

C.3.2 Electron Beam Sterilization

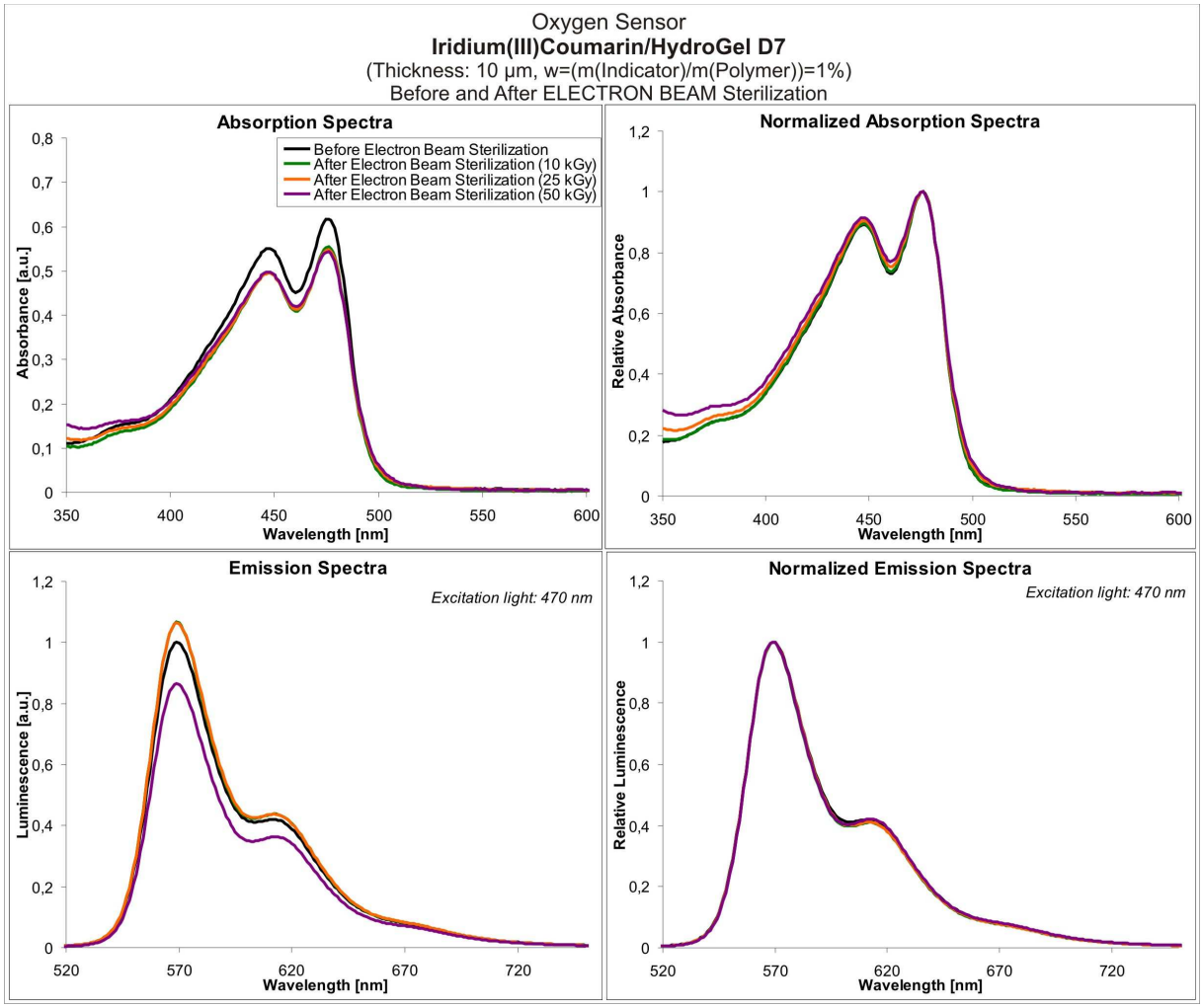

ELECTRON BEAM Sterilization	Absorption Spectra		Emission Spectra	
Alterations in Absorption/Emission Intensity	10kGy	10,27% decrease	10kGy	6,21% increase
	25 kGy	11,32% decrease	25 kGy	6,01% increase
	50 kGy	12,01% decrease	50 kGy	13,57% decrease
Alterations in Absorption/Emission Curve Form	10kGy	Unaltered	10kGy	Unaltered
	25 kGy	Unaltered	25 kGy	Unaltered
	50 kGy	Altered absorption between 350-415 nm.	50 kGy	Unaltered

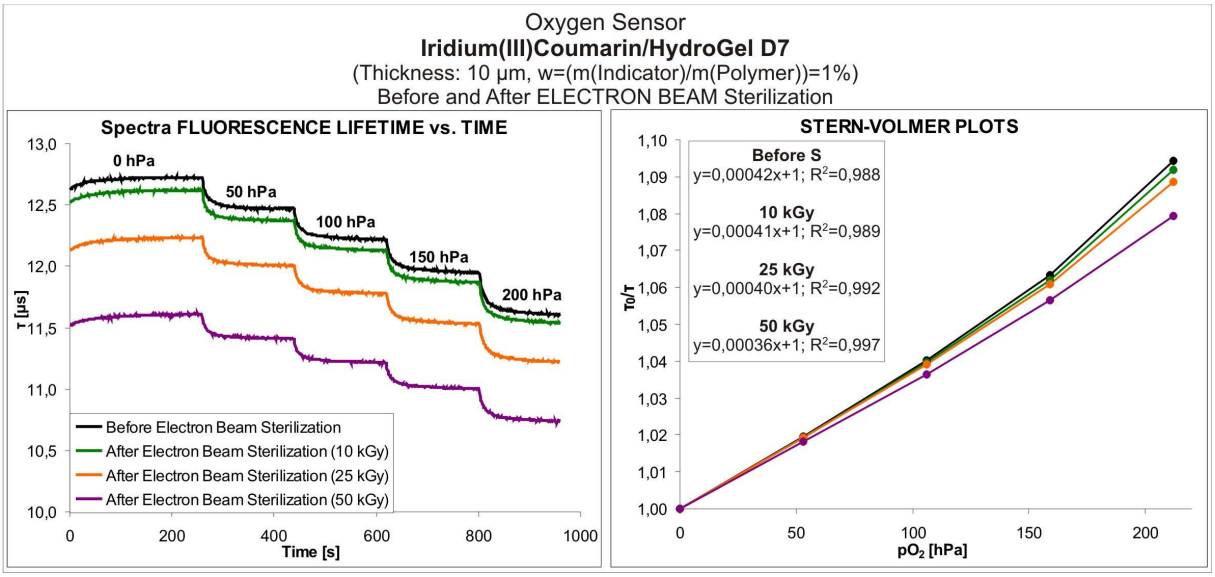

GAMMA Sterilization	Luminescence Lifetime		Stern-Volmer Plot	
Alterations in Luminescence Lifetime and Slope	10kGy	1,57% decrease of τ_0	10kGy	2,38% decrease of slope
		1,59% decrease of τ at 50 hPa		
		1,64% decrease of τ at 100 hPa		
		0,83% decrease of τ at 150 hPa		
		1,72% decrease of τ at 200 hPa		
	25 kGy	5,51% decrease of τ_0	25 kGy	4,76% decrease of slope
		5,56% decrease of τ at 50 hPa		
		4,92% decrease of τ at 100 hPa		
		3,33% decrease of τ at 150 hPa		
		5,17% decrease of τ at 200 hPa		
	50 kGy	8,66% decrease of τ_0	50 kGy	14,29% decrease of slope
		7,94% decrease of τ at 50 hPa		
		8,20% decrease of τ at 100 hPa		
		8,33% decrease of τ at 150 hPa		
		7,76% decrease of τ at 200 hPa		

C.4 Iridium(III) Coumarin Complex immobilized in HydroThane with 5% water content

C.4.1 Gamma Sterilization

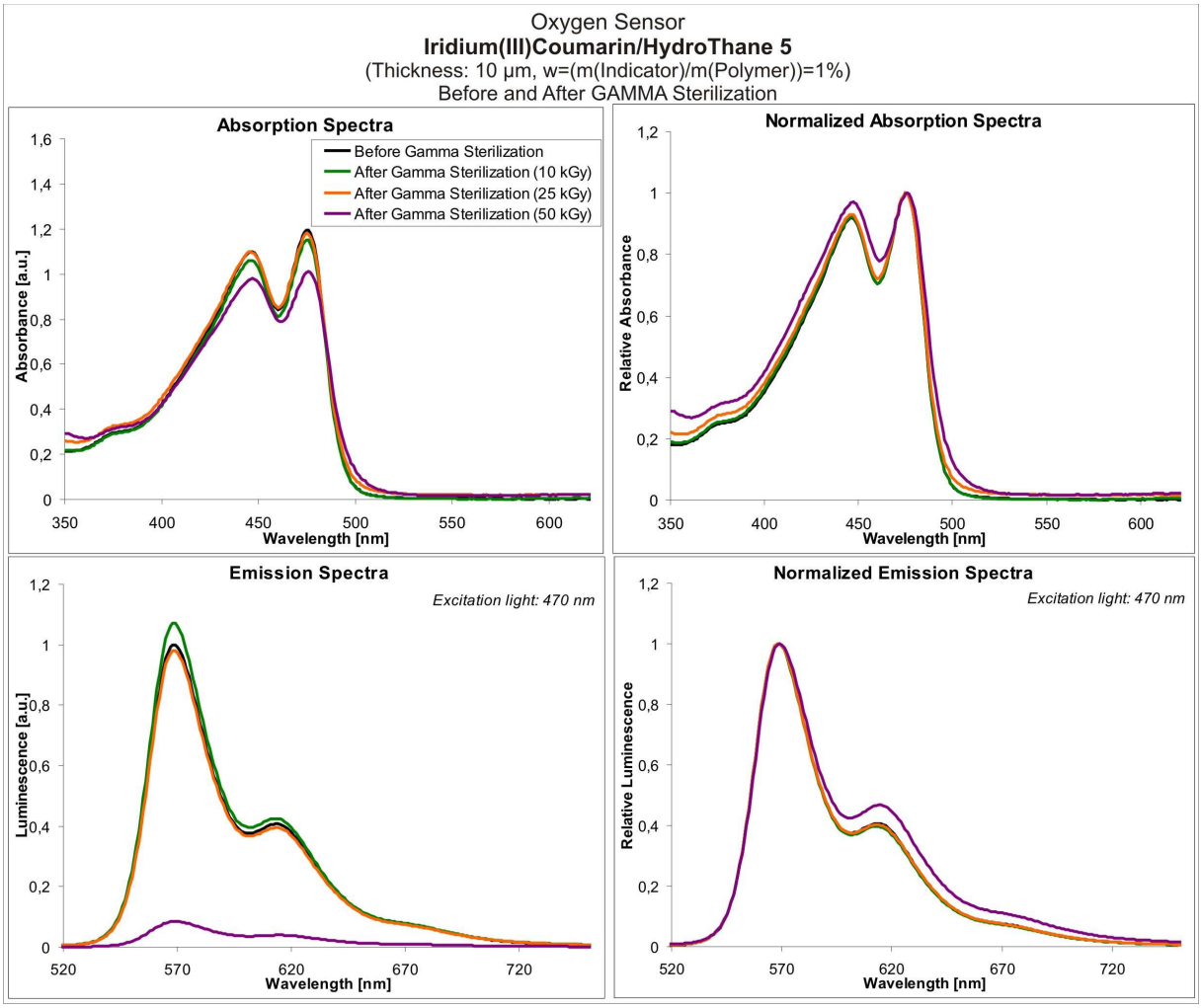

GAMMA Sterilization	Absorption Spectra		Emission Spectra	
Alterations in Absorption/Emission Intensity	10kGy	3,75% decrease	10kGy	6,64% increase
	25 kGy	1,33% decrease	25 kGy	2,00% decrease
	50 kGy	15,56% decrease	50 kGy	91,54% decrease
Alterations in Absorption/Emission Curve Form	10kGy	Unaltered	10kGy	Unaltered
	25 kGy	Altered absorption between 350-400 nm and 500-520 nm.	25 kGy	Unaltered
	50 kGy	Altered absorption between 350-470 nm and 490-520 nm.	50 kGy	Altered emission between 590-740 nm

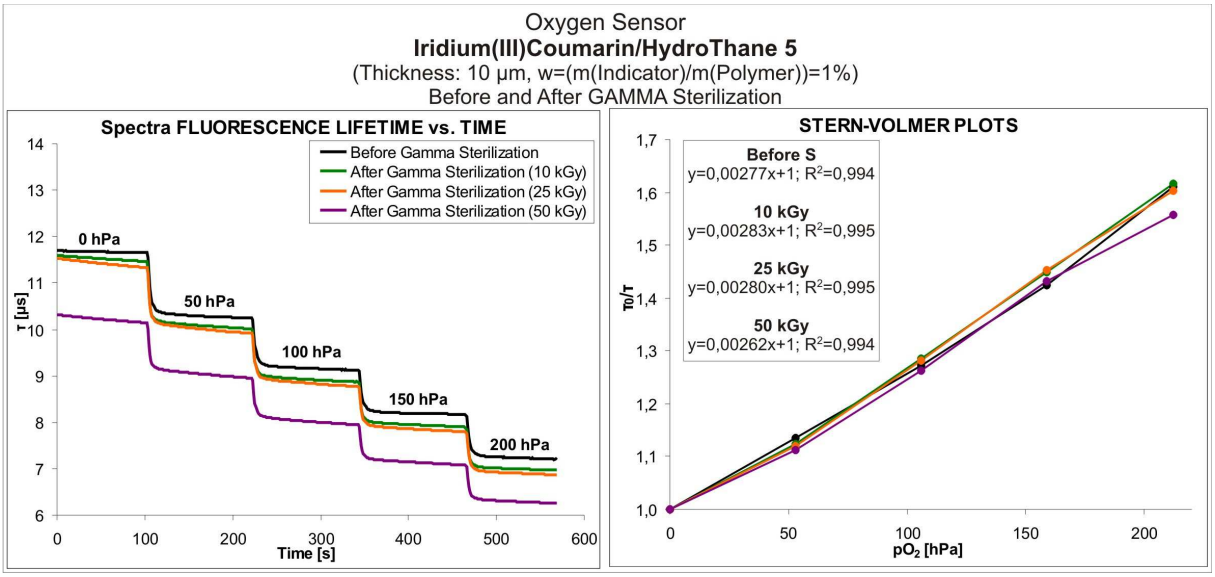

GAMMA Sterilization	Luminescence Lifetime		Stern-Volmer Plot	
Alterations in Luminescence Lifetime and Slope	10kGy	1,71% decrease of τ_0	10kGy	2,12% increase of slope
		1,94% increase of τ at 50 hPa		
		2,62% increase of τ at 100 hPa		
		3,05% increase of τ at 150 hPa		
		3,45% increase of τ at 200 hPa		
	25 kGy	2,56% decrease of τ_0	25 kGy	1,07% increase of slope
		2,91% increase of τ at 50 hPa		
		3,60% increase of τ at 100 hPa		
		4,27% increase of τ at 150 hPa		
		4,70% increase of τ at 200 hPa		
	50 kGy	12,82% decrease of τ_0	50 kGy	5,42% decrease of slope
		12,33% increase of τ at 50 hPa		
		12,55% increase of τ at 100 hPa		
		12,94% increase of τ at 150 hPa		
		13,12% increase of τ at 200 hPa		

C.4.2 Electron Beam Sterilization

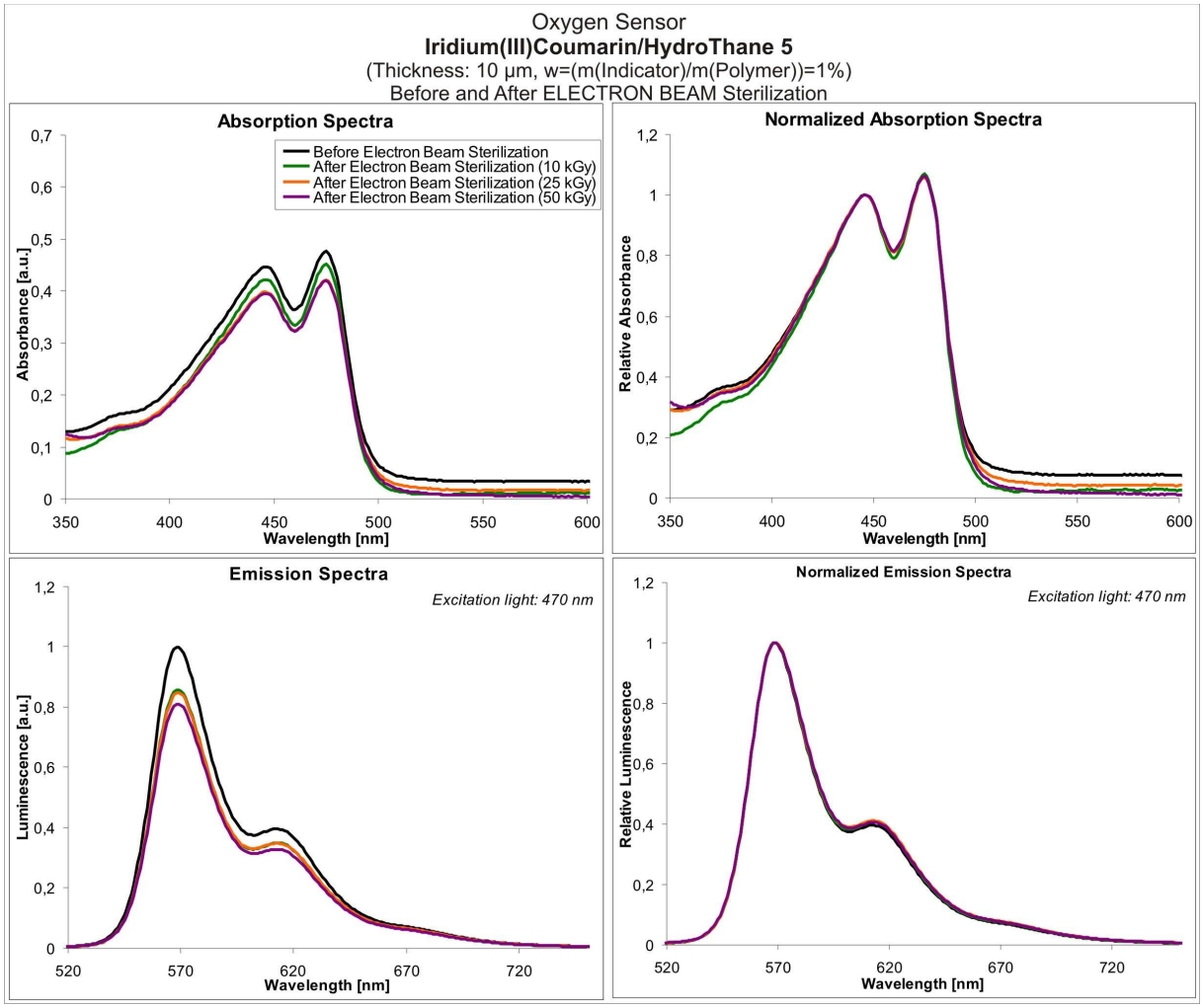

E-BEAM Sterilization	Absorption Spectra		Emission Spectra	
Alterations in Absorption/Emission Intensity	10kGy	5,39% decrease	10kGy	14,18% decrease
	25 kGy	10,75% decrease	25 kGy	15,20% decrease
	50 kGy	11,36% decrease	50 kGy	18,93% decrease
Alterations in Absorption/Emission Curve Form	10kGy	Altered absorption between 350-400 nm and 500-800 nm..	10kGy	Unaltered
	25 kGy	Altered absorption between 500-800 nm.	25 kGy	Unaltered
	50 kGy	Altered absorption between 500-800 nm.	50 kGy	Unaltered

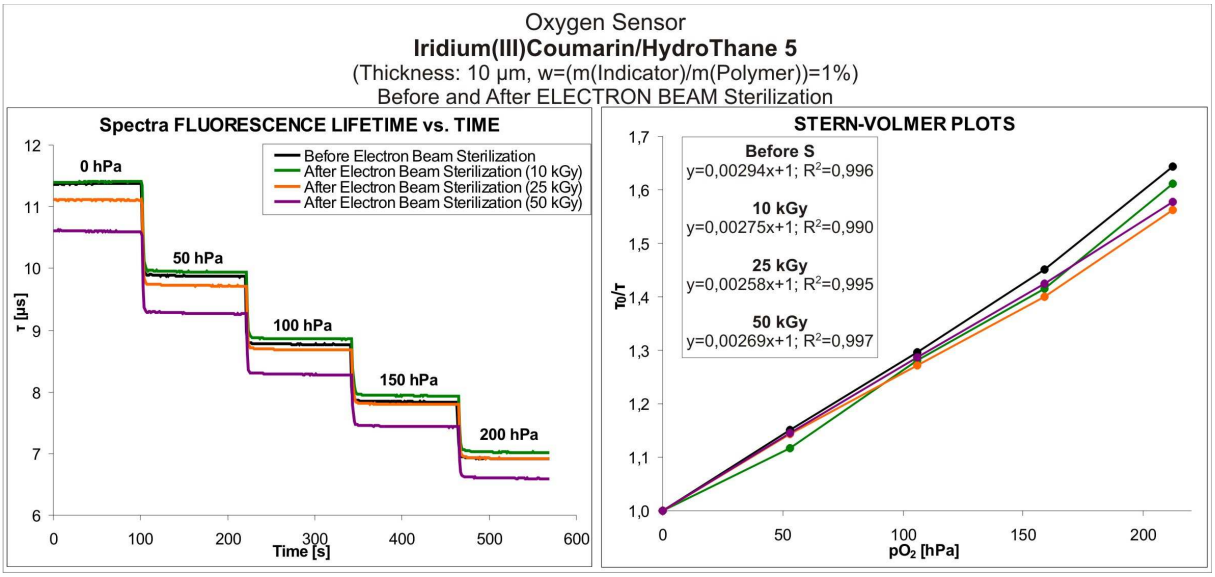

GAMMA Sterilization	Luminescence Lifetime		Stern-Volmer Plot	
Alterations in Luminescence Lifetime and Slope	10 kGy	0,88% decrease of τ_0	10kGy	6,46% decrease of slope
		0,71% increase of τ at 50 hPa		
		1,03% increase of τ at 100 hPa		
		1,15% increase of τ at 150 hPa		
		1,45% increase of τ at 200 hPa		
	25 kGy	2,63% decrease of τ_0	25 kGy	12,24% decrease of slope
		1,52% decrease of τ at 50 hPa		
		0,91% decrease of τ at 100 hPa		
		0,64% decrease of τ at 150 hPa		
		0,14% decrease of τ at 200 hPa		
	50 kGy	7,02% decrease of τ_0	50 kGy	8,50% decrease of slope
		6,07% decrease of τ at 50 hPa		
		5,47% decrease of τ at 100 hPa		
		5,23% decrease of τ at 150 hPa		
		4,77% decrease of τ at 200 hPa		

C.5 Iridium(III) Coumarin Complex immobilized in Poly(Sulfone)

C.5.1 Gamma Sterilization

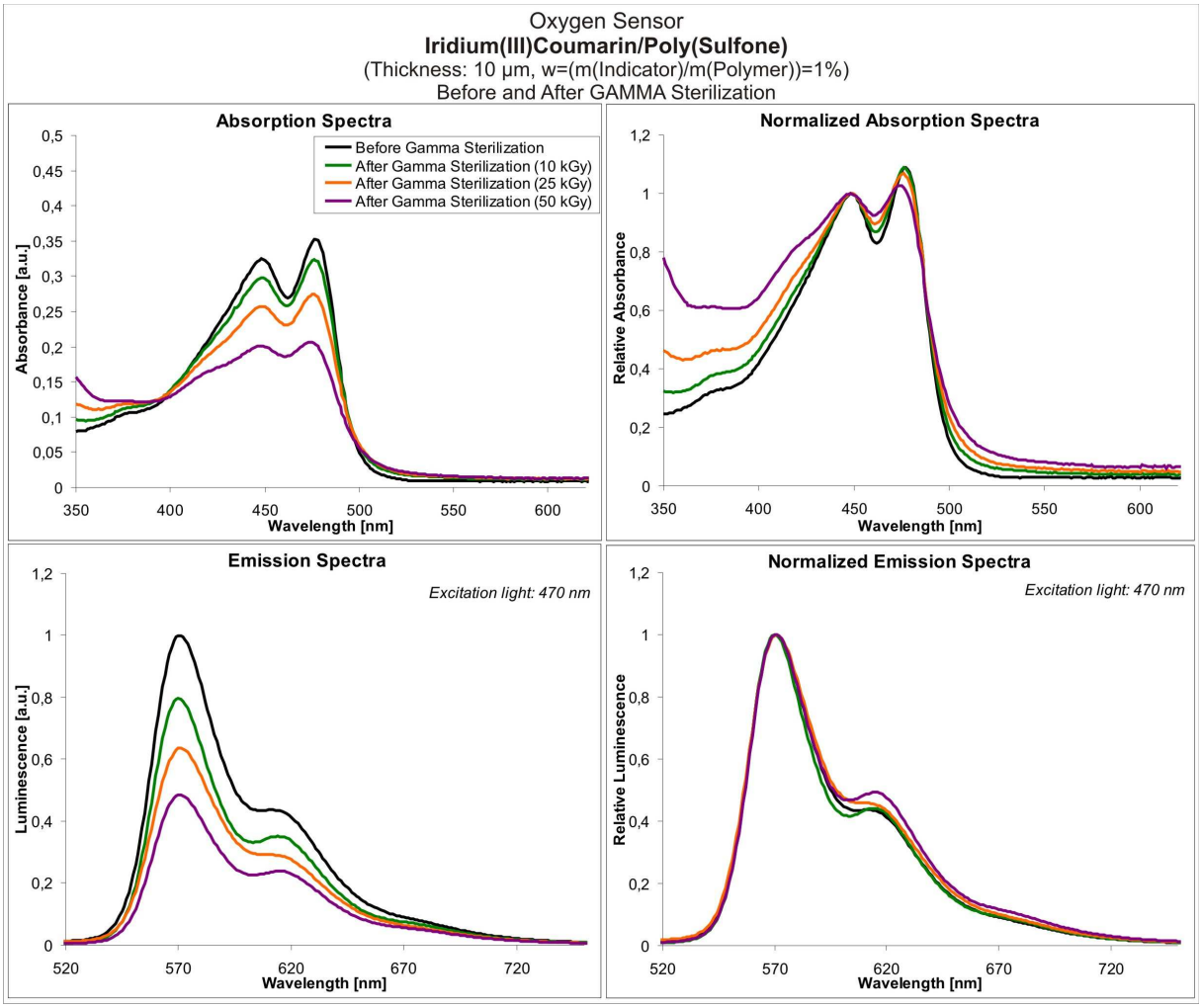

GAMMA Sterilization	Absorption Spectra		Emission Spectra	
Alterations in Absorption/Emission Intensity	10kGy	8,26% decrease	10kGy	20,33% increase
	25 kGy	20,70% decrease	25 kGy	36,38% decrease
	50 kGy	38,05% decrease	50 kGy	51,50% decrease
Alterations in Absorption/Emission Curve Form	10kGy	Altered absorption between 350-430 nm; 460-470 nm and 500-580 nm.	10kGy	Altered emission between 585-610 nm.
	25 kGy	Altered absorption between 350-430 nm; 455-480 nm and 500-800 nm. The ratio between the two absorption maximums has changed.	25 kGy	Altered emission between 590-670 nm.
	50 kGy	Altered absorption between 350-430 nm; 455-490 nm and 490-800 nm. The ratio between the two absorption maximums has changed.	50 kGy	Altered emission between 600-720 nm.

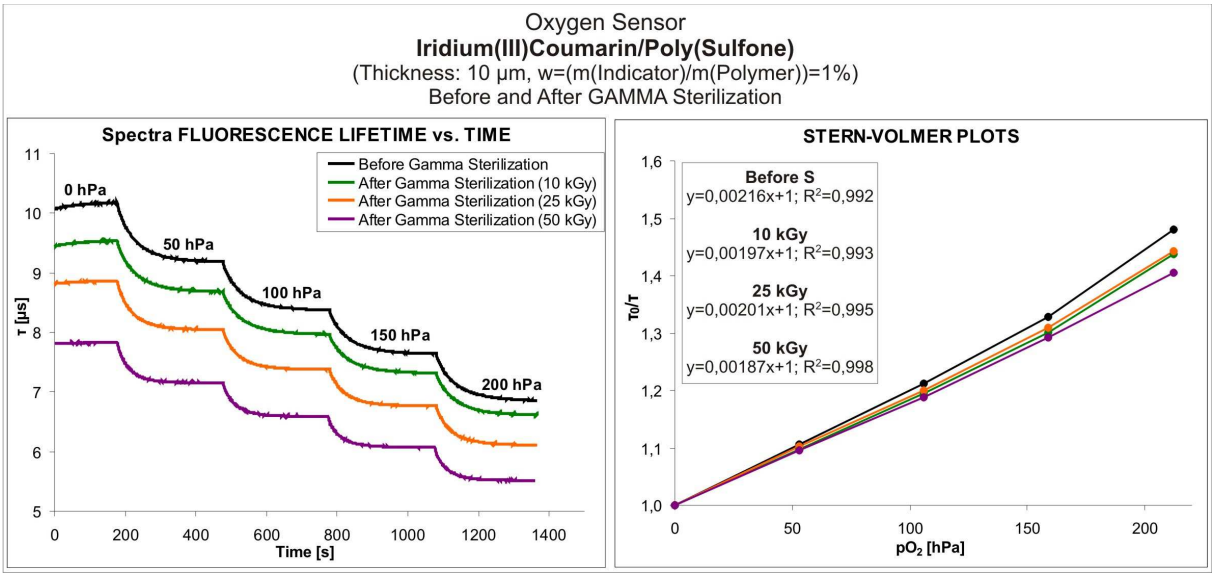

GAMMA Sterilization	Luminescence Lifetime		Stern-Volmer Plot	
Alterations in Luminescence Lifetime and Slope	10kGy	6,67% decrease of τ_0	10kGy	8,80% decrease of slope
		5,43% increase of τ at 50 hPa		
		4,77% increase of τ at 100 hPa		
		4,18% increase of τ at 150 hPa		
		3,35% increase of τ at 200 hPa		
	25 kGy	13,14% decrease of τ_0	25 kGy	6,94% increase of slope
		12,50% increase of τ at 50 hPa		
		11,92% increase of τ at 100 hPa		
		11,50% increase of τ at 150 hPa		
		10,92% increase of τ at 200 hPa		
	50 kGy	23,14% decrease of τ_0	50 kGy	13,43% decrease of slope
		22,17% increase of τ at 50 hPa		
		21,33% increase of τ at 100 hPa		
		20,65% increase of τ at 150 hPa		
		19,65% increase of τ at 200 hPa		

C.5.2 Electron Beam Sterilization

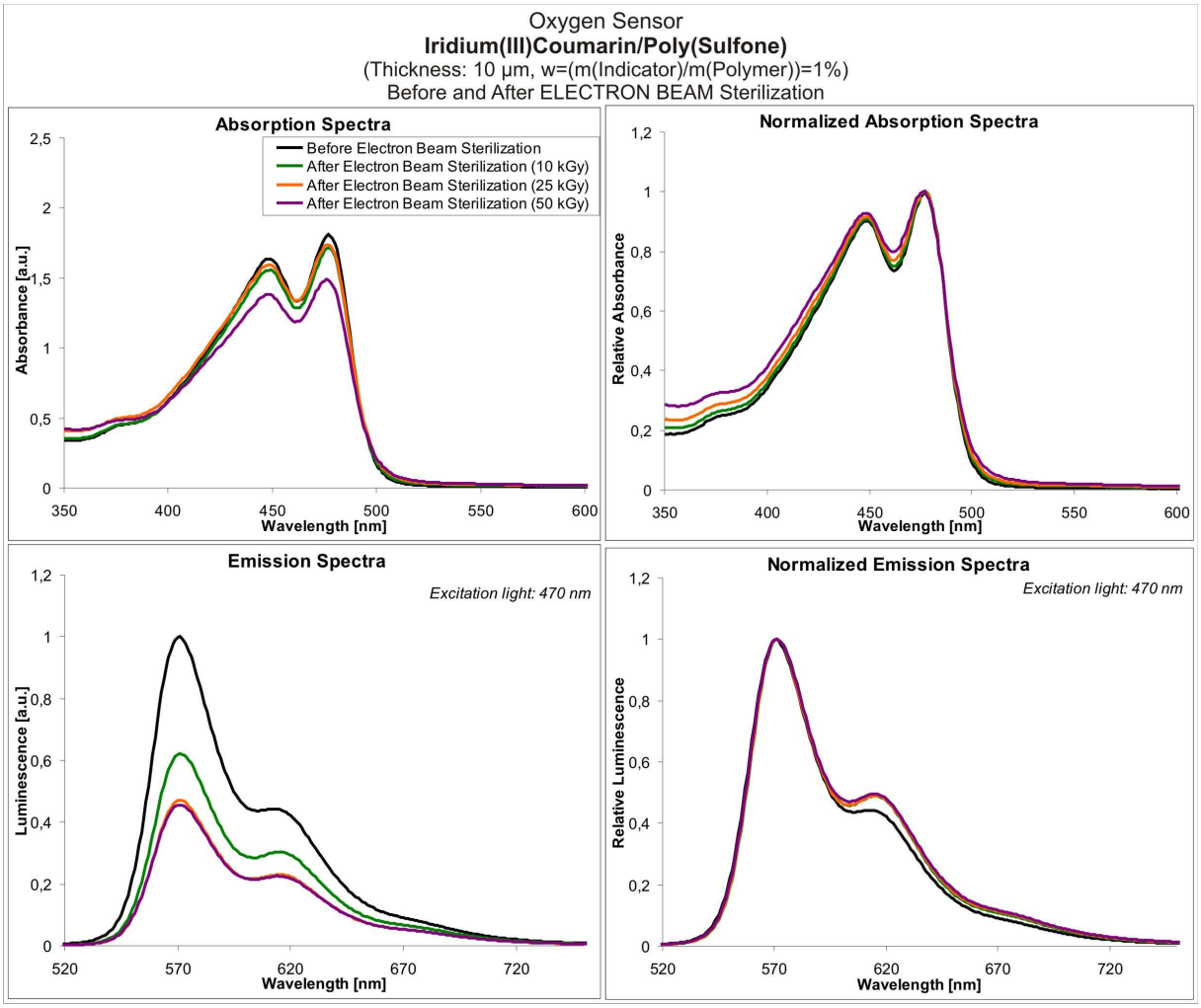

E-BEAM Sterilization	Absorption Spectra		Emission Spectra	
Alterations in Absorption/Emission Intensity	10kGy	5,40% decrease	10kGy	37,89% decrease
	25 kGy	4,08% decrease	25 kGy	52,97% decrease
	50 kGy	17,89% decrease	50 kGy	54,51% decrease
Alterations in Absorption/Emission Curve Form	10kGy	Altered absorption between 350-400 nm and 455-465 nm.	10kGy	Altered emission between 595-720 nm.
	25 kGy	Altered absorption between 350-410 nm and 455-470 nm.	25 kGy	Altered emission between 595-720 nm.
	50 kGy	Altered absorption between 350-440 nm,, 455-480 nm and 500-530 nm.	50 kGy	Altered emission between 595-720 nm.

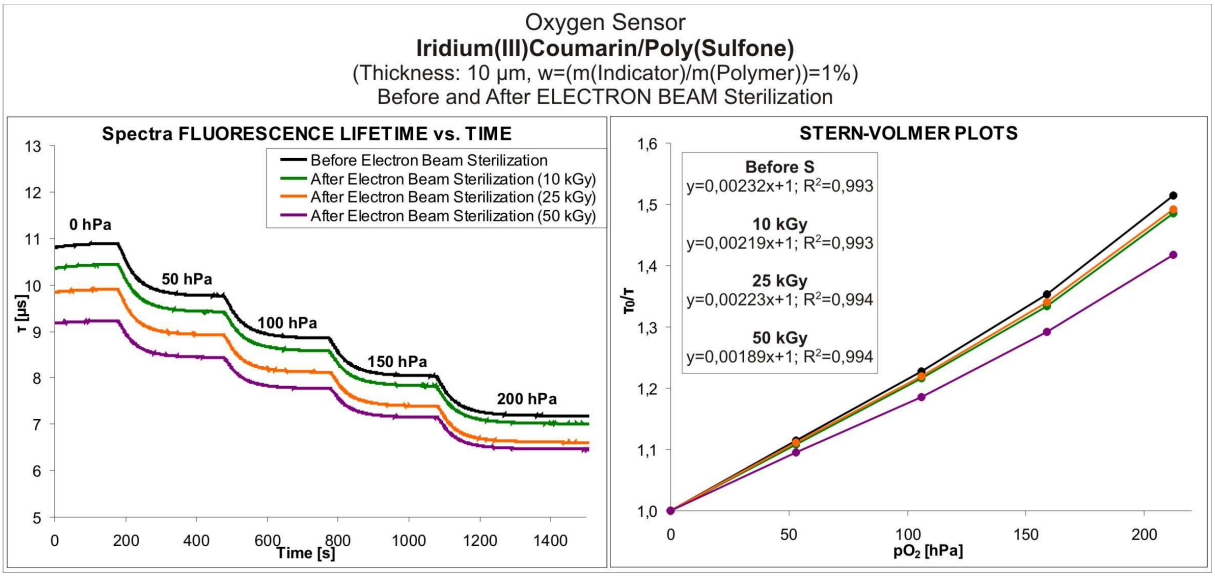

E-BEAM Sterilization	Luminescence Lifetime		Stern-Volmer Plot	
Alterations in Luminescence Lifetime and Slope	10 kGy	3,70% decrease of τ_0	10kGy	5,60% decrease of slope
		3,58% decrease of τ at 50 hPa		
		2,91% decrease of τ at 100 hPa		
		2,61% decrease of τ at 150 hPa		
		2,36% decrease of τ at 200 hPa		
	25 kGy	8,24% decrease of τ_0	25 kGy	3,88% decrease of slope
		8,68% decrease of τ at 50 hPa		
		8,52% decrease of τ at 100 hPa		
		7,96% decrease of τ at 150 hPa		
		7,92% decrease of τ at 200 hPa		
	50 kGy	14,54% decrease of τ_0	50 kGy	18,53% decrease of slope
		13,69% decrease of τ at 50 hPa		
		12,33% decrease of τ at 100 hPa		
		11,07% decrease of τ at 150 hPa		
		10,00% decrease of τ at 200 hPa		

C.6 Iridium(III) Coumarin Complex immobilized in Poly(PhenylSilsesQuioxane)

C.6.1 Gamma Sterilization

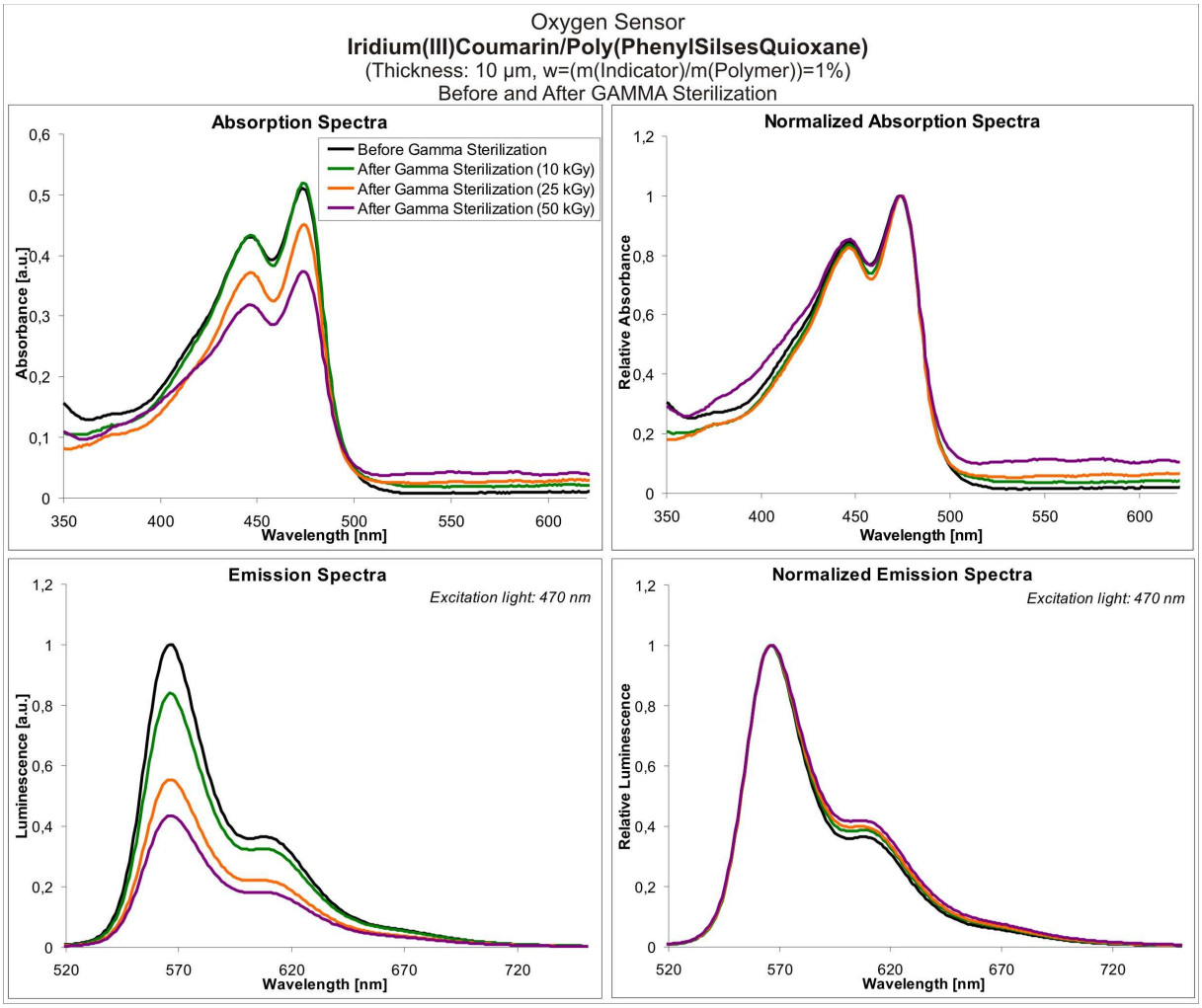

GAMMA Sterilization	Absorption Spectra		Emission Spectra	
Alterations in Absorption/Emission Intensity	10kGy	1,61% increase	10kGy	16,06% increase
	25 kGy	11,65% decrease	25 kGy	44,59% decrease
	50 kGy	26,86% decrease	50 kGy	56,48% decrease
Alterations in Absorption/Emission Curve Form	10kGy	Altered absorption between 350-430 nm; 453-462 nm and 500-800 nm.	10kGy	Altered emission between 590-650 nm.
	25 kGy	Altered absorption between 350-430 nm; 453-462 nm and 500-800 nm.	25 kGy	Altered emission between 590-650 nm.
	50 kGy	Altered absorption between 350-430 nm and 490-800 nm.	50 kGy	Altered emission between 590-700 nm.

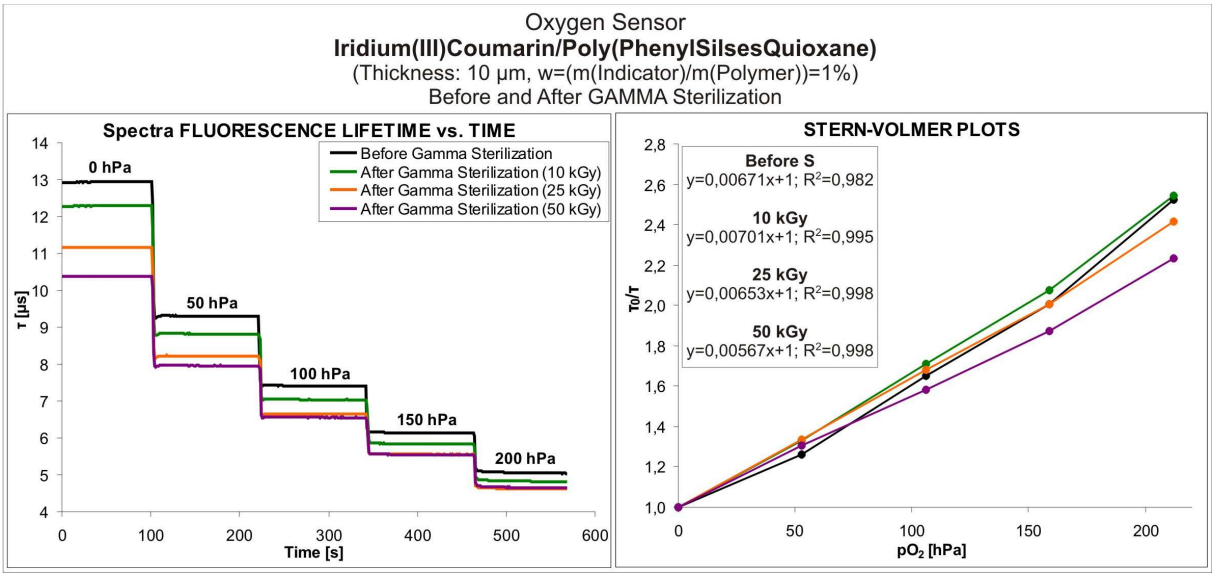

GAMMA Sterilization	Luminescence Lifetime		Stern-Volmer Plot	
Alterations in Luminescence Lifetime and Slope	10kGy	4,65% decrease of τ_0	10kGy	4,28% increase of slope
		5,16% decrease of τ at 50 hPa		
		4,99% decrease of τ at 100 hPa		
		4,88% decrease of τ at 150 hPa		
		4,36% decrease of τ at 200 hPa		
	25 kGy	13,18% decrease of τ_0	25 kGy	2,68% decrease of slope
		11,61% decrease of τ at 50 hPa		
		10,39% decrease of τ at 100 hPa		
		9,45% decrease of τ at 150 hPa		
		8,51% decrease of τ at 200 hPa		
	50 kGy	19,38% decrease of τ_0	50 kGy	15,50% decrease of slope
		14,40% decrease of τ at 50 hPa		
		11,47% decrease of τ at 100 hPa		
		9,61% decrease of τ at 150 hPa		
		7,92% decrease of τ at 200 hPa		

C.6.2 Electron Beam Sterilization

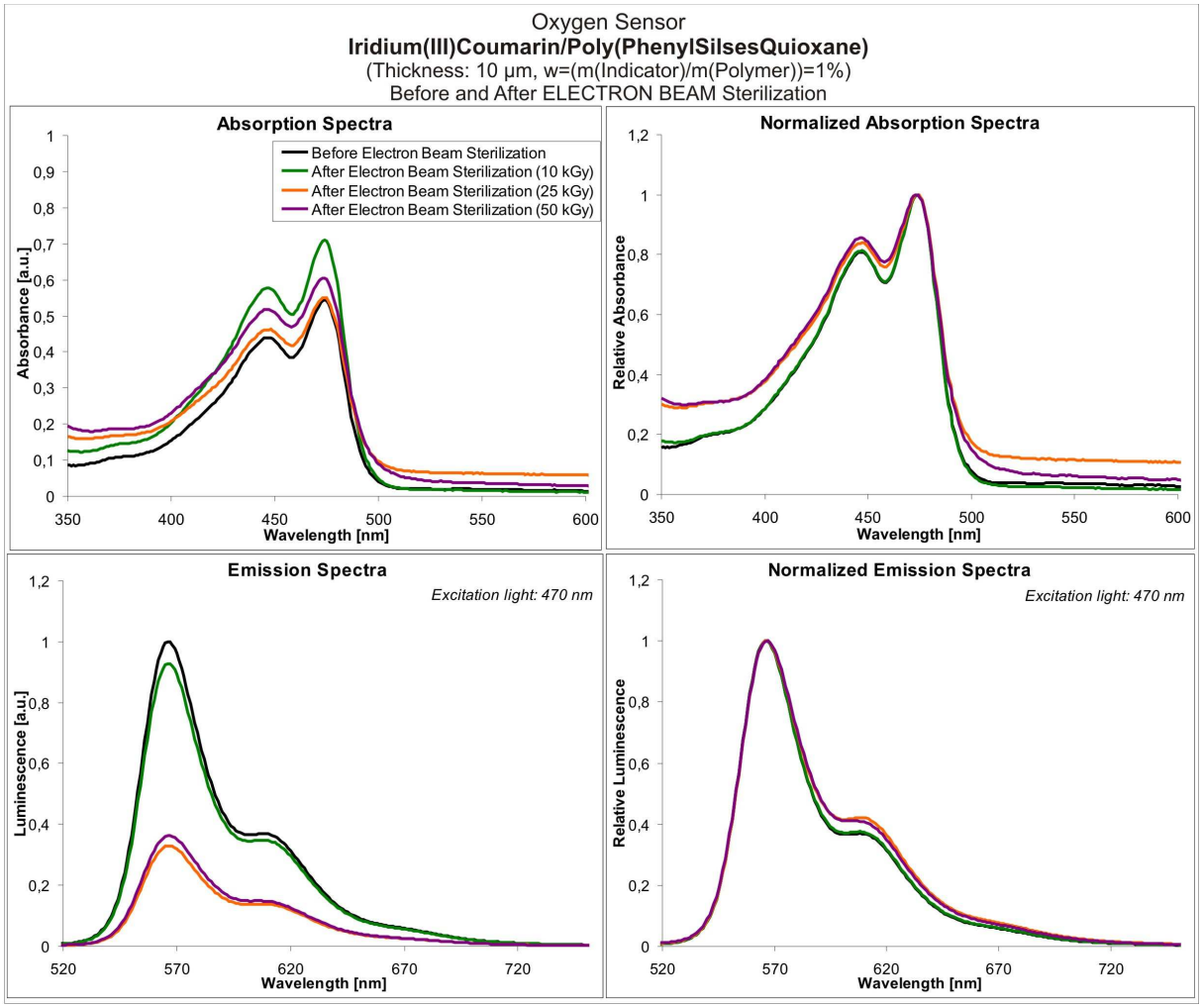

E-BEAM Sterilization	Absorption Spectra		Emission Spectra	
Alterations in Absorption/Emission Intensity	10kGy	30,72% increase	10kGy	7,12% decrease
	25 kGy	1,25% increase	25 kGy	66,99% decrease
	50 kGy	11,27% increase	50 kGy	63,71% decrease
Alterations in Absorption/Emission Curve Form	10kGy	Unaltered.	10kGy	Unaltered.
	25 kGy	Altered absorption between 350-465 nm and 490-800 nm.	25 kGy	Altered emission between 585-670 nm.
	50 kGy	Altered absorption between 350-465 nm and 490-800 nm.	50 kGy	Altered emission between 585-670 nm.

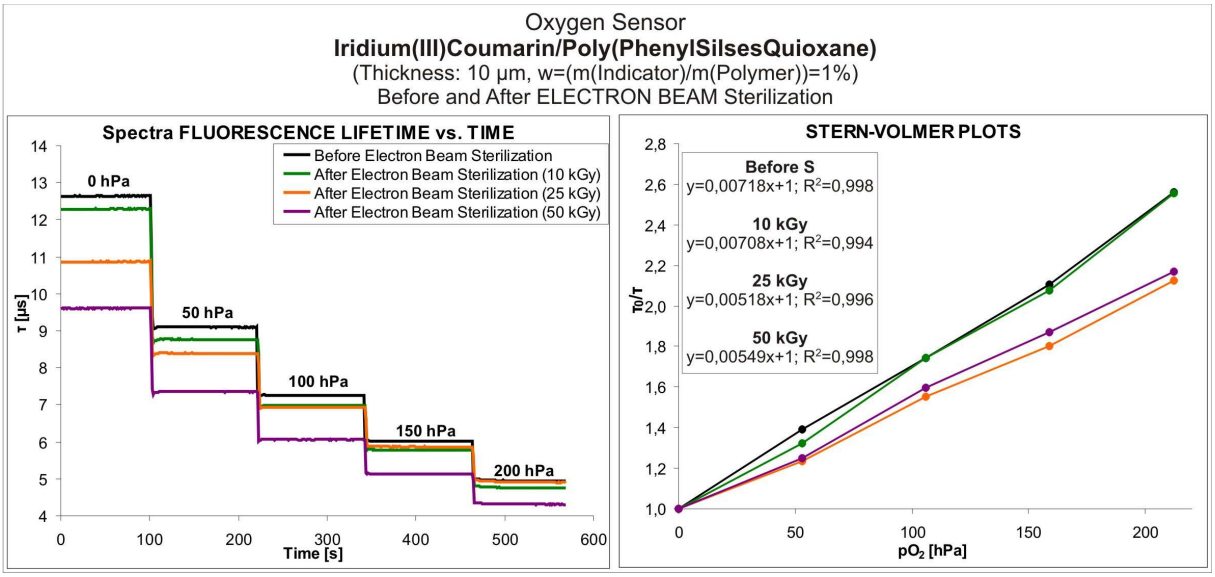

E-BEAM Sterilization	Luminescence Lifetime		Stern-Volmer Plot	
Alterations in Luminescence Lifetime and Slope	10 kGy	2,38% decrease of τ_0	10kGy	1,39% decrease of slope
		3,63% decrease of τ at 50 hPa		
		3,86% decrease of τ at 100 hPa		
		3,83% decrease of τ at 150 hPa		
		3,65% decrease of τ at 200 hPa		
	25 kGy	13,49% decrease of τ_0	25 kGy	27,86% decrease of slope
		7,69% decrease of τ at 50 hPa		
		4,55% decrease of τ at 100 hPa		
		2,33% decrease of τ at 150 hPa		
		0,61% decrease of τ at 200 hPa		
	50 kGy	23,81% decrease of τ_0	50 kGy	23,54% decrease of slope
		19,12% decrease of τ at 50 hPa		
		16,53% decrease of τ at 100 hPa		
		14,33% decrease of τ at 150 hPa		
		12,57% decrease of τ at 200 hPa		

C.7 Iridium(III) Coumarin Complex immobilized in Poly(Styrene)

C.7.1 Gamma Sterilization

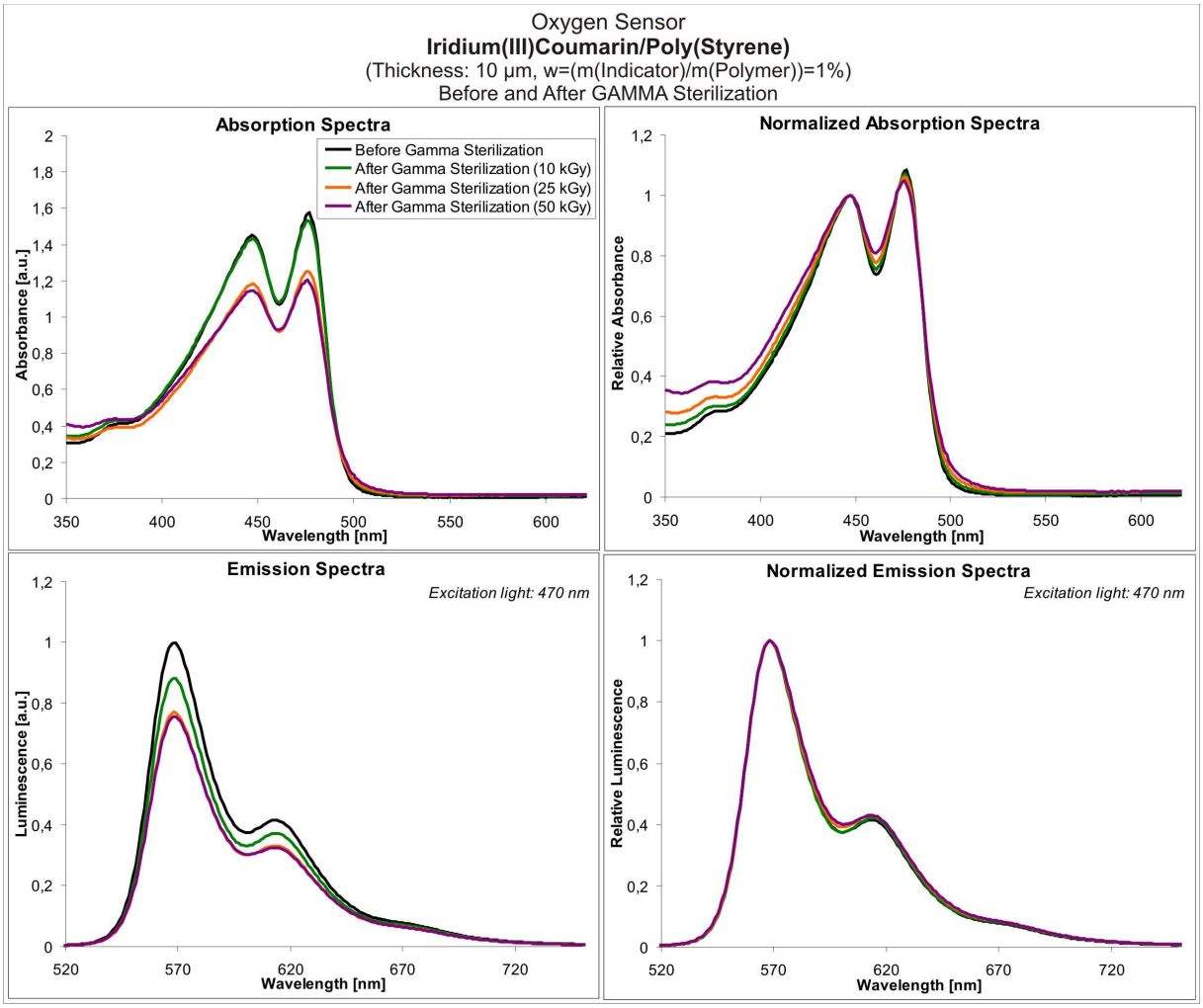

GAMMA Sterilization	Absorption Spectra		Emission Spectra	
Alterations in Absorption/Emission Intensity	10kGy	1,43% decrease	10kGy	11,69% decrease
	25 kGy	18,58% decrease	25 kGy	22,93% decrease
	50 kGy	20,97% decrease	50 kGy	24,33% decrease
Alterations in Absorption/Emission Curve Form	10kGy	Altered absorption between 350-390 nm and 460-465 nm.	10kGy	Altered emission between 595-605 nm.
	25 kGy	Altered absorption between 350-425 nm; 455-465 nm and 495-525 nm.	25 kGy	Altered emission between 595-615 nm.
	50 kGy	Altered absorption between 350-430 nm; 455-470 nm and 495-550 nm.	50 kGy	Altered emission between 595-615 nm.

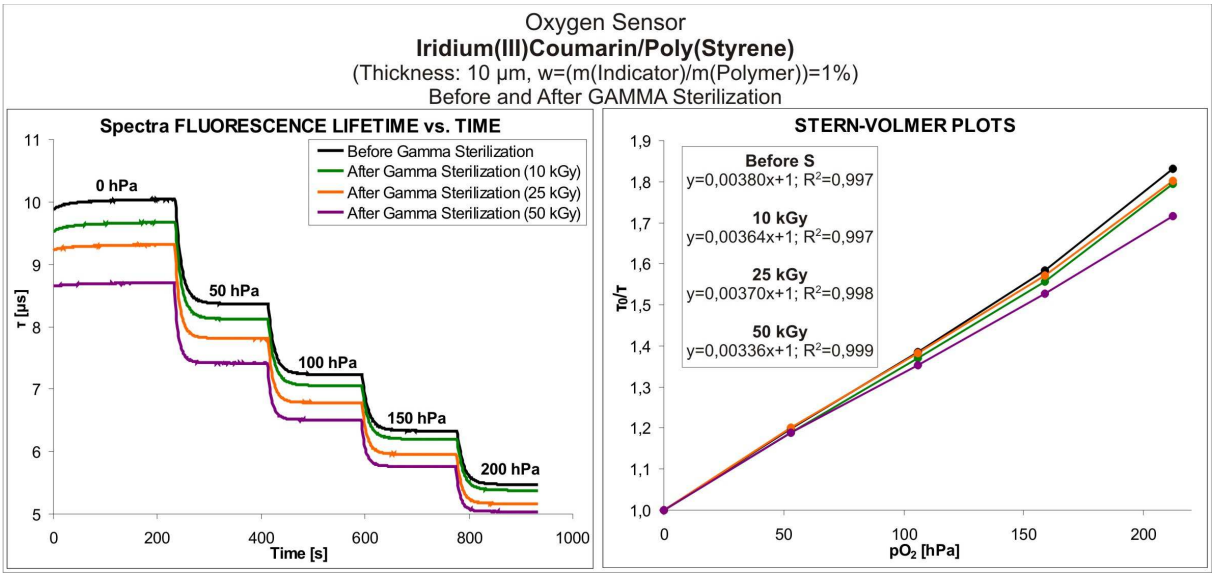

GAMMA Sterilization	Luminescence Lifetime		Stern-Volmer Plot	
Alterations in Luminescence Lifetime and Slope	10kGy	3,40% decrease of τ_0	10kGy	4,21% decrease of slope
		2,99% decrease of τ at 50 hPa		
		2,35% decrease of τ at 100 hPa		
		2,05% decrease of τ at 150 hPa		
		1,64% decrease of τ at 200 hPa		
	25 kGy	6,90% decrease of τ_0	25 kGy	2,63% decrease of slope
		6,69% decrease of τ at 50 hPa		
		6,22% decrease of τ at 100 hPa		
		5,84% decrease of τ at 150 hPa		
		5,67% decrease of τ at 200 hPa		
	50 kGy	13,00% decrease of τ_0	50 kGy	11,58% decrease of slope
		11,47% decrease of τ at 50 hPa		
		9,96% decrease of τ at 100 hPa		
		9,00% decrease of τ at 150 hPa		
		7,86% decrease of τ at 200 hPa		

C.7.2 Electron Beam Sterilization

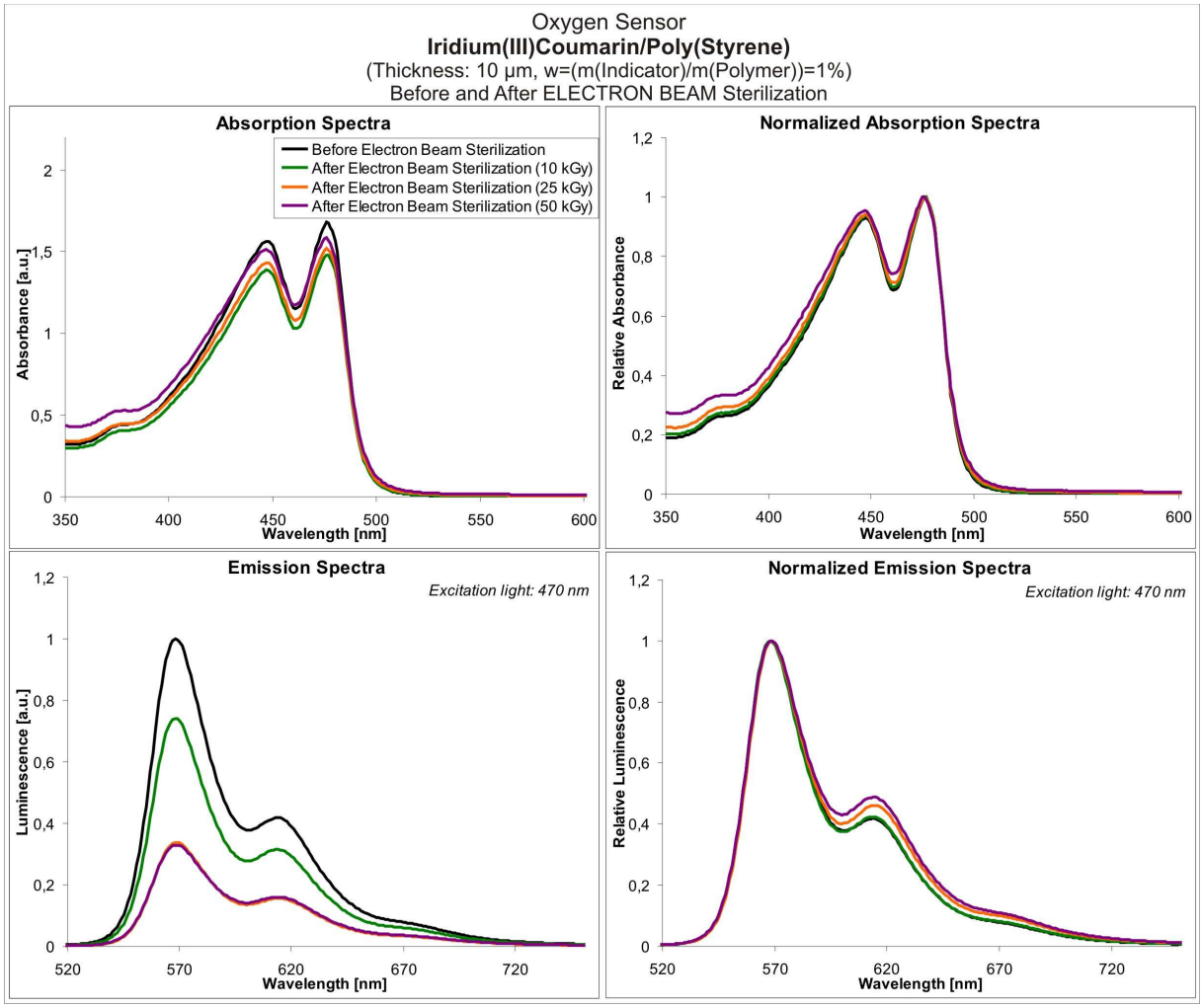

E-BEAM Sterilization	Absorption Spectra		Emission Spectra	
Alterations in Absorption/Emission Intensity	10kGy	12,03% decrease	10kGy	25,83% decrease
	25 kGy	9,51% decrease	25 kGy	66,17% decrease
	50 kGy	5,80% decrease	50 kGy	67,04% decrease
Alterations in Absorption/Emission Curve Form	10kGy	Unaltered.	10kGy	Unaltered.
	25 kGy	Unaltered.	25 kGy	Altered emission between 590-720 nm.
	50 kGy	Altered absorption between 350-430 nm and 460-465 nm.	50 kGy	Altered emission between 590-720 nm.

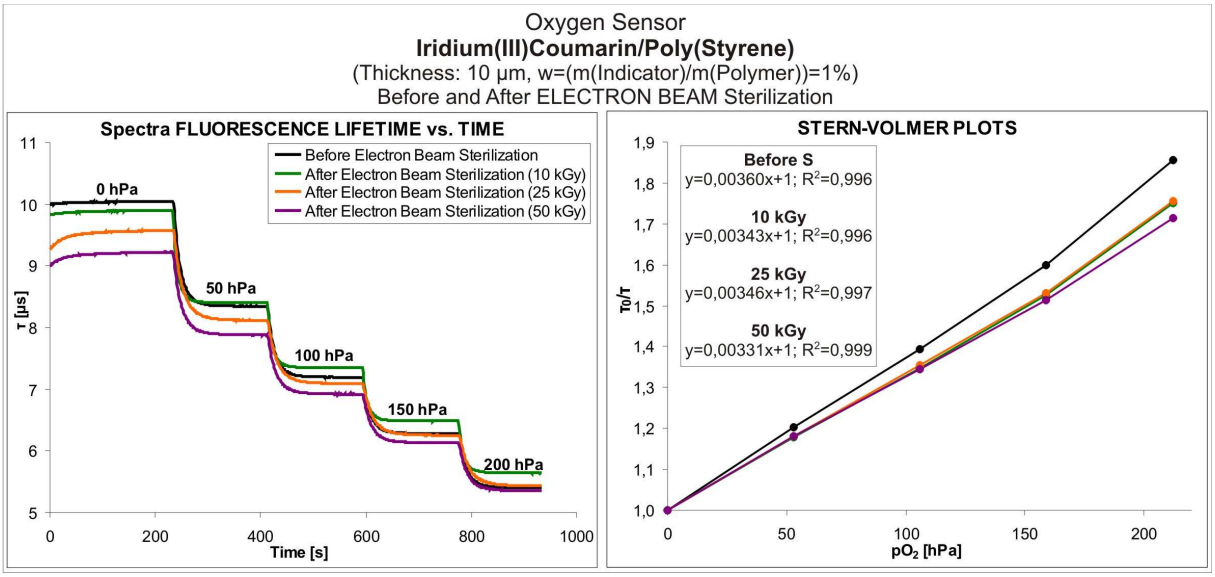

E-BEAM Sterilization	Luminescence Lifetime		Stern-Volmer Plot	
Alterations in Luminescence Lifetime and Slope	10 kGy	1,20% decrease of τ_0	10kGy	4,72% decrease of slope
		0,60% increase of τ at 50 hPa		
		2,08% increase of τ at 100 hPa		
		3,18% increase of τ at 150 hPa		
		4,44% increase of τ at 200 hPa		
	25 kGy	4,70% decrease of τ_0	25 kGy	3,89% decrease of slope
		2,75% decrease of τ at 50 hPa		
		1,39% decrease of τ at 100 hPa		
		0,48% decrease of τ at 150 hPa		
		0,74% increase of τ at 200 hPa		
	50 kGy	8,20% decrease of τ_0	50 kGy	8,06% decrease of slope
		5,51% decrease of τ at 50 hPa		
		3,75% decrease of τ at 100 hPa		
		2,39% decrease of τ at 150 hPa		
		0,26% decrease of τ at 200 hPa		

C.8 Iridium(III) Coumarin Complex immobilized in Poly(Styrene-co-AcryloNitrile)

C.8.1 Gamma Sterilization

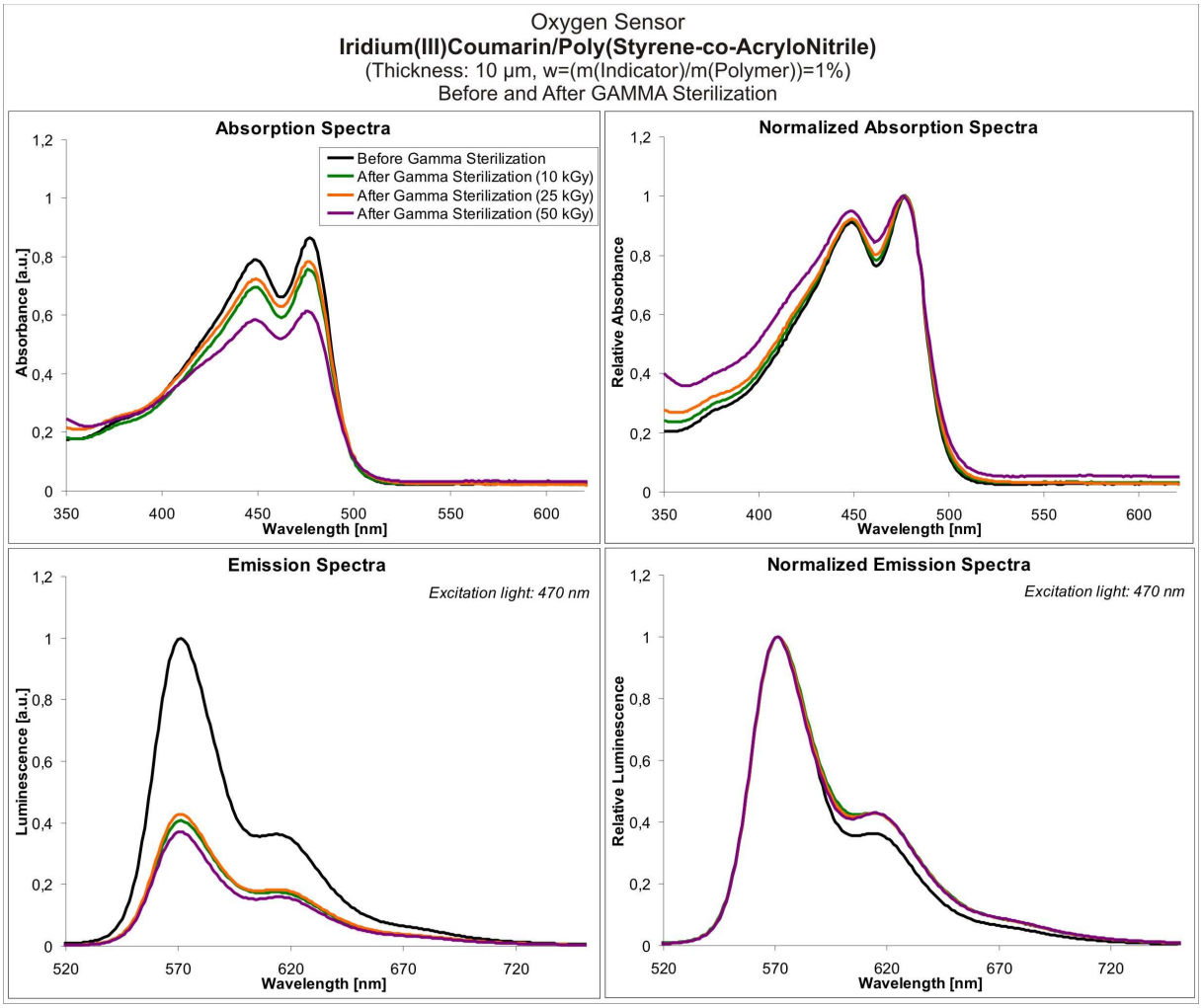

GAMMA Sterilization	Absorption Spectra		Emission Spectra	
Alterations in Absorption/Emission Intensity	10kGy	12,68% decrease	10kGy	59,27% decrease
	25 kGy	9,46% decrease	25 kGy	57,15% decrease
	50 kGy	28,90% decrease	50 kGy	62,94% decrease
Alterations in Absorption/Emission Curve Form	10kGy	Altered absorption between 350-400 nm and 460-465 nm.	10kGy	Altered emission between 590-720 nm.
	25 kGy	Altered absorption between 350-420 nm and 455-466 nm.	25 kGy	Altered emission between 590-720 nm.
	50 kGy	Altered absorption between 350-470 nm and 500-800 nm.	50 kGy	Altered emission between 590-720 nm.

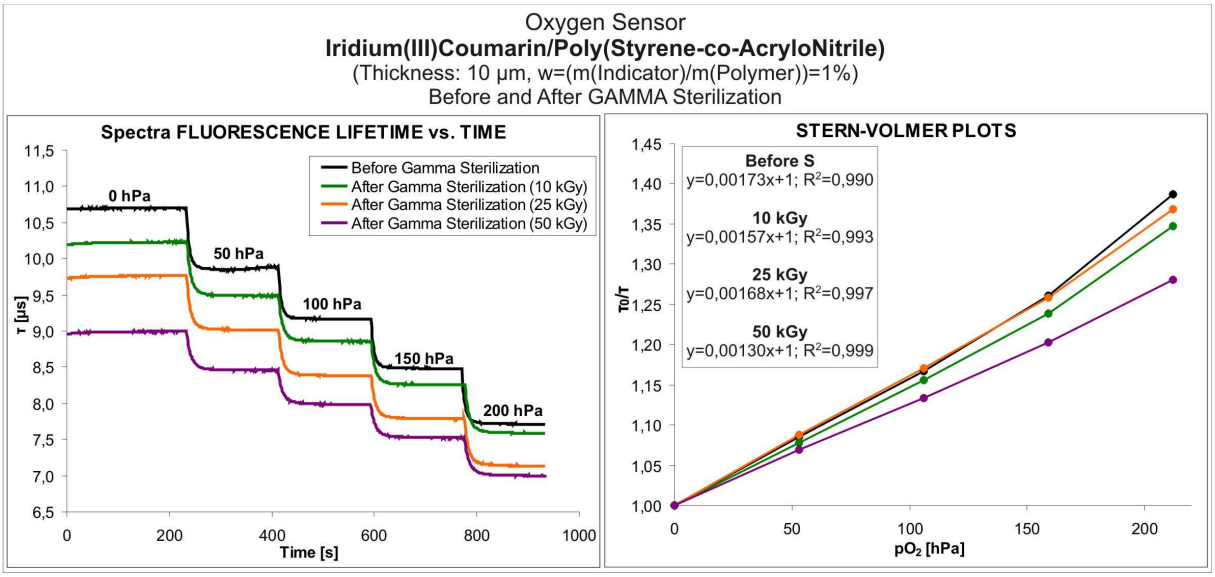

GAMMA Sterilization	Luminescence Lifetime		Stern-Volmer Plot	
Alterations in Luminescence Lifetime and Slope	10kGy	4,67% decrease of τ_0	10kGy	9,25% decrease of slope
		3,65% decrease of τ at 50 hPa		
		3,38% decrease of τ at 100 hPa		
		2,71% decrease of τ at 150 hPa		
		1,56% decrease of τ at 200 hPa		
	25 kGy	8,69% decrease of τ_0	25 kGy	2,89% decrease of slope
		8,43% decrease of τ at 50 hPa		
		8,51% decrease of τ at 100 hPa		
		8,24% decrease of τ at 150 hPa		
		7,39% decrease of τ at 200 hPa		
	50 kGy	15,98% decrease of τ_0	50 kGy	24,86% decrease of slope
		13,81% decrease of τ at 50 hPa		
		12,87% decrease of τ at 100 hPa		
		11,31% decrease of τ at 150 hPa		
		9,21% decrease of τ at 200 hPa		

C.8.2 Electron Beam Sterilization

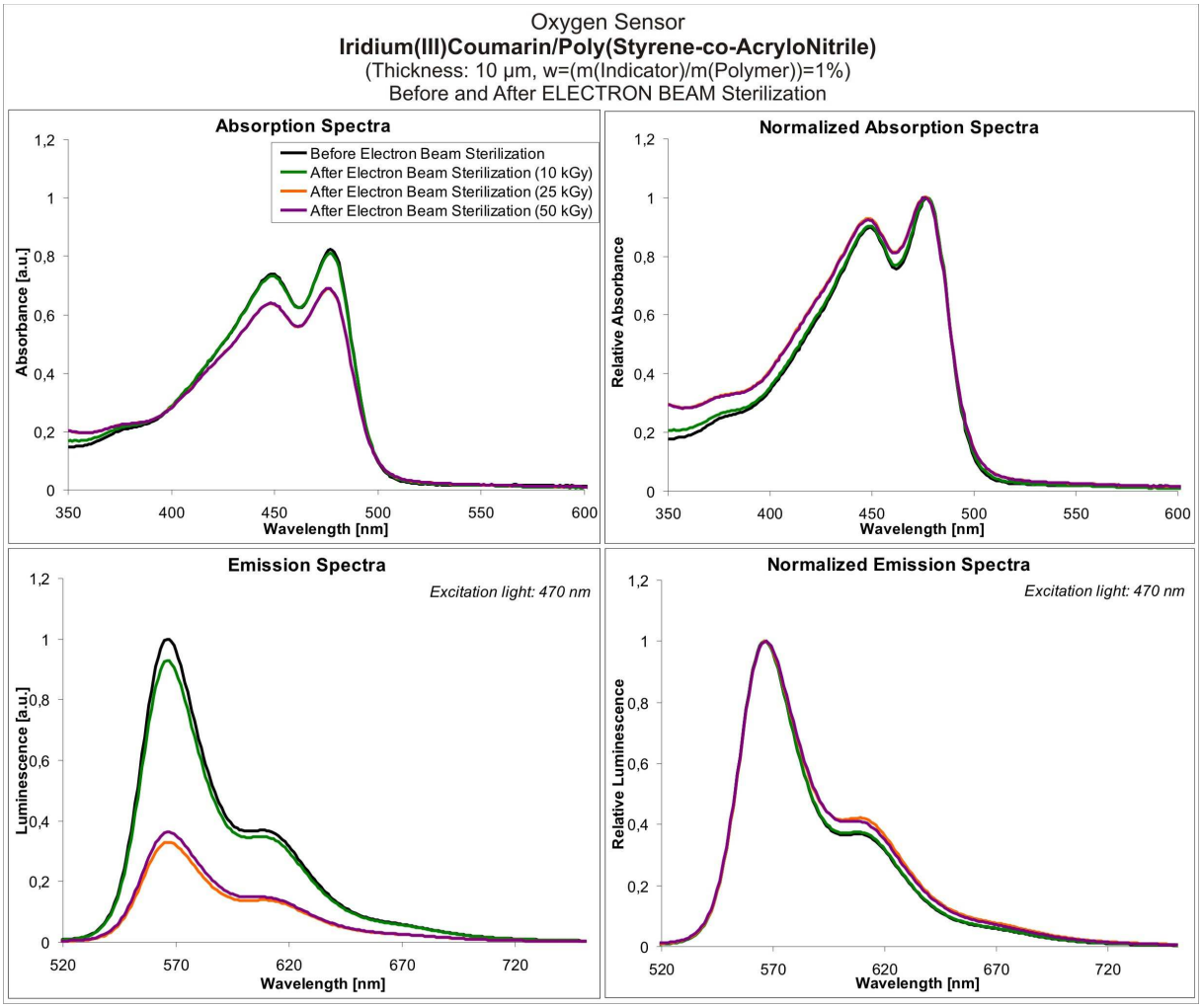

GAMMA Sterilization	Absorption Spectra		Emission Spectra	
Alterations in Absorption/Emission Intensity	10kGy	1,59% decrease	10kGy	7,12% decrease
	25 kGy	16,58% decrease	25 kGy	66,99% decrease
	50 kGy	16,07% decrease	50 kGy	63,71% decrease
Alterations in Absorption/Emission Curve Form	10kGy	Altered absorption between 350-390 nm.	10kGy	Unaltered
	25 kGy	Altered absorption between 350-470 nm and 495-545 nm.	25 kGy	Altered emission between 580-700 nm.
	50 kGy	Altered absorption between 350-470 nm and 495-545 nm.	50 kGy	Altered emission between 580-700 nm.

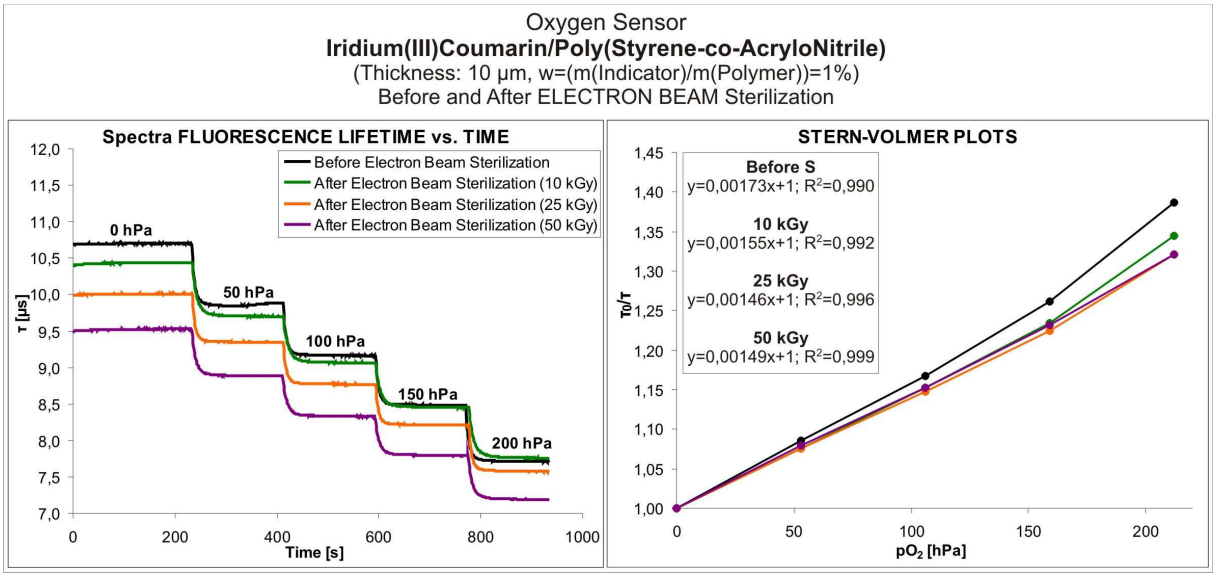

E-BEAM Sterilization	Luminescence Lifetime		Stern-Volmer Plot	
Alterations in Luminescence Lifetime and Slope	10kGy	2,80% decrease of τ_0	10kGy	10,40% decrease of slope
		1,82% decrease of τ at 50 hPa		
		1,09% decrease of τ at 100 hPa		
		0,35% decrease of τ at 150 hPa		
		0,77% increase of τ at 200 hPa		
	25 kGy	6,54% decrease of τ_0	25 kGy	15,60% decrease of slope
		5,36% decrease of τ at 50 hPa		
		4,36% decrease of τ at 100 hPa		
		3,18% decrease of τ at 150 hPa		
		1,69% decrease of τ at 200 hPa		
	50 kGy	10,93% decrease of τ_0	50 kGy	13,87% decrease of slope
		10,02% decrease of τ at 50 hPa		
		9,16% decrease of τ at 100 hPa		
		8,02% decrease of τ at 150 hPa		
		6,61% decrease of τ at 200 hPa		

C.9 Iridium(III) Coumarin Complex immobilized in Poly(Styrene-co-MaleicAnhydride)

C.9.1 Gamma Sterilization

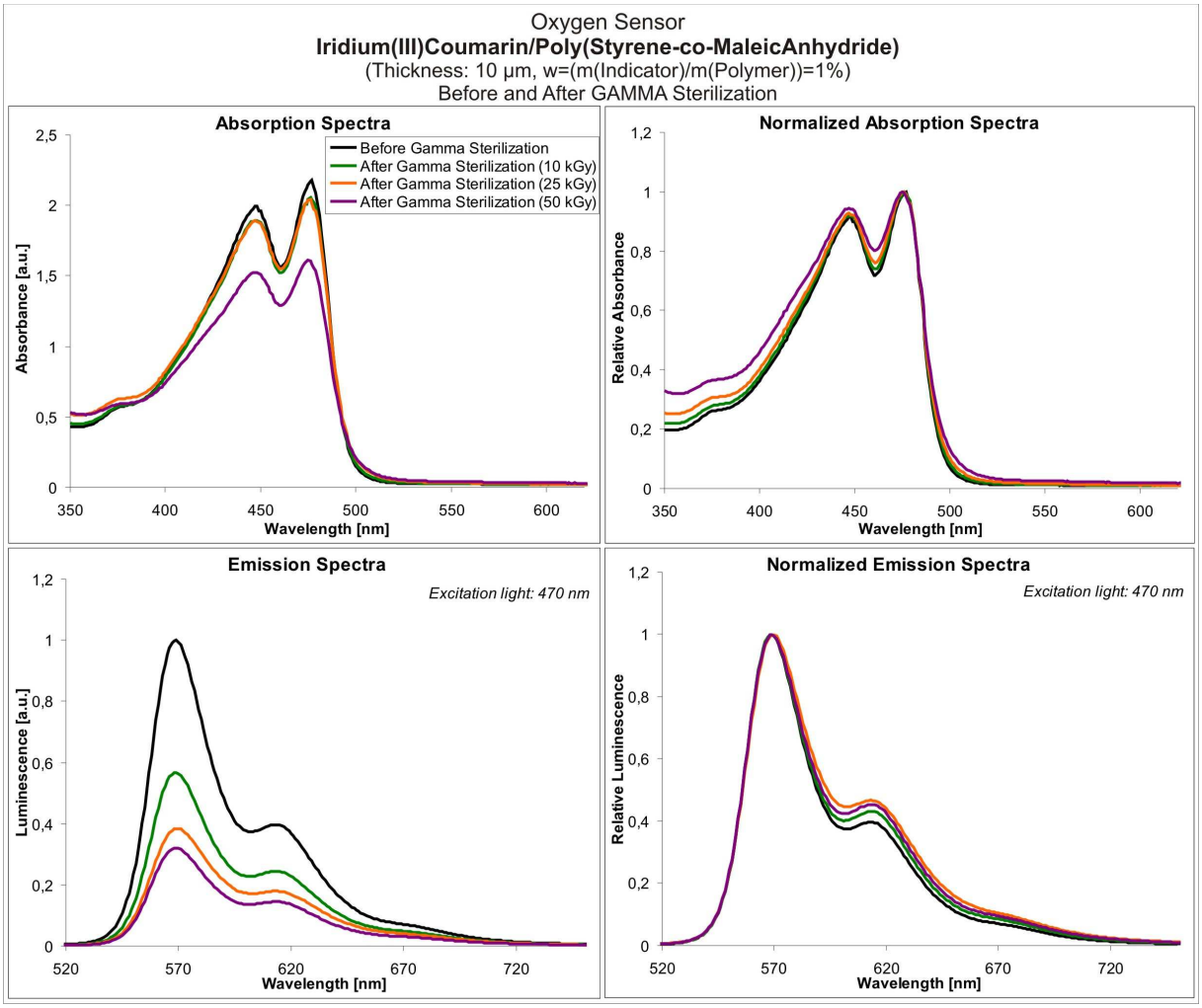

GAMMA Sterilization	Absorption Spectra		Emission Spectra	
Alterations in Absorption/Emission Intensity	10kGy	5,51% decrease	10kGy	43,35% decrease
	25 kGy	6,40% decrease	25 kGy	61,57% decrease
	50 kGy	25,99% decrease	50 kGy	68,03% decrease
Alterations in Absorption/Emission Curve Form	10kGy	Altered absorption between 350-400 nm and 460-463 nm.	10kGy	Altered emission between 590-720 nm.
	25 kGy	Altered absorption between 350-415 nm; 455-465 nm and 495-535 nm.	25 kGy	Altered emission between 585-720 nm.
	50 kGy	Altered absorption between 350-470 nm and 490-560 nm.	50 kGy	Altered emission between 585-720 nm.

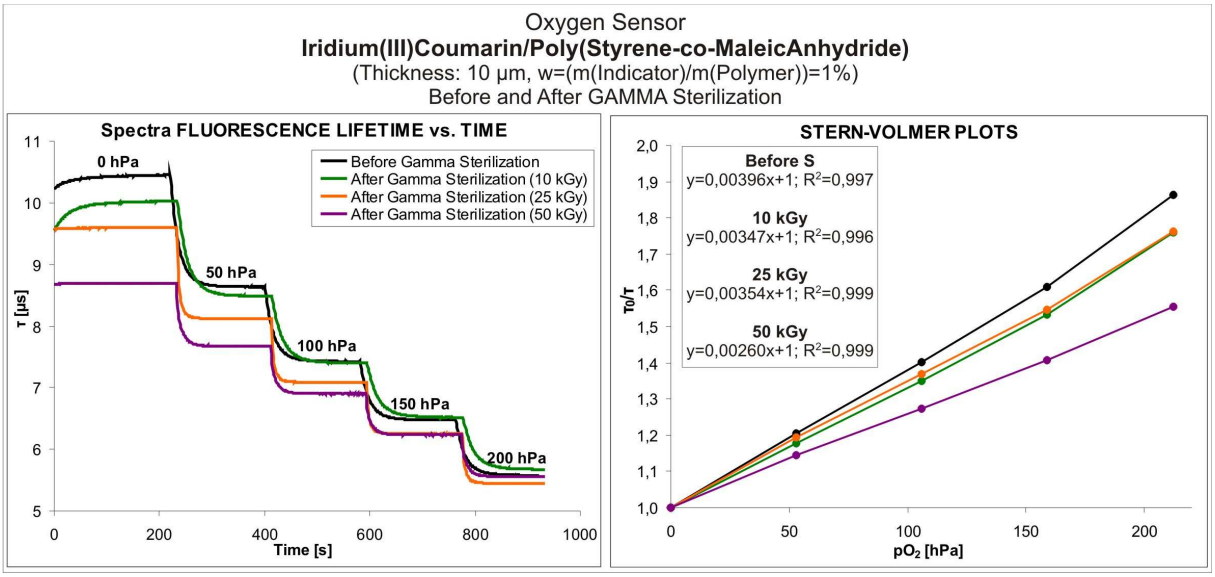

GAMMA Sterilization	Luminescence Lifetime		Stern-Volmer Plot	
Alterations in Luminescence Lifetime and Slope	10kGy	3,85% decrease of τ_0	10kGy	12,37% decrease of slope
		1,74% decrease of τ at 50 hPa		
		0,27% decrease of τ at 100 hPa		
		0,77% increase of τ at 150 hPa		
		1,58% increase of τ at 200 hPa		
	25 kGy	7,69% decrease of τ_0	25 kGy	10,61% decrease of slope
		6,02% decrease of τ at 50 hPa		
		4,45% decrease of τ at 100 hPa		
		3,55% decrease of τ at 150 hPa		
		2,68% decrease of τ at 200 hPa		
	50 kGy	16,44% decrease of τ_0	50 kGy	34,34% decrease of slope
		11,11% decrease of τ at 50 hPa		
		7,00% decrease of τ at 100 hPa		
		3,70% decrease of τ at 150 hPa		
		0,72% decrease of τ at 200 hPa		

C.9.2 Electron Beam Sterilization

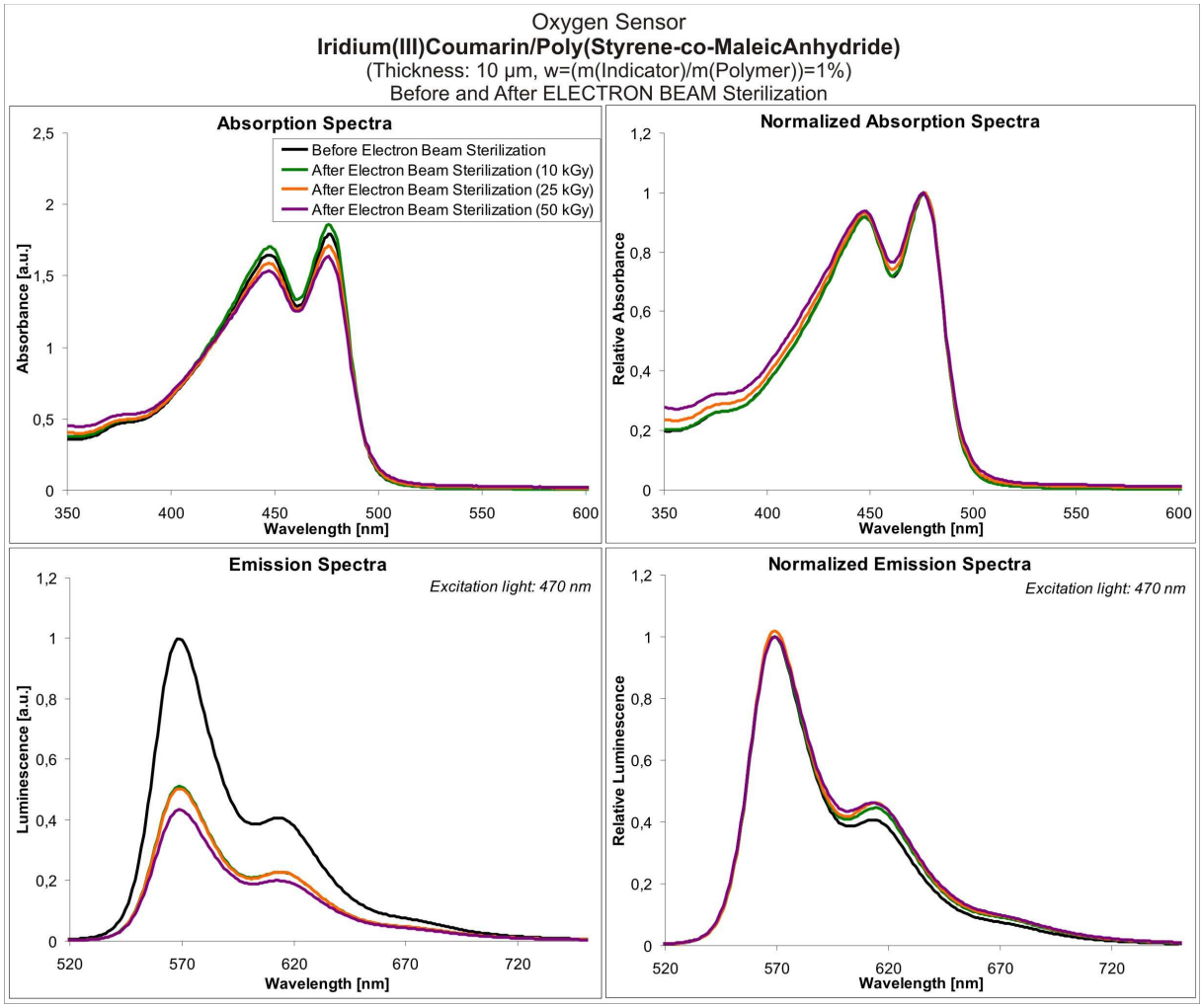

E-BEAM Sterilization	Absorption Spectra		Emission Spectra	
Alterations in Absorption/Emission Intensity	10kGy	3,37% increase	10kGy	48,82% decrease
	25 kGy	4,81% decrease	25 kGy	50,56% decrease
	50 kGy	8,93% decrease	50 kGy	56,62% decrease
Alterations in Absorption/Emission Curve Form	10kGy	Unaltered	10kGy	Altered emission between 595-720 nm.
	25 kGy	Altered absorption between 350-430 nm and 460-465 nm.	25 kGy	Altered emission between 590-720 nm.
	50 kGy	Altered absorption between 350-430 nm; 455-465 nm and 500-530 nm.	50 kGy	Altered emission between 590-720 nm.

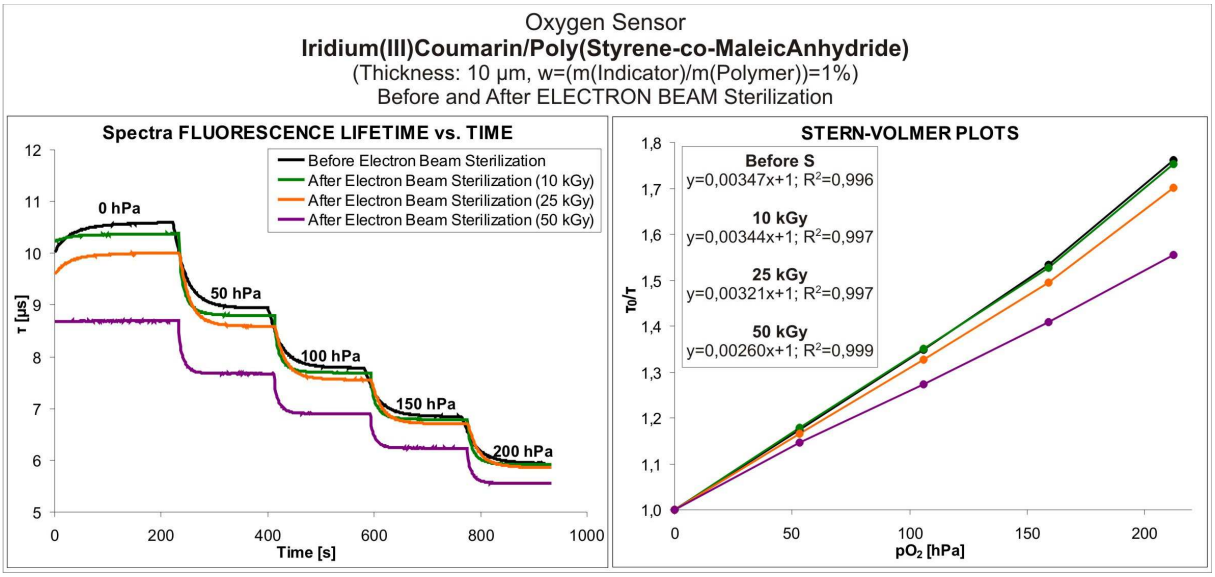

E-BEAM Sterilization	Luminescence Lifetime		Stern-Volmer Plot	
Alterations in Luminescence Lifetime and Slope	10kGy	1,88% decrease of τ_0	10kGy	0,86% decrease of slope
		1,68% decrease of τ at 50 hPa		
		1,28% decrease of τ at 100 hPa		
		0,88% decrease of τ at 150 hPa		
		0,67% decrease of τ at 200 hPa		
	25 kGy	5,66% decrease of τ_0	25 kGy	7,49% decrease of slope
		4,02% decrease of τ at 50 hPa		
		2,95% decrease of τ at 100 hPa		
		2,19% decrease of τ at 150 hPa		
		1,51% decrease of τ at 200 hPa		
	50 kGy	18,12% decrease of τ_0	50 kGy	25,07% decrease of slope
		14,19% decrease of τ at 50 hPa		
		11,42% decrease of τ at 100 hPa		
		8,91% decrease of τ at 150 hPa		
		6,72% decrease of τ at 200 hPa		

C.10 Platinum(II)Tetrakis(PentaFluorPhenyl)Porphyrin (PtTFPP) immobilized in Cellulose Acetate

C.10.1 Gamma Sterilization

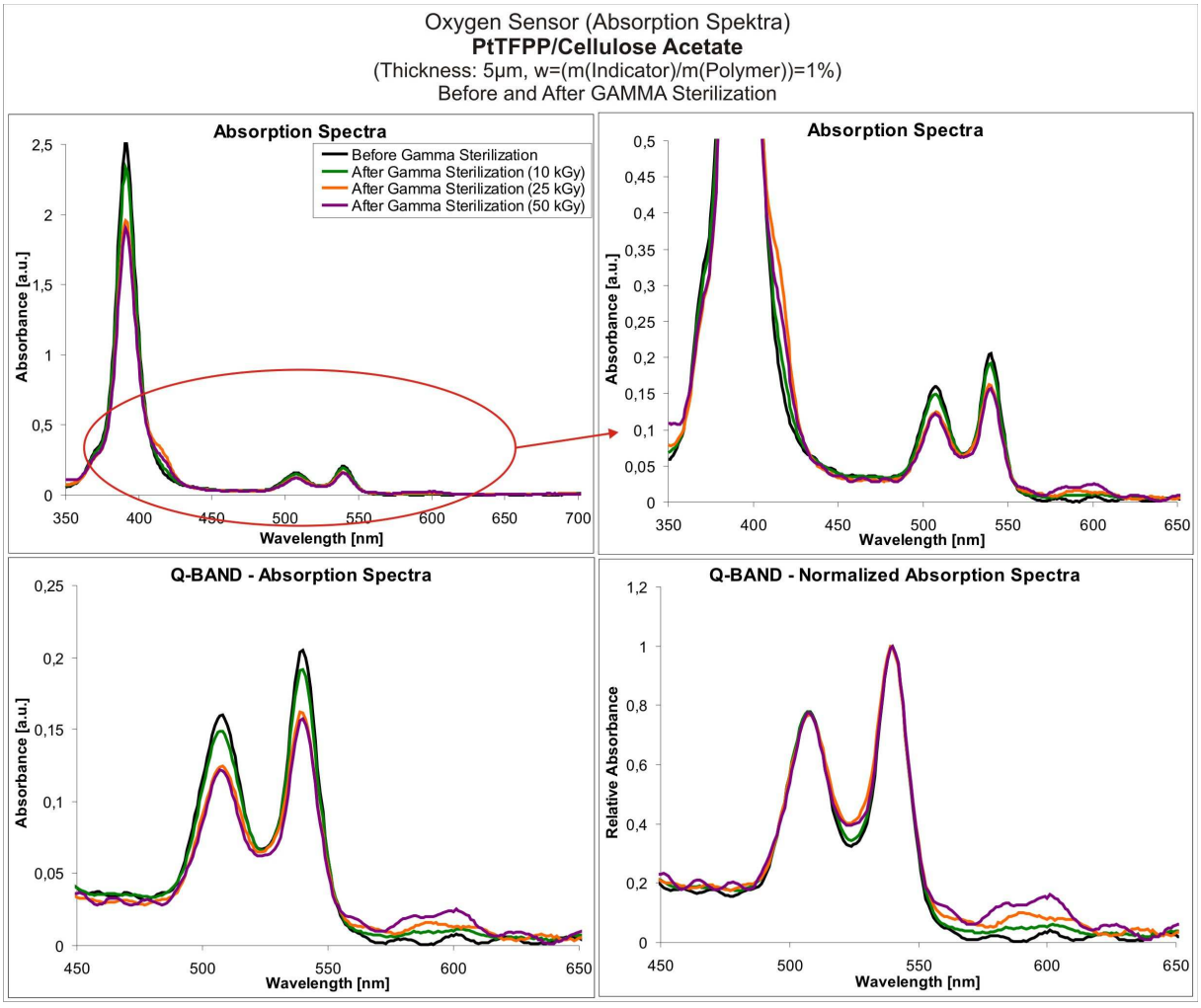

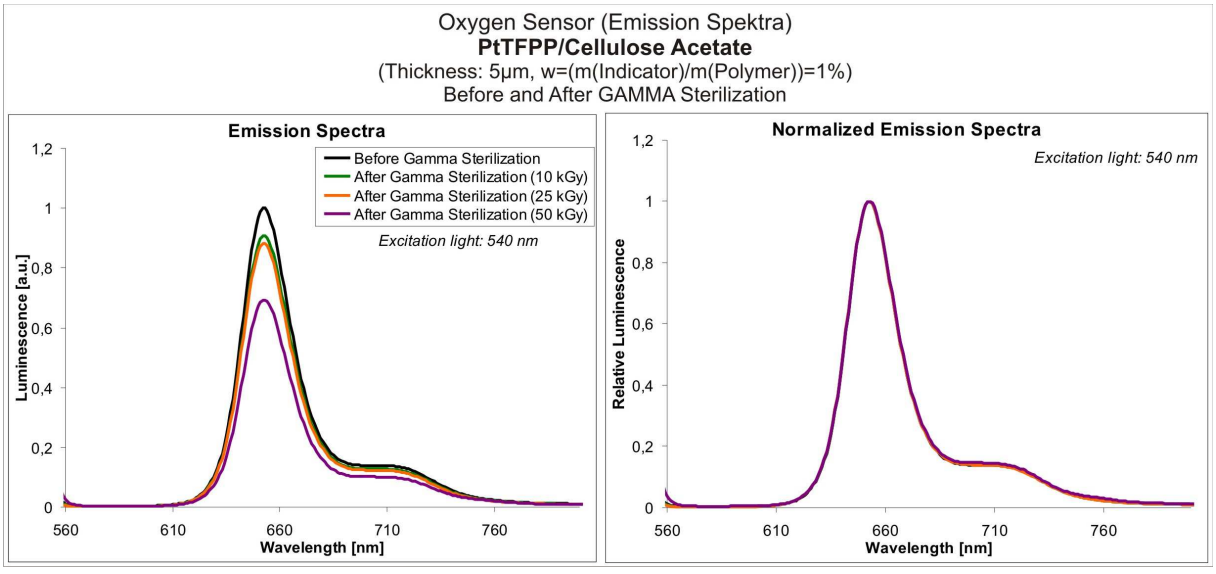

GAMMA Sterilization	Absorption Spectra		Emission Spectra	
Alterations in Absorption/Emission Intensity	10kGy	6,47% decrease	10kGy	9,16% decrease
	25 kGy	20,97% decrease	25 kGy	11,75% decrease
	50 kGy	23,22% decrease	50 kGy	30,76% decrease
Alterations in Absorption/Emission Curve Form	10kGy	Unaltered.	10kGy	Unaltered.
	25 kGy	Altered absorption between 405-430 nm; 515-530 nm and 570-620 nm.	25 kGy	Unaltered.
	50 kGy	Altered absorption between 405-430 nm; 515-530 nm and 570-620 nm. New peak with λ_{max}=600 nm.	50 kGy	Unaltered.

Oxygen Sensor
PtTFPP/Cellulose Acetate
(Thickness: 5 µm, w=(m(Indicator)/m(Polymer))=1%)
Before and After GAMMA Sterilization

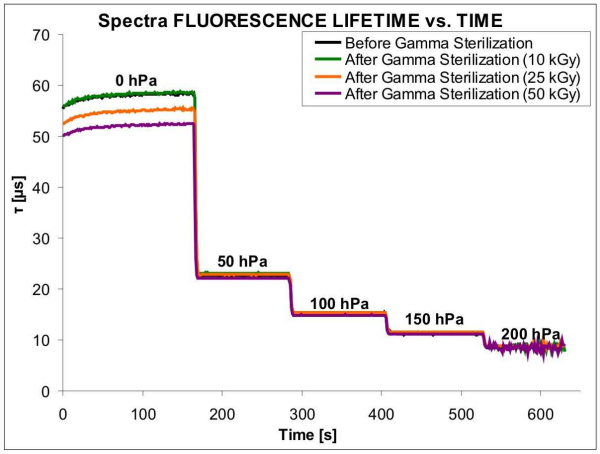

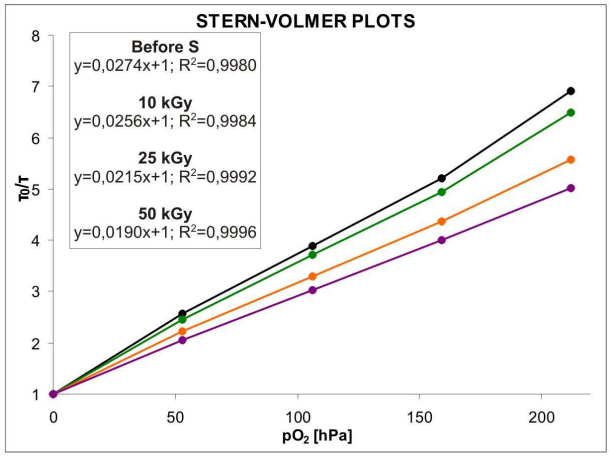

GAMMA Sterilization	Luminescence Lifetime		Stern-Volmer Plot	
Alterations in Luminescence Lifetime and Slope	10kGy	2,58% decrease of τ_0	10kGy	6,57% decrease of slope
		1,95% increase of τ at 50 hPa		
		1,32% increase of τ at 100 hPa		
		2,79% increase of τ at 150 hPa		
		3,77% increase of τ at 200 hPa		
	25 kGy	15,81% decrease of τ_0	25 kGy	21,53% decrease of slope
		2,38% decrease of τ at 50 hPa		
		1,33% decrease of τ at 100 hPa		
		0,71% increase of τ at 150 hPa		
		4,21% increase of τ at 200 hPa		
	50 kGy	27,15% decrease of τ_0	50 kGy	30,66% decrease of slope
		9,13% decrease of τ at 50 hPa		
		6,67% decrease of τ at 100 hPa		
		5,02% decrease of τ at 150 hPa		
		0,59% increase of τ at 200 hPa		

C.10.2 Electron Beam Sterilization

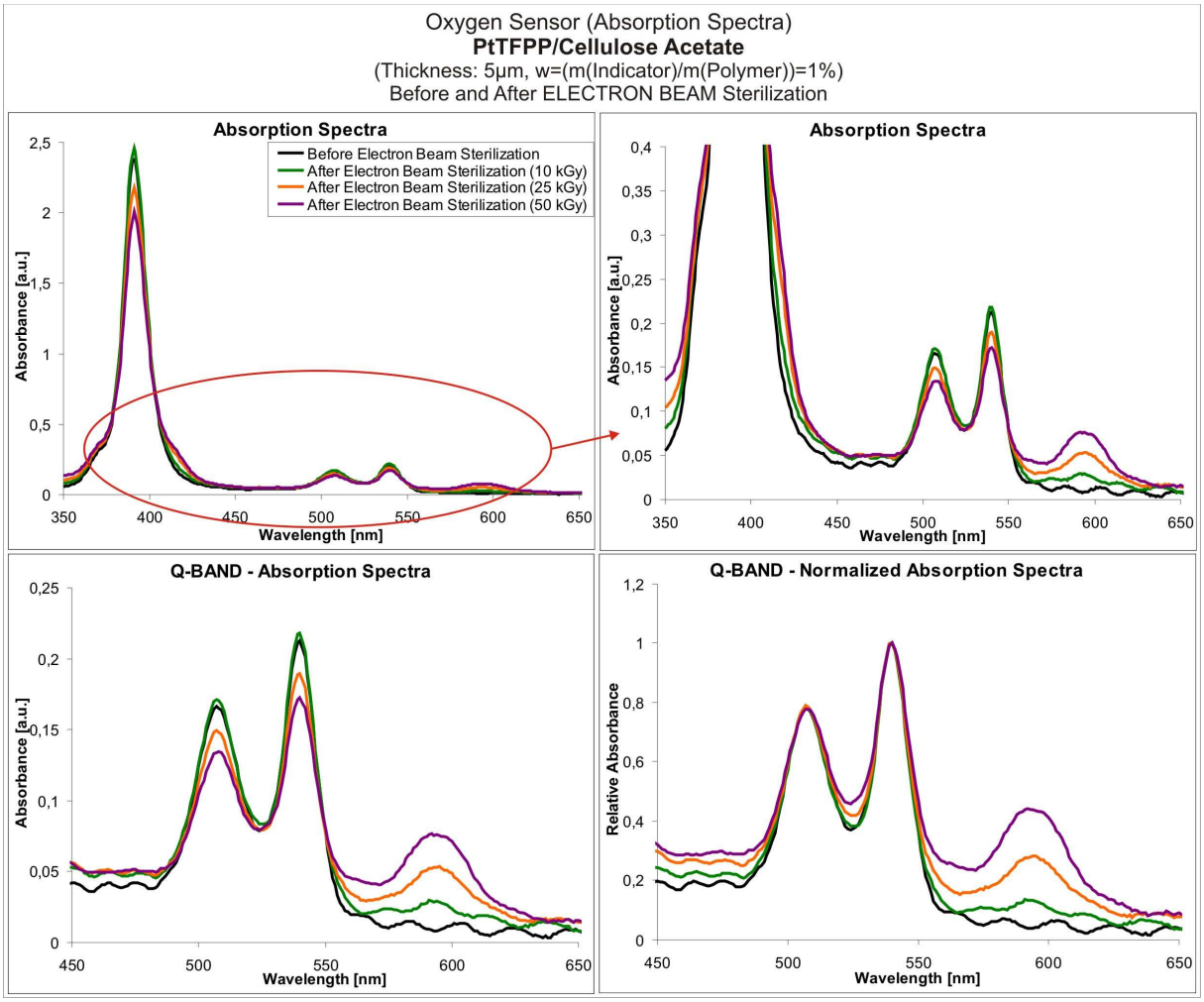

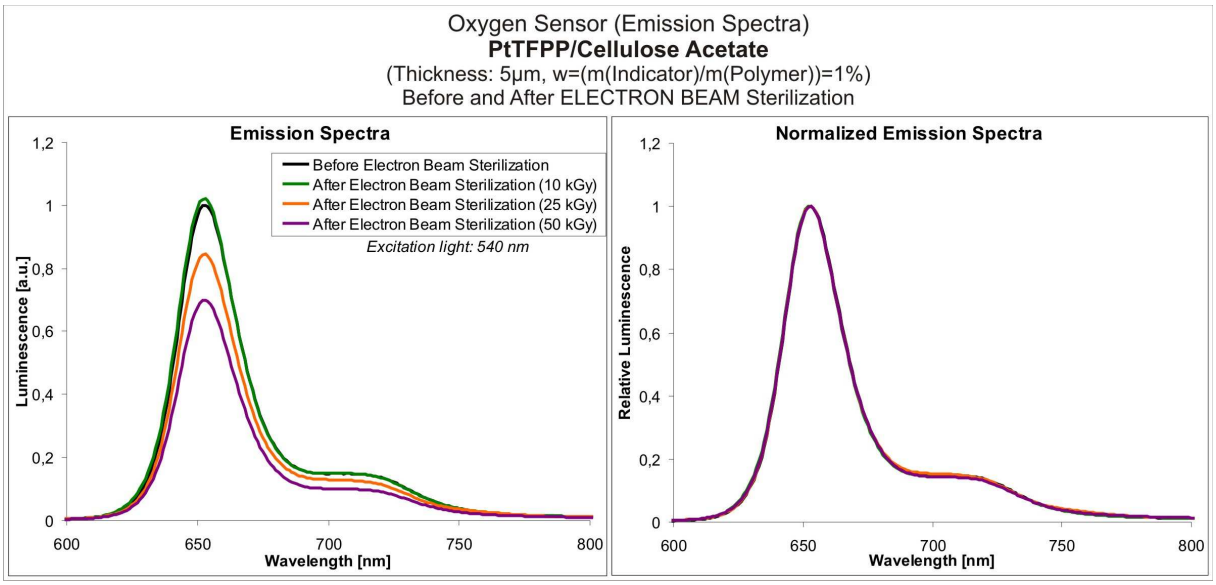

E-BEAM Sterilization	Absorption Spectra		Emission Spectra	
Alterations in Absorption/Emission Intensity	10kGy	2,44% increase	10kGy	1,96% increase
	25 kGy	11,00% decrease	25 kGy	15,52% decrease
	50 kGy	18,86% decrease	50 kGy	30,02% decrease

Alterations in Absorption/Emission Curve Form	10kGy	Altered absorption between 405-490nm and 515-530 nm.	10kGy	Unaltered.
	25 kGy	Altered absorption between 405-490nm and 515-530 nm. New peak with λ_{max}=593 nm.	25 kGy	Unaltered.
	50 kGy	Altered absorption between 405-490nm and 515-530 nm. New peak with λ_{max}=593 nm.	50 kGy	Unaltered.

Oxygen Sensor
PtTFPP/Cellulose Acetate
(Thickness: 5 µm, w=(m(Indicator)/m(Polymer))=1%)
Before and After ELECTRON BEAM Sterilization

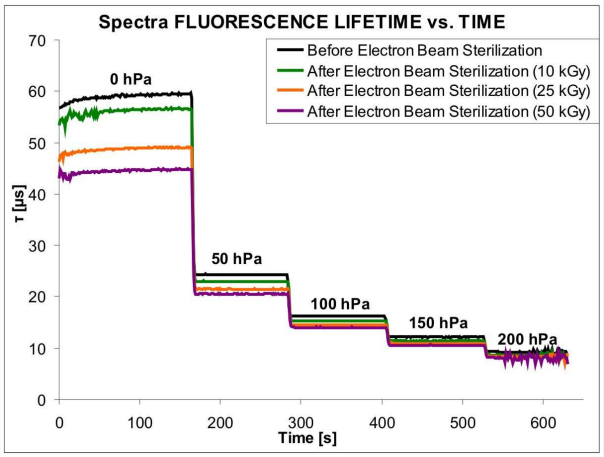

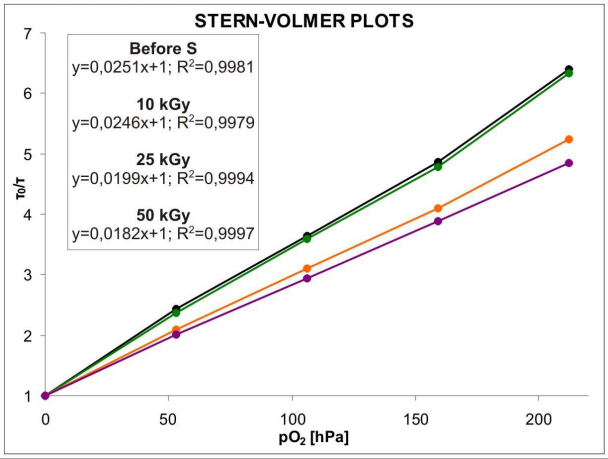

E-BEAM Sterilization	Luminescence Lifetime		Stern-Volmer Plot	
Alterations in Luminescence Lifetime and Slope	10kGy	8,11% decrease of τ_0	10kGy	1,99% decrease of slope
		5,64% decrease of τ at 50 hPa		
		6,75% decrease of τ at 100 hPa		
		6,41% decrease of τ at 150 hPa		
		7,24% decrease of τ at 200 hPa		
	25 kGy	26,35% decrease of τ_0	25 kGy	20,72% decrease of slope
		14,40% decrease of τ at 50 hPa		
		14,11% decrease of τ at 100 hPa		
		12,42% decrease of τ at 150 hPa		
		10,15% decrease of τ at 200 hPa		
	50 kGy	32,09% decrease of τ_0	50 kGy	27,49% decrease of slope
		16,71% decrease of τ at 50 hPa		
		15,95% decrease of τ at 100 hPa		
		14,72% decrease of τ at 150 hPa		
		10,26% increase of τ at 200 hPa		

C.11 Platinum(II)Tetrakis(PentaFluorPhenyl)Porphyrin (PtTFPP) immobilized in Ethyl Cellulose

C.11.1 Gamma Sterilization

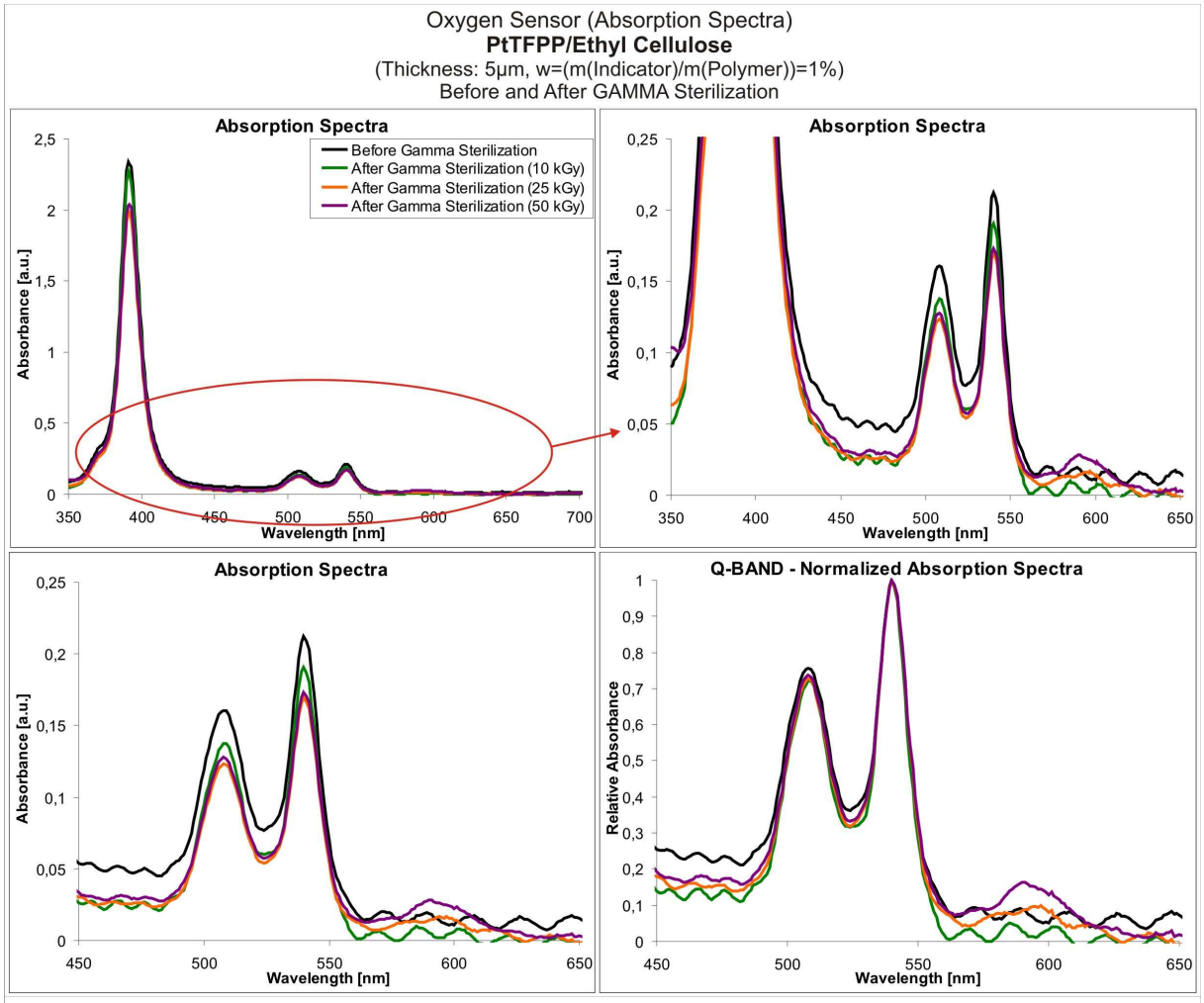

GAMMA Sterilization	Absorption Spectra		Emission Spectra	
Alterations in Absorption/Emission Intensity	10kGy	9,26% decrease	10kGy	14,87% decrease
	25 kGy	20,17% decrease	25 kGy	11,53% decrease
	50 kGy	18,54% decrease	50 kGy	77,68% decrease
Alterations in Absorption/Emission Curve Form	10kGy	Unaltered.	10kGy	Unaltered.
	25 kGy	Unaltered.	25 kGy	Unaltered.
	50 kGy	New absorption peak with λ_{max} = 590 nm.	50 kGy	Altered emission between 685-760 nm.

Oxygen Sensor
PtTFPP/Ethyl Cellulose
(Thickness: 5 µm, w=(m(Indicator)/m(Polymer))=1%)
Before and After GAMMA Sterilization

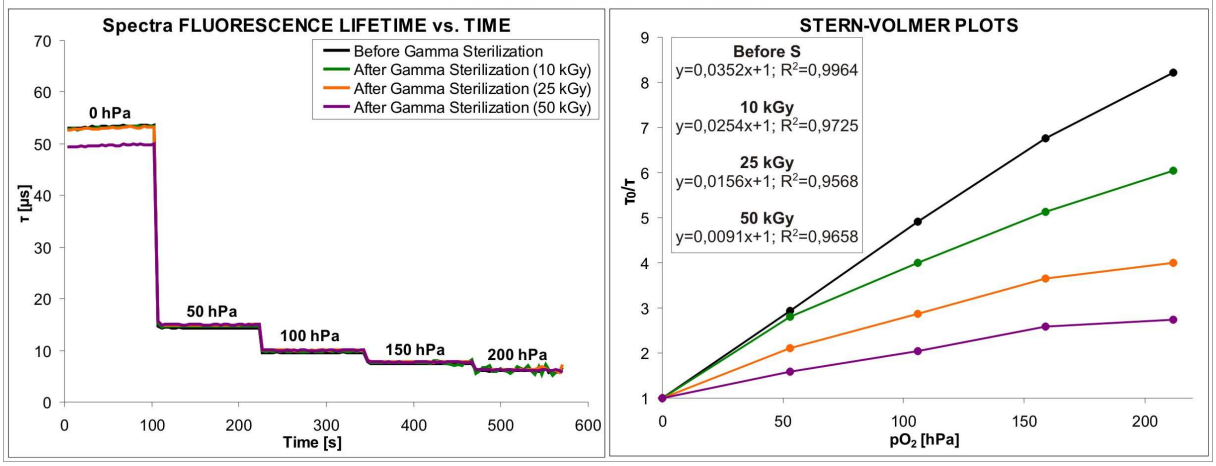

GAMMA Sterilization	Luminescence Lifetime		Stern-Volmer Plot	
Alterations in Luminescence Lifetime and Slope	10kGy	29,75% decrease of τ_0	10kGy	27,84% decrease of slope
		26,64% decrease of τ at 50 hPa		
		13,70% decrease of τ at 100 hPa		
		7,39% decrease of τ at 150 hPa		
		4,34% decrease of τ at 200 hPa		
	25 kGy	51,79% decrease of τ_0	25 kGy	55,68% decrease of slope
		33,48% decrease of τ at 50 hPa		
		17,40% decrease of τ at 100 hPa		
		10,96% decrease of τ at 150 hPa		
		1,08% decrease of τ at 200 hPa		
	50 kGy	68,36% decrease of τ_0	50 kGy	74,15% decrease of slope
		41,75% decrease of τ at 50 hPa		
		23,43% decrease of τ at 100 hPa		
		17,58% decrease of τ at 150 hPa		
		5,27% increase of τ at 200 hPa		

C.11.2 Electron Beam Sterilization

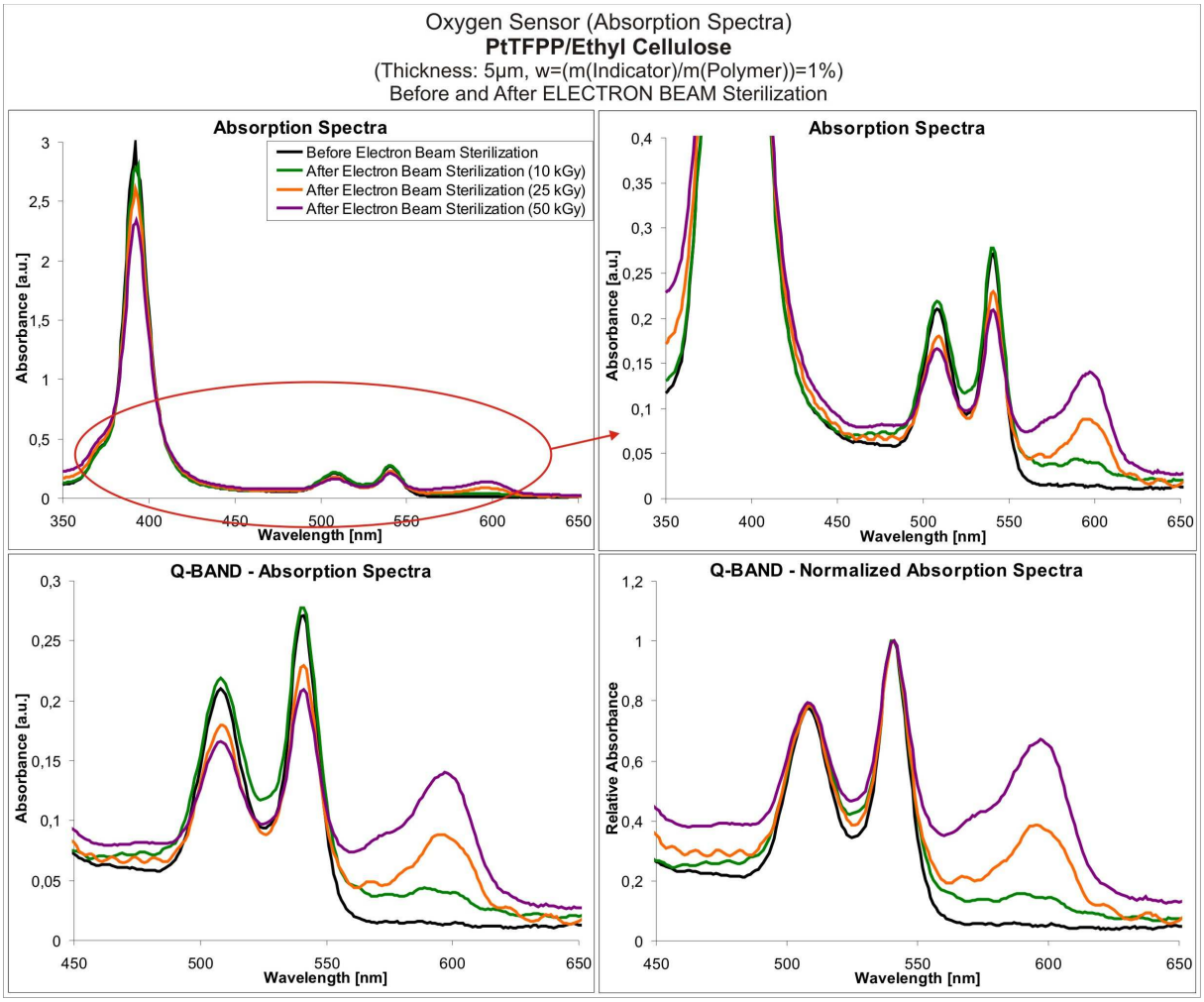

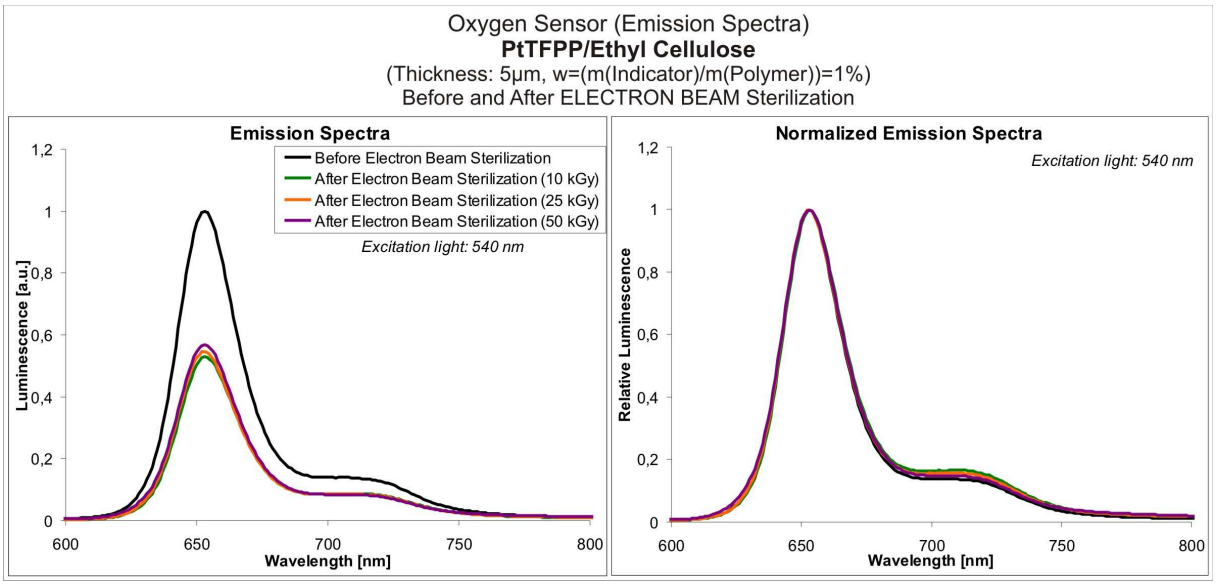

E-BEAM Sterilization	Absorption Spectra		Emission Spectra	
Alterations in Absorption/Emission Intensity	10kGy	2,46% increase	10kGy	47,14% decrease
	25 kGy	15,23% decrease	25 kGy	45,38% decrease
	50 kGy	22,88% decrease	50 kGy	43,18% decrease

Alterations in Absorption/Emission Curve Form	10kGy	Altered absorption between 520-530 nm.	10kGy	Altered emission between 685-750 nm.
	25 kGy	Altered absorption between 350-380 nm, 410-490 nm and 520-530 nm. New absorption peak with λ_{max} = 594 nm.	25 kGy	Altered emission between 685-750 nm..
	50 kGy	Altered absorption between 350-380 nm, 410-490 nm and 520-530 nm. New absorption peak with λ_{max} = 596 nm.	50 kGy	Unaltered.

Oxygen Sensor
PtTFPP/Ethyl Cellulose
(Thickness: 5 µm, w=(m(Indicator)/m(Polymer))=1%)
Before and After ELECTRON BEAM Sterilization

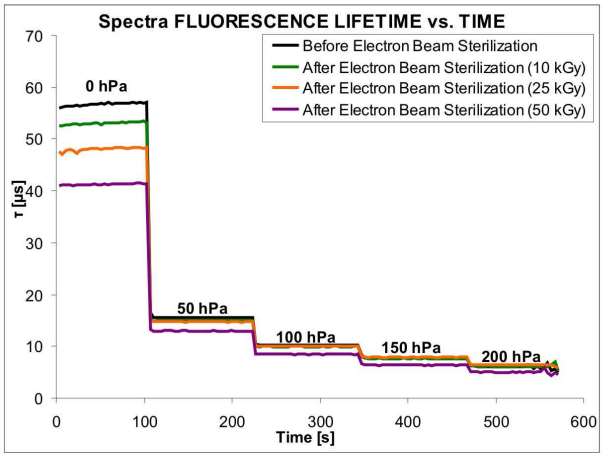

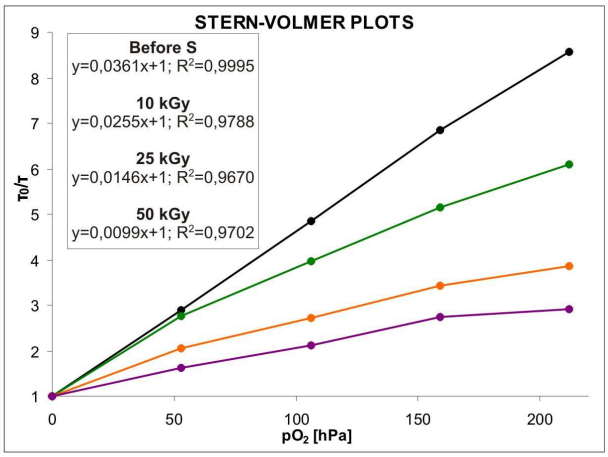

E-BEAM Sterilization	Luminescence Lifetime		Stern-Volmer Plot	
Alterations in Luminescence Lifetime and Slope	10kGy	33,69% decrease of τ_0	10kGy	29,36% decrease of slope
		30,30% decrease of τ at 50 hPa		
		18,88% decrease of τ at 100 hPa		
		11,66% decrease of τ at 150 hPa		
		6,84% decrease of τ at 200 hPa		
	25 kGy	56,56% decrease of τ_0	25 kGy	59,56% decrease of slope
		38,47% decrease of τ at 50 hPa		
		22,67% decrease of τ at 100 hPa		
		13,24% decrease of τ at 150 hPa		
		3,65% decrease of τ at 200 hPa		
	50 kGy	74,11% decrease of τ_0	50 kGy	72,58% decrease of slope
		53,93% decrease of τ at 50 hPa		
		40,77% decrease of τ at 100 hPa		
		29,53% decrease of τ at 150 hPa		
		24,32% decrease of τ at 200 hPa		

C.12 Platinum(II)Tetrakis(PentaFluorPhenyl)Porphyrin (PtTFPP) immobilized in HydroGel D4/D7

C.12.1 Gamma Sterilization

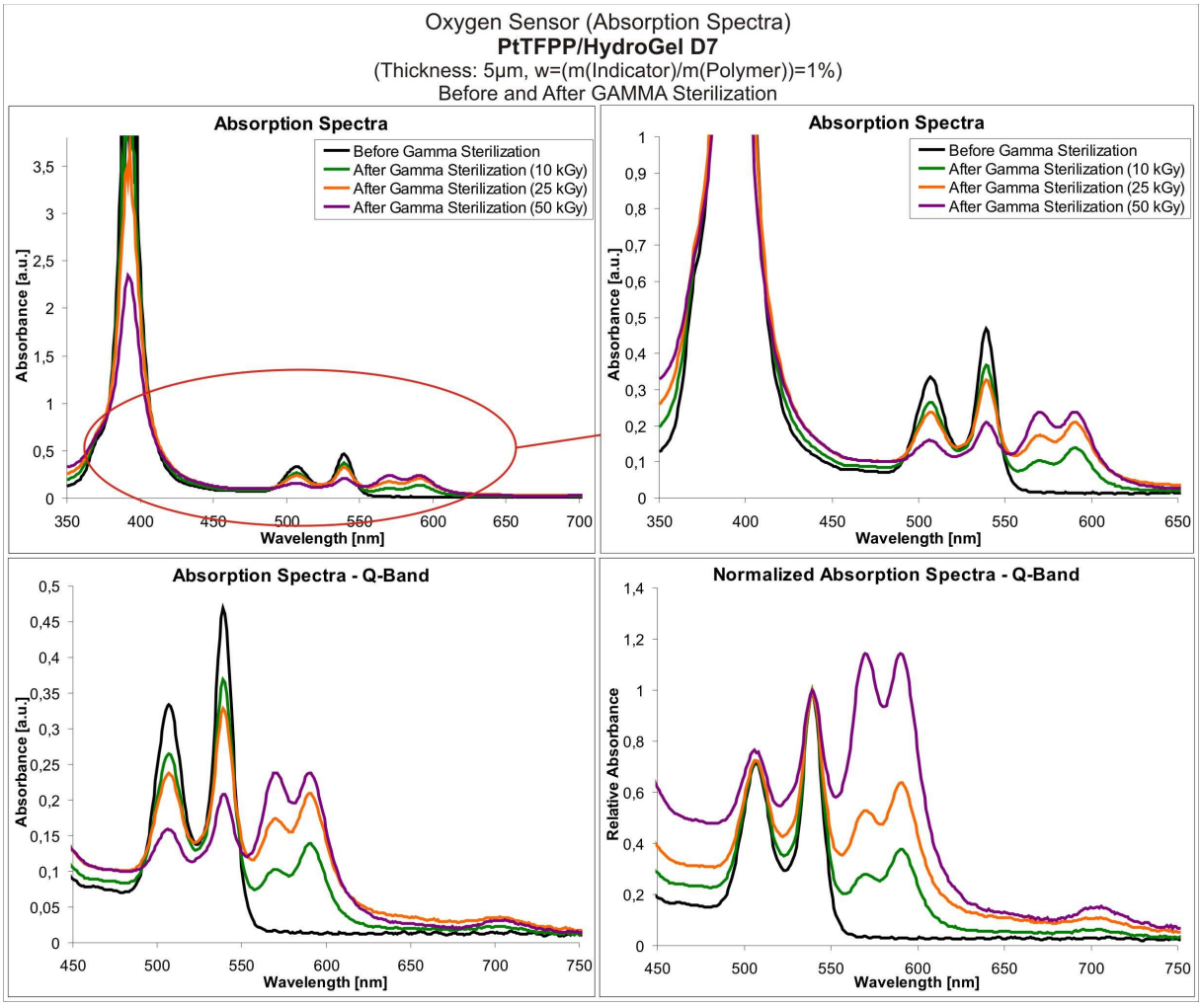

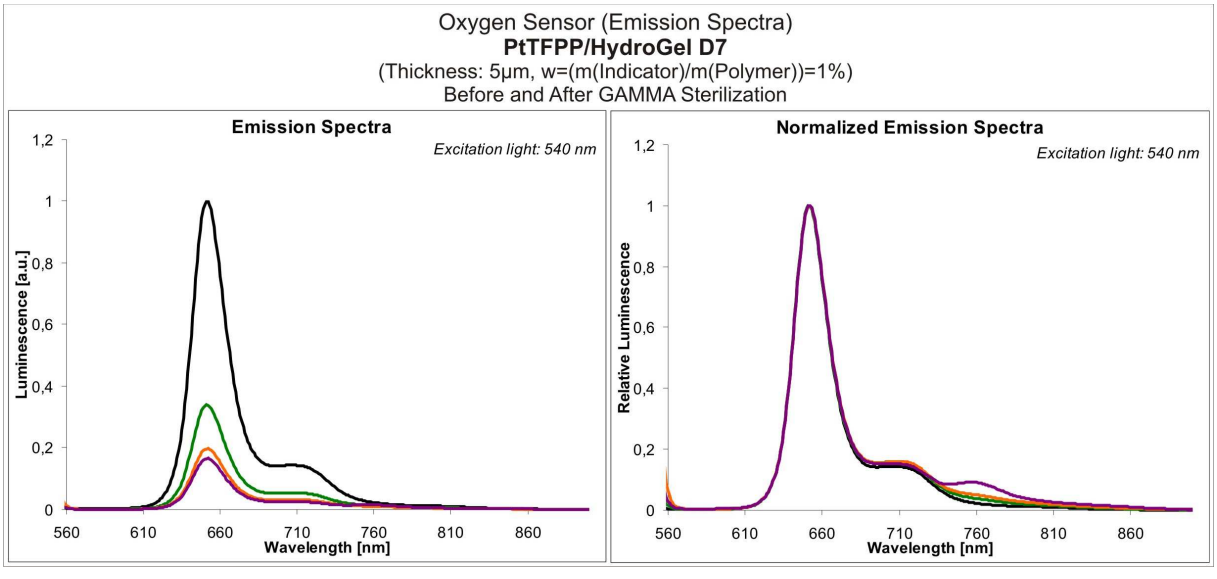

GAMMA Sterilization	Absorption Spectra		Emission Spectra	
Alterations in Absorption/Emission Intensity	10kGy	21,34% decrease	10kGy	66,09% decrease
	25 kGy	30,07% decrease	25 kGy	80,30% decrease
	50 kGy	55,50% decrease	50 kGy	83,45% decrease
Alterations in Absorption/Emission Curve Form	10kGy	Altered absorption curve form between 350-360 nm and 420-485 nm, New absorption peaks with λ_{max}= 567 nm, λ_{max}= 588 nm and λ_{max}= 700 nm.	10kGy	Altered emission curve form between 740-810 nm.
	25 kGy	Altered absorption curve form between 350-360 nm and 420-485 nm, New absorption peaks with λ_{max}= 568 nm, λ_{max}= 589 nm and λ_{max}= 701 nm.	25 kGy	Altered emission curve form between 740-810 nm.
	50 kGy	Altered absorption curve form between 350-360 nm and 420-485 nm, New absorption peaks with λ_{max}= 568 nm, λ_{max}= 589 nm and λ_{max}= 701 nm.	50 kGy	Altered emission curve form between 740-810 nm. New emission peak with λ_{max}= 764 nm.

Oxygen Sensor
PtTFPP/HydroGel D7
(Thickness: 5 µm, w=(m(Indicator)/m(Polymer))=1%)
Before and After GAMMA Sterilization

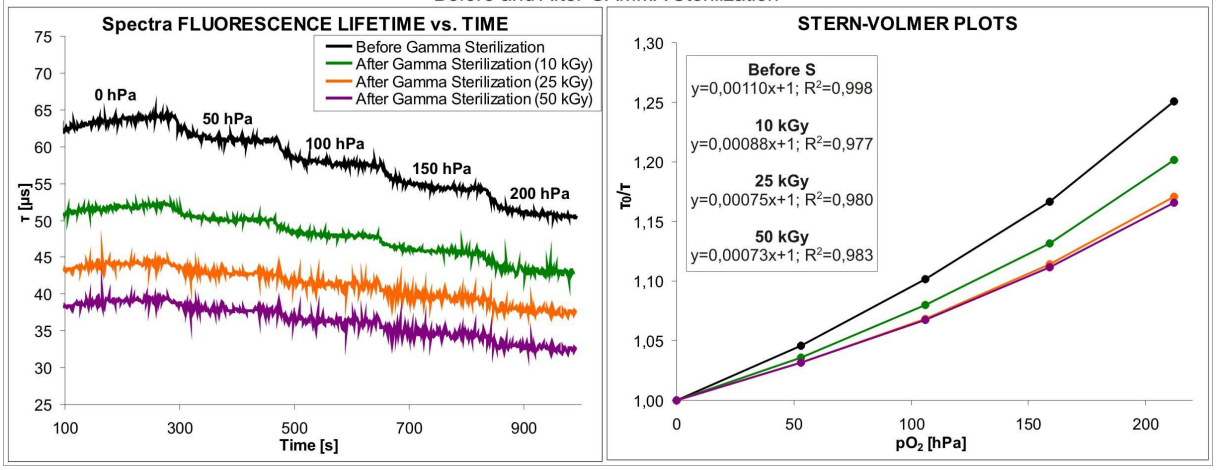

GAMMA Sterilization	Luminescence Lifetime		Stern-Volmer Plot	
Alterations in Luminescence Lifetime and Slope	10kGy	18,68% decrease of τ_0	10kGy	20,24% decrease of slope
		17,87% decrease of τ at 50 hPa		
		16,95% decrease of τ at 100 hPa		
		16,11% decrease of τ at 150 hPa		
		15,32% decrease of τ at 200 hPa		
	25 kGy	30,77% decrease of τ_0	25 kGy	31,76% decrease of slope
		29,86% decrease of τ at 50 hPa		
		28,72% decrease of τ at 100 hPa		
		27,54% decrease of τ at 150 hPa		
		26,13% decrease of τ at 200 hPa		
	50 kGy	42,23% decrease of τ_0	50 kGy	33,66% decrease of slope
		41,46% decrease of τ at 50 hPa		
		40,31% decrease of τ at 100 hPa		
		39,36% decrease of τ at 150 hPa		
		37,92% decrease of τ at 200 hPa		

C.12.2 Electron Beam Sterilization

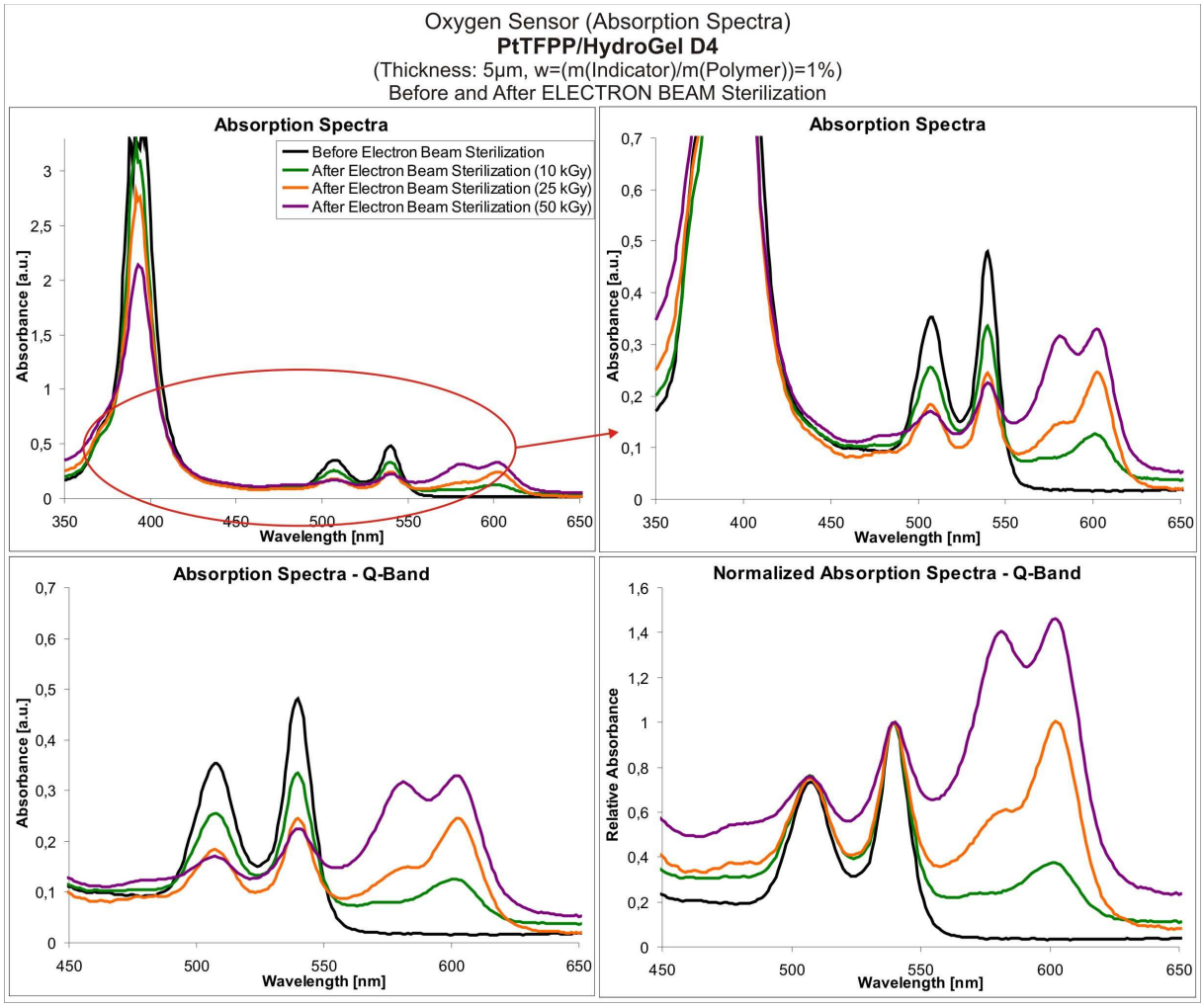

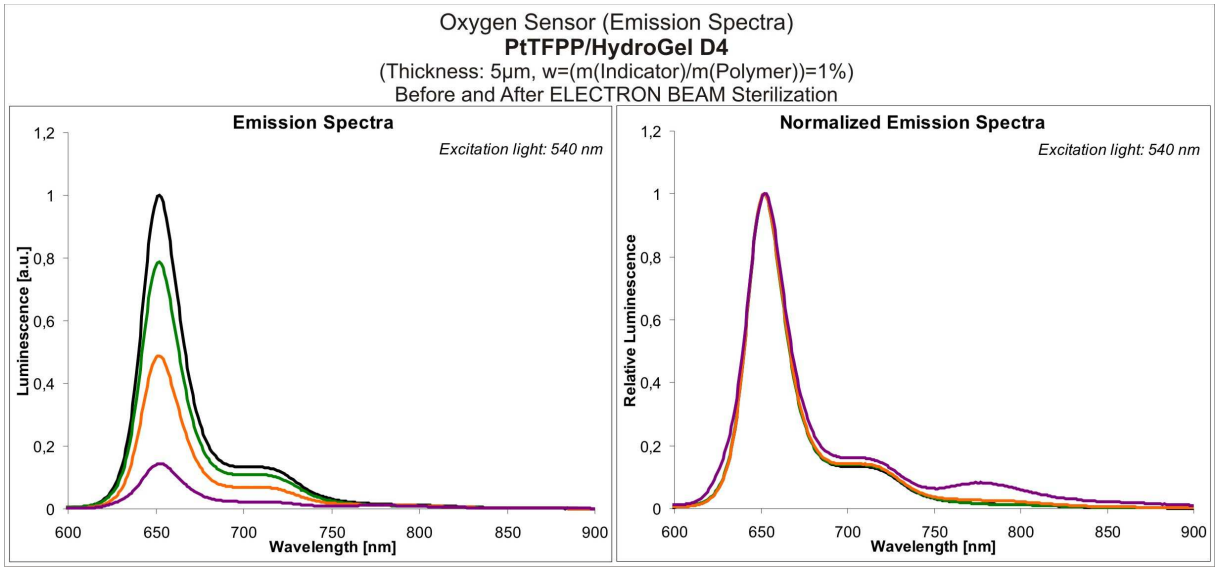

E-BEAM Sterilization	Absorption Spectra		Emission Spectra	
Alterations in Absorption/Emission Intensity	10kGy	30,09% decrease	10kGy	21,30% decrease
	25 kGy	49,11% decrease	25 kGy	51,10% decrease
	50 kGy	53,09% decrease	50 kGy	85,61% decrease

Alterations in Absorption/Emission Curve Form	10kGy	Altered absorption curve form between 350-360 nm, 430-500 nm and 510-535 nm. New absorption peak with λ_{max}= 600 nm.	10kGy	Unaltered.
	25 kGy	Altered absorption curve form between 350-365 nm, 430-500 nm and 510-535 nm. New absorption peaks with λ_{max}= 579 nm and λ_{max}= 601 nm.	25 kGy	Unaltered.
	50 kGy	Altered absorption curve form between 350-370 nm, 430-500 nm and 510-535 nm, New absorption peaks with λ_{max}= 581 nm and λ_{max}= 601 nm.	50 kGy	Altered emission curve form between 620-630 nm and 670-740 nm. New emission peak with λ_{max}= 780 nm.

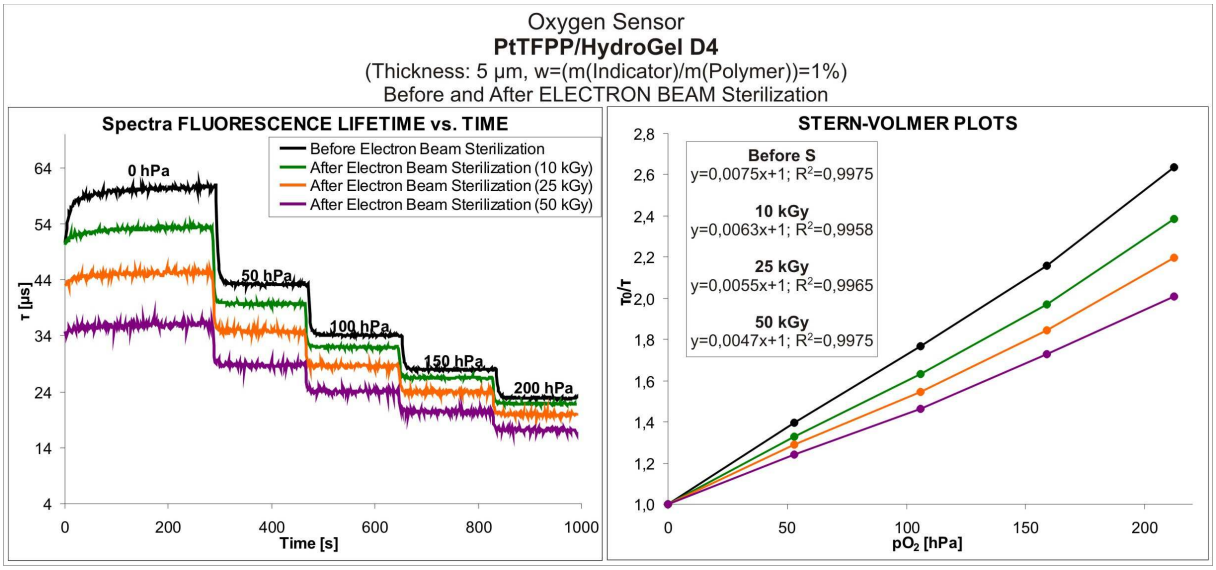

E-BEAM Sterilization	Luminescence Lifetime		Stern-Volmer Plot	
Alterations in Luminescence Lifetime and Slope	10kGy	13,60% decrease of τ_0	10kGy	16,00% decrease of slope
		9,01% decrease of τ at 50 hPa		
		7,33% decrease of τ at 100 hPa		
		5,33% decrease of τ at 150 hPa		
		4,37% decrease of τ at 200 hPa		
	25 kGy	27,53% decrease of τ_0	25 kGy	26,67% decrease of slope
		21,56% decrease of τ at 50 hPa		
		17,01% decrease of τ at 100 hPa		
		15,30% decrease of τ at 150 hPa		
		13,10% decrease of τ at 200 hPa		
	50 kGy	42,79% decrease of τ_0	50 kGy	37,33% decrease of slope
		35,78% decrease of τ at 50 hPa		
		31,08% decrease of τ at 100 hPa		
		28,57% decrease of τ at 150 hPa		
		24,89% decrease of τ at 200 hPa		

C.13 Platinum(II)Tetrakis(PentaFluorPhenyl)Porphyrin (PtTFPP) immobilized in HydroThane 5

C.13.1 Gamma Sterilization

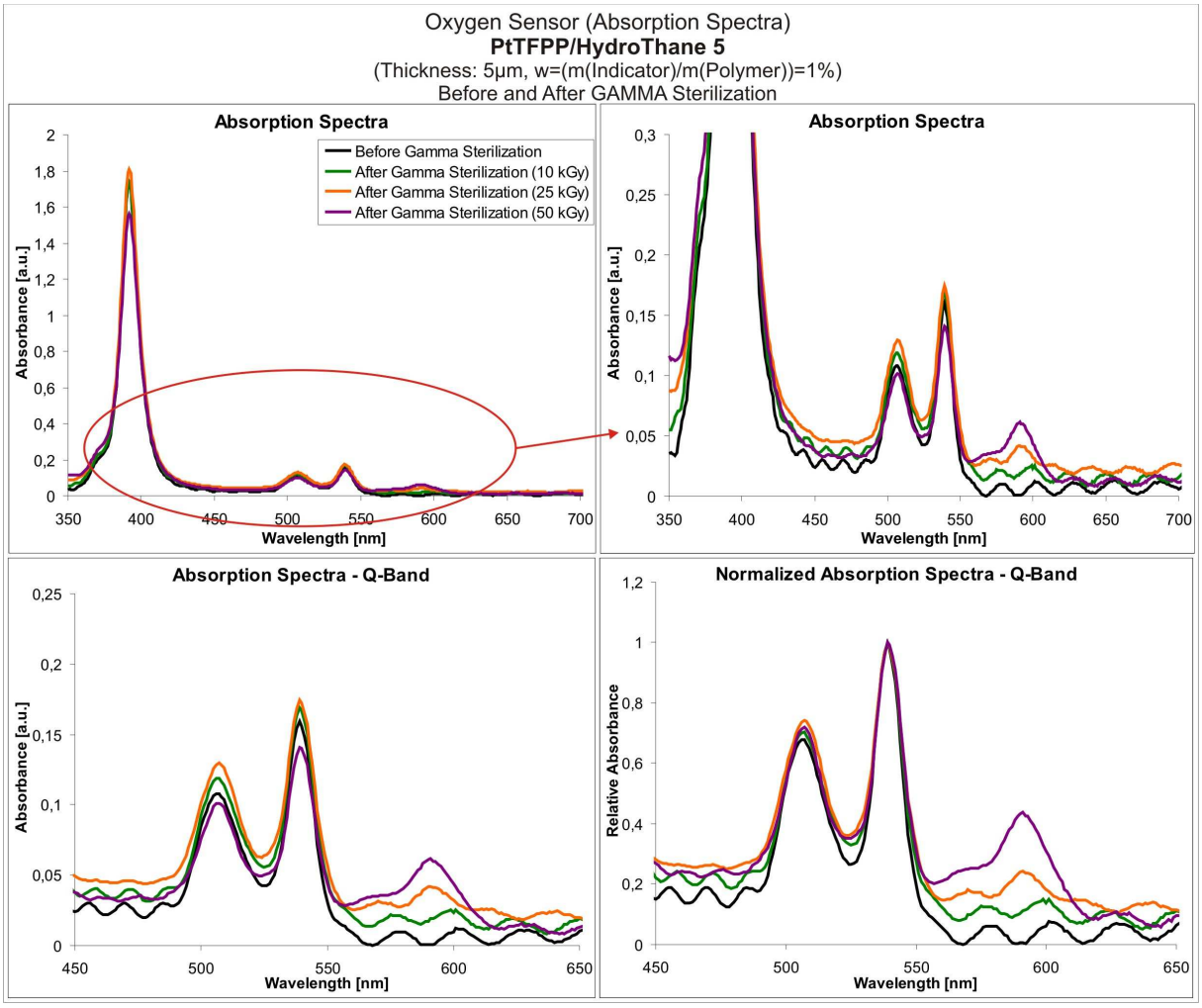

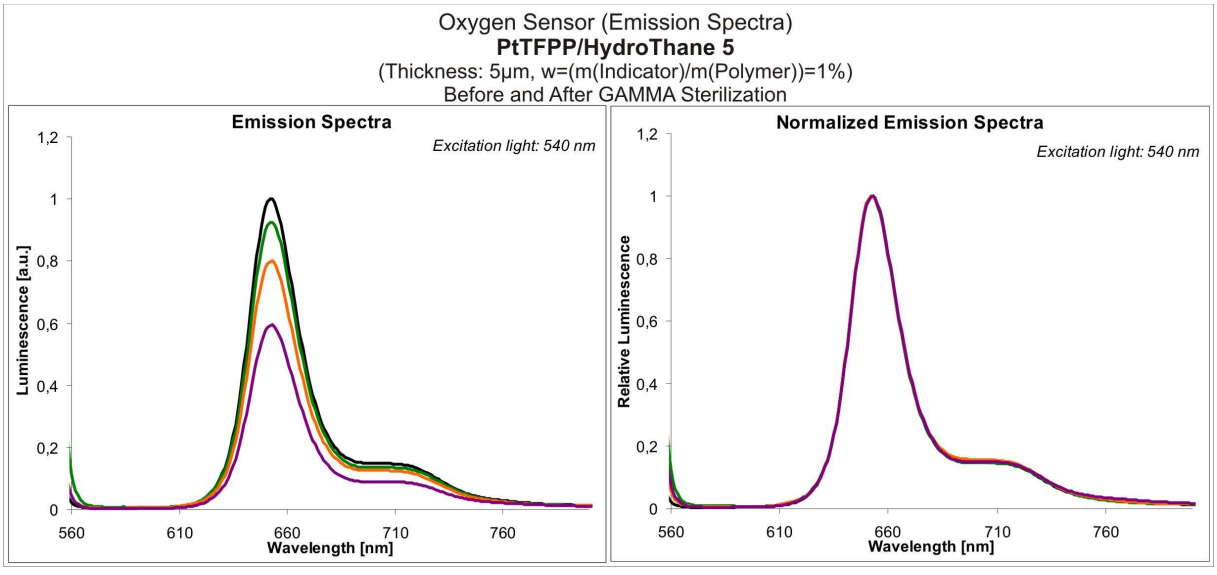

GAMMA Sterilization	Absorption Spectra		Emission Spectra	
Alterations in Absorption/Emission Intensity	10kGy	5,66% increase	10kGy	7,39% decrease
	25 kGy	8,46% increase	25 kGy	7,39% decrease
	50 kGy	11,62% decrease	50 kGy	40,57% decrease
Alterations in Absorption/Emission Curve Form	10kGy	Altered absorption curve form between 350-360 nm, 420-490 nm and 520-530 nm.	10kGy	Unaltered.
	25 kGy	Altered absorption curve form between 350-360 nm, 420-490 nm and 520-530 nm. New absorption peak with λ_{max}= 590 nm.	25 kGy	Unaltered.
	50 kGy	Altered absorption curve form between 350-360 nm, 420-490 nm and 520-530 nm. New absorption peak with λ_{max}= 588 nm.	50 kGy	Unaltered.

Oxygen Sensor
PtTFPP/HydroThane 5
(Thickness: 5 µm, w=(m(Indicator)/m(Polymer))=1%)
Before and After GAMMA Sterilization

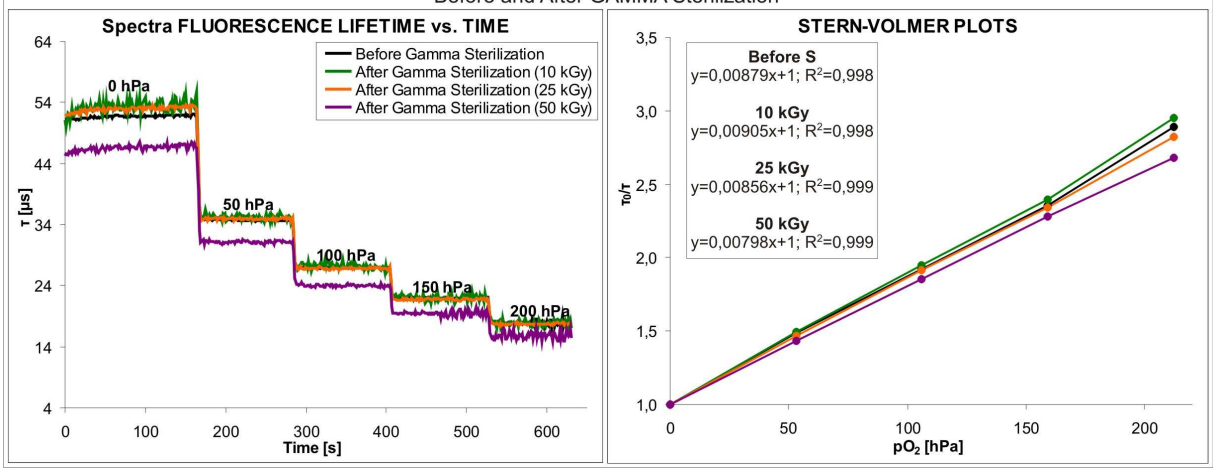

GAMMA Sterilization	Luminescence Lifetime		Stern-Volmer Plot	
Alterations in Luminescence Lifetime and Slope	10kGy	1,52% increase of τ_0	10kGy	2,73% increase of slope
		1,28% increase of τ at 50 hPa		
		Equaly τ at 100 hPa before and after sterilization.		
		0,14% increase of τ at 150 hPa		
		0,56% decrease of τ at 200 hPa		
	25 kGy	3,67% decrease of τ_0	25 kGy	2,62% decrease of slope
		1,89% decrease of τ at 50 hPa		
		3,33% decrease of τ at 100 hPa		
		3,00% decrease of τ at 150 hPa		
		1,12% decrease of τ at 200 hPa		
	50 kGy	18,15% decrease of τ_0	50 kGy	9,22% decrease of slope
		14,68% decrease of τ at 50 hPa		
		15,19% decrease of τ at 100 hPa		
		15,29% decrease of τ at 150 hPa		
		11,73% decrease of τ at 200 hPa		

C.13.2 Electron Beam Sterilization

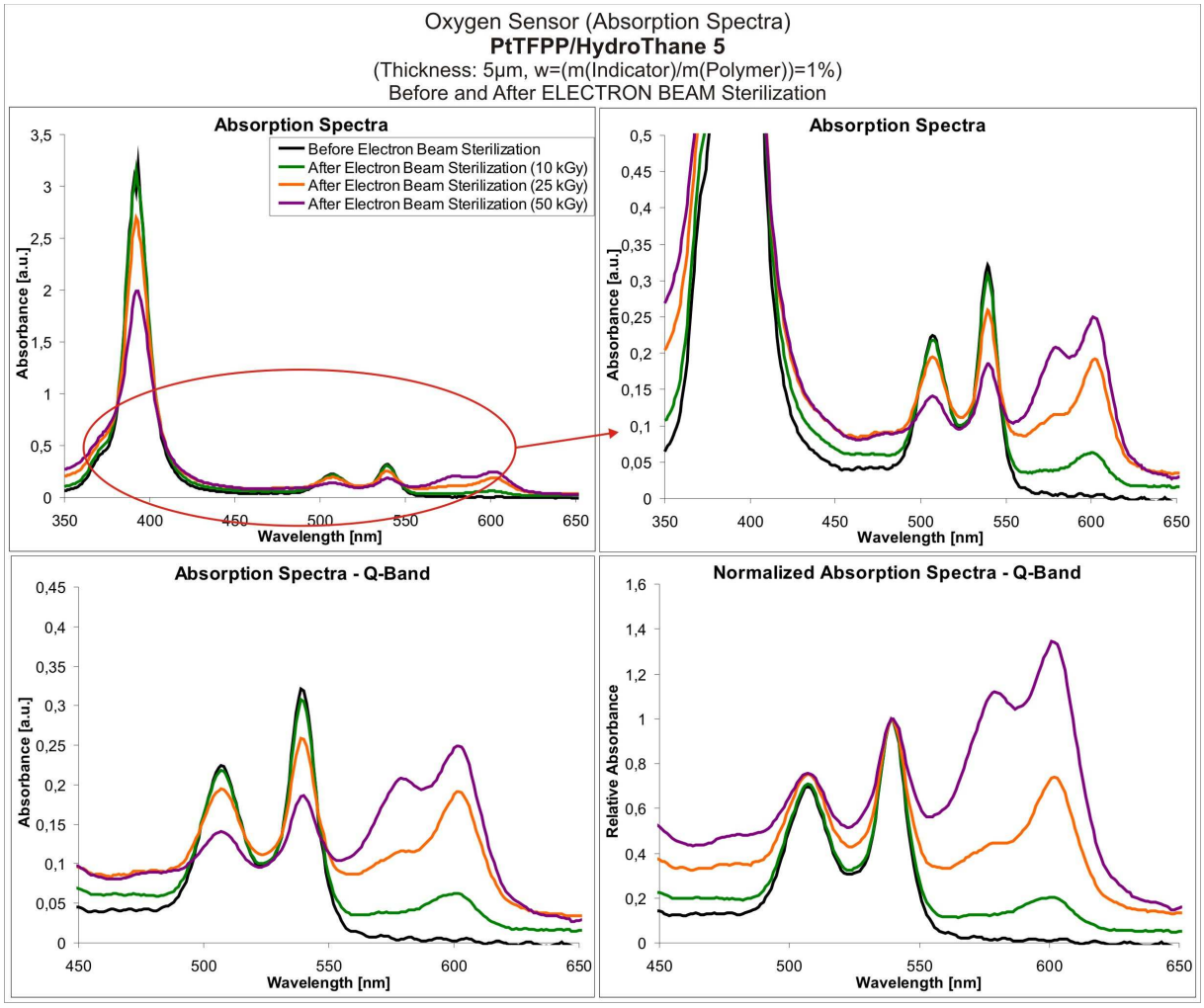

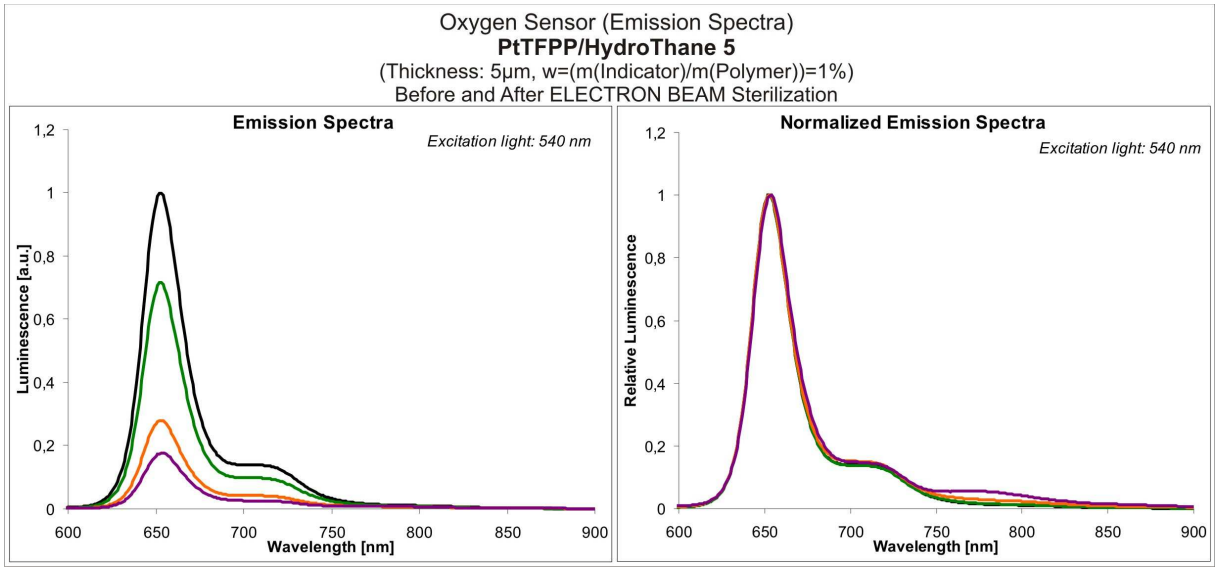

E-BEAM Sterilization	Absorption Spectra		Emission Spectra	
Alterations in Absorption/Emission Intensity	10kGy	4,38% decrease	10kGy	28,42% decrease
	25 kGy	19,42% decrease	25 kGy	71,99% decrease
	50 kGy	42,22% decrease	50 kGy	82,32% decrease

Alterations in Absorption/Emission Curve Form	10kGy	Altered absorption curve form between 350-360 nm, 410-500 nm. New absorption peak with λ_{max}= 600 nm.	10kGy	Unaltered.
	25 kGy	Altered absorption curve form between 350-365 nm, 410-500 nm and 510-535 nm. New absorption peaks with λ_{max}= 577 nm and λ_{max}= 601 nm.	25 kGy	Unaltered.
	50 kGy	Altered absorption curve form between 350-370 nm, 410-500 nm and 510-535 nm, New absorption peaks with λ_{max}= 578 nm and λ_{max}= 601 nm.	50 kGy	New emission peak with λ_{max}= 782 nm.

Oxygen Sensor
PtTFPP/HydroThane 5
(Thickness: 5 µm, w=(m(Indicator)/m(Polymer))=1%)
Before and After ELECTRON BEAM Sterilization

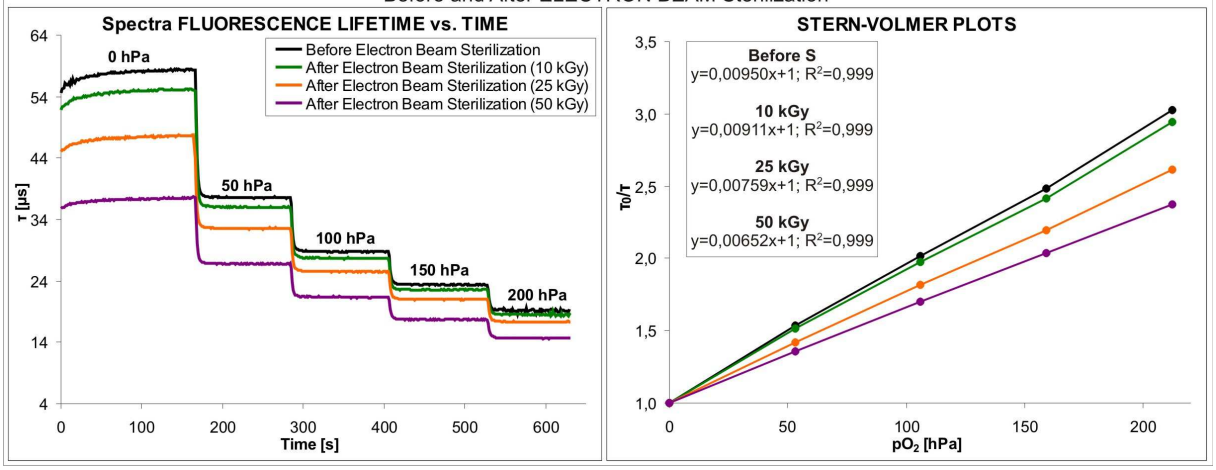

E-BEAM Sterilization	Luminescence Lifetime		Stern-Volmer Plot	
Alterations in Luminescence Lifetime and Slope	10kGy	6,19% decrease of τ_0	10kGy	4,11% decrease of slope
		4,51% decrease of τ at 50 hPa		
		4,51% decrease of τ at 100 hPa.		
		3,63% decrease of τ at 150 hPa		
		3,65% decrease of τ at 200 hPa		
	25 kGy	22,20% decrease of τ_0	25 kGy	20,10% decrease of slope
		15,38% decrease of τ at 50 hPa		
		13,54% decrease of τ at 100 hPa		
		11,79% decrease of τ at 150 hPa		
		9,89% decrease of τ at 200 hPa		
	50 kGy	40,10% decrease of τ_0	50 kGy	31,37% decrease of slope
		31,75% decrease of τ at 50 hPa		
		28,82% decrease of τ at 100 hPa		
		27,01% decrease of τ at 150 hPa		
		23,44% decrease of τ at 200 hPa		

C.14 Platinum(II)Tetrakis(PentaFluorPhenyl)Porphyrin (PtTFPP) immobilized in PolySulfone

C.14.1 Gamma Sterilization

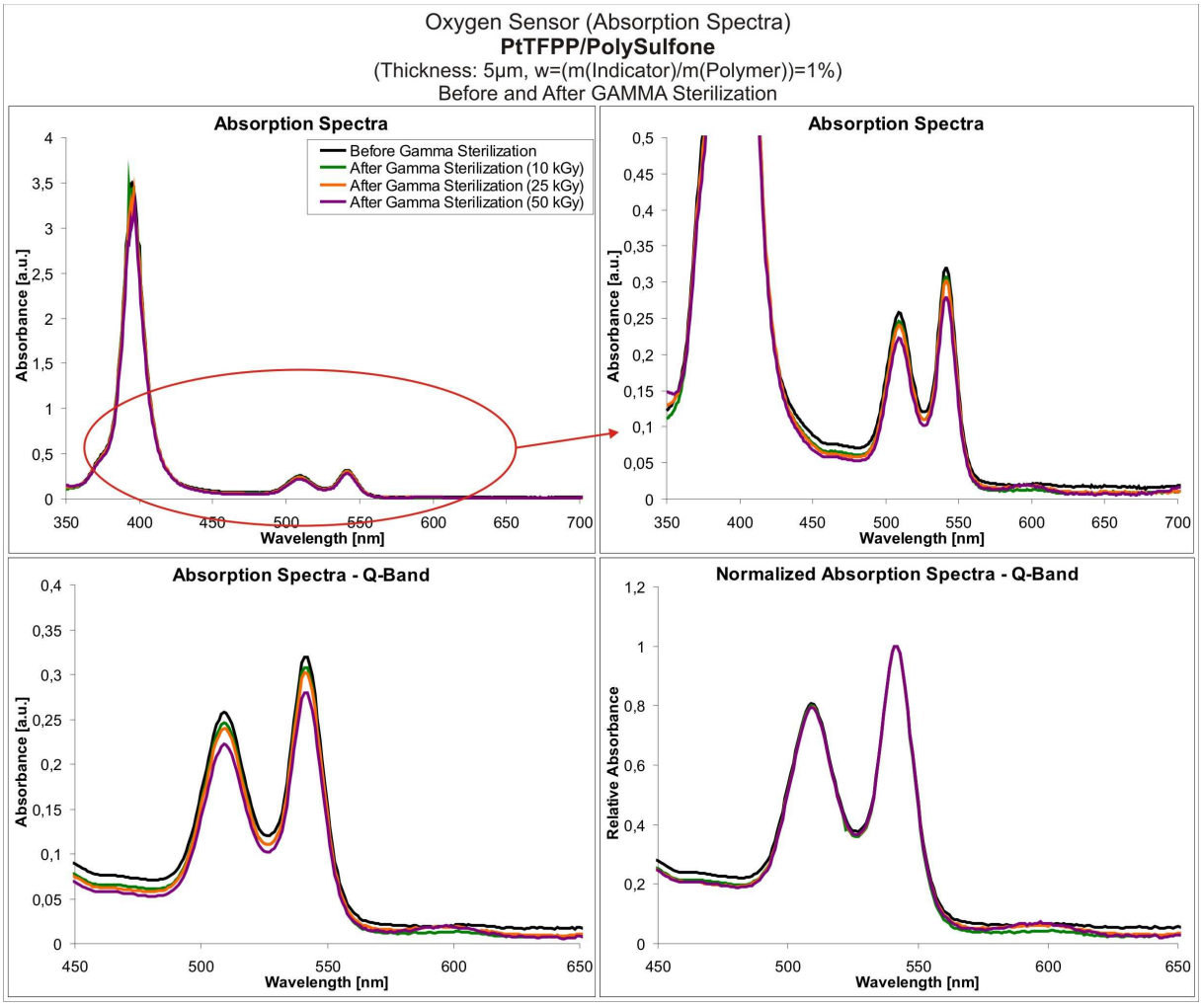

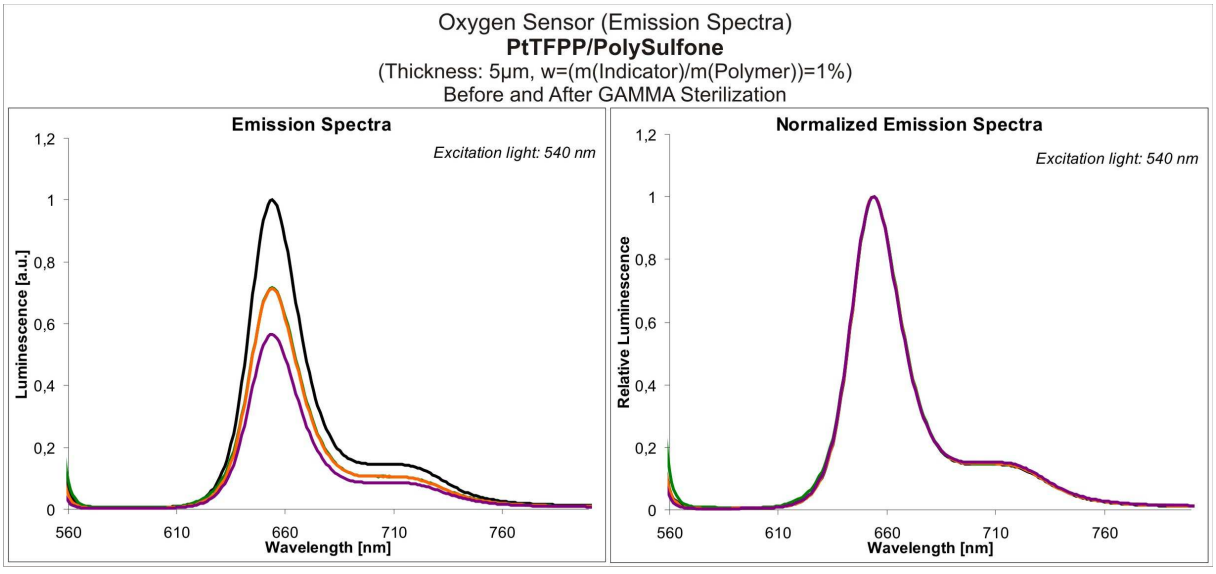

GAMMA Sterilization	Absorption Spectra		Emission Spectra	
Alterations in Absorption/Emission Intensity	10kGy	3,80% decrease	10kGy	28,25% decrease
	25 kGy	5,58% decrease	25 kGy	28,75% decrease
	50 kGy	12,71% decrease	50 kGy	43,42% decrease
Alterations in Absorption/Emission Curve Form	10kGy	Altered absorption curve form between 430-490 nm.	10kGy	Unaltered.
	25 kGy	Altered absorption curve form between 430-490 nm.	25 kGy	Unaltered.
	50 kGy	Altered absorption curve form between 430-490 nm.	50 kGy	Unaltered.

Oxygen Sensor
PtTFPP/PolySulfone
(Thickness: 5 µm, w=(m(Indicator)/m(Polymer))=1%)
Before and After GAMMA Sterilization

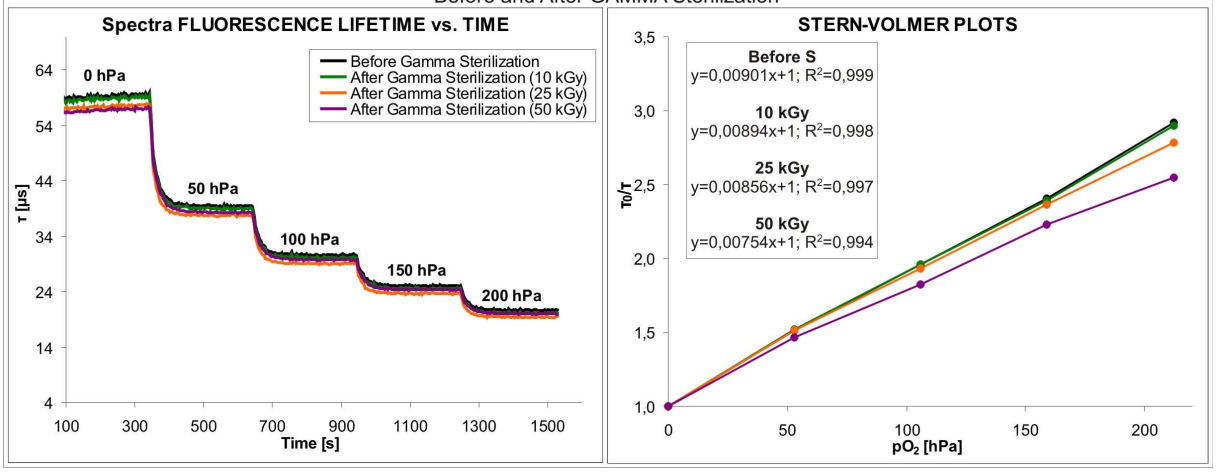

GAMMA Sterilization	Luminescence Lifetime		Stern-Volmer Plot	
Alterations in Luminescence Lifetime and Slope	10kGy	2,83% decrease of τ_0	10kGy	0,78% decrease of slope
		3,13% decrease of τ at 50 hPa		
		2,93% decrease of τ at 100 hPa		
		2,48% decrease of τ at 150 hPa		
		1,94% decrease of τ at 200 hPa		
	25 kGy	10,15% decrease of τ_0	25 kGy	4,99% decrease of slope
		10,16% decrease of τ at 50 hPa		
		8,79% decrease of τ at 100 hPa		
		8,67% decrease of τ at 150 hPa		
		5,83% decrease of τ at 200 hPa		
	50 kGy	31,71% decrease of τ_0	50 kGy	16,31% decrease of slope
		12,40% decrease of τ at 50 hPa		
		9,12% decrease of τ at 100 hPa		
		8,79% decrease of τ at 150 hPa		
		2,91% decrease of τ at 200 hPa		

C.14.2 Electron Beam Sterilization

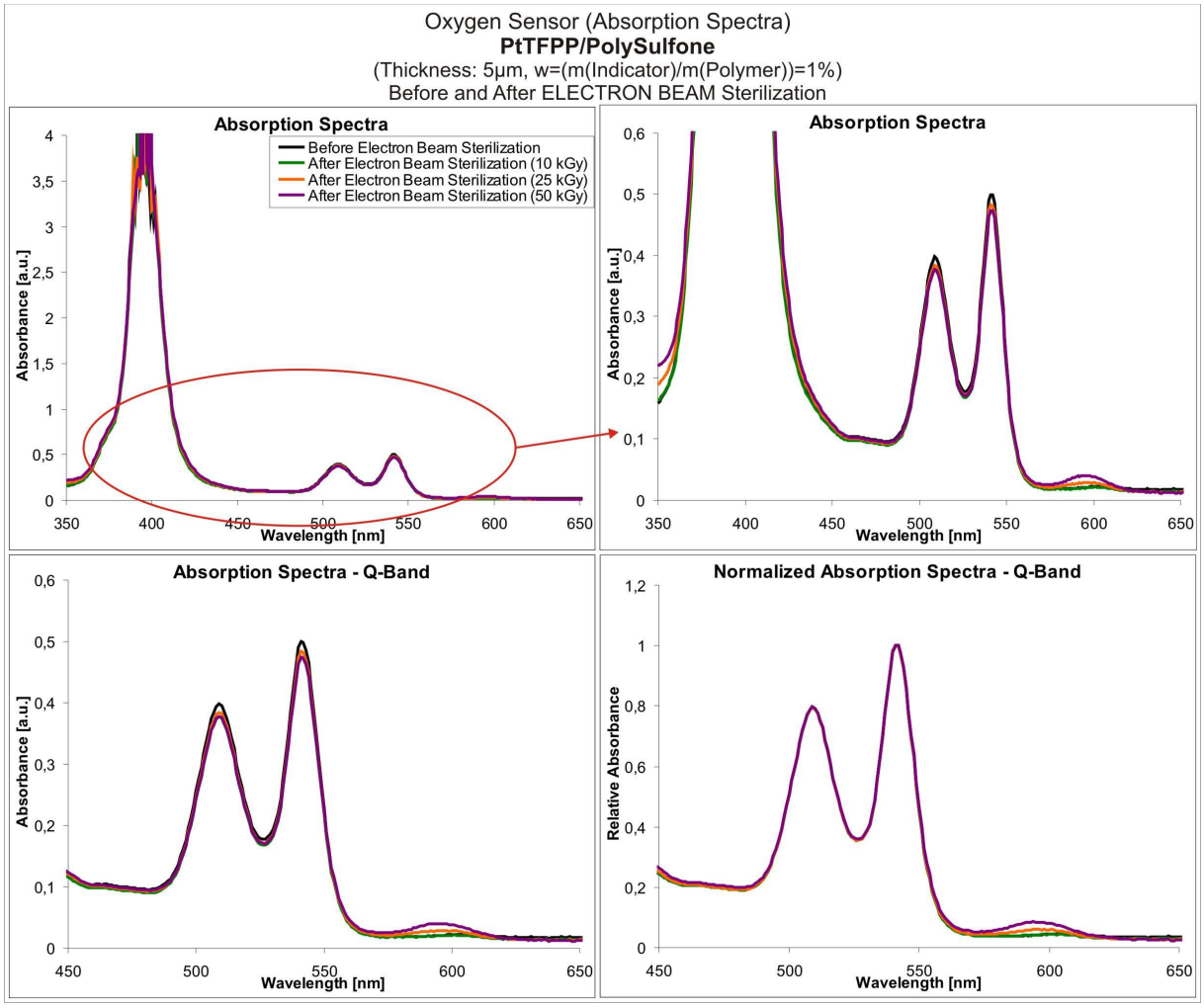

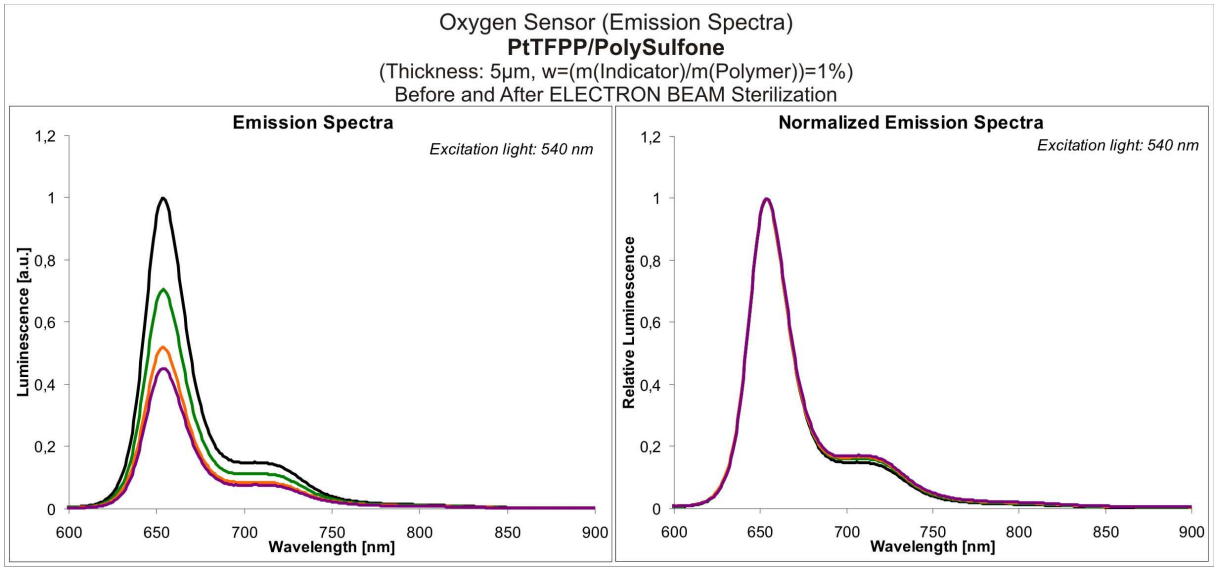

E-BEAM Sterilization	Absorption Spectra		Emission Spectra	
Alterations in Absorption/Emission Intensity	10kGy	5,19% decrease	10kGy	29,58% decrease
	25 kGy	3,19% decrease	25 kGy	48,17% decrease
	50 kGy	5,11% decrease	50 kGy	54,86% decrease

Alterations in Absorption/Emission Curve Form	10kGy	Unaltered.	10kGy	Unaltered.
	25 kGy	New absorption peak with λ_{max} = 594 nm.	25 kGy	Unaltered.
	50 kGy	New absorption peak with λ_{max} = 594 nm.	50 kGy	Unaltered.

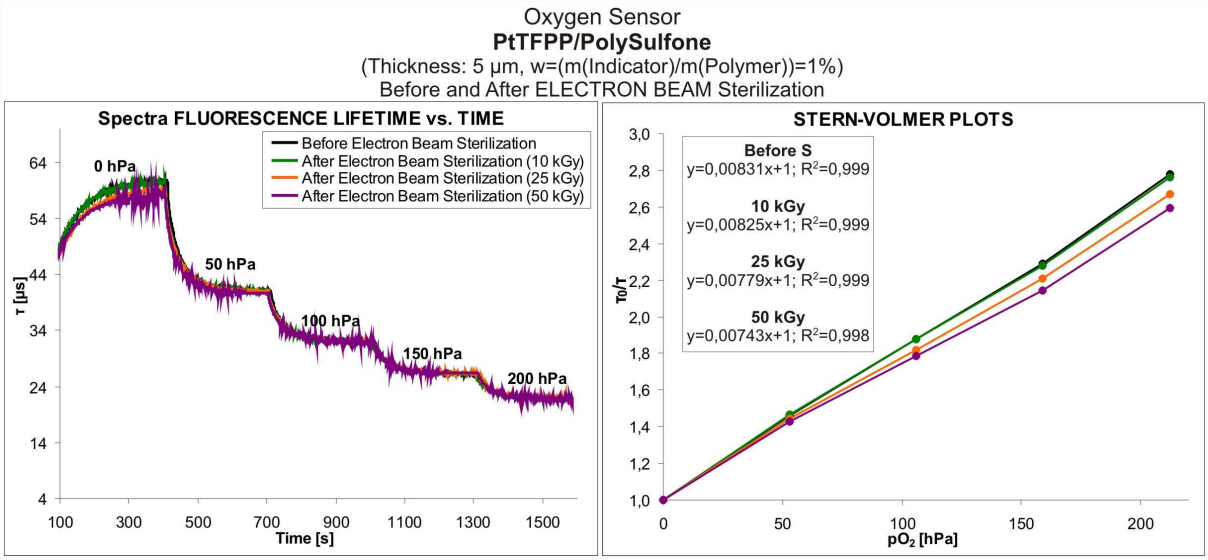

E-BEAM Sterilization	Luminescence Lifetime		Stern-Volmer Plot	
Alterations in Luminescence Lifetime and Slope	10kGy	0,16% decrease of τ_0	10kGy	0,72% decrease of slope
		0,19% decrease of τ at 50 hPa		
		0,31% increase of τ at 100 hPa		
		0,49% increase of τ at 150 hPa		
		0,46% increase of τ at 200 hPa		
	25 kGy	2,82% decrease of τ_0	25 kGy	6,26% decrease of slope
		1,43% decrease of τ at 50 hPa		
		0,31% increase of τ at 100 hPa		
		0,83% increase of τ at 150 hPa		
		0,91% increase of τ at 200 hPa		
	50 kGy	5,98% decrease of τ_0	50 kGy	10,59% decrease of slope
		3,69% decrease of τ at 50 hPa		
		0,94% decrease of τ at 100 hPa		
		0,42% increase of τ at 150 hPa		
		0,46% increase of τ at 200 hPa		

C.15 Platinum(II)Tetrakis(PentaFluorPhenyl)Porphyrin (PtTFPP) immobilized in PolyPhenylSilses Quioxane

C.15.1 Gamma Sterilization

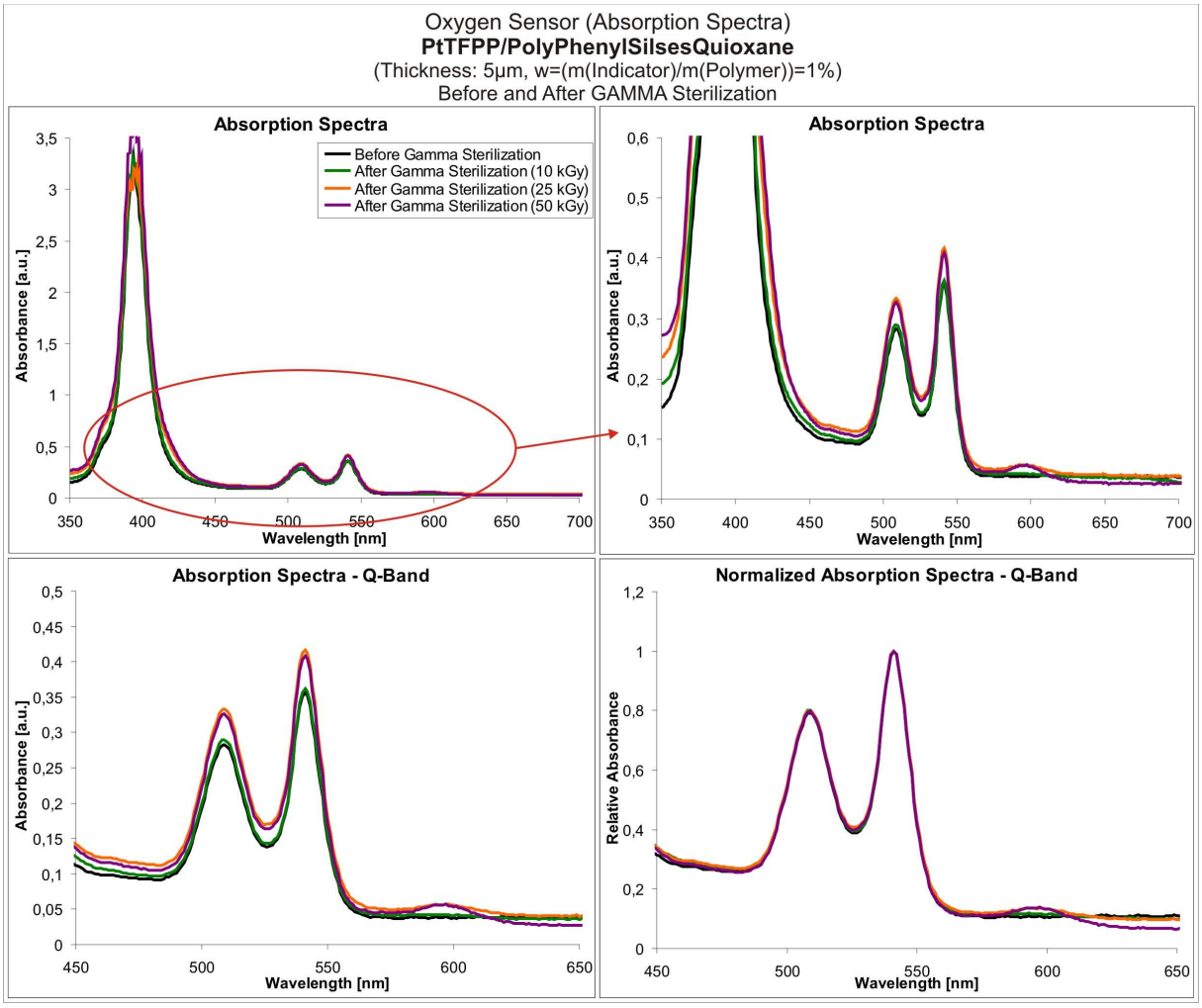

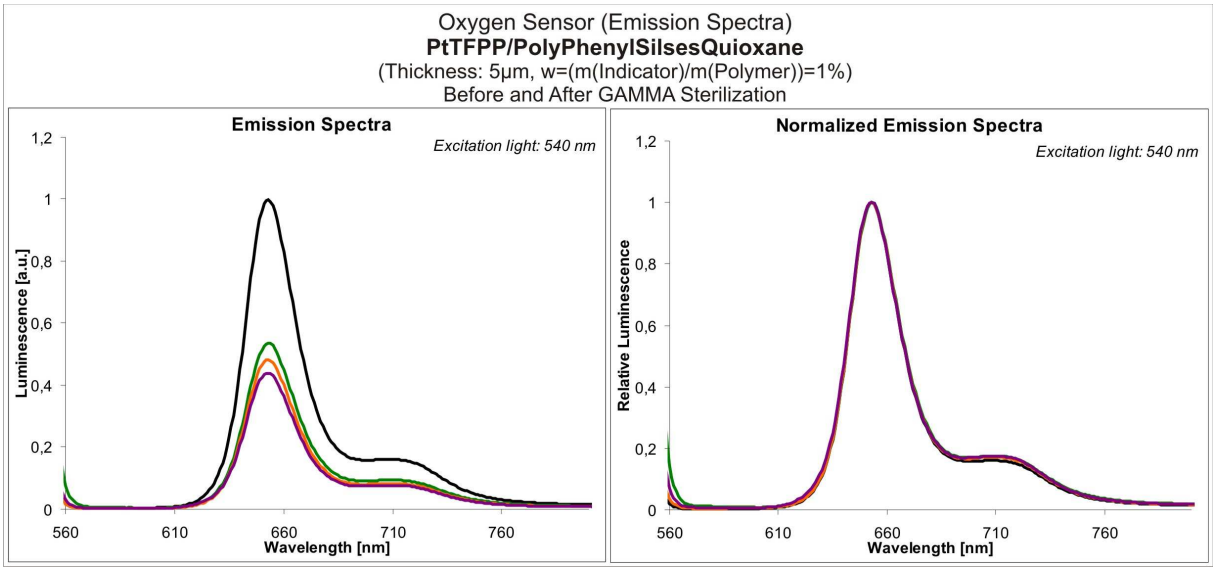

GAMMA Sterilization	Absorption Spectra		Emission Spectra	
Alterations in Absorption/Emission Intensity	10kGy	1,46% increase	10kGy	44,25% decrease
	25 kGy	14,48% increase	25 kGy	49,87% decrease
	50 kGy	12,74% increase	50 kGy	54,34% decrease
Alterations in Absorption/Emission Curve Form	10kGy	Unaltered.	10kGy	Unaltered.
	25 kGy	New absorption peak with λ_{max}=596 nm.	25 kGy	Unaltered.
	50 kGy	New absorption peak with λ_{max}=596 nm.	50 kGy	Unaltered.

Oxygen Sensor
PtTFPP/PolyPhenylSilsesQuioxane
(Thickness: 5 µm, w=(m(Indicator)/m(Polymer))=1%)
Before and After GAMMA Sterilization

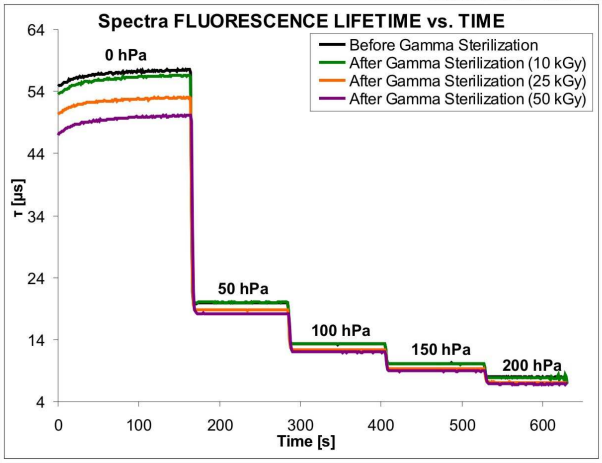

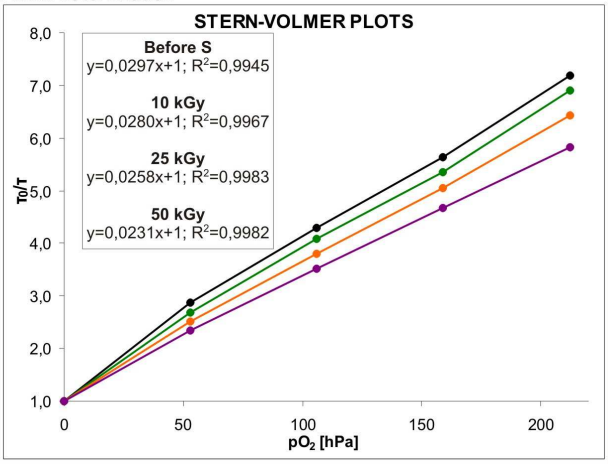

GAMMA Sterilization	Luminescence Lifetime		Stern-Volmer Plot	
Alterations in Luminescence Lifetime and Slope	10kGy	5,77% decrease of τ_0	10kGy	5,72% decrease of slope
		0,45% increase of τ at 50 hPa		
		0,75% decrease of τ at 100 hPa		
		0,30% decrease of τ at 150 hPa		
		1,63% decrease of τ at 200 hPa		
	25 kGy	20,28% decrease of τ_0	25 kGy	13,13% decrease of slope
		8,84% decrease of τ at 50 hPa		
		9,77% decrease of τ at 100 hPa		
		10,76% decrease of τ at 150 hPa		
		10,94% decrease of τ at 200 hPa		
	50 kGy	30,42% decrease of τ_0	50 kGy	22,22% decrease of slope
		14,82% decrease of τ at 50 hPa		
		15,04% decrease of τ at 100 hPa		
		15,79% decrease of τ at 150 hPa		
		14,09% decrease of τ at 200 hPa		

C.15.2 Electron Beam Sterilization

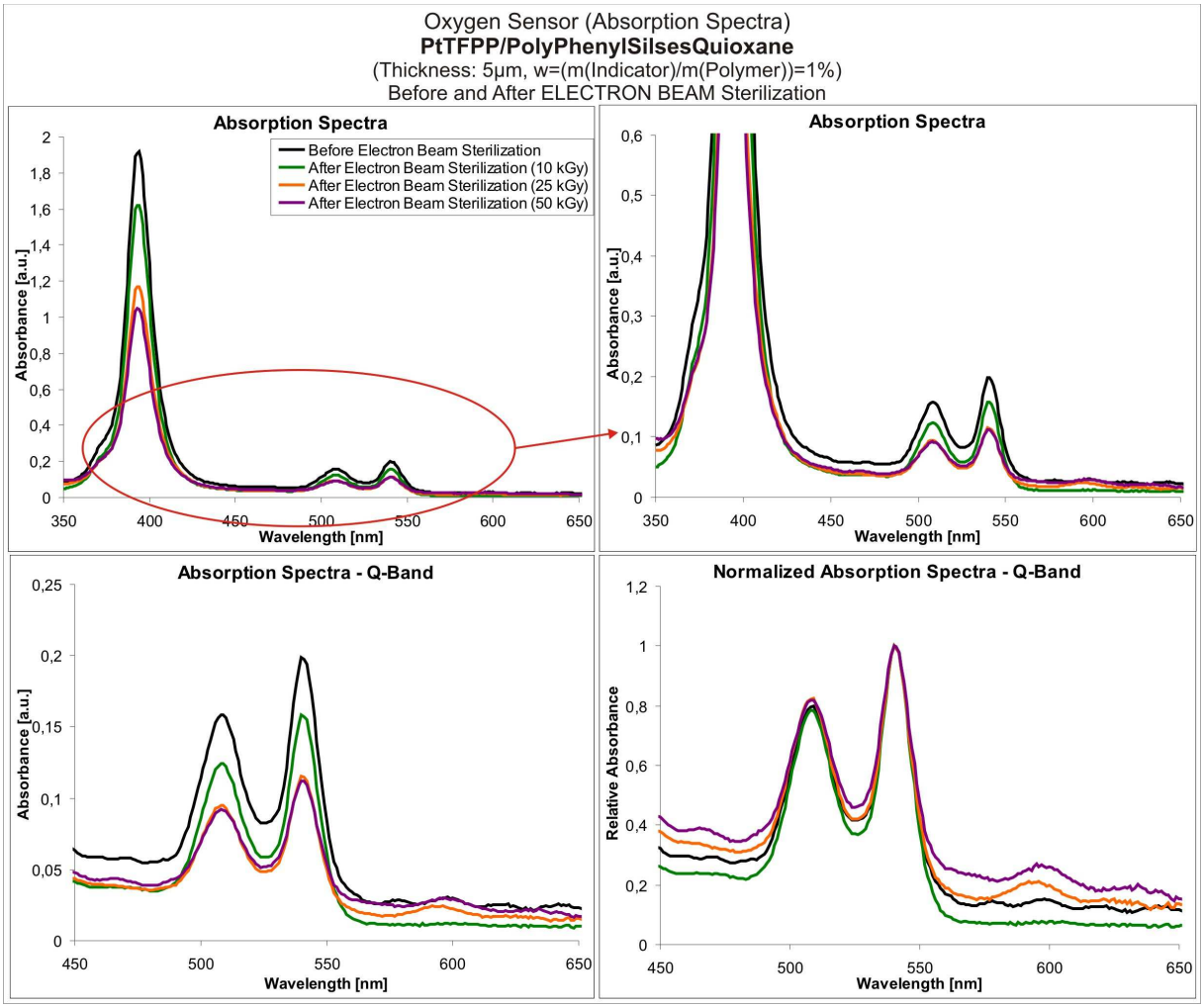

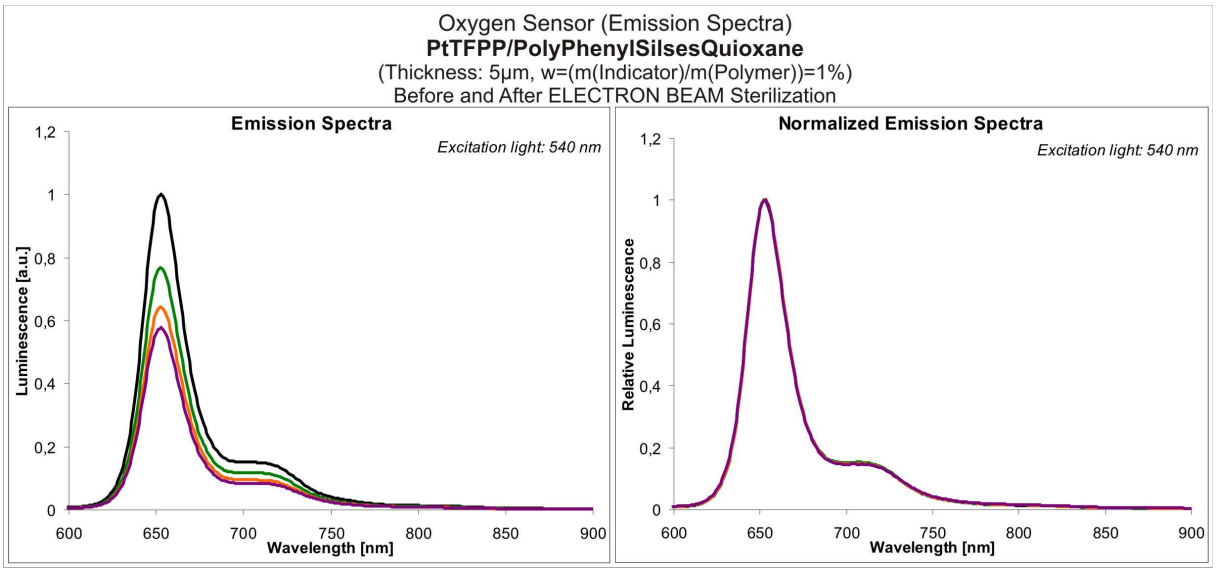

E-BEAM Sterilization	Absorption Spectra		Emission Spectra	
Alterations in Absorption/Emission Intensity	10kGy	20,26% decrease	10kGy	23,09% decrease
	25 kGy	41,98% decrease	25 kGy	35,70% decrease
	50 kGy	43,50% decrease	50 kGy	42,27% decrease

Alterations in Absorption/Emission Curve Form	10kGy	Altered absorption curve form between 360-380 nm, 410-490 nm, 520-530 nm and 565-800 nm	10kGy	Unaltered.
	25 kGy	Altered absorption curve form between 360-380 nm, 410-490 nm, 520-530 nm and 565-800 nm New absorption peak with λ_{max}=593 nm.	25 kGy	Unaltered.
	50 kGy	Altered absorption curve form between 360-380 nm, 410-490 nm, 520-530 nm and 565-800 nm New absorption peak with λ_{max}=597 nm.	50 kGy	Unaltered.

Oxygen Sensor
PtTFPP/PolyPhenylSilsesQuioxane
(Thickness: 5 µm, w=(m(Indicator)/m(Polymer))=1%)
Before and After ELECTRON BEAM Sterilization

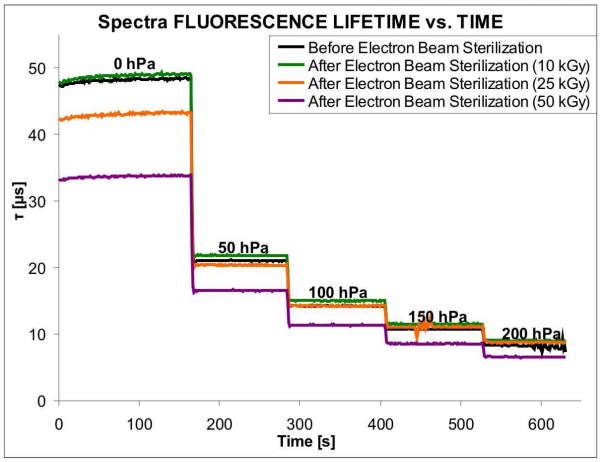

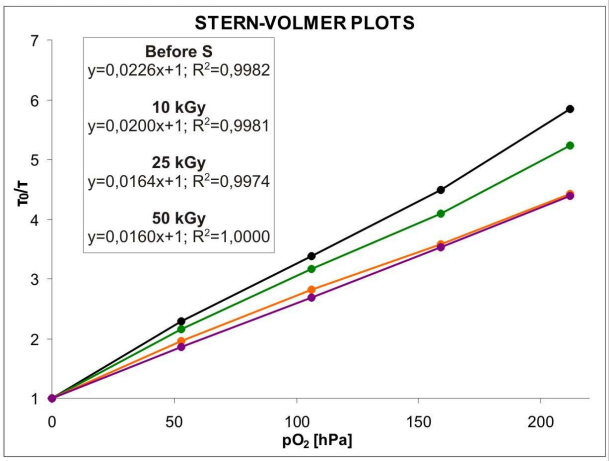

E-BEAM Sterilization	Luminescence Lifetime		Stern-Volmer Plot	
Alterations in Luminescence Lifetime and Slope	10kGy	2,28% decrease of τ_0	10kGy	11,50% decrease of slope
		3,62% increase of τ at 50 hPa		
		4,03% increase of τ at 100 hPa		
		6,59% increase of τ at 150 hPa		
		8,64% increase of τ at 200 hPa		
	25 kGy	19,46% decrease of τ_0	25 kGy	27,43% decrease of slope
		6,08% decrease of τ at 50 hPa		
		3,50% decrease of τ at 100 hPa		
		0,83% increase of τ at 150 hPa		
		6,14% increase of τ at 200 hPa		
	50 kGy	40,37% decrease of τ_0	50 kGy	29,20% decrease of slope
		26,46% decrease of τ at 50 hPa		
		25,17% decrease of τ at 100 hPa		
		24,33% decrease of τ at 150 hPa		
		20,48% decrease of τ at 200 hPa		

C.16 Platinum(II)Tetrakis(PentaFluorPhenyl)Porphyrin (PtTFPP) immobilized in PolyStyrene

C.16.1 Gamma Sterilization

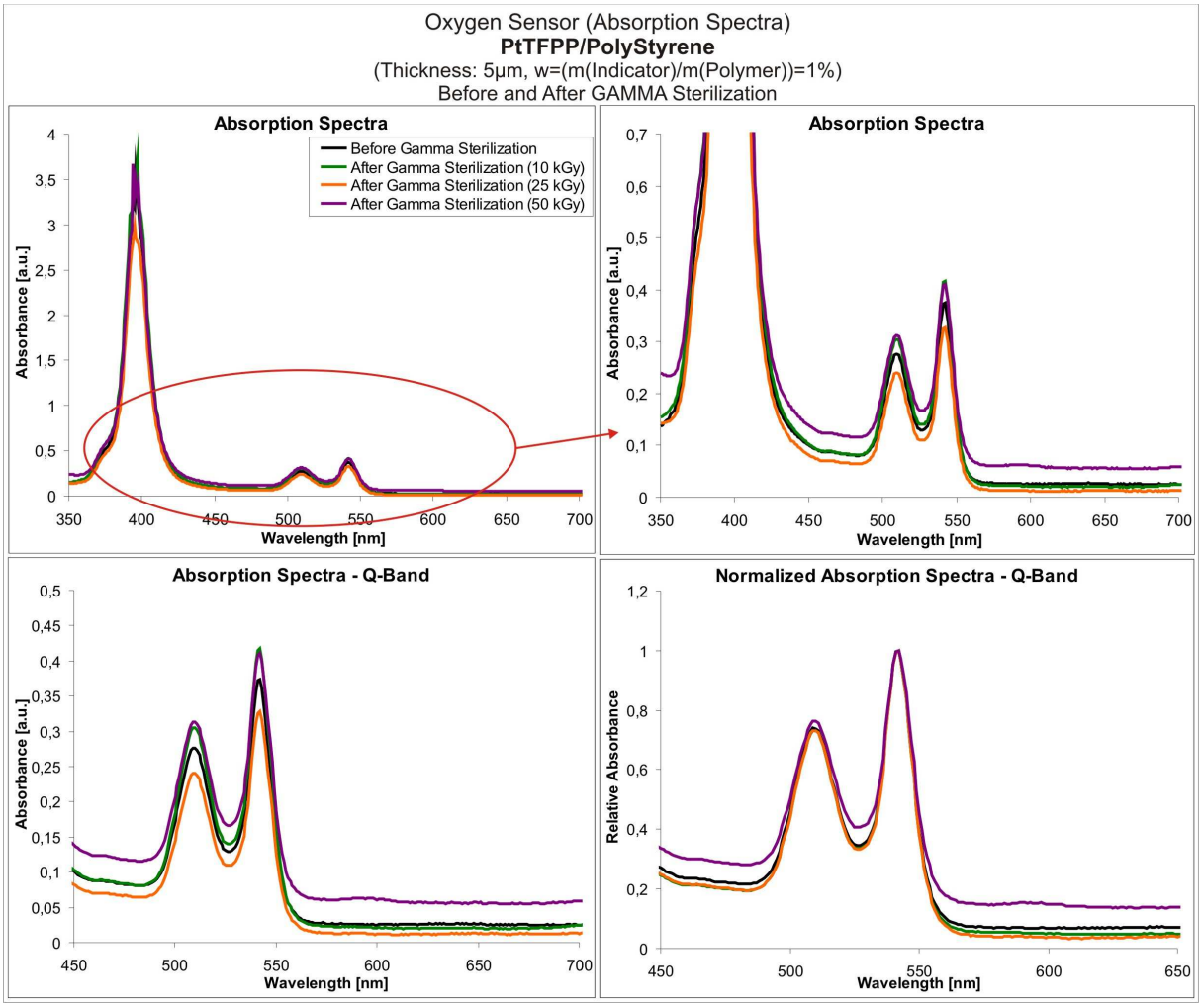

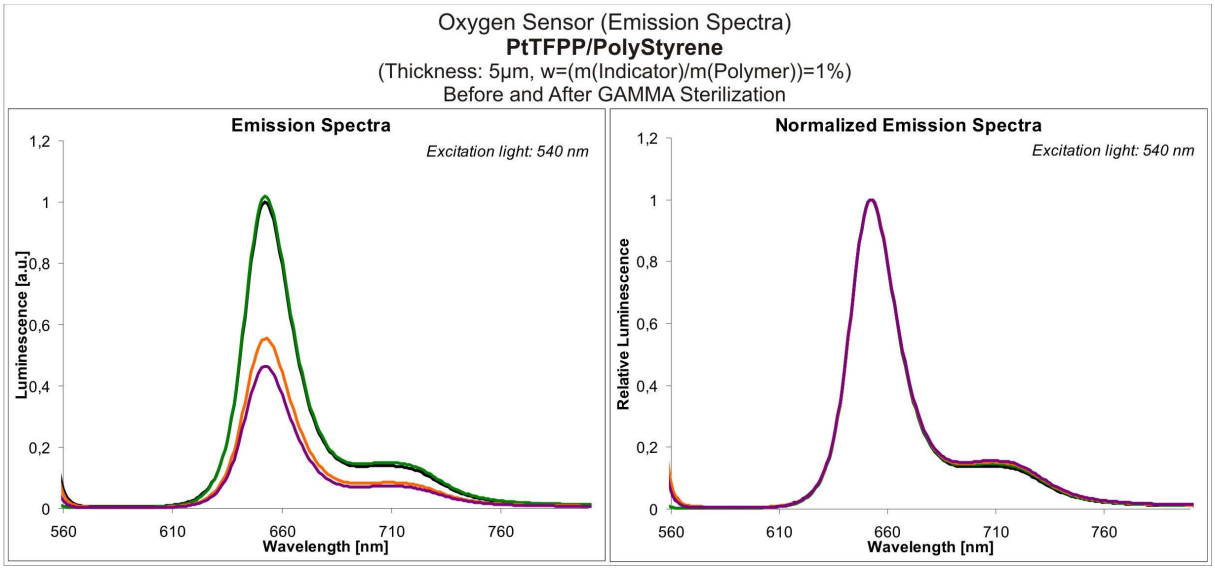

GAMMA Sterilization	Absorption Spectra		Emission Spectra	
Alterations in Absorption/Emission Intensity	10kGy	9,29% increase	10kGy	1,81% increase
	25 kGy	12,31% decrease	25 kGy	44,54% decrease
	50 kGy	8,83% increase	50 kGy	53,55% decrease
Alterations in Absorption/Emission Curve Form	10kGy	Unaltered.	10kGy	Unaltered.
	25 kGy	Unaltered.	25 kGy	Unaltered.
	50 kGy	Altered absorption curve form between 425-500 nm, 520-535 nm and 550-900 nm.	50 kGy	Unaltered.

Oxygen Sensor
PtTFPP/PolyStyrene
(Thickness: 5 µm, w=(m(Indicator)/m(Polymer))=1%)
Before and After GAMMA Sterilization

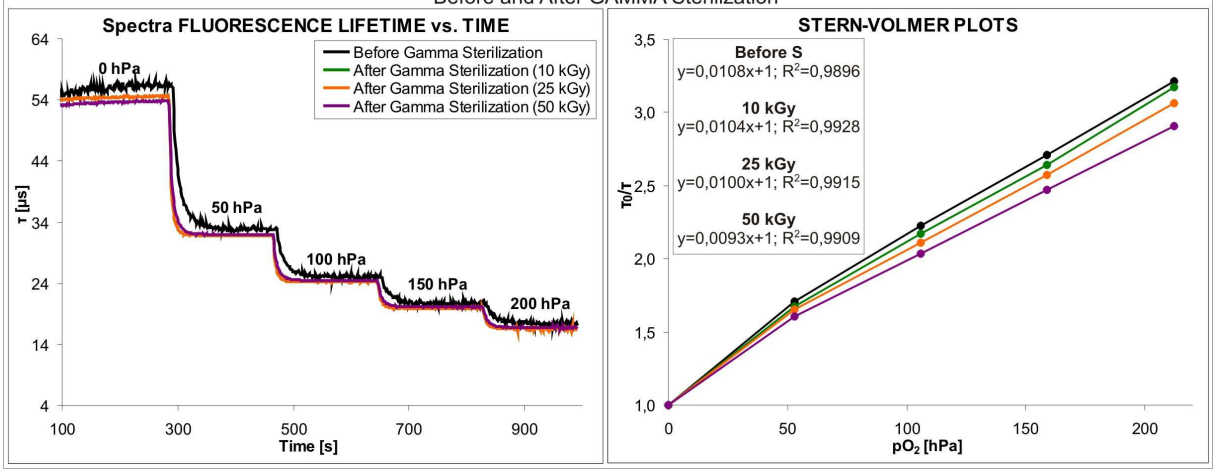

GAMMA Sterilization	Luminescence Lifetime		Stern-Volmer Plot	
Alterations in Luminescence Lifetime and Slope	10kGy	6,42% decrease of τ_0	10kGy	3,70% decrease of slope
		4,41% decrease of τ at 50 hPa		
		3,97% decrease of τ at 100 hPa		
		3,95% decrease of τ at 150 hPa		
		5,14% decrease of τ at 200 hPa		
	25 kGy	9,63% decrease of τ_0	25 kGy	7,41% decrease of slope
		6,66% decrease of τ at 50 hPa		
		4,76% decrease of τ at 100 hPa		
		4,77% decrease of τ at 150 hPa		
		5,14% decrease of τ at 200 hPa		
	50 kGy	13,01% decrease of τ_0	50 kGy	13,89% decrease of slope
		7,64% decrease of τ at 50 hPa		
		4,76% decrease of τ at 100 hPa		
		4,73% decrease of τ at 150 hPa		
		4,00% decrease of τ at 200 hPa		

C.16.2 Electron Beam Sterilization

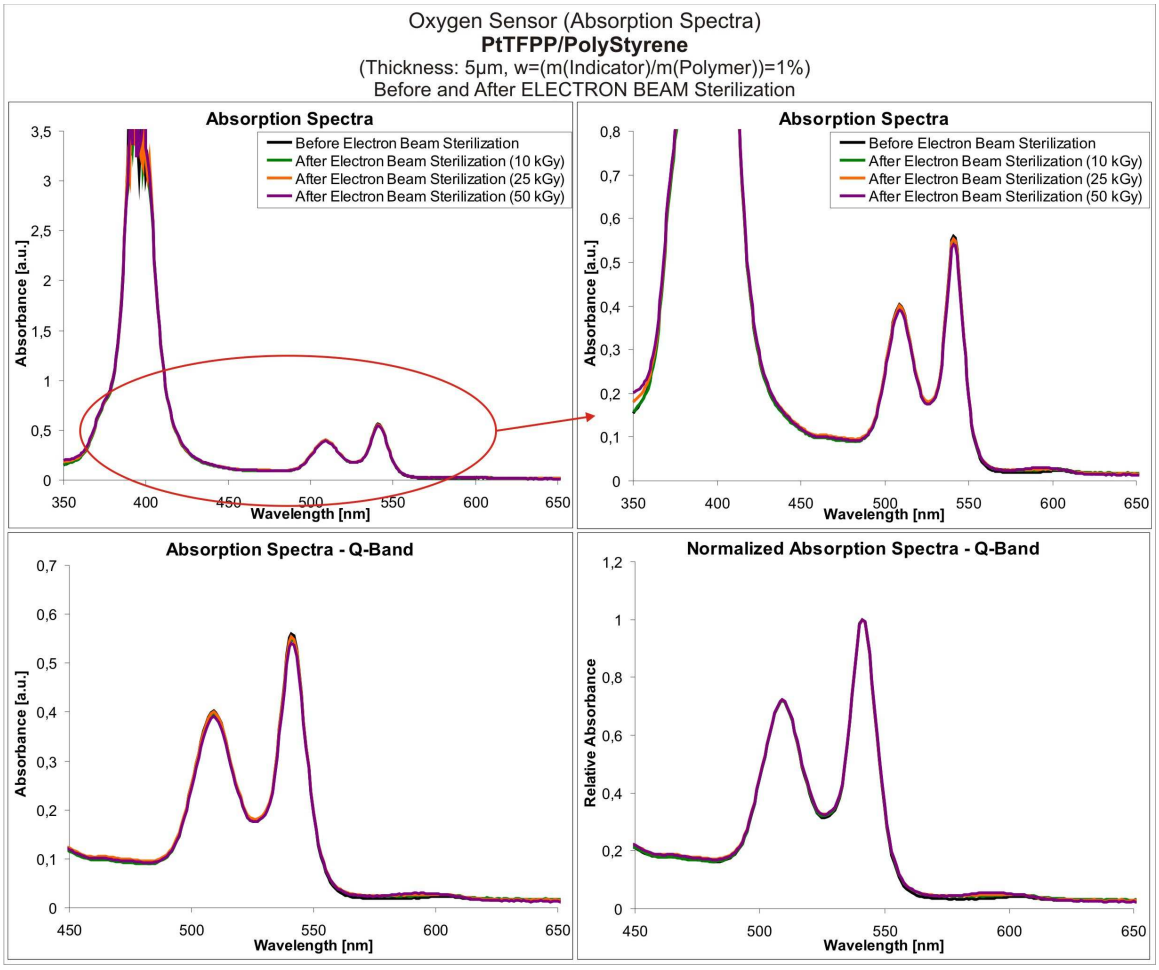

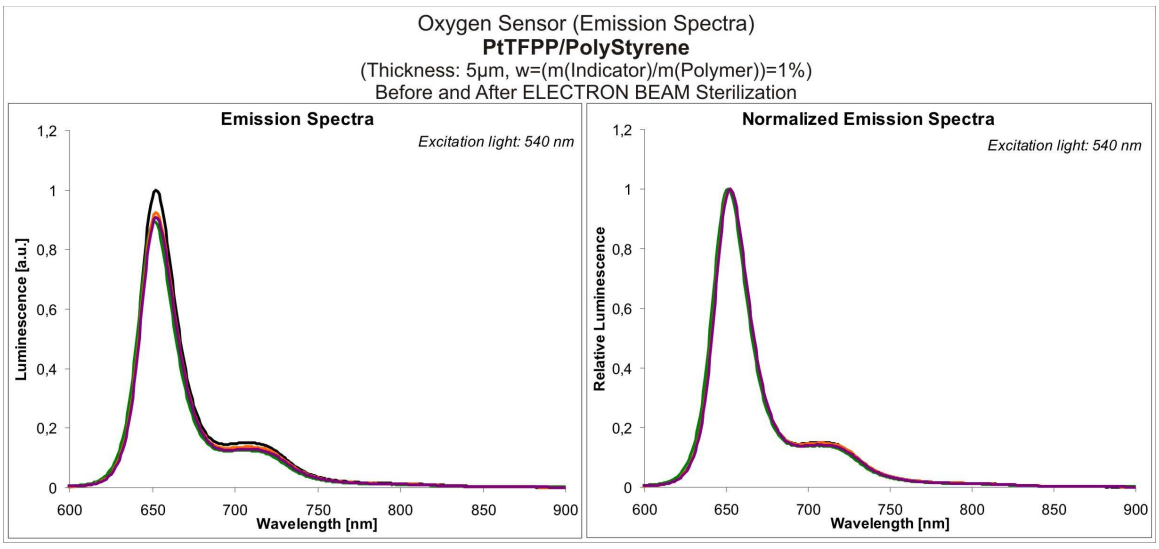

E-BEAM Sterilization	Absorption Spectra		Emission Spectra	
Alterations in Absorption/Emission Intensity	10kGy	1,98% decrease	10kGy	9,45% decrease
	25 kGy	1,02% decrease	25 kGy	7,77% decrease
	50 kGy	3,31% decrease	50 kGy	9,25% decrease
Alterations in Absorption/Emission Curve Form	10kGy	Unaltered.	10kGy	Unaltered.
	25 kGy	Unaltered.	25 kGy	Unaltered.
	50 kGy	New absorption peak with λ_{max}=593 nm.	50 kGy	Unaltered.

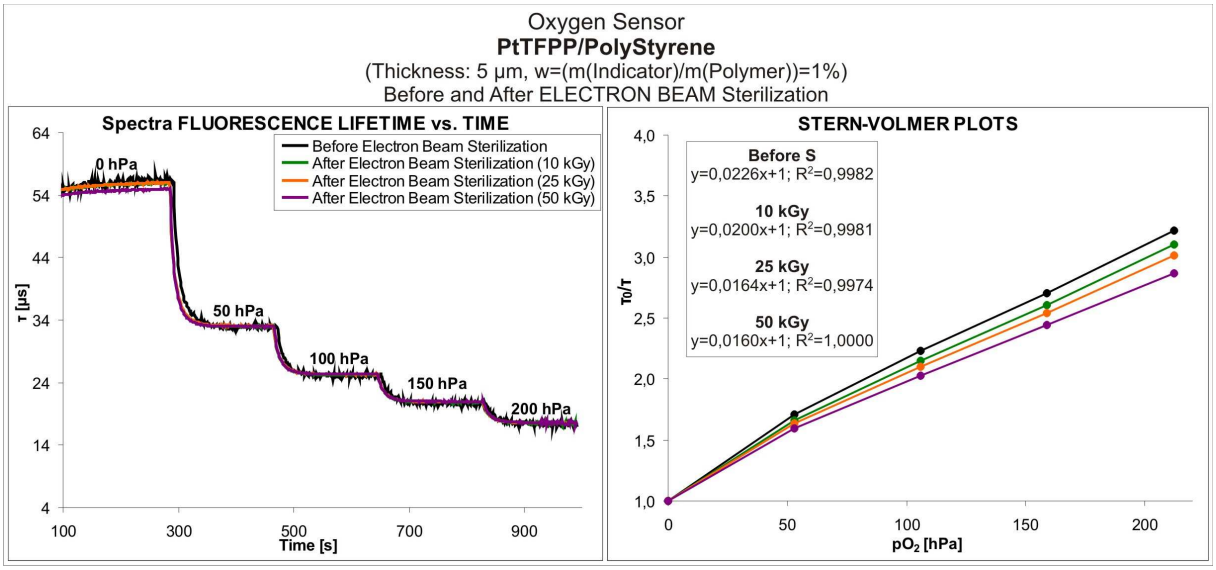

E-BEAM Sterilization	Luminescence Lifetime		Stern-Volmer Plot	
Alterations in Luminescence Lifetime and Slope	10kGy	2,28% decrease of τ_0	10kGy	5,55% decrease of slope
		3,62% increase of τ at 50 hPa		
		4,03% increase of τ at 100 hPa		
		6,59% increase of τ at 150 hPa		
		8,64% increase of τ at 200 hPa		
	25 kGy	19,46% decrease of τ_0	25 kGy	9,26% decrease of slope
		6,08% decrease of τ at 50 hPa		
		3,49% decrease of τ at 100 hPa		
		0,83% increase of τ at 150 hPa		
		6,14% increase of τ at 200 hPa		
	50 kGy	40,37% decrease of τ_0	50 kGy	15,74% decrease of slope
		26,46% decrease of τ at 50 hPa		
		25,17% decrease of τ at 100 hPa		
		24,33% decrease of τ at 150 hPa		
		20,48% decrease of τ at 200 hPa		

C.17 Platinum(II)Tetrakis(PentaFluorPhenyl)Porphyrin (PtTFPP) immobilized in PolyStyrene-co- Acrylonitrile

C.17.1 Gamma Sterilization

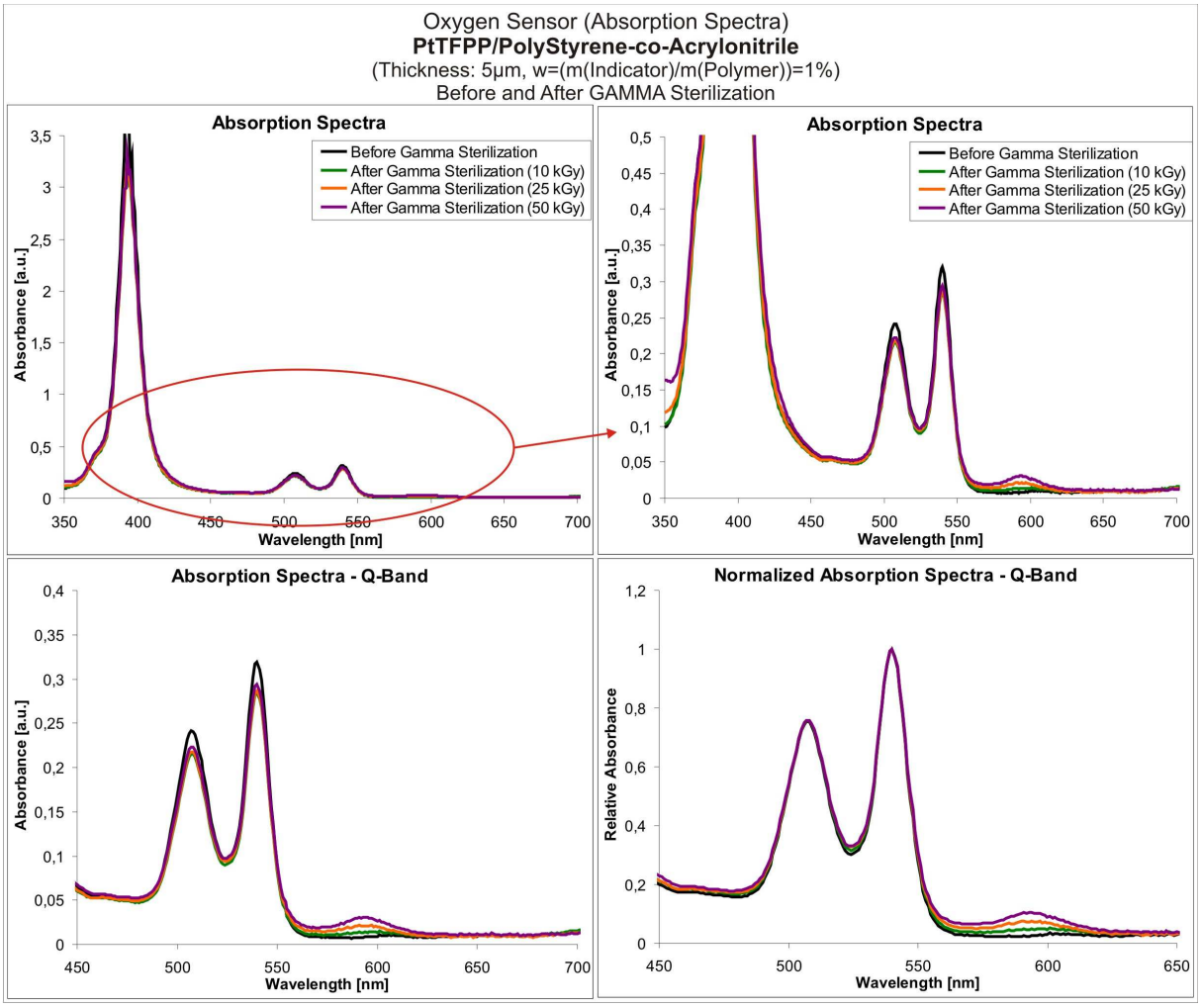

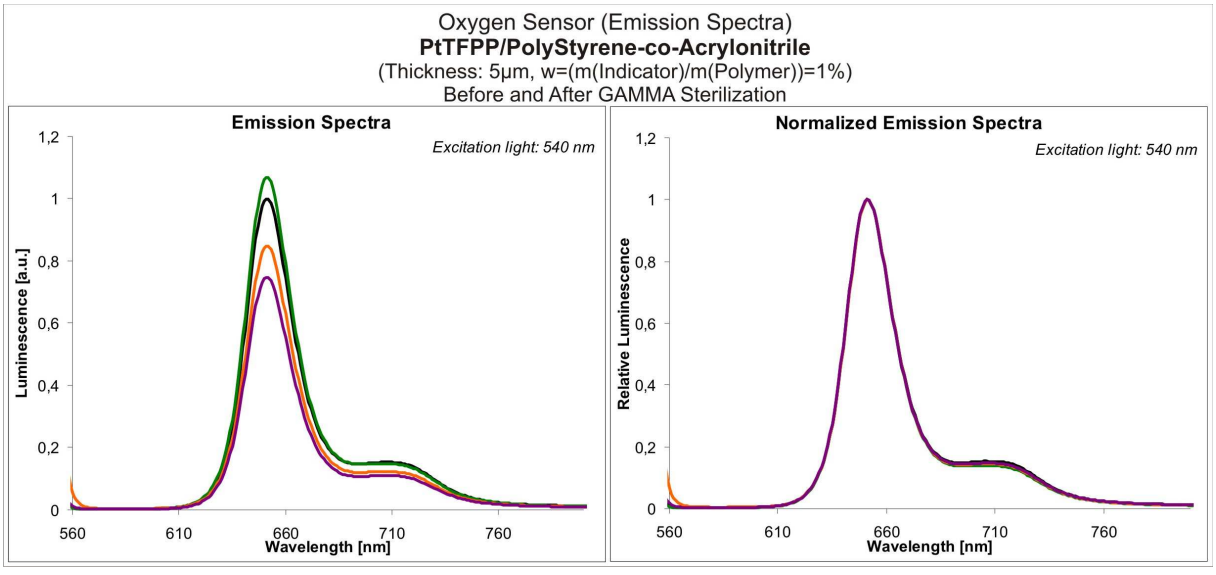

GAMMA Sterilization	Absorption Spectra		Emission Spectra	
Alterations in Absorption/Emission Intensity	10kGy	10,09% decrease	10kGy	6,41% increase
	25 kGy	10,31% decrease	25 kGy	15,16% decrease
	50 kGy	8,04% decrease	50 kGy	25,20% decrease
Alterations in Absorption/Emission Curve Form	10kGy	Unaltered.	10kGy	Unaltered.
	25 kGy	New absorption peak with λ_{max}=592 nm.	25 kGy	Unaltered.
	50 kGy	New absorption peak with λ_{max}=592 nm.	50 kGy	Unaltered.

Oxygen Sensor
PtTFPP/PolyStyrene-co-Acrylonitrile
(Thickness: 5 µm, w=(m(Indicator)/m(Polymer))=1%)
Before and After GAMMA Sterilization

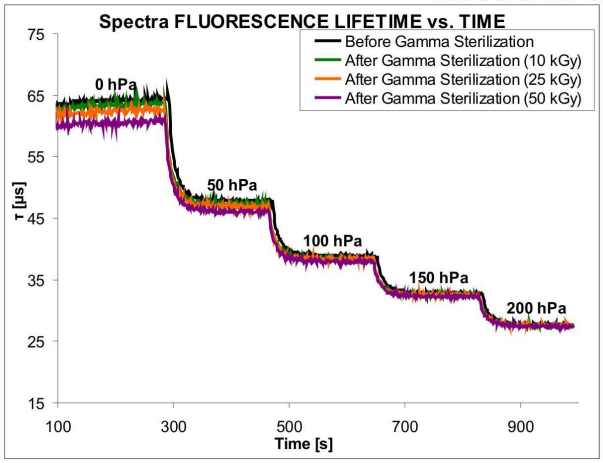

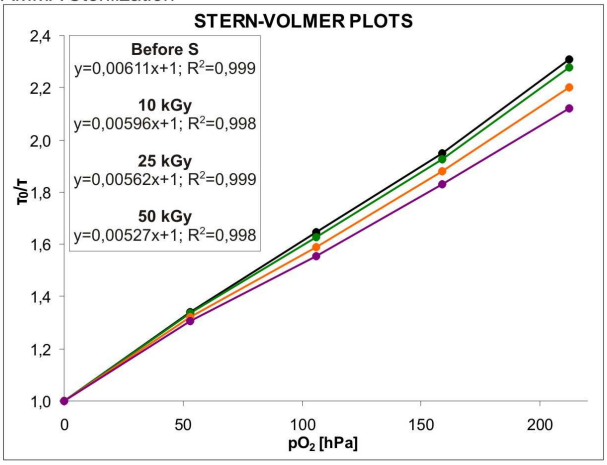

GAMMA Sterilization	Luminescence Lifetime		Stern-Volmer Plot	
Alterations in Luminescence Lifetime and Slope	10kGy	2,34% decrease of τ_0	10kGy	2,45% decrease of slope
		1,76% decrease of τ at 50 hPa		
		1,28% decrease of τ at 100 hPa		
		1,00% decrease of τ at 150 hPa		
		1,08% decrease of τ at 200 hPa		
	25 kGy	5,30% decrease of τ_0	25 kGy	8,02% decrease of slope
		1,79% decrease of τ at 50 hPa		
		1,79% decrease of τ at 100 hPa		
		1,61% decrease of τ at 150 hPa		
		0,72% decrease of τ at 200 hPa		
	50 kGy	9,34% decrease of τ_0	50 kGy	13,75% decrease of slope
		6,76% decrease of τ at 50 hPa		
		4,10% decrease of τ at 100 hPa		
		3,28% decrease of τ at 150 hPa		
		1,44% decrease of τ at 200 hPa		

C.17.2 Electron Beam Sterilization

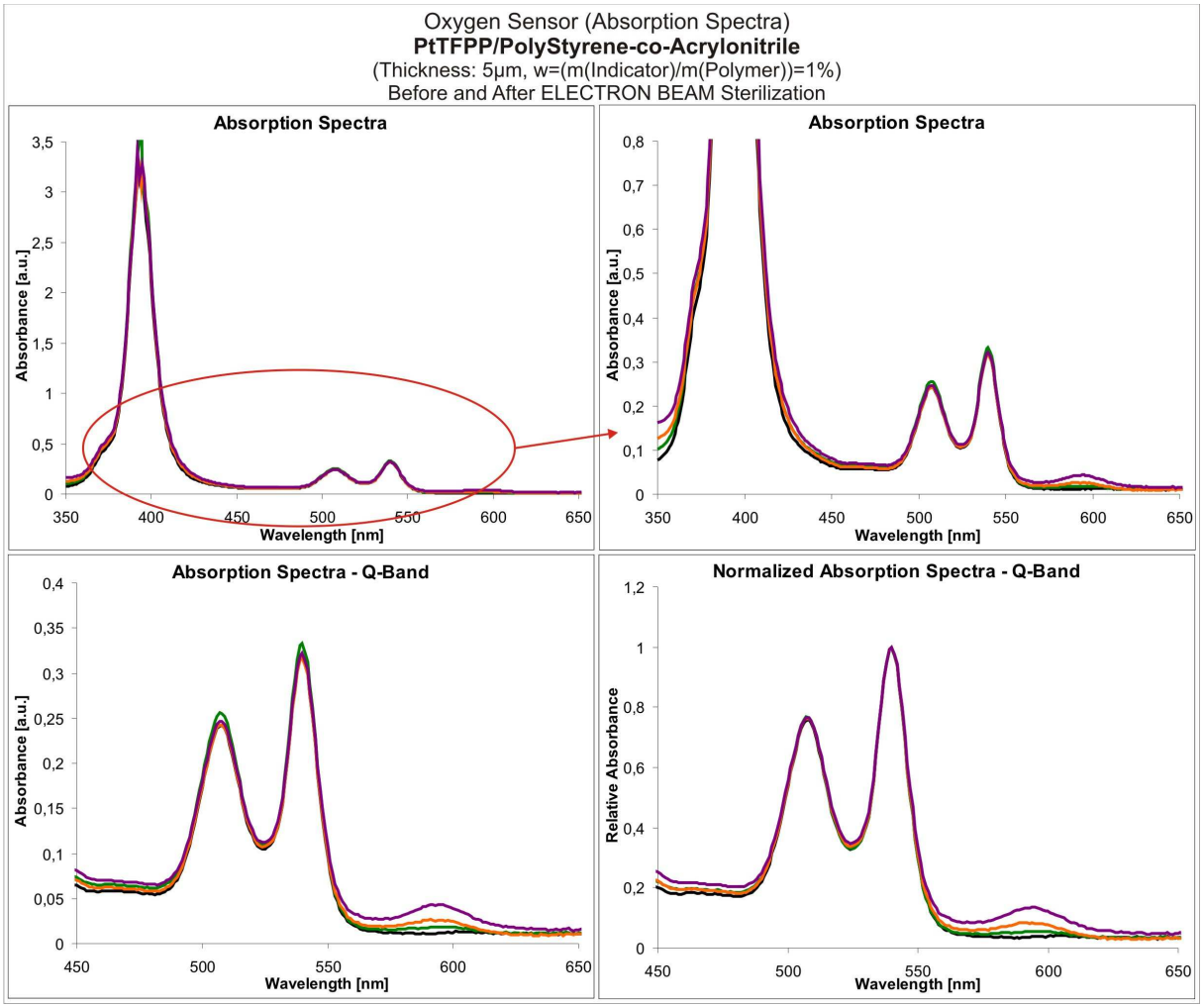

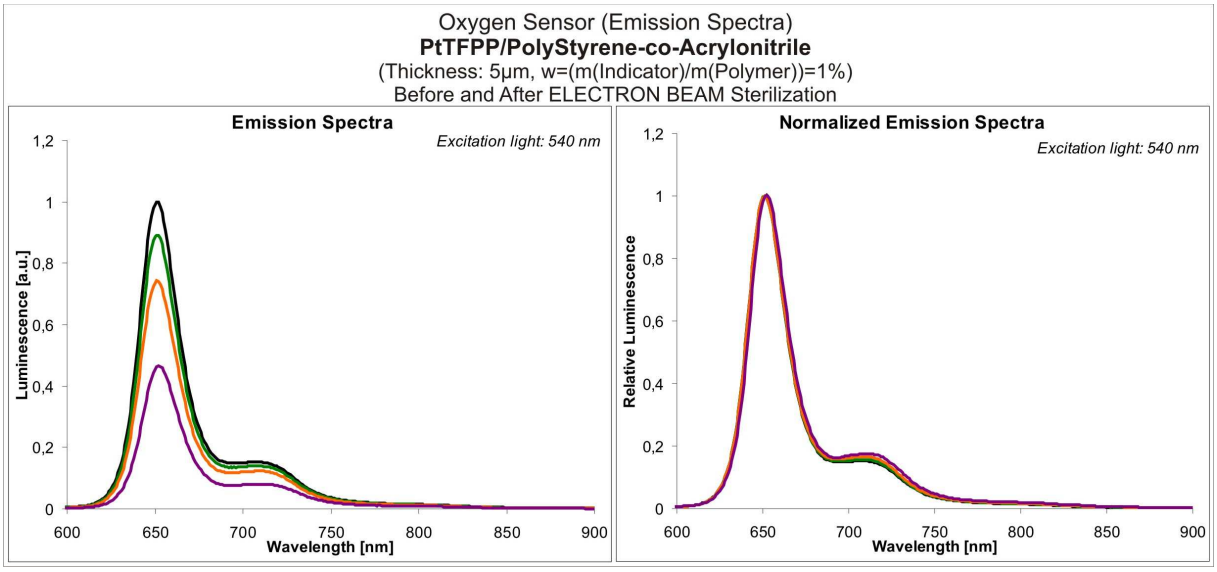

E-BEAM Sterilization	Absorption Spectra		Emission Spectra	
Alterations in Absorption/Emission Intensity	10kGy	4,27% increase	10kGy	9,83% decrease
	25 kGy	0,52% decrease	25 kGy	25,77% decrease
	50 kGy	0,92% increase	50 kGy	53,30% decrease
Alterations in Absorption/Emission Curve Form	10kGy	Unaltered.	10kGy	Unaltered.
	25 kGy	New absorption peak with λ_{max}=592 nm	25 kGy	Unaltered.
	50 kGy	Altered absorption curve form between 350-360 nm and 420-490 nm. New absorption peak with λ_{max}=593 nm.	50 kGy	Altered emission curve form between 695-760 nm.

Oxygen Sensor
PtTFPP/PolyStyrene-co-Acrylonitrile
(Thickness: 5 µm, w=(m(Indicator)/m(Polymer))=1%)
Before and After ELECTRON BEAM Sterilization

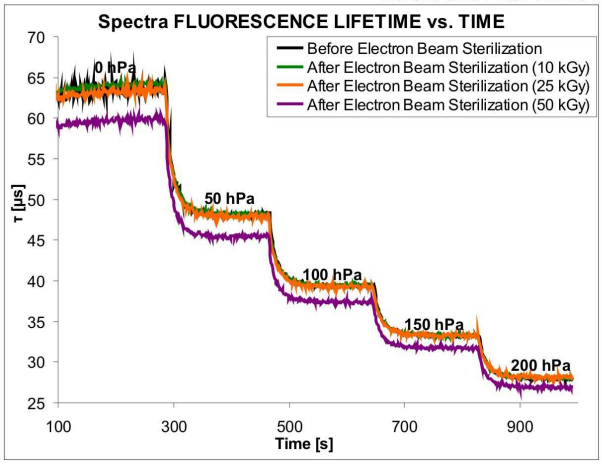

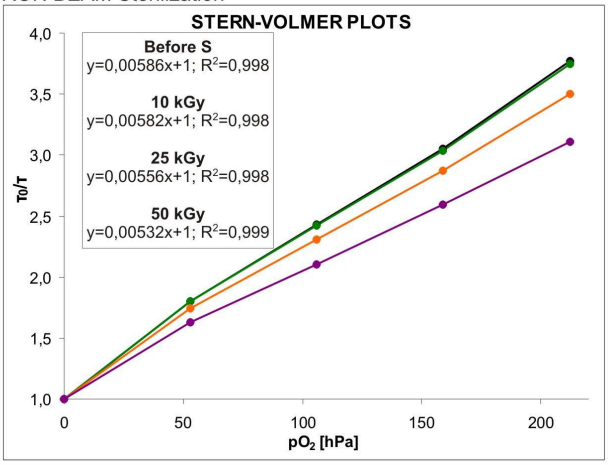

E-BEAM Sterilization	Luminescence Lifetime		Stern-Volmer Plot	
Alterations in Luminescence Lifetime and Slope	10kGy	0,16% decrease of τ_0	10kGy	0,68% decrease of slope
		0,29% decrease of τ at 50 hPa		
		0,02% decrease of τ at 100 hPa		
		0,05% increase of τ at 150 hPa		
		0,36% increase of τ at 200 hPa		
	25 kGy	2,83% decrease of τ_0	25 kGy	5,12% decrease of slope
		2,37% decrease of τ at 50 hPa		
		1,01% decrease of τ at 100 hPa		
		0,72% decrease of τ at 150 hPa		
		0,71% increase of τ at 200 hPa		
	50 kGy	9,61% decrease of τ_0	50 kGy	9,22% decrease of slope
		8,59% decrease of τ at 50 hPa		
		6,58% decrease of τ at 100 hPa		
		6,12% decrease of τ at 150 hPa		
		3,93% decrease of τ at 200 hPa		

C.18 Platinum(II)Tetrakis(PentaFluorPhenyl)Porphyrin (PtTFPP) immobilized in PolyStyrene-co-MaleicAnhydride (PSMA93)

C.18.1 Gamma Sterilization

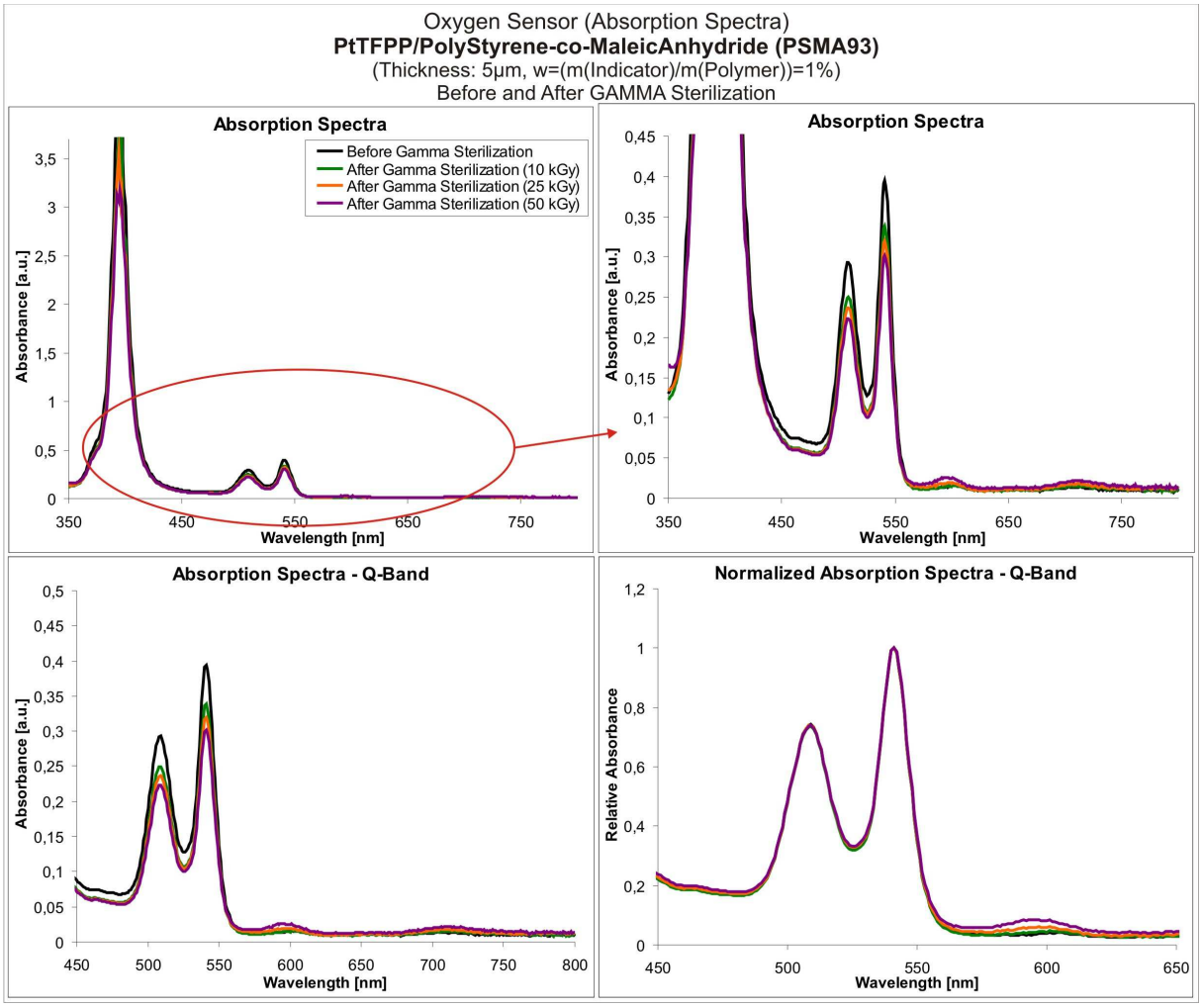

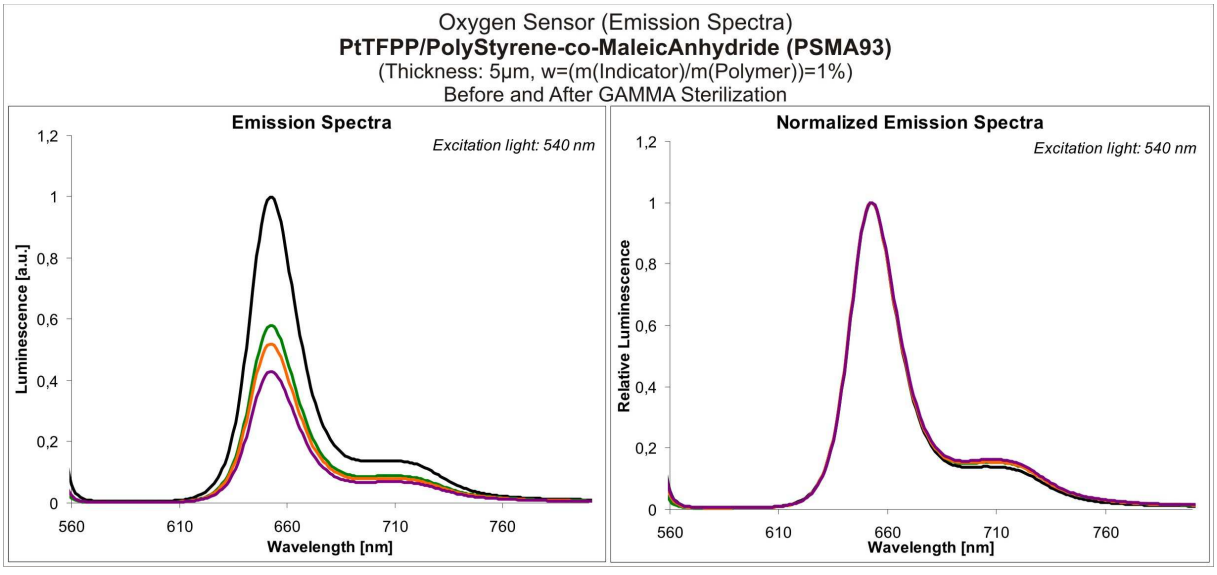

GAMMA Sterilization	Absorption Spectra		Emission Spectra	
Alterations in Absorption/Emission Intensity	10kGy	14,22% decrease	10kGy	41,94% decrease
	25 kGy	19,01% decrease	25 kGy	48,02% decrease
	50 kGy	23,56% decrease	50 kGy	57,04% decrease
Alterations in Absorption/Emission Curve Form	10kGy	Unaltered.	10kGy	Altered emission curve form between 685-760 nm.
	25 kGy	New absorption peak with λ_{max}=596 nm.	25 kGy	Altered emission curve form between 685-760 nm.
	50 kGy	New absorption peak with λ_{max}=596 nm.	50 kGy	Altered emission curve form between 685-760 nm.

Oxygen Sensor
PtTFPP/PolyStyrene-co-MaleicAnhydride (PSMA93)
(Thickness: 5 µm, w=(m(Indicator)/m(Polymer))=1%)
Before and After GAMMA Sterilization

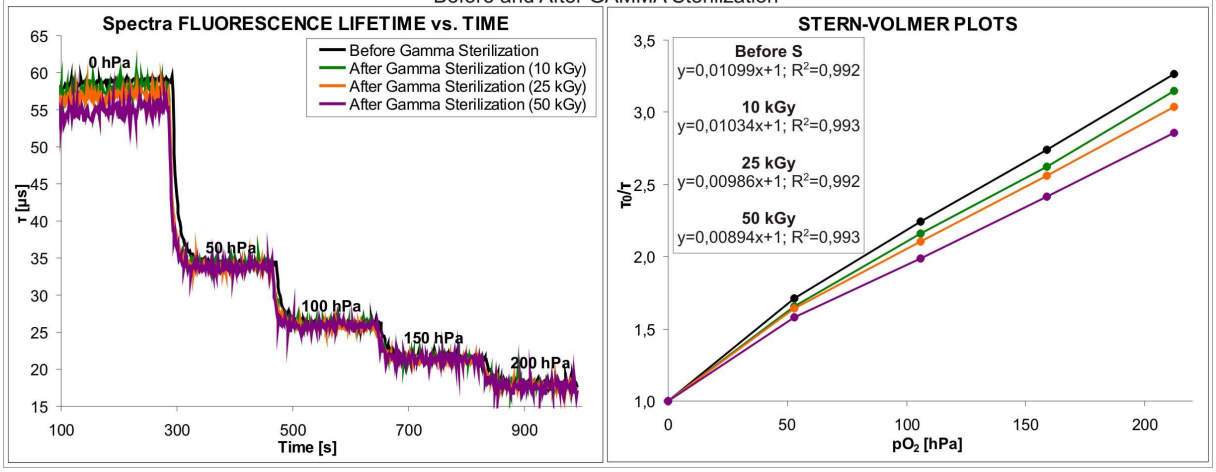

GAMMA Sterilization	Luminescence Lifetime		Stern-Volmer Plot	
Alterations in Luminescence Lifetime and Slope	10kGy	4,08% decrease of τ_0	10kGy	5,91% decrease of slope
		1,19% decrease of τ at 50 hPa		
		0,38% decrease of τ at 100 hPa		
		0,46% decrease of τ at 150 hPa		
		0,55% decrease of τ at 200 hPa		
	25 kGy	8,50% decrease of τ_0	25 kGy	10,28% decrease of slope
		4,62% decrease of τ at 50 hPa		
		2,29% decrease of τ at 100 hPa		
		2,28% decrease of τ at 150 hPa		
		1,67% decrease of τ at 200 hPa		
	50 kGy	14,28% decrease of τ_0	50 kGy	18,65% decrease of slope
		7,23% decrease of τ at 50 hPa		
		3,05% decrease of τ at 100 hPa		
		2,84% decrease of τ at 150 hPa		
		1,67% decrease of τ at 200 hPa		

C.18.2 Electron Beam Sterilization

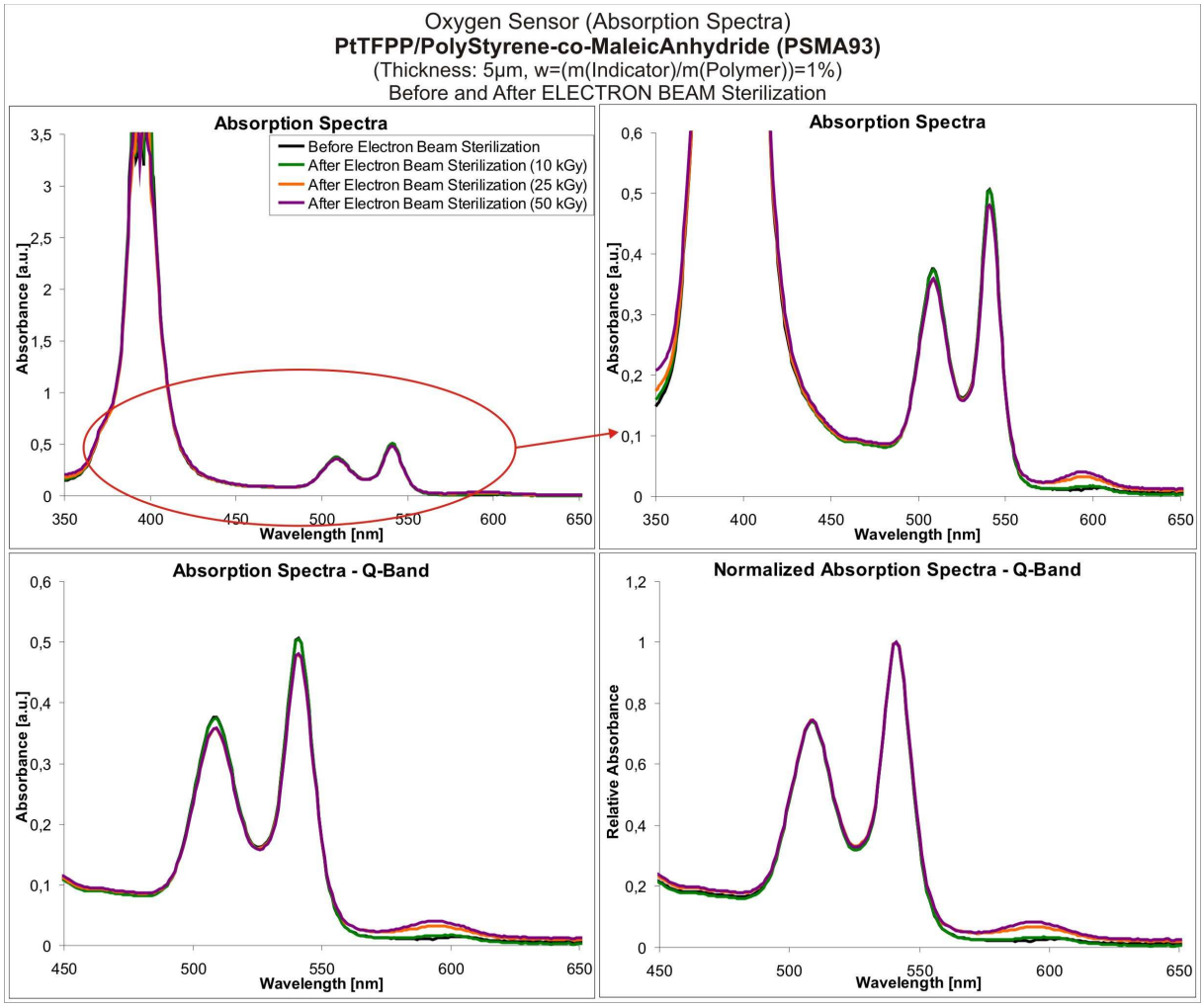

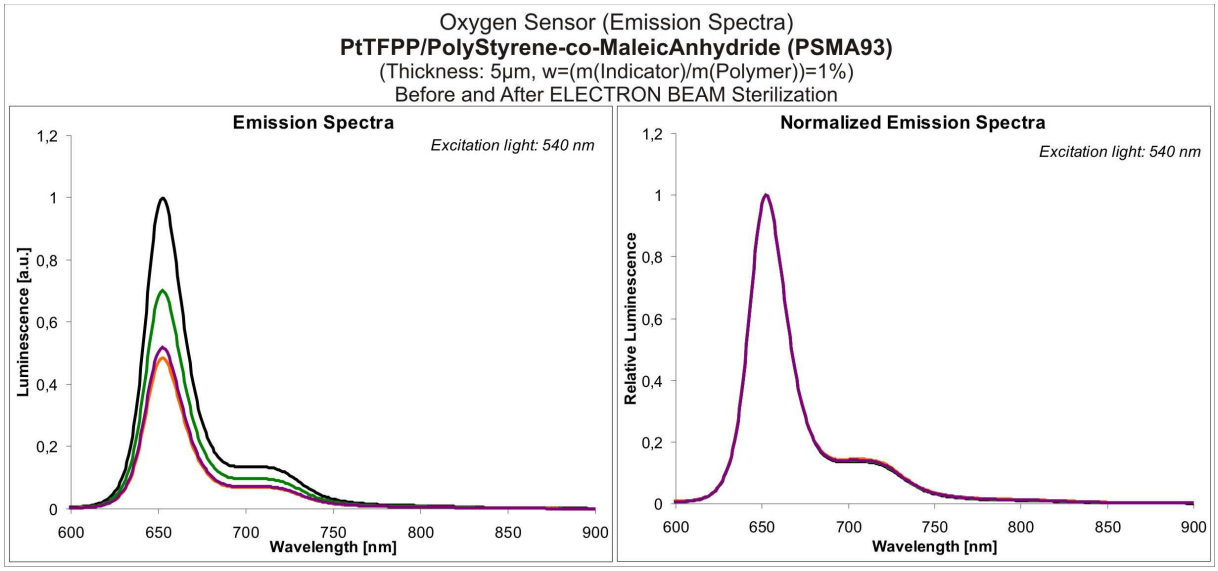

GAMMA Sterilization	Absorption Spectra		Emission Spectra	
Alterations in Absorption/Emission Intensity	10kGy	1,17% decrease	10kGy	29,08% decrease
	25 kGy	5,41% decrease	25 kGy	51,49% decrease
	50 kGy	5,07% decrease	50 kGy	48,10% decrease

Alterations in Absorption/Emission Curve Form	10kGy	Unaltered.	10kGy	Unaltered.
	25 kGy	New absorption peak with λ_{max}=594 nm.	25 kGy	Unaltered.
	50 kGy	New absorption peak with λ_{max}=592 nm.	50 kGy	Unaltered.

Oxygen Sensor
PtTFPP/PolyStyrene-co-MaleicAnhydride (PSMA93)
(Thickness: 5 µm, w=(m(Indicator)/m(Polymer))=1%)
Before and After ELECTRON BEAM Sterilization

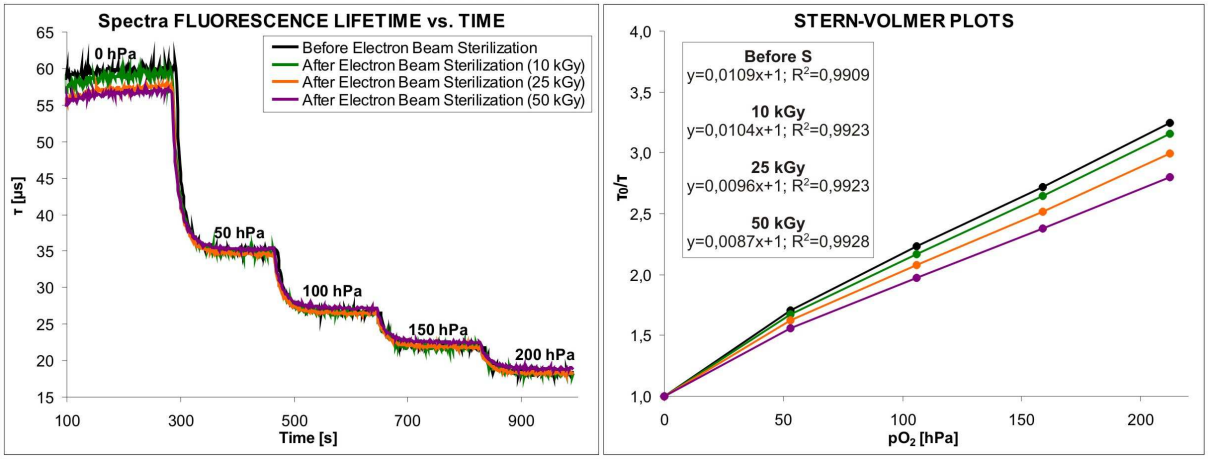

GAMMA Sterilization	Luminescence Lifetime		Stern-Volmer Plot	
Alterations in Luminescence Lifetime and Slope	10kGy	3,18% decrease of τ_0	10kGy	4,59% decrease of slope
		1,06% decrease of τ at 50 hPa		
		0,74% decrease of τ at 100 hPa		
		0,64% decrease of τ at 150 hPa		
		0,54% decrease of τ at 200 hPa		
	25 kGy	8,21% decrease of τ_0	25 kGy	11,93% decrease of slope
		3,40% decrease of τ at 50 hPa		
		1,49% decrease of τ at 100 hPa		
		1,00% decrease of τ at 150 hPa		
		1,09% decrease of τ at 200 hPa		
	50 kGy	11,39% decrease of τ_0	50 kGy	20,18% decrease of slope
		3,03% decrease of τ at 50 hPa		
		0,03% decrease of τ at 100 hPa		
		0,90% increase of τ at 150 hPa		
		2,64% increase of τ at 200 hPa		

C.19 Platinum(II) OctaEthyl Porphyrin (=PtOEP) immobilized in PolyStyrene

C.19.1 Gamma Sterilization

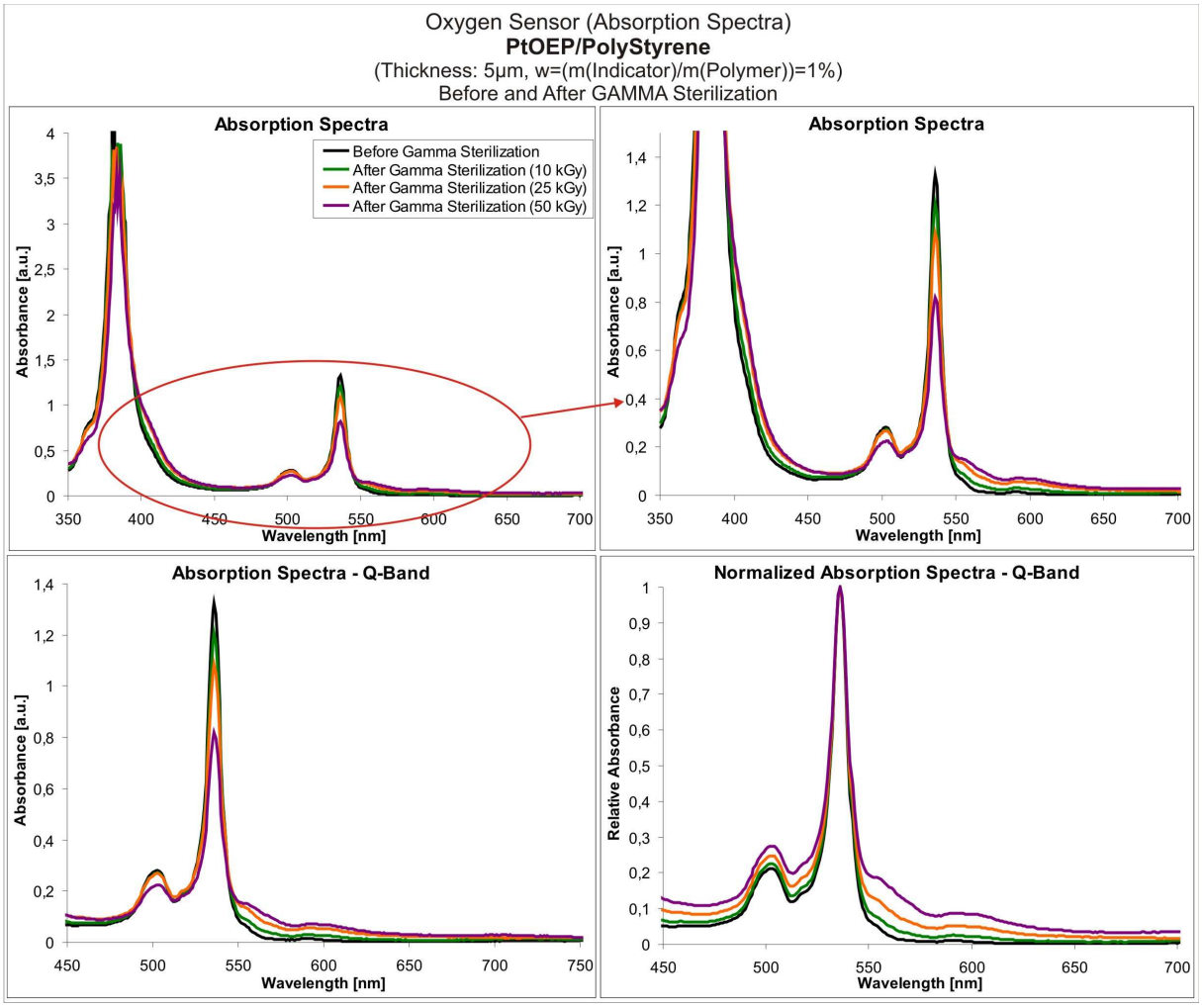

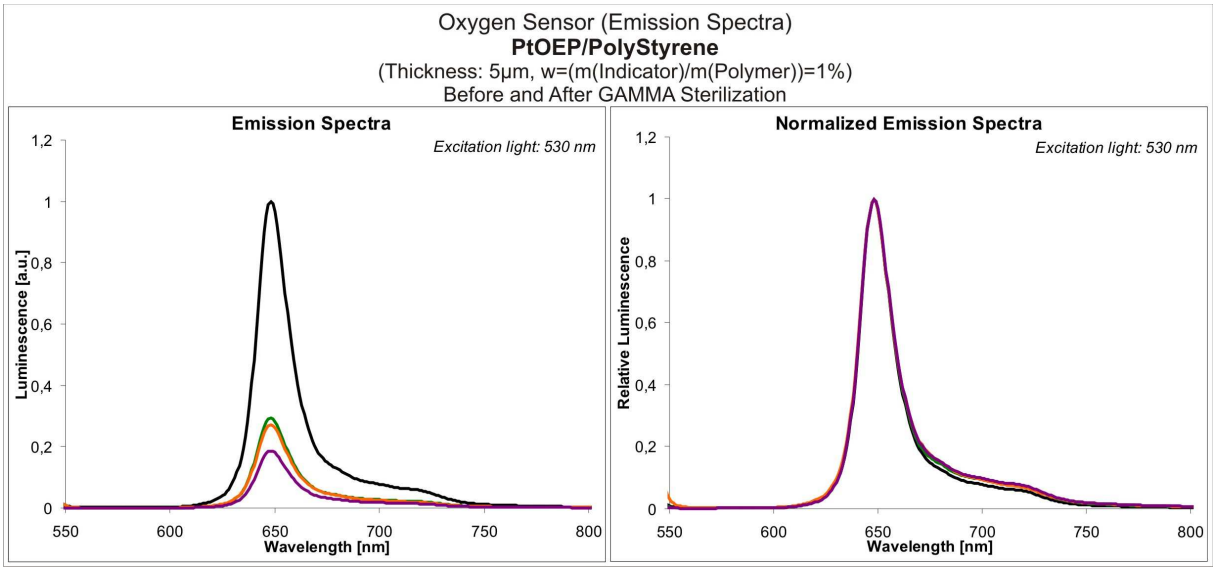

GAMMA Sterilization	Absorption Spectra		Emission Spectra	
Alterations in Absorption/Emission Intensity	10kGy	9,01% decrease	10kGy	70,73% decrease
	25 kGy	18,21% decrease	25 kGy	72,80% decrease
	50 kGy	38,29% decrease	50 kGy	81,36% decrease
Alterations in Absorption/Emission Curve Form	10kGy	Altered absorption curve form between 400-480 nm and 550-625 nm.	10kGy	Altered emission curve form between 670-740 nm.
	25 kGy	Altered absorption curve form between 350-370 nm, 400-520 nm and 550-800 nm.	25 kGy	Altered emission curve form between 670-740 nm.
	50 kGy	Altered absorption curve form between 350-370 nm, 400-520 nm and 550-800 nm.	50 kGy	Altered emission curve form between 670-740 nm.

Oxygen Sensor
PtOEP/PolyStyrene
(Thickness: 5 µm, w=(m(Indicator)/m(Polymer))=1%)
Before and After GAMMA Sterilization

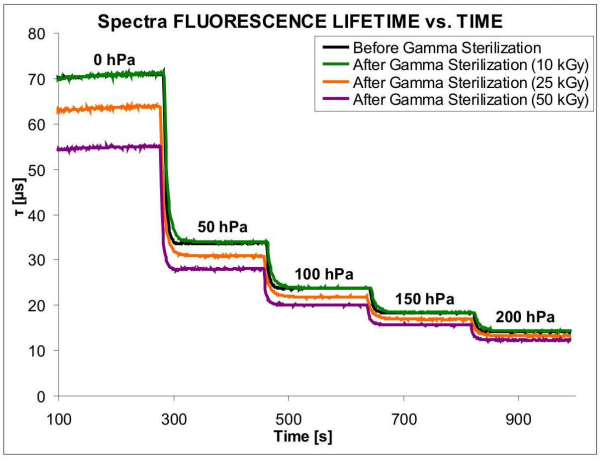

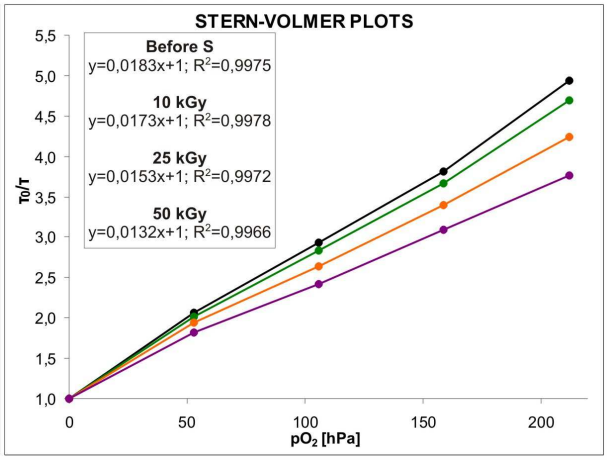

GAMMA Sterilization	Luminescence Lifetime		Stern-Volmer Plot	
Alterations in Luminescence Lifetime and Slope	10kGy	3,44% decrease of τ_0	10kGy	5,46% decrease of slope
		1,18% decrease of τ at 50 hPa		
		0,42% increase of τ at 100 hPa		
		0,54% increase of τ at 150 hPa		
		2,08% increase of τ at 200 hPa		
	25 kGy	19,37% decrease of τ_0	25 kGy	16,39% decrease of slope
		14,24% decrease of τ at 50 hPa		
		10,13% decrease of τ at 100 hPa		
		9,84% decrease of τ at 150 hPa		
		5,67% decrease of τ at 200 hPa		
	50 kGy	33,57% decrease of τ_0	50 kGy	27,87% decrease of slope
		24,33% decrease of τ at 50 hPa		
		18,98% decrease of τ at 100 hPa		
		18,03% decrease of τ at 150 hPa		
		12,76% decrease of τ at 200 hPa		

C.19.2 Electron Beam Sterilization

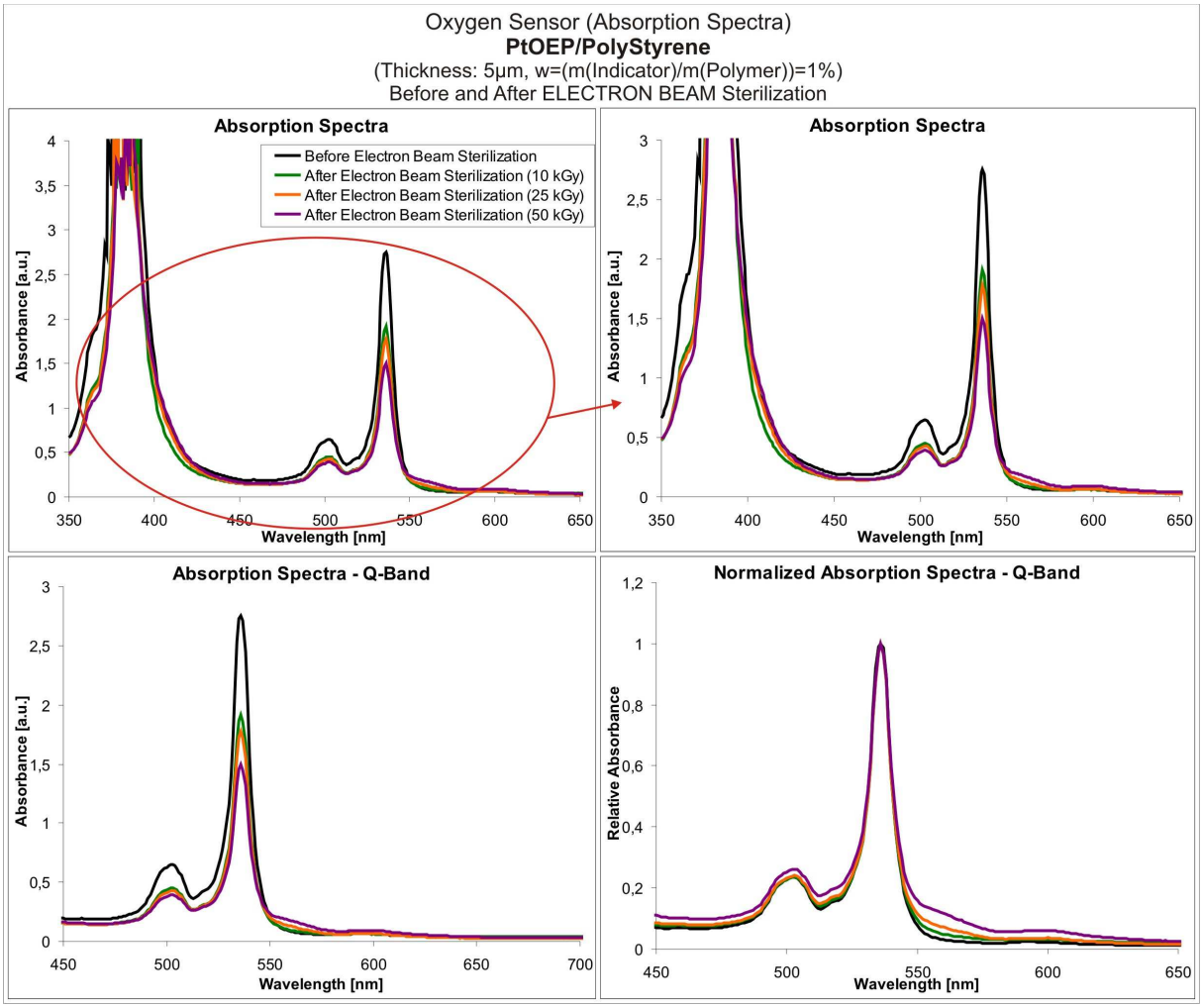

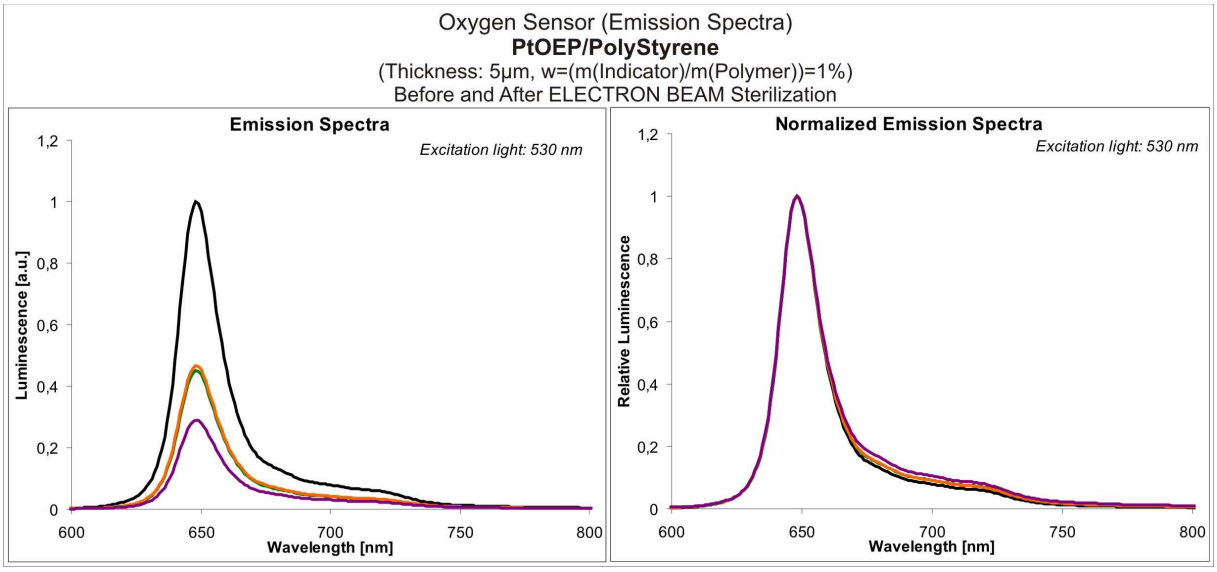

E-BEAM Sterilization	Absorption Spectra		Emission Spectra	
Alterations in Absorption/Emission Intensity	10kGy	30,55% decrease	10kGy	54,95% decrease
	25 kGy	35,45% decrease	25 kGy	53,26% decrease
	50 kGy	45,70% decrease	50 kGy	71,03% decrease

Alterations in Absorption/Emission Curve Form	10kGy	Unaltered.	10kGy	Unaltered.
	25 kGy	Altered absorption curve between 400-450 nm and 550-580 nm.	25 kGy	Altered emission curve between 670-750 nm.
	50 kGy	Altered absorption curve between 350-365 nm, 400-520 nm and 550-630 nm.	50 kGy	Altered emission curve between 670-750 nm.

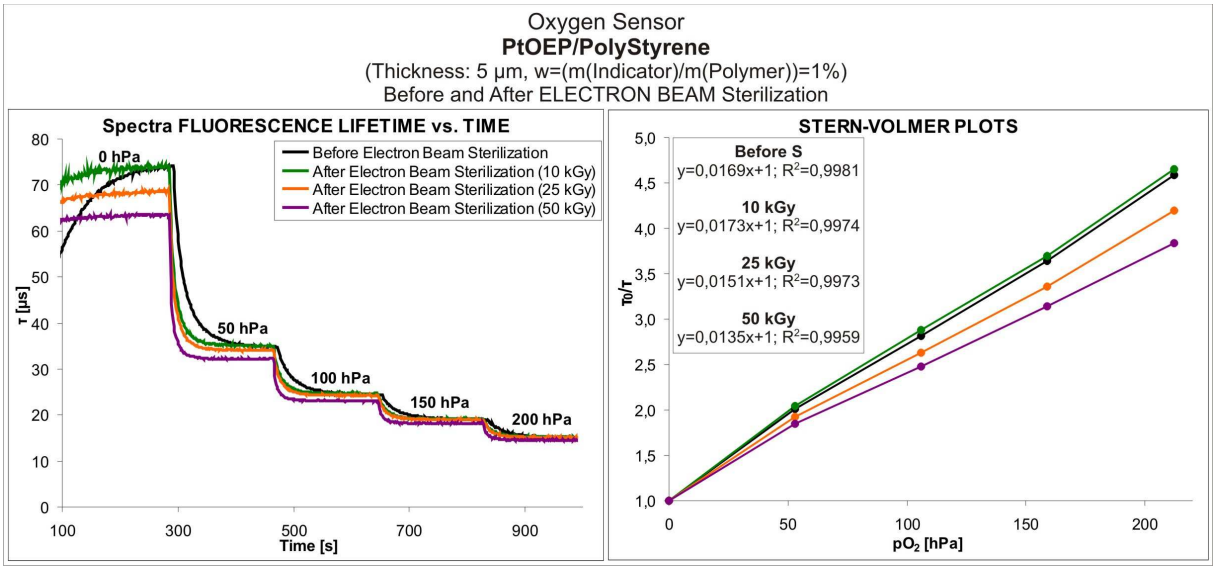

E-BEAM Sterilization	Luminescence Lifetime		Stern-Volmer Plot	
Alterations in Luminescence Lifetime and Slope	10kGy	0,56% increase of τ_0	10kGy	2,31% increase of slope
		1,14% decrease of τ at 50 hPa		
		0,80% decrease of τ at 100 hPa		
		0,93% decrease of τ at 150 hPa		
		0,78% decrease of τ at 200 hPa		
	25 kGy	10,20% decrease of τ_0	25 kGy	10,65% decrease of slope
		6,25% decrease of τ at 50 hPa		
		3,20% decrease of τ at 100 hPa		
		2,58% decrease of τ at 150 hPa		
		1,68% decrease of τ at 200 hPa		
	50 kGy	20,96% decrease of τ_0	50 kGy	20,12% decrease of slope
		14,20% decrease of τ at 50 hPa		
		9,60% decrease of τ at 100 hPa		
		8,45% decrease of τ at 150 hPa		
		5,58% decrease of τ at 200hPa		

C.20 Platinum(II) meso-tetra(4-FluoroPhenyl) TetraBenzoPorphyrin (=PtTPTBPF) immobilized in PolyStyrene

C.20.1 Gamma Sterilization

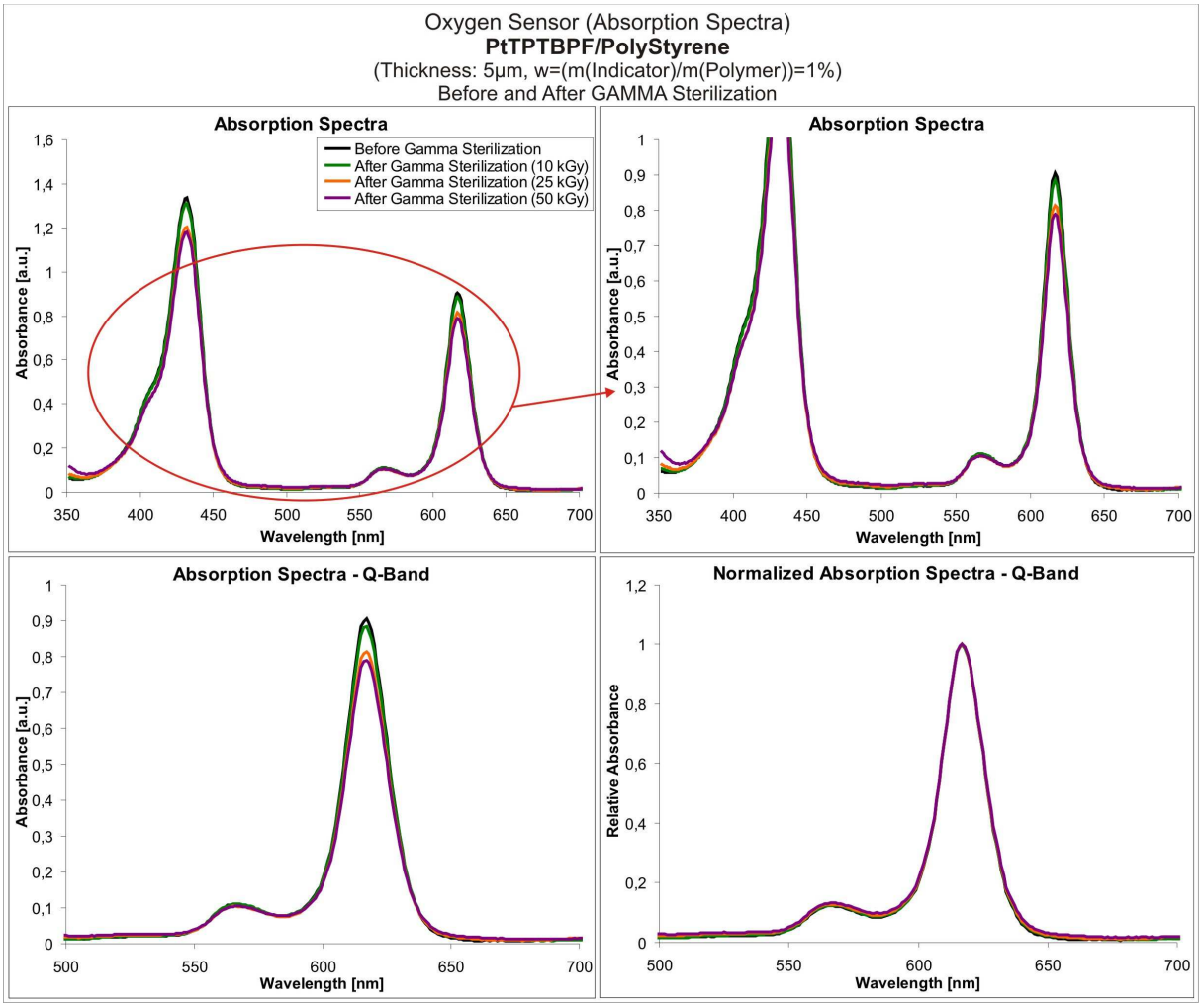

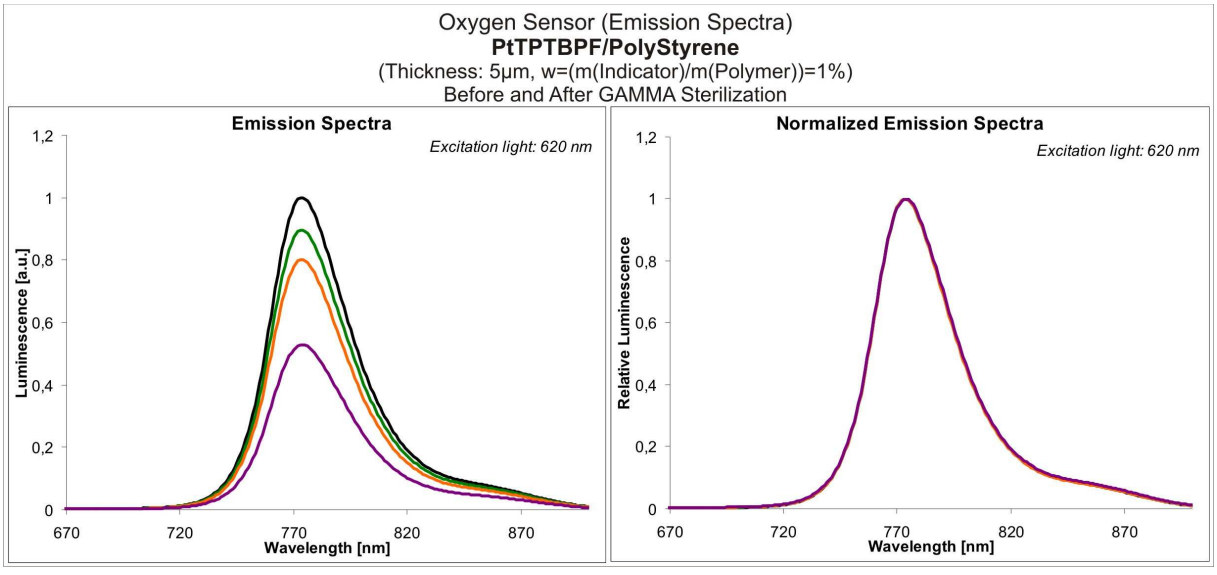

GAMMA Sterilization	Absorption Spectra		Emission Spectra	
Alterations in Absorption/Emission Intensity	10kGy	2,20% decrease	10kGy	9,32% decrease
	25 kGy	9,99% decrease	25 kGy	19,87% decrease
	50 kGy	12,75% decrease	50 kGy	47,16% decrease
Alterations in Absorption/Emission Curve Form	10kGy	Unaltered.	10kGy	Unaltered.
	25 kGy	Unaltered.	25 kGy	Unaltered.
	50 kGy	Altered absorption curve form between 350-365 nm.	50 kGy	Unaltered.

Oxygen Sensor
PtTPTBPF/PolyStyrene
(Thickness: 5 µm, w=(m(Indicator)/m(Polymer))=1%)
Before and After GAMMA Sterilization

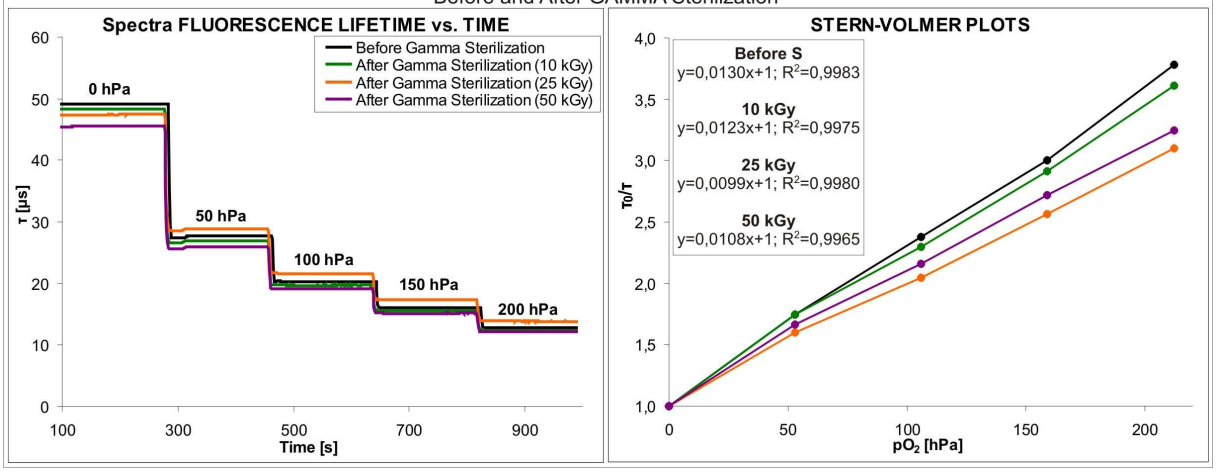

GAMMA Sterilization	Luminescence Lifetime		Stern-Volmer Plot	
Alterations in Luminescence Lifetime and Slope	10kGy	7,64% decrease of τ_0	10kGy	5,38% decrease of slope
		7,58% decrease of τ at 50 hPa		
		3,94% decrease of τ at 100 hPa		
		4,97% decrease of τ at 150 hPa		
		3,12% decrease of τ at 200 hPa		
	25 kGy	11,16% decrease of τ_0	25 kGy	23,84% decrease of slope
		2,89% decrease of τ at 50 hPa		
		3,33% increase of τ at 100 hPa		
		4,17% increase of τ at 150 hPa		
		7,91% increase of τ at 200 hPa		
	50 kGy	18,80% decrease of τ_0	50 kGy	16,92% decrease of slope
		15,16% decrease of τ at 50 hPa		
		10,34% decrease of τ at 100 hPa		
		10,56% decrease of τ at 150 hPa		
		5,47% decrease of τ at 200 hPa		

C.20.2 Electron Beam Sterilization

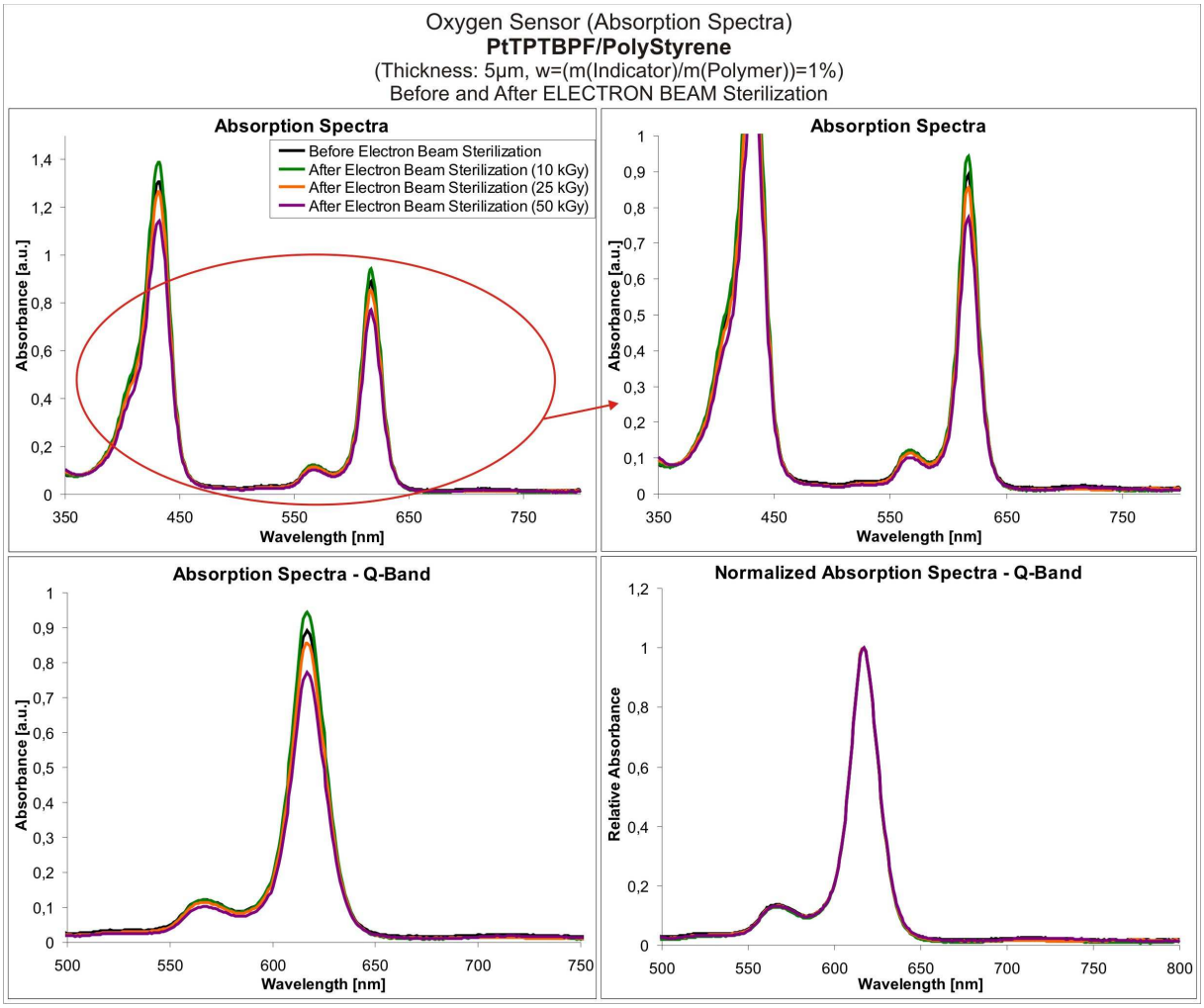

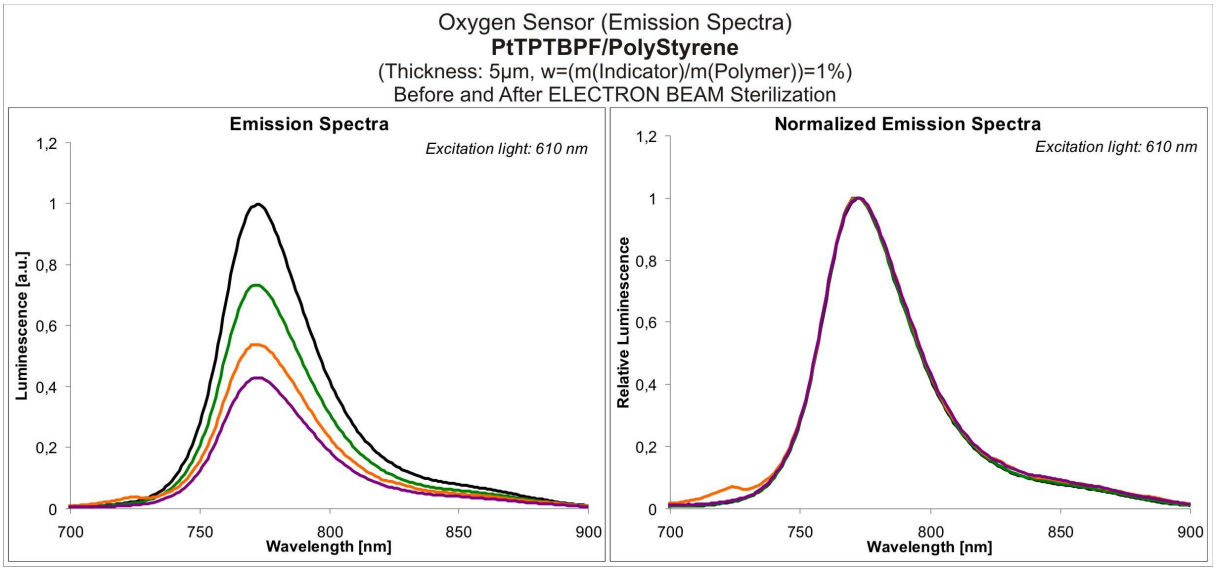

E-BEAM Sterilization	Absorption Spectra		Emission Spectra	
Alterations in Absorption/Emission Intensity	10kGy	5,58% increase	10kGy	26,82% decrease
	25 kGy	3,96% decrease	25 kGy	46,14% decrease
	50 kGy	13,33% decrease	50 kGy	57,12% decrease

Alterations in Absorption/Emission Curve Form	10kGy	Unaltered.	10kGy	Unaltered.
	25 kGy	Unaltered.	25 kGy	Altered emission curve between 700-740 nm.
	50 kGy	Altered absorption curve between 350-360 nm.	50 kGy	Altered emission curve between 825-855 nm.

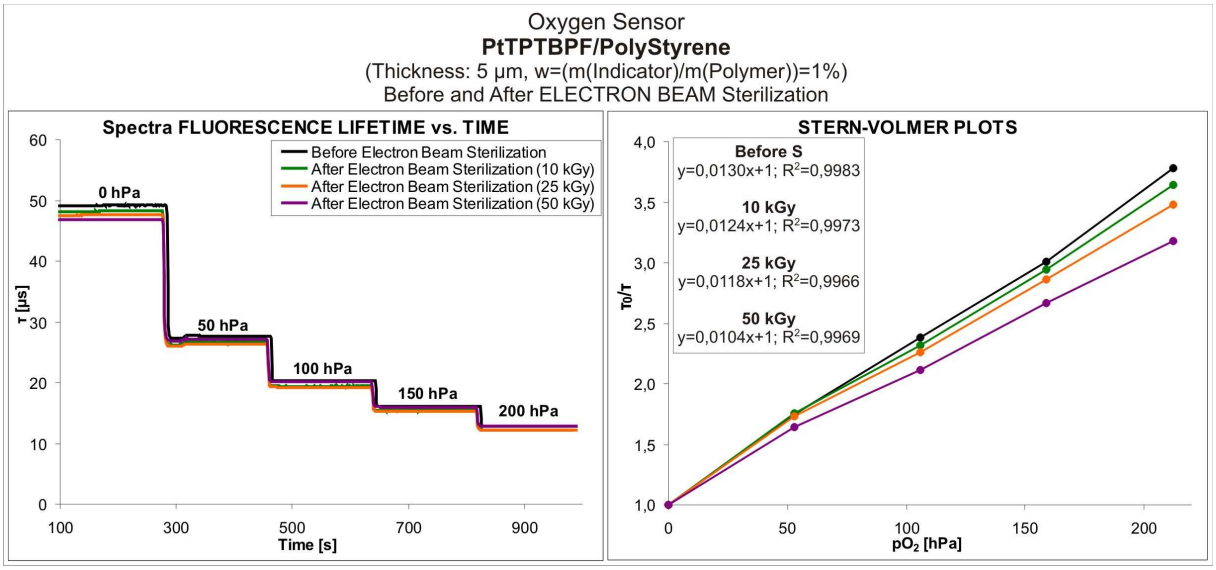

E-BEAM Sterilization	Luminescence Lifetime		Stern-Volmer Plot	
Alterations in Luminescence Lifetime and Slope	10kGy	7,85% decrease of τ_0	10kGy	4,62% decrease of slope
		8,63% decrease of τ at 50 hPa		
		5,98% decrease of τ at 100 hPa		
		5,96% decrease of τ at 150 hPa		
		4,38% decrease of τ at 200 hPa		
	25 kGy	12,81% decrease of τ_0	25 kGy	9,23% decrease of slope
		12,23% decrease of τ at 50 hPa		
		8,43% decrease of τ at 100 hPa		
		8,20% decrease of τ at 150 hPa		
		5,00% decrease of τ at 200 hPa		
	50 kGy	16,11% decrease of τ_0	50 kGy	20,00% decrease of slope
		10,79% decrease of τ at 50 hPa		
		5,98% decrease of τ at 100 hPa		
		5,34% decrease of τ at 150 hPa		
		0,16% decrease of τ at 200hPa		

C.21 Palladium(II)meso-tetra(4-FluoroPhenyl) TetraBenzoPorphyrin (=PdTPTBPF) immobilized in PolyStyrene

C.21.1 Gamma Sterilization

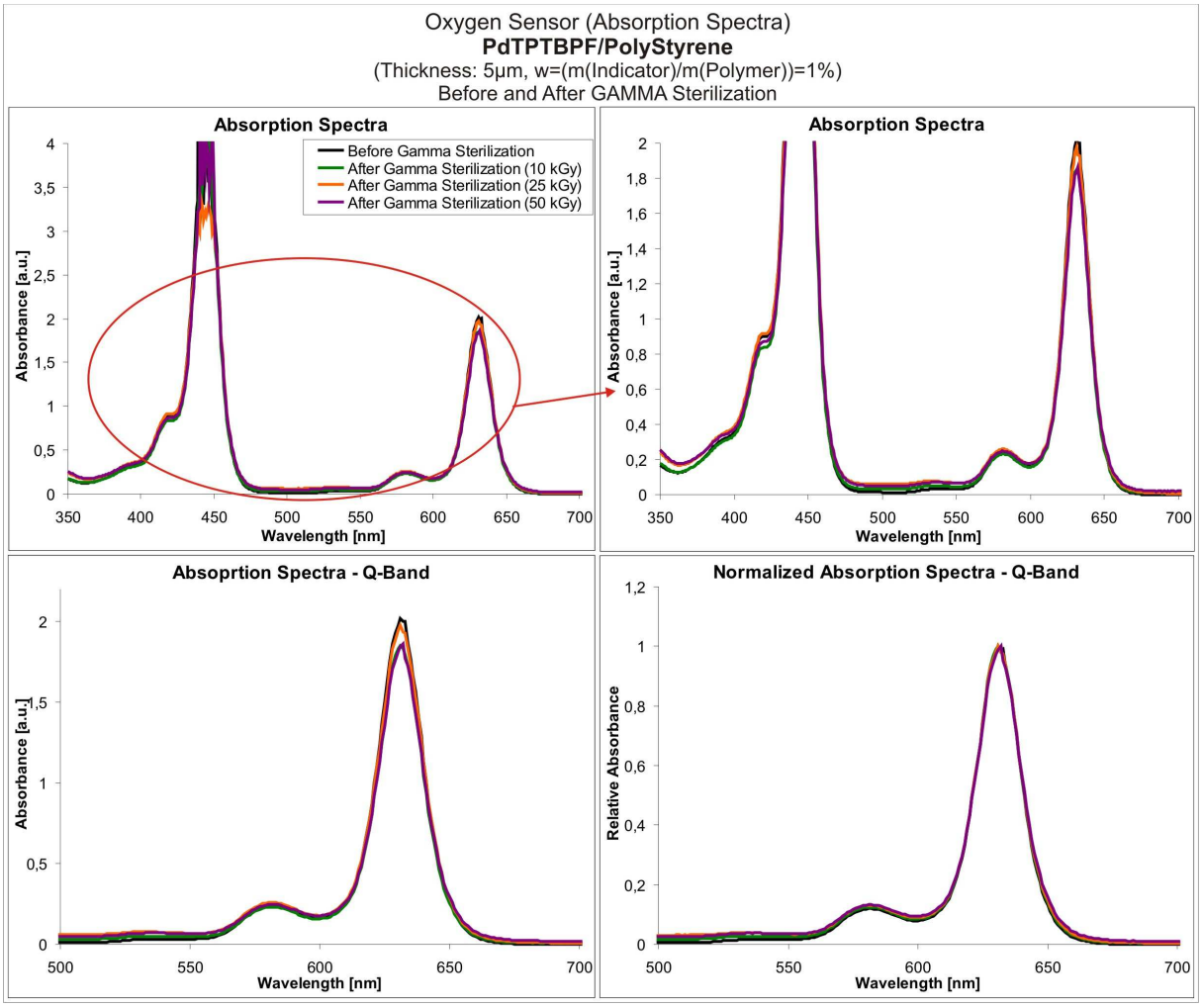

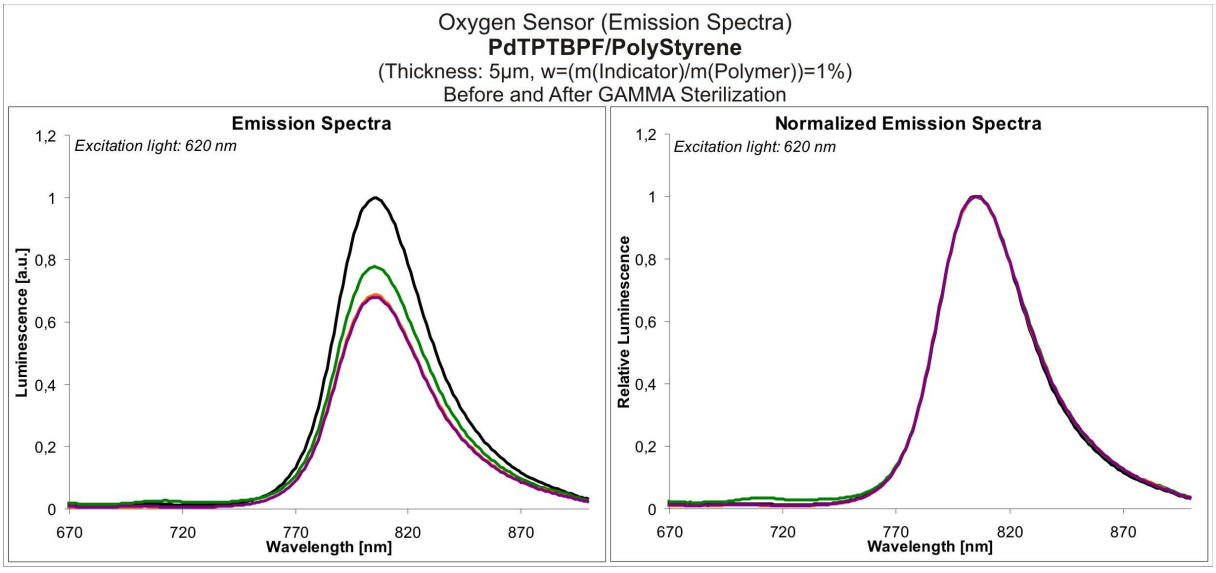

GAMMA Sterilization	Absorption Spectra		Emission Spectra	
Alterations in Absorption/Emission Intensity	10kGy	8,41% decrease	10kGy	22,25% decrease
	25 kGy	2,26% decrease	25 kGy	31,35% decrease
	50 kGy	7,81% decrease	50 kGy	32,17% decrease
Alterations in Absorption/Emission Curve Form	10kGy	Unaltered.	10kGy	Unaltered.
	25 kGy	Unaltered.	25 kGy	Unaltered.
	50 kGy	Unaltered.	50 kGy	Unaltered.

Oxygen Sensor
PdTPTBPF/PolyStyrene
(Thickness: 5 µm, w=(m(Indicator)/m(Polymer))=1%)
Before and After GAMMA Sterilization

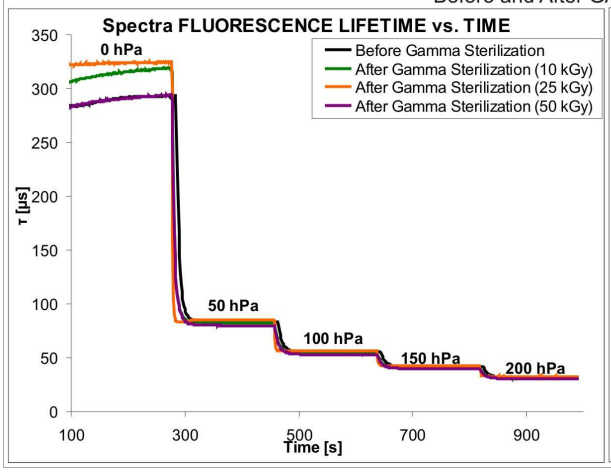

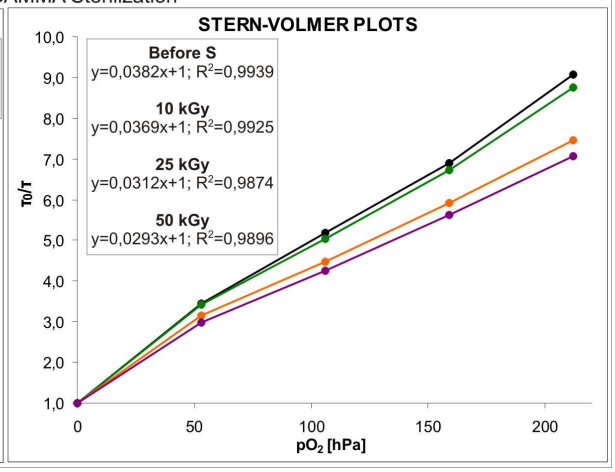

GAMMA Sterilization	Luminescence Lifetime		Stern-Volmer Plot	
Alterations in Luminescence Lifetime and Slope	10kGy	5,90% decrease of τ_0	10kGy	3,40% decrease of slope
		5,04% decrease of τ at 50 hPa		
		3,06% decrease of τ at 100 hPa		
		3,12% decrease of τ at 150 hPa		
		2,52% decrease of τ at 200 hPa		
	25 kGy	15,28% decrease of τ_0	25 kGy	18,32% decrease of slope
		7,20% decrease of τ at 50 hPa		
		1,62% decrease of τ at 100 hPa		
		0,96% decrease of τ at 150 hPa		
		3,35% increase of τ at 200 hPa		
	50 kGy	25,00% decrease of τ_0	50 kGy	23,30% decrease of slope
		13,08% decrease of τ at 50 hPa		
		8,65% decrease of τ at 100 hPa		
		8,15% decrease of τ at 150 hPa		
		3,47% decrease of τ at 200hPa		

C.21.2 Electron Beam Sterilization

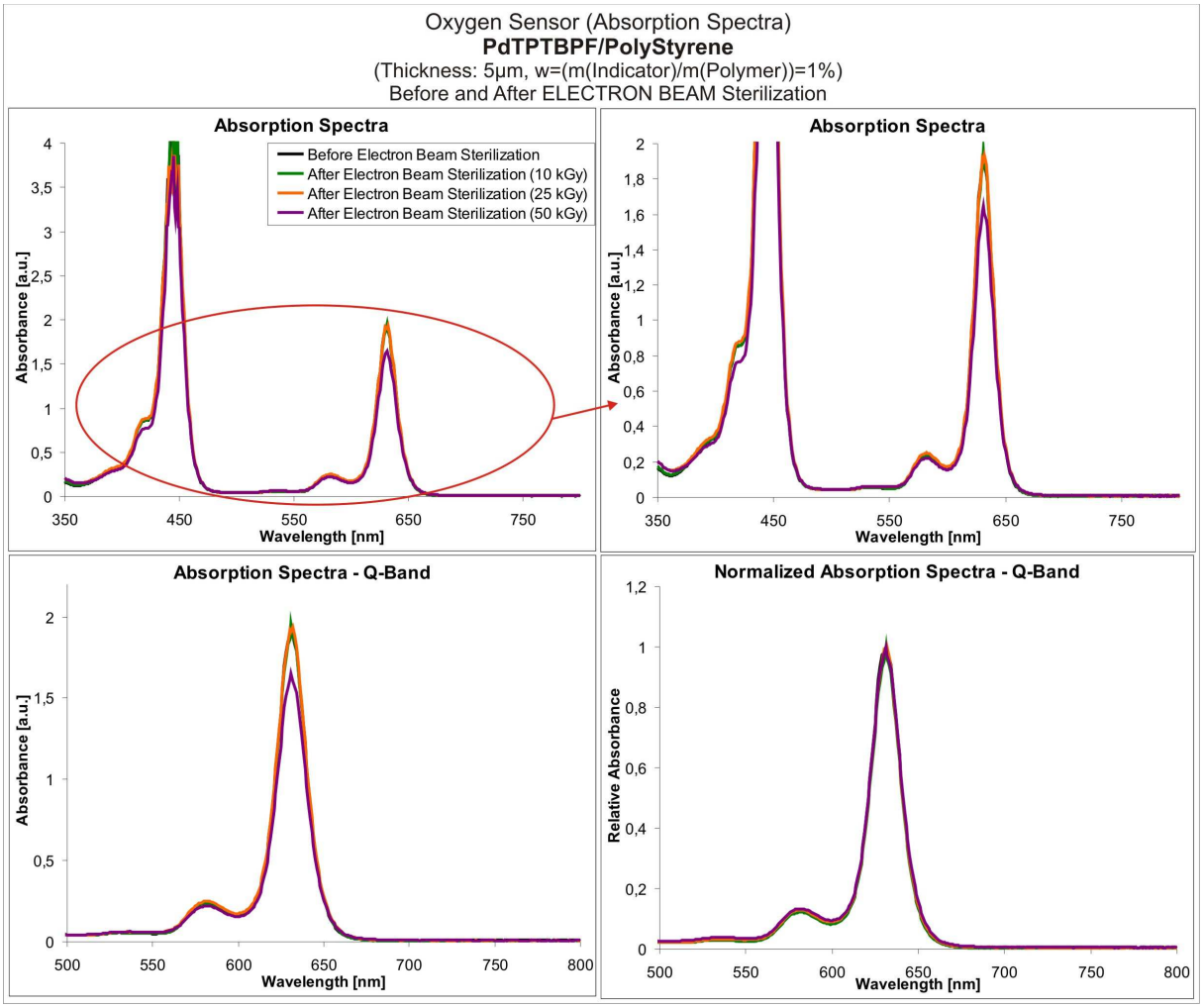

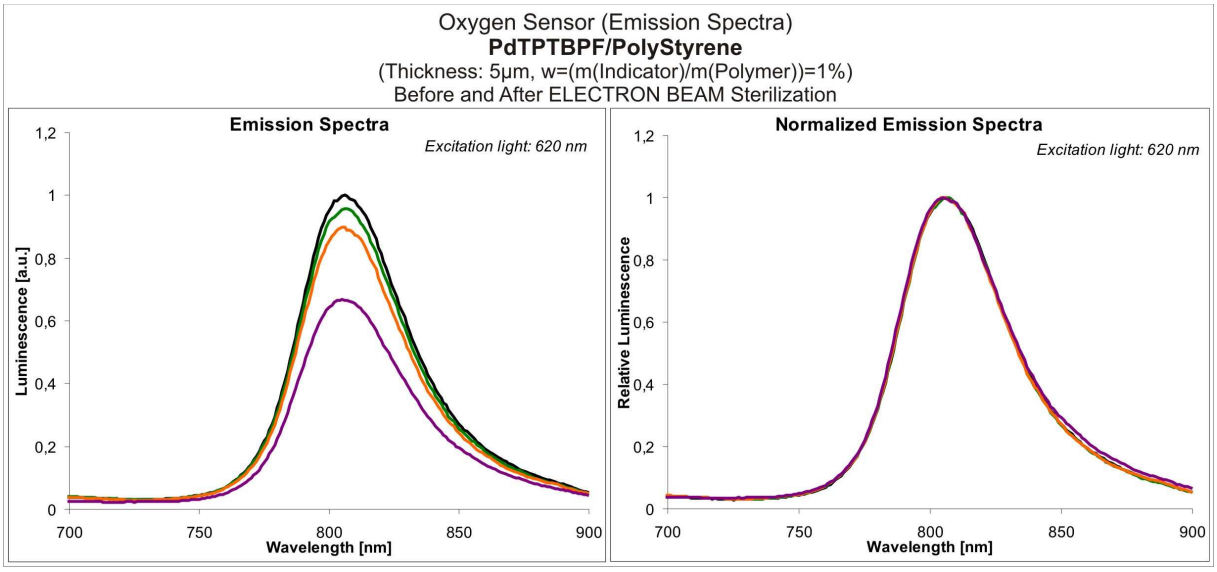

E-BEAM Sterilization	Absorption Spectra		Emission Spectra	
Alterations in Absorption/Emission Intensity	10kGy	2,95% increase	10kGy	4,18% decrease
	25 kGy	1,88% increase	25 kGy	10,30% decrease
	50 kGy	13,16% decrease	50 kGy	33,16% decrease

Alterations in Absorption/Emission Curve Form	10kGy	Unaltered.	10kGy	Unaltered.
	25 kGy	Altered absorption curve between 350-370 and 415-425 nm.	25 kGy	Unaltered.
	50 kGy	Altered absorption curve between 350-370 and 415-425 nm.	50 kGy	Altered emission curve between 850-900 nm.

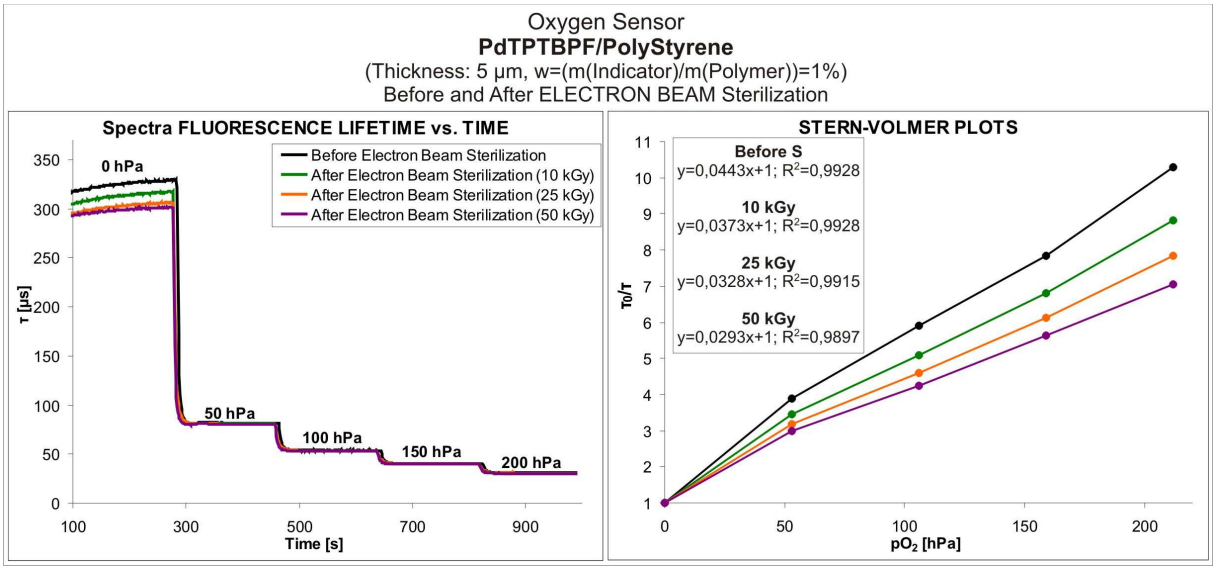

E-BEAM Sterilization	Luminescence Lifetime		Stern-Volmer Plot	
Alterations in Luminescence Lifetime and Slope	10kGy	15,46% decrease of τ_0	10kGy	15,80% decrease of slope
		5,13% decrease of τ at 50 hPa		
		2,04% decrease of τ at 100 hPa		
		2,47% decrease of τ at 150 hPa		
		1,62% decrease of τ at 200 hPa		
	25 kGy	24,60% decrease of τ_0	25 kGy	25,96% decrease of slope
		8,31% decrease of τ at 50 hPa		
		3,35% decrease of τ at 100 hPa		
		3,46% decrease of τ at 150 hPa		
		0,97% decrease of τ at 200 hPa		
	50 kGy	24,61% decrease of τ_0	50 kGy	33,86% decrease of slope
		8,31% decrease of τ at 50 hPa		
		3,34% decrease of τ at 100 hPa		
		5,69% decrease of τ at 150 hPa		
		0,97% decrease of τ at 200hPa		

C.22 Ruthenium(II) DiPhenylPhenanthroline DiChloride ($Ru(dpp)_3Cl_2$) immobilized in Cellulose Acetate

C.22.1 Gamma Sterilization

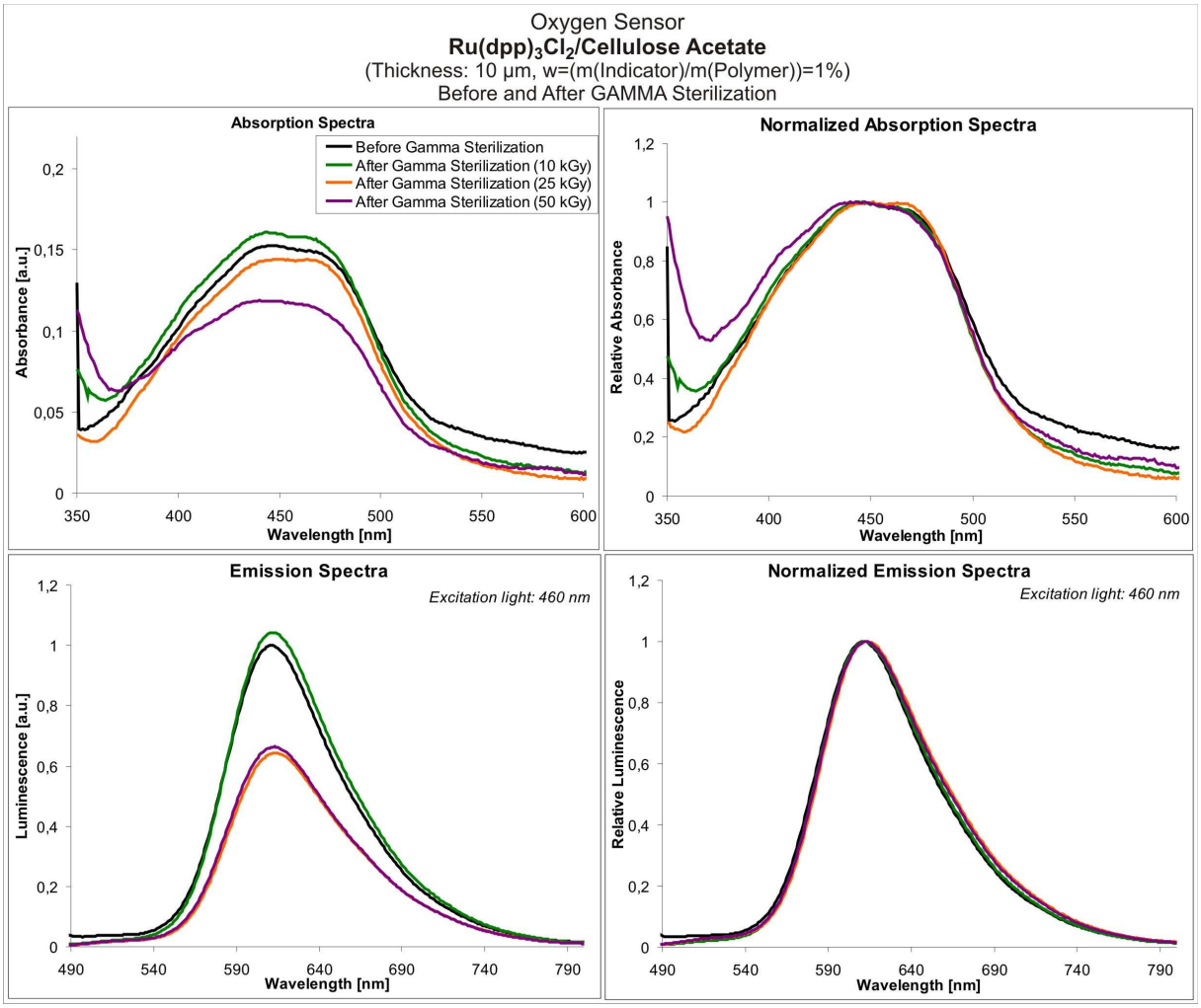

GAMMA Sterilization	Absorption Spectra		Emission Spectra	
Alterations in Absorption/Emission Intensity	10kGy	4,89% increase	10kGy	4,12% increase
	25 kGy	5,49% decrease	25 kGy	35,77% decrease
	50 kGy	22,37% decrease	50 kGy	33,65% decrease
Alterations in Absorption/Emission Curve Form	10kGy	Altered absorption between 350-370 nm and 500-800 nm.	10kGy	Bathochromic shift of the emission maximum for 2 nm.
	25 kGy	Altered absorption between 350-390 nm and 500-800 nm.	25 kGy	Bathochromic shift of the emission maximum for 3 nm.
	50 kGy	Altered absorption between 350-435 nm and 500-800 nm.	50 kGy	Bathochromic shift of the emission maximum for 3 nm.

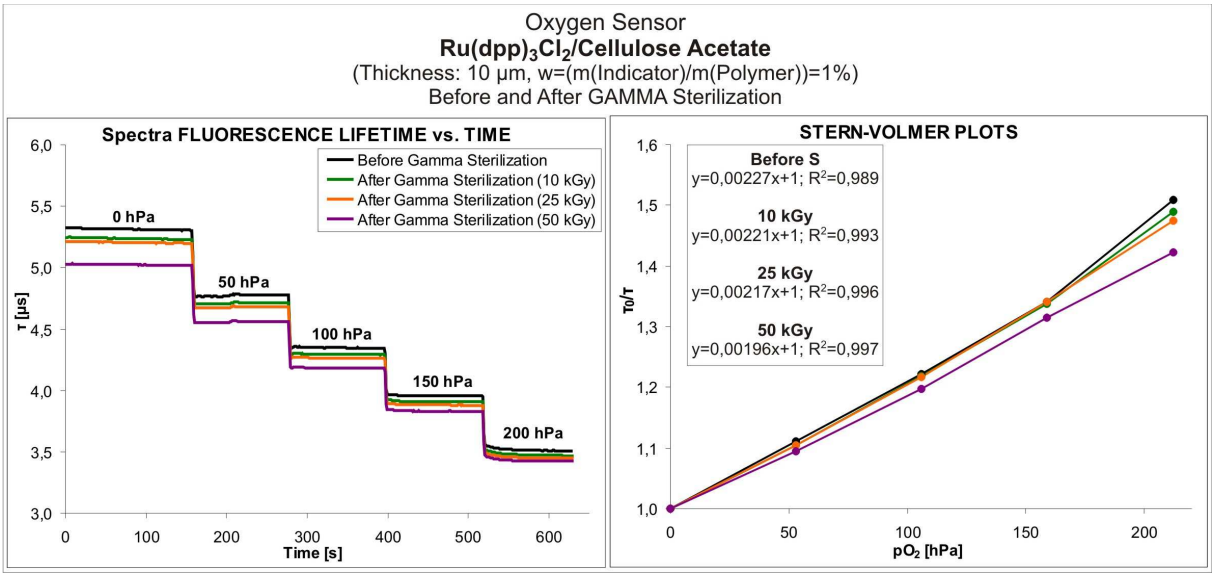

GAMMA Sterilization	Luminescence Lifetime		Stern-Volmer Plot	
Alterations in Luminescence Lifetime and Slope	10kGy	2,45% decrease of τ_0	10kGy	2,64% decrease of slope
		1,89% decrease of τ at 50 hPa		
		2,07% decrease of τ at 100 hPa		
		2,27% decrease of τ at 150 hPa		
		1,14% increase of τ at 200 hPa		
	25 kGy	4,15% decrease of τ_0	25 kGy	4,40% decrease of slope
		3,35% decrease of τ at 50 hPa		
		3,89% decrease of τ at 100 hPa		
		4,29% decrease of τ at 150 hPa		
		1,71% decrease of τ at 200 hPa		
	50 kGy	8,11% decrease of τ_0	50 kGy	13,66% decrease of slope
		6,71% decrease of τ at 50 hPa		
		6,22% decrease of τ at 100 hPa		
		6,56% decrease of τ at 150 hPa		
		2,56% decrease of τ at 200 hPa		

C.22.2 Electron Beam Sterilization

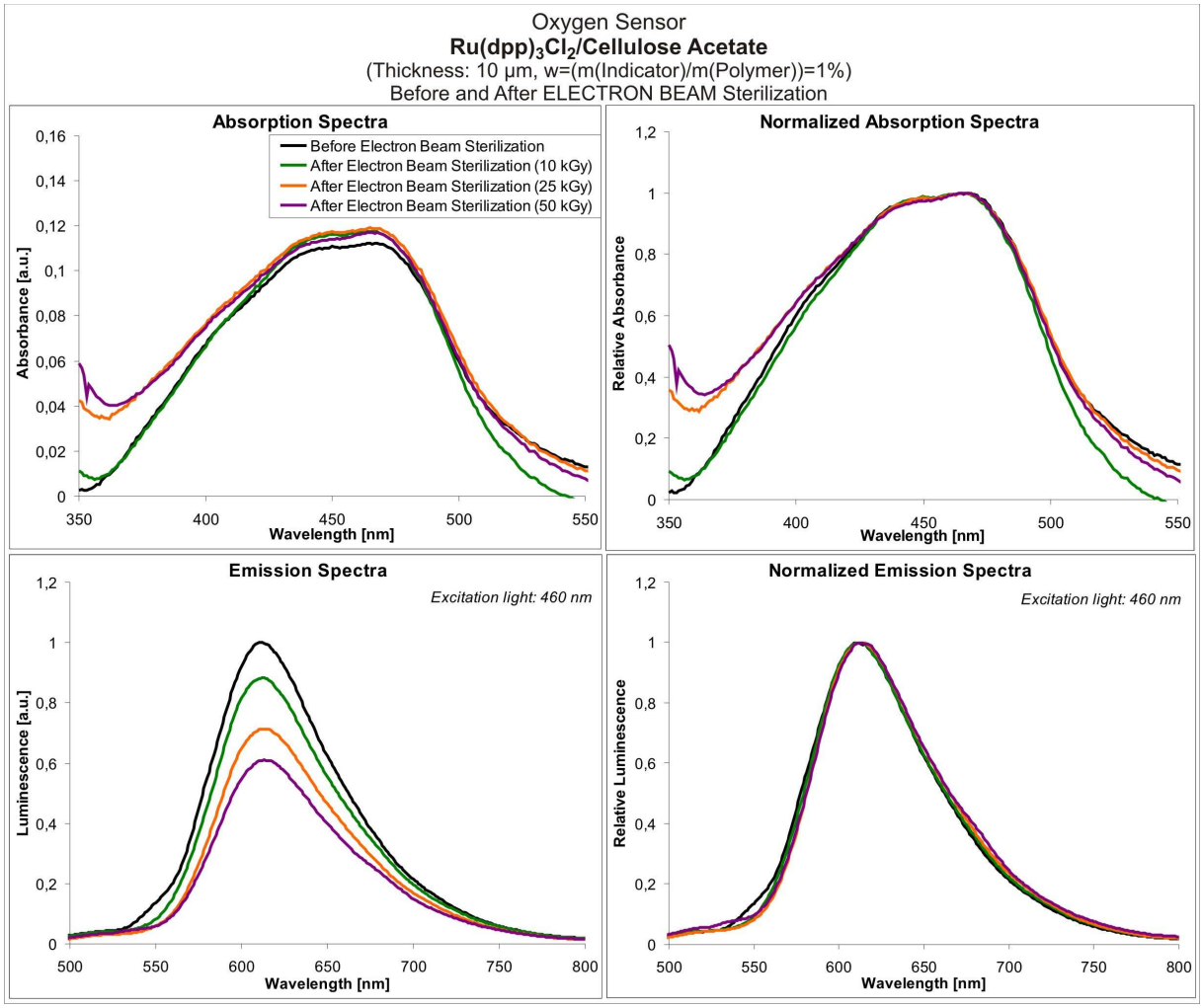

E-BEAM Sterilization	Absorption Spectra		Emission Spectra	
Alterations in Absorption/Emission Intensity	10kGy	4,46% increase	10kGy	9,74% decrease
	25 kGy	5,64% increase	25 kGy	28,63% decrease
	50 kGy	3,99% increase	50 kGy	39,03% decrease
Alterations in Absorption/Emission Curve Form	10kGy	Altered absorption between 350-360 nm and 490-800 nm.	10kGy	Unaltered.
	25 kGy	Altered absorption between 350-420 nm.	25 kGy	Bathochromic shift of the emission maximum for 2 nm.
	50 kGy	Altered absorption between 350-420 nm and 520-800 nm-	50 kGy	Bathochromic shift of the emission maximum for 2 nm. Altered absorption between 670-730 nm.

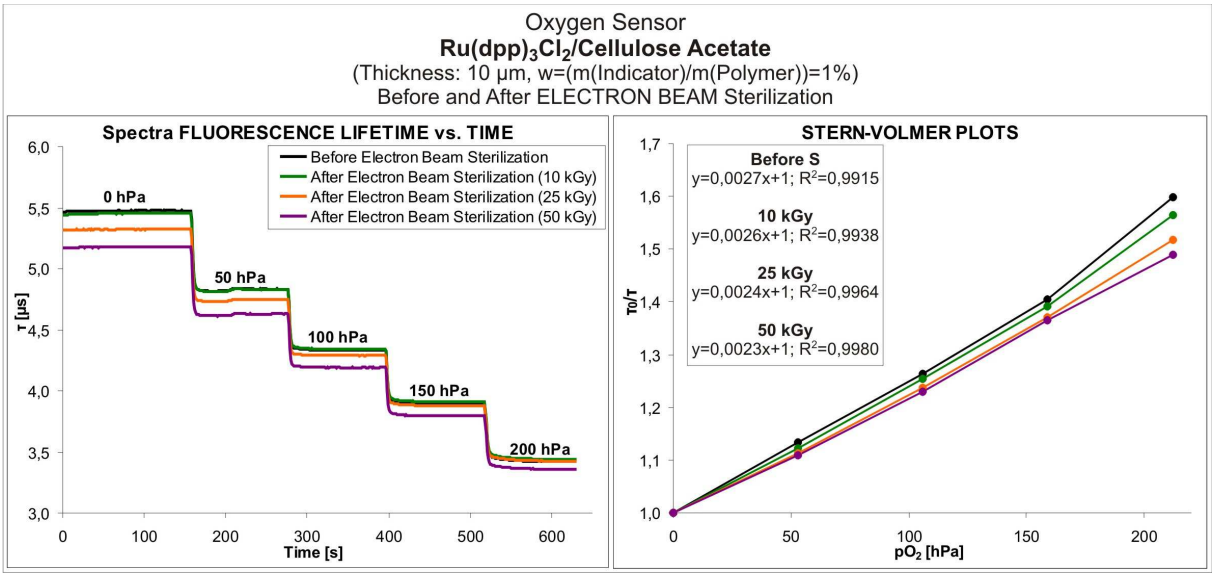

E-BEAM Sterilization	Luminescence Lifetime		Stern-Volmer Plot	
Alterations in Luminescence Lifetime and Slope	10kGy	1,64% decrease of τ_0	10kGy	3,70% decrease of slope
		0,62% decrease of τ at 50 hPa		
		0,92% decrease of τ at 100 hPa		
		0,77% decrease of τ at 150 hPa		
		0,29% increase of τ at 200 hPa		
	25 kGy	5,11% decrease of τ_0	25 kGy	11,11% decrease of slope
		3,31% decrease of τ at 50 hPa		
		3,22% decrease of τ at 100 hPa		
		2,82% decrease of τ at 150 hPa		
		0,29% decrease of τ at 200 hPa		
	50 kGy	8,76% decrease of τ_0	50 kGy	14,81% decrease of slope
		6,62% decrease of τ at 50 hPa		
		6,22% decrease of τ at 100 hPa		
		5,90% decrease of τ at 150 hPa		
		2,04% decrease of τ at 200 hPa		

C.23 Ruthenium(II) DiPhenylPhenanthroline DiChloride ($Ru(dpp)_3Cl_2$) immobilized in Ethyl Cellulose

C.23.1 Gamma Sterilization

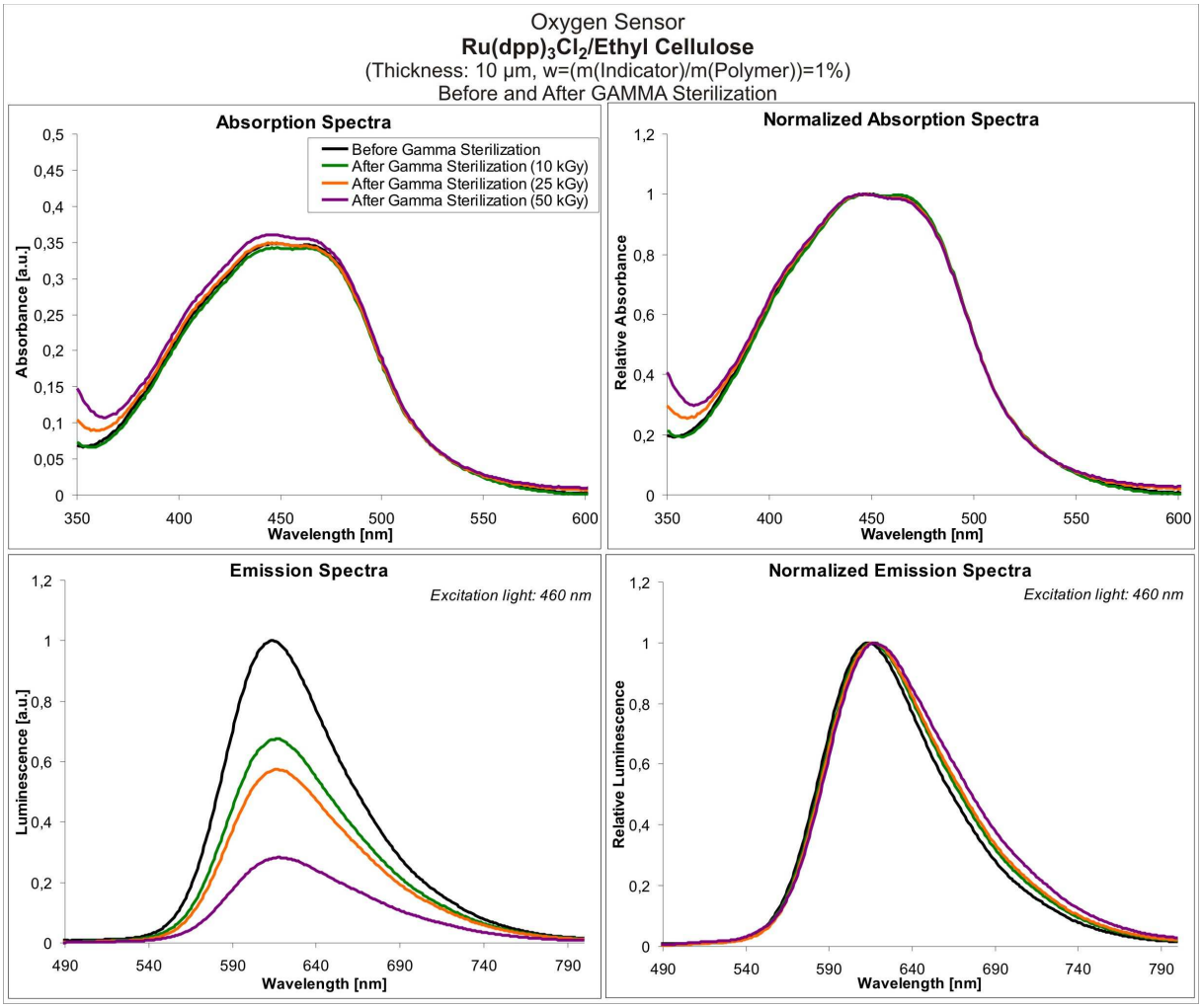

GAMMA Sterilization	Absorption Spectra		Emission Spectra	
Alterations in Absorption/Emission Intensity	10kGy	1,51% decrease	10kGy	32,55% decrease
	25 kGy	0,32% decrease	25 kGy	42,59% decrease
	50 kGy	3,43% increase	50 kGy	71,70% decrease
Alterations in Absorption/Emission Curve Form	10kGy	Unaltered.	10kGy	Bathochromic shift of the emission maximum for 3 nm.
	25 kGy	Altered absorption between 350-380 nm.	25 kGy	Bathochromic shift of the emission maximum for 3 nm.
	50 kGy	Altered absorption between 350-380 nm.	50 kGy	Bathochromic shift of the emission maximum for 5 nm.

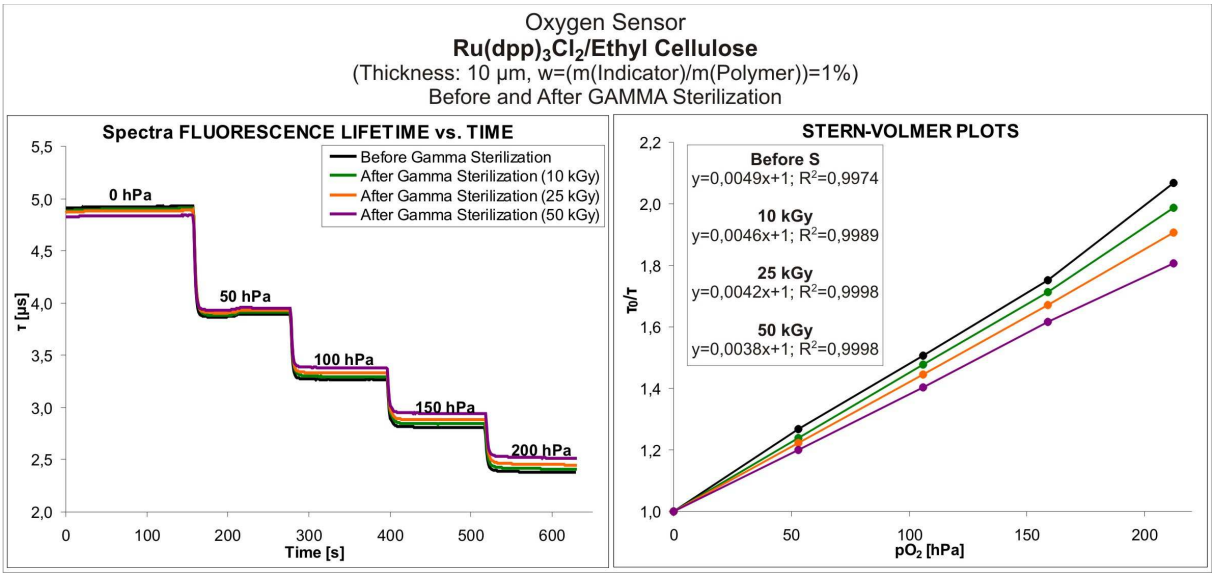

GAMMA Sterilization	Luminescence Lifetime		Stern-Volmer Plot	
Alterations in Luminescence Lifetime and Slope	10kGy	2,44% decrease of τ_0	10kGy	6,12% decrease of slope
		0,26% decrease of τ at 50 hPa		
		0,61% decrease of τ at 100 hPa		
		0,36% decrease of τ at 150 hPa		
		1,24% increase of τ at 200 hPa		
	25 kGy	4,88% decrease of τ_0	25 kGy	14,28% decrease of slope
		1,29% decrease of τ at 50 hPa		
		0,92% decrease of τ at 100 hPa		
		0,71% decrease of τ at 150 hPa		
		2,86% increase of τ at 200 hPa		
	50 kGy	7,52% decrease of τ_0	50 kGy	22,45% decrease of slope
		2,32% decrease of τ at 50 hPa		
		0,61% decrease of τ at 100 hPa		
		0,35% increase of τ at 150 hPa		
		5,56% increase of τ at 200 hPa		

C.23.2 Electron Beam Sterilization

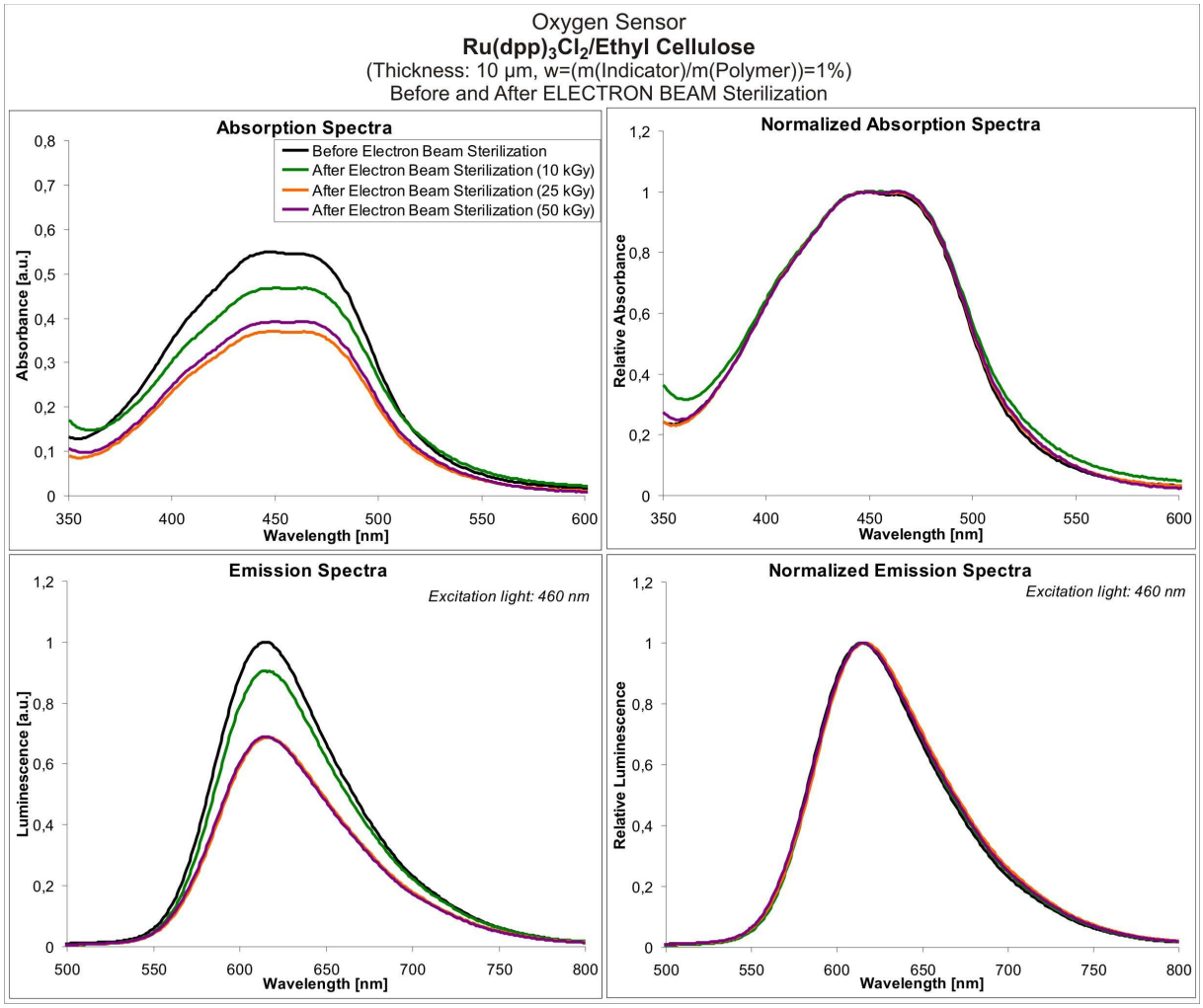

E-BEAM Sterilization	Absorption Spectra		Emission Spectra	
Alterations in Absorption/Emission Intensity	10kGy	15,00% decrease	10kGy	9,37% decrease
	25 kGy	32,55% decrease	25 kGy	31,27% decrease
	50 kGy	28,66% decrease	50 kGy	30,97% decrease
Alterations in Absorption/Emission Curve Form	10kGy	Altered absorption between 350-390 nm and 510-800 nm.	10kGy	Unaltered.
	25 kGy	Unaltered.	25 kGy	Unaltered.
	50 kGy	Unaltered.	50 kGy	Unaltered.

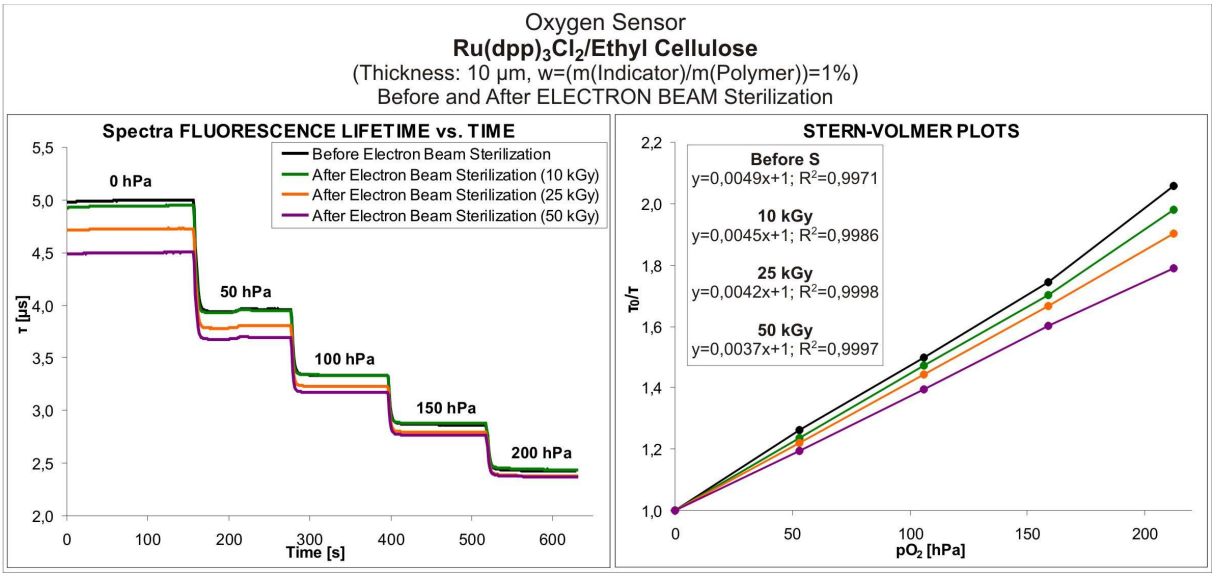

E-BEAM Sterilization	Luminescence Lifetime		Stern-Volmer Plot	
Alterations in Luminescence Lifetime and Slope	10kGy	3,40% decrease of τ_0	10kGy	8,16% decrease of slope
		1,01% decrease of τ at 50 hPa		
		1,20% decrease of τ at 100 hPa		
		1,04% decrease of τ at 150 hPa		
		0,41% increase of τ at 200 hPa		
	25 kGy	9,60% decrease of τ_0	25 kGy	14,28% decrease of slope
		6,33% decrease of τ at 50 hPa		
		5,71% decrease of τ at 100 hPa		
		5,57% decrease of τ at 150 hPa		
		2,06% decrease of τ at 200 hPa		
	50 kGy	15,20% decrease of τ_0	50 kGy	24,49% decrease of slope
		10,13% decrease of τ at 50 hPa		
		8,71% decrease of τ at 100 hPa		
		7,66% decrease of τ at 150 hPa		
		2,47% decrease of τ at 200 hPa		

C.24 Ruthenium(II) DiPhenylPhenanthroline DiChloride ($Ru(dpp)_3Cl_2$) immobilized in HydroGel D4/D7

C.24.1 Gamma Sterilization

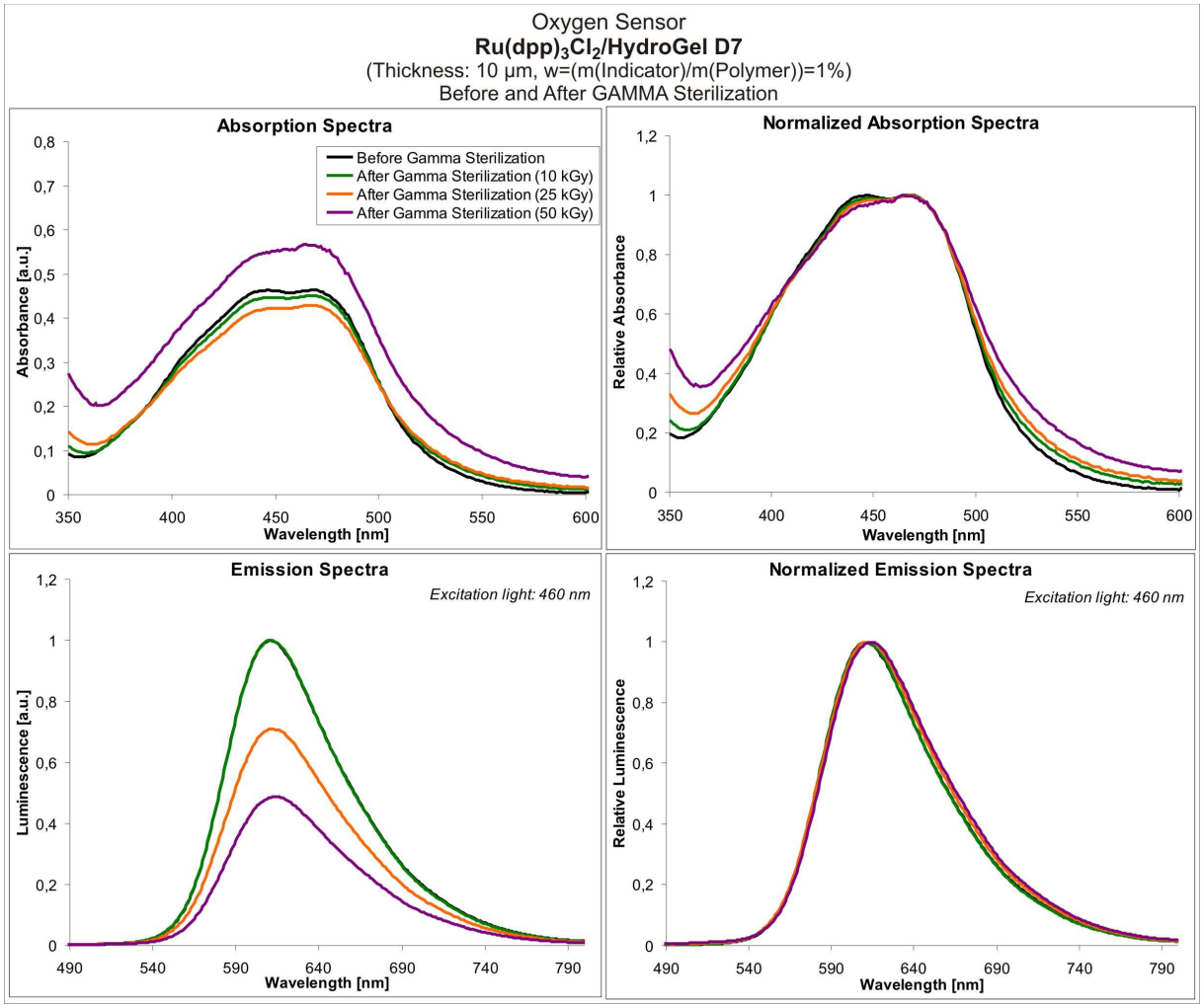

GAMMA Sterilization	Absorption Spectra		Emission Spectra	
Alterations in Absorption/Emission Intensity	10kGy	2,52% decrease	10kGy	0,08% increase
	25 kGy	7,32% decrease	25 kGy	29,14% decrease
	50 kGy	18,33% increase	50 kGy	51,28% decrease
Alterations in Absorption/Emission Curve Form	10kGy	Altered absorption between 350-360 nm and 510-800 nm.	10kGy	Unaltered.
	25 kGy	Altered absorption between 350-390 nm and 505-800 nm.	25 kGy	Bathochromic shift of the emission maximum for 1 nm.
	50 kGy	Sensor became turbid after sterilization. Altered absorption between 350-400 nm and 495-800 nm.	50 kGy	Bathochromic shift of the emission maximum for 3 nm.

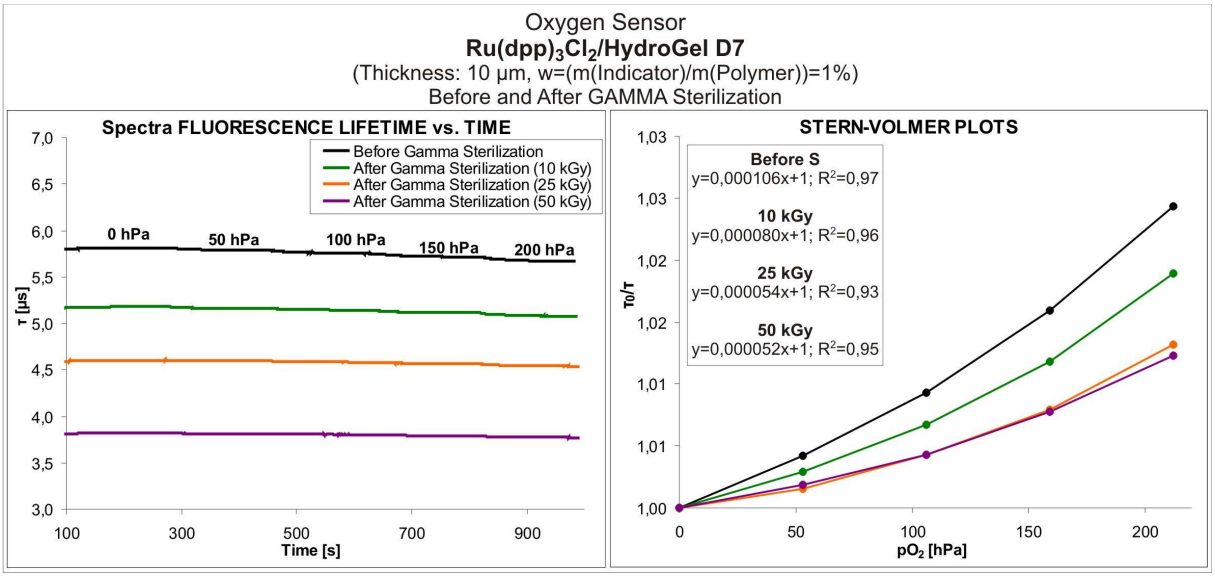

GAMMA Sterilization	Luminescence Lifetime		Stern-Volmer Plot	
Alterations in Luminescence Lifetime and Slope	10kGy	10,84% decrease of τ_0	10kGy	24,34% decrease of slope
		10,88% decrease of τ at 50 hPa		
		10,76% decrease of τ at 100 hPa		
		10,49% decrease of τ at 150 hPa		
		10,40% decrease of τ at 200 hPa		
	25 kGy	20,83% decrease of τ_0	25 kGy	48,77% decrease of slope
		20,55% decrease of τ at 50 hPa		
		20,49% decrease of τ at 100 hPa		
		20,10% decrease of τ at 150 hPa		
		19,93% decrease of τ at 200 hPa		
	50 kGy	34,25% decrease of τ_0	50 kGy	50,75% decrease of slope
		34,20% decrease of τ at 50 hPa		
		34,03% decrease of τ at 100 hPa		
		33,74% decrease of τ at 150 hPa		
		33,35% decrease of τ at 200 hPa		

C.24.2 Electron Beam Sterilization

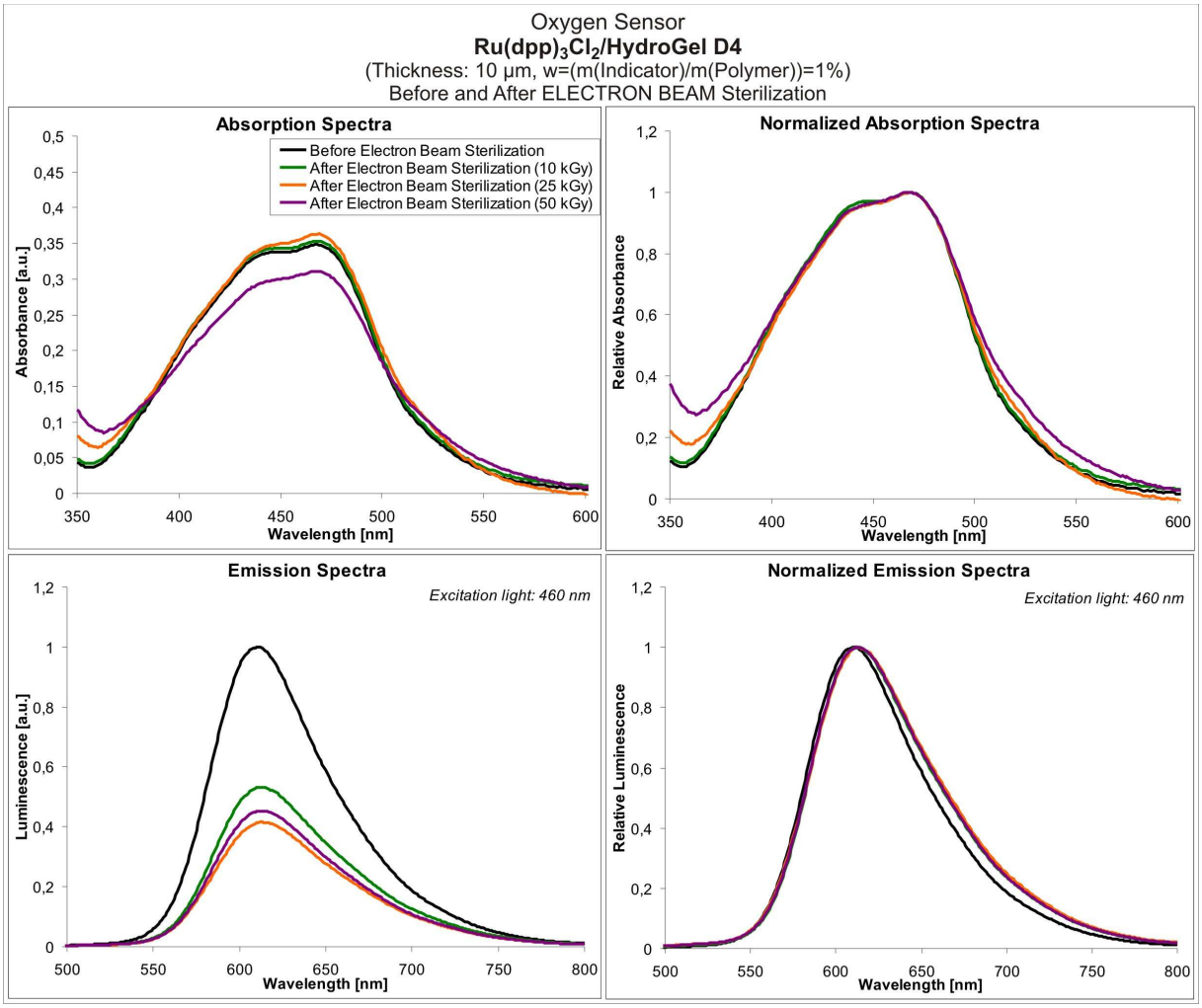

E-BEAM Sterilization	Absorption Spectra		Emission Spectra	
Alterations in Absorption/Emission Intensity	10kGy	1,41% increase	10kGy	46,82% decrease
	25 kGy	4,13% increase	25 kGy	58,40% decrease
	50 kGy	9,77% decrease	50 kGy	54,64% decrease
Alterations in Absorption/Emission Curve Form	10kGy	Unaltered.	10kGy	Bathochromic shift of the emission maximum for 3 nm.
	25 kGy	Altered absorption between 350-375 nm.	25 kGy	Bathochromic shift of the emission maximum for 2 nm.
	50 kGy	Altered absorption between 350-395 nm and 500-600 nm.	50 kGy	Bathochromic shift of the emission maximum for 1 nm.

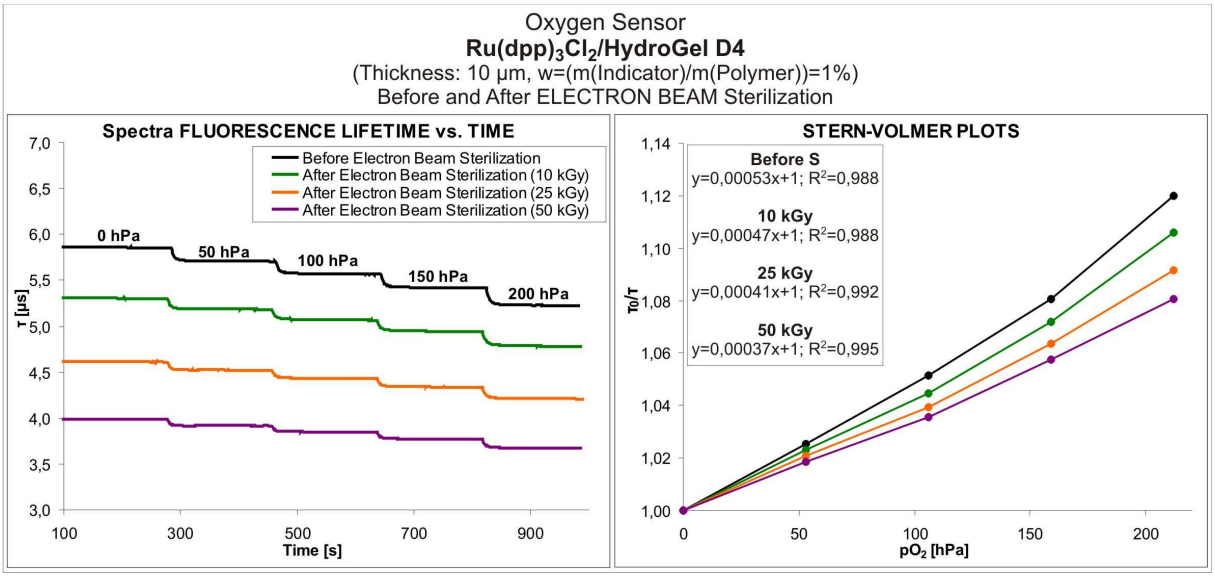

E-BEAM Sterilization	Luminescence Lifetime		Stern-Volmer Plot	
Alterations in Luminescence Lifetime and Slope	10kGy	9,57% decrease of τ_0	10kGy	11,32% decrease of slope
		9,46% decrease of τ at 50 hPa		
		9,16% decrease of τ at 100 hPa		
		8,86% decrease of τ at 150 hPa		
		8,60% increase of τ at 200 hPa		
	25 kGy	21,37% decrease of τ_0	25 kGy	22,64% decrease of slope
		21,19% decrease of τ at 50 hPa		
		20,64% decrease of τ at 100 hPa		
		20,29% decrease of τ at 150 hPa		
		19,50% decrease of τ at 200 hPa		
	50 kGy	31,14% decrease of τ_0	50 kGy	30,19% decrease of slope
		31,70% decrease of τ at 50 hPa		
		31,24% decrease of τ at 100 hPa		
		31,81% decrease of τ at 150 hPa		
		29,83% decrease of τ at 200 hPa		

C.25 Ruthenium(II) DiPhenylPhenanthroline DiChloride ($Ru(dpp)_3Cl_2$) immobilized in HydroThane5

C.25.1 Gamma Sterilization

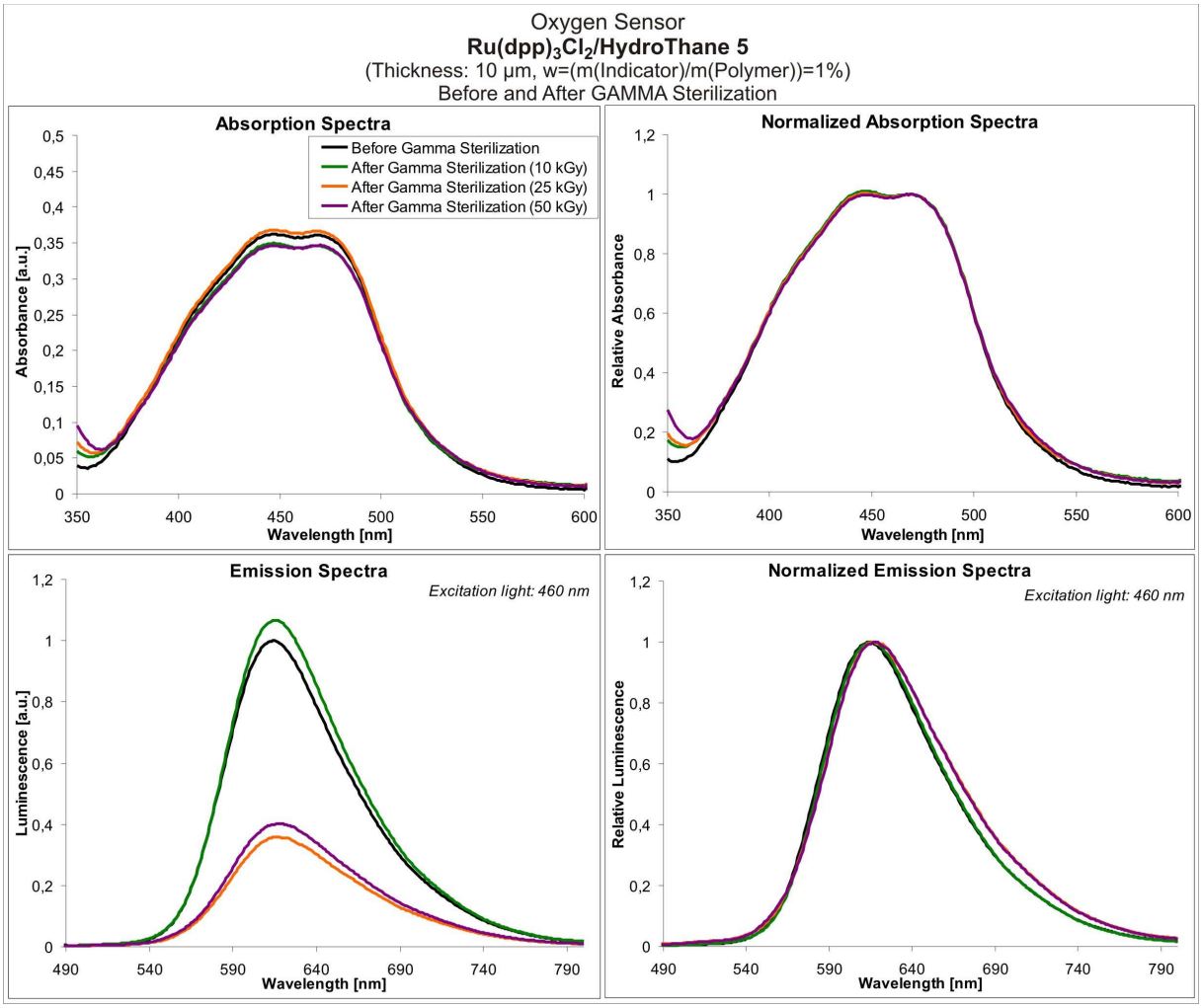

GAMMA Sterilization	Absorption Spectra		Emission Spectra	
Alterations in Absorption/Emission Intensity	10kGy	4,14% decrease	10kGy	6,27% increase
	25 kGy	0,07% decrease	25 kGy	64,20% decrease
	50 kGy	3,88% decrease	50 kGy	60,75% decrease
Alterations in Absorption/Emission Curve Form	10kGy	Altered absorption between 350-370 nm.	10kGy	Unaltered.
	25 kGy	Altered absorption between 350-370 nm.	25 kGy	Bathochromic shift of the emission maximum for 1 nm.
	50 kGy	Altered absorption between 350-370 nm.	50 kGy	Bathochromic shift of the emission maximum for 3 nm.

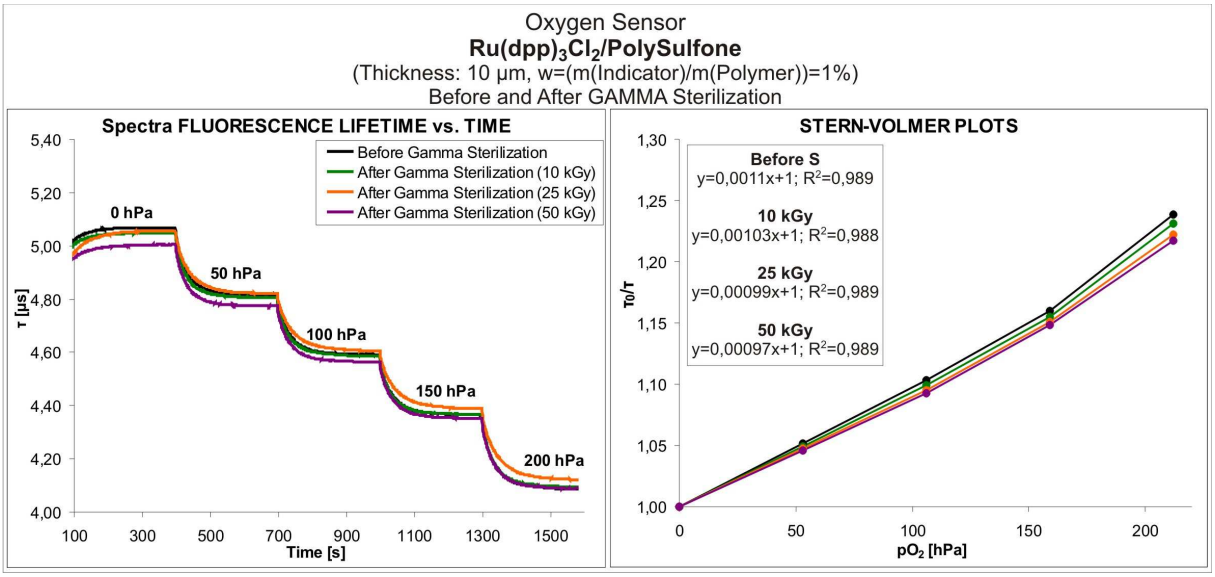

GAMMA Sterilization	Luminescence Lifetime		Stern-Volmer Plot	
Alterations in Luminescence Lifetime and Slope	10kGy	0,84% decrease of τ_0	10kGy	6,72% increase of slope
		1,20% decrease of τ at 50 hPa		
		1,42% decrease of τ at 100 hPa		
		1,64% decrease of τ at 150 hPa		
		1,33% decrease of τ at 200 hPa		
	25 kGy	2,87% decrease of τ_0	25 kGy	9,31% decrease of slope
		3,28% decrease of τ at 50 hPa		
		3,72% decrease of τ at 100 hPa		
		4,01% decrease of τ at 150 hPa		
		3,42% decrease of τ at 200 hPa		
	50 kGy	6,41% decrease of τ_0	50 kGy	11,48% decrease of slope
		6,91% decrease of τ at 50 hPa		
		7,44% decrease of τ at 100 hPa		
		8,03% decrease of τ at 150 hPa		
		7,22% decrease of τ at 200 hPa		

C.25.2 Electron Beam Sterilization

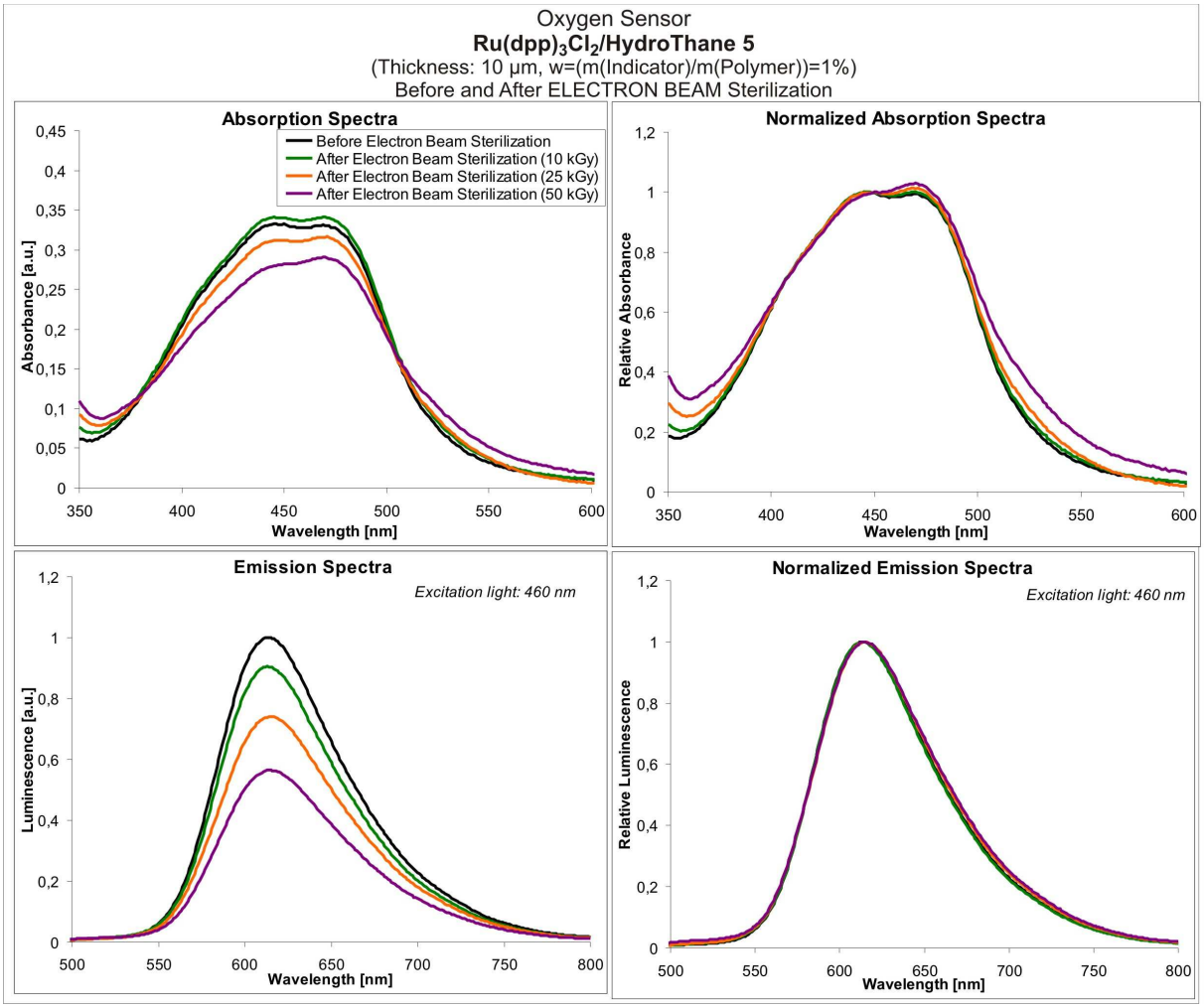

E-BEAM Sterilization	Absorption Spectra		Emission Spectra	
Alterations in Absorption/Emission Intensity	10kGy	2,26% increase	10kGy	9,46% decrease
	25 kGy	6,24% decrease	25 kGy	25,88% decrease
	50 kGy	15,23% decrease	50 kGy	43,53% decrease
Alterations in Absorption/Emission Curve Form	10kGy	Unaltered.	10kGy	Unaltered.
	25 kGy	Altered absorption between 350-380 nm and 510-550 nm.	25 kGy	Bathochromic shift of the emission maximum for 1 nm.
	50 kGy	Altered absorption between 350-395 nm, 455-480 nm and 500-800 nm.	50 kGy	Bathochromic shift of the emission maximum for 1 nm.

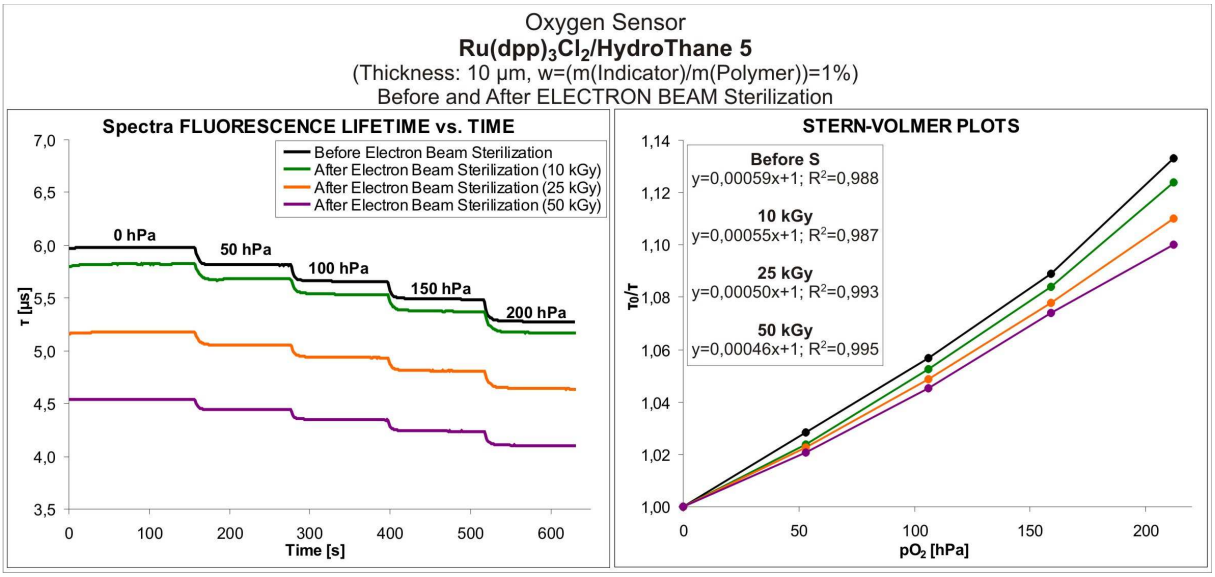

E-BEAM Sterilization	Luminescence Lifetime		Stern-Volmer Plot	
Alterations in Luminescence Lifetime and Slope	10kGy	2,84% decrease of τ_0	10kGy	7,82% decrease of slope
		2,41% decrease of τ at 50 hPa		
		2,47% decrease of τ at 100 hPa		
		2,37% decrease of τ at 150 hPa		
		2,08% increase of τ at 200 hPa		
	25 kGy	13,88% decrease of τ_0	25 kGy	15,68% decrease of slope
		13,40% decrease of τ at 50 hPa		
		13,25% decrease of τ at 100 hPa		
		12,93% decrease of τ at 150 hPa		
		12,12% decrease of τ at 200 hPa		
	50 kGy	24,58% decrease of τ_0	50 kGy	22,09% decrease of slope
		24,05% decrease of τ at 50 hPa		
		23,67% decrease of τ at 100 hPa		
		23,50% decrease of τ at 150 hPa		
		22,35% decrease of τ at 200 hPa		

C.26 Ruthenium(II) DiPhenylPhenanthroline DiChloride ($Ru(dpp)_3Cl_2$) immobilized in PolySulfone

C.26.1 Gamma Sterilization

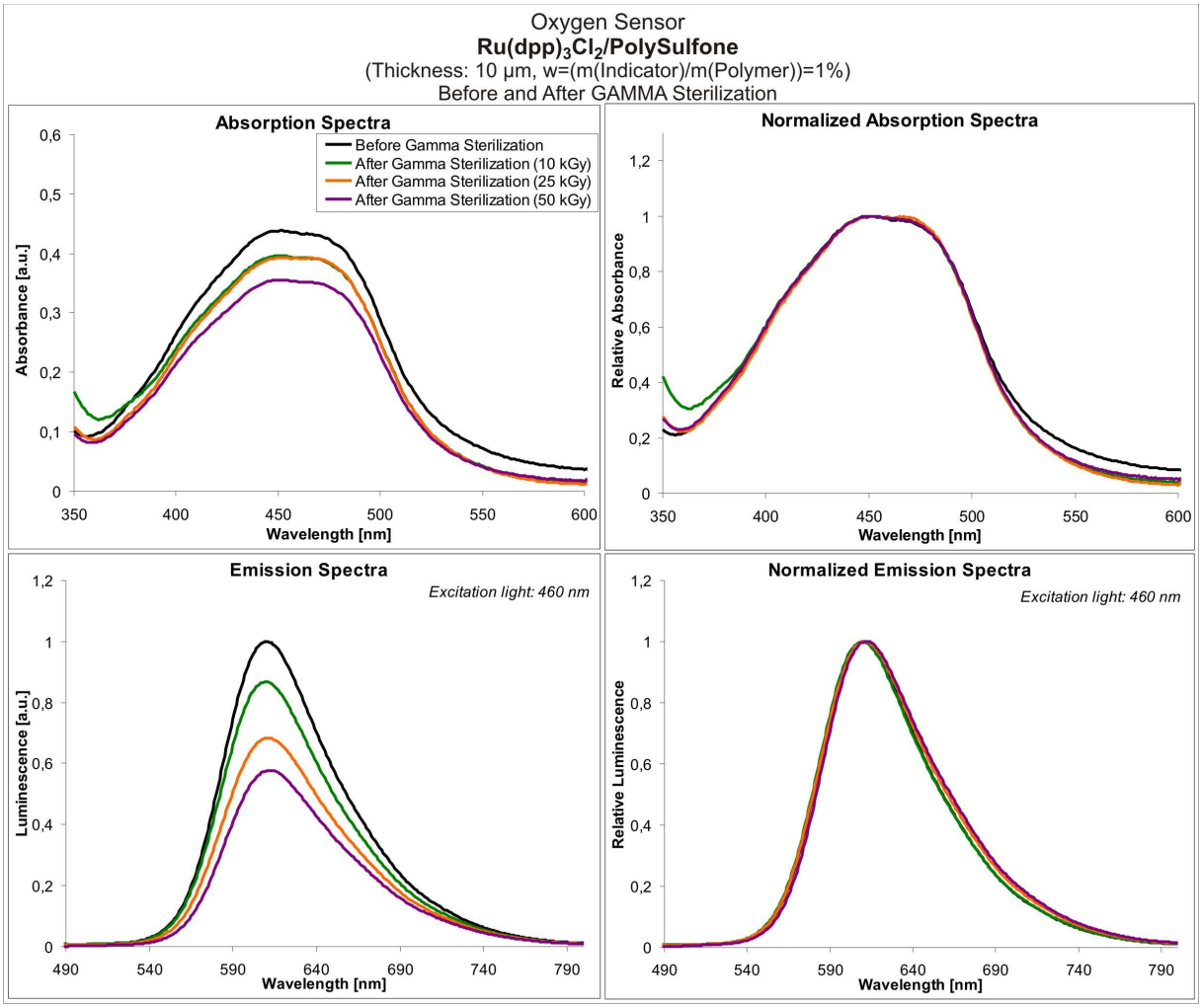

GAMMA Sterilization	Absorption Spectra		Emission Spectra	
Alterations in Absorption/Emission Intensity	10kGy	9,76% decrease	10kGy	13,22% decrease
	25 kGy	10,39% decrease	25 kGy	31,65% decrease
	50 kGy	19,00% decrease	50 kGy	42,32% decrease
Alterations in Absorption/Emission Curve Form	10kGy	Altered absorption between 350-390 nm and 520-800 nm.	10kGy	Unaltered.
	25 kGy	Altered absorption between 520-800 nm	25 kGy	Bathochromic shift of the emission maximum for 1 nm.
	50 kGy	Altered absorption between 520-800 nm	50 kGy	Bathochromic shift of the emission maximum for 3 nm.

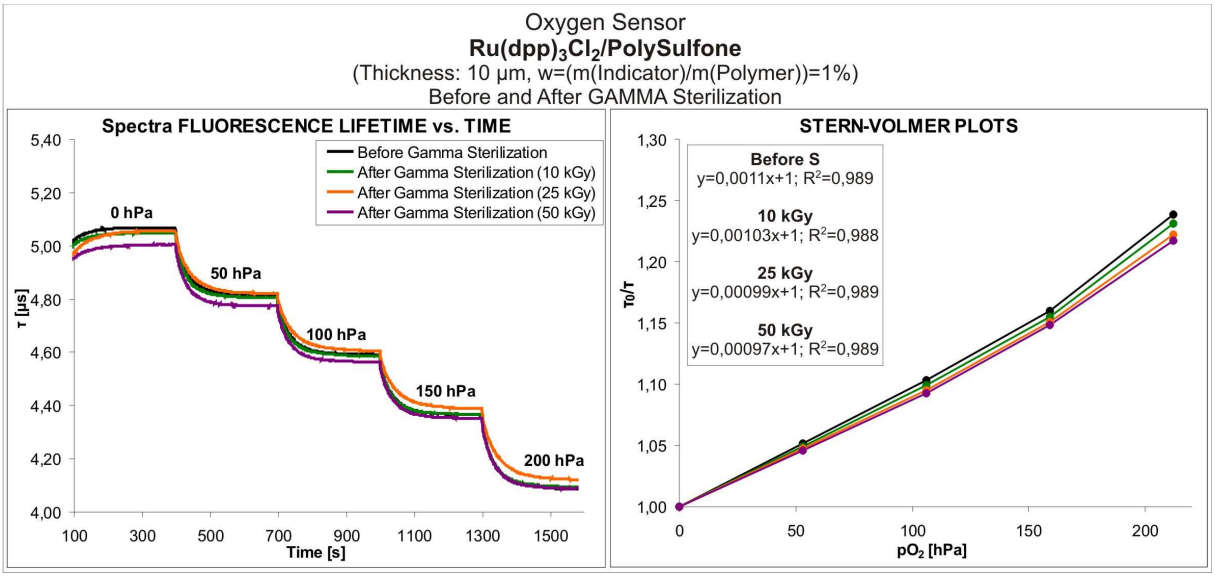

GAMMA Sterilization	Luminescence Lifetime		Stern-Volmer Plot	
Alterations in Luminescence Lifetime and Slope	10kGy	0,59% decrease of τ_0	10kGy	6,36% decrease of slope
		0,41% decrease of τ at 50 hPa		
		0,22% decrease of τ at 100 hPa		
		0,23% decrease of τ at 150 hPa		
		0,24% increase of τ at 200 hPa		
	25 kGy	0,59% decrease of τ_0	25 kGy	10,00% decrease of slope
		0,21% decrease of τ at 50 hPa		
		0,43% increase of τ at 100 hPa		
		0,23% increase of τ at 150 hPa		
		0,97% increase of τ at 200 hPa		
	50 kGy	1,77% decrease of τ_0	50 kGy	11,82% decrease of slope
		1,24% decrease of τ at 50 hPa		
		0,65% decrease of τ at 100 hPa		
		0,91% decrease of τ at 150 hPa		
		0,24% decrease of τ at 200 hPa		

C.26.2 Electron Beam Sterilization

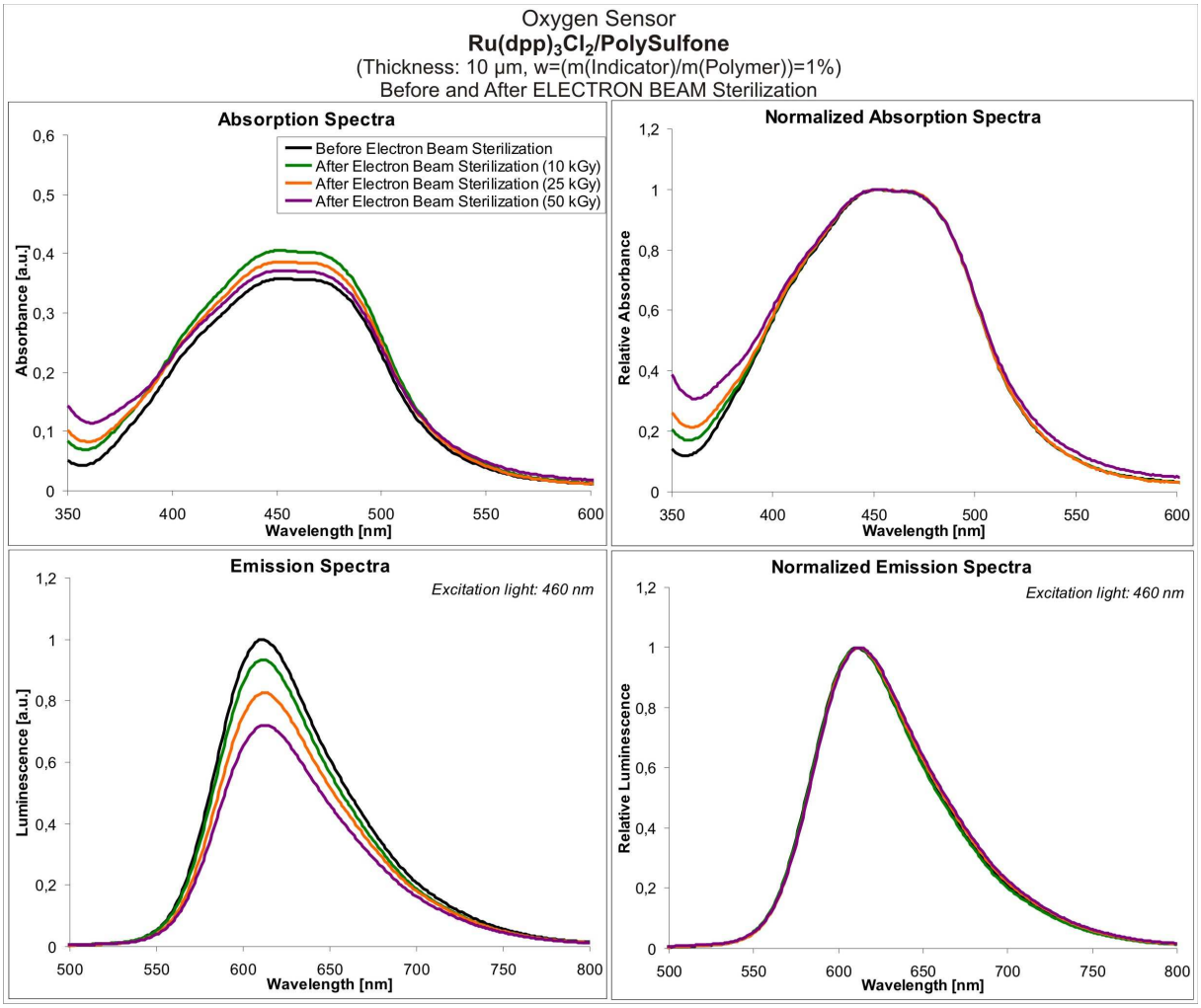

E-BEAM Sterilization	Absorption Spectra		Emission Spectra	
Alterations in Absorption/Emission Intensity	10kGy	9,63% increase	10kGy	6,57% decrease
	25 kGy	7,25% increase	25 kGy	17,37% decrease
	50 kGy	3,51% increase	50 kGy	27,96% decrease
Alterations in Absorption/Emission Curve Form	10kGy	Altered absorption between 350-380 nm.	10kGy	Unaltered.
	25 kGy	Altered absorption between 350-390 nm.	25 kGy	Bathochromic shift of the emission maximum for 1 nm.
	50 kGy	Altered absorption between 350-400 nm and 510-600 nm,	50 kGy	Bathochromic shift of the emission maximum for 1 nm.

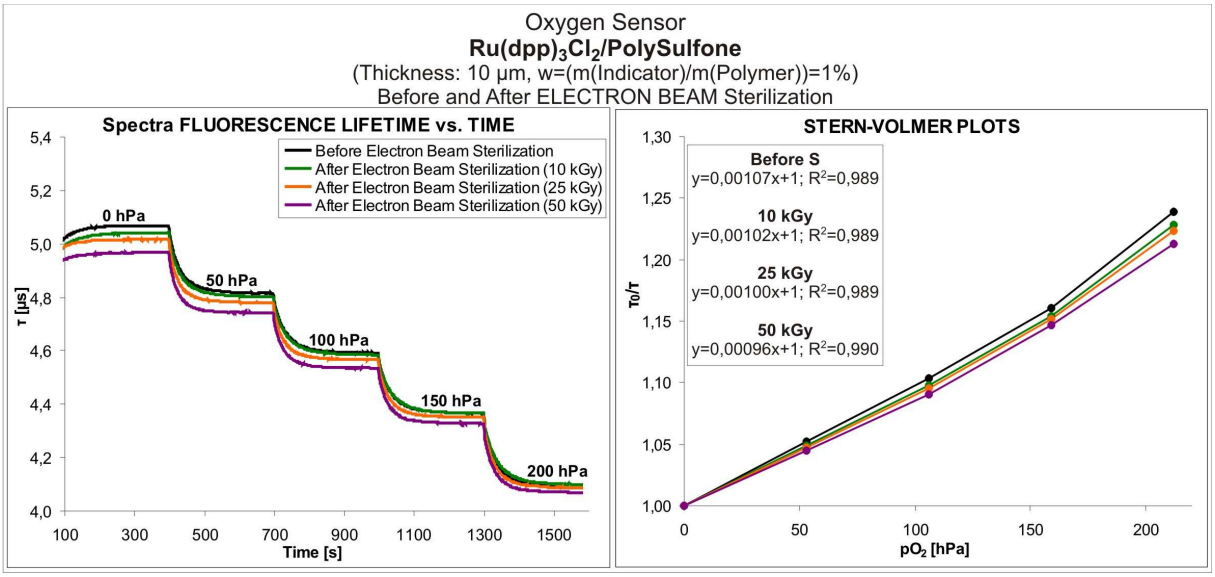

E-BEAM Sterilization	Luminescence Lifetime		Stern-Volmer Plot	
Alterations in Luminescence Lifetime and Slope	10kGy	0,59% decrease of τ_0	10kGy	4,67% decrease of slope
		0,41% decrease of τ at 50 hPa		
		0,22% decrease of τ at 100 hPa		
		0,23% decrease of τ at 150 hPa		
		0,24% increase of τ at 200 hPa		
	25 kGy	1,38% decrease of τ_0	25 kGy	6,54% decrease of slope
		1,04% decrease of τ at 50 hPa		
		0,65% decrease of τ at 100 hPa		
		0,69% decrease of τ at 150 hPa		
		0,24% decrease of τ at 200 hPa		
	50 kGy	2,56% decrease of τ_0	50 kGy	10,28% decrease of slope
		2,07% decrease of τ at 50 hPa		
		1,31% decrease of τ at 100 hPa		
		1,37% decrease of τ at 150 hPa		
		0,49% decrease of τ at 200 hPa		

C.27 Ruthenium(II) DiPhenylPhenanthroline DiChloride ($Ru(dpp)_3Cl_2$) immobilized in PolyPhenyl SilsesQuioxane

C.27.1 Gamma Sterilization

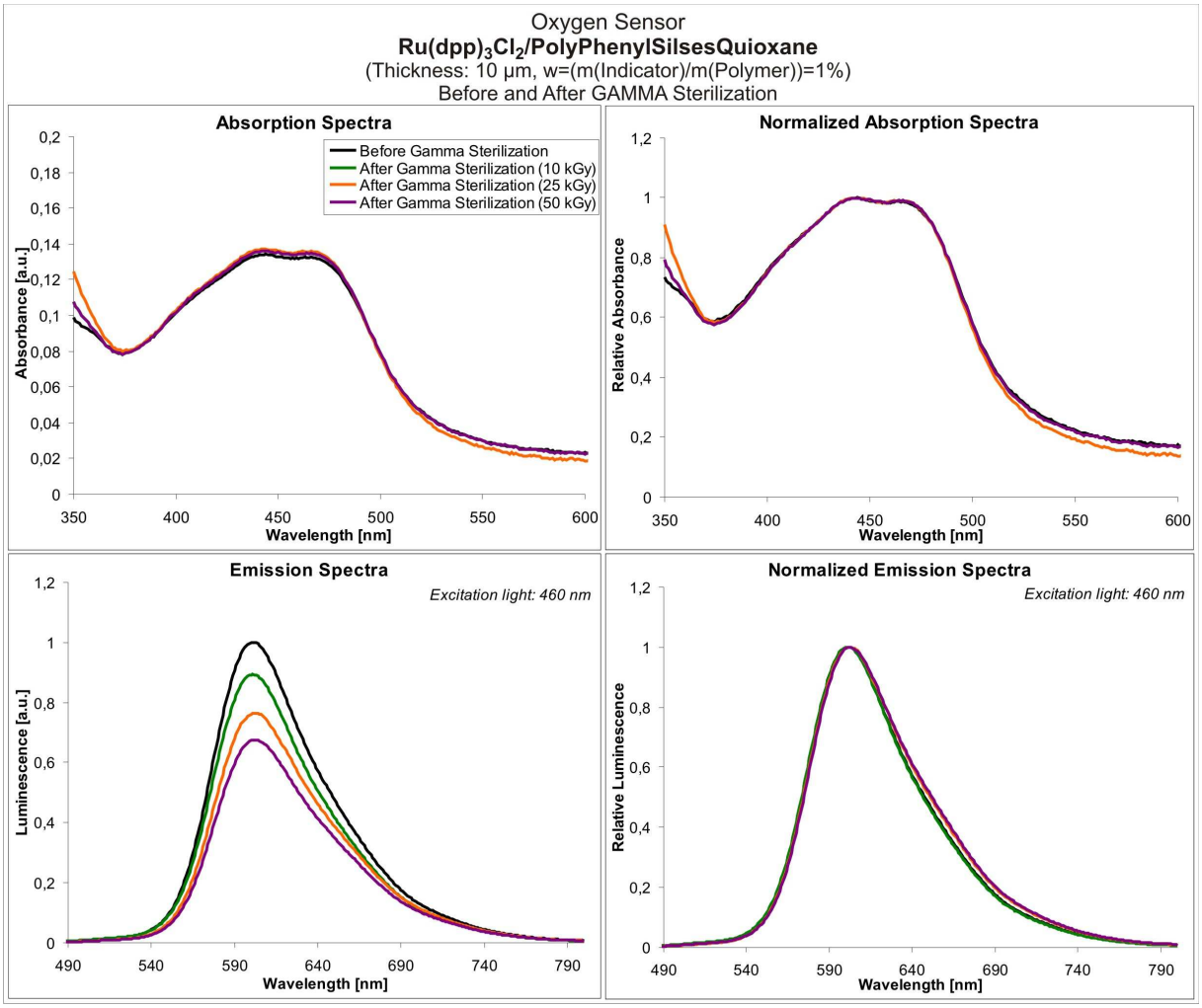

GAMMA Sterilization	Absorption Spectra		Emission Spectra	
Alterations in Absorption/Emission Intensity	10kGy	1,36% increase	10kGy	10,71% decrease
	25 kGy	2,07% increase	25 kGy	23,54% decrease
	50 kGy	1,36% increase	50 kGy	32,40% decrease
Alterations in Absorption/Emission Curve Form	10kGy	Unaltered.	10kGy	Unaltered.
	25 kGy	Unaltered.	25 kGy	Bathochromic shift of the emission maximum for 1 nm.
	50 kGy	Unaltered.	50 kGy	Bathochromic shift of the emission maximum for 1 nm.

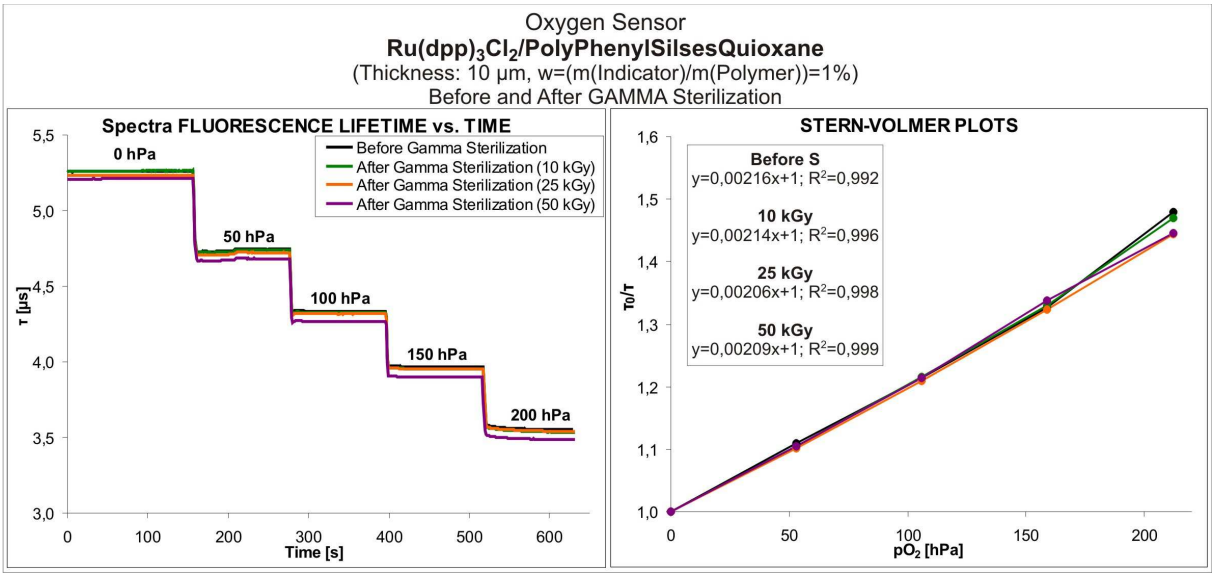

GAMMA Sterilization	Luminescence Lifetime		Stern-Volmer Plot	
Alterations in Luminescence Lifetime and Slope	10kGy	1,14% decrease of τ_0	10kGy	0,93% decrease of slope
		0,62% decrease of τ at 50 hPa		
		1,38% decrease of τ at 100 hPa		
		1,51% decrease of τ at 150 hPa		
		0,56% decrease of τ at 200 hPa		
	25 kGy	2,66% decrease of τ_0	25 kGy	4,63% decrease of slope
		1,90% decrease of τ at 50 hPa		
		2,52% decrease of τ at 100 hPa		
		2,30% decrease of τ at 150 hPa		
		0,84% decrease of τ at 200 hPa		
	50 kGy	4,18% decrease of τ_0	50 kGy	3,24% decrease of slope
		3,80% decrease of τ at 50 hPa		
		4,38% decrease of τ at 100 hPa		
		5,04% decrease of τ at 150 hPa		
		1,97% decrease of τ at 200 hPa		

C.27.2 Electron Beam Sterilization

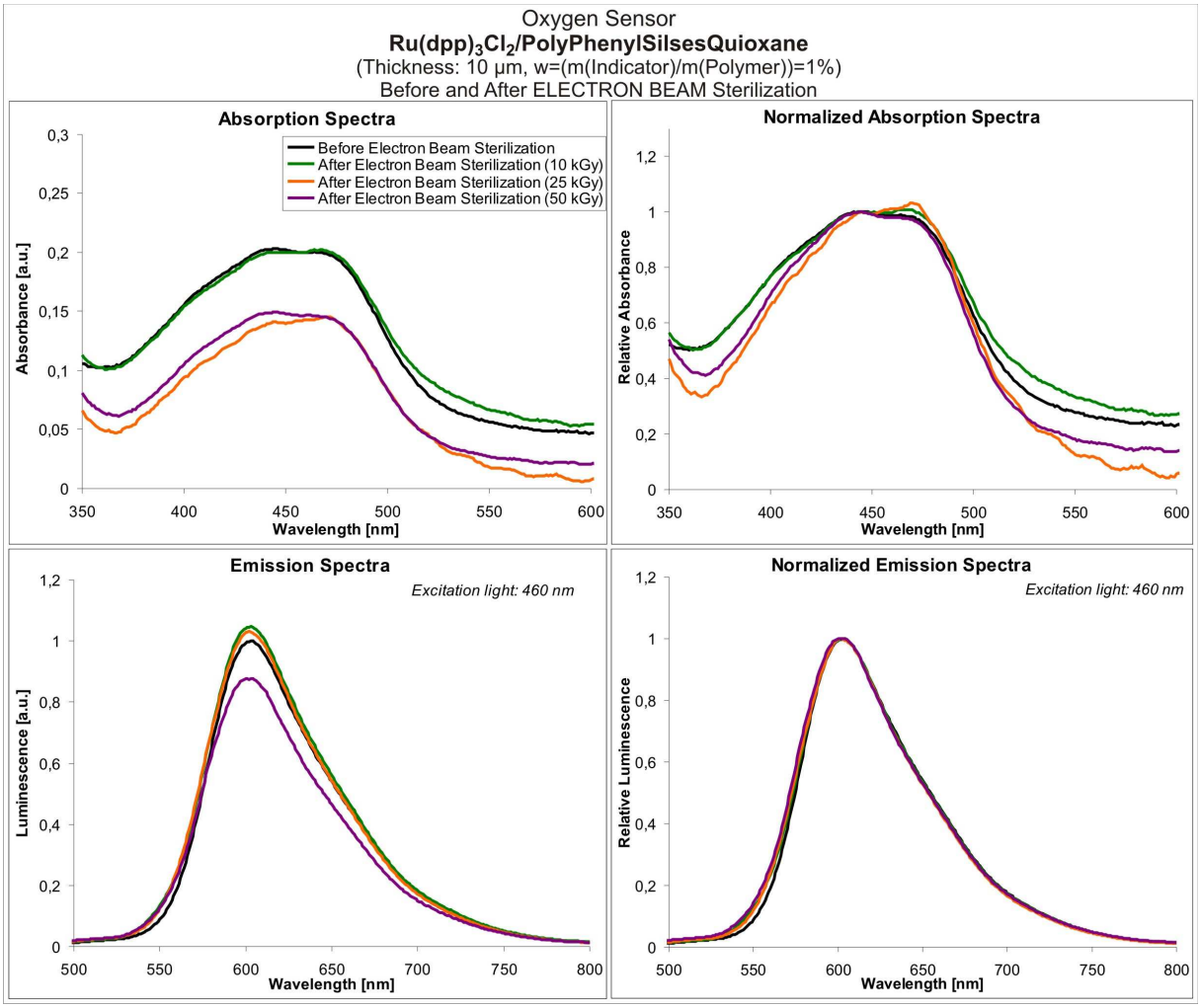

E-BEAM Sterilization	Absorption Spectra		Emission Spectra	
Alterations in Absorption/Emission Intensity	10kGy	1,20% decrease	10kGy	4,47% increase
	25 kGy	30,40% decrease	25 kGy	2,98% increase
	50 kGy	26,22% decrease	50 kGy	12,41% decrease
Alterations in Absorption/Emission Curve Form	10kGy	Altered absorption between 490-800 nm,	10kGy	Unaltered.
	25 kGy	Altered absorption between 350-430 nm and 500-800 nm.	25 kGy	Hypsochromic shift of the emission maximum for 1 nm.
	50 kGy	Altered absorption between 350-425 nm and 500-800 nm,	50 kGy	Hypsochromic shift of the emission maximum for 2 nm.

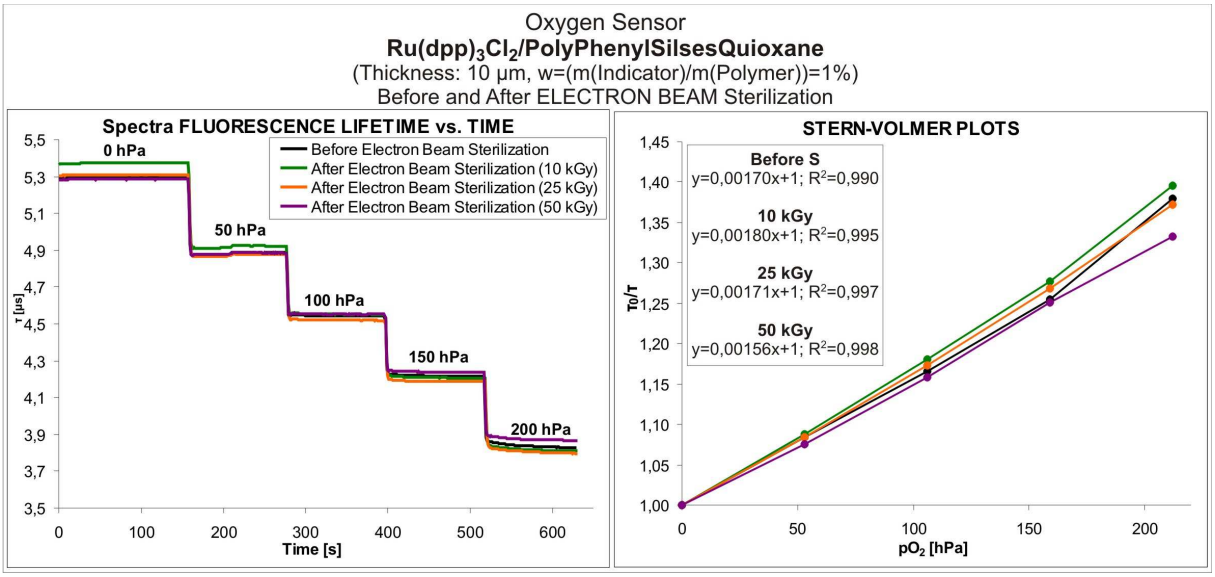

E-BEAM Sterilization	Luminescence Lifetime		Stern-Volmer Plot	
Alterations in Luminescence Lifetime and Slope	10kGy	0,56% increase of τ_0	10kGy	5,55% increase of slope
		0,41% increase of τ at 50 hPa		
		0,66% decrease of τ at 100 hPa		
		0,23% decrease of τ at 150 hPa		
		1,18% decrease of τ at 200 hPa		
	25 kGy	1,51% decrease of τ_0	25 kGy	0,58% increase of slope
		1,43% decrease of τ at 50 hPa		
		1,98% decrease of τ at 100 hPa		
		2,61% decrease of τ at 150 hPa		
		1,04% decrease of τ at 200 hPa		
	50 kGy	2,46% decrease of τ_0	50 kGy	8,23% decrease of slope
		1,84% decrease of τ at 50 hPa		
		2,20% decrease of τ at 100 hPa		
		2,37% decrease of τ at 150 hPa		
		0,77% increase of τ at 200 hPa		

C.28 Ruthenium(II) DiPhenylPhenanthroline DiChloride ($Ru(dpp)_3Cl_2$) immobilized in PolyStyrene

C.28.1 Gamma Sterilization

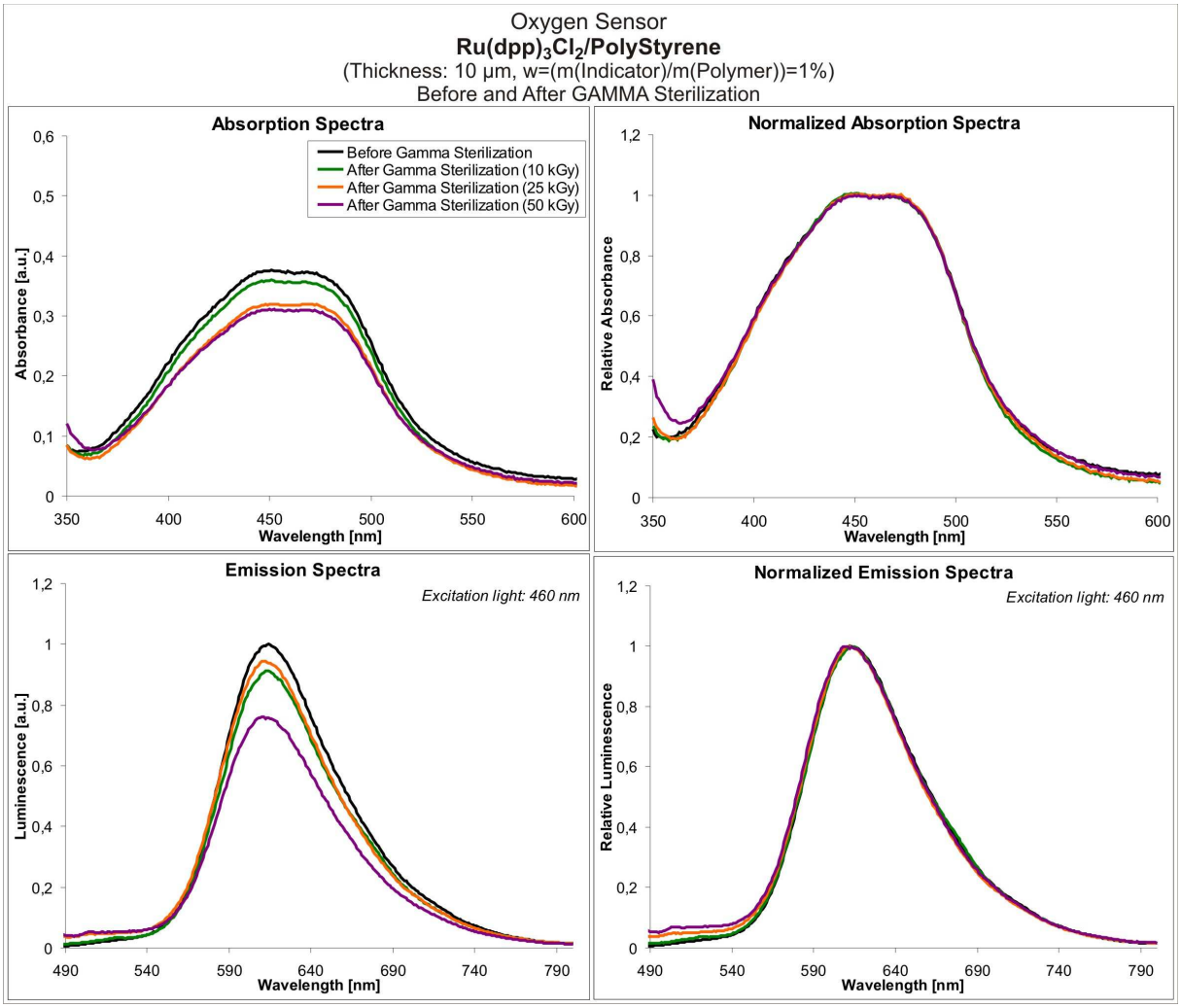

GAMMA Sterilization	Absorption Spectra		Emission Spectra	
Alterations in Absorption/Emission Intensity	10kGy	4,61% decrease	10kGy	8,82% decrease
	25 kGy	14,86% decrease	25 kGy	5,54% decrease
	50 kGy	16,86% decrease	50 kGy	23,92% decrease
Alterations in Absorption/Emission Curve Form	10kGy	Unaltered.	10kGy	Unaltered.
	25 kGy	Unaltered.	25 kGy	Unaltered.
	50 kGy	Altered absorption between 350-390 nm.	50 kGy	Unaltered.

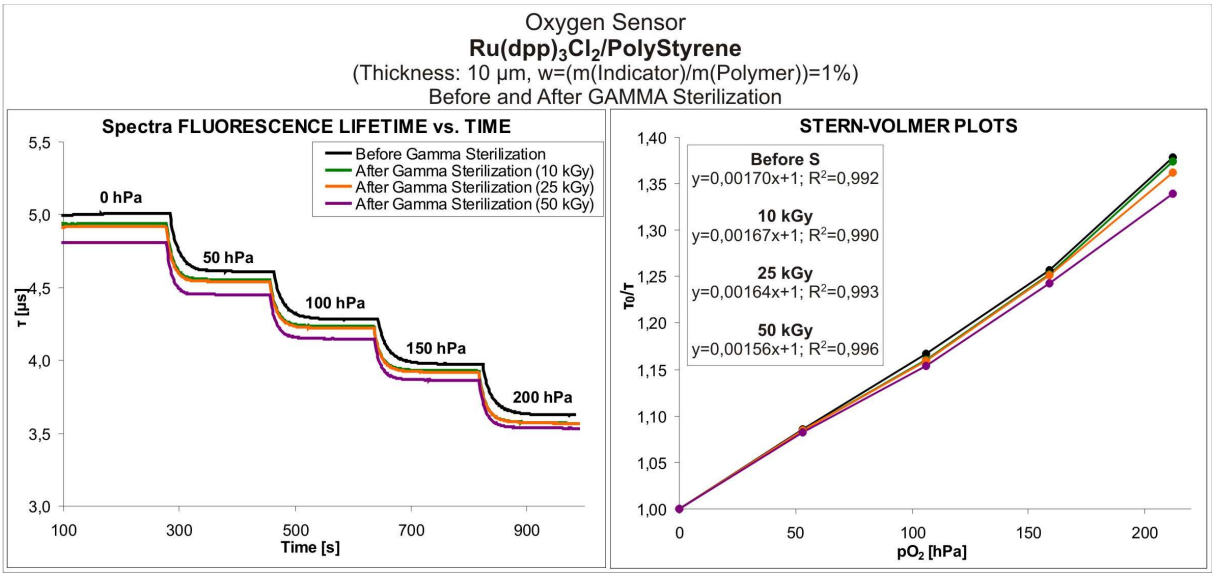

GAMMA Sterilization	Luminescence Lifetime		Stern-Volmer Plot	
Alterations in Luminescence Lifetime and Slope	10kGy	1,80% decrease of τ_0	10kGy	1,76% decrease of slope
		1,95% decrease of τ at 50 hPa		
		1,39% decrease of τ at 100 hPa		
		1,51% decrease of τ at 150 hPa		
		1,65% decrease of τ at 200 hPa		
	25 kGy	2,80% decrease of τ_0	25 kGy	3,53% decrease of slope
		2,82% decrease of τ at 50 hPa		
		2,10% decrease of τ at 100 hPa		
		2,26% decrease of τ at 150 hPa		
		1,93% decrease of τ at 200 hPa		
	50 kGy	5,20% decrease of τ_0	50 kGy	8,23% decrease of slope
		4,99% decrease of τ at 50 hPa		
		4,43% decrease of τ at 100 hPa		
		4,27% decrease of τ at 150 hPa		
		2,48% decrease of τ at 200 hPa		

C.28.2 Electron Beam Sterilization

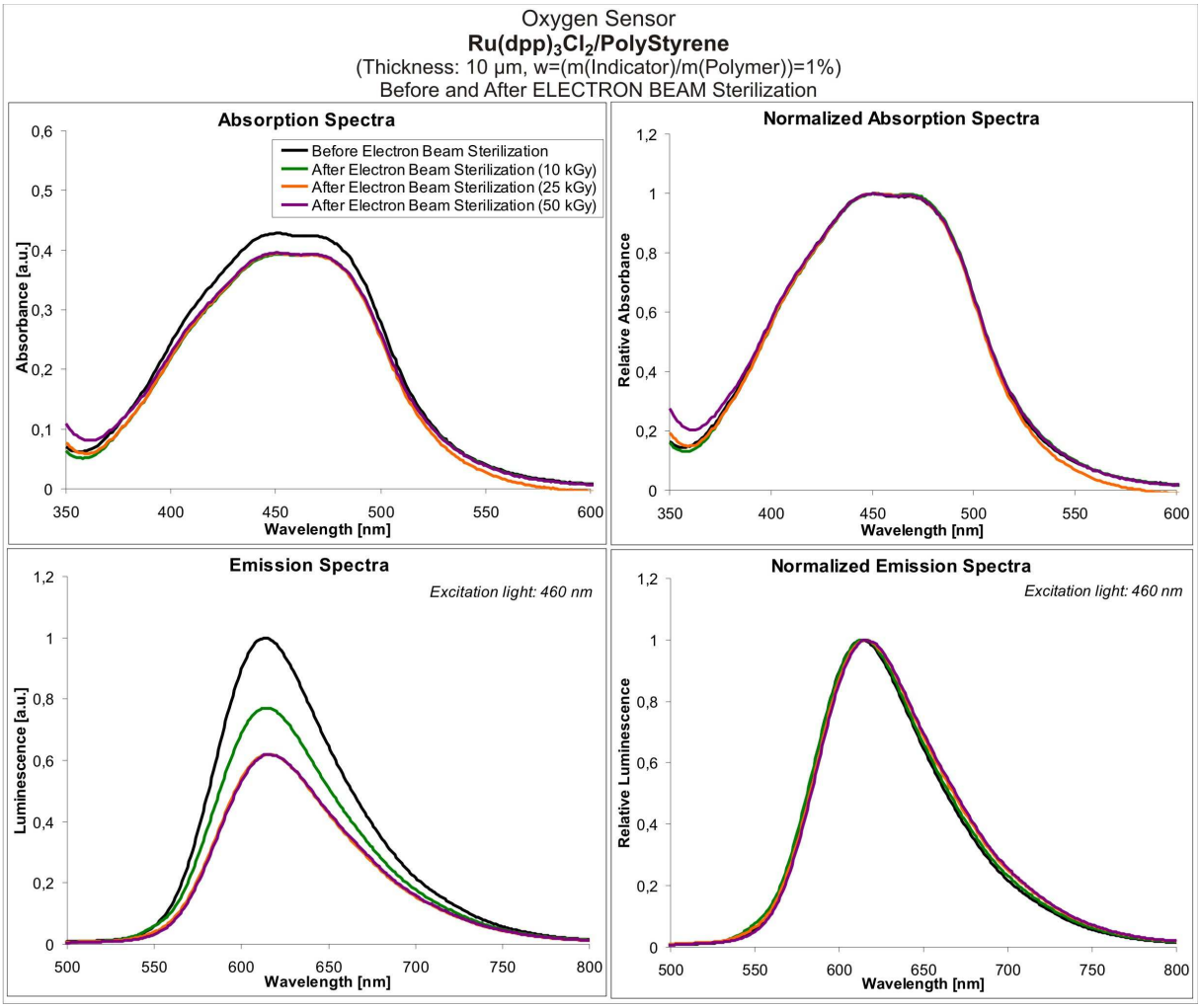

E-BEAM Sterilization	Absorption Spectra		Emission Spectra	
Alterations in Absorption/Emission Intensity	10kGy	8,15% decrease	10kGy	23,05% decrease
	25 kGy	7,87% decrease	25 kGy	37,96% decrease
	50 kGy	7,61% decrease	50 kGy	38,00% decrease
Alterations in Absorption/Emission Curve Form	10kGy	Unaltered.	10kGy	Bathochromic shift of the emission maximum for 1 nm.
	25 kGy	Altered absorption between 530-600 nm.	25 kGy	Bathochromic shift of the emission maximum for 2 nm.
	50 kGy	Altered absorption between 350-380 nm.	50 kGy	Bathochromic shift of the emission maximum for 2 nm..

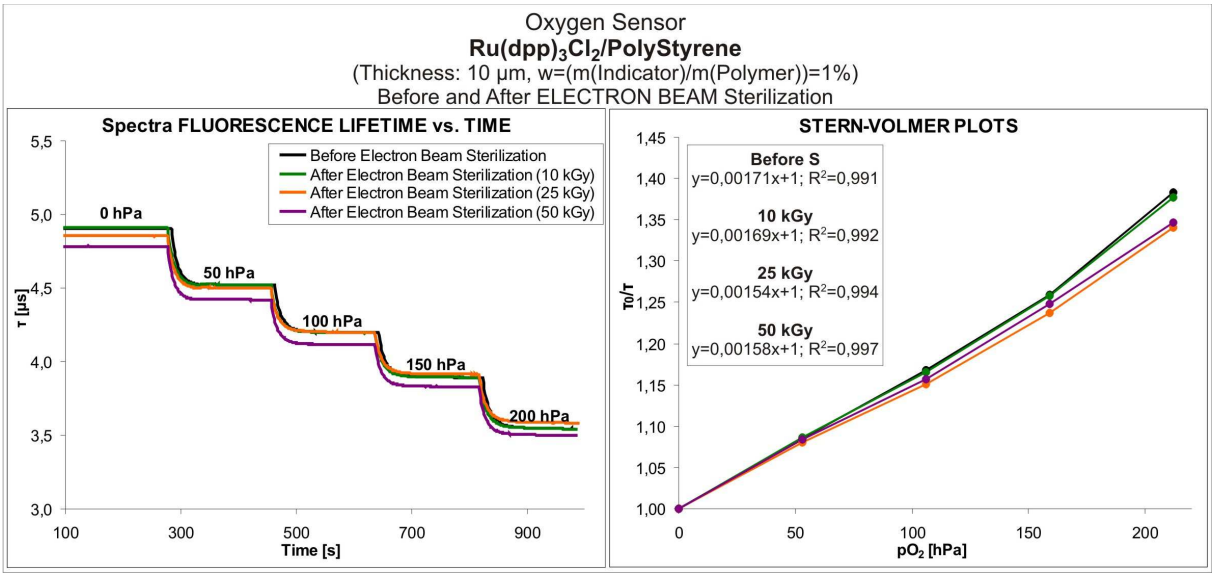

E-BEAM Sterilization	Luminescence Lifetime		Stern-Volmer Plot	
Alterations in Luminescence Lifetime and Slope	10kGy	0,41% decrease of τ_0	10kGy	1,17% decrease of slope
		0,66% decrease of τ at 50 hPa		
		0,24% decrease of τ at 100 hPa		
		0,51% decrease of τ at 150 hPa		
		0,28% decrease of τ at 200 hPa		
	25 kGy	2,04% decrease of τ_0	25 kGy	9,94% decrease of slope
		1,55% decrease of τ at 50 hPa		
		0,48% decrease of τ at 100 hPa		
		0,26% decrease of τ at 150 hPa		
		1,11% increase of τ at 200 hPa		
	50 kGy	3,88% decrease of τ_0	50 kGy	7,60% decrease of slope
		3,76% decrease of τ at 50 hPa		
		3,09% decrease of τ at 100 hPa		
		3,08% decrease of τ at 150 hPa		
		1,41% decrease of τ at 200 hPa		

C.29 Ruthenium(II) DiPhenylPhenanthroline DiChloride ($Ru(dpp)_3Cl_2$) immobilized in PolyStyrene-co-Acrylonitrile

C.29.1 Gamma Sterilization

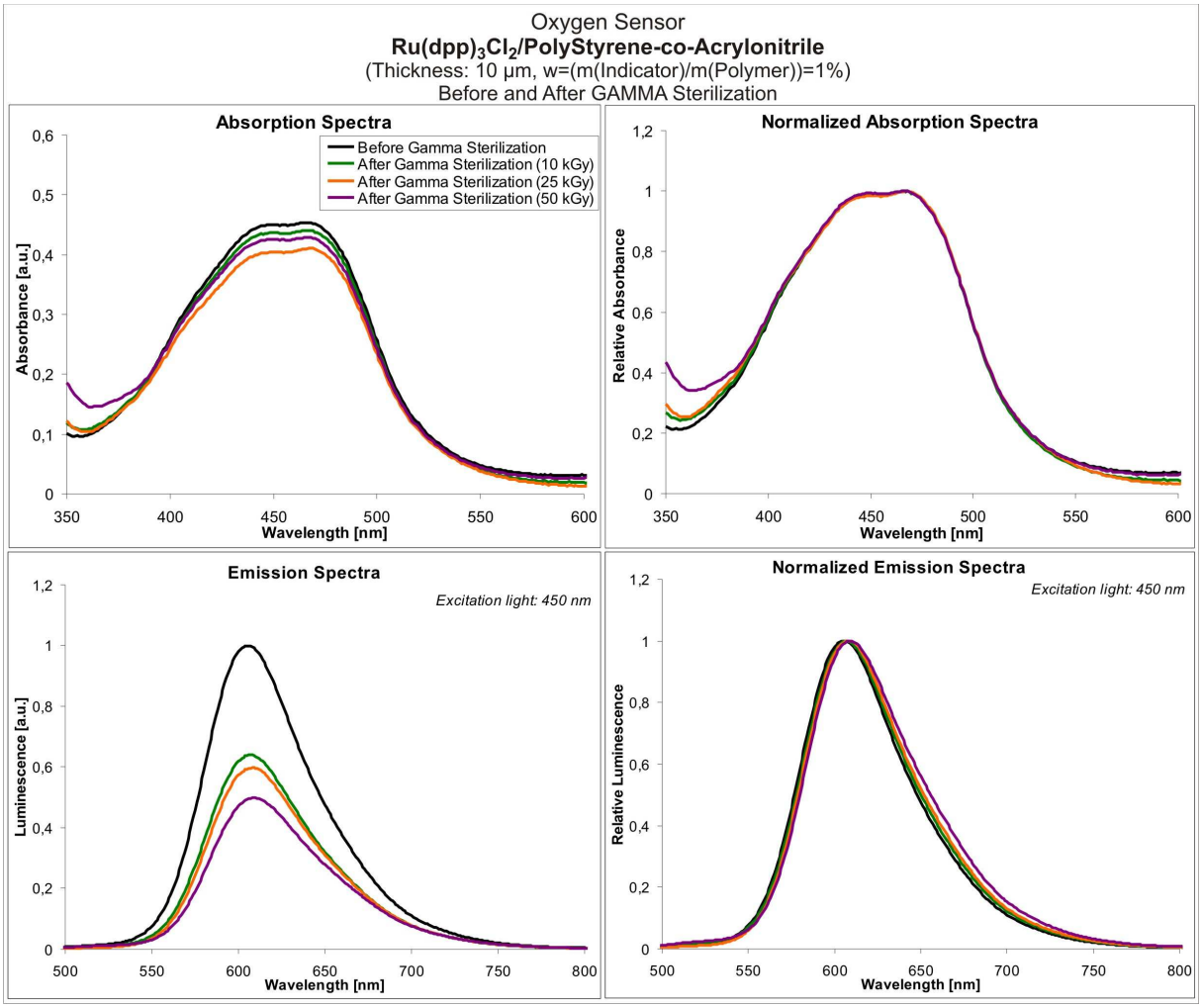

GAMMA Sterilization	Absorption Spectra		Emission Spectra	
Alterations in Absorption/Emission Intensity	10kGy	2,87% decrease	10kGy	35,98% increase
	25 kGy	9,54% decrease	25 kGy	40,26% decrease
	50 kGy	5,61% decrease	50 kGy	50,23% decrease
Alterations in Absorption/Emission Curve Form	10kGy	Unaltered.	10kGy	Bathochromic shift of the emission maximum for 2 nm.
	25 kGy	Unaltered.	25 kGy	Bathochromic shift of the emission maximum for 4 nm.
	50 kGy	Altered absorption between 350-390 nm.	50 kGy	Bathochromic shift of the emission maximum for 5 nm.

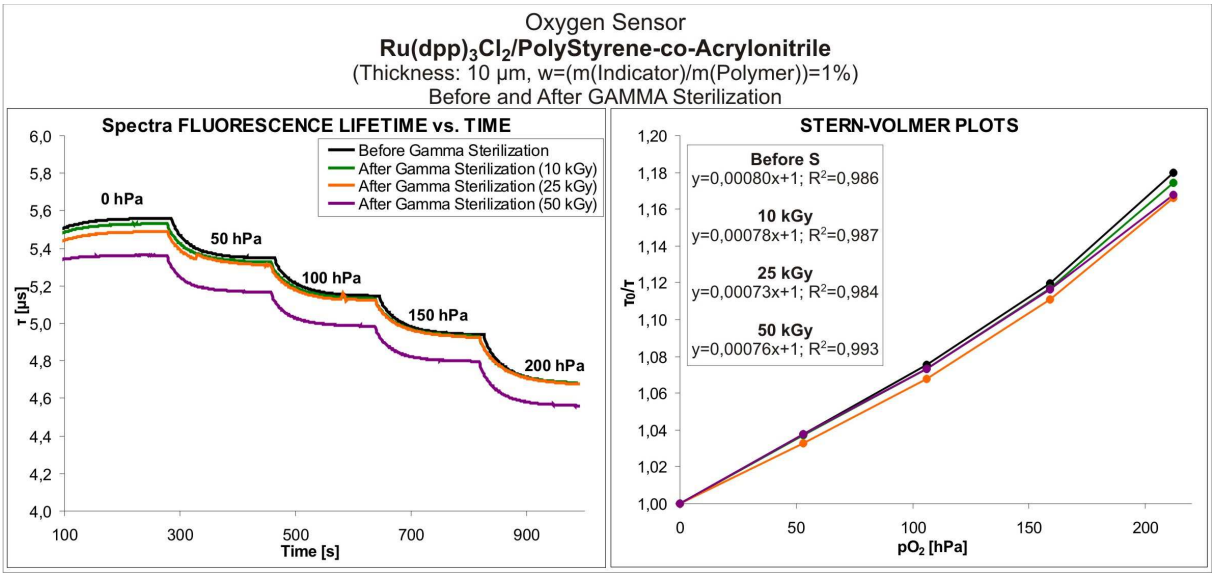

GAMMA Sterilization	Luminescence Lifetime		Stern-Volmer Plot	
Alterations in Luminescence Lifetime and Slope	10kGy	0,54% decrease of τ_0	10kGy	2,50% decrease of slope
		0,56% decrease of τ at 50 hPa		
		0,39% decrease of τ at 100 hPa		
		0,40% decrease of τ at 150 hPa		
		0,21% decrease of τ at 200 hPa		
	25 kGy	1,44% decrease of τ_0	25 kGy	8,75% decrease of slope
		0,93% decrease of τ at 50 hPa		
		0,78% decrease of τ at 100 hPa		
		0,81% decrease of τ at 150 hPa		
		0,42% decrease of τ at 200 hPa		
	50 kGy	3,96% decrease of τ_0	50 kGy	5,00% decrease of slope
		3,92% decrease of τ at 50 hPa		
		3,68% decrease of τ at 100 hPa		
		3,63% decrease of τ at 150 hPa		
		2,97% decrease of τ at 200 hPa		

C.29.2 Electron Beam Sterilization

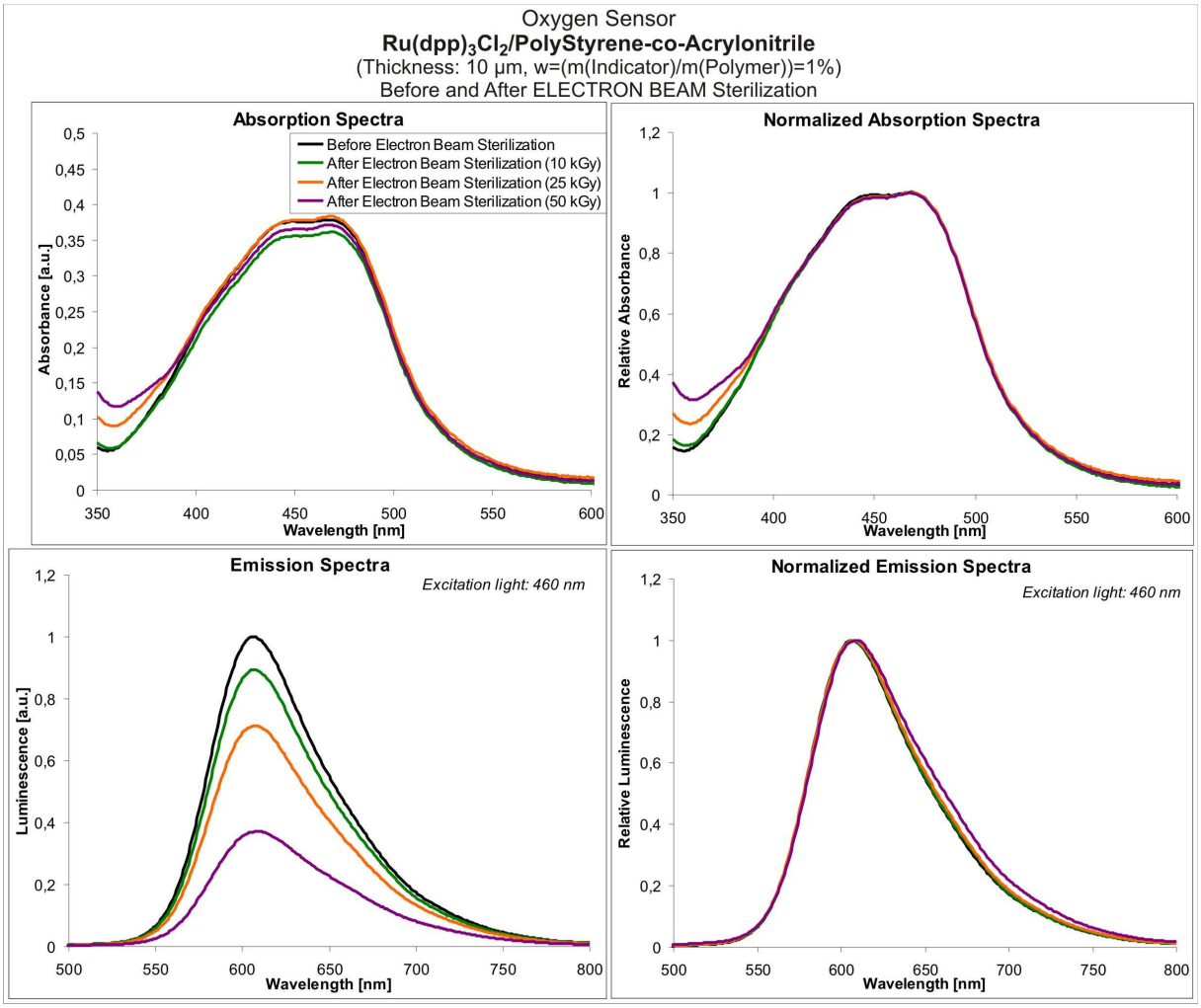

E-BEAM Sterilization	Absorption Spectra		Emission Spectra	
Alterations in Absorption/Emission Intensity	10kGy	4,76% decrease	10kGy	23,05% decrease
	25 kGy	1,09% increase	25 kGy	37,96% decrease
	50 kGy	1,87% decrease	50 kGy	38,00% decrease
Alterations in Absorption/Emission Curve Form	10kGy	Unaltered.	10kGy	Unaltered.
	25 kGy	Unaltered.	25 kGy	Unaltered.
	50 kGy	Altered absorption between 350-390 nm,	50 kGy	Bathochromic shift of the emission maximum for 3 nm.

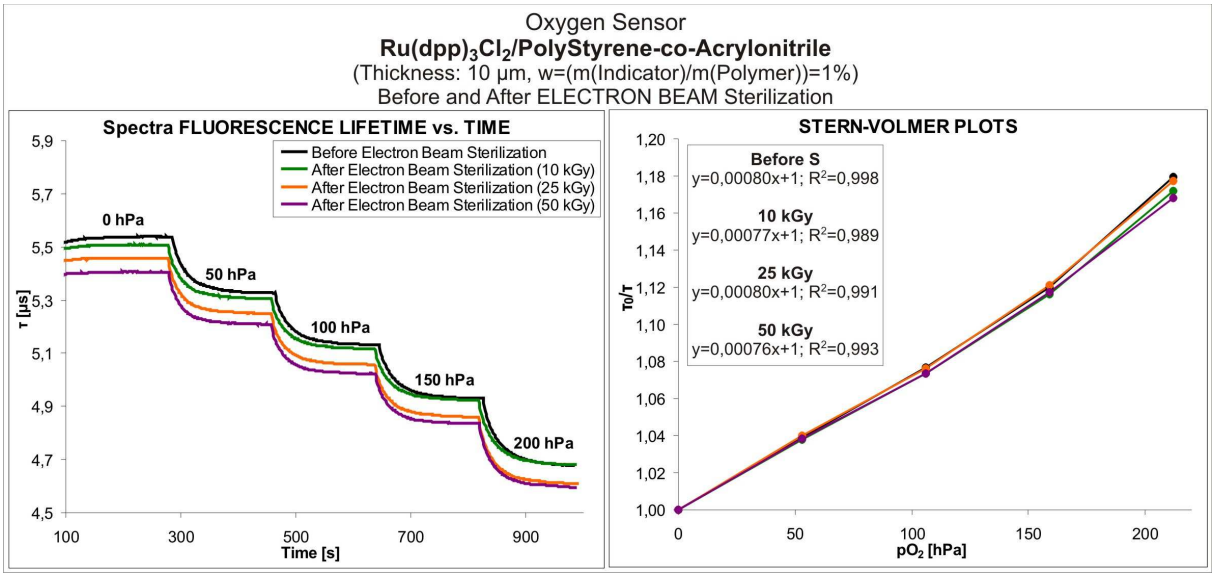

E-BEAM Sterilization	Luminescence Lifetime		Stern-Volmer Plot	
Alterations in Luminescence Lifetime and Slope	10kGy	0,72% decrease of τ_0	10kGy	3,76% decrease of slope
		0,56% decrease of τ at 50 hPa		
		0,39% decrease of τ at 100 hPa		
		0,20% decrease of τ at 150 hPa		
		0,21% decrease of τ at 200 hPa		
	25 kGy	1,80% decrease of τ_0	25 kGy	0,25% decrease of slope
		2,81% decrease of τ at 50 hPa		
		1,75% decrease of τ at 100 hPa		
		1,82% decrease of τ at 150 hPa		
		1,49% decrease of τ at 200 hPa		
	50 kGy	2,89% decrease of τ_0	50 kGy	4,76% decrease of slope
		2,81% decrease of τ at 50 hPa		
		2,53% decrease of τ at 100 hPa		
		2,63% decrease of τ at 150 hPa		
		1,92% decrease of τ at 200 hPa		

C.30 Ruthenium(II) DiPhenylPhenanthroline DiChloride ($Ru(dpp)_3Cl_2$) immobilized in PolyStyrene-co-MaleicAnhydride (PSMA93)

C.30.1 Gamma Sterilization

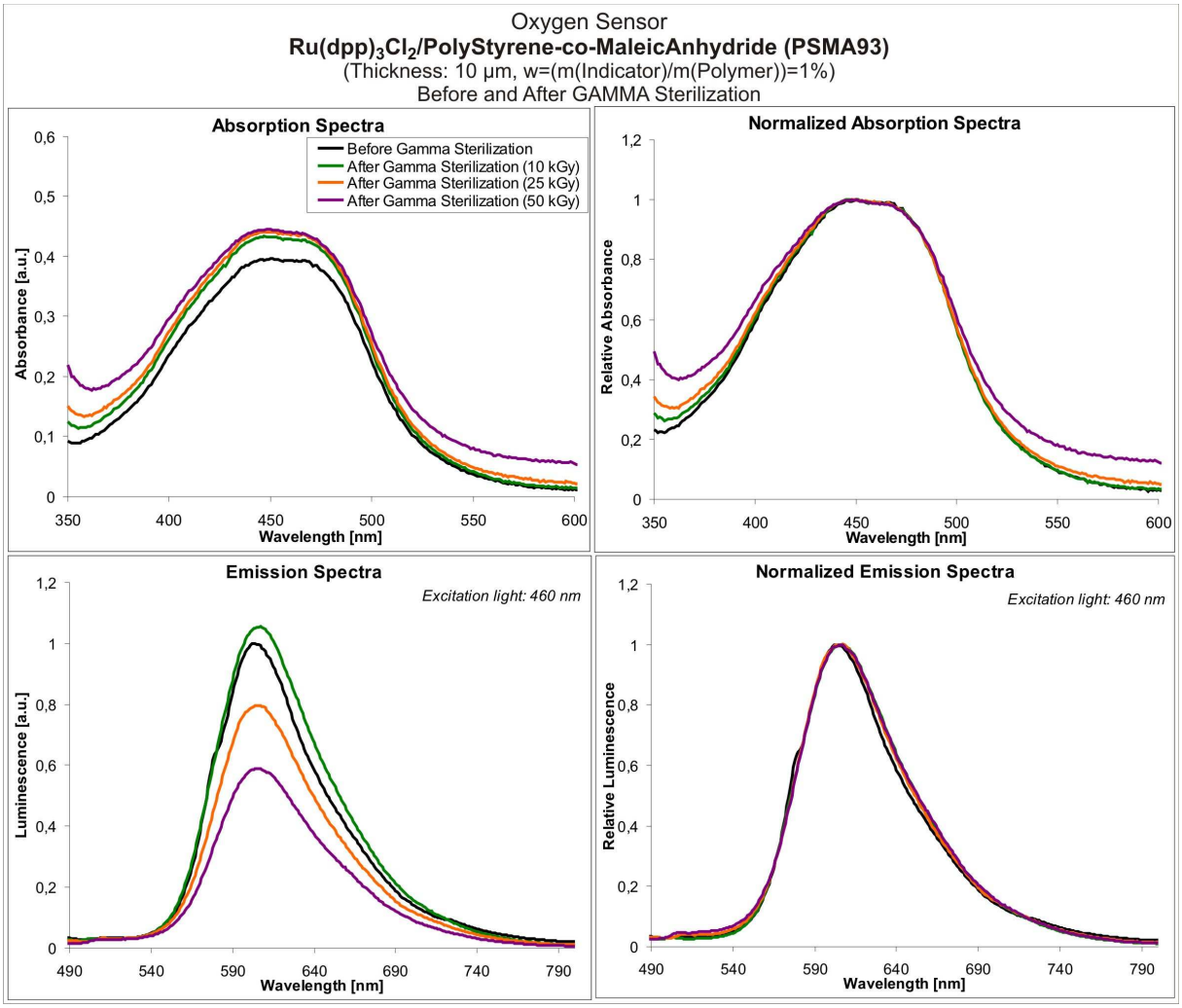

GAMMA Sterilization	Absorption Spectra		Emission Spectra	
Alterations in Absorption/Emission Intensity	10kGy	9,12% increase	10kGy	5,49% increase
	25 kGy	11,23% increase	25 kGy	20,46% decrease
	50 kGy	12,29% increase	50 kGy	40,98% decrease
Alterations in Absorption/Emission Curve Form	10kGy	Altered absorption between 350-370 nm,	10kGy	Bathochromic shift of the emission maximum for 4 nm.
	25 kGy	Altered absorption between 350-385 nm,	25 kGy	Bathochromic shift of the emission maximum for 3 nm.
	50 kGy	Altered absorption between 350-420 nm and 500-800 nm.	50 kGy	Bathochromic shift of the emission maximum for 3 nm.

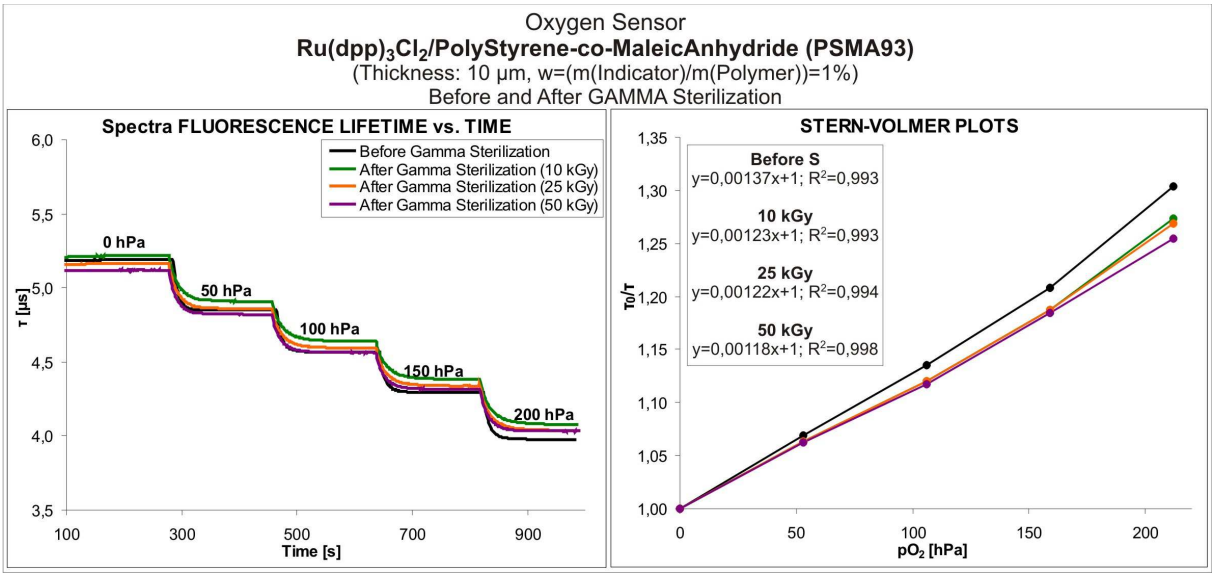

GAMMA Sterilization	Luminescence Lifetime		Stern-Volmer Plot	
Alterations in Luminescence Lifetime and Slope	10kGy	0,19% increase of τ_0	10kGy	10,22% decrease of slope
		0,82% increase of τ at 50 hPa		
		1,51% increase of τ at 100 hPa		
		1,83% increase of τ at 150 hPa		
		2,45% increase of τ at 200 hPa		
	25 kGy	1,16% decrease of τ_0	25 kGy	10,95% decrease of slope
		0,62% decrease of τ at 50 hPa		
		0,22% increase of τ at 100 hPa		
		0,46% increase of τ at 150 hPa		
		1,48% increase of τ at 200 hPa		
	50 kGy	2,50% decrease of τ_0	50 kGy	13,87% decrease of slope
		1,86% decrease of τ at 50 hPa		
		0,88% decrease of τ at 100 hPa		
		0,70% decrease of τ at 150 hPa		
		1,24% increase of τ at 200 hPa		

C.30.2 Electron Beam Sterilization

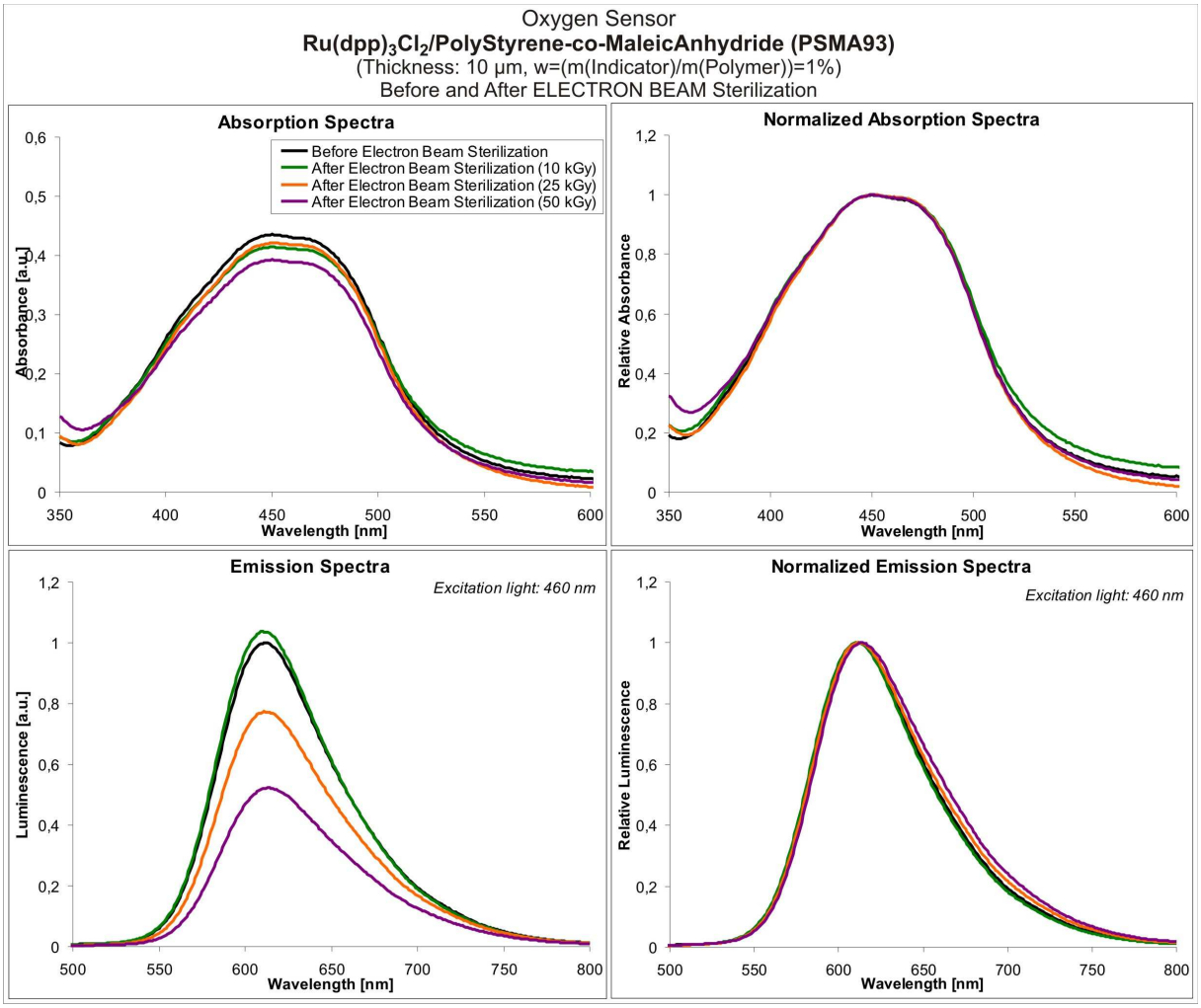

E-BEAM Sterilization	Absorption Spectra		Emission Spectra	
Alterations in Absorption/Emission Intensity	10kGy	4,76% decrease	10kGy	3,59% increase
	25 kGy	3,26% decrease	25 kGy	22,63% decrease
	50 kGy	9,50% decrease	50 kGy	47,71% decrease
Alterations in Absorption/Emission Curve Form	10kGy	Altered absorption between 510-800 nm,	10kGy	Unaltered.
	25 kGy	Altered absorption between 540-800 nm,	25 kGy	Unaltered.
	50 kGy	Altered absorption between 350-380 nm,	50 kGy	Bathochromic shift of the emission maximum for 3 nm.

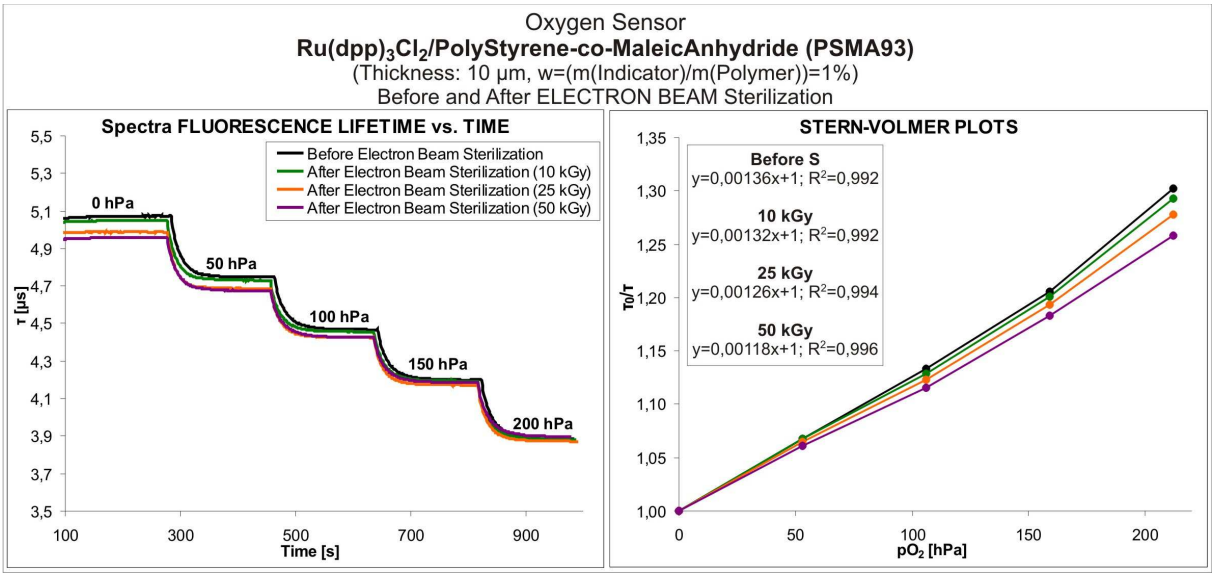

E-BEAM Sterilization	Luminescence Lifetime		Stern-Volmer Plot	
Alterations in Luminescence Lifetime and Slope	10kGy	0,79% decrease of τ_0	10kGy	2,94% decrease of slope
		0,84% decrease of τ at 50 hPa		
		0,45% decrease of τ at 100 hPa		
		0,48% decrease of τ at 150 hPa		
		0,26% decrease of τ at 200 hPa		
	25 kGy	2,37% decrease of τ_0	25 kGy	7,35% decrease of slope
		2,11% decrease of τ at 50 hPa		
		1,34% decrease of τ at 100 hPa		
		1,43% decrease of τ at 150 hPa		
		0,51% decrease of τ at 200 hPa		
	50 kGy	3,16% decrease of τ_0	50 kGy	13,14% decrease of slope
		2,53% decrease of τ at 50 hPa		
		1,56% decrease of τ at 100 hPa		
		1,66% decrease of τ at 150 hPa		
		0,26% increase of τ at 200 hPa		

Optical pH SENSORS

C.31 HPTS(DHA$_3$) immobilized in HydroGel D4

C.31.1 Gamma Sterilization

Absorption Spectra

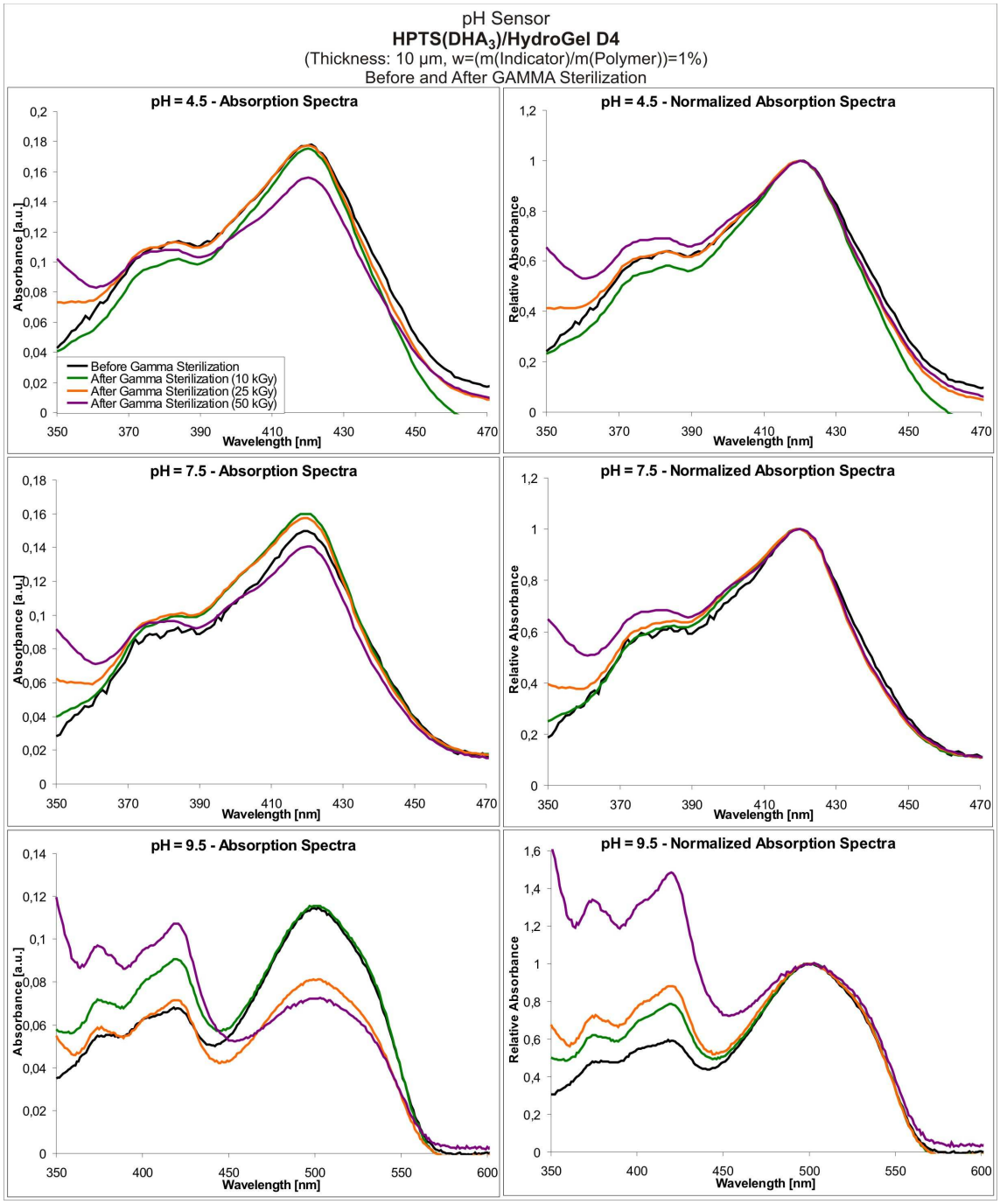

Emission Spectra

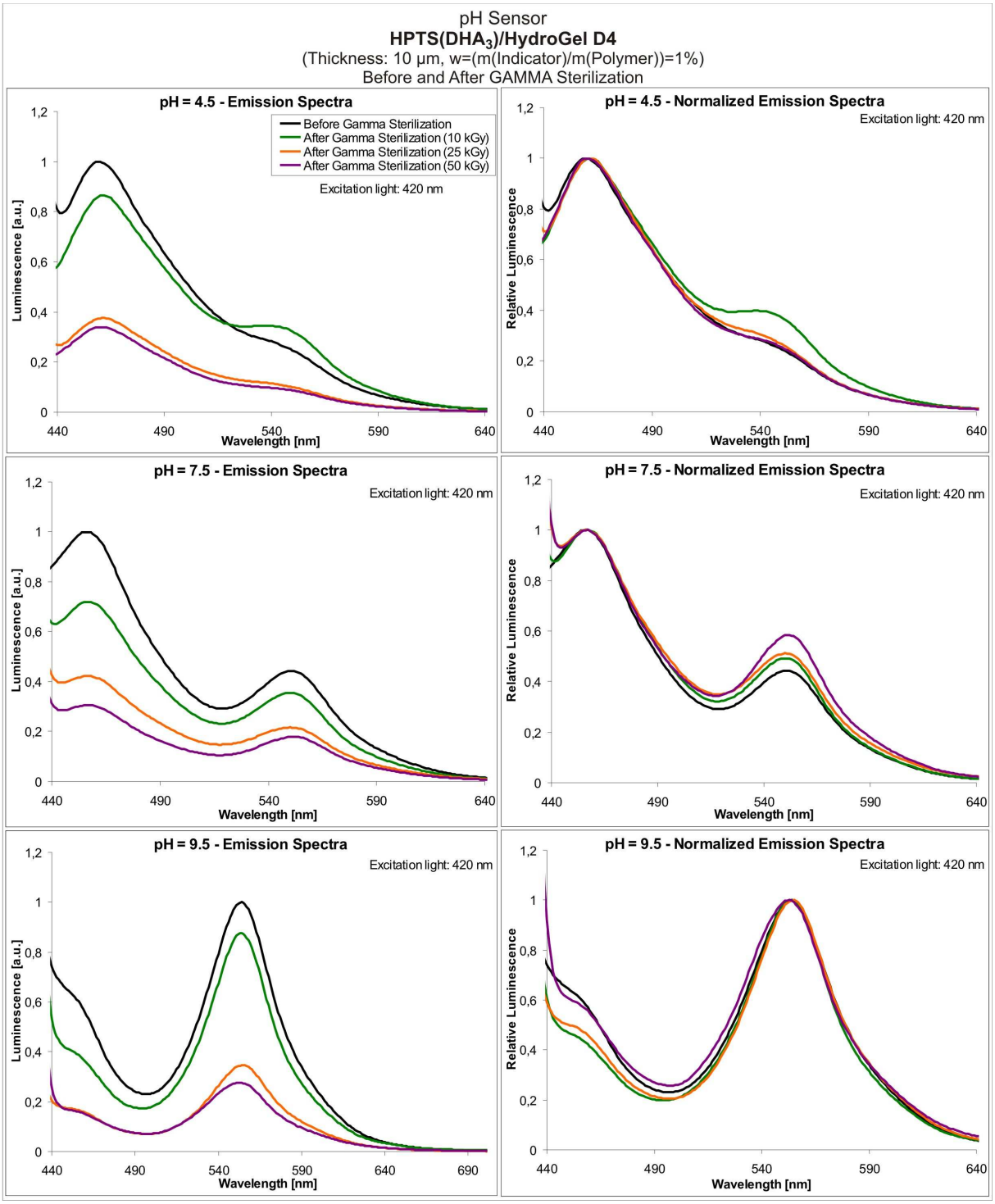

GAMMA S.	Absorption Spectra			Emission Spectra		
		pH	Alterations		pH	Alterations
Alterations in Absorption/ Emission Intensity	10 kGy	4.5	1,52% decrease	10 kGy	4.5	13,42% decrease
		7.5	6,34% increase		7.5	27,97% decrease
		9.5	0,74% increase		9.5	12,48% decrease
	25 kGy	4.5	0,27% decrease	25 kGy	4.5	62,50% decrease
		7.5	4,85% increase		7.5	57,78% decrease
		9.5	29,18% decrease		9.5	65,38% decrease
	50 kGy	4.5	12,20% decrease	50 kGy	4.5	66,03% decrease
		7.5	5,98% decrease		7.5	69,36% decrease
		9.5	36,75% decrease		9.5	72,31% decrease

Alterations in Absorption/ Emission Curve Form	10 kGy	4.5	Unaltered	10 kGy	4.5	The ratio between protonation/deprotonation emission peaks is altered..
		7.5	Unaltered		7.5	The ratio between protonation/deprotonation emission peaks is altered.
		9.5	The ratio between protonation/deprotonation absorption peaks is altered.		9.5	Altered emission between 440-530 nm.
	25 kGy	4.5	Increased absorption between 350-365 nm.	25 kGy	4.5	Unaltered
		7.5	Increased absorption between 350-375 nm.		7.5	The ratio between protonation/deprotonation emission peaks is altered.
		9.5	The ratio between protonation/deprotonation absorption peaks is altered.		9.5	Altered emission between 440-530 nm.
	50 kGy	4.5	Increased absorption between 350-400 nm.	50 kGy	4.5	Unaltered
		7.5	Increased absorption between 350-400 nm.		7.5	The ratio between protonation/deprotonation emission peaks is altered.
		9.5	The ratio between protonation/deprotonation absorption peaks is altered.		9.5	Altered emission between 440-540 nm.

Calibration Curves

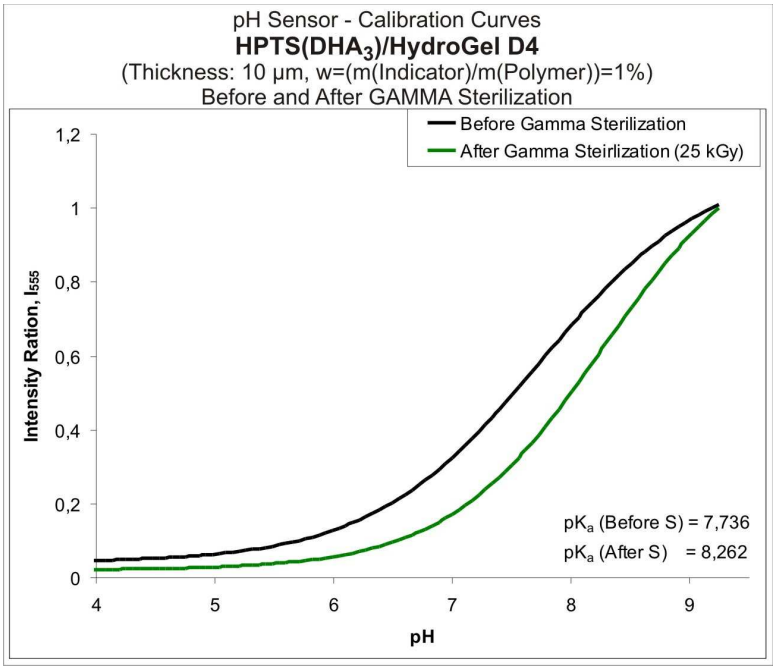

GAMMA S.	Alterations in Calibration Curve Shape	Alterations in pK_a
	Altered curve shape after sterilization. The response to the proton still observed – re-calibration of sensor response.	Increase of pK_a (for 0,526)

C.31.1.1 Sterilization in Buffer Solution

Absorption Spectra

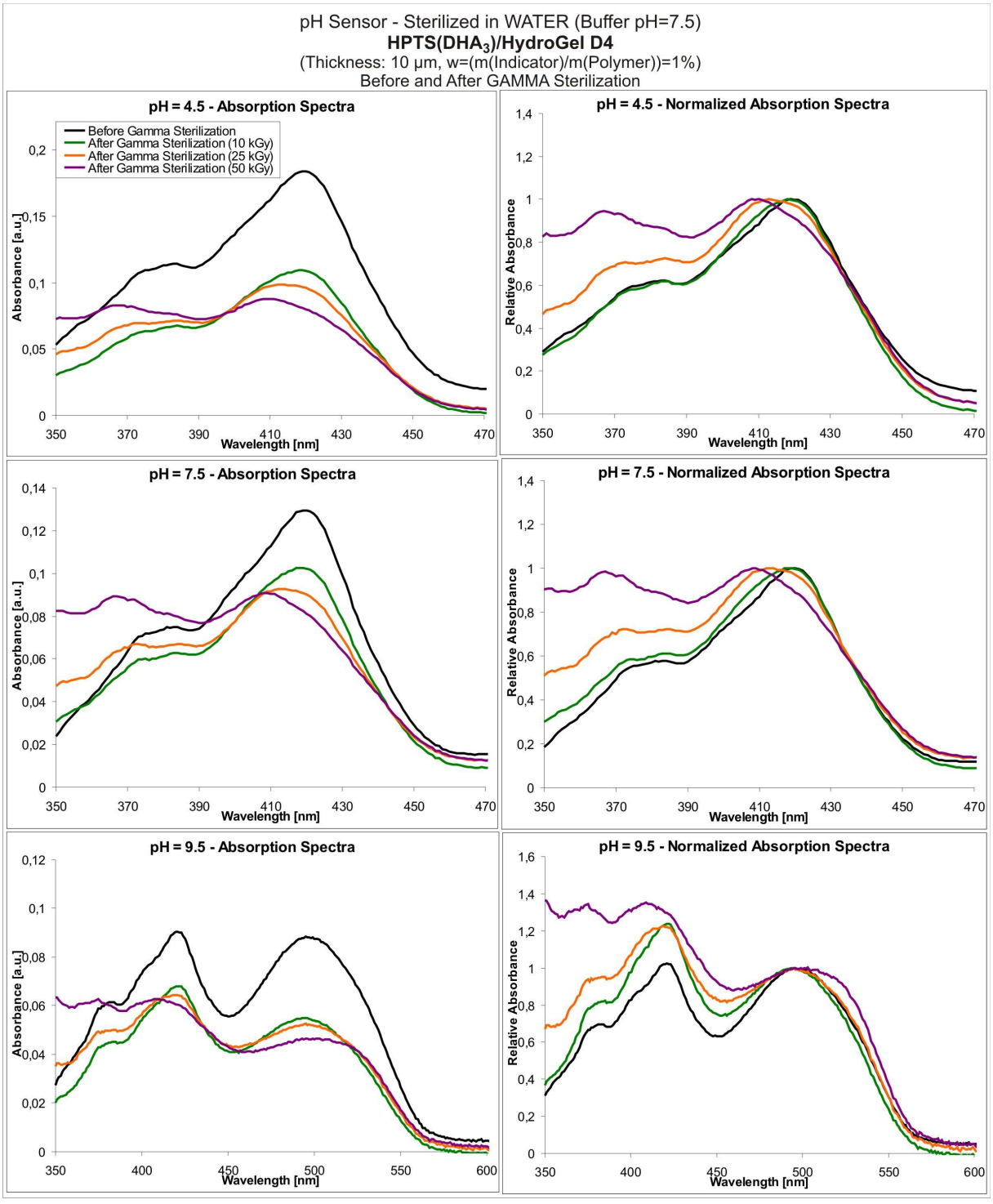

Emission Spectra

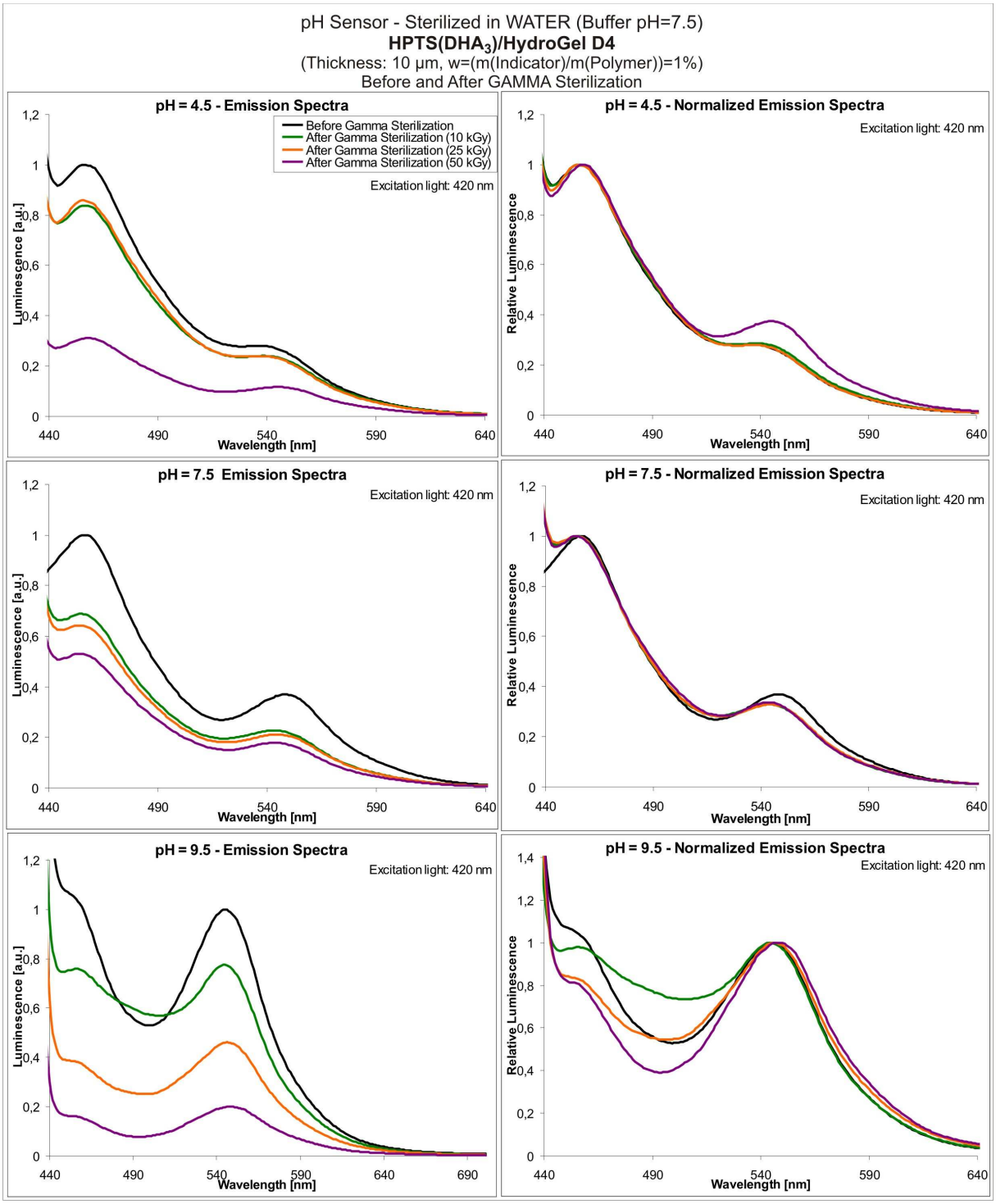

GAMMA S.	Absorption Spectra			Emission Spectra		
		pH	Alterations		pH	Alterations
Alterations in Absorption/ Emission Intensity	10 kGy	4.5	40,58% decrease	10 kGy	4.5	16,16% decrease
		7.5	20,72% decrease		7.5	31,15% decrease
		9.5	37,74% decrease		9.5	22,45% decrease
	25 kGy	4.5	46,26% decrease	25 kGy	4.5	14,21% decrease
		7.5	28,33% decrease		7.5	35,75% decrease
		9.5	40,44% decrease		9.5	53,90% decrease
	50 kGy	4.5	52,12% decrease	50 kGy	4.5	68,92% decrease
		7.5	29,74% decrease		7.5	46,91% decrease
		9.5	47,31% decrease		9.5	80,06% decrease

Alterations in Absorption/ Emission Curve Form	10 kGy	4.5	Unaltered	10 kGy	4.5	Unaltered
		7.5	Altered absorption curve form between 350-415 nm.		7.5	The ratio between protonation/deprotonation emission peaks is slightly altered.
		9.5	Altered absorption curve form between 350-490 nm.		9.5	Altered emission curve form between 440-530 nm.
	25 kGy	4.5	Altered absorption curve form between 350-365 nm. Hypsochromic shift of the absorption maximum for 7 nm.	25 kGy	4.5	Unaltered
		7.5	Altered absorption curve form between 350-415 nm Hypsochromic shift of the absorption maximum for 6 nm.		7.5	The ratio between protonation/deprotonation emission peaks is slightly altered.
		9.5	Altered absorption curve form between 350-490 nm.		9.5	Altered emission curve form between 440-530 nm. Bathochromic shift of the absorption maximum for 1 nm.
	50 kGy	4.5	Altered absorption curve form between 350-415 nm Hypsochromic shift of the absorption maximum for 12 nm.	50 kGy	4.5	The ratio between protonation/deprotonation emission peaks is altered.
		7.5	Altered absorption curve form between 350-415 nm Hypsochromic shift of the absorption maximum for 10 nm.		7.5	The ratio between protonation/deprotonation emission peaks is slightly altered.
		9.5	Altered absorption curve form between 350-490 nm and 505-550 nm.		9.5	Altered emission curve form between 440-535 nm. Bathochromic shift of the absorption maximum for 1 nm.

Calibration Curves

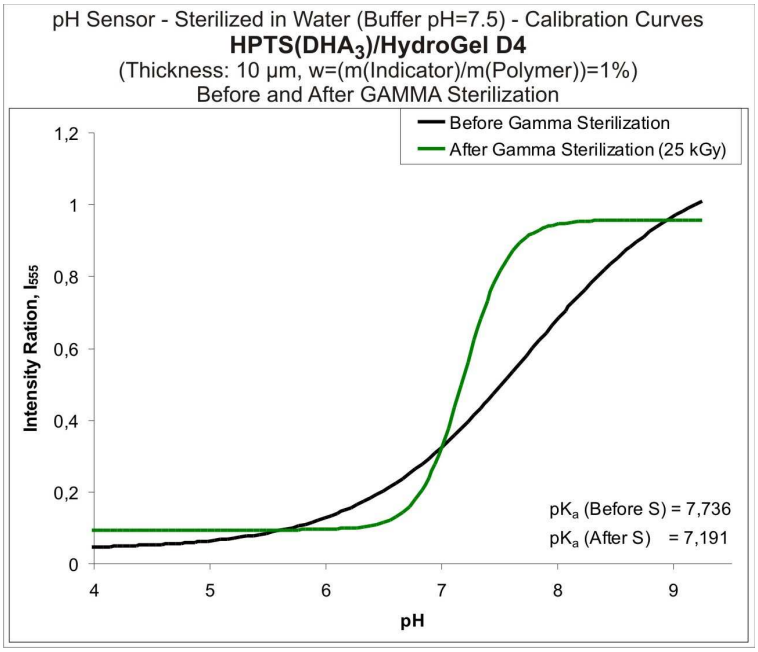

GAMMA S.	Alterations in Calibration Curve Shape	Alterations in pK_a
	Altered curve shape after sterilization. The response to the proton still observed – re-calibration of sensor response.	Decrease of pK_a (for 0,545)

C.31.2 Electron Beam Sterilization

Absorption Spectra

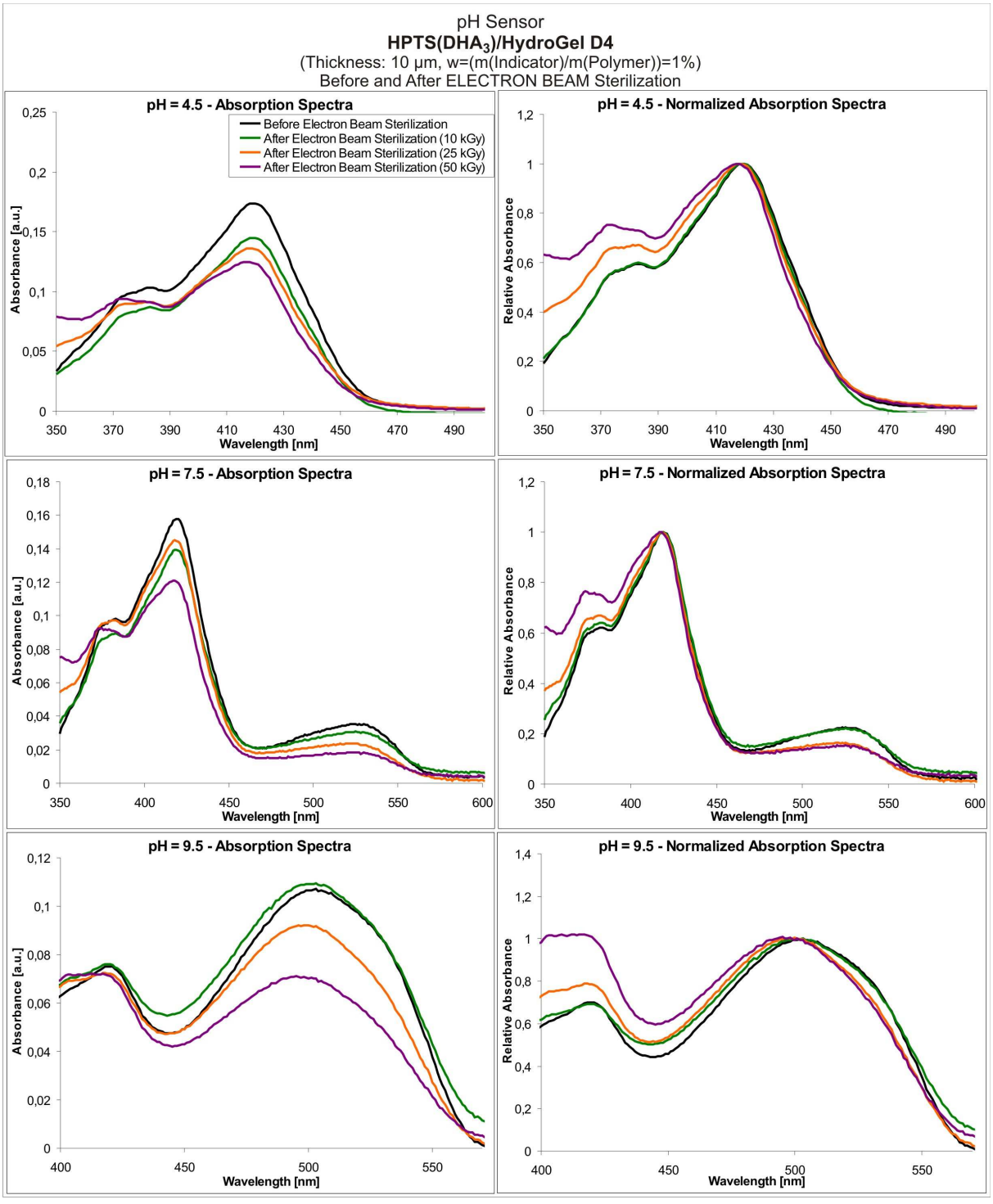

Emission Spectra

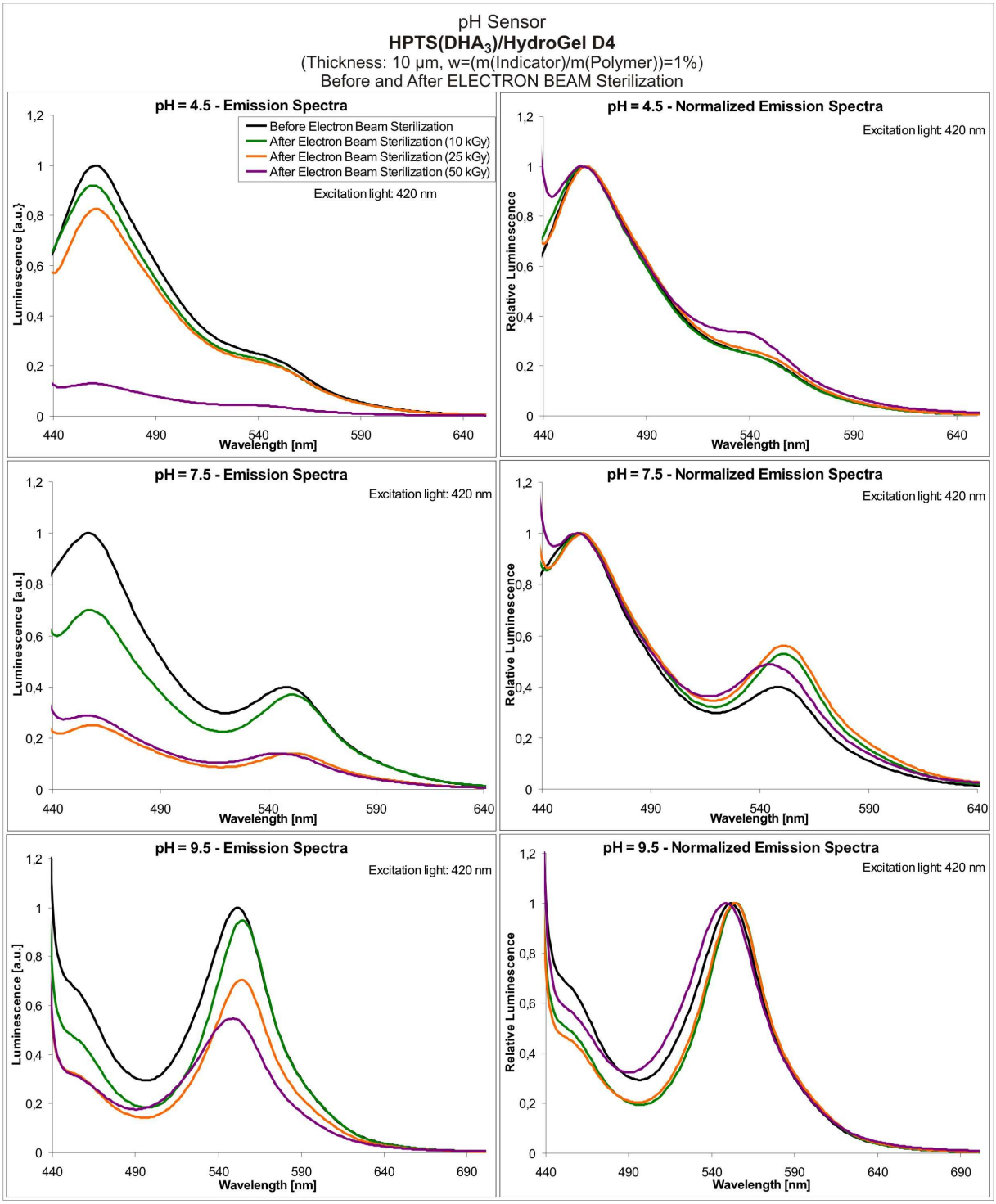

E-BEAM S.	Absorption Spectra			Emission Spectra		
		pH	Alterations		pH	Alterations
Alterations in Absorption/ Emission Intensity	10 kGy	4.5	16,55% decrease	10 kGy	4.5	7,96% decrease
		7.5	11,56% decrease		7.5	30,02% decrease
		9.5	2,17% increase		9.5	5,26% decrease
	25 kGy	4.5	21,56% decrease	25 kGy	4.5	17,32% decrease
		7.5	7,88% decrease		7.5	74,85% decrease
		9.5	14,21% decrease		9.5	29,69% decrease
	50 kGy	4.5	28,06% decrease	50 kGy	4.5	87,00% decrease
		7.5	23,21% decrease		7.5	71,20% decrease
		9.5	34,12% decrease		9.5	45,30% decrease

Alterations in Absorption/ Emission Curve Form	10 kGy	4.5	Unaltered	10 kGy	4.5	Unaltered.
		7.5	Unaltered		7.5	The ratio between protonation/deprotonation emission peaks is altered.
		9.5	Altered absorption curve form between 430-495 nm.		9.5	Bathochromic shift of the emission maximum for 3 nm.
	25 kGy	4.5	Altered absorption curve form between 350-415 nm.	25 kGy	4.5	Unaltered
		7.5	Altered absorption curve form between 350-415 nm. The ratio between protonation/deprotonation absorption peaks is altered.		7.5	The ratio between protonation/deprotonation emission peaks is altered.
		9.5	Altered absorption curve form between 350-445 nm. Hypsochromic shift of the absorption maximum for 2 nm.		9.5	Bathochromic shift of the emission maximum for 3 nm.
	50 kGy	4.5	Altered absorption curve form between 350-415 nm. Hypsochromic shift of the absorption maximum for 2 nm.	50 kGy	4.5	Altered emission curve form between 505-575 nm.
		7.5	Altered absorption curve form between 350-415 nm. The ratio between protonation/deprotonation absorption peaks is altered. Hypsochromic shift of the absorption maximum for 2 nm.		7.5	The ratio between protonation/deprotonation emission peaks is altered.
		9.5	Altered absorption curve form between 350-475 nm. Hypsochromic shift of the absorption maximum for 5 nm.		9.5	Hypsochromic shift of the absorption maximum for 2 nm.

Calibration Curves

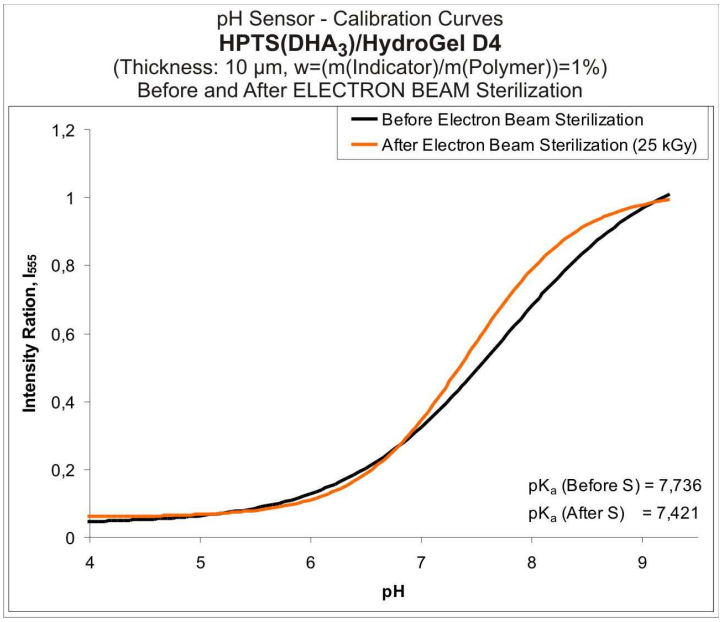

E-BEAM S.	Alterations in Calibration Curve Shape	Alterations in pK_a
	Comparable curve shapes before and after sterilization.	Decrease of pK_a (for 0,315)

C.31.2.1 Sterilization in Water

Absorption Spectra

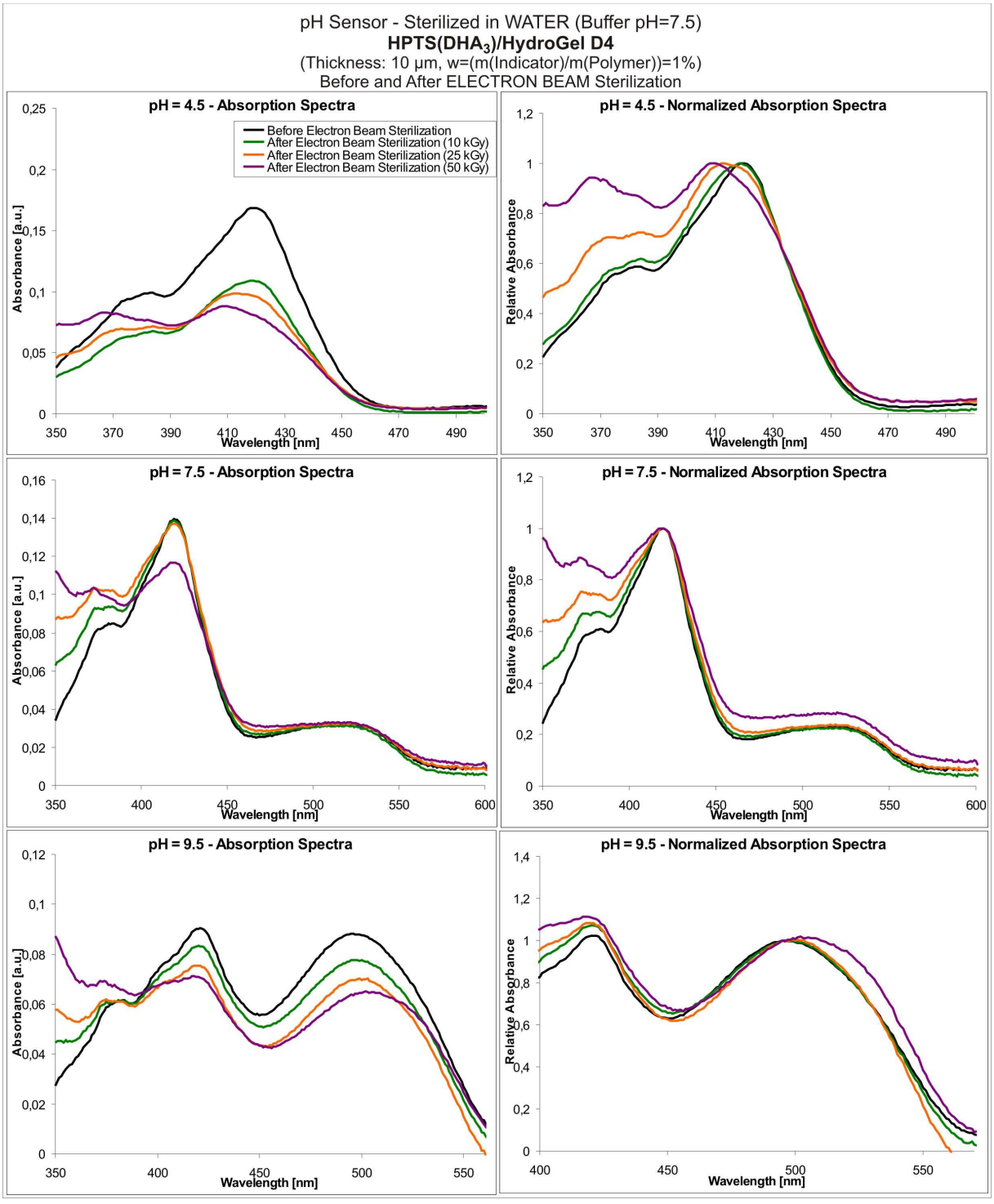

Emission Spectra

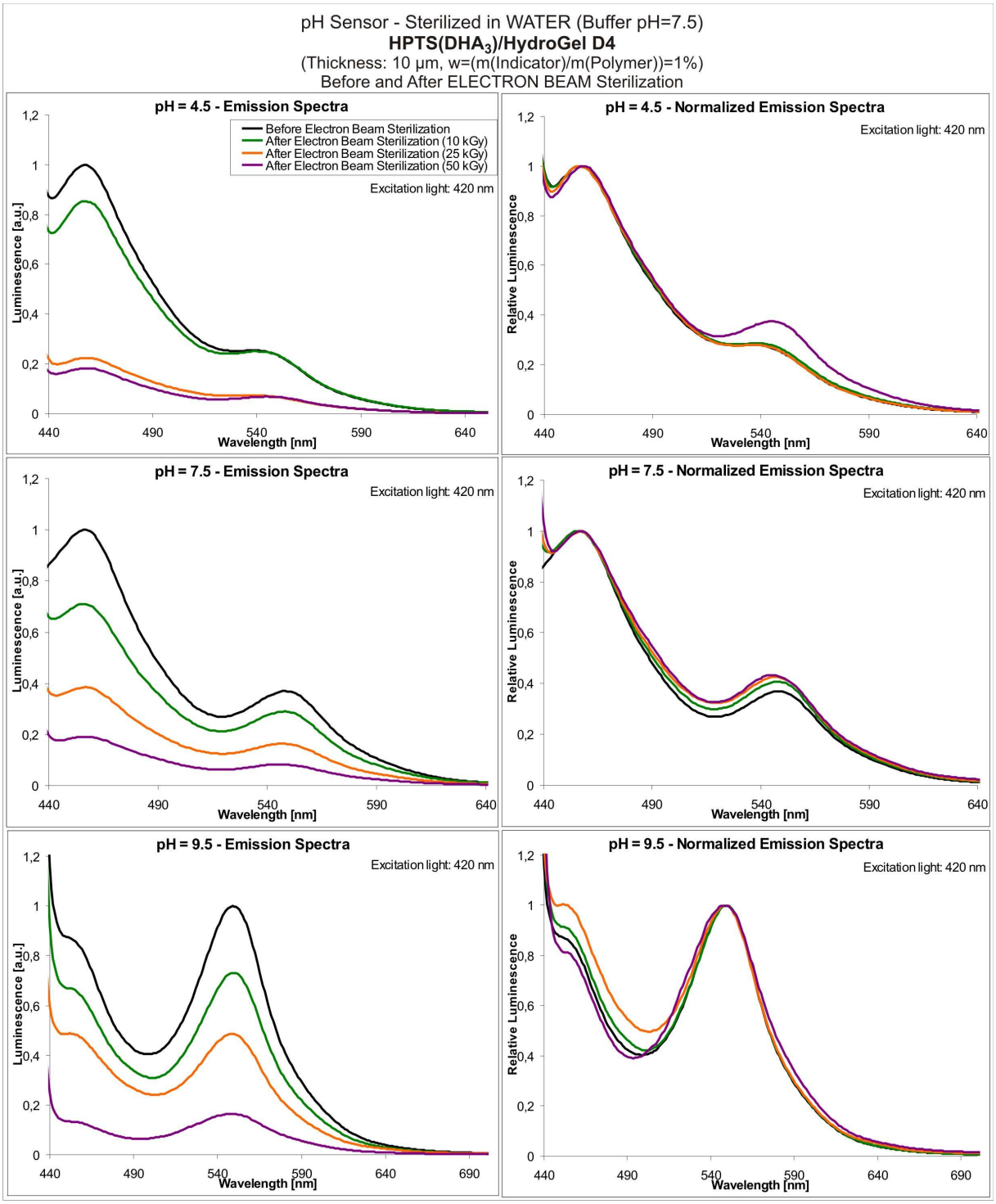

E-BEAM S.	Absorption Spectra			Emission Spectra		
		pH	Alterations		pH	Alterations
Alterations in Absorption/ Emission Intensity	10 kGy	4.5	35,23% decrease	10 kGy	4.5	14,64% decrease
		7.5	0,59% decrease		7.5	29,05% decrease
		9.5	12,03% decrease		9.5	26,83% decrease
	25 kGy	4.5	41,47% decrease	25 kGy	4.5	77,63% decrease
		7.5	1,68% decrease		7.5	61,48% decrease
		9.5	21,03% decrease		9.5	39,81% decrease
	50 kGy	4.5	47,86% decrease	50 kGy	4.5	81,73% decrease
		7.5	16,31% decrease		7.5	80,85% decrease
		9.5	27,74% decrease		9.5	83,60% decrease

Alterations in Absorption/ Emission Curve Form	10 kGy	4.5	Unaltered	10 kGy	4.5	The ratio between protonation/deprotonation emission peaks is altered.
		7.5	Altered absorption curve form between 350-410 nm.		7.5	The ratio between protonation/deprotonation emission peaks is altered.
		9.5	The ratio between protonation/deprotonation absorption peaks is altered.		9.5	Altered emission curve form between 440-510 nm.
	25 kGy	4.5	Altered absorption curve form between 350-400 nm. Hypsochromic shift of the absorption maximum for 6 nm.	25 kGy	4.5	The ratio between protonation/deprotonation emission peaks is altered.
		7.5	Altered absorption curve form between 350-410 nm.		7.5	The ratio between protonation/deprotonation emission peaks is altered.
		9.5	The ratio between protonation/deprotonation absorption peaks is altered.		9.5	Altered emission curve form between 440-530 nm.
	50 kGy	4.5	Altered absorption curve form between 350-400 nm. Hypsochromic shift of the absorption maximum for 11 nm.	50 kGy	4.5	The ratio between protonation/deprotonation emission peaks is altered.
		7.5	Altered absorption curve form between 350-420 nm and 435-800 nm.		7.5	The ratio between protonation/deprotonation emission peaks is altered.
		9.5	Altered absorption curve form between 500-600 nm. The ratio between protonation/deprotonation absorption peaks is altered.		9.5	Altered emission curve form between 440-500 nm. Hypsochromic shift of the absorption maximum for 2 nm.

Calibration Curves

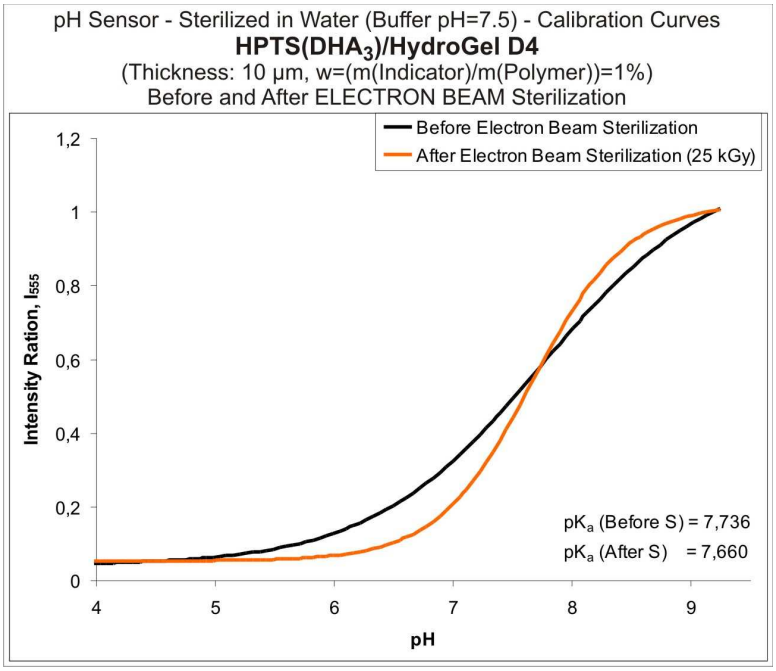

E-BEAM S.	Alterations in Calibration Curve Shape	Alterations in pK_a
	Altered curve shape after sterilization. The response to the proton still observed – re-calibration of sensor response.	Decrease of pK_a (for 0,076)

C.32 2´,7´-DiHexylFluorescein OctadecylEster immobilized in HydroMed Hydrogel D4

C.32.1 Gamma Sterilization

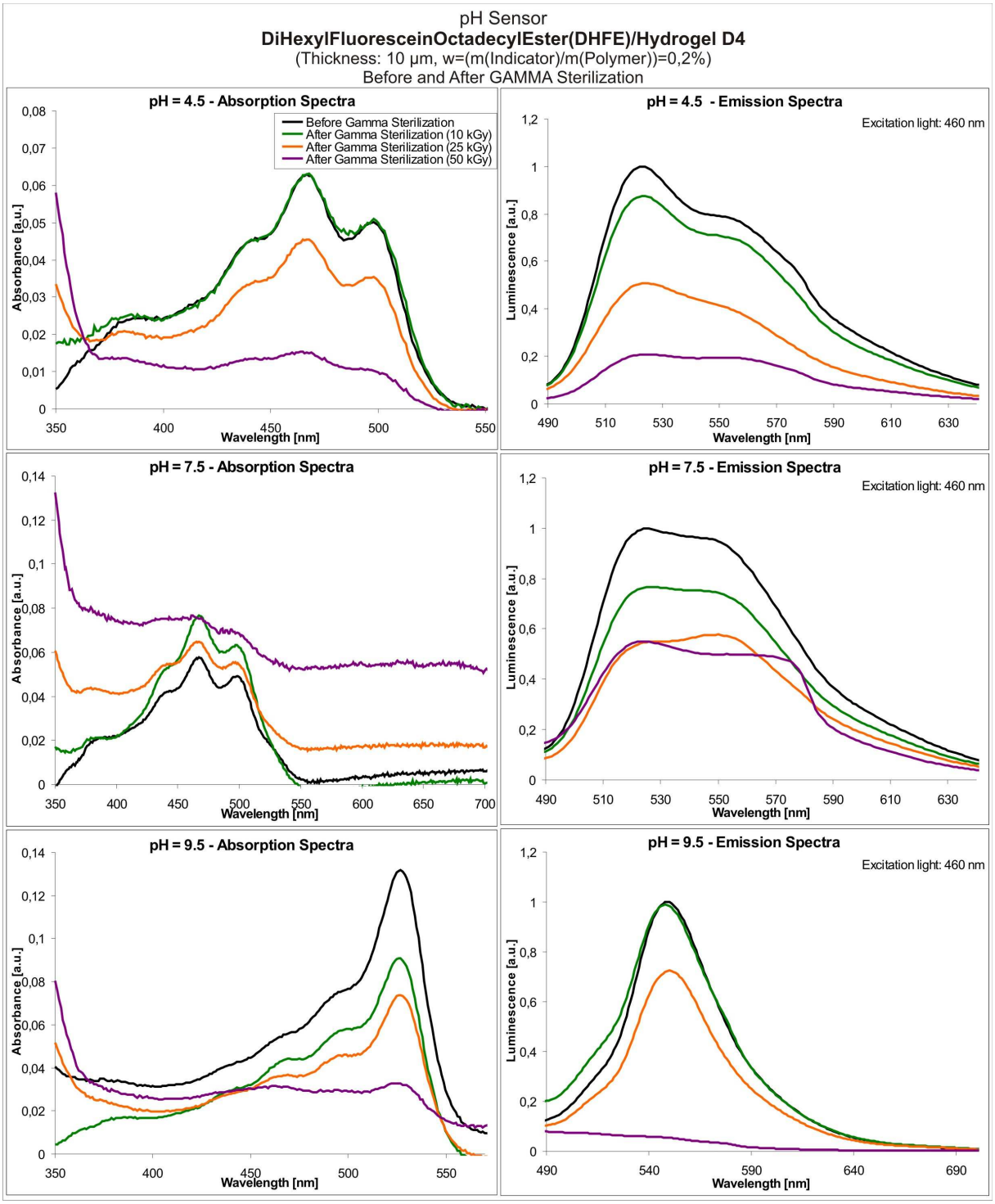

GAMMA S.	Absorption Spectra			Emission Spectra		
		pH	Alterations		pH	Alterations
Alterations in Absorption/ Emission Intensity	10 kGy	4.5	2,05% increase	10 kGy	4.5	12,56% decrease
		7.5	24,97% increase		7.5	23,41% decrease
		9.5	31,02% decrease		9.5	1,05% decrease
	25 kGy	4.5	26,25% decrease	25 kGy	4.5	50,07% decrease
		7.5	11,42% increase		7.5	44,43% decrease
		9.5	44,10% decrease		9.5	27,62% decrease
	50 kGy	4.5	75,59% decrease	50 kGy	4.5	79,22% decrease
		7.5	Increase		7.5	45,17% decrease
		9.5	75,10% decrease		9.5	Decrease
Alterations in Absorption/ Emission Curve Form	10 kGy	4.5	Altered absorption curve form between 350-380 nm.	10 kGy	4.5	Unaltered
		7.5	Altered absorption curve form between 350-370 nm.		7.5	Unaltered.
		9.5	Unaltered.		9.5	Altered emission curve form between 490-530 nm.
	25 kGy	4.5	Altered absorption curve form between 350-370 nm.	25 kGy	4.5	Altered emission curve form between 530-800 nm.
		7.5	Altered absorption curve form between 350-450 nm and 520-800. Sensor became turbid after sterilization.		7.5	Altered emission curve form between 530-560 nm. Emission maximum became peak with λ_{max}=551 nm.
		9.5	Altered absorption curve form between 350-380 nm.		9.5	Altered emission curve form between 490-520 nm.
	50 kGy	4.5	Disappearance of characteristic absorption curve form.	50 kGy	4.5	Altered emission curve form between 535-800 nm. New peak with maximum λ_{max}=557 nm
		7.5	Disappearance of characteristic absorption curve form.		7.5	New peak with maximum λ_{max}=572 nm
		9.5	Disappearance of characteristic absorption curve form.		9.5	Disappearance of characteristic absorption curve form.

Calibration Curves

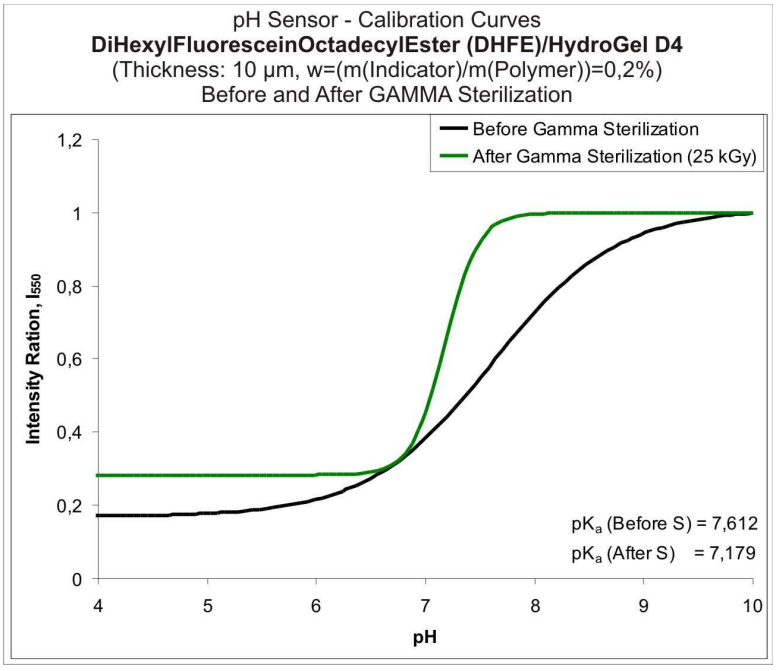

GAMMA S.	Alterations in Calibration Curve Shape	Alterations in pK_a
	Altered curve shape after sterilization. The response to the proton still observed – re-calibration of sensor response.	Decrease of pK_a (for 0,433)

C.32.1.1 Sterilization in Water

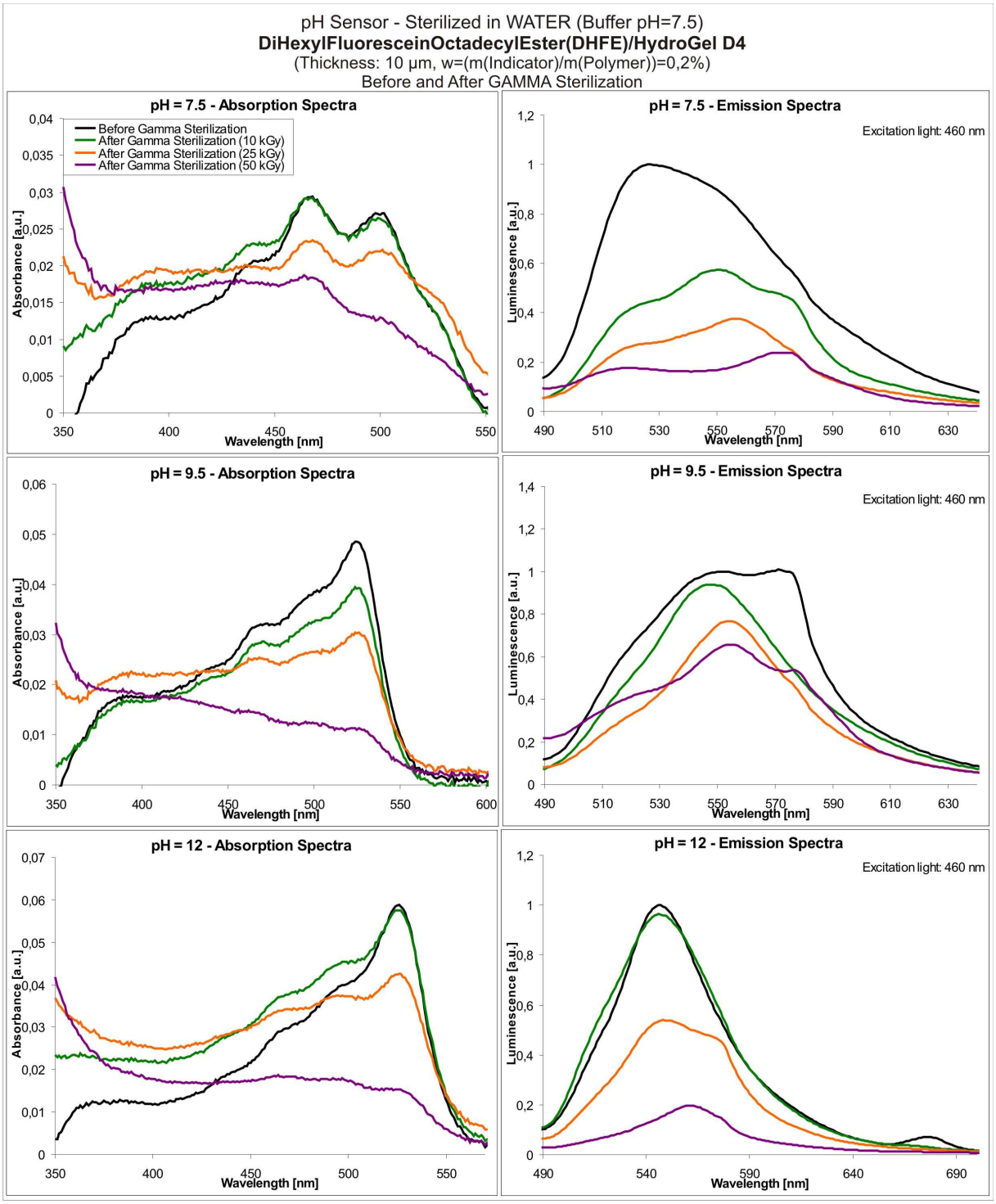

GAMMA S.	Absorption Spectra			Emission Spectra		
Alterations in Absorption/ Emission		pH	Alterations		pH	Alterations
	10 kGy	4.5	0,17% decrease	10 kGy	4.5	56,05% decrease
		7.5	18,66% increase		7.5	7,23% decrease
		9.5	1,69% decrease		9.5	3,76% decrease

Intensity	25 kGy	4.5	20,07% decrease	25 kGy	4.5	72,71% decrease
		7.5	37,37% decrease		7.5	23,22% decrease
		9.5	27,53% decrease		9.5	46,28% decrease
	50 kGy	4.5	36,56% decrease	50 kGy	4.5	82,29% decrease
		7.5	76,69% decrease		7.5	34,30% decrease
		9.5	73,85% decrease		9.5	80,32% decrease
Alterations in Absorption/ Emission Curve Form	10 kGy	4.5	Altered absorption curve form between 350-450 nm.	10 kGy	4.5	Altered emission curve form. Emission maximum became peak with λ_{max}=552 nm.
		7.5	Unaltered.		7.5	Altered emission curve form. Emission maximum became peak with λ_{max}=549 nm.
		9.5	Altered absorption curve form between 350-510 nm.		9.5	Altered emission curve form between 490-540 nm and 550-590 nm.
	25 kGy	4.5	Altered absorption curve form between 350-430 nm. And 520-800 nm.	25 kGy	4.5	Altered emission curve form. Emission maximum became peak with λ_{max}=558 nm.
		7.5	Altered absorption curve form between 350-440 nm.		7.5	Altered emission curve form. Emission maximum became peak with λ_{max}=554 nm.
		9.5	Altered absorption curve form between 350-480 nm.		9.5	Altered emission curve form between 550-610 nm.
	50 kGy	4.5	Disappearance of characteristic absorption curve form.	50 kGy	4.5	Altered emission curve form. Emission maximum became peak with λ_{max}=574 nm.
		7.5	Disappearance of characteristic absorption curve form.		7.5	Altered emission curve form. Emission maximum became peak with λ_{max}=555nm.
		9.5	Disappearance of characteristic absorption curve form.		9.5	Altered emission curve form. Emission maximum became peak with λ_{max}=562nm.

Calibration Curves

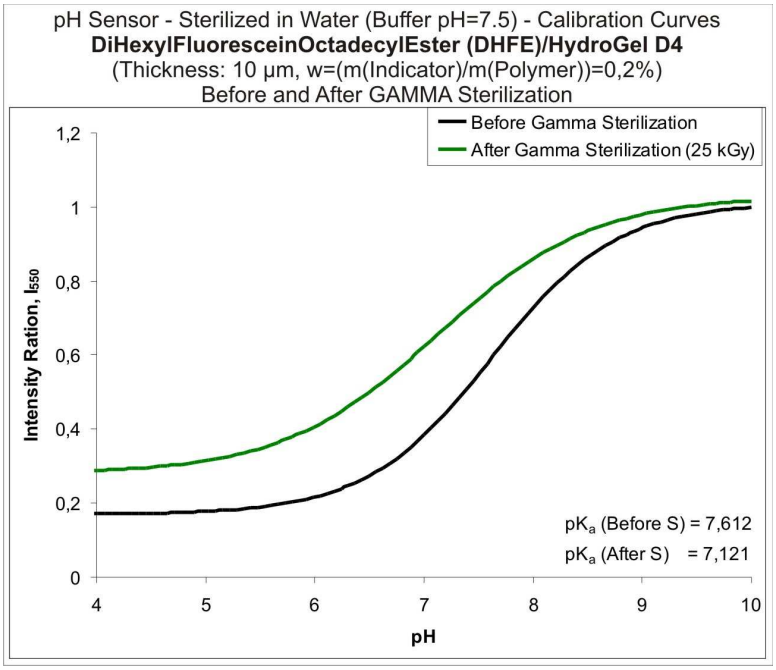

GAMMA S.	Alterations in Calibration Curve Shape	Alterations in pK_a
	Altered curve shape after sterilization. The response to the proton still observed – re-calibration of sensor response.	Decrease of pK_a (for 0,491)

C.32.2 Electron Beam Sterilization

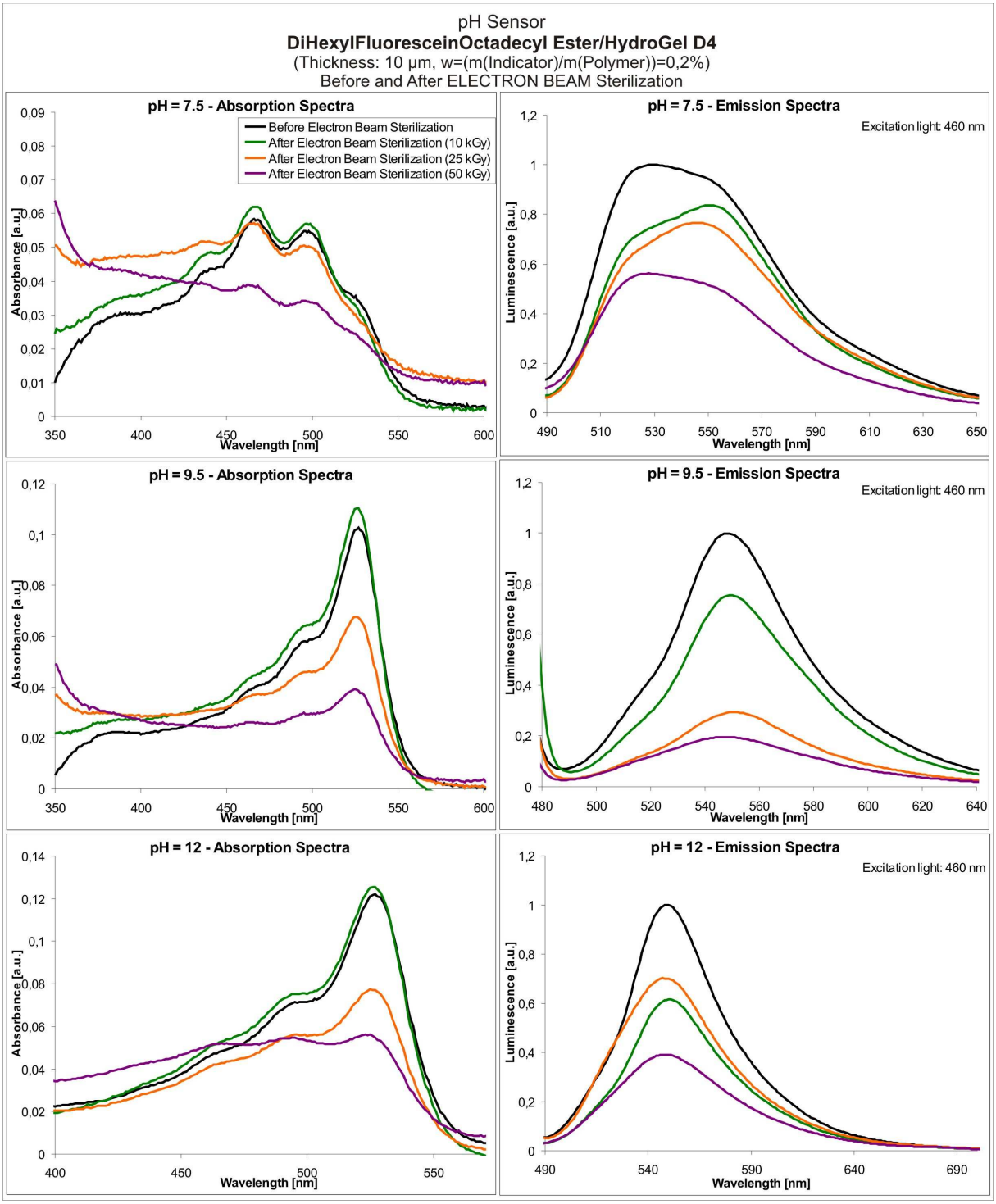

E-BEAM S.	Absorption Spectra			Emission Spectra		
		pH	Alterations		pH	Alterations
Alterations in Absorption/ Emission Intensity	10 kGy	4.5	7,86% decrease	10 kGy	4.5	16,22% decrease
		7.5	7,00% decrease		7.5	24,57% decrease
		9.5	2,68% decrease		9.5	38,43% decrease
	25 kGy	4.5	1,58% decrease	25 kGy	4.5	23,31% decrease
		7.5	34,03% decrease		7.5	70,59% decrease
		9.5	36,58% decrease		9.5	29,81% decrease
	50 kGy	4.5	33,30% decrease	50 kGy	4.5	43,83% decrease
		7.5	61,87% decrease		7.5	80,32% decrease
		9.5	53,94% decrease		9.5	60,93% decrease

Alterations in Absorption/ Emission Curve Form	10 kGy	4.5	Unaltered.	10 kGy	4.5	Emission maximum became peak with λ_{max}=553 nm.
		7.5	Unaltered.		7.5	Altered emission curve form between 480-500 nm and 565-600 nm.
		9.5	Unaltered.		9.5	Unaltered.
	25 kGy	4.5	Altered absorption curve form between 350-450 nm and 540-800 nm.	25 kGy	4.5	Emission maximum became peak with λ_{max}=546 nm.
		7.5	Altered absorption curve form between 350-510 nm.		7.5	Altered emission curve form between 480-525 nm and 560-650 nm.
		9.5	Altered absorption curve form between 350-520 nm.		9.5	Altered emission curve form between 490-550 nm.
	50 kGy	4.5	Altered absorption curve form.	50 kGy	4.5	Unaltered.
		7.5	Altered absorption curve form between 350-515 nm and 550-800 nm. Hypsochromic shift of the absorption maximum for 2 nm.		7.5	Altered emission curve form between 480-540 nm and 565-650 nm. Hypsochromic shift of the absorption maximum for 2 nm.
		9.5	Altered absorption curve form.		9.5	Altered emission curve form between 490-550 nm and 560-650 nm.

Calibration Curves

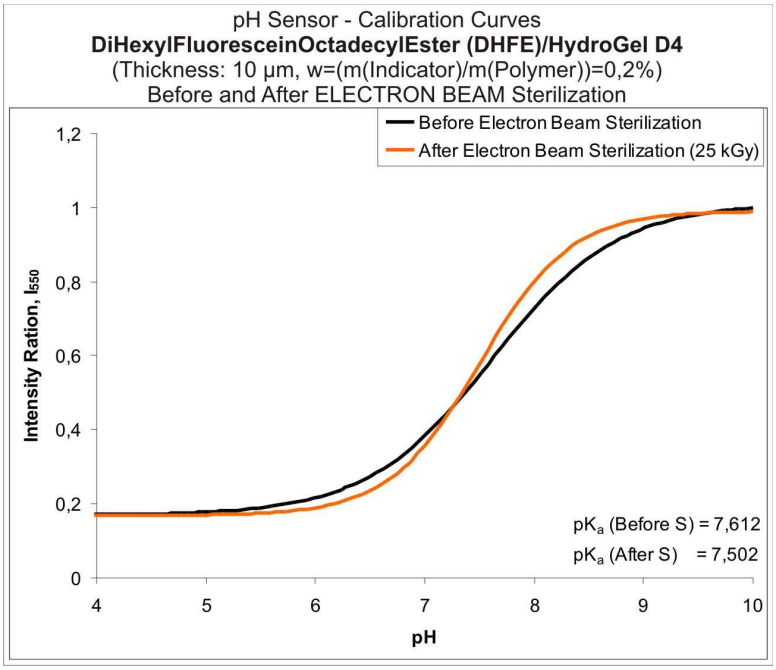

E-BEAM S.	Alterations in Calibration Curve Shape	Alterations in pK_a
	Comparable curve shapes before and after sterilization.	Decrease of pK_a (for 0,110)

C.32.2.1 Sterilization in Water

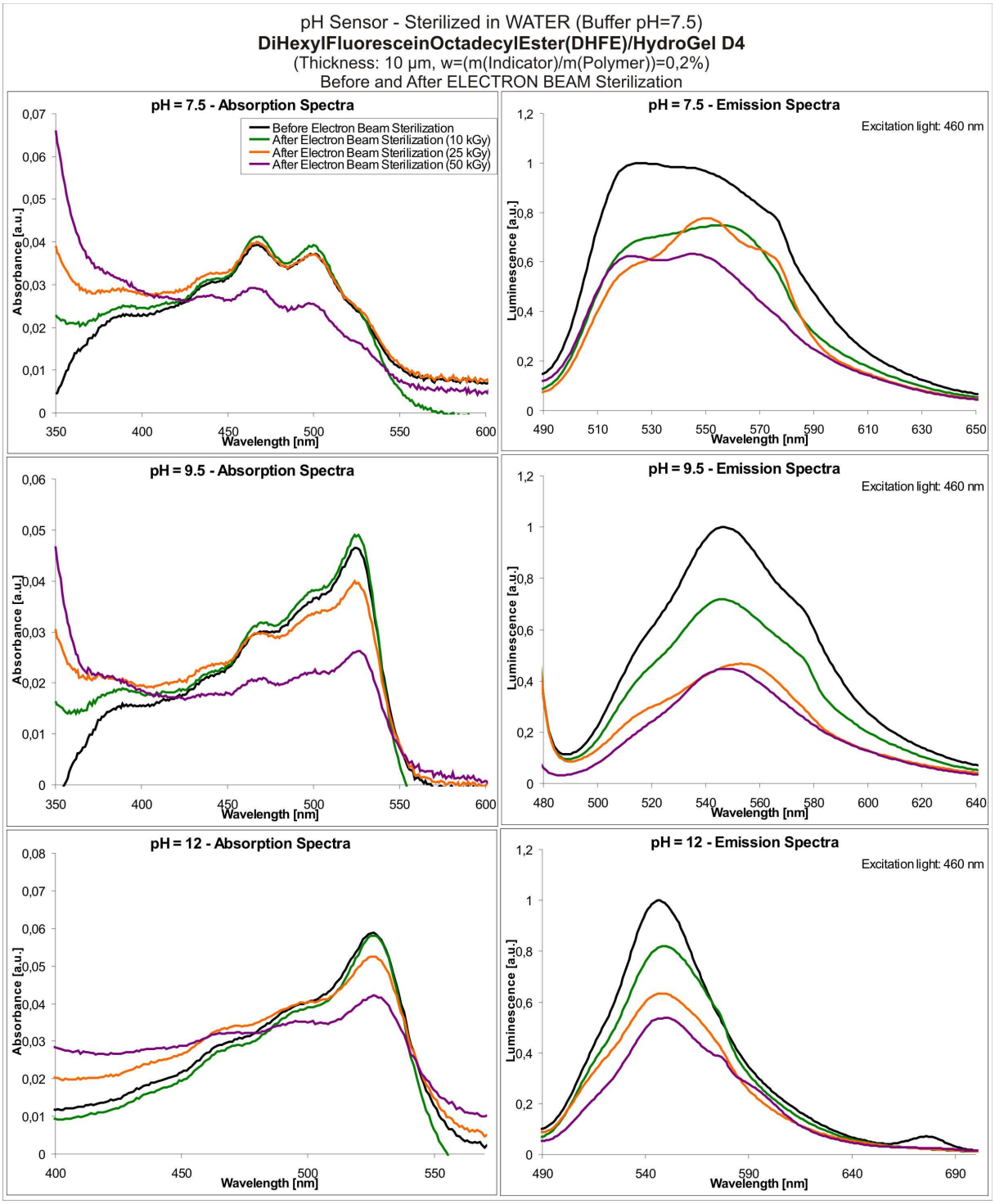

E-BEAM S.	Absorption Spectra			Emission Spectra		
		pH	Alterations		pH	Alterations
Alterations in Absorption/ Emission Intensity	10 kGy	4.5	5,30% increase	10 kGy	4.5	25,04% decrease
		7.5	5,29% decrease		7.5	27,98% decrease
		9.5	1,18% decrease		9.5	18,04% decrease
	25 kGy	4.5	3,07% decrease	25 kGy	4.5	22,29% decrease
		7.5	14,19% decrease		7.5	53,23% decrease
		9.5	10,80% decrease		9.5	36,53% decrease
	50 kGy	4.5	24,82% decrease	50 kGy	4.5	36,65% decrease
		7.5	59,45% decrease		7.5	55,20% decrease
		9.5	28,36% decrease		9.5	46,19% decrease

Alterations in Absorption/ Emission Curve Form	10 kGy	4.5	Altered absorption curve form between 350-420 nm and 535-600 nm.	10 kGy	4.5	Emission maximum became peak with λ_{max}=559 nm.
		7.5	Altered absorption curve form between 350-400 nm.		7.5	Altered emission curve form between 560-590 nm.
		9.5	Unaltered.		9.5	Altered emission curve form between 550-620 nm.
	25 kGy	4.5	Altered absorption curve form between 350-450 nm.	25 kGy	4.5	Emission maximum became peak with λ_{max}=550 nm.
		7.5	Altered absorption curve form between 350-510 nm.		7.5	Emission maximum became peak with λ_{max}=555 nm.
		9.5	Altered absorption curve form between 400-510 nm and 540-600 nm.		9.5	Altered emission curve form between 490-530 nm and 550-620 nm.
	50 kGy	4.5	Altered absorption curve form.	50 kGy	4.5	Emission maximum became peak with λ_{max}=545 nm.
		7.5	Altered absorption curve form between 350-510 nm and 540-600 nm.		7.5	Altered emission curve form between 480-540 nm and 560-590 nm.
		9.5	Altered absorption curve form between 400-515 nm and 535-800 nm.		9.5	Altered emission curve form between 560-620 nm. Bathochromic shift of the emission maximum for 3 nm.

Calibration Curves

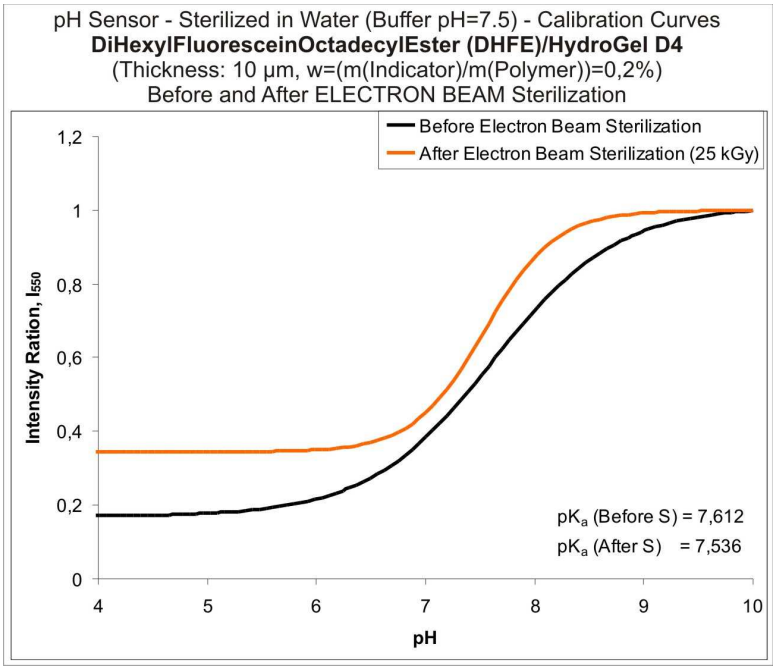

E-BEAM S.	Alterations in Calibration Curve Shape	Alterations in pK_a
	Altered curve shape after sterilization. The response to the proton still observed – re-calibration of sensor response.	Decrease of pK_a (for 0,076)

C.33 2´,7´-DiHexylFluorescein OctadecylEster immobilized in Poly(2-HydroxyEthyl MethAcrylate) (=pHEMA)

C.33.1 Gamma Sterilization

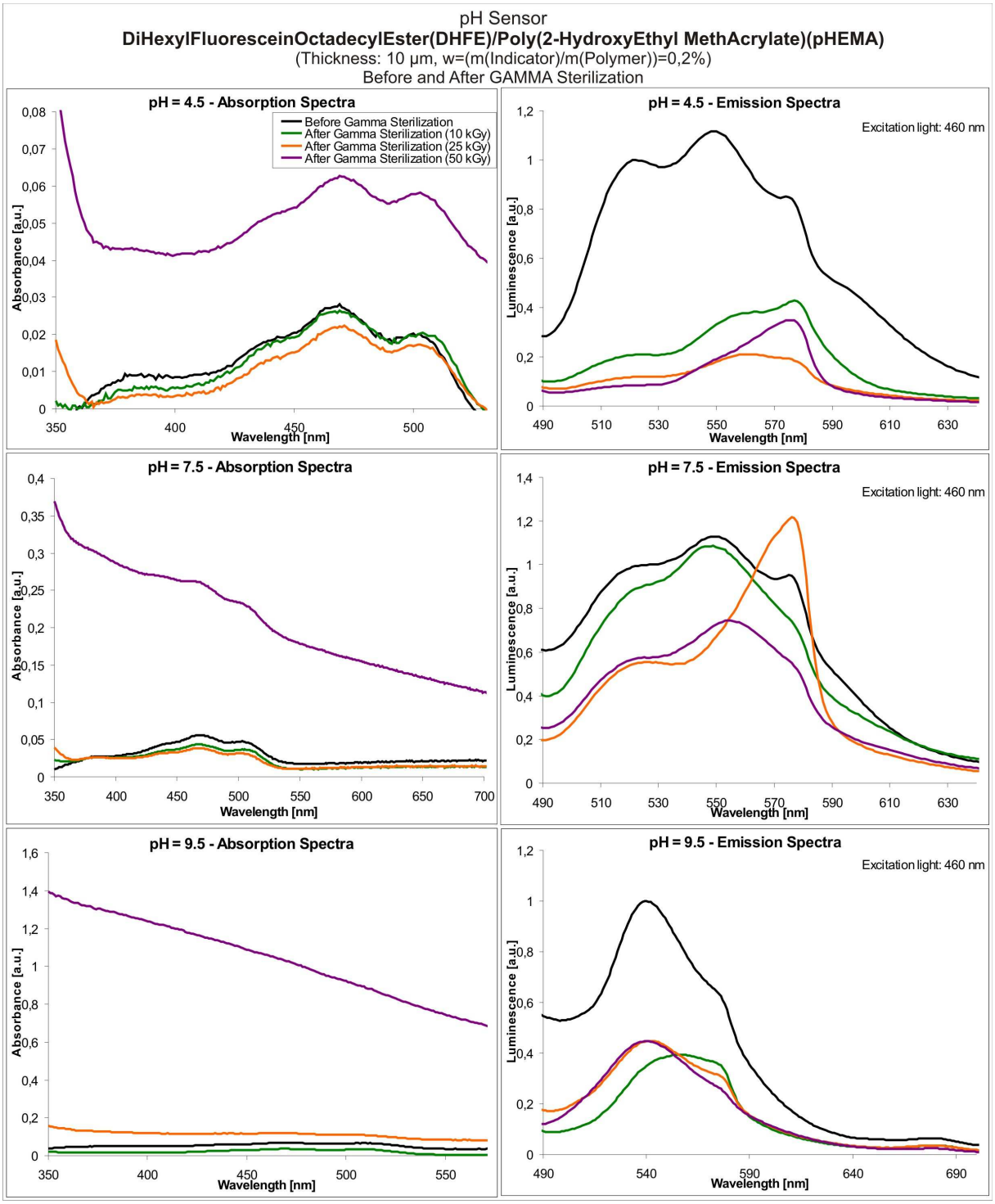

GAMMA S.	Absorption Spectra			Emission Spectra		
		pH	Alterations		pH	Alterations
Alterations in Absorption/ Emission Intensity	10 kGy	4.5	1,11% decrease	10 kGy	4.5	79,42% decrease
		7.5	22,57% decrease		7.5	11,15% decrease
		9.5	28,42% decrease		9.5	64,38% decrease
	25 kGy	4.5	17,93% decrease	25 kGy	4.5	88,17% decrease
		7.5	30,76% decrease		7.5	44,73% decrease
		9.5	80% increase		9.5	55,43% decrease
	50 kGy	4.5	165% increase	50 kGy	4.5	91,51% decrease
		7.5	370% increase		7.5	42,49% decrease
		9.5	1400% increase		9.5	55,87% decrease
Alterations in Absorption/ Emission Curve Form	10 kGy	4.5	Unaltered.	10 kGy	4.5	Altered emission curve form. Emission maximum became peak with λ_{max}=578 nm.
		7.5	Unaltered.		7.5	Altered emission curve form.
		9.5	Unaltered.		9.5	Altered emission curve form. Emission maximum became peak with λ_{max}=558 nm.
	25 kGy	4.5	Altered absorption curve form between 350-360 nm.	25 kGy	4.5	Altered emission curve form. Emission maximum became peak with λ_{max}=563 nm.
		7.5	Altered absorption curve form between 350-360 nm.		7.5	Altered emission curve form. Emission maximum became peak with λ_{max}=577 nm.
		9.5	Sensor became turbid after sterilization and characterization in buffer – more water uptake.		9.5	Altered emission curve form.
	50 kGy	4.5	Altered absorption curve form between 350-360 nm. Sensor became turbid after sterilization and characterization in buffer – more water uptake.	50 kGy	4.5	Altered emission curve form. Emission maximum became peak with λ_{max}=577 nm.
		7.5	Sensor became turbid after sterilization and characterization in buffer – more water uptake.		7.5	Altered emission curve form.
		9.5	Sensor became turbid after sterilization and characterization in buffer – more water uptake.		9.5	Altered emission curve form.

Calibration Curves

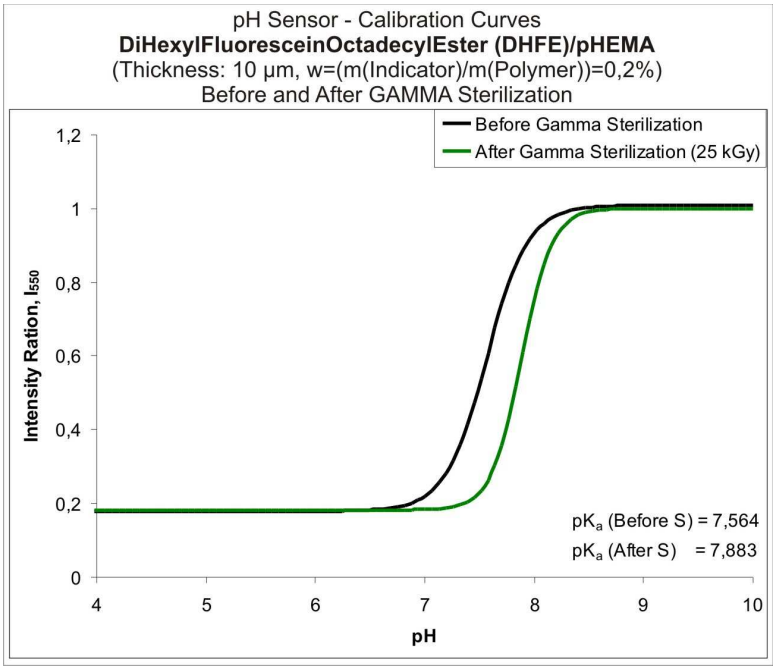

GAMMA S.	Alterations in Calibration Curve Shape	Alterations in pK_a
	The response to the proton still observed – re-calibration of sensor response.	Increase of pK_a (for 0,319)

C.33.1.1 Sterilization in Water

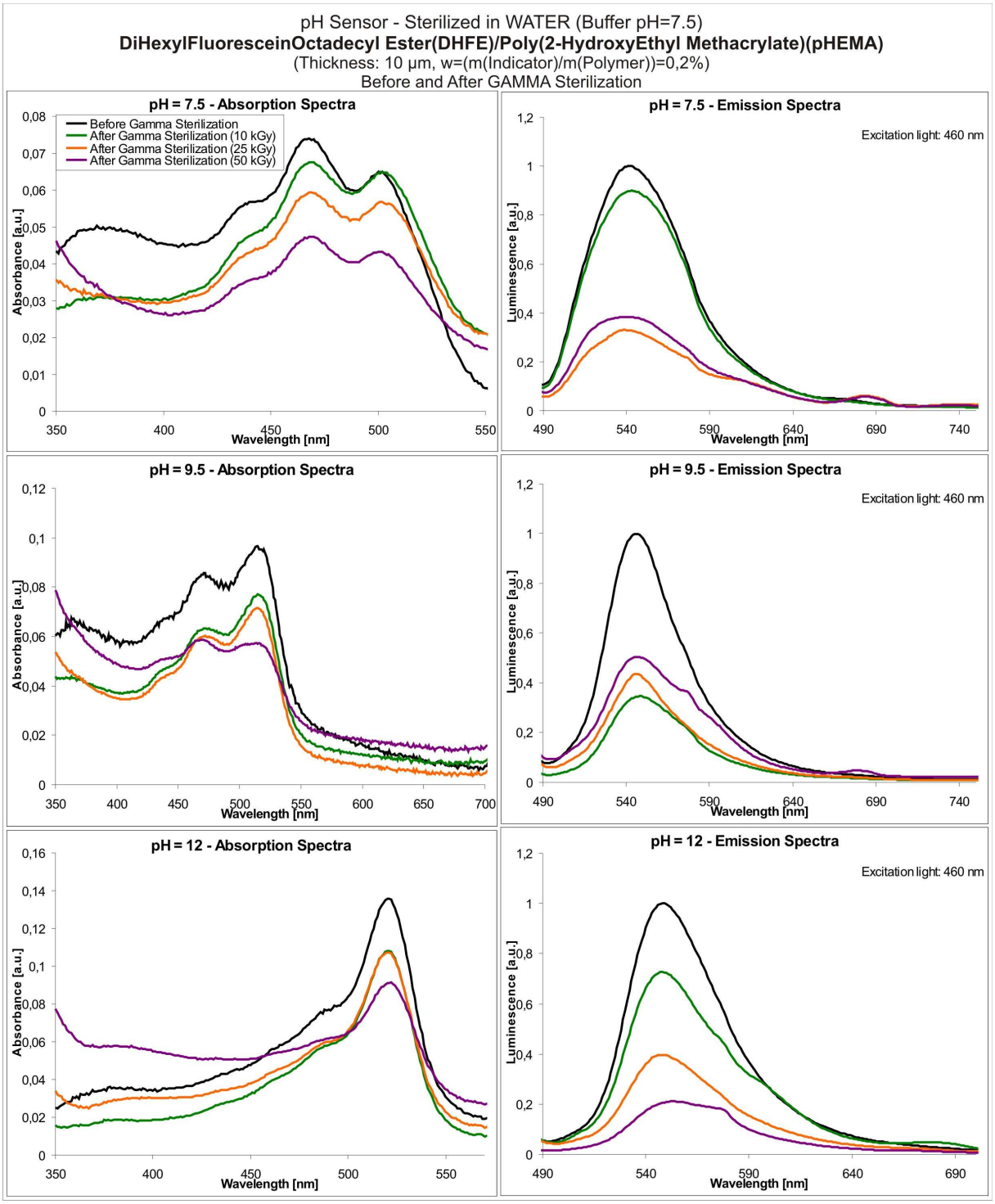

GAMMA S.	Absorption Spectra			Emission Spectra		
		pH	Alterations		pH	Alterations
Alterations in Absorption/ Emission Intensity	10 kGy	7.5	8,19% decrease	10 kGy	7.5	10,04% decrease
		9.5	20,34% decrease		9.5	65,36% decrease
		12	21,02% decrease		12	64,38% decrease
	25 kGy	7.5	19,32% decrease	25 kGy	7.5	66,87% decrease
		9.5	26,25% decrease		9.5	56,34% decrease
		12	21,35% decrease		12	55,43% decrease
	50 kGy	7.5	35,56% decrease	50 kGy	7.5	61,58% decrease
		9.5	40,61% decrease		9.5	49,46% decrease
		12	33,39% decrease		12	55,87% decrease

Alterations in Absorption/ Emission Curve Form	10 kGy	7.5	Altered absorption curve form between 350-380 nm and 510-800 nm.	10 kGy	7.5	Unaltered.
		9.5	Unaltered.		9.5	Altered emission curve form between 550-750 nm.
		12	Unaltered.		12	Altered emission curve form between 570-700 nm.
	25 kGy	7.5	Altered absorption curve form between 350-380 nm and 520-800 nm.	25 kGy	7.5	Altered emission curve form between 490-500 nm and 540-800 nm. New emission peak with λ_{max}=685 nm.
		9.5	Altered absorption curve form between 350-380 nm.		9.5	Altered emission curve form between 490-520 nm and 590-750 nm.
		12	Altered absorption curve form between 350-370 nm.		12	Altered emission curve form between 490-520 nm and 590-700 nm.
	50 kGy	7.5	Altered absorption curve form between 350-390 nm and 530-800 nm.	50 kGy	7.5	Altered emission curve form between 490-540 nm and 580-800 nm. New emission peak with λ_{max}=685 nm.
		9.5	Altered absorption curve form between 350-460 nm and 500-800 nm.		9.5	Altered emission curve form between 490-525 nm and 550-750 nm. New emission peak with λ_{max}=680 nm.
		12	Altered absorption curve form between 350-450 nm and 540-800 nm		12	Bathochromic shift of the emission maximum for 5 nm. New emission peak with λ_{max}=680 nm.

Calibration Curves

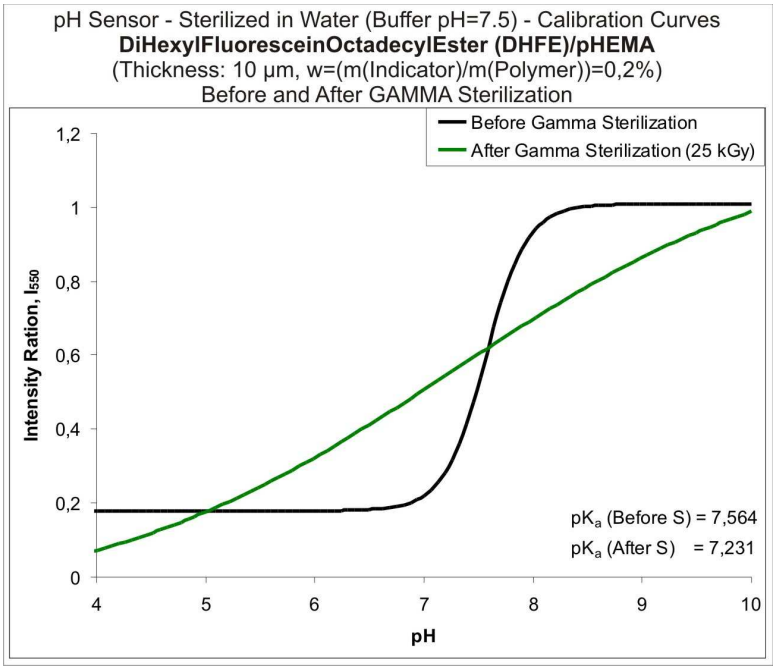

GAMMA S.	Alterations in Calibration Curve Shape	Alterations in pK_a
	Greatly altered curve shape after sterilization.	Decrease of pK_a (for 0,333)

C.33.2 Electron Beam Sterilization

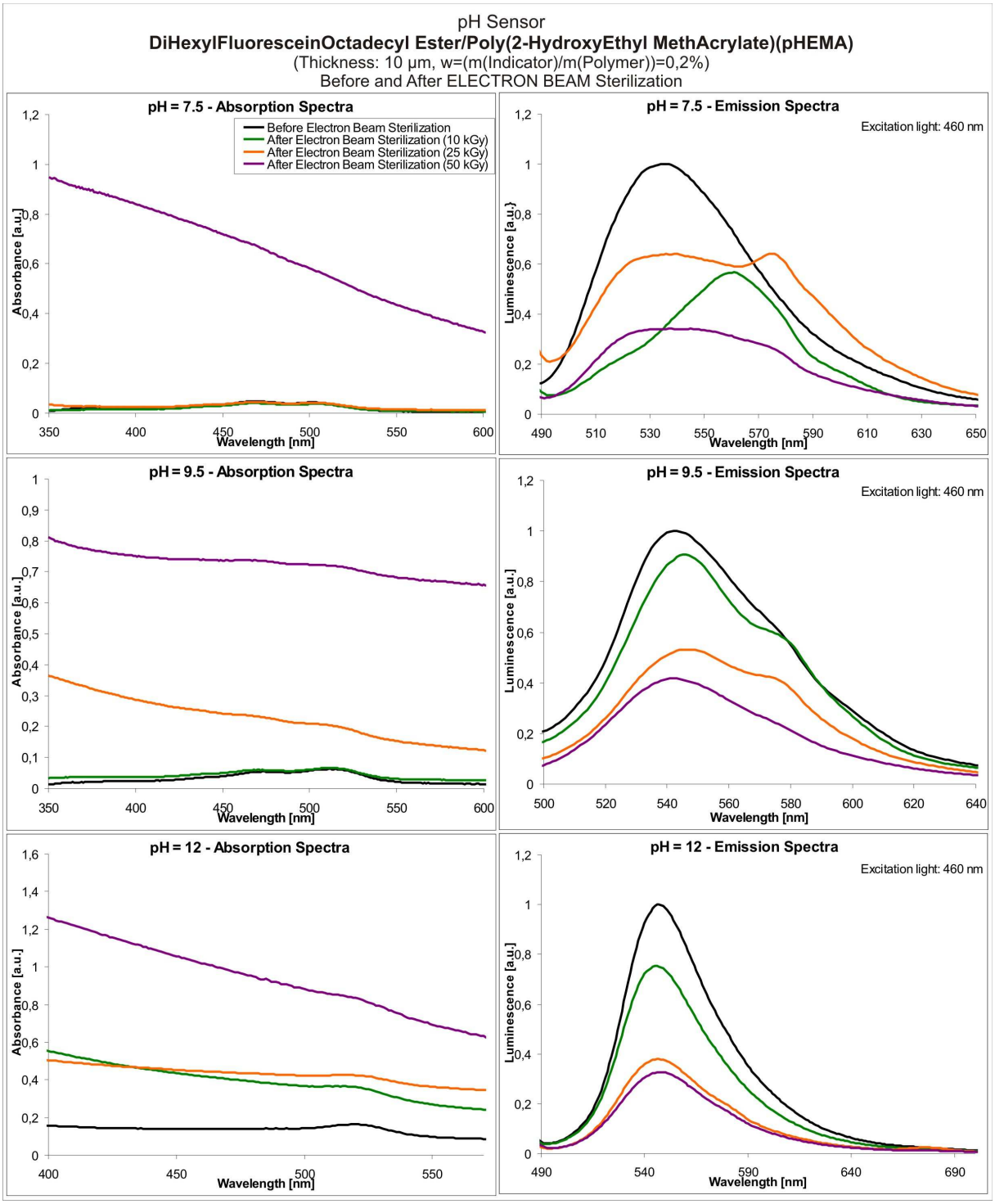

E-BEAM S.	Absorption Spectra			Emission Spectra		
		pH	Alterations		pH	Alterations
Alterations in Absorption/ Emission Intensity	10 kGy	4.5	14,34% decrease	10 kGy	4.5	43,30% decrease
		7.5	5,92% increase		7.5	24,64% decrease
		9.5	120% increase		9.5	9,27% decrease
	25 kGy	4.5	6,42% decrease	25 kGy	4.5	35,93% decrease
		7.5	230% increase		7.5	62,12% decrease
		9.5	160% increase		9.5	46,81% decrease
	50 kGy	4.5	1300% increase	50 kGy	4.5	65,86% decrease
		7.5	1060% increase		7.5	67,35% decrease
		9.5	410% increase		9.5	58,22% decrease

Alterations in Absorption/ Emission Curve Form	10 kGy	4.5	Unaltered.	10 kGy	4.5	Emission maximum became peak with λ_{max}=561 nm.
		7.5	Sensor became slightly turbid after sterilization and characterization in buffer – more water uptake.		7.5	Unaltered.
		9.5	Sensor became slightly turbid after sterilization and characterization in buffer – more water uptake.		9.5	Altered emission curve form between 560-600 nm. Bathochromic shift of the emission maximum for 4 nm.
	25 kGy	4.5	Altered absorption curve form between 350-440 nm and 520-800 nm.	25 kGy	4.5	Emission maximum became peak with λ_{max}=567 nm.
		7.5	Sensor became turbid after sterilization and characterization in buffer – more water uptake.		7.5	New emission peak with λ_{max}=677 nm.
		9.5	Sensor became slightly turbid after sterilization and characterization in buffer – more water uptake.		9.5	Altered emission curve form between 550-620 nm. Bathochromic shift of the emission maximum for 4 nm.
	50 kGy	4.5	Altered absorption curve form. Sensor became turbid after sterilization and characterization in buffer – more water uptake.	50 kGy	4.5	Altered emission curve form.
		7.5	Sensor became turbid after sterilization and characterization in buffer – more water uptake.		7.5	Bathochromic shift of the emission maximum for 1 nm.
		9.5	Sensor became slightly turbid after sterilization and characterization in buffer – more water uptake.		9.5	Altered emission curve form between 500-530 nm.

Calibration Curves

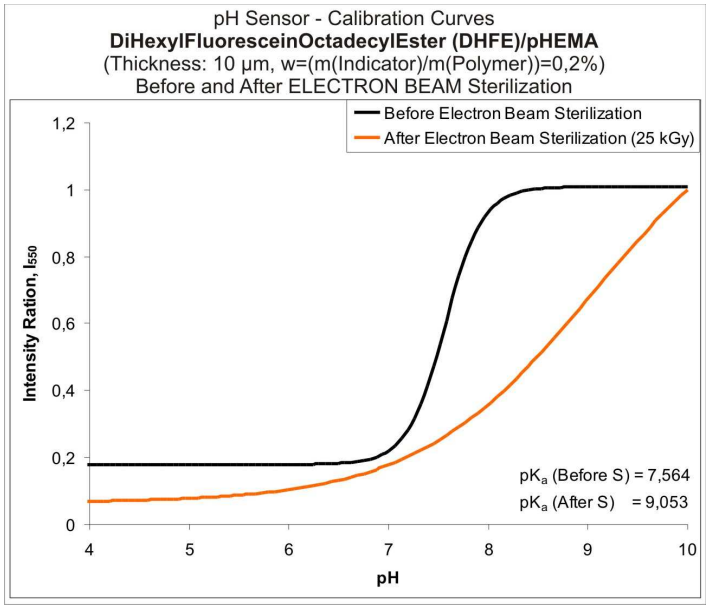

E-BEAM S.	Alterations in Calibration Curve Shape	Alterations in pK_a
	Greatly altered curve shape after sterilization.	Increase of pK_a (for 0,835)

C.33.2.1 Sterilization in Water

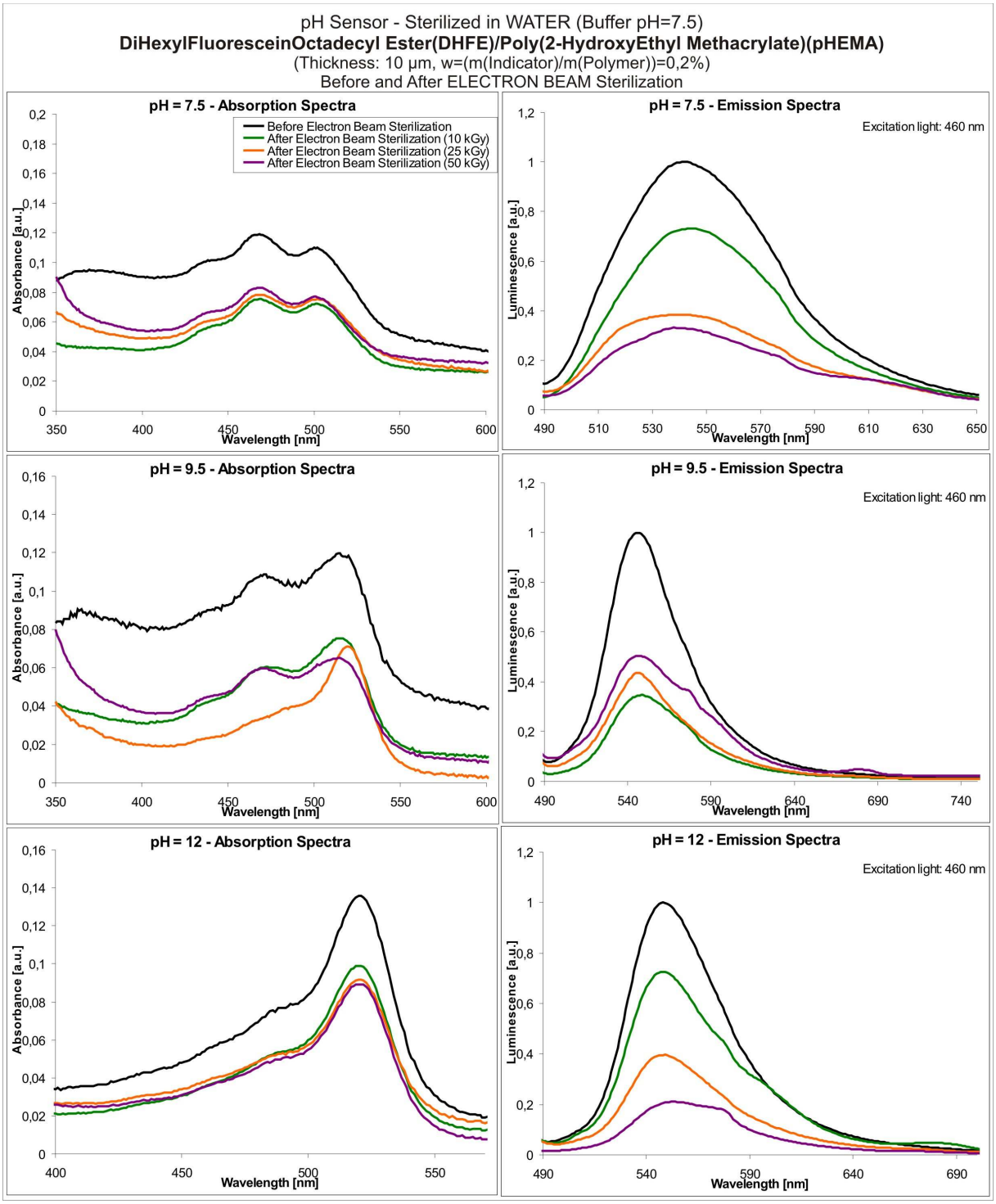

E-BEAM S.	Absorption Spectra			Emission Spectra		
		pH	Alterations		pH	Alterations
Alterations in Absorption/ Emission Intensity	10 kGy	7.5	36,71% decrease	10 kGy	7.5	26,78% decrease
		9.5	36,86% decrease		9.5	49,46% decrease
		12	27,14% decrease		12	9,27% decrease
	25 kGy	7.5	34,27% decrease	25 kGy	7.5	61,59% decrease
		9.5	40,65% decrease		9.5	56,34% decrease
		12	32,47% decrease		12	46,81% decrease
	50 kGy	7.5	30,17% decrease	50 kGy	7.5	66,87% decrease
		9.5	45,55% decrease		9.5	67,30% decrease
		12	35,28% decrease		12	58,22% decrease

Alterations in Absorption/ Emission Curve Form	10 kGy	7.5	Altered absorption curve form between 350-450 nm.	10 kGy	7.5	Bathochromic shift of the emission maximum for 3 nm.
		9.5	Altered absorption curve form between 350-505 nm and 530-800 nm.		9.5	Altered emission curve form between 480-530 nm.
		12	Altered absorption curve form between 350-490 nm and 540-800 nm.		12	Altered emission curve form between 570-700 nm.
	25 kGy	7.5	Altered absorption curve form between 350-450 nm.	25 kGy	7.5	Altered emission curve form between 490-540 nm and 580-700 nm. Bathochromic shift of the emission maximum for 1 nm.
		9.5	The absorption curve has a form of deprotonated state of indicator.		9.5	Altered emission curve form between 480-520 nm and 550-650 nm.
		12	Altered absorption curve form between 550-800 nm.		12	Altered emission curve form between 490-520 nm and 590-700 nm.
	50 kGy	7.5	Altered absorption curve form between 350-450 nm.	50 kGy	7.5	Altered emission curve form between 490-560 nm and 570-700 nm. Hypsochromic shift of the emission maximum for 4 nm.
		9.5	Altered absorption curve form between 550-800 nm.		9.5	Altered emission curve form between 550-600 nm. Bathochromic shift of the emission maximum for 3 nm.
		12	Altered absorption curve form between 540-800 nm.		12	Altered emission curve form between 560-630 nm. Bathochromic shift of the emission maximum for 6 nm.

Calibration Curves

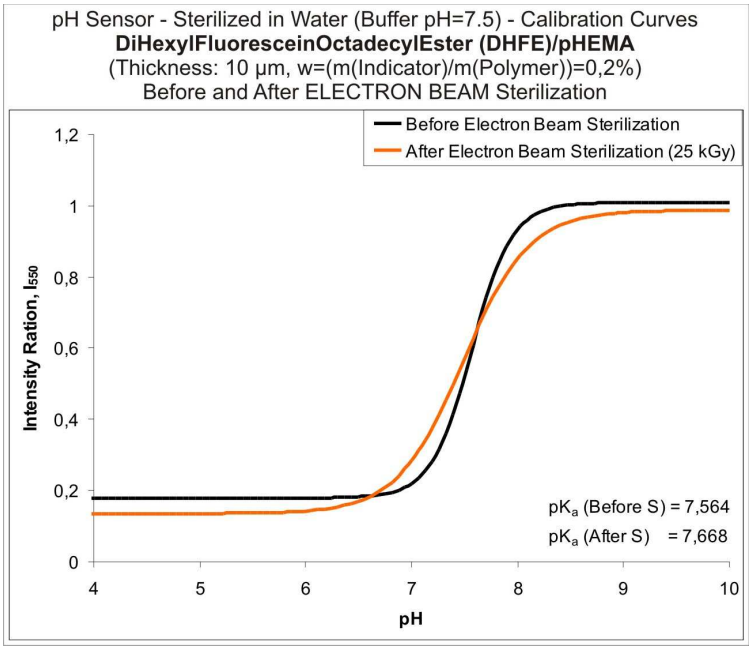

E-BEAM S.	Alterations in Calibration Curve Shape	Alterations in pK_a
	Comparable curve shapes before and after sterilization.	Increase of pK_a (for 0,104)

C.34 2´,7´-DiHexyl-N-Octadecyl-CarboxAmidoFluorescein (=DHFA) immobilized in HydroMed Hydrogel D4

C.34.1 Gamma Sterilization

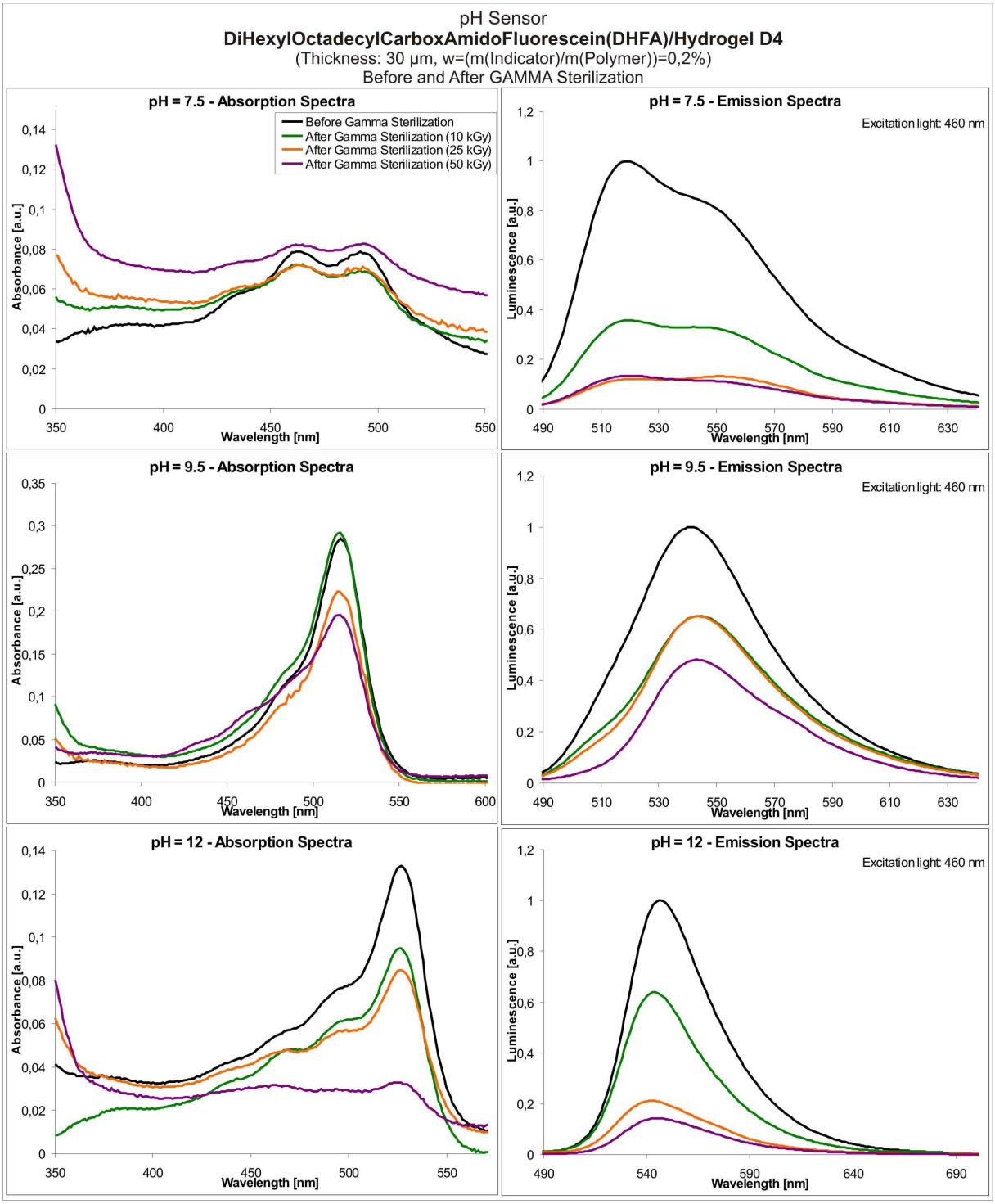

GAMMA S.	Absorption Spectra			Emission Spectra		
		pH	Alterations		pH	Alterations
Alterations in Absorption/ Emission Intensity	10 kGy	7.5	8,28% decrease	10 kGy	7.5	64,12% decrease
		9.5	2,38% increase		9.5	34,67% decrease
		12	28,75% decrease		12	36,09% decrease
	25 kGy	7.5	7,78% decrease	25 kGy	7.5	87,79% decrease
		9.5	21,73% decrease		9.5	34,80% decrease
		12	36,27% decrease		12	78,80% decrease
	50 kGy	7.5	4,40% increase	50 kGy	7.5	86,43% decrease
		9.5	31,21% decrease		9.5	51,77% decrease
		12	75,17% decrease		12	85,66% decrease
Alterations in Absorption/ Emission Curve Form	10 kGy	7.5	Altered absorption curve form between 350-440 nm and 530-800 nm.	10 kGy	7.5	Altered emission curve form between 530-610 nm.
		9.5	Altered absorption curve form between 350-370 nm.		9.5	Bathochromic shift of the emission maximum for 3 nm.
		12	Altered absorption curve form between 350-380 nm.		12	Hypsochromic shift of the emission maximum for 2 nm.
	25 kGy	7.5	Altered absorption curve form between 350-440 nm and 520-800 nm.	25 kGy	7.5	Altered emission curve form between 530-610 nm.
		9.5	Altered absorption curve form between 350-370 nm.		9.5	Bathochromic shift of the emission maximum for 3 nm.
		12	Altered absorption curve form between 350-390 nm.		12	Hypsochromic shift of the emission maximum for 2 nm.
	50 kGy	7.5	Altered absorption curve form between 350-450 nm and 515-800 nm. Sensor became turbid after sterilization.	50 kGy	7.5	Altered emission curve form between 530-610 nm.
		9.5	Altered absorption curve form between 350-505 nm.		9.5	Bathochromic shift of the emission maximum for 3 nm. Altered emission curve form between 490-530 nm.
		12	Disappearance of characteristic absorption curve form.		12	Hypsochromic shift of the emission maximum for 2 nm.

Calibration Curves

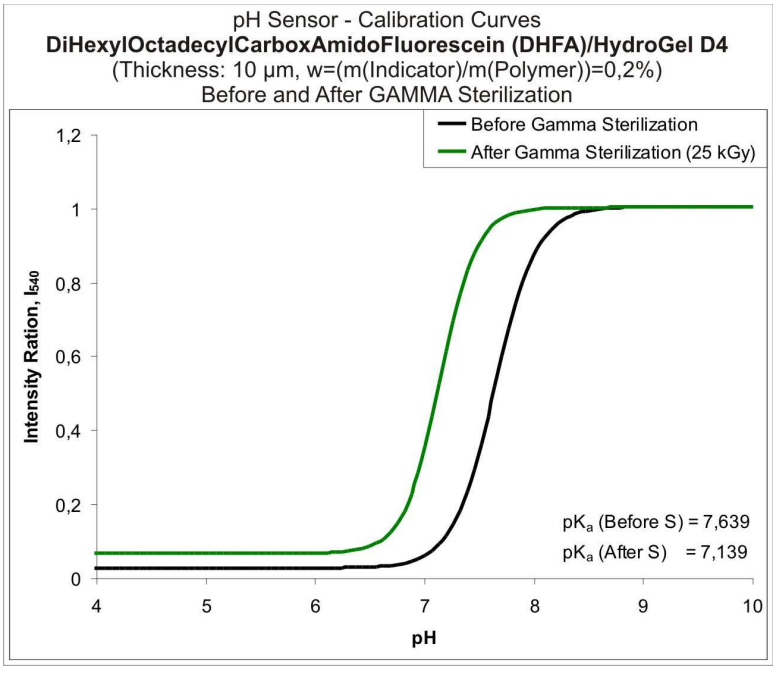

GAMMA S.	Alterations in Calibration Curve Shape	Alterations in pK_a
	Altered curve shape after sterilization. The response to the proton still observed – re-calibration of sensor response.	Decrease of pK_a (for 0,500)

C.34.1.1 Sterilization in Water

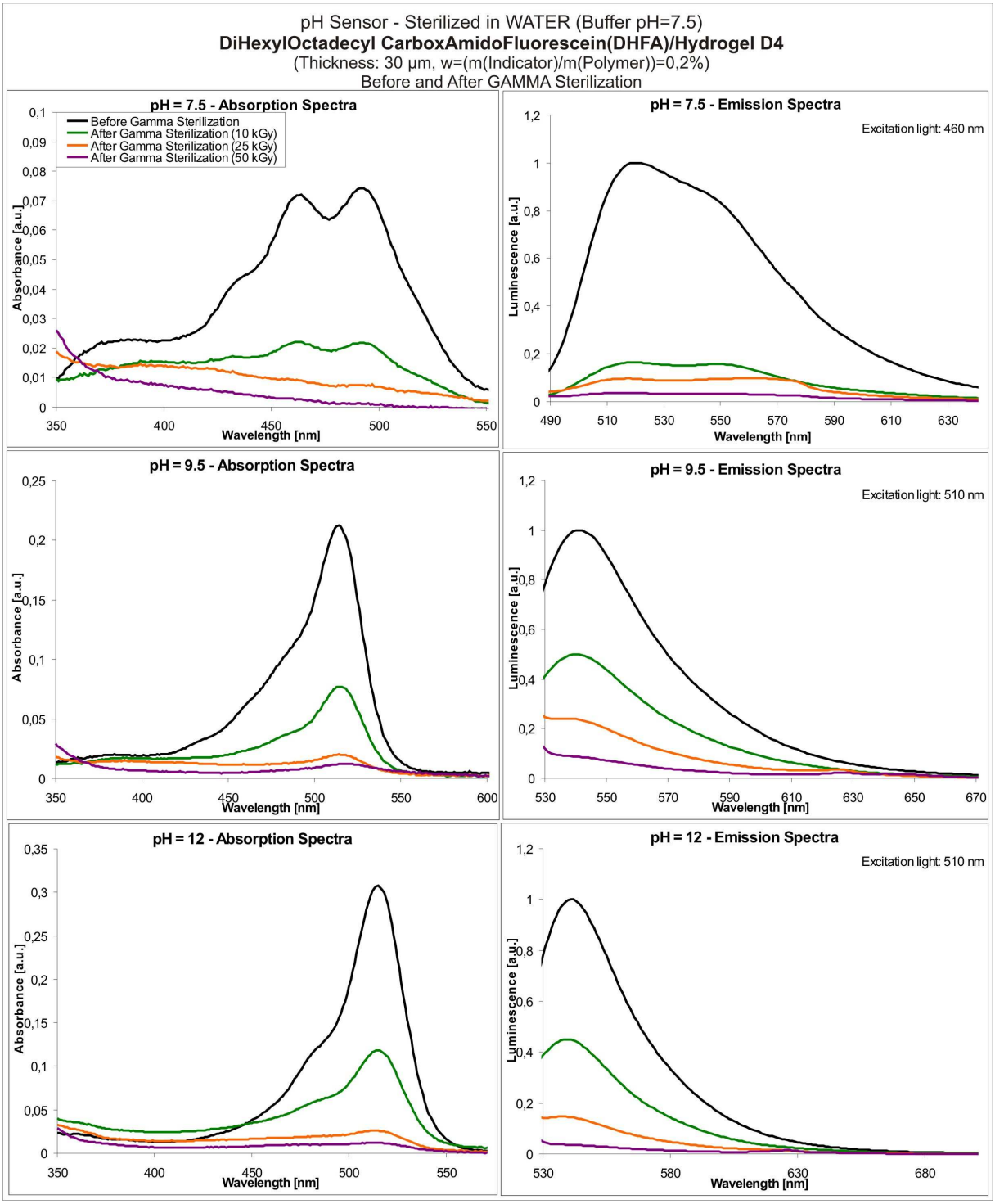

GAMMA S.	Absorption Spectra			Emission Spectra		
Alterations in Absorption/ Emission		pH	Alterations		pH	Alterations
	10 kGy	7.5	69,46% decrease	10 kGy	7.5	83,62% decrease
		9.5	63,64% decrease		9.5	50,06% decrease
		12	61,63% decrease		12	55,14% decrease

Intensity	25 kGy	7.5	87,57% decrease	25 kGy	7.5	90,27% decrease
		9.5	90,56% decrease		9.5	75,89% decrease
		12	91,52% decrease		12	85,33% decrease
	50 kGy	7.5	96,39% decrease	50 kGy	7.5	96,33% decrease
		9.5	94,34% decrease		9.5	90,27% decrease
		12	96,10% decrease		12	96,54% decrease
Alterations in Absorption/ Emission Curve Form	10 kGy	7.5	Unaltered.	10 kGy	7.5	Disappearance of the characteristic emission curve form.
		9.5	Unaltered.		9.5	Unaltered.
		12	Unaltered.		12	Unaltered.
	25 kGy	7.5	Disappearance of the characteristic absorption curve form.	25 kGy	7.5	Disappearance of the characteristic emission curve form.
		9.5	Disappearance of the characteristic absorption curve form.		9.5	Disappearance of the characteristic emission curve form.
		12	Disappearance of the characteristic absorption curve form.		12	Disappearance of the characteristic emission curve form.
	50 kGy	7.5	Disappearance of the characteristic absorption curve form.	50 kGy	7.5	Disappearance of the characteristic emission curve form.
		9.5	Disappearance of the characteristic absorption curve form.		9.5	Disappearance of the characteristic emission curve form.
		12	Disappearance of the characteristic absorption curve form.		12	Disappearance of the characteristic emission curve form.

Calibration Curves

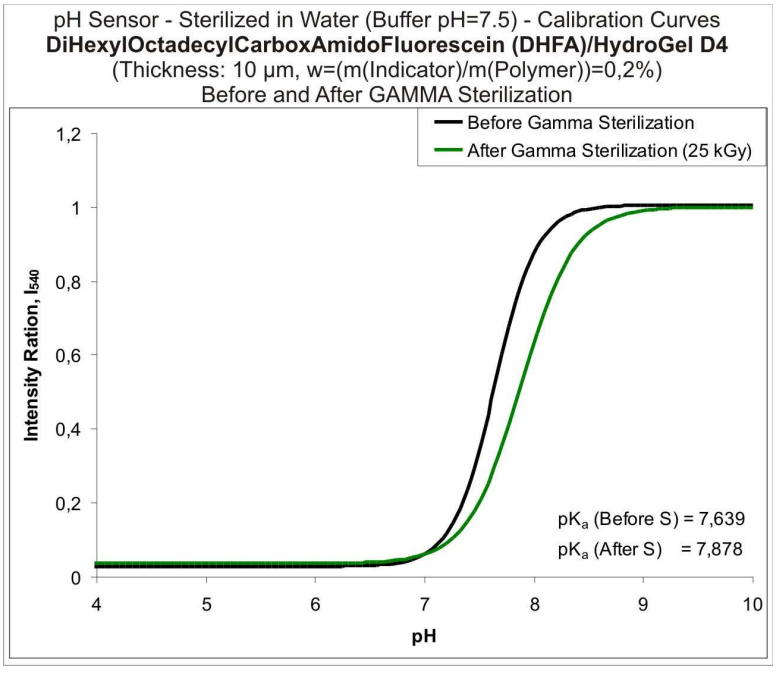

GAMMA S.	Alterations in Calibration Curve Shape	Alterations in pK_a
	Altered curve shape after sterilization. The response to the proton still observed – re-calibration of sensor response.	Increase of pK_a (for 0,239)

C.34.2 Electron Beam Sterilization

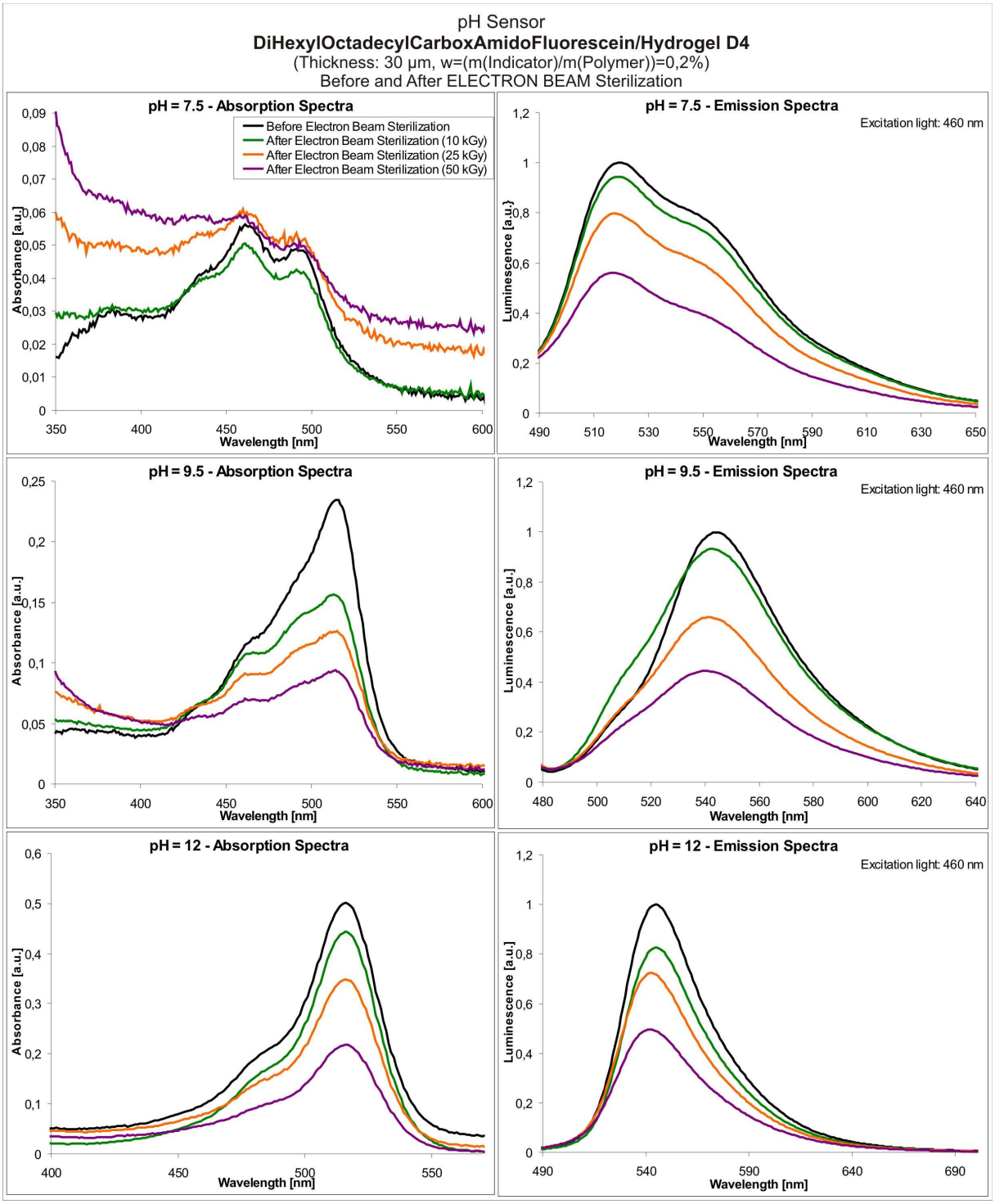

E-BEAM S.	Absorption Spectra			Emission Spectra		
		pH	Alterations		pH	Alterations
Alterations in Absorption/ Emission Intensity	10 kGy	7.5	11,59% decrease	10 kGy	7.5	5,52% decrease
		9.5	33,40% decrease		9.5	6,76% decrease
		12	11,47% decrease		12	17,36% decrease
	25 kGy	7.5	7,53% increase	25 kGy	7.5	20,29% decrease
		9.5	46,34% decrease		9.5	34,04% decrease
		12	30,51% decrease		12	27,66% decrease
	50 kGy	7.5	60,29% increase	50 kGy	7.5	44,03% decrease
		9.5	60,04% decrease		9.5	55,50% decrease
		12	56,63% decrease		12	50,39% decrease

Alterations in Absorption/ Emission Curve Form	10 kGy	7.5	Unaltered.	10 kGy	7.5	Hypsochromic shift of the emission maximum for 2 nm.
		9.5	Altered absorption curve form between 350-505 nm.		9.5	Altered emission curve form between 480-540 nm. Hypsochromic shift of the emission maximum for 1 nm.
		12	Altered absorption curve form between 350-500 nm.		12	Unaltered.
	25 kGy	7.5	Altered absorption curve form. Sensor became slightly turbid after sterilization.	25 kGy	7.5	Altered emission curve form between 540-590 nm. Hypsochromic shift of the emission maximum for 2 nm.
		9.5	Altered absorption curve form between 350-505 nm and 540-800 nm.		9.5	Altered emission curve form between 480-540 nm. Hypsochromic shift of the emission maximum for 3 nm.
		12	Altered absorption curve form between 540-800 nm.		12	Hypsochromic shift of the emission maximum for 2 nm.
	50 kGy	7.5	Altered absorption curve form. Sensor became slightly turbid after sterilization.	50 kGy	7.5	Altered emission curve form between 490-505 nm and 530-570 nm. Hypsochromic shift of the emission maximum for 3 nm.
		9.5	Altered absorption curve form between 350-505 nm and 540-800 nm.		9.5	Altered emission curve form between 480-540 nm. Hypsochromic shift of the emission maximum for 4 nm.
		12	Altered absorption curve form between 350-495 nm and 540-800 nm.		12	Hypsochromic shift of the emission maximum for 3 nm.

Calibration Curves

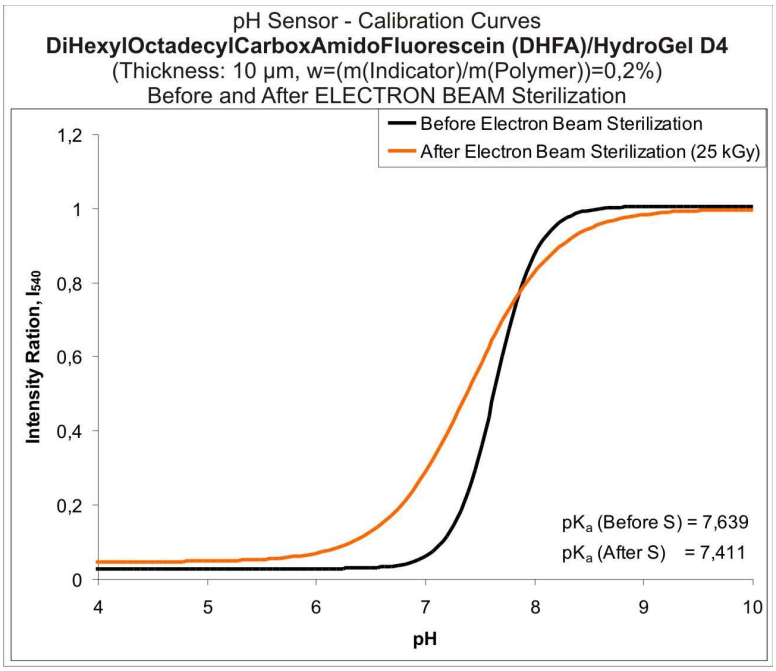

E-BEAM S.	Alterations in Calibration Curve Shape	Alterations in pK_a
	Altered curve shape after sterilization. The response to the proton still observed – re-calibration of sensor response.	Increase of pK_a (for 0,228)

C.34.2.1 Sterilization in Water

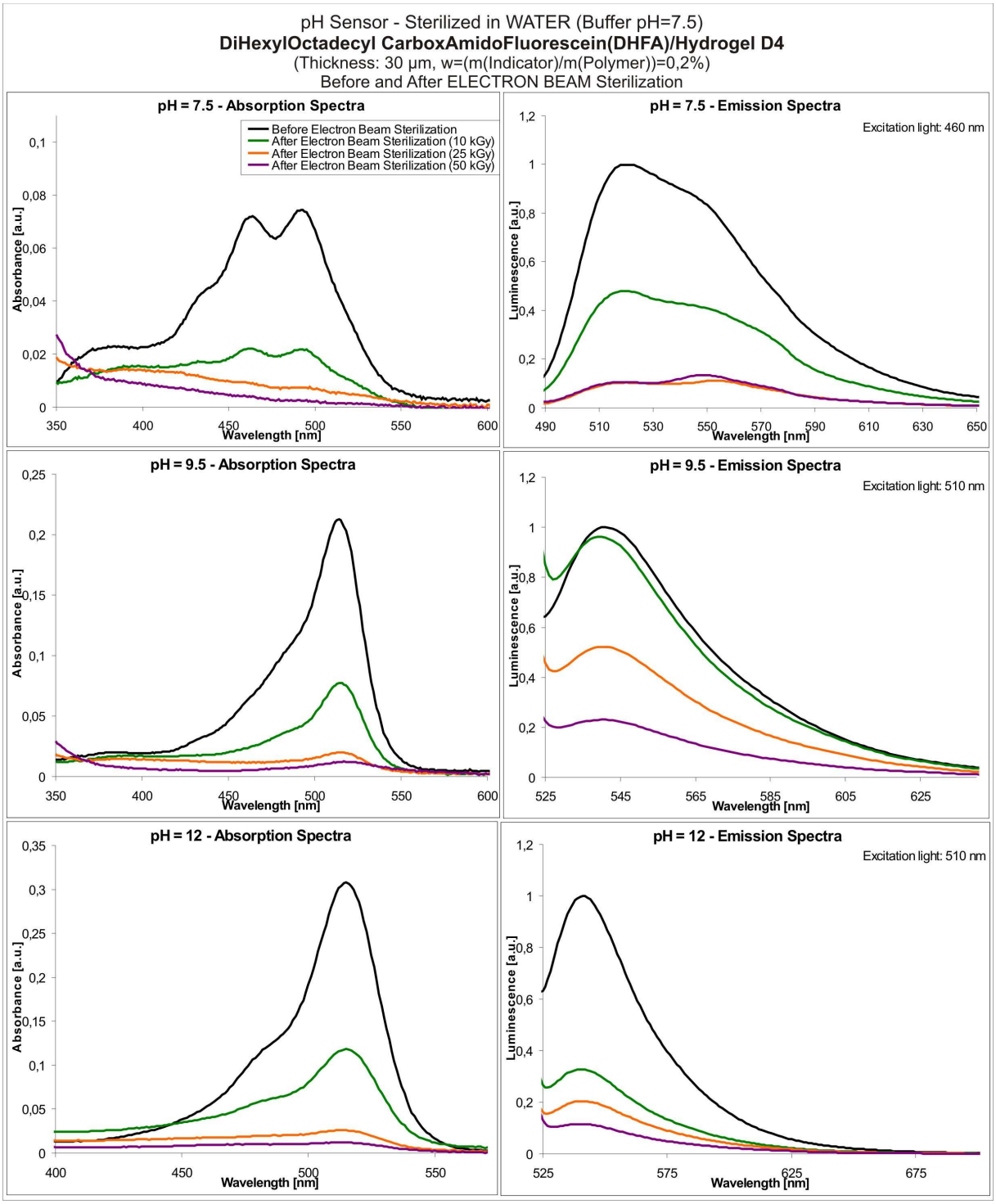

E-BEAM S.	Absorption Spectra			Emission Spectra		
		pH	Alterations		pH	Alterations
Alterations in Absorption/ Emission Intensity	10 kGy	7.5	70,71% decrease	10 kGy	7.5	51,91% decrease
		9.5	33,40% decrease		9.5	3,85% decrease
		12	61,51% decrease		12	67,29% decrease
	25 kGy	7.5	90,08% decrease	25 kGy	7.5	89,59% decrease
		9.5	46,34% decrease		9.5	47,89% decrease
		12	91,66% decrease		12	79,54% decrease
	50 kGy	7.5	96,99% decrease	50 kGy	7.5	89,37% decrease
		9.5	60,04% decrease		9.5	76,98% decrease
		12	96,06% decrease		12	88,43% decrease

Calibration Curves

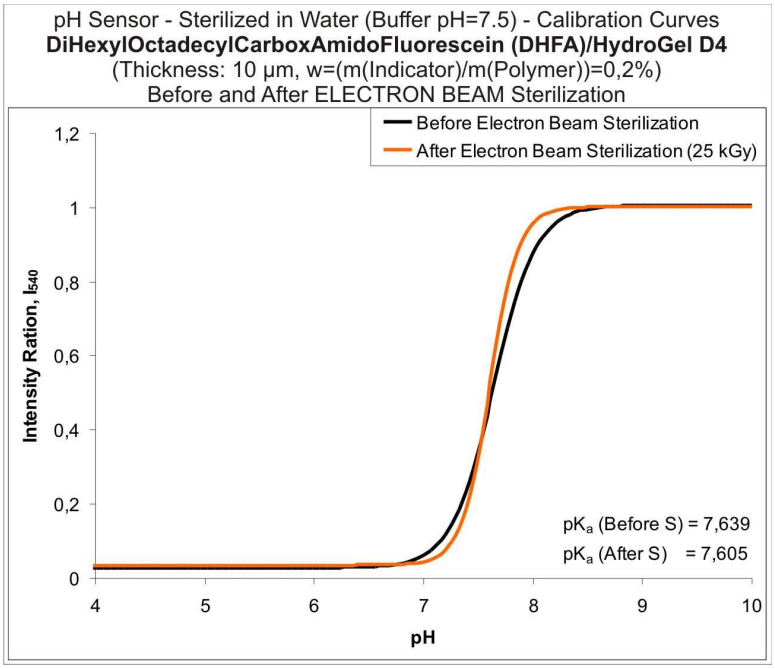

E-BEAM S.	Alterations in Calibration Curve Shape	Alterations in pK_a
	Comparable curve shapes before and after sterilization.	Decrease of pK_a (for 0,034)

C.35 2´,7´-DiHexyl-N-Octadecyl-CarboxAmidoFluorescein (=DHFA) immobilized in Poly(2-HydroxyEthyl Methacrylate) (=pHEMA)

C.35.1 Gamma Sterilization

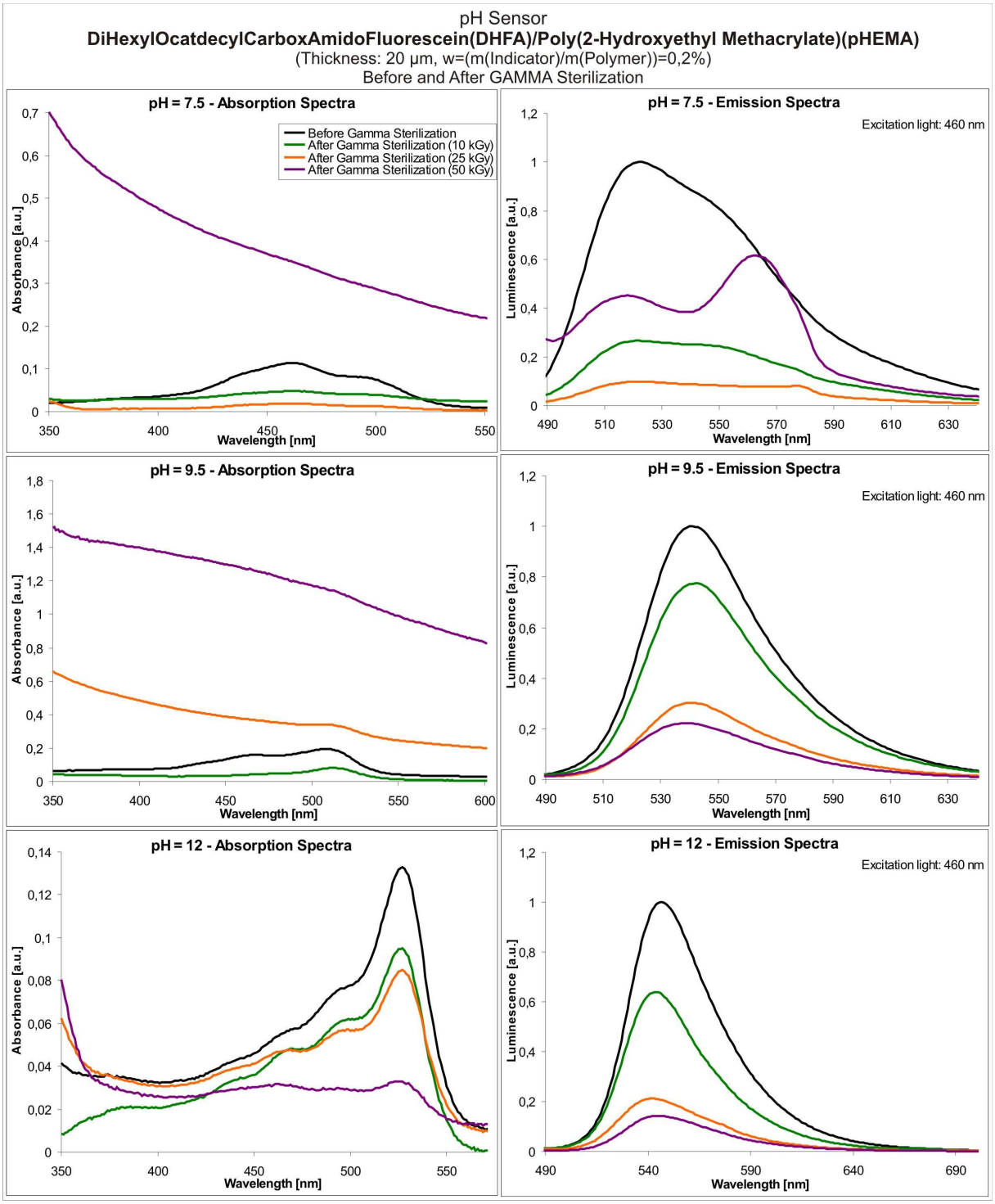

GAMMA S.	Absorption Spectra			Emission Spectra		
		pH	Alterations		pH	Alterations
Alterations in Absorption/ Emission Intensity	10 kGy	7.5	57,78% decrease	10 kGy	7.5	73,47% decrease
		9.5	57,87% decrease		9.5	22,52% decrease
		12	28,75% decrease		12	36,10% decrease
	25 kGy	7.5	83,01% decrease	25 kGy	7.5	90,23% decrease
		9.5	70% increase		9.5	69,77% decrease
		12	36,27% decrease		12	78,80% decrease
	50 kGy	7.5	200% increase	50 kGy	7.5	54,79% decrease
		9.5	490% increase		9.5	77,74% decrease
		12	79,00% decrease		12	85,66% decrease
Alterations in Absorption/ Emission Curve Form	10 kGy	7.5	Disappearance of the characteristic absorption curve form.	10 kGy	7.5	Disappearance of the characteristic emission curve form.
		9.5	Altered absorption curve form between 350-500 nm.		9.5	Unaltered.
		12	Altered absorption curve form between 350-400 nm.		12	Hypsochromic shift of the emission maximum for 2 nm.
	25 kGy	7.5	Disappearance of the characteristic absorption curve form.	25 kGy	7.5	Disappearance of the characteristic emission curve form.
		9.5	Disappearance of the characteristic absorption curve form. Sensor became turbid after sterilization and characterization in buffer – more water uptake.		9.5	Unaltered.
		12	Altered absorption curve form between 350-390 nm.		12	Hypsochromic shift of the emission maximum for 5 nm.
	50 kGy	7.5	Disappearance of the characteristic absorption curve form. Sensor became turbid after sterilization and characterization in buffer – more water uptake.	50 kGy	7.5	Disappearance of the characteristic emission curve form.
		9.5	Disappearance of the characteristic absorption curve form. Sensor became turbid after sterilization and characterization in buffer – more water uptake.		9.5	Hypsochromic shift of the emission maximum for 2 nm.
		12	Disappearance of characteristic absorption curve form.		12	Hypsochromic shift of the emission maximum for 2 nm.

Calibration Curves

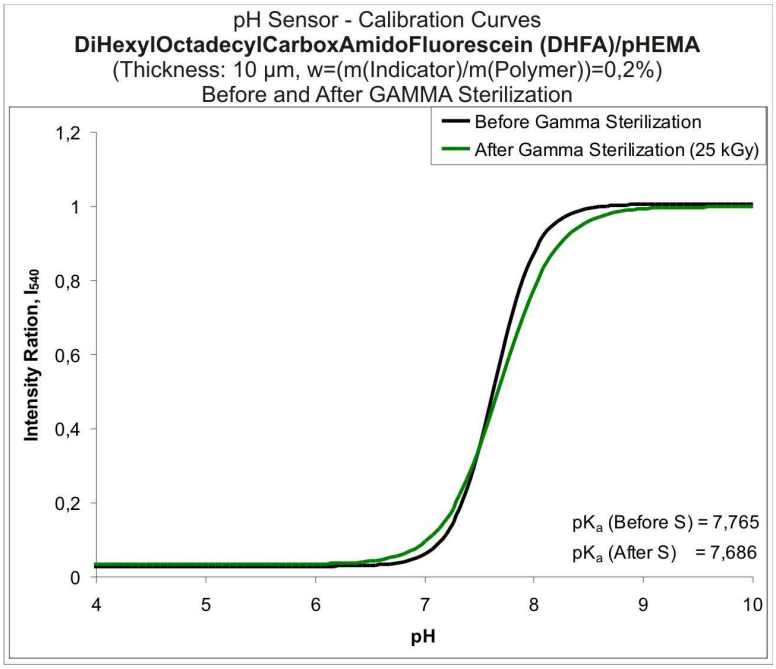

GAMMA S.	Alterations in Calibration Curve Shape	Alterations in pK_a
	Comparable curve shapes before and after sterilization.	Decrease of pK_a (for 0,079)

C.35.1.1 Sterilized in Water

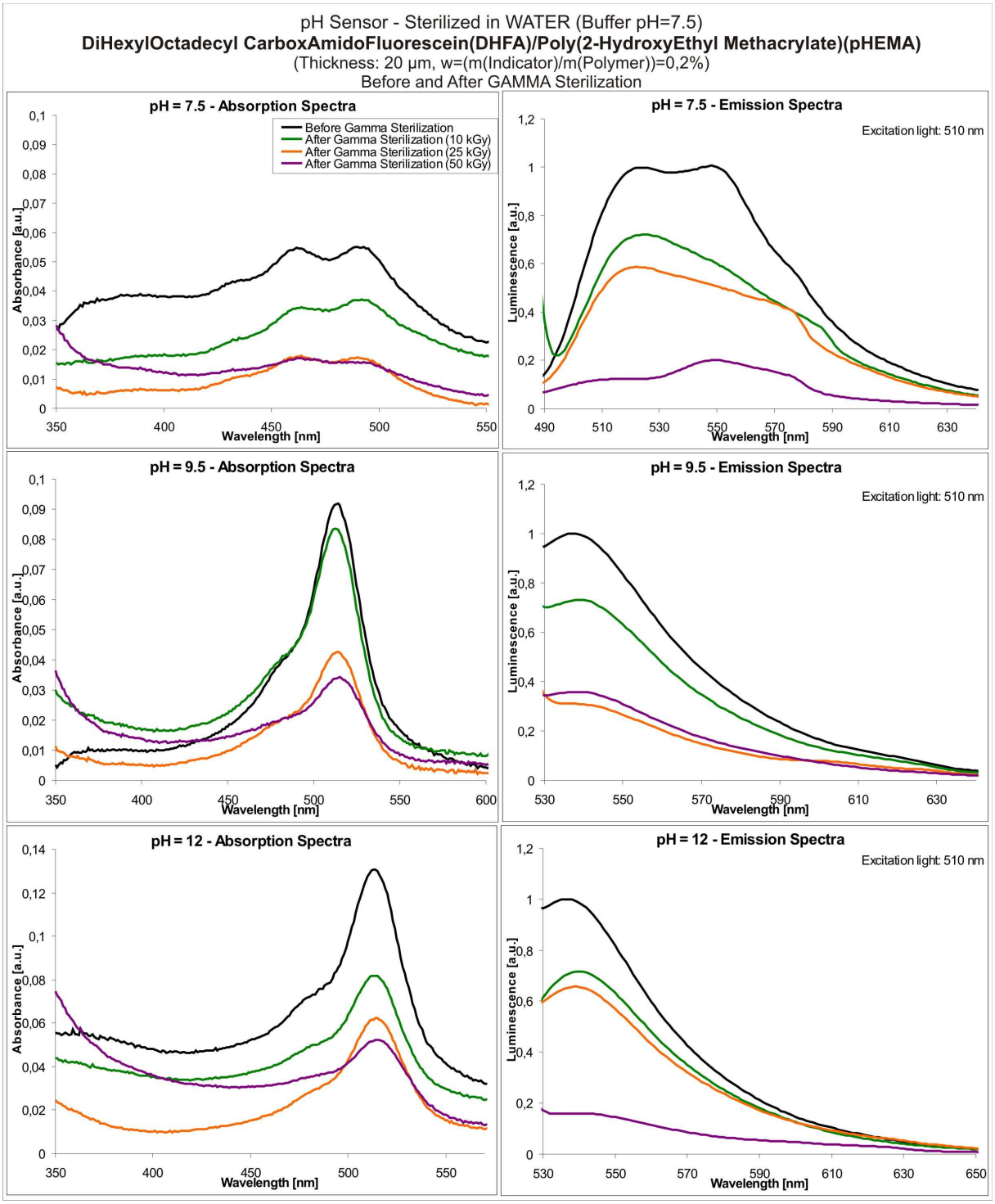

GAMMA S.	Absorption Spectra			Emission Spectra		
		pH	Alterations		pH	Alterations
Alterations in Absorption/ Emission Intensity	10 kGy	7.5	37,34% decrease	10 kGy	7.5	27,66% decrease
		9.5	8,55% decrease		9.5	26,74% decrease
		12	37,12% decrease		12	28,29% decrease
	25 kGy	7.5	67,64% decrease	25 kGy	7.5	41,22% decrease
		9.5	53,39% decrease		9.5	68,94% decrease
		12	52,12% decrease		12	34,26% decrease
	50 kGy	7.5	69,42% decrease	50 kGy	7.5	79,91% decrease
		9.5	63,03% decrease		9.5	64,16% decrease
		12	59,79% decrease		12	83,95% decrease

Alterations in Absorption/ Emission Curve Form	10 kGy	7.5	Unaltered.	10 kGy	7.5	Altered emission curve form between 530-590 nm.
		9.5	Altered absorption curve form between 350-470 nm.		9.5	Bathochromic shift of the emission maximum for 2 nm.
		12	Unaltered.		12	Bathochromic shift of the emission maximum for 4 nm.
	25 kGy	7.5	Unaltered.	25 kGy	7.5	Altered emission curve form between 530-650 nm.
		9.5	Altered absorption curve form between 550-800 nm.		9.5	Altered emission curve form between 590-700 nm.
		12	Unaltered.		12	Bathochromic shift of the emission maximum for 3 nm.
	50 kGy	7.5	Altered absorption curve form between 350-450 nm and 510-800 nm.	50 kGy	7.5	Disappearance of the characteristic emission curve form.
		9.5	Altered absorption curve form between 350-470 nm and 550-800 nm.		9.5	Bathochromic shift of the emission maximum for 1 nm.
		12	Altered absorption curve form between 350-500 nm.		12	Altered emission curve form between 570-650 nm. Bathochromic shift of the emission maximum for 5 nm.

Calibration Curves

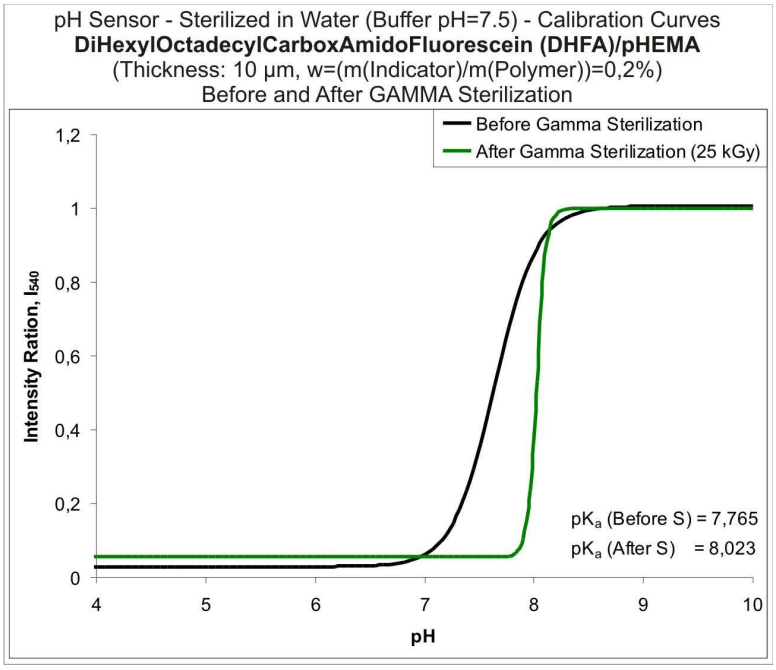

GAMMA S.	Alterations in Calibration Curve Shape	Alterations in pK_a
	Altered curve shape after sterilization. The response to the proton still observed – re-calibration of sensor response.	Increase of pK_a (for 0,322)

C.35.2 Electron Beam Sterilization

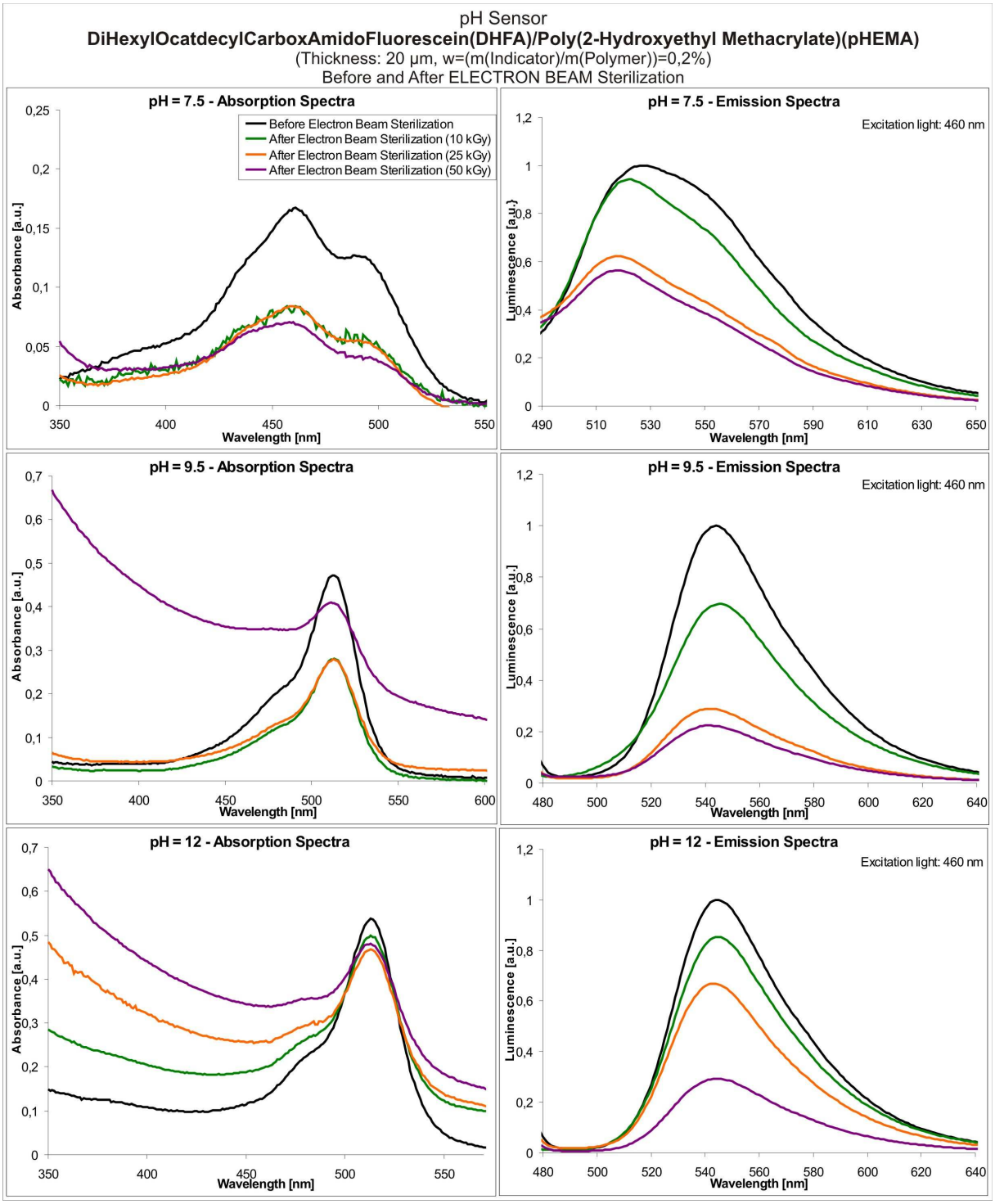

E-BEAM S.	Absorption Spectra			Emission Spectra		
		pH	Alterations		pH	Alterations
Alterations in Absorption/ Emission Intensity	10 kGy	7.5	51,14% decrease	10 kGy	7.5	5,89% decrease
		9.5	40,68% decrease		9.5	6,76% decrease
		12	6,38% decrease		12	14,72% decrease
	25 kGy	7.5	49,39% decrease	25 kGy	7.5	37,75% decrease
		9.5	41,52% decrease		9.5	64,04% decrease
		12	12,16% decrease		12	33,12% decrease
	50 kGy	7.5	58,13% decrease	50 kGy	7.5	43,62% decrease
		9.5	13,22% decrease		9.5	55,50% decrease
		12	10,31% decrease		12	70,72% decrease

Alterations in Absorption/ Emission Curve Form	10 kGy	7.5	Unaltered.	10 kGy	7.5	Hypsochromic shift of the emission maximum for 5 nm.
		9.5	Unaltered.		9.5	Altered emission curve form between 480-530 nm.
		12	Sensor became slightly turbid after sterilization and characterization in the buffer solution - – greater water uptake after sterilization.		12	Unaltered.
	25 kGy	7.5	Unaltered.	25 kGy	7.5	Hypsochromic shift of the emission maximum for 9 nm.
		9.5	Sensor became slightly turbid after sterilization and characterization in the buffer solution - – greater water uptake after sterilization.		9.5	Altered emission curve form between 480-500 nm. Hypsochromic shift of the emission maximum for 3 nm.
		12	Sensor became slightly turbid after sterilization and characterization in the buffer solution - – greater water uptake after sterilization.		12	Hypsochromic shift of the emission maximum for 2 nm.
	50 kGy	7.5	Altered absorption curve form between 350-400 nm and 470-500 nm.	50 kGy	7.5	Hypsochromic shift of the emission maximum for 9 nm.
		9.5	Sensor became turbid after sterilization and characterization in the buffer solution – greater water uptake after sterilization.		9.5	Altered emission curve form between 480-500 nm. Hypsochromic shift of the emission maximum for 3 nm.
		12	Sensor became slightly turbid after sterilization and characterization in the buffer solution - – greater water uptake after sterilization.		12	Hypsochromic shift of the emission maximum for 1 nm.

Calibration Curves

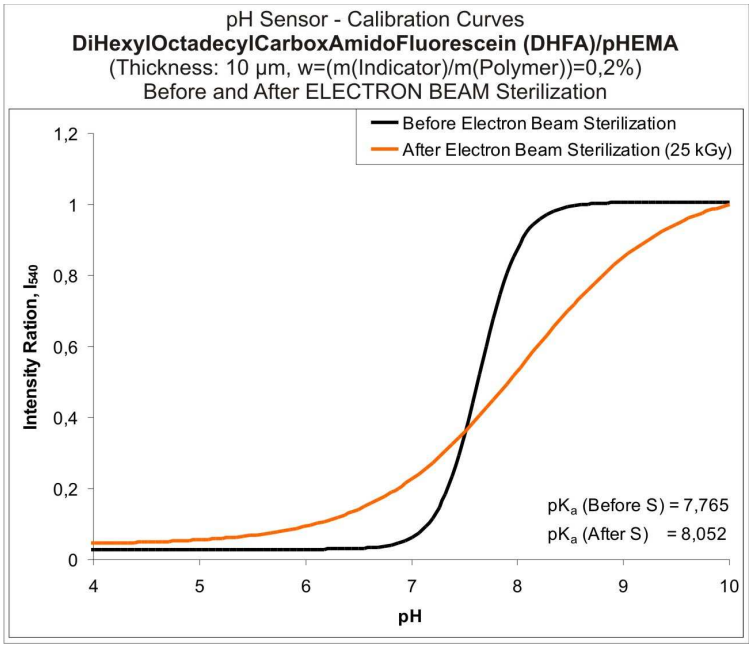

E-BEAM S.	Alterations in Calibration Curve Shape	Alterations in pK_a
	Altered curve shape after sterilization. The response to the proton still observed – re-calibration of sensor response.	Increase of pK_a (for 0,287)

C.35.2.1 Sterilization in Water

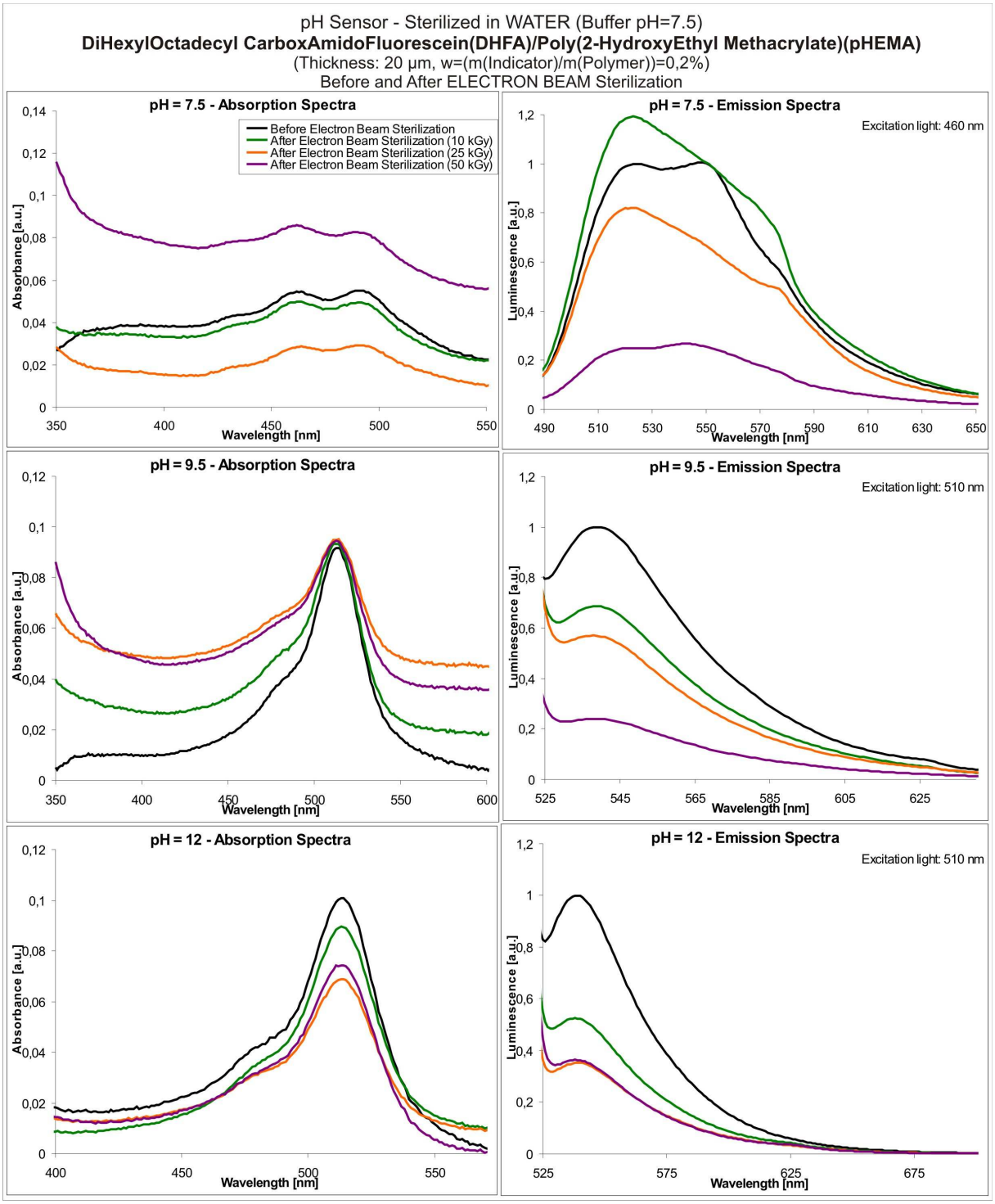

E-BEAM S.	Absorption Spectra			Emission Spectra		
		pH	Alterations		pH	Alterations
Alterations in Absorption/ Emission Intensity	10 kGy	7.5	9,95% decrease	10 kGy	7.5	16,19% increase
		9.5	2,35% increase		9.5	31,39% decrease
		12	11,22% decrease		12	47,52% decrease
	25 kGy	7.5	47,00% decrease	25 kGy	7.5	18,08% decrease
		9.5	4,03% increase		9.5	42,98% decrease
		12	31,77% decrease		12	64,70% decrease
	50 kGy	7.5	37% increase	50 kGy	7.5	75,02% decrease
		9.5	3,22% increase		9.5	76,07% decrease
		12	26,19% decrease		12	63,61% decrease

Alterations in Absorption/ Emission Curve Form	10 kGy	7.5	Unaltered.	10 kGy	7.5	Altered emission curve form between 530-590 nm. Disappearance of the emission peak with λ_{max}=551 nm
		9.5	Sensor became slightly turbid after sterilization and characterization in the buffer solution - – greater water uptake after sterilization.		9.5	Altered emission curve form between 525-535 nm.
		12	Altered absorption curve form between 350-485 nm and 535-700 nm.		12	Altered emission curve form between 525-530 nm and 605-645 nm.
	25 kGy	7.5	Altered absorption curve form between 350-460 nm.	25 kGy	7.5	Altered emission curve form between 530-590 nm. Disappearance of the emission peak with λ_{max}=551 nm
		9.5	Sensor became slightly turbid after sterilization and characterization in the buffer solution - – greater water uptake after sterilization.		9.5	Altered emission curve form between 525-535 nm.
		12	Altered absorption curve form between 535-700 nm.		12	Altered emission curve form between 525-530 nm and 605-645 nm.
	50 kGy	7.5	Sensor became turbid after sterilization and characterization in the buffer solution - – greater water uptake after sterilization.	50 kGy	7.5	Altered emission curve form between 530-590 nm. New emission peak with λ_{max}=543 nm
		9.5	Sensor became turbid after sterilization and characterization in the buffer solution – greater water uptake after sterilization.		9.5	Altered emission curve form between 525-535 nm and 575-610 nm.
		12	Altered absorption curve form between 540-570 nm.		12	Altered emission curve form between 525-530 nm and 605-645 nm.

Calibration Curves

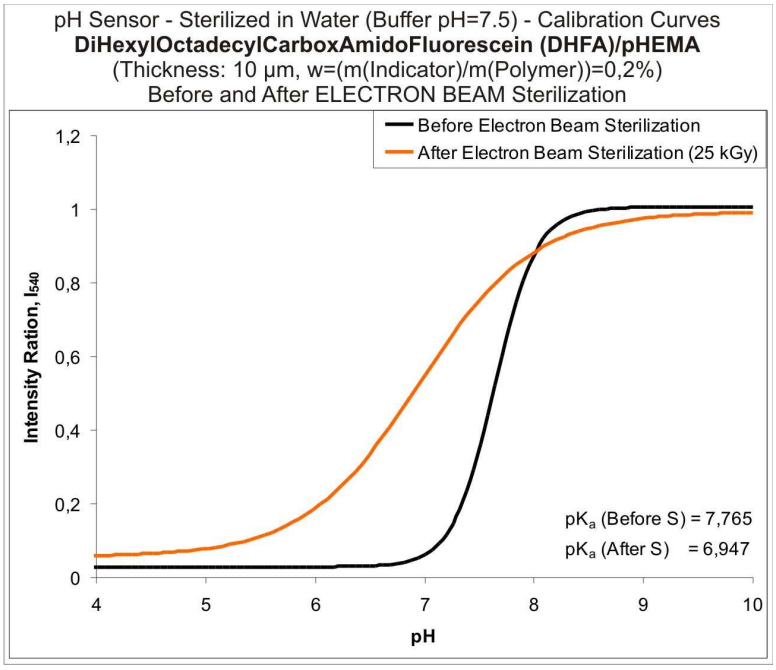

E-BEAM S.	Alterations in Calibration Curve Shape	Alterations in pK_a
	Greatly altered curve shape after sterilization.	Decrease of pK_a (for 0,818)

C.36 pH Sensitive Coumarin immobilized in HydroMed Hydrogel D4

C.36.1 Gamma Sterilization

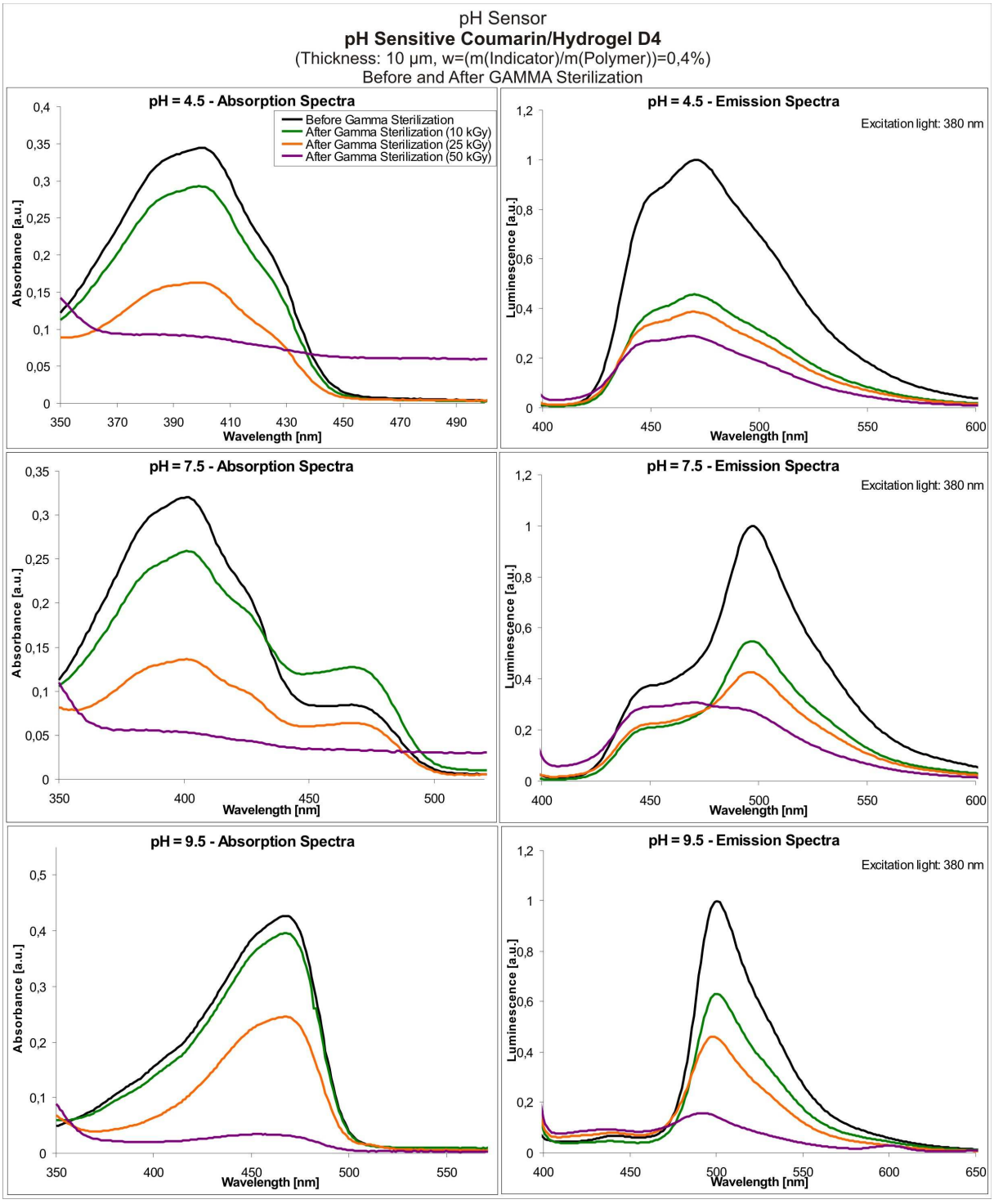

GAMMA S.	Absorption Spectra			Emission Spectra		
		pH	Alterations		pH	Alterations
Alterations in Absorption/ Emission Intensity	10 kGy	4.5	15,10% decrease	10 kGy	4.5	54,30% decrease
		7.5	19,19% decrease		7.5	45,10% decrease
		9.5	7,34% decrease		9.5	36,88% decrease
	25 kGy	4.5	52,86% decrease	25 kGy	4.5	61,29% decrease
		7.5	57,63% decrease		7.5	57,33% decrease
		9.5	42,56% decrease		9.5	53,86% decrease
	50 kGy	4.5	73,58% decrease	50 kGy	4.5	71,12% decrease
		7.5	83,24% decrease		7.5	69,20% decrease
		9.5	92,21% decrease		9.5	84,55% decrease
Alterations in Absorption/ Emission Curve Form	10 kGy	4.5	Unaltered.	10 kGy	4.5	Hypsochromic shift of the emission maximum for 2 nm.
		7.5	The ratio between protonation/deprotonation absorption peaks is altered.		7.5	Unaltered.
		9.5	Unaltered.		9.5	Unaltered.
	25 kGy	4.5	Unaltered.	25 kGy	4.5	Hypsochromic shift of the emission maximum for 2 nm.
		7.5	The ratio between protonation/deprotonation absorption peaks is altered.		7.5	Altered emission curve form between 400-490 nm.
		9.5	Unaltered.		9.5	Altered emission curve form between 400-470 nm Hypsochromic shift of the emission maximum for 2 nm.
	50 kGy	4.5	Disappearance of the characteristic absorption curve form.	50 kGy	4.5	Altered emission curve form between 400-470 nm. Hypsochromic shift of the emission maximum for 2 nm.
		7.5	Disappearance of the characteristic absorption curve form.		7.5	The emission spectrum shows the emission curve of protonated form of indicator.
		9.5	Disappearance of the characteristic absorption curve form.		9.5	Altered emission curve form between 400-470 nm. Hypsochromic shift of the emission maximum for 2 nm. New emission peak with λ_{max}=602 nm.

Calibration Curves

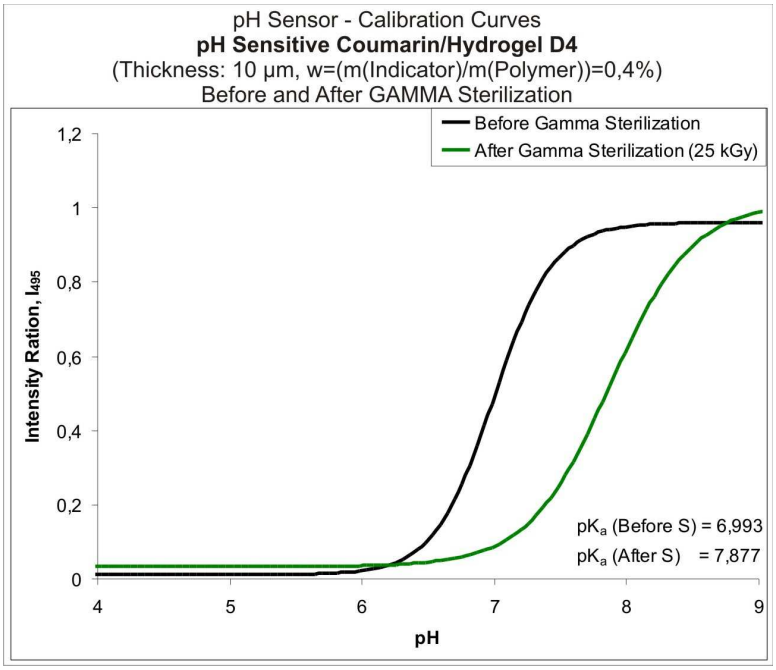

GAMMA S.	Alterations in Calibration Curve Shape	Alterations in pK_a
	Greatly altered curve shape after sterilization.	Increase of pK_a (for 0,884)

C.36.1.1 Sterilized in Water

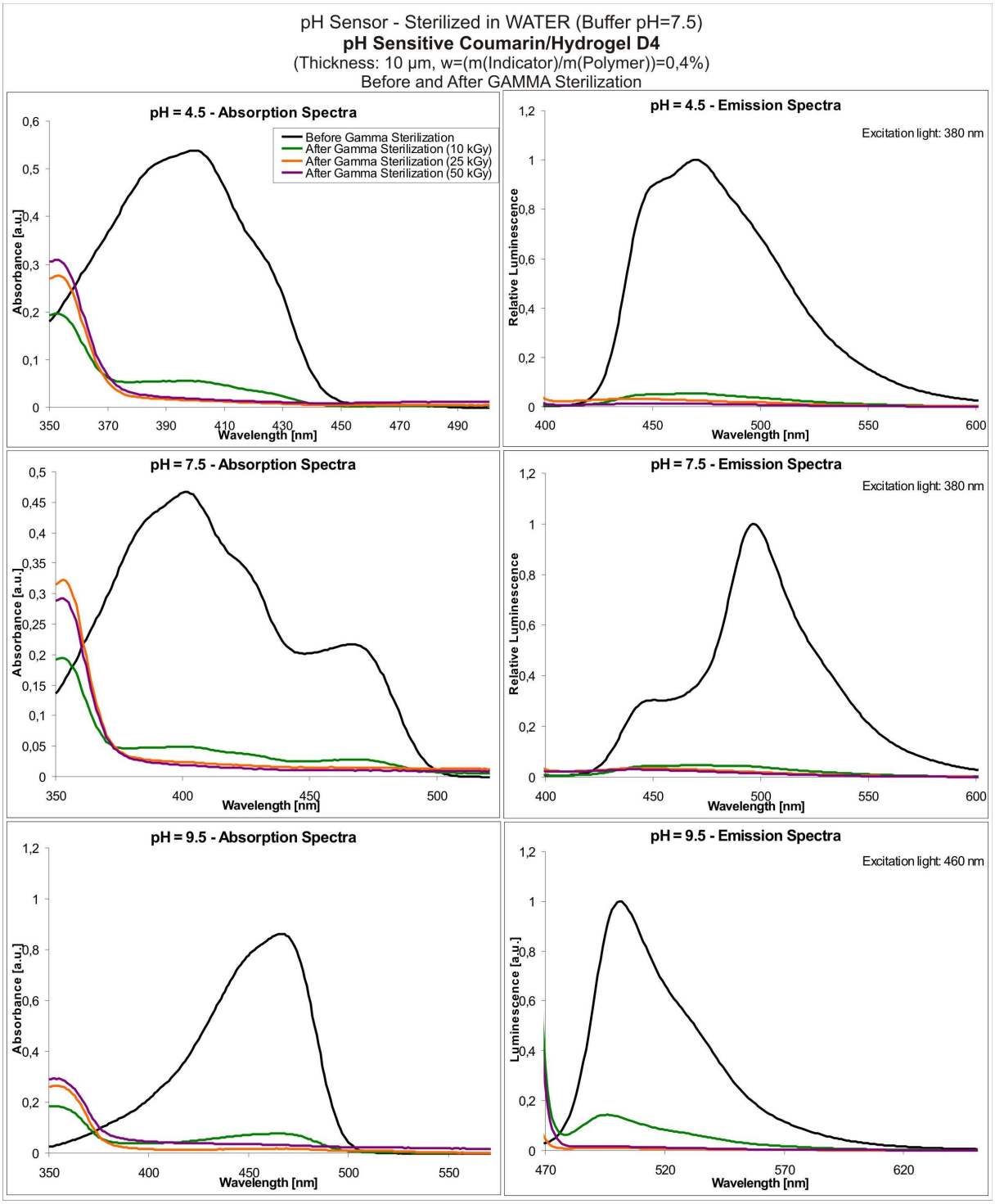

GAMMA S.	Absorption Spectra			Emission Spectra		
		pH	Alterations		pH	Alterations
Alterations in Absorption/ Emission Intensity	10 kGy	4.5	89,81% decrease	10 kGy	4.5	94,56% decrease
		7.5	89,43% decrease		7.5	95,24% decrease
		9.5	91,30% decrease		9.5	85,68% decrease
	25 kGy	4.5	96,41% decrease	25 kGy	4.5	96,71% decrease
		7.5	94,99% decrease		7.5	96,40% decrease
		9.5	98,14% decrease		9.5	98,92% decrease
	50 kGy	4.5	96,58% decrease	50 kGy	4.5	98,68% decrease
		7.5	96,13% decrease		7.5	96,95% decrease
		9.5	96,13% decrease		9.5	98,26% decrease

Calibration Curves

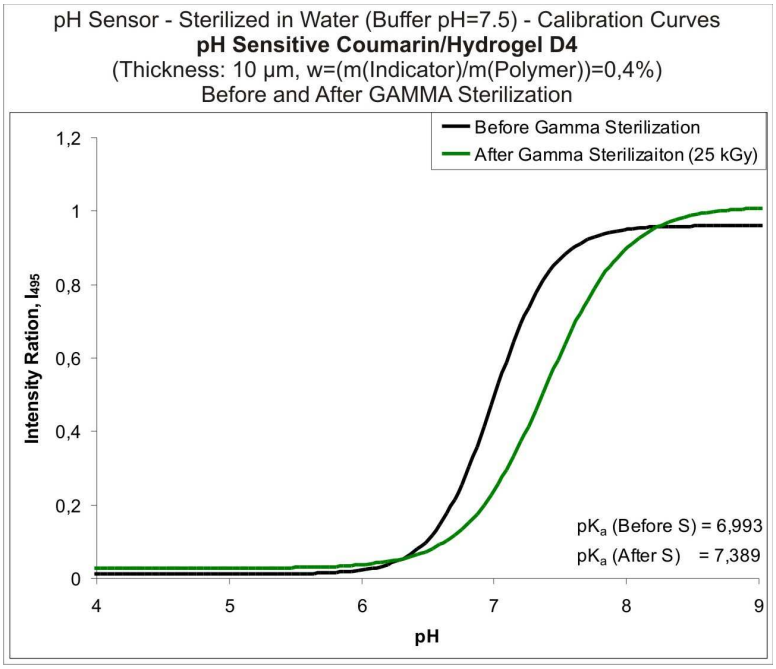

GAMMA S.	Alterations in Calibration Curve Shape	Alterations in pK_a
	Greatly altered curve shape after sterilization.	Decrease of pK_a (for 0,396)

C.36.2 Electron Beam Sterilization

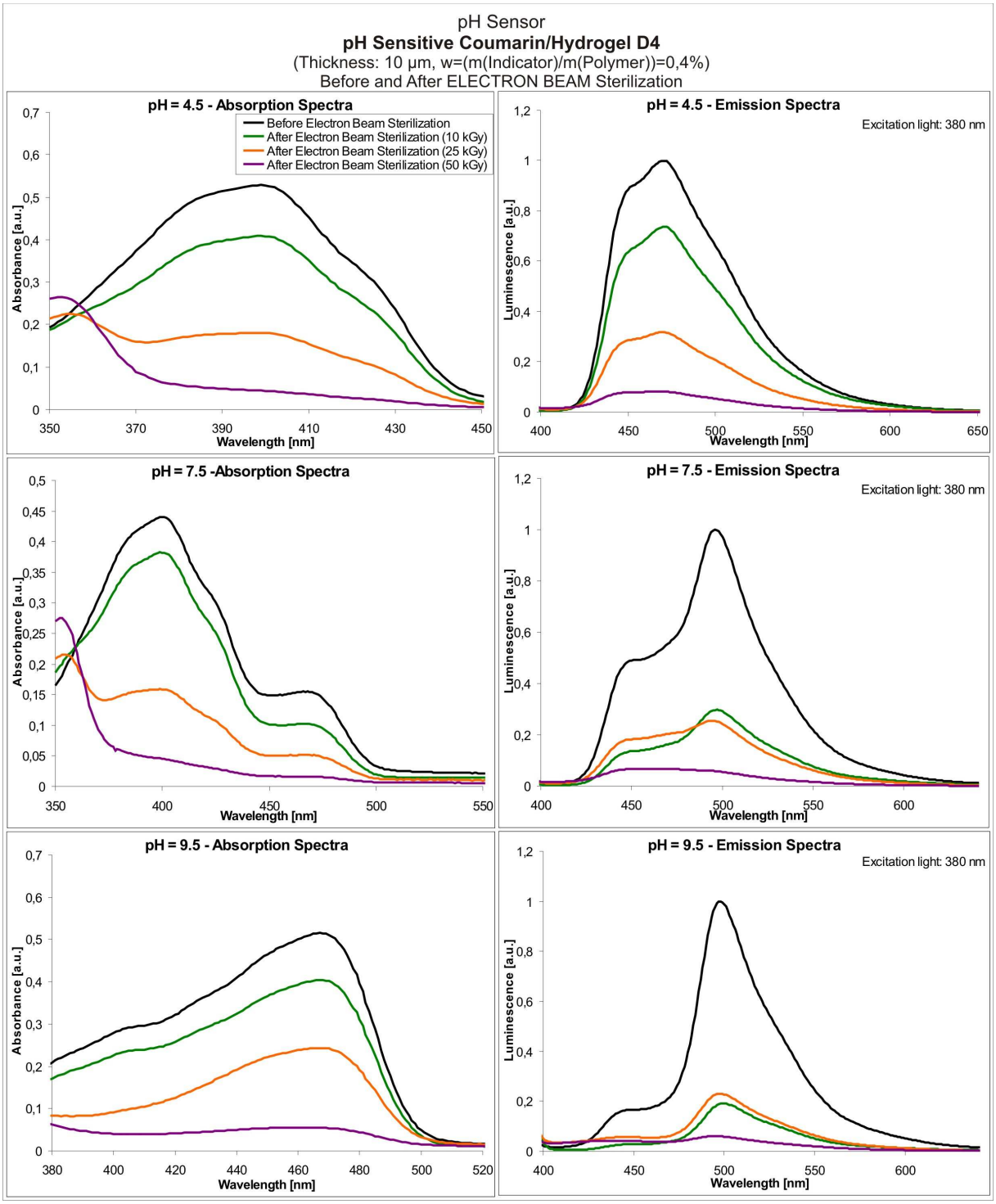

E-BEAM S.	Absorption Spectra			Emission Spectra		
		pH	Alterations		pH	Alterations
Alterations in Absorption/ Emission Intensity	10 kGy	4.5	22,73% decrease	10 kGy	4.5	26,36% decrease
		7.5	12,96% decrease		7.5	70,31% decrease
		9.5	21,80% decrease		9.5	80,76% decrease
	25 kGy	4.5	66,05% decrease	25 kGy	4.5	68,22% decrease
		7.5	63,84% decrease		7.5	74,54% decrease
		9.5	52,69% decrease		9.5	76,93% decrease
	50 kGy	4.5	91,98% decrease	50 kGy	4.5	91,71% decrease
		7.5	89,32% decrease		7.5	93,21% decrease
		9.5	89,29% decrease		9.5	93,90% decrease

Alterations in Absorption/ Emission Curve Form	10 kGy	4.5	Unaltered.	10 kGy	4.5	Unaltered.
		7.5	Unaltered.		7.5	Unaltered.
		9.5	Unaltered.		9.5	Unaltered.
	25 kGy	4.5	Disappearance of the characteristic absorption curve form.	25 kGy	4.5	Altered emission curve form between 400-440 nm.
		7.5	Altered emission curve form between 350-370 nm The ratio between protonation/deprotonation absorption peaks is altered.		7.5	The ratio between protonation/deprotonation absorption peaks is altered.
		9.5	Unaltered.		9.5	Altered emission curve form between 400-480 nm Hypsochromic shift of the emission maximum for 2 nm.
	50 kGy	4.5	Disappearance of the characteristic absorption curve form.	50 kGy	4.5	Altered emission curve form between 400-460 nm. Hypsochromic shift of the emission maximum for 3 nm.
		7.5	Disappearance of the characteristic absorption curve form.		7.5	The emission spectrum shows the emission curve of protonated form of indicator.
		9.5	Disappearance of the characteristic absorption curve form.		9.5	Altered emission curve form between 400-490 nm Hypsochromic shift of the emission maximum for 4 nm.

Calibration Curves

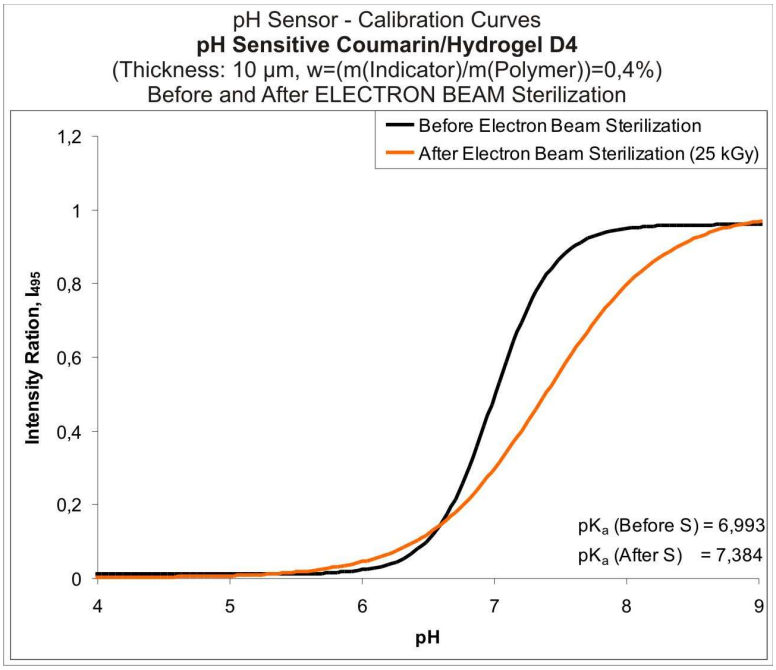

E-BEAM S.	Alterations in Calibration Curve Shape	Alterations in pK_a
	Greatly altered curve shape after sterilization.	Increase of pK_a (for 0,391)

C.36.2.1 Sterilization in Water

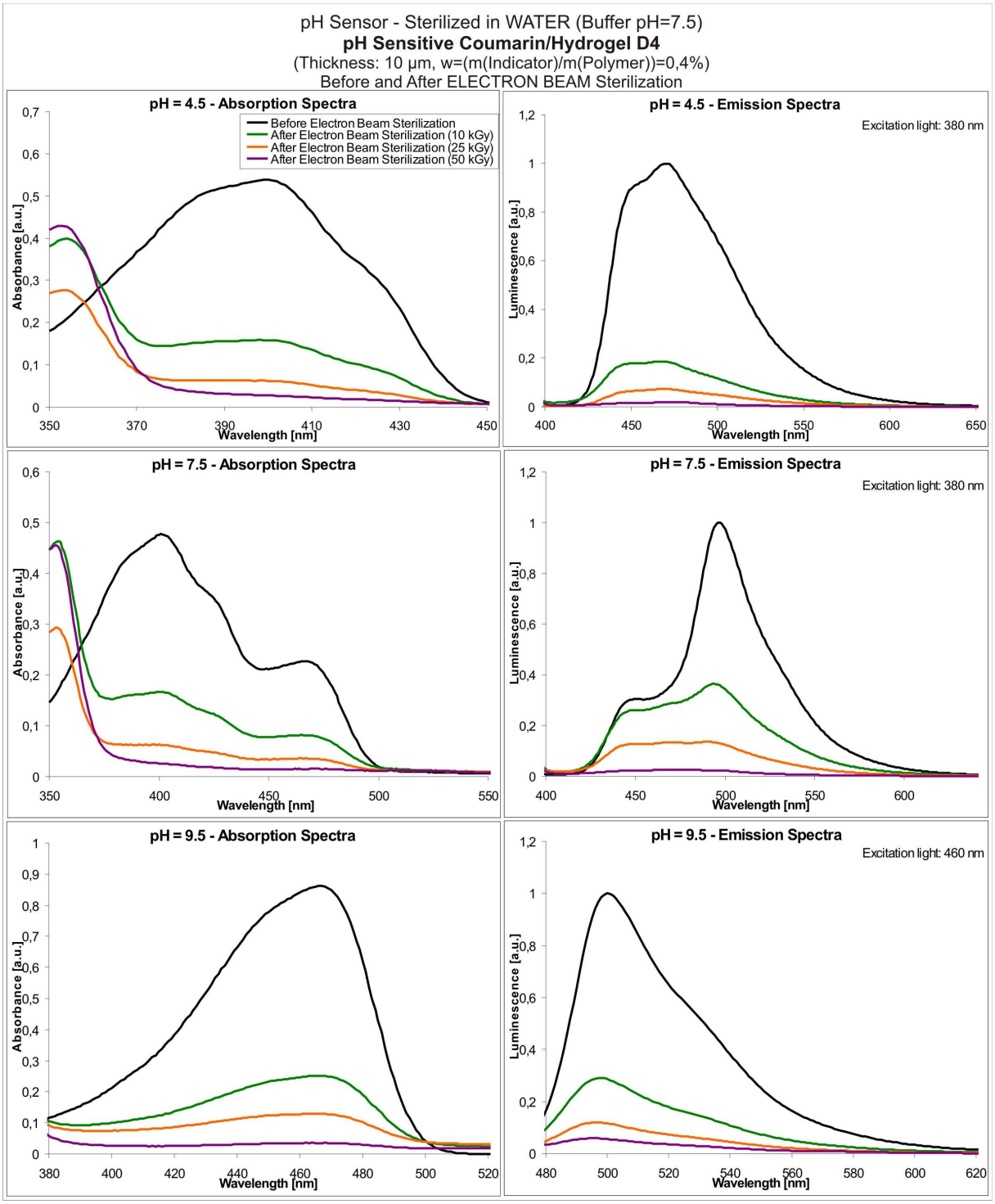

E-BEAM S.	Absorption Spectra			Emission Spectra		
		pH	Alterations		pH	Alterations
Alterations in Absorption/ Emission Intensity	10 kGy	4.5	70,56% decrease	10 kGy	4.5	81,33% decrease
		7.5	65,10% decrease		7.5	63,60% decrease
		9.5	70,82% decrease		9.5	70,09% decrease
	25 kGy	4.5	88,46% decrease	25 kGy	4.5	92,67% decrease
		7.5	86,99% decrease		7.5	86,46% decrease
		9.5	85,02% decrease		9.5	87,97% decrease
	50 kGy	4.5	94,50% decrease	50 kGy	4.5	97,96% decrease
		7.5	94,78% decrease		7.5	97,42% decrease
		9.5	95,86% decrease		9.5	94,09% decrease

Calibration Curves

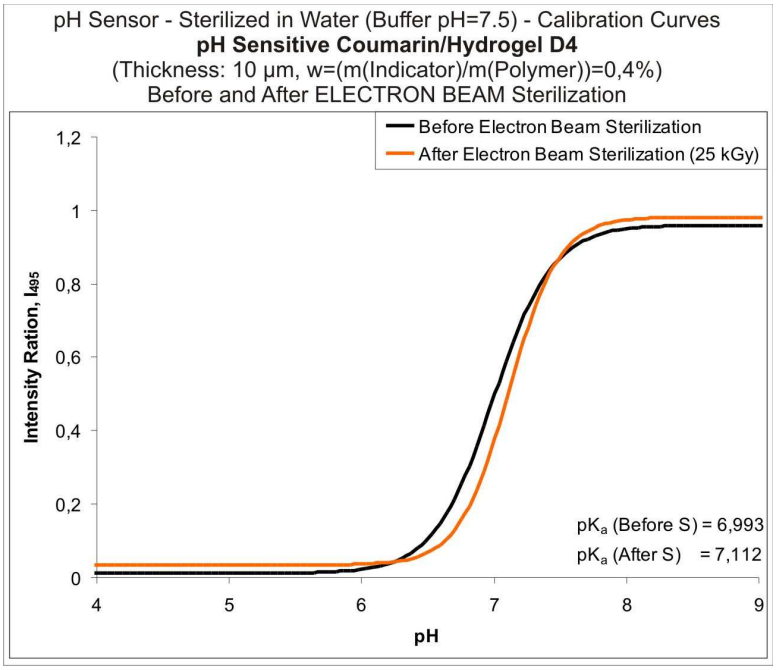

E-BEAM S.	Alterations in Calibration Curve Shape	Alterations in pK_a
	Comparable curve shapes before and after sterilization.	Decrease of pK_a (for 0,119)

C.37 pH Sensitive Coumarin immobilized in Poly(2-HydroxyEthyl Methacrylate) (=pHEMA)

C.37.1 Gamma Sterilization

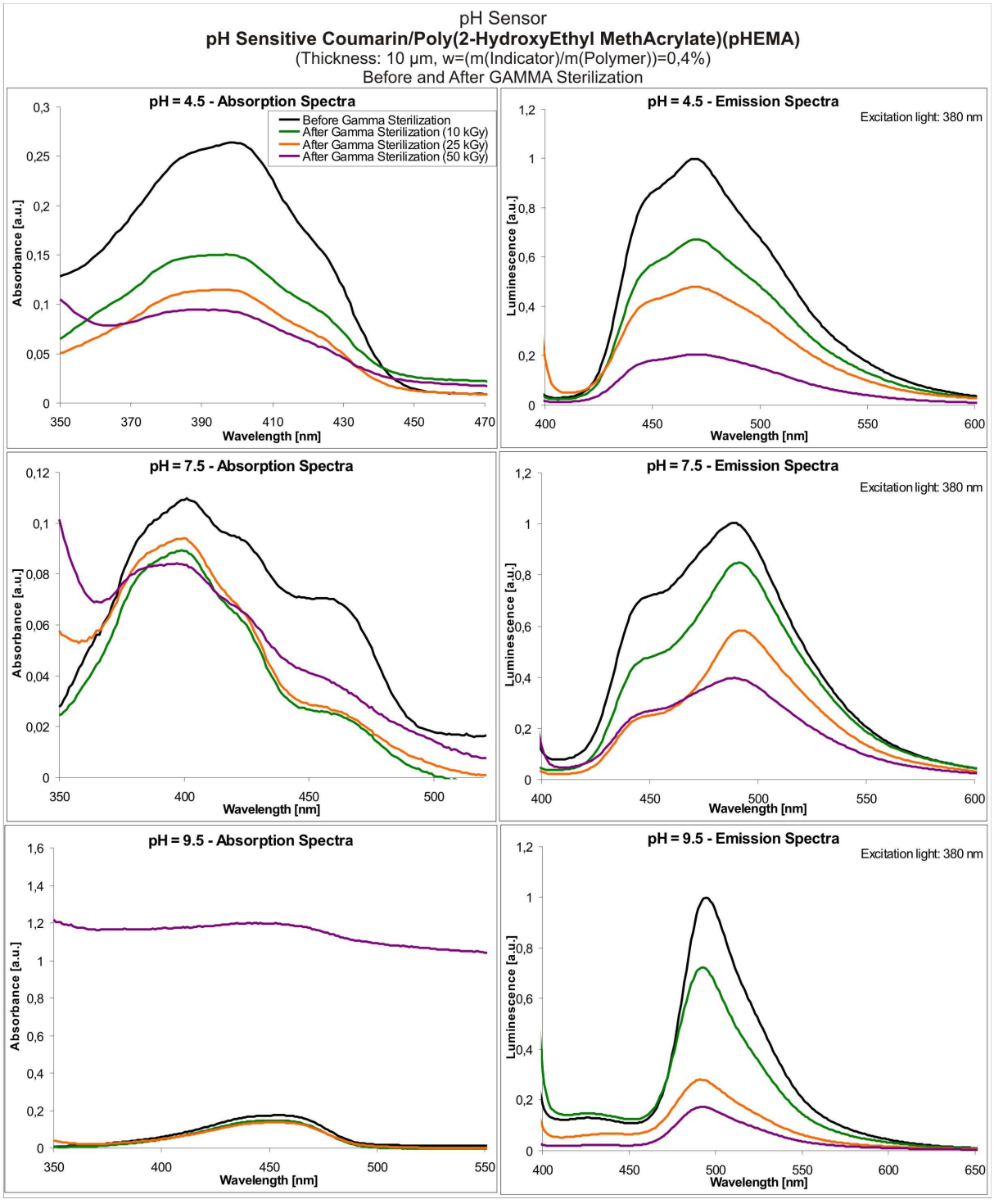

GAMMA S.	Absorption Spectra			Emission Spectra		
Alterations in Absorption/ Emission Intensity		pH	Alterations		pH	Alterations
	10 kGy	4.5	42,70% decrease	10 kGy	4.5	32,75% decrease
		7.5	18,59% decrease		7.5	45,10% decrease
		9.5	15,46% decrease		9.5	27,72% decrease
	25 kGy	4.5	56,41% decrease	25 kGy	4.5	51,96% decrease
		7.5	14,26% decrease		7.5	57,33% decrease
		9.5	21,85% decrease		9.5	71,97% decrease

	50 kGy	4.5	64,39% decrease	50 kGy	4.5	79,37% decrease
		7.5	22,99% decrease		7.5	69,20% decrease
		9.5	580% increase		9.5	82,75% decrease
Alterations in Absorption/ Emission Curve Form	10 kGy	4.5	Altered absorption curve form between 430-800 nm.	10 kGy	4.5	Altered emission curve form between 475-580 nm.
		7.5	The ratio between protonation/deprotonation absorption peaks is altered.		7.5	Altered emission curve form between 400-490 nm. Bathochromic shift of the emission maximum for 4 nm.
		9.5	Unaltered.		9.5	Altered emission curve form between 400-470 nm. Hypsochromic shift of the emission maximum for 3 nm.
	25 kGy	4.5	Altered absorption curve form between 430-800 nm.	25 kGy	4.5	Altered emission curve form between 400-420 nm and 475-580 nm.
		7.5	The ratio between protonation/deprotonation absorption peaks is altered.		7.5	Altered emission curve form between 400-490 nm. Bathochromic shift of the emission maximum for 4 nm.
		9.5	Unaltered.		9.5	Altered emission curve form between 400-470 nm. Hypsochromic shift of the emission maximum for 4 nm.
	50 kGy	4.5	Altered absorption curve form between 350-390 nm and 430-800 nm. Hypsochromic shift of the absorption maximum for 2 nm.	50 kGy	4.5	Altered emission curve form between 400-440 nm and 475-580 nm. Bathochromic shift of the emission maximum for 2 nm.
		7.5	Disappearance of the characteristic absorption curve form.		7.5	Altered emission curve form between 400-490 nm. Bathochromic shift of the emission maximum for 4 nm.
		9.5	The sensor became turbid after sterilization and characterization in the buffer – greater water uptake.		9.5	Altered emission curve form between 400-470 nm. Hypsochromic shift of the emission maximum for 3 nm.

Calibration Curves

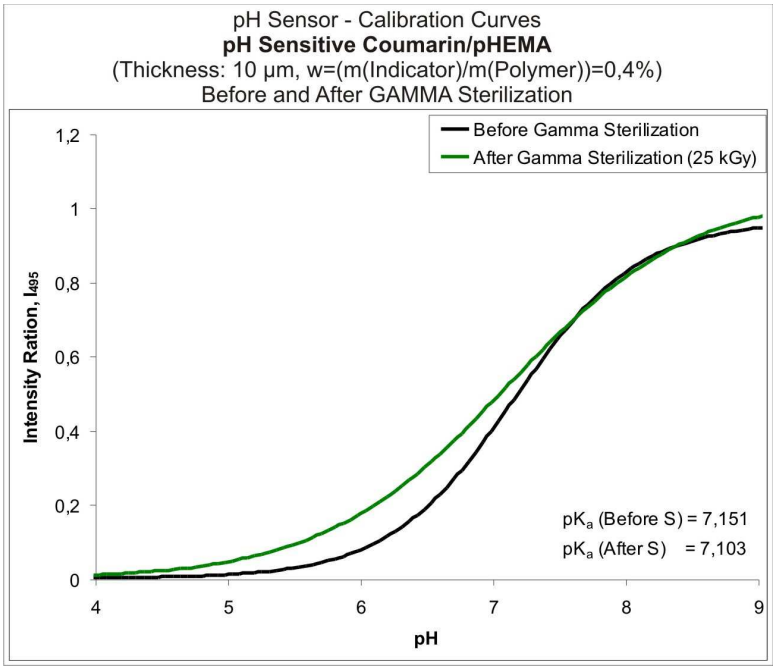

GAMMA S.	Alterations in Calibration Curve Shape	Alterations in pK_a
	Altered curve shape after sterilization. The response to the proton still observed – re-calibration of sensor response.	Decrease of pK_a (for 0,048)

C.37.1.1 Sterilization in Water

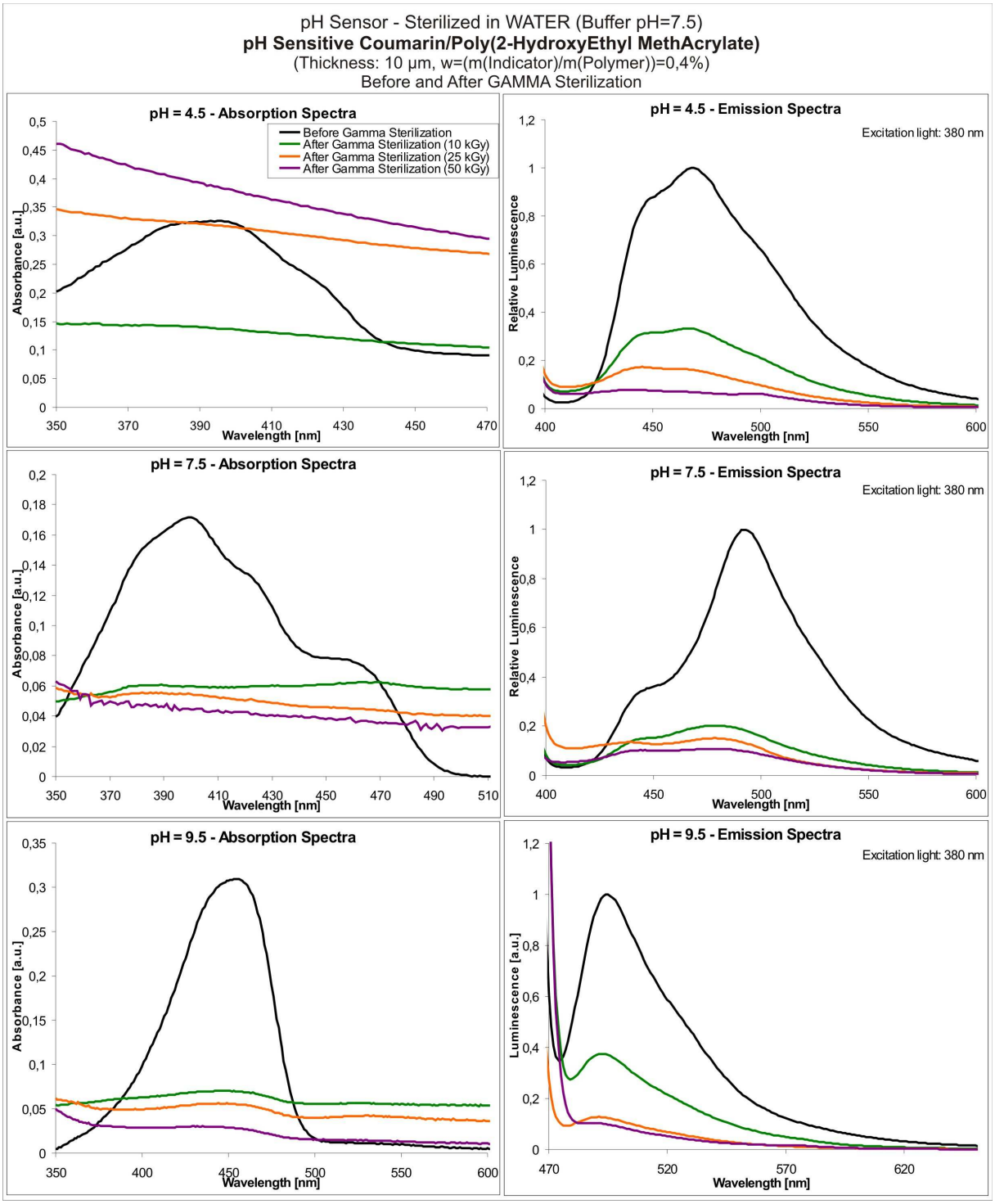

GAMMA S.	Absorption Spectra			Emission Spectra		
		pH	Alterations		pH	Alterations
Alterations in Absorption/ Emission Intensity	10 kGy	4.5	57,70% decrease	10 kGy	4.5	66,73% decrease
		7.5	65,11% decrease		7.5	79,68% decrease
		9.5	77,36% decrease		9.5	62,43% decrease
	25 kGy	4.5	1,97% decrease	25 kGy	4.5	83,54% decrease
		7.5	67,99% decrease		7.5	84,86% decrease
		9.5	81,89% decrease		9.5	87,25% decrease
	50 kGy	4.5	20% increase	50 kGy	4.5	92,21% decrease
		7.5	73,98% decrease		7.5	89,20% decrease
		9.5	90,51% decrease		9.5	89,68% decrease

Calibration Curves

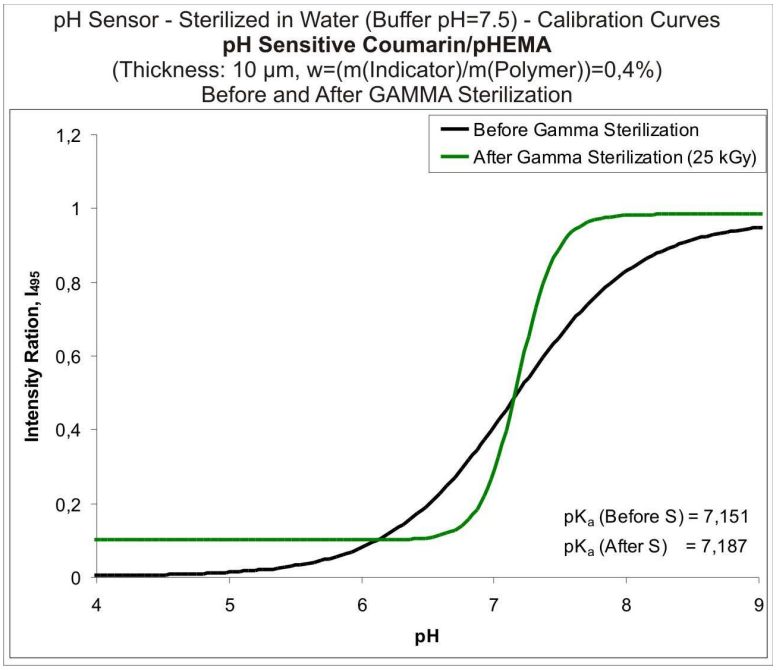

GAMMA S.	Alterations in Calibration Curve Shape	Alterations in pK_a
	Altered curve shape after sterilization. The response to the proton still observed – re-calibration of sensor response.	Decrease of pK_a (for 0,036)

C.37.2 Electron Beam Sterilization

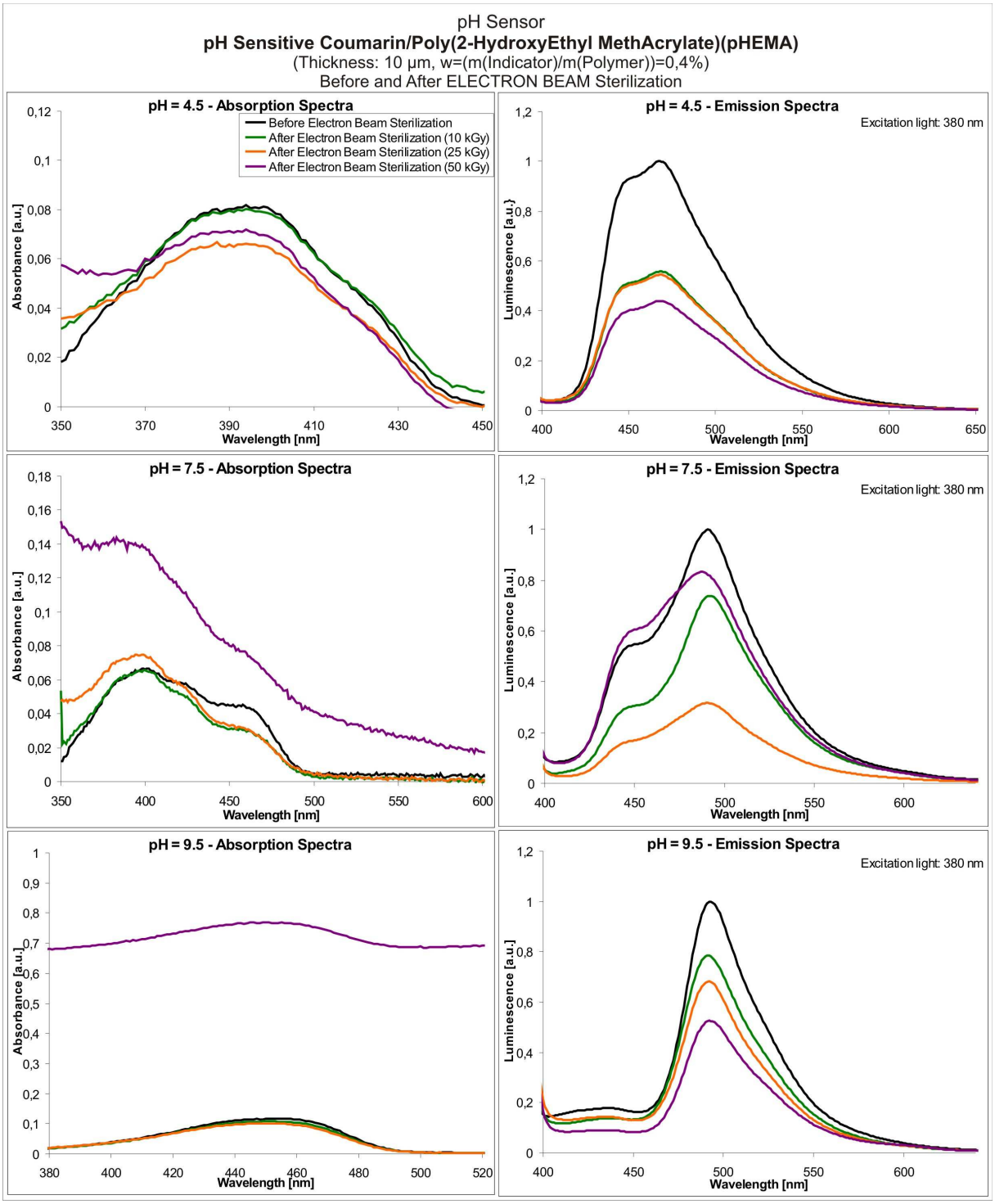

E-BEAM S.	Absorption Spectra			Emission Spectra		
		pH	Alterations		pH	Alterations
Alterations in Absorption/ Emission Intensity	10 kGy	4.5	1,89% decrease	10 kGy	4.5	44,23% decrease
		7.5	0,26% increase		7.5	26,15% decrease
		9.5	8,86% decrease		9.5	21,56% decrease
	25 kGy	4.5	19,79% decrease	25 kGy	4.5	45,45% decrease
		7.5	11,65% increase		7.5	68,33% decrease
		9.5	14,16% decrease		9.5	31,84% decrease
	50 kGy	4.5	12,25% decrease	50 kGy	4.5	55,97% decrease
		7.5	115% increase		7.5	16,61% decrease
		9.5	560% increase		9.5	47,34% decrease

Alterations in Absorption/ Emission Curve Form	10 kGy	4.5	Unaltered.	10 kGy	4.5	Altered emission curve form between 480-570 nm.
		7.5	The ratio between protonation/deprotonation absorption peaks is altered.		7.5	Altered emission curve form between 480-570 nm.
		9.5	Unaltered.		9.5	Hypsochromic shift of the emission maximum for 2 nm.
	25 kGy	4.5	Altered emission curve form between 350-360 nm.	25 kGy	4.5	Altered emission curve form between 480-570 nm.
		7.5	Altered emission curve form between 350-430 nm.		7.5	Altered emission curve form between 480-570 nm. Hypsochromic shift of the emission maximum for 1 nm.
		9.5	Unaltered.		9.5	Altered emission curve form between 400-450 nm Hypsochromic shift of the emission maximum for 2 nm.
	50 kGy	4.5	Altered emission curve form between 350-370 nm.	50 kGy	4.5	Altered emission curve form between 480-570 nm.
		7.5	Disappearance of the characteristic absorption curve form. The sensor became turbid after sterilization and characterization in the buffer – greater water uptake after sterilization.		7.5	Altered emission curve form between 480-570 nm. Hypsochromic shift of the emission maximum for 3 nm.
		9.5	The sensor became turbid after sterilization and characterization in the buffer – greater water uptake after sterilization.		9.5	Hypsochromic shift of the emission maximum for 2 nm.

Calibration Curves

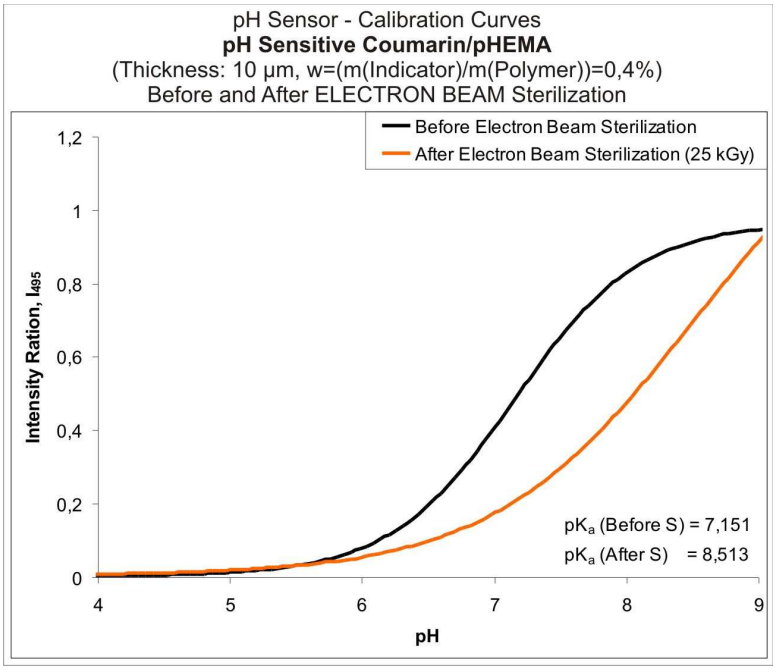

E-BEAM S.	Alterations in Calibration Curve Shape	Alterations in pK_a
	Greatly altered curve shape after sterilization.	Increase of pK_a (for 1,362)

C.37.2.1 Sterilization in Water

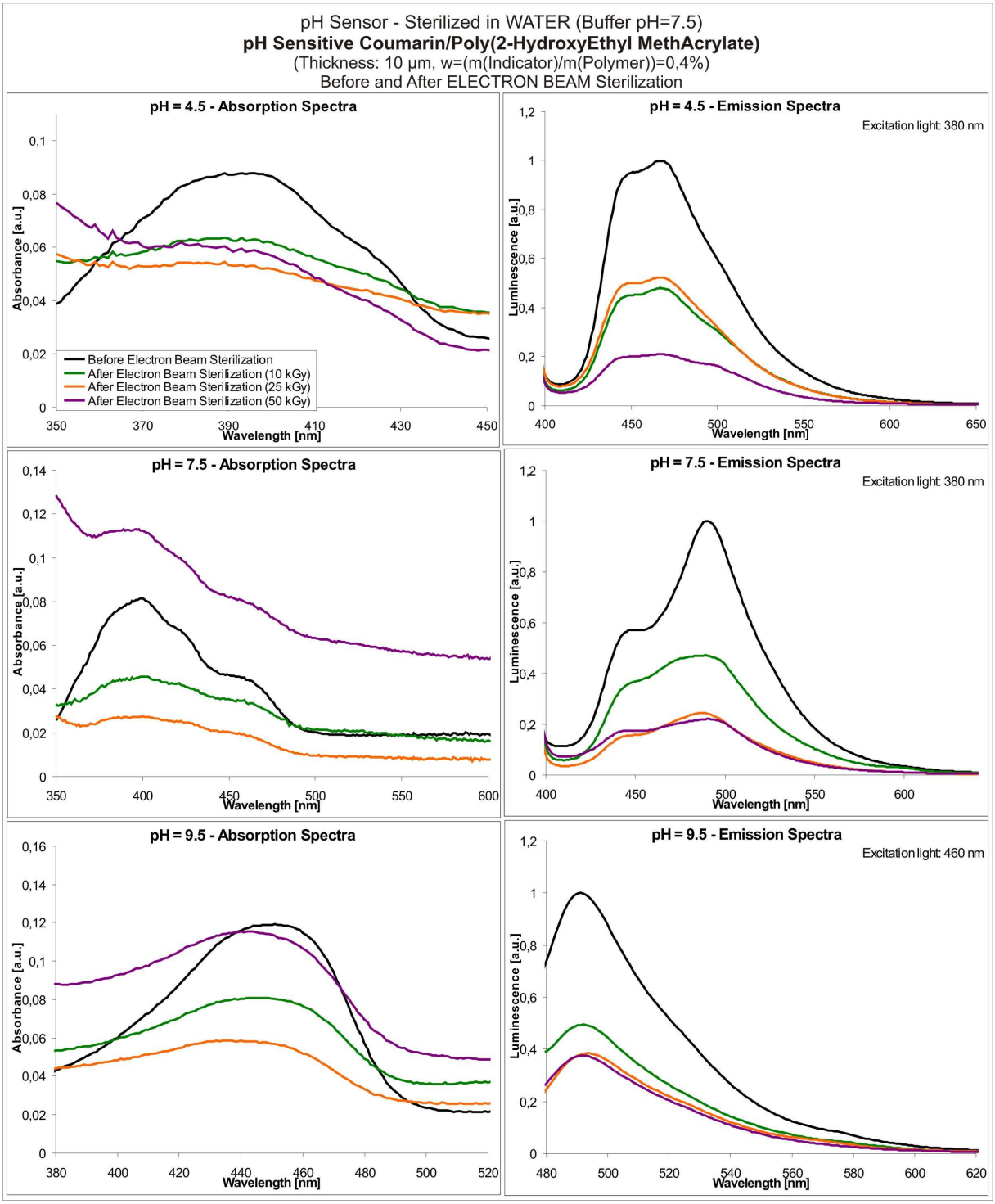

E-BEAM S.	Absorption Spectra			Emission Spectra		
		pH	Alterations		pH	Alterations
Alterations in Absorption/ Emission Intensity	10 kGy	4.5	29,58% decrease	10 kGy	4.5	51,92% decrease
		7.5	43,87% decrease		7.5	52,84% decrease
		9.5	32,32% decrease		9.5	50,53% decrease
	25 kGy	4.5	39,62% decrease	25 kGy	4.5	47,66% decrease
		7.5	66,32% decrease		7.5	75,56% decrease
		9.5	51,92% decrease		9.5	61,56% decrease
	50 kGy	4.5	33,74% decrease	50 kGy	4.5	78,80% decrease
		7.5	37,85% increase		7.5	77,93% decrease
		9.5	4,33% decrease		9.5	62,41% decrease

Calibration Curves

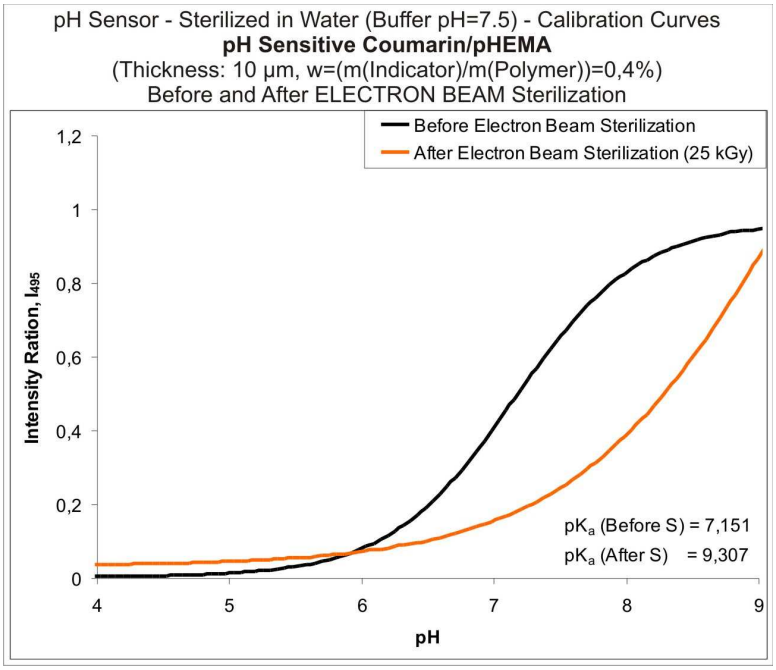

E-BEAM S.	Alterations in Calibration Curve Shape	Alterations in pK_a
	Greatly altered curve shape after sterilization.	Increase of pK_a (for 2,156)

C.38 PET Perylene BisImide immobilized in HydroMed Hydrogel D4

C.38.1 Gamma Sterilization

Absorption Spectra

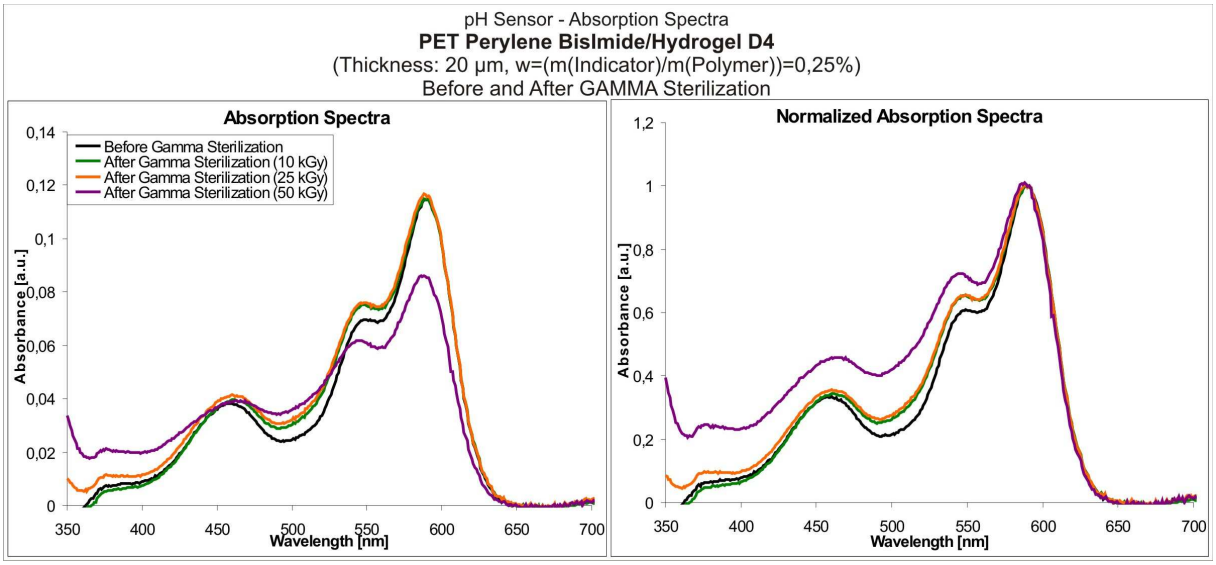

GAMMA Sterilization	Absorption Spectra	
Alterations in Absorption/Emission Intensity	10kGy	0,39% increase
	25 kGy	1,38% increase
	50 kGy	25,46% decrease

Alterations in Absorption/Emission Curve Form	10kGy	Altered absorption between 460-570 nm.
	25 kGy	Altered absorption between 460-570 nm
	50 kGy	Altered absorption between 350-570 nm

Emission Spectra

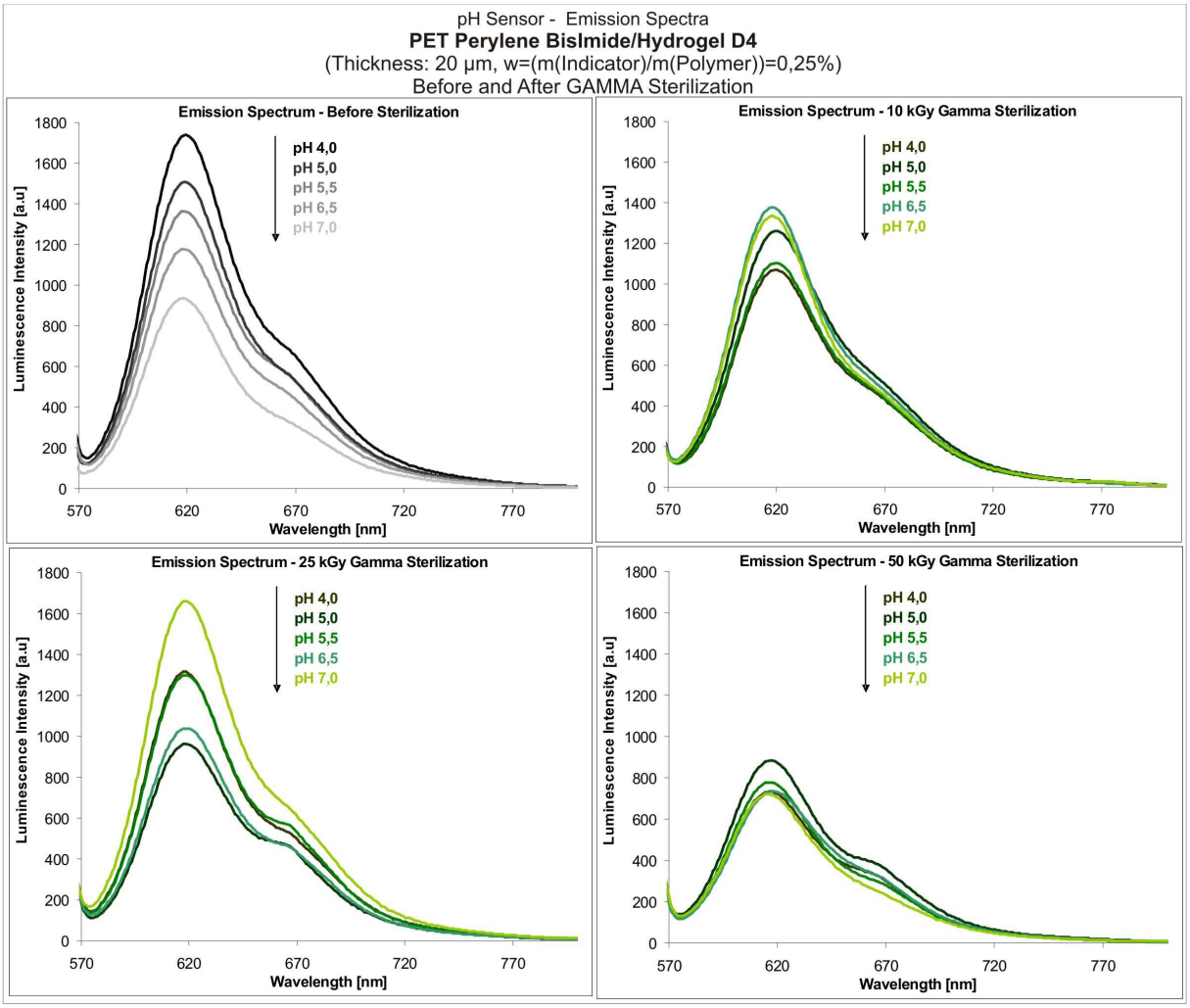

GAMMA S	Emission Spectra					
	Decrease of the Luminescence Intensity in dependence of the Intensity at lower pH			Decrease of the Luminescence Intensity at define pH in dependence of the Intensity Before Sterilization		
BEFORE S	**pH**	**Max. Intensity**				
Alterations in Absorption/ Emission Intensity	4	1739	/			
	5	1509	13,22% decrease			
	5.5	1363	21,62% decrease			
	6.5	1176	32,37% decrease			
	7	933,6	46,31% decrease			
PET Efficiency	1.86					
10 kGy	**pH**	**Max. Intensity**		**pH**	**Compared Intensity**	
Alterations in Absorption/ Emission Intensity	4	1066	/	4	1739	38,70% decrease
	5	1100	3,19% increase	5	1509	27,10% decrease
	5.5	1254	17,64% increase	5.5	1363	8,00% decrease
	6.5	1377	29,17% increase	6.5	1176	17,09% increase
	7	1333	25,05% increase	7	933,6	42,78% increase

25 kGy	pH	Max. Intensity		pH	Compared Intensity	
Alterations in Absorption/ Emission Intensity	4	1315	/	4	1739	24,38% decrease
	5	1300	1,14% decrease	5	1509	13,85% decrease
	5.5	963	26,77% decrease	5.5	1363	29,35% decrease
	6.5	1039	20,99% decrease	6.5	1176	11,65% decrease
	7	1662	26,39% increase	7	933,6	78,02% increase
50 kGy	**pH**	**Max. Intensity**		**pH**	**Compared Intensity**	
Alterations in Absorption/ Emission Intensity	4	731,5	/	4	1739	57,93% decrease
	5	775,8	6,06% increase	5	1509	48,59% decrease
	5.5	882,6	20,66% increase	5.5	1363	35,25% decrease
	6.5	735	0,48% increase	6.5	1176	37,50% decrease
	7	714,3	2,35% decrease	7	933,6	23,49% decrease

Calibration Curves

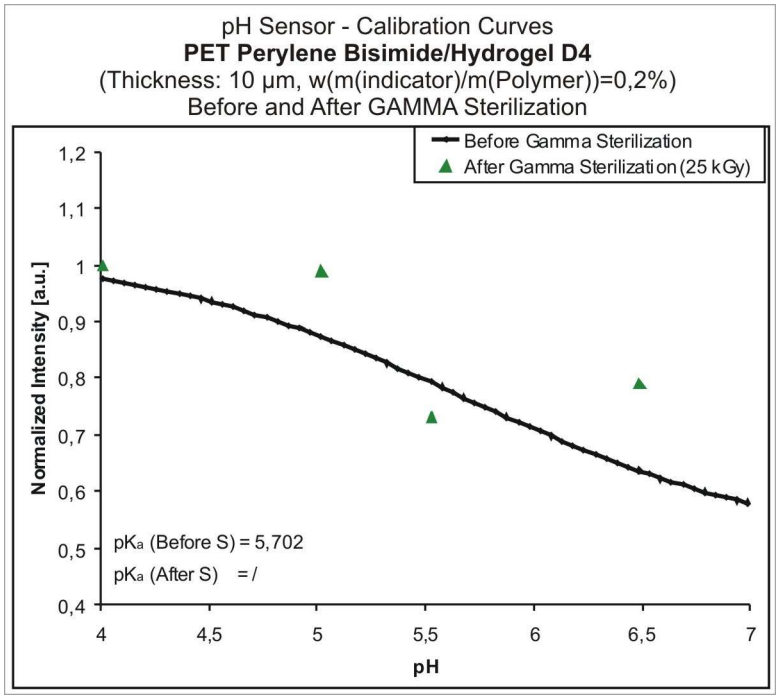

GAMMA S.	Alterations in Calibration Curve Shape	Alterations in pK_a
	The calibration curve no longer observed.	

C.38.1.1 Sterilization in Water

Absorption Spectra

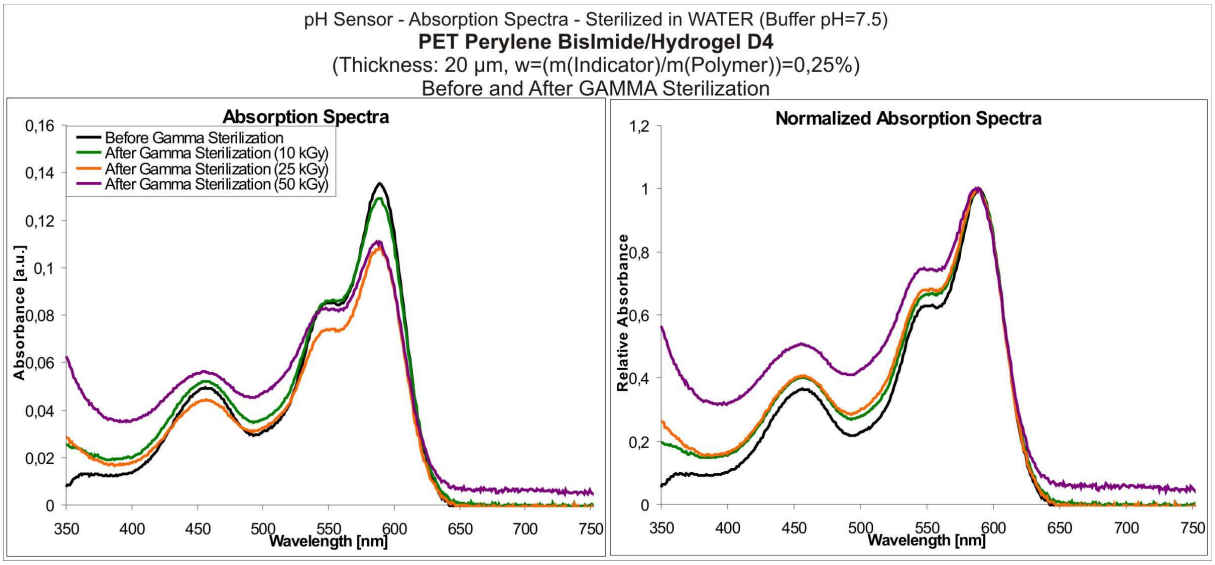

GAMMA Sterilization	Absorption Spectra	
Alterations in Absorption/Emission Intensity	10kGy	4,54% decrease
	25 kGy	19,80% decrease
	50 kGy	18,24% decrease
Alterations in Absorption/Emission Curve Form	10kGy	Altered absorption between 350-570 nm.
	25 kGy	Altered absorption between 350-570 nm
	50 kGy	Altered absorption between 350-570 nm

Emission Spectra

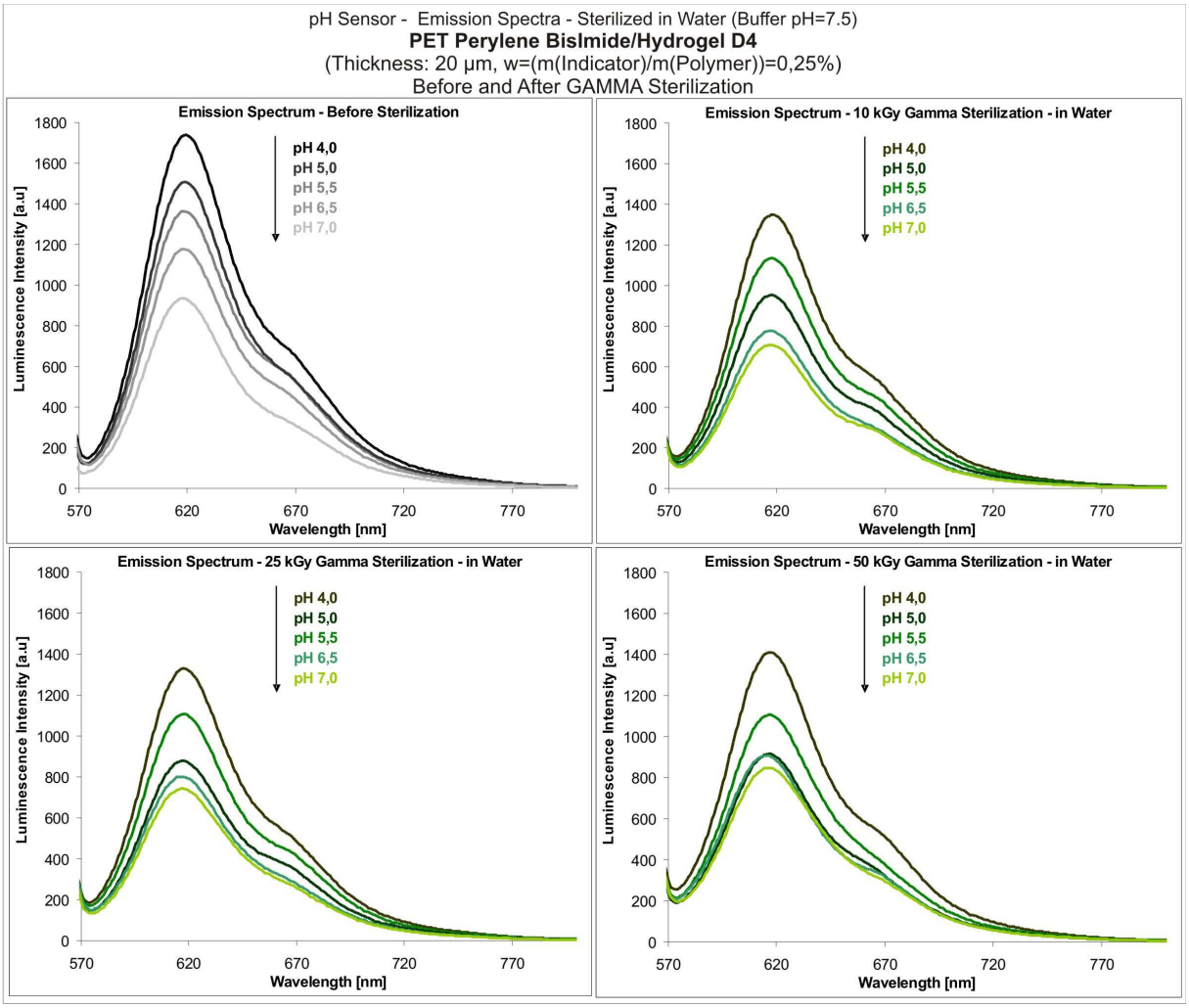

GAMMA S	Emission Spectra					
	Decrease of the Luminescence Intensity in dependence of the Intensity at lower pH			Decrease of the Luminescence Intensity at define pH in dependence of the Intensity Before Sterilization		
BEFORE S	**pH**	**Max. Intensity**				
Alterations in Absorption/ Emission Intensity	4	1739	/			
	5	1509	13,22% decrease			
	5.5	1363	21,62% decrease			
	6.5	1176	32,37% decrease			
	7	933,6	46,31% decrease			
PET Efficiency	1.86					
10 kGy	**pH**	**Max. Intensity**		**pH**	**Compared Intensity**	
Alterations in Absorption/ Emission Intensity	4	1347	/	4	1739	22,54% decrease
	5	1134	15,81% decrease	5	1509	24,85% decrease
	5.5	951,3	17% decrease	5.5	1363	30,21% decrease
	6.5	775,1	29,17% decrease	6.5	1176	34,09% decrease
	7	705,6	25,05% decrease	7	933,6	24,42% decrease
PET Efficiency	1.91					

25 kGy	pH	Max. Intensity		pH	Compared Intensity	
Alterations in Absorption/ Emission Intensity	4	1329	/	4	1739	23,58% decrease
	5	1108	16,63% decrease	5	1509	26,57% decrease
	5.5	877,7	33,96% decrease	5.5	1363	35,60% decrease
	6.5	799,2	39,86% decrease	6.5	1176	32,04% decrease
	7	740,6	44,27% decrease	7	933,6	20,67% decrease
PET Efficiency	1.79					
50 kGy	**pH**	**Max. Intensity**		**pH**	**Compared Intensity**	
Alterations in Absorption/ Emission Intensity	4	1408	/	4	1739	19,03% decrease
	5	1102	21,73% decrease	5	1509	26,97% decrease
	5.5	911,5	35,26% decrease	5.5	1363	33,13% decrease
	6.5	904,8	35,74% decrease	6.5	1176	23,06% decrease
	7	845,3	39,96% decrease	7	933,6	9,46% decrease
PET Efficiency	1.66					

Calibration Curves

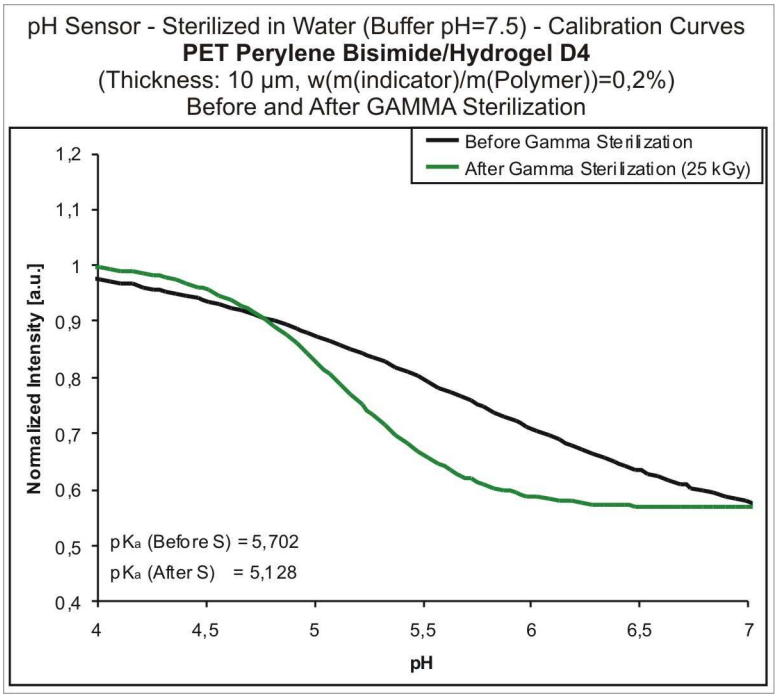

GAMMA S.	Alterations in Calibration Curve Shape	Alterations in pK_a
	Greatly altered curve shape after sterilization.	Decrease of pK_a (for 0,574)

C.38.2 Electron Beam Sterilization

Absorption Spectra

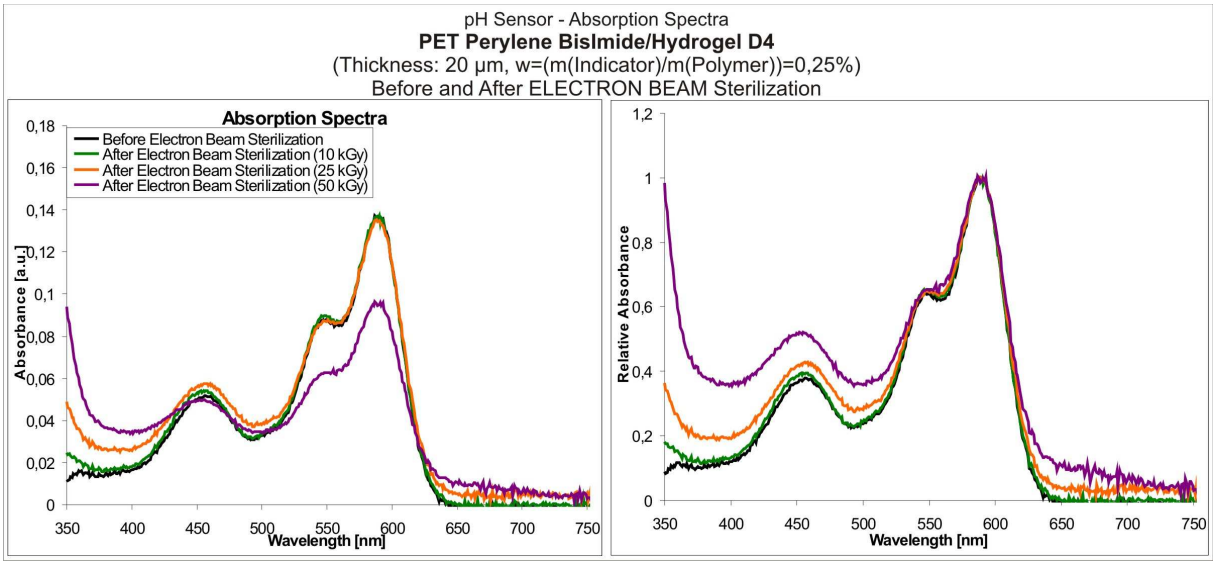

E-BEAM Sterilization	Absorption Spectra	
Alterations in Absorption/Emission Intensity	10kGy	0,02% decrease
	25 kGy	1,58% decrease
	50 kGy	29,97% decrease
Alterations in Absorption/Emission Curve Form	10kGy	Altered absorption between 350-530 nm.
	25 kGy	Altered absorption between 350-530 nm
	50 kGy	Altered absorption between 350-530 nm

Emission Spectra

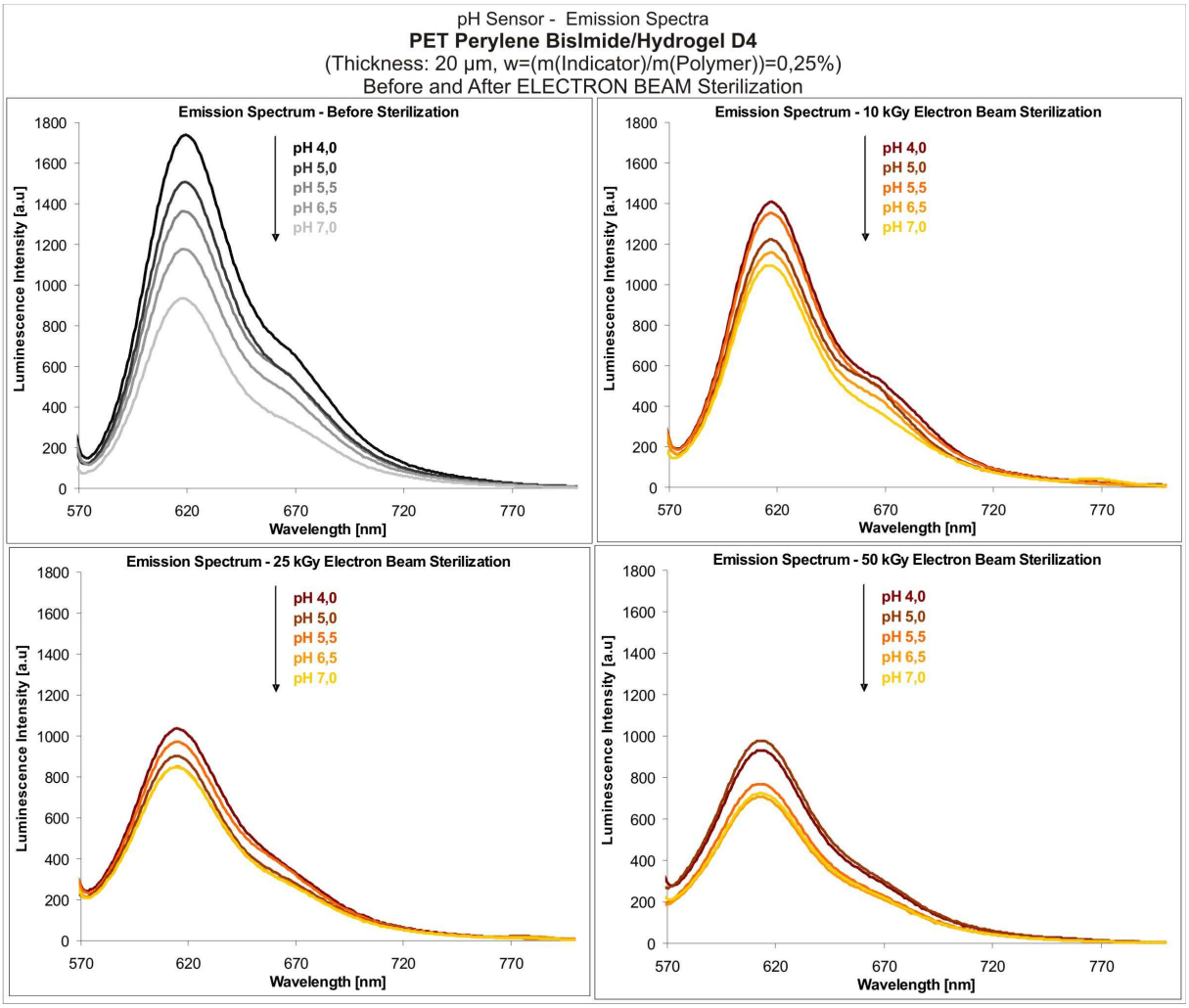

E-BEAM S.	Emission Spectra					
	Decrease of the Luminescence Intensity in dependence of the Intensity at lower pH			Decrease of the Luminescence Intensity at define pH in dependence of the Intensity Before Sterilization		
BEFORE S	**pH**	**Max. Intensity**				
Alterations in Absorption/ Emission Intensity	4	1739	/			
	5	1509	13,22% decrease			
	5.5	1363	21,62% decrease			
	6.5	1176	32,37% decrease			
	7	933,6	46,31% decrease			
PET Efficiency	1.86					
10 kGy	**pH**	**Max. Intensity**		**pH**	**Compared Intensity**	
Alterations in Absorption/ Emission Intensity	4	1406	/	4	1739	19,15% decrease
	5	1350	3,98% decrease	5	1509	10,54% decrease
	5.5	1219	13,30% decrease	5.5	1363	10,56% decrease
	6.5	1156	17,78% decrease	6.5	1176	1,70% decrease
	7	1092	22,33% decrease	7	933,6	16,97% decrease
PET Efficiency	1.29					

25 kGy	pH	Max. Intensity		pH	Compared Intensity	
Alterations in Absorption/ Emission Intensity	4	1022	/	4	1739	41,23% decrease
	5	960,3	6,04% decrease	5	1509	36,36% decrease
	5.5	890	12,92% decrease	5.5	1363	34,70% decrease
	6.5	837,1	18,09% decrease	6.5	1176	28,82% decrease
	7	834,9	18,31% decrease	7	933,6	10,57% decrease
PET Efficiency	1.29					
50 kGy	**pH**	**Max. Intensity**		**pH**	**Compared Intensity**	
Alterations in Absorption/ Emission Intensity	4	910,5	/	4	1739	47,64% decrease
	5	750,2	17,61% decrease	5	1509	50,28% decrease
	5.5	956,4	5,04% decrease	5.5	1363	29,83% decrease
	6.5	687,8	25,46% decrease	6.5	1176	41,51% decrease
	7	707,1	22,34% decrease	7	933,6	24,26% decrease
PET Efficiency	1.29					

Calibration Curves

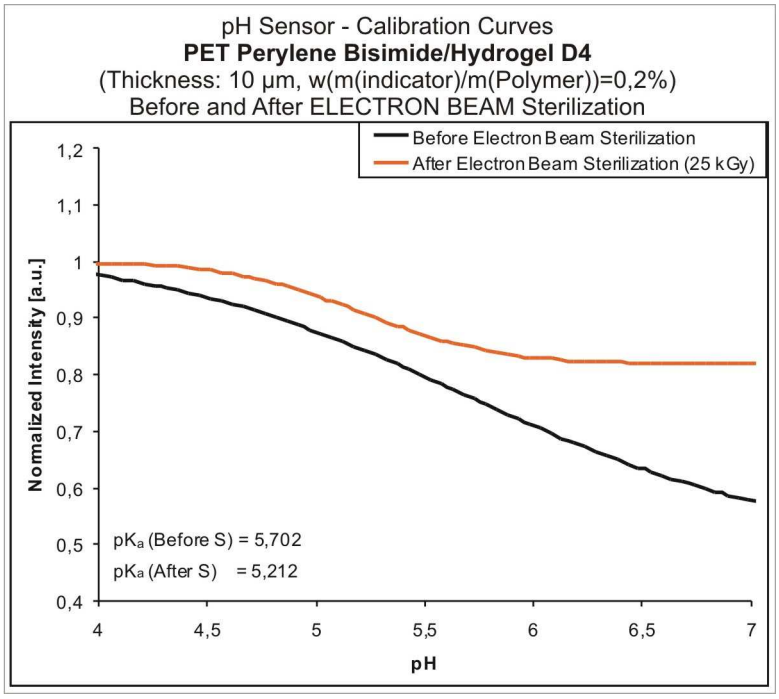

E-BEAM S.	Alterations in Calibration Curve Shape	Alterations in pK_a
	Greatly altered curve shape after sterilization.	Decrease of pK_a (for 0,490)

C.38.2.1 Sterilization in Water

Absorption Spectra

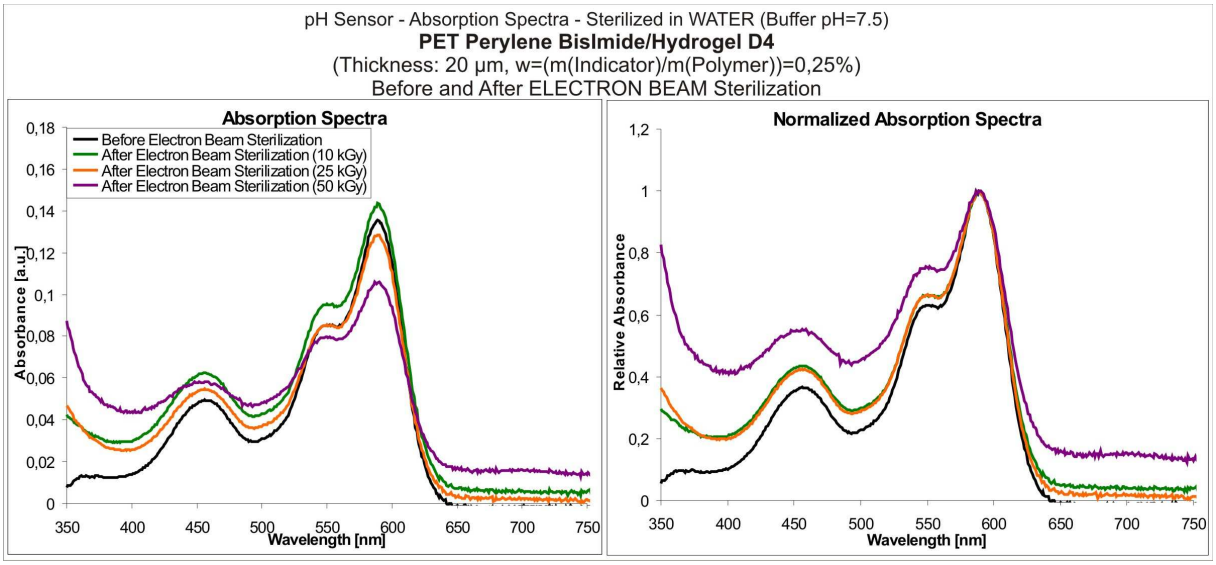

E-BEAM Sterilization	Absorption Spectra	
Alterations in Absorption/Emission Intensity	10kGy	6,00% increase
	25 kGy	4,98% decrease
	50 kGy	21,88% decrease
Alterations in Absorption/Emission Curve Form	10kGy	Altered absorption between 350-570 nm.
	25 kGy	Altered absorption between 350-570 nm
	50 kGy	Altered absorption between 350-570 nm

Emission Spectra

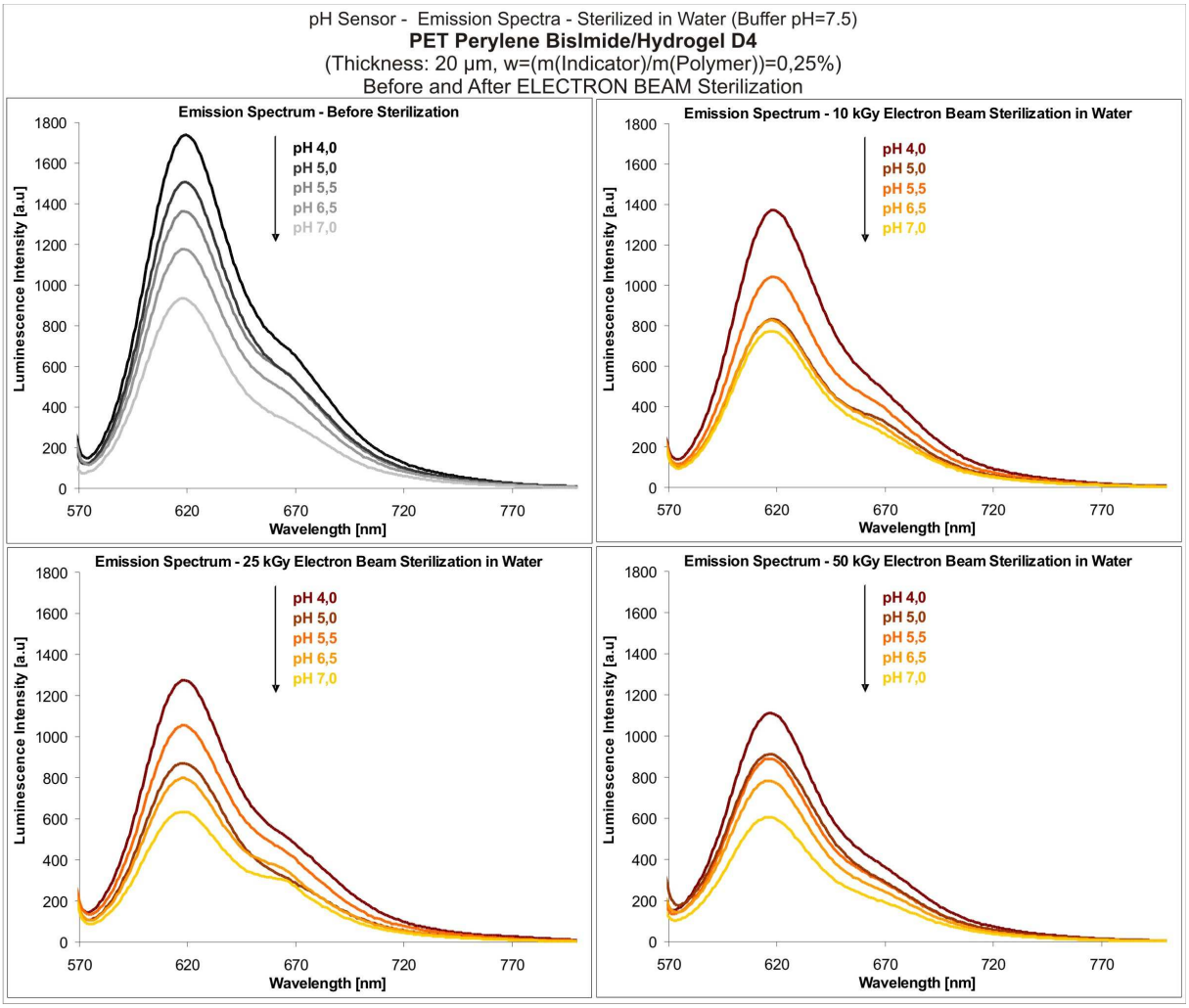

E-BEAM S.	Emission Spectra					
	Decrease of the Luminescence Intensity in dependence of the Intensity at lower pH			Decrease of the Luminescence Intensity at define pH in dependence of the Intensity Before Sterilization		
BEFORE S	**pH**	**Max. Intensity**				
Alterations in Absorption/ Emission Intensity	4	1739	/			
	5	1509	13,22% decrease			
	5.5	1363	21,62% decrease			
	6.5	1176	32,37% decrease			
	7	933,6	46,31% decrease			
PET Efficiency	1.86					
10 kGy	**pH**	**Max. Intensity**		**pH**	**Compared Intensity**	
Alterations in Absorption/ Emission Intensity	4	1370	/	4	1739	21,22% decrease
	5	1040	24,09% decrease	5	1509	31,08% decrease
	5.5	833,5	39,16% decrease	5.5	1363	38,85% decrease
	6.5	826,3	39,69% decrease	6.5	1176	29,74% decrease
	7	772,9	43,58% decrease	7	933,6	17,21% decrease
PET Efficiency	1.77					

25 kGy	pH	Max. Intensity		pH	Compared Intensity	
Alterations in Absorption/ Emission Intensity	4	1274	/	4	1739	26,74% decrease
	5	1054	17,27% decrease	5	1509	30,15% decrease
	5.5	871,9	31,56% decrease	5.5	1363	36,03% decrease
	6.5	798,2	37,35% decrease	6.5	1176	32,13% decrease
	7	633,6	50,27% decrease	7	933,6	32,13% decrease
PET Efficiency	2.01					
50 kGy	**pH**	**Max. Intensity**		**pH**	**Compared Intensity**	
Alterations in Absorption/ Emission Intensity	4	1109	/	4	1739	36,23% decrease
	5	888	19,93% decrease	5	1509	41,15% decrease
	5.5	910,4	17,91% decrease	5.5	1363	33,21% decrease
	6.5	778,5	29,80% decrease	6.5	1176	33,80% decrease
	7	603,9	45,55% decrease	7	933,6	35,31% decrease
PET Efficiency	1.84					

Calibration Curves

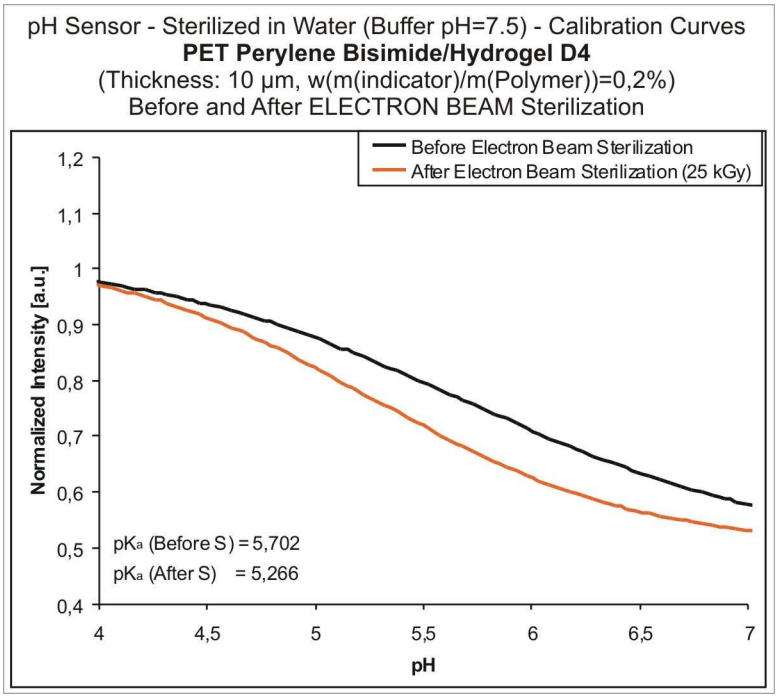

E-BEAM S.	Alterations in Calibration Curve Shape	Alterations in pK_a
	Altered curve shape after sterilization. The response to the proton still observed – re-calibration of sensor response.	Decrease of pK_a (for 0,436)

C.39 BromoPhenol Blue immobilized in HydroMed Hydrogel D4

C.39.1 Gamma Sterilization

Absorption Spectra

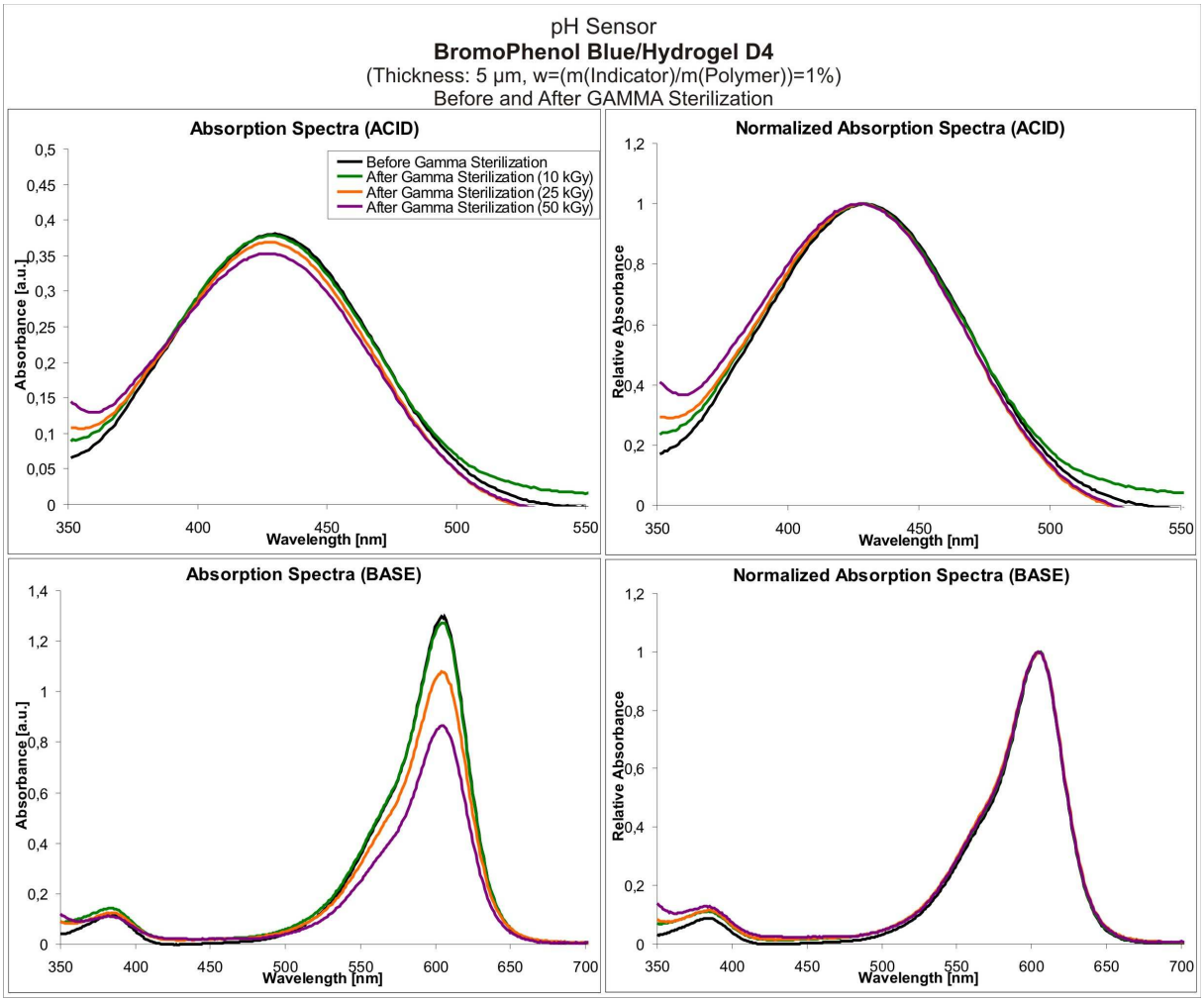

GAMMA S.	Absorption Spectra					
Alterations in Absorption /Emission Intensity		pH	Alterations	Alterations in Absorption /Emission Curve Form		pH	Alterations
	10 kGy	ACID	0,52% decrease		10 kGy	ACID	Altered absorption curve form between 350-380 nm.
		BASE	2,01% decrease			BASE	Altered absorption curve form between 350-400 nm.
	25 kGy	ACID	2,99% decrease		25 kGy	ACID	Altered absorption curve form between 350-380 nm.
		BASE	16,93% decrease			BASE	Altered absorption curve form between 350-400 nm.

	50 kGy	ACID	7,21% decrease		50 kGy	ACID	Altered absorption curve form between 350-400 nm.
		BASE	33,45% decrease			BASE	Altered absorption curve form between 350-400 nm.

C.39.2 Electron Beam Sterilization

Absorption Spectra

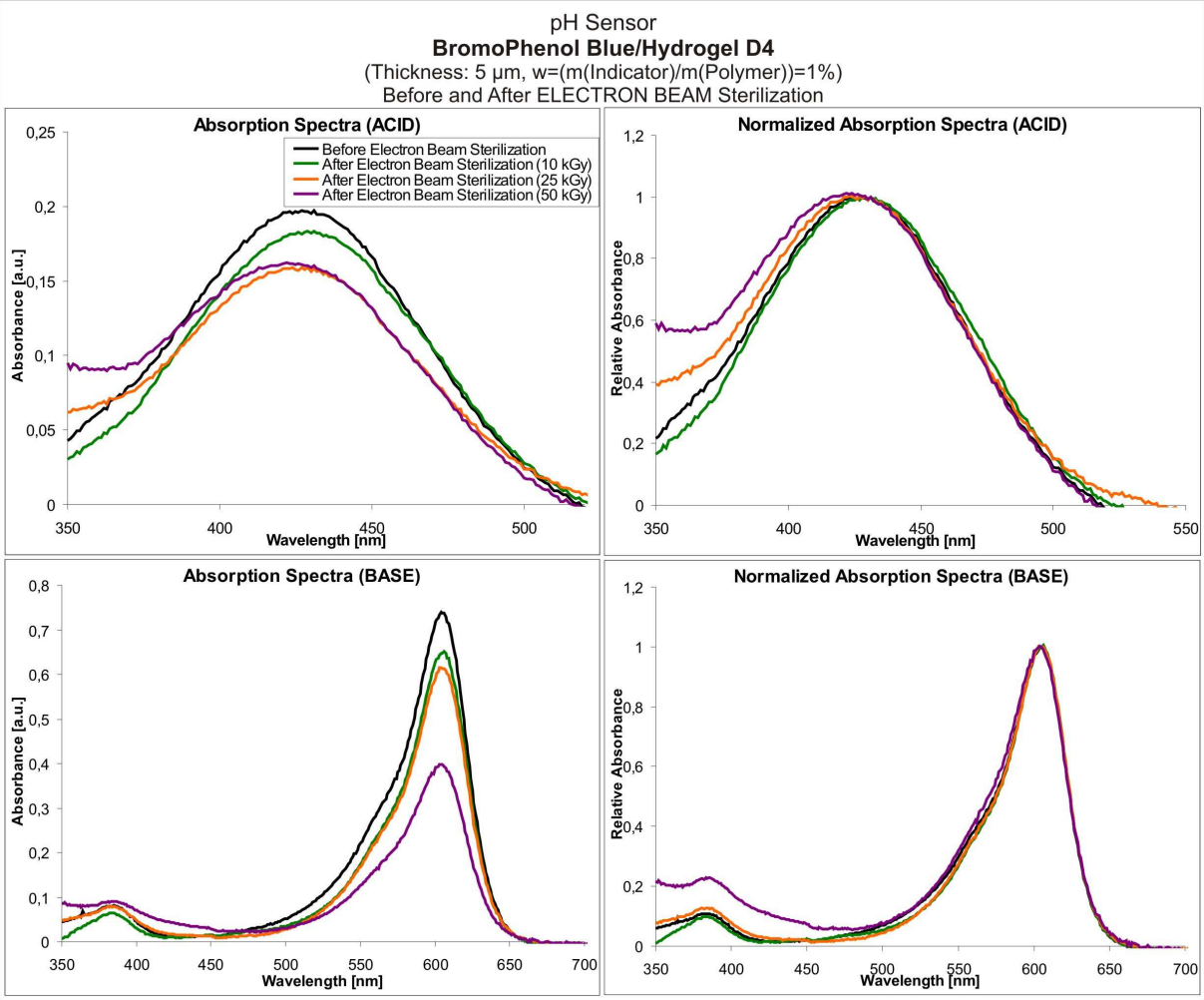

E-BEAM S.	Absorption Spectra					
Alterations in Absorption /Emission Intensity		pH	Alterations	Alterations in Absorption /Emission Curve Form		pH	Alterations
	10 kGy	ACID	7,20% decrease		10 kGy	ACID	Unaltered.
		BASE	12,46% decrease			BASE	Unaltered.

	25 kGy	ACID	19,80% decrease		25 kGy	ACID	Altered absorption curve form between 350-415 nm. Hypsochromic shift of the absorption maximum for 4 nm.
		BASE	17,03% decrease			BASE	Unaltered.
	50 kGy	ACID	18,97% decrease		50 kGy	ACID	Altered absorption curve form between 350-420 nm. Hypsochromic shift of the absorption maximum for 4 nm.
		BASE	46,37% decrease			BASE	Altered absorption curve form between 350-490 nm.

C.40 Thymol Blue immobilized in HydroMed Hydrogel D4

C.40.1 Gamma Sterilization

Absorption Spectra

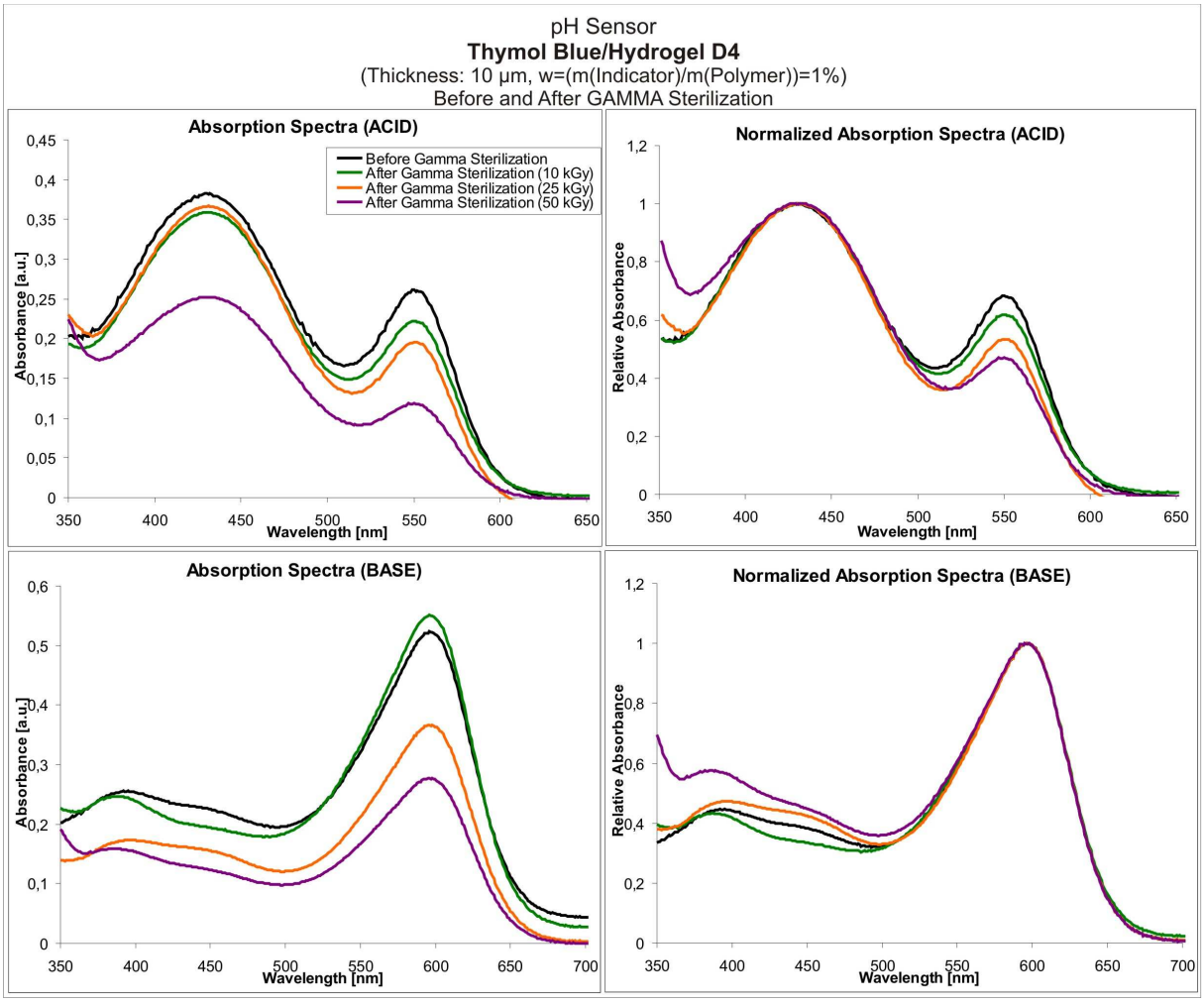

GAMMA S.	Absorption Spectra						
		pH	Alterations			pH	Alterations
Alterations in Absorption /Emission Intensity	10 kGy	ACID	6,14% decrease	Alterations in Absorption /Emission Curve Form	10 kGy	ACID	Ratio between protonated/ deprotonated peak is changed after sterilization.
		BASE	9,88% decrease			BASE	Altered absorption curve form between 350-500 nm.
	25 kGy	ACID	4,15% decrease		25 kGy	ACID	Ratio between protonated/ deprotonated peak is changed after sterilization. Altered absorption curve form between 350-365 nm
		BASE	24,10% decrease			BASE	Altered absorption curve form between 350-500 nm.
	50 kGy	ACID	34,18% decrease		50 kGy	ACID	Ratio between protonated/ deprotonated peak is changed after sterilization. Altered absorption curve form between 350-400 nm.
		BASE	42,17% decrease			BASE	Altered absorption curve form between 350-540 nm.

C.40.2 Electron Beam Sterilization

Absorption Spectra

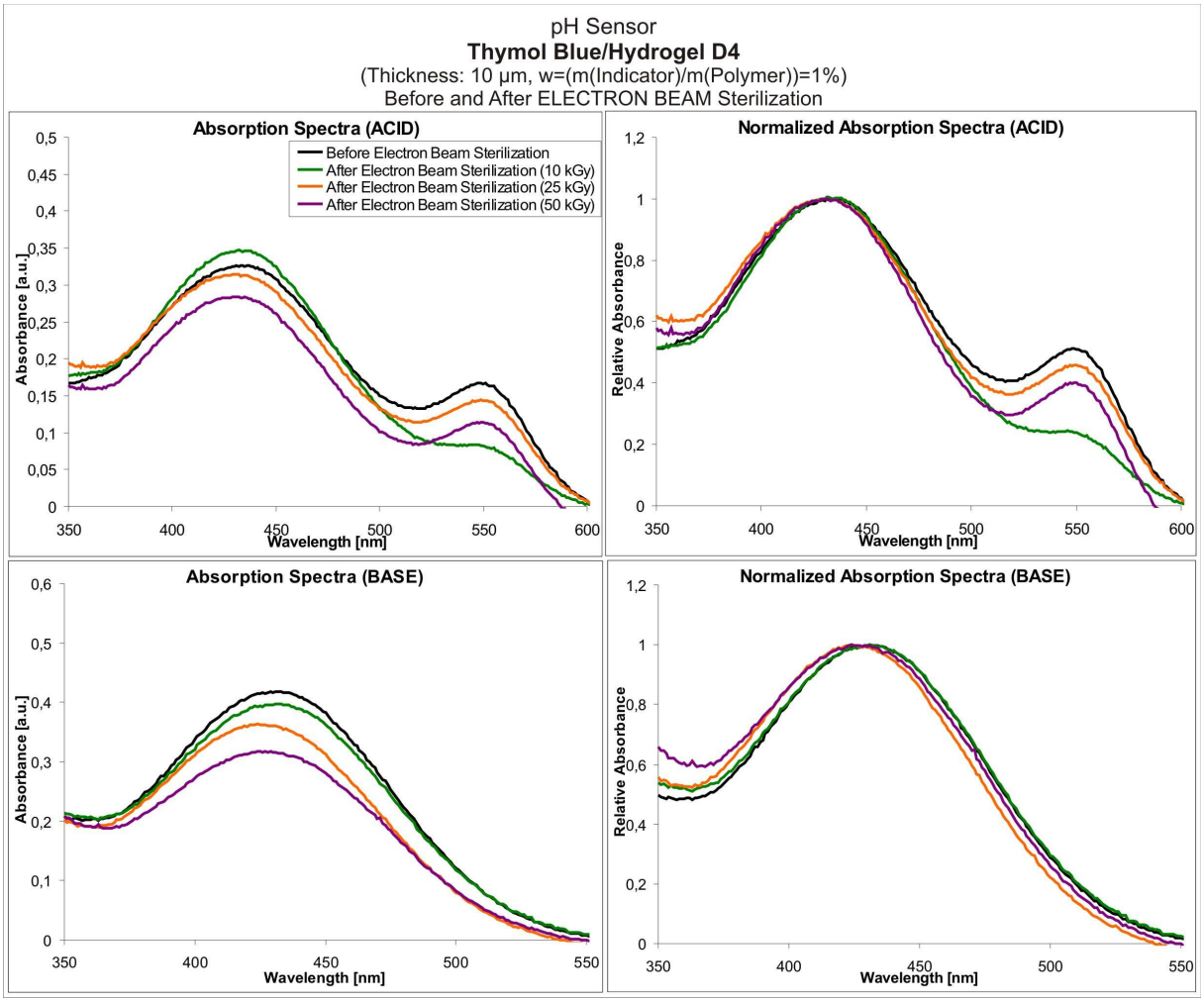

E-BEAM S.	Absorption Spectra					
Alterations in Absorption /Emission Intensity		pH	Alterations	Alterations in Absorption /Emission Curve Form	pH	Alterations
	10 kGy	ACID	5,39% increase	10 kGy	ACID	Ratio between protonated/ deprotonated peak is changed after sterilization. Altered absorption curve form between 500-600 nm.
		BASE	5,02% decrease		BASE	Unaltered.
	25 kGy	ACID	3,63% decrease	25 kGy	ACID	Ratio between protonated/ deprotonated peak is changed after sterilization. Altered absorption curve form between 350-390 nm.
		BASE	13,16% decrease		BASE	Hypsochromic shift of the absorption maximum for 7 nm.

	50 kGy	ACID	12,83% decrease		50 kGy	ACID	Ratio between protonated/ deprotonated peak is changed after sterilization. Altered absorption curve form between 350-370 nm.
		BASE	24,20% decrease			BASE	Altered absorption curve form between 350-370 nm. Hypsochromic shift of the absorption maximum for 7 nm.

C.41 BromoThymol Blue immobilized in HydroMed Hydrogel D4

C.41.1 Gamma Sterilization

Absorption Spectra

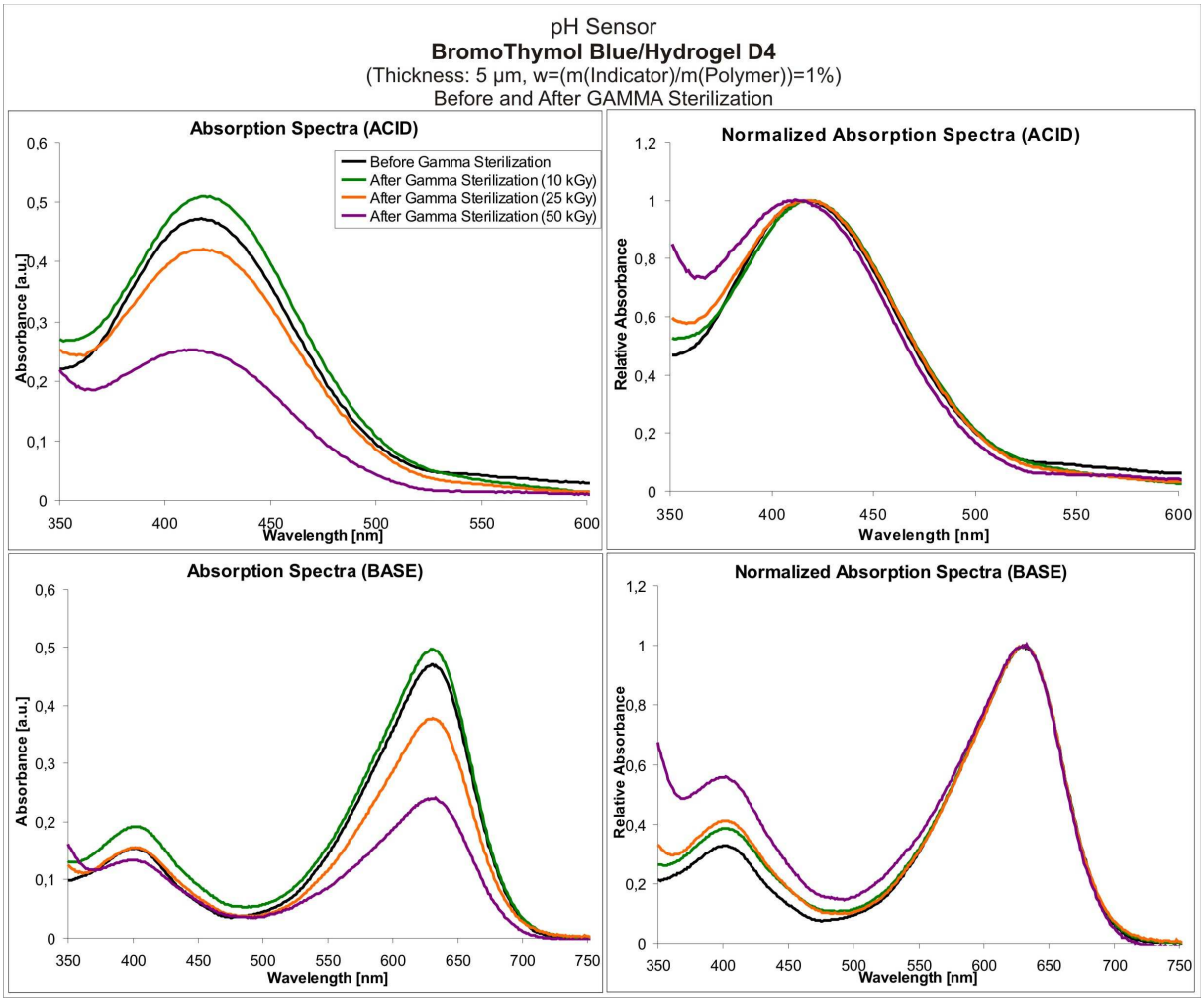

GAMMA S.	Absorption Spectra						
		pH	Alterations			pH	Alterations
Alterations in Absorption /Emission Intensity	10 kGy	ACID	7,42% increase	Alterations in Absorption /Emission Curve Form	10 kGy	ACID	Altered absorption curve form between 350-370 nm.
		BASE	5,37% decrease			BASE	Altered absorption curve form between 350-505 nm.
	25 kGy	ACID	10,90% decrease		25 kGy	ACID	Altered absorption curve form between 350-380 nm.
		BASE	19,75% decrease			BASE	Altered absorption curve form between 350-500 nm.
	50 kGy	ACID	46,61% decrease		50 kGy	ACID	Altered absorption curve form between 350-405 nm. Hypsochromic shift of the absorption maximum for 3 nm.
		BASE	49,05% decrease			BASE	Altered absorption curve form between 350-570 nm.

C.41.2 Electron Beam Sterilization

Absorption Spectra

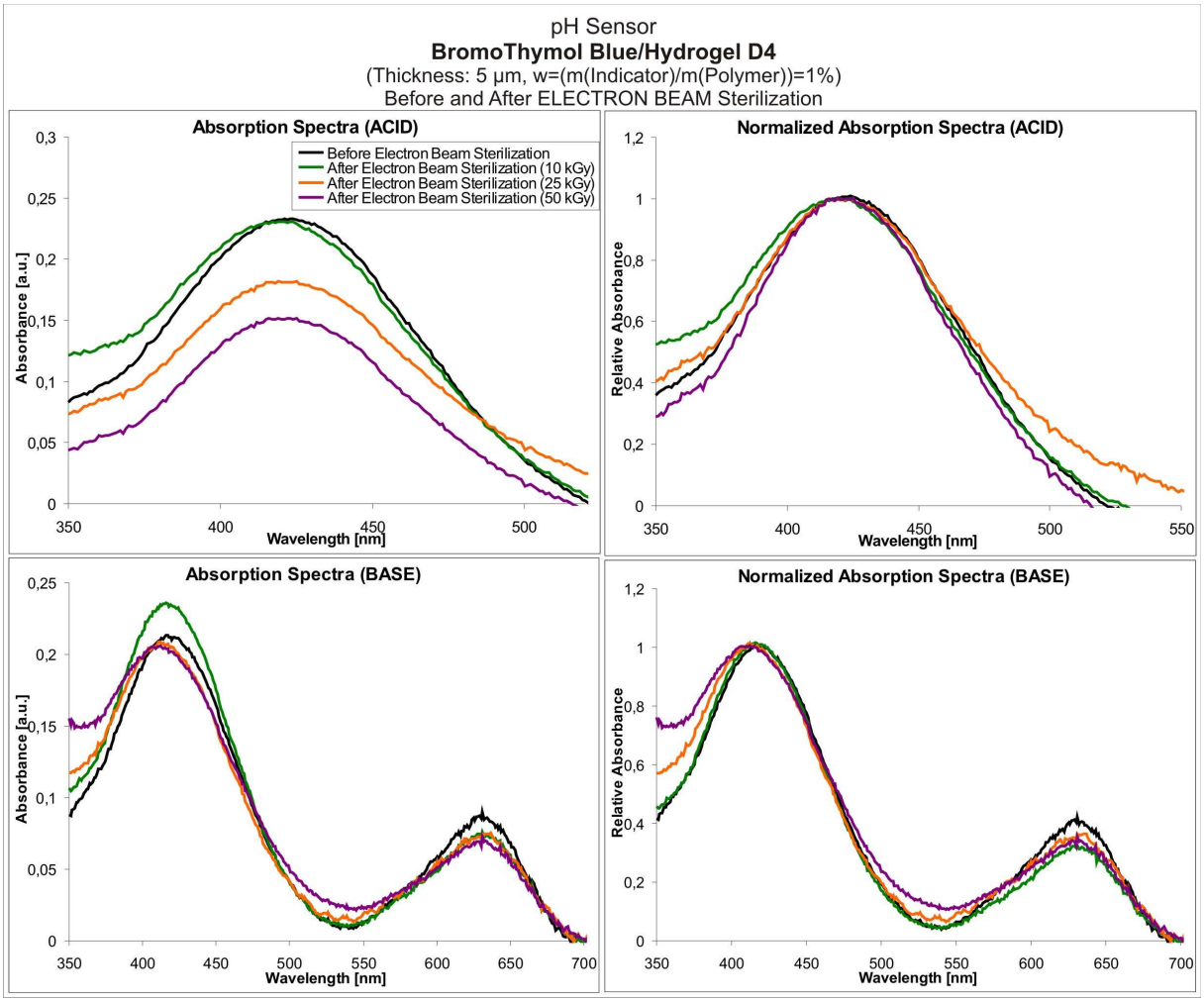

E-BEAM S.	Absorption Spectra					
Alterations in Absorption /Emission Intensity		pH	Alterations	Alterations in Absorption /Emission Curve Form		pH	Alterations
	10 kGy	ACID	0,21% decrease		10 kGy	ACID	Altered absorption curve form between 350-410 nm.
		BASE	8,68% decrease			BASE	Unaltered.
	25 kGy	ACID	21,45% decrease		25 kGy	ACID	Altered absorption curve form between 350-400 nm. Hypsochromic shift of the absorption maximum for 3 nm.
		BASE	2,83% decrease			BASE	Unaltered.
	50 kGy	ACID	34,51% decrease		50 kGy	ACID	Altered absorption curve form between 350-400 nm.

		BASE	3,58% decrease			BASE	Altered absorption curve form between 350-400 nm. Hypsochromic shift of the absorption maximum for 6 nm.

C.42 Methyl Orange immobilized in HydroMed Hydrogel D4

C.42.1 Gamma Sterilization

Absorption Spectra

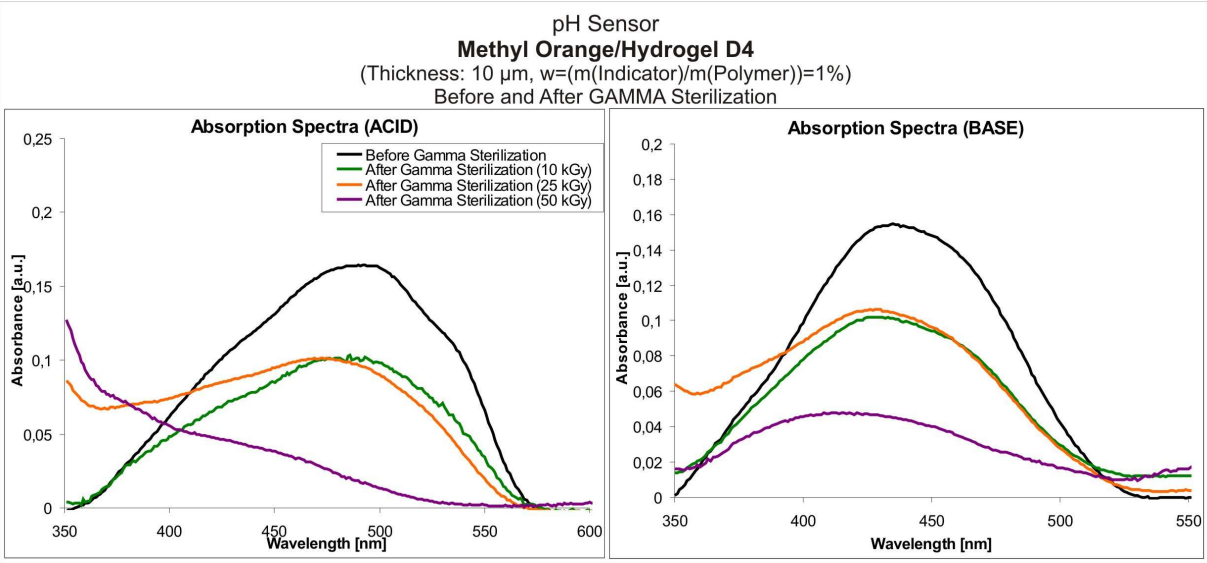

GAMMA S.	Absorption Spectra						
		pH	Alterations			pH	Alterations
Alterations in Absorption /Emission Intensity	10 kGy	ACID	38,98% decrease	Alterations in Absorption /Emission Curve Form	10 kGy	ACID	Unaltered.
		BASE	33,83% decrease			BASE	Unaltered.
	25 kGy	ACID	39,76% decrease		25 kGy	ACID	Altered absorption curve form.
		BASE	31,12% decrease			BASE	Altered absorption curve form.
	50 kGy	ACID	85,81% decrease		50 kGy	ACID	Disappearance of the characteristic absorption curve form.
		BASE	69,02% decrease			BASE	Disappearance of the characteristic absorption curve form.

C.42.2 Electron Beam Sterilization

Absorption Spectra

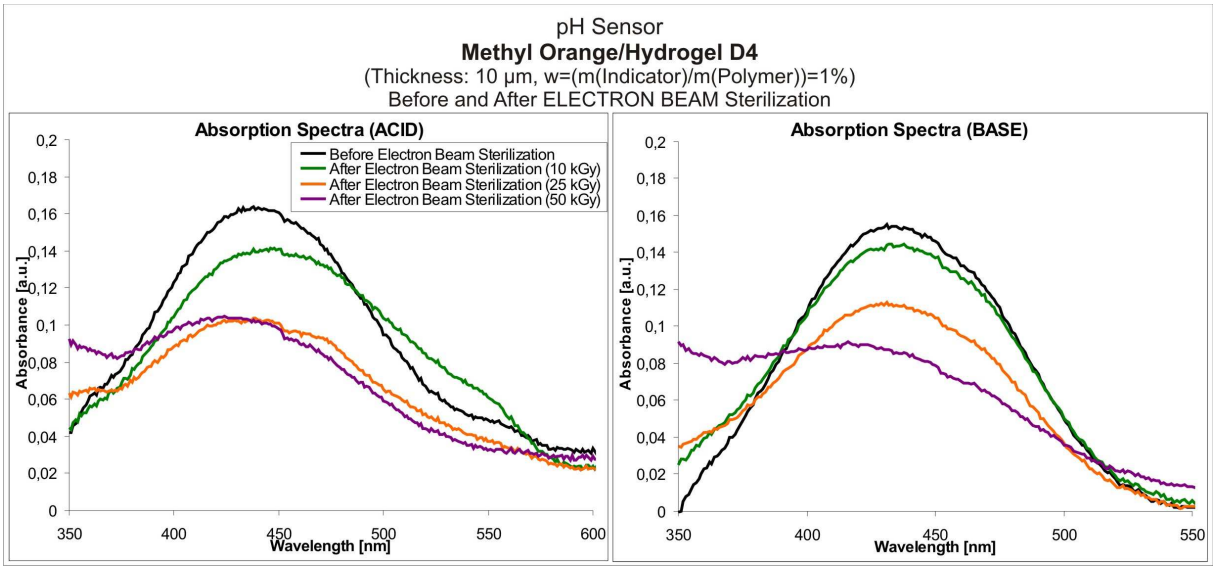

E-BEAM S.	Absorption Spectra						
		pH	Alterations			pH	Alterations
Alterations in Absorption /Emission Intensity	10 kGy	ACID	13,47% decrease	Alterations in Absorption /Emission Curve Form	10 kGy	ACID	Altered absorption curve form between 450-800 nm.
		BASE	5,02% decrease			BASE	Altered absorption curve form between 350-380 nm.
	25 kGy	ACID	37,28% decrease		25 kGy	ACID	Altered absorption curve form between 350-430 nm and 460-800 nm.
		BASE	13,16% decrease			BASE	Altered absorption curve form between 350-380 nm.
	50 kGy	ACID	35,93% decrease		50 kGy	ACID	Altered absorption curve form between 350-380 nm and 550-800 nm. Hypsochromic shift of the absorption maximum for 14 nm.
		BASE	24,20% decrease			BASE	Disappearance of the characteristic absorption curve form.

Optical TEMPERATURE SENSORS

C.43 Europium(III) Complex with 4-(4,6-di(1H-indazol-1-yl)-1,3,5-triazin-2-yl)-N,N-DiEthyl Benzen Amine (=Eu(tta)$_3$DEADIT) immobilized in PolyStyrene-co-Acrylonitrile

C.43.1 Gamma Sterilization

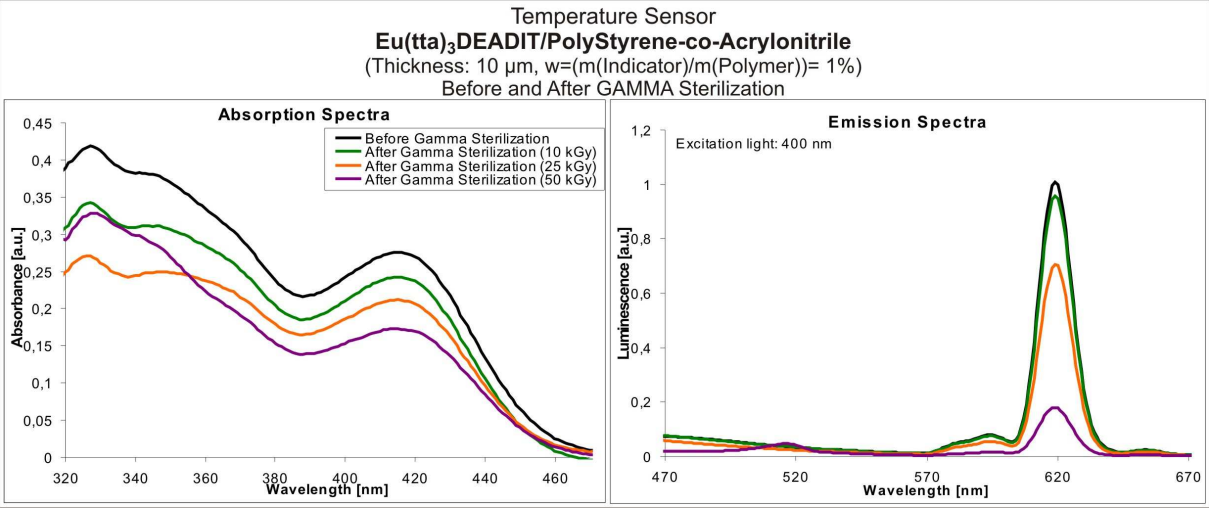

GAMMA Sterilization	Absorption Spectra		Emission Spectra	
Alterations in Absorption/Emission Intensity	10kGy	12,00% decrease	10kGy	5,18% decrease
	25 kGy	22,95% decrease	25 kGy	30,10% decrease
	50 kGy	37,25% decrease	50 kGy	82,21% decrease
Alterations in Absorption/Emission Curve Form	10kGy	The ratio between peaks with λ_{max1}=327 nm and λ_{max1}=416 nm changed after sterilization.	10kGy	Unaltered
	25 kGy	The ratio between peaks with λ_{max1}=327 nm and λ_{max1}=416 nm changed after sterilization.	25 kGy	Unaltered
	50 kGy	The ratio between peaks with λ_{max1}=327 nm and λ_{max1}=416 nm changed after sterilization.	50 kGy	Appearance of new emission peak with λ_{max}=517 nm.

Calibration Curves

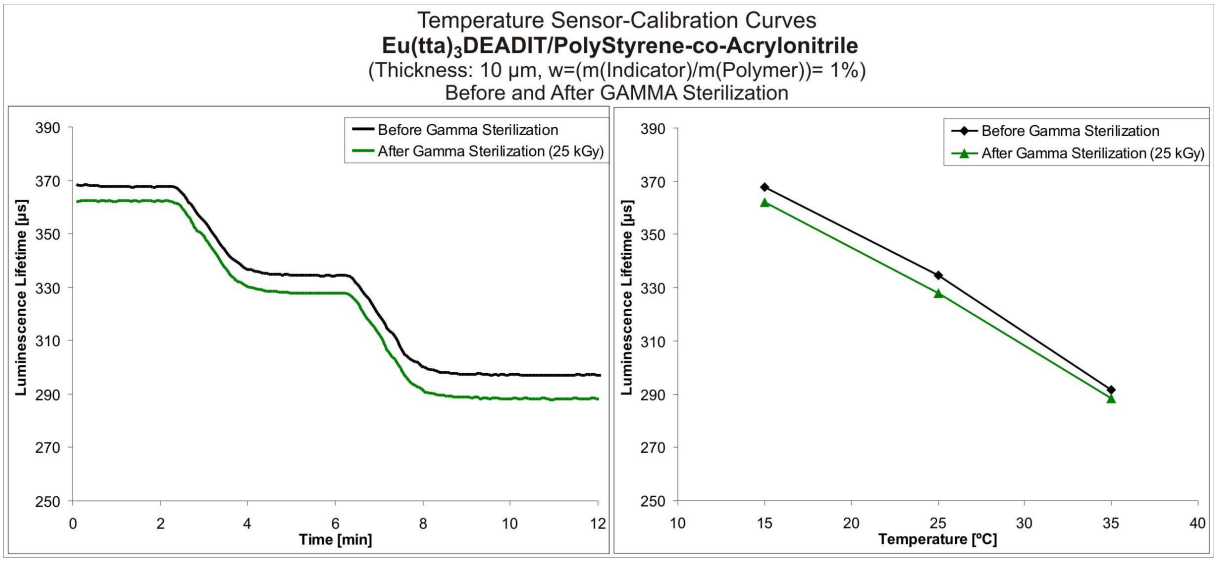

GAMMA S.	Luminescence Lifetime		Alterations of Slope
Alterations in Luminescence Lifetime and Slope	15 °C	1,63% decrease	2,81% decrease of slope
	25 °C	2,09% decrease	
	35 °C	3,03% decrease	

C.43.2 Electron Beam Sterilization

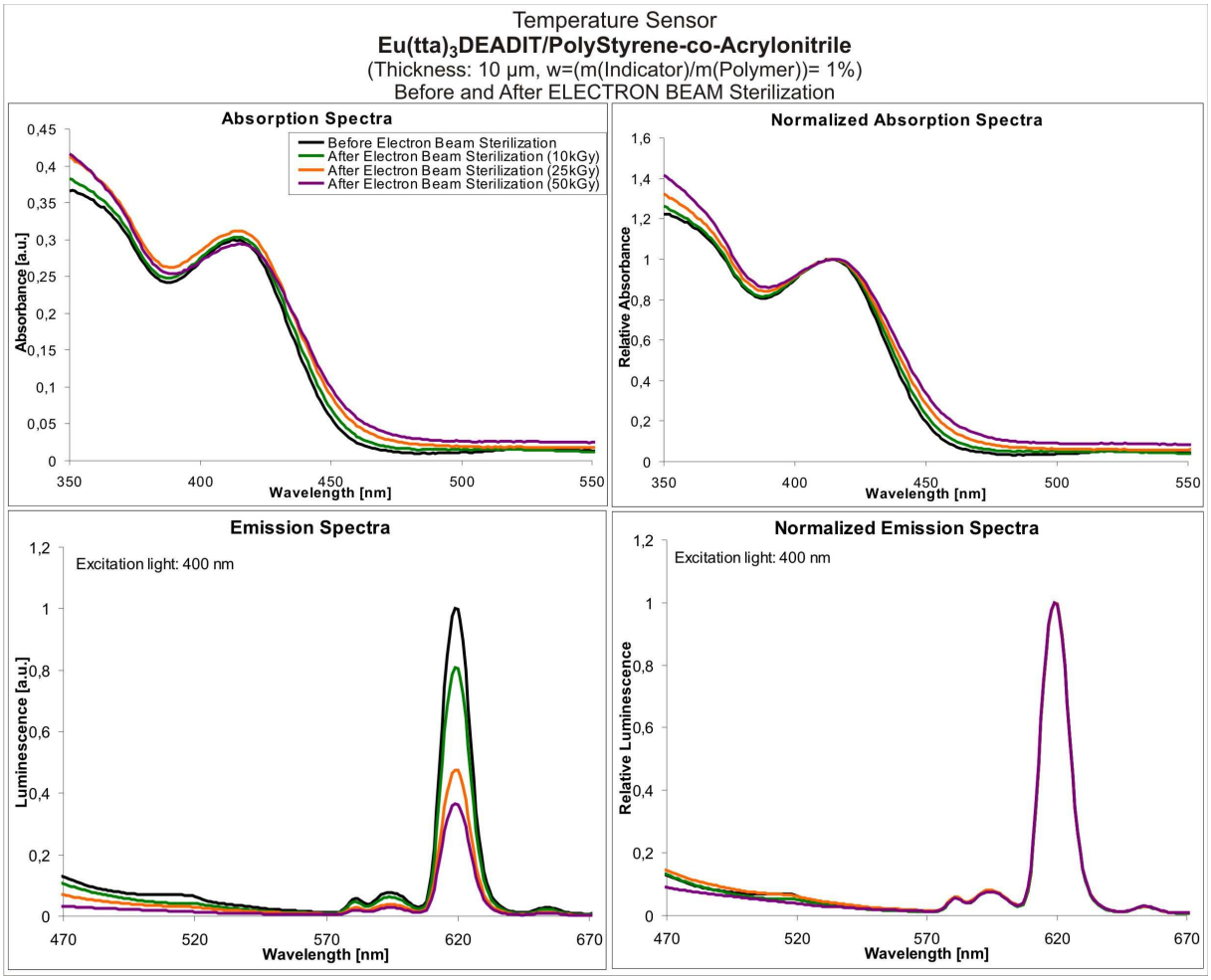

E-BEAM Sterilization	Absorption Spectra		Emission Spectra	
Alterations in Absorption/Emission Intensity	10kGy	1,31% increase	10kGy	19,26% decrease
	25 kGy	4,07% increase	25 kGy	52,35% decrease
	50 kGy	1,74% decrease	50 kGy	63,33% decrease
Alterations in Absorption/Emission Curve Form	10kGy	Unaltered.	10kGy	Unaltered
	25 kGy	Altered absorption between 350-400 nm and 420-600 nm.	25 kGy	Altered emission between 350-400 nm and 420-800 nm.
	50 kGy	Altered absorption between 350-400 nm and 420-800 nm.	50 kGy	Altered emission between 350-400 nm and 420-800 nm.

Calibration Curves

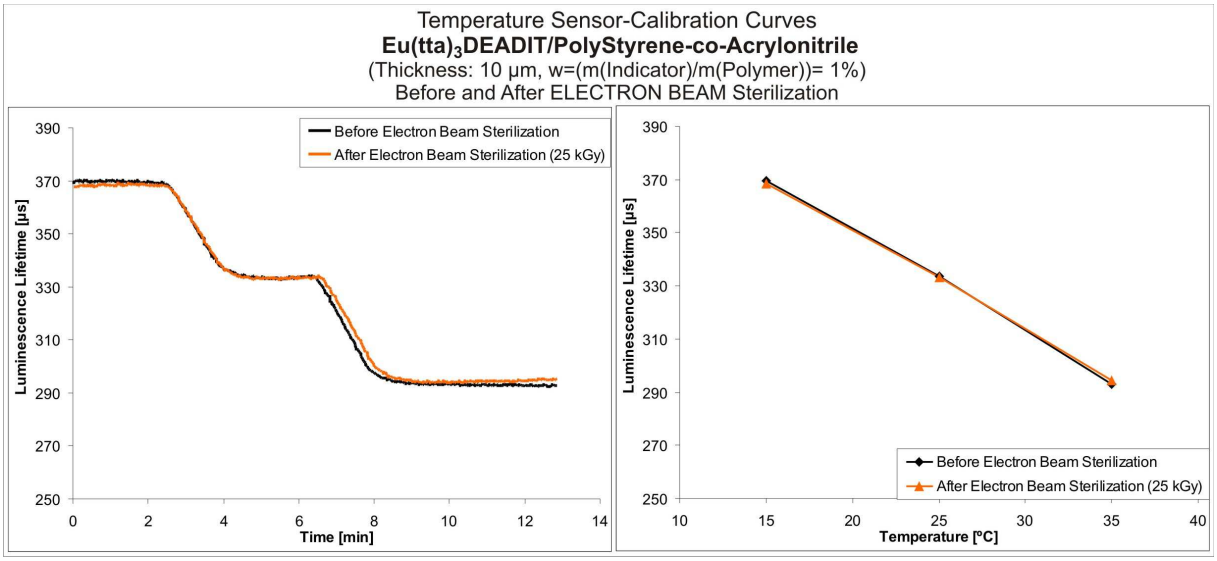

E-BEAM S.	Luminescence Lifetime		Alterations of Slope
Alterations in Luminescence Lifetime and Slope	15℃	0,54% decrease	The same slope before and after sterilization.
	25℃	0,30% decrease	
	35℃	0,34% increase	

C.44 Europium(III) Complex with 4-(4,6-di(1H-indazol-1-yl)-1,3,5-triazin-2-yl)-N,N-DiEthyl Benzen Amine (=Eu(tta)$_3$DEADIT) immobilized in PolyVinylideneChloride-co-Acrylonitrile

C.44.1 Gamma Sterilization

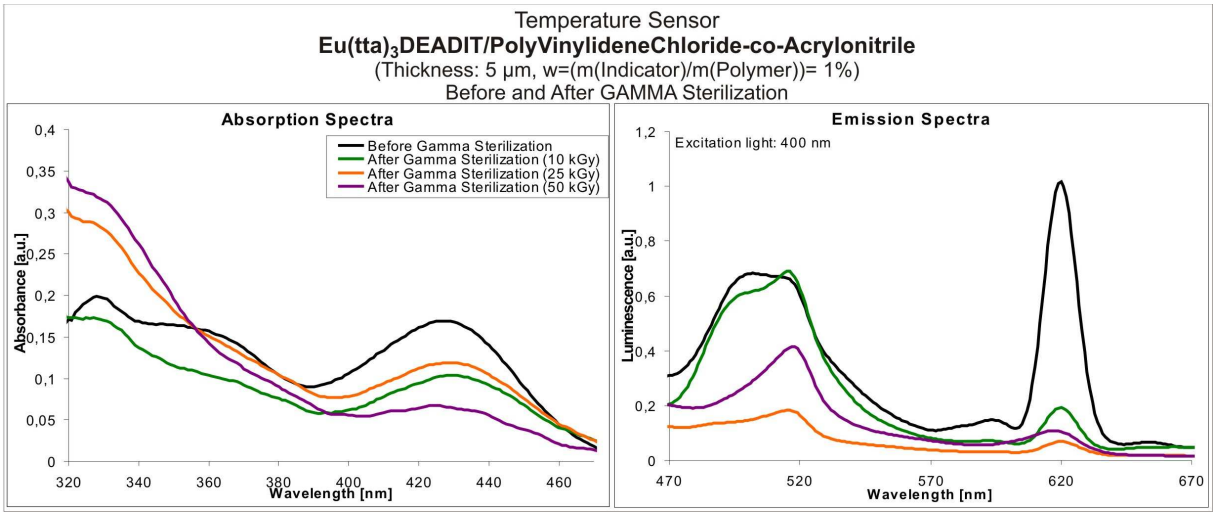

GAMMA Sterilization	Absorption Spectra		Emission Spectra	
Alterations in Absorption/Emission Intensity	10 kGy	38,53% decrease	10 kGy	81,05% decrease (at peak λ_{max1}=620)
	25 kGy	29,53% decrease	25 kGy	93,09% decrease (at peak λ_{max1}=620)
	50 kGy	61,54% decrease	50 kGy	89,45% decrease (at peak λ_{max1}=620)
Alterations in Absorption/Emission Curve Form	10 kGy	Altered absorption curve form between 320-350 nm.	10 kGy	Altered emission curve form. The ratio between peaks with λ_{max1}=501 nm and λ_{max2}=620 nm changed after sterilization.
	25 kGy	Altered absorption curve form between 320-350 nm.	25 kGy	Altered emission curve form. The ratio between peaks with λ_{max1}=501 nm and λ_{max2}=620 nm changed after sterilization.
	50 kGy	Altered absorption curve form between 320-350 nm.	50 kGy	Altered emission curve form. The ratio between peaks with λ_{max1}=501 nm and λ_{max2}=620 nm changed after sterilization.

Calibration Curves

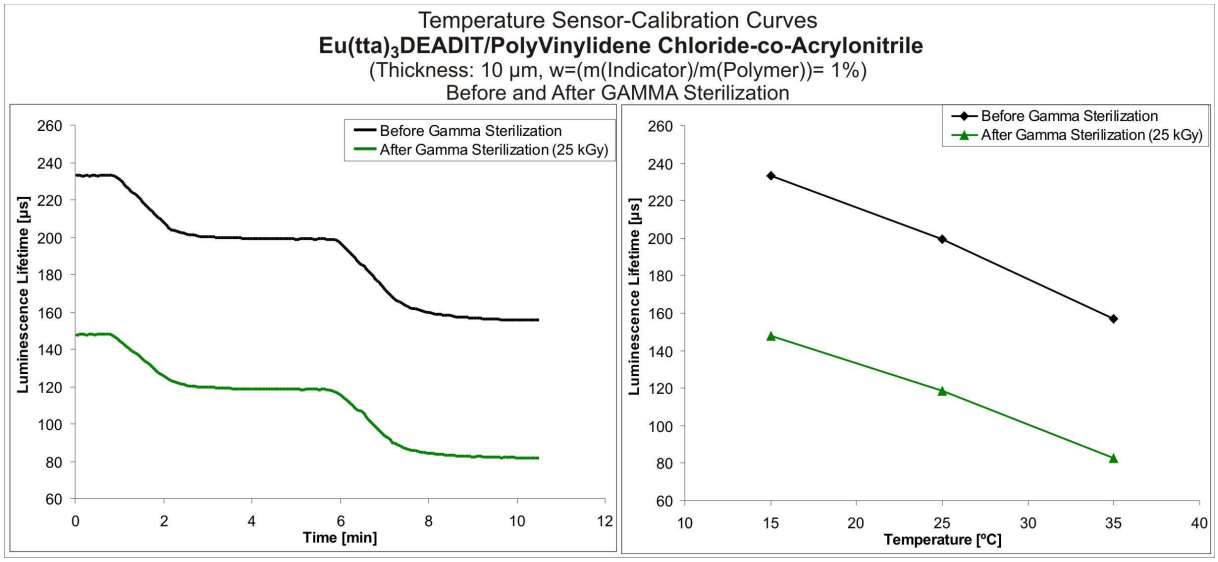

GAMMA S.	Luminescence Lifetime		Alterations of Slope
Alterations in Luminescence Lifetime and Slope	15℃	36,48% decrease	14,28% decrease of slope
	25℃	40,20% decrease	
	35℃	47,32% decrease	

C.44.2 Electron Beam Sterilization

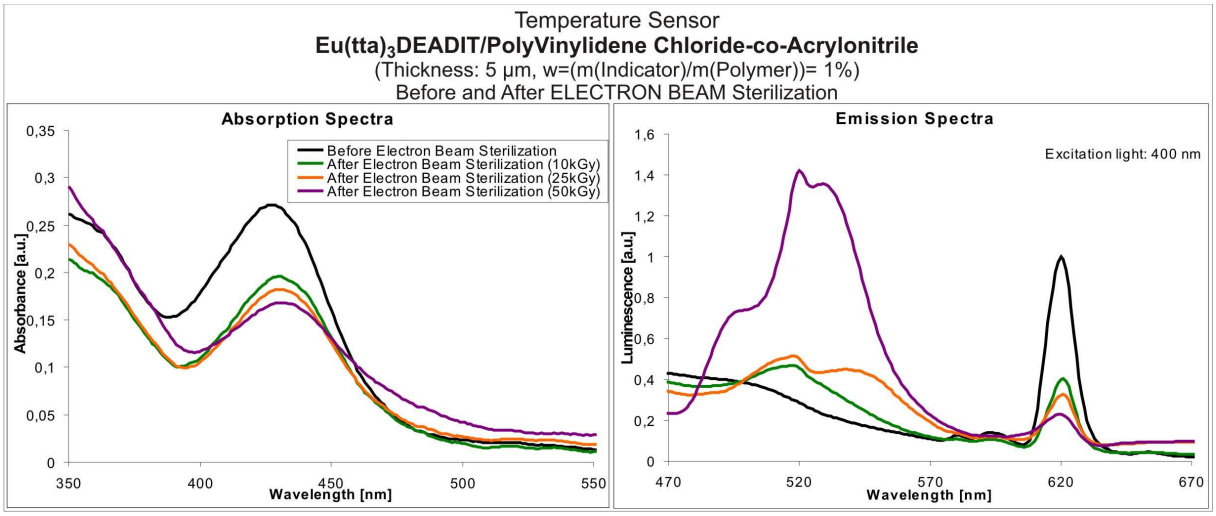

E-BEAM Sterilization	Absorption Spectra		Emission Spectra	
Alterations in Absorption/Emission Intensity	10 kGy	27,88% decrease	10 kGy	59,49% decrease (at peak λ_{max1}=620)
	25 kGy	32,79% decrease	25 kGy	67,31% decrease (at peak λ_{max1}=620)
	50 kGy	38,08% decrease	50 kGy	77,34% decrease (at peak λ_{max1}=620)
Alterations in Absorption/Emission Curve Form	10 kGy	Altered absorption curve form. Bathochromic shift of the absorption maximum for 4 nm.	10 kGy	Altered emission curve form. The ratio between peaks with λ_{max1}=519 nm and λ_{max2}=620 nm changed after sterilization.
	25 kGy	Altered absorption curve form. Bathochromic shift of the absorption maximum for 4 nm.	25 kGy	Altered emission curve form. The ratio between peaks with λ_{max1}=520 nm and λ_{max2}=620 nm changed after sterilization.
	50 kGy	Altered absorption curve form. Bathochromic shift of the absorption maximum for 4 nm.	50 kGy	Altered emission curve form. The ratio between peaks with λ_{max1}=521 nm and λ_{max2}=620 nm changed after sterilization.

Calibration Curves

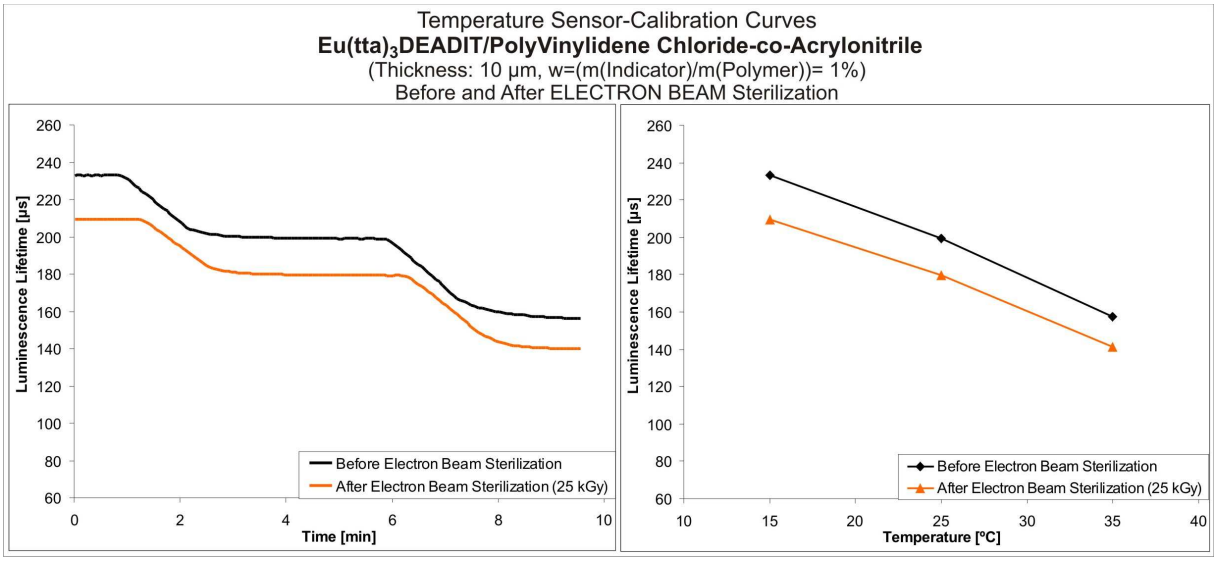

E-BEAM S.	Luminescence Lifetime		Alterations of Slope
Alterations in Luminescence Lifetime and Slope	15℃	10,30% decrease	9,70% decrease of slope
	25℃	9,55% decrease	
	35℃	10,76% decrease	

C.45 Europium(III) Complex with 4-(4,6-di(1H-indazol-1-yl)-1,3,5-triazin-2-yl)-N,N-DiEthyl Benzen Amine (=Eu(tta)$_3$DEADIT) immobilized in PolyMethAcryloNitrile

C.45.1 Gamma Sterilization

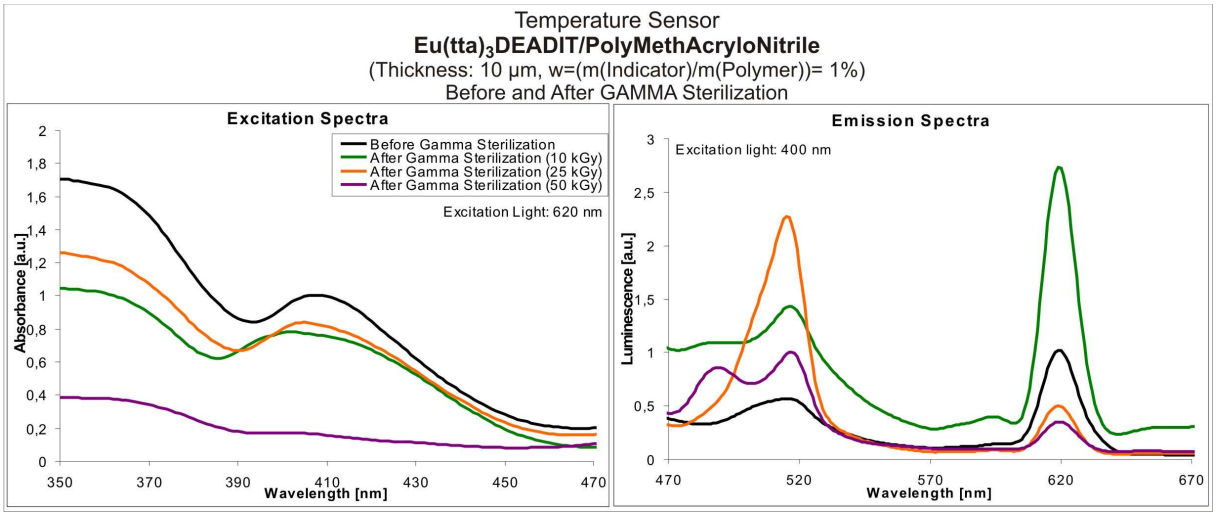

GAMMA Sterilization	Absorption Spectra		Emission Spectra	
Alterations in Absorption/Emission Intensity	10 kGy	24,03% decrease	10 kGy	170% increase (at peak λ_{max1}=620)
	25 kGy	17,16% decrease	25 kGy	50,38% decrease (at peak λ_{max1}=620)
	50 kGy	84,56% decrease	50 kGy	65,51% decrease (at peak λ_{max1}=620)
Alterations in Absorption/Emission Curve Form	10 kGy	Altered absorption curve form between 350-400 nm.	10 kGy	Altered emission curve form. The ratio between peaks with λ_{max1}=501 nm and λ_{max2}=620 nm changed after sterilization.
	25 kGy	Altered absorption curve form between 350-400 nm.	25 kGy	Altered emission curve form. The ratio between peaks with λ_{max1}=501 nm and λ_{max2}=620 nm changed after sterilization.
	50 kGy	Dissapearance of characteristic absorption curve form.	50 kGy	Altered emission curve form. The ratio between peaks with λ_{max1}=501 nm and λ_{max2}=620 nm changed after sterilization.

Calibration Curves

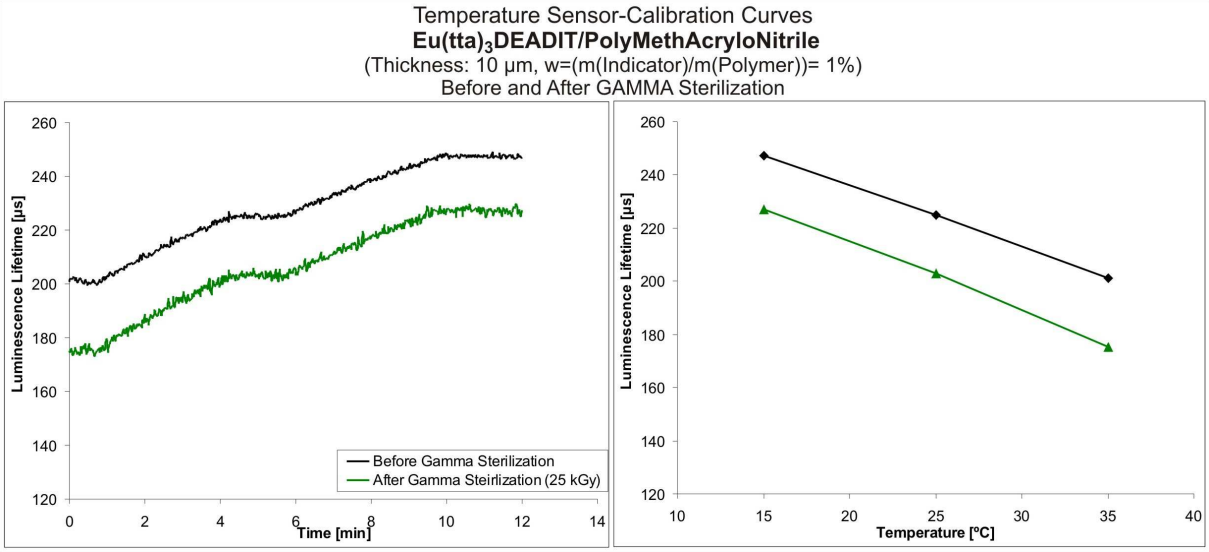

GAMMA S.	Luminescence Lifetime		Alterations of Slope
Alterations in Luminescence Lifetime and Slope	15 °C	8,10% decrease	10,66% increase of slope
	25 °C	9,78% decrease	
	35 °C	12,94% decrease	

C.45.2 Electron Beam Sterilization

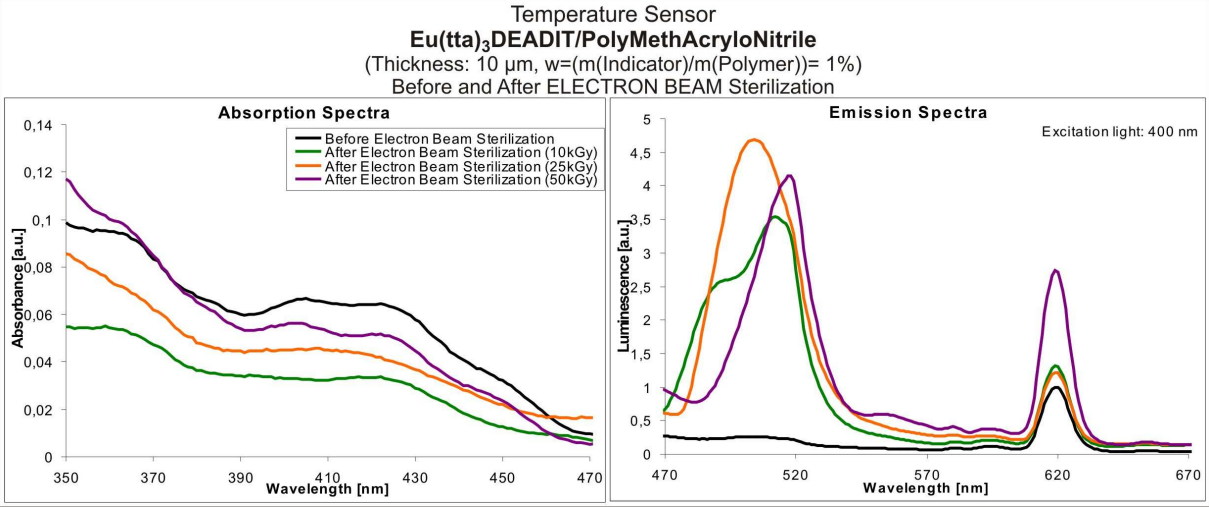

E-BEAM Sterilization	Absorption Spectra		Emission Spectra	
Alterations in Absorption/Emission Intensity	10 kGy	48,22% decrease	10 kGy	30,48% increase (at peak λ_{max1}=620)
	25 kGy	34,48% decrease	25 kGy	21,01% increase (at peak λ_{max1}=620)
	50 kGy	20,22% decrease	50 kGy	170% increase (at peak λ_{max1}=620)

Alterations in Absorption/Emission Curve Form	10 kGy	Altered absorption curve form.	10 kGy	Altered emission curve form. The emission of peaks with λ_{max1}=510 nm and λ_{max2}=620 nm increase after sterilization.
	25 kGy	Altered absorption curve form.	25 kGy	Altered emission curve form. The emission of peaks with λ_{max1}=504 nm and λ_{max2}=620 nm increase after sterilization.
	50 kGy	Altered absorption curve form.	50 kGy	Altered emission curve form. The emission of peaks with λ_{max1}=518 nm and λ_{max2}=620 nm increase after sterilization.

Calibration Curves

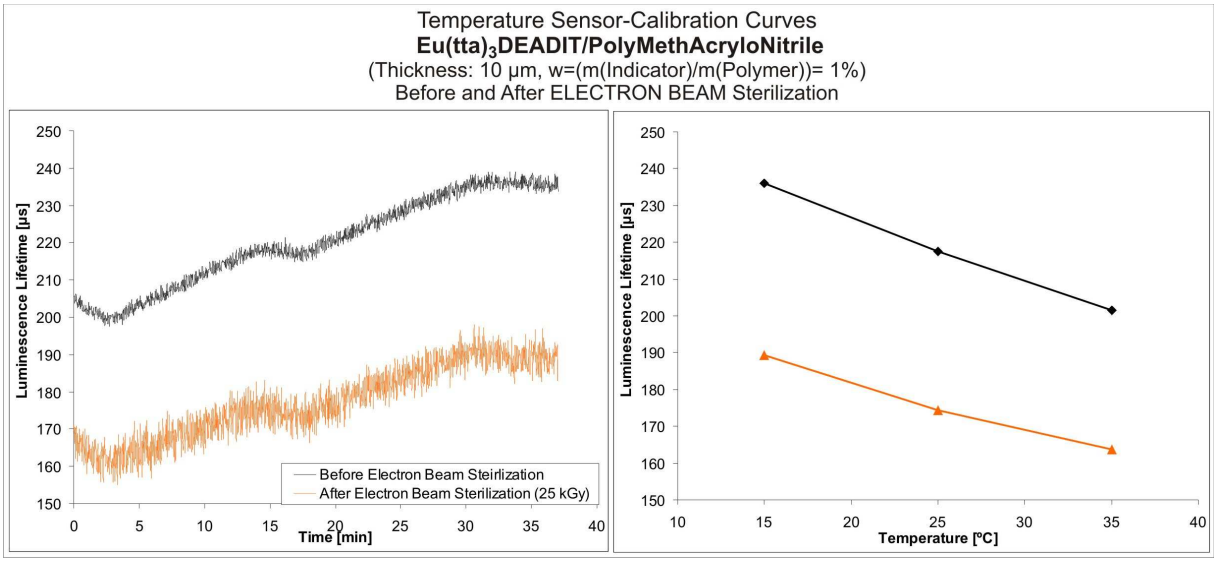

E-BEAM S.	Luminescence Lifetime		Alterations of Slope
Alterations in Luminescence Lifetime and Slope	15 ℃	19,92% decrease	24,91% decrease of slope
	25 ℃	20,18% decrease	
	35 ℃	18,81% decrease	

C.46 DiChloroTrisPhenanthroline Ruthenium(II)Hydrate immobilized in PolyVinylideneChloride-co-Acrylonitrile

C.46.1 Gamma Sterilization

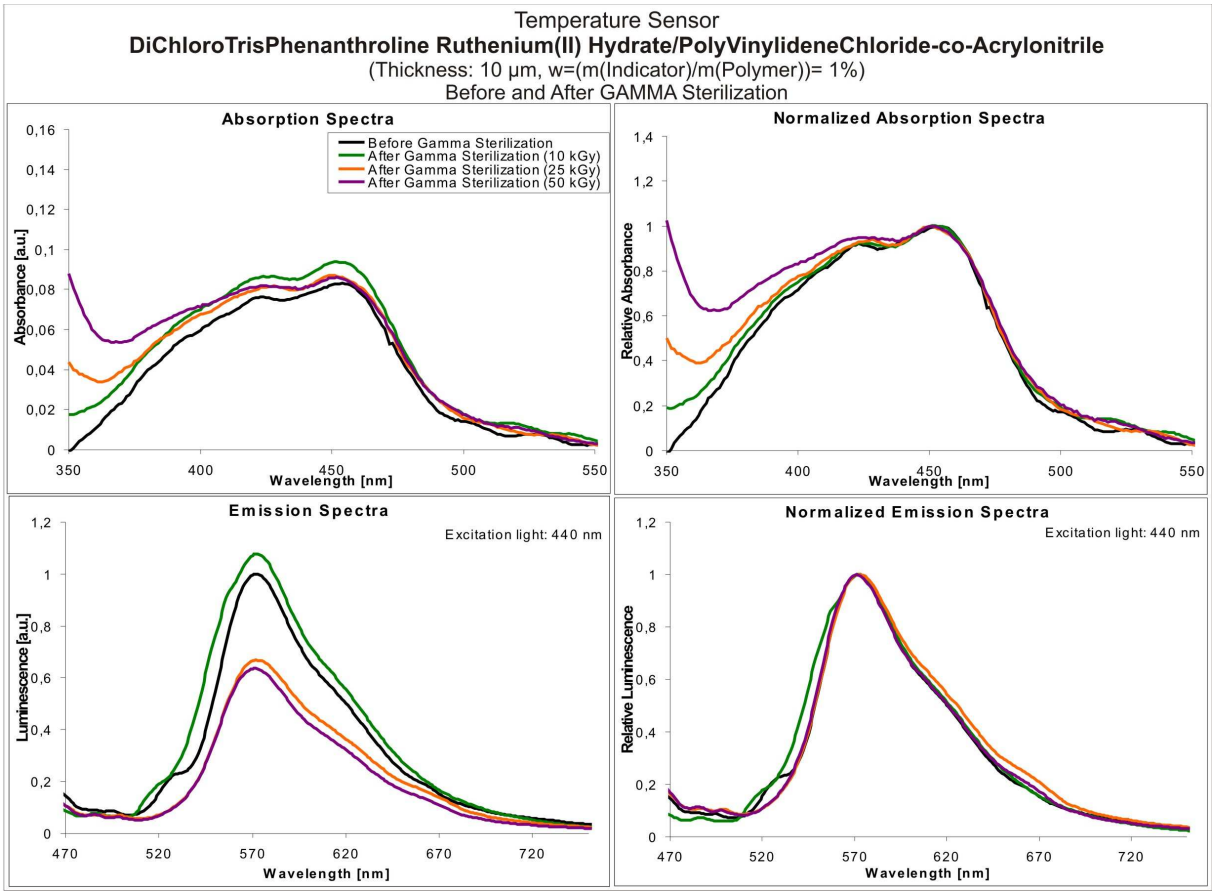

GAMMA Sterilization	Absorption Spectra		Emission Spectra	
Alterations in Absorption/Emission Intensity	10kGy	11,30% increase	10kGy	7,27% increase
	25 kGy	4,70% increase	25 kGy	33,46% decrease
	50 kGy	3,49% increase	50 kGy	36,21% decrease
Alterations in Absorption/Emission Curve Form	10kGy	Altered absorption curve form between 350-400 nm.	10kGy	Altered emission curve form between 470-570 nm.
	25 kGy	Altered absorption curve form between 350-420 nm.	25 kGy	Altered emission curve form between 600-700 nm.
	50 kGy	Altered absorption curve form between 350-430 nm.	50 kGy	Unaltered.

Calibration Curves

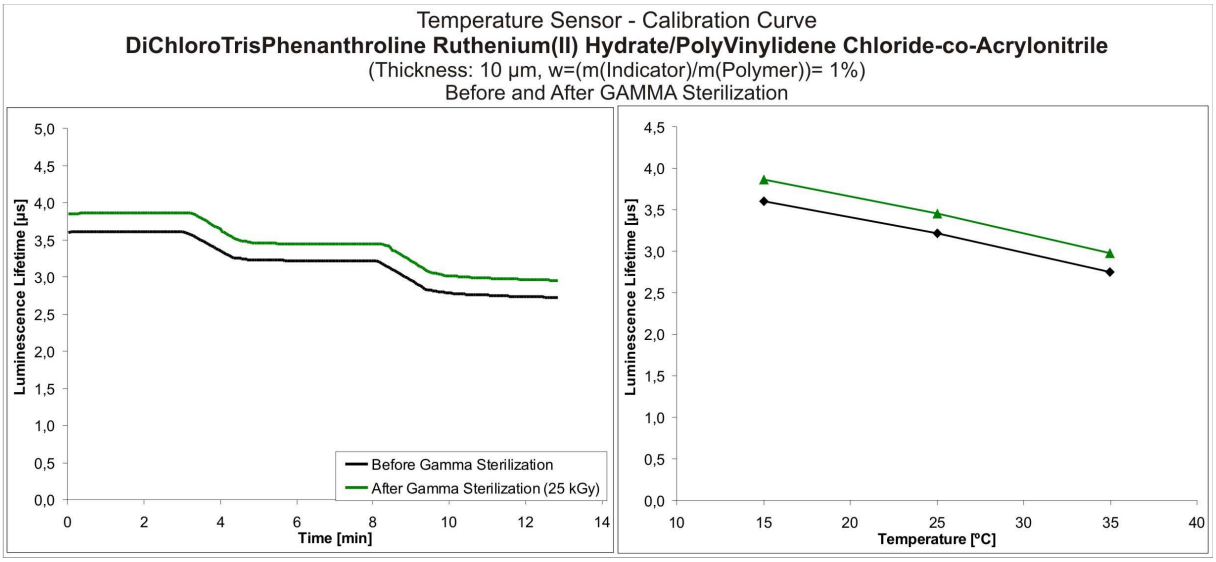

GAMMA S.	Luminescence Lifetime		Alterations of Slope
Alterations in Luminescence Lifetime and Slope	15 °C	6,93% increase	2,81% increase of slope
	25 °C	7,14% increase	
	35 °C	8,36% increase	

C.46.2 Electron Beam Sterilization

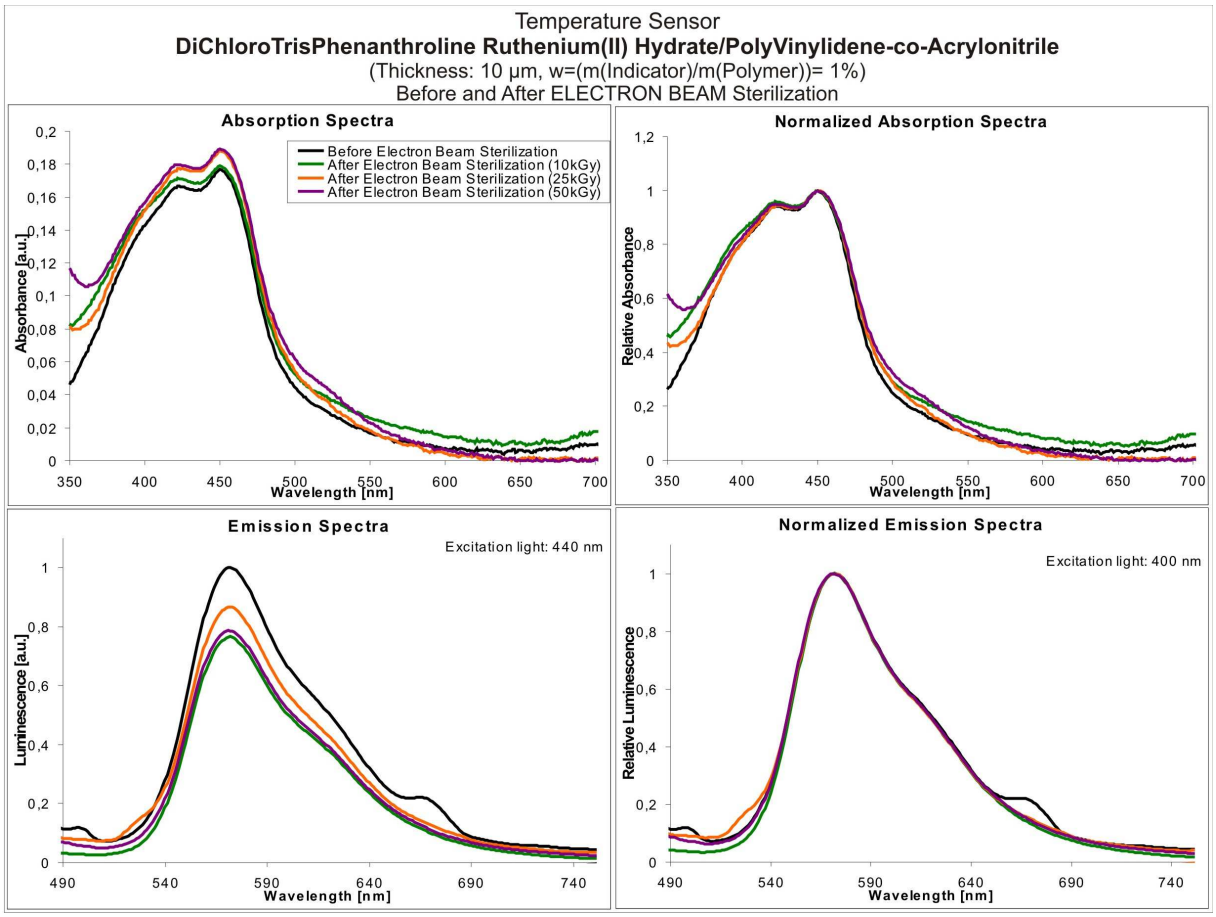

E-BEAM Sterilization	Absorption Spectra		Emission Spectra	
Alterations in Absorption/Emission Intensity	10kGy	1,09% increase	10kGy	23,50% decrease
	25 kGy	5,88% increase	25 kGy	13,39% decrease
	50 kGy	6,63% increase	50 kGy	21,36% decrease
Alterations in Absorption/Emission Curve Form	10kGy	Altered absorption curve form between 350-410 nm and 510-800 nm.	10kGy	Disappearance of emission peak with λ_{max}=669 nm.
	25 kGy	Altered absorption curve form between 350-370 nm.	25 kGy	Disappearance of emission peak with λ_{max}=669 nm.
	50 kGy	Altered absorption curve form between 350-400 nm and 480-560 nm.	50 kGy	Disappearance of emission peak with λ_{max}=669 nm.

Calibration Curves

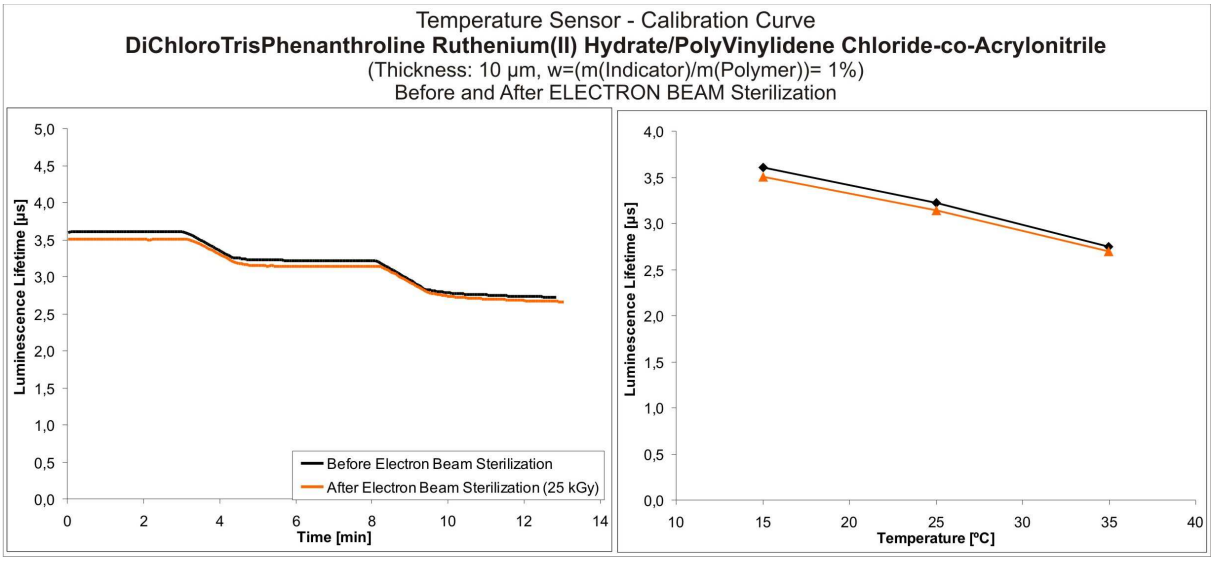

E-BEAM S.	Luminescence Lifetime		Alterations of Slope
Alterations in Luminescence Lifetime and Slope	15 ºC	3,05% decrease	6,09% decrease of slope
	25 ºC	2,48% decrease	
	35 ºC	1,82% decrease	

C.47 DiChloroTrisPhenanthroline Ruthenium(II)Hydrate immobilized in PolyMethAcryloNitrile

C.47.1 Gamma Sterilization

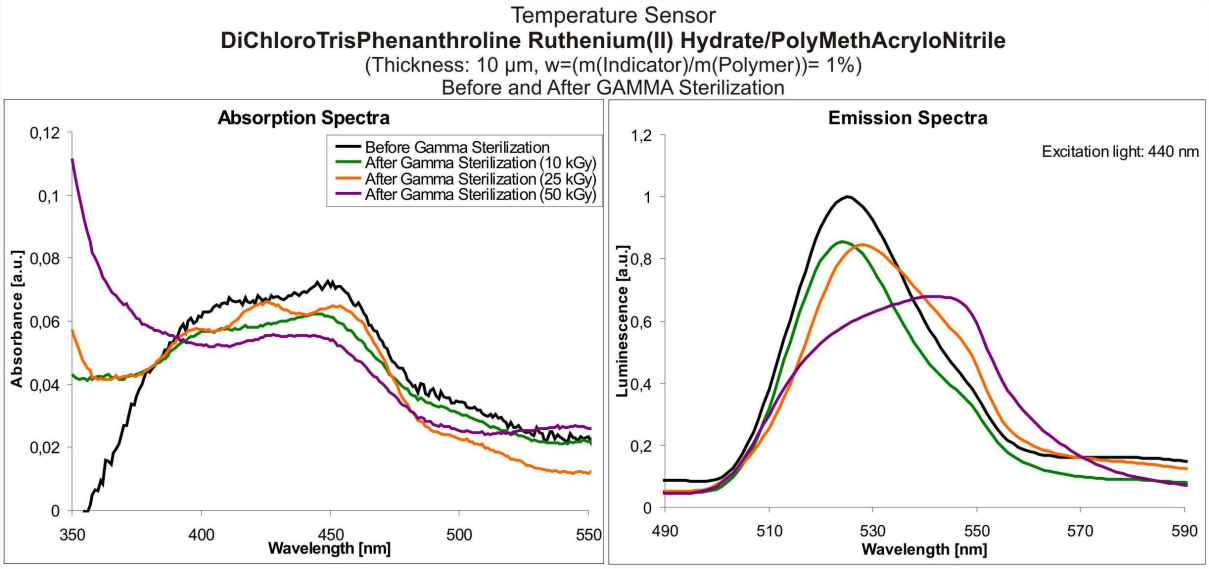

GAMMA Sterilization	Absorption Spectra		Emission Spectra	
Alterations in Absorption/Emission Intensity	10kGy	Decrease	10kGy	Decrease
	25 kGy	Decrease	25 kGy	Decrease
	50 kGy	Decrease	50 kGy	Decrease
Alterations in Absorption/Emission Curve Form	10kGy	Altered absorption curve form.	10kGy	Altered emission curve form
	25 kGy	Altered absorption curve form.	25 kGy	Altered emission curve form.
	50 kGy	Disappearance of the characteristic curve form.	50 kGy	Disappearance of the characteristic curve form.

Calibration Curves

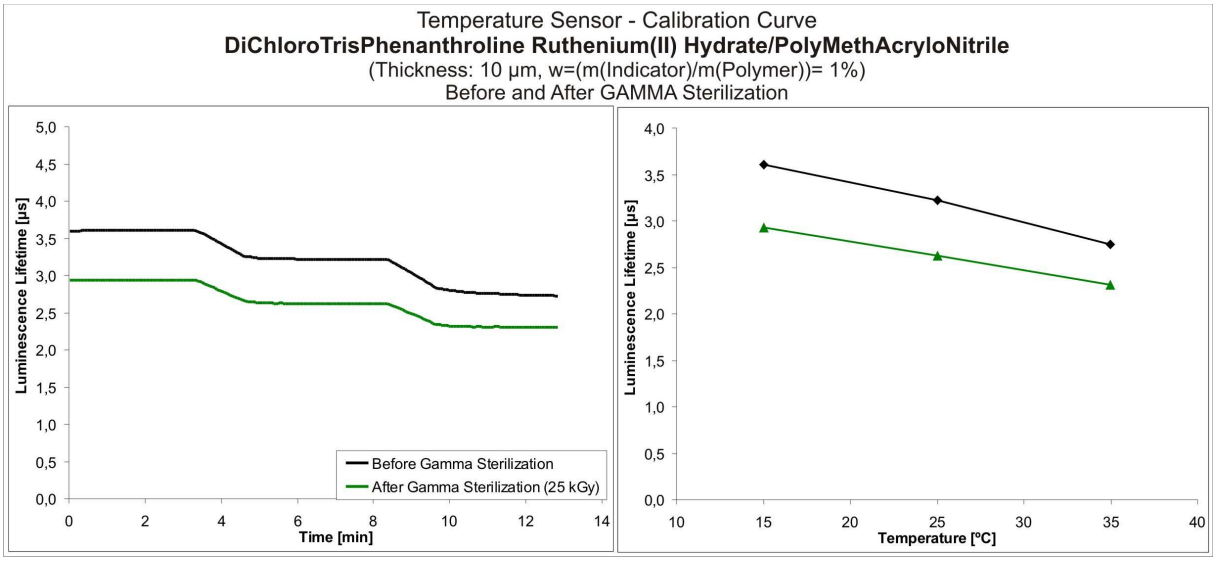

GAMMA S.	Luminescence Lifetime		Alterations of Slope
Alterations in Luminescence Lifetime and Slope	15 ºC	18,61% decrease	26,76% decrease of slope
	25 ºC	18,32% decrease	
	35 ºC	16,00% decrease	

C.47.2 Electron Beam Sterilization

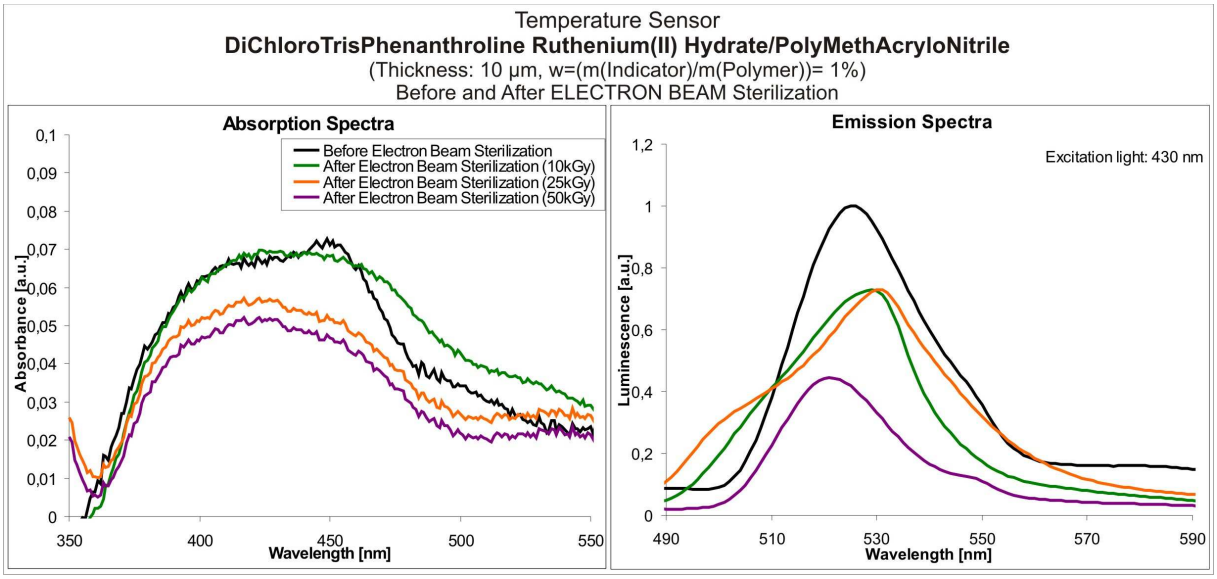

E-BEAM Sterilization	Absorption Spectra		Emission Spectra	
Alterations in Absorption/Emission Intensity	10kGy	Decrease	10kGy	7,60% increase
	25 kGy	Decrease	25 kGy	17,95% decrease
	50 kGy	Decrease	50 kGy	Decrease
Alterations in Absorption/Emission Curve Form	10kGy	Altered absorption curve form.	10kGy	Altered emission curve form
	25 kGy	Altered absorption curve form.	25 kGy	Altered emission curve form.
	50 kGy	Disappearance of the characteristic curve form.	50 kGy	Disappearance of the characteristic curve form.

Calibration Curves

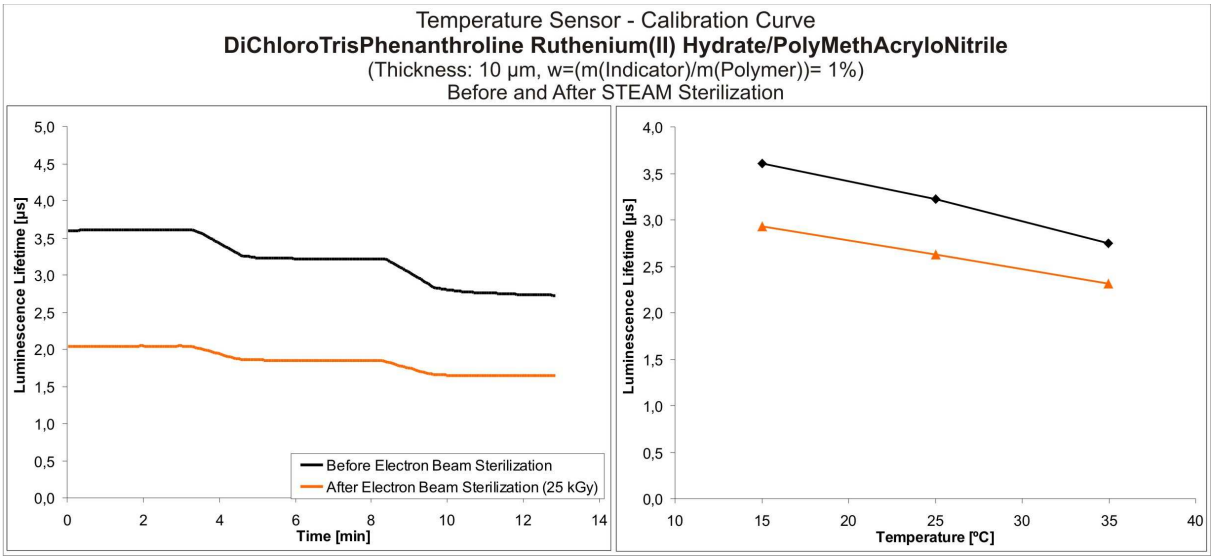

E-BEAM S.	Luminescence Lifetime		Alterations of Slope
Alterations in Luminescence Lifetime and Slope	15 °C	43,33% decrease	26,76% decrease of slope
	25 °C	42,55% decrease	
	35 °C	40,00% decrease	

Optical AMMONIA SENSORS

C.48 Eosin EthylEster immobilized in Cellulose Acetate

C.48.1 Gamma Sterilization

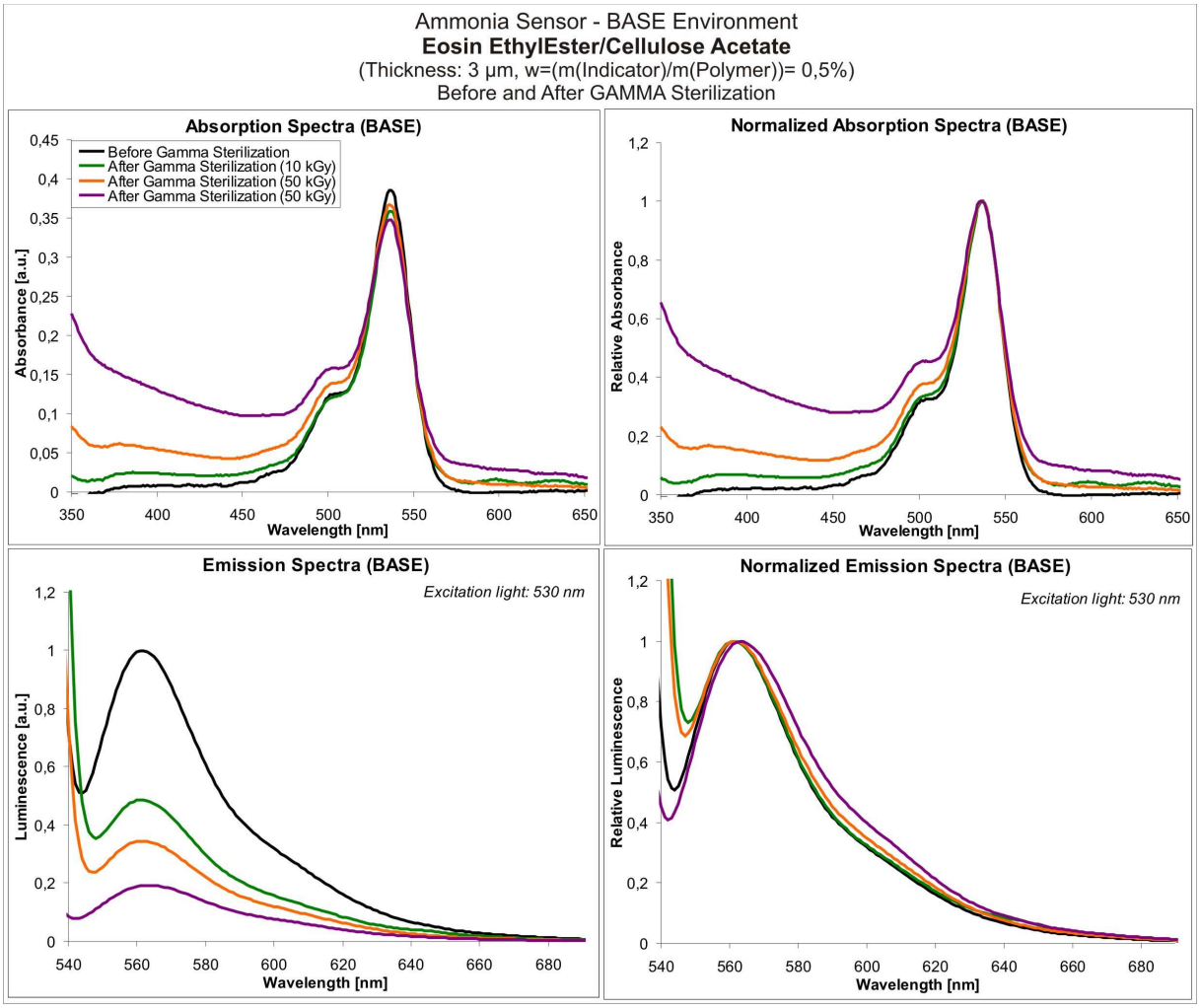

GAMMA S.	Absorption Spectra			Emission Spectra		
			Alterations			Alterations
Alterations in Absorption/ Emission Intensity	10 kGy	Base	6,96% decrease	10 kGy	Base	51,38% decrease
	25 kGy	Base	5,05% decrease	25 kGy	Base	65,51% decrease
	50 kGy	Base	9,88% decrease	50 kGy	Base	80,72% decrease

Alterations in Absorption/ Emission Curve Form	10 kGy	Base	Altered absorption curve form between 350-480 nm and 570-800 nm. The sensor became slightly turbid.	10 kGy	Base	Unaltered.
	25 kGy	Base	Altered absorption curve form between 350-520 nm and 570-800 nm. The sensor became slightly turbid.	25 kGy	Base	Unaltered.
	50 kGy	Base	Altered absorption curve form between 350-520 nm and 560-800 nm. The sensor became slightly turbid.	50 kGy	Base	Altered emission curve form between 570-660 nm. Bathochromic shift of the emission maximum for 2 nm.

C.48.2 Electron Beam Sterilization

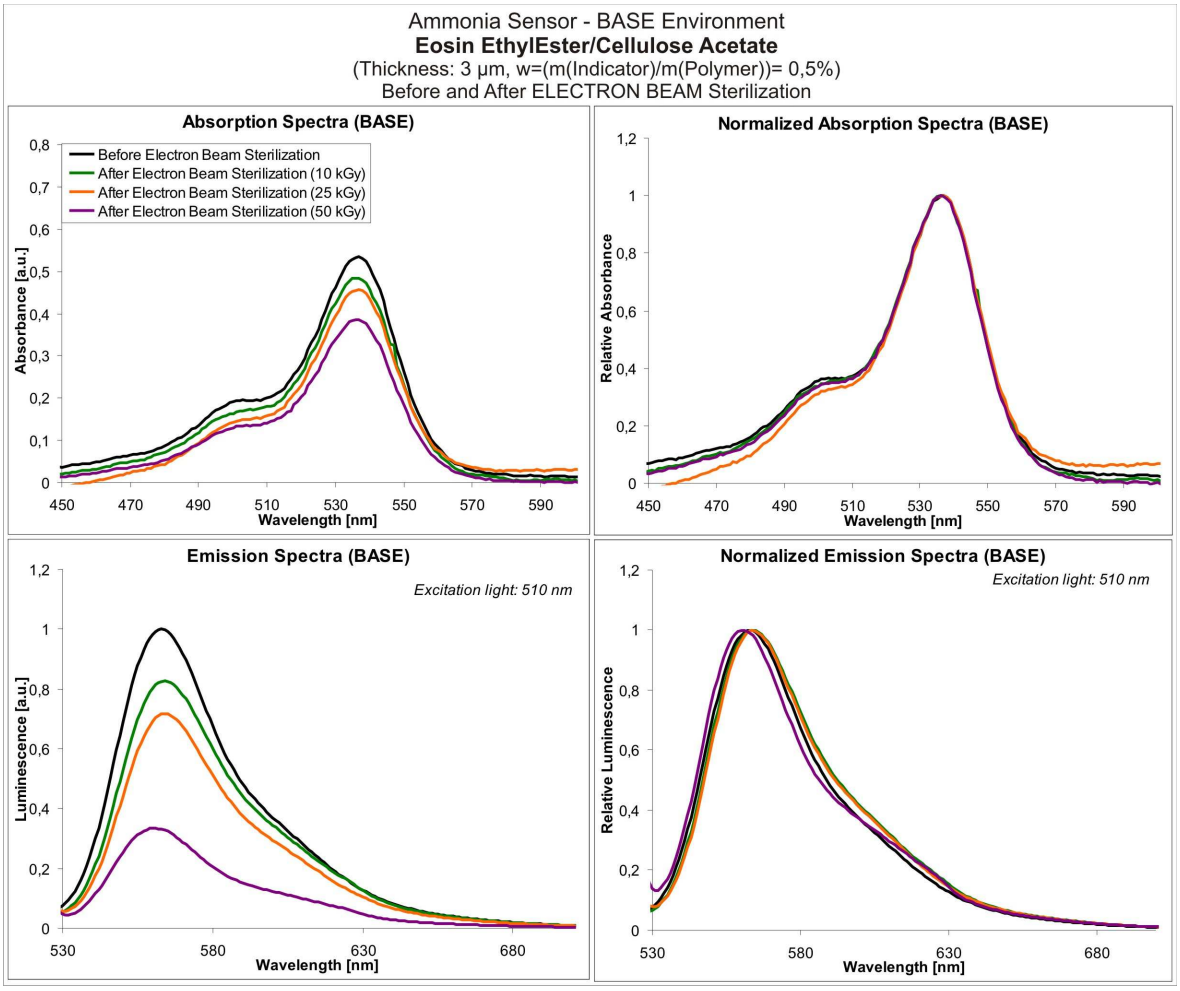

E-BEAM S.	Absorption Spectra			Emission Spectra		
			Alterations			Alterations
Alterations in Absorption/ Emission Intensity	10 kGy	Base	9,36% decrease	10 kGy	Base	17,31% decrease
	25 kGy	Base	14,72% decrease	25 kGy	Base	28,20% decrease
	50 kGy	Base	27,80% decrease	50 kGy	Base	66,56% decrease
Alterations in Absorption/ Emission Curve Form	10 kGy	Base	Altered absorption between 450-515 nm.	10 kGy	Base	Altered emission curve form between 580-630 nm.
	25 kGy	Base	Altered absorption between 450-515 nm and 560-800 nm.	25 kGy	Base	Altered emission curve form between 580-630 nm.
	50 kGy	Base	Altered absorption between 450-515 nm.	50 kGy	Base	Hypsochromic shift of the emission maximum for 3 nm.

C.49 Eosin EthylEster immobilized in Hydrogel D7

C.49.1 Gamma Sterilization

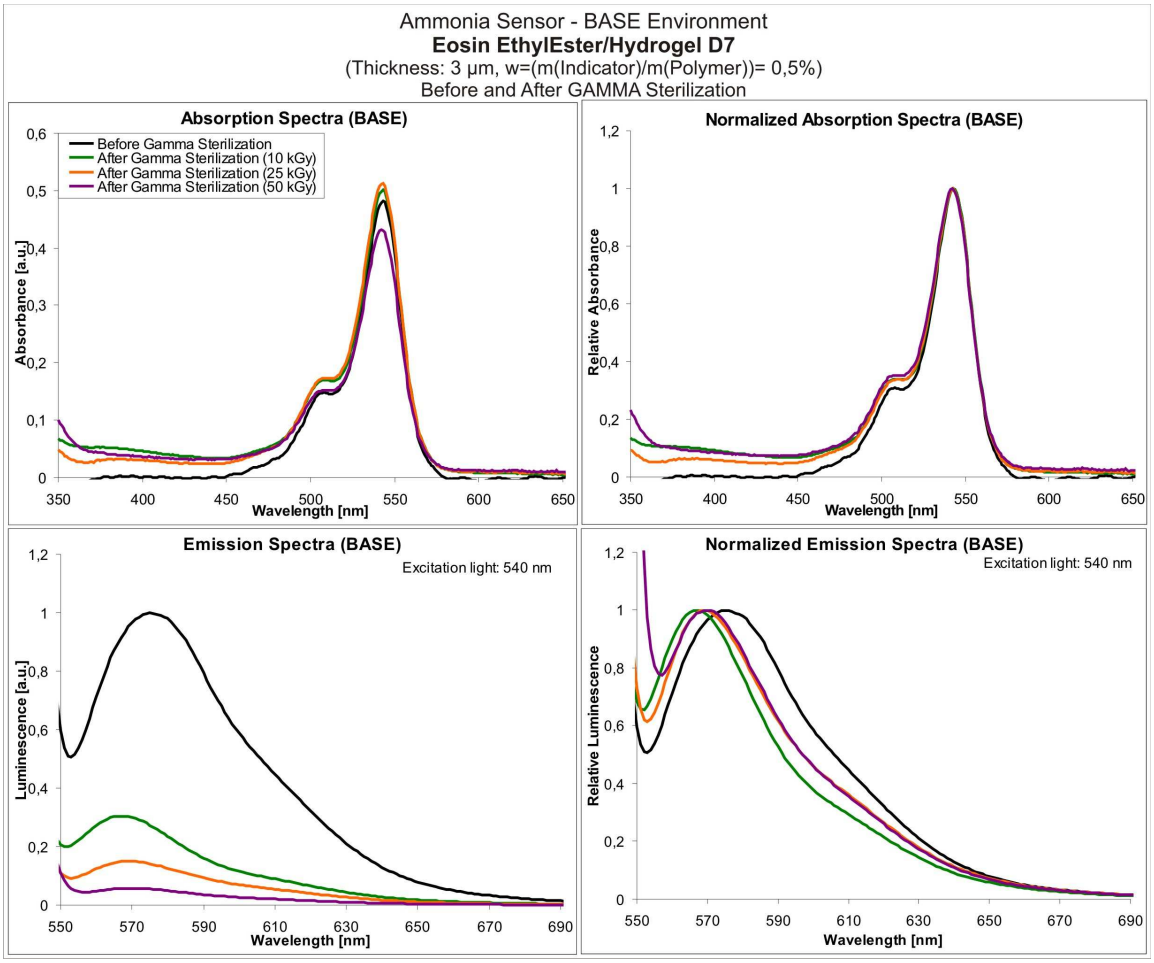

GAMMA S.	Absorption Spectra			Emission Spectra		
			Alterations			Alterations
Alterations in Absorption/ Emission Intensity	10 kGy	Base	3,83% increase	10 kGy	Base	69,58% decrease
	25 kGy	Base	6,12% increase	25 kGy	Base	84,98% decrease
	50 kGy	Base	10,40% decrease	50 kGy	Base	94,24% decrease
Alterations in Absorption/ Emission Curve Form	10 kGy	Base	Altered absorption curve form between 350-520 nm.	10 kGy	Base	Hypsochromic shift of the emission maximum for 8 nm.
	25 kGy	Base	Altered absorption curve form between 350-520 nm.	25 kGy	Base	Hypsochromic shift of the emission maximum for 6 nm.
	50 kGy	Base	Altered absorption curve form between 350-520 nm.	50 kGy	Base	Hypsochromic shift of the emission maximum for 5 nm.

C.49.2 Electron Beam Sterilization

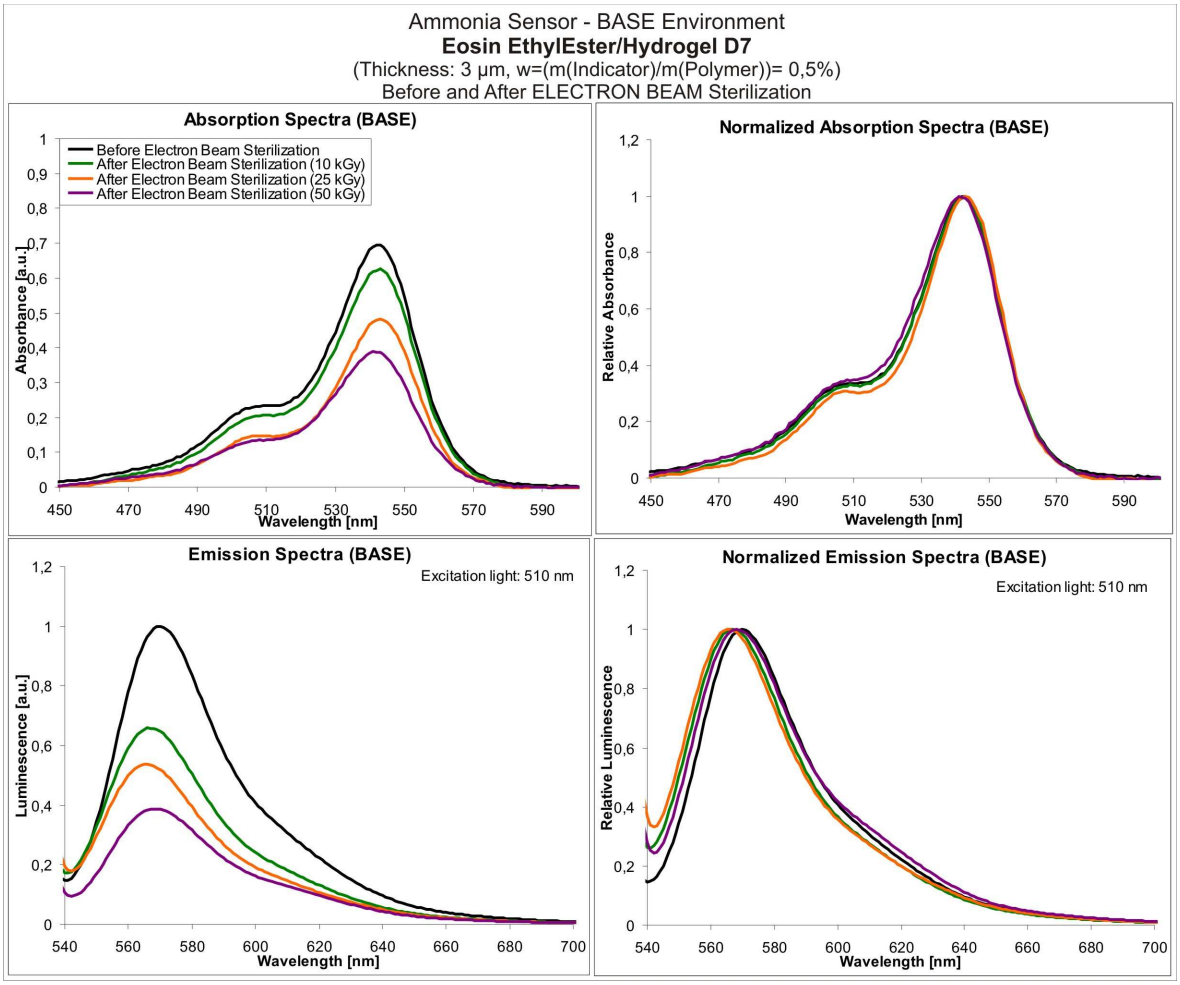

E-BEAM S.	Absorption Spectra			Emission Spectra		
			Alterations			Alterations
Alterations in Absorption/ Emission Intensity	10 kGy	Base	9,80% decrease	10 kGy	Base	34,18% decrease
	25 kGy	Base	30,70% decrease	25 kGy	Base	46,38% decrease
	50 kGy	Base	44,07% decrease	50 kGy	Base	61,21% decrease
Alterations in Absorption/ Emission Curve Form	10 kGy	Base	Unaltered.	10 kGy	Base	Hypsochromic shift of the emission maximum for 4 nm.
	25 kGy	Base	Unaltered.	25 kGy	Base	Hypsochromic shift of the emission maximum for 4 nm.
	50 kGy	Base	Hypsochromic shift of the absorption maximum for 2 nm.	50 kGy	Base	Altered emission curve form between 600-660 nm. Hypsochromic shift of the emission maximum for 2 nm.

C.50 Eosin EthylEster immobilized in Ethyl Cellulose

C.50.1 Gamma Sterilization

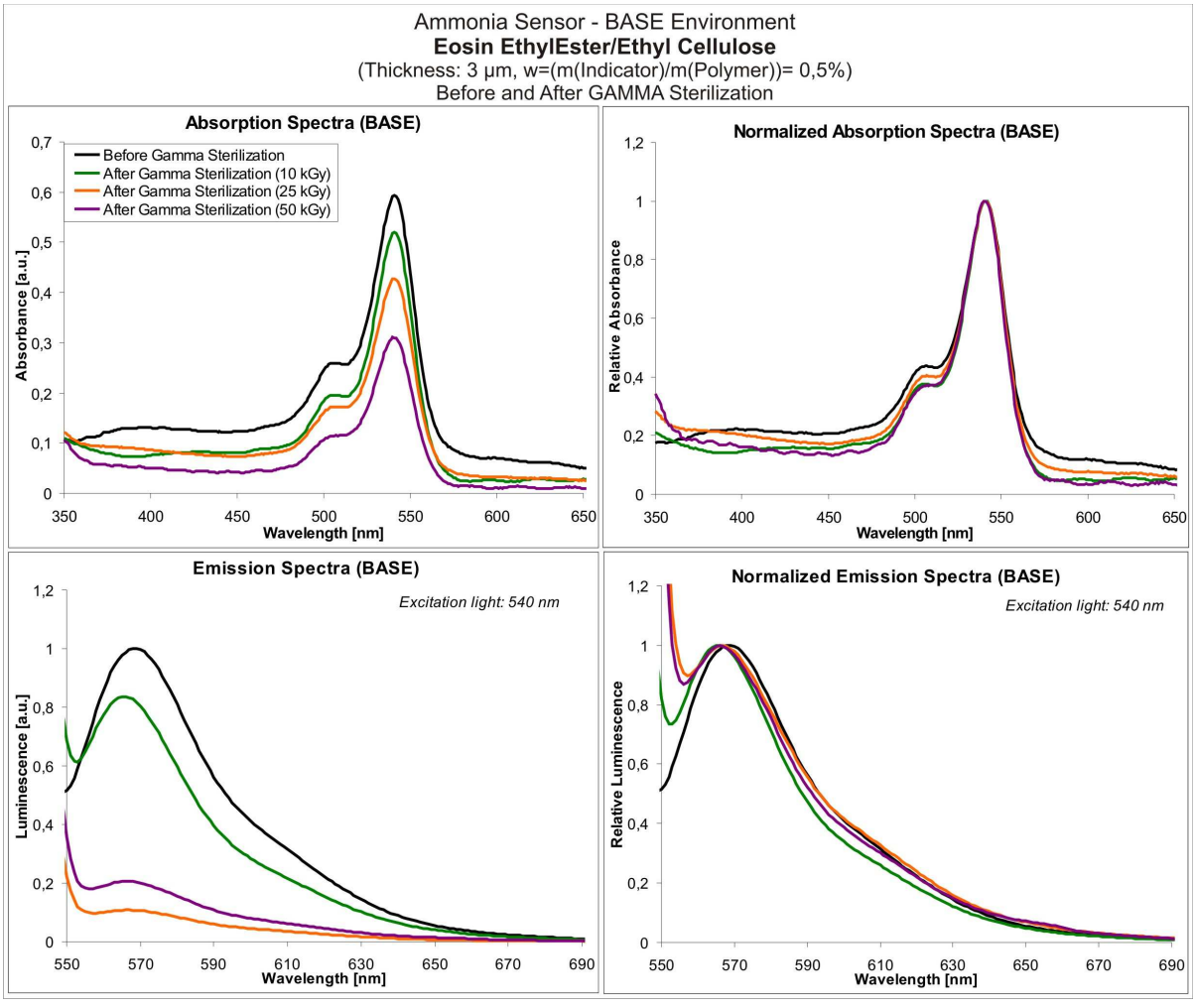

GAMMA S.	Absorption Spectra			Emission Spectra		
			Alterations			Alterations
Alterations in Absorption/ Emission Intensity	10 kGy	Base	12,32% decrease	10 kGy	Base	16,39% decrease
	25 kGy	Base	27,88% decrease	25 kGy	Base	89,16% decrease
	50 kGy	Base	47,64% decrease	50 kGy	Base	79,30% decrease
Alterations in Absorption/ Emission Curve Form	10 kGy	Base	Altered absorption curve form between 350-520 nm and 560-800 nm.	10 kGy	Base	Hypsochromic shift of the emission maximum for 2 nm.
	25 kGy	Base	Altered absorption curve form between 350-520 nm and 560-800 nm.	25 kGy	Base	Hypsochromic shift of the emission maximum for 2 nm.
	50 kGy	Base	Altered absorption curve form between 350-520 nm and 560-800 nm.	50 kGy	Base	Hypsochromic shift of the emission maximum for 2 nm.

C.50.2 Electron Beam Sterilization

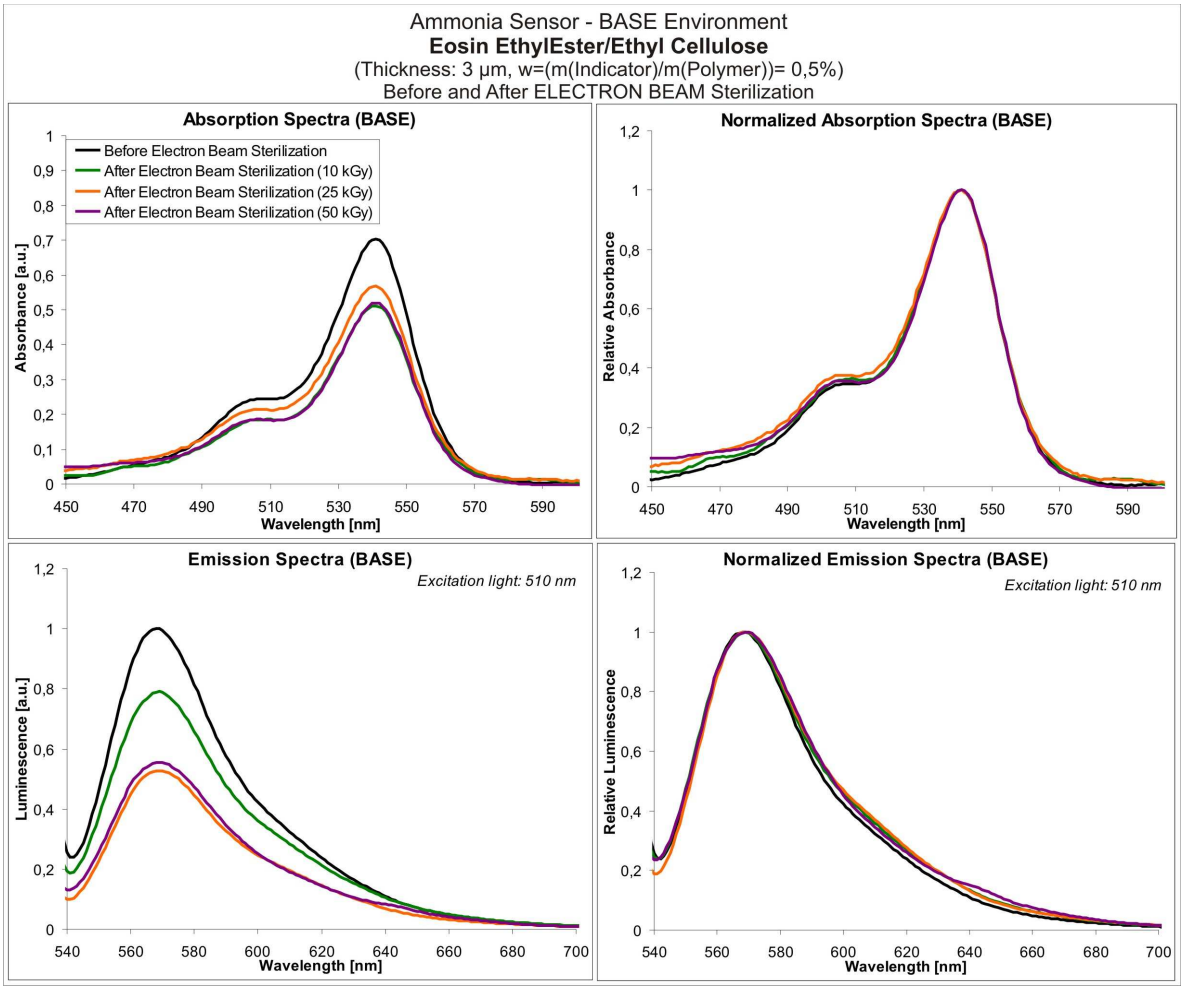

E-BEAM S.	Absorption Spectra			Emission Spectra		
			Alterations			Alterations
Alterations in Absorption/ Emission Intensity	10 kGy	Base	27,23% decrease	10 kGy	Base	20,93% decrease
	25 kGy	Base	19,32% decrease	25 kGy	Base	47,30% decrease
	50 kGy	Base	26,24% decrease	50 kGy	Base	44,50% decrease
Alterations in Absorption/ Emission Curve Form	10 kGy	Base	Unaltered.	10 kGy	Base	Bathochromic shift of the emission maximum for 2 nm.
	25 kGy	Base	Unaltered.	25 kGy	Base	Bathochromic shift of the emission maximum for 2 nm.
	50 kGy	Base	Unaltered.	50 kGy	Base	Bathochromic shift of the emission maximum for 2 nm.

C.51 Eosin EthylEster immobilized in PolyMethylMethAcrylate (=PMMA)

C.51.1 Gamma Sterilization

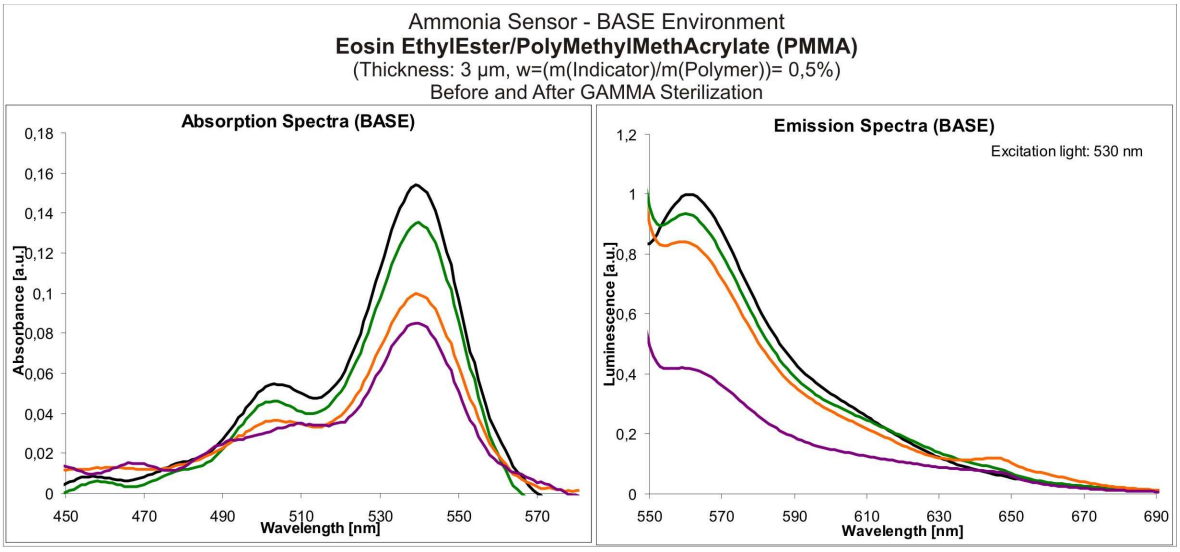

GAMMA S.	Absorption Spectra			Emission Spectra		
			Alterations			Alterations
Alterations in Absorption/ Emission Intensity	10 kGy	Base	12,13% decrease	10 kGy	Base	6,56% decrease
	25 kGy	Base	35,10% decrease	25 kGy	Base	15,93% decrease
	50 kGy	Base	44,66% decrease	50 kGy	Base	57,91% decrease
Alterations in Absorption/ Emission Curve Form	10 kGy	Base	Unaltered.	10 kGy	Base	Altered emission between 615-660 nm.
	25 kGy	Base	Altered absorption curve form between 350-500 nm.	25 kGy	Base	New emission peak with λ_{max} = 648 nm.

	50 kGy	Base	Altered absorption curve form between 350-500 nm.	50 kGy	Base	New emission peak with λ_{max} = 646 nm.

C.51.2 Electron Beam Sterilization

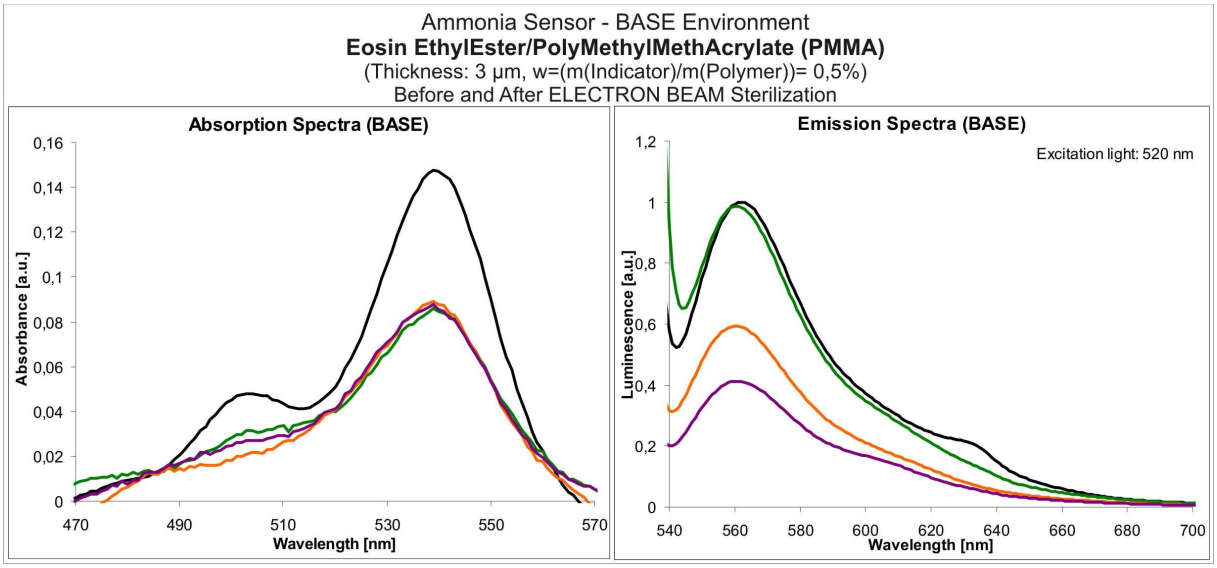

E-BEAM S.	Absorption Spectra			Emission Spectra		
			Alterations			Alterations
Alterations in Absorption/ Emission Intensity	10 kGy	Base	41,81% decrease	10 kGy	Base	1,25% decrease
	25 kGy	Base	39,70% decrease	25 kGy	Base	40,62% decrease
	50 kGy	Base	40,50% decrease	50 kGy	Base	58,68% decrease
Alterations in Absorption/ Emission Curve Form	10 kGy	Base	Altered absorption curve form between 470-530 nm.	10 kGy	Base	Altered emission between 610-660 nm.
	25 kGy	Base	Altered absorption curve form between 470-530 nm.	25 kGy	Base	Altered emission between 610-660 nm.
	50 kGy	Base	Altered absorption curve form between 470-530 nm.	50 kGy	Base	Altered emission between 590-620 nm.

C.52 DiChloroFluorescein immobilized in Cellulose Acetate

C.52.1 Gamma Sterilization

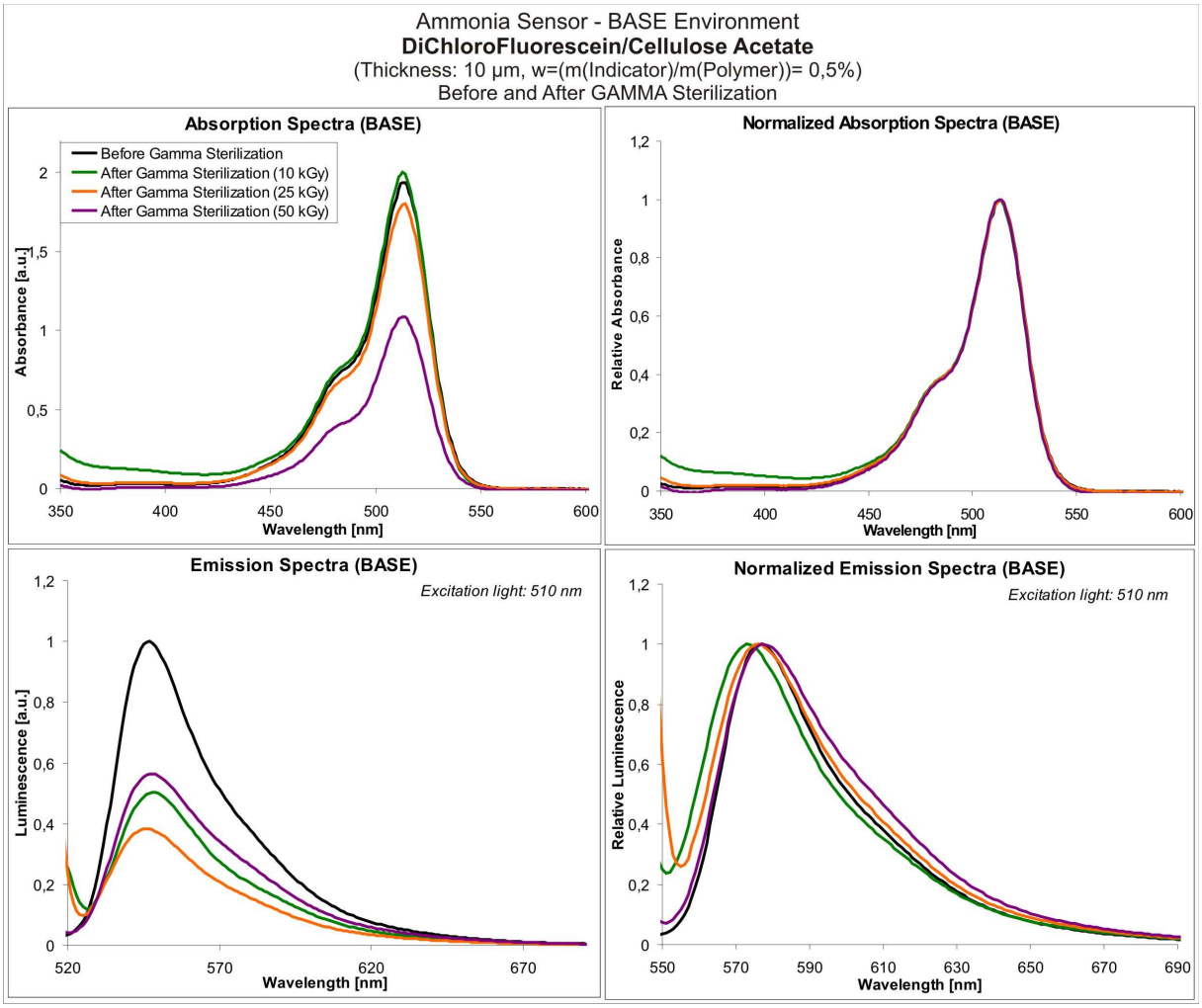

GAMMA S.	Absorption Spectra			Emission Spectra		
			Alterations			Alterations
Alterations in Absorption/ Emission Intensity	10 kGy	BASE	3,18% increase	10 kGy	BASE	49,59% decrease
	25 kGy		7,12% decrease	25 kGy		61,66% decrease
	50 kGy		44,02% decrease	50 kGy		43,49% decrease
Alterations in Absorption/ Emission Curve Form	10 kGy	BASE	Unaltered.	10 kGy	BASE	Hypsochromic shift of the emission maximum for 4 nm.
	25 kGy		Unaltered.	25 kGy		Altered emission between 590-670 nm. Hypsochromic shift of the emission maximum for 2 nm.
	50 kGy		Unaltered.	50 kGy		Altered emission between 580-670 nm.

C.52.2 Electron Beam Sterilization

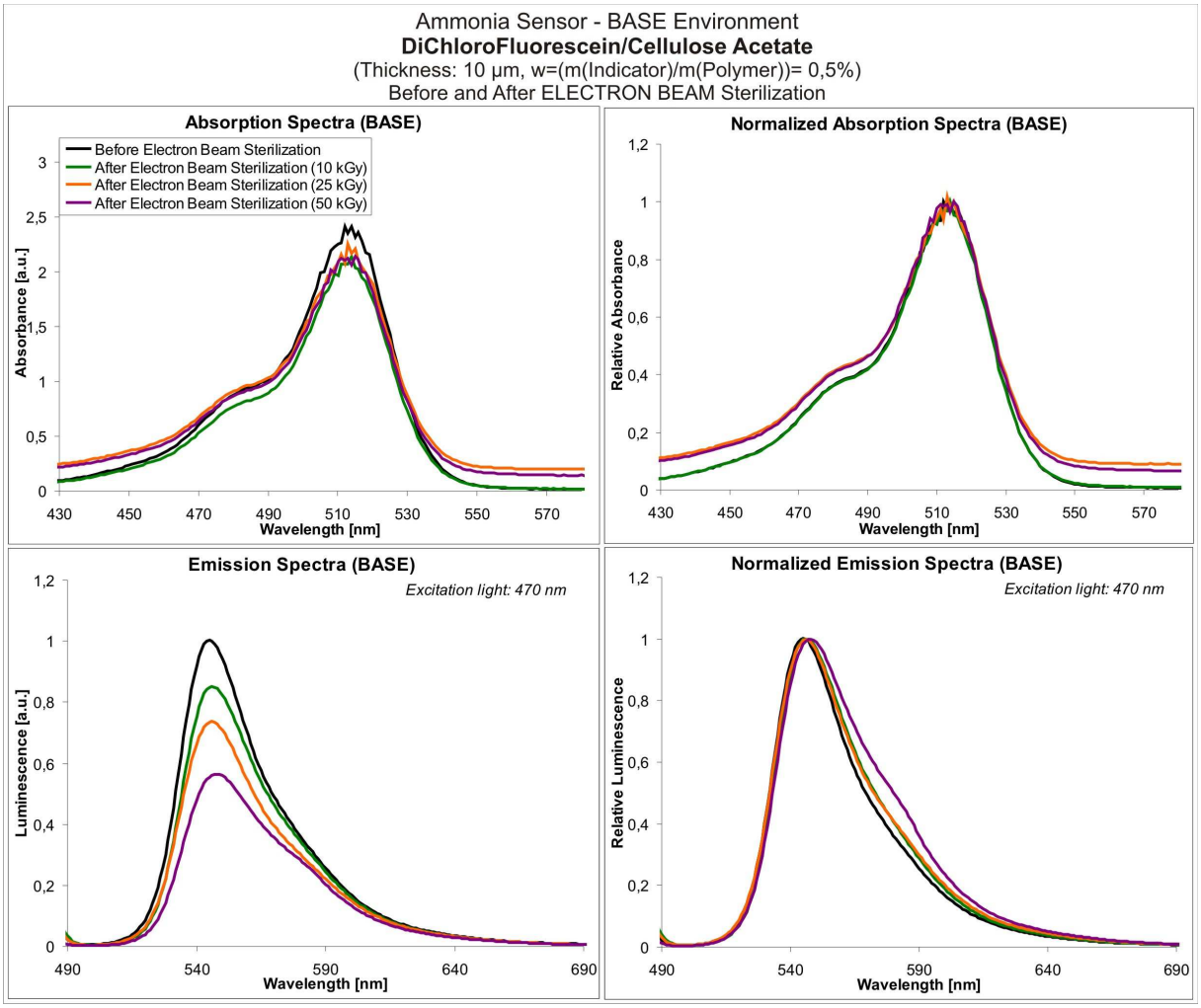

E-BEAM S.	Absorption Spectra			Emission Spectra		
			Alterations			Alterations
Alterations in Absorption/ Emission Intensity	10 kGy	BASE	11,51% decrease	10 kGy	BASE	14,94% decrease
	25 kGy		8,40% decrease	25 kGy		26,21% decrease
	50 kGy		11,32% decrease	50 kGy		43,57% decrease
Alterations in Absorption/ Emission Curve Form	10 kGy	BASE	Unaltered.	10 kGy	BASE	Altered emission between 560-620 nm.
	25 kGy		Altered absorption between 350-500 nm and 530-800 nm.	25 kGy		Altered emission between 560-620 nm.
	50 kGy		Altered absorption between 350-500 nm and 530-800 nm.	50 kGy		Altered emission between 560-640 nm. Bathochromic of emission maximum for 2 nm.

C.53 DiChloroFluorescein immobilized in Hydrogel D7

C.53.1 Gamma Sterilization

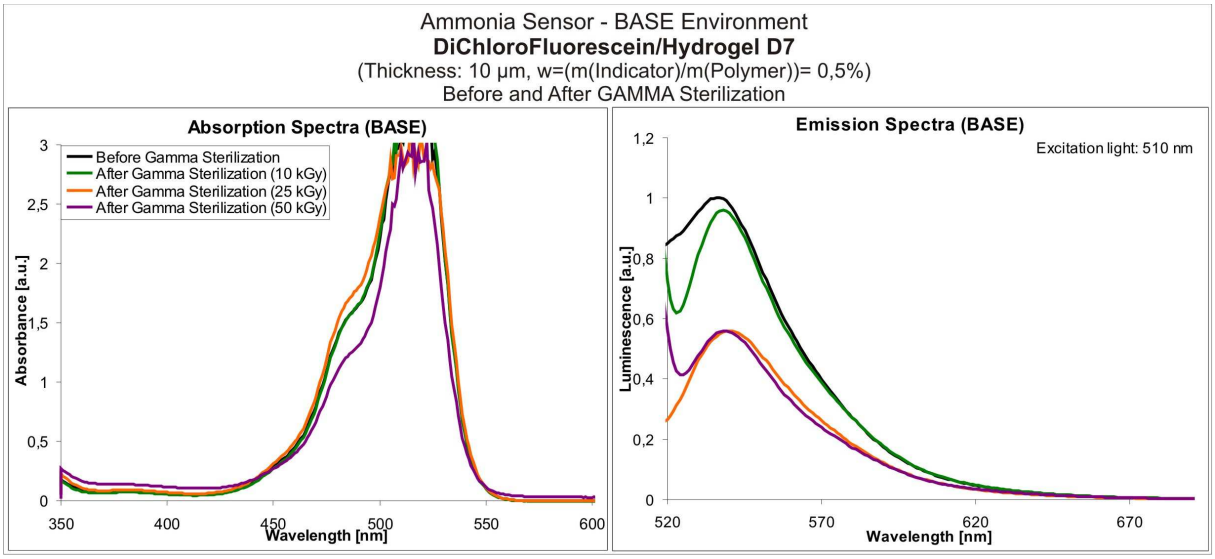

GAMMA S.	Absorption Spectra			Emission Spectra		
			Alterations			Alterations
Alterations in Absorption/ Emission Intensity	10 kGy	BASE	5,99% decrease	10 kGy	BASE	3,92% decrease
	25 kGy		19,54% decrease	25 kGy		43,97% decrease
	50 kGy		21,10% decrease	50 kGy		44,09% decrease
Alterations in Absorption/ Emission Curve Form	10 kGy	BASE	Unaltered.	10 kGy	BASE	Unaltered.
	25 kGy		Unaltered.	25 kGy		Bathochromic shift of the emission maximum for 3 nm.
	50 kGy		Unaltered.	50 kGy		Unaltered.

C.53.2 Electron Beam Sterilization

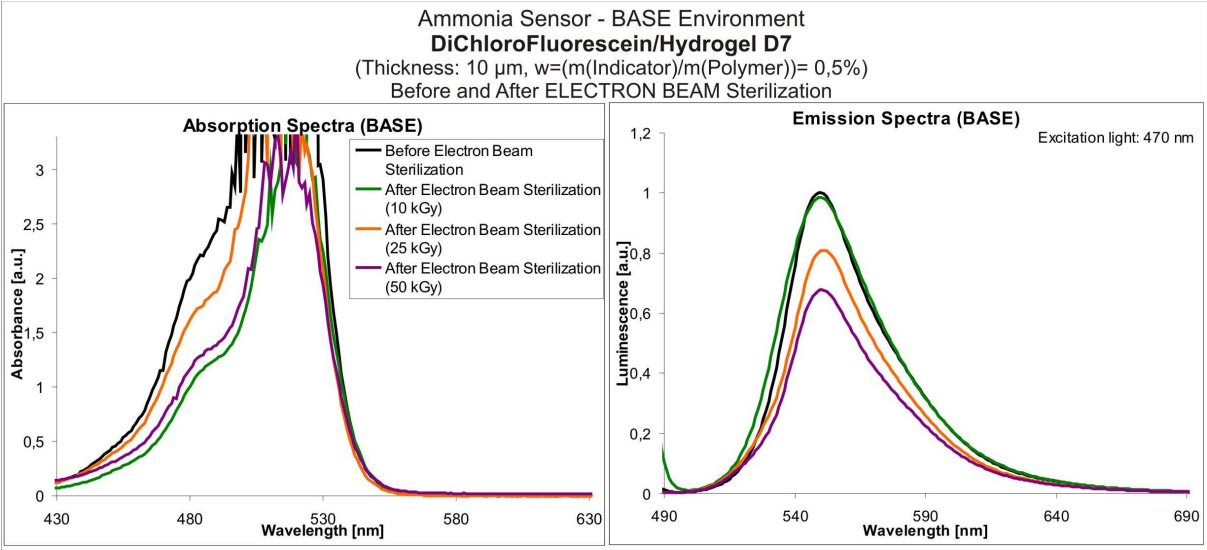

EBEAM S.	Absorption Spectra			Emission Spectra		
			Alterations			Alterations
Alterations in Absorption/ Emission Intensity	10 kGy	BASE	54,73% decrease	10 kGy	BASE	1,34% decrease
	25 kGy		25,44% decrease	25 kGy		19,10% decrease
	50 kGy		48,05% decrease	50 kGy		32,23% decrease
Alterations in Absorption/ Emission Curve Form	10 kGy	BASE	Unaltered.	10 kGy	BASE	Altered emission between 490-540 nm.
	25 kGy		Unaltered.	25 kGy		Unaltered.
	50 kGy		Unaltered.	50 kGy		Unaltered.

C.54 DiChloroFluorescein immobilized in Ethyl Cellulose

C.54.1 Gamma Sterilization

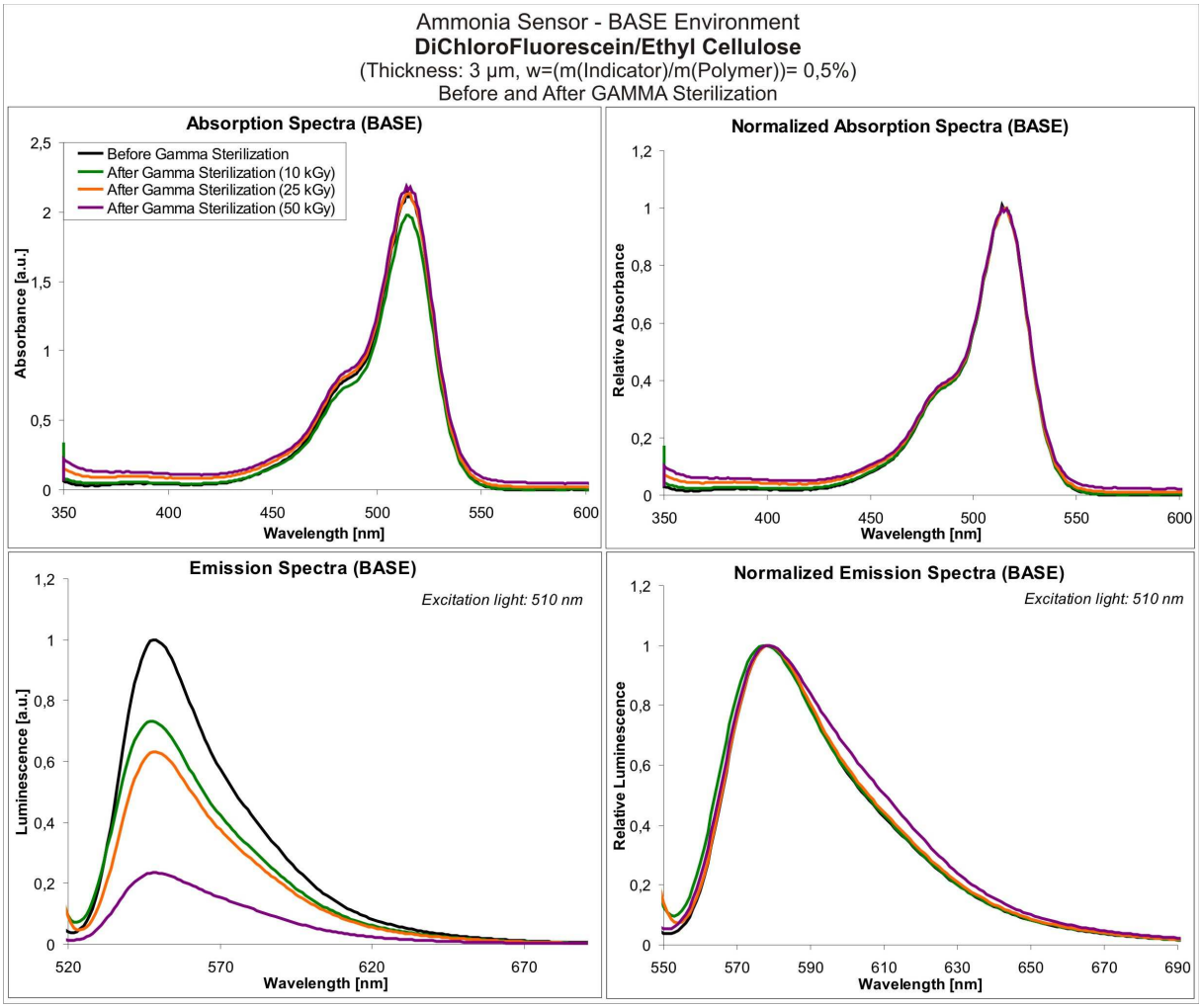

GAMMA S.	Absorption Spectra			Emission Spectra		
			Alterations			Alterations
Alterations in Absorption/ Emission Intensity	10 kGy	BASE	6,56% decrease	10 kGy	BASE	26,79% decrease
	25 kGy		0,83% increase	25 kGy		36,71% decrease
	50 kGy		3,06% increase	50 kGy		76,56% decrease
Alterations in Absorption/ Emission Curve Form	10 kGy	BASE	Unaltered.	10 kGy	BASE	Unaltered.
	25 kGy		Unaltered.	25 kGy		Unaltered.
	50 kGy		Unaltered.	50 kGy		Altered emission between 590-660 nm.

C.54.2 Electron Beam Sterilization

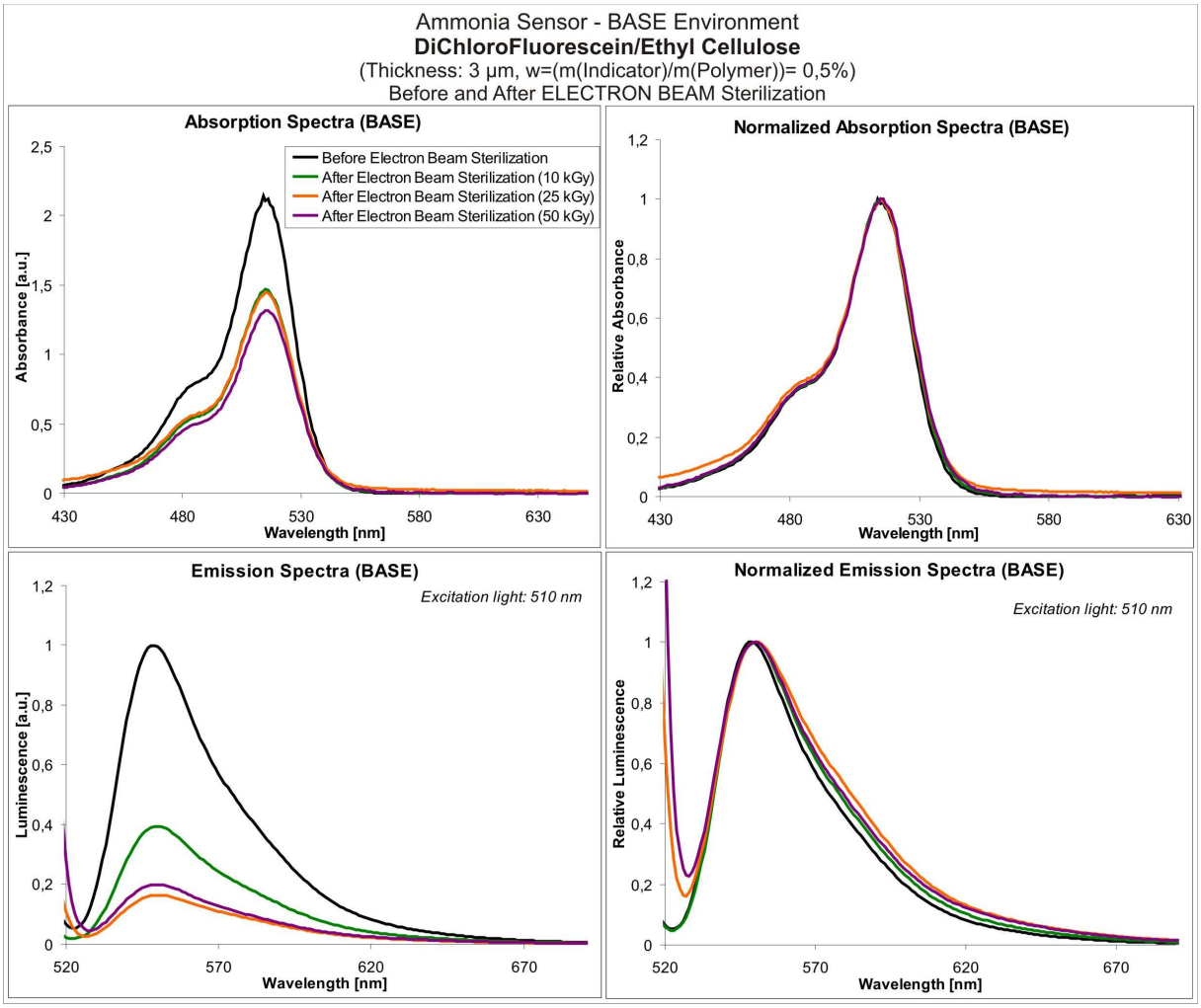

EBEAM S.	Absorption Spectra			Emission Spectra		
			Alterations			Alterations
Alterations in Absorption/ Emission Intensity	10 kGy	BASE	31,48% decrease	10 kGy	BASE	60,62% decrease
	25 kGy		32,15% decrease	25 kGy		83,57% decrease
	50 kGy		38,48% decrease	50 kGy		80,05% decrease
Alterations in Absorption/ Emission Curve Form	10 kGy	BASE	Unaltered.	10 kGy	BASE	Bathochromic shift of the emission maximum for 2 nm.
	25 kGy		Altered absorption between 430-490 nm.	25 kGy		Bathochromic shift of the emission maximum for 2 nm.
	50 kGy		Unaltered.	50 kGy		Bathochromic shift of the emission maximum for 2 nm.

C.55 BromoPhenolBlue immobilized in Cellulose Acetate

C.55.1 Gamma Sterilization

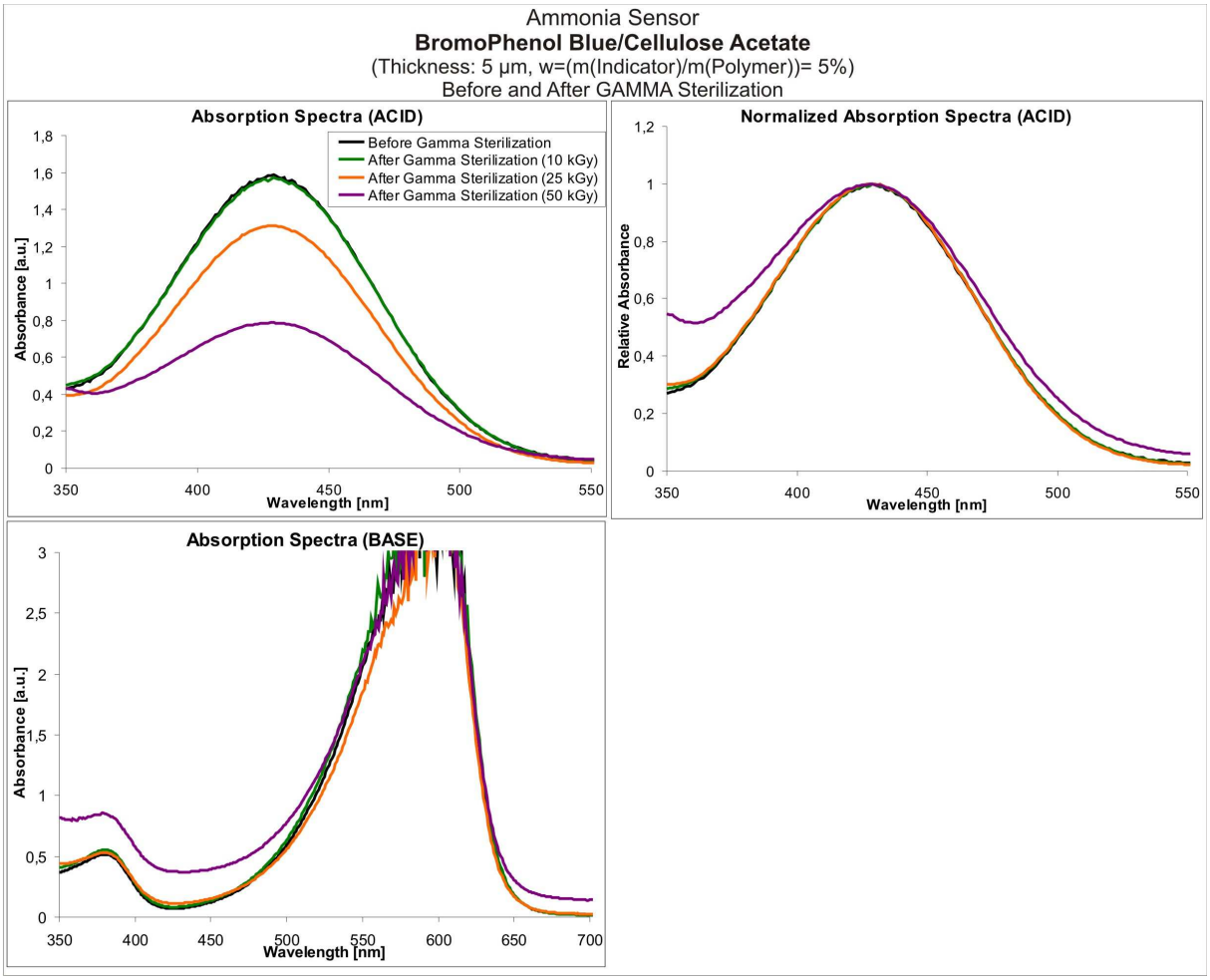

GAMMA S.	Absorption Spectra						
			Alterations				Alterations
Alterations in Absorption /Emission Intensity	10 kGy	ACID	0,90% decrease	Alterations in Absorption /Emission Curve Form	10 kGy	ACID	Unaltered.
		BASE	6,66% decrease			BASE	Unaltered.
	25 kGy	ACID	17,37% decrease		25 kGy	ACID	Unaltered.
		BASE	11,31% decrease			BASE	Unaltered.
	50 kGy	ACID	50,31% decrease		50 kGy	ACID	Altered absorption curve form between 350-415 nm and 460-800 nm.
		BASE	18,37% decrease			BASE	Altered absorption curve form between 350-525 nm and 650-800 nm.

C.55.2 Electron Beam Sterilization

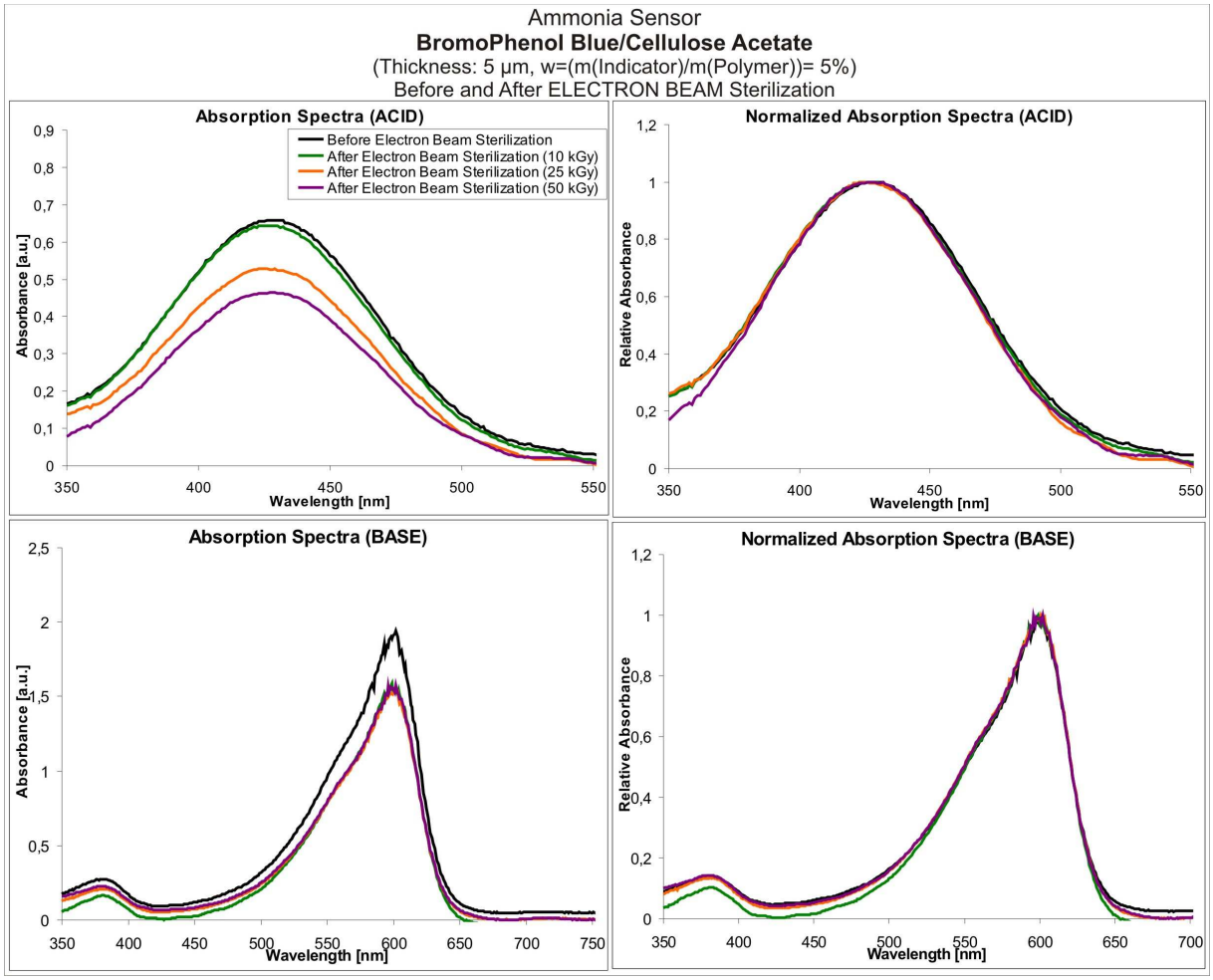

EBEAM S.	Absorption Spectra						
			Alterations				Alterations
Alterations in Absorption /Emission Intensity	10 kGy	ACID	8,57% decrease	Alterations in Absorption /Emission Curve Form	10 kGy	ACID	Unaltered,
		BASE	7,30% decrease			BASE	Unaltered,
	25 kGy	ACID	22,57% decrease		25 kGy	ACID	Unaltered,
		BASE	11,50% decrease			BASE	Unaltered,
	50 kGy	ACID	25,08% decrease		50 kGy	ACID	Altered absorption between 350-375 nm.
		BASE	18,02% decrease			BASE	Unaltered,

C.56 BromoPhenolBlue immobilized in Hydrogel D7

C.56.1 Gamma Sterilization

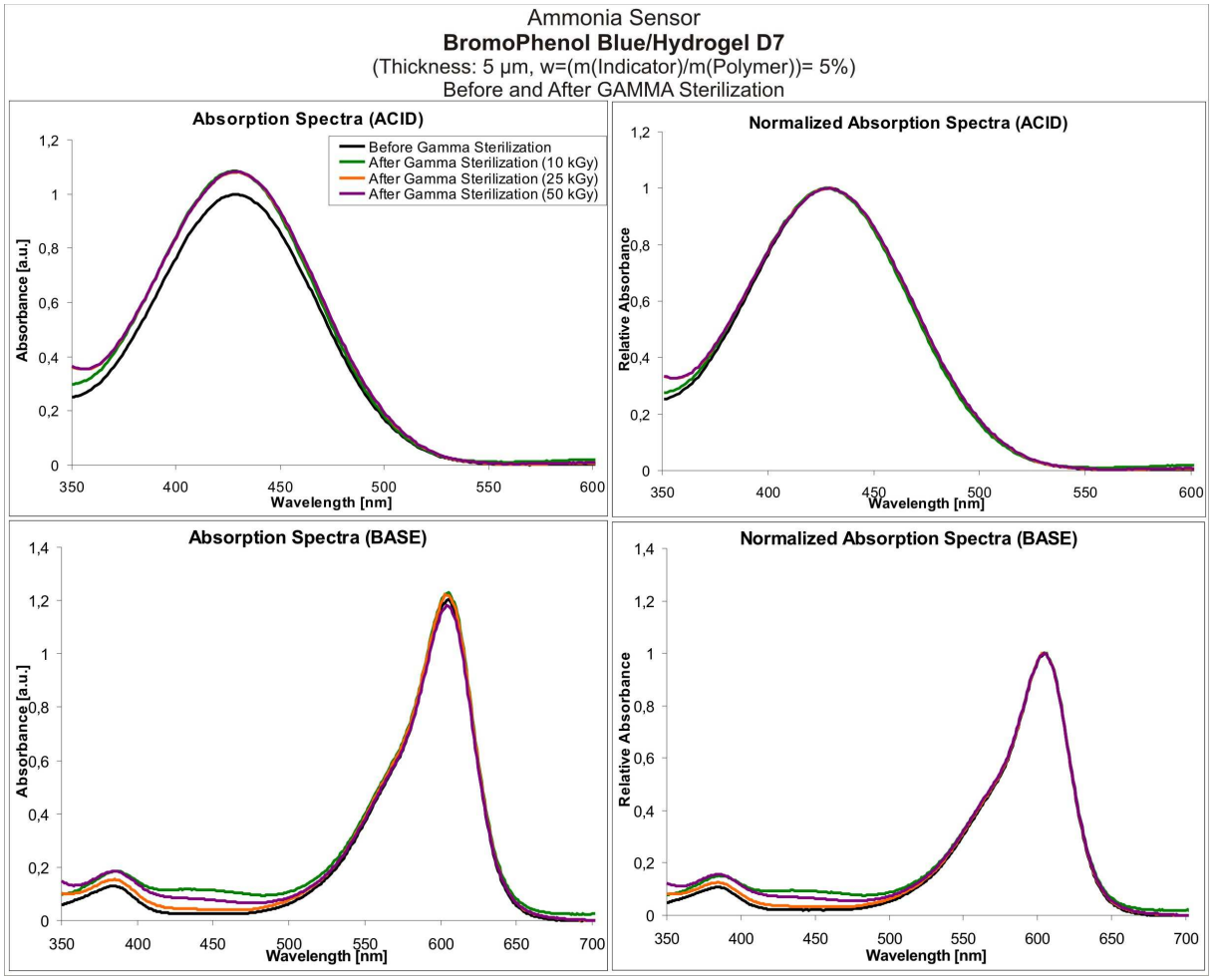

GAMMA S.	Absorption Spectra						
			Alterations				Alterations
Alterations in Absorption /Emission Intensity	10 kGy	ACID	7,93% increase	Alterations in Absorption /Emission Curve Form	10 kGy	ACID	Unaltered.
		BASE	2,07% increase			BASE	Altered absorption curve form between 350-500 nm.
	25 kGy	ACID	7,79% increase		25 kGy	ACID	Unaltered.
		BASE	1,55% increase			BASE	Altered absorption curve form between 350-500 nm.
	50 kGy	ACID	7,79% increase		50 kGy	ACID	Unaltered.
		BASE	1,84% decrease			BASE	Altered absorption curve form between 350-500 nm.

C.56.2 Electron Beam Sterilization

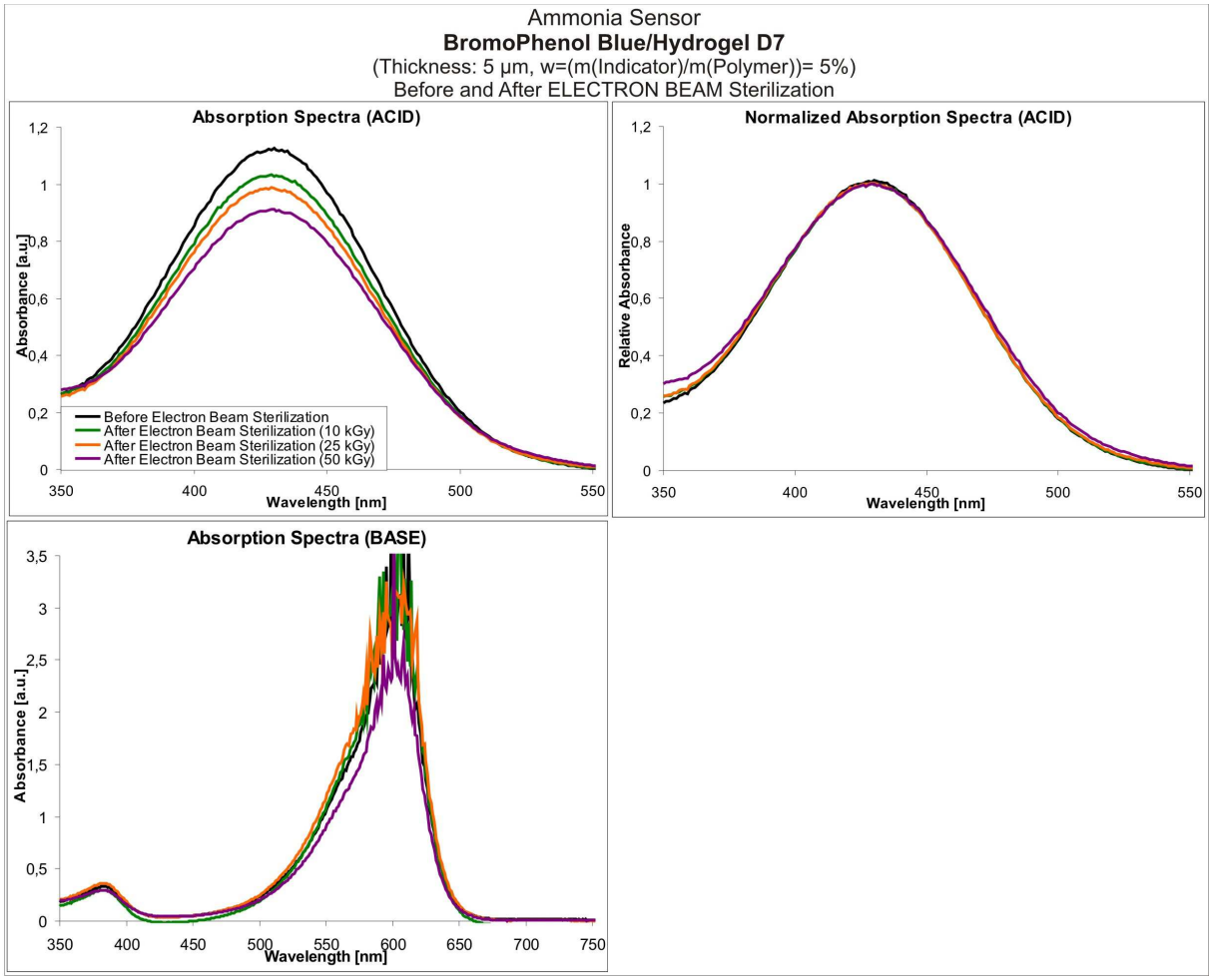

EBEAM S.	Absorption Spectra					
			Alterations			Alterations
Alterations in Absorption /Emission Intensity	10 kGy	ACID	8,57% decrease	Alterations in Absorption /Emission Curve Form	10 kGy	ACID	Unaltered,
		BASE	7,30% decrease			BASE	Unaltered,
	25 kGy	ACID	22,57% decrease		25 kGy	ACID	Unaltered,
		BASE	11,50% decrease			BASE	Unaltered,
	50 kGy	ACID	25,08% decrease		50 kGy	ACID	Altered absorption between 350-375 nm.
		BASE	18,02% decrease			BASE	Unaltered,

C.57.BromoPhenolBlue immobilized in Ethyl Cellulose

C.57.1 Gamma Sterilization

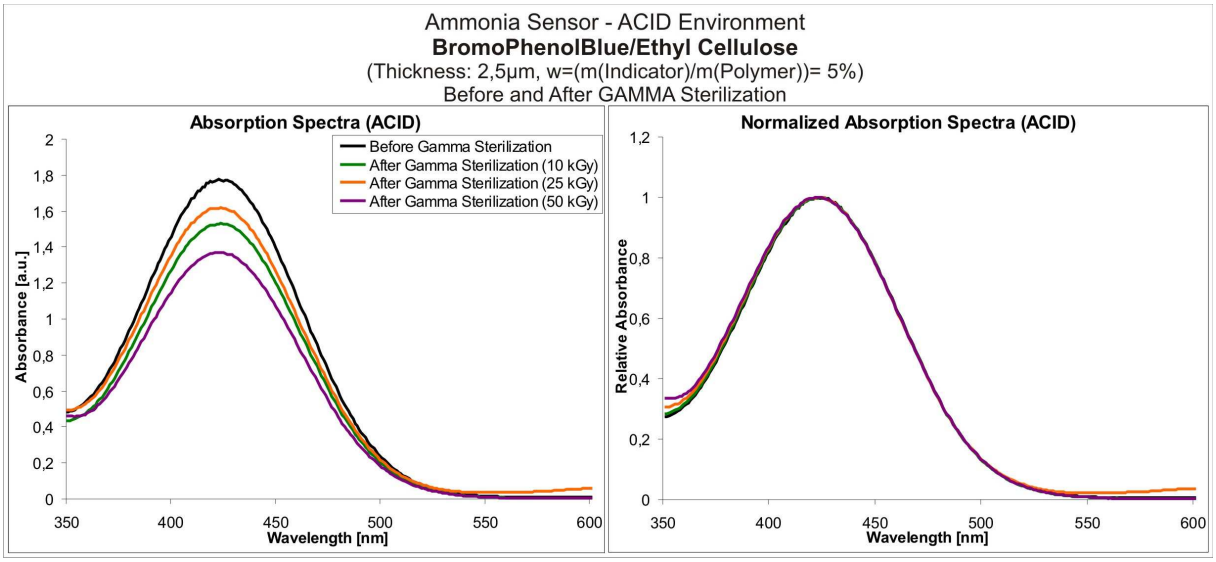

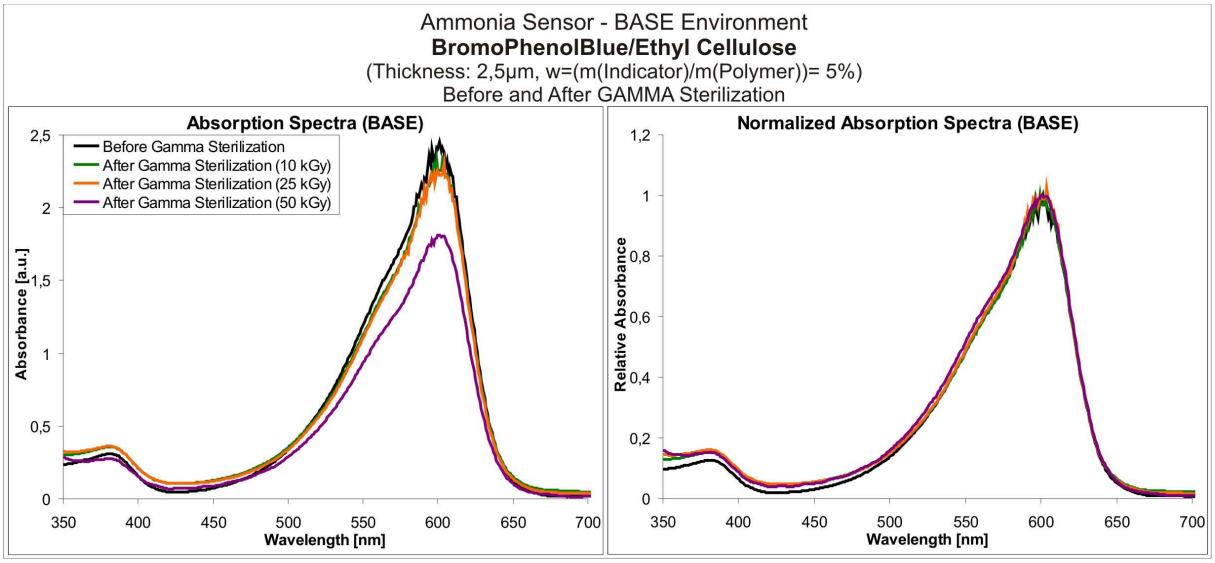

GAMMA S.	Absorption Spectra						
Alterations in Absorption /Emission Intensity			Alterations	Alterations in Absorption /Emission Curve Form			Alterations
	10 kGy	ACID	13,71% decrease		10 kGy	ACID	Unaltered.
		BASE	4,91% decrease			BASE	Unaltered.
	25 kGy	ACID	8,81% decrease		25 kGy	ACID	Unaltered.
		BASE	8,12% decrease			BASE	Unaltered.

	50 kGy	ACID	22,82% decrease		50 kGy	ACID	Unaltered.
		BASE	26,16% decrease			BASE	Unaltered.

C.57.2 Electron Beam Sterilization

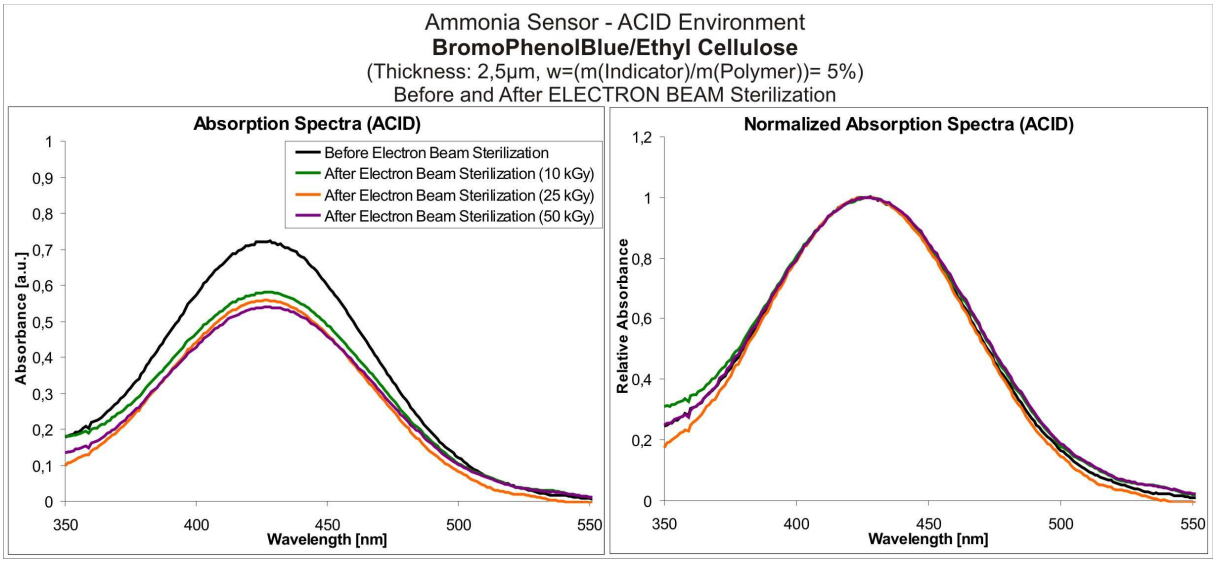

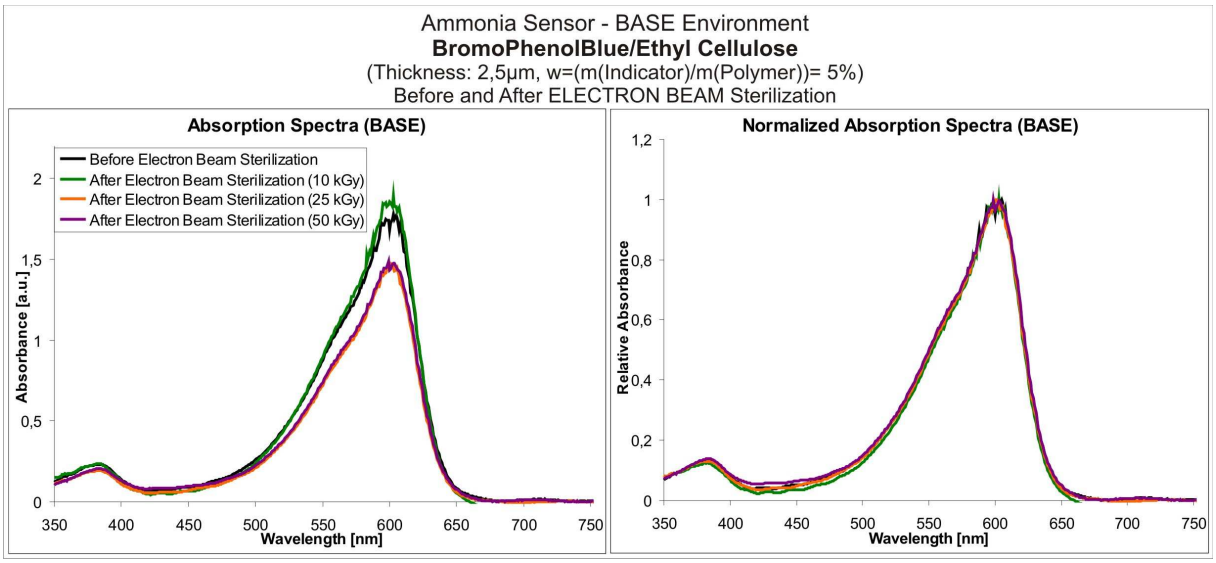

EBEAM S.	Absorption Spectra						
Alterations in Absorption /Emission Intensity			Alterations	Alterations in Absorption /Emission Curve Form			Alterations
	10 kGy	ACID	19,43% decrease		10 kGy	ACID	Altered absorption between 350-375 nm.
		BASE	6,25% increase			BASE	Unaltered,

	25 kGy	ACID	22,57% decrease		25 kGy	ACID	Altered absorption between 350-380 nm.
		BASE	16,76% decrease			BASE	Unaltered,
	50 kGy	ACID	25,08% decrease		50 kGy	ACID	Unaltered,
		BASE	16,27% decrease			BASE	Unaltered,

C.58 BromoPhenol Blue immobilized in PolyMethylMethAcrylate (=PMMA)

C.58.1 Gamma Sterilization

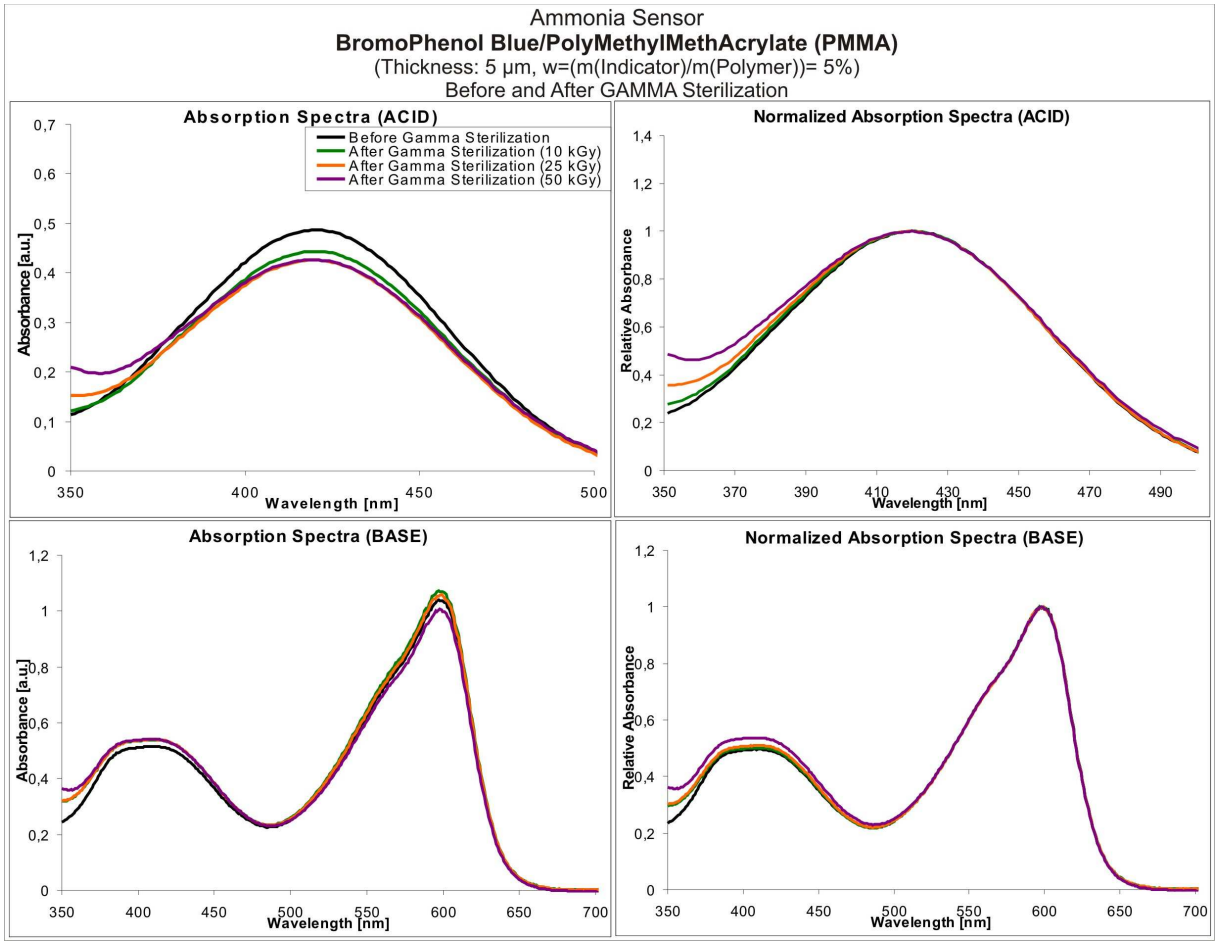

GAMMA S.	Absorption Spectra						
			Alterations				Alterations
Alterations in Absorption /Emission Intensity	10 kGy	ACID	8,87% decrease	Alterations in Absorption /Emission Curve Form	10 kGy	ACID	Unaltered.
		BASE	3,26% increase			BASE	Altered absorption between 350-370 nm.
	25 kGy	ACID	12,50% decrease		25 kGy	ACID	Altered absorption between 350-380 nm.
		BASE	2,04% increase			BASE	Altered absorption between 350-370 nm.
	50 kGy	ACID	12,25% decrease		50 kGy	ACID	Altered absorption between 350-390 nm.
		BASE	2,97% decrease			BASE	Altered absorption between 350-470 nm.

C.58.2 Electron Beam Sterilization

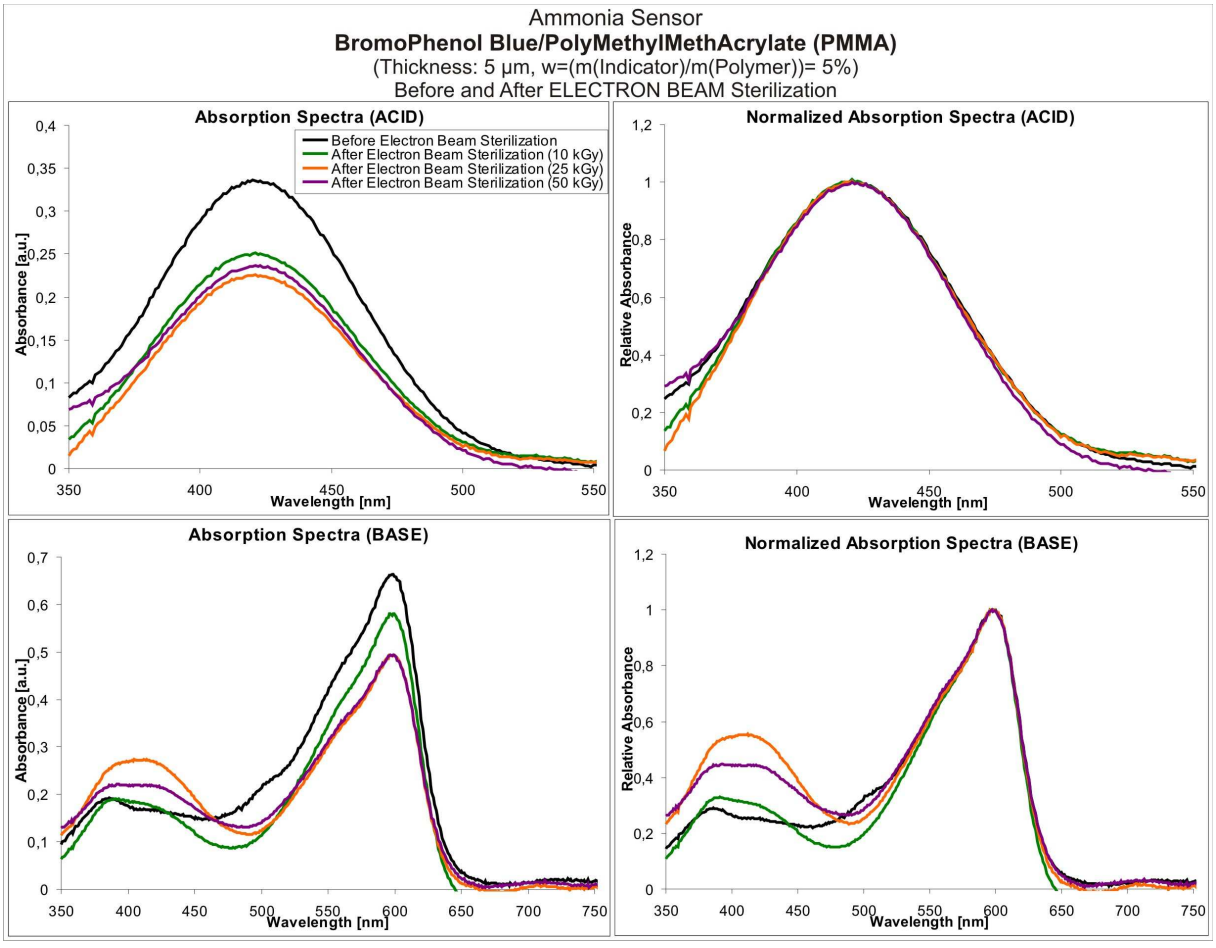

EBEAM S.	Absorption Spectra						
			Alterations				Alterations
Alterations in Absorption /Emission Intensity	10 kGy	ACID	25,70% decrease	Alterations in Absorption /Emission Curve Form	10 kGy	ACID	Altered absorption between 350-375 nm.
		BASE	12,44% decrease			BASE	Altered absorption between 350-500 nm.
	25 kGy	ACID	32,85% decrease		25 kGy	ACID	Altered absorption between 350-375 nm.
		BASE	25,65% decrease			BASE	Altered absorption between 350-500 nm.
	50 kGy	ACID	29,37% decrease		50 kGy	ACID	Altered absorption between 475-550 nm.
		BASE	25,50% decrease			BASE	Altered absorption between 350-500 nm.

D
Steam Sterilization of Optical Sensors

TABLE OF CONTENTS

D STEAM STERILIZATION OF OPTICAL SENSORS 528

Optical OXYGEN SENSORS 571

D.1 Iridium(III) Coumarin Complex immobilized in Cellulose Acetate 571

D.2 Iridium(III) Coumarin Complex immobilized in Ethyl Cellulose 572

D.3 Iridium(III) Coumarin Complex immobilized in HydroGel HydroMed D4/D7 573

D.4 Iridium(III) Coumarin Complex immobilized in HydroThane with 5% water content 574

D.5 Iridium(III) Coumarin Complex immobilized in Poly(Sulfone) 575

D.6 Iridium(III) Coumarin Complex immobilized in Poly(PhenylSilsesQuioxane) 576

D.7 Iridium(III) Coumarin Complex immobilized in Poly(Styrene) 577

D.8 Iridium(III) Coumarin Complex immobilized in Poly(Styrene-co-AcryloNitrile) 579

D.9 Iridium(III) Coumarin Complex immobilized in Poly(Styrene-co-MaleicAnhydride) 581

D.10 Platinum(II)Tetrakis(PentaFluorPhenyl)Porphyrin (PtTFPP) immobilized in Cellulose Acetate 582

D.11 Platinum(II)Tetrakis(PentaFluorPhenyl)Porphyrin (PtTFPP) immobilized in Ethyl Cellulose 583

D.12 Platinum(II)Tetrakis(PentaFluorPhenyl)Porphyrin (PtTFPP) immobilized in HydroGel D4/D7 585

D.13 Platinum(II)Tetrakis(PentaFluorPhenyl)Porphyrin (PtTFPP) immobilized in HydroThane 5 587

D.14 Platinum(II)Tetrakis(PentaFluorPhenyl)Porphyrin (PtTFPP) immobilized in PolySulfone 589

D.15 Platinum(II)Tetrakis(PentaFluorPhenyl)Porphyrin (PtTFPP) immobilized in PolyPhenylSilses Quioxane 590

D.16 Platinum(II)Tetrakis(PentaFluorPhenyl)Porphyrin (PtTFPP) immobilized in PolyStyrene 592

D.17 Platinum(II)Tetrakis(PentaFluorPhenyl)Porphyrin (PtTFPP) immobilized in PolyStyrene-co- Acrylonitrile 594

D.18 Platinum(II)Tetrakis(PentaFluorPhenyl)Porphyrin (PtTFPP) immobilized in PolyStyrene-co-MaleicAnhydride (PSMA93) 596

D.19 Platinum(II) OctaEthyl Porphyrin (=PtOEP) immobilized in PolyStyrene 598

D.20 Platinum(II) meso-tetra(4-FluoroPhenyl) TetraBenzoPorphyrin (=PtTPTBPF) immobilized in PolyStyrene 600

D.21 Palladium(II)meso-tetra(4-FluoroPhenyl) TetraBenzoPorphyrin (=PdTPTBPF) immobilized in PolyStyrene 602

D.22 Ruthenium(II) DiPhenylPhenanthroline DiChloride ($Ru(dpp)_3Cl_2$) immobilized in Cellulose Acetate 603

D.23 Ruthenium(II) DiPhenylPhenanthroline DiChloride ($Ru(dpp)_3Cl_2$) immobilized in Ethyl Cellulose 604

D.24 Ruthenium(II) DiPhenylPhenanthroline DiChloride ($Ru(dpp)_3Cl_2$) immobilized in HydroGel D4/D7 606

D.25 Ruthenium(II) DiPhenylPhenanthroline DiChloride ($Ru(dpp)_3Cl_2$) immobilized in HydroThane5 607

D.26 Ruthenium(II) DiPhenylPhenanthroline DiChloride ($Ru(dpp)_3Cl_2$) immobilized in PolySulfone 609

D.27 Ruthenium(II) DiPhenylPhenanthroline DiChloride ($Ru(dpp)_3Cl_2$) immobilized in PolyPhenyl SilsesQuioxane 611

D.28 Ruthenium(II) DiPhenylPhenanthroline DiChloride ($Ru(dpp)_3Cl_2$) immobilized in PolyStyrene 612

D.29 Ruthenium(II) DiPhenylPhenanthroline DiChloride ($Ru(dpp)_3Cl_2$) immobilized in PolyStyrene-co-Acrylonitrile 613

D.30 Ruthenium(II) DiPhenylPhenanthroline DiChloride ($Ru(dpp)_3Cl_2$) immobilized in PolyStyrene-co-MaleicAnhydride (PSMA93) 614

Optical pH SENSORS 616

D.31 HPTS(DHA_3) immobilized in HydroGel D4 616

D.32 2´,7´-DiHexylFluorescein OctadecylEster immobilized in HydroMed Hydrogel D4 619

D.33 2´,7´-DiHexylFluorescein OctadecylEster immobilized in Poly(2-HydroxyEthyl MethAcrylate) (=pHEMA) 622

D.34 2´,7´-DiHexyl-N-Octadecyl-CarboxAmidoFluorescein (=DHFA) immobilized in HydroMed Hydrogel D4 622

D.35 pH Sensitive Coumarin immobilized in HydroMed Hydrogel D4 624

D.36 PET Perylene BisImide immobilized in HydroMed Hydrogel D4 627

D.37 BromoPhenol Blue immobilized in HydroMed Hydrogel D4 629

D.38 Thymol Blue immobilized in HydroMed Hydrogel D4 630

D.39 BromoThymol Blue immobilized in HydroMed Hydrogel D4 631

D.40 Methyl Orange immobilized in HydroMed Hydrogel D4 632

Optical TEMPERATURE SENSORS 633

D.41 Europium(III) Complex with 4-(4,6-di(1H-indazol-1-yl)-1,3,5-triazin-2-yl)-N,N-DiEthyl Benzen Amine (=Eu(tta)$_3$DEADIT) immobilized in PolyStyrene-co-Acrylonitrile 633

D.42 Europium(III) Complex with 4-(4,6-di(1H-indazol-1-yl)-1,3,5-triazin-2-yl)-N,N-DiEthyl Benzen Amine (=Eu(tta)$_3$DEADIT) immobilized in PolyVinylideneChloride-co-Acrylonitrile 634

D.43 Europium(III) Complex with 4-(4,6-di(1H-indazol-1-yl)-1,3,5-triazin-2-yl)-N,N-DiEthyl Benzen Amine (=Eu(tta)$_3$DEADIT) immobilized in PolyMethAcryloNitrile 635

D.44 DiChloroTrisPhenanthroline Ruthenium(II)Hydrate immobilized in PolyVinylideneChloride-co-Acrylonitrile 637

D.45 DiChloroTrisPhenanthroline Ruthenium(II)Hydrate immobilized in PolyMethAcryloNitrile 638

Optical AMMONIA SENSORS 640

D.46 EosinEthylEster immobilized in Cellulose Acetate 640

D.47 EosinEthylEster immobilized in Hydrogel D7 640

D.48 Eosin EthylEster immobilized in Ethyl Cellulose 641

D.49 EosinEthylEster immobilized in PolyMethylMethAcrylate (=PMMA) 642

D.50 DiChloroFluorescein immobilized in Cellulose Acetate 643

D.51 DiChloroFluorescein immobilized in Hydrogel D7 644

D.52 DiChloroFluorescein immobilized in Ethyl Cellulose 645

D.53 BromoPhenolBlue immobilized in Cellulose Acetate 646

D.54 BromoPhenolBlue immobilized in Hydrogel D7 646

D.55 BromoPhenolBlue immobilized in Ethyl Cellulose 647

D.56 BromoPhenol Blue immobilized in PolyMethylMethAcrylate (=PMMA) 648

Optical OXYGEN SENSORS

D.1 Iridium(III) Coumarin Complex immobilized in Cellulose Acetate

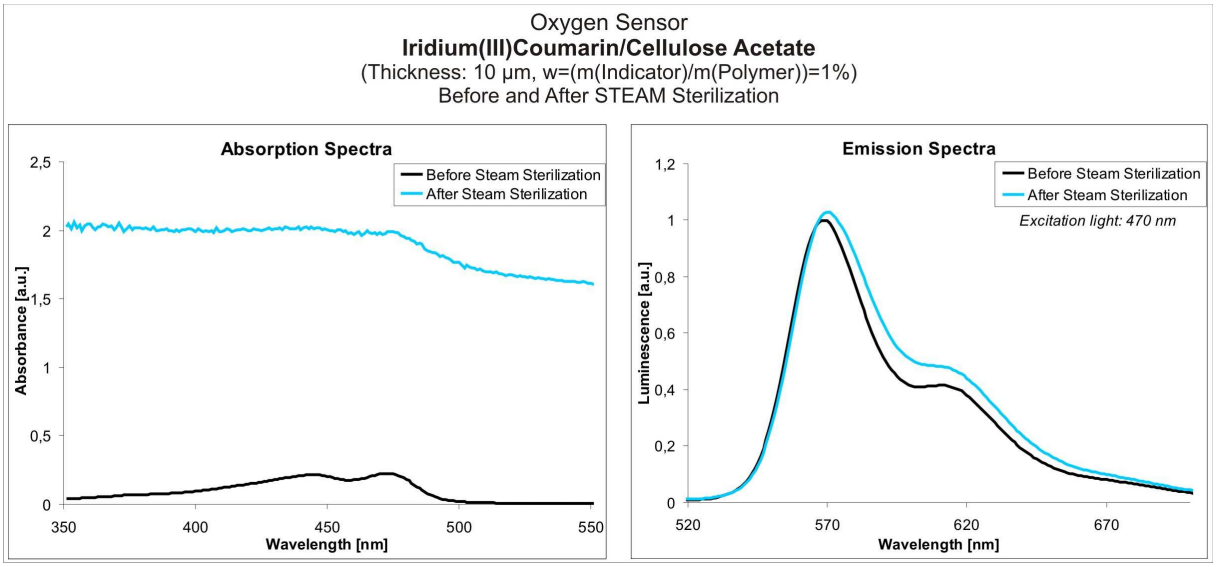

STEAM Sterilization	Absorption Spectra	Emission Spectra
Alterations in Absorption/Emission Intensity	880% increase	2,30% increase
Alterations in Absorption/Emission Curve Form	Polymers become turbid after sterilization.	Hypsochromic shift of emission maximum for 2 nm.

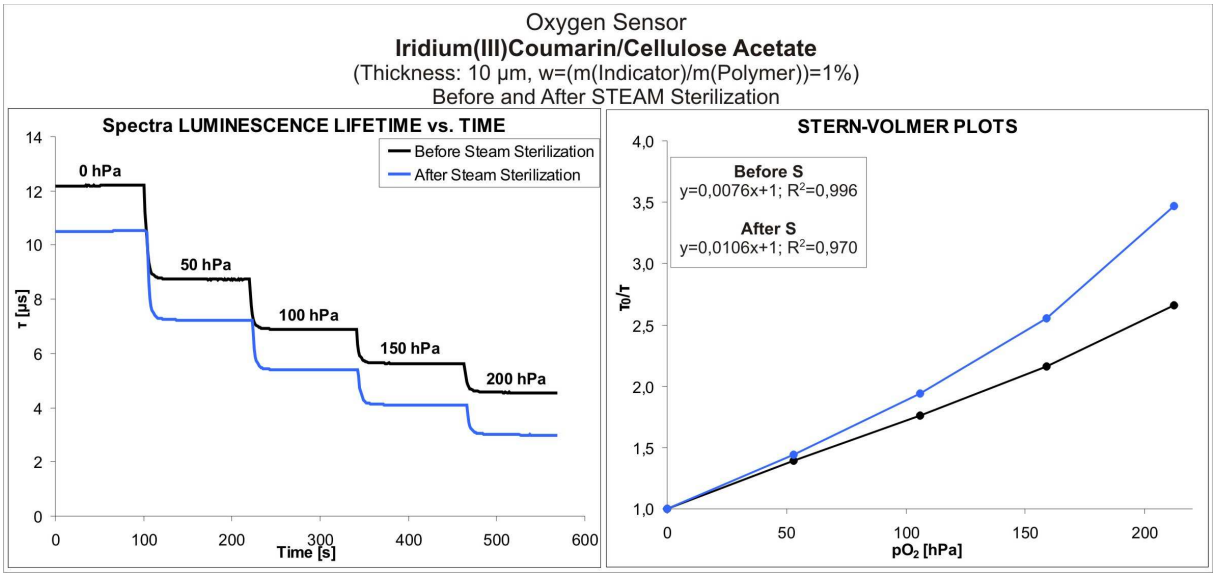

STEAM Sterilization	Luminescence Lifetime	Stern-Volmer Plot
Alterations in Luminescence Lifetime and Slope	13,93% decrease of τ_0	39,47% increase of slope
	17,30% decrease of τ at 50 hPa	
	21,91% decrease of τ at 100 hPa	
	27,18% decrease of τ at 150 hPa	
	34,29% decrease of τ at 200 hPa	

D.2 Iridium(III) Coumarin Complex immobilized in Ethyl Cellulose

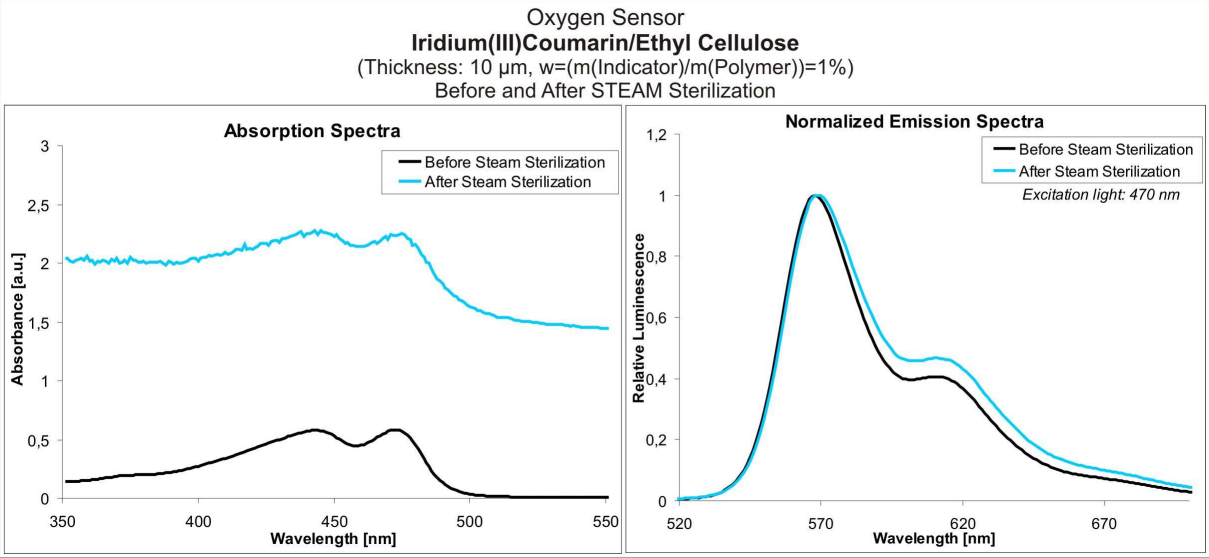

STEAM Sterilization	Absorption Spectra	Emission Spectra
Alterations in Absorption/Emission Intensity	380% increase	80,04% decrease
Alterations in Absorption/Emission Curve Form	Polymers become turbid after sterilization.	Bathochromic shift of emission maximum for 1 nm. Altered emission between 570-670 nm.

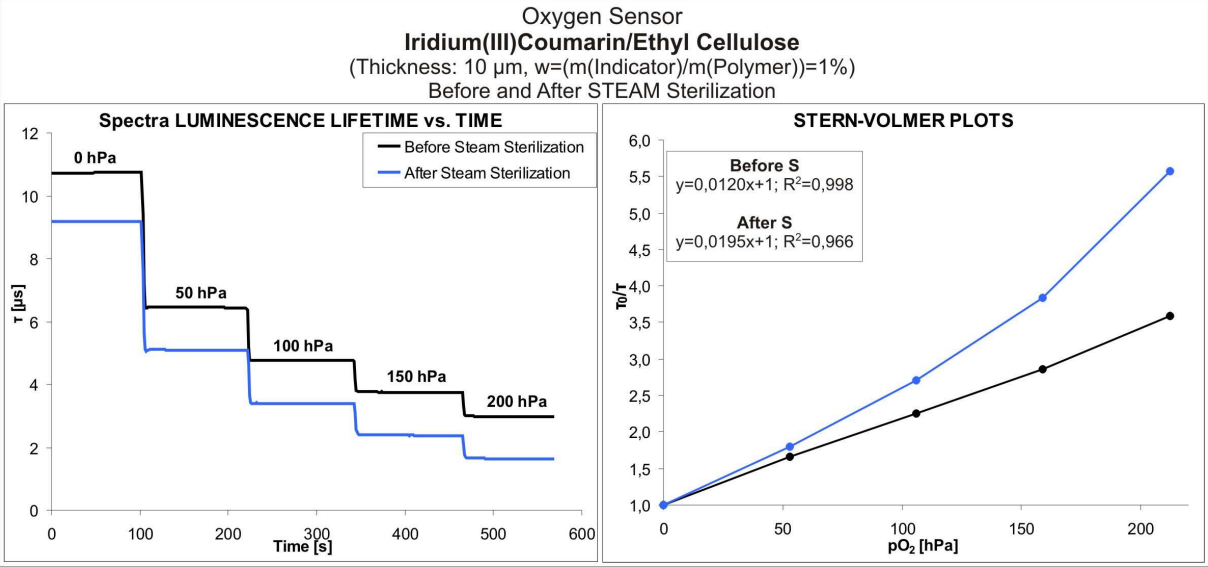

STEAM Sterilization	Luminescence Lifetime	Stern-Volmer Plot
Alterations in Luminescence Lifetime and Slope	14,21% decrease of τ_0	62,50% increase of slope
	20,96% decrease of τ at 50 hPa	
	28,78% decrease of τ at 100 hPa	
	36,36% decrease of τ at 150 hPa	
	45,12% decrease of τ at 200 hPa	

D.3 Iridium(III) Coumarin Complex immobilized in HydroGel HydroMed D4/D7

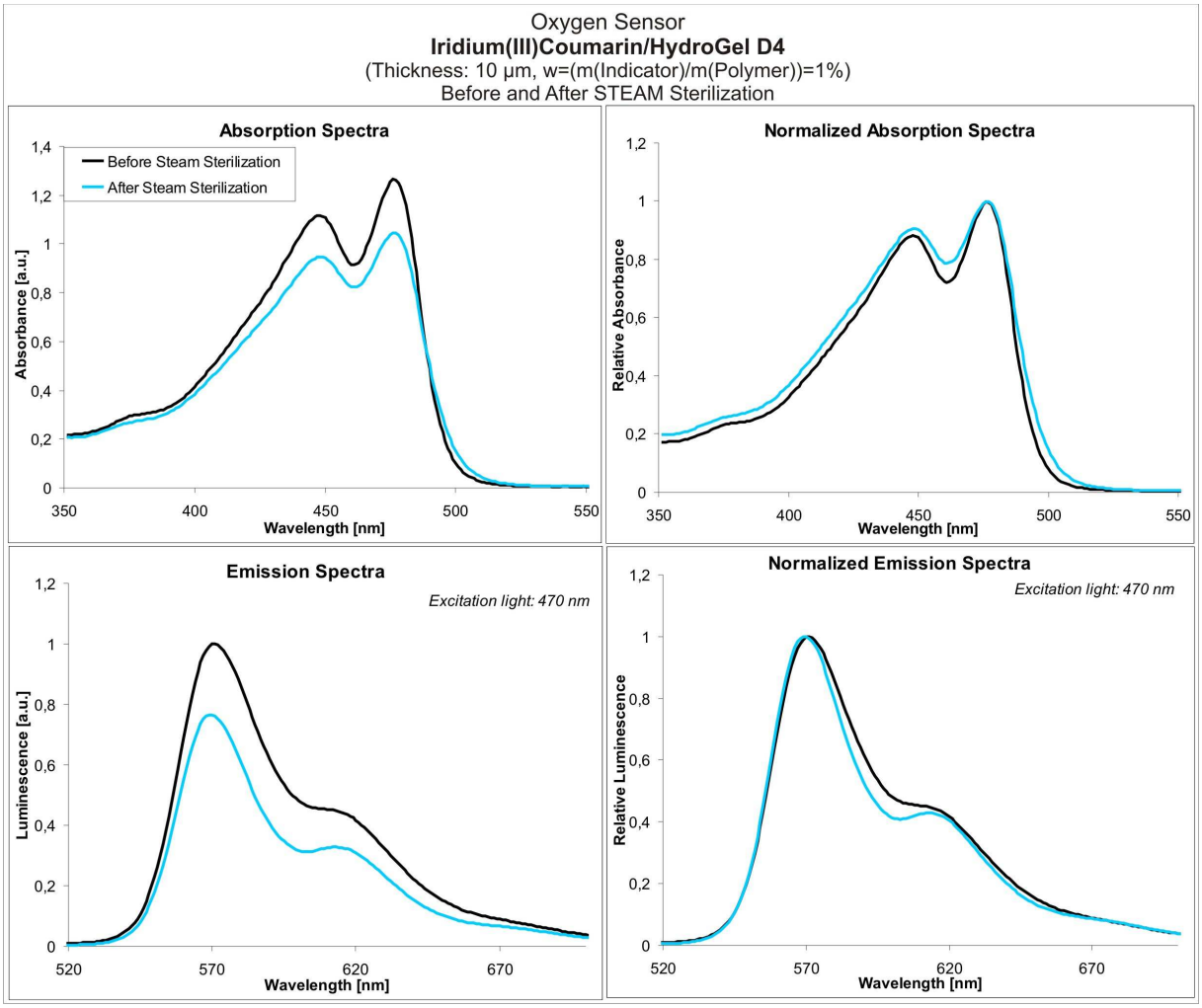

STEAM Sterilization	Absorption Spectra	Emission Spectra
Alterations in Absorption/Emission Intensity	17,47% decrease	23,56% decrease
Alterations in Absorption/Emission Curve Form	Slightly altered absorption between 350-470 nm and 490-520 nm.	Hypsochromic shift of emission maximum for 2 nm. Altered emission between 570-670 nm.

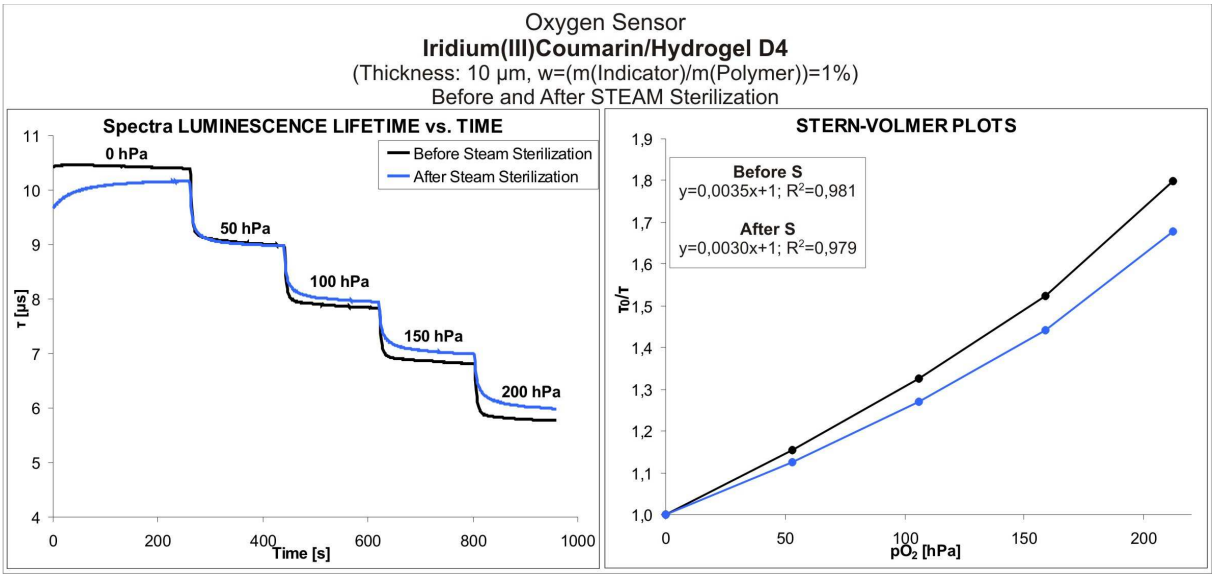

STEAM Sterilization	Luminescence Lifetime	Stern-Volmer Plot
Alterations in Luminescence Lifetime and Slope	4,76% decrease of τ_0	14,29% decrease of slope
	0,22% decrease of τ at 50 hPa	
	1,40% increase of τ at 100 hPa	
	2,64% increase of τ at 150 hPa	
	3,81% increase of τ at 200 hPa	

D.4 Iridium(III) Coumarin Complex immobilized in HydroThane with 5% water content

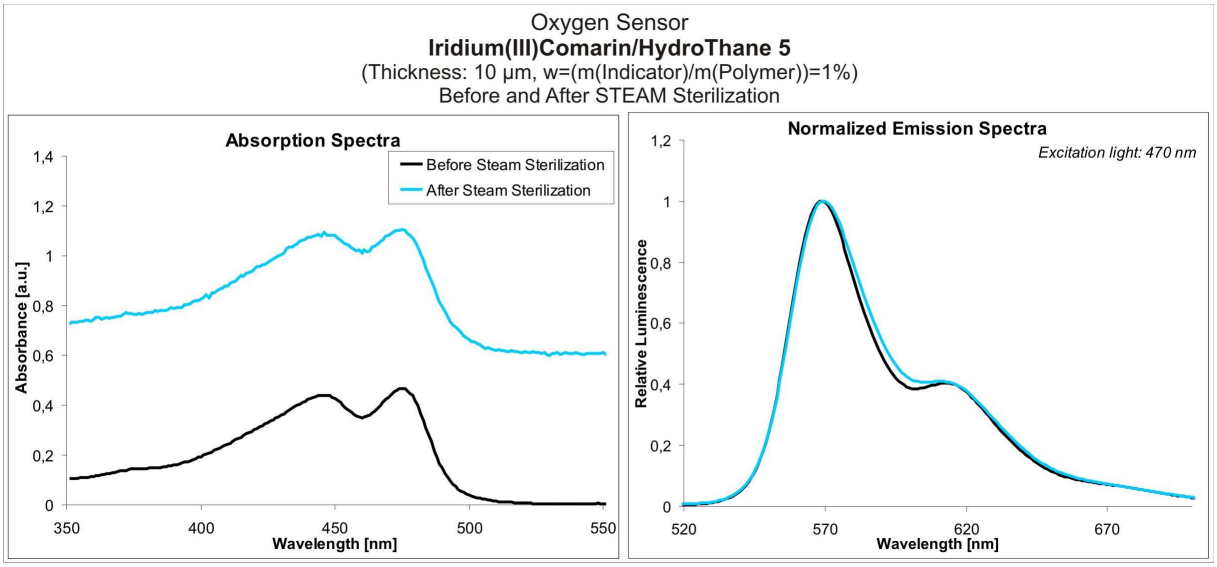

STEAM Sterilization	Absorption Spectra	Emission Spectra
Alterations in Absorption/Emission Intensity	242% increase	16,32% decrease
Alterations in Absorption/Emission Curve Form	Polymer became turbid after sterilization.	Slightly altered emission between 575-610 nm.

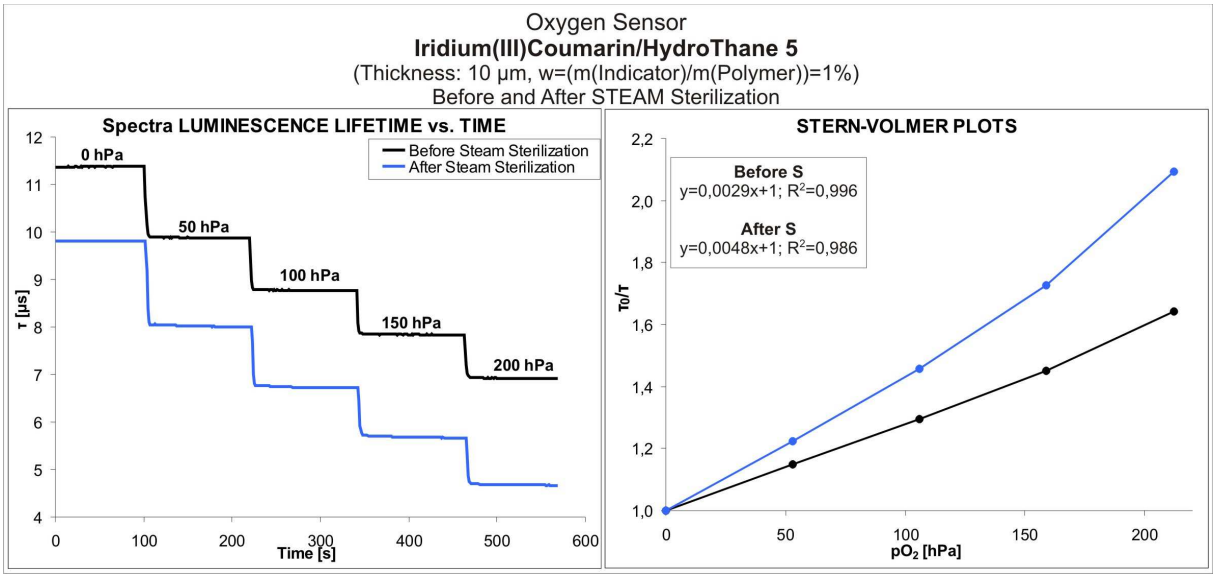

STEAM Sterilization	Luminescence Lifetime	Stern-Volmer Plot
Alterations in Luminescence Lifetime and Slope	13,95% decrease of τ_0	65,52% increase of slope
	18,50% decrease of τ at 50 hPa	
	23,01% decrease of τ at 100 hPa	
	27,42% decrease of τ at 150 hPa	
	32,51% decrease of τ at 200 hPa	

D.5 Iridium(III) Coumarin Complex immobilized in Poly(Sulfone)

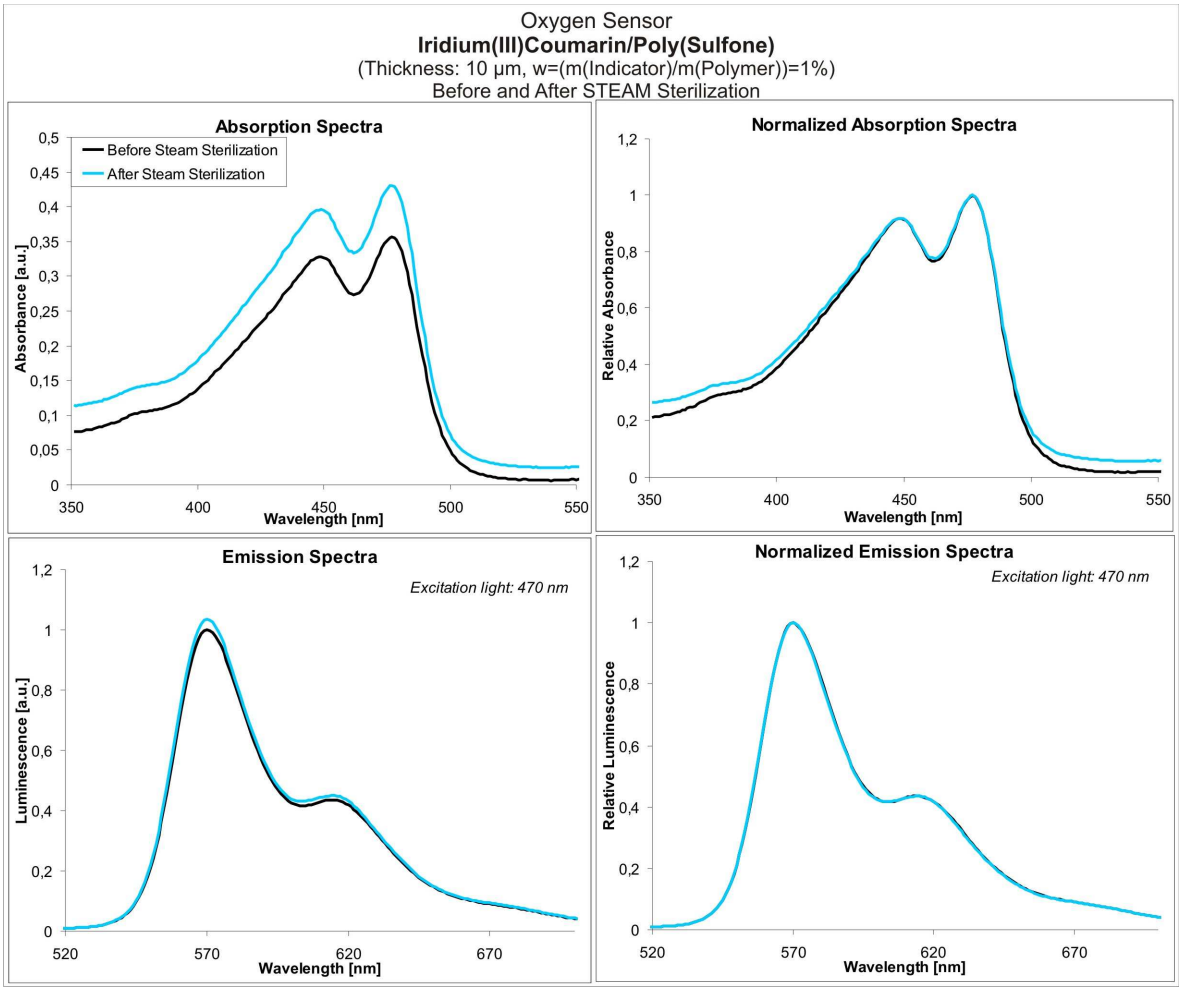

STEAM Sterilization	Absorption Spectra	Emission Spectra
Alterations in Absorption/Emission Intensity	20,67% increase	3,28% increase
Alterations in Absorption/Emission Curve Form	Polymer became turbid after sterilization.	Unaltered

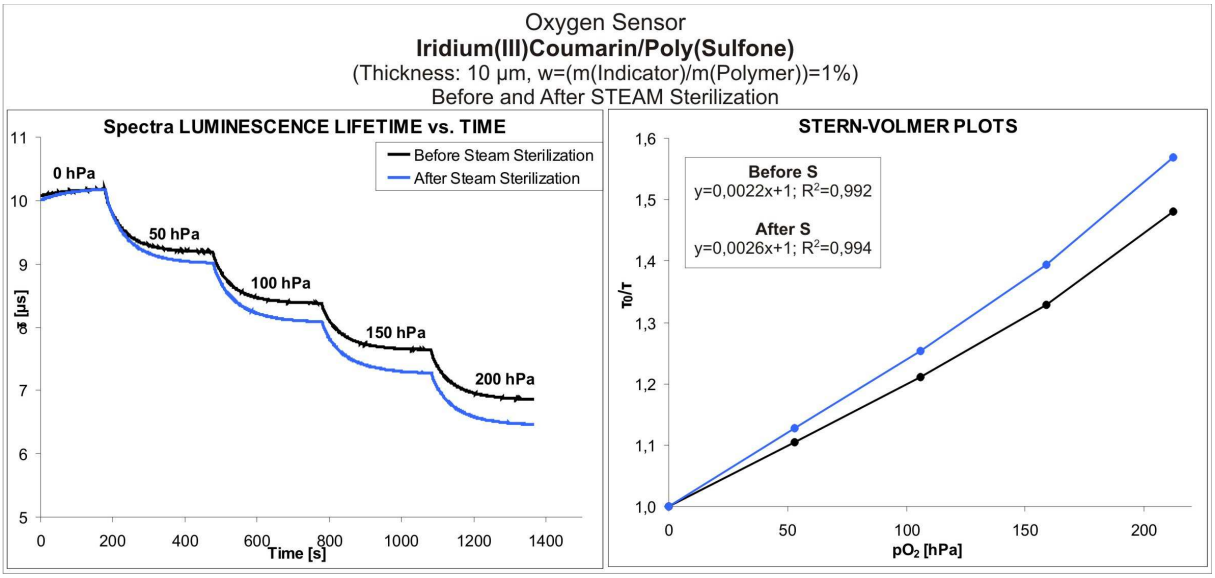

STEAM Sterilization	Luminescence Lifetime	Stern-Volmer Plot
Alterations in Luminescence Lifetime and Slope	0,99% decrease of τ_0	18,18% increase of slope
	1,74% decrease of τ at 50 hPa	
	3,13% decrease of τ at 100 hPa	
	5,36% decrease of τ at 150 hPa	
	5,83% decrease of τ at 200 hPa	

D.6 Iridium(III) Coumarin Complex immobilized in Poly(PhenylSilsesQuioxane)

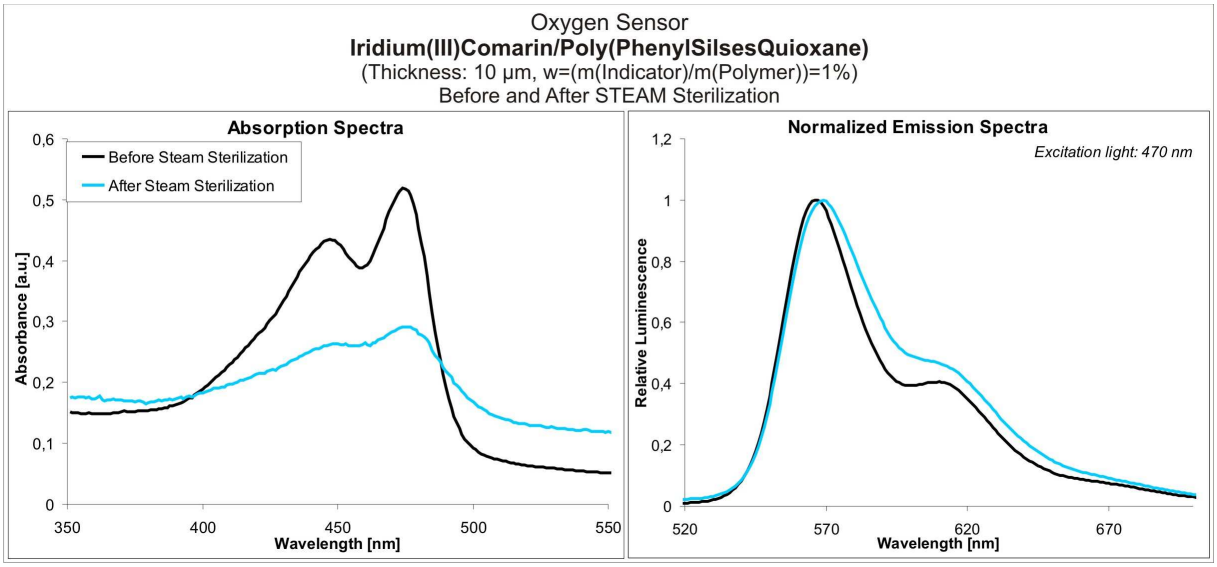

STEAM Sterilization	Absorption Spectra	Emission Spectra
Alterations in Absorption/Emission Intensity	44,00% decrease	47,59% decrease
Alterations in Absorption/Emission Curve Form	Disappearance of characteristic absorption curve form of Iridium(III)Coumarin	Bathochromic shift of emission maximum for 3 nm. Altered emission between 570-670 nm.

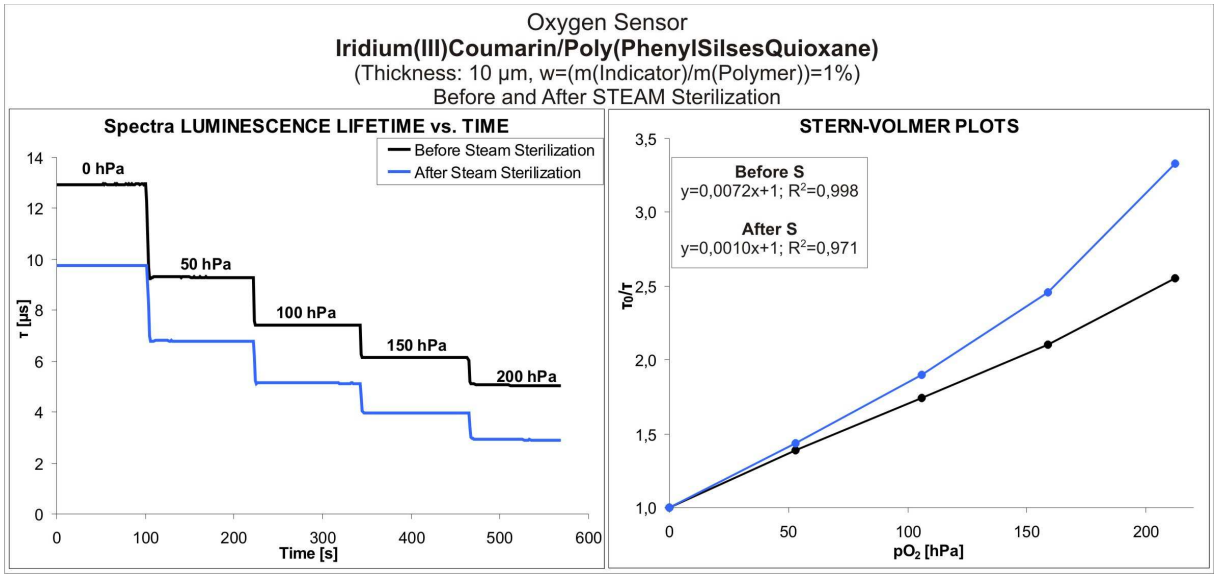

STEAM Sterilization	Luminescence Lifetime	Stern-Volmer Plot
Alterations in Luminescence Lifetime and Slope	24,34% decrease of τ_0	38,89% increase of slope
	26,96% decrease of τ at 50 hPa	
	30,59% decrease of τ at 100 hPa	
	35,40% decrease of τ at 150 hPa	
	42,38% decrease of τ at 200 hPa	

D.7 Iridium(III) Coumarin Complex immobilized in Poly(Styrene)

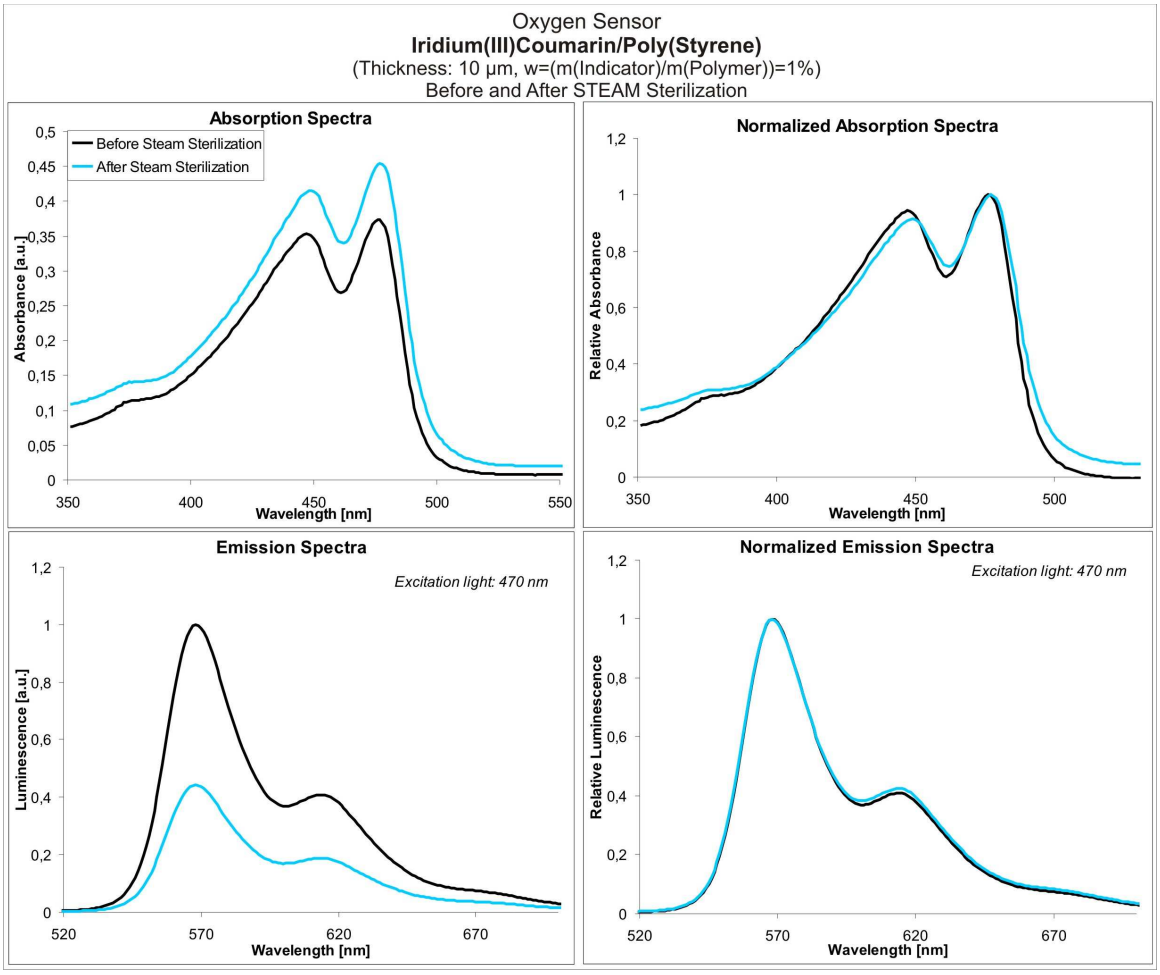

STEAM Sterilization	Absorption Spectra	Emission Spectra
Alterations in Absorption/Emission Intensity	24,94% increase	55,70% decrease
Alterations in Absorption/Emission Curve Form	Altered absorption between 350-465 nm and 480-550 nm. Polymer became slightly turbid after sterilization.	Unaltered

Oxygen Sensor
Iridium(III)Coumarin/PolyStyrene
(Thickness: 10 µm, w=(m(Indicator)/m(Polymer))=1%)
Before and After STEAM Sterilization

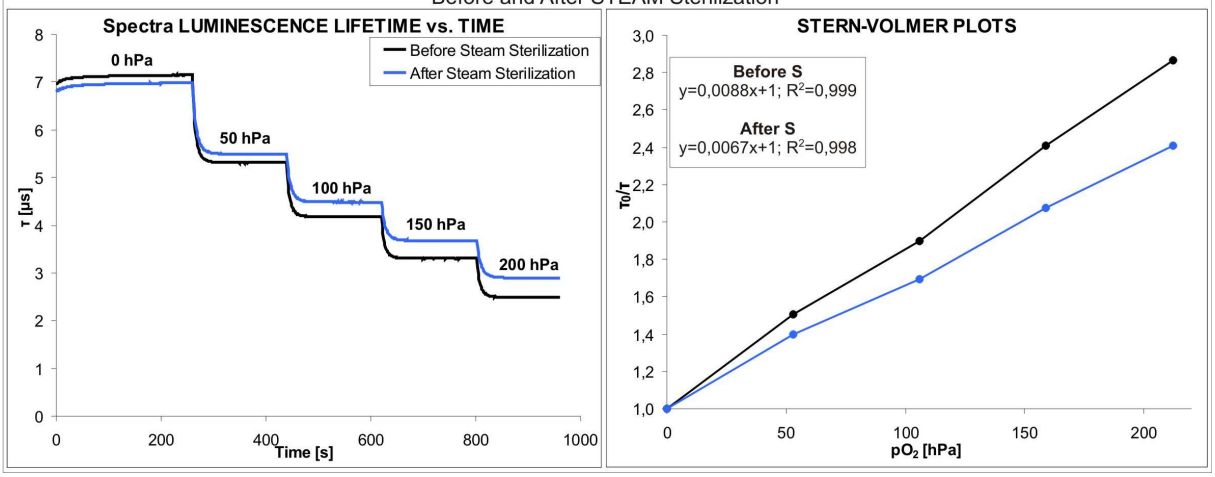

STEAM Sterilization	Luminescence Lifetime	Stern-Volmer Plot
Alterations in Luminescence Lifetime and Slope	2,24% decrease of τ_0	23,86% decrease of slope
	3,00% increase of τ at 50 hPa	
	7,18% increase of τ at 100 hPa	
	10,57% increase of τ at 150 hPa	
	16,06% increase of τ at 200 hPa	

D.8 Iridium(III) Coumarin Complex immobilized in Poly(Styrene-co-AcryloNitrile)

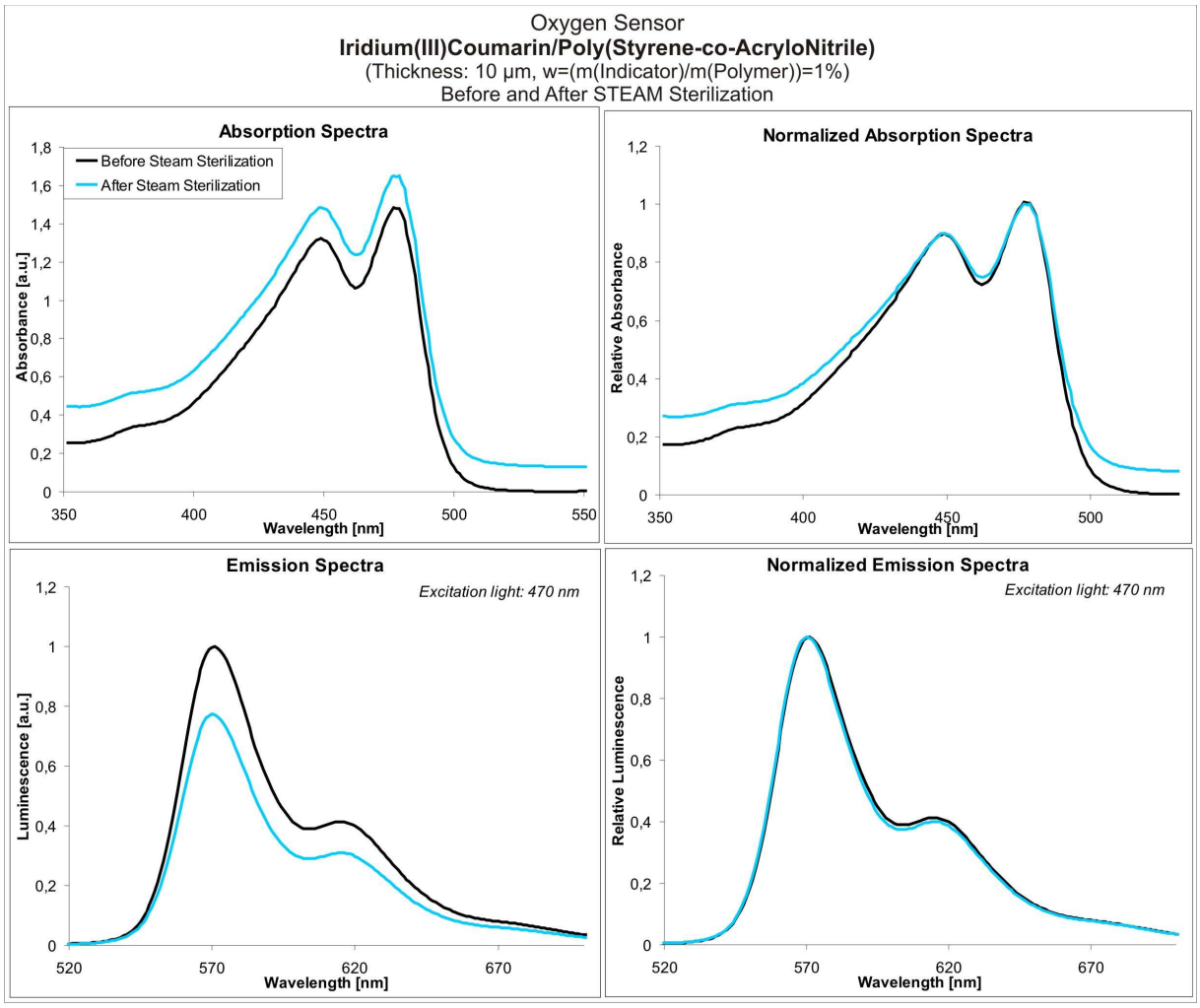

STEAM Sterilization	Absorption Spectra	Emission Spectra
Alterations in Absorption/Emission Intensity	12,13% increase	22,70% decrease
Alterations in Absorption/Emission Curve Form	Altered absorption between 350-430 nm and 490-550 nm. Polymer became slightly turbid after sterilization.	Unaltered

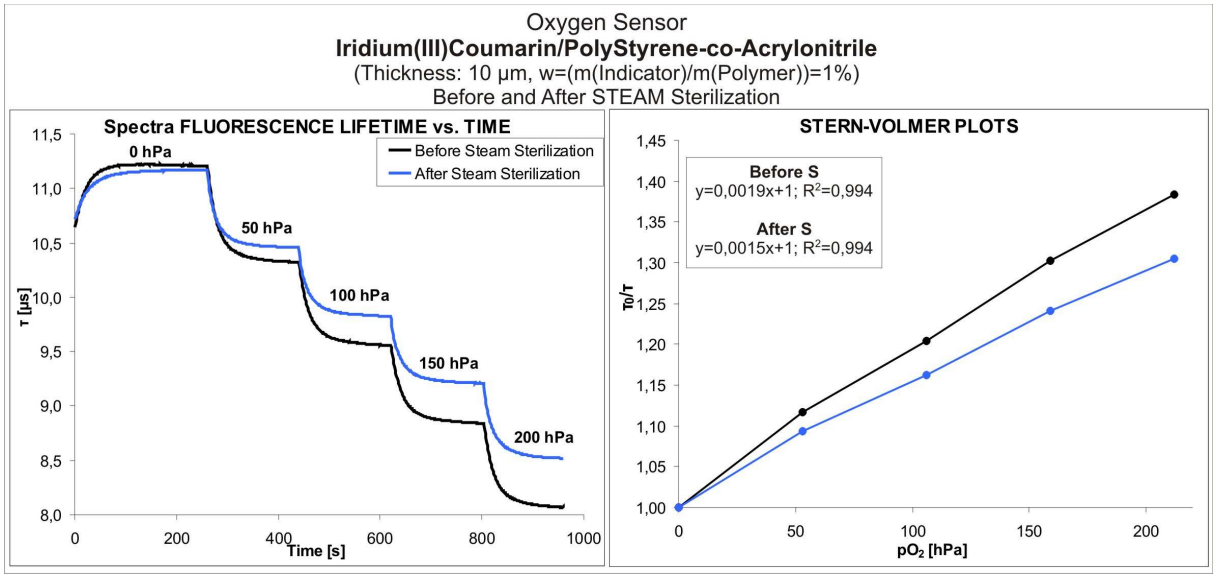

STEAM Sterilization	Luminescence Lifetime	Stern-Volmer Plot
Alterations in Luminescence Lifetime and Slope	0,89% decrease of τ_0	21,05% decrease of slope
	1,94% increase of τ at 50 hPa	
	2,82% increase of τ at 100 hPa	
	4,19% increase of τ at 150 hPa	
	5,58% increase of τ at 200 hPa	

D.9 Iridium(III) Coumarin Complex immobilized in Poly(Styrene-co-MaleicAnhydride)

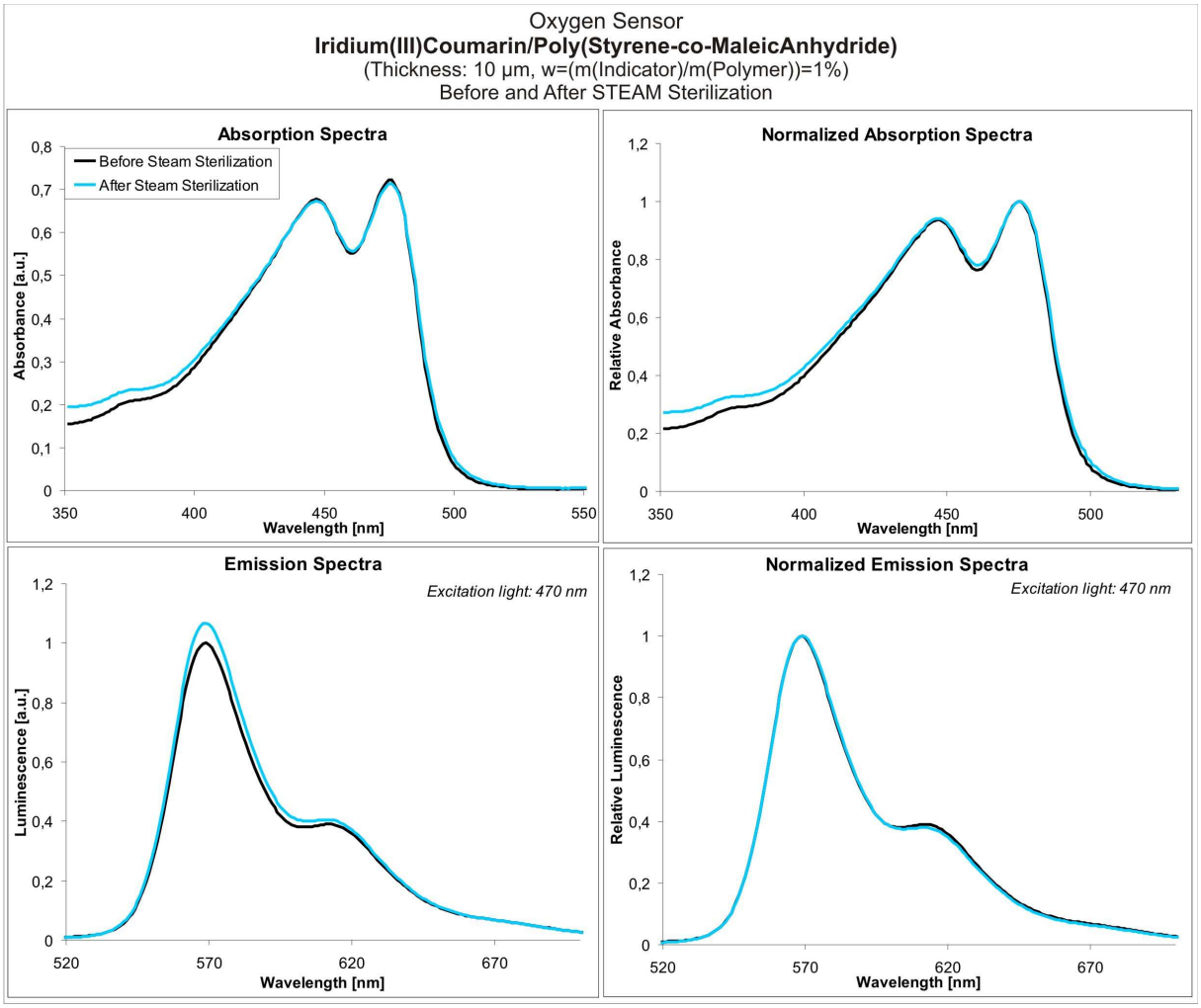

STEAM Sterilization	Absorption Spectra	Emission Spectra
Alterations in Absorption/Emission Intensity	1,13% decrease	6,34% increase
Alterations in Absorption/Emission Curve Form	Slightly altered absorption between 350-410 nm.	Unaltered

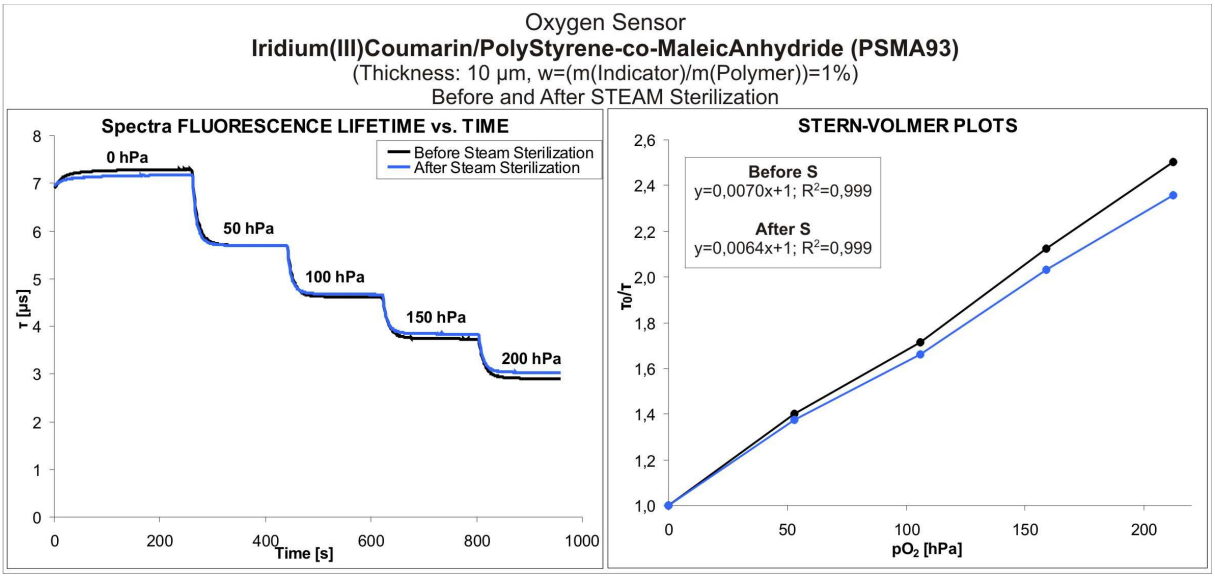

STEAM Sterilization	Luminescence Lifetime	Stern-Volmer Plot
Alterations in Luminescence Lifetime and Slope	2,47% decrease of τ_0	8,57% decrease of slope
	0,18% decrease of τ at 50 hPa	
	1,28% increase of τ at 100 hPa	
	2,67% increase of τ at 150 hPa	
	4,48% increase of τ at 200 hPa	

D.10 Platinum(II)Tetrakis(PentaFluorPhenyl)Porphyrin (PtTFPP) immobilized in Cellulose Acetate

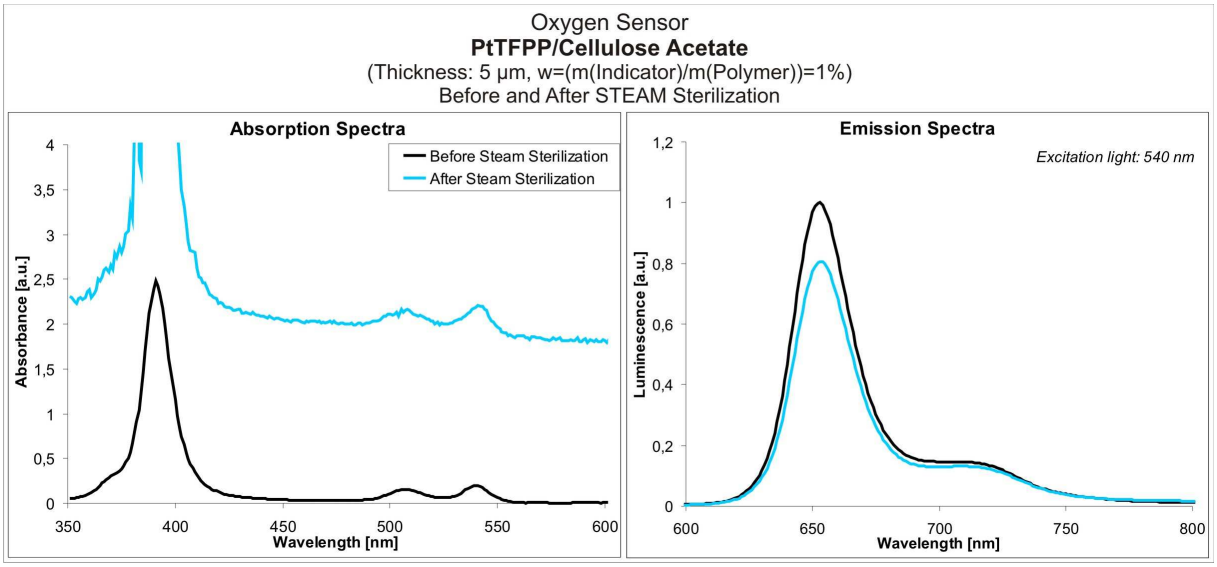

STEAM Sterilization	Absorption Spectra	Emission Spectra
Alterations in Absorption/Emission Intensity	400% increase	19,37% decrease
Alterations in Absorption/Emission Curve Form	Polymers became turbid after sterilization.	Unaltered.

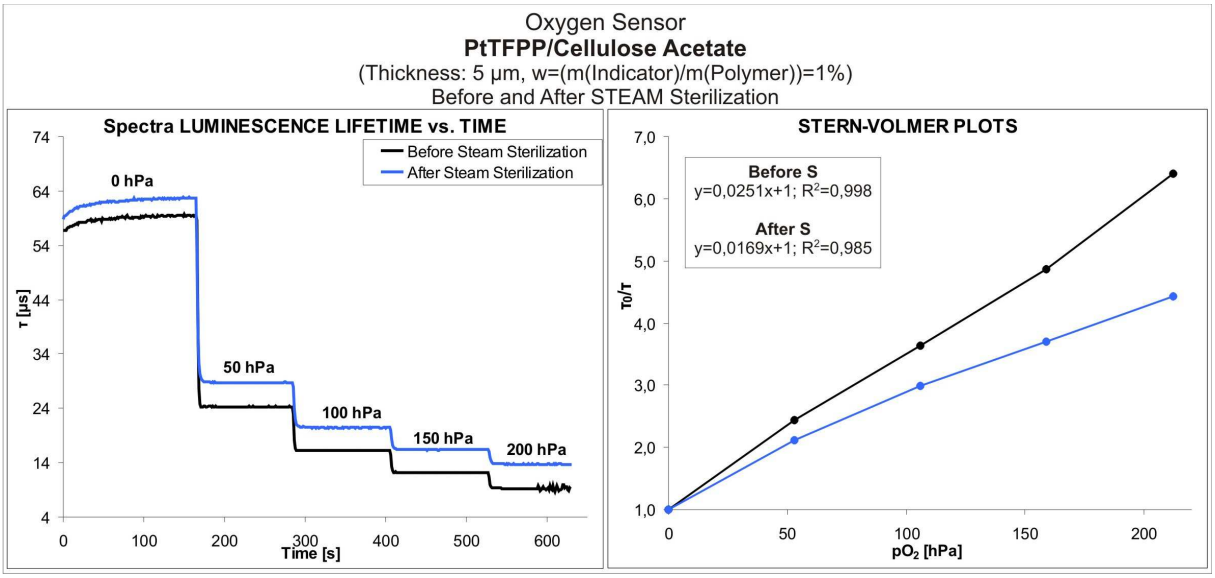

STEAM Sterilization	Luminescence Lifetime	Stern-Volmer Plot
Alterations in Luminescence Lifetime and Slope	5,84% increase of τ_0	32,67% decrease of slope
	18,03% increase of τ at 50 hPa	
	26,08% increase of τ at 100 hPa	
	35,27% increase of τ at 150 hPa	
	47,12% increase of τ at 200 hPa	

D.11 Platinum(II)Tetrakis(PentaFluorPhenyl)Porphyrin (PtTFPP) immobilized in Ethyl Cellulose

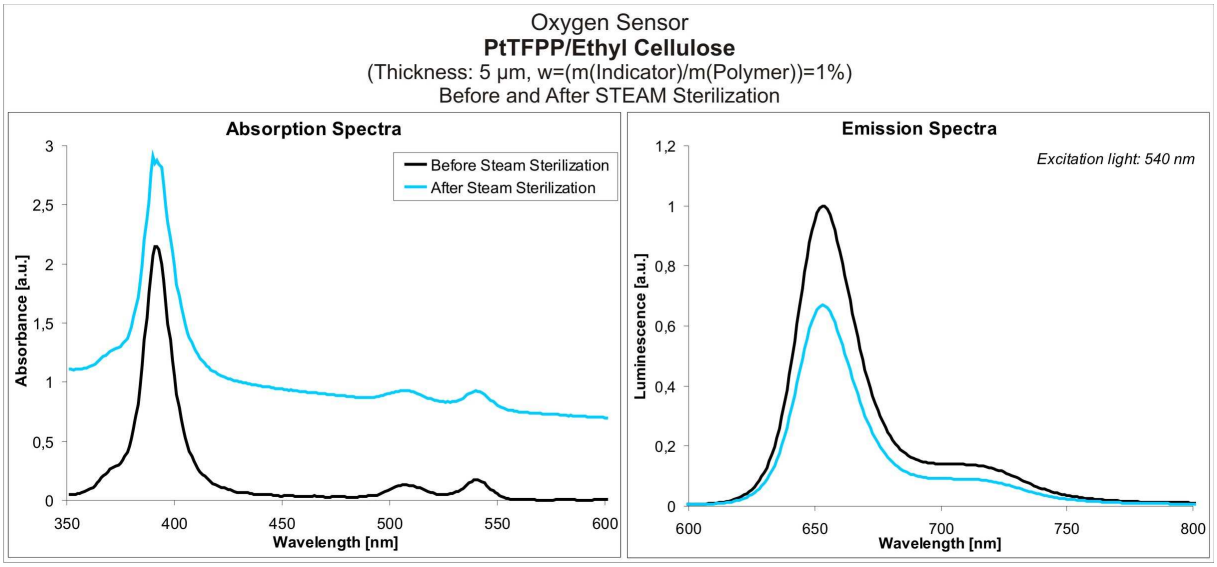

STEAM Sterilization	Absorption Spectra	Emission Spectra
Alterations in Absorption/Emission Intensity	33,00% increase	33,06% decrease
Alterations in Absorption/Emission Curve Form	Polymers became turbid after sterilization.	Unaltered.

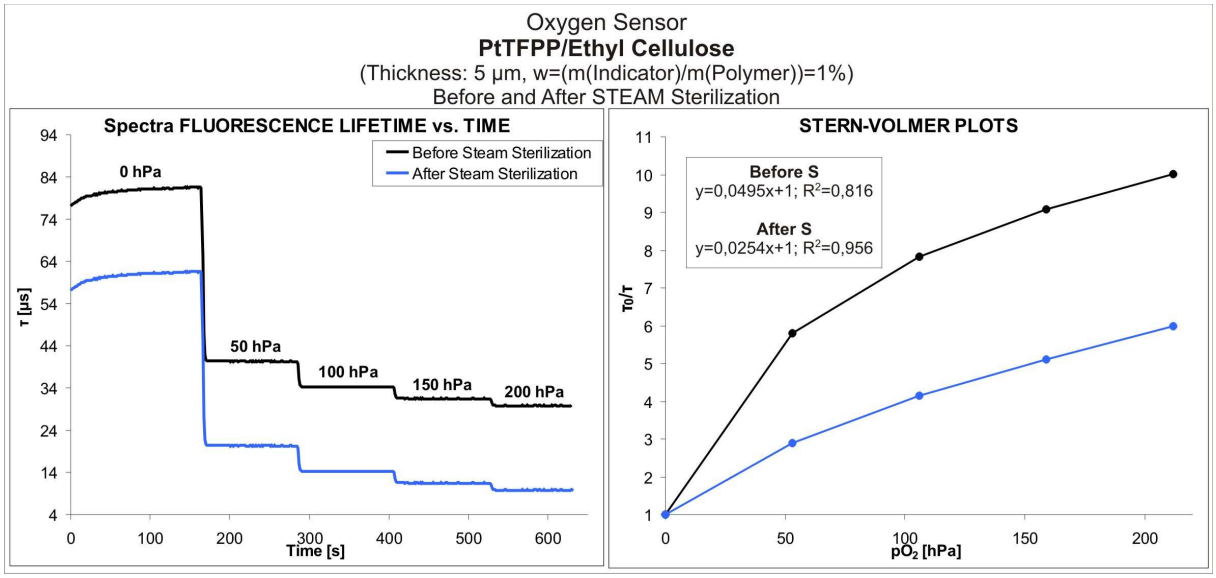

STEAM Sterilization	Luminescence Lifetime	Stern-Volmer Plot
Alterations in Luminescence Lifetime and Slope	24,54% decrease of τ_0	50,50% decrease of slope
	49,65% decrease of τ at 50 hPa	
	58,46% decrease of τ at 100 hPa	
	63,66% decrease of τ at 150 hPa	
	67,11% decrease of τ at 200 hPa	

D.12 Platinum(II)Tetrakis(PentaFluorPhenyl)Porphyrin (PtTFPP) immobilized in HydroGel D4/D7

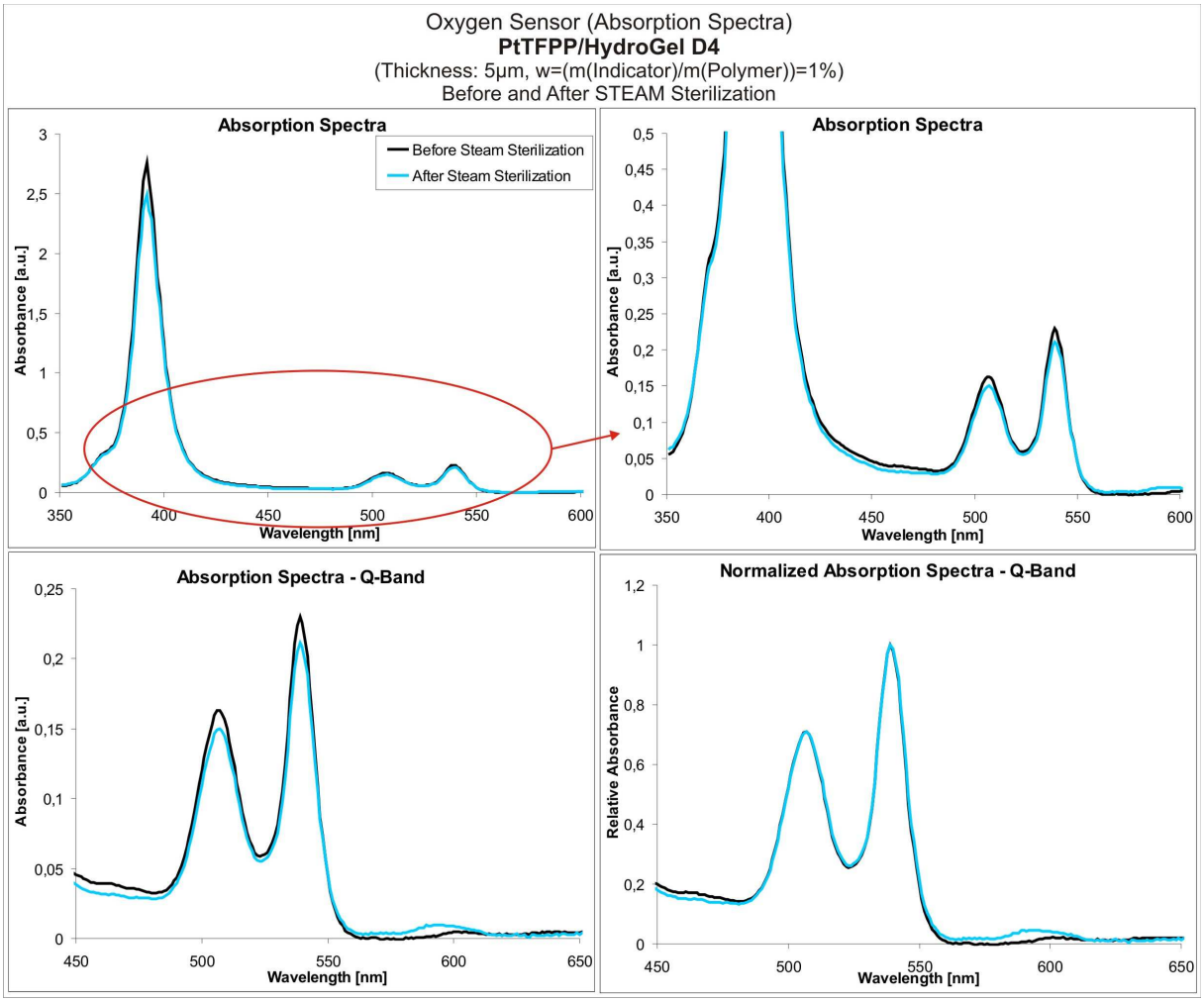

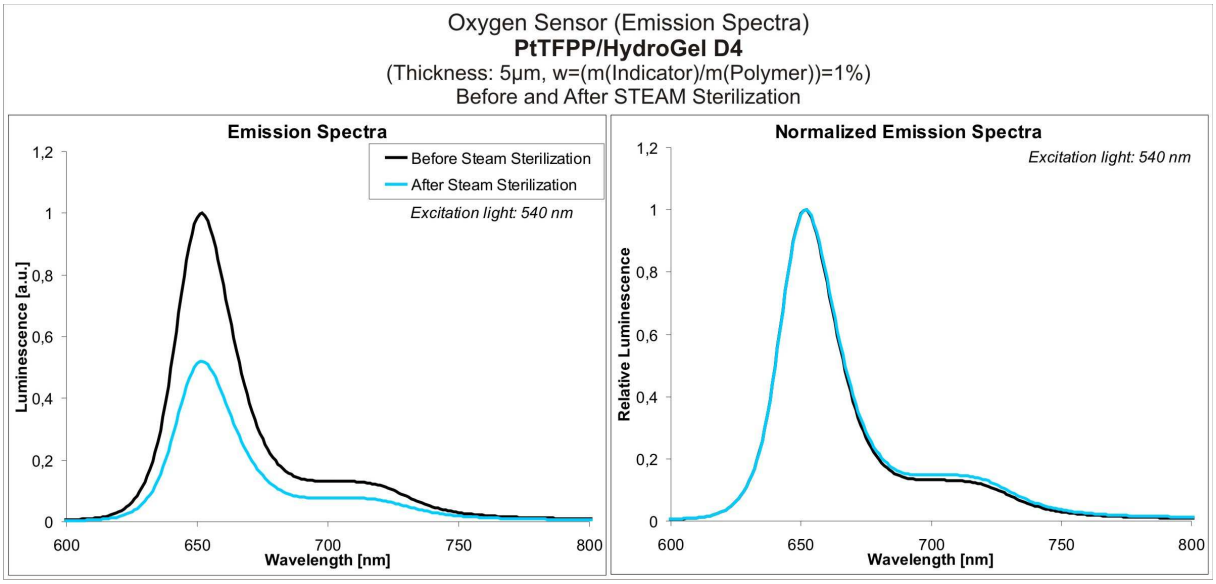

STEAM Sterilization	Absorption Spectra	Emission Spectra
Alterations in Absorption/Emission Intensity	8,02% decrease	47,94% decrease

Alterations in Absorption/Emission Curve Form	Altered absorption curve form between 425-490 nm and 560-620 nm,	Altered emission curve form between 680-750 nm.

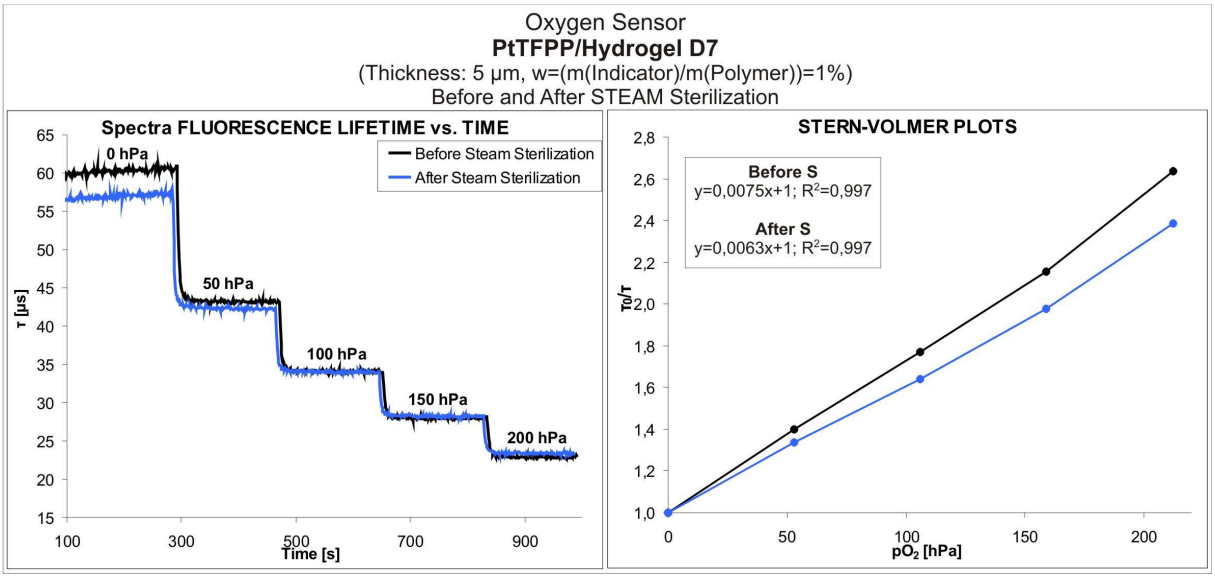

STEAM Sterilization	Luminescence Lifetime	Stern-Volmer Plot
Alterations in Luminescence Lifetime and Slope	5,27% decrease of τ_0	16,00% decrease of slope
	2,14% decrease of τ at 50 hPa	
	1,02% decrease of τ at 100 hPa	
	1,19% increase of τ at 150 hPa	
	1,80% increase of τ at 200 hPa	

D.13 Platinum(II)Tetrakis(PentaFluorPhenyl)Porphyrin (PtTFPP) immobilized in HydroThane 5

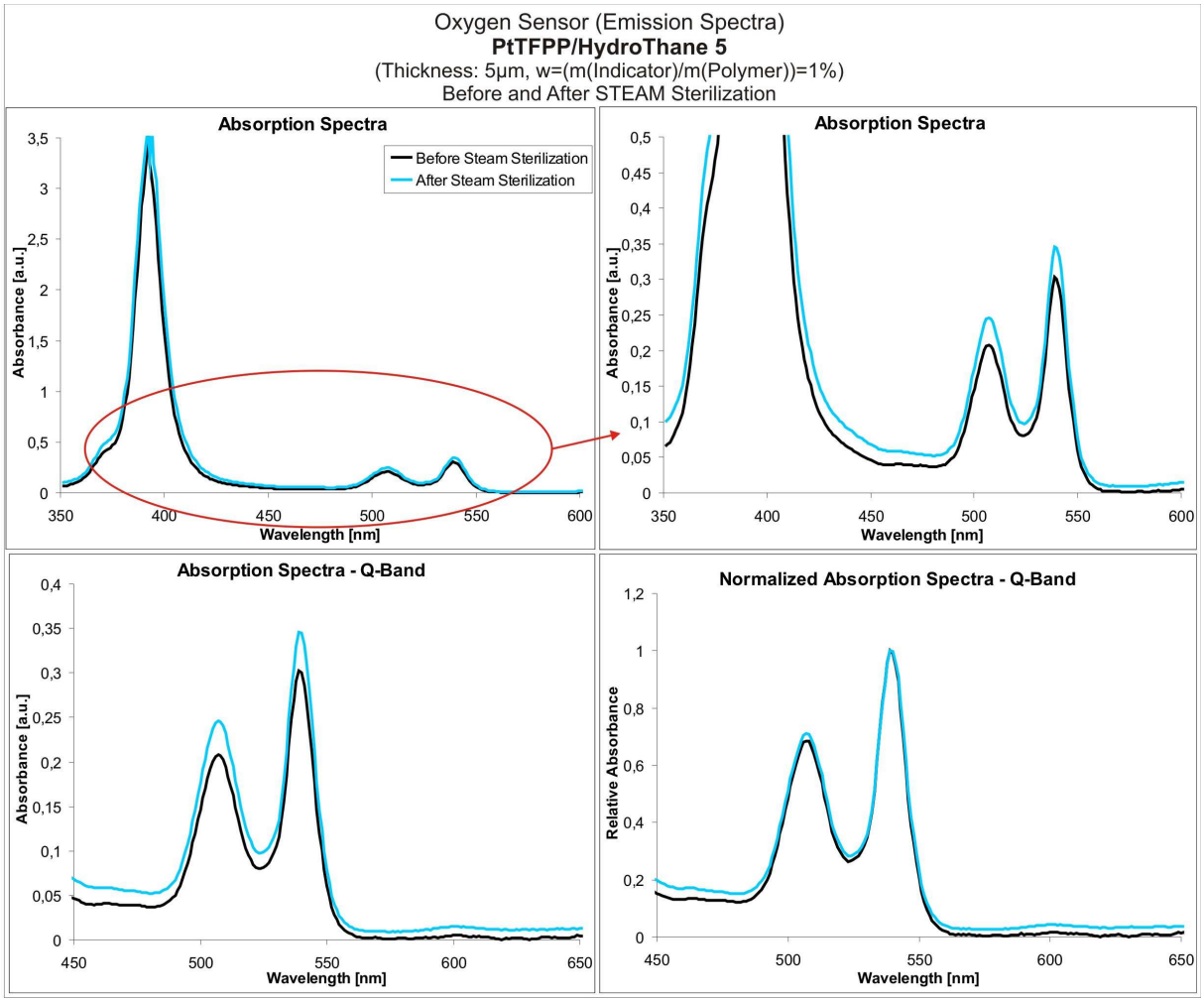

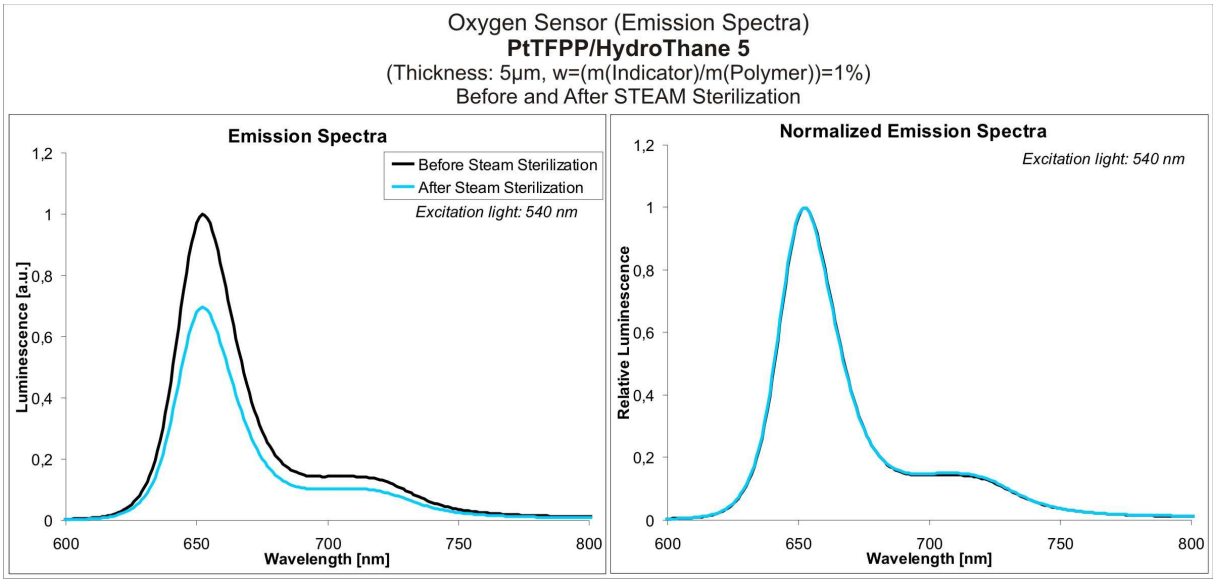

STEAM Sterilization	Absorption Spectra	Emission Spectra
Alterations in Absorption/Emission Intensity	12,40% increase	30,30% decrease

Alterations in Absorption/Emission Curve Form	Altered absorption curve form between 370-380 nm, 415-490 nm and 555-800 nm,	Unaltered.

Oxygen Sensor
PtTFPP/HydroThane 5
(Thickness: 5 µm, w=(m(Indicator)/m(Polymer))=1%)
Before and After STEAM Sterilization

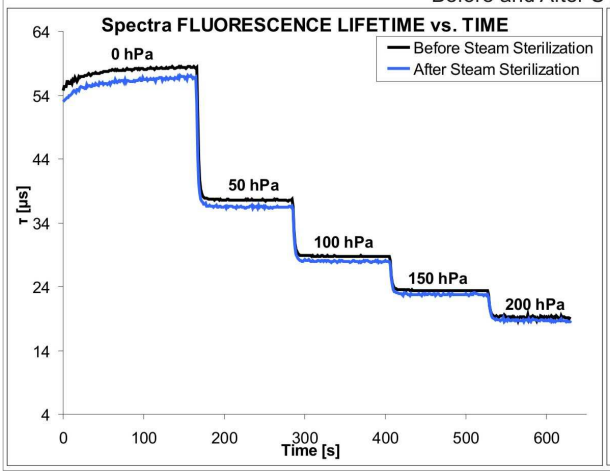

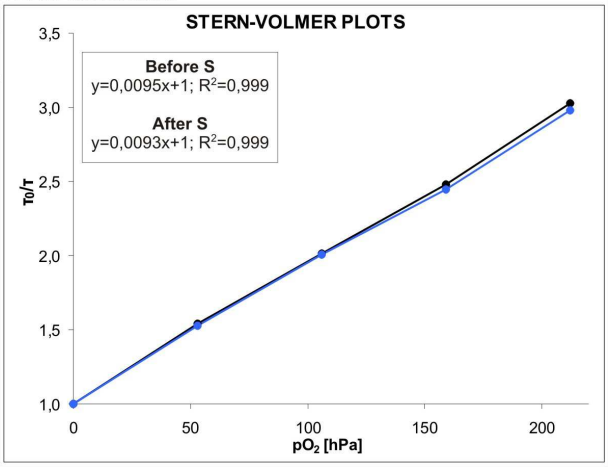

STEAM Sterilization	Luminescence Lifetime	Stern-Volmer Plot
Alterations in Luminescence Lifetime and Slope	2,46% decrease of τ_0	2,10% decrease of slope
	3,04% decrease of τ at 50 hPa	
	2,83% decrease of τ at 100 hPa	
	2,29% decrease of τ at 150 hPa	
	2,55% decrease of τ at 200 hPa	

D.14 Platinum(II)Tetrakis(PentaFluorPhenyl)Porphyrin (PtTFPP) immobilized in PolySulfone

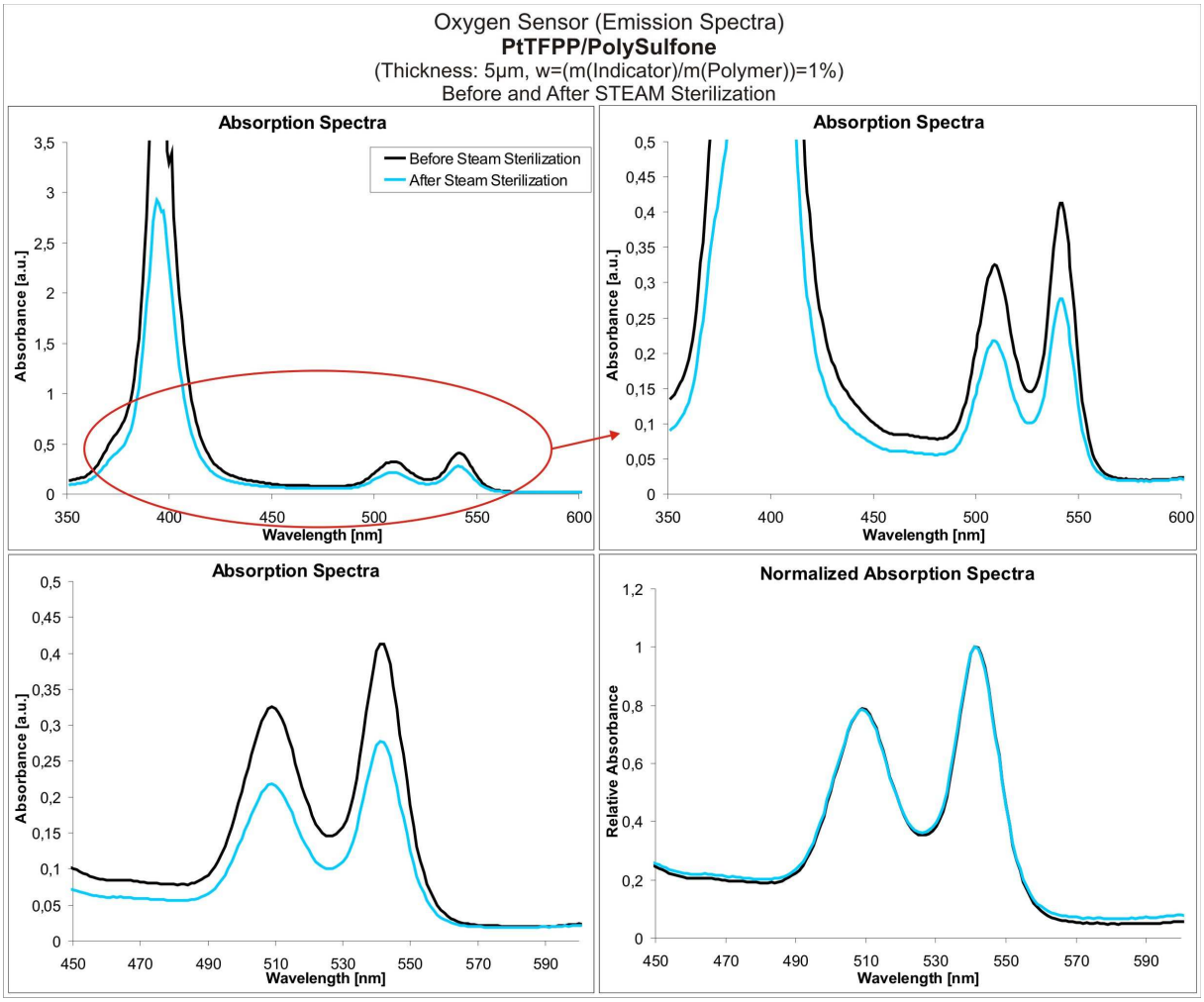

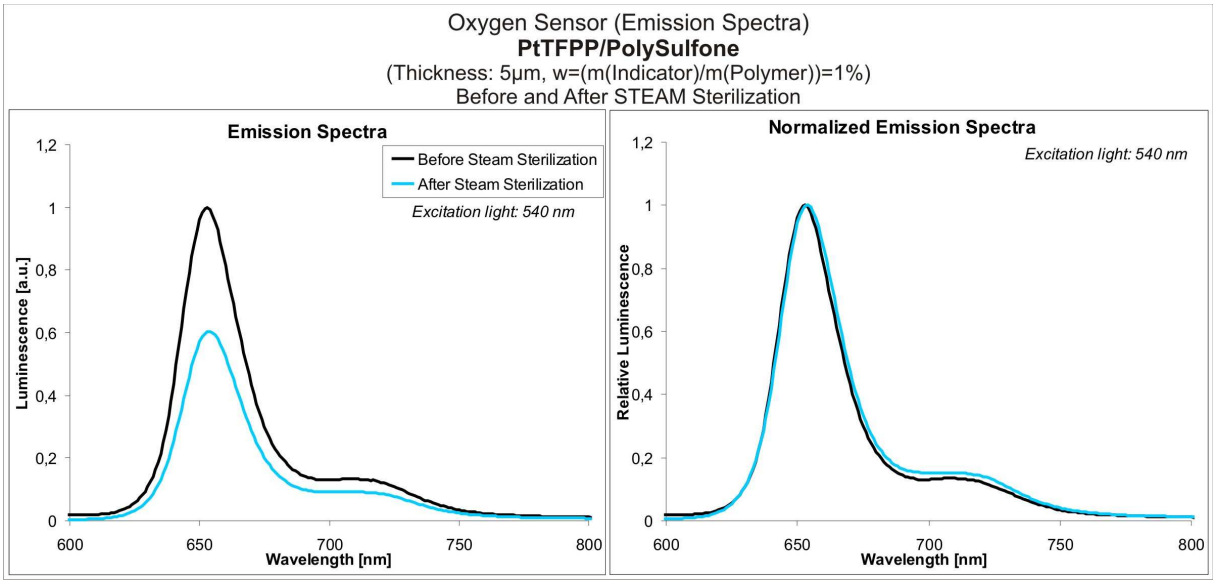

STEAM Sterilization	Absorption Spectra	Emission Spectra
Alterations in Absorption/Emission Intensity	32,69% increase	39,53% decrease

Alterations in Absorption/Emission Curve Form	Unaltered.	Altered emission curve form between 675-750 nm.

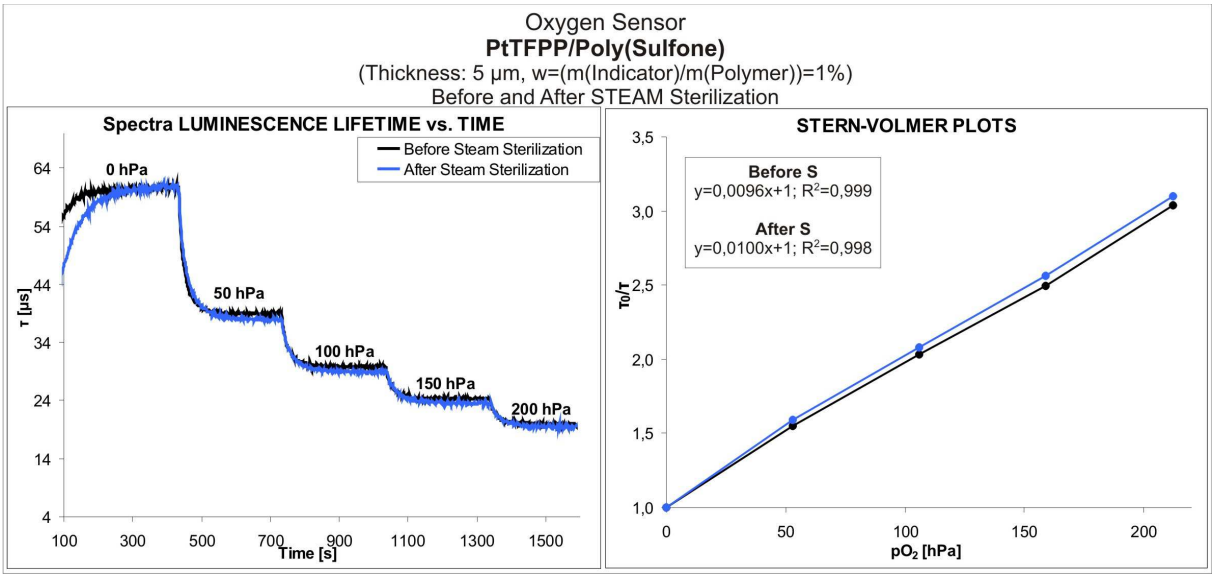

STEAM Sterilization	Luminescence Lifetime	Stern-Volmer Plot
Alterations in Luminescence Lifetime and Slope	0,13% decrease of τ_0	4,17% increase of slope
	0,96% decrease of τ at 50 hPa	
	1,89% decrease of τ at 100 hPa	
	3,49% decrease of τ at 150 hPa	
	1,92% decrease of τ at 200 hPa	

D.15 Platinum(II)Tetrakis(PentaFluorPhenyl)Porphyrin (PtTFPP) immobilized in PolyPhenylSilses Quioxane

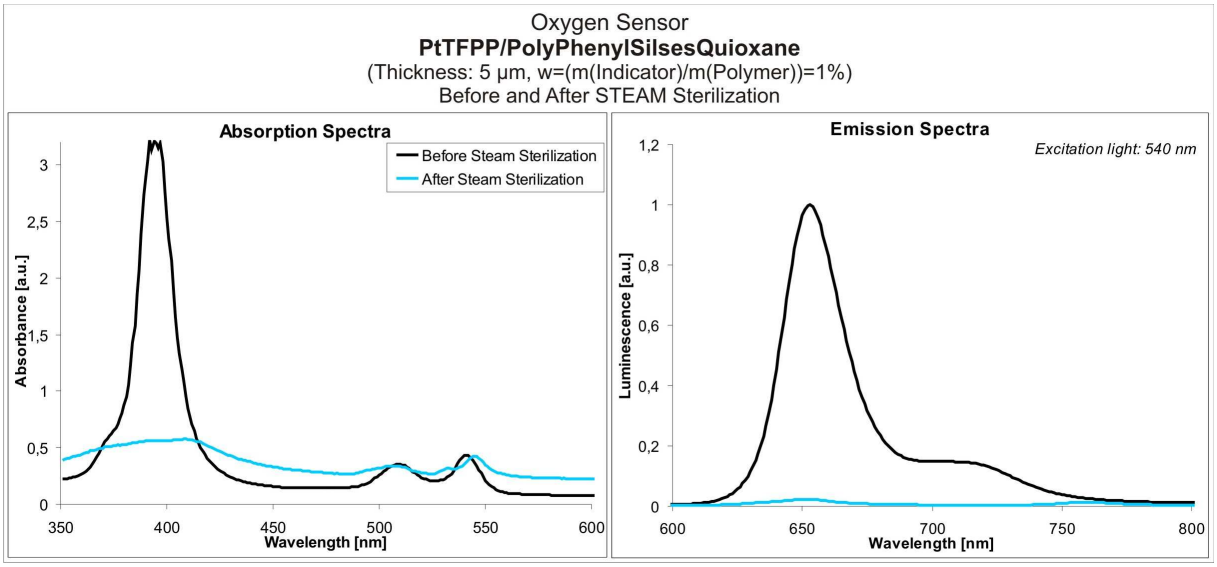

STEAM Sterilization	Absorption Spectra	Emission Spectra
Alterations in Absorption/Emission Intensity	Decrease	Decrease.
Alterations in Absorption/Emission Curve Form	Altered.	Altered.

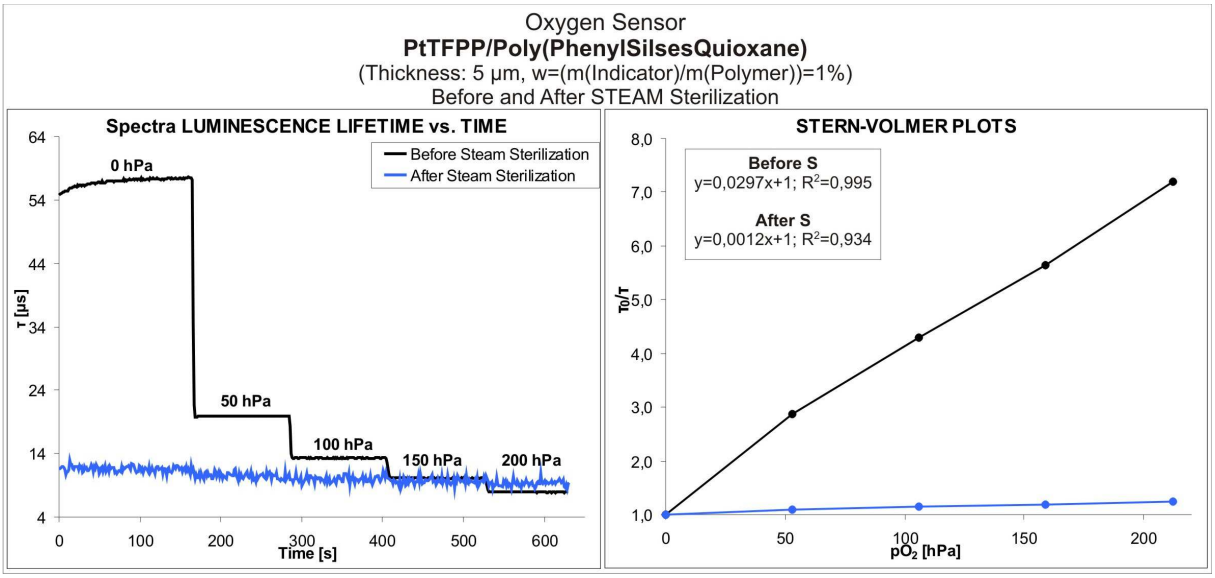

STEAM Sterilization	Luminescence Lifetime	Stern-Volmer Plot
Alterations in Luminescence Lifetime and Slope	Decrease	95,96% decrease of slope

D.16 Platinum(II)Tetrakis(PentaFluorPhenyl)Porphyrin (PtTFPP) immobilized in PolyStyrene

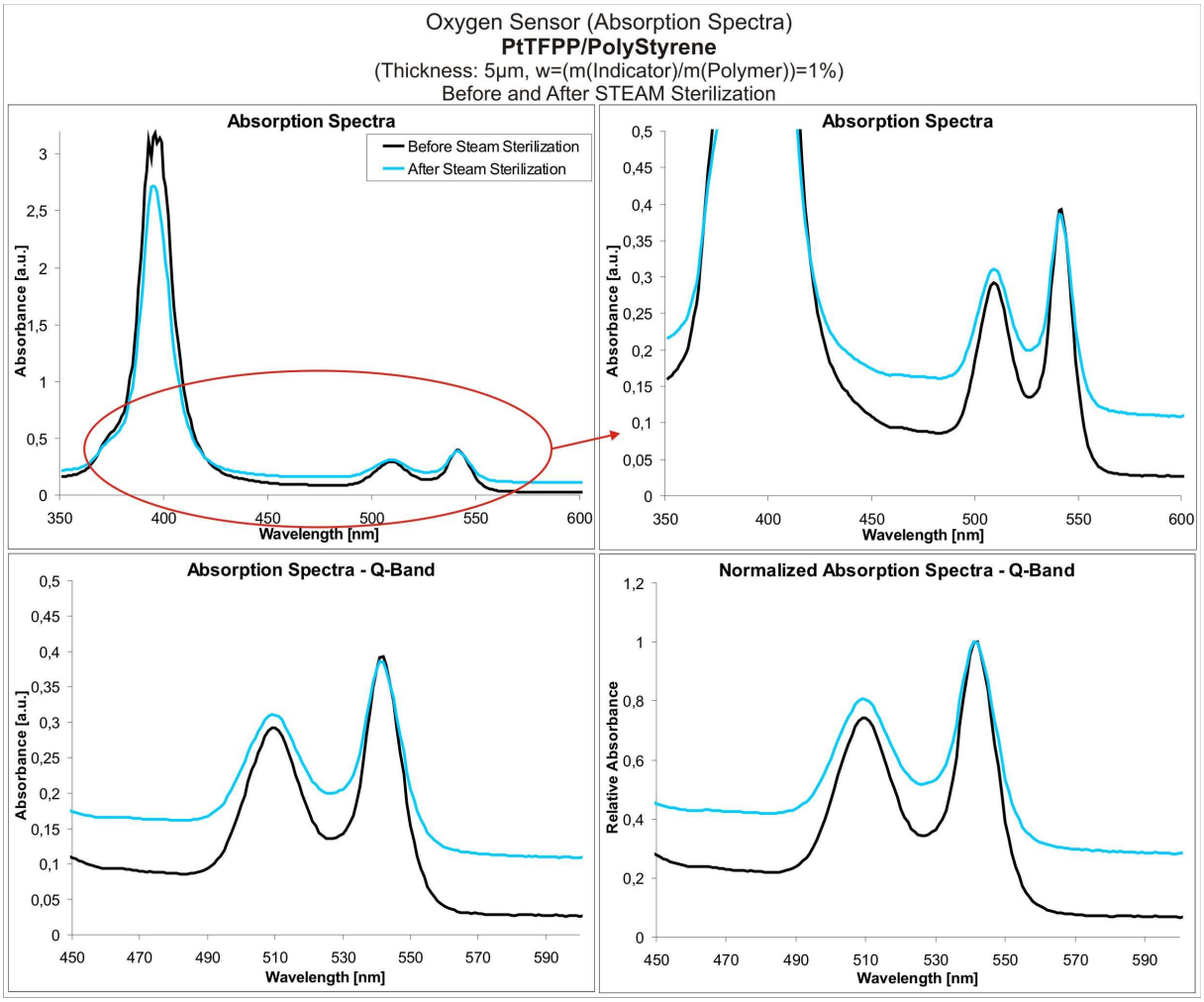

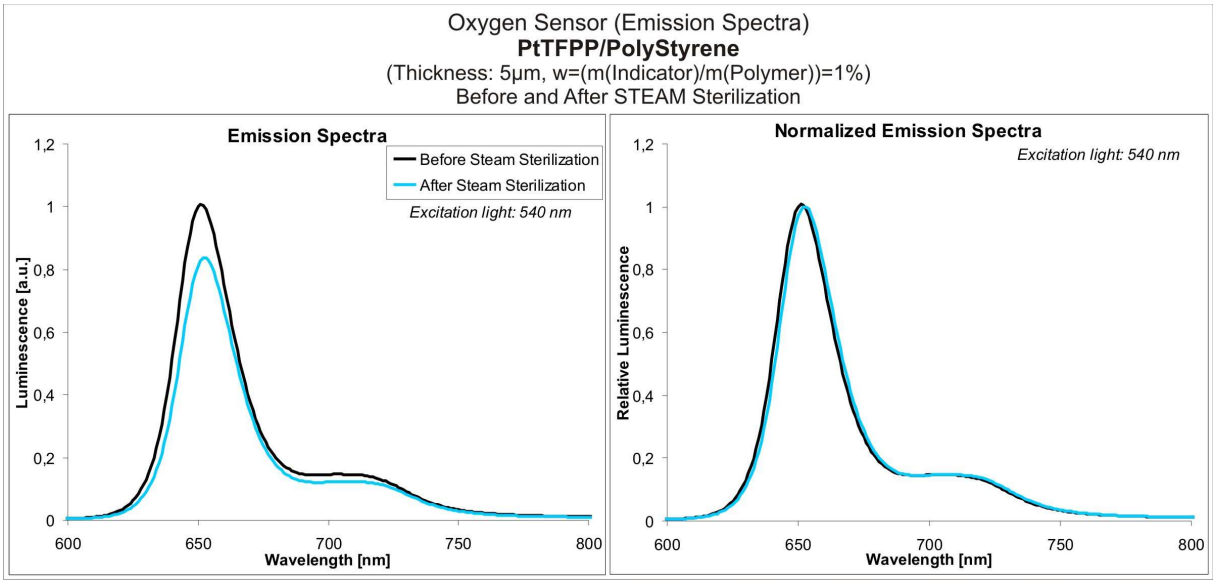

STEAM Sterilization	Absorption Spectra	Emission Spectra
Alterations in Absorption/Emission Intensity	12,45% decrease	16,32% decrease

Alterations in Absorption/Emission Curve Form	Polymer became turbid after sterilization. Altered absorption curve form between 350-365 nm, 425-535 nm and 550-800 nm.	Hypsochromic shift of emission maximum for 3 nm.

Oxygen Sensor
PtTFPP/PolyStyrene
(Thickness: 5 µm, w=(m(Indicator)/m(Polymer))=1%)
Before and After STEAM Sterilization

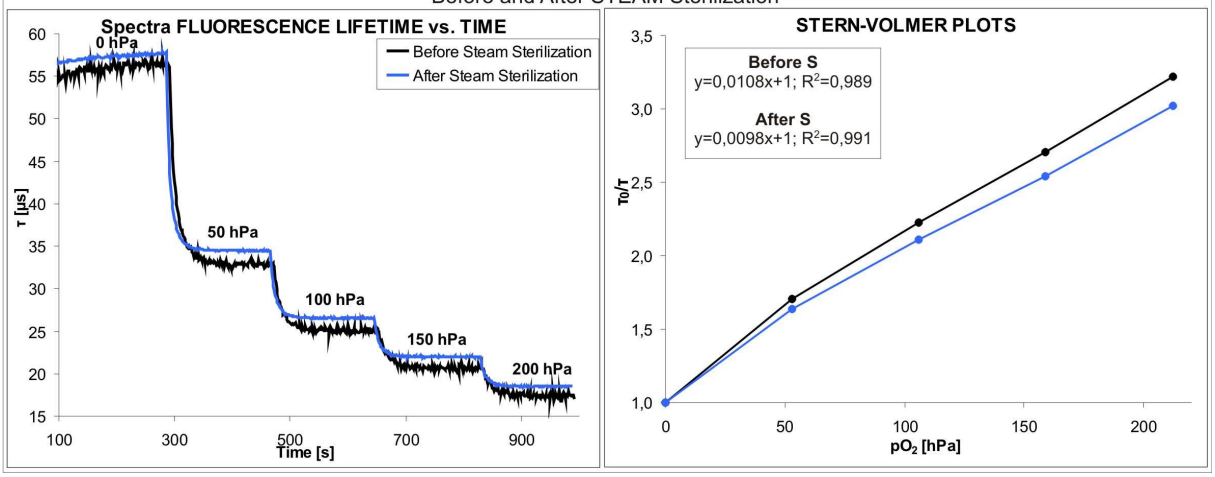

STEAM Sterilization	Luminescence Lifetime	Stern-Volmer Plot
Alterations in Luminescence Lifetime and Slope	3,47% increase of τ_0	9,26% decrease of slope
	5,12% increase of τ at 50 hPa	
	5,07% increase of τ at 100 hPa	
	6,82% increase of τ at 150 hPa	
	5,33% increase of τ at 200 hPa	

D.17 Platinum(II)Tetrakis(PentaFluorPhenyl)Porphyrin (PtTFPP) immobilized in PolyStyrene-co- Acrylonitrile

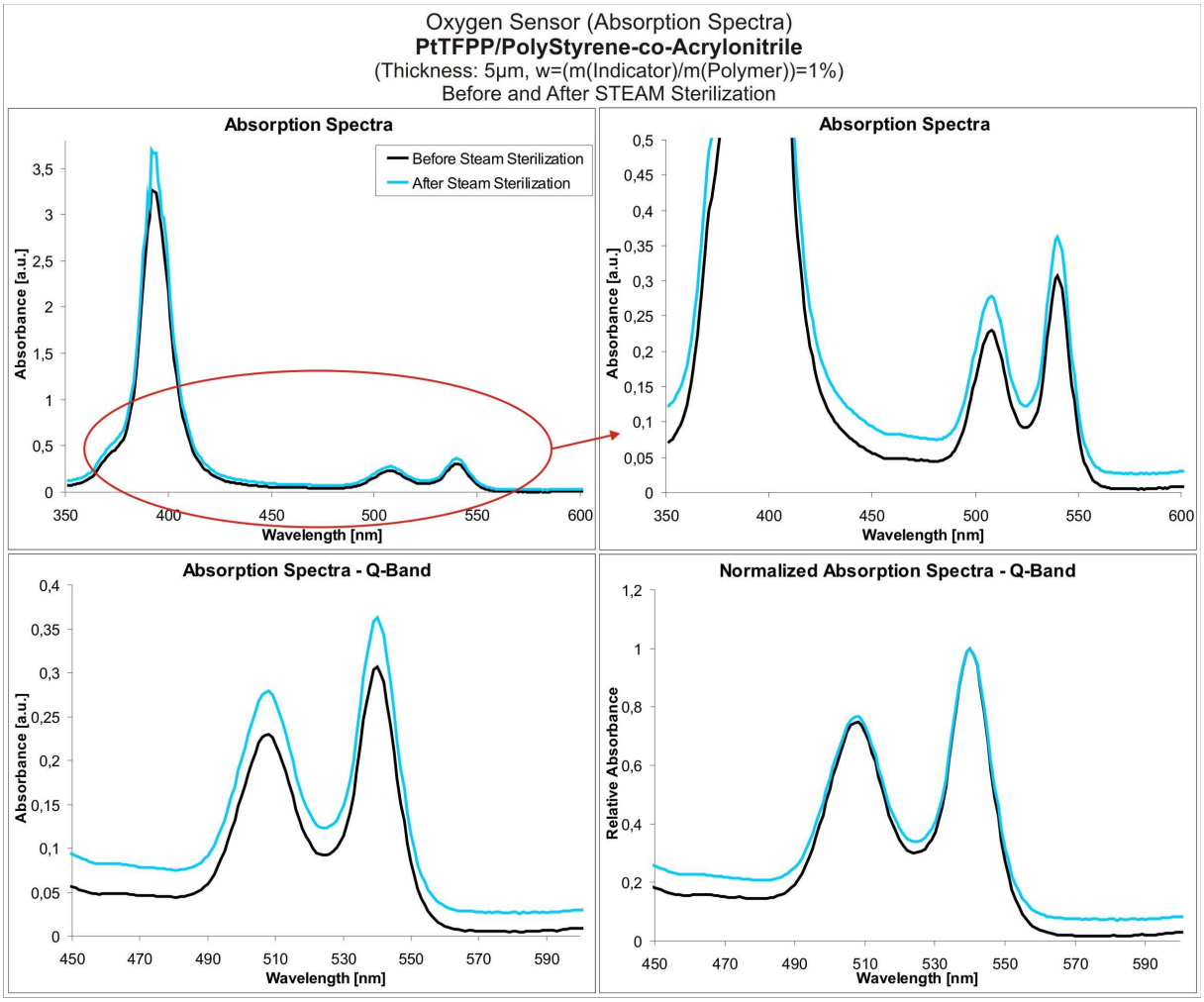

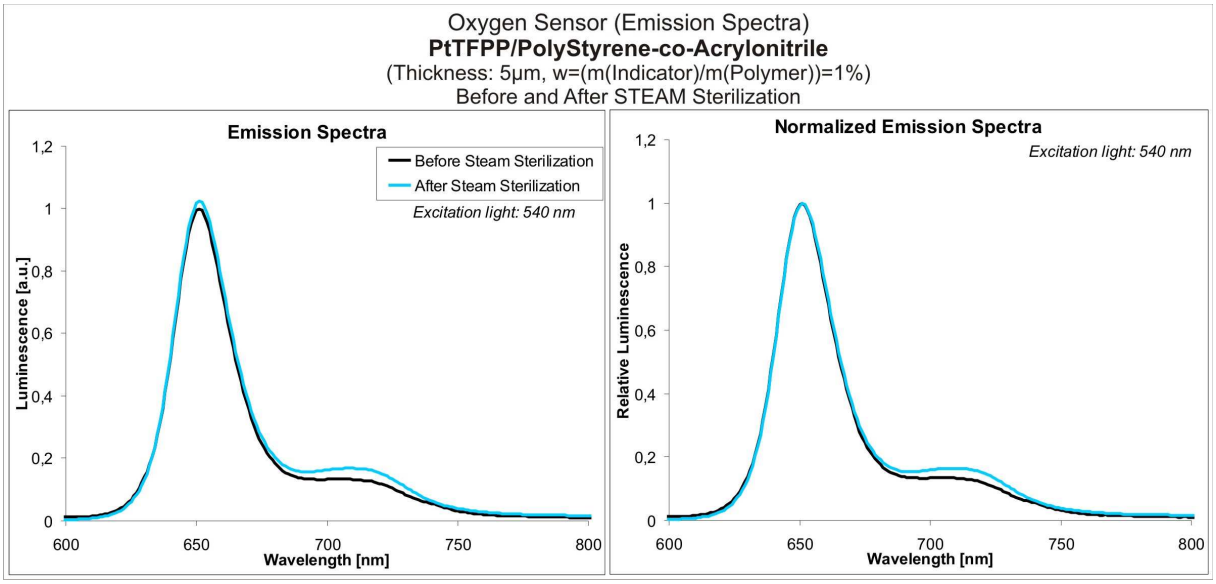

STEAM Sterilization	Absorption Spectra	Emission Spectra
Alterations in Absorption/Emission Intensity	15,42% increase	2,38% increase

Alterations in Absorption/Emission Curve Form	Polymer became turbid after sterilization. Altered absorption curve form between 350-380 nm, 415-490 nm, 520-530 nm and 550-800 nm.	Altere emission curve form between 680-740 nm.

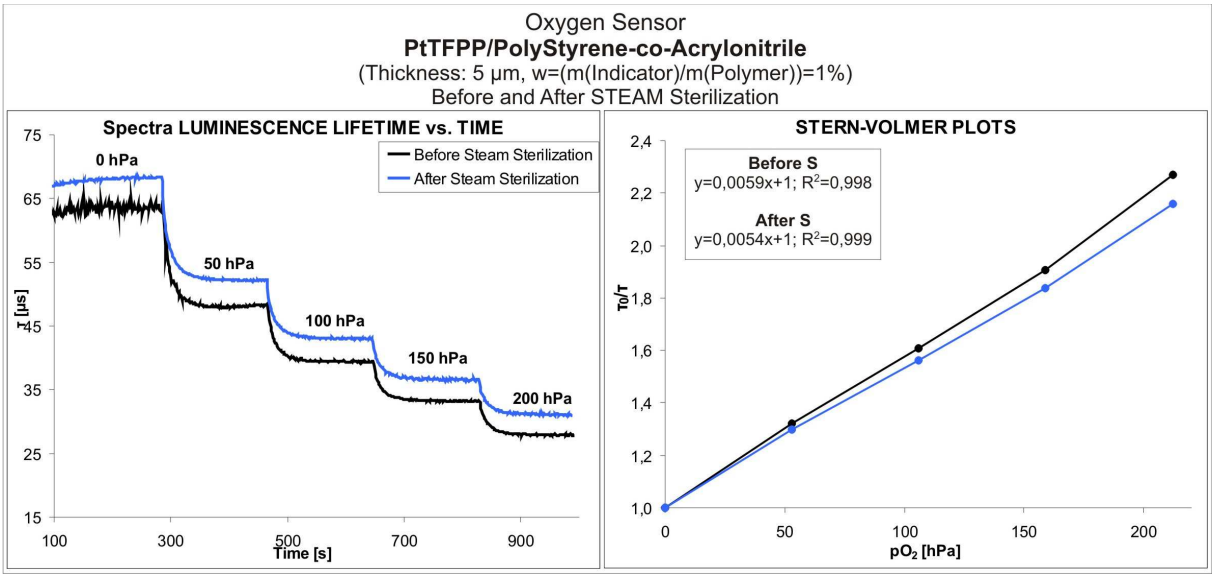

STEAM Sterilization	Luminescence Lifetime	Stern-Volmer Plot
Alterations in Luminescence Lifetime and Slope	6,04% increase of τ_0	8,47% decrease of slope
	8,72% increase of τ at 50 hPa	
	9,37% increase of τ at 100 hPa	
	10,02% increase of τ at 150 hPa	
	12,11% increase of τ at 200 hPa	

D.18 Platinum(II)Tetrakis(PentaFluorPhenyl)Porphyrin (PtTFPP) immobilized in PolyStyrene-co-MaleicAnhydride (PSMA93)

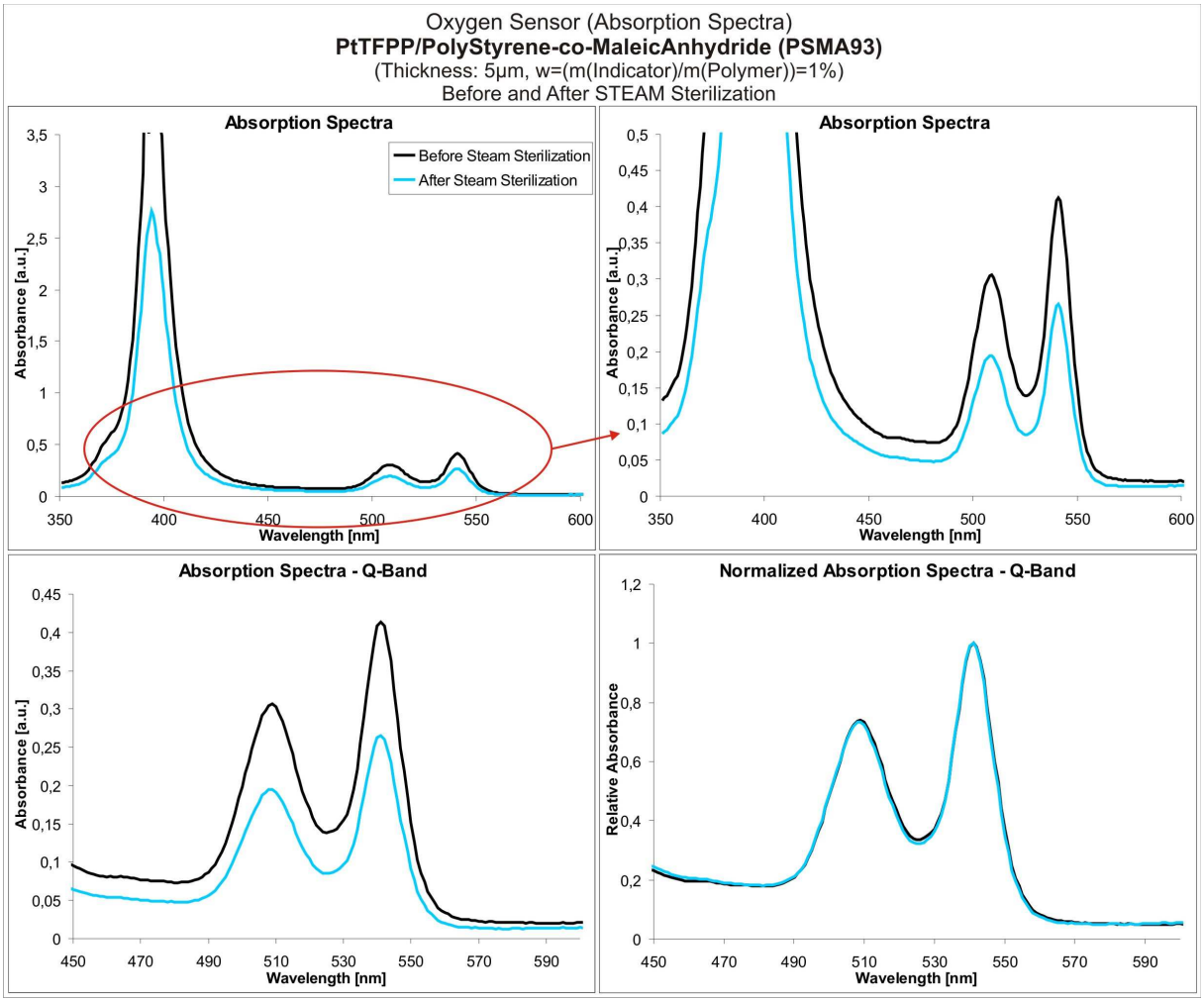

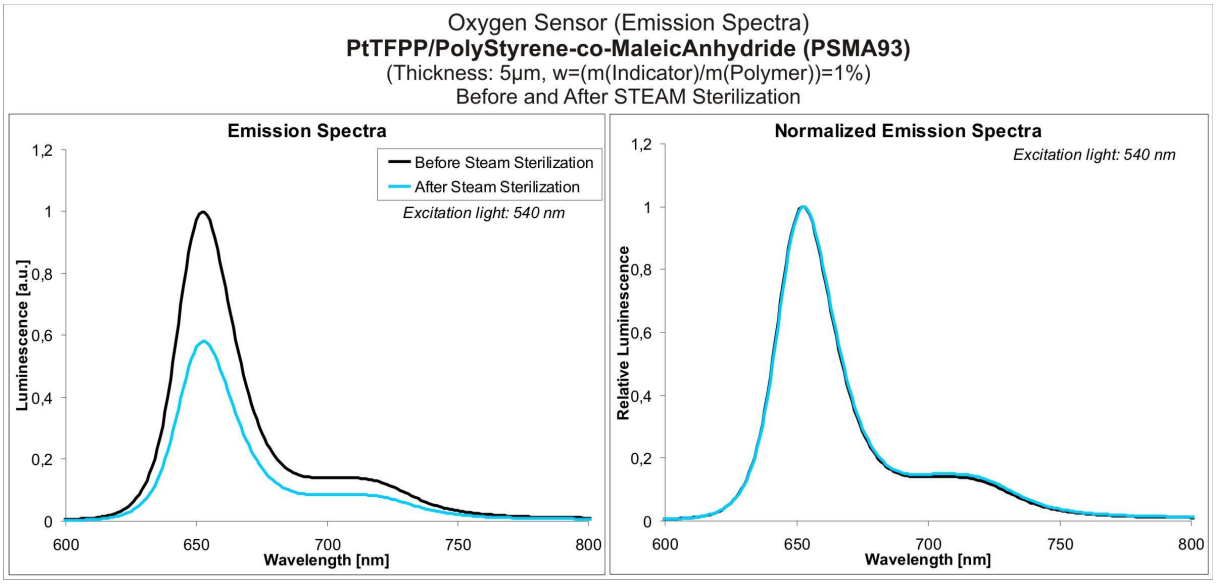

STEAM Sterilization	Absorption Spectra	Emission Spectra
Alterations in Absorption/Emission Intensity	35,86% decrease	56,99% decrease

Alterations in Absorption/Emission Curve Form	Unaltered.	Unaltered.

Oxygen Sensor
PtTFPP/PolyStyrene-co-MaleicAnhydride (PSMA93)
(Thickness: 5 µm, w=(m(Indicator)/m(Polymer))=1%)
Before and After STEAM Sterilization

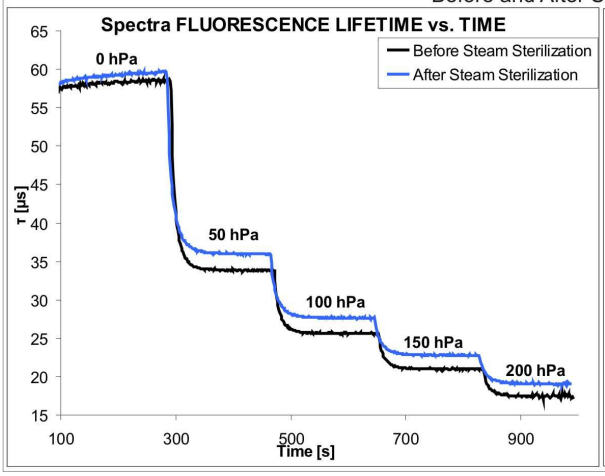

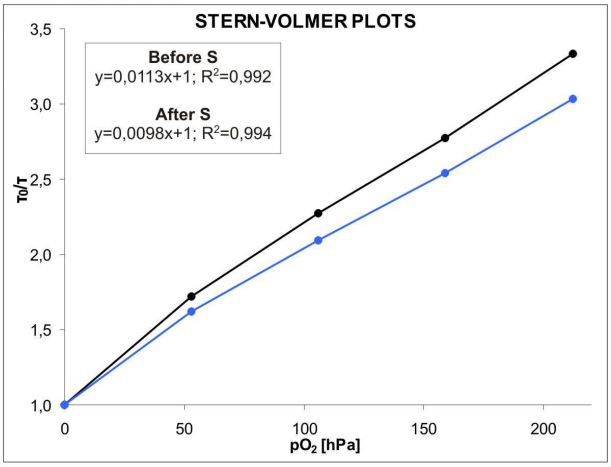

STEAM Sterilization	Luminescence Lifetime	Stern-Volmer Plot
Alterations in Luminescence Lifetime and Slope	1,19% increase of τ_0	13,27% decrease of slope
	6,36% increase of τ at 50 hPa	
	8,12% increase of τ at 100 hPa	
	8,33% increase of τ at 150 hPa	
	8,47% increase of τ at 200 hPa	

D.19 Platinum(II) OctaEthyl Porphyrin (=PtOEP) immobilized in PolyStyrene

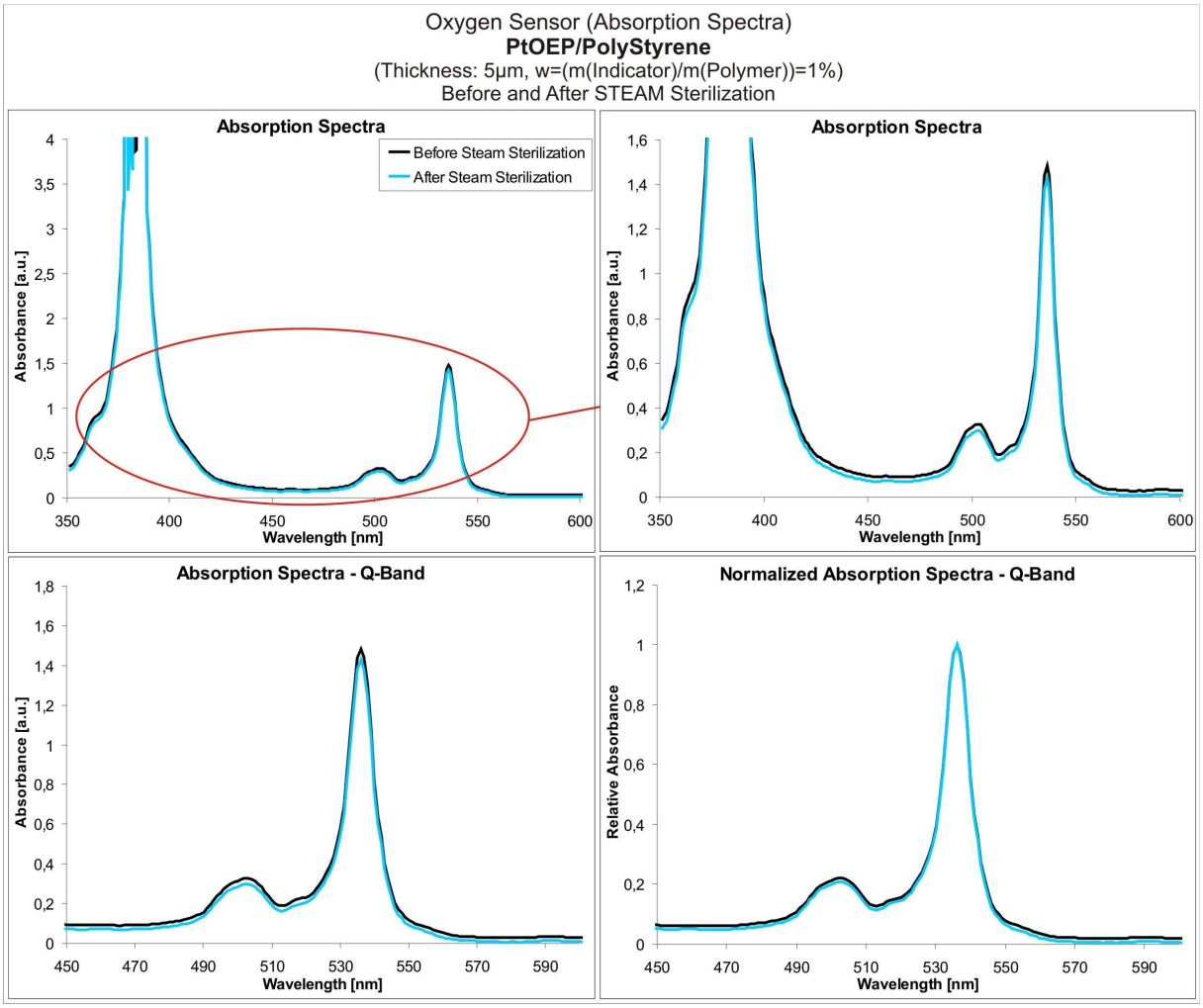

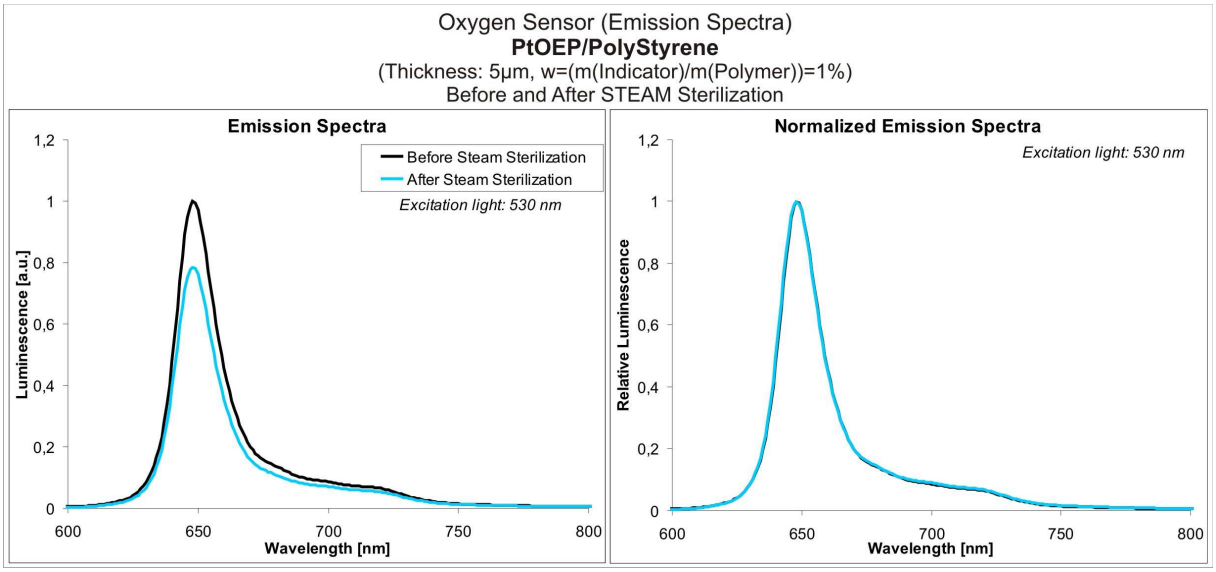

Sterilization with Ethylene Oxide	Absorption Spectra	Emission Spectra
Alterations in Absorption/Emission Intensity	3,80% decrease	21,43% decrease

Alterations in Absorption/Emission Curve Form	Slightly altered absorption curve form between 425-520 nm and 550-800 nm.	Unaltered.

Oxygen Sensor
PtOEP/PolyStyrene
(Thickness: 5 µm, w=(m(Indicator)/m(Polymer))=1%)
Before and After STEAM Sterilization

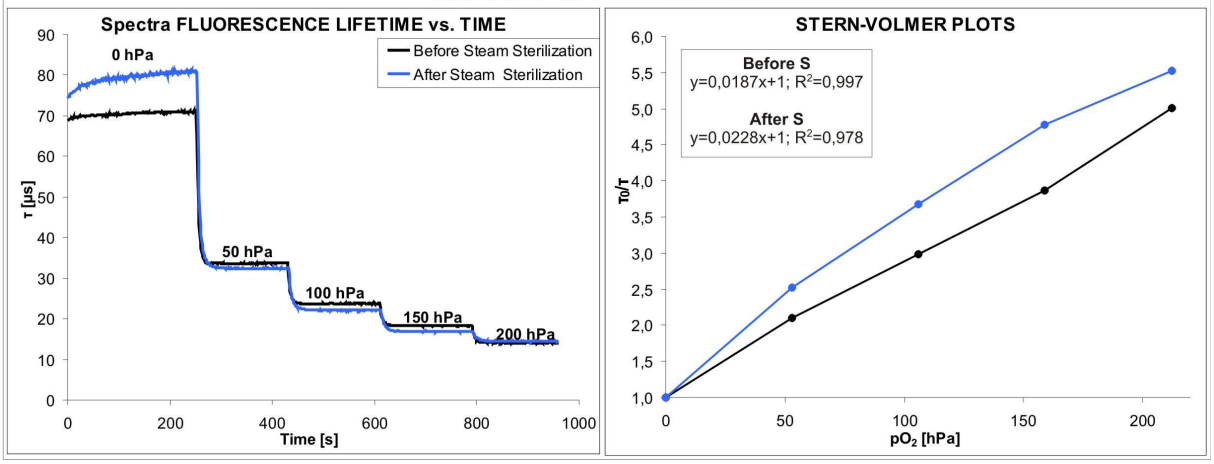

STEAM Sterilization	Luminescence Lifetime	Stern-Volmer Plot
Alterations in Luminescence Lifetime and Slope	12,25% increase of τ_0	54,01% increase of slope
	3,27% decrease of τ at 50 hPa	
	8,79% decrease of τ at 100 hPa	
	8,20% decrease of τ at 150 hPa	
	2,84% decrease of τ at 200 hPa	

D.20 Platinum(II) meso-tetra(4-FluoroPhenyl) TetraBenzoPorphyrin (=PtTPTBPF) immobilized in PolyStyrene

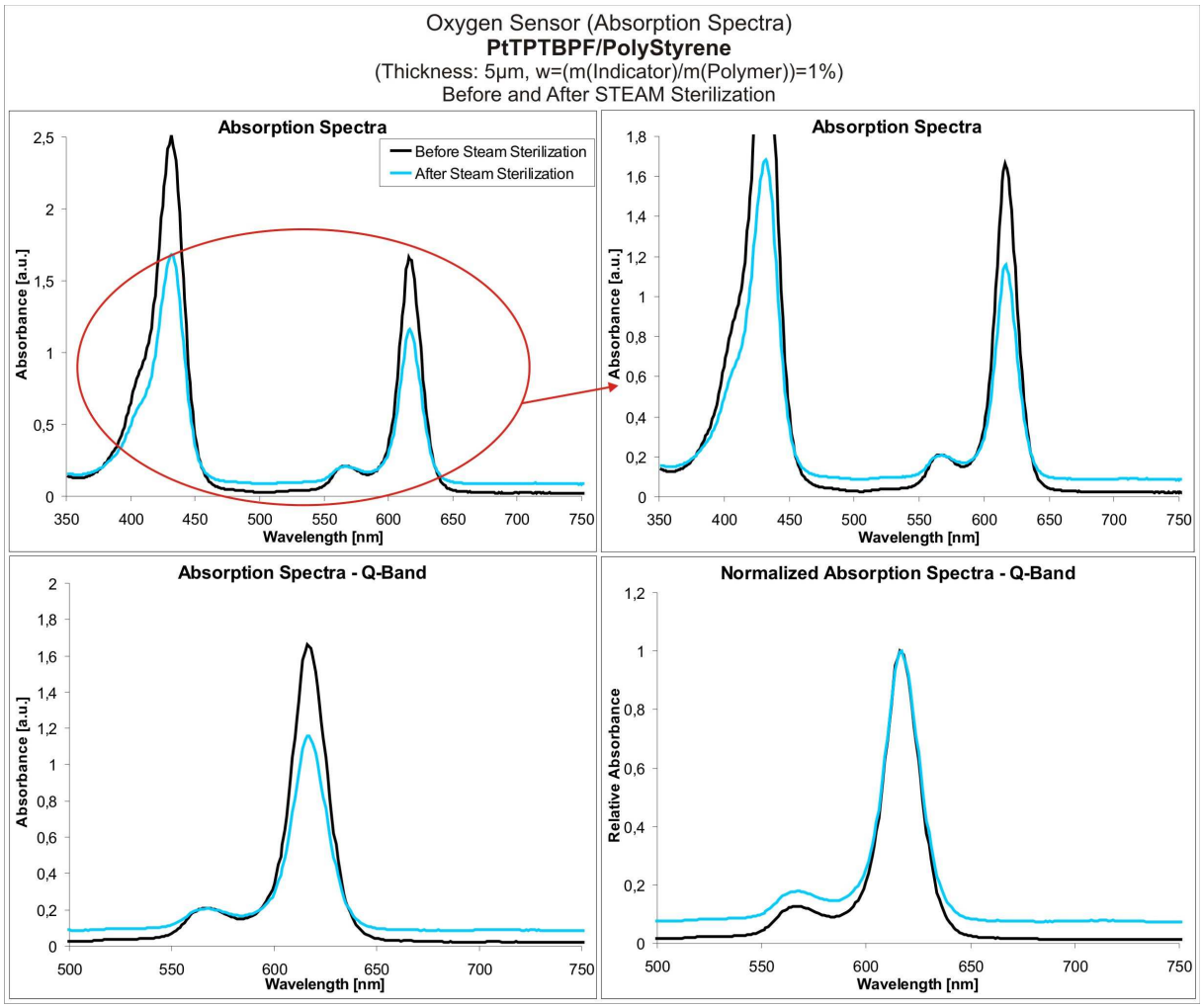

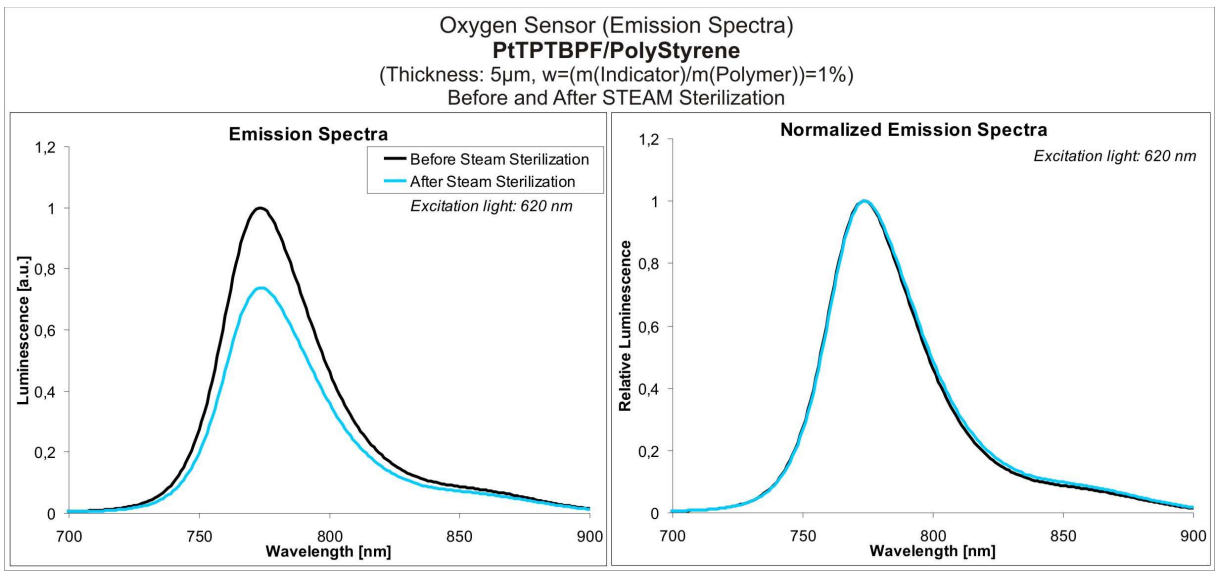

Sterilization with Ethylene Oxide	Absorption Spectra	Emission Spectra
Alterations in Absorption/Emission Intensity	30,18% decrease	26,15% decrease

Alterations in Absorption/Emission Curve Form	Polymer became slightly turbid after sterilization. Altered absorption curve form between 450-600 nm and 635-800 nm.	Unaltered.

Oxygen Sensor
PtTFTBPF/PolyStyrene
(Thickness: 5 µm, w=(m(Indicator)/m(Polymer))=1%)
Before and After STEAM Sterilization

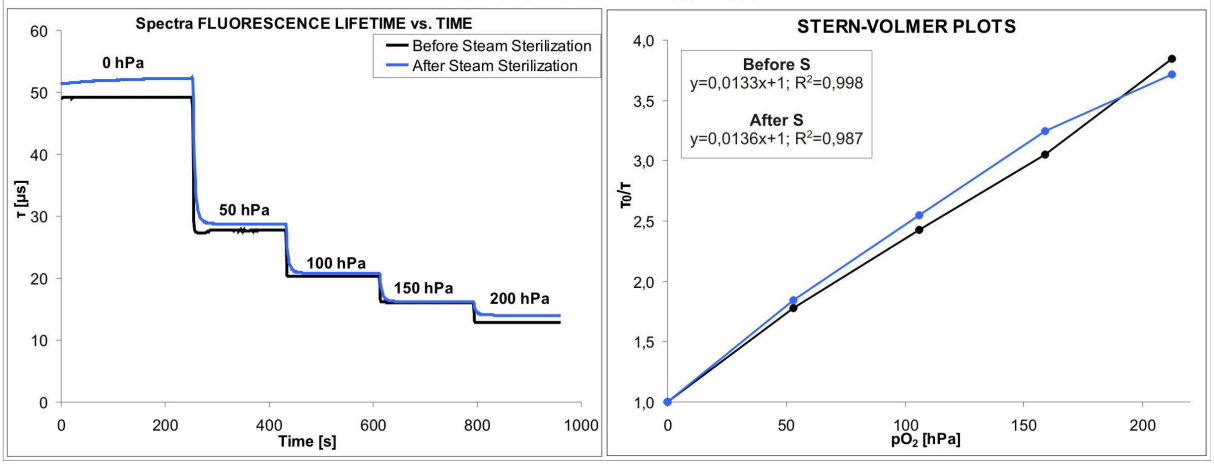

STEAM Sterilization	Luminescence Lifetime	Stern-Volmer Plot
Alterations in Luminescence Lifetime and Slope	5,89% increase of τ_0	2,26% increase of slope
	2,17% increase of τ at 50 hPa	
	0,49% increase of τ at 100 hPa	
	0,62% increase of τ at 150 hPa	
	9,38% increase of τ at 200 hPa	

D.21 Palladium(II)meso-tetra(4-FluoroPhenyl) TetraBenzoPorphyrin (=PdTPTBPF) immobilized in PolyStyrene

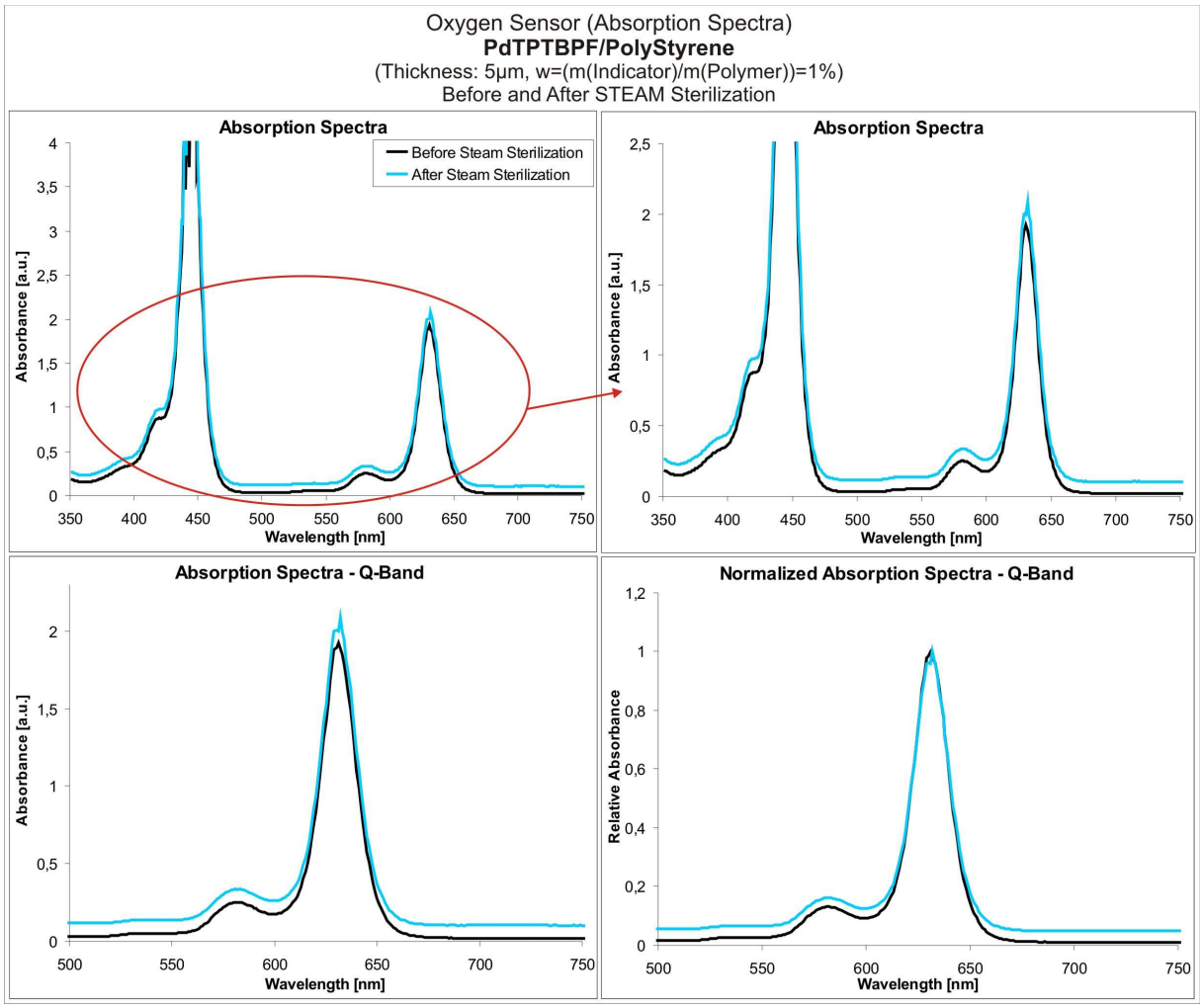

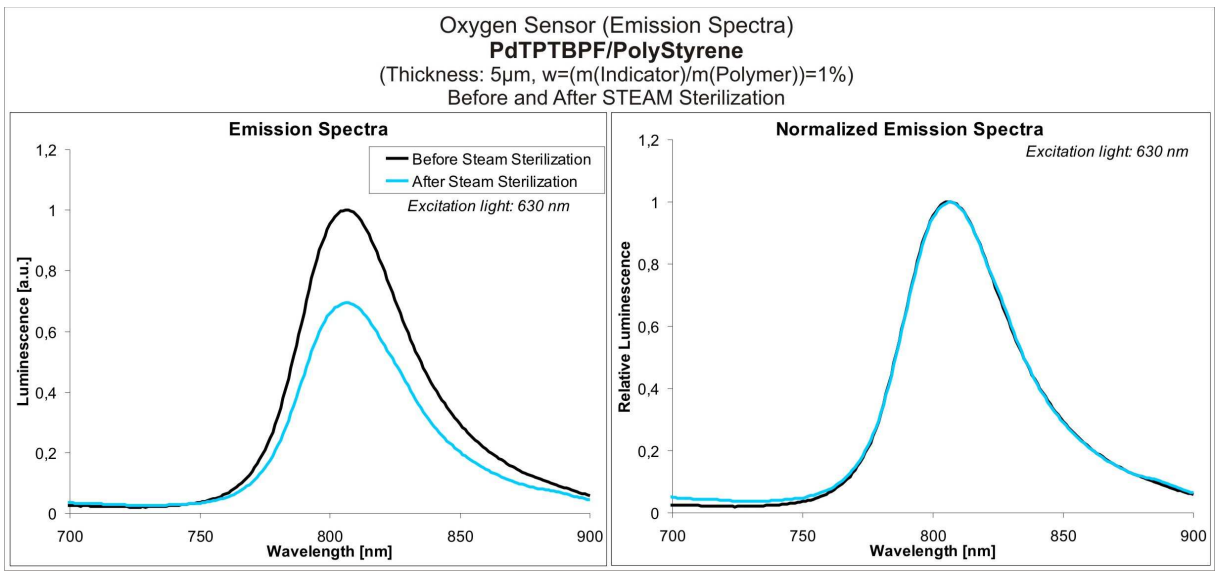

STEAM Sterilization	Absorption Spectra	Emission Spectra
Alterations in Absorption/Emission Intensity	7,80% decrease	30,50% decrease

Alterations in Absorption/Emission Curve Form	Polymer became slightly turbid after sterilization. Altered absorption curve form between 350-425 nm, 470-610 nm and 650-800 nm.	Unaltered.

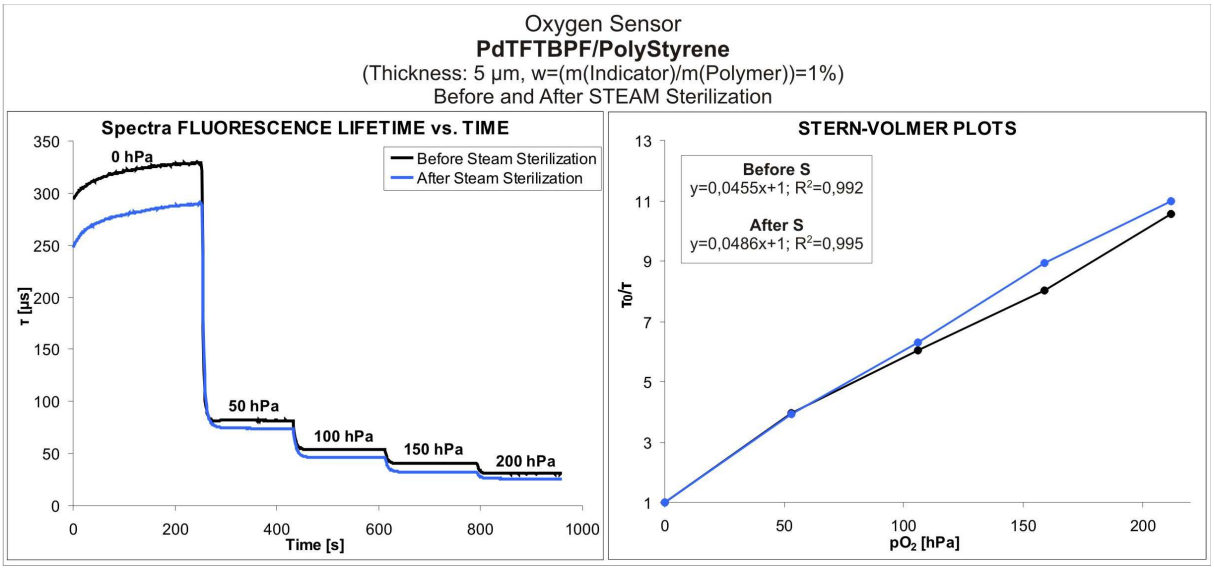

STEAM Sterilization	Luminescence Lifetime	Stern-Volmer Plot
Alterations in Luminescence Lifetime and Slope	12,31% decrease of τ_0	6,81% increase of slope
	11,00% decrease of τ at 50 hPa	
	15,83% decrease of τ at 100 hPa	
	21,29% decrease of τ at 150 hPa	
	15,91% decrease of τ at 200 hPa	

D.22 Ruthenium(II) DiPhenylPhenanthroline DiChloride ($Ru(dpp)_3Cl_2$) immobilized in Cellulose Acetate

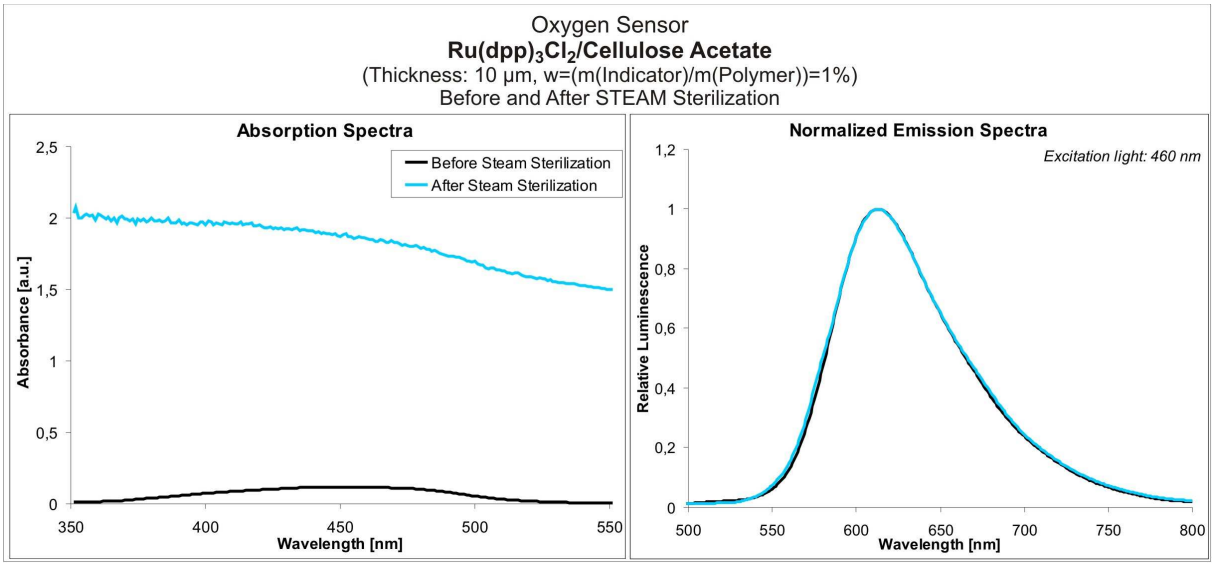

STEAM Sterilization	Absorption Spectra	Emission Spectra
Alterations in Absorption/Emission Intensity	Increase	65% increase

Alterations in Absorption/Emission Curve Form	Polymer became turbid after sterilization. Disappearance of the characteristic absorption curve form.	Unaltered.

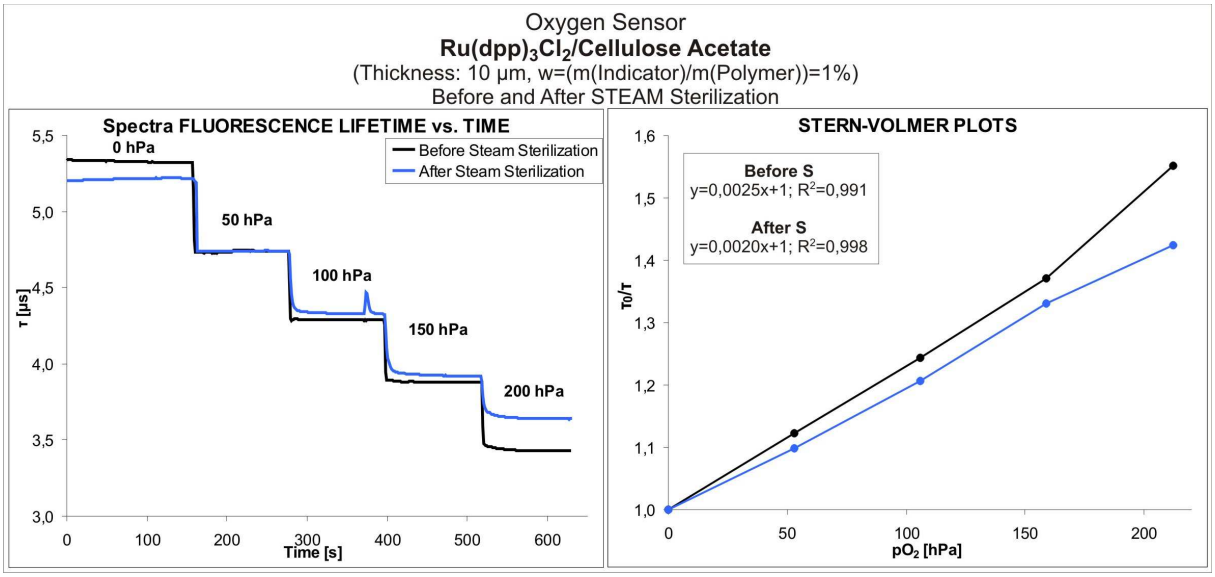

STEAM Sterilization	Luminescence Lifetime	Stern-Volmer Plot
Alterations in Luminescence Lifetime and Slope	2,63% decrease of τ_0	20,00% decrease of slope
	0,42% decrease of τ at 50 hPa	
	0,47% decrease of τ at 100 hPa	
	0,52% increase of τ at 150 hPa	
	6,12% increase of τ at 200 hPa	

D.23 Ruthenium(II) DiPhenylPhenanthroline DiChloride ($Ru(dpp)_3Cl_2$) immobilized in Ethyl Cellulose

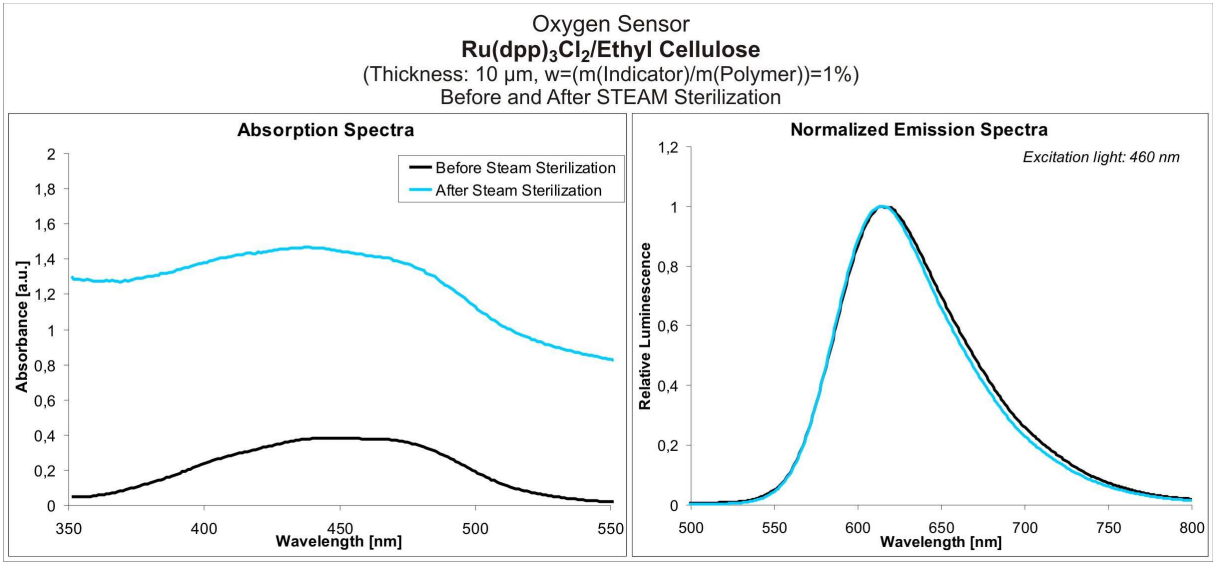

STEAM Sterilization	Absorption Spectra	Emission Spectra
Alterations in Absorption/Emission Intensity	Increase	115% increase
Alterations in Absorption/Emission Curve Form	Polymer became turbid after sterilization.	Altered emission curve form between 620-750 nm.

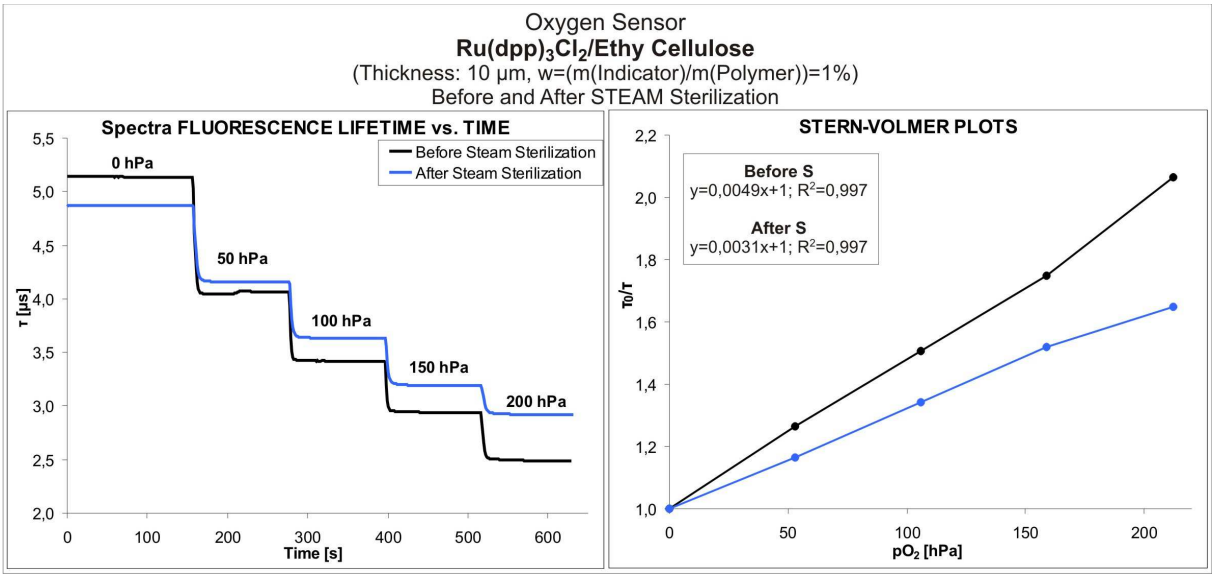

STEAM Sterilization	Luminescence Lifetime	Stern-Volmer Plot
Alterations in Luminescence Lifetime and Slope	6,24% decrease of τ_0	36,73% decrease of slope
	1,72% increase of τ at 50 hPa	
	5,28% increase of τ at 100 hPa	
	7,82% increase of τ at 150 hPa	
	17,27% increase of τ at 200 hPa	

D.24 Ruthenium(II) DiPhenylPhenanthroline DiChloride ($Ru(dpp)_3Cl_2$) immobilized in HydroGel D4/D7

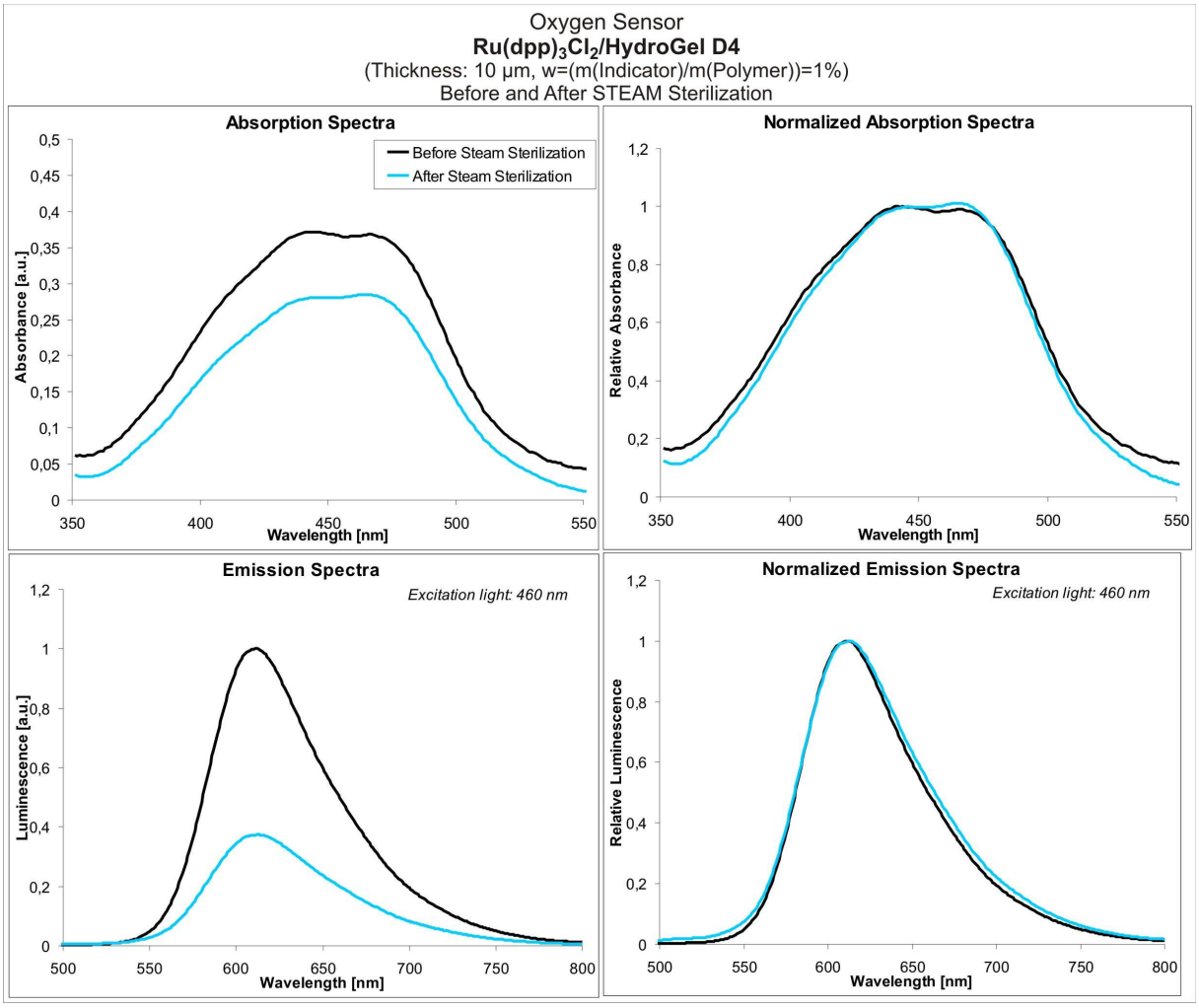

STEAMSterilization	Absorption Spectra	Emission Spectra
Alterations in Absorption/Emission Intensity	25,29% decrease	62,60% decrease
Alterations in Absorption/Emission Curve Form	Altered absorption curve form between 350-420 nm, 420-470 nm and 500-800 nm.	Altered emission curve form between 500-565 nm and 630-750 nm.

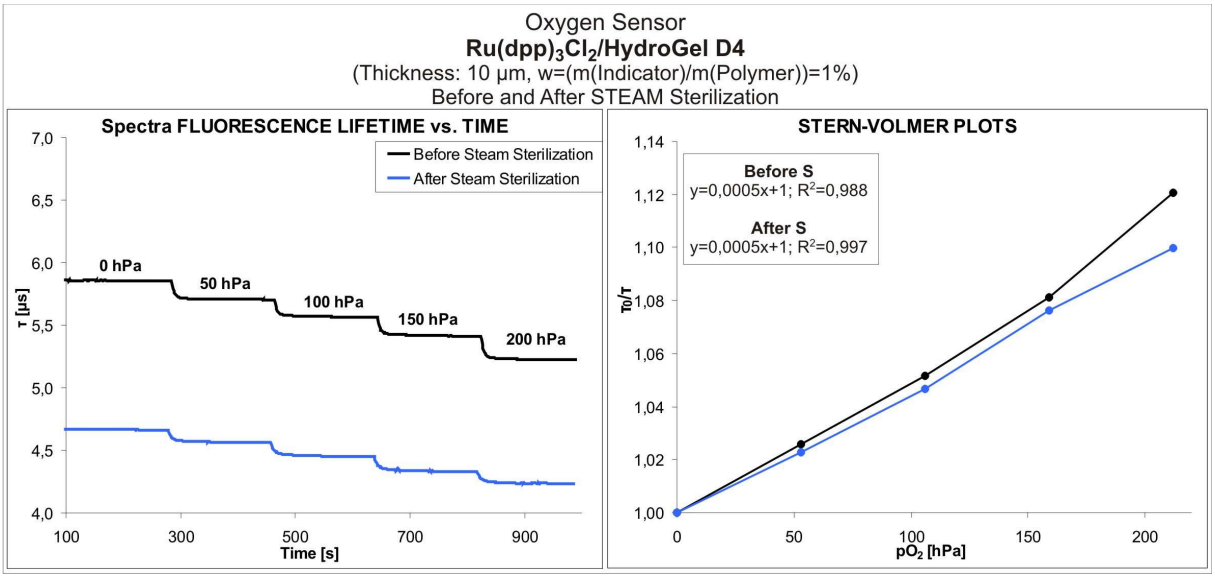

STEAM Sterilization	Luminescence Lifetime	Stern-Volmer Plot
Alterations in Luminescence Lifetime and Slope	20,34% decrease of τ_0	11,45% decrease of slope
	20,32% decrease of τ at 50 hPa	
	20,11% decrease of τ at 100 hPa	
	20,11% decrease of τ at 150 hPa	
	18,93% decrease of τ at 200 hPa	

D.25 Ruthenium(II) DiPhenylPhenanthroline DiChloride ($Ru(dpp)_3Cl_2$) immobilized in HydroThane5

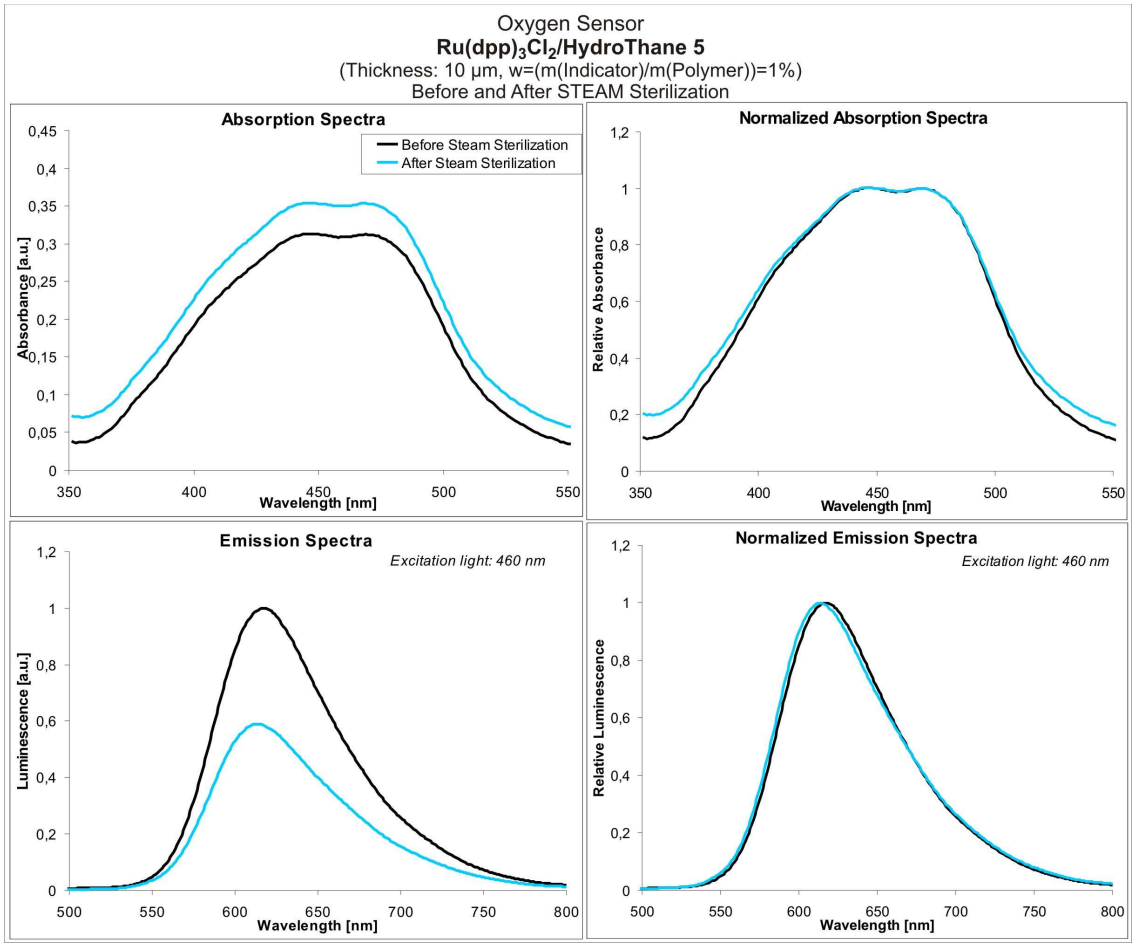

STEAMSterilization	Absorption Spectra	Emission Spectra
Alterations in Absorption/Emission Intensity	13,09% increase	41,02% decrease
Alterations in Absorption/Emission Curve Form	Polymer became slightly turbid after sterilization. Altered absorption curve form between 350-410 nm and 505-800 nm.	Hypsochromic shift of the emission curve maximum for 4 nm.

Oxygen Sensor
$Ru(dpp)_3Cl_2$/HydroThane 5
(Thickness: 10 µm, w=(m(Indicator)/m(Polymer))=1%)
Before and After STEAM Sterilization

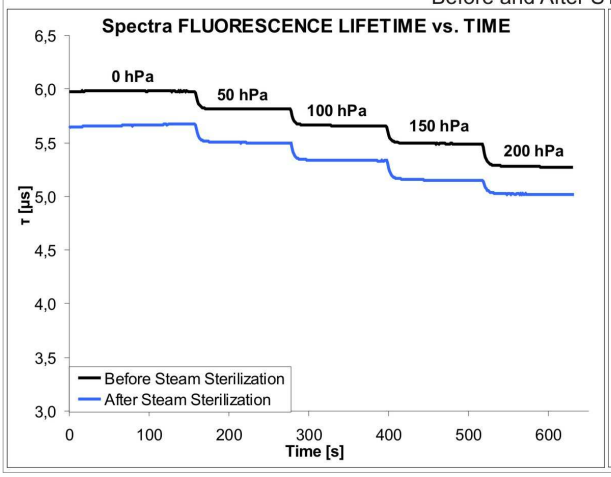

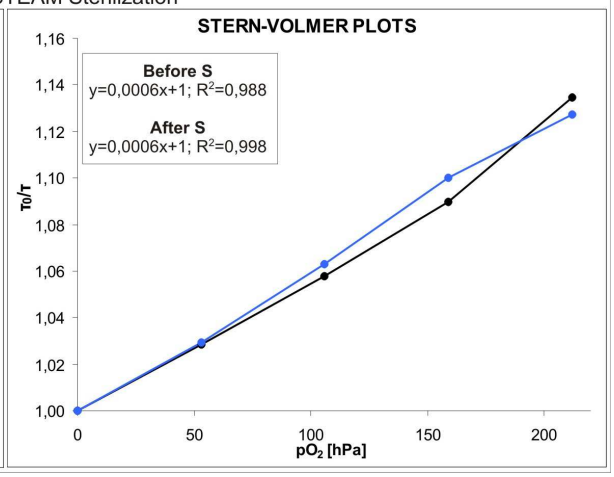

STEAM Sterilization	Luminescence Lifetime	Stern-Volmer Plot
Alterations in Luminescence Lifetime and Slope	5,52% decrease of τ_0	1,46% increase of slope
	5,67% decrease of τ at 50 hPa	
	6,01% decrease of τ at 100 hPa	
	6,38% decrease of τ at 150 hPa	
	4,92% decrease of τ at 200 hPa	

D.26 Ruthenium(II) DiPhenylPhenanthroline DiChloride ($Ru(dpp)_3Cl_2$) immobilized in PolySulfone

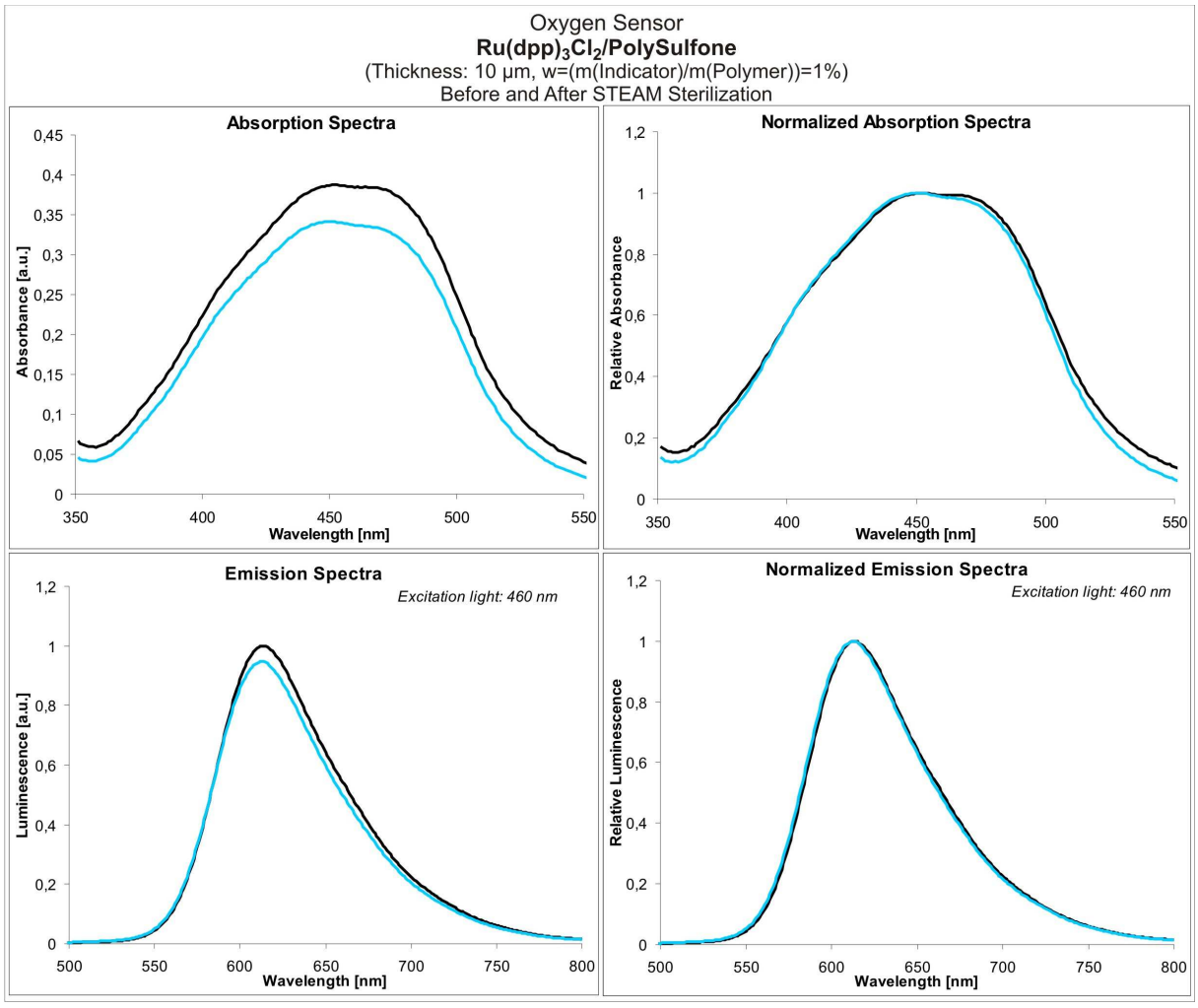

Sterilization with Ethylene Oxide	Absorption Spectra	Emission Spectra
Alterations in Absorption/Emission Intensity	11,92% decrease	5,19% decrease
Alterations in Absorption/Emission Curve Form	Altered absorption curve form between 350-380 nm, 465-495 nm and 510-800 nm.	Unaltered.

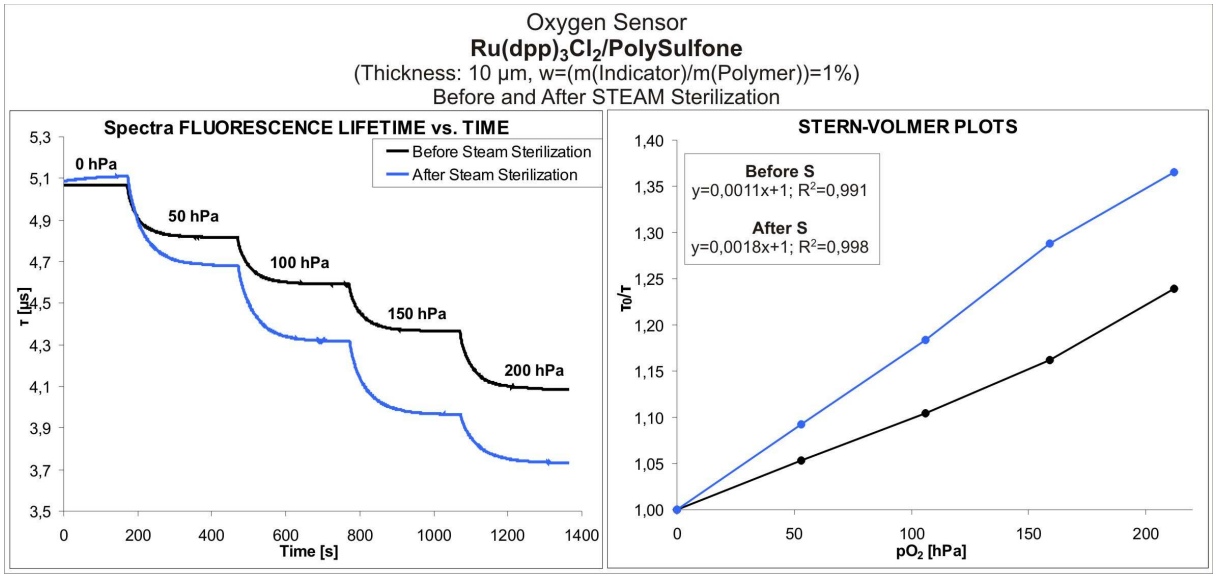

STEAM Sterilization	Luminescence Lifetime	Stern-Volmer Plot
Alterations in Luminescence Lifetime and Slope	0,78% increase of τ_0	63,64% increase of slope
	2,90% decrease of τ at 50 hPa	
	5,88% decrease of τ at 100 hPa	
	9,15% decrease of τ at 150 hPa	
	8,80% decrease of τ at 200 hPa	

D.27 Ruthenium(II) DiPhenylPhenanthroline DiChloride ($Ru(dpp)_3Cl_2$) immobilized in PolyPhenyl SilsesQuioxane

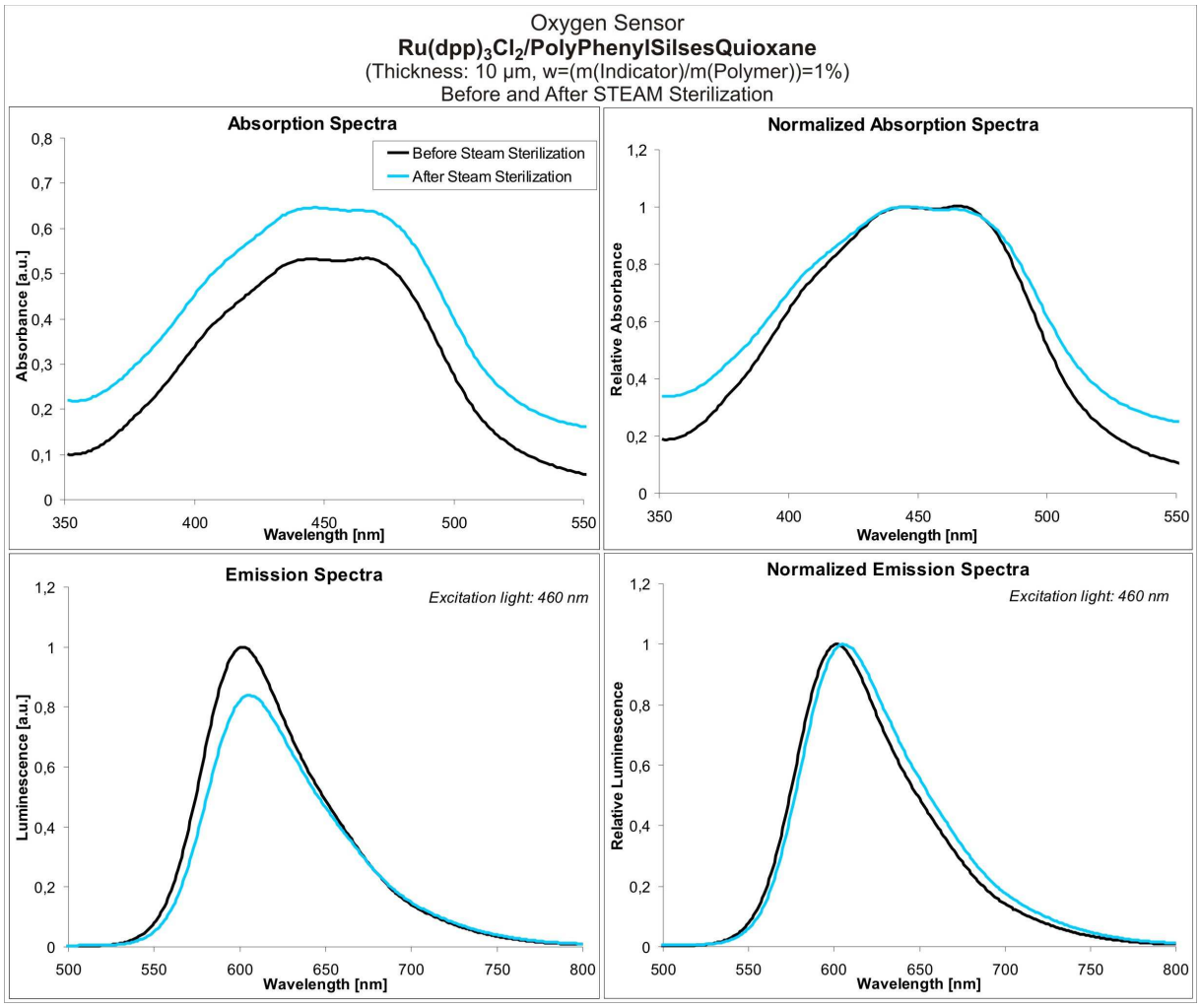

Sterilization with Ethylene Oxide	Absorption Spectra	Emission Spectra
Alterations in Absorption/Emission Intensity	17,51% increase	16,08% decrease
Alterations in Absorption/Emission Curve Form	Altered absorption curve form between 350-425 nm and 485-800 nm.	Bathochromic shift of emission maximum for 4 nm.

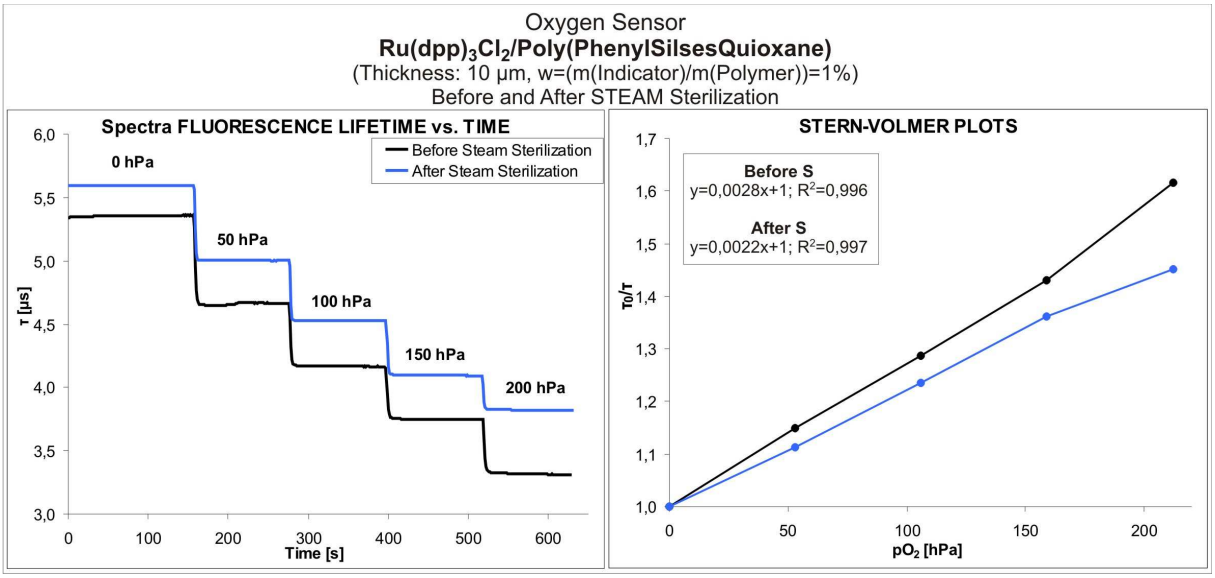

STEAM Sterilization	Luminescence Lifetime	Stern-Volmer Plot
Alterations in Luminescence Lifetime and Slope	3,36% increase of τ_0	21,43% decrease of slope
	6,65% increase of τ at 50 hPa	
	7,69% increase of τ at 100 hPa	
	8,53% increase of τ at 150 hPa	
	15,06% increase of τ at 200 hPa	

D.28 Ruthenium(II) DiPhenylPhenanthroline DiChloride ($Ru(dpp)_3Cl_2$) immobilized in PolyStyrene

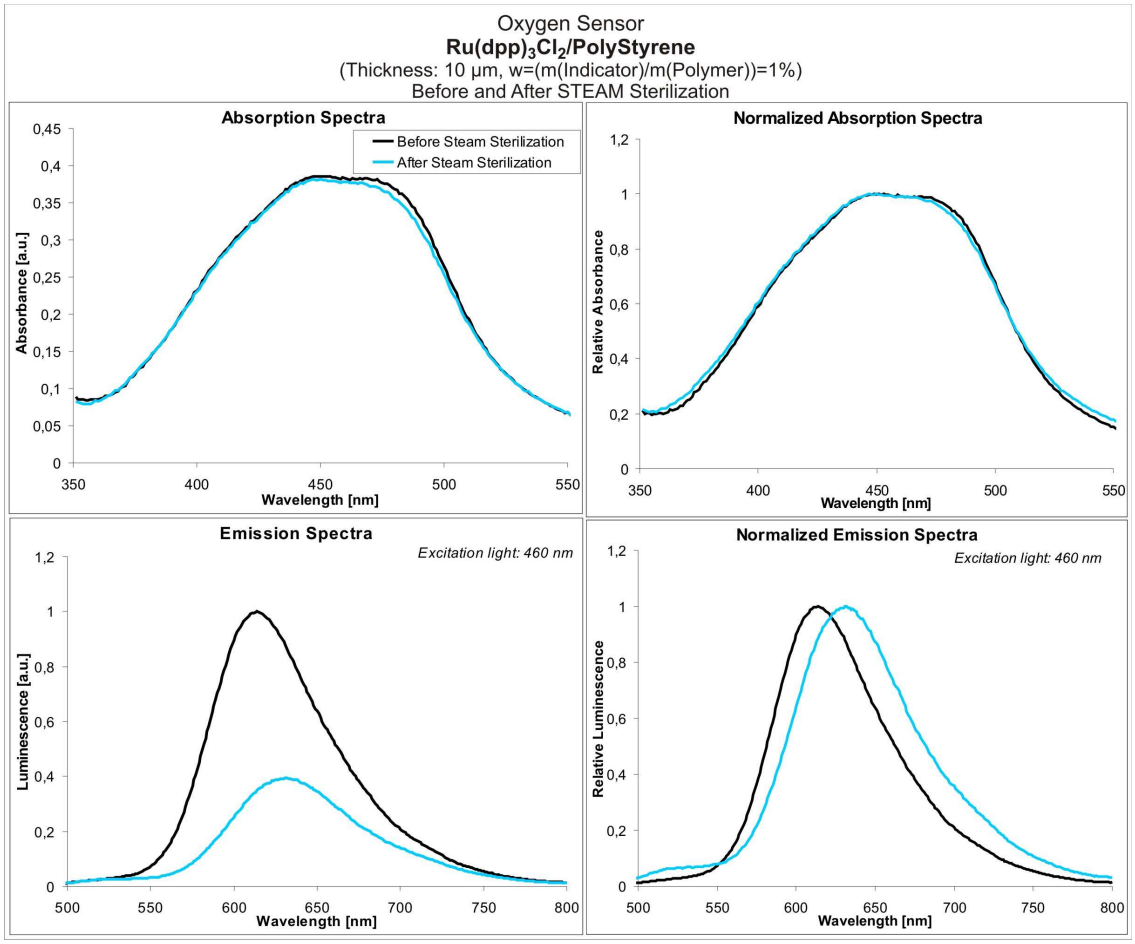

STEAM Sterilization	Absorption Spectra	Emission Spectra
Alterations in Absorption/Emission Intensity	1,45% increase	60,61% decrease
Alterations in Absorption/Emission Curve Form	Unaltered.	Bathochromic shift of the emission curve macimum for 18 nm.

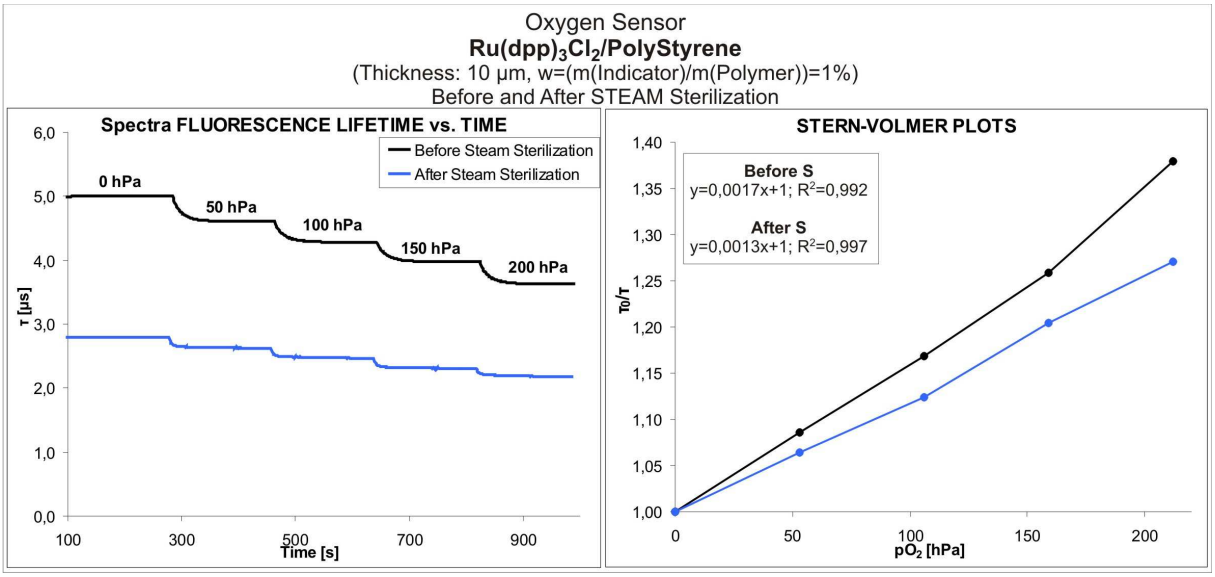

STEAM Sterilization	Luminescence Lifetime	Stern-Volmer Plot
Alterations in Luminescence Lifetime and Slope	44,60% decrease of τ_0	23,53% decrease of slope
	43,38% decrease of τ at 50 hPa	
	42,42% decrease of τ at 100 hPa	
	42,21% decrease of τ at 150 hPa	
	39,94% decrease of τ at 200 hPa	

D.29 Ruthenium(II) DiPhenylPhenanthroline DiChloride ($Ru(dpp)_3Cl_2$) immobilized in PolyStyrene-co-Acrylonitrile

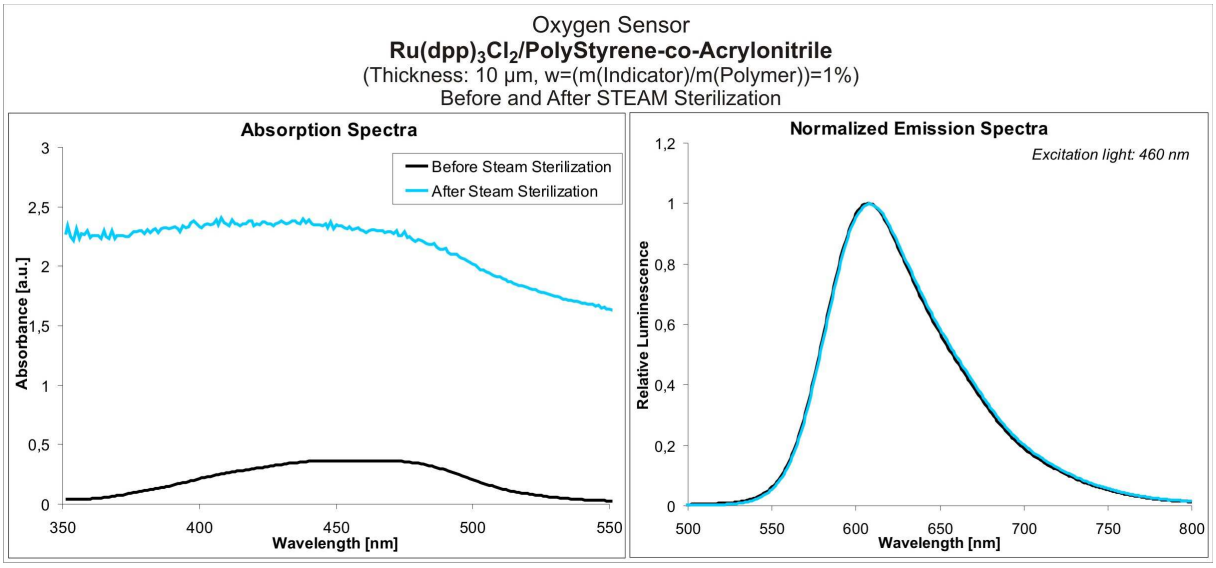

STEAM Sterilization	Absorption Spectra	Emission Spectra
Alterations in Absorption/Emission Intensity	Increase	85,94% increase

Alterations in Absorption/Emission Curve Form	Disappearance of characteristic absorption curve form. .	Unaltered

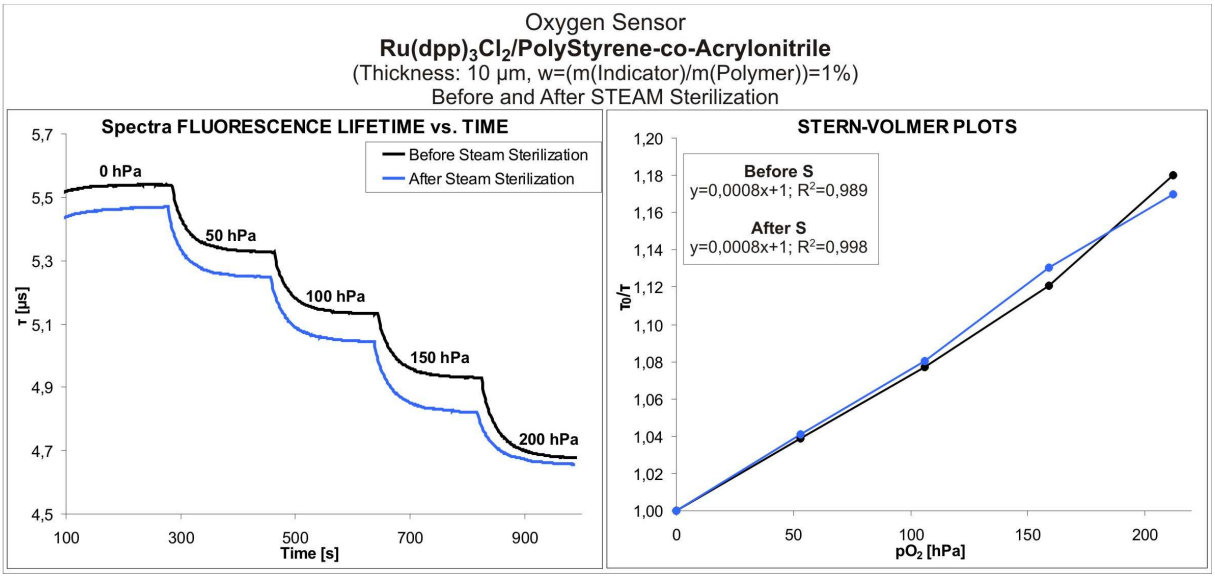

STEAM Sterilization	Luminescence Lifetime	Stern-Volmer Plot
Alterations in Luminescence Lifetime and Slope	1,62% decrease of τ_0	0,43% decrease of slope
	1,69% decrease of τ at 50 hPa	
	1,75% decrease of τ at 100 hPa	
	2,23% decrease of τ at 150 hPa	
	0,43% decrease of τ at 200 hPa	

D.30 Ruthenium(II) DiPhenylPhenanthroline DiChloride ($Ru(dpp)_3Cl_2$) immobilized in PolyStyrene-co-MaleicAnhydride (PSMA93)

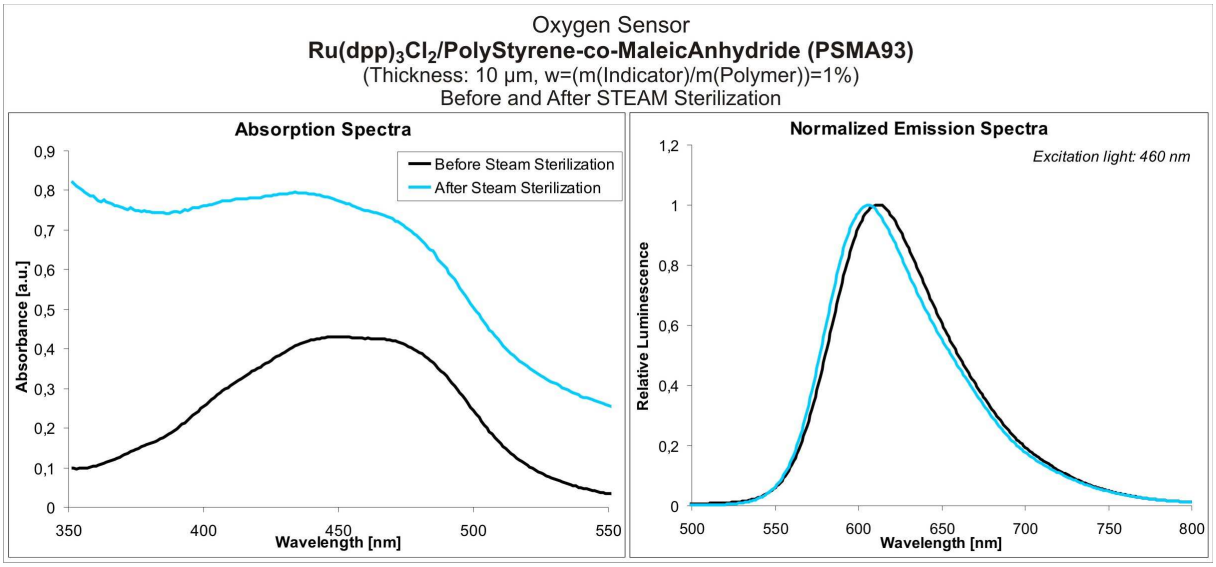

Sterilization with Ethylene Oxide	Absorption Spectra	Emission Spectra
Alterations in Absorption/Emission Intensity	Increase	28,52% increase
Alterations in Absorption/Emission Curve Form	Disappearance of characteristic absorption curve form. .	Hypsochromic shift of the emission maximum for 7 nm.

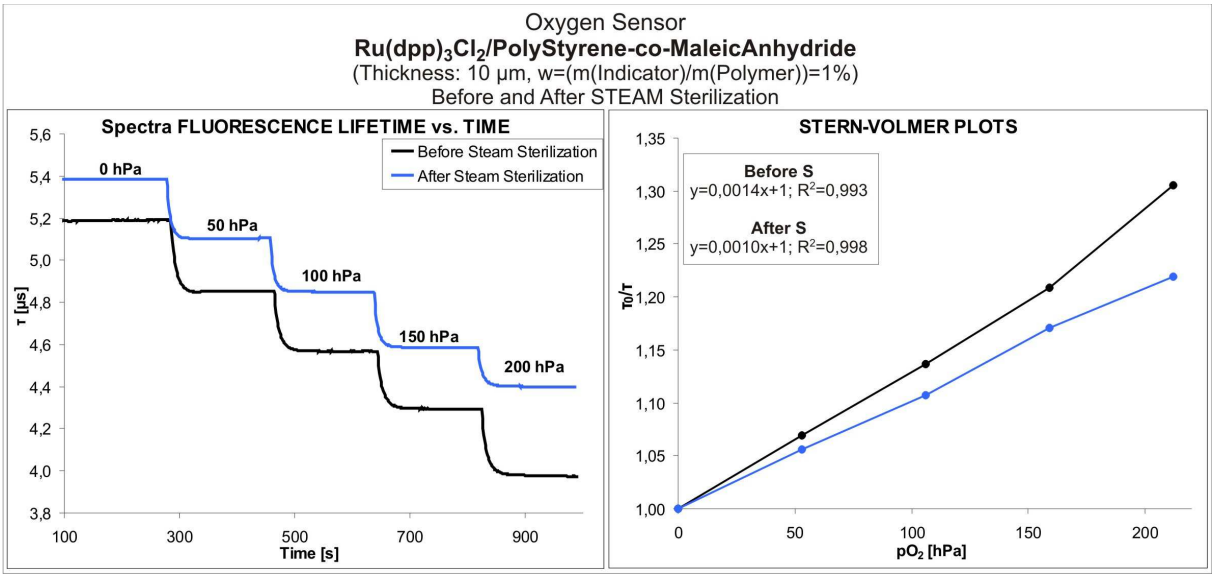

STEAM Sterilization	Luminescence Lifetime	Stern-Volmer Plot
Alterations in Luminescence Lifetime and Slope	3,28% increase of τ_0	28,57% decrease of slope
	4,54% increase of τ at 50 hPa	
	5,91% increase of τ at 100 hPa	
	6,51% increase of τ at 150 hPa	
	10,55% increase of τ at 200 hPa	

Optical pH SENSORS

D.31 HPTS(DHA$_3$) immobilized in HydroGel D4

Absorption Spectra

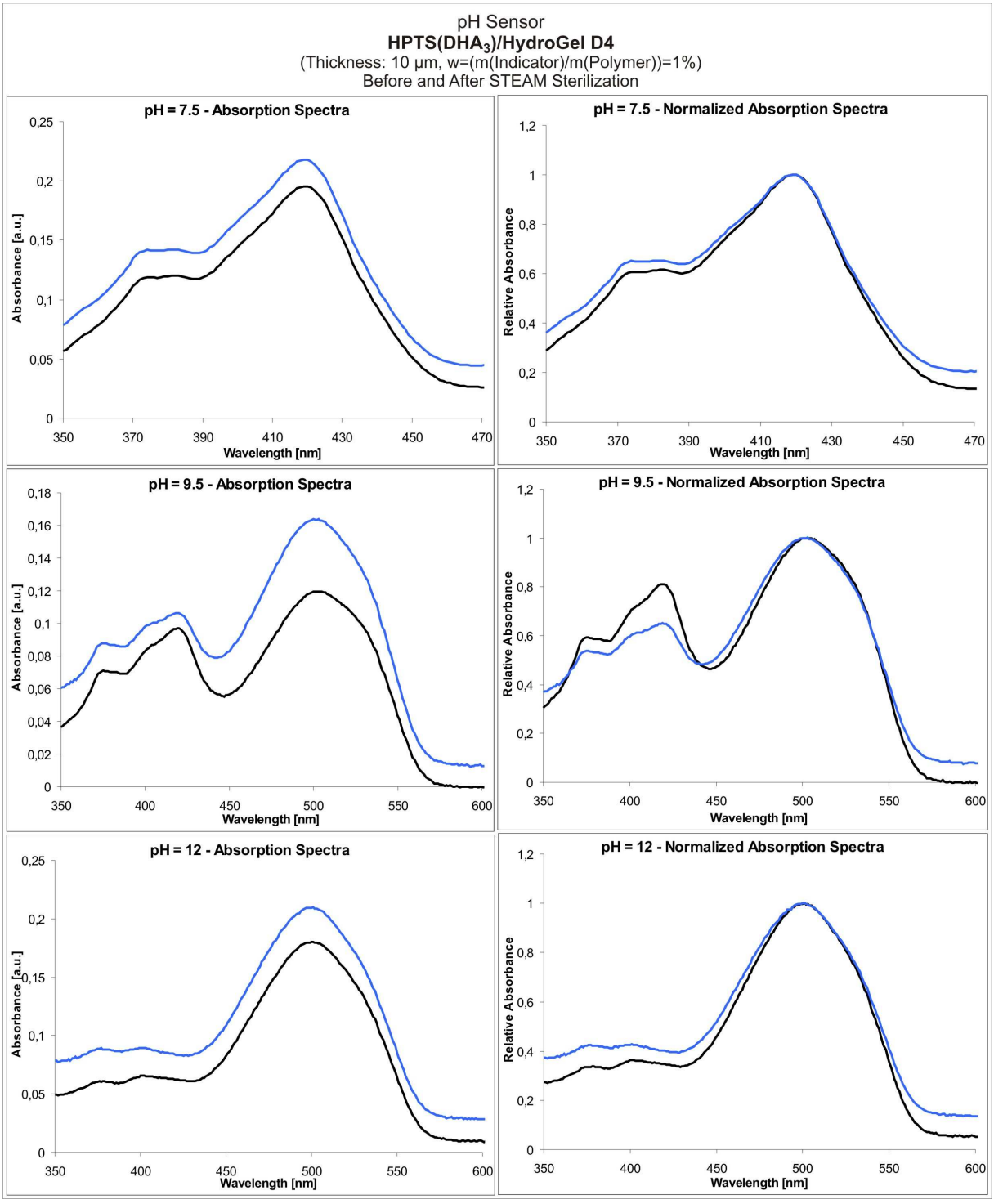

Emission Spectra

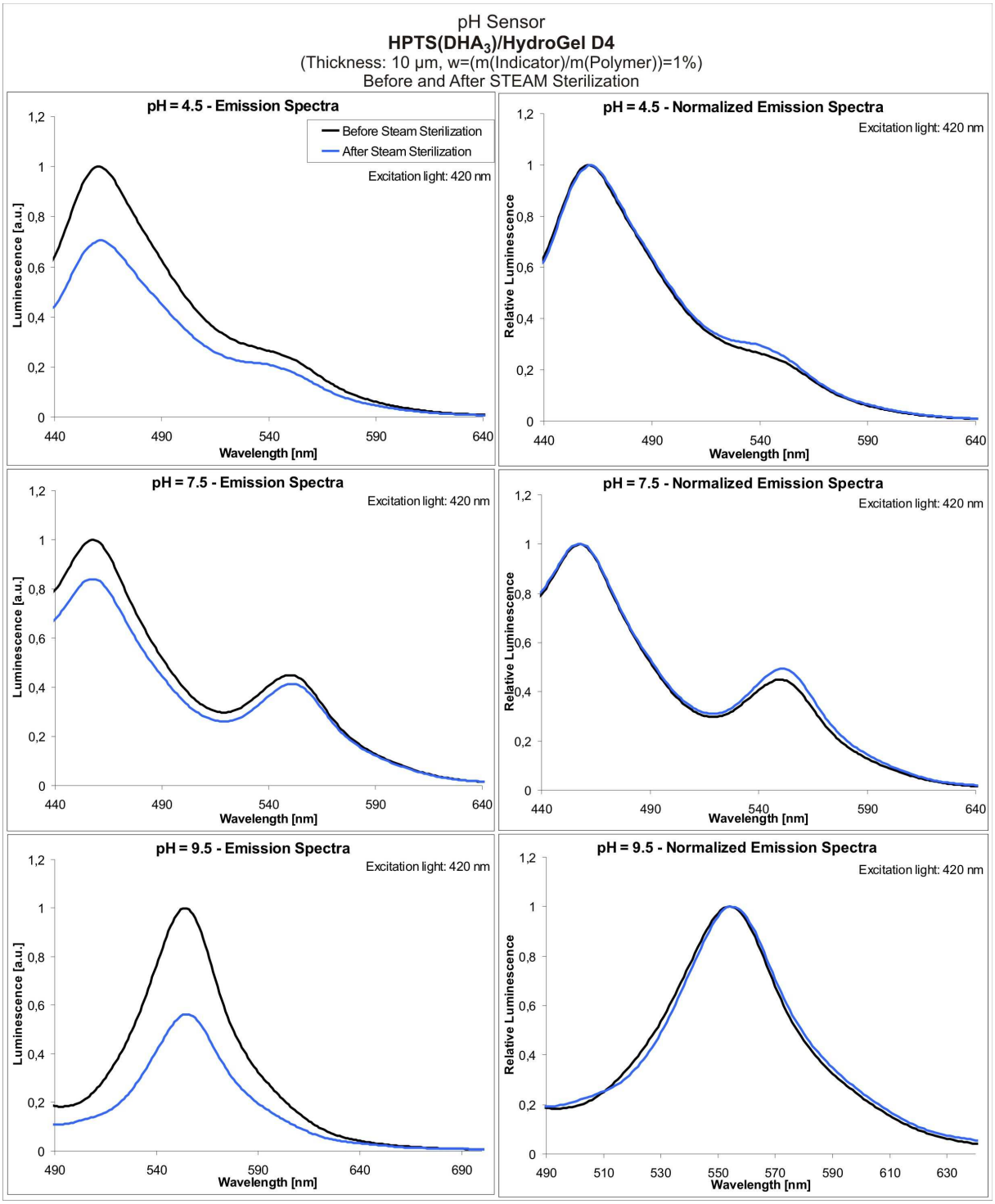

STEAM S.	Absorption Spectra			Emission Spectra		
		pH	Alterations		pH	Alterations
Alterations in Absorption/ Emission Intensity	AFTER S	4.5	15,42% Increase	AFTER S	4.5	29,38% decrease
		7.5	10,28% Increase		7.5	16,08% decrease
		9.5	26,94% Increase		9.5	43,68% decrease

Alterations in Absorption/ Emission Curve Form	AFTER S	4.5	Altered absorption between 350-410 nm and 440-800 nm. The sensor became turbid after sterilization.	AFTER S	4.5	Altered emission between 510-560 nm.
		7.5	Altered absorption between 350-490 nm and 550-800 nm. The ratio between protonation/deprotonation emission peaks is altered. The sensor became turbid after sterilization.		7.5	The ratio between protonation/deprotonation emission peaks is altered.
		9.5	Altered absorption between 350-490 nm and 550-800 nm. The sensor became turbid after sterilization.		9.5	Altered emission between 490-550 nm and 580-650 nm.

Calibration Curves

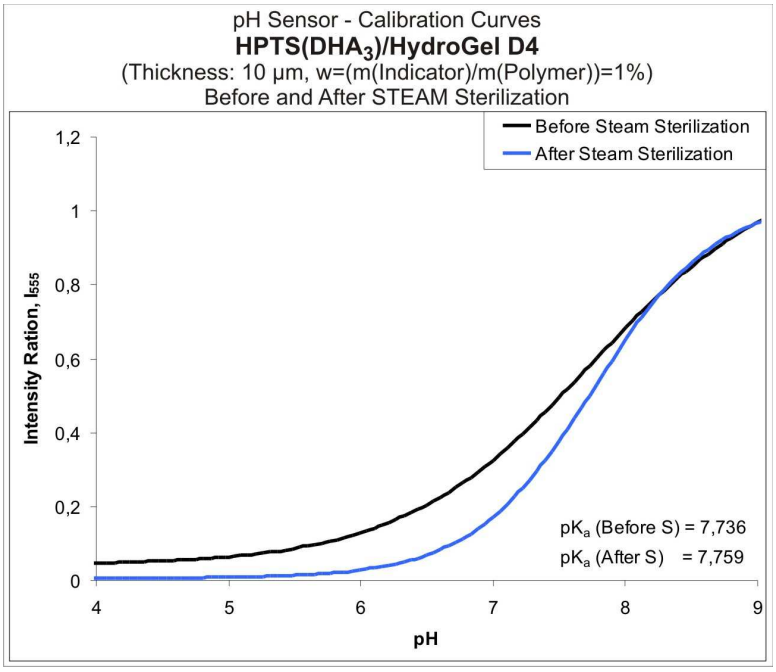

STEAM S.	Alterations in Calibration Curve Shape	Alterations in pK_a
	Altered curve shape after sterilization. The response to the proton still observed – re-calibration of sensor response.	Increase of pK_a (for 0,023)

D.32 2´,7´-DiHexylFluorescein OctadecylEster immobilized in HydroMed Hydrogel D4

Absorption Spectra

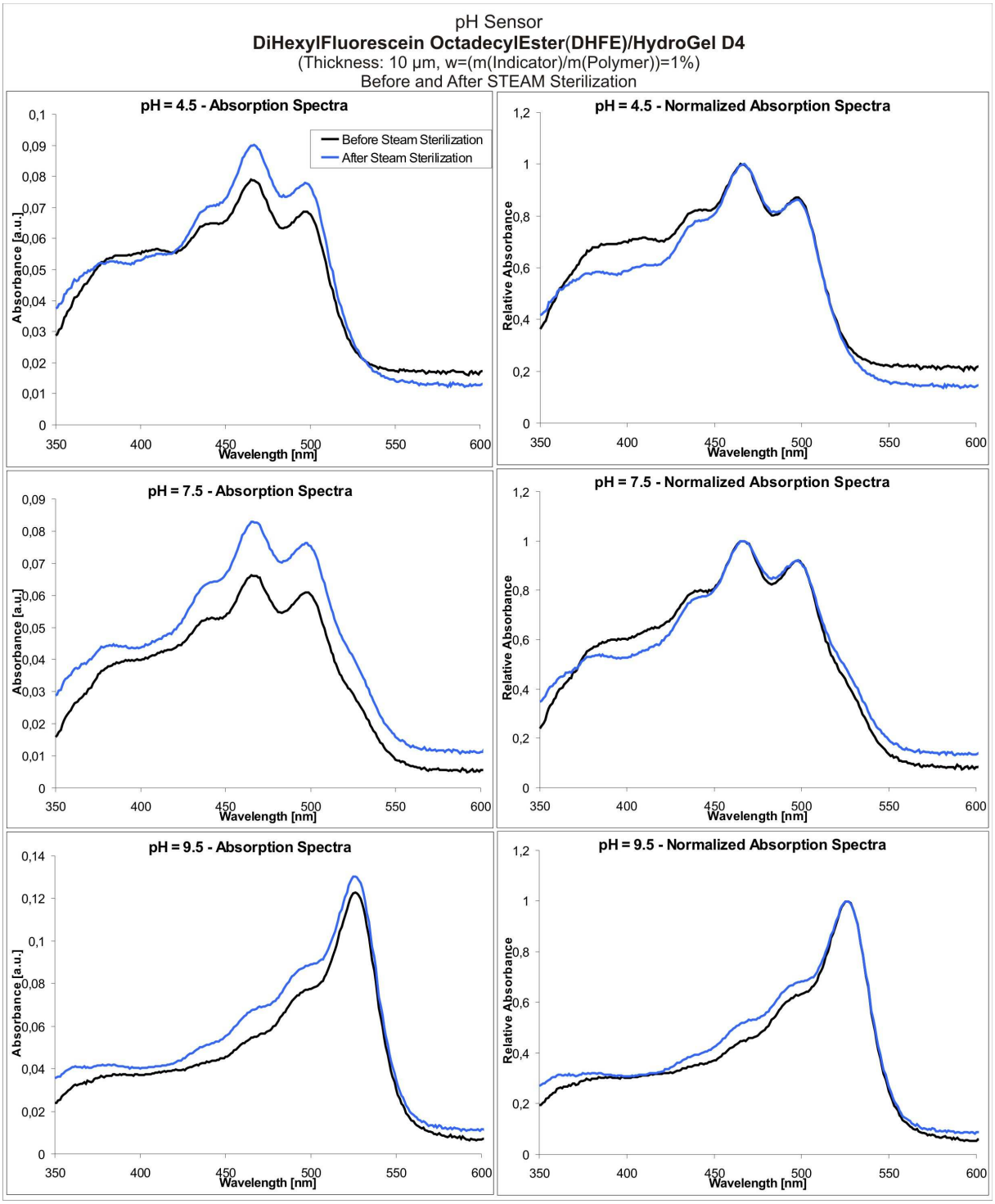

Emission Spectra

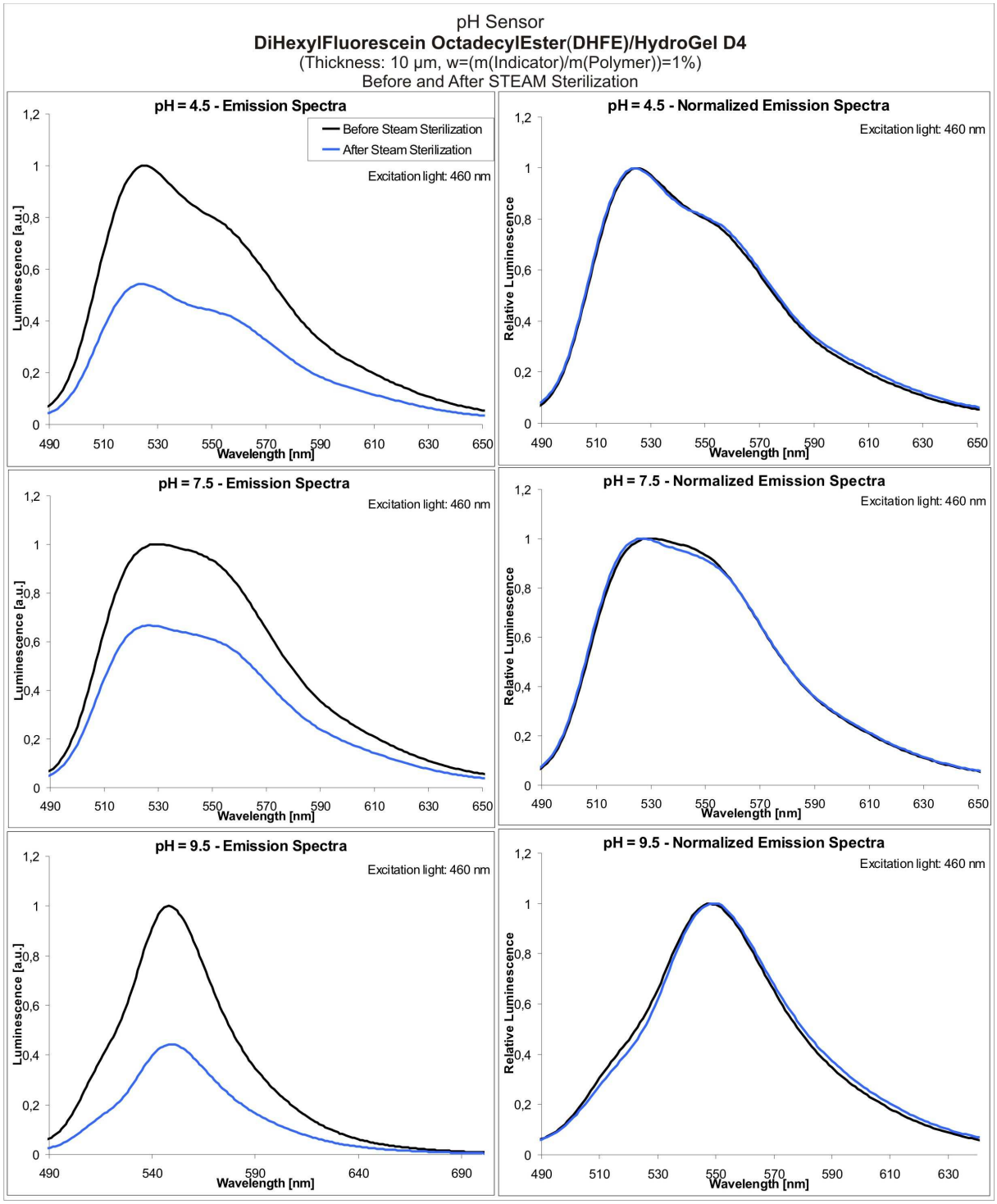

STEAM S.	Absorption Spectra			Emission Spectra		
		pH	Alterations		pH	Alterations
Alterations in Absorption/ Emission Intensity	AFTERS	4.5	12,49% Increase	AFTERS	4.5	45,69% decrease
		7.5	20,20% Increase		7.5	33,32% decrease
		9.5	5,89% Increase		9.5	55,59% decrease

Alterations in Absorption/ Emission Curve Form	AFTER S	4.5	Altered absorption between 350-450 nm and 525-800 nm. The sensor became slightly turbid after sterilization.	AFTER S	4.5	Unaltered.
		7.5	Altered absorption between 350-450 nm and 520-800 nm. The sensor became slightly turbid after sterilization.		7.5	Altered emission between 530-560 nm.
		9.5	Altered absorption between 350-400 nm, 420-510 and 520-800 nm. The sensor became slightly turbid after sterilization.		9.5	Altered emission between 500-540 nm and 570-630 nm.

Calibration Curves

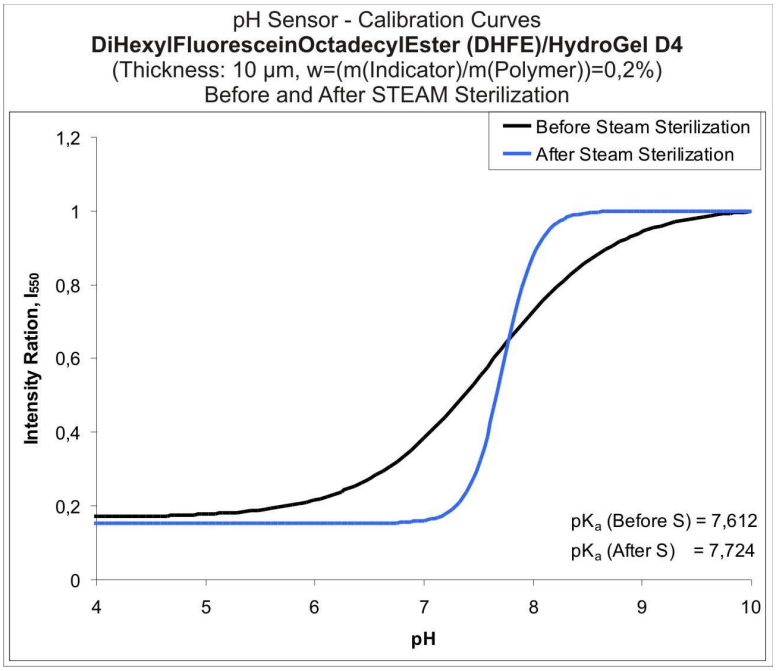

STEAM S.	Alterations in Calibration Curve Shape	Alterations in pK_a
	Altered curve shape after sterilization. The response to the proton still observed – re-calibration of sensor response.	Increase of pK_a (for 0,112)

D.33 2´,7´-DiHexylFluorescein OctadecylEster immobilized in Poly(2-HydroxyEthyl MethAcrylate) (=pHEMA)

Poly(2-HydroxyEthyl MethAcrylate) (=pHEMA) melts after steam sterilization.

D.34 2´,7´-DiHexyl-N-Octadecyl-CarboxAmidoFluorescein (=DHFA) immobilized in HydroMed Hydrogel D4

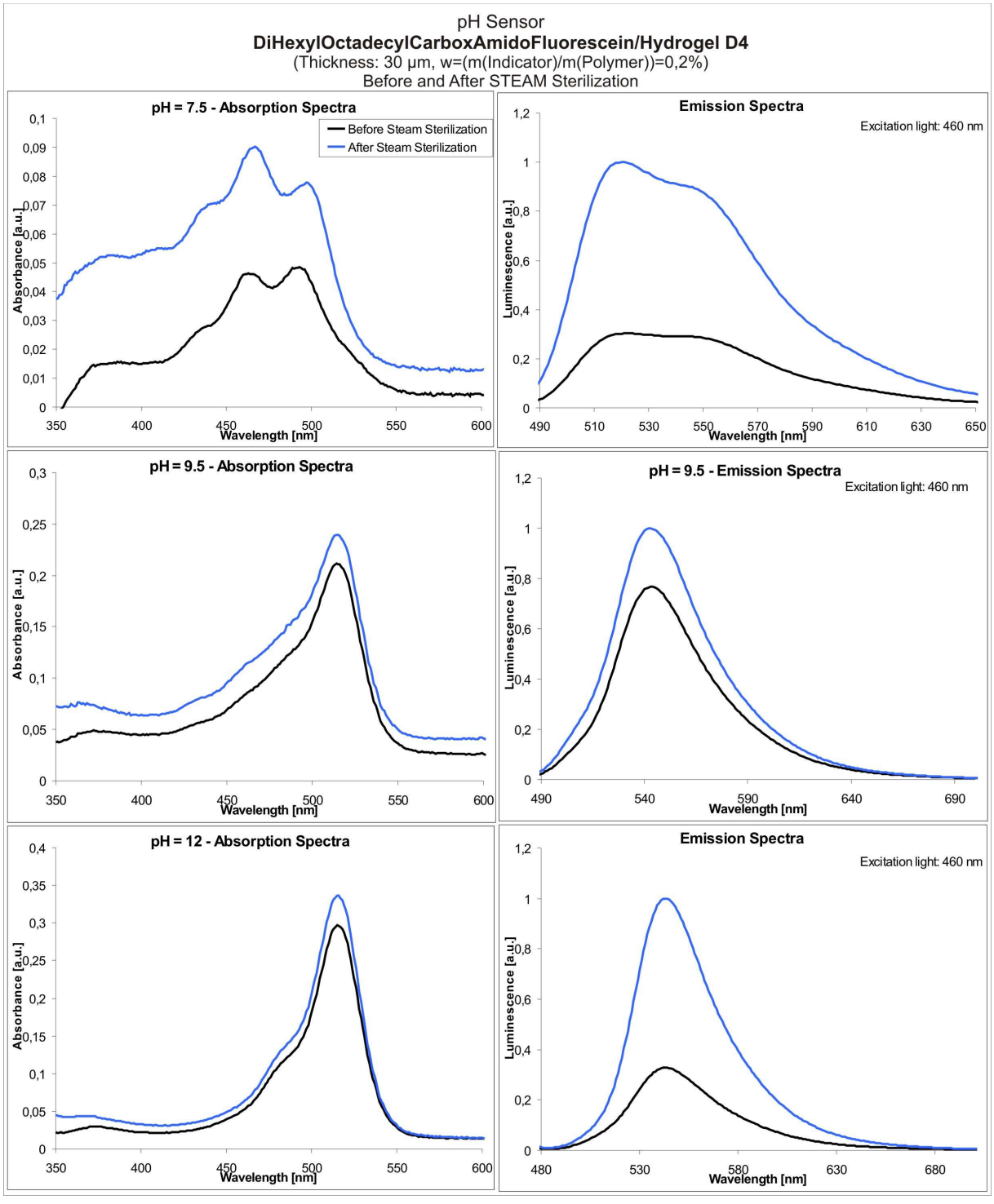

STEAM S.	Absorption Spectra			Emission Spectra		
		pH	Alterations		pH	Alterations
Alterations in Absorption/ Emission Intensity	AFTER S	7.5	53,18% Increase	AFTER S	7.5	230% increase
		9.5	11,73% Increase		9.5	30% increase
		12	11,70% Increase		12	200% increase
Alterations in Absorption/ Emission Curve Form	AFTER S	7.5	Altered absorption curve form. The sensor became turbid after sterilization.	AFTER S	7.5	Altered emission curve form between 525-700 nm.
		9.5	Altered absorption curve form between 350-500 nm and 550-800 nm. The sensor became slightly turbid after sterilization.		9.5	Altered emission curve form between 490-530 nm.
		12	Altered absorption curve form between 350-460 nm. The sensor became slightly turbid after sterilization.		12	Altered emission curve form between 520-530 nm and 560-660 nm.

Calibration Curves

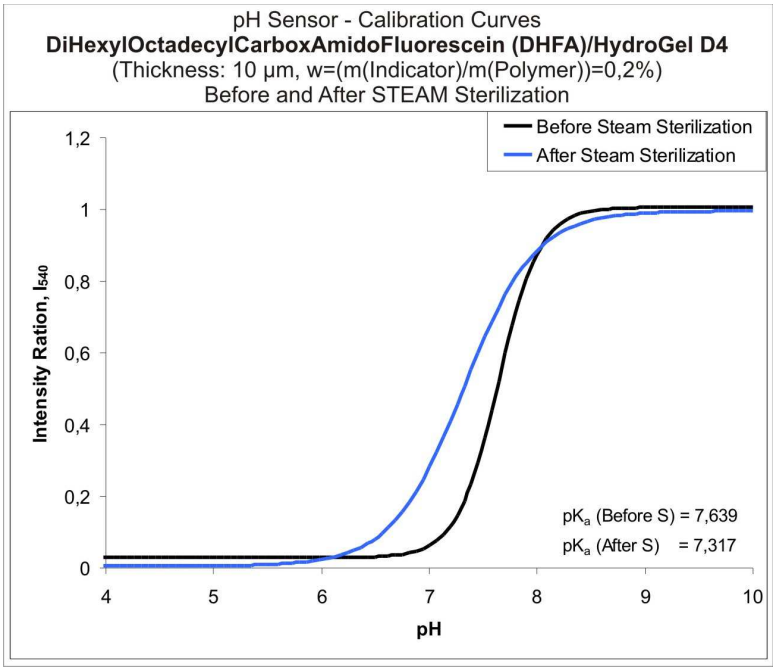

STEAM S.	Alterations in Calibration Curve Shape	Alterations in pK_a
	Altered curve shape after sterilization. The response to the proton still observed – re-calibration of sensor response.	Decrease of pK_a (for 0,322)

D.35 pH Sensitive Coumarin immobilized in HydroMed Hydrogel D4

Absorption Spectra

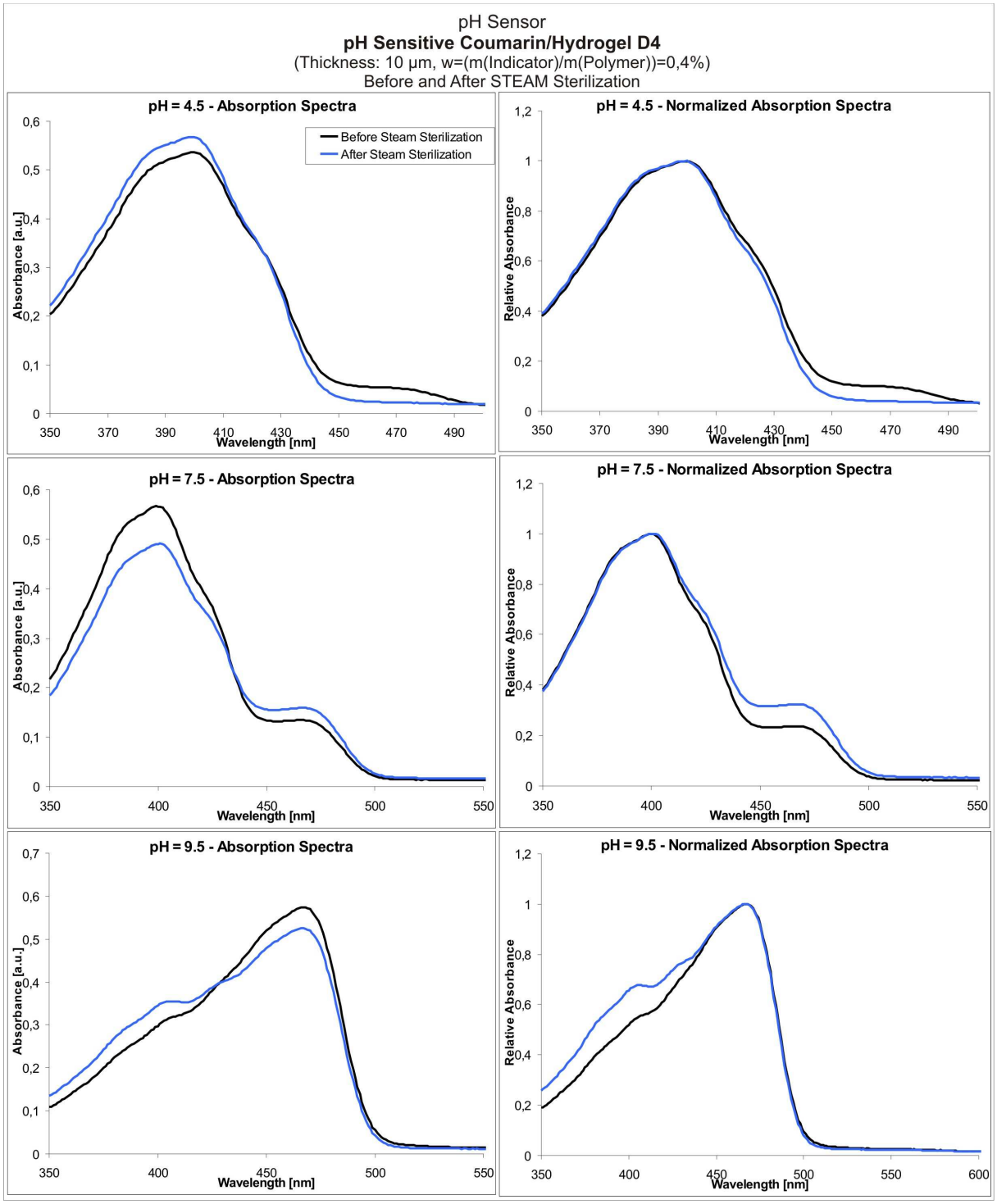

Emission Spectra

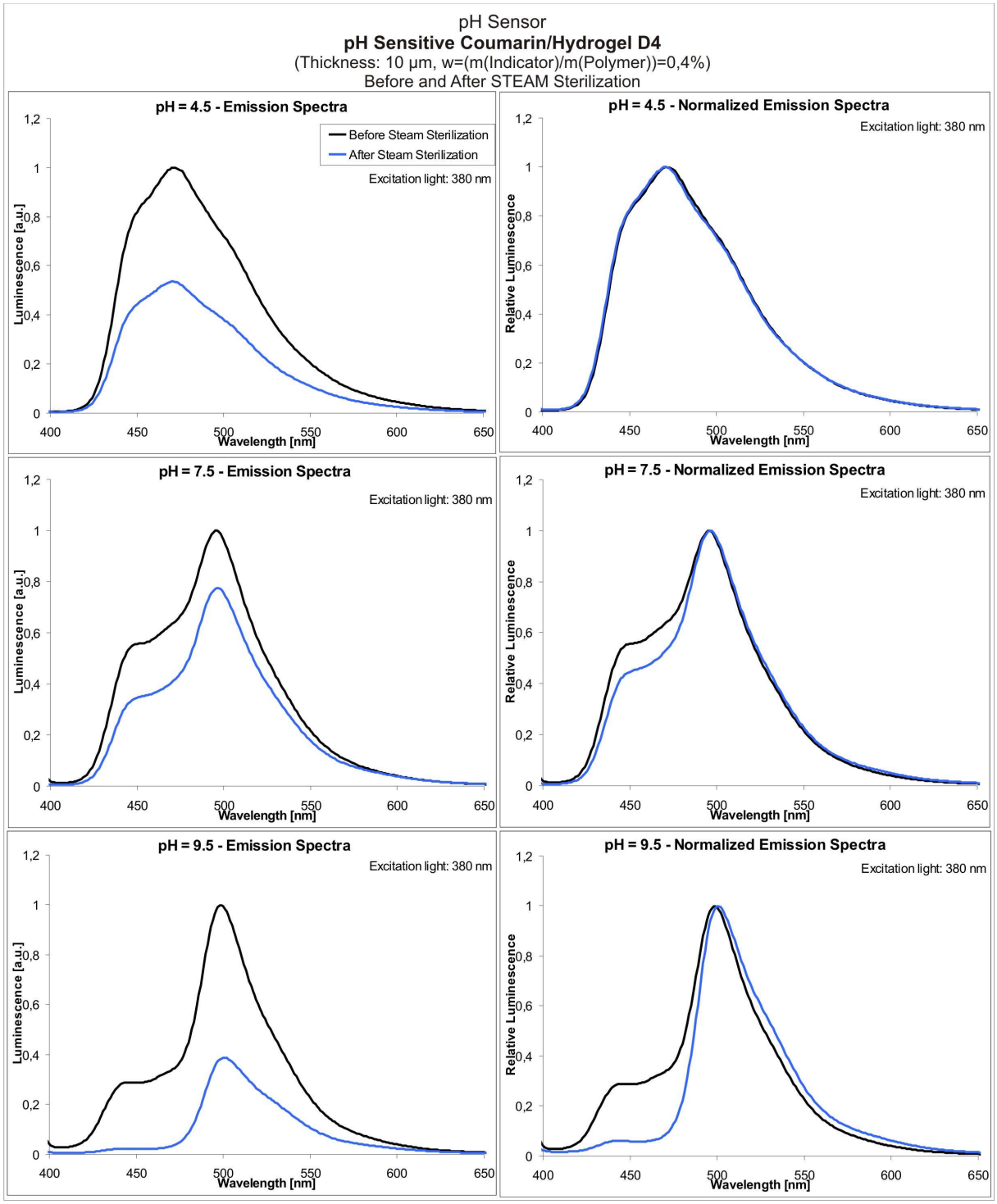

STEAM S.	Absorption Spectra			Emission Spectra		
		pH	Alterations		pH	Alterations
Alterations in Absorption/ Emission Intensity	AFTER S	7.5	5,54% Increase	AFTER S	7.5	46,43% decrease
		9.5	13,47% decrease		9.5	22,46% decrease
		12	8,48% decrease		12	61,25% decrease

Alterations in Absorption/ Emission Curve Form	AFTER S	7.5	Altered absorption curve form between 410-500 nm. The sensor became slightly turbid after sterilization.	AFTER S	7.5	Unaltered.
		9.5	The ratio between protonation/deprotonation absorption peaks is altered.		9.5	Altered emission curve form between 400-490 nm.
		12	Altered absorption curve form between 350-440 nm.		12	Altered emission curve form between 400-490 nm. Bathochromic shift of the emission maximum for 2 nm.

Calibration Curves

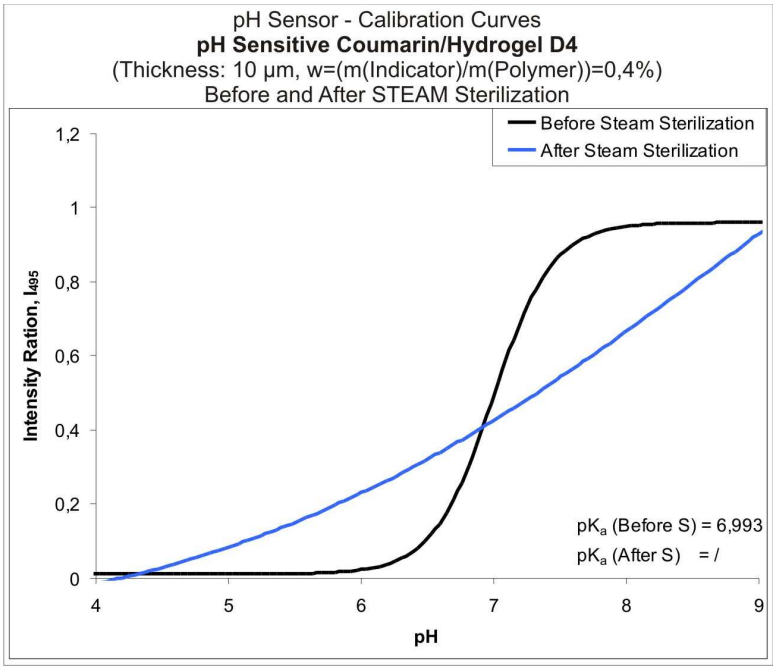

GAMMA S.	Alterations in Calibration Curve Shape	Alterations in pK_a
	Greatly altered curve shape after sterilization.	/

D.36 PET Perylene BisImide immobilized in HydroMed Hydrogel D4

Absorption Spectra

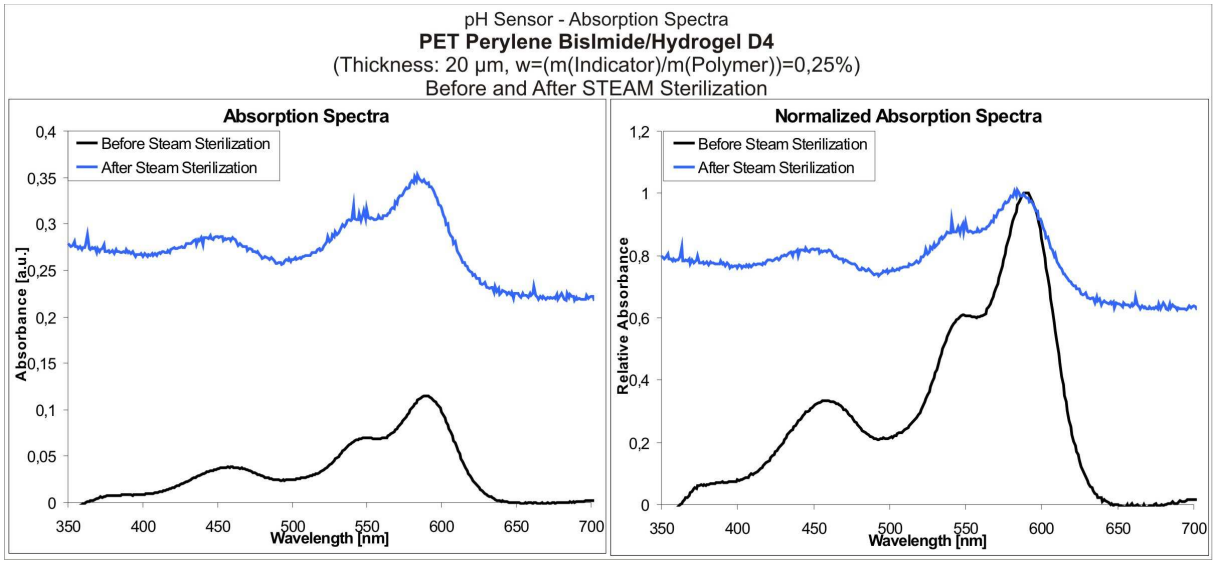

STEAM Sterilization	Absorption Spectra
Alterations in Absorption/Emission Intensity	200% increase
Alterations in Absorption/Emission Curve Form	Polymer became turbid after sterilization.

Emission Spectra

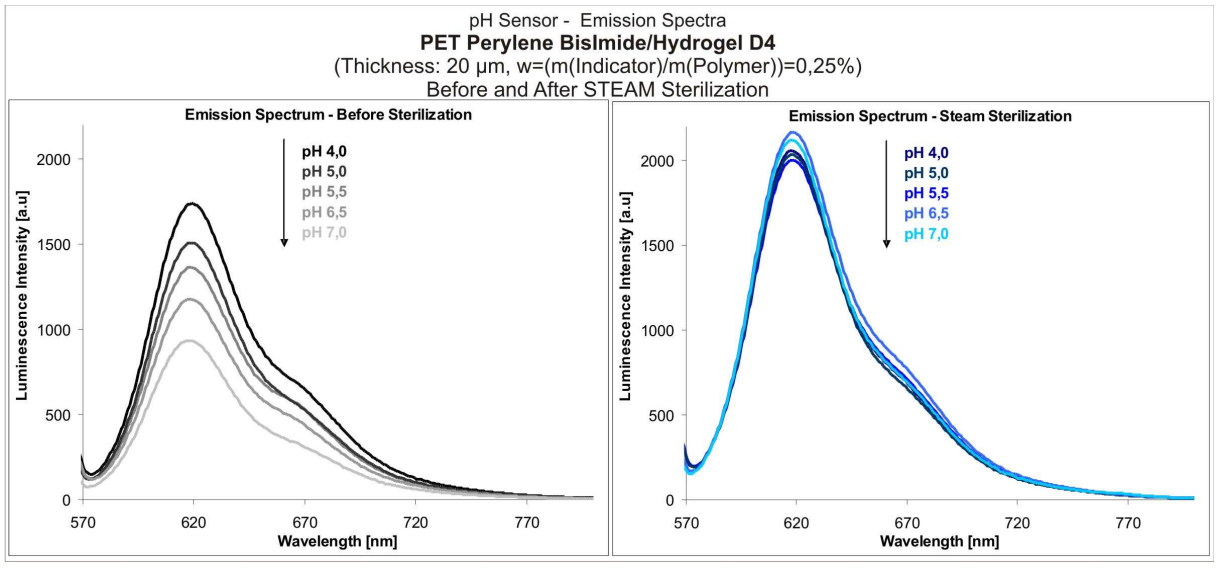

STEAM S	Emission Spectra					
	Decrease of the Luminescence Intensity in dependence of the Intensity at lower pH			Decrease of the Luminescence Intensity at define pH in dependence of the Intensity Before Sterilization		
BEFORE S	**pH**	**Max. Intensity**				
Alterations in Absorption/ Emission Intensity	4	1739	/			
	5	1509	13,22% decrease			
	5.5	1363	21,62% decrease			
	6.5	1176	32,37% decrease			
	7	933,6	46,31% decrease			
PET Efficiency	1.86					
AFTER S	**pH**	**Max. Intensity**		**pH**	**Compared Intensity**	
Alterations in Absorption/ Emission Intensity	4	2059	/	4	1739	18,40% increase
	5	2002	2,77% decrease	5	1509	32,67% increase
	5.5	2034	1,21% decrease	5.5	1363	49,23% increase
	6.5	2168	5,29% increase	6.5	1176	84,35% increase
	7	2120	2,96% decrease	7	933,6	127% increase

Calibration Curves

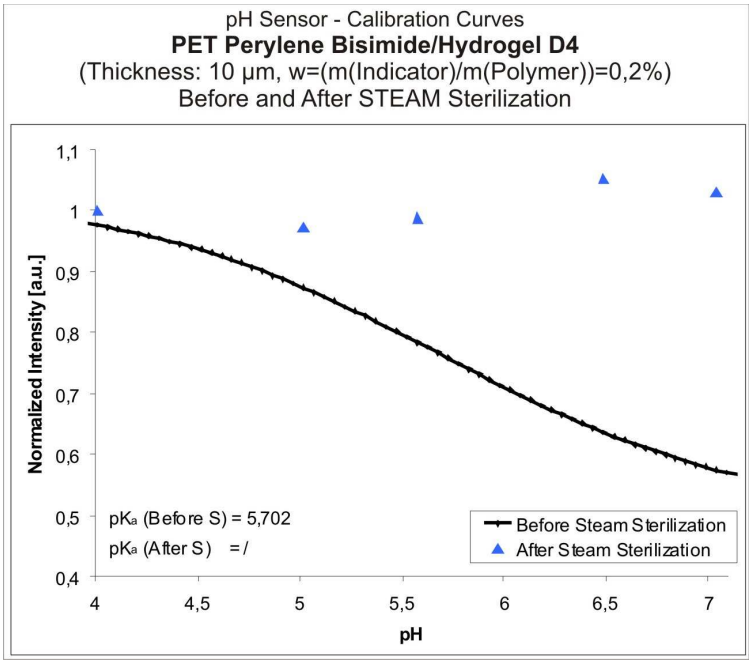

STEAM S.	Alterations in Calibration Curve Shape	Alterations in pK_a
	The calibration curve no longer observed.	

D.37 BromoPhenol Blue immobilized in HydroMed Hydrogel D4

Absorption Spectra

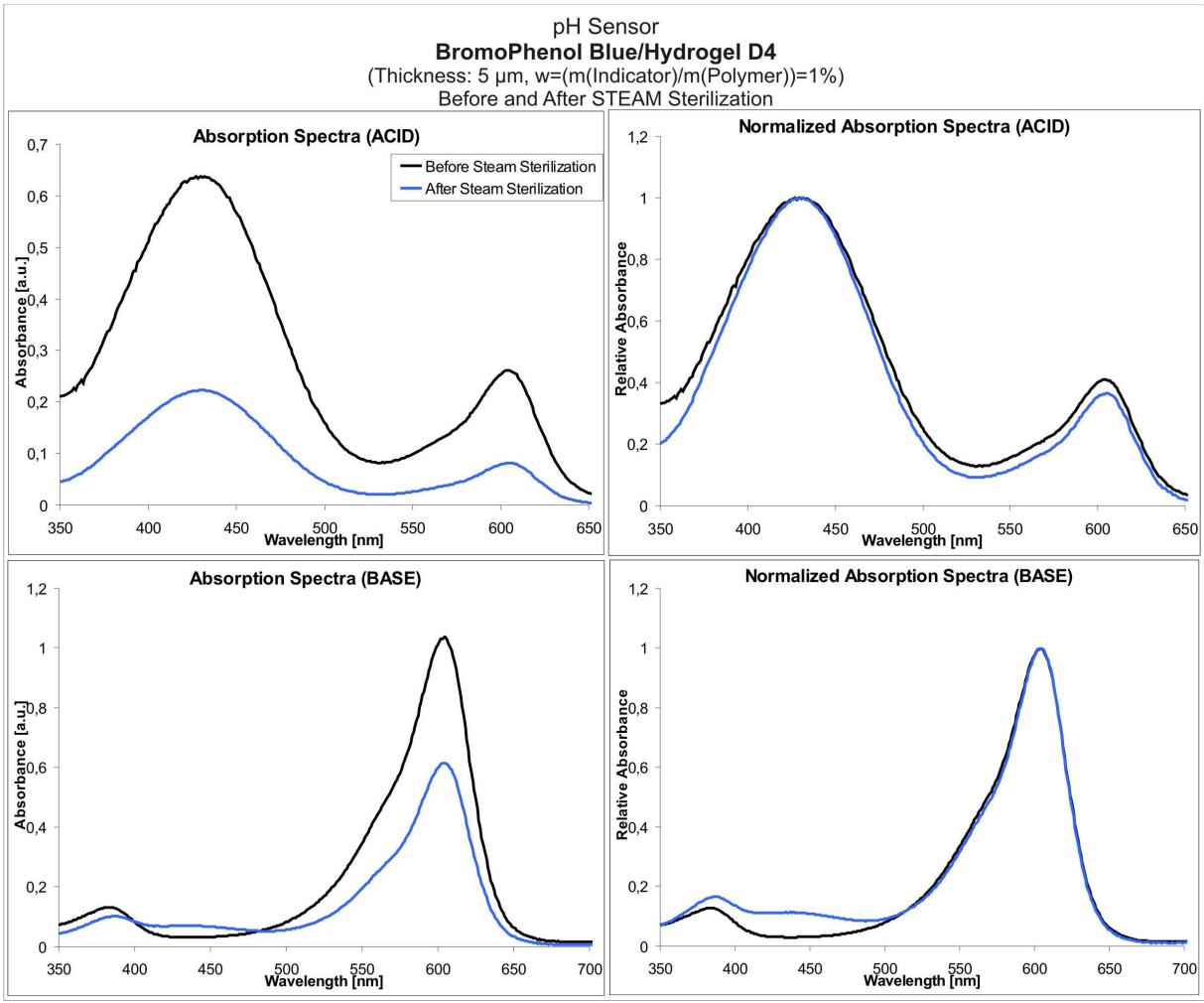

STEAM S.	Absorption Spectra					
		pH	Alterations		pH	Alterations
Alterations in Absorption /Emission Intensity	AFTERS	ACID	65,07% decrease	Alterations in Absorption /Emission Curve Form	AFTERS	ACID	Altered absorption curve form between 350-400 nm and 470-650 nm.
		BASE	40,62% decrease			BASE	Altered absorption curve form between 350-500 nm.

D.38 Thymol Blue immobilized in HydroMed Hydrogel D4

Absorption Spectra

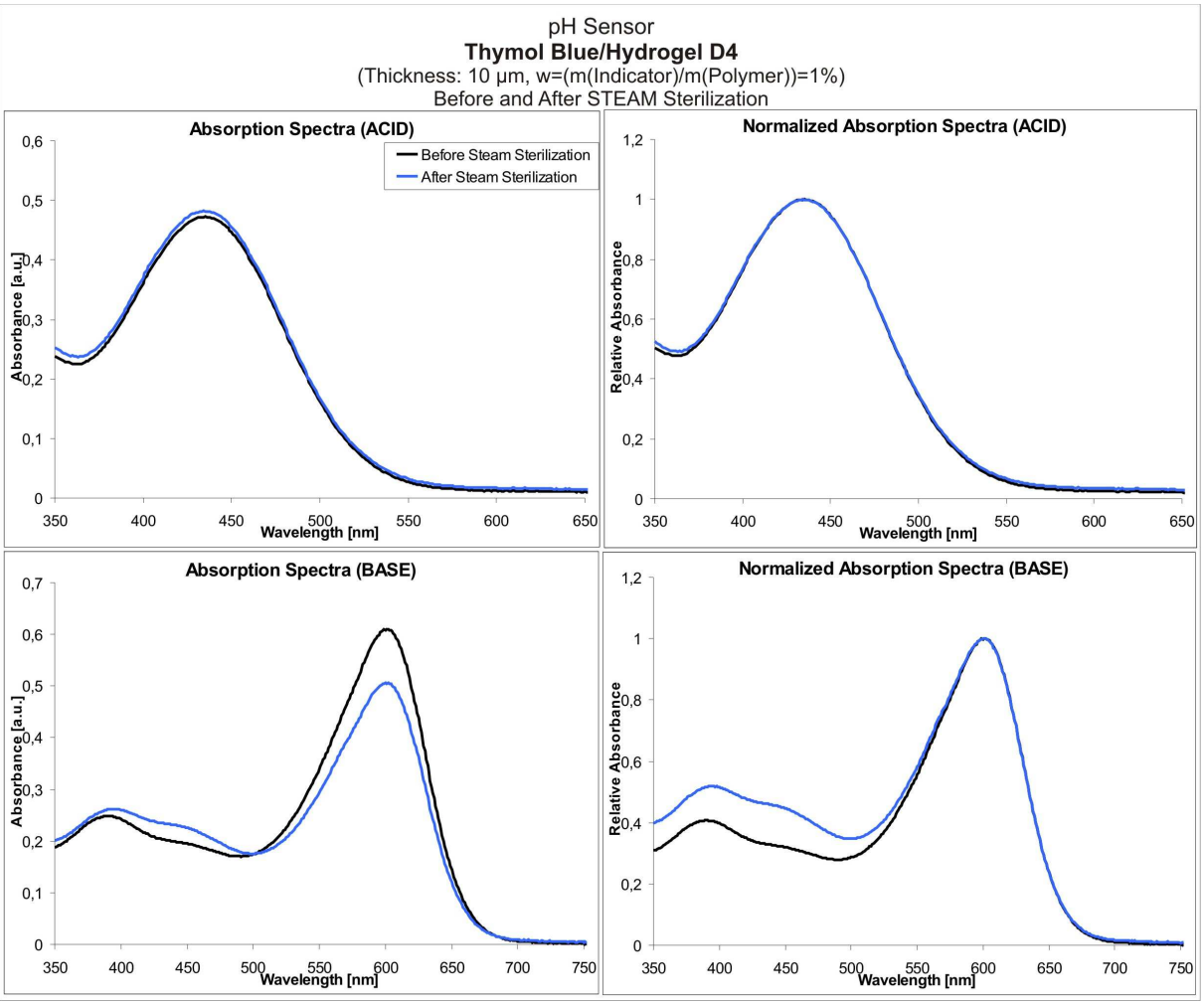

STEAM S.	Absorption Spectra						
		pH	Alterations			pH	Alterations
Alterations in Absorption /Emission Intensity	AFTER S	ACID	6,11% increase	Alterations in Absorption /Emission Curve Form	AFTER S	ACID	Unaltered.
		BASE	17,12% decrease			BASE	Altered absorption curve form between 350-550 nm.

D.39 BromoThymol Blue immobilized in HydroMed Hydrogel D4

Absorption Spectra

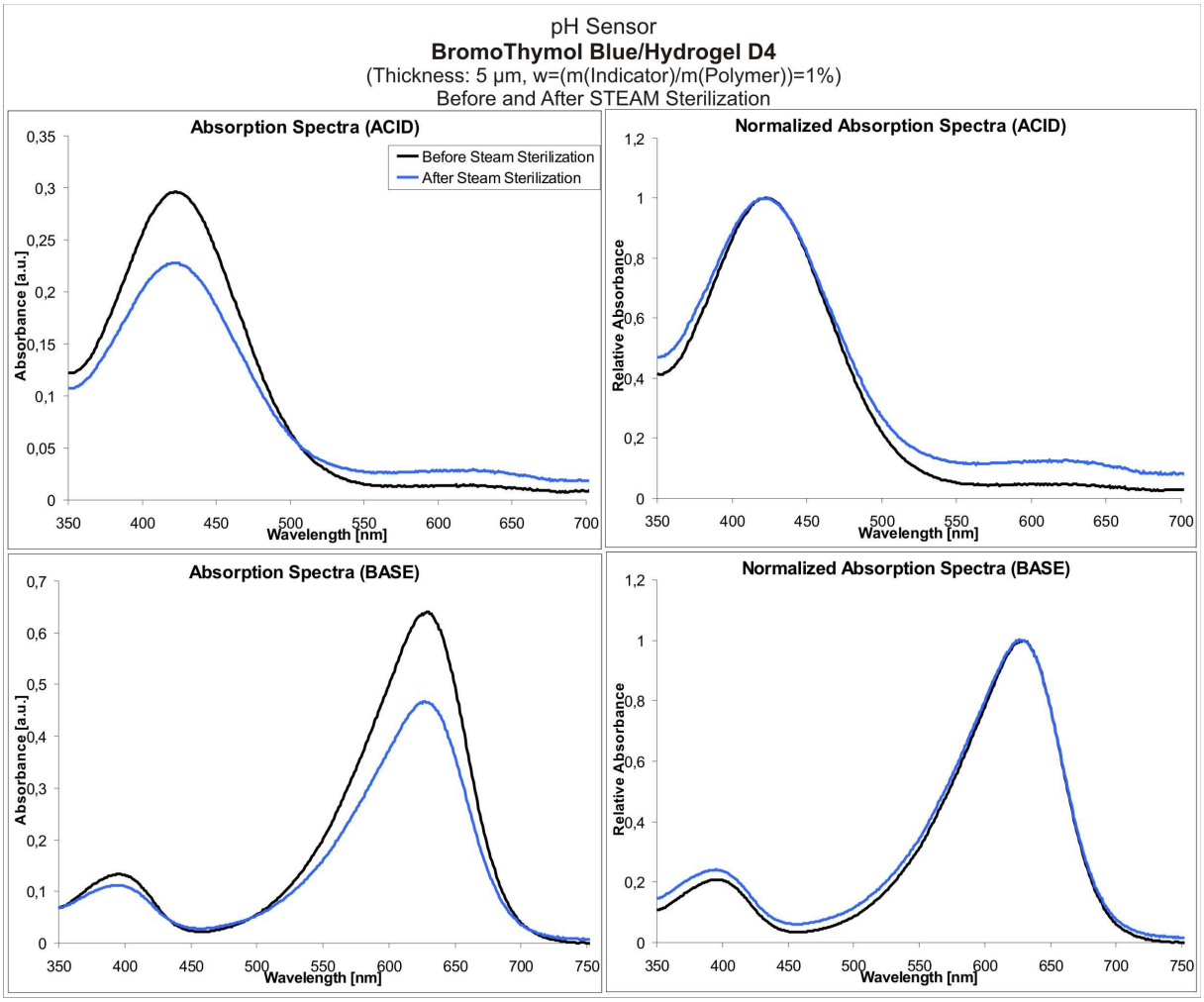

STEAM S.	Absorption Spectra					
Alterations in Absorption /Emission Intensity		pH	Alterations	Alterations in Absorption /Emission Curve Form		pH	Alterations
	AFTER S	ACID	23,03% increase		AFTER S	ACID	Altered absorption curve form between 350-400 nm and 500-800 nm.
		BASE	27,21% decrease			BASE	Altered absorption curve form between 350-600 nm.

D.40 Methyl Orange immobilized in HydroMed Hydrogel D4

Absorption Spectra

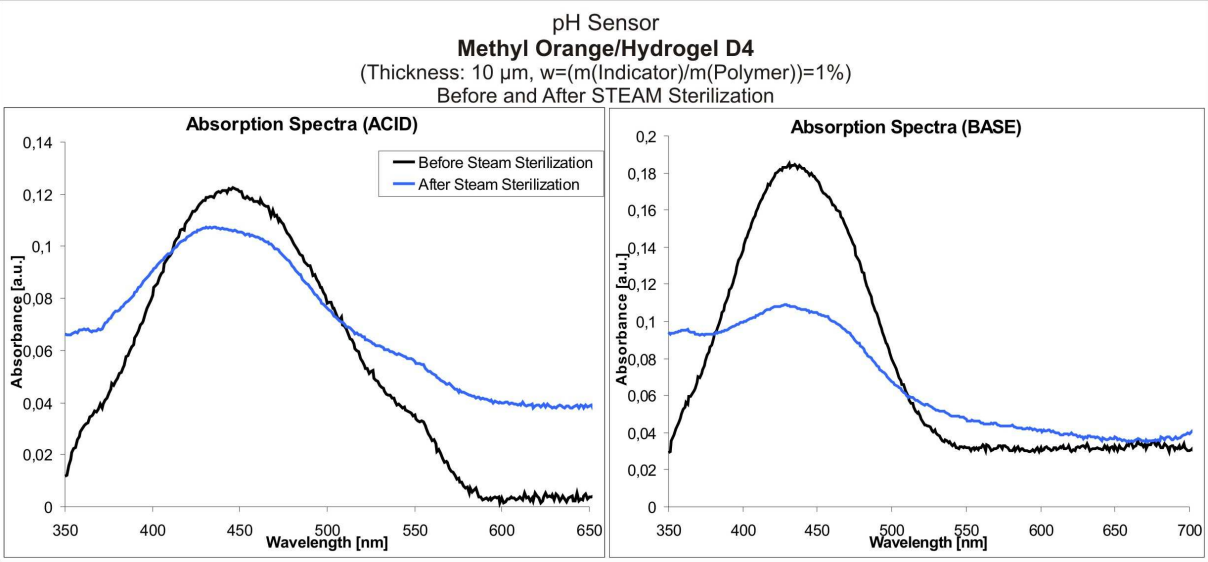

STEAM S.	Absorption Spectra						
		pH	Alterations			pH	Alterations
Alterations in Absorption /Emission Intensity	AFTER S	ACID	13,45% decrease	Alterations in Absorption /Emission Curve Form	AFTER S	ACID	Altered absorption curve form. The sensor became turbid after sterilization.
		BASE	41,17% decrease			BASE	Disappearance of the characteristic absorption curve form.

Optical TEMPERATURE SENSORS

D.41 Europium(III) Complex with 4-(4,6-di(1H-indazol-1-yl)-1,3,5-triazin-2-yl)-N,N-DiEthyl Benzen Amine (=Eu(tta)$_3$DEADIT) immobilized in PolyStyrene-co-Acrylonitrile

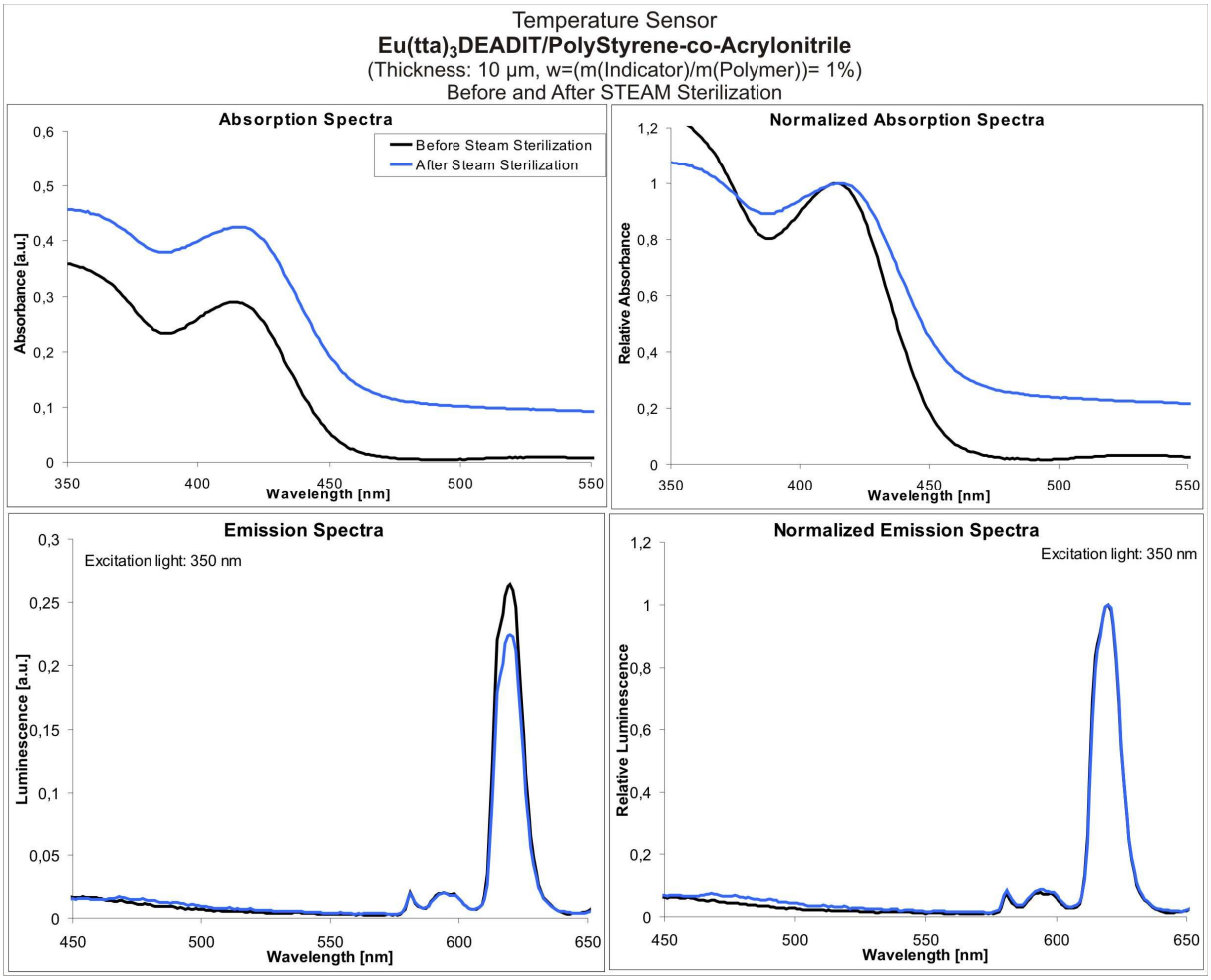

STEAM Sterilization	Absorption Spectra	Emission Spectra
Alterations in Absorption/Emission Intensity	33,88% increase	14,85% decrease
Alterations in Absorption/Emission Curve Form	Polymers become turbid after sterilization.	Unaltered.

Calibration Curves

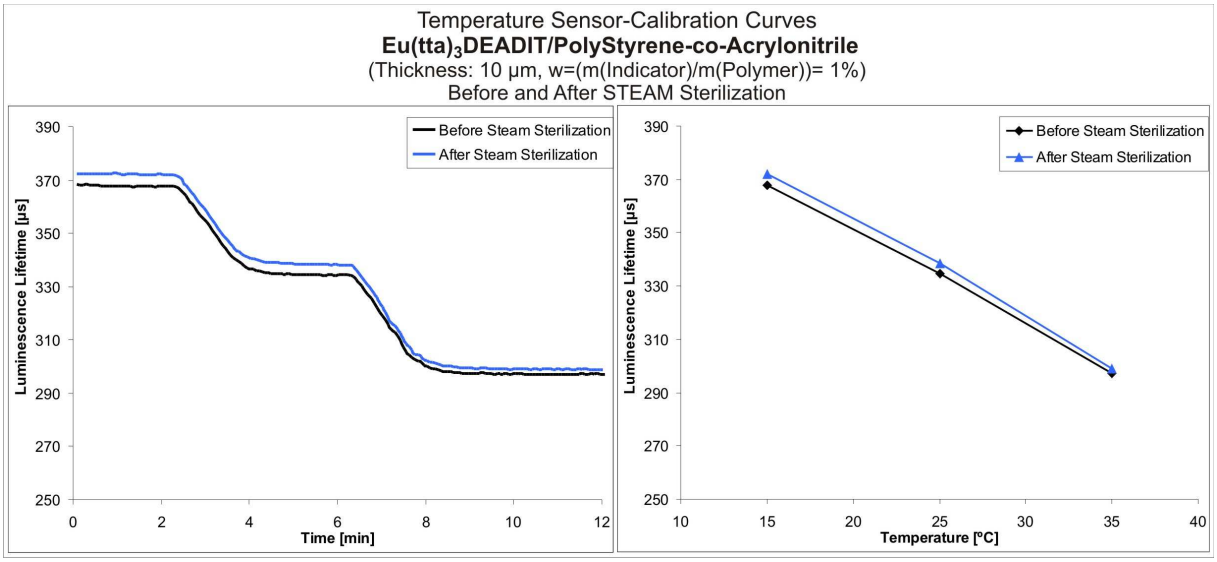

STEAM S.	Luminescence Lifetime		Alterations of Slope
Alterations in Luminescence Lifetime and Slope	15 °C	1,09% increase	3,38% increase of slope
	25 °C	0,90% increase	
	35 °C	0,67% increase	

D.42 Europium(III) Complex with 4-(4,6-di(1H-indazol-1-yl)-1,3,5-triazin-2-yl)-N,N-DiEthyl Benzen Amine (=Eu(tta)$_3$DEADIT) immobilized in PolyVinylideneChloride-co-Acrylonitrile

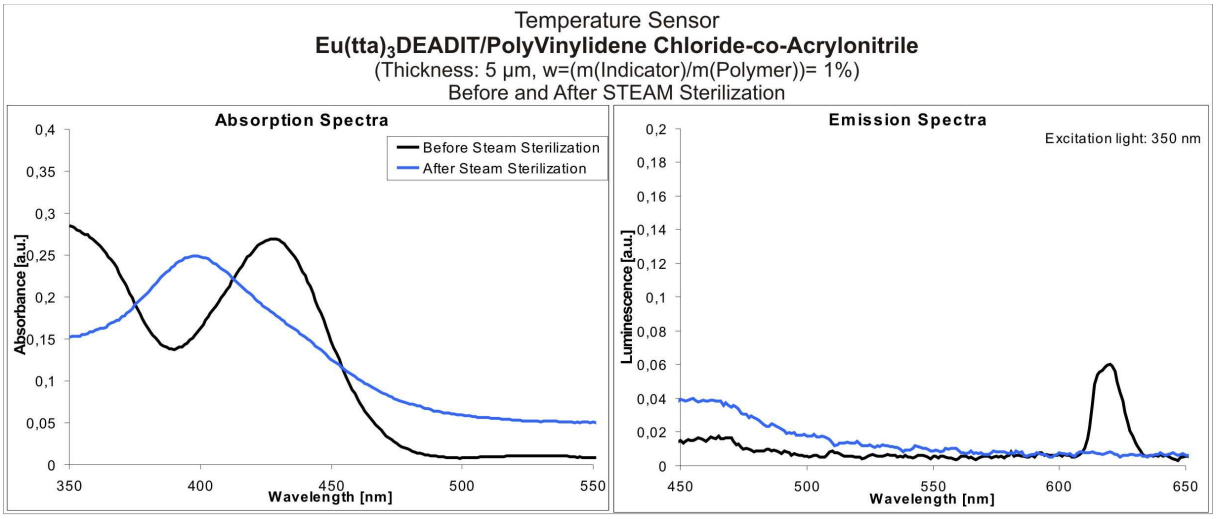

STEAM Sterilization	Absorption Spectra	Emission Spectra
Alterations in Absorption/Emission Intensity	Decrease	Decrease
Alterations in Absorption/Emission Curve Form	New absorption maximum peak with λ_{max}=398 nm Polymers become slightly turbid after sterilization.	Dissapearance of the characteristic emission curve form.

Calibration Curves

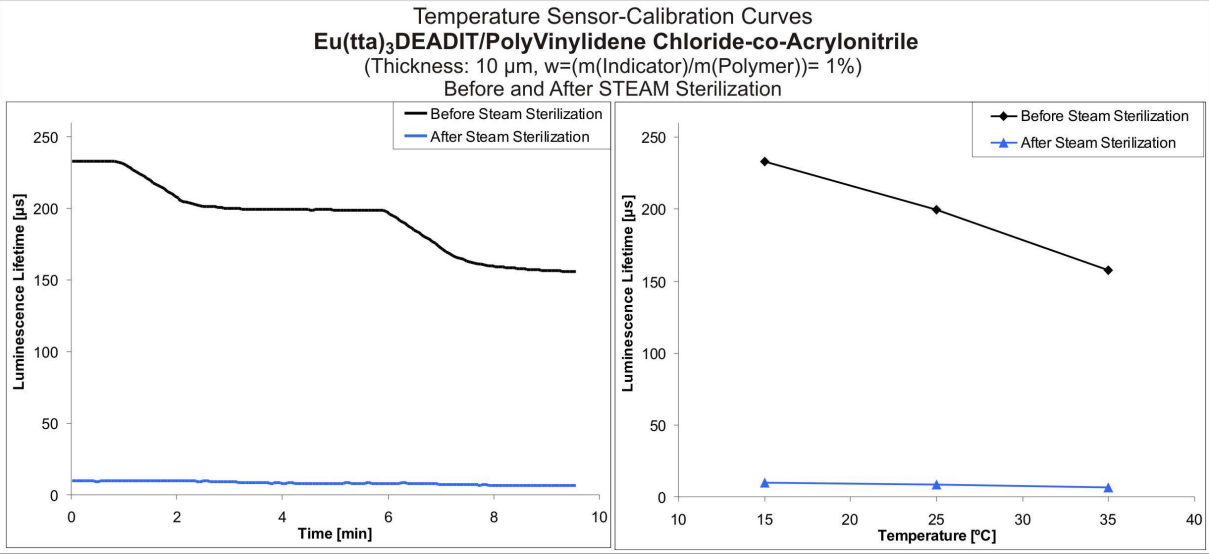

STEAM S.	Luminescence Lifetime		Alterations of Slope
Alterations in Luminescence Lifetime and Slope	15 °C	Decrease – no response	Decrease – no response
	25 °C	Decrease – no response	
	35 °C	Decrease – no response	

D.43 Europium(III) Complex with 4-(4,6-di(1H-indazol-1-yl)-1,3,5-triazin-2-yl)-N,N-DiEthyl Benzen Amine (=Eu(tta)$_3$DEADIT) immobilized in PolyMethAcryloNitrile

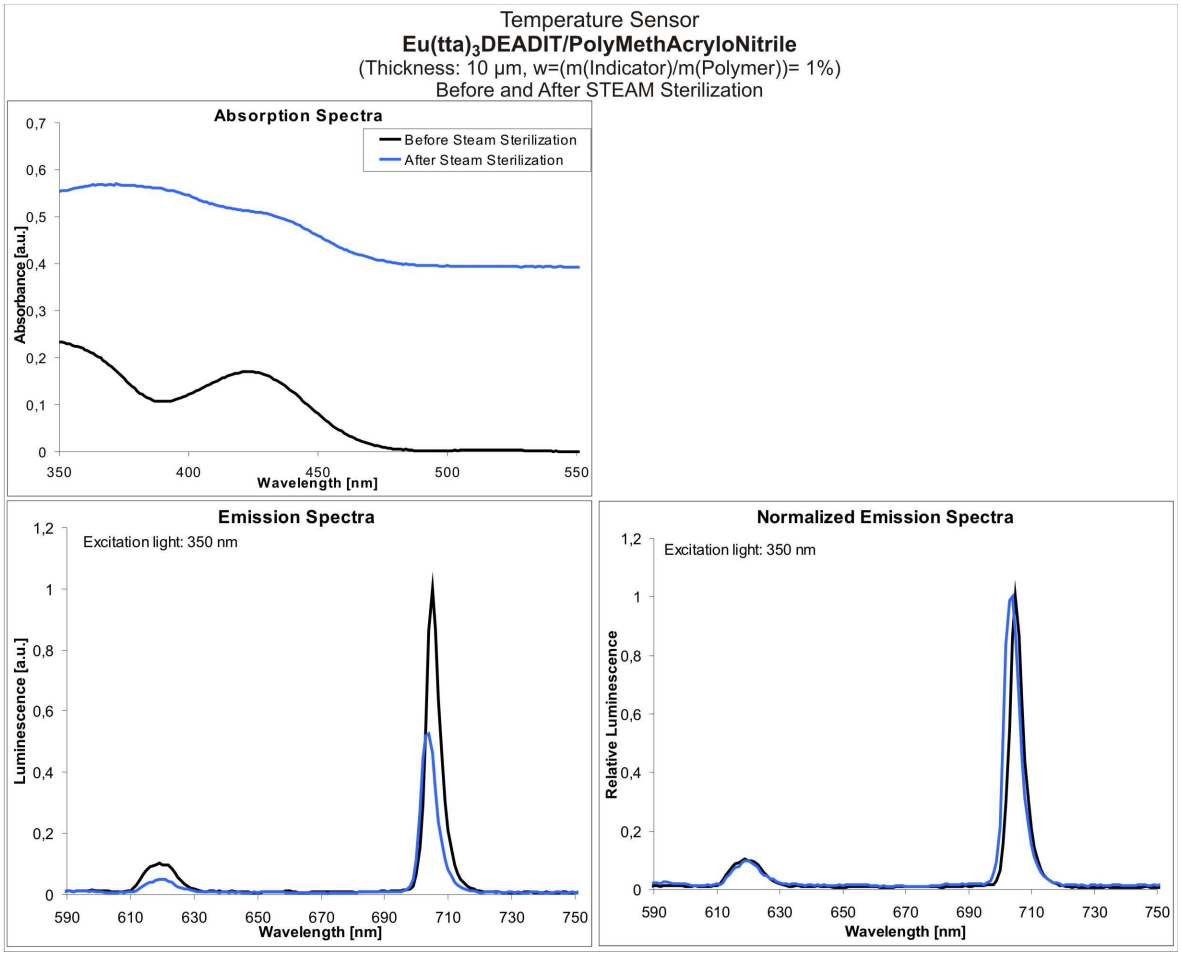

STEAM Sterilization	Absorption Spectra	Emission Spectra
Alterations in Absorption/Emission Intensity	200% increase	47,21% decrease
Alterations in Absorption/Emission Curve Form	Polymers become turbid after sterilization.	Hypsochromic shift of the emission maximum peak for 2 nm.

Calibration Curves

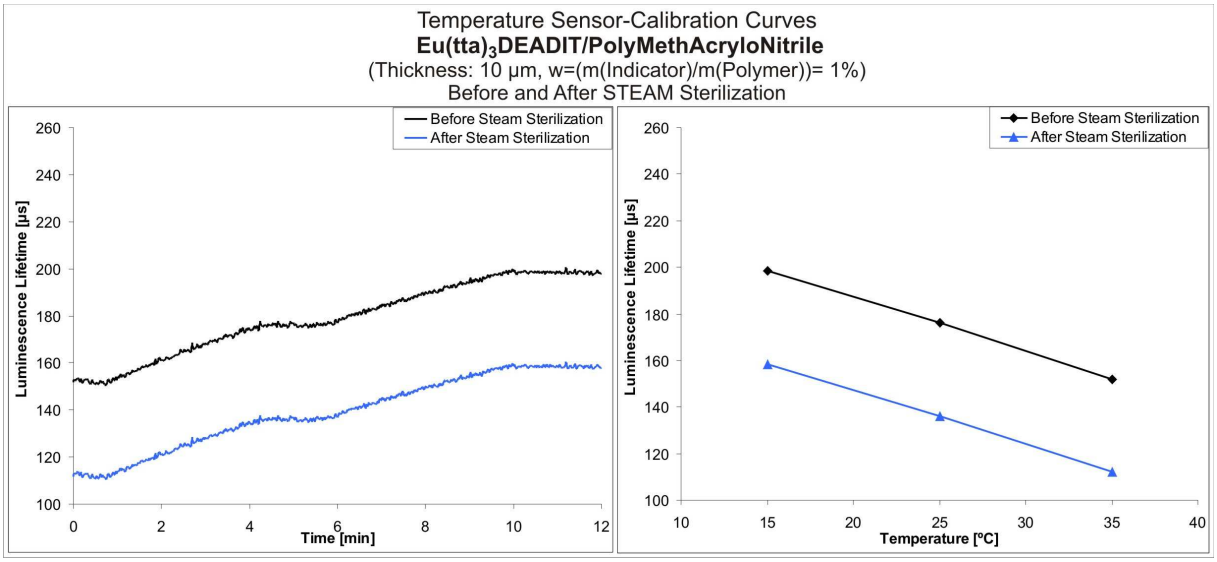

STEAM S.	Luminescence Lifetime		Alterations of Slope
Alterations in Luminescence Lifetime and Slope	15 °C	20,20% decrease	Unaltered
	25 °C	22,73% decrease	
	35 °C	26,32% decrease	

D.44 DiChloroTrisPhenanthroline Ruthenium(II)Hydrate immobilized in PolyVinylideneChloride-co-Acrylonitrile

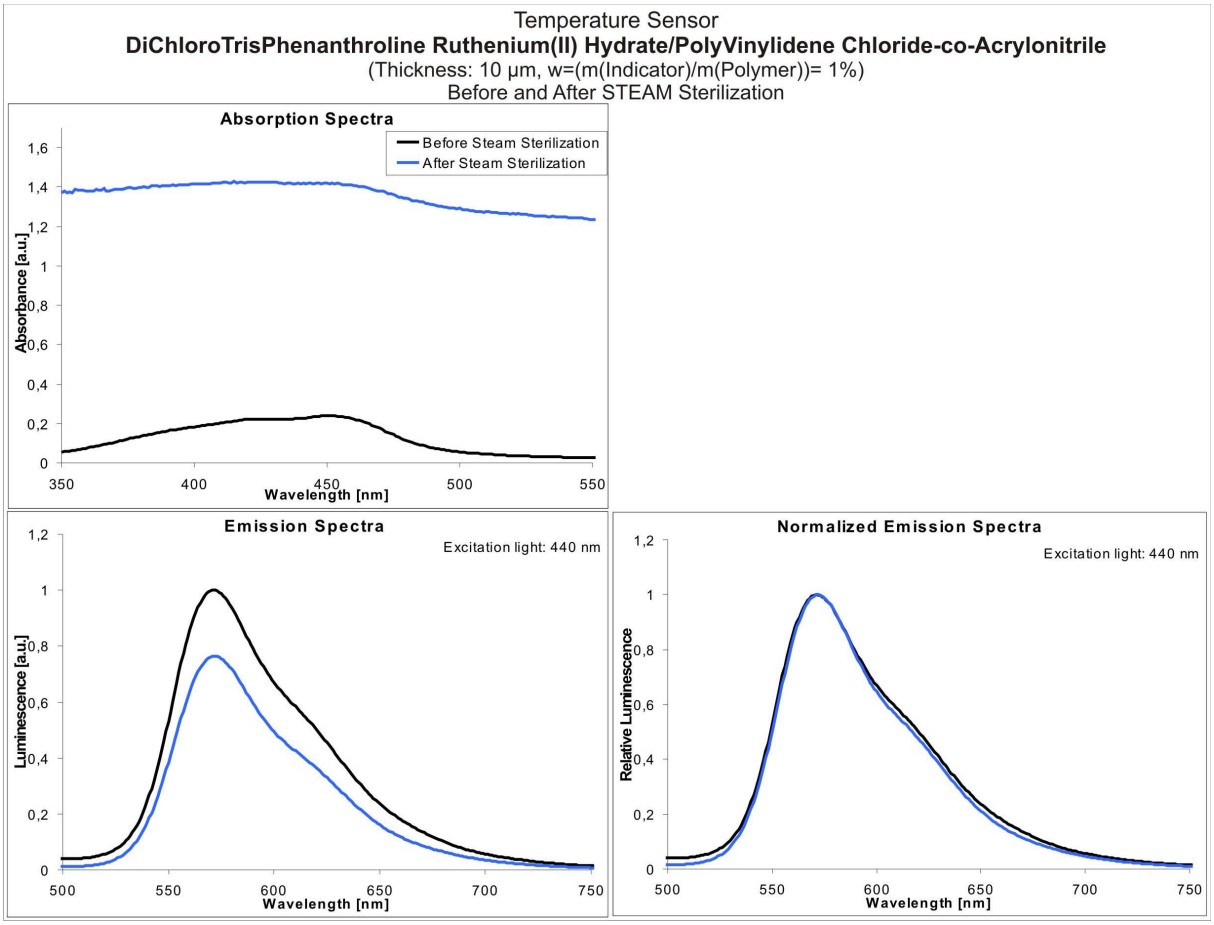

STEAM Sterilization	Absorption Spectra	Emission Spectra
Alterations in Absorption/Emission Intensity	490% increase	23,52% decrease
Alterations in Absorption/Emission Curve Form	Polymers become turbid after sterilization.	Unaltered.

Calibration Curves

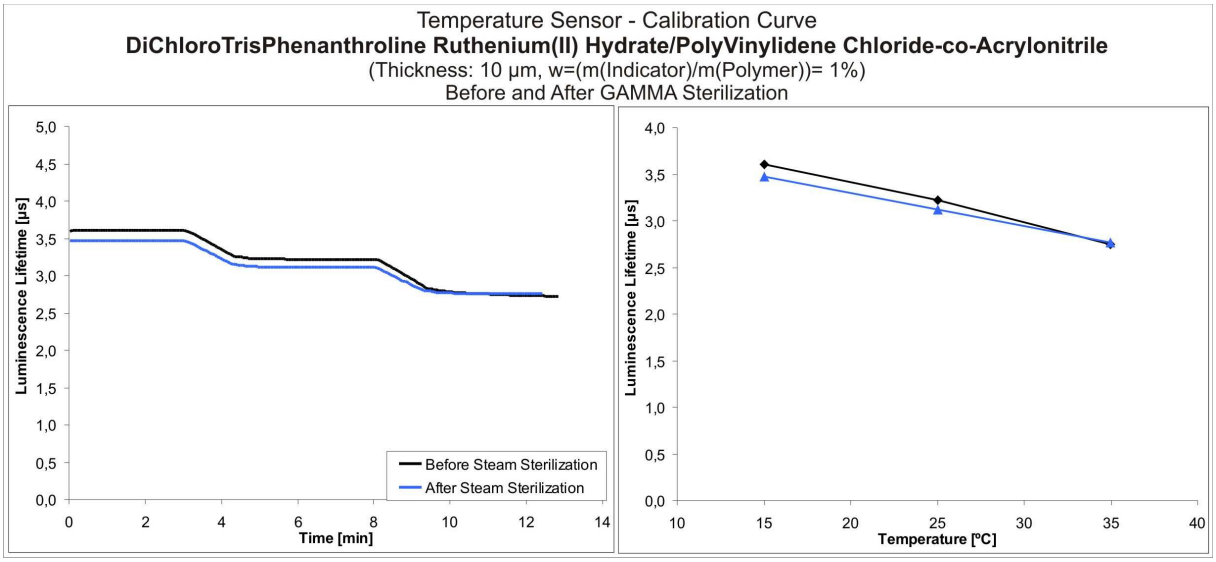

STEAM S.	Luminescence Lifetime		Alterations of Slope
Alterations in Luminescence Lifetime and Slope	15 ºC	3,88% decrease	17,10% decrease of slope
	25 ºC	3,10% decrease	
	35 ºC	0,36% increase	

D.45 DiChloroTrisPhenanthroline Ruthenium(II)Hydrate immobilized in PolyMethAcryloNitrile

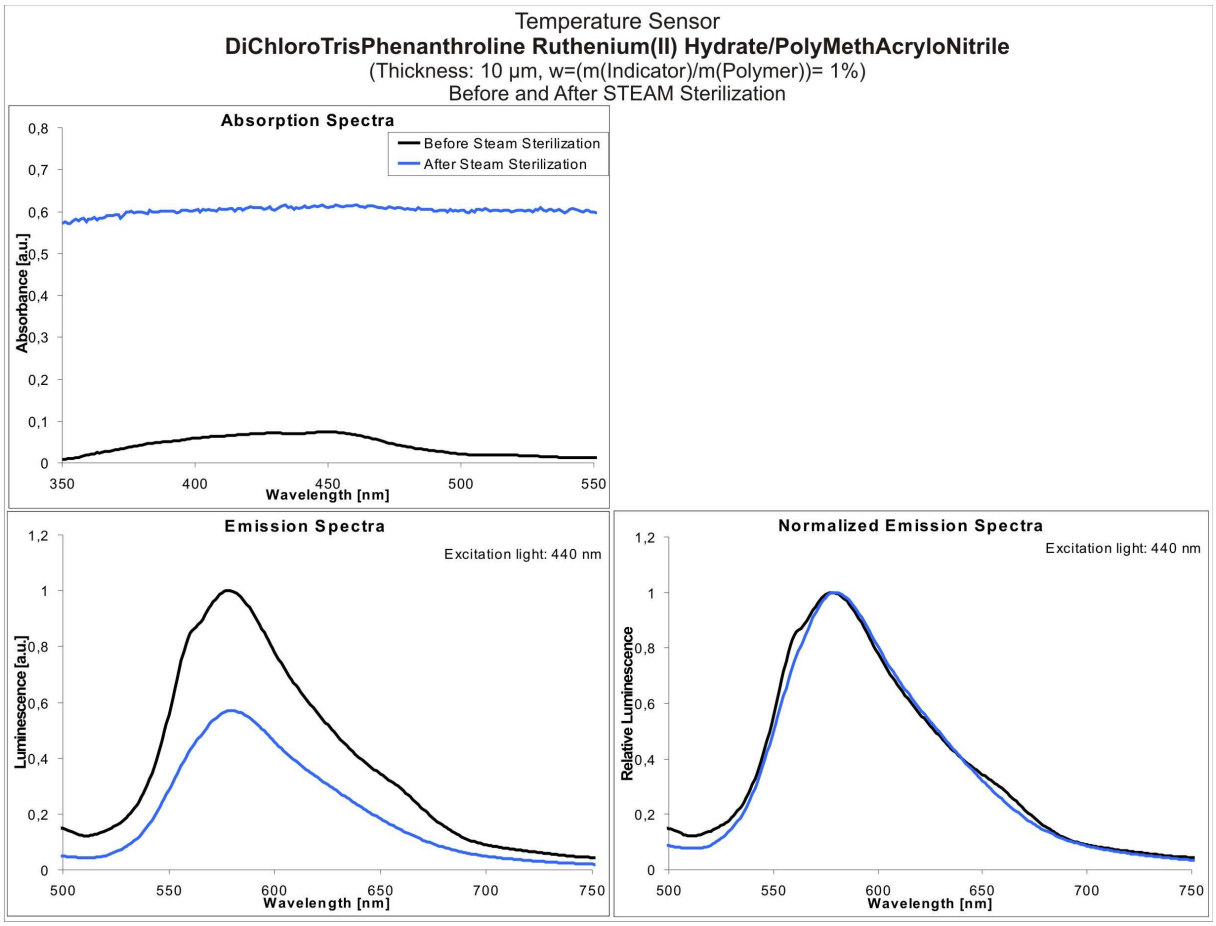

STEAM Sterilization	Absorption Spectra	Emission Spectra
Alterations in Absorption/Emission Intensity	730% increase	42,95% decrease
Alterations in Absorption/Emission Curve Form	Polymers become turbid after sterilization.	Altered emission between 500-570 nm.

Calibration Curves

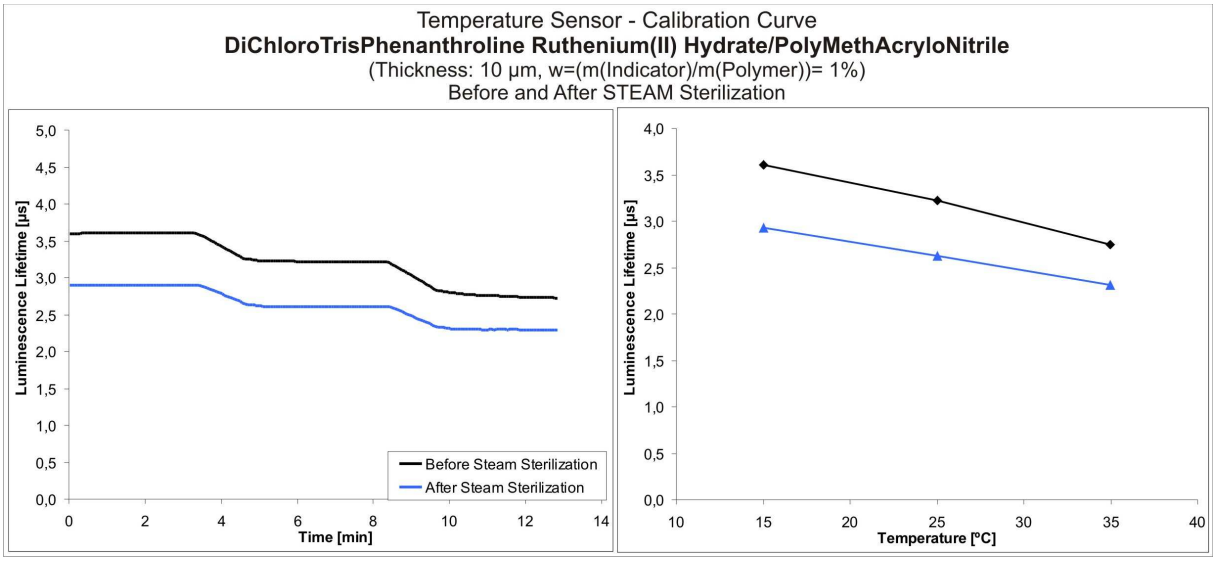

STEAM S.	Luminescence Lifetime		Alterations of Slope
Alterations in Luminescence Lifetime and Slope	15℃	19,44% decrease	26,76% decrease of slope
	25℃	18,94% decrease	
	35℃	16,36% decrease	

Optical AMMONIA SENSORS

D.46 EosinEthylEster immobilized in Cellulose Acetate

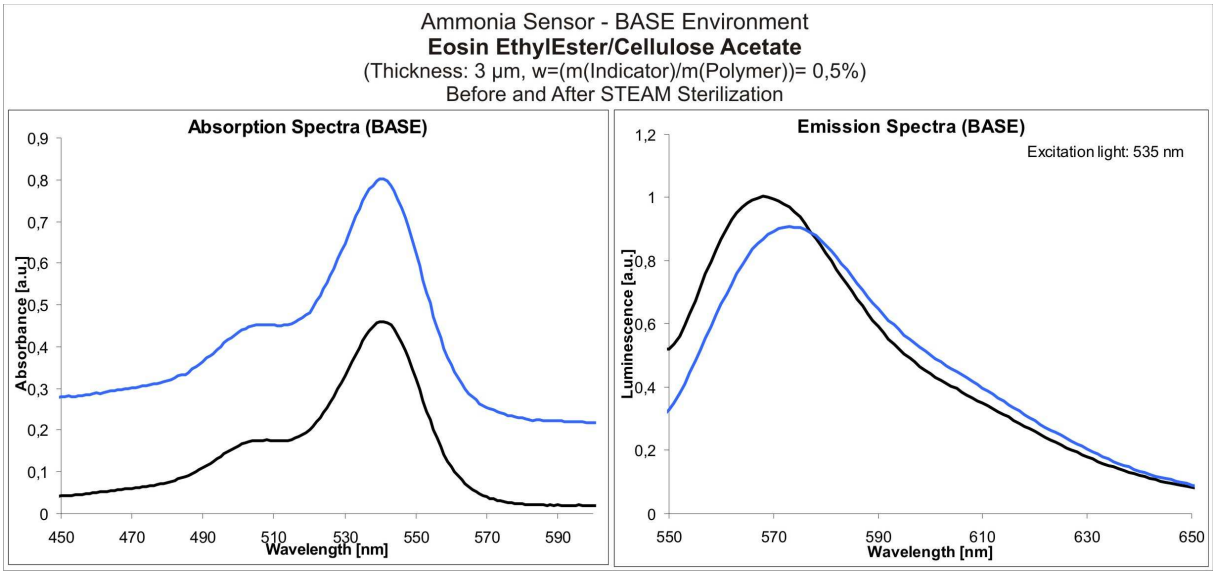

STEAM S.	Absorption Spectra		Emission Spectra	
		Alterations		Alterations
Alterations in Absorption/ Emission Intensity	BASE	Increase	BASE	9,30% decrease
Alterations in Absorption/ Emission Curve Form	BASE	Polymer became turbid after sterilization.	BASE	Bathochromic shift of the emission maximum for 6 nm.

D.47 EosinEthylEster immobilized in Hydrogel D7

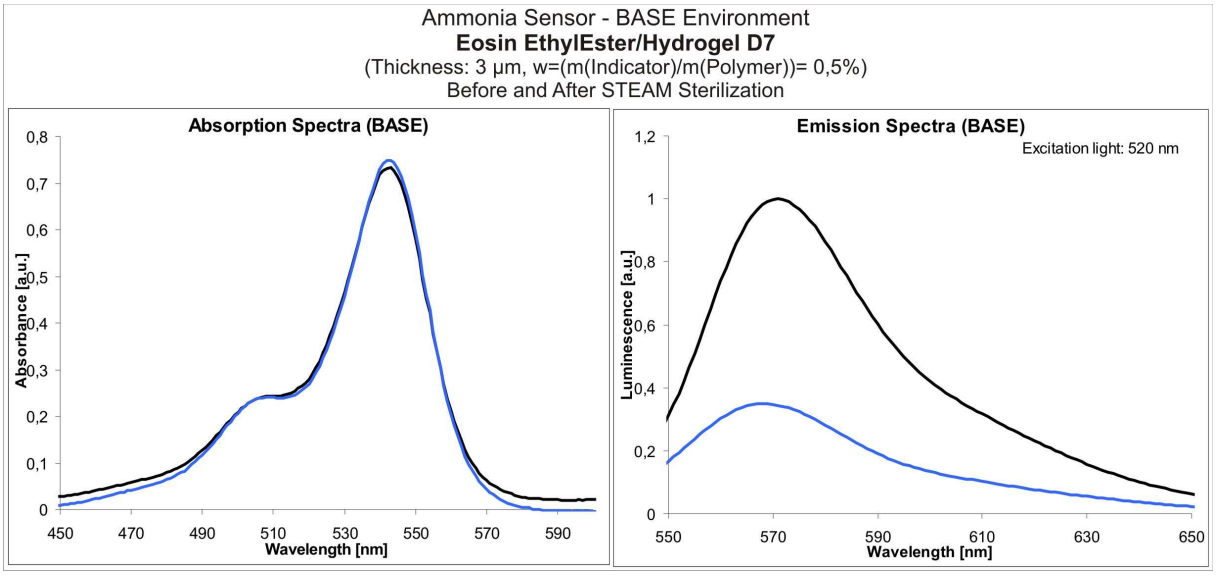

STEAM S.	Absorption Spectra		Emission Spectra	
		Alterations		Alterations
Alterations in Absorption/ Emission Intensity	BASE	2,24% increase	BASE	65,10% decrease
Alterations in Absorption/ Emission Curve Form	BASE	Unaltered.	BASE	Hypsochromic shift of the emission maximum for 3 nm.

D.48 Eosin EthylEster immobilized in Ethyl Cellulose

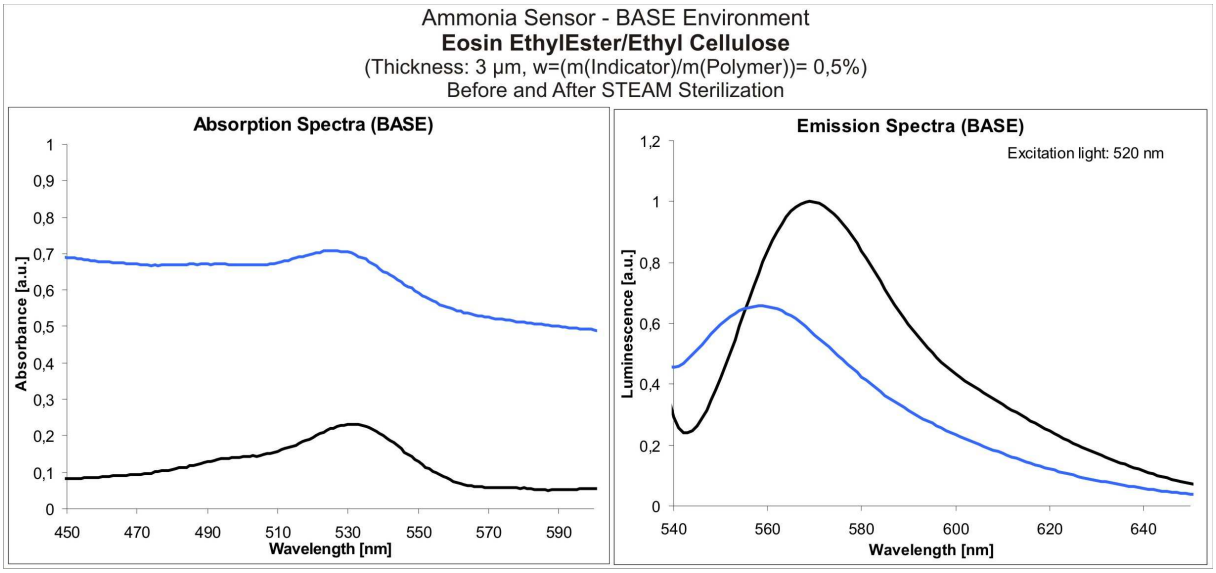

STEAM S.	Absorption Spectra		Emission Spectra	
		Alterations		Alterations
Alterations in Absorption/ Emission Intensity	BASE	200% increase	BASE	34,31% decrease
Alterations in Absorption/ Emission Curve Form	BASE	Polymer became turbid after sterilization.	BASE	Hypsochromic shift of the emission maximum for 11 nm.

D.49 EosinEthylEster immobilized in PolyMethylMethAcrylate (=PMMA)

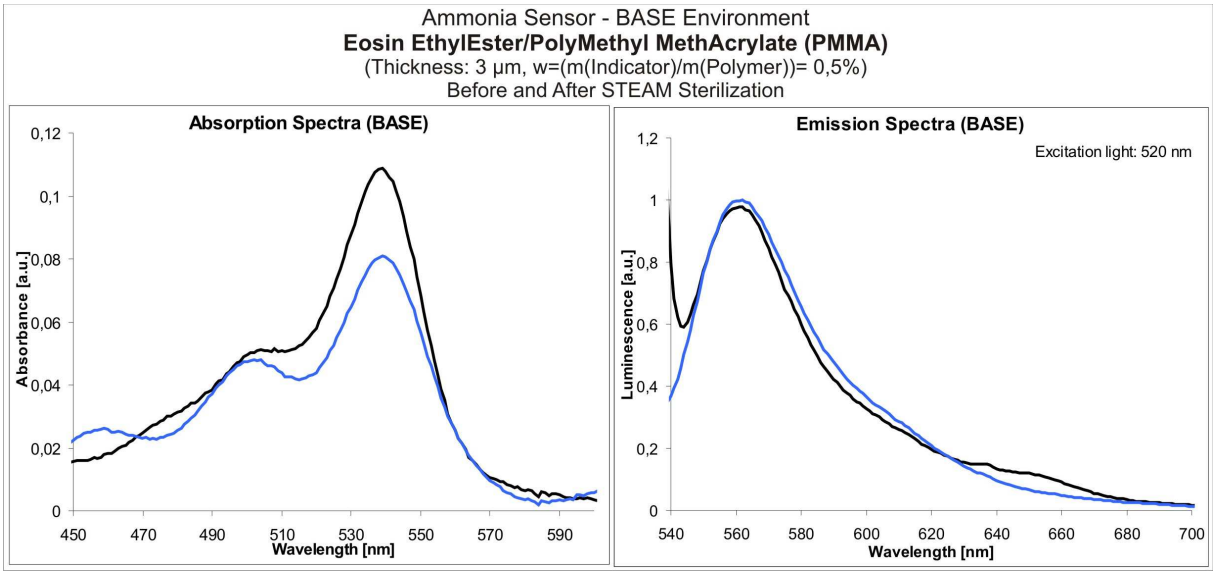

STEAM S.	Absorption Spectra		Emission Spectra	
		Alterations		Alterations
Alterations in Absorption/ Emission Intensity	BASE	25,83% decrease	BASE	2,18% increase
Alterations in Absorption/ Emission Curve Form	BASE	Altered absorption between 450-520 nm and 570-590 nm.	BASE	Altered emission between 545-570 nm.

D.50 DiChloroFluorescein immobilized in Cellulose Acetate

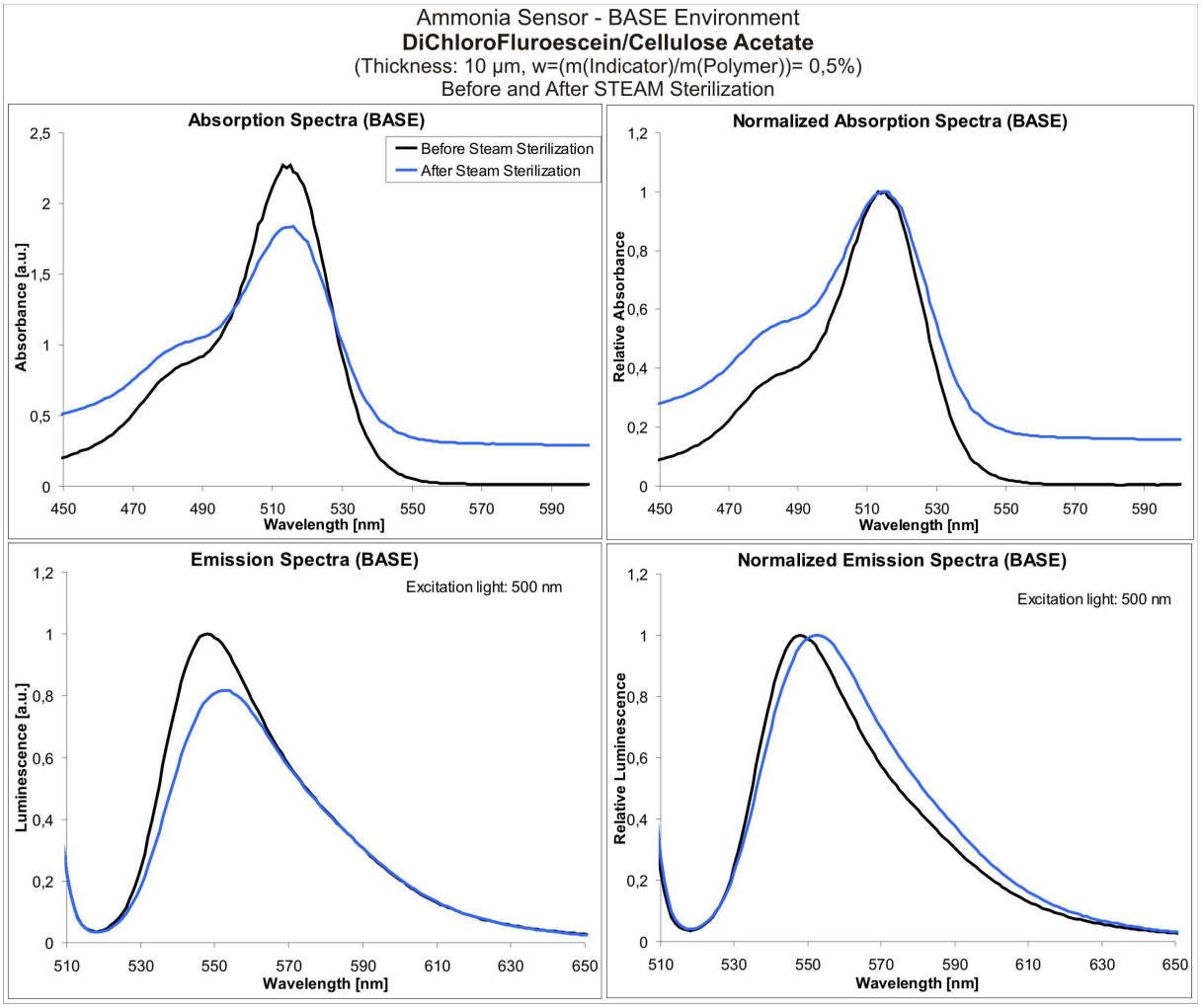

STEAM S.	Absorption Spectra		Emission Spectra	
		Alterations		Alterations
Alterations in Absorption/ Emission Intensity	BASE	19,10% decrease	BASE	18,25% decrease
Alterations in Absorption/ Emission Curve Form	BASE	Sensor became turbid after sterilization.	BASE	Bathochromic shift of the emission maximum for 4 nm.

D.51 DiChloroFluorescein immobilized in Hydrogel D7

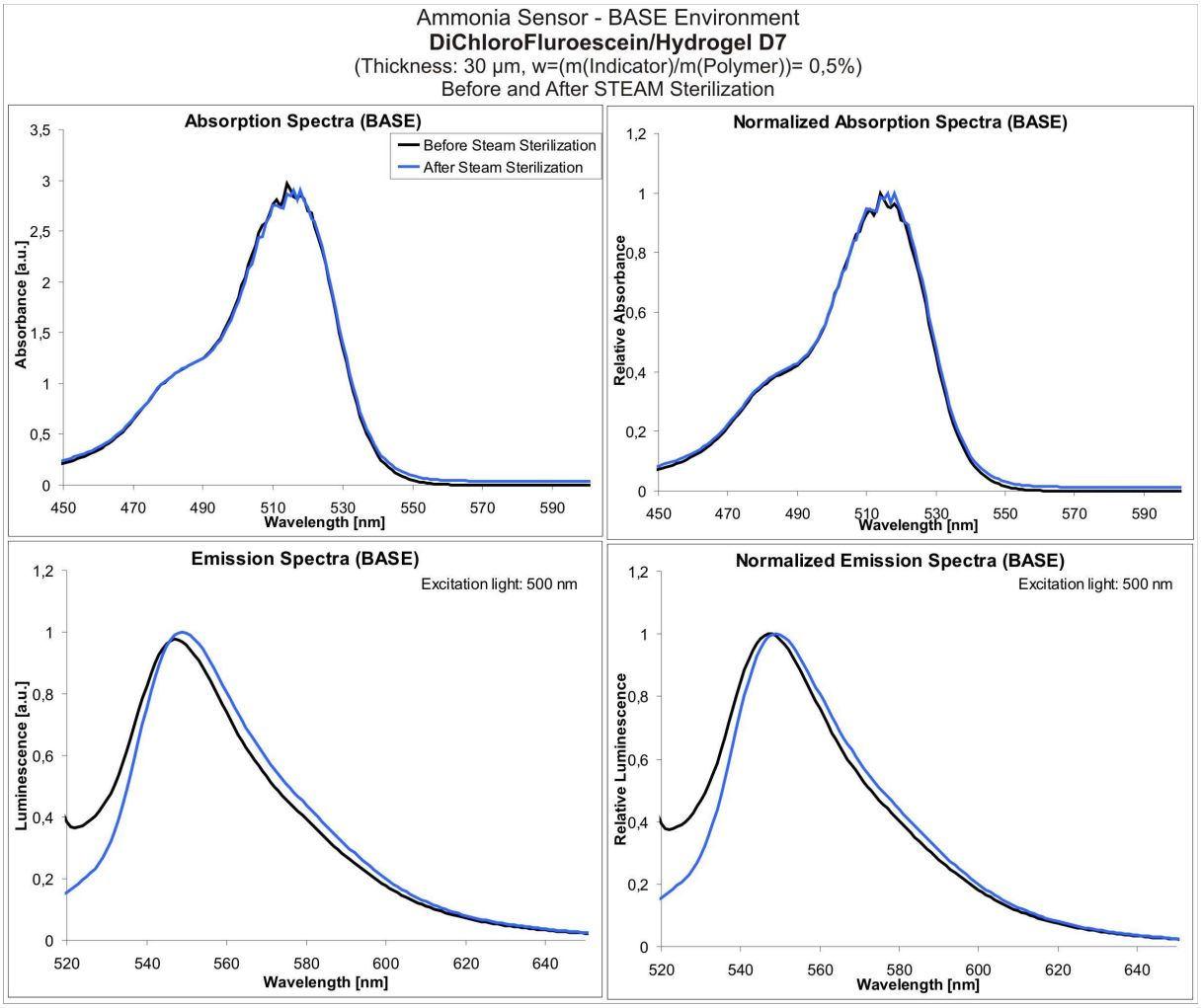

STEAM S.	Absorption Spectra		Emission Spectra	
		Alterations		Alterations
Alterations in Absorption/ Emission Intensity	BASE	2,16% decrease	BASE	2,38% increase
Alterations in Absorption/ Emission Curve Form	BASE	Unaltered.	BASE	Bathochromic shift of the emission maximum for 2 nm.

D.52 DiChloroFluorescein immobilized in Ethyl Cellulose

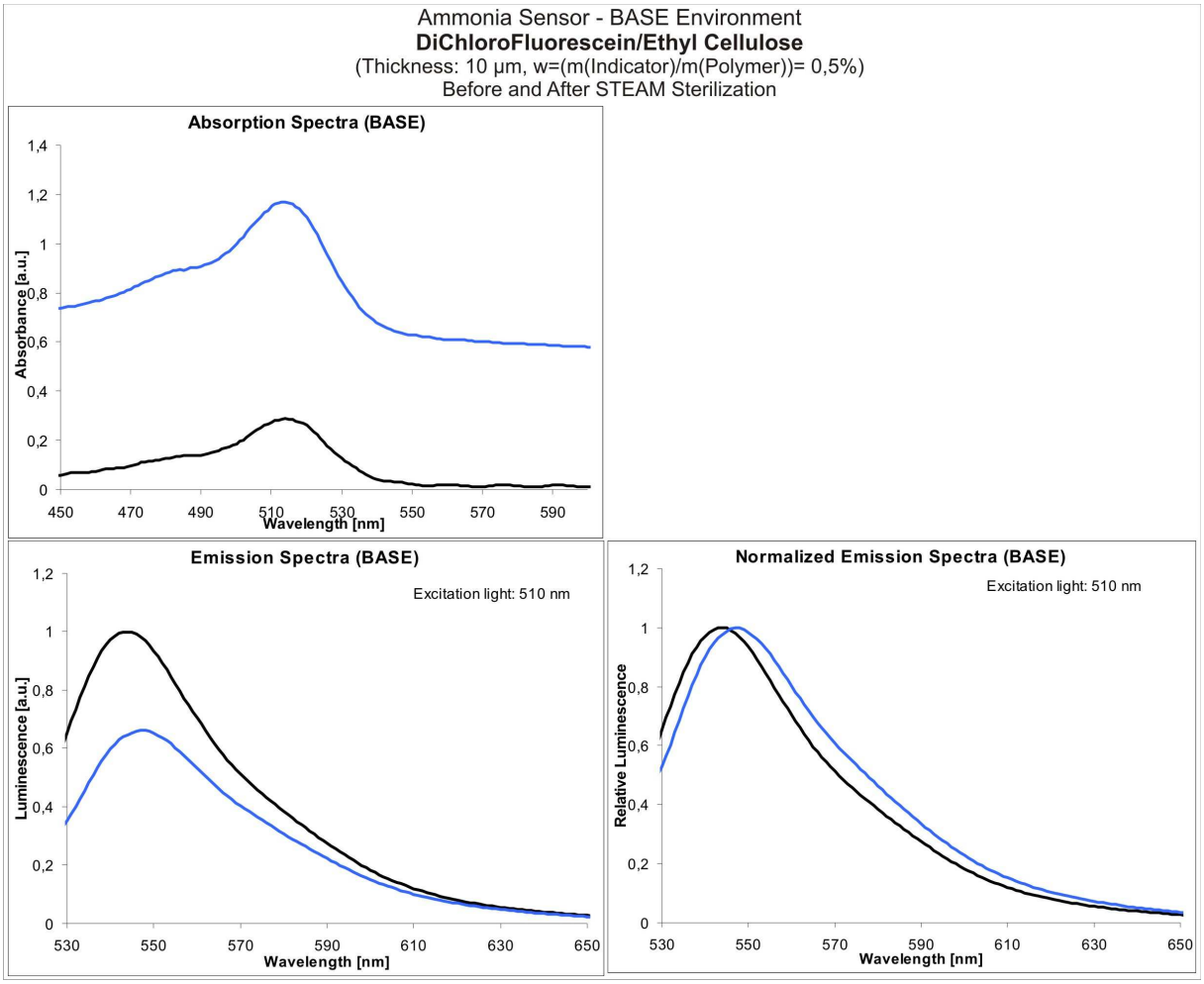

STEAM S.	Absorption Spectra		Emission Spectra	
		Alterations		Alterations
Alterations in Absorption/ Emission Intensity	BASE	315% increase	BASE	33,74% decrease
Alterations in Absorption/ Emission Curve Form	BASE	The sensor became turbid after sterilization.	BASE	Bathochromic shift of the emission maximum for 3 nm.

D.53 BromoPhenolBlue immobilized in Cellulose Acetate

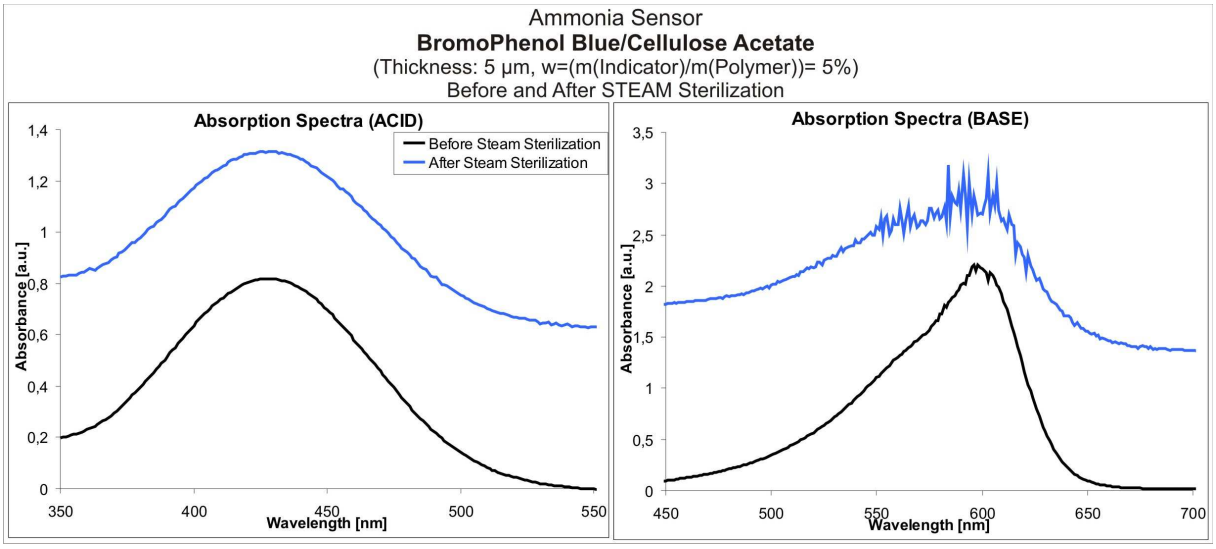

STEAM S.	Absorption Spectra				
		Alterations			Alterations
Alterations in Absorption /Emission Intensity	ACID	60% increase	Alterations in Absorption /Emission Curve Form	ACID	The sensor became turbid after sterilization.
	BASE	40% increase		BASE	The sensor became turbid after sterilization.

D.54 BromoPhenolBlue immobilized in Hydrogel D7

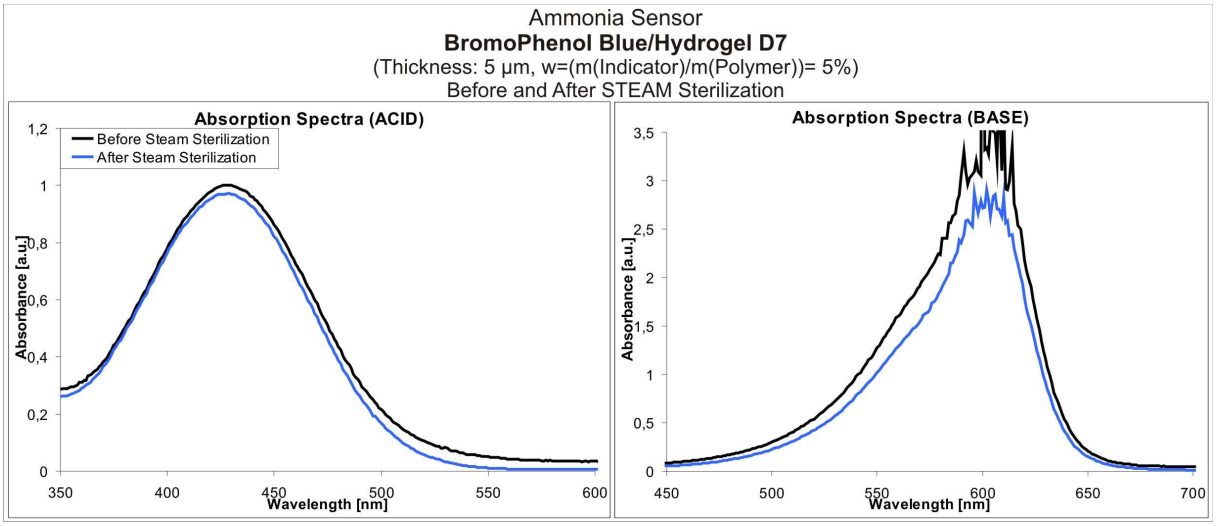

STEAM S.	Absorption Spectra				
		Alterations			Alterations
Alterations in Absorption /Emission Intensity	ACID	2,65% decrease	Alterations in Absorption /Emission Curve Form	ACID	Unaltered.
	BASE	11,31% decrease		BASE	Unaltered.

D.55 BromoPhenolBlue immobilized in Ethyl Cellulose

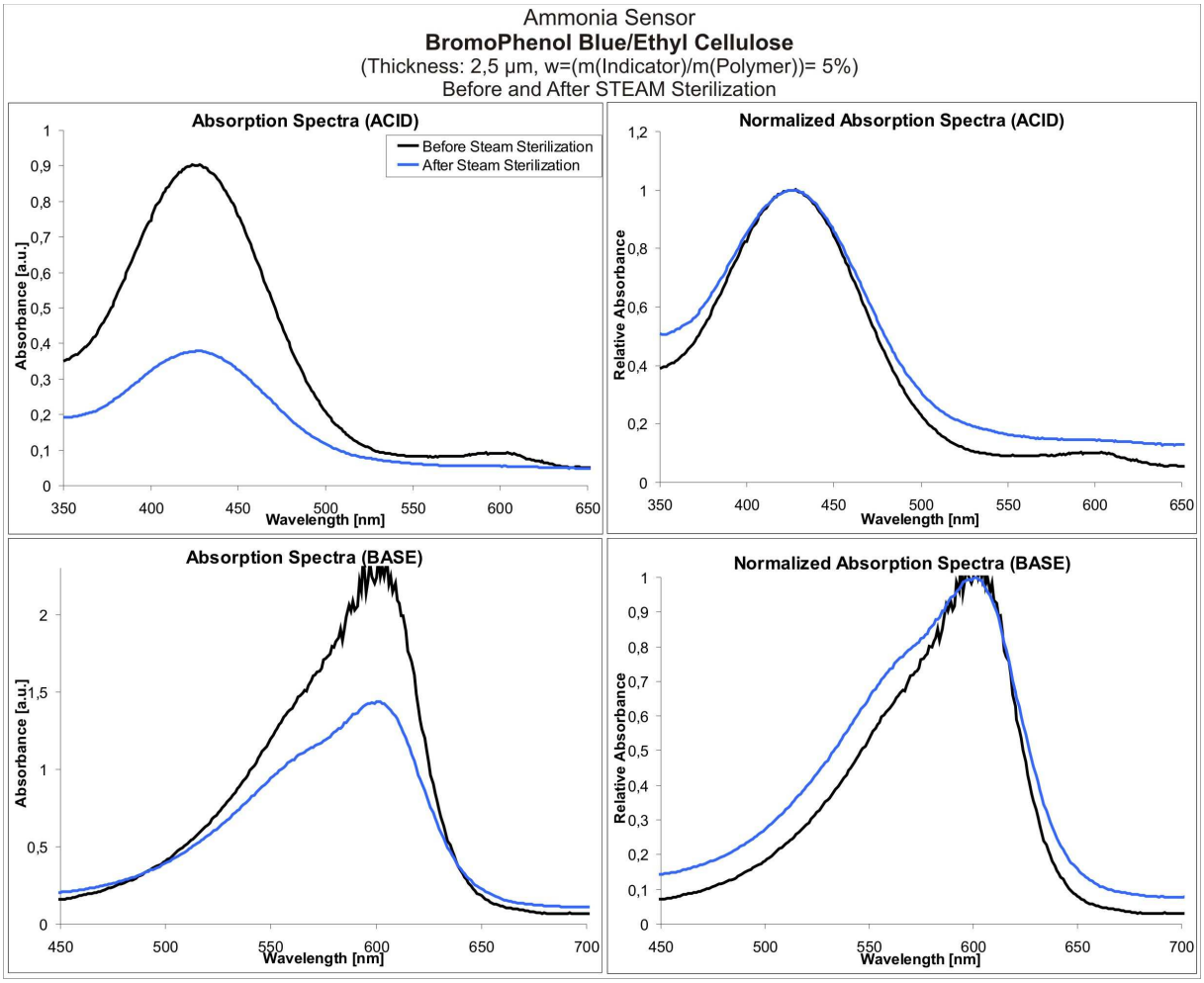

STEAM S.	Absorption Spectra			
Alterations in Absorption /Emission Intensity		Alterations	Alterations in Absorption /Emission Curve Form	Alterations
	ACID	58,07% decrease		ACID: The sensor became slightly turbid after sterilization.
	BASE	35,74% decrease		BASE: The sensor became slightly turbid after sterilization.

D.56 BromoPhenol Blue immobilized in PolyMethylMethAcrylate (=PMMA)

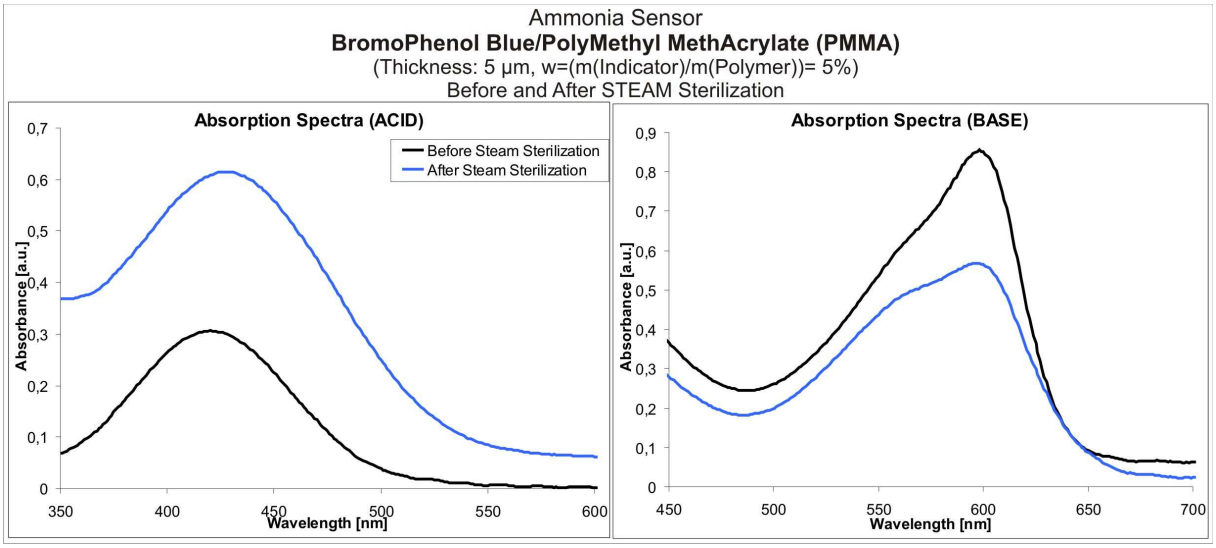

STEAM S.	Absorption Spectra				
		Alterations			Alterations
Alterations in Absorption /Emission Intensity	ACID	100% increase	Alterations in Absorption /Emission Curve Form	ACID	The sensor became turbid after sterilization.
	BASE	33,59% decrease		BASE	The sensor became slightly turbid after sterilization.

E
Sterilization of Optical Sensors with Ethylene Oxide

TABLE OF CONTENTS

E STERILIZATION OF OPTICAL SENSORS WITH ETHYLENE OXIDE 649

Optical OXYGEN SENSORS 655

E.1 Iridium(III) Coumarin Complex immobilized in Cellulose Acetate 655

E.2 Iridium(III) Coumarin Complex immobilized in Ethyl Cellulose 656

E.3 Iridium(III) Coumarin Complex immobilized in HydroGel HydroMed D4/D7 658

E.4 Iridium(III) Coumarin Complex immobilized in HydroThane with 5% water content 659

E.5 Iridium(III) Coumarin Complex immobilized in Poly(Sulfone) 661

E.6 Iridium(III) Coumarin Complex immobilized in Poly(PhenylSilsesQuioxane) 662

E.7 Iridium(III) Coumarin Complex immobilized in Poly(Styrene) 664

E.8 Iridium(III) Coumarin Complex immobilized in Poly(Styrene-co-AcryloNitrile) 665

E.9 Iridium(III) Coumarin Complex immobilized in Poly(Styrene-co-MaleicAnhydride) 667

E.10 Platinum(II)Tetrakis(PentaFluorPhenyl)Porphyrin (PtTFPP) immobilized in Cellulose Acetate 669

E.11 Platinum(II)Tetrakis(PentaFluorPhenyl)Porphyrin (PtTFPP) immobilized in Ethyl Cellulose 671

E.12 Platinum(II)Tetrakis(PentaFluorPhenyl)Porphyrin (PtTFPP) immobilized in HydroGel D4/D7 673

E.13 Platinum(II)Tetrakis(PentaFluorPhenyl)Porphyrin (PtTFPP) immobilized in HydroThane 5 675

E.14 Platinum(II)Tetrakis(PentaFluorPhenyl)Porphyrin (PtTFPP) immobilized in PolySulfone 677

E.15 Platinum(II)Tetrakis(PentaFluorPhenyl)Porphyrin (PtTFPP) immobilized in PolyPhenylSilses Quioxane 679

E.16 Platinum(II)Tetrakis(PentaFluorPhenyl)Porphyrin (PtTFPP) immobilized in PolyStyrene 681

E.17 Platinum(II)Tetrakis(PentaFluorPhenyl)Porphyrin (PtTFPP) immobilized in PolyStyrene-co- Acrylonitrile 683

E.18 Platinum(II)Tetrakis(PentaFluorPhenyl)Porphyrin (PtTFPP) immobilized in PolyStyrene-co-MaleicAnhydride (PSMA93) 685

E.19 Platinum(II) OctaEthyl Porphyrin (=PtOEP) immobilized in PolyStyrene 687

E.20 Platinum(II) meso-tetra(4-FluoroPhenyl) TetraBenzoPorphyrin (=PtTPTBPF) immobilized in PolyStyrene 689

E.21 Palladium(II)meso-tetra(4-FluoroPhenyl) TetraBenzoPorphyrin (=PdTPTBPF) immobilized in PolyStyrene 691

E.22 Ruthenium(II) DiPhenylPhenanthroline DiChloride ($Ru(dpp)_3Cl_2$) immobilized in Cellulose Acetate 693

E.23 Ruthenium(II) DiPhenylPhenanthroline DiChloride ($Ru(dpp)_3Cl_2$) immobilized in Ethyl Cellulose 694

E.24 Ruthenium(II) DiPhenylPhenanthroline DiChloride ($Ru(dpp)_3Cl_2$) immobilized in HydroGel D4/D7 696

E.25 Ruthenium(II) DiPhenylPhenanthroline DiChloride ($Ru(dpp)_3Cl_2$) immobilized in HydroThane5 697

E.26 Ruthenium(II) DiPhenylPhenanthroline DiChloride ($Ru(dpp)_3Cl_2$) immobilized in PolySulfone 699

E.27 Ruthenium(II) DiPhenylPhenanthroline DiChloride ($Ru(dpp)_3Cl_2$) immobilized in PolyPhenyl SilsesQuioxane 700

E.28 Ruthenium(II) DiPhenylPhenanthroline DiChloride ($Ru(dpp)_3Cl_2$) immobilized in PolyStyrene 702

E.29 Ruthenium(II) DiPhenylPhenanthroline DiChloride ($Ru(dpp)_3Cl_2$) immobilized in PolyStyrene-co-Acrylonitrile 703

E.30 Ruthenium(II) DiPhenylPhenanthroline DiChloride ($Ru(dpp)_3Cl_2$) immobilized in PolyStyrene-co-MaleicAnhydride (PSMA93) 705

Optical pH SENSORS 707

E.31 HPTS(DHA_3) immobilized in HydroGel D4 707

E.32 2´,7´-DiHexylFluorescein OctadecylEster immobilized in HydroMed Hydrogel D4 710

E.33 2´,7´-DiHexylFluorescein OctadecylEster immobilized in Poly(2-HydroxyEthyl MethAcrylate) (=pHEMA) 713

E.34 2´,7´-DiHexyl-N-Octadecyl-CarboxAmidoFluorescein (=DHFA) immobilized in HydroMed Hydrogel D4 715

E.35 2´,7´-DiHexyl-N-Octadecyl-CarboxAmidoFluorescein (=DHFA) immobilized in Poly(2-HydroxyEthyl Methacrylate) (=pHEMA) 717

E.36 pH Sensitive Coumarin immobilized in HydroMed Hydrogel D4 719

E.37 pH Sensitive Coumarin immobilized in Poly(2-HydroxyEthyl Methacrylate) (=pHEMA) 722

E.38 PET Perylene BisImide immobilized in HydroMed Hydrogel D4 724

E.39 BromoPhenol Blue immobilized in HydroMed Hydrogel D4 726

E.40 Thymol Blue immobilized in HydroMed Hydrogel D4 **727**

E.41 BromoThymol Blue immobilized in HydroMed Hydrogel D4 **728**

E.42 Methyl Orange immobilized in HydroMed Hydrogel D4 **729**

Optical TEMPERATURE SENSORS **730**

E.43 Europium(III) Complex with 4-(4,6-di(1H-indazol-1-yl)-1,3,5-triazin-2-yl)-N,N-DiEthyl Benzen Amine (=Eu(tta)$_3$DEADIT) immobilized in PolyStyrene-co-Acrylonitrile **730**

E.44 Europium(III) Complex with 4-(4,6-di(1H-indazol-1-yl)-1,3,5-triazin-2-yl)-N,N-DiEthyl Benzen Amine (=Eu(tta)$_3$DEADIT) immobilized in PolyVinylideneChloride-co-Acrylonitrile **731**

E.45 Europium(III) Complex with 4-(4,6-di(1H-indazol-1-yl)-1,3,5-triazin-2-yl)-N,N-DiEthyl Benzen Amine (=Eu(tta)$_3$DEADIT) immobilized in PolyMethAcryloNitrile **733**

E.46 DiChloroTrisPhenanthroline Ruthenium(II)Hydrate immobilized in PolyVinylideneChloride-co-Acrylonitrile **734**

E.47 DiChloroTrisPhenanthroline Ruthenium(II)Hydrate immobilized in PolyMethAcryloNitrile **735**

Optical AMMONIA SENSORS **737**

E.48 EosinEthylEster immobilized in Cellulose Acetate **737**

E.49 EosinEthylEster immobilized in Hydrogel D7 **738**

E.50 Eosin EthylEster immobilized in Ethyl Cellulose **739**

E.51 EosinEthylEster immobilized in PolyMethylMethAcrylate (=PMMA) **740**

E.52 DiChloroFluorescein immobilized in Cellulose Acetate **741**

E.53 DiChloroFluorescein immobilized in Hydrogel D7 **742**

E.54 DiChloroFluorescein immobilized in Ethyl Cellulose **743**

E.55 BromoPhenolBlue immobilized in Cellulose Acetate **744**

E.56 BromoPhenolBlue immobilized in Hydrogel D7 **745**

E.57.BromoPhenolBlue immobilized in Ethyl Cellulose **746**

E.58 BromoPhenol Blue immobilized in PolyMethylMethAcrylate (=PMMA) **747**

Optical OXYGEN SENSORS

E.1 Iridium(III) Coumarin Complex immobilized in Cellulose Acetate

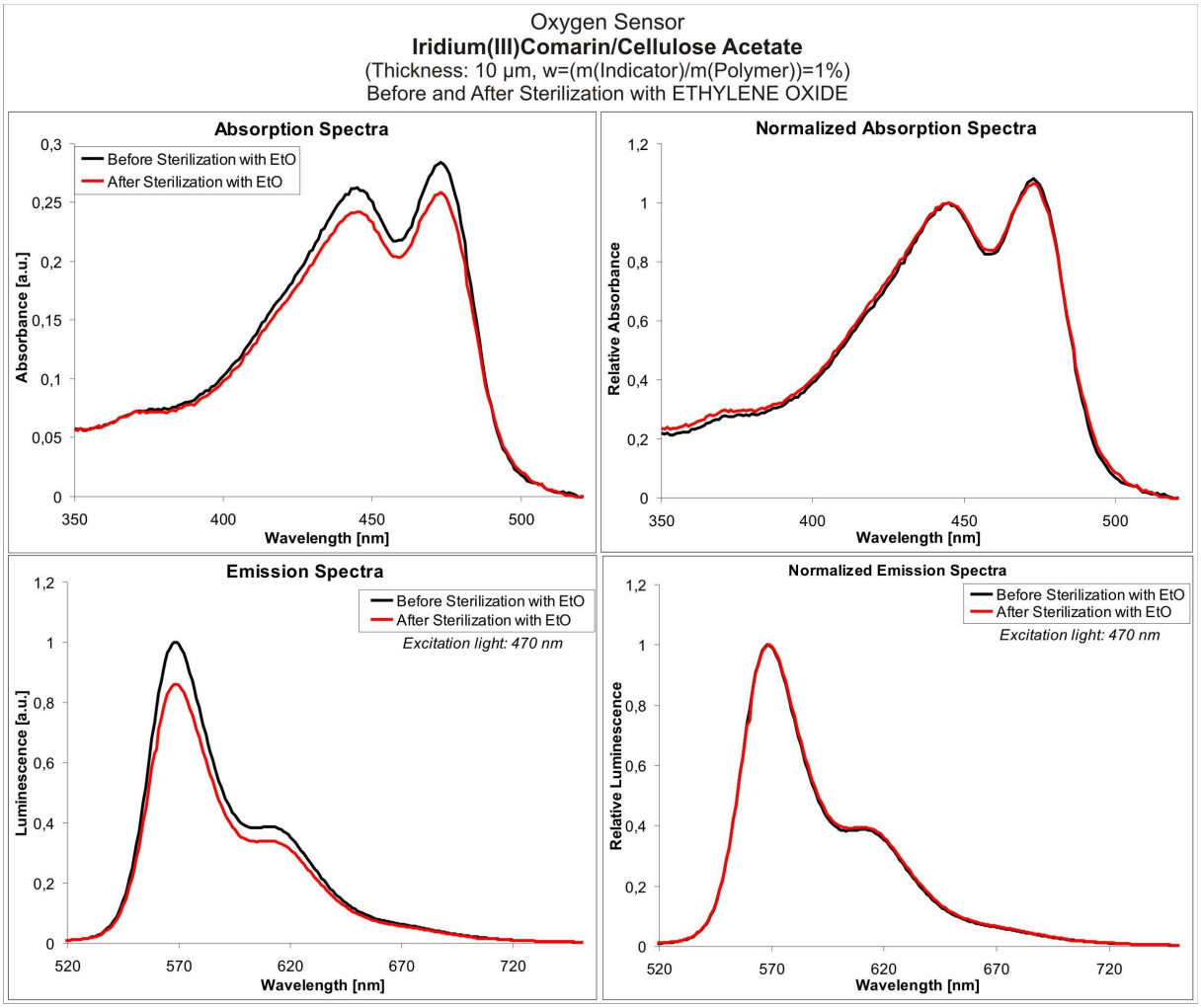

Sterilization with ETHYLENE OXIDE	Absorption Spectra	Emission Spectra
Alterations in Absorption/Emission Intensity	7,84% decrease	13,88% decrease
Alterations in Absorption/Emission Curve Form	Unaltered.	Unaltered.

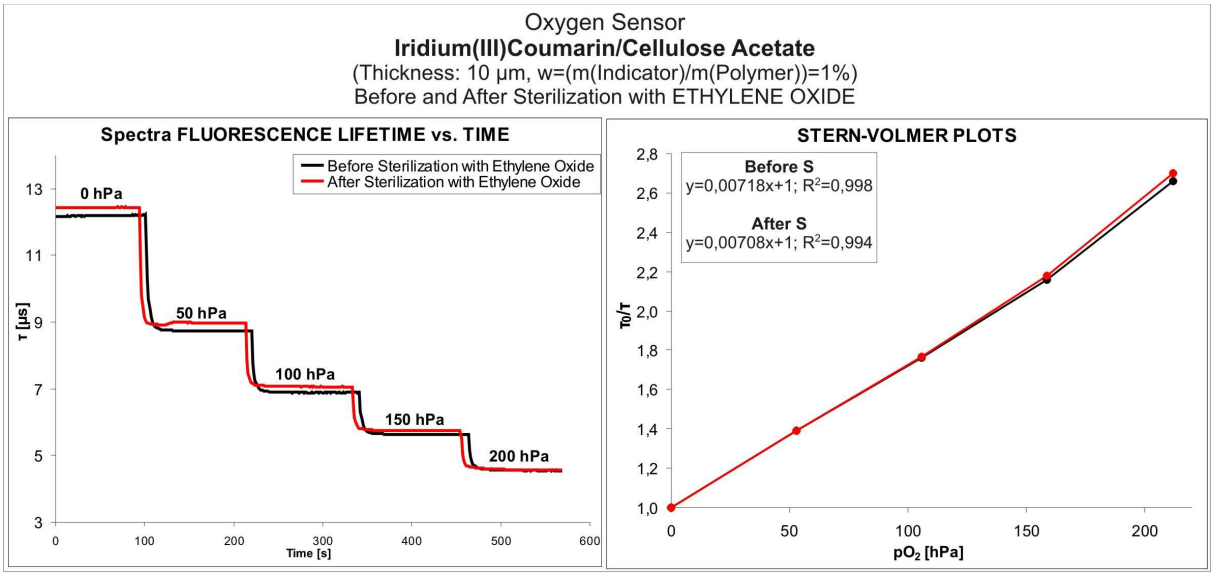

Sterilization with ETHYLENE OXIDE	Luminescence Lifetime	Stern-Volmer Plot
Alterations in Luminescence Lifetime and Slope	1,61% increase of τ_0	1,39% decrease of slope
	2,78% increase of τ at 50 hPa	
	0,14% increase of τ at 100 hPa	
	1,91% increase of τ at 150 hPa	
	0,65% increase of τ at 200 hPa	

E.2 Iridium(III) Coumarin Complex immobilized in Ethyl Cellulose

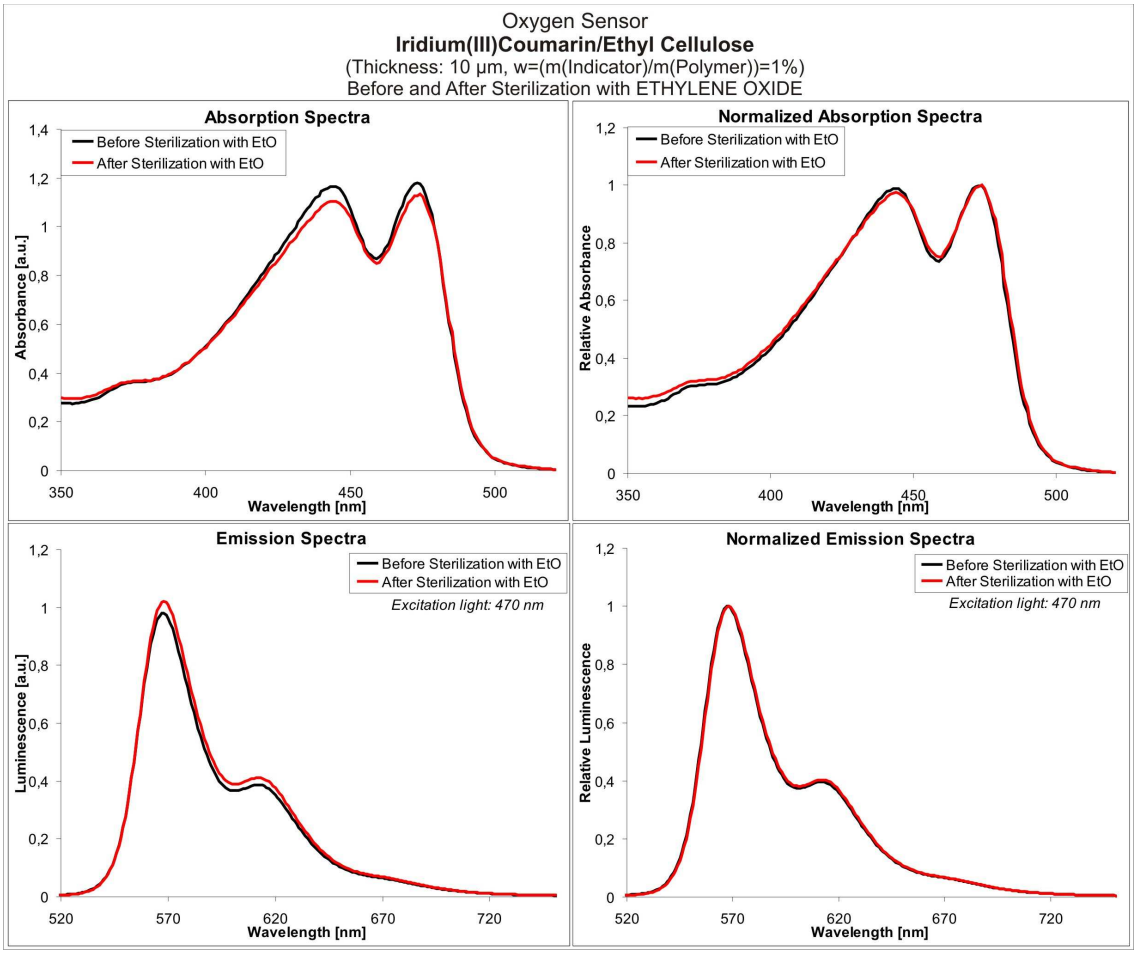

Sterilization with ETHYLENE OXIDE	Absorption Spectra	Emission Spectra
Alterations in Absorption/Emission Intensity	3,79% decrease	2,02% increase
Alterations in Absorption/Emission Curve Form	Unaltered.	Unaltered.

Oxygen Sensor
Iridium(III)Coumarin/Ethyl Cellulose
(Thickness: 10 µm, w=(m(Indicator)/m(Polymer))=1%)
Before and After Sterilization with ETHYLENE OXIDE

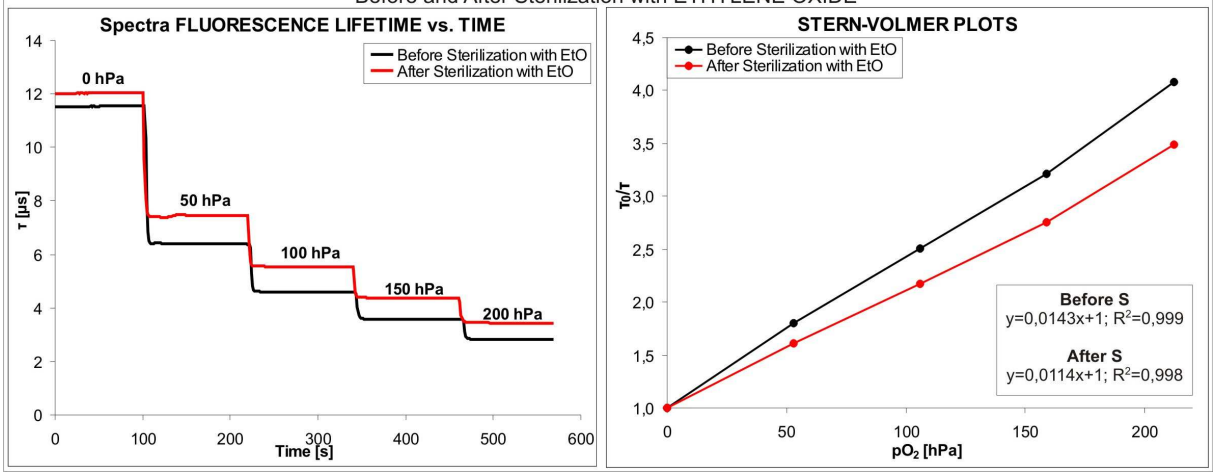

Sterilization with ETHYLENE OXIDE	Luminescence Lifetime	Stern-Volmer Plot
Alterations in Luminescence Lifetime and Slope	4,17% increase of τ_0	20,28% decrease of slope
	14,34% increase of τ at 50 hPa	
	17,00% increase of τ at 100 hPa	
	18,08% increase of τ at 150 hPa	
	18,07% increase of τ at 200 hPa	

E.3 Iridium(III) Coumarin Complex immobilized in HydroGel HydroMed D4/D7

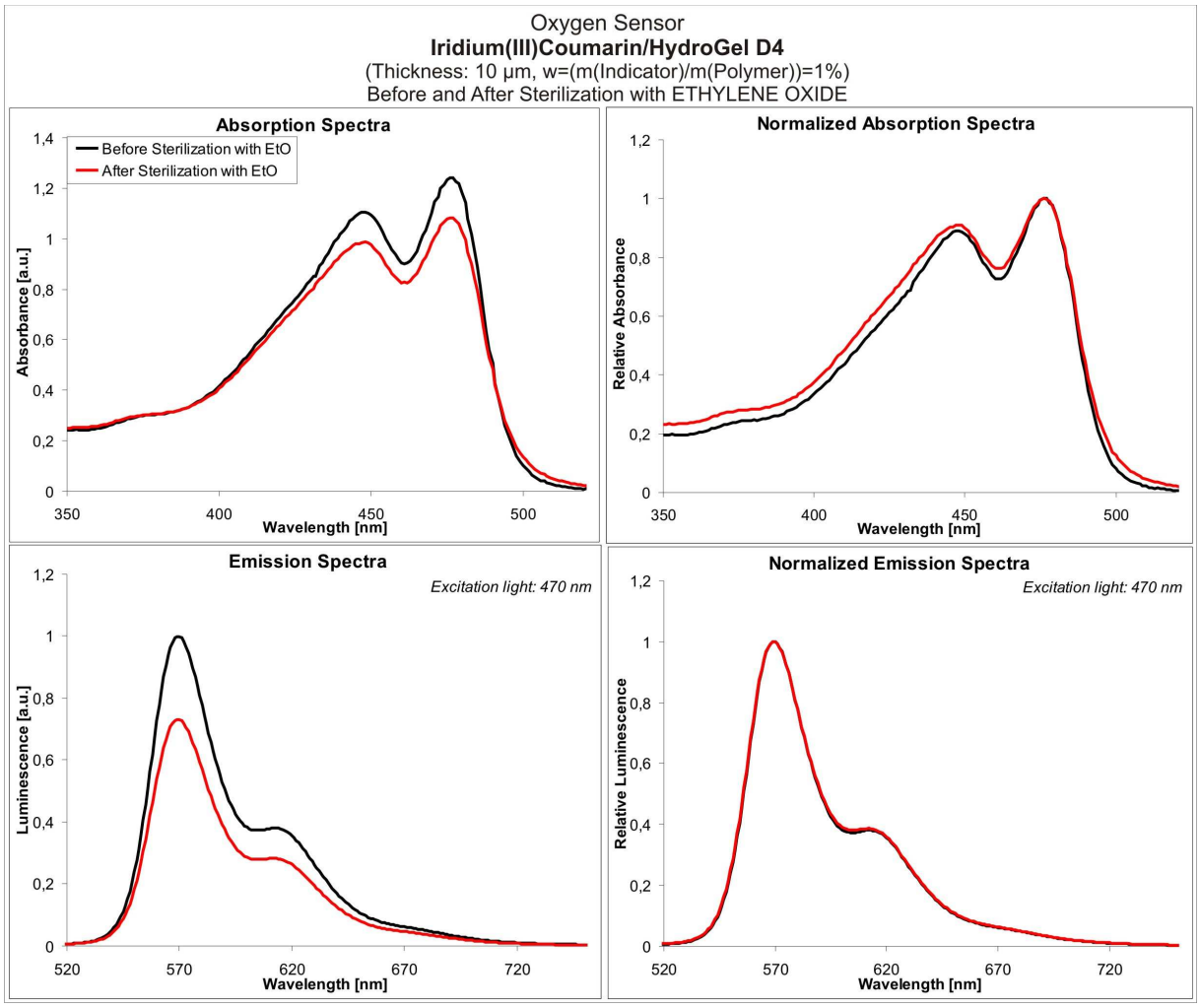

Sterilization with ETHYLENE OXIDE	Absorption Spectra	Emission Spectra
Alterations in Absorption/Emission Intensity	12,80% decrease	26,83% decrease
Alterations in Absorption/Emission Curve Form	Altered absorption between 350-460 nm and 490-520 nm.	Unaltered.

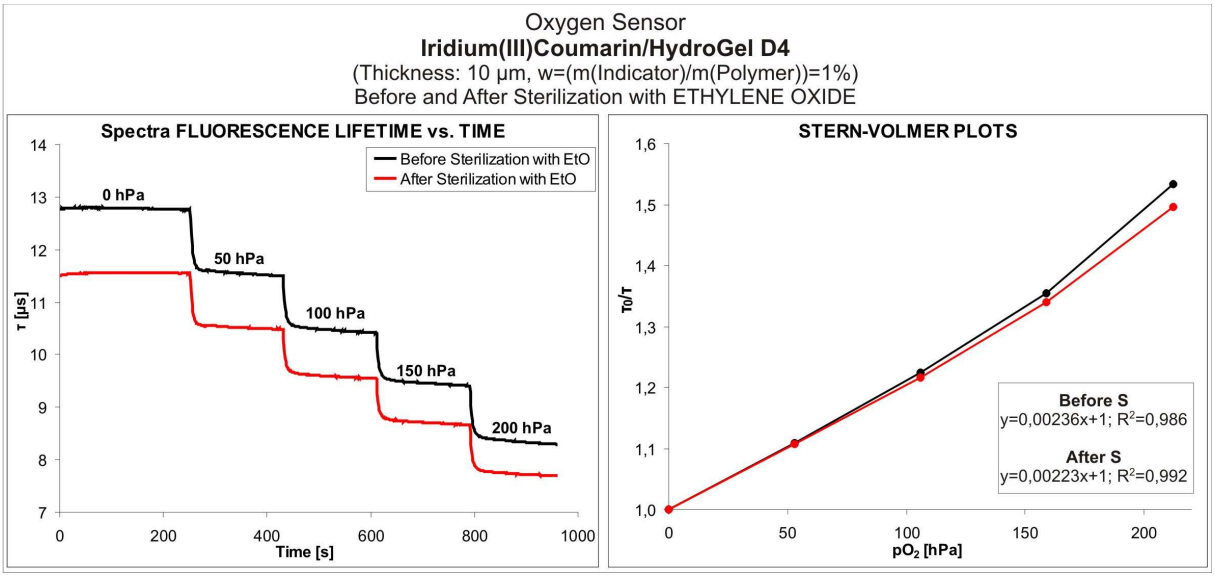

Sterilization with ETHYLENE OXIDE	Luminescence Lifetime	Stern-Volmer Plot
Alterations in Luminescence Lifetime and Slope	9,37% decrease of τ_0	5,51% decrease of slope
	8,70% decrease of τ at 50 hPa	
	8,67% decrease of τ at 100 hPa	
	7,93% decrease of τ at 150 hPa	
	7,54% decrease of τ at 200 hPa	

E.4 Iridium(III) Coumarin Complex immobilized in HydroThane with 5% water content

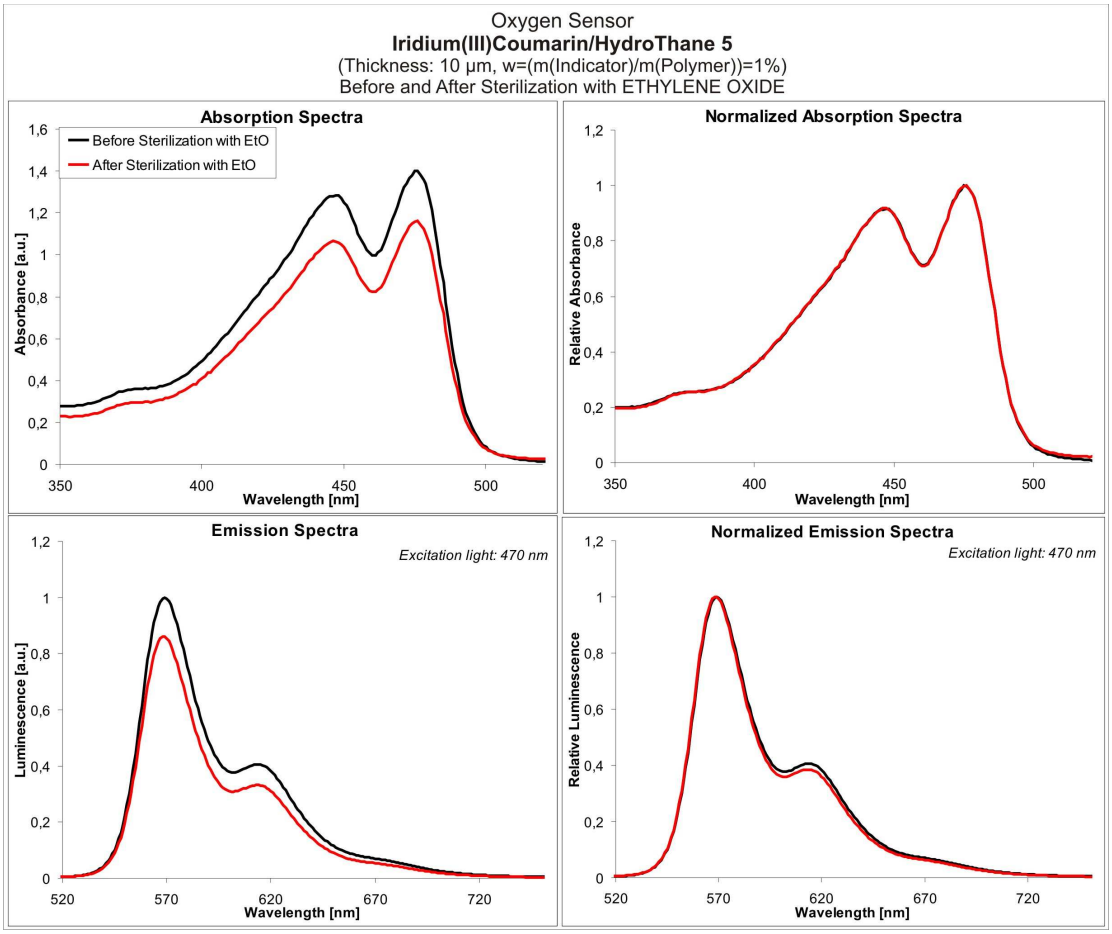

Sterilization with ETHYLENE OXIDE	Absorption Spectra	Emission Spectra
Alterations in Absorption/Emission Intensity	17,21% decrease	14,00% decrease
Alterations in Absorption/Emission Curve Form	Unaltered.	Unaltered.

Oxygen Sensor
Iridium(III)Coumarin/HydroThane 5
(Thickness: 10 µm, w=(m(Indicator)/m(Polymer))=1%)
Before and After Sterilization with ETHYLENE OXIDE

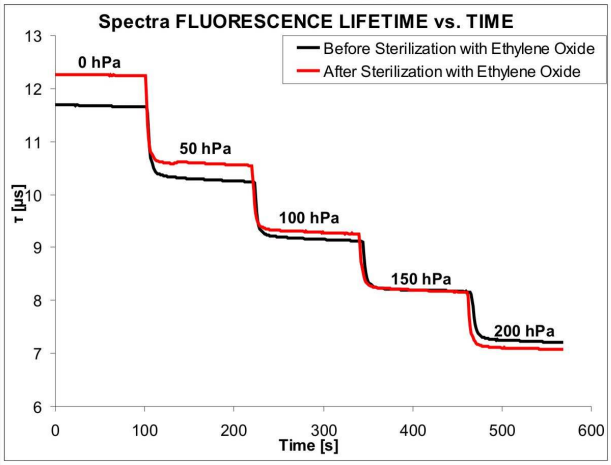

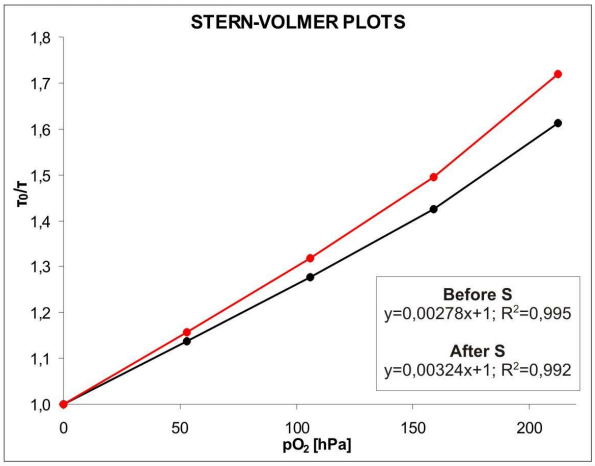

Sterilization with ETHYLENE OXIDE	Luminescence Lifetime	Stern-Volmer Plot
Alterations in Luminescence Lifetime and Slope	4,88% increase of τ_0	14,20% increase of slope
	2,83% increase of τ at 50 hPa	
	1,40% increase of τ at 100 hPa	
	0,85% increase of τ at 150 hPa	
	1,94% decrease of τ at 200 hPa	

E.5 Iridium(III) Coumarin Complex immobilized in Poly(Sulfone)

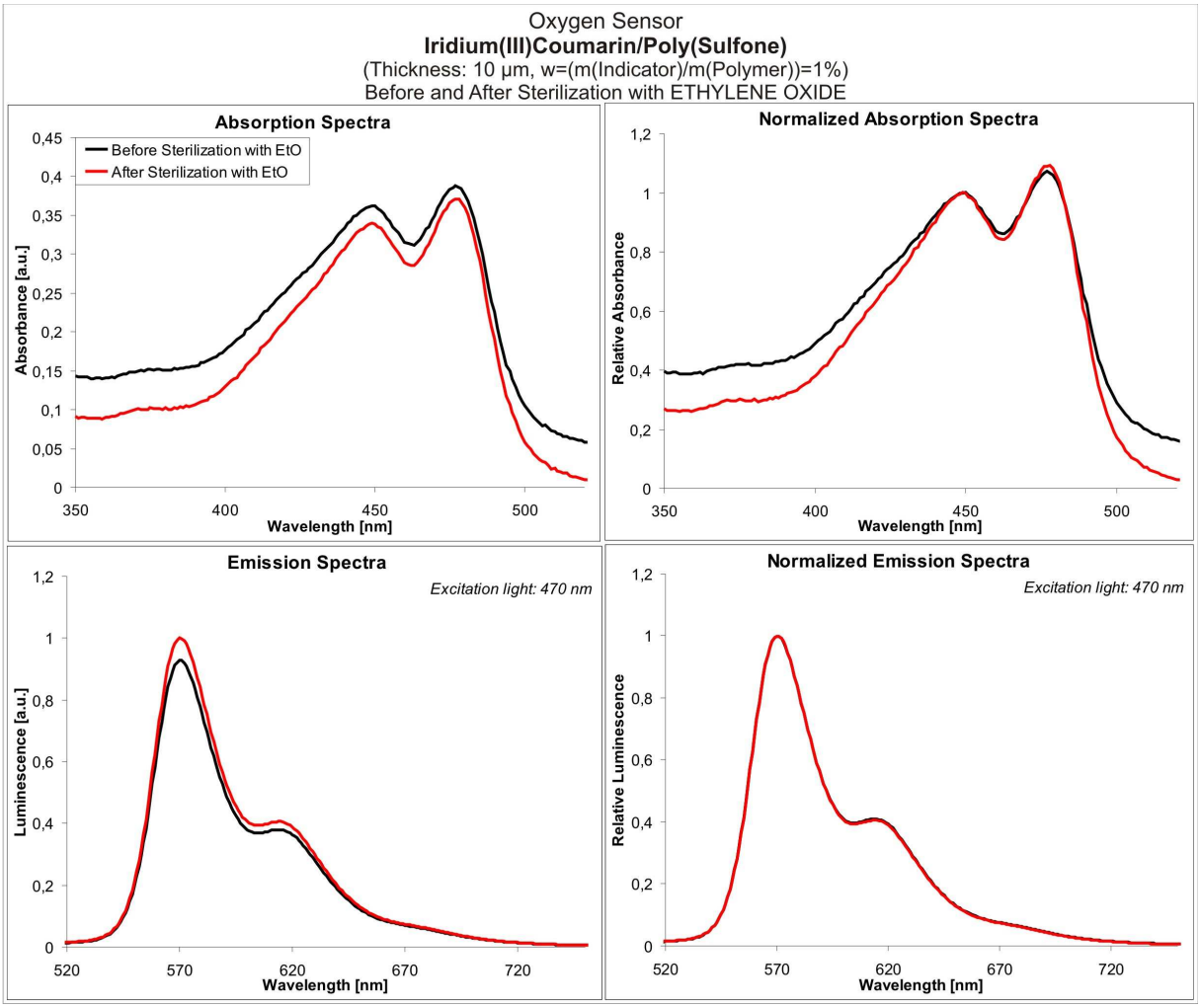

Sterilization with ETHYLENE OXIDE	Absorption Spectra	Emission Spectra
Alterations in Absorption/Emission Intensity	6,19% decrease	7,19% decrease
Alterations in Absorption/Emission Curve Form	Altered absorption between 350-440 nm and 490-520 nm.	Unaltered.

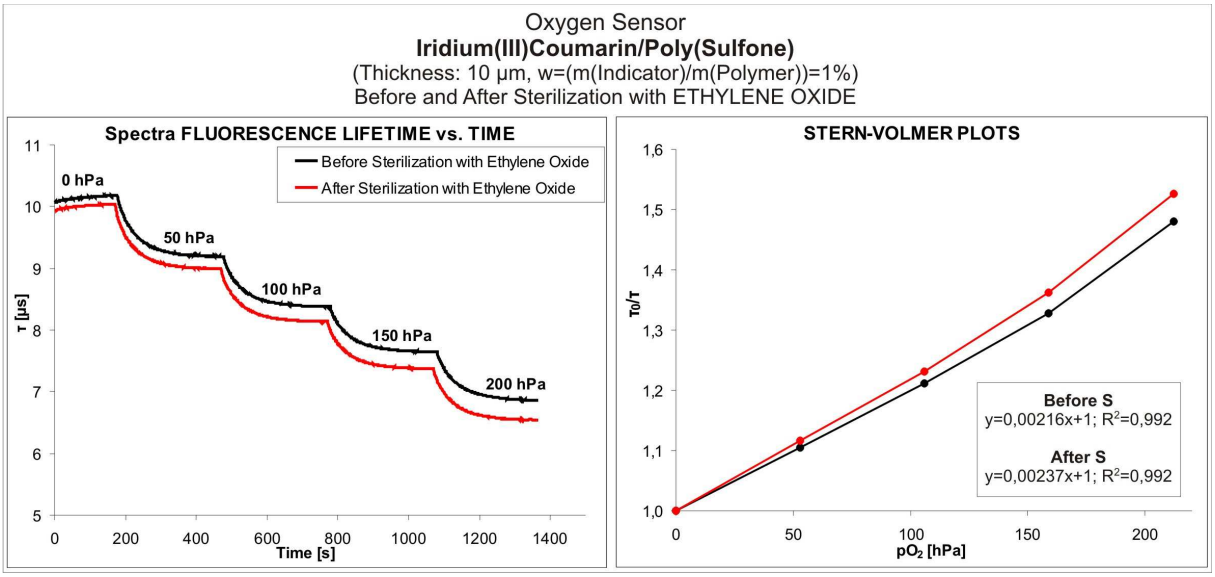

Sterilization with ETHYLENE OXIDE	Luminescence Lifetime	Stern-Volmer Plot
Alterations in Luminescence Lifetime and Slope	1,96% decrease of τ_0	8,86% increase of slope
	2,07% decrease of τ at 50 hPa	
	2,86% decrease of τ at 100 hPa	
	3,66% decrease of τ at 150 hPa	
	4,80% decrease of τ at 200 hPa	

E.6 Iridium(III) Coumarin Complex immobilized in Poly(PhenylSilsesQuioxane)

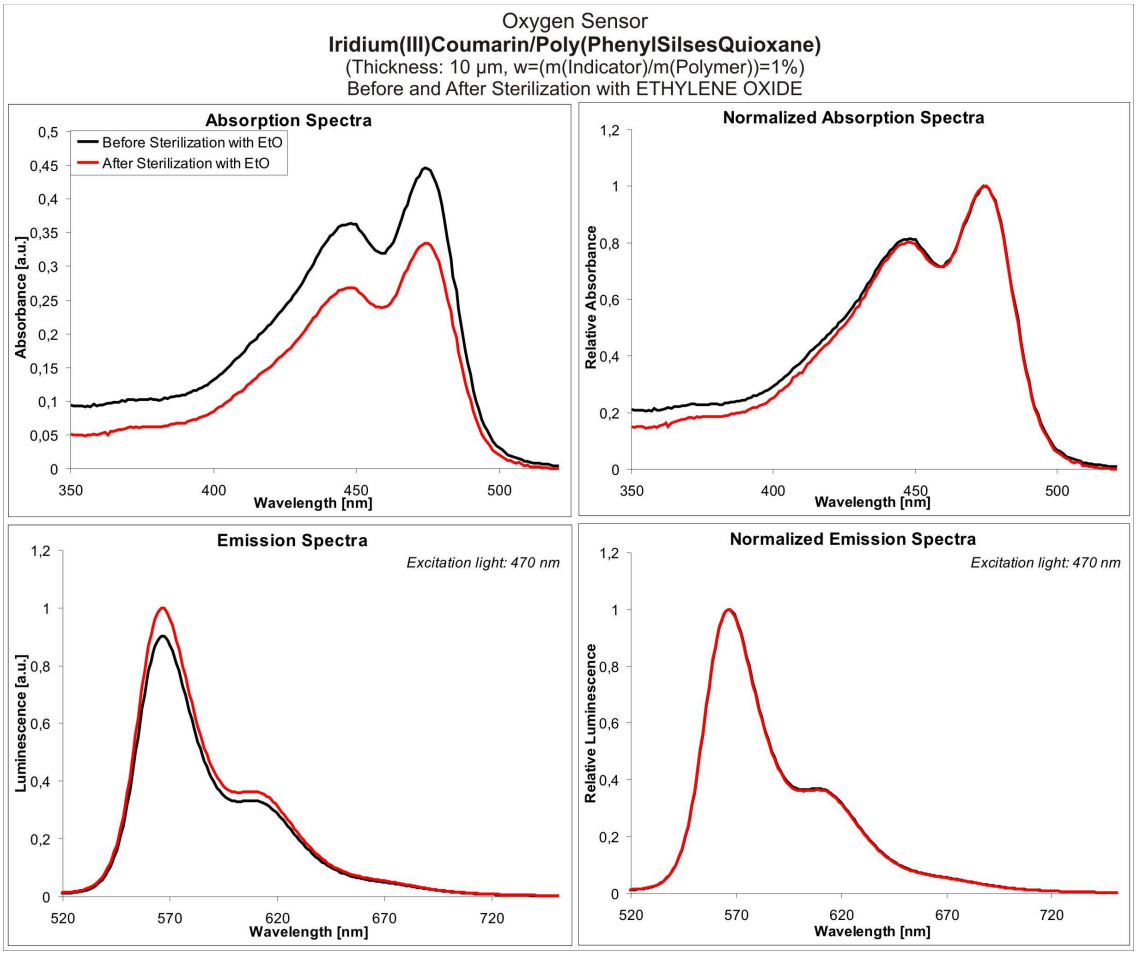

Sterilization with ETHYLENE OXIDE	Absorption Spectra	Emission Spectra
Alterations in Absorption/Emission Intensity	25,03% decrease	9,72% increase
Alterations in Absorption/Emission Curve Form	Slightly altered absorption between 350-430 nm.	Unaltered.

Oxygen Sensor
Iridium(III)Coumarin/Poly(PhenylSilsesQuioxane)
(Thickness: 10 µm, w=(m(Indicator)/m(Polymer))=1%)
Before and After Sterilization with ETHYLENE OXIDE

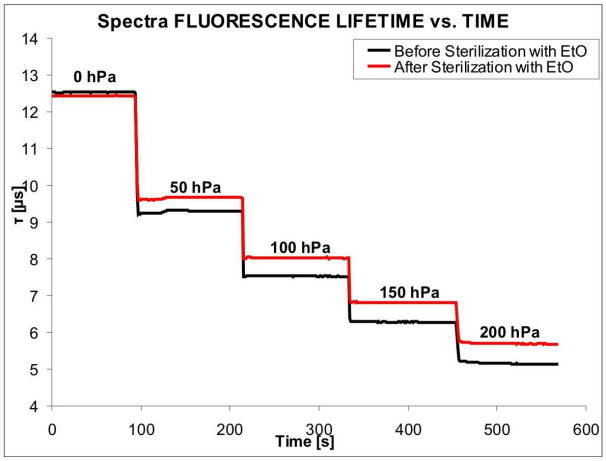

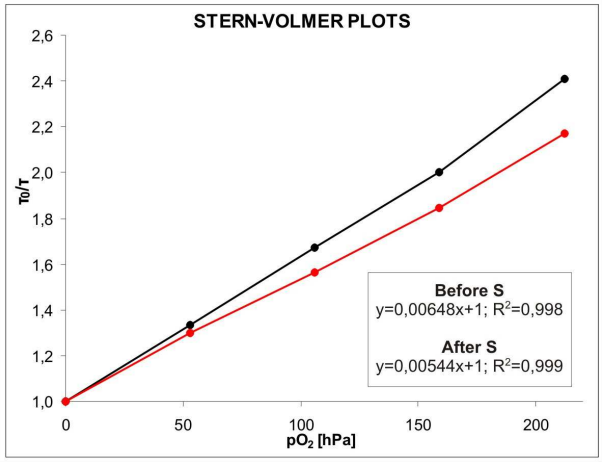

Sterilization with ETHYLENE OXIDE	Luminescence Lifetime	Stern-Volmer Plot
Alterations in Luminescence Lifetime and Slope	0,80% decrease of τ_0	16,05% decrease of slope
	3,83% increase of τ at 50 hPa	
	6,11% increase of τ at 100 hPa	
	7,78% increase of τ at 150 hPa	
	9,49% increase of τ at 200 hPa	

E.7 Iridium(III) Coumarin Complex immobilized in Poly(Styrene)

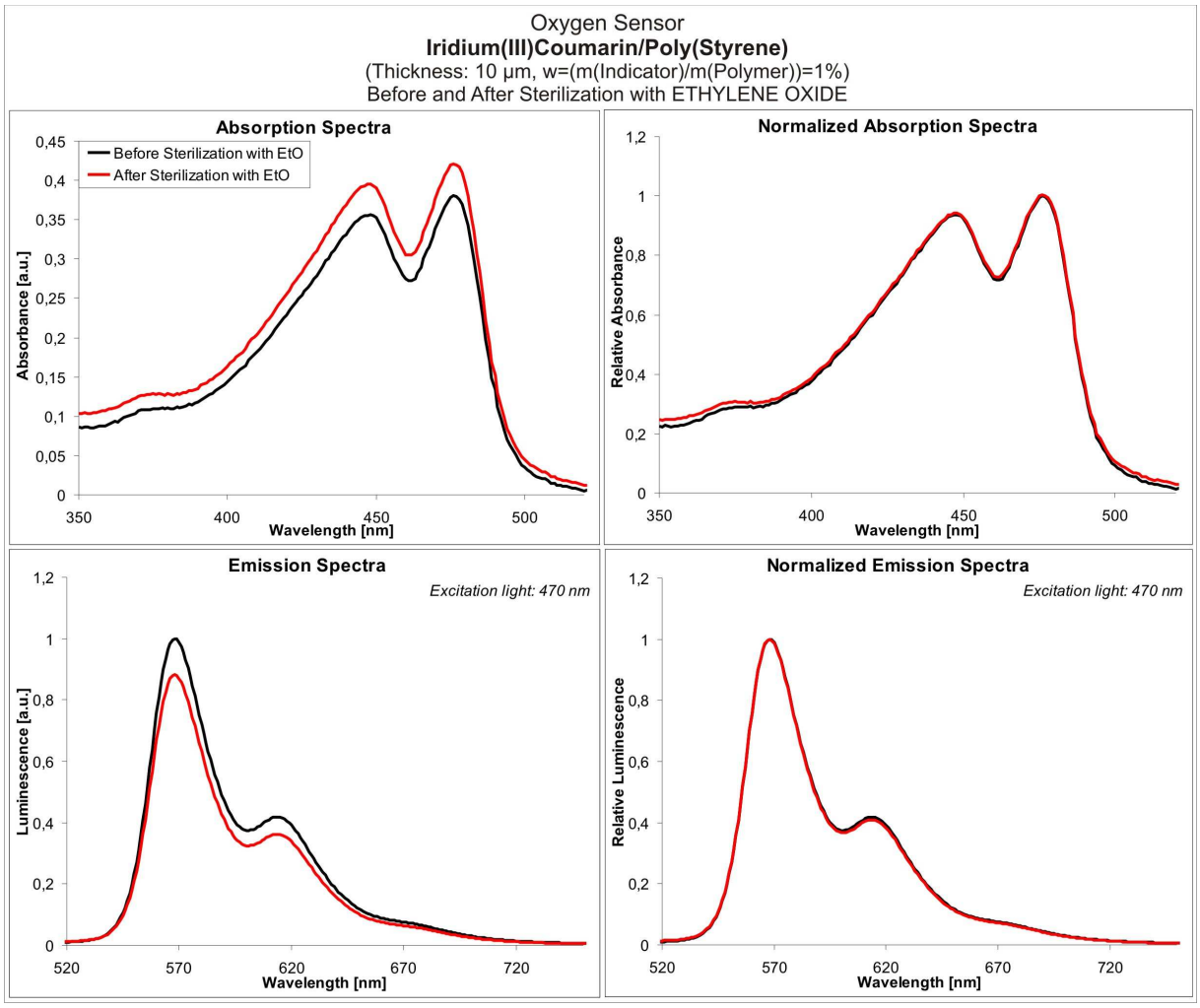

Sterilization with ETHYLENE OXIDE	Absorption Spectra	Emission Spectra
Alterations in Absorption/Emission Intensity	9,31% decrease	11,69% decrease
Alterations in Absorption/Emission Curve Form	Unaltered.	Unaltered.

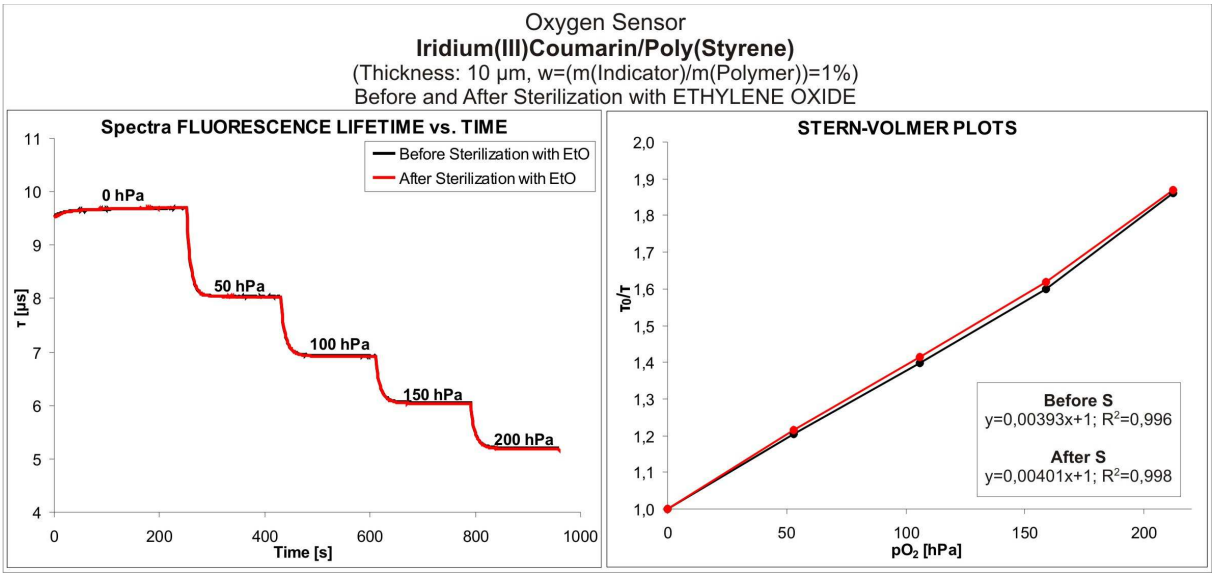

Sterilization with ETHYLENE OXIDE	Luminescence Lifetime	Stern-Volmer Plot
Alterations in Luminescence Lifetime and Slope	0,10% increase of τ_0	1,99% increase of slope
	0,87% decrease of τ at 50 hPa	
	0,87% decrease of τ at 100 hPa	
	0,99% decrease of τ at 150 hPa	
	0,38% decrease of τ at 200 hPa	

E.8 Iridium(III) Coumarin Complex immobilized in Poly(Styrene-co-AcryloNitrile)

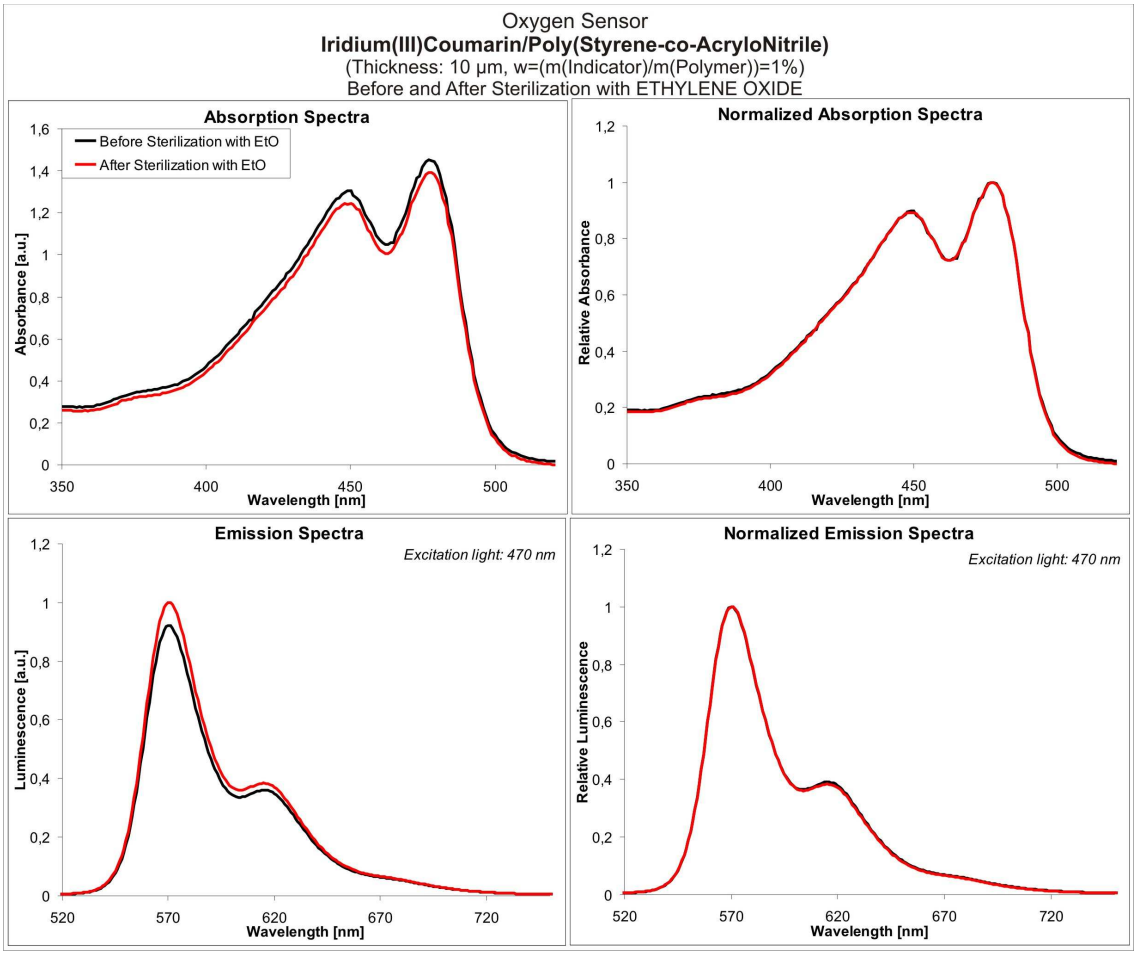

Sterilization with ETHYLENE OXIDE	Absorption Spectra	Emission Spectra
Alterations in Absorption/Emission Intensity	4,04% decrease	7,80% increase
Alterations in Absorption/Emission Curve Form	Unaltered.	Unaltered.

Oxygen Sensor
Iridium(III)Coumarin/Poly(Styrene-co-AcryloNitrile)
(Thickness: 10 µm, w=(m(Indicator)/m(Polymer))=1%)
Before and After Sterilization with ETHYLENE OXIDE

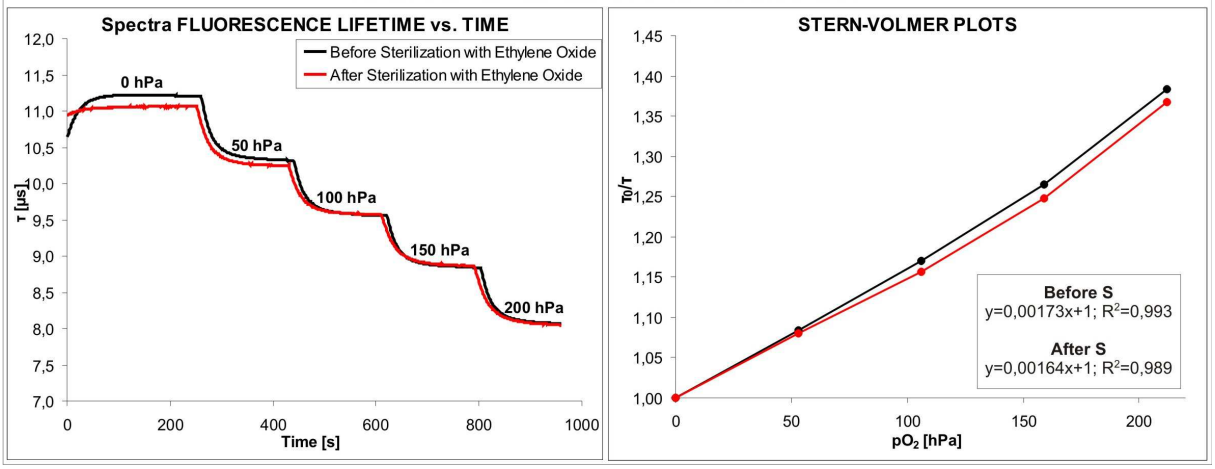

Sterilization with ETHYLENE OXIDE	Luminescence Lifetime	Stern-Volmer Plot
Alterations in Luminescence Lifetime and Slope	0,89% decrease of τ_0	5,20% decrease of slope
	1,06% decrease of τ at 50 hPa	
	0,21% decrease of τ at 100 hPa	
	0,11% decrease of τ at 150 hPa	
	0,25% decrease of τ at 200 hPa	

E.9 Iridium(III) Coumarin Complex immobilized in Poly(Styrene-co-MaleicAnhydride)

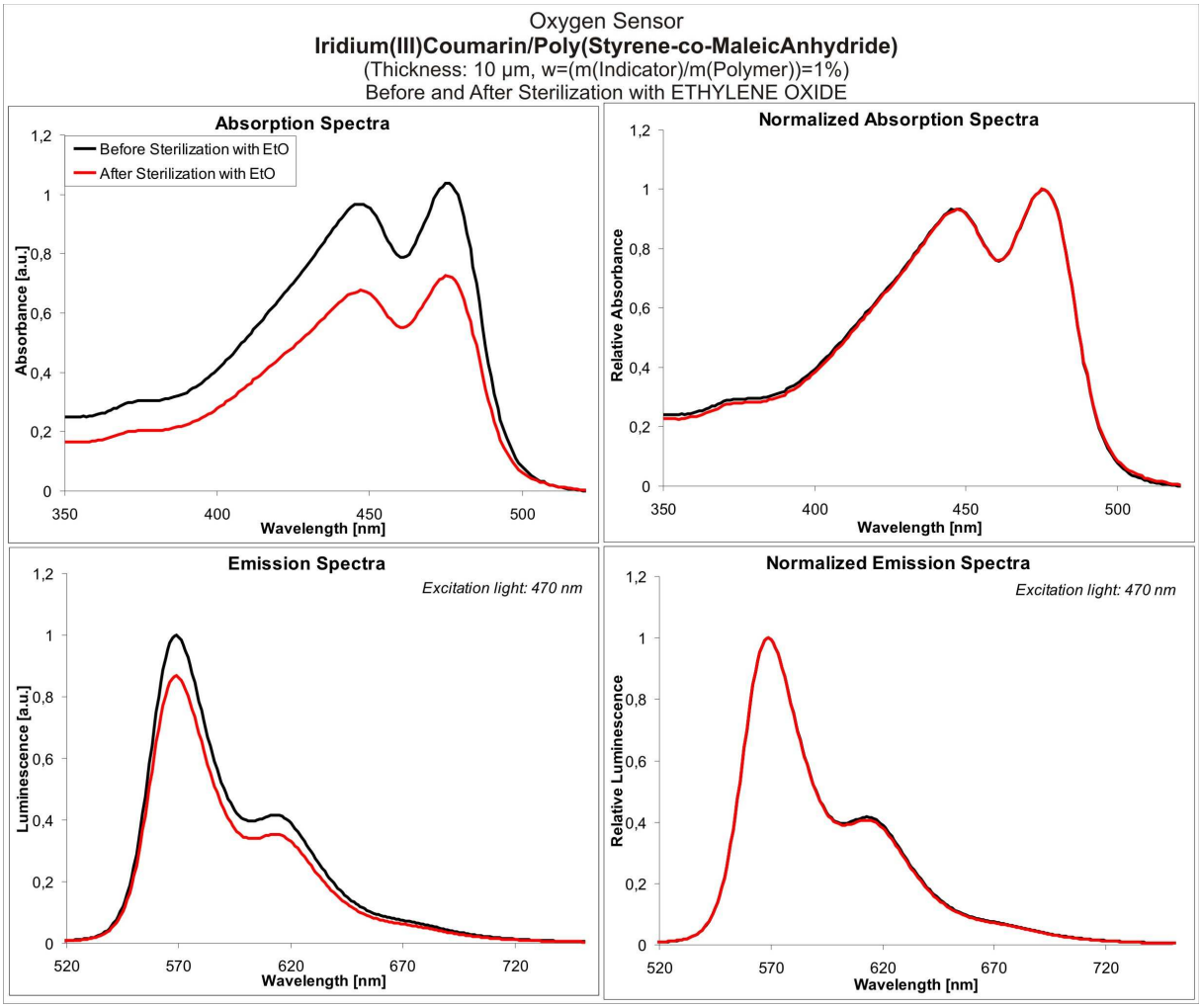

Sterilization with ETHYLENE OXIDE	Absorption Spectra	Emission Spectra
Alterations in Absorption/Emission Intensity	30,02% decrease	13,20% decrease
Alterations in Absorption/Emission Curve Form	Unaltered.	Unaltered.

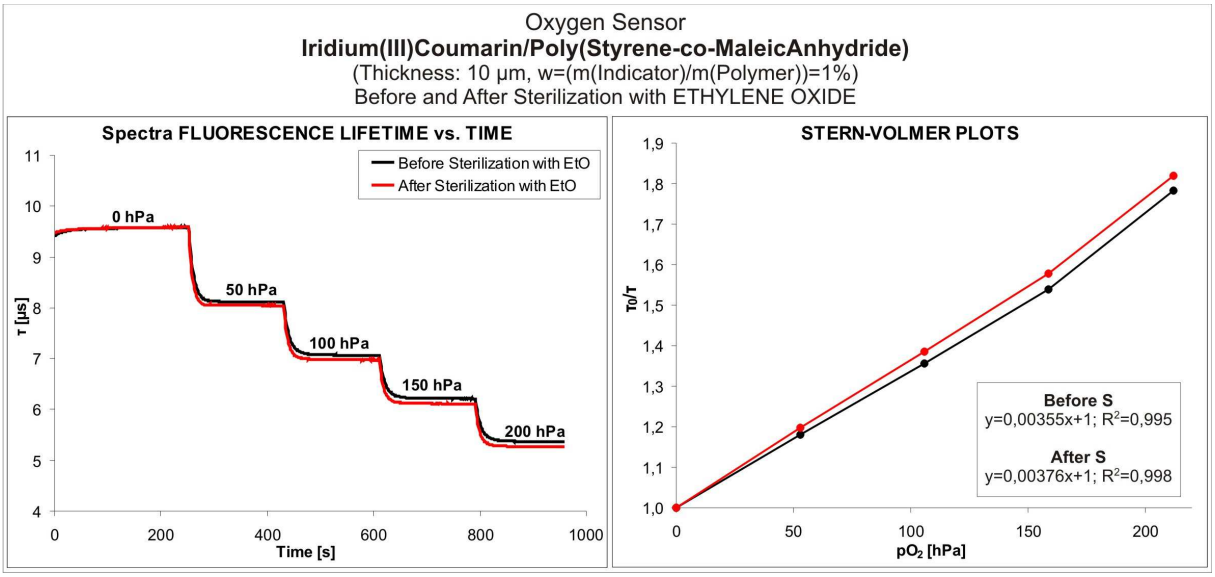

Sterilization with ETHYLENE OXIDE	Luminescence Lifetime	Stern-Volmer Plot
Alterations in Luminescence Lifetime and Slope	0,10% increase of τ_0	5,59% increase of slope
	1,48% decrease of τ at 50 hPa	
	2,12% decrease of τ at 100 hPa	
	2,25% decrease of τ at 150 hPa	
	1,86% decrease of τ at 200 hPa	

E.10 Platinum(II)Tetrakis(PentaFluorPhenyl)Porphyrin (PtTFPP) immobilized in Cellulose Acetate

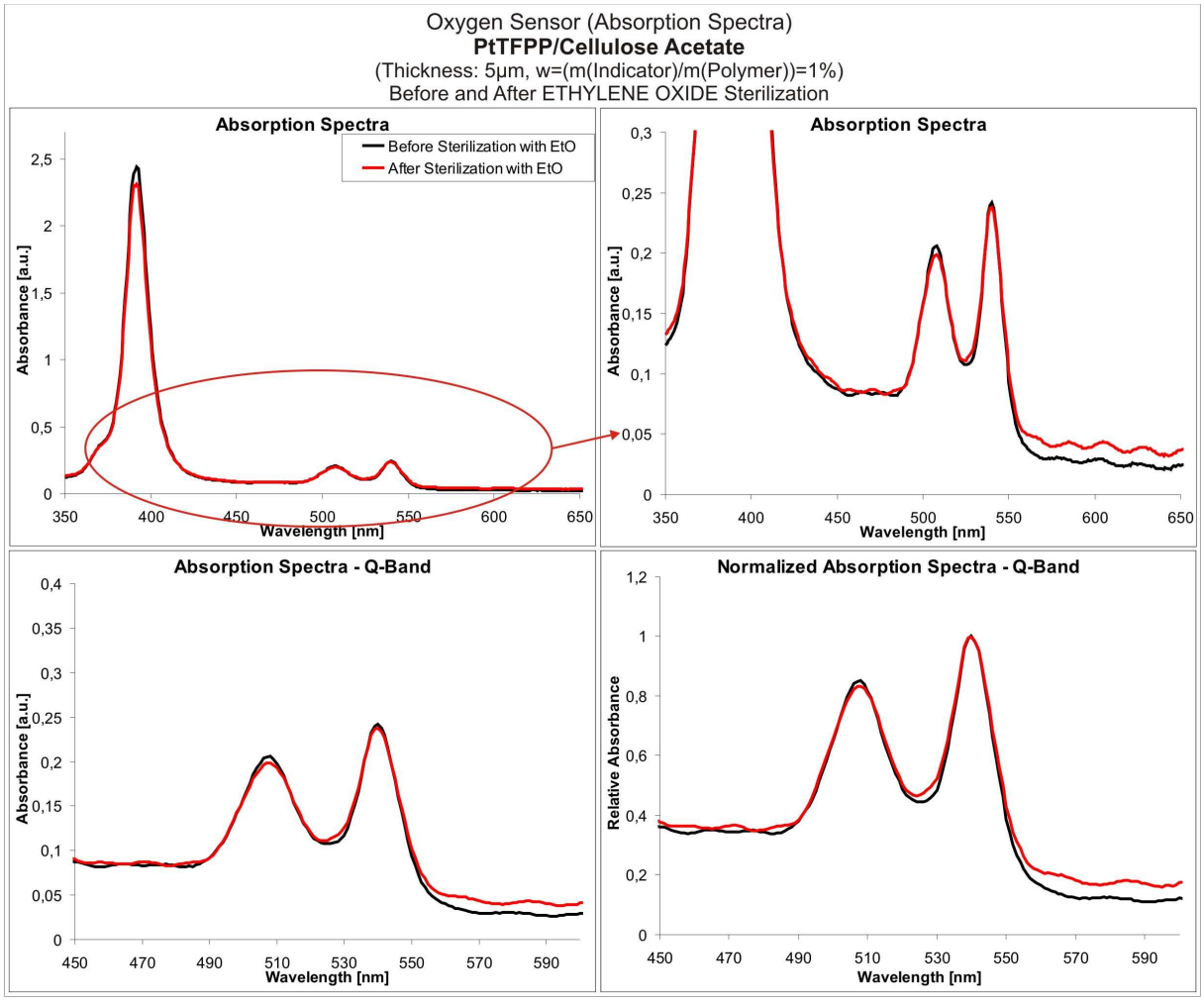

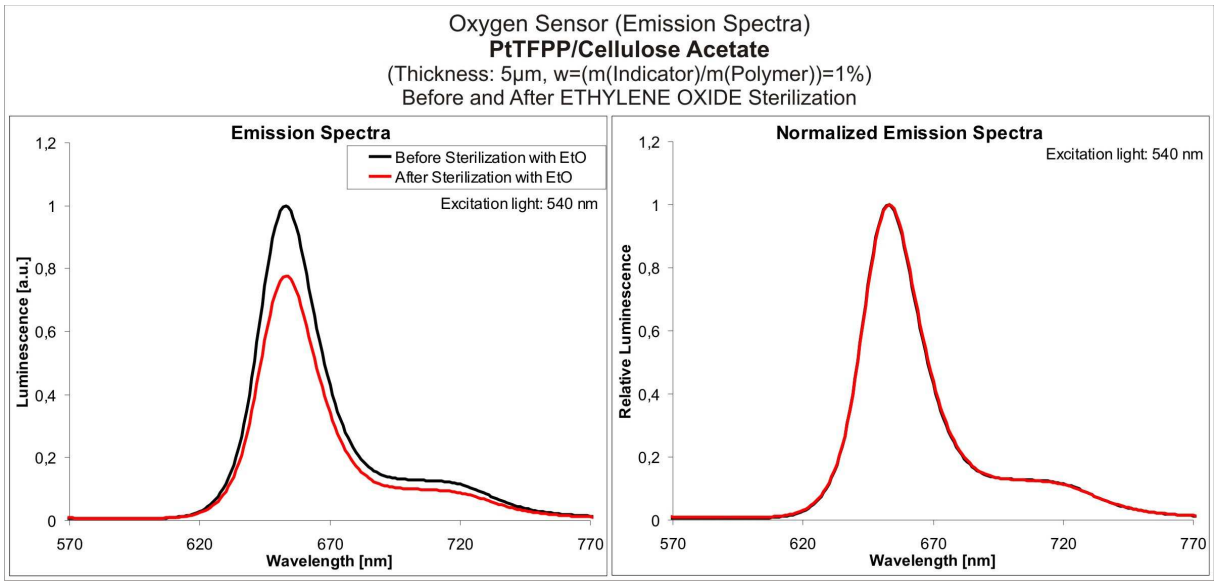

Sterilization with ETHYLENE OXIDE	Absorption Spectra	Emission Spectra
Alterations in Absorption/Emission Intensity	1,51% decrease	22,28% decrease
Alterations in Absorption/Emission Curve Form	Altered absorption curve form between 520-530 nm and 550-800 nm,	Unaltered.

Oxygen Sensor
PtTFPP/Cellulose Acetate
(Thickness: 5 µm, w=(m(Indicator)/m(Polymer))=1%)
Before and After ETHYLENE OXIDE Sterilization

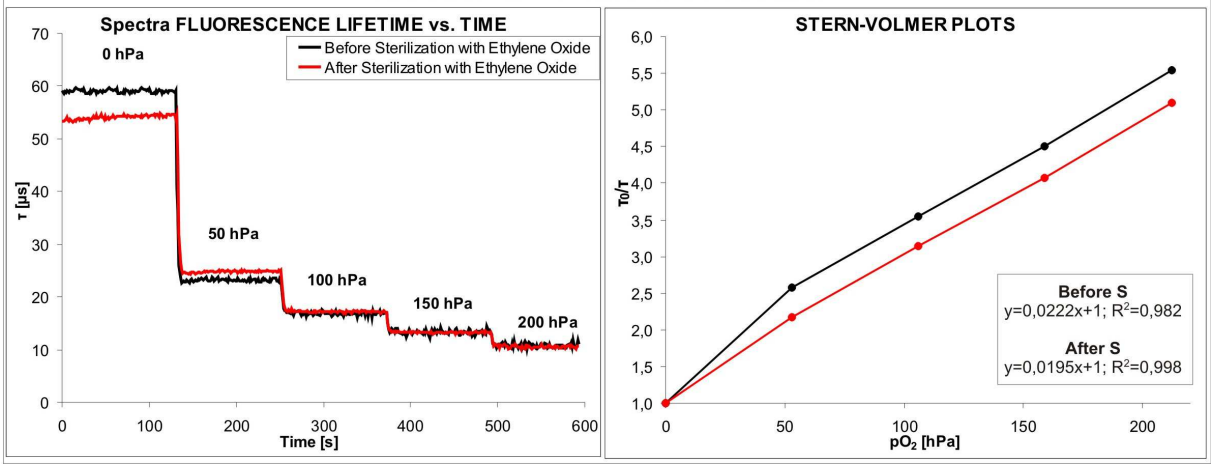

Sterilization with ETHYLENE OXIDE	Luminescence Lifetime	Stern-Volmer Plot
Alterations in Luminescence Lifetime and Slope	9,86% decrease of τ_0	12,16% decrease of slope
	6,45% increase of τ at 50 hPa	
	1,74% increase of τ at 100 hPa	
	0,75% increase of τ at 150 hPa	
	1,85% decrease of τ at 200 hPa	

E.11 Platinum(II)Tetrakis(PentaFluorPhenyl)Porphyrin (PtTFPP) immobilized in Ethyl Cellulose

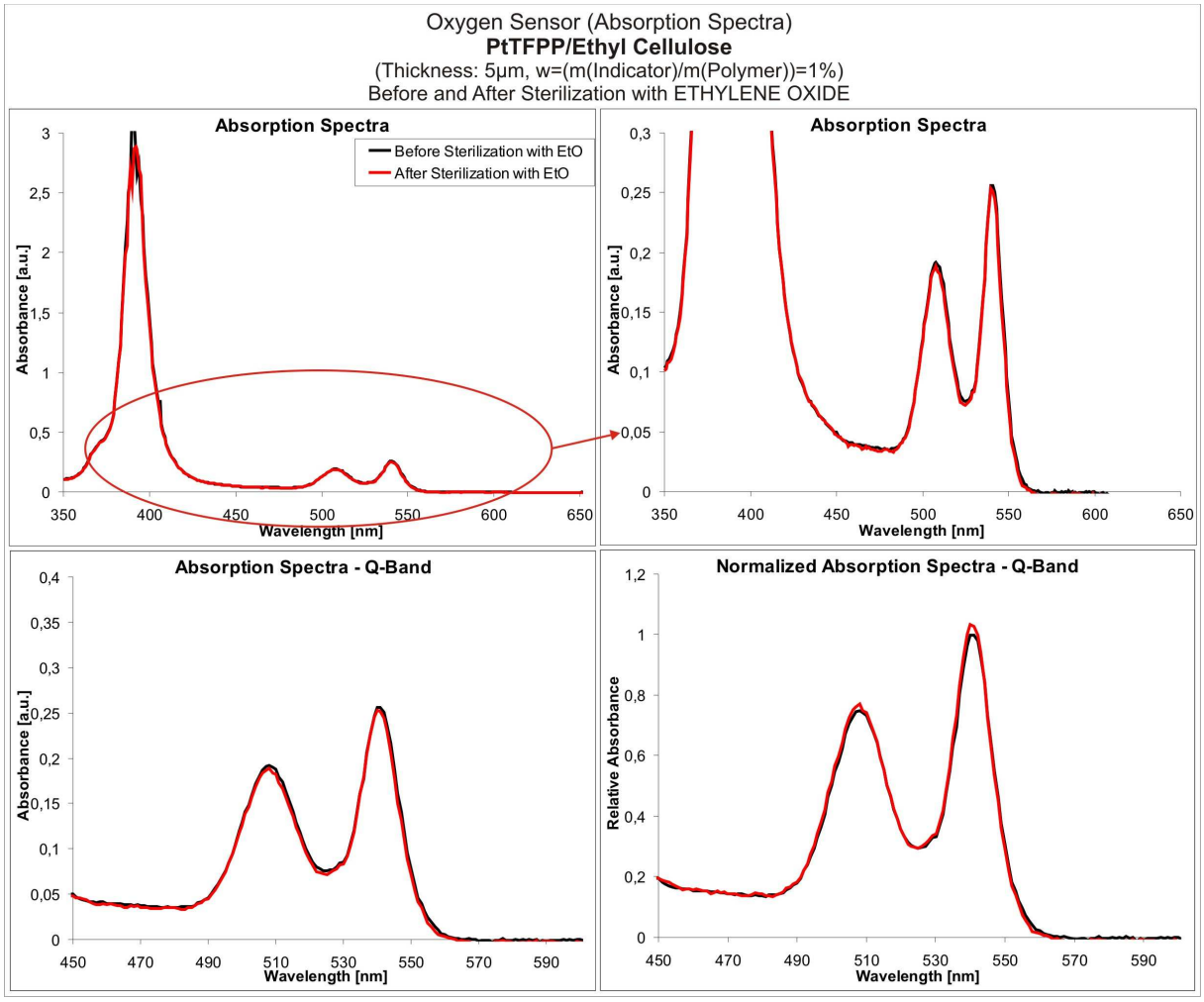

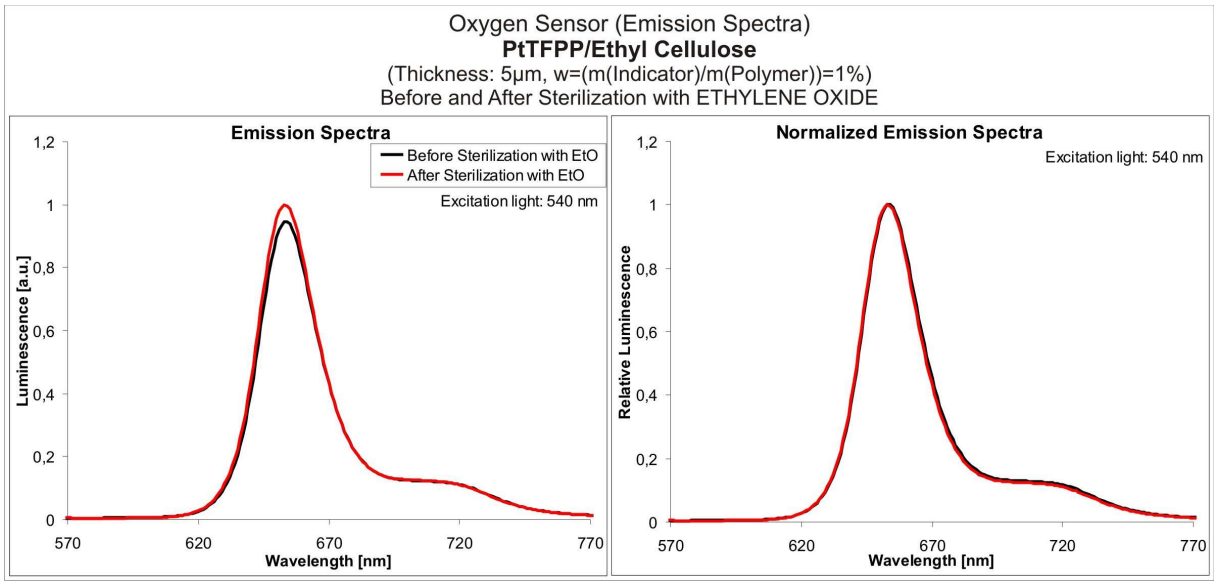

Sterilization with ETHYLENE OXIDE	Absorption Spectra	Emission Spectra
Alterations in Absorption/Emission Intensity	4,32% decrease	5,39% increase

Alterations in Absorption/Emission Curve Form	Unaltered.	Unaltered.

Oxygen Sensor
PtTFPP/Ethyl Cellulose
(Thickness: 5 µm, w=(m(Indicator)/m(Polymer))=1%)
Before and After ETHYLENE OXIDE Sterilization

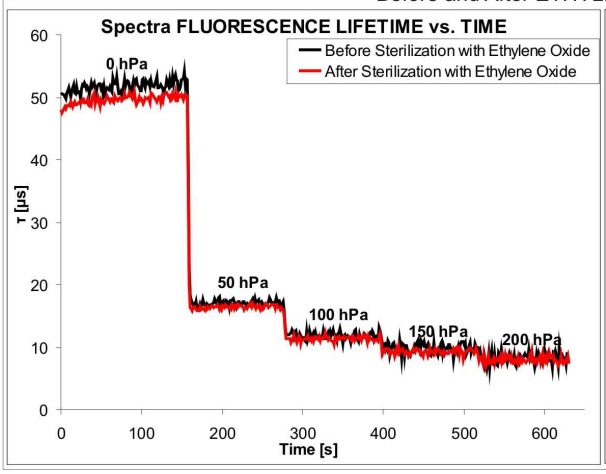

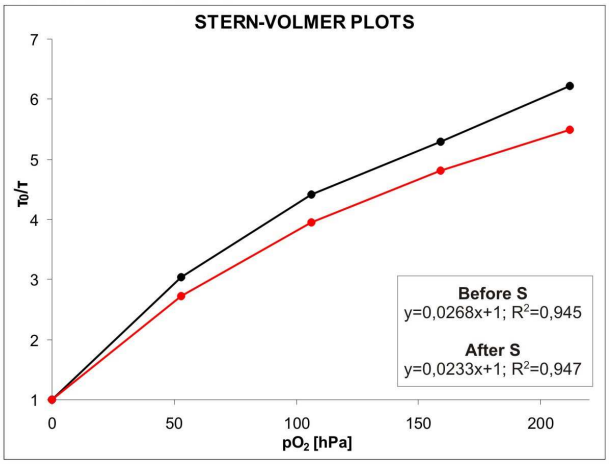

Sterilization with ETHYLENE OXIDE	Luminescence Lifetime	Stern-Volmer Plot
Alterations in Luminescence Lifetime and Slope	4,32% decrease of τ_0	13,06% decrease of slope
	5,62% decrease of τ at 50 hPa	
	5,93% decrease of τ at 100 hPa	
	6,73% decrease of τ at 150 hPa	
	4,08% decrease of τ at 200 hPa	

E.12 Platinum(II)Tetrakis(PentaFluorPhenyl)Porphyrin (PtTFPP) immobilized in HydroGel D4/D7

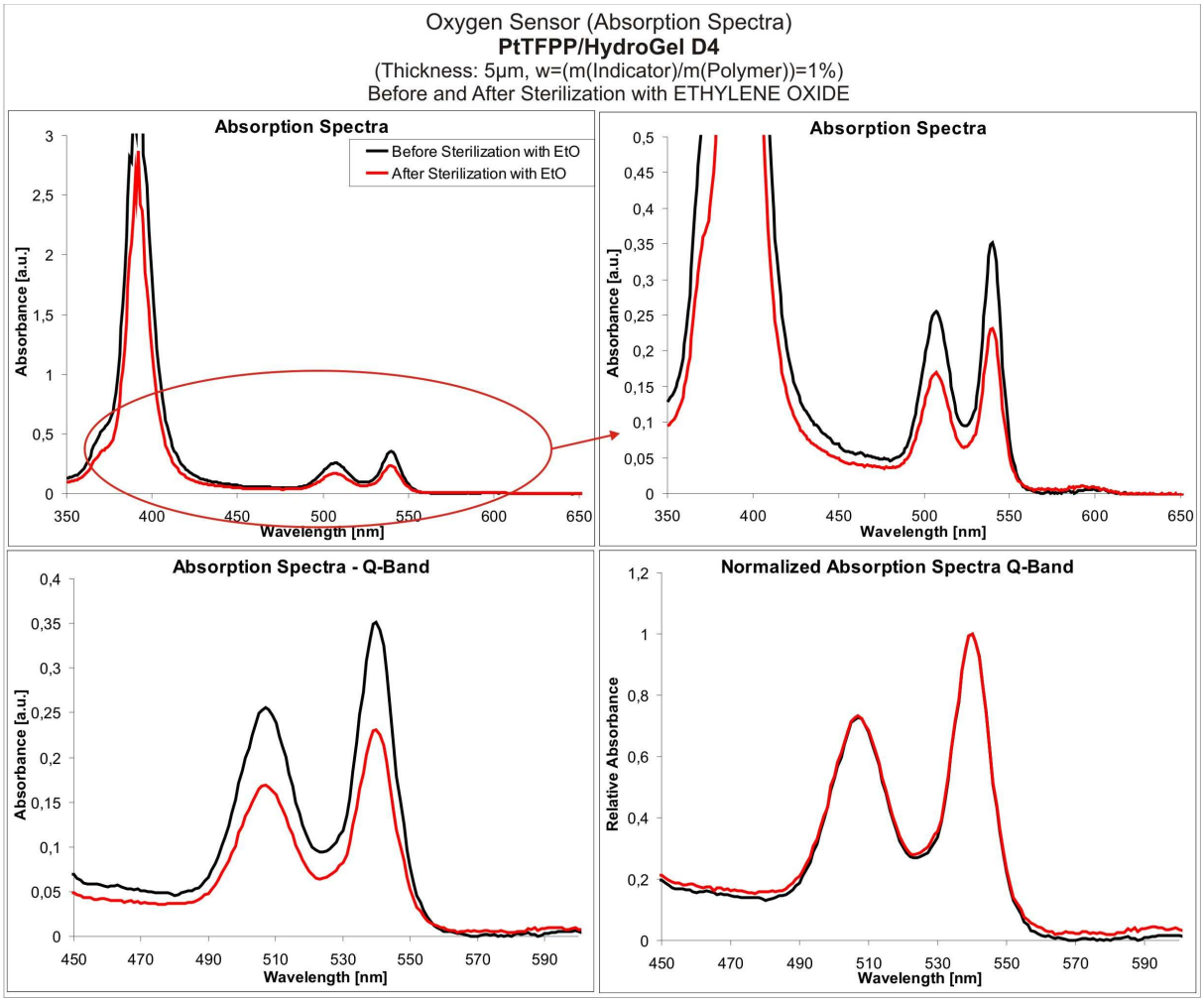

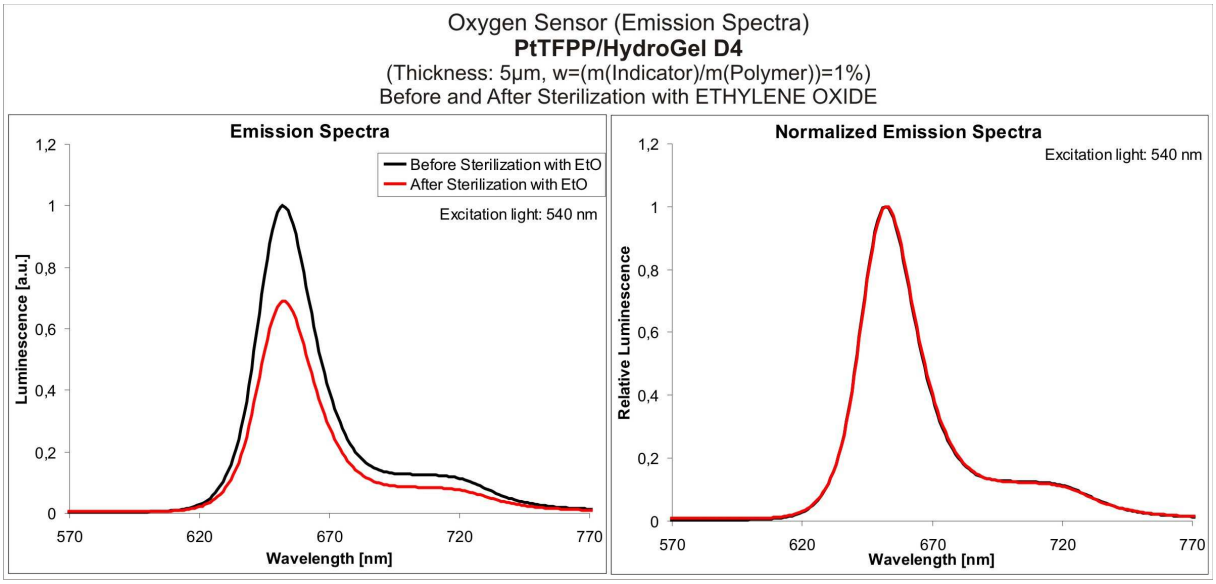

Sterilization with ETHYLENE OXIDE	Absorption Spectra	Emission Spectra
Alterations in Absorption/Emission Intensity	34,18% decrease	31,08% decrease

Alterations in Absorption/Emission Curve Form	Unaltered.	Unaltered.

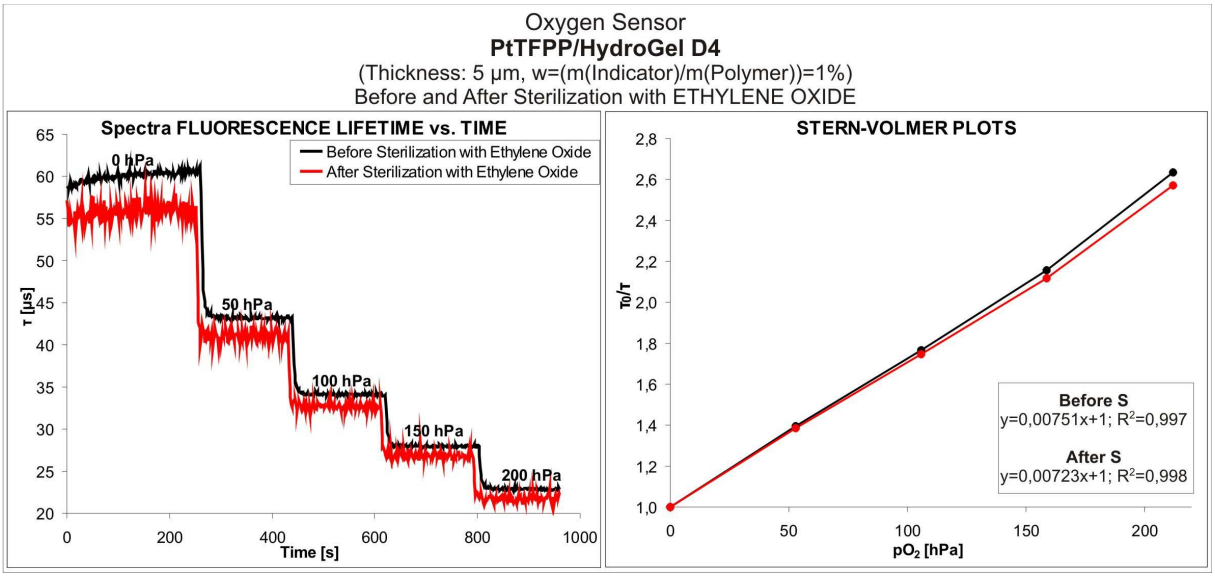

Sterilization with ETHYLENE OXIDE	Luminescence Lifetime	Stern-Volmer Plot
Alterations in Luminescence Lifetime and Slope	7,13% decrease of τ_0	3,73% decrease of slope
	6,48% decrease of τ at 50 hPa	
	5,87% decrease of τ at 100 hPa	
	5,71% decrease of τ at 150 hPa	
	4,80% decrease of τ at 200 hPa	

E.13 Platinum(II)Tetrakis(PentaFluorPhenyl)Porphyrin (PtTFPP) immobilized in HydroThane 5

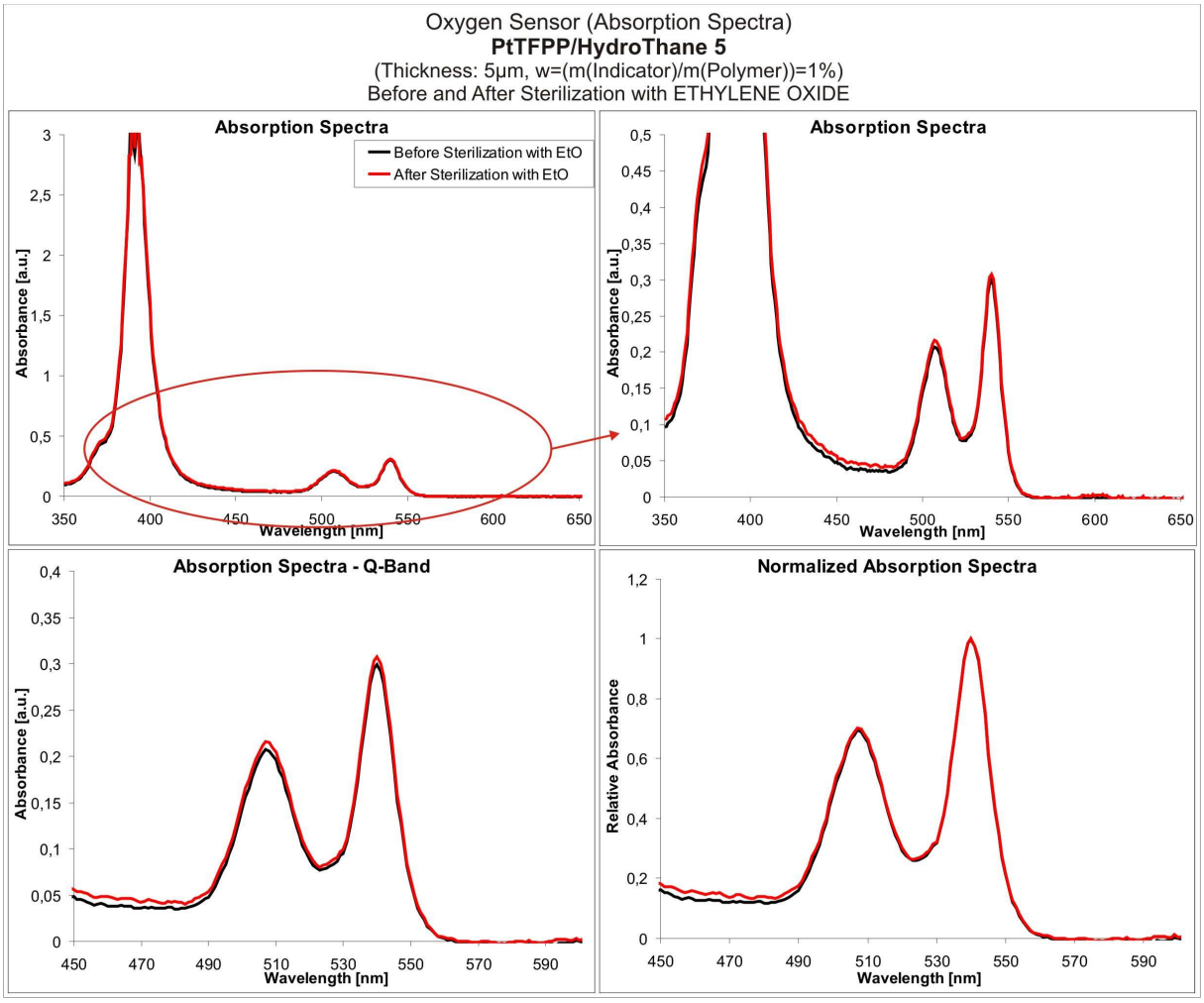

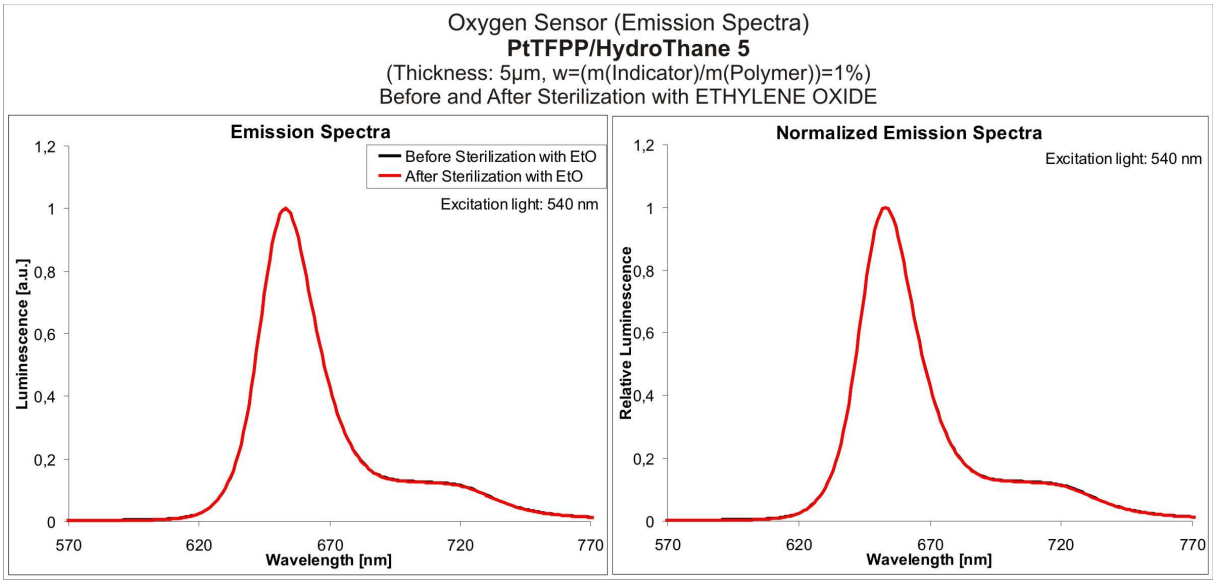

Sterilization with ETHYLENE OXIDE	Absorption Spectra	Emission Spectra
Alterations in Absorption/Emission Intensity	2,68% increase	0,08% increase

Alterations in Absorption/Emission Curve Form	Unaltered.	Unaltered.

Oxygen Sensor
PtTFPP/HydroThane 5
(Thickness: 5 µm, w=(m(Indicator)/m(Polymer))=1%)
Before and After Sterilization with ETHYLENE OXIDE

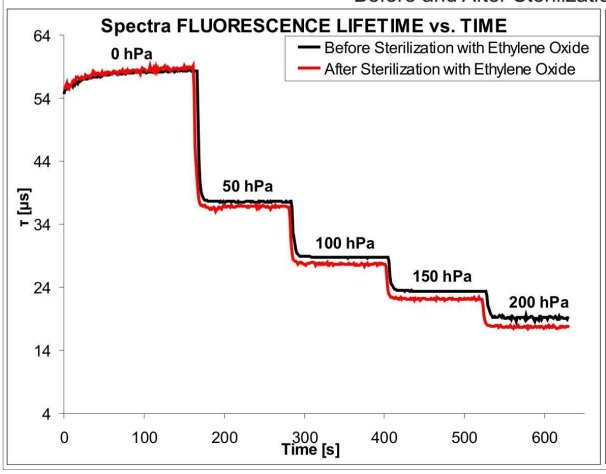

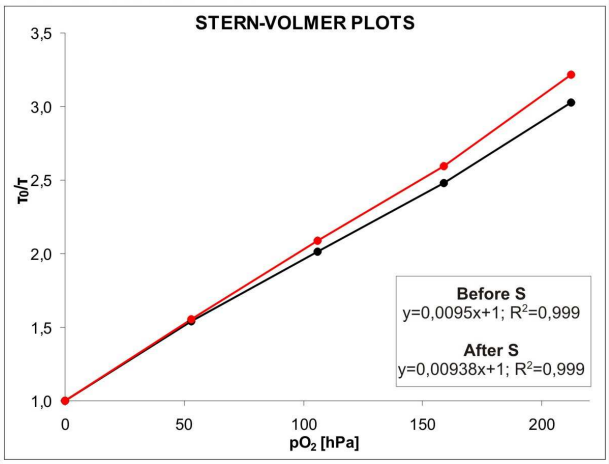

Sterilization with ETHYLENE OXIDE	Luminescence Lifetime	Stern-Volmer Plot
Alterations in Luminescence Lifetime and Slope	1,89% decrease of τ_0	7,77% increase of slope
	2,92% decrease of τ at 50 hPa	
	5,21% decrease of τ at 100 hPa	
	6,20% decrease of τ at 150 hPa	
	7,81% decrease of τ at 200 hPa	

E.14 Platinum(II)Tetrakis(PentaFluorPhenyl)Porphyrin (PtTFPP) immobilized in PolySulfone

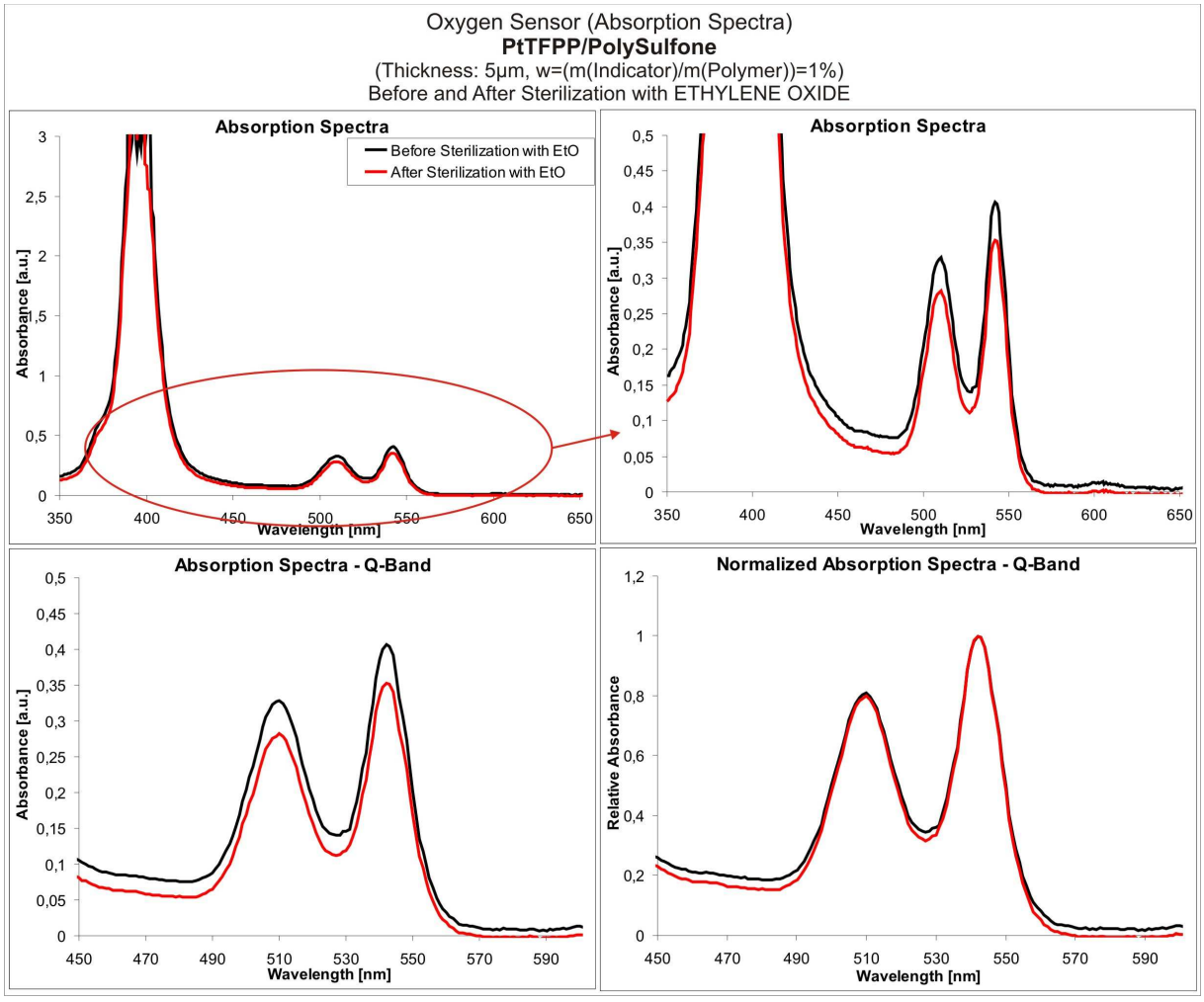

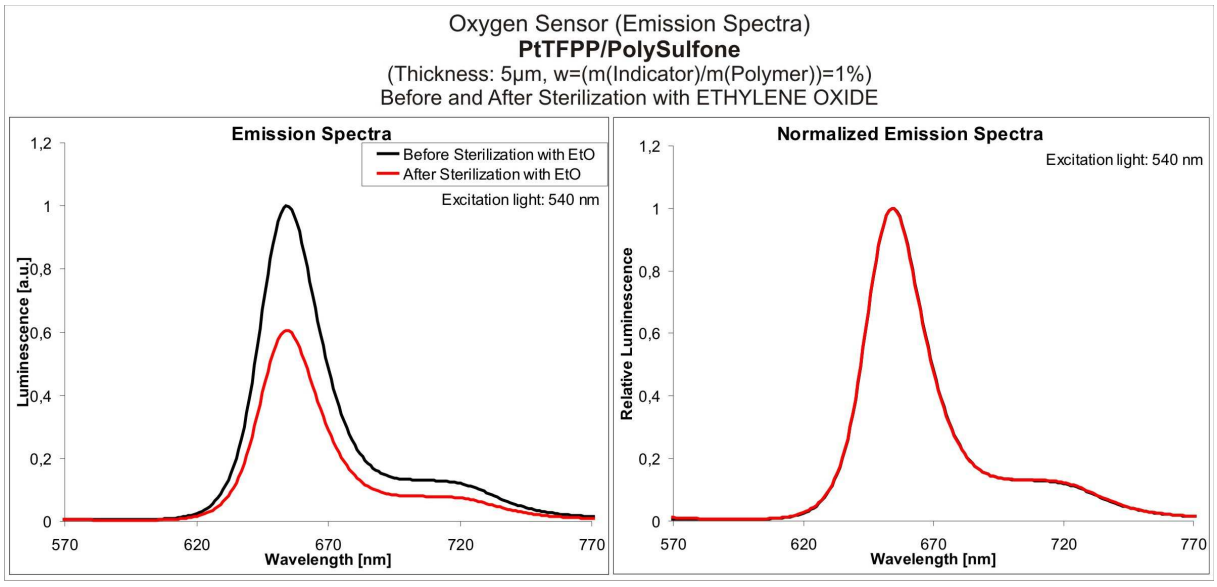

Sterilization with ETHYLENE OXIDE	Absorption Spectra	Emission Spectra
Alterations in Absorption/Emission Intensity	13,18% decrease	39,52% decrease

Alterations in Absorption/Emission Curve Form	Lower absorption after sterilization between 350-380 nm, 420-495 nm, 520-530 nm and 560-800 nm.	Unaltered.

Oxygen Sensor
PtTFPP/PolySulfone
(Thickness: 5 µm, w=(m(Indicator)/m(Polymer))=1%)
Before and After Sterilization with ETHYLENE OXIDE

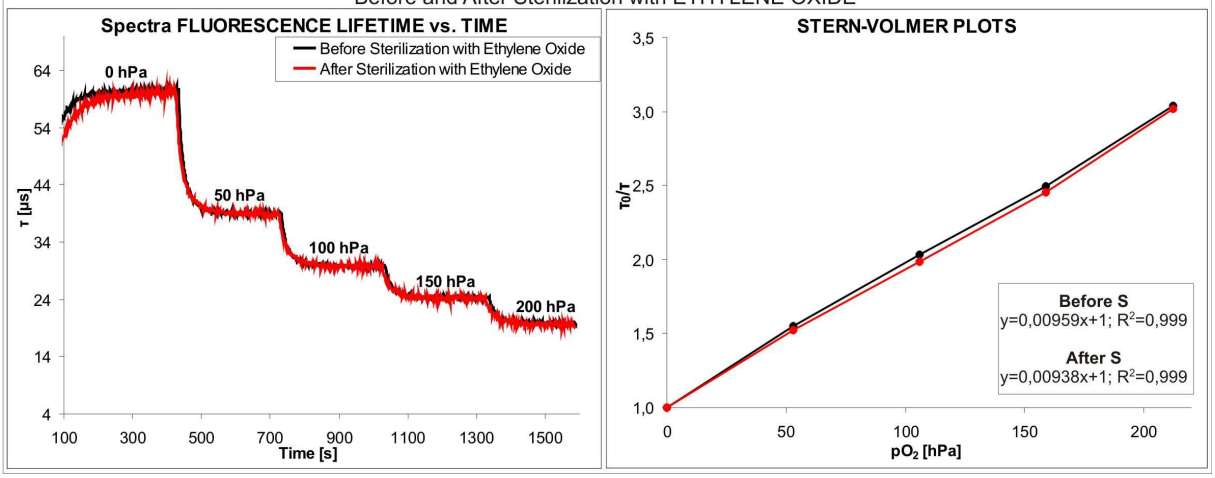

Sterilization with ETHYLENE OXIDE	Luminescence Lifetime	Stern-Volmer Plot
Alterations in Luminescence Lifetime and Slope	2,48% decrease of τ_0	2,19% decrease of slope
	0,44% decrease of τ at 50 hPa	
	0,33% decrease of τ at 100 hPa	
	1,11% decrease of τ at 150 hPa	
	1,51% decrease of τ at 200 hPa	

E.15 Platinum(II)Tetrakis(PentaFluorPhenyl)Porphyrin (PtTFPP) immobilized in PolyPhenylSilses Quioxane

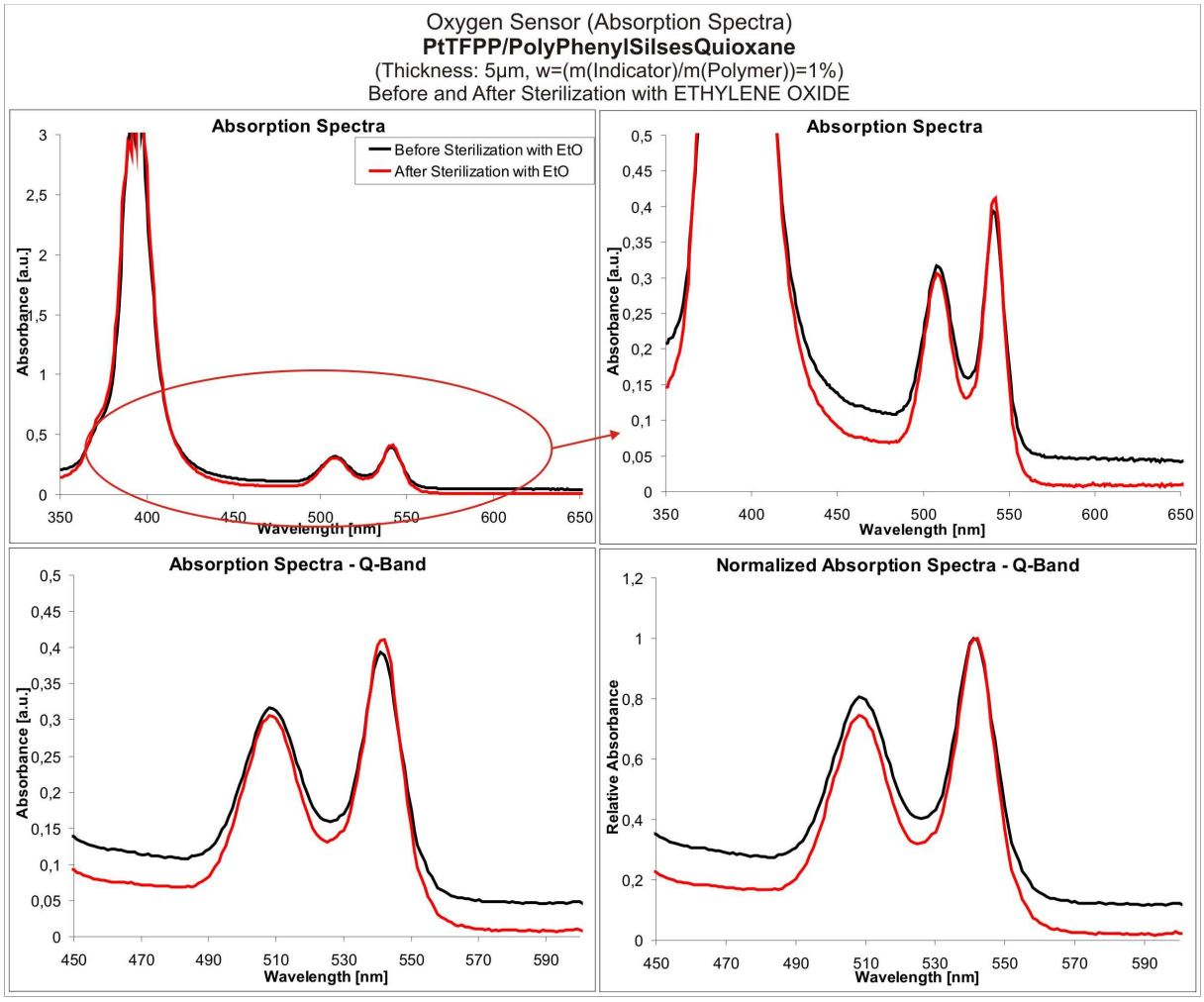

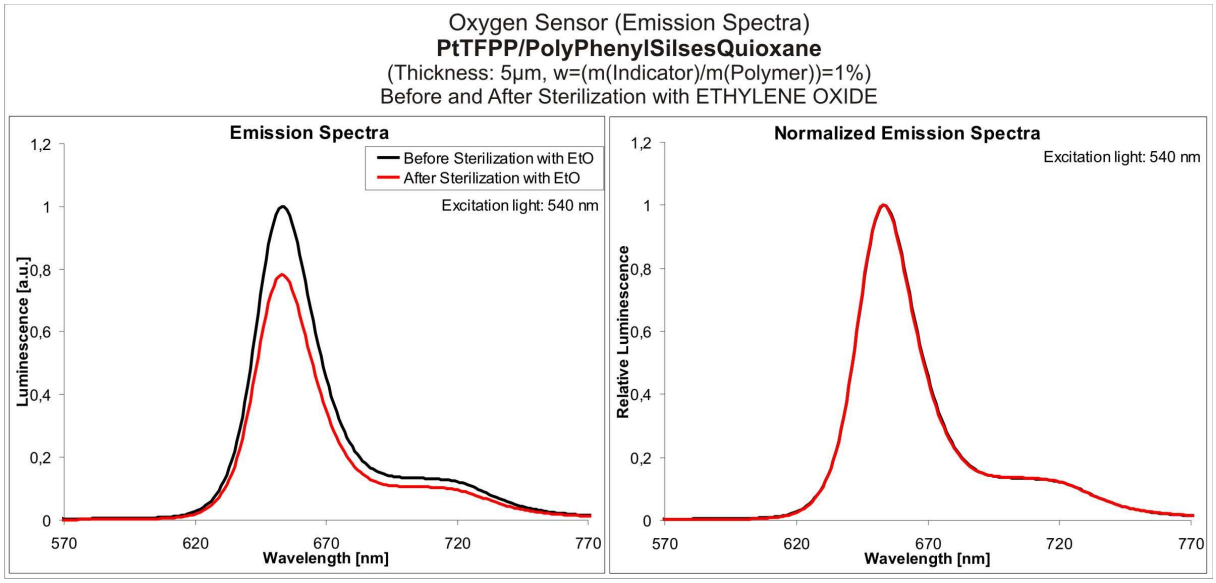

Sterilization with ETHYLENE OXIDE	Absorption Spectra	Emission Spectra
Alterations in Absorption/Emission Intensity	4,42% increase	21,64% decrease

Alterations in Absorption/Emission Curve Form	Lower absorption after sterilization between 350-360 nm, 425-500 nm, 520-530 nm and 550-800 nm.	Unaltered.

Oxygen Sensor
PtTFPP/PolyPhenylSilsesQuioxane
(Thickness: 5 µm, w=(m(Indicator)/m(Polymer))=1%)
Before and After Sterilization with ETHYLENE OXIDE

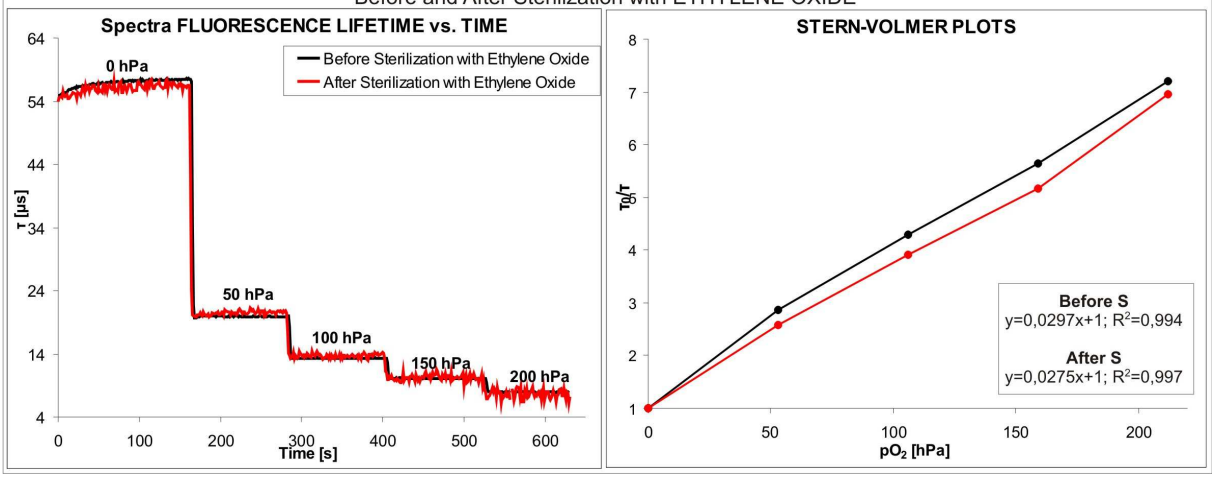

Sterilization with ETHYLENE OXIDE	Luminescence Lifetime	Stern-Volmer Plot
Alterations in Luminescence Lifetime and Slope	8,22% decrease of τ_0	7,41% increase of slope
	2,50% increase of τ at 50 hPa	
	1,48% increase of τ at 100 hPa	
	0,49% increase of τ at 150 hPa	
	4,91% decrease of τ at 200 hPa	

E.16 Platinum(II)Tetrakis(PentaFluorPhenyl)Porphyrin (PtTFPP) immobilized in PolyStyrene

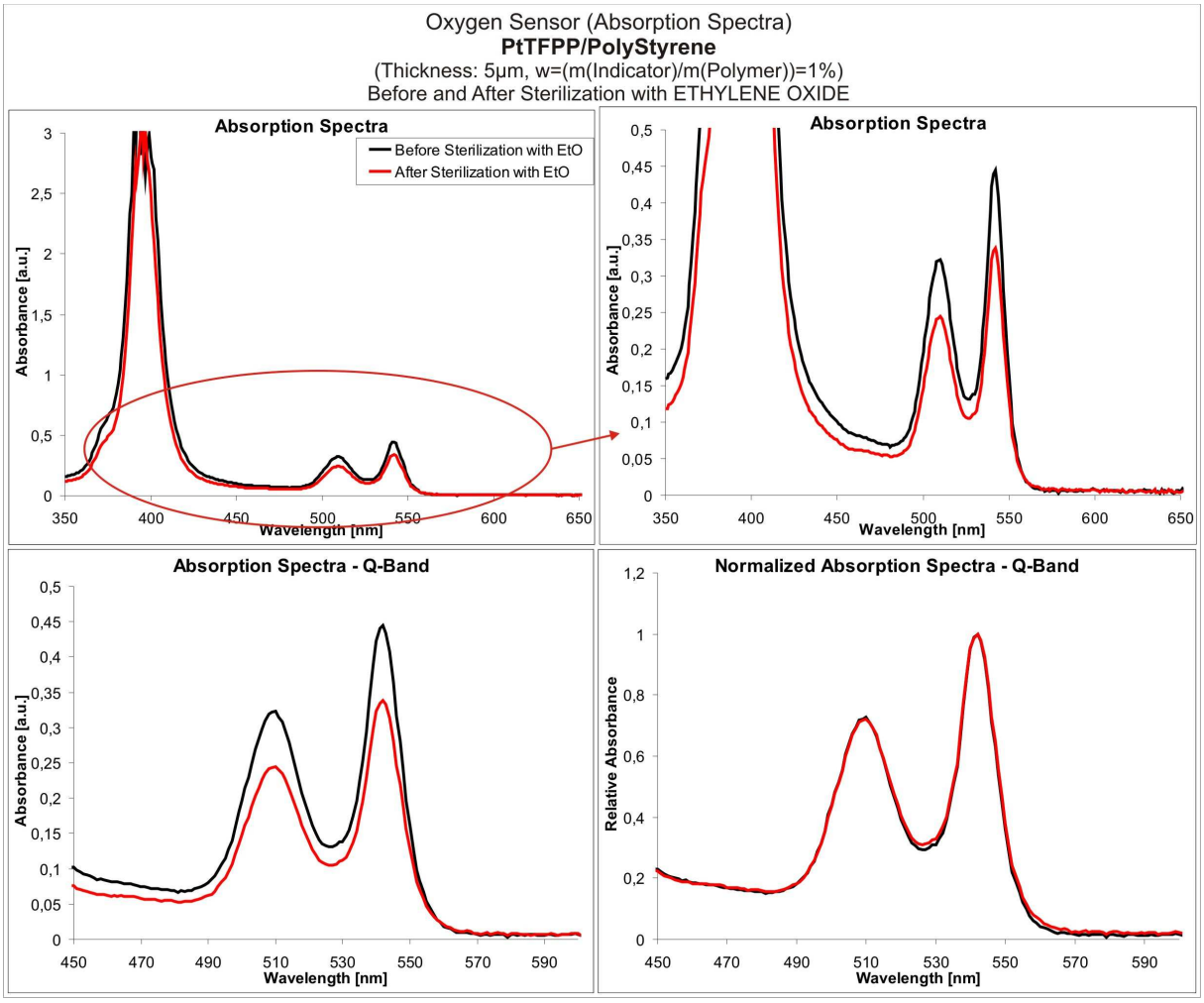

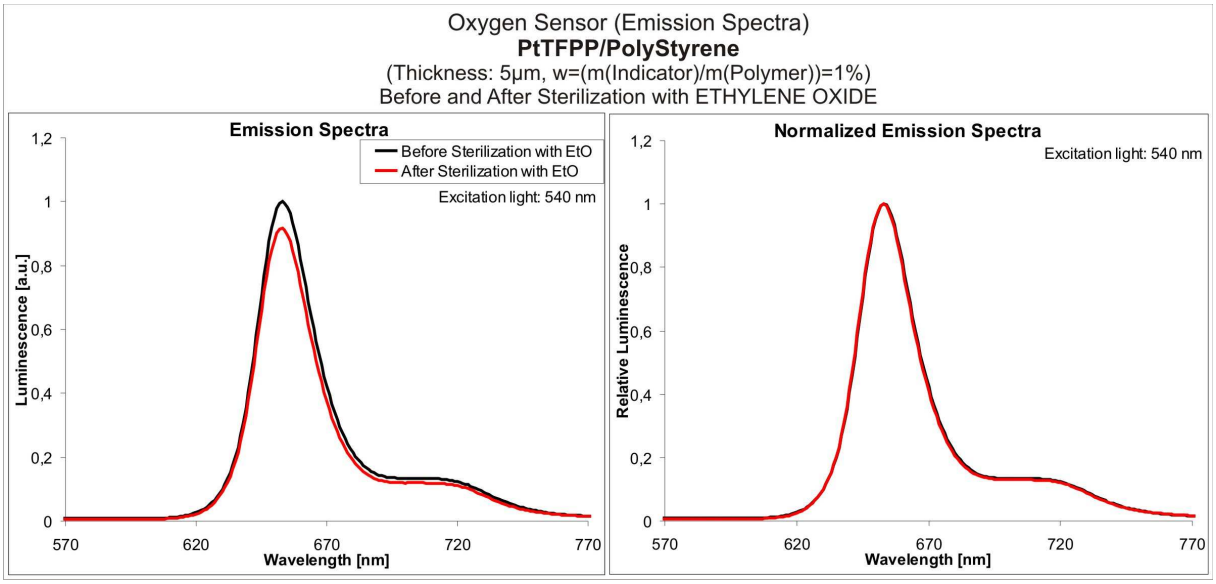

Sterilization with ETHYLENE OXIDE	Absorption Spectra	Emission Spectra
Alterations in Absorption/Emission Intensity	23,82% decrease	8,30% decrease

Alterations in Absorption/Emission Curve Form	Unaltered	Unaltered.

Oxygen Sensor
PtTFPP/PolyStyrene
(Thickness: 5 µm, w=(m(Indicator)/m(Polymer))=1%)
Before and After Sterilization with ETHYLENE OXIDE

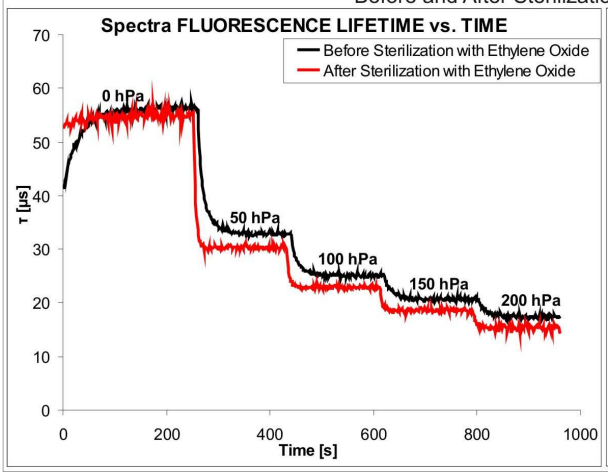

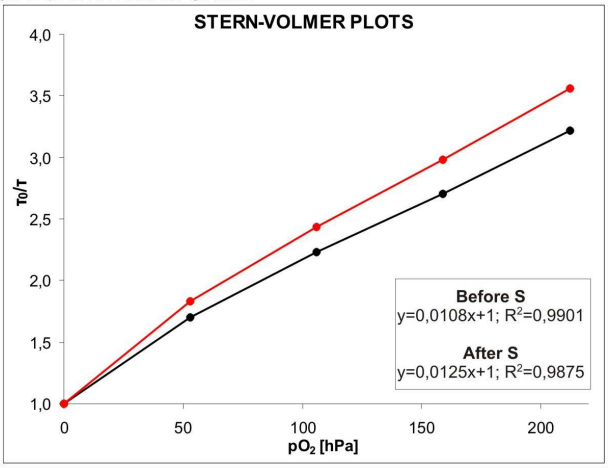

Sterilization with ETHYLENE OXIDE	Luminescence Lifetime	Stern-Volmer Plot
Alterations in Luminescence Lifetime and Slope	2,14% decrease of τ_0	13,60% increase of slope
	9,12% decrease of τ at 50 hPa	
	10,36% decrease of τ at 100 hPa	
	11,11% decrease of τ at 150 hPa	
	11,49% decrease of τ at 200 hPa	

E.17 Platinum(II)Tetrakis(PentaFluorPhenyl)Porphyrin (PtTFPP) immobilized in PolyStyrene-co- Acrylonitrile

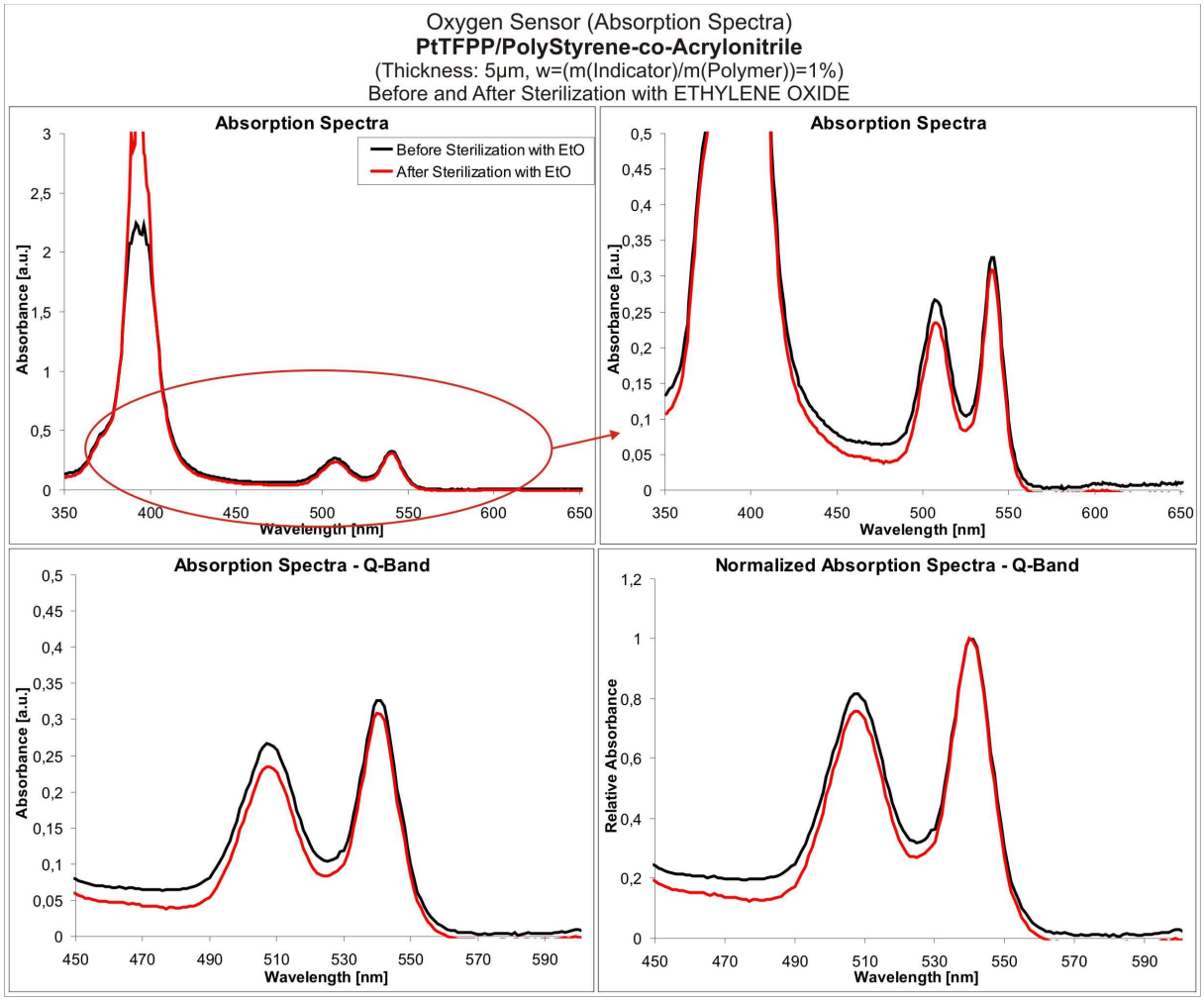

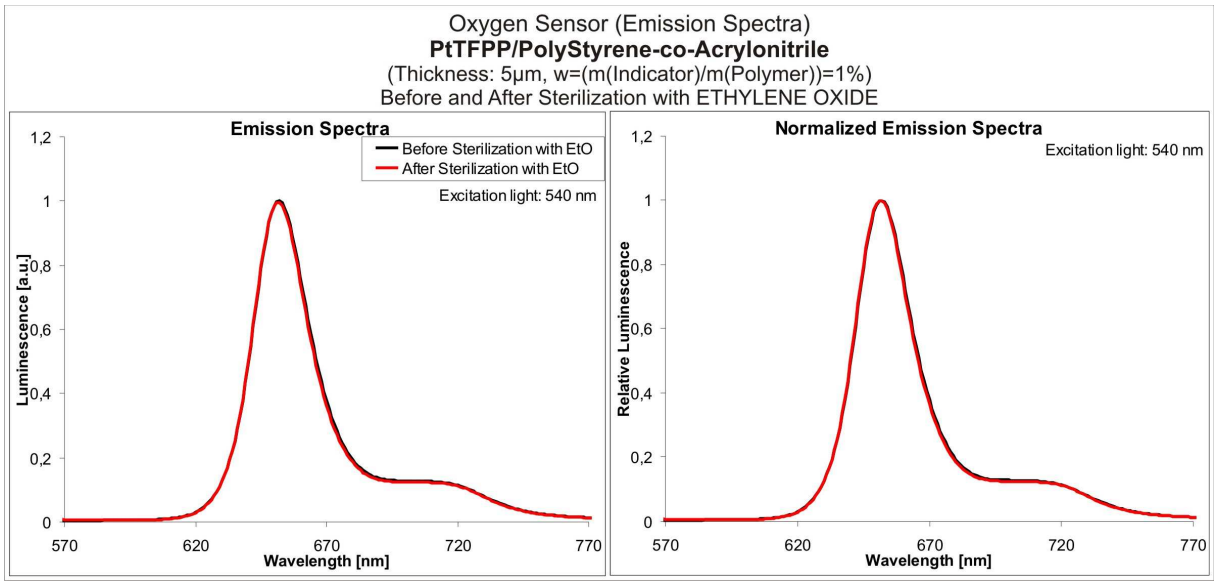

Sterilization with ETHYLENE OXIDE	Absorption Spectra	Emission Spectra
Alterations in Absorption/Emission Intensity	5,18% decrease	0,45% decrease

Alterations in Absorption/Emission Curve Form	Altered absorption curve form between 350-360 nm and 425-530 nm.	Unaltered.

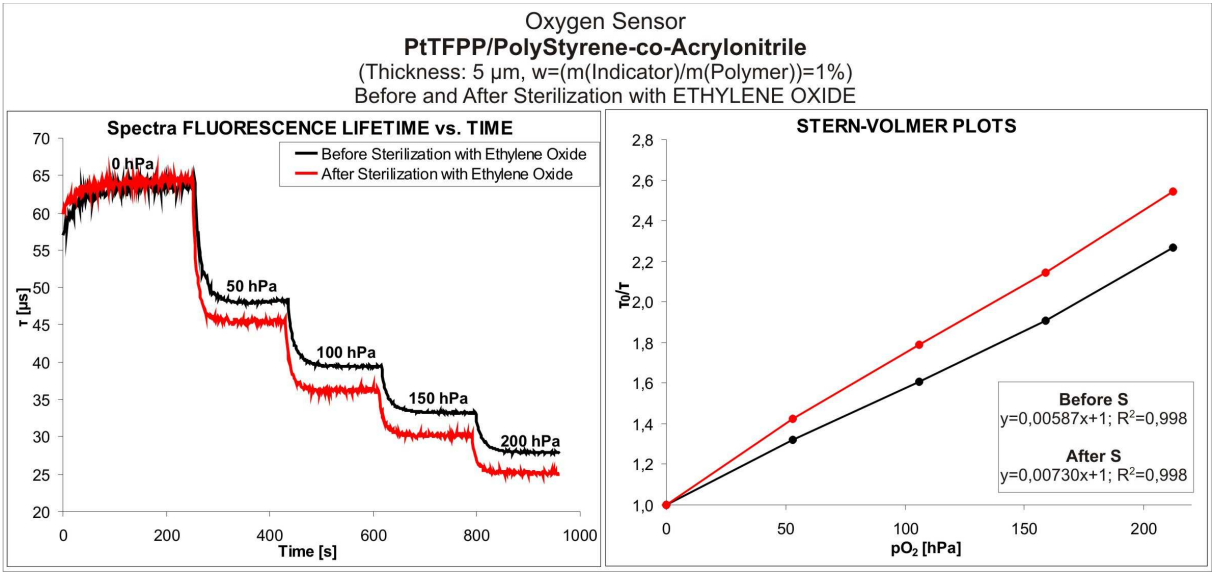

Sterilization with ETHYLENE OXIDE	Luminescence Lifetime	Stern-Volmer Plot
Alterations in Luminescence Lifetime and Slope	1,25% increase of τ_0	19,84% increase of slope
	6,24% decrease of τ at 50 hPa	
	8,88% decrease of τ at 100 hPa	
	9,91% decrease of τ at 150 hPa	
	10,00% decrease of τ at 200 hPa	

E.18 Platinum(II)Tetrakis(PentaFluorPhenyl)Porphyrin (PtTFPP) immobilized in PolyStyrene-co-MaleicAnhydride (PSMA93)

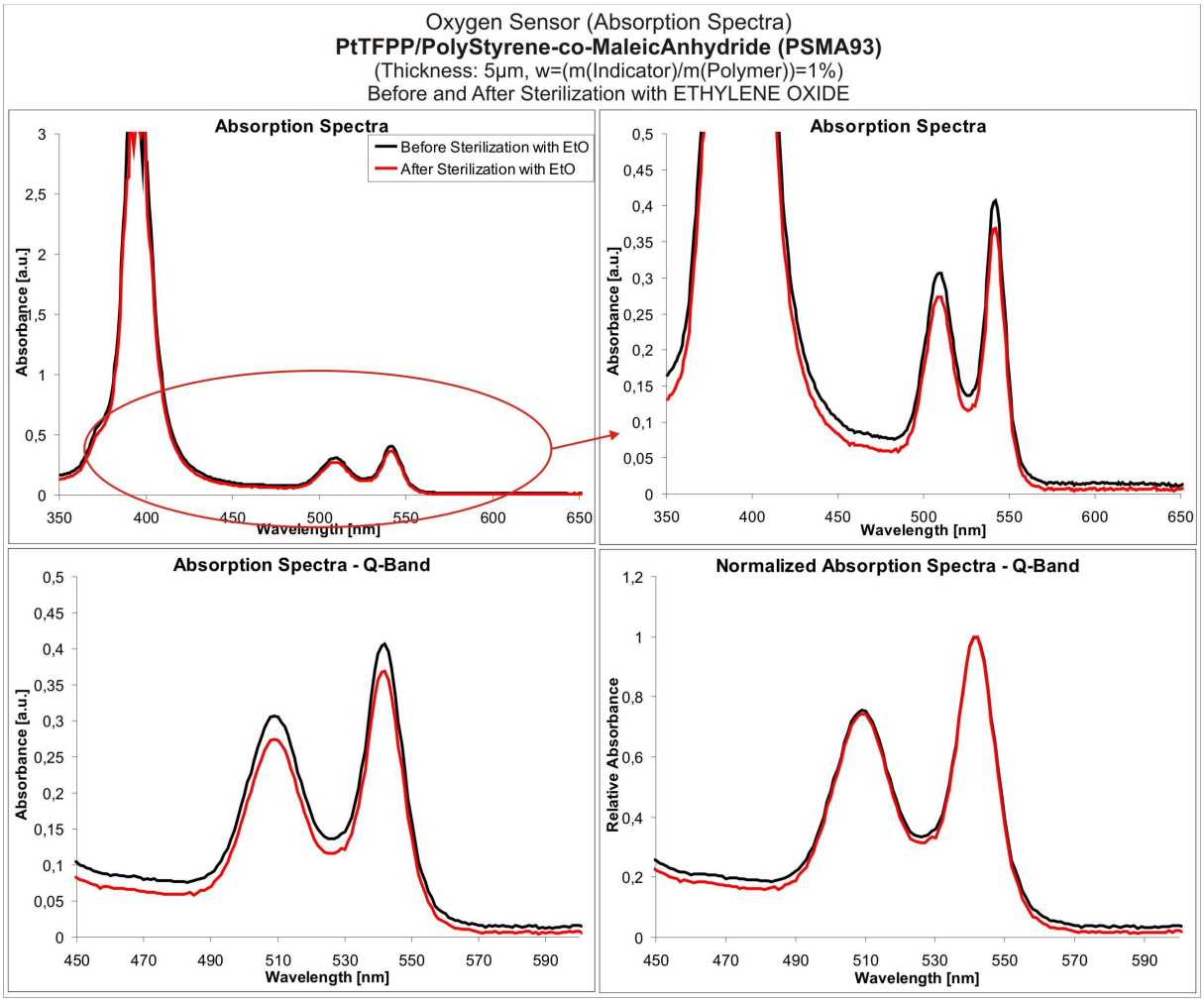

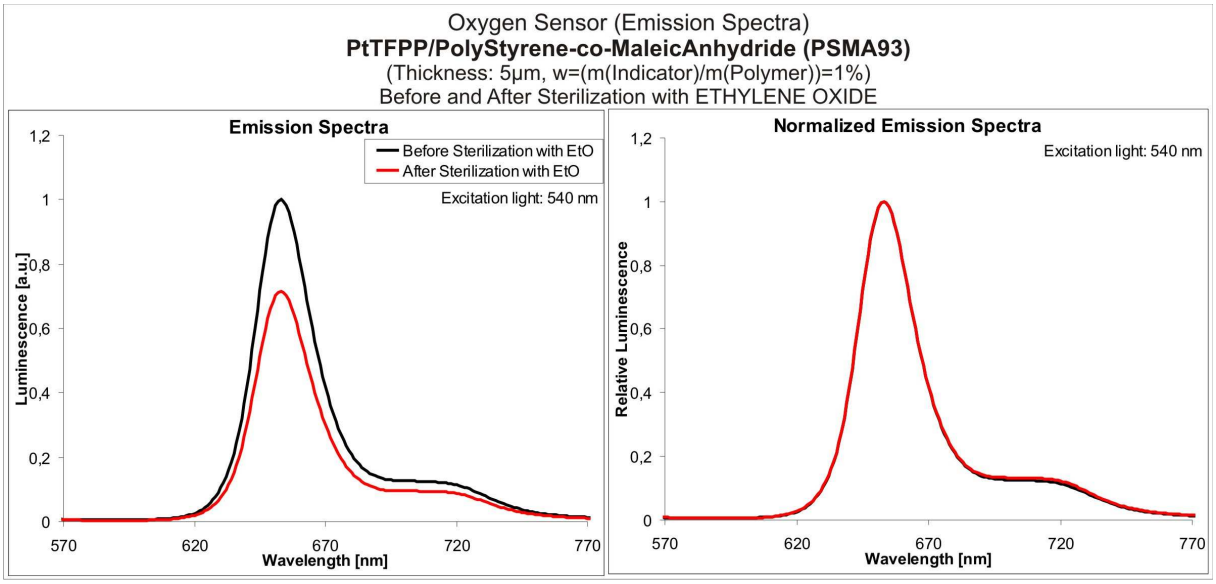

Sterilization with ETHYLENE OXIDE	Absorption Spectra	Emission Spectra
Alterations in Absorption/Emission Intensity	9,46% decrease	28,55% decrease

Alterations in Absorption/Emission Curve Form	Unaltered.	Unaltered.

Oxygen Sensor
PtTFPP/PolyStyrene-co-MaleicAnhydride (PSMA93)
(Thickness: 5 µm, w=(m(Indicator)/m(Polymer))=1%)
Before and After Sterilization with ETHYLENE OXIDE

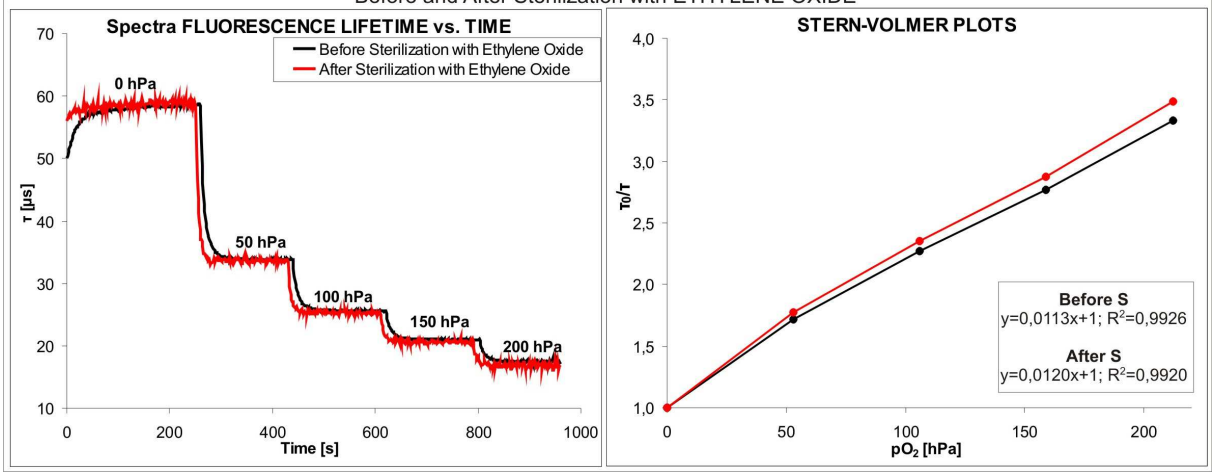

Sterilization with ETHYLENE OXIDE	Luminescence Lifetime	Stern-Volmer Plot
Alterations in Luminescence Lifetime and Slope	1,02% increase of τ_0	5,83% increase of slope
	2,36% decrease of τ at 50 hPa	
	2,73% decrease of τ at 100 hPa	
	2,86% decrease of τ at 150 hPa	
	4,00% decrease of τ at 200 hPa	

E.19 Platinum(II) OctaEthyl Porphyrin (=PtOEP) immobilized in PolyStyrene

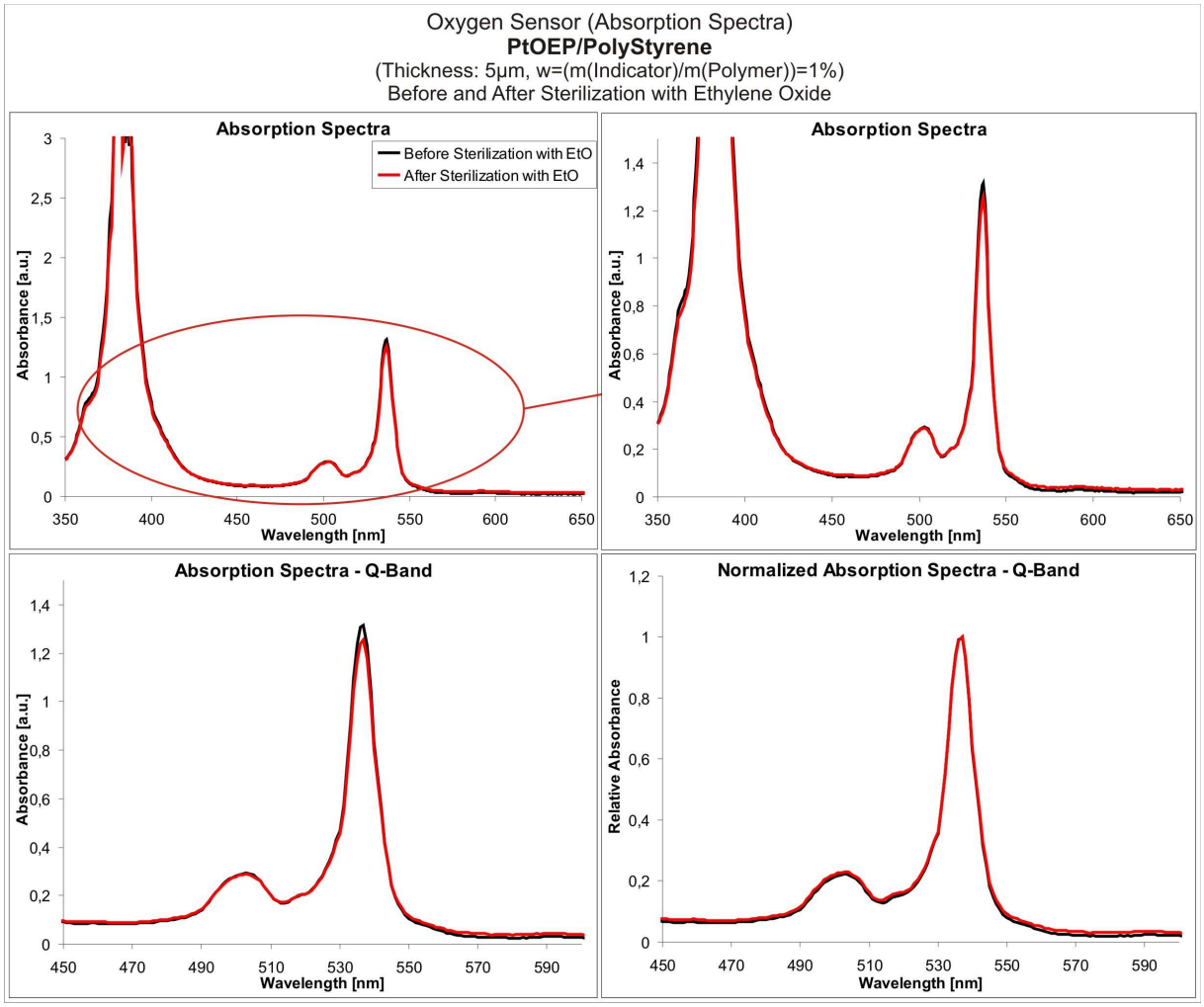

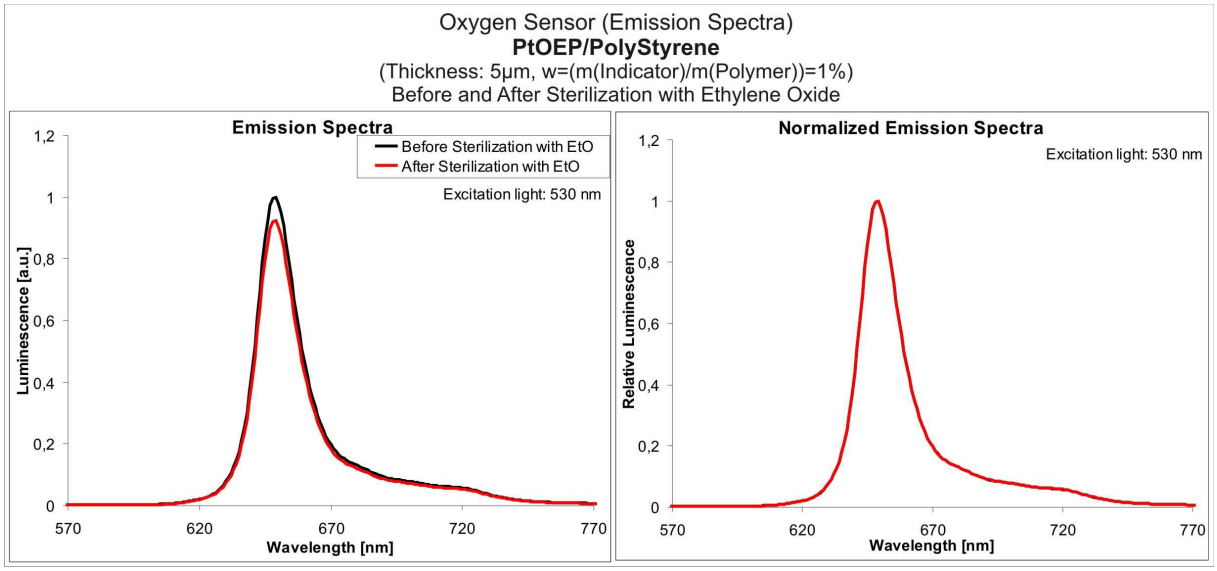

Sterilization with Ethylene Oxide	Absorption Spectra	Emission Spectra
Alterations in Absorption/Emission Intensity	4,68% decrease	7,65% decrease

Alterations in Absorption/Emission Curve Form	Unaltered.	Unaltered.

Oxygen Sensor
PtOEP/PolyStyrene
(Thickness: 5 µm, w=(m(Indicator)/m(Polymer))=1%)
Before and After Sterilization with ETHYLENE OXIDE

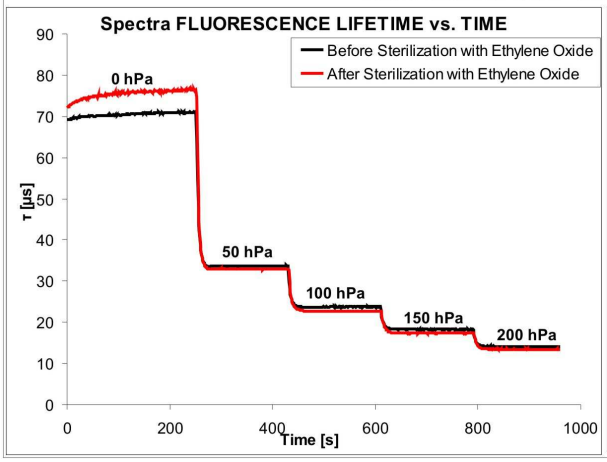

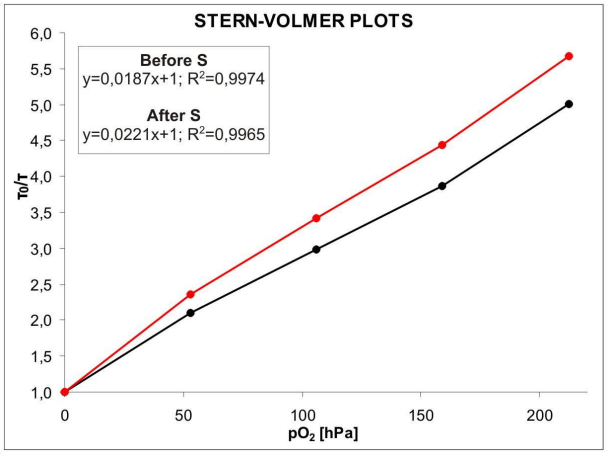

Sterilization with Ethylene Oxide	Luminescence Lifetime	Stern-Volmer Plot
Alterations in Luminescence Lifetime and Slope	6,97% increase of τ_0	15,38% increase of slope
	3,87% decrease of τ at 50 hPa	
	5,91% decrease of τ at 100 hPa	
	6,56% decrease of τ at 150 hPa	
	4,96% decrease of τ at 200 hPa	

E.20 Platinum(II) meso-tetra(4-FluoroPhenyl) TetraBenzoPorphyrin (=PtTPTBPF) immobilized in PolyStyrene

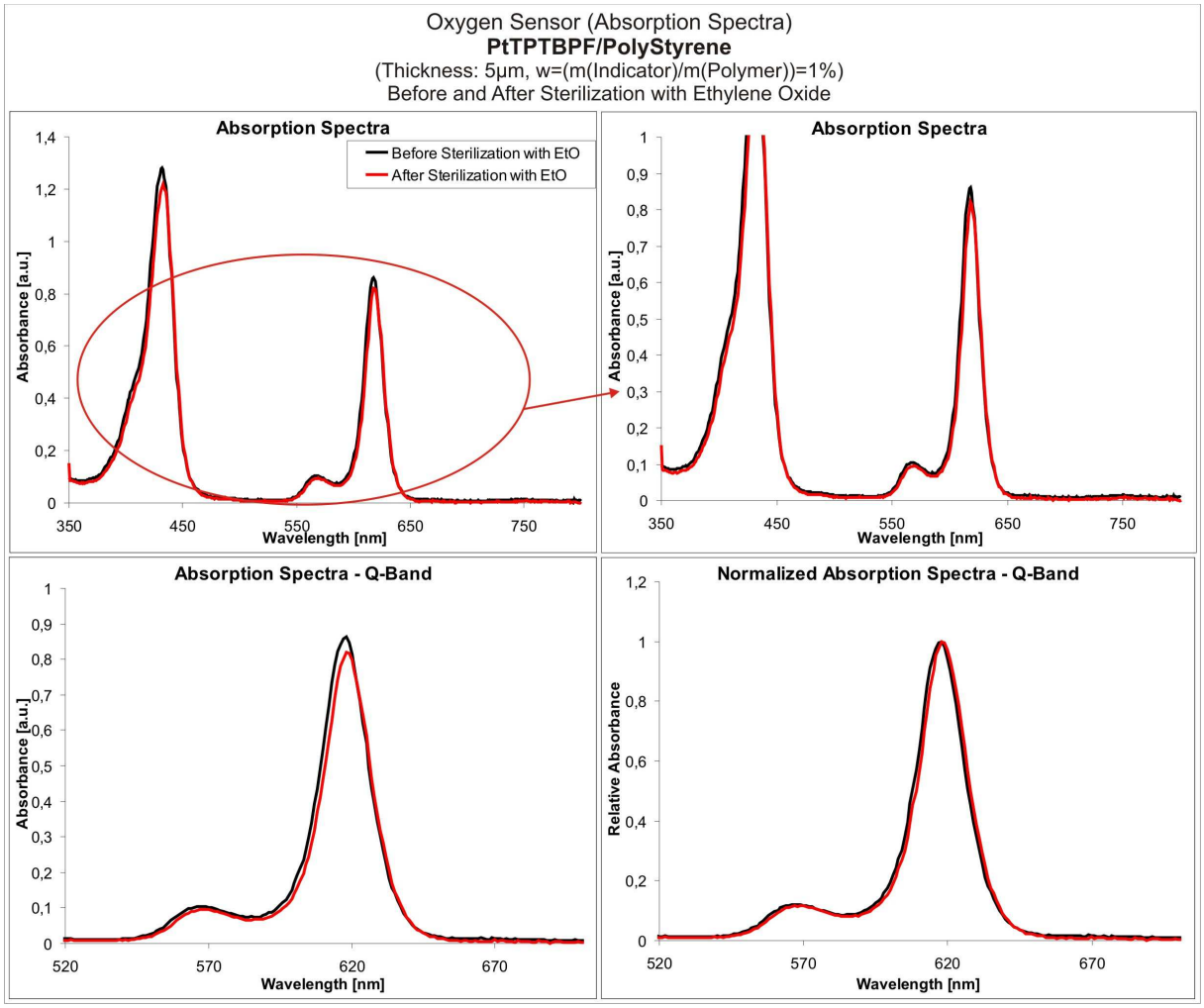

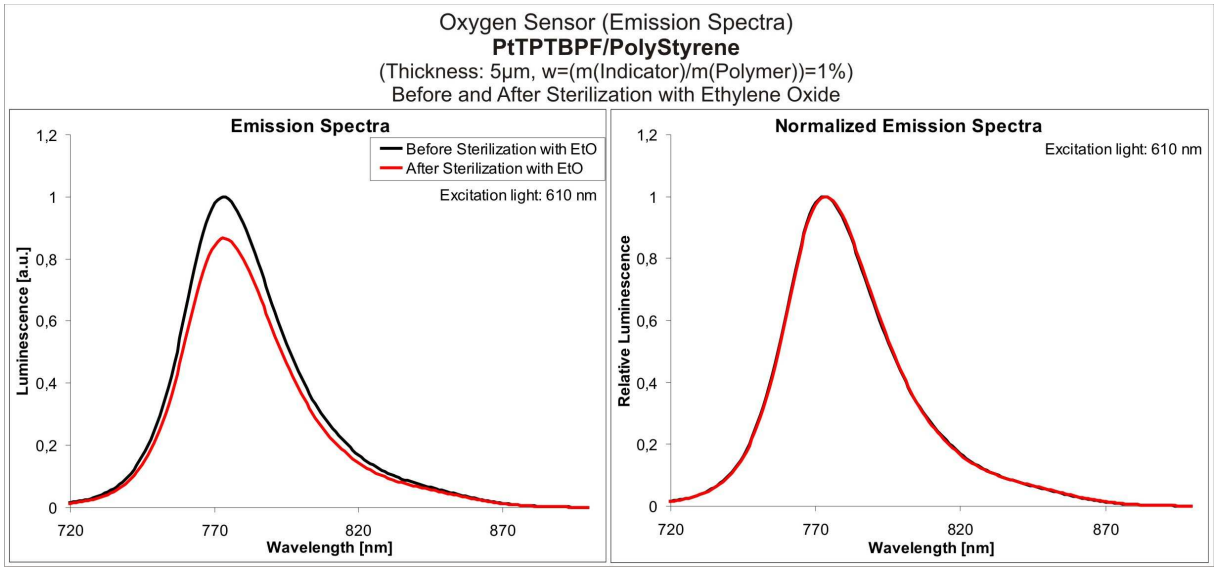

Sterilization with Ethylene Oxide	Absorption Spectra	Emission Spectra
Alterations in Absorption/Emission Intensity	4,85% decrease	13,29% decrease

Alterations in Absorption/Emission Curve Form	Unaltered.	Unaltered.

Oxygen Sensor
PtTPTBPF/PolyStyrene
(Thickness: 5 µm, w=(m(Indicator)/m(Polymer))=1%)
Before and After Sterilization with ETHYLENE OXIDE

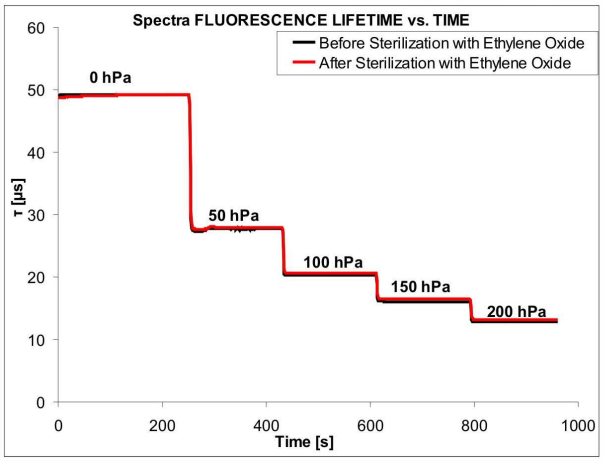

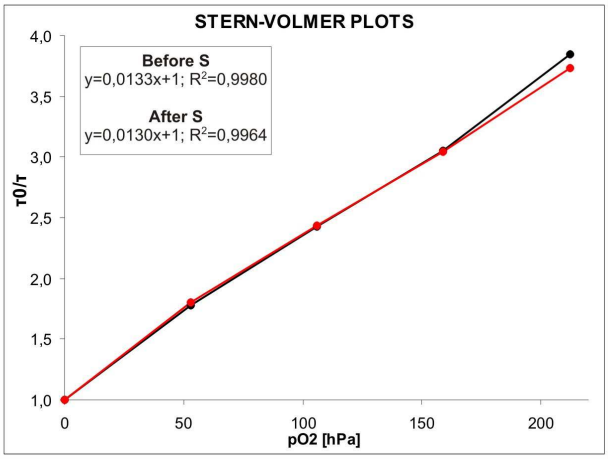

Sterilization with Ethylene Oxide	Luminescence Lifetime	Stern-Volmer Plot
Alterations in Luminescence Lifetime and Slope	τ_0 the same before and after sterilization	2,26% decrease of slope
	1,44% decrease of τ at 50 hPa	
	0,49% decrease of τ at 100 hPa	
	0,62% increase of τ at 150 hPa	
	3,03% increase of τ at 200 hPa	

E.21 Palladium(II)meso-tetra(4-FluoroPhenyl) TetraBenzoPorphyrin (=PdTPTBPF) immobilized in PolyStyrene

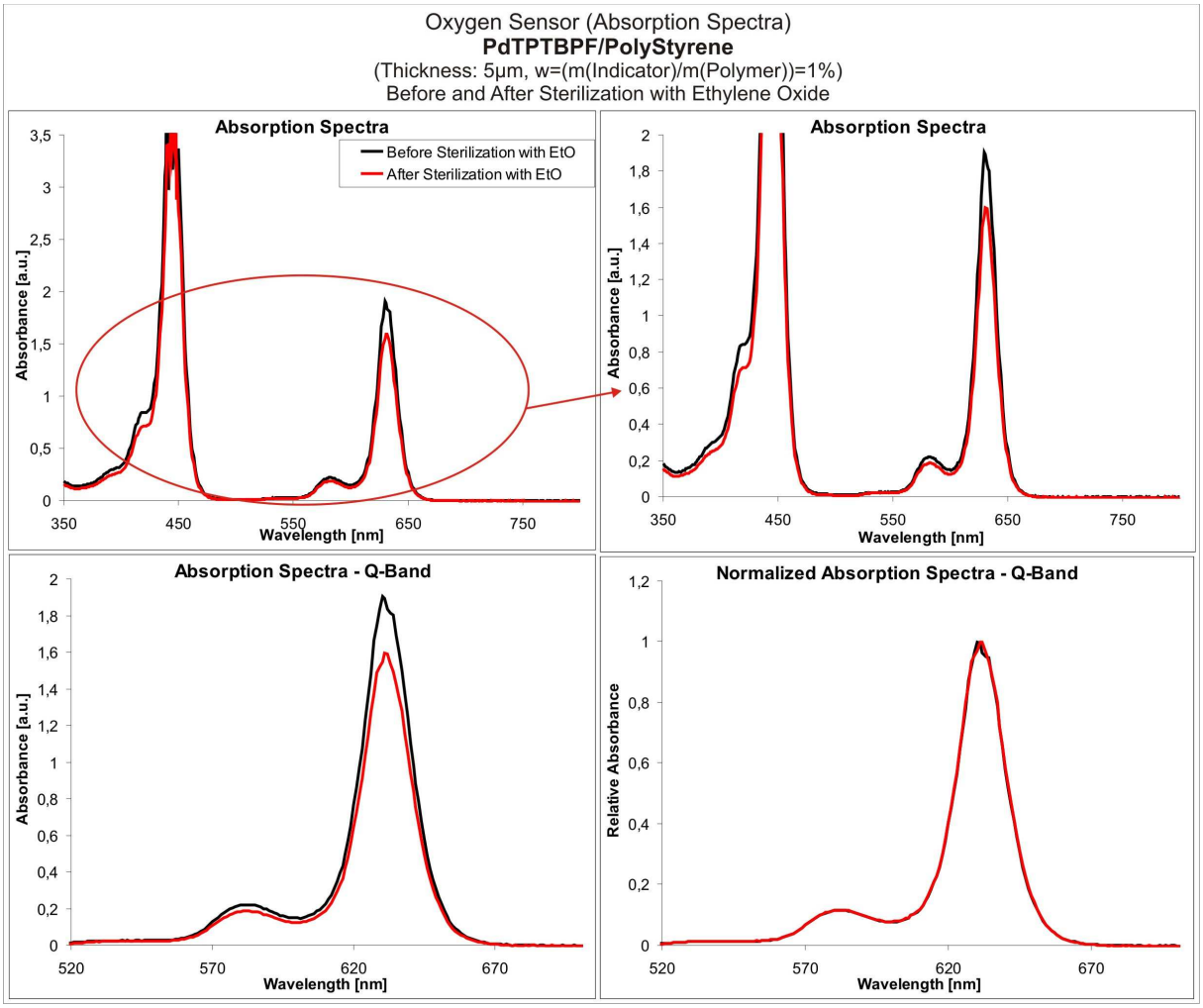

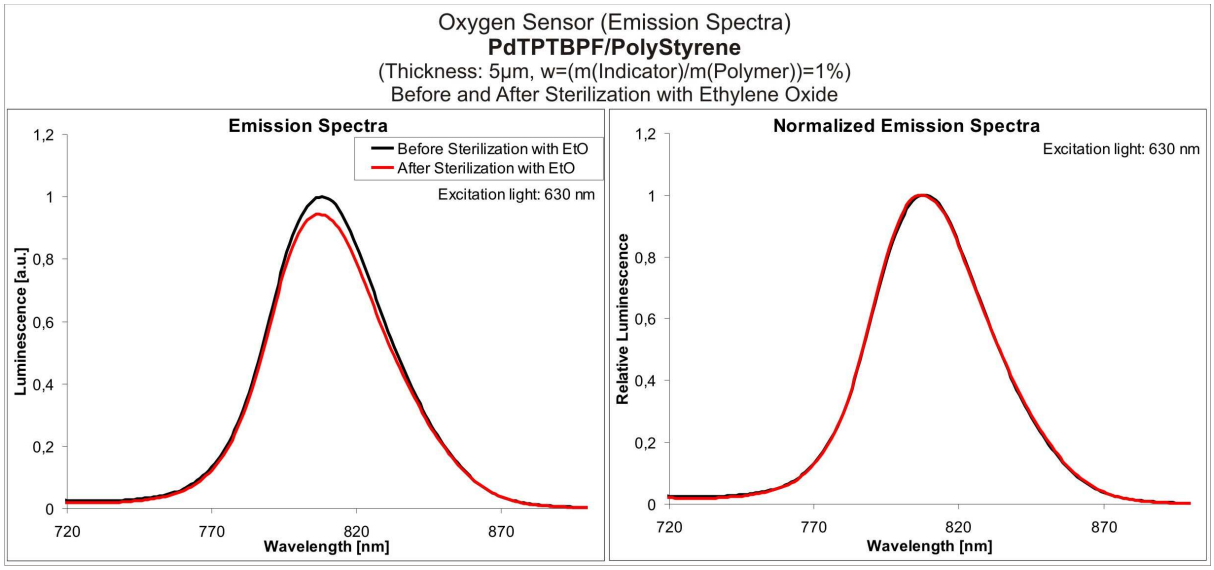

Sterilization with Ethylene Oxide	Absorption Spectra	Emission Spectra
Alterations in Absorption/Emission Intensity	16,19% decrease	5,66% decrease

Alterations in Absorption/Emission Curve Form	Unaltered.	Unaltered.

Oxygen Sensor
PdTPTBPF/PolyStyrene
(Thickness: 5 µm, w=(m(Indicator)/m(Polymer))=1%)
Before and After Sterilization with ETHYLENE OXIDE

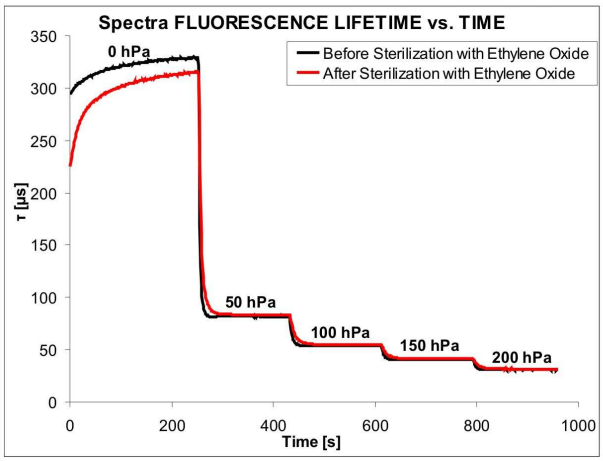

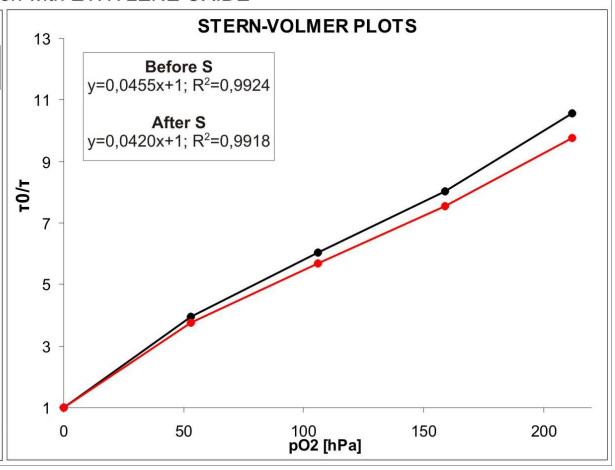

Sterilization with Ethylene Oxide	Luminescence Lifetime	Stern-Volmer Plot
Alterations in Luminescence Lifetime and Slope	4,92% decrease of τ_0	1,32% increase of slope
	0,61% increase of τ at 50 hPa	
	0,92% increase of τ at 100 hPa	
	0,15% increase of τ at 150 hPa	
	0,25% increase of τ at 200 hPa	

E.22 Ruthenium(II) DiPhenylPhenanthroline DiChloride ($Ru(dpp)_3Cl_2$) immobilized in Cellulose Acetate

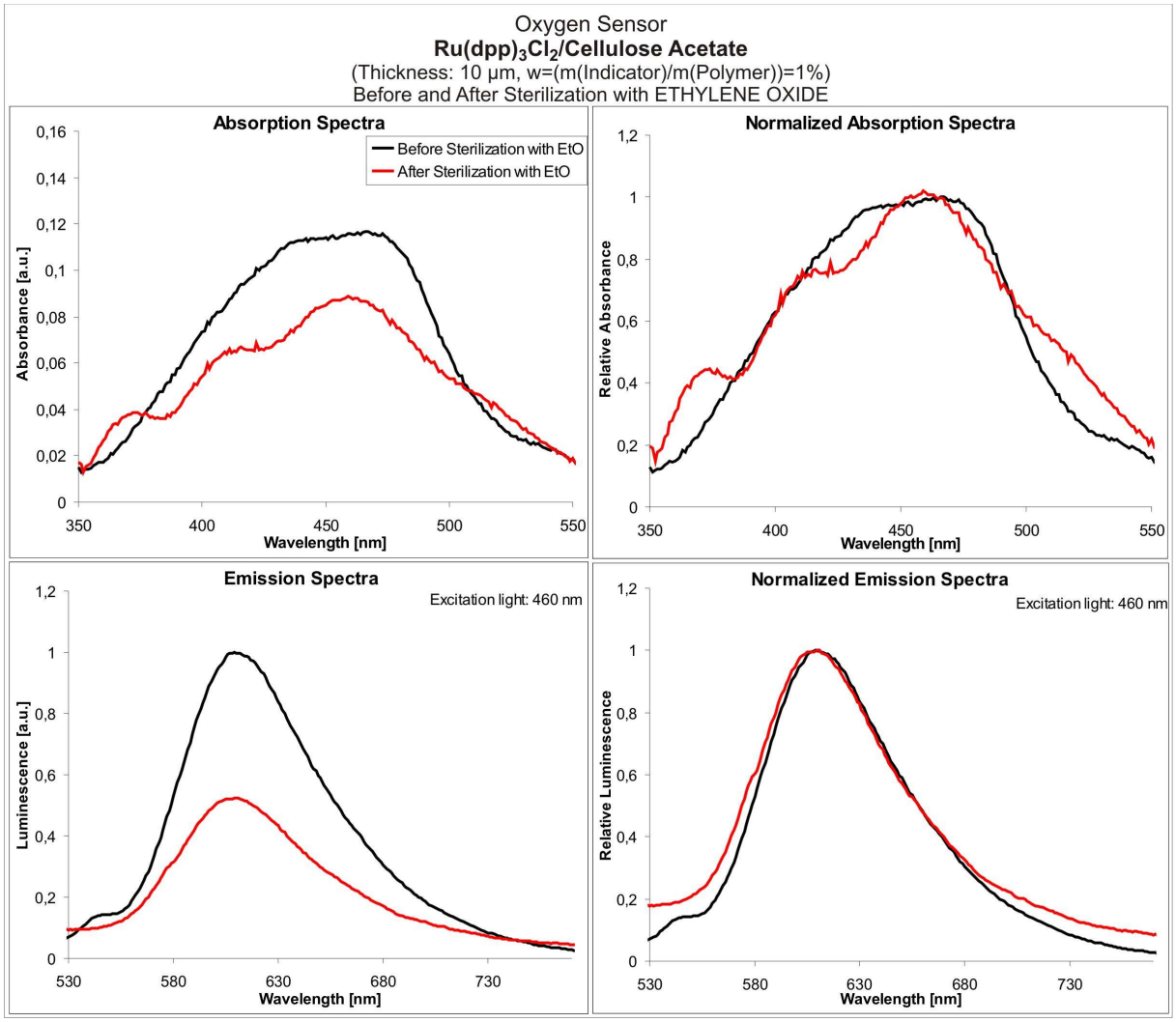

Sterilization with Ethylene Oxide	Absorption Spectra	Emission Spectra
Alterations in Absorption/Emission Intensity	25,40% decrease	47,68% decrease
Alterations in Absorption/Emission Curve Form	Altered absorption curve form.	Altered emission curve form between 550-580 nm and 680-800 nm.

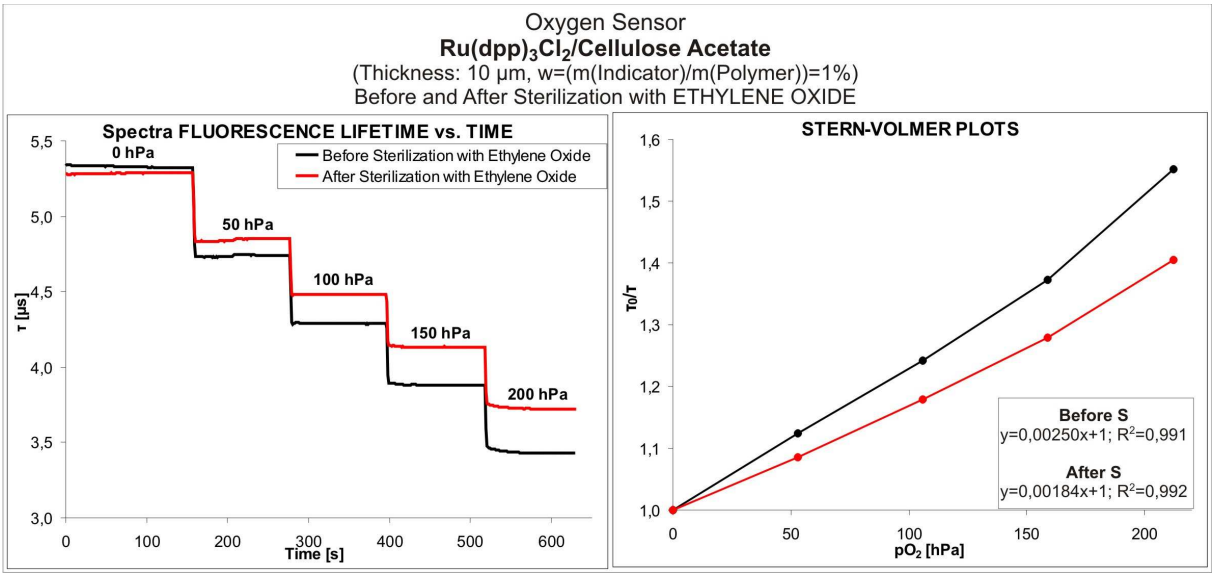

Sterilization with Ethylene Oxide	Luminescence Lifetime	Stern-Volmer Plot
Alterations in Luminescence Lifetime and Slope	1,67% decrease of τ_0	28,00% decrease of slope
	1,84% increase of τ at 50 hPa	
	3,26% increase of τ at 100 hPa	
	5,16% increase of τ at 150 hPa	
	7,76% increase of τ at 200 hPa	

E.23 Ruthenium(II) DiPhenylPhenanthroline DiChloride ($Ru(dpp)_3Cl_2$) immobilized in Ethyl Cellulose

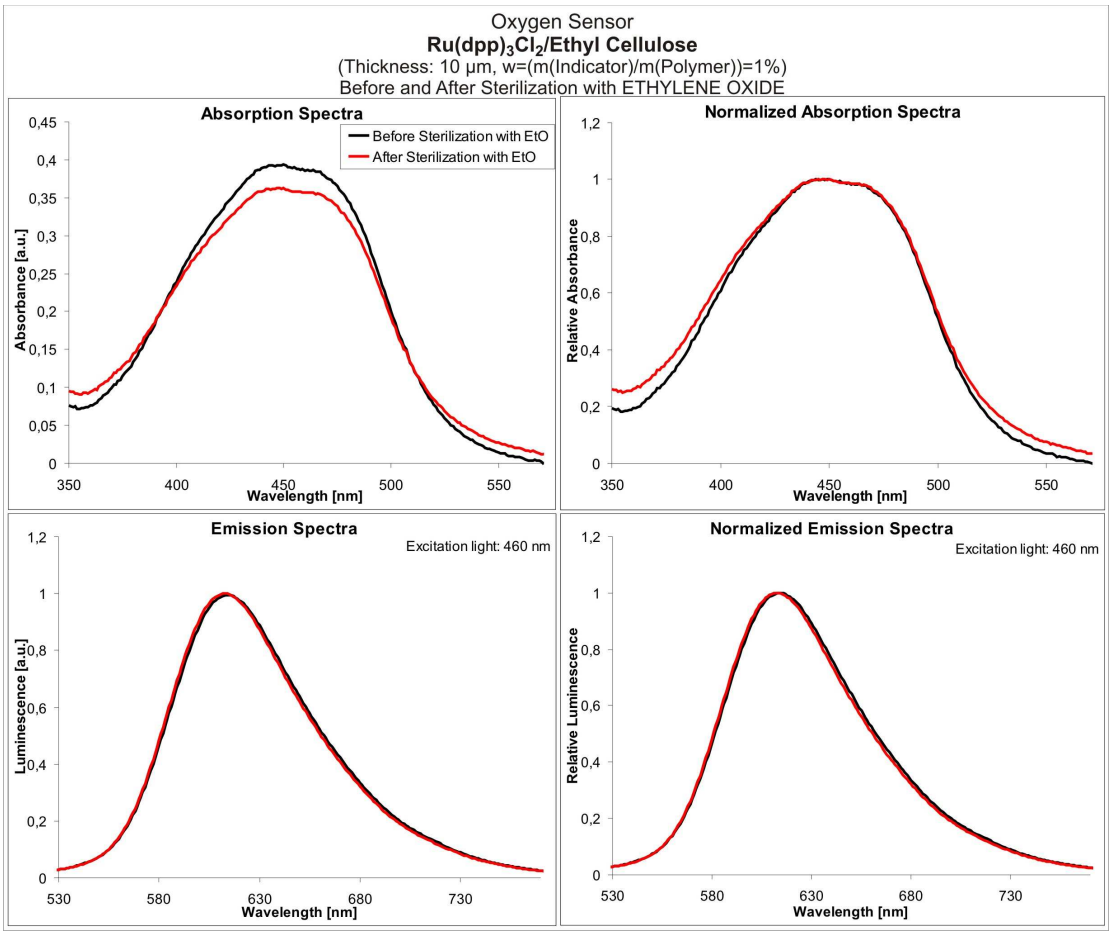

Sterilization with Ethylene Oxide	Absorption Spectra	Emission Spectra
Alterations in Absorption/Emission Intensity	7,79% decrease	0,52% increase
Alterations in Absorption/Emission Curve Form	Altered absorption curve form between 350-420 nm and 510-800 nm.	Unaltered.

Oxygen Sensor
$Ru(dpp)_3Cl_2$/Ethyl Cellulose
(Thickness: 10 µm, w=(m(Indicator)/m(Polymer))=1%)
Before and After Sterilization with ETHYLENE OXIDE

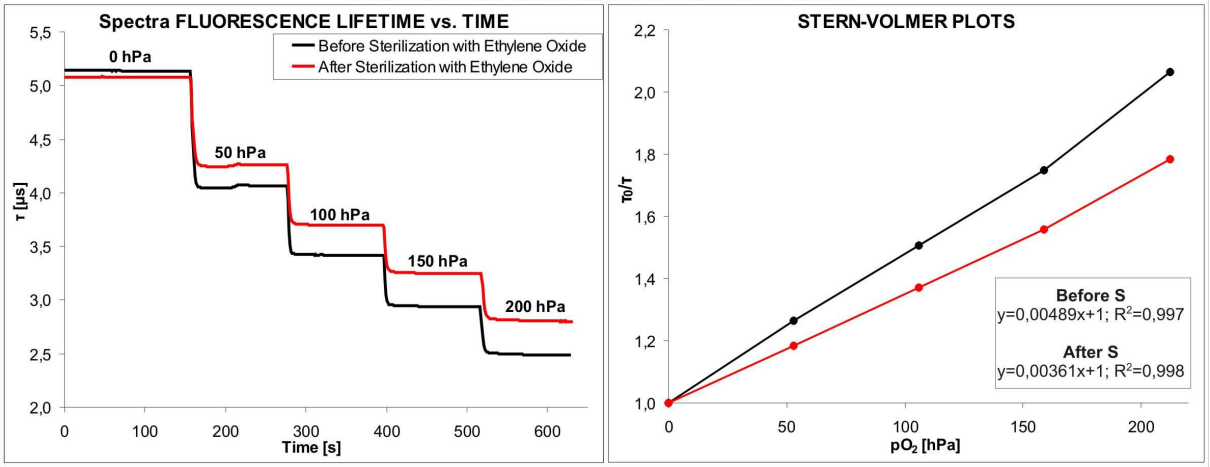

Sterilization with Ethylene Oxide	Luminescence Lifetime	Stern-Volmer Plot
Alterations in Luminescence Lifetime and Slope	2,81% decrease of τ_0	26,53% decrease of slope
	3,92% increase of τ at 50 hPa	
	6,09% increase of τ at 100 hPa	
	8,37% increase of τ at 150 hPa	
	11,46% increase of τ at 200 hPa	

E.24 Ruthenium(II) DiPhenylPhenanthroline DiChloride ($Ru(dpp)_3Cl_2$) immobilized in HydroGel D4/D7

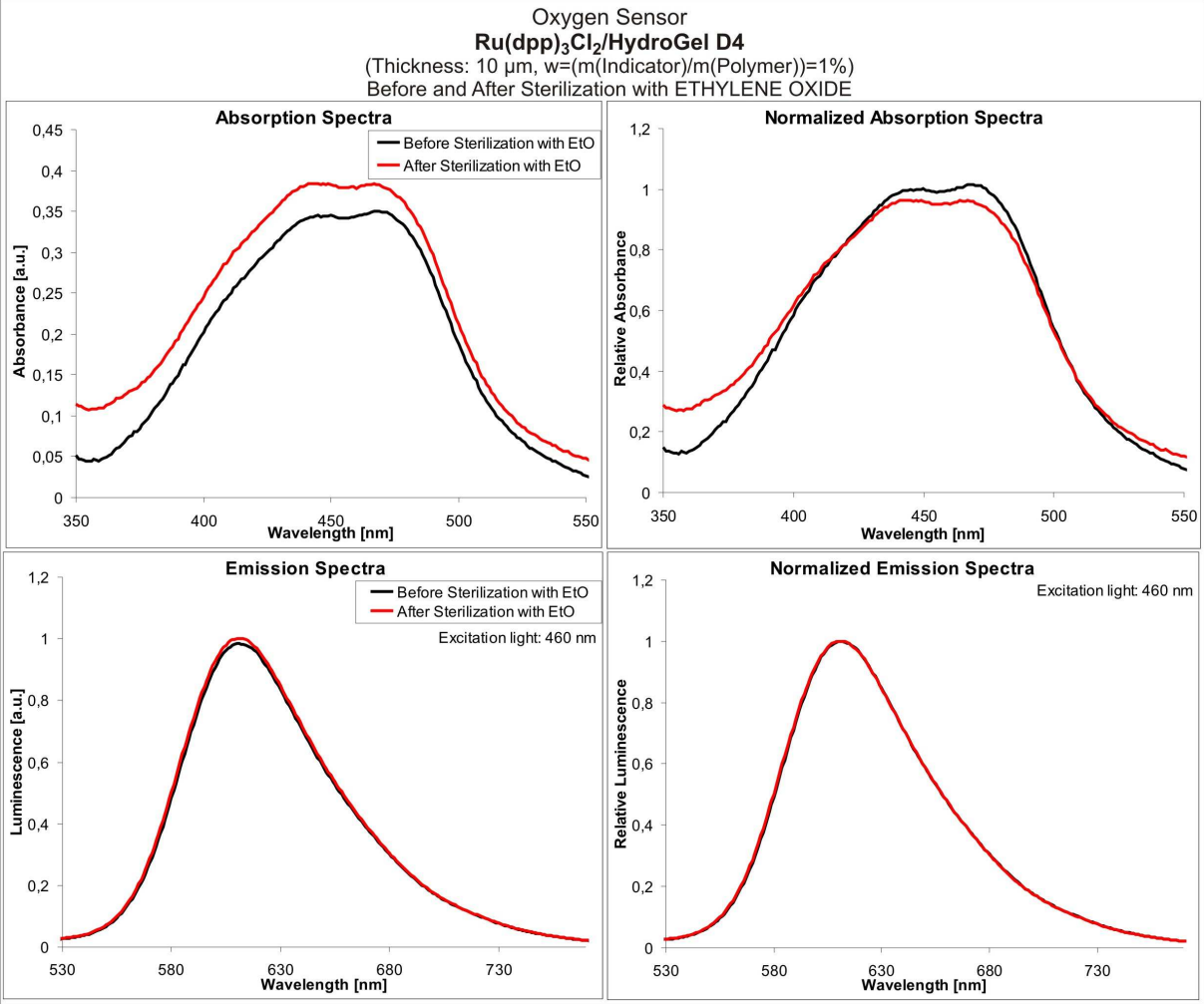

Sterilization with Ethylene Oxide	Absorption Spectra	Emission Spectra
Alterations in Absorption/Emission Intensity	13,41% increase	1,52% increase
Alterations in Absorption/Emission Curve Form	Altered absorption curve form between 350-400 nm, 430-490 nm and 520-800 nm.	Unaltered.

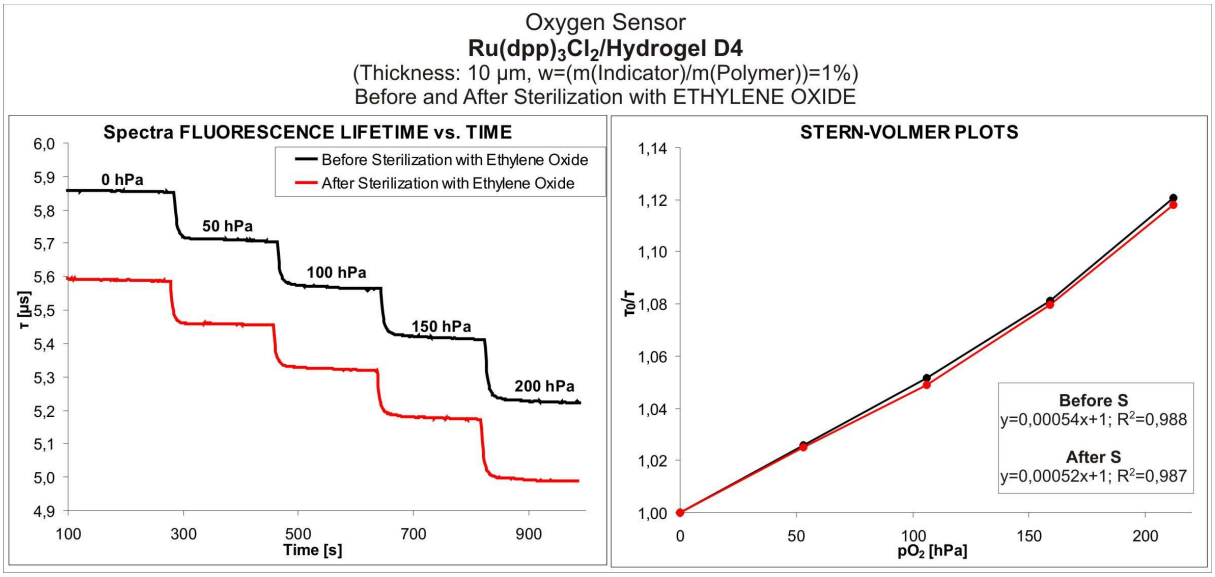

Sterilization with Ethylene Oxide	Luminescence Lifetime	Stern-Volmer Plot
Alterations in Luminescence Lifetime and Slope	4,74% decrease of τ_0	2,43% decrease of slope
	4,68% decrease of τ at 50 hPa	
	4,39% decrease of τ at 100 hPa	
	4,52% decrease of τ at 150 hPa	
	4,47% decrease of τ at 200 hPa	

E.25 Ruthenium(II) DiPhenylPhenanthroline DiChloride ($Ru(dpp)_3Cl_2$) immobilized in HydroThane5

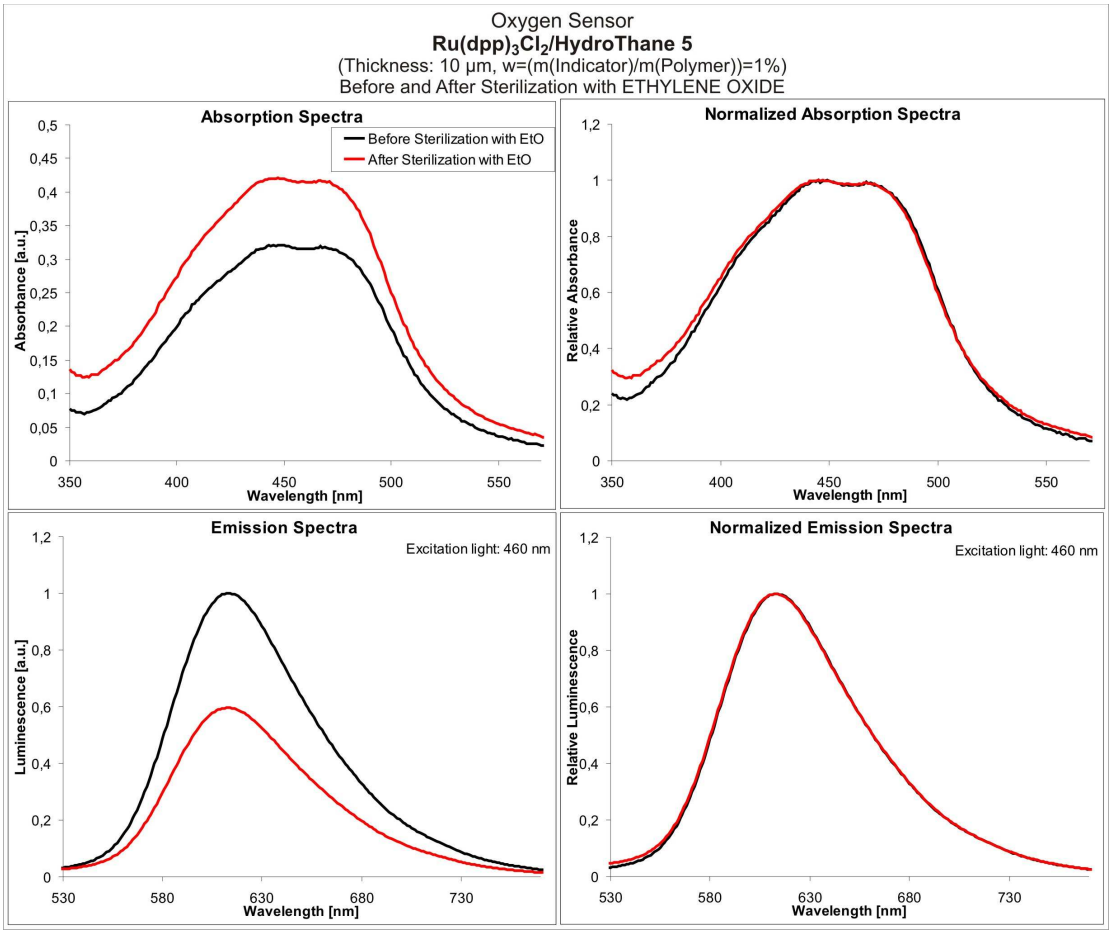

Sterilization with Ethylene Oxide	Absorption Spectra	Emission Spectra
Alterations in Absorption/Emission Intensity	23,58% increase	40,36% decrease
Alterations in Absorption/Emission Curve Form	Sensor became turbid after sterilization. Altered absorption curve form between 350-410 nm and 540-800 nm.	Unaltered.

Oxygen Sensor
$Ru(dpp)_3Cl_2$/HydroThane 5
(Thickness: 10 µm, w=(m(Indicator)/m(Polymer))=1%)
Before and After Sterilization with ETHYLENE OXIDE

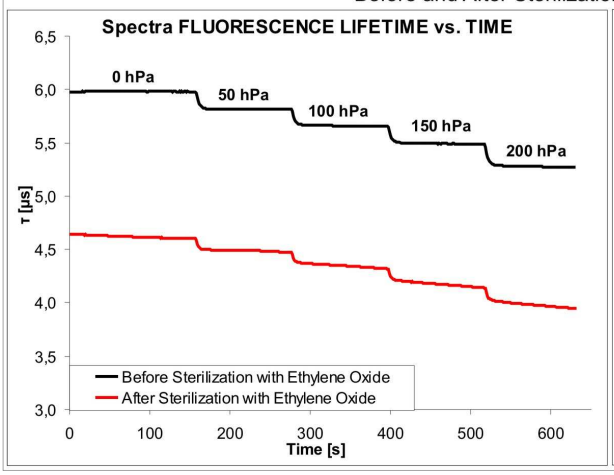

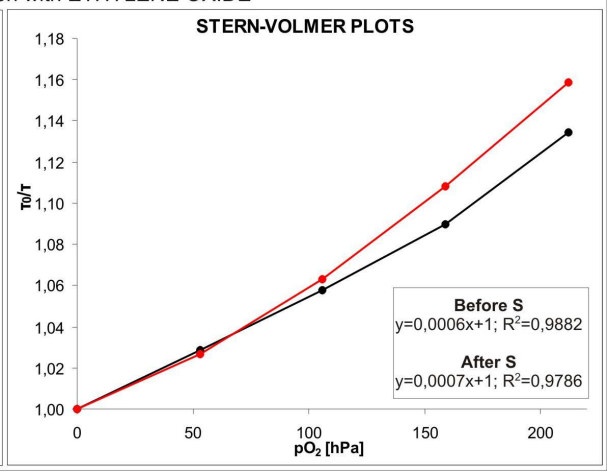

Sterilization with Ethylene Oxide	Luminescence Lifetime	Stern-Volmer Plot
Alterations in Luminescence Lifetime and Slope	23,05% decrease of τ_0	15,71% increase of slope
	22,94% decrease of τ at 50 hPa	
	23,38% decrease of τ at 100 hPa	
	24,29% decrease of τ at 150 hPa	
	24,63% decrease of τ at 200 hPa	

E.26 Ruthenium(II) DiPhenylPhenanthroline DiChloride ($Ru(dpp)_3Cl_2$) immobilized in PolySulfone

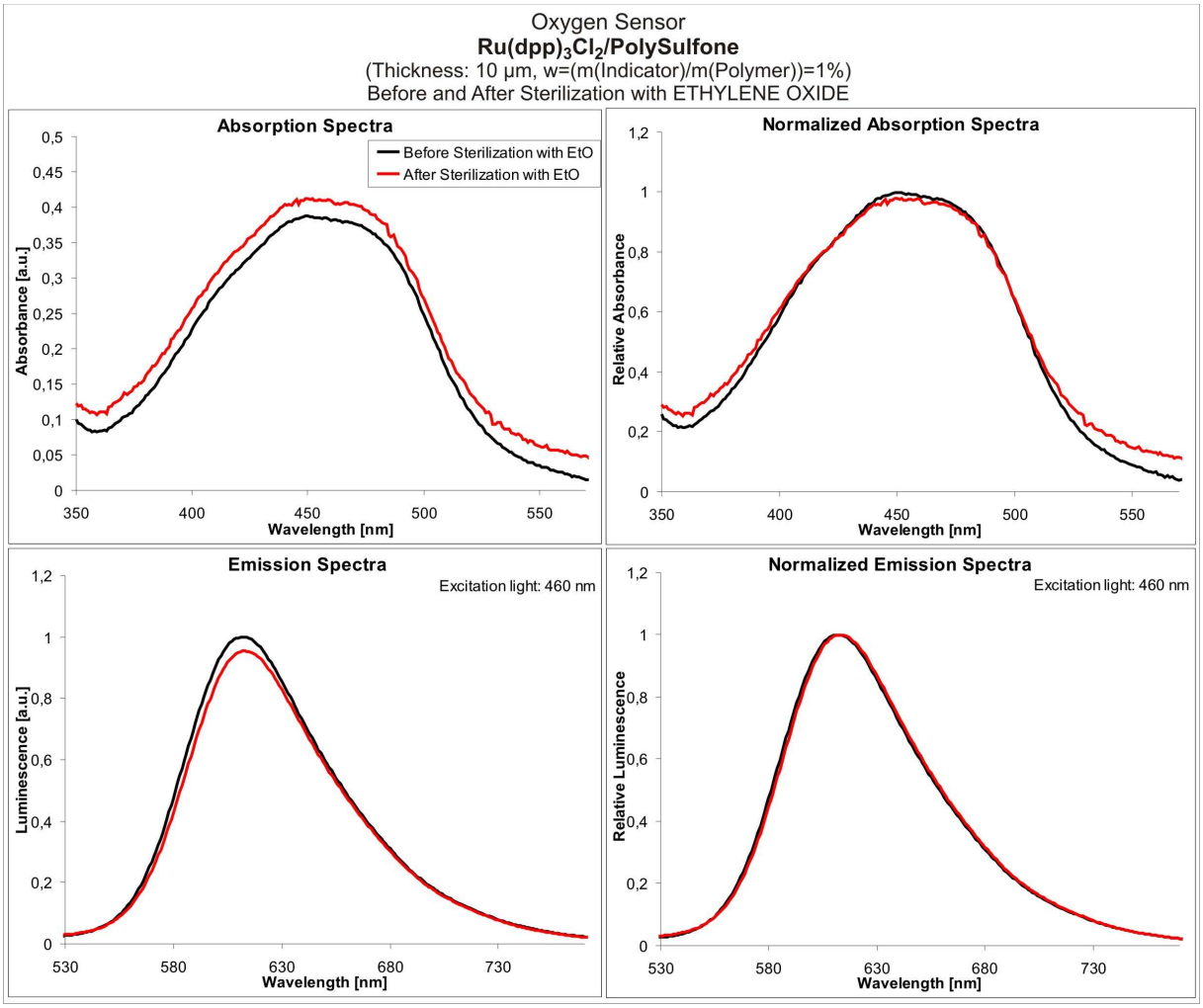

Sterilization with Ethylene Oxide	Absorption Spectra	Emission Spectra
Alterations in Absorption/Emission Intensity	7,81% increase	4,57% decrease
Alterations in Absorption/Emission Curve Form	Sensor became slightly turbid after sterilization. Altered absorption curve form between 350-400 nm, 440-450 nm and 510-800 nm.	Unaltered.

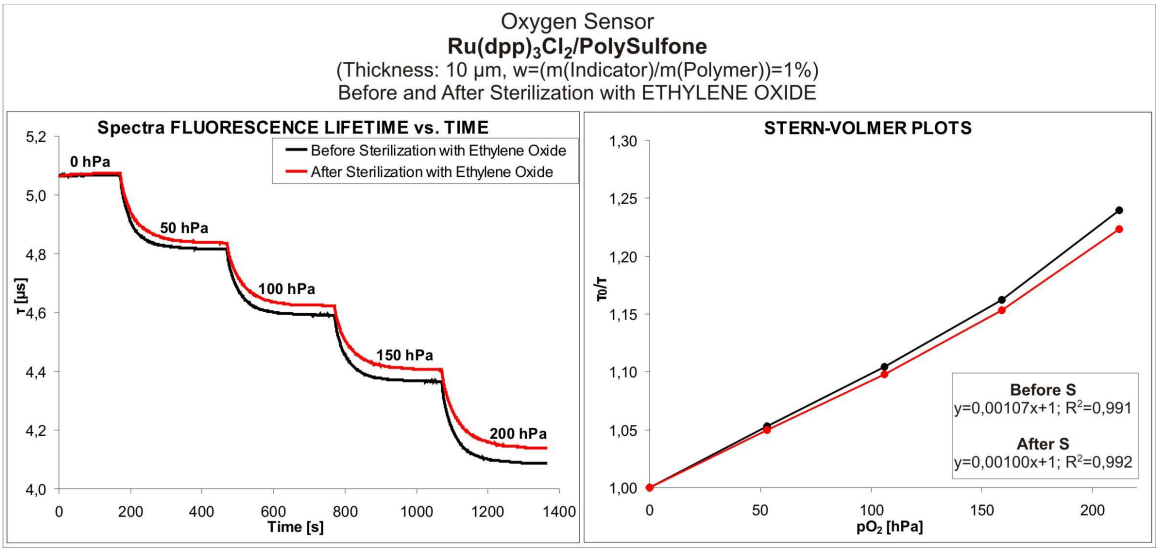

Sterilization with Ethylene Oxide	Luminescence Lifetime	Stern-Volmer Plot
Alterations in Luminescence Lifetime and Slope	0,19% decrease of τ_0	9,10% decrease of slope
	0,21% increase of τ at 50 hPa	
	0,43% increase of τ at 100 hPa	
	0,68% increase of τ at 150 hPa	
	1,21% increase of τ at 200 hPa	

E.27 Ruthenium(II) DiPhenylPhenanthroline DiChloride ($Ru(dpp)_3Cl_2$) immobilized in PolyPhenyl SilsesQuioxane

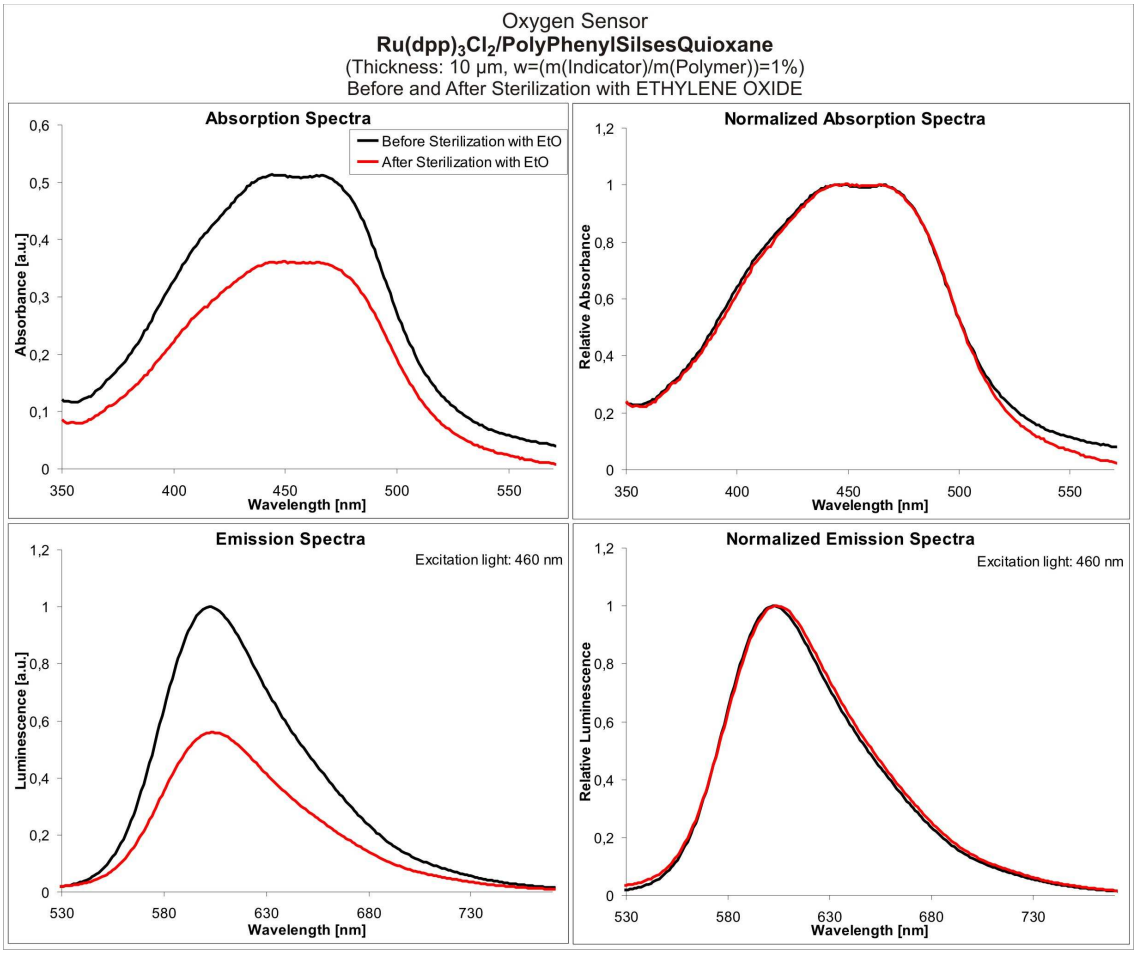

Sterilization with Ethylene Oxide	Absorption Spectra	Emission Spectra
Alterations in Absorption/Emission Intensity	29,70% increase	44,07% decrease
Alterations in Absorption/Emission Curve Form	Altered absorption curve form between 510-800 nm.	Unaltered.

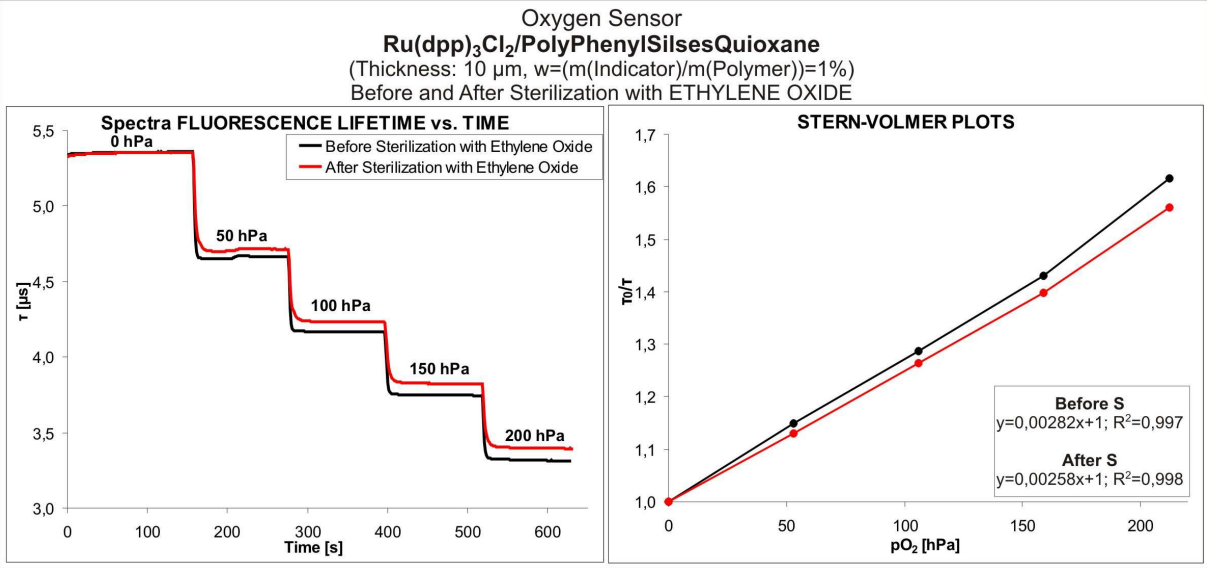

Sterilization with Ethylene Oxide	Luminescence Lifetime	Stern-Volmer Plot
Alterations in Luminescence Lifetime and Slope	1,24% decrease of τ_0	7,14% decrease of slope
	0,71% increase of τ at 50 hPa	
	0,53% increase of τ at 100 hPa	
	1,17% increase of τ at 150 hPa	
	2,28% increase of τ at 200 hPa	

E.28 Ruthenium(II) DiPhenylPhenanthroline DiChloride ($Ru(dpp)_3Cl_2$) immobilized in PolyStyrene

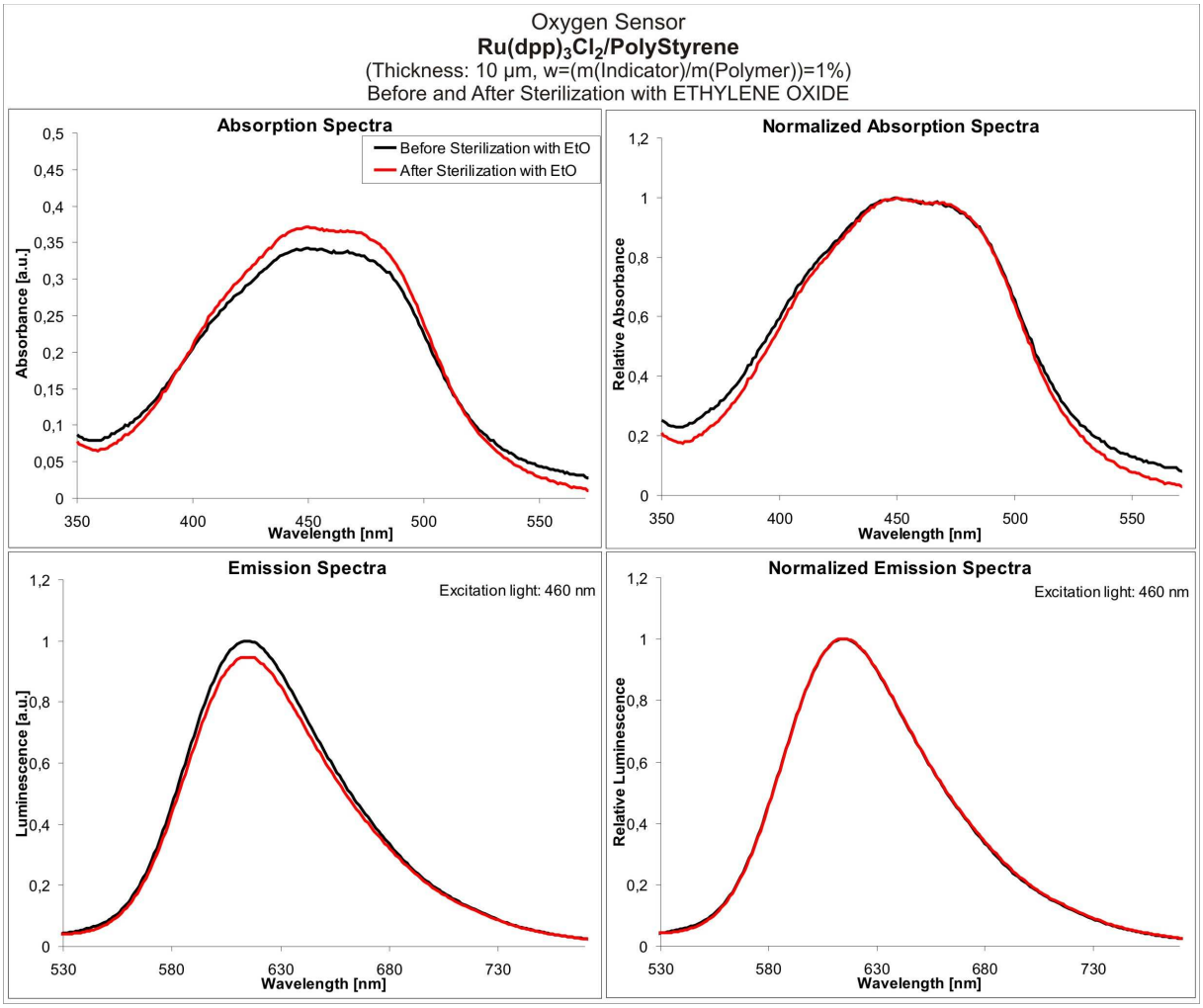

Sterilization with Ethylene Oxide	Absorption Spectra	Emission Spectra
Alterations in Absorption/Emission Intensity	7,80% increase	5,32% decrease
Alterations in Absorption/Emission Curve Form	Altered absorption curve form between 350-430 nm and 510-800 nm,	Unaltered.

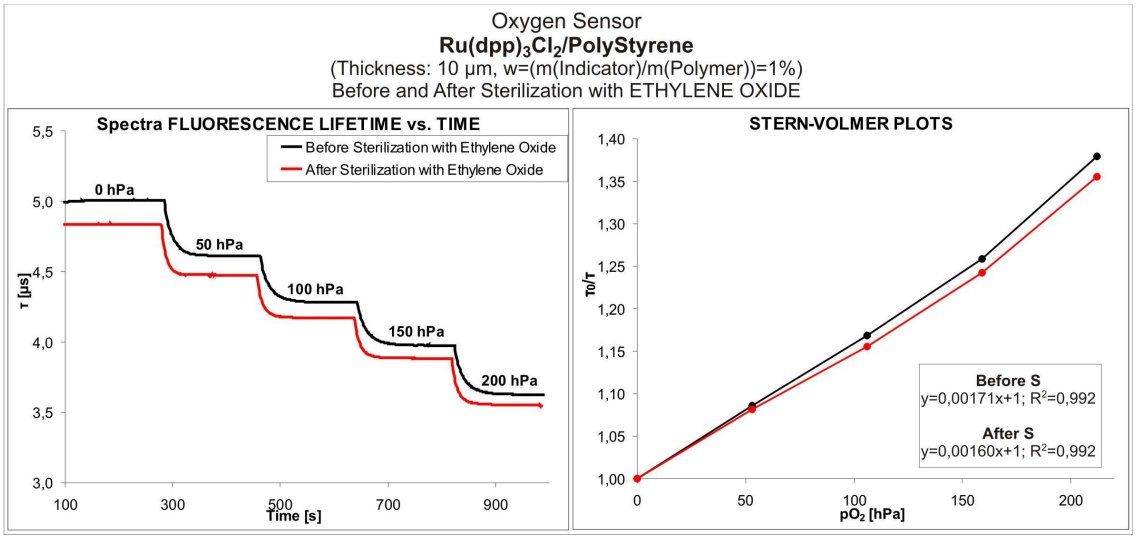

Sterilization with Ethylene Oxide	Luminescence Lifetime	Stern-Volmer Plot
Alterations in Luminescence Lifetime and Slope	3,80% decrease of τ_0	5,88% decrease of slope
	3,69% decrease of τ at 50 hPa	
	3,03% decrease of τ at 100 hPa	
	2,76% decrease of τ at 150 hPa	
	2,20% decrease of τ at 200 hPa	

E.29 Ruthenium(II) DiPhenylPhenanthroline DiChloride ($Ru(dpp)_3Cl_2$) immobilized in PolyStyrene-co-Acrylonitrile

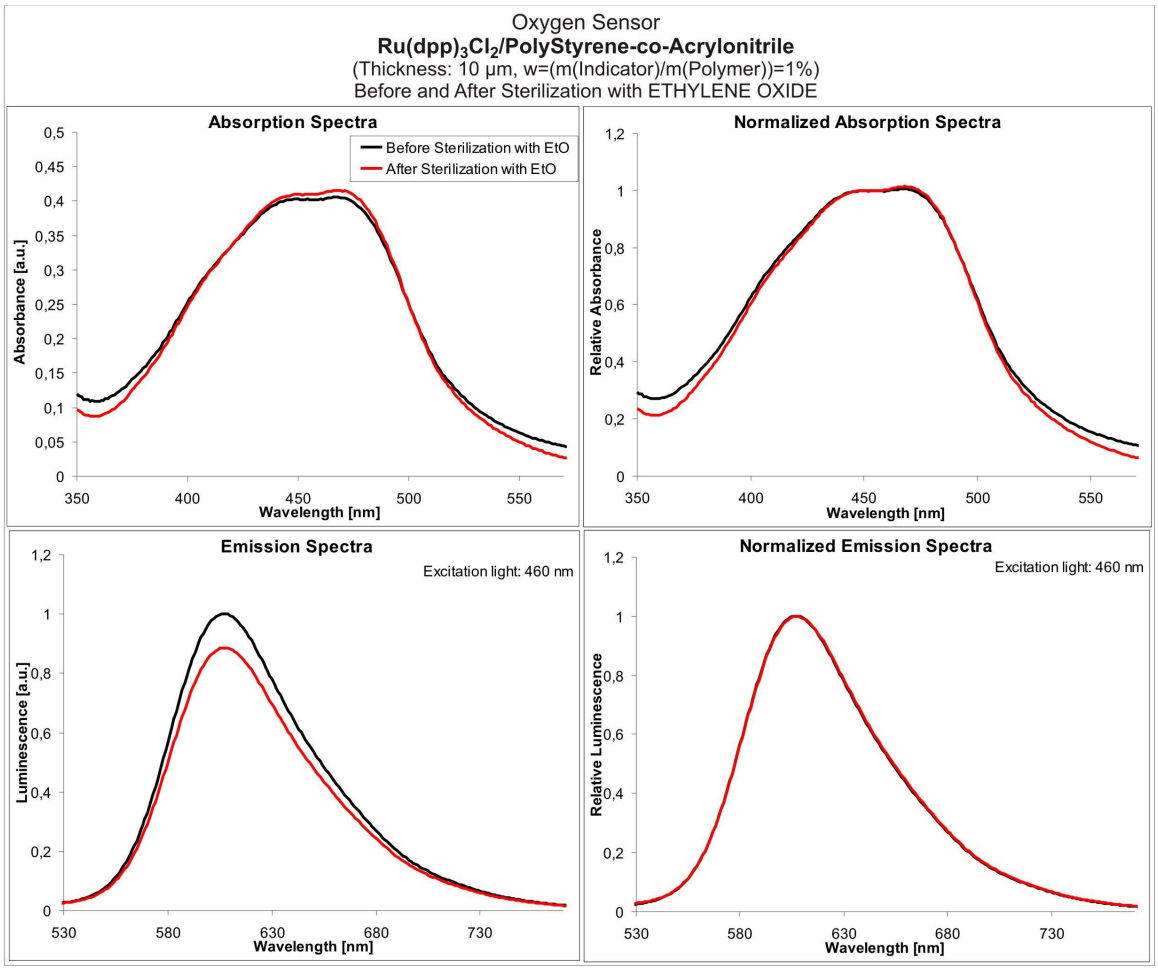

Sterilization with Ethylene Oxide	Absorption Spectra	Emission Spectra
Alterations in Absorption/Emission Intensity	1,68% increase	11,34% decrease
Alterations in Absorption/Emission Curve Form	Altered absorption curve form between 350-410 nm and 510-800 nm.	Unaltered.

Oxygen Sensor
$Ru(dpp)_3Cl_2$/PolyStyrene-co-Acrylonitrile
(Thickness: 10 µm, w=(m(Indicator)/m(Polymer))=1%)
Before and After Sterilization with ETHYLENE OXIDE

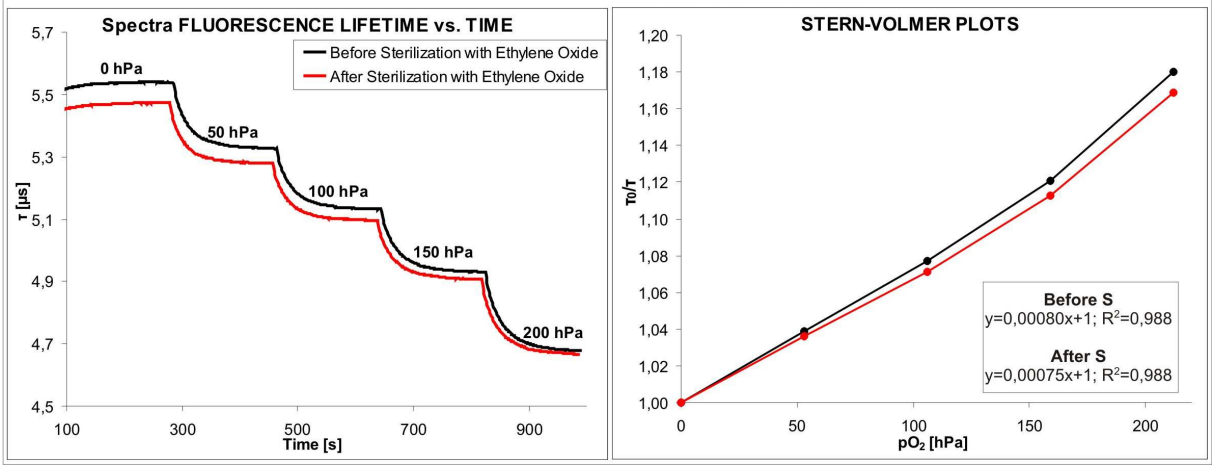

Sterilization with Ethylene Oxide	Luminescence Lifetime	Stern-Volmer Plot
Alterations in Luminescence Lifetime and Slope	1,44% decrease of τ_0	12,50% decrease of slope
	1,23% decrease of τ at 50 hPa	
	0,78% decrease of τ at 100 hPa	
	0,61% decrease of τ at 150 hPa	
	0,21% decrease of τ at 200 hPa	

E.30 Ruthenium(II) DiPhenylPhenanthroline DiChloride ($Ru(dpp)_3Cl_2$) immobilized in PolyStyrene-co-MaleicAnhydride (PSMA93)

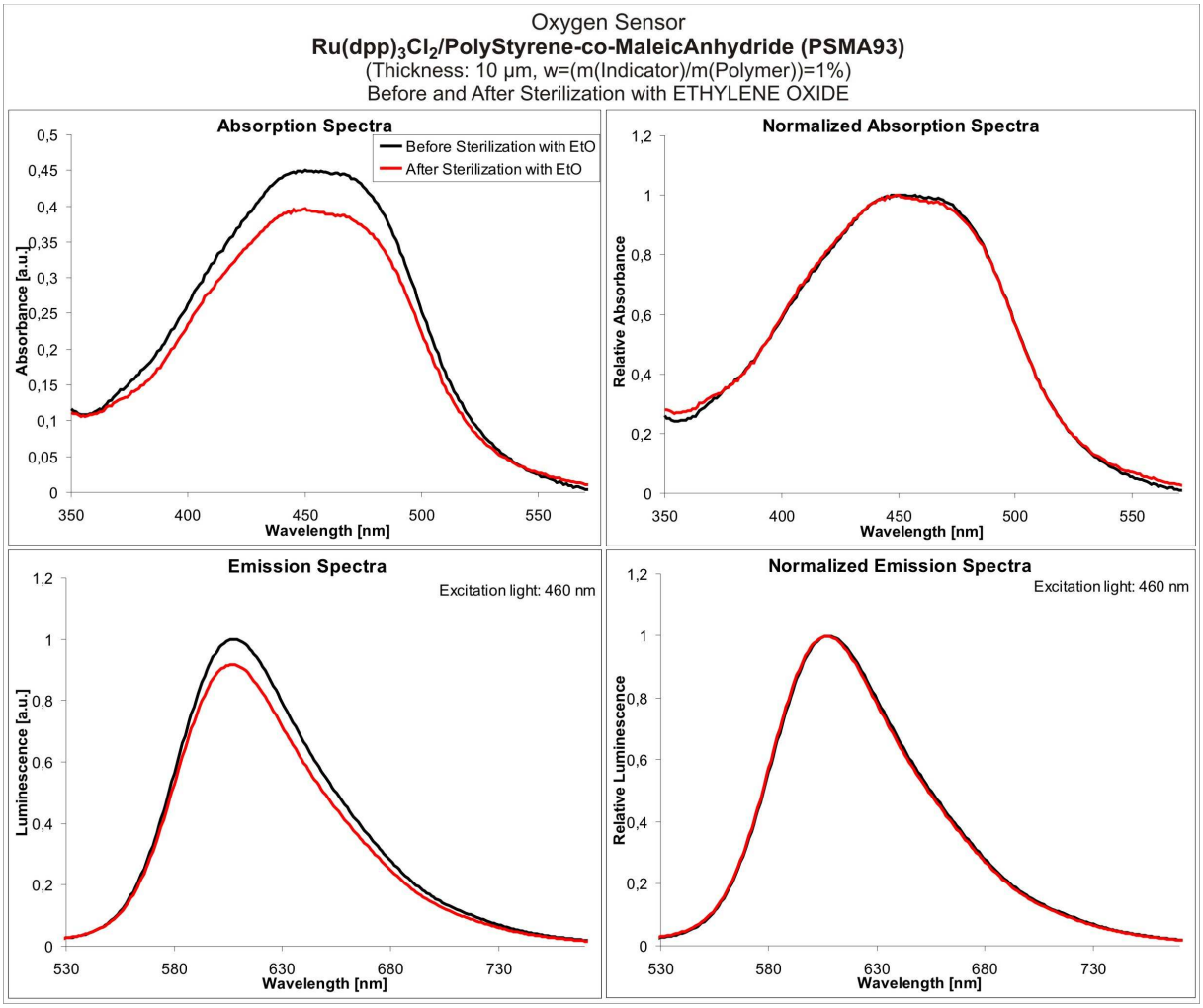

Sterilization with Ethylene Oxide	Absorption Spectra	Emission Spectra
Alterations in Absorption/Emission Intensity	11,87% decrease	8,15% decrease
Alterations in Absorption/Emission Curve Form	Altered absorption curve form between 350-370 nm and 550-800 nm.	Unaltered.

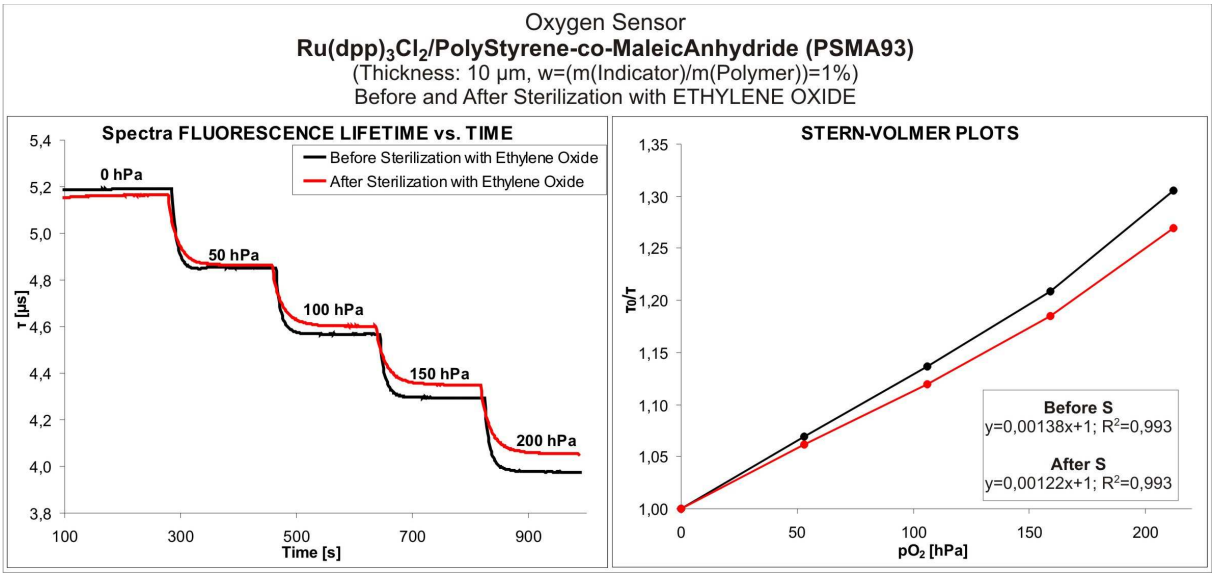

Sterilization with Ethylene Oxide	Luminescence Lifetime	Stern-Volmer Plot
Alterations in Luminescence Lifetime and Slope	0,96% decrease of τ_0	14,28% decrease of slope
	0,21% decrease of τ at 50 hPa	
	0,65% increase of τ at 100 hPa	
	1,15% increase of τ at 150 hPa	
	1,97% increase of τ at 200 hPa	

Optical pH SENSORS

E.31 HPTS(DHA$_3$) immobilized in HydroGel D4

Absorption Spectra

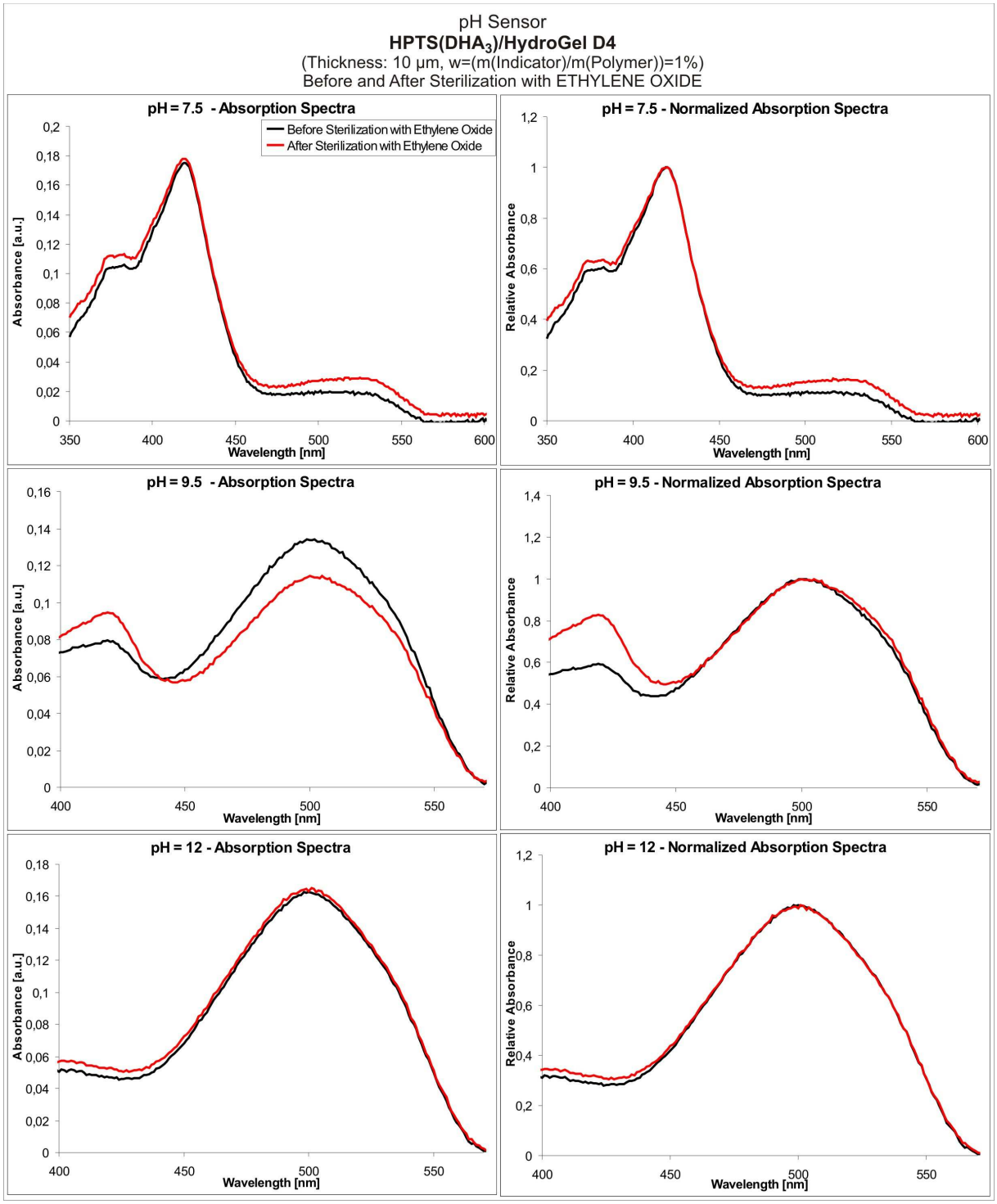

Emission Spectra

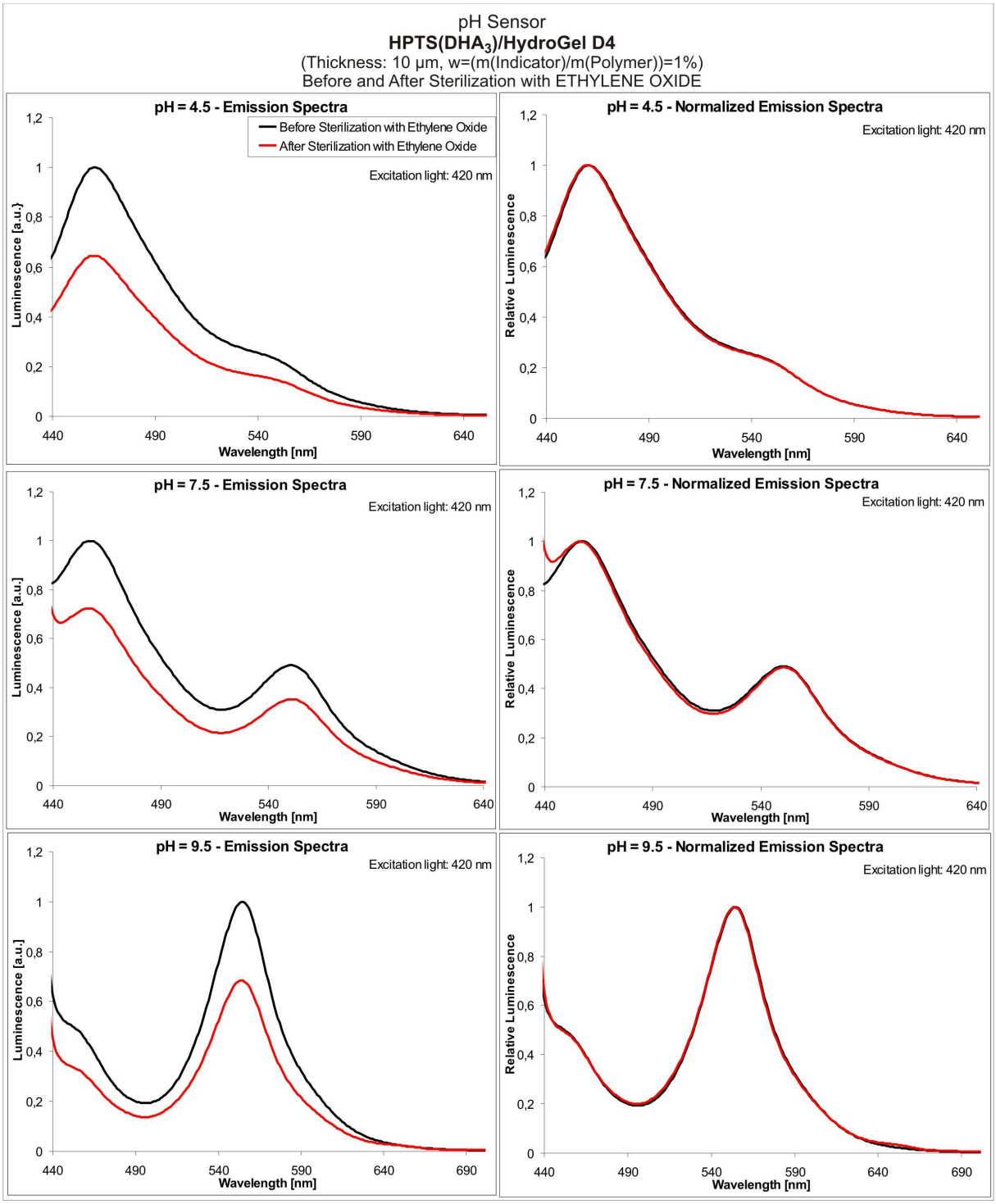

Sterilization with EtO	Absorption Spectra			Emission Spectra		
		pH	Alterations		pH	Alterations
Alterations in Absorption/ Emission Intensity	AFTERS	4.5	1,83% increase	AFTERS	4.5	35,42% decrease
		7.5	1,58% increase		7.5	27,54% decrease
		9.5	14,81% decrease		9.5	31,48% decrease

Alterations in Absorption/ Emission Curve Form	AFTER S	4.5	Unaltered.	AFTER S	4.5	Unaltered.
		7.5	Altered absorption between 350-400 nm. The ratio between protonation/deprotonation emission peaks is altered.		7.5	Unaltered.
		9.5	The ratio between protonation/deprotonation emission peaks is altered.		9.5	Unaltered.

Calibration Curves

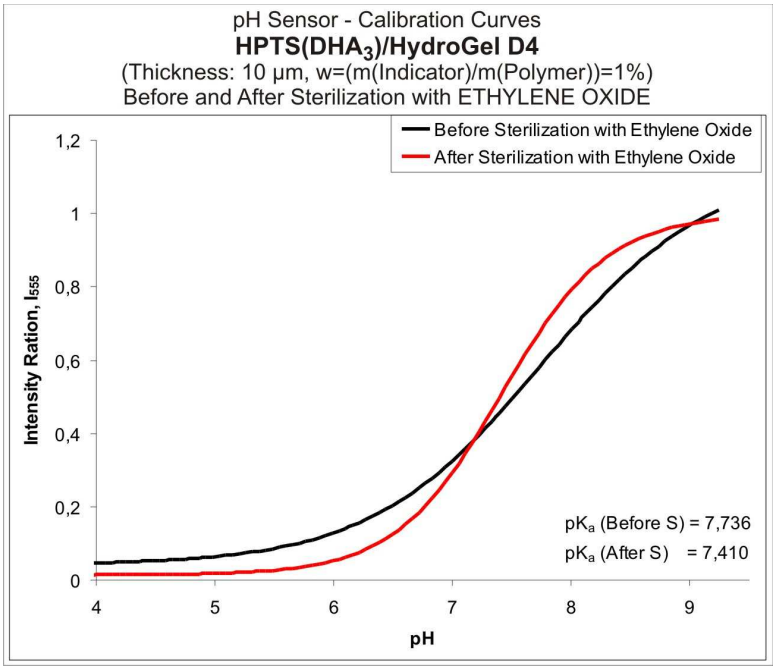

EtO	Alterations in Calibration Curve Shape	Alterations in pK_a
	Altered curve shape after sterilization. The response to the proton still observed – re-calibration of sensor response.	Decrease of pK_a (for 0,326)

E.32 2´,7´-DiHexylFluorescein OctadecylEster immobilized in HydroMed Hydrogel D4

Absorption Spectra

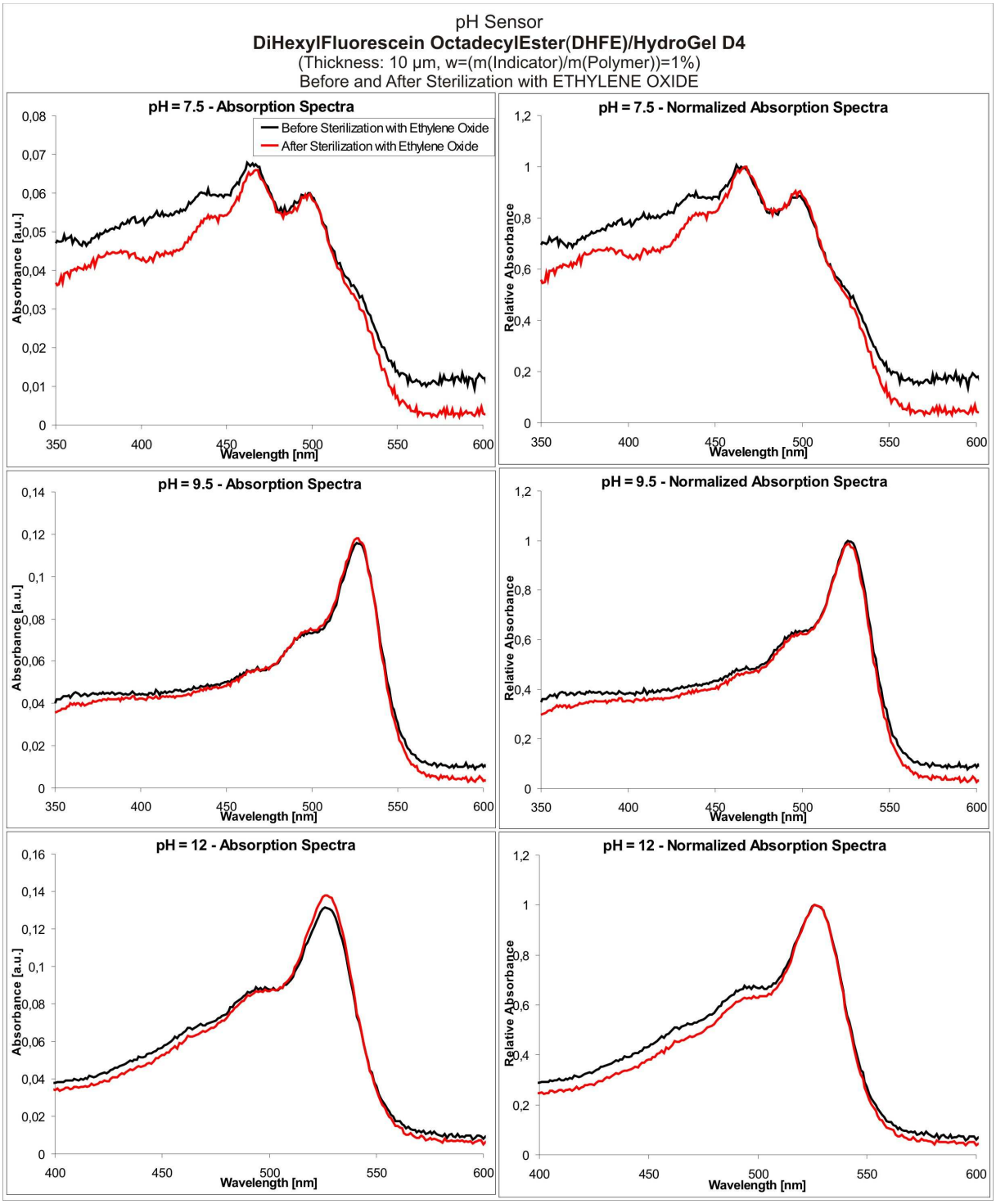

Emission Spectra

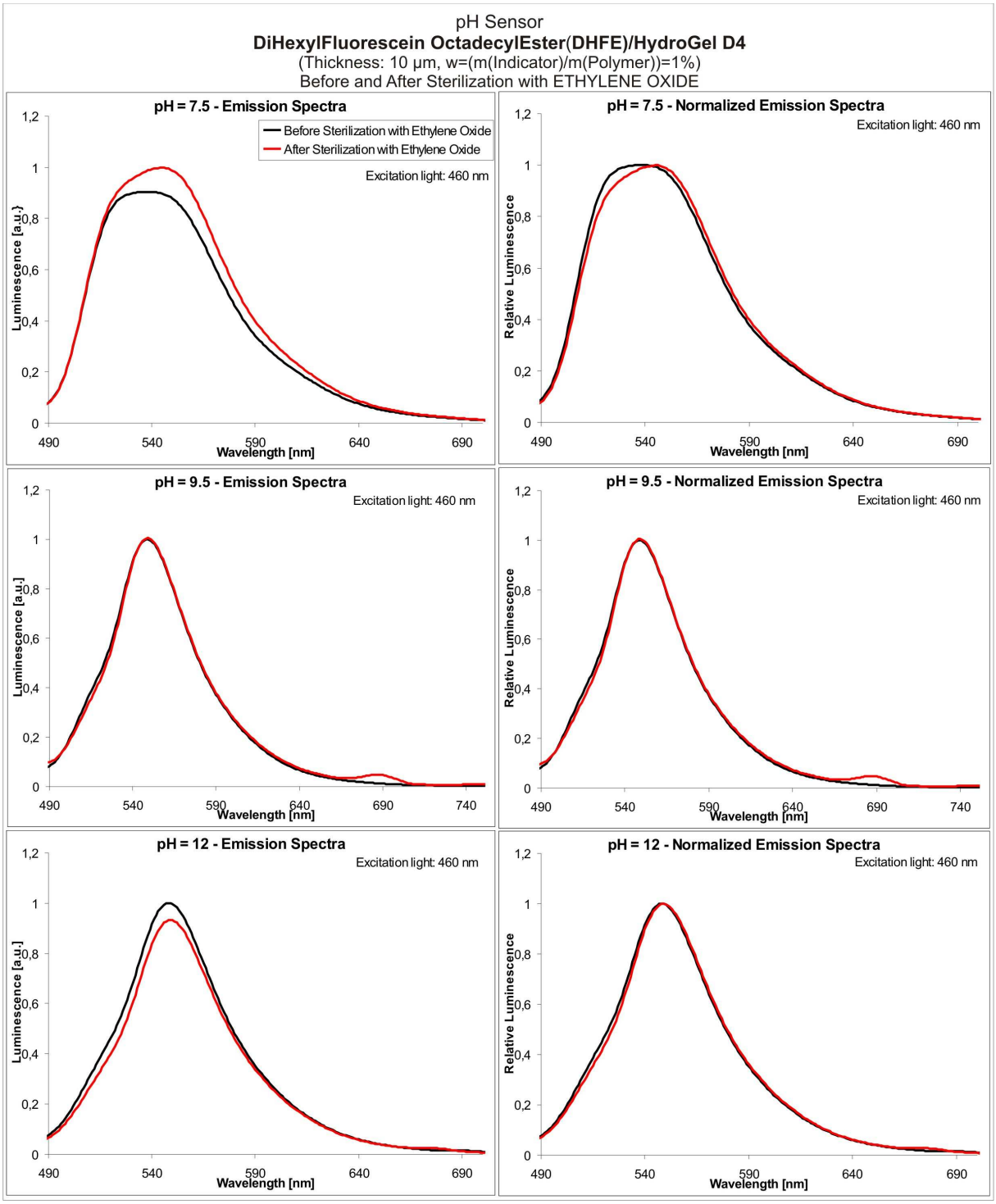

Sterilization with EtO	Absorption Spectra			Emission Spectra		
		pH	Alterations		pH	Alterations
Alterations in Absorption/ Emission Intensity	AFTERS	4.5	2,42% decrease	AFTERS	4.5	10,59% increase
		7.5	3,23% increase		7.5	0,46% decrease
		9.5	4,80% decrease		9.5	6,57% decrease

Alterations in Absorption/ Emission Curve Form	AFTER S	4.5	Altered absorption curve form between 350-450 nm and 550-800 nm.	AFTER S	4.5	Altered emission curve form between 515-555 nm. Bathochromic shift of the emission maximum for 6 nm.
		7.5	Altered absorption curve form between 350-470 nm and 550-800 nm.		7.5	New emission peak with λ_{max}=687 nm.
		9.5	Altered absorption curve form between 400-520 nm and 550-800 nm.		9.5	Bathochromic shift of the emission maximum for 1 nm.

Calibration Curves

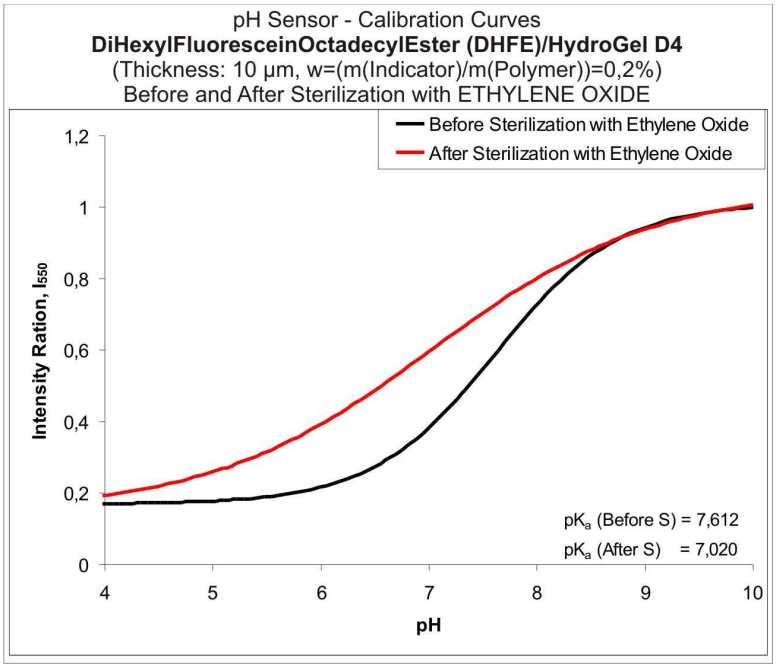

EtO	Alterations in Calibration Curve Shape	Alterations in pK_a
	Altered curve shape after sterilization. The response to the proton still observed – re-calibration of sensor response.	Decrease of pK_a (for 0,592)

E.33 2´,7´-DiHexylFluorescein OctadecylEster immobilized in Poly(2-HydroxyEthyl MethAcrylate) (=pHEMA)

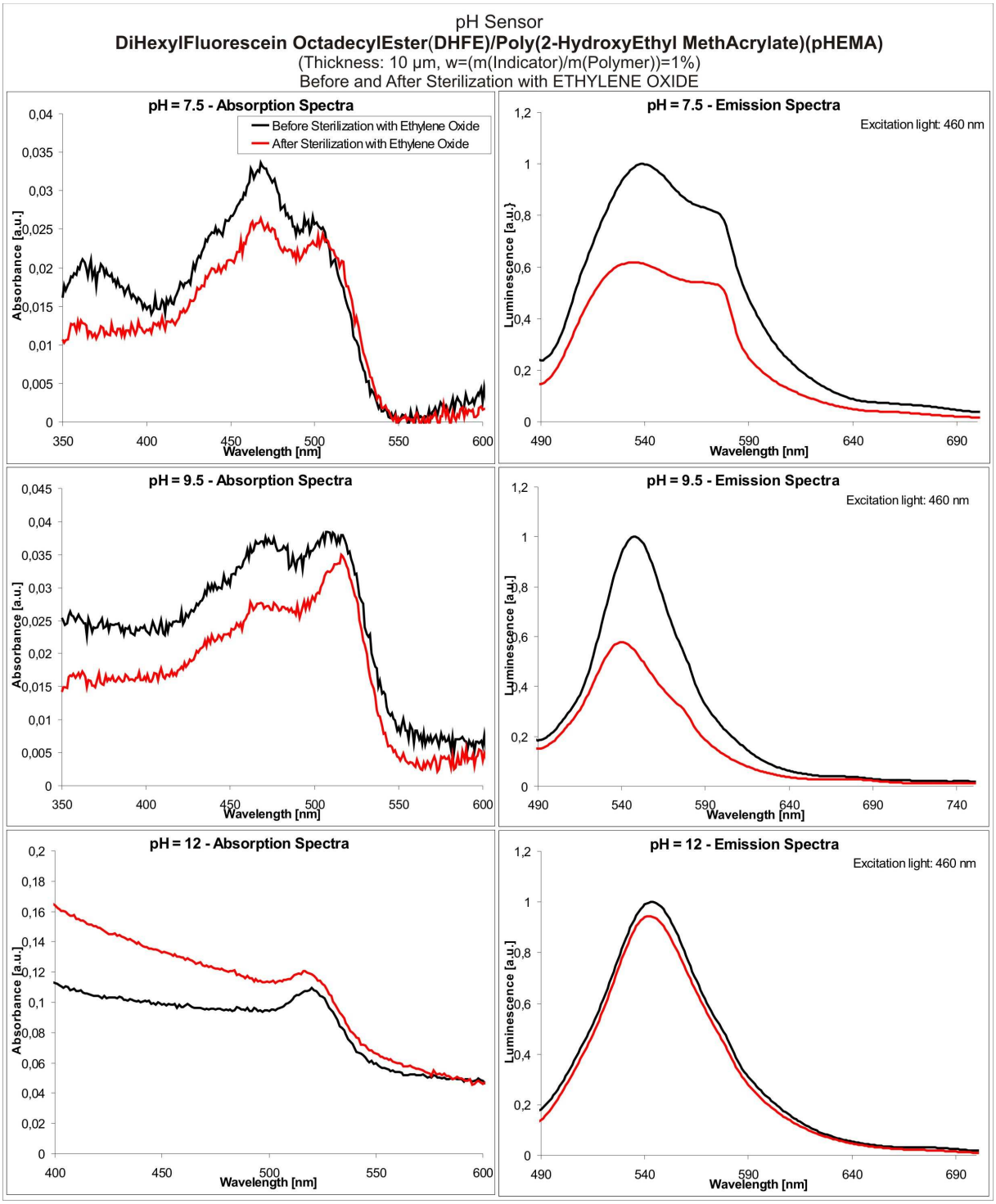

Sterilization with EtO	Absorption Spectra			Emission Spectra		
		pH	Alterations		pH	Alterations
Alterations in Absorption/ Emission Intensity	AFTER S	7.5	20,32% decrease	AFTER S	7.5	38,28% decrease
		9.5	11,62% decrease		9.5	42,28% decrease
		12	9,29% increase		12	5,52% decrease

Alterations in Absorption/ Emission Curve Form	AFTER S	7.5	Altered absorption curve form between 350-400 nm.	AFTER S	7.5	Altered emission curve form between 560-630 nm. Hypsochromic shift of the emission maximum for 5 nm.
		9.5	Altered absorption curve form between 490-530 nm.		9.5	Altered emission curve form between 565-590 nm. Hypsochromic shift of the emission maximum for 7 nm.
		12	Altered absorption curve form.		12	Unaltered.

Calibration Curves

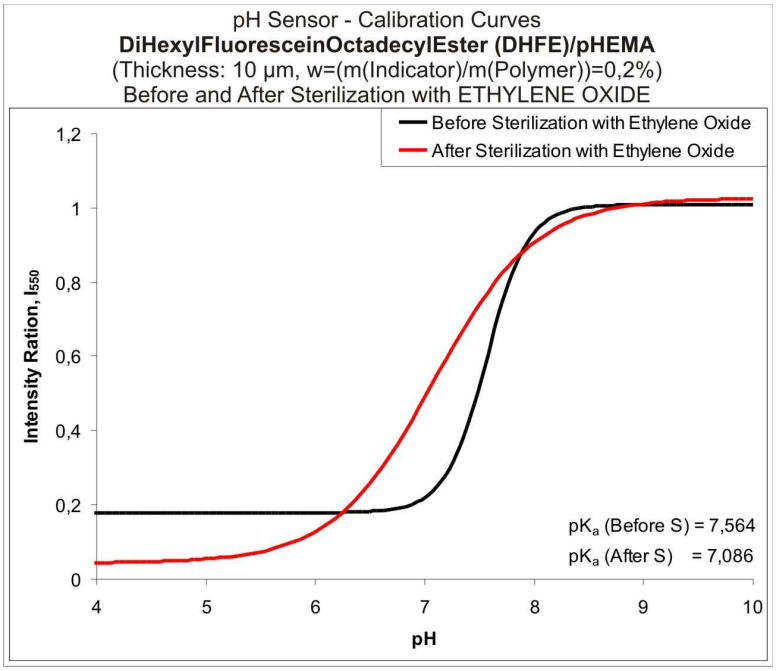

EtO	Alterations in Calibration Curve Shape	Alterations in pK_a
	Altered curve shape after sterilization. The response to the proton still observed – re-calibration of sensor response.	Decrease of pK_a (for 0,478)

E.34 2´,7´-DiHexyl-N-Octadecyl-CarboxAmidoFluorescein (=DHFA) immobilized in HydroMed Hydrogel D4

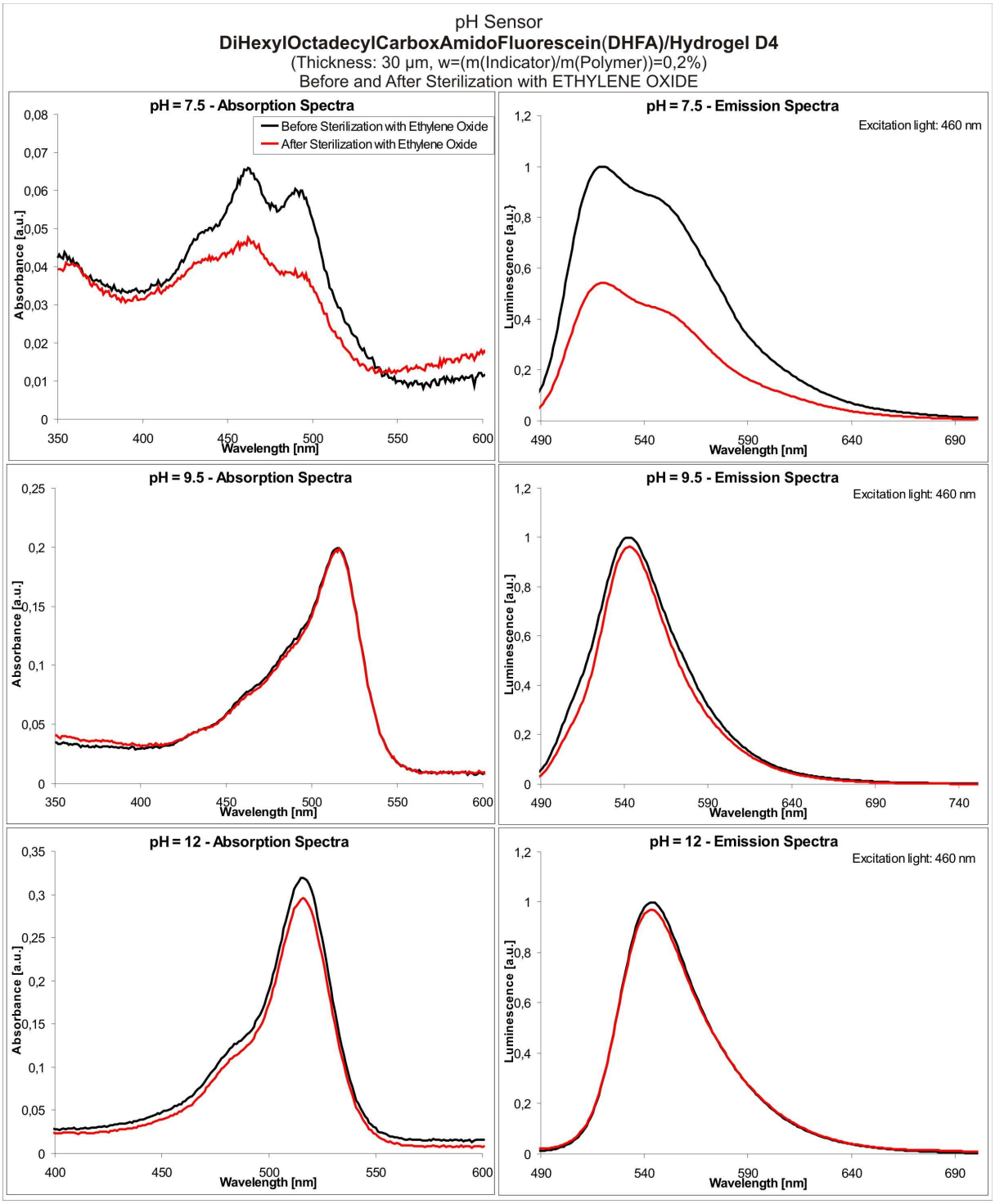

Sterilization with EtO	Absorption Spectra			Emission Spectra		
		pH	Alterations		pH	Alterations
Alterations in Absorption/ Emission Intensity	AFTERS	4.5	28,94% decrease	AFTERS	4.5	45,74% decrease
		7.5	1,17% increase		7.5	3,78% decrease
		9.5	7,22% decrease		9.5	3,04% decrease

Alterations in Absorption/ Emission Curve Form	AFTER S	4.5	Altered absorption curve form.	AFTER S	4.5	Altered emission curve form between 530-590 nm.
		7.5	Altered absorption curve form between 350-400 nm.		7.5	Altered emission curve form between 490-540 nm and 570-640 nm.
		9.5	Unaltered.		9.5	Unaltered.

Calibration Curves

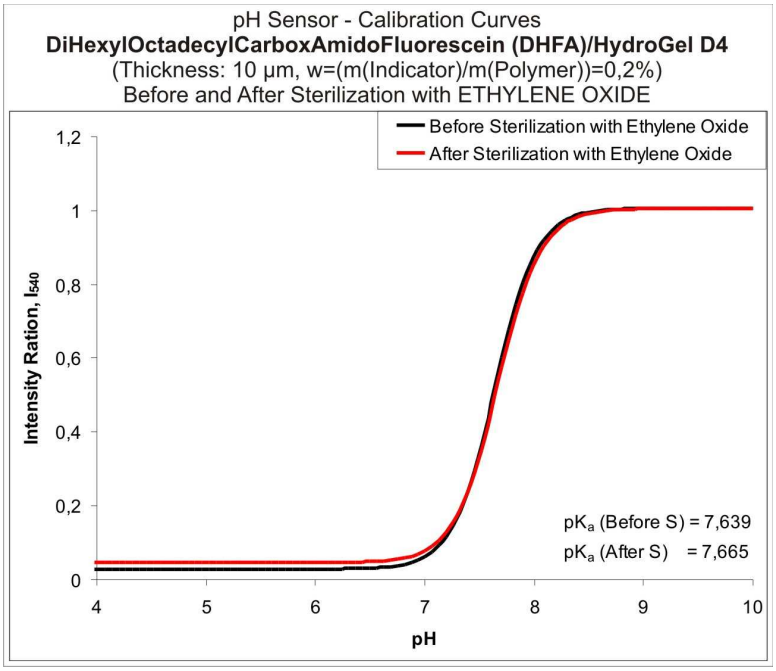

EtO	Alterations in Calibration Curve Shape	Alterations in pK_a
	Unaltered curve shape after sterilization.	Decrease of pK_a (for 0,026)

E.35 2´,7´-DiHexyl-N-Octadecyl-CarboxAmidoFluorescein (=DHFA) immobilized in Poly(2-HydroxyEthyl Methacrylate) (=pHEMA)

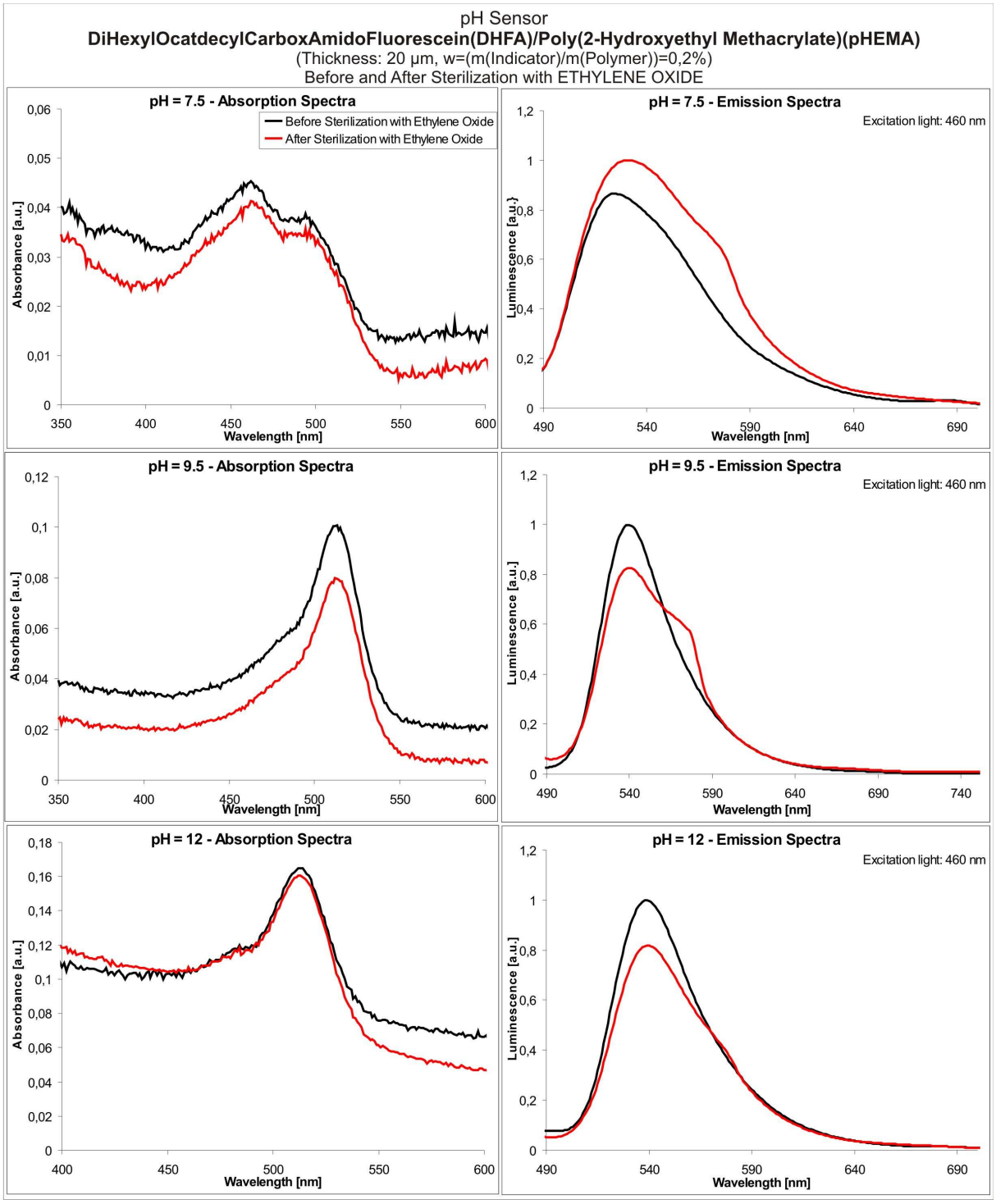

Sterilization with EtO	Absorption Spectra			Emission Spectra		
		pH	Alterations		pH	Alterations
Alterations in Absorption/ Emission Intensity	AFTERS	4.5	10,37% decrease	AFTERS	4.5	13,40% increase
		7.5	20,66% decrease		7.5	17,24% decrease
		9.5	2,63% decrease		9.5	18,26% decrease

Alterations in Absorption/ Emission Curve Form	AFTER S	4.5	Unaltered	AFTER S	4.5	Altered emission curve form between 540-640 nm. Bathochromic shift of the emission maximum for 7 nm.
		7.5	Altered absorption between 350-500 nm and 550-800 nm.		7.5	Altered emission curve form between 550-640 nm.
		9.5	Altered absorption between 400-450 nm and 530-800 nm.		9.5	Altered emission curve form between 550-630 nm.

Calibration Curves

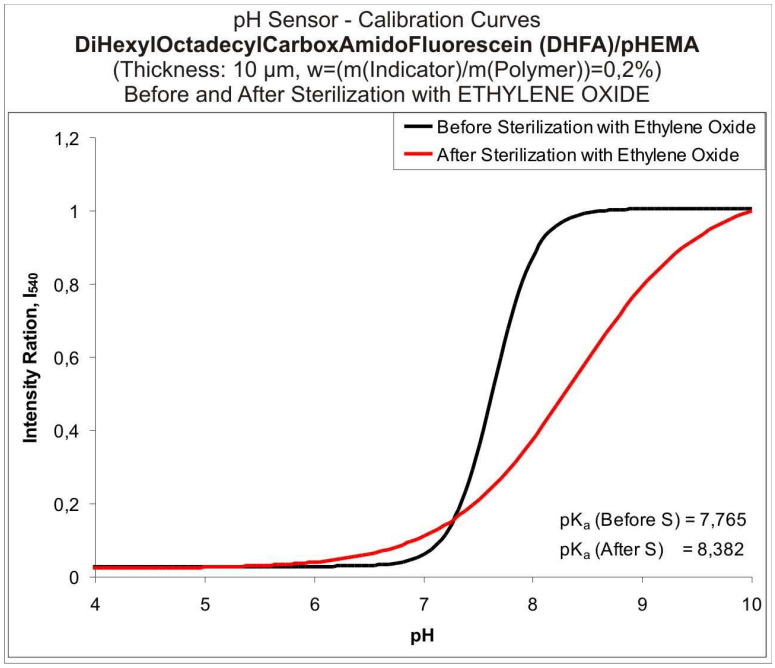

EtO	Alterations in Calibration Curve Shape	Alterations in pK_a
	Altered curve shape after sterilization. The response to the proton still observed – re-calibration of sensor response.	Increase of pK_a (for 0,617)

E.36 pH Sensitive Coumarin immobilized in HydroMed Hydrogel D4

Absorption Spectra

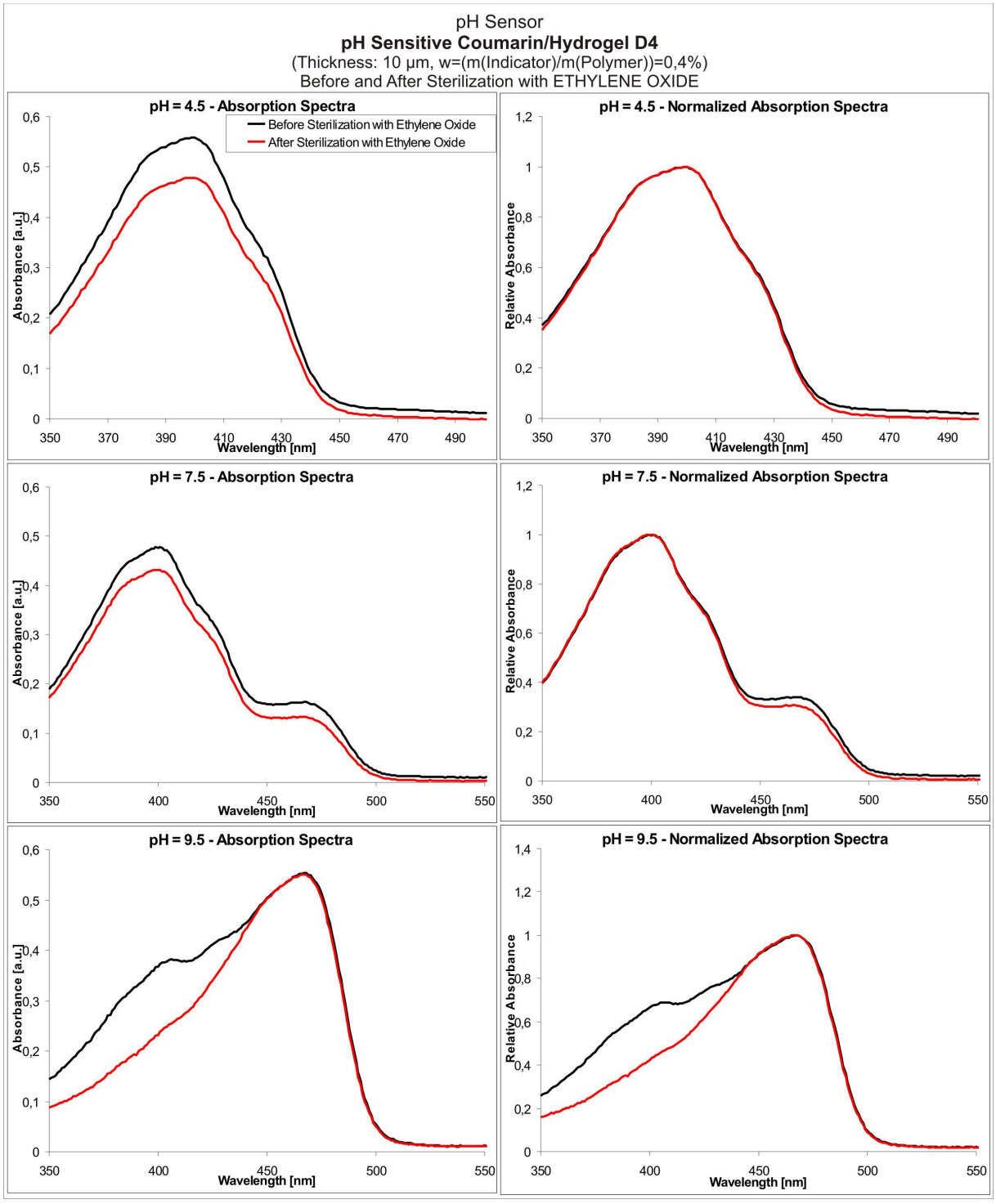

Emission Spectra

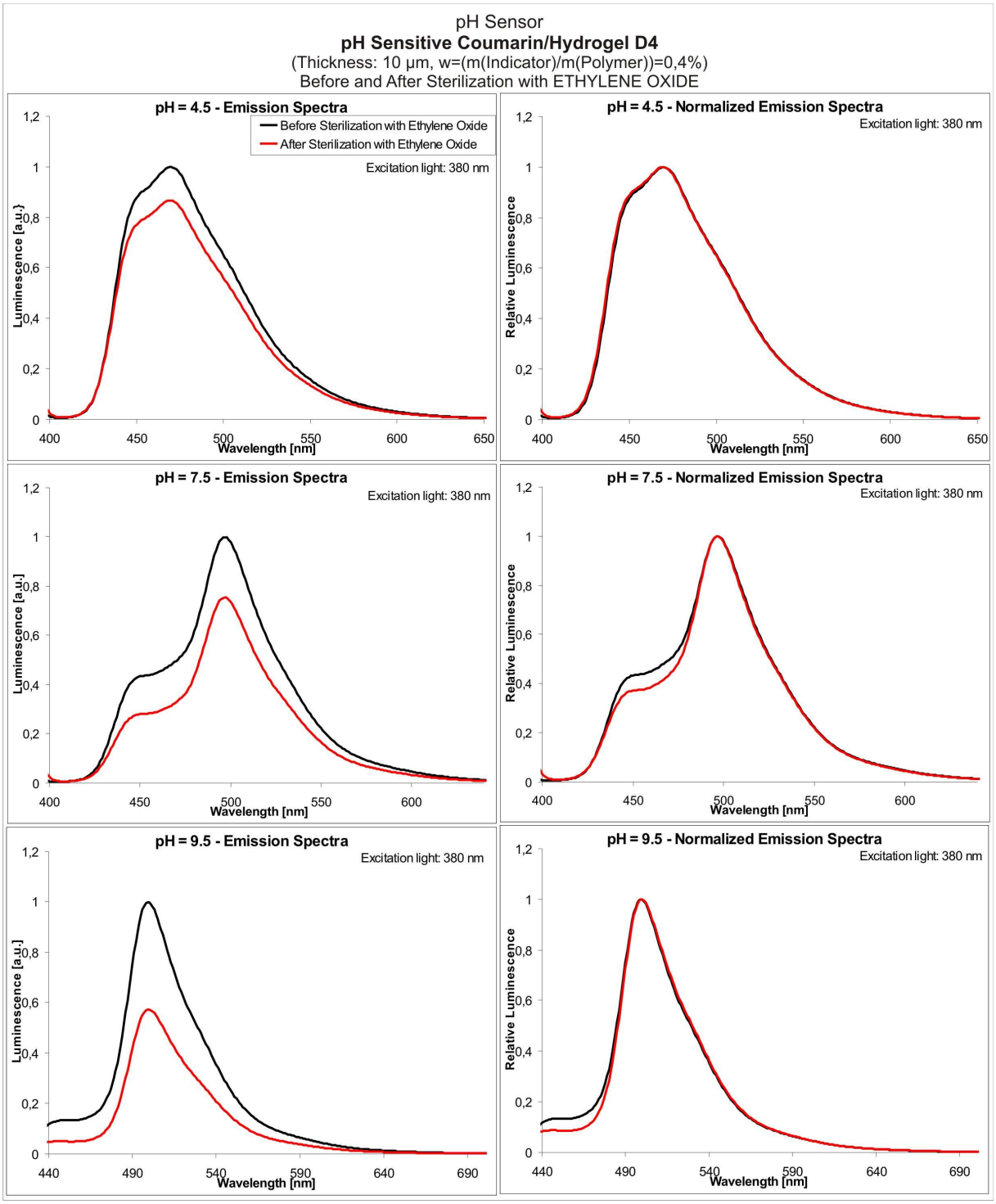

Sterilization with EtO	Absorption Spectra			Emission Spectra		
		pH	Alterations		pH	Alterations
Alterations in Absorption/ Emission Intensity	AFTERS	4.5	14,28% decrease	AFTERS	4.5	13,30% decrease
		7.5	9,51% decrease		7.5	24,63% decrease
		9.5	0,63% decrease		9.5	42,60% decrease

Alterations in Absorption/ Emission Curve Form	AFTER S	4.5	Unaltered	AFTER S	4.5	Unaltered
		7.5	The ratio between protonation/deprotonation absorption peaks is altered.		7.5	The ratio between protonation/deprotonation absorption peaks is altered.
		9.5	Altered absorption between 350-440 nm.		9.5	Altered absorption between 350-490 nm.

Calibration Curves

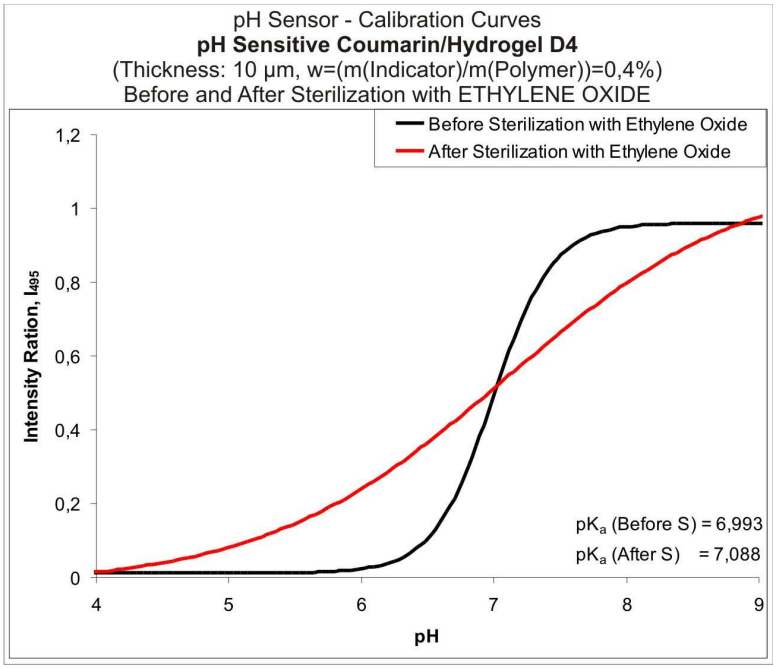

EtO	Alterations in Calibration Curve Shape	Alterations in pK_a
	Altered curve shape after sterilization. The response to the proton still observed – re-calibration of sensor response.	Increase of pK_a (for 0,095)

E.37 pH Sensitive Coumarin immobilized in Poly(2-HydroxyEthyl Methacrylate) (=pHEMA)

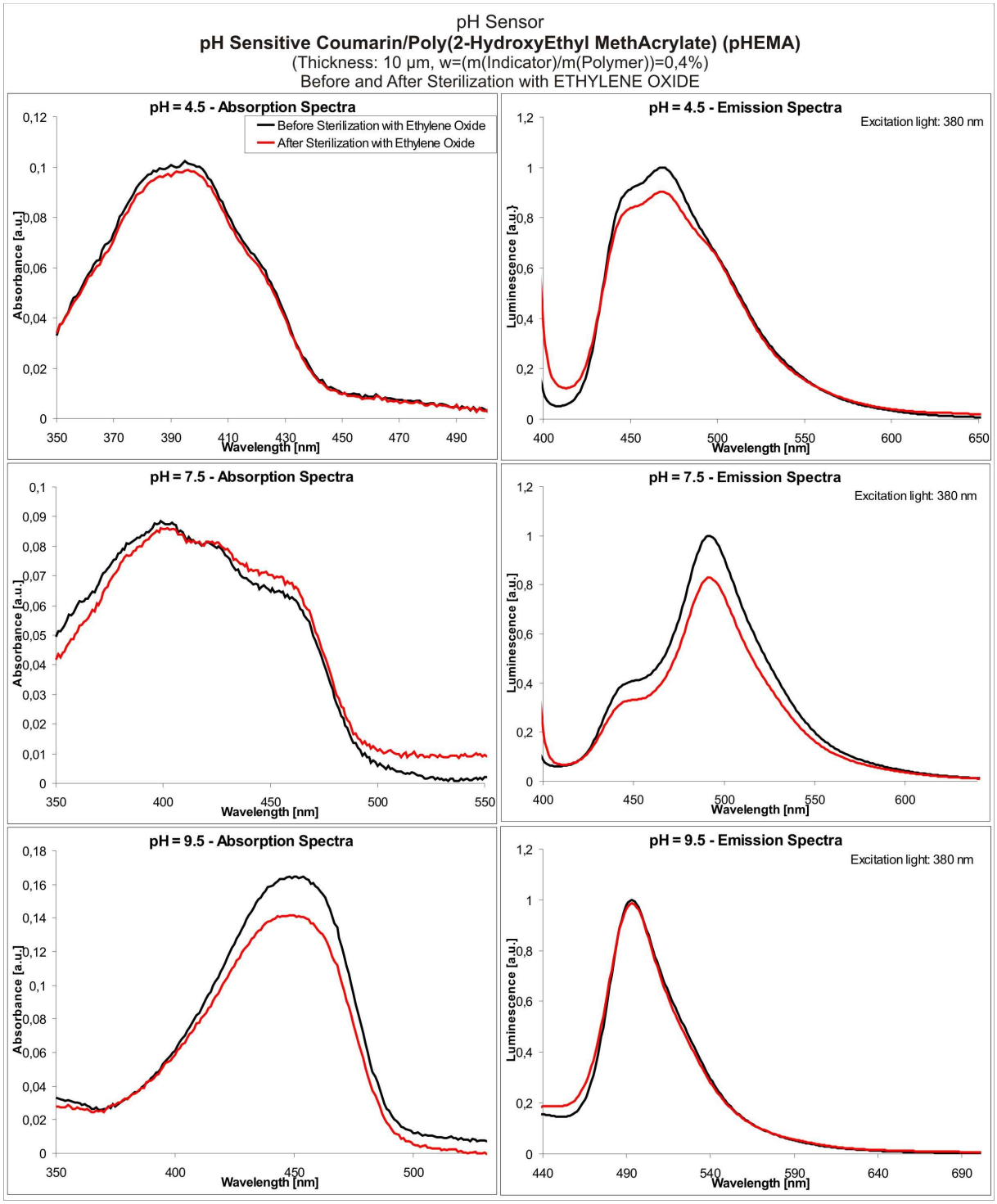

Sterilization with EtO	Absorption Spectra			Emission Spectra		
		pH	Alterations		pH	Alterations
Alterations in Absorption/ Emission Intensity	AFTERS	4.5	3,33% decrease	AFTERS	4.5	9,60% decrease
		7.5	2,35% decrease		7.5	17,08% decrease
		9.5	13,88% decrease		9.5	1,46% decrease

Alterations in Absorption/ Emission Curve Form	AFTER S	4.5	Unaltered	AFTER S	4.5	Altered emission curve form between 400-400 nm and 480-530 nm.
		7.5	Altered absorption curve form.		7.5	Unaltered
		9.5	Altered absorption between 480-800 nm. Hypsochromic shift of the absorption maximum for 4 nm.		9.5	Altered emission curve form between 440-490 nm.

Calibration Curves

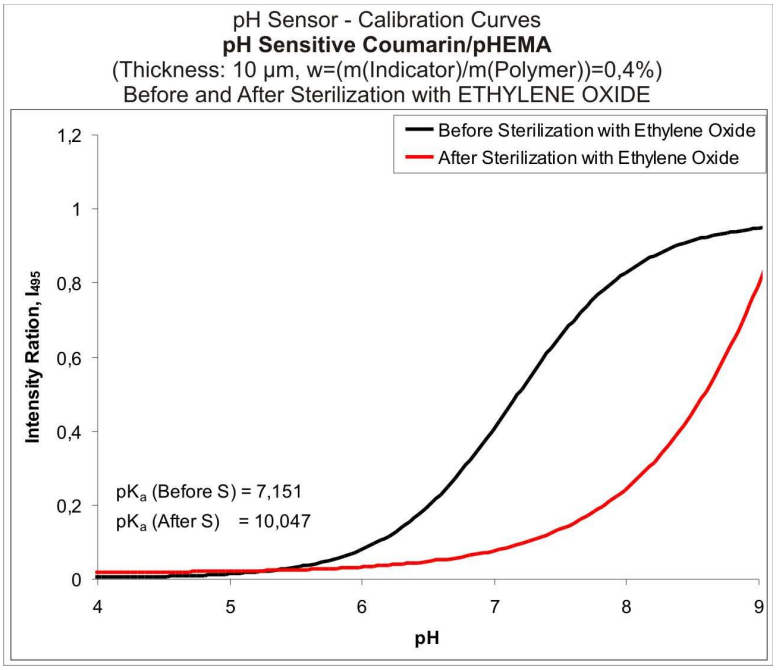

EtO	Alterations in Calibration Curve Shape	Alterations in pK_a
	Greatly altered curve shape after sterilization.	Increase of pK_a (for 2,896)

E.38 PET Perylene BisImide immobilized in HydroMed Hydrogel D4

Absorption Spectra

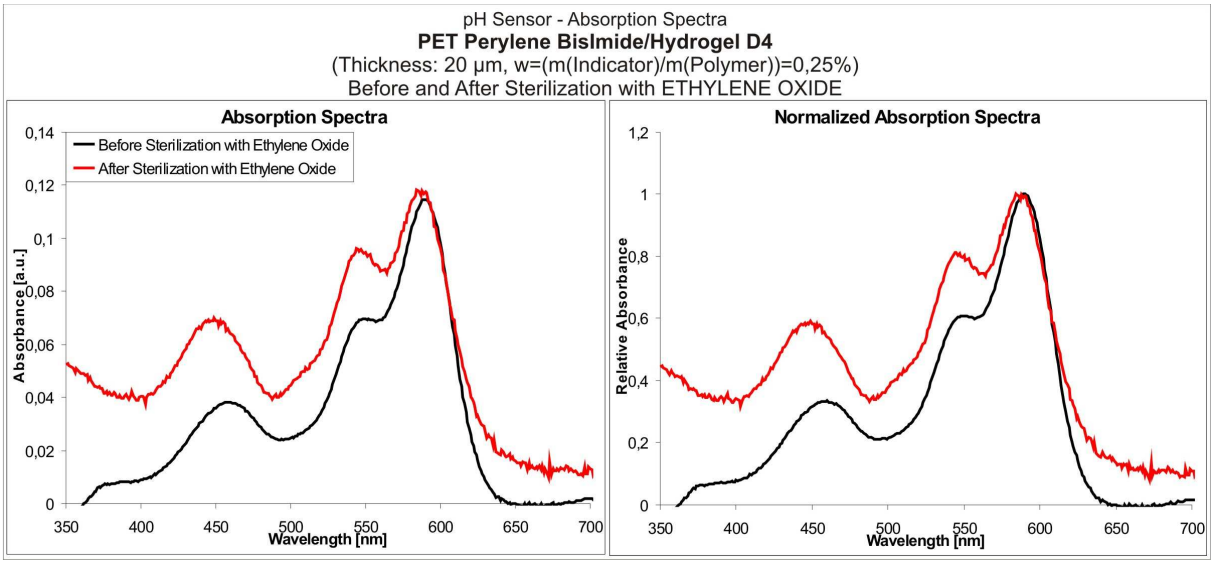

EtO Sterilization	Absorption Spectra
Alterations in Absorption/Emission Intensity	0,24% increase
Alterations in Absorption/Emission Curve Form	Altered absorption curve form. Hypsochromic shift of the absorption maximum for 3 nm.

Emission Spectra

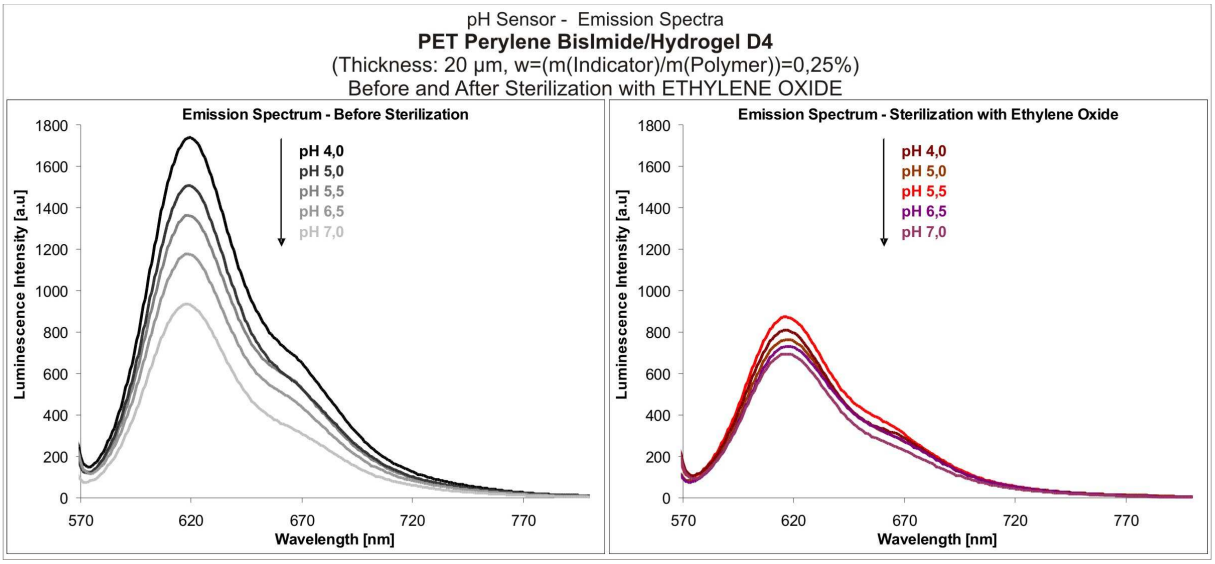

EtO	Emission Spectra					
	Decrease of the Luminescence Intensity in dependence of the Intensity at lower pH			Decrease of the Luminescence Intensity at define pH in dependence of the Intensity Before Sterilization		
BEFORE S	**pH**	**Max. Intensity**				
Alterations in Absorption/ Emission Intensity	4	1739	/			
	5	1509	13,22% decrease			
	5.5	1363	21,62% decrease			
	6.5	1176	32,37% decrease			
	7	933,6	46,31% decrease			
PET Efficiency	1.86					
AFTER S	**pH**	**Max. Intensity**		**pH**	**Compared Intensity**	
Alterations in Absorption/ Emission Intensity	4	763,9	/	4	1739	56,07% decrease
	5	870,2	13,91% increase	5	1509	42,33% decrease
	5.5	806,6	5,59% increase	5.5	1363	40,82% decrease
	6.5	732,1	4,16% decrease	6.5	1176	37,75% decrease
	7	694,1	9,14% decrease	7	933,6	25,65% decrease

Calibration Curves

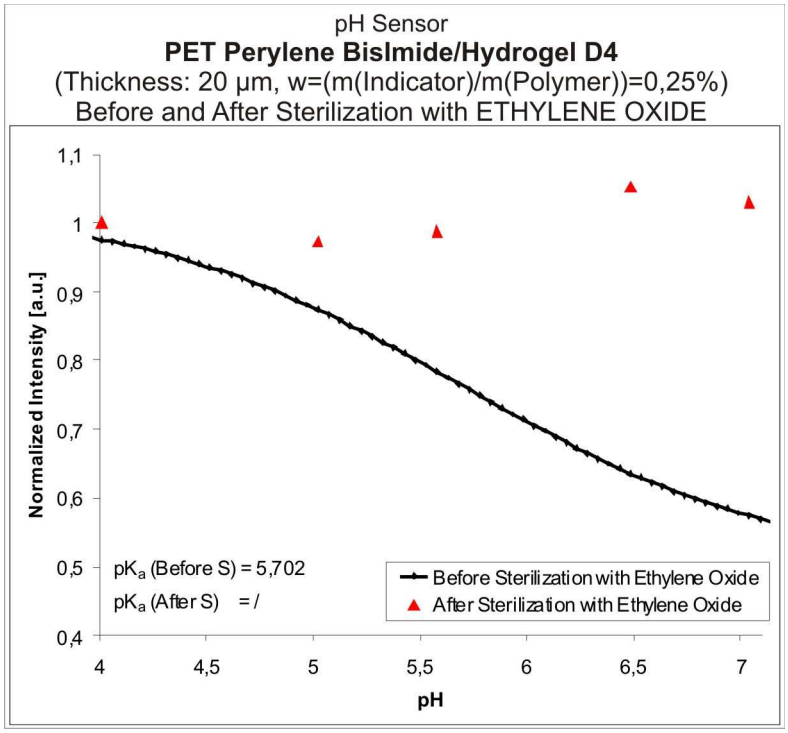

EtO	Alterations in Calibration Curve Shape	Alterations in pK_a
	The calibration curve no longer observed.	

E.39 BromoPhenol Blue immobilized in HydroMed Hydrogel D4

Absorption Spectra

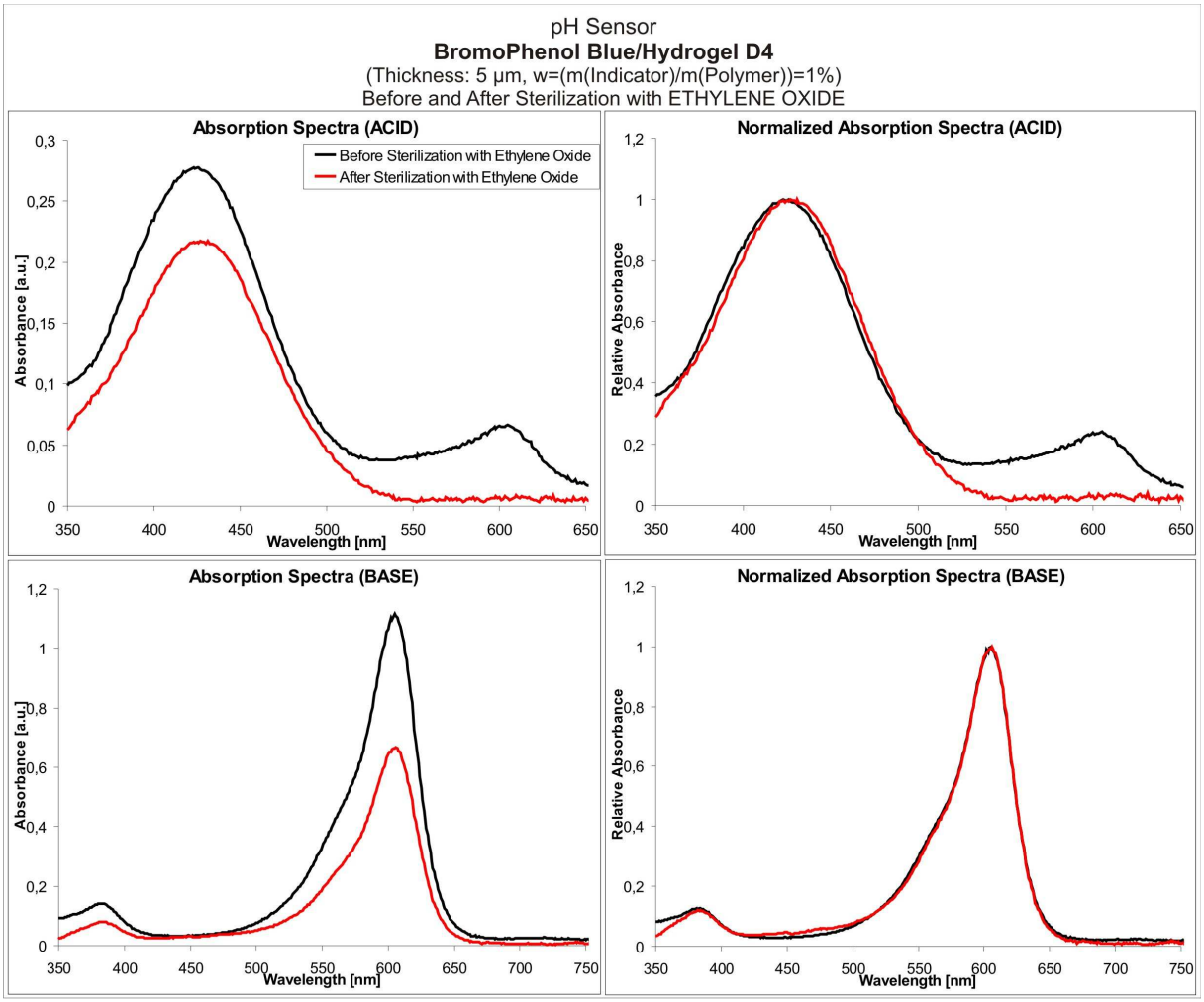

EtO	Absorption Spectra						
		pH	Alterations			pH	Alterations
Alterations in Absorption /Emission Intensity	AFTERS	ACID	21,75% decrease	Alterations in Absorption /Emission Curve Form	AFTERS	ACID	The ratio between protonation/deprotonation absorption peaks is altered.
		BASE	40,19% decrease			BASE	Unaltered.

E.40 Thymol Blue immobilized in HydroMed Hydrogel D4

Absorption Spectra

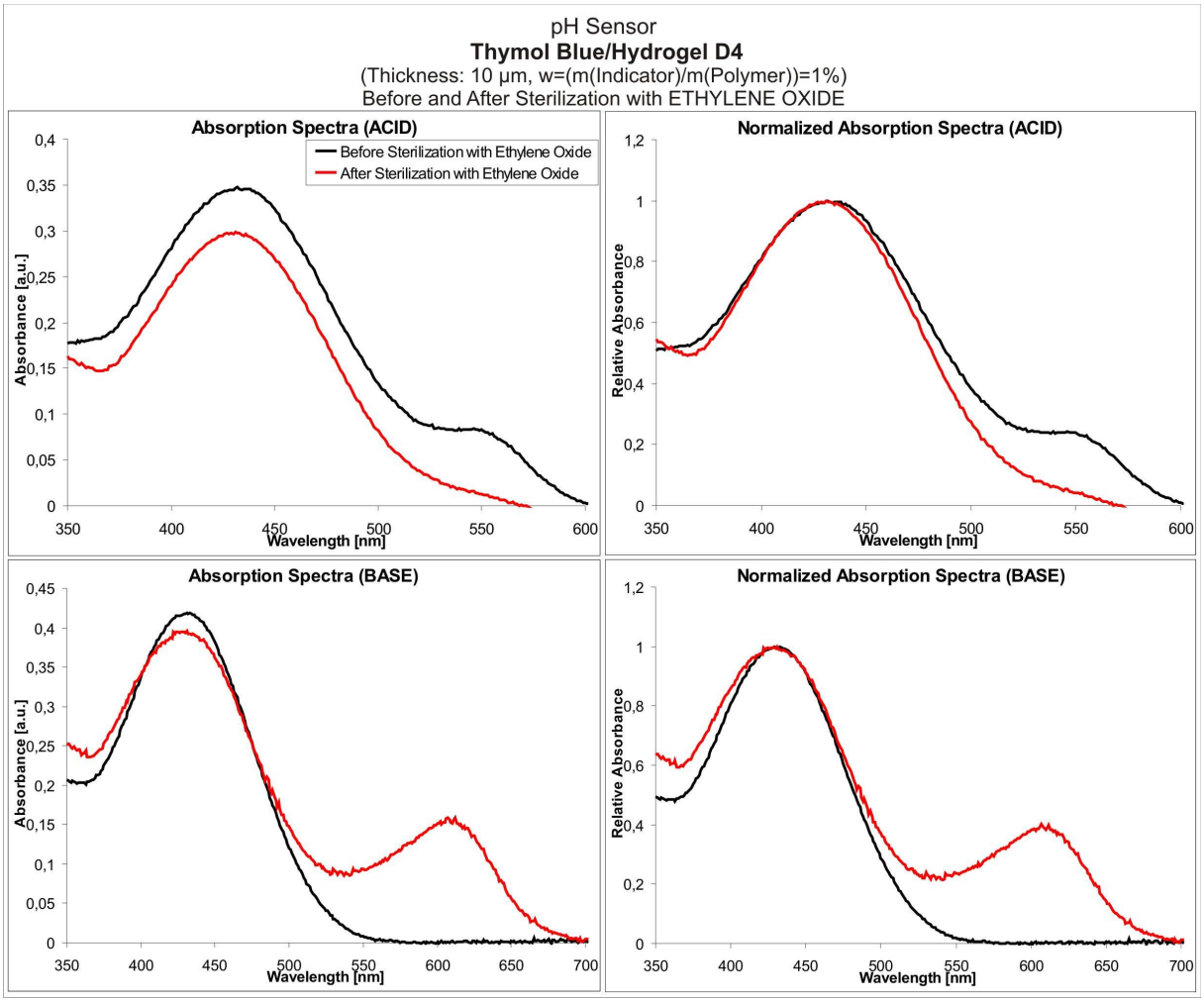

EtO	Absorption Spectra						
		pH	Alterations			pH	Alterations
Alterations in Absorption /Emission Intensity	AFTERS	ACID	14,03% decrease	Alterations in Absorption /Emission Curve Form	AFTERS	ACID	Altered emission between 440-600 nm.
		BASE	5,33% decrease			BASE	The ratio between protonation/deprotonation absorption peaks is altered.

E.41 BromoThymol Blue immobilized in HydroMed Hydrogel D4

Absorption Spectra

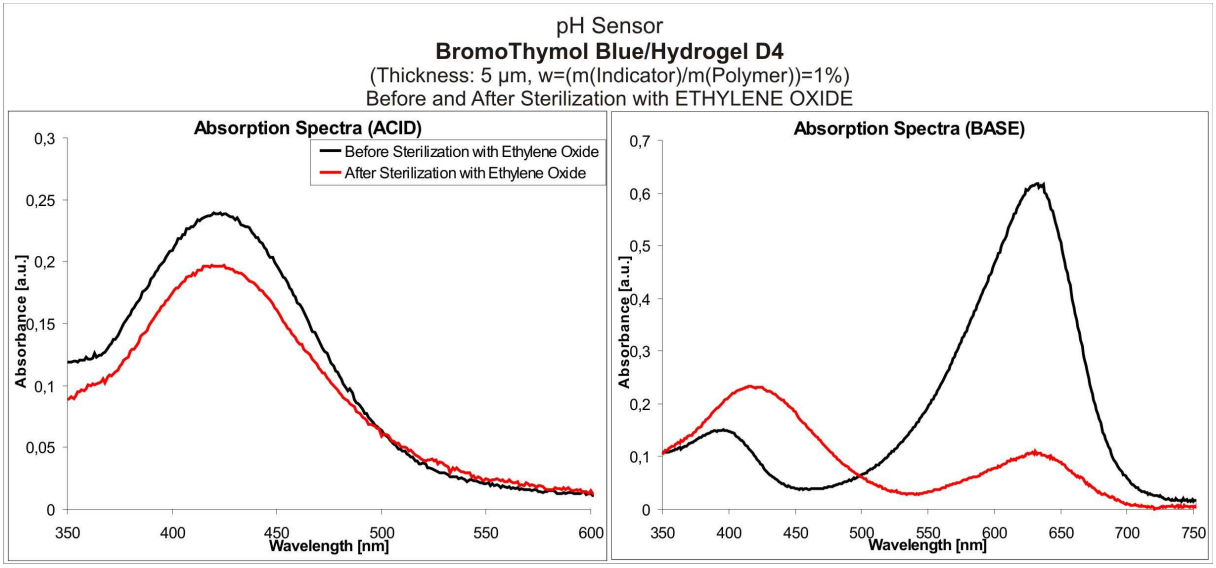

EtO	Absorption Spectra						
		pH	Alterations			pH	Alterations
Alterations in Absorption /Emission Intensity	AFTERS	ACID	17,78% decrease	Alterations in Absorption /Emission Curve Form	AFTERS	ACID	Altered emission between 470-600 nm.
		BASE	82,85% decrease			BASE	The ratio between protonation/deprotonation absorption peaks is altered.

E.42 Methyl Orange immobilized in HydroMed Hydrogel D4

Absorption Spectra

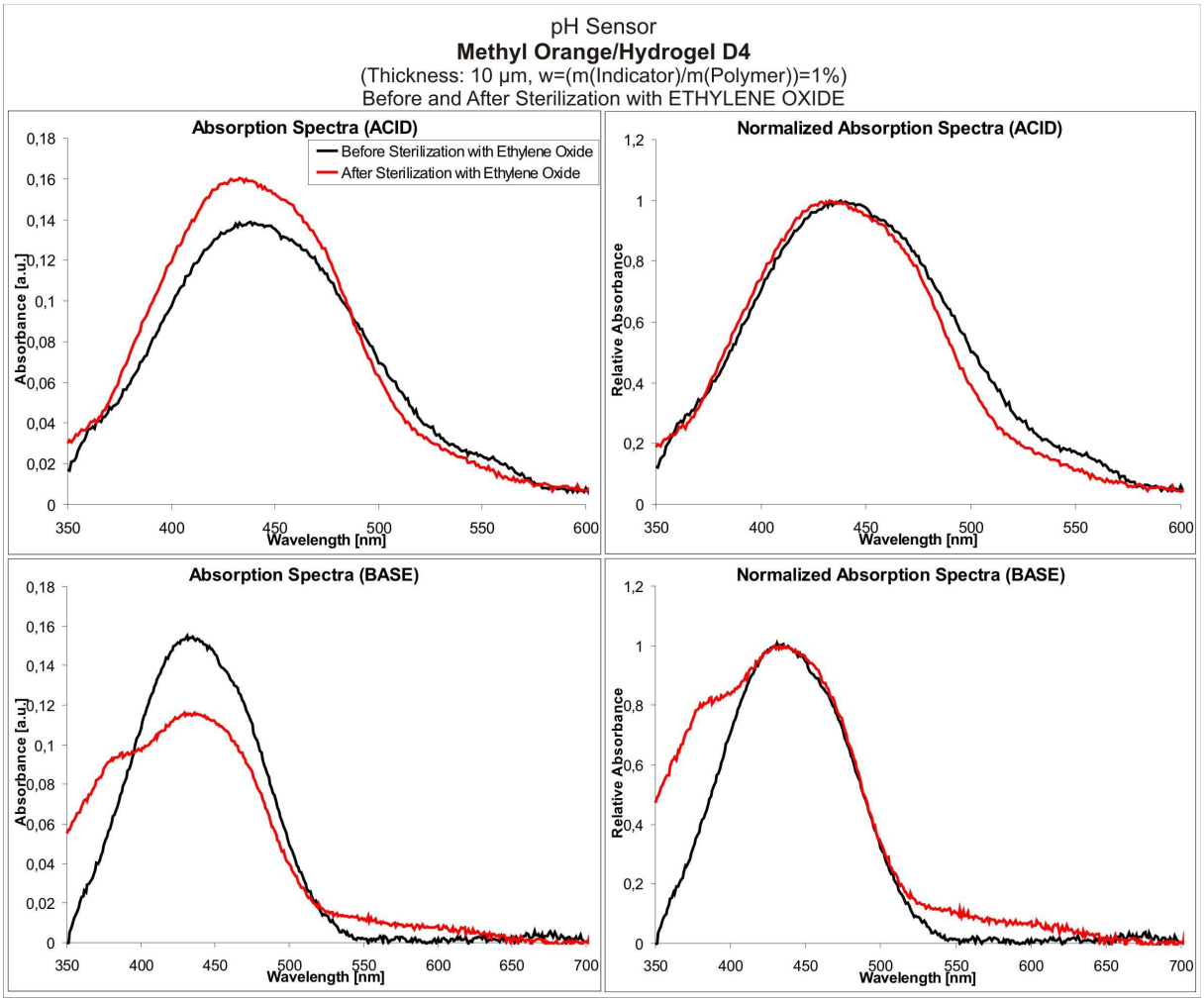

EtO	Absorption Spectra						
		pH	Alterations			pH	Alterations
Alterations in Absorption /Emission Intensity	AFTERS	ACID	13,42% decrease	Alterations in Absorption /Emission Curve Form	AFTERS	ACID	Altered absorption curve form between 460-600 nm. Hypsochromic shift of the absorption maximum for 5 nm,
		BASE	24,53% decrease			BASE	Altered absorption curve form between 350-400 nm and 520-650 nm.

Optical TEMPERATURE SENSORS

E.43 Europium(III) Complex with 4-(4,6-di(1H-indazol-1-yl)-1,3,5-triazin-2-yl)-N,N-DiEthyl Benzen Amine (=Eu(tta)$_3$DEADIT) immobilized in PolyStyrene-co-Acrylonitrile

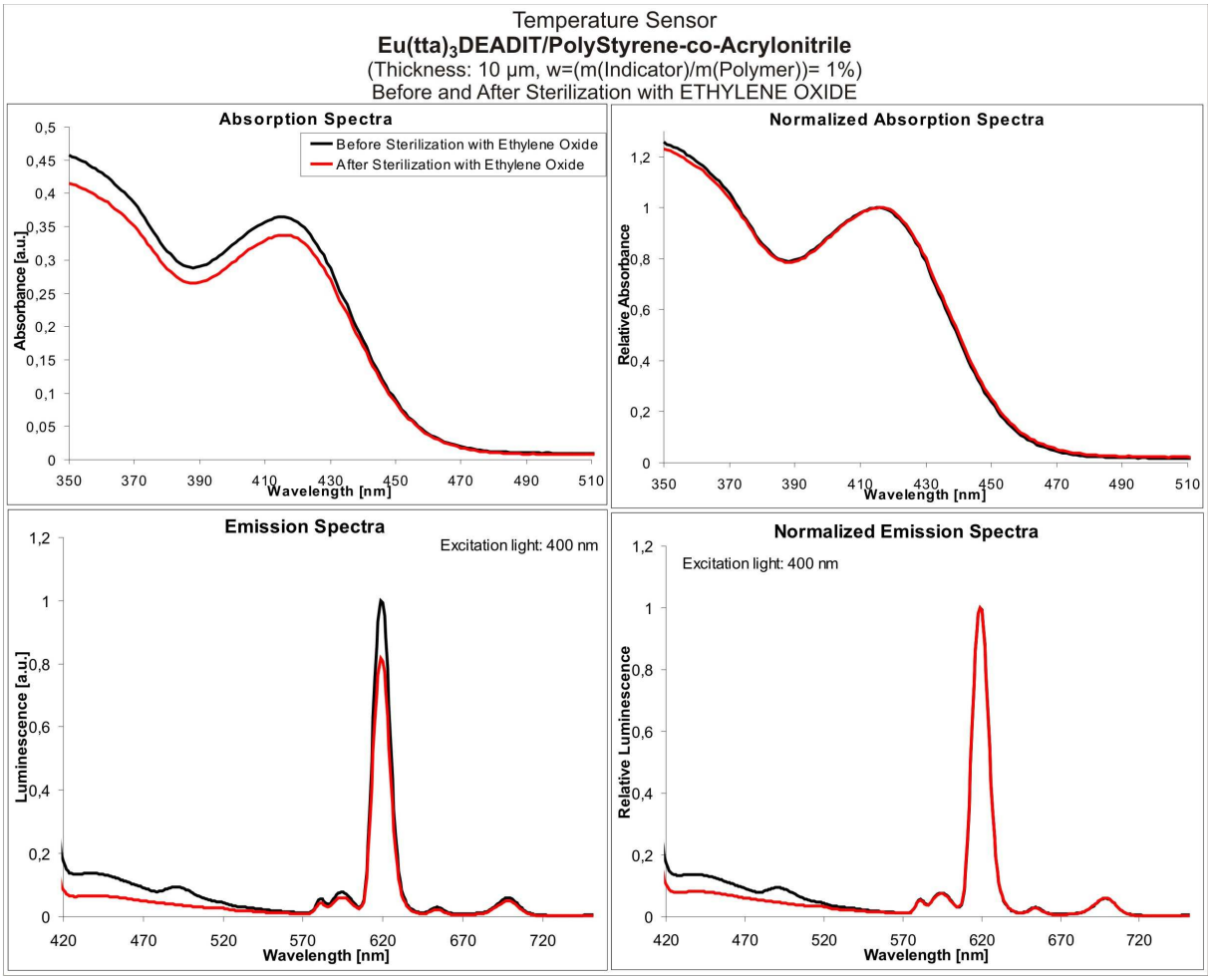

EtO	Absorption Spectra	Emission Spectra
Alterations in Absorption/Emission Intensity	6,72% decrease	18,19% decrease
Alterations in Absorption/Emission Curve Form	Unaltered.	Altered emission between 420-520 nm.

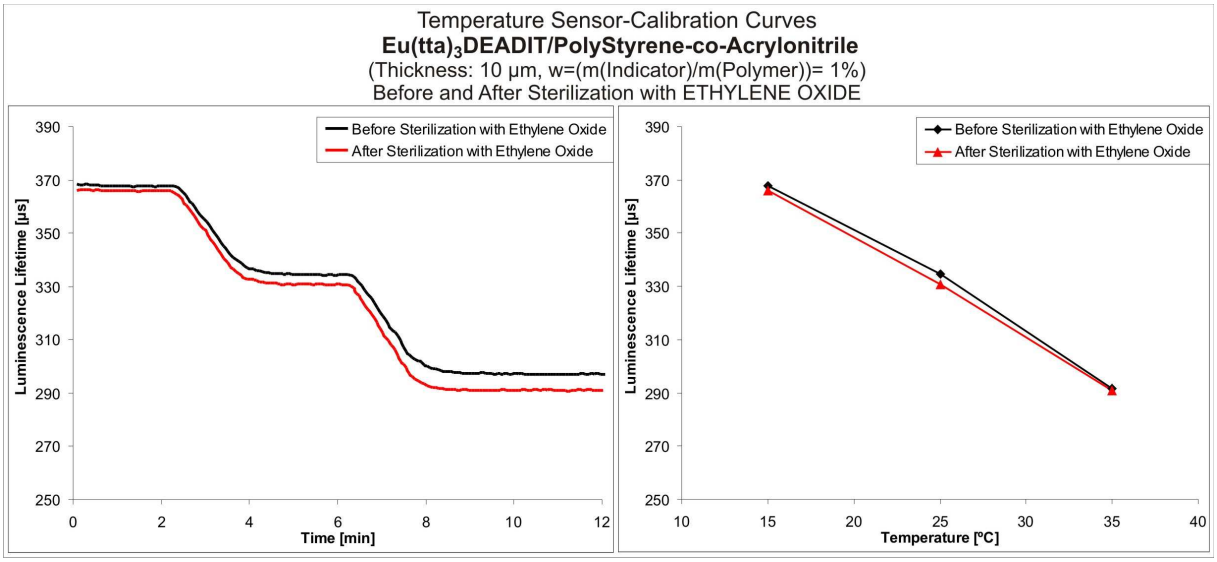

EtO	Luminescence Lifetime		Alterations of Slope
Alterations in Luminescence Lifetime and Slope	15 °C	0,54% decrease	1,42% decrease of slope
	25 °C	1,19% decrease	
	35 °C	0,34% decrease	

E.44 Europium(III) Complex with 4-(4,6-di(1H-indazol-1-yl)-1,3,5-triazin-2-yl)-N,N-DiEthyl Benzen Amine (=Eu(tta)$_3$DEADIT) immobilized in PolyVinylideneChloride-co-Acrylonitrile

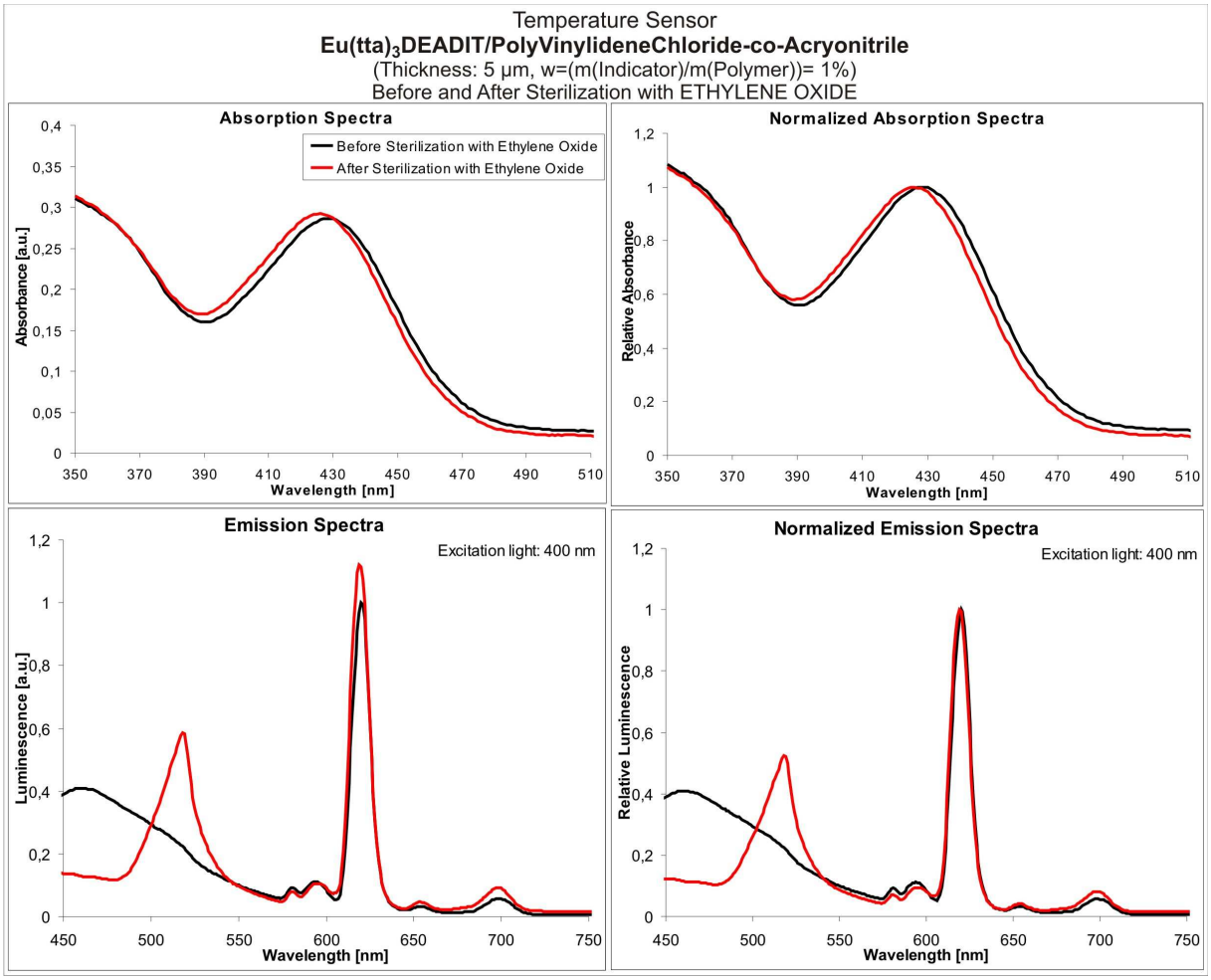

EtO	Absorption Spectra	Emission Spectra
Alterations in Absorption/Emission Intensity	2,08% increase	12,11% increase (at peak λ_{max1}=620)
Alterations in Absorption/Emission Curve Form	Hypsochromic shift of the absorption maximum for 2 nm.	New emission peak with λ_{max}=519 nm observed after sterilization.

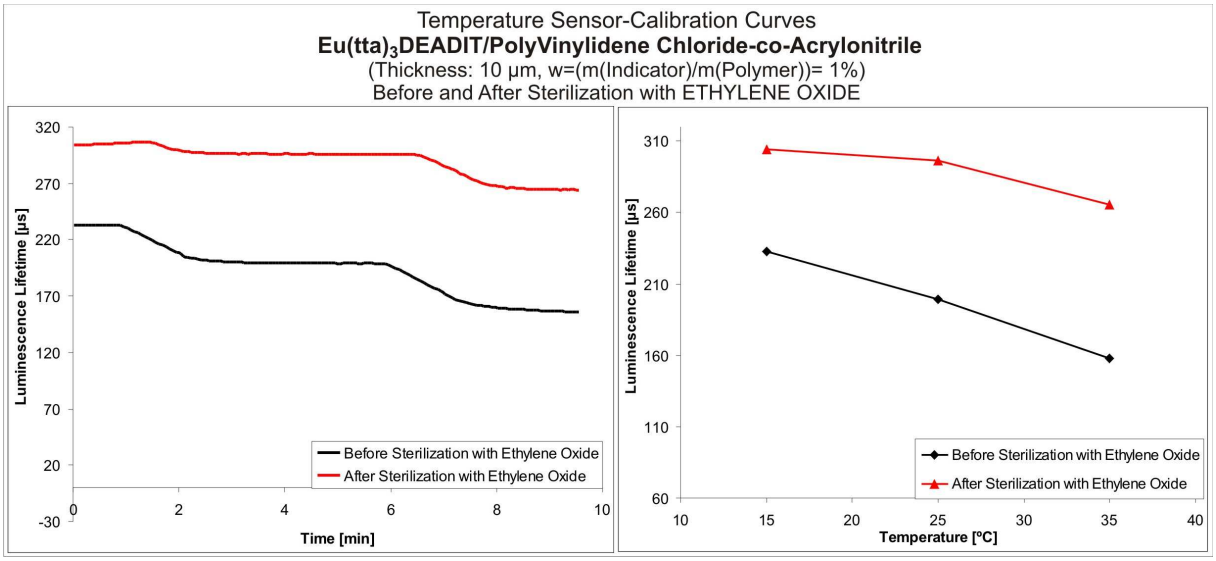

EtO	Luminescence Lifetime		Alterations of Slope
Alterations in Luminescence Lifetime and Slope	15 °C	30,47% increase	48,17% decrease of slope
	25 °C	48,74% increase	
	35 °C	67,72% increase	

E.45 Europium(III) Complex with 4-(4,6-di(1H-indazol-1-yl)-1,3,5-triazin-2-yl)-N,N-DiEthyl Benzen Amine (=Eu(tta)$_3$DEADIT) immobilized in PolyMethAcryloNitrile

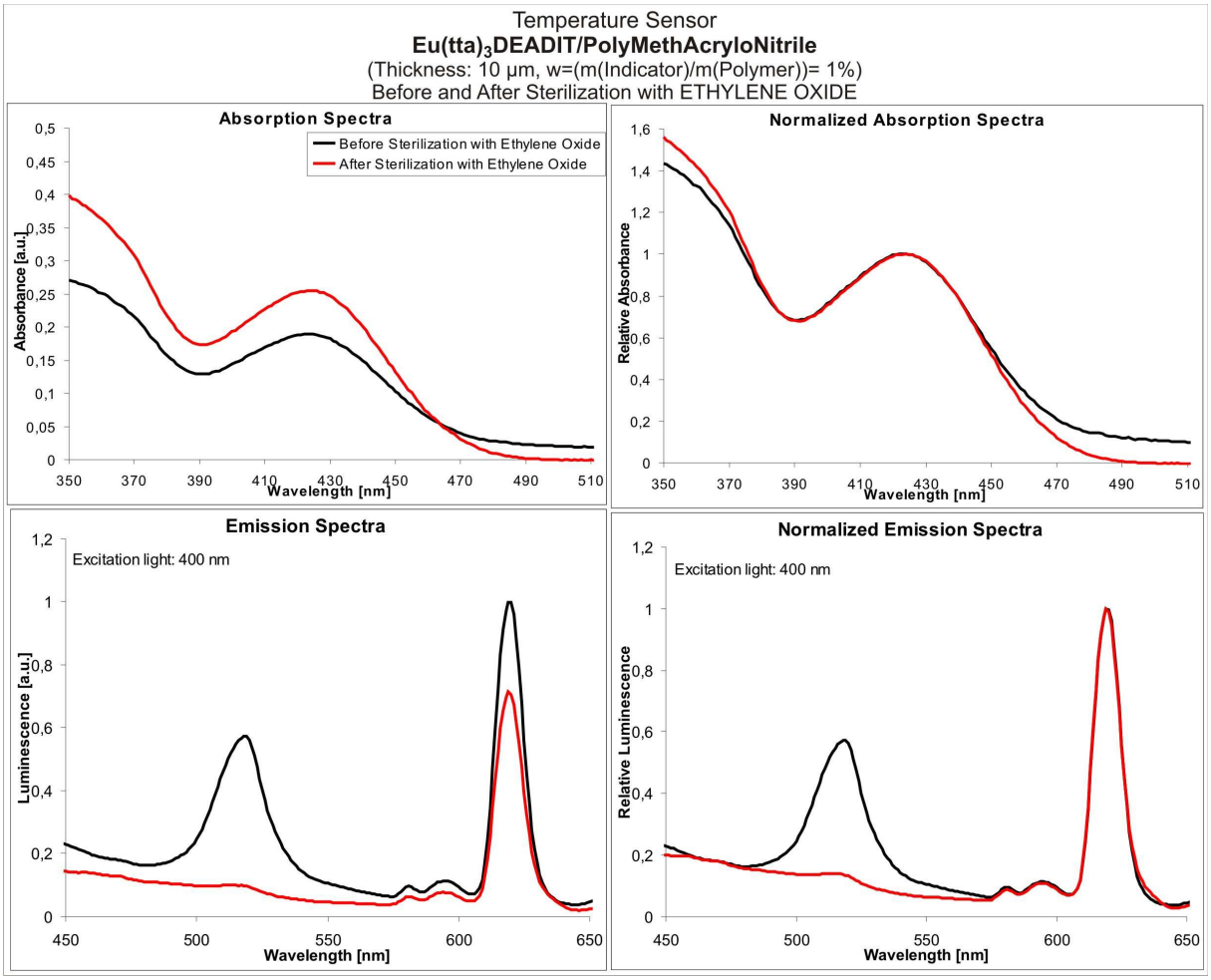

EtO	Absorption Spectra	Emission Spectra
Alterations in Absorption/Emission Intensity	25,92% increase	36,10% decrease (at peak λ_{max1}=620)
Alterations in Absorption/Emission Curve Form	Altered absorption curve form between 350-380 nm and 450-800 nm.	The emission peak with λ_{max}=496 nm no longer observed after sterilization.

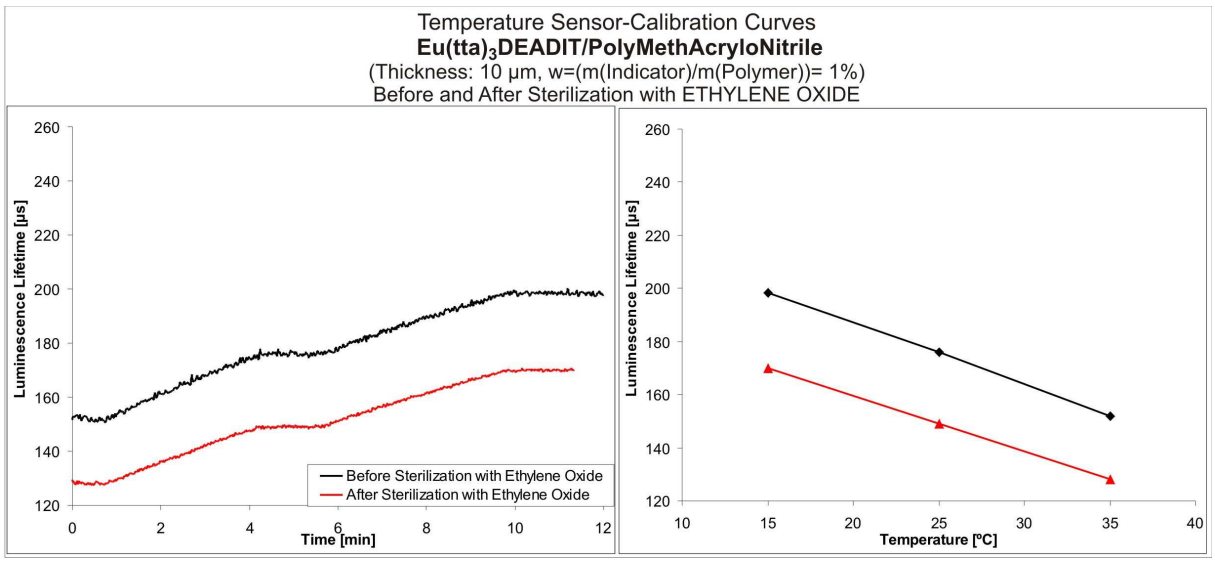

EtO	Luminescence Lifetime		Alterations of Slope
Alterations in Luminescence Lifetime and Slope	15℃	14,14% decrease	9,98% decrease of slope
	25℃	15,34% decrease	
	35℃	15,79% decrease	

E.46 DiChloroTrisPhenanthroline Ruthenium(II)Hydrate immobilized in PolyVinylideneChloride-co-Acrylonitrile

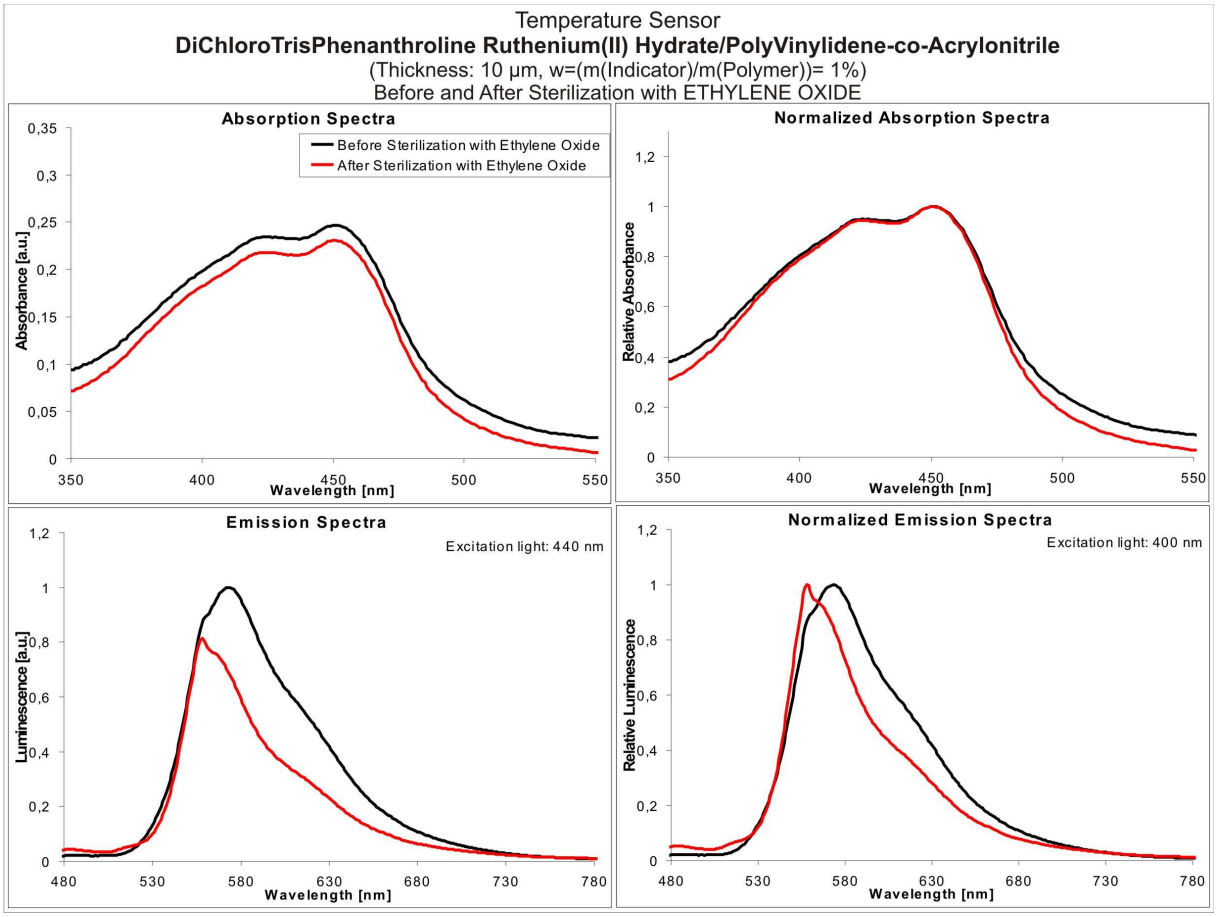

EtO	Absorption Spectra	Emission Spectra
Alterations in Absorption/Emission Intensity	6,50% decrease	18,50% decrease
Alterations in Absorption/Emission Curve Form	Altered absorption curve form between 350-380 nm and 470-800 nm.	Altered emission curve form between 560-680 nm. Hypsochromic shift of the emission maximum for 15 nm.

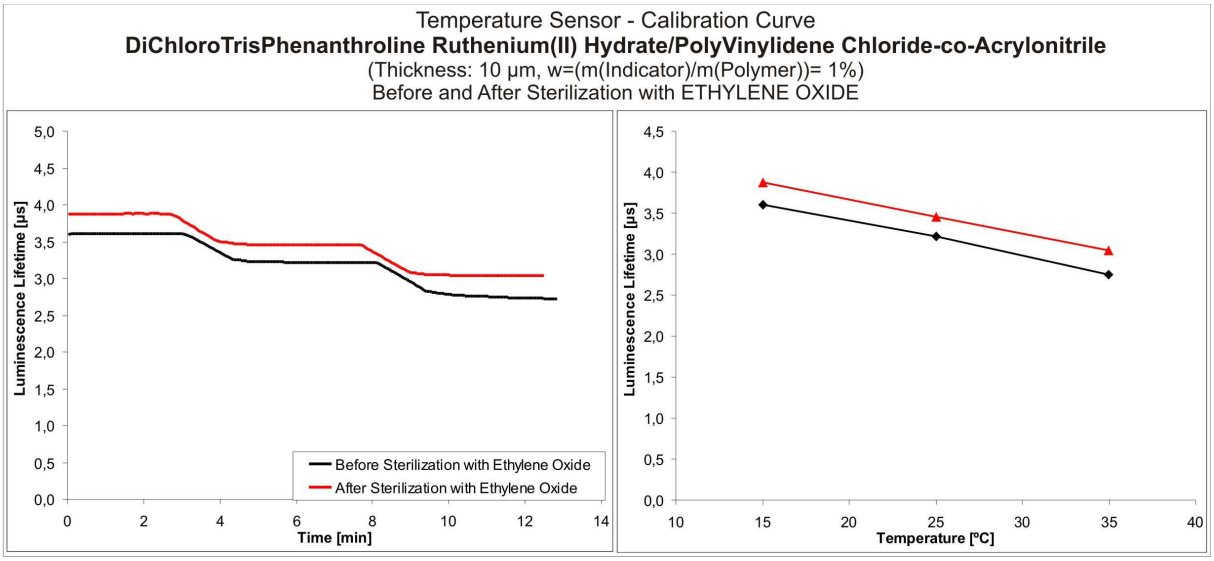

EtO	Luminescence Lifetime		Alterations of Slope
Alterations in Luminescence Lifetime and Slope	15 °C	7,48% increase	1,87% decrease of slope
	25 °C	11,80% increase	
	35 °C	9,54% increase	

E.47 DiChloroTrisPhenanthroline Ruthenium(II)Hydrate immobilized in PolyMethAcryloNitrile

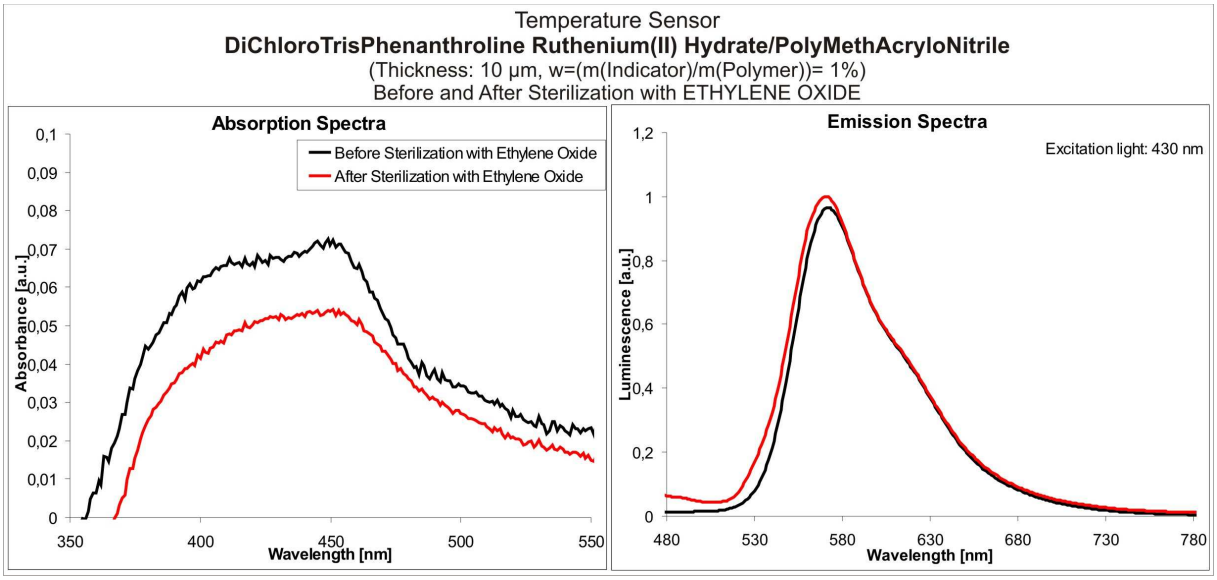

EtO	Absorption Spectra	Emission Spectra
Alterations in Absorption/Emission Intensity	27,93% decrease	3,52% increase
Alterations in Absorption/Emission Curve Form	Altered absorption curve form.	Hypsochromic shift of the emission maximum for 2 nm.

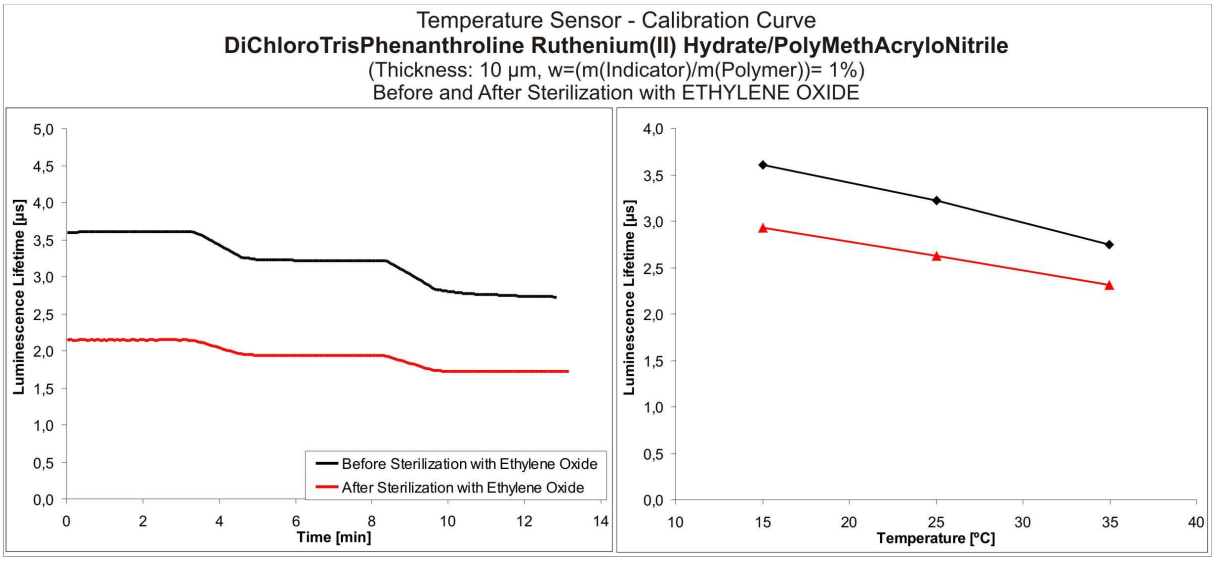

EtO	Luminescence Lifetime		Alterations of Slope
Alterations in Luminescence Lifetime and Slope	15℃	40,28% decrease	26,76% decrease of slope
	25℃	39,75% decrease	
	35℃	37,45% decrease	

Optical AMMONIA SENSORS

E.48 EosinEthylEster immobilized in Cellulose Acetate

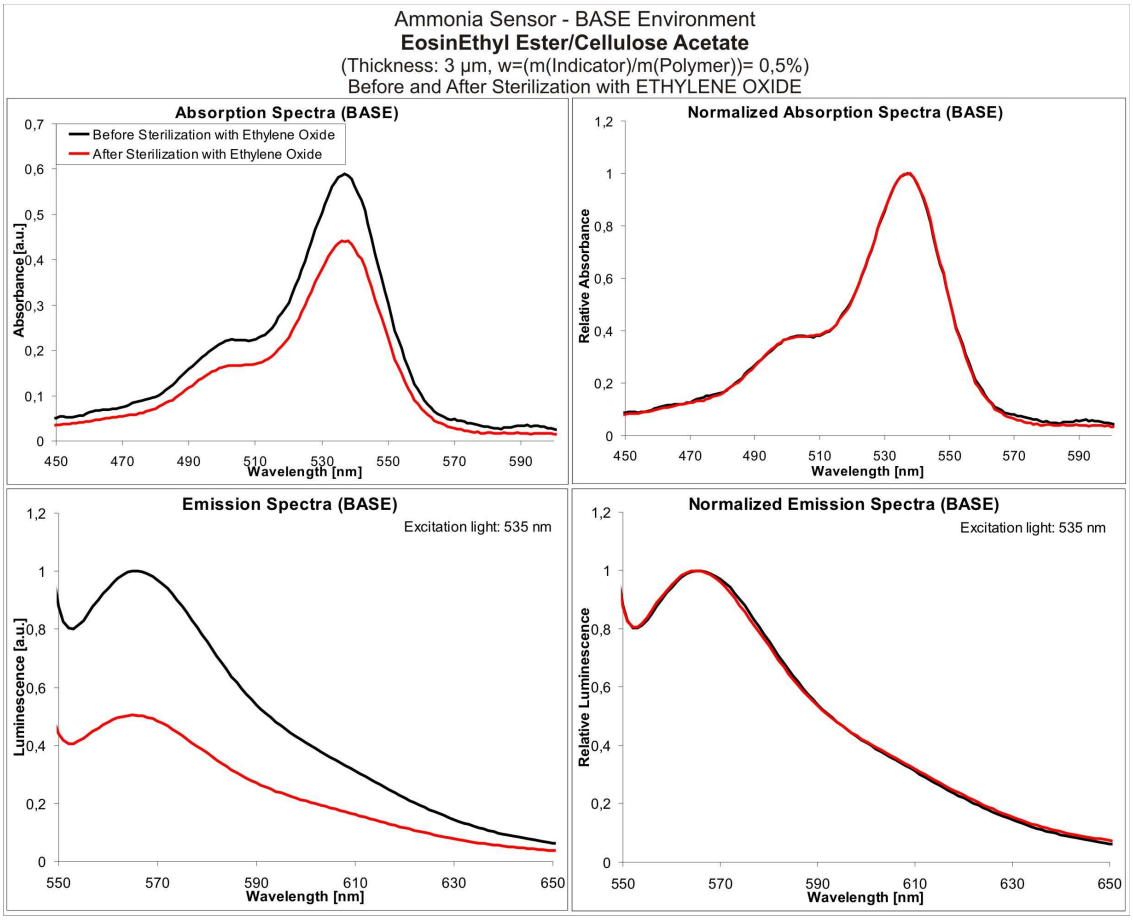

EtO S.	Absorption Spectra		Emission Spectra	
		Alterations		Alterations
Alterations in Absorption/ Emission Intensity	BASE	25,05% decrease	BASE	49,59% decrease
Alterations in Absorption/ Emission Curve Form	BASE	Unaltered.	BASE	Unaltered.

E.49 EosinEthylEster immobilized in Hydrogel D7

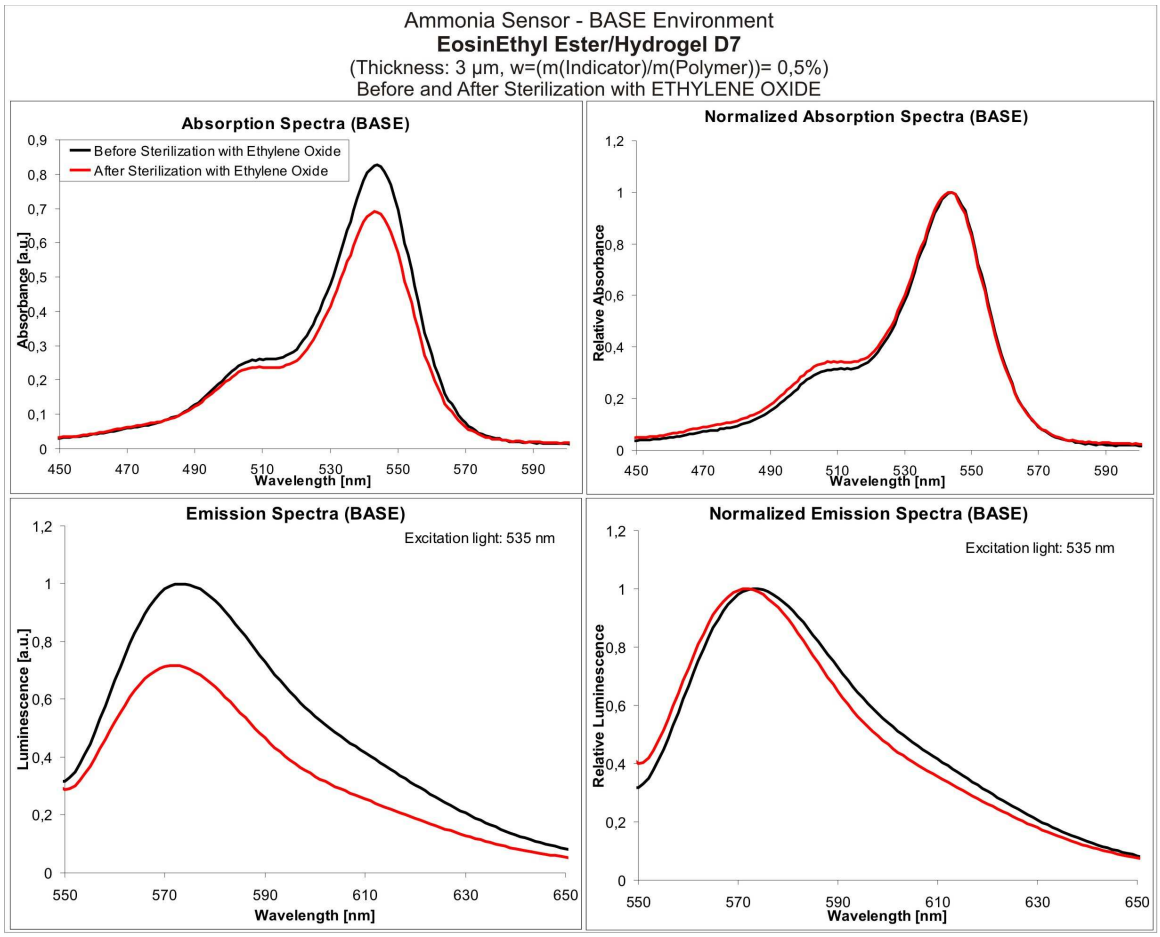

EtO S.	Absorption Spectra		Emission Spectra	
		Alterations		Alterations
Alterations in Absorption/ Emission Intensity	BASE	16,51% decrease	BASE	28,17% decrease
Alterations in Absorption/ Emission Curve Form	BASE	Altered absorption between 450-530 nm.	BASE	Altered emission between 580-630 nm. Hypsochromic shift of the emission maximum for 2 nm.

E.50 Eosin EthylEster immobilized in Ethyl Cellulose

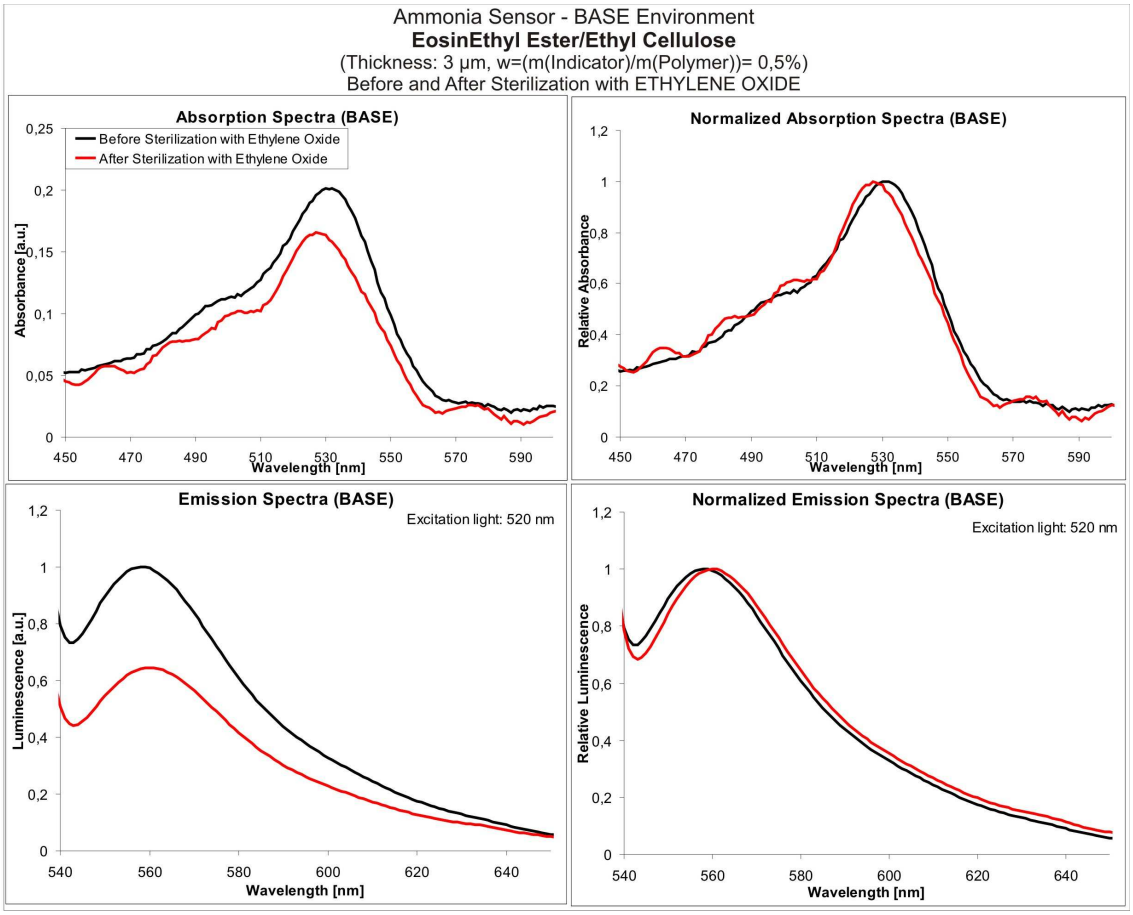

EtO S.	Absorption Spectra		Emission Spectra	
		Alterations		Alterations
Alterations in Absorption/ Emission Intensity	BASE	17,77% decrease	BASE	35,40% decrease
Alterations in Absorption/ Emission Curve Form	BASE	Hypsochromic shift of the absorption maximum for 5 nm.	BASE	Bathochromic shift of the emission maximum for 2 nm.

E.51 EosinEthylEster immobilized in PolyMethylMethAcrylate (=PMMA)

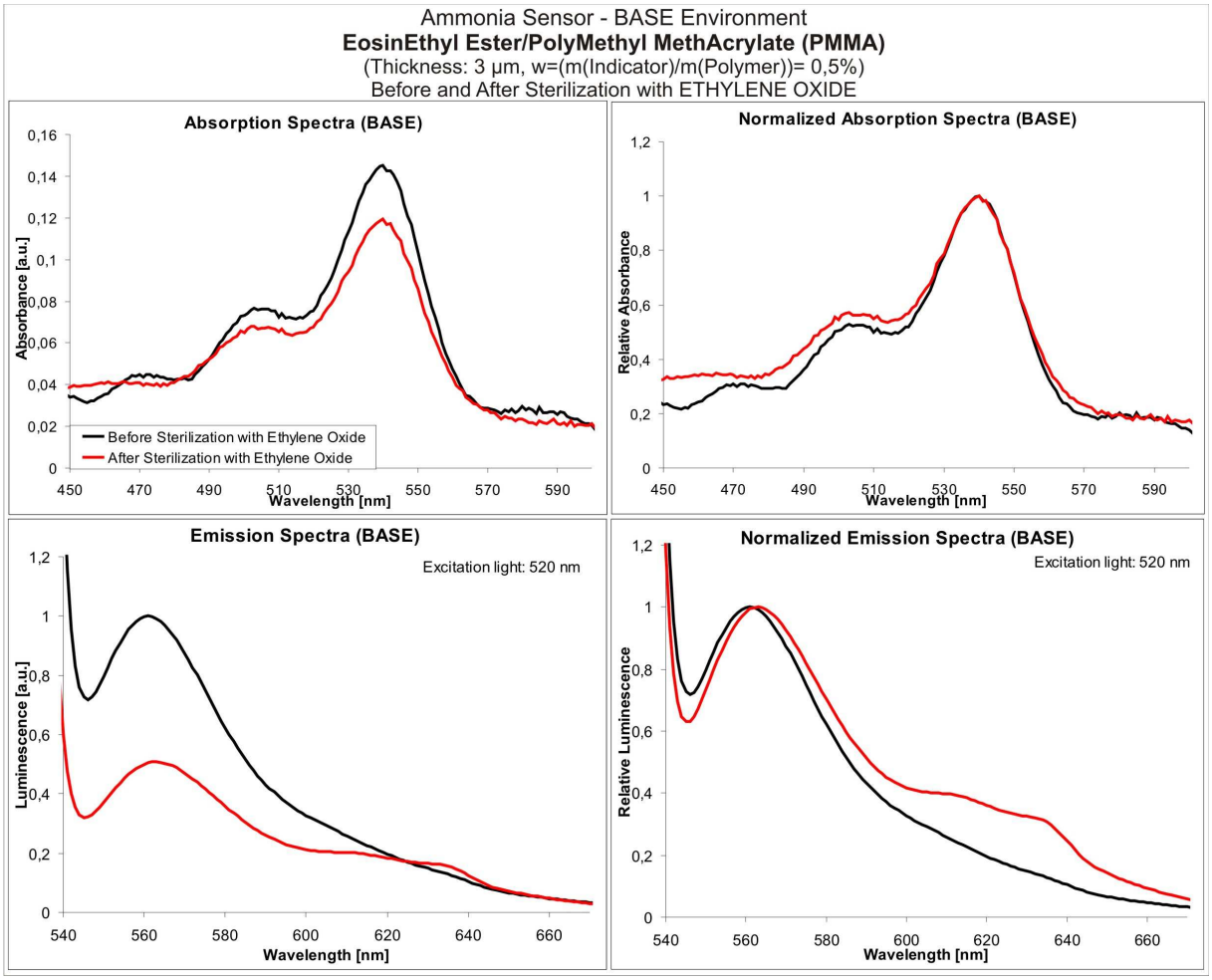

EtO S.	Absorption Spectra		Emission Spectra	
		Alterations		**Alterations**
Alterations in Absorption/ Emission Intensity	BASE	17,90% decrease	BASE	49,17% decrease
Alterations in Absorption/ Emission Curve Form	BASE	Altered absorption between 350-530 nm.	BASE	Altered absorption between 600-680 nm. Bathochromic shift of the emission maximum for 2 nm.

E.52 DiChloroFluorescein immobilized in Cellulose Acetate

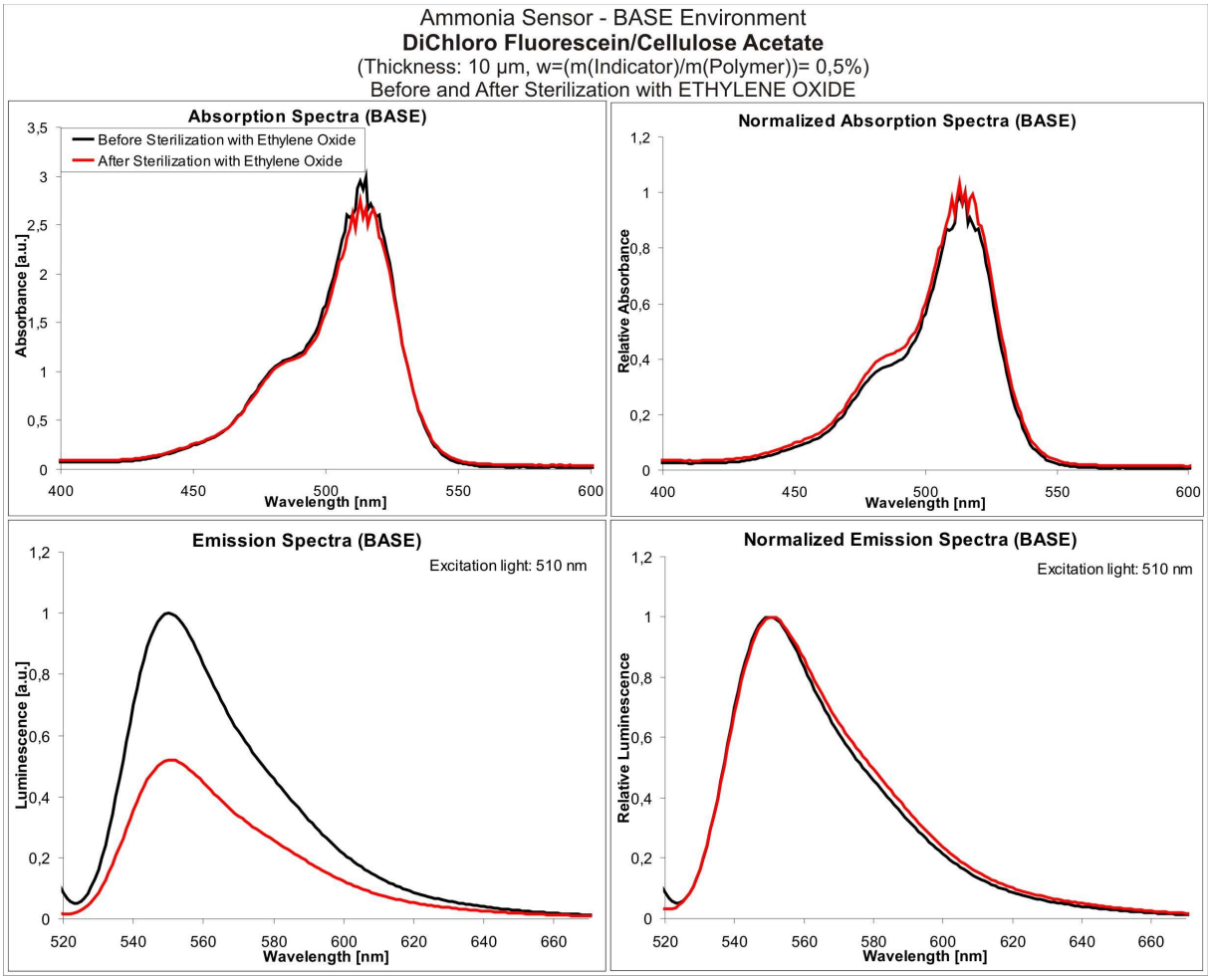

EtO S.	Absorption Spectra		Emission Spectra	
		Alterations		Alterations
Alterations in Absorption/ Emission Intensity	BASE	11,23% decrease	BASE	48,06% decrease
Alterations in Absorption/ Emission Curve Form	BASE	Unaltered.	BASE	Altered emission between 560-640 nm.

E.53 DiChloroFluorescein immobilized in Hydrogel D7

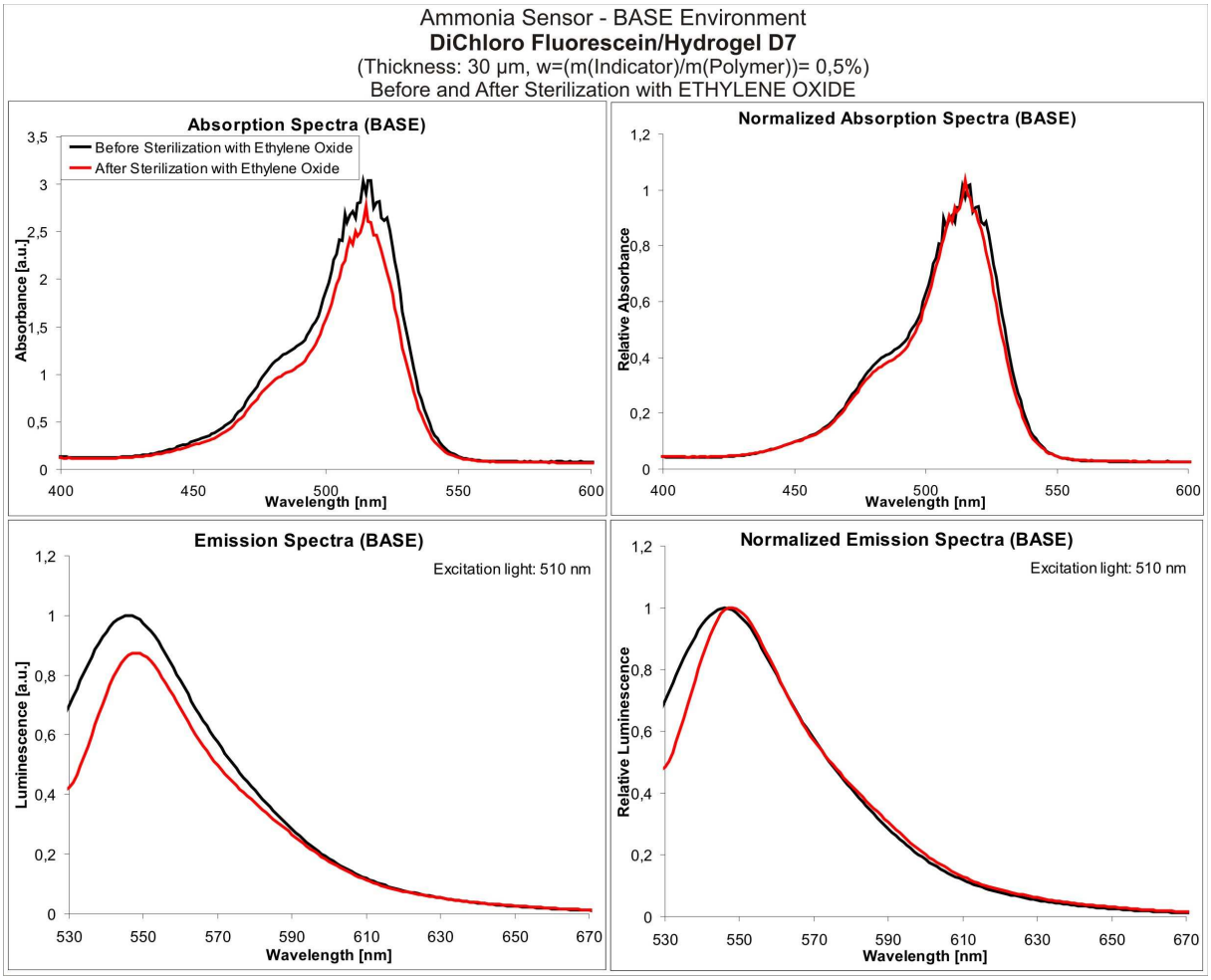

EtO S.	Absorption Spectra		Emission Spectra	
		Alterations		Alterations
Alterations in Absorption/ Emission Intensity	BASE	10,70% decrease	BASE	12,54% decrease
Alterations in Absorption/ Emission Curve Form	BASE	Unaltered.	BASE	Altered emission between 530-545 nm. Bathochromic shift of the emission maximum for 2 nm.

E.54 DiChloroFluorescein immobilized in Ethyl Cellulose

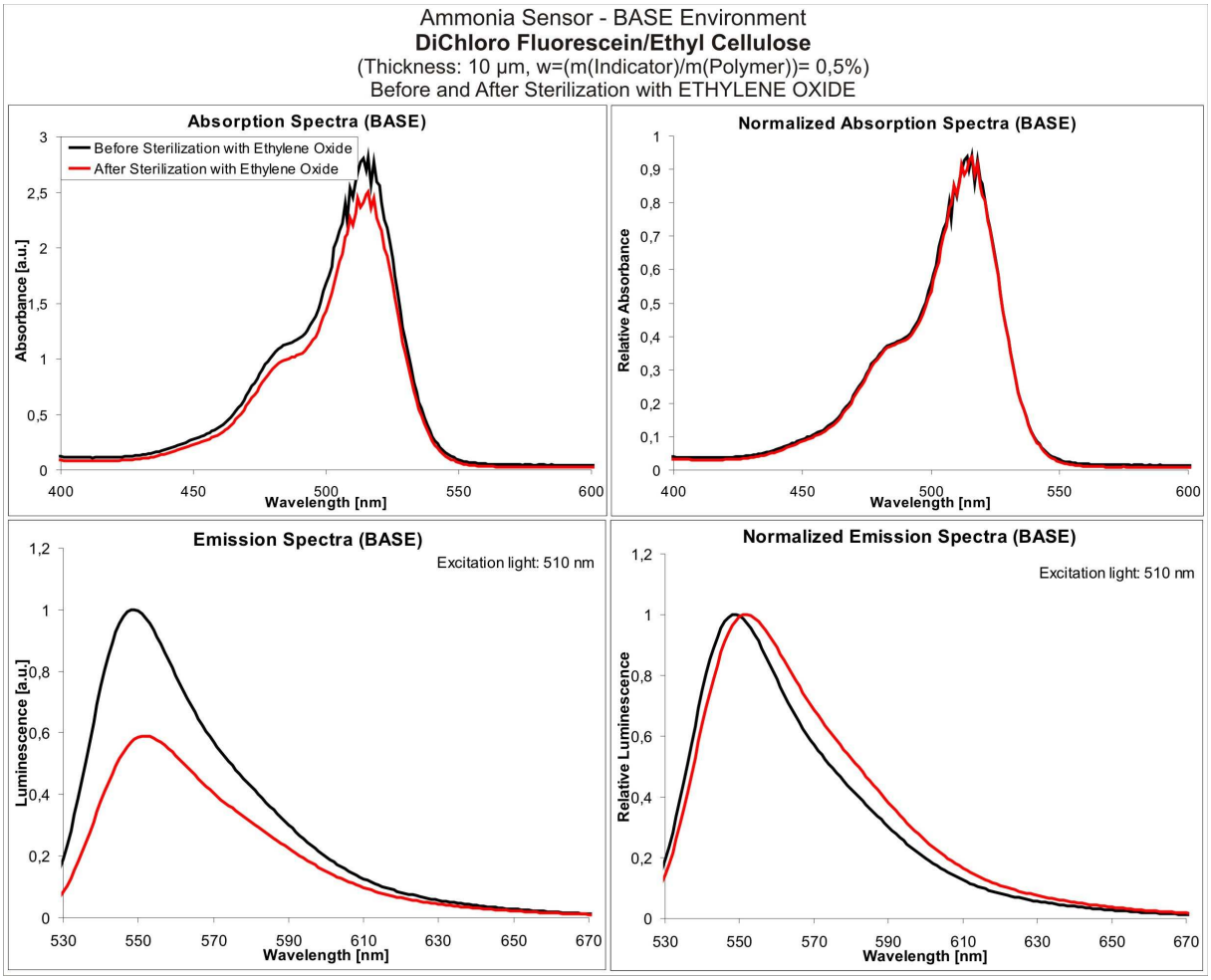

EtO S.	Absorption Spectra		Emission Spectra	
		Alterations		Alterations
Alterations in Absorption/ Emission Intensity	BASE	10,70% decrease	BASE	41,04% decrease
Alterations in Absorption/ Emission Curve Form	BASE	Unaltered.	BASE	Bathochromic shift of the emission maximum for 3 nm.

E.55 BromoPhenolBlue immobilized in Cellulose Acetate

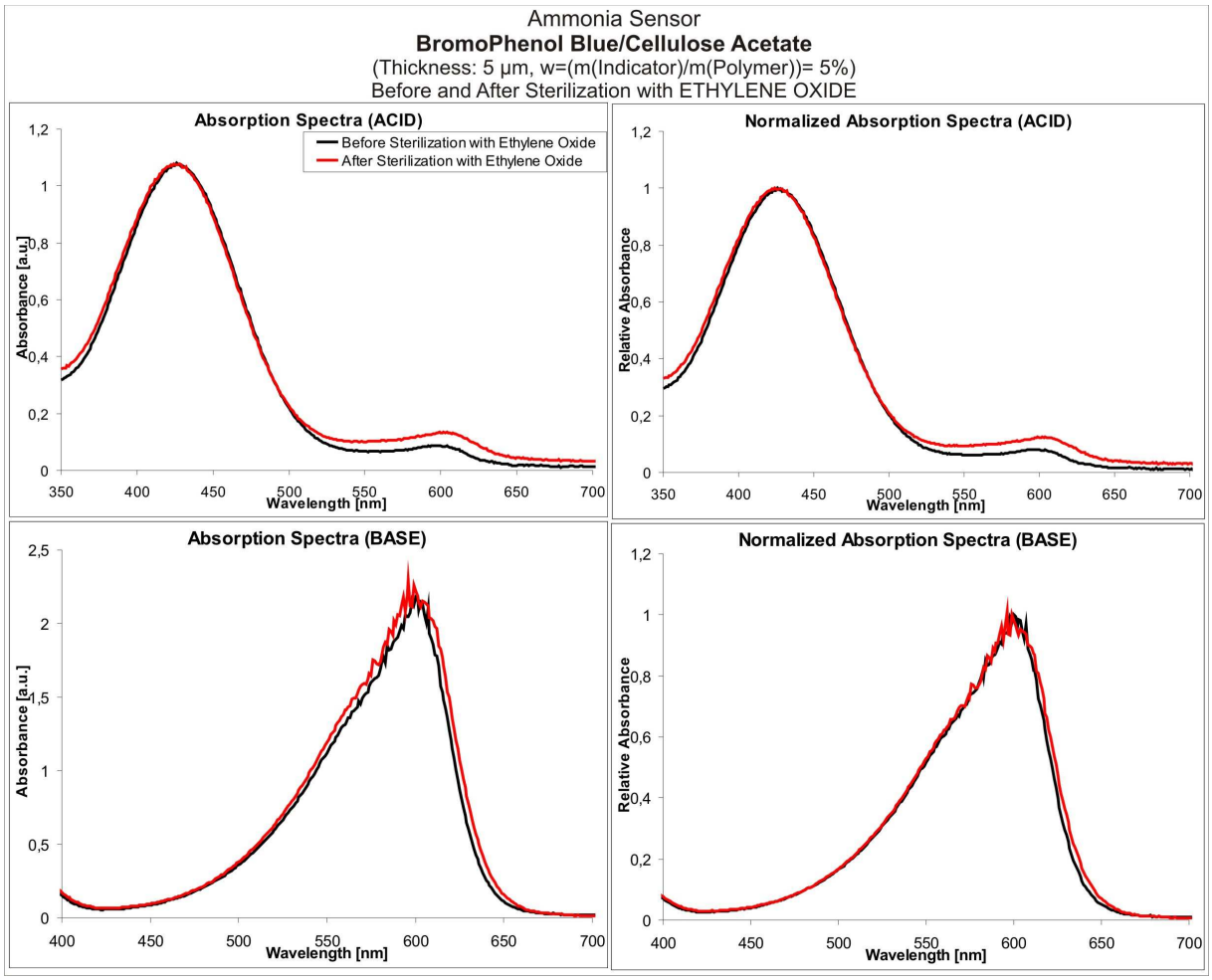

EtO S.	Absorption Spectra			
		Alterations		Alterations
Alterations in Absorption /Emission Intensity	ACID	0,19% decrease	Alterations in Absorption /Emission Curve Form	ACID: Altered emission between 500-700 nm.
	BASE	3,92% increase		BASE: Unaltered.

E.56 BromoPhenolBlue immobilized in Hydrogel D7

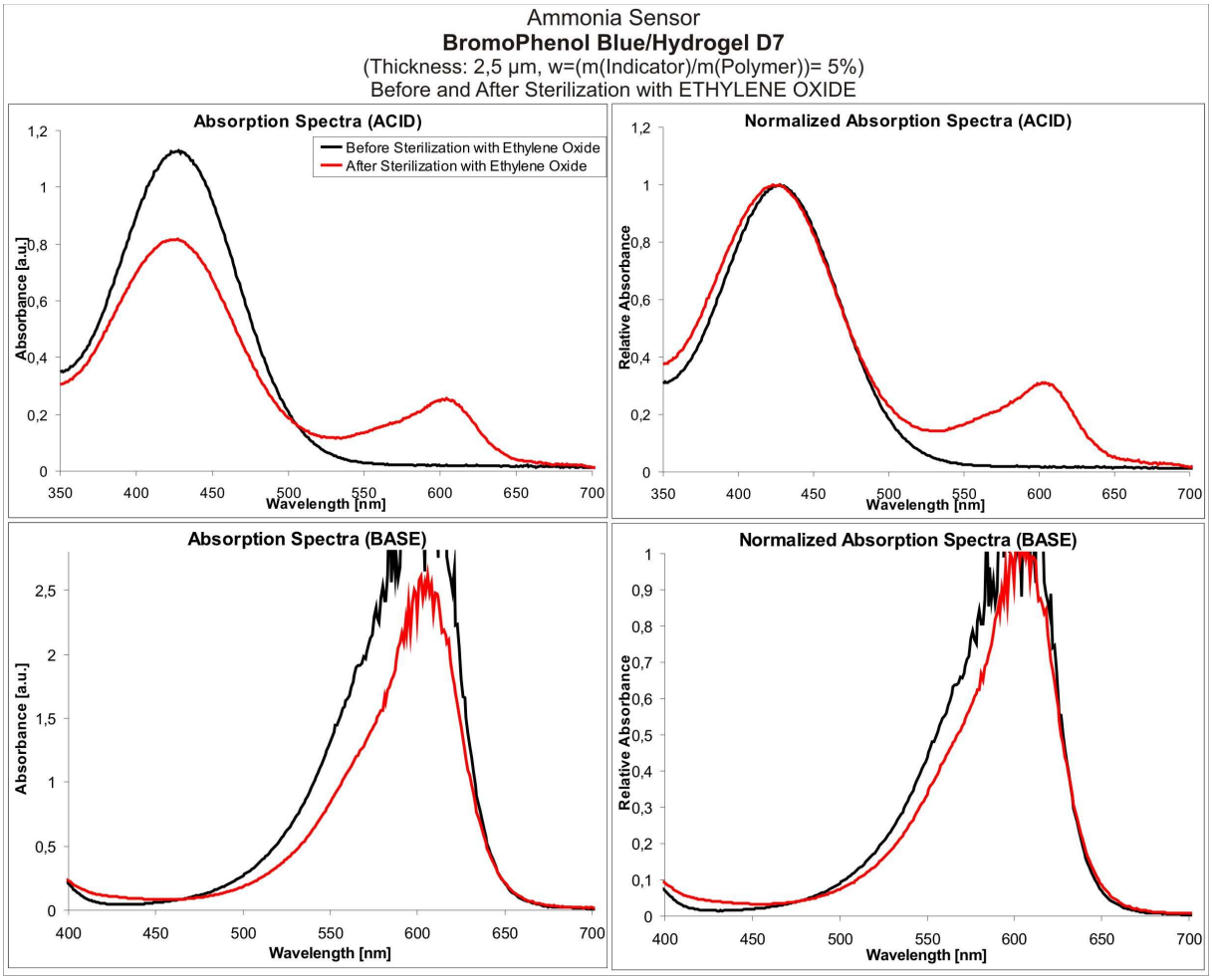

EtO S.	Absorption Spectra			
		Alterations		Alterations
Alterations in Absorption /Emission Intensity	ACID	27,67% decrease	Alterations in Absorption /Emission Curve Form	ACID: The ratio of protonation/ deprotonation peaks is altered after sterilization.
	BASE	24,06% decrease		BASE: Altered emission between 400-550 nm.

E.57.BromoPhenolBlue immobilized in Ethyl Cellulose

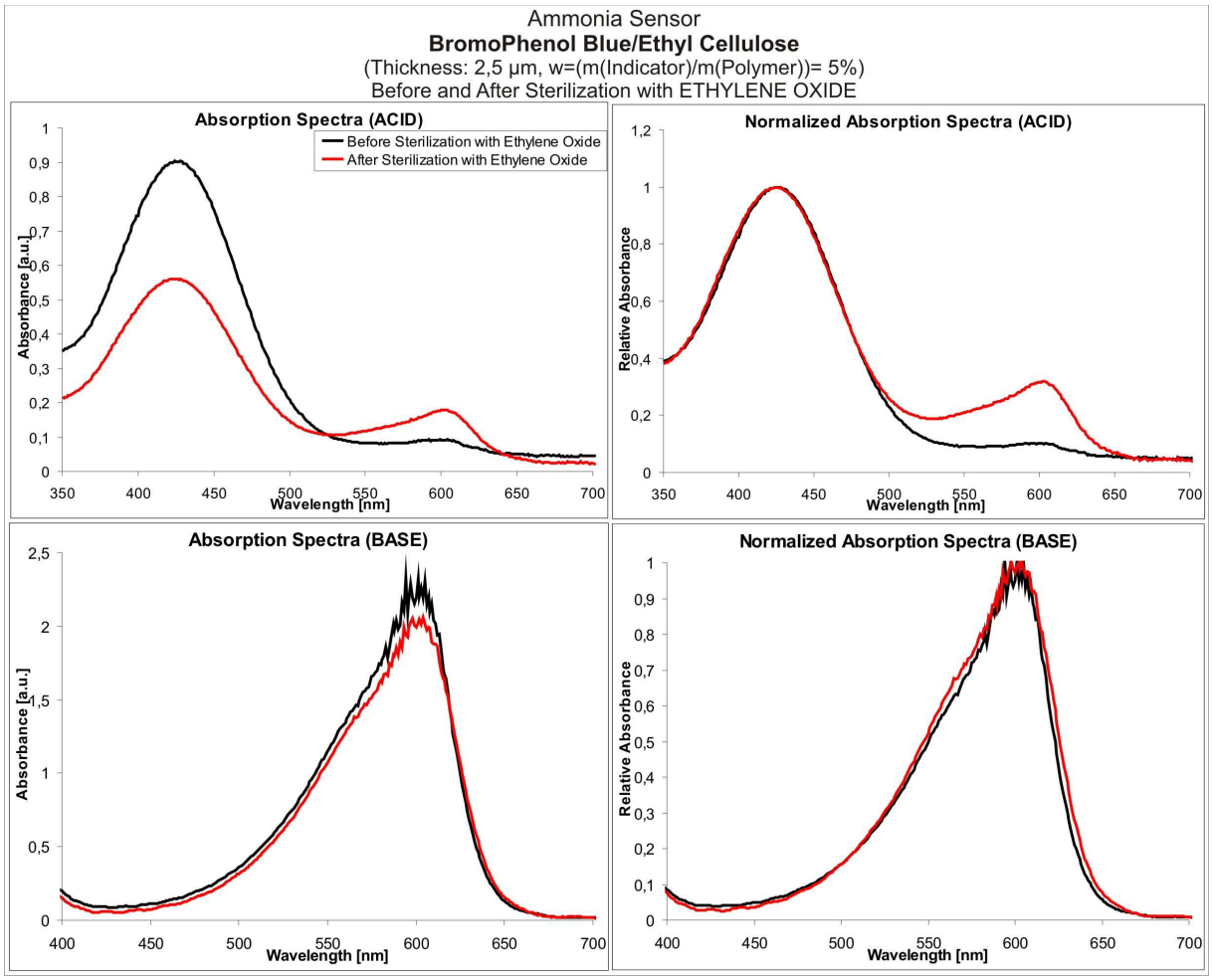

EtO S.	Absorption Spectra			
		Alterations		Alterations
Alterations in Absorption /Emission Intensity	ACID	37,85% decrease	Alterations in Absorption /Emission Curve Form	ACID	The ratio of protonation/ deprotonation peaks is altered after sterilization.
	BASE	11,36% decrease		BASE	Unaltered.

E.58 BromoPhenol Blue immobilized in PolyMethylMethAcrylate (=PMMA)

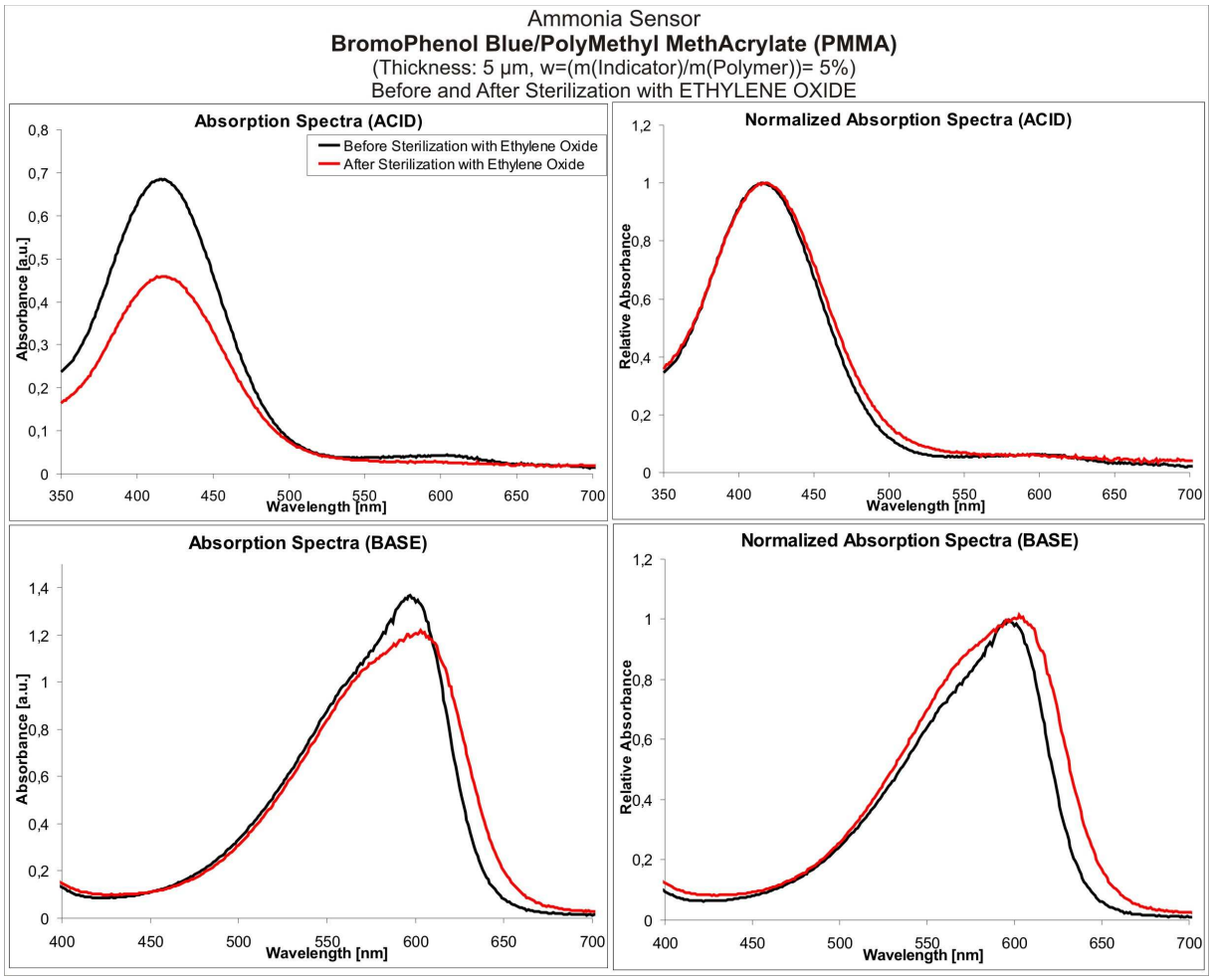

EtO S.	Absorption Spectra				
		Alterations			Alterations
Alterations in Absorption /Emission Intensity	ACID	33,04% decrease	Alterations in Absorption /Emission Curve Form	ACID	Altered absorption between 440-550 nm.
	BASE	12,21% decrease		BASE	Altered form of absorption maximum peak between 550-700 nm.

F
Sterilization of Optical Sensors with Hydrogen Peroxide (Gas and Plasma)

TABLE OF CONTENTS

F STERILIZATION OF OPTICAL SENSORS WITH HYDROGEN PEROXIDE (GAS AND PLASMA) 749

Optical OXYGEN SENSORS 755

F.1 Iridium(III) Coumarin Complex immobilized in HydroGel HydroMed D4/D7 755
F.1.1 Sterilization with Hydrogen Peroxide Gas 755
F.1.2 Sterilization with Low-Temperature Hydrogen Peroxide Plasma 756

F.2 Iridium(III) Coumarin Complex immobilized in HydroThane with 5% water content 758
F.2.1 Sterilization with Hydrogen Peroxide Gas 758
F.2.2 Sterilization with Low-Temperature Hydrogen Peroxide Plasma 759

F.3 Iridium(III) Coumarin Complex immobilized in Poly(Sulfone) 761
F.3.1 Sterilization with Hydrogen Peroxide Gas 761
F.3.2 Sterilization with Low-Temperature Hydrogen Peroxide Plasma 762

F.4 Iridium(III) Coumarin Complex immobilized in Poly(PhenylSilsesQuioxane) 764
F.4.1 Sterilization with Hydrogen Peroxide Gas 764
F.4.2 Sterilization with Low-Temperature Hydrogen Peroxide Plasma 765

F.5 Iridium(III) Coumarin Complex immobilized in Poly(Styrene) 767
F.5.1 Sterilization with Hydrogen Peroxide Gas 767
F.5.2 Sterilization with Low-Temperature Hydrogen Peroxide Plasma 768

F.6 Iridium(III) Coumarin Complex immobilized in Poly(Styrene-co-AcryloNitrile) 770
F.6.1 Sterilization with Hydrogen Peroxide Gas 770
F.6.2 Sterilization with Low-Temperature Hydrogen Peroxide Plasma 771

F.7 Iridium(III) Coumarin Complex immobilized in Poly(Styrene-co-MaleicAnhydride) 773
F.7.1 Sterilization with Hydrogen Peroxide Gas 773
F.7.2 Sterilization with Low-Temperature Hydrogen Peroxide Plasma 774

F.8 Platinum(II)Tetrakis(PentaFluorPhenyl)Porphyrin (PtTFPP) immobilized in HydroGel D4/D7 776
F.8.1 Sterilization with Hydrogen Peroxide Gas 776
F.8.2 Sterilization with Low-Temperature Hydrogen Peroxide Plasma 778

F.9 Platinum(II)Tetrakis(PentaFluorPhenyl)Porphyrin (PtTFPP) immobilized in HydroThane 5 780
F.9.1 Sterilization with Hydrogen Peroxide Gas 780
F.9.2 Sterilization with Low-Temperature Hydrogen Peroxide Plasma 782

F.10 Platinum(II)Tetrakis(PentaFluorPhenyl)Porphyrin (PtTFPP) immobilized in PolySulfone 784
F.10.1 Sterilization with Hydrogen Peroxide Gas 784
F.10.2 Sterilization with Low-Temperature Hydrogen Peroxide Plasma 786

F.11 Platinum(II)Tetrakis(PentaFluorPhenyl)Porphyrin (PtTFPP) immobilized in PolyPhenylSilses Quioxane 788
F.11.1 Sterilization with Hydrogen Peroxide Gas 788
F.11.2 Sterilization with Low-Temperature Hydrogen Peroxide Plasma 790

F.12 Platinum(II)Tetrakis(PentaFluorPhenyl)Porphyrin (PtTFPP) immobilized in PolyStyrene **792**
F.12.1 Sterilization with Hydrogen Peroxide Gas 792
F.12.2 Sterilization with Low-Temperature Hydrogen Peroxide Plasma 794

F.13 Platinum(II)Tetrakis(PentaFluorPhenyl)Porphyrin (PtTFPP) immobilized in PolyStyrene-co- Acrylonitrile **796**
F.13.1 Sterilization with Hydrogen Peroxide Gas 796
F.13.2 Sterilization with Low-Temperature Hydrogen Peroxide Plasma 798

F.14 Platinum(II)Tetrakis(PentaFluorPhenyl)Porphyrin (PtTFPP) immobilized in PolyStyrene-co-MaleicAnhydride (PSMA93) **800**
F.14.1 Sterilization with Hydrogen Peroxide Gas 800
F.14.2 Sterilization with Low-Temperature Hydrogen Peroxide Plasma 802

F.15 Platinum(II) OctaEthyl Porphyrin (=PtOEP) immobilized in PolyStyrene **804**
F.15.1 Sterilization with Hydrogen Peroxide Gas 804
F.15.2 Sterilization with Low-Temperature Hydrogen Peroxide Plasma 806

F.16 Platinum(II) meso-tetra(4-FluoroPhenyl) TetraBenzoPorphyrin (=PtTPTBPF) immobilized in PolyStyrene **808**
F.16.1 Sterilization with Hydrogen Peroxide Gas 808
F.16.2 Sterilization with Low-Temperature Hydrogen Peroxide Plasma 810

F.17 Palladium(II)meso-tetra(4-FluoroPhenyl) TetraBenzoPorphyrin (=PdTPTBPF) immobilized in PolyStyrene **812**
F.17.1 Sterilization with Hydrogen Peroxide Gas 812
F.17.2 Sterilization with Low-Temperature Hydrogen Peroxide Plasma 814

F.18 Ruthenium(II) DiPhenylPhenanthroline DiChloride ($Ru(dpp)_3Cl_2$) immobilized in HydroGel D4/D7 **816**
F.18.1 Sterilization with Hydrogen Peroxide Gas 816
F.18.2 Sterilization with Low-Temperature Hydrogen Peroxide Plasma 817

F.19 Ruthenium(II) DiPhenylPhenanthroline DiChloride ($Ru(dpp)_3Cl_2$) immobilized in HydroThane5 **819**
F.19.1 Sterilization with Hydrogen Peroxide Gas 819
F.19.2 Sterilization with Low-Temperature Hydrogen Peroxide Plasma 820

F.20 Ruthenium(II) DiPhenylPhenanthroline DiChloride ($Ru(dpp)_3Cl_2$) immobilized in PolySulfone **822**
F.20.1 Sterilization with Hydrogen Peroxide Gas 822
F.20.2 Sterilization with Low-Temperature Hydrogen Peroxide Plasma 823

F.21 Ruthenium(II) DiPhenylPhenanthroline DiChloride ($Ru(dpp)_3Cl_2$) immobilized in PolyPhenyl SilsesQuioxane **825**
F.21.1 Sterilization with Hydrogen Peroxide Gas 825
F.21.2 Sterilization with Low-Temperature Hydrogen Peroxide Plasma 826

F.22 Ruthenium(II) DiPhenylPhenanthroline DiChloride ($Ru(dpp)_3Cl_2$) immobilized in PolyStyrene **828**
F.22.1 Sterilization with Hydrogen Peroxide Gas 828
F.22.2 Sterilization with Low-Temperature Hydrogen Peroxide Plasma 829

F.23 Ruthenium(II) DiPhenylPhenanthroline DiChloride ($Ru(dpp)_3Cl_2$) immobilized in PolyStyrene-co-Acrylonitrile **831**
F.23.1 Sterilization with Hydrogen Peroxide Gas 831

F.23.2 Sterilization with Low-Temperature Hydrogen Peroxide Plasma 832

F.24 Ruthenium(II) DiPhenylPhenanthroline DiChloride ($Ru(dpp)_3Cl_2$) immobilized in PolyStyrene-co-MaleicAnhydride (PSMA93) 834
F.24.1 Sterilization with Hydrogen Peroxide Gas 834
F.24.2 Sterilization with Low-Temperature Hydrogen Peroxide Plasma 835

Optical pH SENSORS 837

F.25 HPTS(DHA_3) immobilized in HydroGel D4 837
F.25.1 Sterilization with Hydrogen Peroxide Gas 837
F.25.2 Sterilization with Low-Temperature Hydrogen Peroxide Plasma 840

F.26 2´,7´-DiHexylFluorescein OctadecylEster immobilized in HydroMed Hydrogel D4 843
F.26.1 Sterilization with Hydrogen Peroxide Gas 843
F.26.2 Sterilization with Low-Temperature Hydrogen Peroxide Plasma 845

F.27 2´,7´-DiHexylFluorescein OctadecylEster immobilized in Poly(2-HydroxyEthyl MethAcrylate) (=pHEMA) 847
F.27.1 Sterilization with Hydrogen Peroxide Gas 847
F.27.2 Sterilization with Low-Temperature Hydrogen Peroxide Plasma 849

F.28 2´,7´-DiHexyl-N-Octadecyl-CarboxAmidoFluorescein (=DHFA) immobilized in HydroMed Hydrogel D4 851
F.28.1 Sterilization with Hydrogen Peroxide Gas 851
F.28.2 Sterilization with Low-Temperature Hydrogen Peroxide Plasma 853

F.29 2´,7´-DiHexyl-N-Octadecyl-CarboxAmidoFluorescein (=DHFA) immobilized in Poly(2-HydroxyEthyl Methacrylate) (=pHEMA) 855
F.29.1 Sterilization with Hydrogen Peroxide Gas 855
F.29.2 Sterilization with Low-Temperature Hydrogen Peroxide Plasma 857

F.30 pH Sensitive Coumarin immobilized in HydroMed Hydrogel D4 860
F.30.1 Sterilization with Hydrogen Peroxide Gas 860
F.30.2 Sterilization with Low-Temperature Hydrogen Peroxide Plasma 863

F.31 pH Sensitive Coumarin immobilized in Poly(2-HydroxyEthyl Methacrylate) (=pHEMA) 866
F.31.1 Sterilization with Hydrogen Peroxide Gas 866
F.31.2 Sterilization with Low-Temperature Hydrogen Peroxide Plasma 869

F.32 PET Perylene BisImide immobilized in HydroMed Hydrogel D4 872
F.32.1 Sterilization with Hydrogen Peroxide Gas 872
F.32.2 Sterilization with Low-Temperature Hydrogen Peroxide Plasa 874

F.33 BromoPhenol Blue immobilized in HydroMed Hydrogel D4 876
F.33.1 Sterilization with Hydrogen Peroxide Gas 876
F.33.2 Sterilization with Low-Temperature Hydrogen Peroxide Plasma 877

F.34 Thymol Blue immobilized in HydroMed Hydrogel D4 878
F.34.1 Sterilization with Hydrogen Peroxide Gas 878
F.34.2 Sterilization with Low-Temperature Hydrogen Peroxide Plasma 879

F.35 BromoThymol Blue immobilized in HydroMed Hydrogel D4 880
F.35.1 Sterilization with Hydrogen Peroxide Gas 880
F.35.2 Sterilization with Low-Temperature Hydrogen Peroxide Plasma 881

F.36 Methyl Orange immobilized in HydroMed Hydrogel D4 **882**
F.36.1 Sterilization with Hydrogen Peroxide Gas 882
F.36.2 Sterilization with Low-Temperature Hydrogen Peroxide Plasma 883

Optical TEMPERATURE SENSORS **884**

F.37 Europium(III) Complex with 4-(4,6-di(1H-indazol-1-yl)-1,3,5-triazin-2-yl)-N,N-DiEthyl Benzen Amine (=Eu(tta)$_3$DEADIT) immobilized in PolyStyrene-co-Acrylonitrile **884**
F.37.1 Sterilization with Hydrogen Peroxide Gas 884
F.37.2 Sterilization with Low-Temperature Hydrogen Peroxide Plasma 885

F.38 Europium(III) Complex with 4-(4,6-di(1H-indazol-1-yl)-1,3,5-triazin-2-yl)-N,N-DiEthyl Benzen Amine (=Eu(tta)$_3$DEADIT) immobilized in PolyVinylideneChloride-co-Acrylonitrile **887**
F.38.1 Sterilization with Hydrogen Peroxide Gas 887
F.38.2 Sterilization with Low-Temperature Hydrogen Peroxide Plasma 888

F.39 Europium(III) Complex with 4-(4,6-di(1H-indazol-1-yl)-1,3,5-triazin-2-yl)-N,N-DiEthyl Benzen Amine (=Eu(tta)$_3$DEADIT) immobilized in PolyMethAcryloNitrile **890**
F.39.1 Sterilization with Hydrogen Peroxide Gas 890
F.39.2 Sterilization with Low-Temperature Hydrogen Peroxide Plasma 891

F.40 DiChloroTrisPhenanthroline Ruthenium(II)Hydrate immobilized in PolyVinylideneChloride-co-Acrylonitrile **893**
F.40.1 Sterilization with Hydrogen Peroxide Gas 893
F.40.2 Sterilization with Low-Temperature Hydrogen Peroxide Plasma 894

F.41 DiChloroTrisPhenanthroline Ruthenium(II)Hydrate immobilized in PolyMethAcryloNitrile **895**
F.41.1 Sterilization with Hydrogen Peroxide Gas 895
F.41.2 Sterilization with Low-Temperature Hydrogen Peroxide Plasma 896

Optical AMMONIA SENSORS **884**

F.42 EosinEthylEster immobilized in Hydrogel D7 **898**
F.42.1 Sterilization with Hydrogen Peroxide Gas 898
F.42.2 Sterilization with Low-Temperature Hydrogen Peroxide Plasma 899

F.43 EosinEthylEster immobilized in PolyMethylMethAcrylate (=PMMA) **900**
F.43.1 Sterilization with Hydrogen Peroxide Gas 900
F.43.2 Sterilization with Low-Temperature Hydrogen Peroxide Plasma 901

F.44 DiChloroFluorescein immobilized in Hydrogel D7 **902**
F.44.1 Sterilization with Hydrogen Peroxide Gas 902
F.44.2 Sterilization with Low-Temperature Hydrogen Peroxide Plasma 903

F.45 BromoPhenolBlue immobilized in Hydrogel D7 **904**
F.45.1 Sterilization with Hydrogen Peroxide Gas 904
F.45.2 Sterilization with Low-Temperature Hydrogen Peroxide Plasma 905

F.46 BromoPhenol Blue immobilized in PolyMethylMethAcrylate (=PMMA) **906**
F.46.1 Sterilization with Hydrogen Peroxide Gas 906
F.46.2 Sterilization with Low-Temperature Hydrogen Peroxide Plasma 907

Optical OXYGEN SENSORS

F.1 Iridium(III) Coumarin Complex immobilized in HydroGel HydroMed D4/D7

F.1.1 Sterilization with Hydrogen Peroxide Gas

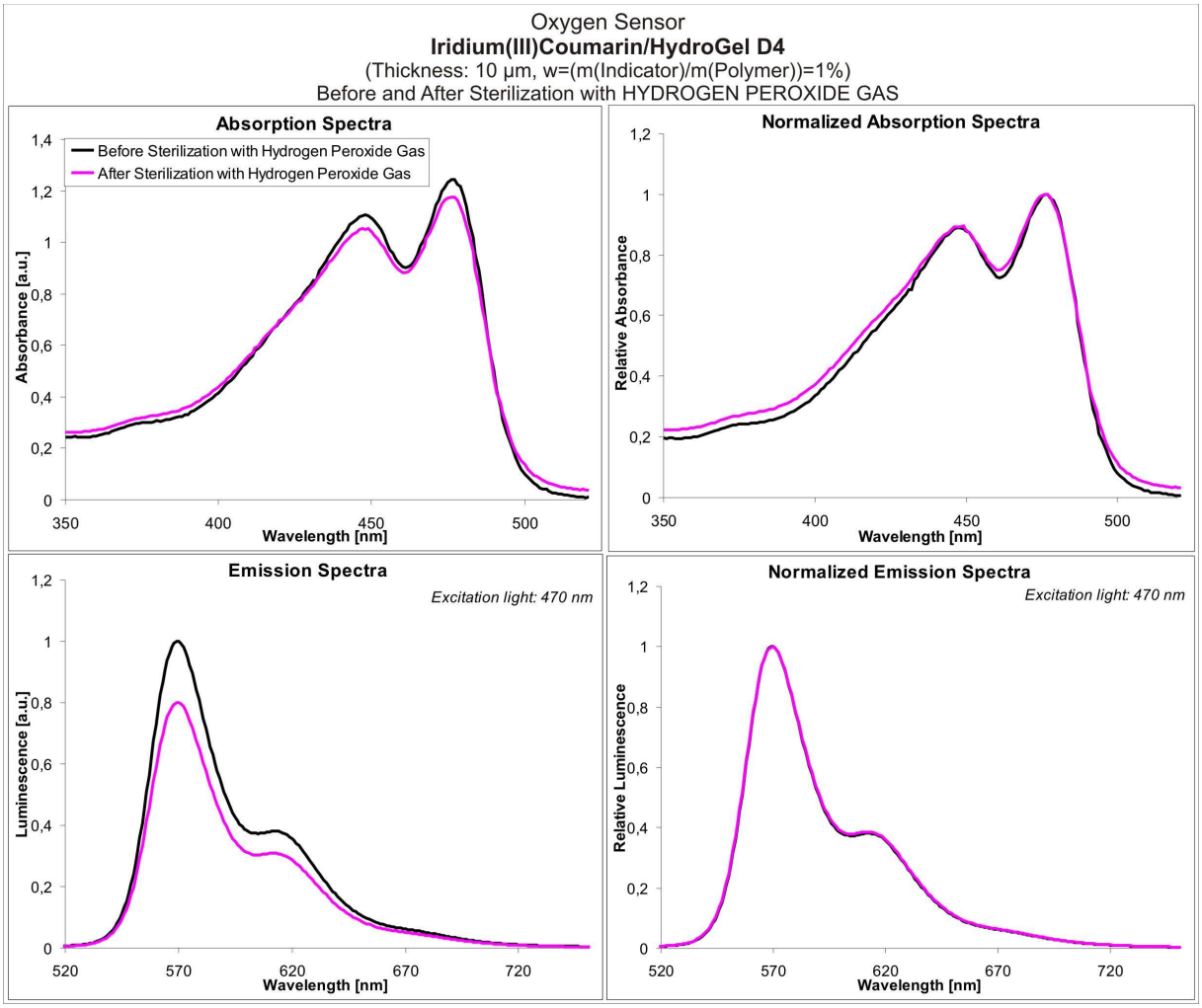

Sterilization with H_2O_2 Gas	Absorption Spectra	Emission Spectra
Alterations in Absorption/Emission Intensity	5,30% decrease	19,94% decrease
Alterations in Absorption/Emission Curve Form	Unaltered.	Unaltered.

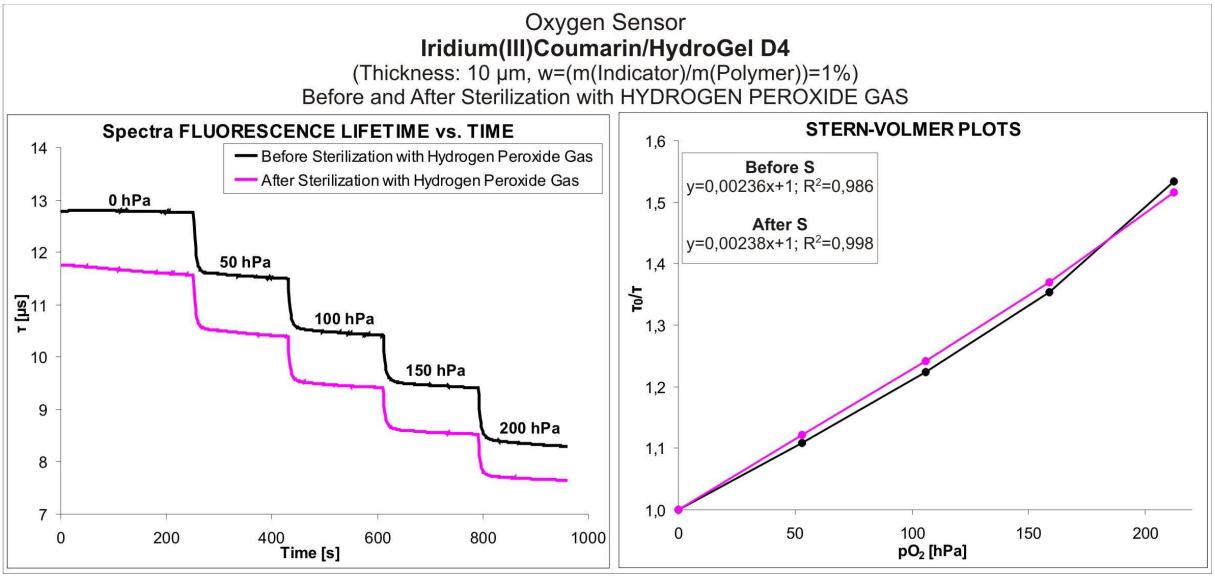

Sterilization with H_2O_2 Gas	Luminescence Lifetime	Stern-Volmer Plot
Alterations in Luminescence Lifetime and Slope	9,38% decrease of τ_0	0,84% increase of slope
	9,91% decrease of τ at 50 hPa	
	10,00 % decrease of τ at 100 hPa	
	10,17 % decrease of τ at 150 hPa	
	8,03 % decrease of τ at 200 hPa	

F.1.2 Sterilization with Low-Temperature Hydrogen Peroxide Plasma

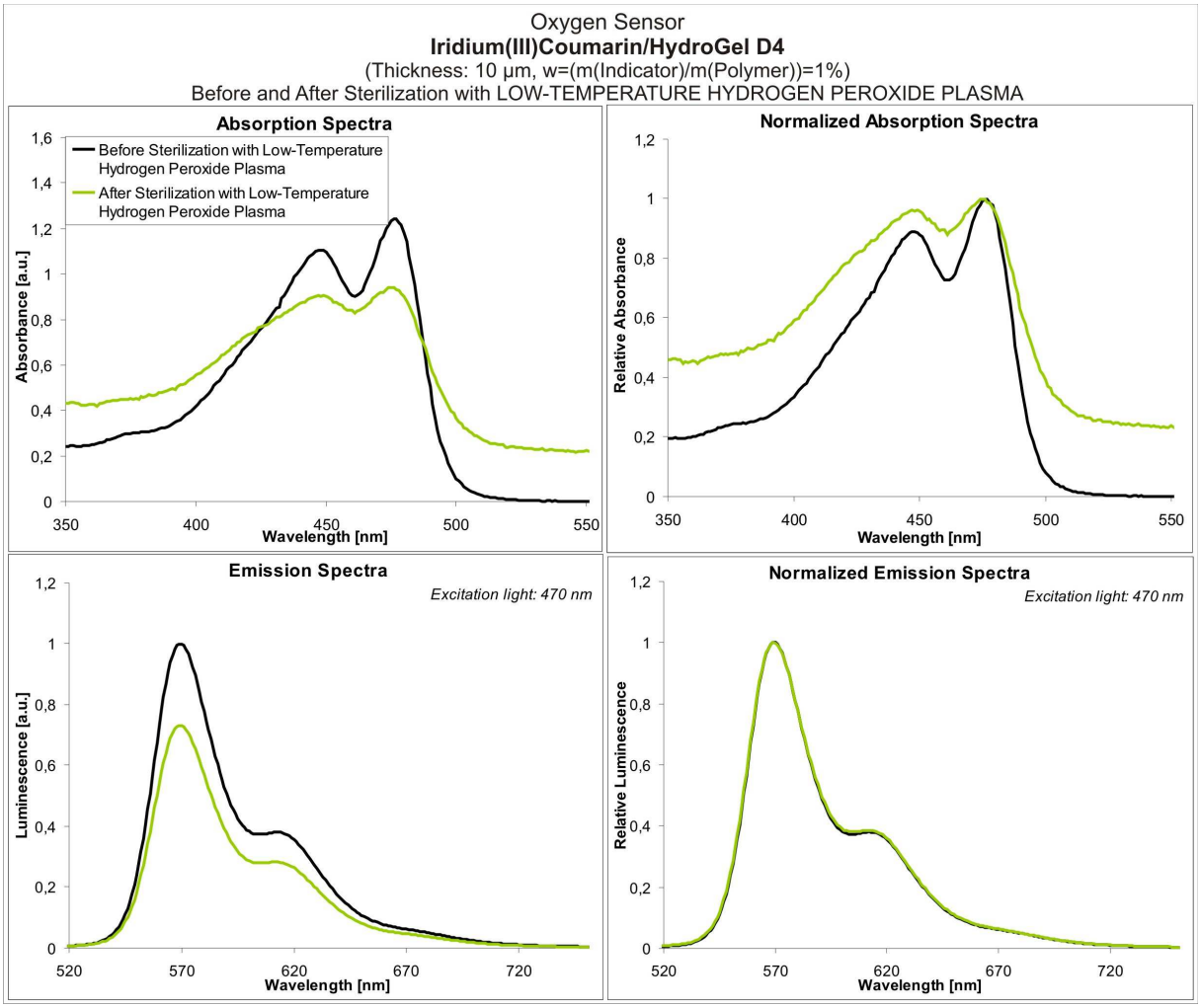

Sterilization with Low-Temperature H_2O_2 Plasma	Absorption Spectra	Emission Spectra
Alterations in Absorption/Emission Intensity	25,27% decrease	26,83% decrease
Alterations in Absorption/Emission Curve Form	Altered absorption curve form between 350-600 nm.	Unaltered.

Oxygen Sensor
Iridium(III)Coumarin/HydroGel D4
(Thickness: 10 µm, w=(m(Indicator)/m(Polymer))=1%)
Before and After Sterilization with LOW-TEMPERATURE HYDROGEN PEROXIDE PLASMA

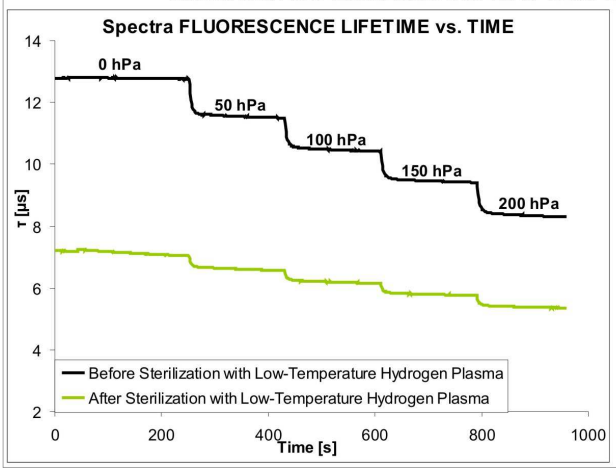

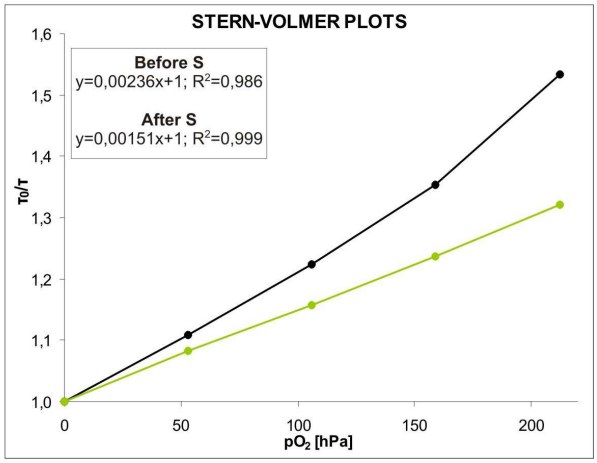

Sterilization with Low-Temperature H_2O_2 Plasma	Luminescence Lifetime	Stern-Volmer Plot
Alterations in Luminescence Lifetime and Slope	44,45% decrease of τ_0	36,02% decrease of slope
	43,10% decrease of τ at 50 hPa	
	40,96% decrease of τ at 100 hPa	
	39,09% decrease of τ at 150 hPa	
	35,49% decrease of τ at 200 hPa	

F.2 Iridium(III) Coumarin Complex immobilized in HydroThane with 5% water content

F.2.1 Sterilization with Hydrogen Peroxide Gas

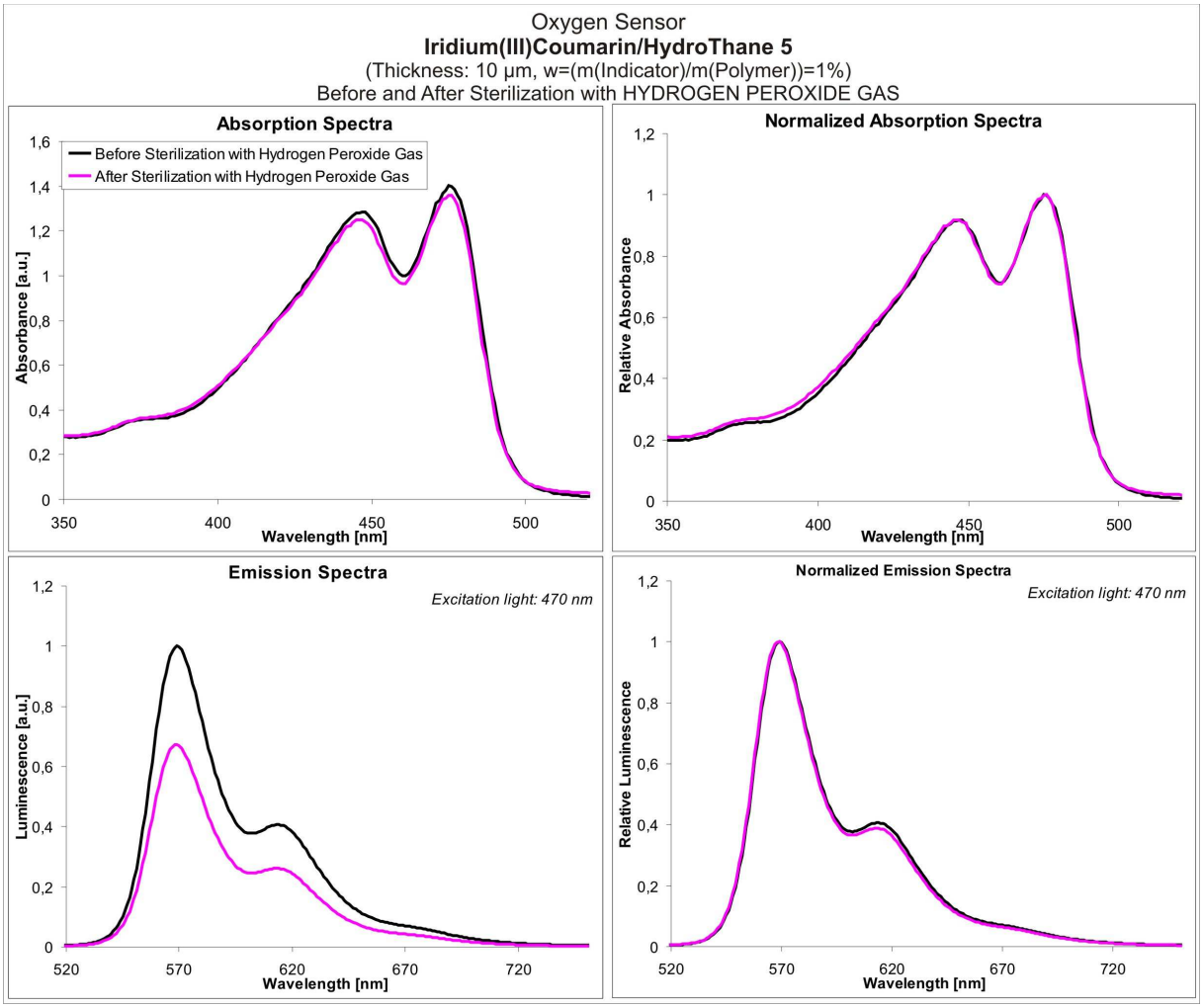

Sterilization with H_2O_2 Gas	Absorption Spectra	Emission Spectra
Alterations in Absorption/Emission Intensity	2,95% decrease	32,72% decrease
Alterations in Absorption/Emission Curve Form	Unaltered.	Unaltered.

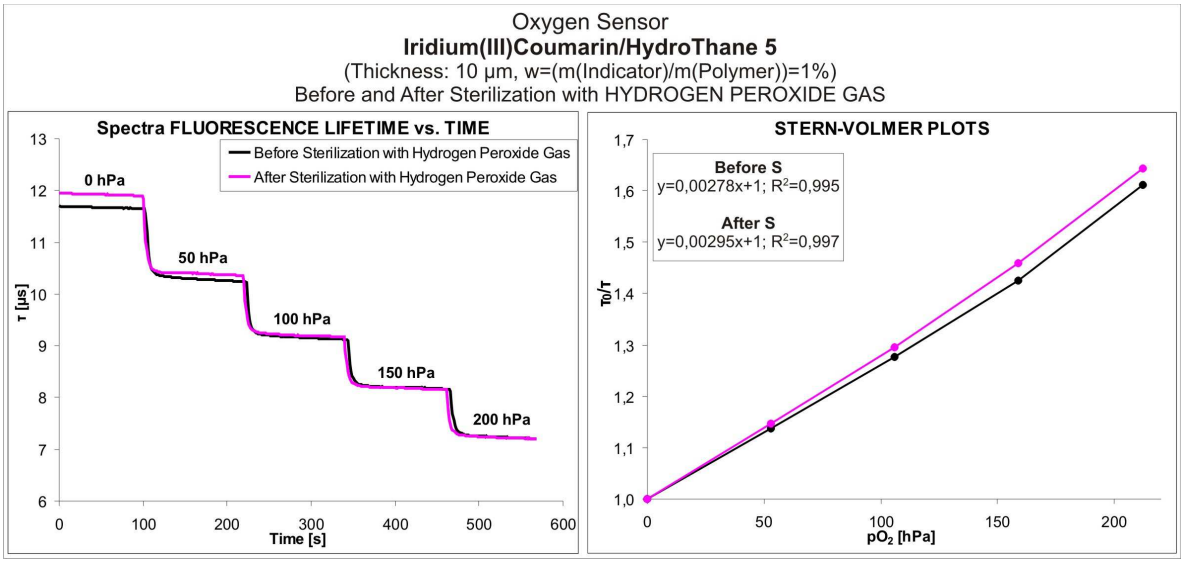

Sterilization with H_2O_2 Gas	Luminescence Lifetime	Stern-Volmer Plot
Alterations in Luminescence Lifetime and Slope	1,68% increase of τ_0	5,76% increase of slope
	1,25% increase of τ at 50 hPa	
	0,43% increase of τ at 100 hPa	
	0,24% decrease of τ at 150 hPa	
	Equal τ at 200 hPa before and after sterilization.	

F.2.2 Sterilization with Low-Temperature Hydrogen Peroxide Plasma

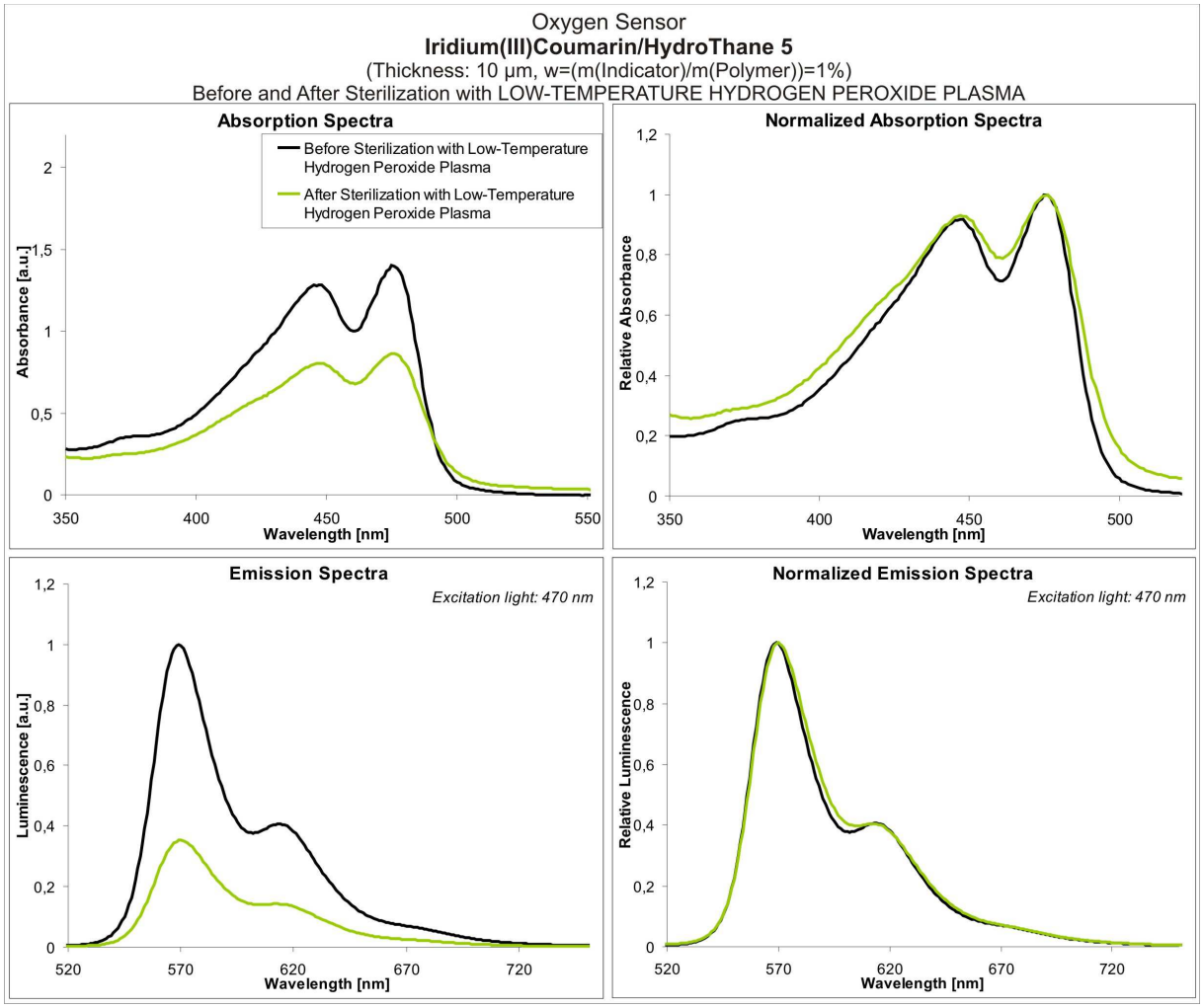

Sterilization with Low-Temperature H_2O_2 Plasma	Absorption Spectra	Emission Spectra
Alterations in Absorption/Emission Intensity	38,29% decrease	64,65% decrease
Alterations in Absorption/Emission Curve Form	Altered absorption curve form between 350-430 nm, 450-470 nm and 480-600 nm.	Altered emission curve form between 570-615 nm.

Oxygen Sensor
Iridium(III)Coumarin/HydroThane 5
(Thickness: 10 µm, w=(m(Indicator)/m(Polymer))=1%)
Before and After Sterilization with LOW-TEMPERATURE HYDROGEN PEROXIDE PLASMA

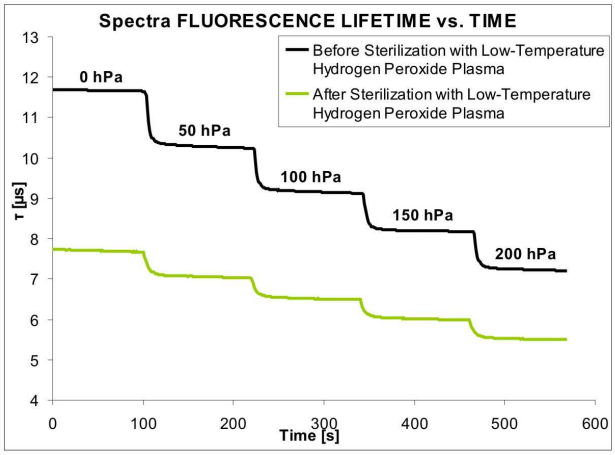

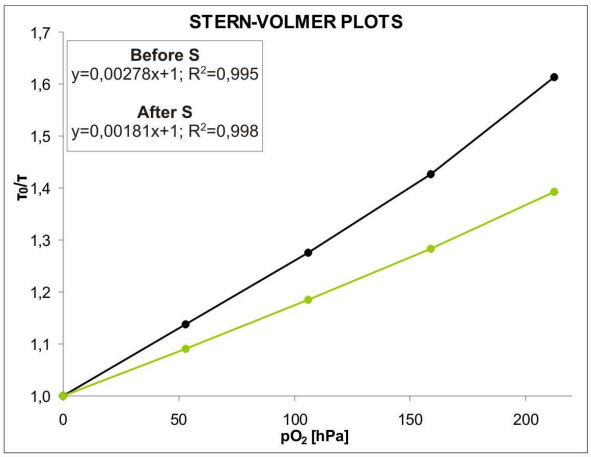

Sterilization with Low-Temperature H_2O_2 Plasma	Luminescence Lifetime	Stern-Volmer Plot
Alterations in Luminescence Lifetime and Slope	34,10% decrease of τ_0	34,89% decrease of slope
	31,20% decrease of τ at 50 hPa	
	28,93% decrease of τ at 100 hPa	
	26,62% decrease of τ at 150 hPa	
	23,59% decrease of τ at 200 hPa	

F.3 Iridium(III) Coumarin Complex immobilized in Poly(Sulfone)

F.3.1 Sterilization with Hydrogen Peroxide Gas

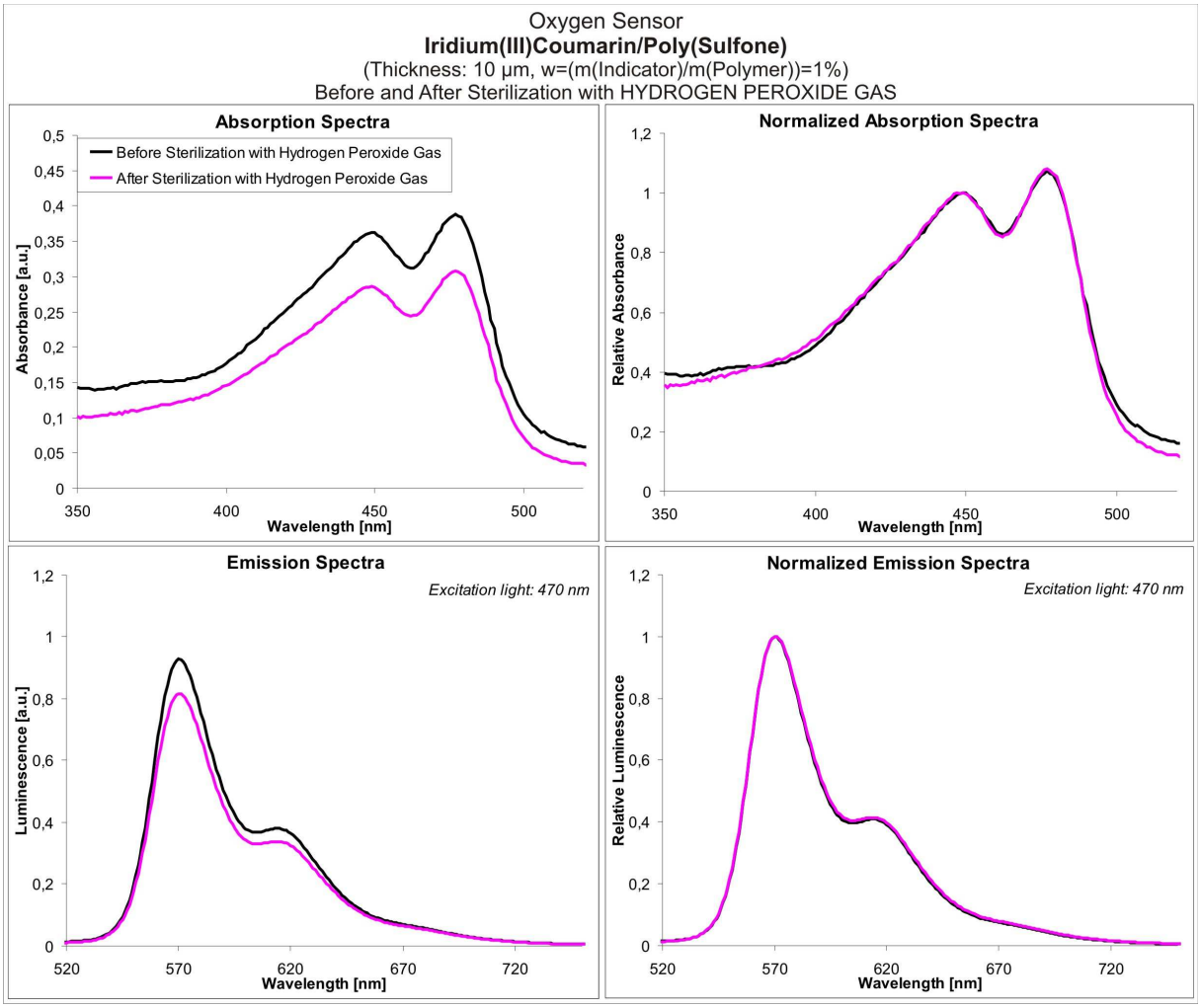

Sterilization with H_2O_2 Gas	Absorption Spectra	Emission Spectra
Alterations in Absorption/Emission Intensity	21,32% decrease	12,06% decrease
Alterations in Absorption/Emission Curve Form	Unaltered.	Unaltered.

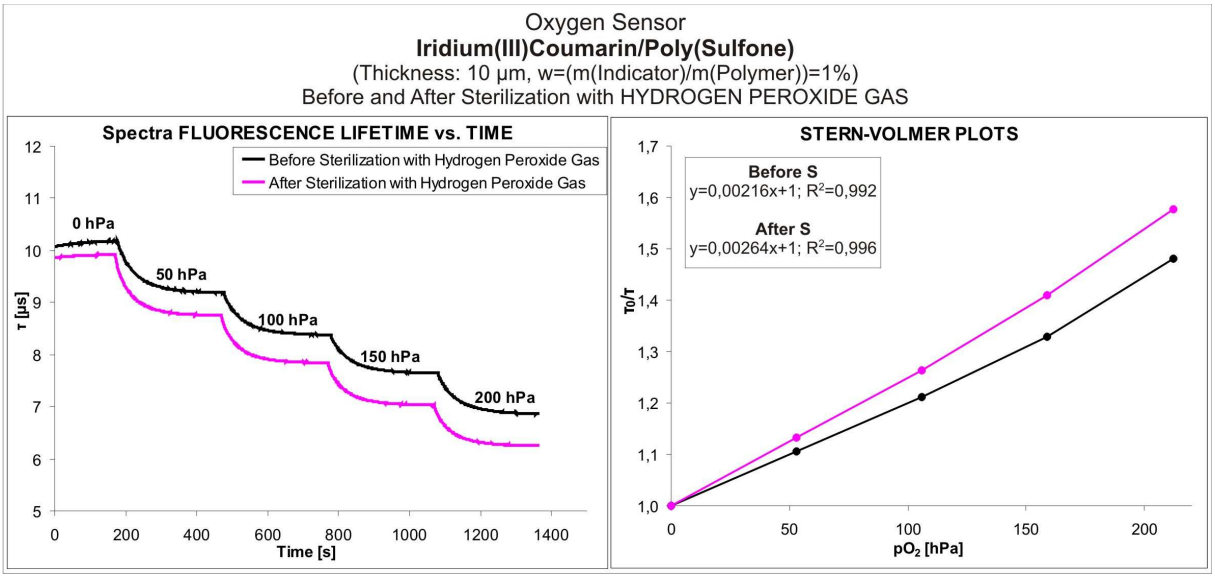

Sterilization with H_2O_2 Gas	Luminescence Lifetime	Stern-Volmer Plot
Alterations in Luminescence Lifetime and Slope	3,23% decrease of τ_0	18,18% increase of slope
	5,33% decrease of τ at 50 hPa	
	6,91% decrease of τ at 100 hPa	
	8,63% decrease of τ at 150 hPa	
	8,88% decrease of τ at 200 hPa	

F.3.2 Sterilization with Low-Temperature Hydrogen Peroxide Plasma

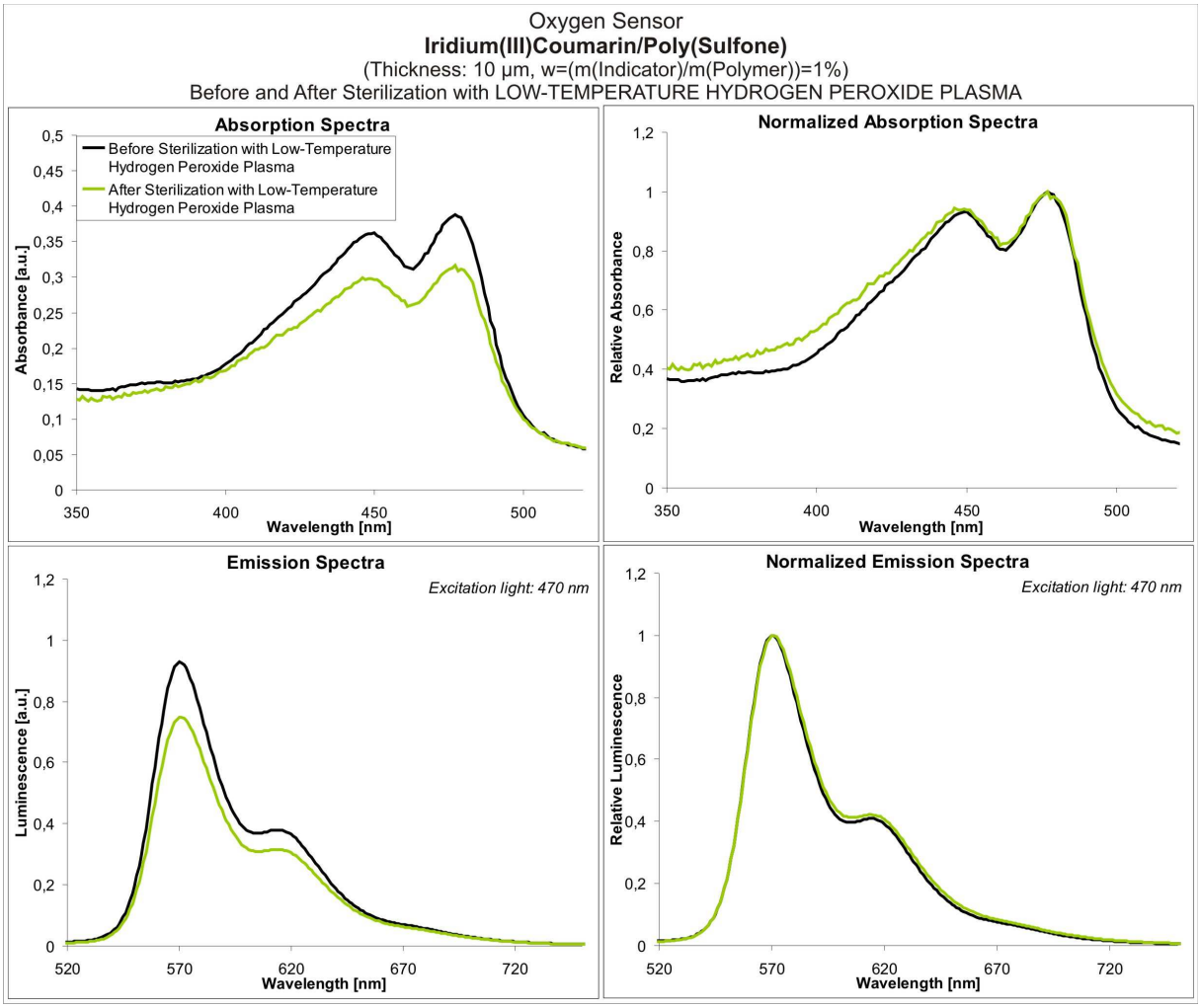

Sterilization with Low-Temperature H_2O_2 Plasma	Absorption Spectra	Emission Spectra
Alterations in Absorption/Emission Intensity	18,58% decrease	19,26% decrease
Alterations in Absorption/Emission Curve Form	Altered absorption curve form between 350-430 nm.	Unaltered.

Oxygen Sensor
Iridium(III)Coumarin/Poly(PhenylSilsesQuioxane)
(Thickness: 10 µm, w=(m(Indicator)/m(Polymer))=1%)
Before and After Sterilization with LOW-TEMPERATURE HYDROGEN PEROXIDE PLASMA

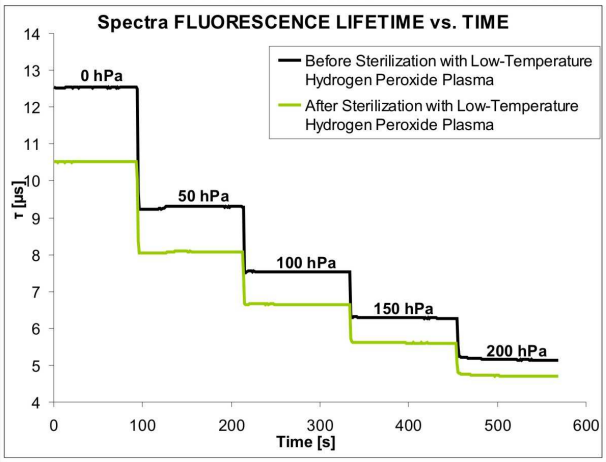

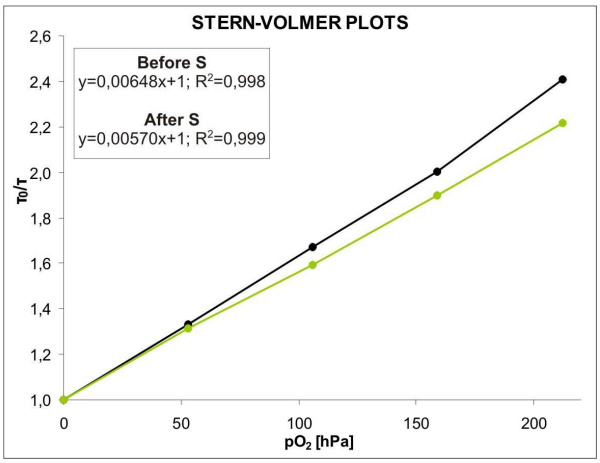

Sterilization with Low-Temperature H_2O_2 Plasma	Luminescence Lifetime	Stern-Volmer Plot
Alterations in Luminescence Lifetime and Slope	10,20% decrease of τ_0	6,49% increase of slope
	10,88% decrease of τ at 50 hPa	
	11,20% decrease of τ at 100 hPa	
	12,03% decrease of τ at 150 hPa	
	11,50% decrease of τ at 200 hPa	

F.4 Iridium(III) Coumarin Complex immobilized in Poly(PhenylSilsesQuioxane)

F.4.1 Sterilization with Hydrogen Peroxide Gas

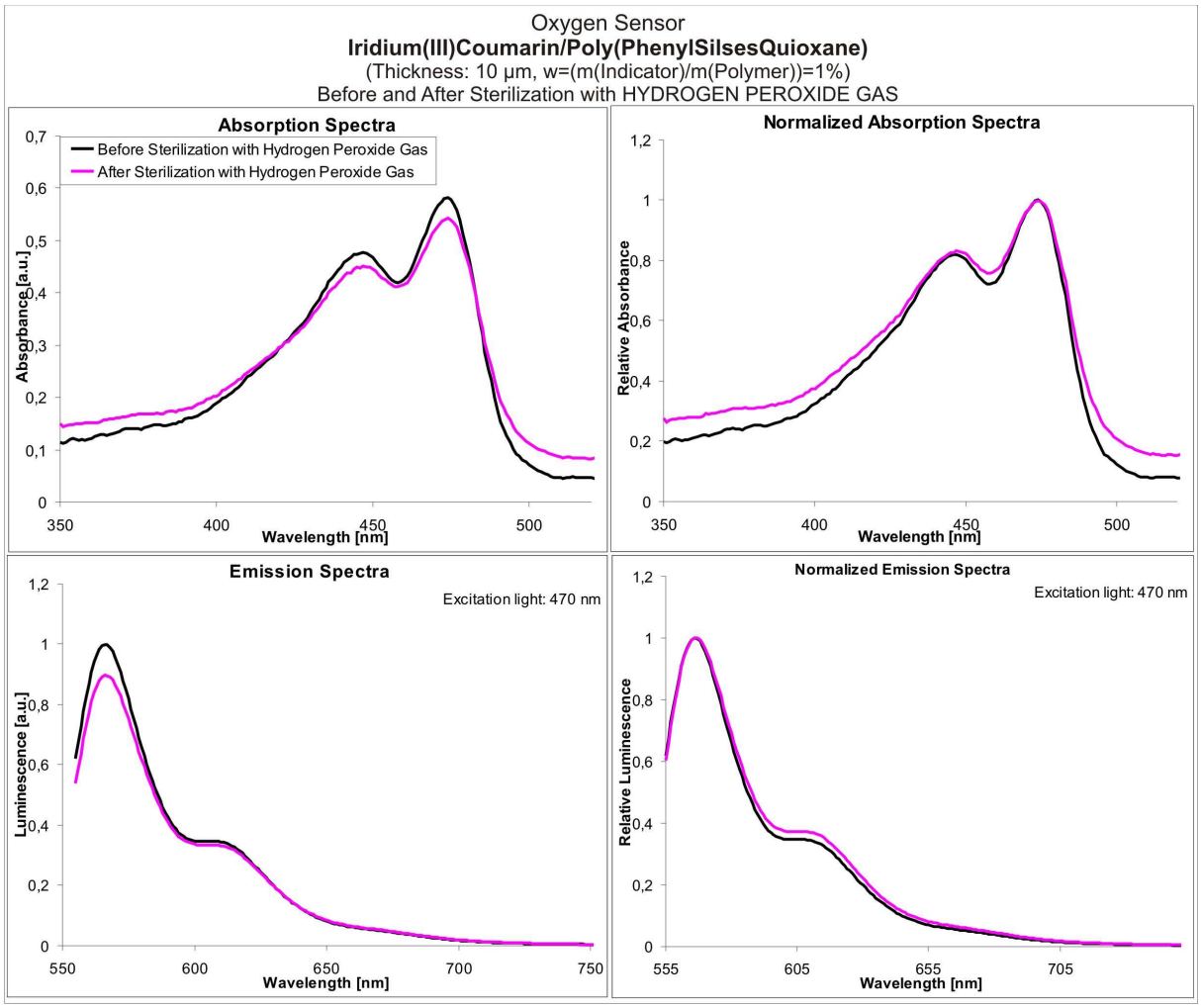

Sterilization with H_2O_2 Gas	Absorption Spectra	Emission Spectra
Alterations in Absorption/Emission Intensity	6,80% decrease	10,38% decrease
Alterations in Absorption/Emission Curve Form	Altered absorption curve form between 350-430 nm, 450-465 nm and 490-800 nm.	Altered emission curve form between 585-655 nm

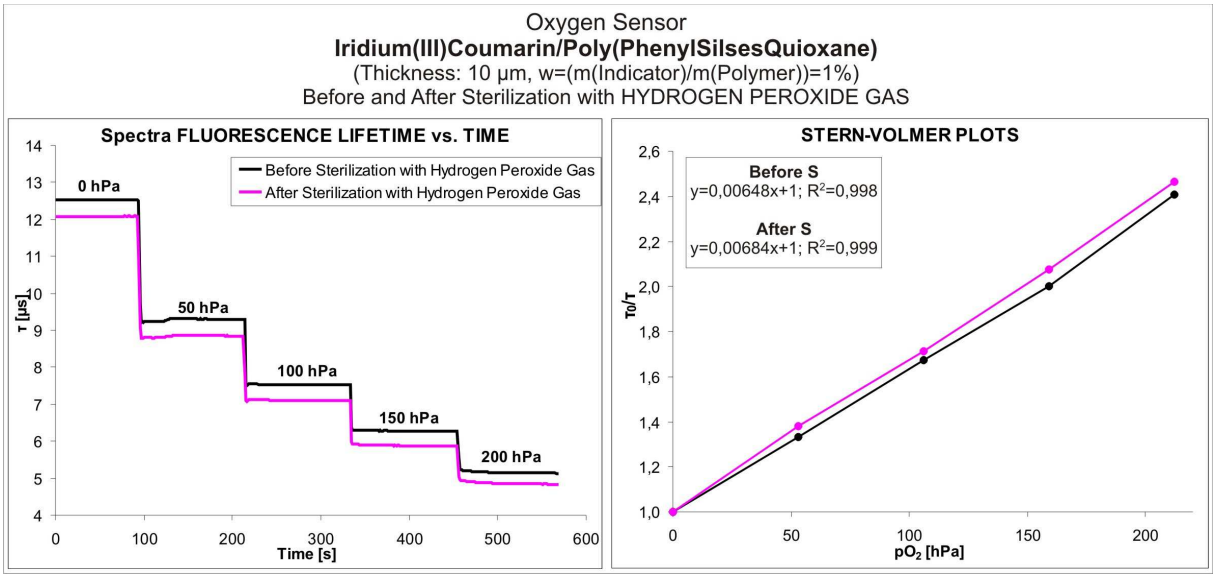

Sterilization with H_2O_2 Gas	Luminescence Lifetime	Stern-Volmer Plot
Alterations in Luminescence Lifetime and Slope	3,23% decrease of τ_0	5,26% increase of slope
	6,49% decrease of τ at 50 hPa	
	5,66% decrease of τ at 100 hPa	
	6,58% decrease of τ at 150 hPa	
	5,44% decrease of τ at 200 hPa	

F.4.2 Sterilization with Low-Temperature Hydrogen Peroxide Plasma

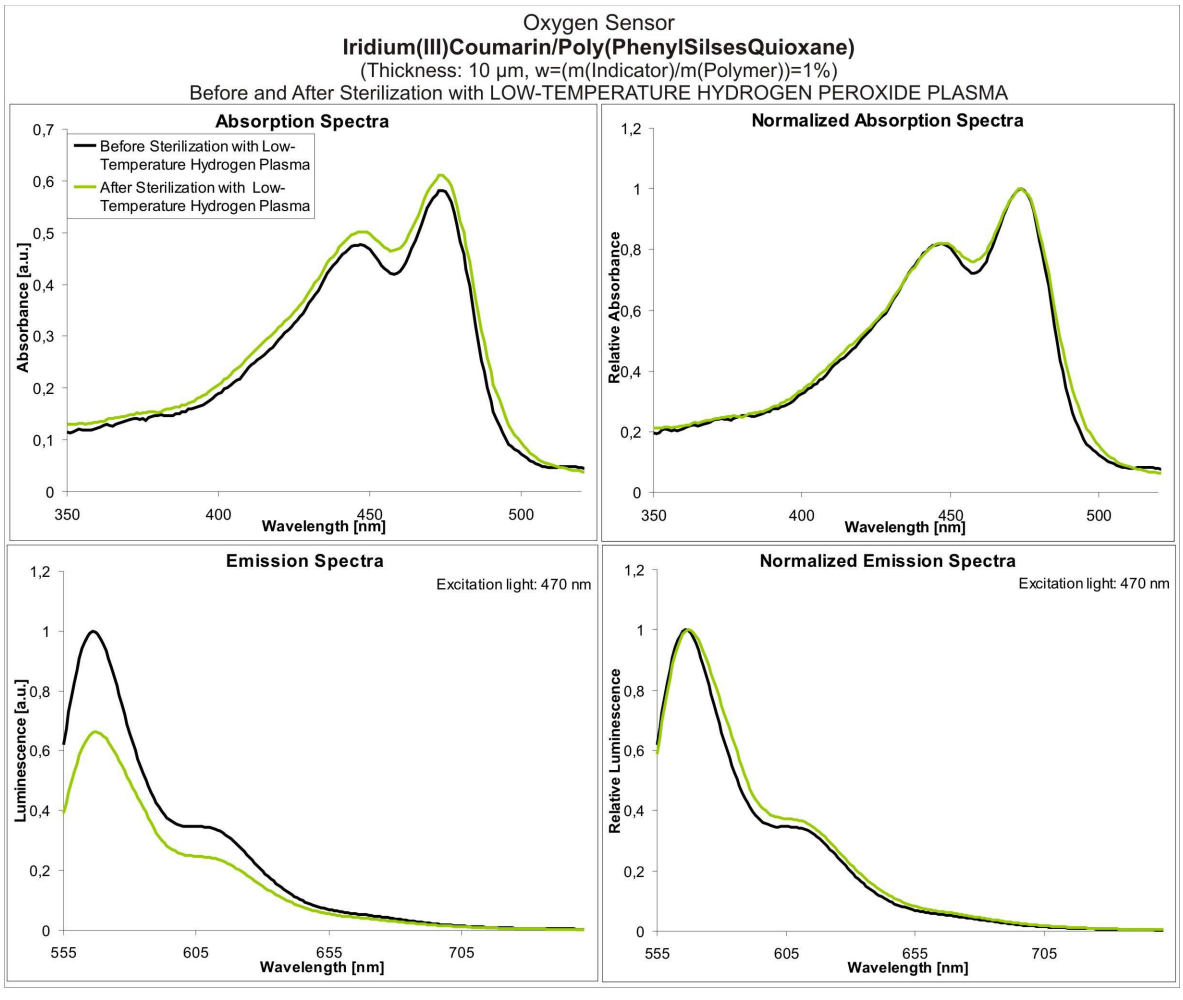

Sterilization with Low-Temperature H_2O_2 Plasma	Absorption Spectra	Emission Spectra
Alterations in Absorption/Emission Intensity	5,04% decrease	33,69% decrease
Alterations in Absorption/Emission Curve Form	Altered absorption curve form between 450-465 nm and 485-510 nm.	Altered emission curve form between 570-655 nm.

Oxygen Sensor
Iridium(III)Coumarin/Poly(PhenylSilsesQuioxane)
(Thickness: 10 µm, w=(m(Indicator)/m(Polymer))=1%)
Before and After Sterilization with LOW-TEMPERATURE HYDROGEN PEROXIDE PLASMA

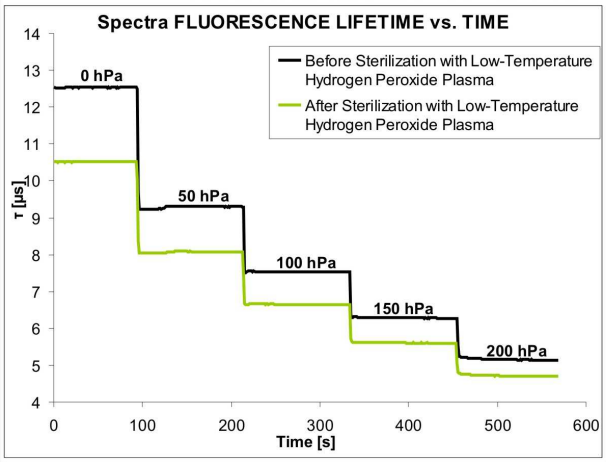

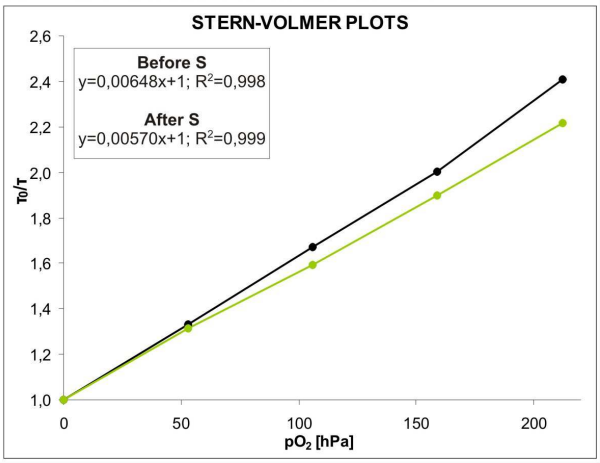

Sterilization with Low-Temperature H_2O_2 Plasma	Luminescence Lifetime	Stern-Volmer Plot
Alterations in Luminescence Lifetime and Slope	16,13% decrease of τ_0	12,04% decrease of slope
	14,41% decrease of τ at 50 hPa	
	11,59% decrease of τ at 100 hPa	
	11,13% decrease of τ at 150 hPa	
	8,35% decrease of τ at 200 hPa	

F.5 Iridium(III) Coumarin Complex immobilized in Poly(Styrene)

F.5.1 Sterilization with Hydrogen Peroxide Gas

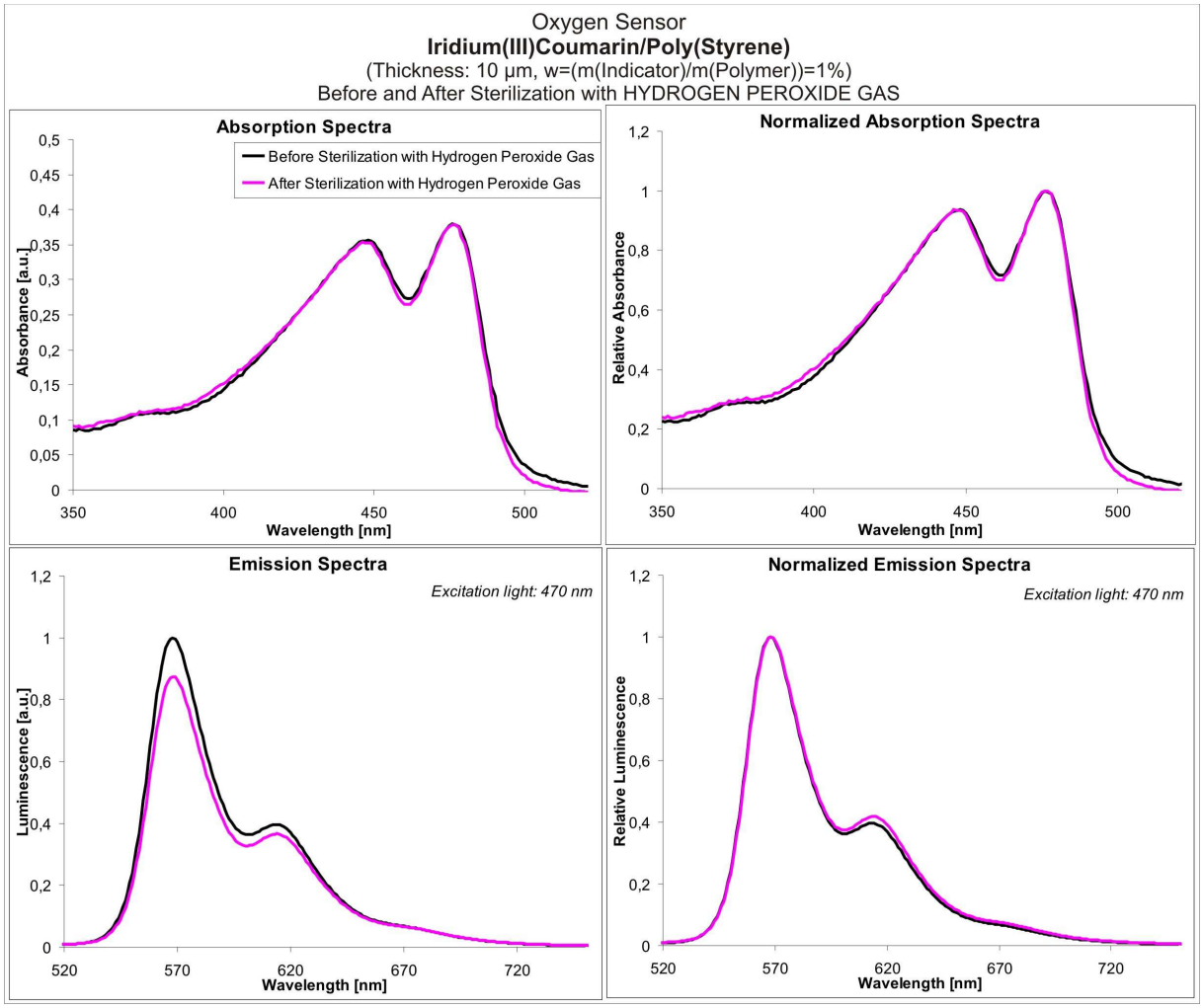

Sterilization with H_2O_2 Gas	Absorption Spectra	Emission Spectra
Alterations in Absorption/Emission Intensity	0,57% decrease	12,54% decrease
Alterations in Absorption/Emission Curve Form	Unaltered.	Unaltered.

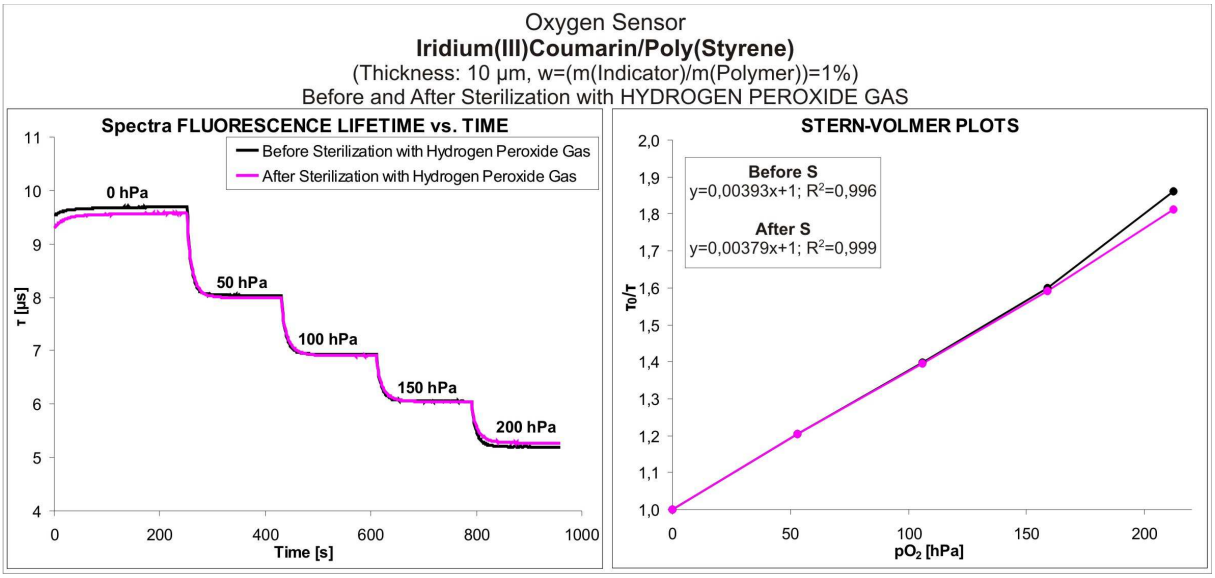

Sterilization with H_2O_2 Gas	Luminescence Lifetime	Stern-Volmer Plot
Alterations in Luminescence Lifetime and Slope	1,24% decrease of τ_0	3,56% decrease of slope
	1,19% decrease of τ at 50 hPa	
	1,01% decrease of τ at 100 hPa	
	0,83% decrease of τ at 150 hPa	
	1,52% increase of τ at 200 hPa	

F.5.2 Sterilization with Low-Temperature Hydrogen Peroxide Plasma

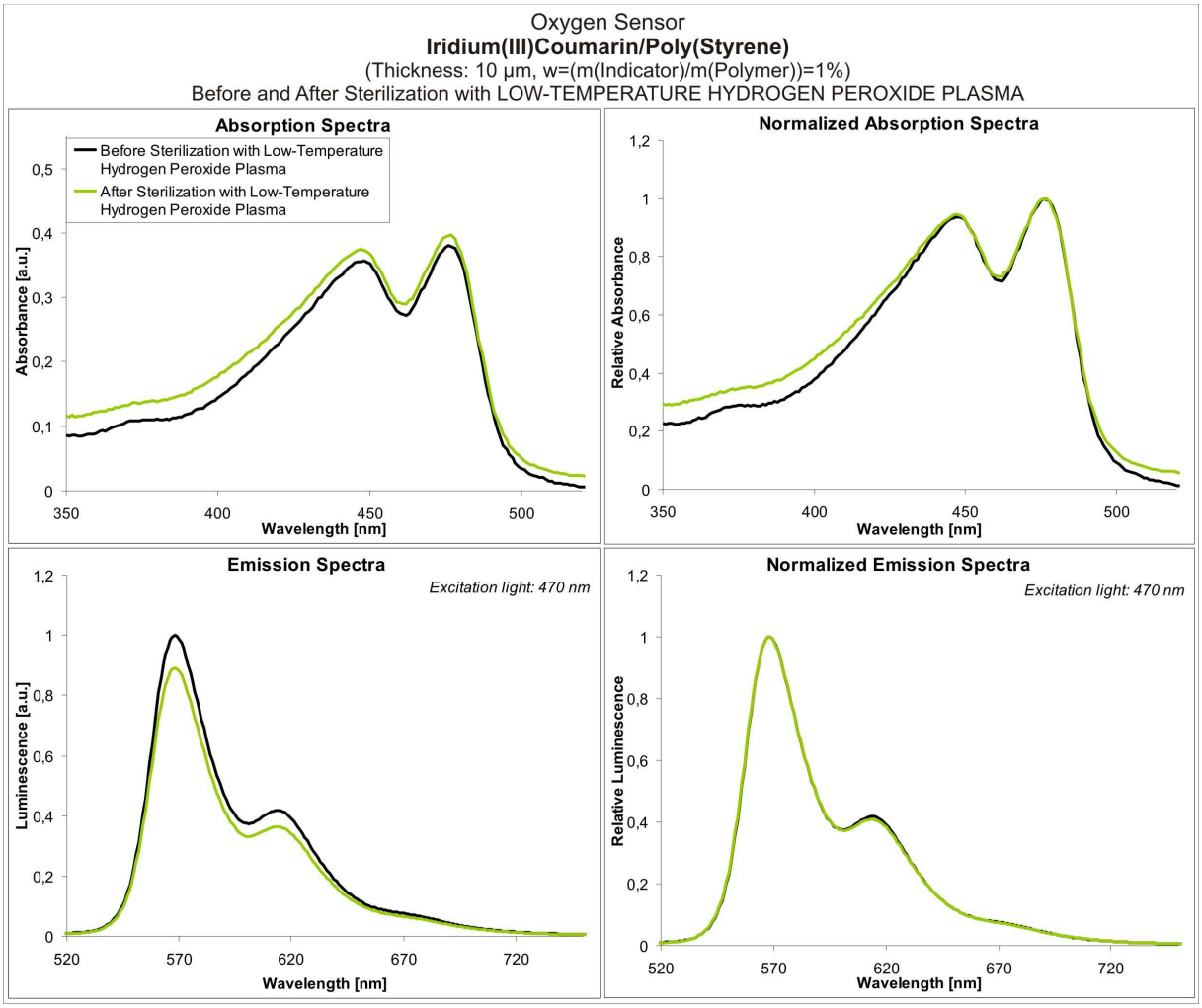

Sterilization with Low-Temperature H_2O_2 Plasma	Absorption Spectra	Emission Spectra
Alterations in Absorption/Emission Intensity	3,98% increase	10,87% decrease
Alterations in Absorption/Emission Curve Form	Altered absorption curve form between 350-430 nm.	Unaltered.

Oxygen Sensor
Iridium(III)Coumarin/Poly(Styrene)
(Thickness: 10 µm, w=(m(Indicator)/m(Polymer))=1%)
Before and After Sterilization with LOW-TEMPERATURE HYDROGEN PEROXIDE PLASMA

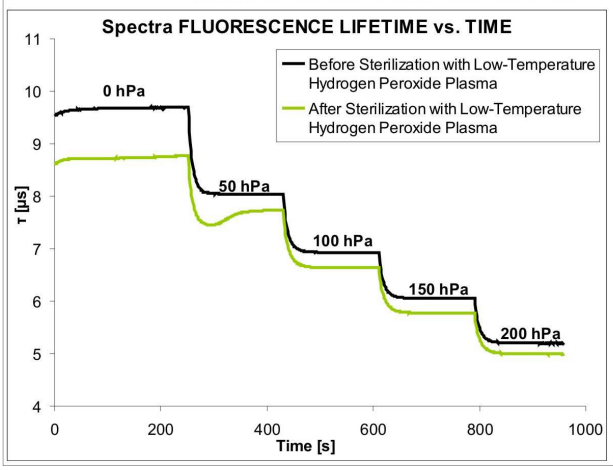

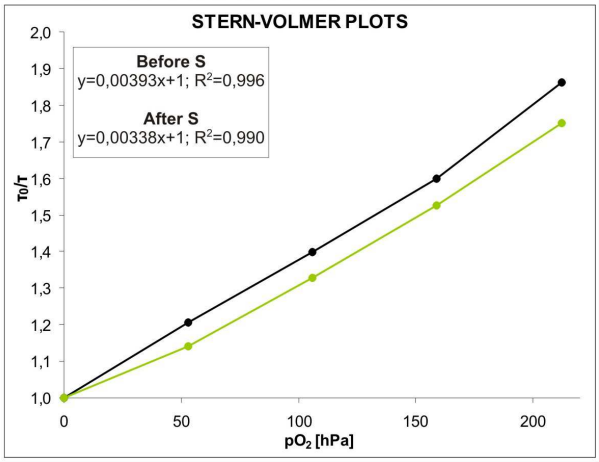

Sterilization with Low-Temperature H_2O_2 Plasma	Luminescence Lifetime	Stern-Volmer Plot
Alterations in Luminescence Lifetime and Slope	9,71% decrease of τ_0	13,99% decrease of slope
	4,73% decrease of τ at 50 hPa	
	4,91% decrease of τ at 100 hPa	
	5,29% decrease of τ at 150 hPa	
	4,04% decrease of τ at 200 hPa	

F.6 Iridium(III) Coumarin Complex immobilized in Poly(Styrene-co-AcryloNitrile)

F.6.1 Sterilization with Hydrogen Peroxide Gas

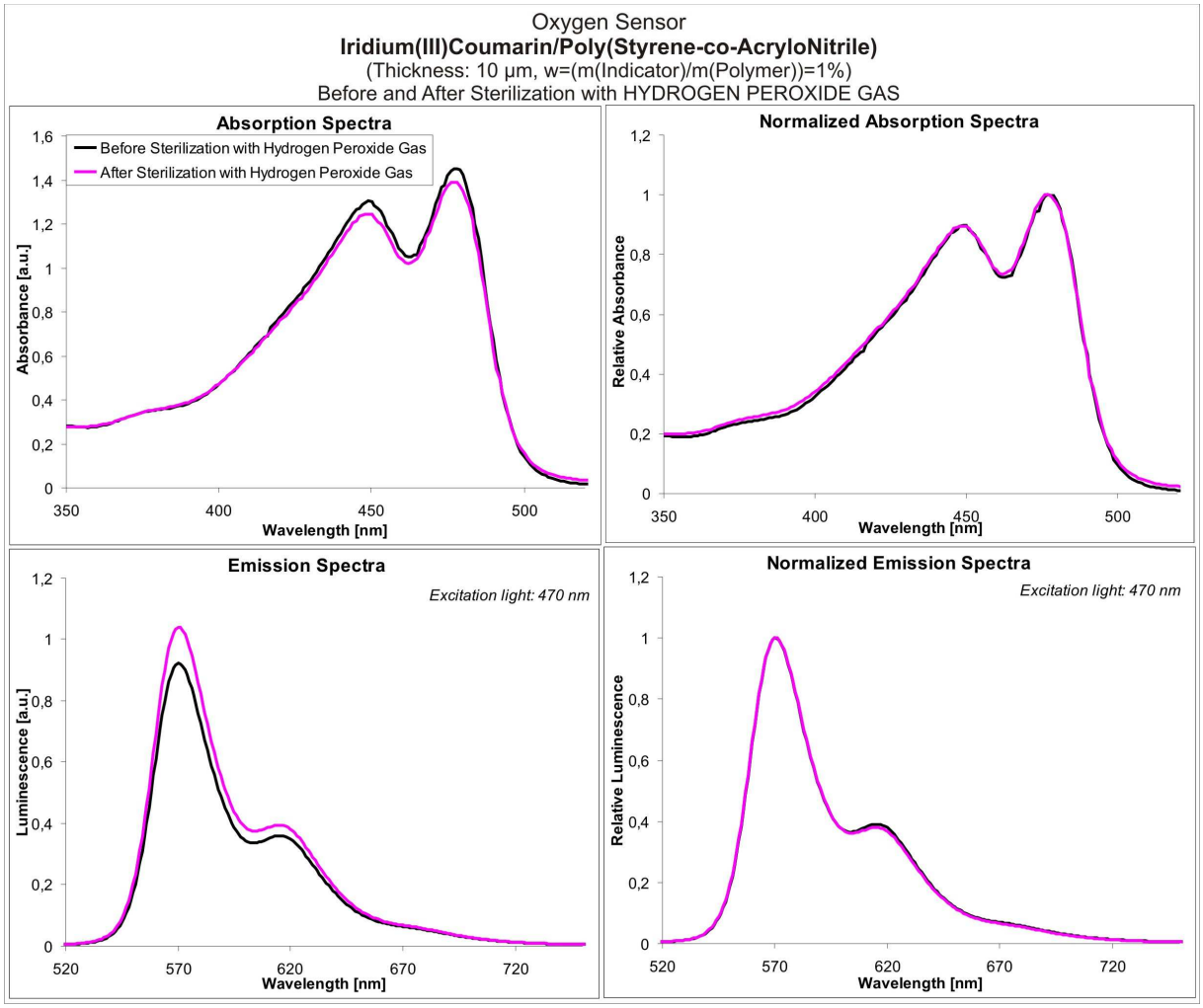

Sterilization with H_2O_2 Gas	Absorption Spectra	Emission Spectra
Alterations in Absorption/Emission Intensity	4,31% decrease	11,26% increase
Alterations in Absorption/Emission Curve Form	Unaltered.	Unaltered.

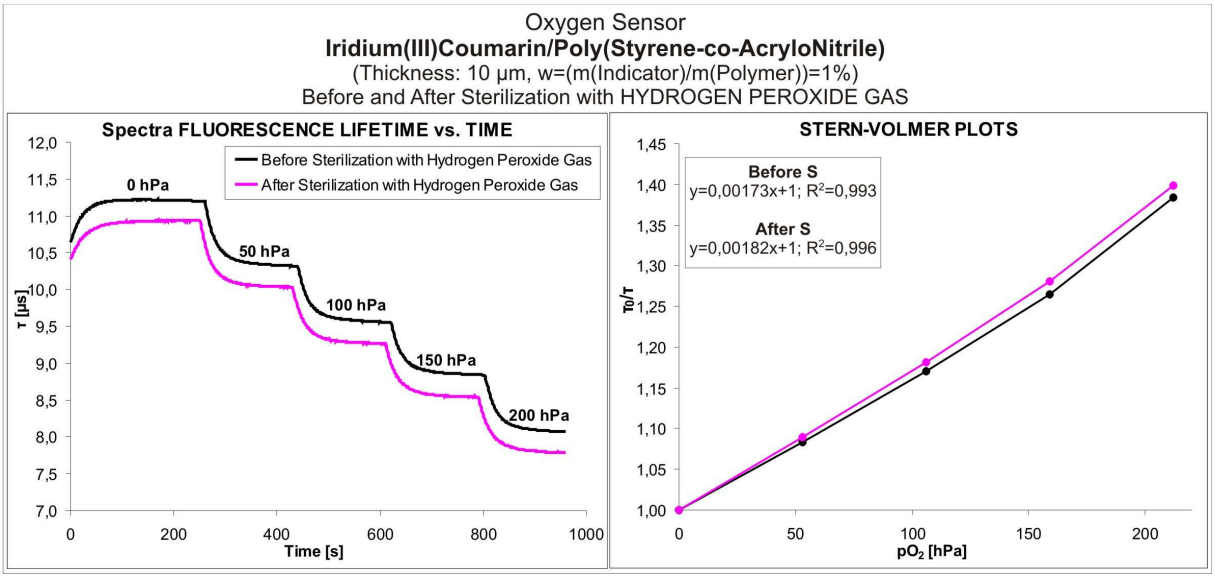

Sterilization with H_2O_2 Gas	Luminescence Lifetime	Stern-Volmer Plot
Alterations in Luminescence Lifetime and Slope	2,68% decrease of τ_0	4,95% increase of slope
	3,09% decrease of τ at 50 hPa	
	3,44% decrease of τ at 100 hPa	
	3,83% decrease of τ at 150 hPa	
	3,57% increase of τ at 200 hPa	

F.6.2 Sterilization with Low-Temperature Hydrogen Peroxide Plasma

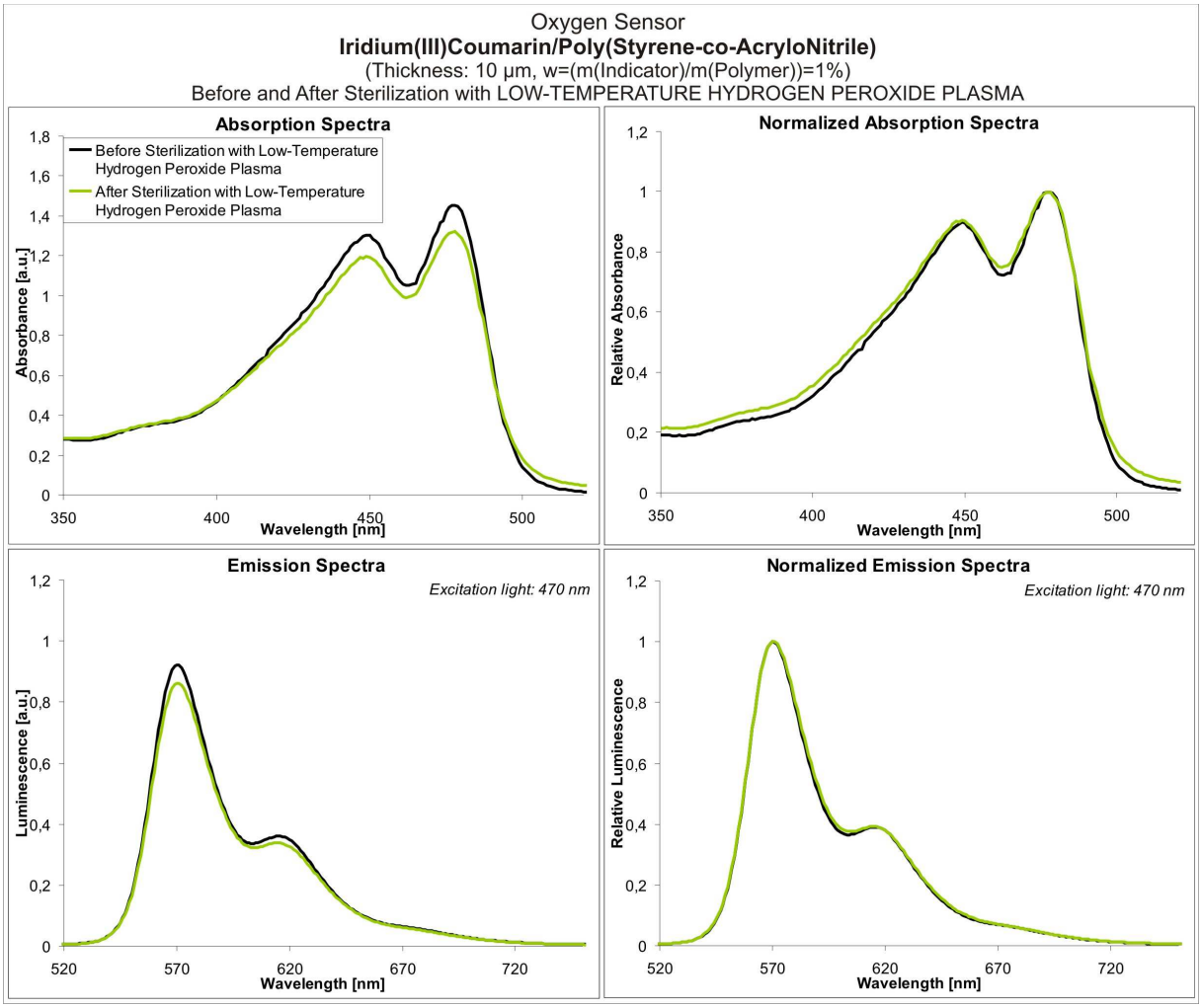

Sterilization with Low-Temperature H_2O_2 Plasma	Absorption Spectra	Emission Spectra
Alterations in Absorption/Emission Intensity	8,97% decrease	6,53% decrease
Alterations in Absorption/Emission Curve Form	Unaltered.	Unaltered.

Oxygen Sensor
Iridium(III)Coumarin/Poly(Styrene-co-AcryloNitrile)
(Thickness: 10 µm, w=(m(Indicator)/m(Polymer))=1%)
Before and After Sterilization with LOW-TEMPERATURE HYDROGEN PEROXIDE PLASMA

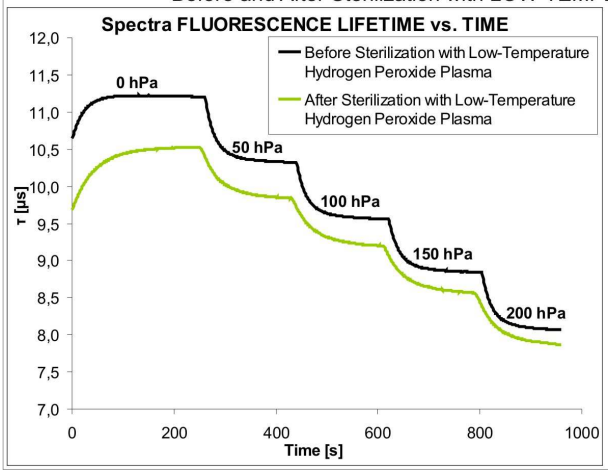

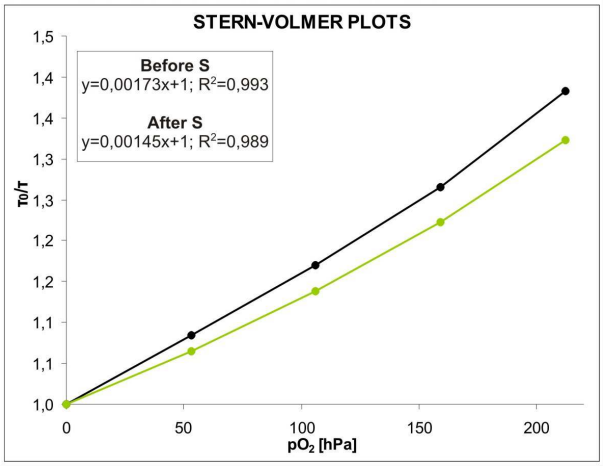

Sterilization with Low-Temperature H_2O_2 Plasma	Luminescence Lifetime	Stern-Volmer Plot
Alterations in Luminescence Lifetime and Slope	6,25% decrease of τ_0	16,18% decrease of slope
	4,73% decrease of τ at 50 hPa	
	3,76% decrease of τ at 100 hPa	
	3,27% decrease of τ at 150 hPa	
	2,22% decrease of τ at 200 hPa	

F.7 Iridium(III) Coumarin Complex immobilized in Poly(Styrene-co-MaleicAnhydride)

F.7.1 Sterilization with Hydrogen Peroxide Gas

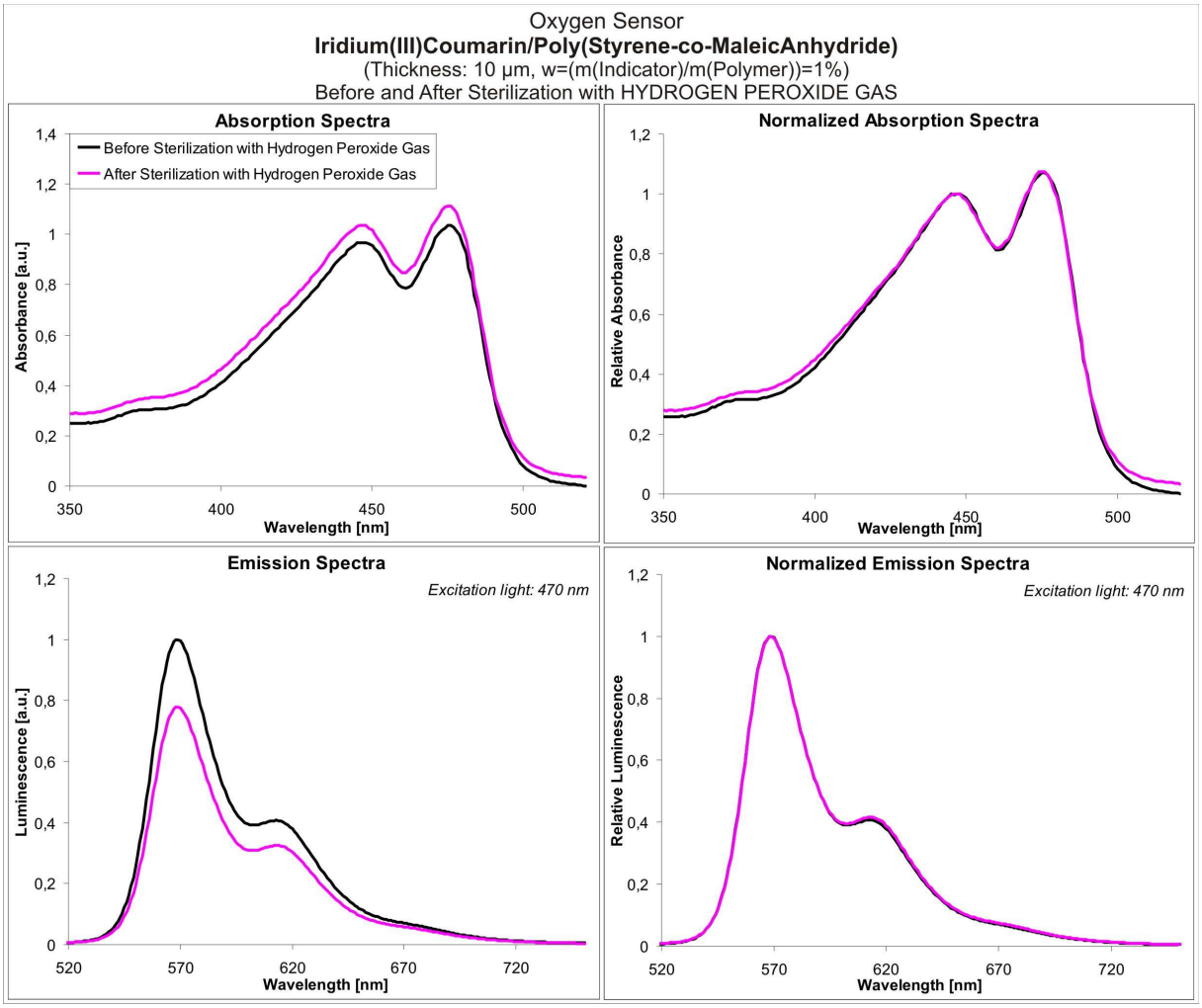

Sterilization with H_2O_2 Gas	Absorption Spectra	Emission Spectra
Alterations in Absorption/Emission Intensity	6,52% increase	22,05% decrease
Alterations in Absorption/Emission Curve Form	Unaltered.	Unaltered.

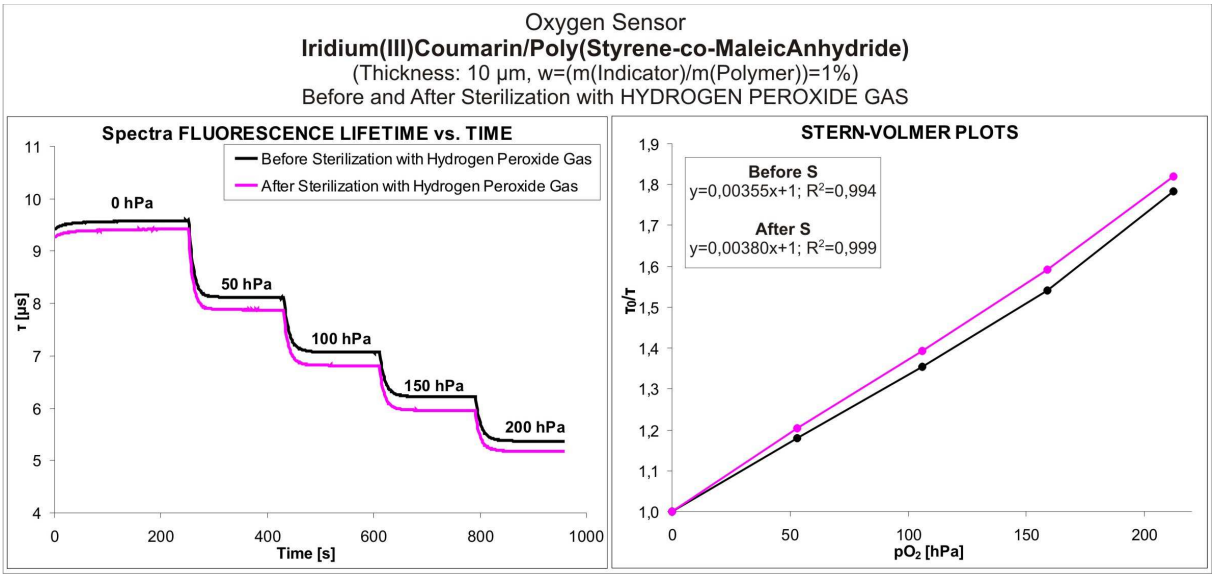

Sterilization with H_2O_2 Gas	Luminescence Lifetime	Stern-Volmer Plot
Alterations in Luminescence Lifetime and Slope	1,67% decrease of τ_0	6,58% increase of slope
	3,45% decrease of τ at 50 hPa	
	4,38% decrease of τ at 100 hPa	
	4,98% decrease of τ at 150 hPa	
	3,54% decrease of τ at 200 hPa	

F.7.2 Sterilization with Low-Temperature Hydrogen Peroxide Plasma

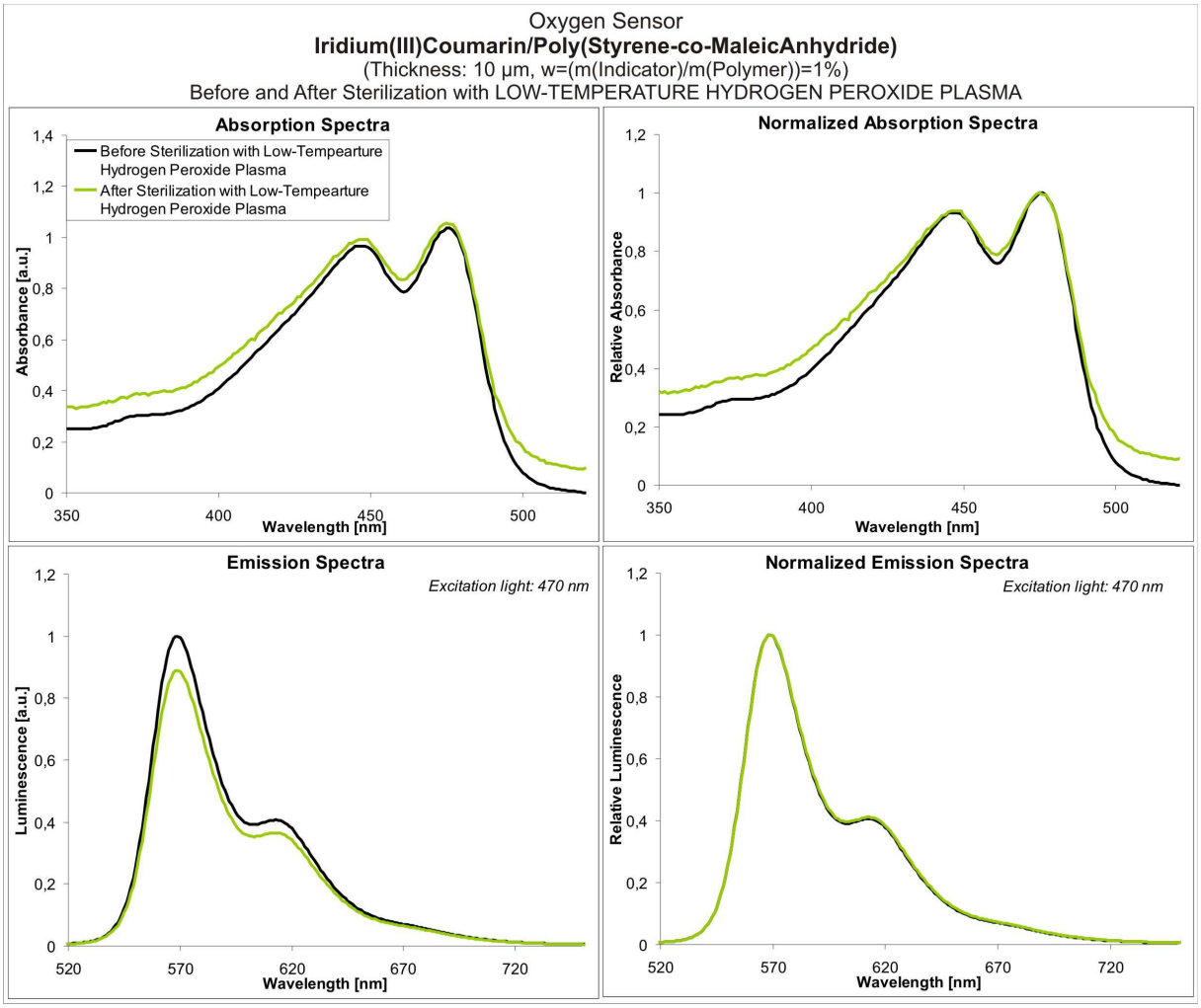

Sterilization with Low-Temperature H_2O_2 Plasma	Absorption Spectra	Emission Spectra
Alterations in Absorption/Emission Intensity	1,83% increase	11,04% decrease
Alterations in Absorption/Emission Curve Form	Altered absorption curve form between 350-430 nm and 490-600 nm.	Unaltered.

Oxygen Sensor
Iridium(III)Coumarin/Poly(Styrene-co-MaleicAnhydride)
(Thickness: 10 µm, w=(m(Indicator)/m(Polymer))=1%)
Before and After Sterilization with LOW-TEMPERATURE HYDROGEN PEROXIDE PLASMA

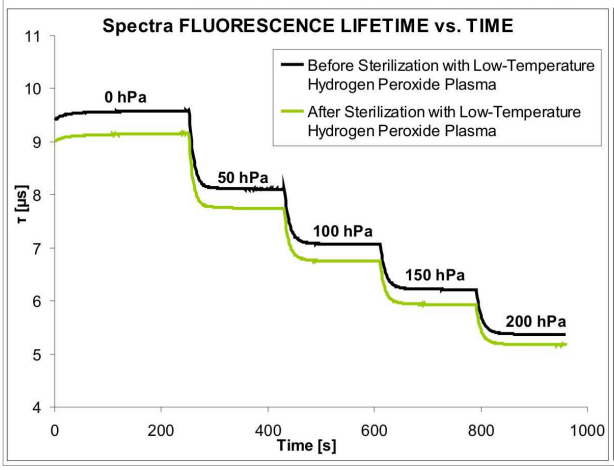

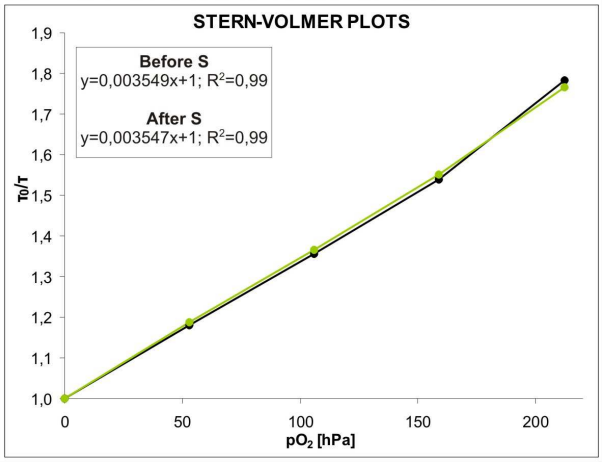

Sterilization with Low-Temperature H_2O_2 Plasma	Luminescence Lifetime	Stern-Volmer Plot
Alterations in Luminescence Lifetime and Slope	4,39% decrease of τ_0	0,056% increase of slope
	5,06% decrease of τ at 50 hPa	
	5,23% decrease of τ at 100 hPa	
	5,15% decrease of τ at 150 hPa	
	3,54% decrease of τ at 200 hPa	

F.8 Platinum(II)Tetrakis(PentaFluorPhenyl)Porphyrin (PtTFPP) immobilized in HydroGel D4/D7

F.8.1 Sterilization with Hydrogen Peroxide Gas

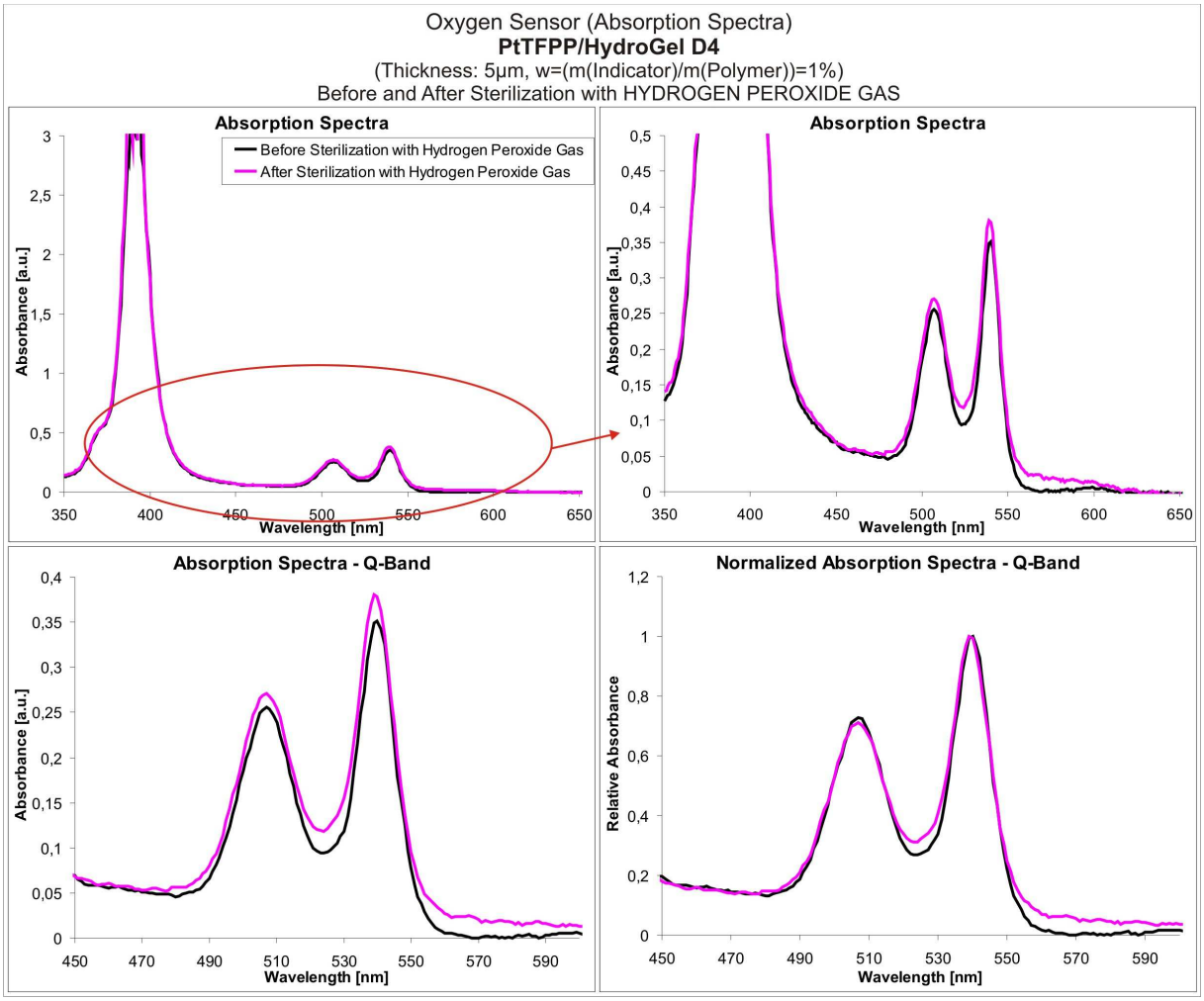

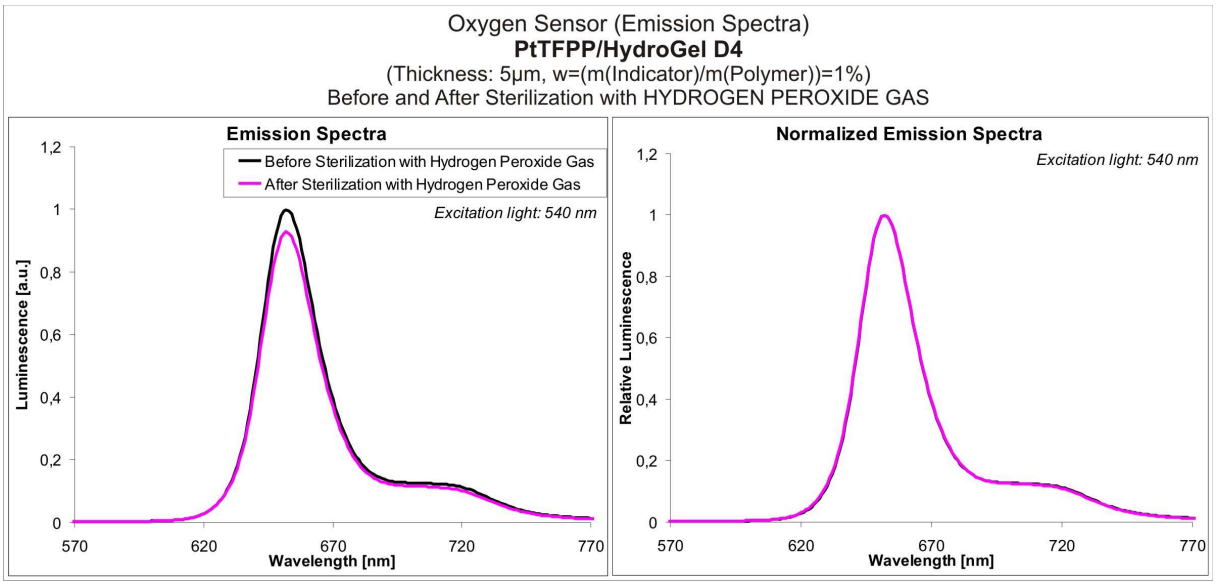

Sterilization with H_2O_2 Gas	Absorption Spectra	Emission Spectra
Alterations in Absorption/Emission Intensity	7,88% increase	7,24% decrease
Alterations in Absorption/Emission Curve Form	Altered absorption curve form between 520-530 nm and 550-800 nm,	Unaltered.

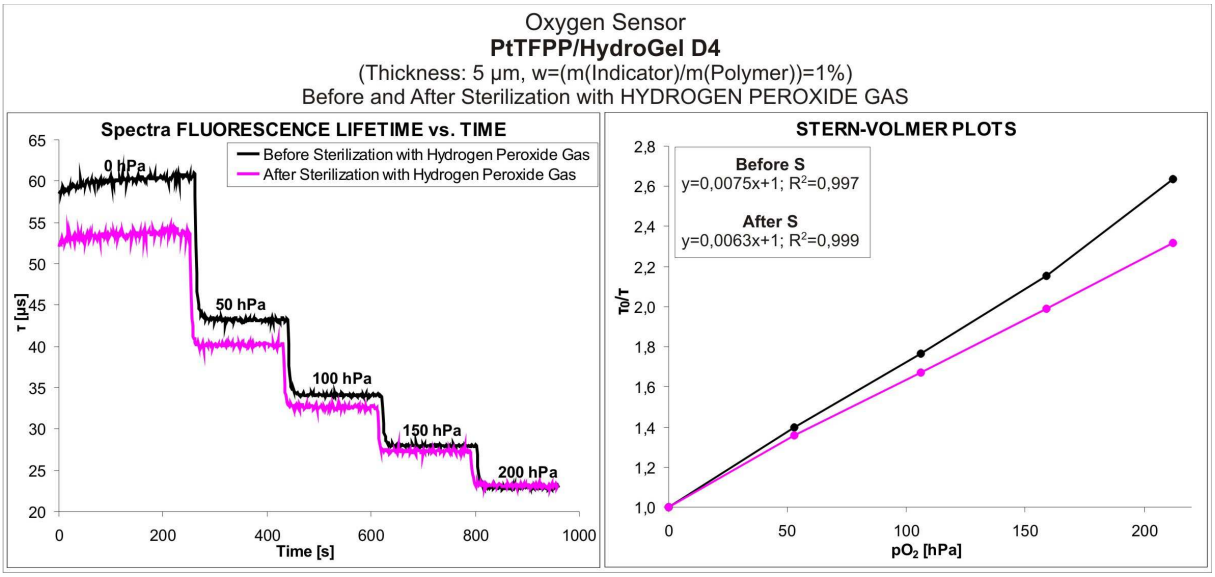

Sterilization with ETHYLENE OXIDE	Luminescence Lifetime	Stern-Volmer Plot
Alterations in Luminescence Lifetime and Slope	10,94% decrease of τ_0	16,00% decrease of slope
	8,33% decrease of τ at 50 hPa	
	5,87% decrease of τ at 100 hPa	
	3,57% decrease of τ at 150 hPa	
	0,86% increase of τ at 200 hPa	

F.8.2 Sterilization with Low-Temperature Hydrogen Peroxide Plasma

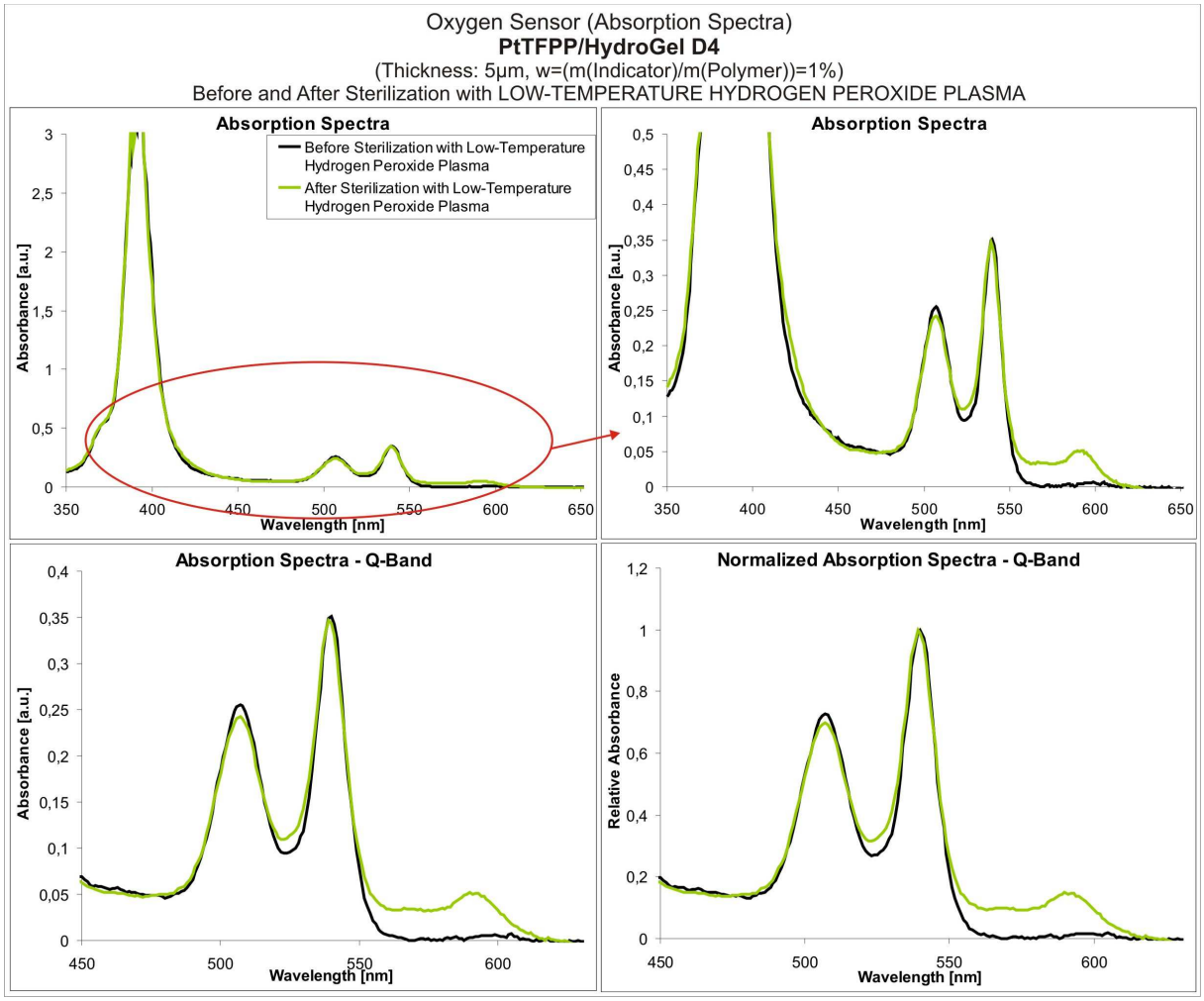

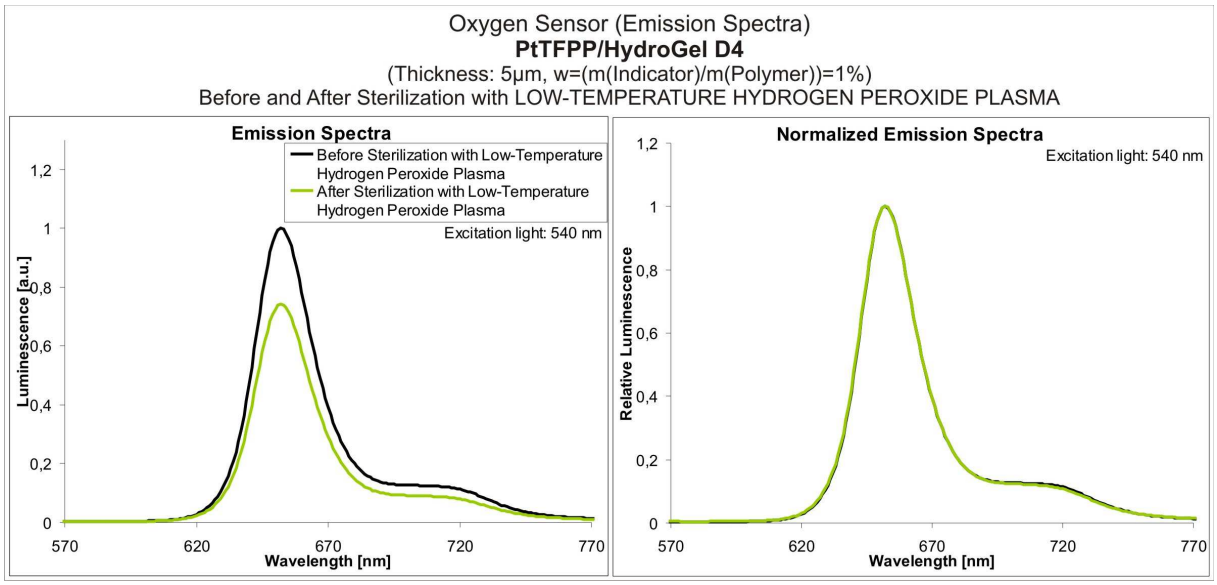

Sterilization with Low-Temperature H_2O_2 Plasma	Absorption Spectra	Emission Spectra
Alterations in Absorption/Emission Intensity	1,10% decrease	24,83% decrease

Alterations in Absorption/Emission Curve Form	Altered absorption curve form between 520-530 nm and 555-620 nm. New absorption peak with λ_{max}=590 nm.	Unaltered.

Oxygen Sensor
PtTFPP/HydroGel D4
(Thickness: 5 µm, w=(m(Indicator)/m(Polymer))=1%)
Before and After Sterilization with LOW-TEMPERATURE HYDROGEN PEROXIDE PLASMA

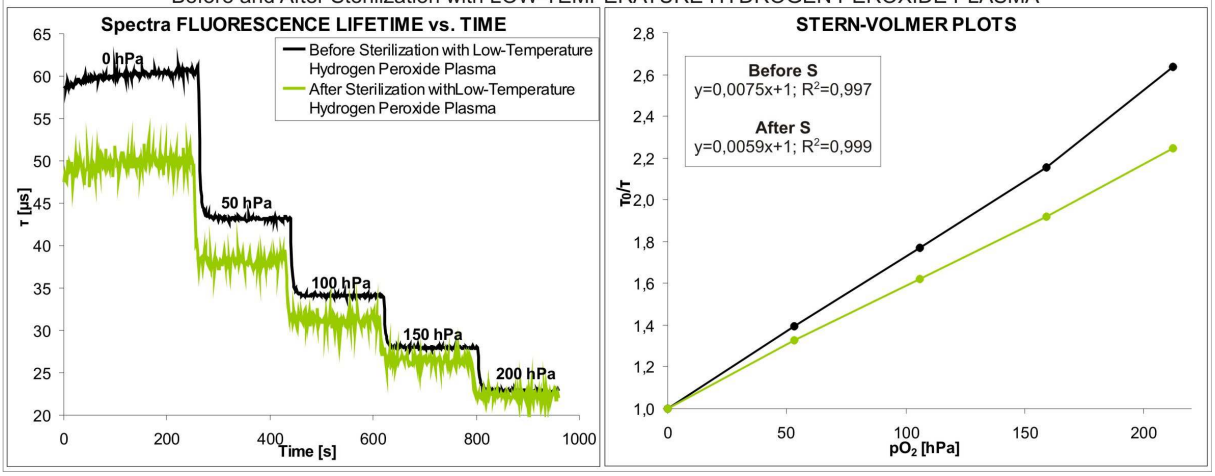

Sterilization with Low-Temperature H_2O_2 Plasma	Luminescence Lifetime	Stern-Volmer Plot
Alterations in Luminescence Lifetime and Slope	17,25% decrease of τ_0	21,33% decrease of slope
	12,96% decrease of τ at 50 hPa	
	9,68% decrease of τ at 100 hPa	
	7,14% decrease of τ at 150 hPa	
	3,06% decrease of τ at 200 hPa	

F.9 Platinum(II)Tetrakis(PentaFluorPhenyl)Porphyrin (PtTFPP) immobilized in HydroThane 5

F.9.1 Sterilization with Hydrogen Peroxide Gas

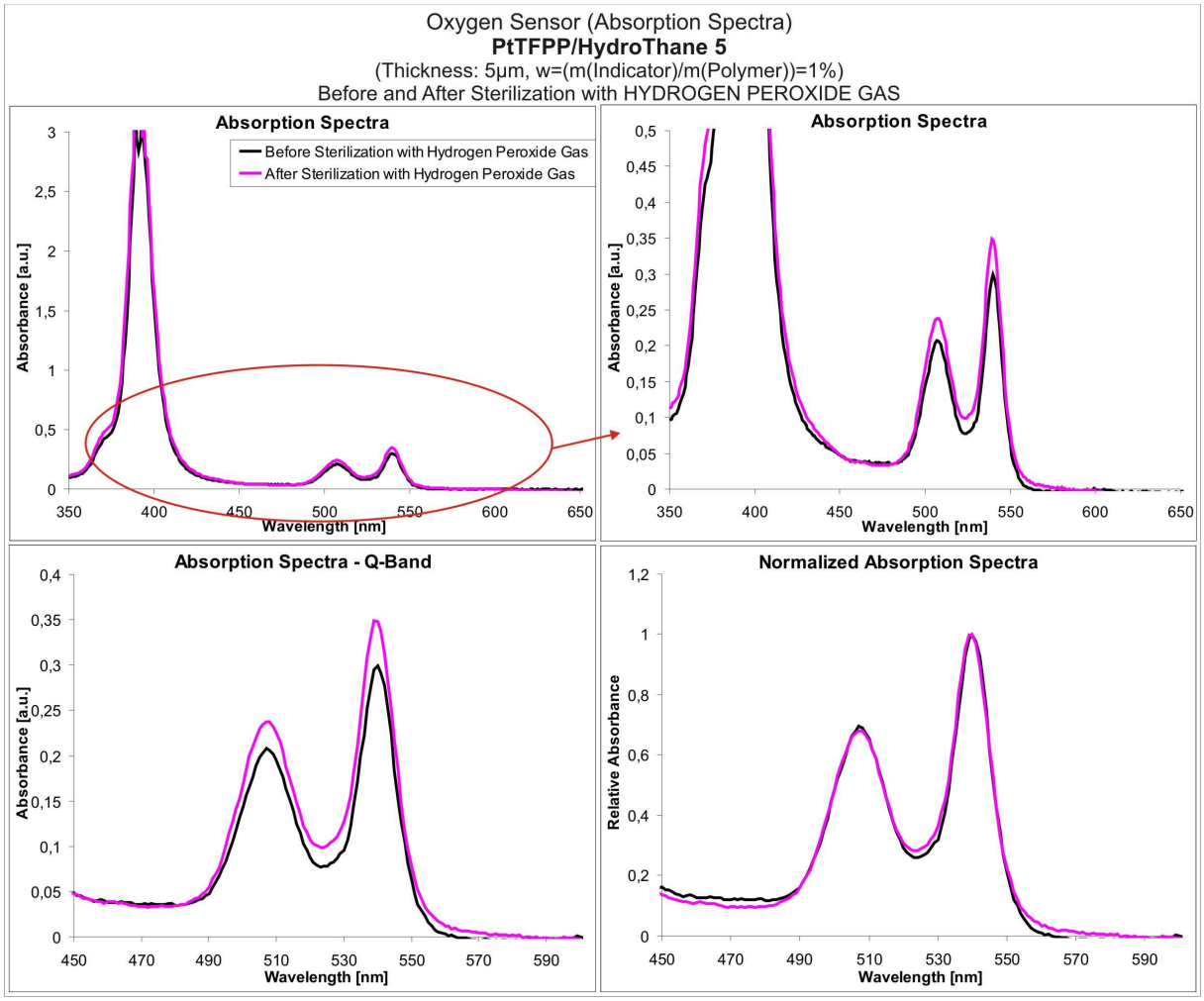

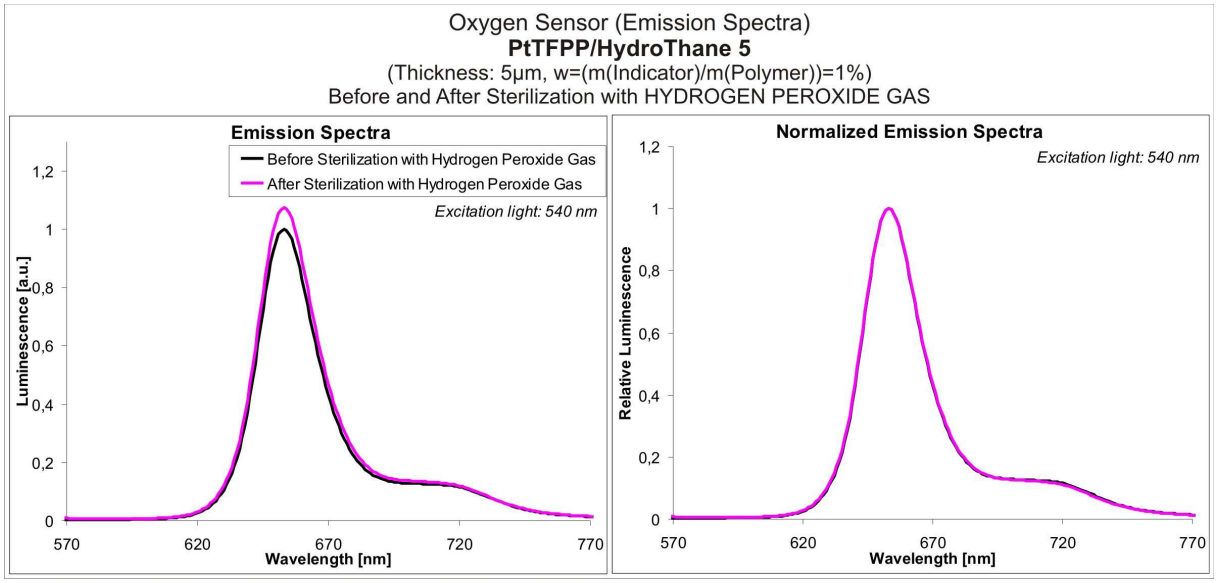

Sterilization with H_2O_2 Gas	Absorption Spectra	Emission Spectra
Alterations in Absorption/Emission Intensity	14,29% decrease	6,88% increase
Alterations in Absorption/Emission Curve Form	Altered absorption curve form between 440-480 nm and 520-530 nm,	Unaltered.

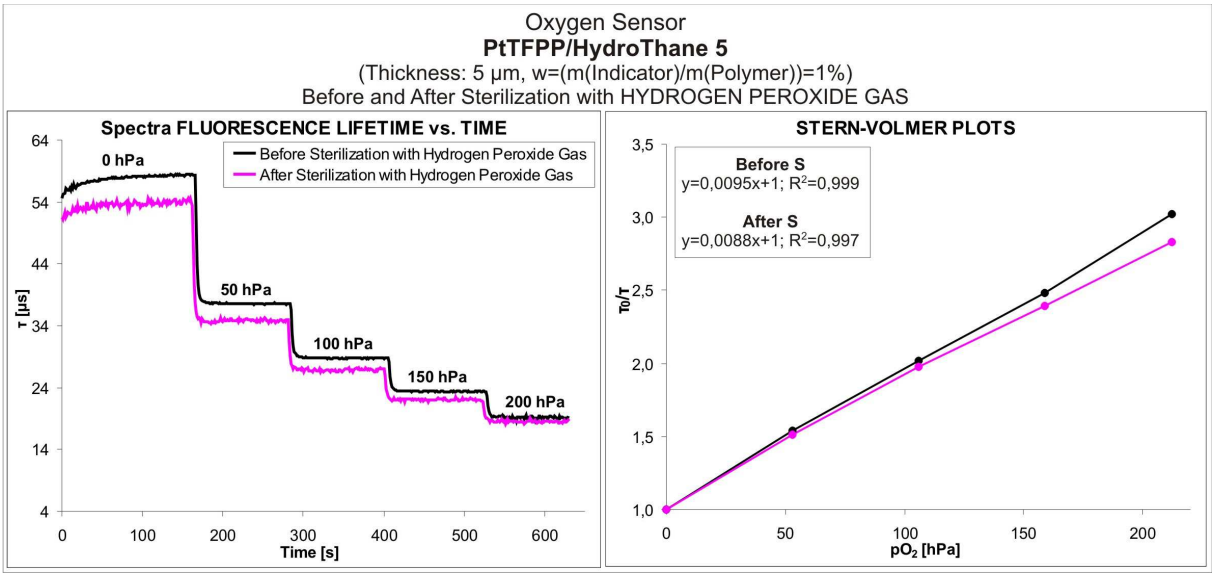

Sterilization with ETHYLENE OXIDE	Luminescence Lifetime	Stern-Volmer Plot
Alterations in Luminescence Lifetime and Slope	9,64% decrease of τ_0	7,37% decrease of slope
	8,10% decrease of τ at 50 hPa	
	7,98% decrease of τ at 100 hPa	
	6,41% decrease of τ at 150 hPa	
	3,65% increase of τ at 200 hPa	

F.9.2 Sterilization with Low-Temperature Hydrogen Peroxide Plasma

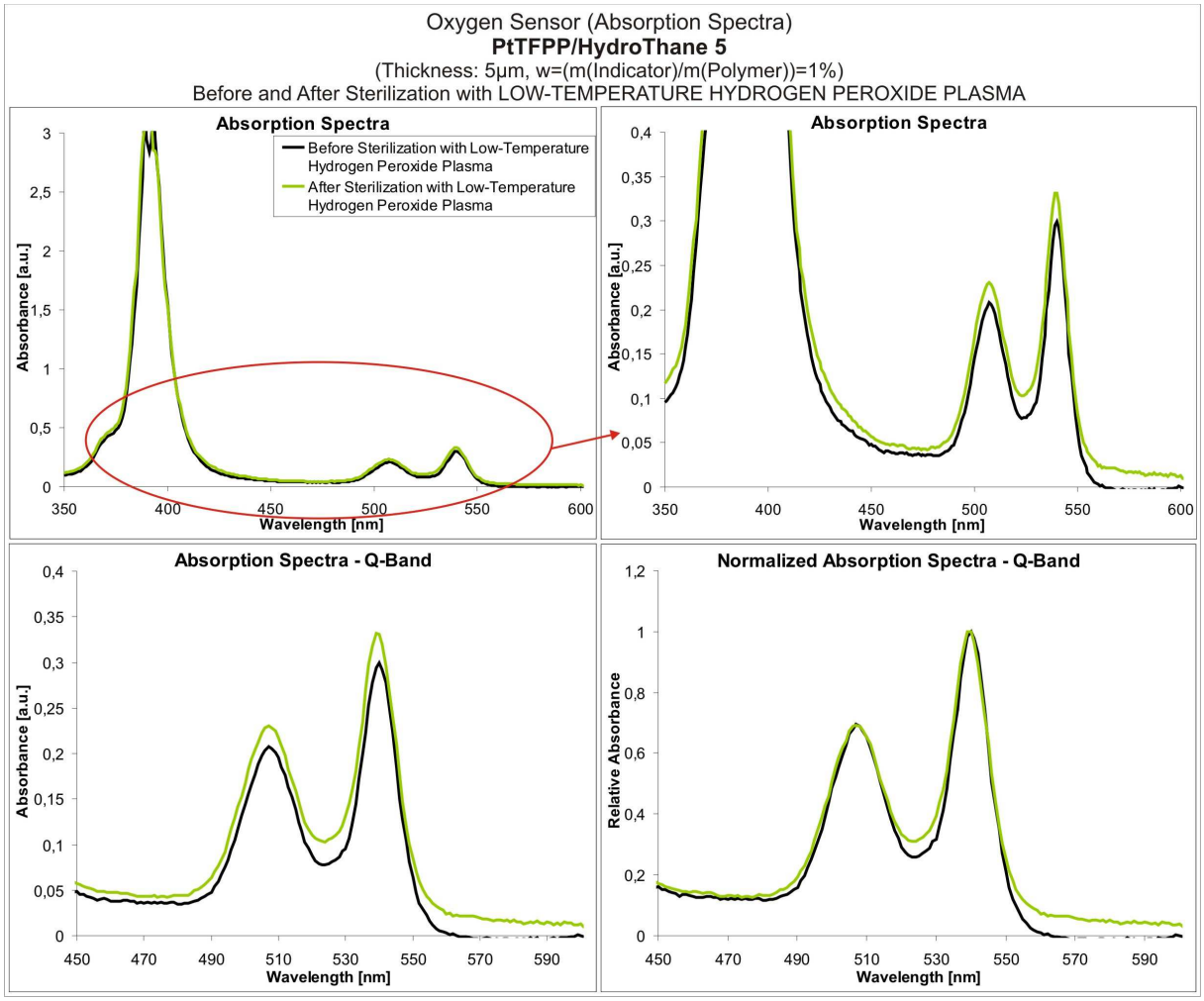

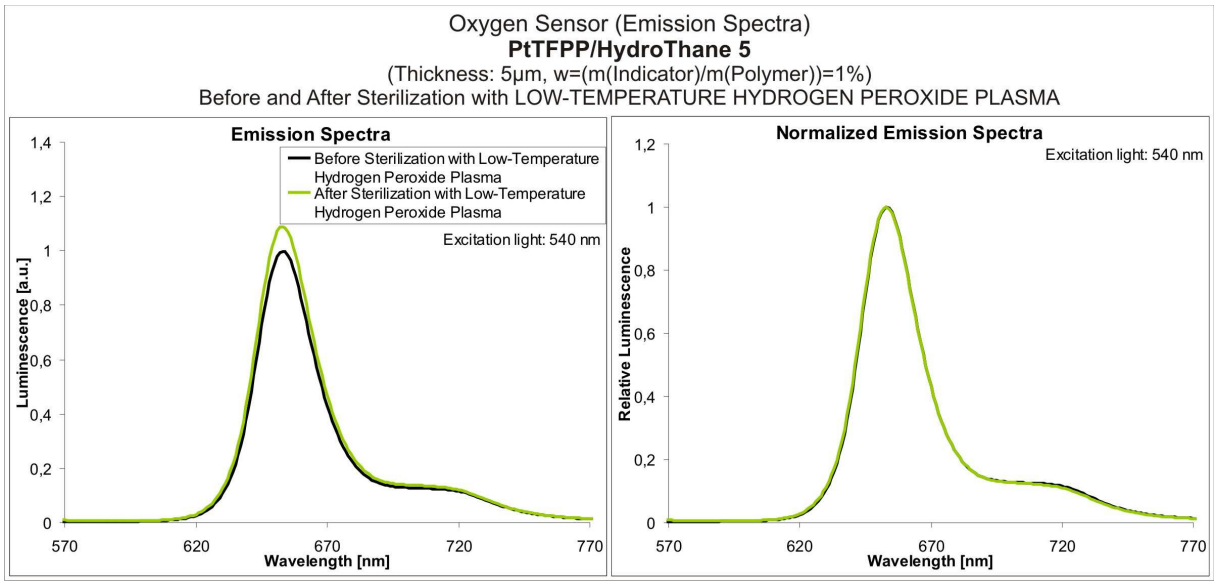

Sterilization with Low-Temperature H_2O_2 Plasma	Absorption Spectra	Emission Spectra
Alterations in Absorption/Emission Intensity	9,85% increase	8,33% increase

Alterations in Absorption/Emission Curve Form	Altered absorption curve form between 520-530 nm and 555-800 nm.	Unaltered.

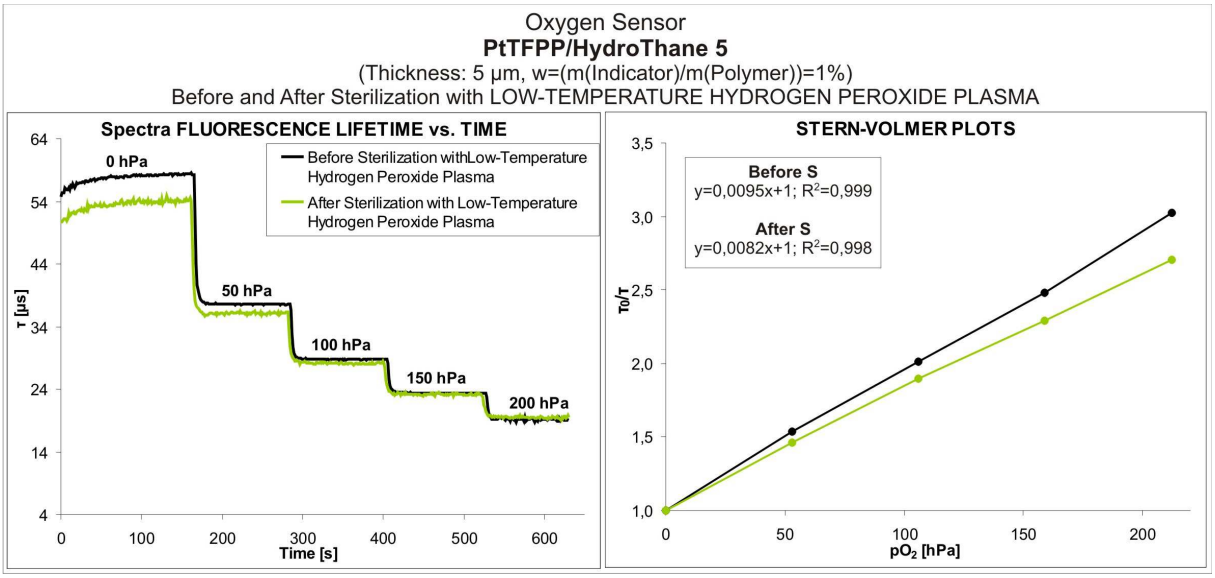

Sterilization with Low-Temperature H_2O_2 Plasma	Luminescence Lifetime	Stern-Volmer Plot
Alterations in Luminescence Lifetime and Slope	9,12% decrease of τ_0	13,68% decrease of slope
	4,43% decrease of τ at 50 hPa	
	3,47% decrease of τ at 100 hPa	
	1,58% decrease of τ at 150 hPa	
	1,54% increase of τ at 200 hPa	

F.10 Platinum(II)Tetrakis(PentaFluorPhenyl)Porphyrin (PtTFPP) immobilized in PolySulfone

F.10.1 Sterilization with Hydrogen Peroxide Gas

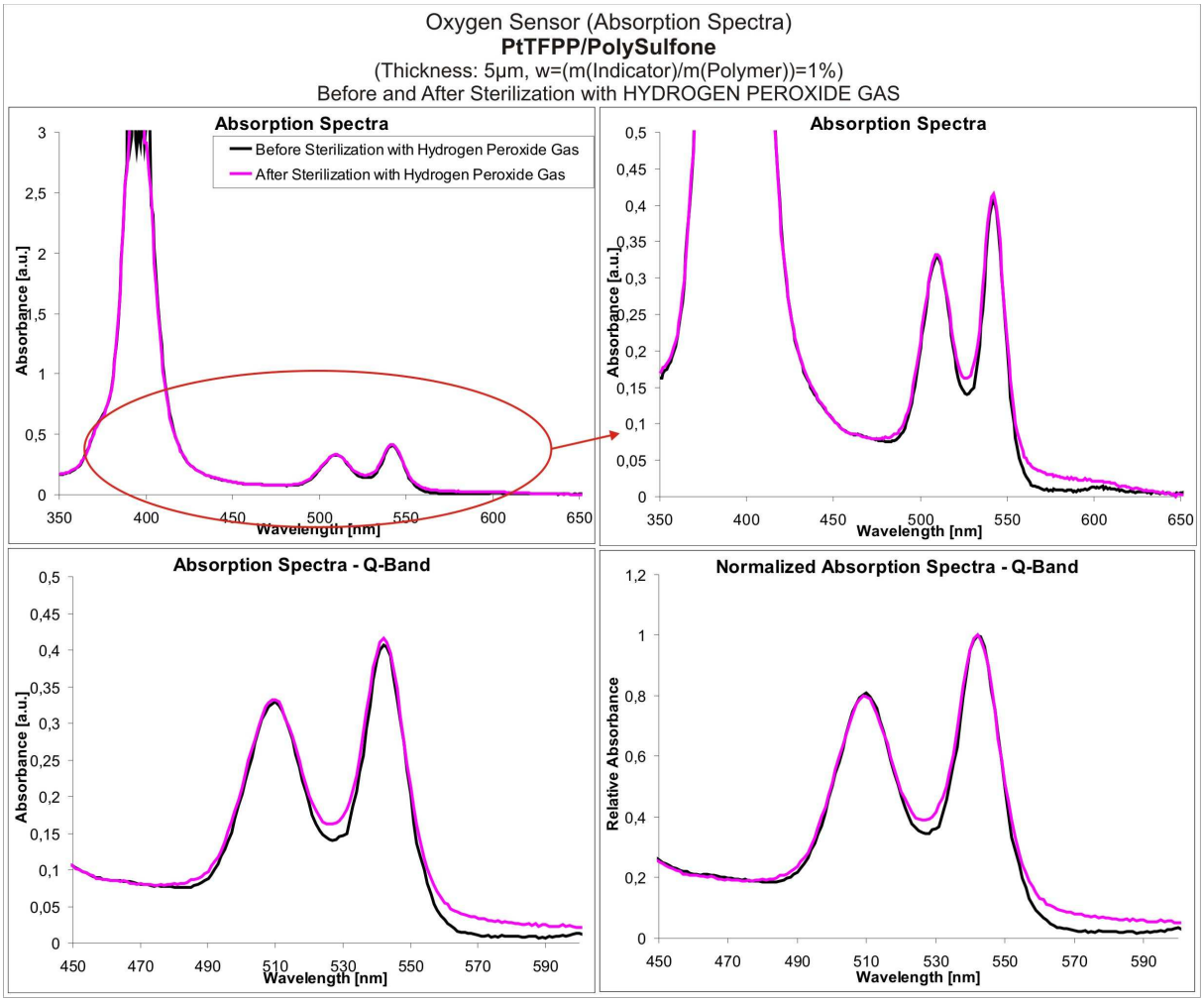

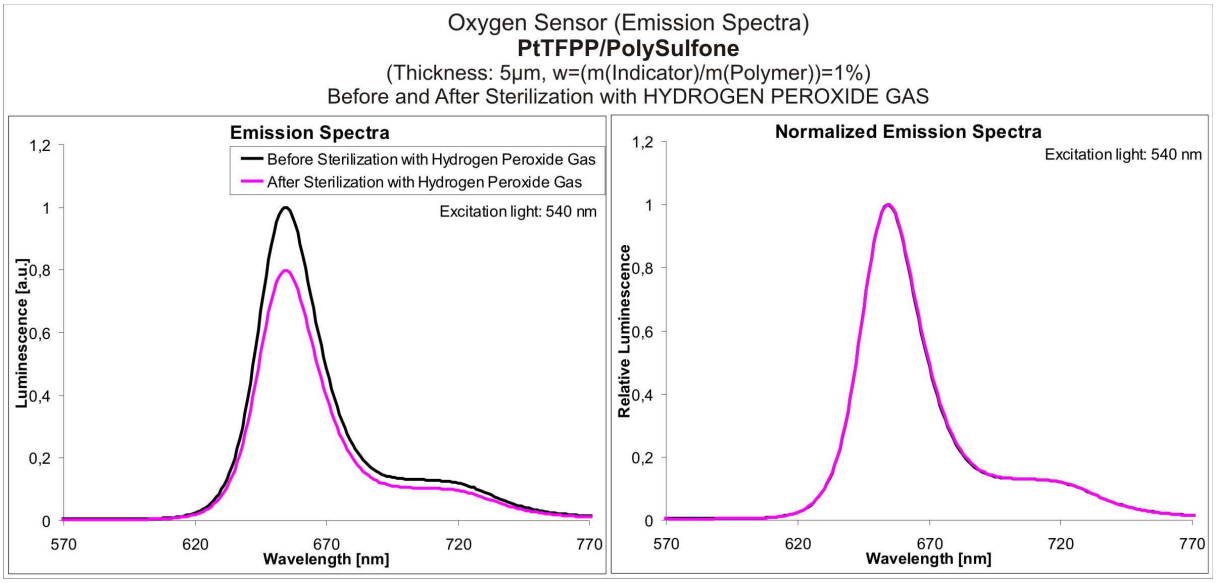

Sterilization with H_2O_2 Gas	Absorption Spectra	Emission Spectra
Alterations in Absorption/Emission Intensity	2,25% increase	20,09% decrease
Alterations in Absorption/Emission Curve Form	Altered absorption curve form between 520-530 nm and 555-800 nm,	Unaltered.

Oxygen Sensor
PtTFPP/PolySulfone
(Thickness: 5 µm, w=(m(Indicator)/m(Polymer))=1%)
Before and After Sterilization with HYDROGEN PEROXIDE GAS

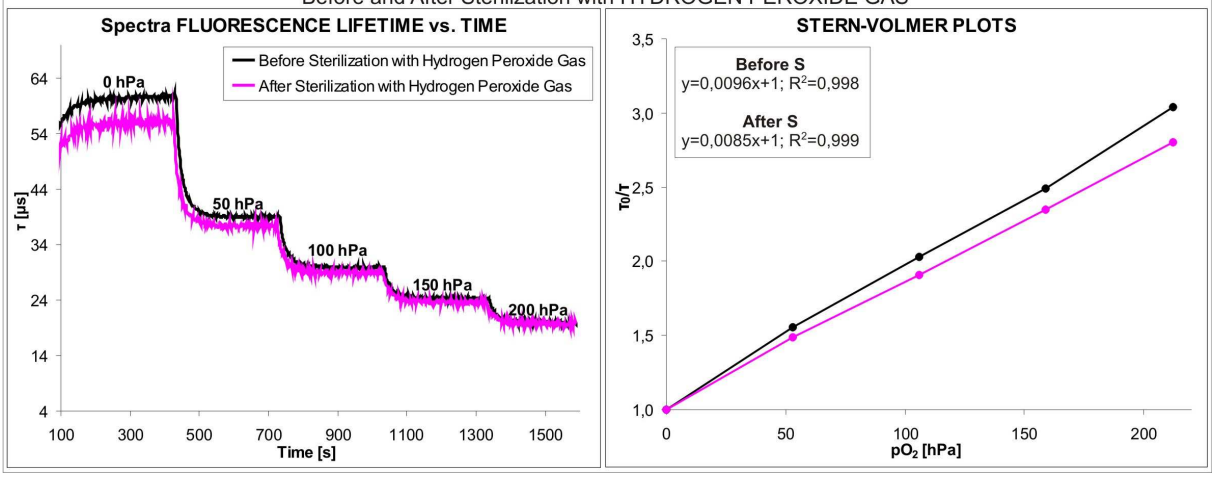

Sterilization with H_2O_2 Gas	Luminescence Lifetime	Stern-Volmer Plot
Alterations in Luminescence Lifetime and Slope	8,74% decrease of τ_0	11,46% decrease of slope
	4,54% decrease of τ at 50 hPa	
	3,01% decrease of τ at 100 hPa	
	3,21% decrease of τ at 150 hPa	
	0,50% decrease of τ at 200 hPa	

F.10.2 Sterilization with Low-Temperature Hydrogen Peroxide Plasma

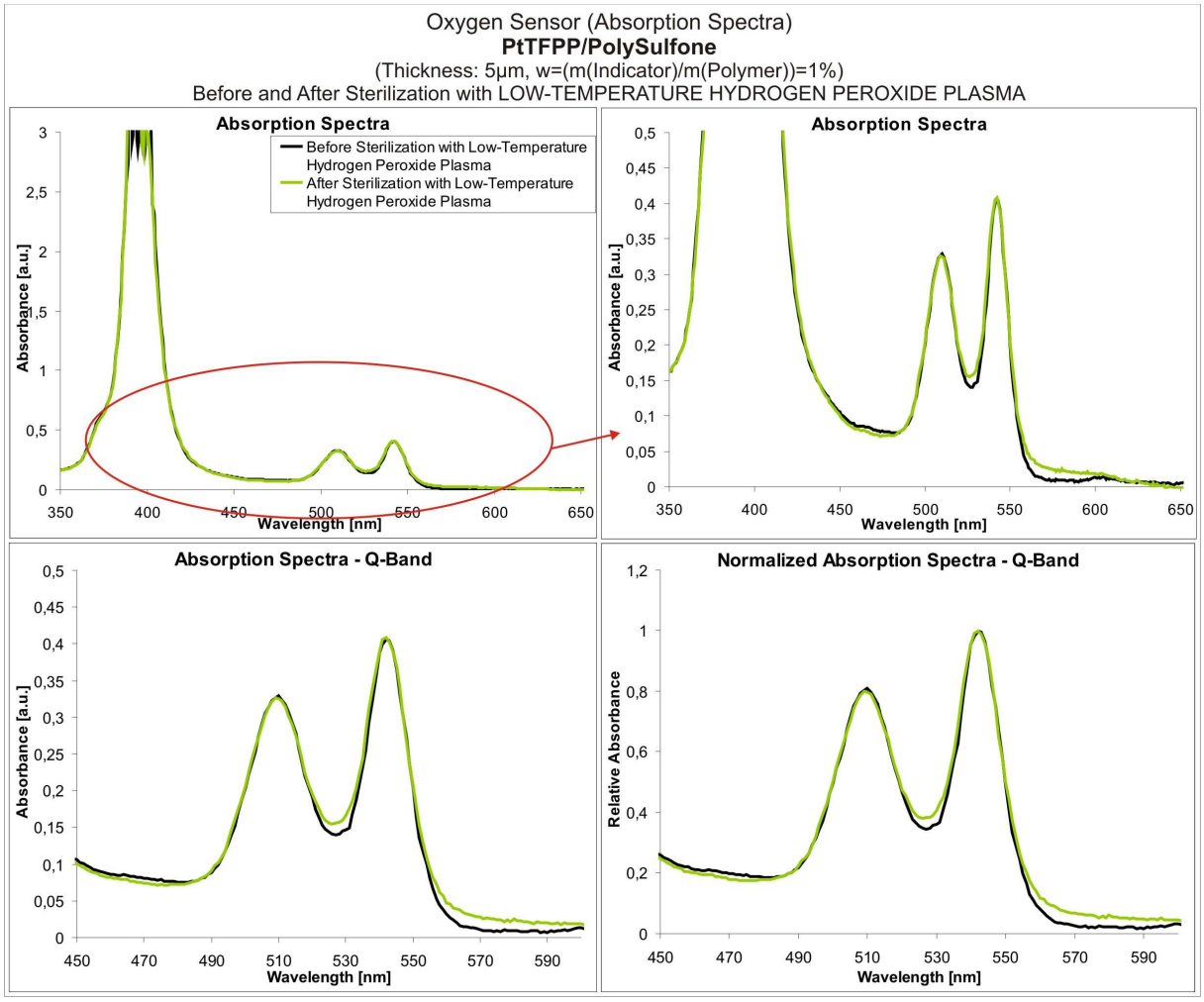

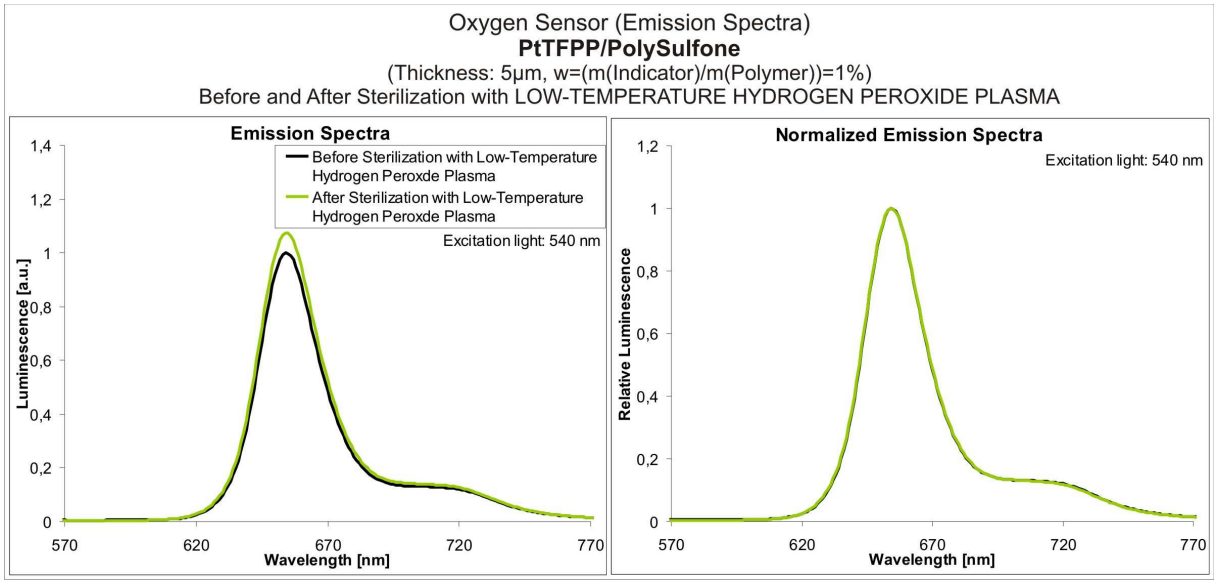

Sterilization with Low-Temperature H_2O_2 Plasma	Absorption Spectra	Emission Spectra
Alterations in Absorption/Emission Intensity	0,41% increase	6,89% increase

Alterations in Absorption/Emission Curve Form	Altered absorption curve form between 520-530 nm and 555-600 nm.	Unaltered.

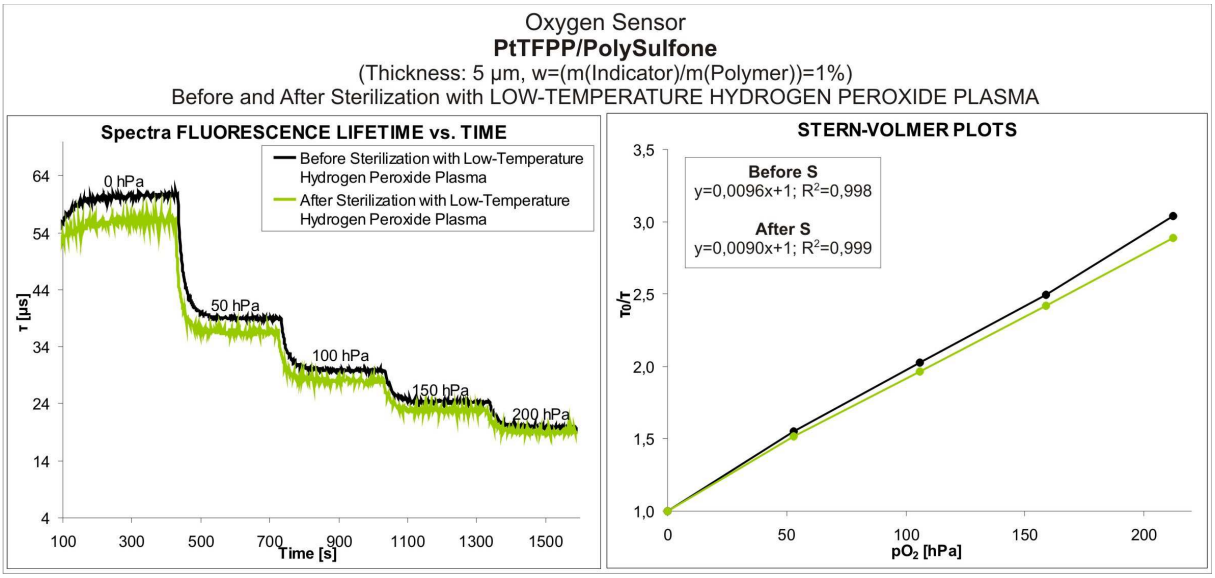

Sterilization with Low-Temperature H_2O_2 Plasma	Luminescence Lifetime	Stern-Volmer Plot
Alterations in Luminescence Lifetime and Slope	8,91% decrease of τ_0	6,46% decrease of slope
	6,66% decrease of τ at 50 hPa	
	6,02% decrease of τ at 100 hPa	
	6,12% decrease of τ at 150 hPa	
	4,02% decrease of τ at 200 hPa	

F.11 Platinum(II)Tetrakis(PentaFluorPhenyl)Porphyrin (PtTFPP) immobilized in PolyPhenylSilses Quioxane

F.11.1 Sterilization with Hydrogen Peroxide Gas

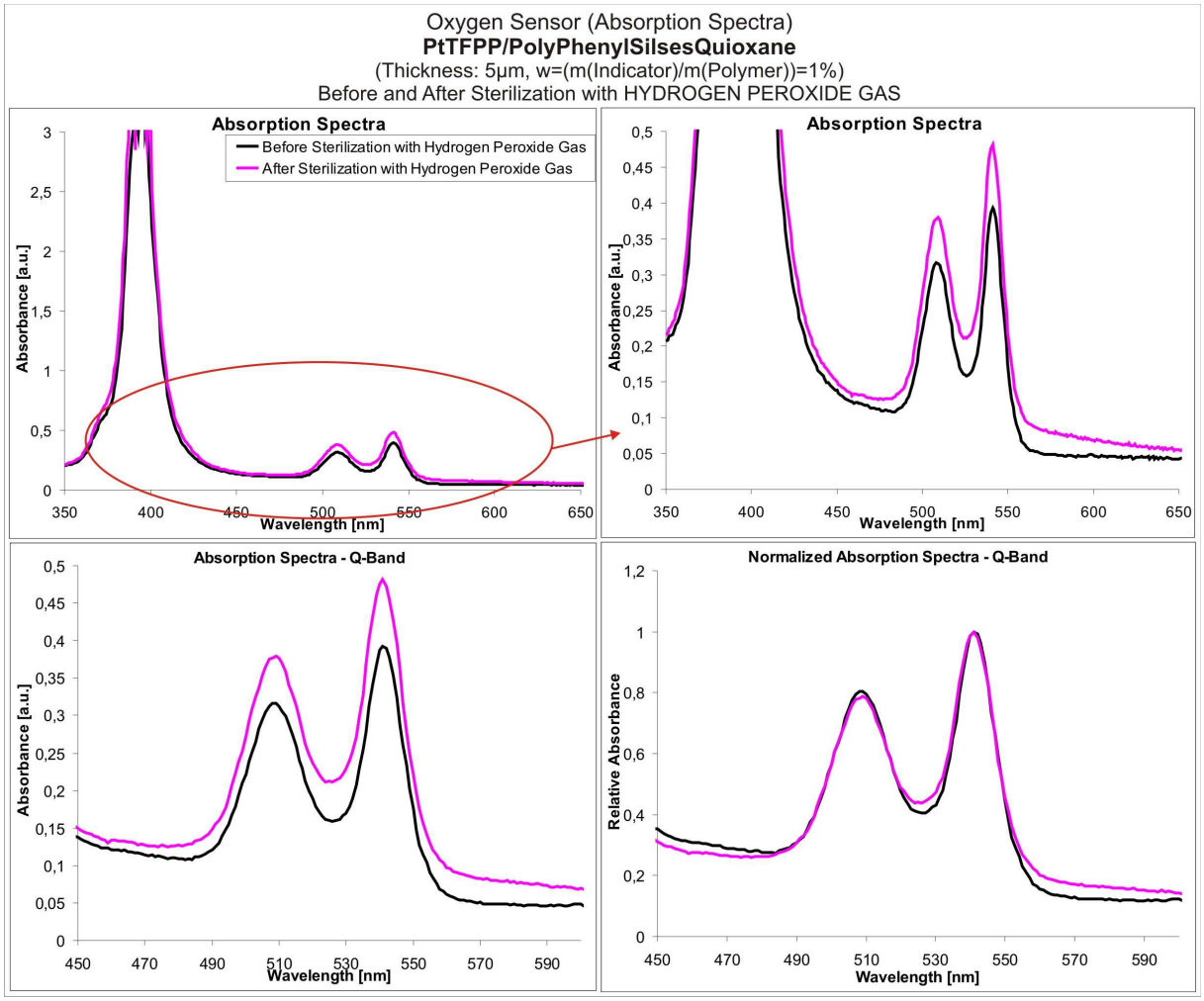

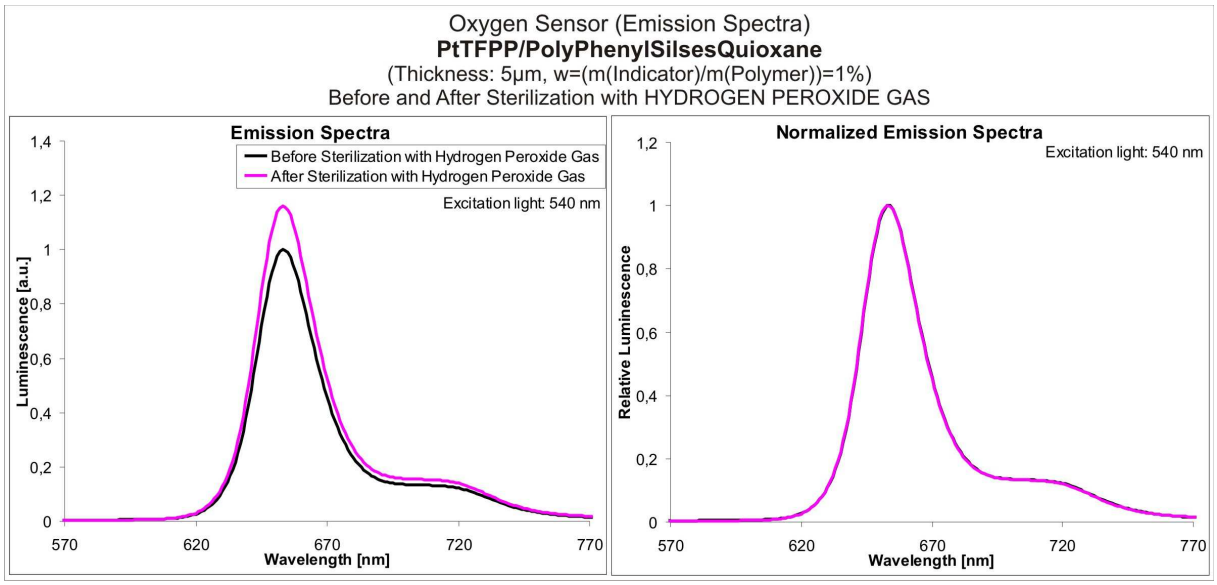

Sterilization with H_2O_2 Gas	Absorption Spectra	Emission Spectra
Alterations in Absorption/Emission Intensity	18,47% increase	13,79% decrease
Alterations in Absorption/Emission Curve Form	Altered absorption curve form between 350-360 nm, 430-480 nm, 520-530 nm and 555-800 nm,	Unaltered.

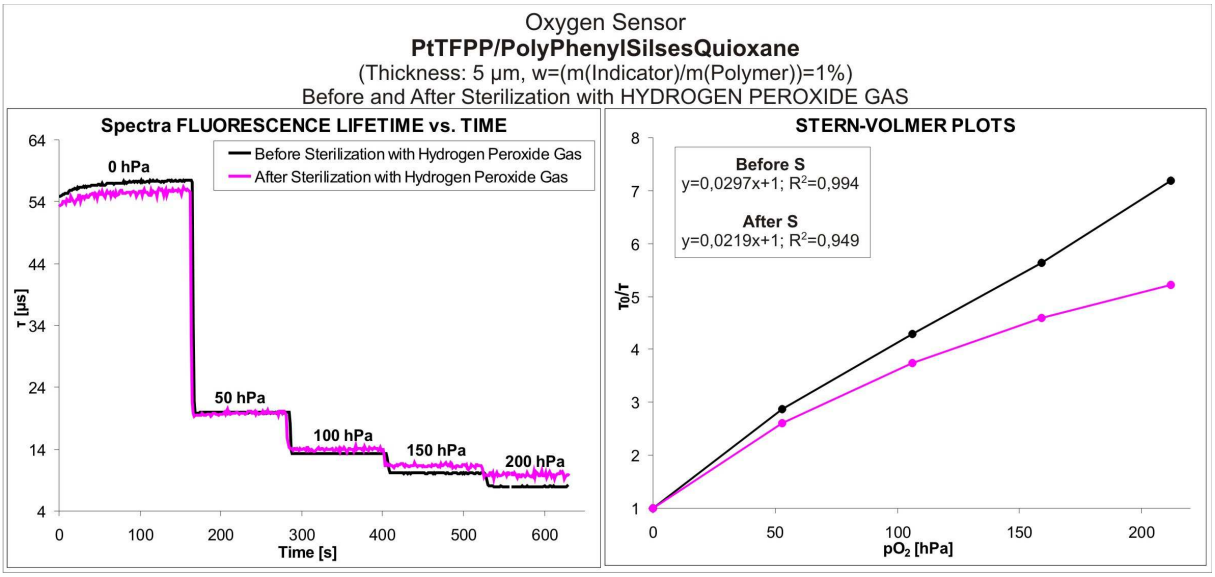

Sterilization with H_2O_2 Gas	Luminescence Lifetime	Stern-Volmer Plot
Alterations in Luminescence Lifetime and Slope	9,96% decrease of τ_0	26,26% decrease of slope
	0,95% decrease of τ at 50 hPa	
	3,62% increase of τ at 100 hPa	
	9,71% increase of τ at 150 hPa	
	19,42% increase of τ at 200 hPa	

F.11.2 Sterilization with Low-Temperature Hydrogen Peroxide Plasma

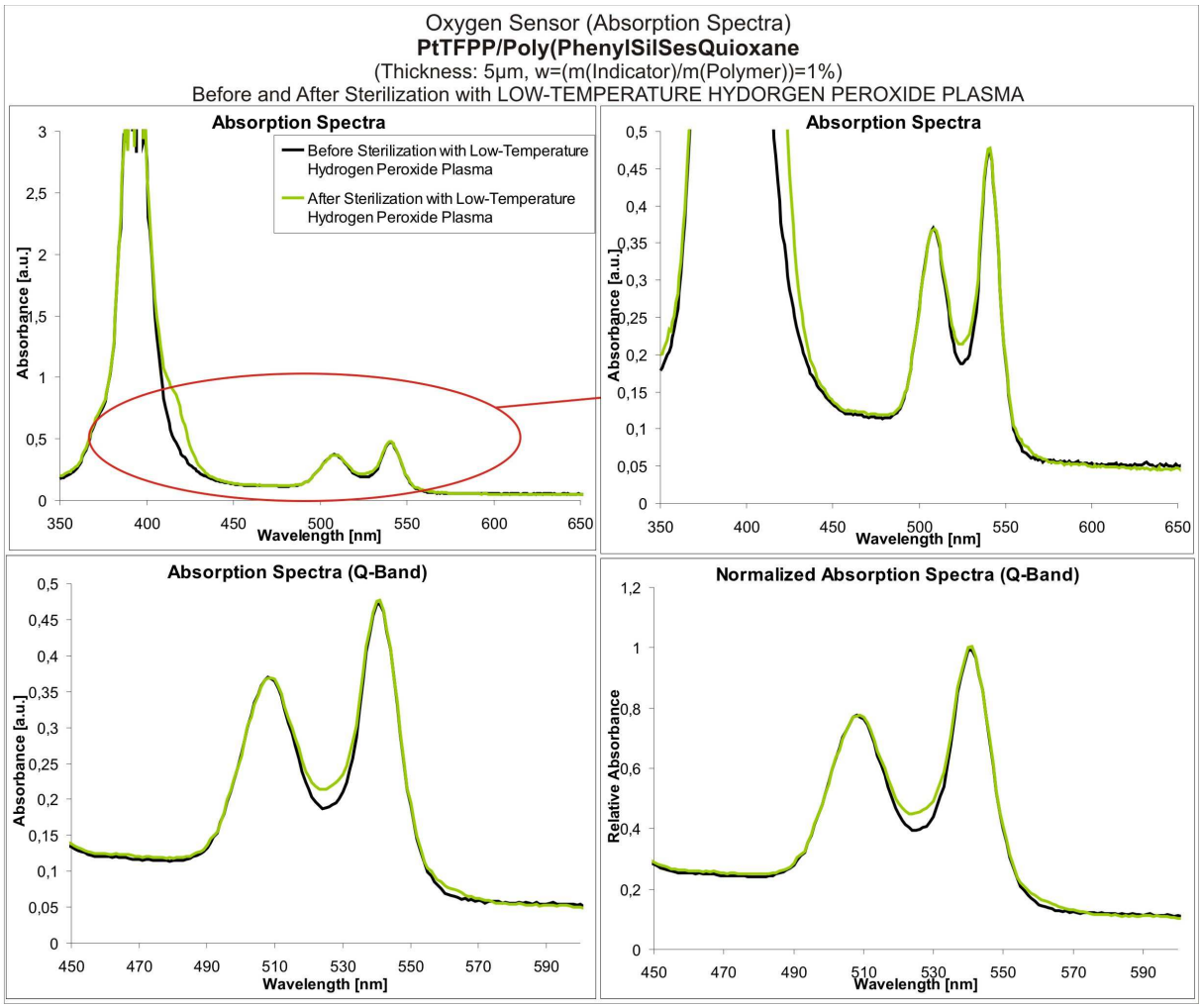

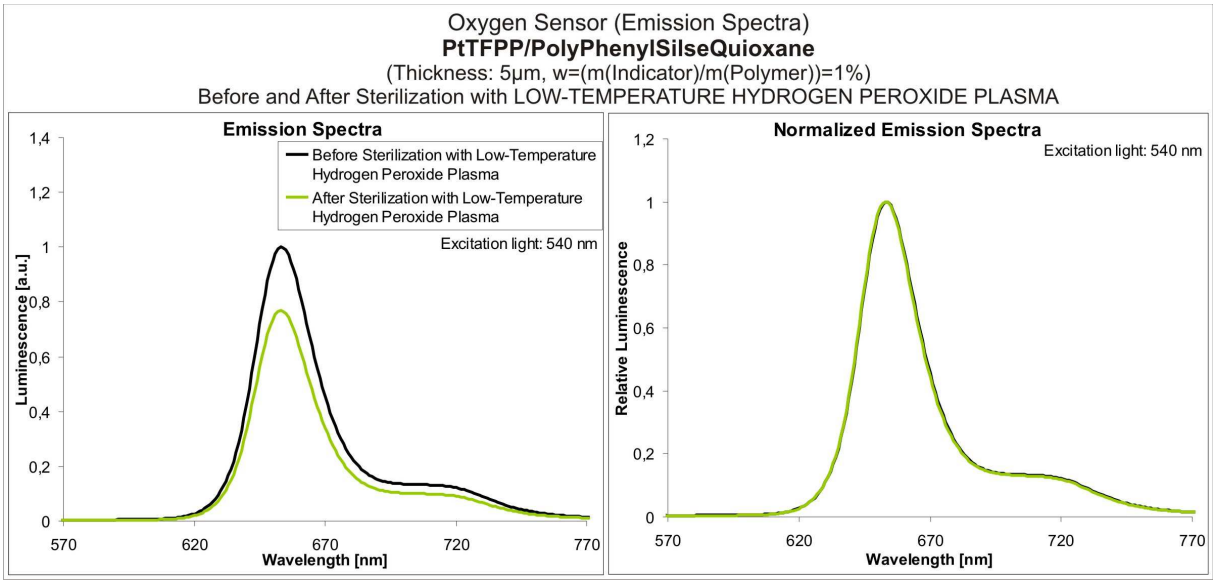

Sterilization with Low-Temperature H_2O_2 Plasma	Absorption Spectra	Emission Spectra
Alterations in Absorption/Emission Intensity	0,58% decrease	23,20% decrease

Alterations in Absorption/Emission Curve Form	Altered absorption curve form between 410-440 nm and 520-530 nm.	Unaltered.

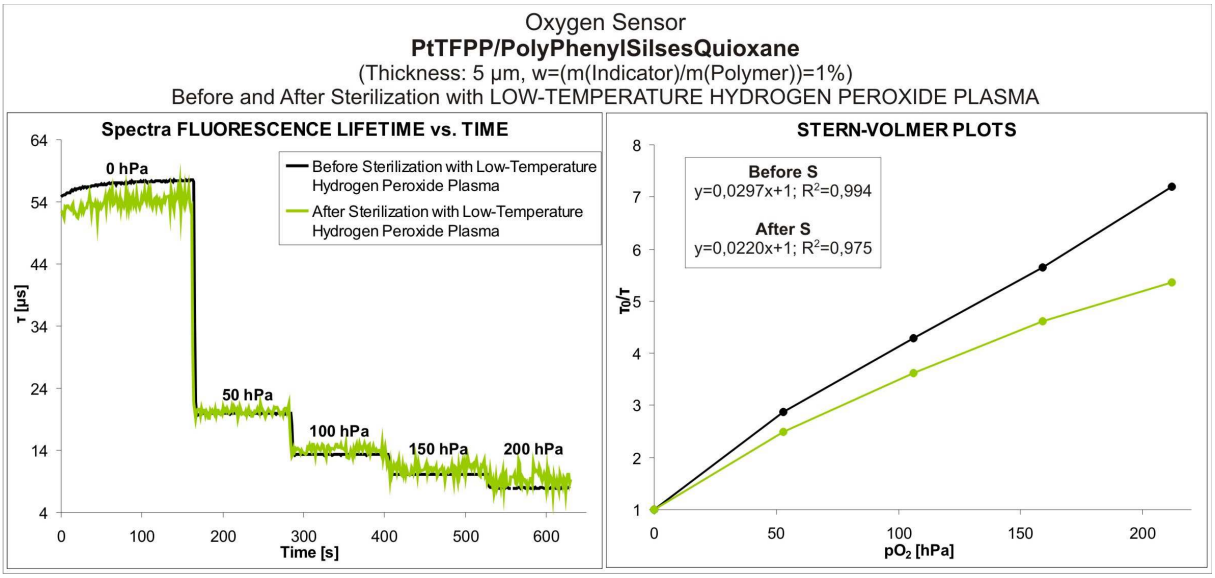

Sterilization with Low-Temperature H_2O_2 Plasma	Luminescence Lifetime	Stern-Volmer Plot
Alterations in Luminescence Lifetime and Slope	11,71% decrease of τ_0	25,92% decrease of slope
	1,34% increase of τ at 50 hPa	
	4,32% increase of τ at 100 hPa	
	7,40% increase of τ at 150 hPa	
	15,61% increase of τ at 200 hPa	

F.12 Platinum(II)Tetrakis(PentaFluorPhenyl)Porphyrin (PtTFPP) immobilized in PolyStyrene

F.12.1 Sterilization with Hydrogen Peroxide Gas

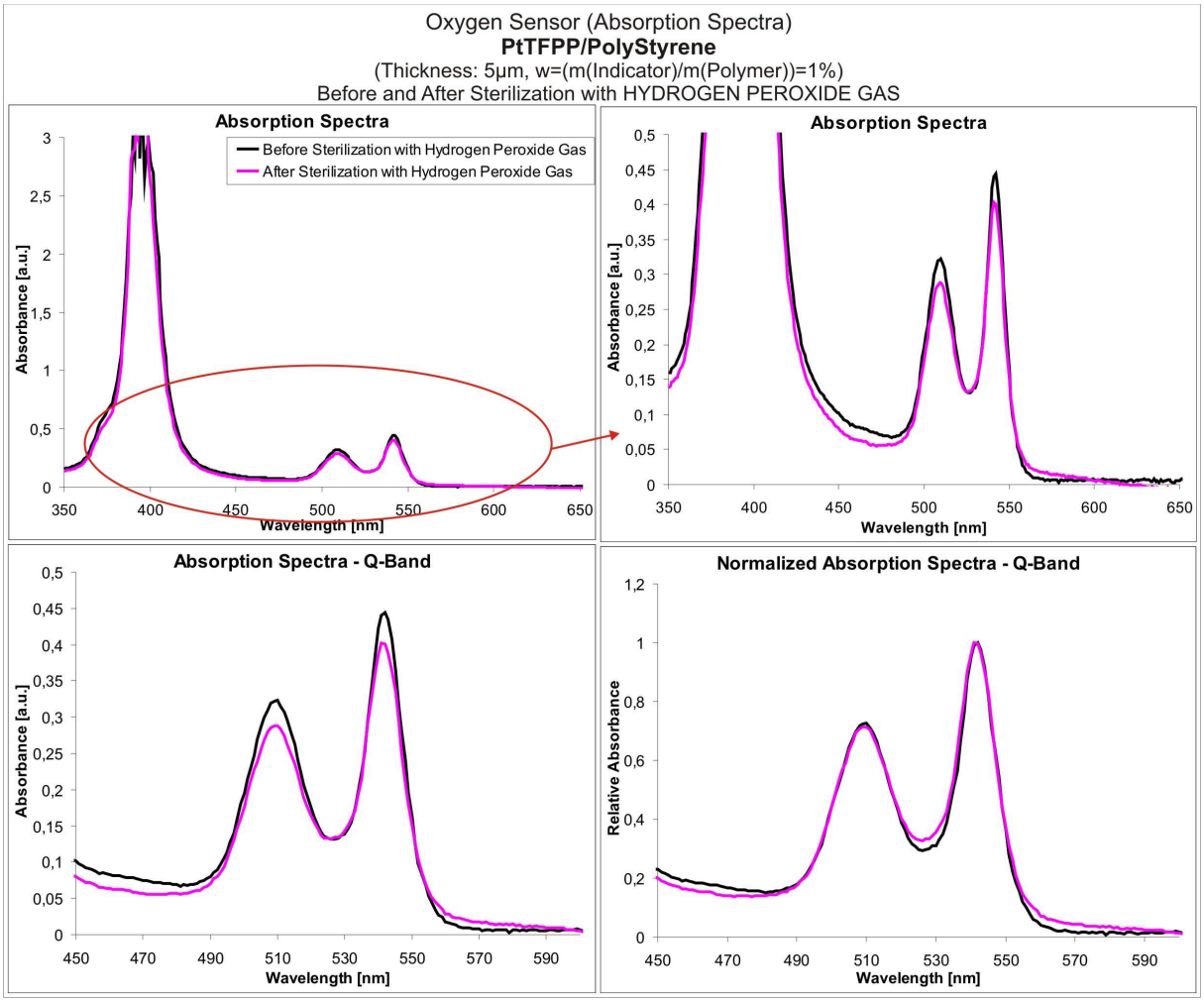

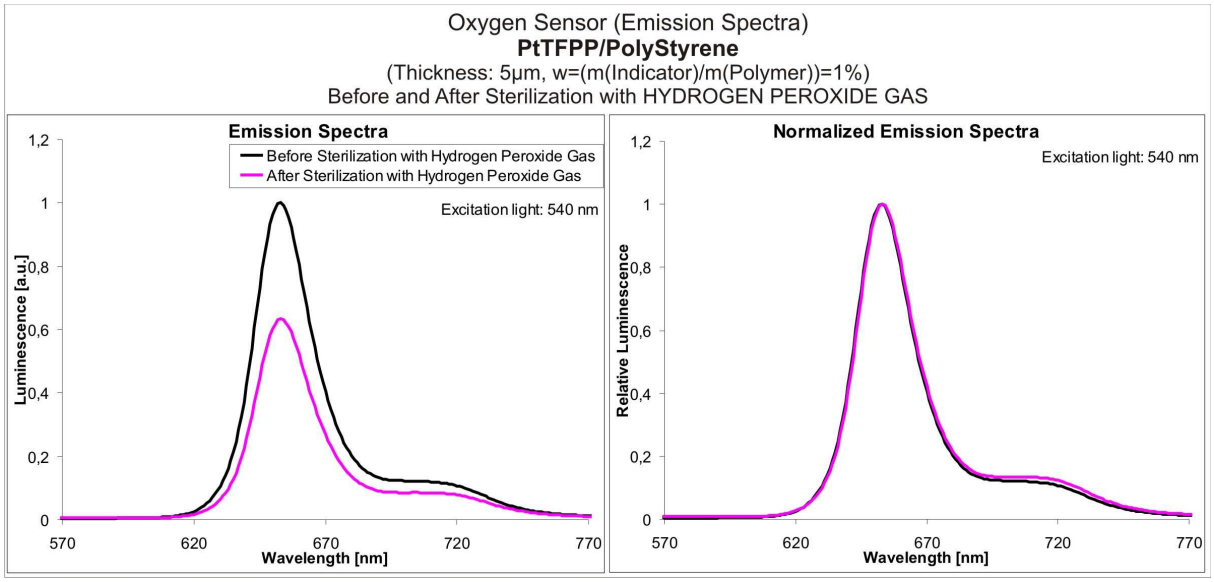

Sterilization with H_2O_2 Gas	Absorption Spectra	Emission Spectra
Alterations in Absorption/Emission Intensity	9,44% decrease	36,63% decrease
Alterations in Absorption/Emission Curve Form	Altered absorption curve form between 350-360 nm, 430-480 nm, 520-530 nm and 555-590 nm,	Unaltered.

Oxygen Sensor
PtTFPP/PolyStyrene
(Thickness: 5 µm, w=(m(Indicator)/m(Polymer))=1%)
Before and After Sterilization with HYDROGEN PEROXIDE GAS

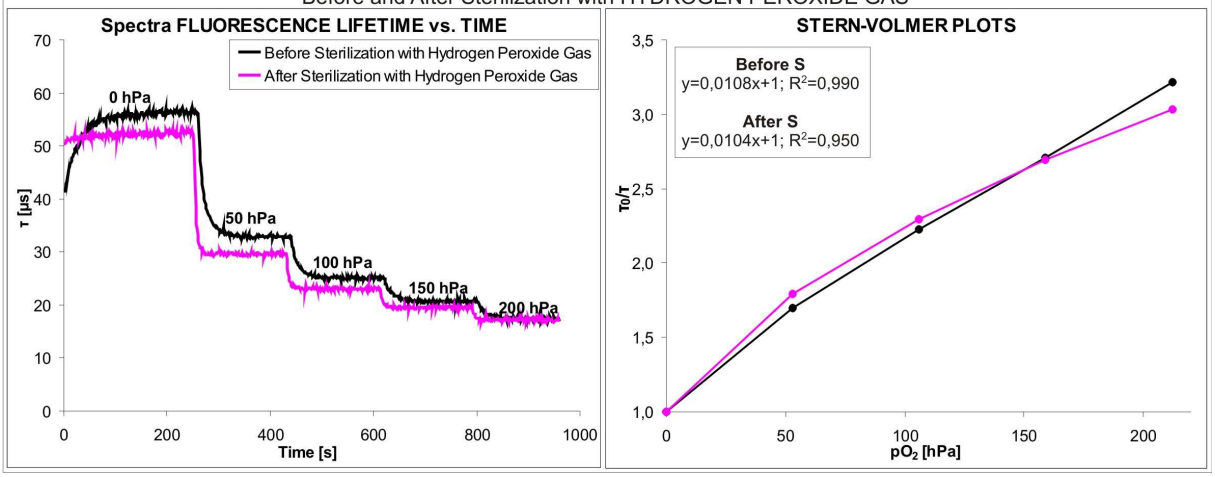

Sterilization with H_2O_2 Gas	Luminescence Lifetime	Stern-Volmer Plot
Alterations in Luminescence Lifetime and Slope	6,61% decrease of τ_0	3,70% decrease of slope
	11,25% decrease of τ at 50 hPa	
	9,16% decrease of τ at 100 hPa	
	6,28% decrease of τ at 150 hPa	
	1,15% decrease of τ at 200 hPa	

F.12.2 Sterilization with Low-Temperature Hydrogen Peroxide Plasma

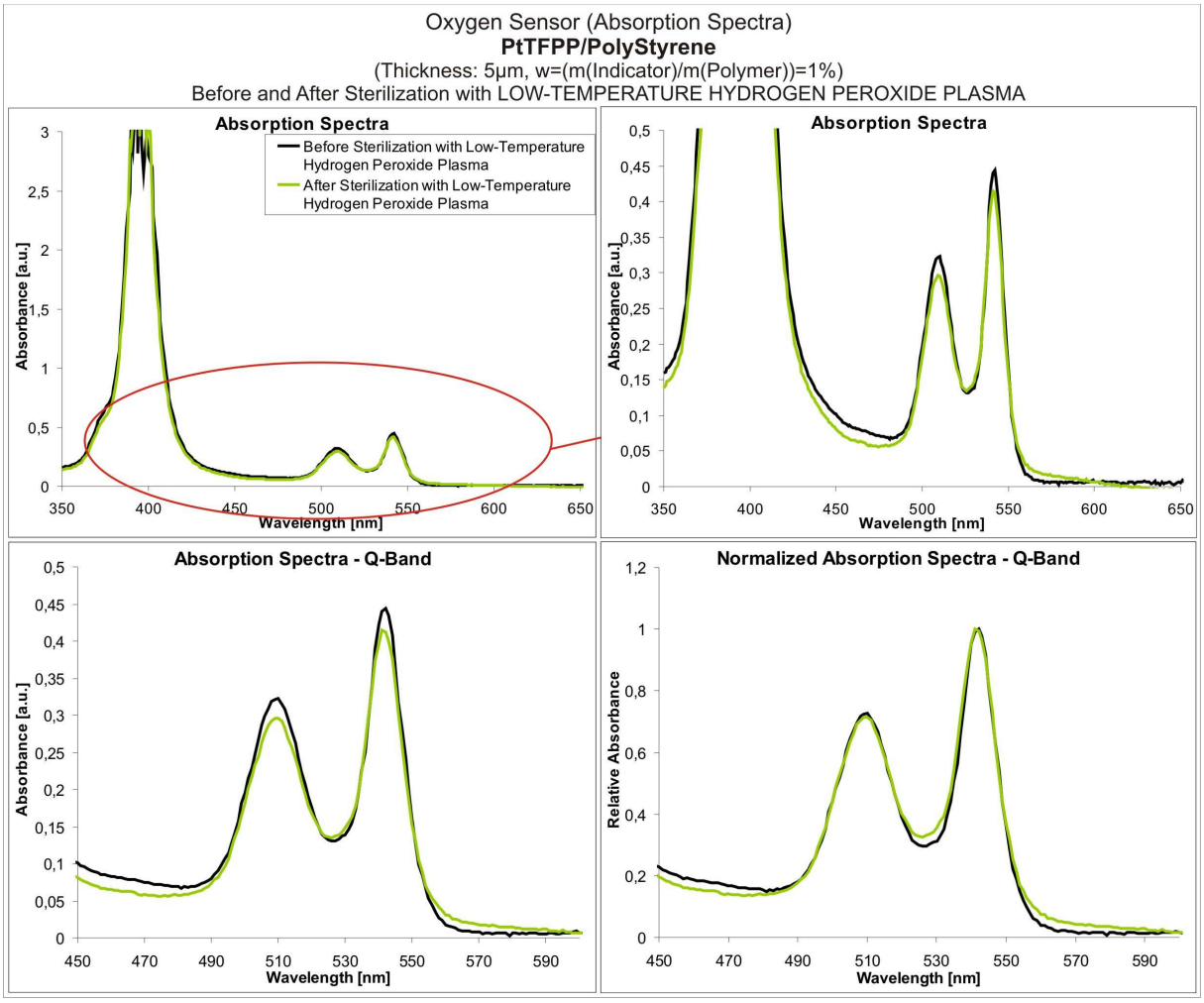

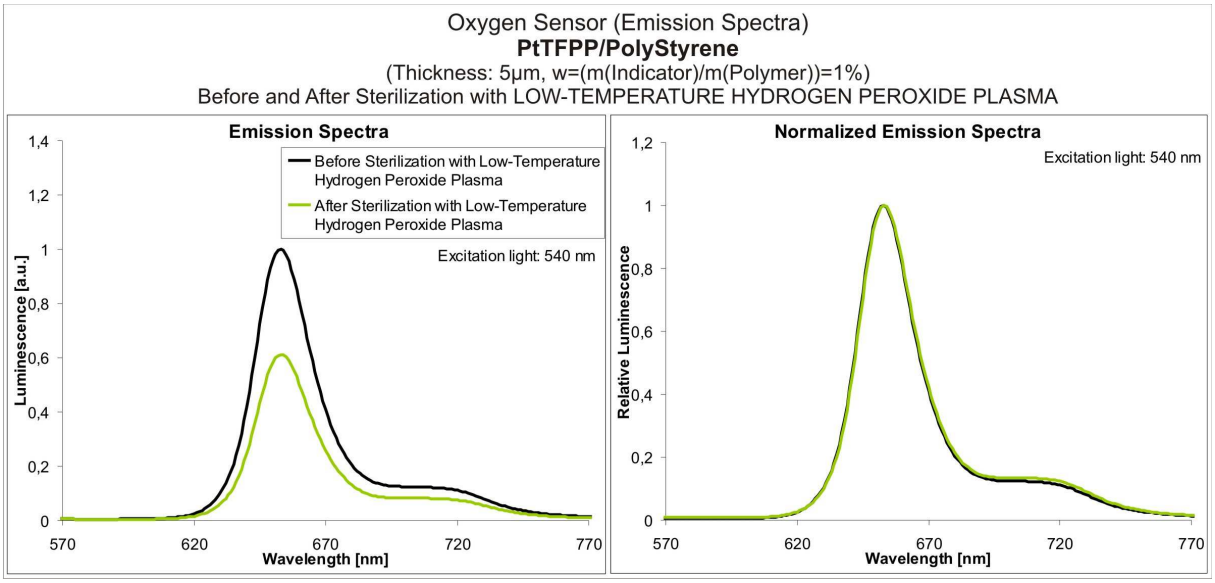

Sterilization with Low-Temperature H_2O_2 Plasma	Absorption Spectra	Emission Spectra
Alterations in Absorption/Emission Intensity	6,76% decrease	38,75% decrease

Alterations in Absorption/Emission Curve Form	Altered absorption curve form between 440-490 nm and 555-590 nm,	Unaltered.

Oxygen Sensor
PtTFPP/PolyStyrene
(Thickness: 5 µm, w=(m(Indicator)/m(Polymer))=1%)
Before and After Sterilization with LOW-TEMPERATURE HYDROGEN PEROXIDE PLASMA

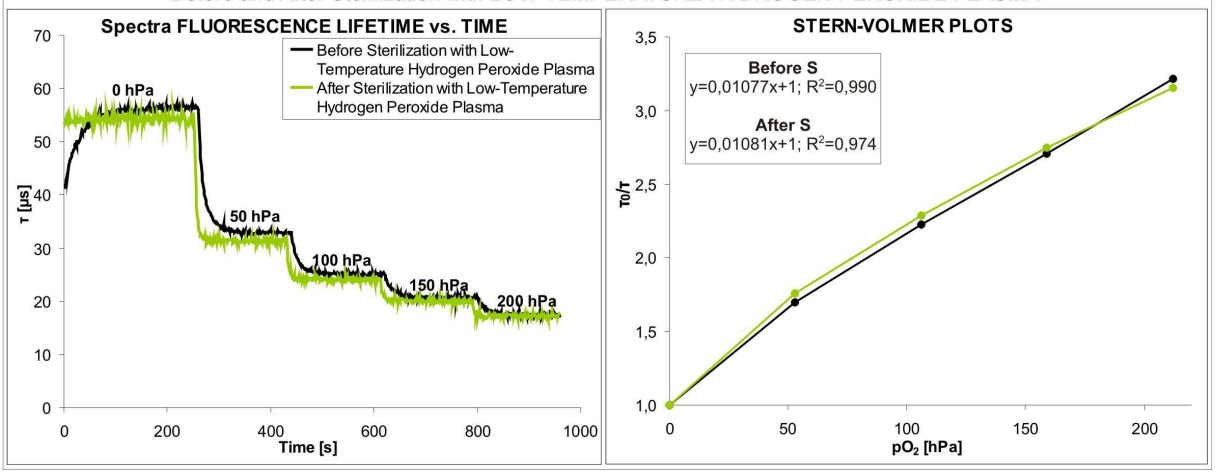

Sterilization with Low-Temperature H_2O_2 Plasma	Luminescence Lifetime	Stern-Volmer Plot
Alterations in Luminescence Lifetime and Slope	3,04% decrease of τ_0	0,37% increase of slope
	6,38% decrease of τ at 50 hPa	
	5,57% decrease of τ at 100 hPa	
	4,34% decrease of τ at 150 hPa	
	1,15% decrease of τ at 200 hPa	

F.13 Platinum(II)Tetrakis(PentaFluorPhenyl)Porphyrin (PtTFPP) immobilized in PolyStyrene-co- Acrylonitrile

F.13.1 Sterilization with Hydrogen Peroxide Gas

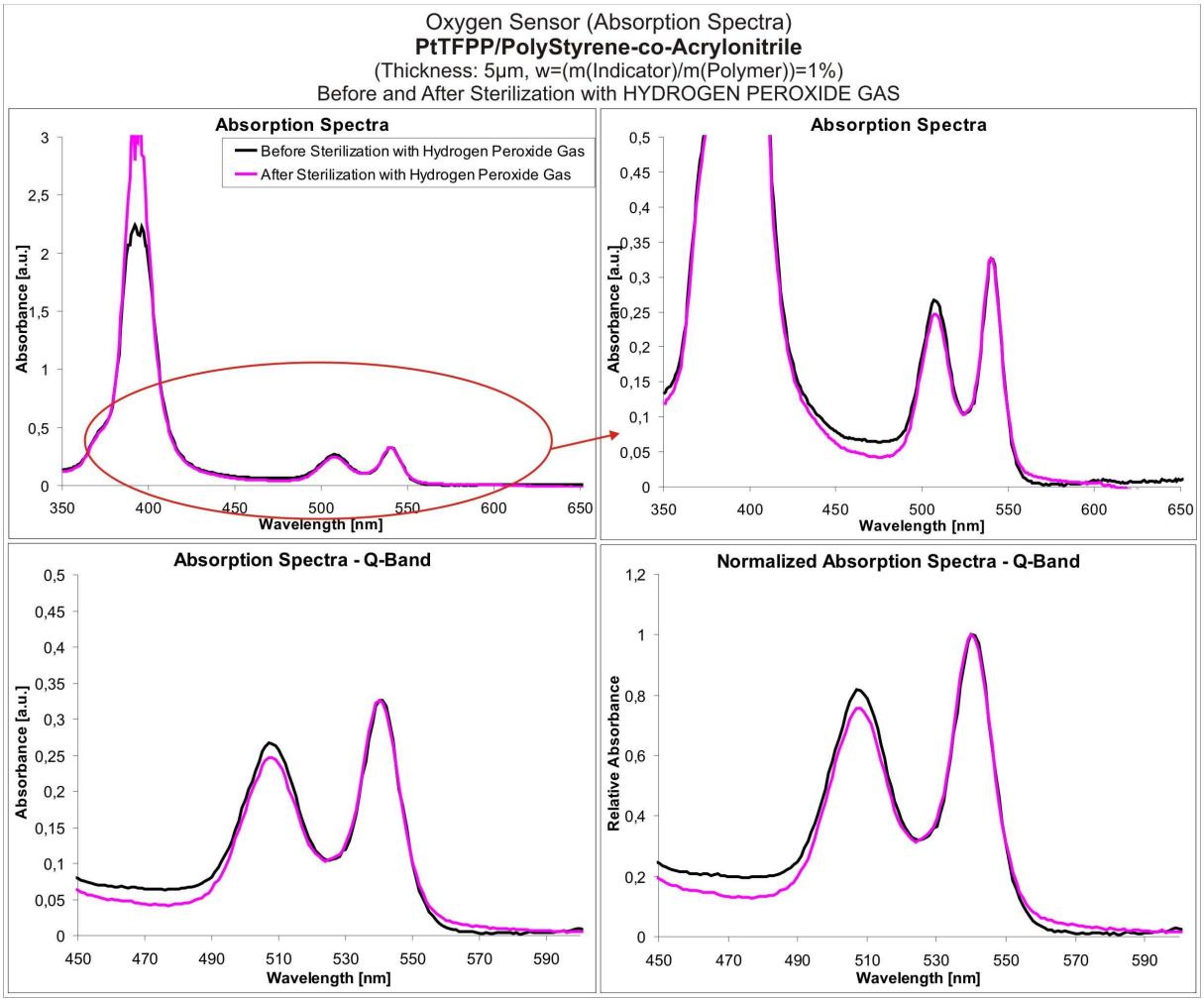

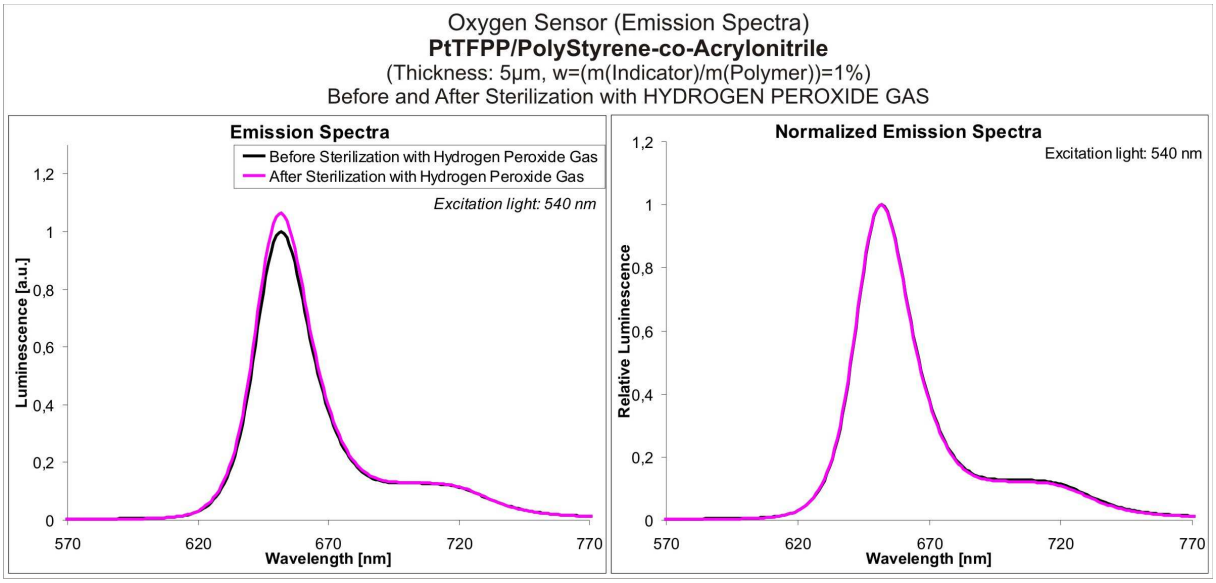

Sterilization with H_2O_2 Gas	Absorption Spectra	Emission Spectra
Alterations in Absorption/Emission Intensity	0,17% increase	6,00% increase
Alterations in Absorption/Emission Curve Form	Altered absorption curve form between 350-360 nm, 430-480 nm and 555-590 nm,	Unaltered.

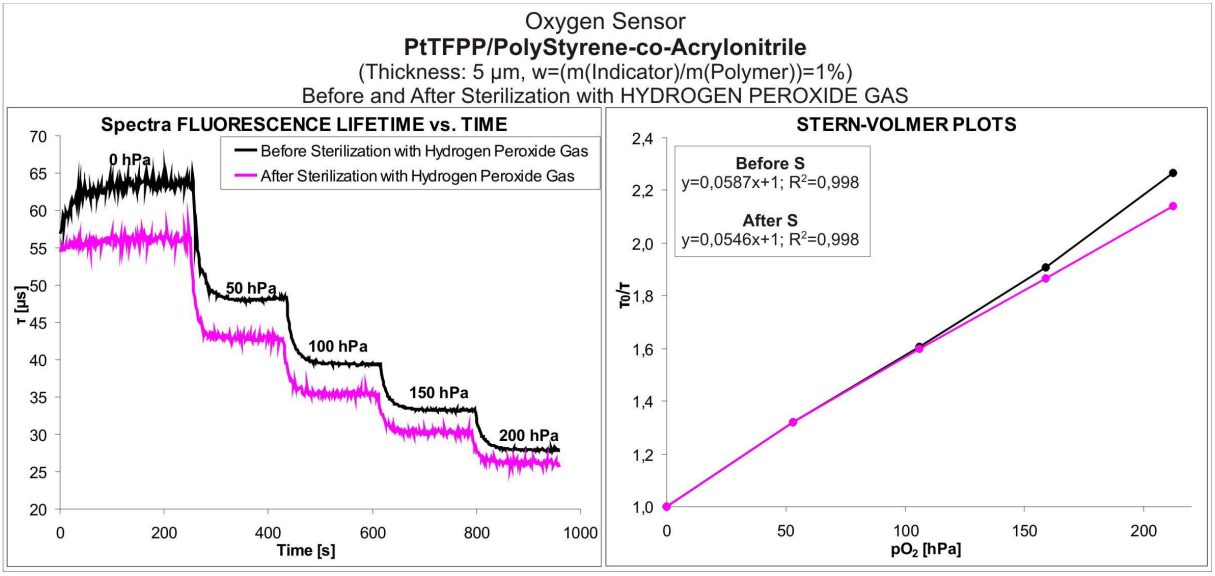

Sterilization with H_2O_2 Gas	Luminescence Lifetime	Stern-Volmer Plot
Alterations in Luminescence Lifetime and Slope	11,36% decrease of τ_0	6,98% decrease of slope
	11,64% decrease of τ at 50 hPa	
	10,91% decrease of τ at 100 hPa	
	9,61% decrease of τ at 150 hPa	
	6,43% decrease of τ at 200 hPa	

F.13.2 Sterilization with Low-Temperature Hydrogen Peroxide Plasma

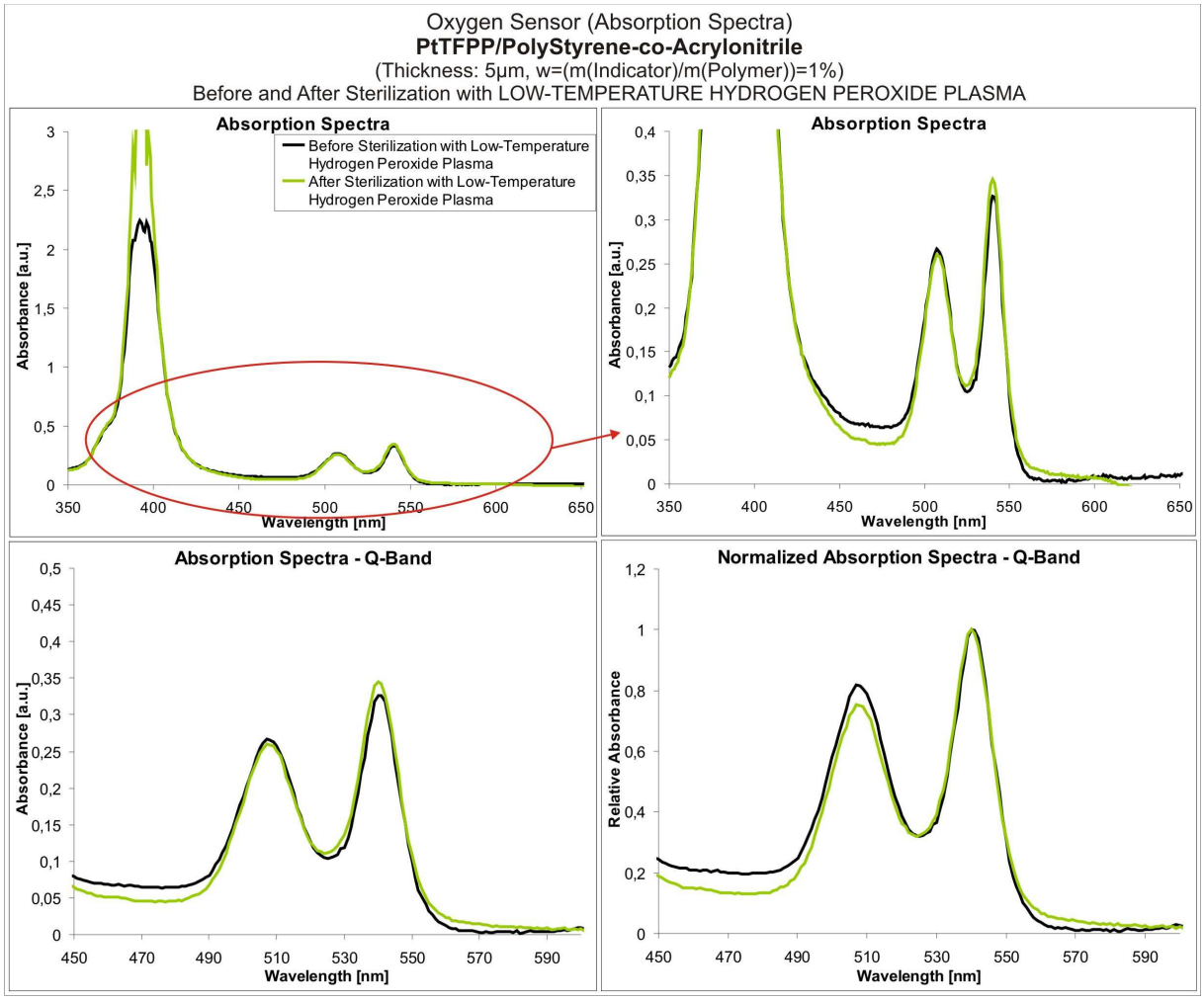

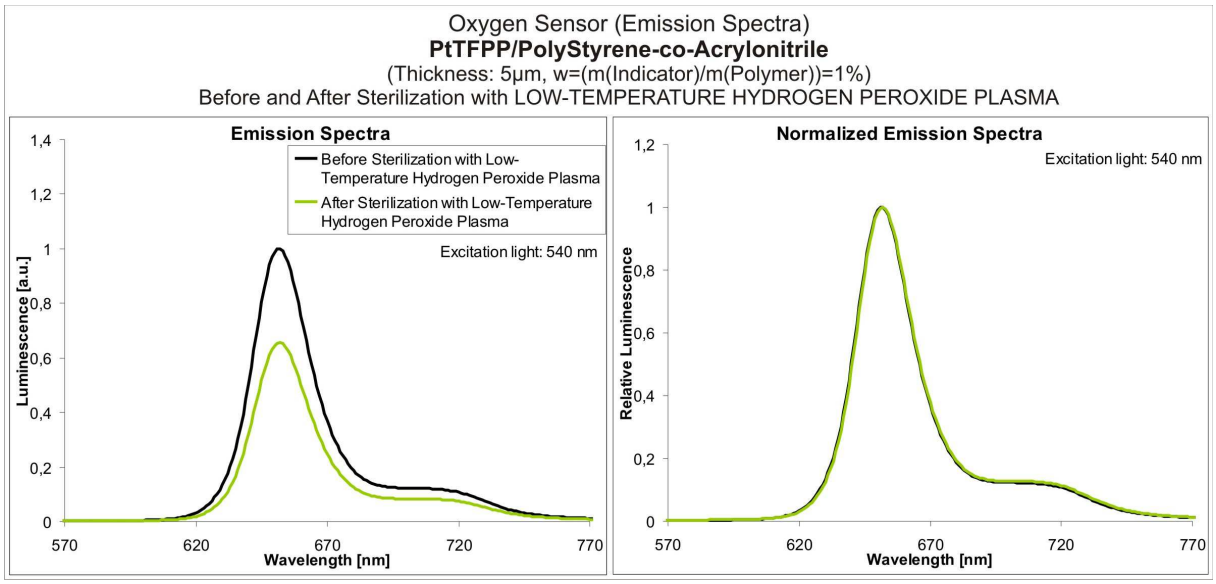

Sterilization with Low-Temperature H_2O_2 Plasma	Absorption Spectra	Emission Spectra
Alterations in Absorption/Emission Intensity	5,65% increase	52,35% decrease

Alterations in Absorption/Emission Curve Form	Altered absorption curve form between 440-510 nm and 555-590 nm,	Unaltered.

Oxygen Sensor
PtTFPP/PolyStyrene-co-Acrylonitrile
(Thickness: 5 µm, w=(m(Indicator)/m(Polymer))=1%)
Before and After Sterilization with LOW-TEMPERATURE HYDROGEN PEROXIDE PLASMA

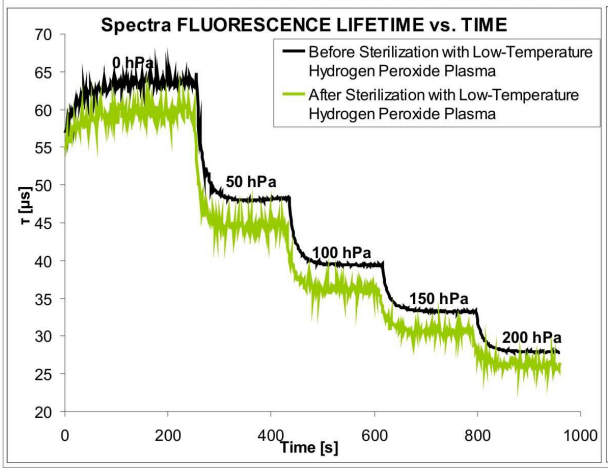

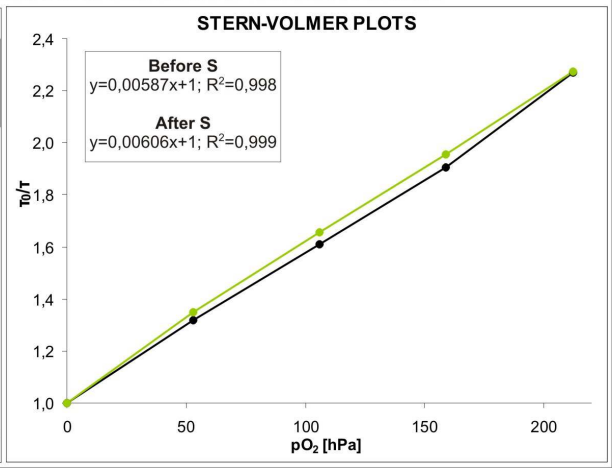

Sterilization with Low-Temperature H_2O_2 Plasma	**Luminescence Lifetime**	**Stern-Volmer Plot**
Alterations in Luminescence Lifetime and Slope	5,99% decrease of τ_0	3,14% increase of slope
	8,11% decrease of τ at 50 hPa	
	8,88% decrease of τ at 100 hPa	
	8,71% decrease of τ at 150 hPa	
	6,43% decrease of τ at 200 hPa	

F.14 Platinum(II)Tetrakis(PentaFluorPhenyl)Porphyrin (PtTFPP) immobilized in PolyStyrene-co-MaleicAnhydride (PSMA93)

F.14.1 Sterilization with Hydrogen Peroxide Gas

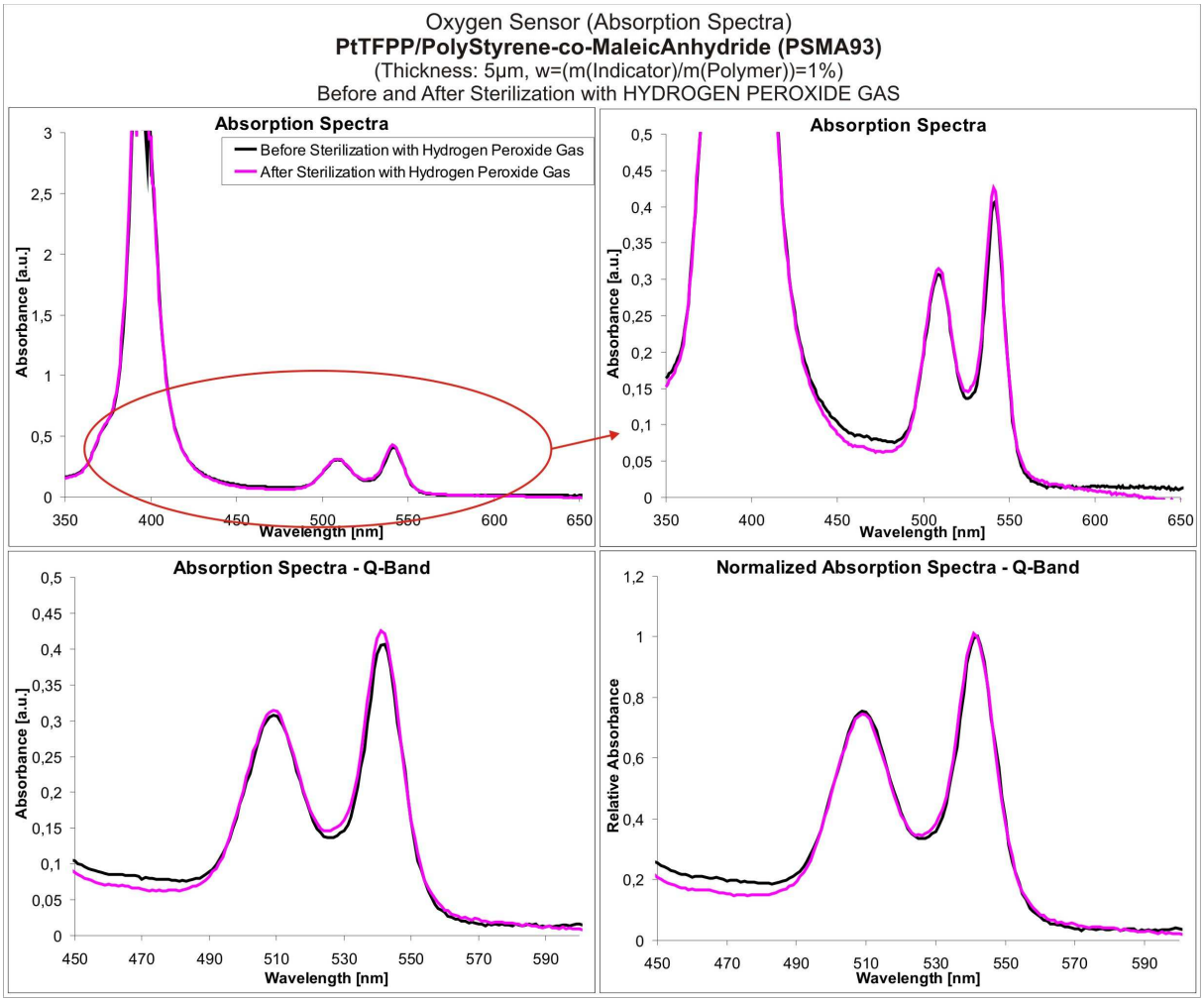

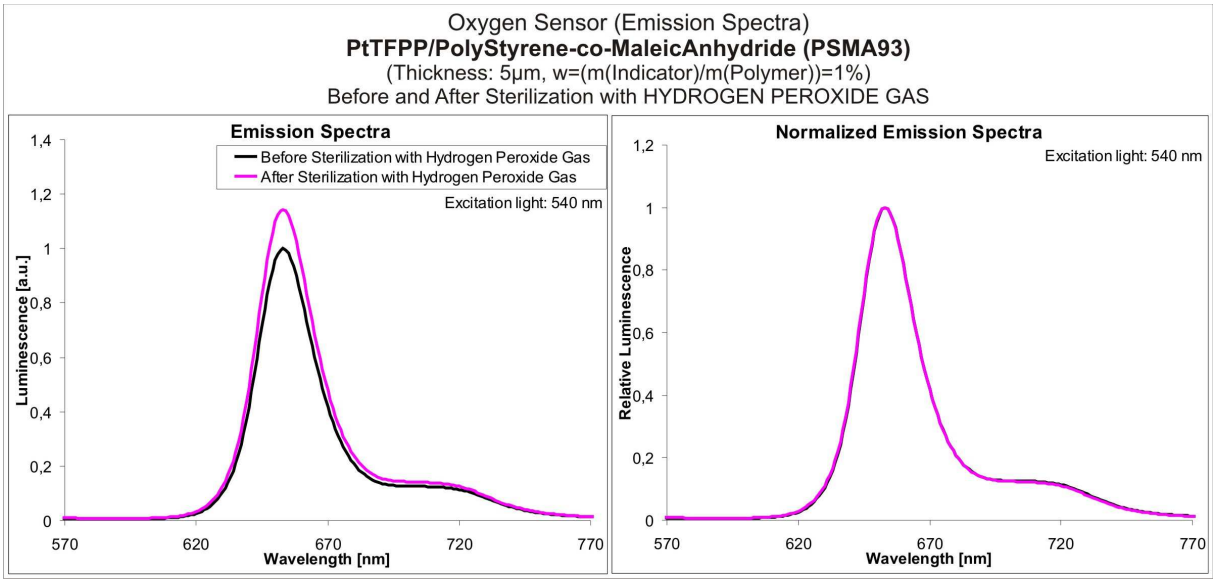

Sterilization with H_2O_2 Gas	Absorption Spectra	Emission Spectra
Alterations in Absorption/Emission Intensity	3,52% increase	12,49% increase
Alterations in Absorption/Emission Curve Form	Altered absorption curve form between 350-360 nm and 430-480 nm.	Unaltered.

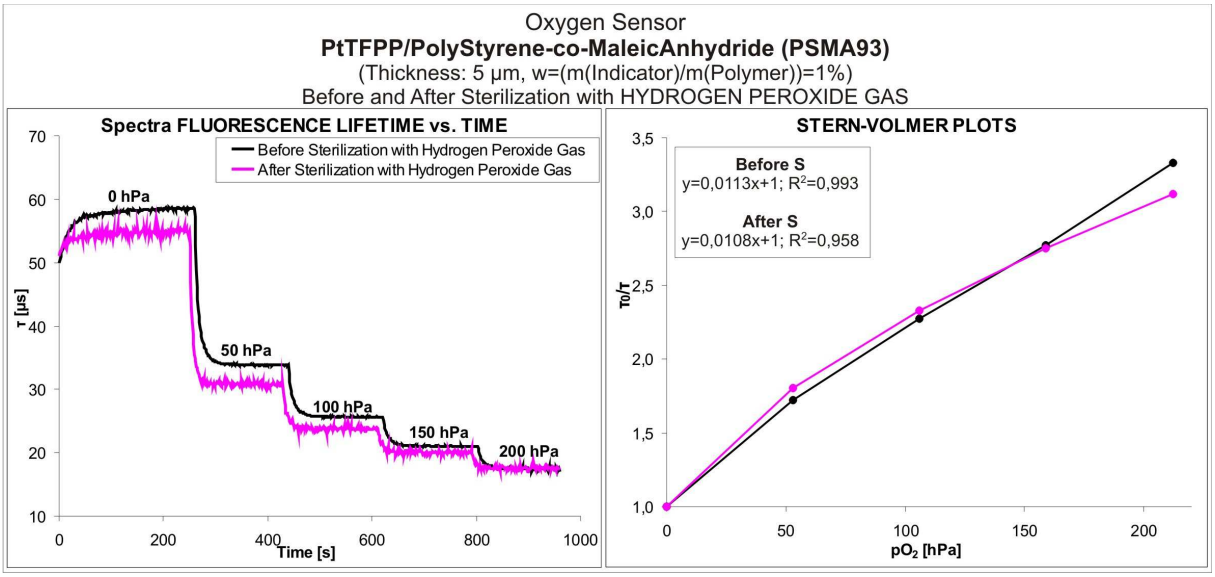

Sterilization with H_2O_2 Gas	Luminescence Lifetime	Stern-Volmer Plot
Alterations in Luminescence Lifetime and Slope	5,84% decrease of τ_0	4,42% decrease of slope
	10,32% decrease of τ at 50 hPa	
	7,81% decrease of τ at 100 hPa	
	5,24% decrease of τ at 150 hPa	
	0,57% increase of τ at 200 hPa	

F.14.2 Sterilization with Low-Temperature Hydrogen Peroxide Plasma

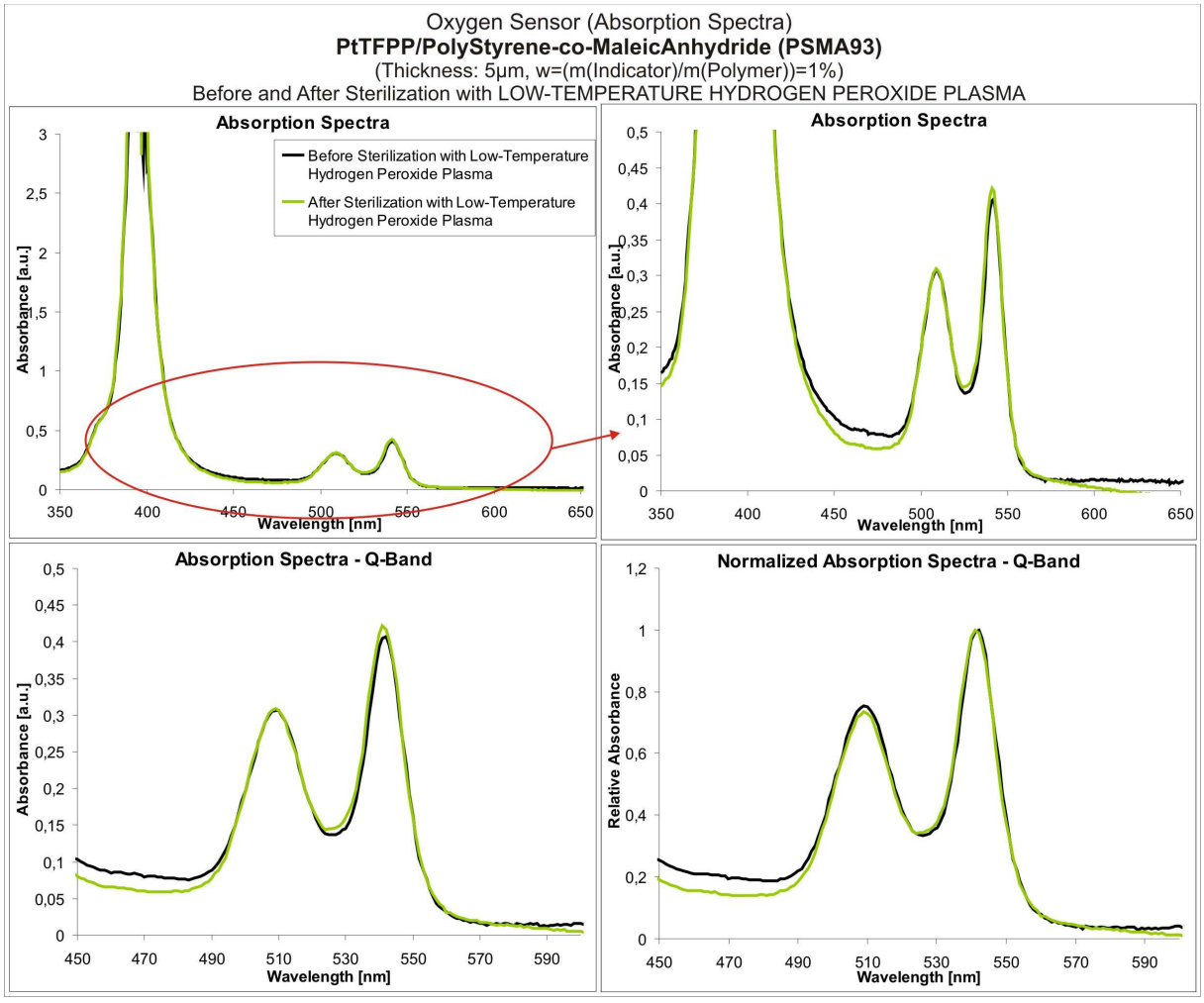

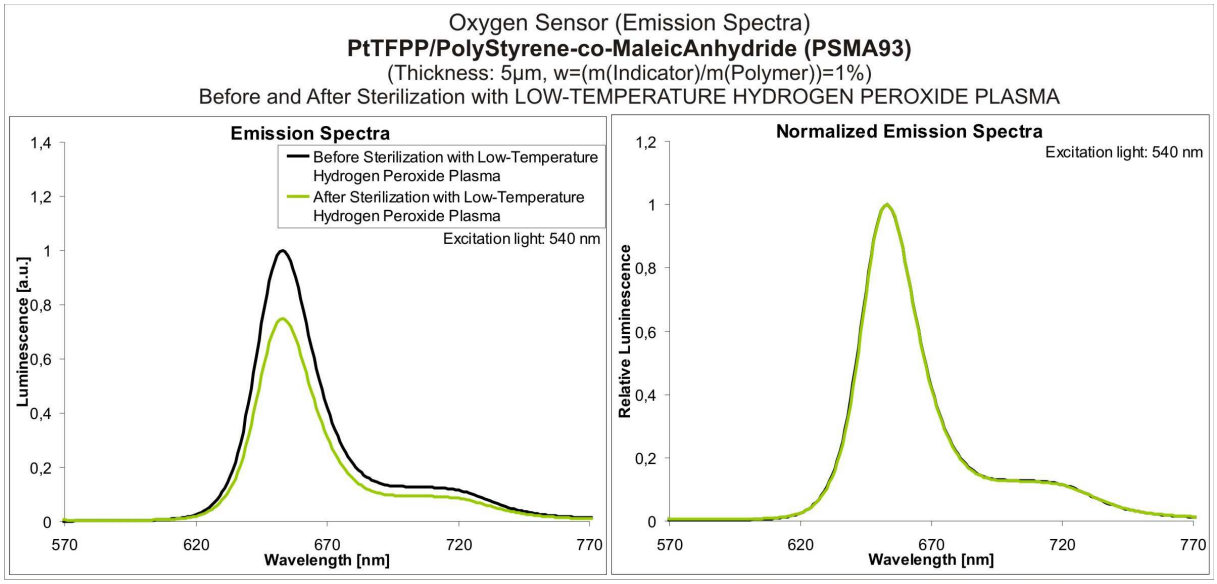

Sterilization with Low-Temperature H_2O_2 Plasma	Absorption Spectra	Emission Spectra
Alterations in Absorption/Emission Intensity	0,26% increase	26,57% decrease

Alterations in Absorption/Emission Curve Form	Altered absorption curve form between 440-490 nm and 600-700 nm.	Unaltered.

Oxygen Sensor
PtTFPP/PolyStyrene-co-MaleicAnhydride (PSMA93)
(Thickness: 5 µm, w=(m(Indicator)/m(Polymer))=1%)
Before and After Sterilization with LOW-TEMPERATURE HYDROGEN PEROXIDE PLASMA

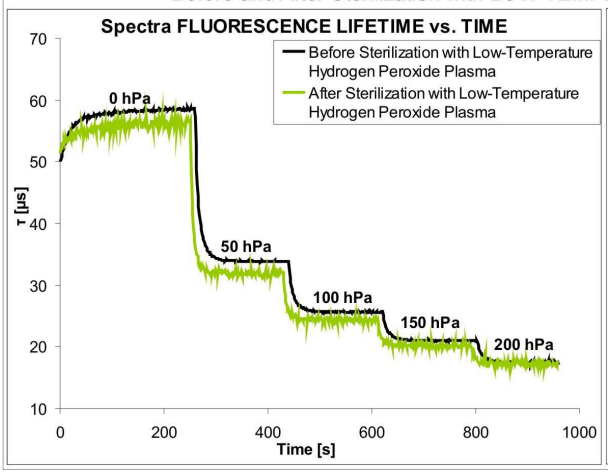

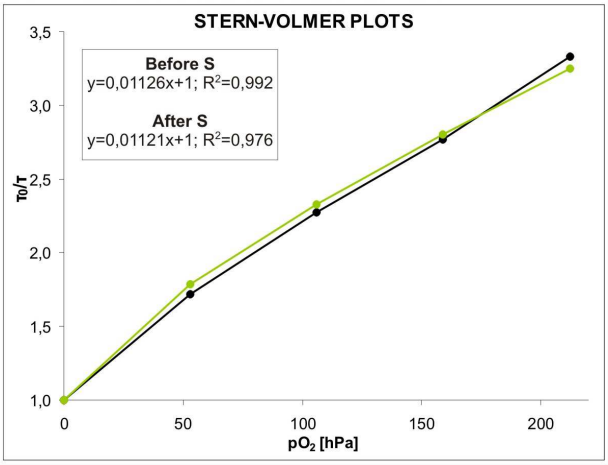

Sterilization with Low-Temperature H_2O_2 Plasma	Luminescence Lifetime	Stern-Volmer Plot
Alterations in Luminescence Lifetime and Slope	3,61% decrease of τ_0	0,44% decrease of slope
	7,37% decrease of τ at 50 hPa	
	6,25% decrease of τ at 100 hPa	
	4,76% decrease of τ at 150 hPa	
	1,14% decrease of τ at 200 hPa	

F.15 Platinum(II) OctaEthyl Porphyrin (=PtOEP) immobilized in PolyStyrene

F.15.1 Sterilization with Hydrogen Peroxide Gas

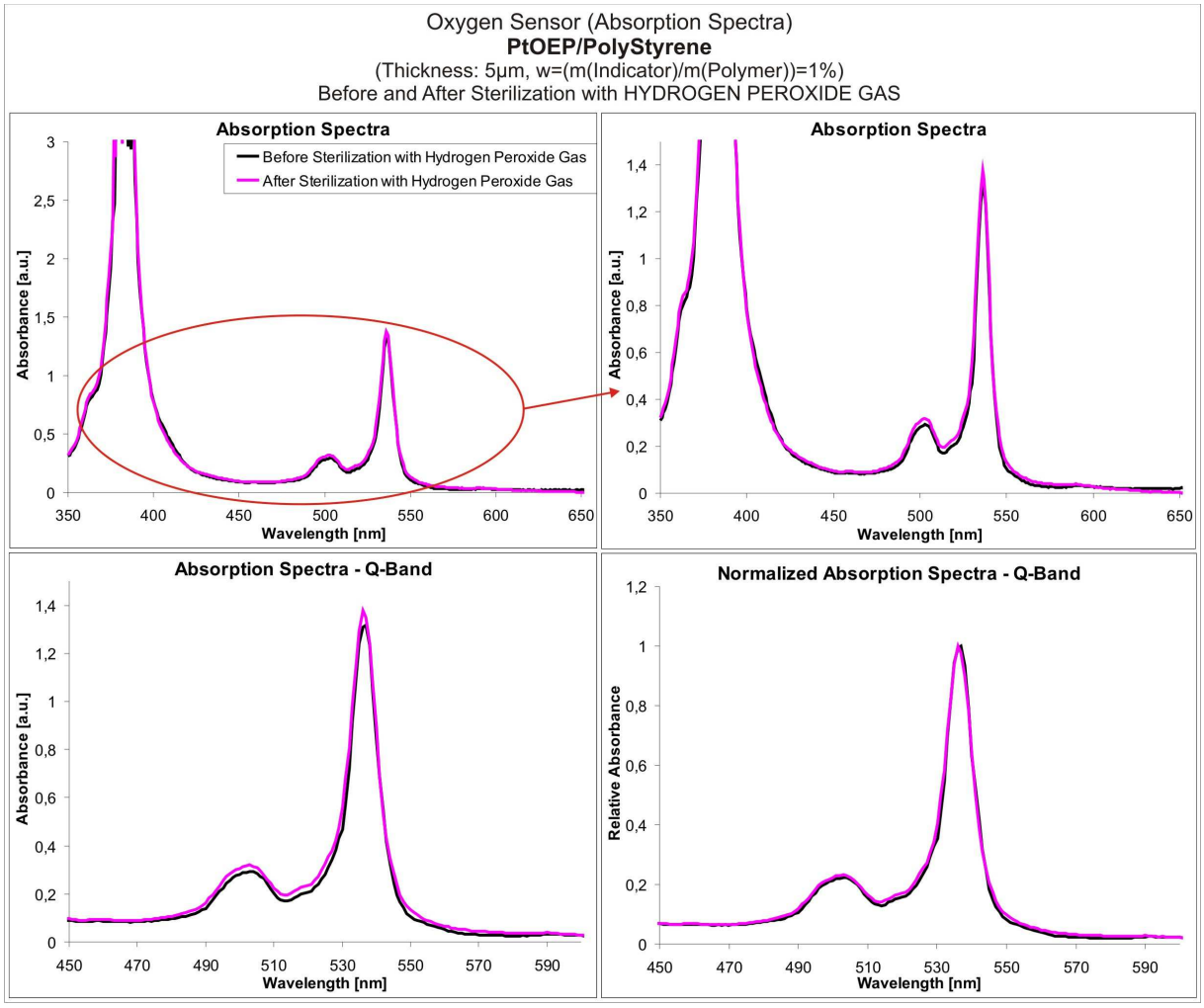

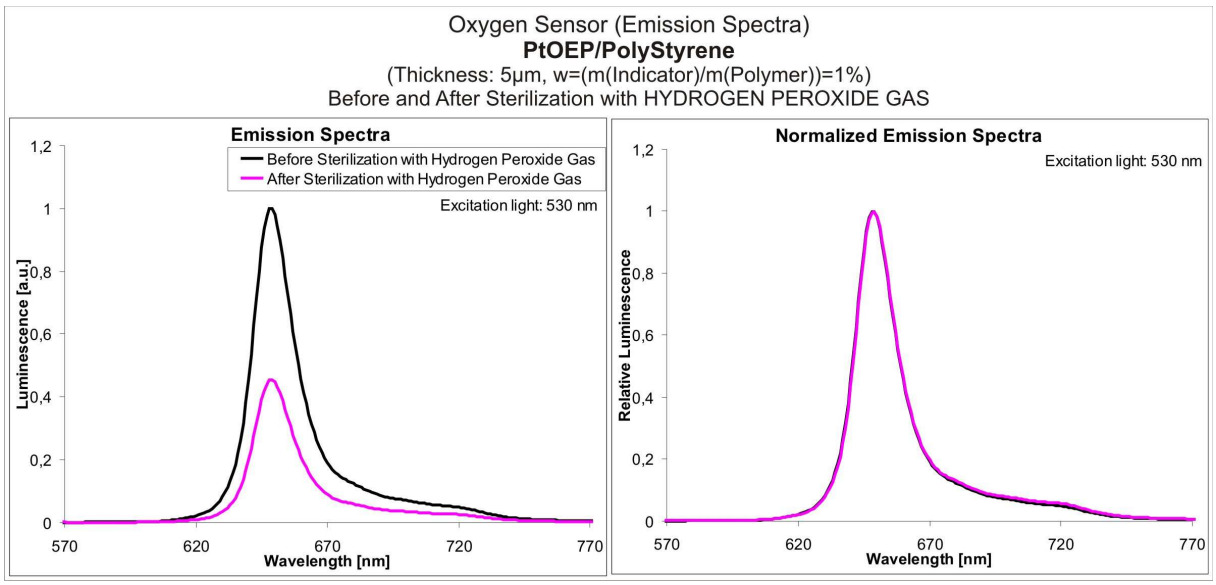

Sterilization with H_2O_2 Gas	Absorption Spectra	Emission Spectra
Alterations in Absorption/Emission Intensity	4,53% increase	54,56% decrease

Alterations in Absorption/Emission Curve Form	Unaltered.	Unaltered.

Oxygen Sensor
PtOEP/PolyStyrene
(Thickness: 5 µm, w=(m(Indicator)/m(Polymer))=1%)
Before and After Sterilization with HYDROGEN PEROXIDE GAS

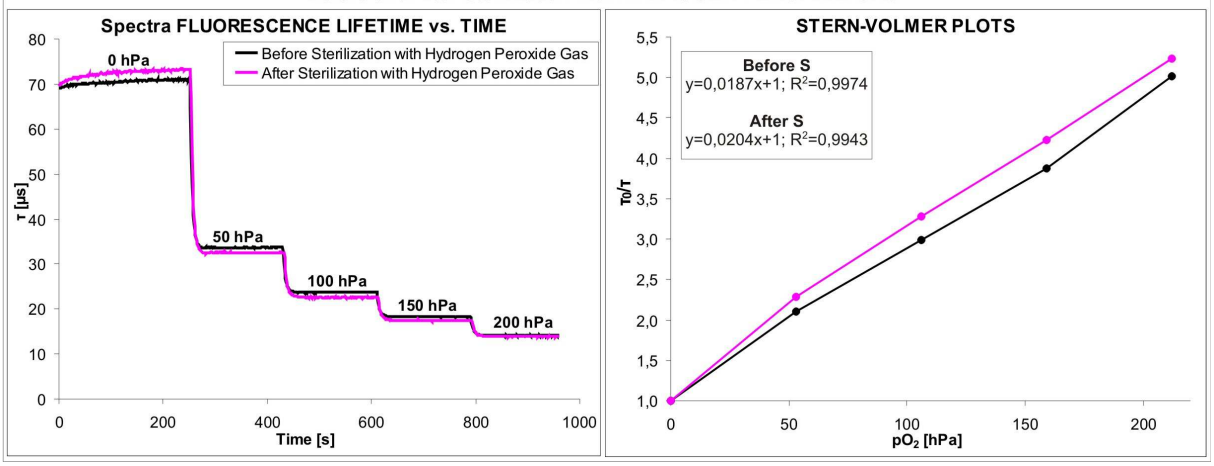

Sterilization with Low-Temperature H_2O_2 Plasma	Luminescence Lifetime	Stern-Volmer Plot
Alterations in Luminescence Lifetime and Slope	3,02% increase of τ_0	8,33% increase of slope
	4,76% decrease of τ at 50 hPa	
	6,33% decrease of τ at 100 hPa	
	6,01% decrease of τ at 150 hPa	
	1,42% decrease of τ at 200 hPa	

F.15.2 Sterilization with Low-Temperature Hydrogen Peroxide Plasma

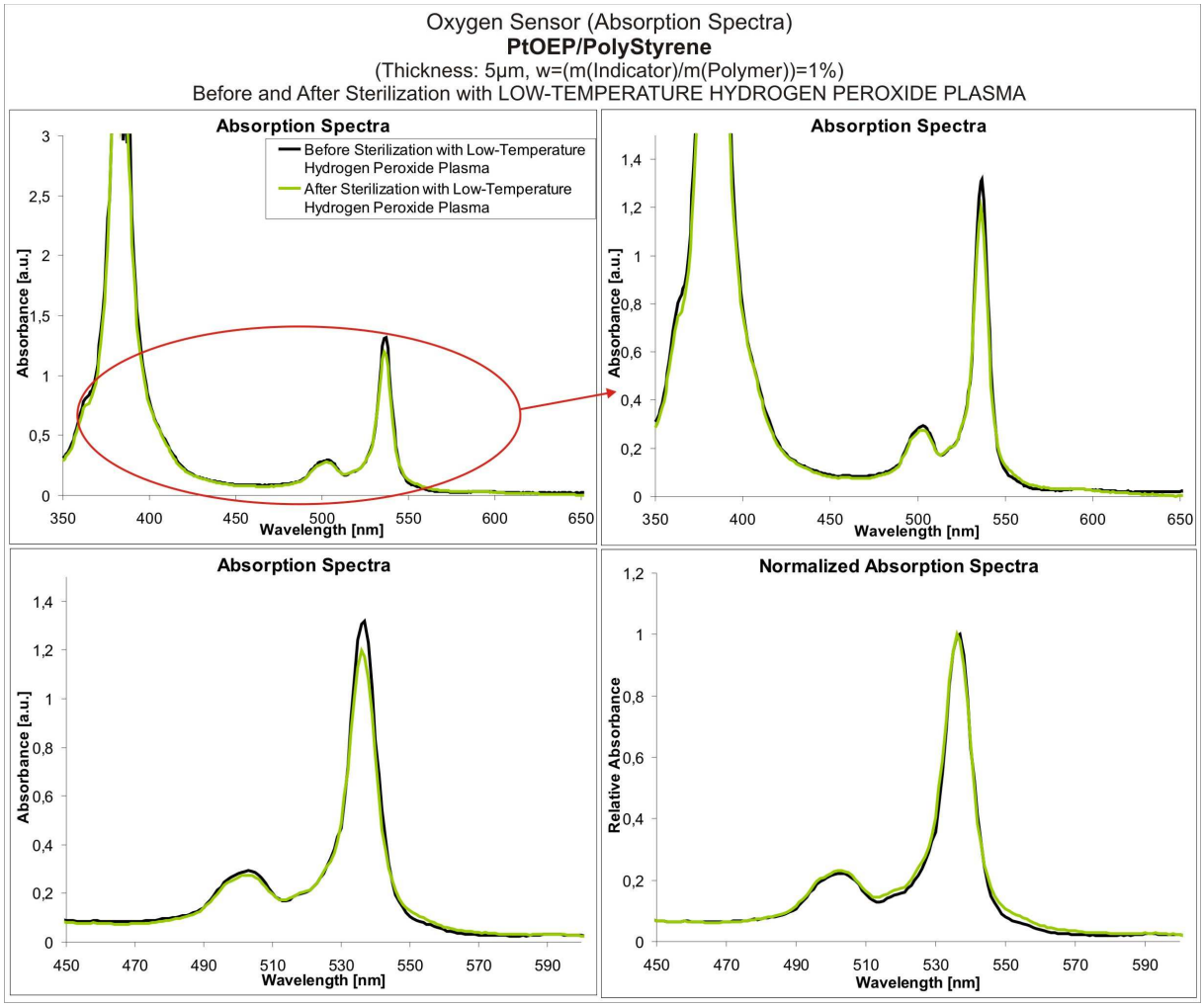

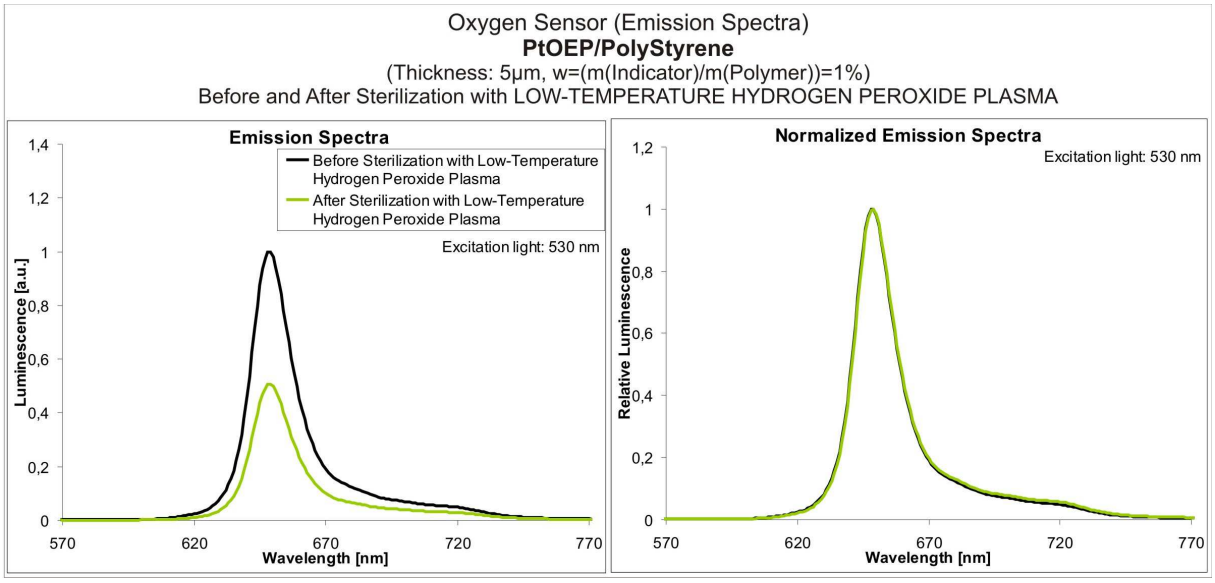

Sterilization with Low-Temperature H_2O_2 Plasma	Absorption Spectra	Emission Spectra
Alterations in Absorption/Emission Intensity	8,94% Decrease	49,23% decrease

Alterations in Absorption/Emission Curve Form	Altered absorption curve form between 515-530 nm and 550-570 nm.	Unaltered.

Oxygen Sensor
PtOEP/PolyStyrene
(Thickness: 5 µm, w=(m(Indicator)/m(Polymer))=1%)
Before and After Sterilization with LOW-TEMPERATURE HYDROGEN PEROXIDE PLASMA

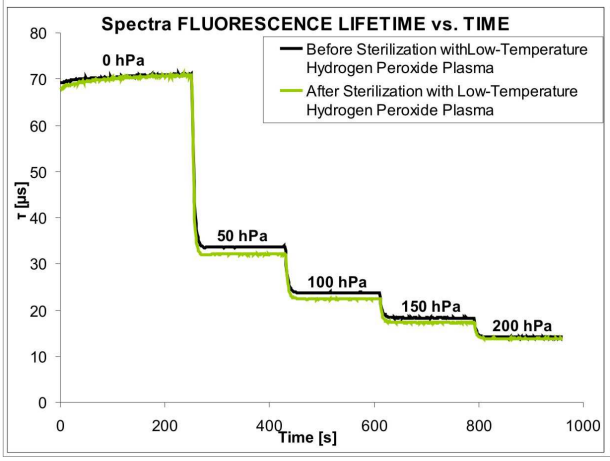

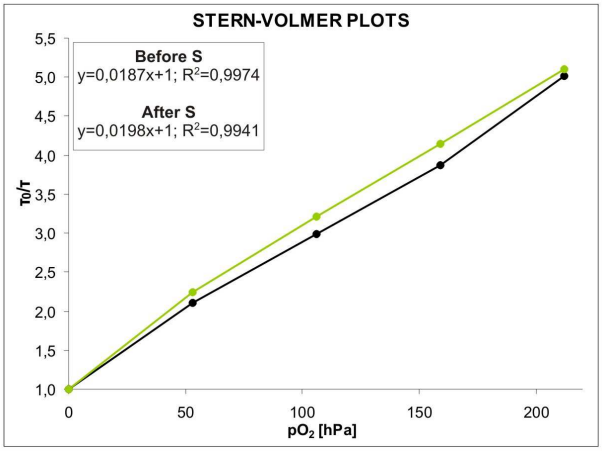

Sterilization with Low-Temperature H_2O_2 Plasma	**Luminescence Lifetime**	**Stern-Volmer Plot**
Alterations in Luminescence Lifetime and Slope	0,28% decrease of τ_0	5,55% increase of slope
	6,55% decrease of τ at 50 hPa	
	7,59% decrease of τ at 100 hPa	
	7,10% decrease of τ at 150 hPa	
	2,13% decrease of τ at 200 hPa	

F.16 Platinum(II) meso-tetra(4-FluoroPhenyl) TetraBenzoPorphyrin (=PtTPTBPF) immobilized in PolyStyrene

F.16.1 Sterilization with Hydrogen Peroxide Gas

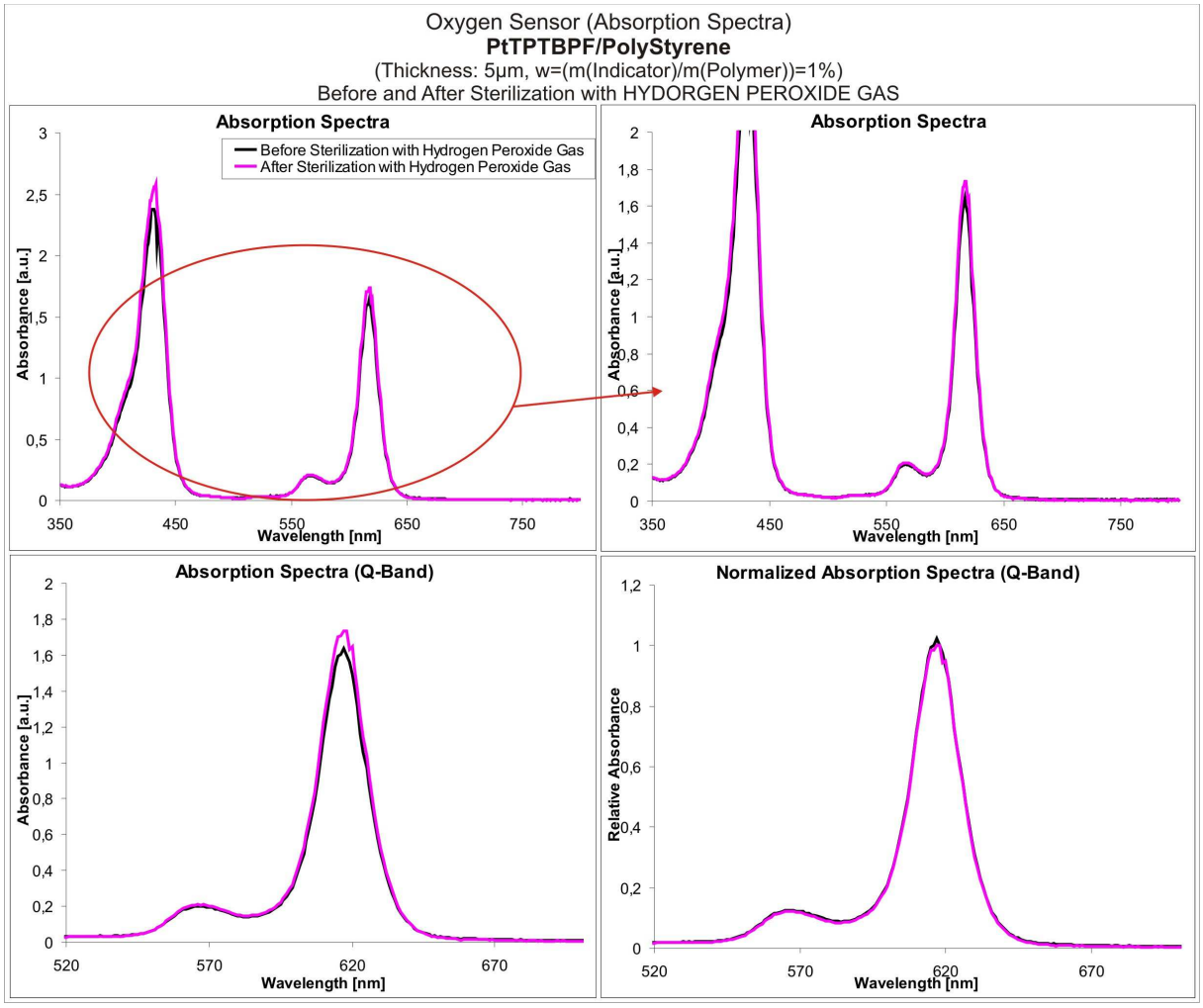

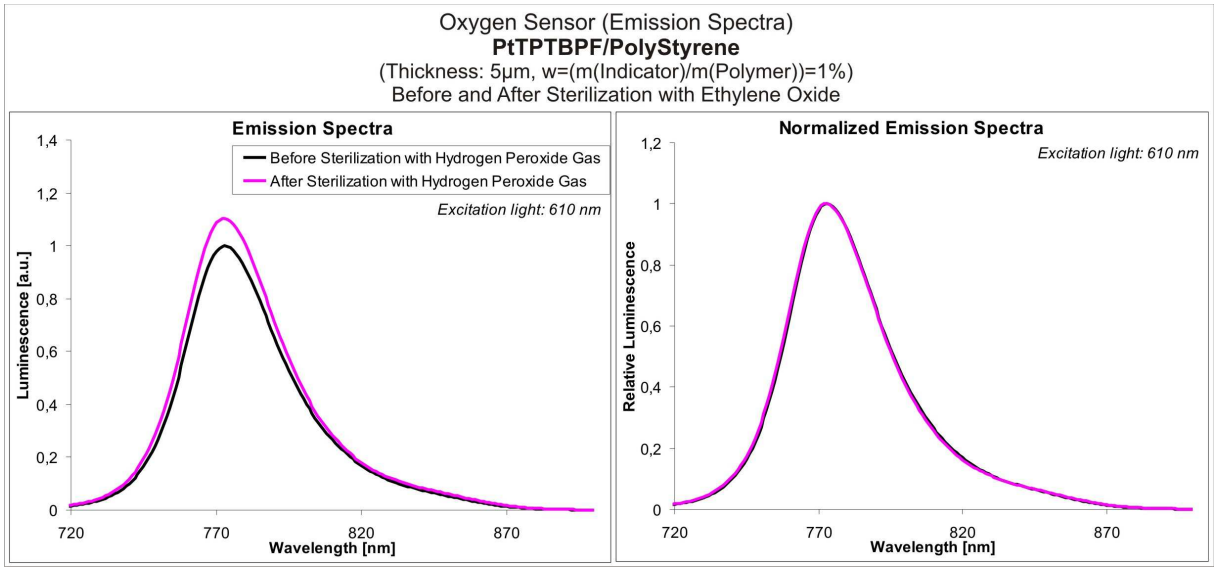

Sterilization with H_2O_2 Gas	Absorption Spectra	Emission Spectra
Alterations in Absorption/Emission Intensity	8,12% increase	9,44% increase
Alterations in Absorption/Emission Curve Form	Unaltered.	Unaltered.

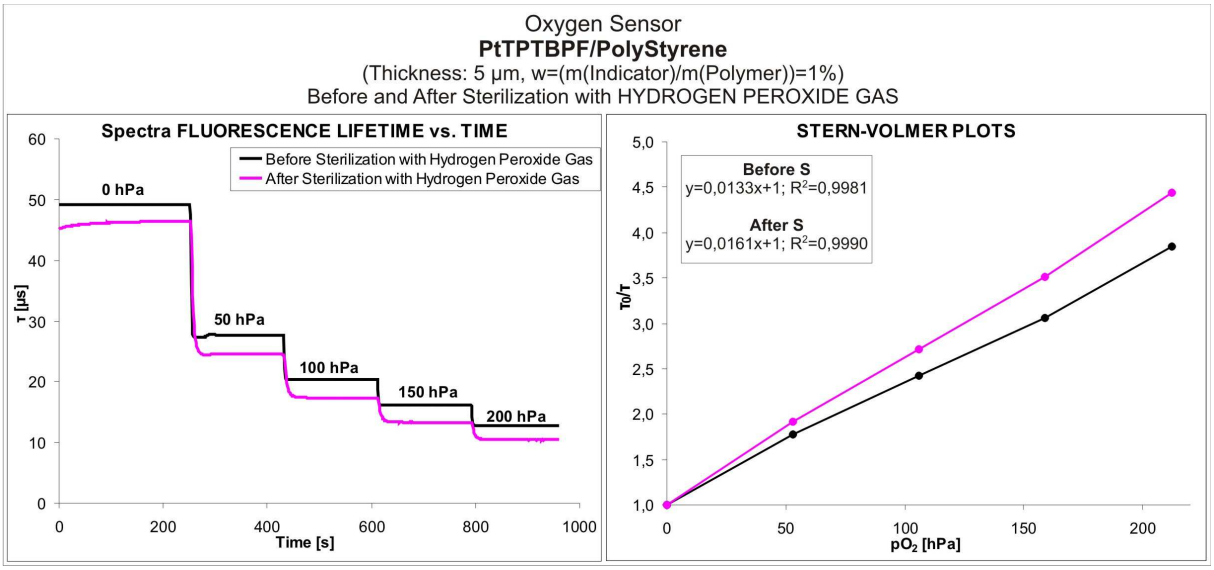

Sterilization with Low-Temperature H_2O_2 Plasma	Luminescence Lifetime	Stern-Volmer Plot
Alterations in Luminescence Lifetime and Slope	5,89% decrease of τ_0	17,39% increase of slope
	13,00% decrease of τ at 50 hPa	
	15,76% decrease of τ at 100 hPa	
	18,01% decrease of τ at 150 hPa	
	18,75% decrease of τ at 200 hPa	

F.16.2 Sterilization with Low-Temperature Hydrogen Peroxide Plasma

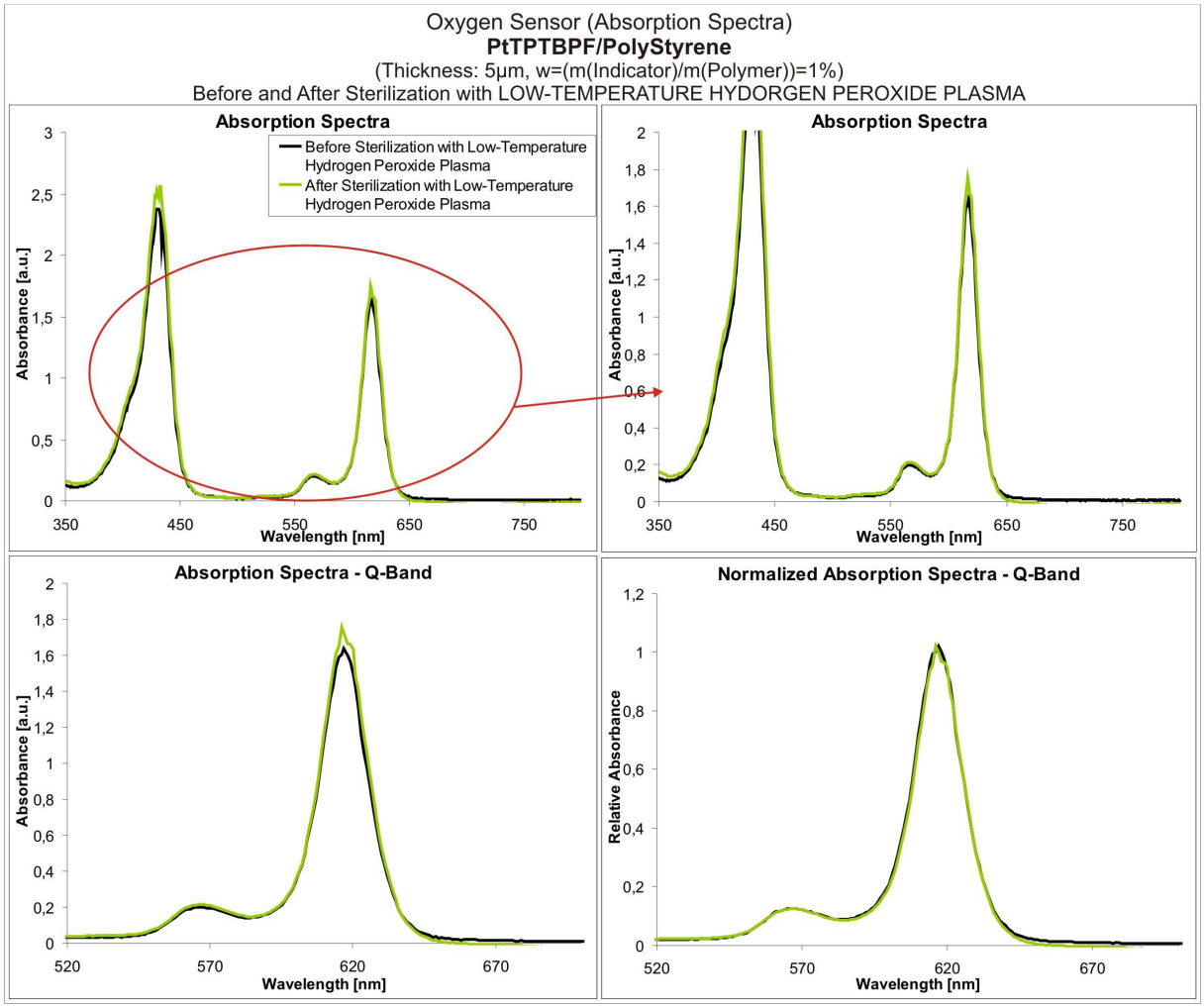

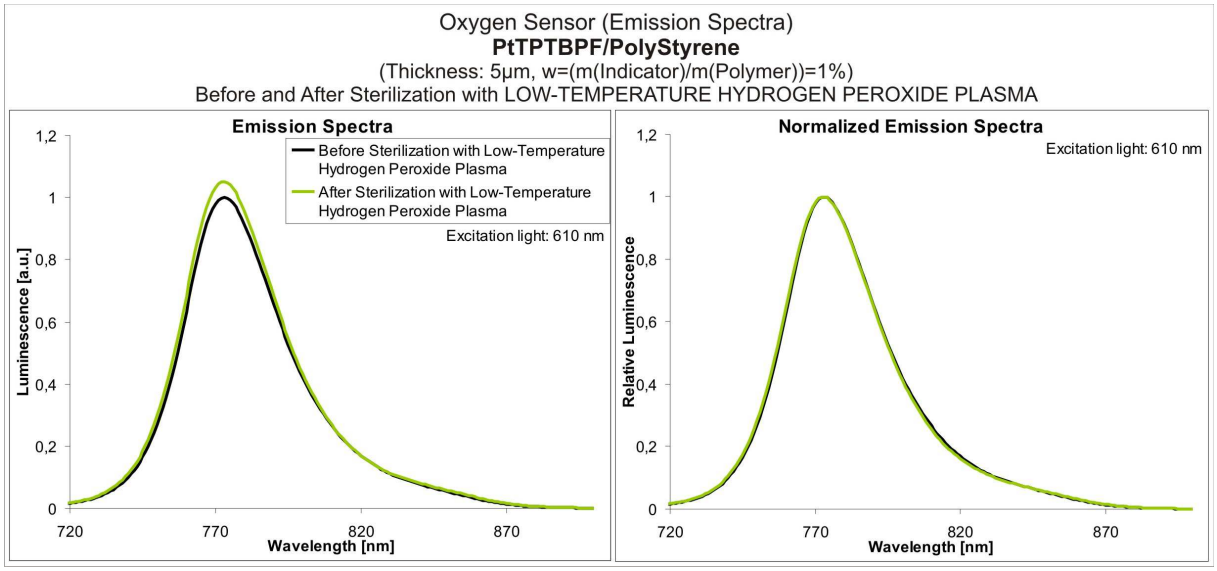

Sterilization with Low-Temperature H_2O_2 Plasma	Absorption Spectra	Emission Spectra
Alterations in Absorption/Emission Intensity	7,86% Increase	4,75 %increase

Alterations in Absorption/Emission Curve Form	Unaltered.	Unaltered.

Oxygen Sensor
PtTPTBPF/PolyStyrene
(Thickness: 5 µm, w=(m(Indicator)/m(Polymer))=1%)
Before and After Sterilization with LOW-TEMPERATURE HYDROGEN PEROXIDE PLASMA

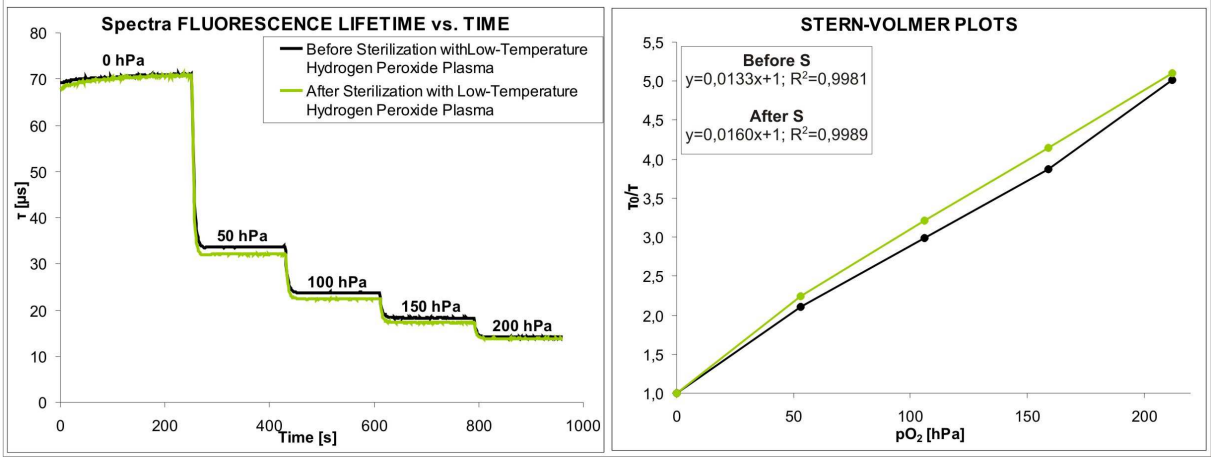

Sterilization with Low-Temperature H_2O_2 Plasma	Luminescence Lifetime	Stern-Volmer Plot
Alterations in Luminescence Lifetime and Slope	6,50% decrease of τ_0	16,87% increase of slope
	13,72% decrease of τ at 50 hPa	
	16,56% decrease of τ at 100 hPa	
	18,01% decrease of τ at 150 hPa	
	18,75% decrease of τ at 200 hPa	

F.17 Palladium(II)meso-tetra(4-FluoroPhenyl) TetraBenzoPorphyrin (=PdTPTBPF) immobilized in PolyStyrene

F.17.1 Sterilization with Hydrogen Peroxide Gas

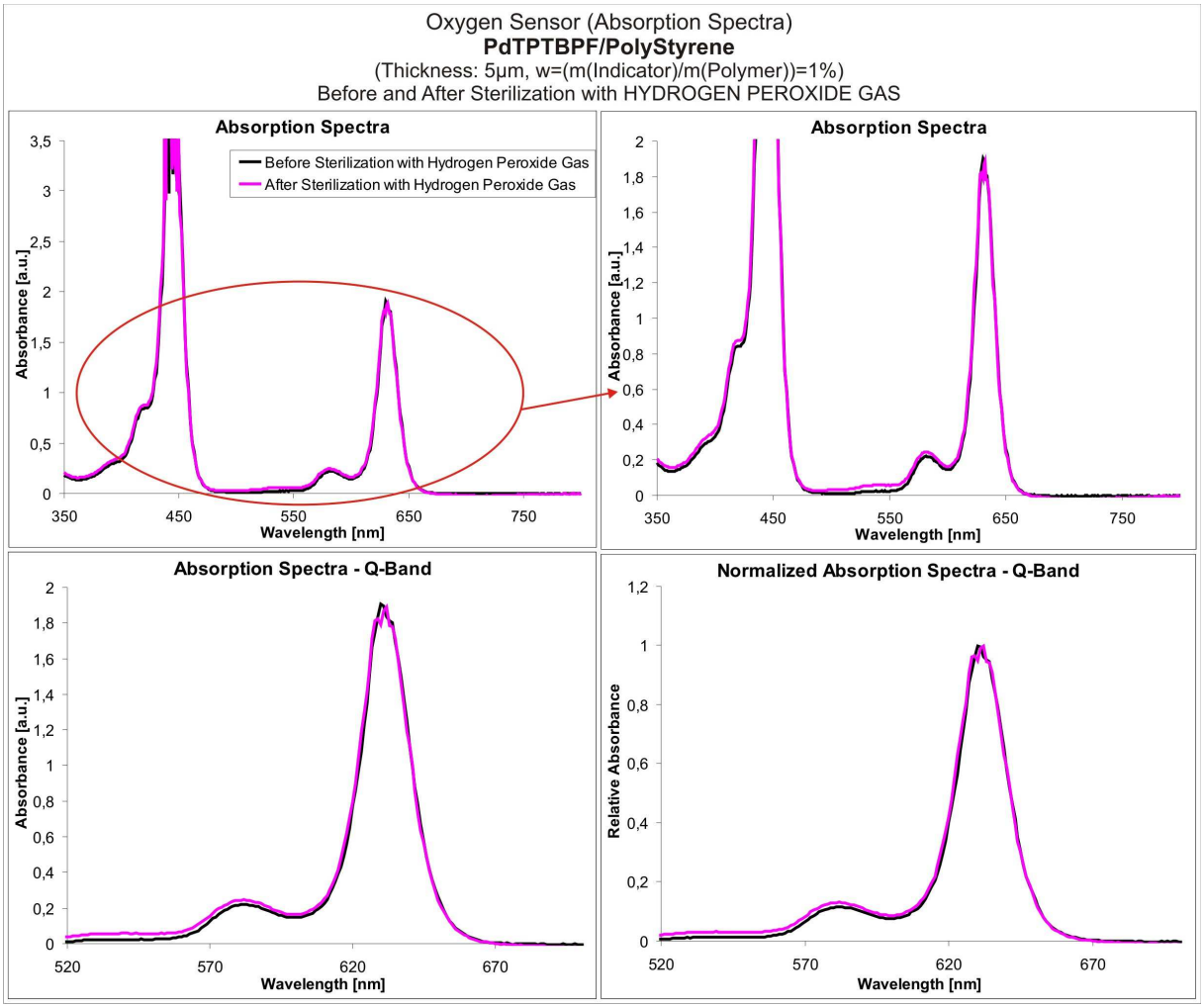

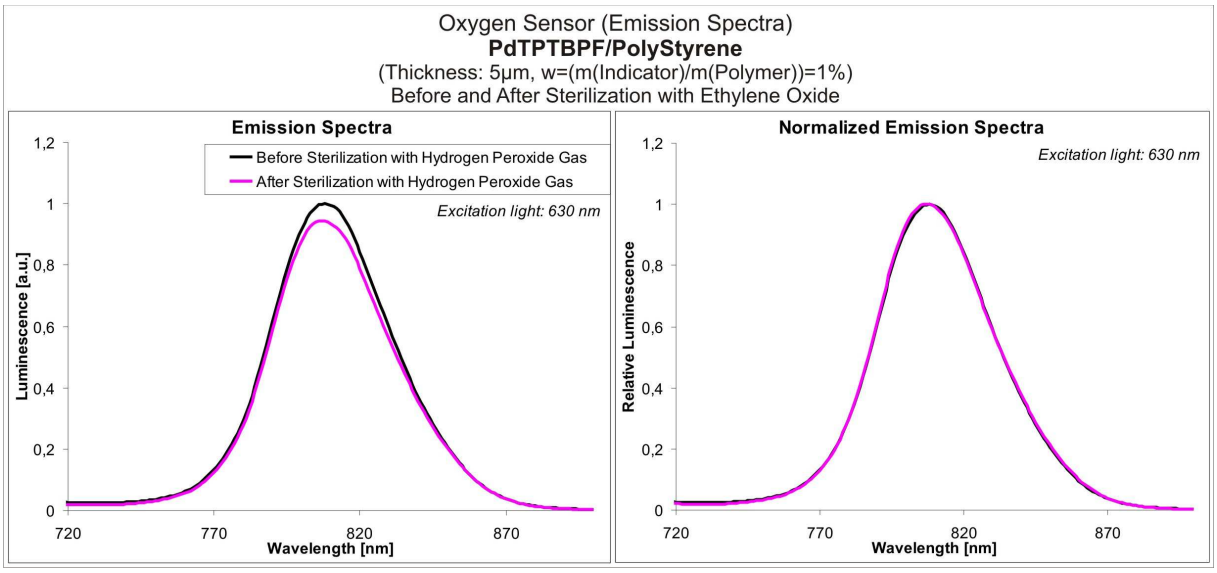

Sterilization with H_2O_2 Gas	Absorption Spectra	Emission Spectra
Alterations in Absorption/Emission Intensity	0,86% decrease	5,66% decrease
Alterations in Absorption/Emission Curve Form	Altered absorption curve form between 490-600 nm.	Unaltered.

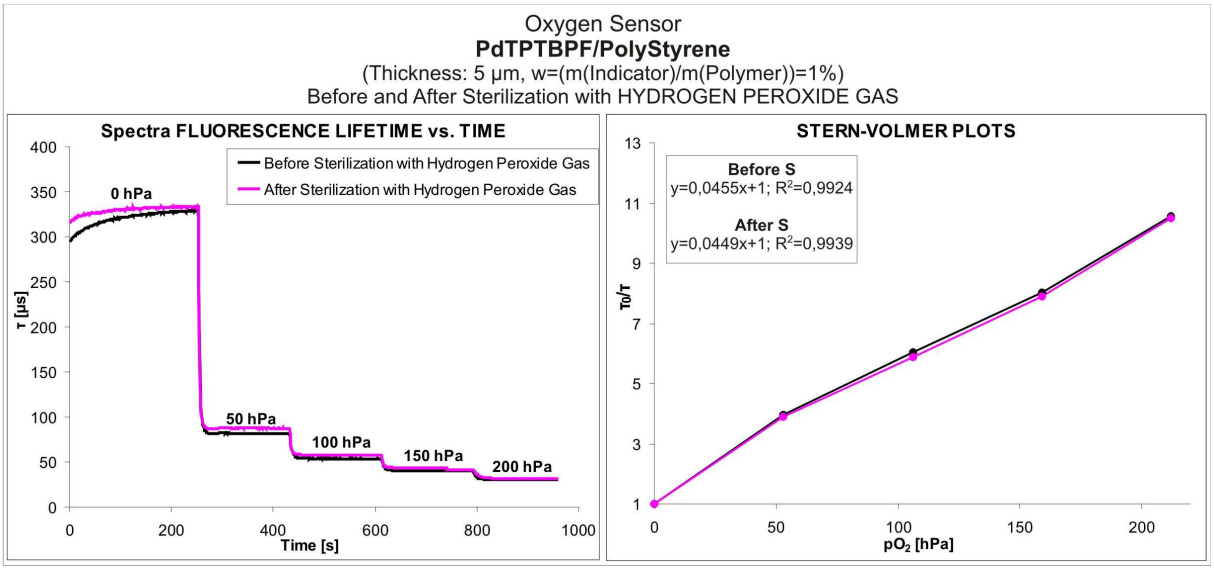

Sterilization with Low-Temperature H_2O_2 Plasma	Luminescence Lifetime	Stern-Volmer Plot
Alterations in Luminescence Lifetime and Slope	2,11% increase of τ_0	1,32% increase of slope
	4,22% increase of τ at 50 hPa	
	5,12% increase of τ at 100 hPa	
	3,81% increase of τ at 150 hPa	
	2,53% increase of τ at 200 hPa	

F.17.2 Sterilization with Low-Temperature Hydrogen Peroxide Plasma

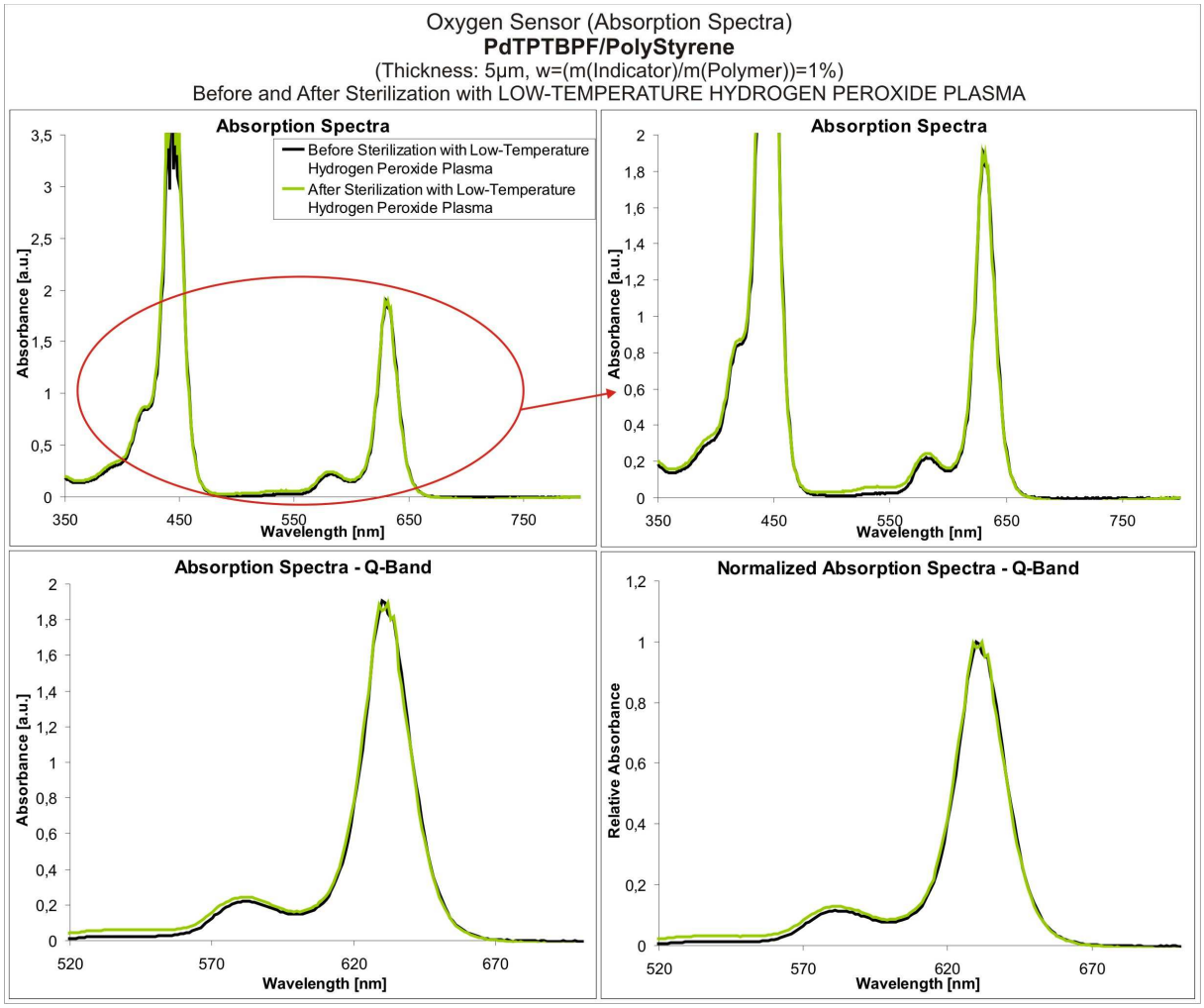

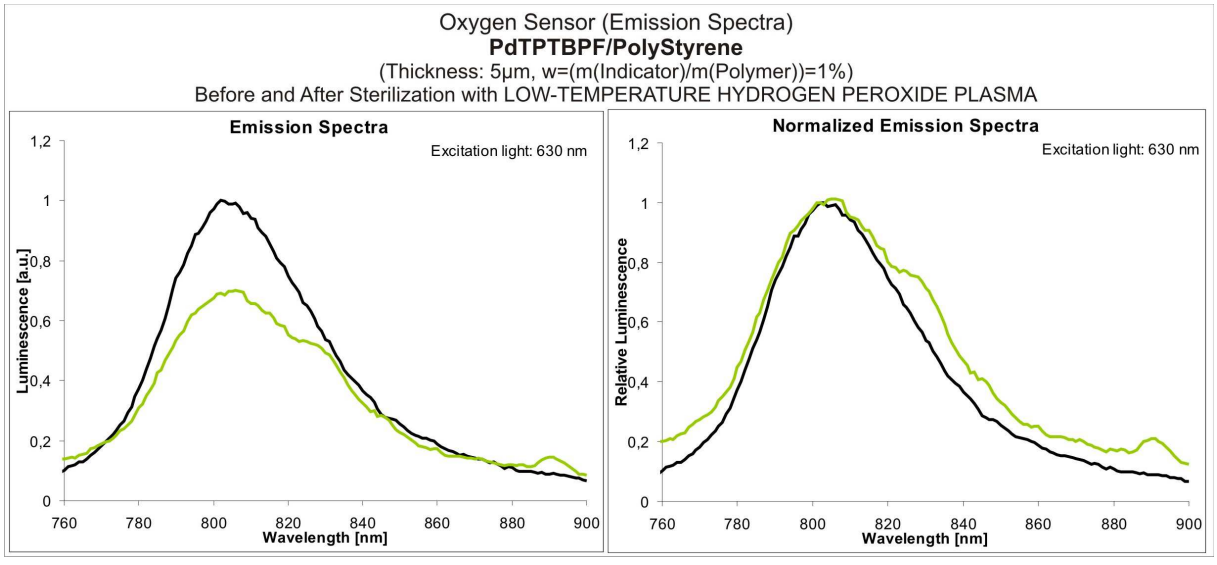

Sterilization with Low-Temperature H_2O_2 Plasma	Absorption Spectra	Emission Spectra
Alterations in Absorption/Emission Intensity	0,59% decrease	30,97% decrease
Alterations in Absorption/Emission Curve Form	Altered absorption curve form between 490-600 nm,	Altere emission curve form between 820-900 nm (probably due to low luminescence intensity.)

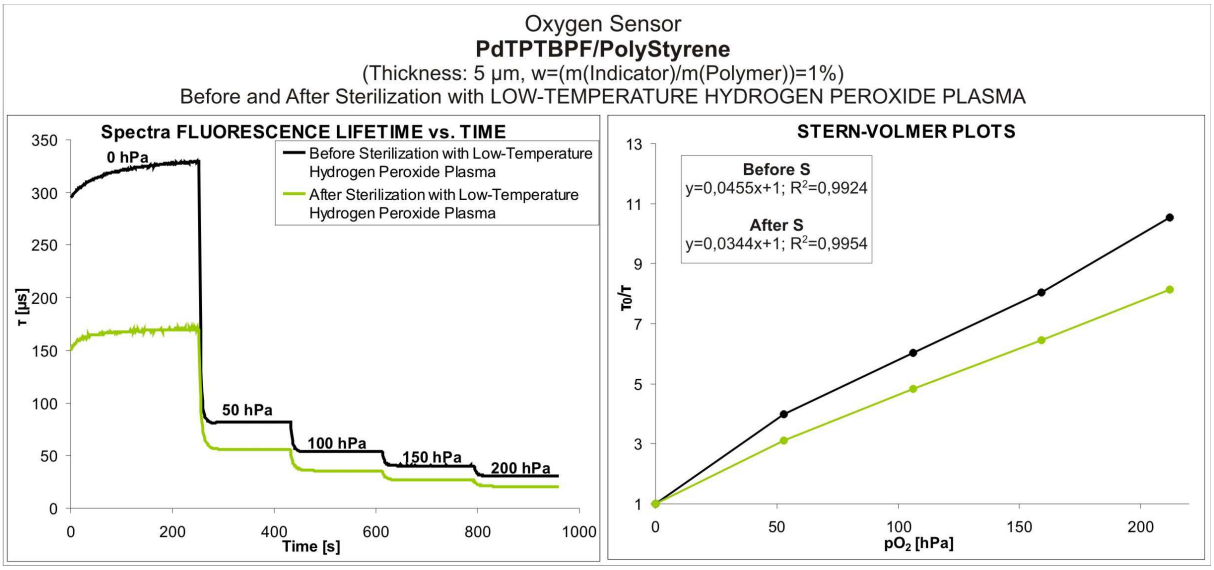

Sterilization with Low-Temperature H_2O_2 Plasma	Luminescence Lifetime	Stern-Volmer Plot
Alterations in Luminescence Lifetime and Slope	73,97% decrease of τ_0	24,40% decrease of slope
	66,75% decrease of τ at 50 hPa	
	67,41% decrease of τ at 100 hPa	
	67,57% decrease of τ at 150 hPa	
	66,23% decrease of τ at 200 hPa	

F.18 Ruthenium(II) DiPhenylPhenanthroline DiChloride ($Ru(dpp)_3Cl_2$) immobilized in HydroGel D4/D7

F.18.1 Sterilization with Hydrogen Peroxide Gas

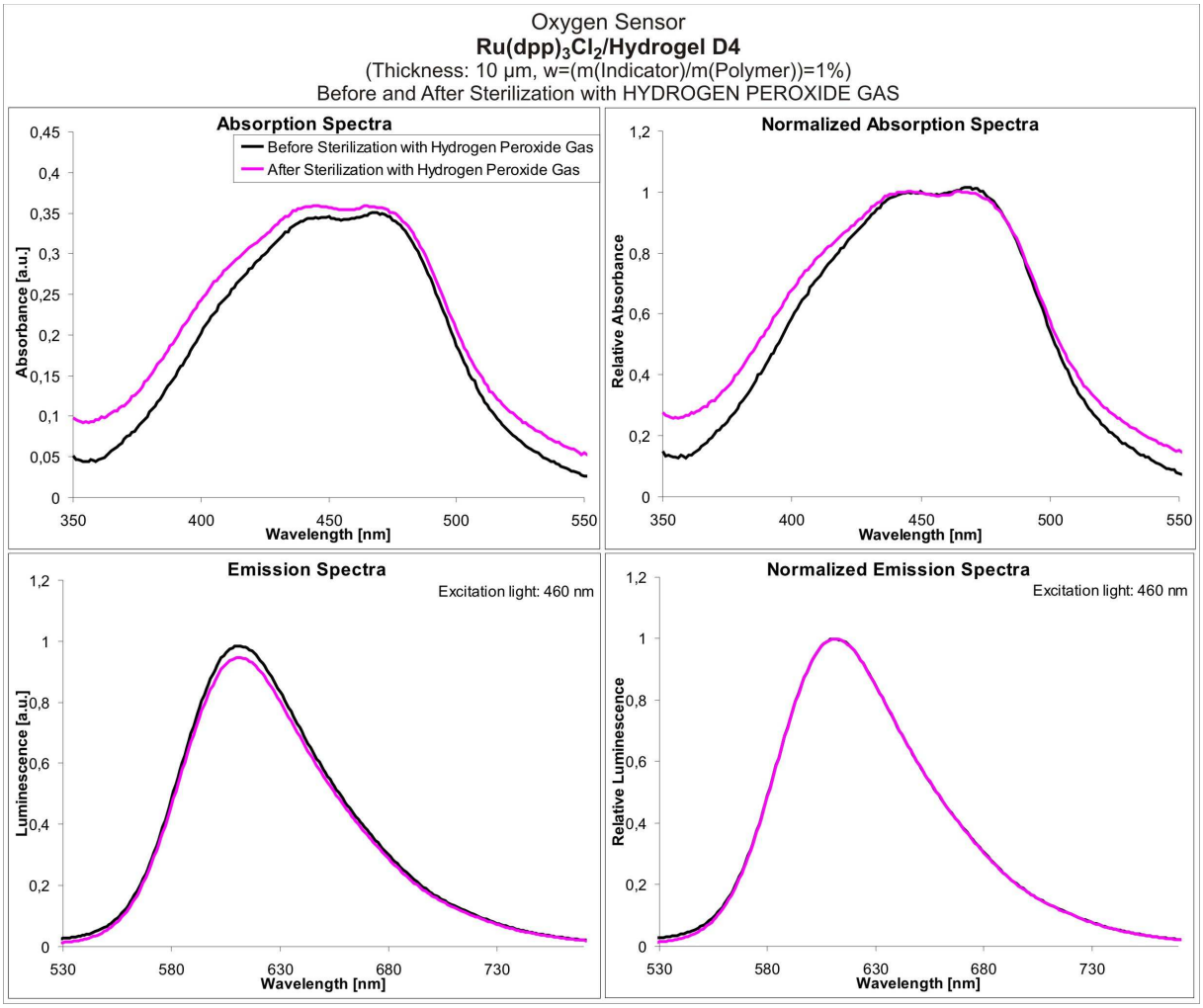

Sterilization with H_2O_2 Gas	Absorption Spectra	Emission Spectra
Alterations in Absorption/Emission Intensity	3,70% increase	3,85% decrease
Alterations in Absorption/Emission Curve Form	Sensor became slightly turbid after sterilization. Altered absorption curve form between 350-440 nm and 500-800 nm.	Unaltered.

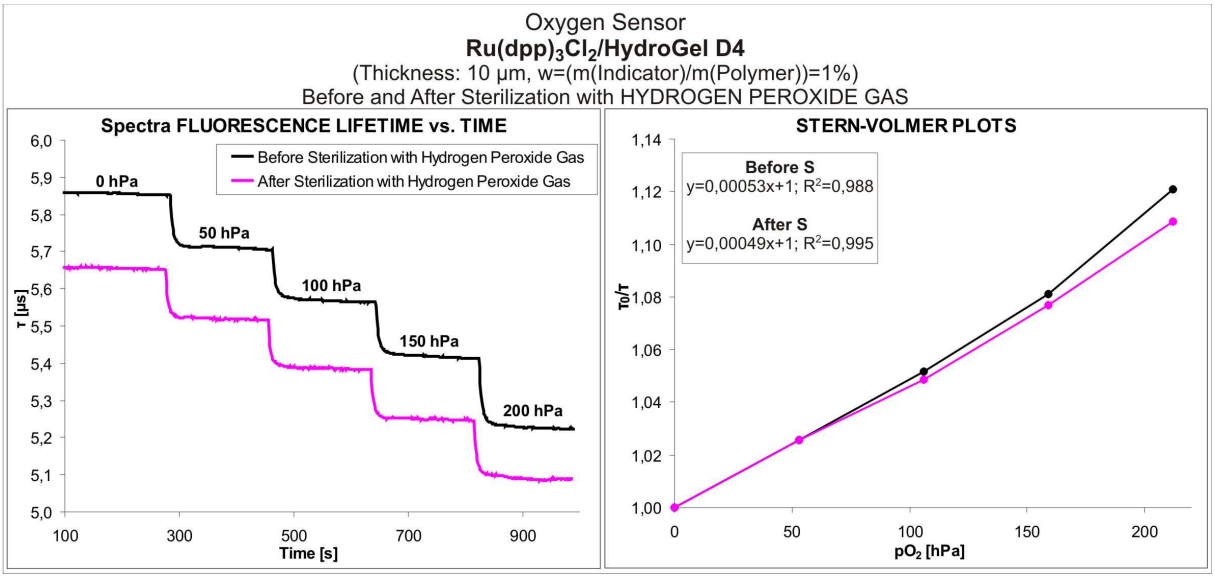

Sterilization with H_2O_2 Gas	Luminescence Lifetime	Stern-Volmer Plot
Alterations in Luminescence Lifetime and Slope	3,80% decrease of τ_0	7,55% decrease of slope
	3,70% decrease of τ at 50 hPa	
	3,39% decrease of τ at 100 hPa	
	3,28% decrease of τ at 150 hPa	
	2,55% decrease of τ at 200 hPa	

F.18.2 Sterilization with Low-Temperature Hydrogen Peroxide Plasma

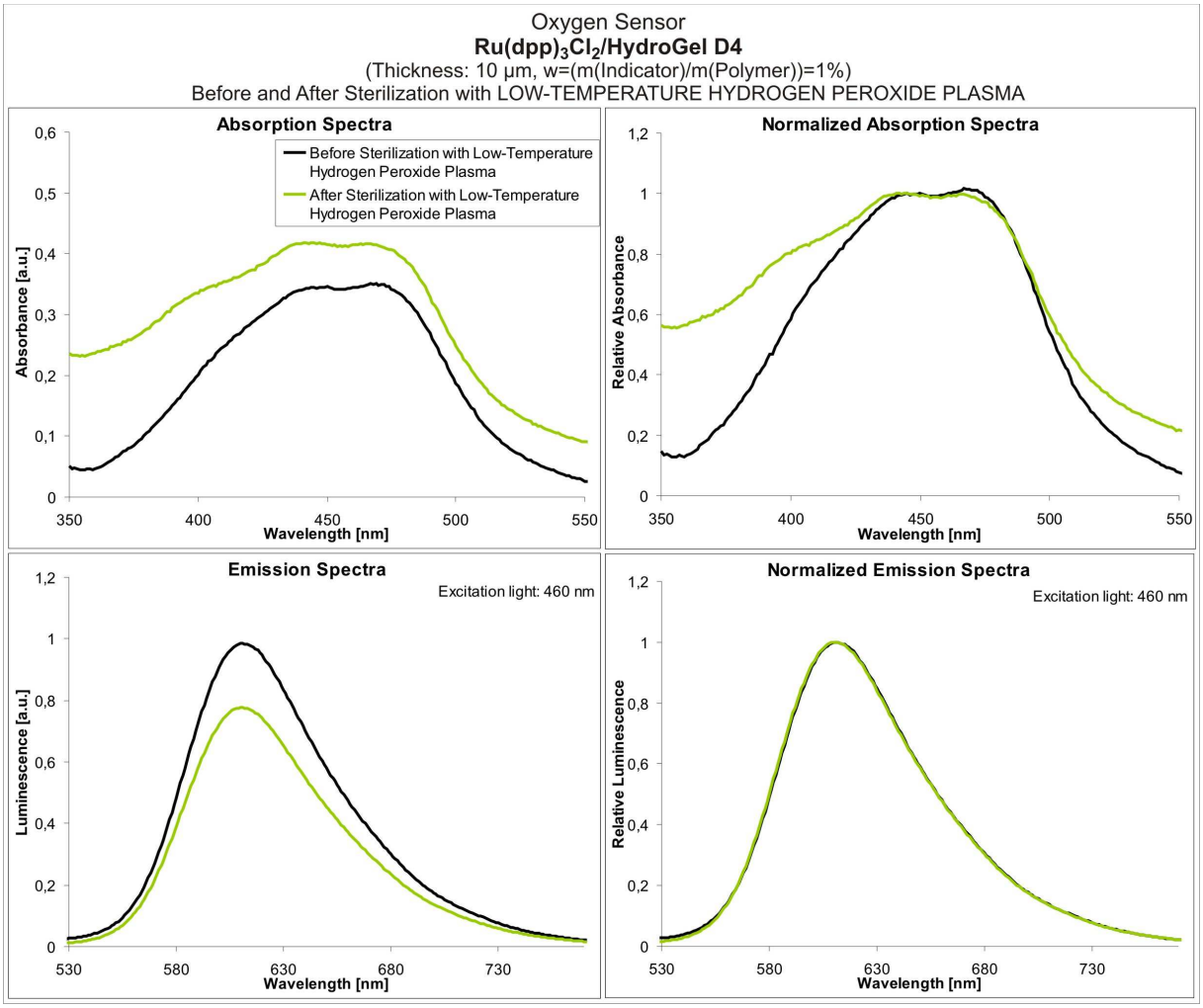

Sterilization with Low-Temperature H_2O_2 Plasma	Absorption Spectra	Emission Spectra
Alterations in Absorption/Emission Intensity	17,43% increase	21,20% decrease
Alterations in Absorption/Emission Curve Form	Sensor became turbid after sterilization. Altered absorption curve form from 350-430 nm, 465-480 nm and 495-800 nm.	Unaltered.

Oxygen Sensor
$Ru(dpp)_3Cl_2$/HydroGel D4
(Thickness: 10 µm, w=(m(Indicator)/m(Polymer))=1%)
Before and After Sterilization with LOW-TEMPERATURE HYDROGEN PEROXIDE PLASMA

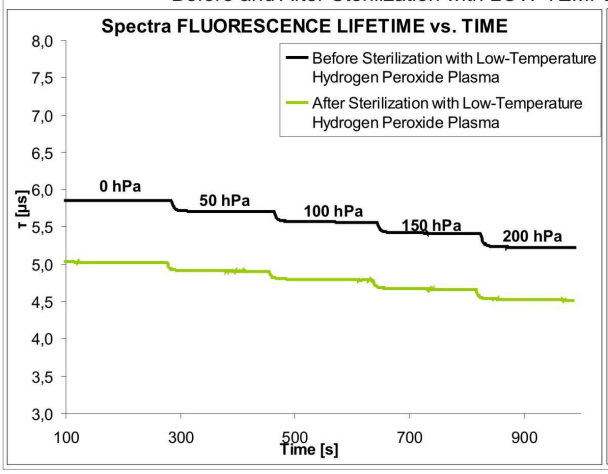

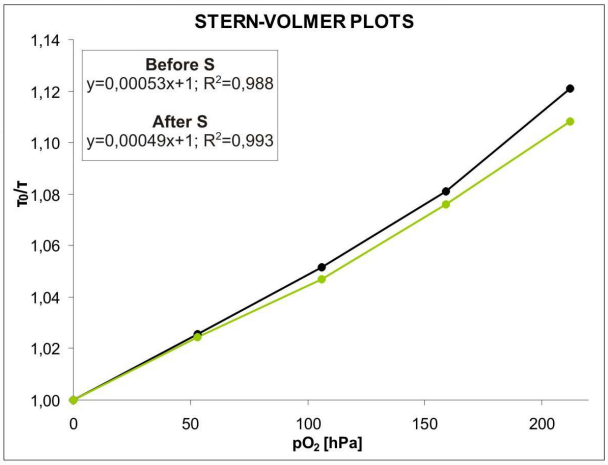

Sterilization with Low-Temperature H_2O_2 Plasma	Luminescence Lifetime	Stern-Volmer Plot
Alterations in Luminescence Lifetime and Slope	14,42% decrease of τ_0	30,61% decrease of slope
	14,15% decrease of τ at 50 hPa	
	13,97% decrease of τ at 100 hPa	
	14,01% decrease of τ at 150 hPa	
	13,40% decrease of τ at 200 hPa	

F.19 Ruthenium(II) DiPhenylPhenanthroline DiChloride ($Ru(dpp)_3Cl_2$) immobilized in HydroThane5

F.19.1 Sterilization with Hydrogen Peroxide Gas

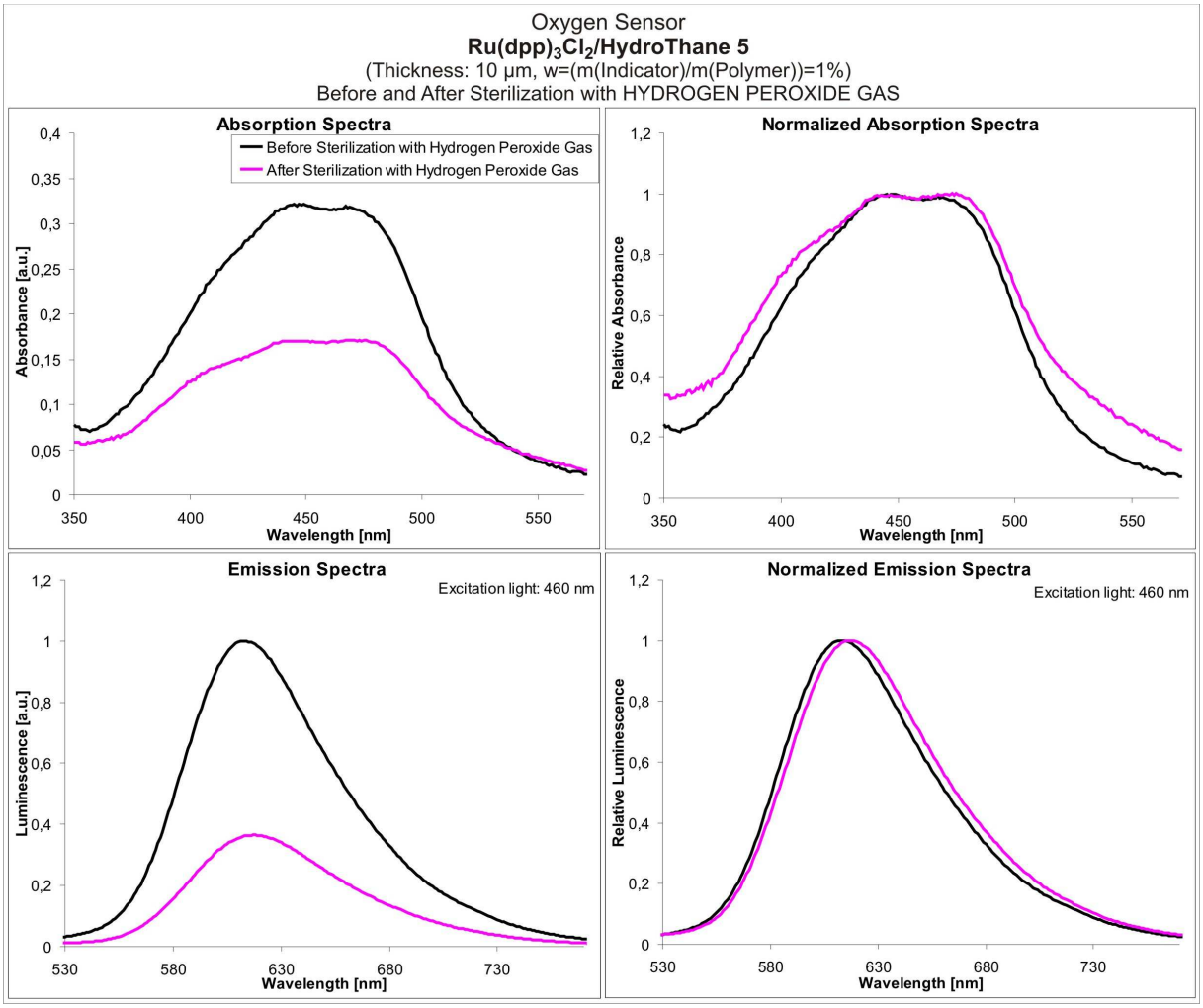

Sterilization with H_2O_2 Gas	Absorption Spectra	Emission Spectra
Alterations in Absorption/Emission Intensity	46,73% decrease	63,48% decrease
Alterations in Absorption/Emission Curve Form	Altered absorption curve form between 350-425 nm and 470-800 nm.	Bathochromic shift of emission maximum for 5 nm.

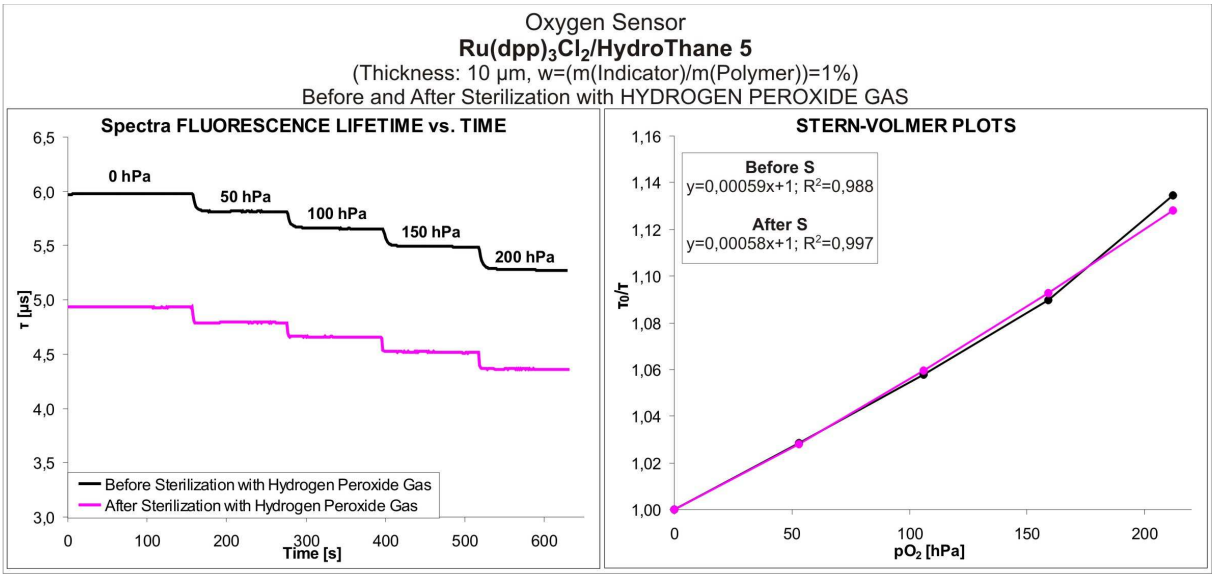

Sterilization with H_2O_2 Gas	Luminescence Lifetime	Stern-Volmer Plot
Alterations in Luminescence Lifetime and Slope	17,84% decrease of τ_0	1,01% decrease of slope
	17,78% decrease of τ at 50 hPa	
	17,88% decrease of τ at 100 hPa	
	18,02% decrease of τ at 150 hPa	
	17,47% decrease of τ at 200 hPa	

F.19.2 Sterilization with Low-Temperature Hydrogen Peroxide Plasma

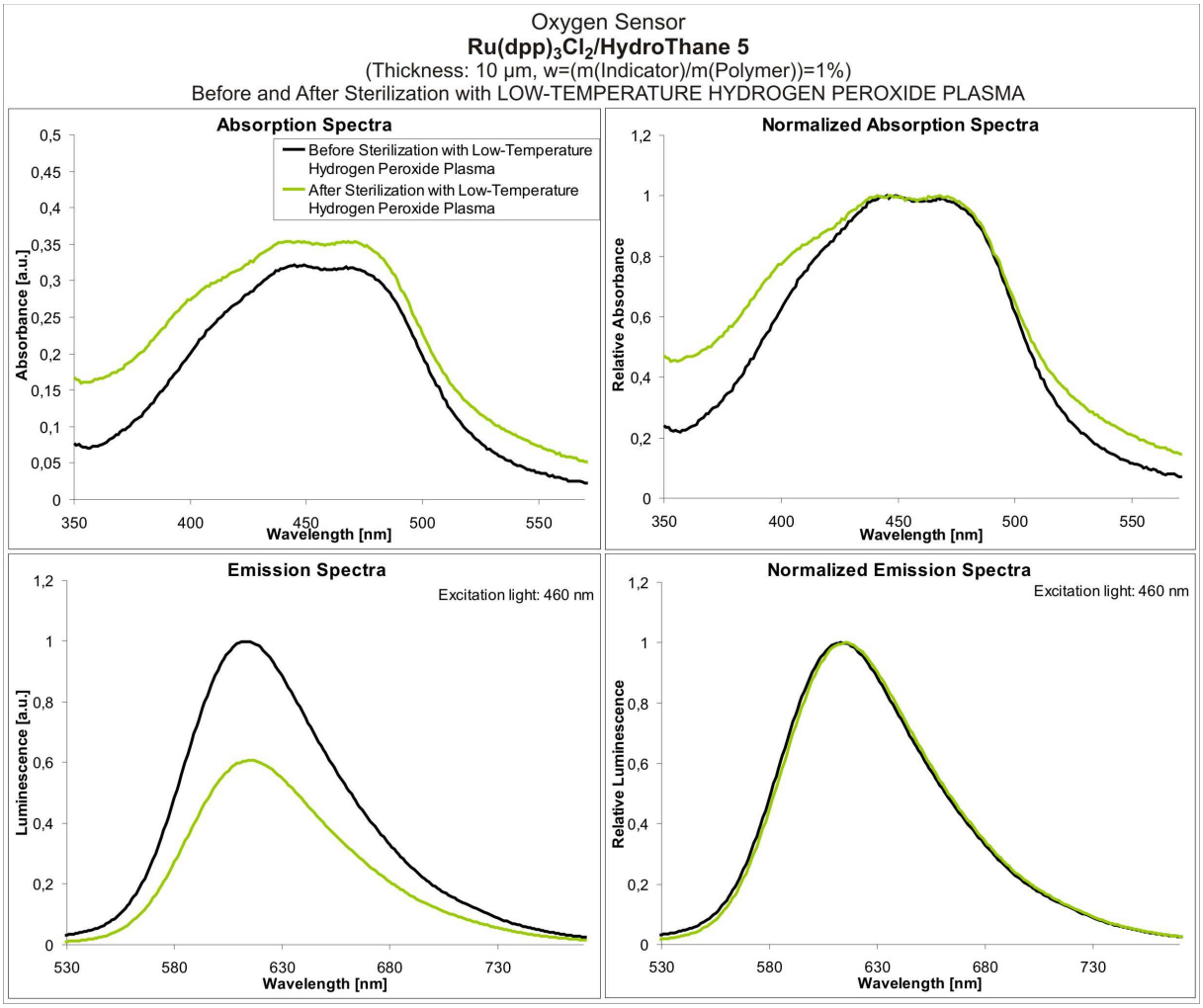

Sterilization with Low-Temperature H_2O_2 Plasma	Absorption Spectra	Emission Spectra
Alterations in Absorption/Emission Intensity	10,27% increase	39,23% decrease
Alterations in Absorption/Emission Curve Form	Sensor became slightly turbid after sterilization. Altered absorption curve form from 350-435 nm and 500-800 nm.	Bathochromic shift of the emission maximum for 3 nm.

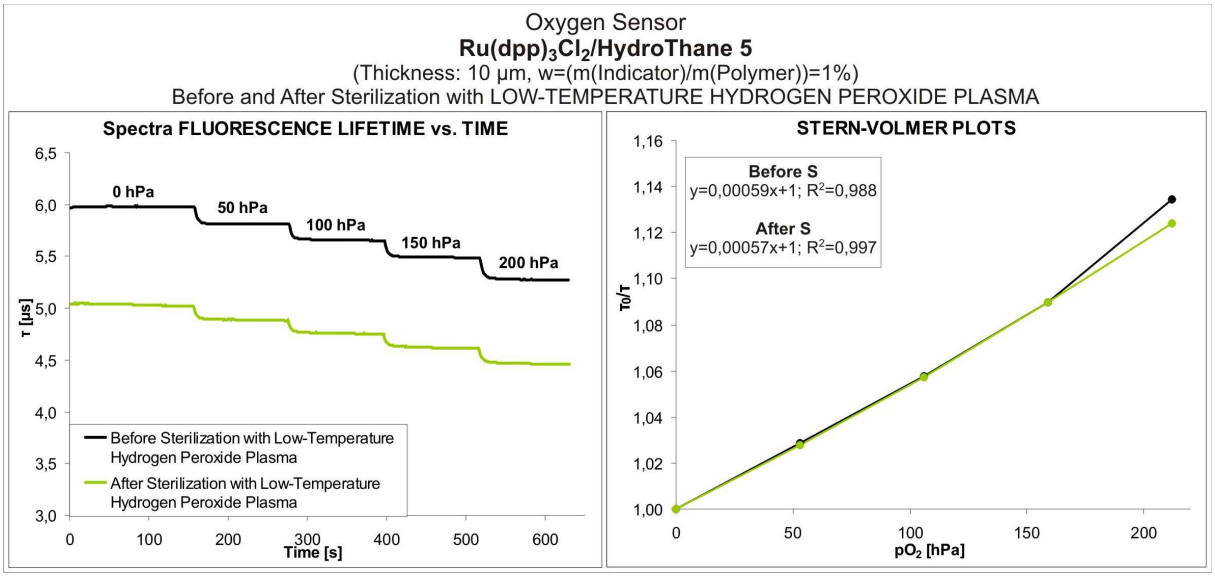

Sterilization with Low-Temperature H_2O_2 Plasma	Luminescence Lifetime	Stern-Volmer Plot
Alterations in Luminescence Lifetime and Slope	16,17% decrease of τ_0	4,21% decrease of slope
	16,04% decrease of τ at 50 hPa	
	16,11% decrease of τ at 100 hPa	
	16,16% decrease of τ at 150 hPa	
	15,37% decrease of τ at 200 hPa	

F.20 Ruthenium(II) DiPhenylPhenanthroline DiChloride ($Ru(dpp)_3Cl_2$) immobilized in PolySulfone

F.20.1 Sterilization with Hydrogen Peroxide Gas

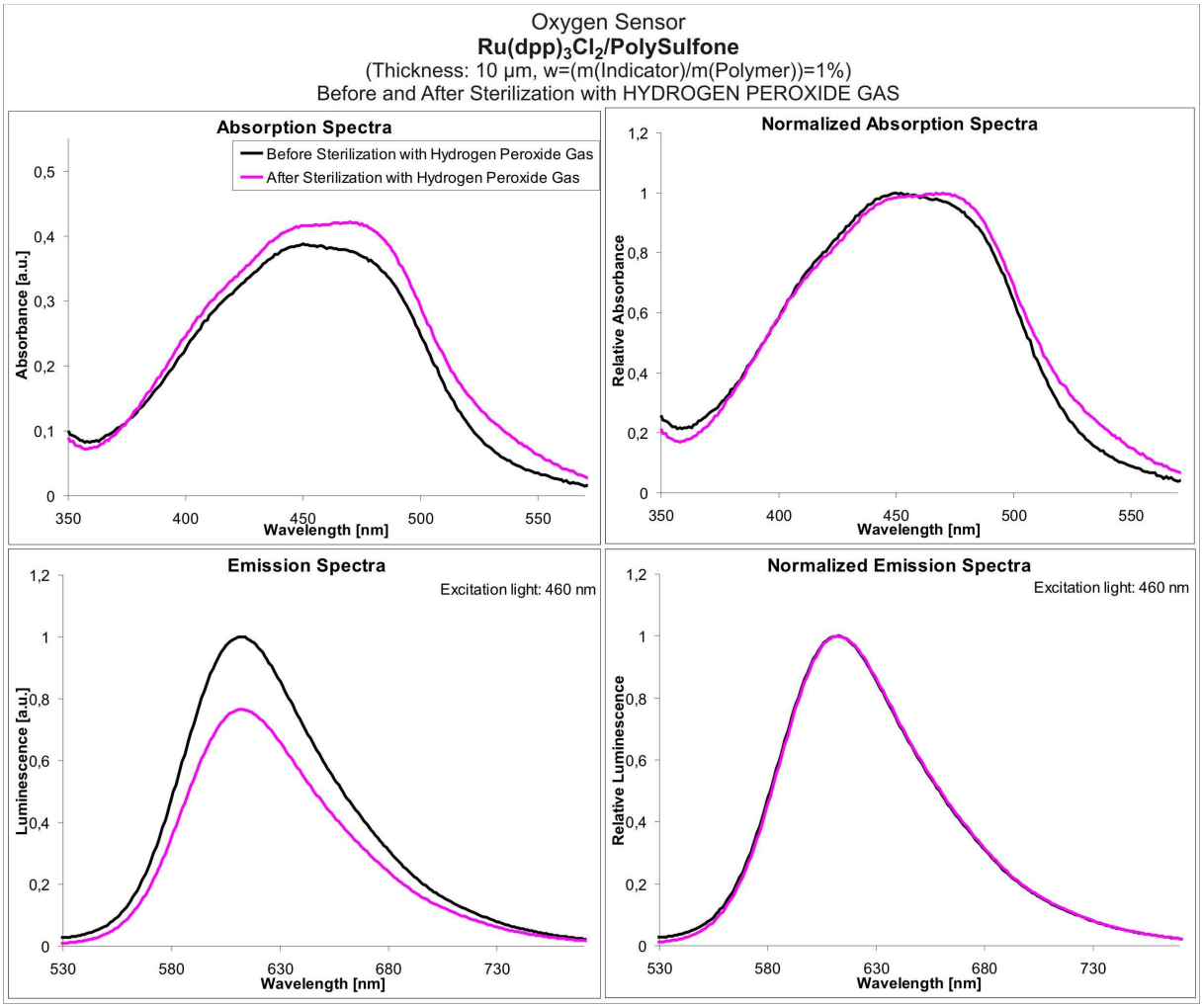

Sterilization with H_2O_2 Gas	Absorption Spectra	Emission Spectra
Alterations in Absorption/Emission Intensity	8,15% increase	23,52% decrease
Alterations in Absorption/Emission Curve Form	Altered absorption curve form between 350-375 nm and 410-800 nm.	Unaltered.

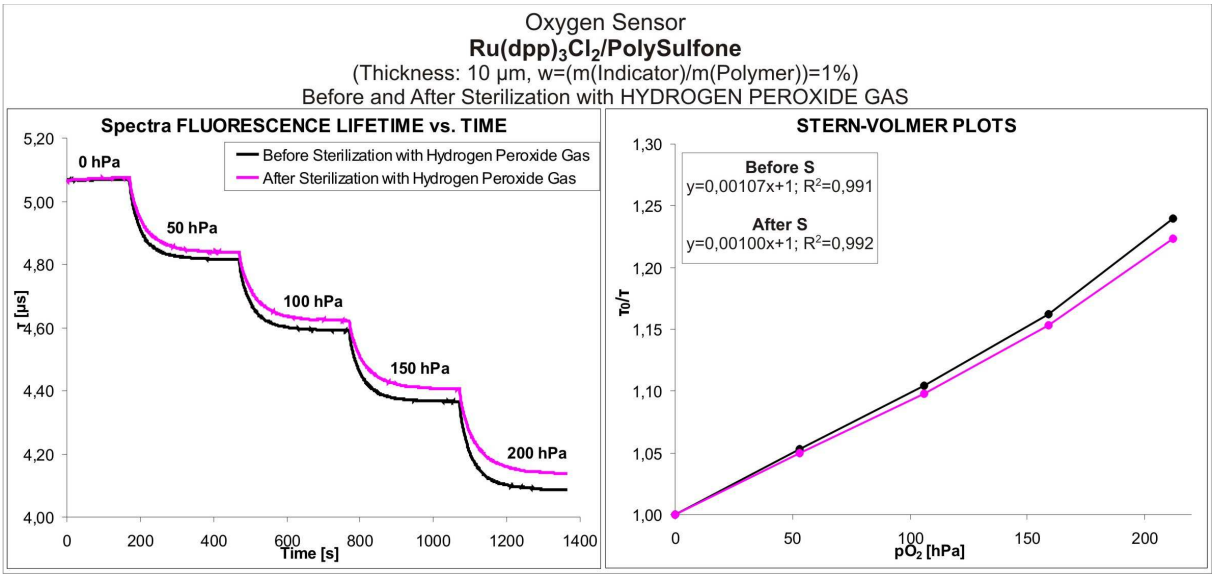

Sterilization with H_2O_2 Gas	Luminescence Lifetime	Stern-Volmer Plot
Alterations in Luminescence Lifetime and Slope	0,19% decrease of τ_0	9,10% decrease of slope
	0,21% increase of τ at 50 hPa	
	0,43% increase of τ at 100 hPa	
	0,68% increase of τ at 150 hPa	
	1,21% increase of τ at 200 hPa	

F.20.2 Sterilization with Low-Temperature Hydrogen Peroxide Plasma

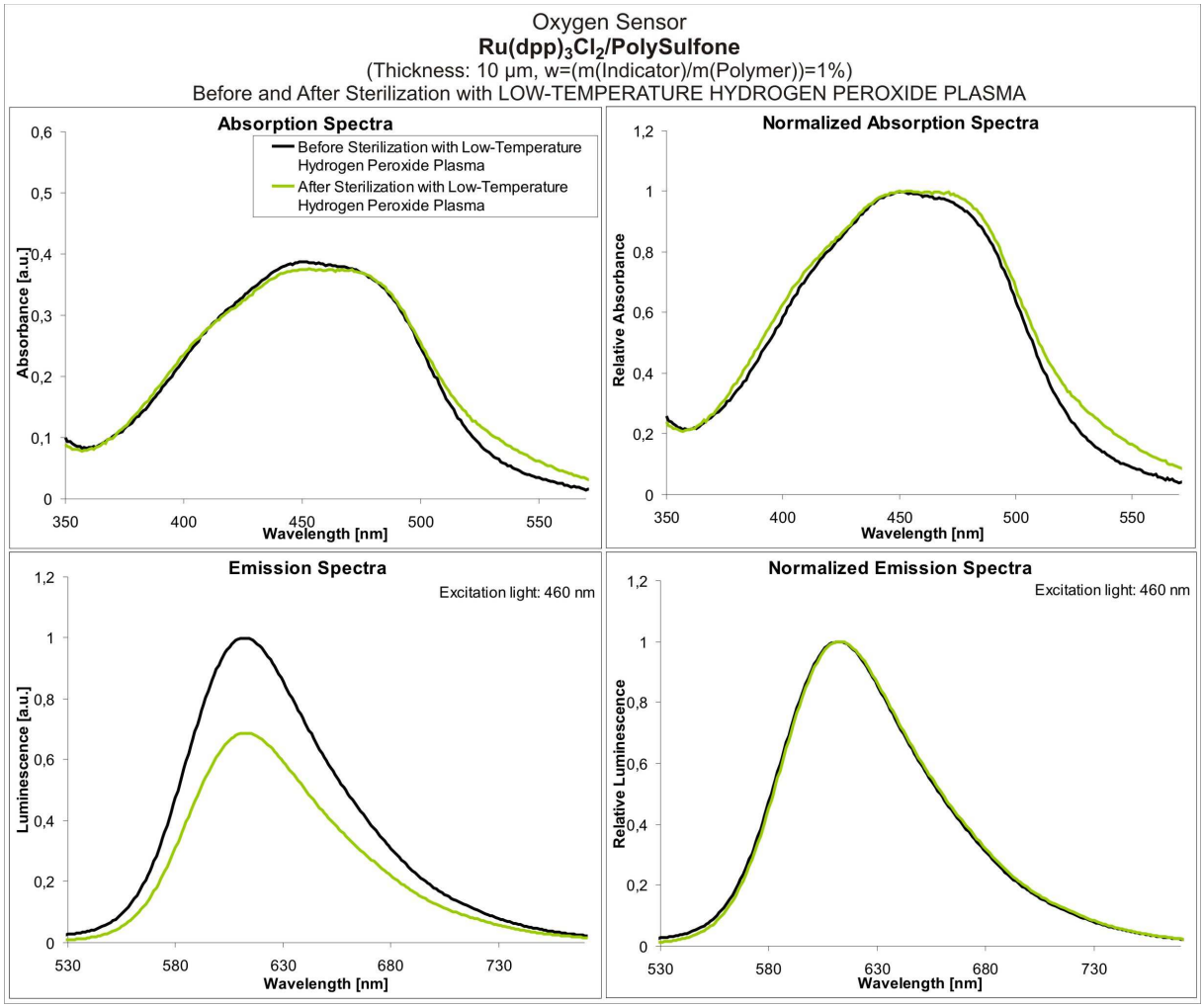

Sterilization with Low-Temperature H_2O_2 Plasma	Absorption Spectra	Emission Spectra
Alterations in Absorption/Emission Intensity	3,33% decrease	31,26% decrease
Alterations in Absorption/Emission Curve Form	Altered absorption curve form from 450-800 nm.	Unaltered.

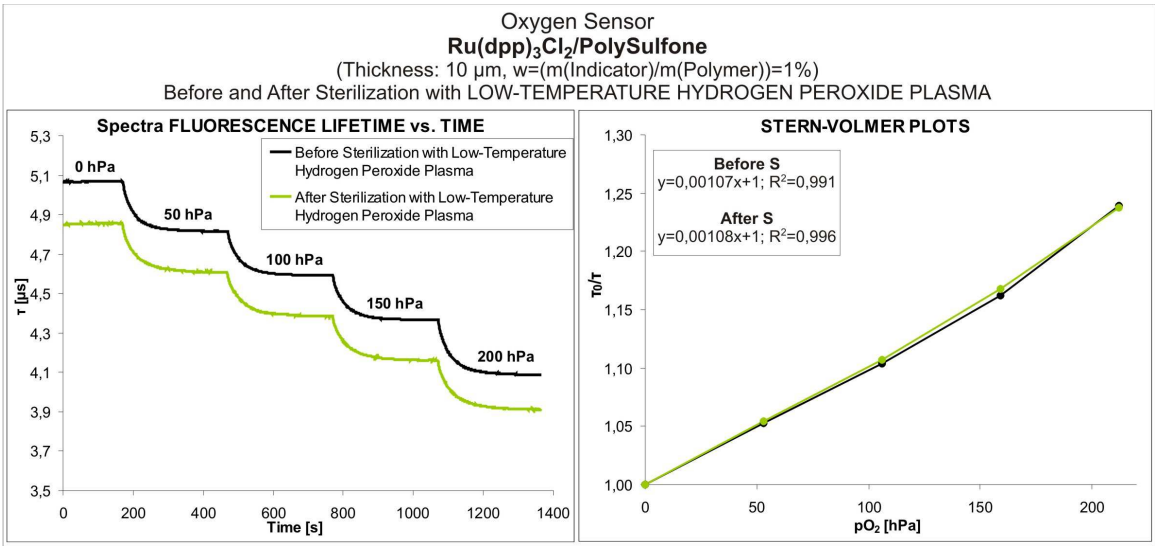

Sterilization with Low-Temperature H_2O_2 Plasma	Luminescence Lifetime	Stern-Volmer Plot
Alterations in Luminescence Lifetime and Slope	4,31% decrease of τ_0	0,93% increase of slope
	4,63% decrease of τ at 50 hPa	
	4,47% decrease of τ at 100 hPa	
	4,90% decrease of τ at 150 hPa	
	4,35% decrease of τ at 200 hPa	

F.21 Ruthenium(II) DiPhenylPhenanthroline DiChloride ($Ru(dpp)_3Cl_2$) immobilized in PolyPhenyl SilsesQuioxane

F.21.1 Sterilization with Hydrogen Peroxide Gas

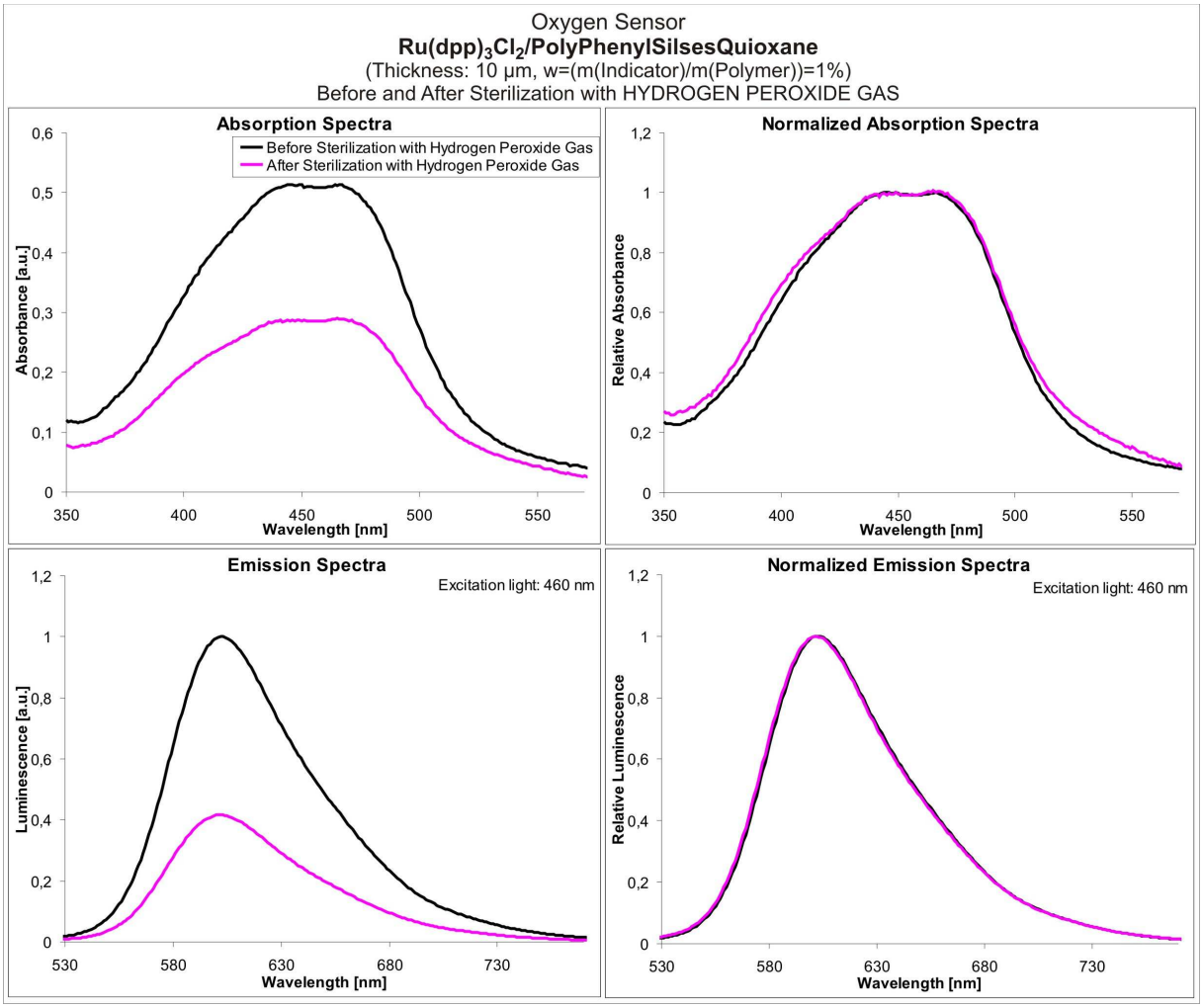

Sterilization with H_2O_2 Gas	Absorption Spectra	Emission Spectra
Alterations in Absorption/Emission Intensity	43,89% decrease	58,37% decrease
Alterations in Absorption/Emission Curve Form	Altered absorption curve form between 350-420 nm and 505-800 nm.	Unaltered.

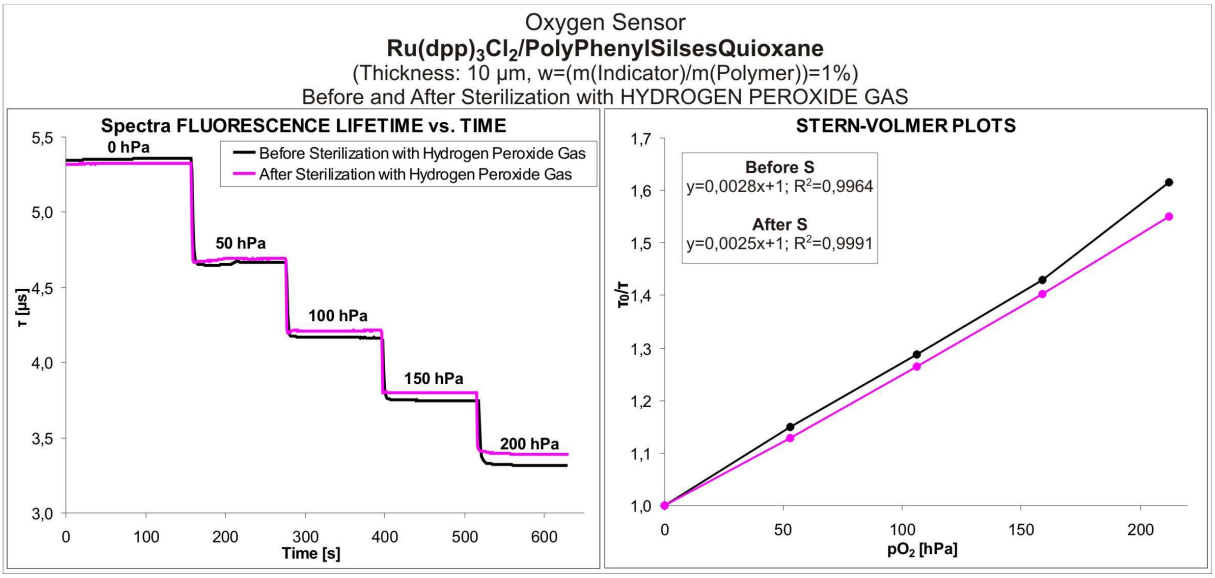

Sterilization with H_2O_2 Gas	Luminescence Lifetime	Stern-Volmer Plot
Alterations in Luminescence Lifetime and Slope	2,07% decrease of τ_0	10,71% decrease of slope
	0,24% decrease of τ at 50 hPa	
	0,26% decrease of τ at 100 hPa	
	0,30% decrease of τ at 150 hPa	
	1,96% increase of τ at 200 hPa	

F.21.2 Sterilization with Low-Temperature Hydrogen Peroxide Plasma

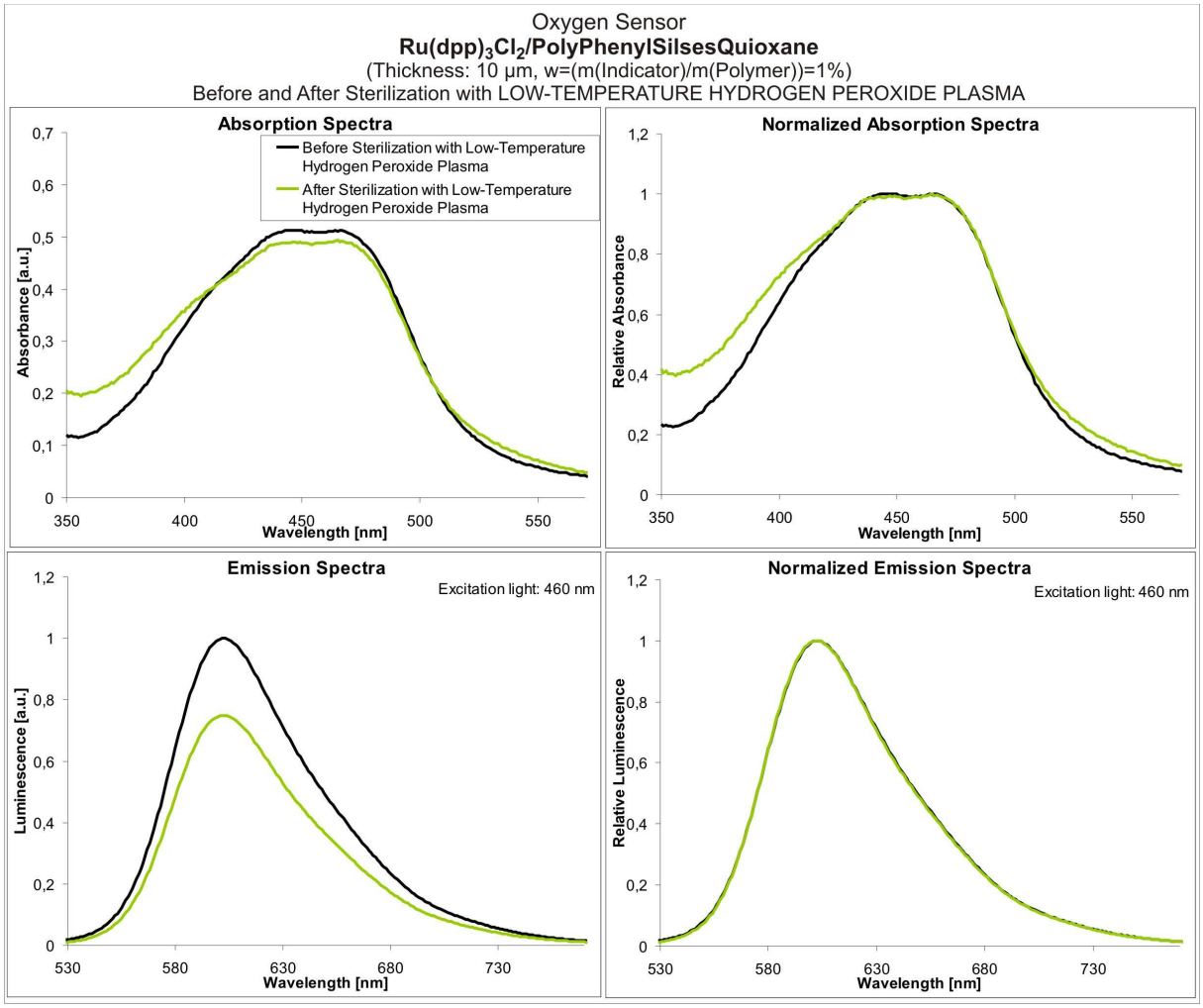

Sterilization with Low-Temperature H_2O_2 Plasma	Absorption Spectra	Emission Spectra
Alterations in Absorption/Emission Intensity	3,76% decrease	25,11% decrease
Alterations in Absorption/Emission Curve Form	Altered absorption curve form from 350-420 nm and 510-800 nm.	Unaltered.

Oxygen Sensor
$Ru(dpp)_3Cl_2$/PolyPhenylSilsesQuioxane
(Thickness: 10 µm, w=(m(Indicator)/m(Polymer))=1%)
Before and After Sterilization with LOW-TEMPERATURE HYDROGEN PEROXIDE PLASMA

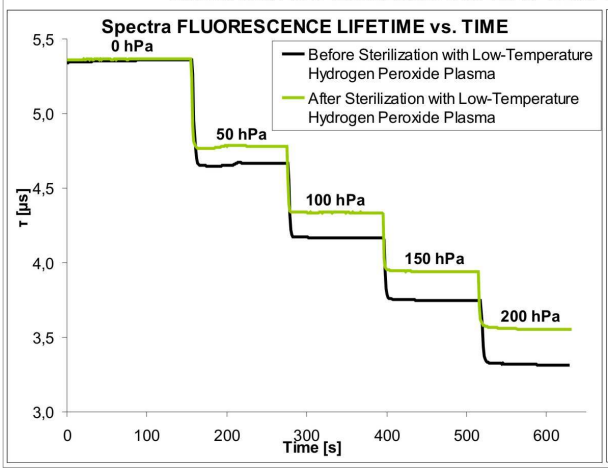

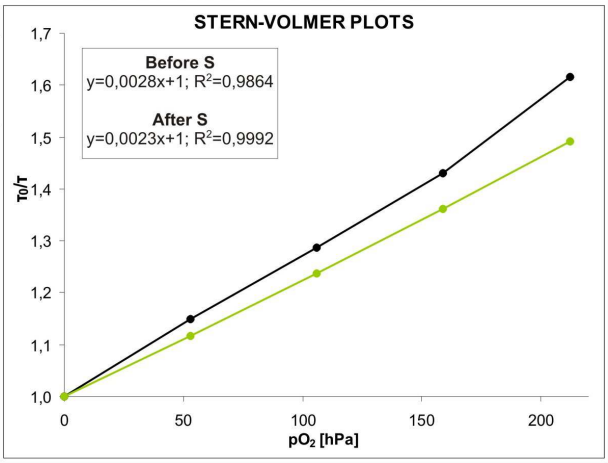

Sterilization with Low-Temperature H_2O_2 Plasma	Luminescence Lifetime	Stern-Volmer Plot
Alterations in Luminescence Lifetime and Slope	1,24% decrease of τ_0	17,86% decrease of slope
	1,87% increase of τ at 50 hPa	
	2,60% increase of τ at 100 hPa	
	3,71% increase of τ at 150 hPa	
	6,56% increase of τ at 200 hPa	

F.22 Ruthenium(II) DiPhenylPhenanthroline DiChloride ($Ru(dpp)_3Cl_2$) immobilized in PolyStyrene

F.22.1 Sterilization with Hydrogen Peroxide Gas

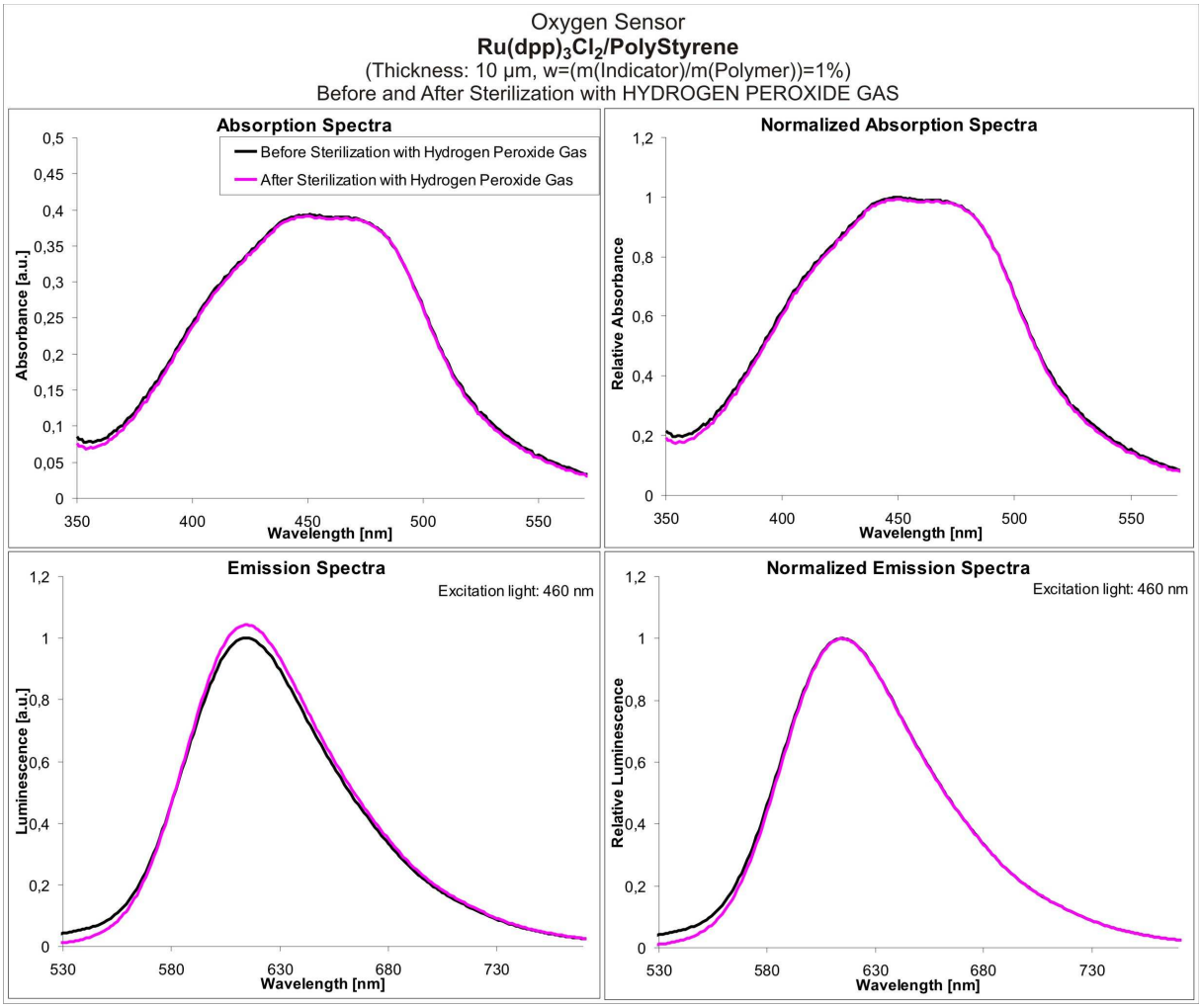

Sterilization with H_2O_2 Gas	Absorption Spectra	Emission Spectra
Alterations in Absorption/Emission Intensity	0,86% increase	4,19% increase
Alterations in Absorption/Emission Curve Form	Unaltered.	Unaltered.

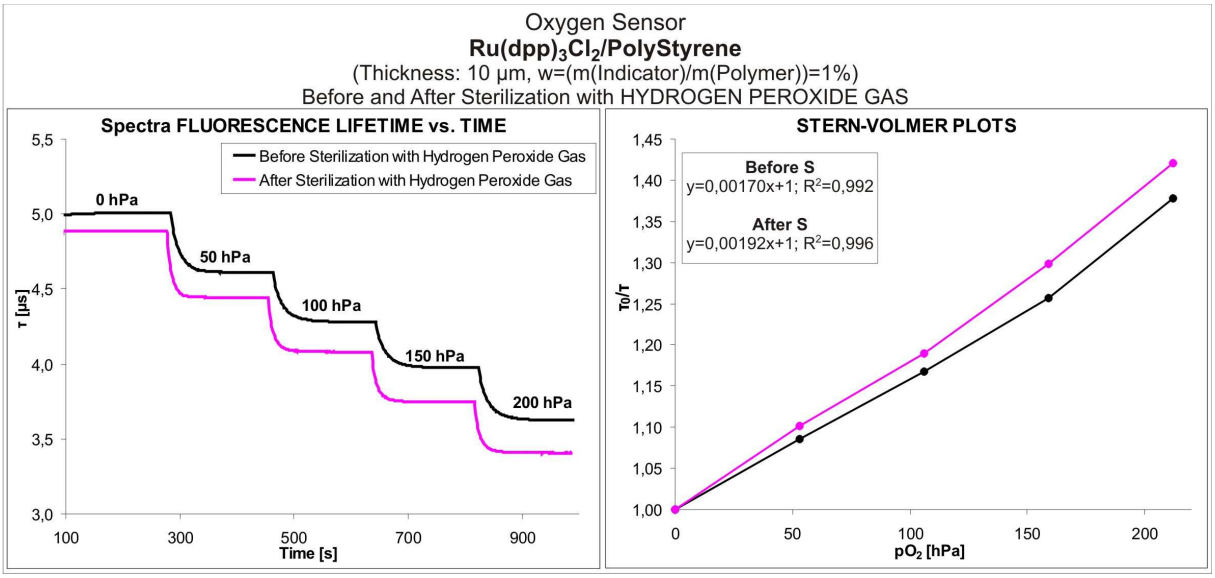

Sterilization with H_2O_2 Gas	Luminescence Lifetime	Stern-Volmer Plot
Alterations in Luminescence Lifetime and Slope	3,11% decrease of τ_0	11,64% increase of slope
	4,58% decrease of τ at 50 hPa	
	5,18% decrease of τ at 100 hPa	
	6,42% decrease of τ at 150 hPa	
	6,11% decrease of τ at 200 hPa	

F.22.2 Sterilization with Low-Temperature Hydrogen Peroxide Plasma

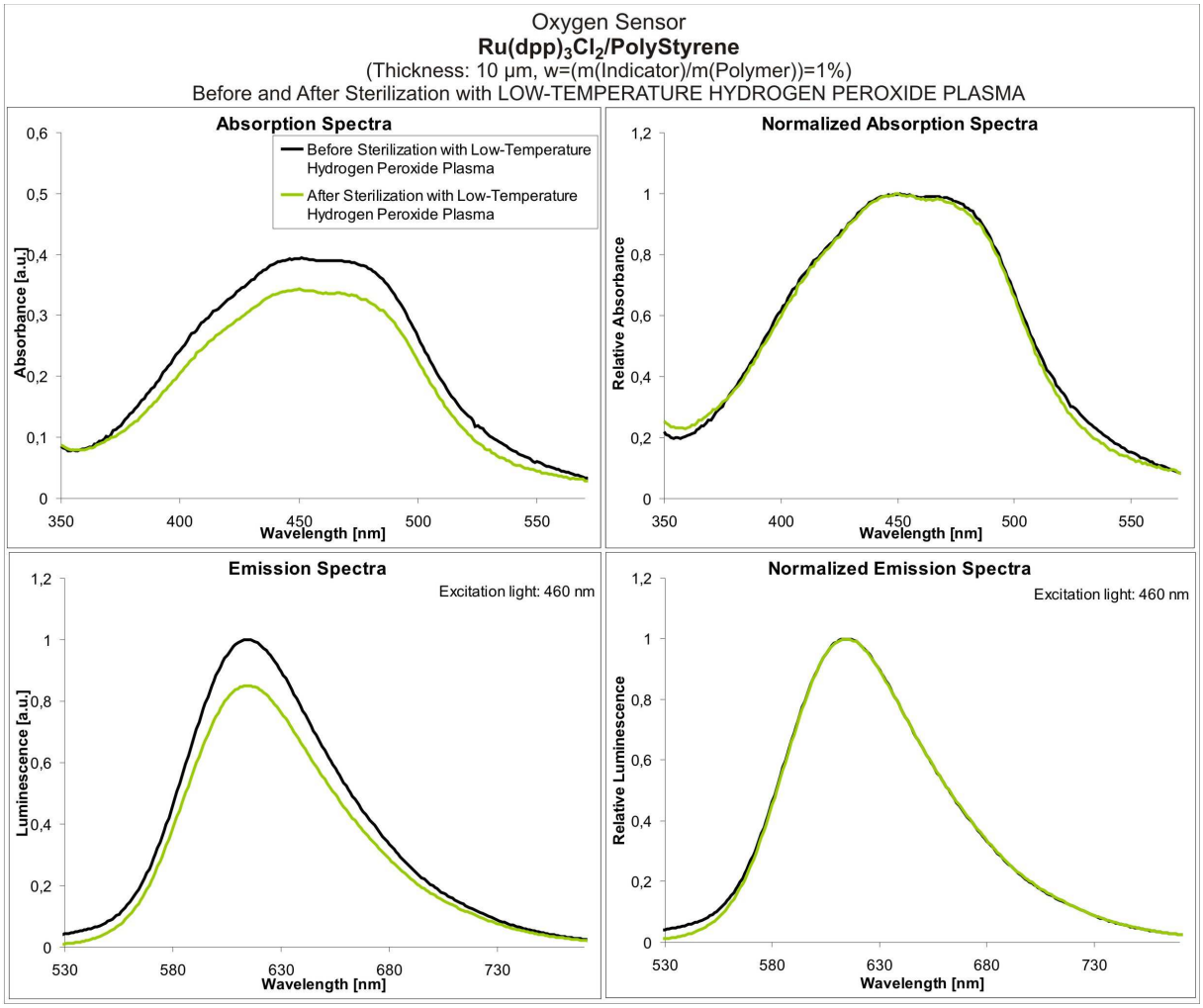

Sterilization with Low-Temperature H_2O_2 Plasma	Absorption Spectra	Emission Spectra
Alterations in Absorption/Emission Intensity	12,91% decrease	14,86% decrease
Alterations in Absorption/Emission Curve Form	Altered absorption curve form from 350-370 nm and 510-560 nm.	Altered emission curve form from 530-570 nm.

Oxygen Sensor
$Ru(dpp)_3Cl_2$/PolyStyrene
(Thickness: 10 µm, w=(m(Indicator)/m(Polymer))=1%)
Before and After Sterilization with LOW-TEMPERATURE HYDROGEN PEROXIDE PLASMA

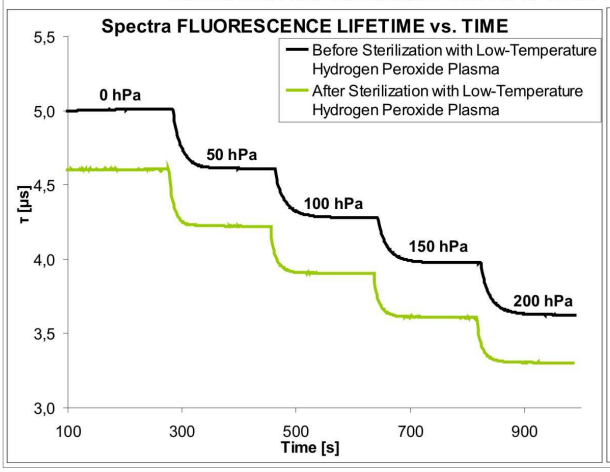

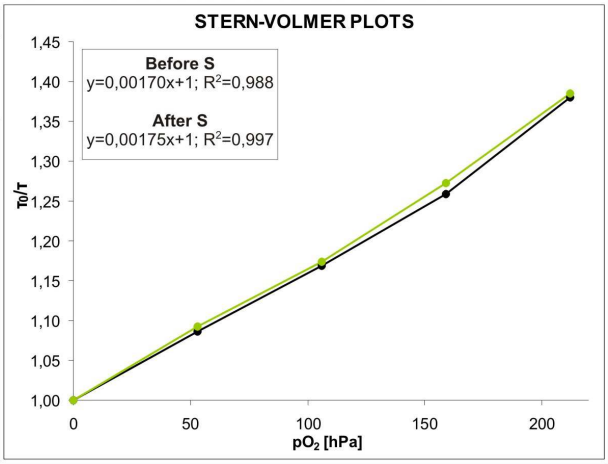

Sterilization with Low-Temperature H_2O_2 Plasma	Luminescence Lifetime	Stern-Volmer Plot
Alterations in Luminescence Lifetime and Slope	8,67% decrease of τ_0	2,86% increase of slope
	9,18% decrease of τ at 50 hPa	
	9,07% decrease of τ at 100 hPa	
	9,77% decrease of τ at 150 hPa	
	9,17% decrease of τ at 200 hPa	

F.23 Ruthenium(II) DiPhenylPhenanthroline DiChloride ($Ru(dpp)_3Cl_2$) immobilized in PolyStyrene-co-Acrylonitrile

F.23.1 Sterilization with Hydrogen Peroxide Gas

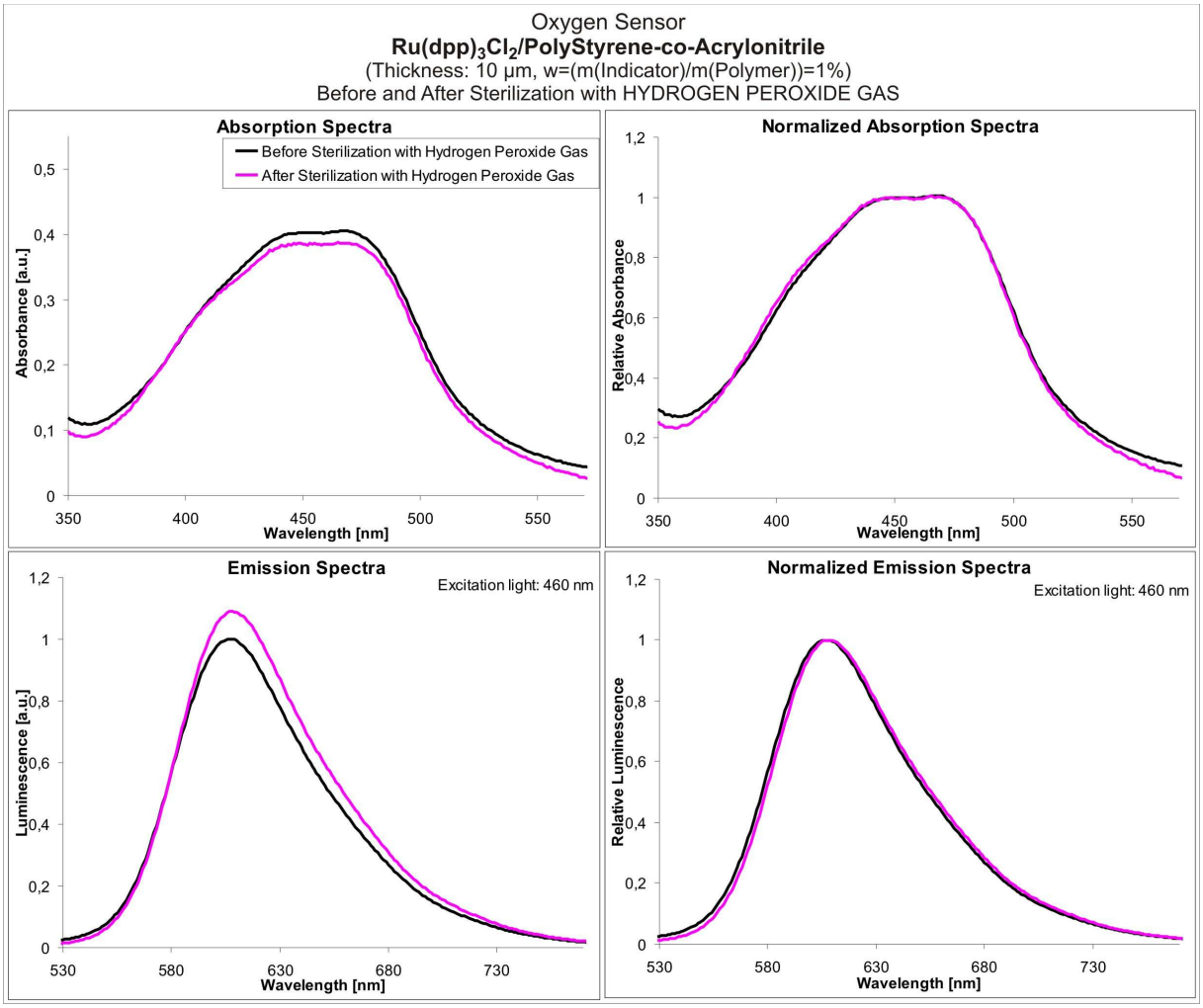

Sterilization with H_2O_2 Gas	Absorption Spectra	Emission Spectra
Alterations in Absorption/Emission Intensity	4,19% decrease	20,06% decrease
Alterations in Absorption/Emission Curve Form	Alteration of absorption curve form between 350-375 nm and 520-800 nm.	Unaltered.

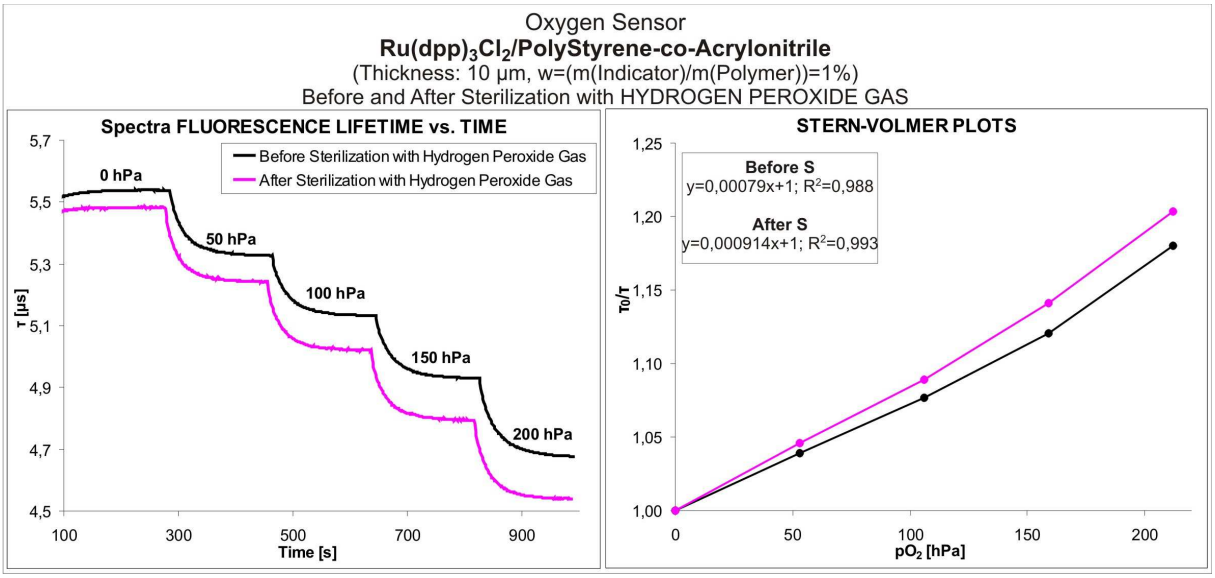

Sterilization with H_2O_2 Gas	Luminescence Lifetime	Stern-Volmer Plot
Alterations in Luminescence Lifetime and Slope	1,20% decrease of τ_0	12,74% increase of slope
	1,88% decrease of τ at 50 hPa	
	2,37% decrease of τ at 100 hPa	
	2,93% decrease of τ at 150 hPa	
	3,08% decrease of τ at 200 hPa	

F.23.2 Sterilization with Low-Temperature Hydrogen Peroxide Plasma

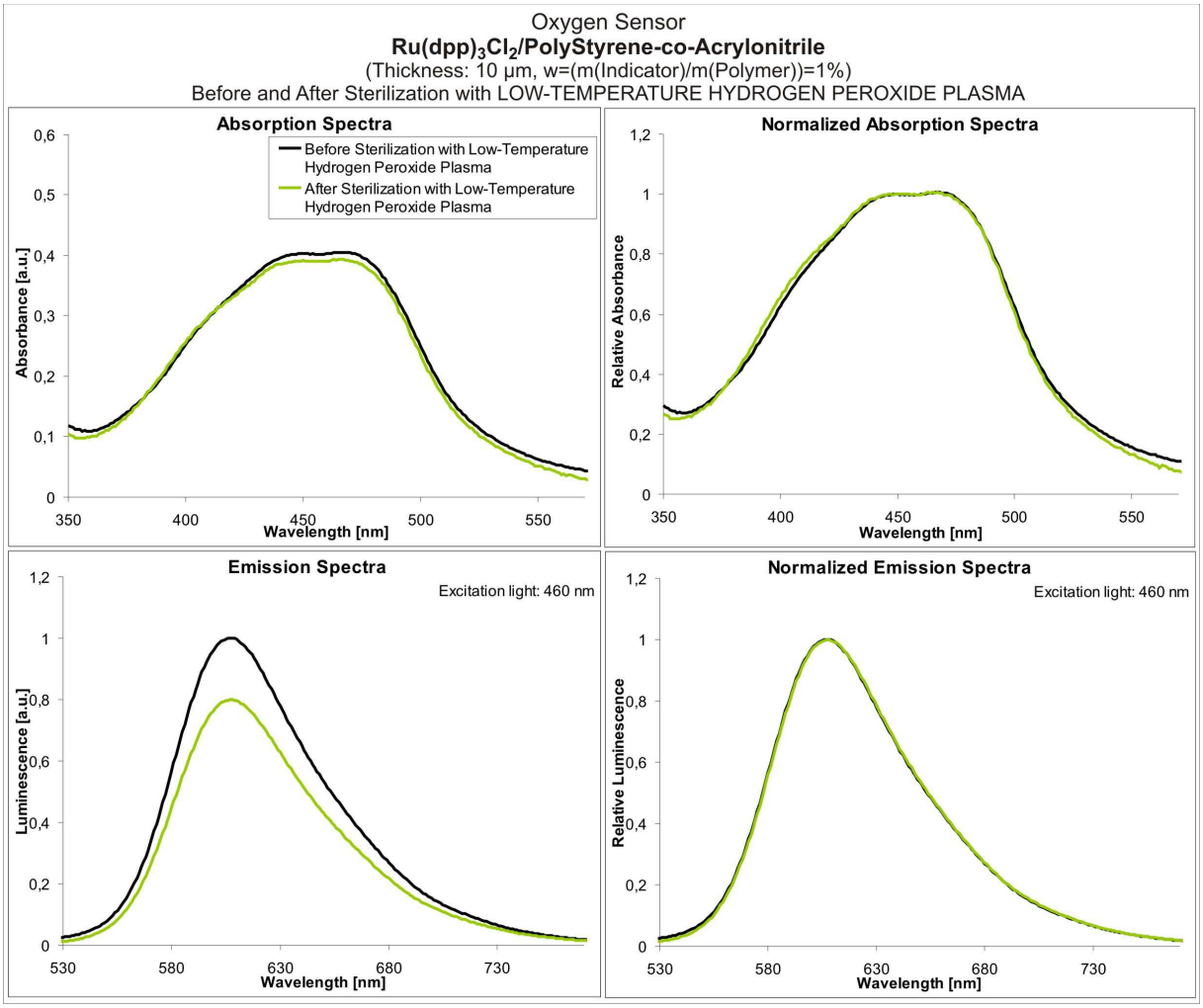

Sterilization with Low-Temperature H_2O_2 Plasma	Absorption Spectra	Emission Spectra
Alterations in Absorption/Emission Intensity	2,99% decrease	20,06% decrease
Alterations in Absorption/Emission Curve Form	Altered absorption curve form from 520-800 nm.	Unaltered.

Oxygen Sensor
$Ru(dpp)_3Cl_2$/PolyStyrene-co-Acrylonitrile
(Thickness: 10 µm, w=(m(Indicator)/m(Polymer))=1%)
Before and After Sterilization with LOW-TEMPERATURE HYDROGEN PEROXIDE PLASMA

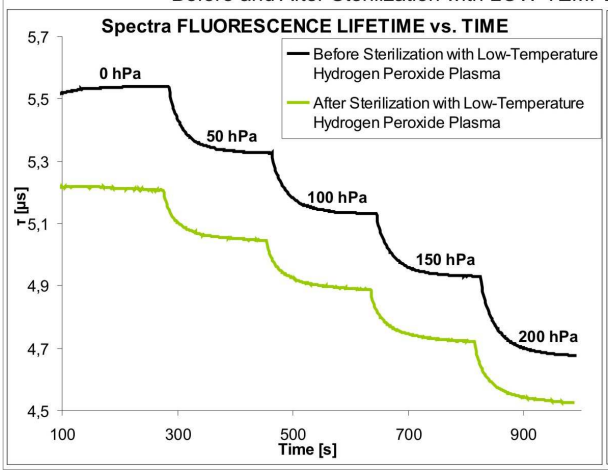

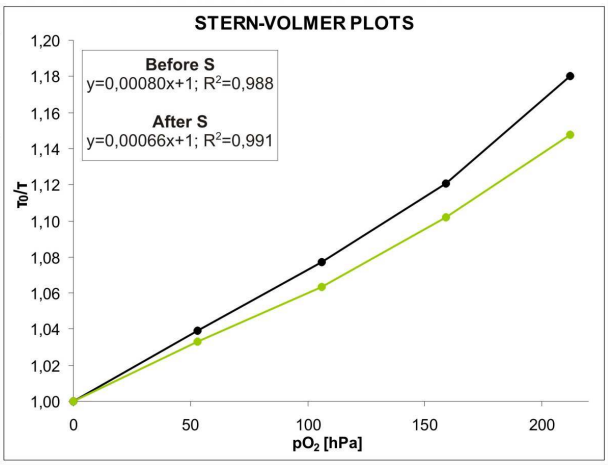

Sterilization with Low-Temperature H_2O_2 Plasma	Luminescence Lifetime	Stern-Volmer Plot
Alterations in Luminescence Lifetime and Slope	6,02% decrease of τ_0	17,29% decrease of slope
	5,43% decrease of τ at 50 hPa	
	4,97% decrease of τ at 100 hPa	
	4,28% decrease of τ at 150 hPa	
	0,97% decrease of τ at 200 hPa	

F.24 Ruthenium(II) DiPhenylPhenanthroline DiChloride ($Ru(dpp)_3Cl_2$) immobilized in PolyStyrene-co-MaleicAnhydride (PSMA93)

F.24.1 Sterilization with Hydrogen Peroxide Gas

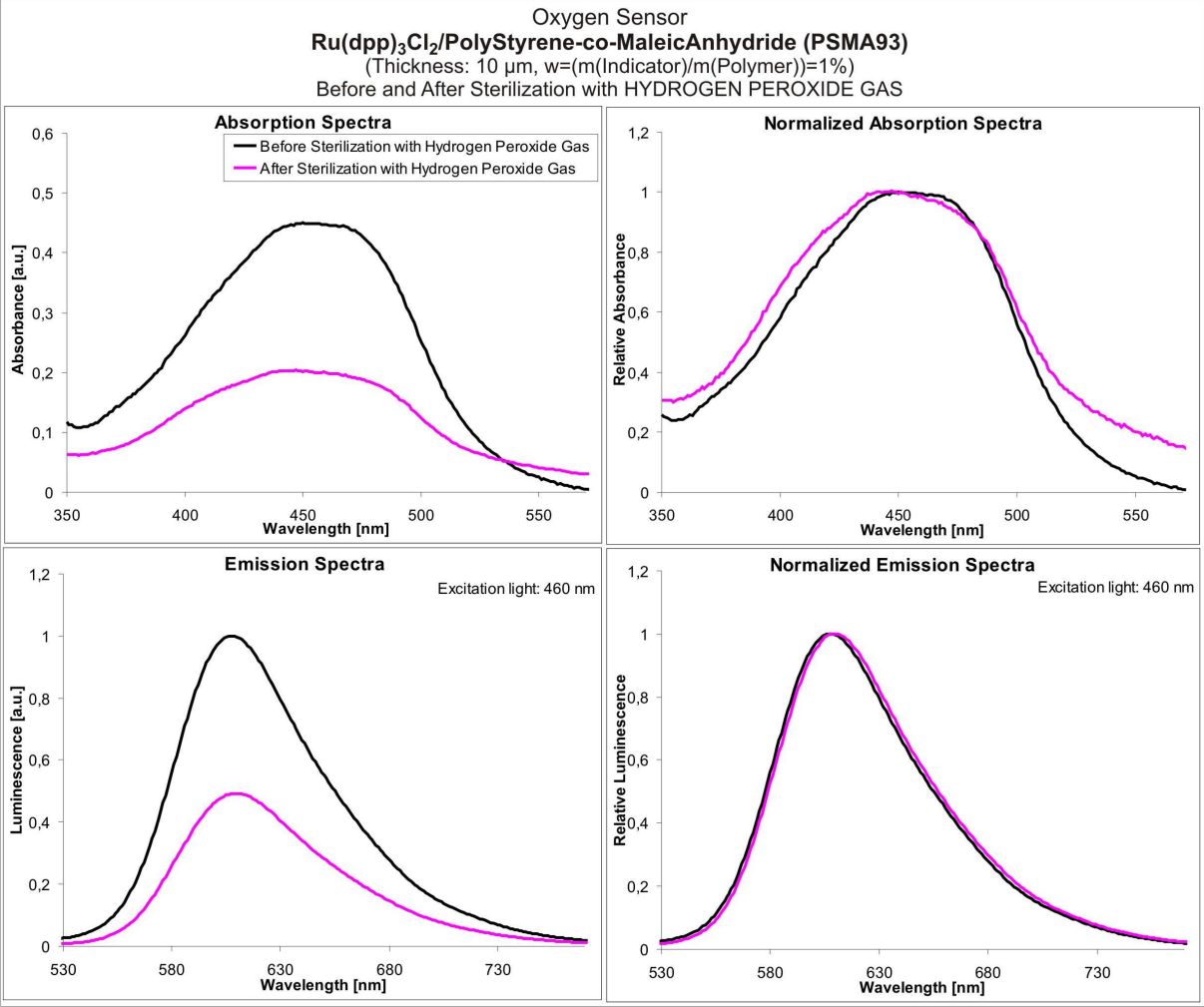

Sterilization with H_2O_2 Gas	Absorption Spectra	Emission Spectra
Alterations in Absorption/Emission Intensity	54,95% decrease	50,74% decrease
Alterations in Absorption/Emission Curve Form	Disapperatance of characteristic curve form after sterilization.	Bathochromic shift of the emission maximum for 2 nm.

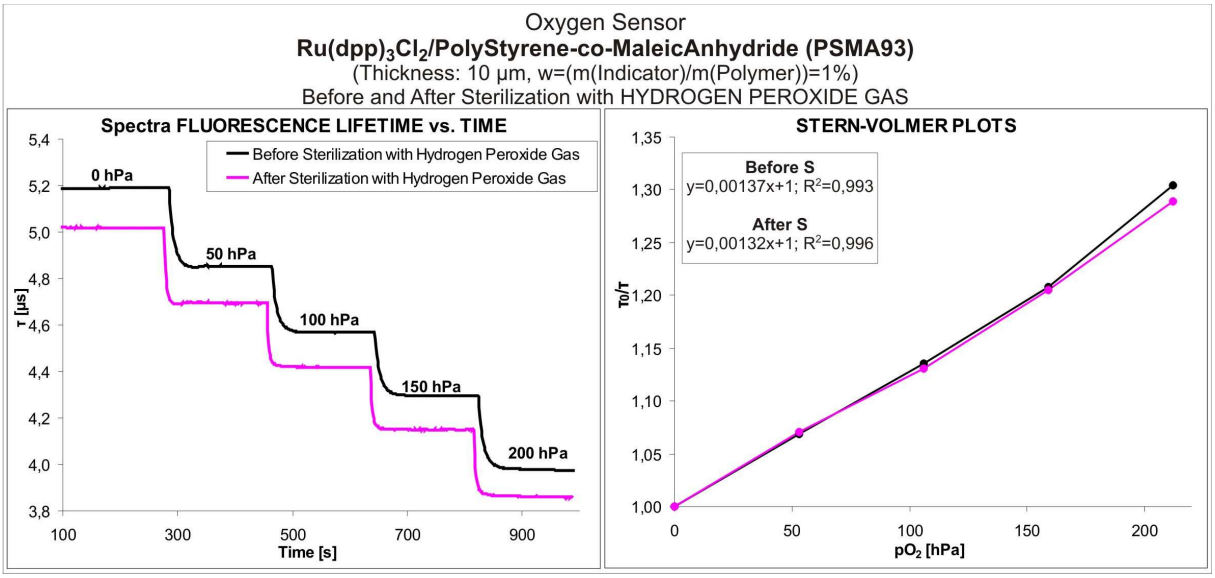

Sterilization with H_2O_2 Gas	Luminescence Lifetime	Stern-Volmer Plot
Alterations in Luminescence Lifetime and Slope	4,07% decrease of τ_0	3,65% decrease of slope
	4,35% decrease of τ at 50 hPa	
	3,65% decrease of τ at 100 hPa	
	3,88% decrease of τ at 150 hPa	
	2,79% decrease of τ at 200 hPa	

F.24.2 Sterilization with Low-Temperature Hydrogen Peroxide Plasma

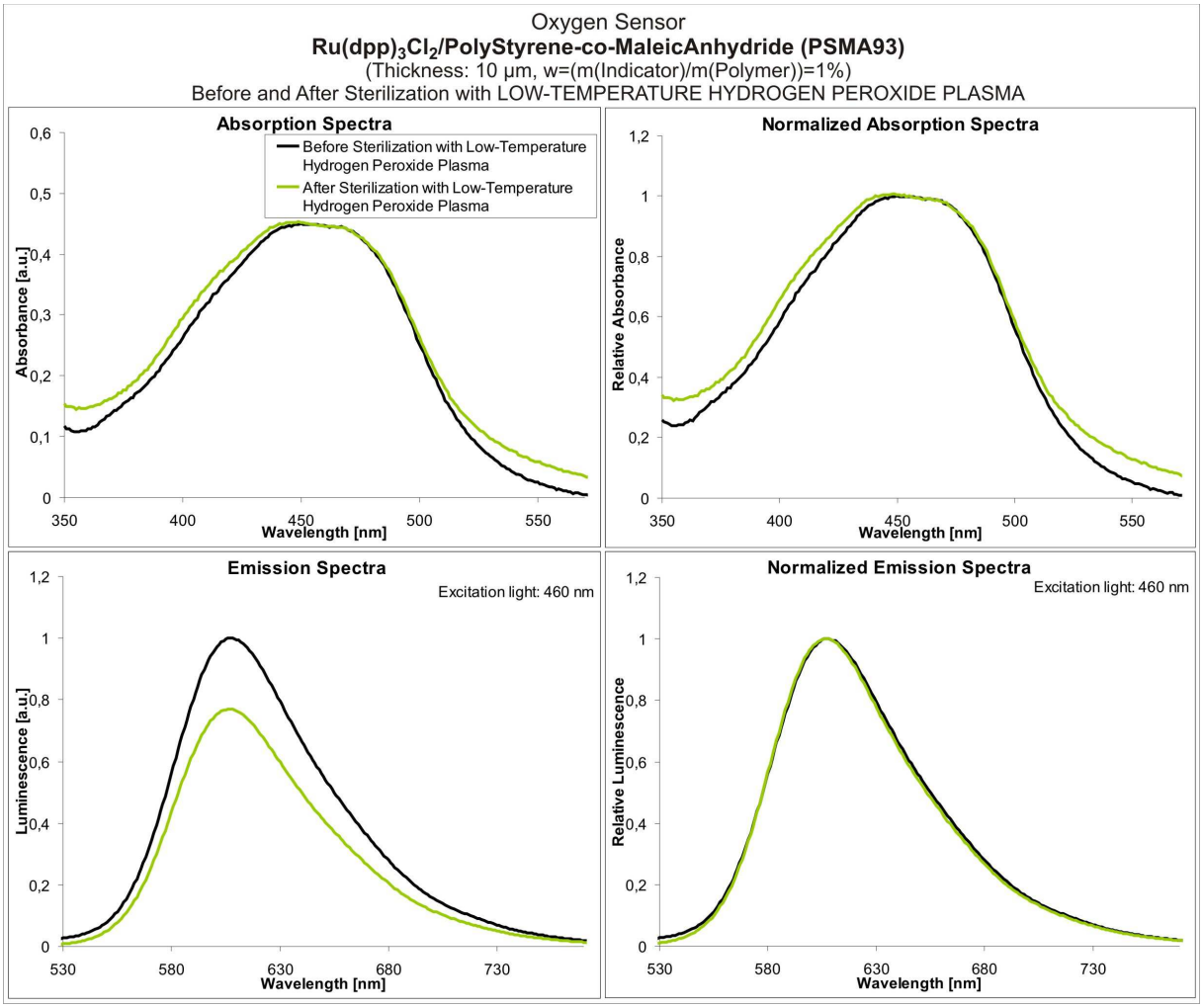

Sterilization with Low-Temperature H_2O_2 Plasma	Absorption Spectra	Emission Spectra
Alterations in Absorption/Emission Intensity	0,07% increase	23,08% decrease
Alterations in Absorption/Emission Curve Form	Altered absorption curve form from 350-450 nm and 500-800 nm.	Unaltered.

Oxygen Sensor
$Ru(dpp)_3Cl_2$/PolyStyrene-co-MaleicAnhydride (PSMA93)
(Thickness: 10 µm, w=(m(Indicator)/m(Polymer))=1%)
Before and After Sterilization with LOW-TEMPERATURE HYDROGEN PEROXIDE PLASMA

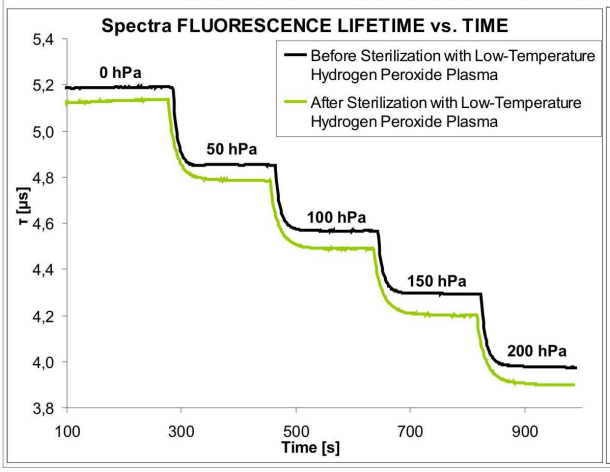

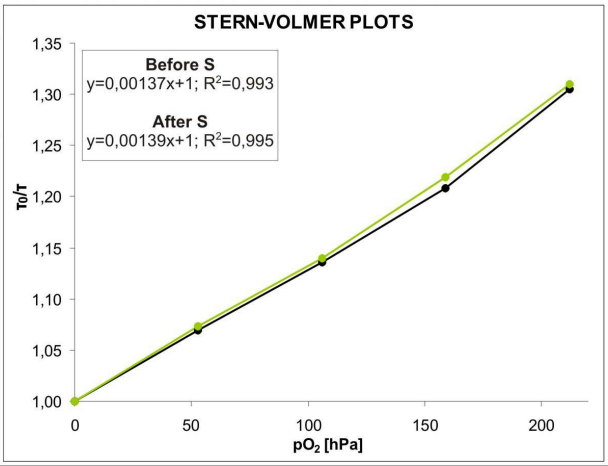

Sterilization with Low-Temperature H_2O_2 Plasma	Luminescence Lifetime	Stern-Volmer Plot
Alterations in Luminescence Lifetime and Slope	1,71% decrease of τ_0	1,44% increase of slope
	2,06% decrease of τ at 50 hPa	
	1,70% decrease of τ at 100 hPa	

Optical pH SENSORS

F.25 HPTS(DHA_3) immobilized in HydroGel D4

F.25.1 Sterilization with Hydrogen Peroxide Gas

Absorption Spectra

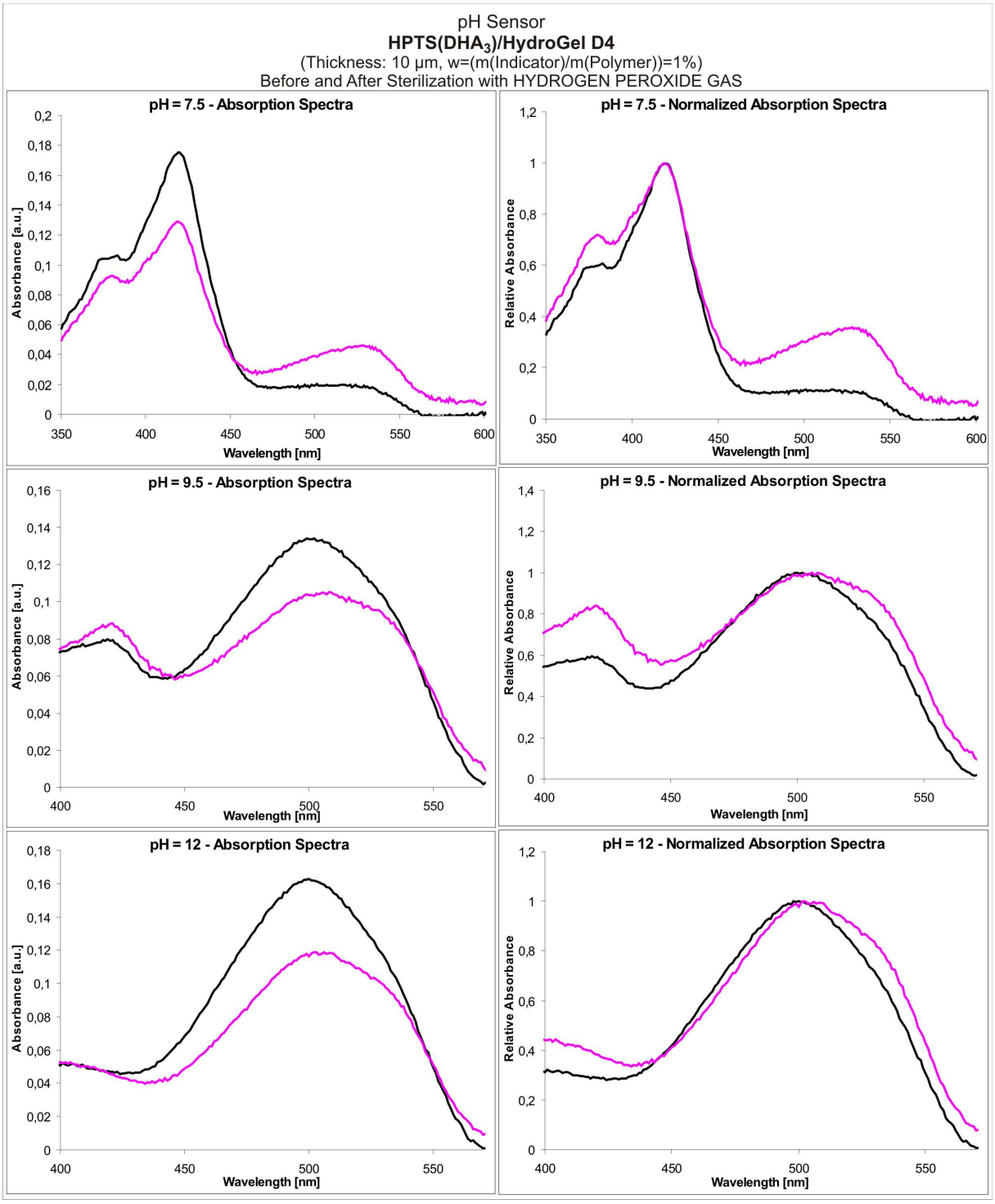

Emission Spectra

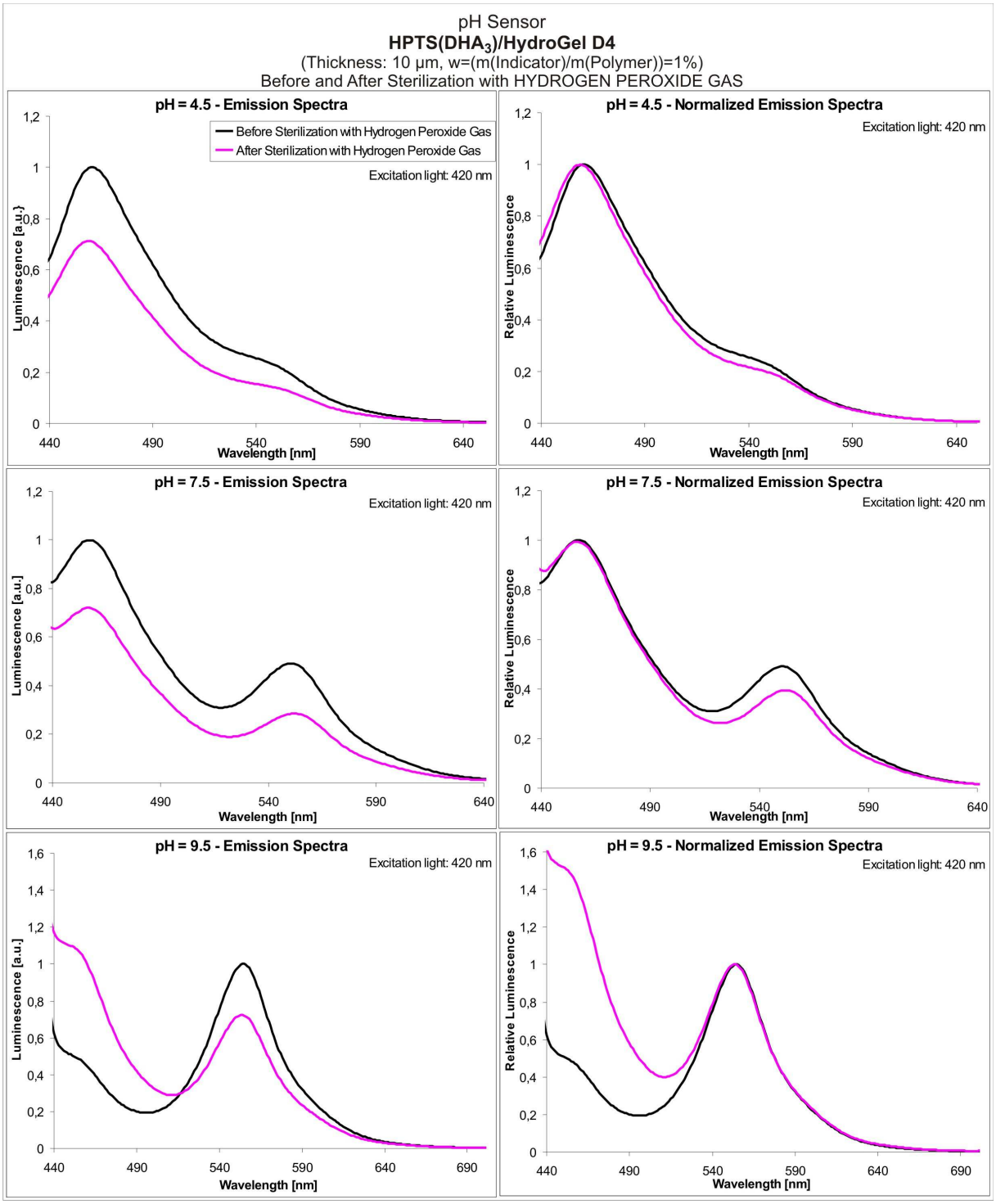

H_2O_2 Gas	Absorption Spectra			Emission Spectra		
		pH	Alterations		pH	Alterations
Alterations in Absorption/ Emission Intensity	AFTER S	4.5	24,93% decrease	AFTER S	4.5	29,00% decrease
		7.5	26,37% decrease		7.5	27,54% decrease
		9.5	21,58% decrease		9.5	27,63% decrease

Alterations in Absorption/ Emission Curve Form	AFTER S	4.5	Altered absorption between 350-410 nm and 430-800 nm.	AFTER S	4.5	Altered emission between 490-580 nm. Bathochromic shift of the emission maximum for 2 nm.
		7.5	Altered absorption between 350-410 nm. The ratio between protonation/deprotonation emission peaks is altered.		7.5	The ratio between protonation/deprotonation emission peaks is altered.
		9.5	Altered absorption between 400-470 nm and 505-600 nm.		9.5	Altered emission between 440-540 nm.

Calibration Curves

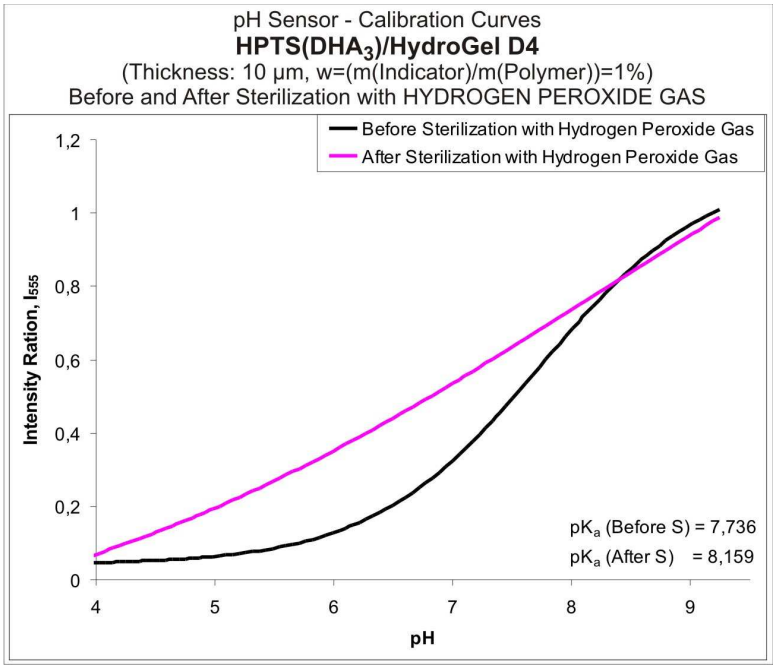

H_2O_2 Gas	Alterations in Calibration Curve Shape	Alterations in pK_a
	Greatly altered curve shape after sterilization.	Increase of pK_a (for 0,423)

F.25.2 Sterilization with Low-Temperature Hydrogen Peroxide Plasma

Absorption Spectra

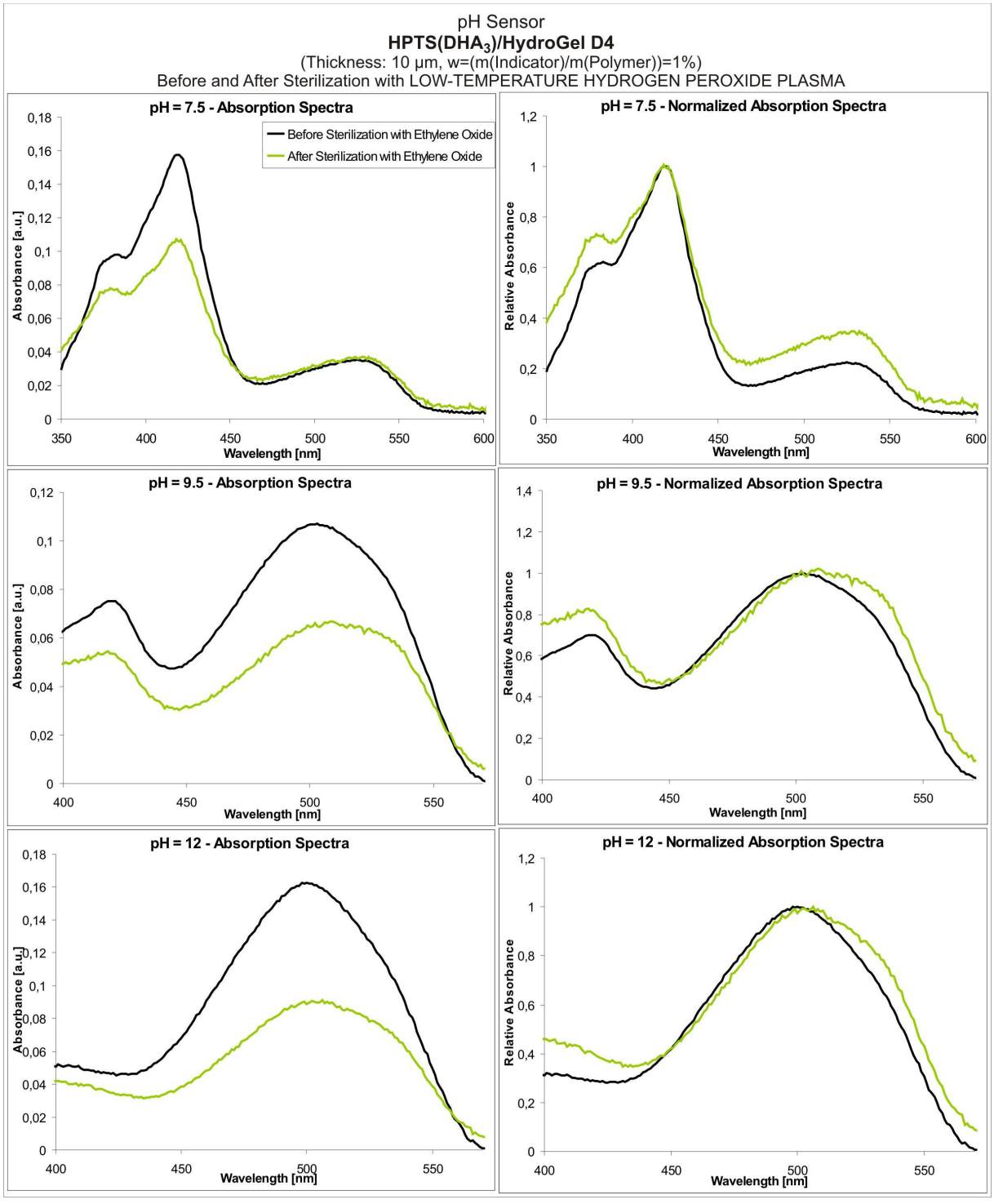

Emission Spectra

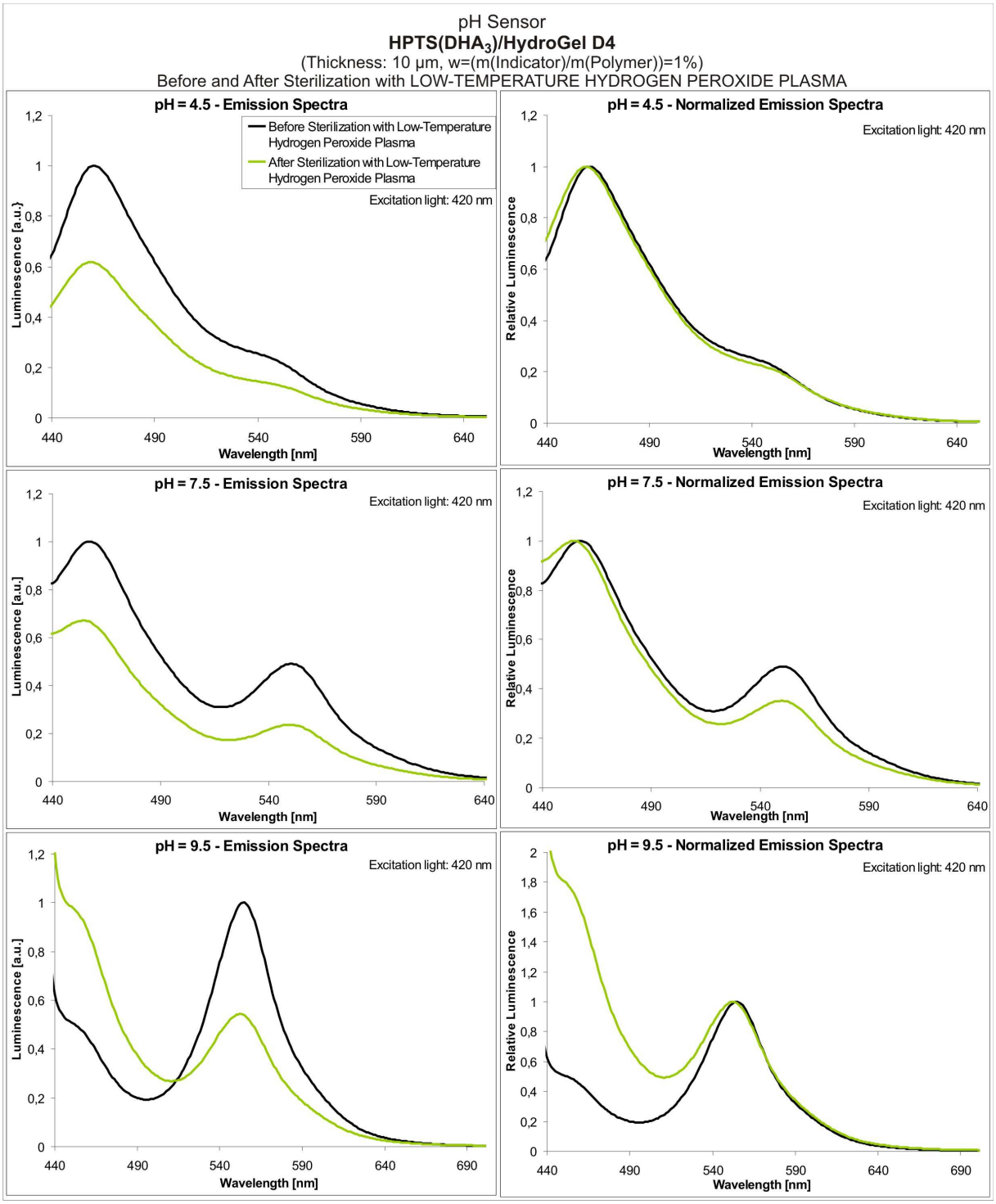

H_2O_2 Gas		Absorption Spectra			Emission Spectra	
		pH	Alterations		pH	Alterations
Alterations in Absorption/ Emission Intensity	AFTER S	4.5	36,53% decrease	AFTER S	4.5	38,20% decrease
		7.5	32,42% decrease		7.5	32,83% decrease
		9.5	38,81% decrease		9.5	45,64% decrease

Alterations in Absorption/ Emission Curve Form	AFTER S	4.5	Altered absorption between 350-410 nm and 430-800 nm.	AFTER S	4.5	Altered emission between 510-550 nm. Hypsochromic shift of the emission maximum for 2 nm.
		7.5	Altered absorption between 350-400 nm. The ratio between protonation/deprotonation emission peaks is altered.		7.5	The ratio between protonation/deprotonation emission peaks is altered. Hypsochromic shift of the emission maximum for 2 nm.
		9.5	Altered absorption between 500-600 nm. The ratio between protonation/deprotonation emission peaks is altered.		9.5	Altered emission between 440-540 nm. Hypsochromic shift of the emission maximum for 2 nm.

Calibration Curves

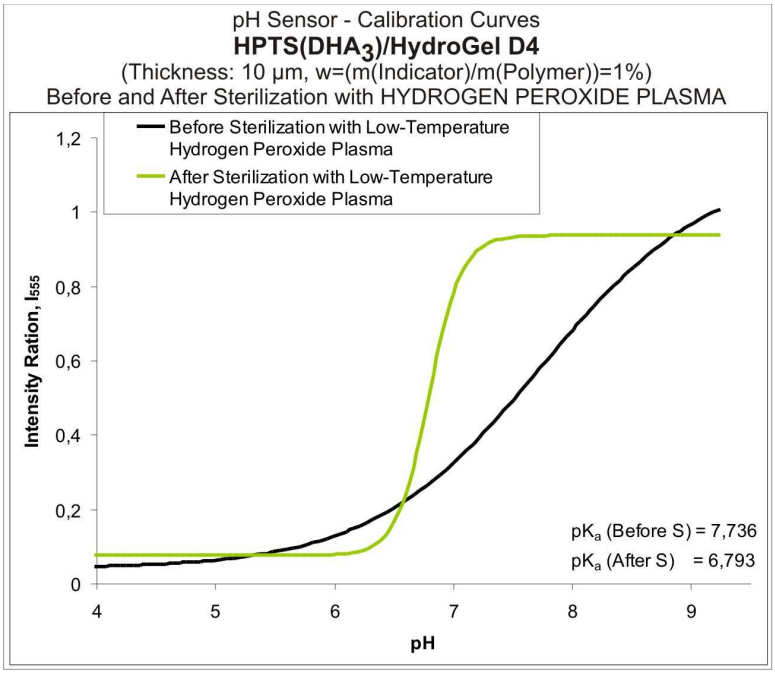

H_2O_2 Plasma	Alterations in Calibration Curve Shape	Alterations in pK_a
	Greatly altered curve shape after sterilization.	Decrease of pK_a (for 0,943)

F.26 2´,7´-DiHexylFluorescein OctadecylEster immobilized in HydroMed Hydrogel D4

F.26.1 Sterilization with Hydrogen Peroxide Gas

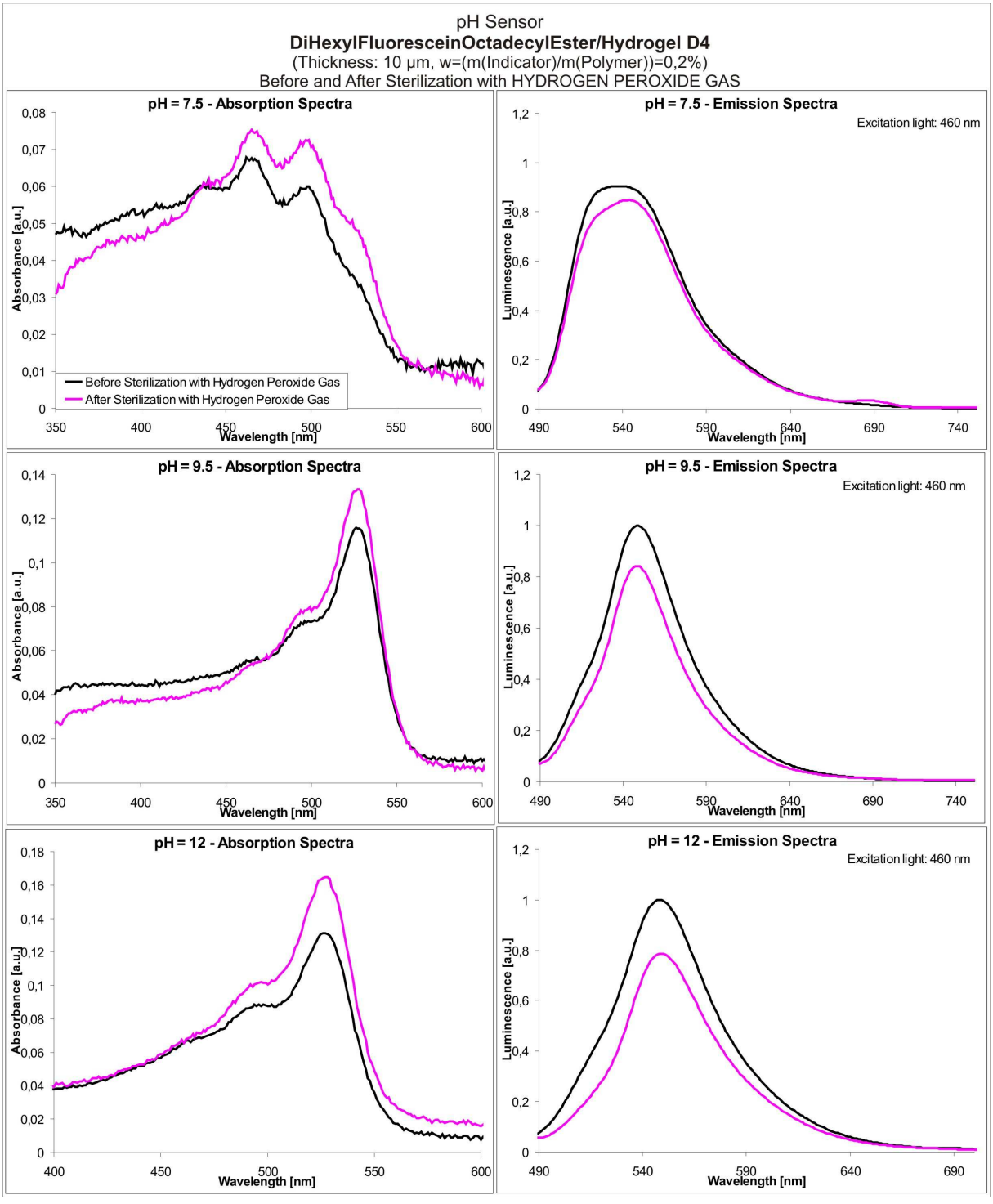

H_2O_2 Gas	Absorption Spectra			Emission Spectra		
		pH	Alterations		pH	Alterations
Alterations in Absorption/ Emission Intensity	AFTERS	4.5	9,28% increase	AFTERS	4.5	15,32% decrease
		7.5	13,51% increase		7.5	16,00% decrease
		9.5	20,04% increase		9.5	21,31% decrease
Alterations in Absorption/ Emission Curve Form	AFTERS	4.5	Altered absorption between 350-430 nm.	AFTERS	4.5	Altered emission between 530-550 nm.
		7.5	Altered absorption between 350-470 nm.		7.5	Unaltered
		9.5	The sensor became slightly turbid after sterilization.		9.5	Unaltered

Calibration Curves

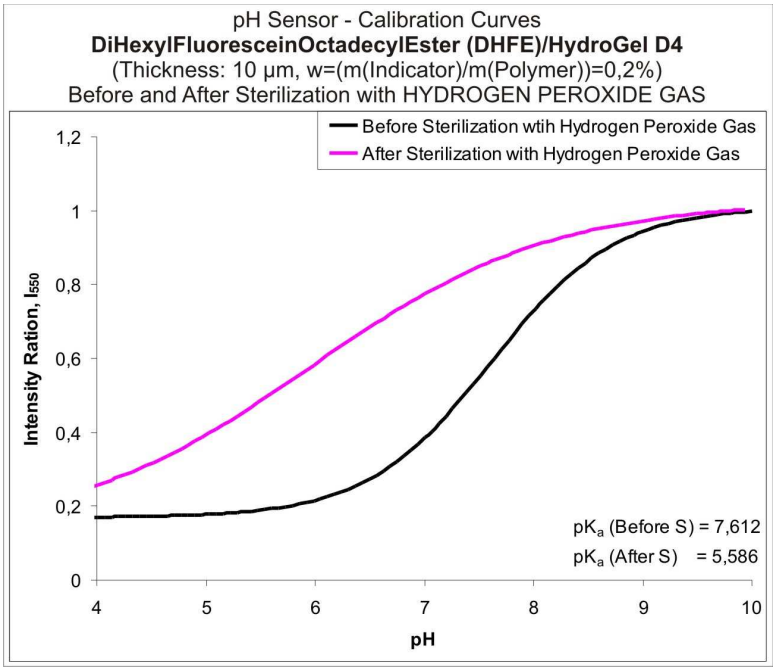

H_2O_2 Gas	Alterations in Calibration Curve Shape	Alterations in pK_a
	Greatly altered curve shape after sterilization.	Decrease of pK_a (for 2,026)

F.26.2 Sterilization with Low-Temperature Hydrogen Peroxide Plasma

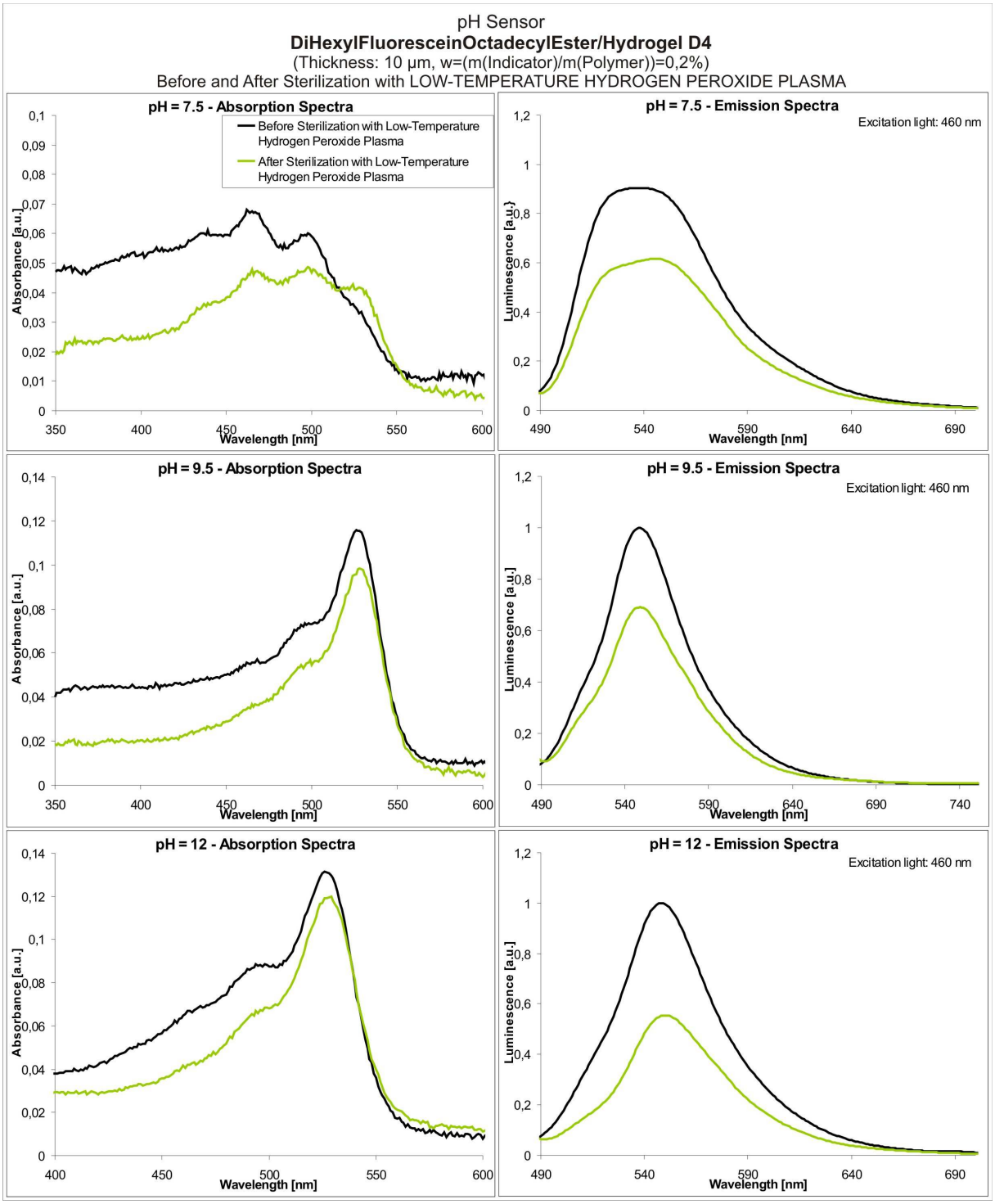

H_2O_2 Plasma	Absorption Spectra			Emission Spectra		
		pH	Alterations		pH	Alterations
Alterations in Absorption/ Emission Intensity	AFTERS	7.5	29,32% decrease	AFTERS	7.5	38,75% decrease
		9.5	15,32% decrease		9.5	30,89% decrease
		12	9,21% decrease		12	44,47% decrease

Alterations in Absorption/ Emission Curve Form	AFTER S	7.5	Altered absorption between 350-430 nm. Bathochromic shift of the absorption maximum for 35 nm.	AFTER S	7.5	Altered emission between 540-560 nm.
		9.5	Altered absorption between 560-800 nm.		9.5	Unaltered
		12	Altered absorption between 560-800 nm.		12	Altered emission between 490-530 nm.

Calibration Curves

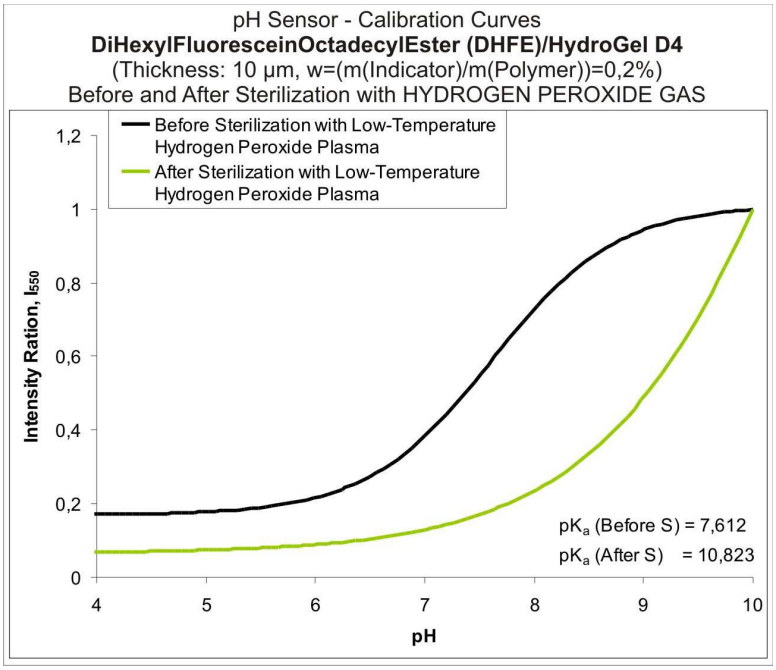

H_2O_2 Plasma	Alterations in Calibration Curve Shape	Alterations in pK_a
	Greatly altered curve shape after sterilization.	Increase of pK_a (for 3,211)

F.27 2´,7´-DiHexylFluorescein OctadecylEster immobilized in Poly(2-HydroxyEthyl MethAcrylate) (=pHEMA)

F.27.1 Sterilization with Hydrogen Peroxide Gas

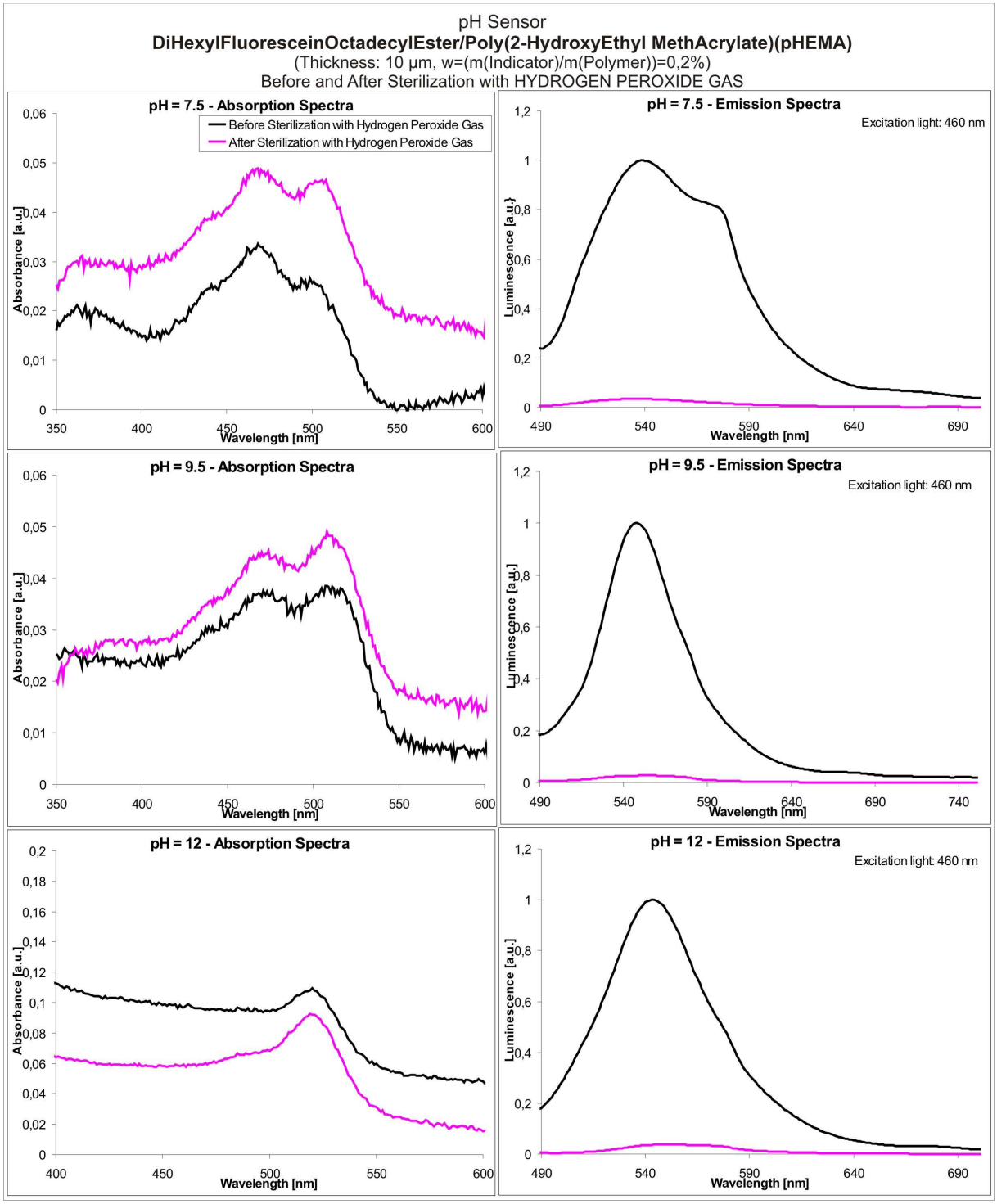

H_2O_2 Gas	Absorption Spectra			Emission Spectra		
		pH	Alterations		pH	Alterations
Alterations in Absorption/ Emission Intensity	AFTERS	4.5	31,36% increase	AFTERS	4.5	96,55% decrease
		7.5	23,56% increase		7.5	97,28% decrease
		9.5	14,23% decrease		9.5	96,25% decrease
Alterations in Absorption/ Emission Curve Form	AFTERS	4.5	The sensor became slightly turbid after sterilization.	AFTERS	4.5	Disappearance of the characteristic emission curve form.
		7.5	The sensor became slightly turbid after sterilization.		7.5	Disappearance of the characteristic emission curve form.
		9.5	Altered absorption curve form.		9.5	Disappearance of the characteristic emission curve form.

Calibration Curves

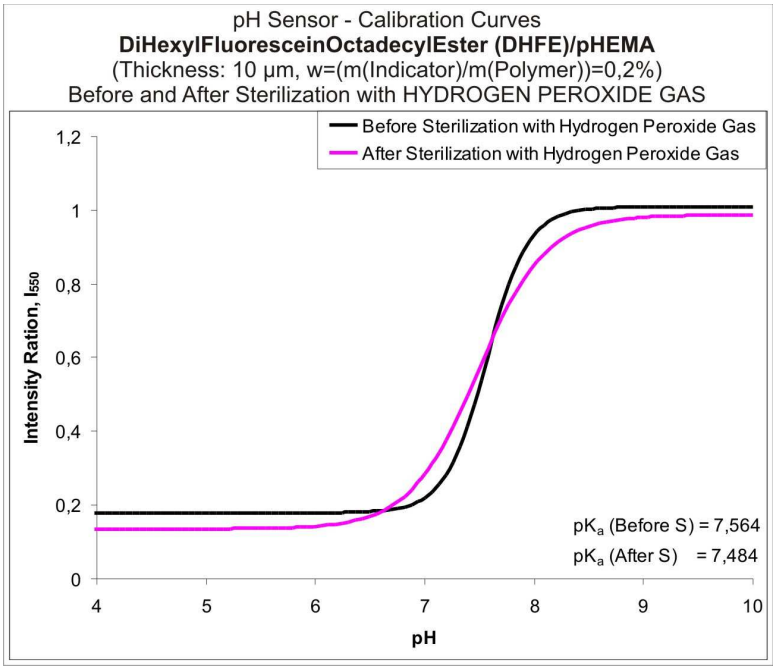

H_2O_2 Gas	Alterations in Calibration Curve Shape	Alterations in pK_a
	Altered curve shape after sterilization. The response to the proton still observed – re-calibration of sensor response.	Decrease of pK_a (for 0,080)

F.27.2 Sterilization with Low-Temperature Hydrogen Peroxide Plasma

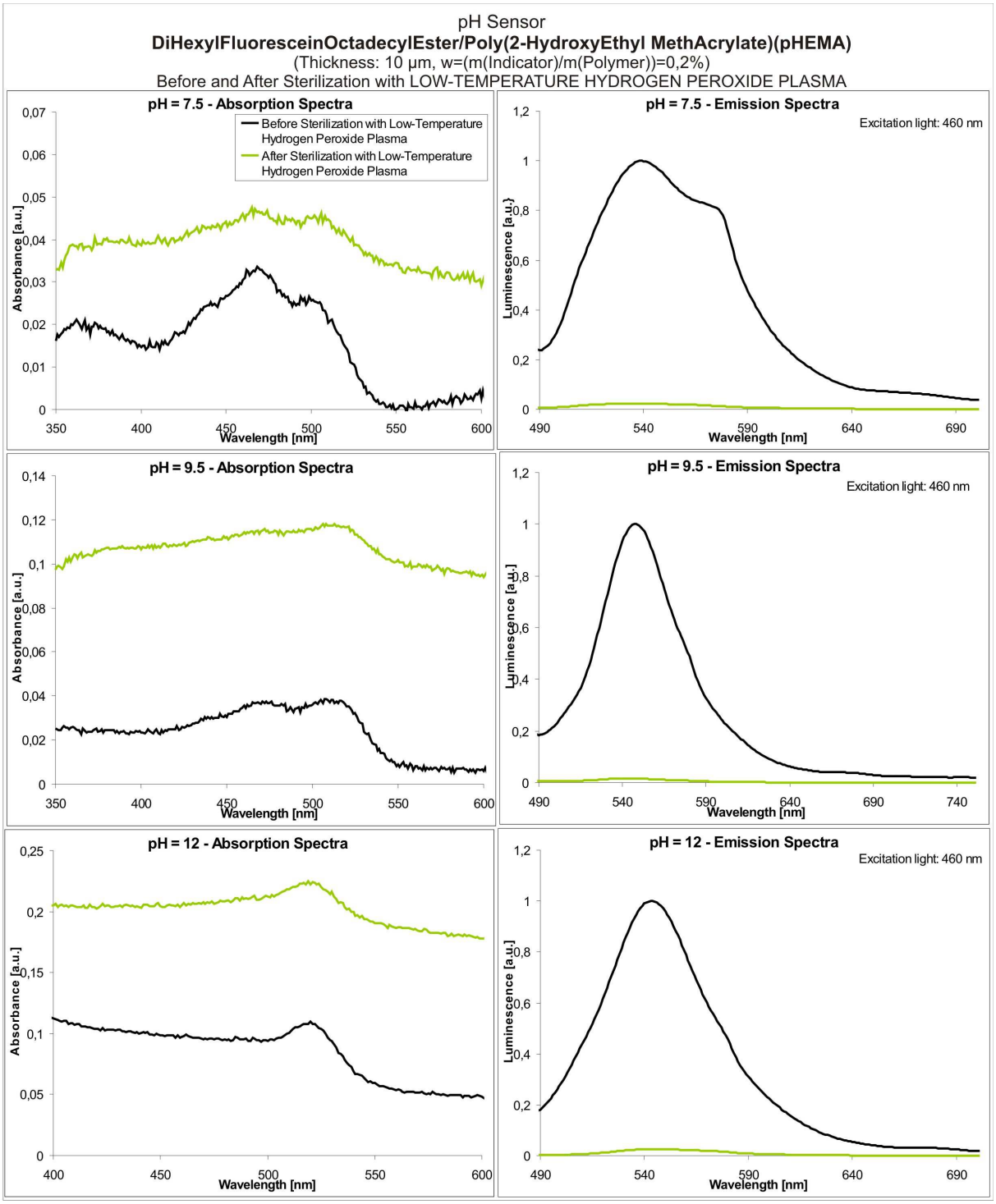

H_2O_2 Gas	Absorption Spectra			Emission Spectra		
		pH	Alterations		pH	Alterations
Alterations in Absorption/ Emission Intensity	AFTERS	7.5	44,80% increase	AFTERS	7.5	97,91% decrease
		9.5	200% increase		9.5	98,27% decrease
		12	105% increase		12	97,56% decrease

Alterations in Absorption/ Emission Curve Form	AFTER S	7.5	The sensor became turbid after sterilization.	AFTER S	7.5	Disappearance of the characteristic emission curve form.
		9.5	The sensor became turbid after sterilization.		9.5	Disappearance of the characteristic emission curve form.
		12	The sensor became turbid after sterilization.		12	Disappearance of the characteristic emission curve form.

Calibration Curves

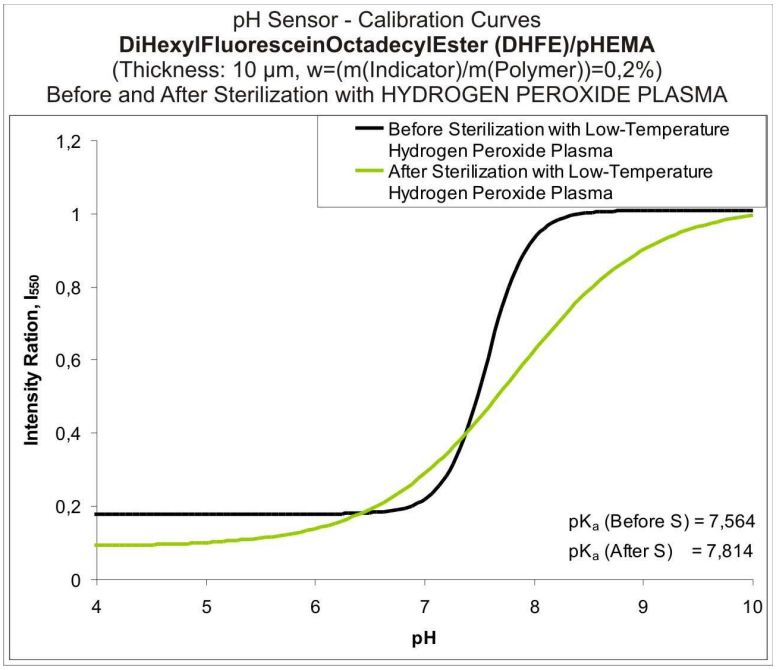

H_2O_2 Plasma	Alterations in Calibration Curve Shape	Alterations in pK_a
	Altered curve shape after sterilization. The response to the proton still observed – re-calibration of sensor response.	Decrease of pK_a (for 0,250)

F.28 2´,7´-DiHexyl-N-Octadecyl-CarboxAmidoFluorescein (=DHFA) immobilized in HydroMed Hydrogel D4

F.28.1 Sterilization with Hydrogen Peroxide Gas

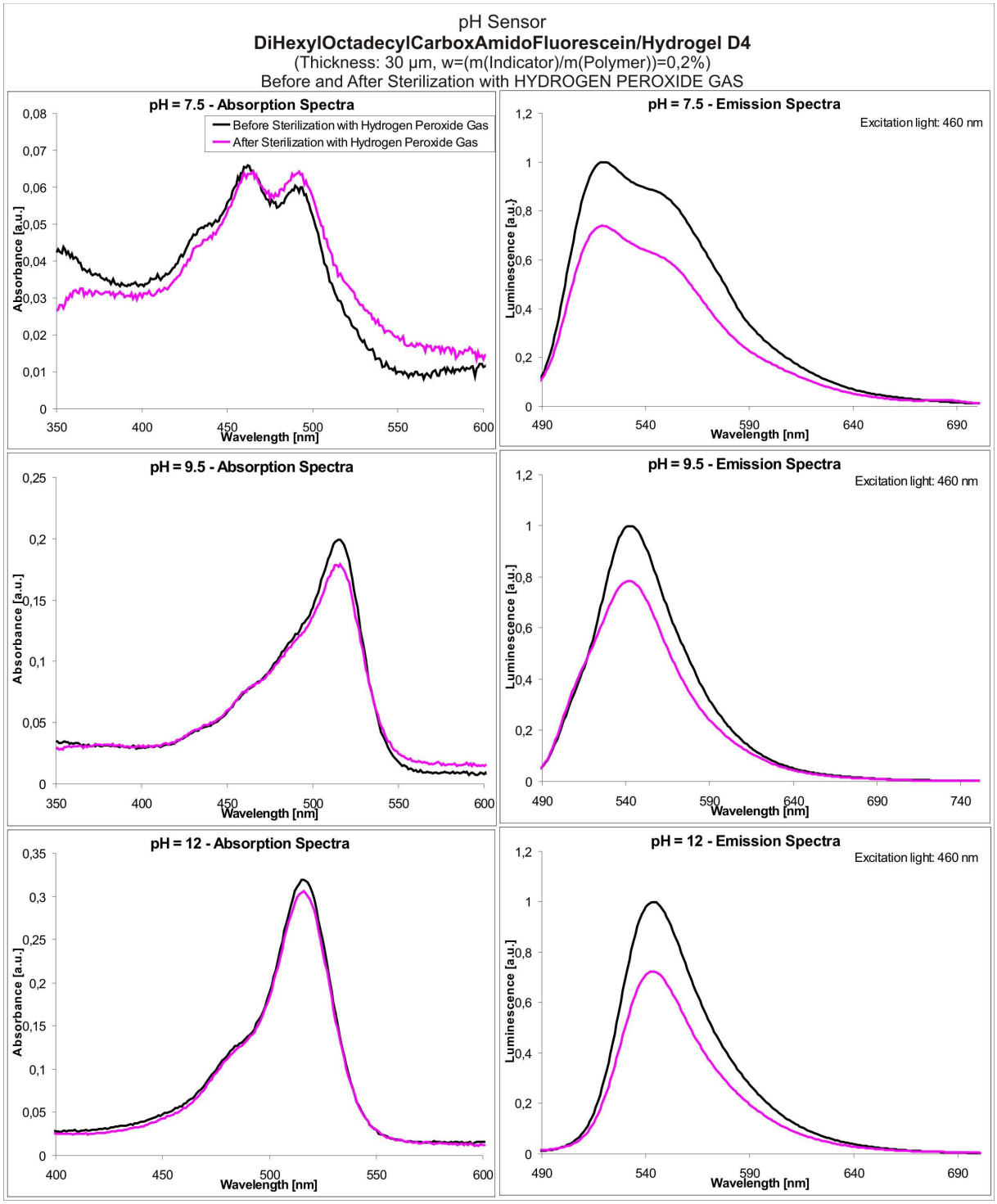

H_2O_2 Gas	Absorption Spectra			Emission Spectra		
		pH	Alterations		pH	Alterations
Alterations in Absorption/ Emission Intensity	AFTERS	4.5	2,40% decrease	AFTERS	4.5	26,16% decrease
		7.5	10,20% decrease		7.5	22,20% decrease
		9.5	4,71% decrease		9.5	27,89% decrease
Alterations in Absorption/ Emission Curve Form	AFTERS	4.5	Altered absorption curve form between 350-440 nm and 500-600 nm.	AFTERS	4.5	Unaltered.
		7.5	Altered absorption curve form between 550-800 nm.		7.5	Unaltered.
		9.5	Unaltered.		9.5	Unaltered.

Calibration Curves

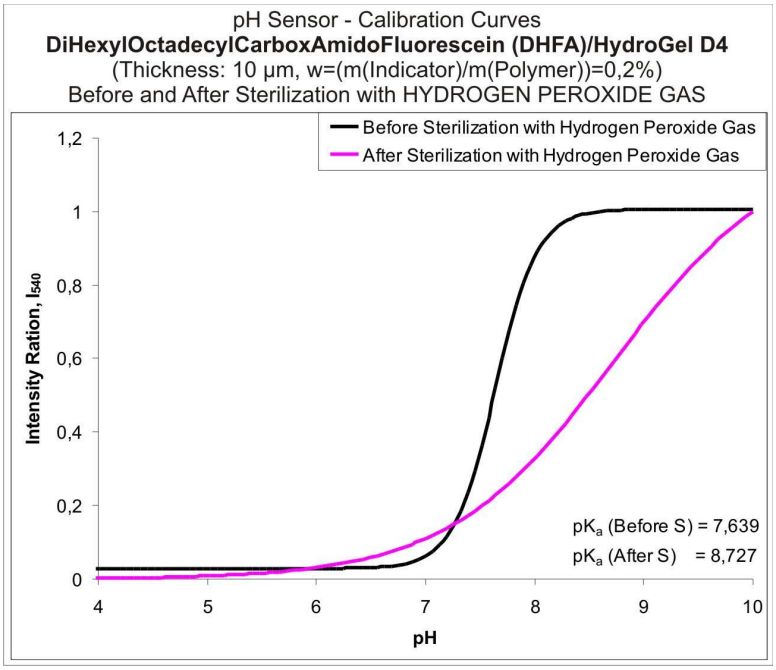

H_2O_2 Gas	Alterations in Calibration Curve Shape	Alterations in pK_a
	Greatly altered curve shape after sterilization.	Increase of pK_a (for 1,088)

F.28.2 Sterilization with Low-Temperature Hydrogen Peroxide Plasma

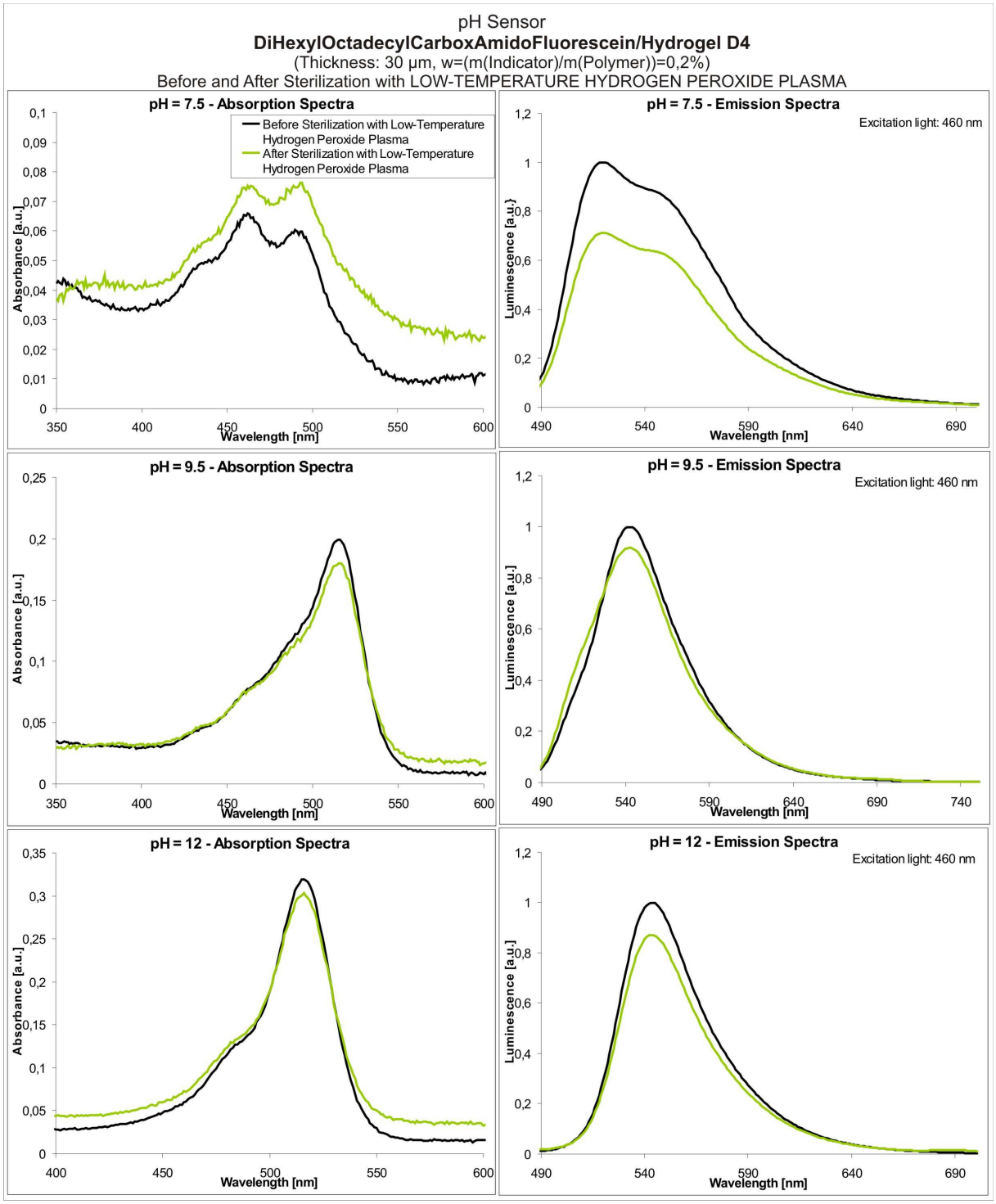

H_2O_2 Plasma	Absorption Spectra			Emission Spectra		
		pH	Alterations		pH	Alterations
Alterations in Absorption/ Emission Intensity	AFTERS	7.5	20,64% increase	AFTERS	7.5	29,13% decrease
		9.5	9,54% decrease		9.5	8,44% decrease
		12	5,71% decrease		12	13,15% decrease

Alterations in Absorption/ Emission Curve Form	AFTER S	7.5	Altered absorption curve form between 520-800 nm.	AFTER S	7.5	Unaltered.
		9.5	Altered absorption curve form between 540-800 nm.		9.5	Altered emission curve form between 490-530 nm.
		12	Altered absorption curve form between 400-500 nm and 550-800 nm.		12	Unaltered.

Calibration Curves

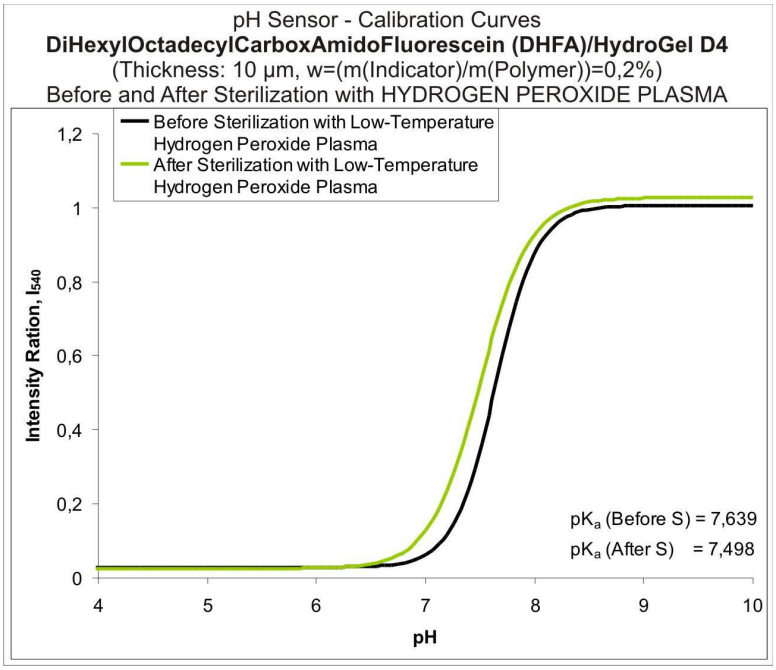

H_2O_2 Plasma	Alterations in Calibration Curve Shape	Alterations in pK_a
	Comparable curve shapes before and after sterilization.	Decrease of pK_a (for 0,141)

F.29 2´,7´-DiHexyl-N-Octadecyl-CarboxAmidoFluorescein (=DHFA) immobilized in Poly(2-HydroxyEthyl Methacrylate) (=pHEMA)

F.29.1 Sterilization with Hydrogen Peroxide Gas

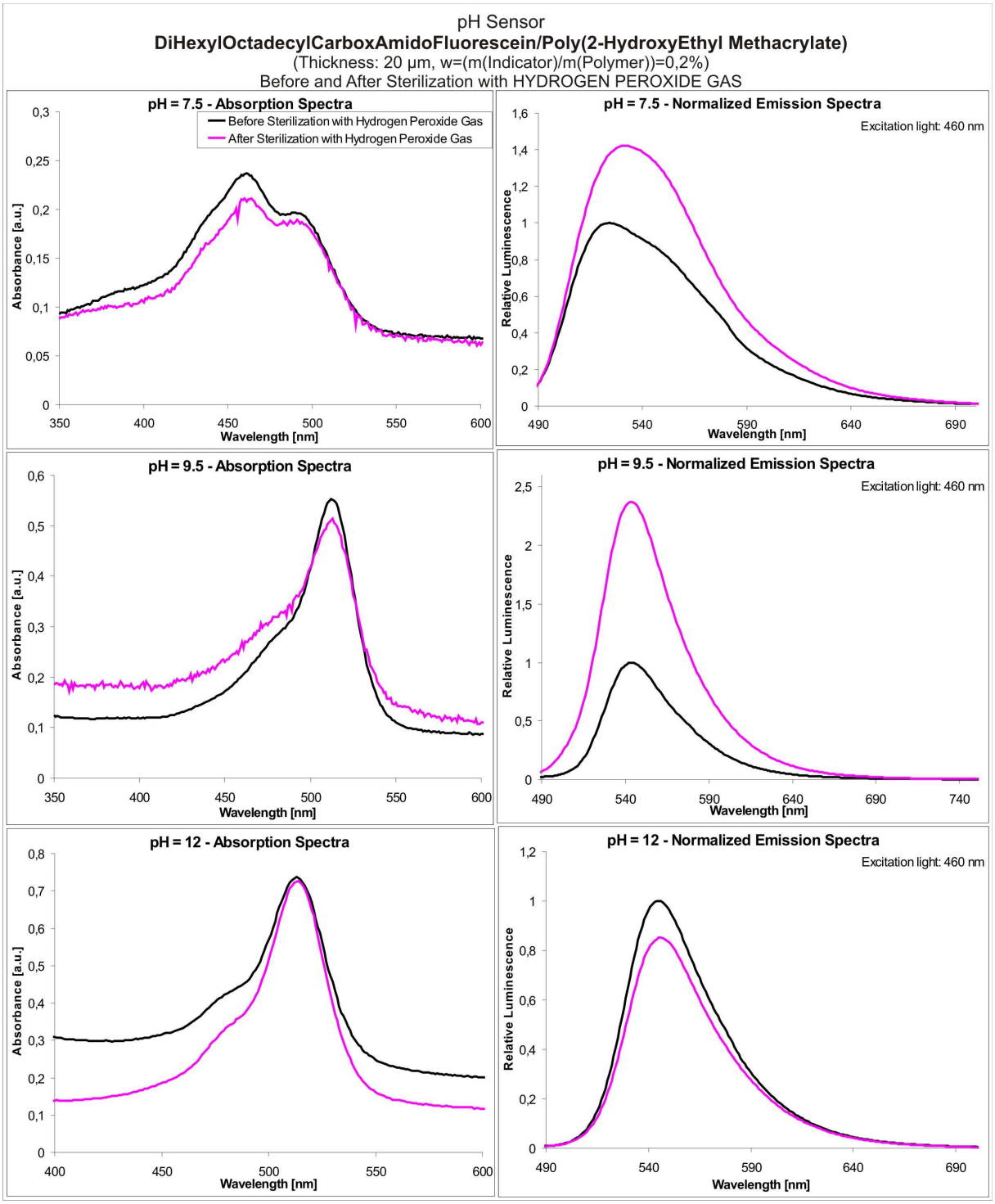

H_2O_2 Gas	Absorption Spectra			Emission Spectra		
		pH	Alterations		pH	Alterations
Alterations in Absorption/ Emission Intensity	AFTERS	7.5	10,67% decrease	AFTERS	7.5	42% increase
		9.5	7,55% decrease		9.5	137% increase
		12	1,36% decrease		12	14,78% decrease
Alterations in Absorption/ Emission Curve Form	AFTERS	7.5	Unaltered	AFTERS	7.5	Altered emission curve form between 540-590 nm.
		9.5	Altered absorption between 350-480 nm and 530-800 nm.		9.5	Unaltered.
		12	Altered absorption between 400-500 nm and 530-800 nm.		12	Unaltered.

Calibration Curves

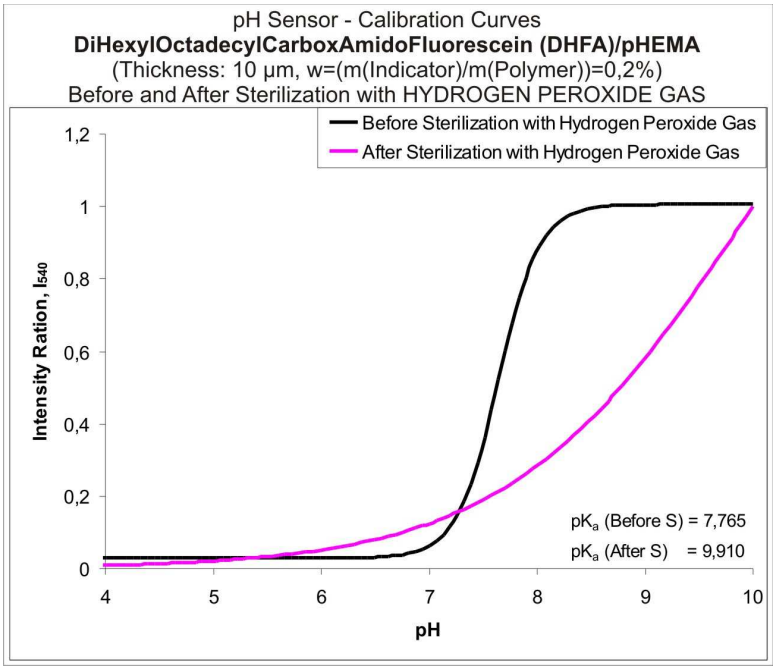

H_2O_2 Gas	Alterations in Calibration Curve Shape	Alterations in pK_a
	Greatly altered curve shape after sterilization.	Increase of pK_a (for 2,145)

F.29.2 Sterilization with Low-Temperature Hydrogen Peroxide Plasma

Absorption Spectra

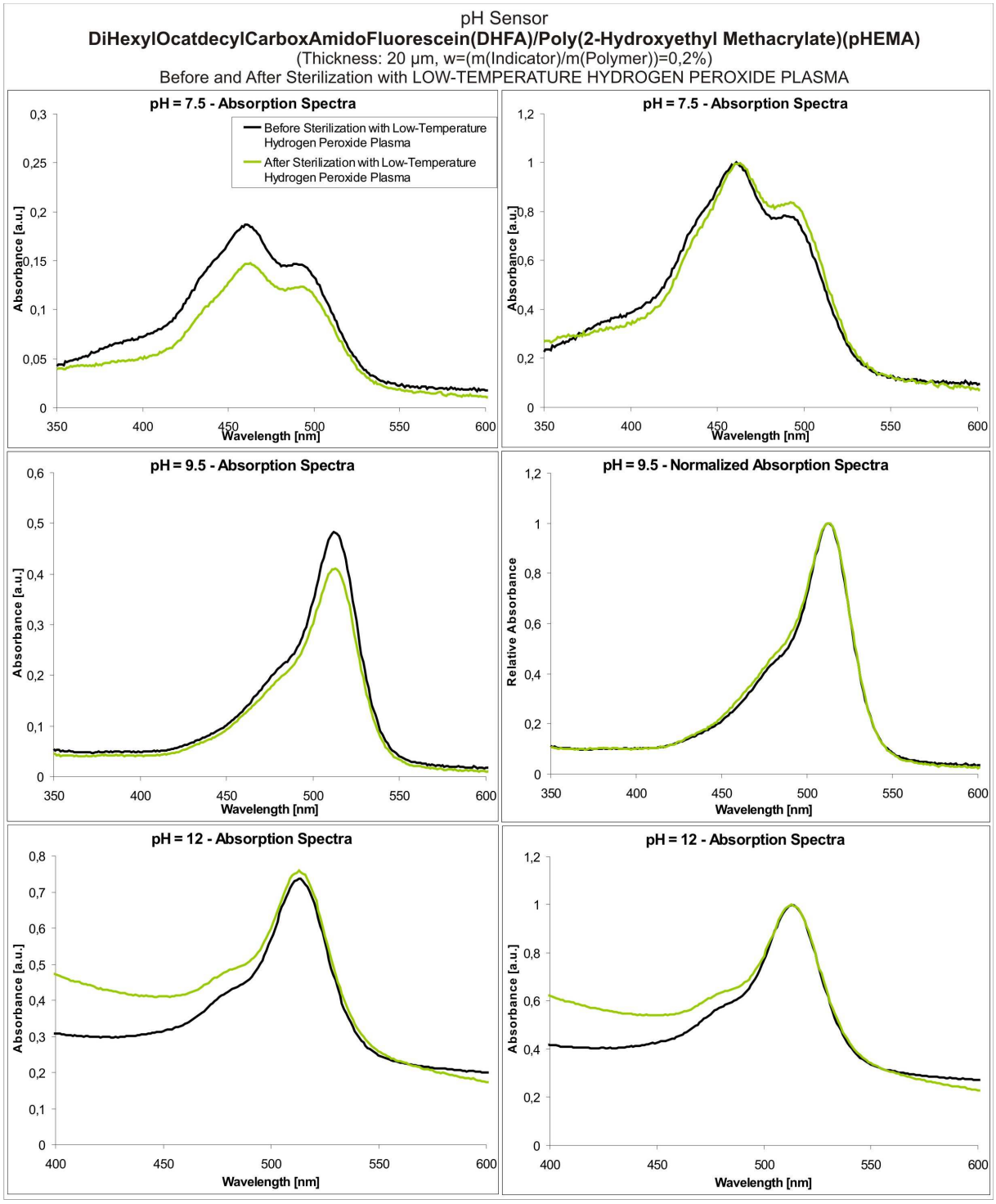

Emission Spectra

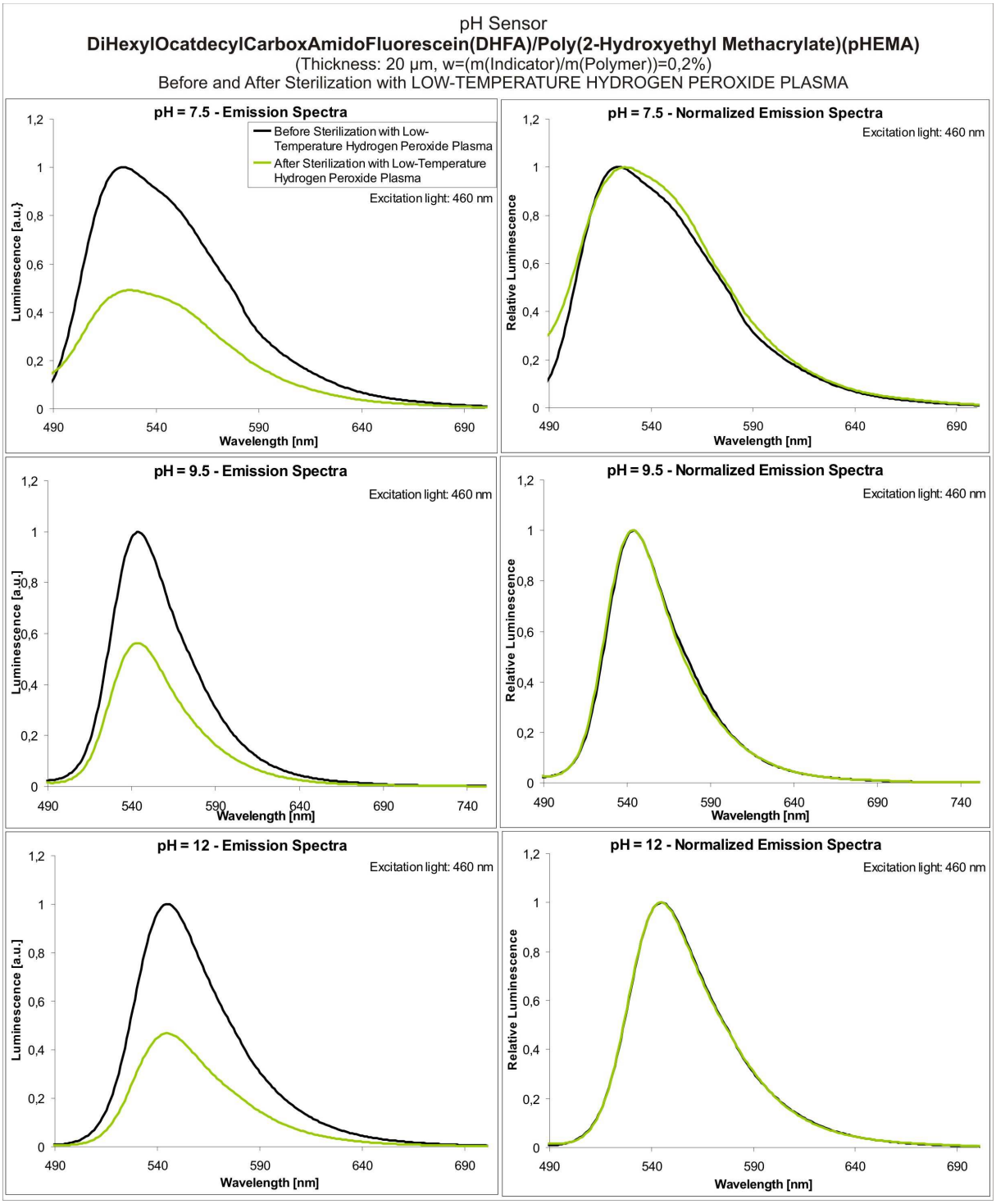

H_2O_2 Plasma	Absorption Spectra			Emission Spectra		
		pH	Alterations		pH	Alterations
Alterations in Absorption/ Emission Intensity	AFTERS	7.5	21,32% decrease	AFTERS	7.5	50,88% decrease
		9.5	15,04% decrease		9.5	43,77% decrease
		12	2,91% decrease		12	53,24% decrease

Alterations in Absorption/ Emission Curve Form	AFTER S	7.5	Altered absorption curve form between 475-510 nm. Bathochromic shift of the absorption maximum for 2 nm.	AFTER S	7.5	Altered emission curve form between 490-505 nm and 530-600 nm.
		9.5	Unaltered.		9.5	Unaltered.
		12	Altered absorption curve form between 400-500 nm and 550-800 nm.		12	Unaltered.

Calibration Curves

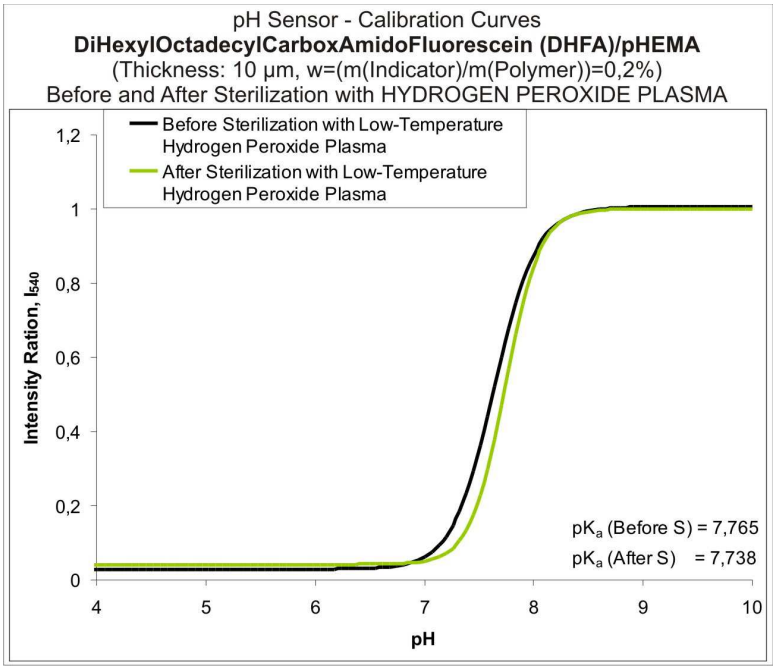

H_2O_2 Plasma	Alterations in Calibration Curve Shape	Alterations in pK_a
	Comparable curve shapes before and after sterilization.	Decrease of pK_a (for 0,027)

F.30 pH Sensitive Coumarin immobilized in HydroMed Hydrogel D4

F.30.1 Sterilization with Hydrogen Peroxide Gas

Absorption Spectra

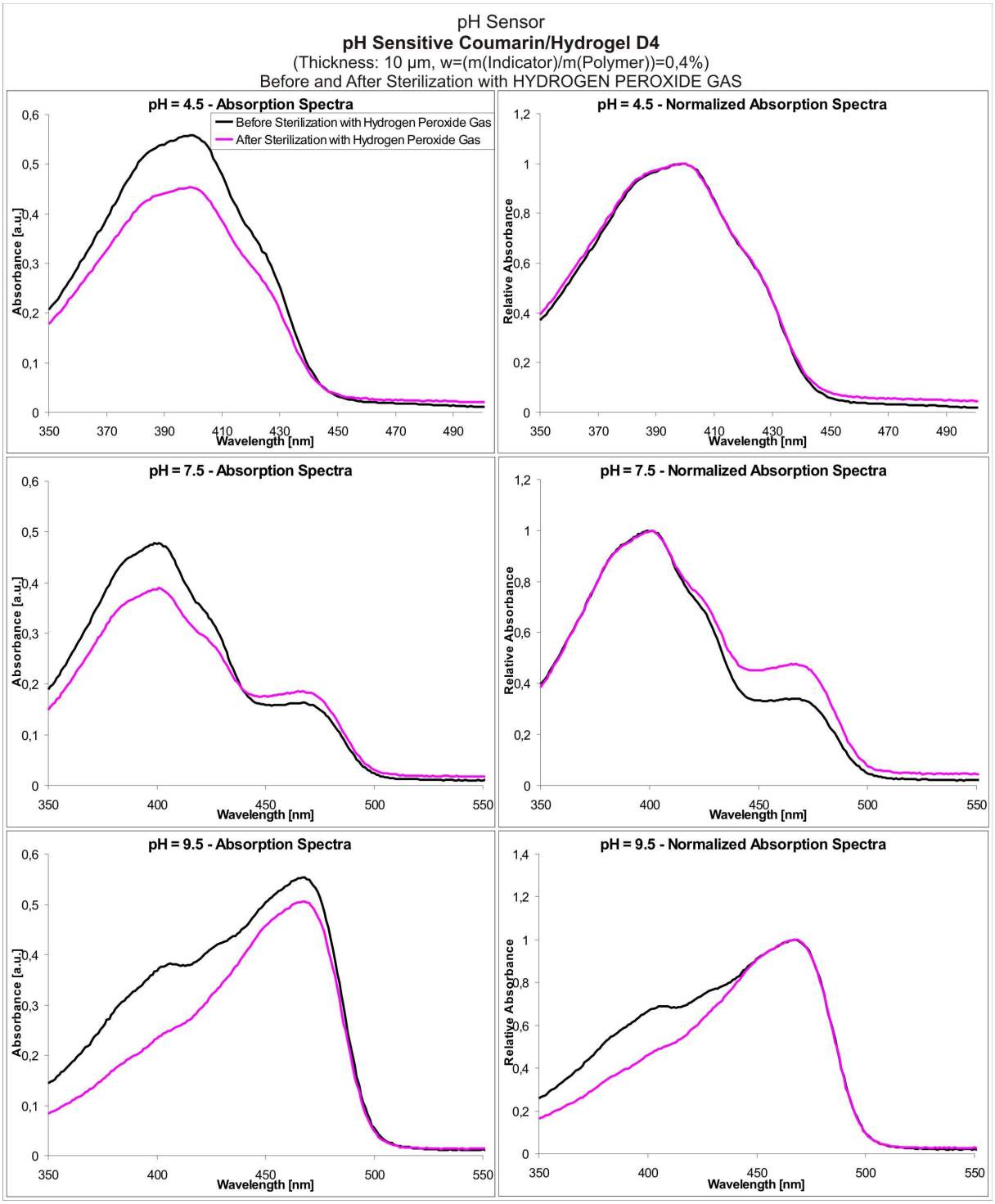

Emission Spectra

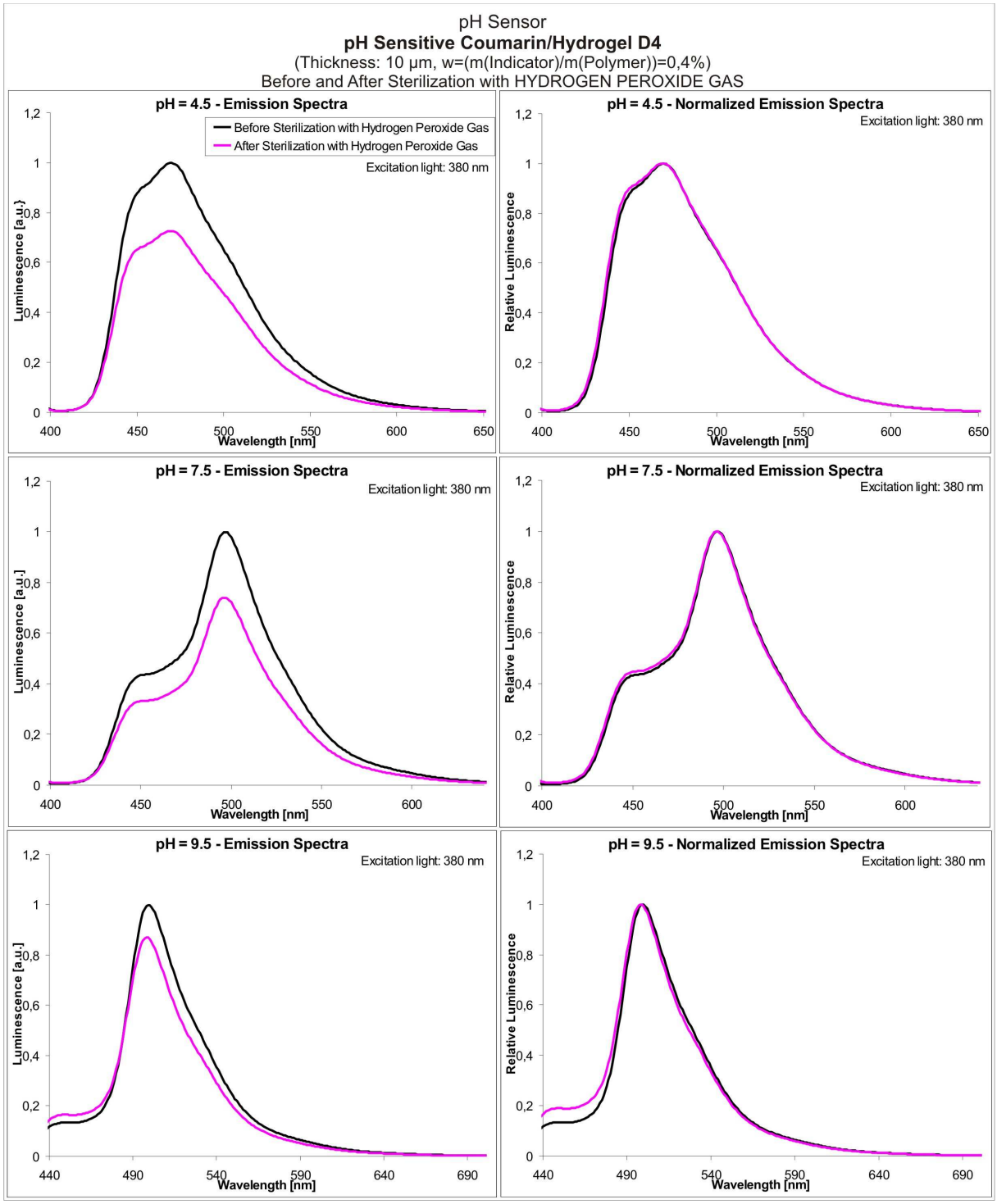

H_2O_2 Gas	Absorption Spectra			Emission Spectra		
		pH	Alterations		pH	Alterations
Alterations in Absorption/ Emission Intensity	AFTERS	4.5	18,83% decrease	AFTERS	4.5	27,42% decrease
		7.5	18,45% decrease		7.5	25,95% decrease
		9.5	8,70% decrease		9.5	12,99% decrease

Alterations in Absorption/ Emission Curve Form	AFTER S	4.5	Unaltered	AFTER S	4.5	Unaltered
		7.5	The ratio between protonation/deprotonation absorption peaks is altered.		7.5	Unaltered
		9.5	Altered absorption between 350-450 nm.		9.5	Altered emission curve form between 440-490 nm.

Calibration Curves

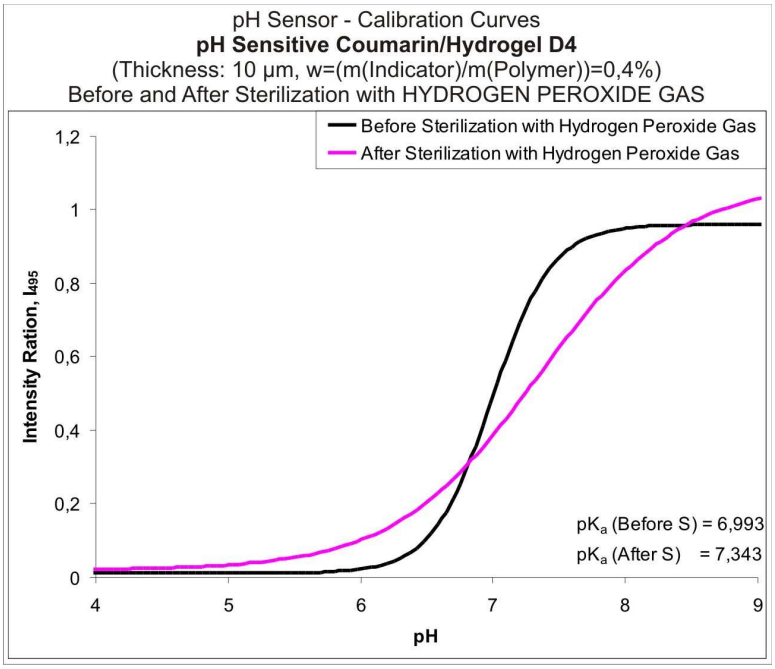

H_2O_2 Gas	Alterations in Calibration Curve Shape	Alterations in pK_a
	Altered curve shape after sterilization. The response to the proton still observed – re-calibration of sensor response.	Increase of pK_a (for 0,350)

F.30.2 Sterilization with Low-Temperature Hydrogen Peroxide Plasma

Absorption Spectra

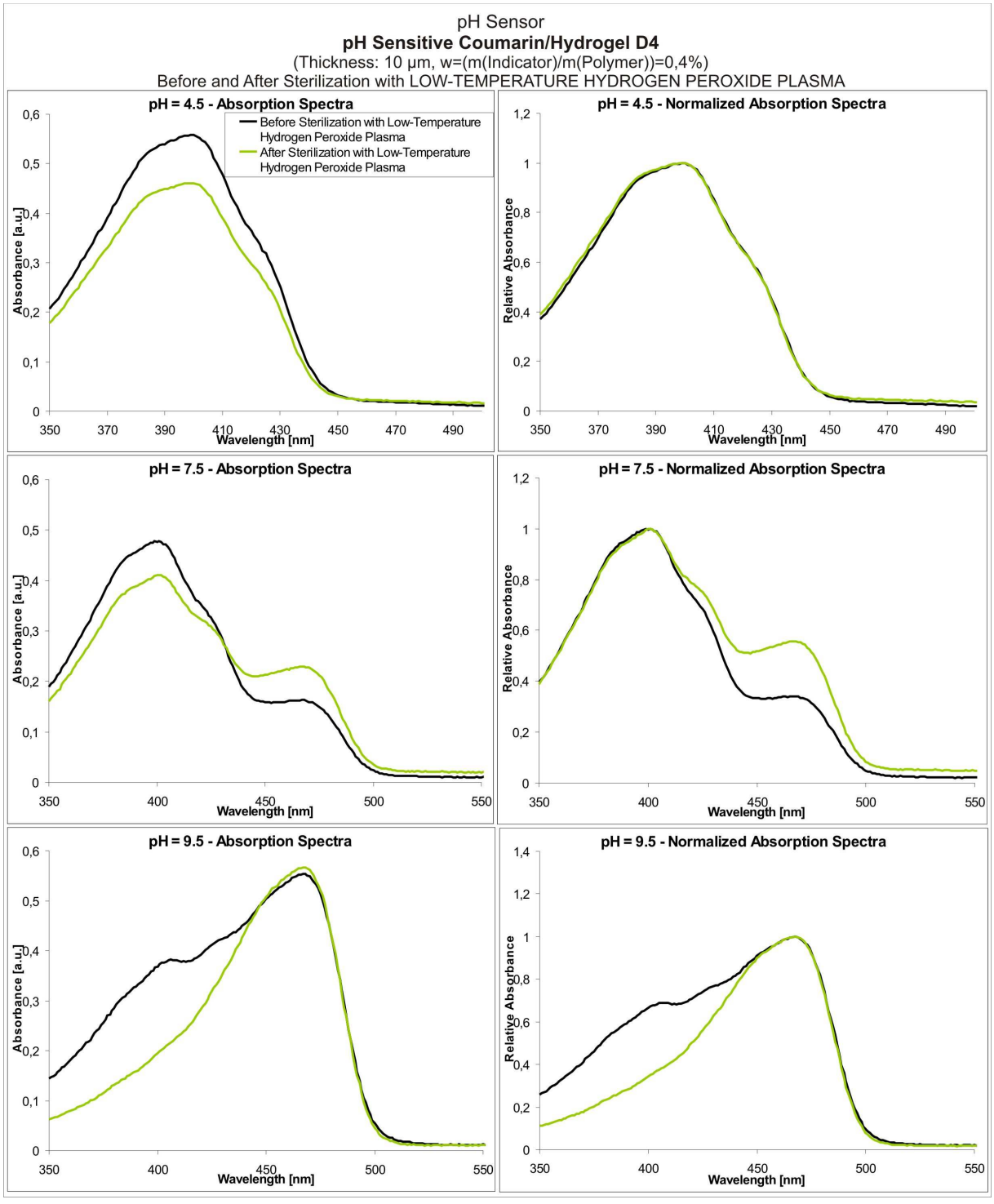

Emission Spectra

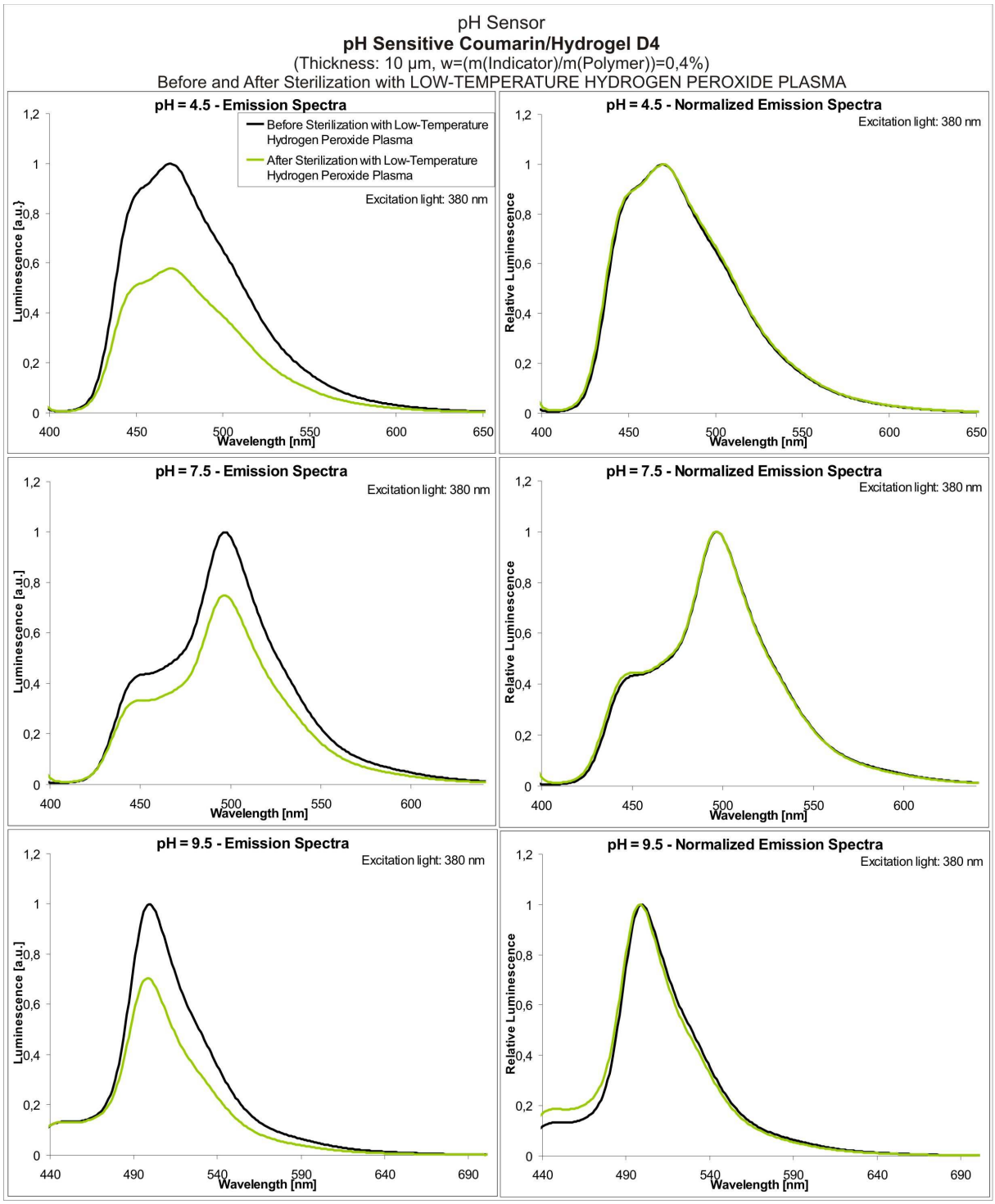

H_2O_2 Plasma	Absorption Spectra			Emission Spectra		
		pH	Alterations		pH	Alterations
Alterations in Absorption/ Emission Intensity	AFTERS	4.5	17,45% decrease	AFTERS	4.5	42,05% decrease
		7.5	13,82% decrease		7.5	25,08% decrease
		9.5	2,13% decrease		9.5	29,55% decrease

Alterations in Absorption/ Emission Curve Form	AFTER S	4.5	Unaltered	AFTER S	4.5	Unaltered
		7.5	The ratio between protonation/deprotonation absorption peaks is altered.		7.5	Unaltered
		9.5	Altered absorption between 350-450 nm.		9.5	Altered emission curve form between 440-490 nm.

Calibration Curves

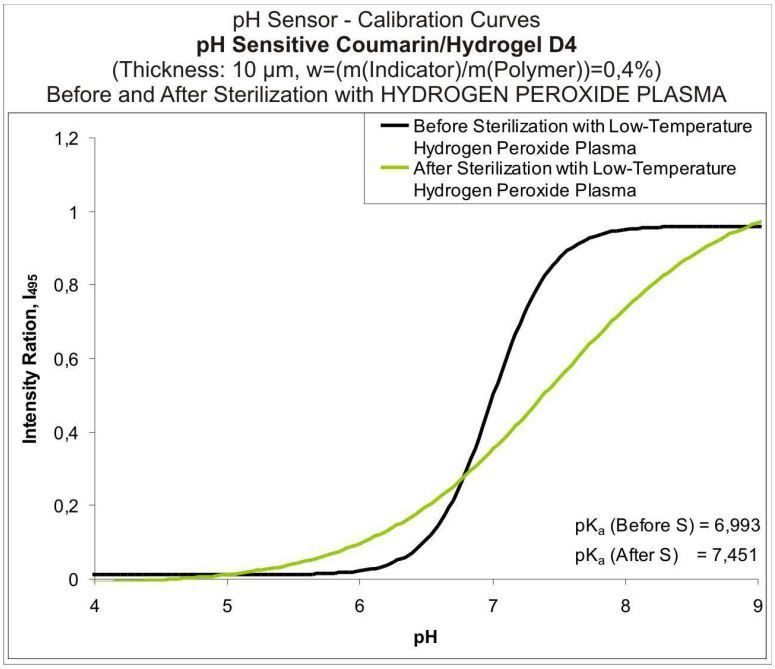

H_2O_2 Plasma	Alterations in Calibration Curve Shape	Alterations in pK_a
	Altered curve shape after sterilization. The response to the proton still observed – re-calibration of sensor response.	Increase of pK_a (for 0,458)

F.31 pH Sensitive Coumarin immobilized in Poly(2-HydroxyEthyl Methacrylate) (=pHEMA)

F.31.1 Sterilization with Hydrogen Peroxide Gas

Absorption Spectra

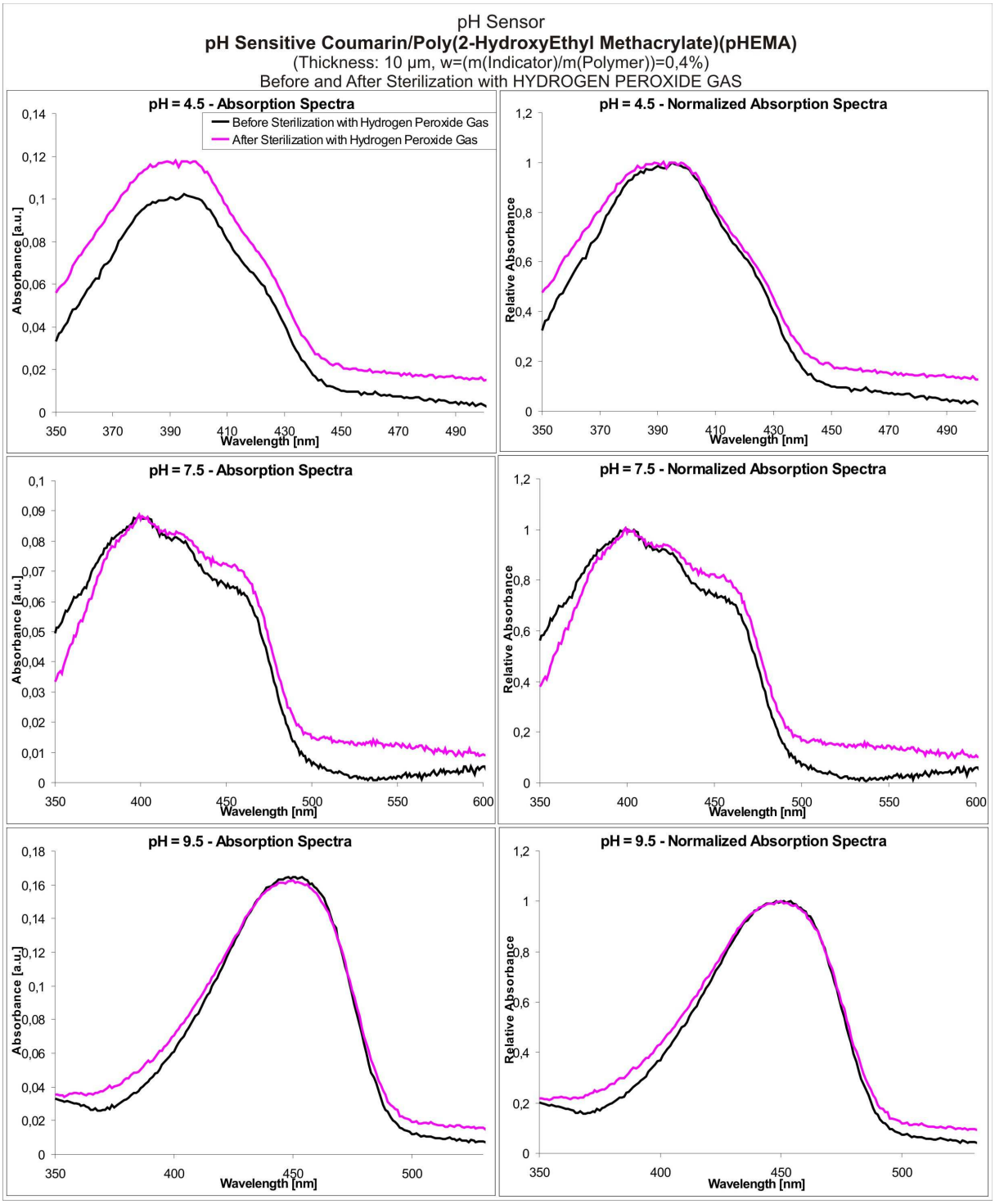

Emission Spectra

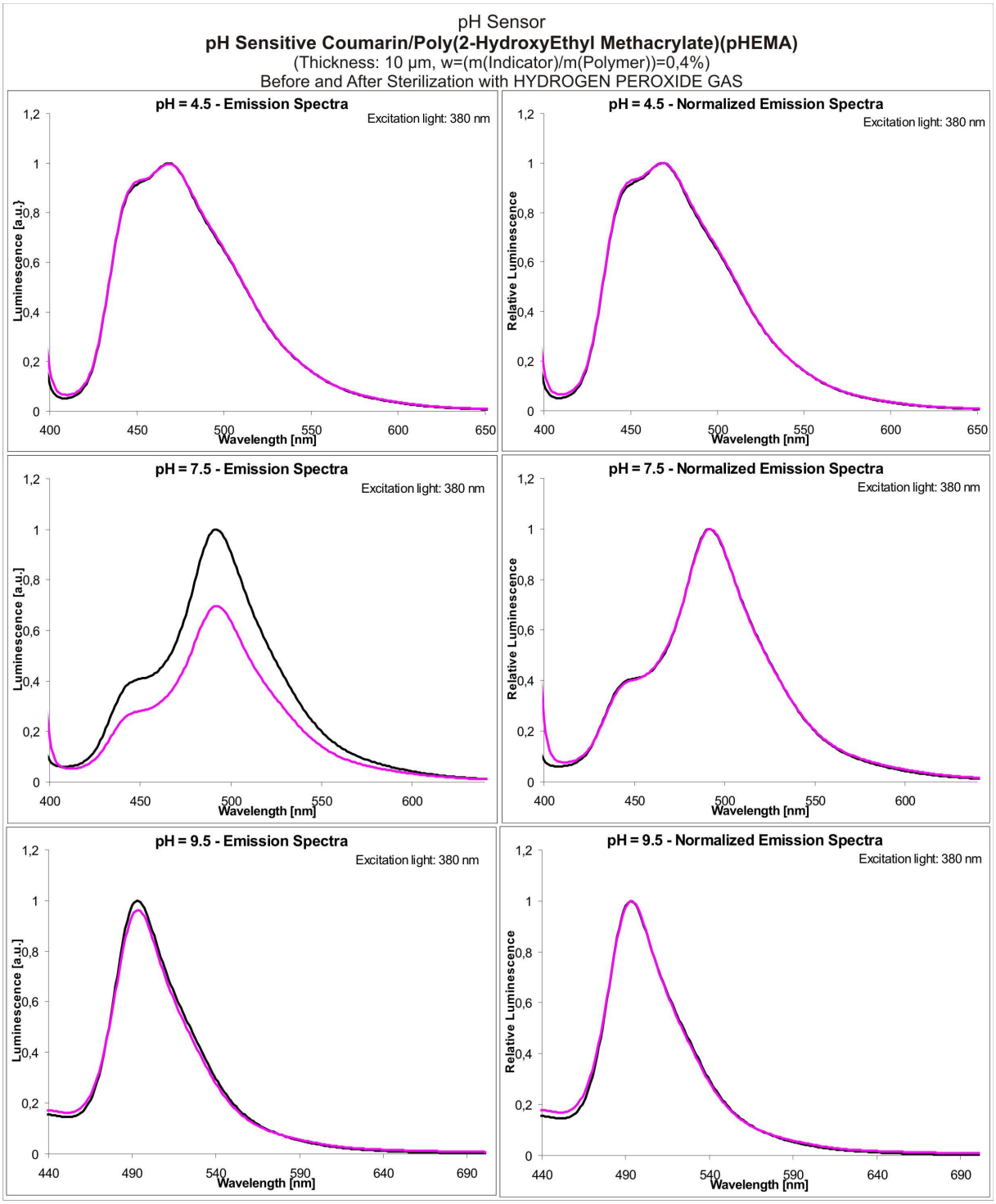

H_2O_2 Gas	Absorption Spectra			Emission Spectra		
		pH	Alterations		pH	Alterations
Alterations in Absorption/ Emission Intensity	AFTER S	4.5	13,15% decrease	AFTER S	4.5	0,30% decrease
		7.5	0,17% decrease		7.5	30,33% decrease
		9.5	1,10% decrease		9.5	3,72% decrease

Alterations in Absorption/ Emission Curve Form	AFTER S	4.5	Altered absorption between 350-390 nm and 430-800 nm. The sensor became slightly turbid after sterilization.	AFTER S	4.5	Unaltered
		7.5	Altered absorption between 350-380 nm and 430-800 nm.		7.5	Unaltered
		9.5	Altered absorption between 350-430 nm and 490-800 nm. The sensor became slightly turbid after sterilization.		9.5	Unaltered

Calibration Curves

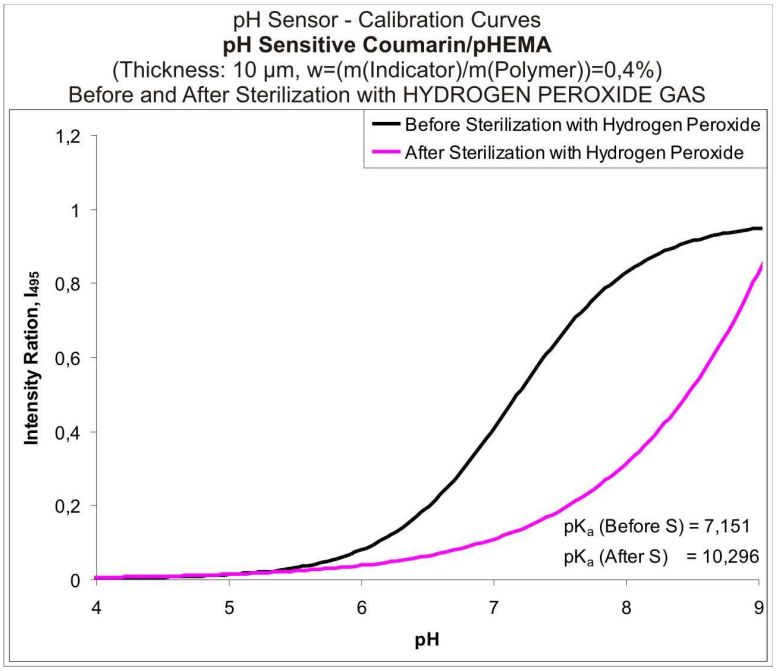

H_2O_2 Gas	Alterations in Calibration Curve Shape	Alterations in pK_a
	Greatly altered curve shape after sterilization.	Increase of pK_a (for 3,145)

F.31.2 Sterilization with Low-Temperature Hydrogen Peroxide Plasma

Absorption Spectra

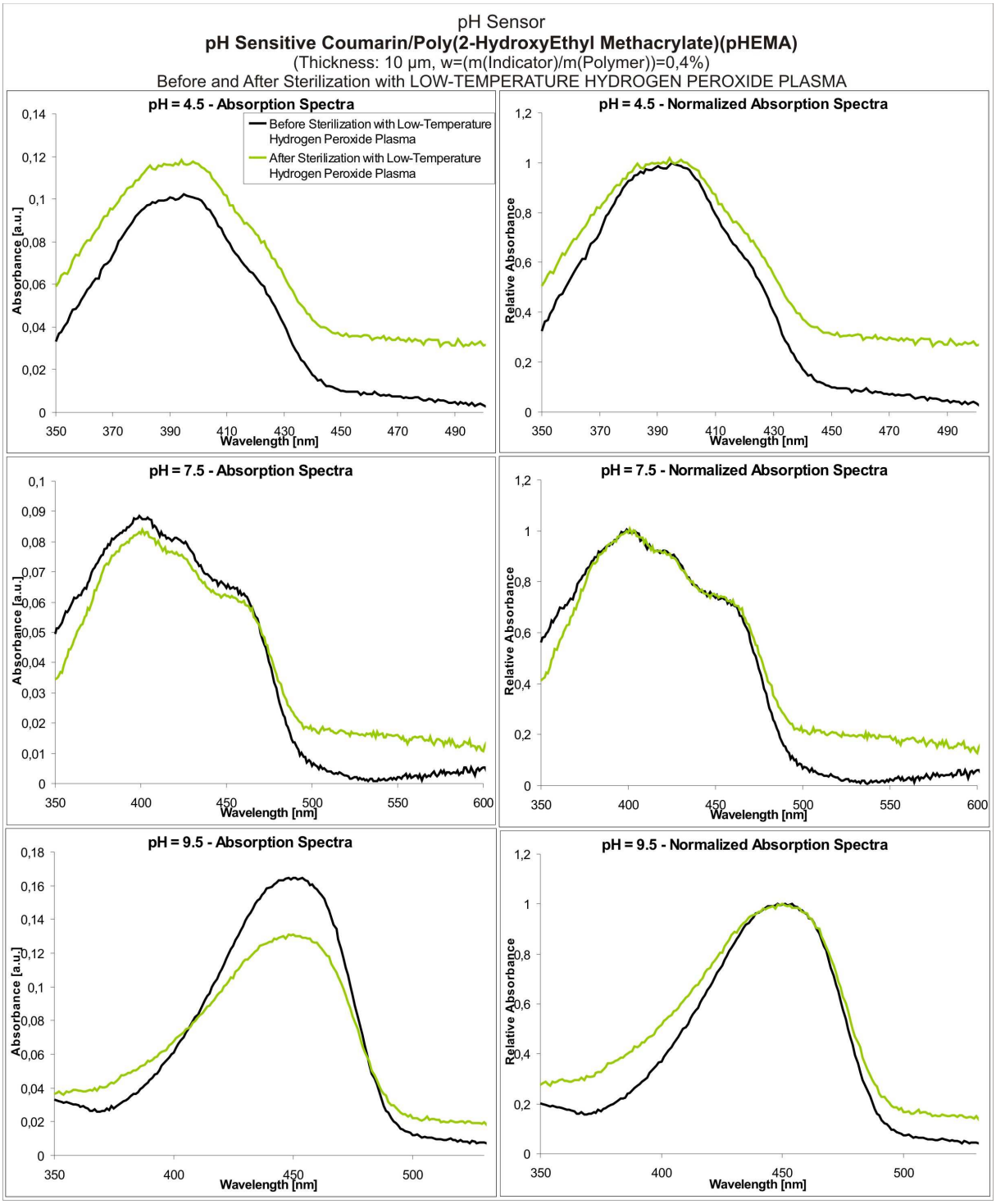

Emission Spectra

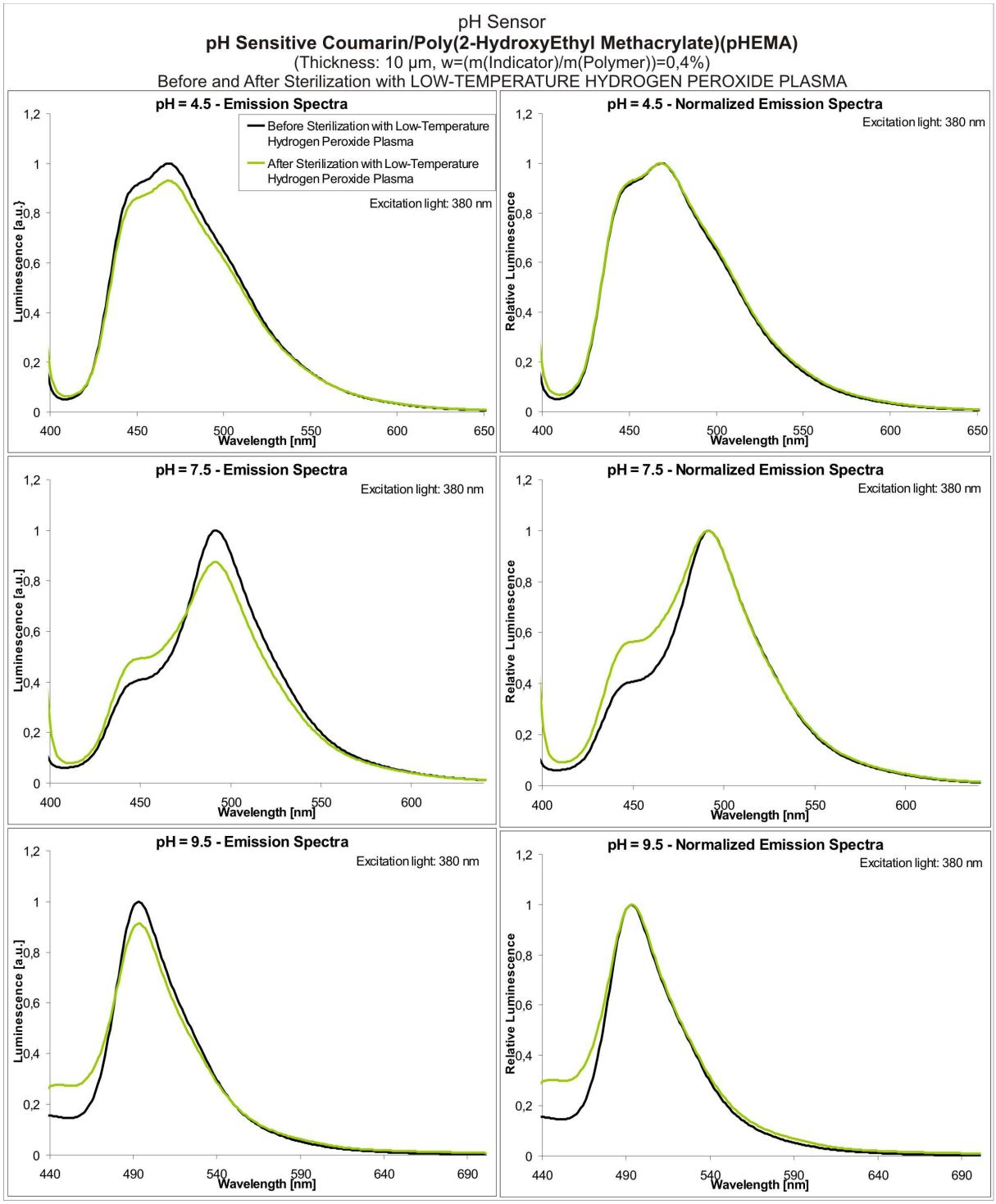

H_2O_2 Plasma	Absorption Spectra			Emission Spectra		
		pH	Alterations		pH	Alterations
Alterations in Absorption/ Emission Intensity	AFTERS	4.5	12,90% increase	AFTERS	4.5	6,97% decrease
		7.5	5,53% decrease		7.5	12,65% decrease
		9.5	25,69% decrease		9.5	8,67% decrease

Alterations in Absorption/ Emission Curve Form	AFTER S	4.5	The sensor became slightly turbid after sterilization.	AFTER S	4.5	Unaltered
		7.5	Altered absorption between 350-380 nm and 500-800 nm.		7.5	Altered emission curve form between 400-500 nm.
		9.5	Altered absorption between 350-430 nm and 470-800 nm.		9.5	Altered emission curve form between 440-490 nm.

Calibration Curves

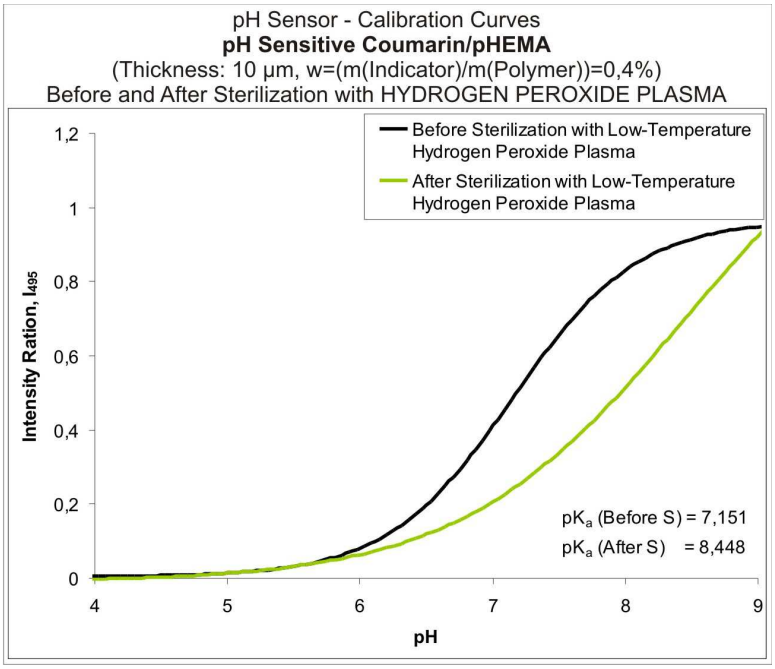

H_2O_2 Plasma	Alterations in Calibration Curve Shape	Alterations in pK_a
	Greatly altered curve shape after sterilization.	Increase of pK_a (for 1,297)

F.32 PET Perylene BisImide immobilized in HydroMed Hydrogel D4

F.32.1 Sterilization with Hydrogen Peroxide Gas

Absorption Spectra

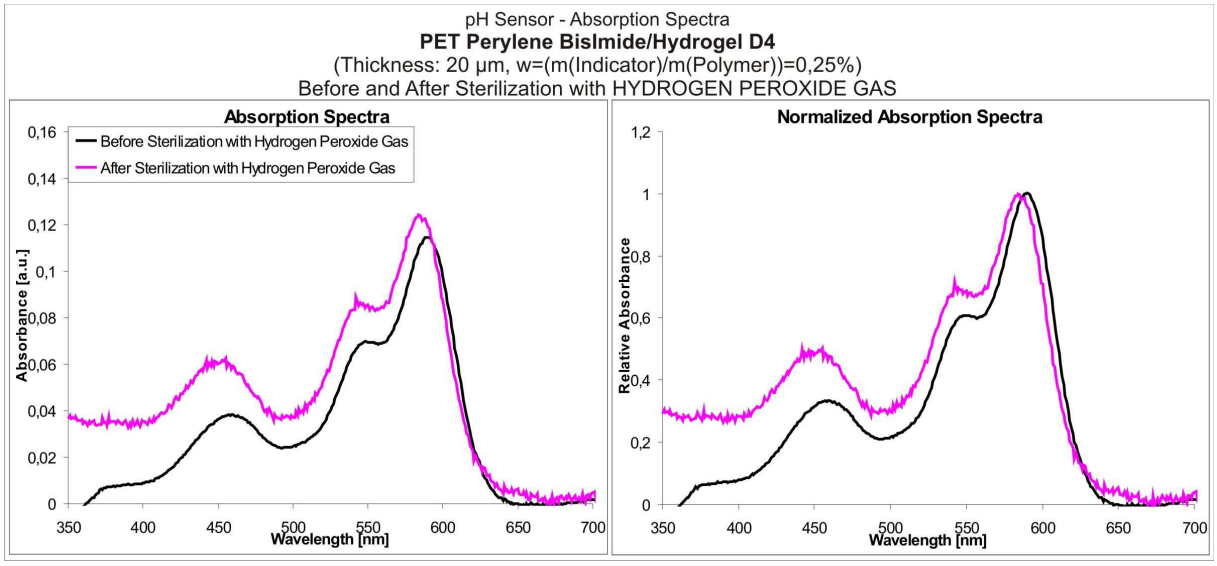

H_2O_2 GAS Sterilization	Absorption Spectra
Alterations in Absorption/Emission Intensity	0,58% increase
Alterations in Absorption/Emission Curve Form	Altered absorption curve form between 350-580 nm. Hypsochromic shift of the absorption maximum for 4 nm.

Emission Spectra

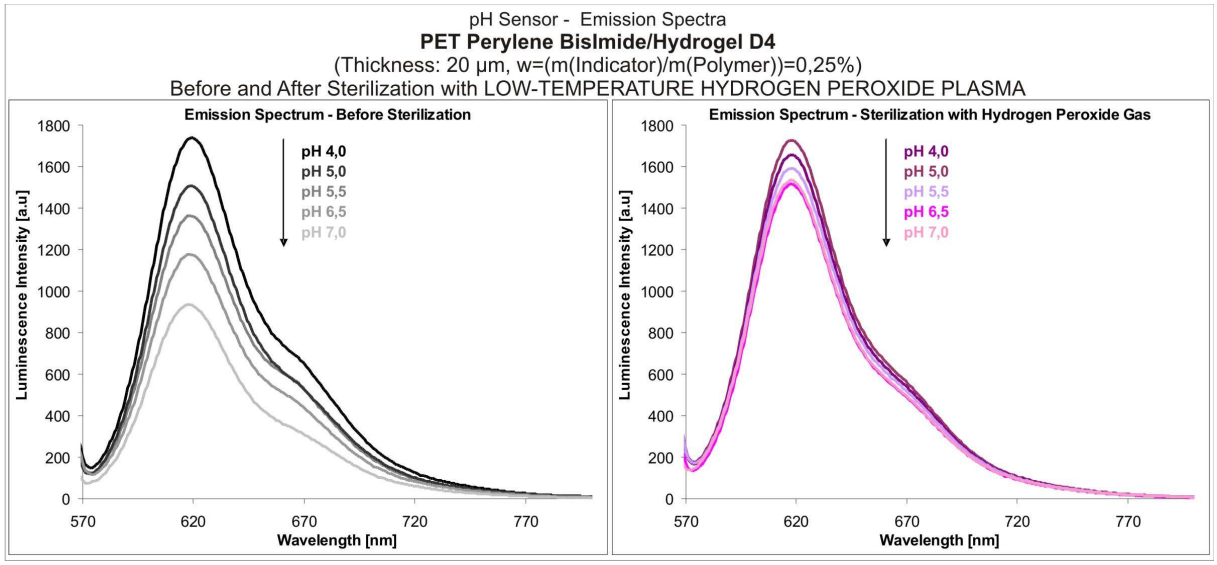

H_2O_2 Gas	Emission Spectra					
	Decrease of the Luminescence Intensity in dependence of the Intensity at lower pH			Decrease of the Luminescence Intensity at define pH in dependence of the Intensity Before Sterilization		
BEFORE S	**pH**	**Max. Intensity**				
Alterations in Absorption/ Emission Intensity	4	1739	/			
	5	1509	13,22% decrease			
	5.5	1363	21,62% decrease			
	6.5	1176	32,37% decrease			
	7	933,6	46,31% decrease			
PET Efficiency	1.86					
AFTER S	**pH**	**Max. Intensity**		**pH**	**Compared Intensity**	
Alterations in Absorption/ Emission Intensity	4	1727	/	4	1739	0,69% decrease
	5	1514	12,33% decrease	5	1509	0,33% increase
	5.5	1657	5,59% decrease	5.5	1363	21,57% increase
	6.5	1592	4,05% decrease	6.5	1176	35,37% increase
	7	1533	11,23% decrease	7	933,6	64,20% increase

Calibration Curves

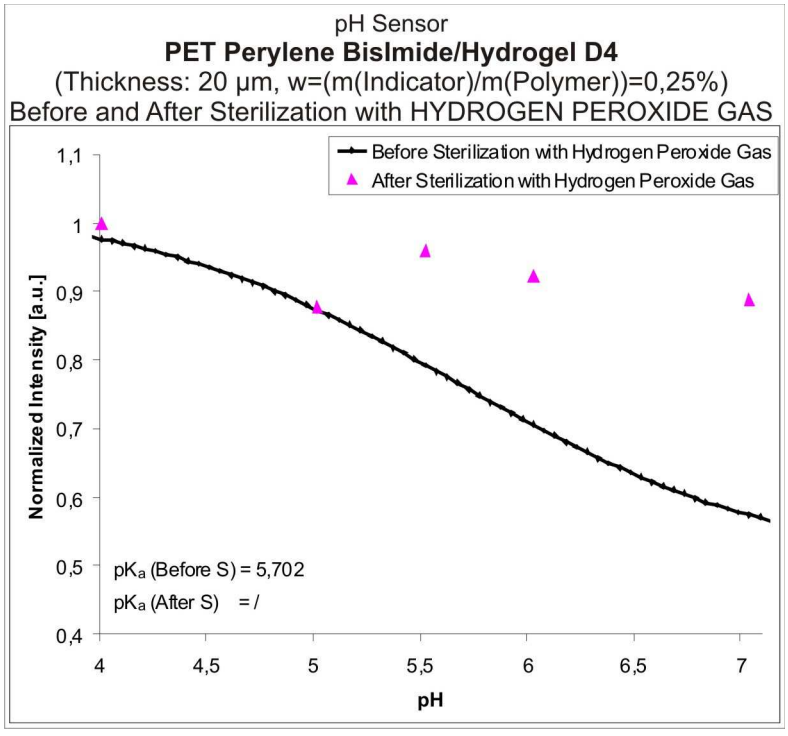

H_2O_2 Gas	Alterations in Calibration Curve Shape	Alterations in pK_a
	The calibration curve no longer observed.	

F.32.2 Sterilization with Low-Temperature Hydrogen Peroxide Plasa

Absorption Spectra

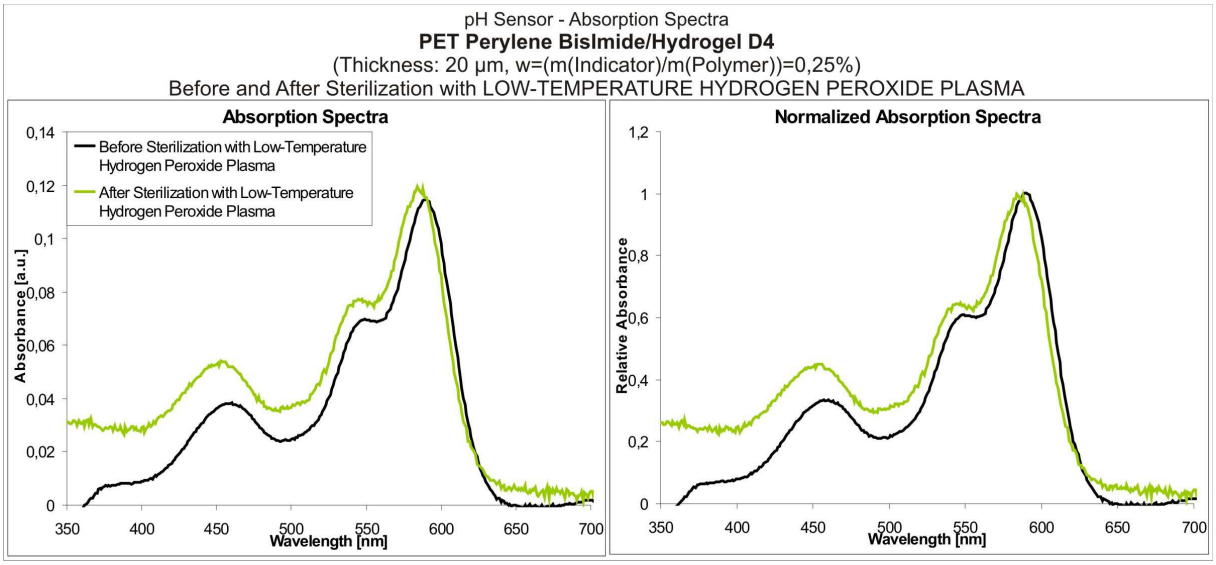

H_2O_2 PLASMA Sterilization	Absorption Spectra
Alterations in Absorption/Emission Intensity	0,47% increase
Alterations in Absorption/Emission Curve Form	Altered absorption curve form between 350-580 nm and 640-700 nm. Hypsochromic shift of the absorption maximum for 3 nm.

Emission Spectra

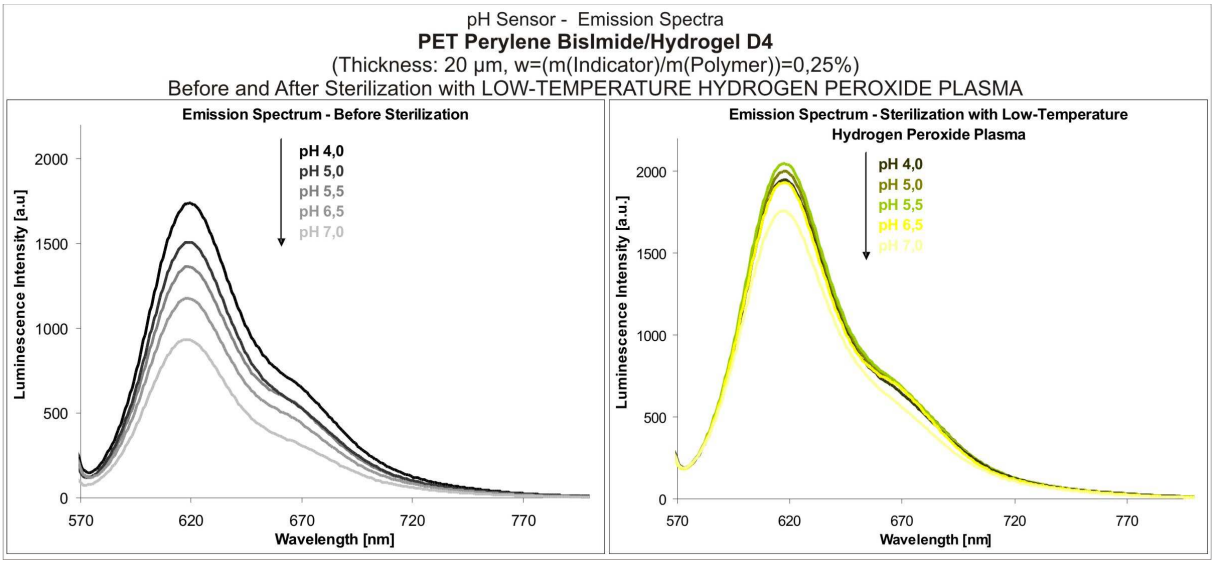

H_2O_2 Plasma	Emission Spectra					
	Decrease of the Luminescence Intensity in dependence of the Intensity at lower pH			Decrease of the Luminescence Intensity at define pH in dependence of the Intensity Before Sterilization		
BEFORE S	**pH**	**Max. Intensity**				
Alterations in Absorption/ Emission Intensity	4	1739	/			
	5	1509	13,22% decrease			
	5.5	1363	21,62% decrease			
	6.5	1176	32,37% decrease			
	7	933,6	46,31% decrease			
PET Efficiency	1.86					
AFTER S	**pH**	**Max. Intensity**		**pH**	**Compared Intensity**	
Alterations in Absorption/ Emission Intensity	4	1999	/	4	1739	14,95% increase
	5	2044	2,25% increase	5	1509	35,45% increase
	5.5	1947	2,60% decrease	5.5	1363	42,85% increase
	6.5	1931	3,45% decrease	6.5	1176	64,20% increase
	7	1756	12,16% decrease	7	933,6	88,09% increase

Calibration Curves

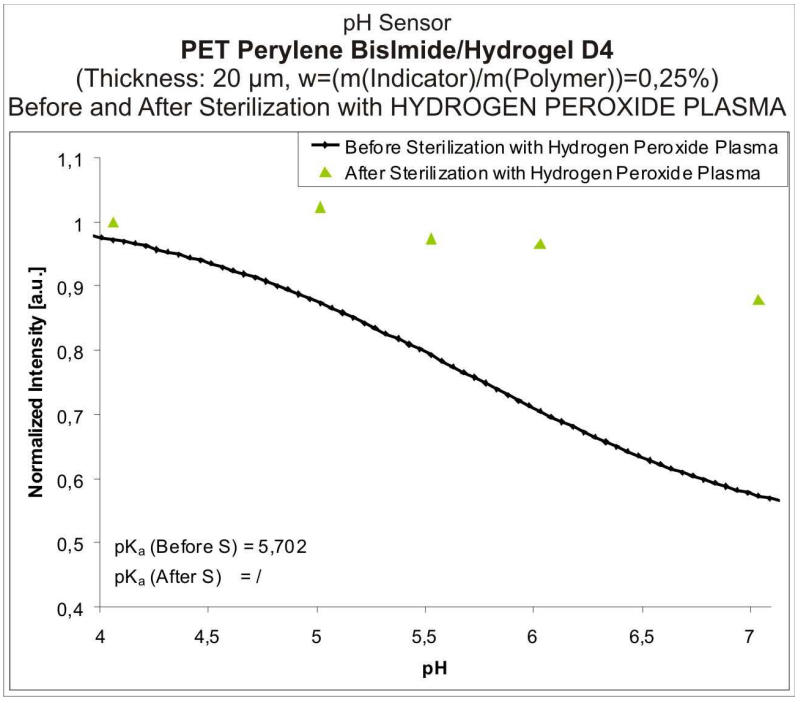

H_2O_2 Plasma	Alterations in Calibration Curve Shape	Alterations in pK_a
	The calibration curve no longer observed.	

F.33 BromoPhenol Blue immobilized in HydroMed Hydrogel D4

F.33.1 Sterilization with Hydrogen Peroxide Gas

Absorption Spectra

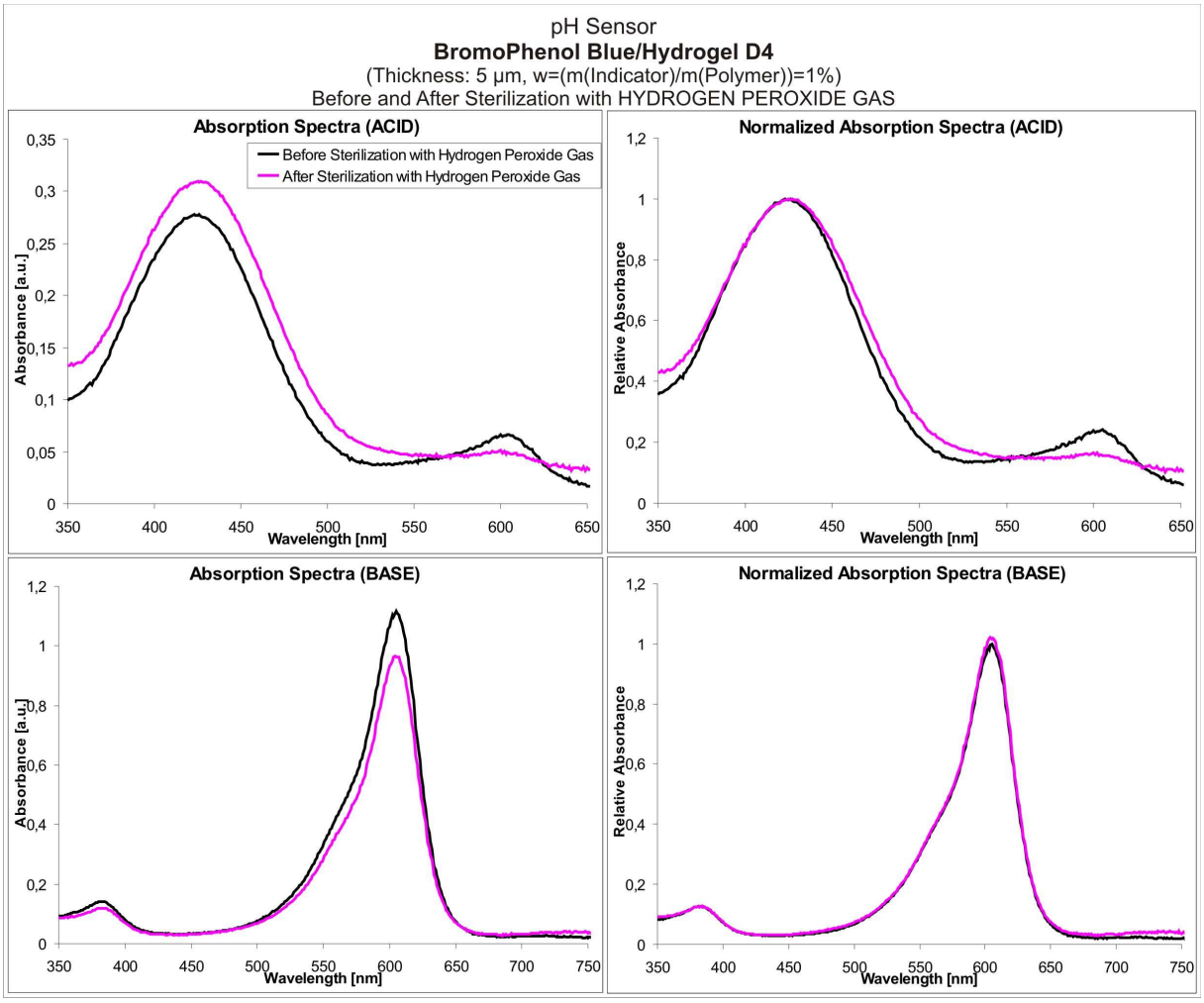

H_2O_2 Gas	Absorption Spectra						
		pH	Alterations			pH	Alterations
Alterations in Absorption /Emission Intensity	AFTERS	ACID	9,89% decrease	Alterations in Absorption /Emission Curve Form	AFTERS	ACID	The ratio between protonation/deprotonation absorption peaks is altered.
		BASE	15,28% decrease			BASE	Unaltered.

F.33.2 Sterilization with Low-Temperature Hydrogen Peroxide Plasma

Absorption Spectra

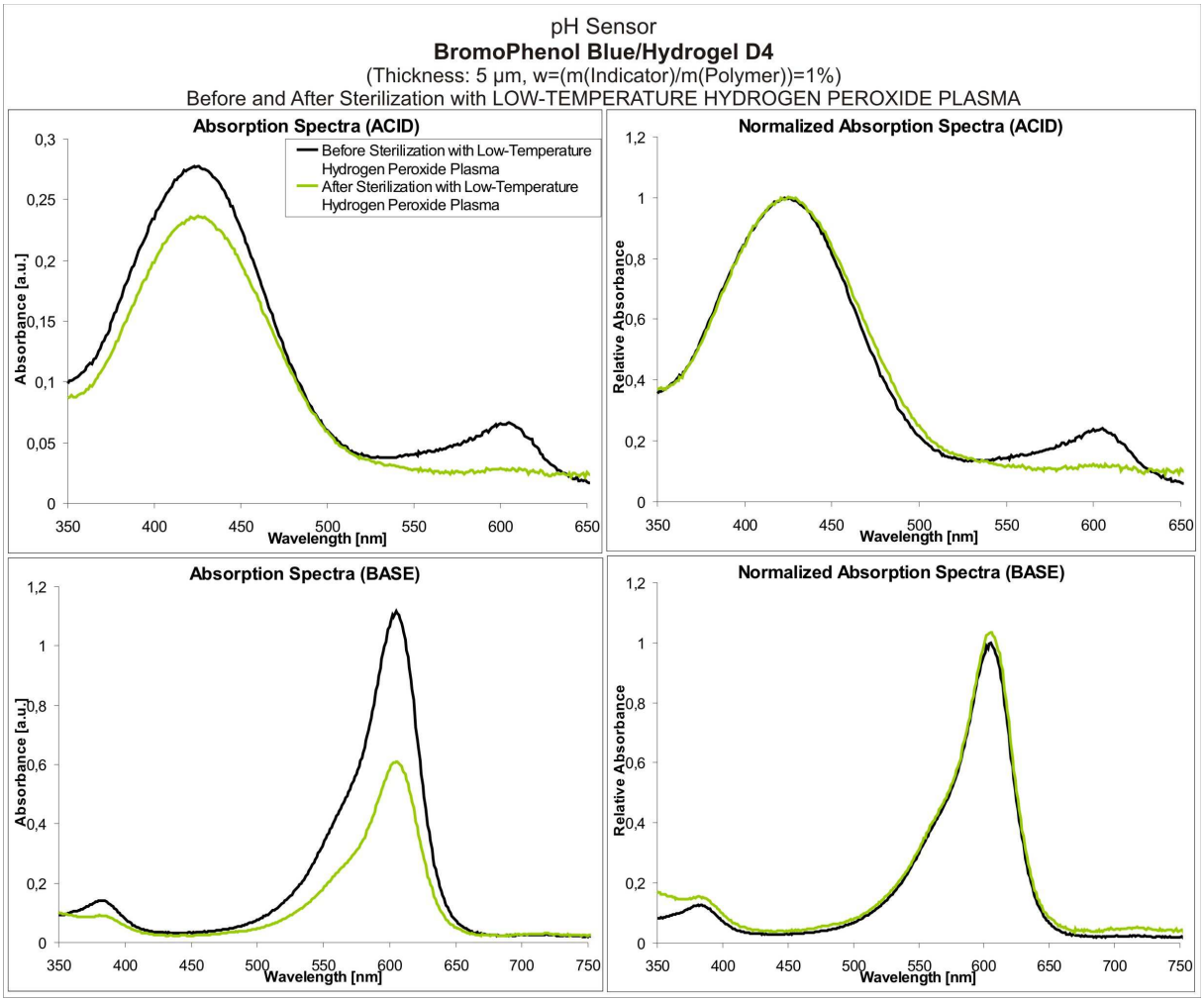

H_2O_2 Plasma	Absorption Spectra						
		pH	Alterations			pH	Alterations
Alterations in Absorption /Emission Intensity	AFTERS	ACID	15,15% decrease	Alterations in Absorption /Emission Curve Form	AFTERS	ACID	The ratio between protonation/deprotonation absorption peaks is altered.
		BASE	47,15% decrease			BASE	Unaltered.

F.34 Thymol Blue immobilized in HydroMed Hydrogel D4

F.34.1 Sterilization with Hydrogen Peroxide Gas

Absorption Spectra

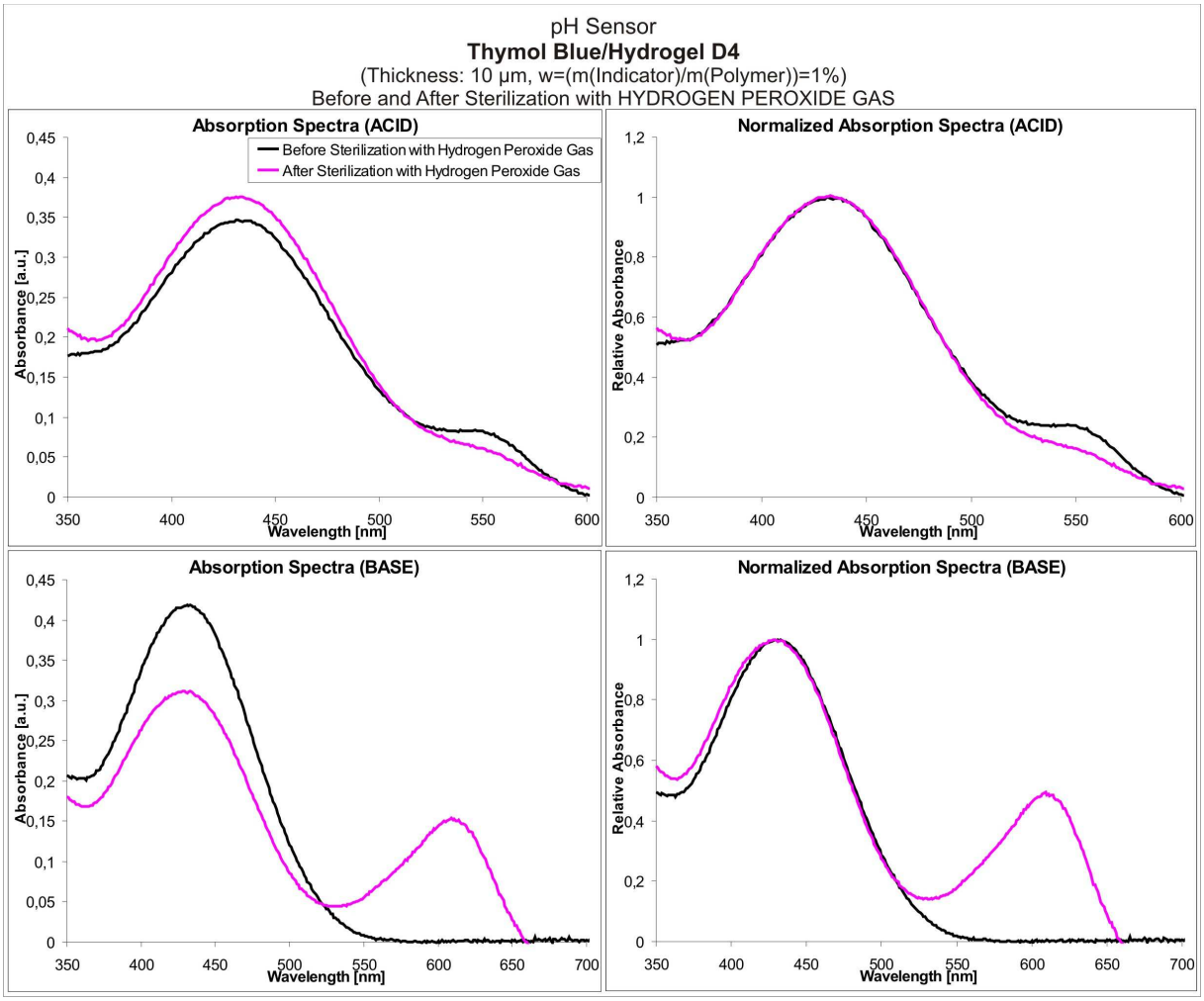

H_2O_2 Gas	Absorption Spectra						
		pH	Alterations			pH	Alterations
Alterations in Absorption /Emission Intensity	AFTERS	ACID	7,23% increase	Alterations in Absorption /Emission Curve Form	AFTERS	ACID	The ratio between protonation/deprotonation absorption peaks is altered.
		BASE	25,46% decrease			BASE	The ratio between protonation/deprotonation absorption peaks is altered.

F.34.2 Sterilization with Low-Temperature Hydrogen Peroxide Plasma

Absorption Spectra

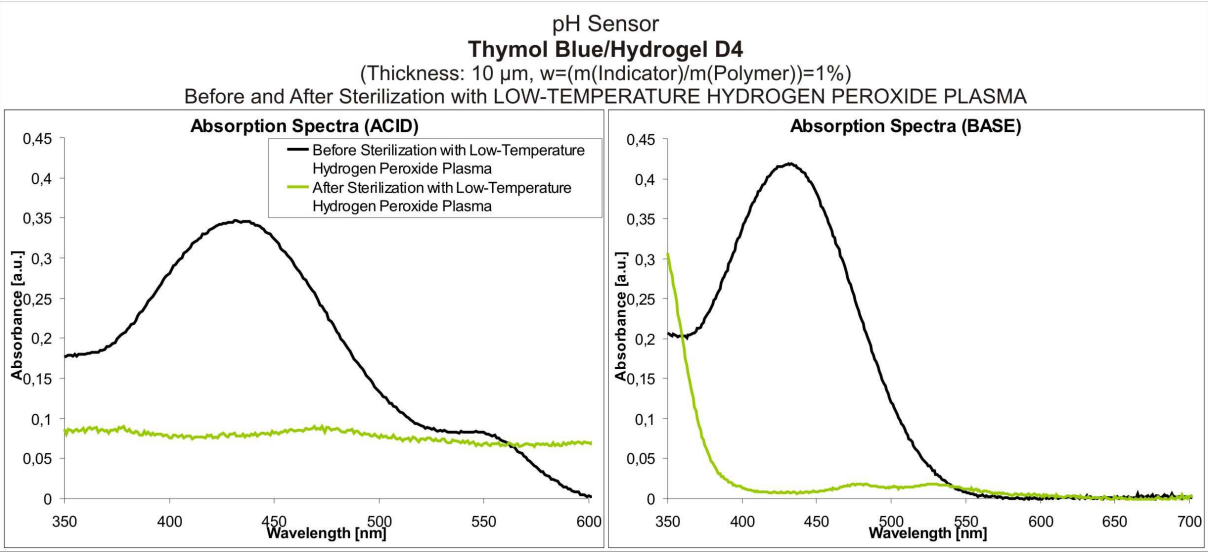

H_2O_2 Plasma	Absorption Spectra						
		pH	Alterations			pH	Alterations
Alterations in Absorption /Emission Intensity	AFTERS	ACID	Decrease	Alterations in Absorption /Emission Curve Form	AFTERS	ACID	Disappearance of the characteristic absorption curve form.
		BASE	Decrease			BASE	Disappearance of the characteristic absorption curve form.

F.35 BromoThymol Blue immobilized in HydroMed Hydrogel D4

F.35.1 Sterilization with Hydrogen Peroxide Gas

Absorption Spectra

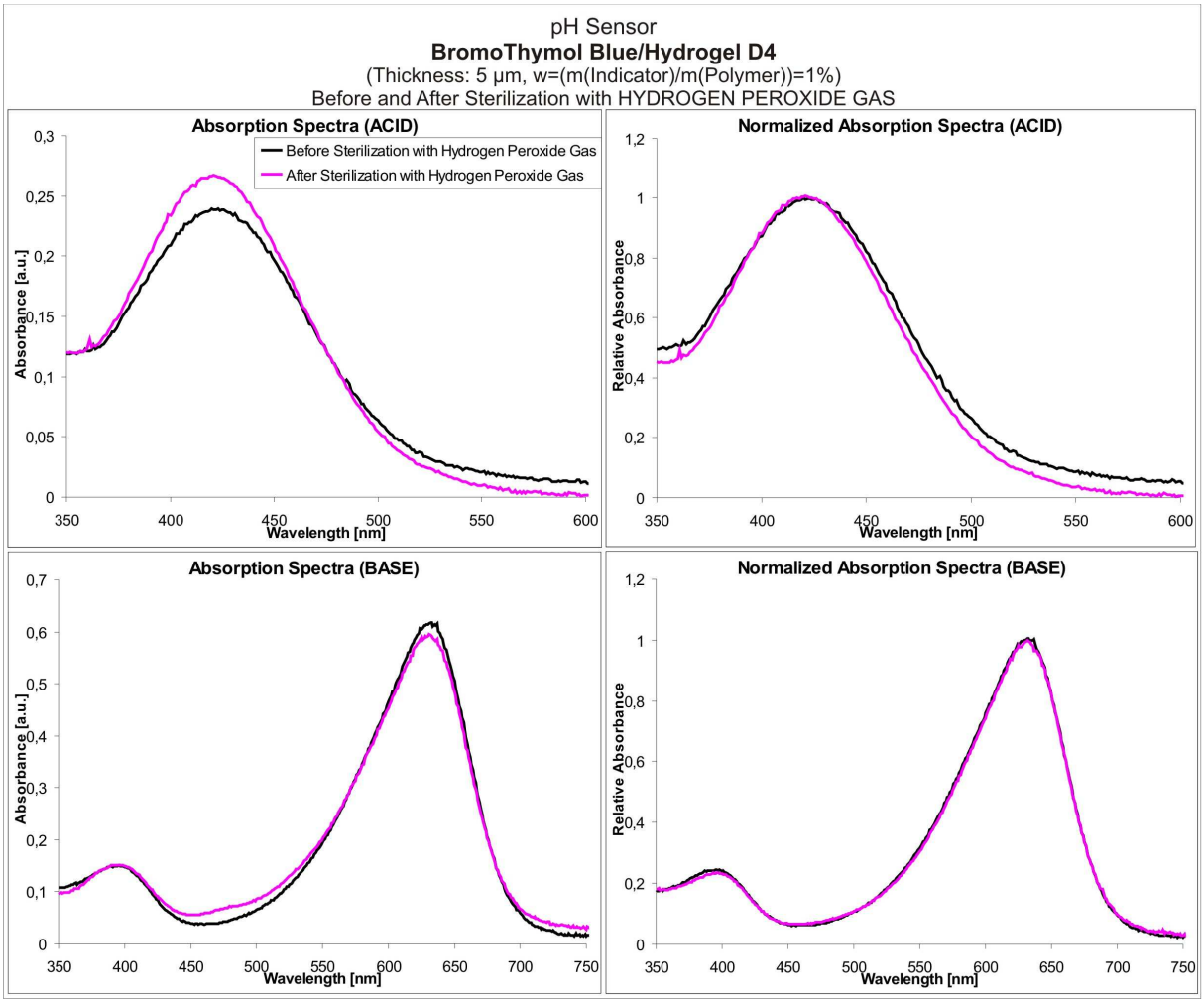

H_2O_2 Gas	Absorption Spectra						
		pH	Alterations			pH	Alterations
Alterations in Absorption /Emission Intensity	AFTERS	ACID	9,79% increase	Alterations in Absorption /Emission Curve Form	AFTERS	ACID	Alteration of the absorption between 500-800 nm. Hypsochromic shift of the absorption maximum for 3 nm.
		BASE	3,10% decrease			BASE	Unaltered.

F.35.2 Sterilization with Low-Temperature Hydrogen Peroxide Plasma

Absorption Spectra

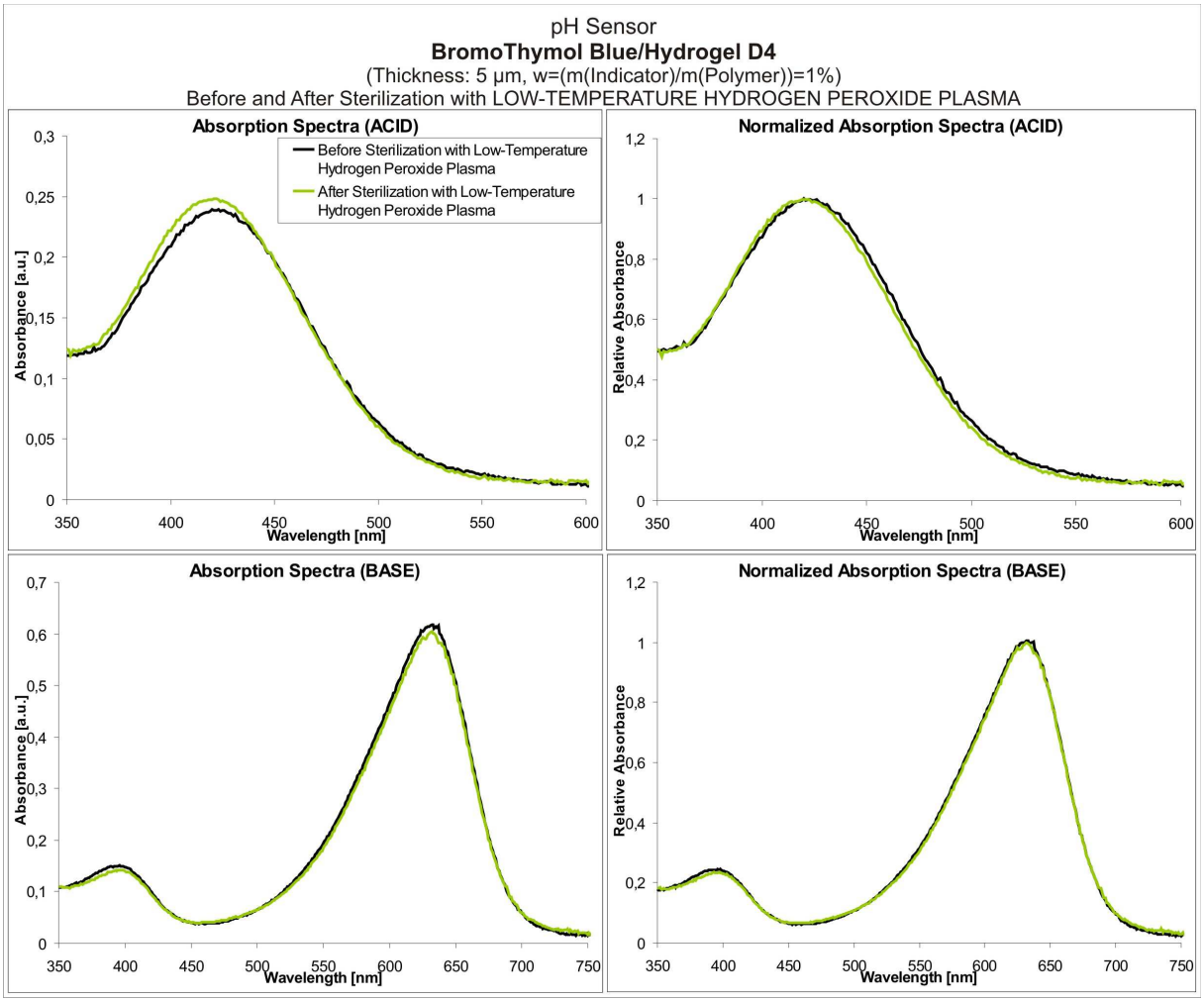

H_2O_2 Plasma	Absorption Spectra						
		pH	Alterations			pH	Alterations
Alterations in Absorption /Emission Intensity	AFTERS	ACID	3,63% decrease	Alterations in Absorption /Emission Curve Form	AFTERS	ACID	Unaltered.
		BASE	1,59% decrease			BASE	Unaltered.

F.36 Methyl Orange immobilized in HydroMed Hydrogel D4

F.36.1 Sterilization with Hydrogen Peroxide Gas

Absorption Spectra

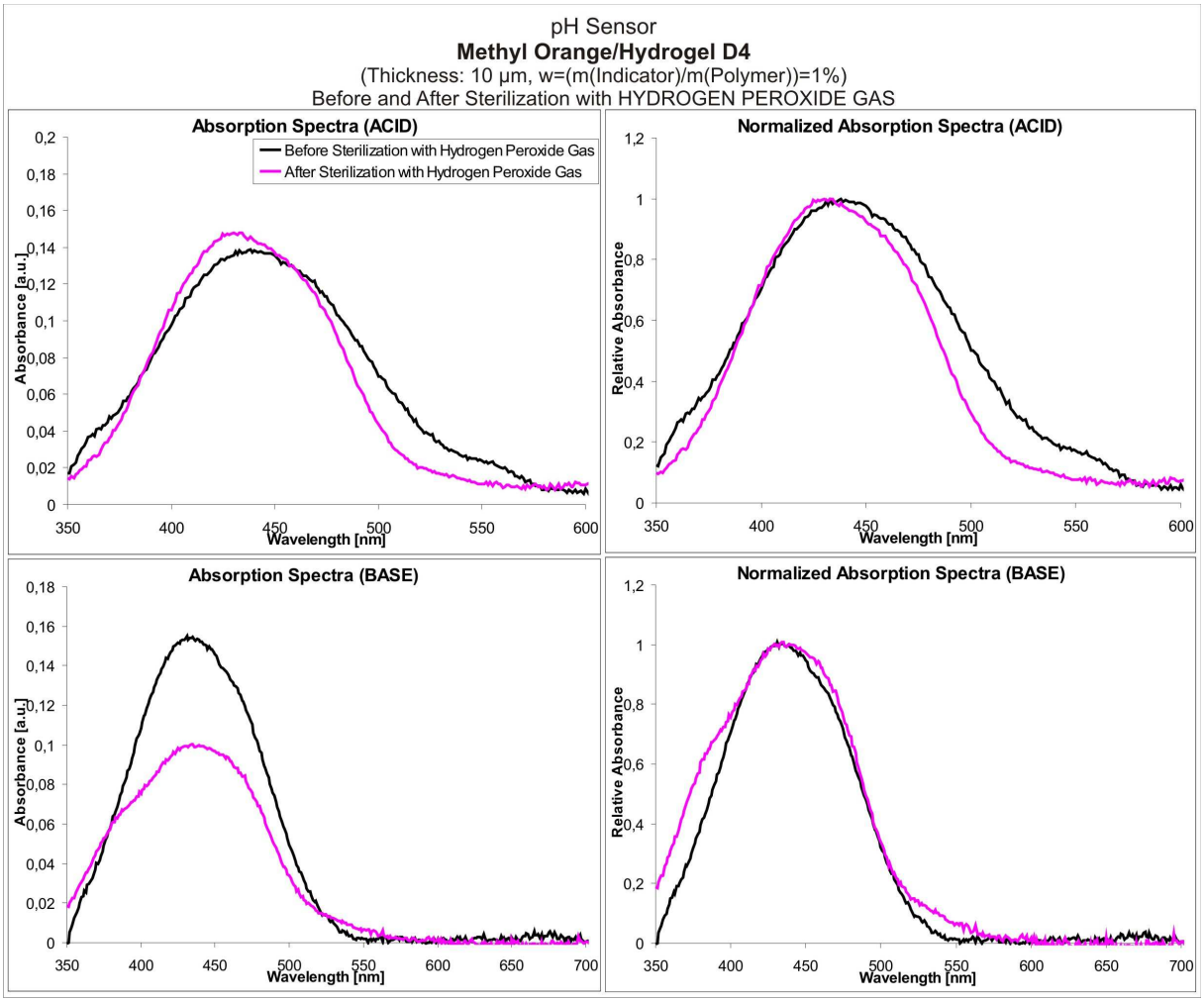

H_2O_2 Gas	Absorption Spectra						
		pH	Alterations			pH	Alterations
Alterations in Absorption /Emission Intensity	AFTERS	ACID	6,11% increase	Alterations in Absorption /Emission Curve Form	AFTERS	ACID	Altered absorption curve form between 350-400 nm, 450-470 nm and 500-600 nm.
		BASE	35,35% decrease			BASE	Altered absorption curve form between 480-600 nm. Hypsochromic shift of the absorption maximum for 8 nm.

F.36.2 Sterilization with Low-Temperature Hydrogen Peroxide Plasma

Absorption Spectra

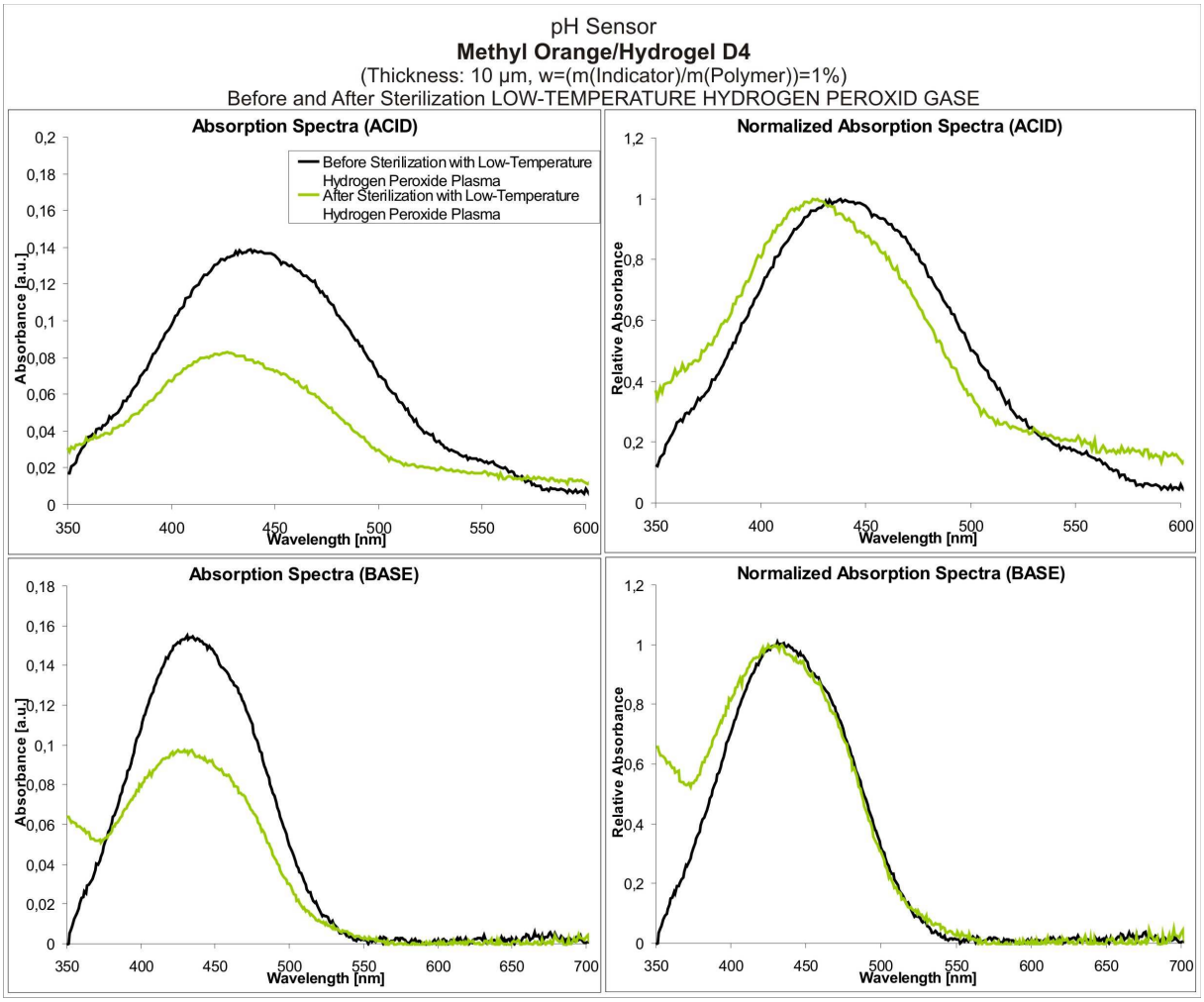

H_2O_2 Plasma	Absorption Spectra						
		pH	Alterations			pH	Alterations
Alterations in Absorption /Emission Intensity	AFTERS	ACID	40,33% decrease	Alterations in Absorption /Emission Curve Form	AFTERS	ACID	Hypsochromic shift of the absorption maximum for 11 nm.
		BASE	36,62% decrease			BASE	Alteration of absorption between 340-410 nm.

Optical TEMPERATURE SENSORS

F.37 Europium(III) Complex with 4-(4,6-di(1H-indazol-1-yl)-1,3,5-triazin-2-yl)-N,N-DiEthyl Benzen Amine (=Eu(tta)$_3$DEADIT) immobilized in PolyStyrene-co-Acrylonitrile

F.37.1 Sterilization with Hydrogen Peroxide Gas

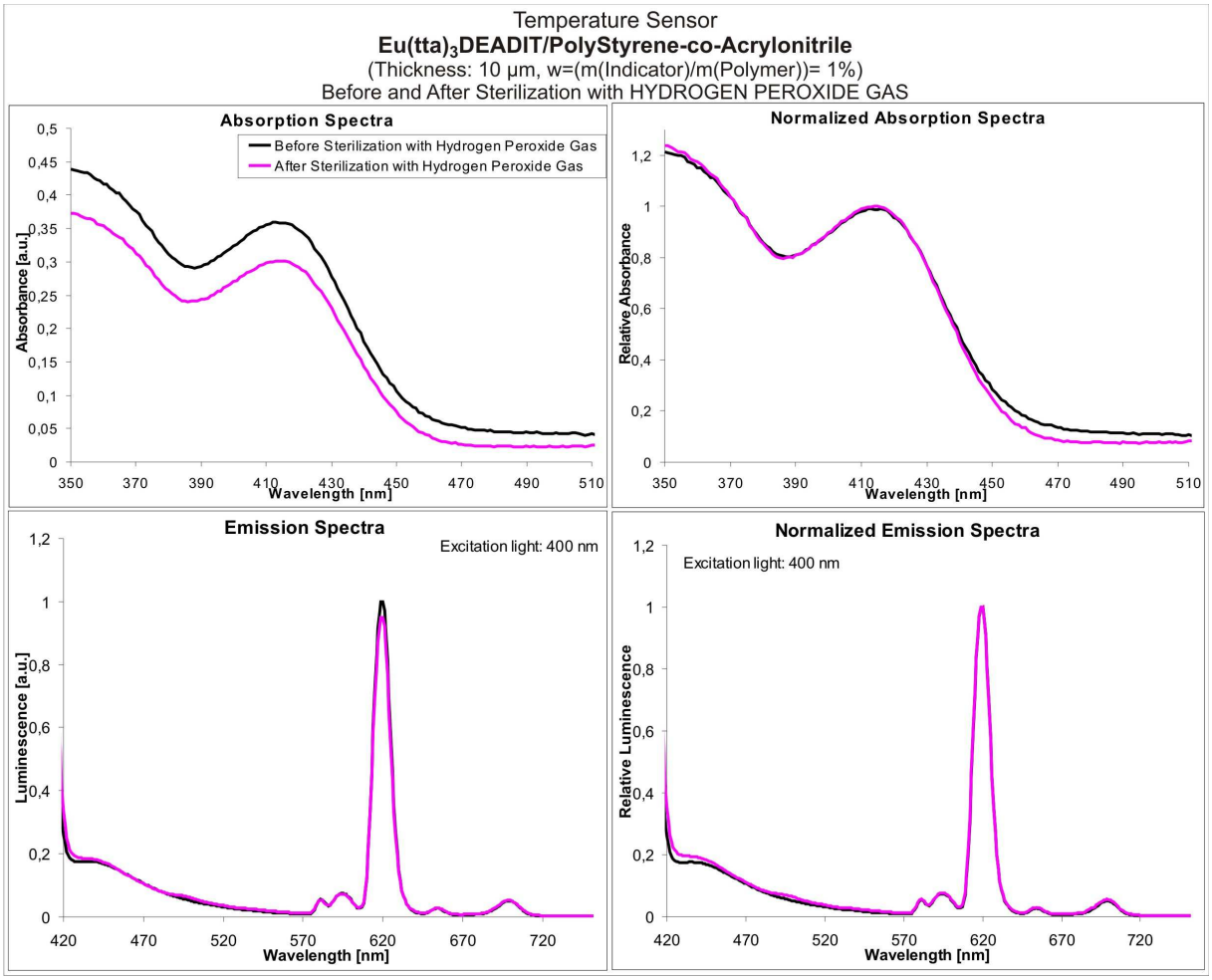

H_2O_2 Gas	Absorption Spectra	Emission Spectra
Alterations in Absorption/Emission Intensity	16,11% decrease	4,98% decrease
Alterations in Absorption/Emission Curve Form	Altered absorption between 450-800 nm	Unaltered.

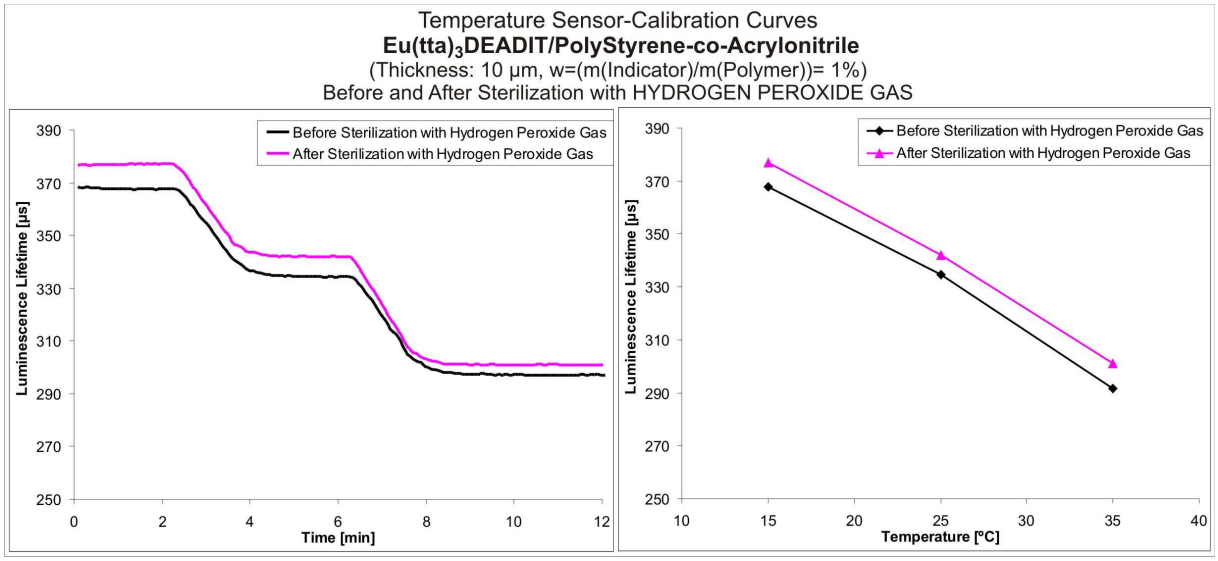

H_2O_2 Gas	Luminescence Lifetime		Alterations of Slope
Alterations in Luminescence Lifetime and Slope	15 °C	2,45% increase	0,07% decrease of slope
	25 °C	2,09% increase	
	35 °C	3,03% increase	

F.37.2 Sterilization with Low-Temperature Hydrogen Peroxide Plasma

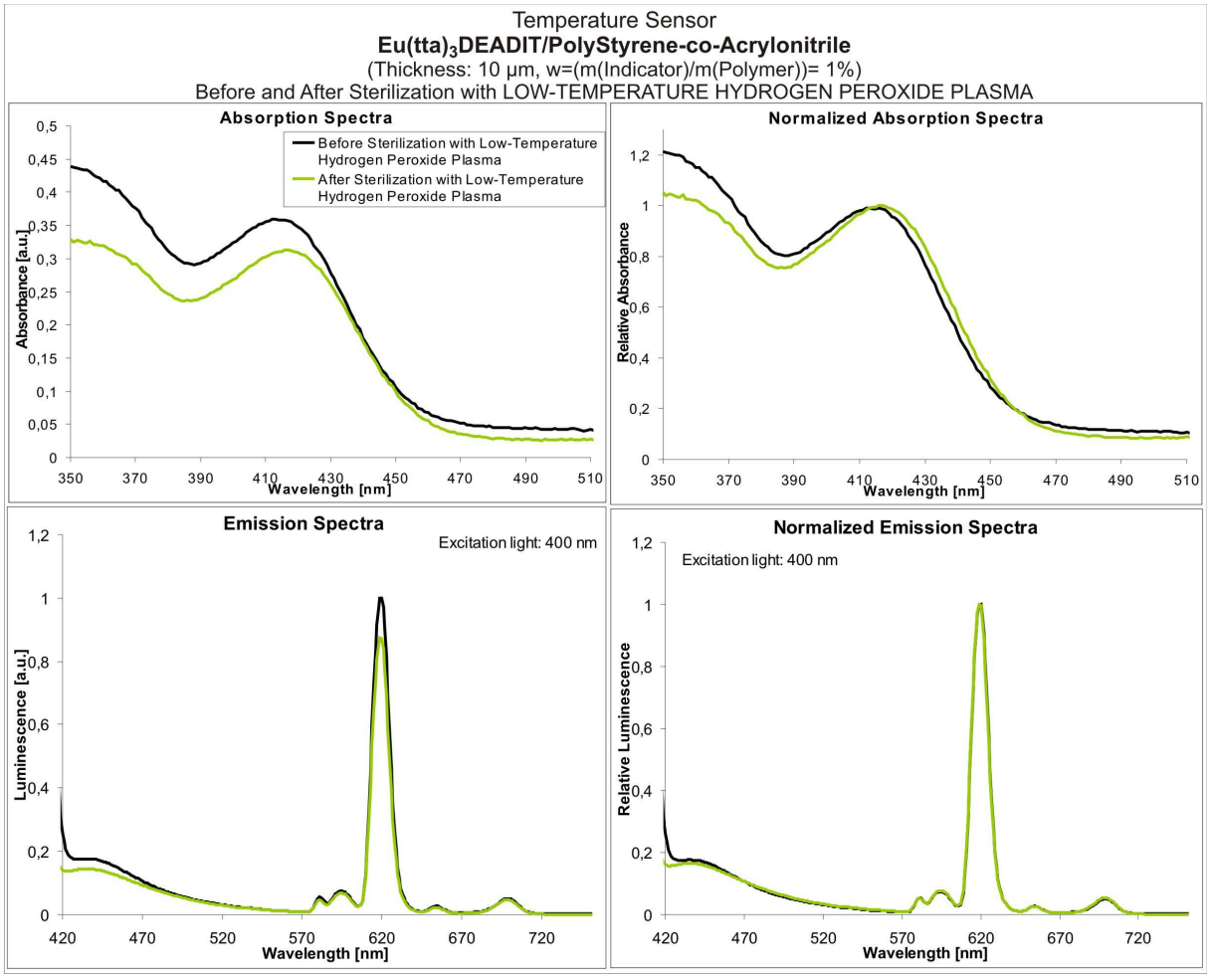

H_2O_2 Plasma	Absorption Spectra	Emission Spectra
Alterations in Absorption/Emission Intensity	12,92% decrease	12,52% decrease
Alterations in Absorption/Emission Curve Form	Bathochromic shift of the absorption maximum for 2 nm.	Unaltered.

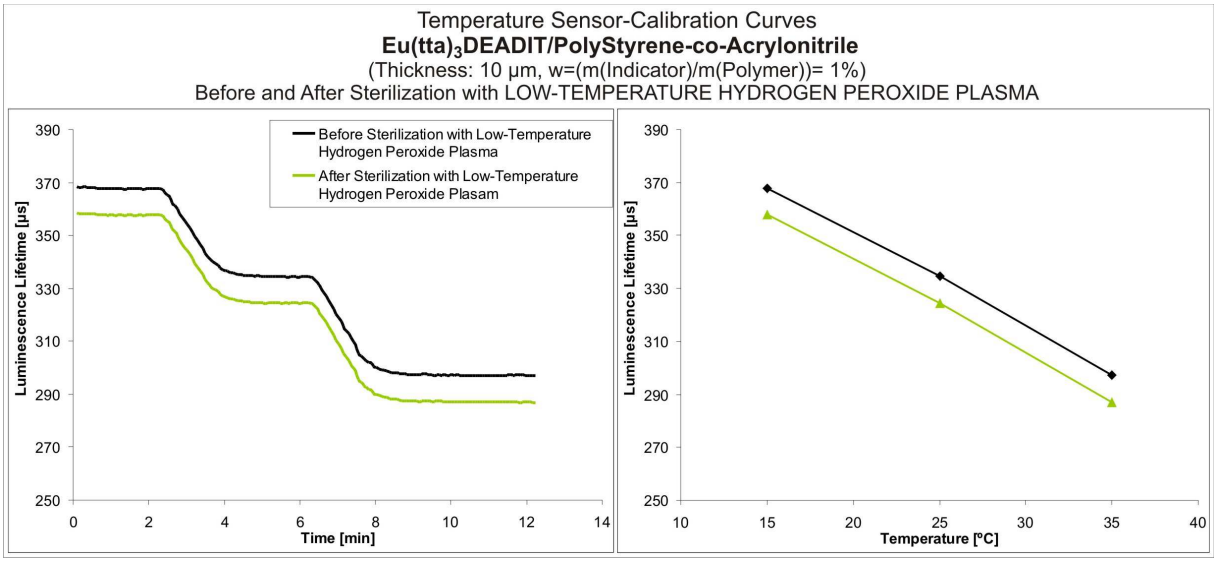

H_2O_2 Plasma	Luminescence Lifetime		Alterations of Slope
Alterations in Luminescence Lifetime and Slope	15℃	2,72% decrease	0,09% decrease of slope
	25℃	2,99% decrease	
	35℃	3,37% decrease	

F.38 Europium(III) Complex with 4-(4,6-di(1H-indazol-1-yl)-1,3,5-triazin-2-yl)-N,N-DiEthyl Benzen Amine (=Eu(tta)$_3$DEADIT) immobilized in PolyVinylideneChloride-co-Acrylonitrile

F.38.1 Sterilization with Hydrogen Peroxide Gas

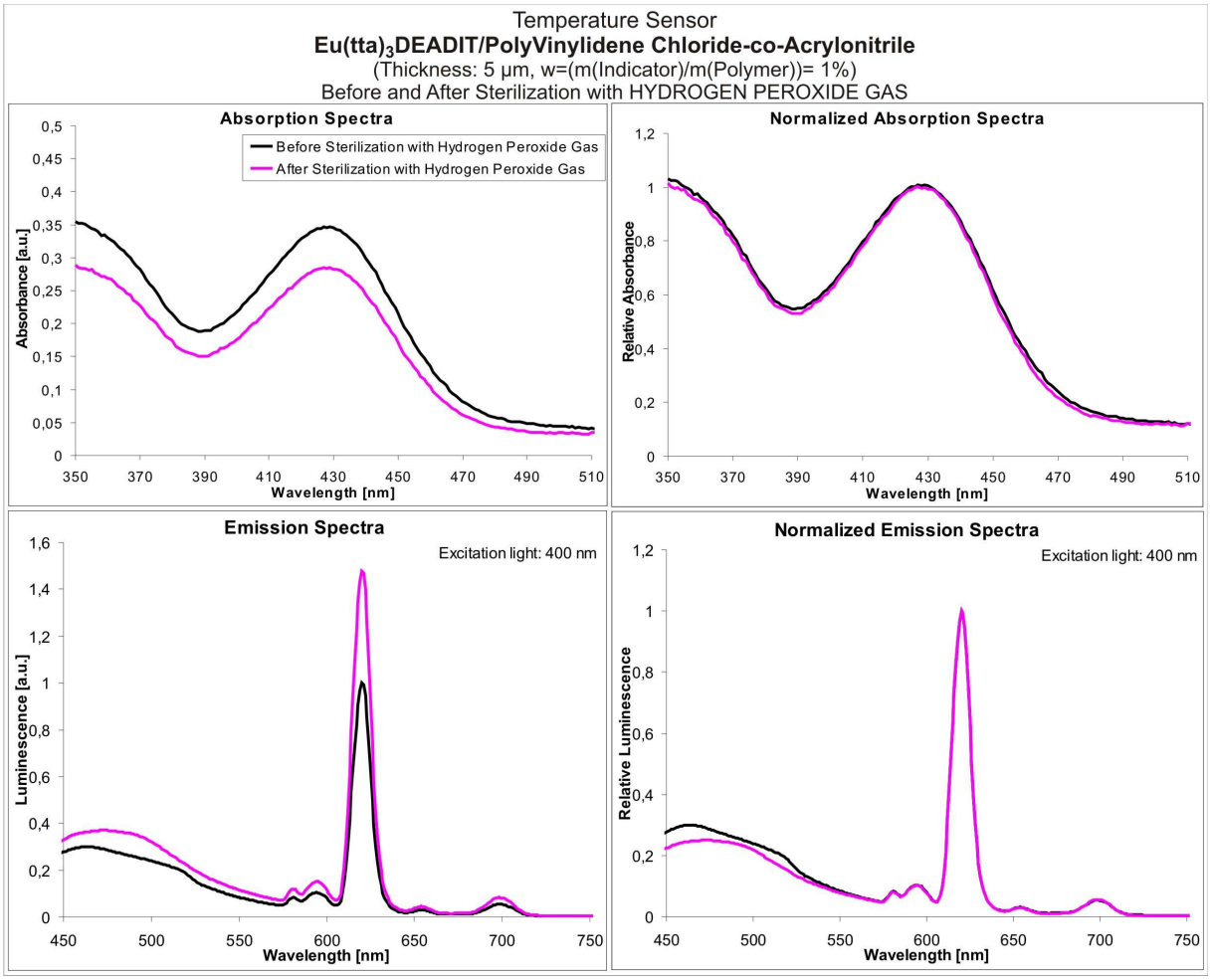

H_2O_2 Gas	Absorption Spectra	Emission Spectra
Alterations in Absorption/Emission Intensity	17,23% decrease	48% increase
Alterations in Absorption/Emission Curve Form	Unaltered.	Altered emission between 450-800 nm.

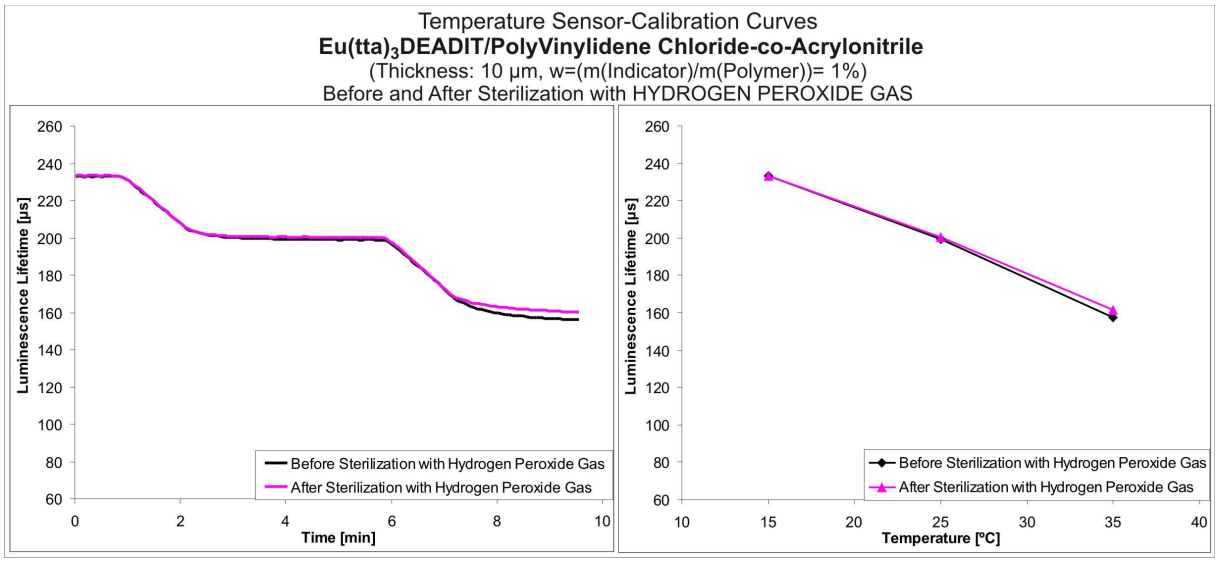

H_2O_2 Gas	Luminescence Lifetime		Alterations of Slope
Alterations in Luminescence Lifetime and Slope	15 °C	Unaltered	4,66% decrease of slope
	25 °C	1,01% increase	
	35 °C	2,53% increase	

F.38.2 Sterilization with Low-Temperature Hydrogen Peroxide Plasma

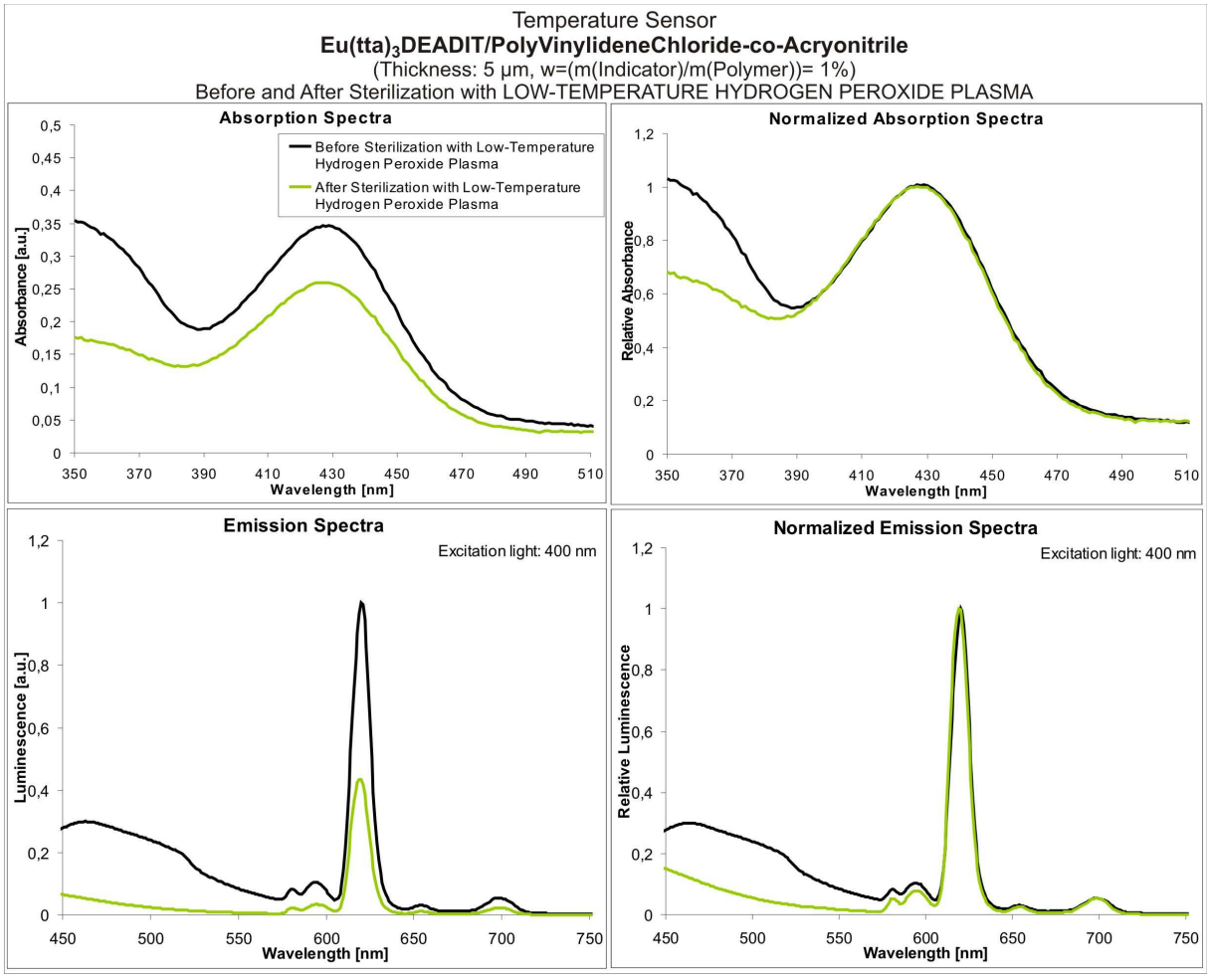

H_2O_2 Plasma	Absorption Spectra	Emission Spectra
Alterations in Absorption/Emission Intensity	24,59% decrease	56,47% decrease
Alterations in Absorption/Emission Curve Form	Altered absorption between 350-390 nm.	Altered emission between 50-600 nm.

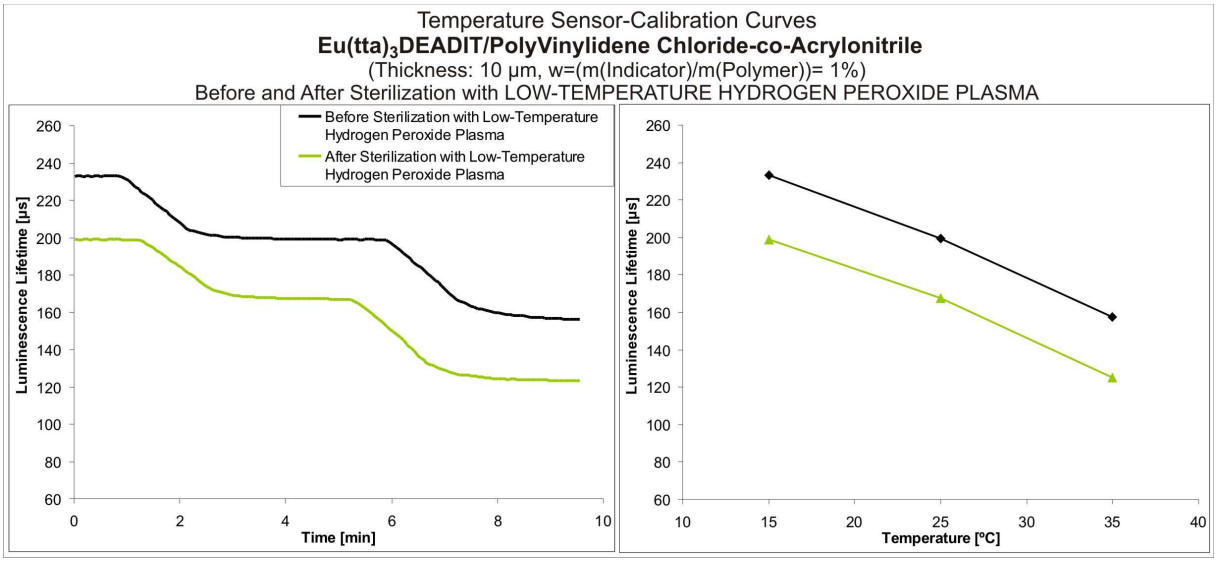

H_2O_2 Plasma	Luminescence Lifetime		Alterations of Slope
Alterations in Luminescence Lifetime and Slope	15℃	14,59% decrease	1,73% decrease of slope
	25℃	15,58% decrease	
	35℃	20,89% decrease	

F.39 Europium(III) Complex with 4-(4,6-di(1H-indazol-1-yl)-1,3,5-triazin-2-yl)-N,N-DiEthyl Benzen Amine (=Eu(tta)$_3$DEADIT) immobilized in PolyMethAcryloNitrile

F.39.1 Sterilization with Hydrogen Peroxide Gas

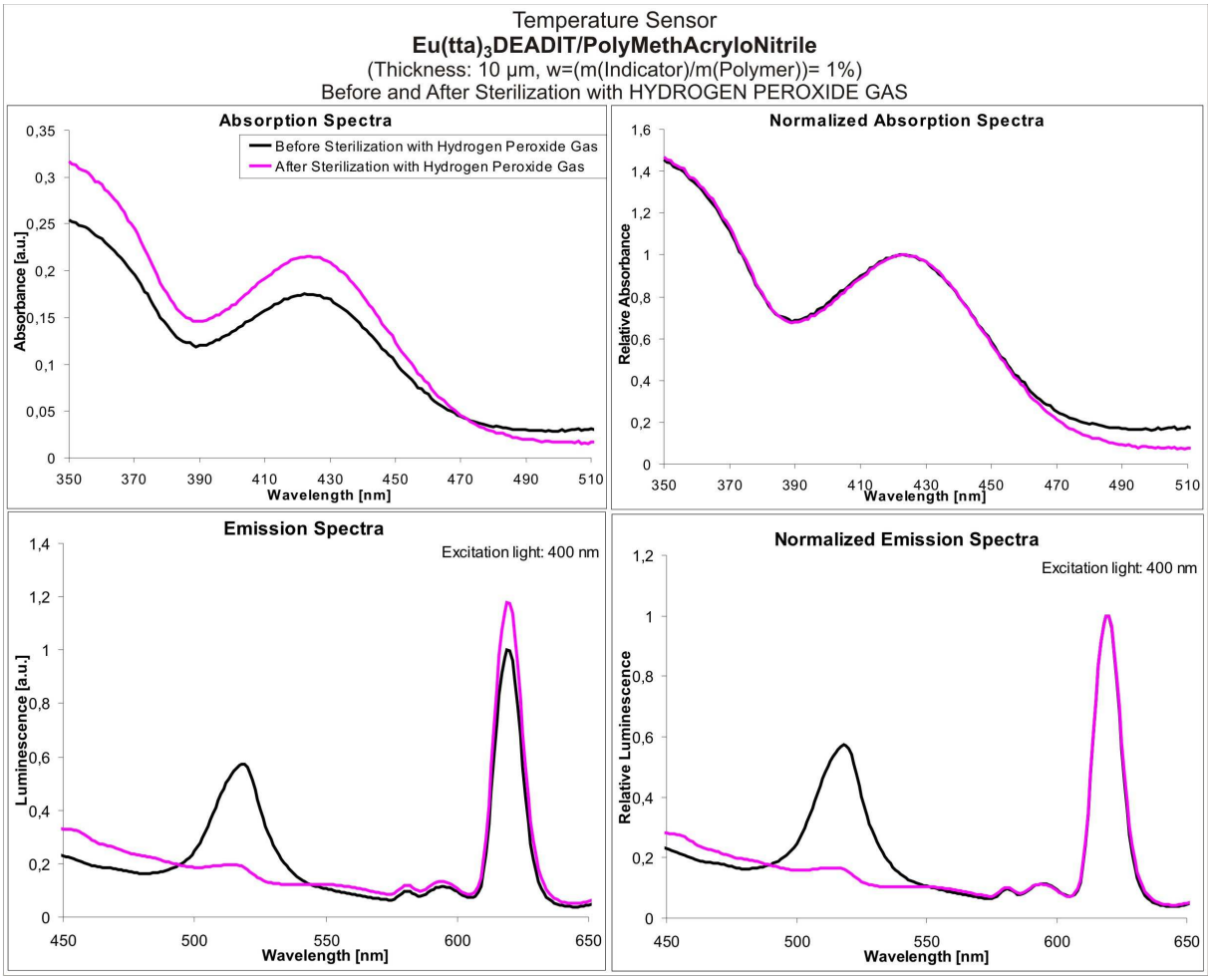

H_2O_2 Gas	Absorption Spectra	Emission Spectra
Alterations in Absorption/Emission Intensity	18,89% increase	17,72% increase
Alterations in Absorption/Emission Curve Form	Altered absorption between 470-800 nm.	The emission peak with λ_{max}=518 nm no longer observed after sterilization.

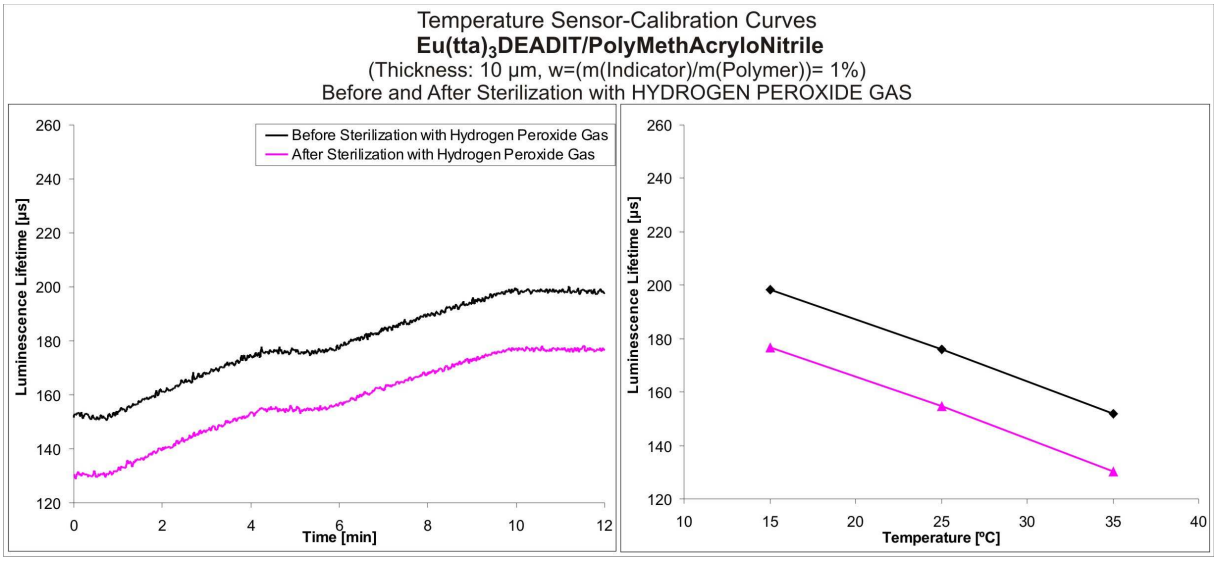

H_2O_2 Gas	Luminescence Lifetime		Alterations of Slope
Alterations in Luminescence Lifetime and Slope	15 °C	10,61% decrease	0,09% decrease of slope
	25 °C	11,93% decrease	
	35 °C	14,47% decrease	

F.39.2 Sterilization with Low-Temperature Hydrogen Peroxide Plasma

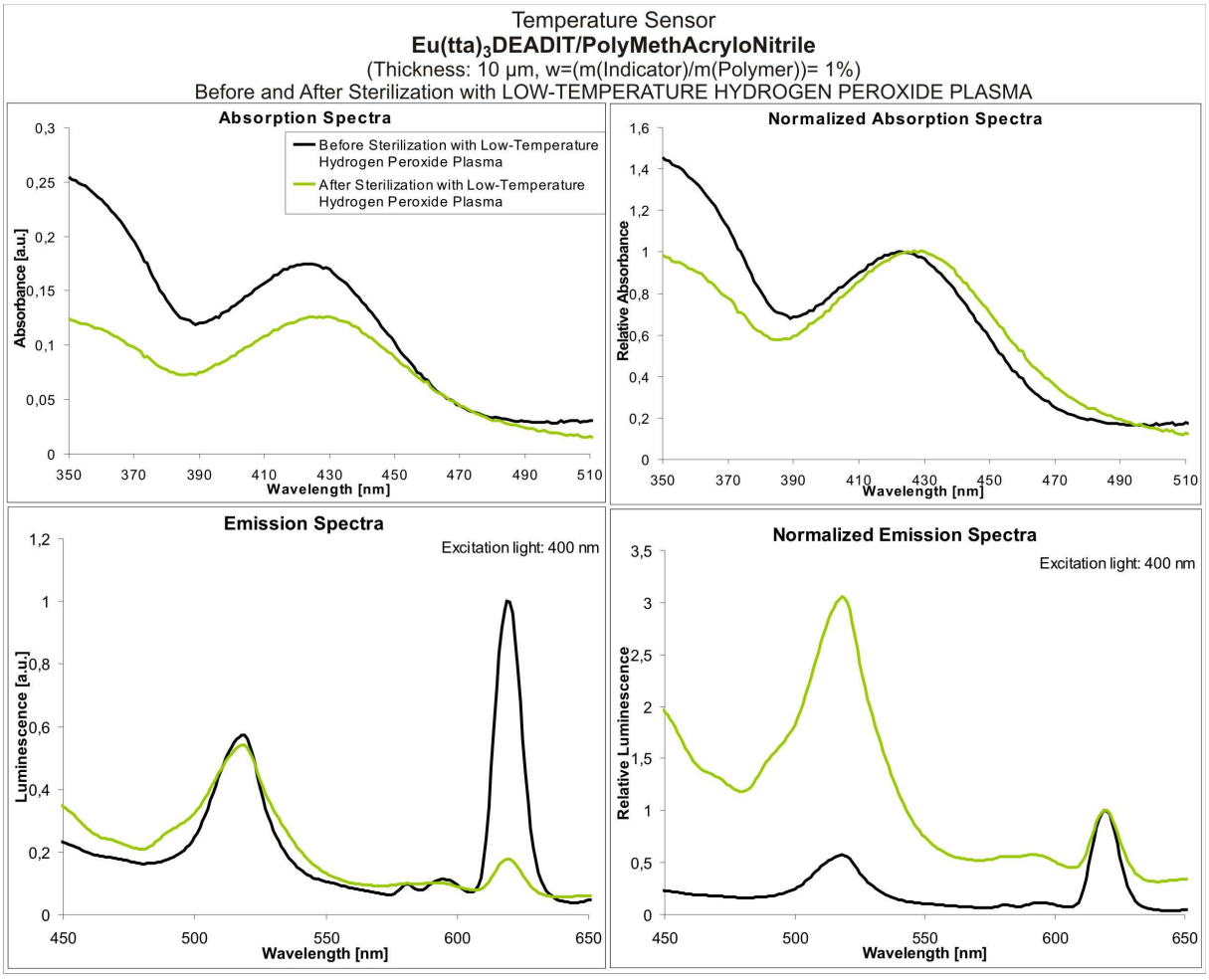

H_2O_2 Plasma	Absorption Spectra	Emission Spectra
Alterations in Absorption/Emission Intensity	28,07% decrease	82,27% decrease
Alterations in Absorption/Emission Curve Form	Bathochromic shift of the absorption maximum for 5 nm.	Altered emission curve form. The emission of peaks with λ_{max1}=519 nm increase after sterilization.

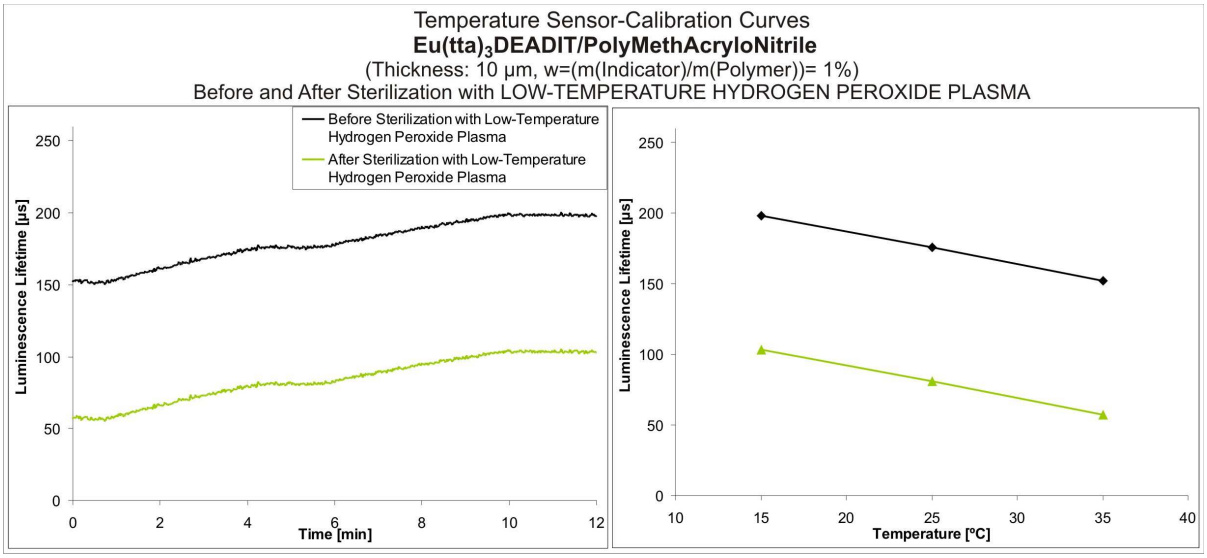

H_2O_2 Plasma	Luminescence Lifetime		Alterations of Slope
Alterations in Luminescence Lifetime and Slope	15°C	47,98% decrease	0,06% decrease of slope
	25°C	53,98% decrease	
	35°C	62,50% decrease	

F.40 DiChloroTrisPhenanthroline Ruthenium(II)Hydrate immobilized in PolyVinylideneChloride-co-Acrylonitrile

F.40.1 Sterilization with Hydrogen Peroxide Gas

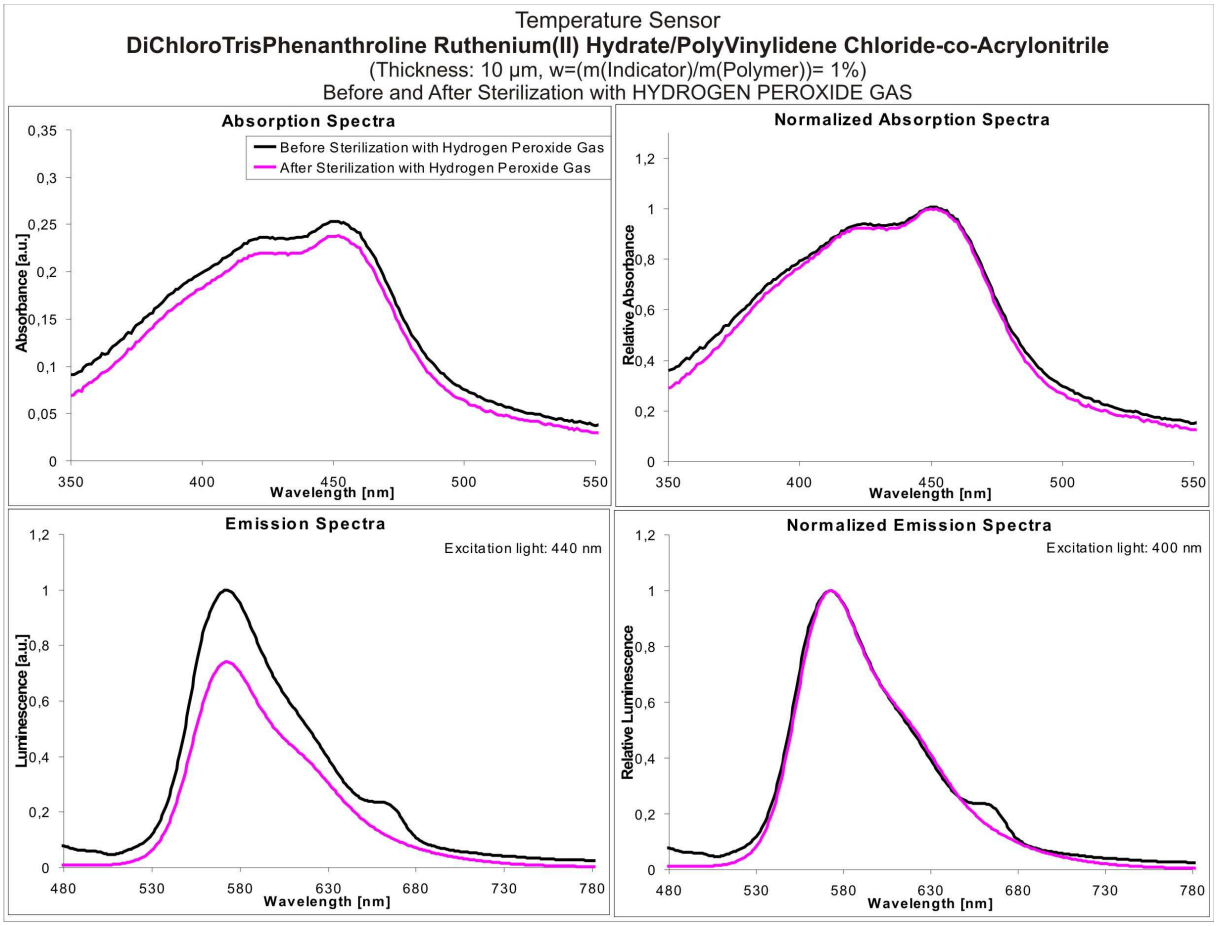

H_2O_2 Gas	Absorption Spectra	Emission Spectra
Alterations in Absorption/Emission Intensity	5,53% decrease	25,93% decrease
Alterations in Absorption/Emission Curve Form	Unaltered.	The emission peak with λ_{max}=664 nm no longer observed.

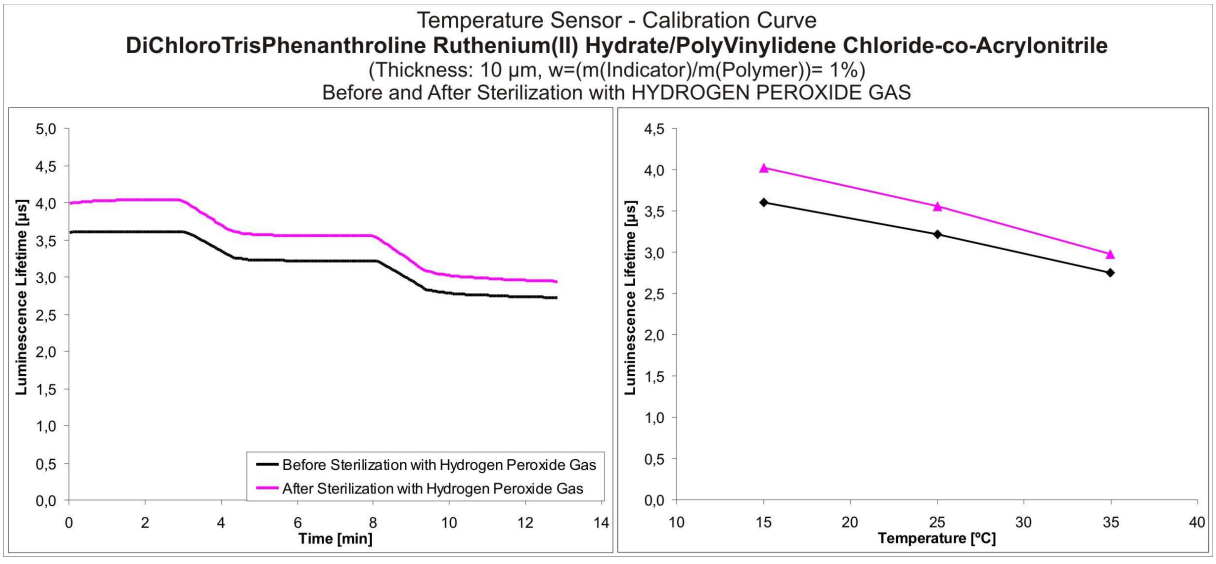

H_2O_2 Gas	Luminescence Lifetime		Alterations of Slope
Alterations in Luminescence Lifetime and Slope	15 ℃	11,63% increase	18,36% increase of slope
	25 ℃	10,56% increase	
	35 ℃	8,36% increase	

F.40.2 Sterilization with Low-Temperature Hydrogen Peroxide Plasma

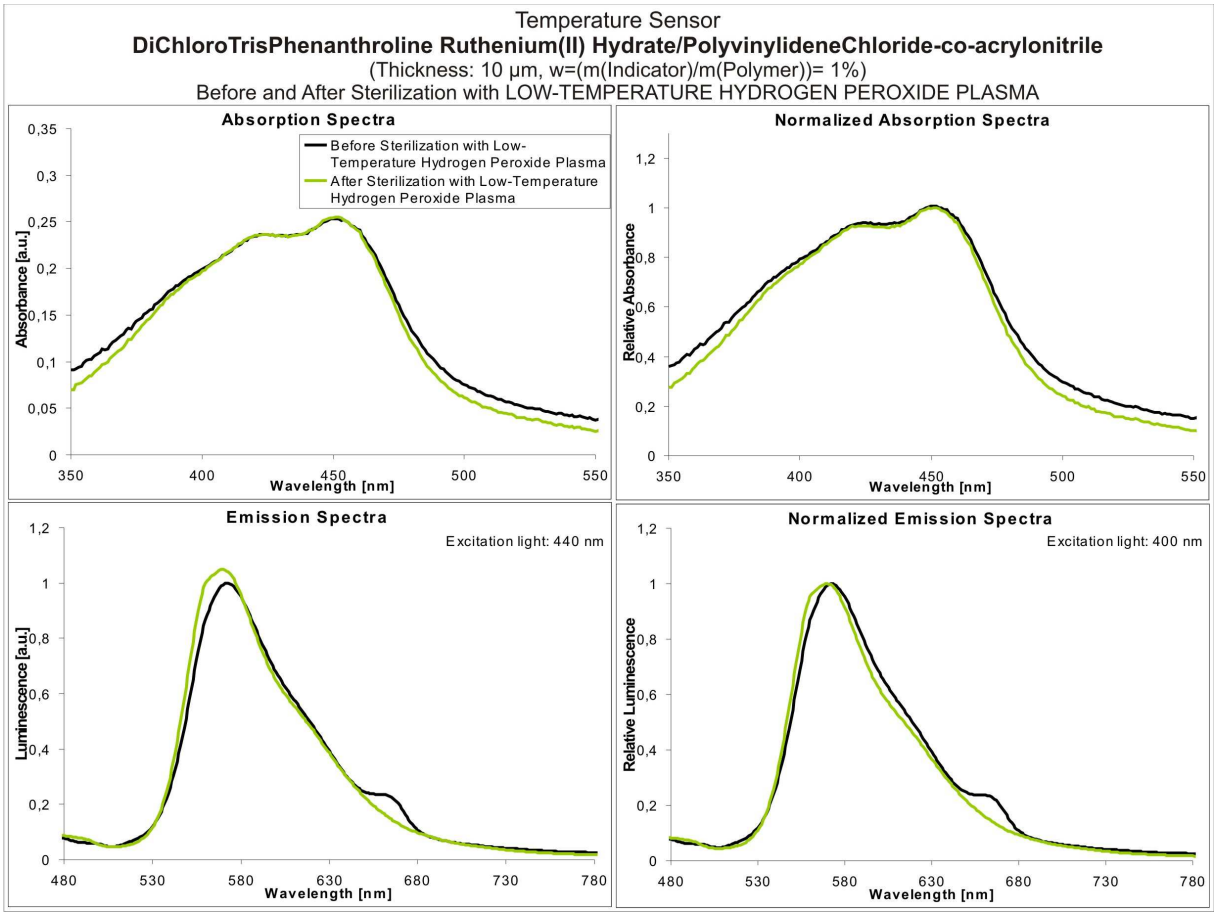

H_2O_2 Plasma	Absorption Spectra	Emission Spectra
Alterations in Absorption/Emission Intensity	1,14% increase	4,82% increase
Alterations in Absorption/Emission Curve Form	Altered absorption curve form between 350-400 nm and 475-800 nm.	Hypsochromic shift of the emission maximum for 3 nm. The emission peak with λ_{max}=664 nm no longer observed.

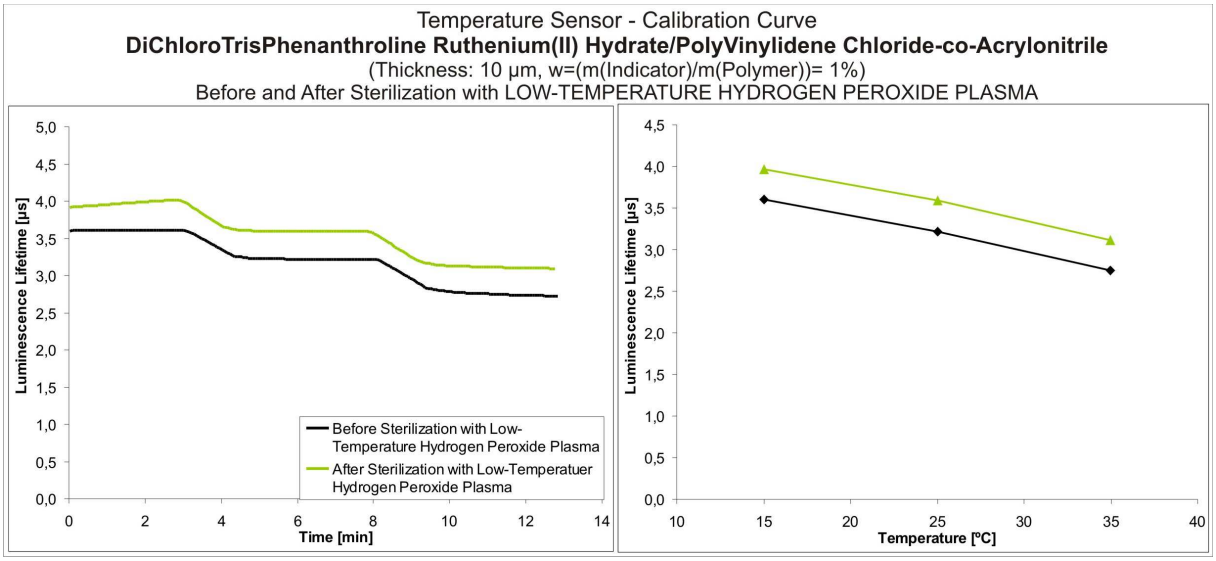

H_2O_2 Plasma	Luminescence Lifetime		Alterations of Slope
Alterations in Luminescence Lifetime and Slope	15 ℃	9,97% increase	0,47% increase of slope
	25 ℃	11,49% increase	
	35 ℃	13,09% increase	

F.41 DiChloroTrisPhenanthroline Ruthenium(II)Hydrate immobilized in PolyMethAcryloNitrile

F.41.1 Sterilization with Hydrogen Peroxide Gas

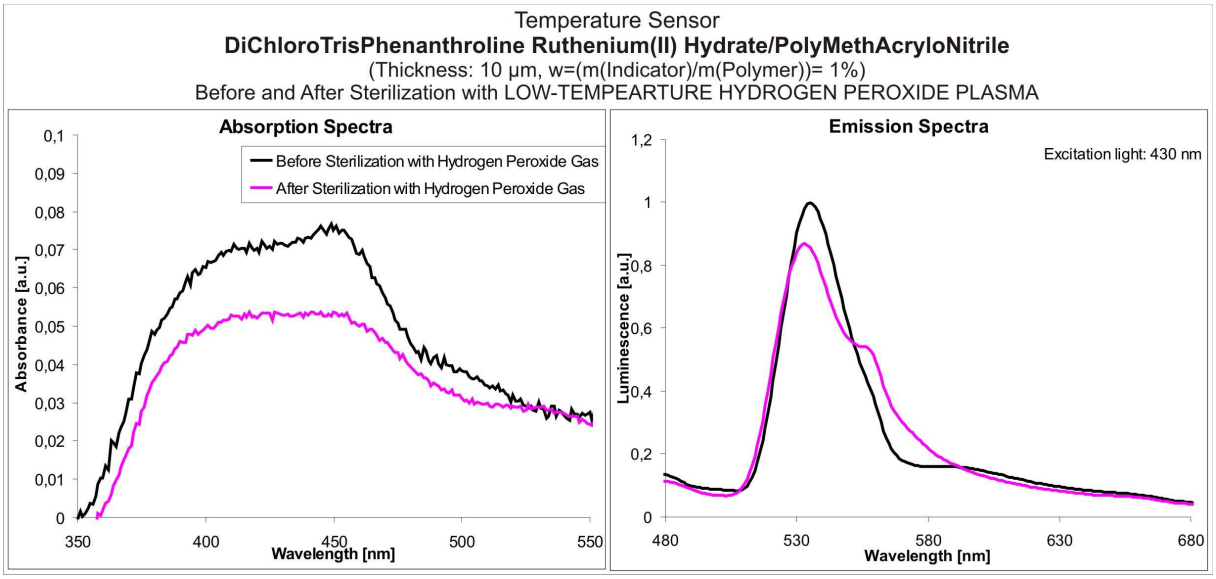

H_2O_2 Gas	Absorption Spectra	Emission Spectra
Alterations in Absorption/Emission Intensity	32,05% decrease	12,34% decrease
Alterations in Absorption/Emission Curve Form	Altered absorption curve form.	Altered emission curve form between 550-630 nm. Hypsochromic shift of the emission maximum for 2 nm.

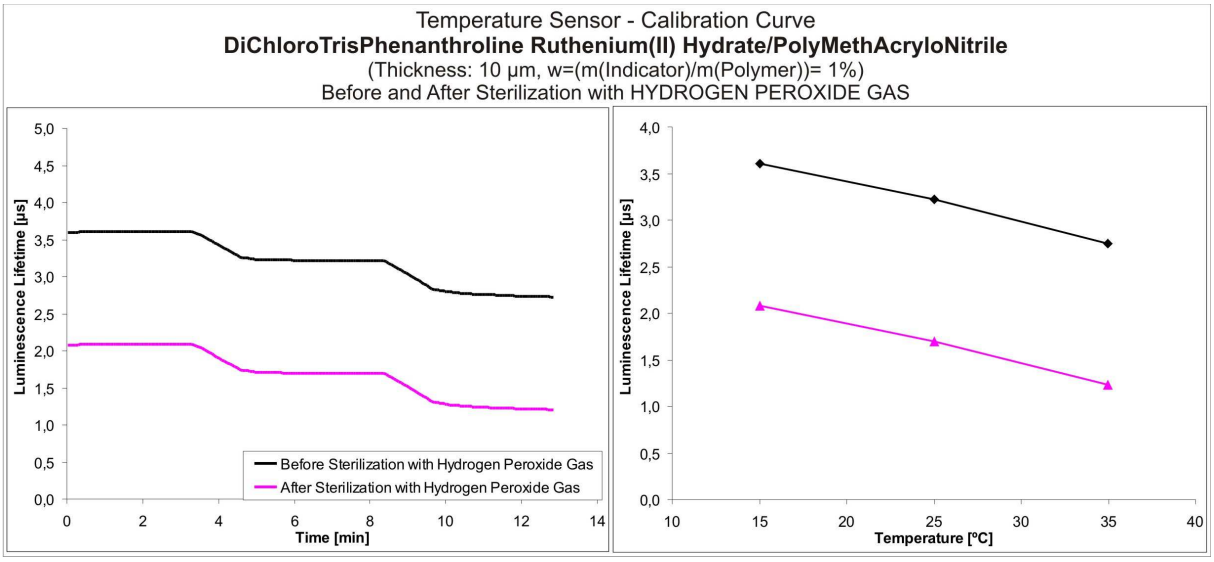

H_2O_2 Gas	Luminescence Lifetime		Alterations of Slope
Alterations in Luminescence Lifetime and Slope	15 °C	42,22% decrease	0,07% decrease of slope
	25 °C	47,20% decrease	
	35 °C	55,27% decrease	

F.41.2 Sterilization with Low-Temperature Hydrogen Peroxide Plasma

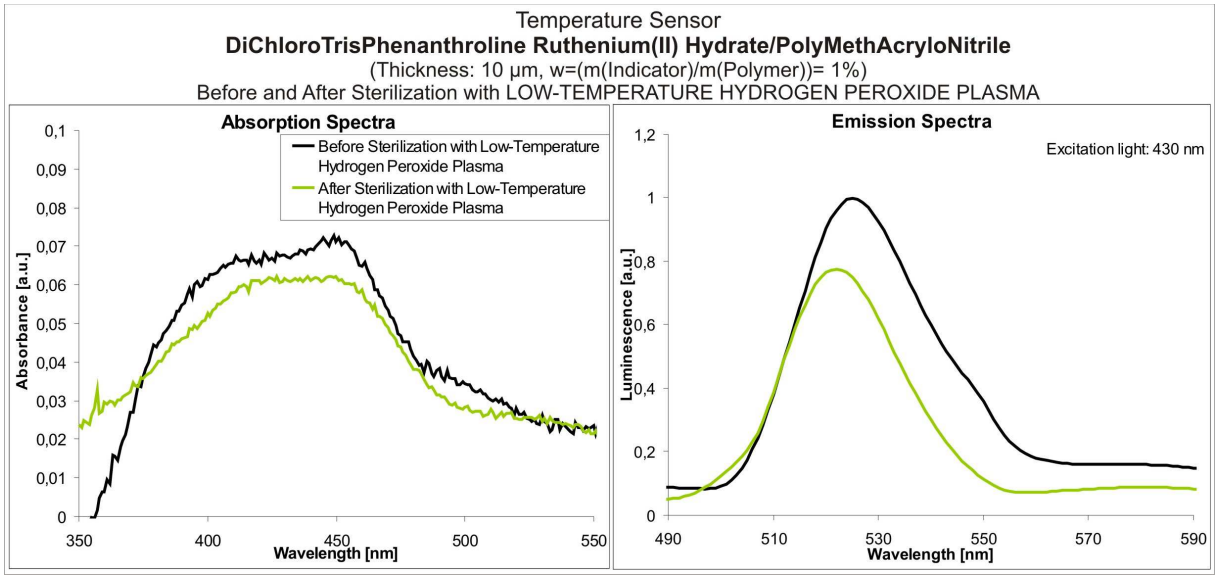

H_2O_2 Plasma	Absorption Spectra	Emission Spectra
Alterations in Absorption/Emission Intensity	15,58% decrease	21,87% decrease
Alterations in Absorption/Emission Curve Form	Altered absorption curve form.	Hypsochromic shift of the emission maximum for 3 nm.

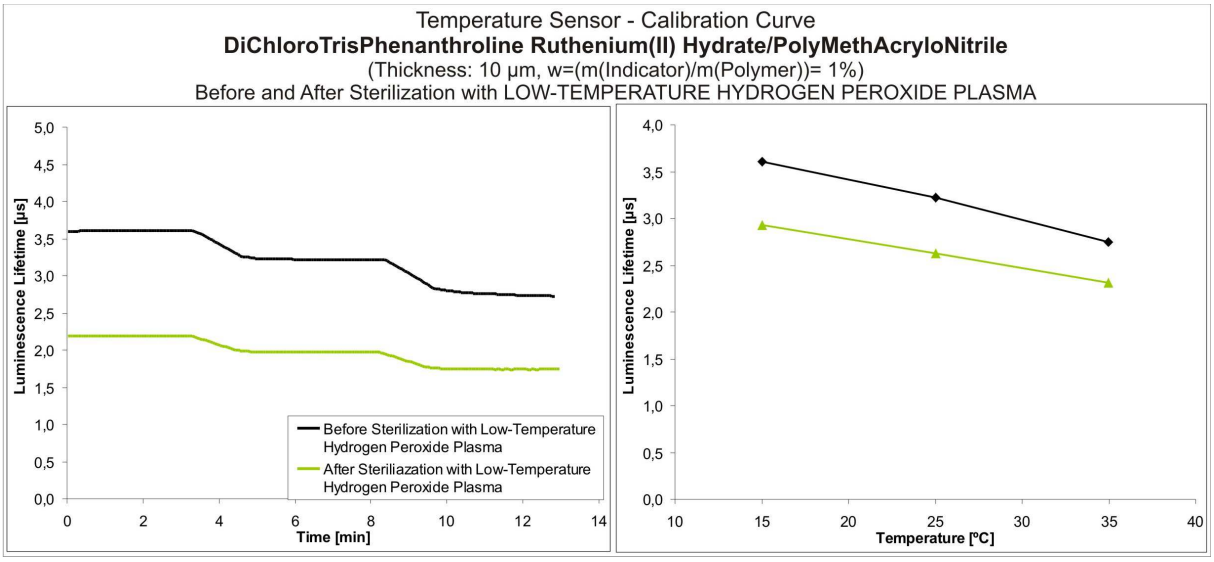

H_2O_2 Plasma	Luminescence Lifetime		Alterations of Slope
Alterations in Luminescence Lifetime and Slope	15 °C	39,17% decrease	26,76% decrease of slope
	25 °C	38,82% decrease	
	35 °C	36,73% decrease	

Optical AMMONIA SENSORS

F.42 EosinEthylEster immobilized in Hydrogel D7

F.42.1 Sterilization with Hydrogen Peroxide Gas

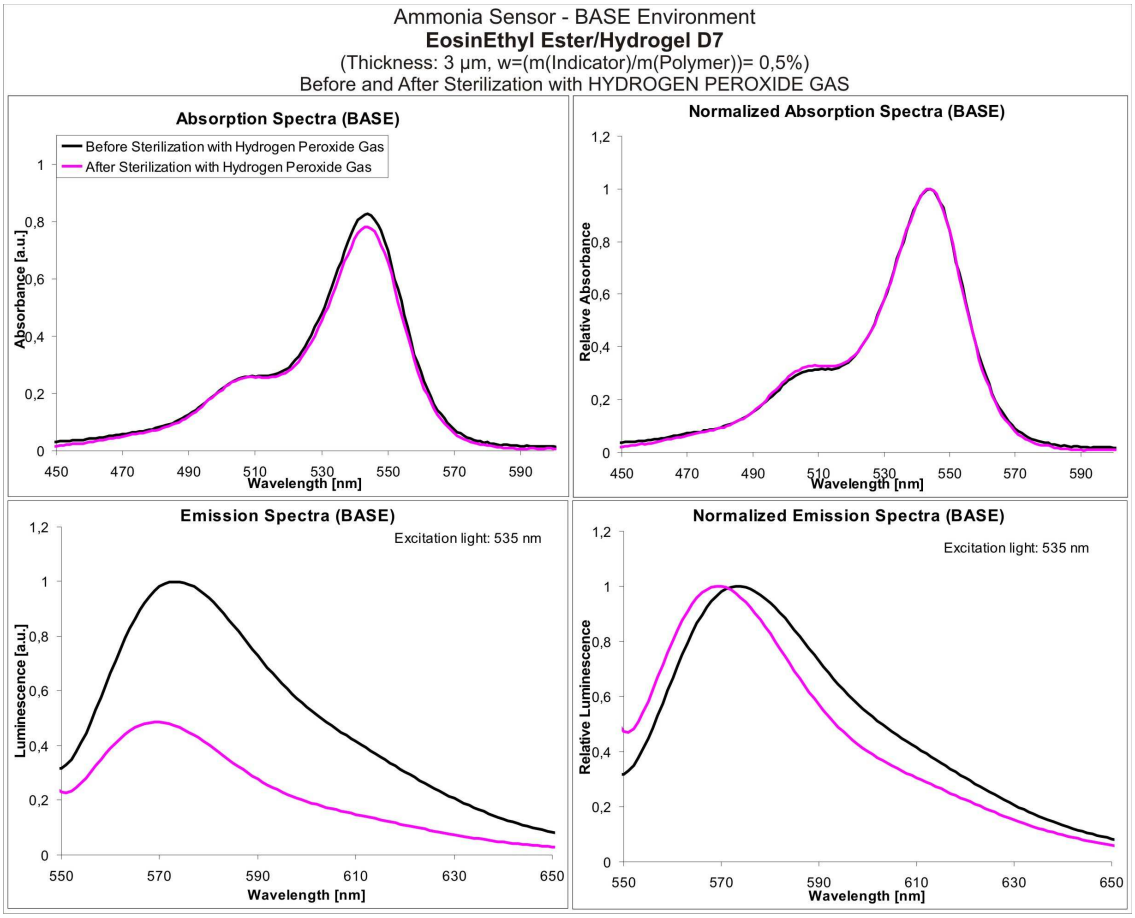

H_2O_2 S.	Absorption Spectra		Emission Spectra	
		Alterations		Alterations
Alterations in Absorption/ Emission Intensity	BASE	5,60% decrease	BASE	51,36% decrease
Alterations in Absorption/ Emission Curve Form	BASE	Unaltered.	BASE	Hypsochromic shift of the emission maximum for 4 nm.

F.42.2 Sterilization with Low-Temperature Hydrogen Peroxide Plasma

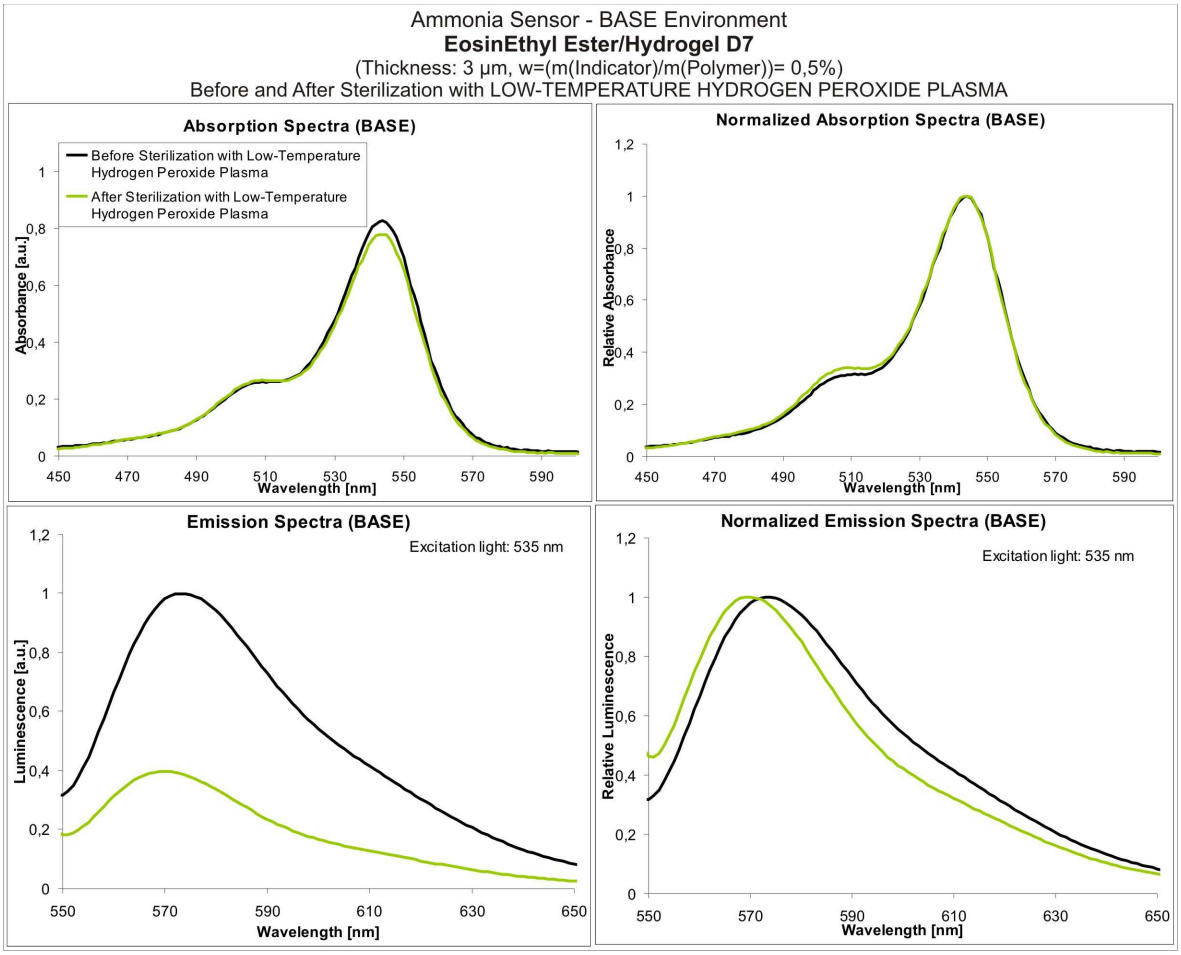

H_2O_2 Plasma	Absorption Spectra		Emission Spectra	
		Alterations		Alterations
Alterations in Absorption/ Emission Intensity	BASE	5,86% decrease	BASE	60,39% decrease
Alterations in Absorption/ Emission Curve Form	BASE	Unaltered.	BASE	Hypsochromic shift of the emission maximum for 3 nm.

F.43 EosinEthylEster immobilized in PolyMethylMethAcrylate (=PMMA)

F.43.1 Sterilization with Hydrogen Peroxide Gas

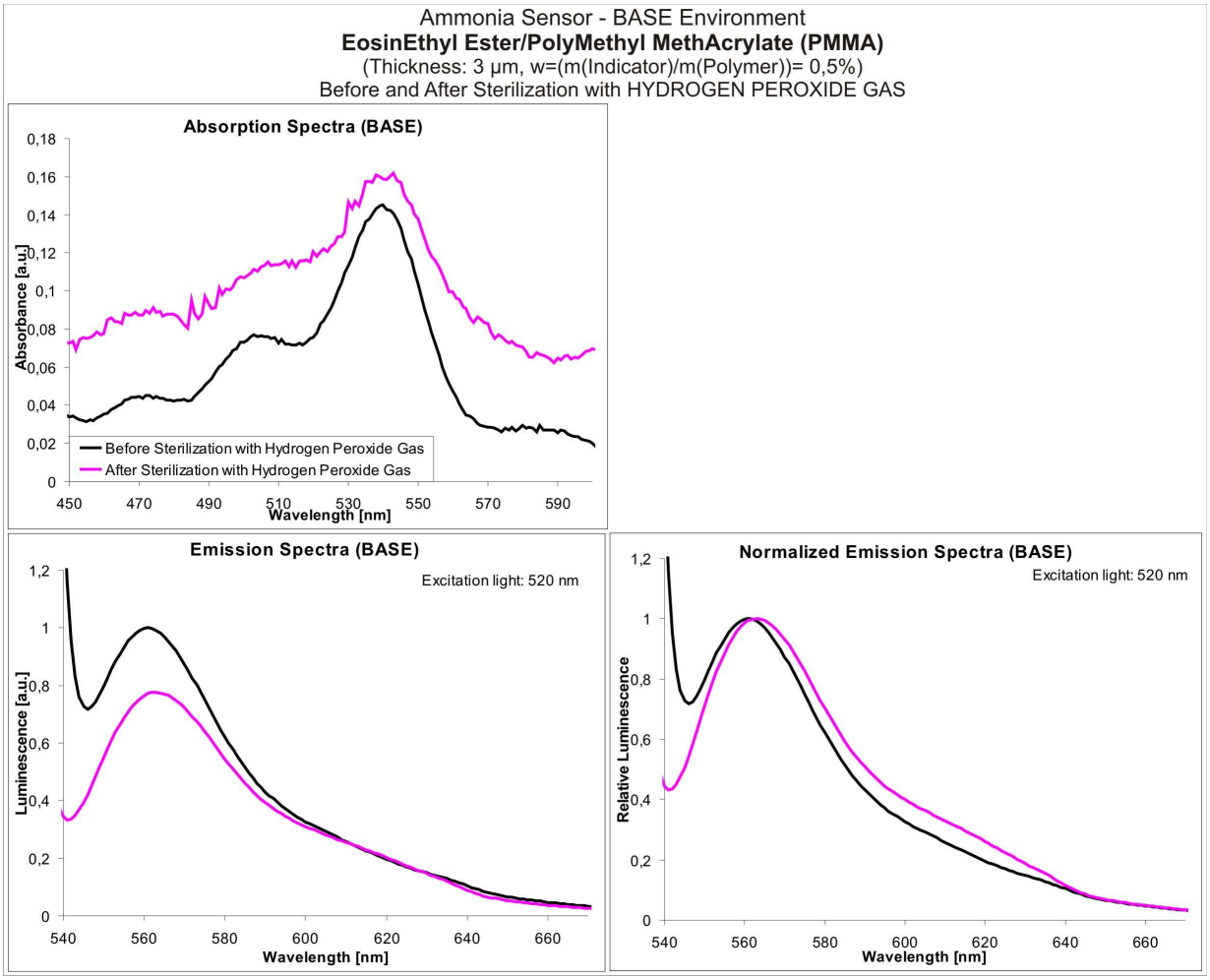

H_2O_2 S.	Absorption Spectra		Emission Spectra	
		Alterations		Alterations
Alterations in Absorption/ Emission Intensity	BASE	10% increase	BASE	22,48% decrease
Alterations in Absorption/ Emission Curve Form	BASE	The sensor became turbid after sterilization. Dissapearance of the characteristic curve form.	BASE	Bathochromic shift of the emission maximum for 2 nm.

F.43.2 Sterilization with Low-Temperature Hydrogen Peroxide Plasma

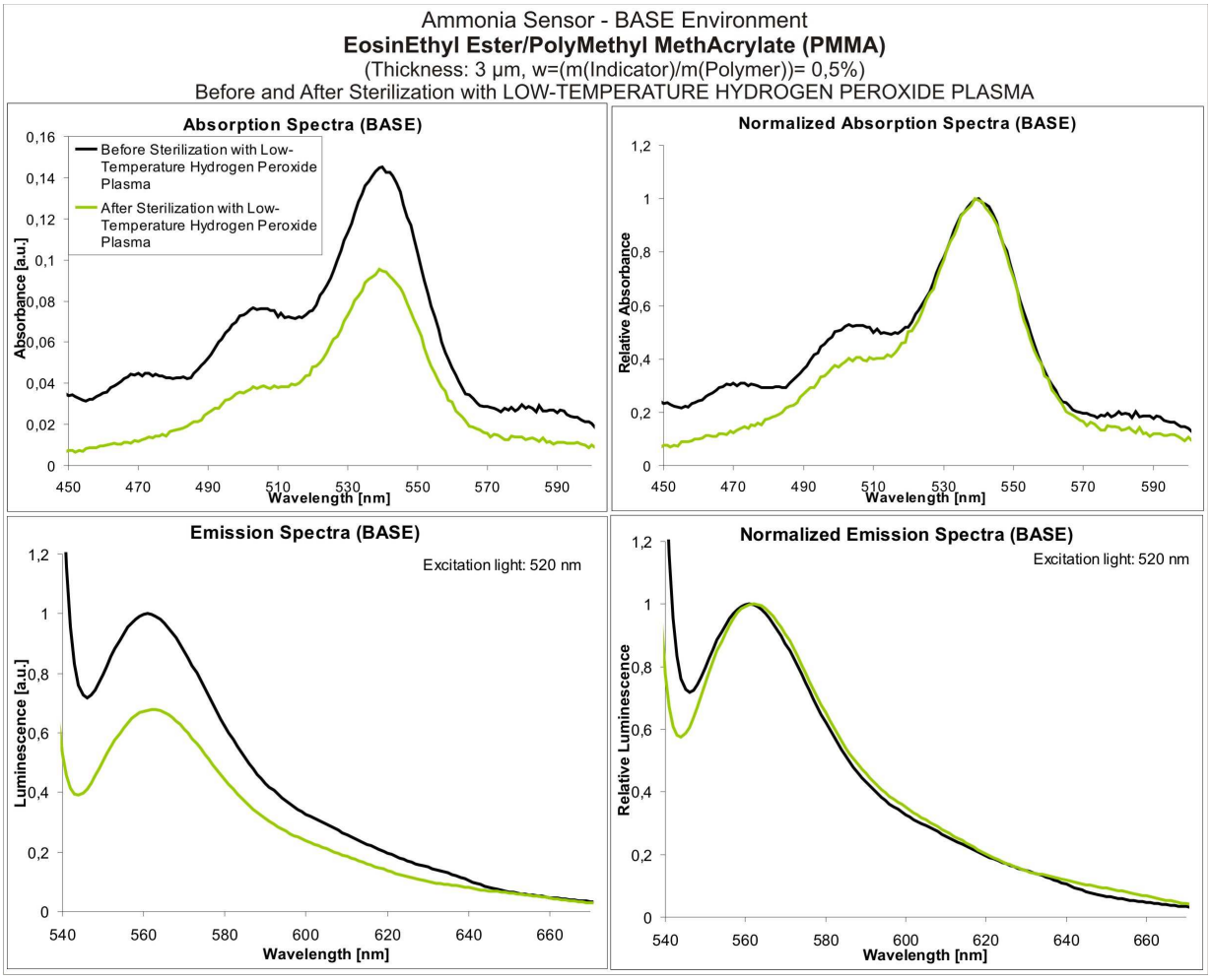

H_2O_2 Plasma	Absorption Spectra		Emission Spectra	
		Alterations		**Alterations**
Alterations in Absorption/ Emission Intensity	BASE	34,37% decrease	BASE	32,14% decrease
Alterations in Absorption/ Emission Curve Form	BASE	Altered absorption between 450-510 nm and 570-600 nm.	BASE	Unaltered.

F.44 DiChloroFluorescein immobilized in Hydrogel D7

F.44.1 Sterilization with Hydrogen Peroxide Gas

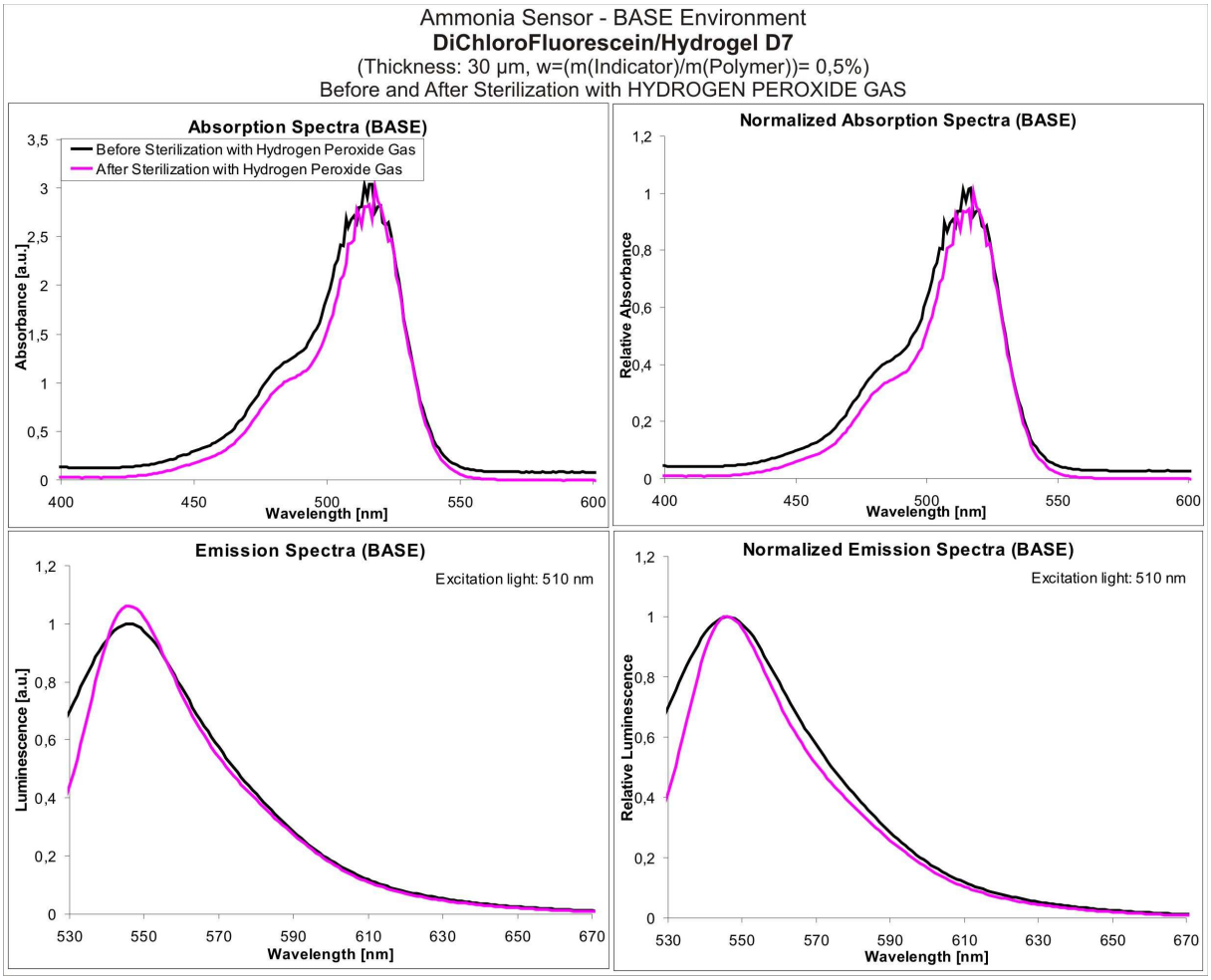

H_2O_2 S.	Absorption Spectra		Emission Spectra	
		Alterations		Alterations
Alterations in Absorption/ Emission Intensity	BASE	7,24% decrease	BASE	5,86% increase
Alterations in Absorption/ Emission Curve Form	BASE	Lower absorption between 400-500 nm and 550-800 nm.	BASE	Altered emission between 530-540 nm and 550-630 nm.

F.44.2 Sterilization with Low-Temperature Hydrogen Peroxide Plasma

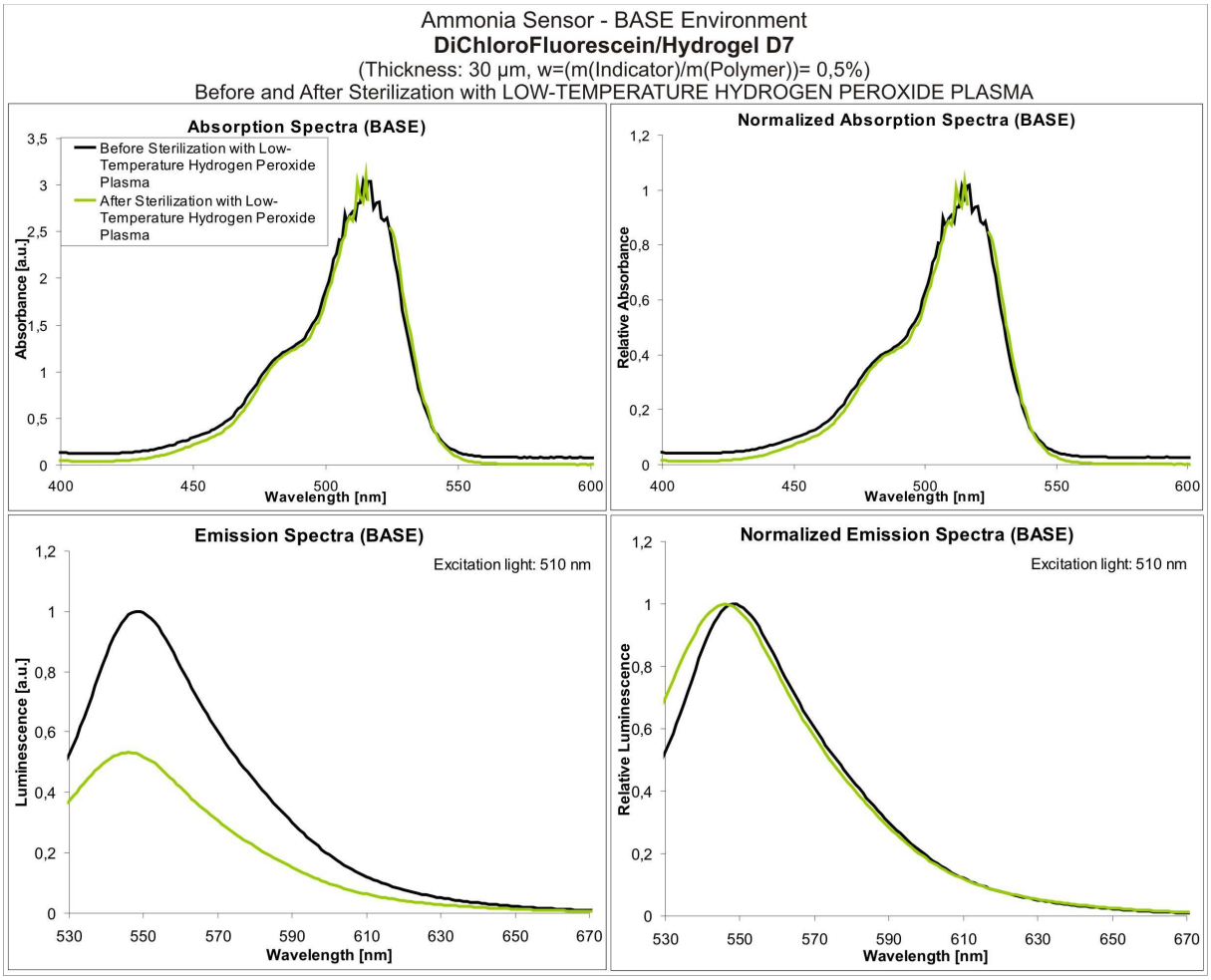

H_2O_2 Plasma	Absorption Spectra		Emission Spectra	
		Alterations		Alterations
Alterations in Absorption/ Emission Intensity	BASE	6,88% decrease	BASE	46,75% decrease
Alterations in Absorption/ Emission Curve Form	BASE	Unaltered.	BASE	Hypsochromic shift of the emission maximum for 2 nm.

F.45 BromoPhenolBlue immobilized in Hydrogel D7

F.45.1 Sterilization with Hydrogen Peroxide Gas

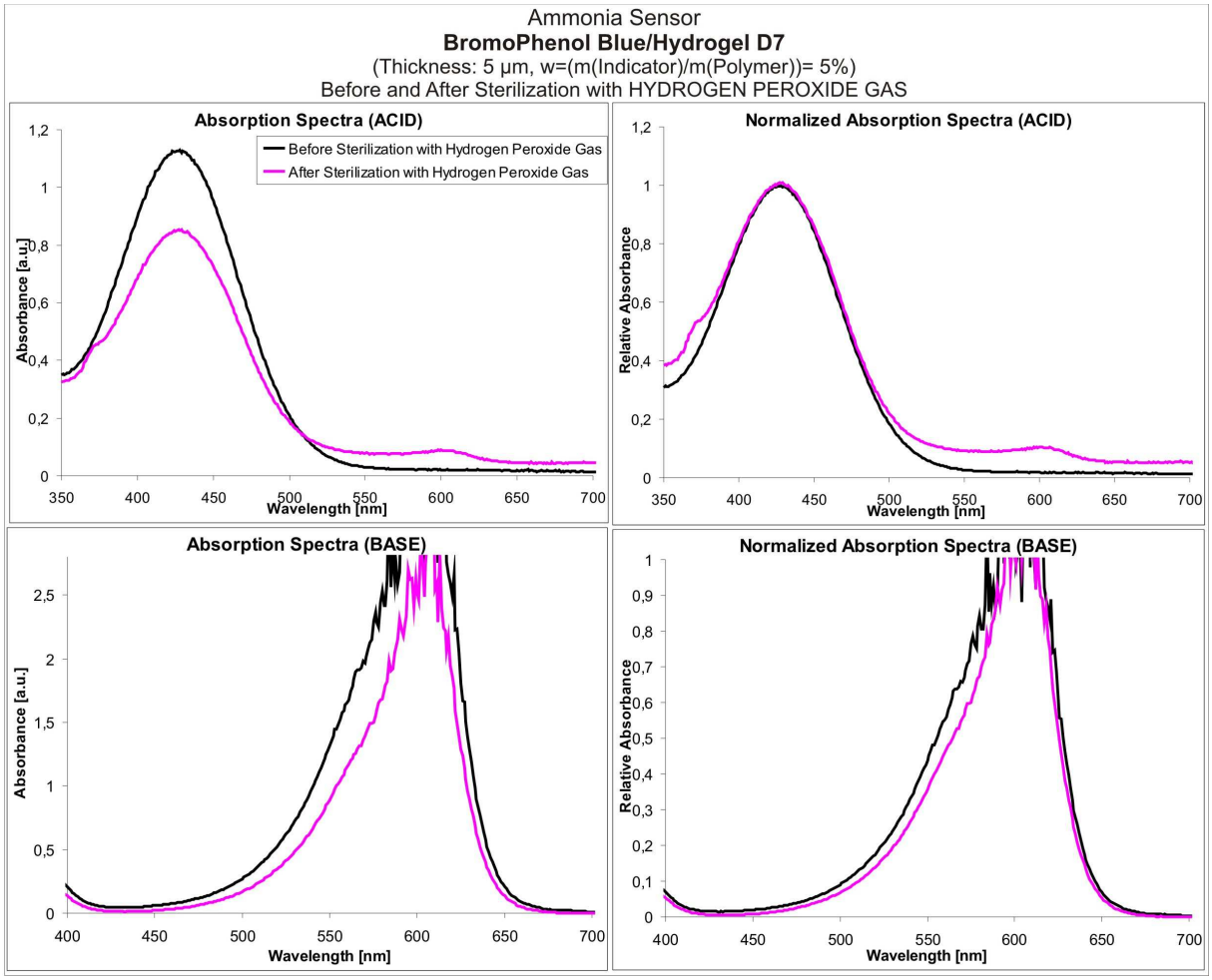

H_2O_2 Gas	Absorption Spectra			
		Alterations		Alterations
Alterations in Absorption /Emission Intensity	ACID	25,12% decrease	Alterations in Absorption /Emission Curve Form	ACID: Altered absorption between 350-400 nm and 500-800 nm.
	BASE	13,01% increase		BASE: Altered absorption between 500-600 nm.

F.45.2 Sterilization with Low-Temperature Hydrogen Peroxide Plasma

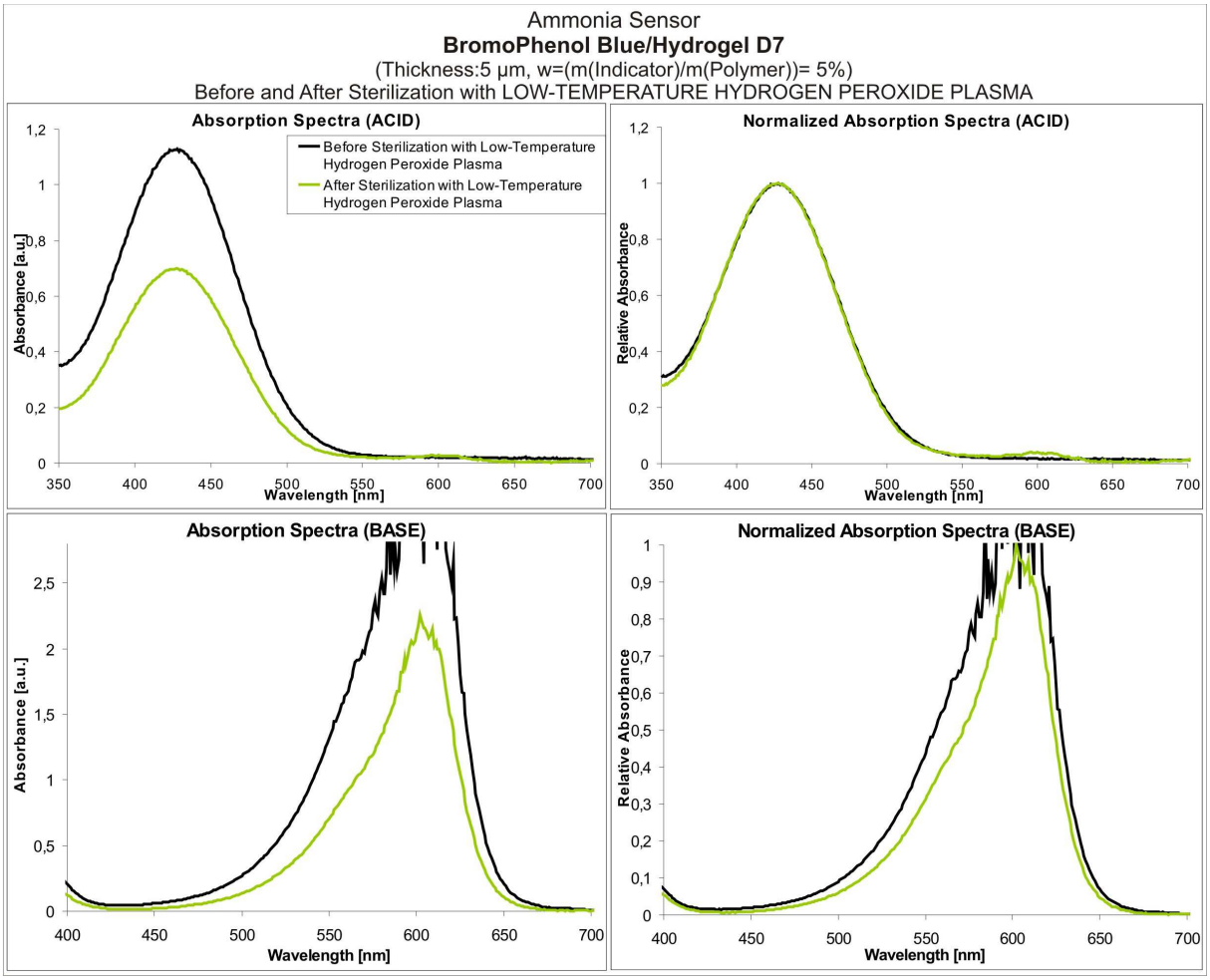

H_2O_2 Plasma	Absorption Spectra				
		Alterations			Alterations
Alterations in Absorption /Emission Intensity	ACID	38,15% decrease	Alterations in Absorption /Emission Curve Form	ACID	Unaltered.
	BASE	37,80% decrease		BASE	Unaltered.

F.46 BromoPhenol Blue immobilized in PolyMethylMethAcrylate (=PMMA)

F.46.1 Sterilization with Hydrogen Peroxide Gas

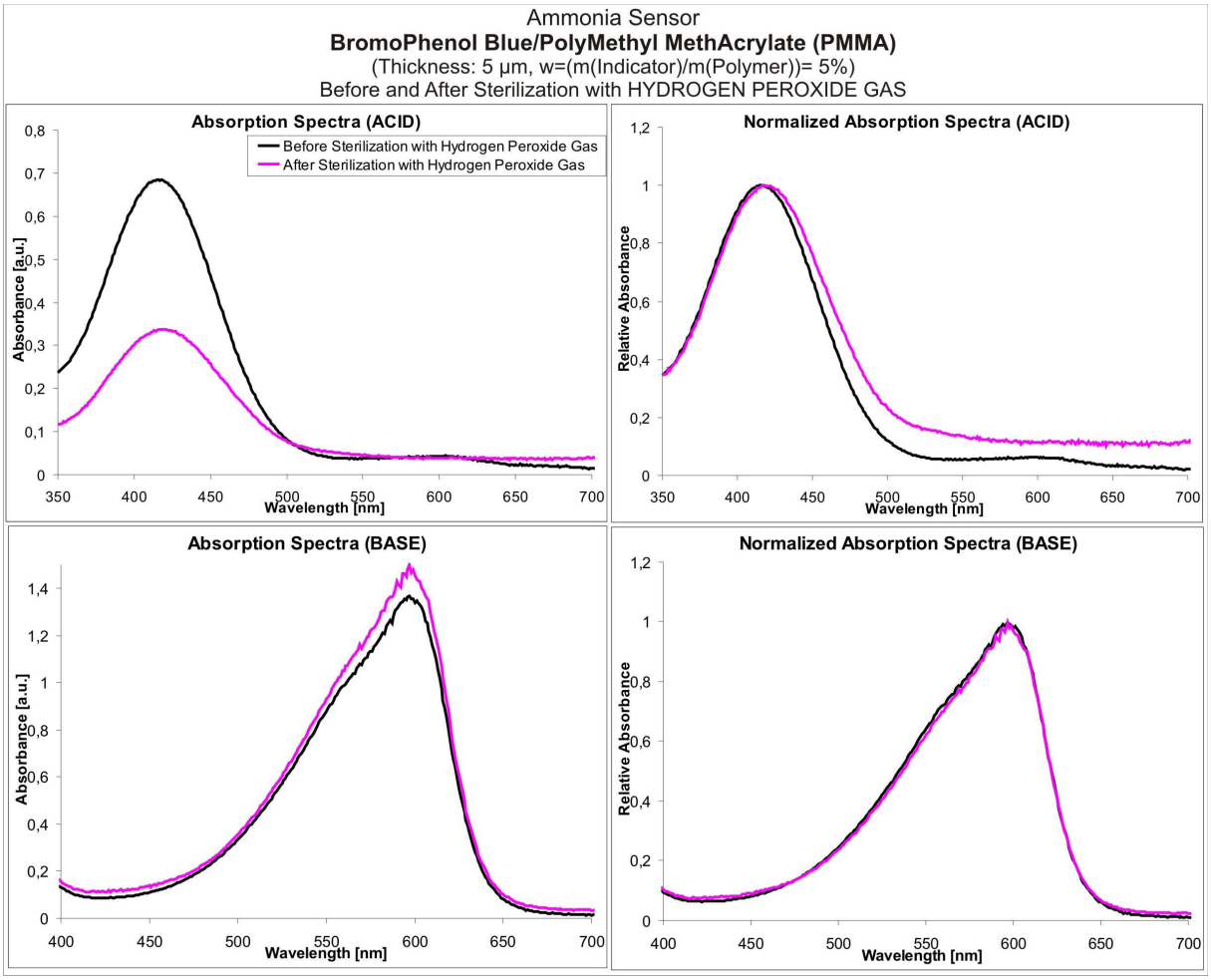

H_2O_2 Gas	Absorption Spectra			
		Alterations		Alterations
Alterations in Absorption /Emission Intensity	ACID	50,78% decrease	Alterations in Absorption /Emission Curve Form	ACID	Increased absorption between 480-800 nm. Bathochromic shift of the absorption maximum for 3 nm.
	BASE	9,53% increase		BASE	Unaltered.

F.46.2 Sterilization with Low-Temperature Hydrogen Peroxide Plasma

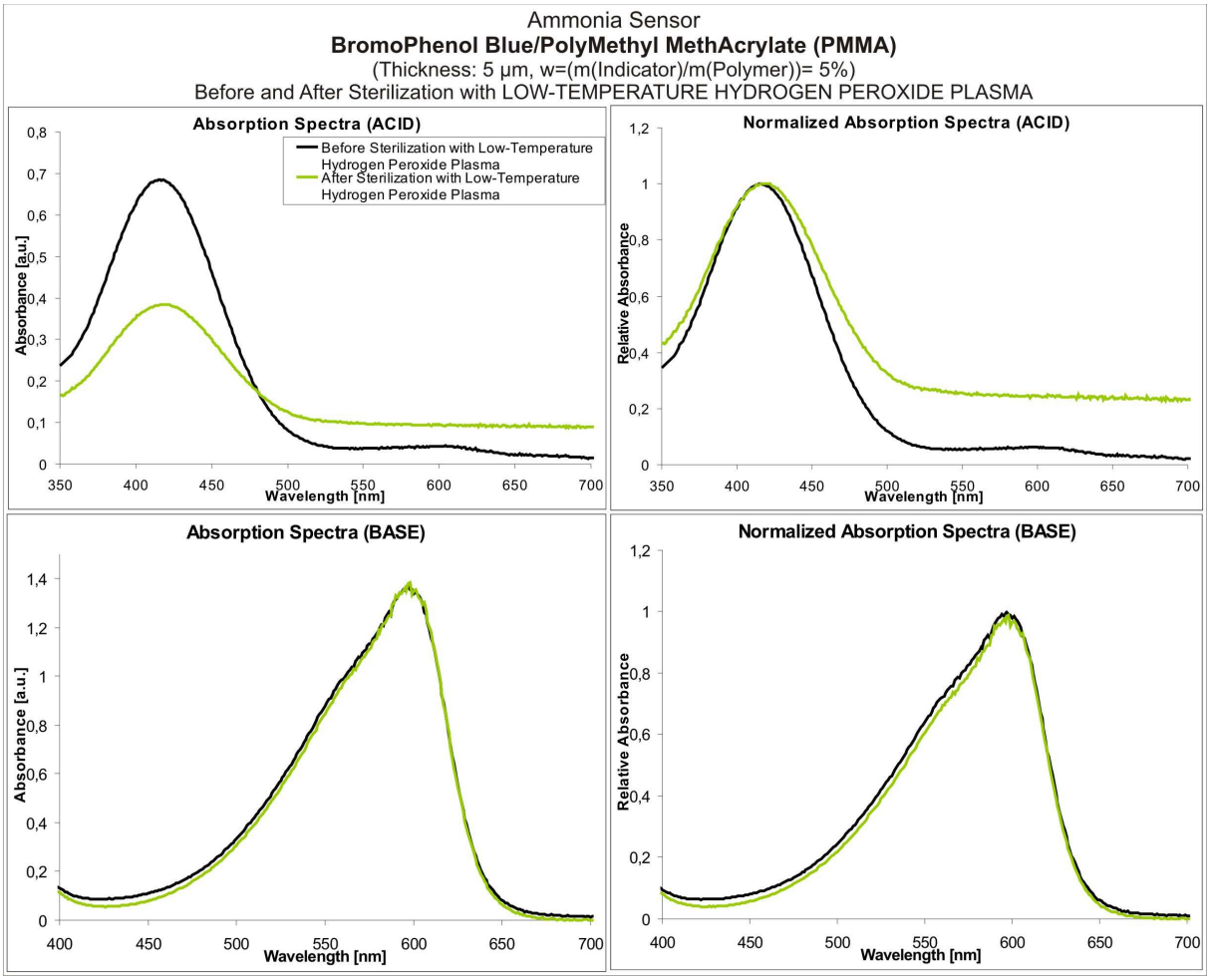

H_2O_2 Gas	Absorption Spectra			
		Alterations		Alterations
Alterations in Absorption /Emission Intensity	ACID	42,65% decrease	Alterations in Absorption /Emission Curve Form	ACID	Increased absorption between 480-800 nm. Bathochromic shift of the absorption maximum for 2 nm.
	BASE	0,02% increase		BASE	Unaltered.

Curriculum Vitae

Personal Information

Name:	Zajko Špela
Address:	Slatinski Dol 23/a, 2201 Zg.Kungota, Slovenia
	Winkelgasse 2/Top 27, 8010 Graz, Austria
E-mail:	spela.zajko@student.tugraz.at
Birth date and place:	23.01.1985, Maribor
Citizenship:	Slovenian

Education

Since 05/2008:	PhD studies at the Institute of Analytical Chemistry and Food Chemistry, Chemo- and Biosensor Workgroup – TU Graz, Austria.
06/2007 – 03/2008:	Diploma thesis at the Institute of Analytical Chemistry and Food Chemistry, TU Graz, Austria in the framework of the EU project CLINICIP; title: "Optimization of optical glucose sensors for monitoring critically ill patients".
10/2003 – 03/2008:	Study on Faculty of Chemistry and Chemical Engineering Maribor.
09/1999 – 09/2003:	Gymnasium, Maribor.
09/1991 – 09/1999:	Elementary school, Kungota.

Professional Experience

10/2011 – 02/2012:	University project assistant at the Institute of Analytical Chemistry and Food Chemistry, Chemo- and Biosensor Workgroup – TU Graz, Austria.
05/2008 – 10/2008:	Project researcher by project "Development of optical glucose sensor" at the Institute of Analytical Chemistry and Food Chemistry, TU Graz, Austria and the company SmartMed, Graz.

Scholarships

09/1999 – 09/2008:	Zois Scholarship for gifted students
10/2008 – 10/2011:	Scholarship for PhD study abroad from Slovene human resources development and scholarship fund Ad Futura

List of Publications

Oral Presentations

"Barrier layers for diffusion eliminated enzyme sensors; HydroThane blended barrier layers"
Zajko Špela, 01.07.2009, Young Investigators´ Seminar on Analytical Chemistry (Yisac), Graz, Austria.

"The effects of gamma sterilization on optical sensors materials"
Zajko Špela, Ingo Klimant. 08.06.2011, DocDays, Graz, Austria.

Poster Presentation

"Comprehensive study of the effects of gamma sterilization on sensor materials"
Zajko Špela, Ingo Klimant. 28 – 31.03.2010, Europtrode X, Prague, Czech Republic,